DEVELOPMENT AND APPLICATION OF GSTAR-1D

Jianchun Huang, vhuang@do.usbr.gov, Blair P. Greimann, bgreimann@do.usbr.gov, Travis Bauer, trbauer@do.usbr.gov, Hydraulic Engineers, Sedimentation and River Hydraulics Group, Technical Service Center, Bureau of Reclamation, Denver, CO 80225

Abstract: GSTAR-1D is a hydraulic and sediment transport numerical model developed to simulate flows in rivers and channels with or without movable boundaries. GSTAR-1D is able to compute water surface profiles in single channels, simple channel networks, and complex channel networks. It has both steady and unsteady flow models, many sediment transport equations, floodplain simulation, and cohesive and non-cohesive sediment transport. Lateral inflows can be simulated along with internal boundary conditions, such as time-stage tables, rating curves, weirs, bridges, and radial gates. GSTAR-1D is applied to a reach of the Rio Grande, from Cochiti Dam to Isleta Diversion Dam from 1972 to 1992 and from 1992 to 2002. The bed profile and sediment cumulative erosion are compared with the field data. After calibration, the model is used to predict future sedimentation in the Cochiti Reach. The application demonstrates the capability of the model in solving practical river engineering problems.

INTRODUCTION

GSTAR-1D is a hydraulic and sediment transport numerical model developed to simulate flows in rivers and channels with or without movable boundaries. It is able to compute water surface profiles in single channels, dendritic, and looped network channels. It has both steady and unsteady flow models, steady and unsteady sediment models. GSTAR-1D uses standard step method to solve the energy equation for steady gradually varied flows. GSTAR-1D uses a modified "NewC" scheme to solve the de St Venant equations for unsteady rapid varied flows. Two methods of sediment transport are used in GSTAR-1D. For a long term simulation, the unsteady terms of the sediment transport continuity equation are ignored, and the non-equilibrium sediment transport method of Han (1980) is used. For a short term simulations, the governing equation for sediment transport is the convection-diffusion equation with a source term arising from sediment erosion/deposition. This equation is solved with an implicit finite-volume method and with the Lax-Wendroff TVD scheme for the convective term and the central difference scheme for the diffusion term. Internal boundary conditions, such as time-stage tables, rating curves, weirs, bridges, and radial gates are simulated. The notation of an active layer, which allows selective erosion, provides an appropriate framework to simulate the bed armoring. Non-cohesive sediment transport equations and cohesive sediment physical processes are applied to calculate the sediment deposition and erosion. The most recent version can be downloaded at: *www.usbr.gov/pmts/sediment*.

GSTAR-1D is applied to the Cochiti Reach of the Middle Rio Grande, New Mexico to study channel geomorphic changes after the construction of the Cochiti Diversion Dam, and project future aggradations/degradation and streambed characteristics to assist river management. Successful management of the Middle Rio Grande relies a great deal on predicting changes in channel geometry, sediment transport, and river plan form while protecting and maintaining habitat for various operation and maintenance alternatives. The reduction of sediment supply to the Middle Rio Grande below Cochiti, Isleta, and San Acacia Dam has increased the recent trend of channel incision and narrowing. This incision and narrowing in the river causes the channel depth and velocity to increase. Thus, the river is providing fewer and fewer areas of good habitat for both the Rio Grande silvery minnow (RGSM) and southwestern willow flycatcher (SWFL). In many areas the river is coarsening from a sand bed to a gravel bed. The model is first calibrated with field measurements/data to two time periods: 1972 through 1992 and 1992 through 2002. Following calibration of the sediment transport model, an analysis of future sedimentation on the Middle Rio Grande is performed.

NUMERICAL MODEL

Hydraulic Model: GSTAR-1D provides both steady and unsteady flow components to handle gradually varied flows and rapidly varied flows, in a simple channel or a complex channel network. GSTAR-1D uses standard step method to solve the energy equation for steady gradually varied flows. GSTAR-1D uses a modified "NewC" scheme to solve the de St Venant equations for unsteady rapid varied flows. Interested readers can refer to the GSTAR-1D user's manual for more details (Yang et al., 2004)

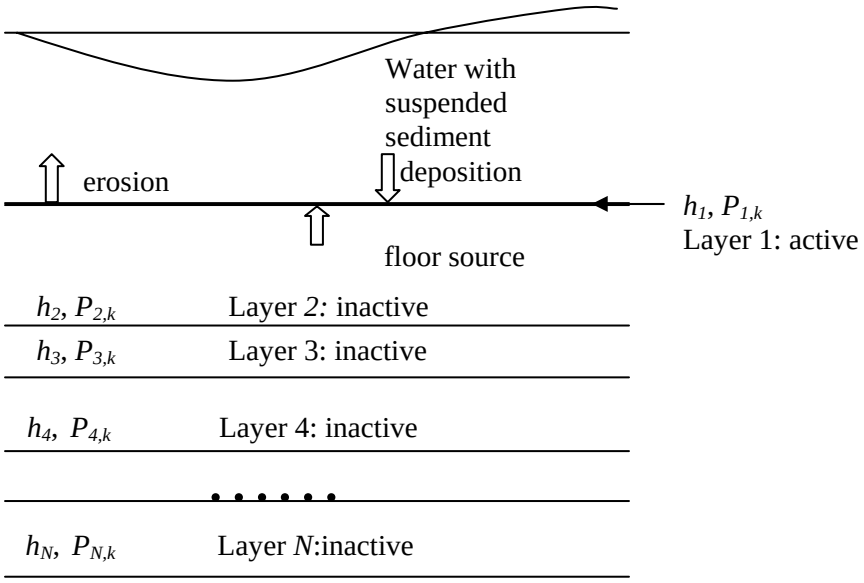


Figure 1 Conceptual model.

Sediment Transport Model: This section describes the conceptual model to simulate sediment transport in natural river systems. Figure 1 is a schematic of the conceptual model, in which the bed is composed of one active layer and N-1 inactive layers. In this figure, h_n = bed thickness of layer n, $P_{n,k}$ = volume fraction of k-th size class in layer n. The model is able to simulate both non-cohesive and cohesive sediment at the same time. A maximum of nf size fractions will be used to represent the sediment size distributions. The model includes cohesive sediment processes, such as settling, deposition, erosion, and consolidation. Consolidation of the sediment bed is modeled using multiple bed layers.

The bed profile is assumed to be composed of a number of layers of various thicknesses and bulk density. In each layer, bulk density of the cohesive sediment increases with time according to empirical consolidation rate, while the bulk density of the non-cohesive sediment remains constant. During consolidation, the bed thickness decreases but no mixing exists between layers.

The notation of an active layer provides an appropriate framework for erosion and deposition modeling. The active layer is defined as a thin upper layer bed of constant thickness, which is proportional to the geometric mean of the largest size class. The constant of proportionality is user defined. Each layer is assumed to have a uniform size distribution and bulk density throughout its depth. It is also assumed that all sediment particles of a given size class inside the active layer are equally exposed to the flow. Experimental results demonstrate that the presence of the fine cohesive sediment in the bed can increase the bed's resistance to erosion. The model used by GSTAR-1D assumes that the erosion rates of silts, sands and gravels are limited by the entrainment rate of the clay if the fraction of clay is above a user specified value.

The notation of an active layer allows size specific erosion on the streambed surface. If the bed shear stress is larger than the critical shear stress for the finer size classes, but smaller than that for coarser size classes, only the finer size classes are eroded. This process of selective erosion will eventually armor the bed surface and prevent further erosion.

The active layer contains the bed material available for transport. During net erosion, the first inactive layer supplies material to the active layer. During net deposition, the additional material is moved to the first inactive layer. A range is set for the thickness of the first inactive layer. The lower limit is set to allow enough sediment to be supplied to the active layer during erosion. The upper limit is set to provide enough resolution of the layers when simulating the bed layer. When it becomes very thin during net erosion, it merges with the second inactive layer. On the other hand, when it becomes very thick during net deposition, it is divided into two layers. All other layers are shifted accordingly.

Two kinds of sediment transport are introduced in GSTAR-1D. For a long term simulation, the unsteady term of the suspended sediment transport continuity equation are ignored. In this method, GSTAR-1D uses the non-equilibrium

sediment transport method of Han (1980). For a short term simulations, the governing equation for sediment transport is the convection-diffusion equation with a source term from sediment erosion/deposition. This equation is solved with an implicit finite-volume method. The Lax-Wendroff TVD scheme is used to discretize the convective term. A central difference scheme is used to discretize the diffusion term.

Both non-cohesive and cohesive sediment can be simulated in GSTAR-1D. GSTAR-1D employs 13 transport functions for non-cohesive sediment transport. Cohesive sediment transport is controlled by user-specified parameters that control the processes of aggregation, deposition, erosion, and consolidation.

GSTAR-1D calculates channel geometry adjustments in two ways: vertical change and width change. A vertical change adjusts the bed geometry under water uniformly. A width change adjusts the bed geometry under water surface linearly according to the local water depth. During a width adjustment, the maximum bed geometry adjustment occurs near the bank. In this way, the channel width is changed without thalweg elevation changing. Whether the adjustment will proceed in the depth or width direction at a given time step of computation depends on a user-specified minimization theory. However, in most cases simulated to date, the width adjustment option has not been used.

MODEL INPUT

The simulations use the original 1972, 1992, and 2002 measured cross section data, average bed material gradation data at cross sections where data were available, daily flow data at Cochiti Diversion Dam, and calibrated Manning's coefficient values for the main channel and the floodplains. After the closure of the Cochiti Diversion Dam, the reservoir trapped more than 99% of the sediment incoming. The model assumes that no sediment incoming from upstream boundary at the Cochiti Diversion Dam. The sediment yield from an ungaged tributary is estimated from the hydrology data and the related watershed. The sediment yield from a gaged tributary is estimated from the Modified Einstein Procedure (Colby and Hembree 1955), which employs the measured suspended sediment concentrations, the bed material particle size distribution, and the measured hydraulic parameters to arrive at a total sediment load. The study reach ends at the Isleta Diversion Dam, where water surface elevations are used as the downstream boundary condition. The model consists of 133 cross sections starting at the Cochiti Diversion Dam and ending at the Isleta Diversion Dam.

1992-2002 model calibration*:* The numerical model reproduces the general shape and magnitude of the cumulative erosion and deposition in the main channel (Figure 2). From Cochiti Diversion Dam to Angostura Diversion Dam, the field measurements show that the main channel were in state of dynamic equilibrium and experienced minimal erosion and deposition. The numerical model reproduces the same trend, but predicts that there was slight aggregation from Tonque Arroyo to Angostura Diversion Dam. From Angostura Diversion Dam to Arroyo de la Baranca, the field measurements show that the main channel experienced erosion. The numerical model reproduces the same trend. From Arroyo de la Baranca to Isleta Diversion Dam, the field measurements show that the main channel experienced no erosion or deposition. The model predicts that there was slight erosion from Arroyo de la Baranca to 10km downstream of Arroyo de las Calabacillas and no erosion and deposition downstream. It should be mentioned that the original model predicted erosion in this reach so the bed material was intentionally coarsened in this reach. In reality, the channel maintains relative equilibrium even though the surface bed material was fine in 1992.. This relative equilibrium was due to a variety of factors. Firstly, coarse sediments from the tributaries were deposited at their confluence with the Rio Grande. These coarse sediments might be moved to the thalweg due to transverse movement of sediment and provided material for the armored layer to prevent further erosion. These circumstances can not be simulated by a 1D model. Secondly, the bed material samples were usually collected in the falling stage of the flood and sand was deposited on the bed, thus, in many cases the coarse sediment controlling the form of the channel could be covered by a finer layer of sand.. The bed was coarsened to reflect the coarser gradation that was assumed to form the channel.

Figure 3 shows the changes in thalweg profile from 1992 to 2002. Overall, the numerical model reproduces the thalweg profile change well. The bed elevations were stable upstream of Angostura Diversion Dam and are simulated fairly accurately, however, the model overpredicts aggregation downstream of the Tonque Arroyo due to lateral sediment input from the arroyo. The model predicts the degradation correctly from Angostura Diversion Dam to Arroyo de los Montoyas. The reach from Arroyo de los Montoyas to Isleta Diversion Dam was relatively stable with a little degradation, which is predicted by the model.

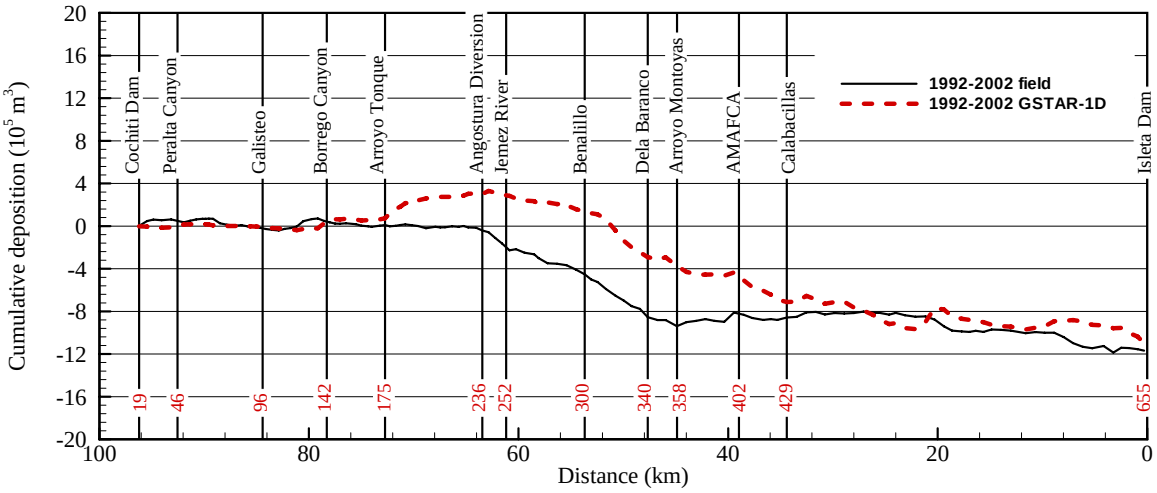


Figure 2 Cumulative total volume of sediment from 1992 to 2002.

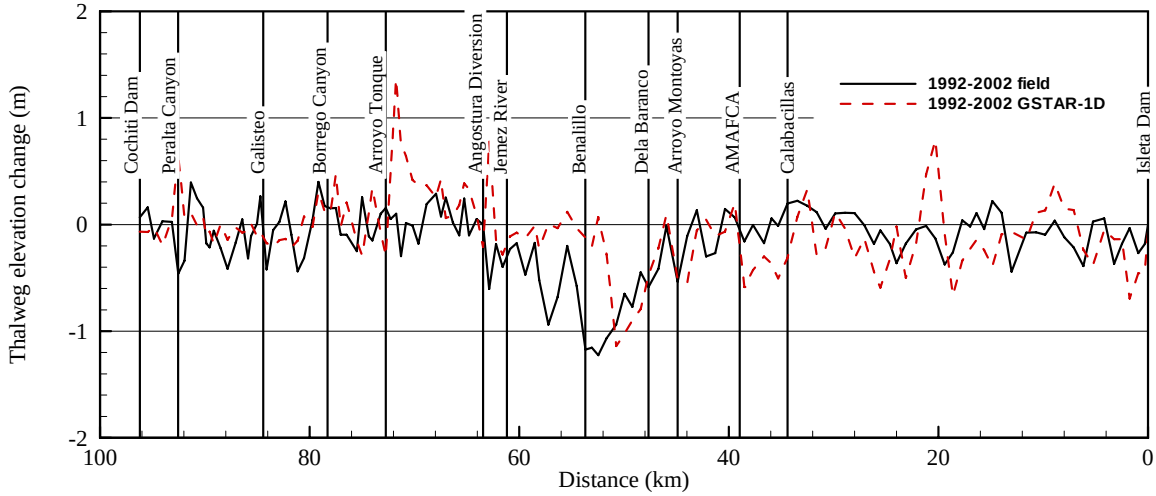


Figure 3 1992-2002 thalweg change.

The median bed material size, d_{50}, of three subreaches is shown in Figure 4. The three subreaches are from Cochiti Dam to Angostura Diversion Dam, from Angostura Diversion Dam to Arroyo de los Montoyas, and from Arroyo de los Montoyas to Isleta Dam, respectively. In all three subreaches, the model results show the bed material became coarser during high flows and finer during low flows. In the first subreach from the Cochiti Dam to Angostura Diversion Dam, the bed material was coarse. Numerical results show that this reach had already reached approximate equilibrium with the upstream sediment supply and the d_{50} was relatively stable and in the range of coarse gravel. In the second subreach from Angostura Diversion Dam to Arroyo de los Montoyas, the median sediment size, d_{50}, was in the range of very fine gravel and fine gravel. The bed material tended to coarsen during a series of floods between 1992 and 1995 and then became a little finer thereafter. In the 10-year period the bed material (d_{50}) coarsened from 2.85 mm in 1992 to 4.36 mm in 2002. In the subreach from Arroyo de los Montoyas to Isleta Diversion Dam, the bed material was fine. Numerical results show that bed material was fine and was relatively stable. The mean bed material (d_{50}) in this reach was in the range of very fine gravel and showed a slow coarsening trend.

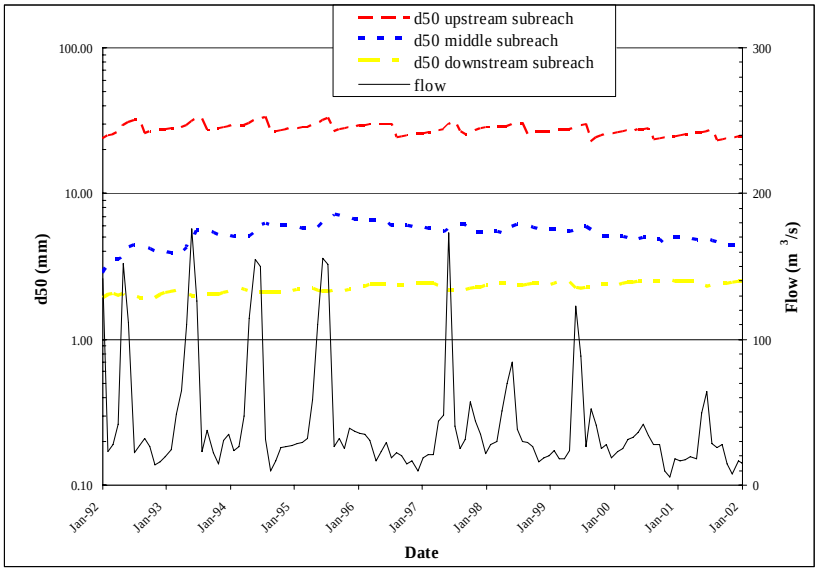


Figure 4 Change in bed material size (d_{50}) during model simulation from 1992 to 2002.

1972-1992 model calibration: The sediment transport from 1972 to 1992 was also simulated with only the river geometry and bed material fractions different and results are compared with the field data. Here only the change in bed material is presented in Figure 5. In the reach from Angostura Diversion Dam to Arroyo de los Montoyas, the bed was coarsening from a sand-bed to a gravel bed. The numerical model shows that the median sediment size, d_{50}, changed from 0.7mm (coarse sand) to 3.8mm (very fine gravel), which is close to the field data of 4.3 mm measured in 1992. The model captures the coarsening of the bed material in whole Cochiti Reach after the closure of the Cochiti Diversion Dam in 1973. The model also reproduced the transition from a sand bed to a gravel bed in the reach from Angostura Diversion Dam to Arroyo de los Montoyas.

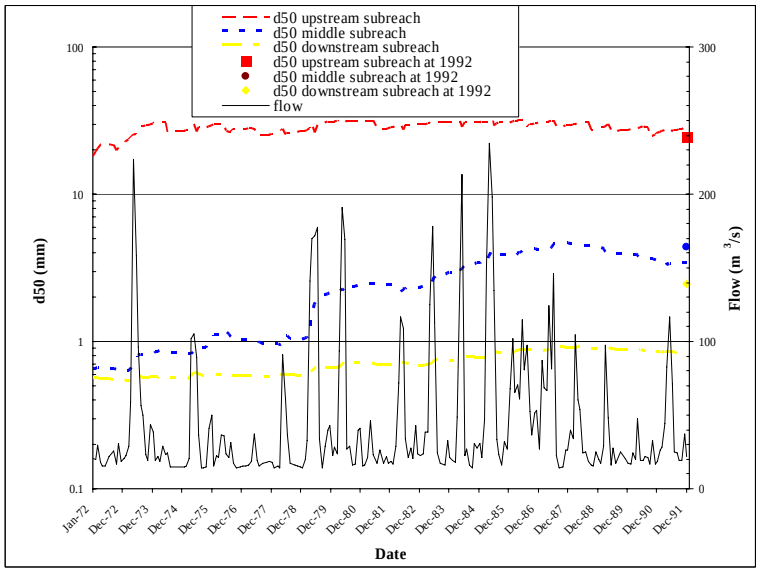


Figure 5 Change in median bed material size (d_{50}) during model simulation from 1972-1992.

2002-2022 PREDICTION

After the model was calibrated using the period from 1972 to 1992 and from 1992 to 2002, the calibrated parameters are used for the 2002 to 2022 predictive model. The model uses 2002 cross-section data and the sediment bed gradation calculated from the end time of the 1992-2002 simulation. The predictive hydrology is based on the historical record of the San Felipe gage, which has the longest data in the reach. Three hydrologic scenarios were simulated: a dry, average, and wet hydrology . The water surface elevation at Isleta Diversion Dam, which is the downstream boundary condition for the model, is calculated according to the predictive hydrology.

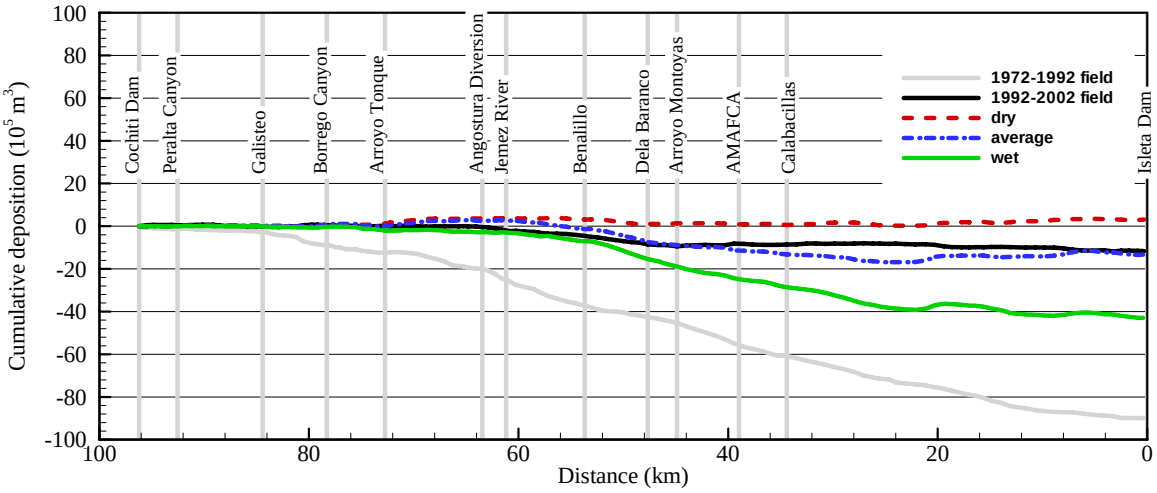


Figure 6 Cumulative main channel volume of sediment 2002-2022.

Figure 6 shows the cumulative erosion in the main channel for the three different hydrological scenarios. The results show the erosion for the entire reach is similar to that of the historic record from 1992 to 2022. However, the erosion zone has moved slightly downstream. From the Cochiti Diversion Dam to Bernalillo, the field measurements show that the main channel will be in an equilibrium state and experience only small amounts of erosion. The main channel volume calculations are dependent upon the hydrology. As the dry hydrology causes essentially slight deposition while the wet hydrology causes the most erosion.

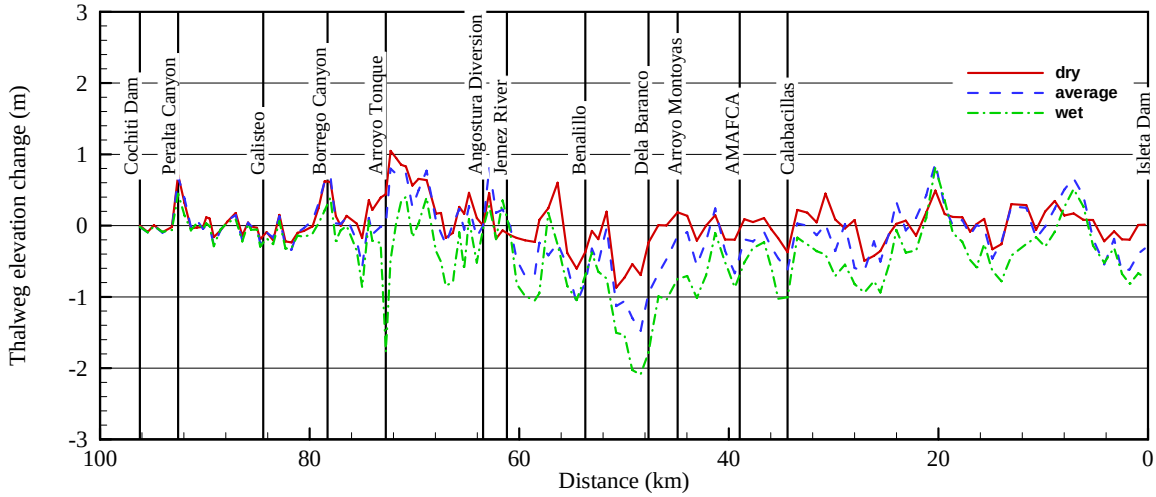


Figure 7 2002-2022 change in thalweg.

Figure 7 shows the total changes in thalweg elevation, from the start (2002) of the simulation to the end (2022) for each hydrology. Overall, the bed elevations will be stable upstream of the Angostura Diversion Dam with slight sediment deposition at the confluences of Borrego Canyon for all hydrologies and erosion upstream of the confluences of Tonque Arroyo during the wet hydrology. Degradation is predicted for an 18 km reach beginning at the confluence of the Jemez River.

Table 1 summarizes the reach-averaged median sediment size, d_{50}, at the beginning and end of the simulation. The bed material becomes coarser in all three subreaches and in all hydrologies. The bed material will encounter greatest coarsening during wet hydrology.

Table 1 Reach-averaged median sediment size d_{50} at the beginning and end of the simulation.

	d_{50} (mm) at year 2002	d_{50} (mm) at year 2022		
		Dry	Average	Wet
upstream subreach	22.55	25.66	26.44	33.56
middle subreach	4.18	4.58	8.24	9.64
downstream subreach	2.10	2.32	2.67	3.36

SUMMARY

The GSTAR-1D model is briefly presented in this paper. GSTAR-1D is a hydraulic and sediment transport numerical model developed to simulate flows in rivers and channels with or without movable boundaries. GSTAR-1D can be used to simulate flows in simple channels and in channel networks, to simulate steady and unsteady flow and sediment transport, and to simulate cohesive and non-cohesive sediment transport.

GSTAR-1D was used to simulate the channel and bed material changes of the Middle Rio Grande from the Cochiti Diversion Dam to Isleta Diversion Dam. The model was calibrated with the data from two time periods; 1972 through 1991 and 1992 through 2001. These two periods covered typical dry and wet hydrologic conditions. From the calibration results it was found that the modified GSTAR-1D model was capable of reproducing the river geometry changes and bed material coarsening caused by the reduced sediment supply. After the model was calibrated for these two time periods, the model was used to predict future sedimentation for various hydrologic regimes: dry, average, and wet.

REFERENCES

Colby, B.R., and Hembree, C.H., (1955). Computation of total sediment discharge, Niobrara River near Cody, Nebraska. U.S. Geological Survey, Water-Supply, p. 1357.

Han, Q. (1980). "A study on the non-equilibrium transportation of suspended load," Proc. of the Int. Symp. on River Sedimentation, Beijing, China, pp. 793–802. (In Chinese.)

Yang, C.T., Huang, J., and Greimann, B.P., (2004). User's Manual for GSTAR-1D 1.0 (Generalized Sediment Transport for Alluvial Rivers – One Dimension, Version 1.0). U.S. Bureau of Reclamation, Technical Service Center, Denver, Colorado.

APPLICATION OF GSTAR-1D SEDIMENT TRANSPORT MODEL ON THE MIDDLE RIO GRANDE, NM - SAN ACACIA DIVERSION DAM TO ELEPHANT BUTTE RESERVOIR

Christopher L. Holmquist-Johnson, Hydraulic Engineer, Sedimentation and River Hydraulics Group, Technical Service Center, Bureau of Reclamation, Denver, CO, cljohnson@do.usbr.gov

Abstract: Sediment transport was modeled for an 80 mile reach of the Rio Grande from San Acacia Diversion Dam to Elephant Butte Reservoir. Operation and maintenance options were evaluated to determine which option would most likely result in a stable river channel and minimize future maintenance requirements, thus improving the effectiveness of the river maintenance program. Future hydraulic geometry and morphology projections are valuable for assessment of river operations, maintenance, and restoration activities such as varying Low Flow Conveyance Channel diversions, adding sediment to degrading reaches, and bank stabilization or terrace lowering. The Generalized Sediment Transport for Alluvial Rivers - One Dimension (GSTAR-1D) computer program, developed by Reclamation, was used to develop the sediment transport model.

Data from two periods, 1972 through 1992 and 1992 through 2002, were available to calibrate the model using historical hydrology and cross-section geometry. These two periods were typical of dry and wet hydrologic conditions, respectively. The general shape and magnitude of the historical cumulative erosion and deposition curves in the main channel and the total cross-section for both calibrations were generally reproduced by the GSTAR-1D model.

The calibrated model was then used to predict future sedimentation for a 20-year period using 2002 data as the starting point with three predicted hydrologic scenarios: wet, average, and dry. Additionally, the predictive model was used to investigate sediment augmentation to assist in channel stabilization along the reach. The predictive model results reveal that additional channel incision may take place in the upper portion of the study reach if the future hydrology is relatively wet or has many high peak flows and that bed material coarsening may continue. The main channel appears to be relatively stable through the middle of the study reach with a general trend towards channel incision in the lower portion of the study reach. The most likely causes of the projected erosion in the main channel are attributed to the large unregulated peak flows present in the predictive hydrology combined with low reservoir levels, the existence of a perched channel system, and the uncertainty of sediment transport and mixing in a bi-modal system.

From these results it is apparent that additional research would help refine the sediment transfer between the main channel and floodplains in a perched system. Similarly, refinement of bed material mixing and armor layer development in a bi-modal system should also be investigated.

INTRODUCTION

The Generalized Sediment Transport for Alluvial Rivers - One Dimension (GSTAR-1D) computer program, developed by Reclamation, and customized specifically for the Middle Rio Grande (Yang et al, 2004), was used to develop a comprehensive calibrated sediment transport model of the Middle Rio Grande from San Acacia Diversion Dam to Elephant Butte Reservoir (Figure 1). The resulting comprehensive sediment model was used to predict future sediment transport trends and provides a valuable tool to analyze the impacts to channel geometry and sediment size from various future operation and maintenance alternatives

.

This paper focuses on sediment models for the Middle Rio Grande for two calibration periods from 1972 through 1992 and 1992 through 2002, and future analysis for a twenty year period assumed to run from 2002 through 2022.

The purpose of modeling time periods 1972 through 1992 and 1992 through 2002 was to calibrate parameters for the predictive model using historical hydrology and cross-section geometry. Following calibration of the study reach, an analysis of future sediment trends on the Middle Rio Grande was performed using a sediment transport model based on 2002 data. The projected aggradation/degradation and streambed characteristics provide information to aid management planning to achieve goals regarding effective water delivery to Elephant Butte Reservoir and

improving habitat for the Rio Grande silvery minnow (RGSM) and southwestern willow flycatcher (SWFL). Scenarios for the prediction of future sediment conditions used dry, wet, and average hydrologic regimes.



Figure 1 Site map of the Middle Rio Grande and the study area.

DATA ANALYSIS AND MODEL CALIBRATION

Data available for use in the model consisted of suspended sediment data, bed material samples, cross-section surveys, flow hydrology, reservoir elevations, lateral sediment inputs, and aerial photography.

USGS gages at San Acacia and San Marcial were used to generate inflow sediment rating curves, bed gradations, and flow hydrology. Data at Elephant Butte Reservoir were used to determine reservoir pool elevations for the downstream boundary condition. Aerial photography from 1972, 1992, and 2002 were used to generate cross-section geometry, calculate depositional/erosional changes, and identify bank locations, levee locations, ineffective flows,

and changes in channel and overbank roughness. Elephant Butte Reservoir surveys were used to provide additional cross-section data downstream of cross section 1792 (Agg/Deg#1792) to provide reservoir water surface elevations used as down stream boundary condition.

Historical (1962, 1972, 1992) and current (2002) cross-section data comparisons were used to determine aggradation/degradation trends along the study reach. Computing the volume change between cross-sections and then generating a cumulative sediment volume plot allowed comparison with the model results. This comparison provided a method for calibrating the sediment model to produce similar results to the measured data. Model calibration also included comparison of model results and field data parameters such as bed material, slope, and mean bed elevations. The model was calibrated for two time periods, 1972-1992 and 1992-2002. Calibration over these two time periods provided verification that the model could be used consistently for two different hydrologic time periods (dry and wet) and provided calibration parameters for the future predictive models.

CALIBRATION RESULTS

The overall results of the final calibration runs reproduce the general shape and magnitude of the cumulative erosion and deposition in both the main channel and the total channel including the floodplains (Figure 2). The results from both sediment models reasonably matched the total historical deposition within the reach (16,741 acre-feet historical vs. 12,036 acre-feet simulated for the 1972 to 1992 model and 4,274 acre-feet historical vs. 4,745 acre-feet simulated for the 1992 to 2002 model) and predicted the overall geometry changes along the reach fairly well. Though the base runs show the deposition for the entire reach is similar to that of the historical record, the reach by reach volumes of deposition differ slightly from the historical volumes of deposition (Figure 3).

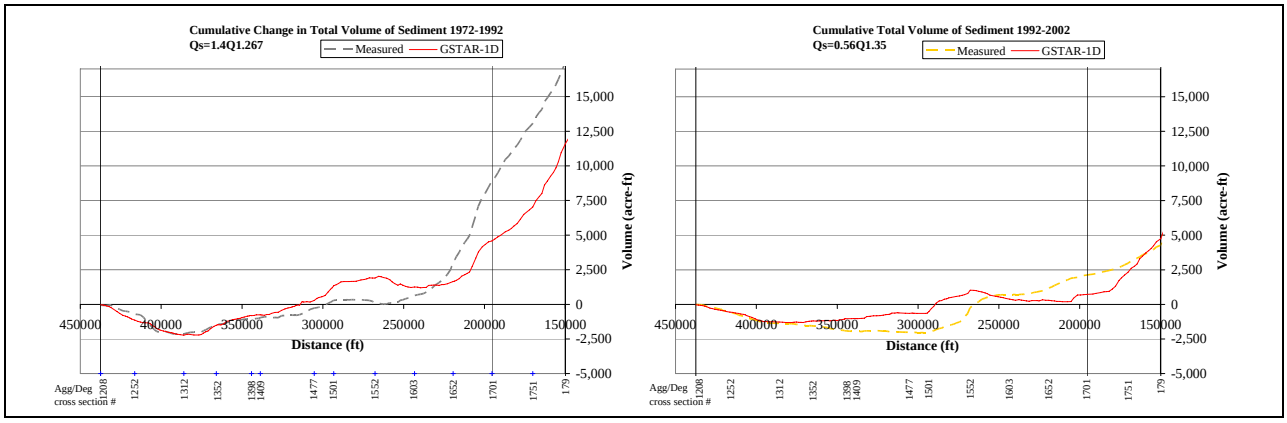


Figure 2 Comparison of cumulative change in total volume of sediment.

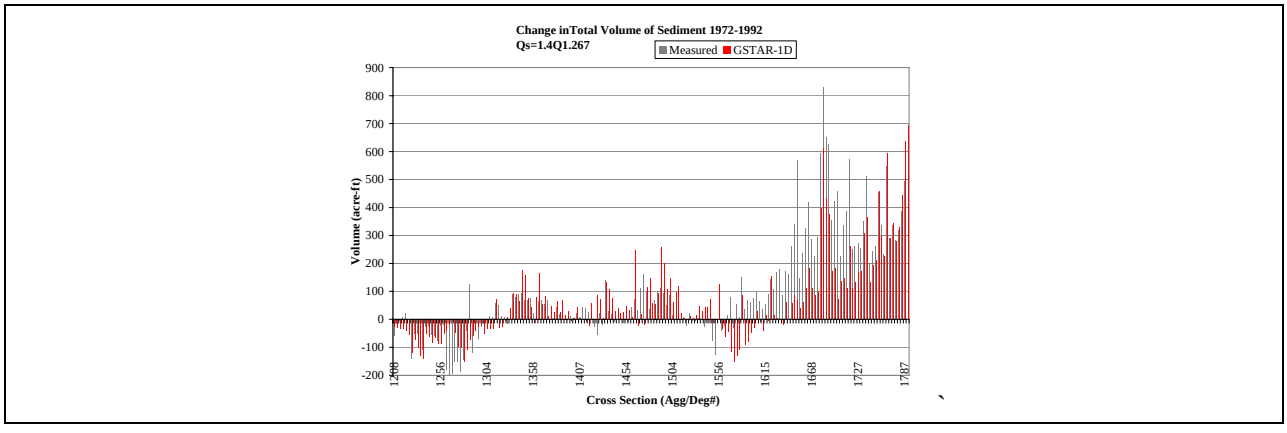


Figure 3 Comparison of change in total volume of sediment.

Figure 4 shows the change in mean bed from the start of each simulation to the end. Overall, the numerical model reproduces the mean bed profile change along the reach. The average difference in mean bed between 1992 measured and the 20 year simulation (1972 to 1992) is 0.26 ft. and has a standard deviation of 1.75 ft. The average difference in mean bed between the 2002 measured and the 10 year simulation (1992 to 2002) is 0.94 ft. and has a standard deviation of 2.05 ft. The degradation of the channel downstream from San Acacia Diversion Dam and the channel aggradation in the reach upstream from Elephant Butte Reservoir has resulted in an overall decrease in channel slope.

While the numerical model reproduces the deposition in the main channel induced by the downstream reservoir fairly well, it tends to over predict the floodplain deposition as a result of the slightly perched channel causing complex interactions between the main channel and the floodplains. In a perched channel system, the interaction between the floodplain and main channel cannot be modeled properly with a 1-dimensional model because a 1-D model assumes a constant water surface for the entire cross-section resulting in a sediment transport capacity that is too low. Additionally, the 1-D model is not able to replicate the tendency to decant overbank flows.

Overall, there is a trend for coarsening, but the model results do not show as much coarsening as the measured data. There are two likely reasons for not capturing the coarsening of the bed: 1) the initial bed material and incoming load does not contain enough coarse sediment, and/or 2) the bed mixing processes may not be represented correctly in the model. Erosion during high flows may leave armoring layers of coarse sediment. As low flows follow a period of high flows, the model will mix the fines with the coarser material. However, in reality the fines may pass over the top of the coarser material and not mix.

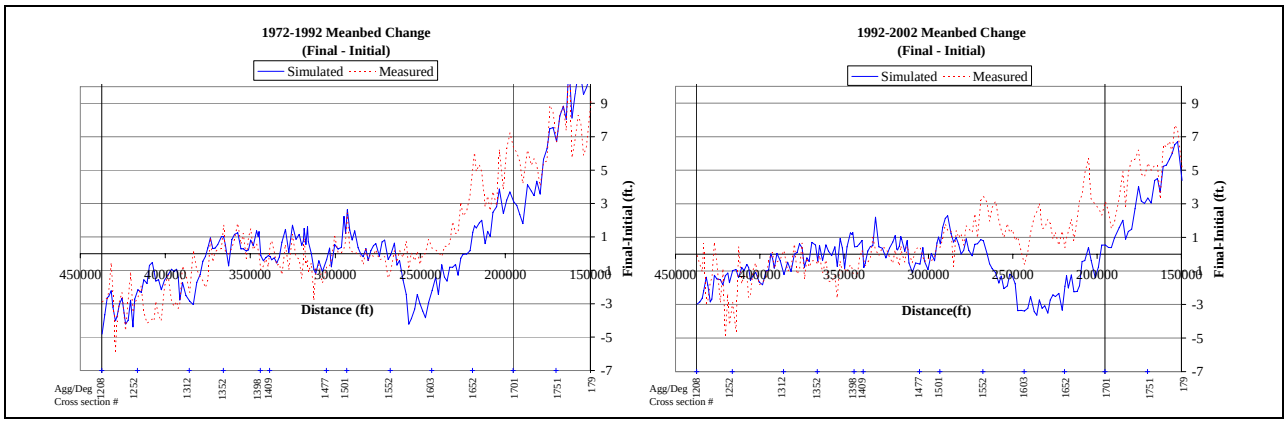


Figure 4 Mean bed change comparison.

PREDICTIVE MODEL RESULTS

No Action Option: The predicted erosion and deposition for the 20-year period are, in general, greater than historical trends (Figure 5). The numerical model shows the main channel to be relatively stable downstream from Agg/Deg#1327 with a general trend towards channel erosion at the furthest downstream cross sections (Figure 6).

The major difference between the different hydrologic scenarios is in the overbanks and the main channel just downstream of San Acacia Diversion Dam at the upper portion of the modeled reach (Figure 7). Floodplain aggradation increases with higher flows as a result of additional channel-floodplain interaction. The lower portion of the study reach exhibits excessive amounts of aggradation in the floodplain for the wet hydrology due to the complex interaction between the floodplain and main channel in a perched channel system (Figure 5).

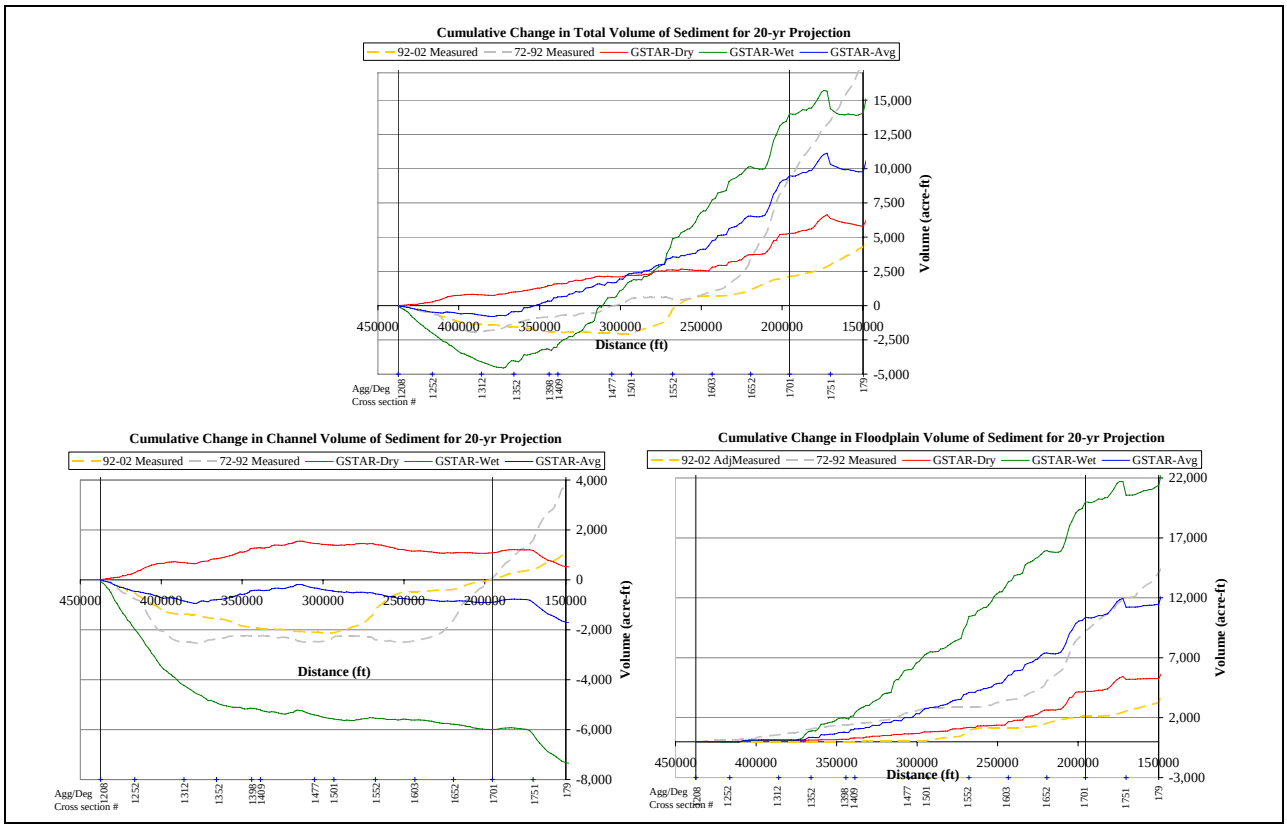


Figure 5 20-Comparison of 20-yr projection of cumulative change in volume of sediment.

Sediment Augmentation Option: It is difficult to predict the effect of sediment augmentation because the sediment loads at the San Acacia floodway gage have not been measured above 4,000 ft^3/s. If the current loads are unknown it is difficult to predict the effect of incremental change. Since the predictive hydrology contains flows up to 21,000 ft^3/s and a large number of flows greater than 5,000 ft^3/s, it is necessary to determine the incoming load for the discharges ranging from 4,000 – 21,000 ft^3/s. Augmentation of fine sediment (fine sand, silt and clay) will increase the aggradation in the floodplains in the lower reaches and augmentation of coarse sand and gravel may prevent some erosion in the upper reaches. Therefore, further work could compute the volume of gravel necessary to maintain the current bed elevations downstream of San Acacia Diversion Dam.

CONCLUSION

The project developed a comprehensive sediment transport model of the Middle Rio Grande from San Acacia Diversion Dam to Elephant Butte Reservoir. The model was calibrated with the data from two time periods: 1972 through 1992 and 1992 through 2002. From the calibration results it was found that the modified GSTAR-1D model was capable of reproducing the general river geometry changes caused by sediment transport. After the model was calibrated for these two time periods, the model was used to predict future sedimentation for three hydrologic regimes: wet, average, and dry. The following can be concluded:

Summary of Calibration Model Results:

- The numerical model reproduced the general shape and magnitude of the cumulative erosion and deposition in the main channel and the total cross-section for both calibration time periods; 1972 through 1992 and 1992 through 2002.

- For both calibration time periods, the numerical model reproduced the degradation in the mean bed profile downstream of San Acacia Diversion Dam as well as the aggradation in the mean bed profile near the reservoir.

- For both calibration time periods, the numerical model reproduced the cross-section geometry changes such as channel width, water surface width, thalweg elevation, and mean bed elevation fairly well. However, due to the limitations of a one-dimensional model, the model cannot predict the uneven deposition in the floodplains, main channel, or the channel meandering and migration.

Summary of 20-year Predictive No Action Model Results:

- The 20-year predictive model results are impacted by the greater magnitude and duration of peak flows in the predictive hydrology and the perched system causing increased floodplain deposition.

- The 20-year predictive model produces deposition in the main channel with the dry hydrology, and main channel erosion with the average and wet hydrology just downstream of San Acacia Diversion Dam.

- Upstream of Agg/Deg#1352, additional channel erosion may take place if the future hydrology is relatively wet or many peak flows are encountered. If large flows are encountered, the coarsening of bed material may continue. Further work could define more precisely the magnitude of flows required to extend the erosion and coarsening of bed material in the upstream reach.

- The 20-year predictive model produces floodplain deposition for all three hydrologic scenarios (dry, average, and wet) due to the unregulated peak flows in the predictive hydrology and the complex interaction of overbank flows in a perched channel system.

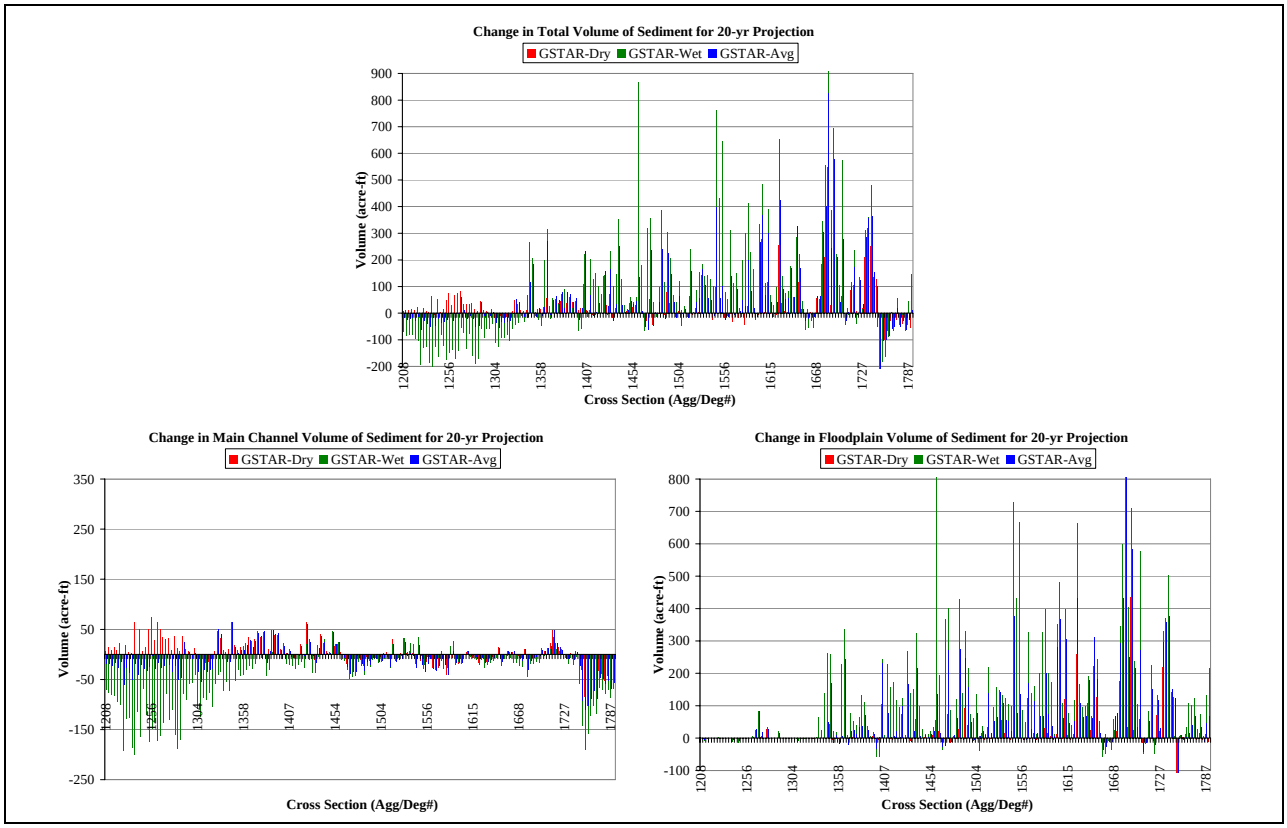


Figure 6 Comparison of change in volume of sediment for 20-year projection.

Figure 7 shows the total change in mean bed from the start (2002) of the simulation to the end of the 20-year modeling period for each hydrology.

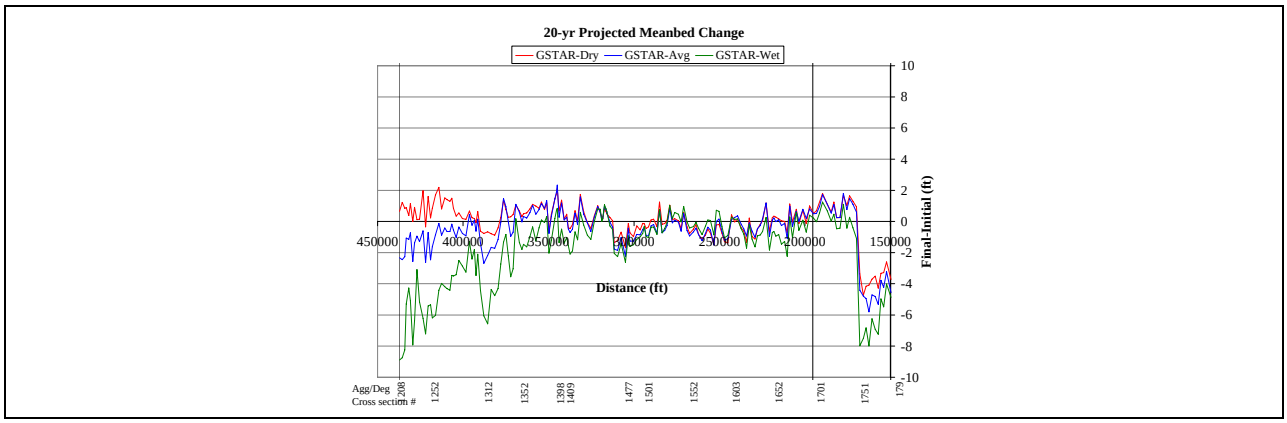


Figure 7 20-year projected change in mean bed.

Summary of 20-year Predictive Sediment Augmentation Model Results:

- Increasing the sand load at San Acacia Diversion Dam has the potential to stop or reverse the erosion occurring in the upper reach. For dry hydrological conditions, no additional sediment may be necessary. For average to wet hydrology, however, the increase in sand load would have to be up to several thousand acre-ft. However, additional modeling of the upper reach is required to predict the volume of sediment currently entering the reach. If fine sediment is added to the system, additional floodplain deposition may occur in the downstream reach, and/or additional deposition will occur in Elephant Butte Reservoir.

Recommendations for future analysis:

- The overall bed changes in the predictive models differ from the historical trends due to the magnitude and duration of the unregulated discharges present in the predictive hydrology. Therefore, additional analysis of the predictive hydrology should be conducted to determine if flow regulation should be included in generating future flows.
- Collection of additional sediment data (suspended and bed material) to further define the incoming sediment rating curve, especially at higher discharges, and further define the bed material gradation variation along the reach.
- Additional calibration work to more closely simulate the change in channel slope and the coarsening of the river bed.
- Additional capabilities that could be introduced into the model would include: refining the sediment diffusion between the main channel and floodplains to better predict the main channel floodplain interaction in a perched system, and refinement of bed material mixing and armor layer development for Rio Grande conditions.

REFERENCES

Holmquist-Johnson, C. L. (2004). Sediment Model for the Middle Rio Grande – Phase 1 San Acacia Diversion Dam to Elephant Butte Reservoir. Draft. U.S. Department of the Interior, Bureau of Reclamation (Reclamation), Sedimentation and River Hydraulics Group, Denver, CO.

Yang, C.T., Huang, J., Greimann, B.P. (2004). User's Manual for GSTAR-1D 1.0 (Generalized Sediment Transport for Alluvial Rivers – One Dimension version 1.0). U.S. Department of the Interior, Bureau of Reclamation (Reclamation), Sedimentation and River Hydraulics Group, Denver, CO.

BUREAU OF RECLAMATION AUTOMATED MODIFIED EINSTEIN PROCEDURE (BORAMEP) PROGRAM FOR COMPUTING TOTAL SEDIMENT LOAD

David Raff PhD, PE, Hydraulic Engineer, Flood Hydrology Group, Technical Service Center, Bureau of Reclamation, Denver, CO, draff@do.usbr.gov; Christopher L. Holmquist-Johnson, Hydraulic Engineer, Sedimentation and River Hydraulics Group, Technical Service Center, Bureau of Reclamation, Denver, CO, cljohnson@do.usbr.gov

INTRODUCTION

Developing a reliable and consistent method of computing total sediment discharge within a river is one of the most important practical objectives of research in fluvial processes (Burkham and Dawdy, 1980). Current techniques for suspended sediment collection do not allow sampling throughout the entire depth of flow and therefore the concentration and particle size distribution in only part of the flow can be determined from the suspended-sediment samples. The unsampled flow near the stream bed normally contains higher concentrations and coarser particle-size distributions than the flow in the sampled zone. Thus, the concentration of suspended-sediment samples is usually lower than the suspended-sediment concentration for the entire depth, and the particle sizes of the samples are usually smaller that the particle sizes for the entire depth.

In 1950, Einstein presented a procedure for computing the total discharge of sediment of sizes found in appreciable quantities in the stream bed for a long reach of a stream channel. However, acquiring the data required by Einstein's procedure was very labor intensive and time consuming. In 1955, Colby and Hembree presented a modified version of Einstein's procedure (MEP) that used data from a single cross section to calculate the total sediment discharge for a particular reach. The MEP is considered an improvement over the original Einstein method because it is simpler in computation and it uses parameters more readily available from actual stream measurements. The modified method, however, requires a great deal of experience and judgment to obtain reliable results and often times the results are not easily replicated by multiple users. Computations are made for several ranges of particle sizes and involve many variables resulting in a very complex process of computing total sediment load. As a result, a more simplified and automated method of computing total sediment discharge for a given reach that can be reproduced by numerous users is of great interest.

The primary objective of this manuscript is to present a reliable and readily automated algorithm for computing total sediment load using Reclamations version of the MEP procedure as described in Reclamations 1955 and 1966 publications. The algorithm has been developed and deployed through a computer program that is applicable to a wide range of flow and sediment conditions and provides information to identify areas where additional research might be needed. This paper describes the Bureau of Reclamation Automated Modified Einstein Procedure (BORAMEP) program and procedures (Holmquist-Johnson and Raff, 2005) that were used to automate the process of calculating total sediment load using the MEP procedure.

METHODS

Modified Einstein Equations and Procedure: The following presents the basic steps required during the calculation of total load using the Modified Einstein Procedure with additional information provided in areas where calculations have been automated.

1) Compute the measured suspended load.

$$Q_s = 0.0027\, Q\, Conc \;\; (tons/day) \tag{1}$$

2) Compute the product of the hydraulic radius and friction slope assuming x = 1.

2a) First, compute the value of $\sqrt{(RS_f}$ using Colby and Hembree 's (1955) equation E.

$$\sqrt{(RS_f} = \frac{V_{avg}}{32.63 \log\left[12.27 \frac{h}{k_s} x\right]} \tag{2}$$

2b) Compute the shear velocity.

$$U_* = \sqrt{g(RS_f)} \tag{3}$$

2c) Compute the laminar sublayer thickness δ.

$$\delta = \frac{11.6v}{U_*} \tag{4}$$

2d) Recheck x to make sure that the initial guess of x = 1 is valid.

Step 2 becomes an iterative process utilizing a newly fit equation to Colby and Hembree 's (1955) Plate 3 describing the relationship between x and $\frac{k_s}{\delta}$. The equation presented in

Figure *1* is considered valid for $0.2 \le \frac{k_s}{\delta} \le 40$.

3) Compute the value of P.

$$P = 2.303 \log\left[30.2 \frac{hx}{k_s}\right] \tag{5}$$

4) Compute the fraction of the flow depth not sampled (A').

$$A' = \frac{d_n}{d_s} \tag{6}$$

5) Compute the sediment discharge Q'$_s$ through the sampled zone. This is calculated using a percentage of the flow sampled determined from the appropriate equation for the value of A' and P. Equations 8 – 11 were calculated by fitting equations to Colby and Hembree 's (1955) Plate 4 and are used to automate the calculations of % *flow sampled*.

$$Q'_{stotal} = Q_s * \%\ \ flow\ sampled \tag{7}$$

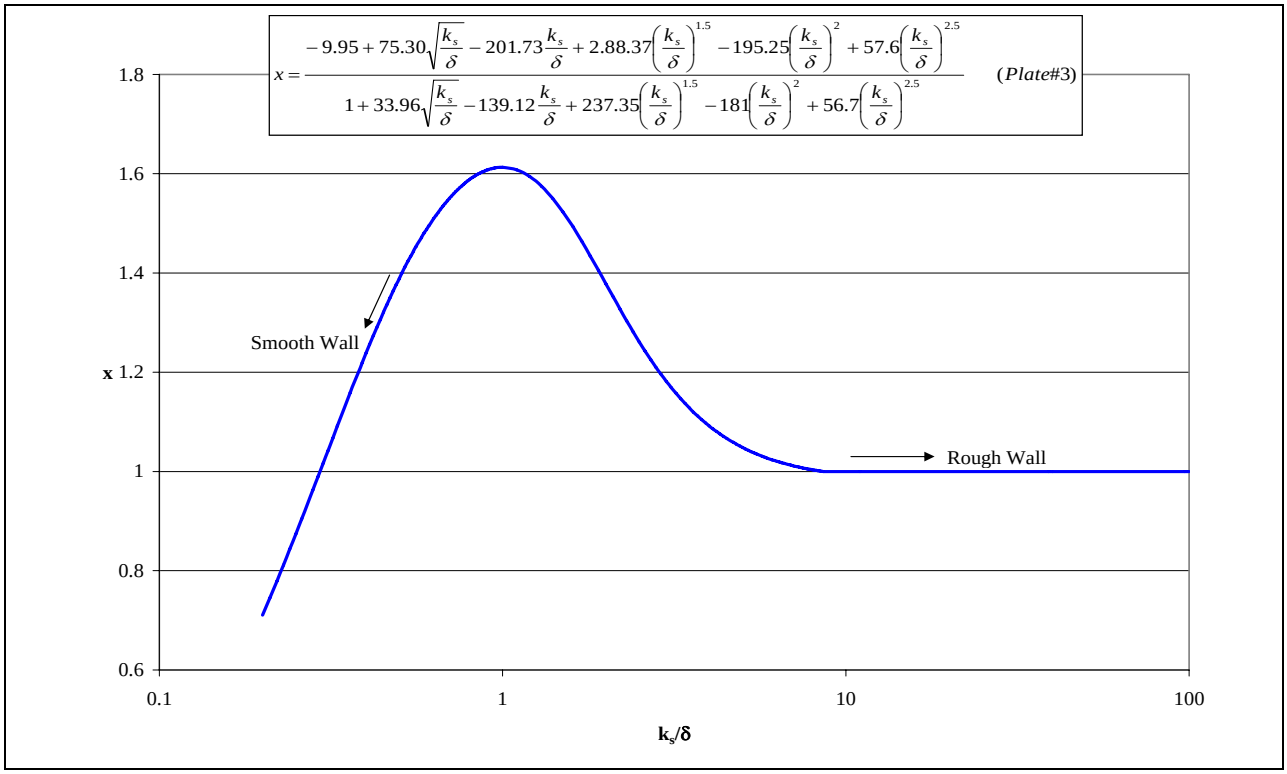


Figure 1 Correction x in the logarithmic friction formula in terms of k_s/δ.

For P=4, % flow sampled=

$$\frac{100 - 2941.79A'^{2} + 265357.48A'^{4} + 64219.08A'^{6} - 325482.24A'^{8}}{1 - 29.38A'^{2} + 2621.48A'^{4} + 5407.23A'^{6} + 157.44A'^{8} + 1272.32A'^{10}} \tag{8}$$

For P=8, % flow sampled=

$$\frac{100 + 30991.16A'^{2} + 21184.18A'^{4} + 211800.14A'^{6} - 263775.36A'^{8}}{1 + 325.87A'^{2} + 1201.21A'^{4} + 1872.11A'^{6} + 5759.38A'^{8} - 2976.45A'^{10}} \tag{9}$$

For P=11, % flow sampled=

$$\frac{100.19 + 31425.83A'^{2} - 54359.86A'^{4} + 1566703.2A'^{6} - 1543898.1A'^{8}}{1 + 336.12A'^{2} + 444.29A'^{4} + 15662.05A'^{6} + 18936.5A'^{8} - 5820.32A'^{10}} \quad (10)$$

For P=14, % flow sampled=

$$\frac{100.31 + 45744.98A'^{2} + 103307.39A'^{4} + 635604.51A'^{6} - 784215.44A'^{8}}{1 + 485A'^{2} + 2934.57A'^{4} + 7640.27A'^{6} + 11737.99A'^{8} - 3015.81A'^{10}} \quad (11)$$

6) Compute the bed-load for each size fraction.

6a) The first step in computing the bedload is to calculate the shear intensity (ψ) for all particle sizes in the analysis by using the minimum of the following two equations, where d_i is the geometric mean for each size class:

$$\psi = 1.65\left(\frac{d_{35}}{RS_f}\right) \quad or \quad 0.66\left(\frac{d_i}{RS_f}\right) \quad (12)$$

6b) Colby and Hembree 's (1955) Plate#2 was used to determine the intensity of bed-load transport for each calculated shear intensity. In order to automate the calculations of the intensity of the bed-load transport (φ), the following equation was used (Yang, 1996):

$$\phi_* = \frac{0.023p}{(1-p)} \quad (13)$$

Where p is the probability a sediment particle is entrained in the flow and is calculated using the following version of the Error Function (Yang,1996):

$$p = 1 - \frac{1}{\sqrt{\pi}}\int_a^b e^{-t^2}dt \quad (14)$$

Note: The Error Function is numerically computed within BORAMEP as the following integral.

$$ERF = \frac{2}{\sqrt{\pi}}\int_a^b e^{-t^2}dt \quad (15)$$

Where:

$$a = -\frac{B_*}{\psi} - \frac{1}{\eta_0}; \text{ and}$$

$$b = \frac{B_*}{\psi} - \frac{1}{\eta_0}.$$

and B_* is equal to a value of 0.143 and η_0 is equal to a value of 0.5.

Therefore, to compute the probability "p", equations 14 and 15 are combined to give:

$$p = 1 - \frac{1}{2} ERF \tag{16}$$

6c) Compute the unit bed-load for each size fraction.

$$i_B q_B = 1200 d_i^{3/2} i_B \frac{\phi_*}{2} \tag{17}$$

6d) Compute the bed-load for each size fraction in Tons/Day.

$$i_B Q_B = i_B q_B (43.2W) \tag{18}$$

7) Compute Suspended Load ($Q_s^{'}$) for each size fraction by multiplying the total sampled suspended load ($Q_{s\,total}^{'}$) by the suspended load fractions for the sample.

$$Q_s^{'} = i_s \, Q^{'}{}_{s\,total} \tag{19}$$

8) Compute the theoretical exponent for vertical distribution of sediment (Z). The original Reclamation MEP method from 1955 used Colby and Hembree's (1955) Plate 8 to determine Z (termed Z' in the initial calculations) by computing the ratio of the suspended load ($Q_s^{'}$) to the bed-load ($i_B Q_B$) for each size class. However, Plate 8 was based solely on data from the Niobrara River near Cody, Nebraska. A subsequent study completed by Reclamation in 1966 determined that using the regression line in Plate 8 produced errors on the order of 20% for the total load. Therefore, the following process determines the Z-values by trial and error. Reasonable assumptions should be bound between approximately 0.01 and 1.8 as this was the range of Z' from the original Plate 8.

8a) Compute the ratio $\frac{Q_s^{'}}{i_B Q_B}$ for all size classes with suspended load transport.

8b) Size classes that have calculated values for the ratio of the suspended load to the bed-load are used as the reference ranges for Z-value computations. However, if any of the ratios is for a size range less than a sand/silt split of 0.0625mm it is not used since the sediment in

this size range is considered wash load and usually not found in large quantities in the bed. The ratio of suspended load to bed-load is set equal to a function with the parameters $I_1^{"}, J_1^{"}, J_1^{"}, J_2^{'}$ (Reclamation,1955).

Due to the lack of computer resources available in 1955 to explicitly solve the integral form of the equations for $I_1^{"}, J_1^{"}, J_1^{"}, J_2^{'}$, these values were read from Plates 9-11 (Colby and Hembree 1955). However, current computer technology allows for an explicit solution to these integrals, which results in a more precise answer to the parameters compared to reading the values off the plates.

For each size class an initial Z-value must be assumed and then the equations given below are used to determine the parameters contained in plates 9-11. To provide some guidance in the initial guess of the Z-value, the equation from Colby and Hembree 's (1955) Plate 8 is used.

$$Z_{guess} = -0.1465 \ln\left(\frac{Q_s^{'}}{i_B Q_B}\right) + 1.0844 \tag{20}$$

Using the initial guess for the Z-values and the equations given below for $I_1^{"}, J_1^{"}, J_1^{"}, J_2^{'}$, a trial and error process is carried out for each size class using a solver routine to determine the value of Z by minimizing the difference between the ratio $\frac{Q_s^{'}}{i_B\ Q_B}$ and $\frac{I_1^{"}}{J_1^{"}}\left(PJ_1^{'} + J_2^{'}\right)$.

$$I_1^{"} = 0.216 \frac{A^{"(z-1)}}{(1-A^{"})^z} J_1^{"} \tag{21}$$

$$J_1^{'} = \int_{A'}^{1} \left(\frac{1-y}{y}\right)^z dy \tag{22}$$

$$J_1^{"} = \int_{A"}^{1} \left(\frac{1-y}{y}\right)^z \log_e(y) dy \tag{23}$$

$$-J_2^{'} = \int_{A'}^{1} \left(\frac{1-y}{y}\right)^z \log_e(y) dy \tag{24}$$

$$-J_2^{"} = \int_{A"}^{1} \left(\frac{1-y}{y}\right)^z \log_e(y) dy \tag{25}$$

8c) Once the Z-values have been determined for the suspended load, a log-log plot is made of the relationship between Z and the fall velocity for each size class. A power function equation is then developed such that $Z = a\,\omega^{b}$. The remaining Z-values for the bed-load are computed using this relationship. The fall velocity is computed using Rubey's Equation.

$$\omega = F\left[d_i\, g\left(\frac{\gamma_s - \gamma}{\gamma}\right)\right]^{1/2} \tag{26}$$

Where F is a mathematical abbreviation for

$$F = \left[\frac{2}{3} + \frac{36\nu^2}{g\,d^3\left(\frac{\gamma_s}{\gamma} - 1\right)}\right]^{1/2} - \left[\frac{36\nu^2}{g\,d^3\left(\frac{\gamma_s}{\gamma} - 1\right)}\right]^{1/2} . \tag{27}$$

9) Compute the total sediment load.

$$Qs_{total} = Qs_{total\ suspended} + Qs_{total\ bed} \tag{28}$$

Where:

$$Qs_{total\ suspended} = Q_s^{'}\frac{\left(P\,J_1^{"} + J_2^{"}\right)}{\left(P\,J_1^{'} + J_2^{'}\right)} \text{ ; and}$$

$$Qs_{total\ bed} = i_B Q_B\left(P\,I_1^{"} + I_2^{"} + 1\right) .$$

BORAMEP Program: To automate the process of calculating the total load using the modified Einstein procedure presented above, a visual basic program was written to calculate the total load for multiple samples at one time. The following sections describe the input to the program and the output that is generated by the program.

. **Program Input:** The BORAMEP program can be used either for a single sample entered by the user or an input file containing multiple samples. A sample of the input data that is required for the program is presented in
Figure 2. Additionally, a value for the minimum percent of sediment contained in a size class that should be used in calculating the z-values must also be specified.

The input file option allows the user to generate a comma separated file that contains the input data for multiple samples and run the program for all the samples at one time. To use the input file option, an input file must be generated prior to running the BORAMEP program and follow a specified format (Holmquist-Johnson and Raff, 2005).

Constants/Properties:			Sediment:		
g =	32.17	ft/s^2	C_s =	2560	PPM
ν =	1.35E-05	ft^2/s	d_{65} =	0.235	mm
γ_w =	62.4	lb/ft^3	d_{35} =	0.199	mm
γ_s =	165	lb/ft^3	d_s =	1.6	ft
d_n =	0.3	ft	Particle Size (mm)	Susp %	Bed %
Hydraulics:					
Q =	777	ft^3/s	0.001 - 0.0625	65.00	0.00
V_{avg} =	3.6	ft/s	0.0625 - 0.125	12.00	5.00
h =	1.6	ft	0.125 - 0.25	18.00	76.00
W =	130	ft	0.25 - 0.5	5.00	18.00
A =	208	ft^2	0.5 - 1	0.00	1.00
T =	51.8	^oF	1 - 2	0.00	0.00

Figure 2 Input data for BORAMEP program.

Program Output: The BORAMEP program generates three output files: .txt, .txt.sum, and .txt.err. The first file called *filename*.txt contains output in a format that is similar to output from a previous single sample program, PSANDS (Reclamation, 1969), used by Reclamation. This output allows previous users of the Psands program to view the output in a format that they are familiar with as well as new users to view the input data for a sample and the results generated from the MEP calculations.

The second file called *filename*.txt.sum (

Figure *3*) contains a comma separated summary of the output data that was generated by the program. This file can easily be imported into a spreadsheet program such as Microsoft Excel and used to view the results of the MEP calculations. The summary file provides data for conducting additional water-sediment discharge analysis such as discharge vs. total load, discharge vs. total load within a specified grain size, suspended vs. total load, etc.

***		Discharge	Conc	Suspended	d65	d35	Temp	Computed total load by size fraction (tons/day)						Total Load
Location	Date	(cfs)	(PPM)	Sample (tons/day)	(mm)	(mm)	F	0.001 - 0.0625	0.0625 - 0.125	0.125 - 0.25	0.25 - 0.5	0.5 - 1		(tons/day)
Trial1	5/24/1968	445	7660	9203.49	0.22	0.17	64.4	6408.83	312.12	181.82	7.06	0.00		6909.83
Trial2	10/1/1968	38	200	20.52	0.23	0.18	66.2	4.32	1.98	4.93	0.92	0.02		12.16
Trial3	10/16/1968	71	250	47.93	0.23	0.19	59	41.99	5.92	7.66	0.41	0.01		55.98
Trial4	4/14/1969	632	8500	14504.40	0.19	0.13	64.4	8977.30	1229.82	944.07	18.15	0.00		11169.34
Trial6	5/19/1969	817	6500	14338.35	0.18	0.12	69.8	7623.59	3023.25	1070.93	43.56	0.00		11761.32

Figure 3 Example filename.sum.txt output.

The third file called filename.txt.err contains a comma separated summary of any errors that were generated by the program as well as output for samples that did not meet the MEP criteria but might be able to be used with additional analysis (

Figure *4*). The most common error encountered in the MEP calculation is “Not enough overlapping bins for MEP”. This error occurs when the overlap between the suspended and bed material samples for a given grain size do not meet the minimum percent of sediment contained

in a size class entered by the user to be used in calculating the z-values. This occurs frequently in fine-grained systems when the overlap between suspended and bed sediment for a given grain size is very small or non-existent.

***		Discharge	Conc	Suspended	d65	d35	Temp	Computed total load by size fraction (tons/day)						Total Load
Location	Date	(cfs)	(PPM)	Sample (tons/day)	(mm)	(mm)	F	0.001 - 0.0625	0.0625 - 0.125	0.125 - 0.25	0.25 - 0.5	0.5 - 1		(tons/day)
Trial5	5/5/1969	-9999	THERE WAS AN ERROR DURING FILE INPUT											
Trial7	5/14/1968	-9999	NOT ENOUGH OVERLAPPING BINS FOR MEP											

Figure 4 Example filename.error.txt.err output.

The output files generated from the BORAMEP program facilitates engineering judgment by calculating results for all possible samples while calling attention to those that may be questionable. Additionally, BORAMEP provides standardizes results and reduces calculation time from 4 samples per hour to ~2000 samples per hour.

CONCLUSIONS

This manuscript has presented revisions to the Modified Einstein Procedure for calculation of total load. The revisions have focused on making the procedure automated, accurate, and reproducible. Key features include the fitting of equations to Plates from the original Einstein documents as well as placing criteria on overlapping bins during the calculation of *Z* values. The new procedure has been developed into a software packaged named BORAMEP. To further ease the implementation of BORAMEP, Reclamation is working with the USGS to make downloads of key variables in the input format of BORAMEP readily accessible. This cost-effective automated method of computing total sediment load, which can be reproduced by numerous users, provides a tool that could be used by other government agencies and the private sector and could decrease technical disagreements.

REFERENCES

Burckham, D.E., and Dawdy, D.R. (1980). General study of the modified Einstein method of computing total sediment discharge, USGS Water Supply Paper 2066.

Colby, B.R., and Hembree, C.H. (1955). Computations of total sediment discharge Niobrara River near Cody, Nebraska. USGS Water Supply Paper 1357.

Einstein, H.A. (1950). The bed-load function for sediment transportation in open channel flows. U.S. Department of Agriculture, Soil Conservation Service, Technical Bulletin No. 1026.

Holmquist-Johnson, C. L. and Raff, D., (2005 draft). Bureau of Reclamation automated modified Einstein procedure (BORAMEP) program for computing total sediment load manual. U.S. Department of the Interior, Bureau of Reclamation (Reclamation), Sedimentation and River Hydraulics Group, Denver, CO.

United States Bureau of Reclamation. (1955 revised). Step method for computing total sediment load by the modified Einstein procedure. Prepared by Sedimentation Section Hydrology Branch Project Investigation Division Bureau of Reclamation.

United States Bureau of Reclamation. (1966). Computation of “Z’s” for use in the modified Einstein procedure. Prepared by Joe Lara, Hydraulic Engineer. Division of Project Investigations Hydrology Branch Sedimentation Section.

United States Bureau of Reclamation. (1969). Guide for application of total sediment load computer program. Prepared by Sedimentation Section Hydrology Branch Project Investigation Division Bureau of Reclamation.

FRAMEWORK OF YEARLY STREAM SEDIMENT INPUT

Aaron Byrd, Research Hydraulic Engineer, Engineer Research and Development Center, US Army Corps of Engineers, Vicksburg, MS, Aaron.R.Byrd@erdc.usace.army.mil

Abstract: The US Army Corps of Engineers has developed a watershed model called Gridded Surface Subsurface Hydrologic Analysis (GSSHA) that also computes sediment erosion and deposition in both overland flow areas and stream reaches. One of the primary problems in using GSSHA for sediment yield studies is a mismatch of temporal resolution. River morphology and sediment yield studies often cover a 30- to 50-year time scale with times steps measured in years while GSSHA typically operates on time steps of seconds and simulation periods usually cover a few months to a year. In order to bridge this gap between simulation time scales another model has been created. This model interfaces with GSSHA and is called the Framework of Yearly Stream Sediment Input (FYSSI.) FYSSI in essence simulates annual yield by running GSSHA for hypothetical storm events, stochastically generating a sequence of storm events, and then aggregating the results of the GSSHA model for each storm event sequence. What is then generated are sediment yield curves that show values of sediment input by grain size into individual stream reaches over the lifetime of the project. This data is a primary input of the SIAM model, a model being developed by USACE to analyze annual stream sediment yield and aggradation and degradation trends over a project lifetime. The nature of this approach lends itself to a stochastic analysis that helps answer another primary concern in sediment yield analysis, namely the uncertainty in sediment runoff produced by seemingly identical precipitation events. FYSSI currently takes into account seasonal effects of cover, variability in soil moisture, and the return period and duration of a given storm when generating a series of hypothetical storm events and input parameters for GSSHA. To produce a distribution of expected sediment input over the project lifetime FYSSI simulates 1000 storm sequence scenarios over the project lifetime and uses the results to create a distribution of values for each year and each grain size for each segment of the stream network. These ranges of values can then be used by SIAM to produce a confidence range on the lifetime of the project. This project is funded as part of the System Wide Water Resources Program funded by Headquarters, U.S. Army Corps of Engineers.

PREDICTING SEDIMENT DISCHARGE FROM FOREST ROADS: THE ROLE OF SURFACE RUNOFF AND RAINFALL INTENSITY

Joseph R. Amann, Hydraulic Engineer, WEST Consultants, Inc., Bellevue, Washington; email: jamann@westconsultants.com; Dr. Arne Skaugset, Associate Professor, Department of Forest Engineering, Oregon State University, Corvallis, Oregon; email: arne.skaugset@oregonstate.edu

Abstract: Unpaved roads can be sources of chronic sediment to streams in forested watersheds. The bare soil on forest roads is subjected to rainfall and overland flow, which lead to surface erosion. Published research on sediment production from forest roads focuses primarily on road and hillslope characteristics. Water drives the mechanics of sediment transport; therefore, hydrologic variables should correlate with sediment production from roads. This project investigated the relationship between parameters representing storms that produced runoff on individual road segments in a forested watershed and the sediment production from those road segments. Rainfall parameters were correlated with sediment production for nine road segments in the upper Oak Creek Watershed in western Oregon near Corvallis from November 2002 through June 2003.

INTRODUCTION

Most running surfaces of roads in managed forests are a mixture of aggregate and soil that has low infiltration capacities. The soil from the road can be transported to streams and can degrade aquatic habitat and water quality. Accurate prediction of the potential of road segments to produce sediment could help focus efforts to reduce erosion from roads. Existing tools that quantify sediment production from roads focus on 1) road design, 2) physical characteristics of the road, 3) the amount and type of traffic on the road, and 4) road maintenance. There are fewer research results available that relate sediment production from roads to hydrologic variables. Since water drives sediment transport mechanics, hydrologic variables, such as rainfall amount as well as intensity and runoff amount, should be good predictors of sediment production from roads. This project assessed sediment production from unpaved roads in a small forested watershed in the Oregon Coast Range. The results of this study are part of ongoing research to understand sediment production from aggregate surfaced forest roads and to minimize the production of this sediment.

Site Description: Upper Oak Creek is an actively managed forested watershed in the eastern foothills of the Oregon Coast Range. It encompasses 824 hectares in McDonald-Dunn Research Forest, the school forest for the College of Forestry at Oregon State University, northwest of Corvallis, Oregon (Figure 1).

The elevation of the watershed ranges from 140 to 600 meters and hillslope gradients range from 20 to 70 percent. Discharge from the watershed is measured at the boundary of the Research Forest. Traffic is light and consists mainly of vehicles involved in research or teaching on the school forest. Other activities in the watershed include hiking, bicycling, and horse-back riding. There are 4,880 meters of stream in the watershed resulting in a drainage density of 5.92 m/ha and there are 4,570 meters of road in the watershed resulting in a road density of 5.55 m/ha. The average width of the roads is five meters. They are crowned with drainage ditches and all are aggregate-surfaced. Most of the road system was built in the 1950's and 1960's using cut-and-fill construction methods.

The watershed is instrumented with four tipping-bucket rain gauges, a micrometeorology station, and capacitance rods (automated water-level recorders) were installed at the inlet of all culverts. Sediment traps were installed at the outlet of nine cross-drain culverts. Data were analyzed on time scales that ranged from individual storms to the complete winter. This was a small-scale, observational case study that describes processes at individual road segments.

METHODS

Sampling sites were selected using a backward elimination process. The process began by using the GIS database developed by Ellingson (2002) to locate the population of cross-drain culverts within the Oak Creek Watershed. The flow data from these culverts from past winters were used to identify fifteen culverts that had experienced the highest flow. Of these fifteen culverts, nine were chosen based on the ease of installing the sampling equipment.

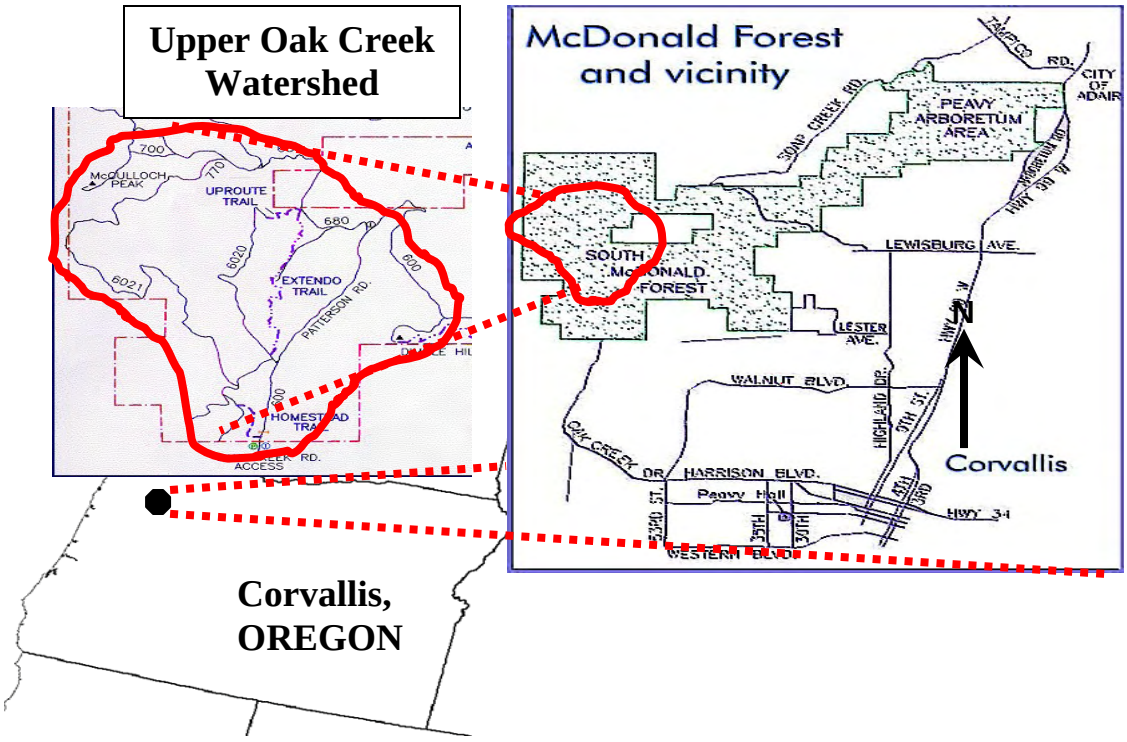


Figure 1 Location of study site.

Hydrology: Precipitation in the upper Oak Creek watershed was measured using four NovaLynx® tipping bucket rain gauges each mated with an Onset® HOBO event data logger. Culvert discharge was measured using depth/discharge relationships. Depth of water at each cross-drain culvert was measured using Tru-Track®, model WT-HR 500 (820 mm length) electronic automated capacitance rods. The location of the rain gauges and culverts is shown in Figure 2.

Sediment: Three types of sediment traps were used to capture sediment during this study. Each type of sediment trap corresponded to a specific size class of sediment observed: coarse, settleable, and suspended. A geotextile sock was attached to the outlet of each study culvert that trapped the coarse fraction ($\geq$ 0.425 mm or #40 U.S. Sieve) of sediment and organic debris. A barrel was installed at the outlet of the geotextile sock that trapped the settleable size fraction that was too small to be trapped by the geotextile sock but large enough to settle out in the barrel. Finally, an ISCO water sampler was used to sample the suspended sediment size fraction that flowed out of the barrel.

RESULTS AND DISCUSSION

Hydrology: During the period of study, November 17, 2002 through June 18, 2003, precipitation was slightly below average for the region. Monthly precipitation during the study period is summarized in Table 1.

Table 1 Monthly 2002 - 2003 total precipitation in upper Oak Creek watershed and Hyslop weather station Corvallis, Oregon. Values are in millimeters of precipitation. Note: "N/A" indicates rain gauge malfunction.

Rain Gauge Location	Elevation (m)	NOV 2002	DEC 2002	JAN 2003	FEB 2003	MAR 2003	APR 2003	MAY 2003	JUN 2003
Dimple Hill	440	146	338	224	N/A	N/A	161	N/A	N/A
McCullough Peak	592	152	367	254	110	248	N/A	N/A	N/A
Oak Creek Meadow	163	141	320	204	99	210	N/A	N/A	N/A
Starker Meadow	324	159	385	247	114	264	182	N/A	N/A
Hyslop	70	137	318	183	91	191	165	34	9
Average (not including Hyslop)		149	353	232	108	241	171	N/A	N/A

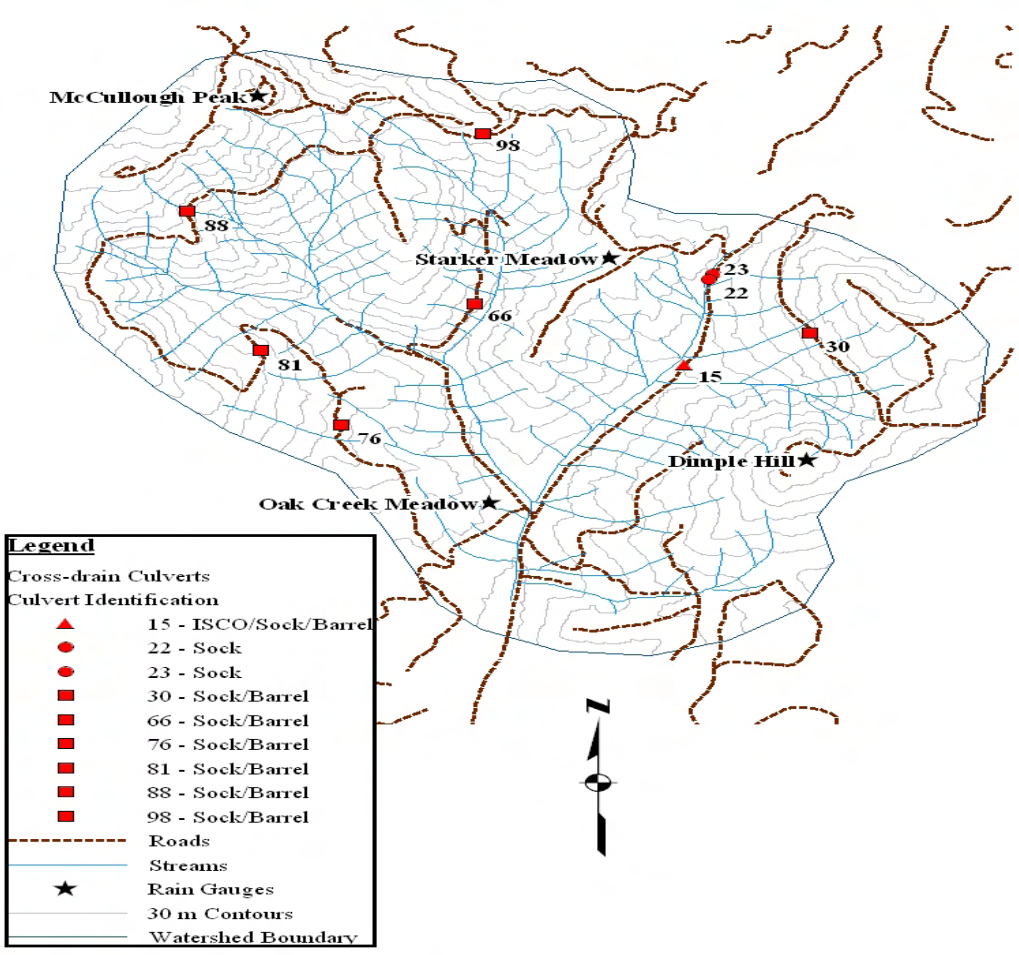


Figure 2 Upper Oak Creek Watershed rain gauge and sediment sampling site locations.

Analysis was carried out for four storms. A storm was defined as any 24-hour period when at least 12.7mm (0.5 inch) of precipitation was recorded. Storms occurred March 5-9, April 11-15, April 23-27, and May 3-5, 2003. Storm attributes are summarized in Table 2.

Table 2 Summarized precipitation and discharge data used for storm analysis. Discharge data is from culvert 15.

Storm Attributes	Storm 1	Storm 2	Storm 3	Storm 4
Date	March 5-9	April 11-15	April 23-27	May 3-5
Duration (hr:min)	97:25	96:24	83:02	31:25
Total Precipitation (mm)	82	28	43	16
1-hr intensity (mm/hr)	5.2	6.1	1.8	2.0
2-hr intensity (mm/hr)	3.2	3.7	1.4	1.7
24-hr intensity (mm/hr)	1.6	0.9	1.4	0.6
Cumulative Discharge (m^3)	33	25	86	24
Depth of runoff from culvert (mm)	63	47	163	46
Average runoff rate (mm/hr)	0.65	0.49	1.96	1.46
Runoff Ratio	3.0	6.7	15.1	11.3
Peak Discharge (L/s)	0.27	0.39	0.43	0.25
Date & Time of peak	3/8/03 2:58	4/12/03 22:22	4/25/03 17:22	5/4/03 6:02

The 1-hour, 2-hour, and 24-hour rainfall intensities from these four storms varied. All storms that occurred during water year (WY) 2003 at Oak Creek had a recurrence interval of less than 1-year (Toman, 2004). The March 5-9 storm had a 24-hour intensity of 1.6 mm/hr and a total storm precipitation of 82 mm. The storm that occurred April 11-15 had the greatest 1-hour intensity of 6.1 mm/hr. These were some of the highest values recorded in Oak Creek during the 2003 WY.

Average discharge for each of the nine culverts during the study period ranged from 0.01 l/s at culvert 81 to 5.96 l/s at culvert 23. A runoff ratio was calculated for each road segment to determine the proportion of the total runoff from the road segment that came from the road surface (Marbet, 2003). The road segment that drained to culvert 81 was the only one where runoff came mainly from the road running surface. Runoff at culvert 23 was, most likely, from the contributing hillslope. These values are summarized for each culvert in Table 3.

Table 3 Summary of discharge data for all culverts.

Culvert Number	Time Span of Record	Average Discharge (L/s)	Total Runoff Volume (m^3)	Cont. Area (m^2)	Runoff Ratio	Peak Q (L/s)	Sediment (g)
15	11/17/02 - 06/18/03	0.05	945	825	5.7	1.2	3550
22	03/10/03 - 06/18/03	0.22	1870	25	16.5	2.3	400
23	03/10/03 - 06/18/03	5.96	52000	31600	173.0	355	15000
30	11/17/02 - 06/18/03	0.05	920	225	5.5	0.9	650
66	11/17/02 - 06/18/03	0.17	2600	150	16.6	1.7	1020
76	11/17/02 - 06/18/03	0.06	960	250	4.0	1.6	570
81	11/17/02 - 06/18/03	0.01	100	75	0.1	4.9	25
88	11/17/02 - 06/18/03	0.26	3960	400	21.8	3.9	80
98	01/11/03 - 06/18/03	0.39	5960	350	7.4	11.6	2510

Culvert 15 was chosen to be monitored intensively during the four storms. The runoff ratio for this road segment for the four storms was not constant. Storm 1 had the most precipitation (82 mm) and 33 m^3 of runoff. Storm 3 had roughly half the precipitation (43 mm) but 2.6 times more runoff (86 m^3). Discharge at culvert 15 for the four storms is shown in Table 4.

Table 4 Summarized discharge values during automated water sampling at culvert 15.

	Storm 1	Storm 2	Storm 3	Storm 4
Cumulative Discharge (m^3)	33	25	86	24
Depth of runoff from culvert (mm)	63	47	163	46
Average runoff rate (mm/hr)	0.65	0.49	1.96	1.46
Runoff Ratio	3.0	6.7	15.1	11.3
Peak Discharge (L/s)	0.27	0.39	0.43	0.25
Date & Time of peak	3/8/03 2:58	4/12/03 22:22	4/25/03 17:22	5/4/03 6:02

Sediment: The sum of coarse and settleable sediment trapped by geotextile socks and barrels was also highly variable and ranged from 25 g at culvert 81 to 15,000 g at culvert 23.

Coarse and Settleable Sediment: The most sediment trapped, 15,000 g, was at culvert 23 (Tables 3 and 5). This culvert may have trapped more sediment had sampling equipment been in place earlier. Culvert 23 also had the greatest total runoff volume and runoff ratio.

Total coarse sediment (geotextile sock) and coarse and settleable sediment (geotextile sock with barrel) were regressed against total runoff. These relationships had comparable R^2-values (0.53 and 0.51, respectively) and p-values (0.003 and 0.004, respectively).

Suspended Sediment: Suspended sediment concentration (SSC) was sampled at culvert 15 at 2-hr intervals. The occurrence of rainfall was recorded for each 0.254 mm (0.01 inches) of rain and discharge was recorded at 10-minute intervals. The sum of the instantaneous suspended sediment concentration (SSC), or ΣSSC, was determined using Equation 1. Storm 1 had the highest ΣSSC (1982 mg/L, Table 6) and storm 2 had the highest maximum SSC (796 mg/L) in a sample.

$$\left(\frac{\text{mg}}{\text{l}}\right) = \sum_{\text{n}}^{1} \text{SSC}\left(\frac{\text{mg}}{\text{l}}\right) \qquad (1)$$

Table 5 Summary of coarse and settleable sediment for all culverts. Note: Blocked, shaded sections correspond to partitioned analysis of culvert. Suspended sediment collected only at culvert 15 was not added to the total amount of sediment for that road segment.

n	Culvert Number	Time Span of Sampling	Oven-dried Weight of Mineral Sediment (g)		
			COARSE (Geotextile Sock)	SETTLEABLE (Barrel)	TOTAL
1	15 Storm 1	03/05/03 - 03/09/03	9	90	99
2	15 Storm 2	04/11/03 - 04/15/03	97	180	277
3	15 Storm 3	04/23/03 - 04/27/03	12	75	87
4	15 Storm 4	05/03/03 - 05/05/03	63	20	83
5	15 I/S	Beg. & End of Season + Interstorm	1110	1900	3010
6	15 Total	11/17/02 - 06/18/03	1290	2260	3550
7	22	03/10/03 - 06/18/03	400	N/A	400
8	23	03/10/03 - 06/18/03	15000	N/A	15000
9	30	11/17/02 - 06/18/03	120	N/A	N/A
10	30	02/03/03 - 06/18/03	N/A	530	650
11	66	11/17/02 - 06/18/03	620	400	1020
12	76	11/17/02 - 06/18/03	430	140	570
13	81	11/17/02 - 06/18/03	0	25	25
14	88	11/17/02 - 06/18/03	35	45	80
15	98	01/11/03 - 06/18/03	2250	260	2510

Table 6 Summarized suspended sediment data during automated water sampling at culvert 15.

	Storm 1	Storm 2	Storm 3	Storm 4
ΣSSC, (mg/L)	1982	1506	717	532
Max. SSC, (mg/L)	598	796	121	189
Date & Time of Max.	3/9/03 12:00	4/12/03 22:00	4/23/03 18:00	5/4/03 6:00

For culvert 15, storm 3 was selected to illustrate some of the findings from this study. Similar results from the three other storms studied can be found in Amann, (2004). A hydrograph for the storm and a graph of SSC are shown in Figure 3. The graph shows that a given value for discharge does not yield a unique value of SSC. There was no

minimum threshold of discharge that initiated the production of suspended sediment. The variability in SSC is not explained by discharge as the independent variable.

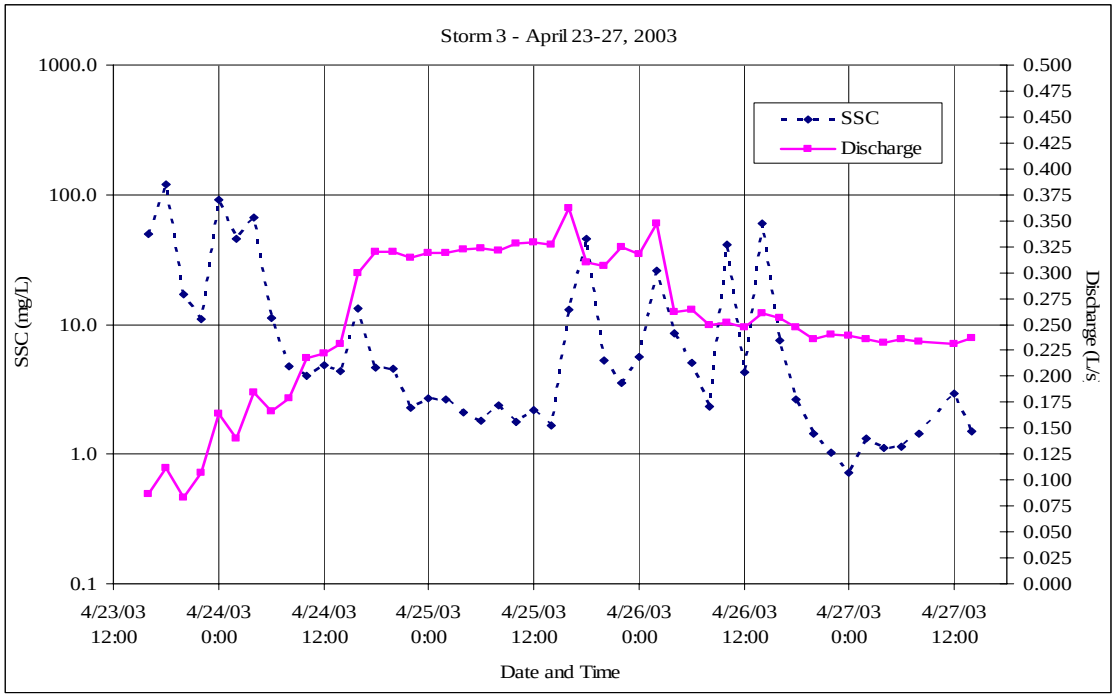


Figure 3 The hydrograph and suspended sediment concentrations at culvert 15 for storm 3. Note: SSC is on log-scale.

Cumulative discharge and ΣSSC were plotted against time to further observe how suspended sediment might be affected by discharge (Figure 4). Discharge accumulated slowly before a linear slope was achieved. However, SSC accumulated over many steps with occasional periods of production. At culvert 15, storm 3 yielded the most discharge and the third most suspended sediment.

Plots of 1-hr and 2-hr rainfall intensities and SSC at culvert 15 showed that changes in SSC are correlated with changes in rainfall intensity. In the upper Oak Creek watershed for the storms that were studied, rainfall intensity is a better predictor of SSC than culvert discharge at culvert 15. Peak 1-hr and peak 2-hr rainfall intensities for all four storms were significantly correlated with peak SSC at culvert 15 (Figure 5), which also demonstrates the close relationship between rainfall intensity and SSC. The quantity of rainfall was also related to suspended sediment (Figure 6). As rainfall accumulated, suspended sediment accumulated proportionally.

CONCLUSIONS

The amount of sediment collected from the nine segments of unpaved forest road in the upper Oak Creek Watershed was variable and ranged from as little as 0.025 kg to as much as 15.0 kg over seven months during the winter of 2002-2003. The volume of runoff measured at cross-drain culverts from the same road segments ranged from 100 m^3 to 52,000 m^3. Total runoff volume was the single most important variable that explained the variability in sediment ($R^2 = 0.51$, $p = 0.004$).

Summed instantaneous SSC (ΣSSC) was correlated with cumulative rainfall during storms 2, 3, and 4. The implications of such data suggest that sediment production from unpaved roads may be minimized if the erosive force from raindrop impact can be attenuated. The ability to predict sediment is an important step toward managing it.

The relationship between sediment production, runoff, and rainfall suggests that the erosion processes from forest roads in the upper Oak Creek Watershed is energy-limited. Rainfall energy detaches soil particles and runoff energy

transports them. Without runoff, soil particles detached by rainfall would be transported only as far as the raindrop splash. Without rainfall, runoff energy would be limited to transporting only soil particles that could not withstand the shear forces of overland flow.

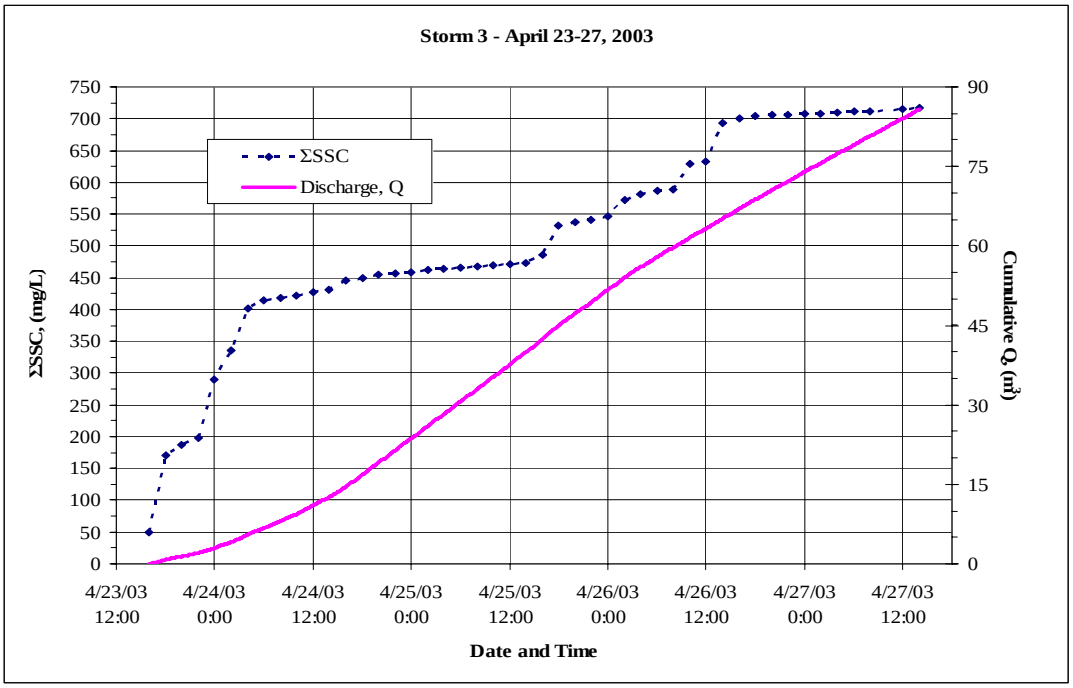


Figure 4 ΣSSC and cumulative discharge at culvert 15 during storm 3.

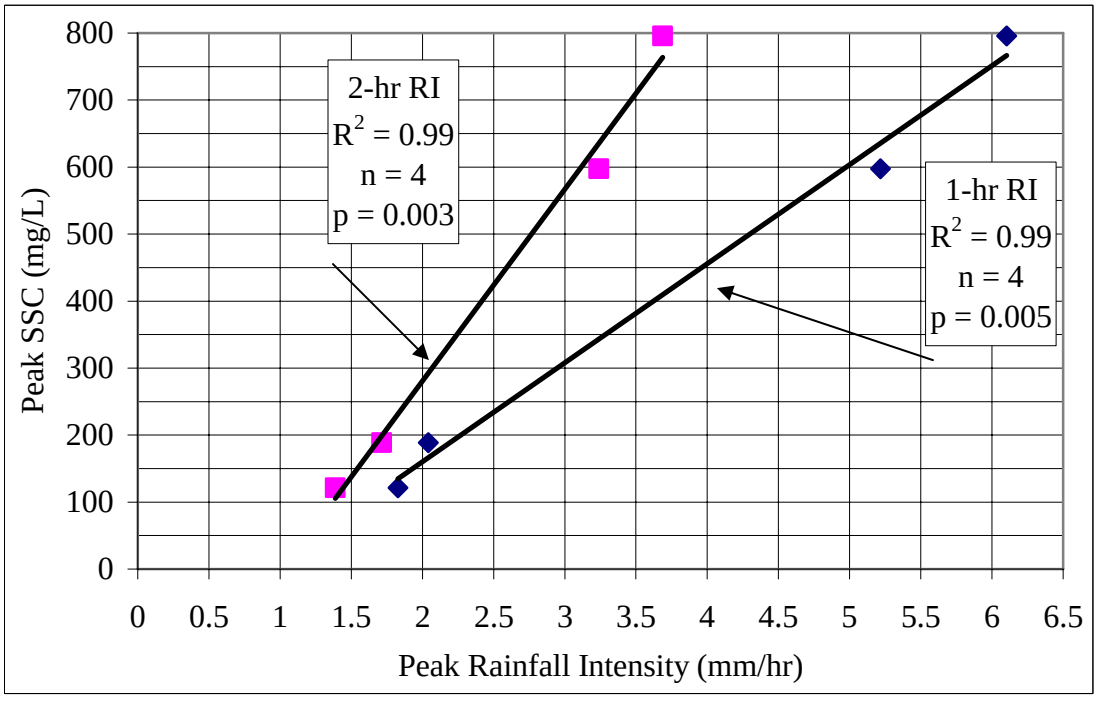


Figure 5 Regression of peak suspended sediment concentration on peak 1- and 2-hr rainfall intensity for storms 1-4 at culvert 15.

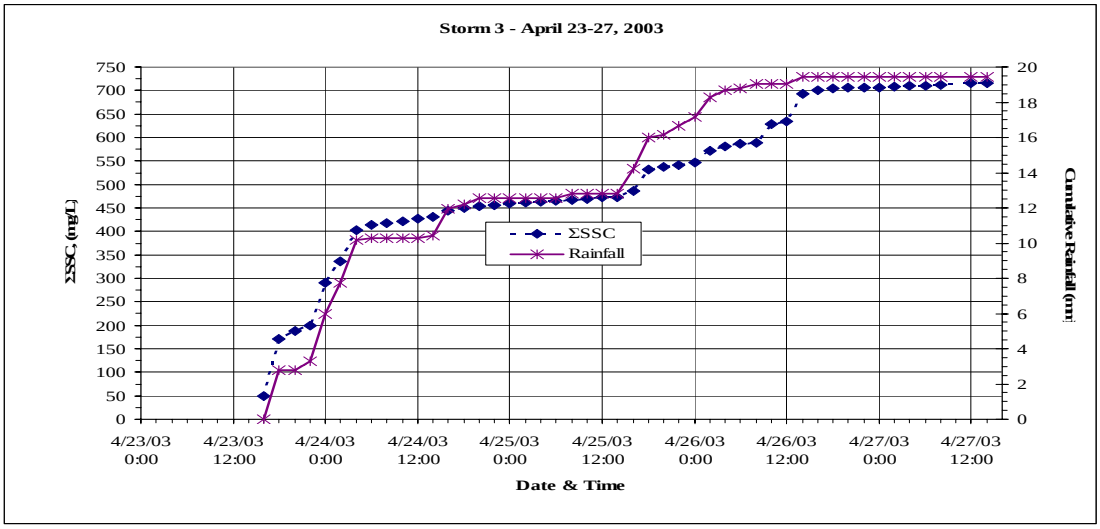


Figure 6 ΣSSC and cumulative rainfall at Culvert 15 for storm 3.

REFERENCES

Amann, J. R. 2004. Sediment production from forest roads in the Upper Oak Creek Watershed of the Oregon Coast Range. M.S. thesis. Forest Engineering Department, Oregon State University. Corvallis, Oregon. 90 pp.

Ellingson, K. 2002. Road surface runoff for the Oak Creek Watershed: the influence of hillslope and road characteristics. M.F. thesis. Forest Engineering Department, Oregon State University. Corvallis, Oregon. 63 pp.

Marbet, C. E. 2003. Hydrology of Five Forest Roads in the Oregon Coast Range. M.S. thesis. Forest Engineering Department, Oregon State University. Corvallis, Oregon. 94 pp.

Toman, E. T. 2004. Forest road hydrology: the influence of forest roads on stream flow at stream crossings. M.S. thesis. Forest Engineering Department, Oregon State University. Corvallis, Oregon. 78 pp.

EROSION CONTROL IN COTTON PRODUCTION THROUGH THE USE OF ULTRA NARROW ROW

R. F. Cullum, USDA-ARS-National Sedimentation Laboratory, 598 McElroy Dr, Oxford, MS, bcullum@ars.usda.gov; G. V. Wilson, USDA-ARS-National Sedimentation Laboratory, 598 McElroy Dr, Oxford, MS, gvwilson@ars.usda.gov; J. R. Johnson, Mississippi State University, North Mississippi Branch Experiment Station,42 MAFES Circle, Holly Springs, MS, jjohnson@ra.msstate.edu; K. C. McGregor, USDA-ARS, National Sedimentation Laboratory, 598 McElroy Dr, Oxford, MS, kmcgregor@ars.usda.gov

Abstract. Grass hedges and no-till cropping systems reduced soil losses on standard erosion plots in ultra narrow-row (20 cm) cotton during a four-year study (1999-2002). No-till cotton with grass hedges, no-till cotton without grass hedges, conventional-till cotton with grass hedges, and conventional-till cotton without grass hedges produced four-year average annual soil losses of 1.8, 2.9, 4.0, and 30.8 t/ha, respectively, and produced four-year average runoff amounts of 226, 364, 338, and 738 mm, respectively. The ratio of annual soil loss with grass hedges to without hedges averaged 0.62 for no-till. The ratio of annual soil loss with grass hedges to without hedges was 0.13 for conventional-till. Averaged over all plots (with and without grass hedges), no-till plots reduced soil loss from conventional-till plots by 86%. No-till plots without grass hedges had 90% less soil loss than conventional-till plots without grass hedges. Grass hedges effectively reduced soil loss on erosion plots with similar cropping practices as compared to plots without hedges. Other studies of contoured grass hedges on field-sized areas are being conducted to determine their applicability on larger areas with greater concentrations of runoff.

INTRODUCTION

Grass hedges are narrow strips of stiff, erect dense grass planted close to the contour that can withstand concentrated flows that would bend and overtop finer vegetation (Dunn and Dabney, 1996). Dabney et al. (1995, 1996) concluded that stiff-grass hedges planted across concentrated flow zones retard and spread out surface runoff, cause deposition of eroded sediment, and control ephemeral gully development.

McGregor et al. (1999) published runoff and soil loss data for no-till and conventional-till cotton plots (with and without stiff-grass hedges) for standard row widths (100 cm) at Holly Springs, MS. These were the same plots as used in this ultra narrow-row (20 cm) study. Hedges were established in the spring of 1991. Original standard-row width treatments consisted of no-till cotton with grass hedges, no-till cotton without grass hedges, conventional-till cotton with grass hedges, conventional-till cotton without grass hedges, and no-till cotton without grass hedges but with a winter wheat cover crop. Average annual crop year soil losses (1992-1994) were highest for conventional-till cotton without grass hedges followed by conventional-till cotton with hedges, no-till cotton without hedges, no-till cotton with hedges, and no-till cotton with winter wheat cover. No-till cropping practices effectively reduced soil losses as compared to conventional-till. Averaged over all plots (with and without grass hedges, but not including winter cover plots), no-till plots reduced soil loss from conventional-till plots by 88%. No-till plots without grass hedges had 57% less soil loss than conventional-till plots with grass hedges.

McGregor and Dabney (1993) reported reduced soil losses during the first growing season (1991) of establishment of grass hedges on these cotton plots, even though completely consolidated hedges were not produced. During the 1991 cotton growing season, soil loss on conventional-till plots with hedges was 31.4 t/ha as compared to 56.0 t/ha for conventional-till plots without hedges. During the same period, soil loss from no-till cotton with hedges averaged 1.8 t/ha as compared to 3.1 t/ha for no-till plots without hedges.

The USDA-ARS National Sedimentation Laboratory conducts other field studies on larger plots and watersheds to evaluate the upper limits of concentrated flow for grass hedges and to evaluate their potential for use in conservation tillage systems in a manner similar to terraces. The conservation objective is to cause sediment deposition above the hedges, disperse concentrated flow, and reduce ephemeral gully development

This paper reports the runoff and soil losses for ultra narrow-row cotton (UNRC) plots during 1999-2002 and evaluates the erosion-control effectiveness of the stiff-grass hedges. Row ridges were not used in any of the ultra narrow-row treatments. Soil loss ratios are estimated for use in the revised universal soil loss equation (RUSLE) for ultra narrow-row cotton planted without row ridges.

Objectives of the study were to: (1) compare runoff from no-till and conventional-till, non-ridged ultra narrow-row, cotton plots with and without stiff-grass hedges; (2) evaluate the effectiveness of fully developed stiff-grass hedges for reducing erosion for cotton; and (3) estimate soil loss ratios for non-ridged ultra narrow-row cotton for use in soil loss prediction.

PROCEDURE

The study was conducted at the North Mississippi Branch of the Mississippi Agricultural and Forestry Experiment Station, Holly Springs, MS. Erosion plots were 4 m wide and 22.1 m long on 5% slopes. Plots were equipped with FW-1 water level recorders, H-flumes, and N-1 Coshocton wheel sampling devices. Soils on the plots were predominantly Providence silt loam (Typic Fragiudalfs).

Stiff grass (*Miscanthus sinesis*) plants that would develop into hedges were transplanted about 0.5 m up slope from the lower ends of standard erosion plots on March 27, 1991 (McGregor and Dabney, 1993). The grass hedge on each plot was a mixture of three accessions (designated 130, 129 and 128) of *Miscanthus sinesis*. Individual plants were about 0.2 m apart. The hedges were transplanted about a month before the initiation of research across four rows of standard row width (100 cm) in 1991. Cotton was planted in 5% sloping rows running perpendicular to the grass hedges on May 3, May 11, May 15, and May 21 and was harvested on October 8, October 13, October 26, and October 24 in 1999, 2000, 2001, and 2002, respectively. UNRC (*Gossypium hirsutum*) treatments included both no-till and conventional-till cotton with and without grass hedges. No-till in this study refers to planting cotton in plots with no tillage operations and only a chemical burndown for weed control. Conventional-till in this study refers to the tillage sequence of two overland passes with a rototiller. Planting on all plots was done with a Marliss no-till drill planter. Cotton was planted on flat beds. Grasses and weeds were controlled with chemicals. Fertilizer and lime additions were based on experiment station recommendations. As part of a related poultry litter efficiency study, nitrogen was applied using an annual application of 3.6 t/ha poultry litter.

In June of each year, all hedges were clipped to a height of 0.5 m. The hedges were clipped using an electric hedge trimmer and hand shears. The lengths of hedge trimmings were about 50 to 80 mm. All grass clippings and cut stems were removed from the plots. In August, the hedges were trimmed again after they had grown to heights averaging from 0.9 to 1.4 m. All clippings were removed from the plots and discarded. All clippings were removed from the plots so the trapping efficiency of the completely developed hedges could be determined.

RESULTS

Grass Hedge Growth Characteristics: Hedges grew well during the first summer after being transplanted into the plots in the spring of 1991. But there were gaps in the hedges about 0.08 m wide at the end of that first growing season (McGregor and Dabney, 1993). Throughout the 1992-1994 study period grass hedges on no-till and conventional-till plots developed in the same manner and with similar characteristics (McGregor *et al.*, 1999). By the end of the 1994 crop year, grass hedges averaged 531 green stems per meter square, 975 dead stems per meter square, and had a base width of 0.6 m. The hedges were well developed by the 1999-2002 study period.

Rainfall, Rainfall Erosion Index, and Runoff: The 4-year average monthly rainfall amounts (Table 1) were fairly evenly distributed throughout the year, except that slightly lower amounts occurred in the summer months. The 4-year average rainfall for the 1999-2002 crop years (May through April) was 1321 mm, similar to the 30-year normal rainfall of 1372 mm for North Central Mississippi (McGregor *et al.*, 1987) and similar to the 1386 mm of rainfall during the earlier 1992-1994 standard row-width cotton study.

The rainfall erosion index, EI, for a storm is a function of the product of storm kinetic energy and the maximum storm 30-minute rainfall intensity. The annual EI used in RUSLE is the expected sum of EI for all storms (McGregor *et al.*, 1995).

The four-year average EI of 7104 MJ•mm•(ha•h)$^{-1}$ was 30% higher than the long-term expected EI used in RUSLE for Holly Springs (Renard *et al.*, 1997). The 3-year average of 7804 MJ•mm•(ha•h)$^{-1}$ during the 1992-1994 study was 43% higher than the long-term expected EI.

Table 1 Four-year average rainfall, erosion index, and runoff by months during the1999 thru 2002 crop years for UNRC.

MONTH	RAIN (mm)	EROSION INDEX (MJ mm (ha h)$^{-1}$)	RUNOFF NT-G† (mm)	NT WOG† (mm)	CT-G† (mm)	CT WOG† (mm)
M	117	495	21	17	34	58
J	100	588	24	24	28	45
J	65	880	9	10	14	25
A	72	506	6	7	13	28
S	77	401	9	7	13	37
O	135	1184	30	41	39	70
N	156	736	44	36	46	70
D	146	623	33	28	32	65
J	87	226	16	11	12	25
F	139	491	33	28	46	75
M	123	206	23	21	33	49
A	104	768	21	17	43	42
Crop year	**1321**	**7104**	**269**	**247**	**353**	**589**

† NT = no-till, CT = conventional-till, G = with grass, and WOG = without grass
Note: During the 19 year period (1982-2000 calendar years), EI at Holly Springs was 91.5% of that at Goodwin Creek Watershed, so values were estimated using this result.

Hedges reduced average annual runoff on conventional-till cotton plots by 40%, but runoff from no-till plots with hedges was 9% higher than from no-till plots without hedges (Table 1). However, the runoff from all no-till plots (with and without hedges) was 45% less than runoff from all conventional-till plots. Average annual runoff was highest (Table 1) for conventional-till cotton without grass hedges followed by conventional-till cotton with hedges, no-till cotton with hedges, and no-till cotton without hedges. The four-year average runoff amounts were 269, 247, 353, and 589 mm for no-till with hedges, no-till without hedges, conventional-till with hedges, and conventional-till without hedges, respectively. The four-year average monthly runoff amounts were lowest in January, July, August, and September for all plots.

Generally, runoff differences from no-till plots with and without hedges were small. The four-year average monthly runoff differences for these plots exceeded 5 mm only during October and November (11 and 8 mm, respectively). Average monthly runoff differences for conventional-till plots exceeded 15 mm in all but four months.

Soil Loss: Hedges reduced average annual soil loss on conventional-till cotton plots by 87% and on no-till plots by 37% during 1999-2002 crop years for UNRC as compared to 76% and 58%, respectively, during the 1992-1994 crop years for standard-row cotton (SRC). Average annual soil losses were highest (Table 2) for conventional-till cotton without grass hedges followed by conventional-till cotton with hedges, no-till cotton without hedges, and no-till cotton with hedges. The average soil losses for UNRC were 1.8, 2.9, 4.0, and 30.8 t/ha as compared to 2.2, 5.2, 12.3, and 48.5 t/ha for SRC (1992-1994) for no-till with grass hedges, no-till without hedges, conventional-till with hedges, and conventional-till without hedges, respectively. The higher soil losses during the standard-row study can be partly attributed to significantly higher erosion index although the rainfall was only slightly higher.

No-till cotton plots with and without grass hedges adequately controlled annual soil losses to less than the tolerance value of 7 t/ha whereas the conventional-till cotton plots did not for standard row cotton years. But for the UNRC, the conventional-till plots with hedges as well as the no-till plots with and without hedges controlled annual soil losses to less than the tolerance value of 7 t/ha.

About 16% and 15% of the annual rainfall and annual erosion index for UNRC occurred during the combined months of May and June, during the early growth stages. But about 56% and 57% of the annual soil loss from

conventional-till plots with hedges and conventional-till plots without hedges occurred during May and June. Soil loss during May and June for the conventional-till plots with hedges averaged only 2.2 t/ha as compared to 17.6 t/ha for conventional-till plots without hedges.

Table 2 Four-year average soil losses by months during the UNRC crop years.

		SOIL LOSS			
MONTH	**RAIN**	**NT-G†**	**NT WOG†**	**CT-G†**	**CT WOG†**
	(mm)	**(t/ha)**	**(t/ha)**	**(t/ha)**	**(t/ha)**
M	117	0.47	0.35	1.13	8.24
J	100	0.37	1.02	1.09	9.32
J	65	0.04	0.17	0.24	3.30
A	72	0.05	0.08	0.12	1.52
S	77	0.02	0.03	0.06	0.49
O	135	0.17	0.27	0.15	1.26
N	156	0.20	0.28	0.17	1.33
D	146	0.17	0.21	0.37	1.22
J	87	0.10	0.11	0.11	0.72
F	139	0.13	0.13	0.28	1.60
M	123	0.05	0.11	0.08	0.62
A	104	0.08	0.16	0.19	1.14
Crop year	**1321**	**1.85**	**2.92**	**3.99**	**30.76**

† NT = no-till, CT = conventional-till, G = with grass, and WOG = without grass hedge

The standard-row study again illustrated the effectiveness of no-till cropping practices in reducing soil losses as compared to conventional-till. Averaged over all plots (with and without grass hedges), no-till plots reduced soil loss from conventional-till plots by 86%. Averaged over all plots, no-till plots reduced soil loss from conventional-till plots by 88% during the earlier 1992-1994 study.

Ratios of Soil Loss With and Without Grass Hedges: The effect of grass hedges in reducing soil loss was determined by dividing the average soil loss of no-till cotton plots with hedges by the average soil loss of no-till cotton plots without hedges. The annual ratio of soil loss for no-till UNRC plots with grass hedges to those without hedges averaged 0.62. The annual ratio of soil loss for conventional-till plots with grass hedges to without hedges was 0.13.

An erosion control practice factor could be used in RUSLE to give some credit for grass hedges. McGregor *et al.* (1999) reported that the ratio of soil loss from plots with grass hedges to soil loss from plots without grass hedges would reflect 100% credit for soil loss trapped above the hedges. McGregor *et al.* (1999) observed that a higher value may need to be used so that credit for soil trapped immediately above hedges will not be considered applied over the entire plot area.

C-Factor Estimates: The cropping and management C-factor used in USLE is defined as the ratio of soil loss from land cropped under specified conditions to the corresponding loss from tilled continuous fallow land (Wischmeier and Smith, 1978). The ratio calculated for a crop stage is referred to as a soil loss ratio (SLR). Mutchler *et al.* 1985 reported that SLR values for the erosion plots at Holly Springs can be computed with the following equation:

$$SLR=33.95(\text{Measured Soil Loss during crop stage})/(\text{Measured EI during crop stage}) \quad (1)$$

where soil loss units are in t/ha, and EI units are in $MJ \bullet mm \bullet (ha \bullet h)^{-1}$.

SLR values using the above equation are not valid for the plots with grass hedges. Part of the credit for lower soil loss with plots with grass hedges should be reflected in an erosion control practice factor (P).

Annual SLR's were 0.007, 0.014, 0.017, and 0.013 for 1999 through 2002 crop years, respectively, for no-till UNRC on flat beds (Table 3). For conventional-till on flat beds, these annual SLR's ratios were 0.327, 0.155, 0.082, and 0.117, respectively. The UNRC average annual SLR's were 0.013 and 0.170 for no-till and conventional-till, respectively.

McGregor *et al.* (1999) published annual SLR's for standard row cotton during the 1992 through 1994 crop years of 0.019, 0.008, and 0.037, respectively, for no-till cotton on flat beds. For conventional-till standard-row cotton on flat beds, these ratios were 0.256, 0.109, and 0.248, respectively. Mutchler *et al.* (1985) reported annual SLR values for conventional-till cotton on ridges to be 0.217 for conventional-cotton after 11 years of no-till, and 0.408 for conventional-till cotton on ridges after 11 years of conventional-till. They reported annual SLR values for no-till cotton after reduced-till soybeans of 0.102.

Cotton Yields and Ground Residues: Cotton yields were not significantly different ($\alpha = 0.05$) for the four treatments; however, a significant year effect was found with higher yields in each of the four treatments during 2001 and 2002 as compared to the yields in 1999 and 2000 (Table 4). The overall average yields and residues for the NT-G, NT-WOG, CT-G, and CT-WOG were 1637, 1642, 1624, and 1442 kg/ha and 4.3, 4.2, 4.2, and 3.2 t/ha, respectively. These yields and residues averages show a trend that conventional-till without grass hedge results in lower yields and residues as compared to no-till with and without grass hedges and conventional-till with grass hedge.

Table 3 Annual soil loss ratios (SLR) computed using measured soil losses and estimated annual EI values.

CROP			NARROW-ROW COTTON STUDY			
YEAR	RAIN	EROSION INDEX	NT-G†	NT WOG†	CT-G†	CT WOG†
	(mm)	(MJ mm (ha h)$^{-1}$)	P(SLR)	SLR	P(SLR)	SLR
1999	990	5110	0.015	0.007	0.037	0.327
2000	1041	4906	0.012	0.014	0.021	0.155
2001	1733	11634	0.007	0.017	0.013	0.082
2002	1516	6756	0.006	0.013	0.015	0.117
4 year-average	**1320**	**7102**	**0.010**	**0.013**	**0.022**	**0.170**
CROP			**STANDARD ROW COTTON STUDY**			
YEAR	**RAIN**	**EROSION INDEX**	**NT-G†**	**NT WOG†**	**CT-G†**	**CT WOG†**
	(mm)	**(MJ mm (ha h)$^{-1}$)**	**P(SLR)**	**SLR**	**P(SLR)**	**SLR**
1992	1464	7984	0.011	0.019	0.052	0.256
1993	1376	6792	0.005	0.008	0.027	0.109
1994	1343	8660	0.013	0.037	0.073	0.248
3 year-average	**1394**	**7812**	**0.010**	**0.021**	**0.051**	**0.204**

† **NT = no-till, CT = conventional-till, WOG = without grass hedge**

Notes: SLR = 33.95(Soil Loss/EI) for plots without hedges, and where P (the erosion control practice value in RUSLE) equals 1.0; but P(SLR)= 33.95(Soil Loss/EI) for plots with hedges and the value of P is less than 1.0. Holly Springs EI estimated as being 91.5% of EI measured at Goodwin Creek Watershed. Based on 19 years of records at both locations. P(SLR) is the product of the P factor and the annual soil loss ratio (or annual C factor). P(SLR) values are shown for plots that had grass hedges. SLR is the crop year annual soil loss ratio or "annual C" factor. SLR values are shown for plots without hedges.

SUMMARY AND CONCLUSIONS

Low soil loss ratios computed for use in soil loss prediction reflected the erosion control potential of non-ridged, no-till, ultra narrow-row cotton. Average annual runoff was highest for ultra narrow-row cotton treatments of conventional-till without grass hedges followed by conventional-till cotton with hedges, no-till cotton with hedges, and no-till cotton without hedges. Runoff from all no-till plots (with and without hedges) was 45% less than runoff from all conventional-till plots. Hedges reduced average annual runoff on conventional-till cotton plots by 40%, but runoff from no-till plots with hedges was 9% higher than from no-till plots without hedges.

Ultra narrow-row cotton conventional-till plots with hedges as well as the no-till plots with and without hedges controlled annual soil losses to less than the tolerance value of 7 t/ha during the 1999-2002 crop years. Average annual soil losses were highest for conventional-till cotton without grass hedges followed by conventional-till cotton with hedges, no-till cotton without hedges, and no-till cotton with hedges. Hedges reduced average annual soil loss on conventional-till cotton plots by 87% and on no-till plots by 37% during the 1999-2002 crop years.

Table 4 Crop Yields and Residues during the 1999-2002 Crop Years.

CROP YEAR	TREATMENT	COTTON YIELD (kg/ha)	RESIDUE (t/ha)
1999	NT-G†	990	4.9
	NT-WOG†	1216	6.0
	CT-G†	1107	5.2
	CT-WOG†	1123	4.9
2000	NT-G†	1339	3.8
	NT-WOG†	1178	3.8
	CT-G†	1172	3.3
	CT-WOG†	1284	2.7
2001	NT-G†	2346	4.1
	NT-WOG†	2167	3.8
	CT-G†	2233	4.1
	CT-WOG†	1655	2.4
2002	NT-G†	1874	4.6
	NT-WOG†	2006	3.4
	CT-G†	1982	4.3
	CT-WOG†	1704	2.9

† NT = no-till, CT = conventional-till, G = grass hedge and WOG = without grass hedge
Crop Residues collected after harvest.

REFERENCES

Dabney, S.M., Meyer, L.D. Harmon, W.C. Alonso, C.V., and Foster, G.R. (1995). "Depositional patterns of sediment trapped by grass hedges," Trans. of the ASAE, 38(6), pp.1719-1729.

Dabney, S.M., Meyer, L.D. Dunn, G.H. Foster, G.R., and Alonso, C.V. (1996). "Stiff-grass hedges a vegetative alternative for sediment control," Proc. of the 1996 Interagency Sedimentation Conf., Las Vegas, NV, pp. X-62 to X-69.

Dunn, G.H. and Dabney, S.M. (1996). "Modulus of elasticity and moment of inertia of grass hedge stems," Trans. of the ASAE 39(3), pp.947-952.

McGregor, K.C., Bingner, R.L. Bowie, A.J., and Foster, G.R. (1995). "Erosivity index values for northern Mississippi," Trans. of ASAE 38(4), pp.1039-1047.

McGregor, K.C. and Dabney, S.M. (1993). "Grass hedges reduce soil loss on no-till and conventional till cotton plots," Proceedings of 1993 Southern Conservation Tillage Conference for Sustainable Agriculture, P. K. Bollich, ed., pp. 16 20.

McGregor, K.C., Dabney, S.M., and Johnson, J.R. (1999). "Runoff and Soil Loss from Cotton Plots with and without Stiff-grass Hedges," Trans. Of the ASAE 42(2), pp.361-368.

McGregor, K.C., Muller, R.A., and Murphree, C.E. (1987). "Comparison of extreme 1-day amounts of rainfall for coastal and north central regions of Mississippi," Proc. of 17th Miss. Water Resources Conf., Jackson, MS, Water Resources Research Institute, Mississippi State, MS, pp. 73, 78.

Mutchler, C.K., McDowell, L.L., and Greer, J.D. (1985). "Soil loss from cotton with conservation tillage," Trans. of the ASAE 28(1), pp. 160-163, & 168.

Renard, K.G., Foster, G.R. Weesies, G.A. McCool, D.K., and Yoder, D.C. (1997). Predicting Soil Erosion by Water: A Guide to Conservation Planning with the Revised Soil Loss Equation (RUSLE). U.S. Dept. of Agriculture, Agric. Handbook No. 703, 404 pp.

Wischmeier, W.H. and Smith, D.D. 1978. Predicting rainfall erosion losses-a guide to conservation planning. Washington, D.C., USDA Agriculture Handbook 537

HILLSLOPE EROSION AND SMALL WATERSHED SEDIMENT YIELD FOLLOWING A WILDFIRE ON THE SAN DIMAS EXPERIMENTAL FOREST, SOUTHERN CALIFORNIA

Peter M. Wohlgemuth, Hydrologist, USDA Forest Service, Pacific Southwest Research Station, Riverside, California, pwohlgemuth@fs.fed.us

Abstract: In 2002, a wildfire burned over an ongoing sediment flux study in the steep San Gabriel Mountains of southern California. The study was conducted on the chaparral-covered San Dimas Experimental Forest, the site of previous vegetation type-conversions and prescribed burning. Hillslope erosion was measured with metal collector traps on unbounded plots in four catchments. Small watershed sediment yield was measured in debris basins in 17 catchments. Annual erosion did not correlate with maximum 15-minute rainfall intensities. Both hillslope erosion and sediment yield showed remarkable similarities in the post-burn environment. Erosion increased by one to two orders of magnitude in the first year after the fire compared to unburned levels, followed by a relatively rapid recovery to baseline values. Prescribed fire and wildfire produced similar post-fire erosion responses.

INTRODUCTION

In southern California chaparral environments, the vegetation communities are adapted to prolonged summer drought. However, these adaptations, which include waxy or resinous leaves, produce fuels that are extremely flammable. In these fire-prone ecosystems, wildfire is a significant disturbance event that incinerates vegetation, alters soil properties, and renders the landscape susceptible to the agents of erosion. Under these conditions, increased sediment transport in upland watersheds is inevitable.

In the mountains of southern California, increased post-fire erosion is accentuated because of steep topography, non-cohesive soils, and intense rainfall events. This accelerated erosion can cause environmental site degradation, can extirpate refugia populations of endangered species, and can seriously harm downstream human communities at the wildland/urban interface. Lives are threatened, property is jeopardized, and corporate infrastructure (roads, bridges, pipelines, utility lines) is placed at risk.

Although the patterns of post-fire erosion on chaparral landscapes in southern California are generally understood, uncertainty about the magnitude of post-fire erosion events limits our ability to predict specific post-fire watershed responses. Unfortunately, prediction, usually in the form of risk assessment and planning that involves numerical modeling, is only possible with a sufficient understanding of the erosion problem along with the quantification of fire effects on erosion processes.

A wildfire on the San Dimas Experimental Forest that burned over an ongoing sediment flux study provided an opportunity to document and quantify the effects of fire on hillslope erosion and sediment yield in small watershed units in a semiarid, chaparral-covered, steepland environment. Results of this research could serve as a benchmark against which to test existing models of post-fire erosion for the southern California area.

Background: Semiarid geomorphic systems are characterized by high rates of sediment production (Langbein and Schumm, 1958), as the erosive rains attack significant areas of bare ground. In the steep mountains of southern California, weathered rock debris combines with organic litter to form thin, colluvial soils (DeBano, 1974). This sediment, stored on the hillslopes, is shed quasi-continuously by the gravitational process of dry ravel and the hydrologic processes of rainsplash and overland flow (Rice, 1974). Sediment accumulates in the ephemeral channels where it is periodically scoured by surface runoff and debris flows, generated by infrequent high magnitude storms, and routed primarily as bedload to the watershed outlet (Scott and Williams, 1978).

Fire magnifies the erosion hazard in mountainous southern California by reducing the resistances to the agents of erosion. The removal of the vegetation canopy and surface organic material decreases rainfall interception, and the denuded hillsides are subjected to unimpeded raindrop impacts (Rice, 1974). In addition, the combustion of soil organic matter can create a subsurface water-repellent layer that restricts infiltration and promotes overland flow (DeBano, 1981), enhancing surface runoff and concomitant sediment yield. In southern California, first-year post-fire sediment yield is 35 times greater on average than comparable unburned annual levels (Rowe et al., 1954).

Study Area: The San Dimas Experimental Forest (SDEF) is a nearly 7000 ha research preserve administered by the USDA Forest Service, Pacific Southwest Research Station (Figure 1). With its headquarters at Tanbark Flat (34^{o} 12' N latitude, 117^{o} 46' W longitude), the SDEF is located in a front range of the San Gabriel Mountains about 45 km northeast of Los Angeles, California. The SDEF was established in the early 1930s to document and quantify wildland hydrology in the semiarid chaparral-covered steeplands of southern California.

Topography in the SDEF consists of a highly dissected mountain block with narrow, steep-walled canyons (slope angles average 68 percent) and steep channel gradients (average of 15 percent). Elevations in the study area range from 750 m to 1050 m. Bedrock geology is dominated by tectonically uplifted Precambrian metamorphics and Mesozoic granitics that produce shallow, azonal, coarse-textured soils (Dunn et al., 1988).

The SDEF experiences a Mediterranean climate, characterized by cool, moist winters and hot, dry summers. Mean annual precipitation, falling almost exclusively as rain, is 714 mm (72-year record), but rain during individual years can range from 252 to 1848 mm. Over 90 percent of the average annual precipitation falls between the months of November and April, with 10 percent of the storms producing over 50 percent of the total rain (Wohlgemuth, 1996).

Native vegetation in the SDEF consists primarily of mixed chaparral. Plant cover on south-facing slopes ranges from dense stands of chamise (*Adenostoma fasciculatum*) and ceanothus (*Ceanothus* spp.) to more open stands of chamise and sage (*Salvia* spp.). North-facing hillsides are dominated by scrub oak (*Quercus berberidifolia*) and ceanothus, with occasional hardwood trees – live oak (*Quercus agrifolia*) and California laurel (*Umbellularia californica*) – occurring on moister shaded slopes and along the riparian corridors (Wohlgemuth, 1996).

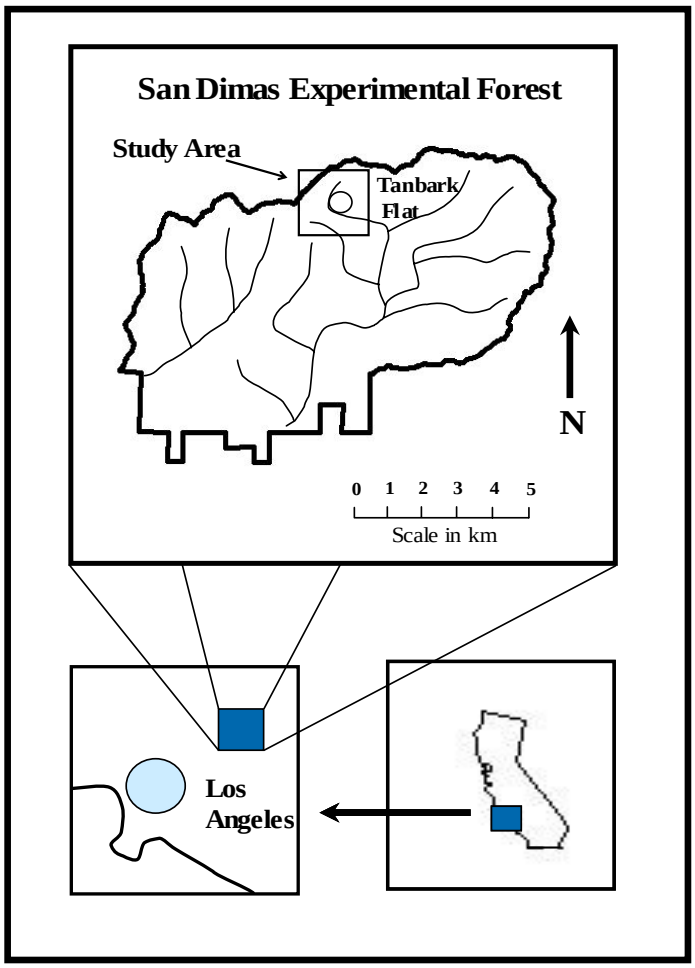


Figure 1 Location map of the San Dimas Experimental Forest.

Management treatments following a wildfire in 1960 involved the vegetation type-conversion of some native chaparral watersheds to a mixture of perennial grasses. Accompanied by herbicide spraying of the re-growing brush vegetation to assist in the grass establishment, these perennials included a variety of wheatgrass species (*Agropyron* spp.), Harding grass (*Phalaris tuberosa* var. *stenoptera*), big bluegrass (*Poa ampla*), smilo grass (*Oryzopsis miliacea*) and blando brome (*Bromus mollis*) (Corbett and Green, 1965).

In 1994, a study was initiated to quantify sediment fluxes through several small (1-3 ha) headwater catchments in the SDEF that last burned in the 1960 wildfire (Wohlgemuth, 1996). Because of differences in the nature of the ground surface vegetation, hillslope erosion was an order of magnitude less in type-converted grass watersheds compared to chaparral catchments. Sediment yield was virtually negligible for both vegetation types in the unburned watersheds. One of these chaparral watersheds was burned in a prescribed fire in 2001. First year post-fire hillslope erosion was twice as great as pre-burn levels during the dry season, and increased by 5-fold in the wet season, despite a record drought year. First-year post-fire sediment yield was 20 times greater than the unburned annual average (Wohlgemuth and Hubbert, in press).

In September 2002 virtually the entire SDEF burned in the Williams Fire, a high severity wildfire that consumed the vegetation on nearly 15,000 ha across the San Gabriel Mountains. The fire burned over the aforementioned sediment flux study, providing a unique opportunity to quantify hillslope erosion and small watershed sediment yield following a wildfire on the same sites for which there were extensive pre-fire measurements. The areas that burned in the 2001 prescribed fire did not re-burn in the 2002 wildfire.

METHODS

In the sediment flux study, four small watersheds were selected to measure hillslope erosion: three in native chaparral vegetation and one in type-converted grass (Wohlgemuth, 1996). Hillslope erosion was sampled using sheet metal collector traps with a 30 cm aperture (Wells and Wohlgemuth, 1987). Seventy-five traps were placed on unbounded plots scattered throughout each watershed. The traps were installed in summer 1994. Sediment was collected for 8 years prior to the Williams Fire and through the third post-fire winter. One of the chaparral watersheds completely burned in the 2001 prescribed fire. Hillslope erosion is expressed as a flux: the air-dried mass of collected debris per unit width of slope contour (kg m^{-1}) per collection period. Although 26 sediment collections have been made to date at irregular intervals over the life of the project, the data are aggregated here into annual erosion periods.

Sediment was trapped and measured behind earth-filled dams constructed after the 1960 wildfire (Rice et al., 1965). Sediment yields were calculated using an engineering end-area formula (Eakin, 1939) based on repeated sag tape surveys of permanent cross sections (Ray and Megahan, 1978). Sediment yield was measured from 15 small watersheds: eight in native chaparral vegetation and seven in type-converted grass. The debris basins were re-activated in winter 1994. Sediment yield was measured for 8 years prior to the Williams Fire and through the third post-fire winter. Two watersheds completely burned in the 2001 prescribed fire, one from each vegetation type. Three watersheds partially burned in the prescribed fire and were discarded from post-fire analysis. Two watersheds were newly re-activated after the Williams Fire. See Table 1 for an accounting of the 17 small watersheds used in this study. To normalize for catchments of different sizes, comparisons in sediment yield were made as cubic meters per hectare. A centrally located weighing rain gage recorded precipitation amounts and intensities throughout the study period.

RESULTS AND DISCUSSION

Results of the annual rainfall, hillslope erosion, and watershed sediment yield by hydrologic year (October to September) over the duration of the project are arrayed in Table 2.

Rainfall: Tabulated values show four years of average to above average precipitation, followed by six years of drought, followed by a very wet year (Table 2). During this study period, the SDEF experienced both the wettest (2005) and driest (2002) years in its 72-year history. Precipitation amounts and rainfall intensities are often related, and the 24-hour maximum generally correlates well with the annual totals. Conversely, the 15-minute maximum shows little relation with the annual amounts (Table 2).

Table 1 Listing of the sediment yield watersheds.

Watershed ID	Area (ha)	Vegetation	Re-activated	Comments
0505	2.49	Brush	2002	Added after the Williams Fire
0506	2.74	Grass	1994	
0507*	3.25	Grass	1994	
0508*	2.38	Brush	1994	
0512	1.95	Brush	1994	Partial burn; discarded 2001
0513	3.21	Grass	1994	Partial burn; discarded 2001
0514	3.28	Grass	1994	Partial burn; discarded 2001
0516	2.04	Grass	1994	
0517	1.57	Brush	1994	
0519	2.27	Grass	1994	Burn in prescribed fire 2001
0520	2.21	Brush	2002	Added after the Williams Fire
0541	0.76	Brush	1994	
0542*	2.13	Brush	1994	
0550	1.28	Brush	1994	
0552	2.22	Brush	1994	BAER treatment; discarded 2002
0554	3.12	Grass	1994	
0560*	1.28	Brush	1994	Burn in prescribed fire 2001

* Hillslope erosion watershed

Short bursts of intense rain often govern the erosion process (Moody and Martin, 2001). Unfortunately, the values for the 15-minute maximum have no relation to annual erosion (hillslope or small watershed) for either vegetation type before or after fire (Table 2). This is understandable on the hillsides, where much of the erosion in southern California steeplands is produced by the mechanism of dry ravel, in the absence of any rain (Wohlgemuth, 1996). Watershed sediment yield, which is strictly rainfall/runoff determined, is evidently related to a more complex relationship of amounts, intensities, and perhaps antecedent moisture conditions. While rainfall is a necessary driver, it appears that increased landscape sensitivity controls accelerated erosion in the post-fire environment.

Hillslope Erosion: Prior to burning, annual hillslope erosion was nearly an order of magnitude greater under brush vegetation compared to type-converted grass (Table 2), confirming previously published results (Wohlgemuth, 1996). However, in the post-fire environment, annual hillslope erosion was roughly equal for the two vegetation types (Table 2), although values were slightly greater in the burned chaparral watersheds. Presumably the fire removed the differential resistances to surface sediment transport, equalizing the erosion response for the two types of vegetation.

Table 2 Annual rainfall, hillslope erosion, and sediment yield over the duration of the study.

Hydrologic Year	1995	1996	1997	1998	1999	2000	2001	2002	2003	2004	2005
Rainfall (mm)											
Total	1227	688	738	1367	347	526	597	252	615	408	1848
24-hour maximum	118	168	85	169	42	83	60	64	86	100	232
15-min maximum	6	17	5	15	6	5	4	9	4	5	13
Average Hillslope Erosion (kg m^{-1} yr^{-1})											
Unburned											
Grass (n=75)	1.0	0.6	0.5	0.9	0.5	0.3	0.4	0.3	-	-	-
Brush (n=225)	6.0	6.0	4.4	6.0	3.9	4.7	3.2	1.8	-	-	-
Prescribed Burn											
Brush (n=75)	-	-	-	-	-	-	5.3	30.9	12.7	2.1	3.6
Wildfire											
Grass (n=75)	-	-	-	-	-	-	-	-	37.9	3.2	6.8
Brush (n=150)	-	-	-	-	-	-	-	-	53.6	4.9	9.8
Average Sediment Yield (m^3 ha^{-1} yr^{-1})											
Unburned											
Grass (n=7)	0	0	0	0.7	0	0	0	0	-	-	-
Brush (n=8)	0	0.8	0	2.8	0	0	0.5	0.2	-	-	-
Prescribed Burn											
Grass (n=1)	-	-	-	-	-	-	-	13.2	0	0	0
Brush (n=1)	-	-	-	-	-	-	-	31.3	6.3	1.6	0.8
Wildfire											
Grass (n=4)	-	-	-	-	-	-	-	-	23.3	0.3	3.9
Brush (n=7)	-	-	-	-	-	-	-	-	37.6	0	5.4

Hillslope erosion in the first-year post-fire was an order of magnitude greater than unburned levels in the brush watersheds, and nearly two orders of magnitude greater under the grass vegetation (Table 2), again reflecting the parity in post-burn response. In subsequent years post-fire, annual hillslope erosion declined dramatically in both vegetation types, attesting to the rapid recovery of the burned hillsides. In part this recovery can be attributed to the re-growing vegetation on the sites, but it also stems from the removal of the easily mobilized sediment from the hillsides and exposing less erodible soil material at the surface. The record rainfall in 2005

produced a modest increase in annual hillslope erosion (Table 2), suggesting a residual landscape sensitivity from the fire, especially in the grass vegetation.

Post-fire annual hillslope erosion on brush vegetation was similar for the prescribed burn and the wildfire (Table 2). The prescribed fire occurred in May 2001, after the rainy season had ceased. Adding the dry season erosion from 2001 to the annual totals for 2002 and 2003, the prescribed burn watershed had a sediment flux of nearly 49 kg m^{-1}, compared to a flux of 59 kg m^{-1} for the first two years after the wildfire (Table 2). While the lower value in the prescribed fire watershed may result from lower fire severities, and hence less watershed disturbance, more probably this response reflects the record low rainfall following the prescribed burn (Wohlgemuth and Hubbert, in press). This is supported by the higher second-year erosion values for the prescribed burn watershed under a wetter year compared to the wildfire (Table 2).

Sediment Yield: Prior to burning, annual small watershed sediment yield was slightly greater under brush vegetation compared to grass, but virtually negligible for most years (Table 2). Presumably this reflects the greater sediment availability for channel transport during wet years because of the higher sediment delivery from the hillslopes under brush vegetation. In the post-fire environment this pattern continued, with the brush catchments generating moderately more annual sediment yield than the grass (Table 2). Again, this can probably be accounted for by greater sediment storage in the channels of the brush watersheds prior to the fire, and thus the greater availability for post-burn channel scour.

In the immediate post-fire year, watersheds of both vegetation types produced two orders of magnitude more sediment yield than the unburned annual average (Table 2). In part this reflects the accelerated hillslope erosion and sediment delivery to the channels, but the increased runoff from water repellent hillsides can also more effectively entrain sediment deposits already in the channels. In subsequent post-fire years, annual sediment yields decreased dramatically, mirroring the hillslope erosion recovery and a relatively rapid return to baseline levels (Table 2). No doubt the easily mobilized channel sediment was flushed out of the watersheds during the floods of the first post-fire year. The record rainfall in 2005 produced a moderate increase in annual sediment yield (Table 2), again suggesting a residual landscape sensitivity from the fire.

Post-fire annual sediment yield under both vegetation types was similar for the prescribed burn and the wildfire (Table 2). Care must be taken not to over-extrapolate these data from the single prescribed burn watershed for each vegetation type. For example, it appears from Table 2 that the inherent site factors of the prescribed burn grass catchment produced anomalously low values of sediment yield. However, the post-fire response over the first two years is virtually identical for the brush watersheds, both prescribed burn and wildfire, despite the differences in rainfall.

CONCLUSIONS

In southern California steeplands, accelerated post-fire erosion is inevitable. A wildfire that burned over an ongoing sediment flux study revealed remarkably similar patterns of both hillslope erosion and small watershed sediment yield: a one to two order of magnitude increase in immediate post-fire erosion followed by a relatively rapid recovery to baseline levels. Annual erosion has little relation to peak rainfall intensities. Post-fire erosion response was very similar

whether the watersheds burned in a prescribed fire or a wildfire. Although rainfall is a necessary driver, post-fire erosion is governed more by the landscape sensitivity to the agents of erosion.

REFERENCES

Corbett, E.S., and Green, L.R. (1965). "Emergency revegetation to rehabilitate burned watersheds in southern California," Research Paper PSW-22, USDA Forest Service, Berkeley, CA.

DeBano, L.F. (1974). "Chaparral soils," Proc. Symposium on Living with the Chaparral, Riverside, CA, Sierra Club, San Francisco, CA. pp 19-26.

DeBano, L.F. (1981). "Water repellent soils: A state-of-the-art," General Technical Report PSW-46, USDA Forest Service, Berkeley, CA.

Dunn, P.H., Barro, S.C., Wells, W.G., II, Poth, M.A., Wohlgemuth, P.M., and Colver, C.G. (1988). The San Dimas Experimental Forest: 50 years of research. General Technical Report PSW-104, USDA Forest Service, Berkeley, CA.

Eakin, H.M. (1939). "Instructions for reservoir sedimentation surveys," in Silting of Reservoirs. U.S. Department of Agriculture, Technical Bulletin 524, pp 153-164.

Langbein, W.B., and Schumm, S.A. (1958). "Sediment yield in relation to mean annual precipitation," Transactions of the American Geophysical Union, 39, pp 1076-1084.

Moody, J.A., and Martin, D.A. (2001). "Initial hydrologic and geomorphic response following a wildfire in the Colorado Front Range," Earth Surface Processes and Landforms, 26(10), pp 1048-1070.

Ray, G.A., and Megahan, W.F. (1978). Measuring cross sections using a sag tape: A generalized procedure. General Technical Report INT-47. USDA Forest Service, Ogden, UT.

Rice, R.M. (1974). "The hydrology of chaparral watersheds," Proc. Symposium on Living with the Chaparral, Riverside, CA, Sierra Club, San Francisco, CA. pp 27-34.

Rice, R.M., Crouse, R.P., and Corbett, E.S. (1965). Emergency measures to control erosion after a fire on the San Dimas Experimental Forest. U.S. Department of Agriculture, Miscellaneous Publication 970, pp 123-130.

Rowe, P.B., Countryman, C.M., and Storey, H.C. (1954). Hydrologic analysis used to determine effects of fire on peak discharge and erosion rates in southern California watersheds. U.S. Department of Agriculture, Forest Service, California Forest and Range Experiment Station.

Scott, K.M., and Williams, R.P. (1978). Erosion and sediment yields in the Transverse Ranges, southern California. U.S. Geological Survey, Professional Paper 1030.

Wells, W.G., II, and Wohlgemuth, P.M. (1987). Sediment traps for measuring onslope surface sediment movement. Research Note PSW-393, USDA Forest Service, Berkeley, CA.

Wohlgemuth, P.M. (1996). "Hillslope erosion, channel routing, and sediment yield in small semiarid watersheds, southern California," Proc. 6th Federal Interagency Sedimentation Conference, Las Vegas, NV, Interagency Advisory Committee on Water Data, Subcommittee on Sedimentation, Washington, D.C., pp X54-X61.

Wohlgemuth, P.M., and Hubbert, K.R. (in press). "The effects of fire on soil hydrologic properties and sediment fluxes in chaparral steeplands, southern California," Proc. California Association for Fire Ecology Conference, San Diego, CA, General Technical Report, USDA Forest Service, Albany, CA.

SIMULATION OF FLOOD FLOW AND SEDIMENT TRANSPORT ON ALLUVIAL FANS OF COACHELLA VALLEY, CALIFORNIA

Andrey Shvidchenko, Northwest Hydraulic Consultants, West Sacramento, CA, ashvidchenko@nhc-sac.com; Brad Hall, Northwest Hydraulic Consultants, West Sacramento, CA, bhall@nhc-sac.com; Joseph Howard, Northwest Hydraulic Consultants, West Sacramento, CA, jhoward@nhc-sac.com; Rene Vermeeren, U.S. Army Corps of Engineers, Los Angeles, CA, rene.a.vermeeren@usace.army.mil; Cuong Ly, U.S. Army Corps of Engineers, Los Angeles, CA, cuong.ly@spl01.usace.army.mil.

Abstract: A two-dimensional hydrodynamic MIKE-21 model was developed for the alluvial fan reach of the Coachella Valley between Thousand Palms and Sun City developments in South California. The model was used to simulate existing conditions flood flow dynamics and quantify the potential effect of proposed flood protection works on flooding pattern in the study area. The MIKE-21 model results were used to calculate sediment transport characteristics under existing and project conditions and to determine the project effects on sedimentation processes within and downstream of the project area. The modeling results indicate that the proposed project structures provide effective protection of Thousand Palms development against flooding and, at the same time, do not increase sediment deposition in the Sun City area.

INTRODUCTION

Flooding and sedimentation on alluvial fans are complex processes that are difficult to simulate numerically. Alluvial fans are typically characterized by irregular surface topography, complex patterns of unconfined, highly dynamic distributary flows, significant flooding and drying areas, and mixed (subcritical, critical, and supercritical) flow regimes. Alluvial fan flooding presents unique problems in terms of quantifying flood hazards, assessing sediment transport characteristics, devising reliable flood protection schemes, and evaluating impact of various projects on flow and sediment dynamics. Standard one-dimensional (1-d) methods developed for flow and sediment routing in confined streams with sufficiently simple channel geometry are usually inadequate for alluvial fan applications. For a numerical model to simulate flow and sediment transport over a fan surface, the model must account for spatial flow patterns, incorporate transient flow conditions, provide stable wetting and drying scheme, and simulate mixed flow regimes.

This paper assesses flood flow dynamics and sediment transport capacities on alluvial fans in the Coachella Valley, California and evaluates potential effects of proposed flood protection works on flow and sediment transport patterns within the project area. Flood flow dynamics was simulated using the Danish Hydraulic Institute (DHI) two-dimensional (2-d) computer model MIKE-21. Sediment transport capacities were calculated using the simulated hydraulic parameters. The sediment transport budgets were determined for both existing and project conditions, and were utilized to assess potential sedimentation impacts and maintenance requirements. The intention of the paper is to inform of the capability of MIKE-21 to simulate complex sheet flows over initially dry fan surfaces, demonstrate a method of assessing sediment transport characteristics using MIKE-21 results, and present the main simulation results of this study. All the results are presented in metric units (1 m = 3.28 ft, 1 km = 0.62 miles, 1 metric ton = 1.10 net tons).

PHYSICAL SETTINGS

The Coachella Valley is located in South California, northwest of the Salton Sea. The fluvial system of the valley consists of ephemeral stream channels (washes), which originate in the surrounding mountains and drain into large unconfined alluvial fans that spread onto the valley floor. Due to the arid environment, runoff events in the valley are infrequent and typically produced by individual high intensity storms. Long periods of several years or more may pass between significant flood events.

The study area includes approximately 12 by 12 km portion of the Coachella Valley between Thousand Palms and Sun City developments (Figure 1). The area is bordered by Indio Hills from the north and Interstate 10 from the southwest. Thousand Palms Wash, the largest Indio Hills drainage, has formed an alluvial fan more than 8 km^2 in size. The surface of the alluvial fan exhibits a network of small, shallow distributary channels that radiate from the fan apex and become indistinct a short distance downstream of the fan apex. Other streams draining the hills have

much smaller watersheds and comparatively small alluvial fans. The alluvial fans are largely devoid of vegetation (Figure 2). Surface deposits primarily consist of stratified silt, sand, and gravel. The median grain sizes range from about 1 mm near the fan apexes to 0.2 mm at the base of the fans, with the area-average size of 0.58 mm (Bechtel 2002). Large dune sand deposits are frequently observed on the valley surface, caused by aeolian (wind-blown) processes that transport sand toward the southeast. The average ground surface slope ranges from about 0.025 in the vicinity of the hills to 0.005 at the valley base.

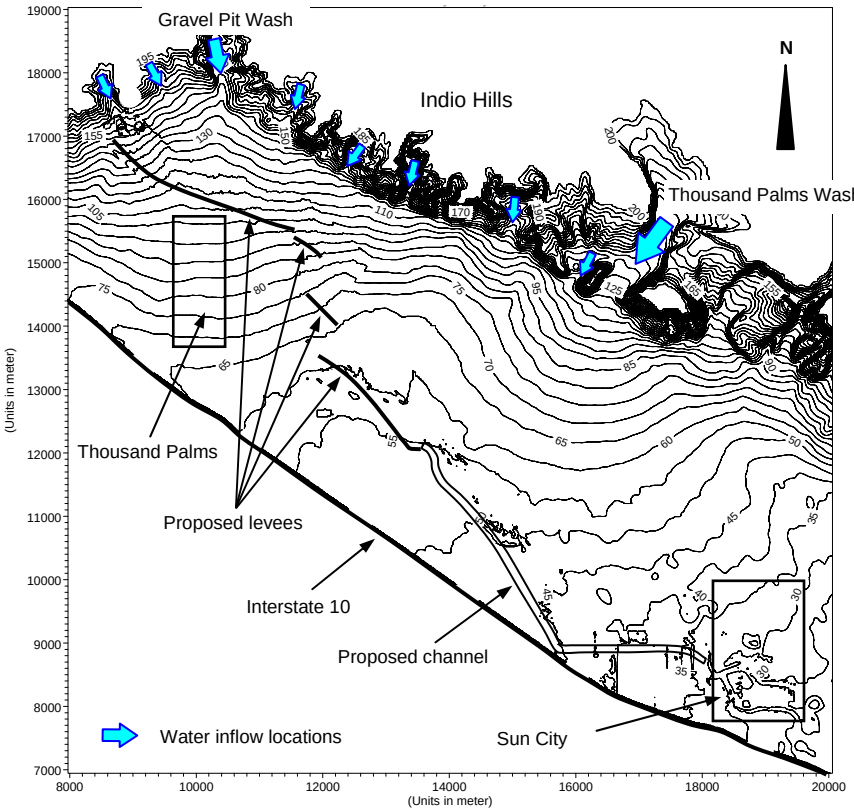


Figure 1 Study area of Coachella Valley.



Figure 2 Typical landscape of alluvial fans in Coachella Valley (left) and Sun City greenbelt channels (right).

Significant storm flows in the study area are extremely rare, typically last for a few hours, and cause widespread sheet flooding. The floodwaters emanating from Indio Hills flow in general southern direction and then southeasterly along Interstate 10. A network of floodway ("greenbelt") channels was constructed in Sun City to protect the development from flooding (Figure 2). The greenbelt channels are dry most of the time and are used for recreational purposes and as a golf course. To provide flood protection to Thousand Palms development, the U.S. Army Corps of Engineers (USACE) has designed a series of levees and a channel that would divert flows away from the developments and convey floodwaters into the Sun City greenbelt channels. The location of the proposed facilities is shown in Figure 1.

MODELING APPROACH

The modeling activities reported in this paper were aimed at the estimation of the effect of the USACE flood control project on flow conditions and sediment transport within the study area, and particularly on water levels and potential sediment deposition in the Sun City greenbelt channels. Hydrodynamic characteristics were simulated with the MIKE-21 model for the 5-, 10-, 25-, 50-, and 100-year flood events. Using the simulated flow data, sediment transport capacities were then calculated for each event. The event-based sediment transport capacities were annualized to develop an average annual sediment transport capacity. The potential impacts of the proposed flood protection project were assessed by analyzing the relative difference between the existing and project conditions flow and sediment transport characteristics.

The sediment modeling approach used in this study does not couple the hydrodynamics with the sediment transport computations. Sediment calculations were conducted for fixed bed topography, sediment was not routed between cells, and it was assumed that there was unlimited sediment supply to each cell. Therefore, the computed sediment loads represented theoretical (potential) capacity of the water flow to transport sediment, which for the sandy deposits of the Coachella Valley, however, is likely to be close to the actual sediment load.

HYDRAULIC MODELING

MIKE-21 Model: MIKE-21 is a 2-d hydrodynamic model used for computation of unsteady open-channel flows. MIKE-21 is applicable to the simulation of hydraulic phenomena in a wide range of environments including shallow sheet flows over initially dry flat surfaces. The computational procedure is based on the solution of the depth-averaged time-dependent non-linear equations of conservation of mass and momentum. The water levels and flows are resolved on a rectangular grid covering the area of interest. The main input parameters for the model are surface topography, bed resistance, location and magnitude of water inflows and outflows, initial water surface elevation, flooding and drying depths, and flow turbulence characteristic. Output parameters include water depth and 2-d water flux components at each grid point for each time step, as well as maximum inundation depths.

Model Parameters: Rectangular grids of the study area were developed for existing and project conditions using the U.S. Geological Survey 30 m Digital Elevation Model of the Coachella Valley, Light Detection and Ranging (LiDAR) data for the project area, Sun City greenbelt channel grading plans, and project structures design parameters. The model grid cell size was set to 15 by 15 m. This grid scale is sufficiently dense to describe the topographic and project features within the study area and at the same time provides manageable model run times. To eliminate any effects of the model boundaries on the solution in the study area, the downstream model limit was extended approximately 16 km below Sun City. The Manning roughness coefficient for the study area was set to 0.05 in accordance with the earlier study of Simons, Li and Associates (2000). Nine isolated time-variant flow sources were specified at the fan apexes to simulate model inflows and a set of sinks was specified at the downstream model extent to remove water mass from the model. Inflow hydrographs were developed by the USACE and employed in the MIKE-21 model. Comparison of the inflow hydrographs for the 100-year flood event is shown in Figure 3. The initial water surface elevation was set at ground level (i.e. the initial bed surface was dry). The simulation time step was set to 3 s to maintain computational stability (Courant numbers less than one) for velocities less than 5 m/s. Flooding and drying depths (0.02 and 0.01 m, respectively), as well as eddy viscosity (1.5 m^2/s) were developed using procedures recommended by DHI. Infiltration water losses were not simulated due to the absence of relevant calibration data. Model results were stored at 10-minute increments to provide sufficient resolution of the output hydrodynamic data. The simulation period was 24 hrs and included the major phase of the simulated flood events.

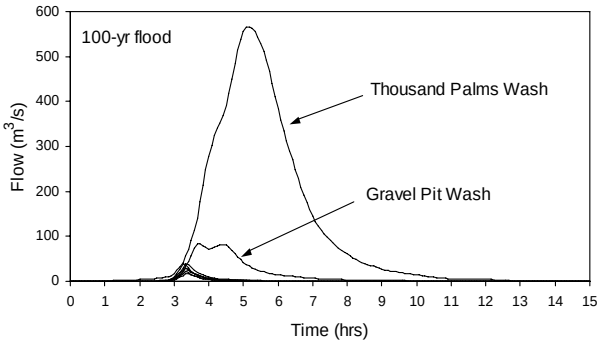


Figure 3 Inflow hydrographs for 100-year flood event.

Existing Conditions Flood Simulations: Under existing conditions, floodwaters spread over vast expanses of the valley between Indio Hills and Interstate 10 (Figure 4). Thousand Palms Wash provides the largest flow magnitude and volume to the study area and inundates larger areas than the other smaller tributaries. The flows from Thousand Palms Wash moving in southern direction comprise the first and the largest flood wave reaching the Sun City area. Floodwaters from the four westerly most drainages flow southward through Thousand Palms development toward Interstate 10 and then continue southeasterly along Interstate 10. Storm flows from the other drainages head in general southeasterly direction towards Sun City. The inundation depths are generally less than 0.5 m for Thousand Palms Wash and Gravel Pit Wash and less than 0.2 m for the other drainages. For higher flood events, the inundation area tends to increase, but the flows remain relatively shallow. Comparison of the inundation limits simulated for the 100-year flood event with aerial photographs of the Thousand Palms September 11, 1977 flood (shown in Figure 5) indicates that the model is capable of simulating complex sheet flows and closely replicates the observed flooding pattern in the study area.

Project Conditions Flood Simulations: Under project conditions, flows emanating from Indio Hills are effectively intercepted by the levees and redirected across the fan surfaces and through the project channel to the Sun City floodway channels (Figure 4). The project provides effective protection of Thousand Palms development, reduces inundation area, and at the same time reduces travel time and attenuation of the flood wave and increases the peak flows delivered to the Sun City greenbelt channels. The peak flow in the greenbelt channels increases under project conditions from about 1 to 20 m^3/s for the 5-year flood event and from 260 to 400 m^3/s for the 100-year event, which results in 0.2-0.6 m increase of maximum water depths Flooding pattern in the northeast part of the study area is not affected by the project structures.

SEDIMENT CAPACITY MODELING

Sediment Transport Calculations: The hydraulic data computed by the MIKE-21 model were used to calculate time-variant sediment fluxes and cumulative event-based sediment volumes (yields) at each grid cell of the computational domain. The calculations were performed for each flow scenario using the Ackers and White (1973) total sediment load function. A single sediment size of 0.58 mm, corresponding to the mean grain size in the project area was used in the calculations. A computer program was written to perform the sediment transport calculations. This program reads hydrodynamic data from the MIKE-21 output file, computes hydraulic parameters, performs sediment transport computations, and creates output data file that can be visualized and analyzed using the MIKE-21 viewing tools.

Existing Conditions Sediment Transport Capacities: The modeling results indicate that sediment transport generally follows water flow patterns, is highly non-uniform, and occurs over large expanses of the alluvial fans (Figure 6). Thousand Palms Wash has the highest sediment transport capacity and is potentially by far the most important contributor of sediment to the project area. Total sediment transport capacity of Thousand Palms Wash at the fan apex ranges from about 200 tons for the 5-year flood to 59000 tons for the 100-year flood, the long-term average annual being 1900 tons. The flow downstream of Thousand Palms Wash outlet spreads over the much flatter valley, which results in the reduction of the flow sediment transport capacity. The calculated sediment delivery to distal fan region near Sun City is less than 12% of sediment transport capacity at the fan apex. Due to their high magnitude, the flows from Thousand Palms Wash are responsible for the most of sediment transport in the

vicinity of and through the Sun City greenbelt channels. Sediment contribution from the other sources is appreciably smaller.

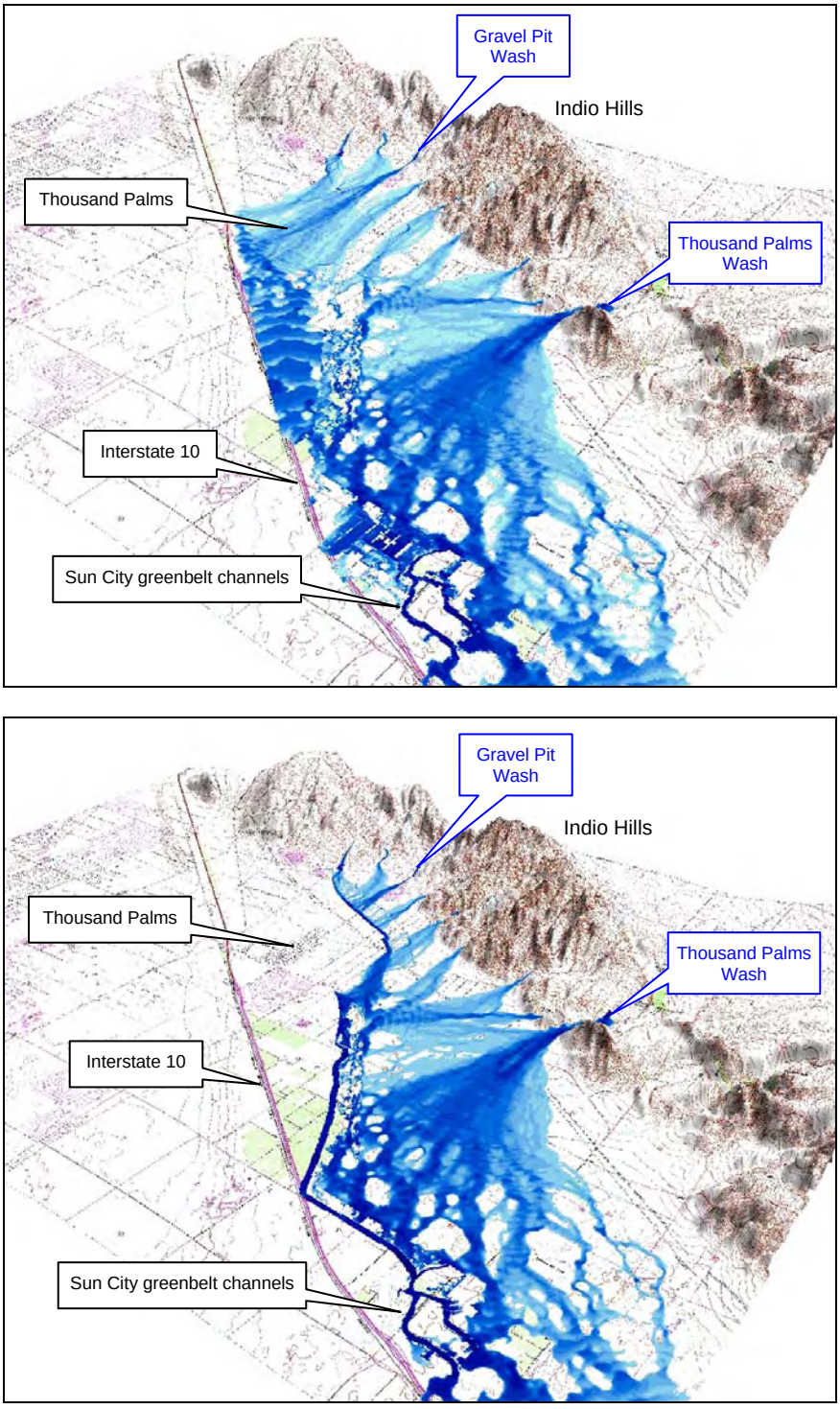


Figure 4 Perspective views of inundation limits simulated for 100-year flood event under existing (top) and project (bottom) conditions. Darker areas indicate deeper flows. Vertical exaggeration = 5.

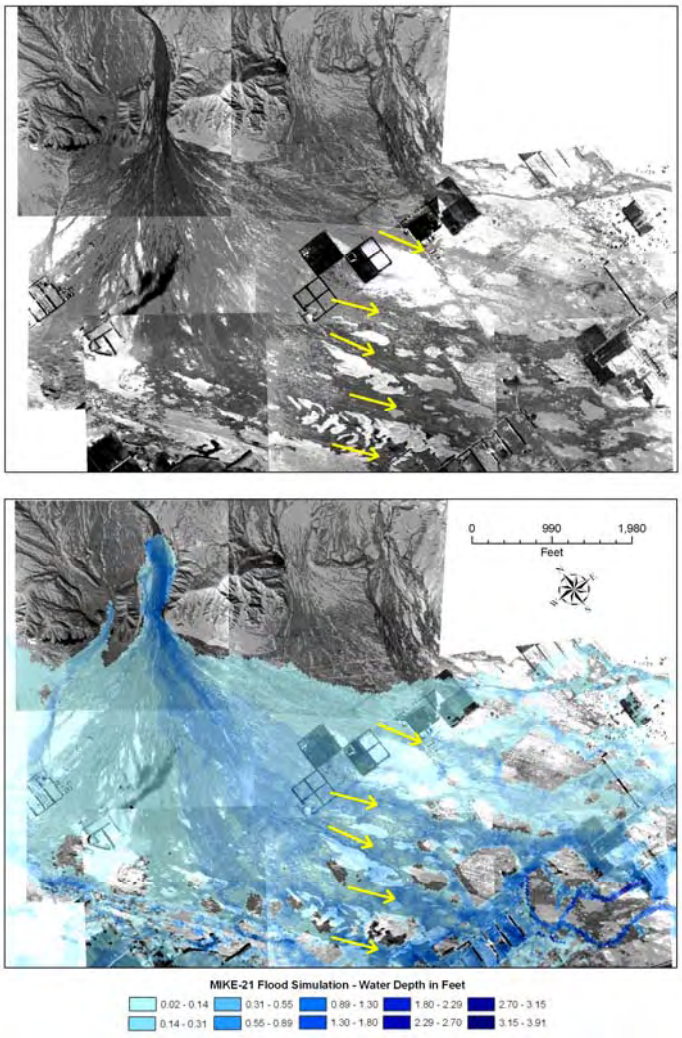


Figure 5 Comparison of simulated 100-year flood inundation limits with September 11, 1977 Thousand Palms flood aerial photographs. According to Exponent (2002), this flood has exceeded the 100-year event. Arrows delineate significant flow paths common to both model results and aerial photographs.

The calculated potential sediment inflow to the greenbelt site ranges from 15 tons for the 5-year flood to 7300 tons for the 100-year floods, the average annual being 172 tons (Table 1). At the same time, capacity of the greenbelt channels is estimated for the same floods at about 1 and 570 tons, respectively, with the average annual capacity of only 12 tons. Thus, under existing conditions, sediment transport capacity of the greenbelt channels is less than 10% of potential sediment inflow. The Sun City greenbelts serve as sinks for inflowing sediment and during floods they will intercept the majority of the sediment supplied to the Sun City area. The amount of sediment that can potentially deposit in the greenbelt channels varies from 14 tons for the 5-year flood event to about 6730 tons for the 100-year event. The long-term, statistically averaged annual deposition in the Sun City greenbelts is estimated at about 160 tons.

Project Conditions Sediment Transport Capacities: The proposed flood control project significantly alters sediment transport patterns in the western and southern parts of the project area and does not affect sediment transport in the northeast portion of the valley. Sediment transport activity is concentrated in a narrow band along the project levees and in the project channel (Figure 6). Sediment transported by Thousand Palms Wash comprise the first sediment input to the Sun City greenbelt area, which is shortly followed by additional concentrated sediment inputs from the other streams originating from Indio Hills.

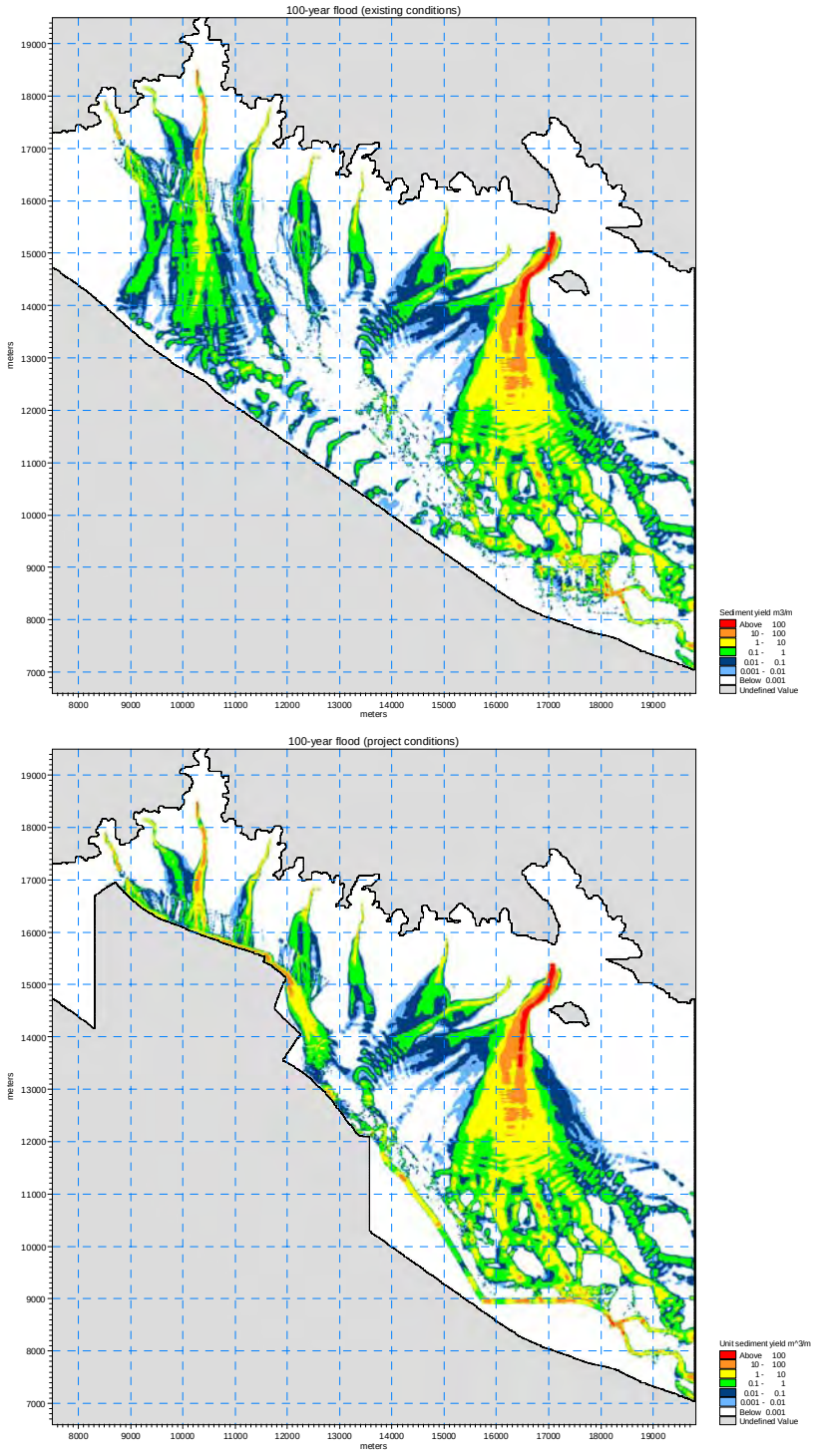


Figure 6 Sediment yields calculated for 100-year flood event under existing (top) and project (bottom) conditions.

The calculated sediment inflow to the greenbelt area varies under project conditions from 16 tons for the 5-year flood to 4700 tons for the 100-year flood, with the average annual sediment inflow of 145 tons (Table 1). Project conditions sediment transport capacity of the greenbelt channels ranges from about 4 tons for the 5-year flood to 1500 tons for the 100-year flood event, the average annual being 34 tons. The potential sediment deposition in the greenbelt channels ranges from 12 tons for the 5-year flood to 3200 tons for the 100-year flood, with the long-term

average annual deposition of 111 tons. Comparison of the existing and project conditions results indicates that that the project has varying effect on event-based sediment loads in the Sun City greenbelt area (see Table 1). The long-term effect, however, is a 16% reduction of the sediment inflow to the greenbelt area, 180% increase of sediment transport capacity of the greenbelt channels, and 30% reduction of potential sediment deposition in the greenbelt channels. The calculated sediment loads do not include infiltration water losses and, therefore, the sediment assessment results presented here should be regarded as conservative estimates.

Table 1 Sediment transport capacities and potential deposition calculated for Sun City greenbelt area.

Flood event	Existing conditions			Project conditions		
	Inflow to greenbelts (tons)	Capacity of greenbelts (tons)	Potential deposition (tons)	Inflow to greenbelts (tons)	Capacity of greenbelts (tons)	Potential deposition (tons)
100-year	7300	570	6730	4700	1500	3200
50-year	1800	150	1650	2000	420	1580
25-year	560	16	544	860	69	791
10-year	90	3	87	91	19	72
5-year	15	1	14	16	4	12
Average annual	172	12	160	145	34	111

Comparison of Fluvial and Aeolian Sediment Yields: High winds blowing in the Coachella Valley in the southeastern direction convey appreciable amounts of sand from the fan aprons towards Sun City. Estimated rates of aeolian sediment transport in the study area range from about 4 to 37 tons/m/year (Weaver 1979). Sun City development extends approximately 800 m across the wind corridor, which gives annual aeolian sediment supply into the Sun City area in the range of 3000 to 30000 tons. This amount is one to two orders of magnitude larger than the calculated average annual fluvial sediment supply to the greenbelt channels. Thus, sediment transport in the study reach of the Coachella Valley is dominated by aeolian processes.

CONCLUSIONS

The results of this study indicate that the proposed flood control project effectively intercepts and redirects floodwaters emanating from Indio Hills and provides effective protection of Thousand Palms development. At the same time, the project reduces travel time of the flood flows from the northwest part of the project area, which increases the peak flows and maximum water depths in the greenbelt channels. Sediment transport is concentrated in a narrow band along the project structures, which generally reduces the potential long-term average annual sediment inflow to and deposition in the greenbelt channels under project conditions. Flooding and sediment transport patterns in the northeast part of the study area are not affected by the project. The calculated fluvial sediment loads in the Sun City area are insignificant compared to the amount of sediment transported by aeolian processes.

ACKNOWLEDGEMENTS

This study was conducted for and funded by the Los Angeles District of the U.S. Army Corps of Engineers.

REFERENCES

Ackers, P., and White, W.R. (1973). “Sediment transport: New approach and analysis,” Journal of the Hydraulics Division, ASCE, 99 (HY11), pp 2041-2060.

Bechtel, Inc. (2002). Coachella Valley Water District Sedimentation Transport Study, Comparison of Annualized Sediment Loads Delivered to Del Webb Sun City Development. Report, Issue 4.0.

Exponent, Inc. (2002). Del Webb, Sun City, Palm Desert, Phase III, Existing Conditions Flood Hazards Along Interstate 10, Morongo Wash Bridges to Washington Street, Coachella Valley, California. Failure Analysis Associates, Civil Group.

Simons, Li and Associates, Inc. (2000). Hydraulic Appendix, Whitewater River Feasibility Study. Report prepared for Los Angeles District, Corps of Engineers by Simons, Li and Associates, Inc., Irvine, California.

Weaver, D.C. (1979). Assessment of Effects of Flood Control Alternatives of Blowsand Conditions in the Coachella Valley - Whitewater River Basin. U.S. Army Corps of Engineers. Contract No. DACW09-78-C-052.

SEDIMENT TRANSPORT COMPUTATIONS WITH HEC-RAS

Stanford Gibson, Research Hydraulic Engineer, US Army Corps of Engineers, Hydrologic Engineering Center, Davis, CA 95616, stanford.a.gibson@usace.army.mil; Gary Brunner, PE, US Army Corps of Engineers, Hydrologic Engineering Center, Davis, CA 95616, gary.w.brunner@usace.army.mil; Steve Piper, Research Hydraulic Engineer, US Army Corps of Engineers, Hydrologic Engineering Center, Davis, CA 95616, steven.s.piper@usace.army.mil; Mark Jensen, Research Hydraulic Engineer, US Army Corps of Engineers, Hydrologic Engineering Center, Davis, CA 95616, mark.r.jensen@usace.army.mil

Abstract: Sediment transport capabilities have been added to the Hydrologic Engineering Center's River Analysis System (HEC-RAS). HEC-RAS can be used to perform sediment routing and mobile bed computations. The initial version of this sediment model will leverage the wide range of hydraulic capabilities existing in HEC-RAS to compute a series of steady flow profiles used to develop hydrodynamic parameters for sediment transport. Hydraulic computations are "explicitly coupled" with transport, erosion, deposition, bed mixing and cross section change computations using the set of initial value-boundary value equations used in HEC-6. The result is a continuous simulation of the change in cross sections as sedimentation processes adjust to the hydraulic conditions imposed by the inflowing water-sediment hydrograph and the base level control boundary conditions.

INTRODUCTION

Sediment routing and mobile boundary simulations are commonly employed in support of various U. S. Army Corp's of Engineer missions. Traditional applications of dredging prediction, reservoir sedimentation and engineered channel stability have been joined by channel restoration and bed gradation response projects. HEC-6 has been the industry standard for one-dimensional mobile bed modeling since 1976. This DOS program has remained widely utilized while other popular HEC hydrologic and hydraulic models (HEC-1, HEC-2, and UNET) have been eclipsed by more powerful and user friendly products (e.g. HEC-RAS and HEC-HMS). However, many of the core capabilities of HEC-6 have recently been incorporated into HEC-RAS, leveraging the robust, existing, hydrodynamic capabilities in RAS and providing helpful user interfaces for one dimensional sediment transport modeling.

SCOPE

Sediment computations in HEC-RAS utilize one dimensional, cross-section averaged, hydraulic properties from RAS's hydraulic engines to compute sediment transport rates and update the channel geometry based on sediment continuity calculations. The initial objective is to replicate the functionalities of HEC-6 within the HEC-RAS framework. Once these capabilities are available new features and model advancements will be implemented.

METHODOLOGIES

Hydrodynamics: Flow specification for sediment transport computations currently follows the "quasi-steady" flow approach of HEC-6. An event or period of record is approximated by computing a series of steady flow profiles (Figure 1). Each of these each steady flow profiles is

then associated with a duration and transport parameters are generated at each cross section. Usually, however, bathymetry updates are required more frequently than the flow increment duration, so a computational time step is specified. The geometry file is updated and new steady flow hydrodynamics are computed at the beginning of each computational time step.

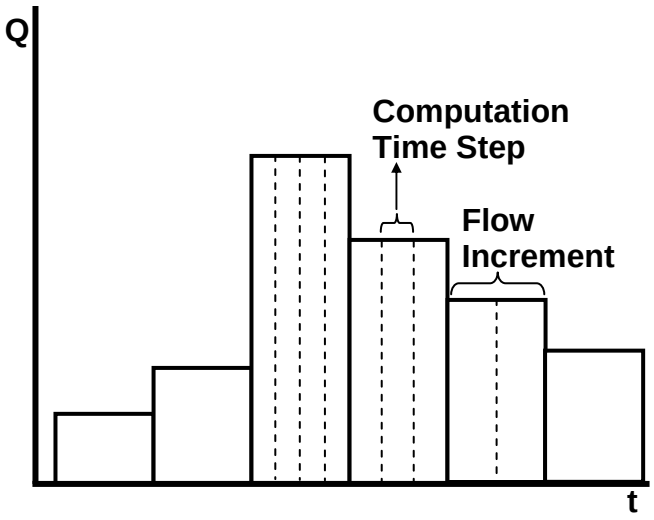


Figure 1 Schematic of quasi-steady flow division.

Transport Calculations: Six different transport functions are currently available in RAS including Ackers and White (1973), Englund-Hansen (1967), Laursen (1958), Myer-Peter-Muller (1948), Toffaleti (1968), and Yang (1972). Total transport capacity is calculated by invoking the *similarity hypothesis* (Armanini, 1992 and Vanoni 1975 after Einstein, 1950) by dividing the sediment gradation curve into discrete size classes, independently computing a transport potential for each size class and then weighted by the relative abundance in the active layer such that:

$$T_c = \sum_{j=1}^{n} \beta_j T_j$$

Where:

T_c=Total transport capacity
n=number of grain size classes
β_j=% of active layer composed of material in grain size class "j"
T_j=Transport potential computed for 100% of the material grain class "j"

The sediment continuity equation can then be solved over the control volume associated with each cross section, computing from upstream to downstream. The Exner equation is solved:

$$(1-\lambda_p)B\frac{\partial \eta}{\partial t} = -\frac{\partial q}{\partial x}$$

Where η is bed elevation, B is the width of the control volume, q is volumetric transport rate, λ_p is bed porosity. Qualitatively, this represents a change in bed elevation in response to a sediment deficit or surplus in the control volume when the capacity is subtracted from the supply. The Exner equation is solved separately for each grain size and material is added or removed to the active layer. At the end of each computational time step, the aggregation or degradation is translated into a uniform bed change over the entire wetted perimeter of the cross section. The cross sectional station-elevation information is updated and new hydraulics performed before the next transport capacity is computed for the next sediment routing iteration.

Physical Constraints to Erosion and Deposition: Physical constraints can result in a fraction of the sediment surplus or deficit computed by the Exner equation translating directly into aggregation or degradation in a given time step. RAS currently follows HEC-6 in applying

temporal erosion and deposition modifiers as well as sorting and armoring routines to augment the simple continuity computations.

Temporal Modifiers: Solution of the Exner equation will result in 100% of the computed surplus or deficit translating immediately into deposition or erosion. This does not reflect actual physical processes, however, as both deposition and erosion are temporal phenomena. Therefore, time dependent modifiers are applied to the surplus or deficit HEC-RAS calculates at each cross section. Deposition efficiency is calculated by grain size based on the computed fall velocity and the expected center of mass of the material in the water column based roughly on Toffeletti's concentration relationships (Vanoni, 1975). The deposition rate as the ratio of sediment surplus that translates into deposition in a given time step is defined as:

$$\text{Deposition Rate} = \frac{V_s(i)\cdot \Delta t}{D_e(i)}$$

Where V_s(i) is the settling velocity for particle size i, D_e(i) is the effective depth for sediment size i (e.g. the midpoint of the depth zone in which transport is expected for the grain class), and Δt is the duration of the computational time step (USACE (1993) and Thomas (1994)).

A similar relationship was implemented to temporally modify erosion. This coefficient invokes "characteristic length" approach found in HEC-6 which includes the assumption that erosion takes a distance of approximately 30 times the depth to fully develop. Therefore, in cases where capacity exceeds supply, the capacity/supply discrepancy is multiplied by an entrainment coefficient (C_e) which limits the amount of material that can be removed from a cross section in a computational time step. The entrainment coefficient is:

$$C_e = 1.368 - e^{\frac{-L}{30\cdot D}}$$

where L is the length of the control volume and D is the effective depth (USACE (1993), Thomas (1994)). As the length of the control volume goes to thirty times the depth, the coefficient approaches unity and erosion approaches the full amount of computed deficit.

Sorting and Armoring: The other major process considered in the computation of continuity is potential supply limitation as a result of bed mixing processes. Currently HEC-RAS employs Exner 5, a "three layer" algorithm from HEC-6 to compute bed sorting mechanisms. Exner 5 divides the active layer into two sub-layers, simulating bed coarsening by removing fines initially from a thin cover layer. During each time step, the composition of this cover layer is evaluated and if, according to a rough empirical relationship, the bed is partially or fully armored, the amount of material available to satisfy excess capacity can be limited.

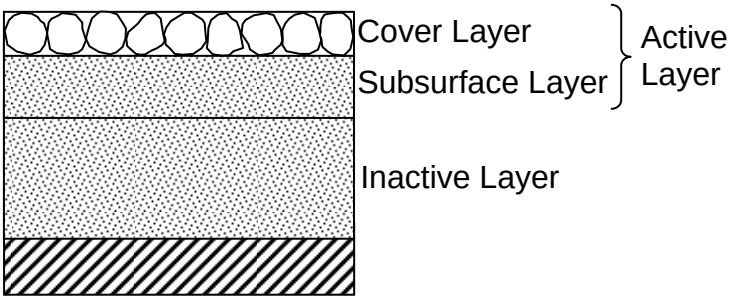


Figure 2 Schematic of 3-layers used in Exner 5 sorting and armoring method.

MODEL TESTING AND VERIFICATION

Comparison to Myer-Peter and Muller Data: Several tests have been conducted to evaluate these methodologies in HEC-RAS. First, HEC worked with Tony Thomas to simulate one of the original Myer-Peter and Muller (MPM) experiments (1948) with HEC-RAS and HEC-6T. Since the MPM transport function was derived from these experiments, they can be simulated with an expectation of reproducing the end result without the standard problems of transport function uncertainty. In the MPM experiment, a constant flow was run through a flat bed flume with a constant rate of gravel feed (grain size diameter 28.5mm) until it reached a stable, equilibrium slope of about 0.0081. This slope is plotted in Figure 3 with the equilibrium bed profiles computed by HEC-6T and HEC-RAS. There was very good agreement between the physical data and both numerical models.

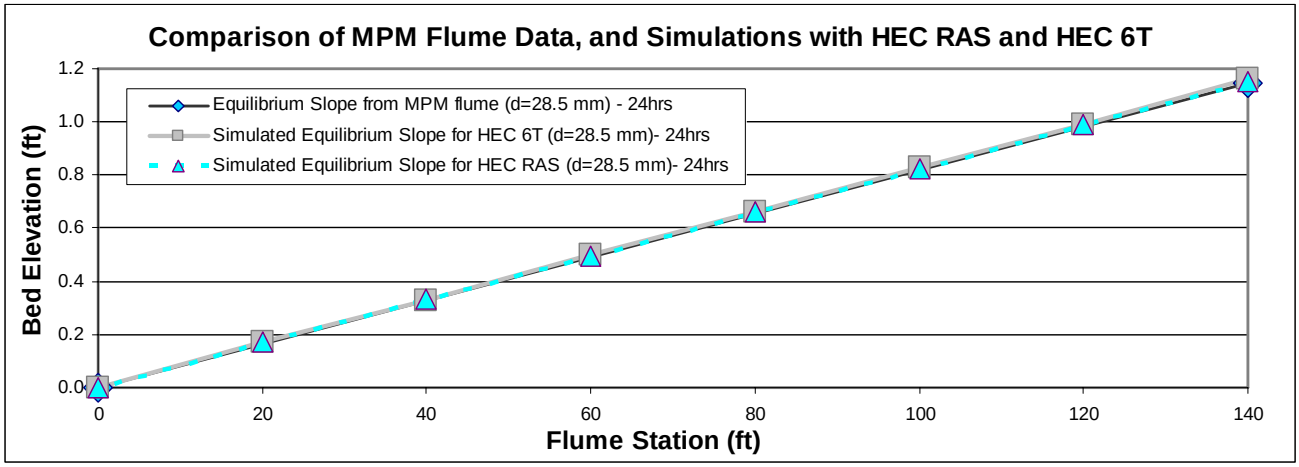


Figure 3 Myer-Peter and Muller flume data with HEC-6 and HEC-RAS simulations.

Comparison to HEC-6: There are several settings between HEC-6 and HEC-RAS that can produce divergent results (e.g. fall velocity method, hydraulic radius vs. hydraulic depth, and friction slope methods). In general, if these settings are harmonized, HEC-RAS does a reasonably good job replicating HEC-6 (e.g. Figure 3). However, sometimes small hydrodynamic differences can result in divergent sediment results. In the example depicted in Figure 4, Yang (1972) was applied to a trapezoidal channel with a single grain size material. Small differences in how HEC-6 and HEC-RAS compute water surface profiles resulted in a minor difference in calculated transport capacity (~0.56%). However, since supply was only slightly larger than capacity, this small capacity discrepancy translated into a 6% difference in total aggradation. Therefore the bed profiles diverge, despite very small calculated differences. It is of note that the computational differences implemented in RAS, though minor, are considered improvements by HEC and, therefore, the sediment responses to these are considered to be improvements as well.

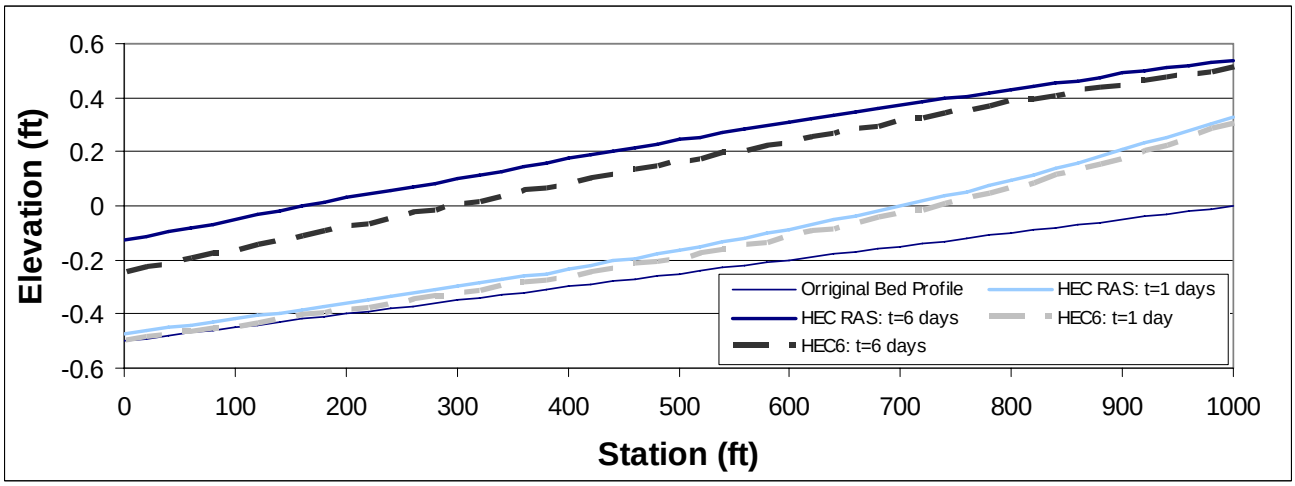


Figure 4 Single grain trapezoidal channel with supply slightly exceeding capacity simulated with HEC-RAS and HEC-6.

Finally, multiple grain size tests were conducted with HEC-6 and HEC-RAS to evaluate the effectiveness of the sorting and armoring routines. The Little and Mayer flume experiment (1972) where clean water was run over a graded bed to investigate armor development was used to test these algorithms. Because the inflowing sediment was set to zero, the sediment load exiting the upstream most cross section during a time step is equal to the eroded mass from that control volume. The material eroded from the upstream cross section is plotted for HEC-6 and HEC-RAS with transport capacities forced equal in Figure 5. As time passes and fine materials are removed from the bed. The bed coarsens and as grain classes are exhausted, there are significant, non-linear drops in the erosion rate. Finally, after approximately two thirds of a day, the armor layer fully forms and prohibits the removal of any more material. HEC-RAS produced the same pattern of grain-specific erosion and armoring as HEC-6 verifying the similarity of the algorithms.

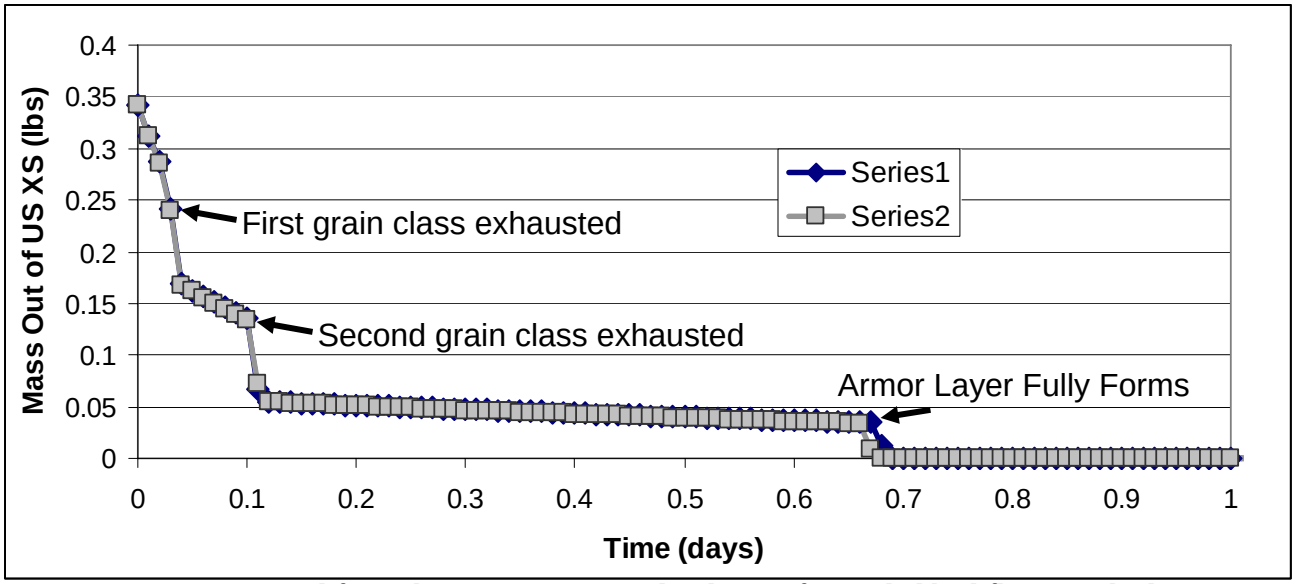


Figure 5 Mass removed from the upstream control volume of a graded bed flume with clear water inflow as simulated with HEC-6 and HEC-RAS.

USER INTERFACE

One of the benefits of implementing sediment transport functionalities into HEC-RAS is the ability to perform these analyses within the framework of the RAS graphical user interface. Sediment input screens have been added to this interface that allow users to specify the limits of their sediment control volumes (Figure 6). Each cross section is attributed with a bed gradation template (Figure 7) in order to allow the initial specification of bed gradation samples which are then associated with the appropriate range of cross sections with drag and click functions. The Flow-load relationships for the upstream boundary conditions and the corresponding gradational breakdowns are also specified through a table in the user interface (Figure 8)

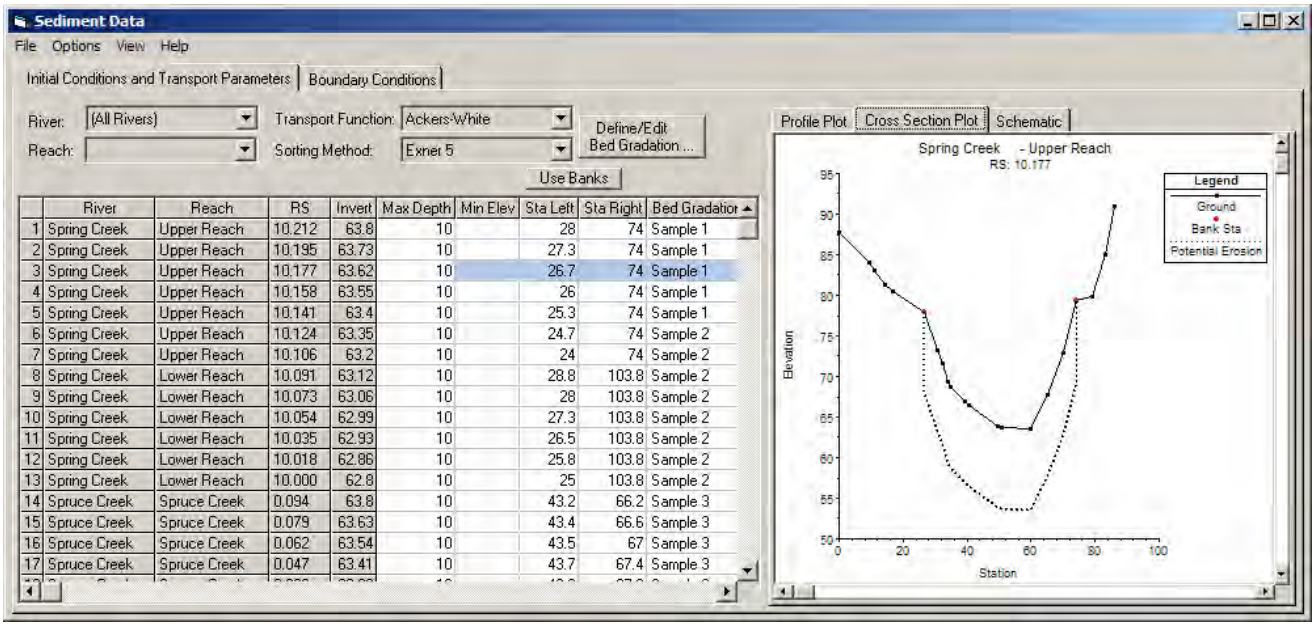


Figure 6 Sediment boundary conditions editor.

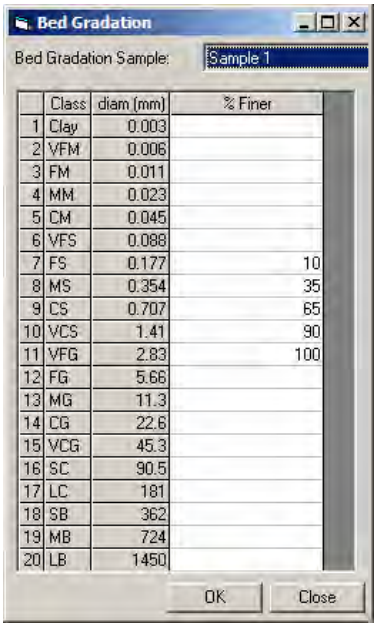


Figure 7 Bed Gradation Template.

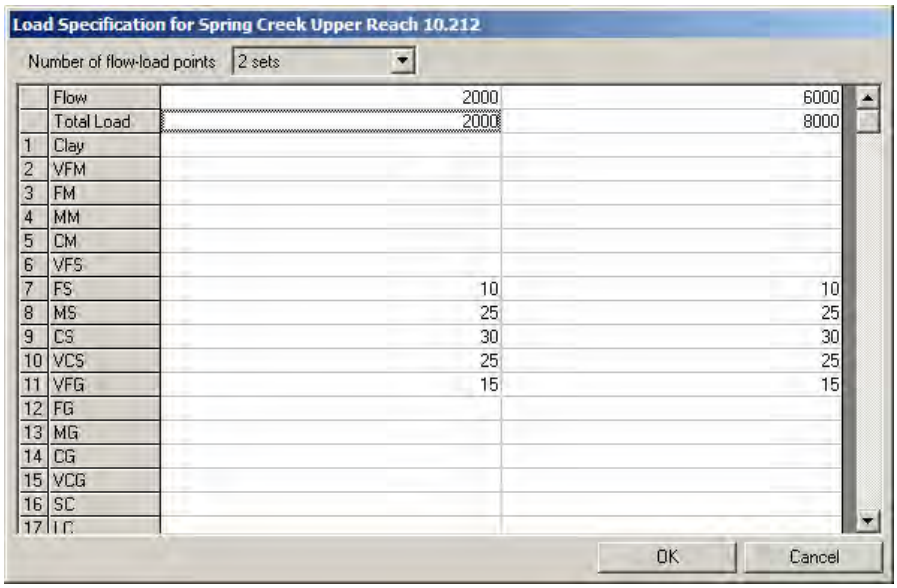


Figure 8 HEC-RAS load specification editor.

OUTPUT

HEC-RAS also has a wide range of variables accessible as output following a run. User output can be viewed as time series or profile data which can be animated.

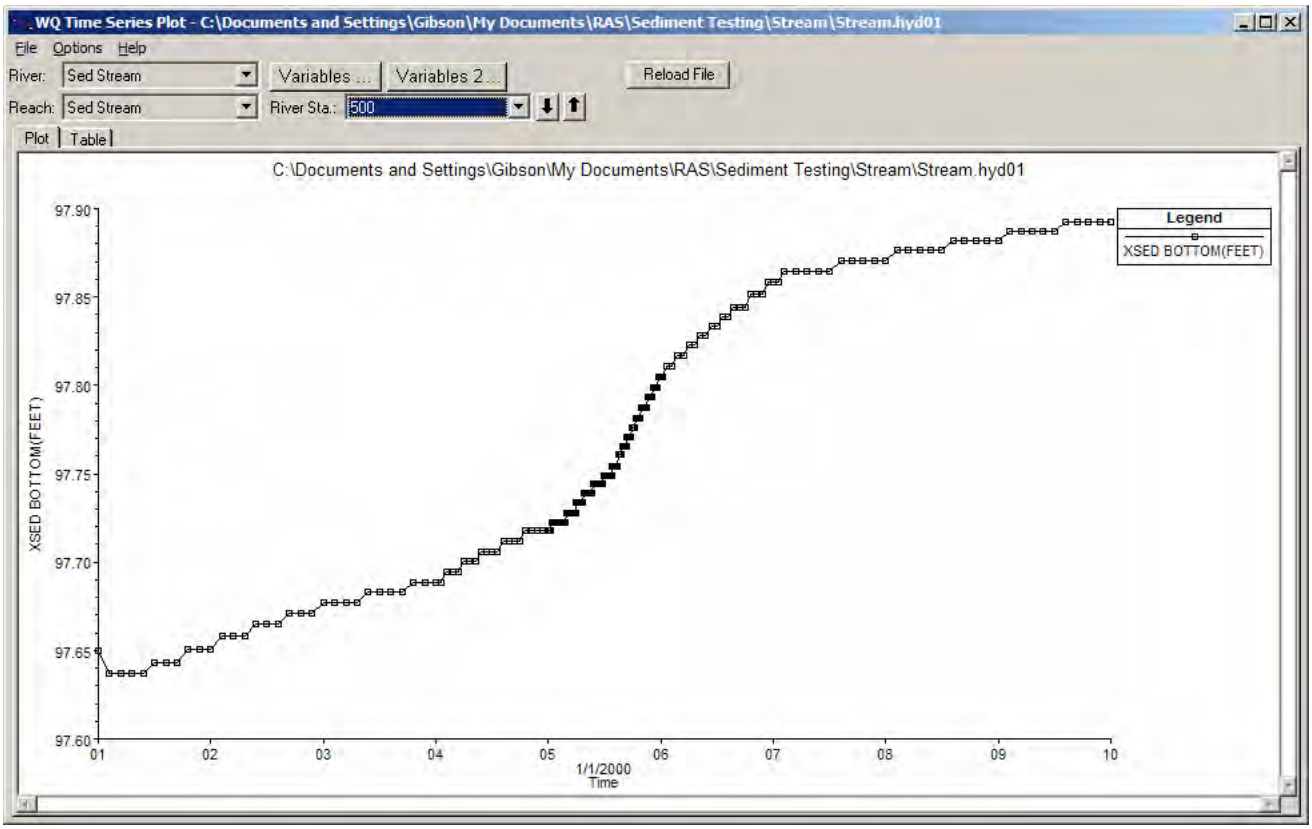


Figure 9 Example of a time series output of bed aggradation at a specified cross section.

CONCLUSION

HEC-RAS now has basic sediment transport capabilities. RAS utilizes quasi-steady hydrodynamics and one of several transport equations to solve the sediment continuity equation. Sediment surpluses and deficits are modified with temporal and physical constraints and translated into bed aggradation and degradation. After each computational time step the RAS geometry file is updated based on bed elevation changes for the hydrodynamics and sediment potential computations to use during the next time step. The model has generally performed well in testing against HEC-6 and flume data, but can differ slightly from HEC-6 in certain conditions due to minor differences in hydraulics. RAS includes a convenient user interface to specify the necessary data for a sediment analysis and a wide range of available outputs for analyzing a simulation.

REFERENCES

Ackers, P., and White, W. R. (1973). "Sediment transport: new approach and analysis," Journal of Hydraulics Division, American Society of Civil Engineers, Vol. 99, No. HY11, pp. 2040-2060.

Armanini, A. (1992). "Variations of bed and sediment load mean diameters due to erosion and deposition processes," Dynamics of Gravel Bed Rivers, Edited by P. Billi, R. G. Hey, C. R. Thorne, and P, Tacconi, pgs. 351-359.

Englund, F. and Hansen, E. (1967). "A monograph on sediment transport in alluvial streams," Teknisk Vorlang, Copenhagen.

Laursen, E. M. (1958). "Total sediment load of streams," Journal of Hydraulics Division, American Society of Civil Engineers, Vol. 84, No. HY 1, pp. 1530:1- 1530:36.

Little and Mayer. (1972). "The role of sediment gradation on channel armoring," Publication ERC-0672, Georgia Institute of Technology: School of Engineering, 105p.

Meyer-Peter, B. and Muller, T. (1948). "Formulas for bed load transport," Report on Second Meeting of International Association for Hydraulics Research, Stockholm Sweden, pp. 39-64.

Toffaleti, F. B. (1968). "Technical report No. 5. A procedure for computation of total river sand discharge and detailed distribution, bed to surface," Committee on Channel Stabilization, U.S. Army Corps of Engineers.

Thomas, W. A. (1994). "Sedimentation in Stream Networks, HEC-6T user's manual," Mobile Boundary Hydraulics Software, Inc., Clinton, MS.

U. S. Army Corps of Engineers. (1993). "Scour and deposition in rivers and reservoirs: HEC-6 user's manual," Hydrologic Engineering Center, Davis, CA.

V. A. Vanoni. (1975). "Sedimentation engineering," ASCE Manuals and Reports on Engineering Practice No. 54, 745 p.

Yang, C. T. (1972). "Unit sream power and sediment transport," Journal of Hydraulics Division, American Society of Civil Engineers, Vol. 98, No. HY10, pp. 1805-1826.

IMPLEMENTATION OF THE SEDIMENT IMPACT ASSESSMENT MODEL (SIAM) IN HEC-RAS

Stanford A Gibson, Research Hydraulic Engineer, U.S. Army Corps of Engineers, Institute for Water Resources, Hydrologic Engineering Center, 609 Second Street, Davis, CA 95616, Stanford.A.Gibson@usace.army.mil; Charles D. Little, Jr., P.E., Research Hydraulic Engineer, U.S. Army Engineer Research and Development Center, Coastal and Hydraulics Laboratory, 3909 Halls Ferry Road, Vicksburg, MS 39180, Charles.D.Little@erdc.usace.army.mil

Abstract: A sediment impact assessment model is being incorporated as part of the Hydrologic Engineering Center's River Analysis System (HEC-RAS) through a joint research and development effort between HEC and the U.S. Army Engineer Research and Development Center's (ERDC) Coastal and Hydraulics Laboratory (CHL). The sediment impact assessment model (SIAM) was initially developed through CHL research activities conducted with Colorado State University. The reach based sediment accounting model has been embedded in the Hydraulic Design module of HEC-RAS, and will provide users with an expedient means of determining average annual sediment impacts for stream networks. The stream network of HEC-RAS provides the conceptual framework for the application of SIAM, and the HEC-RAS user interface expedites data entry. HEC-RAS hydraulic and sediment transport calculations are coupled with user defined bed material and wash material descriptions, sediment sources, and flow duration information to compute reach averaged sediment supply, transport capacity, and local balance by grain size. Input data include bed material gradation, flow duration representative of an average annual hydrologic cycle, sediment properties, sediment source loading by grain size, and reach averaged hydraulic parameters. Results are reported by grain size and in total for each reach, and include local bed material balance, average annual sediment transport capacity, bed material and wash material supply, and local source supply. Use of the HEC-RAS interfaces to generate and execute SIAM runs will be discussed and illustrated.

INTRODUCTION

As water resource projects become more complex, there is a growing emphasis on the ability to implement effective regional sediment management. A common goal of many regional sediment management projects is the reduction of sediment loading from the watershed. This is often accomplished with rehabilitation features such as grade control structures, bank stabilization, drop pipes, dams, and land treatments. While these features are often implemented to reduce sediment yields to downstream areas, the spatial and temporal impacts of these features on the sediment regime of the system are far from straightforward, and often result in unexpected morphologic changes in the channel system. Therefore, the challenge in regional sediment management projects is to select the appropriate sediment management features that produce the desired reductions in sediment delivery while minimizing the disruption to the stability of the channel systems. In order to facilitate this decision-making process, ERDC and HEC are currently developing a Sediment Impact Assessment Model (SIAM), which provides for rapid assessment of the impact of sediment management activities on downstream sedimentation trends. SIAM is viewed as a screening tool for the assessment of multiple rehabilitation alternatives, particularly in the reconnaissance and feasibility phases of a project. It provides a

framework to combine sediment sources and computed sediment transport capacities into a model that can evaluate sediment imbalances and downstream sediment yields for different alternatives. The development of SIAM includes the incorporation of the model into the Hydraulic Design module of HEC-RAS, which is an on-going task at the time of this writing. The implementation of SIAM into HEC-RAS will allow users to utilize the popular, widely used hydraulic modeling system for stream network development and data entry for SIAM applications. In addition, sediment impact assessments with SIAM can easily be conducted for systems where existing HEC-RAS models are available.

SIAM DESCRIPTION

SIAM was initially developed through CHL research activities conducted with Colorado State University on channel stability in small watersheds. The objective of model development was to create a tool that would combine sediment, hydrologic, and hydraulic information for a channel network and determine the average annual sediment budget for the system. In general, SIAM performs reach average sediment transport computations by grain size class, and integrates the computed transport rates with flow duration information to compute an average annual sediment transport capacity in tons per year. Computed average annual sediment transport capacity is compared with the average annual inflowing sediment load to evaluate sediment continuity for the reaches in the system. This provides the means to assess the potential impact of local alterations to the sediment regime on channel stability.

Model Computation Methodology: SIAM treats a stream network as a series of user defined sediment reaches. Sediment reaches are typically delineated based on observed locations of significant geomorphic change such as tributary locations, changes in channel gradient, plan form and geometry, and shifts in sediment composition. Computations of sediment supply and transport are conducted on a reach-by-reach basis and are representative of the average annual conditions for each reach.

In addition to reach-based computations, SIAM sediment computations are also conducted by grain size class. The sediment gradations are divided into fractions with a single representative grain diameter, and sediment transport and supply calculations are conducted independently for each fraction. This accounting by grain size allows the fate of specific size sediments to be observed throughout the system.

The grain size accounting also allows the tracking of wash material and bed material within the system. SIAM determines whether sediments within a system are wash material or bed material based on a user defined wash load threshold diameter. Changes in the wash load threshold diameter permit sediment that is wash material in one reach to transition into bed material in a downstream reach, and vice versa. The wash load threshold diameter is typically determined following Einstein (1950). The value of this model feature is illustrated by considering a channel where the upstream reach is very steep and the channel bed material is correspondingly very coarse, but the downstream reach is significantly less steep and the bed material is much finer. Coarse sands may be included in the wash material of the upstream reach due to a larger wash load threshold diameter. In the downstream reach that is less steep, the wash load threshold diameter is smaller, thus the coarse sand will transition into the bed material. The coarse sand

load would have little morphological impact on stability of the upstream reach as wash material, but would have much more impact on the downstream reach as bed material. This demonstrates how modification of a sediment source by a given management practice could have little effect on channel stability in one reach but have significant effect on stability in reaches farther downstream.

Data Requirements: The SIAM process requires developing input records for each sediment reach that describe bed material composition, sediment properties, hydrology, hydraulics, and sediment loading from local sources (Figure 1). The bed material records define the percentage of sediment present in the channel bed for each grain size class. Sediment property records are used to set the threshold between wash material and bed material, and to select the sediment transport function. Hydrology records define the discharges and corresponding durations that are representative of an average annual hydrologic cycle. The hydrology records are populated with discharge values corresponding to each flow profile in the HEC-RAS model. Hydraulic records list the reach averaged HEC-RAS hydraulic parameters of depth, area, velocity, hydraulic radius, wetted perimeter, top width, friction slope and roughness for each flow profile. The local source records define the sediment sources and corresponding loadings from channel and watershed sources such as eroding channel banks, gullies, upland surface erosion, and point sources such as sand and gravel mining operations.

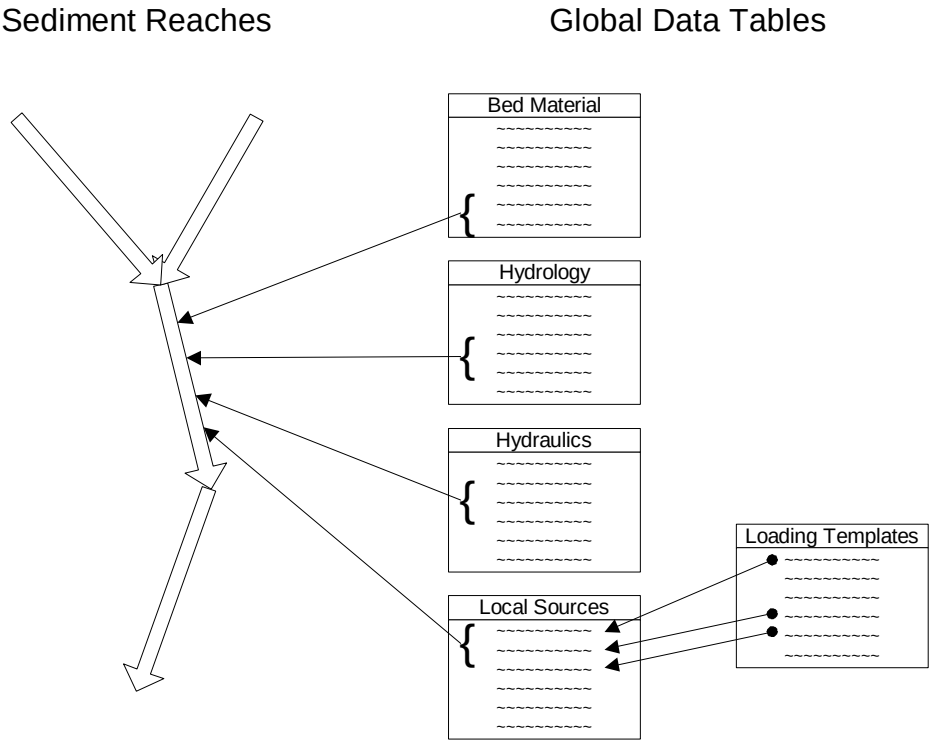


Figure 1 Input data requirements for SIAM

Model Output: The SIAM output consists of local bed material balance, average annual transport capacities, bed material and wash material supplies, and local sediment supply totals for each sediment reach. Local bed material balance is defined as the difference in the bed

material supply and the average annual transport capacity for a sediment reach. A negative local balance indicates excess transport capacity and thus erosion potential for a reach, whereas a positive local balance indicates excess supply and potential for deposition. All output is listed by grain size class as well as total values for each sediment reach.

Capabilities and Limitations: SIAM provides sediment managers an intermediate assessment tool between qualitative evaluations and comprehensive mobile boundary numerical models. Funding constraints and limited resources often preclude the wide-scale use of complex numerical models in a study. With SIAM, users can rapidly evaluate the effectiveness of proposed sediment management techniques and identify which techniques may be candidates for more detailed investigation, thus providing cost savings to the project. Also, the data input structure of SIAM allows individual sediment sources to be easily entered and/or modified, allowing the user to quickly alter sediment loadings to reflect various sediment management techniques. The incorporation of SIAM into HEC-RAS makes the model available to the engineering community in a familiar format with continuing user support.

SIAM is not an event-based sediment routing model, which limits its applicability to investigations where average annual sediment budget calculations are sufficient. SIAM computations are based on annual flow duration, which makes modeling of individual events difficult. Channel geometry is not updated based on erosion or deposition, so the results are only indicative of a single channel configuration for the entire period of record being analyzed. Since SIAM is a reach-based model that uses reach-averaged parameters and produces reach-averaged results, information on specific locations of erosion/deposition cannot be determined.

INCORPORATING SIAM INTO HEC-RAS

Since SIAM directly utilizes HEC-RAS outputs it was advantageous to incorporate SIAM directly into the HEC-RAS framework. This enables a SIAM user to conduct the entire study in a single program, and utilize existing HEC-RAS models, which commonly exist, as a foundation for new SIAM evaluations. The combination of these programs also facilitates integrated output and results analysis capabilities.

SIAM Input: SIAM can be accessed through the "Hydraulic Design" menu in HEC-RAS versions 3.2 and later. The user interface populates the HEC-RAS schematic and provides a series of tabs under which the pertinent SIAM input data can be entered (Figure 2). Sediment reaches are specified and appropriate bed materials, sediment properties and sources are attributed to each sediment reach. Most of these data sets can have a one-to-one relationship with the reaches (e.g. each sediment reach has its own bed material gradation) or can be specified once and applied globally (e.g. a single sediment properties designation, including transport function and fall velocity method, is applied to all reaches).

The five major templates for input data are depicted in Figures 2 through 4. Each sediment reach must have a bed gradation to compute proportional grain fractions for transport capacity computations (Figure 2). HEC-RAS will populate the hydrology dialog (Figure 3a) with the flows corresponding to the sediment reach for each specified profile. The user then associates a duration with each profile to distribute this hydrologic record over a statistically average year.

Next a few basic sediment properties including a transport function are specified on the sediment properties tab (Figure 3b). The hydraulic tab is automatically populated by HEC-RAS (Figure 3c). A single set of hydraulic parameters is associated with each reach for each profile. HEC-RAS computes weighted averages of hydraulic parameters by prorating the value at each cross section by the length of the associated control volume as a percentage of the total reach length. Finally, users specify sediment sources (Figure 4). Annual load by grain size is entered for each source, which can then be associated with multiple sediment reaches and modified by means of a multiplier. Following complete specification of the input data, the "Compute" button will write a SIAM input file and launch the stand-alone program.

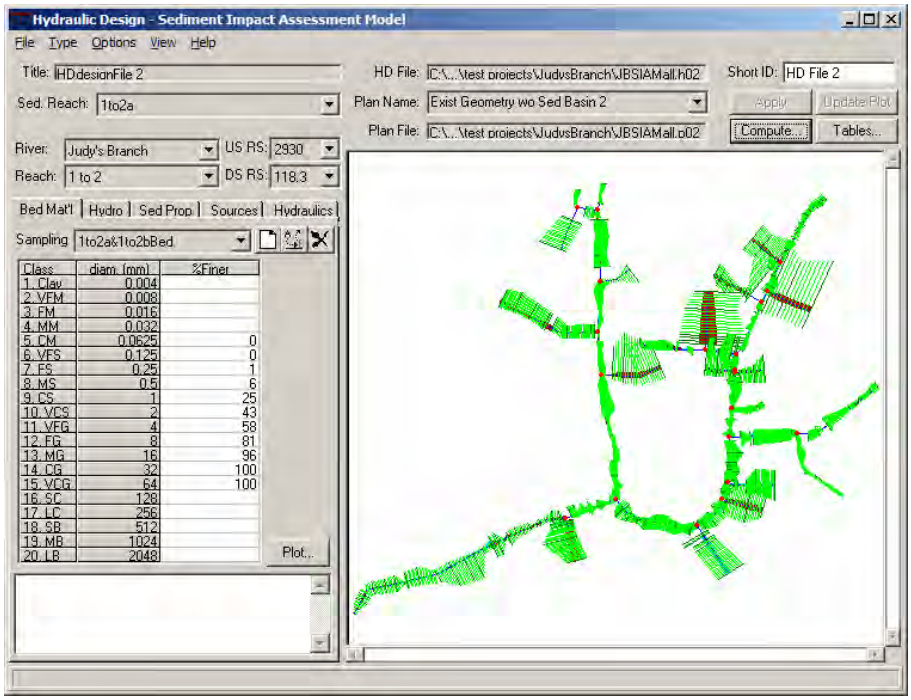
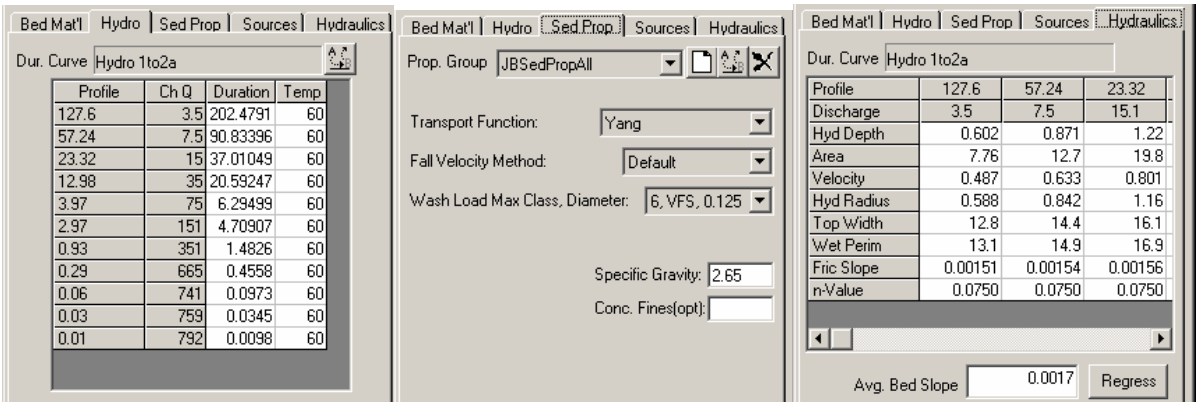


Figure 2 HEC-RAS interface for SIAM with the bed material input tab



(a) (b) (c)

Figure 3 SIAM data tabs in the HEC-RAS interface for (a) hydrology, (b) sediment properties and (c) hydraulics

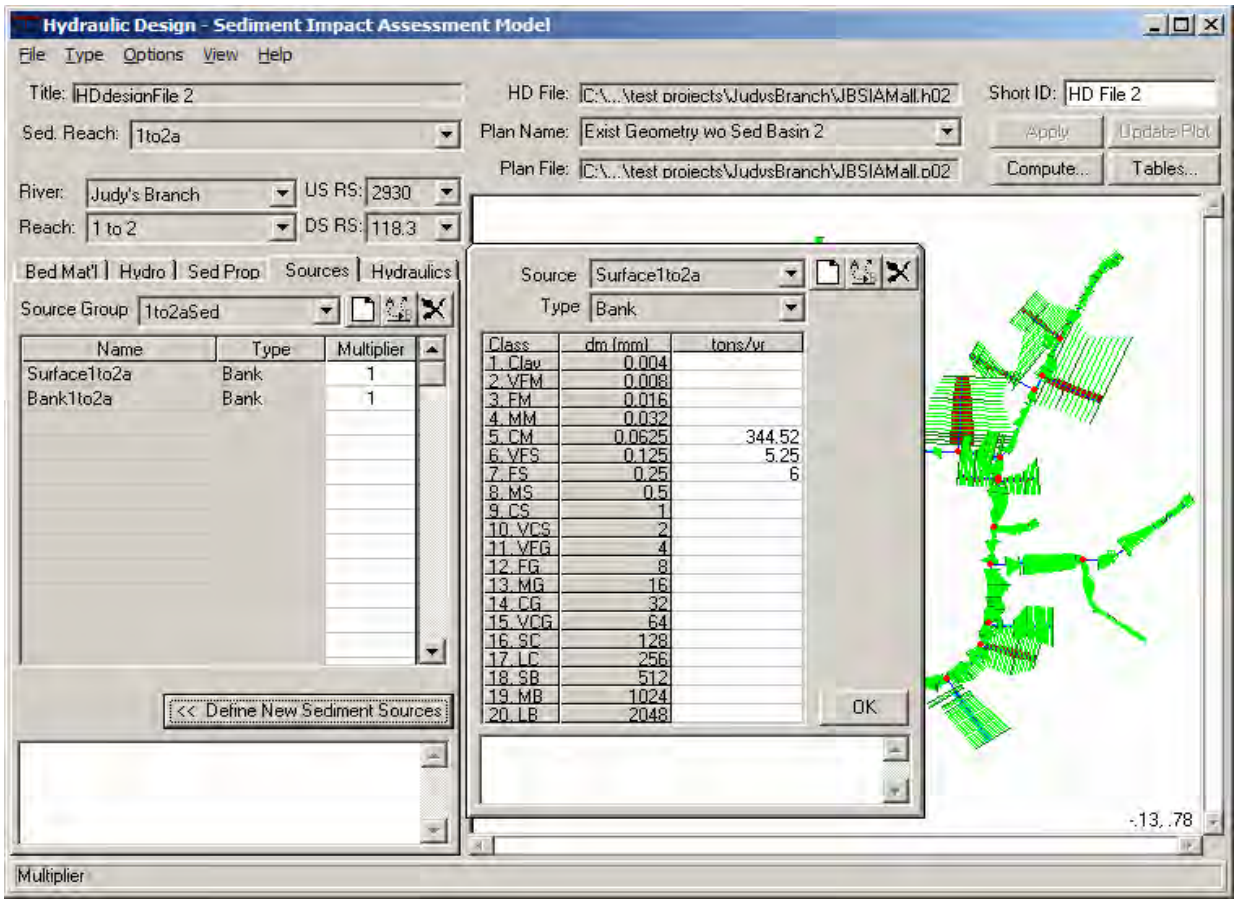
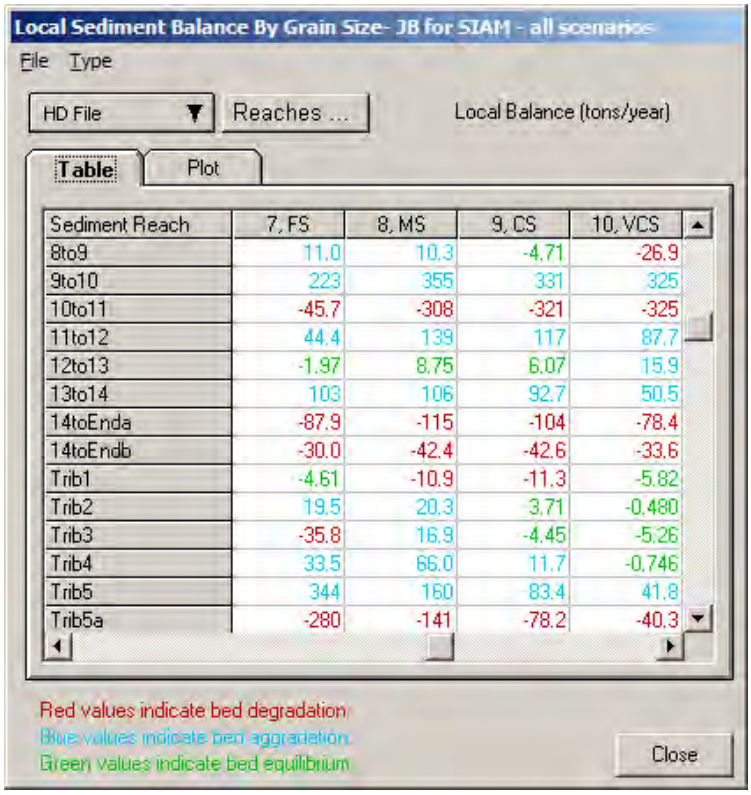


Figure 4 Source specification dialog and tab in the HEC-RAS interface for SIAM.

SIAM Output: SIAM currently generates a binary output file that HEC-RAS reads and makes available through several user output options. A range of tables and graphs are available for analysis of results following a computation. The primary SIAM output is "Local Balance" which reports magnitude of the average annual tendency of a reach to fill or scour. The local bed material balance plot for two alternatives, reported by reach, is depicted in Figure 5. HEC-RAS can also report SIAM output in graphical or tabular form by grain size as shown in Figure 6. Deficits and surpluses reported in tabular form are color coded to quickly identify expected aggradation or degradation, with any computed intervals falling within a user specified "equilibrium tolerance" reported in a third color (Figure 6). Since the local balance can be driven by reach length, a user can also select output by "Normalized Local Balance" which translates reach deficits or surpluses into tons/year/linear foot of channel. This output is more directly relatable to aggradation and degradation and allows more general comparison of impact between reaches. Other output options include grain-specific transport potentials, sediment source and supply information, and breakdowns of wash and bed material.



Figure 5 SIAM output plot of local bed material balance



Sediment Reach	7, FS	8, MS	9, CS	10, VCS
8to9	11.0	10.3	-4.71	-26.9
9to10	223	355	331	325
10to11	-45.7	-308	-321	-325
11to12	44.4	139	117	87.7
12to13	-1.97	8.75	6.07	15.9
13to14	103	106	92.7	50.5
14toEnda	-87.9	-115	-104	-78.4
14toEndb	-30.0	-42.4	-42.6	-33.6
Trib1	-4.61	-10.9	-11.3	-5.82
Trib2	19.5	20.3	3.71	-0.480
Trib3	-35.8	16.9	-4.45	-5.26
Trib4	33.5	66.0	11.7	-0.746
Trib5	344	160	83.4	41.8
Trib5a	-280	-141	-78.2	-40.3

Figure 6 SIAM output table of local balance by grain size

CONCLUSION

SIAM is being implemented into HEC-RAS with the aim of providing planners and designers an easily usable means of integrating sediment continuity concepts into stream rehabilitation and best management practices. It has the capability to be a very effective and easily applied tool for evaluating sediment management alternatives on a watershed scale where the application of complex numerical routing models may be impractical. The incorporation of SIAM into the proven and user-friendly environment of HEC-RAS greatly enhances the option for managers to address the impacts of sediment supply and transport in an expedient and cost effective manner.

REFERENCES

Einstein, H.A. (1950). "The bed-load function for sediment transport in open channel flows", U.S. Dept. of Agriculture, Soil Conservation Service, Technical Bulletin No. 1026.

SEDIMENT INVESTIGATION AND STABLE CHANNEL DESIGN FOR THE LOWER MUD RIVER

Martin J. Teal, Vice President, WEST Consultants, Inc., 16870 West Bernardo Drive, Suite 340, San Diego, CA 92127, mteal@westconsultants.com; Phillip E. Anderson, Hydraulic Engineer, U.S. Army Corps of Engineers, Huntington District, 502 Eighth Street, Huntington, WV 25701, phillip.e.anderson@usace.army.mil

Abstract: The U.S. Army Corps of Engineers, Huntington District (COE or the District) is currently developing a feasibility level investigation to determine viable alternatives for local flood protection for the town of Milton and vicinity in Cabell County, West Virginia. The principal flooding source is the Lower Mud River. In the current investigations several alternatives are being evaluated to determine the most cost effective project. These alternatives consist of a levee and channel widening/channel diversion as well as combinations of these options. A detailed stable channel and sediment transport analysis for the project was warranted to determine the aggradation/degradation tendencies that may have adverse impacts on the operational and functionality characteristics of the local protection project. The objectives of this study were to define both the long-term and short-term aggradation/degradation tendencies associated with the project. This information would be used as a basis for determining expected channel maintenance. Part of the scope for this study was to perform initial design of a new stable channel. Design of the new channel using an innovative combination of geomorphic and sediment transport analyses is described in the paper.

INTRODUCTION

The U.S. Army Corps of Engineers, Huntington District (COE or the District) is currently developing a feasibility level investigation to determine local flood protection alternatives for the town of Milton and vicinity in Cabell County, West Virginia. The principal flooding source is the Mud River.

Within the feasibility study conducted by the COE, several alternatives are being evaluated to determine the most cost effective project. These alternatives consist of a levee (with varying levels of protection) and channel widening/channel diversion as well as combinations of these options. One such alternative, consisting of a levee providing a 250-year level of protection and a new river channel, was identified as the preferred alternative (or PA) for purposes of this study.

A detailed sediment transport analysis for the project was warranted to determine the aggradation/degradation tendencies that may have adverse impacts on the operational and functionality characteristics of the local protection project. While hydrologic and hydraulic tasks were performed as part of the study, this paper will focus primarily on the efforts related to stable channel design with mention as well of the sedimentation analyses.

EXISTING DATA

The available data included an existing HEC-RAS hydraulic model of the study area, historic average daily flow data, historic flood hydrographs, current and historic stage-discharge rating

curves, limited historic suspended sediment measurements, and historic aerial photography. WEST substantially modified portions of the hydraulic model in order to perform hydraulic and sediment transport simulations for this study. The corrected existing conditions model was used as a basis for the preferred alternative HEC-RAS model as well as both existing condition and preferred alternative HEC-6T sediment transport models (MBH, 2002). Historic stream discharge data were available from the U.S. Geological Survey (USGS) gage "Mud River near Milton, WV," active from 1938 until it was abandoned in 1980. No historical aerial photography was available from the COE. However, digital orthographic quadrangle maps (DOQs) for the project and model areas were available from the West Virginia Department of Environmental Protection. These photos were taken in April 1996 and April 1997. Additional aerial photography from March 1988 was available through the TerraServer website (MSN, no date). The COE provided copies of the Milton and Hurricane USGS 7.5 minute topographic maps. Raster graphic images of these same quadrangles were downloaded to use as background images within ArcView GIS. The GIS (geographic information system) was also used to overlay other information provided by the COE such as 1999 and 2001 elevation contours, levee alignment, and "new" cross section locations.

HYDROLOGY

Hydrologic data included both long-term flow data with a period of record equal to the 50-year design life of the project and a short-term flood hydrograph. The long-term data were used to develop an understanding of the long-term trends in aggradation/degradation that should be expected as a result of the project. The short-term data were used to understand the potential magnitude of aggradation/degradation associated with large flood events and what impact this may have on the hydraulics of the channel during a flood. Frequency flows were developed through statistical analysis, and used for fixed bed calibration of the HEC-6T models.

STABLE CHANNEL DESIGN

The preferred alternative developed by the COE consisted of a levee offering a 250-year level of protection and a reach of new river channel within the project limits. Part of the scope for this study was to perform initial design of the new channel such that, on average, it would neither aggrade nor degrade over time. The following sections describe the qualitative evaluation of the sediment transport characteristics of the river [in this discussion, the terms "bypassed channel" or "bypassed reach" refer to that portion of the river that will be cut off and no longer convey flow; the terms "new channel" or "new reach" refer to the newly constructed channel that will take the place of the bypassed channel].

The design of the new channel is presented here in four steps. The first step is the analysis of overall river stability. This evaluation is based on changes in the historic planform of the river, site observations, and a specific gage analysis for the Mud River gage. The second step is analysis of the current planform and hydraulic characteristics of the bypassed reach. The third step is the calculation of the theoretical planform for a "stable channel," using predictive techniques. The fourth step is the determination of a proposed alignment and cross sectional shape for the new channel.

RIVER STABILITY

Historic Planform: The available historic data showed little change in the planform of the Lower Mud River at Milton. Other than minor changes in vegetation, no significant channel movement or bar development was noted. Comparisons of March 1988 aerial photography with 1999/2001 mapping, and 1972 USGS topographic mapping with 1999/2001 mapping, revealed that the channel banks had no significant movement. Minor differences that were seen could be attributed to the water level at the time of each photograph or drawing. Comparison of this information with conditions observed in the field led to the conclusion that the planform of the Lower Mud River has remained relatively constant over the last 30 years.

Site Observations: An extensive field reconnaissance was performed to encompass both the project area and modeled reaches of the river. In general, the Lower Mud River appeared to be a stable river with little signs of active aggradation or degradation. Bank erosion was almost nonexistent.

Specific Gage Analysis: The USGS gage was located near a bridge about five miles upstream of Milton. The site of the gage was visited during the field reconnaissance and no hydraulic controls were noted at the site. Forty-four rating curves were obtained from the COE which cover the time period 1938 to 1978. Each rating curve was examined to determine the stage over time for a series of given flows from 50 to 10,000 cfs. The results of the specific gage analysis show that the Mud River near Milton was relatively stable between 1937 and 1980 (42 years).

EXISTING PLANFORM AND HYDRAULIC CHARACTERISTICS:

Channel Profile: The HEC-RAS model was used to determine the existing longitudinal slope in the bypassed reach. Water surface elevations at the ends of the bypassed reach were used to calculate a slope through the reach. Because determination of the in-bank channel slope was the objective, the highest discharge at which flow was in-bank at all cross sections was used. Based on model results, this discharge was found to be about 800 cfs. At 800 cfs, the average water surface slope is 0.00044.

Cross Section Geometry: The cross sections in the existing conditions HEC-RAS model from about river mile 20.144 to 19.413 were examined. This region includes nine cross sections. The approximate top of bank, toe of slope, and top of slope were estimated at each cross section. There was no discernable trend in the top width changes, except for a narrowing of the channel near the Fairgrounds Road Bridge. It was also found that the average bottom width is 49.4 feet, and the median bottom width is 41.5 feet. The average side slope for left and right banks is 2.2:1 (horizontal to vertical), and the median side slope is 2.28:1.

Amplitude, Meander Length and Radii of Curvature: These parameters were identified via use of a geographic information system for the existing reach to be bypassed.

STABLE CHANNEL PARAMETERS

The next step was to use predictive methods to calculate stable channel dimensions and expected planform parameters. A comparison of the predicted stable channel parameters with the actual parameters in the bypassed reach provides an indication of whether the bypassed reach is stable.

Predictions of stable dimensions for channel width, depth, and longitudinal slope were generated using two "regime" methods. The first method is Copeland's procedure (Copeland, 1994), which balances inflowing and outflowing sediment transport to predict stable channel dimensions. The second method is Julien and Wargadalam's method (Julien and Wargadalam, 1995), which uses a series of equations to predict channel dimensions. Predictions of meander length and amplitude were made using formulas developed by Leopold and Wolman, which predict these parameters based on channel width (Leopold and Wolman, 1960).

Channel Forming Discharge: The use of regime equations or SAM (USACE, 1998) to predict channel geometry requires specification of a channel-forming discharge. This discharge is a single representative flow that will theoretically produce (for stable rivers in regime) the same bankfull dimensions as the natural sequence of flow events.

Biedenharn et al., (2000) describe three ways to estimate channel-forming discharge. The first estimate is the bankfull discharge, the maximum discharge a stream can convey without overflowing its banks. Dunne recommends a 1.5-year recurrence interval as an estimate of bankfull discharge (Dunne et al., 1978). Another, less common, method to estimate bankfull discharge is through the use of the exceedance percentage. Nixon (1959) found that for rivers in England, the average bankfull discharge was equal to the 0.6% exceedance discharge of the mean daily discharges. When a hydraulic model is available, as is the case for this study, the bankfull discharge can also be estimated by modeling the highest discharge where the water stays in bank at each cross section.

The second estimate of channel-forming discharge described by Biedenharn et al., is based on flood recurrence intervals. The channel-forming discharge is generally between the 1-year and 5-year floods. Unfortunately, it is difficult to estimate precisely from this very wide range of discharges.

The third estimate of channel-forming discharge suggested by Biedenharn et al. is the effective discharge. Effective discharge is that discharge which transports the largest fraction of the average annual bed-material load.

The most practical approach, and the most common practice, is to use bankfull discharge to estimate the channel-forming discharge. That approach was adopted here. For this reach of the Lower Mud River, the 1.5-year flood (as suggested by Dunne to estimate bankfull) was not calculated, but the 1-year flood is 5,481 cfs and the 5-year flood is 11,259 cfs. It was found, however, than even the 1-year flood of 5,481 cfs caused most of the cross sections in the bypassed reach to overtop their banks in the HEC-RAS model. The hydraulic model results indicated that discharges somewhere between 3,500 to 4,500 cfs resulted in a bankfull condition at most cross sections in the bypassed reach. The exceedance percentage method of estimating bankfull showed that the 0.6% exceedance discharge equaled 4,080 cfs. Because both the HEC-RAS model and the exceedance discharge method indicate a lower channel-forming discharge than the 1.5-year flood method, these results were

considered more reliable. The 4,080 cfs bankfull discharge obtained from the exceedance method was in the range of the bankfull discharges observed from the HEC-RAS model, and was adopted as the bankfull discharge and the channel-forming discharge for the purposes of this study.

Comparison of Predictions with Existing Conditions:

(1) Copeland Method. The agreement between cross section parameters in the bypassed channel reach and the SAM predictions is excellent. However, this is to be expected. The HEC-6T model was used to generate the sediment transport rates used as an input into SAM. It is therefore not surprising that SAM predicts stable channel parameters which are similar to the actual cross sections found in the bypassed reach. The SAM results are useful, however, for verifying the trapezoidal dimensions and slopes which provide similar sediment transport rates to the natural channel in the bypassed reach.

(2) Julien and Wargadalam's Method. Julien and Wargadalam's formulas provide a more independent prediction of stable channel parameters than the SAM method, since they do not depend on sediment transport rates calculated in HEC-6T. The predicted channel slope of 0.00045 is very close to the average slope of about 0.00044. The Julien and Wargadalam method, however, predicts a somewhat wider and shallower channel than found in the bypassed reach. The actual average depth is about 10 feet versus a predicted 7.2 feet. The actual widths range from below 100 feet to about 145 feet, versus a predicted 187 feet. One possible reason why the existing channel is narrower and deeper than the method's predictions may be the presence of cohesive bank material along much of the Lower Mud River (cohesive material is not considered in the method).

(3) Meander Wavelength and Amplitude. Empirical relations were used to predict the planform variables meander length and amplitude using channel width (w) as the input. The equations used were both from Leopold and Wolman (1960): $8=10.9w^{1.01}$ for meander length and $A=2.7w^{1.1}$ for meander amplitude.

The average existing meander length is 937 feet. The predicted stable meander length of 1234 feet is reasonably close to this value. The meanders in the bypassed reach have amplitudes of 77, 89, 154, 166, 194, and 298 feet. The average of these is 163 feet. The predicted meander amplitude of 466 feet is considerably higher than the existing values.

NEW REACH

Because the bypassed reach is apparently stable, the primary objective of the design of the new reach was to duplicate the parameters in the bypassed reach. For ease of design and analysis, a trapezoidal cross section was used for the new reach. Observation of cross sections from the HEC-RAS model shows that existing sections can also be reasonably approximated by a trapezoid.

The design of the new reach had the primary objectives of preserving the length and slope of the bypassed reach, and preserving the approximate channel geometry of sections in the bypassed reach. Secondary objectives were duplication of meander lengths and meander amplitudes of the existing

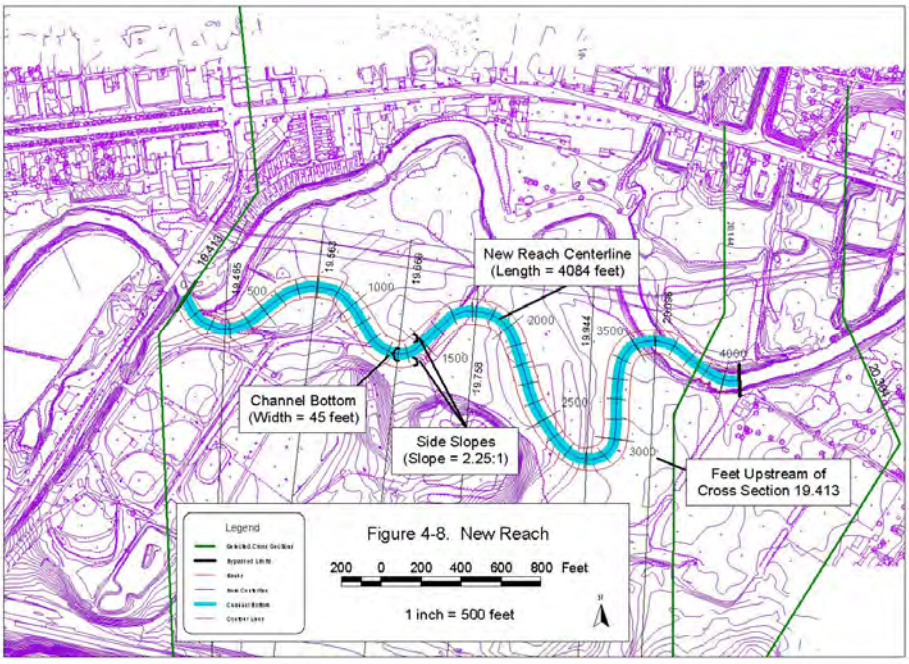


Figure 1 New reach layout.

channel. Another objective was that the meanders should maintain the left-right alternation found in natural channels. This last objective required, for example, that the first meander at the upstream limit of the new reach turn to the right since the previous upstream meander turned to the left.

Alignment: In addition to duplicating the previously measured parameters of the bypassed reach, the vertical position of the new channel needed to be established. The cross section of the existing (bypassed) channel near the upstream limit of the bypassed channel was used to establish the elevation of the new channel. For simplicity, the longitudinal slope of the new reach was set to a constant value, as was the bottom width and sides slopes. This was reasonable, as the existing slope of the bypassed reach is also more or less constant.

The proposed channel centerline is shown in Figure 1. This alignment is based on a 0.00045 longitudinal slope, 45 foot bottom width, 2.25:1 side slopes, and an elevation of 560.00 at cross section 20.144. The bank lines shown are based on where the side slopes would intersect the existing topography, assuming that the bypassed channel is filled in where it does not overlap the new channel. Meander amplitudes, lengths, and radii of curvature were kept within reasonable values as determined from analysis of the existing bypassed channel. Table 1 summarizes how the parameters of the new channel compare to those of the bypassed channel. Generally, the agreement between the new channel parameters and the bypassed channel parameters is good. The depth and width of the new channel depend on the existing terrain; because the terrain elevations were generally higher in the new reach than in the old, the channel tended to be slightly deeper and wider.

SEDIMENT TRANSPORT

Several HEC-6T models were developed to analyze sediment continuity in the Lower Mud River for two scenarios: future without project (FWOP) and future with the preferred alternative (PA).

Models were developed for long-term and single event hydrology, and for sensitivity analyses. Bed material samples were collected at various locations along the Lower Mud River and representative gradations were used in the modeling. From the field reconnaissance and plots of the cross sections, the lateral limits of erosion and deposition were determined at individual cross sections and input to the HEC-6T model. All cross sections were allowed to erode with the exception of those located at two weirs. For inflowing sediment load, the Colby method (Vanoni, 1975) was used to estimate total bed sediment discharge based on the stream measurements of suspended discharge. The values of mean channel velocity, stream width, and mean depth, necessary input for the method, were taken from the HEC-RAS results for the upstream most cross sections.

Table 1 Parameters of bypassed channel versus new channel.

Parameter	**Bypassed Channel ***	**New Channel ****
Channel Length	4,082 feet	4,084 feet
Longitudinal Slope	0.00042 – 0.00046 average across reach	0.00045 constant
Bottom Width	Average about 49 feet Median about 41 feet	45 feet
Side Slope	Average about 2.2:1 Median about 2.28: 1	2.25:1
Width From Top of Left Bank to Top of Right Bank	From about 71 to 141 feet. Average 108 feet	From 96 to 133 feet Average 117 feet
Vertical Position of Channel	Varies	Channel bottom at 560.00 feet at cross section 20.144
Average Depth	From about 6.1 to 11.8 feet Average 10.1 feet	From 4.6 to 12.9 feet*** Average 10.8 feet
Width to Average Depth Ratio at Bankfull	From 7.7:1 to 13.4:1 Average 10.8:1	From 10.2:1 to 15.2:1 Average 10.7:1
Meander Amplitude	From 77 to 298 feet Average 195 feet	From 162 to 356 feet Average 208 feet
Meander Length	From 643 to 1102 feet Average 890 feet	From 643 to 1102 feet Average 903 feet
Radius of Curvature of Bends	From 120 to 500 feet Average 228 feet	From 138 to 260 feet Average 194 feet

* Based on cross sections from the HEC-RAS model.

** Based on cross sections every 10 feet from 10 feet upstream of RM 19.413 to the upstream limit of the new reach.

*** A very low right bank for the first 100 feet upstream of RM 19.413, gives the lowest depths and top widths.

Hydraulic calibration of the sediment models was achieved by running the HEC-6T model in fixed bed mode and making adjustments to model parameters such as roughness values. The calibrated HEC-6T model was used for a long term simulation representative of “future without project” conditions.

Sediment and hydrologic data were added to the geometric data set to create the model. Time steps were adjusted as needed to allow the model to converge to reasonable solutions. The 100-year event hydrograph previously described was also simulated with the calibrated HEC-6T model to gage the response of the system to a single flood event. Because of the great deal of uncertainty in sediment transport modeling, a sensitivity analysis was performed to quantify the affects of several assumptions upon model results. Future without Project (FWOP) results were analyzed for variation of the following parameters: Manning's 'n', inflowing sediment load, and transport equation.

Preferred Alternative: The existing conditions models (HEC-RAS and HEC-6T) were adjusted to reflect the addition of the new channel and levee. Cross sections falling between RM 19.45 and RM 20.2 in the old model were replaced by new cross sections. Water surface and velocity profiles for the calibrated PA HEC-6T model also compared very well with the HEC-RAS model results, except again for expected discrepancies near the bridge locations. Manning's 'n' values were adjusted at these locations to help compensate for this known issue. Differences in channel velocities between the HEC-RAS and HEC-6T model were typically on the order of +/- 5% while water surface elevations were generally within +/- 2%. The 50-year synthetic hydrology record was used with the PA geometry to create the preferred alternative HEC-6T model. Similar to the FWOP results, a general lowering trend is predicted for the bed in the model reach and in the project reach. The PA model was also executed using the 100-year flood hydrograph described previously. The results closely resembled those found for the existing conditions single event model.

CONCLUSIONS

The study revealed that the Mud River in the vicinity of Milton, West Virginia appears to be a stream in quasi-equilibrium based upon historic data, a specific gage analysis and field observations. Numerical simulations of the stream behavior over the next 50 years (FWOP alternative) showed periods of erosion and deposition that varied over time. Overall, results showed that the stream will degrade slightly over much of its length during this period. However, given sensitivity analysis results and the above conclusion, the slight degradational trend may be caused by uncertainties in roughness values and inflowing sediment load and not necessarily by instability in the river system. Considering the long term numerical results in light of historic behavior suggests that the stream will be relatively stable over the next 50 years for the FWOP alternative.

The new channel was designed using geomorphic and engineering methods and is expected to be stable. Because the portion of the existing channel that will be bypassed appears to be stable, the new channel was also designed to match as closely as possible (within project constraints) the hydraulic and geomorphic parameters of the bypassed reach. Sedimentation modeling results support the assertion that the new channel will be stable in that the preferred alternative (PA) results show the same stable to slightly degradational trends as the FWOP results.

REFERENCES

Biedenharn, D.S. Copeland, R.R., Fischenich, J.C. (2000). "Channel-forming discharge," USACE, Engineering Research and Development Center, ERDC/CHL HETN-II-5, Washington, DC.

Copeland, R.R. (1994). "Application of channel stability methods – case studies," Technical Report HL-94-11, USACE, Waterways Experiment Station, Vicksburg, MS.

Dunne, T., and Leopold, L. B. (1978). "Water in environmental planning," W. H. Freeman and Company, San Francisco, CA.

Julien, P.Y., and Wargadalam, J. (1995). "Alluvial channel geometry: theory and applications," Journal of Hydraulic Engineering, ASCE, 121(4), 312-325.

Leopold, L. B., and Wolman, M.G. (1960). "River meanders," Geol. Soc. Am Bull. v. 71, pp. 769-794.

MBH Software, Inc. (2002). "Sedimentation in stream networks (HEC-6T)," Clinton, MS.

MSN (no date). http://terraserver.microsoft.com/

Nixon, M. (1959). "A study of bankfull discharges of rivers in England and Wales," Proceedings of the Institution of Civil Engineers, vol. 12, pp. 157-175.

USACE. (1998). "Draft user's manual for the SAM hydraulic design package for channels," Vicksburg, MS.

Vanoni, V.A. (editor, 1975). Sedimentation engineering. ASCE Manuals and Reports on Engineering Practice Number 54, ASCE, New York, NY.

SEDIMENT IMPACT ANAYSIS FOR THE LOWER THAMES FLOOD STRATEGY STUDY

Ian M Tomes, SE Area Flood Risk Manager, Environment Agency (Thames Region), Frimley, Surrey, UK, ian.tomes@environment-agency.gov.uk; Oliver P. Harmar, Consultant Geomorphologist, Halcrow Group, Leeds, UK, HarmarO@halcrow.com; Colin R. Thorne, Professor of Physical Geography, University of Nottingham, Nottingham, UK, colin.thorne@nottingham.ac.uk,

INTRODUCTION

Sediment impact assessment was performed during the Lower Thames Flood Strategy Study to assess the geomorphological sustainability of river-bed re-profiling to reduce flood risk in the reach between Datchet and Teddington. The specific objectives of the sediment study were to:

i. estimate how much sediment is likely to be deposited in, or eroded from, the study reach by flows up to and including long return interval flood events for 'do minimum' and 'bed reprofiling' options that would lower the bed by 0.5 to 1 m;

ii. estimate an average annual rate of sedimentation for the 'do minimum' and 'bed reprofiling' options.

MORPHOLOGY OF THE RIVER THAMES

The study reach of the River Thames has the characteristics of a mature, lowland river with well developed meanders and reaches divided by stable, mid-channel islands. The movement of water and sediment along the river has been controlled by locks and weirs for over a century. These structures present obstructions to the natural movement of sediment and dredging was, historically, required to maintain a navigable channel. The banks along much of the navigable river have been stabilised by revetment and, therefore, the river is unable to adjust its planform.

SEDIMENTATION AND SEDIMENT TRANSPORT

Analysis of dredging records: Dredging records for the Lower Thames, investigated as part of the Lower Thames Dredging Study (Mott MacDonald, 1998), show that dredging has declined from the high activity of the late 1940s to the late 1990s, following the 1947 flood, and that since 1997, there has been very little dredging in the study reach. The reduction in dredging over recent years may be related to a reduction in sediment supply due to river engineering throughout the Thames basin. The recent cessation of dredging reflects not only a reduced need, but also stringent new environmental controls on the disposal of dredged material, coupled with increased costs of disposal.

It is believed that the quantities of sediment dredged annually in the study reach were broadly in balance with annual rates of sedimentation for the 10-20 year period prior to 1997, when dredging ceased, suggesting a sedimentation rate of about 37 000 tonnes/year. Since then, bed elevations are thought to have increased somewhat, in response to the lack of dredging (Smith, pers. comm., 2005).

Suspended sediment concentration from the Thames: No long term record of suspended sediment concentration has been published for the Lower Thames. However, HR Wallingford (1988) report measurements over a 3-month period in 1987 (Figure 1).

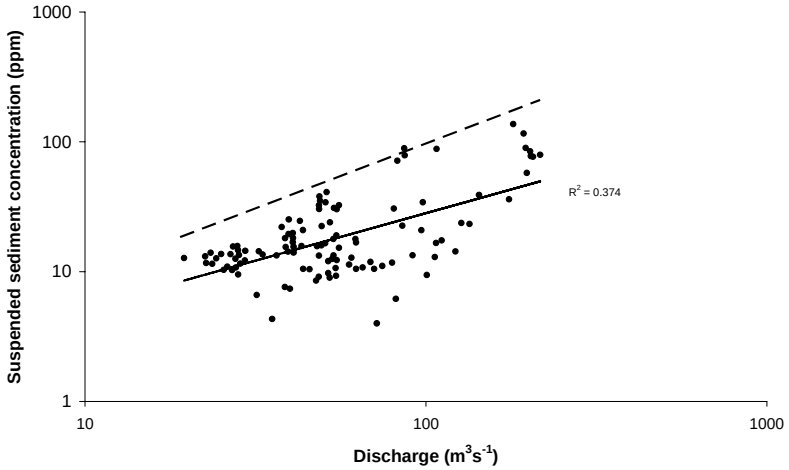


Figure 1 Sediment rating curve at Boulters Weir from HR Wallingford (1988).

The best-fit regression line for the data in Figure 1 has the form: $C = aQ^b$, where, $a = 0.97$ and $b = 0.78$. This equation gives a sediment concentration at near bankfull flow of only 91.5 ppm. On most river systems, the value for the exponent b, typically falls in the range 1 to 2 (Walling and Webb, 1992). Hence, the above relation probably under-estimates suspended sediment concentrations, particularly at high flows. Des Walling (pers. comm. 2005) suggests that suspended sediment concentrations in the Lower Thames may reach 250-300ppm at bankfull flow. If a value of unity were used for exponent *b* in the above equation, a suspended sediment concentration of 250 ppm would be obtained for a bankfull flow of 256 m^3s^{-1}, which may be more reliable than the value based on the limited measured data. Hence, in the modelling section of this study, the Q-C relation obtained using this higher exponent was used as well as the Q-C relation for the measured data, to specify *upper* and *lower-bound* estimates of sediment inflow concentration.

Sediment load estimates: Q-C relations can be used to estimate the total suspended sediment load transported during a specific time period by combining the sediment concentration with the discharge record. The upper and lower bound sediment concentrations from Figure 1 were converted to sediment loads in tonnes/day and the sediment transport for each discharge class was multiplied by the frequency of occurrence at the Windsor gauge between 1979 and 2004 to estimate the suspended sediment load transported during that period. Dividing these totals by the number of years of record gives a lower-bound annual sediment load estimate of 45 000 tonnes and an upper bound estimate of 158 000 tonnes. This equates to an upstream sediment yield in the range 6-22 t km^{-1} which is considered appropriate given the land use characteristics and sediment control upstream (Halcrow, 2001). These sediment loads are, however, considerably higher than the estimated average annual rate of sedimentation (37 000 tonnes/year). This indicates not only that some of the bed material load passes through the study reach, but also that at least 70% of the total granular load is actually 'wash load', which is held permanently in suspension and hence, does not accumulate on the river bed. If 25% of this material is assumed to deposit in the study reach (75% being through-put load and washload), 11- 40 000 tonnes will be deposited in the channel (not including sediment contributions from the tributaries). When considered

alongside the estimate of 37 000 tonnes from dredging/hydrographic survey analysis, it suggests that the measured Q-C relation may indeed underestimate sediment concentration.

Suspended sediment concentrations from the Jubilee River and tributaries: In addition to specifying the upstream Q-C relation for the River Thames, Q-C relations must be specified for tributary and other inflowing channels for the purposes of sediment impact assessment. The tributaries and inflowing channels in the study reach are listed below in downstream order. As no measured sediment concentrations are available for these watercourses Q-C relations were formulated from available, qualitative information.

- Jubilee River (flood diversion channel)
- River Colne (tributary)
- River Wraysbury (tributary)
- Colne Brook (tributary)
- River Wey (tributary)
- River Mole (tributary)

The Jubilee River diversion channel carries a high proportion of the total flow in the Thames during a 5-year event and, therefore, represents a potentially important sediment inflow. Analysis of aerial photographs during the 2003 flood on the Lower Thames indicate that the sediment concentration in the Jubilee River diversion channel was higher than that in the main river. However, the concentration may have been elevated because it was the first time the channel was operational. In the modelling, the suspended sediment concentration inflow from the Jubilee was, therefore, assumed to be the same as the inflow from the main Thames. The Rivers Wey and Mole are the most important tributaries in terms of discharge. In the River Wey Environmental Management Strategy (Mott MacDonald, 1997), the sediment concentration is estimated to be 200 ppm at 10 m^3s^{-1} and 400 ppm for a mean annual flood flow of 28.4 m^3s^{-1}. To obtain a Q-C relation for the tributary inflow boundary, higher and lower flow concentrations were extrapolated based on these estimates. Since the River Mole has some similar catchment characteristics to the River Wey, this Q-C relation was also used as the inflow boundary for the Mole tributary. There is no published information regarding sediment concentrations for the remaining tributaries and so Q-C inflow relations were assumed to be the same as in the main river. Errors resulting from this assumption are not significant because their collective discharge contribution is minor (12 m^3s^{-1} for the 5 year design event) and, therefore, their collective contribution of sediment will also be small.

Suspended sediment composition: The only reported information on suspended sediment composition in the Lower Thames is provided from a 25 litre water sample collected from the silt monitoring station just upstream of Boulters Weir as part of the Maidenhead Morphological Study (HR Wallingford, 1988). The D_{50} and D_{75} of the silt-sized fraction were found to be 0.005mm and 0.017mm, respectively. Since material of sand-sized or coarser (>0.063 mm) was not analysed, these values represent only the finer fraction of the sediment load. It is likely that the D_{50} and D_{75} would have been somewhat coarser if the whole particle size distribution had been analysed, better representing suspended sediment characteristics in the River Thames. Since there is little reported information on the suspended sediment composition of the tributaries, they are assumed to be the same as those in the main river.

Surface bed material: A series of bed material gradation curves arising from the available data are plotted in Figure 2. Bed material is generally dominated by fine-medium gravel (70-

95%) and medium-coarse sand (5-25%), although individual samples range from fine-medium sand dominated (with some silt/clay material) to coarse gravels-dominated. The degree of variability is shown by the 'min' and 'max' curves representing the finest and coarsest of 40 samples analysed (HR Wallingford, 1988).

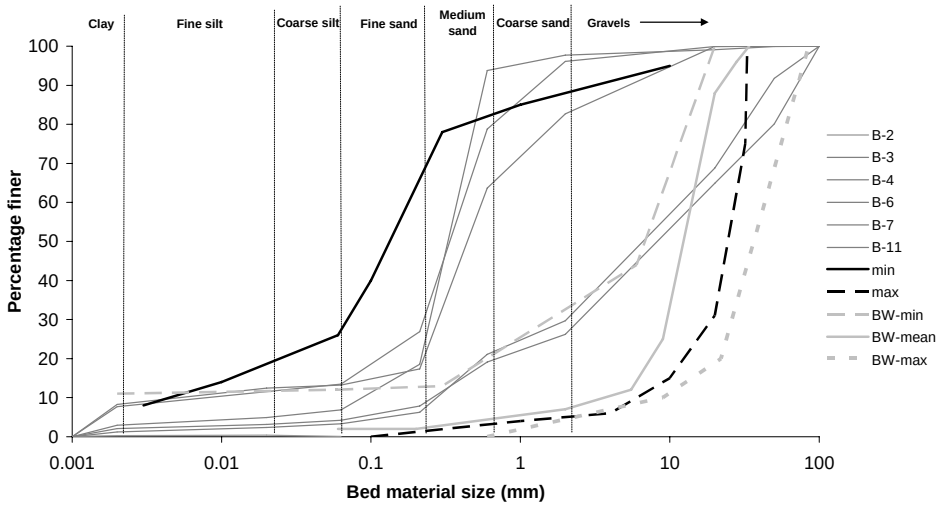


Figure 2 Bed material gradation curves for samples taken from the Lower Thames.

Subsurface bed material: The sediment stratigraphy from borehole logs was used to infer the composition and variability of subsurface material. The upper layer is floodplain alluvium, which is typically composed of fine silt, sand and clay and has an average thickness of approximately 3 m. This is underlain by a much coarser, gravel-dominated complex. The Lower Thames flows across these gravels for most (if not all) of the study reach. The thickness of the gravel unit averages 4.2 metres, although this ranges from about 1 metre to over 6 metres. Hence, deepening the river by re-profiling the bed is likely to expose gravel similar to the existing bed material in most locations. However, there is a risk of underlying London Clay being exposed in some downstream locations, where the gravel unit only about 1 m thick.

iSIS-SEDIMENT MODELLING

The 1-D iSIS sediment transport model was used to estimate the sediment impacts in the study reach of 'do minimum' and 'bed re-profiling' options. Modelling involved three stages:

1. assessing the sensitivity of model output to sediment boundary conditions; inflow suspended sediment concentrations; inflow suspended sediment composition; and bed material composition.
2. simulating the geomorphological impact of design flow events with return periods of 2, 5 and 20-years and a constant lower flow (25% exceedance at Teddington) for 'do minimum' and 're-profiling' options.
3. predicting the long-term average annual rate of erosion/deposition from the event-based analyses described above.

iSIS-sediment uses equations for sediment transport and sediment continuity to calculate sediment transport rates, erosion/deposition and bed elevation changes within a modelled reach. Cross-sections are updated according to predicted quantities of erosion/deposition and the hydraulic model is updated accordingly at the end of each timestep. Sediments can be divided into as many as 10 particle size classes. Transport rates for each size fraction are predicted using one of four sediment transport equations. Fractions can be specified as either cohesive or non-cohesive. In this study, the Westrich-Jurashek sediment transport equation was used for cohesive sediments (< 0.032 mm) and the revised Ackers-White sediment transport equations were used for all coarser fractions.

A base iSIS-sediment transport model was completed and tested, with gate movement rules added to the model to ensure water levels stay above the Standard Head Water Levels at each of the lock reaches (i.e. the levels retained for navigation). This is necessary as much of the sediment deposition is likely to occur as the flows recede after an event, as well as possibly during lower flow periods.

iSIS-sediment was run for the 2, 5 and 20-year return period flows, and a constant in-bank flow to account for lower flows. Sediment boundary conditions were specified for the channel bed and for all upstream inflow boundaries. Suspended sediment inflows into the Lower Thames (upstream, Jubilee and tributaries) were specified as Q-C boundaries. It was assumed that the density of all sediments was 2650 kg m^{-3} and a constant bed porosity of 0.6 was used.

To predict event-based and longer-term average rates of erosion/deposition, the upper and lower bound estimates of sediment concentration were applied for sediment inflow boundaries. Sensitivity analyses were undertaken to identify model response to variations in bed material and suspended material composition.
Based on the results of sensitivity analyses, it was decided to appraise options for the range of flow boundaries using three sets of sediment boundary conditions:

1. measured (lower bound) inflow sediment concentration and coarse bed material.
2. high (upper bound) inflow sediment concentration and coarse bed material.
3. measured inflow sediment concentration and intermediate bed material.

Sediment Impact of events for 'do minimum' option: In Figure 3, net deposition amounts are plotted for the three return period events and the constant, in-bank flow. There is greater uncertainty in the reach response for higher return period events. Both model runs with coarse bed material result in aggradation, but when the bed material has the intermediate composition, net aggradation is recorded at the constant flow and 2-year event, but the study reach degrades for longer return period events. Given that the bed material is composed of approximately 70-95% gravel, it is unlikely that net degradation would actually occur in the study reach. However, the intermediate bed results do suggest that areas of the bed in which there are high proportions of sand sized material (>20%) may scour during events with return periods of 5-years or longer.

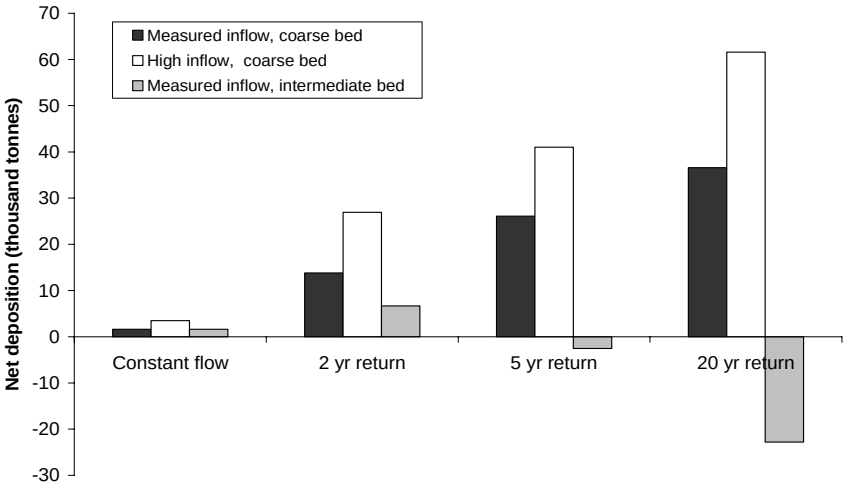


Figure 3 Net deposition at Teddington for the 'do minimum' option.

Based on these results, average rates of sedimentation would be in the range 23 to 44 000 tonnes/yr for a lower and upper bound inflow sediment concentrations with a coarse bed, but only about 7 000 tonnes/yr for a lower bound inflow concentrations with an intermediate bed material. Since the analysis of hydrographic surveys and historic dredging records yielded an average annual rate of sedimentation of 37 000 tonnes, the coarse bed estimates seem to provide more reasonable upper and lower bound estimates of sedimentation rates. Assuming an active bed width of 30 m and uniform deposition throughout the study reach, these estimates represent siltation rates of approximately 12 to 25 mm/yr. These are however only estimates because actual rates of deposition will vary between sub-reaches and more locally around shoals and hydraulic structures.

Sediment impact of bed re-profiling: The bed re-profiling option was modelled by taking the iSIS model representing existing conditions and lowering the bed of the river to 4.0m below the Standard Head Water Level (SHWL: the navigation water level maintained by the downstream weir and sluice structures at each lock). The depth below SHWL is constant between the lock, weir and sluice structures, resulting in a stepped profile (Figure 4). The re-profiled sections of river bed are roughly trapezoidal, with an increased depth of 0.5 -1 metre. Although the degree of bed lowering varies across the cross-section, deepening has only been applied between bank toes to prevent over-steepening of the banks and so maintain bank stability. Hence, deepening has been applied to roughly the central third of the river.

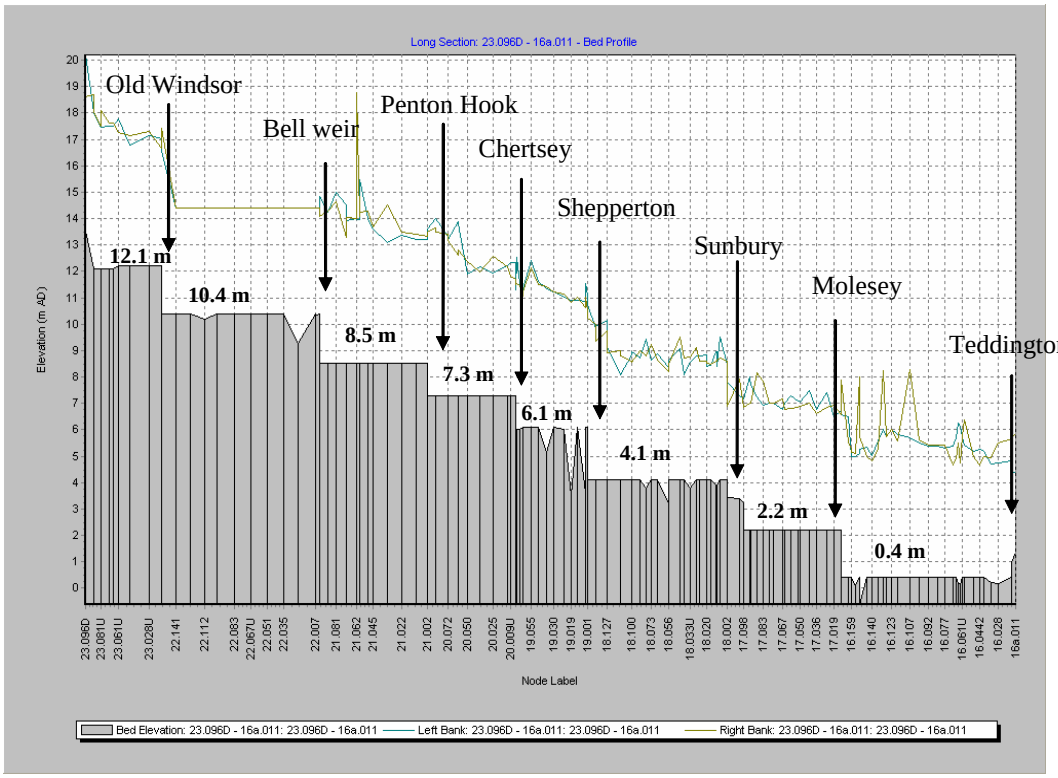


Figure 4 Long section of the study reach after bed re-profiling in the model.

In Figure 5, net rates of deposition are compared for the three return period events and the constant in-bank flow for the 'do minimum' and 're-profiling reach 3' options. The inflow sediment concentration is the measured (lower bound) Q-C relation, with the coarse bed composition, since this better represents bed composition through most of the study reach. Net deposition rates for the are similar for the 'do minimum' and 're-profiling' options. This suggests that sediment impacts associated with bed re-profiling are not serious and that the longterm average annual rate of sedimentation is unlikely to increase dramatically.

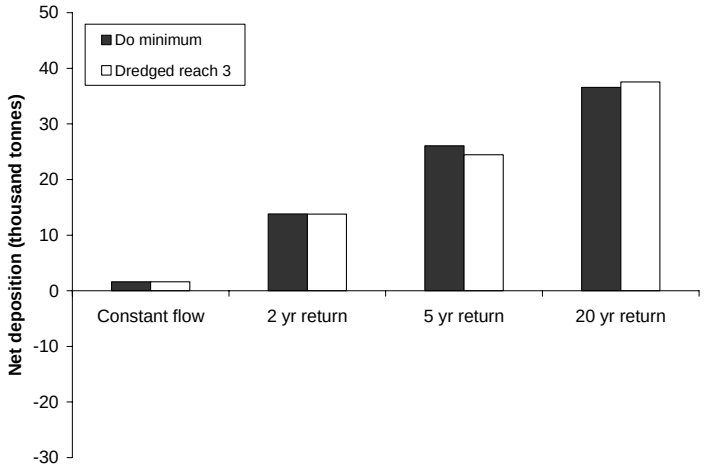


Figure 5 Net deposition for the 'do minimum' and 'bed re-profiling options'.

CONCLUSIONS

Dredging records, measured sediment transport data, and iSIS-sediment transport modelling used in the Lower Thames Flood Strategy Study indicate a long-term annual rate of sedimentation in the range 23-44 000 tonnes or 12-25 mm/yr. iSIS-sediment modelling results suggest that river bed re-profiling will not lead to a significant increase in the rate of sedimentation providing that bed lowering is restricted to between bank toes. The sediment impact assessment used here was developed in conjunction with the UK Flood Risk Management Research Consortium www.floodrisk.org.uk funded by the EPSRC under grant GR/S76304/01, jointly with NERC, the Joint Defra/EA R&D programme, the Scottish Executive, the Rivers Agency (Northern Ireland) and UK Water Industry Research.

REFERENCES

HR Wallingford. (1988). "Maidenhead, Windsor and Eton flood study: morphological model studies," Wallingford, Oxfordshire.

Mott MacDonald. (1997). "River Wey environmental management study," Report prepared for the Environment Agency, Frimley, UK.

Mott MacDonald. (1998). "River Thames dredging study scoping study," Prepared for the Environment Agency, Frimley, UK.

Halcrow (2001). "Sedimentation in storage reservoirs," Report to the Department of the Environment, Transport and the Regions, Halcrow Group Ltd, Swindon.

PERFORMANCE OF BED LOAD TRANSPORT EQUATIONS IN MOUNTAIN GRAVEL-BED RIVERS: A RE-ANALYSIS

Jeffrey J. Barry, Water Resource Engineer, University of Idaho and CH2M Hill, Boise, Idaho, email (jeffrey.barry@ch2m.com); John M. Buffington, Research Geomorphologist, University of Idaho and USDA Forest Service, Rocky Mountain Research Station, Boise, Idaho, email (jbuffington@fs.fed.us); John G. King, retired Research Hydrologist, USDA Forest Service, Rocky Mountain Research Station, Boise, Idaho; Peter Goodwin, Professor of Civil Engineering, University of Idaho, Boise, Idaho, email (pgoodwin@uidaho.edu)

Abstract: Our recent examination of bed load transport data from mountain gravel-bed rivers in the western United States shows that the data can be fit by a simple power function of discharge, with the coefficient being a function of drainage area (a surrogate for basin sediment supply) and the exponent being a function of supply-related channel armoring (transport capacity in excess of sediment supply) (Barry et al., 2004). We also compared the performance of our proposed equation to that of five commonly used bed load transport equations. Here, we explore the sensitivity of equation performance to differences in how the statistical assessment of error is parameterized. We also consider the performance of these bed load transport equations in terms of geomorphic significance. Over the past two decades numerous studies have assessed the performance of various equations for predicting bed load transport; however, these analyses have been based on paired observations of measured and predicted bed load transport, the majority of which were taken at low flows (including Barry et al. (2004)). Consequently, formula performance is weighted toward low discharges which may not have geomorphic significance. Here, we consider equation performance at a number of gravel-bed rivers in mountain basins of the western United States in terms of the accuracy with which the equations are able to predict the effective discharge.

INTRODUCTION

In previous work, we examined bed load transport in 24 mountain gravel bed-rivers in central Idaho, using an extensive dataset recently compiled by King et al (2004). This data set included over 2,100 bed load transport observations collected over a range of flows from 2 to 181% of the 2-year flood flow (Q_2). We showed that the observed bed load transport could be fit by a simple power function of discharge and that the coefficient of this equation is a function of drainage area (a surrogate for basin sediment supply), while the exponent is a function of supply-related armoring, parameterized by Dietrich et al.'s (1989) q^* ratio (Barry et al., 2004). We evaluated the performance of this bed load transport equation and four other commonly used equations in terms of their ability to predict the observed bed load transport rates at 17 test sites outside of Idaho, thereby providing a test of our equation independent from the sites from which it was developed. The 17 test sites are mountain gravel-bed rivers in Oregon, Wyoming and Colorado, and are further described by Barry et al. (2004). The selected bed load transport equations were those of 1) Meyer-Peter and Müller (1948), 2) Ackers and White (1973) (as modified by Day (1980)), 3) Bagnold (1980), 4) Parker (1990), and Barry et al. (2004).

To examine formula performance, we calculated the critical error, e^*, at each of the 17 test sites, where e^* is the smallest amount of error that will lead to adequate model performance (i.e.,

acceptance of the null hypothesis of equal distributions of observed and predicted bed load transport rates assessed via Freese's (1960) χ^2 test at a significance level of 0.05). Hence, we are asking how much error would have to be tolerated to accept a given bed load transport equation (Reynolds, 1984). Freese's (1960) χ^2 test is calculated as

$$\chi^2 = \frac{\sum_{i=1}^{n} (x_i - \mu_i)^2}{\sigma^2} \tag{1}$$

where x_i is the i^{th} predicted value, μ_i is the i^{th} observed value, n is the number of observations, and σ^2 is the required accuracy defined as

$$\sigma^2 = \frac{E^2}{(1.96)^2} \tag{2}$$

where E is the user-specified acceptable error, and 1.96 is the value of the standard normal deviate corresponding to a two-tailed probability of 0.05. We evaluate χ^2 using log-transformed values of bed load transport, with ε added to both x_i and μ_i prior to taking the logarithm, and E defined as one log unit (i.e., ± an order of magnitude error). We use ε in our analysis because the Meyer-Peter and Müller (1948), Ackers and White (1973) and Bagnold (1980) equations contain a transport threshold. Formulae of this sort often erroneously predict zero transport at low to moderate flows that are below the predicted threshold for transport. To include the incorrect zero-transport predictions in our log-transformed assessment of formula performance, we added a constant ε (equal to the lowest predicted transport rate of $1 \cdot 10^{-15}$ kg/m·s) to all predicted bed load transport rates. We find that both the Meyer-Peter and Müller (1948) equation and the Bagnold (1980) equation typically under predict total transport due to the large number of incorrect zero predictions, with the magnitude of this under prediction set by ε. Figures 1 and 2 (modified from Barry et al. (2004)) show the prediction error and the critical error, e^*, at each of the 17 test sites. The effect of ε set to $1 \cdot 10^{-15}$ kg/m·s is illustrated by the extent of under-prediction, with the magnitude of the under-prediction set by ε (Figure 1), and in the high values of critical error associated with both the Meyer-Peter and Müller (1948) and the Bagnold (1980) equations (Figure 2). Because the effect of ε is evident in the both the prediction errors (Fig. 1) and the critical errors (Fig. 2) for the Meyer-Peter and Müller (1948) and the Bagnold (1980) equations, we examine the sensitivity of formula performance to ε in this paper.

Moreover, our previous analysis considered formula performance based on paired observations of measured and predicted bed load transport, similar to approaches used in other studies (e.g., Gomez and Church, 1989; Yang and Huang, 2001). Because the majority of bed load transport measurements are typically taken during low flows, the assessment of formula performance may be biased toward low discharges which generally do not have geomorphic significance. Geomorphically significant sediment transport in sand- and gravel-bed rivers typically occurs at bankfull flow, which is recognized as both the effective discharge (Q_e, that which transports the most sediment over time (Wolman and Miller, 1960; Andrews and Nankervis, 1995)) and the channel forming discharge (that which controls channel morphology (e.g., Henderson, 1963; Parker, 1978)).

Here, we examine sensitivity of formula performance to selection of ε, and we explore the geomorphic performance of bed load transport equations in terms of their ability to accurately predict the effective discharge.

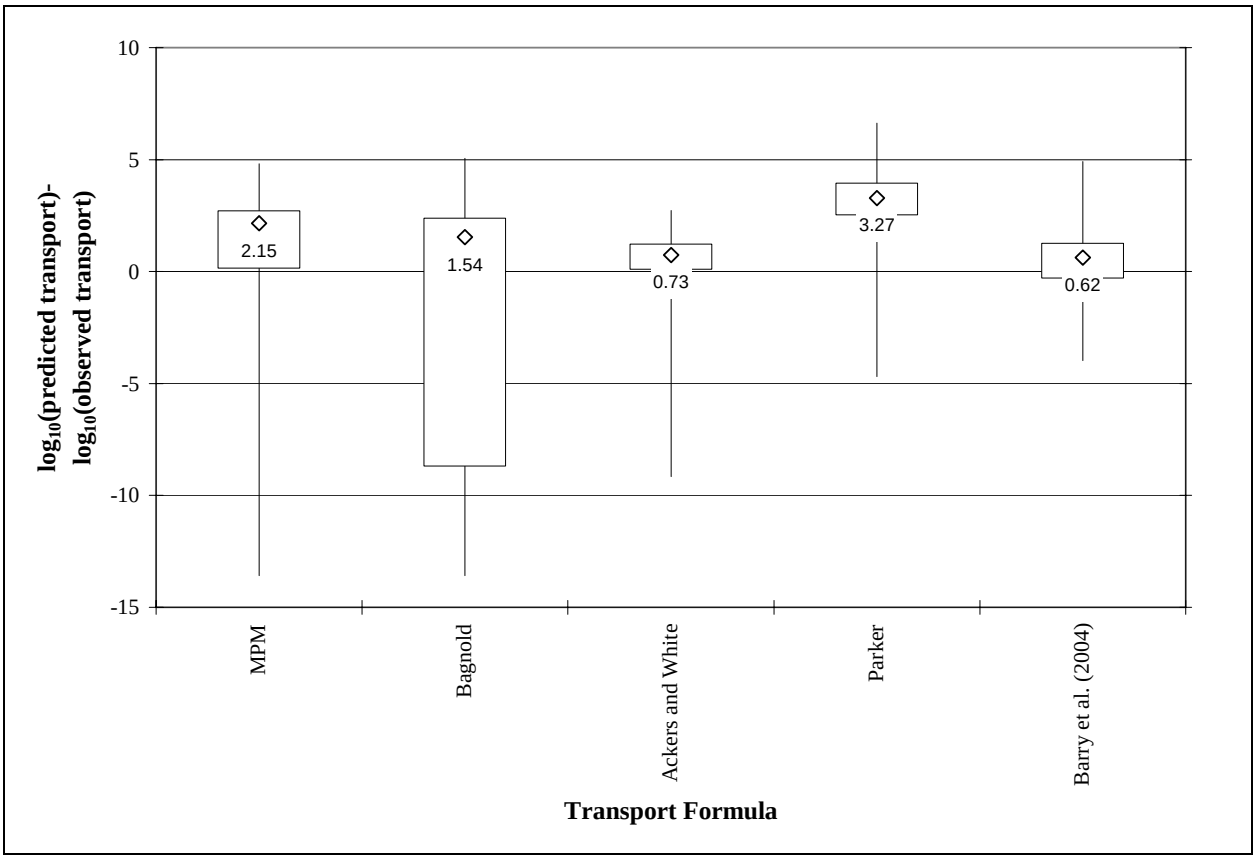


Figure 1 Box plots of the distribution of $\log_{10}$ differences between observed and predicted bed load transport rates for Barry et al.'s (2004) 17 test sites. Median values are specified. Extent of whiskers indicates maximum and minimum values. Upper and lower ends of each box indicate the inter-quartile range. MPM stands for Meyer-Peter and Müller.

FORMULA PERFORMANCE AND THE SELECTION OF ε

Figure 3 illustrates the effect of varying ε between values of $1 \cdot 10^{-15}$ kg/m·s to 10 kg/m·s, demonstrating that formula performance is sensitive to ε, particularly for the Meyer-Peter and Müller (1948) and Bagnold (1980) equations. The performance of these equations improves significantly as ε increases up to values of $1 \cdot 10^{-4}$ kg/m·s. In contrast, performance of the Ackers and White (1973), Parker (1990) and Barry et al. (2004) equations does not respond until ε becomes greater than $1 \cdot 10^{-4}$ kg/m·s, after which the median value of the critical error, e^*, for all five equations begins to increase. The difference in behavior between the two sets of equations has to do with the number of incorrect zero bed load transport rates predicted by each equation. Significant numbers of incorrect zero predictions make e^* a function of ε, rather than an indicator of actual formula performance. This is particularly evident for the results of the Meyer-

Peter and Müller (1948) and Bagnold (1980) equations due to the high number of incorrect zero predictions for those equations at our study sites (Fig. 3, Barry et al. 2004). In contrast, the Ackers and White (1973), Parker (1990) and Barry et al. (2004) equations predict some degree of transport at most discharges, which makes their e^* values less susceptible to choice of ε (at least up to values of $1 \cdot 10^{-4}$ kg/m·s). Prediction of transport at most discharges agrees with Paintal's (1971) notion that there is no critical shear stress for incipient motion, just different degrees of motion as discharge is increased. However, transport rates in these equations become vanishingly small at low discharges.

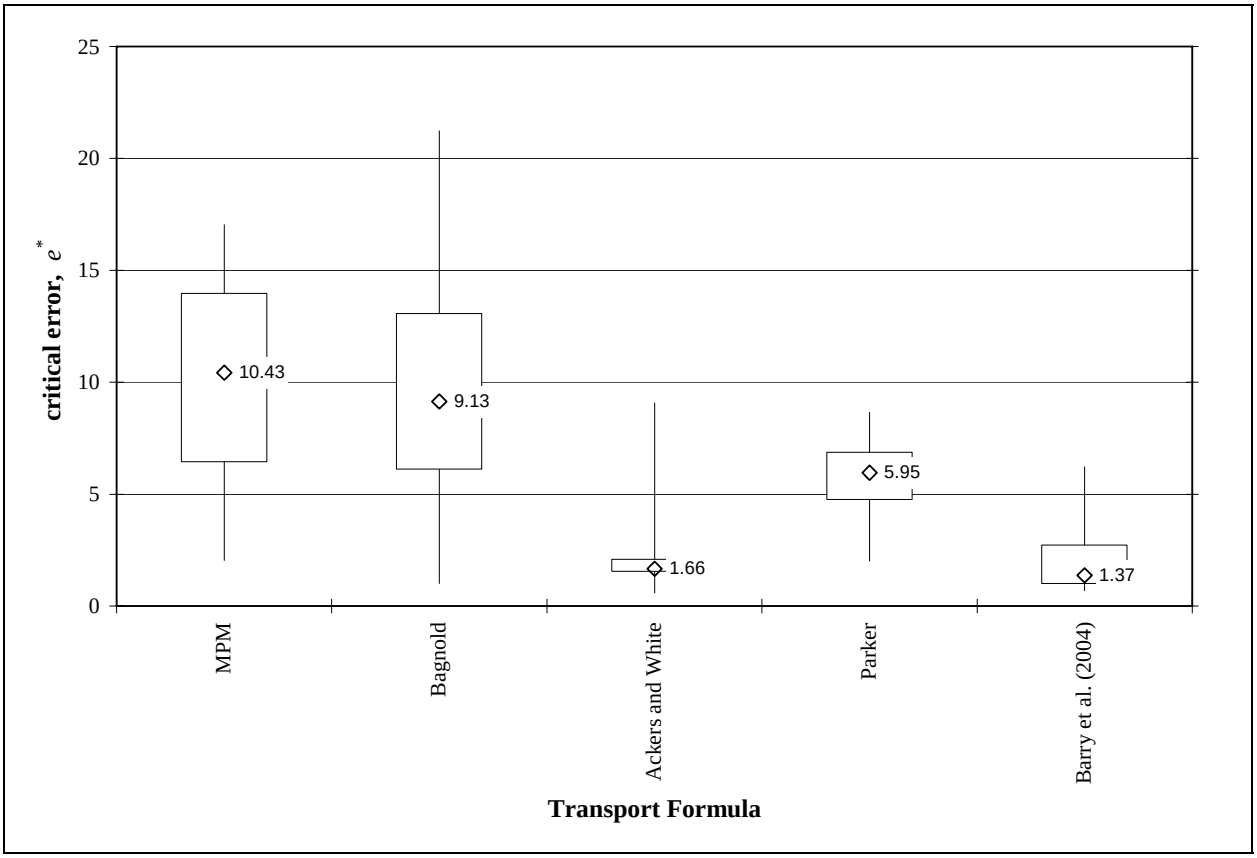


Figure 2 Box plots of the distribution of critical error, e^*, for the 17 test sites. Median values are specified. Extent of whiskers indicates maximum and minimum values. Upper and lower extents of box illustrate the inter-quartile range. MPM stands for Meyer-Peter and Müller.

Both the Ackers and White (1973) and Barry et al. (2004) equations out-perform the other equations included in this analysis until the value of ε increases to 1 kg/m·s. Furthermore, as ε increases to values greater than 10 kg/m·s all equations show similar values of e^*. The similarity in critical error as ε increases to 10 kg/m·s and larger is because such large values of ε are greater than the majority of the observed transport rates. Consequently, the magnitude of error (i.e., the degree of over-prediction) is similar for all equations and is set by the value of ε.

Figure 3 illustrates that the influence of ε on the median critical errors, e^*, of the Meyer-Peter and Müller [1948] and the Bagnold [1980] equations is least when ε is between $1 \cdot 10^{-3}$ and $1 \cdot 10^{-4}$

kg/m·s. Similarly, ε only begins to influence the critical errors, e^*, of the other equations when ε is greater than $1 \cdot 10^{-4}$ kg/m·s. Together, these observations indicate that an ε value between $1 \cdot 10^{-3}$ and $1 \cdot 10^{-4}$ kg/m·s is perhaps a more appropriate value than $1 \cdot 10^{-15}$ kg/m·s, as was selected in Barry et al. (2004).

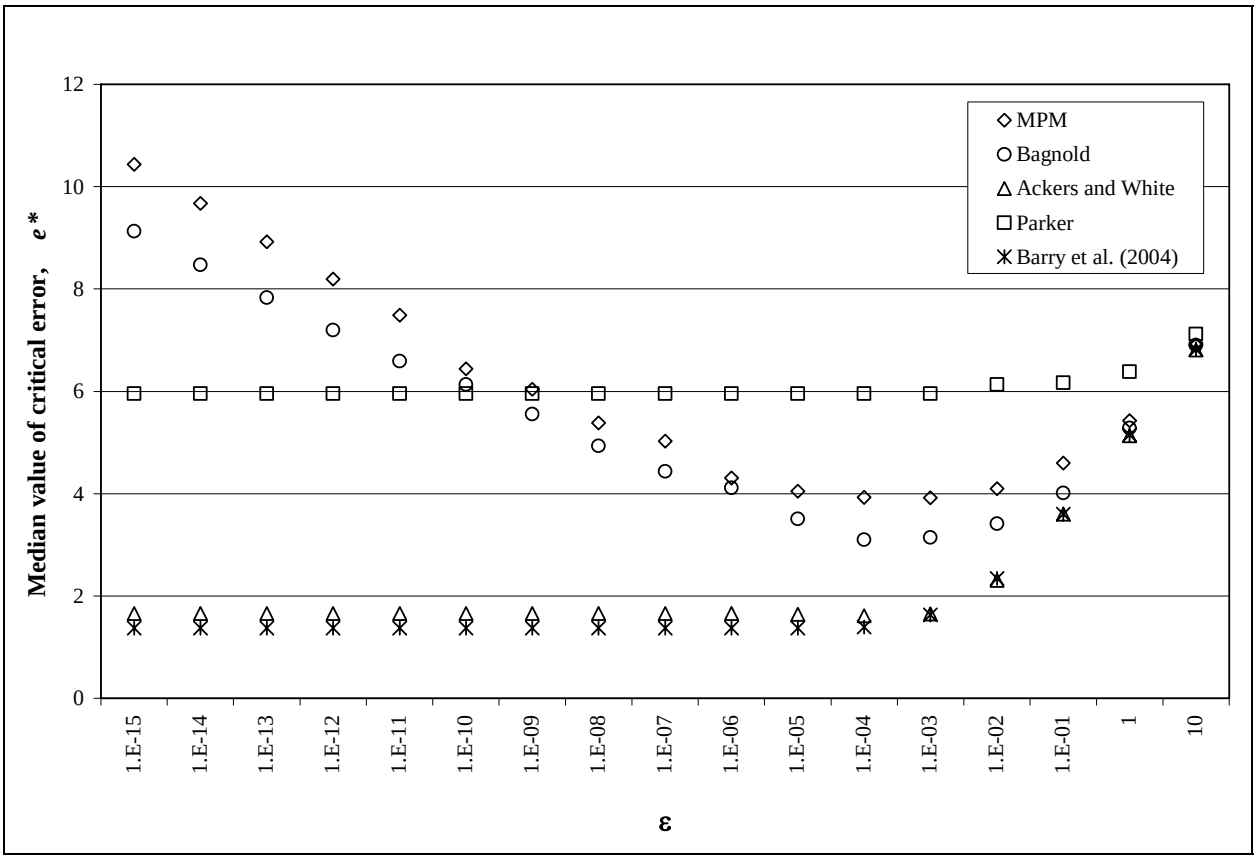


Figure 3 Sensitivity of median critical error values, e^*, to changes in ε. MPM stands for Meyer-Peter and Müller.

ASSESSMENT OF GEOMORPHIC SIGNIFICANCE

In this portion of the paper, we assess the accuracy with which each equation is able to predict the effective discharge (Q_e) (Wolman and Miller, 1960) at each site. The observed bed load rating curve at each site was used to determine Q_e, with the rating curve expressed as a power function of discharge (Barry et al., 2004)

$$q_b = \alpha Q^{\beta} \tag{3}$$

where q_b is bed load transport per unit width, and α and β are empirical values (Leopold et al., 1964, Smith and Bretherton, 1972; Vanoni, 1975). We only included those sites where 1) the observed bed load transport data are well described by Equation (3) (i.e., where the correlation coefficient (r^2) of the rating curve is greater than 0.70, and there is no obvious non-linearity to the observed transport data in $\log_{10}$ space) and 2) where the observed record of discharge covers

at least 10 years (Biedenharn et al., 2001). Only 22 of the 41 sites examined by Barry et al. (2004) met these criteria and were examined here.

At each of the 22 sites, we followed the method proposed by Biedenharn et al. (2001) to calculate flow frequency distributions. This approach divides the range of observed discharges into 25 arithmetic discharge class intervals. The "true" bed load transport rate for each discharge interval is determined by applying the site-specific rating curve to each discharge class. Similarly, predicted transport rates for each discharge class are determined from the five transport equations discussed above. Shear stress and other necessary equation parameters were determined for each discharge following an approach similar to that used by Barry et al. (2004). The product of the bed load transport and flow frequency within each discharge interval is the total bed load transport for that interval. The effective discharge occurs where this product is maximized.

To facilitate comparison of predicted and "true" values of effective discharge across watersheds of widely varying size, we normalized both values by drainage area, producing values of unit effective discharge for each site. Figure 4 shows the distribution of the differences between the predicted and "true" values of unit effective discharge across the 22 sites using the 5 equations included here. The median error is close to zero for all equations included in this analysis. However, there are substantial differences between the 5 equations in terms of both the width of the inter-quartile ranges and the 95% prediction intervals. To illustrate the potential absolute error in the predicted value of effective discharge at a site, an error of 0.05 in unit effective discharge at the Selway River site would translate to an absolute error of 248 m^3/sec. By way of comparison, the "true" value of effective discharge at this site is 677 $m^3\ s^{-1}$.

CONCLUSION

We find that formula performance is sensitive to ε. In particular, the statistical assessment of both the Meyer-Peter and Müller (1948) and Bagnold (1980) equations is in large part determined by ε due to the large number of incorrect predictions of zero transport for those equations at our sites. The influence of ε is minimized between $1 \cdot 10^{-3}$ and $1 \cdot 10^{-4}$ kg/m·s, and with ε set between these values the assessment of formula performance differs from that presented in Barry et al. (2004). That is, both the Meyer-Peter and Müller (1948) and Bagnold (1980) equations out-perform that of Parker (1990). However, the equations of Ackers and White (1973) and Barry et al. (2004) out-perform the other equations included in this analysis, and this result is insensitive to changes to the value of ε between $1 \cdot 10^{-15}$ and $1 \cdot 10^{-1}$ kg/m·s.

We also find that prediction of the effective discharge is not particularly sensitive to one's choice of bed load transport equation (at least for those examined here). This result corroborates the analytical results of Goodwin (2004), demonstrating why the effective discharge estimate tends to be a reliable and robust indicator. That is, even when one cannot predict the absolute value of sediment transport accurately it is possible to estimate the "channel forming" or "effective discharge". Consequently, the selection of an appropriate sediment transport equation depends on the intended application. For example, in channel restoration work, estimates of the cross-sectional area are usually obtained from empirical relations based on the effective discharge, rather than the magnitude of sediment transport at different flow conditions. However, if one

were interested in modeling landscape evolution or the effective storage life of a dam, accurate prediction of the magnitude of sediment transport is critical and, therefore, more care may be needed in selecting an appropriate transport equation.

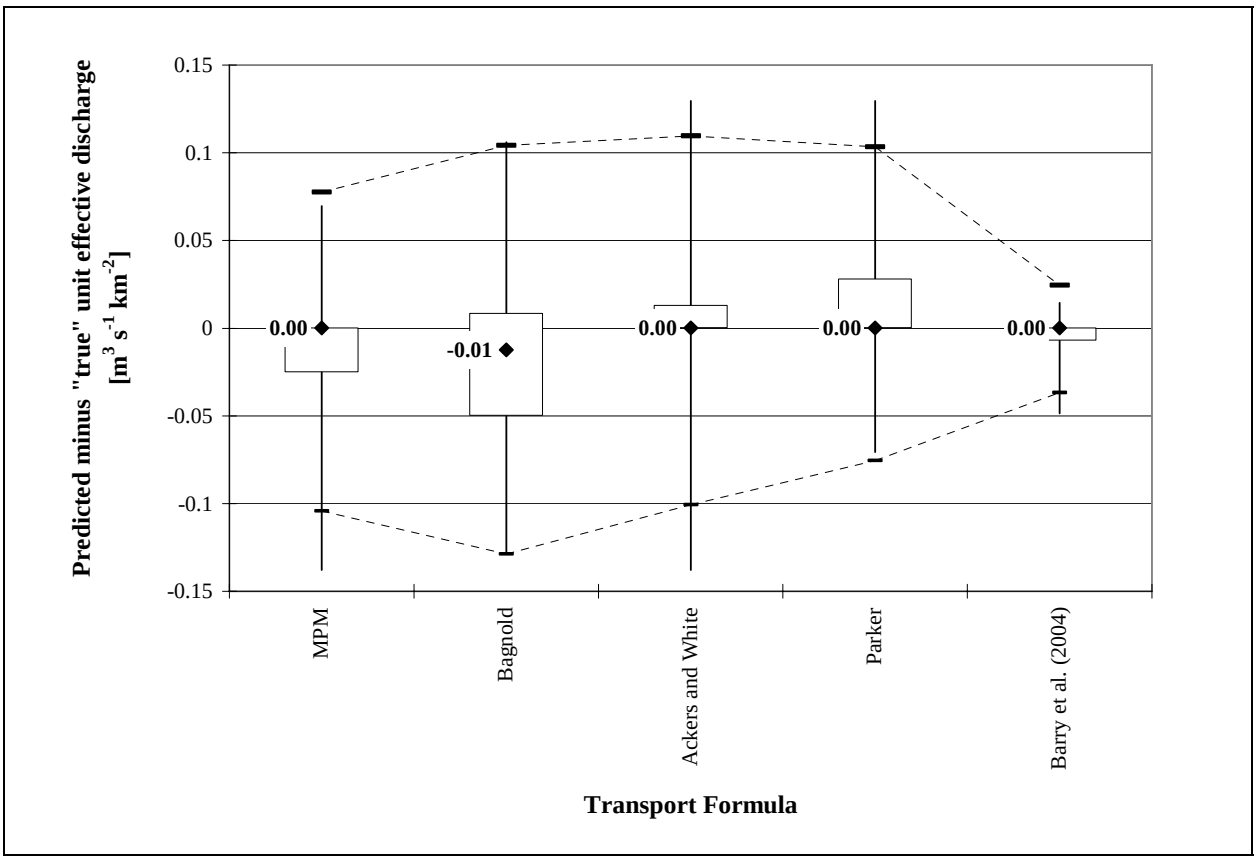


Figure 4 Box plots of the distribution of differences between predicted and "true" unit effective discharge. Median values are specified. Extent of whiskers indicates maximum and minimum values. Upper and lower extents of box illustrate the inter-quartile range. Also shown (dashed lines) are the 95% prediction intervals [Neter et al., 1974; Zar, 1974]. MPM stands for Meyer-Peter and Müller.

REFERENCES

Ackers, P. and White, W.R. (1973). "Sediment transport: New approach and analysis." J. Hydraul. Div., Am. Soc. Civ. Eng., 99, 2041-2060.

Andrews, E. and Nankervis, (1980). "Effective discharge and the design of channel maintenance flows for gravel-bed rivers." In: Natural and Anthropogenic Influences in Fluvial Geomorphology, edited by Costa, J. E., Miller, A. J., Potter, K. W. and Wilcock, P. R., pp. 151-164, Amer. Geophys. Union, Washington, DC.

Bagnold, R.A. (1980). "An empirical correlation of bedload transport rates in flumes and natural rivers." Proc. R. Soc. London, 372, 453-473.

Barry, J.J., Buffington, J.M. and King, J.G. (2004). "A general power equation for predicting bed load transport rates in gravel bed rivers." Water Resour. Res., 40, doi:10.1029/2004WR003190.

Biedenharn, D.S., Thorne, C.R., Soar, P.J., Hey, R.D. and Watson, C.C. (2001). "Effective discharge calculation guide." Int. J. Sediment Res., 16(4), 445-459.

Day, T.J. (1980). "A study of the transport of graded sediments." Hydraul. Res. Stat. Rep. IT 190, Wallingford, England, 10 pp.

Dietrich, W.E., J. Kirchner, H. Ikeda, and F. Iseya (1989). "Sediment supply and the development of the coarse surface layer in gravel-bedded rivers," Nature, 340, 215-217.

Freese, F. (1960). "Testing accuracy." Forest Science., 6, 139-145.

Gomez, B., and Church, M. (1989). "An assessment of bedload sediment transport formulae for gravel bed rivers." Water Resour. Res., 25, 1161-1186.

Goodwin, P. (2004). "Analytical solutions for estimating effective discharge." J. Hydraul. Eng., 130 (8), 729-738.

Henderson, F. M. (1963). "Stability of alluvial channels." Amer. Soc. Civ. Eng. Trans., 128, 657-720.

King, J. G., W. W. Emmett, P. J. Whiting, R. P. Kenworthy, and J. J. Barry (2004). "Sediment transport data and related information for selected gravel-bed streams and rivers in Idaho." U.S. For. Serv. Gen. Tech. Rep. RM, RMRS-GTR-131, 26 pp.

Leopold, L.B., M.G. Wolman, and J.P. Miller (1964). Fluvial Processes in Geomorphology. 552 pp., W.H. Freeman, San Francisco, California.

Meyer-Peter, E. and Müller, R. (1948). "Formulas for bed-load transport." In: Proceedings of the 2nd Meeting of the International Association for Hydraulic Structures Research, pp. 39-64, Int. Assoc. Hydraul. Res., Delft, Netherlands.

Neter, J., Wasserman, W. and Kutner, M.H. (1974). Applied Linear Statistical Models. Richard D. Irwin, Inc., Burr Ridge, Illinois.

Paintal, A.S. (1971). "Concept of critical shear stress in loose boundary open channels". J. Hydraul. Res., 9, 91-113.

Parker, G. (1978). "Self-formed straight rivers with equilibrium banks and mobile bed. Part 2. The gravel river." J. Fluid Mech., 89(1), 127-146.

Parker, G. (1990). "Surface-based bedload transport relation for gravel rivers." J. Hydraul. Res., 28, 417-436.

Reynolds, M.R. (1984). "Estimating error in model prediction." Forest Science., 30, 454-469.

Smith, T.R., and F.P. Bretherton (1972). "Stability and the conservation of mass in drainage basin evolution." Water Resour. Res., 8, 1506-1528.

Vanoni, V.A. (1975). "Sediment discharge formulas." In: Sedimentation Engineering, edited by V.A. Vanoni, pp. 190-229, Amer. Soc. Civ. Eng., New York.

Wolman, M.G. and Miller, J.P. (1960). "Magnitude and frequency of forces in geomorphic processes." J. Geol., 68, 54-74.

Yang, C.T., and Huang, C. (2001). "Applicability of sediment transport formulas." Int. J. Sed. Res., 16, 335-353.

Zar, J.H. (1974). Biostatistical analysis. Prentice Hall, Englewood Cliffs, New Jersey.

PREDICTABILITY OF BEDLOAD RATING AND FLOW COMPETENCE CURVES FROM BED ARMORING, STREAM WIDTH AND BASIN AREA

Kristin Bunte, Engineering Research Center, Colorado State University, Fort Collins, CO, kbunte@engr.colostate.edu; Steven R. Abt, Engineering Research Center, Colorado State University, Fort Collins, CO, sabt@engr.colostate.edu; and Kurt W. Swingle, Boulder, CO, kskb@ix.netcom.com

Abstract: In mountain gravel- and cobble-bed streams, relationships between discharge, bedload transport rates and the largest bedload particle size are typically not well predictable from bedload transport or shear stress equations. This study explored the prediction of gravel transport rates and particle sizes from watershed and streambed characteristics. Exponents and coefficients of the rating and flow competence curves obtained from bedload trap samples were significantly correlated to easily measurable parameters such as stream width, basin area size and the area-gradient product. High correlations indicating good predictability were obtained from the degree of bed armoring.

INTRODUCTION

Prediction of the bedload transport – discharge relationship in mountain gravel- and cobble bed streams is problematic. Transport rates for specified flows are typically predicted from a bedload transport equation that is applied to measured cross-sectionally averaged flow hydraulics (e.g., mean flow depth) and local bed material size. However, for coarse-bedded mountain streams, predictions from different bedload equations commonly vary by orders of magnitude, and only rarely do modeled results match measured gravel transport rates with satisfactory accuracy (e.g., Bathurst et al. 1987; Gomez and Church 1989; Weinhold 2001; Bravo-Espinosa et al. 2004; Barry et al. 2004). A similar problem exists with the prediction of flow competence, i.e., the largest bedload particle size transported at a specified flow. Shear stress or dimensionless critical shear stress equations often do not predict critical flow for the onset of motion of a specified particle size with sufficient accuracy. Given this, one may reasonably ask whether relationships of bedload transport and flow competence with flow can be predicted using a different approach.

Our field data measured in several mountain streams suggested that bedload rating and flow competence curves in mountain streams vary with parameters that scale streambed and stream size. This led us to pursue an approach that predicts bedload rating and flow competence curves from these characteristics. Observations and suggestions regarding the variability of bedload rating curves in streams of different sediment sizes, geological conditions, sediment supply, armoring, and channel gradient are also beginning to emerge from other sources (e.g., Barry et al. 2004; Ryan et al. 2002, 2005; as well as in several contributions to the 2005 Gravel-Bed Rivers Meeting (e.g., Hassan et al.; Diplas; and Lisle).

METHODS

Field procedures: Over the past 8 years, we have measured 10 data sets of bedload transport rates and flow competence by intensive sampling of gravel bedload over the snowmelt runoff

season at 9 study sites in 8 Rocky Mountain gravel- and cobble-bedded streams. All streams were relatively undisturbed and had step-pool, cascade, plane-bed and pool-riffle morphologies. Basin area sizes ranged from 8 to 105 km^2, channel gradients from 1 to 9%, bankfull flows from 0.8 to 6.2 m^3/s, bankfull widths from 3.7 to 15 m, bed material surface D_{50} particle sizes from 45 to 108 mm, and subsurface D_{50s} sizes from 26 to 42 mm. The streams were typically incised, such that flows of 1.5 times bankfull caused very little overbank flooding. Samples were collected using bedload traps and a similarly designed large net-frame sampler. Bedload traps consist of an aluminum frame 0.3 by 0.2 m in size that is fastened onto a ground plate that is anchored to the stream bottom. Bedload is collected in a 0.9-1.6 m long net with a 3.5 mm mesh width. Four to six bedload traps are typically installed across the stream spaced 1-2 m apart (Bunte et al. 2003, 2004, 2005) (Figure 1). The net-frame sampler has a 1.5 by 0.3 m opening to which a 3 m long net with a 1 cm mesh width is attached (Bunte 1996) (Figure 2). Both samplers have large openings and a large sampler capacity that permits sampling over a long duration (typically 1 hr).



Figure 1 Bedload traps installed in a stream

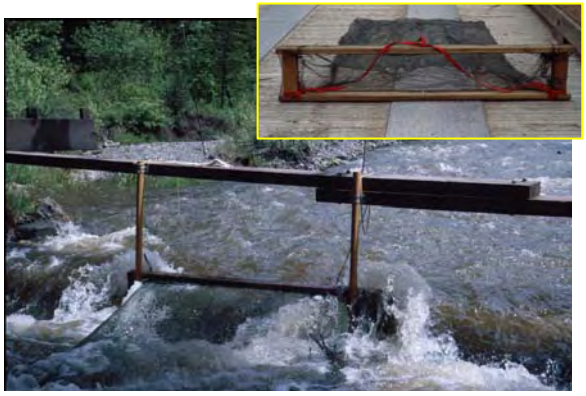


Figure 2: Net-frame sampler installed

Power function regressions were fitted to the relationships between measured gravel transport rates (Q_B, in g/s) and discharge (Q, in m^3/s) as well as to the relationships between the largest measured bedload particle sizes (D_{max}, in mm) and discharge. This yielded bedload rating curves and flow competence curves in the form of

$$Q_B = a \cdot Q^b \quad \text{and} \quad D_{max} = f \cdot Q^g$$

Exponents (b and g) indicate the curve steepness. Steeper curves have a higher rate of increase in transport rates or in the D_{max} particle size with flow. Coefficients (a and f) indicate the vertical position of the curves and thus the magnitude of transport or the size of D_{max} particles. Bedload rating curves fitted to transport rates obtained from bedload trap samples were generally steep with exponents of 8 to18. Flow competence curves had exponents of 1.5 to 4.3. All rating curves used in this study were well established, with r^2-values of 0.49 to 0.90 and a mean of 0.77. Flow competence curves were likewise well established ($0.40 < r^2 < 0.90$, mean $r^2 = 0.65$).

Regression analyzes: Exponents and coefficients of the bedload rating curves (b and a) and flow competence curves (g and f) established for the 10 data sets were regressed against several watershed and streambed parameters that included: basin area size (A, from maps), bankfull stream width (w_{bkf}, field measured), stream gradient (S, field survey), bankfull flow (Q_{bkf}, field determined or from 1.5-year recurrence interval flood), bankfull stream power (simplified to Q_{bkf}

$\cdot S$), median surface bed material size (D_{50}, reach-spanning pebble count exceeding 400 particles), surface bed material sorting (Inman sorting coefficient $\sigma_I = |\phi_{16}-\phi_{84}|/2$), median subsurface bed material size (D_{50s}, several volumetric samples with a mass exceeding 10 times the mass of the sample D_{max} particle, typically 150-200 kg), the percent sand and fines in the subsurface sediment (from volumetric samples) and the degree of bed armoring (ratio of surface D_{50} to subsurface D_{50s} size). Power function regressions in the form of $b = \alpha_1 \cdot X^{\beta 1}$, $a = \alpha_2 \cdot X^{\beta 2}$, $f = \alpha_3 \cdot X^{\beta 3}$, and $g = \alpha_4 \cdot X^{\beta 4}$ generally obtained the best fit (where X denotes a watershed or streambed parameter, and α and β are the coefficients and exponents of the fitted functions).

RESULTS

Results from our study showed that exponents and coefficient of the rating and flow competence curves where significantly and in some cases very well correlated to parameters describing the bed material and the stream size. Exponents decreased with the degree of bed armoring, percent sand and fines in the subsurface sediment, surface bed material sorting coefficient, D_{50} surface and D_{50s} subsurface bed material size, and stream gradient. Exponents increased with bankfull stream width, basin area, bankfull stream power, as well as bankfull flow. Since exponents and coefficients of bedload rating and flow competence curves are inversely related, stream parameters that have positive relationships with the exponents have negative ones with the coefficients and vice versa. Exponents and coefficients had only weak relationships with stream gradient, the D_{50} surface and D_{50s} subsurface bed material sizes, and the surface bed material sorting coefficient.

Exponents of bedload transport rating and flow competence curves: Exponents of bedload transport rating and flow competence curves were found to be highly correlated to the degree of bed armoring (Table 1) (Figure 3). Both, bedload rating and flow competence curves were less steep in more heavily armored streams. The matching trends of the bedload rating and flow competence curves, and the well defined negative functions (with r^2-values of 0.91 and 0.82, and p-values of 0.0001 and 0.005, respectively) with bed armoring are not unexpected when one considers that the degree of armoring is a direct result of the interaction between flow and bedload transport. Streams that are lightly or not armored (i.e., $D_{50}/D_{50s} \approx 1$) transport particle size-distributions that are similar to the subsurface bed material size-distribution near bankfull flow (Lisle 1995), while heavily armored streams (i.e., $D_{50}/D_{50\,sub} \geq 2$) transport bedload that is

Table 1 Regression parameters α and β and the r^2-value for relationships between exponents of the bedload rating and flow competence curves and parameters describing the streambed and stream size. r^2-values > 0.80 are printed in bold, and those between 0.50 and 0.80 in bold italics.

	Exponents ***b*** of bedload transport rating curve				Exponents ***g*** of flow competence curve			
Parameter	α	β	r^2	p-value	α	β	r^2	p-value
D_{50} surface/D_{50} subsurf. [-]	30.2	-1.89	**0.91**	0.00097	7.34	-2.10	**0.82**	0.0049
Bankfull stream width [m]	3.86	0.483	***0.55***	0.014	0.716	0.557	***0.54***	0.016
% subsurface fines <8 [%]	465	-1.17	***0.58***	0.048	142	-1.28	***0.50***	0.074
Basin area [km^2]	5.11	0.199	0.31	0.096	0.976	0.233	0.31	0.093
Stream power [$Q_{bkf} \cdot S$; m^3/s]	51.1	0.621	0.43	0.040	11.3	0.614	0.31	0.095
Bankfull flow [m^3/s]	8.41	0.184	0.23	0.16	1.77	0.205	0.21	0.18

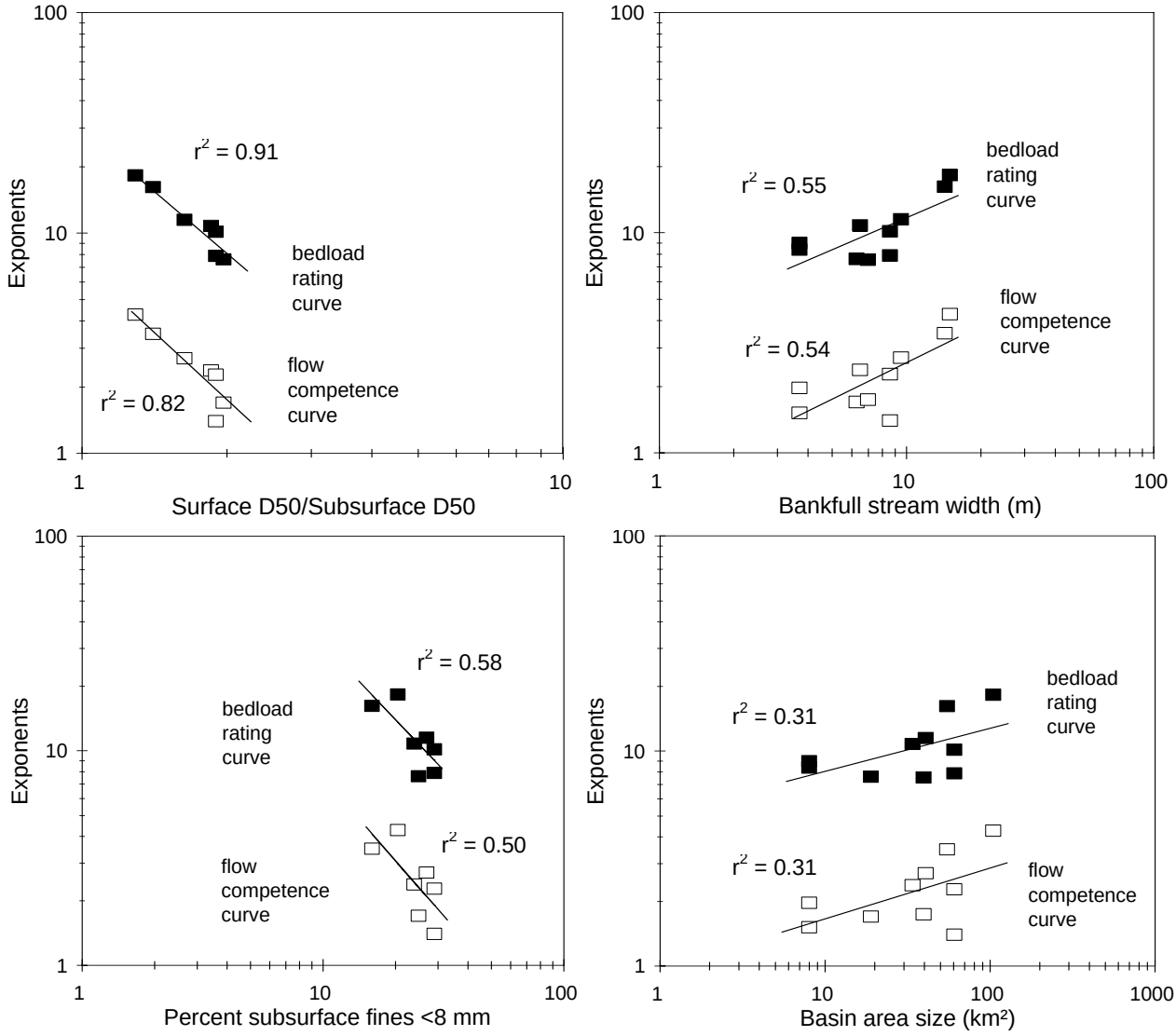


Figure 3 Relationship of exponents of bedload rating and flow competence curves with streambed and stream size parameters.

finer than the bed. Highly armored coarse-bedded mountain streams have only a limited number of transportable particles available on the stream bed such that increasing flow is not likely to find particles of transportable sizes on the bed. The result is a relatively flat rating curve with a low exponent. By contrast, lightly armored streams are likely to have more transportable coarse surface particles, and transport rates can easily respond to increasing flow.

Exponents were also found to decrease with the percent fines <8 mm in the subsurface sediment, which is positively correlated to bed armoring. Streams with a high percent of subsurface fines have an ample supply of small gravel particles available for transport at low flows at the very onset of fine gravel motion. This low-flow transport elevates the lower end of the rating and flow competence curves, thus reducing the overall slopes and resulting in lower exponents. However, with r^2-values of 0.58 and 0.50, respectively, the percent surface fines is not as good a predictor of the exponents as the degree of armoring. Exponents were also found to increase

with bankfull stream width. Wider streams typically have a larger mobile bed area in which transport rates and bedload particle sizes can increase strongly with flow. Although the r^2-values are only 0.55 and 0.54, respectively, the bankfull stream width is easy enough to measure in the field that it could serve as a first estimator of the rating and flow competence curve exponents. Exponents also increase with basin area, stream power, and bankfull flow, but the relationships are not as tightly defined.

Coefficients of bedload transport rating and flow competence curves: Coefficients of bedload transport rating and flow competence curves were generally better correlated with streambed and stream size parameters than the exponents (Table 2). Coefficients were highly and positively correlated to bed armoring (r^2 values of 0.95 and 0.96, and p-values of 0.0002 and 0.0001, respectively) (Figure 4). The tight relationship of both exponents and coefficients with bed armoring indicates that the degree of armoring reflects gravel transport processes quite well. Armoring is thus a good predictor of both the rating curve and flow competence curve response to increasing flows in coarse-bedded mountain streams. Coefficients are also related to the percent subsurface fines, but the correlations (r^2 of 0.60 and 0.62) are only moderate. In contrast to exponents, coefficients are highly, but negatively, correlated to the bankfull stream width (r^2-values of 0.91 and 0.88, respectively and p-values <0.0001) and thus predictable from an easy to measure field parameter. Coefficients also decrease with parameters indicating stream size such as bankfull flow, basin area, and adjusted basin area. However, with r^2-values of 0.52 to 0.71, the relationships are not as well defined as those for armoring and stream width and are less well suited as predictors.

Table 2 Regression parameters α and β and the r^2-value for relationships between coefficients of the bedload rating and flow competence curves and parameters describing the streambed and stream size. r^2-values > 0.80 are printed in bold, and those between 0.50 and 0.80 in bold italics.

	Coefficients *a* of bedload transport rating curve				Coefficients *f* of flow competence curve			
	α	β	r^2	p-value	α	β	r^2	p-value
D_{50} surface/D_{50} subsurf. [-]	3.04E-18	45.9	**0.95**	0.00017	4.04E-03	10.1	**0.96**	0.00012
Bankfull stream width [m]	7.54E+12	-20.3	**0.91**	<0.0001	1.33E+04	-4.31	**0.88**	<0.0001
Basin area [km^2]	1.13E+10	-9.93	***0.71***	0.0022	2.97E+03	-2.06	***0.67***	0.0039
Bankfull flow Q_{bkf} [m^3/s]	0.619	-10.2	***0.67***	0.0040	21.7	-2.12	***0.62***	0.0070
% subsurface fines <8 [%]	6.17E-47	28.4	***0.60***	0.040	1.59E-09	6.31	***0.62***	0.036
Stream power, $Q_{bkf} \cdot S$ [m^3/s]	5.64E-25	-17.1	0.30	0.099	2.51E-04	-3.51	0.28	0.12

DISCUSSION AND CONCLUSION

Results from intensive sampling of gravel bedload transport using bedload traps in several Rocky Mountain gravel- and cobble-bed streams showed that exponents and coefficients of both bedload transport rating and flow competence curves vary systematically with stream size and bed material characteristics. Exponents have a strong negative correlation with the degree of bed armoring, and to a lesser extent with the percentage of subsurface sand and fines, and there is a moderate positive correlation with stream width. Coefficients have a significantly positive relationship to the degree of bed armoring and are negatively related to stream width. There are moderate, negative relationships with bankfull flow, basin area, and percent subsurface sand. It

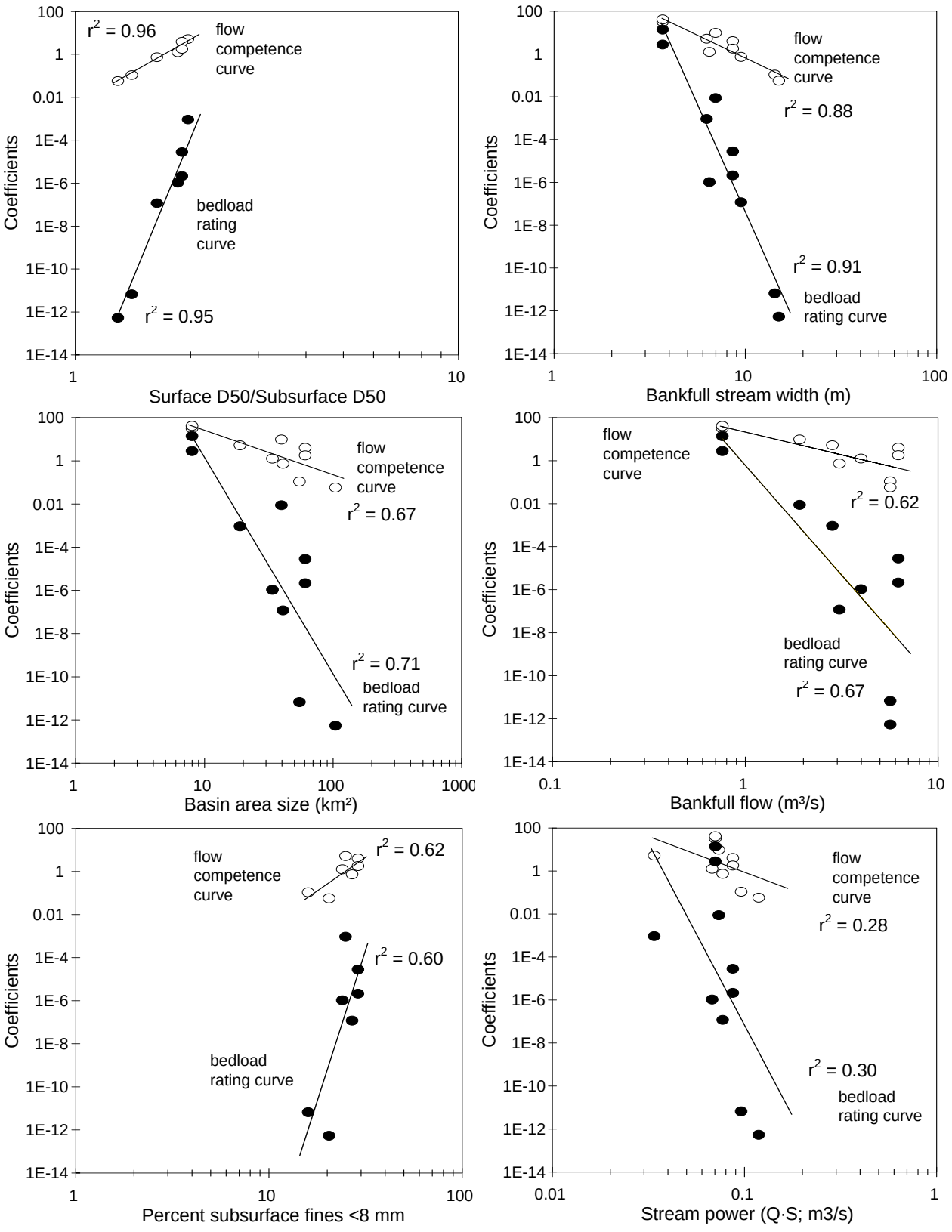


Figure 4 Relationship of the bedload rating and flow competence curve coefficients with streambed and stream size parameters.

is notable that exponents and coefficients of both the bedload rating and the flow competence curves follow the same trend, suggesting that the mobility of the bedload D_{max} particle size and high bedload transport rates are positively correlated.

Computational, procedural, and natural variability in bedload rating curves: Ideally, a large number of streams should be used for an analysis of this type to show that results apply to gravel-bed streams in general. A large sample size can also include and highlight variability between streams or watersheds of different characteristics. However, including data sets from the literature in the analyses is problematic because exponents and coefficients of bedload rating and flow competence curves are affected by computational differences, natural variability, and sampling methods. Computational difference that arise from computations of transport rates, the D_{max} particle size, and discharge using different units can easily be fixed. Those arising from the curve fitting procedure and the measured data range pose larger problems. Exponents and coefficients vary depending on whether measured zero-transport values were excluded from a power function regression or included after a small numerical value (e.g., 0.1 times the smallest measured transport rate) has been assigned to them. The range of flow over which transport rates are measured also affects the fitted rating curve due to the scatter of transport rates around discharge. Exponents are higher and coefficients lower in large data ranges (e.g., with flows from 30 and 130% Q_{bkf}) compared to small data ranges with flows of 30 to 80% or 80 to 130% of bankfull. These factors may change a rating curve exponent by up to approximately ±20% and a coefficient by a factor of up to ±5. Attempts to determine correlations of exponents and coefficients with stream parameters are necessarily compromised by this uncertainty.

By far the greatest variability in measured rating curve exponents and coefficients is due to the difference in transport rates obtained from using different samplers. For example, transport rates collected during low transport at 50% bankfull flow with a 0.076 m Helley-Smith sampler are several orders of magnitude higher than those collected with bedload traps, while both samplers produce similar results when a large number of bedload particles are moving near bankfull flow. Bedload rating curves computed from Helley-Smith samples are thus less steep. Exponents typically range from 2 to 5 in coarse-bedded mountain streams (compare to exponents from bedload trap rating curves of 8 to 18 (Bunte et al. 2004)). Helley-Smith rating curve coefficients, by contrast, are many orders of magnitude higher than those obtained from bedload traps. To avoid sampler specific differences in bedload transport rates and particle sizes, our study was solely based on data obtained from bedload traps and the similarly designed net-frame sampler. Results from a comparable study that used a different bedload sampler deviate to some degree from results in our study. Based on a large data set of Helley-Smith samples compiled primarily by King et al. (2004), Barry et al. (2004) found a significant negative correlation between bedload rating curve coefficients and basin area size (r^2 = 0.79) which is a similar but better defined relationship than in this study. They also found a moderately well defined relationship between exponents and the dimensionless bedload transport rate q^* (Dietrich et al. 1989) (r^2 = 0.56). The parameter q^* includes some ratio of the D_{50} and D_{50s} particle sizes, however, no relationship was found with the field-measured degree of bed armoring.

Using bedload traps, our field study showed relationships between rating curve exponents and coefficients with the degree of bed armoring that are sufficiently well developed to predict bedload rating and flow competence curves. This finding could lead to tremendous savings in

time and labor. The field and lab work required for a careful analysis of the degree of bed armoring can be completed within several days (Bunte and Abt 2001). This is much faster and more convenient than intensive bedload sampling over a snowmelt highflow season. Bankfull stream width is even more easily measurable stream and is well suited to predict coefficients of the rating and flow competence curves, but is only moderately well suited to estimate exponents (steepness of the rating curve). A first estimate of exponents and coefficients of the bedload transport rating and flow competence curves can be obtained from the basin area size which is obtainable from detailed topographic maps.

Acknowledgement: Funding for the field work of this study was provided by the USDA Forest Service Stream Systems Technology Center, Fort Collins, CO. We thank John Potyondy for good advice, foresight, and encouragement.

REFERENCES

Barry, J.J., Buffington, J.M., and King, J.G. (2004). "A general power equation for predicting bed load transport rates in gravel bed rivers", Water Resour. Res., 40, W10401, doi:10.1029/2004WR003190.

Bathurst, J.C., Graf, W.H., and Cao, H.H. (1987). "Bed load discharge equations for steep mountain rivers". In: Sediment Transport in Gravel-Bed Rivers. C.R. Thorne, J.C. Bathurst and R.D. Hey (eds.), John Wiley and Sons, Chichester, pp 453-491.

Bravo-Espinosa, M., Osterkamp, W.R., and Lopes, V.L (2003). "Bedload transport in alluvial channels", Journal of Hydraulic Engineering 129(10), pp 783-795.

Bunte, K., and Abt, S.R. (2001). Sampling Surface and Subsurface Particle-Size Distributions in Wadable Gravel- and Cobble-Bed Streams for Analysis in Sediment Transport, Hydraulics, and Streambed Monitoring. USDA Forest Service, Rocky Mountain Research Station, Fort Collins, CO, General Technical Report RMRS-GTR-74, 428 pp. http://www.fs.fed.us/rm/pubs/rmrs/gtr_74.html

Bunte, K., (1996). Analyses of the temporal variation of coarse bedload transport and its grain size distribution (Squaw Creek, Montana, USA). U.S.D.A., Forest Service, Rocky Mountain Forest and Range Experiment Station, General Technical Report RM-GTR-288, 124 pp.

Bunte, K. and Abt, S.R. (2003). "Sampler size and sampling time affect measured bedload transport rates and particle sizes measured with bedload traps in gravel-bed streams". In: Erosion and Sediment Transport Measurement in Rivers: Technological and Methodological Advances. J. Bogen, T. Fergus and D.E. Walling (eds.), IAHS-Publication No. 283, pp 126-133.

Bunte, K., Abt, S.R., Potyondy, J.P., and Ryan, S.E. (2004). "Measurement of coarse gravel and cobble transport using a portable bedload trap", Journal of Hydraulic Engineering 130(9), pp 879-893.

Bunte, K., Swingle, K.W., and Abt, S.R. (2005). Guidelines for using bedload traps in coarse-bedded mountain streams: Construction, installation, operation and sample processing. Report submitted to Stream Systems Technology Center, USDA Forest Service, Rocky Mountain Research Station, Fort Collins, CO, 79 pp.

Dietrich, W.E., Kirchner, J.W., Ikeda, H. and Iseya, F. (1989). "Sediment supply and the development of the coarse surface layer in gravel-bedload rivers", Nature, 340, pp 215-217.

Gomez, B., and Church, M. (1989). "An assessment of bed load sediment transport formulae for gravel bed rivers", Water Resources Research 25(6), pp 1161-1186.

King, J.G., Emmett, W.W., Whiting, P.J., Kenworthy, R.P., and Barry, J.J. (2004). Sediment transport data and related Information for Selected Coarse-Bed Streams and Rivers in Idaho. USDA Forest Service, Rocky Mountain Research Station, General Technical Report RMRS-GTR 131, 26 pp.

Lisle, T.E. (1995). "Particle size variations between bed load and bed material in natural gravel bed channels", Water Resources Research 31(4), pp 1107-1118.

Ryan, S.E., Porth, L.S., and Troendle, C.A. (2002). "Defining phases of bedload transport using piecewise regression", Earth Surface Processes and Landforms, 27(9), pp 971-990.

Ryan S.E., Porth, L.S., and Troendle, C.A. (2005). "Coarse sediment transport in mountain streams in Colorado and Wyoming, USA", Earth Surface Processes and Landforms 30, pp 269-288. DOI: 10.1002/esp.1128.

Weinhold, M.R. (2001). " Application of a site-calibrated Parker-Klingeman bedload transport model", M.S. Thesis, Department of Civil Engineering, Colorado State University, Fort Collins, Colorado, 99 pp.

RADIONUCLIDE AND RARE EARTH ELEMENT TRACERS OF EROSIONAL PROCESSES ON THE PLOT SCALE

A.P. Stubblefield, Dept. Geological Sciences, Case Western Reserve University, Cleveland, OH, aps12@case.edu; C. Fondran, Dept. Geological Sciences, Case Western Reserve University, Cleveland, OH, lorimor@darwin.epbi.cwru.edu; M.E. Ketterer, Dept. Chemistry, Northern Arizona University, Flagstaff, AZ, Michael.Ketterer@nau.edu; G. Matisoff, Dept. Geological Sciences, Case Western Reserve University, Cleveland, OH, gxm4@case.edu; P.J. Whiting, Dept. Geological Sciences, Case Western Reserve University, Cleveland, OH, pjw5@case.edu.

INTRODUCTION

Soil erosion results in the loss of primary productivity for agriculture and silviculture and contributes to the degradation of aquatic ecosystems. The two dominant processes of erosion, sheetwash and rill erosion, can have very different impacts. Sheetwash can remove nutrients concentrated near the surface. Rilling can quickly excavate large volumes of soil and initiate unstable conditions. Typical management prescriptions differ as well. Rilling is best treated by contour planting, and by reducing concentrated flows with buffer strips and grassy swales. Sheetwash is better addressed by maintaining soil cover, and enhancing soil porosity. For example, the application of no-till agriculture has been shown to increase infiltration by maintaining macropores, organic matter and the size of soil-aggregates (Holland 2004).

The goal of this work is to develop tools to better understand sheetwash erosion processes and the development of rill networks. We seek to quantify the contributions of rill versus sheetwash erosion in agricultural settings. By developing a signal of rill erosion, we hope to be able to more completely understand the hydrological and geomorphological factors that lead to rill initiation. Better understanding of process is also important for the improvement of soil erosion models (Takken et al. 2005). The results will be directly relevant to land managers.

The first technique presented here is the use of the naturally-occurring radionuclide Be-7 as a tracer of soil movement. Created in the atmosphere by the spallation of nitrogen and oxygen, Be-7 is washed onto the landscape by wet and dry precipitation. Upon contact with the soil surface, it adsorbs onto soil particles with a very high partitioning coefficient (Kd ~10^4-10^5, Hawley et al. 1986). Because of its atmospheric source and short-half life ($t_{1/2}$=53 d) Be-7 tags only the top 1-5 mm of the soil surface. Once eroded, soil retains its diagnostic radionuclide activity. Thus high Be-7 content in sediment can be used as an indicator of sheetwash erosion and low Be-7 content can indicate rill erosion (Whiting et al. 2001, Matisoff et al. 2002).

A complementary technique in tracer studies is the use of soil labeled with rare earth elements (REE). While the radionuclides can serve as tracers of soil originating from specific depths, REEs can be used to tag soil from specific spatial regions. REE is co-precipitated onto soil taken from the study area in the laboratory, and then reapplied in the field setting (Matisoff et al. 2001). Measurements from the soil surface downslope of application sites or in suspended sediment (SS) from captured runoff samples can then indicate particle transport distances, travel

times, and rates of deposition. Suites of different REEs can be applied to identify regions of the plot such as topslopes, side slopes, rills and depositional areas (Polyakov et al. 2004).

In this report we present findings from a study that used both REEs and fallout radionuclides to provide a more comprehensive view of spatial and temporal contributions to soil loss.



Figure 1 View of the erosion plot looking upslope.

METHODS

In June 2004, a 4 x 9 meter erosion plot was installed at the USDA Agricultural Research Service Deep Loess Research Station near Treynor, IA. The plot was located in a field with a slope of 8% (Figure 1). While planted to corn, the field was in rotation with soybeans, and no-till practices had been utilized for the previous two years. Borders prevented entry of runoff from regions above and to the side of the plot. A gutter pipe and cement sill were installed flush to the ground surface to collect runoff without causing erosion of the soil near the collection interface. Six cores were collected adjacent to the plot to establish inventories and depth-profiles for Be-7 prior to the study. Soil tagged with the REEs Tb, Ho, and Eu were applied in thin strips (0.25 x 4m) at 1, 4 and 7 meters, respectively, upslope from the bottom of the plot. We then waited for thunderstorm activity. All runoff was collected from the plot in 20-L sample containers. Precipitation was collected to determine Be-7 flux. After the event, 6 cores were taken from within the plot to determine change in radionuclide inventory. Sediment was extracted from runoff samples with settling and flow-through centrifugation. Samples were analyzed for suspended sediment yield, Be-7 activity and yield, and concentration and yield of REEs. Be-7 activity was determined with high efficiency germanium-drifted gamma spectrometry (Matisoff

et al. 2002). REE concentration was measured by quadrupole, inductively coupled plasma mass spectrometry (Matisoff et al. 2001).

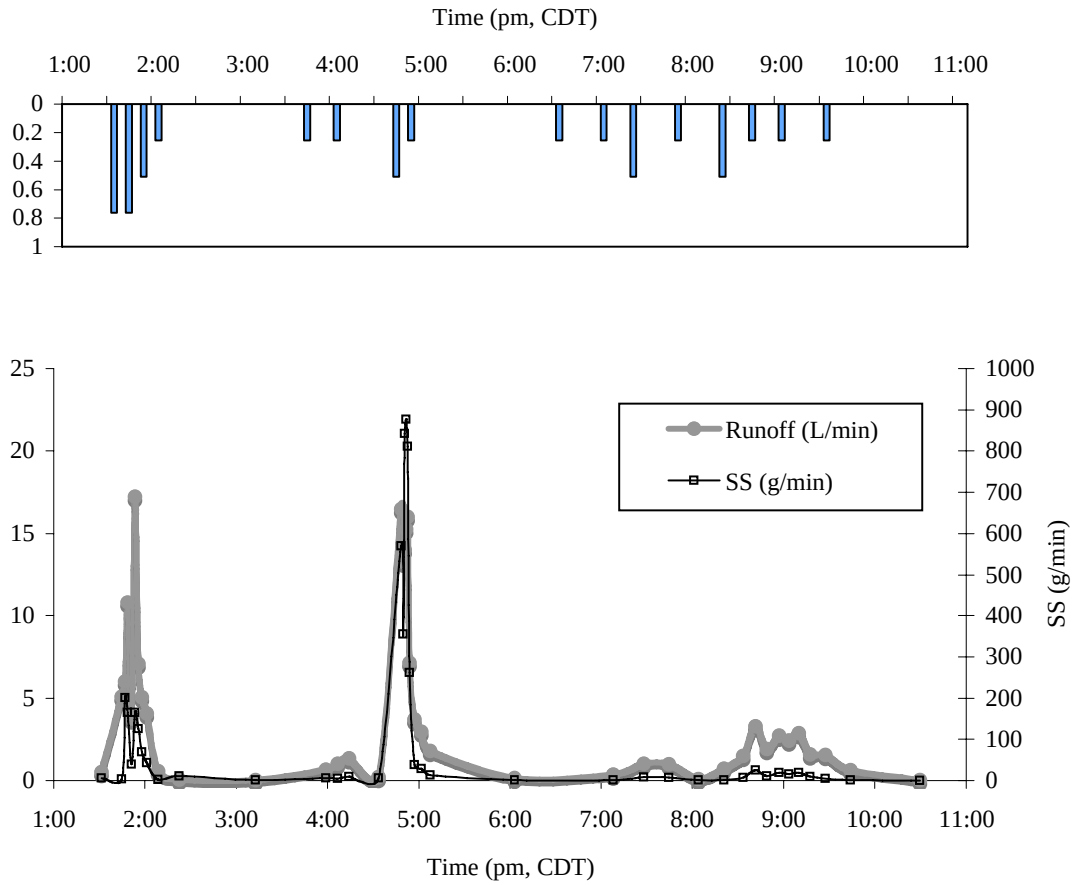


Figure 2 Rainfall, discharge and suspended sediment delivery over time.

RESULTS

The thunderstorm yielded 10 cm of precipitation in three distinct pulses of gradually lessening intensity over twelve hours (Figure 2). The largest suspended sediment yield and concentrations occurred during the second pulse (Figure 2). The sustained, but less intense, rains of the third pulse produced large runoff volumes but less suspended sediment yield.

Be-7 profiles from before and after the event show concentrations of Be-7 and the increment of the radionuclide added during the thunderstorm (Figure 3). The highest concentration is found at the surface. Levels decay exponentially with depth. The increment added by the thunderstorm is found entirely in the top sample (0-0.4 cm). In Figure 4, Be-7 activity of the suspended sediment and cumulative suspended sediment yield are plotted against time. During periods of highest sediment yield, Be-7 activities drop. In pulse two, starting at 4:00, Be-7 activity drops from 0.5 to 0.1 Bq/g. In pulse three, starting at 7:20, activity drops from 0.62 to 0.2 Bq/g. After each rainfall pulse subsides, Be-7 activity, per gram of runoff sediment, rises.

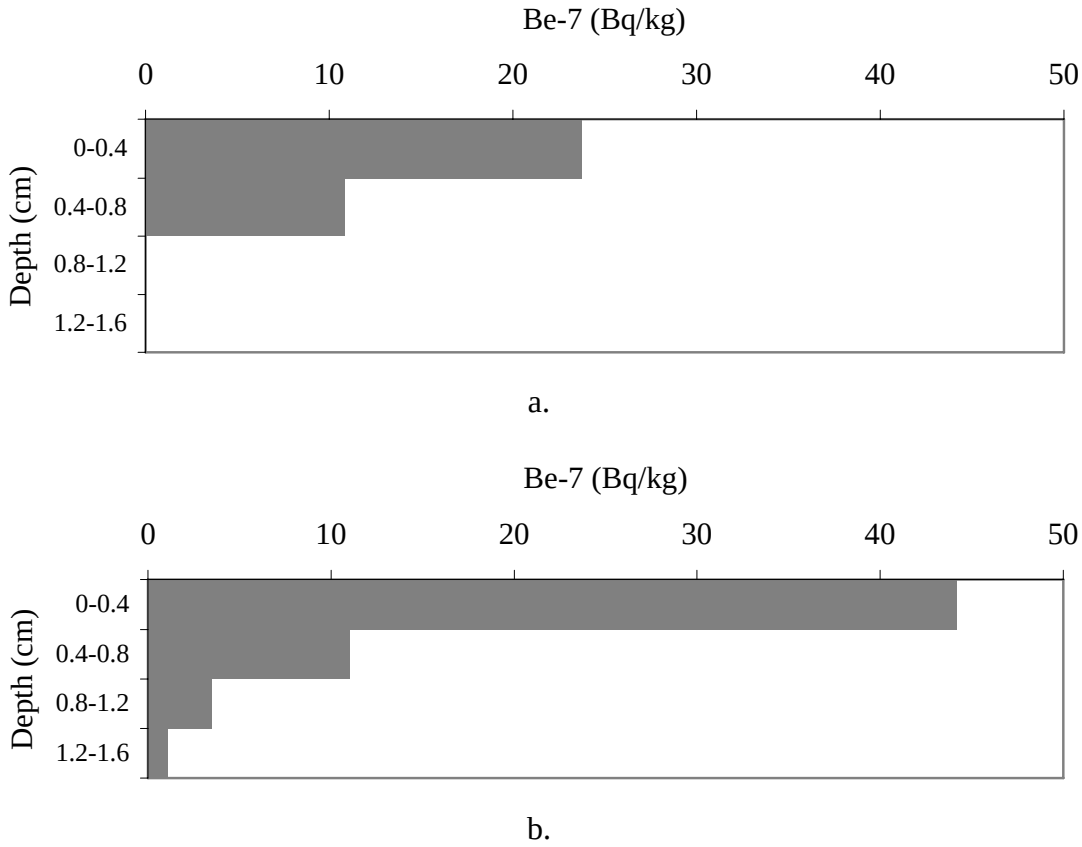


Figure 3 Be-7 activity with depth. a. Before rainstorm; b. after rainstorm.

In Figure 5, REE concentrations in runoff are plotted against time. Above background concentrations from all three REEs are detected during the first pulse, with the magnitude of the concentration inversely related to the distance to the outlet. During the second pulse, all three REEs are detected; however Tb remains high, while Ho concentration drops. During the third pulse, at 5:06, Tb drops relative to earlier concentrations, Ho attains the concentration of the first pulse and Eu reaches its highest concentration.

DISCUSSION

The results presented above present a consistent picture of the sequence of erosional processes. At the onset of precipitation, rain infiltrates into the soil. As the rainstorm continues, the soil becomes locally saturated, resulting in local overland flow and sheetwash erosion. During the first pulse of rainfall, relatively intense rains produce a modest amount of sediment (as compared to later pulses of rain and runoff). The sediment collected during runoff from this first event has a relatively low activity of Be-7 (0.15-0.25 Bq/g) (Fig 3). An exception is at the end of the runoff from the first pulse when the activity of Be-7 in sediment increases to near 0.4 Bq/g. As observed in our earlier work at this site (Whiting et al. 2001), such an increase in activity is associated with sediment produced by more shallow erosion of the soil column – sheetwash erosion. After the onset of the second pulse of precipitation (at ~4:50), sediment yield increases.

Initially the activity of Be-7 associated with runoff during this second event is high, indicating sheetwash erosion. During the peak of runoff, the activity of Be-7 in sediment drops to less than 0.1 Bq/g. This low value indicates a shift to more of the sediment being produced by deeper rill erosion. As sediment yield wanes after the second event, the activity of Be-7 climbs again to above 0.3 Bq/g, indicating a sheetwash source. The third pulse of rainfall is distributed over a longer time period than the first two pulses and the runoff volumes and sediment yields are lower. High Be-7 activity in runoff sediment suggests that sheetwash is the initial source of much of this sediment. During the period 8:30-9:40, Be-7 activity again decreases to 0.1-0.2 Bq/g. This time period corresponds to an interval of substantial production of sediment which we infer to be primarily by rilling.

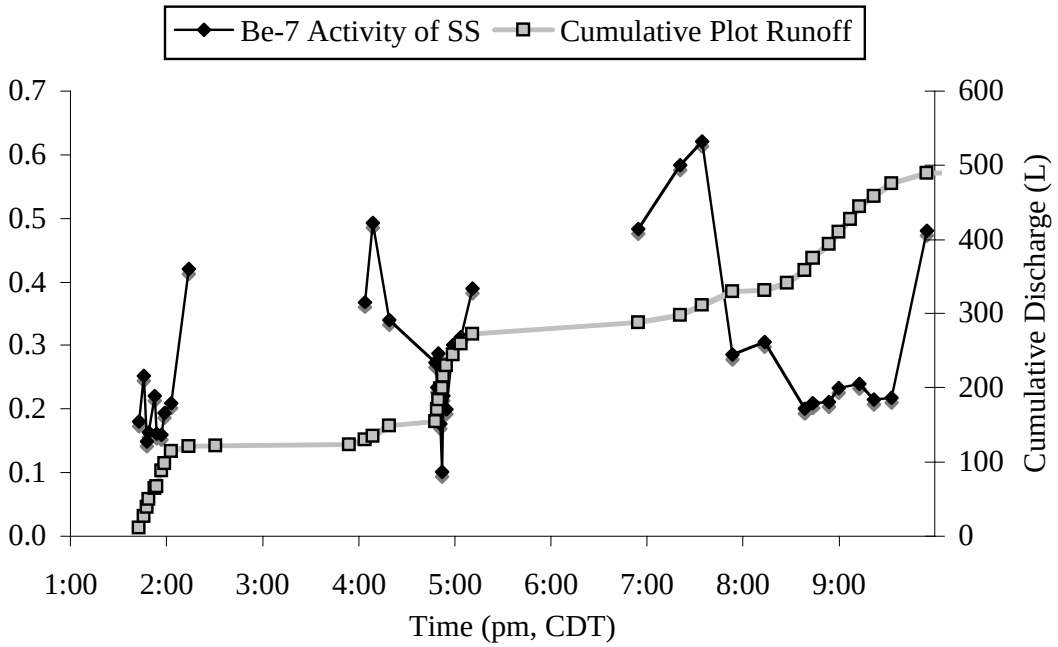


Figure 4 Be-7 activity in sediment and cumulative runoff with time.

Evidence of the gradual expansion of flow networks over the course of the event is provided by REE data (Figure 5). During the first rain pulse (~1:40) REE signal is detected for all three bands. However the concentration of REE in the runoff suspended sediment is related to the distance from the outlet; with Tb, 1 m from the outlet reaching 80 ug/g; Ho at 4 m reaching 40 ug/g; and Eu, 7 m from the outlet, peaking at 20 ug/g. As the second event begins (4:00) the same relative concentration pattern is observed. Then the rainfall intensifies and the sediment yield increases (~4:50, Figure 5). Concentrations of all REEs drop. This reflects dilution by sediments derived from rill erosion as identified by the Be-7 concentrations. Since the REEs were applied to the soil surface, decreasing concentrations in the suspended sediment imply deeper erosion. As the rainfall abates and sediment yield drops (~5:00), there is an increase in the Eu concentration to an event maximum of 44 ug/g. The farthest upslope band now contributes substantially to the sediment load. This indicates that the entire plot is hydrologically linked. REE concentrations were diluted during the period of maximum rill cutting and this may have masked high inputs of Eu occurring at this time. The third pulse of rainfall (~7:00) has

consistently low REE levels. This may reflect reduced sediment transport as a result of lower intensity rainfall, or depletion of available stores of REE-labeled sediment.

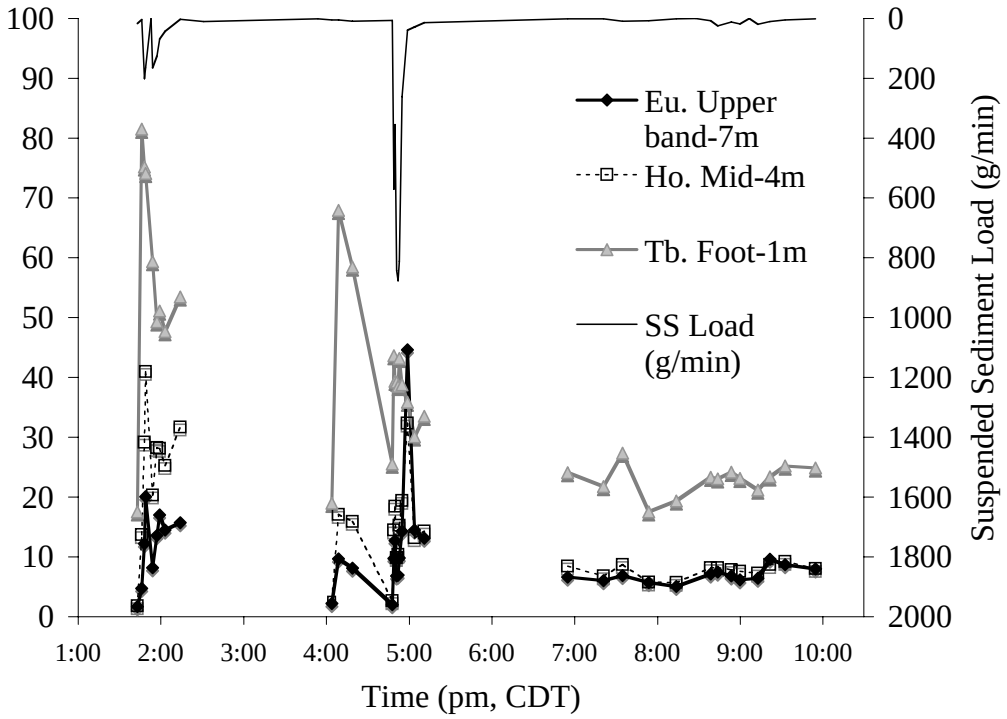


Figure 5 REE concentrations in sediment versus time. Second axis is suspended sediment loading versus time.

REFERENCES

Hawley, N., Robbins, J.A., and Eadie, B.J. (1986). "The partitioning of 7-Beryllium in fresh water," Geochim. Cosmochim. Acta, 50: 1127-1131.

Holland, J.M. (2004). "The environmental consequences of adopting conservation tillage in Europe: reviewing the evidence," Agriculture Ecosystems and Environment. 103: 1-25.

Matisoff, G., Ketterer, M.E., Wilson, C.G., Layman, R., and Whiting, P.J. (2001). "Transport of rare earth element - tagged soil particles in response to thunderstorm runoff," Environmental Science and Technology. 35: 3356-3362.

Matisoff, G., Bonniwell, E.C., and Whiting, P.J. (2002). "Soil erosion and sediment sources in an Ohio watershed using Beryllium-7, Cesium-137, and Lead-210," Journal of Environmental Quality. 31:54-61.

Polyakov, V.O., Nearing, M.A., and Shipitalo, M.J. (2004). "Tracking sediment redistribution in a small watershed: implications for agro-landscape evolution," Earth Surfaces Processes and Landforms. 29: 1275-1291.

Takken, I., Covers, G., Jetten, V., Nachtergaele, J., Steegen, A., and Poesen, J. (2005). "The influence of both process descriptions and runoff patterns on predictions from a spatially distributed soil erosion model," Earth Surface Processes and Landforms. 30: 213-229.

Whiting, P.J., Bonniwell, E.C., and Matisoff, G. (2001). "Depth and areal extent of sheet wash and rill erosion from radionuclides in soils and suspended sediment," Geology, 29:1131-134.

DREDGED MATERIAL MANAGEMENT IN A WATERSHED CONTEXT: SEEKING INTEGRATED SOLUTIONS

Craig Vogt, U.S. Environmental Protection Agency, EPA West (4504t), 1200 Pennsylvania Ave. NW, Washington, DC 20460, Vogt.Craig@epa.gov; Barry Holiday, U.S. Army Corps Of Engineers, 441 G Street NW, Washington, DC 20314, Barry.Holiday@usace.army.mil; Elizabeth Kim, U.S. Environmental Protection Agency, EPA West (4504t), 1200 Pennsylvania Ave., NW, Washington, DC 20460, Kim.Elizabeth@epa.gov; Molly Madden, U.S. Environmental Protection Agency, EPA West (4504t), 1200 Pennsylvania Ave., NW, Washington, DC 20460, Madden.Molly@epa.gov

Abstract: Dredged material management historically utilizes site-specific solutions to address what are essentially the results of watershed-wide problems. The National Dredging Team is seeking to incorporate a broader watershed perspective into dredged material planning. Dredged material managers are primarily affected by sediment deposition in navigational waterways that result from sediment overloading. Watershed managers also face problems stemming from sediment overloading, such as water quality and loss of flood-carrying capacity. Possible solutions for dredged material managers that reduce the amount of sediment deposited can lead to sediment shortage for the watershed and result in coastal and stream bank erosion, as well as wetland loss. Coordination between dredged material and watershed managers is necessary. The National Dredging Team plans to bring the dredged material, sediment, and watershed managers together at a national conference to discuss dredged material management in a watershed context in order to create a coordinated approach to solving these problems.

A FARM SEDIMENT TRAP AND POND IN COLUSA COUNTY, CALIFORNIA

Jack Alderson, Agricultural Engineer, USDA Natural Resources Conservation Service, Colusa, California, jack.alderson@ca.usda.gov

INTRODUCTION

Two brothers wanted to reduce the quantity of sediment leaving their farm, build a farm pond, and reestablish a corner of native habitat. Their project now includes a sediment trap, pond, and plantings of native grasses, trees, and shrubs spread across a four-acre site. These new features were integrated into an intensively managed farmscape without disrupting the existing farming patterns. The transformation of the site was managed by the Colusa County Resource Conservation District as a demonstration project. Funding was provided by the landowners and by the CALFED Bay-Delta Program. The field office of the USDA Natural Recourses Conservation Service designed and managed the construction of the earthworks. The landowners, the Conservation District, and local high school students planted the site.

The immediate transformation of the site was dramatic. Over time, there will be a second transformation as the tree canopy arches over the plantings. Energy flow and structural diversity will be greatly altered. The flora and fauna of the site will continue to shift as the canopy matures. The results of sediment trapping have also been dramatic. The immediate effects have been an over-filled sediment trap and a consequent reduction in the quantity of sediment leaving the farm, one of the original goals of the project. Over time, sediment trapping may provide feedback that helps growers reduce the volume of sediment generated in the field.

This paper describes the design and implementation of the project and reports some initial observations and measurements made at the site. The functioning of the sediment trap is emphasized.

SITE DESIGN

The site is on the former flood plain of Sycamore Slough about one-half mile north of the old channel. Sycamore Slough was cut off from its source, overflow from the Sacramento River, early in the last century as the surrounding land was developed for farming. Parts of the channel remain as narrow strands of mature riparian vegetation. Other sections have been completely filled, their locations unmarked in uniform, laser-leveled fields.

The project was located at this site because it is the low point in the constructed topography of 230 acres of cropland and because it has had a history of poor germination and low yields. A shallow surface drainage ditch ran the length of the west edge of the site and emptied into a farm drainage system. Farm drainage flows into the Colusa Basin Drain, and eventually into the Sacramento River. The site is favorably located for capturing water and sediment. Three sides of the site were bounded by existing farm roads. The new boundary between habitat and cropland was established as a straight line orthogonal to the farming direction. This simple geometry facilitates the use of large equipment in the crop field.

Within the site, the constructed features are curvilinear. The general nature of the earthwork is shown in Figure 1. We chose these shapes to introduce contrasting elements into the landscape and to suggest natural physiographic forms, but they also have a functional basis. The sediment trap has two long arms that bow out from the road at their centers. Constructing these as relatively narrow, linear channels helps to distribute flow through the full volume of the trap and

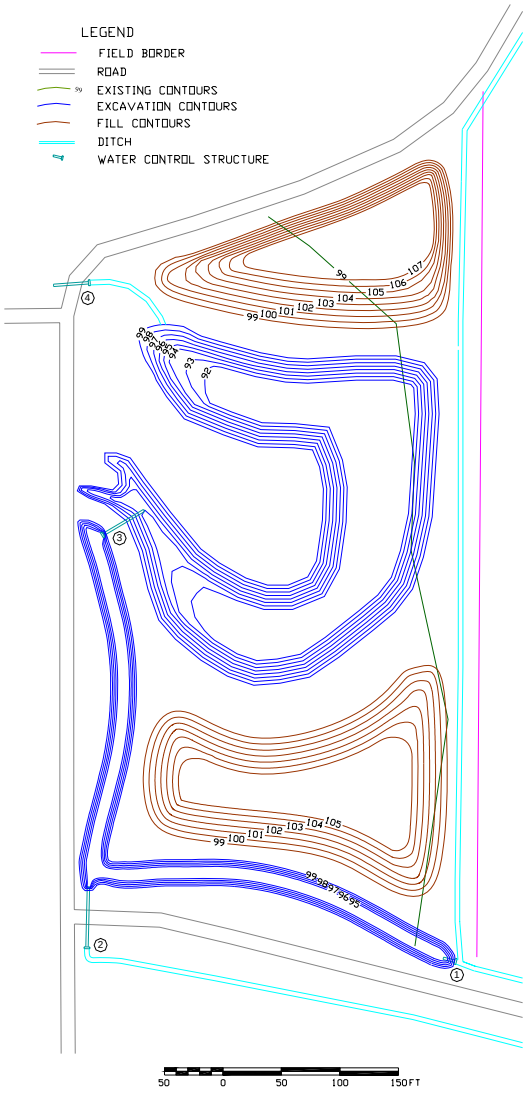


Figure 1 Plan of earthwork.

allows them to be cleaned from one side by a small excavator. The arc of land between the road and the bowed channel provides space for the sediment to be piled for drying. The two arms of the sediment trap each start at the road where they connect to the existing field ditches. The sediment trap has two curved segments, each 300 feet long with a ten-foot bottom width and four-foot depth. The total excavated volume is 1320 cubic yards and the useable storage volume is 890 cubic yards with a surface area of 9600 square feet.

The primary function of the pond is to provide wildlife habitat, but it also traps sediment, and it too is designed to reduce short-circuit flows between the inlet and outlet without the use of baffles. The shape is from a 1905 topographic map of the area. It is a mirrored and scaled transformation of an oxbow lake along the Sacramento River. The pond was designed with a bottom depth that is seven feet below field level. This depth was chosen to assure a large area of open water. The pond is filled by runoff from winter rains and summer irrigations. Even at low water levels, the depth of water is three to four feet, sufficient to prevent the establishment of emergent vegetation. Emergent vegetation is expected to establish around the perimeter of the pond and especially at the two ends where there are bands with a relatively shallow and fluctuating water depth.

The pond has a flow length of 600 feet. The width varies from less than 30 feet to more than 100 feet. The total excavated volume is 8,700 cubic yards. Filled to a depth one foot below field level, the pond covers one acre and holds 4.8 acre-feet of water.

Four water control structures regulate the water depths in the pond, sediment trap, and field ditches. The structures are flashboard weirs with high-density polyethylene corrugated pipe conduits. The conduits allow for field road crossings. The weirs were installed so that the invert of the flow lines could be maintained at the levels that existed before installation of the project or the inverts could be raised independently to near field level. Sediment trapping is maximized when the flashboards are maintained at the highest level. Rapid field drainage is maintained with the boards at the lowest level. With an active strategy, the pond could be drawn down before an irrigation to provide more capacity for short-term tailwater storage.

Excavation spoils were used on site to build contoured mounds. The slopes are gentle; we designed them to allow planting and mowing with normal farm equipment. The two mounds were placed on the north and south sides of the pond to provide shelter from the prevailing strongest winds.

CONSTRUCTION AND PLANTING

The pond and sediment trap were built by a contractor. Excavation was started in the fall of 2002, but rains delayed completion until the following spring. The contractor used a long-reach excavator and off-road dump truck to move the soil. The mounds were built without compaction. The landowners finished the grading of the mounds with a dozer.

The landowners seeded the flats and mounds with native grasses in the fall of 2003. Native trees and shrubs were planted as container stock the following winter. The featured trees are California sycamore (*Platanus racemosa*) and valley oak (*Quercus lobata*), the two dominants of the riparian strand along Sycamore Slough. The landowners, the Resource Conservation District, and an environmental science class from Colusa High School worked together on the plantings.

OBSERVATIONS AND MEASUREMENTS

Near the end of the second growing season after the pond was installed, the landowner reported that there was a danger that the sediment trap would overflow. The trap did not overflow, but by the end of the season the tailwater was running in rivulets over the top of an accumulated mass of sediment. Figure 2 is a photo of the trap at the end of the growing season. The bulk of the sediment came from a tomato field that drained into the downstream arm of the trap. Erosion was evident in the tailwater ditch at the end of this field and in the ends of the furrows where head cutting had occurred. Winter wheat had been grown in this field the previous year, and there had been no evidence of erosion in the field or of sediment accumulation in the trap.



Figure 2 Sediment accumulated in trap.

At the end of the second growing season, we resurveyed the sediment trap to determine how much sediment had accumulated. We also took samples for determining the bulk density and particle size distribution of the sediment and the particle size distribution of the field soil. Four hundred and fifty cubic yards of sediment with an average bulk density of 79 pounds per cubic feet, or 480 tons of sediment, accumulated in the two arms of the sediment trap during the two year period. Figure 3 shows the particle size distributions for the sediment and for the field soil, a silt loam. Based on the difference between the sand fraction of the sediment compared to that of the field soil, the estimated trap efficiency was 23 percent, and the estimated sediment delivery from the fields was 2100 tons. The sediment production is 4.6 tons per acre averaged over the two-year period and the full 230 acres draining into the sediment trap. However, approximately two-thirds of the sediment was delivered from a single 85-acre tomato field during one growing season, a production rate of 16 tons per acre.

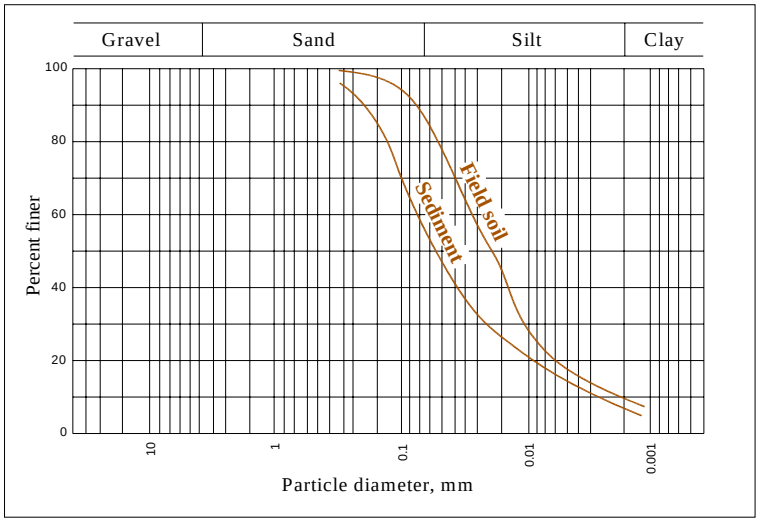


Figure 3 Particle size distributions for field soil and for sediment from the sediment trap.

One reason for the low trap efficiency is that the arm of the trap that captured the most sediment filled. The Yolo County Resource Conservation District (2002) used inlet and outlet water samples to study sediment trap efficiency. They found that efficiency declined during the season as the trap filled. Mid-season efficiencies varied from 33 to 55 percent in their study. There is relatively little guidance available for sizing sediment traps for agricultural operations where sediment is generated by irrigation water rather than stormwater. The California Regional Water Quality Control Board, San Francisco Bay Region (1999) suggests a general method for sizing silting basins and sediment traps based on flow and the particle size to be trapped. For the Colusa site, the maximum anticipated tailwater flow would be three cubic feet per second, and a sediment trap with 15,000 square feet of area would be required to remove fine silt (0.01 millimeter particle size). This is larger than the useable area of the empty sediment trap, but only about one-third the size of the pond downstream of the sediment trap.

Two years after the start of the project 480 tons of sediment that might have entered the Sacramento River was returned to the field. Even over this short monitoring period, the variation in sediment production from different fields and crops has been striking. For the two-year period, approximately two-thirds of the sediment came from one crop on one-third of the land area in one year. The landowners have not had to do calculations to realize this; they saw the sediment clog the trap. Hopefully we will be able to use this knowledge to find the most effective ways to keep the sediment in the field.

REFERENCES

California Regional Water Quality Control Board, San Francisco Bay Region (1999). Erosion & Sediment Control Field Manual, 3rd Edition.

Yolo County Resource Conservation District (2002). Final Report, CALFED Water Use Efficiency Program, Yolo County Resource Conservation District Pilot Program, 2001.

USE OF MONITORING DATA TO EVALUATE WATERSHED MANAGEMENT PRACTICES IN A MIXED-LAND USE WATERSHED IN NORTHERN IDAHO

Krzysztof M. Ostrowski, Graduate Research Assistant, Department of Biological and Agricultural Engineering, University of Idaho, Moscow, ID 83844-2060, ostr0120@uidaho.edu; Jan Boll, Dr., Associate Professor, Department of Biological and Agricultural Engineering, University of Idaho, Moscow, ID 83844-2060, jboll@uidaho.edu; William J. Price, Dr., Statistical Programs, University of Idaho, Moscow, ID 83844-2337, bprice@uidaho.edu; Erin S. Brooks, Dr., Department of Biological and Agricultural Engineering, University of Idaho, Moscow, ID 83844-2060, broo2789@uidaho.edu; Jeremy Newson, Graduate Research Assistant, Department of Biological and Agricultural Engineering, University of Idaho, Moscow, ID 83844-2060, news2880@uidaho.edu

Abstract: The accuracy of sediment load estimates is critical to the detection of watershed effects including changes in watershed management practices, road building and maintenance, and stream restoration. We combined fixed-time interval monitoring at multiple locations with continuous monitoring at one location to determine the effectiveness of conservation practices at multiple locations. In 2000, we established a monitoring program in the Paradise Creek watershed near Moscow, Idaho including 15-minute average stage height and turbidity at a continuous station and bi-weekly monitoring of discharge (Q) and total suspended sediment (TSS) at eight locations. Event-based sampling of total suspended sediment concentrations and discharge was conducted at the continuous station. We applied standard linear regression to Q and turbidity data at the continuous station and Q and TSS at bi-weekly monitoring points for 2001, 2002, and 2005. Using regression equations, we established 15-minute time series at the bi-weekly monitoring points. Flow and TSS correlated well when bi-weekly monitoring points were close to the continuous station. Because bi-weekly data collection occurred during low flow conditions, the relationships between the continuous station and each bi-weekly monitoring point exhibited large errors at high flow events. When calculating sediment loads as the product of Q and TSS, the errors associated with regression alone became substantial. Despite these errors, we applied a trend analysis that shows effects of conservation practices during different years following implementation. Ongoing research attempts to reduce the regression errors include increased frequency of data collection at bi-weekly monitoring points to capture peak flow events, use of particle size distribution in TSS-turbidity relationships, and establishing a continuous flow record at monitoring points using a hydrologic model.

INTRODUCTION

Increasing emphasis on non-point sources (NPS) of pollution such as agriculture and forestry has initiated a growing need for procedures to estimate the effects of all sources of pollution within a watershed (MacDonald, 2005). These effects include changes in watershed management practices, road building and maintenance, stream restoration, and construction development sites. The routing and possible downstream accumulation of sediment from those management activities is of particular concern because it affects aquatic resources by clogging spawning beds, shortening the life of reservoirs, and degrading drinking water. Most studies relate these effects to adverse impact of land use activities. The effects of typical forest and agricultural land activities are increased runoff and sediment transport, higher peak streamflows, increased channel scouring and streambank undercutting (Queen et al., 1995).

Paradise Creek (IDHW-DEQ, 1997) requires a 75% reduction in NPS sediment loading to meet the TMDL. The impact of agricultural land use and other activities can be changed using conservation practices such as conservation tillage, buffer strips or gully plugs. To evaluate the effectiveness of conservation practices and understand the impact of other pollution sources, a monitoring program needs to include multiple sampling locations in the watershed (Mostaghimi et al., 1997). While continuous monitoring is known to provide the most accurate sediment load estimates, a typical monitoring design may use a fixed-time interval (e.g., bi-weekly) for economical reasons. Spatially distributed monitoring using continuous sampling is expensive. In this paper, we present a methodology, which combines fixed time interval monitoring at multiple locations and continuous monitoring at one location. We use this methodology to determine the effectiveness of conservation practices in the watershed at multiple locations.

METHODOLOGY

Watershed description: Paradise Creek watershed (PCW) is located in the Palouse River hydrologic basin in northern Idaho. The headwaters of the creek are located on Moscow Mountain in the Palouse Range. The watershed in total is 50,684 ha. The upper portion of the watershed is steeply sloped, with the majority of the drainage basin consisting of moderately steep rolling hills. Elevations range from 1330m to 770m. The Palouse hills are very susceptible to erosion due to their topography, soil texture, climate and land use practices. Agriculture occupies 66% of the watershed. Nearly 40% of annual precipitation falls during November through January. Most soils are deep, moderately to well-drained silt loam soils formed in loess (Brooks et al., 2002). In 2000 a monitoring program in PCW was established. This program includes continuous stream monitoring in a nested watershed system at three locations (number 20, 30 and 40 in Figure 1). Spatial monitoring on a bi-weekly basis "before" (2001 water year) and "after" (2002 and 2005 water years) implementation of conservation practices occurred at twelve locations. A set of conservation practices was implemented during 2001 including conversion to direct seeding (15% of area converted), gully plugs (25), buffer strips, rock chutes and stream restoration.

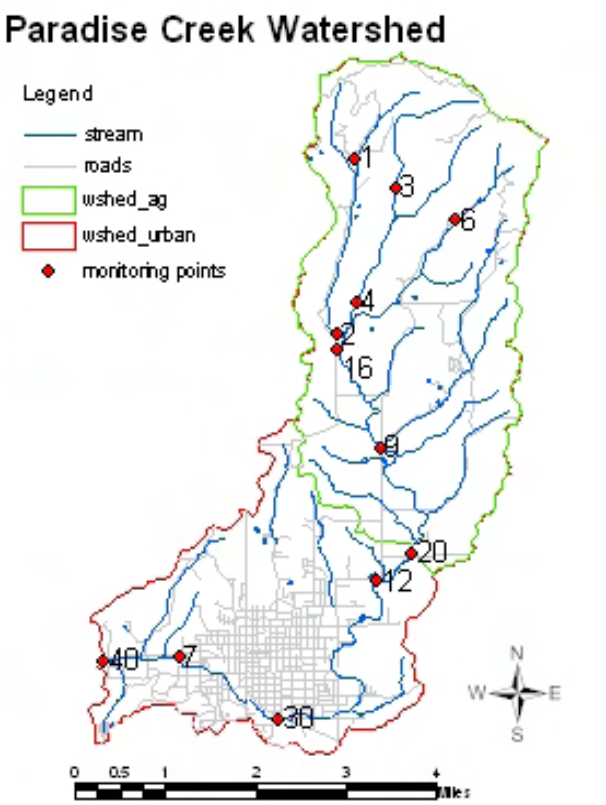


Figure 1 Map of Paradise Creek watershed showing monitoring points.

Available data: Continuous data since October, 2000 include: 15-minute average values of stream stage height, turbidity, electrical-conductivity and water temperature, event-based sampling of total suspended sediment (TSS) concentrations, and periodic discharge measurements. Data from the continuous station at location 20 (Figure 1), below agricultural land will be used in this paper. This station will be referred to as "continuous." The same set of parameters was measured manually on a bi-weekly basis at eight monitoring points within the agricultural part of the watershed (green bordered area in Figure 1) during water years 2001-2002 and 2005. Table 1 shows total precipitation, total flow volume, and maximum daily flow for the continuous station. In 2001 and 2005 total precipitation was much less than the average for the area (ca. 610mm) resulting in low flows (Figure 2) and low sediment loads (Table 1).

Table 1 Summary of hydrologic information for the continuous station for monitoring years 2001, 2002, and 2005.

Water year	Total precip. (mm)	Total flow volume (10^6 m^3)	Max daily flow (m^3/s)	Sediment loads (tons/year)
2001	422	0.51	0.60	42
2002	694	5.13	3.10	1143
2005	467	0.39	0.57	27

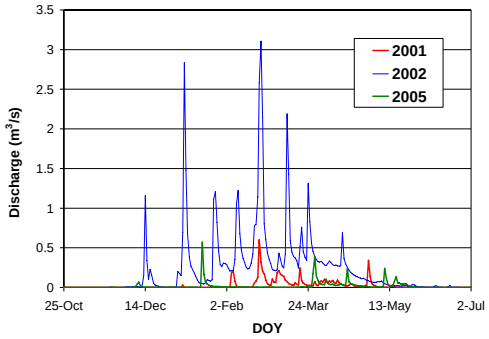


Figure 2 Daily flows at automated recording the continuous station in years 2001, 2002, and 2005.

Data analysis: Raw stage height (H) and turbidity ($NTU_{continuous}$) at the continuous station were checked for quality before analysis. Extremely high $NTU_{continuous}$ observed before regular probe cleaning were set to post-cleaning values. Continuous (15-min average) discharges ($Q_{continuous}$) were determined from H-Q rating curves. Flow lag times were evaluated between the continuous station and each of eight bi-weekly monitoring points, but were negligible. Time series were constructed consisting of data pairs of $Q_{continuous}$ and $NTU_{continuous}$, respectively, and Q_i and TSS_i, respectively, where i is a bi-weekly monitoring point, in each of the years 2001, 2002 and 2005 using standard linear regression. The coefficient of determination and 95% confidence intervals were calculated for each regression equation.

A 15-minute time series of Q_i and TSS_i was constructed separately for each bi-weekly monitoring point in each year using the general linear relationships (Equation 1 and 2):

$$Q_i = aQ_{continuous} + b + e_i \quad (1)$$

$$TSS_i = aNTU_{continuous} + b + e_i \quad (2)$$

where Q_i and TSS_i are the responses at time i, a and b are slope and intercept terms, respectively, and e_i is an error term assumed $N(0, \sigma^2)$. Annual sediment loads for every monitoring point were subsequently calculated by multiplying the predicted 15-minute Q_i and TSS_i values and summing the result over the water year. The error in these load calculations was determined using the standard formula for the variance of the product of two random variables for each 15-minute data and summed over the specified time (Mood et al., 1974) assuming statistical independence and normality of the data.

An exploratory data analysis was performed to check data quality and to see if the data were in the proper form for further statistical analysis. Log-transformations were applied to normalize the data. Autocorrelation was eliminated by aggregating data into daily time steps (Grabow et al., 1998). Discharge was selected as explanatory variable for a selected single downstream station approach. Comparisons of all 15-minute TSS_i data series were carried out using reduced model dummy variable regression following Grabow et al. (1999). The single watershed approach was used ("before/after") for each monitoring point so the comparisons allowed detection of discrete water quality changes due to land treatment changes (Grabow et al., 1998) as well as the magnitude of this change.

RESULTS AND DISCUSSION

Regression analysis: The linear relationships for Q_i and TSS_i at each monitoring point and year are summarized in Table 2 showing the estimates for slope (a) and intercept (b), the coefficient of determination (R^2), and number of observations (n). In general, R^2 for the linear regressions between $Q_{continuous}$ and Q_i for 2002 (0.44-0.94) are better than for 2001 and 2005 (0.18-0.88). In 2002, a greater range of flows (see max Q in Table 2) was observed at the monitoring points than in 2001 and 2005. The R^2 for points further upstream from the continuous station are lower than for points closer to the continuous station, reflecting the differences in hydrologic behavior of subwatersheds and subsequent flow regimes in the upper watershed relative to the lower watershed.

Table 2 Estimated regression parameters, maximum discharge, and maximum total suspended solids for bi-weekly monitoring points in years 2001, 2002, and 2005.

		Regression: $Q_i = a*(Q_{continuous})+b$						Regression: $TSS_i = a*(NTU_{continuous})+b$				
Monitoring site		slope (a)	intercept (b)	R^2	n	max Q (m^3/s)		slope (a)	intercept (b)	R^2	n	max TSS (mg/l)
2001												
PC-16		0.38	0.012	0.79	8	0.127		0.72	-4.24	0.55	9	150
PC-12		0.52	0.015	0.82	12	0.396		0.54	10.84	0.78	12	120
PC-9		0.07	0.003	0.88	9	0.048		0.15	9.60	0.29	9	40
PC-6*		0.03	0.004	0.36	11	0.017		-0.03	11.81	0.06	5	20
PC-4		0.11	0.001	0.71	11	0.105		1.79	-18.46	0.44	10	300
PC-3*		0.05	0.001	0.81	10	0.014		-0.06	19.37	0.42	4	20
PC-2		0.05	0.005	0.78	11	0.057		1.01	22.86	0.38	9	200
PC-1*		0.04	0.001	0.72	10	0.014		0.00	15.51	0.00	12	20
2002												
PC-16		0.76	0.011	0.94	11	0.765		0.09	8.78	0.24	10	25
PC-12		1.80	-0.031	0.92	16	1.982		0.32	4.59	0.70	11	35
PC-9		0.23	-0.009	0.93	16	0.227		0.05	8.45	0.09	11	15
PC-6*		0.08	0.004	0.47	13	0.057		-0.01	11.46	0.01	7	15
PC-4		0.23	0.011	0.86	11	0.255		0.07	6.67	0.19	11	20
PC-3*		0.08	0.002	0.44	12	0.042		1.38	-58.89	0.65	5	100
PC-2		0.25	-0.015	0.88	12	0.255		0.23	8.11	0.22	11	40
PC-1		0.08	0.005	0.58	16	0.085		0.09	6.29	0.76	8	30
2005												
PC-16		0.44	0.003	0.72	11	0.028		0.11	7.13	0.45	12	20
PC-12		0.80	0.001	0.82	13	0.048		0.80	-1.85	0.89	11	50
PC-9		0.12	0.003	0.18	11	0.011		0.85	1.13	0.74	8	60
PC-6*		0.07	0.002	0.27	13	0.008		-0.15	6.46	0.17	11	6
PC-4		0.10	0.004	0.28	13	0.011		0.22	12.06	0.08	12	40
PC-3*		0.07	0.000	0.62	4	0.006		-0.13	14.13	0.55	4	10
PC-2*		0.04	0.002	0.55	10	0.008		-0.01	12.74	0.00	8	15
PC-1*		0.12	0.002	0.62	13	0.011		-0.04	6.86	0.14	12	10

The R^2 for the $NTU_{continuous}$-Tes_{sa} relationships (0.0 to 0.89) are lower than for the $Q_{continuous}$-Q_i relationships. In addition to differences in flow regimes, which affected *TSS* and turbidity, at different locations in the watershed, differences in sediment characteristics also appeared to affect the $NTU_{continuous}$-TSS_i relationships. According to Gippel (1989), the *NTU-TSS* relationship is usually site specific. Just below forest land (points PC-1, PC-3 and PC-6 in Figure 1) and at point PC-2, $NTU_{continuous}$ is not or negative correlated to TSS_i. In further analysis, therefore, the $NTU_{continuous}$-TSS_i relationships for these points (marked with * in Table 2) were not used. Given the relatively even TSS_i concentrations at these points, the average observed TSS_i were used instead.

An evaluation of the errors in the 15-minute Q_i and TSS_i time series shows, as expected, that if the R^2 is lower, the corresponding 95% confidence interval on the predicted lines is greater. As an example, Figure 3 shows the $Q_{continuous}$-Q_i and $NTU_{continuous}$-TSS_i relationships with 95% confidence intervals for point PC-9 in 2002. Results from

point PC-9 are shown in this paper, because a substantial number of gully plugs were installed in the subwatershed in 2001 (Dansart, 2002). For the $Q_{continuous}$-Q_i data (R^2 = 0.93), the confidence interval is relatively small over the range of measurements (Figure 3a), while for the $NTU_{continuous}$-TSS_i data (R^2 = 0.29), the confidence interval widens as the points become more scattered (Figure 3b). When applying the regression equations to obtain 15-minute time series at individual monitoring points, observed $Q_{continuous}$ and $NTU_{continuous}$ outside the range of observed Q_i and TSS_i have large errors and, thus, are less reliable. A drawback of bi-weekly monitoring designs is the tendency to collect data primarily during low flow conditions, as was experienced also in this study in all three years (Figure 4).

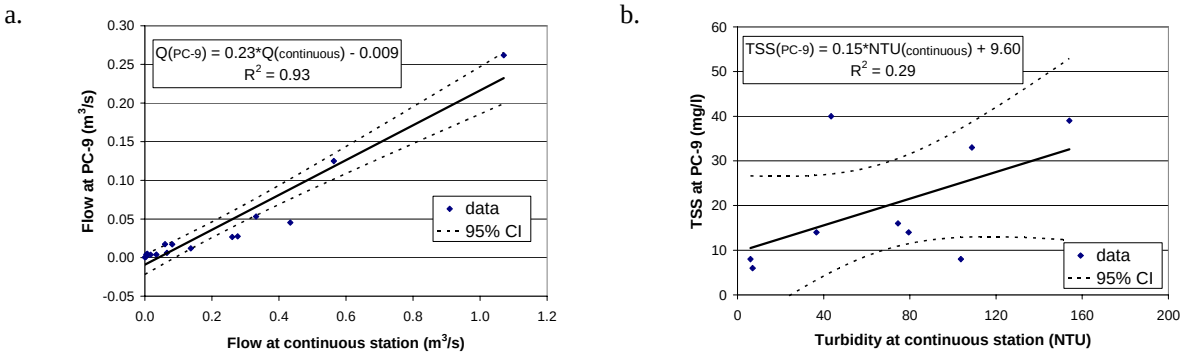


Figure 3 Regression lines with 95% confidence intervals for PC-9 (a. Q_i vs. $Q_{continuous}$, b. TSS_i vs. $NTU_{continuous}$).

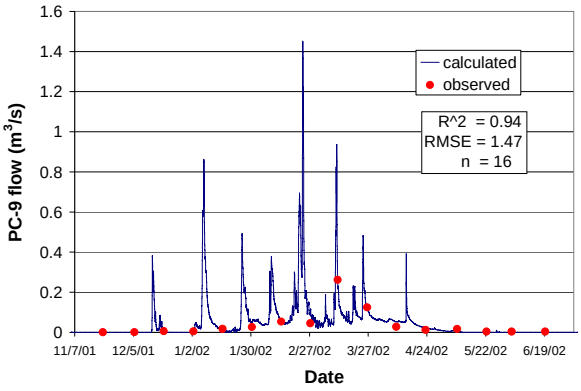


Figure 4 Comparison of calculated and observed discharges for point PC-9 in 2002 year.

Sediment loads: Sediment loads, cumulative errors, and sediment yields for all monitoring points are summarized in Table 3. The sediment loads for point PC-12 were expected to be similar to sediment loads at the continuous station given they are in close proximity (Figure 1). Indeed, the results approximately match the sediment loads at the continuous station for dry years (Table 1). However, for 2002 the sediment load was greatly underestimated (695 vs. 1143 tons/year at the continuous station). The most probable reason is the lack of high Q_i values at PC-12 in 2002 causing large errors at high $Q_{continuous}$ values. Thus, the method of data generation based on bi-weekly sampling for these data underestimated the annual sediment loads.

Cumulative errors for sediment load in Table 2 were substantial for several points. These large errors resulted when Q_i and TSS_i were extrapolated in regions with large errors of prediction. Figure 5 shows magnitudes of error up to 3000% (in kg/15-minute time step) as a function of 15-minute instantaneous discharges at point PC-9 in 2002. To decrease the cumulative errors and, in turn, increase the accuracy of the calculated loads, the measurement frequency should increase. Most importantly, more measurements must be taken at high flows.

Sediment yields for all subwatersheds above bi-weekly monitoring points are included in Table 3 and displayed in Figure 6. Dramatic increases in sediment yield in 2002 were followed by the strong decreases in 2005 at all

monitoring points showing the influence of climate variability (see Table 1) between years. Overall, based on these data, no definitive conclusions can be drawn about true reductions in sediment concentrations and the evaluation of conservation practices. If we consider the average sediment yield estimates, however, the subwatershed above PC-9, appears to have a sediment yield similar to the subwatersheds in the upper watershed (e.g., PC-1, PC-3 and PC-6), where agricultural impacts were much less.

Table 3 Sediment load characteristics for all monitoring points in years 2001, 2002, and 2005.

Monitoring point	Area (ha)	Sediment loads (tons/year)			Cumulative error +/- (tons/year)			Sediment yield (kg/ha/year)		
		2001	2002	2005	2001	2002	2005	2001	2002	2005
PC-16	214.2	25.6	121.2	4.4	579	1919	54	119.7	565.9	20.3
PC-12	1047.4	35.3	694.5	31.8	710	5584	225	33.7	663.0	30.3
PC-9	409.9	2.5	22.3	6.9	66	530	168	6.1	54.5	16.8
PC-6	189.3	1.2	6.0	0.3	32	135	5	6.6	31.9	1.6
PC-4	307.9	14.8	31.0	3.0	588	555	86	47.9	100.8	9.8
PC-3	160.0	0.7	4.7	0.3	22	461	15	4.5	29.4	2.0
PC-2	353.9	11.6	71.1	0.7	299	1446	12	32.9	201.0	1.9
PC-1	172.6	0.9	12.1	0.4	38	149	6	5.0	69.9	2.6

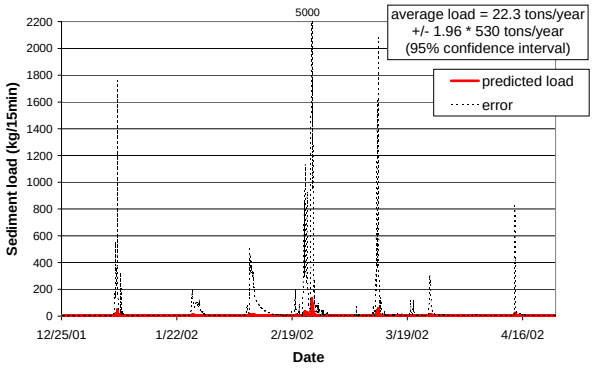


Figure 5 Calculated 15-minute sediment load estimates with possible errors at point PC-9 for 2002 water year.

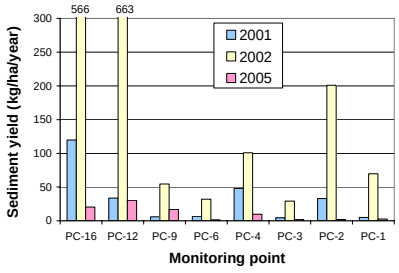


Figure 6 Sediment yields at all monitoring points for monitoring years 2001, 2002, and 2005.

Comparison of trends: A reduced model dummy variable regression analysis was performed on the 15-minute Q_i and TSS_i data series for each monitoring point. Data were aggregated into daily flows excluding periods of time when the creek was dry. Comparisons were made for 2005 vs. 2001, 2002 vs. 2001 and 2005 vs. 2002. Analyses were not applied to points marked with a * in Table 2 since TSS_i were relatively constant throughout the year at these locations. Table 4 lists the average change in TSS concentration, parameters B2 and B3 (difference in

intercepts and difference in slopes between regression lines, respectively) and their statistical significance reflected by p-values. In general, a significant percent reduction in sediment concentrations (from 64 to 97%) was observed in 2002 vs. 2001 for all points (bold values in Table 4, negative sign indicates the reduction). In 2005, TSS_i increased to levels higher than in 2001, except at PC-4.

Table 4 Comparison of regression parameters B2 and B3 and average change in TSS concentrations for all monitoring points in monitored years.

	PC-16	PC-12	PC-9	PC-4
2005 vs. 2001				
B2	0.50	0.03	0.57	-0.68
B3	-0.78	0.09	0.40	-0.16
p-value B2	0.0000	0.4661	0.0000	0.0000
p-value B3	0.0000	0.3163	0.0003	0.1449
Average change in TSS (%)	19	12	60	**-76**
2002 vs. 2001				
B2	0.31	-0.49	-0.46	-1.42
B3	-0.88	-0.24	-0.38	-0.39
p-value B2	0.0024	0.0000	0.0000	0.0000
p-value B3	0.0000	0.0277	0.0000	0.0000
Average change in TSS (%)	**-65**	**-80**	**-64**	**-97**
2005 vs. 2002				
B2	0.19	0.52	1.04	0.74
B3	0.11	0.33	0.78	0.23
p-value B2	0.0000	0.0000	0.0000	0.0000
p-value B3	0.0714	0.0002	0.0000	0.0037
Average change in TSS (%)	46	85	91	84

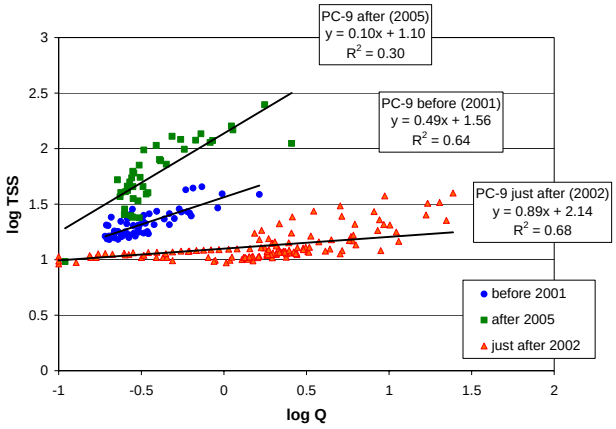


Figure 7 Log-log plot of total suspended sediment (TSS) versus discharge (Q) and best-fit lines for point PC-9.

Results of analyses for TSS_i at point PC-9 are shown in Figure 7. For 2002 (red triangles) vs. 2001 (blue dots) the p-value for the B2 parameter (Table 4) indicates that a statistically significant difference in TSS intercepts between year 2002 and 2001 exists at the 99% confidence level. The B2 value of -0.46 represents the magnitude of the difference while the negative sign indicates a reduction. The negative value of B3 indicates greater reductions occurred at higher TSS_i (also at the 99% confidence level; p-value for B3). The overall 64 percent average reduction in TSS_i exists for PC-9 in 2002 vs. 2001.

Despite the increased sediment yields and loads for all monitoring points in 2002 a significant reduction in TSS_i concentrations was observed. It may indicate that the conservation practices were the most effective in 2002

throughout the watershed, just after installation. The increase in TSS_i in 2005 may be explained by increased human impact observed in the watershed such as dredging the stream channels or road and ditch maintenance which masked the effectiveness of applied conservation practices.

CONCLUSION

A new methodology for the spatial evaluation of conservation practices was presented. The method is based on the generation of spatial time series data from discrete sampling and continuous data recorded at an automated stream station using linear regression. Bi-weekly sampling data collected primarily during low to medium flows used in this paper were not satisfactory for accurate assessment of sediment loads. The extrapolations for high flows produced large errors. To decrease the cumulative errors and, in turn, increase the accuracy of the calculated loads, the measurement frequency should increase. Most importantly, more measurements must be taken at high flows. Comparison of trends revealed that conservation practices were most effective just after their implementation. The increase in sediment concentrations recorded recently is most likely due to increased anthropogenic impact that masked the effectiveness of applied conservation practices.

As a next step to improve the regressions, and thus the sediment load estimates, we will be following three strategies. (i) We will collect discharge and sediment data more frequently at the bi-weekly monitoring points, especially during higher flows, to improve the regressions. During the 2006 water year, we will add a storm chasing procedure to the existing bi-weekly monitoring program as recommended by Robertson and Roerish (1999). (ii) We will improve the TSS-NTU relationships by incorporating changes in particle size distribution during rising and falling limbs of the hydrograph. (iii) We will use flows simulated with a GIS-based hydrologic modeling at the bi-weekly monitoring points to augment the discharge time series.

Acknowledgements: This research was funded by the National Science Foundation through the CAREER program (award 9985194), the USDA Forest Service (agreement number 03-JV-11222065-068), and USDA-CSREES through the CEAP program (award 2004-48619-03119).

REFERENCES

Brooks, E.S., and Boll, J. (2002). "Evaluation of a distributed hydrology model to support restoration efforts in small watersheds with limited data: from research scale to management scale," UNESCO technical reports, presented at the 2002 ERB/Friend 5 conference, Demanovska dolina, Slovakia, 6 p.

Dansart, W. (2002). "Paradise Creek Water and Sediment Control Structure Efficiency," Idaho Soil Conservation Commission, Moscow, Draft Report, August 1. 7 p.

Gippel, C.J. (1989). "The Use of Turbidity Instruments to Measure Stream Water Suspended Sediment Concentrations," Monograph Series No. 4. Department of Geography and Oceanography, University College, The University of New South Wales and Australian Defense Force Academy, 204 p.

Grabow, G.L., Spooner, J., Lombardo, L.A, and Line, D.E. (1998). "Detecting water quality changes before and after BMP implementation: Use of a spreadsheet for statistical analysis," NWQEP Notes, No. 92.

Grabow, G.L., Lombardo, L.A., Line, D.E., and Spooner, J. (1999). "Detecting water quality improvement as BMP effectiveness changes over time: use of SAS for trend analysis," NWQEP Notes, No. 95.

IDHW-DEQ. (1997). Paradise Creek TMDL.

MacDonald, L.H. (2005). "Predicting and Managing Cumulative Watershed Effects," College of Natural Resources, University of Minnesota. http://www.cnr.umn.edu/FR/courses/fr5153/MacDonald.pdf, accessed on May 27, 2005.

Mood, A.M., Graybill, F.A., and Boes., D.C. (1974). Introduction to the Theory of Statistics. Third Edition. McGraw-Hill Book Company, pp 175-181.

Mostaghimi, S., Park, S.W., Cooke, R.A., Wang, S.Y. (1997). "Assessment of management alternatives on a small agricultural watershed," Water Resources, 31(8), pp 1867-1878.

Queen, L.P., Brooks, K.N., Wold, W.L. (1995). "Assessing cumulative effects in the Nemadji River Basin, Minnesota," Proceedings of the 1995 Watershed Management Symposium, August 14-16, San Antonio, TX, USA, ASCE, pp 239-249.

Robertson, D.M., and Roerish, E.D. (1999). "Influence of various water quality sampling strategies on load estimates for small streams," Water Resources Research, 35(12), pp 3747-3759.

A NEW METHOD FOR ESTIMATING SUSPENDED SEDIMENT LOAD AND ITS APPLICATION TO THE REGULATED SOUTH SASKATCHEWAN RIVER

Robert Thomas, Schools of Geography and Earth Sciences, University of Leeds, Leeds, UK, r.thomas@earth.leeds.ac.uk; Stuart Lane, Department of Geography, University of Durham, Durham, UK, S.N.Lane@durham.ac.uk

Abstract: The determination of suspended sediment loads that are both accurate and precise is a continuing problem facing fluvial geomorphologists, engineers and riparian managers. Faced with only intermittent measurements of suspended sediment concentration (*C*), many researchers have utilized least squares regression to determine a log-log rating relationship between coincident values of *C* and water discharge (*Q*) measured at intervals ranging from days to several weeks. Continuous data for *C* are then modeled using (relatively) high frequency measurements of *Q*. The suspended sediment load is then estimated as the product *CQ*. Unfortunately, a large number of factors may introduce error into load estimates derived from rating curves, potentially leading to incorrect interpretation and understanding.

In this paper, an enhanced new method for estimating suspended sediment loads that allows the propagation of uncertainty associated with potential sources of error in measurements of *C* and *Q* is detailed. Uncertainties associated with discharge records, such as variations in the stage-discharge curve and rounding error, are propagated through the simulation by perturbing within the possible bounds of *Q*. LOcally-WEighted Scatter plot Smoother (LOWESS) relationships allow each perturbed ln *Q*-value to be transformed to an estimated value of ln *C*. The resulting estimate of ln *C* and its local standard deviation allow for Monte Carlo simulation of a possible value of ln *C* for the river discharge on that day. Each simulated value of ln *C* is then transformed into real space, and multiplied by the corresponding discharge. This procedure is undertaken for each day within a calendar year, and then repeated for each year within a 250-run Monte Carlo framework. The entire procedure allows uncertainties inherent both in discharge measurement and in suspended-sediment rating curves to propagate through to estimates of annual loads.

The new method has been applied to a reach of the South Saskatchewan River, Saskatchewan, Canada, in order to study the impact of Gardiner Dam, a 64 m-high and 4.8 km-wide earth fill dam. It impounds about 9.36×10^9 m^3 of water to form the 225 km-long Lake Diefenbaker. A reservoir of this size can be expected to have a 100% sediment trapping efficiency and this is borne out by the available data. Pre-closure (1911-1965), the median annual load 140 km downstream of the dam was 3,704,000 tonnes; post-closure (1968–2003), this reduced by 93% to 248,500 tonnes. 262 km upstream of the dam, the median annual load for the period 1917–2003 was 8,922,580 tonnes. Using annual load estimates from this location, and assuming a mean deposit density of 911 kg m^{-3}, it is estimated herein that 1.66×10^8 m^3 of reservoir volume was lost between 1966 and 1980 (90% confidence limits 1.35–2.06 $\times 10^8$ m^3). This compares to a value of 1.27×10^8 m^3 derived from a series of repeated cross-sections. It is hypothesized that this discrepancy is caused by error in the assumed deposit density, error in the earliest surveys or a cross-section spacing (mean ≈ 7.3 km) that was too large to sufficiently capture morphological change.

CALIBRATION OF THE WATBAL SEDIMENT AND WATER YIELD MODEL CLEARWATER NATIONAL FOREST

Dick Jones, Forest Hydrologist, Clearwater National Forest, Orofino, Idaho. rmjones@fs.fed.us; Rick Patten, Forest Hydrologist, Idaho Panhandle National Forests, Coeur d'Alene, Idaho. rpatten@fs.fed.us

Abstract: WATBAL is the Clearwater National Forest watershed response model used to simulate the likely cumulative sediment and water yield effects of roads, timber harvest and fire. The model estimates are based upon the soil, hydrologic and geomorphic characteristics of over 160 landtypes on the Clearwater National Forest. This paper documents a recent calibration of the model to improve its accuracy and predictability for the Forest. Two previous validations of the WATBAL model, the first in 1997 and the last in 2002 showed the model tending to under-predict sediment delivery. The 1997 validation indicated the model estimated only 27 percent of the measured sediment in Lolo Creek and 56 percent of measured sediment in Pete King Creek. The 2002 validation examined six watersheds and found the model estimating between 32 and 78 percent of the actual sediment measured.

In 2005, over 18,000 suspended sediment and 600 bedload sediment measurements collected between 1978 and 2004 were analyzed from seven different watersheds. Watersheds were selected with a variety of management intensity, underlying geology and long-term data sets that could be paired to evaluate WATBAL model runs. Validation tests of sediment data collected showed the model estimating between 31 percent of measured sediment in Elk Creek, a watershed dominated by general granitic and grussic-granitic parent materials associated with the Idaho Batholith and low relief rolling hills landforms; and 103 percent in Swamp Creek, a watershed dominated by Belt Series quartzite parent materials. Overall, the model estimated 62 percent of the measured sediment in the seven watersheds with a correlation coefficient of the regression (r^2) for predicted versus measured sediment of 0.46.

Three adjustments were made to WATBAL's landtype input files to recalibrate the model. On five landtypes that have a high occurrence of landslides related to a 20-year flood event, the mass wasting coefficients were increased from "high" (40 t/mi^2/yr.) to "very high" (80 t/mi^2/yr.); on highly erosive grussic-granitic and micaceous schist parent materials the landtype surface and mass wasting coefficients were doubled; and on general granitic landtypes, the surface and mass wasting coefficients were increased by 150 percent. When the model was run with the calibrated landtype coefficients, it estimated 64 percent of measured sediment in Lolo Creek to 126 percent in Deadman Creek. The overall mean accuracy for the seven watersheds combined improved to 99 percent. The resulting r^2 was 0.60.

The WATBAL model continues to under-predict sediment in watersheds such as Lolo Creek and Elk Creek with high percentages of low relief rolling hills and over-predicts sediment in watersheds such as Deadman Creek with higher percentages of over-steepened breaklands. Watershed predictive models, including WATBAL, are not expected to be perfect due to the extraordinary variability of natural watershed systems; however the accuracy has improved as long-term sediment data became available. In any case, the value of the model for its primary purpose of identifying change and comparing watersheds or alternatives is improved.

INTRODUCTION

WATBAL is the Clearwater National Forest cumulative watershed response model used to simulate the likely cumulative sediment and water yield effects that result from typical forest management disturbances, such as roads, timber harvest and fire. The model estimates are based upon the watershed characteristics of over 160 landtypes characterized on the Clearwater National Forest, Wilson, et al. (1983). The purpose of this paper is to document the calibration of the Clearwater National Forest's WATBAL sedimentation model as recommended in *Validation of the WATBAL Sediment Model*, Jones (2002). The intent of this paper is not to explain the concepts of the R1-R4 or WATBAL watershed model. These are well documented in *Guide for Predicting Sediment Yields from Forested Watersheds*, Cline, et al. (1981) and in *Watershed Response Model for Forest Management, WATBAL Technical Users Guide*, Patten (1989); Patten and Jones (2001); and Patten and Jones (2005).

Two previous papers dealt with the validation of WATBAL; *Evaluating the WATBAL Sediment Loading Model, Clearwater National Forest, Idaho*, Hickey (1997) and *Validation of the WATBAL Sediment Model, Clearwater National Forest*, Jones (2002). Both validations indicated that WATBAL was tending to under-predict sediment.

Hickey performed his test of predicted versus actual sediment in two watersheds; Lolo Creek and Pete King Creek. The Lolo Creek test included nine years of predicted versus measured sediment between 1984 and 1994. The Pete King test included 19 years of predicted versus measured sediment between 1975 and 1994. Hickey found that, for the periods of records analyzed, WATBAL under-predicted sediment by 22.1 t/mi^2/yr in Lolo Creek (27% of measured sediment) and 28.0 t/mi^2/yr in Pete King Creek (56% of measured sediment).

In *Validation of the WATBAL Sediment Model*, Jones analyzed predicted versus actual sediment in six watersheds; Fish, Swamp, Deadman, Pete King, Lolo and Canyon creeks. Between nine and 23 years of discharge and sediment data were used depending on the length of record in each watershed. WATBAL under-predicted sediment from 20.6 t/mi^2/yr (32% of measured sediment) in Lolo Creek to 4.5 t/mi^2/yr (78% of measured sediment) in Swamp Creek. For all six test watersheds combined, WATBAL under-predicted measured sediment by 14.9 t/mi^2/yr (56%). Because WATBAL consistently under-predicted sediment in all watersheds, these recommendations were made to calibrate the model:

- Re-calculate the runoff coefficients and distributions in the model to reflect the annual hydrograph for the most representative gauging stations Jones (2002). This step was completed as part of *Validation of the WATBAL Sediment Model in 2002;*

- Adjust the natural surface and mass erosion coefficients in the external WATBAL support files for landtypes (the subject of this paper).

METHODOLOGY

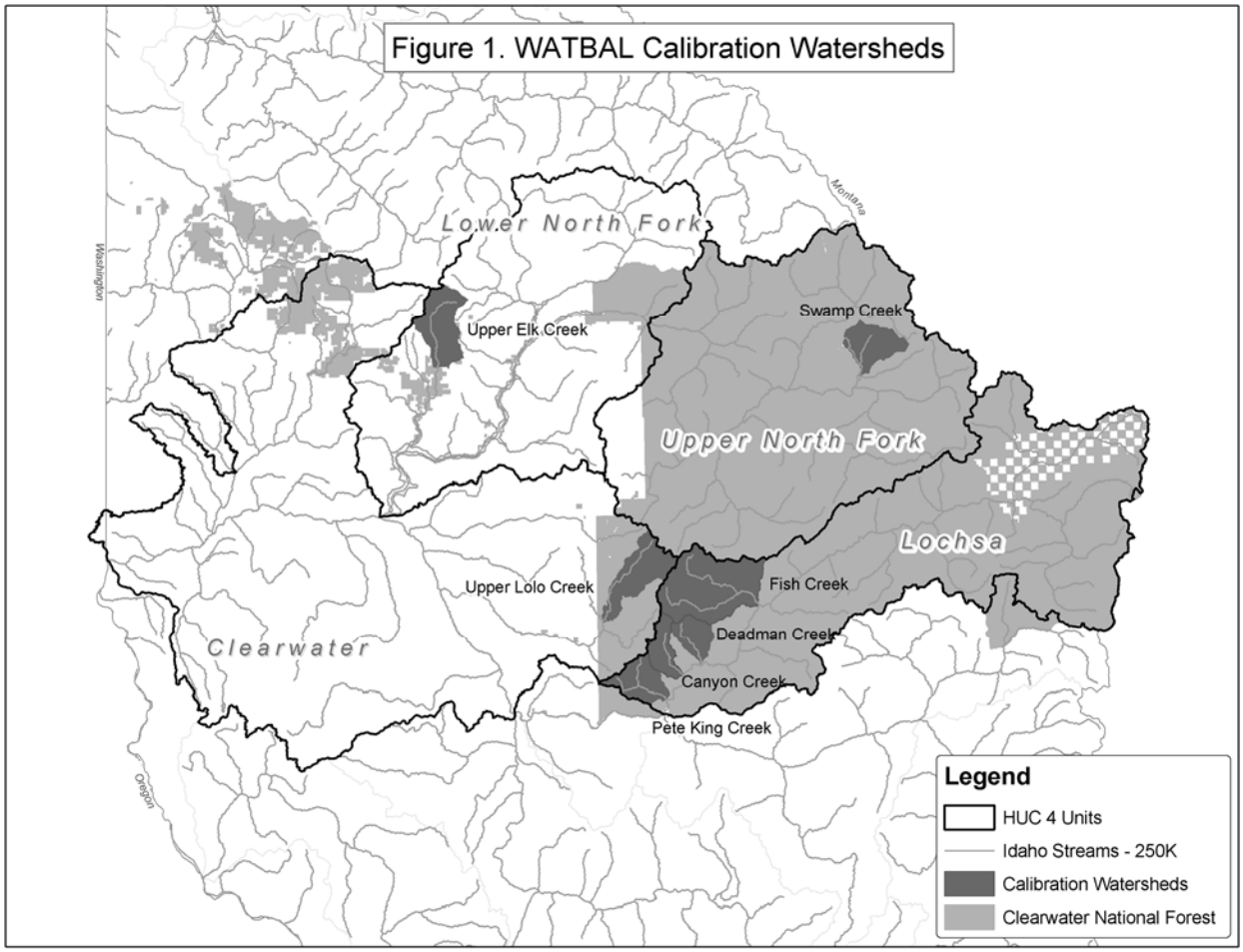
The Clearwater National Forest is rich in stream discharge and suspended sediment data. In 1978, the first automated suspended sediment sampler was installed at the Pete King Creek gaging station. Since that time, stage recorders and automated suspended sediment samplers have been installed in six other watershed for the purpose of model calibration. In this calibration, over 18,000 suspended and 600 bedload sediment samples were used from seven different established water quality stations. To derive the total annual sediment load at a station, both bedload and suspended load samples were analyzed. First, each bedload measurement (with a Helley-Smith sampler) was converted to its relative percent of the depth integrated suspended load measured (with a DH-48 sampler) that same day. Since far fewer bedload measurements were taken than suspended load, this bedload ratio was then added to the daily composited suspended load measurements (from an automated ISCO device) for each day when no bedload measurement was taken to determine the *total* load estimate for that day. The annual calculation of these total load estimates was then compared to the WATBAL estimates.

For selecting calibration watersheds, the criteria used were: 1) a broad range of management intensities; 2) a variety of parent materials and landforms; 3) long-term periods of record of stream discharge and suspended sediment; and 4) a WATBAL run driven by a comprehensive set of disturbance activities. Seven watersheds met these requirements and they were used for this calibration exercise. The calculated total sediment, derived from measured instream data, was compared to WATBAL modeled outputs of total sediment. Data are presented in *tons per square mile of watershed per year* (t/mi^2/yr) and ratios as percentages. The analysis included the watersheds in Figure 1.

The *Fish Creek* watershed is located within the Lochsa River Subbasin. Fish Creek was the largest watershed analyzed at 88 square miles (mi^2). Management intensity is light (e.g., road density is less than 0.1 miles per square mile of watershed (mi/mi^2) and harvest intensity is less than 2 percent of the watershed). The geology is dominated by undifferentiated parent materials[1] (38%) and grussic[2] and other granitic rocks of the Idaho Batholith (58%). Landforms consist of low relief rolling hills (33%), mountain slopelands (31%) and steep breaklands (31%). A

[1] Undifferentiated parent materials consist of mapping units where the type of parent material does not influence the interpretative criteria for the units.
[2] Highly weathered granitic rocks.

combination of WATBAL runs on upper Fish Creek (below Hungery Creek) was used to compare to the measured data at the Fish Creek gaging station near its mouth.



The *Swamp Creek* watershed is located within the Upper North Fork Clearwater River Subbasin. The watershed area is 16 mi^2. Management intensity is light (e.g., road density is less than 1 mi/mi^2 and harvest intensity is less than 1 percent of the watershed). The geology is dominated by Belt series quartzites (47%) and undifferentiated parent material (52%). Landforms consist of low relief rolling hills (18%), mountain slopelands (55%) and steep breaklands (27%).

The *Deadman Creek* watershed is located within the Lochsa River Subbasin. The watershed area is 20 mi^2. Management intensity is moderate (e.g., road density is nearly 2 mi/mi^2 and harvest intensity 13 percent). The geology is dominated by granitic and grussic-granitic rocks (79%) and undifferentiated parent material (20%). Landforms consist of low relief rolling hills (49%), mountain slopelands (15%) and steep breaklands (34%).

The *Elk Creek* watershed (above Partridge Creek) is located within the Lower North Fork Clearwater River Subbasin. The watershed area is 35 mi^2. Management intensity is heavy (e.g., road density is nearly 4 mi/mi^2 and harvest intensity greater than 20 percent). The geology is a mixture of granitic and grussic-granitic rocks (52%), Belt series quartzites (21%), Border Zone micaceous schists (19%) and alluvial deposition (5%). Landforms consist of low relief rolling hills (52%) and mountain slopelands (44%).

The *Pete King Creek* watershed is located within the Lochsa River Subbasin. The watershed area is 28 mi^2. Management intensity is heavy (e.g., road density greater than 5 mi/mi^2 and harvest intensity is nearly 30 percent).

The geology is dominated by Border Zone[3] micaceous schist parent material (75%). Landforms consist of low relief rolling hills (41%), mountain slopelands (19%), steep breaklands (34%) and mass wasted slopes (5%). This was the most erosive watershed studied for both surface and mass erosion.

The *Lolo Creek* watershed (above Musselshell Creek) is located within the Clearwater River Subbasin. The watershed area is 32 mi^2. Management intensity is heavy (e.g., road density is 5 mi/mi^2 and harvest intensity greater than 40 percent). The geology is dominated by granitic rocks (66%) and alluvial deposition (15%). Landforms consist of low relief rolling hills (72%) and mountain slopelands (26%).

The *Canyon Creek* watershed is located within the Lochsa River Subbasin. The watershed area is 20 mi^2. Management intensity is heavy (e.g., road density greater than 5 mi/mi^2 and harvest intensity near 50 percent). The geology is dominated by granitic and grussic-granitic rocks (78%) and Border Zone micaceous schist parent material (15%). Landforms consist of low relief rolling hills (56%), mountain slopelands (14%), mass wasted slopes (7%) and steep breaklands (21%).

RESULTS

The *Fish Creek* water quality station was in operation in 1980 for one year and continuously from 1992 through 2004. During the same period, mean annual discharge was 216 *cubic feet per second* (cfs) with a standard deviation of 61.2 cfs and a coefficient of variation of 28 percent (Table 1). Over 2,000 suspended sediment samples collected between 1980 and 2004 were used in this composite analysis. Thirteen sets of bedload and suspended load sediment samples collected between 1980 and 1994 indicated that the bedload component was 8.1 percent of the total sediment load. Measured mean annual sediment was 21.9 $t/mi^2/yr$ for the period of record. Standard deviation was 29.9 $t/mi^2/yr$ while the coefficient of variation was 136 percent. WATBAL-2002 under-predicted sediment seven out of 14 years, estimating 54.8 percent of measured sediment over the period of record (Table 2)

Table 1 Management intensity, mean annual discharge, and sediment load for all stations.

Watershed	Management Intensity	Annual Discharge (cfs)			Annual Sediment Load ($t/mi^2/yr$)		
		Mean	Std	CV %	Mean	Std	CV %
Fish Creek	Light	216	61.2	28	21.9	29.9	136
Swamp Creek	Light	36.5	10.2	28	19.0	15.8	83
Deadman Creek	Moderate	37.5	9.4	25	28.1	28.0	100
Elk Creek	Heavy	81.4	29.9	37	24.3	18.8	77
Pete King Creek	Heavy	43.5	13.9	32	46.6	42.0	90
Lolo Creek	Heavy	91.1	26.6	29	27.5	15.7	57
Canyon Creek	Heavy	44.7	16.8	38	28.9	49.4	171

The *Swamp Creek* water quality station was in operation between 1980 and 1994. During the same period, mean annual discharge was 36.5 cfs with a standard deviation of 10.2 cfs and a coefficient of variation of 28 percent. Over 1,700 suspended sediment samples collected between 1980 and 1994 were used in the analysis. Over 50 sets of bedload and suspended load sediment samples collected between 1979 and 1991 indicated that the bedload component was 10.1 percent of total sediment load. Measured mean annual sediment was 19.0 $t/mi^2/yr$ for the period of record. Standard deviation was 15.8 $t/mi^2/yr$ while the coefficient of variation was 83 percent. WATBAL-2002 under-predicted sediment five out of 15 years, estimating 102.6 percent of measured sediment over the period of record.

The *Deadman Creek* water quality station has been in operation since 1989.[4] During the same period, mean annual discharge was 37.5 cfs with a standard deviation of 9.4 cfs and coefficient of variation of 25 percent. Over 2,000 suspended sediment samples collected between 1989 and 2004 were used in the analysis. Over 100 sets of bedload and suspended load sediment samples collected between 1979 and 1992 indicated that the bedload component was

[3] The contact between intrusive granites and metasediments in north Idaho.
[4] Data was not collected at Deadman Creek in 1996 because a flood destroyed the station.

30.7 percent of total sediment load. Measured mean annual sediment was 28.1 t/mi^2/yr for the period of record. Standard deviation was 28.0 t/mi^2/yr while the coefficient of variation was 100 percent. WATBAL-2002 under-predicted sediment nine out of 15 years, estimating 68.2 percent of measured sediment over the period of record.

Table 2 Measured versus WATBAL-2002 modeled sediment for all stations.

Watershed	Total Measured Sediment (t/mi^2/yr)	WATBAL-2002 Predicted Sediment (t/mi^2/yr)	WATBAL-2002 Predicted Sediment (%)
Fish Creek	21.9	12.0	54.8
Swamp Creek	19.0	19.5	102.6
Deadman Creek	28.1	19.1	68.2
Elk Creek	24.3	7.4	30.6
Pete King Creek	46.6	29.8	63.9
Lolo Creek	27.5	10.3	37.5
Canyon Creek	28.9	23.8	82.3
Mean for all watersheds	28.0	17.4	62.1

The *Elk Creek* water quality station was in operation between 1982 and 1987 and 1990 and 2003.[5] During the same period, mean annual discharge was 81.4 cfs with a standard deviation of 29.2 cfs and coefficient of variation of 37 percent. Over 3,000 suspended sediment samples collected between 1982 and 2003 were used in the analysis. Over 150 sets of bedload and suspended load sediment samples collected between 1978 and 2004 indicated that the bedload component was 8.8 percent of total sediment load. Measured mean annual sediment was 24.3 t/mi^2/yr for the period of record. Standard deviation was 18.8 t/mi^2/yr while the coefficient of variation was 77 percent. WATBAL-2002 under-predicted sediment 19 out of 20 years, estimating 30.6 percent of measured sediment over the period of record.

The *Pete King Creek* water quality station has been in operation since 1978. During the same period, mean annual discharge was 43.5 cfs with a standard deviation of 13.9 cfs and coefficient of variation of 32 percent. Over 4,000 suspended sediment samples collected between 1978 and 2004 were used in the analysis. Over 100 sets of bedload and suspended load sediment samples collected between 1975 and 1993 indicated that the bedload component was 40.3 percent of total sediment load. Measured mean annual sediment was 46.6 t/mi^2/yr for the period of record. Standard deviation was 42.0 t/mi^2/yr while the coefficient of variation was 90 percent. WATBAL-2002 under-predicted sediment 17 out of 27 years, estimating 63.9 percent of measured sediment over the period of record.

The *Lolo Creek* water quality station has been in operation since 1985. During the same period, mean annual discharge was 91.1 cfs with a standard deviation of 26.6 cfs and coefficient of variation of 29 percent. Nearly 3,000 suspended sediment samples collected between 1985 and 2004 were used in the analysis. Over 150 sets of bedload and suspended load sediment samples collected between 1980 and 2004 indicated that the bedload component was 16.1 percent of total sediment load. Measured mean annual sediment was 27.5 t/mi^2/yr for the period of record. Standard deviation was 15.7 t/mi^2/yr while the coefficient of variation was 57 percent. WATBAL-2002 under-predicted sediment 19 out of 20 years, estimating 37.3 percent of measured sediment over the period of record.

The *Canyon Creek* water quality station has been in operation since 1992. During the same period, mean annual discharge was 44.7 cfs with a standard deviation of 16.8 cfs and coefficient of variation of 38 percent. Over 2,000 suspended sediment samples collected between 1992 and 2000 were used in the analysis. Eighteen sets of bedload and suspended load sediment samples collected between 1992 and 1994 indicated that the bedload component was 19.4 percent of total sediment load. Measured annual sediment was 28.9 t/mi^2/yr for the period of record. Standard deviation was 49.4 t/mi^2/yr while the coefficient of variation was 171 percent. WATBAL-2002 under-predicted sediment six out of 13 years, estimating 82.3 percent of measured sediment over the period of record.

[5] All discharge data was lost in 2004 because the stage recorder failed.

It was noted that for all stations, WATBAL-2002 estimates of annual sediment were always within the range of variability of the annual measured total sediment load; however, WATBAL-2002 consistently under-predicted sediment in six of the seven watersheds. The model estimates for total sediment was best for the Swamp Creek watershed and least accurately in the Lolo Creek and Elk Creek watersheds. The overall mean of predicted versus measured sediment was 62.1 percent, with a range of 30.6 percent (Elk Creek) to 102.6 percent (Swamp Creek).

WATBAL-2002 appeared to have the largest discrepancies in terms of total sediment in watersheds with alluvial deposition and granitic and grussic parent materials in combination with low relief rolling hills and mountain slopeland landforms i.e., Elk Creek and Lolo Creek watersheds. WATBAL-2002 predicted adequately in the Pete King Creek and Canyon Creek watersheds, despite high levels of mass wasting in those watersheds. This suggests that the existing accelerated mass wasting coefficients in WATBAL-2002 are performing well.

The predictability of the pre-calibrated WATBAL-2002 model, or the correlation coefficient of the regression of measured versus predicted sediment (r^2), was 0.46. Based upon the preceding results, a decision was made to calibrate the model to improve its overall performance.

CALIBRATION

WATBAL uses the mass and surface erosion coefficients from an external support file for landtypes. Natural sediment yield coefficients for each landtype are based on the landtype risk factors (e.g., potentials for debris avalanche and rotational mass wasting; and erosion hazards for surface soils, sub soils, and parent materials). The risk factors are used to adjust known sediment rates to develop one mass erosion sediment coefficient and one surface sediment coefficient for each landtype. The landtype coefficients are combined and then they are weighted by landtype area and aggregated for the watershed by WATBAL to provide an estimate of natural sediment production. Natural sediment from mass wasting processes is assumed to vary from essentially zero to 80 t/mi^2/yr (very high). Natural sediment from surface erosion processes varies from 5 (low) to 25 t/mi^2/yr (very high). When the watershed is disturbed from roads, harvest or fire, the mass erosion is assumed to be accelerated up to 250 times the natural erosion rate in WATBAL. The same disturbances are assumed in WATBAL to induce sediment from surface erosion that varies from 0 to 67,500 t/mi^2/yr., depending on the activity type, landtype and time since the disturbance, Patten and Jones (2005).

Three adjustments were made to the external support file for landtypes to calibrate the WATBAL-2005 model:

1) For each landtype, the frequency of landslides that occurred during the 1995-1996 flood events was determined McClelland, et al. (1997). Five landtypes had very high mass wasting frequencies, ranging from 0.64 to 2.69 landslides per square mile[6], yet the mass erosion hazard was only rated "high" in the external support file. All other landtypes had landslide densities of 0.38 or less. The authors have chosen to increase the mass erosion hazard from "high" (40 t/mi^2/yr) to "very high" (80 t/mi^2/yr) on these five landtypes.

2) The authors have chosen to increase the mass and surface erosion coefficients for grussic granitic and micaceous schist parent materials landtypes by 100 percent. A revised value up to 80 t/mi^2/yr was used for mass wasting for each landtype with those parent materials.

3) The authors have chosen to increase the mass and surface erosion coefficients for general granitic parent material landtypes by 150 percent. A revised value up to 80 t/mi^2/yr was used for mass wasting for each landtype with that parent material.

Pre- and Post Calibration results for each of the seven test watersheds are compared in Table 3.

After calibration, WATBAL-2005 accuracy improved from 55 to 101 percent of measured sediment in Fish Creek. The calibrated WATBAL-2005 under-predicted sediment five out of 14 years.

[6] The number of landslides that occurred on each landtype on the Forest was divided by the total area in square miles of the landtype to determine the frequency. Stream breaklands with undifferentiated or grussic-granitic parent materials were the landtypes with the highest frequency of landslides.

Table 3 Measured versus original and calibrated WATBAL modeled sediment for all stations.

Watershed	Total Measured Sediment ($t/mi^2/yr$)	Original WATBAL-2002 Predicted Sediment ($t/mi^2/yr$)	Original WATBAL-2002 Predicted Sediment (%)	Calibrated WATBAL-2005 Predicted Sediment ($t/mi^2/yr$)	Calibrated WATBAL-2005 Predicted Sediment (%)
Fish Creek	21.9	12.0	54.8	22.0	100.5
Swamp Creek	19.0	19.5	102.6	21.5	113.2
Deadman Creek	28.1	19.1	68.0	35.5	126.3
Elk Creek	24.3	7.4	30.5	17.8	73.3
Pete King Creek	46.6	29.8	63.9	43.4	93.1
Lolo Creek	27.5	10.3	37.5	17.6	64.0
Canyon Creek	28.9	23.8	82.4	36.1	124.9
Mean for all watersheds	28.0	17.4	62.1	27.7	98.8

After calibration, WATBAL-2005 went from estimating 103 to 113 percent of measured sediment in Swamp Creek. The calibrated WATBAL-2005 under-predicted sediment six out of 15 years.

After calibration, WATBAL-2005 accuracy improved from 68 to 126 percent of measured sediment in Deadman Creek. The calibrated WATBAL-2005 under-predicted sediment three out of 15 years.

After calibration, WATBAL-2005 accuracy improved from 31 to 73 percent of measured sediment in Elk Creek. The calibrated WATBAL-2005 under-predicted sediment ten out of 20 years.

After calibration, WATBAL-2005 accuracy improved from 64 to 93 percent of measured sediment in Pete King Creek. The calibrated WATBAL-2005 under-predicted sediment nine out of 27 years.

After calibration, WATBAL-2005 accuracy improved from 38 to 64 percent of measured sediment in Lolo Creek. The calibrated WATBAL-2005 under-predicted sediment 14 out of 20 years.

After calibration, WATBAL-2005 went from estimating 82 to 125 percent of measured sediment in Canyon Creek. The calibrated WATBAL-2005 under-predicted sediment two out of 13 years.

By modifying the mass and surface erosion coefficients, WATBAL-2005 estimates improved from 62 to 99 percent of measured sediment for all watersheds combined. Under predictions improved from six to only three of seven test watersheds. The model's predictability (correlation coefficient of the regression - r^2) of measured versus calibrated sediment improved from 0.46 to 0.60.

CONCLUSIONS

Modifying the mass and surface erosion coefficients in the external landtype file improved the predictability of the WATBAL model from 62 to 99 percent when the results of the seven stations were averaged together. The correlation of measured versus calibrated sediment (r^2), improved from 0.46 to 0.60. WATBAL-2005 most accurately predicts the long-term average sediment in Fish Creek (100.5%), Pete King Creek (93.1%) and Swamp Creek (113.2%). It somewhat over-predicts long-term average sediment in Canyon Creek (124.9%) and Deadman Creek (126.3%) and under-predicts sediment in Lolo Creek (64.0%) and Elk Creek (73.3%).

The WATBAL-2005 user and land management decision maker should recognize that the model estimates sediment within a range of 60 percent to 130 percent of long-term measured averages for watersheds similar to the test watersheds. The model still tends to somewhat under-predict sediment in watersheds with extensive rolling hills and

mountain slopeland landforms and over-predict sediment in watersheds with high percentages of breakland landforms.

We recommend that calibration re-assessments should occur every five years as data becomes available and test watersheds meet the calibration selection criteria.

REFERENCES

Cline, R., Cole, G., Megahan, W., Patten R., Potyondy J. (1981). "Guide for Predicting Sediment Yields from Forested Watersheds," (Commonly referred to as the R1/R4 Sediment Guidelines), USDA Forest Service, Northern and Intermountain Regions.

Hickey, R. (1997). "Evaluating the WATBAL Sediment Loading Model, Clearwater National Forest, Idaho," Northwest Science, Vol. 71, No. 3, Page 233-242.

Jones, R. M. (2002). Validation of the WATBAL Sediment Model, Clearwater National Forest, Orofino, Idaho.

McClelland, D., Foltz, R., Wilson, D., Cundy, T., Heinemann, R., Saubier, J., Schuster, R. (1997). "Assessment of the 1995 & 1996 Floods and Landslides on the Clearwater National Forest. Part 1: Landslide Assessment," USDA Forest Service, Northern Region.

Patten, R. (1989). Watershed Response Model for Forest Management. WATBAL Technical User Guide. Clearwater National Forest. Orofino, Idaho.

Patten, R. and Jones, R. (2001). Watershed Response Model for Forest Management. WATBAL Technical User Guide. Clearwater National Forest. Orofino, Idaho.

Patten, R. and Jones, R. (2005). Watershed Response Model for Forest Management. WATBAL Technical User Guide. Clearwater National Forest. Orofino, Idaho.

Wilson, D., Coyner, J., Deckert, T. (1983). Land System Inventory of the Clearwater National Forest. First Review Draft. Orofino, Idaho.

ESTIMATING SEDIMENT YIELD IN THE SOUTHERN APPALACHIANS USING WCS-SED

Paul Bolstad, University of Minnesota, 1530 Cleveland Ave. St Paul MN 55108, pbolstad@umn.edu; Andrew Jenks, University of Minnesota, jenk008@umn.edu; Mark Riedel, USFS Coweeta Hydrologic Lab, 3160 Coweeta Lab Rd., Otto, NC 28763, mriedel@baird.com; James M. Vose, USFS Coweeta Hydrologic Lab, jvose@fs.fed.us

Abstract: We measured and modeled sediment yield over two months on five watersheds in the southern Appalachian Mountains of North Carolina. These watersheds contained first and second-order streams and are primarily forested, but span the development gradient common in this region, with up to 10 percent in suburban and transitional development and up to 27% low-intensity agriculture. Sediment yield was measured using automated pumped samplers, continuous depth measurements, and gravimetric analysis. Sediment yield was predicted using WCS-SED for the coincident period employing fine and medium-resolution elevation, soils, and land use data. Mean sediment yield varied from 0.025 to 0.344 t/ha/yr and was strongly related to the proportion of non-forest area in the watershed. Sediment yield was not related to road density within the watershed or in near-stream areas. Predicted sediment yield was several times higher than observed sediment yield on four of five watersheds, with the most agriculturally developed watershed serving as the exception. Sediment yield was high over the plausible range of USLE land use and cropping factors that underlie the sediment yield predictions.

INTRODUCTION

Section 303(b) of the Clean Water Act requires that states identify water bodies that are unlikely to meet ambient water quality standards. The states must also identify a Total Maximum Daily Load (TMDL) for each constituent pollutant, and develop a plan to maintain inputs below these values. Sediment from erosion is the most common pollutant in many streams of the southeastern United States. Suspended sediment levels above 20-30 mg/L have been shown to degrade stream biotic integrity (Walters et al., 2001), and impairment may occur at lower concentrations.

Models may be used to estimate sediment generation in uplands and sediment transport to streams. However, model accuracy, appropriate parameters, and sensitivity to input data quality must be determined prior to accepting sediment yield predictions as a monitoring or management tool. When these models are spatially explicit and run in a grid-cell environment, the appropriate cell size, data sources, and model parameters must be identified.

We report on a test of one widely-use sediment model, the Watershed Characterization System – Sediment Tool (WCS-SED), developed by Tetra Tech, Inc., in cooperation with the US Environmental Protection Agency, Region 4. This model is representative of cell-based erosion generation and transport models that use the Universal Soil Loss Equation (USLE) and derivatives (Kinnell and Risse 1998, Hood et al., 2002). We measured suspended sediment transport in five small watersheds in the southern Appalachian Mountains, and compared these to sediment yield predicted with WCS-SED. We evaluated the impact of input data resolution by varying the cell size for elevation data, and the cell size and categorical detail for land use and soils data within each watershed. We estimated the importance of stream network specification, and the sensitivity of predicted sediment yield to variation in the cropping factors for each land use type.

METHODS

Study Watersheds: Analyses were conducted on five study watersheds spanning a range of areas and land use practices in the southern Appalachian Mountains, USA (Figure 1, Table 1). These watersheds represented the current and past land uses typical of many first and second order streams in the southern Appalachian. Watersheds were predominantly forested with varying histories of prior agriculture in near stream portions, and current increases in road and residential development. Two watersheds (Addie Branch and Dryman Fork) were on US Forest Service land and differed primarily in road density, two were forested with light residential development (Reed Mill and Watauga Creek), and one was primarily forested with moderate pasture agriculture and light residential development. Roads were predominantly unpaved gravel, and road density varied within the ranges typical of the region.

Table 1: Characteristics of Study Watersheds

Name	Area (ha)	Road density (m/ha)	Forest (%)	Agric. (%)
Addie Branch	574	6.54	100.0	0
Dryman Fork	153	42.57	100.0	0
Sutton Branch	132	14.97	72.6	26.2
Reed Mill	440	11.12	95.8	0
Watauga Creek	1,675	40.64	87.3	4.9

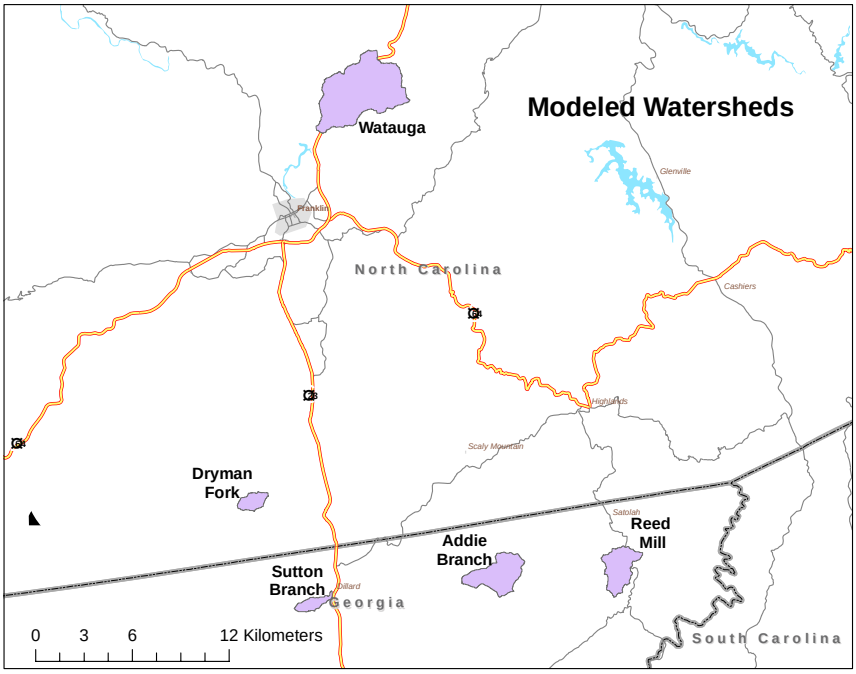


Figure 1 Watersheds in this study

Spatial Data Collection: Watershed boundaries were delineated from US Geological Survey (USGS) National Elevation Datasets (NED), 10 meter resolution, using a flowpath analysis (Bolstad, 2005). These boundaries were used to extract elevation, slope, roads, soils, stream, and land use data from developed and new sources.

Elevation data were derived from three sources. Ten meter (NED) and 30 meter (1:24,000 scale quad-based) resolution raster data were extracted from USGS sources, and slope derived using a third-order finite difference algorithm (Bolstad, 2005) for all study watersheds. A three-meter resolution DEM was created from digitized contours of a 1:7,200 paper map produced by the US Forest Service for the Dryman Fork basin. Roads were extracted from 1:24,000 scale USGS digital line graph data, and updated based on interpretation of May 2003

SPOT 2.5 meter satellite images. Soils data were digitized from US Natural Resource Conservation Service soil survey data, both county-level (SSURGO) and statewide (STATSGO).

Land use data were derived from two sources. Moderate resolution data were extracted from the 1990s National Land Cover Dataset (NLCD, Vogelman et al., 1998). Landcover was resolved into one of 21 potential classes for 30 meter cells for the entire United States based primarily on early 1990s Landsat satellite images, 30 meter DEMs, and US Census data. Data were extracted for each study watershed. From four to 10 categories were present in the watersheds. Classification accuracies were above 60% for all watersheds, and above 86% when aggregating mature forest classes.

High resolution land use (UMN) data were manually interpreted from resolution-merged SPOT satellite images collected in May 2003. Panchromatic 2.5 meter data were merged with 10 meter multispectral data using a principal component transform (Pohl and Van Generen, 1998). Land use was assigned to NLCD categories. Withheld points indicate the classification accuracy above 96% when aggregating mature forest classes.

Water Sampling: Flow data and water quality samples were gathered with automated pumping samplers, as described in Riedel et al., (2004). Stream stage was logged on 15 minute intervals with submerged pressure transducers. Data were checked via manual gauging on a weekly basis. Samplers collected water samples, calibrated via manual depth integrated sampling, under baseline conditions and storm flow conditions. Samples were analyzed gravimetrically to determine total suspended solids (TSS) to 1.5 μm and combusted to determine ash-free dry weight (USGS, 1978).

Field Data Analysis: Sediment concentration data were paired with discharge data based upon sediment/discharge rating curves to calculate sediment transport during the calibration period. Due to a hysteretic relationship between sediment and discharge on Addie Branch and Dryman Fork, separate rating curves were generated for rising and falling limbs of stormflow hydrographs. The curves were generated using filtered data. Filtering was based on hydrograph regime, dQ/dt, computed as the percent difference in stream flow over three consecutive intervals; a one percent threshold for dQ/dt most consistently differentiated hydrograph regime. The reader is directed to Riedel, et al., (2004) for a complete discussion of the methods. A summary of filtering is shown in Table 2. Cumulative sediment transport was estimated for an approximate two-month period spanning June and July, 2003.

Table 2 Filtering limits for defining hydrographs and sediment regimes

Percent change in slope	Hydrograph regime	Sediment regime
$dQ/dt > 1$	Rising Limb	Proportional increase with flow.
$-1 < dQ/dt < 1$	Baseflow	Low (<10 ppm)
$dQ/dt < -1$	Recession Limb	Disproportional decrease with flow, then low (<10ppm).

Model Runs: Sediment yield was estimated through application of the WCS model, sediment tool module (Tetra Tech, 2000). WCS-SED uses the USLE to calculate surface erosion and variable transport equations to estimate delivery to water courses (Yagow 1988, Sun and McNulty 1998). Sediment yield is assumed equal to delivery, thereby assuming no bank erosion or net in-stream source or sink. All model runs were conducted for the two-month sampling period, adjusting period rainfall from annual sums based on observed relative rainfall intensity.

Multiple model runs were performed, varying the source of elevation (and hence slope), soils, and land use data. Precipitation amount and characteristics derived from the nearby Coweeta Hydrologic Lab weather station were used to specify the USLE R factor, held constant across all runs. Soil erodibility factors (K) were derived from NRCS source materials for digital soils data, slope factors (LS) from digital elevation models, and cropping management factors (C) from NRCS entries that matched the land use categories.

Models were run across a coarse and fine-resolution elevation (30 m and 10 m), soils (STATSGO and SSURGO), and land use data (NLCD from Landsat 30 m, and UMN from SPOT 2.5 m).

Stream network was held constant across a primary set of runs at a threshold. The stream network is defined in WCS-SED by a contributing area threshold. First order streams are initiated when an upstream, contributing area exceeds a specific area. Streams accrue downstream, joining to form higher order streams in a network. We varied the threshold to best match the stream network observed in the field, arriving at a value of 1600 for a 10 meter resolution DEM to match the observed stream density. All the initial runs over the combinations of soils, DEM resolution, and land use data were conducted at this threshold. A second set of runs were performed to estimate the impact of inferred stream density on estimated sediment yield, using the highest resolution data (SSURGO soils, 10 m DEM, and UMN-SPOT based 2.5 meter land use data). Stream thresholds were varied at 50, 450, 1600, and 2500 10 m cells, all other data constant.

RESULTS

Land Use: Forest land use dominated the study watersheds, with between approximately 73 to 100% forest extent (Table 2). Estimates of forest area varied only slightly between the NLCD and UMN-SPOT high resolution data sources, although there were substantial differences when resolving forest types. Differences among forest types are minor when estimating erosion in this region of the southern Appalachians, as rates are effectively zero in most closed-canopy forest types.

There were substantial differences in the amount of urban and transitional urban land uses when comparing the NLCD and higher resolution UMN-SPOT data (Table 2).

Table 2 Land use data for the five study watersheds, based on an interpretation of 2003 SPOT high-resolution satellite images (UMN) or 1990s NLCD data (NLCD). Land use classes are reported in percent.

	UMN	NLCD	UMN	NLCD	UMN	NLCD	UMN	NLCD	UMN	NLCD
Low Dense Urban	0.00	0.00	0.00	0.00	4.22	0.00	1.16	0.00	2.54	0.13
High Dense Urban	0.00	0.00	0.00	0.00	0.00	0.00	0.00	0.00	0.00	0.89
Transitional Urban	0.00	0.00	0.00	0.00	0.00	1.40	0.00	0.00	2.36	0.06
Deciduous Forest	0.00	0.00	0.00	93.64	0.00	16.02	72.64	42.06	0.00	69.49
Evergreen Forest	0.00	0.00	0.00	0.37	0.00	36.18	0.00	4.59	0.00	7.84
Mixed Forest	100.0	100.0	100.0	5.93	95.78	45.36	0.00	28.33	87.35	14.64
Pasture/Hay	0.00	0.00	0.00	0.06	0.00	0.82	26.18	24.34	7.18	4.52
Row Crops	0.00	0.00	0.00	0.00	0.00	0.22	0.00	0.68	0.51	0.88
Other Grasses	0.00	0.00	0.00	0.00	0.00	0.00	0.00	0.00	0.00	1.55
Woody Wetlands	0.00	0.00	0.00	0.00	0.00	0.00	0.02	0.00	0.06	0.01

Observed Sediment Yield: Sediment yields for the two-month monitoring period were generally within limits observed in previous studies in the region, with mean baseflow sediment concentrations typically varying between 1 and 7 ppm, and maximum stormflow concentrations ranging from approximately 15 to 40 ppm. Two-month observed yields vary between 4.2 and 57.3 kg/ha (Figure 2), equivalent to approximate annualized yields of 0.025 to 0.344 t/ha/year. These fall within the ranges observed for eastern forests.

Sediment yield was strongly influenced by percent non-forest, primarily agricultural and low density residential development. Sutton Branch is the only watershed with substantial areas in agriculture, primarily pasture and hayfields in near-stream areas. Despite nearly 100% perennial vegetation in this watershed, substantially higher

sediment yield values were observed than in predominantly forested watersheds and in watersheds with lower levels of development. Two watersheds, Reed Mill and Watauga Creek, were characterized by low density and transitional suburban/rural land uses in less 2 to 5% of their surface area, and pasture and hay in 1 to 7% of their surface, and these watersheds exhibited commensurately lower sediment yields than Sutton Branch. Road density was not well correlated with sediment yield, with Watauga Creek and Dryman Fork exhibiting the highest values (4.0 and 4.2 km/km^2, respectively), Sutton Branch and Reed Mill intermediate (0.11 and 0.14 km/km^2), and Addie Branch the lowest density (0.065 km/km^2).

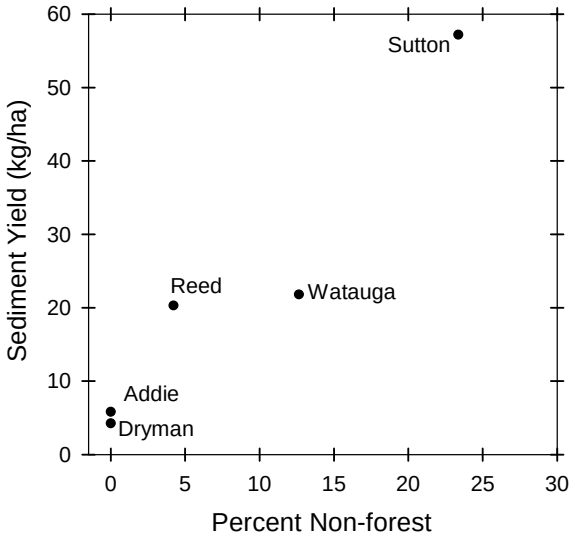


Figure 2 Observed sediment yield during June and July, 2003, plotted vs. percent non-forest in each study watershed

Modeled Sediment Yield: Predicted WCS-SED sediment yield was higher than observed yield for four of the five measured watersheds, typically by a factor of three to four (Figure 3). Modeled sediment yield for Sutton Branch was approximately one-third lower than observe sediment yield. Modeled sediment yield followed these patterns irrespective of the combination of digital elevation model resolution, land use data source, and soils data used. Previous work has found that modeled sediment yield is often higher than observed yield when using the USLE and related functions, both within the framework of WCS-SED, and within other systems (Ward and Trimble 2003, Wu et al., 2004, Riedel et al. 2005).

There may be many sources for this over prediction, including overestimation of erosion via the constituent USLE factors and erroneous estimation of transport. USLE factors have been developed and validated over a large range of conditions, and assume a field length 72.6 ft, or approximately 22 m. This dimension is spanned by the range of DEM cell sizes used in these calculations. However, slopes may not be accurately represented at this resolution, with elevation errors on the order of a few meters common. Previous work has shown more accurate estimates of yield when finer-grained DEMs are used (Riedel et al., 2004); however, it is not clear whether this increased accuracy is due to improved estimates of erosion or improved estimates of sediment transport.

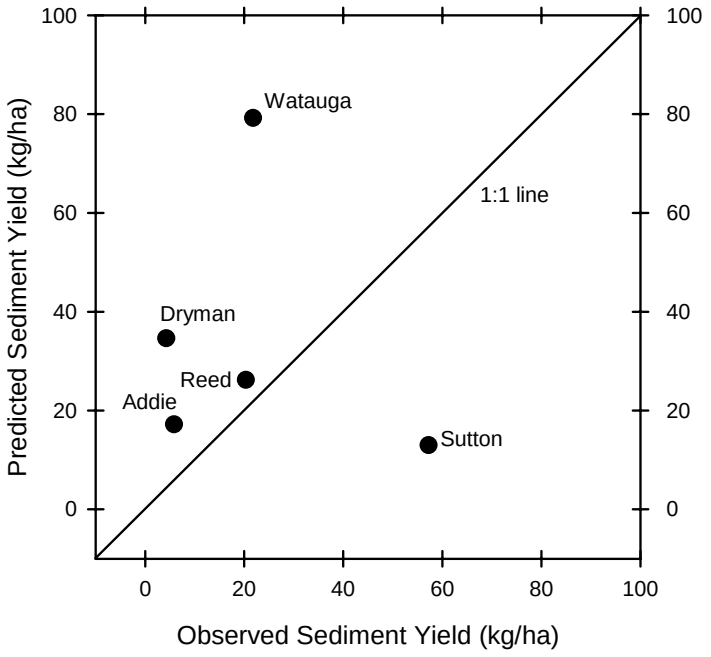


Figure 3 Predicted and observed sediment yield for five study watersheds for the period encompassing June and July, 2003. Predicted values were based on USGS 10 meter DEMs, NRCS SSURGO data, and 2003 land use data derived from a manual interpretation of SPOT 2.5-10m pan sharpened image data.

Estimated sediment yield was only inconsistently sensitive to cell resolution, with higher, lower, and similar yield predictions among 10 and 30 meter DEMs. Yield was sensitive to soil source with SSURGO-based predictions consistently 10 to 30% lower than STATSGO-based predictions. Yield was most sensitive to the C factors used in the USLE, and plausible C values resulted in substantially improved predictions for the agriculturally-dominated watershed, Sutton Branch (Figure 4). Initial model runs employed the best estimated C values for the predominant land uses given the site conditions and published tables (0.005 and 0.003 for pasture and forest, respectively). USLE C values span a wide range of values to reflect the density and stature of vegetation. Forest areas in this study were characterized by greater than 85% crown cover, and pasture by greater than 95% vegetation cover, and standard model runs employed the appropriate C values. Our initial runs may have used inappropriately high C values on forested sites and low C values on pasture sites, which might lead to the observed errors. However, sediment yield was overpredicted by a factor of more than two at extremely low C values (0.0005/0.0003) on predominantly forested sites, and as expected, sediment yields for higher than indicated C values increased overprediction on Dryman, Addie, Watauga, and Reed watersheds accordingly. We conclude that no plausible range of C values in forested sites are likely to improve estimation of sediment yield. However, an increase in C values for agricultural lands improved agreement between predicted and observed sediment yield on Sutton Branch (Figure 4), the lone watershed with substantial agricultural lands.

Predicted sediment yields were also strongly dependent on the threshold that established stream network density. Increasing the threshold substantially reduced the stream network, with a substantial reduction in estimated sediment. Sediment yield varied from 10 to 37 kg/ha as the stream threshold varied from 2500 to 50 10-meter cells. The lowest threshold generated approximately one-half the known reaches in the study watersheds, and still predicted more than twice the observed sediment yield for our study period.

We suspect sediment transport equations or poor estimates of road-generated sediment are primarily responsible for the large errors observed in estimated sediment yield, particularly on the four watersheds with little agriculture. Transport equations used in WCS-SED rest on a narrow empirical base, and need be tested over a wider range of conditions. The equations have been developed in one to a few studies, with a limited range of soils, land uses, terrain, and soil conditions. In addition, the study areas have high road densities for predominantly rural areas, a legacy of dispersed small holdings and active forest management. A majority of the roads are unpaved and are significant sources of sediment to streams (Riedel et al., 2005).

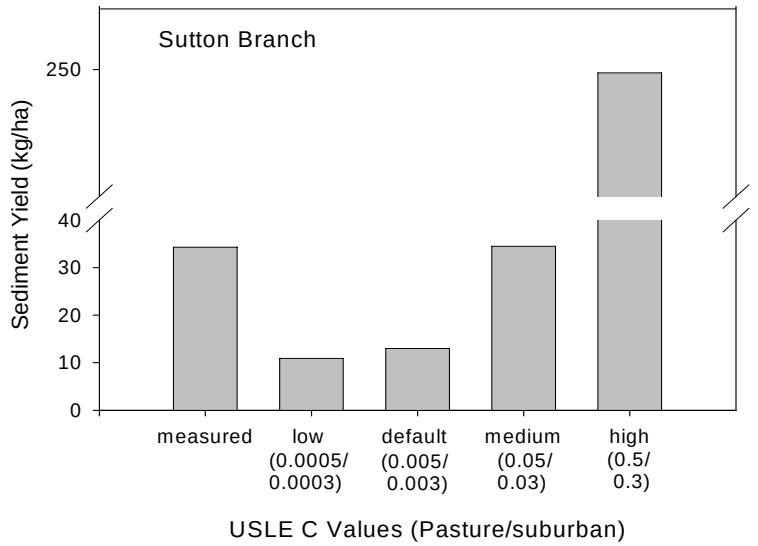


Figure 4 Sediment yield by USLE C values used in estimating sediment deliver to streams. Implausibly low C values did not substantially improve estimated yield, while plausibly high values substantially degraded model performance.

CONCLUSIONS

Sediment yields predicted by WCS-SED were substantially higher than observed values over a summer study period on four of five study watersheds in the southern Appalachian Mountains. The general trends in observed sediment yield were replicated in predictions, but predicted values were generally three to four times higher than observed sediment yields. This increase was consistent across completely forested watersheds, and across watersheds with significant near-stream development. Predicted values were lower than observed values for Sutton Branch, the study watershed with the highest proportion of non-forest land use.

Predicted sediment yield was only slightly dependent on source data resolution. While predictions were generally better when using finer resolution SSURGO soils, SPOT-based land use and 10 m DEMs, improvements were slight relative to the observed error.

Acknowledgements: This work was supported by NSF via the Coweeta Long-Term Ecological Research Project, and by the University of Minnesota Agricultural Experiment Station. We thank Charles Marshall and Ryan Kirk for primary data collection.

REFERENCES

Bolstad, P.V. (2005). GIS Fundamentals: A first text on geographic information systems. Eider Press, White Bear Lake, 543 p.

Hood, S. M., Zedaker, S.M., Aust, W. M., and Smith, D.W. (2002). "Universal Soil Loss Equation (USLE)-Predicted Soil Loss for Harvesting Regimes in Appalachian Hardwoods," Northern Journal of Applied Forestry, Society of American Foresters, v. 19, no. 2, p. 53-58.

Kinnell, P.I.A., and Risse, L.M. (1998). :USLE-M: Empirical Modeling Rainfall Erosion Through Runoff and Sediment Concentration." Soil Science Society of America Journal, v. 62, no. 6, p. 1667-1672.

Pohl, C., Van Genderen J.L. (1998. "Multisensor image fusion in remote sensing: concepts, methods and applications," International Journal of Remote Sensing 19:832-854.

Riedel, M.S.,Vose, J.M., and Bolstad P.V. (2004). "Characterizing Hysteretic Water Quality in southern Appalachian Stream," in Proc. 2004 National Water Quality Monitoring Conference, United States Advisory Committee on Water Information – National Water Quality Monitoring Council, Chattanooga, TN, May 17th – 20th.

Riedel, M.S., Jenks, A.C., Bolstad, P.V., and Vose, J. M. (2005). "Application and Validation of a Sediment Yield Model in Developing Regions of the Southern Appalachians," in Watershed Management to Meet Water Quality Standards and Emerging TMDL (Total Maximum Daily Load), Third Conference, Atlanta, GA.

Sun, G., McNulty, S. (1998). "Modeling soil erosion and transport on forest landscapes," in Proceedings of Conference 29, International Erosion Control Association, February 16-20, Reno, Nevada, 187-198.

Tetra Tech. (2000). Watershed Characterization System, Sediment Tool User's Guide. Fairfax, VA.

U.S.G.S. (1978). Laboratory Analysis – Suspended-Sediment Concentration. Section 3.F.2.a. in Chapter 3 – Sediment of the National Handbook of Recommended Methods for Water Data Acquisition. United Stages Geological Survey, Office of Water Data Coordination, Reston, VA.

Vogelmann, J.E., Sohl,T., Campbell, P.V., and Shaw D.M. (1998). "Regional land cover characterization using Landsat Thematic Mapper data and ancillary data sources," Environmental Monitoring and Assessment 51: 415-428.

Walters, D.M., Freeman, M.C., Leigh, D.S., Freeman, B.J., Paul, M.J., and Pringle, C.M. (2001). "Bed texture and turbidity as indicators of fish biotic integrity in the Etowah River System," in K.J. Hatcher (ed.) Proceedings of the 2001 Georgia Water Resources Conference. March 26-27, 2001. Athens, Georgia. p. 233-236.

Ward, A.D., and Trimble, S.W. (2003). Chapter 9, Soil Conservation and Sediment Budgets, Environmenat Hydrology: Boca Raton, FL, CRC Press LLC, p. 448.

Wu, S., Li, J., and Huang, G. (2004). "Effect of Digital Elevation Model Resolution on Empirical Estimation of Soil Loss and Sediment Transport with GIS," International Journal of Sediment Research, v. 19, no. 1, p. 28-36.

Yagow, E.R., Shanholtz, V.O., Julian, B.A., and Flagg, J.M. (1988). "A water quality module for CAMPS," International Winter Meeting of ASAE, December 13-16, 1988, Chicago, Il.

RECONSTRUCTING RESERVOIR STRATIGRAPHY FROM HYDROLOGIC HISTORY AND SIMPLE TRANSPORT CALCULATIONS: ENGLEBRIGHT LAKE, YUBA RIVER, NORTHERN CALIFORNIA

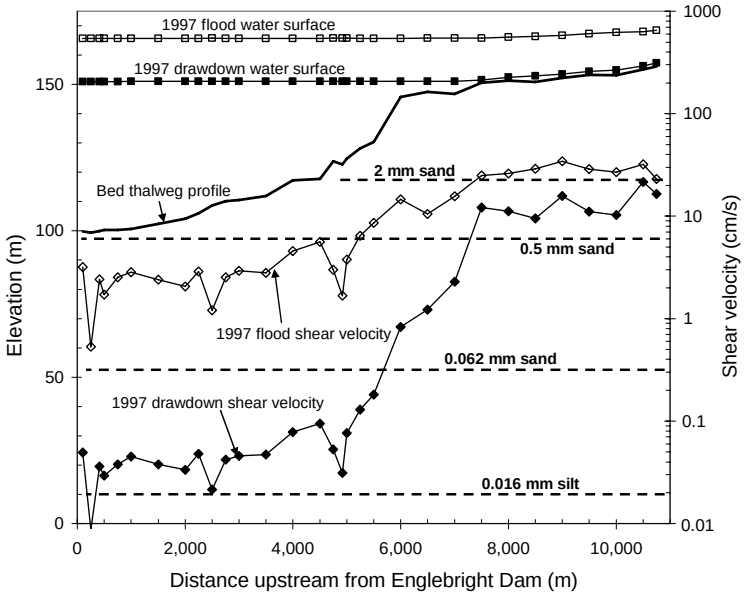
Scott A. Wright, Hydrologist, U.S. Geological Survey, Flagstaff, AZ, sawright@usgs.gov; Noah P. Snyder, Assistant Professor, Boston College, Boston, MA, noah.snyder@bc.edu

Abstract: Englebright Dam impounds the Yuba River in the foothills of the Sierra Nevada, creating a 14-kilometer long reservoir. The dam is 80 meters tall and was completed in December 1940 by the California Debris Commission, with the primary purpose of trapping sediment from hydraulic mining activity in the Yuba River watershed and thus reducing flood risk downstream. In 2001-2003, the U.S. Geological Survey conducted an extensive bathymetric survey and coring project of Englebright Lake. Cores were extracted along the length of the reservoir and analyzed for grain size, providing a detailed stratigraphic cross section. Between 1940 and 2001, accumulation of sediment in the lake reduced the original storage capacity by about 26%. This accumulation amounts to 24.8 million metric tons of sediment, which is approximately 20% gravel, 49% sand, 25% silt, and 6% clay. The reservoir longitudinal profile exhibits the classic deltaic configuration, with a topset composed primarily of gravel and sand, a foreset composed mostly of sand and silt, and a bottomset of silt and clay with a small fraction of fine sand.

Prior to construction of New Bullards Bar Dam in 1970, Englebright Lake was drawn down about 20 meters annually during the summer irrigation season. The reservoir has also experienced several very large floods during its history (1995, 1964, and 1997). In order to analyze the relative importance of floods and drawdowns in building the deposit, we performed some simple calculations of reservoir hydraulics and sediment transport. The procedure consisted of backwater calculations (yielding the shear velocity) for two conditions, one representative of floods and one of drawdowns. The shear velocities in the reservoir were then compared with the settling velocities for a range of grain sizes in order to determine the approximate extent of suspended transport of a given grain size.

The computed shear-velocity profiles (inset figure) for representative events from 1997 indicate that both floods (Q=3,821 m^3/s, lake elevation=166 m) and drawdowns (Q=37 m^3/s, lake elevation=151 m) have the potential to transport sand in suspension in the upper reach of the reservoir (the topset and foreset), with floods somewhat more vigorous. In this upper topset reach, shear velocities easily exceed the settling velocity (dashed horizontal lines in the figure) for fine sands and indeed approach the settling velocity for coarse sands; thus, both types of events have the potential to transport and rework sand in topset and foreset sections of the delta. The short duration of floods (hours to days) compared to drawdowns (weeks to months) suggests that although floods may initially transport much of the coarse sediment to the topset and foreset region, significant reworking occurs during drawdown periods.

The calculations indicate that the effects of floods and drawdowns differ downstream from the delta front. The drawdown shear velocities in the bottomset region exceed the settling velocities for clay and fine silt, but not sand. In contrast, shear velocities under flood conditions exceed the settling velocity for fine sand throughout the reservoir, suggesting that most of the fine sand in the bottomset was deposited during floods and not during drawdowns. These results are also consistent with the sedimentological observation that sand finer than ~0.5 mm is not deposited downstream of the delta front. Furthermore, the calculations suggest that fine sediment bypass may be important during large floods.



CHESTER MORSE LAKE OUTLET CHANNEL ALTERNATIVES EVALUATION

Hans R. Hadley, Geomorphologist, WEST Consultants, Inc., Salem, OR, hhadley@westconsultants.com; Thomas R. Grindeland, Vice President, WEST Consultants, Inc., Salem, OR, tomg@westconsultants.com; Dalong "Daniel" Huang, Supervising Civil Engineer, Seattle Public Utilities, Seattle, WA, daniel.huang@seattle.gov

Abstract: Chester Morse Lake is a naturally formed reservoir located on the western slope of the Cascade Mountains in King County, Washington. The Chester Morse Lake Outlet Channel (CMLOC) connects Chester Morse Lake to the downstream Masonry Pool reservoir. The reservoir system, operated by Seattle Public Utilities, stores two-thirds of the regional supply water for the 1.3 million people in the Seattle metropolitan area. At high Masonry Pool stages, water backwaters into Chester Morse Lake, inundating the CMLOC. Under normal operating conditions the stage in Chester Morse Lake is maintained at a higher elevation than the Masonry Pool by a control structure located at the downstream limit of the CMLOC. Under drought conditions, water must be pumped from the available dead storage within Chester Morse Lake to the upstream inlet of the CMLOC. A Discharge Dike was constructed to a crest elevation of 1535 feet at the upstream inlet to the CMLOC as a head wall for the pump discharge lines in 1992.

Sedimentation in the CMLOC, as measured in 2002, has resulted in a channel bottom elevation up to five feet higher as compared to 10 years earlier. Consequently, the geometry of the channel reduces the flow capacity of the channel and dictates the water surface elevations at the Discharge Dike that are capable of providing sufficient flow by gravity along the CMLOC. A minimum flow capacity along the channel of 279 cfs (180 mgd) is required and a high flow capacity of 371 cfs (240 mgd) is desired. To achieve the desired flow capacity, a portion of the channel was deepened in December 2002 and construction was completed on a new Discharge Dike with a crest elevation of about 1538 ft at the pump discharge location.

Hydraulic modeling, using channel surveys conducted in 2004, showed that sedimentation has again significantly reduced the flow capacity of the CMLOC. With continued uncertainties regarding the channel discharge capacity, various channel improvement alternatives were proposed. This paper will review the CMLOC discharge capacity under drought conditions and discuss the associated hydraulic uncertainties. More importantly, this paper will present the results of our investigation of the hydraulic and sediment transport characteristics of five proposed channel improvement alternatives to ensure adequate discharge capacity of the CMLOC.

SEDIMENT TRANSPORT RESEARCH IN SHALLOW OVERLAND FLOW

M. J. M. Römkens, Laboratory Director, USDA ARS National Sedimentation Laboratory, Oxford, MS 38655, mromkens@ars.usda.gov; S. Madhusudana Rao, Research Associate, Dept. of Civil Engineering, University of Mississippi, University, MS 38677, MSuryadevara@msa-oxford.ars.usda.gov; S. N. Prasad, Professor, Dept. of Civil Engineering, University of Mississippi, University, MS 38677, cvprasad@olemiss.edu

Abstract: Hydraulic induced sediment movement is a highly complex process influenced by many factors of a hydraulic and sediment property nature. This process is even more complicated in shallow overland flow, where the hydraulic regime as well as the sediment characteristics can be highly variable. Research to better understand the micro-mechanical nature of sediment movement in shallow flow has been underway for several years. Studies were conducted to examine this process both in the absence (gravity flow) and presence of water. Experiments consisted of measurements of particle velocity and particle concentration on the mode of transport and the corresponding associated transport rates. Results show that the sediment movement is not a random phenomenon but occurs in a highly organized manner ranging from saltation of sediment particles at very low concentrations to movement in a sediment wave like pattern. These waves may transgress into meanders depending on the channel bed conditions and the grain addition rate into the stream. As a consequence, the sediment transport capacity of shallow flow is severely impacted. This paper discusses the experimental findings from a steady state flow regime to which sediment was added at a controlled rate at the upstream of a 7 m long and 10 cm wide channel of about 1º slope steepness. The analytical interpretations are based on a two-phase flow model involving the St. Venant equations of shallow water flow and granular flow.

INTRODUCTION

At the Seventh Federal Interagency Sedimentation Conference results of a study were reported (Pal et al., 2001) that concerned the development of organizational structures in granular gravity flow, when sand grains and glass beads were dropped at a constant rate into an inclined plane of 30^o to 38^o. That paper focused on possible similarities and dissimilarities between the origins of structured flow of granular material in a gravity flow field in air or water. The study was motivated by the observations that grains, dropped into a constant flow regime, changed their mode of transport when the concentration increased and exceeded the transportation capacity. This mode consisted of the development of clusters, which subsequently grew larger to become domains, and finally formed grain waves (Fig. 1). Similar experiments were conducted with different granular materials: glass beads between 200-250 μm, and two classes of sand of 200-250 and 300-350 μm. In all cases, sediment waves developed and a critical concentration threshold value was reached.

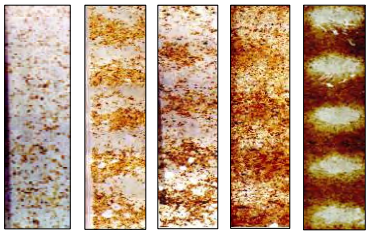


Figure 1 Granular organization with increasing sediment seeding rates.

The conventional view is that detachment and subsequent transport of sediment particles in overland flow exclusively depends on the sheer stress generated by the velocity profile. Incipient motion requires a minimum of critical shear stress at the bed (Foster and Meyer, 1975). Others (Rose et al., 1983) prefer to use the stream power concept and its critical value in describing sediment detachment and subsequent transport. It is also routinely assumed that variations in the free surface profiles in channel flow are the cause of the evolution of bed features. However, no adequate explanation has been given for the regularity in length and time scales of these bed features. In effect, the issue whether the surface waves in shallow flow are the sole driving mechanism for the organized mode of sediment transport is very much an open question. This issue motivated granular gravity flow experiments without the presence of water.

GRAVITY DRIVEN GRANULAR FLOW

Our granular flow studies (Prasad et al., 2000; Pal et al., 1999) have indicated that the particles themselves show under certain conditions, a strong tendency of a high degree of organization in terms of identifiable waves with distinct density characteristics. These waves can move upslope or downslide depending on the prevailing conditions of slope, particle size, etc. In these experiments several modes of sediment movement were noted. They have been schematically illustrated in Fig. 2. They are: (1) Uniform flow, in which the granular material moves in a near uniform concentration, downslide. This flow does not show any evidence of differences in the density of the granular material. This is the prevalent condition in low concentration regimes where the dominant movement is by saltation. (2) A mid-inertial flow regime, where flow exhibits zones of higher densities or waves in which the individual particle velocity has a smaller velocity than that in the rarefied zone between waves. These waves have a higher volumetric solid fraction though the flow depth does not change in the longitudinal flow direction. (3) A fully-inertial flow regime, in which the waves move faster than the individual particles. The waves are zones with a higher density and the free surface varies substantial in the flow direction.

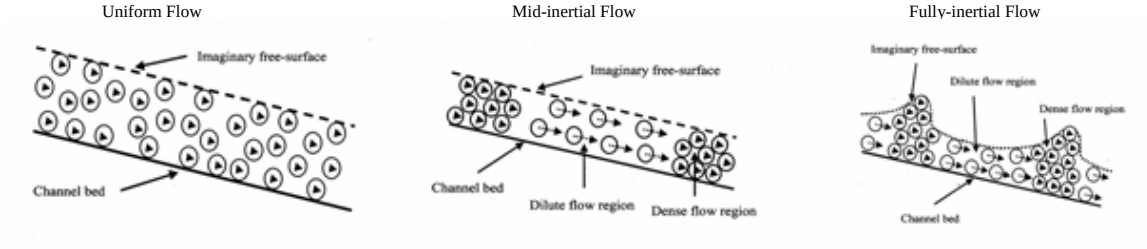


Figure 2 Shallow granular flow mode.

In light of these findings of a micro-mechanical nature of sediment particle interactions and energy flow changes in gravity flow it was postulated that the sediment dynamics in channel with fluid flow must be governed, at least to some degree, by similar kinetic processes, though the presence of water may have a strong moderating influence on the organizational nature of the particulate matter. Open channel flow exhibits a wide variety of velocity details with turbulent scales in the range of a fraction of a mm to several cms. It is assumed that flow with supercritical conditions with waves has sufficiently small turbulent scales. Thus the transport of sediments with diameter larger than 200 μm will tend to preserve the mode and mechanisms observed in gravity dominated granular flows. To address these issues, detailed laboratory tests were conducted in which sediment was added at a known rate at an upstream point into a constant flow regime and its movement was followed.

Table 1 Properties of Materials and Flow Characteristics.

Material	Diameter (d_s)	Density (ρ_s)	Packing Factor	Flow Rate	Froude Number
	μm	kg m^{-3}	(-)	l min^{-1}	(-)
Coarse Sand	1000-1400	2.52	0.64	21.6; 15.7	1.92 & 1.45
Medium Sand	600-850	2.67	0.61	21.6; 15.7	1.92 & 1.45
Glass Beads	600-1000	1.52	0.68	21.6; 15.7	1.92 & 1.45

SEDIMENT TRANSPORT IN SHALLOW FLOW

Briefly, the experiments were conducted in a 7 m x 10.7 cm x 4.4 cm deep rectangular open aluminum channel with an inclination < 1^o. A known, but controlled rate of water entered at the upstream end of the channel and also sediment particles of a desired size range, were seeded to the flow at a constant rate at the upstream end of the channel. Sediment movement was followed by a set of Fotonic probes located about 4 m from the upstream end. Both particle velocity and the solid concentration at the point of observation were determined. Two flow rates and three particle size ranges were studied (Table 1). Details of the velocity and solid concentration measurement have

been given by Suryadevara et al. (2004) and Prasad et al. (2004). A schematic of the experimental set up is given in Figure 3.

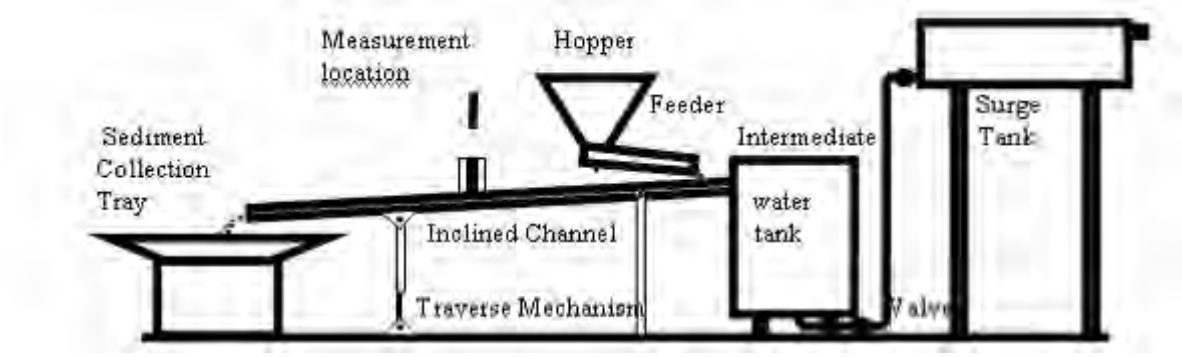


Figure 3 Experimental setup of sediment transport in shallow flow.

Experiments show that at low feed rates, the sediment transport rate measured at the downstream end of the channel equals the addition rate thus suggesting that the transport-capacity of the flow has not yet been reached. Also, visual observations indicate that the mode of sediment transport is by saltation. While the grain addition rate is gradually increased until a critical value beyond which solid grains started clustering. These clusters gradually organized by a natural selection process into particle wave structures of distantly spaced stripes. While the stripes are gradually spreading in the entire channel the measured transport rates started declining thus exhibiting an asymptotic (Fig. 4) behavior. Further increases in the addition rate while the particles are in stripe mode do not significantly change the

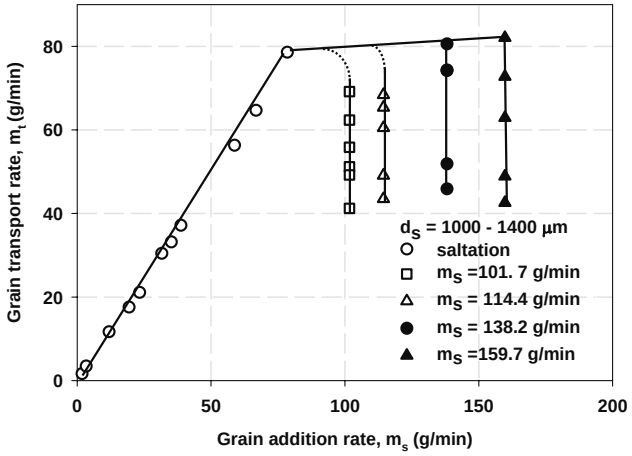


Figure 4 Sediment transport rates in relation to sediment addition rates. Coarse sand (d_s = 1000-1400 μm) water flow rate q_l = 15.7 liters/min (Fr_l = 1.45).

transport rate. The added material is stored in the channel bed and the flow regime in terms of the free surface boundary is materially impacted. Continuing the experiment for longer duration results in a wave pocketed bed into a meandering bed (Fig. 4). For a flow regime of 15.7 ℓ/min with Froude number 1.45 and feed rates beyond 101.7 g/min of coarse sand these changes takes place. Though the bed patterns seem to be similar with different grain addition rates the time scales in developing the structures seem to vary largely with the grain addition rates. As the grains organized into meanders the associated transport mass rate seem to be reduced largely. Meander formation was observed with four values of grain addition rates, 101.7, 114.4, 138.2 and 159.7 g/min and the corresponding transport rates were denoted by four fork shaped trends (Fig. 4). Similar observations were made with other flow rates (Fr_l = 1.92) and particle sizes.

In reality, when the sediment transport is forming into the wave propagation mode by meanders the transport rate associated with a given grain addition rate varies with time. Such a transient nature of the transport rate for a grain

addition value of 143.6 g/min for coarse sand is observed in Figure 5. Visual observations indicated that until 6min stripe packets are prevalent and until 14min both stripe and meanders existed together and the later periods the prevalent sediment waves are only meanders. In all these modes the minima indicated by solitary grain transport by saltation, sliding or creeping when the tail of the wave packet is barely touching the tip of the transport end. Maxima occur when the wave packets are in to the measurement sample.

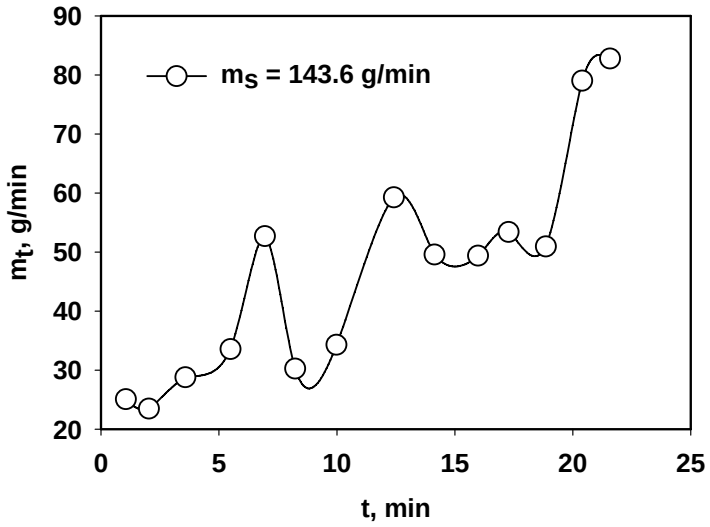


Figure 5 Transient variation of measured transport rates (t = 0 corresponds to addition of grains into the water stream). Solids addition rate is kept constant, m_s = 143.6 g/min. Coarse sand (d_s = 1000 - 1400 μm) and Froude number, Fr_l = 1.45.

In our experiments we have captured the meander evolution and its growth by placing camera at a fixed location. Various stages of a meander formation for coarse sand are shown in Figure. 6. When grains are introduced into the

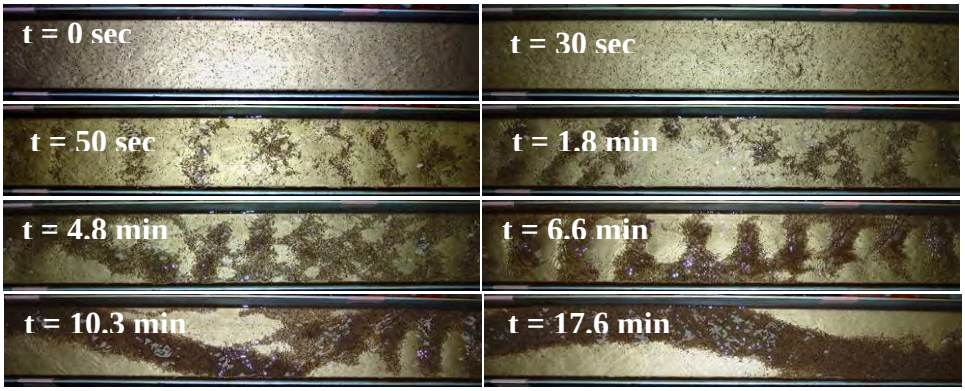


Figure 6. Meander formation in an open channel transport of water-sand system (all the figures correspond to a fixed camera location). Particle size, d_s = 1000 – 1400 μm; water flow rate = 21.6 l/min and the solids addition rate, m_s = 170.3 g/min.

clear water stream at 170.3 g/min, initially saltating grains quickly starts clustering in less than a half minute and in less than a minute they organize into distinctly spaced stripes. Further evolution of the channel bed is noticed by widening and multiplication of these strips with more grain joining into them. This strip wave propagation continues for about 18-20 min, at which a clear meander is formed. A clear picture on transport rates in these modes is till lacking and needs further investigation.

From these observations, it was concluded, that particle interactions during transport have a major impact on the mode and velocity and thus on the transport capacity of the flow regime. Therefore, information about the solid concentration and the velocity of the individual particles in the flow field is essential in developing an understanding of the observed phenomena. To that end, two closely spaced optical probes aligned in the direction of flow with an 8 mm diameter sensor hooked up to a signal analyzer were placed in the flow 4.3 m from the upstream end of the channel. This arrangement allowed for concentration and velocity measurements. The measurements indicated that at very low concentration, the velocity of the saltating particle consistently increased with increasing particle concentrations reaching fairly quickly a maximum value. Thereafter, a rapid decrease in the particle velocity was noted with further increases in the particle concentrations (Fig. 7). The initial increase is attributed to a redistribution of the streamline pattern in the neighborhood of sediment particles. However, it is well known that the boundary layer is distorted due to the sediment near the bed. The subsequent decrease is the result of kinetic energy loss through collisions of individual particles. Thus increasing the sediment addition rate leads to more frequent collisions and reduced particle velocities. Just, as we have seen in the case of gravity flow, a "pile-up" occurs at the upstream end of the wave packet while at the downstream end, particles are swept up again by the flow, gain momentum until the next series collisions lead to a new wave packet development. It was also observed that in the flow, the sediment particles were mainly concentrated in a shallow layer near the channel bottom of which the thickness appears to be decreasing with increasing concentrations. This phenomenon was also observed in the gravity flow experiments. The remainder of the shallow flow layer was particle free.

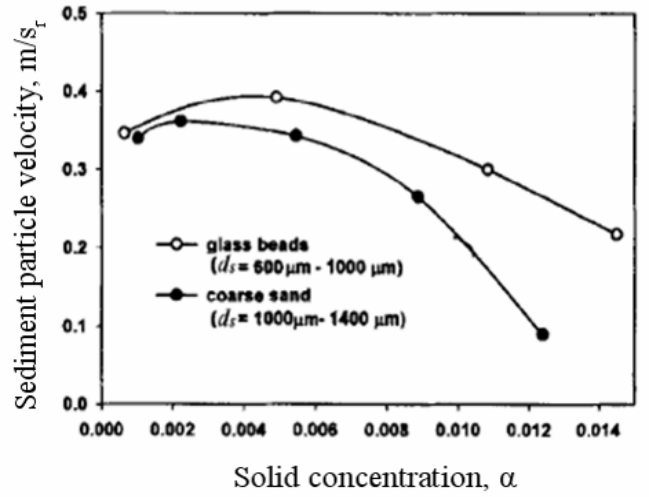


Figure 7 Observed relationship between sediment particle velocity and solid concentration for different glass beads and coarse sand and a flow rate of Fr_l = 1.92.

The observation of two zones of flow, the bottom zone with sediment and the upper one without sediment was the impetus of formulating a mathematical model, in which to each zone the mass and momentum balance equation were applied (Fig. 8). The momentum equation for the sediment some includes components for pressure, gravitation, and the dispersive stress between particles and the water phase, while the momentum equation for the sediment free zone includes the gravity and flow resistance effect. The details of this treatise has been given by Prasad et al. (Submitted). Briefly, the relationships for the sediment zone are:

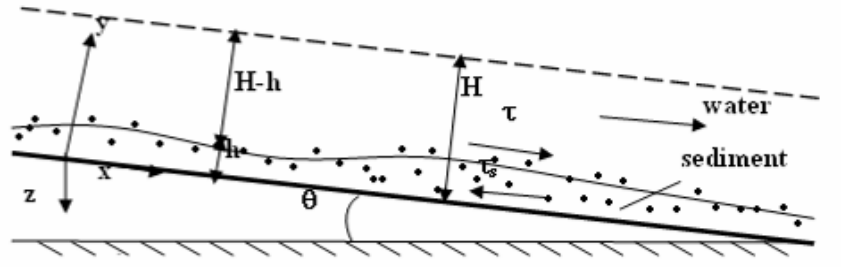


Figure 8 Sediment transport in water over an inclined channel. τ_s - unit width dispersive stress in the sediment ,τ - unit width tractive hydro-dynamic stress on the sediment, h - saltation height, H - water depth (flow), θ - bed slope and x,y,z are coordinates.

$$\frac{\partial}{\partial t}(\rho_m h) + \frac{\partial}{\partial x}(\rho_m h u) = 0 \tag{1}$$

$$\frac{\partial}{\partial t}(\rho_m h u) + \frac{\partial}{\partial x}(\rho_m h u^2) = -h\frac{\partial p}{\partial x} + \rho_m g h \sin\theta - h(\tau_s - \tau) \tag{2}$$

and for the sediment free zone are:

$$\frac{\partial \eta}{\partial t} + U\frac{\partial \eta}{\partial x} + \eta\frac{\partial U}{\partial x} = 0 \tag{3}$$

$$\frac{\partial U}{\partial t} + U\frac{\partial U}{\partial X} + g\frac{\partial \eta}{\partial x} - g\sin\theta = -T \tag{4}$$

where ρ_m is the effective continuum density of the solid, h is the thickness of the sediment zone or saltation height, u is the grain velocity, p is the pressure on the sediment particle and consists of the hydrodynamic pressure p_h of the overland flow plus the dispersive pressure p_d of the sediment, θ is the channel slope, T is the effective flow resistance, U is the depth-average flow velocity, τ is the shear stress, and $\eta = H - h$ with H being the flow depth.

The dispersive pressure p_d is ascribed to dilatational effects while the hydrodynamic pressure is readily accounted for by the relationship:

$$p_h = \rho_w\, g(H - y) \tag{5}$$

Where ρ_w is the water density. The dispersive stress is quantified based on Bagnold's work (1954), where it is assumed that for small shear rates, the case behaves like a Newtonian fluid, in which the normal (P_d) and tangential (τ_s) stresses are linearly proportional to the fluid dynamic viscosity μ, the shear rate γ and the volumetric solid factor α_v. Here the stresses varied with the solid concentration as $\alpha^{3/2}$, where α is the linear concentration which is defined as the ratio of the grain diameter to the mean radial separation distance.

From the above information, the concentration profile $\alpha(X)$ can be determined in terms of its spatial derivative (Prasad et al., 2005):

$$3\rho_o \frac{(u-c)^2}{\alpha^2}\left(1+\frac{1}{\alpha}\right)^{-4}\frac{d\alpha}{dX} - \frac{5h}{\rho_s d_s}\mu\gamma\alpha^{1/2}\frac{d\alpha}{dX} = \frac{\rho_w h g}{\rho_s d_s}\frac{d\eta}{dX} - \rho_o g\left(1+\frac{1}{\alpha}\right)^{-3}\sin\theta + \frac{h}{\rho_s d_s}\left[2.25\mu\gamma\alpha^{3/2} - \tau\right] \quad (6)$$

where the moving coordinate X = (x-ct), c is the velocity of the solid density wave.

In evaluating this model, the shear rate γ must be known and this can be derived from particle velocity gradients. Given the difficulty of obtaining this information, an alternative method was used to obtain an analytical expression for the solid fraction based on the hydrodynamic stress with the drag coefficient and slip velocity being the difference between free water velocity of the sediment free zone and the water velocity moving through the solid particles in the saltation layer. The slip velocity is a measure of the mean fluid thrust on the sediment layer on the saltation layer (Eames *et al*., 2004). The hydrodynamic stress between fluid and solids was derived as:

$$\tau = \frac{24\rho_w \nu C_o U \alpha^3}{h d_s} \quad (7)$$

and the particle velocity u relationship in terms of α is given by:

$$u = 10.7 C_m C_o U \alpha^{3/2}\frac{h}{d_s} \quad (8)$$

Where C_o is the maximum possible volumetric concentration (~0.78 for spheres) and C_m is the added mass coefficient due to the particles matrix (Eames *et al*., 2004).

Figure 9 shows the calculated relationship between the particle velocity and the solid concentrations for different ratios of saltation height over particle diameter and flow velocities for low solid concentrations.
The transition from saltation to a strip mode transport capacity is obtained for the condition dα/dx = 0 in Eq. (6).

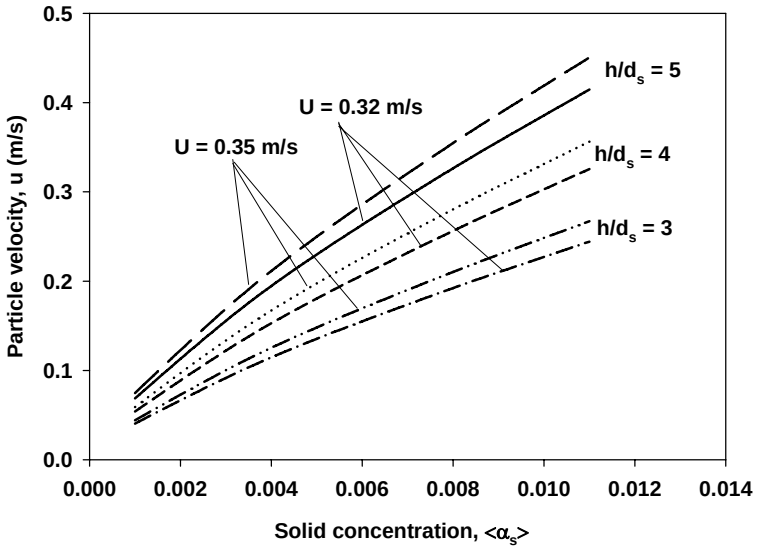


Figure 9 Particle velocity predictions relationships as a function of the solid concentration for h/d_s ratios.

This leads to the following relationship for the solid concentration.

$$\frac{\alpha^6}{\left(1+\alpha^2\right)} = \frac{3 q_m{}^2}{48 \left(\frac{h}{d_s}\right) C_0{}^2 \rho_s \rho_w \nu U} \tag{9}$$

SUMMARY

Sediment movement in a laboratory scale demonstrated several features of the overland shallow flow in a controlled manner. Existence of density waves has a tremendous impact on the transport rates of sediment in the channel. The measured transport rates with meander formation are transient in nature and a detailed investigation is required. A small amount of solids in water are initially uniformly dispersed and their movement is by saltation. However a gradual increase in the grain addition to the water stream caused the development of a large dispersive stress component due to intense grain collisions up to a critical value beyond which the flow developed into organized mode. A mathematical model was developed and formulated based on observations of sediment movement in shallow flow which provide a better understanding of the mechanism of sediment transport modes from saltation to wave packets.

REFERENCES

Bagnold, R.A. (1954). "Experiments on a gravity free dispersion of large solid spheres in a Newtonian fluid under shear," Proc. Roy. Soc. London. A 225, pp 49-63.

Eames, I., Hunt, J.C.R., and Belcher, S.E. (2004). "Inviscid mean flow through and around groups of bodies," J Fluid Mechanics. 115, pp 371-389.

Foster, G., and Meyer, L.D. (1975). "A mathematical simulation of upland erosion using fundamental erosion mechanics," In: Present and Prospective Technology for Predicting Sediment Yield and Sources, Proc. Sed. Yield Workshop. ARS-5-40, Oxford, MS 190-207.

Pal, D., Prasad, S.N., and Römkens, M.J. M.(2001). "Modes of shallow and dispersed particulate transport in sloping channels," Proc. Seventh Interagency Sed. Conf. I-16 to I-17. Reno Nevada.

Pal, D., Prasad, S.N, and Römkens, M.J.M. (1999). "Periodic waves in shallow granular flows," Proc. 3rd ASME/JSME Joint Fluids Engineering Conf., San Francisco, California. FED-Vol. 248.

Prasad, S.N., Suryadevara, M.R. and M.J.M. Römkens. "Granular process controlled evolutions and sediment transport rates in shallow overland flow." (Submitted, J. Fluid Mechanics).

Prasad, S.N., Pal, D., and Römkens, M.J.M. (2000). "Wave formation on a shallow layer of flowing grains," J. Fluid Mechanics. 413: 89-110.

Prasad, S.N., Suryadevara, M.R., and Römkens, M.J.M. (2004). "A sediment transport capacity of shallow flows in upland areas," 13th International Soil Conservation Organization Conf., 4 pp. July , Brisbaine, Australia.

Rose, C.W., Williams, J.R., Sander, G.C., and Barry, B.A. (1983). "A mathematical model of soil erosion and deposition: I. theory for a plane land element," Soil Sci. Soc. Am. J. 47: 991-995.

Suryadevara, M.R., Prasad, S.N., and Römkens, M.J.M. (2004). "Optical measurements of grain velocity and sediment concentration in shallow upland flow," Proc. 9th International Symp. on River Sedimentation. pp 1222-1226. Oct. Yichang, P.R. China.

BED FORMS IN THE LOW FLOW CONVEYANCE CHANNEL

Drew C. Baird, Hydraulic Engineer, U.S. Bureau of Reclamation, Denver, Colorado, dbaird@do.usbr.gov

Abstract: Plane bed and symmetric dunes were found to occur in the Low Flow Conveyance Channel near Socorro, New Mexico. The ability to determine bed types in fluvial channels is important for estimating flow resistance and sediment and hydraulic modeling. The flow resistance and sediment transport can ultimately affect flood stage. There are long primary dunes in the Low Flow Conveyance Channel. Superposed on the large primary dunes are secondary dunes. The data set used for this study consists of primary and secondary dunes collected at 5 discharges. Bed form population data shows a large number of primary dunes in the 500 to 1000 ft. long range, with stoss and lee side angles of about 1 degree. Secondary dunes range in length from 50 to 200 ft. The dune height ranged from 0.8 ft. to about 2.5 ft. The dune height and length are reported and compared with other data sets. The dune symmetry ratio (stoss side length divided by the lee side length) was also reported and it was found that the primary dune symmetry ratios are less than 3 while secondary dunes fall between 0.8 and 1.4. The symmetry ratio of asymmetrical dunes is generally greater than 5. The measured bed forms are compared with existing methods to predict bed form based upon sediment size and flow characteristic. Using the measured Low Flow Conveyance Channel dune data, $k_s^{'}$ is calculated and compared with the available literature. Conclusions are drawn about the general applicability of bed form phase predictive methods and methods to estimate $k_s^{'}$, to the Low Flow Conveyance Channel.

INTRODUCTION

Bed features develop naturally in alluvial sand channels whenever the velocity of flow and shear stress exceed threshold values. These bed forms affect resistance to flow, sediment transport, turbulence, flood stage estimates, and velocity and depth for habitat characterization. Various authors have generally shown that dunes have an asymmetrical shape, with a long stoss side slope, sharp crest, short steep lee side slope, and lee side flow separation (Chien and Wan, 1999; Nelson and Smith, 1989, and Bennett and Best, 1995). Laboratory and field evidence also shows that dunes can be symmetrical with stoss and lee side slopes having approximately equal length, without flow separation (Sanderson and Lockett, 1983: Kostaschuk and Villard, 1996; and Smith and McLean, 1997). Smith and McLean (1977) suggest that symmetrical dunes occur in situations where suspended sediment transport dominates so that suspended sediment settles on the lee side slope causing a more symmetrical shape. Sanderson and Lockett (1983) also observed humpback dunes that have symmetrical shape with a nearly flat dune crest. Several methods and diagrams have been developed, designed to predict the conditions under which plane beds, dunes, ripples and anti-dunes would occur. These bed phase diagrams are based mostly on flume data and may not be applicable to field conditions (Kostashuk and Villard, 1996). Secondary dunes can also be superposed on larger underlying primary dunes (Ashley, 1990; Harbor, 1998; Carling et al, 2000). The ratio of dune height/length can be related to the equivalent roughness of Nikuradse ($k_s^{'}$) (Van Rijn, 1982). The objective of this paper is to summarize the LFCC bed form data, compare these data with published bed form phase

diagrams, compare the measured $k_s^{'}$ with the method of Van Rijn (1982) and draw conclusions about the applicability of published methods to the LFCC..

Field Data: Measurements of hydraulics, bed forms and sediment transport have been made on the Low Flow Conveyance Channel (LFCC) near Socorro New Mexico (Figure 1). Field tests were conducted during May or June of 1997, 1998, 1999, and 2001 in a straight reach of the LFC near Socorro, New Mexico, USA. Figure 1 shows a plan view of the channel and the experimental cross section. The experimental program included measurements of bed material particle-size distribution, bed form, water surface slope as well as standard measurements of flow rate, and cross sections. The bed form and some of the channel hydraulics portion of the experimental testing procedure are reported herein. Target discharges ranged from 300 cfs to 1,500 cfs. Cross-sectional shape of the channel is trapezoidal with riprap side slopes and a mobile sand bottom. The side slopes are about 2.2 horizontal to 1 vertical, and the riprap size is D_{50}=152 mm (6 in) and D_{84}=250 mm (9.8 in).

The LFCC discharges were controlled at the inlet works located at San Acacia Diversion Dam (Figure 1). Table 1 contains the cross-sectional averaged hydraulic parameters for the various data sets. The Manning's roughness coefficients (n values) were determined by matching the measured water surface elevations with those estimated in a HEC-RAS (USACOE, 2001) model. The hydraulic parameters reported in Table 1 were computed by HEC-RAS once the calibration was complete. The mean suspended sediment transport for the plane bed 1999-600 cfs case was 636 mg/l, while the mean concentration dune bed 2001-585 cfs data set was

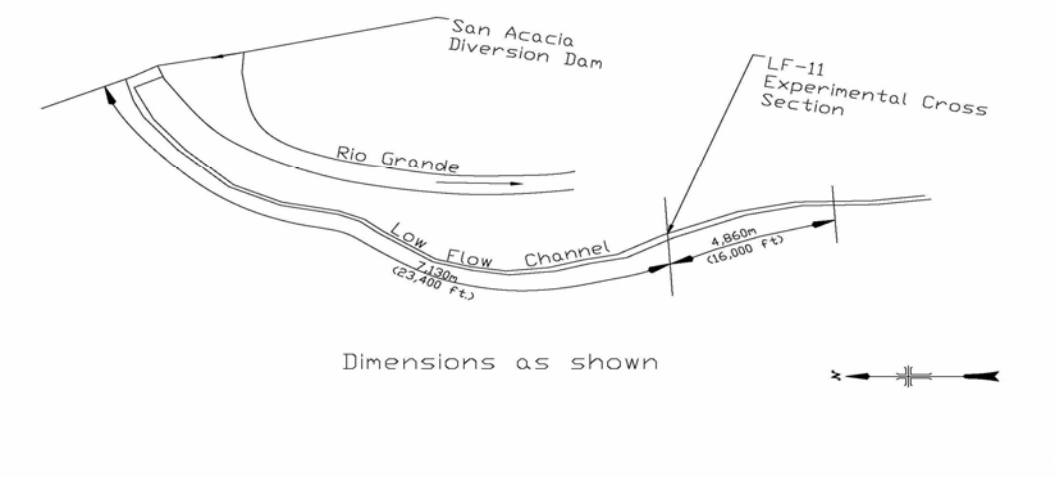


Figure 1 Plan view of the test reach.

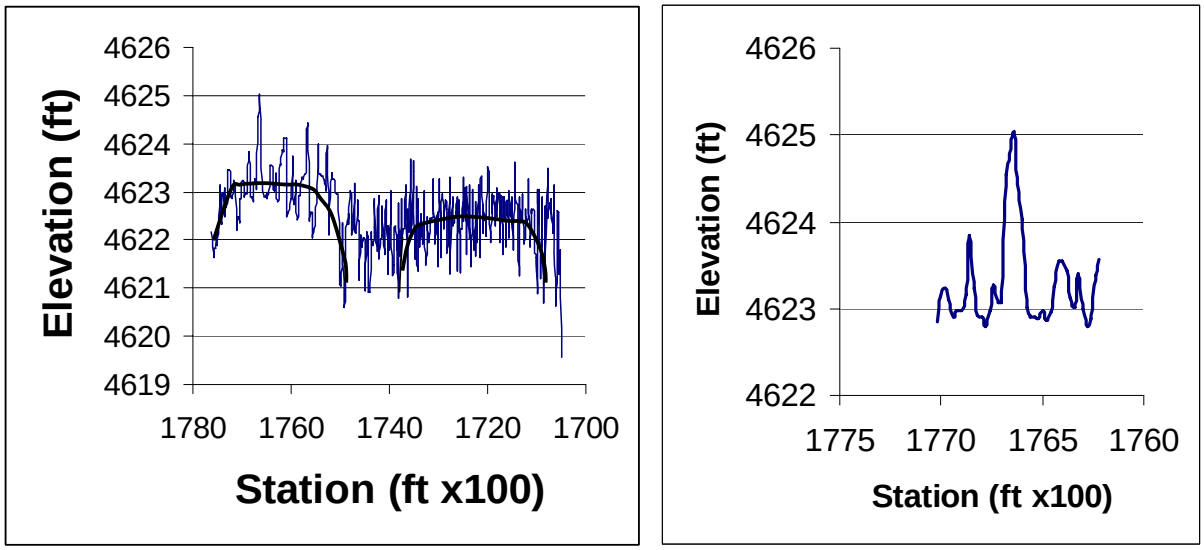
599 mg/l, or about 6% less. The bed elevation in all of the dune bed data sets remained about the same with the water surface elevation increasing with discharge.

Table 1 Hydraulic data for cross section LF-11. The measured flow is for the period during which the ADV and cross section measurements were made.

Year	Target Flow Cfs	Measured Flow cfs	Hydraulic Radius ft	Hydraulic Depth ft	Main Channel Avg. Depth ft	Energy Slope	Froude Number	Calculated Manning's N	Bed Forms
1997	1200	1191	4.86	5.3	7.63	0.000647	0.38	0.026	Dune
1998	1500	1552	5.70	6.15	9.55	0.000616	0.32	0.026	Dune
1999	600	625	3.95	4.03	5.04	0.000382	0.33	0.020	Plane
2001	600	585	4.04	4.77	7.34	0.000413	0.28	0.035	Dune
2001	300	1390	3.66	3.81	5.48	0.000260	0.23	0.024	Dune

DATA ANALYSIS

Dune Data: The LFCC dunes were symmetrical with stoss and lee sides of nearly equal steepness (Figure 2). Humpback dunes with flat tops with equal steepness stoss and lee sides also occurred. The primary symmetrical and humpback dunes had average lengths from 630 to 890 ft. (Table 2). Primary dunes are on average 7 to 10 times longer than secondary dunes (Table 2). The length of the flat top on humpback dunes for primary dunes ranges from 110 to 360 ft. and for secondary dunes the range is 10-100 ft. Primary dune lengths were "very large" (dune length > 330 ft.) while dune heights ranged from the "small" (0.25 < dune height < 1.3 ft.) to "medium" (1.3 < dune height < 2.5 ft.) based on the classification of Ashley (1990). Secondary dunes lengths were "large" and the height was "small" or "medium" based on the classification. The stoss and lee side slope angles were less than 1 degree, while symmetrical dunes reported on the Rhine river had lee side slopes of about 10 degrees with some as low as 1-2 degrees (Carling, et al., 2000). Fraser river dunes had stoss and lee side angles ranging from 2.4 to 18.9 degrees (Kostachuk and Villard, 1996). Dune symmetry ratio is defined as the stoss side length (L_s) divided by the lee side length (L_l). The majority of secondary dunes had a symmetry ratio ranging from 0.8 to 1.4(Figure 3), falling in the same range of symmetry ratios of symmetrical dunes found on the Fraser River (Kostachuk and Villard, 1996). By comparison, asymmetrical dunes on the Fraser River had symmetry ratios ranging from 5.67 to 8.17 (Kostachuk and Villard, 1996).

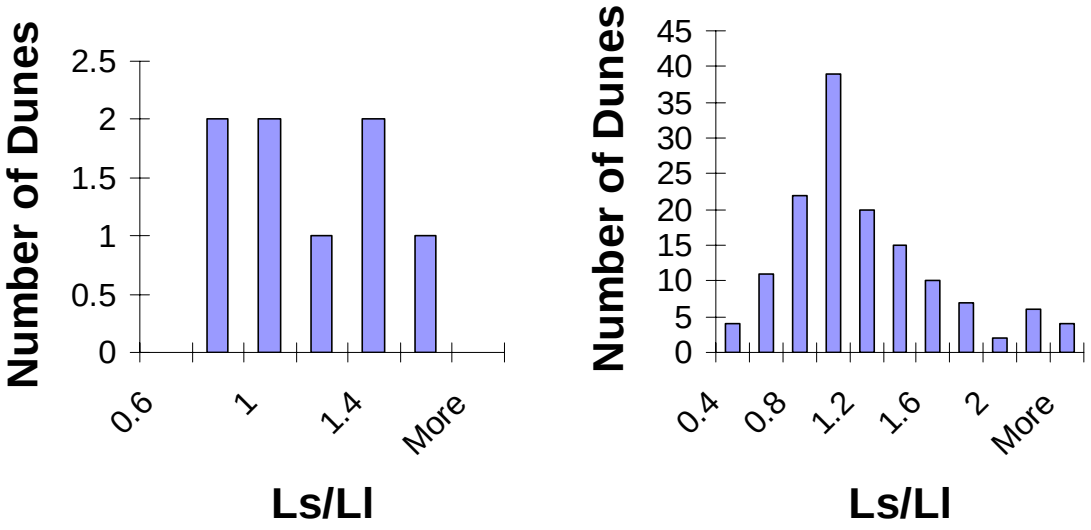


(a) (b)

Figure 2 Dune Profiles (a) Primary Dunes (the line denotes the approximate crest of the primary dunes) and (b) Secondary Dunes.

Table 2 Dune properties for 300, 600, 1,200, and 1,500 cfs discharges.

Date/Discharge	Average Dune Height/Length Ratio	Average Dune Height (ft.)	Average Dune Length (ft.)	Average Stoss Side Angle ($\sin^{-1}(H/L_s)$)	Average Lee Side Angle ($\sin^{-1}(H/L_l)$)
1997 1200 cfs					
Primary Dunes	0.00149	0.82	630	0.169	0.145
Secondary Dunes	0.00459	1.05	230	0.402	0.398
1998 1500 cfs					
Primary Dunes	0.0018	1.625	890	0.172	0.323
Secondary Dunes	0.0247	1.628	94	0.555	0.533
2001 600 cfs					
Primary Dunes	0.00583	2.78	730	0.515	0.413
Secondary Dunes	0.006978	0.767	111	0.458	0.454
2001 300 cfs					
Primary Dunes	0.00464	2.5	666	0.529	0.508
Secondary Dunes	0.01796	0.831	58	0.579	0.597



(a) (b)

Figure 3 Dune Symmetry Ratio (a) primary dunes, and (b) secondary dunes.

Five bed form phase diagrams were selected to examine the stability fields of the LFCC dunes: stream power diagram of Simons and Richardson (1963, 1966), shear stress diagram of Chabert and Chauvin (1963), Froude number diagram of Simons and Senturk (1992), mean velocity diagram of Ashley (1990), and the modified sediment mobility parameter diagram of Van den Berg and Van Gelder (1993). These five phase diagrams each have fundamentally different physical parameters to estimate bed form phases. Dunes were measured in all data sets except the 1999 data set, while the published stability fields showed anti-dunes, upper regime plane bed, transition between lower and upper regime, or transition between dunes and anti-dunes, Only the dunes measured in the 2001 300 cfs data set matched the prediction by Simons and Richardson (1963, 1966). In the Chabert and Chauvin's (1963) shear stress diagram and the velocity based method of Ashley (1990), the measured LFCC velocity exceeded the reported range of the methods. These data support the conclusion of Kostachuk and Villard (1996) that "flume based bed form phase diagrams are not applicable to dunes in deep natural flows." Laboratory models do not scale the same for sediment size, flow hydraulics and turbulence (Kostachuk and Villard, 1996), and results from such models may not be applicable to field conditions. Regardless of the interpretation of these results, it is apparent that published bed form phase diagrams cannot be readily applied to the LFCC data set.

Equivalent Roughness of Nikuradse (k_s')

Using the log law given as

$$\frac{\bar{u}}{u_*} = \frac{1}{\kappa}\ln(\frac{y}{y_0}) \qquad (1)$$

Table 3 Comparison of Measured LFCC Bed forms with Bed Forms Predicted by various Bed Form Phase Diagrams.

Data Set	Measured	Simons And Richardson (1963,1966)	Chabert And Chauvin (1963)	Simons And Senturk (1992)	Ashley (1990)	Van den Berg and Van Gelder (1993) Flume	Van den Berg and Van Gelder (1993) River
1997 (1200 cfs)	Dune	Anti-dune and Plane Bed	Shear Stress Exceeded the diagram	Transition[1]	Velocity Exceeded The Diagram	Upper Regime Plane Bed	Upper Regime Plane Bed
1998 (1500 cfs)	Dune	Transition between dunes and anti-dunes	Shear Stress Exceeded the diagram	Transition	Velocity Exceeded The Diagram	Dunes to Upper Regime Plane Bed	Upper Regime Plane Bed
1999 (600 cfs)	Plane	Dunes	Shear Stress Exceeded the diagram	Transition	Velocity Exceeded The Diagram	Upper Regime Plane Bed	Upper Regime Plane Bed
2001 (600 cfs)	Dune	Anti-dunes and Plane Bed	Shear Stress Exceeded the diagram	Transition	Velocity Exceeded The Diagram	Upper Regime Plane Bed	Upper Regime Plane Bed
2001 (300 cfs)	Dune	Dunes	Shear Stress Exceeded the diagram	Dunes	Velocity Exceeded The Diagram	Upper Regime Plane Bed	Upper Regime Plane Bed

[1]Transition between Lower Regime and Upper Regime

where $\bar{u}$ is the time average velocity at depth y, u_* is the shear velocity, κ is the Von-Karman parameter, and y_o is the zero velocity roughness height. The slope of the logarithmic portion of the stream wise velocity profiles was used to obtain the values of shear velocity u_* and the zero velocity roughness height y_o. By regressing u on to $ln\ y$ the zero velocity roughness heights (y_0) (Bergeron, and Abrahams 1992) is found from

$$u = m \ln y + c \tag{2}$$

$$y_o = e^{(-c/m)} \quad (3)$$

where *m* is the regression line slope, and *c* is the intercept. The grain roughness height is found using (Julien, 1995)

$$k_s^{'} = 30.2 y_o \quad (4)$$

where $k_s^{'}$ is the equivalent grain roughness height. For dune beds, Van Rijn (1982) developed an empirical equation for estimating $k_s^{'}$ using dune length and height

$$k_s^{'} = 1.1H(1 - e^{-25H/L}) \quad (5)$$

applicable in the range $0.01 \le H/L \le 0.2$. The majority of the LFCC data has *H*/L values less than this range except the secondary dunes in 1998 at 1500 cfs and in 2001 at 300 cfs, and somewhat compares with the method of Van Rijn (1982) (Table 4).

Table 4. Comparison of Predicted and measured.

	$k_s^{'}$ Van Rijn (1982) Eq. 5 (mm)	$k_s^{'}$ from the measured velocity profile (mm)
1998 1500 cfs Secondary Dunes	250	230
2001 300 cfs Secondary Dunes	100	140

CONCLUSIONS AND RECOMMENDATIONS

It has been shown that dunes on the LFCC are symmetrical shaped with long, low height geometry that sometimes have flat or humpback crests. LFCC bed forms are not well represented by existing bed form phase diagrams and the equivalent grain roughness height for dunes is somewhat represented by the method of Van Rijn (1982). It is recommended that the bed form phase diagrams and the method for predicting the equivalent grain roughness height be adjusted to apply to the LFCC to estimate hydraulic and sediment transport conditions.

ACKNOWLEDGEMENTS

The author wishes to acknowledge the contributions of Tetra Tech Inc, who collected the field data, Maria Bullard and Dwight Slaugh for measuring some of the dune properties from the field data, Mark Nemeth for computing some of the hydraulic variables, Anita Wood for preparing one of the figures, and to Yong Lai and Kent Collins for reviewing the document.

REFERENCES

Ashley, G. M., (Syposium Chairperson), (1990). "Classification of large-scale subaqueous bedforms: a new look at an old problem," Journal of Sedimentary Petrology, Vol. 60, No. 1 January, pp 160-172.

Bennett, S.J., and Best, J.L., (1995). "Mean flow and turbulence structure over fixed, two-dimensional dunes: implications for sediment transport and bed form stability," Sedimentology, 42, pp 491-513.

Bergeron, N.E., and Abrahams, A.D., (1992). "Estimating shear velocity and roughness length from velocity profiles," Water Resources Research, Vol. 28, No. 8, pp. 2155-2158.

Carling, P.A., Williams, J.J., Golz, E., and Kelsey, A.D., (2000) "The Morphodynamics of Fluvial Sand Dunes in the River Rhine, Near Mainz, Germany. II. Hydrodynamics and Sediment Transport," Sedimentology, 47, pp. 253-278.

Chabert, J., and Chauvin, J.L., (1963), "Formation de Dunes et de Rides Dans Les Modeles Fluviaux", Bull. Cen. Rech. Ess. Chatau, No. 4. (From Julien, 1995).

Chien, N, and Wan, Z., (1999) Mechanics of Sediment Transport. ASCE Press.

Harbor, D., (1998), "Dynamics of Bedforms in the Lower Mississippi River," Journal of Sedimentary Research, Vol. 68, No. 5, September, pp. 750-762.

Julien, P.Y., (1995) Erosion and Sedimentation. Cambridge University Press.

Kostaschuk, R., and Villard, P., (1996), "Flow and Sediment Transport Over Large Subaqueous Dunes: Fraser River, Canada," Sedimentology, 43, pp 849-863.

Nelson, J.M., and Smith, J.D., (1989), "Mechanics of Flow Over Ripples and Dunes," Journal of Geophysical Research, Vol. 94, No. C6, pp 8146-8162.

Sanderson H.C., and Lockett, F.P.J., (1983) "Flume Experiments On Bedforms and Structures at the Dune-Plane Bed Transition," Spec. Publs, Int. Assoc. Sedimentologists, vol. 6, pp. 49-58.

Simons, D.B., and Richardson, E.V., (1963), "Form of Bed Roughness in Alluvial Channels," Transactions ASCE, 128, pp 284-323.

Simons, D.B., and Richardson, E.V., (1966), Resistance to Flow in Alluvial Channels. U.S.G.S. Professional Paper 422-J, Washington D.C.

Simons, D.B., and Senturk,F., (1992) Sediment Transport Technology. Water Resources Publications, Littleton, CO.

Smith, J.D., and McLean, S.R., (1977), "Spatially Averaged Flow Over A Wavy Surface," Journal of Geophysical Research, Vol. 82, No. 12, pp 1735-1746.

US Army Corps of Engineers (2001), HEC-RAS River Analysis System User's Manual Version 3.0. Hydrologic Engineering Center, Davis California.

Van Den Berg, J.H., and Van Gelder, A., (1993), "A New Bedform Stability Diagram, with Emphasis on the Transition of Ripples to Plane Bed In Flows Over Fine Sand and Silt," Spec. Publis. Int. Ass. Sediment. 17, pp 11-21.

Van Rijn, L. C., (1982), "Equivalent Roughness of Alluvial Bed," J. Hydr. Engrg., ASCE Vol. 108, No. HY10, pp 1215-1219.

PATH OF GRAVEL MOVEMENT IN A COARSE STREAM CHANNEL

Kristin Bunte, Engineering Research Center, Colorado State University, Fort Collins, CO, kbunte@engr.colostate.edu, John P. Potyondy, Stream Systems Technology Center, USDA Forest Service, Fort Collins, CO, jpotyondy@fs.fed.us, Steven R. Abt, Engineering Research Center, Colorado State University, Fort Collins, CO, sabt@engr.colostate.edu and Kurt W. Swingle, Boulder, CO, kskb@ix.netcom.com

INTRODUCTION

Little is known about the path of gravel transport within a mountain stream, and it is often assumed that gravel bedload generally follows the thalweg where flow is deepest and fastest. However, field studies have shown this not to be the case. Based on the forces of flow and gravity acting on bedload particles in a meander bend, Dietrich and Smith (1984), Parker and Andrews (1985) and Bridge (1992) concluded that coarse and fine bedload followed different paths. The coarse portion approaches a stream bend along the inside bank and crosses over to the outside bank near the bend apex. Measured bedload travel paths in sand-bedded meandering streams by Bridge and Jarvis (1976; 1982), Dietrich and Whiting (1989), Anthony and Harvey (1991) and Julien and Anthony (2002) also showed that the fine and coarse portion of bedload followed different paths. The coarse fraction, coarse sand and pea gravel, traveled laterally over the head of the point bar close to the inside bank, shifted towards the stream center at the bend apex and towards the thalweg in the outside bank at the bend exit. This path coincided approximately with the location of highest grain shear stress. We may reasonably ask whether gravel transport in coarse-bedded mountain streams with a meandering thalweg also follows a similar distinct and predictable path.

Knowing where within a stream cross-section most of the gravel travels not only furthers our general understanding of how gravel transport and stream morphology work together, but the ability to identify the location of maximum transport by simply looking at the local stream morphology would also be helpful for planning field measurements of gravel transport. Sampling could be focused at the locations of highest transport within a cross-section and thus increase the accuracy obtained from a specified number of samples. If wadeability was an issue, sampling could be focused at locations within a cross-section where most of the transport occurs in relatively shallow flow. In order to find out where within a stream most of the gravel bedload is transported we examined the lateral positions of gravel bedload measured in eight individual cross-sections in different gravel- and cobble-bed streams, as well as the gravel transport path over a point bar.

METHODS

Gravel bedload transport was measured at eight sites in six different streams that were classified as having plane-bed and step-pool morphology. Although not generally meandering, all streams had a meandering thalweg and gravel bars that were mostly submerged during low and moderate flows. Gravel transport was measured using bedload traps. Bedload traps consist of an aluminum frame 0.3 by 0.2 m in size that is fastened onto a ground plate that is anchored to the stream bottom. Bedload is collected in a 0.9-1.6 m long net with a 3.5 mm mesh width.

Sampling time was typically 1 hour, but was reduced when transport rates were high. Four to six bedload traps were typically installed across the stream spaced 1-2 m apart (Bunte et al. 2003, 2004, 2005) (Figure 1). Four to 9 samples of gravel bedload transport were collected almost every day over the snowmelt highflow season that typically lasted 4-7 weeks. This amounted to 21-163 samples per site with an average of 80. At one stream, Halfmoon Creek, near Leadville, CO, gravel bedload was measured with 6 bedload traps installed in two neighboring cross-sections. One spanned a riffle close to the pool exit, while the other was located about 8 m downstream and spanned a point bar-thalweg cross-section (Figure 1).



Figure 1 Bedload traps installed at two neighboring cross-sections at Halfmoon Creek.

Gravel transport rates were computed for each trap per cross-section individually and then assigned to the portion of stream width represented by each trap. Summing across the stream yielded the cross-sectionally averaged transport rate. The proportion of total transport passing through individual stream sections during a highflow season can be computed for each measuring site.

Although none of the streams were classified as meandering, all of the measuring sites were situated within reaches that had a meandering thalweg. In some cross-sections, the thalweg was near one of the banks, in others the thalweg was near the center of the stream. Assuming an idealized reach with a meandering thalweg (see center part of Figure 2), the measured cross-sections from different streams can be longitudinally arranged over an idealized meandering reach such that the lateral location of the thalweg in the measured cross-sections matches the one in the idealized reach. Each individual cross-section then represents a specified location, i.e., some cross-sections represent the upstream part of a submerged point bar, some the downstream

part, and some the riffle or crossing (Figure 2). For each of the cross-sections, the lateral position of maximum annual gravel bedload transport is known from the field measurements.

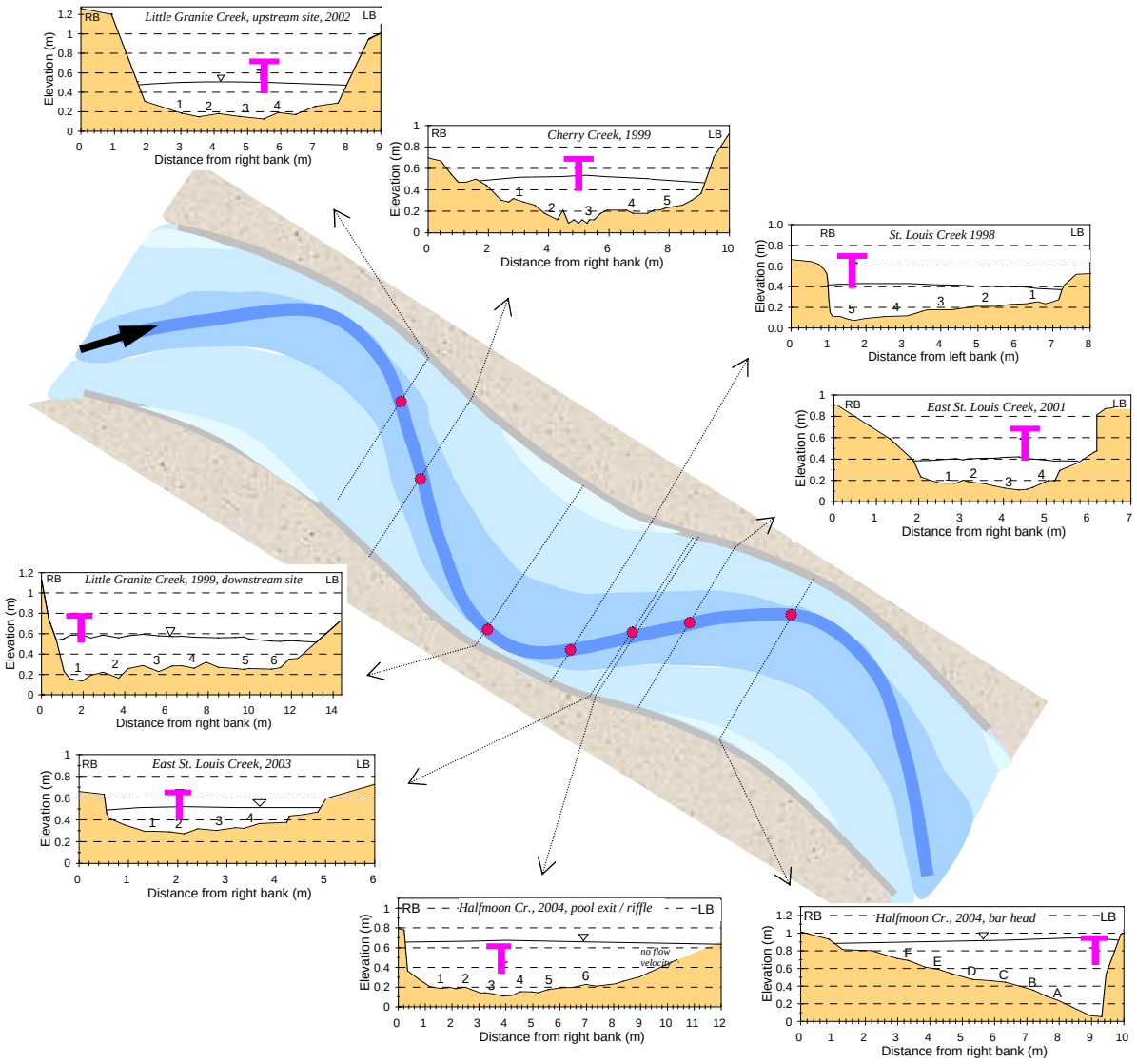


Figure 2 Longitudinal arrangement of measured cross-sections from different streams to represent locations within an idealized reach that has a meandering thalweg. The pink "T" indicates the thalweg. Darker blue colors indicate deeper flow. Numbers and letters in the cross-sections indicate bedload trap locations.

RESULTS

Transport locations in eight cross-sections representing a meandering thalweg reach: Results from our field studies showed that for cross-sections that extended from a bar on one bank to a thalweg on the other bank, most of the gravel traveled over the bar. At a pool exit, most gravel traveled through the thalweg, and at a riffle or crossing, transport was focused toward the side of the stream at which the next downstream bar appeared. Knowing the lateral

position of major gravel transport for each of the 8 cross-sections that cover an idealized meandering thalweg reach, a picture of the downstream travel path can be developed. The combined results from the individual field studies strongly suggested that gravel transport in coarse-bedded streams with a meandering thalweg follows the path taken by the coarsest particles in sand-bedded streams indicated by the yellow stippled band in Figure 3: over the bankward side of the bar head, then diagonally across the bar and towards the pool near the bend apex.

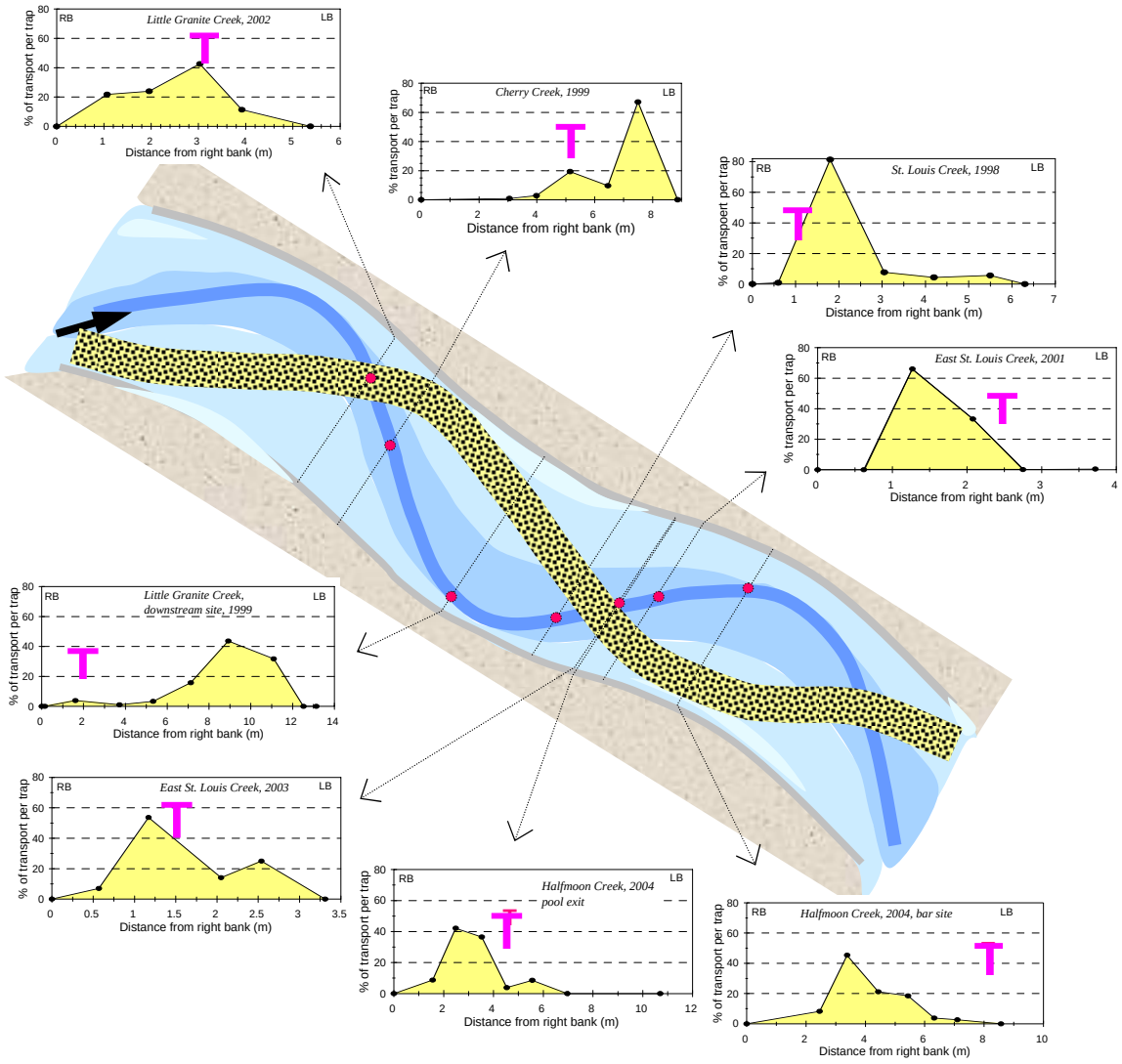


Figure 3 Lateral positions of maximum annual transport in eight cross-sections representing different locations within a meandering thalweg reach. The stippled yellow band indicates the travel path for gravel transport.

Transport path between the pool exit and the bar head: To confirm the gravel transport path along the inside bank between the pool exit and the head of a point bar, the lateral location of gravel transport was evaluated over two neighboring cross-sections in a pool-riffle section of a mountain gravel-bed stream (Halfmoon Creek). Integrated over the entire highflow season, most of the gravel was transported adjacent to the thalweg towards the inside bend in the pool exit/riffle cross-section. In the point bar cross-section, most gravel traveled over the shallow parts of the bar (compare the two lower right plots for Halfmoon Creek in Figures 2 and 3).

The lateral locations of gravel transport were not static over the highflow season but shifted laterally with the magnitude flow. At the lowest gravel transporting flows (14-27% of bankfull), most of the pea gravel in transport moved near the thalweg in the pool exit/riffle. At higher flows, gravel transport shifted towards the inside bank (Figure 4). At the bar head, most gravel transport occurred over the center of the bar at low flows and moved higher onto the bar as flows increased to 80% Q_{bkf}. The location of maximum transport rates were also the locations where the largest gravel particles were transported. Experiments with mobile tracer gravels confirmed the curved transport path along the inside bend. Gravel transport rates and the largest gravel bedload particle sizes had a secondary maximum closer to the thalweg, but transport rates there attained only 10% of the maximum rates. Almost no transport took place through the thalweg.

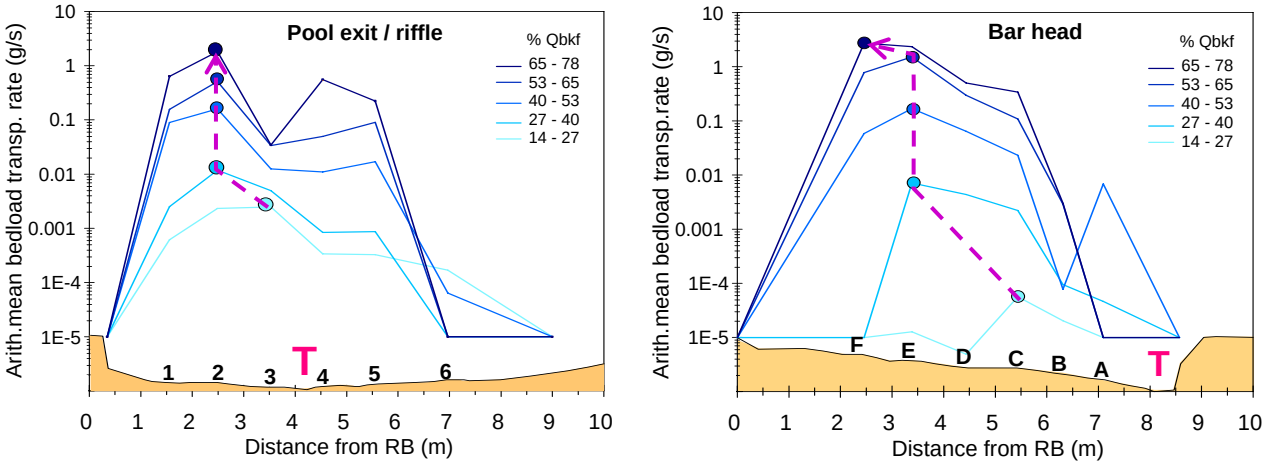


Figure 4 Lateral shift of gravel transport from near the center of the bankfull stream width at the lowest transporting flows towards the inside bank at the highest measured flows. Bold numbers and letters along the bottom of the plots indicate locations of bedload traps in the cross-section. The dashed arrows indicate the bankward shift in the locations of maximum transport with increasing flow.

Predictability of the lateral distribution of gravel transport rates from flow hydraulics and bed material size: Of several measured and computed parameters of flow hydraulics, the maximum mean flow velocity per vertical (v) measured in 0.6 of the water depth (d) coincided with the locations of maximum transport rates (Figure 5). By contrast, local water depth, discharge per unit width (q) and boundary shear stress (τ_o) were always largest at the thalweg and did not predict the lateral variation in gravel transport rates. Grain shear stress τ_g computed from $\rho_f \cdot[(v_d \cdot \kappa)/\ln(d/0.1\ D_{84})]^2$ (Dietrich and Whiting 1989) (where κ is a constant that is usually taken as 0.4, and D_{84} is the size for which 84% of the sediment is smaller) as well as

dimensionless shear stress $\tau^* = \tau_o/(\rho_s-\rho_f)\cdot g\cdot D_{50}$ (with ρ_s = sediment density) which within a cross-section is a function of d/D_{50} both had their maxima in the thalweg, but secondary maxima were noticeable for the two parameters over the bar.

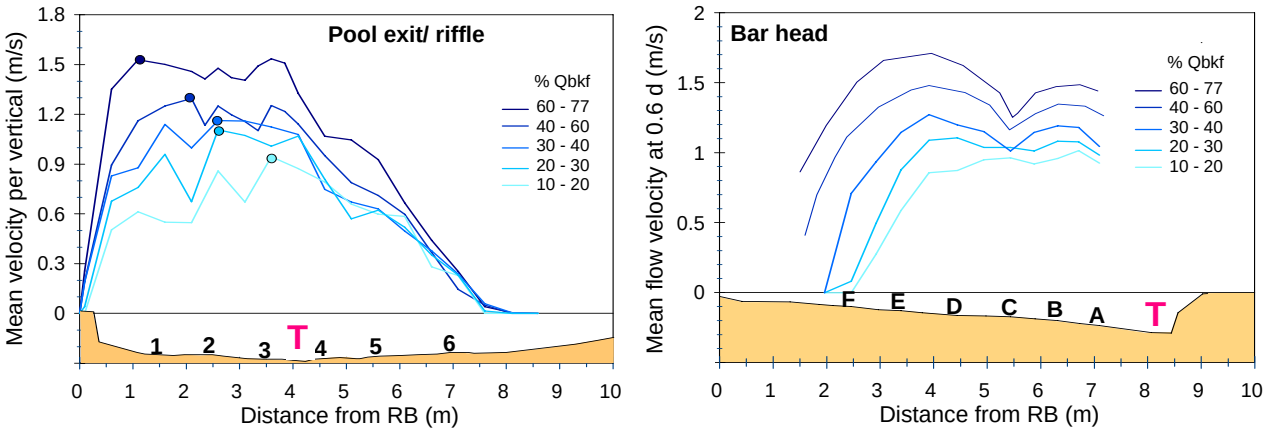


Figure 5 Lateral distribution of the mean vertical flow velocity in the pool exit/riffle (left) and the point bar-thalweg cross-section (right). Velocities at the point bar-thalweg cross-section for flows above 50% of bankfull are extrapolated and printed in dashed lines.

The bed material size and structure, by comparison, were good predictors of the bedload transport locations at Halfmoon Creek. At the bankward side of the bar, the local surface D_{50} bed-material particle size was 8 mm and increased to 46 mm in the thalweg. Besides a strong bankward fining trend, the bed on the bar was unarmored and easily erodible. The bed material in the thalweg was not only considerably coarser and devoid of surface fines but also strongly imbricated and thus quite erosion resistant. The surface bed material size in the pool exit/riffle cross-section did not show bankward fining except for a silty backwater deposit on the far bank.

Making use of the asymmetrical travel path for bedload sampling in deeper streams: Bedload transport in mountain streams is often collected using hand operated samplers such as a Helley-Smith-type sampler, bedload traps, basket-type samplers or non-recording pit traps (Ryan et al. 2005). These samplers are typically deployed in a straight reach with a symmetrical cross-section. All of these samplers require flows that are wadeable during sampler operation. Wadeability can be defined as the product of flow depth and mean vertical flow velocity in English units (Abt et al. 1989). Depending on a person's height and weight (as well as athletic skills and the slipperiness of the bed), values of 7-12 pose a limit to safe wading. At flows near bankfull or larger, even small streams often become difficult to wade, while wading may become next to impossible for many people in most cross-sections of larger streams.

Results from the study at Halfmoon Creek indicated that most gravel travels over the head of submerged point bars along the inside bend. This stream location – the upstream end of a submerged point bar – is generally likely to remain wadeable over much of the stream width when the riffle or crossing has become unwadeable at high flow. In our study, 90-95% of the cross-sectional gravel transport was collected within the 50% of the bankfull stream width at the inside bend during flows 40-80% of bankfull (Figure 6, left). This means that at the head of a point bar,

the majority of all gravel bedload is transported within the wadeable portion of the stream (Figure 6, right).

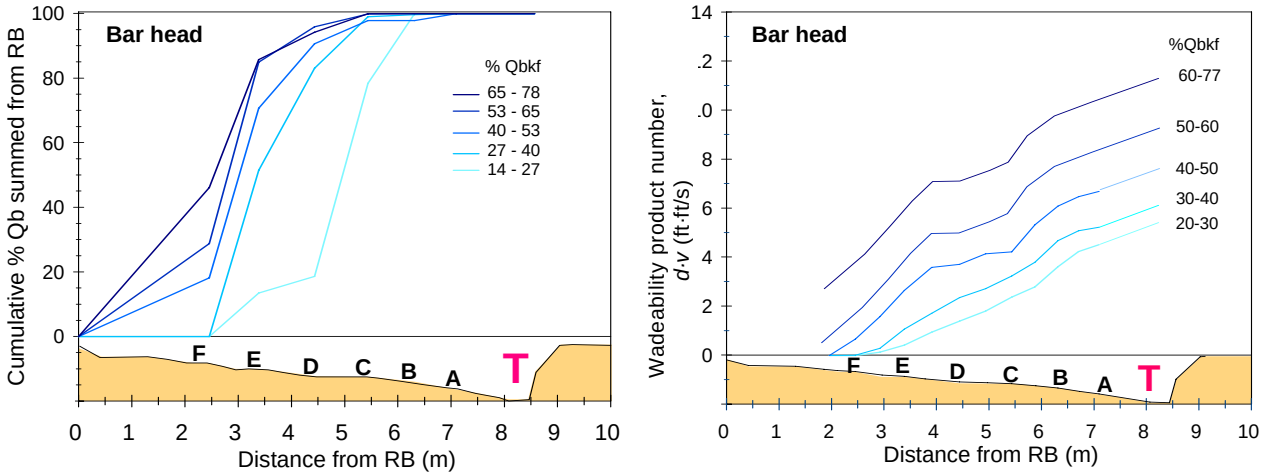


Figure 6 Cumulative percent of total cross-sectional gravel transport (summed over sampling locations starting at the shallow part of the stream) for flows 20 to 70% of bankfull (left). Wadeability of the cross-section for increasing flow (right).

DISCUSSION AND CONCLUSION

Combined results from our field studies suggested that in a coarse gravel-bedded mountain stream with a meandering thalweg, gravel travels over the head of the submerged bar along the inside bankward side, proceeds diagonally over the bar and then towards the thalweg near the bar apex. Detailed measurements on two neighboring cross-sections between a pool exit and the head of the point bar in a mountain stream verified this transport path. The path of gravel transport in mountain streams with a meandering thalweg thus is predictable from stream morphology and generally follows the path modeled and measured for the coarsest bedload in sand-bedded streams.

The observed shift in gravel transport towards the inside bank occurred when flows increased from 20 to 80% of bankfull flow. It is unknown whether this bankward trend continues for flows larger than bankfull or when transport rates are very high. The observed gravel transport path may change during high sediment supply when subsequent high transport rates may change the local channel morphology. Gravel transport may also deviate from its predicted path in stream bends if local hydraulics are influenced by non-moveable boundaries such as bedrock outcrops or large woody debris, which may cause different spatial patterns of bedload transport. However, under moderate flow and transport conditions that formed freely in a moveable gravel bed, knowledge of the gravel transport path over a submerged bar can be used when designing a sampling scheme. Measurements of gravel bedload could be concentrated or intensified at the location of maximum transport in order to increase the accuracy obtained from a preset number of samples. If wadeability is an issue, sampling can be limited to the shallow portion of the stream over the upstream part of a submerged point bar, where wading is possible while other parts of the stream no longer permit this, without neglecting a substantial portion of bedload.

A few caveats are associated with sampling across a bar head, though. Flow hydraulics at this location are influenced by the asymmetrical cross-sectional shape; they are subject to strong secondary flows and thus not well suited to characterize the general hydraulic conditions of the reach which are customarily measured within a straight reach or across a riffle. Note also that sand follows a downstream path that is different from the one followed by gravel. The majority of sand does not travel over the bankward part of the bar head but rather the bar tail. Bedload transport rates measured for a specified flow across the bar head may also differ slightly from those measured on a nearby riffle. In our study, the rating curve across the bar head was slightly steeper, because the very onset of fine gravel particle motion occurred at somewhat higher flows than on the riffle, while during the largest measured flows transport rates on the bar were slightly higher. However, compared to not being able to collect samples at all, the slight shift in the rating curve poses a relatively small inaccuracy.

Acknowledgement: This study was funded by the USDA Forest Service, Stream Systems Technology Center, Fort Collins, CO.

REFERENCES

Abt, S.R., Wittler, R.J., Taylor, A. and Love, D.J. (1989). "Human stability in a high flood hazard zone," Water Resources Bulletin 25 (4), pp 881-890.

Anthony, D.J., and Harvey, M.D. (1991). "Stage-dependent cross-section adjustments in a meandering reach of Fall River, Colorado," Geomorphology 4, pp. 187-203.

Bridge, J.S. (1992). "A revised model for water flow, sediment transport, bed topography and grain size sorting in natural river bends," Water Resources Research 28(4), pp 999-1013.

Bridge, J.S. and Jarvis, J. (1976). "Flow and sedimentary processes in the meandering river South Esk, Glen Clova, Scotland," Earth Surface Processes and Landforms 1, pp 303-336.

Bridge, J.S. and Jarvis, J. (1982). "The dynamics of a river bend: a study in flow and sedimentary processes," Sedimentology 29, pp 499-543.

Bunte, K. and Abt, S.R. (2003). "Sampler size and sampling time affect measured bedload transport rates and particle sizes measured with bedload traps in gravel-bed streams," In: Erosion and Sediment Transport Measurement in Rivers: Technological and Methodological Advances. J. Bogen, T. Fergus and D.E. Walling (eds.), IAHS-Publication No. 283, pp 126-133.

Bunte, K., Abt, S.R., Potyondy, J.P., and Ryan, S.E. (2004). "Measurement of coarse gravel and cobble transport using a portable bedload trap," Journal of Hydraulic Engineering 130(9), pp 879-893.

Bunte, K., Swingle, K.W., and Abt, S.R. (2005). Guidelines for using bedload traps in coarse-bedded mountain streams: Construction, installation, operation and sample processing. Report submitted to Stream Systems Technology Center, USDA Forest Service, Rocky Mountain Research Station, Fort Collins, CO, 79 pp.

Dietrich, W.E. and Smith, J.D. (1984). "Bed load transport in a river meander," Water Resources Research 20(10), pp 1355-1380.

Dietrich, W.E and Whiting, P. (1989). "Boundary shear stress and sediment transport in river meanders of sand and gravels," In: River Meandering. S. Ikeda and G. Parker (eds.), Water Resources Monograph 12, American Geophysical Union, Washington, DC, p. 1-50.

Julien, P.Y. and Anthony, D.J. (2002). "Bed load motion and grain sorting in a meandering stream," Journal of Hydraulic Research 40(2), pp 125-133.

Parker, G. and Andrews, E.D. (1985). "Sorting of bedload sediment by flow in meander bends," Water Resources Research 21, pp 1361-1373.

Ryan, S.E., Bunte, K. and Potyondy, J.P. (2005). "Breakout Session II: Bedload Transport Measurements, Data Uncertainty, and New Technologies," Proceedings of the Federal Interagency Sedimentation Monitoring Instrument and Analysis Workshop, September 9-11, 2003, Flagstaff, Arizona, J.R.Gray (ed.). U.S. Geological Survey Circular 1276, p. 16-28. http://water.usgs.gov/pubs/circ/2005/circ1276/

COMPARISON OF SEDIMENT-TRANSPORT AND BAR-RESPONSE RESULTS FROM THE 1996 AND 2004 CONTROLLED-FLOOD EXPERIMENTS ON THE COLORADO RIVER IN GRAND CANYON

David J. Topping, Research Hydrologist, U.S. Geological Survey, Golden, Colorado, dtopping@usgs.gov; David M. Rubin, Research Geologist, U.S. Geological Survey, Santa Cruz, California, drubin@usgs.gov; John C. Schmidt, Professor, Department of Aquatic, Watershed, and Earth Resources, Utah State University, Logan, Utah, jschmidt@cc.usu.edu; Joseph E. Hazel, Jr., Research Associate, Department of Geology, Northern Arizona University, Flagstaff, Arizona, joe.hazel@nau.edu; Theodore S. Melis, Physical Scientist, U.S. Geological Survey, Flagstaff, Arizona, tmelis@usgs.gov; Scott A. Wright, Hydrologist, U.S. Geological Survey, Flagstaff, Arizona, sawright@usgs.gov; Matt Kaplinski, Research Associate, Department of Geology, Northern Arizona University, Flagstaff, Arizona, matt.kaplinski@nau.edu; Amy E. Draut, Research Geologist, U.S. Geological Survey, Santa Cruz, California, adraut@usgs.gov; and Michael J. Breedlove, Research Associate, Department of Aquatic, Watershed, and Earth Resources, Utah State University, Logan, Utah, mbreedlove@usgs.gov

INTRODUCTION

Sandbars and other sandy deposits in and along the Colorado River in Grand Canyon National Park (Fig. 1) were an integral part of the natural riverscape, and are important for riparian habitat, fish habitat, protection of archeological sites, and recreation (Rubin et al., 2002). Recent work has shown that these sandbars in lateral recirculation eddies contain the bulk of the sand, silt, and clay in storage (Hazel et al., in press), and the surface grain size of these sandbars is the dominant regulator of sand transport over multi-year timescales (Topping et al., 2005). These deposits have eroded substantially following the 1963 closure of Glen Canyon Dam that reduced the supply of sand at the upstream boundary of Grand Canyon National Park by about 94% (Topping et al., 2000a). In response to this reduction in sand supply and the alteration of the natural hydrograph by dam operations (Topping et al., 2003), sandbars in Marble Canyon and the upstream part of Grand Canyon have substantially decreased in size since closure of the dam (Schmidt et al., 2004) and are still in decline under normal powerplant operations at the dam (Wright et al., 2005).

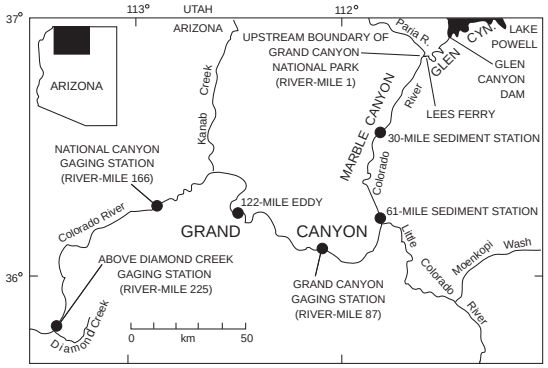


Figure 1 Map of the study area showing the locations where sediment-transport measurements were made during either the 1996 or 2004 controlled-flood experiments (solid circles). Formal names and station numbers of the Grand Canyon, National Canyon, and above Diamond Creek gaging stations are in Webb et al. (1999). By convention, locations along the Colorado River in Marble and Grand Canyons are referred to by river mile. Marble Canyon extends from Lees Ferry to the mouth of the Little Colorado River; Grand Canyon begins at the mouth of the Little Colorado River.

Prior to the 7-day 1,270 m^3/s 1996 controlled-flood experiment (Webb et al., 1999), the sediment-transport paradigm for the regulated Colorado River in Marble and Grand Canyons was that, under normal powerplant releases from Glen Canyon Dam, tributary-supplied sand would accumulate in the channel over multi-year timescales and that this accumulated sand could be transferred from the channel bed to eddies during controlled floods, increasing both the total area and volume of eddy sandbars. As summarized in Rubin et al. (2002), work conducted during and

subsequent to the 1996 controlled flood indicated that this paradigm was based on assumptions that were either false or only partially true. First, sand did not accumulate in the channel of the river over multi-year time scales. Second, during the 1996 flood, sand deposited at higher elevations in eddy sandbars was eroded mostly from the lower parts of upstream sandbars (not from the channel bed) causing a net decrease in total sandbar area and volume (although sandbars did gain sand at higher elevations). Tributary inputs of new sand were relatively low in the year preceding the 1996 flood and dam releases were moderate to high. Thus, the 1996 flood experiment was conducting during a period when the Colorado River in Marble and Grand Canyons was relatively depleted with respect to sand.

The 2004 controlled-flood experiment was designed to, first, keep dam releases relatively low (<280 m^3/s) during September-November 2004 to allow the accumulation and retention of new tributary sand inputs in the channel, and, second, if more than 800,000 metric tons of new sand were retained in Marble Canyon, follow this period of lower dam releases by a 60-hour controlled-flood release of 1,160 m^3/s in November 2004 to redistribute this new sand from the channel bed into the eddies. Between July 1, 2004, and the November 2004 controlled flood, 760,000-1,200,000 (range in values results from uncertainties in calculations) metric tons of new tributary-supplied sand and 190,000-380,000 metric tons of new tributary-supplied silt and clay were retained in the Colorado River in Marble Canyon upstream from river-mile 30[1]. Virtually all of this retention of new tributary-supplied sediment occurred after dam releases were decreased to $\leq$280 m^3/s on September 1. No appreciable transport of sand was measured at river-mile 30 after this date, in spite of the fact that the Paria River supplied about 920,000$\pm$180,000 metric tons of sand between September 1, 2004, and the November 2004 controlled flood.

SEDIMENT TRANSPORT DURING THE TWO FLOODS

Substantially more sand, silt, and clay was present in suspension in the 99-km-long reach of the Colorado River in Marble Canyon during the 2004 controlled flood than during the 1996 controlled flood, with the enrichment in sand, silt, and clay during the 2004 controlled flood being greatest in the upstream half of Marble Canyon. Likewise, substantially more silt and clay was present in suspension in the 300-km-long reach of the Colorado River in Grand Canyon during the 2004 controlled flood than during the 1996 controlled flood. During the 2004 controlled flood, however, less sand was present in suspension in this downstream reach than during the 1996 controlled flood.

Suspended silt and clay concentrations measured at all sites during the 2004 controlled flood were substantially higher than those measured during the 1996 controlled flood (Fig. 2). Suspended-sand concentrations measured in Marble Canyon during the 2004 flood were 160-240% higher than those estimated at river-mile 30 during the 1996 flood, and 60-90% higher than those measured at river-mile 61 during the 1996 flood (Fig. 2). This resulted from the lower dam releases between September 1, 2004, and the November 2004 flood retaining much of the silt and clay and almost all of the sand supplied from the Paria River and other tributaries after September 1.

Suspended-sediment data were collected during the early part of the first day of the 2004 flood in a Lagrangian scheme designed to sample the same "parcel" of water as it moved downstream. These data indicate that suspended-sand concentrations increased rapidly from river-mile 0 to 7, and then increased more slowly to river-mile 23 (Fig. 3). This rapid increase in sand concentration indicates that the highest erosion rate occurred in the first 6 river miles below the mouth of the Paria River (at river-mile 1). Thus, at the beginning of the 2004 flood, most of the newly supplied sand from the Paria River was located, not only upstream from river-mile 30, but upstream from river-mile 7. In fact, analysis of multi-beam bathymetric surveys conducted before and after the flood indicates that a large part of this new sand was retained on the bed of the channel upstream from river-mile 3. Downstream from this erosional reach, sand concentrations decreased from river-mile 23 to about river-mile 43, indicating deposition of sand in this reach, presumably in eddies. From river-mile 43 through the downstream end of Marble Canyon at river-mile 62, sand concentrations increased again. Erosion in this second reach of increasing sand concentration likely occurred by erosion of sand stored in eddies because: (1) sediment-transport data collected prior to the flood indicate that little accumulation of new tributary-supplied sand occurred in this reach, and (2) recent work by Hazel et al. (in press) has shown that most of the "background" storage of sand in Marble Canyon occurs in the

[1] River-mile 30 is the location of one of four sediment stations using conventional, pump, laser-diffraction, and acoustic methods to measure sediment transport at a resolution of 15 minutes. Laser-acoustic instrumentation at the 30-mile sediment station, 61-mile sediment station, and above Diamond Creek gaging station are similar to those at Grand Canyon gaging station described in Topping et al. (this volume).

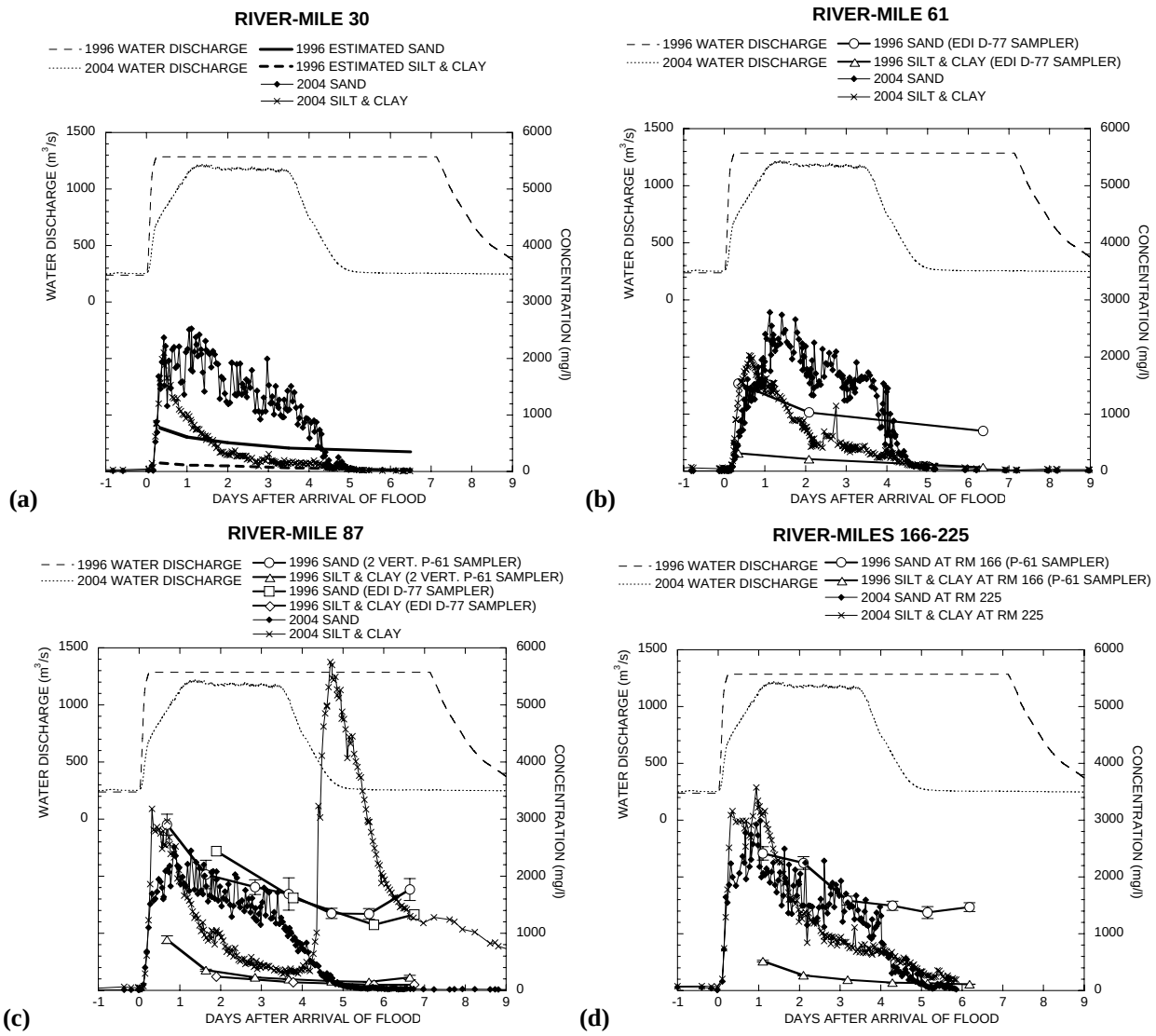


Figure 2 Hydrographs and suspended-sediment concentrations during the 1996 and 2004 controlled-flood experiments at **(a)** river-mile 30, **(b)** river-mile 61 at the lower end of Marble Canyon, **(c)** the Grand Canyon gaging station at river-mile 87 (second peak in silt and clay concentration in 2004 due to Little Colorado River flood during recession of 2004 controlled flood), and **(d)** the National Canyon gaging station (now decommissioned) at river-mile 166 in 1996 and the above Diamond Creek gaging station at river-mile 225 in 2004. Suspended-silt and clay, and suspended-sand concentrations estimated for river-mile 30 in 1996 based on sampling trip conducted in spring 2000 under sediment-depleted conditions similar to those that existed during the 1996 controlled-flood experiment. Under such conditions, silt and clay, and sand concentrations increase approximately linearly in a downstream direction from river-mile 1 to river-mile 61. Thus, 1996 silt and clay, and 1996 sand concentrations at river-mile 30 were estimated to be half of those measured at river-mile 61. Error bars for 1996 P-61 measurements are one standard error.

lower-elevation parts of eddy sandbars. Sand concentrations increased rapidly again downstream from the Little Colorado River presumably by erosion of the ~50,000 metric tons of sand supplied by this tributary between September 1, 2004, and the November 2004 controlled flood. Finally, sand concentrations decreased from river-mile 72 to the Grand Canyon gaging station at river-mile 87, where the Lagrangian sampling effort ended.

Construction of a “mass-balance” sediment budget using sediment-transport data from the tributaries, 30-mile sediment station, 61-mile sediment station, Grand Canyon gaging station (river-mile 87), and above Diamond Creek

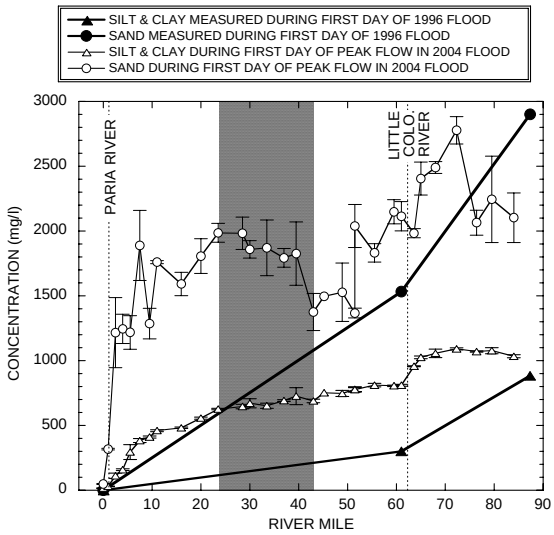


Figure 3 Cross-sectionally averaged suspended-silt and clay, and sand concentrations measured during the Lagrangian sampling program in the 2004 flood compared to cross-sectionally averaged suspended-silt and clay, and sand concentrations measured on the first day of the 1996 flood. Linear interpolation between the sparse 1996 measurements is justified in Fig. 2. Error bars are one standard error. Gray shaded region indicates reach in Marble Canyon that was net depositional with respect to sand early on the first day of the 2004 flood.

gaging station (river-mile 225) indicate that, of the 760,000-1,200,000 metric tons of the new tributary-supplied sand retained in uppermost Marble Canyon prior to the 2004 controlled flood, at least 130,000 metric tons were deposited above river-mile 30 during the 2004 flood (probably in eddy sandbars). In contrast, these data suggest that the change in the mass balance of sand during the 2004 flood was either zero or slightly negative in the downstream half of Marble Canyon and all of Grand Canyon, depending on the level of uncertainty included in the analysis. Therefore, either no change in the amount of sand in background storage or slight erosion of sand from background storage occurred downstream from river-mile 30. The total amount of sand eroded between river-miles 30 and 225 during the 2004 flood, however, was much less than the amount of new tributary-supplied sand deposited upstream from river-mile 30 during the 2004 flood. Thus, the sand budget for the period from July 1, 2004, through the end of the November 2004 flood was positive throughout the entire length of Marble and Grand Canyons.

Suspended-sand concentrations at the Grand Canyon gaging station and above Diamond Creek gaging station were approximately equal throughout the 2004 controlled flood, but about 20-45% lower than measured in this reach at the Grand Canyon gaging station, 122-mile eddy, and the National Canyon gaging station during the 1996 controlled flood (Fig. 2). This difference can be explained only in part by the fact that the peak discharge during the 2004 flood was slightly less than that during the 1996 flood. Thus, unlike the sand-enriched conditions in Marble Canyon, the sand supply in Grand Canyon was less during the 2004 flood than during the 1996 flood. This indicates that more sand was eroded from Grand Canyon between the 1996 and 2004 floods than could be replenished by the 760,000-1,200,000 metric tons of new tributary-supplied sand that were retained in uppermost Marble Canyon between July 1, 2004, and the beginning of the November 2004 controlled flood.

GRAIN-SIZE EVOLUTION ON THE BED AND IN SUSPENSION DURING THE TWO FLOODS

As observed during the 1996 controlled flood, the grain size of the sand on the bed and in suspension coarsened as the upstream supply of sand became depleted during the 60-hours of peak flow during the 2004 controlled flood (Fig. 4). In addition, during both floods, the concentration of silt and clay decreased rapidly over time (Fig. 2). Because the concentration of silt and clay decreased more rapidly than the concentration of sand, the silt and clay content of the total suspended load available to be deposited in eddies decreased over time during both floods. The median grain size of the bed sand at the Grand Canyon gaging station (the only place where bed-sand grain size was measured in 1996) was slightly finer during the 2004 flood than during the 1996 flood, despite the fact that less sand was present in suspension during the 2004 flood at this site. Regardless of whether more or less sand was present in

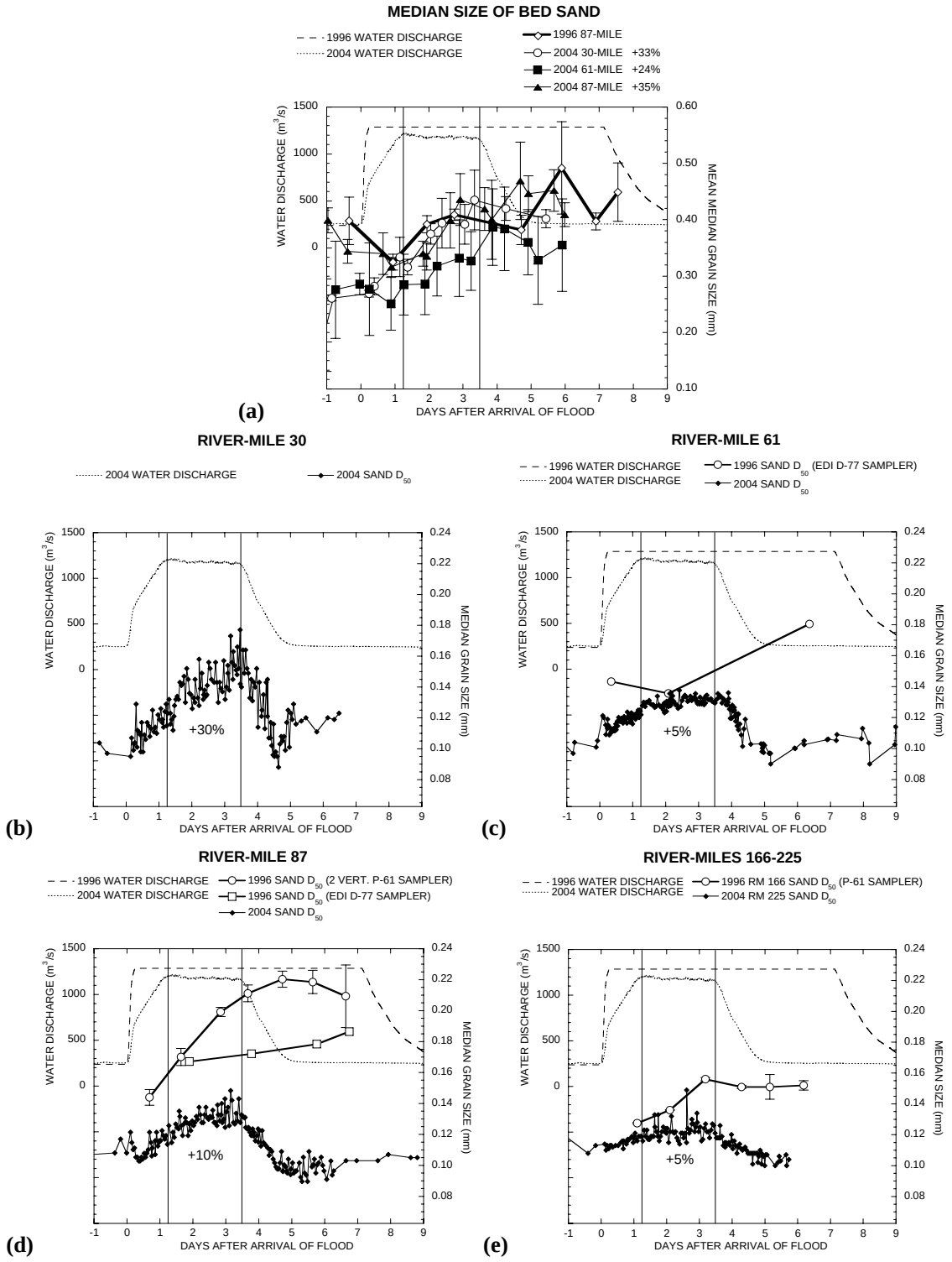


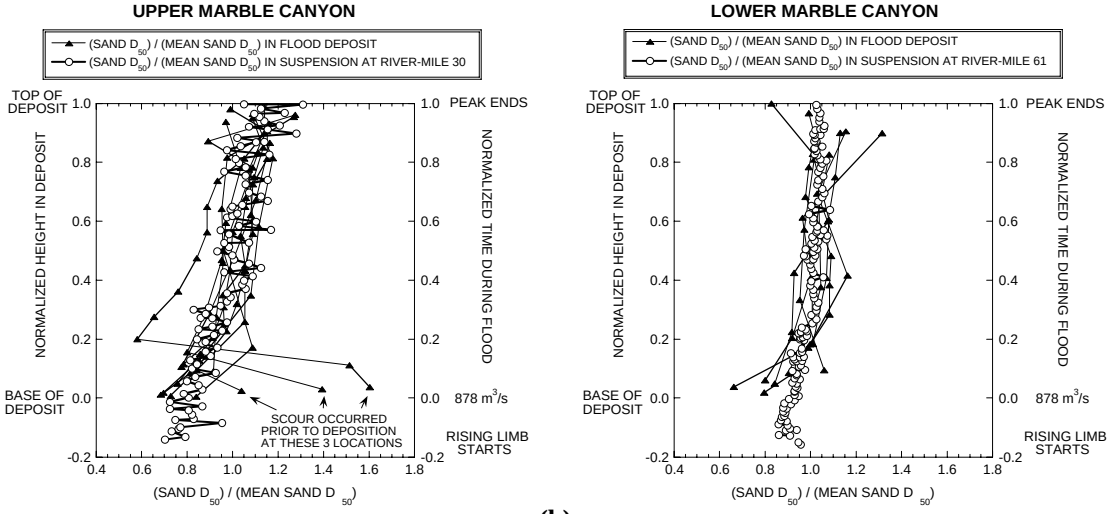
Figure 4 Hydrographs and median grain size (D_{50}) of sand during the 1996 and 2004 floods. Two vertical lines denote duration of peak-flow part of 2004 flood; degree of coarsening during peak-flow part of 2004 flood is indicated for each site in percent. Error bars are one standard error. **(a)** On the bed. **(b)** In suspension at river-mile 30. **(c)** In suspension at river-mile 61. **(d)** In suspension at the Grand Canyon gaging station at river-mile 87. **(e)** In suspension at either the National Canyon gaging station at river-mile 166 (in 1996 flood) or at the above Diamond Creek gaging station at river-mile 225 (in 2004 flood).

suspension, however, the median grain size of the suspended sand (like the bed sand) was finer at all sites where measurements were made during the 2004 flood. At the Grand Canyon and above Diamond Creek gaging stations, this difference (like the lower sand concentrations during the 2004 flood) can be explained only in part by the fact that the peak discharge during the 2004 flood was slightly lower than it was during the 1996 flood. Thus, not only was the supply of sand during the 2004 flood slightly less below about river-mile 75 (Figs. 2 & 3), the supply of sand available to be transported in suspension also was slightly finer than it was during the 1996 flood (Fig. 4).

Although Marble Canyon was enriched with respect to sand during the 2004 flood relative to during the 1996 flood, this enrichment was not sufficient to prevent the occurrence during the 2004 flood of the grain-size-evolution effects of sand-supply limitation observed during the 1996 flood (Rubin et al., 1998; Topping et al., 1999; Topping et al., 2000b). In both floods, the bed winnowed, suspended sand coarsened, and suspended-sand concentration decreased. The greatest amounts of suspended-sand coarsening occurred in the reaches most enriched with respect to finer sand prior to the 2004 flood, i.e., the reaches downstream from the two key sand-supplying tributaries, the Paria River (which enters the Colorado River at river-mile 1) and the Little Colorado River (which enters the Colorado River at river-mile 62). During the peak-flow part of the 2004 flood, the median grain size of the suspended sand coarsened by 30% at river-mile 30 (downstream from the reach most highly enriched in finer sand prior to the flood) and 10% at river-mile 87. The least amount of coarsening of the suspended sand occurred at river-miles 61 and 225, where the median grain size coarsened by only 5% during the peak-flow part of the 2004 flood. These two measurement locations were the farthest downstream from the sand-enriched reaches below the Paria and Little Colorado Rivers.

SEDIMENTOLOGIC AND TOPOGRAPHIC RESPONSE OF EDDY SANDBARS

As during the 1996 flood (Rubin et al., 1998; Topping et al., 2000b, Fig. 8), the eddy deposits produced during the 2004 flood coarsened upward by both a coarsening of the sand (Fig. 5) and a decrease in the silt and clay content. Unlike during the 1996 flood, however, in areas where scour preceded deposition during the 2004 flood, 2-10 cm of clean, horizontally laminated sand (with the same, coarser grain size as the underlying pre-flood bar surface) was



(a) **(b)**

Figure 5 Median grain size of the sand in a deposit (normalized by the mean median grain size of the sand in each deposit) as a function of normalized height within a deposit, and the median grain size of the sand in suspension (normalized by the mean median grain size of the sand in suspension during the flood) as a function of normalized time (0 = time at which the flood rises above 878 m^3/s and bars are mostly inundated, 1 = time of end of peak flow): **(a)** in deposits between river-miles 21 and 31 and in suspension at river-mile 30, **(b)** in deposits between river-miles 43 and 60 and in suspension at river-mile 61.

sometimes deposited prior to the coarsening-upward part of the deposit. The deposits produced during both floods tracked the coarsening of the suspended sediment through time (Topping et al., 2000b, Fig. 8; Fig. 5). In the ten deposits sampled between river-miles 21 and 31, after the first arrival of the silt and clay, the median grain size of the sand coarsened upward on average by 46%, and the silt and clay content decreased on average by about 93%. At river-mile 30, the median grain size of the suspended sand coarsened by 50% and the silt and clay content of the

suspended load decreased by 85% during the rising-limb and peak-flow part of the flood. In the eight deposits sampled between river-miles 43 and 60, the median grain size of the sand coarsened upward on average by 20%, and the silt and clay content decreased on average by about 87%. At river-mile 61, the median grain size of the suspended sand coarsened by 18% and the silt and clay content of the suspended load decreased by 79% during the rising-limb and peak-flow part of the flood. Because more silt and clay was present in suspension during the 2004 flood, more silt and clay was present in the 2004 deposits (16%) than in the 1996 deposits (~5%) in Marble Canyon.

In the upstream half of Marble Canyon (the reach with the greatest degree of sand enrichment relative to the 1996 flood), sandbars produced during the 2004 flood were much larger in total area and volume than those produced during the 1996 flood. The topographic response of eddy sandbars in this reach during the 2004 flood correlates well with: (1) the observed spatial pattern in suspended-sand concentration during the Lagrangian sampling trip showing net deposition of sand between river-miles 23 and 43, and (2) the sediment budget showing post-flood retention of at least 130,000 metric tons of the new tributary-supplied sand upstream from river-mile 30. Half of the sandbars surveyed in this reach were substantially larger in both area and volume above the stage associated with 227 m^3/s (i.e., base flow for daytime dam operations) than they were immediately following the 1996 flood. In addition, analysis of combined multi-beam bathymetric, ground-based, and airborne LiDAR surveys indicates that, during the 2004 flood, the eddy sandbars between river-miles 21 and 32 increased in total area and volume. In contrast, during the 1996 flood, eddy sandbars increased in area and volume only at higher elevations, with larger amounts of erosion of the lower-elevation parts of the bars (Hazel et al., 1999; Schmidt, 1999). Thus, eddy sandbars in Marble Canyon decreased in total area and volume during the 1996 flood.

In contrast to the results in the upstream half of Marble Canyon, only 18% of the sandbars surveyed in the downstream half of Marble Canyon and the upstream part of Grand Canyon (above river-mile 87) were larger in both area and volume above the stage associated with 227 m^3/s immediately following the 2004 flood than they were immediately following the 1996 flood. Furthermore, analysis of combined multi-beam bathymetric, ground-based, and airborne LiDAR surveys indicates that the total area and volume of eddy sandbars downstream from river mile 42 generally decreased during the 2004 flood. The topographic response of the eddy sandbars during the 2004 flood in this reach also correlates well with: (1) the observed spatial pattern in suspended-sand concentration during the Lagrangian sampling trip showing general erosion of sand downstream from river-mile 43, and (2) the sediment budgets showing no change or slightly negative change in the reaches downstream from river-mile 30.

CONCLUSIONS

Results from the 2004 controlled-flood experiment indicate that substantial increases in total eddy-sandbar area and volume in the Colorado River in Marble and Grand Canyons are possible only during controlled floods conducted under the sediment-enriched conditions that follow large tributary floods. Results from the 1996 controlled-flood experiment indicate that, during sediment-depleted conditions, sand deposited at higher elevations in downstream eddy sandbars is derived from the lower-elevation parts of upstream sandbars. Thus, controlled floods conducted under these conditions result in decreases in total eddy-sandbar area and volume (especially in Marble Canyon). Analysis of surveys conducted one to four times per year during the 1990s indicates that sandbars in Marble Canyon and the upstream part of Grand Canyon contained ~25% less sand at lower elevations in 2000 than in 1991, and that the lower-elevation parts of these sandbars and the adjacent channel bed never fully recovered in sand volume after scouring during the 1996 flood (Schmidt et al., 2004). Thus, controlled floods conducted under sediment-depleted conditions, such as those that existed in 1996, cannot be used to sustain sandbar area and volume. Under the lower dam releases that preceded the 2004 flood, most of the new tributary-supplied sand was retained in the uppermost part of Marble Canyon. During the 2004 flood, this sand was eroded from the channel bed and transported downstream, with a fraction transferred into eddies. This resulted in a net increase in the total area and volume of eddy sandbars in the upstream half of Marble Canyon. In addition, about half of the sandbars surveyed in this reach following the 2004 flood were substantially larger at higher elevations than they were following the 1996 flood. Downstream reaches were not as enriched with new tributary-supplied sand, however. During the 2004 flood, sand concentrations in Grand Canyon were lower than they were during the 1996 flood. The total area and volume of eddy sandbars downstream from about river-mile 42 generally decreased during the 2004 flood. Only 18% of the sandbars surveyed following the 2004 flood between river-miles 42 and 87 were larger at higher elevations than they were following the 1996 flood. Therefore, the amount of new sand in retention prior to the 2004 controlled flood was sufficient to result in substantial increases in sandbar area and volume in only the first 50 km of the 400-km long reach of the Colorado River in Marble and Grand Canyons. Only a relatively small amount of the new

tributary-supplied sand in retention prior to the flood was deposited in the upstream half of Marble Canyon during the 2004 flood, resulting in the observed increases in total eddy-sandbar area and volume in this reach. Lengthening the hydrograph of a future controlled flood with a similar amount of sand as the 2004 flood, thus, would likely drive the sediment budget in the upstream half of Marble Canyon negative, resulting in either no change or a decrease in total eddy-sandbar area and volume. Therefore, in future controlled floods, more sand is required to achieve increases in the total area and volume of eddy sandbars throughout all of Marble and Grand Canyons. Annual tributary inputs of sand much larger than one million metric tons occur, but are relatively rare. Therefore, "more sand" could be achieved directly by augmentation from sand trapped in the reservoir impounded by Glen Canyon Dam or perhaps indirectly by following each large tributary input of sand with short-duration controlled floods. Frequent short-duration controlled floods under sand-enriched conditions could result in the downstream propagation (into the downstream half of Marble Canyon and into Grand Canyon) of the gains in total eddy-sandbar area and volume observed in the upstream half of Marble Canyon during the 2004 controlled-flood experiment.

REFERENCES

Hazel, J.E., Jr., Kaplinski, M., Parnell, R., Manone, M., and Dale, A., 1999, "Topographic and bathymetric changes at thirty-three long-term study sites," in Webb, R.H., Schmidt, J.C., Marzolf, G.R., and Valdez, R.A., eds., The 1996 controlled flood in Grand Canyon. Washington, D.C., American Geophysical Union, Geophysical Monograph 110,, p 161-184.

Hazel, J.E., Jr., Topping, D.J., Schmidt, J.C., and Kaplinski, M., in press, "Influence of a dam on fine-sediment storage in a canyon river," Journal of Geophysical Research-Earth Surface.

Rubin, D.M., Nelson, J.M., and Topping, D.J., 1998, "Relation of inversely graded deposits to suspended-sediment grain-size evolution during the 1996 Flood Experiment in Grand Canyon," Geology, v. 26, p. 99-102.

Rubin, D.M., Topping, D.J., Schmidt, J.C., Hazel, J., Kaplinski, K., and Melis, T.S., 2002, "Recent sediment studies refute Glen Canyon Dam hypothesis," EOS, Trans., American Geophysical Union, v. 83, n. 25, p. 273, 277-278.

Schmidt, J.C., 1999, "Summary and synthesis of geomorphoric studies conducted during the 1996 controlled flood in Grand Canyon," in Webb, R.H., Schmidt, J.C., Marzolf, G.R., and Valdez, R.A., eds., The 1996 controlled flood in Grand Canyon. Washington, D.C., American Geophysical Union, Geophysical Monograph 110, p. 329-342.

Schmidt, J.C., Topping, D.J., Grams, P.E., and Hazel, J.E., Jr., 2004, System-wide changes in the distribution of fine sediment in the Colorado River corridor between Glen Canyon Dam and Bright Angel Creek, Arizona: Final report submitted to the U.S. Geological Survey Grand Canyon Monitoring and Research Center, Flagstaff, AZ.

Topping, D.J., Rubin, D.M., Nelson, J.M., Kinzel, P.J., III, and Bennett, J.P., 1999, "Linkage between grain-size evolution and sediment depletion during Colorado River floods," in Webb, R.H., Schmidt, J.C., Marzolf, G.R., and Valdez, R.A., eds., The 1996 controlled flood in Grand Canyon. Washington, D.C., American Geophysical Union, Geophysical Monograph 110, p. 71-98.

Topping, D.J., Rubin, D.M., and Vierra, Jr., L.E., 2000a, "Colorado River sediment transport 1. Natural sediment supply limitation and the influence of Glen Canyon Dam," Water Resources Research, v. 36, p.515-542.

Topping, D.J., Rubin, D.M., Nelson, J.M., Kinzel, III, P.J., and Corson, I.C., 2000b, C"olorado River sediment transport 2. Systematic bed-elevation and grain-size effects of sand supply limitation," Water Resources Research, v. 36, p. 543-570.

Topping, D.J., J.C. Schmidt, and L.E. Vierra, Jr., 2003, Computation and Analysis of the Instantaneous-Discharge Record for the Colorado River at Lees Ferry, Arizona -- May 8, 1921, through September 30, 2000. U.S. Geological Survey Professional Paper 1677, 118 p.

Topping, D.J., Rubin, D.M., and Schmidt, J.C., 2005, "Regulation of sand transport in the Colorado River by changes in the surface grain size of eddy sandbars over multi-year timescales," Sedimentology, v. 52, p. 1133-1153.

Topping, D.J. Wright, S.A., Melis, T.S., and Rubin, D.M., this volume, "High-resolution monitoring of suspended-sediment concentration and grain size in the Colorado River using laser-diffraction instruments and a three-frequency acoustic system," Proceedings of the 8th Interagency Sedimentation Conference.

Webb, R.H., Schmidt, J.C., Marzolf, G.R., and Valdez, R.A., eds., 1999, The 1996 controlled flood in Grand Canyon. Washington, D.C., American Geophysical Union, Geophysical Monograph 110, 367 p.

Wright, S.A., Melis, T.S., Topping, D.J., and Rubin, D.M., 2005, "Influence of Glen Canyon Dam operations on downstream sand resources of the Colorado River in Grand Canyon," in Gloss, S.P., Lovich, J.E., and Melis,

T.S., eds., The state of the Colorado River ecosystem in Grand Canyon: U.S. Geological Survey Circular 1282, p. 17-31.

STREAM BANK STABILITY ASSESSMENT IN GRAZED RIPARIAN AREAS

Mark S. Riedel, PhD, Baird & Associates, Madison, WI, mriedel@baird.com; Kenneth N. Brooks, PhD, U. of MN, Forest Resources, St. Paul, MN, kbrooks@umn.edu; Elon S. Verry, PhD, Ellen River Partners, Grand Rapids, MN,sverry@mchsi.com

Abstract: Streams in the Nemadji River Watershed of east-central Minnesota are deeply incised in lacustrine clay and glacial till. This region is naturally erosive because of recent glacial activity (~10,000 years ago). Indeed, the Nemadji River is the largest source of fluvial sediments to Lake Superior. While natural land cover was predominantly coniferous forest, riparian areas were commonly converted to pasture by the late 1800's. We investigated stream bank stability under a variety of riparian cattle traffic scenarios to determine the impacts of cattle traffic on stream bank stability over a 3-year period. Grazing significantly reduced stream bank stability. In response, grazed streams adopted "stable" stream bank geometry. While root tensile strength of riparian species dominated resisting forces, the cohesive strength of the lacustrine clay channels was generally sufficient to maintain stable channel geometry in ungrazed streams. The "Pfankuch" method of rating stream bank stability in the field was very consistent with mechanistic estimates and measured values of stream bank stability.

INTRODUCTION

Streams in the Nemadji River Watershed of east central Minnesota and northwestern Wisconsin cut into glacially derived cohesive, lacustrine clay and clay till (Figure 1). This is important

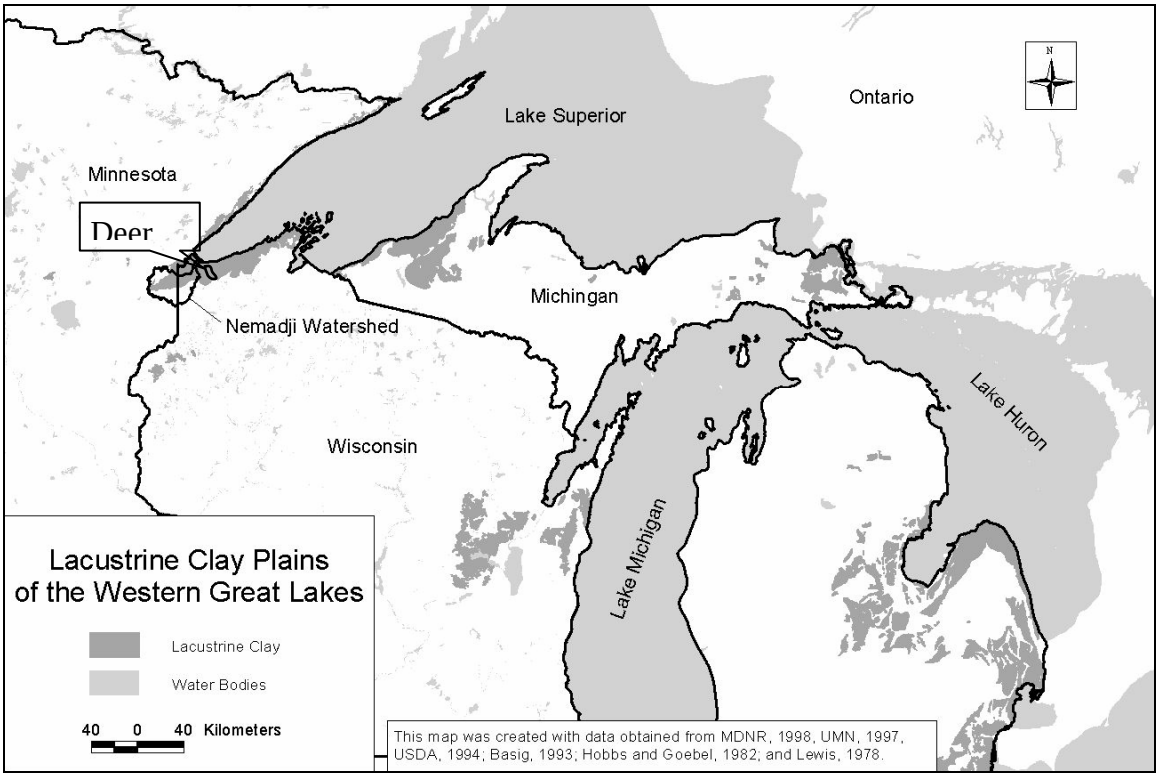


Figure 1 Location of Nemadji Watershed and Lacustrine Clay deposits.

because clay increases the strength and stability of streams (Schumm, 1960). Smith (1998) and Grissinger, et al (1981) found channels in flumes shifted to stable meandering forms when cohesive clays were present. Grissinger, et al observed erosion decreased 50% as clay content increased by 33%. Similarly, Dunaway, et al, (1994) reported bank erosion rates decreased as clay to silt ratios increased and noted root density limited bank erosion. Riparian land use conversion often reduces the stability of "natural" gravel and sand bed streams (Abernethy and Rutherford, 2000; Millar, 2000; Hupp, 1999; Hupp, 1992; and Charlton, et al., 1978) and causes morphologic response (Osman and Thorne, 1998 and Huang and Nanson, 1998). In-situ influences of streamside land use on stability and morphology in cohesive clay channel streams is largely undocumented. We observed morphology and stability on a cohesive clay channel stream experiencing cattle disturbance over three consecutive summers.

Site Description: Three study reaches were installed on Deer Creek (Figure 2). The upstream Reach I (50 m long, 4 cross sections, 3.47 km^2 watershed), separated a barn and adjacent 16 ha pasture. The stream experienced frequent traffic (many times/day) from 40 beef cattle and 25 sheep. Most native cover was gone and streambanks were 20% vegetated with perennial grasses and herbs. Flood plain vegetation consisted of herbaceous plants and perennial grasses, and a 30 % deciduous tree canopy dominated by quaking aspen (*Populus tremuloides*), black ash (*Fraxinus nigra*) and paper birch (*Betula papyrifera*) with diameters ranging from 20 – 50 cm at breast height (dbh).

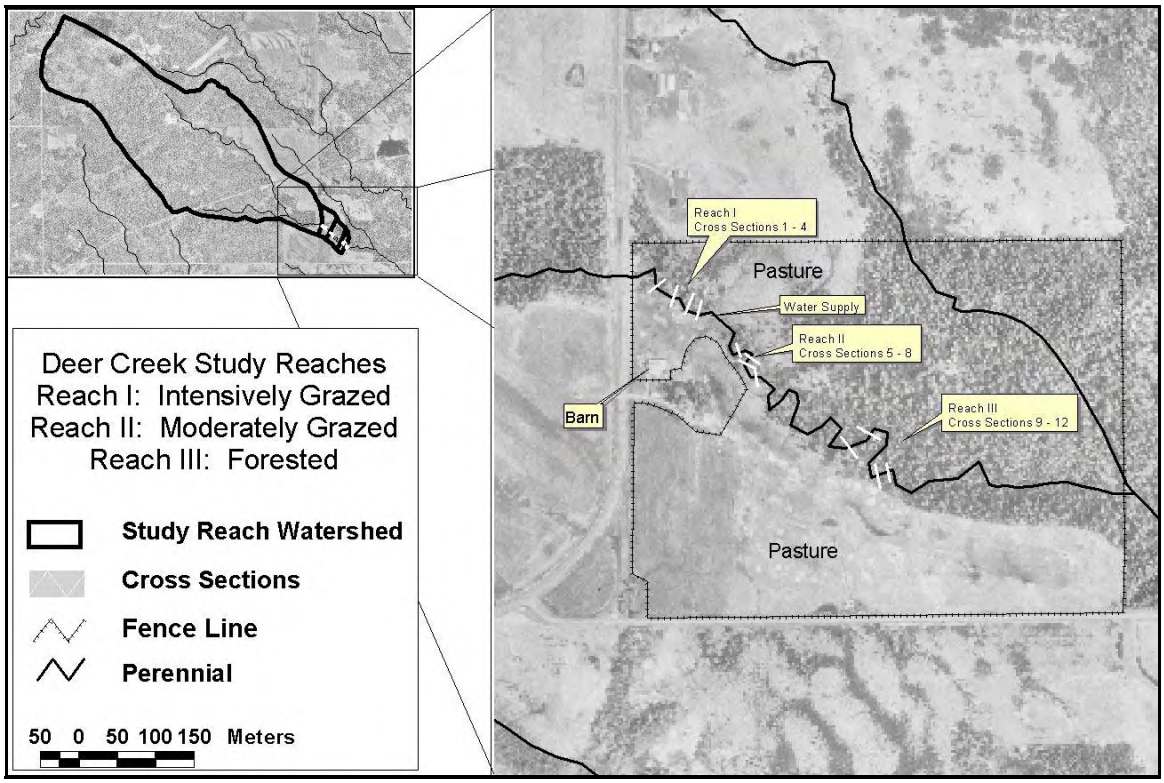


Figure 2 Location of Deer Creek study reaches.

Downstream, Reach II (75 m long, 4 cross sections, 3.52 km^2 watershed) flowed through a forested pasture. Native vegetation was largely absent, cattle access infrequent (few times/day),

and ground cover well established. Stream banks were 40% covered with grasses and shrubs. Forest canopy of aspen, black ash, white pine (*Pinus strobus*), birch, jack pine (*Pinus banksiana*) and balsam fir (*Abies balsamea*) covered 80% of the floodplain (trees from30 to 70 cm dbh).

Reach III (150 m long, 4 cross sections, 3.58 km^2 watershed) was another half kilometer downstream. The flood plain and valley forest had 100% canopy closure by aspen, balsam fir, birch, black ash, white pine, and white spruce (*Picea glauca*). Herbaceous vegetation, hazel (*Alnus serrulata*), and balsam fir covered more than 60% of the stream banks. There was no cattle traffic and stream morphology was similar to natural reference streams with watersheds that were completely forested for at least 70 years (Riedel, et al, 2005 and Riedel, et al, 2002).

METHODS

We analyzed stability for stream banks and beds using two methods:
1. Pfankuch's (1975) empirically based stream bank stability index (PSI);
2. Mechanistically based estimates.

PSI Rating: The PSI for each reach was determined according to the methods of Pfankuch (1975). Stream bank characteristics include bankfull channel capacity, bank rock content, channel obstructions, channel incision, and channel aggradation. Channel substrate was rated by rock angularity, rock brightness, degree of substrate armoring, substrate grain size distribution, occurrence of localized scour and deposition, and the existence and vigor of aquatic vegetation.

Mechanistic Stream Stability Analysis: We estimated mechanistic stability by comparing shear strength (resisting) and shear stress (driving) forces as the factor of safety (FSh):

$$FSh = S / H*(\gamma t) \quad (1)$$

where S = Shear strength (kPa), H = bank height (m), γt = saturated weight of soil (kN/m^3).

Stream Banks: We adapted the Mohr-Coulomb equation to include soil cohesive strength (adapted from Millar and Quick 1998) and the contribution of root tensile strength;

$$S = (Ns)cu + \sigma * \tan(\phi) + Cr \quad (2)$$

where
Ns = saturated dimensionless stability (Huang, 1983) = $3.83 + 0.052 (90 - \theta) - 0.0001 (90 - \theta)^2$ (Taylor, 1948);
cu = Soil cohesive strength (kPa) = 1.93 + 0.1444(PI) (lbs/ft^2, Cousins, 1984),
PI = Plastic Index = plastic limit – liquefaction limit
σ = Bank shear strength (kPa),
ϕ = Internal friction angle = angle of repose for stable banks,
Cr = root cohesion (kPa) (Gray and Megahan, 1981) = $tr * (\cos(\theta) * \tan(\phi) + \sin(\theta))$ (Wu, 1976),
tr = root tensile strength per unit area (kPa m^{-2}) and θ = angle of root shear distortion.

Taylor's (1948) method to estimate Ns has been tested for stream bank applications (Millar and Quick, 1998). Undrained cohesive strength was estimated from PI, plasticity and liquefaction data (Mengel and Brown, 1979 and Lewis, 1978). Estimates of soil cohesion were consistent with published values (Huang, 1983 and Bjerrum and Simons, 1960). We computed shear

strength under saturated conditions, the $\phi = 0$ approach (Huang, 1983), to remove the dependence on soil moisture content and pore water pressure ($\sigma \tan(\phi) =$ zero) (Spangler and Handy, 1982 and Peck and Lowe, 1960). Such conditions often preclude bank failure and occur following bankfull or larger flows (Alabyan and Chalov, 1998; Hickin, 1995; Leopold, et al., 1992; and Chang, 1979).

We estimated tr by Wu's (1976) "theoretical model of a fiber-reinforced soil" which accounts for lateral and normal force components (Hammond, et al, 1992). This approach is valid when roots shear rather than slip and is applicable in cohesive soils (Abe and Ziemer, 1991 and Megahan, et al 1978). We obtained root mass and tensile strength data from a field study of 40+ sites in the Nemadji Watershed (Kaputska and Davidson, 1979). Root distributions were limited to 0.5 m depth by the cohesive clay soils. Roots greater than 8 mm in diameter were not tested so we assigned these tensile strengths equivalent to those in the 8 mm size class.

Stream Beds: Bankfull average bed shear stress was estimated as;

$$\tau \text{ bed} = \gamma * R * S \qquad (3)$$

where
γ = Specific weight of water (kg/m^3),
R = Bankfull hydraulic radius (m) = Ax / Wp, Ax = channel area (m^2), Wp = wetted perimeter (m),
S = Bankfull water surface slope (m/m),

Estimates were consistent with those from dimensionless values (ASCE, 1998; Ritter, et al., 1995; and Schumm, 1960). Shear stress distribution between the stream bed and banks was estimated with the empirical relationship of shear stress distribution in trapezoidal channels developed by Knight, et al (1984) and Flintham and Carling (1988):

$$SFbank = 1.77 * (Pbed / Pbank + 1.5)^{\wedge(-1.4)} \qquad (4)$$

where
SFbank = Proportion of total shear stress acting on channel banks;
Pbed, Pbank = Wetted perimeter of stream bed and banks, respectively (m).

Critical shear stress for the cohesive clay was estimated by two methods: 1. by sodium adsorption ratio (SAR), pore fluid salt concentrations, and conductivity (Arulanandan, et al, 1980). These data were obtained from the red clay study of Bahnick, et al, (1979); 2. Chow's unit tractive force relationships for cohesive soils (Chow, 1959). Estimated values were 3.61 Pa, and 4.79 Pa, respectively; we used the geometric mean, 4.16 Pa. Stream bank stability with respect to fluvial erosion was estimated as the factor of safety with respect to bank shear, FSτ.

$$FS\tau = \tau \text{ crit} / \tau \text{ bed} \qquad (5)$$

where
τ crit = shield's critical shear stress for bank sediments (kPa),
τ bed = mean bed fluvial shear stress (kPa).

RESULTS

Width-depth ratios were largest and stability lowest on grazed reaches (Figure 3).

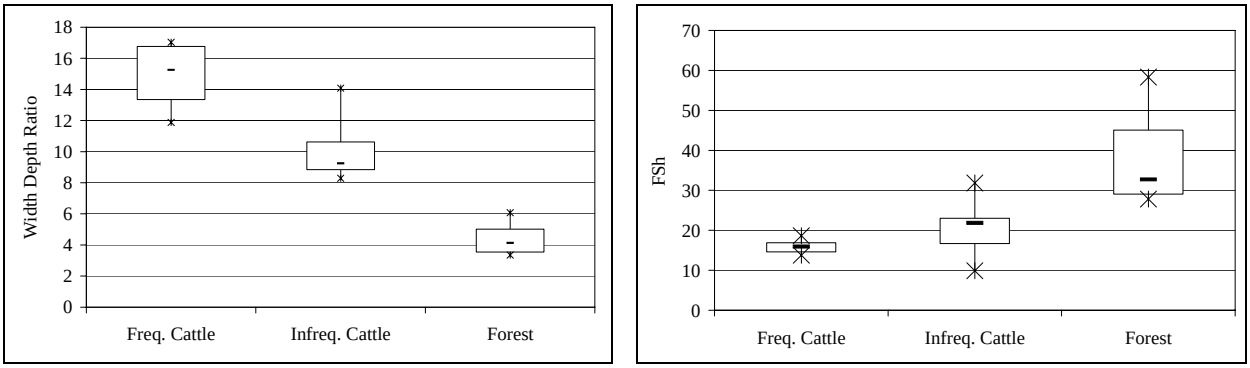


Figure 3 Stem and whisker plots of width depth ratios and mechanistic stream bank stability by reach (n=16/reach) (adapted from Riedel, et al, in review).

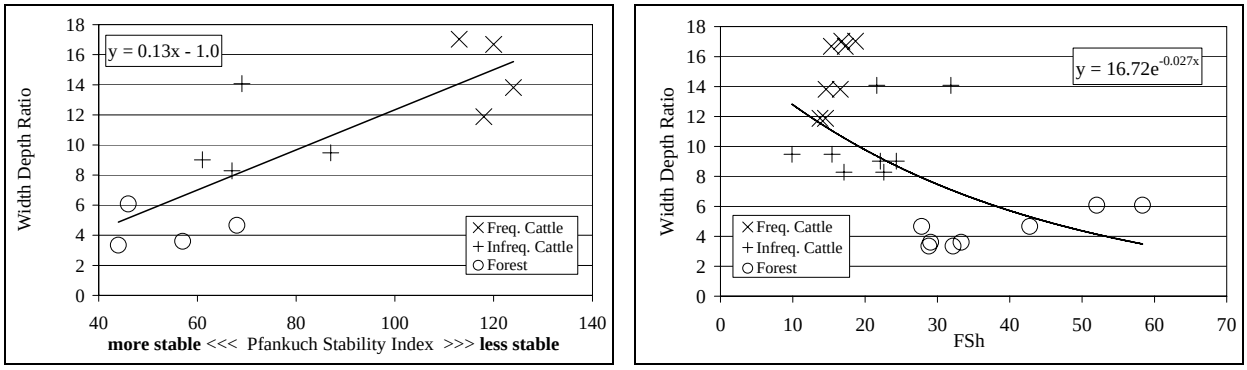


Figure 4 Scatter plots of width depth ratio by PSI and FSh. Note - PSI is inversely related to stability. Upstream / Downstream (dependence) arrangement of sites precludes regression and correlation analyses.

The width-depth ratio of streams increased with PSI (decreasing stability) in the study reaches (Figure 4). Width-depth increased as FSh decreased from forest to cattle sites (Figure 4). While stream banks were fluvially stable, stream beds were generally not stable (Figure 5). Bed stability was near the threshold at the frequent cattle site and declined slightly to the forest site.

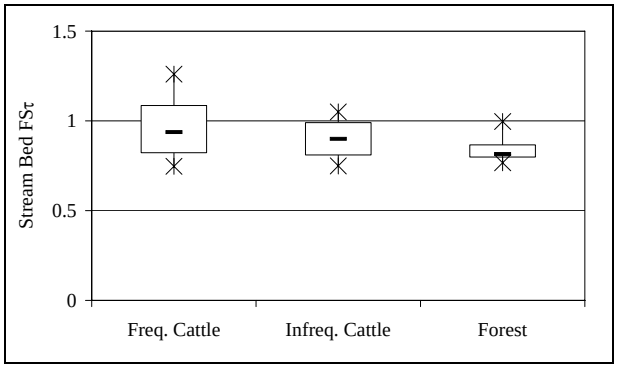


Figure 5 FSτ of stream beds for each reach (n=16/reach)

PSI was inversely correlated to FSh (Figure 6) but independent of stream bed and bank FSτ.

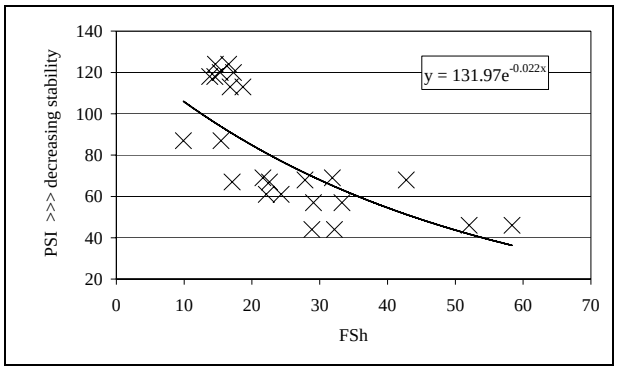


Figure 6 Pfankuch Stability Index (PSI) as related to calculated FSh There are 2 FSh values per reach. Upstream / Downstream (dependence) arrangement of sites precludes regression and correlation analyses.

DISCUSSION

Mechanisms which alter the riparian land use condition have consistently been found to reduce the stability of the stream banks and induce erosion. Platts (1981) noted that stream banks had eroded, channels widened, and mean depth decreased in response to disturbance by sheep. Hupp and Simon (1986) attributed stream widening to reduced bank stability caused by vegetation removal and channelization. Millar and Quick (1998) found that riparian vegetation increased the critical bank shear stress of natural streams and allowed them to be narrower and have steeper bank angles. Burckhardt and Todd (1998) reported riparian forests stabilized the outside bank of meandering streams - unvegetated banks eroded three times faster. Numerous authors have found that the width-depth ratio of a stream increases in response to decreased bank stability. Schumm (1960) documented the tendency of normally narrow clay channel streams to widen in response to destabilization such as changes in stream bank vegetation. On Deer Creek, the width-depth ratio increased as bank stability decreased with cattle traffic. The width-depth ratios in the grazed riparian areas is controlled by frequency of cattle traffic because the cohesive banks have sufficient strength to resist gravitational failure. Conversely, the width-depth ratios of the forested stream reaches are dependent upon the factors of safety with respect to stream bank and streambed shear.

CONCLUSIONS

Width-depth ratio of the study reaches were strongly related to both the Pfankuch (1976) and mechanistically estimated measures of streambank stability. Hoof shear from cattle traffic had the largest impact on stream bank stability because even with the loss of riparian vegetation, FSh was normally not exceeded. The FSτ indicated that the stream bank materials were generally stable from fluvial erosion. It was the factor of safety for fluvial shear, FSτ, of the stream bed materials that was commonly found to be exceeded. Instability of the stream banks only occurred with the removal of riparian vegetation and subsequent bank erosion caused by cattle traffic. The fluvial erosion thresholds for the stream bank materials were exceeded once materials were introduced into the streambed. The stream morphology and subsequent erosion

of stream bank and streambed materials were due to the destabilizing effects of cattle grazing and traffic on the stream banks. Consequently, stabilization of cohesive clay stream banks in this region may be accomplished by simply excluding cattle.

AKNOWLEDGEMENTS

Funding was provided by the US Forest Service, North Central Res. Sta., Grand Rapids, MN and the Univ. of MN, Dept. of Forest Resources, Ag. Exp. Sta., St. Paul, MN. The authors thank Jason Tidwell and Zhou XangQing for their field support. This project was conducted while Dr. Riedel worked at the Univ. of MN, Dept. of Forest Resources, St. Paul, MN and Dr. Verry served as Research Hydrologist, US Forest Service North Central Res. Sta., Grand Rapids, MN.

REFERENCES

Abe, K. and Ziemer, R.R. (1991). "Effect of tree roots on a shear zone: modeling reinforced shear stress," Canadian Journal of Forest Research, 21:1012–1019.

Abernethy, B. and Rutherford, I.D. (2000). "The effect of riparian tree roots on the mass-stability of riverbanks," Earth Surface Process and Landforms, 25:921–93.

Alabyan, A.M. and Chalov, R.S. (1998). "Types of river patterns and their natural controls," Earth Surface Processes and Landforms, 23:467–474.

Arulanandan, K., Gillogley, E., and Tully, R. (1980). Development of a Quantitative Method to Predict Critical Shear Stress and Rate of Erosion of Natural Undisturbed Cohesive Soils, Report GL-80-5, USACOE Waterways Experiment Station, Vicksburg, MS.

ASCE. (1998). "River Width Adjustment.I: Processes and Mechanisms," ASCE Task Comm. on Hydraulics, Bank Mechanics, and Modeling of River Width Adjustment, Journal of Hydraulic Engineering, 124(9):881–902.

ASTM. (1997). "Standard classification of soils for engineering purposes, Annual Book of ASTM Standards, 4.08, Soil and Rock (I): D420–D4914.

Bahnick, D.A., Markee, T.P. and Roubal, R.K. (1979). Chemical Effects of Red Clays on Western Lake Superior. USEPA #EPA-905/9-79-003, January.

Basig, E.J. (1993). "Nemadji River Watershed - Carlton County 1:50,000 Map of Surficial Glacial Geology".

Bjerrum, L. and Simons, N.E. (1960). "Comparison of shear strength characteristics of normally consolidated clays, Proc. The Research Conference on Shear Strength of Cohesive Soils. American Society of Civil Engineers, University of Colorado, Boulder, CO.

Chang, H.H. (1979). "Minimum stream power and river channel patterns," J. Hydrology, 41:303–327.

Charlton, F.G., Brown, P.M., and Benson, R.W. (1978). The Hydraulic Geometry of Some Gravel Rivers in Britain.

Chow, V.T. (1959). Open Channel Hydraulics. McGraw-Hill, New York, NY.

Cousins, F. (1984). Empirical relationships as reported by written communication to Simon and Hupp (1986). USDA Soil Conservation Service.

Downs, P.W. and Thorne, C.R. (2000). "Rehabilitation of a lowland river: reconciling flood defense with habitat diversity and geomorphological sustainability," Journal of Environmental Management, 58:249–268.

Dunaway, D., Swanson, S.R., Wendel, J., and Clary, W. (1994). "The effect of herbaceous plant communities and soil textures on particle erosion of alluvial stream banks," Geomorphology, 9:47–56.

Flintham, T.P. and Caring, P.A. (1988). "The prediction of mean bed and wall boundary shear in uniform and compositely roughened channels," International Conference on River Regime. W.P. White ed. John Wiley & Sons, Inc. England. 367–287.

Gray, D.H. and Megahan, W.F. (1981). Forest Vegetation Removal and Slope Stability in the Idaho Batholith, USDA Forest Service Intermountain Forest and Range Experiment Station Research Paper INT-271.

Grissinger, E.H., Little, W.C., and Murphey, J.B. (1981). "Erodibility of stream bank materials of low cohesion," Transactions of the American Society of Agricultural Engineers, 24(3):624–630.

Hammond, C., Hall, D., Miller, S., and Swetik, P. (1992). "Appendix B – root strength: a detailed literature review," Level I Stability Analysis (LISA) Documentation for Version 2.0. USDA Forest Service Intermountain Research Station Gen. Tech. Report INT-285.

Hickin, E.J. (1995). "Hydraulic geometry and channel scour, Fraser River, British Columbia, Canada," River Geomorphology, Hickin, E.J. (ed), John Wiley & Sons.

Hobbs, H.C. and J.E. Goebel. (1982). "Geologic Map of Minnesota: Quaternary Geology," Minnesota Geological Survey State Map Series Map S-1. Minnesota Geological Survey.

Huang, H.Q. and Nanson, G.C. (1998). "The influence of bank strength on channel geometry: an integrated analysis of some observations," Earth Surface Process and Landforms, 23:865–876.

Huang, Y.R. (1983). "Shear strength," Stability Analysis of Earth Slopes, Reinhold Publishing, NY, NY.

Hupp, C.R. (1999). "Relations among riparian vegetation, channel incision processes and forms, and large woody debris," Incised River Channels, Processes, Forms, Engineering and Management, Darby, S.E. and Simon, A. (eds.), John Wiley & Sons.

Hupp, C.R. (1992). "Riparian vegetation recovery patterns following stream channelization: a geomorphic perspective," Ecology, 73(4):1209–1226.

Kaputska, L.A., and Davidson, D.W. (1979). "Role of plant roots in red clay erosion," Impact of Nonpoint Pollution Control on Western Lake Superior, Red Clay Project Final Report Part II. U. S. Environmental Protection Agency Report, EPA 905/9-76-002-B.

Knight, D.W., Demetrious, J.D., and Hamed, M.E. (1984). "Boundary shear in smooth rectangular channels," Journal of Hydraulics, 110(4):405–422.

Leopold, L.B., Wolman, M.G., and Miller, J.P. (1992). Fluvial Processes in Geomorphology.

Lewis, R.R. (1978). "Soil Survey of Carlton County, Minnesota," USDA and MN Agricultural Experiment Station.

MDNR. (1998). "Quaternary Geology of Michigan," Michigan Dept. of Natural Resources. Lansing, MI. 2nd ed.

Megahan, W.F., Day, N.F., and Bliss, T.M. (1978). "Landslide occurrence in the western and central northern Rocky Mountain physiographic province in Idaho," 5th Annual North American Forest Soils Conference, Colorado State Univeristy, Fort Collins, CO. 1116 – 139.

Mengel, J.T. and Brown, B.E. (1979). "Red clay slope stability factors," Impact of Nonpoint Pollution Control on Western Lake Superior, Red Clay Project Final Report Part II, U. S. Environmental Protection Agency Report, EPA 905/9-76-002-B.

Millar, R.G. (2000). "Influence of bank vegetation on alluvial channel patterns," Water Resources Research, 36(4):1109–1118.

Millar, R.G. and Quick, M.C. (1998). "Stable width and depth of gravel-bed rivers with cohesive banks," Journal Hydraulic Engineering, 124(10):1005–1013.

Millar, R.G. and Quick, M.C. (1993). "Effect of bank stability on geometry of gravel rivers," Journal Hydraulic Engineering, 119(12):1343–1363.

Osman, A.M. and Thorne, C.R. (1998). "Riverbank stability analysis. I: theory," Journal of Hydraulic Engineering, 114(2):134–150.

Peck, R.B. and Lowe, J., III. (1960). "Moderator's report - session 4: shear strength of undisturbed cohesive soils," The Research Conference on Shear Strength of Cohesive Soils. American Society of Civil Engineers, June, 1960, University of Colorado, Boulder, CO.

Pfankuch, D.J. (1975). Stream Reach Inventory and Channel Stability Evaluation: A Watershed Management Procedure, USFS general technical report R1-75-002, USDA Forest Service, Northern Region.

Platts, W.S. (1981). Effects of Sheep Grazing on a Riparian-Stream Environment, USDA Forest Service Research Note INT307.

Rhoads, B.L. and Welford, M.R. (1991). "Initiation of river meandering – instability and meander initiation," Progress in Physical Geography, 15(2)127–156.

Riedel, M.S., Verry, E.S., and Brooks, K.N. In Review. Riparian land use impacts on fluvial processes and the morphology of clay channel streams. J. Int. Assoc. of Great Lakes Research.

Riedel, M.S., Brooks, K.N. and Verry, E.S. (2005). "Impacts of land use conversion on bankfull discharge and mass wasting," Journal of Environmental Management, 76(2005)326–337.

Riedel, M.S., Verry, E.S. and Brooks, K.N. (2002). "Land use impacts on fluvial processes in the Nemadji River watershed." Hydrologic Science and Technology, 18(1-4):197-205.

Ritter, D.F., Kochel, R.C., and Miller, J.R. (1995). "Fluvial processes," in Process Geomorphology, 3rd edition, chpt. 6, Wm. C. Brown Publishers, Dubuque, IA.

Schumm, S.A. (1960). The Shape of Alluvial Rivers in Relation to Sediment Type, USGS Prof. Paper 352 – B.

Shields, F.D., Knight, S.S., and Cooper, C.M. (2000). "Cyclic perturbation of lowland river channels and ecological response," Regulated Rivers: Reservoir Management, 16:307–325.

Simon, A. and Hupp, C.R. (1986). Channel Widening Characteristics and Bank Slope Development Along a Reach of Cane Creek, West Tennessee, USGS Water Supply Paper 2290.

Smith, C.H. (1998). "Modeling high sinuosity meanders in a small flume," Geomorphology, 25:19–30.

Spangler, M.G. and Handy, R.L. (1982). Soil Engineering. 4th ed. Harper and Row Publishing, Inc., NY.

Taylor, D.W. (1948). Fundamentals of Soil Mechanics, John Wiley and Sons, Inc., NY, NY.

Trimble, S.W. (1994). "Erosional effects of cattle on stream banks in Tennessee, U.S.A.," Earth Surface Processes and Landforms, 19:451–464.

UMN. (1997). "Geomorphology of Minnesota," Univ. of MN-Duluth, MN Geo. Surv., and MN Dept. of Nat. Res.

USDA. (1994). State Soil Geographic (STATSGO) data for Wisconsin. USDA, Fort Worth, TX.

Wu, T.U. (1976). Investigation of Landslides on Prince of Wales Island, Alaska, Geotechnical Report No. 5, Dept. of Civil Engineering, Ohio State University, Columbus, OH.

Ziemer, R.R. (1978). "An apparatus to measure the crosscut shearing strength of roots," Canadian Journal of Forest Research, 8:–144.

GEOMORPHIC RESPONSE TO A DAM FAILURE IN THE DEAD RIVER WATERSHED, MICHIGAN: INTEGRATION OF EMPIRICAL AND ANALYTICAL TECHNIQUES IN A GIS FRAMEWORK

Alex Brunton, Geoscientist; W.F. Baird & Associates, Oakville, ON, abrunton@baird.com; Rob Nairn, Principal, W.F. Baird & Associates, Oakville, ON, rnairn@baird.com; Jim Selegean, Hydraulic Engineer, U.S. Army Corps of Engineers - Detroit District, James.P.Selegean@lre02.usace.army.mil

Abstract: The Dead River in the upper peninsula of Michigan was subject to a large flood resulting from a reservoir fuse plug failure in May 2003. Approximately one million cubic meters of sediment was mobilized during the flood event, which was equivalent to a 500-year precipitation-driven flow event. Extensive redistribution of alluvial and bedrock material took place during the event as the river channel realigned, widened and deepened in response to the extreme flow. In places, material deposited on the floodplain in the middle reaches of the river exceeded 2 meters in depth. Processes of channel readjustment in response to the flood morphological adjustment, including bank erosion, avulsion and braiding are ongoing, and present significant challenges to channel and watershed sediment management. Removal of the storage basin (the dam has not been rebuilt) in the headwaters of the watershed has led to a flashier river regime in the upper reaches of the river system, upstream from the next major storage basin, which presents an additional challenge to assessing channel stability.

Several empirical and analytical techniques were applied in order to gain an understanding of the nature of river adjustment in the system, and to aid in producing a suite of watershed sediment management tools as part of the USACE 516e Great Lakes Tributary Modeling Program. A walking survey of the entire river system was undertaken to collect detailed, post-event geomorphic baseline data, including channel morphology, substrate, in-channel features such as bars, pools and riffles and the location, extent, and mechanisms of contemporary bank erosion. This information was combined in a geodatabase with hydrologic, hydrodynamic and sediment transport models, along with analytical assessments of channel stability based on established geomorphic principles. Results from the geomorphic analysis are presented, along with a discussion of the challenges and benefits of integrating water and sediment management tools on a single platform.

TEMPORAL VARIATIONS OF SCOUR AND FILL PROCESSES AT SELECTED BRIDGE SITES IN ALASKA

Conaway, J.S., Hydrologist, U.S. Geological Survey, Alaska Science Center, 4230 University Dr. Suite 201, Anchorage AK, 99508, jconaway@usgs.gov

Abstract: Streambed-scour monitoring at selected sites in Alaska is being used to assess real-time hazards, but also illustrates the complexities of scour and the difficulty of predicting scour using existing methods. Pier-mounted sonar transducers and stage sensors installed on 16 bridges in Alaska measure the distance to the streambed and water stage every 30 minutes during the open-water season. Data have been collected for over 3 years at 5 of the bridges. Near real-time transmission of these data allow state engineers to monitor bed elevations during high flows at scour-critical bridges. A wide range of hydraulic and sediment regimes are represented by the monitoring network. Annual peak discharges range from approximately 1,000 ft^3/s to nearly 70,000 ft^3/s and median grain size diameter of bed material ranges from about 1 mm to over 50 mm. Measured local scour ranged from no change in bed elevation at some sites to nearly 20 ft of scour at 1 location. The sonar data together with hydraulic variables measured during high flows will be used to evaluate a range of predictive equations for scour. Initial results suggest that scour and fill conditions are generally site specific as well as being dependent upon timing and duration of high flows. Discharge peaks of similar magnitude did not always produce corresponding scour depths of similar magnitude at individual sites. Scour magnitude was more dependent on flow duration, seasonal timing, and source of the high flow. These factors all have an influence on the availability of sediment in the river. Four years of stage and bed elevation data at the Knik River near Palmer show an annual cycle of channel aggradation and degradation to an equilibrium level that is punctuated by shorter periods of scour and fill. The annual cycle of channel change at this site is an interplay of sediment supply, discharge, and the influence of instream hydraulic structures.

INTRODUCTION

Streambed scour followed by fill after a flood passage is a well documented process at locations where regular cross section measurements are made. Data describing the timing and duration of this process are limited by the frequency of field visits. To better understand this process and to monitor bed elevation at bridge piers, the U.S. Geological Survey and the Alaska Department of Transportation and Public Facilities operate a network of streambed scour-monitoring stations in Alaska. Currently 16 bridges are instrumented with sonars for measuring distance to the streambed and pressure transducers for measuring river stage (Figure 1). These stations provide state engineers with near real-time bed elevation data to remotely assess scour at bridge piers during high flows. The data also provide a nearly continuous record of bed elevation and responses to changes in discharge and sediment supply. Seasonal changes as well as shorter duration scour and fill have been recorded. The monitoring network covers a wide range of streamflow and sediment regimes across Alaska. Annual peak streamflow discharges range from less than 1,000 ft^3/s to near 70,000 ft^3/s and median grain-size diameter of the bed material ranges from 1 mm to over 50 mm. In addition to the near real-time data, channel bathymetry and

velocity profiles are collected at each site several times per year. This paper focuses on 4 years of hydraulic and sonar data collected at the Knik River.

INSTRUMENTATION

Each bridge was instrumented with a retractable, pier-mounted 235 kHz echosounder. At locations with multiple scour-critical piers, sonar transducers were mounted on each pier. Sonar transducers were mounted either at an angle on the side of piers near the nose or on the pier nose in order to collect data just upstream of the pier footing. Data are collected every thirty minutes and transmitted every six hours via satellite. When bed elevation or stage thresholds are exceeded satellite transmissions increase in frequency. These near real-time data are available on the web at http://ak.water.usgs.gov/usgs_scour. Streambed elevation and stage data accuracies are ±0.5 ft and ±0.1 ft, respectively.

STREAMBED-SCOUR DATA

Changes in bed elevation at the monitored bridge piers and stage, represented by the maximum annual value less the minimum annual value, are presented in Table 1 for all stations. The network of pier scour-monitoring sites is dynamic, with locations being added and removed annually based on monitoring priority and installation of scour countermeasures. Instrumentation is subject to damage by high flows, debris, and ice and repairs at some sites can only be made during low-flow conditions.

Little to no change in bed elevation was observed at most sites. Streambed scour typically occurs during high flows and only one significant event affecting a single basin occurred during the period of data collection. Intense rainfall in July 2003 in the Tanana River Basin resulted in a rapid increase in stage at three sites. Discharge on the Chena River was near the 10-year recurrence interval and the 5-year recurrence interval was exceeded at both the Tanana and Salcha Rivers (Meyer and others, 2004). Despite the high streamflows, relatively little bed elevation change occurred at these sites. The Knik River near Palmer was the only site with large changes in bed elevation each year. Annual scour ranged from 17.2 ft to 20.0 ft.

Streambed Scour at the Knik River: The Knik River is a braided sand and gravel channel that transports large quantities of sediment from the Knik Glacier. It drains an area of approximately 1,200 mi^2, over half of which consists of glaciers. The braided channel narrows from approximately 3 mi wide at the glacier mouth to just over 400 ft at the Old Glenn Highway bridge where the channel is subject to a 4:1 contraction during summer high flows. Current morphological and alluvial characteristics of the river can be partially attributed to large glacial outburst floods that occurred nearly every year from 1914-1966. The maximum measured discharge from these events was 359,000 ft^3/s. At a discharge of 30,000 ft^3/s on July 12, 2003, suspended sediment concentration was measured at 711 mg/L and bedload discharge was 9,010 tons/d. Median grain size of the bedload was 1.5 mm.

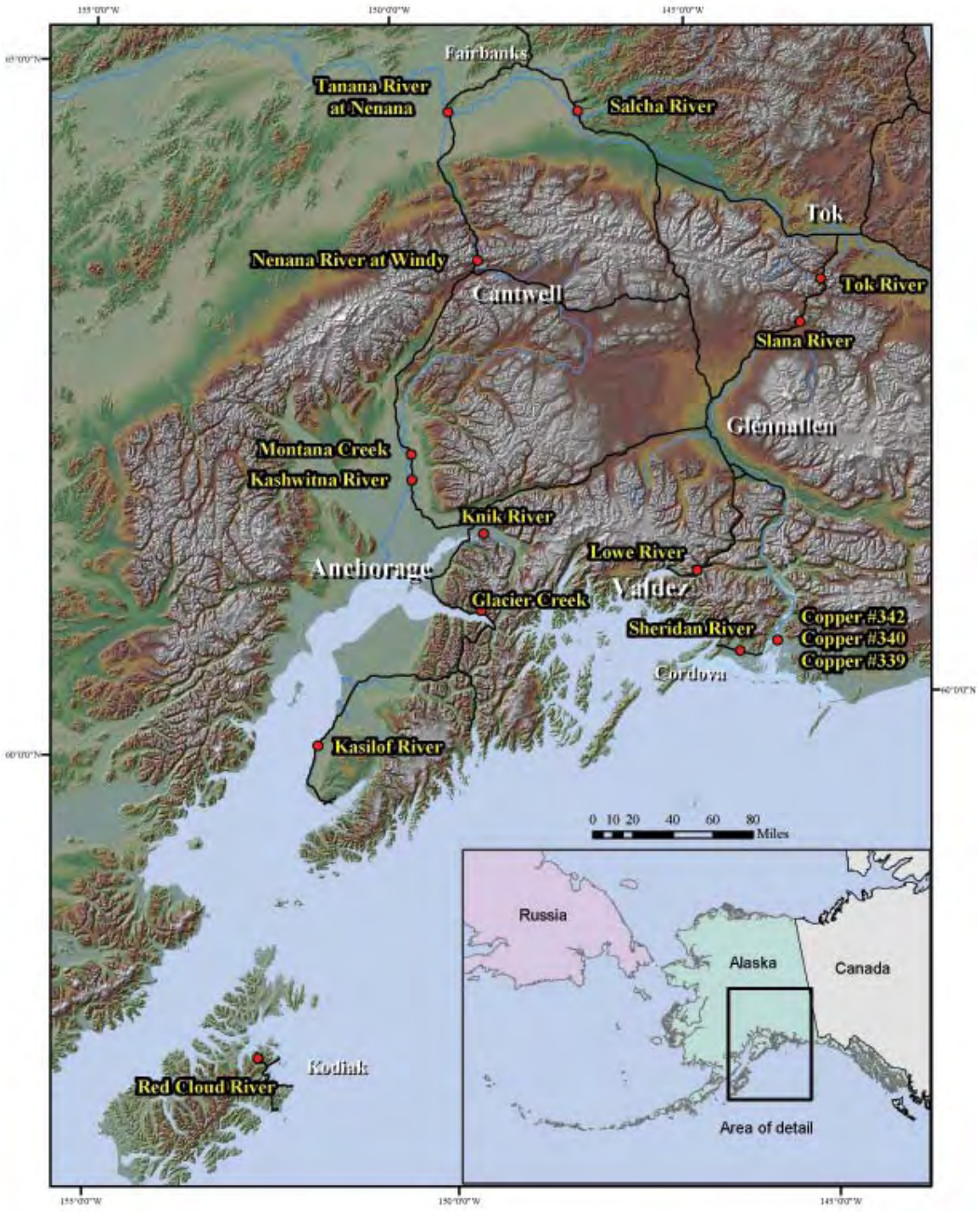


Figure 1 Active U.S. Geological Survey streambed-scour monitoring locations in Alaska.

Since the installation of the monitoring equipment, streamflows at the Knik River ranged from 600 ft^3/s to 60,400 ft^3/s for water years 2002-2005. During the winter months, the streambed at the monitored bridge pier aggraded to an elevation of between 29 and 31 ft (local datum) each year (Figure 2). From the beginning of data collection each year in early May until the latter part

of June, the bed degraded at an average rate of 0.2 ft/day, about 8 ft each year. Over this same period of time, the stage increased at a rate of 0.07 ft/day, 0.09 ft/day, and 0.06 ft/day for 2003, 2004, and 2005, respectively. Following this period of seasonal channel degradation the bed elevation at the pier remains relatively stable, with brief periods of scour and fill. Stability in the bed elevation can be interpreted as an equilibrium in the sediment transport rather than a lack of sediment transport. The channel begins to aggrade in September as stage decreases.

Table 1 Changes in bed elevation at the monitored bridge piers and stage at streambed-scour monitoring stations. (All values are in feet and represent changes during open water, - indicates no data)

	2003		2004		2005	
Location	**Stage**	**Bed**	**Stage**	**Bed**	**Stage**	**Bed**
Tanana River at Nenana	9.9	3.5	-	-	-	-
Nenana River at Windy	5.5	2.0	2.1	3.0	-	0.5
Montana Creek	-	-	2.1	1.0	3.3	0
Kashwitna River	-	-	2.1	4.0	3.1	3.5
Red Cloud River	-	-	-	-	1.1	0.0
Salcha River	7.7	2.0	3.6	1.5	2.0	1.5
Tok River	0.7	0.0	0.9	0.0	1.5	4.0
Chena River	8.0	3.0	-	-	-	-
Slana River	-	-	-	-	2.8	1.5
Lowe River	-	-	-	-	4.2	2.0
Knik River	6.2	19.7	6.1	17.2	5.1	20.0
Kenai River	3.5	0.5	1.0	1.0	-	-
Kasilof River	2.4	1.0	2.3	1.5	4.6	1.0
Sheridan River	-	-	-	-	9.8	9.0
Copper River #339	-	-	-	-	3.5	7.5
Copper River #340	-	-	-	-	3.3	10.5
Copper River #342	-	-	-	-	5.4	8.0
Glacier Creek	-	-	2.5	0.0	2.7	0.0

The mean bed elevation at a river cross section is not only dependent upon discharge, but is also related to changes in width, depth, velocity, and sediment load during the passage of a flood (Leopold and others, 1964). Streambed scour in the bridge reach is an interplay of discharge, sediment transport and the flow hydraulics associated with the channel contraction, upstream guide banks, and piers. Although the sonar only measures the bed elevation in front of the right-bank pier, the measured changes in bed elevation represent channel change from all the above factors. The cross section defined by the upstream bridge opening was surveyed periodically to document changes in bed elevation across the channel (Figure 3). These cross sections and the sonar data show an annual cycle in channel change.

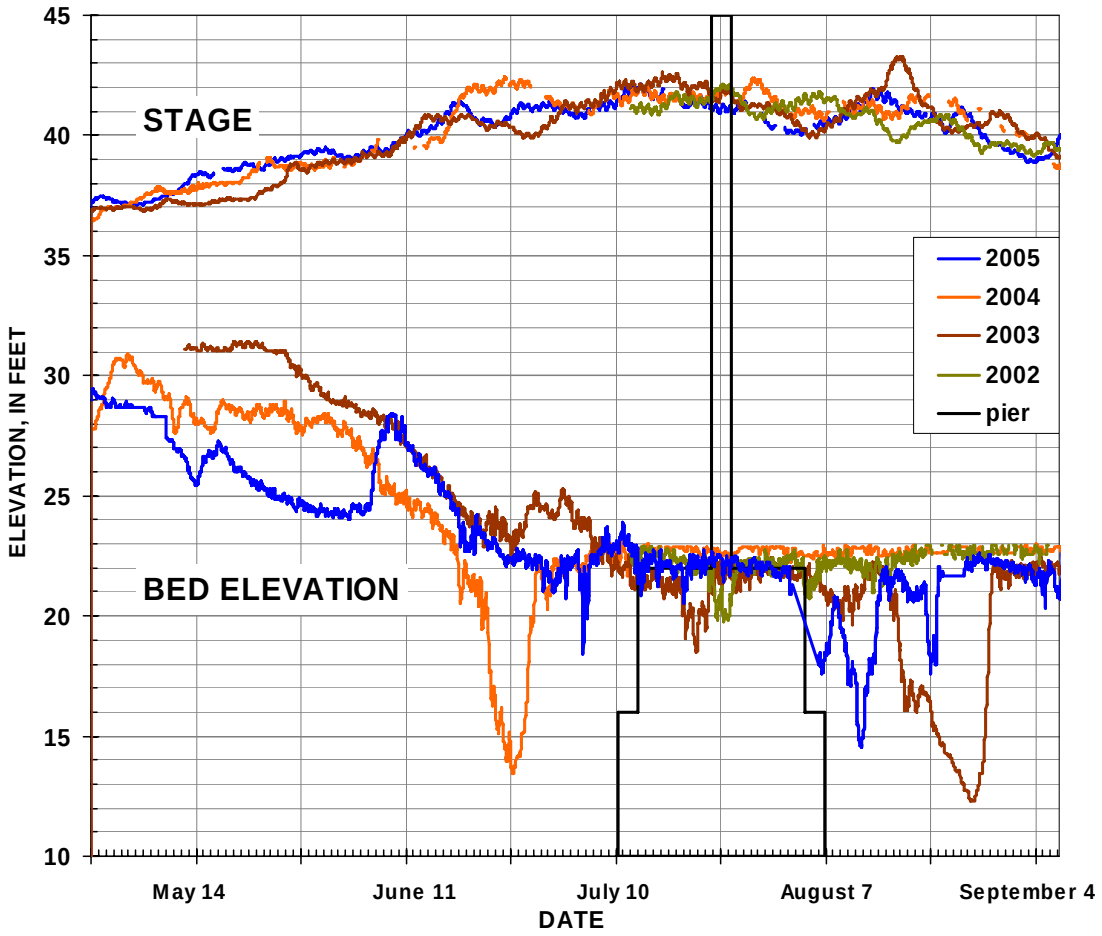


Figure 2 Stage and bed elevation at the monitored bridge pier for 2002-2005 at the Knik River near Palmer, Alaska. The bridge pier and footings are plotted for reference.

Flow vortices that develop as flow is routed around the guide banks erode the channel along the banks. Increases in stage result in larger flow vortices and progressive deepening of the channel from the banks towards the center of the channel. At higher stages this scour along the channel margins is thought to override the effects of local scour at the pier where the sonar is mounted. The pier is supported by a 24 ft wide footing and 30 ft wide sub footing. These footings appear to armor the local bed and bed elevation remained near the elevation of the top of the footing for extended periods (Figure 2). Parola and others (1996) found that rectangular pier footings protect the streambed from the scouring of vortex systems formed by the pier until the footing is above the streambed and then vortices from the footing induce scour. The channel scours vertically and laterally towards the center to accommodate increased summer streamflow. Vertical and lateral scour are concurrent until the footing of the pier is reached, at which point vertical scour is limited and increases in channel area are made by lateral scour. This process is illustrated in the successive cross sections plotted in Figure 3.

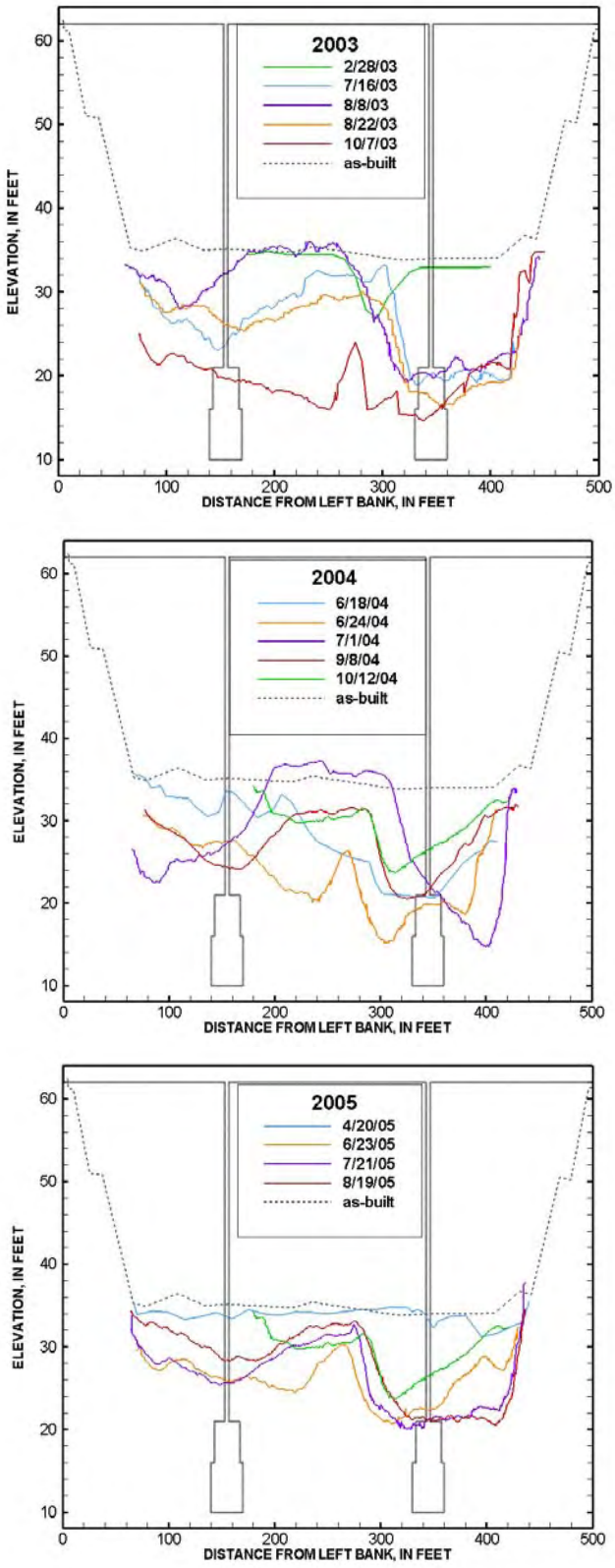


Figure 3 Upstream bridge cross sections at the Knik River for 2003-2005.

Two distinct scour and fill cycles from 2003 and 2004 highlight differences in timing and duration of scour (Figure 4). Both scour events were associated with a period of high temperatures and subsequent increased glacial melt, but in 2003 the warm weather was followed by 10 days of rainfall and cooler temperatures. The maximum scour occurred slightly after the peak in stage in 2003 and in 2004 maximum scour was concurrent with peak stage. The duration of scour, measured from when the bed elevation begins to decrease until fill begins, was 11.5 days in 2003 and 4 days in 2004. The scour in 2003 was of greater duration because the discharge and sediment supply from the glacier was reduced by the cooler temperatures. The channel filled 10 ft in two days after warmer temperatures resumed, likely accompanied by an increase in sediment load. In 2004, stage increased rapidly prior to scour and was then steady with diurnal fluctuations. The scour began after the bed had degraded to the elevation of the top of the pier footing. Filling of the channel began before the stage began to decrease. Bed elevation changes in alluvial systems are the response to changes in sediment supply and flow hydraulics. Since flow hydraulics were relatively constant, an increase in sediment supply is thought to have initiated the filling.

SUMMARY

Streambed-scour monitoring at bridges across Alaska provides state engineers with a tool to remotely evaluate the stability of these structures during high flows. The data sets also are providing a nearly continuous record of stage and bed elevation across a range of hydrologic regimes. Large changes in bed elevation were recorded each year at the Knik River. The bed elevation data recorded both a seasonal channel aggradation and degradation pattern and shorter duration cycles of scour and fill. The channel aggraded to the same relative elevation each winter and then degraded to an equilibrium elevation that is coincident with the elevation of the top of the pier footing. The bed scoured beyond this elevation for short periods as a result of prolonged high flow and possibly fluctuations in sediment supply. The onset of scour occurred on the falling limb of a hydrograph in 2003 and at the peak in 2004. Fill began after the recession in the hydrograph in 2003 and before it in 2004. The timing and duration of scour and fill at the Knik River is believed to be attributed more to sediment supply and the source of high flows rather than discharge alone.

REFERENCES

Leopold, L.B., Wolman, M.G, and Miller, J.P., 1964, Fluvial Processes in Geomorphology. San Francisco, CA, W.H. Freeman and Company.

Meyer, D.F., Bartu, D.P., Eash, J.D., and Swenson, W.A., 2004, Water resources data for Alaska, water year 2003. U.S. Geological Survey Water-Data Report AK-03-1.

Parola, A.C., Mahavadi, S.K., Brown, B.M., and El Khoury, A., 1996, “Effects of rectangular foundation geometry on local pier scour,” Journal of Hydraulic Engineering, v. 122, no. 1, p. 35-40.

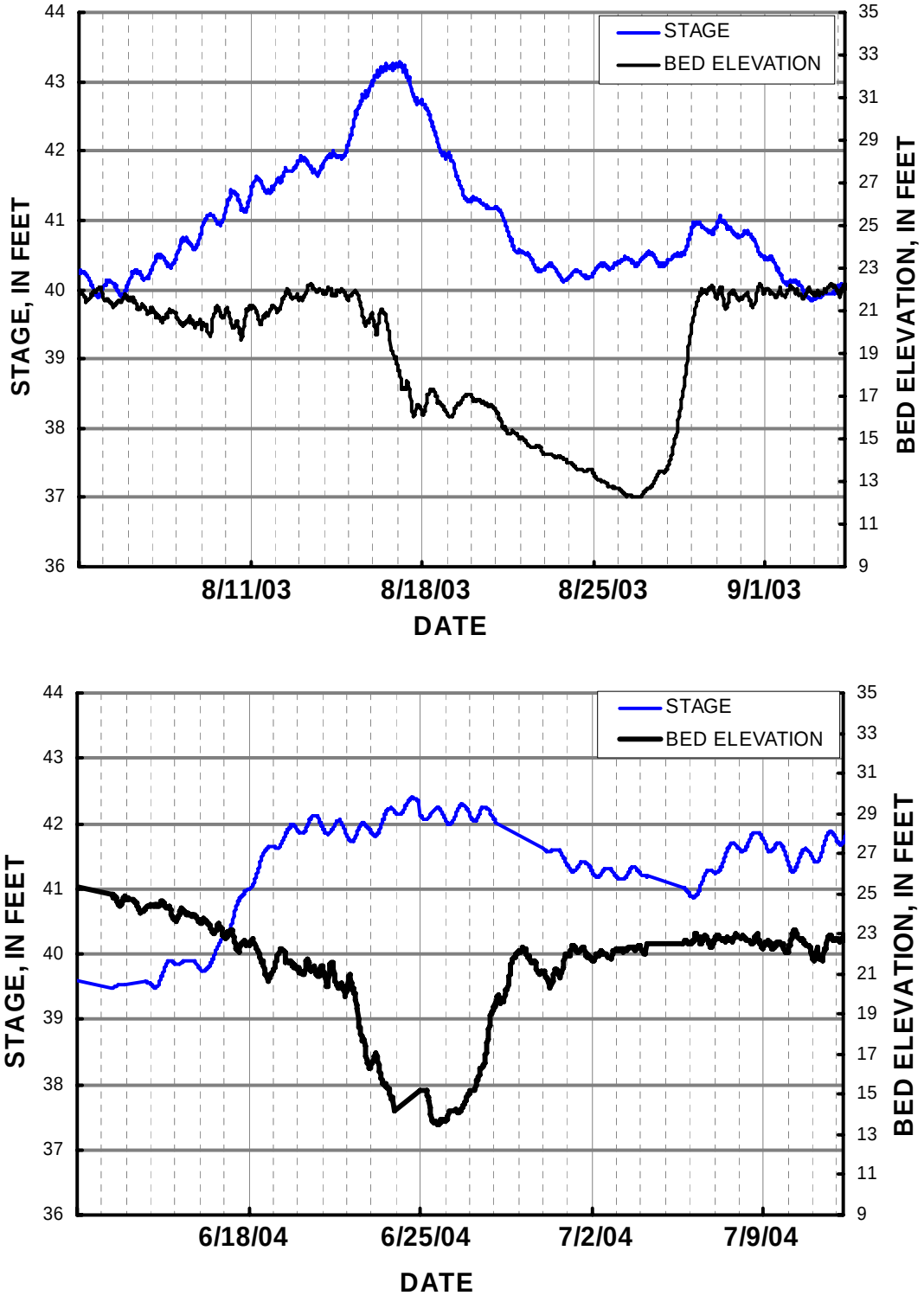


Figure 4 Stage and bed elevation at monitored bridge pier from two scour and fill events on the Knik River near Palmer, Alaska. Stage increases were the result of rainfall (2003, upper plot) and glacial melting from a prolonged period of warm weather (2004, lower plot).

GEOMORPHIC CONTEXT FOR HISTORICAL DETERMINATION OF SEDIMENT SOURCES, TRANSPORT, AND DEPOSITION IN THE BAD RIVER WATERSHED, BAD RIVER RESERVATION, WISCONSIN

Faith A. Fitzpatrick, Research Hydrologist, U.S. Geological Survey, Middleton, WI, fafitzpa@usgs.gov; Kirsten A. Cahow-Scholtes, Water Resources Specialist, Bad River Band of the Chippewa Tribe, Odanah, WI, water@badriver.com; and Marie C. Peppler, U.S. Geological Survey, Middleton, WI, peppler@usgs.gov

Abstract: The Bad River in northern Wisconsin is thought to be the largest U.S. contributor of sediment to Lake Superior (19 percent of the suspended load). Previous studies have shown that the average suspended sediment load for the Bad River is 2.81 kg/ha/d or 1,030 kg/ha/yr. In 2001, a study was begun by the U.S. Geological Survey and Bad River Band of the Chippewa Tribe to better understand the major sediment source areas and historical geomorphic processes in the Bad River watershed related to erosion, transport, and deposition of sediment throughout the watershed. Initially, historical aerial photographs, maps, documents, low altitude video footage, and GIS overlays of watershed-scale thematic maps of land cover, surficial deposits, and bedrock geology were examined. Data gathered from these sources indicated that the majority of sediment and surface runoff originated from the lower half of the watershed. The upper half of the watershed is mainly forested, with a poorly developed drainage network developed on sandy and loamy surficial deposits. The lower part of the watershed has a mix of agriculture and forested land and a well-developed drainage network on clayey surficial deposits. In the lower half of the watershed, erosion is evident along approximately 150-ft high bluffs as the entrenched Bad River valley and tributary valleys intersect an early Holocene sandy glacial lake shoreline. Ridges of quartzite bedrock, mainly buried by surficial deposits, crop out along the lower main stems and act as intermediate base level controls, limiting any potential incision. Topographic surveys were done and cores collected along valley cross sections along the Bad River and its major tributary main stems in selected reaches dominated by erosion or deposition. Sandy historical overbank deposits along middle and lower main stems are about 7-10 feet thick, making the channels look entrenched even though little historical incision has occurred. At a USGS streamflow gaging station on the Bad River, the flood-plain sedimentation record is being compared to 80 years of flood record to determine overbank sedimentation rates in the context of climate and land cover changes. Total sediment load samples were collected at the gaging station in the spring of 2005 and data were compared to previous suspended sediment data and overbank deposition rates.

A RIVER EVOLUTION COMPARISON OF ADJACENT STABLE AND UNSTABLE URBAN WATERSHEDS IN SAN JOSE, CALIFORNIA

Brett Jordan, Graduate Student, Department of Civil Engineering, Colorado State University, Fort Collins, Colorado, bjordan@engr.colostate.edu; W.K. Annable, Professor, Department of Civil Engineering, University of Waterloo, Waterloo, Ontario; C.C. Watson, Professor, Department of Civil Engineering, Colorado State University, Fort Collins, Colorado

Abstract: Berryessa Creek, located at the base of the Diablo mountain range on the east side of San Jose, California, has experienced significant channel instability and sedimentation problems over the past 40 years of urban sprawl. As late as the early 1900s, a defined stream channel was not present throughout the entire watershed, as overland flow infiltrated into alluvial fan deposits upon reaching the Santa Clara Valley. By 1943, a constructed channel was developed by farmers to increase agricultural productivity and was later altered for residential development along the valley floor. As urbanization proceeded in the San Jose area, the channel has undergone a series of realignments, catchment alterations and channelization practices, resulting in an aggrading man-made canal at the downstream end of the watershed and severe erosion problems in the middle and upper reaches.

Conversely, the adjacent watershed of Upper Penitencia Creek has a similar watershed area, land use, geology and relief and has undergone comparable urbanization over the same time period, and a stable channel planform and outlet condition has persisted since the early 1900s. This study examines the comparative geomorphic, river mechanics and hydraulic processes occurring in these two urbanizing watersheds resulting in an understanding of the processes governing channel stability and instability of two adjacent watersheds with vastly differing morphological response to urbanization. Methods of investigation include: morphometric analysis, time trend urbanization analysis, storm sewer network characterization, and hydraulic and sediment transport analysis by both numerical modeling and field investigations (including longitudinal profiles, cross-section erosion surveys, discharge measurement, bed load and suspended load sediment transport sampling and bed material sedimentological analysis).

INTEGRATING TWO SEDIMENTATION RATE METHODS TO DETERMINE PAST CHANNEL ADJUSTMENT RATES

Laura L. Keefer, Hydrologist, Illinois State Water Survey, Champaign, IL, lkeefer@uiuc.edu; Richard A. Cahill, Geochemist, Illinois State Geological Survey, Champaign, IL, cahill@isgs.uiuc.edu; Richard L. Allgire, Support Hydrologist, Illinois State Water Survey, Carbondale, IL, sws1495@siu.edu

Abstract: Channel adjustment and sedimentation rates are needed when determining stream management activities to reduce erosion and sedimentation. Channel adjustment rates are typically determined using historical channel geometry, channel profiles, and air photos, or dendrogeomorphic techniques. When this information is not available, sediment deposition rates of a downstream waterbody may be used as a surrogate for long-term channel adjustment rates in the watershed. Methods of determining sediment deposition rates include developing sediment budgets and/or radiometric (^{137}Cs) analysis. Using these two methods, short-term and long-term depositional rates within the Lower Cache River-Cypress Creek Wetland in southern Illinois were computed and compared. Results provide insights into the historical rate of upstream channel adjustments in the watershed. Specifically, based on sediment core data collected in 2000, the radiometric (^{137}Cs) analysis determined that the wetland has a long-term sediment deposition rate of 0.86 cm/yr (1963-2000). The sediment budget method, based upon sediment monitoring data collected between 1986 and 2002, computed a nearly identical short-term sediment deposition rate of 0.79 cm/yr. Since the depositional rates determined by the two methods are very similar, it is reasonable to assume that the sediment deposition in the wetland, as well as the channel adjustment rates in Big Creek, have been steady since at least 1963.

INTRODUCTION

Identifying the prevailing channel response processes to disturbances is needed for predicting the rates and magnitudes of channel adjustments. Conceptual models of channel evolution (i.e. Schumm et al., 1984; Simon, 1989) are used to identify these processes and focused geomorphic assessments utilize historical analyses and field measurements to quantitatively predict the channel response rates (Simon et al., 2005). Channel adjustment rates are typically determined by measuring changes in channel geometry over time using channel gradient profiles and cross-section surveys (Trimble, 1998). Maps and aerial photography integrated with GIS technology has improved the ability to inspect changes in channel planform and measure channel meander rates (Urban and Rhoads, 2003). Dendrogeomorphic indicators have also been used to establish stages of channel evolution, rates of channel widening, and floodplain accretion (Hupp and Bornette, 2003). In the absence of these types of data, depositional (sedimentation) rates in lakes or wetlands can be used as a reflection of erosion responses, one of which is channel adjustment, in a watershed. Generating a sediment budget based on annual yields measured at the inflows and outflows of a reservoir is a common technique to determine sedimentation rates. Other techniques include sedimentation surveys or radiometric analysis using cesium-137 (^{137}Cs). Sedimentation rates based on radiometric ^{137}Cs analysis has been reviewed by Crickmore et al., 1990) Ritchie and McHenry (1990), and Santschi and Honeyman, 1989). Brown et al. (1981), Lance et al. (1986), and McHenry et al. (1973) have demonstrated the application of ^{137}Cs to measure accumulation patterns in small watersheds and Kadlec and Robbins (1984) in a wetland area. Cesium-137 measurements were used to determine in-channel, wetland, and reservoir sediment storage for erosion response studies in small catchments (Zhang et al., 1997; Walling et al., 2002).

The ^{137}Cs measurement technique has been successfully used in Illinois to study sedimentation processes in backwater lakes associated with the Illinois and Mississippi Rivers (Cahill and Autrey, 1987). Demissie et al. (1992) determined sedimentation rates for the Lower Cache River-Cypress Creek Wetland in southern Illinois by comparing two methods: ^{137}Cs analysis in the wetland and a sediment budget generated from measured sediment yield data for the watershed. The objective of their study was to determine the sedimentation rates for various depositional environments of the Lower Cache River-Cypress Creek Wetland. The two sedimentation rate methods were used because each had some limitations for achieving that objective. The sediment budget method provided the sedimentation rate over the entire area and identified high sediment yield sub-watersheds but was not capable of providing the spatial distribution of sediment deposition within the wetland. The radiometric method provided the site-specific data of the sedimentation rates for various depositional environments. The combination of these two methods provided a more complete picture of the sedimentation pattern in the wetland.

Demissie and others (1990b) identified Big Creek as the tributary that contributes a significant portion (nearly 70%) of the suspended sediment load to the Lower Cache River-Cypress Creek Wetland. Subsequently, several investigations have been conducted in the Big Creek watershed to determine the magnitude of the sedimentation and the erosion processes responsible for the high sediment loads (Allgire, 1991; Demissie and Xia, 1991; Demissie et al., 1992; Allgire and Cahill, 2001; Demissie et al., 2001). A geomorphic assessment was recently conducted in the Big Creek watershed to determine and quantify the prevailing erosion processes. The study found that there was significant channel straightening in the lower reaches of Big Creek, bedrock controls in the upper reaches, and historical land use changes throughout the watershed. This resulted in two styles of channel adjustment responses distributed between upper and lower regions of the Big Creek watershed. Data typically used to directly measure channel adjustments rates was unavailable for the Big Creek watershed which made it difficult to estimate potential channel adjustment rates. Therefore, sedimentation rates in the wetland were examined as a surrogate to determine an average channel adjustment rate in Big Creek. This paper presents the results of an investigation that determined the rates of sediment deposition in the wetland using the two methods as described by Demissie et al. (1992). This investigation utilized the sedimentation rates for the Lower Cache River-Cypress Creek Wetland as reported by Allgire and Cahill (2001). They determined the rates from 1963 to 2000 based on ^{137}Cs measurements of cores collected for a sedimentation survey conducted in 2000. Based on eight years of monitoring data in the Lower Cache River watershed collected by the Illinois State Water Survey, annual sediment budgets were generated by this investigation to determine the average wetland sedimentation rate between 1986 and 2002. The 1986-2002 sedimentation rate determined by the sediment budget method will be contrasted with the 1963-2000 rate reported by Allgire and Cahill (2001) to identify the adjustment rate leading up to the current character of the Big Creek watershed.

BACKGROUND

Study Watershed Description: The Cache River Basin is located in extreme southern Illinois near the confluence of the Ohio and Mississippi Rivers (figure 1). During the first half of the 1900s, intensive drainage, flooding, and water-level control projects here implemented to facilitate "reclamation" of the land for agricultural use that resulted in the division of the Cache River into two distinct drainage basins (Hutchison, 1984). The Upper Cache River watershed (953 km^2 drainage area) drains directly into the Ohio River, but farther upstream from the original outlet, and the Lower Cache River watershed (927 km^2) drains westward into the Mississippi River through a diversion channel. During high flows the Lower Cache River can also drain eastward to the Upper Cache River-Post Creek Cutoff through one-way culverts in a levee. The Lower Cache River-Cypress Creek Wetland is recognized by state, national, and international organizations as a "biologically significant" natural area and a RAMSAR "wetland of importance". The wetlands are known for being the northern most extent of cypress-tupelo gum tree stands of the Coastal Plains Province, some more than 1,000 years old. The wetland has two major tributaries: Big Creek and Cypress. Each of these tributaries drains a high-relief headwater area and flows into the nearly flat valley bottom of the Lower Cache River. Logging, conversion of forest to agriculture, and many drainage alterations projects have led to substantial changes in runoff and sediment supply, which set into motion adjustment processes that have caused erosion of the uplands and channel perimeter and delivery of high suspended-sediment loads to the Lower Cache River-Cypress Creek Wetland (Demissie et al., 1990). The position of the wetland and changes to the river's hydraulic characteristics due to drainage alterations causes the wetland to act much like a sedimentation basin. This has produced deposition and high levels of turbidity in the wetland, endangering the sensitive components of the ecosystem.

Geomorphic Assessment: The geomorphic assessment established the temporal and spatial context of the stream channel character through a combination of historical analysis and multi-scale field reconnaissance for the entire watershed. The study identified the major disturbances and two responding channel adjustment processes in the lower and upper regions of Big Creek. The major disturbance in Big Creek was the 58% reduction in channel length due to channel straightening in the 1930s and 1940s. Inspection of maps and air photos show no significant lateral channel movement outside of the straightened reaches. The other was a major shift from virtually all forest to agricultural production by the 1930s. Currently, 18% of the land cover is in forest. Watershed area in agricultural use has increased slightly from 1925 (26%) to present (34%) due to increase in row crops. Pasture and

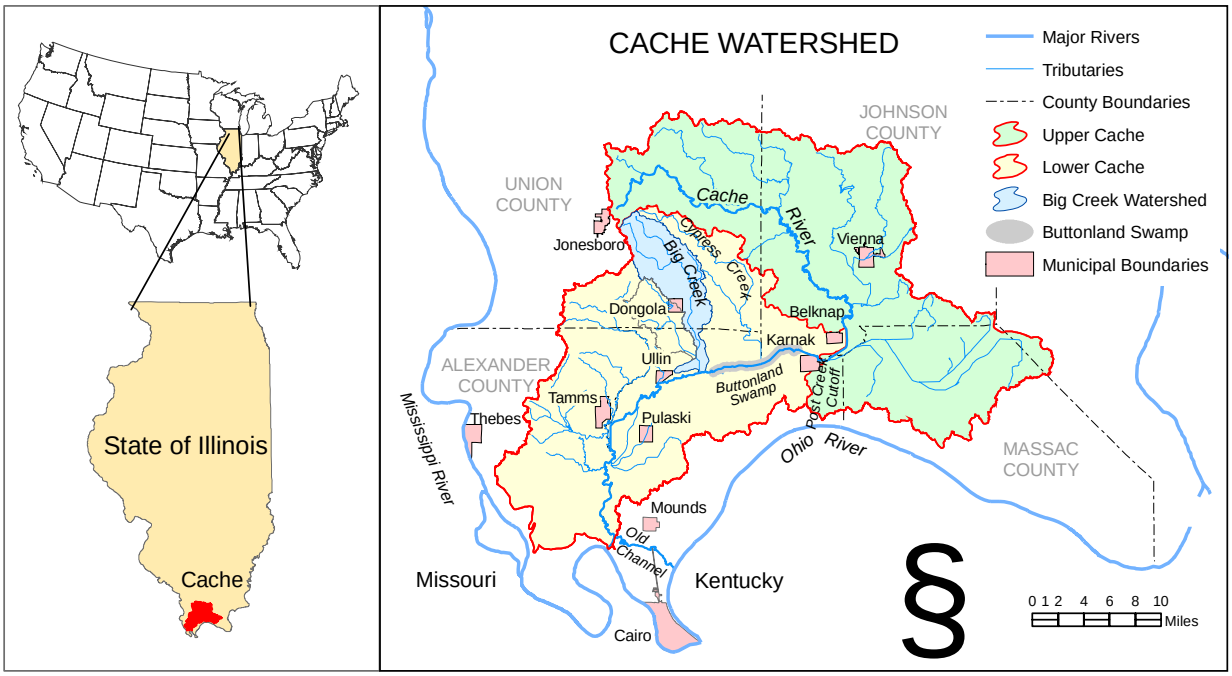


Figure 1 Location of study area in the Cache River Basin, Illinois.

open lands comprise the remaining area for agricultural use. The channel straightening projects included six major flow control structures to compensate for the increased slope (figure 2). However, field reconnaissance has identified incision and widening throughout the channel in the lower region which currently exhibits Stages IV (threshold) and V (aggradation) of channel evolution (Simon, 1989). Historical channel geometry confirms that incision and widening occurred within straightened reaches (figure 3). Although it is the reaches further upstream

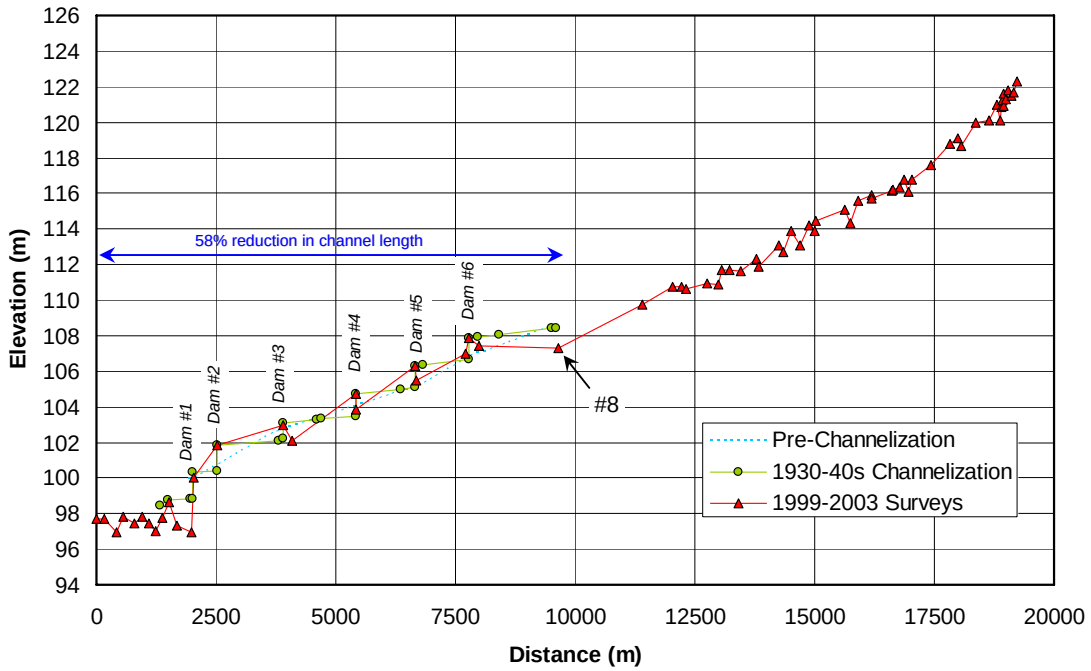


Figure 2 Channel profiles for 1944-2003

that have significant bank instabilities (rotational slips, toe erosion, and major large woody debris) indicative of active channel widening. Hydraulic modeling shows the absence of energy for further significant channel incision which infers that the channel may be entering Stage V (aggradation) of evolution. The channel in the upper region is underlain by Mississippian limestone bedrock and Quaternary gravel lake deposits which has interrupted any incision processes. Gravel is the major bed material and forms mid-channel bars that tend to deflect flow into the channel banks. The entire watershed is covered by 1-2 meters of Peoria loess which is exposed at all channel banks. Particle size analyses show that the sediment deposited in the wetlands is the same as the material found in the banks.

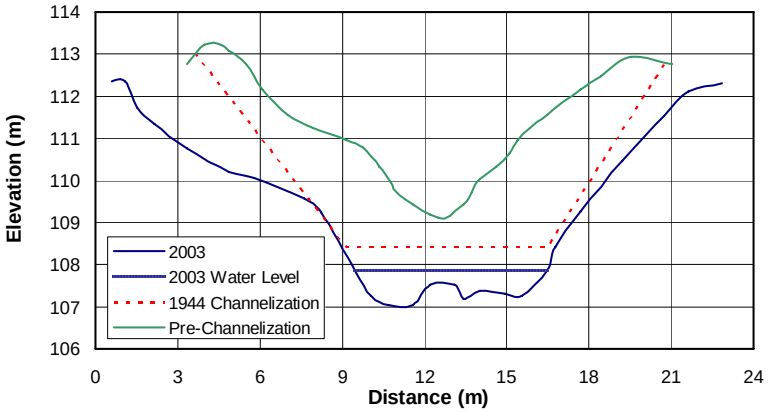


Figure 3 Change in channel geometry from at Site #8 1944-2003

METHOD

This investigation uses a combination of two sedimentation rate methods as described by Demissie et al., (1992). The first is a sediment budget generated from sediment yields measured at streamgaging stations monitoring the inflow and outflow of the wetland. The volume of sediment deposited in the wetland is determined from the sediment budget by dividing the sediment weight by the sediment density. The rate of vertical deposition is then calculated by dividing the sediment volume by the area of sediment deposition. The second method determines sedimentation rate by ^{137}Cs measurement of sediment cores collected from various locations within the wetland. The ^{137}Cs method and results of the Lower Cache River-Cypress Creek Wetland 2000 sedimentation survey as reported by Allgire and Cahill (2001) are presented below. The method for determining sedimentation rate by sediment budget and results will follow.

Sedimentation Rates Based on Radiometric Dating: Allgire and Cahill (2001) performed a sedimentation survey of the Lower Cache River-Cypress Creek Wetland in 2000. Sediment cores were collected along 10 transects through the river channel, sloughs, and floodplain deposits as well as areas not disturbed by dredging or tillage operations. A piston-type and Wildco gravity core samplers were used to sample submerged sediments in the wetlands while a stainless steel soil probe was used to collect sediment cores in aerated sediments. The piston-type core sampler was used to collect submerged sediment cores for unit weight, particle size, and chemistry analyses. Several representative 5-centimeter (cm) sub-samples were sectioned from the core for laboratory analyses.

The Wildco gravity core sampler, with lexan core tubes, was used to collect submerged sediment cores for analysis by the Cesium-137 (^{137}Cs) dating technique. Sediment cores collected using the soil probe were sub-sampled in the field, prepared and packaged, and transported to the analytical laboratory for unit weight, particle size, and radiometric analysis. Sediment cores for radiometric analysis were extruded, cut into detailed 5 cm intervals, and sub-sampled for ^{137}Cs analysis. Sediments were weighed and then air-dried in a Class 100 laminar-flow clean bench. Sediment sub-samples were ground using a ceramic mortar and pestle and sieved to pass a 1.0-mm stainless steel sieve. Ten grams (g) of sediment were weighed into polystyrene petri dishes, which were then sealed.

The long radioactive half-life (30.174 years) and the distinct pattern of ^{137}Cs in the environment make it a very useful tracer of recent hydrologic and sedimentologic processes. The atmospheric testing of nuclear weapons that produced ^{137}Cs began to be deposited worldwide in significant quantities in 1952. About 90 percent of the total flux of ^{137}Cs in the Northern Hemisphere was deposited between 1954 and 1963, prior to the signing of the Limited Nuclear Test Ban Treaty of 1963. Despite sporadic inputs in recent years, the amount of ^{137}Cs in the atmosphere has decreased since 1966 to near zero (Ritchie and McHenry, 1990).

Gamma activity of sediment samples was measured using high-purity germanium and lithium-drifted germanium [Ge (Li)] crystals. Sediment samples were counted for an average of 45 hours. Peak analysis software was use to calculate net peak area. The sample activity relative to NIST 4350B was then calculated in milli-becquerel per gram (mBq/g). The lowest specific activity that could be detected in a 10-g sample was approximately 0.003 mBq/g. Figure 4 illustrates the ^{137}Cs activity versus depth plotted for each core to select the position in the sedimentation record when fallout from testing of nuclear weapons (1954) in the atmosphere began or the peak time of fallout from nuclear testing (1963). Sedimentation rates then were calculated with these dates as a marker. All sedimentation rates obtained by this technique are based on the assumption of a constant rate of sedimentation over the time interval of interest (37 or 46 years). However, computing a sedimentation rate between the depths of 1954 and 1963 can be highly suspect unless there is good evidence of no significant shifting or scouring of bottom sediments.

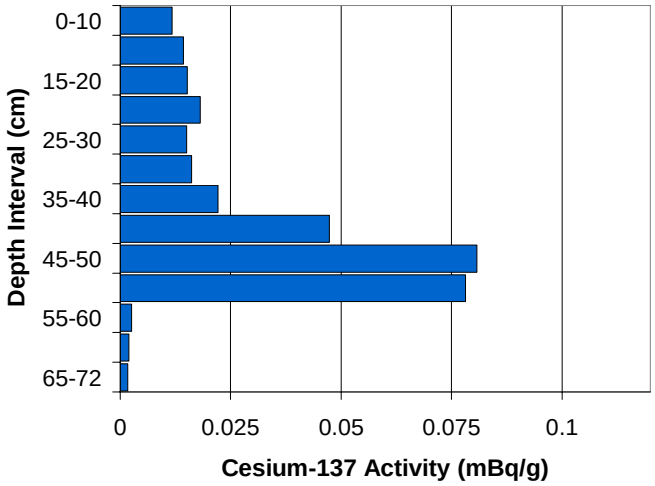


Figure 4 Example 137Cesium core results from transect 9-10 in the Cache River wetland.

Allgire and Cahill (2001) reported that the wetland sedimentation rates for the 1963-2000 period averaged 0.86 cm/yr and ranged from 0.2 to >2 cm/yr. In general, the side channels had the highest rate of sedimentation followed by backwater sloughs, ponds, and wetland meadows. The samples collected from the floodplain showed the lowest rate of sedimentation, and the sites directly connected to the main channel in the wetland had the highest sedimentation rates.

Sedimentation Rates Based on Sediment Budget: A sediment budget was generated from suspended sediment data collected from stream gaging stations during water years 1986-1990 and 2000-2002 by the Illinois State Water Survey. Sediment load was computed for three stations in the Lower Cache River-Cypress Creek Wetland area. The wetland has two major tributaries, Big and Cypress Creeks, and each has a station that monitored sediment inflow. The third station, Lower Cache River at Ullin, monitored the sediment outflow from the wetland. Using the sediment yields at Big and Cypress Creek to estimate yields for non-monitored watersheds, a sediment budget was generated using the total sediment inflow into the wetland area and sediment outflow at Ullin. Sediment yield from the entire area draining into the wetland was determined by dividing the area into nine sub-watersheds (figure 5). Sub-watersheds 1 and 8 are the Big Creek and Cypress Creek monitored watersheds, respectively. The sediment yields at the Cypress Creek gage was used to determined yields for sub-watersheds 3-7 and 9. Big Creek's sediment yield rate was used for sub-watershed 2 due to similarity of physical characteristics with Big Creek. Once the yields were determined, the sediment budget for the Lower Cache River wetland area was calculated by using an equation similar to one used by Parker (1988):

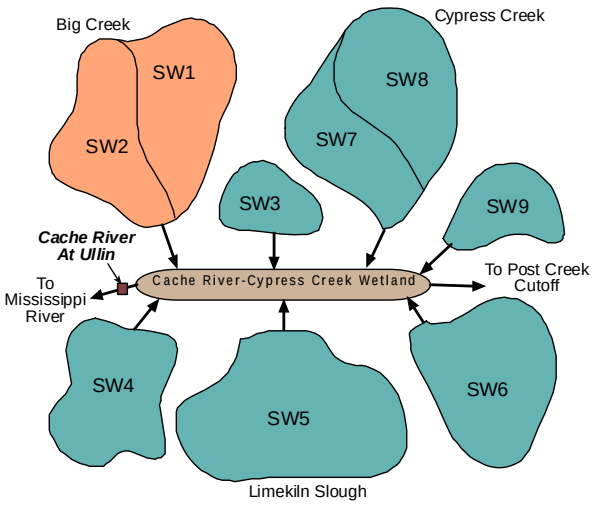


Figure 5 Sub-watersheds draining into the Cache River-Cypress Creek Wetland

$$\Delta Qs = \sum_{i=1}^{n} Qs_{Ti} - Qs_o \qquad (1)$$

where ΔQs = sediment trapped/scoured from the study area; Qs_o = sediment outflow from the study area; Qs_{Ti} = sediment inflow from tributary stream; and n = number of tributary streams.

Table 1 Sediment Budget of the Cache River-Cypress Creek Wetland

		Sediment Yields (tons x 10^3)							
Subwatersheds	*Hectares ($x10^3$)*	*1986*	*1987*	*1988*	*1989*	*1990*	*2000*	*2001*	*2002*
SW1 (Big)	8.1	8.1	74.6	14.3	16.1	46.6	36.4	18.9	4.5
SW2	4.8	4.8	44.0	8.5	9.5	27.5	21.5	11.1	2.7
SW3	3.3	3.3	3.8	1.9	2.8	5.2	5.8	2.7	0.7
SW4	1.6	1.6	1.9	0.9	1.4	2.5	2.8	1.3	0.3
SW5	5.7	5.7	6.8	3.3	4.9	9.1	10.2	4.8	1.2
SW6	3.0	3.0	3.6	1.7	2.6	4.8	5.4	2.5	0.6
SW7	5.7	5.7	6.7	3.3	4.9	9.1	10.2	4.8	1.1
SW8 (Cypress)	6.3	6.3	7.4	3.6	5.4	10.1	11.2	5.3	1.3
SW9	1.7	1.7	2.0	1.0	1.5	2.8	3.1	1.5	0.3
Total Sediment Inflow:	40.2	150.8	38.5	49.1	117.8	106.6	52.9	12.7	246.5
Cache R. @ Ullin		23.3	7.9	14.0	41.2	32.2	8.7	2.4	25.4
Total Sediment Outflow:*		25.6	8.7	15.4	45.3	35.4	9.6	2.6	27.9
Total Sediment Deposited		**125.2**	**29.8**	**33.8**	**72.5**	**71.2**	**43.3**	**10.1**	**218.6**

*Adjusted sediment yield at Cache River at Ullin x 1.10

The total sediment yield into the wetland was calculated by summing the yields for all nine sub-watersheds. However, the total sediment discharge from the wetland area was calculated by increasing the measured sediment load at Ullin by 10 percent to account for some outflow of sediment through the levee culverts to Post Creek Cutoff (Demissie et al., 1992). Using this approach, the sediment yield rates for the sub-watersheds, presented in table 1, are considered conservative and would tend to underestimate the sediment yield from the entire area but should provide a reasonable estimate.

With the total sediment deposited in the wetland for each year determined, the annual vertical rate of sediment deposition was calculated using the equation used by Demissie, et al. (1992):

$$\Delta Z = \frac{S_{wt}}{S_d \bullet A_s} \tag{2}$$

where ΔZ = vertical sedimentation rate; S_{wt} = weight of sediment deposited; S_d = density of the deposited sediment; and A_s = area of sediment deposition.

An average sediment density of 800 kilograms per cubic meter (kg/m^3) for the entire area was estimated from densities determined in the laboratory of several submerged (641 kg/m^3) and exposed (1,442-1,602 kg/m^3) samples (Demissie et al., 1992). To determine the area of deposition, Demissie et al. (1992) generated stage exceedence curves using water level records in the wetland. Based on these curves, and knowledge of the river valley, they determined an area that included all stream channels, backwaters, sloughs, and the wetlands along the streambanks. These areas are generally flooded every year and took into account natural variability of flood water-levels from year to year. The area was estimated by using an elevation-surface area curve also developed by Demissie et al. (1992).

Results: The results of the sedimentation rate calculations based on the sediment budget method are summarized in table 2. The annual sedimentation based on sediment budget ranges from 0.3 to 2.3 inch with an overall average rate of 0.79 inch for the eight years. The average sedimentation rate for water years 1986-1990 is 0.69 and 2000-2002 is 0.95 cm/yr. However, it should be noted that water years 1987, 1988, 2000, and 2001 were dryer years, while water years 1986, 1989, and 1990 varied near normal and 2002 was extremely wet. The variation of wet and dry years is not evenly distributed and consequently cannot be used to infer a change in sedimentation rate between these two periods. Therefore, the 0.79 average sedimentation rate will be assumed to be the representative rate for the entire 17-year period (1986-2002).

Table 2 Sedimentation Rates Based on Sediment Budget

Water Year	*Sediment Accumulation (tons x 10^3)*	*Volume of Sediment (m^3 x 10^3)*	*Area of Wetland Sedimentation (ha x 10^3)*	*Wetland Sedimentation Rates (cm)*
1986	125.2	156.5	1.2	1.30
1987	29.8	37.3	1.2	0.31
1988	33.8	42.2	1.2	0.35
1989	72.5	90.6	1.2	0.76
1990	71.2	89.0	1.2	0.74
2000	43.3	54.1	1.2	0.45
2001	10.1	12.6	1.2	0.11
2002	218.6	273.2	1.2	2.28

DISCUSSION

The sedimentation rate as determined by sediment budget for the more recent 17-year period (WY1986-2002) is on average 0.79 cm/yr and ranges from 0.3 to 2.3 cm/yr, depending in the year. The radiometric analysis determined the rate in the wetland for the 38-year period of 1963-2000 to be 0.86 cm/yr with a range of 0.2 to >2 cm/yr, depending on the depositional environment. Based on the sediment budget and radiometric analysis, the average sedimentation rate for the wetland, as well as the range of rates, is very similar. Therefore, it is reasonable to assume that since the rate from the recent period is nearly the same as the longer 40-year period, sedimentation in the wetland has been steady since at least 1963. The sedimentation rates for the wetland are lower than nearby lakes such as Horseshoe Lake, a natural oxbow lake in the Mississippi River valley, and the Vienna Correctional Center Lake, which had sedimentation of 1.3 cm/yr during the 1951-84 (Horseshoe Lake) and 1965-96 (Vienna Lake) periods (Bogner et al., 1985; Bogner et al., 1997). However, the wetland rates are higher than those for wetlands in other Coastal Plain rivers, which range from 0.15-0.54 cm/yr (1.5-5.4 mm/yr) (Hupp, 2000).

Since Big Creek was identified as contributing 70% of sediment to the wetland (Demissie et al., 1990), the wetland sedimentation rate was assumed to be representative of sediment delivery from Big Creek. Based on the similar rates between the two time periods, this implies that Big Creek has been steadily adjusting for the last 40 years. Although, sedimentation rates between the 1940s and 1963 are unknown, the influence of the six flow control structures installed during the channel straightening is assumed to have slowed upstream adjustments during this period similar to the effect constructed pool/riffle sequences would have on improving channel stability. Without these structures, the 58% reduction in stream length, doubling of slope, would have resulted in much higher initial sediment transport rates. Field reconnaissance and modeling information has established that Big Creek is currently transitioning out of a Stage IV of channel evolution (incision and widening process). This is 60 years from the initial disturbance (Stage II), which implies that the channel may take many years to evolve through the Stage V phase of widening to restabilization (Stage VI). The integration of disturbance history, identification of the active channel response processes (CEM), and determination of sedimentation rates as a surrogate for channel adjustment rates allows for reasonable determination of future channel response. Combining sedimentation rates as determined by sediment budget and radiometric analysis methods is an alternative for estimating average channel adjustment rates when typical data and information are not available.

REFERENCES

Allgire, R. (1991). "Comparison of 1987 and 1989 bed profile surveys of the Lower Cache River," Illinois State Water Survey, Contract Report 508, Champaign, IL, 8 p.

Allgire, R. L. and Cahill, R. A. (2001). "Benchmark sedimentation survey of the Lower Cache River wetlands," Illinois State Water Survey, Contract Report 2001-17, 42 p.

Bogner, W. C., Fitzpatrick, W. P. and Blakley, D. S. (1985). "Sedimentation rates in Horseshoe Lake, Alexander County, Illinois," Illinois State Water Survey, Contract Report 364, 55 p.

Bogner, W. C., Lin, S. D., Hullinger, D. L. and Raman, R. K. (1997). "Diagnostic-feasibility study of Vienna Correctional Center Lake, Johnson County, Illinois," Illinois State Water Survey, Contract Report 619, 113 p.

Cahill, R. A. and Autrey, A. D. (1987). "Measurement of 210-Pb and 137-Cs, organic carbon and trace elements in sediments of the Illinois and Mississippi Rivers," Journal of Radioanalytical and Nuclear Chemistry, 110:197-205.

Crickmore, M. J., Tazioli, G. S., Appleby, P. G. and Oldfield, F., Eds. (1990). "The use of nuclear techniques in sediment transport and sedimentation problems," IHP-III Project 5.2 SC-90/WS-49, UNESCO, Paris, France.

Demissie, M., Fitzpatrick, W. F. and Cahill, R. A. (1992). "Sedimentation in the Cache River wetlands: comparison of two methods," Illinois State Water Survey, Miscellaneous Publication 129, Champaign, IL, 43 p.

Demissie, M., Knapp, H. V., Parmar, P. and Kriesant, D. (2001). "Hydrology of the Big Creek watershed and its influence on the Lower Cache River," Illinois State Water Survey, Contract Report 2001-06, Champaign, IL, 114 p.

Demissie, M., Soong, T. W., Allgire, R., Keefer, L. and Makowski, P. (1990). "Cache River Basin: hydrology, hydraulics, and sediment transport. Volume 1: Background, data collection, and analysis," Illinois State Water Survey, Contract Report 484, Champaign, IL, 173 p.

Demissie, M. and Xia, R. (1991). "Channel stabilizing structures for the Upper Cache River," Illinois State Water Survey, Contract Report 511, Champaign, IL, 21 p.

Hupp, C. R. (2000). "Hydrology, geomorphology, and vegetation of coastal plain rivers in South-Eastern USA," Hydrological Processes, 14:2991-3010.

Hupp, C. R. and Bornette, G. (2003). Vegetation as a Tool in the Interpretation of Fluvial Geomorphic Processes and Llandforms in Humid Temperate Areas. Tools in Fluvial Geomorphology. Edited by G. M. Kondolf and H. Piegay. John Wiley & Sons, Ltd. p. 269-288.

Hutchison, M. D. (1984). "Lower Cache preservation plan," The Nature Conservancy, Chicago, IL, 97 p.

Ritchie, J. C. and McHenry, J. R. (1990). "Application of radioactive fallout ^{137}Cs for measuring soil erosion and sediment accumulation rates and patterns: A review," Journal of Environmental Quality, 19:215-233.

Santschi, P. H. and Honeyman, B. D. (1989). "Radionuclides in aquatic environments," International Journal of Radiation and Applied Instrumentation, Part C, Radiation Physics and Chemistry, 32(2):213-240.

Schumm, S. A., Harvey, M. D. and Watson, C. C. (1984). Incised Channels: Morphology, Dynamics and Control. Water Resources Publications. 200 p.

Simon, A. (1989). "A model of channel response in disturbed alluvial channels," Earth Surface Processes and Landforms, 14:11-26.

Simon, A., Doyle, M. W., Kondolf, G. M., Shields, F. D., Jr., Rhoads, B. L., Grant, G. E., Fitzpatrick, F. A., Juracek, K. E., McPhillips, M. and MacBroom, J. (2005). "How well do the Rosgen Classification and associated "Natural Channel Design" methods integrate and quantify fluvial processes and channel response?" Proc. of World Water and Environmental Resources Congress 2005, Anchorage, AK, ASCE p. 12.

Trimble, S. W. (1998). "Dating fluvial processes from historical data and artifacts," Catena, 31:283-304.

Urban, M. A. and Rhoads, B. L. (2003). "Catastrophic human-induced change in stream-channel planform and geometry in an agricultural watershed, Illinois, USA," Annals of the Association of American Geographers, 94(3):783-796.

Walling, D. E., Russell, M. A., Hodgkinson, R. A. and Zhang, Y. (2002). "Establishing sediment budgets for two small lowland agricultural catchments in the UK," Catena, 47:323-353.

Zhang, Y., Walling, D. E., Quine, T. A. and Wen, A. (1997). "Use of reservoir deposits and caesium-137 measurments to investigate the erosional response of a small drainage basin in the Rolling Loess Plateau Region of China," Land Degradataion & Development, 8:1-16.

EFFECTS OF REGULARLY REVERSING ENERGY GRADIENTS ON SEDIMENT TRANSPORT IN A TIDAL WETLAND SYSTEM

Kevin Knuuti, P.E., U.S. Army Engineer Research and Development Center, Vicksburg, Mississippi, knuutik@wes.army.mil

INTRODUCTION

During the past two decades, people have become much more aware of the biological importance of tidal wetlands. This awareness has led to a dramatic increase in the number of tidal wetland restoration projects being planned and constructed around the United States. In planning and constructing these projects, engineers and geomorphologists often design or predict the morphology of the channel networks that exist in the wetlands. These channels are critical to the habitat zones that will develop in the restored wetlands because they control the depth and frequency of inundation of the different areas of the wetlands and thus control the types of plant communities that can survive in those habitat zones.

Tidal wetland restoration projects frequently begin with ecological goals based on an optimum mix of habitat zones. The habitat zones usually progress out from the wetland channels, with the channel bottoms supporting subtidal or intertidal plant species and the areas farthest away from the channels supporting transitional or upland plant species. The types of species that can survive in an area of the wetland are determined by the depth and frequency of tidal inundation of that area. As an example, a tidal wetland in New England may be designed to support *Zostera marina (*eel-grass, a subaquatic species) habitat in the wetland channels, to support *Spartina alterniflora* (cord grass, an intertidal species that typically colonizes an area between mean sea level (MSL) and mean high water (MHW)) habitat in the zone immediately adjacent to the wetland channels and on the marsh surface, and to support a zone of mixed *Juncus gerardii* (black grass) and *Distichlis spicata* (spike grass) (both upper high marsh species that typically colonize an area between MHW and mean spring high water (MSHW)) habitat between the *alterniflora* zone and the upland (non-tidal) zone.

Unfortunately, due to insufficient understanding of the physical processes involved in shaping tidal wetlands, many of these projects fail to meet their habitat restoration goals. One manner of failure is excessive erosion or deposition of sediments in various areas of the wetlands. If the wetland channels are not properly designed or if their morphology is not properly anticipated, zones that were planned to be intertidal may end up actually becoming subtidal or upland habitat. Current methods of designing wetland channels and anticipating morphologic characteristics such as channel width and depth are commonly based on empirical relationships (Coats, 1995) with high levels of uncertainty. This paper presents the initial methods, along with some preliminary results, of a physics-based approach to describing how reversing tidal flows affect erosion and deposition in tidal wetland channels. Since this paper describes what is, at this point, work in progress, it is somewhat incomplete. The conference presentation and subsequent papers will provide more detail and more results, based on the data collected and additional analysis.

Within this paper, tidal wetlands are defined as wetlands that are subjected to regular inundation by salt or brackish water due to astronomical tides. Wetlands which are normally unaffected by astronomical tides, but which are periodically inundated by meteorological tides (surges) are not included in this definition or in this paper.

TIDAL WETLAND MORPHOLOGY AND DESIGN

Tidal Wetland Morphology: Tidal wetlands can take many forms, depending on the percent area of emergent land, the tidal range, and the depth and frequency of submergence of the subtidal and intertidal areas. Wetlands with a relatively small (percentage) emergent area, and with a relatively large (percentage) subtidal area often take the form of lagoons interspersed with connected and unconnected islands. Wetlands with a relatively large (percentage) emergent or intertidal area and a relatively small (percentage) subtidal area often take the form of marshes interlaced with a dendritic network of channels. Flooding of the marsh surface in these types of wetlands may be by transmission of water through the wetland channels to interior areas or by submergence of the marsh and transmission of tidal waters over the entire marsh surface at higher tide stages. Channels in these types of wetlands

are often highly sinuous (Fagherazzi, 2004) with widths and depths that usually decrease as distance from the channel mouth increases.

Influencing Factors: Channel morphology in tidal wetlands is influenced by many of the same factors that influence upland rivers and streams, but is complicated by the varying and dynamic nature of tides. Tidal range, regime (diurnal, semidiurnal, or mixed), and asymmetry determine the depths, durations, and frequencies for which various land-surface elevations are submerged. Tidal range and regime can be partially characterized by tidal datums, such as mean lower low water (MLLW), mean low water (MLW), mean tide level (MTL), MHW, mean higher-high water (MHHW), and mean spring high water (MSHW). These datums are determined and published by the National Ocean Service (NOS) for tide gauge locations around the United States. Tidal asymmetry can be estimated by comparing the relative times of high tides and low tides or by examining the tidal harmonic constituents calculated by NOS for various tide gauge locations.

The topography and elevation of the marsh surface (with respect to the local tidal datums), the marsh size, and the type of vegetative cover on the marsh surface all affect the boundary shear stresses in the wetland channels. These boundary shear stresses, and the marsh surface and channel bed and bank material characteristics, govern the potential for erosion and sediment transport throughout the wetland system.

Tidal Wetland Channel Design: In areas where tidal wetlands have been completely eliminated or severely degraded, the restoration (or creation) process involves designing, or at least anticipating, the locations, widths, depths, and sinuosities of the wetland channels. The wetlands may be designed and constructed to their planned final form prior to reintroducing tidal action or they may be only partially restored with the final wetland form shaped by the erosion and deposition of sediments that will occur after reintroducing tidal action. In the case of the tidal wetland that is constructed to its final or near final form prior to reintroducing tidal action, the channel design is critical to ensuring the wetland system is successful and does not dramatically change from its desired (and constructed) form. In the case of the tidal wetland that is only partially restored prior to reintroducing tidal action, understanding how the wetland channels will evolve and being able to accurately predict which areas of the wetland will experience significant erosion or deposition of sediments is also critical to a successful restoration project. For each of these cases, understanding how to design or predict the form of the wetland channels is essential.

General Assumptions: Several assumptions related to tidal characteristics, tidal currents, tidal prism, channel velocities and channel form are common, though not necessarily accurate, in tidal wetland channel design. Some of these common assumptions are:

- Horizontal tidal currents can be anticipated based on the rate of rise or fall of the tides and used to estimate the direction of net sediment transport (Walker, 1988),

- Peak velocities in a channel are uniform along the entire channel length for both ebb and flood flows (Pestrong, 1965; Myrick, 1963; Fagherazzi, 2004).

Ebb/Flood Dominance: Determining whether a tidal wetland is dominated by ebb or flood tides by comparing the rates of tidal rise to tidal fall assumes that the velocity of horizontal tidal currents is primarily due to the rate of change of the water level. While this may initially seem reasonable, analysis of measurements taken by NOS indicates it is not necessarily true. In its published tidal current tables, NOS (2005) explains that "the relation of current to tide is not constant, but varies from place to place" and that "the time of maximum speed of the current [does not] usually coincide with the time of most rapid change in the vertical height of the tide." Assuming flood or ebb dominance, based on predicted tides for a given location, can thus lead to incorrect conclusions that a wetland system experiences a net loss or gain of sediment due to tidal currents.

Empirical Relationships: Channel characteristics, such as width and depth, are sometimes designed based on empirically-derived relationships between tidal prism and channel width and depth (Coats, 1995). These relationships are similar to those developed in early work on upland rivers and streams that related drainage area or discharge to channel width and slope (Leopold, 1964 and Julien, 1995). Many of these relationships, however, fail to include such critical factors as bed material and bank material characteristics and the elevation of the wetland surface with respect to the local tidal datums. The result is that many of these relationships have extremely high

levels of uncertainty associated with them and can, at best, only be used for very crude estimations of channel width and depth (Knuuti, 2000).

Application of Fluvial Hydraulics Methods: Stable channel design for stream and river restoration projects is often based on calculations of sediment transport over a channel's full range of discharges (Watson, 2005; Copeland, 2001; and Soar, 2001). This method involves using the channel bed material characteristics, the discharge hydrograph, and the physical features of the channel to design a stable cross section and planform. This method may also be applicable in tidal wetland channels, but is significantly complicated by the fact that the energy grade line of the water in the channels is constantly changing and reversing. Channel beds in tidal wetlands almost always slope down toward the channel mouths, but the energy grade line only slopes in this direction during an ebbing tide. During a flood tide, the energy grade line slopes is in the opposite direction. The result of this varying and reversing energy gradient is that bed material in a tidal wetland channel is alternately transported into (during a flood tide) and out of (during an ebb tide) the wetland channel. Stable design of a tidal wetland channel must take this into account in order to be effective.

ONGOING WORK

Background: Designing tidal wetland channels using a physics-based approach that is similar to the approach used in traditional fluvial hydraulics may allow designers to be more certain of their results than they would be using empirical relationships and general assumptions. This type of approach requires a thorough understanding of the hydraulic processes in tidal wetland channels. Various previous studies have examined suspended sediment processes (Ward, 1981), discharge asymmetries (Boon, 1975 and Reed, 1987), and velocity surges (Pethick, 1980) in tidal wetlands. None of these studies, however, have comprehensively examined the full range of physical processes, based on wetland characteristics and tidal range and regime, involved in tidal wetland channel hydraulics and stability. A new effort, under the U.S. Army Corps of Engineers' System-Wide Water Resources (research) Program (SWWRP), is beginning to study this range of physical processes in an attempt to better guide tidal wetland restoration projects.

Approach: Initial work involved collecting data for use in documenting and explaining the hydraulic processes in the wetland channels by measuring channels characteristics, water stage and water velocities at several locations, simultaneously, in several different tidal wetland channels. Tidal wetland channel planform was measured and recorded using newly collected, high-resolution, digital ortho-rectified aerial photographs. Tidal wetland topography was mapped using a combination of differential global positioning system (DGPS) and traditional (total station and optical level) surveying methods. Tidal wetland channel cross sections were surveyed at numerous locations and tied into the wetland topographic mapping. Vegetation types, within the wetland channels and on the marsh surface, were recorded and measured. Sediment characteristics, to include grain-size distributions for bed material, thickness of peat layers on the marsh surface, and organic content of bed and bank materials were recorded at each surveyed channel cross section. Water stage was monitored using both traditional staff gauges and acoustic water-level meters. Water-velocity profiles were recorded using bed-mounted acoustic Doppler current profilers (ADCPs). Some channels in the study areas were only surveyed, while others were surveyed and monitored for water stage and velocity. Each channel that was monitored for water stage and velocity had staff plates and ADCPs mounted at several locations simultaneously. ADCP time clocks were synchronized so both the temporal the spatial variations in the water levels and velocities could be determined. Tide and weather (wind speed and direction and barometric pressure) conditions were monitored at each location using newly installed weather stations and tide gauges.

Study Sites: Initial data collection efforts have been completed in four different tidal wetlands, all within New England. The wetland locations are in Wells, Maine; Seabrook, New Hampshire (Figure 1); Revere, Massachusetts; and Duxbury, Massachusetts. In each of these wetlands, numerous measurements of wetland topography and channel geometry have been made. More detailed data collection, to include water stage and water velocity profiles, has been completed in four of the surveyed wetland channels in Wells, Maine and Seabrook, New Hampshire. Although many of the tidal wetlands in New England have undergone severe ditching over the past century, as part of hay farming and mosquito-control efforts, the four wetland channels selected for detailed study are in areas that have never been ditched or otherwise altered by unnatural influences.



Figure 1 Tidal wetland in Seabrook, New Hampshire

Methods: After collecting aerial photographs and examining the wetland sites in person, the wetland areas were surveyed and sediment samples were collected. Several channels were selected and ranked in order of priority for more detailed data collection. Water levels and velocity profiles were monitored for periods of time varying from thirteen hours to five days, depending on how the times of high and low tide coincided with daylight hours. Each period of data collection closely coincided with a full moon, in order to obtain the highest tides and the best variation in successive high tides possible, in the shortest amount of time. With the sites all being in New England, detailed data collection efforts were also planned to avoid the extreme low temperatures that occur between December and March, due to equipment limitations and freezing water in the channels.

Tide gauges in the estuaries, but near the mouths of the channels, were used to measure the tide stage outside the wetlands. The varying tide stage at these locations is what drives the hydraulics in the wetland channels and can be used to examine water surface slope. After installing staff gauges at the desired channel cross sections, low-profile ADCPs were installed on the channel beds at low tide. Each channel studied had three to four ADCPs installed, at various locations successively farther up the channel from the mouth. ADCPs were installed in channel locations that appeared to be dominated by one-dimensional flows, along the channel axis, with minimal secondary circulation effects. These locations were determined by considering channel planform, channel cross-sectional geometry, and channel bed-form orientation. After installation, the ADCPs were surveyed to record their elevations and the staff gauges were monitored throughout the tidal cycle. ADCPs were removed during another low tide, at the end of the sampling period.

Data Collection: For each channel with detailed data collection, basic parameters such as wind speed, wind direction, and estuarine tide stage were recorded. Within the channels, water level, water-velocity profiles and water temperature were continuously recorded. In order to be able to assess the quality of the data collected with the ADCPs, the signal strength, acoustic backscatter, standard error, and flow direction were also collected and examined. ADCP data were sampled at a rate of 1 Hz and were later averaged over continuous 60-second periods to remove small-scale turbulent fluctuations and wind-wave effects.

Data Analysis: Prior to beginning field data collection, it was anticipated that the hydraulics in the channels would be driven by the long-wave mechanics associated with tidal propagation. For each of the channels studied, however, it was apparent that the time of slack water coincided almost exactly with the time of high tide. One possible reason to explain this was that the small tidal channels may have attenuated the propagating tide wave enough to allow the

time of slack water to coincide with the time of high tide. Because the channels were relatively short and because this attenuation and phase lag was not seen in the estuary near the mouth of each channel, an alternative explanation was considered. That explanation was that flow in the wetland channels was driven primarily by the head difference between the channel mouth and the upper reaches of the channel. If that was the case, it might be possible to consider the flow in the wetland channels to be steady, uniform flow and to apply the methods commonly used to examine sediment transport in rivers and streams to the wetland channels.

Considering the flow in the wetland channels to be steady and uniform seemed somewhat far-reaching, at first. The channels are not prismatic since they have horizontal banks and sloping beds and taper from wide mouths to narrow upper reaches in only a few thousand meters. Flow in the channels includes velocities that regularly change and water depth is constantly cycling from low tide to high tide. Still, the velocity changes, depth changes, and channel narrowing were gradual so quasi-steady, gradually-varied flow seemed possible. To test this assumption, the hydraulic grade line along a channel reach was assumed to be parallel to the energy grade line. The slope of this measured line, as it varied throughout a tidal-day in one-minute increments, was used along with the measured water depths to predict the mean water velocity in the channel, using Manning's equation. This series of one-minute velocity calculations was compared to the measured mean velocities, also in one-minute increments, in the same reach of channel. The agreement between measured and calculated velocities was quite good so the assumptions of head-driven, quasi-steady, gradually-varied flow were considered reasonable for basic analysis.

Data were then analyzed to determine how the constantly changing and reversing energy grade line affected boundary shear stress at the bed (bed shear stress) and sediment transport potential throughout a tidal cycle (one flood and one ebb). Bed shear stress τ_o was calculated using

$$\tau_o = \gamma R_h S_f \tag{1}$$

where γ is specific weight of water, R_h is channel hydraulic radius, and S_f is energy slope. The median bed-material particle diameter was determined from the bed material grain size distribution and converted to a dimensionless particle diameter d_* using

$$d_* = d_{50}[(G-1)g/\upsilon^2_m]^{1/3} \tag{2}$$

where d_{50} is the median grain diameter for the bed material, G is specific gravity, g is gravitational acceleration, and υ_m is kinematic viscosity of water. Shields parameter τ_* was then calculated using

$$\tau_* = \tau_o/[(\gamma_s-\gamma)d_{50}] \tag{3}$$

where γ_s is the specific weight of a sediment particle. Shields parameter values were calculated for every minute of the measured tidal cycle and compared to the critical value of the Shields parameter to determine if the boundary shear stress was great enough to mobilize the median grain size of the bed. The critical value of the Shields parameter τ_{*c} was approximated using

$$\tau_{*c} = 0.25 d_*^{0.4} \tan\varphi \tag{4}$$

where φ is the angle of repose for the median bed material size. The total time durations of the median bed material being mobilized during flood and ebb tides were then compared in order to provide a very quick estimate of whether the net time of transport was into or out of the wetland channels. This method is, admittedly, fairly crude but provided a relatively quick method for initial assessment and for assessing the feasibility of more rigorous methods.

INITIAL RESULTS

Velocities: Velocities in the tidal channels were generally asymmetrical about high tide for each cross section. All velocity plots were significantly different, in terms of asymmetry and surges, than the plots of predicted tidal currents in the estuaries near the mouths of the tidal channels. One important aspect of the channel velocities was the obvious surge in velocity corresponding to the time when the rising tide overtops the upper limit of the channel banks and begins to flood the marsh surface. A corresponding, though less intense, velocity surge occurs on the

falling tide. This velocity surge can be clearly seen in Figure 2. In this figure, the thin horizontal line represents the channel bank elevation and the vertical red lines show how the time when the tide level meets the bank height corresponds to the surges in velocity. The intensity of this overbank velocity surge varied with maximum depth of water above the bank at high tide, and with location of the channel cross section. Initial analysis indicates the overbank velocity surges are less dramatic closer to the mouths of the channels. Mean channel velocities varied slightly with location along the channel axis, but not dramatically.

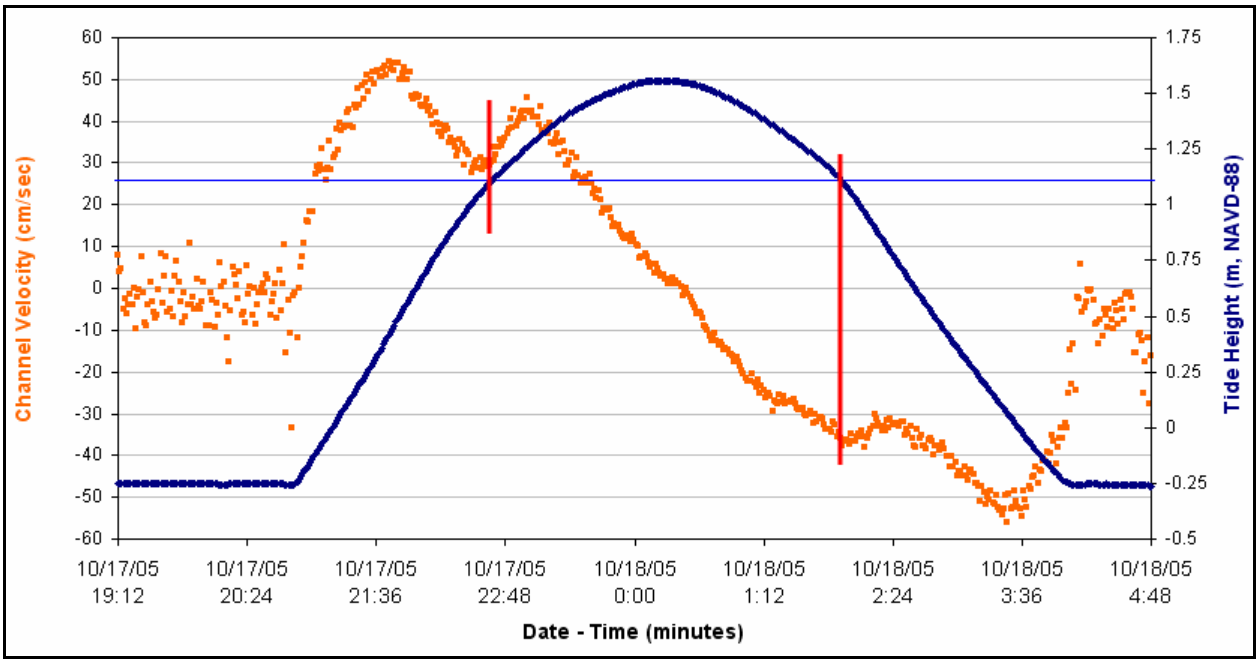


Figure 2 Mean channel velocity variations with time (Seabrook XS-B7)

Water Levels and Energy Gradients: Water levels varied both spatially and temporally throughout each wetland channel. With only small variations in velocity, the energy grade line closely paralleled the hydraulic grade line. Figure 3 shows the variation in the energy grade line at one channel cross section measured in the wetland in Seabrook, New Hampshire. Horizontal portions of the energy grade line, at the beginning, in the middle, and at the end represent times when the channel was dry or the water level was low enough that it could not be accurately measured. Short-term variability in the energy grade line, and spikes immediately adjacent to the horizontal portions of the plot, are due to noise in the data

Shear Stress and Sediment Transport: Preliminary calculations of bed material transport potential in the tidal wetland channels were based only on the median bed material grain size. Times of flood and ebb transport were used as a quick estimate of the direction of net sediment transport and were determined by comparing the total number of minutes when the Shields parameter exceeded the critical Shields parameter for the flood and ebb portions of the tide. For the two low-high-low tidal cycles recorded and presented in Figure 3 and Figure 4, the first cycle indicated a possible net sediment export from the channel with the time of sediment export exceeding the time of sediment import by 44 minutes. The second cycle of this series, however, indicated a possible net sediment import to the channel, with the time of sediment import exceeding the time of sediment export by 36 minutes. Together, the two low-high-low cycles had a net time of sediment export from the channel of only eight minutes, or very close to equilibrium. It is important to remember that the net volume of sediment transport may or may not be similar to the net time of transport into or out of the channels. To properly estimate net sediment transport volumes, sediment transport rates and distances would have to be considered, along with lengths of time for slack water periods, and transport would have to be calculated for much longer tidal cycles, such as the 365-day solar year or the 4.4-year lunar perigee modulation cycle. It is also important to note that the channels chosen for this study were selected, in part, due to their apparent long-term stabilities (based on aerial photo analysis and interviews with local residents) and equilibrium natures.

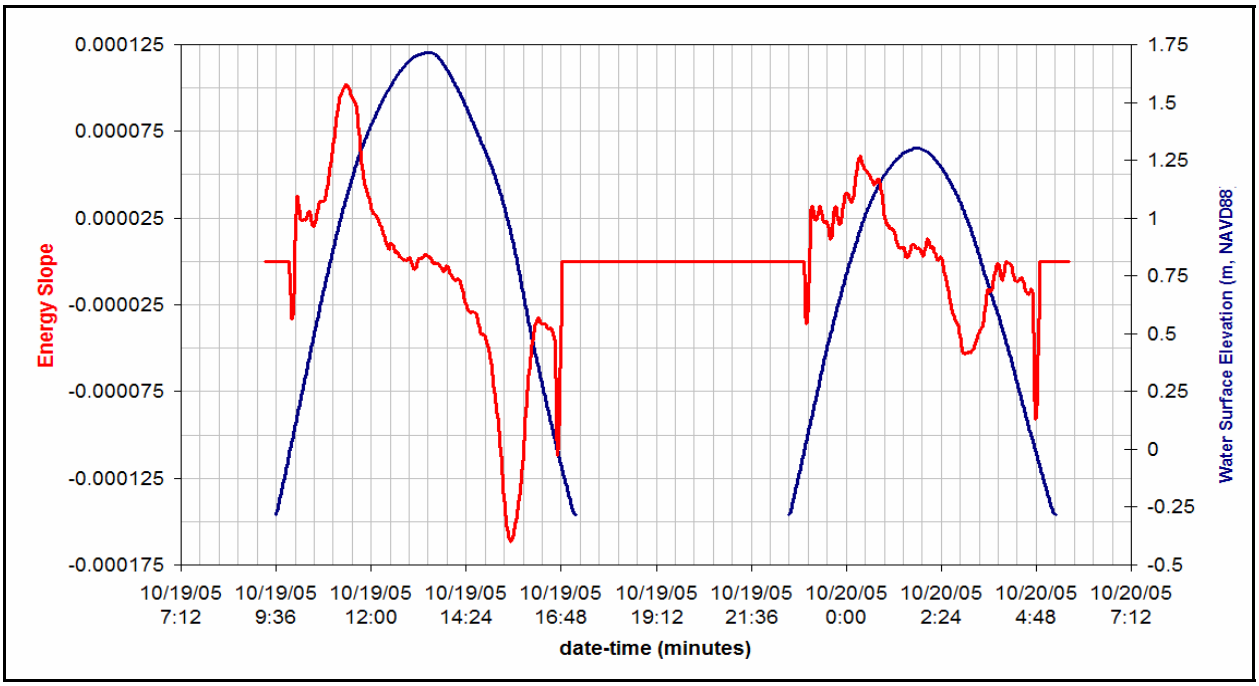


Figure 3 Energy grade line variations over two successive tidal cycles (Seabrook XS-A2)

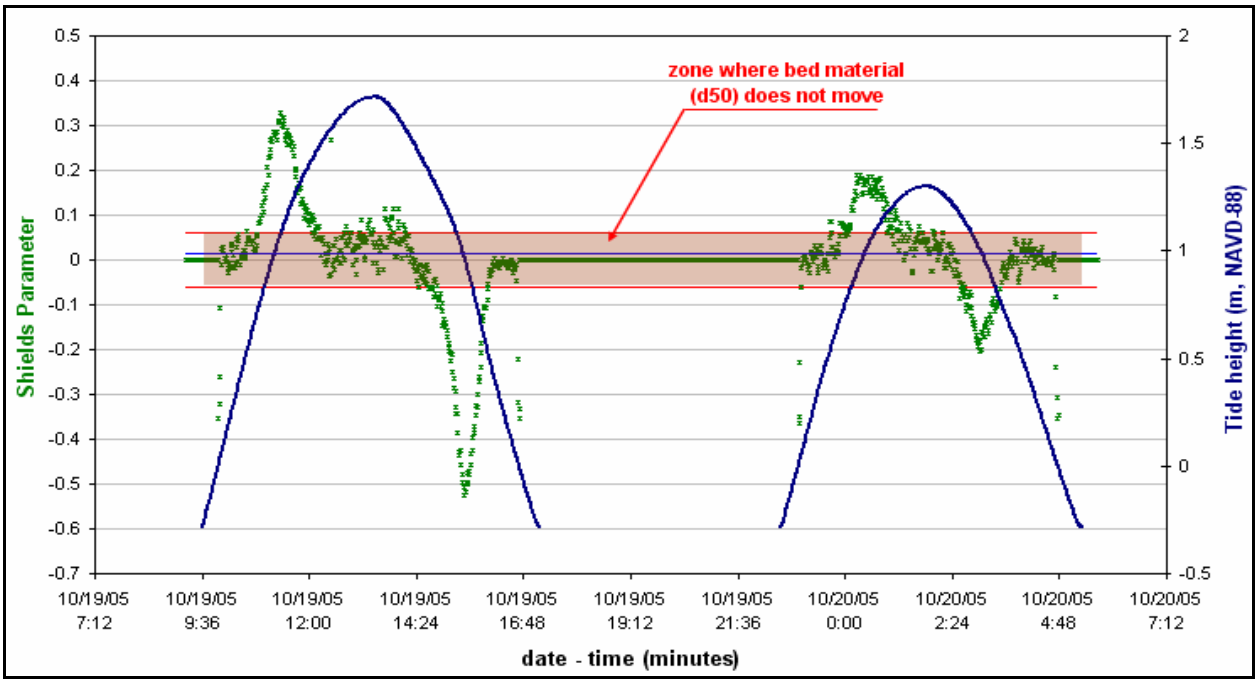


Figure 4 Calculated Shields parameter values compared to critical Shields parameter (Seabrook XS-A2)

FUTURE WORK

Data Analysis: Work on this topic should continue, under the SWWRP, for at least the remainder of this fiscal year and possibly throughout fiscal year 2007, as well. Initially, additional work will focus on continuing to analyze the existing data from the three study sites but using much more rigorous methods. In particular, the effect of tidal range (between different tidal datums) on velocity and shear stress will be examined as will the effect of changing

bedforms (throughout the tidal cycle) on velocity profiles. Net sediment transport calculations will be expanded to include transport of the full range of sediment sizes present in the bed material. In order to improve on some of the geomorphic relationships between tidal prism and channel width and depth that have been developed by others, detailed calculations of tidal prism will be made and compared to several different channel cross sections.

Numerical Modeling: Numerical models of tidal wetlands are most commonly developed using estuarine circulation and water level models. Many of these models have difficulty modeling the processes in tidal wetlands due to rapid land surface variations and severe wetting and drying. Two numerical models have already been developed for the estuary in Seabrook, New Hampshire and will be modified in an attempt to see how well they can model the processes occurring in the tidal wetland channels. A third numerical model, which is currently under development at the U.S. Army's Engineer Research and Development Center, will be modified and used in an attempt to improve on the results currently possible with existing numerical models.

Use of Remote Sensing Data: Part of the data collection effort that has already been completed included collecting topographic and bathymetric LIDAR data for each of the study sites. The LIDAR data will be compared to the DGPS and traditional survey data collected at each site to determine how accurate the LIDAR system is for mapping ground elevations in densely vegetated coastal wetlands. If the LIDAR data proves to be reasonably accurate, it will be used to develop topographic maps of the wetland sites which will then be used for tidal prism calculations and numerical model development.

REFERENCES

Boon, J.D. (1975). "Tidal discharge asymmetry in a salt marsh drainage system," Limnology and Oceanography, 20(1), pp 71-80.

Coats, R.N., et. al. (1995). Design Guidelines for Tidal Channels in Coastal Wetlands. Unpublished report prepared for the U.S. Army Corps of Engineers Waterways Experiment Station.

Copeland, R.R., et. al. (2001). Hydraulic Design of Stream Restoration Projects. U.S. Army Corps of Engineers Report ERDC/CHL TR-01-28, Vicksburg, Mississippi.

Fagherazzi S., et al. (2004). "The effect of bidirectional flow on tidal channel planforms," Earth Surface Processes and Landforms, (29), pp 295–309.

Julien, P.Y. and Wargadalam, J. (1995). "Alluvial channel geometry: theory and applications," Journal of Hydraulic Engineering, ASCE, 121 (4), pp 312-325.

Julien, P.Y. (1998). Erosion and Sedimentation. Cambridge University Press. New York.

Knuuti, K. (2000). "Assessment of using hydraulic geometry relationships to estimate channel characteristics in San Francisco Bay coastal wetland restoration projects," U.S. Army Corps of Engineers internal report.

Leopold, L.B., Wolman, M.G., and Miller, J.P. (1964). Fluvial Processes in Geomorphology. Dover Publications, Inc., New York.

Leopold, L.B., Collins, J.N. and Collins, L.M. (1993). "Hydrology of some tidal channels in estuarine marshland near San Francisco," CATENA, Cremlingen, 20, pp 469-493.

Myrick R.M, Leopold L.B. (1963). "Hydraulic geometry of a small tidal estuary," U.S. Geological Survey Professional Paper 422-B.

National Ocean Service (2005). Tidal Current Tables 2005. International Marine. Camden, Maine.

Pestrong R. (1965). "The development of drainage patterns on tidal marshes," Stanford University, Publications in Geological Science (10).

Pethick, J.S. (1980). "Velocity surges and asymmetry in tidal channels," Estuarine and Coastal Marine Science, (11), pp 331-345.

Reed, D.J. (1987). "Temporal sampling and discharge asymmetry in salt marsh creeks," Estuarine, Coastal and Shelf Science (25), pp 459-466.

Soar, P.J., and Thorne, C.R. (2001). Channel Restoration Design for Meandering Rivers. U.S. Army Corps of Engineers Report ERDC/CHL CR-01-01, Vicksburg, Mississippi.

Walker, J.R., et al. (1988). "Hydraulic aspects of wetland design," Proceedings of the Twenty-first Coastal Engineering Conference, American Society of Civil Engineers, pp 2666-2680.

Ward, L.G. (1981). "Suspended-material transport in marsh tidal channels," Marine Geology (40), pp 139-154.

Watson, C.C., Biedenharn, D.S., and Thorne, C.R. (2005). Stream Rehabilitation. Cottonwood Research LLC, Fort Collins, Colorado.

RECENT CHANNEL INCISION AND FLOODPLAIN EVOLUTION WITHIN THE MIDDLE RIO GRANDE, NM

Tamara Massong, Hydrologist, Bureau of Reclamation, Albuquerque, NM, tmassong@uc.usbr.gov; Paul Tashjian, Hydrologist, Fish and Wildlife Service, Albuquerque, NM, Paul_Tashjian@fws.gov; Paula Makar, Hydraulic Engineer, Bureau of Reclamation, Denver, CO, pmakar@do.usbr.gov .

INTRODUCTION

The Rio Grande was historically an aggrading river system with a wide, sandy, braided planform with an even more extensive floodplain/wetland system inundated during high flows (Scurlock 1998). Consecutive flooding of irrigated and inhabited lands prompted the Middle Rio Grande Project to create a series of large dams on the Rio Grande and its major tributaries (1950s-1970s) to control flooding and sedimentation (Lagasse 1980). Much of the Middle Rio Grande (MRG) today is no longer flooding and aggrading, but rather is evolving at a rapid rate in the opposite direction. For example, the active channel width, which has been decreasing since the 1930s, had a measurable decrease between the 2001-2002 data sets (Makar et al., 2006). The historical floodplain is in many places abandoned, with the formation of vegetated bars constituting the majority of flooded surfaces in these areas (Tashjian et al., 2006). As much of the floodplain became abandoned through degradation of the channel bed (a.k.a., incision), bank heights grew, but their growth has not appeared systematic as they change throughout the MRG (Klawon and Makar 2002, Massong et al. 2002, Ortiz 2004, and Massong 2005).

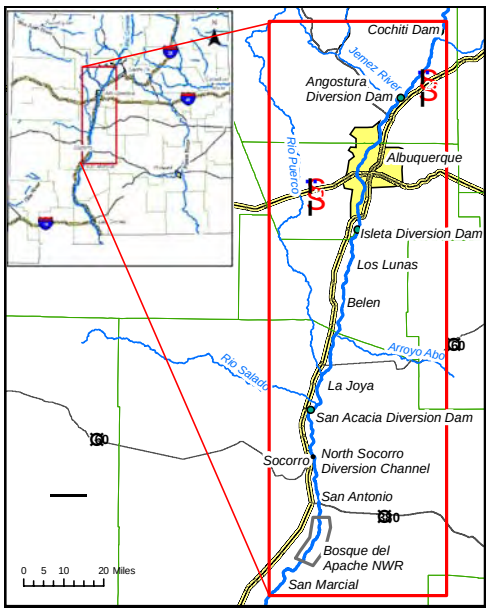


Figure 1 Location of the Middle Rio Grande (MRG) within the state of New Mexico.

The main purpose of this paper is to describe the current pattern of floodplain abandonment through examining bed incision data and terrace formation within the MRG and secondly to

discuss possible governing processes that are influencing the channel bed elevations. The study extends from Cochiti dam at Cochiti, NM to the head of Elephant Butte Reservoir at the historic town of San Marcial, NM (Figure 1), a river reach of approximately 170 river miles (RM).

DATA AND METHODS

A variety of data were used to assess the degree of channel incision throughout the MRG. These data include: terrace maps in the high incision areas, field observations of bank heights where terrace maps do not currently exist, historical bed elevation data, current (2002) bed and bank elevation data, aerial photography, and existing GIS base layer/map data.

Data collected from field visits and plane flights determined location and degree of historical floodplain abandonment. Spring 2005 aerial photography, accomplished through a cooperative effort lead by the U.S. Fish and Wildlife Service, the New Mexico Interstate Stream Commission, and the U.S. Army Corps of Engineers, funded through the ESA Collaborative Program, the U.S. Army and the State of New Mexico, was also reviewed. Floodplains that remained dry throughout the runoff were confirmed abandoned. In the locations where the floodplain became inundated, an attempt was made to determine the river discharge at the time of flooding, as the 2005 runoff peak was greater than a 2-year event.

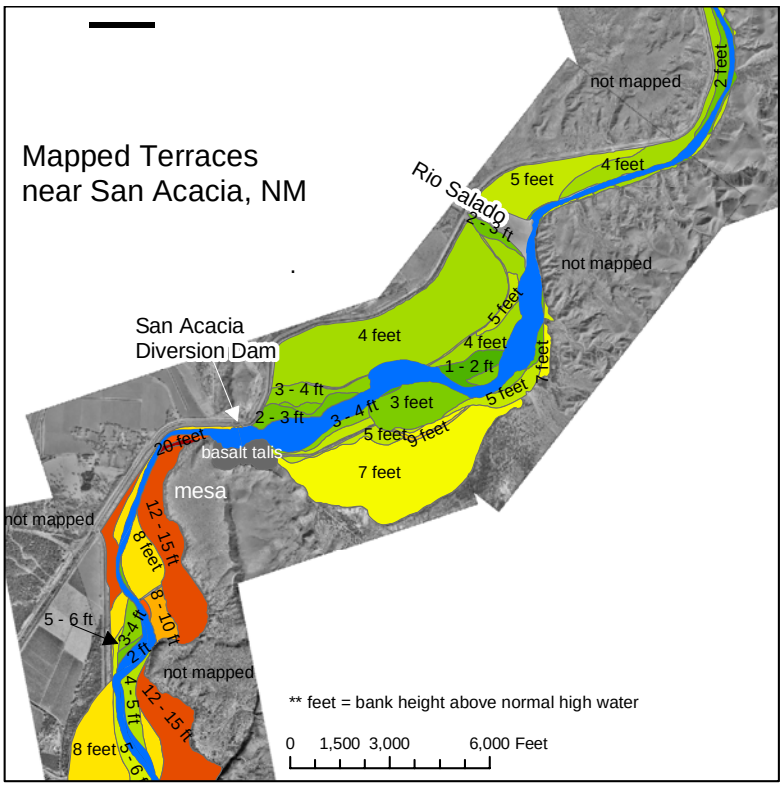


Figure 2 Sample of the abandoned floodplain data in the San Acacia, NM area that shows terrace height data associated with each polygon; partial data set from Massong 2005.

A series of historical terraces/abandoned floodplains exist throughout the MRG (Figure 2), some of which have been mapped; riverine terraces have recently been mapped near Bernalillo-Corrales, NM (Ortiz 2004) and from the Rio Puerco confluence to the head of Elephant Butte (Massong 2005, Klawon and Makar 2002). For locations where data are not available, field visits have been made to observe bank heights and floodplain characteristics.

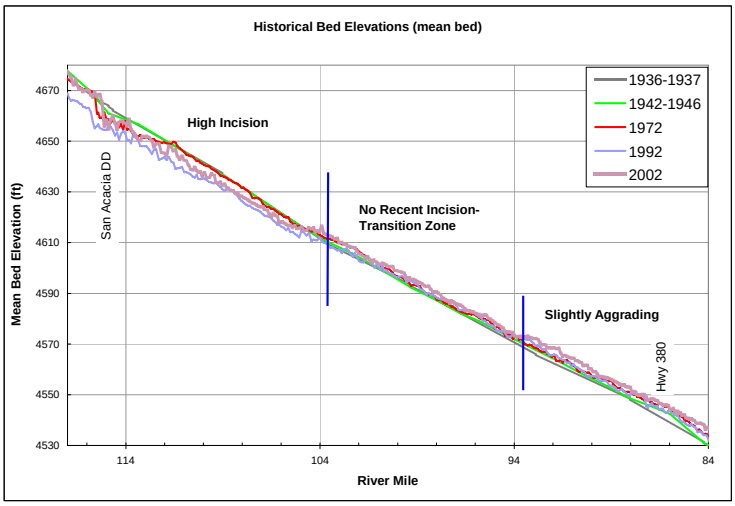


Figure 3 Sample of the Rio Grande bed elevation data available for the Middle Rio Grande; San Acacia Diversion Dam to the U.S. Highway 380 crossing near San Antonio, NM.

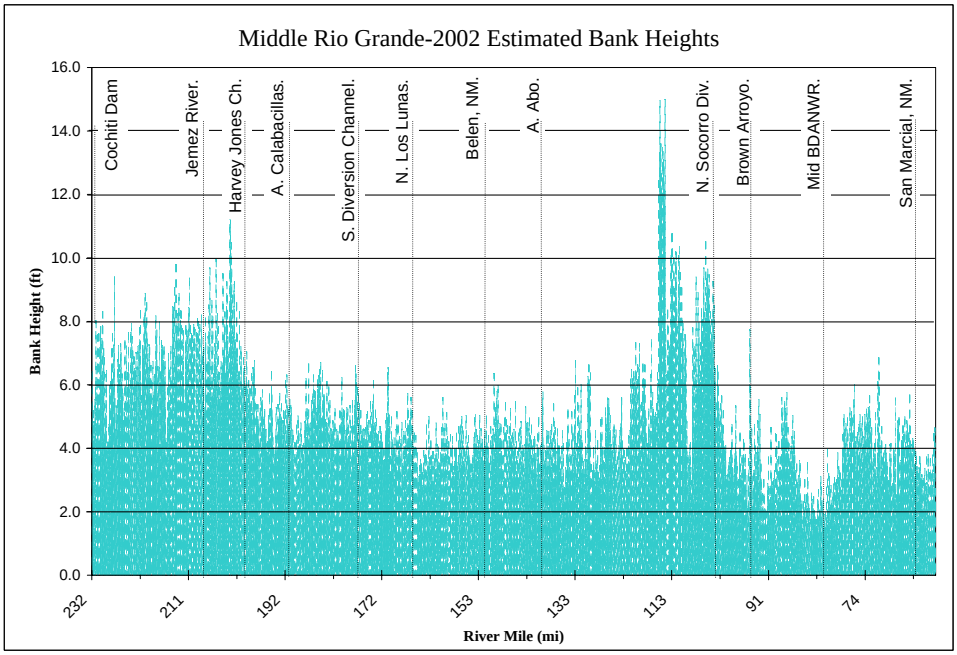


Figure 4 Estimated bank height for the MRG based on cross section data.

Historical and current cross section data (bed elevation data) were compiled by Chris Holmquist-Johnson (Reclamation-TSC, Sedimentation Group, Denver, CO) for: 1936-7, 1942-46, 1952-54,

1962, 1972, 1992, and 2002. Changes in bed elevation were used to initially define incision boundaries (Figure 3). Boundary refinements were made using the 2002 estimated bank height data (Figure 4) and field observations. Historical channel location data and channel outlines were digitized from Reclamation aerial photographs by Jan Oliver (Reclamation-TSC, Remote Sensing Group, Denver, CO). Spatial analyses were performed with ArcMap 9.0.

Incision was estimated first on whether the historic floodplain was currently active, which was assessed predominantly through field observations. Additional field inspections occurred in 2005, when the spring runoff flow exceeded the 2-year return period (peaking at almost 7,000 cfs in Albuquerque, NM). Bed and bank elevation data were used to better define boundaries between different amounts of incision (Figure 3).

RESULTS

Through comparisons of the bank heights and bed degradation data, the study area is divided into eleven reaches that either describes the amount of incision or aggradation present (Figures 4 & 5). The amount of incision ranged from no incision to high with bank heights greater than 6 ft.. In the active floodplain areas, the channel bed aggradation is described as either slightly (<10 ft. since 1935) or rapidly aggrading (>10 ft. since 1935). Reach descriptions follow.

1. Cochiti Dam to Jemez River (24 RM)-Moderate-High Incision: After operations began at Cochiti Dam in 1973, the channel bed immediately began to erode and coarsen (Lagasse 1980) which has continued to the present (Massong 2004). The large grain size that emerged quickly after 1973 is suspected in retarding incision (Lagasse, 1980), such that the floodplain although quickly abandoned, is not more than 6 ft. higher than the current channel elevation.

2. Jemez River to Harvey Jones Channel (10 RM)-High Incision: Bed degradation and coarsening have also been ongoing processes here since 1973, however the bank heights are higher than upstream. Unlike upstream, an extensive series of mid-channel bars emerged in the 1990s, and now act as floodplain surfaces.

3. Harvey Jones Channel to Arroyo Calabacillas (7 RM)-Moderate Incision: Bank height varies from 3-5 ft., decreasing in the downstream direction (Ortiz 2004). The channel planform is in transition from the wide, sand-bar-braided channel so characteristic of the Rio Grande prior to 1973 to a vegetated-island-braided channel with a gravel bed.

4. Arroyo Calabacillas to the South Diversion Channel (14 RM)-Low-Moderate Incision: Channel planform conversion is also ongoing in this section with islands becoming a dominant in-channel feature. However, the incision is less than upstream, with maximum 4 ft. bank height.

5. South Diversion Channel to Northern Los Lunas, NM (13 RM)-Low Incision: Although the historical floodplain is predominantly abandoned, relatively small sections flood at very high flows, as seen in 2005. Numerous mid-channel islands have also evolved in the last 5 years and now act as in-channel floodplains.

6. Northern Los Lunas, NM to Belen, NM (15 RM)-No Recent Incision: The recently formed, vegetated islands and bars as well as the historical floodplain areas became inundated at the highest 2005 flows. The bed elevation data indicates relative stability.

7. Belen, NM to Arroyo Abo (10 RM)-Low-Moderate Incision: Although bank heights are only slightly higher than found upstream, the historical floodplain is abandoned. Extensive vegetated island complexes now flood during the high flows.

8. Arroyo Abo to North Socorro Diversion Channel (36 RM)-High Incision: Unlike in the upstream reaches where one or maybe two historical floodplain surfaces existed, a series of floodplain surfaces are present. Review of historical photos, however, shows that many of the terraces formed prior to 1973 but within the last 100 years. The tallest terraces in this reach exist just downstream from San Acacia, NM (Massong 2005), with a distinct change in terrace heights at the San Acacia Diversion Dam (Figure 2).

9. North Socorro Diversion Channel to Brown Arroyo (9 RM)-No Recent Incision: Within a very short distance, the high upstream incision ends (Klawon and Makar 2002), and the channel bed elevation becomes somewhat stable (Figure 3). This transition reach separates the degradation upstream and aggradation downstream in a very short distance that acts almost as a 'pivot point'.

10. Brown Arroyo to the middle of Bosque Del Apache National Wildlife Refuge (13 RM)-Slightly Aggrading: This section is and has been gradually aggrading since the 1930s; bank heights are low and the floodplain along with newly formed islands are flood prone.

11. Middle of Bosque Del Apache National Wildlife Refuge to San Marcial, NM (15 RM)-Rapidly Aggrading: Although the Rio Grande has a long-term history of aggradation (Lagasse 1980), this reach is aggrading excessively. Bed accretion is about 15 ft. in the last 65 years. The historical floodplain located within the levee system is active and noticeably aggrading along with the channel bed; islands and bars are uncommon.

DISCUSSION

In 117 miles of the 170 river miles of the Middle Rio Grande, the channel bed is incising and has largely abandoned its historical floodplain. Although recently developed islands and bars flood during high flows, the loss of the large floodplain system indicates a change in governing processes. Based on the bed elevation/bank height information, the eleven reaches have been combined into sections that attempt to link processes to the channel patterns (Figure 5). Section 1, Sediment Supply Influenced Section, extends from Cochiti Dam to South Diversion Channel, joining Reaches 1-4, about 57 RM. Section 2, Uplift Influenced Section, extends from the Arroyo Abo confluence to North Socorro Diversion Channel, combining Reaches 7 and 8, about 48 RM. Section 3, Aggrading Section, groups Reaches 10 & 11, about 30 RM.

The influence of dams on river systems is a well discussed and documented topic throughout the world. Most Rio Grande studies (Lagasse 1980, Richard, 2001, Ortiz 2004, Massong and Porter

2004, Massong and Porter 2005) document a dramatic reduction in sand-sized sediments which is resulting in an increasing grain size and localized bed degradation. Section 1 shows a

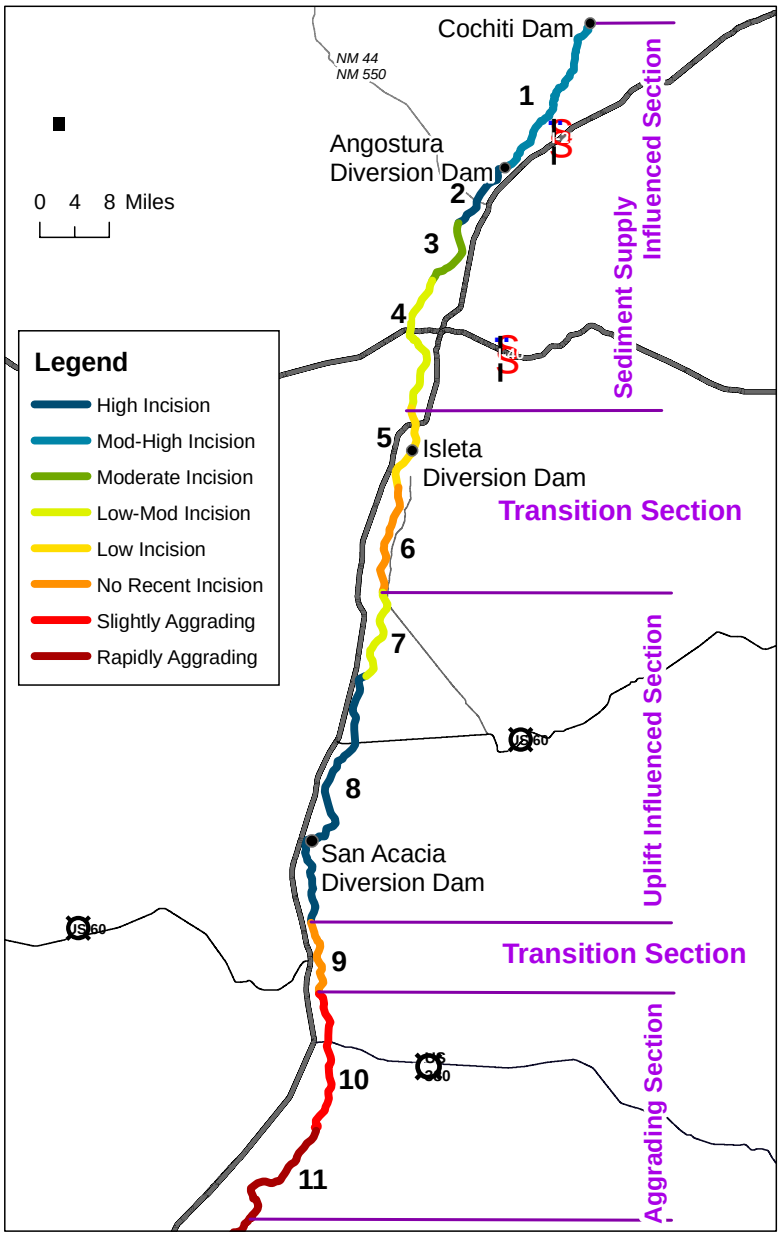


Figure 5 Summary figure showing incision trends from Cochiti Dam to Elephant Butte Reservoir, NM; numbers correspond to reach descriptions in the text. Channel descriptions are as follows: **high incision** has bank heights >6 ft.; **moderate incision** has bank heights 3-5 ft.; **low incision** has bank heights <3 ft.; **slightly aggrading** channels have <10 ft. of aggradation since 1935, while the **rapidly aggrading** is >10 ft. of aggradation; combination descriptions (i.e., Mod-High) indicates a mixture of bank heights.

degrading river system downstream from Cochiti Dam, in which the highest incision is near the dam. The incision systematically decreases downstream such that about 60 miles downstream

from the dam near the Isleta Diversion Dam the floodplain is at least in part active. The floodplain inundation increases downstream to the Los Lunas, NM area, about 70 miles downstream of Cochiti Dam. Section 1 incision is distinct from Section 2; only one historical floodplain appears to have been abandoned in Section 1, creating only one terraced surface. Only one terrace supports the concept of a single event, such as a permanently reduced supply of sediment changing the governing process. Lagasse (1980) found that the reduction in sediment supply quickly reversed the historically aggrading Rio Grande to a degrading system directly downstream of Cochiti Dam; this process/mechanism now appears to be influencing almost 60 miles downstream from the dam outlet. As a significant increase in sediment supply is unlikely, channel bed degradation will likely continue to increase bank heights and migrate downstream.

A series of riverine terraces centered near San Acacia, NM is an obvious signature of the Socorro Magma Body crustal uplift. Ouchi (1983) discussed the influence of this uplift through a review of bed elevation data (1930s-1970s) which showed a persistent 'bulge' in the river's longitudinal profile located over the magma body. Recent investigations by Klawon and Makar (2002) and Massong (2005) focused on mapping the variations in bank heights in the Socorro, NM area; they found that a series of terraces extend from approximately Arroyo Abo to the North Socorro Diversion Channel. These terraces peak in height near San Acacia, NM (Figure 2 and Massong 2005), which is also the approximate center of uplift (Larsen and Relinger 1983). Since the outline of terraces in Section 2 closely mirrors the estimated uplift associated with the magma body, geology appears to be dominating floodplain abandonment in this Section. However, Massong (2005) also clearly shows that several terraces have formed since the early 1970s, some are already as high as 6 feet. These data likely indicate additional processes (i.e., reduced supply of sediment) are influencing the recently abandoned floodplains in this Section.

Downstream from the transition zone (Reach 9), aggradation is ongoing and increases in a downstream direction. Reclamation archive data/studies (Scurlock 1998, and Makar and Strand 2002) show that this section of the MRG has been subject to aggradation dating back to the earliest records (pre-1900). USGS Rio Grande gage data clearly show that all gages in the Middle Rio Grande, even the gage at San Marcial (Massong et al., 2002), have a reduced suspended sediment supply since Cochiti Dam began operating; however, the bed elevation data shows a steadily aggrading channel in Section 3, a system obviously laden with sediment. The lack of channel response in this Section to the change in sediment supply is not well understood. For the continued aggradation, one thought is that the aggradation may be geologic; Larsen and Relinger (1983) suggest that just south of the Socorro Magma Body, the crust could be sinking. The theorized subsidence is a secondary effect of the uplifting 'bulge' of the Socorro Magma Body which could account for the continued and constant aggradation in this Section. Interestingly, bank height increases with the aggradation (Figure 4), such that the higher bank heights occur with the high aggradation; unfortunately, the process controlling this channel response is also not well understood.

This incision study is a clear example illustrating the effects of two processes that influence the Rio Grande. One of the most noticeable changes over the last 10 years is the emergence of stable, vegetated bars and islands throughout the MRG. As the historical floodplain is predominantly abandoned in the upper MRG, these features now act as floodplains, even though they are within the active channel. Interestingly, bar/island formation is independent of changes

in the bed elevation, as they form in both the degrading and aggrading channel sections. Along with the curious channel features at San Marcial, NM, a variety of processes are obviously influencing the MRG, creating the complicated riverine system found today.

ACKNLOWLEDGEMENTS

We would like to thank others that contributed to this study: Travis Bauer, Chris Holmquist-Johnson, Charlene Nelson, Mark Nemeth, K. Jan Oliver, Robert Padilla, and Nancy Umbreit.

REFERENCES

Klawon, J., and Makar, P. (2002). "Historical terrace mapping: Escondida Bridge to Pool of Elephant Butte Reservoir," U.S. Department of the Interior, Bureau of Reclamation Technical Report, Technical Services Center, Sedimentation and River Hydraulics Group, Denver, Colorado.

Lagasse, P.F. (1980). "An assessment of the response of the Rio Grande to dam construction-Cochiti to Isleta," U. S., Army Corps of Engineers Technical Report, Albuquerque, NM.

Larsen, S., and Reilinger, R. (1983). "Recent measurements of crustal deformation related to the Socorro Magma Body, New Mexico," 34th Field Conference of the New Mexico Geological Society (guidebook), New Mexico, pp 119-121.

Makar, P., and Strand R.I. (2002). "Geomorphological assessment of the Rio Grande: Escondida Bridge to near Fort Craig," U.S. Department of the Interior, Bureau of Reclamation Draft Technical Report, Technical Services Center, Sedimentation and River Hydraulics Group, Denver, Colorado.

Makar, P., Massong, T., Bauer, T., Tashjian, P., and Oliver, K J. (2006). "Channel sidth and flow regime changes along the Middle Rio Grande, NM," Joint 8th Federal Interagency Sedimentation Conference and 3rd Federal Interagency Hydrologic Modeling Conference, Reno, Nevada.

Massong, T.M, (2004). "Rio Grande River maintenance priority sites on the Pueblo of Cochiti: historical channel information," U.S. Department of the Interior, Bureau of Reclamation Technical Report, Environment Division, Albuquerque, New Mexico.

Massong, T.M. (2005). "Mapped Rio Grande terraced floodplain surfaces from the Arroyo Abo confluence to Escondida, NM," U.S. Department of the Interior, Bureau of Reclamation unpublished Technical Report (draft), Environment Division, Albuquerque, New Mexico.

Massong, T., Smith, K.I., Glover, A., Candelaria, K., and Bullard, M. (2002). "Overview of geomorphology for the Middle Rio Grande," U.S. Department of the Interior, Bureau of Reclamation unpublished Technical Note, River Analysis Team, Albuquerque, NM.

Massong, T.M., and Porter, M D. (2004). "Changes in the Middle Rio Grande due to the altered hydrology," Geological Society of America Abstracts with Programs, Denver, Colorado, Vol. 36, No. 5, p. 12

Massong, T.M., and Porter, M D. (2005). "Predicting future fish nursery habitat using geomorphology," Proc. 2005 American Fisheries Society Annual Meeting, Anchorage, Alaska.

Ortiz R.M. (2004). "A river in transition: geomorphic and bed sediment response to Cochiti Dam on the Middle Rio Grande, Bernalillo to Albuquerque, New Mexico," M.S. Thesis,

University of New Mexico, Department of Earth and Planetary Sciences, Albuquerque, New Mexico.

Ouchi, S. (1983). "Response of alluvial rivers to active tectonics," Ph.D. Dissertation, Colorado State University, Earth Resources Department, Fort Collins, Colorado.

Scurlock, D. (1998). "From the Rio to the Sierra: an environmental history of the Middle Rio Grande Basin," U. S. Department of Agriculture, Forest Service, Rocky Mountain Research Station, Fort Collins, Colorado, General Technical Report RMRS-GTR-5.

Tashjian, P., Massong, T., and Makar, P. (2006). "The implications of recent floodplain evolution on habitat," Joint 8th Federal Interagency Sedimentation Conference and 3rd Federal Interagency Hydrologic Modeling Conference, Reno, Nevada.

Richard, G.A. (2001). "Quantification and prediction of lateral channel adjustments downstream from Cochiti Dam, Rio Grande, NM," Ph.D. Dissertation, Colorado State University, Department of Civil Engineering, Fort Collins, Colorado.

TEMPORAL AND SPATIAL VARIABILITY IN ROOT-REINFORCEMENT OF STREAMBANKS: ACCOUNTING FOR GEOTECHNICAL PROPERTIES AND MOISTURE.

Natasha Pollen, Research Associate, USDA-ARS National Sedimentation Laboratory, Oxford, MS, npollen@ars.usda.gov; Andrew Simon, Research Geologist, USDA-ARS National Sedimentation Laboratory, Oxford, MS, asimon@ars.usda.gov

Abstract: Riparian vegetation exerts a number of mechanical and hydrologic controls on streambank stability, which affect the delivery of sediment to channels. Estimates of root-reinforcement of soils have commonly been attained using perpendicular root models that simply sum root tensile strengths and consider these as an add-on factor to soil strength. A major limitation of such perpendicular models is that the effect of variations in soil moisture and bank geotechnical properties on root-reinforcement are omitted as root tensile strengths are considered to be independent of soil type and moisture. In reality, during mass failure of a streambank, some roots break, and some roots are pulled out of the soil intact; the relative proportions of roots that break or pull out are determined by soil moisture and shear strength, and root strengths. In this paper an equation to predict the frictional resistance of root-soil bonds was tested against field data collected at Long Creek, MS, under two soil moisture conditions. The root pullout equations were then included in the root-reinforcement model, RipRoot, and bank stability model runs for Goodwin Creek, MS, were carried out in order to examine the effects of spatial and temporal variations in soil shear strength and rooting density, on streambank factor of safety. Model results and collected filed data showed that at low root diameters breaking forces exceeded pullout forces, but at higher root diameters pullout forces exceed breaking forces. The threshold diameter between root pullout and root breaking varied with soil shear strength, with increasing soil shear strength leading to a greater proportion of roots failing by breaking instead of pullout. Root-reinforcement estimates were shown to reflect changes in soil shear-strength, for example, brought about by variations in soil matric suction. Resulting Factor of Safety (F_S) values for the bank during the period modeled ranged from 1.36 to 1.74 with 1000 grass roots/m^2, compared to a range of 0.97 to 1.37 for the non-vegetated bank. Root-reinforcement was shown to increase bank stability under the entire range of soil moisture conditions modeled. However, the magnitude of root reinforcement varied in both space and time as determined by soil geotechnical properties and soil moisture.

INTRODUCTION

Streambank instability poses a number of economic and ecological problems including land loss, and destabilizing of structures (e.g. bridges). The resulting delivery of excessive sediment to channels can cause downstream aggradation and impairment of water quality. Sediment is one of the principal pollutants of surface waters in the United States and recent studies have shown that stream bank materials are a significant if not dominant source (USEPA, 2002). It is therefore important to understand and quantify the controlling processes and the role vegetation can play in stabilizing streambanks and thereby reducing sediment erosion from this source.

Riparian areas are an important component of the overall landscape mosaic, particularly in terms of species diversity (Malanson, 1993). The presence of riparian vegetation on streambanks not only provides ecological benefits, but is also widely believed to increase the stability of stream-banks (Abernethy and Rutherfurd, 1998; Simon and Collison, 2002). As a result of the potential benefits for stability and environmental quality, interest in the use of riparian vegetation in stream restoration and stabilizing schemes has grown in recent years. However, quantification of the interactions between vegetation and bank erosion processes has been unreliable due to limited knowledge regarding the way in which roots affect the geotechnical, hydrological and hydraulic processes within a bank and its adjoining channel. Current stream-restoration designs are, therefore, based on empirical methods and standardized practices (Gregory and Gurnell, 1988; Wynn et al. 2004), as process based models examining vegetation effects are unavailable.

Riparian vegetation exerts a number of controls on bank stability. These controls can be separated into mechanical and hydrologic effects, some beneficial and some negative to bank stability. To quantify vegetation effects, several properties regarding the root network need to be established. Possibly the most challenging aspect of root investigations is the acquisition of data pertaining to root architecture and root-distributions throughout the bank. Despite the difficulties concerned with obtaining root data, a number of papers have attempted to measure and quantify the physical properties of riparian root networks and relate these properties to streambank stability. These include the studies conducted in Mississippi by Simon and Collison (2002), Easson and Yarbrough (2002), in Virginia by Wynn et al. (2004), in California by Simon et al. (in press), in various parts of the USA by Pollen et al. (2004), and in Australia by Abernethy and Rutherfurd (1998; 2000). In addition, the hydrologic effects of riparian vegetation on bank stability have been explored by Simon and Collison (2002), Simon and Pollen (2004) and Pollen (2004).

Quantifying Root-Reinforcement of Soil: It is generally accepted that plant roots provide reinforcement to a soil matrix due to the dramatically different physical properties of roots, and the soil they are embedded in (Greenway, 1987). Soil is strong in compression but weak in tension. Conversely, roots are weak in compression but strong in tension. The presence of roots in the soil thus produces a reinforced matrix in which stress is transferred to the roots during loading of the soil (Thorne, 1990). Estimates of root-reinforcement of soils have commonly been attained using simple perpendicular root models such as those of Waldron (1977) and Wu et al. (1979), which calculate root-reinforcement as an add-on factor to soil strength. The root reinforcement model of Waldron is based on the Coulomb equation in which soil-shearing resistance is calculated from cohesive and frictional forces:

$$S = c + \sigma_N \tan\phi \quad (1)$$

where S is soil shearing resistance (kPa), σ_N is the normal stress on the shear plane (Pa), ϕ is soil friction angle (degrees), and c is the cohesion (kPa).

Waldron (1977) extended Equation 1 for root-permeated soils, by assuming that all roots extended vertically across a horizontal shearing zone, and that the roots act like laterally loaded piles, so tension is transferred to them as the soil is sheared. The modified Coulomb equation becomes:

$$S = c + \Delta S + \sigma_N \tan\phi \quad (2)$$

where ΔS is increased shear strength due to roots (kPa).

In the Waldron model (1977), the tension developed in the root as the soil is sheared is resolved with a tangential component resisting shear and a normal component increasing the confining pressure on the shear plane. ΔS can be represented by:

$$\Delta S = T_r (\sin\theta + \cos\theta \tan\phi) (A_R/A) \quad (3)$$

where T_r is average tensile strength of roots per unit area of soil (kPa), A_R/A is the root area ratio (no units), and θ is the angle of shear distortion in the shear zone.

Gray (1974) reported the angle of internal friction of the soil appeared to be affected little by the presence of roots. Sensitivity analyses carried out by Wu et al. (1979) showed that the value of the first bracketed term in (3) is fairly insensitive to normal variations in θ and ϕ (40-90° and 25-40° respectively) with values ranging from 1.0 to 1.3. A value of 1.2 was therefore selected by Wu et al. (1979) to replace the bracketed term and the simplified equation becomes:

$$\Delta S = T_r (A_R/A) \times 1.2 \quad (4)$$

Thus, according to the simple perpendicular root model of Wu et al. (1979), the magnitude of reinforcement simply depends on the amount and strength of roots present in the soil. However, Pollen et al. (2004) and Pollen and Simon (2005), found that these perpendicular root models tend to overestimate root-reinforcement due to the inherent assumption that the full tensile strength of each root is mobilized during soil shearing, and that the roots all break simultaneously. This overestimation was largely corrected

by Pollen and Simon (2005), by constructing a fiber-bundle model (RipRoot) to account for progressive breaking during mass failure.

However, observations of incised streambanks suggest that when a root-reinforced soil shears, two mechanisms of root failure occur: 1) root breaking and 2) root pullout. The anchorage of individual leek roots was studied by Ennos (1990), who developed a function for pullout forces based on the strength of the bonds between the roots and soil:

$$F_P = S * L * 2\pi r \quad (5)$$

where F_P is the pullout force for an individual root (N), S is soil shear strength (kPa), r is the radius of the root (m) and L is the length of the root (m). L can be estimated in the absence of field data using (Waldron and Dakessian, 1981):

$$L = R\, r^g \quad (6)$$

where the constants g and R have ranges: $0.5 < g < 1.0$; $200 < R < 1000$.

For the saturated part of the bank profile the Coulomb equation is used to calculate S (Equation 1). For the unsaturated part of the bank profile the criterion as modified by Fredlund et al. (1978) is used:

$$S = c' + (\sigma - \mu_a) \tan \phi' + (\mu_a - \mu_w) \tan \phi^b \quad (7)$$

where c' is effective cohesion (kPa), σ is normal stress (kPa), μ_a is pore air pressure (kPa), μ_w is pore-water pressure (kPa), $(\mu_a - \mu_w)$ is matric suction, or negative pore-water pressure (kPa), and $\tan \phi^b$ is the rate of increase in shear strength with increasing matric suction.. The quantity $(\mu_a - \mu_w) \tan \phi^b$ represents the additional strength provided by matric suction along the unsaturated part of the failure plane and is reflected in the apparent or total cohesion (c_a) term (although this does not signify that matric suction is a true form of cohesion) (Fredlund and Rahardjo, 1993):

$$c_a = c' + (\mu_a - \mu_w) \tan \phi^b \quad (8)$$

Although root breaking may be independent of soil moisture, root pullout forces are a function of soil shear strength, which is determined by effective cohesion, soil friction angle, and soil matric suction. Thus, the forces required for root-pullout vary spatially with material type, and temporally with variations in soil moisture. The original version of RipRoot (Pollen and Simon, 2005) did not take into account root pullout forces, and as such could not take into account the effect of differing soil types and moistures on estimates of root-reinforcement. This was considered to be a major deficiency of the model and the perpendicular root models that preceded it. In this paper, the forces required to pullout roots were investigated in a field study, and the results tested against Equation 5 (Ennos, 1990). Root pullout forces were then compared to root breaking forces obtained from tensile strength testing, and the RipRoot model was modified to account for both root-failure mechanisms. Results from the newly constructed model are presented to show the variability in root-reinforcement as soil matric suction changed through a wetting and drying cycle following a storm event.

METHODS

Root tensile strengths and root pullout forces were measured using a Root-Puller (based on a design by Abernethy, 1999). The puller is comprised of a metal frame, with a winch attached to a load cell and displacement transducer,and connected to a datalogger. A trench was dug using an excavator, to expose the roots of a stand of mature river birch (*Betula nigra*) trees located on the banks of Long Creek, MS. The Root-Puller was attached to the side of the trench opposite each tree, so that the roots being tested were no longer anchored by the tree. The excavation process may have loosened the bond between the roots and the soil at the trench interface, but any disturbance did not appear to extend more than a few millimeters into the soil, thus limiting the effect on the root-soil friction forces measured. The device was attached to the

side of the trench by tying a rope around metal stakes hammered into the ground along the top of the trench. The load cell measured the force required to either pull the root out of the soil, or for it to break. Root-soil friction experiments were carried out at the same site (Long Creek, N. Mississippi), at different times of the year (April and July 2002) to test under varying soil moisture conditions. In each experiment 70 to 80 roots were tested to have sufficient data to distinguish any trends in the data from natural variability.

RESULTS AND DISCUSSION

Hypothetical pullout forces were estimated using Equation 5 and compared to root breaking forces (calculated from tensile strength-diameter relations of the form $y = ax^{-b}$ previously published in Pollen et al., 2004 and Pollen and Simon, 2005). Comparison of the variation in pullout and breaking forces with increasing root diameters (range of root diameters was 0.5 to 8 mm) showed.that smaller diameter roots are more likely to be pulled out of the soil, and larger diameter roots are more likely to break as a soil shears. The threshold between the two failure mechanisms is a function of the shear strength of the soil and thus the strength of frictional bonds between the roots and soil, and the species specific tensile strength curves.

River birch field data: The field data collected from Long Creek, MS were used to examine whether a clear threshold existed between the two root-failure mechanisms (Figure 1). The data show that above a certain root diameter, all of the roots broke. However, below this threshold diameter some of the roots broke and some were pulled out of the soil intact. The breaking of roots below the threshold diameter may have been due to the presence of root branching, causing the friction forces to vary from the idealized situation of straight, un-branched roots as assumed in Equation 5.

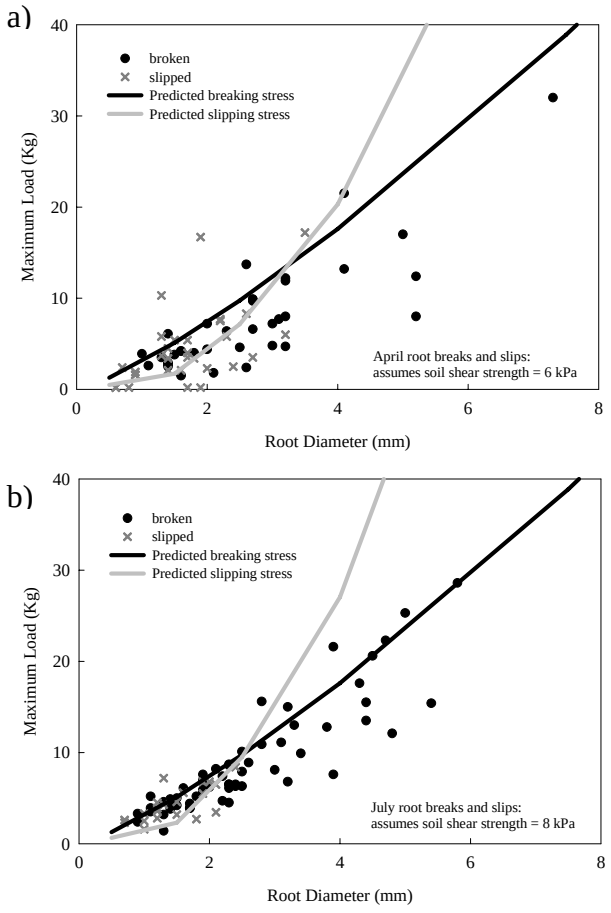


Figure 1 Field data for root breaking and root pullout at the Long Creek site, MS. In a) April and b) July. Also shown are the predicted breaking and pullout forces calculated for the apparent soil cohesion at the site assuming the constants $R = 200$ and $g = 0.7$ (Equation 6).

The root-soil friction tests conducted in April and July 2002, experienced moisture contents of 21.1% and 11.3% respectively. Statistical analysis confirmed that there was not a significant difference between the median root breaking forces for the April and July data (Mann-Whitney Rank Sum Test, p = 0.220). This result confirms that the tensile strengths of the roots studied, and therefore their breaking forces, were largely independent of soil moisture. Changes in soil moisture did, however, affect the threshold diameter between root pullout and breaking. Although the mean diameters of roots that pulled out of the soil during the April and July tests were not significantly different (t-test, p = 0.221), the range of root diameters that were pulled out of the soil was less in July than in April (range of 1.7 mm and 2.9 mm respectively), and the maximum root diameters that could be pulled out of the soil were different. During the April tests, the threshold value was approximately 3.5 mm whereas in the July tests the threshold value was approximately 2.4 mm. This change in threshold diameter for root pullout suggests that as the soil dries out the frictional bonds between the roots and the soil become stronger, as apparent cohesion of the soil increases with increasing soil matric suction. Root breaking is therefore likely to be the predominant mode of root-failure in dry soils, or those with higher shear strengths, whereas soils that are moist, or have lower shear strength will exhibit greater root-pullout than breaking.

Inclusion of pullout forces in the RipRoot model: Root-pullout forces were included in the progressive breaking algorithm of the RipRoot model using Equations 5 and 6. Root lengths for all species were calculated using values in the suitable range outlined by Waldron and Dakessian (1981) (R = 200 and g = 0.7). Root tensile strength curves used to calculate root breaking forces for each species were obtained from Pollen and Simon (2005). The first set of model runs adding pullout forces, were conducted using a specified number of roots for each species, using varying soil shear-strengths. As soil shear strength increased, the threshold diameter between root pullout and root breaking decreased. Therefore, at higher soil shear strengths, more roots were predicted to break than be pulled out of the soil, and above a certain soil shear strength all roots were predicted to break, similar to the field data collected. Using Figures 2a and 2b it is possible to determine the threshold diameter above which all roots are predicted to break (indicated by a leveling off above a certain soil shear-strength). Thus, the effects of both soil type and soil moisture can now be accounted for in the RipRoot model.

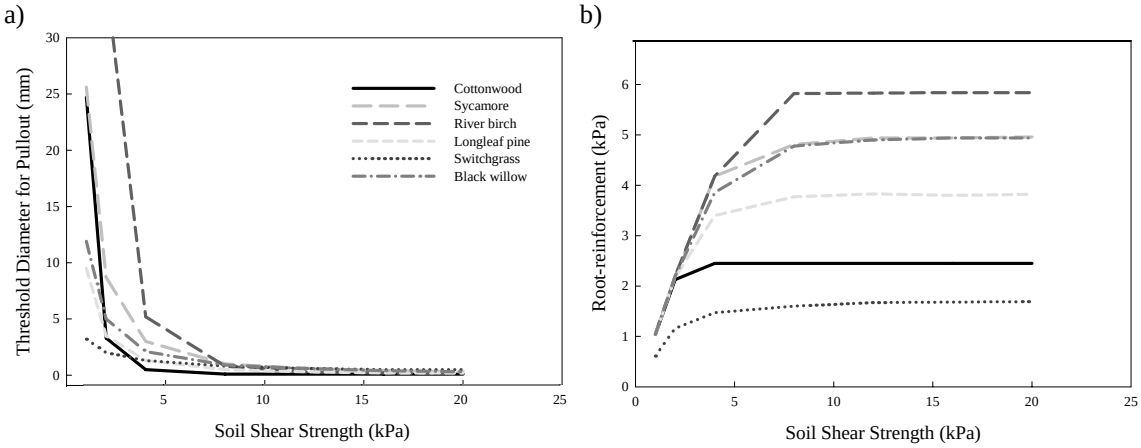


Figure 2 Variations in a) threshold root diameter for pullout with changing soil shear strength and b) root-reinforcement for each riparian species, with changing soil shear strength.

Effect of changing soil matric suction on root-reinforcement values: An additional set of model runs were performed using data from the Goodwin Creek Experimental Bendway (GCEB), to examine temporal variability in root-reinforcement estimates before and after a storm event (December 7th - 23rd 2004). The period of study was chosen because the tensiometer data exhibited a drying curve followed by a large storm event during which the soil matric suction dropped rapidly. To estimate soil shear strength (using Equation 7), the following variables were required: effective soil cohesion, pore-water pressure, σ, ϕ' and ϕ^b. The GCEB was used for these model runs because geotechnical properties were available (c' = 1.4 kPa, ϕ^b = 17 degrees , ϕ' = 28.5 degrees for the upper 1m of the bank profile that contains the root zone, Simon et al., 1999). In addition, detailed matric-suction data were available from nests of tensiometers installed in

different vegetative treatments (Simon and Collison, 2002). Normal stress (σ) was calculated for a soil depth of 0.5 m (the assumed center of the root-reinforced zone), using the regression equation established in Simon et al. (1999) that relates soil matric suction to soil unit weight for the upper 1m of the modeled bank.

Mean daily soil shear strength was calculated using the bank-geotechnical properties and mean matric suction value for each day in the top layer of the grass plot, during the period (December 7th to December 23rd, 2004). The values of soil shear strength were used in the RipRoot model to calculate daily root-reinforcement values for root densities of 500 and 1000 roots/m^2. In the case of the upper 1m of the Goodwin Creek bank profile, *c'* was small (1.4 kPa), and values of matric suction recorded by the tensiometers, in combination with soil friction angle produced soil shear-strength values ranging from 7.3 to 10.7 kPa during the period. Soil shear strength was therefore in the range of soil strengths in which most of the roots were predicted to break during soil shearing, with very few roots being pulled out from the soil (Figure 2a and 2b). Variations in this range of soil strengths produced almost indistinguishable (approximately 1-2%) variations in root-reinforcement, ranging from 5.55 to 5.61 kPa (500 root/m^s) and 11.10 to 11.22 kPa (1000 roots/m^2). Slight increases in root-reinforcement were seen with increasing soil matric suction until soil shear strength increased above 10 kPa, at which point root-reinforcement values leveled off because all roots were predicted to break (as seen in Figure 2). Further increases in matric suction above 10 kPa, therefore, had no effect on root-reinforcement.

To test the effect of changing matric suction on a soil with weaker shear strength, RipRoot runs were repeated using mean, daily shear-strength values that were half those calculated for the first set of runs. The results of this second set of runs showed that because soil strength values were in the range where both root breaking and root pullout occurred (Figure 2a and 2b), any variation in matric suction had more of an effect on calculated root-reinforcement values. In this case, changes in matric suction were reflected in root-reinforcement values, with no plateau in root-reinforcement values as soil shear strengths were not great enough to force all roots to break. Root-reinforcement estimates for the lower range of soil shear strengths (3.66 to 5.36 kPa) varied from 9.12 to 11.2 kPa at a root density of 1000 roots/m^2. Therefore, the effect of soil type and moisture on root-reinforcement depends on spatial and temporal variability, and relative contributions of effective and apparent cohesion, matric suction and soil friction angle to soil shear strength.

Effect of dynamic root-reinforcement values on Streambank Factor of Safety (F_S): The streambank stability model of Simon et al. (1999) was run for the grass plot at Goodwin Creek for the period December 7th through December 23rd 2004. Previously published model runs using this bank stability model have included root-reinforcement as a static add-on factor, assuming that all roots broke and that root-reinforcement was independent of soil type and moisture (Simon and Collison, 2002; Pollen et al., 2004). As such, the addition of vegetation to any bank produces F_S for bare and vegetated banks that show sets of parallel lines, with vegetated banks having higher F_S values. Root-reinforcement estimates including root pullout as well as root breaking, result in root-reinforcement forces that vary with soil shear strength. The effect of temporal variability in root-reinforcement values on streambank F_S values is shown in Figure 3. The F_S for vegetated and non-vegetated banks diverges slightly as F_S increases (Figure 3). This trend occurs because root reinforcement is greatest when matric suction and thus F_S are high. Root reinforcement is lowest when bank F_S conditions are critical, although some reinforcement is still provided through soil-root friction forces even when pullout is the dominant root failure mechanism.

F_S values where soil shear strength was high and root-reinforcement thus varied only slightly, showed that F_S for the vegetated and non-vegetated bank diverged slowly as F_S increased. The difference in minimum F_S being 0.35 and the difference in maximum F_S being 0.36 for a density of 1000 roots/m^2 (Figure 3). Figure 3 also shows the F_S runs repeated with root reinforcement estimates for the soil of lower shear strength. In this second set of model runs, at minimum F_S the difference in F_S between the bare bank and the bank with 1000 roots/m^2 was 0.31, but at maximum F_S, the difference was 0.36. At lower soil shear strengths the range of root reinforcement values was thus reflected in a wider range of F_S values. Results of model runs show that for a specified rooting density, the range of root-reinforcement values is dependent on soil shear strengths and how they affect the predominance of species specific root pullout and root breaking mechanisms. Figure 3 shows that the variations in model runs for soil of lower and higher shear

strengths were greatest at lower F_S values. This suggests that the inclusion of pullout forces is particularly important when bank stability conditions are critical.

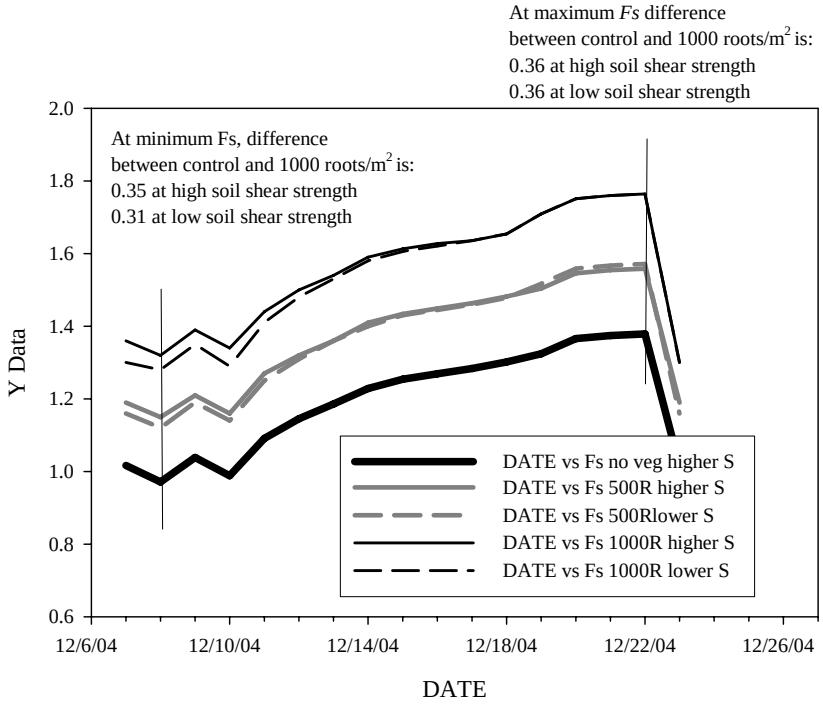


Figure 3 Factor of safety values for the grass plot at Goodwin Creek, MS during December 2004, with no roots, 500 roots per m^2 and 1000 roots per m^2 at high soil shear strengths (7.3 to 10.7 kPa) and lower soil shear strengths (3.66 to 5.36 kPa).

CONCLUSIONS

Field tests confirmed the presence of a threshold root-diameter, above which all roots broke under applied stress, and below which, both root breaking and pullout occurred. The threshold diameter between root-failure mechanisms is determined by the shear strength of the soil. Model results have thus shown that the effect of soil type and moisture on root-reinforcement is dependent on spatial and temporal variability in several factors including soil matric suction and geotechnical properties.

When soil shear strengths were calculated for Goodwin Creek, root reinforcement values during December 2004 ranged from 5.55 to 5.61 kPa (500 grass roots/m^2) and 11.10 to 11.22 kPa (1000 grass roots/m^2). The root-reinforcement values varied very little throughout the period of time modeled because root-breaking was predominant at that range of soil shear strengths; changes in matric suction therefore had little or no effect on root-reinforcement estimates. When soil shear-strength was halved, root-reinforcement estimates decreased correspondingly, but the range of values was greater as both root pullout and root breaking occurred in this range of soil shear strengths. Any changes in soil matric suction therefore affected the proportion of roots that would break or pullout of the soil, thereby causing larger variations in root-reinforcement estimates.

Quantification of spatial and temporal variability in root-reinforcement can now be taken into account in RipRoot by changing input variables such as root density, species assemblage, and soil shear strength. In the first version of RipRoot the roots and soil were considered separately as root breaking was assumed to be independent of soil properties. The addition of root pullout forces in the new version allows for interaction between the root-soil matrix, thereby improving the representation of the processes occurring during mass-failure of a streambank. Future work will use field data to validate the level of improvement made by using varying root-reinforcement estimates instead of static add-on values. More accurate

estimates of root-reinforcement of streambanks will ultimately aid in future studies of bank stability, and may help explain and quantify rates of channel widening, and lateral migration of channels with riparian corridors of various species compositions.

REFERENCES

Abernethy, B. and Rutherfurd, I.D. (1998). "Where along a river's length will vegetation most effectively stabilize stream-banks?" Geomorphology, **23**: 55-75.

Abernethy, B. (1999). "On the Role of Woody Vegetation in Riverbank Stability", PhD Thesis. Monash University: Melbourne.

Abernethy, B. and Rutherfurd, I.D. (2000). "The effect of riparian tree roots on the mass-stability of riverbanks", Earth Surface Processes and Landforms, **25**: 921-937.

Easson, G. and Yarbrough, L.D. (2002). "The Effects of Riparian Vegetation on Bank Stability", Environmental and Engineering Geoscience, **8(4)**: 247-260.

Ennos, A.R. (1990). "The Anchorage of leek Seedlings: The Effect of Root Length and Soil Strength", Annals of Botany, **65**: 409-416.

Fredlund, D.G., Morgenstern, N.R., and Widger, R.A. (1978). "The shear strength of unsaturated soils", Canadian Geotechnical Journal. 15: 313-321.

Fredlund, D.G. and Rahardjo, H. (1993) Soil Mechanics of Unsaturated Soils. John Wiley and Sons, New York.

Gray, D.H. (1974). "Reinforcement and Stabilization of Soil by Vegetation", Journal of Geotechnical Engineering ASCE (100(GT6)), 695-699.

Greenway, D.R. (1987). "Vegetation and Slope Stability", In: Anderson, M.G and Richards, K.S., eds. Slope Stability John Wiley and Sons Ltd, New York, 187-230.

Gregory, K.J. and Gurnell, A.M. (1988). "Vegetation and river channel form and process", In: H. Viles, ed. Biogeomorphology. Blackwell, Oxford, 11-42.

Malanson, G.P. (1993). Riparian Landscapes. Cambridge University Press, Cambridge.

Pollen, N. (2004). "The Effects of Riparian Vegetation on streambank stability: Mechanical and Hydrological interactions", Ph.D. Thesis. King's College, University of London, 320pp

Pollen, N., and Simon, A. (2005). "Estimating the mechanical effects of riparian vegetation on streambank stability using a fiber bundle model", Water Resour. Res., 41, W07025, doi:10.1029/2004WR003801

Pollen, N., Simon, A., and Collision, A.J.C. (2004). "Advances in Assessing the Mechanical and Hydrologic Effects of Riparian Vegetation on Streambank Stability", In: S. Bennett and A. Simon, eds. Riparian Vegetation and Fluvial Gomorphology, Water Science and Applications 8, AGU, 125-139.

Simon, A. and Pollen, N. (2004). "Hydrologic controls of riparian vegetation on the geotechnical stability of streambanks: experimental results", Proceedings of the 6th Int. Conf. on Hydroscience and Engineering (ICHE-2004).

Simon, A., Pollen, N. and Langendoen, E. (in press, JAWRA special edition on riparian zones)

Simon, A., and Collison, A.J.C. (2002). "Quantifying the mechanical and hydrologic effects of riparian vegetation on stream-bank stability", Earth Surface Processes and Landforms, **27**(5): 527-546.

Simon, A., Curini, A., Darby, S., and Langendoen, E. (1999). "Stream-bank Mechanics and the Role of Bank and Near-Bank Processes in Incised Channels", In: Darby, S. and Simon, A., eds. Incised River Channels. John Wiley and Sons, New York. 123-152.

Thorne, C.R. (1990). "Effects of Vegetation on riverbank erosion and stability", In: Thornes, J.B., ed. Vegetation and Erosion. John Wiley and Sons Inc, Chichester, 125-143.

USEPA, (2002) http://www.epa.gov/OWOW/tmdl/sed_miles.html

Waldron, L.J. (1977). "The shear resistance of root-permeated homogeneous and stratified soil", J. Soil Science Soc. Amer., **41**: 843-849.

Waldron, L.J. and Dakessian, S. (1981). "Soil Reinforcement by Roots: Calculation of increased soil shear resistance from root properties", Soil Science. **132**: 427-435.

Wu, T.H., McKinnell, W.P. III, and Swanston, D.N. (1979). "Strength of tree roots and landslides on Prince of Wales Island, Alaska", Canadian Geotechnical Journal. **16:** 19-33.

Wynn, T, Mostaghimi, S., Burger, J.A., Harpold, A.A., Henderson, M.B. and Henry, L. (2004). "Variation in Root Density along Stream Banks", J. Environ. Qual., **33**: 2030-2039.

MORPHOLOGIC EVOLUTION IN THE USGS SURFACE-WATER MODELING SYSTEM

Jonathan Nelson, Hydrologist, U.S. Geological Survey Geomorphology and Sediment Transport Laboratory, Golden, Colorado, jmn@usgs.gov; Richard McDonald, Hydrologist, USGS, Golden, Colorado, rmcd@usgs.gov; Paul Kinzel, Hydrologist, USGS, Golden, Colorado, pjkinzel@usgs.gov

Abstract: The morphology of an alluvial channel adjusts in response to variations in the volume and timing of water and sediment supplied to the channel. For example, hydrograph alterations due to anthropogenic causes, such as dams and diversions, produce channel adjustments over a wide variety of length and time scales; similarly, extreme flow events associated with natural variability can have profound effects on channel morphology that may produce morphologic adjustment over days to decades. For these and other important problems, geomorphologists and engineers are asked to provide quantitative assessment of the morphologic impacts of hypothetical or planned alterations in flow and/or sediment supply. Because the flow field and the morphology are intricately linked with each other and the processes of sediment transport, predicting channel form and its temporal changes in response to a known hydrograph is difficult, and better tools to address these types of problems are needed.

The USGS Multidimensional Surface Water Modeling System (MD_SWMS) was originally created as a public-domain tool for surface-water modeling in rivers and streams. The software comprises topography filtering and editing tools, grid-generation tools, two- and three-dimensional surface water models, and a wide spectrum of flexible two- and three-dimensional graphics routines for visualizing inputs to and outputs from the models. To extend MD-SWMS capabilities to providing quantitative predictions of morphologic adjustment in rivers, we incorporated routines for the prediction of sediment transport and the stepwise prediction of changes in bed elevation produced by predicted patterns of erosion and deposition. Thus, given an initial channel geometry, grain sizes making up the bed, and a hydrograph, the new version of MD_SWMS can predict the time evolution of bed morphology.

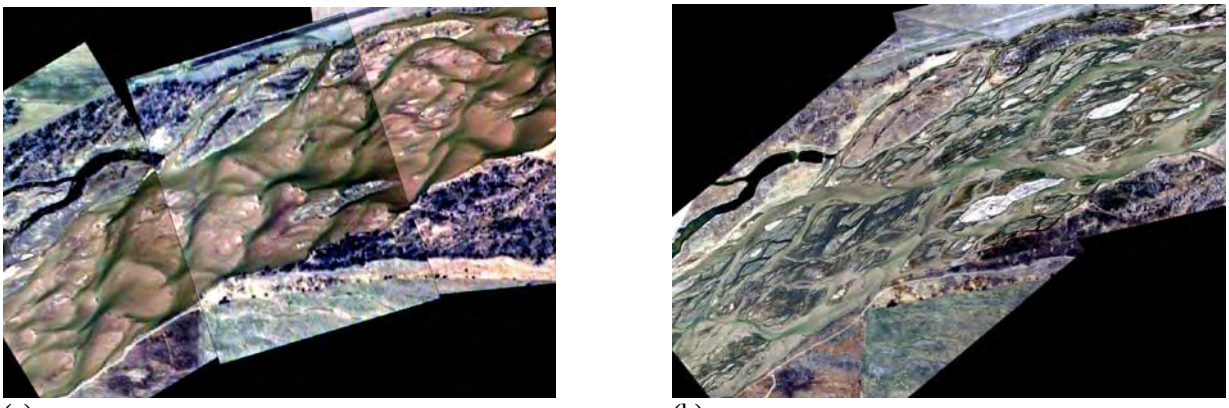
To test the approach for well-known simple geometries, we verified that MD_SWMS predicts realistic point bars in curved channels, alternate bars in straight channels with low width-to-depth ratios, and higher-mode braid bars in straight channels with higher width-to-depth ratios. The approach also predicts the formation of mid-channel bars and/or separation bars in channels with rapid expansions. A simple example of the role of discharge variations on topographic adjustment of a point bar is shown to illustrate how the new module can be used to examine such effects. We believe MD-SWMS now includes a good methodology for making quantitative predictions of channel responses to changes in flow and sediment supply and that, in the future, this and other similar approaches could be more widely used to evaluate and predict the temporal adjustment of river channels.

INTRODUCTION

The use of multidimensional flow models to predict flow in rivers and streams has increased dramatically over the past decade. This has primarily been driven by the increasingly detailed nature of the questions scientists and engineers have been trying to answer and has been facilitated by the evolution of computational power available in low-cost computers. The need for increased detail is especially clear in the areas of channel maintenance and habitat assessment in rivers; these problems are inherently tied to spatially distributed information that simple one-dimensional approaches cannot provide, so two- or three-dimensional models are required. As the application of multidimensional flow models for practical problems in rivers has become more common, the importance of considering the temporal change of erodible beds in rivers has become increasingly obvious, not just as a research goal to understand channel behavior, but as a critical part of applied problems. For example, the standard methodology in using a multidimensional model for the evaluation of channel maintenance or restoration consists of computing flows (and typically sediment transport) through a given channel form for a variety of discharges or hydrographs to evaluate the capability of the channel to carry the prescribed water and sediment discharges. Similarly, habitat assessments are generally made by taking a “snapshot” of the channel planform and bathymetry, and applying a multidimensional model for a variety of discharges in order to compute local quantities (such as velocity and depth) for comparison to some measure of habitat quality or preference. In both cases, the channel morphology is assumed to be static, whereas in reality the channel morphology will change in response to changing flow or sediment supply. Thus, for all but the simplest static channels in which morphology never changes,

predictions are strongly dependent on the actual bathymetry used for making model predictions; that bathymetry may in fact be a very poor approximation of the bathymetry for certain discharges or hydrographs. This simple point is illustrated in Figure 1, which shows two aerial photograph mosaics of a reach of the Platte River in Nebraska; the two photos were taken at similar discharges, but (a) shows the topography after a prolonged period of high flow and (b) shows the topography after a long period of low flow. Use of either set of topography for the assessment of habitat (crane roosting habitat in this case, see Kinzel et al., 2005) over a variety of discharges may yield different results, as the morphology changes dramatically depending on flow history. In this and many other similar problems, the key to improved predictions is the inclusion of temporal changes in bed morphology (i.e., morphodynamics) in multidimensional flow modeling codes.

In this paper, we present results from the new morphodynamics module recently incorporated into the U.S. Geological Survey's Multi-Dimensional Surface-Water Modeling System (MD_SWMS). The module consists of a suite of algorithms for computing local sediment transport along with a time-stepping procedure for computing the temporal evolution of the morphology of a channel bed. The components of the approach are briefly described in the sections below. To verify the behavior of the coupled models for flow, sediment transport, and bed evolution, results for the time evolution of several simple channels during a period of constant discharge also are shown below. In addition, bed evolution results for a suite of simple hydrographs for the same initial bed configuration are shown in order to exemplify how the model can be used to examine the role of real or hypothetical hydrographs in creating, maintaining, or altering channel bed morphology. In a companion paper (McDonald et al., 2006; this volume), an example of the application of the MD_SWMS morphodynamics capability for a field application is described. The new module offers a simple way to predict the temporal changes in bed morphology along with two- and three-dimensional flow patterns as required for a wide variety of practical problems.



(a) (b)

Figure 1 Aerial photograph mosaic of the Platte River near Kearney Nebraska after a prolonged period of high flow (a) and a prolonged period of low flow (b). All photos taken at a discharge of approximately 1000 cfs.

THE MD_SWMS MODELING INTERFACE

The MD_SWMS modeling interface was developed by the U.S. Geological Survey as a public-domain tool for surface-water modeling in rivers and streams. The software comprises topography filtering and editing tools, grid-generation tools, two- and three-dimensional surface water models, and a wide spectrum of flexible two- and three-dimensional graphics routines for visualizing inputs to and outputs from the models. This software development program was intended to provide a means to allow both internal and public access to research models currently in use within the USGS National Research Program. MD_SWMS and its application are described in detail in the User's Guide developed by McDonald et al. (2005); the interface is available for download from the USGS at the following URL: http://wwwbrr.cr.usgs.gov/projects/SW_Env_Fluid/.

THE FASTMECH MODEL

One of the models currently available within MD-SWMS is the Flow and Sediment Transport with Mechanical Evolution of Channels (FASTMECH) model originally described in Nelson and McDonald (1996). Originally, only the flow modeling portion of the FASTMECH code was available in MD-SWMS; the module described here

incorporates the sediment transport and bed evolution components of that code with some expansion and improvements. Although the length of this paper precludes a complete description of the model development, the basic equations are given here; further details can be found in Nelson and McDonald (1996) and Nelson et al. (2003). Assuming flow is hydrostatic and incompressible and that momentum fluxes associated with vertical correlations between velocity and stress components are negligible, the vertically averaged equations of motion expressing conservation of mass and momentum in a curvilinear coordinate system with centerline radius of curvature R and streamwise and cross-stream coordinates *s* and *n* can be written as follows

$$\frac{1}{1-N}\frac{\partial}{\partial s}\left(<u>h\right)-\frac{<v>h}{(1-N)R}+\frac{\partial}{\partial n}\left(<v>h\right)=0 \tag{1}$$

$$\begin{aligned}\frac{1}{1-N}\frac{\partial}{\partial s}\left(<u>^2 h\right)+\frac{\partial}{\partial n}\left(<u><v>h\right)-\frac{2<u><v>h}{(1-N)R}=-\frac{gh}{1-N}\frac{\partial E}{\partial s}+\\ \frac{1}{\rho}\left[\frac{1}{1-N}\frac{\partial}{\partial s}\left(<\tau_{ss}>h\right)+\frac{\partial}{\partial n}\left(<\tau_{ns}>h\right)-\frac{2<\tau_{ns}>h}{(1-N)R}\right]+\\ \frac{1}{\rho}\left[\frac{1}{1-N}\left(\tau_{ss}\right)_B\frac{\partial B}{\partial s}+\left(\tau_{ns}\right)_B\frac{\partial B}{\partial n}-\left(\tau_{zs}\right)_B\right]\end{aligned} \tag{2}$$

$$\begin{aligned}\frac{1}{1-N}\frac{\partial}{\partial s}\left(<u><v>h\right)+\frac{\partial}{\partial n}\left(<v>^2 h\right)+\frac{\left(<u>^2-<v>^2\right)h}{(1-N)R}=-\frac{gh}{1-N}\frac{\partial E}{\partial n}+\\ \frac{1}{\rho}\left[\frac{1}{1-N}\frac{\partial}{\partial s}\left(<\tau_{ns}>h\right)+\frac{\partial}{\partial n}\left(<\tau_{nn}>h\right)-\frac{<\tau_{ss}-\tau_{nn}>h}{(1-N)R}\right]+\\ \frac{1}{\rho}\left[\frac{1}{1-N}\left(\tau_{ns}\right)_B\frac{\partial B}{\partial s}+\left(\tau_{nn}\right)_B\frac{\partial B}{\partial n}-\left(\tau_{zn}\right)_B\right]\end{aligned} \tag{3}$$

where < > denotes vertical averaging, *u* and *v* are the streamwise and cross-stream components of Reynolds-averaged velocity, *E* is the water surface elevation, *B* is the bed elevation, *h* is the local depth, *g* is the gravitational constant, ρ is the fluid density, $N=n/R$ and the components of the Reynolds stress tensor are given by

$$\begin{aligned}&\tau_{ss}=2\rho K\left[\frac{1}{1-N}\frac{\partial u}{\partial s}-\frac{v}{(1-N)R}\right] \qquad \tau_{nn}=2\rho K\left[\frac{\partial v}{\partial n}\right] \qquad \tau_{ns}=\rho K\left[\frac{1}{1-N}\frac{\partial v}{\partial s}+\frac{u}{(1-N)R}+\frac{\partial u}{\partial n}\right]\\ &\tau_{zn}=\rho K\left[\frac{\partial w}{\partial n}+\frac{\partial v}{\partial z}\right] \qquad \tau_{zs}=\rho K\left[\frac{1}{1-N}\frac{\partial w}{\partial s}-\frac{\partial u}{\partial z}\right] \qquad \tau_{zz}=2\rho K\left[\frac{\partial w}{\partial z}\right].\end{aligned} \tag{4}$$

In Equation 4, *K* is the value of the kinematic eddy viscosity and *w* is the vertical velocity. Because rivers are predominantly like turbulent boundary layers, *K* is set using turbulent open-channel flow results. For the solution of the vertically averaged equations above, *K* is assigned a typical vertically averaged value as follows

$$K=\frac{ku_*h}{\beta}+\alpha_H \tag{5}$$

where *k* is an empirical constant of proportionality called von Karman's constant (≈ 0.408, see Long et al. 1993), *h* is the local flow depth, β is a constant (see below), $u_*=\sqrt{\tau_B}/\rho$ and α_H is an empirical constant related to lateral diffusive processes (Nelson and McDonald, 1996)**.** The boundary shear stress, τ_B is expressed in terms of the vertically averaged velocity components using a drag coefficient closure as follows, where C_d is the drag coefficient

$$\tau_B = \rho C_d (< u >^2 + < v >^2) \,. \tag{6}$$

Splitting Equation 6 into components in the streamwise and cross-stream directions yields

$$(\tau_{zs})_B = \rho C_d \sqrt{< u >^2 + < v >^2} < u > \qquad (\tau_{zn})_B = \rho C_d \sqrt{< u >^2 + < v >^2} < v > \tag{7}$$

which allows complete closure of Equations 1 through 3. These equations are solved for the water-surface elevation and the components of vertically averaged velocity (and bed stress, through Equation 7) using the semi-implicit method for pressure linked equations (SIMPLE) presented by Patankar (1980) to iteratively solve for the water-surface elevation while solving the momentum equations for <u> and <v> using an explicit finite-difference scheme. Both schemes are used with differential relaxation to converge to a solution that satisfies the momentum equations and conserves mass both at each point and by matching the assigned discharge at each cross-section. This procedure yields the full vertically-averaged solution.

In order to develop a three-dimensional solution including the effect of secondary flows driven by channel and streamline curvature, an eddy viscosity profile is assigned along the streamlines of the vertically-averaged flow determined from the numerical solution as follows

$$K = k u_* h \kappa(\xi) \tag{8}$$

where $\kappa(\xi)$ is a shape function giving the vertical distribution of K between the bed and the water surface, using $\xi = z/h$ where h is the local flow depth and z is distance from the boundary. The choice of this function sets the value of β in Equation 5 and, along with the assumption that the vertical stress profile is approximately linear along the streamlines of the vertically averaged flow (see Nelson and Smith, 1989a), it also yields the vertical structure of the velocity along those streamlines as

$$u = u_* f(z, z_o) \tag{9}$$

where z_0, the so-called roughness length, is a constant of integration that depends on the boundary shear stress, the fluid viscosity, and/or the size of the roughness elements on the bed (see Middleton and Southard 1984, or any text on wall-bounded shear flows for a discussion of roughness lengths). Note that if $\kappa(\xi)$ is chosen to be parabolic between the bed and surface, Equation 9 is the well-known logarithmic velocity profile. In practice, slightly better results (compared to data) are found using the shape function suggested by Rattray and Mitsuda (1974), which is given by

$$\begin{aligned} \kappa(\xi) &= \xi(1-\xi) \qquad \xi < 0.2 \\ \kappa(\xi) &= 0.16 \qquad\quad \xi \geq 0.2 \end{aligned} \,. \tag{10}$$

This yields a logarithmic profile near the bed and a parabolic velocity profile in the flow interior; this shape function was used for the results shown below.

Equation 9 provides a direct relation between roughness length and the value of the boundary shear stress for a given choice of $\kappa(\xi)$. In addition, it can be used along with scaled versions of the full momentum equations to compute secondary flows perpendicular to the direction of the vertically averaged streamlines, as described by Nelson and Smith (1989b). These flows are driven by curvature of the flow streamlines and have no vertically averaged mass flux; they include the typical helical flow associated with flow in curved channels as well as the alteration in the direction of the bed stress produced by those flows. Although some aspects of this approach can at best be approximate, it does allow the computation of vertical structure and secondary flows without resorting to a full three-dimensional model, which is prohibitively slow for computing bed evolution in realistic cases.

As implemented in MD-SWMS, the FASTMECH model offers several tools for the computation of sediment flux given the solution of the flow field described above, including a variety of bedload equations, total load equations,

and advection-diffusion schemes for suspended sediment. A complete discussion of these options is outside the scope of this short paper, but all the results shown below were carried out for the case of bedload only using the so-called modified Meyer-Peter Müller equation, given by

$$(q_b)_* = 8\left[\tau_* - (\tau_*)_c\right]^{3/2} \tag{11}$$

where $(q_b)_* = \dfrac{q_b}{\left[\left(\dfrac{\rho_s - \rho}{\rho}\right) g D^3\right]^{1/2}}$, $\tau_* = \dfrac{\tau_b}{\left[(\rho_s - \rho) g D\right]}$, q_b is sediment flux per unit width in the direction of the boundary shear stress, ρ_s is sediment density, D is the sediment grain size, and $(\tau_*)_C$ is the Shields critical shear stress for sediment motion. The last component of the sediment computation algorithm is a gravitational correction to treat the effect of lateral bed slope on the direction of sediment transport. There are many such corrections, but most (e.g., those by Engelund (1974), Kikkawa et al. (1976), Hasegawa (1984) and Parker (1984)) take the form

$$q_n = q_s\left[\frac{\tau_s}{\tau_n} + \Gamma f\left(\frac{\tau_c}{\tau_b}\right)\frac{\partial B}{\partial n}\right] \tag{12}$$

where τ_s and τ_n refer to the streamwise and cross-stream components of the boundary shear stress, q_s and q_n are the streamwise and cross-stream components of bedload sediment flux, Γ is a coefficient, and f is a simple function of the ratio of critical to boundary shear stress. For details of the values of these parameters, the reader is referred to Nelson (1990). For the results here, the method of Hasegawa (1984) is used.

The final component of the bed evolution model described here is the so-called erosion equation that relates sediment flux and concentration to rates of change of the local bed elevation as follows

$$\frac{\partial B}{\partial t} = -\frac{1}{c_b}\left[\nabla \cdot \vec{q}_B + \frac{\partial}{\partial t}\int_B^E c_s dz\right] \tag{13}$$

where c_b is the concentration of sediment in the bed (taken here as 0.65) and c_s is the suspended sediment concentration. Using Equation 13 along with an assumed time step allows prediction of the evolution of channel bed topography. Thus, starting with some initial topography, the flow field is found from the numerical flow model which is, in turn, used to compute the sediment fluxes. Those values are used in Equation 13 to predict the bed morphology one time step in the future. The process is repeated iteratively to predict the temporal evolution of the bed. Time steps must be chosen such that stability is maintained, which dictates that bed changes be relatively small (typically a small fraction of the flow depth) at each time step. In practice, some experimentation with time steps is usually the best method to optimize computational time while preserving stability. For further discussion of model assumptions and limitations, the reader is referred to Nelson et al. (2003).

SIMPLE CHANNEL RESPONSE

To carry out a preliminary test of the bed evolution module that has been added to MD_SWMS, calculations were performed for a few simple channel geometries. These geometries are ones for which the basic morphological response is well known; the idea behind this simple verification was to ensure that the bed evolution model reproduced important basic responses in bed topography. There are two basic types of bar responses in rivers. First, there are bar forms that are coupled to the planform geometry of the channel such as point bars and, second, there are bar forms that arise spontaneously as a result of an instability in the coupled flow and sediment transport system, such as alternate bars. To test the model, bed evolution calculations were performed for both types of bar forms. To facilitate this, a sub-model for creating simple channels was created within MD_SWMS (the so-called "channel builder") in order to create simple initial channel forms for evolution calculations.

In Figure 2, a curved channel with initially parabolic topography is shown in plan view along with the topography predicted after 1000 minutes of bed evolution. The model predicts the formation of point bars, as expected.

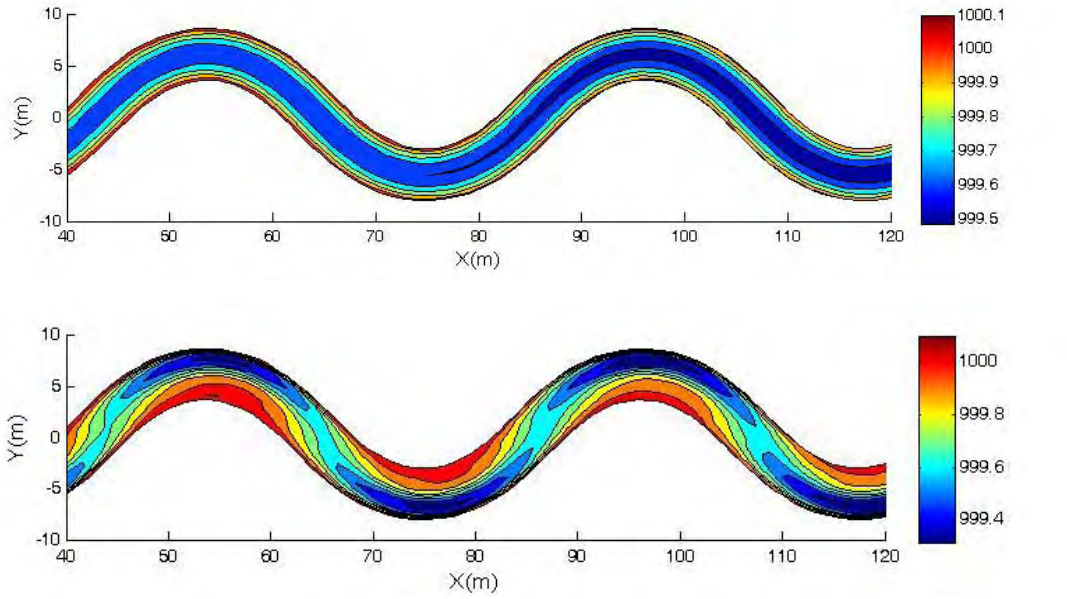


Figure 2 Initial (top) and final (bottom) topography for a simple channel described by a sine-generated curve with crossing angle of 45^o and an initially parabolic bed. The discharge is 1.0 m^3/s and the grain size is 0.5 mm.

In Figure 3, initial and final topography for a simple one-sided rectilinear channel expansion are shown. In this case, the flow in the upstream narrower channel produces much higher sediment transport in that area which is subsequently deposited downstream. Over time, the downstream deposit migrates downstream leaving a higher bed elevation so that the cross-sectional areas above and below the expansion become much more similar over time. At the same time, sediment is deposited in the eddy region, as discussed in more detail by Nelson and McDonald (1996). As in the case of the point bar, this feature is coupled to the channel planform.

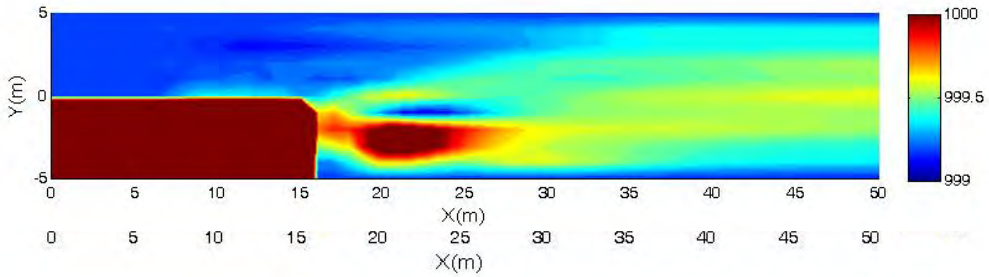


Figure 3 Initial (top) and final (bottom, after 1000 minutes) topography for a simple one-sided rectilinear expansion with discharge of 2.0 m^3/s and grain size of 0.5mm.

In Figure 4, two examples are shown for the case where planform does not force the development of bars; the bars arise from a more basic instability. In both cases, the initial channel is straight and flat-bedded, but a small

perturbation is introduced near the upstream end of the reach. This perturbation is less than 10% of the flow depth, but it is sufficient to excite the fundamental bar instability. In the upper panel, where the channel width is 20 times the depth, this results in the growth of alternate bars, but in the lower panel, where the width is 100 times the depth, a higher mode bar instability occurs, as expected.

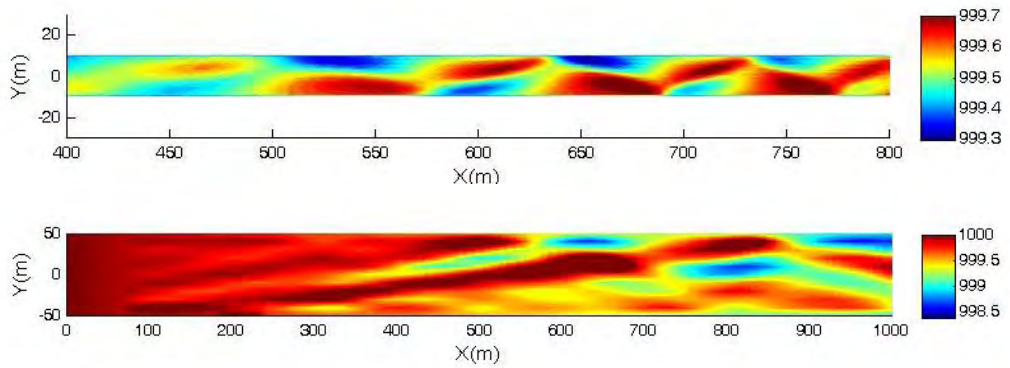


Figure 4 Topography after 1000 minutes for initially straight, flat-bedded channels with width-to-depth ratios of 20 (top) and 100 (bottom) with grain size of 0.5 mm and discharge of 5.0 and 25.0 m^3/s, respectively.

Figures 2-4 support the hypothesis that the simple bar evolution model module in MD_SWMS is capable of predicting appropriate basic behavior for well-known cases. In order to illustrate a simple case with variable discharge, channel evolution calculations were made for a simple meander (similar to that in Figure 2) for three different hydrographs, each using the same total volume of water, as shown in Figure 5.

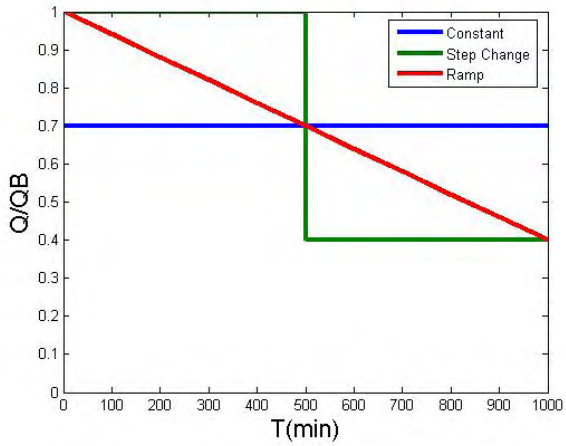


Figure 5 Three hydrographs used for examination of the effects of discharge variations on point bar growth. Q_B is the bankfull discharge for the channel.

In Figure 6, results are shown for two of the three hydrographs shown in Figure 5. As in Figure 2, the initial channel was a sine-generated planform with a parabolic bed. Note that the case where the discharge has a step change has a higher and broader point bar relative to the case where the discharge is a linear ramp. This occurs because the period of high flow allows the bar to grow higher than in the ramp case, even though the same volume of water is used. In the case with constant discharge, the bar is even smaller. This shows how the bed evolution module in MD_SWMS can be used to examine the role of hydrograph shape on resulting topography.

CONCLUSIONS

In situations where evolution of a river or stream bed is an important part of habitat or channel maintenance issues, the new bed evolution module in MD_SWMS can be used to investigate the changes in bed morphology. With further development and testing at the field scale (see McDonald et al., 2006, this volume), this new capability

expands the applicability of MD_SWMS, and allows investigation of more complex problems. Current efforts are directed at treating the formation and evolution of bedforms (ripples and dunes, see Nelson et al., 2005) and treating bank erosion and planform evolution within MD_SWMS.

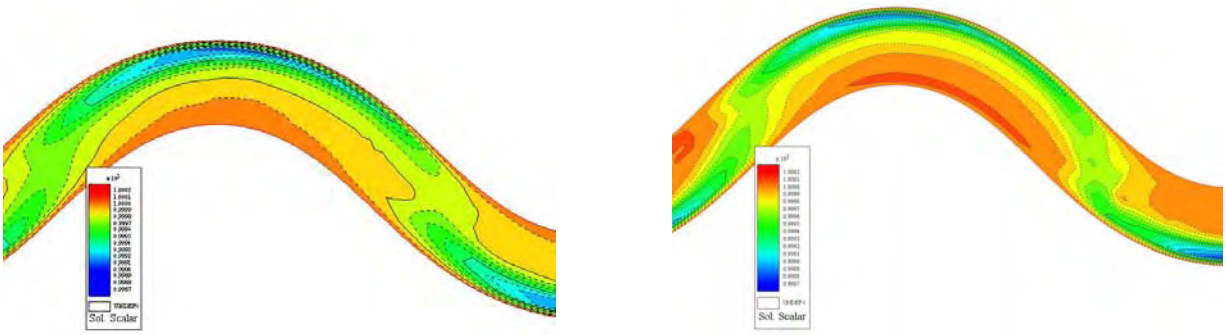


Figure 6 Bed topography in a simple meander bend after 1000 minutes of evolution using a linear ramp hydrograph (left panel) and a step hydrograph (right panel) with the same total volume.

REFERENCES

Engelund, F. (1974). "Flow and bed topography in channel bends," J. Hyd. Div. ASCE, 100(HY11): 1631-1648.

Hasegawa, K. (1984). "Hydraulic Research on Planimetric Forms, Bed Topographies, and Flow in Alluvial Channels," Ph.D. Dissertation, Hokkaido University, Sapporo, Japan.

Kikkawa, H., Ikeda, S. and Kitagawa, A. (1976). "Flow and bed topography in curved open channels," J. Hyd. Div. ASCE, 102(HY9): 1327-1342.

Kinzel, P.J., Nelson, J.M., and R.S. Parker. (2005). "Assessing sandhill crane roosting habitat along the Platte River, Nebraska," U.S. Geological Survey Factsheet 05-3029. 2p.

Long, C.E., Wiberg, P.L. and Nowell, A.R.M. (1993). "Evaluation of von Karman's constant from integral flow parameters," Journal of Hydrologic Engineering, ASCE, 119(10): 1182-1190.

McDonald, R.R., Nelson, J.M., and Bennett, J.P. (2005). "Multi-Dimensional Surface-Water Modeling System User's Guide," U.S. Geological Survey Techniques in Water Resources Investigations 11-B2, 136 p.

McDonald, R.M., Barton, G., and Nelson, J.M., in press, "Modeling hydraulic and sediment-transport processes in white sturgeon spawning habitat on the Kootenai River," Proceedings of the Federal Interagency Sedimentation Conference, this volume.

Middleton, G.V. and Southard, J.B. (1984). "Mechanics of Sediment Movement," SEPM, Tulsa. 401 pp.

Nelson, J.M., Burman, A.R., Shimizu, Y., McLean, S.R., Shreve, R.L., Schmeeckle, M.W. (2005). "Computing flow and sediment transport over bedforms," Proceedings of River Coastal and Estuarine Morphodynamics, IAHR.

Nelson, J.M., Bennett, J.P., and Wiele, S.M. (2003). "Flow and Sediment Transport Modeling," Chapter 18, p. 539-576. In: Tools in Geomorphology, eds. G.M. Kondolph and H. Piegay, Wiley and Sons, Chichester, 688 pp.

Nelson, J.M., and McDonald R.R. (1996). "Mechanics and modeling of flow and bed evolution in lateral separation eddies," Glen Canyon Environmental Studies Report, 69 pp.

Nelson, J.M. (1990). "The initial instability and finite-amplitude stability of alternate bars in straight channels," Earth-Science Reviews, 29: 97-115.

Nelson, J.M. and Smith, J.D. (1989a). "Flow in meandering channels with natural topography," In: S. Ikeda and G. Parker (eds), River Meandering, AGU Water Resources Monograph 12, Washington, D.C. 69-102.

Nelson, J.M. and Smith, J.D. (1989b). "Evolution and stability of erodible channel beds," In: S. Ikeda and G. Parker (eds), River Meandering, AGU Water Resources Monograph 12, Washington, D.C. 321-377.

Parker, G. (1984). "Discussion of: Lateral bedload transport on side slopes (by S. Ikeda, Nov., 1982)," J. Hyd. Div. ASCE, 110(2): 197-203.

Patankar, S.V. (1980). "Numerical Heat Transfer and Fluid Flow," Hemisphere, Washington, D.C. 197 pp.

Rattray, M. Jr and Mitsuda, E. (1974). "Theoretical analysis of conditions in a salt wedge," Estuarine and Coastal Marine Science, 2: 375-394

CHANNEL MIGRATION MODEL FOR MEANDERING RIVERS

Timothy J. Randle, Supervisory Hydraulic Engineer,
U.S. Department of the Interior, Bureau of Reclamation,
Sedimentation and River Hydraulics Group
Denver, Colorado, trandle@do.usbr.gov

INTRODUCTION

The migration of river channels across their floodplains and the occasional erosion of terrace banks is a natural process (Leopold et al., 1964; Yang, 1971; Dunne and Leopold, 1978; Leopold, 1994; and Thorne, 1992 and 2002). This process becomes especially important to people living in or near the floodplain or to organizations planning or maintaining infrastructure within or along the edge of the floodplain. Natural rates of channel migration can be accelerated by human or natural disturbance. For example, the clearing of floodplain vegetation can accelerate the rate of channel migration. This paper provides a summary of a channel migration model for meandering rivers (Randle, 2004).

METHODOLOGY

Meandering river bends are observed in natural river channels, at all scales, and in all parts of the world (Leopold et al., 1964; Thorne, 1992; and Leopold, 1994). The channel migration model assumes that the river is able to adjust its channel alignment, slope, width, and depth between the non-erodible boundaries of the river valley. These adjustments occur so that the sediment transport capacity of the river channel matches the upstream sediment supply rate without deposition or erosion along the channel bed. The channel continually evolves because the upstream rates of water and sediment are continually changing.

Bank Erosion Rate: The model simulates channel migration by computing bank erosion as a function of the sediment transport capacity, the radius of channel curvature, and the bank material properties acting to resist the erosion including vegetation, large woody debris, cohesion, and armoring. The equation for bank erosion is based on dimensional analysis of the controlling variables and the use of empirical coefficients. Equation 1 is proposed to predict the rate of bank erosion and channel migration.

$$B_e = \left\{ \left[a_1 C_s \left(\frac{W_b}{R_c} \right) \right]_{at\ L} - \left[a_2 \left(r_\gamma \frac{r_d}{h_b} \right) + a_3 \left(LWD \frac{d_W}{D} \right) + a_4 (PI) + a_5 \left(d_c \frac{h_b}{D} \right) \right]_{\text{at } L + \text{Phase Lag}} \right\} a_6 V \qquad (1)$$

where B_e = rate of bank erosion [L/T],
C_s = bed-material sediment concentration [ppm]
W_b = bankfull channel width [L]
R_c = channel radius of curvature [L]
L = distance along the channel
Phase Lag = planform phase lag along the channel (see Figure1)
r_γ = fraction of bank area covered by vegetation roots [%]
r_d = vegetation root depth [L]

h_b = bank height [L]
LWD = fraction of bank area covered by trees or large woody debris [%]
d_W = average height of large woody debris jams [L]
D = hydraulic depth of the channel [L]
PI = plastic index
d_c = portion of bank sediment too coarse for incipient motion [%]
V = mean channel velocity [L/T]
a_1 and a_6 are empirical coefficients and a_2, $a3$, a_4, and a_5, are weighting factors

All the parameters on the right-hand side of Equation 1 produce dimensionless terms except for the average channel velocity, which provides dimensions for the bank erosion rate [L/T]. The first set of terms in Equation 1 [a_1, C_s, (W_b/R_c)] are computed at some distance L along the channel. The following terms of Equation 1 act to resist the bank erosion and are computed at a phase lag distance downstream from point L. The velocity term of Equation 1 (a_6 V) is computed at a distance L along the channel. The computed rate of bank erosion from Equation 1 is multiplied by a time step (Δt) and then applied to the channel at a distance equal to L + phase lag.

The equation coefficients a_1 and a_6 must be determined empirically through calibration. Coefficients a_2, a_3, a_4, and a_5 are used to weight the relative importance of the terms acting to resist bank and erosion and can be set so that the weighting is equal. Not all of these coefficients may be important for a particular river reach.

The root structure of riparian vegetation can add cohesive properties to the river bank and reduce the rates of bank erosion if the roots are at least as deep as the bank is high. Otherwise, the bank can become undercut by erosion underneath the vegetation roots, which may cause the top portion of the bank to collapse. Trees that fall into the river from an eroding bank can add large woody debris to the bank and channel. Large woody debris, present along the river bank, tends to increase the channel roughness, slow velocity, and also reduces the rates of bank erosion. However, the woody debris may be floated away if the flow depths are larger than the cumulative height of the large woody debris jam.

The presence of riparian vegetation can be expressed as the root density along the local bank area (r_γ). The effectiveness of these roots can be expressed as the ratio of the root length to the bank height (r_d /h_b). A ratio much less than unity would mean that the roots are not deep enough to prevent erosion at the bank toe from undercutting the vegetation. The presence of riparian forests and large woody debris along the eroding bank can be expressed as a percentage of the local bank area occupied by trees and large woody debris (LWD). The ability of large woody debris to remain along the river bank can be expressed as the average ratio of the height of large woody debris jams to the hydraulic depth of the river channel (d_W /D). A ratio much less than unity would indicate that the woody debris would be floated away.

The plasticity index (PI) is used to characterize the cohesive properties of the bank material. The percentage of bank sediment that is too coarse for incipient motion in the river channel (d_c) is used to characterize the ability of coarse bank material to armor the toe of an eroding river bank. The ratio of bank height to hydraulic depth (h_b/D) accounts for the greater mass of armoring

material when a river bank is higher than normal. For alluvial banks within the floodplain, this ratio is normally equal to unity, but the ratio can be significantly greater in the case of high terrace banks.

Planform Phase Lag: River meander bends induce secondary currents that increase the flow velocities and shear stresses along the outer bank and decrease them along the inner bank. Consequently, sediment erosion occurs along the outer bank and deposition occurs along the inner bank (Leopold et al., 1964; Thorne, 1992; and Leopold, 1994). The tendency to erode the outer bank and deposit sediment along the inner bank causes the channel to migrate laterally.

Typically, the maximum rate of bank erosion along the outer bank is located some phase-lag distance downstream of the meander bend apex, which causes the river channel to migrate both across the floodplain and downstream along the river valley (see Figure 1). If there were no phase lag, the meander bends would only migrate laterally across the floodplain and increase in amplitude. If the phase lag were equal to the channel distance along one-fourth of a meander wavelength, then the meander bends would only migrate downstream without any increase in amplitude.

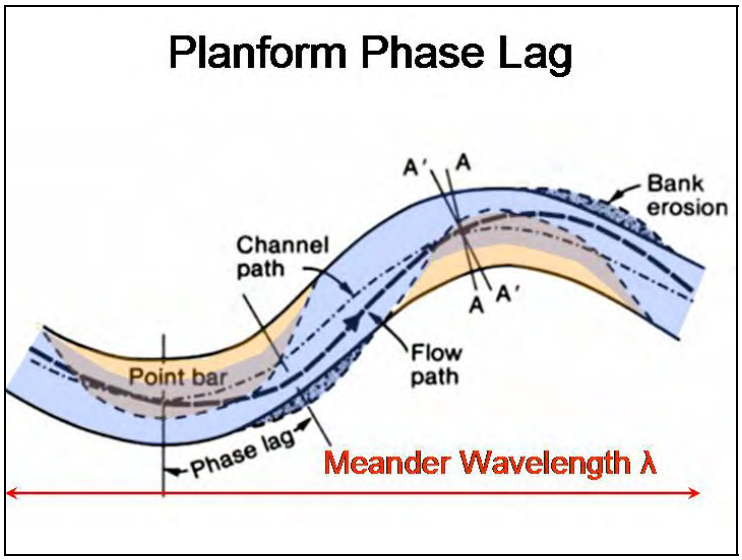


Figure 1 The greater the planform phase lag, the greater downstream migration of the meander bend along the valley axis.

In the model, the variable phase lag is determined by evaluating the river channel slope relative to the valley slope and the limiting channel slope associated with the minimum unit stream power. As the channel slope begins to approach the slope at the minimum unit stream power (*VS*), the migration of the meander bends will be primarily down valley. Since the channel slope is limited by both the valley slope and the slope at minimum *VS*, the planform phase lag should be proportional to the differences in these slopes (see Equation 2).

$$\text{Phase Lag} = \frac{\left(S_v - S_c\right)}{\left(S_v - S_{\min VS}\right)} C_{PL} \left(\frac{\Omega}{4}\right) \lambda \qquad (2)$$

where S_v = valley slope
S_c = channel slope
$S_{\min VS}$ = channel slope at minimum *VS*
λ = meander wavelength
Ω = channel sinuosity
C_{PL} = a phase-lag coefficient, normally equal to 1.0

The model keeps track of the changing alignment throughout the simulation. At the beginning of each time step, the model computes the radius of curvature for each point along the channel alignment.

Model Input Requirements: The meander model input requirements include both initial conditions and boundary conditions. The initial conditions describe the river channel alignment and the material properties (vegetation, large woody debris, cohesion, and armor material) of the floodplain and terraces, including any lateral limits of channel migration. The boundary conditions describe the upstream inputs of water and sediment.

Initial Conditions The initial alignment of the river channel thalweg is digitally measured, in some Cartesian coordinate system, from rectified aerial photographs or from channel surveys. The river valley alignment and longitudinal slope are also measured from ortho-rectified aerial photography and topographic surveys. Channel cross-section data are not part of the model input. The model computes a channel width and depth for each time step and for each point along the channel alignment (Randle, 2004). The computation of cross section width and depth is based on the upstream inputs of water and sediment, Manning's equation for normal depth, a sediment transport capacity equation, and the minimum rate of energy dissipation theory (Yang and Song, 1979). However, the rate of change in channel width is limited to a certain percentage per time step.

Boundary Conditions The upstream boundary conditions include the discharge hydrograph and corresponding sediment supply. The model assumes that the upstream sediment supply is equal to the transport capacity for a specified cross section shape and channel slope.

Model Calibration and Validation: Measurements of historical channel migration should be used to calibrate and then validate the model results before the model is used for future predictions. The historic measurements of channel alignment could be divided into two independent time periods: one for model calibration and one for model validation.

EXAMPLE RESULTS

A 4.2-mile reach of the Hoh River, Washington was used to demonstrate the calibration and validation of the model. This reach is 5.5 miles downstream from the boundary of Olympic National Park and between river miles 21.4 and 25 (Piety et al., 2004). Historical aerial photographs of the Hoh River are available for the following years: 1950, 1960, 1971, 1977, 1981, 1994, 2001, and 2002. The initial channel alignment, for the model simulation, was digitized from the 1950 aerial photograph (see Figure 2).

The 27-year time period, from 1950 to 1977, was selected for model calibration. The 25-year time period, from 1977 to 2002, was selected for model validation. The 57-year record of mean-daily stream flow and annual peak flow is presented in Figure 3. Since there are no measurements of sediment load, the upstream sediment supply to the study reach was set equal to the sediment transport capacity (Randle, 2004).

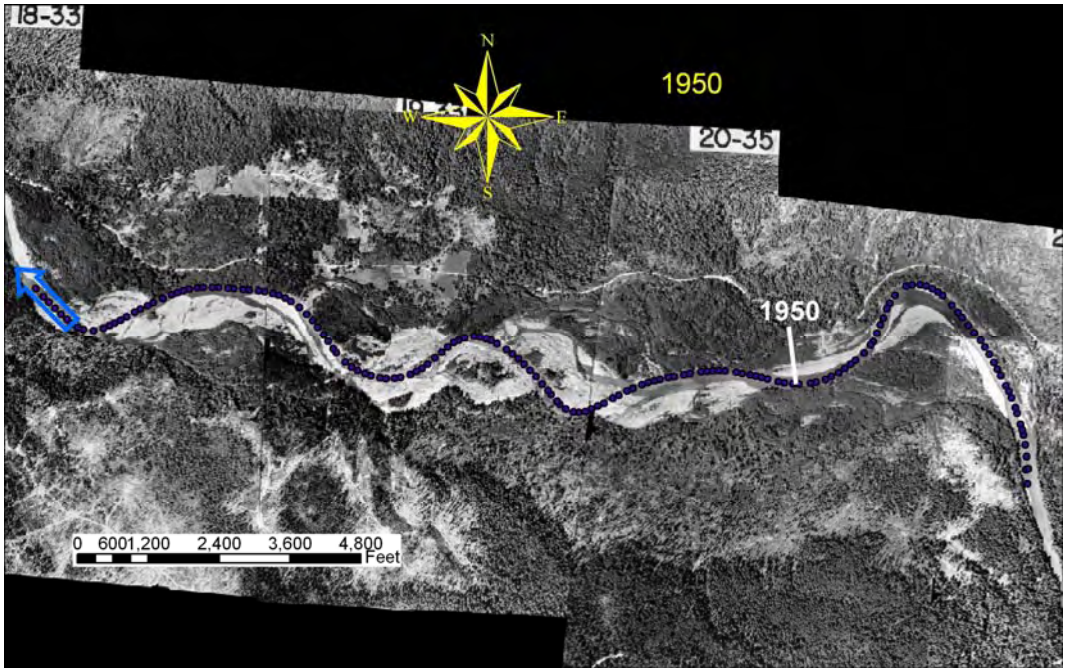


Figure 2 1950 aerial photograph and initial channel alignment.

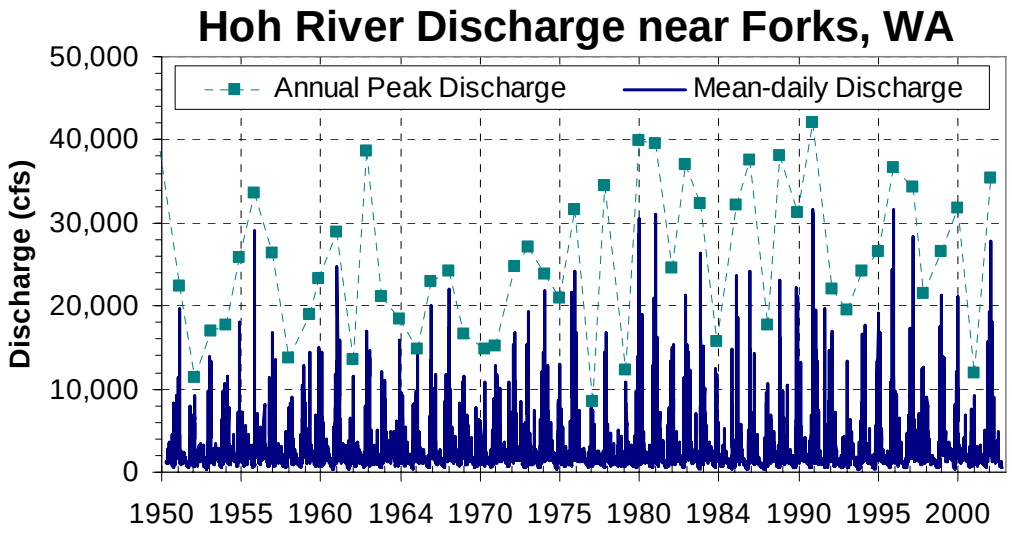


Figure 3 Mean-daily and annual-peak discharge of the Hoh River.

The bank material properties were globally defined for the modeled area and locally defined for seven smaller areas of the channel, floodplain, and terraces. The material properties for vegetation, large woody debris, cohesion, and armoring were determined for each area based on field inspection and were not subsequently adjusted during the calibration process.

Figure 4 shows a series of predicted channel alignments over the period 1950 to 2002. The model was not able to predict the meander-bend cutoff that occurred sometime between 1971 and 1977 (see Figure 5). Therefore, the predicted channel alignment was calibrated for the first two meander bends. The combination of coefficients a_1 and a_6 and the phase-lag coefficient that provided the best match between the predicted and measured channel alignments was determined by visual inspection of the model results compared to the 1977 aerial photographs.

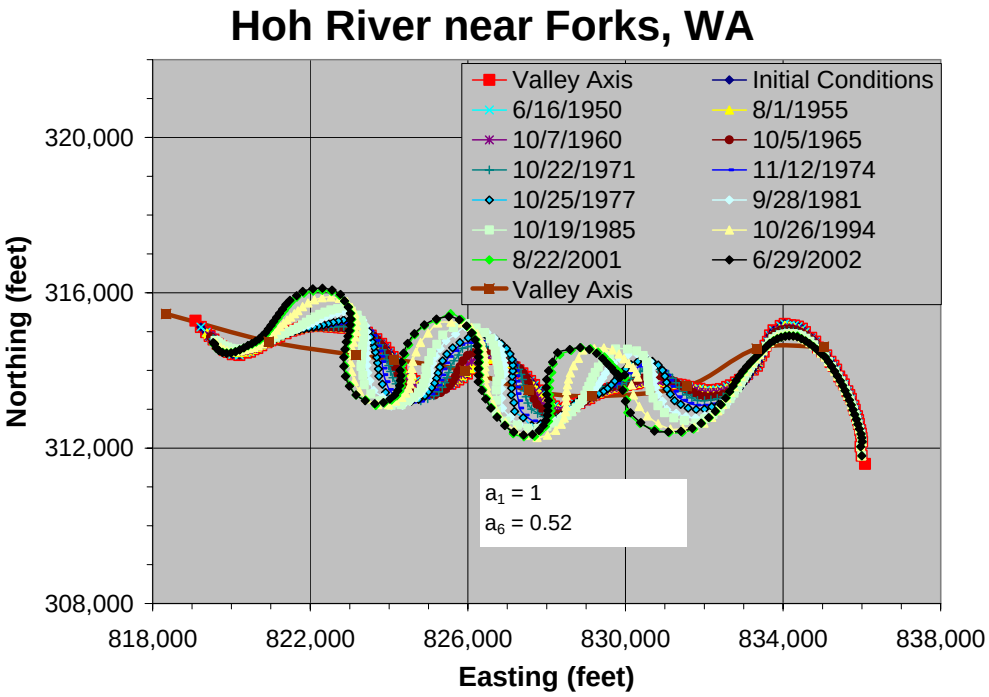


Figure 4 Predicted channel alignments for the period 1950 to 2002.

The model simulation was continued for the entire period (1950 to 2002). Although the model is not yet capable of predicting a meander-bend cutoff, the relatively short radius of curvature of the predicted meander bends would suggest that a cutoff is likely (see Figure 6).

DISCUSSION

Calibration was required for only two coefficients (a_1, a_6,) of Equation 1. The model was able to correctly predict the direction and approximate magnitude of channel migration for a least 10 years, until the cutoff of meander bends that first occurred between 1960 and 1971. Although the model is not yet able to predict the meander-bend cutoffs, they can be inferred from the tight radius of curvature from the predicted channel alignments.

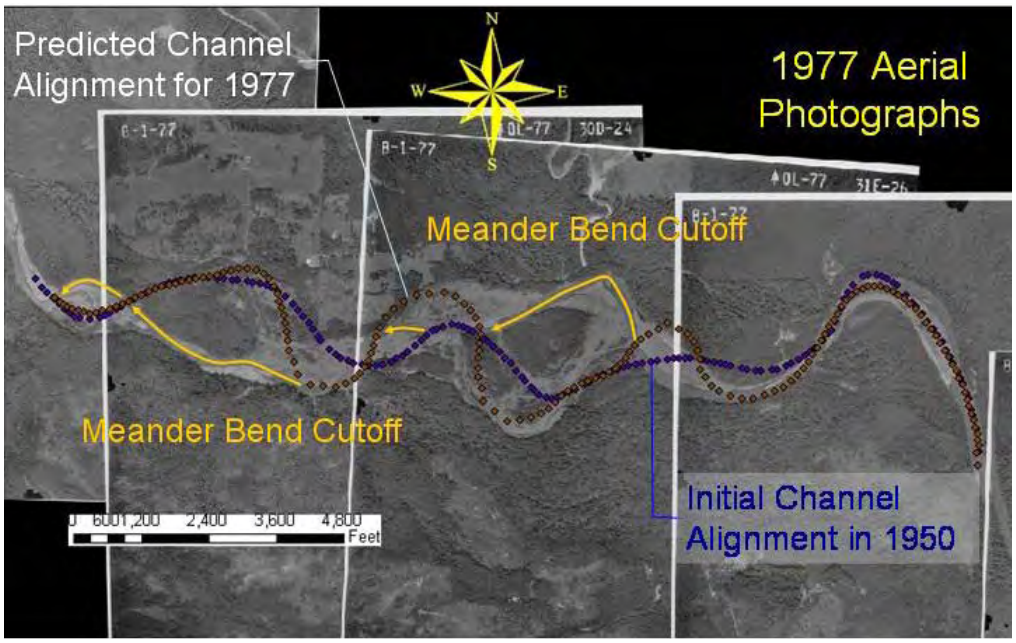


Figure 5 1977 aerial photograph and the initial (1950) and predicted (1977) channel alignments. A meander bend cutoff occurred sometime between 1971 and 1977.

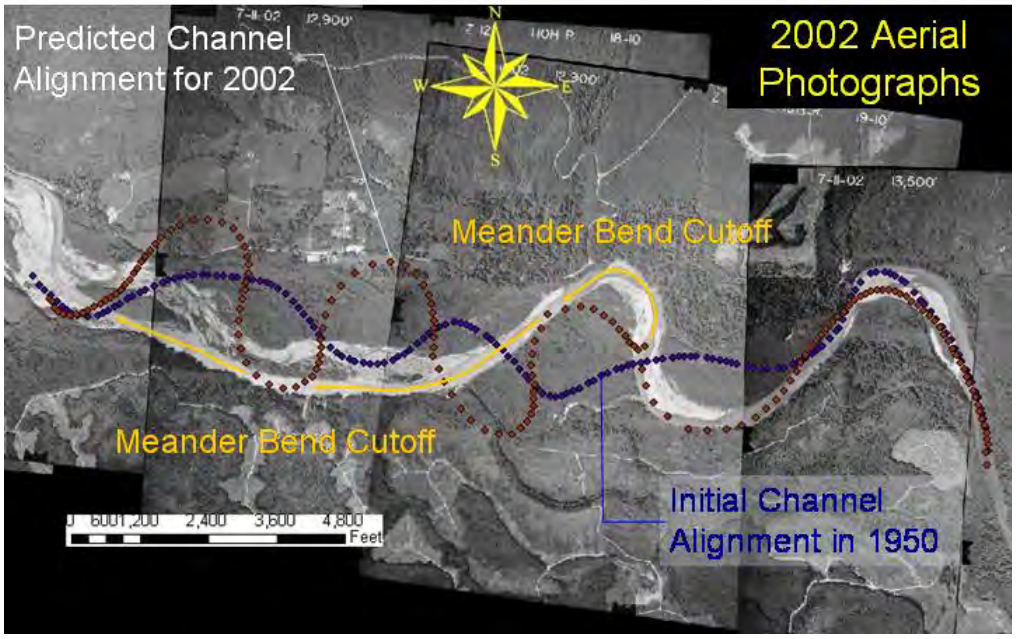


Figure 6 Initial (1950) and predicted (2002) channel alignments plotted on the 2002 aerial photograph.

The model correctly predicted that the initial direction of channel migration was in the lateral direction, across the floodplain. As the meander-bend amplitude increased, more of the meander-bend migration was in the down-valley direction (see Figure 4).

CONCLUSIONS

The channel migration model described in this paper does show promise as a tool for predicting future channel alignments. The model could be used to compare different hydrologic scenarios and alternative land use plans. The model could also be used to evaluate proposed highway and bridge alignments in the vicinity of the river channel and floodplain.

Additional research is needed to develop and implement criteria for the occurrence of meander-bend cutoffs. Future versions of the model could track the age of floodplain and terrace vegetation over time. As the model simulates the creation of point bars along the inside curves of meander bends, the model could also simulate the growth of vegetation on these point bars. Young vegetation could either be scoured by subsequent floods or grow to maturity and potentially protect the bank from future erosion. A future version of the model could also account for the increase in sediment supply caused by the erosion of terrace banks because they are higher in elevation than the floodplain surface.

REFERENCES

Dunne, T. and Leopold, L. B. (1978). "Water in environmental planning," W.H. Freeman and Company, New York, New York.

Leopold, L. B. (1994). A Vew of the River. Harvard University Press, Cambridge, Massachusetts.

Leopold, L. B., Wolman, M. G., and Miller, J. P. (1964). "Fluvial processes in geomorphology," W. H. Freeman and Company, San Francisco, California.

Piety, L. A., Bountry, J. A., Randle, T. J., and Lyon E. W. (2004). "Geomorphic assessment of the Hoh River, Washington, river miles 17 to 40 between Oxbow Canyon and Mount Tom Creek," U.S. Department of the Interior, Bureau of Reclamation, Denver, Colorado.

Randle, T.J. (2004). "Channel Migration Model For Meandering Rivers," A thesis submitted to the University of Colorado at Denver in partial fulfillment of the requirements for the degree of Masters of Science, Civil Engineering.

Thorne, C. R. (1992). "Inaugural lecture, River meanders: Nature's answer to the straight line," University of Nottingham, Department of Physical Geography, Nottingham, England.

Thorne, C. R., (2002). "Geomorphic analysis of large alluvial rivers," Geomorphology, 44, 203-219.

Yang, C. T. (1971). "On river meanders," Journal of Hydrology, 13, 231-253.

Yang, C. T. and Song, C. C. (1979). "Theory of minimum rate of energy dissipation," Journal of the Hydraulics Division, American Society of Civil Engineers, 105 (7), 769-784.

ENVIRONMENTALLY SENSITIVE GRAVEL BAR SCALPING

Frank Reckendorf, Fluvial Geomorphologist, 950 Market St. NE, Salem, OR 97301, frecken@open.org

INTRODUCTION

This paper evaluates and summarizes previous studies and presents the results of four years of evaluation of scalping along the Wilson and Kilchis Rivers in Tillamook Co. OR. Data concerning the Donaldson, Barker, Dill and Gomes Bars will be shown. These are two of the four rivers in the basin that have been periodically scalped for many years. Bar scalping does not exceed the annual recruitment rate, consistent with Oregon Department of Fish and Wildlife policy. To reduce any potential impact on salmonids, particularly chum salmon, the scalping is done under a state-county-private coordinated agreement that scalping is only allowed if there is active erosion on the opposite streambank. This agreement was signed in 1992 and had some minor word amendments in 1999

SETTING

Landscape Conditions: Sea level occupied the lowlands of the Tillamook Basin as late as about 6,000 years ago. Stratigraphic sections can be characterized as a mixed sequence of marine gravels and gravely clay, overlaid by a thick sequence of marine sand, possibly volcanic ash and some organic rich zones, overlaid by sandy gravel, overlain by sand, silt and clay estuary deposits. Various units, but in particular the estuary deposits have thin sand layers that are likely to be tsunami deposits from subduction zone earthquakes. A recent published (Reckendorf and Peterson, 2003) list of coseismic events shows subduction zone earthquake events in radio carbon years before present as 3,200; 2,800; 2,500; 1,700; 1,300; 1,100; and 1700AD. With each event would have been subsidence and additions of tsunami sands of various thickness, Once sea level started to drop, alluvial fans and landsides developed around the margin of the basin. Over time the streams developed that meandered and deposited gravelly lateral accretion deposits. During floods some of the lateral accretion deposits were overlain by sandy and silty vertical accretion deposits. As the river downcut to present sea level, the rivers developed new food plains, leaving older flood plains as terraces along the stream banks. This results today in a stepped sequence of low flood plains flooded in ordinary high water (also called bankfull flow); flood plains a few feet higher called intermediate flood plains that are only flooded occasionally, and high flood plains that are only flooded in rare flood events. All of these flood plains, as well as un-flooded terrace, and alluvial fans, which are a combination of stratified sandy, silty, and gravel deposits, are encountered by the Wilson, and Kilchis Rivers at any given location. Of critical importance is that the lateral accretion flood plain gravel deposits that are overlain by vertical accretion finer textured deposits are incised within the fan and terrace deposits. Fines and sand are frequently washed out of the gravel matrix causing the gravel to slough and de-stabilize the overlying material. The tsunami sand layers are also easily washed out causing failure above.

In the 1800's, the Wilson River was much narrower than today such as shown in Figures 10 and 29 in Coulton et al (1996) and in Figure 6-3 in Coulton, (1998). It is estimated that the Wilson River and its bars had a width of roughly 70 feet in the early 1900's. The channel width, including the bar, in 1939 at the Donaldson, and Barker Bars on the Wilson River and Middle Gomes, Lower Gomes, and Dill Bars on the Kilchis River are about 147 ft, 107 ft., 67 ft., 53 ft. and 80 ft., respectively. In 2000 the width measured is 280 ft., 180 ft., 178 ft., 290 ft., and 290 ft., respectively. Widening along the Wilson, and Kilchis Rivers has occurred primarily from lateral erosion of the sandy and silty vertical accretion deposits of the low flood plain, apparent on old (1939) aerial photographs. Once the vertical accretion deposits are eroded off the underlying lateral accretion deposits are exposed as gravel bar. These new gravels have than been taken as gravel scalping in gravel removal operation. In other words, much of the gravel being taken in scalping is from areas that were historically low flood plains, rather than natural bars.

Stream Hydrology and Sediment in Gravel Bars: The Wilson River has had a recording stream gage at RM 11.4 since 1937. This 74 years of record allows for the development of an excellent discharge frequency curve for the Wilson stream gage. A frequency curve (Reckendorf, 2004a) for the Wilson River Gage was developed based on the data in USGS Open File Report 93-63 (Wellman et al, 1993). This frequency curve was extended at the low flows between the 80% chance (2 year average recurrence interval) and 99% chance (1.0 year average recurrence interval), using unpublished data provided by the US Geological Survey.

Based on field evidence along the Wilson and Kilchis Rivers of the first flat flooded depositional surface, and high water marks of six recent floods, as well as the frequency-discharge curve best break in slope, a bankfull flow at the gage is proposed that has a provisional discharge of 11,500 cfs. This has a stage of 12.5 ft. at the stream gage. Since the gage has a one foot offset, the bankfull depth at the gage is 11.5 ft. The bankfull flood event has an average recurrence interval flood frequency of 1.16 years. However for the Donaldson Bar at RM 5.0 there is an additional 31 sq. mi. of drainage area. The gage has a drainage area of 161 sq. mi. Therefore the additional drainage area represents 19% of the gage drainage area, so all discharges for the Donaldson Bar could be increased for evaluation purposes by as much as 19% as was done in some past studies (Reckendorf, 2005a, 2004) However increasing the bankfull flow by 19% probably overestimates the bankfull flow condition at the Donaldson Bar, because much of the additional watershed comes from lower elevations In addition increasing the bankfull flow by 19% made little difference in the velocity used in the analysis of pre and post scalp incipient motion of particles (Reckendorf 2005a)

The largest flood peak in 2002-2003 was on January 31, 2003 and had a discharge of 17,800 cfs. and a stage of 14.8 feet. That flood has about a 2-year average recurrence interval. A flood occurred on March 22, 2003 that has a provisional discharge of 11,500 cfs and a stage of about 12.5 ft. This flood has an average recurrence of 1.16 years. In the 2003-2004 the largest flood was on January 29, 2004. This flood has a provisional discharge of 12,600 cfs with a stage of 12.8 with an average recurrence interval of 1.23yrs. In the 2004-2005 there was a flood on December 11, 2004 that has a provisional discharge of 11,100 cfs. with a stage of 12.1 ft. This flood has an average recurrence interval of 1.19 yrs. The largest flood of the 2004-2005 occurred on January 18, 2005. It has a provisional discharge of 15,500 cfs. with a stage of 14.0 ft. This flood has and average recurrence interval of 1.6 yrs. Another large flood occurred on March 27, 2005. This flood had a discharge of 12,000 and stage of 12.6 ft. Of the last five floods three of them were between 11,100 and 12,000 cfs. Therefore the bankfull flow of 11,500 cfs. fits the average for the field conditions of ordinary high water. The overall flood history of the Tillamook Basin is reflected in the Wilson River gage or the last 12 years, (and to some degree the debris flow history). has been shown in Reckendorf, 2005a. Almost all of the winter floods shown are close to or above bankfull discharge except the runoff event on December 23, 2000 of 3,750 cfs. and one on 2/24/94 of 8,180 cfs. Several years show three or more floods greater than bankfull in a given year, and it is no surprise the 1996 is one of those years, as a 1% chance event occurred that year.

The Kilchis River Watershed is the adjacent watershed to the Wilson River watershed on its north side. The Kilchis River had at short-term stream gage at approximately river mile 2.5. The Oregon Water Resources Department provided me with a rating curve for the Kilchis River gage (14301450). This rating curve did not extend far enough to include discharges above 8,400 cfs. Therefore for the January 31, 2003, March 23, 2003 or January 29, 2004 floods, I extended the rating curve for these higher observed stages to determine a higher discharges Reckendorf, (2004b), even though there was no field measurement to support these discharges. The January 31, 2003 flood has a discharge of 17,500 cfs. associated with a stage of 14.6 feet. Another flood on March 22, 2003 has a flood discharge of 12,500 cfs. associated with a stage of 12.3 feet. The January 29, 2004 flood has a provisional discharge of 16,700 cfs. associated with a stage of 14.3 feet. Assuming that the Kilchis floods would be operating at about the same flood frequency 1.16 yr., a 11,500 cfs. event on the Wilson River would have a provisional discharge of 11,500 cfs. on the Kilchis River which has a stage of 11.7 (no offset) based on the Kilchis rating curve.

A study by Stinson and Stinson, (1998) looked (1993-1997) at the effects of gravel bar scalping on the morphology of gravel bars and particle size distribution of the bar gravel and gravel armor layer in four watersheds in Tillamook County.. The study, which took repeated samples at the same location for particle size distribution, showed no consistent downstream decrease in particle size for either the Wilson, or the Kilchis River. The Stinson's (1998) concluded that there was no correlation between gravel bar harvesting and the variability in particle size. They found no trend in any particle size class increasing or decreasing consistently over the course of the study. There was no correlation between the particle size distributions and gravel bars in the same watershed. They found no correlation between the flows in the watershed and the particle size distributions as shown in the lack of a corresponding shift in the particle size distributions between 1994 and 1996 to match the flow pattern shift. The variability encountered in particle size is consistent with a landslide-debris flow-debris torrent dominated system. It depends on the variability in size of source material, and on debris flow occurrence and movement for local storms conditions on where any given sediment debris has moved and distributed downstream.

Dynamic Equilibrium: The natural dynamic equilibrium condition along the Wilson, and Kilchis, Rivers in the Tillamook Bay Watershed, has been severely altered over the years by alteration of sediment load and size as well as the channel slope, and probably the discharges. These alterations have come about because of initial logging and log drives down the rivers, forest fires, roads and railroads built for salvage logging, woody debris accumulations and blowouts of woody debris accumulations, removing channel large woody debris, and channel straightening and alterations by the Corps of Engineers and local landowners, especially after floods. These changed conditions along with a landslide-debris flow-debris torrent driven system, have resulted in over-widened streams with mixed bed material load that is not in equilibrium with flow conditions. The over widen width with a bed material load that did not increase with flow or decrease with distance downstream (Stinson and Stinson 1998) is evidence that the Wilson and Kilchis Rivers are operating in a "chaos condition" and are not in a dynamic equilibrium condition. There have been gravel operations along the Wilson, Trask, Kilchis, and Miami River in the Tllamook Bay Basin that have removed some gravel sediment from some channels and bars for over 50 years. however, in about the last 10 years there has only been bar scalping. The over widen condition existed 70 ft. to 147 ft. by 1939, and 200 ft. by 1953) prior to most of the gravel removal operations. The gravel removal does not appear to be the cause that created the dis-equilibrium condition. It is the excess sediment supply (Reckendorf, 2005a, 2004, 1995) from landslide-debris flows-debris torrents along with the over-widen channel and bar area that prevents the discharge and slope from re-establishing a dynamic equilibrium condition. Part of the over widened channel may have been caused because of past large and repetitive log debris jams moved down the channels (Coulton et al 1996), and by disturbances along the channel for salvage logging after the Tillamook Burn fires. The excess sediment supply in the watersheds of rivers keeps bars replenished and growing. Un-scalped bars through sedimentation keep growing in width and height. However, it takes a flood larger than a bankfull event to add much sediment height once the bars grow in height up to the level of the low flood plain.

Landslides, Debris Flows, and Debris Torrents: The term landslides denotes "the movement of a mass of rock, debris, or earth down a slope" (Cruden, 1991). One study (USDA, 1978) stated that there were 1,870 human caused landslides in the Wilson Watershed verses 86 natural landslide. On the Kilchis they (USDA, 1978) stated that there were 828 human caused landslides verses 28 natural landslides. Sometimes landslides are converted to debris flows, which are landslides where, "considerable amounts of loose material are suddenly moved by an excessive amount of water and transported in an extremely fast and destructive flow through a valley." (TRB, NRS, 1996). Debris torrents are likely the most important means of sediment transport in the upper watersheds in the Tillamook Bay Watershed (TBNEP, Chapter 6 Sedimentation, Charland and Reckendorf, 1998). Debris torrents are rapid movements of water-charged debris confined to steep headwater channels. They begin as landslides and debris flows and can transport up to 100 times more than the initiated slide when fully developed (Mills, 1997a, and 1997b). The most common triggering mechanism for debris torrents are extreme water discharge, either heavy rainfall or temporary damming of a channel (Van Dine, 1985). Debris flows and torrents tend to deposit there material where channel gradients decline. Once the debris flow or debris torrent reaches a stream they can stop and develop a local sediment debris jam in a channel, or at a tributary junction. Once they have formed a plug in the channel they cause the stream to severely erode the streambank to get around the plug of sediment. The plug of sediment debris does not move all at once but moves downstream as a pulse only under high runoff conditions. Therefore the streambanks are progressively eroded out in a downstream direction, as the stream finds more easily eroded material in the streambanks than the coarse material in the sediment debris in the channel. One statewide study (Hofmeister, 2000) associated severe storms, that cause flood peaks, with landslides (all forms of upland slope failure were included). The severe storms were February 1996, November 1996, and December 1996/January 1997 which generated 9,582 landslides in Oregon that were reported in the inventory. Tillamook County accounted for 836 landslides, of which 212 landslides were inventoried in the Wilson Watershed, and 159 in the Kilchis Watershed.

Active Erosion: Gravel scalping has been allowed in the Tillamook Basin since 1992, based on a state-county-private coordinated agreement. According to that agreements scalping is only allowed if there is active erosion. Active erosion over the years has caused stream widening as reflected in Tables 1 and 2. Table 2 is based on average conditions between aerial photo dates, except for the year 2000 which is based on cross section width. As shown in Table 2 rates are very high in some time periods for some time periods or locations. For example high erosion rates between 1939-1953 likely reflect the impact of the Tillamook Burn, salvage logging operations, log drives and breached log jams. Between 1994-200 rates are quite high likely reflecting the 1996-1997 flood runoff and related debris flows and torrents. Local conditions of very high erosion rates are shown for Tannler Bar on the Wilson River., between 1939 and 1953. These high rates are attributed to debris flow deposition and associated log jams causing local dams in the river that were flanked by the Wilson River by eroding its streambanks. The

immediately upstream Barker Bar erosion rates are also high but not nearly as high as the Tannler Bar rates, and the Barker Bar would lie in the backwater of any debris flow plug along the downstream Tannler Bar. Erosion rates were also quite high along the Kilchis River between 1939 and 1953, also reflecting salvage logging as well as excess sediment supply from debris flows. The length of active streambank erosion is shown in Table 1, for the streambanks across from the bar stated. All areas of active erosion have weak stratigraphic layers, sloughing of gravels as fines and sand are washed out effectively decreasing matrix material, overhanging layers, and slump blocks at the base of the streambanks. All of these areas have essentially no effective vegetative cover, but have overhanging vegetative cover from above of Japanese Knapweed, Himalaya Blackberry, and Morning Glory. These vegetative materials provide essentially no erosion control protection, or a rooting system that binds the soil together, and hang out as much as 9 feet from the bank.

Stream Bar, Bed, and Bank Scour Conditions: At the Donaldson bar along the Wilson river, the competent average erosive velocity (Simon and Senturk, 1977, Figure 9.8) for pre and post-scalped conditions are reflected in Table 3. Using the gage discharge of 11,500 cfs., and a bankfull of 11.5 ft., the average velocity is 11.7 ft./sec. for pre-scalped conditions, and 7.9 ft./sec. for post-scalped conditions. The median bar size is 12.5 mm. and the median streambed size is 13 mm. The leave armour area (105 ft.) has an armour d50 of 27 mm. and the leave side of the upper bar has a d50 of 35 mm. As shown the average velocity for the pre-scalped conditions can cause incipient movement of particles up to 90 mm. at the 11 ft./sec. velocity, but only up to 30 mm. in the post-scalped condition. Therefore for the post scalped condition the average velocity will not cause particle movement of the buffer at the upped end or side of the bar. Although the post-scalped condition is shown to be high enough to move the median bar d50 there is no field evidence during floods or in post flood evaluation that scour, especially a scoured back channel, has developed. In contrast re-deposition is occurring with each runoff event with the amount varying with discharge and debris flow activity. As shown in Table 3, the results are little different if adjusted for a drainage area correction of 19%. The discharge is 13,385 cfs. and the average velocity 11.3 ft./sec. The incipient motion of particles is essential the same. The gravel basal stratigraphy along the right streambank that is undermining the right streambank, has an estimated d100 of less than 90 mm. with a sand and silt matrix material that is much smaller. This means that the pre-scalp velocity can readily scour out all of the gravel material, to undermine the overlying materials. This does not happen uniformly along the 575 feet of active eroded streambank, but instead results in an overhanging or vertical streambank along some areas and sloughed gravels. Under both conditions there are failed slump blocks at the base of the slope that are slowly reworked during flood runoff conditions. For the Barker Bar the 15.6 ft./sec pre-scalp velocity can cause significant d50 bed material movement, or streambed scour of material smaller than 200 mm. It is significant that there are many slump blocks along the 250 feet of 10 foot high eroding streambank. The Barker Bar was not scalped for three years (2001-2003), and the vertical streambanks with slump blocks may reflect the lack scalping in those years. For the Barker Bar post-scalping average velocity is shown to be high enough to cause significant movement of median d50 of 9.7 mm. However there are no scour areas or back channel scour channels developed after scalping in 2004. The upstream buffer leave area has a d50 of 42 mm., which is likely preventing downstream scour from occurring. For the Dill Bar on the Kilchis River the leave buffer armour is 53 mm. which is substantially above the bar median d50 of 17 mm. Post scalping average velocity will only cause incipient motion of particles with a d50 of less than 6 mm., which indicates essentially little incipient motion of particles on the post-scalped bar. For the Lower Gomes the leave area buffer armour is 26 mm. In addition the average size of the pebbles in the basal sloughing along the opposite streambank is less than 20 mm. Therefore the average velocity conditions for pre-scalped conditions, which can cause significant bed movement of particles with a d50 of up to 37 mm. is more erosive in the pre-scalp than post-scalp conditions where significant movement of particles will only occur for particles smaller than 7 mm.

Table 1 Channel and bar widths and active erosion length

BAR	RIVER	1939	1944	1953	1994	2000	Length
		ft.	ft.	ft.	ft.	ft.	ft.
DONALD.	WILSON	147		200	260	280	575
BARKER	WILSON	107	136	155	170	180	250
TANNLER	WILSON		136	150	160		
DILL	KILCHIS	80	89	140	180	290	345
L. GOMES	KILCHIS	55	92	120	150	223	385
M. GOMES	KILCHIS	67	91	130	160	178	120

Table 2 Average erosion rates

BAR	RATE	RATE	RATE	RATE	RATE
	1939-1944	1939-1953	1944-1953	1953-1994	1994-2000
	ft./yr.	ft./yr	ft./yr	ft./yr	ft./yr
DONALD.		3.8		1.46	2.2
BARKER	5.8	4.8	2.1	0.37	1.7
TANNLER	16.6	14	1.56	0.2	
DILL	6.3	4.28	5.7	0.98	12.2
L. GOMES	4.3	4.78	3.11	0.61	8.1
M. GOMES	4.8	4.5	4.3	0.73	3

Table 3 Stream bar and bed characteristics.

BAR	Bank full	Bank full	Velocity	Bar d50	Bed d50	Signifi-cant d50 Mov.	Buffer d50	Leave Buffer
	cfs.	ft.	ft./sec.	mm	mm	mm	mm	ft.
Don. Pre.	11500	11.5	11	12.5	13	90	27-35	105
Post Scalp			7.9			30		
Don. Pre.	13385	12	11.3	12.5	13	93	27-35	105
Post Scalp			8			30		
Bark. Pre.	11500	11.5	12	9.7		95	42	20
Post Scalp			8			32		
Dill Pre.	11500	11.7	7.5	17-26	14	25	53	100
Post Scalp			5.2	12		7		
LGom Pre.	11500	11.7	8.4	13-15		37	26	80
Post Scalp			5.3	9		8		

ENVIRONMENTAL ISSUES AND CONCERNS

A number of environmental issues have been raised concerning gravel scalping Castor and Cluer, (2003); Kondolf et al (2002); and Oregon Water Resources Institute (OWRRI,1995). Castro and Cluer (2003) referenced other authors that streambanks derive their strengthened resistance from vegetation and to a lesser degree from their composition, height and slope. The concept that weak units cause failure by streambank scour, which undermine overlying materials, is ignored. Castro and Cluer (2003) in general ignore the confining condition caused by bars and higher velocities in pre-scalp verses post-scalp. Castro and Cluer (2003) state, "Using shear equations and the flow continuity equation, one can expect that shear stress will increase most in the upper part of the sediment removal areas where the slope increase is most pronounced.. Laboratory experiments by Begin et al (1981) verified the effect." The difference in slope on the Donaldson Bar is 0.5% down the bar to 0.16% down the channel. No increase in scour has occurred. The Begin et al (1981) flume experiment was for a 1% slope with a base level lowering that allowed a headcut to form and migrate upstream . No such condition occurs for the four bars evaluated. Kondolf et al (2002) state that "bar scalping typically reduces preferred salmonid spawning and rearing habitat by removing riparian vegetation and woody debris, reducing the area of adjacent pools and riffles, and causing channel bed degradation." No vegetation has been removed by gravel operations in the last four years, no additions of large woody debris (LWD), and any LWD that was present has not been disturbed. The pools and riffles have remained at the same location, there is no change in the depth of the streambed based on comparing 2000 and 2004 cross sections. Kondolf et al (2000) state, "By removing most of the gravel above the water lever,

the confinement of the low water channel is reduced or eliminated, changing the patterns of flow and sediment transport through the reach." The channels along the four scalped bars all have thalwegs, and the bars are scalped at a cross slope There is no evidence, in the last 4 years of evaluation, that the thalweg has moved or that there has been any change in flow pattern or sediment transport through the reach because of the scalping. Castro and Cluer (2003) state, "Disturbing or harvesting the armour layer of streambeds and bar deposits provides the stream readily erodible sediment supply because relatively finer grained sediment are now available for transport at a lower discharge. The new supply of sediment derived from the streambed will be moved downstream where it can adversely affect aquatic habitats. " The streambeds are not disturbed along the four bars discussed, and an armour layer is left at the upped end , and side of each bar as discussed and reflected in Table 3. However, even where there is data on post scalp particle size, for the Dill Bar a d50 of 12 mm present, is still higher than the 7 mm size for a velocity of 5.2. ft./sec.. For the Lower Gomes Bar the post scalping size of 9 mm is marginal to have significant incipient motion by the 5.3 ft./sec., and no field evidence of significant movement. The upstream armour is probably a control in preventing scour from starting.

CRITERIA FOR EVALUATION AND RECOMMENDATIONS

The criteria for evaluation are: (1) bankfull discharge; (2) stream slope; (3) bar slope; (4) bed and bar d50 particle size; (5) buffer d50 particle size; (6) bar depositional slope; (7) cross sectional area for pre-and post scalp conditions; (8) documented erosion condition based on average erosion rate from aerial photographs, and documented photographs and or notes of sloughing, and slump blocks; (9) documentation of eroding streambank materials and stratigraphy across from the bar, (11) document growing vegetation on eroding streambank, (11) documentation of overhanging vegetation materials on streambank; (12) documented LWD on bar and along streambank; (13) document rip rap, barbs, and veins; (14) documented woody material and soil bioengineering installations; (15) use cross sections to determine area for bankfull condition, and with bankfull discharge calculate average velocity to cause significant motion of pre and post scalp particles; (16) determine the primary source of sediment and (17) evaluate potential solutions and recommend most viable to reduce streambank erosion with minimal aquatic habitat impact.

The criteria recommended for carrying out environmental sensitive bar scalping are: (1) work in the dry and leave upper and side bar buffer at low flow; (2) scalp bar at approximately the slope of depositional bar; (3) leave the scalped bar with a roughened surface; (4) remove all scalped materials from the bar; (5) do not place or leave upper or side bar berms, (6) do not scalp bars at a higher level than the annual recruitment rate (OWRRI, 1995). Bar berms recommended by fish agencies in the past have caused split flows and development of back channels that have trapped downstream migrating fry when back channels dewater. Bar scalping has not caused the rivers to scour back channels and the bars are scalped with a leave armour area that prevents a scoured back channel from forming. The bars have not caused downstream alterations such as scour or deposition along the Wilson and Kilchis Rivers. and there has been essentially no change in the stream slope or thalweg along the bars in the four years of evaluation. A few downstream migrating fry have been trapped in dewatered back channels created by berms on the Donaldson and Dill Bars in 2000. These back channels continue to fill in by natural depositions. In addition a few chum fry were documented in June 2005 to be tapped in a natural spit channel on the Lower Gomes Bar in the buffer area above the scalping The conclusion for the velocity data is that the pre-scalped velocity can cause significant movement of the bar particle sizes verses the armor protected post-scalped condition where the runoff spreads out over a much broader area. In other words if the bars are allowed to build up to constrict flow between the bar and the opposite streambank than erosion will be much higher along the sides of the un-scalped bar as well as the opposite streambank.

REFERENCES

Begin, Z. B., Meyer, D. F., and Schumn, S. A. (1981) "Development of longitudinal profiles of alluvial channels in response to baseline lowering," Earth Sciences Processes and Landforms 6, pp 49-68.

Castro, J and Cluer, B. (2003). "Instream Aggregate Mining Issues in Oregon," Draft White Paper, October 2003. U. S. Fish and Wildlife Service, Portland , OR.

Chaland, J. and Reckendorf, F. (1998). "Chapter 5, Sedimentation, Tillamook Bay Environmental Characterization: A Scientific and Technical Summary," Tillamook Bay National Estuary Program (NEP), Garibaldi, OR.

Coulton, K. G., Williams, P & Benner, P. (1996). "An Environmental History of the Tillamook Bay Estuary Watershed," Tillamook Bay, NEP, Garibaldi, OR.

Coulton, K, (1998). "Chapter 6, Flooding, Tillamook Bay Environmental Characterization: A Scientific and Technical Summary," Tillamook Bay NEP, Garibaldi, OR.

Cruden, D. M. (1991). "A simple definition of a landslide," Bulletin of the International Association of Engineering Geology, No.43, pp 27-29.

Hofmeister, R.J. (2000). "Slope Failures in Oregon: GIS Inventory for three 1996-1997 Storm Events,"Oregon Department of Geology and Mineral Industries Special Paper 34, Portland, OR.

Kondolf, G. M., Smeltzer, M., and Kimball, L. (2001). "Freshwater Gravel Mining and Dredging Issues," White Paper, December 10, 2002, Center For Env. Design Res. CEDR-01, Berkeley, CA

Mills, K. (1997a). " Landslides and their association to forest practices for the storm," Proceedings of the Pacific NW Water Issues Conf., American Institute of Hydrology, Portland, OR, pp 185-199.

Mills, K. (1997b). "Forest Roads, Drainage, and Sediment Delivery in the Kilchis River Watershed," Tillamook Bay NEP, Garibaldi, OR.

Oregon Water Resources Research Institute (OWRRI). (1995). "Gravel Disturbance Impacts on Salmon Habitat and Stream Health," Volume 1, Summary Report, Volume 2, Technical Background Report. A Report for the Division of State Lands, OWRRI, Corvallis, OR.

Reckendorf, F. F. (2005). "Second Revision, Active Erosion Along Streambanks across from Donaldson and Barker Bars along Wilson River; Waldron Bar along Miami River, and Gomes Bars along Kilchis River," Reckendorf and Associates, Salem, OR.

Reckendorf, F. F.. (2004). "Evaluation of White Paper, Instream Aggregate Mining Issues in Oregon. by Janine Castro, and Brian Cluer," March, 2004. Report for Coastwide Readymix, Reckendorf and Associates, Tillamook, OR.

Reckendorf, F. F. and Peterson, C. (2003). "Holocene Coastal Processes in the Columbia River Cell," Northwest Cell of the Friends of the Pleistocene, Field Tour,. Reckendorf and Associates, Salem, OR

Reckendorf, F. F. (1995). "Sources and characteristics of sediments in the Tillamook Bay Watershed, Impacts of erosion and sedimentation in Tillamook Bay Watershed. " White paper prepared for, Scientific Technical Advisory Committee Forum, Tillamook Bay NEP, Garibaldi, OR.

Simon, D. B. and Senturk, F. (1977). "Sediment Transport Technology," Water Resources Publications, Fort Collins, CO.

Stinson, R and Stinson, S. (1998). "Affect of Gravel Bar Harvesting on Gravel Bar Armour Layer and Substrata Material in Four Watersheds on the North Oregon Coast," Tillamook County Soil & Water Conservation District and Natural Resources Conservation Service, Tillamook OR.

Transportation Research Board (TRB), and National Research Council (NRC). (1996). "Landslides Investigations and Mitigation," Special Report 247, Washington D. C.

USDA, Soil Conservation Service. (1978). "Tillamook Bay Drainage Basin Erosion and Sediment Study," USDA, SCS, Portland, OR.

Wellman R., Gordon, J., and Moffatt, R. (1993). "Statistical Summary of Streamflow Data in Oregon, Volume 2, Annual Low, High Flow, and Instantaneous Peak Flow," U.S. Geological Survey, Open File Report 93-63, Portland, OR.

VanDine, D. (1985). "Debris flows and debris torrents in Southern Canadian Cordella," Canadian Geotechnical Journal 22(1), pp 44-68.

COMPUTATIONAL MODEL FOR THE DEVELOPMENT OF SEDIMENT PLUGS IN ALLUVIAL RIVERS

Craig B. Boroughs, Senior Project Engineer, BH&H Engineering, Inc., Dillon, Colorado, Boroughs@BHandH.com; Steven R. Abt, Professor, Department of Civil Engineering, Colorado State University, Fort Collins, Colorado, sabt@engr.colostate.edu; Drew C. Baird, Hydraulic Engineer, Sedimentation and River Hydraulics Group, Bureau of Reclamation, Denver, Colorado, dbaird@do.usbr.gov

Abstract: Historical cases for sediment plug formation in alluvial rivers have been documented, but often plug development is attributed to such factors as a sudden decline in sediment transport capacity, the effect of debris in a channel, or human factors such as watershed management. These qualitative explanations are pertinent, but a study was conducted to identify the specific processes occurring at the location where plugs develop. A theory regarding plug formation was formulated following an extensive literature review, evaluation of data, and discussions with other researchers. Sediment plugs form at significant constrictions in alluvial rivers. As flows are lost to the overbank areas at these constrictions during higher flow events, sediment transport capacity decreases, but the total sediment load in the main channel does not reduce by the same proportion. As a result, deposition ensues in the main channel. If flows continue to overbank for weeks, the deposition will eventually completely clog the main channel of the river. An original numerical sediment transport/movable bed computer model was developed to test the theory. The one-dimensional, open channel, numerical model performs hydraulic calculations, computes sediment transport rates, and determines erosion/deposition. The sediment transport/movable bed numeric model was developed solely to analyze the development of sediment plugs with specific focus on the effects of the loss of flow to the overbank areas, the corresponding loss to the total sediment load, and the subsequent effects on erosion/deposition in the main channel. The model was calibrated and validated against plug formation in the Middle Rio Grande during 1995 and 1991. Ultimately, the model will be used to develop simplified criteria for the development of sediment plugs in alluvial rivers.

INTRODUCTION

There are several documented cases of sediment plugs forming in alluvial rivers. While there are general qualitative conclusions as to why these plugs formed, there has not been extensive study of the specific processes occurring at the locations where plugs develop. Research was conducted to identify the specific processes that cause plug formation. A theory on the cause of sediment plug formation was formulated. That theory was tested using an original sediment transport/movable bed computational model.

Definition: A sediment plug is aggradation (that may include debris) in a river which completely blocks the original channel (Diehl, 1994) and grows upstream by accretion (Diehl, 2000). The plugs, or local channel filling, may result from an obstruction combined with sediments derived from upstream (Shields *et al.*, 2000). Sediment plugs historically form over short periods – a matter of weeks in some cases (USBR, 1992). Plugs can grow to be miles in length and can cause numerous problems for river managers.

PLUG FORMATION THEORY

Several processes, associated parameters, and site characteristics exist that may influence the development of sediment plugs. After evaluating available information on historical sediment plug formation, a theory was formulated for the prediction of plug development (Boroughs, 2005). This theory focuses on the key processes that ultimately lead to the entire main channel of the river becoming clogged with sediment (i.e. a sediment plug) for a specified channel morphology.

For a reach of an alluvial river that is prone to sediment plug development due to a significant constriction such as a bend, structure, or debris snag that ultimately causes a reduction in conveyance capacity greater than 50%, a sediment plug will form if the following series of events occurs:

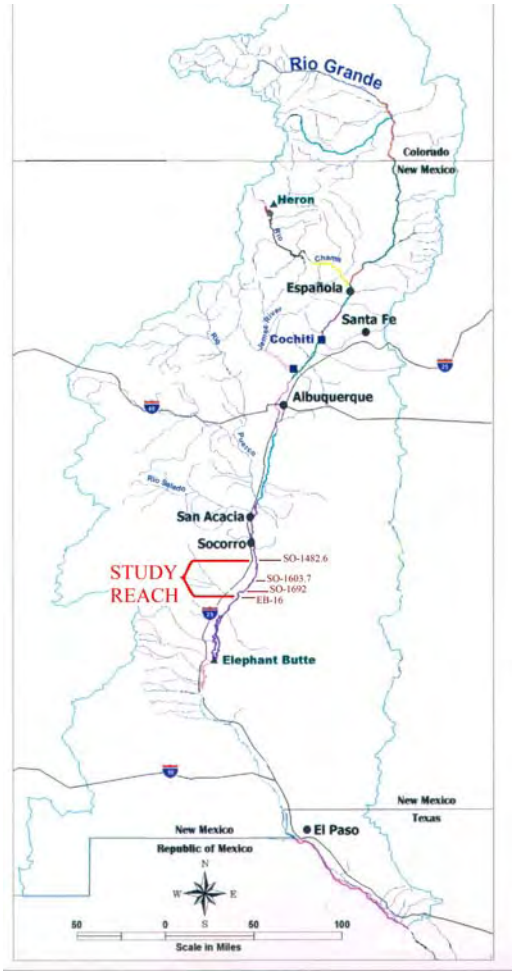
- daily total sediment load into the reach exceeds the historical average daily total sediment load (corresponding with above average flows),
- a significant portion of the flow abruptly overbanks (within a few thousand feet longitudinally along the river) combined with a non-uniform vertical distribution for the total sediment load – the sediment transport

capacity is reduced without the same proportional reduction in the total sediment load causing deposition to ensue in the main channel, and

- higher flows are prolonged, causing deposition to continue until the entire main channel of the river becomes completely clogged (i.e. a sediment plug has formed).

FOCUS STUDY REACH

The focus study reach (Figure 1) for calibrating and validating the computational model for sediment plug formation is the Tiffany Junction Reach of the Middle Rio Grande that extends from the Highway 380 bridge south of Socorro, New Mexico to below the railroad bridge near the United State Geological Survey (USGS) streamflow gage Rio Grande at San Marcial (ID# 08358400) (USGS, 1988-2003). An expansive set of USGS data was referenced which would also most closely represent conditions around the time of historical plug formation. The first upstream cross section is at the U.S. Bureau of Reclamation's (Reclamation) rangeline SO-1482.6 located just below the Highway 380 bridge, and the last downstream cross section is at Reclamation's rangeline EB-16 located below the San Marcial gage. The study reach is approximately 22 river miles in length.





Vicinity Map

Figure 1 Rio Grande Map with the Tiffany Junction Reach Depicted (w/ Vicinity Map)

Aerial photography (USBR, 2003) is available for reviewing the channel geometry along the study reach at the time of plug formation. The main channel is wider with widths exceeding 1000 feet through much of the upper portion of the reach, but the channel is narrower toward the southern end of the reach where the width does not exceed 300 feet. The sediment plugs that formed in 1991 and 1995 initiated in the narrowest portion of the reach immediately above Reclamation's rangeline SO-1692. The constriction at this location provides the key set-up condition for plug development.

COMPUTER MODEL METHODS

The theory of sediment plug formation was tested using a sediment transport/movable bed computer model of the Tiffany Junction Reach of the Middle Rio Grande. The one-dimensional, open channel, numerical model performs hydraulic calculations, computes sediment transport rates, and determines erosion/deposition. The sediment transport/movable bed numeric model was developed solely to analyze the development of sediment plugs with specific focus on the effects of the loss of flow to the overbank areas, the corresponding loss to the total sediment load, and the subsequent effects on erosion/deposition in the main channel. The model is referred to as the SPAR model for this discussion as an acronym for the Sediment Plug formation in Alluvial Rivers simulation model.

Hydraulics: Within the numerical model, information on the hydraulics is determined by solution of the unsteady flow equations. These calculations are completed using a timestep chosen with consideration for the Courant-Friedrich-Levy condition (Julien, 2002) to assure stability while reducing numerical diffusion.

Unsteady Flow Calculations: One-dimensional hydraulic calculations are completed in the SPAR model using the double sweep procedure to solve the linearized unsteady flow equations determined using the Preissman scheme (Hromadka *et al.*, 1985). Unsteady flow calculations are completed primarily to allow the effects of flow losses to the overbank areas to be considered. A stage-discharge curve is input for the downstream boundary condition. An inflow hydrograph is used for the upstream boundary condition. A weighting coefficient, θ, of 0.7 is utilized in the Preissmann scheme (Julien, 2002). An appropriate timestep is selected within the model to assure the Courant-Friedrich-Levy condition is satisfied (Julien, 2002):

$$C = c\frac{\Delta t}{\Delta x} = \beta V \frac{\Delta t}{\Delta x} \le 1.0 \tag{1}$$

where C is the Courant Number,
c is the wave celerity,
Δt is the timestep,
Δx is the spatial step,
β is the exponent in the Q (discharge) vs. A (cross sectional area) relationship for the study reach, and
V is the mean velocity.

The spacing between the input cross sections, Δx, is known, and an input inflow hydrograph is referenced to determine an estimate for the highest expected mean velocity during a simulation. The corresponding wave celerity, c, is then computed assuming β equals 5/3 based on the Manning equation. The highest Δt is then computed such that the Courant number will be equal to 1.0 for the determined highest expected wave celerity. The Courant-Friedrich-Levy criterion will assure computational stability while reducing numerical diffusion as a result of the computational scheme.

Losses to the Overbank Areas: The lateral loss of flow to overbank areas is computed using the broad crested weir equation (Henderson, 1966):

$$Q = C\Delta x H^{3/2} \tag{2}$$

where Q is the flow over the weir (cfs),
C is the broad crested weir coefficient,
Δx is the width of the weir (ft), and
H is the head over the weir crest (ft).

The head over the weir is the elevation of the water surface over the bank elevation (velocity head is neglected for this computation of lateral outflow). The width of the weir is equal to the incremental spatial step in the computer model. As discussed later, the broad crested weir coefficient is the primary calibration parameter in the model. The

elevation of the banks along each incremental spatial step is determined using the main channel cross section endpoints. The computed loss to the overbank areas is then included in the solution of the unsteady flow equations.

Sediment Transport: Sediment transport is computed in the SPAR model using an input power function rating curve:

$$Q_S = aQ^b \tag{3}$$

where Q_S is the total sediment load (tons/day),
a is the coefficient from the regression relationship,
Q is the flow (cfs), and
b is the exponent from the regression relationship.

Parameters a and b in Equation 3 were determined by a regression analysis relating computed total sediment loads to flowrates measured at the USGS gage at San Marcial. Total sediment loads were computed using the Modified Einstein procedure (Yang, 2003) and data collected at San Marcial.

Vertical Distribution of Sediment Load: The vertical distribution of the total sediment load is computed in the SPAR model based on a computed vertical velocity profile and a vertical profile for the sediment concentration. The vertical distribution of the total sediment load is the product of the velocity and concentration profiles. The percentage of the total sediment load carried above a specific elevation can then be determined.

The vertical velocity profile, $v_x(z)$, is computed based on the equation for flow over a rough boundary (Julien, 1995):

$$\frac{v_x}{u_*} = \frac{2.3}{\kappa}\log\left(\frac{z}{k_s'}\right) \tag{4}$$

where v_x is the velocity (ft/s),
u_* is the shear velocity (ft/s),
κ is the von Kármán constant,
z is the elevation above the bed (ft), and
k_s' is the mean grain roughness height (ft).

The shear velocity, u_*, is computed during the model simulation along with the friction slope and hydraulic radius. The von Kármán constant, κ, is set to 0.4. A mean grain roughness height, k_s', is input.

The vertical distribution of the sediment concentration is computed using the Rouse equation (Julien, 1995):

$$C = C_a\left[\left(\frac{h-z}{z}\right)\left(\frac{a}{h-a}\right)\right]^{Ro} \tag{5}$$

where C is the concentration at elevation z,
C_a is the concentration at reference elevation a,
z is the elevation above a datum elevation,
h is the flow depth, and
Ro is the Rouse number.

A Rouse number, Ro, is input. The concentration, C_a, at a distance, a, above the channel bed is determined such that the total sediment load along the vertical at the deepest depth in a cross section matches that same parameter computed using the sediment transport power function (Equation 3). The distance, a, is set to $4/20^{th}$ of the depth where the concentration is appreciably greater than zero but not too close to the bed where the concentration approaches infinity based on the Rouse equation. (The concentration is assumed to be uniform for the bottom $1/20^{th}$

of the vertical to prevent a concentration of infinity at the bed surface as computed using the Rouse Equation). The value of C_a is determined by dividing the total sediment load by the top width, then multiplying by the deepest depth and dividing by the hydraulic depth to determine the total sediment load along the vertical at the location of the maximum depth.

Loss of Sediment to Overbank Areas: As flows overbank, the river stage above the bank elevation at each cross section is referenced for determining the percentage of the total sediment load transported above that bank elevation. It is assumed that this portion of the total sediment load is lost to the overbank areas with the loss of flow. The lower total sediment load at the downstream node for an incremental spatial step – due to the reduction in flow – is computed using the power function rating curve; however, the amount of sediment lost to the overbank areas needs to be known before determining the amount of erosion/deposition along the incremental spatial step (i.e. any sediment lost to the overbank areas is not available for deposition in the main channel). The influx of sediment to the upstream node for an incremental spatial step is reduced by the amount of sediment lost to overbank areas.

Erosion/Deposition: After the appropriate sediment transport magnitudes are known for each cross section for a given timestep, the amount of erosion or deposition is computed and the cross section geometry is modified before progressing to the next timestep. The erosion/deposition is computed in the SPAR model using an immediate erosion/deposition method (or the Exner equation with a trap efficiency of 100%) (Julien, 2002):

$$T_{Ei}\frac{\partial Q_{txi}}{\partial x}+(1-p_0)\frac{W\partial z_i}{\partial t}=0 \tag{6}$$

where T_{Ei} is the trap efficiency,
Q_{txi} is the sediment discharge,
∂x is the incremental spatial step,
p_0 is the porosity of the bed material,
W is the channel width,
∂z is the vertical change in bed elevation (deposition or erosion), and
∂t is the timestep.

The lateral distribution of erosion/deposition is based on the depth along the cross section divided by the hydraulic depth (Cunge *et al.*, 1980). If the water surface elevation is above the bank elevation, the calculation is the same but the bank elevation is utilized as opposed to the water surface elevation when computing the depth along the cross section and the hydraulic depth (Cunge *et al.*, 1980). The erosion/deposition is evenly split longitudinally between the two adjacent cross sections bounding the incremental spatial step being analyzed (Julien, 2002).

MODEL CALIBRATION AND VALIDATION

The SPAR model developed to simulate sediment plug formation was created in FORTRAN using all the methods/procedures just discussed. Since software packages are not available that include all the necessary components, the original SPAR program was developed. The hydraulic calculations in the SPAR model were validated against the commonly used program, HEC-RAS, that is routinely used to solve the unsteady flow equations (USACE HEC, 2002). The SPAR model was then calibrated for sediment plug development along the Tiffany Junction Reach in 1995. The model was then validated against information from the Tiffany Junction Reach that plugged in 1991.

Calibration to Plug Formation in 1995: The SPAR model was calibrated for the 1995 plug formation event along the Tiffany Junction Reach. The input information consisted of a total sediment load power function, a downstream stage discharge curve, an inflow hydrograph, a constant Manning n roughness value of 0.017, a porosity of 0.43, a mean particle size of 0.25 mm, a corresponding particle fall velocity of 0.113 ft/s, and a Rouse number of 1.15. Data from cross section surveys completed prior to 1995 were utilized for the calibration simulation. The input initial depths at each cross section were determined by completing a steady state simulation with HEC-RAS with the initial inflow.

All the parameters input into the model are initially known except for the broad crested weir coefficient for computing the lateral loss of flow to the overbank areas. This value was determined such that the plug that developed in the SPAR model matched the plug that formed along the Tiffany Junction Reach in 1995. In addition to predicting the deposition in the main channel at individual cross sections, the calibration was completed to match the longitudinal extent of the plug as it existed in August of 1995.

The calibrated broad crested weir coefficient used for simulation is 0.5. This value represents the degree of submergence for flow over a weir. The lateral loss of flow over the banks of the main channel of an alluvial river simulates flow over a submerged weir. As the water surface elevation on the downstream side of a weir approaches the water surface elevation on the upstream side of a weir, the broad crested weir coefficient approaches zero (Davis, 1952), so the 0.5 value, which is lower than the typical value of 3.09 for free flow over a broad crested weir, reflects the effect of a higher water surface elevation on the downstream side of a weir.

A comparison of bed elevations predicted with the SPAR model versus bed elevations measured during 1995 is presented in Figure 2. Based on anecdotal information and data, the plug extended nearly five miles as of August 5, 1995. Deposition continued through 1996 before a pilot channel was dredged and the plug washed out in 1997. A plot of predicted deposition at Reclamation's cross section SO-1652.7 along the reach is presented in Figure 3. The SPAR model was successfully calibrated for plug formation along the Tiffany Junction Reach during 1995.

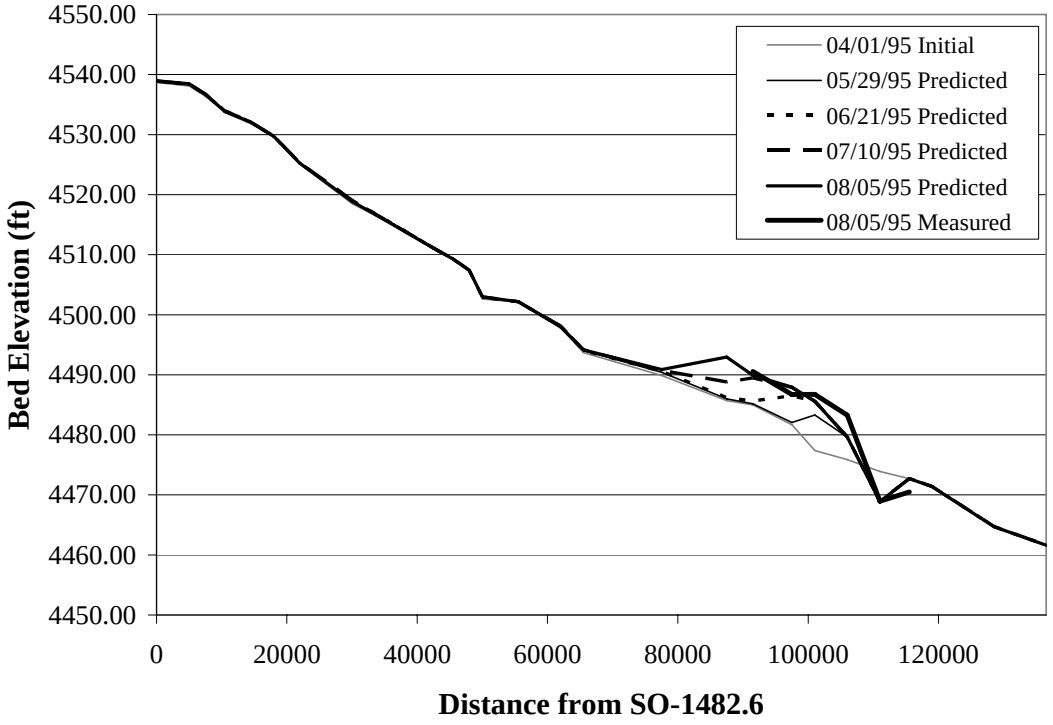


Figure 2 Plot of 1995 Initial, Predicted, and Measured Bed Elevations

Validation against Conditions in 1991: After the SPAR model was developed and calibrated with data from 1995, a model run was prepared for conditions along the Tiffany Junction Reach in 1991. The most recent cross section survey data prior to plug formation in 1991 were used and the upstream hydrograph was developed based on gaged flows. The simulation yielded a plug that, although was approximately 40% smaller by volume, matched the reported extents of the plug that developed in 1991 (USBR, 1992).

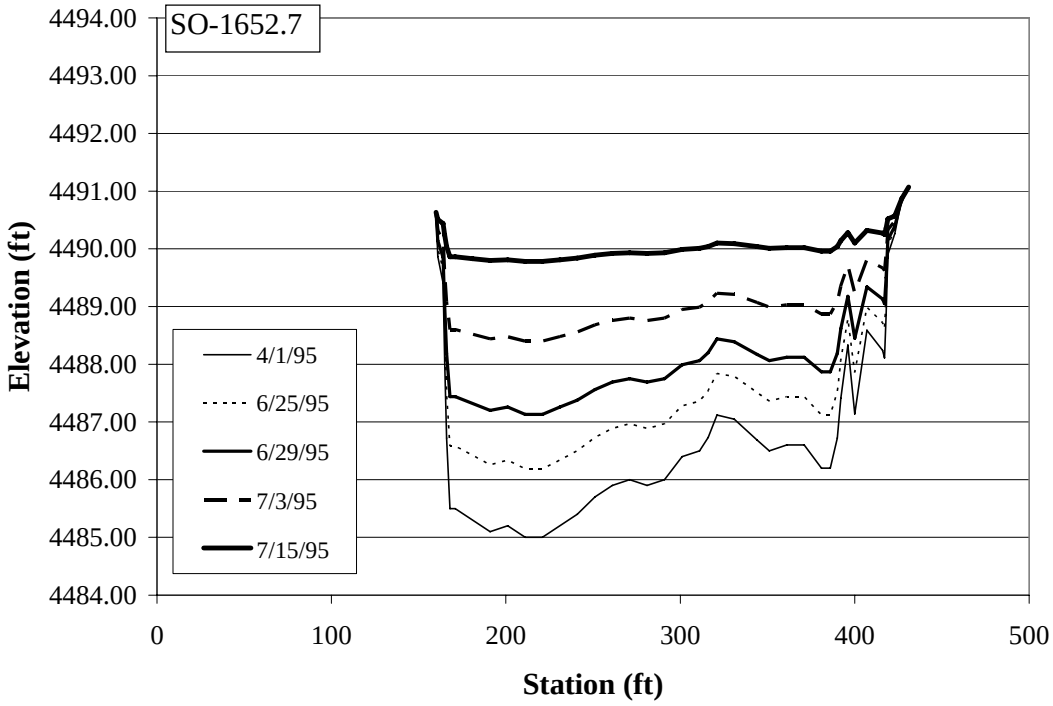


Figure 3 Plot of Predicted Deposition during 1995 at Cross Section SO-1652.7

The SPAR model was successfully calibrated and validated. While this program was calibrated and validated using data for the Tiffany Junction Reach of the Middle Rio Grande, this program is applicable to other alluvial river systems. The SPAR model can now be used to simulate different conditions along an alluvial river in regards to channel cross sections, reach inflows, river slope, etc. and analyze values of different parameters during plug formation.

SUMMARY AND CONCLUSIONS

An investigation was conducted to better understand why, how, where, and when sediment plugs form. A theory on sediment plug development was formulated. For a reach of an alluvial river that is prone to sediment plug development due to a significant constriction such as a bend, structure, or debris snag that ultimately causes a reduction in conveyance capacity greater than 50%; a sediment plug will form if the following series of events occurs:

- daily total sediment load into the reach exceeds the historical average daily total sediment load (corresponding with above average flows),
- a significant portion of the flow abruptly overbanks (within a few thousand feet longitudinally along the river) combined with a non-uniform vertical distribution for the total sediment load – the sediment transport capacity is reduced without the same proportional reduction in the sediment load causing deposition to ensue in the main channel, and
- higher flows are prolonged causing deposition to continue until the entire main channel of the river becomes completely clogged (i.e. a sediment plug has formed).

The theory regarding sediment plug formation was tested using a general sediment transport/movable bed computer model. The model includes methods for completing unsteady flow calculations while satisfying the Courant-Friedrich-Levy condition. The lateral loss of flow to the overbank areas is computed using the broad crested weir equation. A corresponding loss to the total sediment load is also determined. After the loss of flow and total sediment load is considered, a resulting immediate deposition/erosion in the main channel is computed based on the change to the sediment transport capacity.

The model was calibrated for plug formation along the Tiffany Junction Reach of the Middle Rio Grande in 1995. The model was then validated for plug development along that reach in 1991. As a result of this study, engineers not only have a better understanding as to how and why sediment plugs form but will be able to use the computer model better predict when and where a plug will develop and ultimately prevent or manage plug development.

REFERENCES

Boroughs, Craig B. (2005). "Criteria for the Formation of Sediment Plugs in Alluvial Rivers," Ph.D. Dissertation, Colorado State University, Fort Collins, CO.

Cunge, J.A., F.M. Holly, and A. Verwey. (1980). Practical Aspects of Computational River Hydraulics. Pittman Publishing Limited, Boston.

Davis, C.V. (Editor). (1952). Handbook of Applied Hydraulics. McGraw-Hill Book Company, New York, New York.

Diehl, T.H. (1994). "Causes and Effects of Valley Plugs in West Tennessee" in Sale, M.J. and R.O. Wadlington *eds.*, Symposium on Responses to Changing Multiple-Use Demands; New Directions for Water Resources Planning and Management, Nashville, Tennessee., April 17-20, 1994, Proceedings of extended abstracts: American Water Resources Association, p. 97-100.

Diehl, T.H. (2000). "Shoals and Valley Plugs in the Hatchie River Watershed," U.S. Geological Survey Water-Resources Investigations Report 00-4279.

Henderson, F.M. (1966). Open Channel Flow. Macmillan Publishing Company, New York, New York.

Hromadka II, Theodore V. II, T.J. Durbin, and J.J. Devries. (1985). Computer Methods in Water Resources. Lighthouse Publications, Mission Viejo, California.

Julien, P.Y. (1995). Erosion and Sedimentation. Cambridge University Press, New York, New York.

Julien, P.Y. (2002). River Mechanics. Cambridge University Press, New York, New York.

Shields Jr., F.D., S.S. Knight, and C.M. Cooper. (2000). "Cyclic Perturbation of Lowland River Channels and Ecological Response," Regulated Rivers: Research and Management, 16: 307-325.

U.S. Army Corps of Engineers (USACE), Hydrologic Engineering Center (HEC). (2002). HEC-RAS, River Analysis System, Hydraulic Reference Manual, Version 3.1. Davis, California.

U.S. Bureau of Reclamation (USBR). 2003. Middle Rio Grande, NM, Velarde to Elephant Butte, River Miles and Rangelines, Index and Maps. Produced by the Remote Sensing and GIS Group. Denver, Colorado.

U.S. Bureau of Reclamation (USBR). (1992). Review of Operation and Maintenance Program, 1991 Project Office Examination Report, Tiffany Levee, Middle Rio Grande Project. Albuquerque Area Office, Albuquerque, New Mexico.

U.S. Geological Survey (USGS). (1988-2003). Water Resources Data – New Mexico. Water Year Data Reports prepared by the Water Resources Division. Albuquerque, New Mexico.

Yang, T.C. (2003). Sediment Transport, Theory and Practice. Krieger Publishing Company, Malabar, Florida.

HOW INCIPIENT MOTION DETERMINATION JUDGMENT AFFECTS DIFFERENT PARAMETERS IN SEDIMENT TRANSPORT INVESTIGATION

Muhammad Ashiq (Ph.D.), JSPS Fellow, Department of Civil Engineering and Urban Management, Faculty of Engineering, Kyoto University, Japan, mashiqk@yahoo.com; John C Doering (Ph.D.), Dean, Faculty of Graduate Studies (& Professor of Civil Engineering), University of Manitoba, Winnipeg, Canada.

Abstract: Incipient condition plays a significant role in the field of sediment transport and channel stability and different parameters based upon it are used in the sediment initiation and transport formulas both for the development and application purposes. Its determination depends upon the subjective judgment of the investigator. Effects of this judgment on sediment transport and flow parameters have been investigated in this paper by considering three flow conditions of M (when small number of particles start to move), M_1 (when large number of particles starts to move), and M_2 (when very large number of particles starts to move). Data used in this paper were collected from a sediment transport study conducted in the hydraulics laboratory of the University of Manitoba (Canada). Effects of each flow condition on sediment transport, critical discharge, critical velocity, and flow depth parameters were investigated and a significant variation in results was found when flow conditions varied. This variation was more pronounced with the smaller sediment sizes as compared to the larger ones. For the critical discharge, a difference between M and M_1, M_1 and M_2 and M and M_2 conditions ranged from 36-118%, 16-129% and 61-211%, respectively. Likewise, other parameters of flow depth, critical velocity, sediment loads were significantly affected when the conditions were altered. Among the three conditions the M_1 appeared to be more reliable and realistic to be used for the incipient motion determination.

INTRODUCTION

Owing to the variation in particle sizes and their positioning in different directions, incipient motion of sediment for all particles does not occur at one time. Vibration of bed-material particles is an indication that movement is about to begin. This indicates the response of particles to the passing flow, which causes pressure differences and shear stresses that lead to lift and drag forces. If these forces increase over time, the in-place vibration may change to motion. Meanwhile, other particles may respond to increasing shear stresses and pressure differences over their surfaces by a more-abrupt initiation of motion, without vibration. As individual particles begin to move, they leave behind vacant spaces that change the local flow field at the bed surface. These alter lift and drag forces acting on other particles and may help to mobilize several particles simultaneously (Matin 1993).

Incipient motion of sediment in channels, natural or man made, has great significance in the field of sedimentation, especially when prediction is desired. It is the beginning of movement of sediment particles that were stationary some time before. As soon as they have initiated their movement they continue to move for an unspecified time and distance. The precise discharge and time at which initial movement occurs is a subjective determination, therefore investigators have different point of views in this regard. Some argue that it takes place when a small number of particles starts to move while others disagree and say this is just a settlement stage and

incipient motion takes place when a significant number of particles starts to move. Some observers consider initiation of sediment transport to occur when the first few particles start moving, whereas others may say that it occurs when a large number of particles starts to move over a large part of the bed surface.

This paper investigates this subjective determination (judgment) issue so that a possible accurate condition could be found when the incipient motion takes place. For this purpose three flow conditions M, M_1 and M_2 were assumed and their effects on flow depth, critical velocity, critical discharge, and sediment load parameters were investigated both qualitatively and quantitatively.

SIGNIFICANCE OF THE STUDY

Threshold parameters like V_c, d_c, and q_c are required in the development of incipient motion and sediment transport formulae, in their application for sediment load prediction, and other sediment related and channel stabilization studies. It is, therefore, a fundamental step to make a right judgment about the incipient motion so that these threshold parameters may be recorded correctly. Importance of the incipient motion can be imagined from the fact that most of the sediment transport formulae developed are based on the premises of sediment transport theories of excess shear $\{q_b \propto f[\tau - \tau_c]\}$, excess stream power $\{q_b \propto f[\omega - \omega_c]\}$, excess discharge $\{q_b \propto f[q - q_c]\}$, and excess velocity $\{q_b \propto f[V - V_c]\}$ which involve a parameter that rely upon the threshold condition. Therefore, a small error regarding the threshold condition judgment could seriously affect the structure of sediment transport formulae based upon them and their predicted results. Nice examples of sediment transport formulas in which threshold parameters were used are Schoklitsch (1962), Bagnold (1966), Wilcock and Southard (1989), Ashiq (1997). Likewise, the threshold condition determination is equally important for the sediment incipient motion prediction formulae (Ashiq and Bathurst (1999), irrespective of the theories used and approach followed for their development i.e. characteristic diameter size (reference particle size) approach [e.g. $q_c = 0.0345 \sqrt{g} D_{50}^{3/2} S^{-1.12}$, Milhous 1982] or fractional sizes approach [e.g. $\tau^*_{ci} = \tau^*_{c50} (D_i/D_{50})^{-1}$, Andrews and Erman 1986].

EXPERIMENTAL METHODOLOGY

For the purpose of data collection an experimental setup (Figure 1) was re-designed and constructed in the hydraulics laboratory of the University of Manitoba, Department of Civil Engineering (Winnipeg, Canada) during 2003. At completion, an adjustable slope flume channel of 10 m long, 0.7 m wide, and 0.945 m deep was available to be used in this study. Further details regarding the construction, equipment used, and problems faced during the study may be found in Ashiq et. al (2004). During this study, five different sediment sizes were used and for each size slopes were varied 6 times. The sediment material sizes used and the corresponding slopes adopted are given in Table 1, whereas the collected sediment data and other related parameters may be seen in Table 2.

For determining the incipient condition at which movement of sediment starts, the data corresponding to three different flow conditions were recorded: a) when small number of particles started to move, M; b) when large number of particles started to move, M_1; and c) when very large number of sediment particles started to move, M_2. Values of the critical velocity, flow rates, flow depth and sediment load parameters were recorded for the M, M_1 and M_2 conditions and are given in Table 2.



Figure 1 Measurements in progress with a flume channel in the hydraulics lab of the University of Manitoba (2003).

Table 1 Sediment sizes used and the corresponding slopes adopted during the experimentation [University of Manitoba, Canada 2003].

Sr. No.	Channel Slope (%)	Bed Material Size (mm)
1	1.16 - 2.13	6.350 - 7.938
2	1.16 - 2.75	4.763 - 6.350
3	1.30 - 3.03	3.175 - 4.763
4	1.14 - 2.86	1.588 - 3.175
5	1.17 - 2.90	0.794 - 1.588

EFFECTS OF THE FLOW CONDITIONS' SELECTION ON FLOW DEPTHS

The general trend of variation between the depths recorded under all the three flow conditions (M, M_1, and M_2), for the five bed sediment sizes used, is evident from the bar chart heights and trend lines as depicted in Figs. 2-6. According to that the depths recorded under the M condition are less than the M_1 and M_2 for all the sediment sizes, except for 6.350-7.938 mm size (largest size, Fig. 2) for which they are greater than the M_2 condition but smaller than M_1 condition. The reason for this anomaly is that during the M and M_1 flow (conditions) period, the transported sediment from the upstream reach deposited at the location of measurements, which reduced the flow depth. Likewise, for the 4.763-6.350 mm size the trend line for the M_1 crossed M_2 when depth exceeded 40 mm, due to the reason that bed surface which was a bit uneven some time ago changed to a plane one, resulting in a decrease in the flow depth under the M_2 condition. Other minor variations in the flow depths for the M, M_1 and M_2 flow conditions for the 3.175-4.763 mm and 1.588 - 3.175 mm sizes were due to: i) a series of pits in the channel bed in the longitudinal direction (Fig.7); and ii) a wavy bed and water surfaces during measurements (Fig.8). Likewise, fluctuations in depths under the M and M_2 conditions for the smallest size (0.794-1.588 mm) were due to the wavy water surface and sediment deposition at the point of measurement (Fig.6).

Table 2 Sediment transport and other related data collected during experimentation at the University of Manitoba (2003).

Sr. No.	Remarks	Channel Width	Temp.	Slope	Flow Depth	Flow Depth	Mini Flow Reading	Critical Vel. (Vc)	Critical Vel. (Vc)	Flow Rate (Q)	Duration of Sediment Collection	Wt. of Sed.	Sediment Load Qs
		(m)	(C)	(%)	(mm)	(m)		(cm/s)	(m/s)	(m3/sec)	(sec)	(kg)	(kg/min)
1- Bed Material Size 6.350 -7.938 mm							28 Aug. 2003						
1 iv	M	0.945	19.5	1.17	80	0.080	38.0	105.0	1.050	0.0794	948	17.273	1.0932
2 iii	M	0.945	19.5	1.3	55	0.055	30.0	84.0	0.840	0.0437	617	3.436	0.3342
3 iii	M	0.945	20	1.55	50	0.050	31.0	86.5	0.865	0.0409	1003	9.150	0.5474
4 iii	M	0.945	20	1.76	44	0.044	30.0	84.0	0.840	0.0349	1243	10.341	0.4992
5 iii	M	0.945	19.5	2.24	34	0.034	27.0	75.5	0.755	0.0243	1119	10.314	0.5530
6 iii	M	0.945	20	2.9	25	0.025	27.0	75.5	0.755	0.0178	542	9.118	1.0094
1 v	M1	0.945	19.5	1.17	85	0.085	40.0	111.0	1.110	0.0892	948	17.273	1.0932
2 iv	M1	0.945	19.5	1.3	62	0.062	33.0	92.0	0.920	0.0539	617	3.436	0.3342
3 iv	M1	0.945	20	1.55	55	0.055	34.0	94.5	0.945	0.0491	1003	9.150	0.5474
4 iv	M1	0.945	20	1.76	47	0.047	32.0	89.0	0.890	0.0395	1243	10.341	0.4992
5 iv	M1	0.945	19.5	2.24	37	0.037	31.0	86.5	0.865	0.0302	1119	10.314	0.5530
6 iv	M1	0.945	20	2.9	28	0.028	29.0	81.0	0.810	0.0214	542	9.118	1.0094
3 v	M2	0.945	20	1.55	59	0.059	38.0	105.0	1.050	0.0585	1003	9.150	0.5474
4 v	M2	0.945	20	1.76	50	0.050	34.0	94.5	0.945	0.0447	1243	10.341	0.4992
5 v	M2	0.945	19.5	2.24	40	0.040	33.0	92.0	0.920	0.0348	1119	10.314	0.5530
6 v	M2	0.945	20	2.9	33	0.033	32.0	89.0	0.890	0.0278	542	9.118	1.0094
2- Bed Material Size 4.763 - 6.350 mm							21 Sept. 2003						
1 iv	M	0.945	19.5	1.14	55	0.055	28.0	78.0	0.780	0.0405	787	8.695	0.6629
4 iii	M	0.945	20	2.13	30	0.030	26.0	73.0	0.730	0.0207	688	7.359	0.6418
5 iv	M	0.945	19.5	2.35	31	0.031	23.5	66.5	0.665	0.0195	890	8.636	0.5822
6 iii	M	0.945	20	2.86	29	0.029	23.5	66.0	0.660	0.0181	766	11.277	0.8833
1 v	M1	0.945	19.5	1.14	58	0.058	30.0	84.0	0.840	0.0460	788	8.695	0.6621
2 v	M1	0.945	20	1.44	45	0.045	29.0	81.0	0.810	0.0344	567	5.568	0.5892
3 iv	M1	0.945	20	1.75	36	0.036	28.0	78.5	0.785	0.0267	444	7.586	1.0252
4 iv	M1	0.945	20	2.13	32	0.032	28.0	78.0	0.780	0.0236	689	7.359	0.6408
5 v	M1	0.945	19.5	2.35	32	0.032	26.5	74.5	0.745	0.0225	891	8.636	0.5816
6 iv	M1	0.945	20	2.86	30	0.030	24.5	69.0	0.690	0.0196	767	11.277	0.8822
1 vi	M2	0.945	19.5	1.14	63	0.063	32.0	89.5	0.895	0.0533	789	8.695	0.6613
2 vi	M2	0.945	20	1.44	48	0.048	31.5	88.0	0.880	0.0399	568	5.568	0.5882
4 v	M2	0.945	20	2.13	34	0.034	29.0	81.0	0.810	0.0260	690	7.359	0.6399
5 vi	M2	0.945	19.5	2.35	34	0.034	28.5	80.0	0.800	0.0257	892	8.636	0.5809
6 v	M2	0.945	20	2.86	31	0.031	27.0	76.0	0.760	0.0223	768	11.277	0.8810
3- Bed Material Size 3.175 - 4.763 mm							2 Oct. 2003						
1 v	M	0.945	20	1.3	45	0.045	24.5	69.0	0.690	0.0293	835	7.132	0.5125
2 iii	M	0.945	19.5	1.61	30	0.030	24.5	66.5	0.665	0.0189	909	5.909	0.3900
3 iv	M	0.945	20	1.95	25	0.025	22.5	64.0	0.640	0.0151	954	17.445	1.0972
4 iii	M	0.945	19.5	2.27	25	0.025	20.5	58.5	0.585	0.0138	304	6.223	1.2282
5 iii	M	0.945	19.5	2.62	17	0.017	19.0	54.0	0.540	0.0087	580	6.336	0.6555
6 ii	M	0.945	20	3.03	16	0.016	16.0	46.0	0.460	0.0070	651	10.427	0.9610
1 vi	M1	0.945	20	1.3	47	0.047	26.5	74.5	0.745	0.0331	836	7.132	0.5119
2 iv	M1	0.945	19.5	1.61	32	0.032	25.5	72.0	0.720	0.0218	910	5.909	0.3896
3 v	M1	0.945	20	1.95	27	0.027	24.0	68.0	0.680	0.0174	955	17.445	1.0960
4 iv	M1	0.945	19.5	2.27	27	0.027	22.5	63.5	0.635	0.0162	305	6.223	1.2241
5 iv	M1	0.945	19.5	2.62	19	0.019	21.0	59.5	0.595	0.0107	581	6.336	0.6544
6 iii	M1	0.945	20	3.03	18	0.018	19.0	54.0	0.540	0.0092	652	10.427	0.9596
1 vii	M2	0.945	20	1.3	55	0.055	28.5	80.0	0.800	0.0416	837	7.132	0.5112
2 v	M2	0.945	19.5	1.61	34	0.034	27.0	75.5	0.755	0.0243	911	5.909	0.3892
3 vi	M2	0.945	20	1.95	29	0.029	27.0	75.5	0.755	0.0207	956	17.445	1.0949
4 v	M2	0.945	19.5	2.27	28	0.028	26.5	74.5	0.745	0.0197	306	6.223	1.2201
5 v	M2	0.945	19.5	2.62	20	0.020	24.0	68.0	0.680	0.0129	582	6.336	0.6532
6 iv	M2	0.945	20	3.03	20	0.020	20.0	57.0	0.570	0.0108	653	10.427	0.9581
4- Bed Material Size 1.588 - 3.175 mm							10 Oct. 2003						
1 iv	M	0.945	20	1.16	19	0.019	11.0	32.0	0.320	0.0057	813	7.614	0.5619
2 ii	M	0.945	20	1.47	13	0.013	11.5	34.0	0.340	0.0042	873	4.659	0.3202
3 iii	M	0.945	19.5	1.81	15	0.015	11.5	34.0	0.340	0.0048	768	7.586	0.5927
1 v	M1	0.945	20	1.16	21	0.021	14.0	40.5	0.405	0.0080	814	7.614	0.5612
2 iii	M1	0.945	20	1.47	15	0.015	14.0	40.5	0.405	0.0057	874	4.659	0.3198
3 iv	M1	0.945	19.5	1.81	17	0.017	14.0	40.5	0.405	0.0065	769	7.586	0.5919
4 iii	M1	0.945	19.5	2.16	14	0.014	13.5	39.5	0.395	0.0052	808	14.973	1.1118
5 ii	M1	0.945	20	2.42	9	0.009	10.0	30.0	0.300	0.0026	570	11.991	1.2622
6 iii	M1	0.945	19.5	2.75	11	0.011	9.5	28.5	0.285	0.0030	586	10.936	1.1198
1 vi	M2	0.945	20	1.16	25	0.025	17.0	49.0	0.490	0.0116	815	7.614	0.5605
2 iv	M2	0.945	20	1.47	16	0.016	15.5	45.0	0.450	0.0068	875	4.659	0.3195
3 v	M2	0.945	19.5	1.81	18	0.018	18.0	51.5	0.515	0.0088	770	7.586	0.5911
4 iv	M2	0.945	19.5	2.16	16	0.016	15.0	43.5	0.435	0.0066	809	14.973	1.1105
5 iii	M2	0.945	20	2.42	10	0.010	15.0	43.5	0.435	0.0041	571	11.991	1.2600
6 iv	M2	0.945	19.5	2.75	13	0.013	16.0	46.0	0.460	0.0057	587	10.936	1.1179
5- Bed Material Size 0.794 - 1.588 mm							25 Oct. 2003						
1 iii	M	0.945	20	1.16	11	0.011	8.5	26.0	0.260	0.0027	1544	2.868	0.1115
3 iii	M	0.945	20	1.72	11.5	0.012	6.5	20.5	0.205	0.0022	1060	5.173	0.2928
4 iii	M	0.945	19.5	1.84	8	0.008	7.5	23.5	0.235	0.0018	1044	5.682	0.3265
5 iv	M	0.945	20	1.96	10	0.010	7.0	21.5	0.215	0.0020	800	6.309	0.4732
6 ii	M	0.945	19.5	2.13	10	0.010	6.0	19.0	0.190	0.0018	690	9.914	0.8621
1 iv	M1	0.945	20	1.16	13	0.013	11.0	32.5	0.325	0.0040	1545	2.868	0.1114
2 iii	M1	0.945	20	1.46	14	0.014	10.0	30.0	0.300	0.0040	821	5.768	0.4215
3 iv	M1	0.945	20	1.72	13	0.013	10.5	31.5	0.315	0.0039	1061	5.173	0.2925
5 v	M1	0.945	20	1.96	12	0.012	11.5	34.0	0.340	0.0039	801	6.309	0.4726
6 iii	M1	0.945	19.5	2.13	11	0.011	7.5	23.5	0.235	0.0024	691	9.914	0.8608
1 v	M2	0.945	20	1.16	15	0.015	12.5	37.0	0.370	0.0052	1546	2.868	0.1113
2 iv	M2	0.945	20	1.46	16	0.016	14.0	40.0	0.400	0.0060	822	5.768	0.4210
3 v	M2	0.945	20	1.72	14	0.014	11.5	34.0	0.340	0.0045	1062	5.173	0.2922
4 iv	M2	0.945	19.5	1.84	11	0.011	10.5	31.5	0.315	0.0033	1045	5.682	0.3262
5 vi	M2	0.945	20	1.96	15	0.015	13.5	39.5	0.395	0.0056	802	6.309	0.4720
6 iv	M2	0.945	19.5	2.13	13	0.013	10.0	30.0	0.300	0.0037	692	9.914	0.8596
Where M = condition when small number of particles started to move.													
M1 = condition when large number of particles started to move.													
M2 = condition when very large number of particles started to move.													

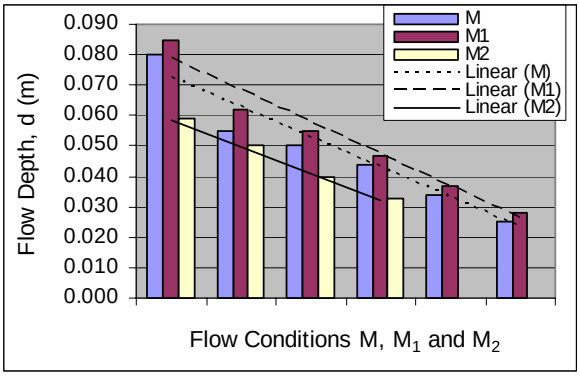


Figure 2 Variation in flow depth for the sediment size of 6.350 -7.938 mm.

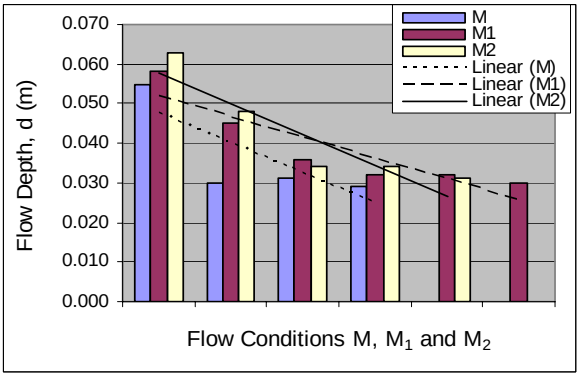


Figure 3 Variation in flow depth for the sediment size of 4.763 - 6.350 mm.

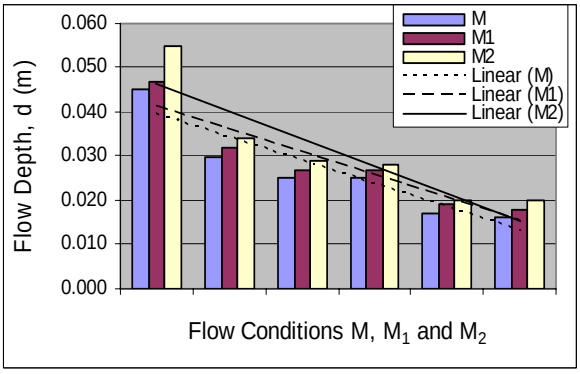


Figure 4 Variation in flow depth for the sediment size of 3.175 - 4.763 mm.

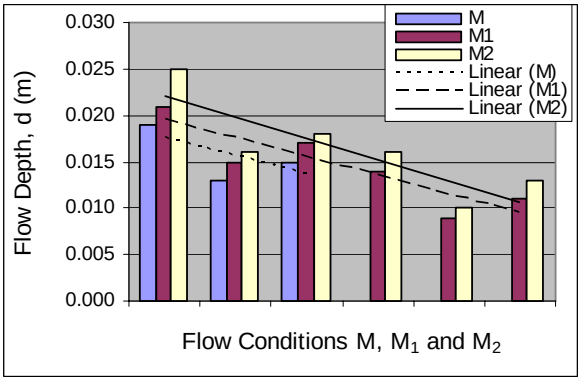


Figure 5 Variation in flow depth for the sediment size of 1.588 - 3.175 mm.

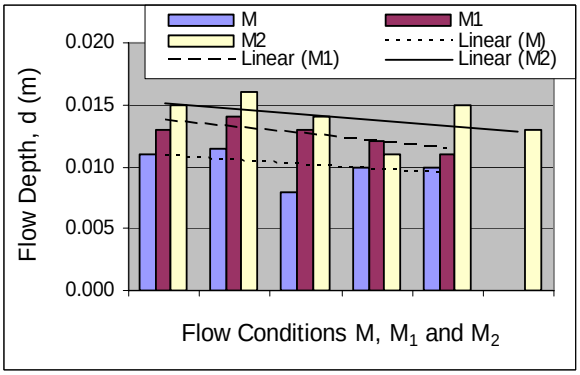


Figure 6 Variation in flow depth for the sediment size of 0.794 - 1.588 mm.



Figure 7 A series of pits in the longitudinal direction observed during the experimentation.

EFFECTS OF FLOW CONDITIONS' SELECTION ON THE SEDIMENT LOAD AND CORRESPONDING FLOW PARAMETERS

To investigate effects of incipient condition determination judgment on the depth, critical vertical, discharge, and sediment load, these parameters were analyzed for all the five sizes used in the study. In this analysis critical discharge vs. sediment load, slope vs. critical velocity, and sediment load vs. critical velocity were plotted and then trend lines were fitted to find the general

trend of relationships among the respective variables. Out of all these plots only 0.794-1.588 mm size plots are presented here for the purpose of demonstration (Figs. 9-11).
In critical discharge vs. sediment load plots, for the largest four sizes which almost belonged to the coarser size of sediment, the relationships were found to be of polynomial nature. While for the smallest size, a size which belonged to the fine sediment material, the linear relationship was found more appropriate. Both for the coarse and fine sizes the sediment loads under the three flow conditions (M, M_1 and M_2) increased from M towards M_2. The only size for which (partly) deviation recorded was the largest size (i.e. 6.350-7.938 mm), for which somewhere in the middle of the plot the M and M_1 lines crossed each other. This deviation from the general trend could be due to aggradations at the point of measurements.

On the other hand for the slope vs. critical velocity plots, for all the five sizes, a linear relationship was found more appropriate and clearly the critical velocity values increased with the flow conditions i.e. from M toward M_2. Nonetheless, in the case of the sediment load vs. critical velocity plots, the best relationships were of polynomial nature for the four coarser sizes and for the fine size the linear relationship was found to be the best one.



Figure 8 A wavy bed surface observed during the experimentation.

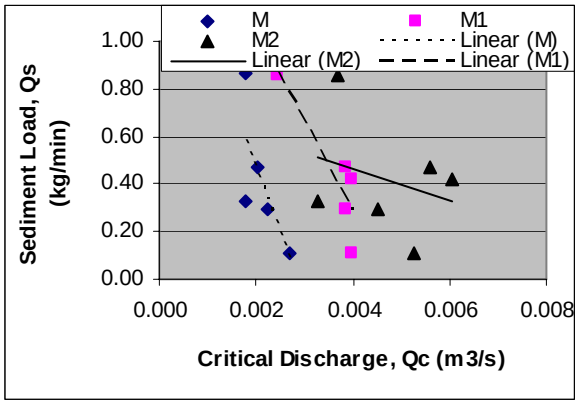


Figure 9 Variation in sediment load under M, M_1, & M_2 flow conditions for sediment size of 0.7941-0.588mm.

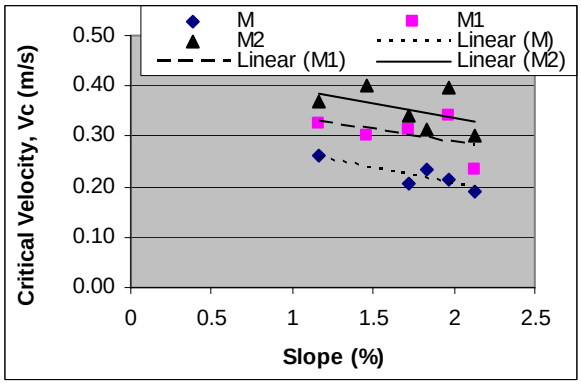


Figure 10 Variation in critical velocity under M, M_1, & M_2 flow conditions for sediment size of 0.794 - 1.588 mm.

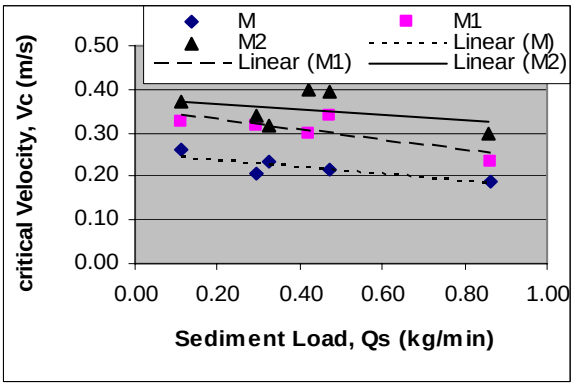


Figure 11 Variation in critical velocity under M, M_1, & M_2 flow conditions for sediment size of 0.794 - 1.588 mm.

QUANTITATIVE EFFECTS OF FLOW CONDITIONS' SELECTION ON CRITICAL DISCHARGE, VELOCITY, AND DEPTH

When the critical discharges were compared under the M and M_2 flow conditions, the variations of 27.84-55.5%, 31.43-92.88%, 28.67-54.89%, and 81.76-101.48% respectively were recorded for the coarse sizes (size 1-4) and 61.16-211.84% for the fine (size 5). The variations between the M and M_1 were found to be 12.32-24.68%, 13.57-66.44%, 12.77-32.07%, and 37.44-39.88% respectively for the coarse sizes and 36.05-117.82% for the fine size of 0.794-1.588 mm. While for the M_1 and M_2 flow conditions the variations ranged between 16.24-129.21% for the fine size and 12.96-29.5%, 8.97-15.88%, 11.41-25.66%, and 18.52-90.75% respectively for the coarse sizes. It showed that the discharge significantly changed with the selection of flow condition when altered from M to M_1, M_1 to M_2 and M to M_2. Likewise, variation in discharge increased with the decrease in sediment size which means that the finer sizes are more susceptible to the variation as compared to the coarse ones. A similar, general trend of variation was also found with the other two parameters of velocity and depth, with a few exceptions. A numeric set of values for variations in critical discharges, velocity and depth under the three flow conditions may be seen in Table 3.

Table 3 Variations (in percentage) in critical discharge, critical velocity, and flow depth under the M, M_1 and M_2 flow conditions for the five sediment sizes used.

Sr. No	Sediment Size (mm)	Critical Discharge			Critical Velocity			Flow Depth		
		M1-M (%)	M2-M (%)	M2-M1 (%)	M1-M (%)	M2-M (%)	M2-M1 (%)	M1-M (%)	M2-M (%)	M2-M1 (%)
1	6.350 - 7.938	12.32-24.68	27.84-55.5	12.96-29.5	5.71-14.57	12.50-21.85	6.18-11.11	6.25-12.73	13.64-32.00	6.38-17.86
2	4.763 - 6.350	13.57-66.44	31.43-92.88	8.97-15.88	7.69-18.18	14.74-21.80	2.01-8.64	5.45-50.00	9.68-60.00	6.25-8.62
3	3.175 - 4.763	12.77-32.07	28.67-54.89	11.41-25.66	6.25-17.39	13.53-27.35	4.86-17.32	4.44-12.50	12.00-25.00	3.70-17.02
4	1.588 - 3.175	37.44-39.88	81.76-101.48	18.52-90.75	19.12-26.56	32.35-53.13	10.13-61.40	10.53-15.38	20.00-31.58	5.88-19.05
5	0.794 - 1.588	36.05-117.82	61.16-211.84	16.24-129.21	23.68-58.14	42.31-107.8	7.94-68.09	10.00-62.50	10.00-75.00	7.69-36.36

CONCLUSIONS

Based upon the study results, the following specific conclusions may be drawn from this study:

- When the determination judgment regarding the incipient motion is not made accurately the recorded data could be significantly underestimated/overestimated, therefore a very careful decision has to be made.

- The coarser sizes were found to be less affected with the subjective judgment as compared to the finer one under these flow conditions. Therefore, for studies in which finer sediments are to be dealt with, more care should be followed. However, it is important to mention that only one fine size sediment material was available for this investigation and further tests with more fine sizes would be helpful to further generalize this part of the conclusion.

- It seemed more appropriate to take the M_1 flow condition for the incipient motion determination, which represents a condition when large number of sediment particles start to move over a large part of the bed surface.

NOTATIONS

D_i = particle size for ith size fraction;
D_{50} = particle size for which 50% of the material is finer.
V = flow velocity;
V_c = critical flow velocity (i.e. velocity at threshold point);
q = water discharge per unit width;
q_c = critical discharge per unit width;
q_b = bed load discharge per unit width;
S = slope;
τ = shear stress;
τ_c = critical shear stress
τ^*_{ci} = Shield's parameter for particle size D_i;
τ^*_{c50} = reference shear stress parameter used in Parker et. al (1982) for D_{50} size;
ω = stream power; and
ω_c = critical stream power.

REFERENCES

Andrews, E. D., and Erman, D.C. (1986). "Persistence in the size distribution of the surficial bed material during an extreme snowmelt flood," Water Resources Research, 22, pp 191-197.

Ashiq, M. (1997). "Bed load transport models for coarse bed material rivers," Ph. D. Thesis submitted to the Department of Civil Engineering, University of Newcastle Upon Tyne, UK, 402 pp

Ashiq, M., and Bathurst, J.C. (1999). "Comparison of bed load sampler and tracer data on initiation of motion," Journal of Hydraulic Engineering, ASCE, 125(6), pp 661- 664.

Bagnold, R. A. (1966). An approach to the sediment transport problem from general Physics. U. S. Geological Survey, Professional Paper 422 - I, 37 pp.

Matin, H. (1993). "Incipient motion and particle transport in a gravel-bed stream," Ph.D. Thesis, Oregon State University, Corvallis (USA).

Milhous, R.T. (1989). "On the selection of sediment transport equations," Proc. International Symposium: Sediment Transport Modeling. Hydraulic Division, ASCE, New Orleans, Louisiana (USA).

Parker, G., Klingeman, P.C., and McLean, D.G. (1982). "Bed load and size distribution in paved gravel-bed stream," Journal of Hydraulic Division, ASCE, 108(HY4), pp 544-571.

Schoklitsch, A. 1962. Handbuch des Wasserbaues. 3rd. Springer-Verlag, Vienna.

Wilcock, P.R., and Southard, J.B. (1989). "Bed load transport of mixed-size sediment fractional transport rates, bed forms, and the development of coarse bed surface layer," Water Resources Research, 24, pp 1629-1641.

A REGIONAL PROTOCOL FOR EVALUATING THE EFFECTIVENESS OF FORESTRY BEST MANAGEMENT PRACTICES AT CONTROLLING EROSION AND SEDIMENTATION

Roger Ryder, Research Associate, Colorado State University, roger.ryder@us.army.mil;
Pamela Edwards, Hydrologist, USDA Forest Service, Parsons, WV, pjedwards@fs.fed.us

Abstract: Forestry operations do not have permitting requirements under the Clean Water Act because there is a "silvicultural exemption" given in that law, as long as best management practices (BMPs) are used to help control non-point source pollution. However, states' monitoring of BMP effectiveness often has been sporadic and anecdotal, and the procedures used have varied widely. Consequently, there are inconsistencies in the rigor used to evaluate BMP effectiveness, and thus, the objectiveness and accuracy of those evaluations. As a result of litigation questioning the "silvicultural exemption", the US Environmental Protection Agency has expressed interest in improving the monitoring of BMP effectiveness. Since 1990, several approaches for developing consistent BMP evaluations and reporting methodologies have had varying degrees of success, utility, and acceptance. Traditionally, monitoring has focused on individual BMP practices in terms of their prescriptive guidelines, which vary by state. But this approach has created an impediment both for developing a consistent methodology and for focusing on whether BMPs are actually effective at controlling erosion and sedimentation. To improve consistency and provide a more universal method of BMP monitoring while maintaining state control of BMPs, a protocol was developed that is based on the underlying principles of BMPs (e.g., controlling water in small amounts) and that focuses on the outcomes of those principles (e.g., did sediment reach the stream). Formal protocol development was funded by the USDA Forest Service and the US Environmental Protection Agency. The protocol was created cooperatively over a number of years with input by a wide variety of stakeholders, including state forestry and watershed agencies, industrial land owners, and university and federal scientists. The protocol was field tested by state forestry and industry personnel in 9 states across the northeastern United States in 2002-2003. This testing provided information for further improvements to wording of the questions and identified where additional questions were needed or where others could be deleted. Following these changes, the protocol again was field tested extensively in 7 northeastern states in 2004. Although testing has focused on states in the Northeast, because the protocol is based on BMP principles and examines outcomes, it is applicable to most of the physiographic and forest conditions nationwide.

INTRODUCTION

Water pollution in the United States is regulated by the US Environmental Protection Agency, primarily through the 1972 Clean Water Act (CWA) and its reauthorization in 1993. While much of the CWA deals with point source pollution, non-point source pollution is addressed in sections 404, 208 and 319. These sections exempt silvicultural and other forest operations from the permitting requirements associated with water pollution as long as best management practices (BMPs) are used. As a result, all states have adopted their own sets of forestry BMPs that are to be employed during and/or after road and landing construction, harvesting, and other forestry operations.

Critics of the silvicultural exemption argue that there is a general lack of evidence that BMPs effectively control non-point source pollution, especially in-stream sedimentation, from roading and harvesting operations. Much of this criticism is attributable to two factors: (1) many purported evaluations of BMP effectiveness are instead evaluations of BMP implementation (i.e., determining whether BMPs were used) and not a review of their effectiveness, and (2) many research studies that have evaluated BMP effectiveness have evaluated surrogates of BMP effectiveness and not the actual effectiveness of BMPs (Edwards 2004). The lack of a substantial body of rigorous evidence showing BMP effectiveness often is given as a reason that there should be no silvicultural exemption in the CWA. Litigation in California requesting that the US Environmental Protection Agency withdraw the silvicultural exemption has demonstrated the need to be able to document rigorously how effective forestry BMPs are at controlling non-point source pollution.

As a result, a joint effort was undertaken by the USDA Forest Service, Maine's Forest Service, and the US Environmental Protection Agency to develop a protocol that would allow credible, consistent, and scientifically-based evaluation of BMP effectiveness. The initial steps in protocol development and versions of the protocol itself actually originated from BMP training sessions for loggers and foresters in Maine and from the Maine Forest Service's intent to modify and improve the state's BMP implementation and effectiveness monitoring program (Ryder and Edwards 2005). Soon thereafter, the USDA Forest Service's Northeastern Watershed Team and the US Environmental Protection Agency became interested in Maine's developing approaches and provided funding to formalize the protocol and expand it to make it applicable to at least the 20 states in the US Forest Service's Northeastern Area and Virginia. This paper describes development and features of the protocol; more detailed information about the steps taken in protocol development is provided in Ryder and Edwards (2005).

UNIQUE CHARACTERISTICS OF THE REGIONAL PROTOCOL

In several ways, the Regional Protocol is unique compared to many past attempts at evaluating BMPs. First and foremost, this protocol is based on evaluating BMP performance, such as determining if sediment reached the channel, rather than focusing on whether prescriptive requirements in BMP manuals were followed (e.g., were cross drains installed on roads at required distances). This differentiation is important because implementation is not synonymous with BMP effectiveness. By focusing on BMP performance and not specific prescriptions, the Regional Protocol can be applied to most types of landscapes and conditions, across states or regions, and it inherently considers the outcomes of good planning, which many prescriptive-based procedures do not.

Outcome-based evaluation is successful because it is founded on the underlying principles of BMPs which are based on the laws of physics and chemistry. For example, covering exposed soil to minimize initiation of soil movement by raindrop impact and retain infiltration rates, and maintaining/establishing root growth to retain infiltration and bind soil particles are well accepted principles of soil physics and soil chemistry (Schwab et al. 1993). Hence, mulching and re-vegetating exposed mineral soil are BMPs that have been developed from these underlying principles. But rather than focusing on whether mulching or revegetation was done according to a specific state's BMPs, the protocol evaluates the outcomes of soil protection, e.g.,

did soil movement occur or did sediment reach the stream. This point is important because every state has its own unique set of BMPs (Edwards and Stuart 2002), with hundreds and perhaps thousands of individual BMPs prescribed nationwide; thus, relying on underlying principles and outcomes allows the Regional Protocol to be applied much more universally than evaluation techniques that are designed around agency-specific or institution-specific prescribed BMPs. Focus on individual BMPs is one reason that many previous attempts at BMP effectiveness protocols have failed to be widely accepted or applied (Ryder and Edwards 2005).

Questions in the Regional Protocol are worded to avoid subjective or value-laden answers. Words, such as "acceptable", "excessive", "short-term", and "low-impact" were avoided, as these can be interpreted differently by different people, agencies, or organizations. Thus, typical questions about BMP effectiveness, such as "Is the BMP practice effective?" were replaced with questions like "Is a rill evident?". The answer to the latter question is much less subjective particularly since the definition of a rill is provided, and the evaluator can use measurements of width, length, and/or depth to determine if an erosion feature meets the definition of a rill. Similarly, a question such as "Is sedimentation on the stream bank and/or in the stream substantial?" can be reworded as "Are sediment accumulations on the stream bank and/or in the stream greater than or equal to [one of the defined answer choice categories or measurements]?" These types of quantifiable question/answer pairs not only reduce subjectivity but they also increase the repeatability of data collection, which is important for assuring data quality.

BMP effectiveness traditionally has been defined in terms of sediment reaching water bodies because in-stream conditions are the emphasis of the CWA; however, the Regional Protocol also identifies erosion and sediment transport problems on the hillside (e.g., in the buffer area around streams), even if sedimentation does not terminate in the stream channel. Identifying these hillside effects is important because erosion and soil movement may not be contributing to in-stream pollution at the time of evaluation, but sediment could reach the stream in the future. Thus, information about potential future problems can be obtained with the Regional Protocol for future follow-up, if desired.

The Regional Protocol also includes questions that address issues which represent more contemporary interpretations and applications of the CWA, including issues of chemical pollution prevention, occurrence of in-stream large woody debris, channel condition, and fish passage (i.e., through stream crossings). While these types of issues generally were not considered in the context of non-point source pollution in the past, many state and federal agencies now recognize and actively consider these issues in terms of the chemical, physical, and biological integrity of water bodies within their interpretations of the CWA.

PROTOCOL DEVELOPMENT

The Regional Protocol is a living document that has undergone multiple iterations based upon general comments, comments obtained during short-term field testing by a variety of end users and researchers, and comments resulting from extensive data collection by various state agency personnel responsible for evaluating BMP effectiveness. The first field testing was done in 9 northeastern states in 2002-2003 by state forestry and industry personnel. This testing provided information for further improvements to wording of the questions and identified where additional

questions were needed or where others could be deleted. Field testing and extensive data collection again occurred in 7 northeastern states in 2004. Participants in the various steps of protocol development included representatives from Maryland, West Virginia, Virginia, Pennsylvania, Ohio, Indiana, Wisconsin, Vermont, Massachusetts, New Hampshire and Maine, the New York City Watershed Council, Maine's Atlantic Salmon Commission, the Chesapeake Bay Project, US Environmental Protection Agency Washington Office Staff, American Forest and Paper Association, Master Logger Program of Maine, Master Logger Program of Maryland, Northeast Area State Foresters Association, Mead Westvaco, International Paper Company, a variety of independent foresters, and other interested stakeholders. To date, more than 250 individuals have seen and reviewed at least a portion of the protocol, and approximately 75 individuals have field tested the protocol. The shaded states in Figure 1 indicate those in which the protocol was tested and/or data were collected for one or more of the versions of the Regional Protocol.

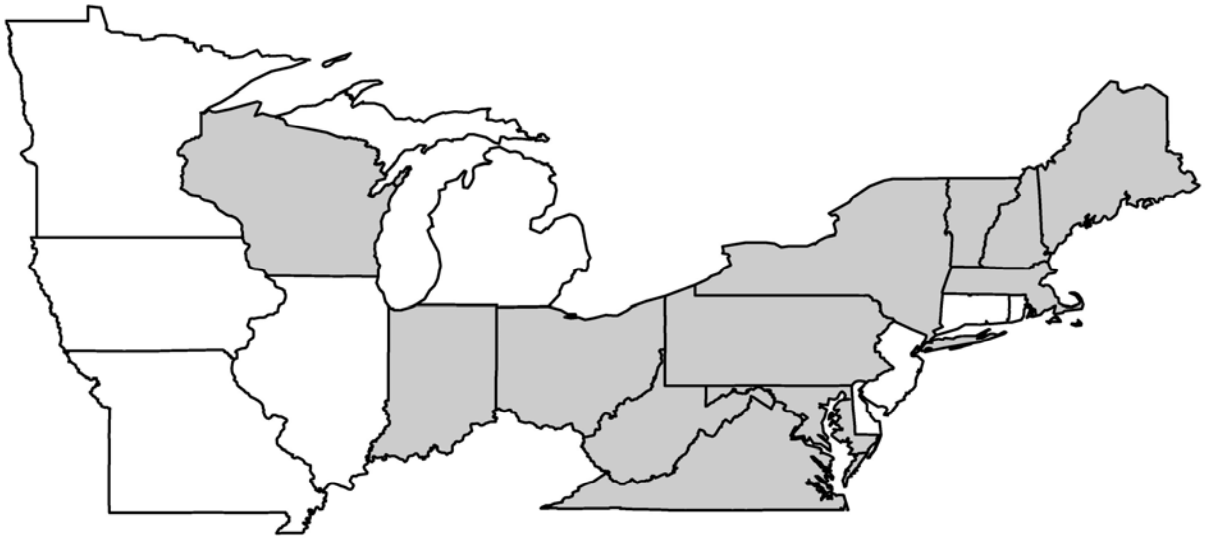


Figure 1 States shown are the 20 states in the US Forest Service's Northeastern Area and Virginia. Shaded states indicate those in which data collection for and testing of the various versions of the Regional BMP Effectiveness Protocol occurred.

PROTOCOL DESIGN

The protocol contains multiple sections: (1) general information, which includes socially focused questions, such as landowner types, harvest unit acreage, and involvement with state stewardship programs, logger training, and certification programs; (2) water body crossings (i.e., haul roads and skidder crossings) and associated approaches; (3) haul roads located within a riparian or buffer area; (4) chemical pollution prevention; and (5) riparian or buffer areas. Where relevant, each section (e.g., a water body crossing) has a subsection with questions about site attributes, such as slope of the land and specific soil information.

The Regional Protocol is structured like a dichotomous key, with each question having associated answer options. The answer for a question determines the subsequent sequence of

questions. Initially the questions and answer choices were programmed into Trimble GEO3 GPS units, but now Palm Pilots™ with Windows®-based pocket PC software are used.

The areas evaluated for BMP effectiveness in each forest operation are those most likely to contribute or control sediment or act as a conduit for sediment delivery to water bodies, influence shading of water bodies, or alter the hydraulics of water (i.e., stream crossings). Consequently, the focus is on the water bodies themselves or areas in close proximity to water bodies – the area immediately outside the riparian buffer, the riparian buffer, and the water body crossing. Together, these areas comprise the sample unit (Figure 2) in the Regional Protocol.

By definition, a sample unit is a "contiguous harvest unit that includes either or both a riparian zone or a water body crossing. It is bounded by any combination of water bodies, the boundary of the harvest area, or a land ownership boundary. The sample unit starts when a water body is crossed or a riparian area is entered [assumes entrance by a road or trail]. A new sample unit begins each time a water body is crossed and ends at the next water body, the edge of the harvest area, or the land ownership boundary, whichever is encountered first." The outer boundary of the sampling area is defined (in feet) by the length of the slope distance outside the riparian buffer where there is greater than a 5 percent change in slope for a minimum distance of 25 ft.

REPEATABILITY OF DATA COLLECTION

Precision and repeatability are important components of the Regional Protocol. One of the goals of having objective questions is to ensure that the answer to each question by different evaluators for a given sample unit will be the same. However, repeatability can be assessed only by the inclusion of duplicate evaluations. Consequently, both "hot checks" and repeated evaluations are a suggested part of protocol use. Hot checks are duplicate evaluations of a subset of sample units performed by a team or individual at the same time but independently of the principal evaluator. Repeated evaluations are done independently by a separate team or individual at a subset of sample units at a later time than the initial evaluation. These latter evaluations must be done within a timely manner after the initial evaluation to ensure that external changes (natural or human) that might affect answers have not occurred (Ryder and Edwards 2005).

The technical team, who has been largely responsible for developing the Regional Protocol, would like an overall answer replication rate of 90 percent, though it is not known from the testing and use that have happened to date if this goal is attainable. In the Regional Protocol's first phase of use, 30 percent of the sample units were revisited for repeated evaluations. There were 620 questions that were replicated in this repeated evaluation, and 71 percent of the replicated questions had identical results from two independent evaluations. Additional improvements to the Regional Protocol are being made to reconcile differences and improve replication in the future.

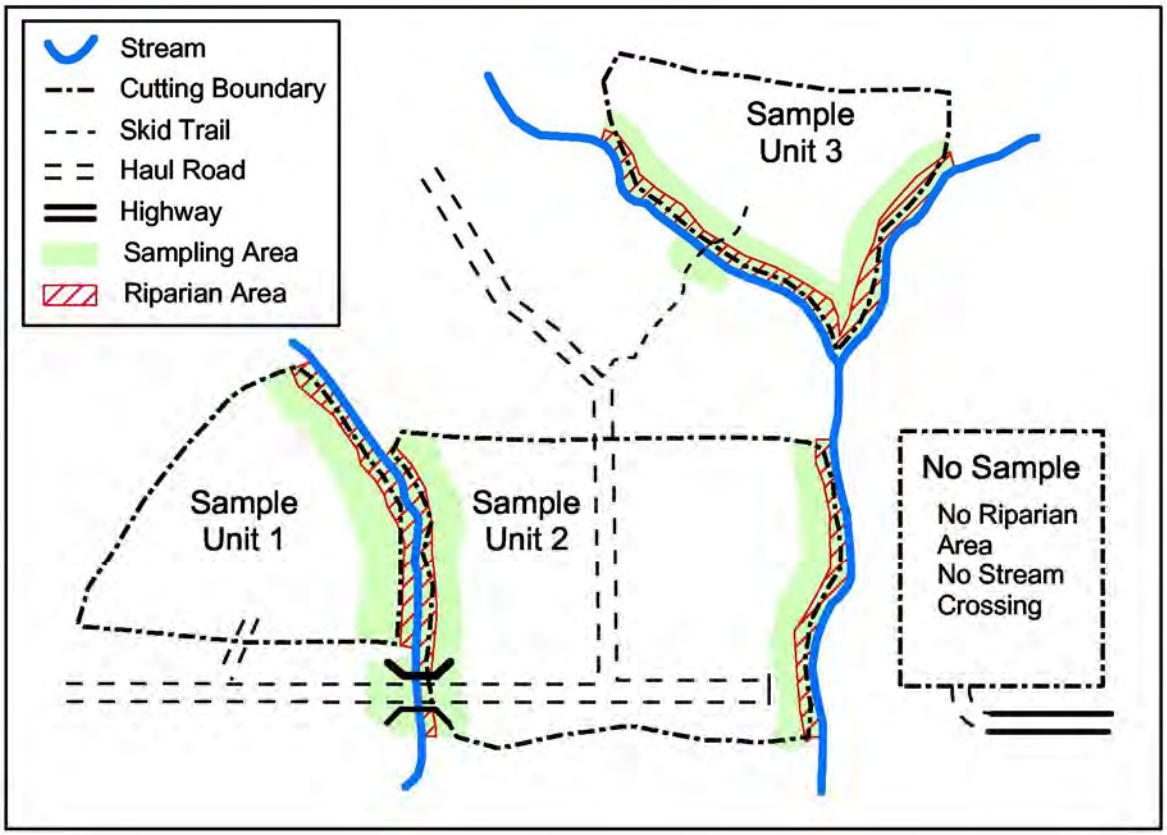


Figure 2 Examples of sample unit boundaries in the Regional BMP Effectiveness Monitoring Protocol.

The shaded sampling area includes the riparian buffer width plus a defined slope distance outside the riparian buffer. Sample Unit 1 has only a riparian buffer and the boundaries of the harvest to delineate the sample unit and no water crossing; Sample Unit 2 has a water crossing and two riparian buffers and the boundaries of the current harvest to delineate the sample unit; Sample Unit 3 has a water crossing, a riparian buffer and the boundaries of the current harvest to delineate the sample unit. When a water body crossing is part of a sample unit, the entire water crossing and the associated approaches are considered part of and evaluated as a component of the water crossing, though one side of the approach may be outside the sample unit.

SUMMARY

A protocol was developed out of the need to be able to objectively evaluate the effectiveness of forestry BMPs. Questions in the protocol are in the form of a dichotomous key, largely with quantitative or objective answer choices. The protocol was developed and tested over several years throughout much of the northeastern United States to ensure broad applicability over the region's many physiographic conditions and myriad of forest operations. Rather than focusing on specific BMPs, this protocol is grounded in the physical and chemical principles from which BMPs have been developed and it focuses on the outcomes of BMPs, such as evaluating whether

in-stream sedimentation occurred. As a result, while the protocol has been developed in the Northeast, it has wide application for much of the nation.

ACKNOWLEDGMENTS

We thank Tim Post of the Maine Forest Service for his extensive work in developing the Regional Protocol. Funding for protocol development and testing was provided by the USDA Forest Service's Northeastern Area and the US Environmental Protection Agency. The use of trade, firm, or corporation names in this paper is for the information and convenience of the user. Such use does not constitute an official endorsement or approval by the US Department of Agriculture or the Forest Service of any product or service to the exclusion of others that may be suitable.

REFERENCES

Ryder, R., and Edwards, P.J. (2005). Development of a Repeatable Regional Protocol for Performance-Based Monitoring of Forestry Best Management Practices. General Technical Report NE-335. USDA Forest Service, Northeastern Research Station, Newtown Square, Pennsylvania.

Edwards, P.J. (2004). "Forestry best management practices: where we've been, where we're going," Proc. 2003 Penn State Forest Resources Issues Conference, Forestry's Role in Integrated Water Management. University Park, Pennsylvania, pp 26-33.

Edwards, P.J., and Stuart, G.W. (2002). "State survey of silvicultural nonpoint source programs: a comparison of the 2000 northeastern and national results," Northern Journal of Applied Forestry 19(3), pp 122-127.

Schwab, G., Fangmeier, D., Elliot, W., and Frevert, R. (1993). Soil and Water Conservation Engineering, Fourth Edition. John Wiley and Sons, Inc., New York.

FLOODS AND SEDIMENT YIELDS FROM RECENT WILDFIRES IN ARIZONA

Daniel G. Neary, Project Leader, USDA Forest Service, Rocky Mountain Research Station, Flagstaff, Arizona, dneary@fs.fed.us; Gerald J. Gottfried, Research Forester, USDA Forest Service, Rocky Mountain Research Station, Phoenix, Arizona, ggottfried@fs.fed.us; Jan L. Beyers, Research Plant Ecologist, USDA Forest Service, Pacific Southwest Research Station, Riverside, California, jbeyers@fs.fed.us; Peter F. Ffolliott, Professor, School of Natural Resources, University of Arizona, Tucson, Arizona, ffolpete@ag.arizona

Abstract: Large area, high severity wildfires have become common in the Southwest since the mid-1990s due to drought, excessive woody fuel buildups, exotic grass invasions, and increasing ignition sources. These fires have alter watershed conditions, resulting in greater storm peakflows and sediment losses. This paper examines information gathered from three Arizona wildfires that burned ponderosa pine or mixed-conifer forests. Previous wildfires produced flood peakflows between 5 and 407 times greater than pre-wildfire peakflows. Erosion rates have ranged from 4.2 to 370 Mg/ha/yr. The Coon Creek Fire burned 3,887 ha in April, 2000. The wildfire was classified as uniform high severity in the mixed-conifer Middle Fork drainage of Workman Creek. A rainfall burst of 66 mm in 15 minutes during a monsoon thunderstorm produced a weir-overtopping peakflow (57.4 m^3/s) of more than seven times the previous 40-year record peakflow (8.2 m^3/s). Two additional peakflows that overtopped the main weir occurred in 2001, and were estimated at 11.9 m^3/s. Sediment yield during the first storm could not be calculated because of the size of the flood flow. After the first flood flow in 2000, sediment yields returned to normal (39.3 m^3/yr). The Rodeo-Chediski Fire of 2002 burned 187,290 ha in the headwaters of the Salt River and Little Colorado River. Two 24-ha experimental watersheds (WS 3 and WS 4) were re-instrumented to document post-wildfire peakflows. Previously-measured peakflows, associated with snowmelt runoff, never exceeded 0.0002 m^3/s. The first rainfall after the wildfire on the high-severity burned watershed WS 3, produced a flow of 0.252 m^3/s, 90 times the pre-fire flood peakflow. A subsequent storm that dropped over 65 mm of rain in 1 hour produced a peakflow (6.6 m^3/s, 2,350 times larger than pre-fire) that overtopped the gaging structure. Hillslope erosion on WS 3, the most severely burned of the two watersheds, was 109.2 Mg/ha the first year after the fire. Erosion on WS 4 with low-to-moderate severity fire was 61% of WS 3. Erosion rates declined significantly the second year. The Indian Fire of 2002 burned 553 ha in chaparral and ponderosa pine hills southwest of Prescott, Arizona. Sediment yields the first year was 64.8 Mg/ha, and it was 49.8 Mg/ha the second year. For these new wildfires, flood peakflows increased considerably and sediment yields were in the mid-range of Arizona wildfires. The recent large area, high severity wildfires have evidently pushed watershed responses out of their historical range of variability.

INTRODUCTION

Erosion and flooding are certainly the most visible and dramatic impact of wildfire apart from the consumption of vegetation. Fire management activities (wildfire suppression, prescribed fire, and post-fire watershed rehabilitation) can affect erosion processes in wildland ecosystems (Neary et al. 2005). Forest floor combustion, fireline construction, temporary roads, and permanent, unpaved roads receiving heavy vehicle traffic will increase storm runoff and associated erosion. Increased storm peakflows after wildfires will also increase erosion rates due to aggravated sheet, rill, and

gully erosion, debris flows, and channel incision. Burned Area Emergency Rehabilitation work on watersheds will decrease potential post-fire erosion to varying degrees depending on the timing and intensity of rainfall (Robichaud et al. 2000).

Erosion: Post-wildfire erosion is a function of fire severity, which occurs primarily with moderate- to high-severity wildfires (DeBano et al. 2005). The most common types are sheet, rill, and gravity erosion. Dry ravel is another post-wildfire erosion type in which the gravity-induced, down slope, surface movement of soil grains, aggregates, and rock material delivers sediment to stream channels. It is a ubiquitous process in semiarid steep-land ecosystems that can be triggered by a number of processes. Dry ravel can equal or exceed rainfall-induced hillslope erosion after fire in chaparral ecosystems of the Southwest. Mass failures include slope creep, falls, topples, rotational and translational slides, lateral spreads, debris flows, and complex movements. Cannon (2001) describes several types of debris flow initiation mechanisms after wildfires in the southwestern United States. Of these, surface runoff, which increases sediment entrainment, was the dominant triggering mechanism.

Sediment yields after fires vary, depending on fire frequency, climate, vegetation, and geomorphic factors such as topography, geology, and soils. In some regions, over 60 percent of the total landscape sediment production is fire-related. Much of that sediment loss can occur the first year after a wildfire (DeBano et al. 2005). Increased side slope erosion after fires can alter channel equilibrium by transporting additional sediment into channels where it is stored until increased peakflows produced after fires erode the channel and move the stored material downstream. Channel geomorphology can be affected, and the deposition of sediments alters aquatic organism habitat.

Soil erosion following wildfires can vary from <0.1 Mg/ha/yr (<0.1 tons/ac/yr) in low-severity wildfire to over 369 Mg/ha/yr (164.6 tons/ac/yr) in high-severity wildfires on steep slopes (DeBano et al. 2005). DeBano et al. (1996) found that, following a wildfire in ponderosa pine, sediment yields from a low severity fire recovered to normal levels after 3 years, but moderate and high severity burned watersheds took 7 and 14 years, respectively. Nearly all fires increase sediment yield, but wildfires in steep terrain produce the greatest amounts. Sediment yields usually are the highest the first year after a fire and then decline in subsequent years. However, if precipitation is below normal, peak sediment delivery might be delayed until years two or three post-fire. In semi-arid areas like the Southwest, postfire sediment transport is very episodic in nature. There is growing evidence that short-duration, high intensity rainfall (>50 mm/hr in 10-to-15 minute bursts) over areas of about 1 km^2 (247 ac) produce flood flows that result in large amounts of sediment transport (Neary et al. 2005).

Peakflows: Peakflows are the maximum discharge during a flood event. They are important events in channel formation, sediment transport, and sediment redistribution in riverine systems. The effects of forest disturbance on storm peakflows are highly variable and complex. The magnitude of increased peakflow following fire is more variable than streamflow discharges, and is usually well out of the range of responses produced by forest harvesting. Increases in peakflow as a result of a high severity wildfire are generally related to the occurrence of intense and short duration rainfall events, slope steepness on burned watersheds, and the formation of soil water repellency during burning (DeBano et al. 1998, 2005; Neary et al. 2005). Fire has the

potential to increase peakflows well beyond the normal range of variability observed in watersheds under fully vegetated conditions.

Neary et al. (2005) provided a good review of peakflow response to disturbance. These responses are influenced by fire severity. Intense, short duration storms have been associated with high stream peakflows and significant erosion events after fires. In the Intermountain West, high intensity, short duration rainfall is relatively common. Five minute rainfall rates of 213 and 235 mm/hr (8.38 and 9.25 in/hr) produced peakflows from newly burned areas that increased 5 times more than flow from adjacent, unburned areas (Croft and Marston 1950). Moody and Martin (2001) reported on a threshold for rainfall intensity (10 mm/hr or 0.39 in/hr in 30 minutes) above which flood peakflows increase rapidly in the Rocky Mountains. Robichaud (2002) collected rainfall intensity data on 12 areas burned by wildfire in the Bitterroot Valley of Montana. He measured precipitation intensities that ranged from 3 to 15 mm in 10 minutes. The high end of the range was equivalent to 75 mm/hr (greater than the 100-year return interval). It is these types of extreme rainfall events, in association with altered watershed condition, that produce large increases in stream peakflows.

Low severity, prescribed fires and wildfires have little or no effect on peakflows since they do not substantially alter watershed condition. Severe wildfires have much larger effects on peakflows. A 127-ha (314 ac) wildfire in Arizona increased summer peakflows by 5- to 150-fold, but had no effect on winter peakflows. Another wildfire in Arizona produced a peakflow 58 times greater than an unburned watershed during record autumn rainfalls (Neary et al. 2005). Campbell et al. (1977) documented the effects of fire severity on peakflows. A moderate severity wildfire increased peakflow 23-fold, but high severity wildfire increased peakflow response three orders of magnitude to 406.6-fold greater than undisturbed conditions. In New Mexico, Bolin and Ward (1987) reported a 100-fold increase in peakflow after wildfire in a ponderosa pine and pinyon-juniper forest. Watersheds in the Southwest are much more prone to these enormous peakflow responses due to interactions of fire regimes and site factors.

Another concern is the timing of stormflows or response time. Burned watersheds respond to rainfall faster, producing more flash floods. They also may increase the number of runoff events. After the Rattle Fire, Campbell et al. (1977) measured 6 events on an unburned watershed and 25 on a high-severity burned watershed. Hydrophobic soil conditions, bare soils, and litter and plant cover loss will cause flood peaks to arrive faster and at higher levels. Flood warning times are reduced by "flashy" flow and higher flood levels can be devastating to property and human life. Recovery times after fires can range from years to many decades. Still another aspect of the postfire peakflow issue is the fact that the largest discharges often occur in small areas. Biggio and Cannon (2001) examined runoff after wildfires in the western United States. They found that specific discharges (flow per unit area) were greatest from relatively small areas 1 km^2 or <0.4 mi^2. The smaller watersheds had peak specific discharges averaging 193.0 $m^3/sec/km^2$ (17,664.3 $ft^3/sec/mi^2$), while those in the next higher sized watershed category (10 km^2 or about 4 mi^2) averaged 22.7 $m^3/sec/km^2$ (2,077.6 $ft^3/sec/mi^2$).

Opportunities to study the impacts of watershed-scale fire on hydrologic processes in Arizona montane forests often present themselves following the occurrence of wildfire. Peak flows deserve special attention because of their impacts on erosion processes, and erosion is important

because of downslope impacts on aquatic habitats (DeBano et al. 1998, Neary 2002). Post-fire erosion and peakflows following summer monsoonal rainfall events are documented in this paper. Case studies are presented from the Coon Creek Fire of 2000, the Indian Fire of 2002, and the historically large Rodeo-Chediski Fire of 2002.

METHODS

Coon Creek Fire 2000: The Coon Creek Fire originated on April 26, 2000, as an unattended campfire in the lower reaches of Coon Creek on the eastern side of the Sierra Ancha Mountains, Tonto National Forest. The wildfire eventually burned approximately 3,887 ha (9,600 ac) including parts of the Workman Creek Experimental Watersheds and the Sierra Ancha Wilderness area. The burned area originally supported a vegetative cover of mixed ponderosa pine and oak, ponderosa pine, and mixed conifer forests and chaparral shrubs. While most of the fire was low severity, approximately 20 percent of the area was burned at high severity. The fire crossed three watersheds (South Fork, Middle Fork, and North Fork) in the headwaters of Workman Creek (Gottfried and Neary 2003). These watersheds, which cover a total of 440 ha (1,087 ac), were established in 1939 and were the sites of several watershed experiments investigating the hydrology of mixed conifer forests and the impacts of forest management treatments on watershed resources. The undisturbed Middle Fork watershed burned at a high severity due to its high fuel load. Vegetation and the soil surface on two-thirds of the watershed were subject to high soil heating where litter, duff, and logs were completely consumed. Burn severities on the other two watersheds were low to moderate. The weirs and a flume at Workman Creek were reopened in June, 2000, to assess the impacts of the Coon Creek Fire on streamflow volumes, peak flows, and soil erosion and sedimentation rates. The Main Dam, a compound 90° V-notch weir and Cipolletti weir, measures streamflows from the entire three-watershed area. The South Fork and North Fork watersheds are gauged by 90° V-notch weirs and streamflows from the main part of Middle Fork are measured at a trapezoidal flume. Sediment export was measured at the Main Dam Workman Creek weir and by means of channel cross-sections.

Indian Fire 2002: This fire occurred from May 15-20, 2002. It started southwest of Prescott, AZ, near Indian Creek Road in the Prescott National Forest and burned into the city limits. The fire consumed 553 ha (1,365 ac) of ponderosa pine and chaparral vegetation. Some areas of high severity fire were instrumented with sediment fences to determine soil loss from 0.4 ha (1 ac) burned but untreated and other burned and rehabilitated areas (Robichaud and Brown 2002). No stream gauges were located within the fire perimeter, so flood peakflows were not assessed.

Rodeo-Chediski Fire 2002: This historic wildfire was actually two fires that ignited on the White Mountain Fort Apache Reservation and then merged into one devastating burn. Burning to the northeast, the merged Rodeo-Chediski fire then moved onto the Apache-Sitgreaves National Forest, along the Mogollon Rim in central Arizona, and into many of the White Mountain communities scattered along the Mogollon Rim from Heber to Show Low. The fire burned 187,300 ha (462,606 ac) in total by July 13th. Two nearly homogeneous watersheds, 24 ha (60 ac) each, had been established along Stermer Ridge at the headwaters of the Little Colorado River in 1972-73. The watersheds were gauged with 91 cm (3-foot H-flumes) that remained in place. Following cessation of the Rodeo-Chediski Fire, the flumes were re-

furbished and re-instrumented with water-level recorders and a weather station to study the impacts of varying fire severities on hydrologic processes. One of the Stermer Ridge watersheds experienced a high severity stand-replacing fire, while the other watershed was exposed to a low-to-medium severity stand-modifying burn. Sediment loss was measured by erosion pins since the H-flumes did not contain any structures or devices for measuring sediment loss. Sixty-five percent of the 635 mm (25 in) of annual precipitation falls from October to April, much of it as snow, and the remainder in rainstorms from July to early September. Summer storms, while often intense, rarely produced significant peakflows before the watersheds were burned.

RESULTS AND DISCUSSION

Coon Creek Fire 2000

Peakflows: Several record peak flows have been estimated at the Workman Creek Main Dam weir site since the wildfire. Middle Fork was gauged by a flume that did not have any sediment-determining structure. Most of the peakflows and sediment yield measured at the main weir originated in the Middle Fork watershed. A 15-minute rainfall burst at an intensity of 66 mm/hr (2.6 in/hr) on Middle Fork in June 2000 produced a peak flow that was more than 7-times (57.3 m^3/sec or 2,023 ft^3/sec) that of the previous highest peak flow of 8.18 m^3/sec (289 ft^3/sec) measured on October 10, 1972 (Neary and Gottfried 2002). The streamflow overtopped the Main dam weir, and, therefore, peak flow was estimated from high water marks. Two other peak flow events were observed in August, 2001. The higher of these peak flows, between 11.6 and 11.9 m^3/sec (409 and 420 ft^3/sec), was recorded on August 11, 2001, when a thunderstorm produced a rainfall event of approximately 33 mm/hr (1.3 in/hr) in intensity.

Sediment Loss: Severe surface soil erosion and sub-channel scouring were observed on Middle Fork following the June 2000 storm but no measurements were made because the control sections had not been instrumented at the time. Currently, erosion and sedimentation information are being measured on a series of channel cross sections that have been established on Middle Fork and on South Fork above the weirs. Sediment also is being measured at the settling basins behind the weirs at Main Dam, South Fork, and North Fork. Measurements are made on series of cross-sections that extend at 1-m (3 ft) intervals parallel to the cutoff walls. Most of these data have not been fully analyzed. However, the August, 2001, storms produced more than 41.3 m^3 (1,456 ft^3) of sediment in the Main Dam basin, which had been cleaned less than two month earlier, compared to 14.9 m^3 (526 ft^3) measured between late June and December of 2000 (Gottfried and Neary 2003). Most of the sediment appeared to originate from Middle Fork although some should be attributed to a main forest system road that runs parallel to the channel below the confluence of the three forks and crosses Middle Fork at one point. For the first 20 months after the fire the yield was 56.2 m^3 (1,982 ft^3), most likely a gross underestimate due to the large weir-overtopping flows. A sediment yield of 148.9 Mg in 20 months from the 440 ha (1,087 ac) of burned area would be considered an average amount even if it all came from the 166.4 ha (411 ac) Middle Fork watershed (Gottfried and Neary 2003). A pebble count of sediment behind the Main Dam in June 2001 indicated that 48% of the sediments were sand and 36% were cobbles. Approximately 3% of the sediments were in the boulder category >256 mm in diameter.

Indian Fire 2002

Peakflows: Flood peakflows were not assessed at this site. However, substantial overland flows were observed by the senior author during the first rainfall event after the fire, and the evidence of high runoff was observed during the forst 3 monsoon seasons after the fire. Due to the limited area of high-severity fire, significant flood flows were not generated off of the area within the fire perimeter.

Sediment Loss: After the first monsoon rain period, sediment yield from plots on the Indian Fire burned at high severity was about 50 Mg/ha (22 tons/ac). Most of this sediment was delivered by one storm event that contained an intense rainfall burst. The maximum rainfall intensity was 117 mm/hr (4.62 in/hr). Addition of wood chips or straw mulch onto the high-severity burned soil reduced erosion by 80%. This rehabilitation technique mimicked the normal forest floor covering and returned most hydrologic function to the site. Total sediment yield from the burned but un-rehabilitated area was 64.8 Mg/ha at the end of 2002, and 49.8 Mg/ha the second year (2003). By 2005, sediment yield had become negligible in treated and untreated burned areas alike due to vegetation regrowth.

Rodeo-Chediski Fire 2002

Peakflows: Following the Rodeo-Chediski Fire of 2002, peakflows were orders of magnitude larger than earlier recorded. The estimated initial peakflow on the WS 3 watershed that experienced high severity stand-replacing fire was almost 0.25 m^3/sec (8.9 ft^3/sec) or nearly 900 times that measured pre-fire (Ffolliott and Neary 2003). The peakflow on the watershed subjected to low-to-medium severity fire was estimated to be <50%, but still far in excess any previously observed ones. A subsequent and higher peakflow on the severely burned watershed was estimated to be 6.57 m^3/sec (232 ft^3/sec) or about 2,232 times that measured in snow-melt runoff prior to the wildfire. This latter peakflow increase represents the highest known relative post-fire peak flow increase that has been measured in the ponderosa pine forest ecosystems of Arizona or, more generally, the southwestern United States. However, the specific discharge of 1.02 m^3/sec/km^2 (94.2 ft^3/sec/mi^2) was on the lower end of range of discharges measured by Biggio and Cannon (2001).

Sediment Loss: The measurements of soil pedestals suggest that 56 to 67 Mg/ha (25 to 30 tons/ac) of soil were eroded from the severely burned watershed in response to the first summer monsoon rains (Garcia et al. 2005). Between 34 to 45 Mg/ha (15 to 20 tons/ac) of soil were lost from the lightly-to-moderately burned watershed (Figure 1). Soil erosion rates on the severely burned and lightly-to moderately burned watersheds after the first winter precipitation and snowmelt-runoff period following the wildfire were 49 to 27 Mg/ha (22 and 12 tons/ac), respectively. Erosion rates following the second summer monsoon rains were statistically similar between watersheds, averaging about 25 Mg/ha (11 tons/ac) for both watersheds. During the second winter, erosion rates increased again to the 40 to 50 Mg/ha range but there was no statistical difference between the burn severities.

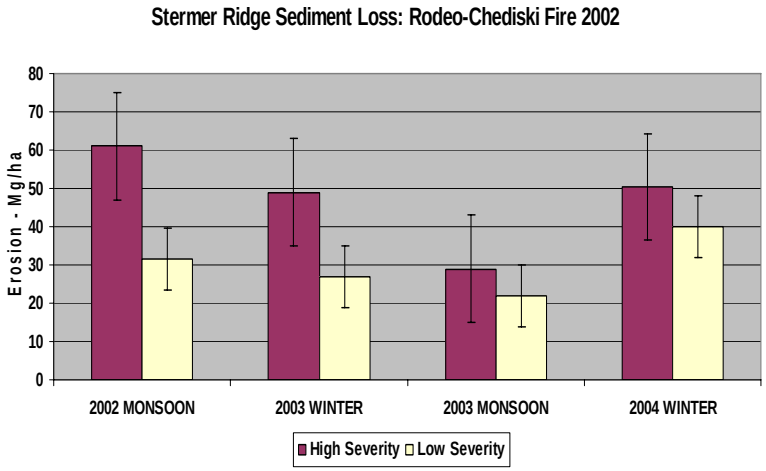


Figure 1 Sediment loss from Stermer Ridge Watersheds, Rodeo-Chediski Wildfire 2002, first four precipitation periods (Adapted from Garcia et al. 2005 and Stropki et al. In Press).

SUMMARY AND CONCLUSIONS

Following wildfires, flood peak flows can increase dramatically, severely affecting stream physical conditions, aquatic habitat, aquatic biota, and sediment yield. The potential exists for peak flood flows to jump to 2,300 times that of pre-wildfire levels as observed after the Rodeo-Chediski Fire. Sediment yields in these study areas were at about the middle of the range observed in other wildfires in the Southwest (Neary et al. 2005). Land managers must be aware of these potential watershed responses in order to adequately and safely manage their lands and water resources in the post-wildfire environment. The recent large-area, high-severity wildfires have evidently pushed watershed peakflow responses out of their historical range of variability, and have the potential to do the same to sediment yield.

REFERENCES

Biggio, E.R., Cannon, S.H. (2001). "Compilation of post-wildfire runoff data from the western United States," Open-file Report 2001-474. U.S. Geological Survey. 24 p.

Bolin, S.B., Ward, T.J. (1987). "Recovery of a New Mexico drainage basin from a forest fire," In: Swanson, R.H.; Bernier, P.Y.; Woodward, P.D. (eds.). Forest hydrology and watershed management. International Association of Hydrological Sciences Publication 167: 191-198.

Campbell, R.E., Baker, M.B., Jr., Ffolliott, P.F., Larson, F.R., Avery, C.C. (1977). Wildfire effects on a ponderosa pine ecosystem: an Arizona case study. Research Paper RM-191. Fort Collins, CO. U.S. Department of Agriculture, Forest Service, Rocky Mountain Forest and Range Experiment Station. 12 p.

Cannon, S.H. (2001). "Debris-flow generation from recently burned watersheds," Environmental & Engineering Geoscience 7(4):321-241.

Croft, A.R., Marston, R.B. (1950). "Summer rainfall characteristics in northern Utah," Transactions, American Geophysical Union. 31(1): 83-95.

DeBano, L.F., Ffolliott, P.F., Baker, M.B., Jr. (1996). "Fire severity effects on water resources," In: Ffolliott, P.F.; DeBano, L.F.; Baker, M.B., Jr.,; Gottfried, G.J.; Solis-Garza, G.;

Edminster, C.B.; Neary, D.G.; Allen, L.S.; Hamre, R.H. (tech. coords.). "Effects of fire on Madrean Province ecosystems - A symposium proceedings," General Technical Report RM-GTR-289. Fort Collins, CO, U.S. Department of Agriculture, Forest Service, Rocky Mountain Forest and Range Experiment Station, pp 77-84.

DeBano, L.F., Neary, D.G., Ffolliott, P.F. (1998). Fire's Effects on Ecosystems. John Wiley & Sons, New York.

DeBano, L.F., Neary, D.G., Ffolliott, P.F. (2005). "Chapter 2: Effects on soil physical properties," In: Neary, D.G., Ryan, K.C., DeBano, L.F. (eds.) 2005. "Fire effects on soil and water," General Technical Report RMRS-GTR-42, Volume 4: Fort Collins, CO, U.S. Department of Agriculture, Forest Service, Rocky Mountain Research Station. 250 p.

Ffolliott, P.F., Neary, D.G. (2003). "Impacts of a historical wildfire on hydrologic processes: A case study in Arizona," Proceedings of the American Water Resources Association International Congress on Watershed Management for Water Supply Systems, New York, NY, June 29 – July 2, 2003. CD-ROM.

Garcia, P., Ffolliott, P.F., Neary, D.G. (2005). "Soil erosion following the Rodeo-Chediski wildfire: an initial assessment," Hydrology and Water Resources in Arizona and the Southwest 34:51-5

Gottfried, G.J., Neary, D.G. (2003). "Preliminary assessment of sediment measurements at weir basins following the Coon Creek Fire in central Arizona," Hydrology and Water Resources in Arizona and the Southwest 33: 103-111.

Moody, J.A., Martin, D.A. (2001). "Hydrologic and sedimentologic response of two burned watersheds," U.S. Geological Survey Water-Resources Investigation Report 01-4122.

Neary, D.G. (2002). "Chapter 6: Environmental sustainability of forest energy production, 6.3 Hydrologic values," In: Richardson, J.; Smith, T; Hakkila, P. (eds.) Bioenergy from sustainable forestry: Guiding principles and practices. Amsterdam: Elsevier; 36-67.

Neary, D.G., Gottfried, G.J. (2002). "Fires and floods: post-fire watershed responses," In: Viegas, D.X. (ed.). Forest fire research and wildland fire safety, Proceedings of the 4th International Forest Fire Research Conference, Luso, Portugal, 18-22 November 2002. Roterdam: Mill Press; 203 and 1-9 in CD version of complete papers.

Neary, D.G., Ryan, K.C., DeBano, L.F. (eds.) (2005). "Fire effects on soil and water," General Technical Report RMRS-GTR-42, Volume 4, Fort Collins, CO, U. S. Department of Agriculture, Forest Service, Rocky Mountain Research Station. 250 p.

Robichaud, P.R. (2002). "Wildfire and erosion: When to expect the unexpected," Symposium on the geomorphic impacts of wildfire. Paper 143-10. Boulder, CO, Geological Society of America.

Robichaud, P.R., Brown, R.E. (2002). "Silt fences: An economical technique for measuring hillslope soil erosion," General Technical Report RMRS-GTR-94. Fort Collins, CO, U.S. Department of Agriculture, Forest Service, Rocky Mountain Research Station. 24 p.

Robichaud, P.R., Beyers, J.L., Neary, D.G. (2000). "Evaluating the effectiveness of post-fire rehabilitation treatments," General Technical Report RMRS-GTR-63. Fort Collins, CO, U. S.Department of Agriculture, Forest Service, Rocky Mountain Research Station. 85 p.

Stropki, C.L., Ffolliott, P.F., DeBano, L.F., Neary, D.G. IN PRESS. "Water repellent soils on the Stermer Ridge watersheds following the Rodeo-Chediski wildfire: A preliminary assessment.," Water Resources in Arizona and the Southwest 34.

ESTIMATION OF SEDIMENT AND NUTRIENT LOADS FROM MIXED LAND USE WATERSHEDS IN THE UPPER MISSISSIPPI RIVER BASIN AND THE ROLE OF WETLANDS IN REDUCING THEM.

J.P. Schubauer-Berigan, US Environmental Protection Agency, National Risk Management Research Laboratory, Cincinnati, OH, schubauer-berigan.joseph@epa.gov; W.B. Richardson, US Geological Survey, La Crosse, WI; P. Hughes, US Geological Survey, Middleton, WI; L. Bartsch, US Geological Survey, La Crosse, WI; J. Cavanaugh, US Geological Survey, La Crosse, WI; R. Kreiling, US Geological Survey, La Crosse, WI; M. Morrison, US Environmental Protection Agency, Cincinnati, OH

Abstract: We present results from our ongoing work examining the role of wetlands in the interception and processing of suspended sediment (SS), nitrogen (N) and phosphorus (P) loads from two suburbanizing watersheds near La Crosse, WI**.** Using field measurements, we estimated SS, N and P loads for each of two small (25 and 100 sq. km) watersheds and loads entering a native (NW) and constructed wetland (CW). Estimates of SS were based on both discrete pumped water samples and monitoring using Laser *In situ* Suspended Sediment Transmissometers (LISST -25X). Continuous *in situ* measurements of water quality (using YSI sondes outfitted with chlorophyll and turbidity probes) were also made. Spatial patterns of SS and C, N and P deposition in the CW were quantified using clay pads. Sediment denitrification (DN) and nitrification (NT) were estimated for the streams and wetlands using acetylene block. SS estimates made using each method will be described and contrasted. Estimates of sediment and nutrient loads will be described for periods of base flow, storm flow, season and annually. Spatial patterns of stream and wetland DN and NT rates and factors limiting rates will be presented and discussed. The amount of sediments and nutrients removed by the wetlands in relation to the loads estimated for the watersheds, will be compared and discussed.

THE ISOKINETIC STREAMLINED SUSPENDED-SEDIMENT PROFILING LISST-SL – STATUS AND FIELD RESULTS

Yogesh C. Agrawal, President, Sequoia Scientific, Inc., yogi.agrawal@sequoiasci.com; H.C. Pottsmith, Vice President, pottsmith@sequoiasci.com, Sequoia Scientific, Inc., 2700 Richards Rd., Bellevue, WA 98005

Abstract: A streamlined isokinetic sediment profiler – the LISST-SL – has been developed by this company in a Cooperative Research and Development Agreement with the U.S. Geological Survey (USGS). This device continuously measures suspended-sediment concentrations, size distributions, depths of measurements (pressure), water velocities, and water temperatures. It is cable-suspended using a standard USGS B-reel. A topside control box provides power and communication. Data are stored on a PC for subsequent windows-based processing. Due to the inclusion of a depth sensor, the wire-angle limitation of the past induced by downstream drag on the instrument is relaxed. The additional simultaneous measurement of velocity permits computation of true horizontal flux of sediment in 32 distinct size classes covering the size range 2.5 to 500 microns. Typical data at a depth are acquired in a few seconds; however, statistical stability requires averaging over several integral scales of the turbulence (this scale is z/U, where z is distance above bed, U is mean velocity). The system employs laser diffraction optics. Bluetooth may be offered.

In this paper, we present LISST-SL technical details and field data from a river in the Northwest US. Influence of shape effects on measurement accuracy is considered in a quantitative way based on new data on small-angle light scattering properties of natural dusts versus spherical particles.

INTRODUCTION

The LISST-SL instrument is a streamlined version of the standard LISST series of particle sizing systems that are now in common use; a partial list of publications appears on the company's website [http://www.sequoiasci.com/library/technical.aspx?SectionName=library]. An earlier report on this device was presented at the last such conference. Since then, field tests, an evaluation at the Federal Interagency Sedimentation Project (FISP) and further engineering development of the isokinetic controller have been performed. Furthermore, shape effects of particles are under study that, when incorporated in the algorithms for inversion of multi-angle scattering, will measurably improve measurement accuracy. These are the subjects of the present report. In the following, we summarize fundamental concepts and the instrument. We then present test results from the field as well as the laboratory. Preliminary indication of shape effects of particles is included.

The LISST series of instruments are based on the small-angle scattering principle, which is more widely recognized as laser diffraction. Briefly, light scattering at small forward angles consists of two parts: light diffracted by the obstruction that is the particle, and light that entered the particle and then emerged in the forward direction, i.e. transmitted or refracted light. Of these, at small

angles, diffracted light is usually dominant, hence the name laser diffraction. This diffraction follows exactly the same form as through an aperture, which is a classical solution due to Airy, and bears his name (see e.g. Born and Wolf, 1975). For circular apertures, the Airy *function* follows the form $a^4[J_1(ka\theta)/(ka\theta)]^2$ where J_1 is the Bessel function of first order, k is $2\pi/\lambda$, a is particle radius and θ is scattering angle. Because diffraction does not concern particle internal properties, the measurement is insensitive to changes in particle composition or color. Thus, this method does not suffer from changed calibrations with changing sediment color – a significant shortcoming of the widely used optical backscatter sensors. Furthermore, since the size distribution is measured, the calibration of the measurement remains fixed, regardless of the sediment-size distribution. This latter advantage is central to the need for alleviating this second source of calibration change with OBS as well as acoustic sensors (Sutherland et al.2000). The full technical details of relevant light scattering theory are presented elsewhere (Agrawal and Pottsmith, 2000).

The method, unlike single particle counting methods, measures scattering of light from an ensemble of particles in a laser beam, all of which contribute to it. Of the illuminated set, each size contributes in proportion to its number and to its own characteristic diffraction form described above. The overall sum becomes the observation of multi-angle scattering. This is inverted to obtain the size distribution. Summing the size distribution produces the total suspended-sediment concentration. The other essential relevant details for this report are that the minimum and maximum scattering angles at which measurements are made determine, respectively, the maximum and minimum particle size that can be included in the inversion. For example, for optimal inversion, we set $ka_{min}\theta_{max} = ka_{max}\theta_{min} = 2$. The LISST-SL instrument is designed with θ_{min} and θ_{max} chosen to cover the size range 2.5 to 500 microns.

The instrument consists of a streamlined hull with a low drag coefficient of <0.2. A coaxial aperture at the nose is fitted with a USGS standard nozzle (Davis and the Federal Interagency Sedimentation Project, 2005) to draw water, through a long drilled conduit. Approximately midway through the passage of this water, laser optics measure multi-angle scattering. These optics consist of a laser, collimating lens, glass windows to separate river water from the optics and electronics, a receiving lens, and a custom detector (Figure 1). As for electronics, although the original prototype, which constitutes the platform for some of the test results included here used an internal micro-computer and data storage capability, the new production models only include a micro-processor. Each includes, in addition, the photo-current amplifiers and a pump controller. The micro-computer (or the micro-processor) communicates with a Topside Controller Box (TCB) where data are stored. The Controller communicates with a PC or laptop computer. For effecting isokinetic withdrawal of water from the stream, a pump assist is included. An external flow sensor is enclosed in a streamlined tube in the 'sail' of the instrument. It measures the local velocity of river flow, it is based on heated thermistor technology. The flow internal to the instrument is monitored with an identical heated thermistor sensor, so that feedback is included. The micro-computer adjusts pump drive voltage to equalize intake velocity to river flow. This also permits an operator to identify flow blockage. The TCB commands the submersible LISST-SL to deliver data according to the program parameters that an operator sets up on a laptop computer.

The system employs a pressure sensor to record the depth at which any measurement is being made. The depth data is integrated into the optical multi-angle scattering data stream that is sent to the TCB. The heated thermistor readings are also transmitted to the TCB as measures of water temperature and river velocity. By integrating the depth, water temperature and velocity data with the optical data, synchronism of data are assured. All communications and power transmission are implemented with the standard USGS B-reel.

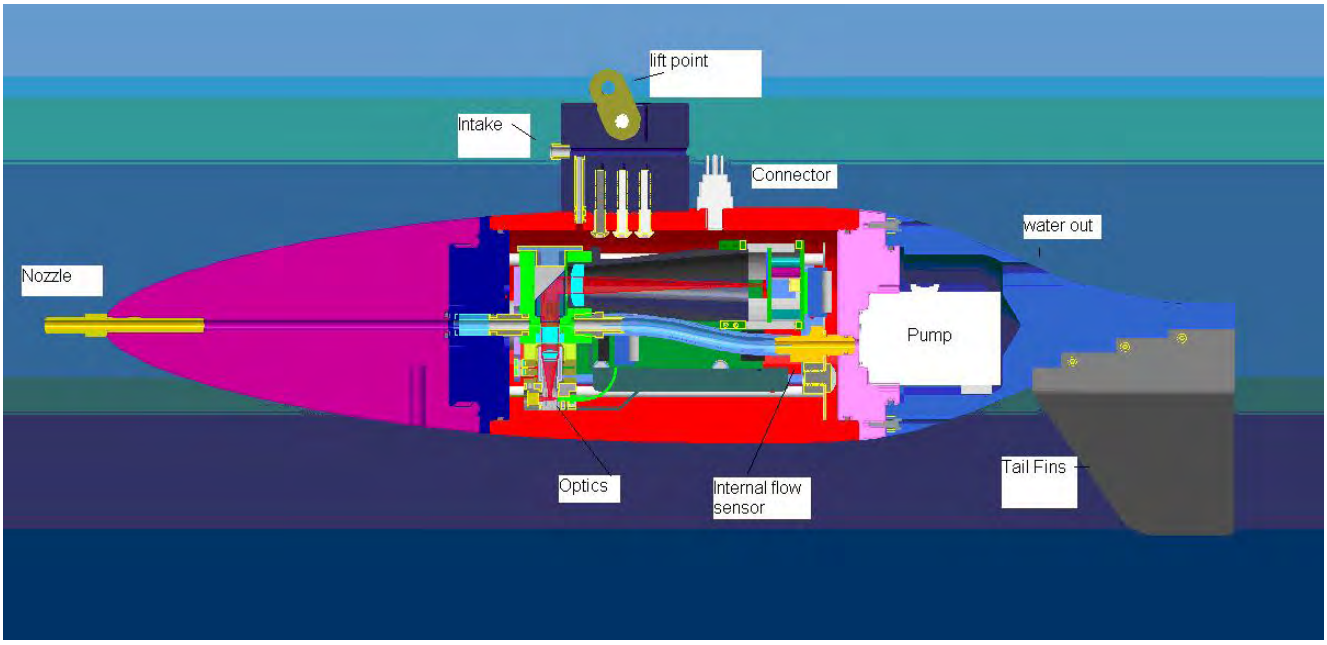


Figure 1 A cut-away of the LISST-SL instrument.

TESTS- LABORATORY

The laboratory tests were performed, both at the FISP facility in Vicksburg, MS, and subsequently again after minor optics improvement incorporated in the first commercial instrument, at the factory. These tests were intended to establish accuracy of measurement of suspended-sediment concentration. Key components of the test set up included a well-stirred reservoir into which measured amounts of sediment samples were inserted. For each sample, as it was the intention to examine accuracy at different flow-through velocities, a set of water samples were collected from the discharge end while measurements of multi-angle scattering were being made. This was meant to ensure that precisely the same water that passed through the instrument is available for physical determination of samples. The system was designed and built by Broderick Davis and Wayne O'Neil of FISP. The results of those tests were not fully within the CRADA's specifications and are not reproduced here. The identical tests were repeated at the company with the improved optics built into the first commercial Unit-001. The improved optics reduced background scattering from optical surfaces, reducing noise contamination of the results. These are displayed in Figure 2.

The true vs. estimated concentrations show a reasonable 1:1 trend, over the range of concentrations from 10-5,000 mg/l, Fig. 2 (*left*). The maximum error is 12%, at both the

extremes of concentrations, i.e. at 10 and 5,000 mg/l. The error is less than 10% throughout the mid range (20-2,500 mg/l). The size distributions for the entire range of tests are displayed in Fig.2 (*right*). Clearly, the size distributions appear consistent, scaling up with increasing concentrations.

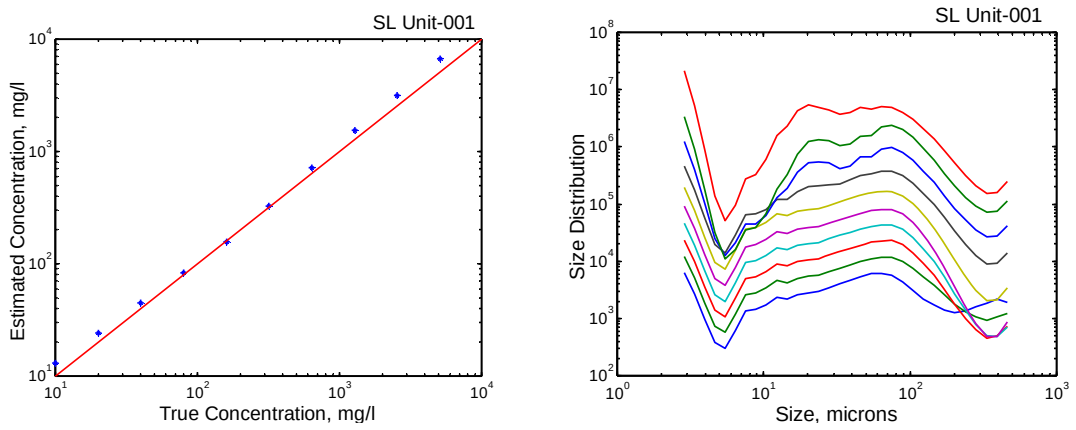


Figure 2 Test of fidelity of concentration (*left*) and size distribution over 1-5000 mg/l, and size distributions (*right*).

It is noteworthy that the rising left edge of the size distributions is attributed to shape effects. More on this is presented later in the paper. Isokinetic tests have not been carried out at the time of this writing (November 2005) but should be available in 2006.

TESTS - FIELD

On June 24, 2004, the prototype LISST-SL (i.e. previous to improved optics) was tested in Puyallup River, Washington. This river carries sediment from Mr. Rainier, a regional dormant volcano. The LISST-SL, shown in Figure 3, was lowered from a USGS standard B-reel into the river. Simultaneously, point-integrated bottle samples were collected isokinetically at the same depth and time as the LISST-SL data. These are compared in Figure 4 below. Note that the data represent less than currently achievable level of performance.

There are two segments in this data, Figure 4. In the first segment, LISST-SL sample numbers 20 to 90, a long time series was taken at a fixed depth, during which time bottle samples were also collected. The second segment shows a detailed vertical profile, between sample numbers 110 and 200 (abscissa). The yellow trace (top) shows river velocity. The dots indicate bottle data that was post processed.

The first segment of this data is preceded by an artifact of high values which may have been contaminated by bubbles in the system, to about sample number 20. Following this, the agreement between concentrations derived from the LISST-SL and P-61 samples is within 20% with the LISST-SL results tending to be biased low. Note also the two sudden discontinuities in the P-61 sample data around sample number 45 and 52. These are unlikely to be correct, and are not supported by nearby measurement, suggesting variability in these samples. The profiled

samples, points 120-200 show a distinct rise in concentration measured by the LISST–SL as it reaches maximum depth (nearest bottom), about 15 cm above bed. The increase in concentration



Figure 3 (*left*) The LISST-SL shown suspended from a bridge on the Puyallup river, Washington, from the B-reel frame. (*right*) View, looking down from the bridge of 'fish in water' shows the instrument aligned with flow, as indicated by the wake.

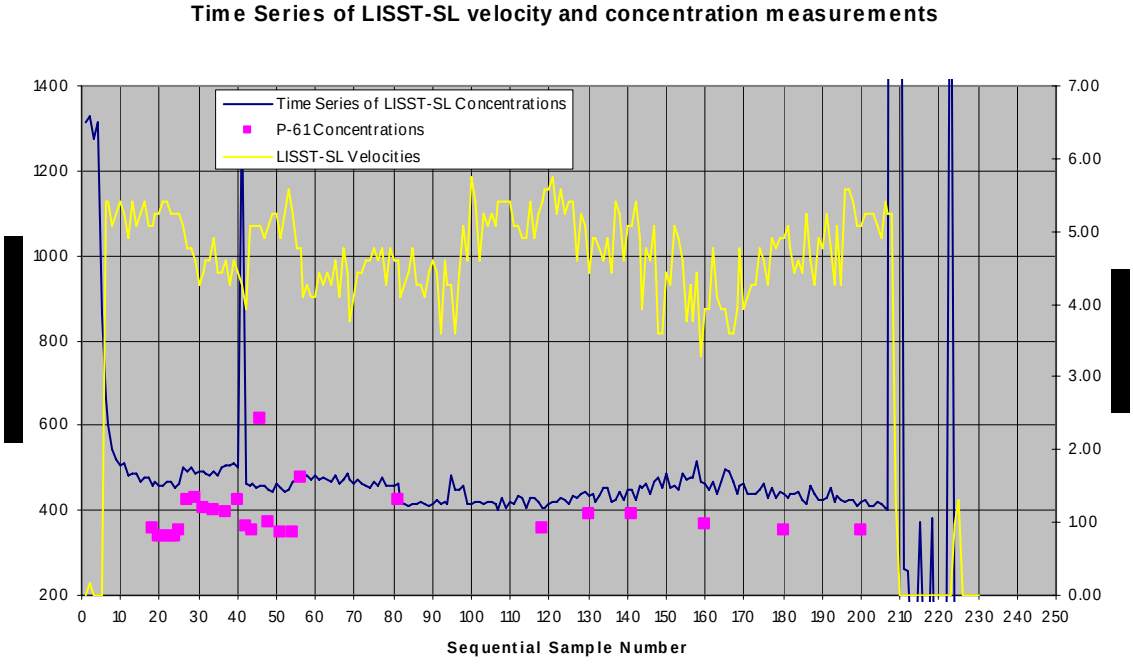


Figure 4 Time series of measurements with the LISST-SL and P-61 samples (dots).

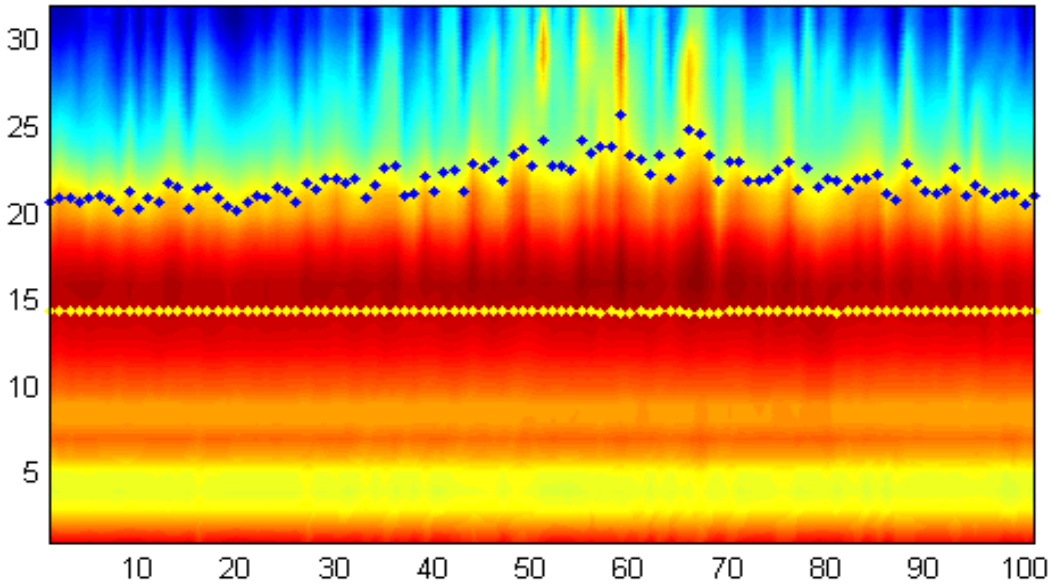


Figure 5 Detailed size distribution, concentration (blue dots) and concentration via optical transmission (yellow dots) through a vertical profile, segment 100-200 of Fig. 4.

coincides with reduced velocity – all characteristic boundary layer patterns. The profile of sediment concentration seen here is expected in any natural environment, it results from the balance of gravitational settling and turbulent diffusion. The phenomenon bears the name of Rouse (1937). The velocity series, top profile, reflects a slowing down of flow near bed. The profile properties recover on the up-cast, approximately 160-200. Strangely, bottle samples do not 'see' the increase of sediment concentration near the bed.

the ordinate is the size class number. Recall that the LISST-SL reports concentration in these 32 size classes. Colors indicate concentration, reds being high, blues low. It is evident that the More detailed analysis of the multi-angle scattering data from LISST-SL supports the suspended-sediment concentration of figure 4. This is displayed in Figure 5. Here, the size distribution during the vertical profile is displayed, expanded. The abscissa is data sequential number, while middle of this pseudo color plot displays the presence of significant concentrations in the high numbered size classes, i.e. large particles. Again, this is consistent with Rouse (1937) formulation – the faster-sinking particles stay near the bed. The blue dots (total concentration) suggest an increased concentration accompanying the large particles nearest bed. The upcast gradually shows the disappearance of large particles, and a return of the concentration to its original downcast starting value. Interestingly, a measure of sediment concentration via beam attenuation (which is similar in properties to optical backscatter), shown as yellow dots in mid-range of the plot, does not pick up this increase of concentration nearest bed. This is a consequence of the inability of such measurements (transmission, nephelometry or optical backscatter) to see large particles with sufficient sensitivity. In other words, had an OBS or beam transmissometer been in use, the concentration would be in error and no details of large grains would show up near the riverbed. To sum, the detailed profile measurement of the LISST-SL consistently finds patterns that are expected in a vertical profile, amply supported by densely populated data points, whereas sampling variability of P-16 seems to miss the detail.

PARTICLE SHAPE EFFECTS

As noted, light scattering theory is not sufficiently developed yet to easily compute the angular scattering or diffraction from arbitrarily shaped particles. In particular, the computations are possible for small sizes but become far too computationally intensive to be useful in practice. Therefore, one uses the scattering-diffraction properties of spheres. We have made strides in characterizing differences that arise from shape effects. In Figure 6, we show the measured light scattering pattern from a size fraction from Arizona dust (size 63-125 microns, obtained by careful multi-wash wet sieving), compared with the same for spheres. The difference is qualitatively evident (*left*). In particular when the scattering signature of AC Sparkplug dust particles is interpreted as a collection of spheres, it produces a size distribution shown in Figure 6 (right), which shows the apparent 'invention' of fines that were in fact absent. This is the essential consequence of shape effect. Far more exhaustive studies are underway, including the variability in scattering from particles of different sources. These data will begin the quantification of errors arising out of changes in shapes of particles from different sources. We hasted to add that these changes are still small compared to the 12% change mentioned in figure 2. These studies are important simply to place fundamental bounds on accuracy.

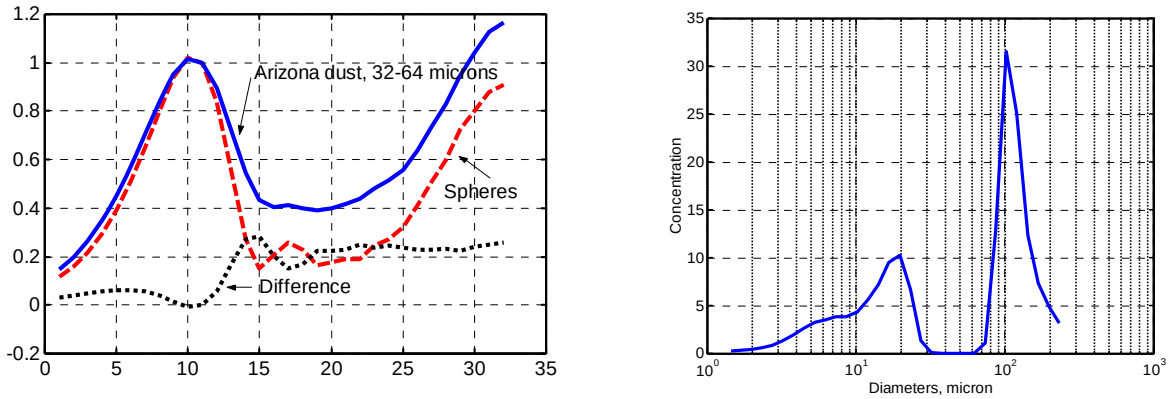


Figure 6 The difference between light scattering by Arizona dust and spheres of equivalent sizes (*left*), and the consequent invention of fines when the dust is interpreted as a set of spheres (*right*, from inversion of the 'difference' in scattering between dust and spheres).

CONCLUSIONS

Provisional results are encouraging. The LISST-SL appears capable of holding calibration within 12% over the concentration range 10-5,000 mg/l, although the accuracy is superior – better than 10% – for 20-2,500 mg/l. Field tests in a river produced an approximate 20% discrepancy with the P-61 samplers, with the original prototype, a differential that would presumably be lower with the improved commercial instrument. Interestingly, the LISST-SL clearly reveals a Rouse-like concentration behavior in concentration profile, not seen by bottle samplers, which begs explanation.

The next tasks are the completion of the isokinetic flow withdrawal system, and the incorporation of shape effects in interpreting multi-angle scattering data. These results may be available by April 2006.

Acknowledgments: This work is funded by internal R&D dollars of Sequoia Scientific, Inc. We gratefully acknowledge the advice and inspiration of USGS personnel, especially John Gray at Reston, VA. We are grateful to Kurt Spicer of USGS Tacoma, Washington for the data collected at Puyallup River, displayed in Figure 4. We also acknowledge the on-going contributions of Broderick Davis and past contributions of Wayne O'Neal at FISP in Vicksburg, MS in laboratory testing. At Sequoia, the team includes Doug Keir, Khanh Le, and Kurt Duclos deserving special recognition.

REFERENCES

Agrawal, Y. C., and H.C. Pottsmith. (2000). "Instruments for particle size and settling velocity observations in sediment transport," Marine Geology 168: 89-114

Born,M. and E. Wolf, (1975) Principles of Optics, 5th Ed. Pergamon.

Davis, B.E., and the Federal Interagency Sedimentation Project, 2005. A guide to the proper selection and use of federally approved sediment and water-quality samplers. U.S. Geological Survey Open-File Report 2005-1087, 20 p., Reston, Virginia (**http://pubs.er.usgs.gov/pubs/ofr/ofr20051087).**

Edwards and Glysson, (1999). USGS TWRI Book 3, Chapter C2.

Rouse, H., (1937) "Modern Conceptions of the Mechanics of Fluid Turbulence, Transactions of the American Society of Civil Engineering," v102, pp 463-554.

Sutherland, T.F, P.M. Lane, C.L. Amos, J. Downing, (2000) "The calibration of optical backscatter sensors for suspended sediment of varying darkness levels," Marine Geology, v162, pp 587-597.

FISP'S SUITE OF FEDERALLY APPROVED SUSPENDED-SEDIMENT/WATER QUALITY COLLAPSIBLE-BAG SAMPLERS

Broderick Davis, Mechanical Engineer, FISP, U.S. Geological Survey, Vicksburg, MS, bedavis@usgs.gov

Abstract: In 1996, the Federal Interagency Sedimentation Project (FISP) began research and development of an isokinetic collapsible-bag suspended-sediment/water-quality depth-integrating sampler. The research has led to the development and approval by the FISP Technical Committee of four collapsible-bag depth-integrating suspended-sediment/water-quality samplers weighing from 30 to 285 lbs (13.6 to 130 kg) and capable of collecting from 1 to 6 liters of sample. The FISP suite of collapsible-bag samplers is capable of sampling stream velocities that range from 2 to 15 ft/sec (0.5 to 4.6 m/sec) and stream depths of up to 220 ft (67 m). The samplers incorporate plastic parts for suspended-sediment sampling and non-contaminating parts that meet the U.S. Geological Survey's (USGS) Office of Water Quality's requirements for collecting non-contaminated water-quality samples for trace-element analysis outlined by Lane and others (2003).

INTRODUCTION

Various investigators including Gluschkoff and the Rhine Works Authority (FISP 1940), Stevens and others (1980) and Szalona (1982) documented research on the use of a collapsible-bag depth-integrating suspended-sediment sampler. Results were encouraging, but the proposed samplers were not able to collect isokinetic samples at all stream velocities typically encountered in natural streams. An isokinetic sampler collects a water-sediment sample from the stream at a rate such that the velocity in the nozzle is equal to the incident stream velocity at the nozzle entrance. In 1996, the Federal Interagency Sedimentation Project (FISP) began research and development of an isokinetic collapsible-bag depth-integrating suspended-sediment/water-quality sampler. A collapsible-bag sampler has several advantages over traditional rigid-container samplers. A primary advantage is sampling depth. Rigid-container samplers are limited to a maximum depth of 15 ft (4.6 m) due to air compressibility. A bag container is flexible and contains essentially no air. As a result, sampling depth is not limited because of air compressibility, meaning the depth to which the sampler can be used is limited only by the intake diameter of the nozzle and the volume of the bag. It also means the maximum transit rate is limited only by the apparent approach angle of the nozzle facing into the stream flow as the sampler makes its vertical traverse, which is 0.4 times the mean stream velocity (FISP 1952). The minimum transit rate is limited by the volume of the collapsible bag. Another advantage is cost savings in the use of collapsible bags as opposed to a rigid container or bottle.

The initial development effort beginning in 1996 resulted in a 3-liter sampler designated the US D-96 and patented by Davis and O'Neal (2001a). The sampler was designed, tested, and approved for use by the FISP Technical Committee as reported by Davis (2001b). The US D-96 sampler weighs 130 lbs (59 kg). In 1999, design and testing of a 6-liter collapsible-bag sampler was initiated. The result was the US D-99, a 285 lb (130 kg) sampler and is described by the FISP (2005). In 2003 an 80 lb (36 kg) version of the US D-96, designated the US D-96-A1, was designed, tested, and approved by the FISP Technical Committee and reported by Davis (2003).

In 2002, development of a bag sampler deployable by handline was initiated. The result was the US DH-2, a 30 lb (13.6 kg), 1-liter sampler described by Davis (2005). The samplers incorporate plastic parts for suspended-sediment sampling and non-contaminating parts that meet the U.S. Geological Survey's (USGS) Office of Water Quality's requirements for collecting non-contaminated water-quality samples for trace-element analysis outlined by Lane and others (2003). These samplers are in wide-spread use throughout the United States and other countries.

US D-96

The US D-96 is 35 in (89 cm) long, 8 in (20 cm) diameter at its widest point, and weighs 130 lbs (59 kg). The nozzle is located at the centerline of the sampler resulting in an unsampled zone (distance from centerline of nozzle to bottom of sampler) of 4 in (10) cm. The sampler (figure 1) is composed of various parts including a top section, bottom section, tail section, nose section with tray, nozzle holder, and nose insert. The top section is made of cast bronze with a plastic liner on its bottom side. The bottom section is a cast aluminum shell that mates with the top section to form the cavity inside the sampler. The inside of the bottom section is lined with plastic. The nose section is cast aluminum and has a slot machined in the front that matches the slot in the top section for the nose insert. The nose section is also fitted with a plastic tray. The tray slides into the cavity formed by the bottom section and is designed to support the bag. All metal parts are plastic coated to minimize the possibility of contamination of samples for trace-

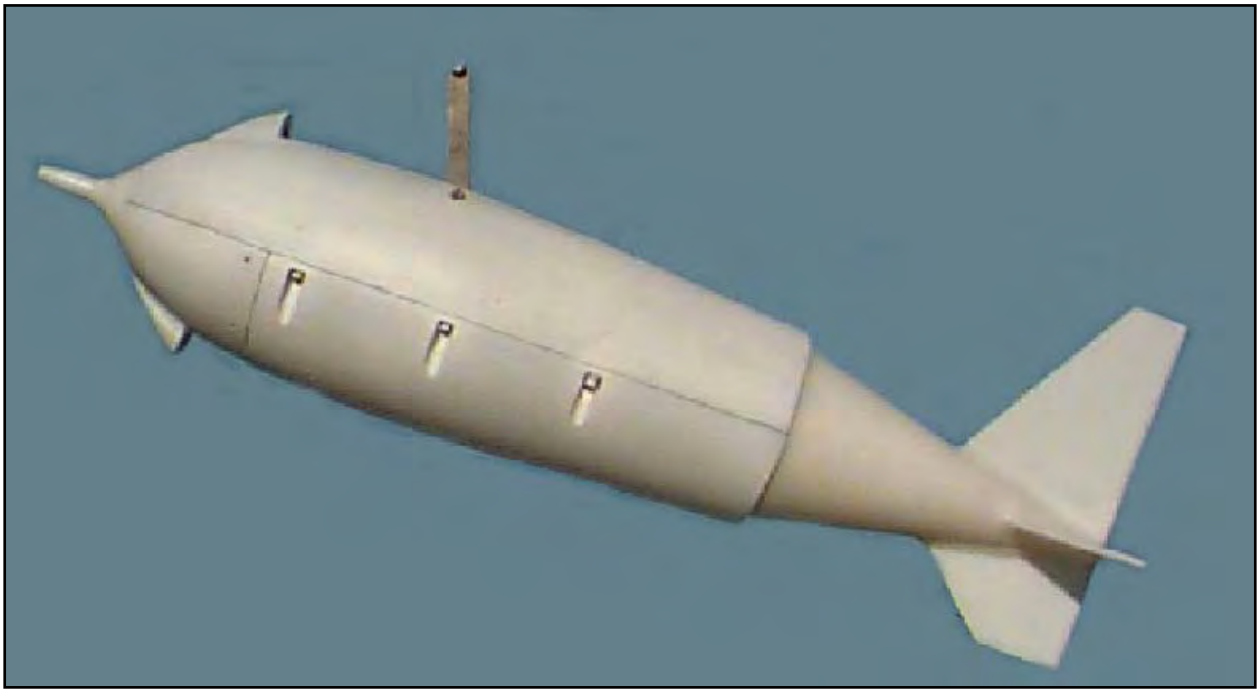


Figure 1 US D-96.

metal analyses. The nose insert is fabricated from plastic and is machined to fit in the slot in the nose section. The nozzle holder is fabricated from either plastic or tetrafluoroethylene (TFE), and mates with the nose insert. A nozzle threads into the front of the nozzle holder and the bag is attached to the rear of the nozzle holder with a hook-and-loop strap. Figure 2 shows the

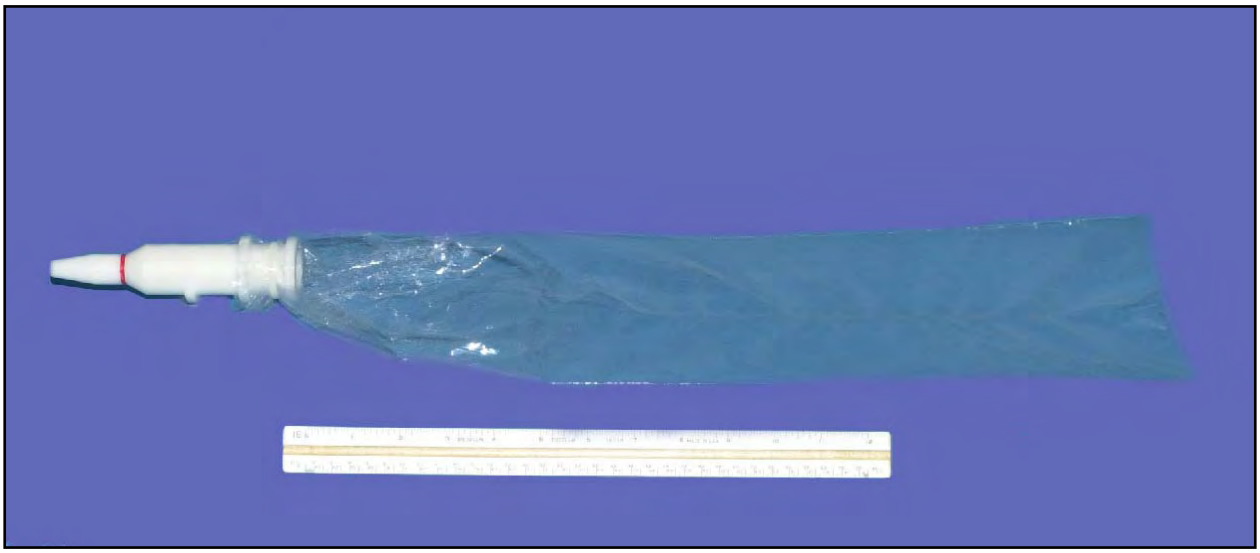


Figure 2 US D-96 nozzle holder with nozzle and bag attached.

nozzle/nozzle holder/bag assembly. The tail section is fabricated from high-density polyethylene plastic (HDPE). HDPE is neutrally buoyant in water, which allows the suspension point of the sampler to be located such that in air, the sampler maintains a tail-down attitude allowing it to orient itself facing into the streamflow. Once submerged, the sampler assumes a horizontal position.

Plastic and perfluoroalkoxy (PFA) bags are available for use with the US D-96. Plastic and TFE nozzles with internal diameters of 3/16, 1/4, and 5/16 in (0.48, 0.64, and 0.79 cm) are available for use with the US D-96. Plastic nozzles and bags are generally used for suspended-sediment sampling, and PFA bags and TFE nozzles for water-quality sampling. The US D-96 can sample to a depth of 110 ft (33.5 m) with a 3/16 in (0.48 cm) internal diameter nozzle, 60 ft (18.3 m) with a 1/4 in (0.64 cm) internal diameter nozzle, and 39 ft (11.9 m) with a 5/16 in (0.79 cm) internal diameter nozzle. The US D-96 sampler will collect flow-weighted samples in streams with velocities that range from 2 to 12.5 ft/sec (0.5 to 3.8 m/sec). An acceptable velocity range is one at which a representative flow-weighted sample is collected at a sampler inflow efficiency between 90 and 110 pct. Inflow efficiency is defined as the ratio of the sample velocity in the nozzle to the ambient stream velocity. An inflow efficiency of 100 pct is referred to as isokinetic.

US D-96-A1

The success and wide-spread use of the US D-96 revealed a need for a lighter version that would still collect a 3-liter sample. Changing the top section material from bronze to aluminum and the bottom section material from aluminum to bronze resulted in a sampler that weighs 80 lbs (36 kg). The sampler is designated the US D-96-A1. The US D-96-A1 is identical in appearance and uses the same parts as the US D-96. The maximum sampling depths are theoretically the same, but in practice the drift angle will determine the useful depth of operation. The recommended stream velocity range for the US D-96-A1 is 2 to 6 ft/sec (0.5 to 1.8 m/sec).

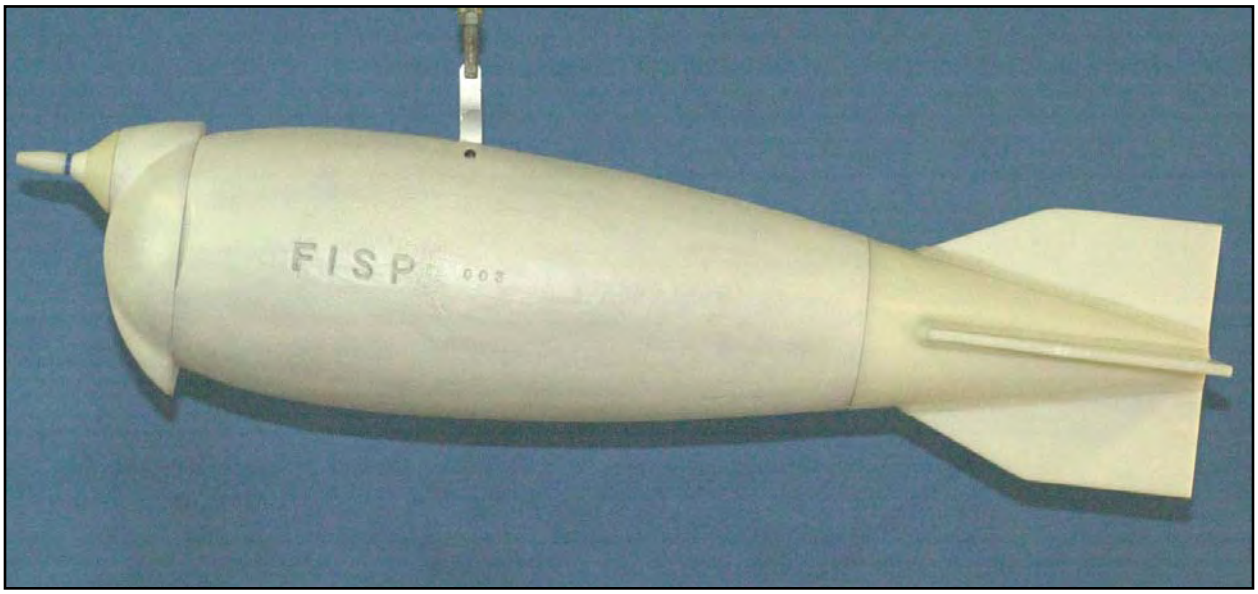


Figure 3 US D-99.

The US D-99 (figure 3) collapsible-bag sampler is capable of collecting up to a 6-liter sample. It is 41 in (104 cm) long, 9.5 in (24 cm) in diameter at its widest point and weighs 285 lbs (130 kg). It has a 5.5 in (14 cm) diameter hollow cavity inside the sampler body. It is fabricated from a bronze casting with a HDPE tail. All metal parts are plastic coated to minimize possible sample contamination. The sampler employs a hinged head with a plastic insert that holds the nozzle holder with nozzle in place. The bag is attached to the nozzle holder with a hook-and-loop strap. Figure 4 shows the sampler head open for insertion of the bag.

The US D-99 uses 3- or 6-liter plastic or PFA bags. Plastic and TFE nozzles with internal diameters of 3/16, 1/4, and 5/16 in (0.48, 0.64, and 0.79 cm) are available for use with the US D-99. With a 6-liter bag, the US D-99 can sample to a depth of 220 ft (67 m) with a 3/16 in (0.48 cm) internal diameter nozzle, 120 ft (37 m) with a 1/4 in (0.64 cm) internal diameter nozzle, and 78 ft (24 m) with a 5/16 in (0.79 cm) internal diameter nozzle. Maximum sampling depth with a 3-liter bag is half that of the 6-liter bag. The acceptable stream velocity range for the US D-99 is 2 to 15 ft/sec (0.5 to 4.6 m/sec). Based on data collected during inflow efficiency test, it is recommended that a 3-liter bag be used with all samples collected in the velocity range of 2 to 3.5 ft/sec (0.5 to 1 m/sec). For samples collected from 3.5 to 15 ft/sec (1 to 4.6 m/sec) the 6-liter bag should be used. The unsampled zone for the US D-99 is 9.5 in (24 cm).

US DH-2

The success of the large-volume collapsible-bag samplers generated the desire for a small, lightweight sampler that would collect a sample volume of 1 liter and sample to a depth of approximately 35 ft (10.7 m). Such a sampler fills the gap between lightweight rigid-container samplers that have a depth limitation of 15 ft (4.6 m), and the heavier collapsible-bag samplers already in use. Research and development resulted in a handline deployable sampler designated the US DH-2 which collects a 1-liter sample. The US DH-2 (Figure 5) is 19 in (48 cm) long

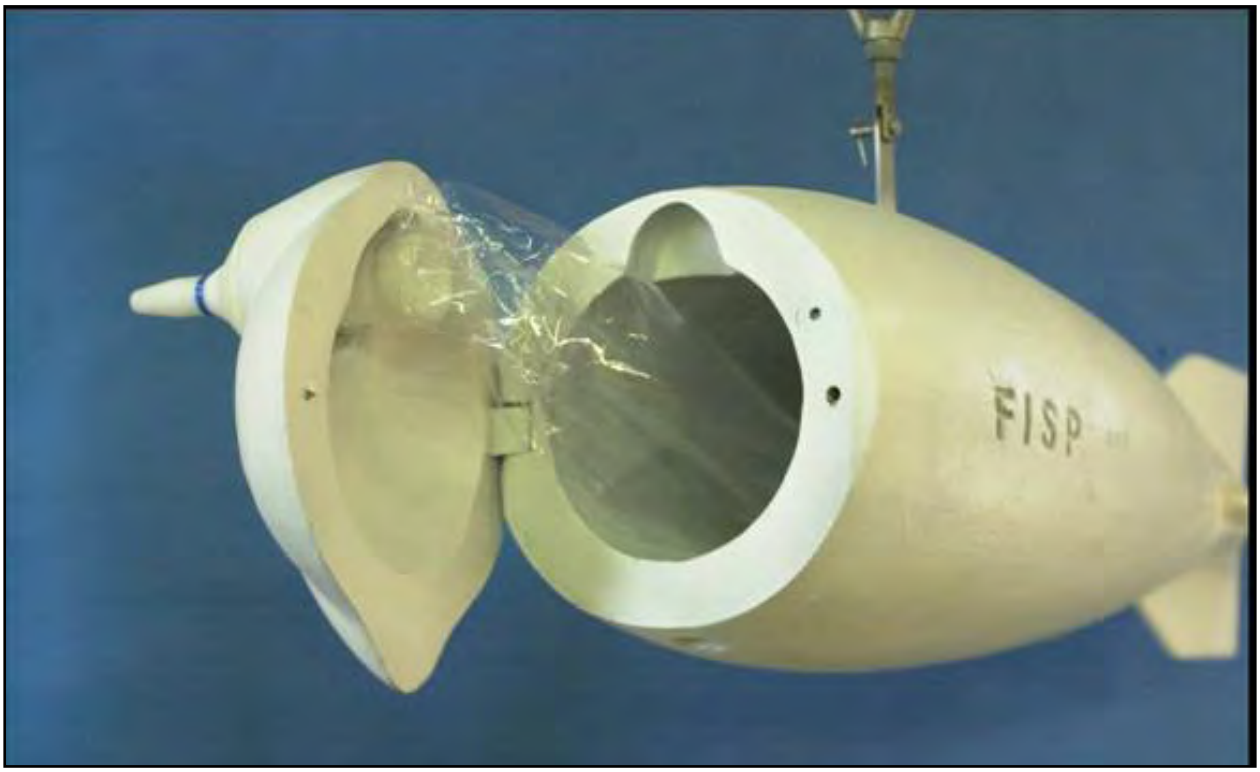


Figure 4 US D-99 with hinged head open.

with a 6 in (15.2 cm) diameter at its widest point, and weighs 30 lbs (13.6 kg). The sampler is composed of a cast bronze body with a 3.75 in (9.5 cm) diameter longitudinal cavity, a neutrally buoyant plastic tail section that has a hollow cavity, and a plastic nose. A nozzle holder fits into the back of the nose. The nozzle threads into the front of the nozzle holder, and the collapsible bag is attached to the rear of the nozzle holder with a hook-and-loop strap (figure 6). The bag slides into the cavity of the sampler and the nose snaps into the front of the sampler body with an O-ring friction fit (Figure 7). The cavity of the bronze body is lined with a clear plastic tube and the outside of the body is plastic coated to minimize possible sample contamination.

The US DH-2 uses plastic or PFA bags. Plastic and TFE nozzles with internal diameters of 3/16, 1/4, and 5/16 in (0.48, 0.64, and 0.79 cm) are available for use with the US DH-2. The US DH-2 can sample to a depth of 35 ft (10.7 m) with a 3/16 in (0.48 cm) internal diameter nozzle, 20 ft (6.1 m) with a 1/4 in (0.64 cm) internal diameter nozzle, and 13 ft (4 m) with a 5/16 in (0.79 cm) internal diameter nozzle. The acceptable stream velocity range for the US DH-2 is 2 to 6 ft/sec (0.5 to 1.8 m/sec). The unsampled zone for the US DH-2 is 3.5 in (9 cm).

Table 1 presents the characteristics and operating parameters of the samplers. Guidance for collecting suspended-sediment samples can be found in Edwards and Glysson (1999). Guidance for collecting water-quality samples can be found in Wilde and others (1999).

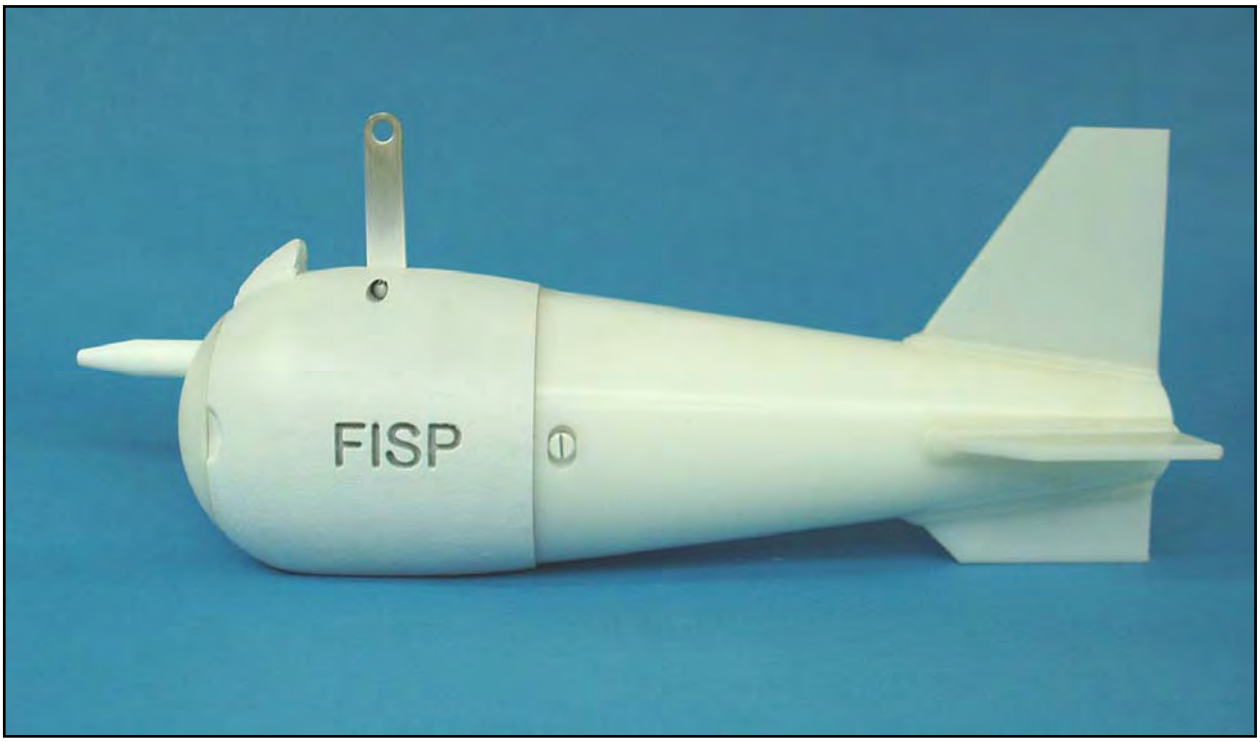


Figure 5 US DH-2.

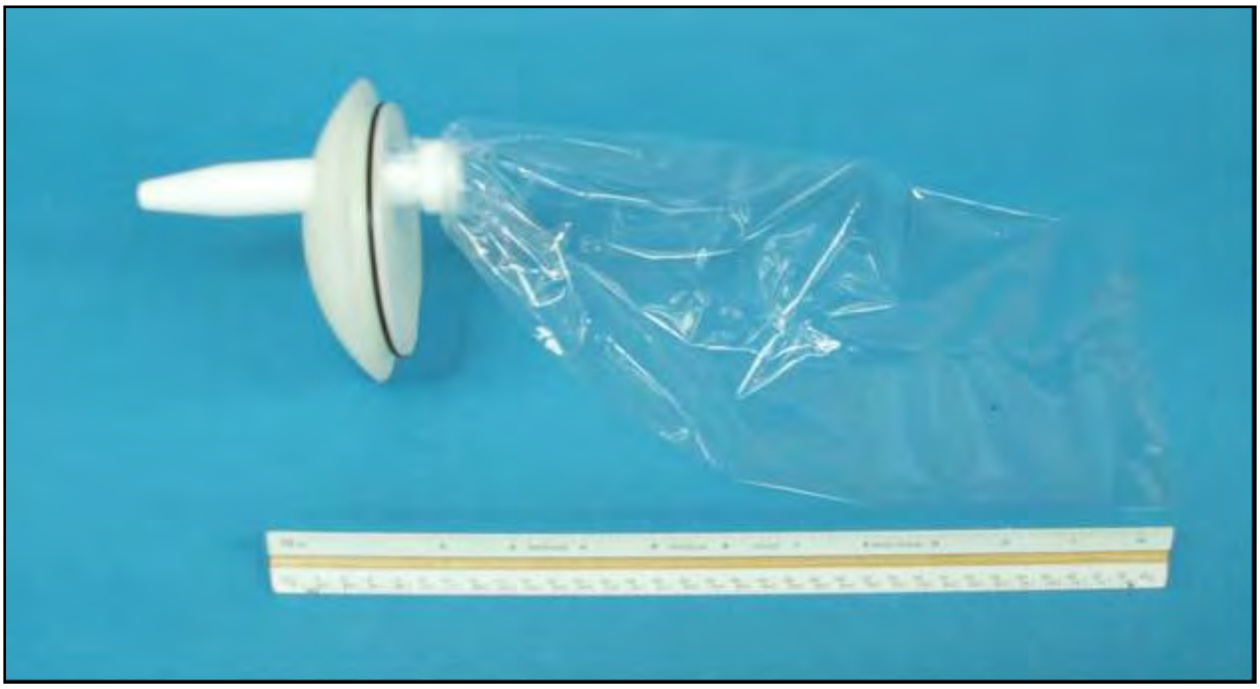


Figure 6 US DH-2 nose, nozzle, nozzle holder and bag assembly.



Figure 7 Insertion of nose with nozzle and bag into US DH-2.

Table 1 Characteristics and operating parameters of FISP bag samplers.

Sampler Designation	Nozzle ID in (cm)	Sample Size liters	Maximum Depth ft (m)	Minimum Velocity ft/sec (m/sec)	Maximum Velocity ft/sec (m/sec)	Weight lbs (kg)
US D-96	3/16 (0.48)	3	110 (33.5)	2 (0.5)	12.5 (3.8)	130 (59)
US D-96	1/4 (0.64)	3	60 (18.3)	2 (0.5)	12.5 (3.8)	130 (59)
US D-96	5/16 (0.79)	3	39 (11.9)	2 (0.5)	12.5 (3.8)	130 (59)
US D-96-A1	3/16 (0.48)	3	110 (33.5)	2 (0.5)	6 (1.8)	80 (36)
US D-96-A1	1/4 (0.64)	3	60 (18.3)	2 (0.5)	6 (1.8)	80 (36)
US D-96-A1	5/16 (0.79)	3	39 (11.9)	2 (0.5)	6 (1.8)	80 (36)
US D-99	3/16 (0.48)	6	220 (67)	2 (0.5)*	15 (4.6)	285 (130)
US D-99	1/4 (0.64)	6	120 (37)	2 (0.5)*	15 (4.6)	285 (130)
US D-99	5/16 (0.79)	6	78 (24)	2 (0.5)*	15 (4.6)	285 (130)
US DH-2	3/16 (0.48)	1	35 (10.7)	2 (0.5)	6 (1.8)	30 (13.6)
US DH-2	1/4 (0.64)	1	20 (6.1)	2 (0.5)	6 (1.8)	30 (13.6)
US DH-2	5/16 (0.79)	1	13 (4)	2 (0.5)	6 (1.8)	30 (13.6)

*A 3-liter bag is used for stream velocities of 2 to 3.5 ft/sec (0.5 to 1 m/sec).

SUMMARY

The FISP has developed a suite of collapsible-bag depth-integrating suspended-sediment/water-quality samplers that make it possible to collect flow-weighted samples from un-wadeable streams and rivers that are typically encountered. The samplers will collect suspended-sediment

and/or water-quality samples in stream velocities ranging from 2 to 15 ft/sec (0.5 to 4.7 m/sec) and depths up to 220 ft (67 m). The samplers have been approved for use by the FISP Technical Committee.

REFERENCES

Davis, Broderick E., and O'Neal, C. Wayne (2001a). Collapsible Bag Sediment/Water-Quality Flow-Weighted Sampler, U.S. Patent 6,216,549 B1

Davis, Broderick E., (2001b). FISP Report PP, The US D-96: An Isokinetic Suspended-Sediment/Water-Quality Collapsible-Bag Sampler, 37 p.

Davis, Broderick E., (2003). FISP Report PP-Addendum II, The US D-96: An Isokinetic Suspended-Sediment/Water-Quality Collapsible-Bag Sampler-- The US D-96-A1: A Lightweight Version of the US D-96, 5 p.

Davis, Broderick E., (2005). FISP Report SS, The US DH-2: A One-Liter Hand-Line Isokinetic Suspended-Sediment/Water-Quality Collapsible-Bag Sampler, 19 p.

Edwards, T.K., and Glysson, G.D., (1999). Field Methods for Measurement of Fluvial Sediment: U.S. Geological Survey Techniques of Water Resources Investigations, Book 3, Chapter C2, 89 p., available at http://water.usgs.gov/pubs/twri/twri3-c2

FISP, (1940). Field Practice and Equipment used in Sampling Suspended-Sediment, Interagency Report 1: Minneapolis, Minnesota, St. Anthony Falls Hydraulic Laboratory, pp.154-155

FISP, (1952). Report 6. The Design of Improved Types of Suspended Sediment Samplers, Minneapolis, Minnesota, St. Anthony Falls Hydraulic Laboratory, 103 p.

FISP, (2005). FISP Report RR, The US D-99 Depth-Integrating Collapsible-Bag Suspended-Sediment Sampler

Lane, S.L., Flanagan, Sarah, and Wilde, F.D., (2003). Selection of Equipment for Water Sampling (ver. 2.0): U.S. Geological Survey Techniques of Water-Resources Investigations, Book 9, chap. A2, accessed August 17, 2005 at http://pubs.water.usgs.gov/twri9A2/

Stevens, H.H. Jr., Lutz. G.A., and Hubbell, D.W., (1980). "Collapsible-bag suspended-sediment sampler," Journal of the Hydraulics Division, ASCE, vol. 106, No. HY4, pp. 611-616

Szalona, J.J., (1982). Development of a Bag-Type Suspended-Sediment Sampler, Interagency Report Y: Minneapolis, Minnesota, St. Anthony Falls Hydraulic Laboratory, 32 p.

Wilde, F.D., Radtke, D.B., Gibs, Jacob, and Iwatsubo, R.T., eds., (1999). Collection of water samples: U.S. Geological Survey Techniques of Water-Resources Investigations, Book 9, Chap. A4, accessed August 17, 2005 at http://pubs.water.usgs.gov/twri9A4/

A TIDALLY AVERAGED SEDIMENT-TRANSPORT MODEL OF SAN FRANCISCO BAY, CALIFORNIA

Megan A. Lionberger, Hydraulic Engineer, U.S. Geological Survey, Sacramento, CA, mlionber@usgs.gov; David H. Schoellhamer, Research Hydrologist, U.S. Geological Survey, Sacramento, CA, dschoell@usgs.gov; John Oram, Environmental Scientist, San Francisco Estuary Institute, Oakland, CA, joram@sfei.org ;Christine May, Senior Associate, Philip Williams and Associates, San Francisco, CA, c.may@pwa-ltd.com

Abstract: A tidally averaged sediment-transport model of San Francisco Bay was incorporated into a tidally averaged salinity box model previously developed and calibrated using salinity, a conservative tracer (Uncles and Peterson 1995). The Bay is represented in the model by 50 segments composed of 2 layers, one representing the channel (>5-meter depth) and the other the shallows (0 to 5-meter depth). Calculations are made using a daily time step and simulations can be made on the decadal time scale.

The new sediment-transport model includes an erosion-deposition algorithm, a bed sediment algorithm, and sediment boundary conditions. Erosion and deposition of bed sediments are calculated explicitly, and suspended sediment is transported by solving the advection-dispersion equation implicitly. The bed sediment model simulates the increase in bed strength with depth owing to consolidation of fine sediments that make up San Francisco Bay mud. The model is calibrated to either net bathymetric change or suspended-sediment concentration. Specified boundary conditions are the tributary fluxes of suspended sediment and suspended-sediment concentration in the Pacific Ocean.

The purpose of developing a tidally averaged sediment transport model is to create a tool to simulate sediment transport and bathymetric change in San Francisco Bay on a decadal time scale. The model has been applied to three resource management issues: 1) to estimate sediment outflow and change in storage on the bed as part of a new sediment budget for the Bay, 2) to evaluate restoration scenarios of the South San Francisco Bay salt ponds, and 3) to better understand the long-term fate of Polychlorinated Biphenyls (PCBs) in San Francisco Bay.

Introduction: Knowledge about long-term sediment movement within San Francisco Bay (Bay) is required to develop sediment budgets for the Bay and various subareas within the Bay (Schoellhamer et al, 2005). Reliable sediment budgets, in turn, are useful for evaluating the long-term fate of various contaminants associated with sediment particles (Leatherbarrow et al. 2005) and proposed wetland restoration projects (PWA in progress).

Accordingly, a model for simulating sediment transport in the Bay was developed. The sediment-transport model was incorporated as a subroutine in a tidally averaged, salinity model previously developed by Uncles and Peterson (1995). The Uncles-Peterson (UP) model uses residual-current, hydrodynamic calculations applied to adjacent segment layers, an approach that also is applicable to sediment transport. The UP model has been calibrated, widely distributed, and used to simulate the long-term effects of global warming on salinity (Knowles and Cayan 2004). This report describes the sediment-transport model and its application to three resource-management issues in the Bay.

Description of the Study Area: The Bay is made up of multiple broad, shallow bays connected by deep, narrow channels. The average depth in the Bay is less than 6 m, with a maximum depth of 100 m at the Golden Gate (Conomos 1979). The Bay receives 90 percent of its mean annual freshwater inflow from the Sacramento-San Joaquin Delta (Delta), which drains 40 percent of California including the agriculturally rich Central Valley. The remaining 10 percent of freshwater inflow comes from local tributaries and waste-water treatment plant effluent. North San Francisco Bay (North Bay) is a partially-mixed estuary with estuarine circulation maintained by the density difference between freshwater river inflow from the Delta and Pacific Ocean seawater (Conomos and Peterson 1977). South San Francisco Bay (South Bay) is typically well-mixed because of small freshwater inflows.

Sediment supply to the Bay varies seasonally with 80 percent of the average annual supply entering the Bay during the winter (Conomos and Peterson 1977). During high winter flows, sediment enters into the slower waters of Suisun and San Pablo Bays and begins to deposit. Coarse-grained and aggregated fine-grained sediments deposit, while the finest particles are exported out the Golden Gate. During the summer, sediment supply to the Bay is drastically reduced. Sediment undergoes a cycle of resuspension by tidal currents and wind waves, transport by tidal currents, and deposition at slack tide.

UP Salinity Model: The UP salinity model (Uncles and Peterson 1995) uses a box-model approach where each segment layer is well mixed. The Bay is represented by 50 width-averaged segments (boxes) (Figure 1) each composed of 2 layers (Figure 2). The upper layer of each segment represents the shallows (0 to 5-meter depth) and the lower layer represents the channel (> 5-meter depth). The two layers allow for density stratification. Tidally averaged residual currents advect water, and theoretical mixing rates constrain the dispersive exchanges of water between segments. A tidally averaged salinity field is solved implicitly using a one-day time step to enable the model to run over a decadal time scale in a relatively short period of time. The model has been calibrated to tidally averaged salinity (Uncles and Peterson 1995).

Input data used in the salinity mass-balance calculations include root-mean-square coastal sea level elevation at the Golden Gate to represent tides, near-bed coastal salinity, precipitation, evaporation, and freshwater outflow from the Delta. Delta outflow is calculated by DAYFLOW (California Department of Water Resources, 1986). Errors are thought to be relatively small (<10%) on a monthly time-scale, except for extreme low, or perhaps, high flows (Uncles and Peterson, 1996).

Salinity boundary conditions are set at the Pacific Ocean (box 46) and the Delta (box 45), and a zero flux boundary condition is applied at the most southern point of South Bay (box 1) to ensure conservation of mass. The lower-layer segment salinity at box 46 is set to coastal salinity, while the upper-layer segment salinity is variable since it is affected more by buoyant freshwater inputs from upstream sources. Delta outflow entering the Bay is relatively fresh water; therefore, salinity is set to zero in both layers of box 45. Additionally, local tributary flows also are relatively fresh and are set to zero salinity.

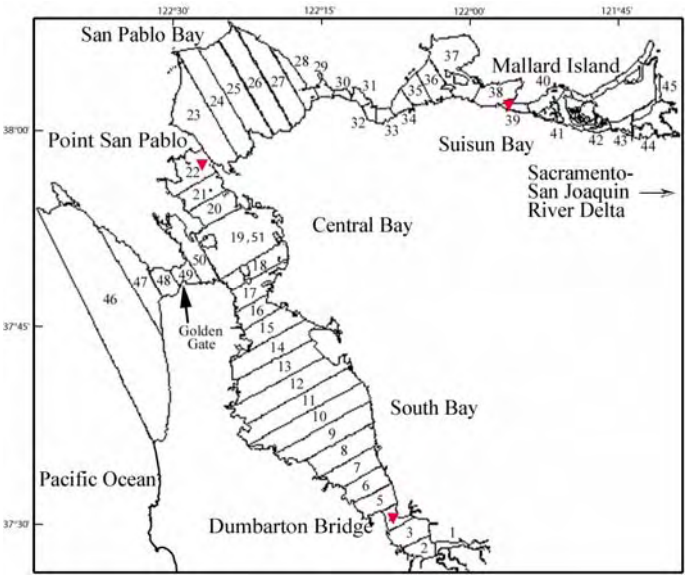


Figure 1 UP model segmentation of the San Francisco Bay (Uncles and Peterson 1995).

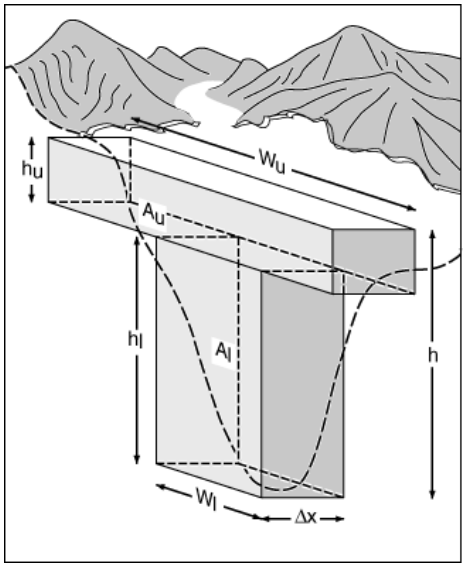


Figure 2 2-layer box composition of the UP box segments (Uncles and Peterson 1995).

Sediment Transport: The sediment-transport model was incorporated as a subroutine into the existing UP salinity model to simulate sediment transport in the Bay on a decadal time scale (1940 – 2004). A daily time step is used to compute daily-average suspended-sediment concentration (SSC) and net sedimentation. Mixing and advection rates calculated by the salinity model are used to simulate suspended sediment exchange between models segments. Exchange between bed sediments and suspended sediments are calculated explicitly with the aid of a simplified bed model.

Additional input data required for the sediment model include daily estimates of average wind velocity, suspended-sediment flux from the Delta, and local tributary sediment loads. Wind-velocity and tide data are used to calculate tidally averaged bed shear ($\overline{\tau_b}$),

$$\overline{\tau_b} = \frac{\rho g \overline{u}^2}{C_z^2} + c_w \frac{1}{2} \rho f \frac{\overline{u_w^2}}{\cosh kh} \qquad (1)$$

Where ρ = density (kg/m3); g = gravity (m/s2); $\overline{u}$ = tidally averaged current speed (m/s); C_z = Chezy coefficient, ($m^{1/2}/s$); c_w = calibration coefficient, f = friction factor, 0.1; $\overline{u_w}$ = daily average wind velocity (m/s); k = wave number, (m^{-1}); and h = average water depth (m). Daily suspended-sediment flux from the Delta is estimated for water years 1995 – 2003 by McKee et al. (2002). For all other simulation periods, a rating curve was developed (not shown) relating SSC at Freeport, Sacramento (station 11447500) and Delta Outflow (DAYFLOW) to suspended-sediment flux from the Delta. Tributary sediment load is simulated for major tributaries in the Bay including Napa River, Walnut Creek, Alameda Creek, San Francisquito Creek, and Guadalupe River (Porterfield 1980).

Sediment boundary conditions are specified at the Delta (box 39) and at the Pacific Ocean (box 46). The suspended-sediment flux at Mallard Island represents the Delta boundary condition and SSC in the lower layer of box 46 is held constant at 5.7 mg/L, the long-term mean concentration from monthly water quality sampling by the USGS (http://sfbay.wr.usgs.gov/access/wqdata). The upper layer of box 46 is left free to vary, as it is affected more by buoyant freshwater inputs from upstream sources. Mass conservation in segment 1, the Southern end of South Bay, is maintained by a no-flux boundary condition.

The daily mass balance sediment algorithm begins by adding tributary sediment load to specific boxes throughout the UP model grid. The tributary loads are mixed within the estuary by implicitly solving the advection-dispersion transport equation using mixing parameters calculated by the salinity model. Mass exchange with the sediment bed (C_n) is simulated by explicit calculation at the end of each time step (n) as

$$C_n = C_o + \left(Fc_E R_E - c_D R_D\right)\frac{\Delta t}{H} \tag{2}$$

where C_o = SSC at the beginning of the time step (mg/L); F = erodibility factor described below; c_E = calibration coefficient; R_E = rate of erosion (g/m^2/s); c_D = calibration coefficient; R_D = rate of deposition (g/m^2/s); Δt = time step (s); and H = total water depth (m).

The rate of erosion is affected by shear strength properties of the sediment bed, which vary with depth and time (Krone 1999). A simplified method was developed to simulate the effect of consolidation of the sediment bed by reducing the erodibility of the bed as a function of depth of sediment and time since deposition. A summary of previous sediment bed studies (Hayter 1984), showed that sediments consolidated over time have properties that vary in the top 4 cm of the bed, but that are essentially uniform below this depth with a critical shear stress roughly four times the critical shear stress at the bed surface. To account for freshly deposited sediments that are still easily eroded, a representation of bed profile incorporating three layers was developed. The top layer is composed of freshly deposited, easily erodible sediment that was deposited to the bed during the present or the previous time steps. The middle layer represents the partially consolidated sediments that become harder to erode with increasing depth. The lowest layer represents consolidated sediments where the erodibility is constant and about four times less than at the bed surface. The erosion rate calculated by the model is multiplied by the erodibility factor, F, whose value depends on the sediment layer and the elevation of the sediment bed surface relative to a vertical datum. The erodability factor, F, varies from 1.0 to 0.25 and is given as

$$F = \begin{cases} 1.0 & z > 0 \\ 1.0e^{34.7z} & 0 \geq z > -0.04 \text{ m} \\ 0.25 & -0.04 \text{ m} \geq z \geq -\infty \end{cases} \tag{3}$$

where z is the sediment bed surface elevation referenced to the bed datum. Sediment remaining in the top layer after one full time step is incorporated into either the middle or lower layers depending on the current bed elevation below the datum and assumes the F value at that depth. If

deposition raises the bed surface elevation above the datum, the datum is reset to the current bed surface elevation.

The model is calibrated by adjusting c_w, c_E, and c_D. The model can be calibrated to either net bathymetric change or SSC, but results show the model cannot simulate both simultaneously.

The sediment transport model was calibrated to SSC by adjusting model coefficients until modeled SSC most closely matched simulated daily-averaged continuously-measured SSC during water year 1999 at two locations in the bay, Point San Pablo in North Bay and Dumbarton Bridge in South Bay (Buchanan and Ruhl 2001). Water year 1999 is classified as having an average annual Sacramento-San Joaquin River basin outflow. Separate sets of calibration parameters were determined for North Bay and for South Bay. Results of the calibration at Dumbarton Bridge (figure 3) show that a tidally averaged sediment transport model can be used to predict the general trends in SSC associated with tidal fluctuations, residual velocity, and wind stress.

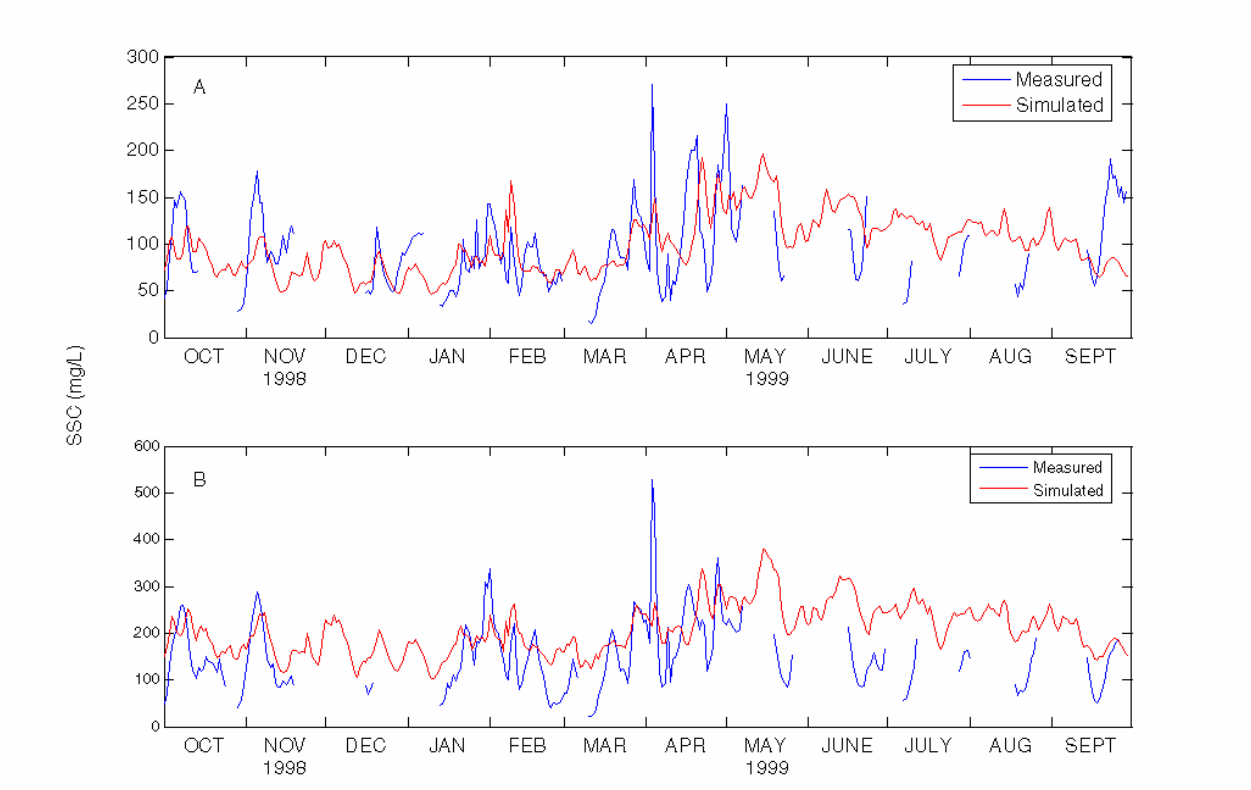


Figure 3 Simulated SSC for water year 1999 at Dumbarton Bridge (A) at mid depth (22 ft below MLLW) and (B) at near bottom (41 ft below MLLW).

Estimates of net bathymetric change are available for Suisun Bay, San Pablo Bay, and South Bay (Jaffe et al. 1998, Cappiella et al. 1999, Foxgrover et al. 2004) for periods ranging from 28 to 49 years. No survey data exists for Central Bay. Regional sediment density data from sediment cores were used to convert net mass change to net volumetric change in order to compare estimated bathymetric change to simulated net sedimentation from the model calibrated to SSC.

Results of the comparisons (Table 1) indicate that the model calibrated to SSC is not able to hindcast bathymetry change accurately. This is most likely the result of small errors compounding over longer simulation periods.

Table 1 Comparison of simulated net sedimentation to estimated bathymetric change for the model calibrated to SSC and for the model calibrated to net sedimentation.

Embayment and Survey Period	UP boxes	USGS Bathymetric Change Estimates (million cubic meters)	UP Net Sedimentation calibrated to SSC (million cubic meters)	UP Net Sedimentation calibrated to net sedimentation (million cubic meters)
Suisun Bay (1942-1990)	29-39	-35	-12	-35
San Pablo Bay (1951-1983)	23-28	-11	-131	-11
South Bay (1956-1983)	1-14	-47	-25	-47
Central Bay (1956-1983)	15-22, 46-50	NA	-185	0

The model also was calibrated to net sedimentation. Model calibration coefficients were adjusted within various bays until the simulated net sedimentation matched estimated bathymetric change in Suisun Bay, San Pablo Bay, and South Bay (Table 1). Because no survey data exists for Central Bay, an assumption of no net change was used. Determining the effectiveness of the model calibrated to long-term net sedimentation requires a validation data set for comparison. Validation data are currently unavailable pending new bathymetric surveys and analyses to determine recent net bathymetric change.

Other Model Applications: Because the model can simulate long periods, it has become a valuable tool for evaluating sediment transport in the San Francisco Bay system. Applications include 1) development of a sediment budget, 2) a landscape-scale analysis of potential sediment change in South Bay resulting from the planned restoration of salt ponds to tidal action and 3) estimation of the time period required for recovery of water quality impairment by polychlorinated biphenyls (PCBs) in bottom sediment.

The UP sediment model was used to estimate the Bay sediment budget for the period of 1995 – 2002 when change in storage of the system and sediment outflow through the Golden Gate is unknown (Schoellhamer et al. 2005). The model was first calibrated for the period 1955 – 1990, when the only unknown is sediment outflow, and then applied to the 1995 – 2002 period, assuming the same calibration coefficients were applicable, to obtain a sediment budget that estimates the two unknown terms.

The South Bay Salt Pond Restoration Project plans to restore over 15,000 acres of former salt ponds, some of which are deeply subsided, to a mosaic of tidal wetland and managed environments to provide habitat for a host of avian, fish, and other endangered and indigenous species. However, a restoration project this large has the potential to significantly alter existing habitats. Therefore, prior to performing restoration actions, it is essential to develop an understanding of the potential long-term system response to restoration actions, such as how the restoration may affect South Bay sediment dynamics, morphology, and ultimately the extent of tidal marsh, mudflat and shallow-water habitats within South Bay and the restored ponds. The use of a sediment budget tool is desirable because it accounts for conservation of mass – sediment that is captured and deposited in the restored ponds is no longer available for deposition and/or redistribution within South Bay (Philip Williams and Associates, PWA, in progress).

The UP Model was chosen as the sediment budget tool for the project, and the model was calibrated to past geomorphic change as determined by Foxgrover et al. (2004). In order to assess the restoration alternatives, the ponds to be restored were divided into clusters associated with each UP model box, and the total area and mean depth of each pond cluster was added to the model to represent a new sediment sink. The model was run forward 50 years and the model outputs were evaluated using a suite of empirical and analytic tools in order to determine the potential year-50 morphology and habitat distribution of the South Bay (PWA in progress).

An ongoing effort jointly funded by the Clean Estuary Partnership and the Regional Monitoring Program further builds on the salinity and sediment transport models to simulate long-term trends in total PCB concentrations in the water column and bedded sediment. A primary objective of this effort is to estimate timescales of recovery with respect to water quality impairment by PCBs as part of a Total Maximum Daily Load allocation.

The PCB model accounts for external inputs of PCBs to the Bay from the Central Valley via the Sacramento-San Joaquin River Delta, local tributaries, atmospheric deposition (wet and dry), and municipal wastewater effluent in a spatially explicit manor (Leatherbarrow et al. 2005). The model includes a post-depositional vertical mixing model that explicitly accounts for storage of PCBs in bed sediment. Along with physical processes that determine PCB transport, this study incorporates the influence of chemical-specific traits of PCBs that govern partitioning between particulate and dissolved fractions, degradation in water and sediment, and volatilization into the atmosphere. The primary application of this model is to develop scenarios of decadal trends in PCB contamination in major segments of the Bay for various reductions in PCB loading.

Conclusions: A tidally averaged sediment transport model was developed that uses the hydrodynamics of the UP model calibrated to salinity, a conservative tracer. The model uses a daily time step and is able to perform simulations on the decadal time scale. The UP sediment model can be calibrated to either SSC or net bathymetric change, but not to both simultaneously, because small errors in the model compound over time. The model is currently being used to simulate changes in sediment dynamics and morphology as a result of the South Bay salt pond restoration project and to forecast decadal trends in PCB contamination.

REFERENCES

Buchanan, P.A., and Ruhl, C.A., 2001, Summary of suspended-sediment concentration data, San Francisco Bay, California, water year 1999, US Geological Survey, Open-File Report 01-0100, 56 p.

California Department of Water Resources (1986). DAYFLOW program documentation and DAYFLOW summary user's guide.

Cappiella, K., Malzone, C., Smith, R.E, and Jaffe, B.E. (1999). Sedimentation and bathymetry changes in Suisun Bay; 1867 – 1990, US Geological Survey, Open-File Report 99-0563.

Conomos, T.J. (1979). San Francisco Bay: The Urbanized Estuary: American Association for the Advancement of Science, Pacific Division, San Francisco.

Conomos, T.J., and Peterson, D.H. (1977). Suspended-Particle Transport and Circulation in San Francisco Bay: An Overview: in Estuarine Processes, Volume II, Academic Press, Inc., New York, NY.

Foxgrover, A.C., Higgins, S.A., Ingraca, M.K., Jaffe., B.E., and Smith, R.E. (2004). Deposition, erosion, and bathymetric change in South San Francisco Bay: 1858-1983, US Geologic Survey, Open-File Report 2004-1192.

Jaffe, B.E., Smith, R.E, and Zink Torresan, L. (1998). Sedimentation and bathymetric change in San Pablo Bay 1856 – 1983, US Geological Survey, Open-File Report 98-0759.

Hayter, E.J. (1984). Estuarial sediment bed model, in A.J. Mehta, ed., Lecture Notes on Coastal and Estuarine Studies, 14, Estuarine Cohesive Sediment Dynamics, pp 326 – 359.

Knowles, N., and Cayan D. (2004). "Elevational Dependence of Projected Hydrologic Changes in the San Francisco Estuary and Watershed," Climatic Change, 62, pp 319-336.

Krone, R.B. (1999) "Effects of Bed Structure on Erosion of Cohesive Sediments," Journal of Hydraulic Engineering, ASCE, 125(12), pp 1297 – 1301.

Leatherbarrow, J.E., Oram, J.J., and Davis, J.A. (2005). Draft Report: A Model of Long-Term PCB Fate and Transport in San Francisco Bay, CA., SFEI Contribution #388, San Francisco Estuary Institute, Oakland, CA.

McKee, L., Ganju, N.K., Schoellhamer, D.H., Davis, J.A., Yee, D., Leatherbarrow, J.E., and Hoenicke, R. (2002). "Estimates of suspended sediment flux entering San Francisco Bay from the Sacramento and San Joaquin Delta," SFEI Contribution 65, San Francisco Estuary Institute.

Porterfield, G. (1980). Sediment transport of streams tributary to San Francisco, San Pablo, and Suisun Bays, California, 1909 – 1966, US Geological Survey, Water-Resources Investigations Report 80-64.

Schoellhamer, D.H., Lionberger, M.A., Jaffe, B.E., Ganju, N.K., Wright, S.A., and Shellenbarger, G.G. (2005). "Bay sediment budgets: sediment accounting 101," Pulse of the Estuary 2005, San Francisco Estuary Institute, 14, pp 58 – 63.

Uncles, R.J. and Peterson, D.H. (1995). "A computer model of long-term salinity in San Francisco Bay: sensitivity to mixing and inflows," Environment International, 21(5), pp 647 – 656.

Uncles, R.J. and Peterson D.H. (1996). "The long-term salinity field in San Francisco Bay, Continental Shelf Research," 16(15), pp 2005 – 2039.

A UNIFIED APPROACH FOR RIVER MORPHOLOGY, SEDIMENT TRANSPORT, AND EROSION STUDIES

Chih Ted Yang, Borland Professor of Water Resources, Colorado State University, Fort Collins, CO 80523-1372, ctyang@engr.colostate.edu

Abstract: Vectorial and variational approaches are the two basic approaches in mechanics. A systematic review of these two approaches concludes that the theory of minimum energy dissipation rate and its simplified versions of minimum stream power and minimum unit stream power can be applied to solve a wide range of problems which are difficult or impossible to be solved from vectorial approach alone. The minimization theories can be derived from thermodynamic laws and theories. They can also be derived from mathematical argument.

The unit stream power theory for sediment transport can be derived from well-established and adopted theories in fluid mechanics. Yang's unit stream power equations based on this theory are easy to apply and are generally more accurate than other equations. These unit stream power equations can be applied for the determination sediment transport in the clay, silt, sand, and gravel size range. The unit stream power theory is applicable to laminar as well as to turbulent flow conditions. The unit stream power equations can be applied to sub-critical, critical, and supercritical flows with or without the influence of wash-load.

Conjunctive use of the theory of minimum energy dissipation rate, or its simplified theories, and unit stream power equations can provide us the theoretical basis of a unified approach for river morphology, sediment transport, and erosion studies of a watershed and its river systems.

Bureau of Reclamation's Generalized Sediment Transport computer models for Alluvial River Simulation (GSTARS 2.0/2.1/3) are based on the unified approach and stream tube concept. These models can simulate and predict semi-three-dimensional erosion, transport, and deposition processes in rivers and reservoirs under quasi-steady flow conditions by solving one-dimensional equations along stream tubes. These models have been successfully applied to solve a wide range of river and reservoir sedimentation problems. The GSTAR-1D model was developed for unsteady flows with cohesive and non-cohesive sediment transport.

A review of Geographic Information System (GIS) and remote sensing technology concludes that they are useful and powerful tools to store and analyze geologic, geographic, land use, and ground cover information. These technologies can be coupled with erosion and sediment transport computer models for solving water resources, environmental, and engineering problems.

The Generalized Sediment Transport model for Alluvial Rivers and Watersheds (GSTAR-W) being developed is base on the unified approach using GSTARS2.0/2.1/3/1-D as building blocks and GIS and remote sensing as tools for the determination of total maximum daily load of sediment in a watershed and its river and reservoir systems. GSTAR-W will be a physically based, process oriented, temporal and spatially distributed model upon its completion.

REGEM: THE REVISED EPHEMERAL GULLY EROSION MODEL

Lee Gordon, Department of Geography, University at Buffalo, New York, lmgordon@buffalo.edu; Sean Bennett, Department of Geography, University at Buffalo, New York, seanb@buffalo.edu; Ron Bingner, USDA-ARS, National Sedimentation Laboratory, Oxford, Mississippi, RBingner@msa-oxford.ars.usda.gov; Fred Theurer, USDA-NRCS, National Water and Climate Center, Gaithersburg, Maryland, Fred_Theurer@verizon.net; Carlos Alonso, USDA-ARS, National Sedimentation Laboratory, Oxford, Mississippi, calonso@msa-oxford.ars.usda.gov

Abstract: Ephemeral gullies serve as effective links transferring sediment and associated agrichemicals from upland areas to stream channels. Current erosion prediction technologies often require the exact topographic position (the length) of an ephemeral gully *a priori*, which greatly limits the utility of such models. The Revised Ephemeral Gully Erosion Model has been developed as a rational approach to predict ephemeral gully erosion and development. REGEM incorporates analytic formulations for plunge pool erosion and headcut retreat within single or multiple storm events in unsteady, spatially-varied flow at the sub-cell scale. The model employs sediment continuity equations for five soil particle-size classes to predict gully evolution and transport capacity. Event-based simulations demonstrate the model's utility for predicting the initial development of an ephemeral gully channel, while continuous simulations allow the channel to evolve over multiple runoff events accounting for seasonal variations in management operations and soil conditions.

REGEM currently functions as a stand alone tool, but it has now been integrated as an additional module within the Annualized Agricultural Non-Point Source (AnnAGNPS) suite of watershed modeling tools developed by the USDA. REGEM allows a more accurate and physically based examination of sediment sources in agricultural catchments, providing practitioners the tools necessary to effectively manage the Nation's water and soil resources.

INTRODUCTION

Over the past several decades the USDA-NRCS has focused its efforts on enhancing and extending the utility of the Universal Soil Loss Equation (USLE) (*Wischmeier and Smith*, 1978) through the development of the revised USLE (RUSLE) (*Renard et al*, 1997). RUSLE technology has been developed using standard runoff plots on which rill and interrill erosion were intensively studied on planar surfaces of uniform slope. When opposing slopes converge, however, overland and subsurface flow is concentrated, resulting in a different hydrologic regime. The channels formed by this concentration of runoff on agricultural lands are known as ephemeral gullies, recognized as a distinct erosion phenomena (*Foster*, 1986) that have been shown to account for more than two-thirds of the total erosion occurring on farmland in a range of environments (*USDA-NRCS*, 1996; *Bennett et al.*, 2000).

The recognized importance of ephemeral gully erosion has prompted the USDA-NRCS to stress its inclusion in future assessment studies because RUSLE-based technologies do not account for such erosion phenomena (*USDA-NRCS*, 1996). The few erosion models that incorporate routines to account for ephemeral gully erosion (EGEM, CREAMS, WEPP) use the same theoretical framework of changing channel dimensions developed by *Foster and Lane*, 1983. While this theory was considered a significant step with respect to the physically-based modeling of ephemeral gully erosion, its applicability is substantially limited by the extensive data requirements, namely the concentrated flow length. That is, the length of an ephemeral gully must be known before the model can be applied. Moreover, these models are limited to the processes of incision and widening only, neglecting the lengthwise growth of an ephemeral gully system within single or over multiple runoff events.

Additional limitations of ephemeral gully erosion routines in EGEM, CREAMS, and WEPP involve the use of the diameter and specific gravity of a representative particle to calculate sediment transport capacity. There are two significant limitations to this approach: (1) for any material to be detached, the amount of sediment carried by the water must be below transport capacity, thus deposition cannot be simulated; and (2) because soil particle diameter and specific gravity are simplified to some representative or dominant value, the soil material delivered to the mouth of the ephemeral gully contains the same ratios of clay, silt, sand and aggregates as the soil *in situ.*

The Revised Ephemeral Gully Erosion Model (REGEM) has been developed with two basic objectives: (1) to overcome some of the limitations of current technology with regard to ephemeral gully erosion; and (2) while functioning as a stand-alone tool, to be incorporated as an individual module within the Annualized Agricultural Non-Point Source Model (*Bingner* and *Theurer*, 2001), giving it the ability to explicitly account for ephemeral gullies in its erosion routines at the sub-cell scale (i.e. field-scale).

MODEL DEVELOPMENT

Four fundamental improvements have been integrated within REGEM to overcome major limitations of current technology. They include: (1) runoff or storm events as unsteady, spatially-varied flows; (2) addressing the upstream migration of a headcut, thereby removing the ephemeral gully length as an input parameter; (3) determining channel width from discharge, allowing channel dimensions to be explicitly predicted at any point in time and space; and (4) routing five distinct particle-class sized (clay, silt, sand, and small and large aggregates) through the gully and the downstream sorting of these sediments.

REGEM has been designed specifically to comply with the computational framework of the Annualized Agricultural Non-Point Source (AnnAGNPS) suite of watershed modeling tools. An AnnAGNPS cell is considered homogeneous in terms of topography, and soil and management conditions. REGEM operates at the sub-cell scale. That is, parameters dealing with topography, soil, and management are singular and static for an modeled ephemeral gully.

Input Requirements: Table 1 lists the input requirements to REGEM, and many of these are available within AnnAGNPS and not unique to the ephemeral gully module. Procedures using Geographic Information Systems to extract data specific to REGEM (drainage area, thalweg slope) are currently being developed to extend the utility of ephemeral gully modeling within AnnAGNPS.

Table 1 Input requirements to REGEM

Notation	Description	Units
Q_p	event peak discharge	m^3 sec^{-1}
V_r	event runoff volume	m^3
S	average thalweg slope	m m^{-1}
n	Manning's roughness	---
D_t	tillage depth	m
A_d	drainage area to gully mouth	ha
R_{clay}	clay ratio in surface soil	---
R_{silt}	silt ratio in surface soil	---
R_{sand}	sand ratio in surface soil	---
R_{sagg}	small aggregate ratio in surface soil	---
R_{lagg}	large aggregate ratio in surface soil	---
B_d	soil bulk density	Mg m^{-3}
τ_c	critical shear stress of surface soil*	N m^{-2}
k_d	headcut erodibility coefficient*	cm^3 N^{-1} sec^{-1}
C_{soil}	integer value classifying current soil condition	1 = no-till, 2 = freshly cultivated 3 = established crop

*calculated internally if not user-defined

Hydrology: The drainage area to the mouth of the ephemeral gully, the event peak discharge, and the runoff volume are required as input parameters used to calculate the time to base of the event hydrograph. A triangular hydrograph is constructed an even number of user-defined timesteps. A specific discharge then can be assigned to represent hydraulic conditions during each of the timesteps. Model hydrology will eventually be passed to REGEM by AnnAGNPS, however for the sensitivity analyses presented below, procedures outlined in the standard TR-55 approach, (*USDA-NRCS*, 1986) have been used.

Erodibility: Defining the erodibility or critical shear stress for a particular soil at a discrete point in time and space is not a simple assessment. If the user cannot specify these erodibility parameters, REGEM calculates them internally. As in the original EGEM, (*Woodward*, 1999) the critical shear stress of a freshly cultivated soil is a function of the soil's clay content. This value is then adjusted for changes in tillage condition or crop growth using one of the three tillage conditions (C_{soil}) in Table 1. Once the critical shear stress has been determined, an erodibility coefficient is calculated based on the relationship developed by *Hanson* and *Simon* [2001]. Procedures are currently being developed to more accurately vary soil erodibility over time and space using certain RUSLE subfactors within AnnAGNPS and will be reported at a later date.

Erosion Components: Ephemeral gully erosion is modeled as a combination of three distinct processes: scour to tillage depth, headcut migration, and sediment transport. Bank processes associated with channel widening are not explicitly addressed. Instead, an empirical relationship between dominant discharge and ephemeral gully width developed by *Nachtergaele et al.* [2002] is used to predict channel width at any point in time and space.

Scour to Tillage Depth: A portion of the ephemeral gully channel at the most downstream location (scour hole) with an undetermined length, but with a defined width and depth is evacuated until the tillage depth (a markedly less-erodible layer) is reached. This portion of the model contains algorithms developed for the original EGEM. Excess stress relationships are used to calculate a detachment capacity, which when multiplied by the timestep duration gives a depth of scour for each timestep. All soil material detached in the scour hole is assumed to be evacuated. That is, transport capacity is not addressed during downward scour. If the depth of the scour hole does not reach the tillage depth during a runoff event, erosion is assumed to be zero.

Headcut Migration: The main process resulting in the development and evolution of ephemeral gullies simulated by REGEM is that of headcut migration. Headcuts are step changes in bed surface elevation where intense, localized erosion takes place (*Bennett et al.* 2000a). While other models of ephemeral gully erosion (e.g., EGEM) require the length of an ephemeral gully as an input parameter, REGEM seeks to more accurately describe the lengthwise growth of an ephemeral gully channel over time. *Foster* [1986] describes the detachment and transport of soil material within an ephemeral gully, that is, the incision of the channel. Recently, *Bennett et al.* [2000] and *Casali et al.* [2003] have identified the formation and migration of headcuts as one of the main processes involved in the formation of an ephemeral gully.

Once the scour hole (modeled as a short section of the gully at its downstream end) is evacuated, a headcut is assumed to have formed at the step between the original soil level and the tillage depth. An overfall now exists at a brinkpoint located where the change in elevation occurs. The algorithms based on realistic, physical approximations governing mass, momentum, and energy transfer developed by *Alonso et al*. [2002] are employed during each timestep to determine a rate of headcut migration, and thus a certain length to which the ephemeral gully has grown. As the gully grows longer, the drainage area contributing runoff to the headcut is reduced. A relationship between channel length and drainage area presented by *Leopold et al.* [1964] is used to define the maximum potential ephemeral gully length for a given drainage area and to partition the spatially varied discharge, which, when used to predict channel width causes the ephemeral gully to be widest at its mouth and most narrow at the location of the headcut. As discharge and headcut migration rate are constant within a given timestep, a single three-dimensional rectangular section of ephemeral gully channel is formed during each timestep having a width proportional to the discharge at the time the section is formed, a length equal to the distance of headcut migration, and a depth equal to the tillage depth.

Sediment Transport: The adjustments in flow discharge over time (the runoff event) and space (the length of the ephemeral gully) are held in a two dimensional array built with each successive runoff event. Water associated with a specific event must be routed through the entire length of the ephemeral gully. An examination of sediment transport capacity along the entire gully is necessary for two reasons: (1) often there will be deposition in downstream gully sections that were formed during a previous event (e.g., *Bennett et al.*, 2000); and (2) previously formed gully sections are allowed to adjust laterally in case a larger channel-forming discharge occurs and widens the downstream sections of the gully (e.g., *Nachtergaele et al*., 2002). The algorithms used by REGEM to calculate sediment transport capacity for each of the five particle-class sizes have been adapted from those used in other modules of the AnnAGNPS model and detailed in *Bingner et al.* [2002].

There are three possible sources of sediment available for transport within a gully section during a timestep: (1) incoming sediment from upstream sections; (2) internal sediment due to headcut migration and/or channel widening within the gully section; and (3) previously deposited sediment that resides on the bed within the gully section. These three possible sources are combined to determine the amount of each particle-class size available for transport in each gully section during a timestep. If this amount is less than the sediment transport capacity for that timestep, all available sediment will be moved to the next downstream section, where it is again compared to that section's transport capacity and so on until the gully mouth is reached. Should transport capacity be exceeded for a particular particle-class size, the excess amount is deposited in a layer on the channel bed, possibly re-entrained during subsequent timesteps. If in a given timestep, the available sediment is less than transport capacity, previously deposited sediment will be entrained and eroded until transport capacity is reached.

Sensitivity Analyses: Simulations using REGEM were conducted to examine the performance of the program as well as its stability, and may be classified into three basic categories: (1) total event simulations designed to represent overall output at the end of a single runoff event; (2) within-event simulations designed to demonstrate variations in model output in time (over the event hydrograph) within a single runoff event; and (3) continuous simulations designed to examine how gullies develop and evolve over several runoff events.

Default Input Parameters: Tables 2, 3, and 4 summarize default values used during the sensitivity analyses. Here we examine a 5.0 ha field, tilled to 0.2 m, with a Manning's roughness of 0.03, at a 1% slope, subjected to rainfalls varying from 1.0 to 5.0 inches, with a default soil containing equal parts clay, silt, and sand, and smaller but equal parts as aggregates.

Table 2 Default hydrologic values calculated by TR-55 for five event rainfall amounts on a 5.0 ha drainage area.

Rainfall mm	**Runoff volume** m^3	**Peak Discharge** m^3/s
25.4 (1.0 in)	5.9	0.00025
38.1 (1.5 in)	106.5	0.01092
50.8 (2.0 in)	305.5	0.06888
76.2 (3.0 in)	907.0	0.27410
101.6 (4.0 in)	1688.5	0.54870
127.0 (5.0 in)	2586.0	0.86330

Table 3 A summary of the default values for field-scale input and the range of values tested.

Input Parameter	**Default Value**	**Range Tested**
slope	0.010 m/m	0.005 to 0.100 m/m
Manning's 'n'	0.030	0.030 to 0.060
tillage depth	0.2 m	0.1 to 0.3 m
drainage area	5.0 ha	0.5 to 20.0 ha

Table 4 A summary of the default values for input soil properties.

Soil Type	R_{clay}	R_{silt}	R_{sand}	R_{sagg}	R_{lagg}	B_d	τ_c	k_d
default	30	30	30	5	5	1.5 g/cm^3	1.09 N/m^2	.096 cm^3/N-s
clay loam	55	28	17	0	0	1.8 g/cm^3	3.12 N/m^2	.057 cm^3/N-s
silt loam	13	73	14	0	0	1.6 g/cm^3	0.54 N/m^2	.137 cm^3/N-s
loam	22	38	40	0	0	1.5 g/cm^3	0.72 N/m^2	.113 cm^3/N-s

RESULTS / DISCUSSION

Figures 1, 2, and 3 present basic results from sensitivity analyses performed on the REGEM model. Overall results from a single simulation, within event variation, and continuous simulation results are given.

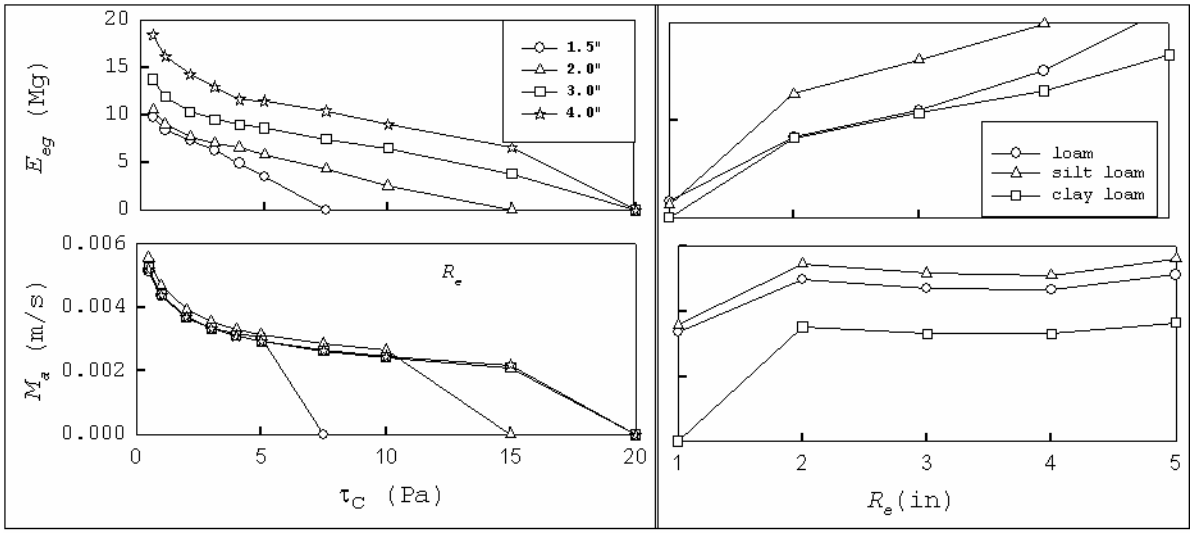


Figure 1 Single event results for different critical shear stresses (τ_c) and rainfall events (R_e) using default storms and soil types, where E_{eg} is total ephemeral gully erosion and M_a is average event headcut migration rate.

For all event rainfalls, slopes, drainage areas, and tillage depths examined, an increase in the critical shear stress reduces the amount of simulated ephemeral gully erosion (Figure 1). A higher critical shear stress not only limits the time for soil detachment, it reduces the rate of headcut migration by decreasing the erodibility coefficient. In fact, the average headcut migration rate appears more dependent on the erodibility of the soil than the magnitude of the runoff. While headcut migration rate remains relatively constant regardless of increased rainfall, ephemeral gully erosion is markedly increased because of the larger channel widths associated with higher discharges.

At the sub-event scale (Figure 2) no erosion occurs until critical shear stress is exceeded and tillage depth is reached, and this occurs more quickly when critical shear stress is low (30 v.70 min, e.g., Figure 2). Headcut migration rate is shown to be relatively constant over the event hydrograph, varying more with differences in erodibility than discharge. Higher critical shear stresses cause headcut migration to begin later during a given event because time devoted to scour is greater.

During continuous simulation (Figure 3), erosion amounts decline after several storm events. This is due to the reduction in drainage area and the corresponding reduction in storm discharge in the upper reaches of an ephemeral gully. Several small events result in a longer and narrower gully than several large events beacuse these smaller events have much longer base times and therefore a longer duration of active headcut migration. This may be due to the nature of the TR-55 calculations and will be investigated further. Smaller magnitude events result in more deposition while larger events are more capable of transporting detached sediment.

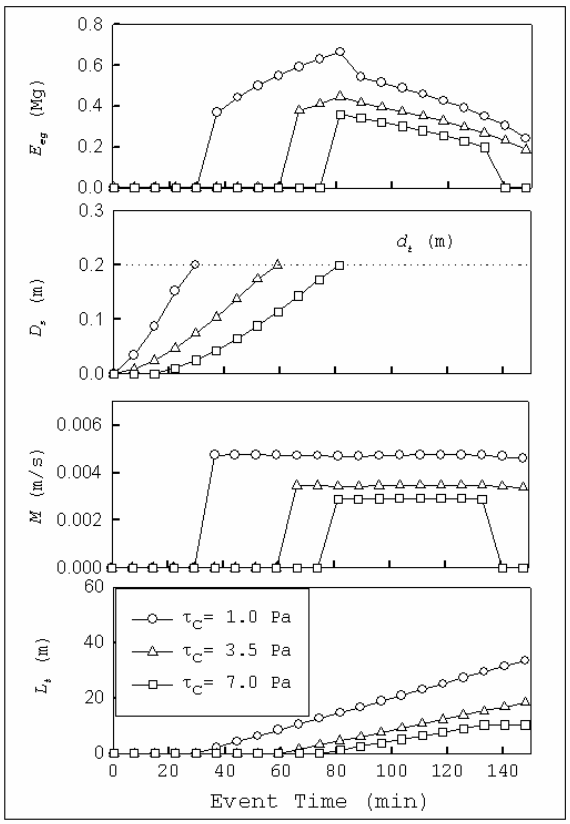


Figure 2 Within event variations in erosion (E_{eg}), scour depth (D_s), where d_t is tillage depth, headcut migration rate (M), and ephemeral gully length (L_t) over a 2.0 inch (50.8mm) rainfall event hydrograph for different critical shear stresses (τ_c).

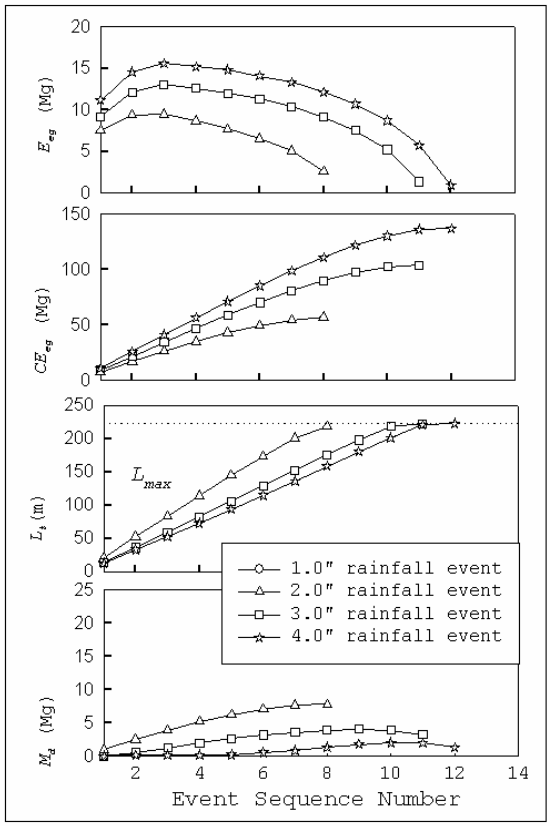


Figure 3 Continuous simulations for different rainfall events showing variations in event erosion (E_{eg}), cumulative erosion (CE_{eg}), total ephemeral gully length (L_t) where L_{max} is maximum possible ephemeral gully length for a 5.0ha drainage area and deposition mass within the ephemeral gully channel (M_d).

CONCLUSION

REGEM effectively overcomes several limitations of previous technology. The ephemeral gully length has been removed as an input parameter as gullies now develop along a given length through headcut migration and plunge-pool erosion processes. Unsteady, spatially-varied flows allow sediment transport and deposition to be examined explicitly. Sediment routing calculations address five particle-size classes accounting for differences between the ephemeral gully sediment flux and the *in situ* soil material. REGEM has been integrated with the AnnAGNPS model, giving AnnAGNPS the ability to explicitly account for ephemeral gully erosion with a minimum of additional input data. Future improvements to REGEM will follow its verification and validation.

REFERENCES

Alonso, C.V., Bennett S.J., and Stein, O.R. (2002). "Predicting head cut erosion and migration in concentrated flows typical of upland areas," Water Resources Research, 38(12),1303.

Bennett, S.J., Casali, J., Robinson, K.M., Kavavy, K.C. (2002). "Characteristics of actively eroding ephemeral gullies in an experimental channel," Transactions of the ASAE, 43(3), 641-649.

Bennett, S.J., Alonso, C.V., Prasad, S.N., and Römkens, M.J.M. (2000a). "Experiments on headcut growth and migration in concentrated flows typical of upland areas," Water Resources Research, 36(7), 1911-1922.

Bingner, R.L and Theurer F.D. (2001). "AnnAGNPS: estimating sediment yield by particle size for sheet and rill erosion," Proceedings of thee Sedimentation, Monitoring, Modeling, and Managing, 7th Federal Interagency Sedimentation Conference, Reno, NV, 25-29 March 2001. I-1 – I-7.

Bingner, R.L., and Theurer F.D. (2002). "Physics of suspended sediment transport in AnnAGNPS," Proceedings of the 2002 Second Federal Interagency Hydrologic Modeling Conference, Las Vegas, NV, July-August, 12 pp.

Casalí, J., Lopez J.J., and Giraldez, J.V. (2003). "A process-based model for channel degradation: application to ephemeral gully erosion," Catena, 50, 435-447.

Foster, G.R. and Lane, L.J. (1983). "Erosion in concentrated flow in farm fields," in Proceedings, D.B. Simons Symposium on erosion and Sedimentation, Colorado State University, Ft. Collins, Colorado, 9.65-9.82.

Foster, G.R. (1986). "Understanding Ephemeral Gully Erosion," Soil Conservation, Assessing the National Resource Inventory, National Academy of Science Press, 2, 90-125.

Hanson, G.J. and Simon, A. (2001). "Erodibility of cohesive streambeds in the loess area of the Midwestern USA," Hydrological Processes, 15, 23-38.

Leopold, L.B., Wolman, M.G., and Miller, J.P. (1964). "Fluvial Processes in Geomorphology," W.H. Freeman and Company, San Francisco.

Nachtergaele, J., Poesen, J., Sidorchuk, A., and Torri, D. (2002). "Prediction of flow width in ephemeral gully channels," Hydrological Processes, 16, 1935-1953.

Renard, K.G., Foster, G.R., Weesies, G.A., McCool, D.K., and Yoder, D.C. (1997). "Predicting soil erosion by water: A guide to conservation planning with the Revised Universal Soil Loss Equation (RUSLE)," U.S. Department of Agriculture, Agricultural Handbook No. 703, 404 pp.

United States Department of Agriculture - Natural Resource Conservation Service (1996). "America's Private Lands: A Geography of Hope," Washington, D.C.

United States Department of Agriculture – Natural Resource Conservation Service (1986). "Urban Hydrology for Small Watersheds," USDA-NRCS Conservation Engineering Division, Technical Release 55.

Wischmeier, W.H. and Smith, D.D. (1978). "Predicting Rainfall Erosion Losses – a Guide to Conservation Planning," USDA, Agriculture Handbook 537.

Woodward, D.E. (1999). "Method to Predict Cropland Ephemeral Gully Erosion," Catena, 37, 393-399.

SEDIMENT INVESTIGATIONS IN THE VICINITY OF THE OLD RIVER COMPLEX, LOUISIANA: RED RIVER ABOVE OLD RIVER OUTFLOW CHANNEL

Nina J. Reins, MS, Shaw Coastal, New Orleans, Louisiana, nina.reins@gmx.de; Tonja L. Koob, PhD, PE, Gaea Consultants, LLC, New Orleans, Louisiana, tonja.koob@gaeaconsultants.com

Abstract: This research introduces the Old River Control Complex (ORCC) and defines the existing problem of disproportionate water versus sediment diversions. Because the ORCC is a water control complex built to keep the Atchafalaya River from taking over the Mississippi River and to generate power, it is crucial for the system to function properly to maintain a balanced sediment regime. The slightest changes in the sediment environment can be critical for the Mississippi, Atchafalaya, and Red Rivers, and for the Old River Outflow Channel itself. Scouring and deposition occur due to an existing imbalance of sediment concentrations. Therefore, analyzing the available sediment data for stations in the vicinity of the ORCC is important to understand the overall shifts of sediment occurring in this area. If the sources for the shifts of sediment can be defined, additional recommendations for future handling methods can be made, and excessive scouring and deposition can be prevented.

Focusing on the station *Red River above Old River Outflow Channel*, this research outlines a method of properly assembling, managing and interpreting the data available from a sediment sampling station in the vicinity of the ORCC. The spreadsheets developed in this study are easy to use for ongoing data management and make updating the analysis and future interpretations much easier. The introduced methods can now be easily implemented for the key stations to draw more detailed conclusions concerning sediment shifts.

INTRODUCTION

The Mississippi River is one of the world's major river systems in size, habitat diversity, and biological productivity. Under natural conditions, the Mississippi River might have switched its course to the Gulf of Mexico via the Atchafalaya distributary between 1965 and 1975. The river has been prevented from doing so by artificial levees and control structures at Old River. Natural diversion of Mississippi River flow to the Atchafalaya has been imminent because the Atchafalaya is both a steeper and shorter route to the Gulf of Mexico than is the Mississippi. The Atchafalaya now drains about 30% of the latitude flow of the Mississippi and the Red Rivers to the Gulf of Mexico.

The structures controlling this flow through the Old River Outflow Channel are referred to as the Old River Control Complex (ORCC), which is located on the west bank of the Mississippi River about 50 miles northwest of Baton Rouge, Louisiana, as shown in Figure 1. This complex is a vital part of the Mississippi River and Tributaries (MR&T) flood control plan.

The initial features were: two mechanically operated control structures, designated as the Low Sill Structure and the Overbank Structure; inflow and outflow channels; a lock for navigation, and other appurtenant works. Construction began in 1955 and was completed in 1963. An Auxiliary Structure was added to the complex in 1986 to provide greater flexibility and to reduce stress on the Low Sill Structure, which was damaged in the 1973 flood. Four years later a privately owned and operated hydropower plant was constructed in the immediate vicinity of the ORCC.

Sediment transport plays an important role in this complex. Accumulation of large grain sediment in some areas within the vicinity of the ORCC and significant accretion in others cause problems for facility operators as well as bank instabilities and failures. U.S. Army Corps of Engineers (USACE) hydraulic experts believe that a continued accumulation of large-grain sediment in the Mississippi River may lead to a deterioration of the MR&T system in the vicinity of the ORCC area, and could ultimately result in a need to increase the height of the Mississippi River levees to provide the required level of flood protection. The numerous bank failures and soil erosion in the lower Red River may require expensive levee setbacks if measures are not implemented to reduce the number of bank failures that are occurring at a progressive rate. There is also concern that the current ratio of large-grain sediment between the Mississippi River and Atchafalaya River is out of the targeted range and will eventually result in navigation problems and an increase in bank failures throughout the system, resulting in regional and national consequences.

There is no unanimity among experts of the cause or significance of the events that are being observed in the lower Red, Old, Mississippi, and Atchafalaya Rivers. This is a very complex river system that requires recognizing subtle changes that will lead to significant problems many years before the problem occurs. Constant vigilance and experience are necessary to understand and perceive minor changes that could ultimately alter the system in a negative way. Part of the difficulty is recognizing the subtle changes and determining if the changes are part of a natural cycle or if they are a detrimental pattern that will destabilize the system. The MR&T system is so important to the region and the nation that every anomaly with a potential to destabilize the system should be investigated thoroughly.

Sediment investigations have been made since the 1930's, but the most recent study, published in 1999, was the "Lower Mississippi Sediment Study" by the Louisiana Hydroelectric Limited Partnership, Vidalia, Louisiana. The study results were reviewed by sediment transport experts in the consulting and academic fields who recommended further and, if possible, more detailed monitoring and analysis, and updating of the reviews about every five years. Because of the broad agreement on this recommendation, especially within the USACE, a new comprehensive study within the vicinity of the Red, Old, Mississippi, and Atchafalaya Rivers (ROMA Study) is in preparation. A draft was established in 2004 to introduce the purpose and the tasks of this study. This research is the first approach towards fulfilling some of the goals established by the ROMA Study draft document. Collecting, processing and managing data is one of the tasks detailed in the draft. Existing data needs to be inventoried and updated, and appropriate databases have to be established for use during the study and in future reviews. Sediment concentration and grain size analyses are a substantial portion of the data to be processed and analyzed. To evaluate the trends in sediment transport within the ORCC and its vicinity, it is necessary to research and compare the stations above and below Old River Outflow Channel and the Outflow Channel itself. The stations 1) Red River above Old River Outflow Channel, 2) Coochie, 3) Simmesport, 4) Tarbert Landing and 5) Old River Outflow Channel fulfill this criterion, and are illustrated in Figure 2.

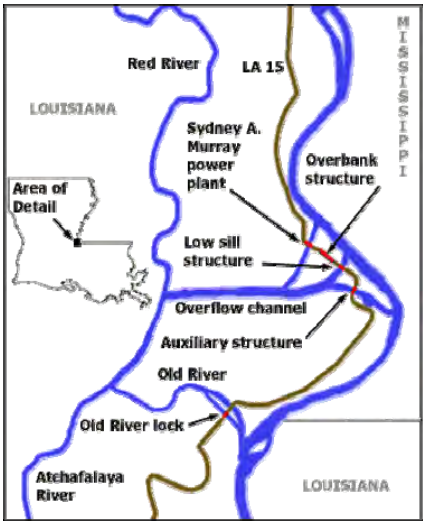


Figure 1 Old River Control Complex



Figure 2 Sediment Sampling Stations in the Vicinity of the ORCC

These sediment sampling stations have long data records, making it possible to evaluate changes over time in the hope of predicting future trends. Due to the overwhelming amount of data for each station, and the effort it takes to verify the data, this research focused on one station, and developed a template for the other stations.

METHODS

Data Collection: Sediment data at all five stations within the vicinity of the ORCC is available in an electronic 3pg format from the USACE from 1973 to 2003 for Tarbert Landing and Simmesport, from 1975 to 2003 for Coochie and Red River above Old River Outflow Channel, and from 1977 to 2003 for the Old River Outflow Channel. Some 3pg files have less information than others, depending on the sampling procedure or whether the soil tests were successful. Missing data was identified and old documents and handwritten data files, which were not available in

electronic form, were researched for needed data. No additional data was found for the Red River above Old River Outflow Channel.

Because of the overwhelming amount of data, which has to be either reviewed closely or manually entered into the computer and analyzed for errors, only the station Red River above Old River Outflow Channel was picked to create all spreadsheets and documents needed for data interpretation because of (a) it experienced lack of sediment resulting in numerous bank failures and soil erosion in the lower Red River due to scouring and (b) because almost all collected data was available in electronic form.

Creation of One Data Summary: In cooperation with the USACE, the decision was made to use the information in the 3pg summaries to create one data summary including all the years of available data. It includes the date of the sampling, gage reading [ft], type of sampler used, number of verticals taken, discharge [cfs], coarse load [tons/day], Fine Load [tons/day], Total Load [tons/day], Coarse Concentration [ppm], Fine Concentration [ppm], Total concentration [ppm], suspended sediment sieve analysis, and bed material sieve analysis. The only year between 1973 and 2003 without any 3pg files is 1990. No sediment samples were taken at this station during that year. Some months are missing in other years, and every water year had a different number of sampling dates, making a comparison of the analyzed data more complicated and more prone to errors.

Creation of Grain Size Distribution Curves: In agreement with the USACE, the decision was made to establish a general spreadsheet for Grain Size Distribution Curves, but not to create a grain size distribution curve for every day measurements were taken. The detailed analysis of the Suspended Sediment and Bed Material, as well as its quality control, is a further, very extensive analysis which will not be covered in this research, but will have to be completed to fulfill the goals set in the Draft of the "Red, Old, Mississippi and Atchafalaya Rivers Comprehensive Study". To still use the provided information to view a trend in the change of bed and suspended material, the available data was divided into four periods of measurement (1973-1979, 1980-1989, 1991-1999, 2000-2003) and average grain size distribution curves for bed material and suspended sediment are shown in Figures 3 and 4.

Creation of Discharge Curves: The maximum, minimum and average daily discharge data from Simmesport and Old River Outflow Channel were combined and formatted in a spreadsheet and QA/QC measures were applied. To determine the daily discharge values for Red River above Old River Outflow Channel, the values of the Old River Outflow Channel had to be subtracted from the values from Simmesport. If either of the values for a specific day was not given, the cell to be calculated remained empty. If a negative value or a value below 4,000 cfs was calculated for Red River above Old River Outflow Channel, it was changed manually to 4,000 cfs, due to information from the USACE, which is based on their experience with the river. Additionally the daily average from water years 1972/1973 to 2003/2004 was calculated. Graphs presenting the calculated discharge values were created for every water year and supplemented with the actual measured values in the field and the average for the entire period of records. An example discharge graph is presented in Figure 5.

With this procedure, calculated values could be compared to actual measured discharge values. Typographical errors in the measured data were detected and resolved in agreement with the USACE. The average helps to define if the specific water year is a high water year, an average water year or a low water year. It also makes it easier to detect the time period of any particular flood. This information, together with the computed loads as introduced later, helps to find a correlation between load and discharge for any given water year.

CREATION OF POWER CURVES

Power Curves for Every Water Year: From the created data summary, power curves were obtained for every water year. The x-axis of the graph is discharge in cfs, and the y-axis is sand concentration in ppm. After all data points for the specific water year were added to the graph, a power curve trendline was generated. The equation and the R-squared value received from this trendline were placed next to each graph. For sampling dates where the sediment concentration equaled zero, the value was changed to one in order to establish the power curve trendline. With a value of one the calculated load for those days is still close to zero and does not appreciably change the outcome of the data analysis.

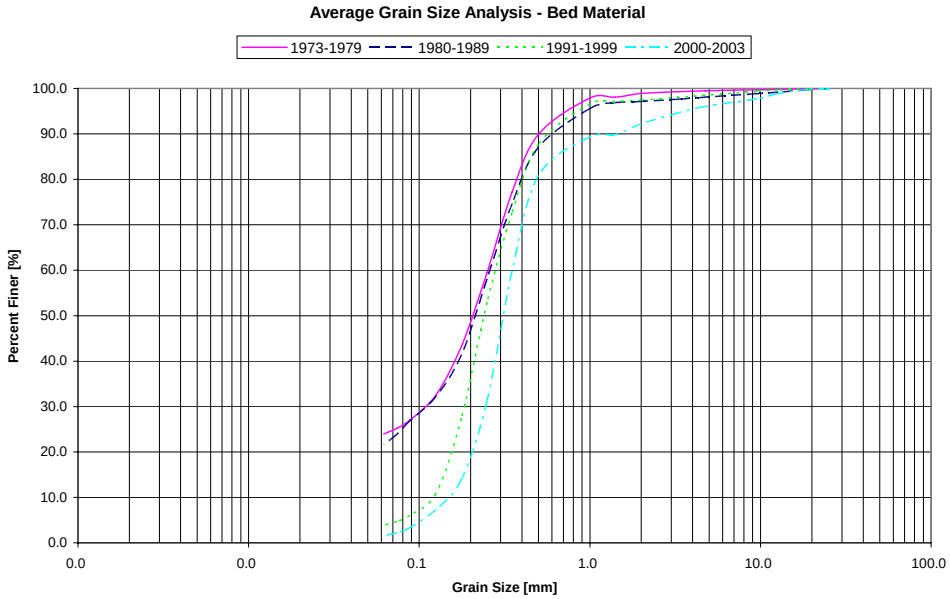


Figure 3 Average Grain Size Analysis for the Bed Material over Time (1973-2003)

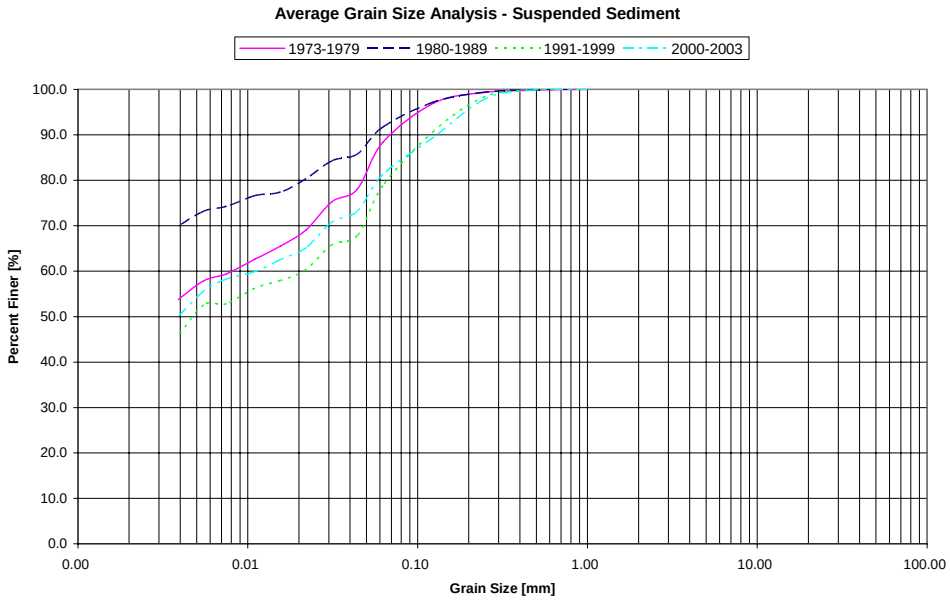


Figure 4 Average Grain Size Analysis for the Suspended Material over Time (1973-2003)

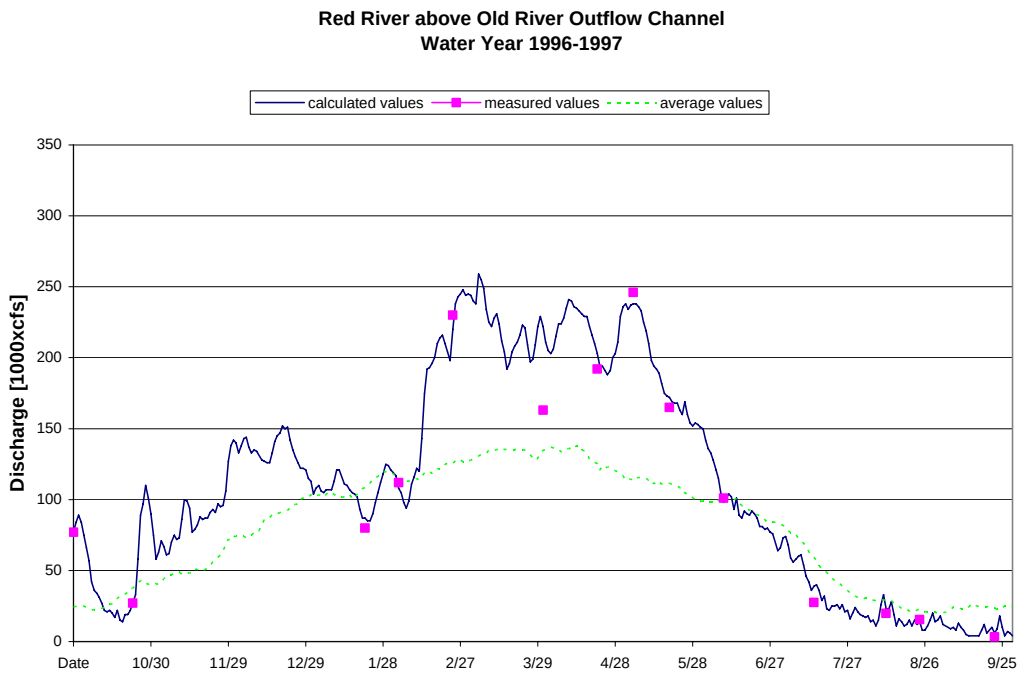


Figure 5 Discharge Graph for the Water Year 1996-1997 at Red River above Old River Outflow Channel, including Calculated and Measured Discharge Values

Combined Power Curves for a Period of Time: Similar to the procedure described above, power curves were established representing a longer period of time, instead of just one particular water year, and were combined in one graph. The periods chosen to be presented intended to cover a period of 10 years each, starting with 1970, 1980, 1990, and 2000. Due to the available period of record from 1973 - 2003, and the fact that no sampling occurred in 1990, the periods chosen were 1973 – 1979, 1980 – 1989, 1991 – 1999, 2000 – 2003. All data points used to create the trendlines were removed from the graph and only the four trendlines are shown in Figure 6 with their equations and R-squared values. These power curves are designed to find overall trends, and because each one is based on more data points than a single water year, the trendlines are more accurate than annual trendlines.

Load Calculation for Water Years 1972/1973 to 2002/2003: Daily discharge data and the power curve results were used to create a daily summary for every water year, including discharge, sand concentration, and coarse load. After calculating the load per day, the annual load for the water year was calculated. To calculate the coarse load in tons/day the following equation provided by the USACE was used:

$$\text{Coarse Load [tons/day]} = \text{Sand Concentration [ppm]} \times \text{Discharge [cfs]} \times 0.00269568 \quad (1)$$

In a final step, the annual load in tons was calculated. To visualize the calculated information, Figure 7 was created to show the Computed Annual Load per Water Year for the entire period of record. The graph was obtained by using all available information of this research.

CONCLUSIONS AND RECOMMENDATIONS

For the Red River above Old River Outflow Channel a correlation exists between annual sand loads and the discharge pattern. Post-1990 high water years produced more load than pre-1990, which is not the case for average or low flows. Because of the continuous high waters in the period 1991-1999, there might have been more sediment uptake upstream from the gage due to more powerful flow and loosened sediment from the lock constructions, which would explain the experienced increase of sand load. Furthermore, because of the scouring problem observed in the Lower Red River after the construction of locks and dams upstream,, high discharges might have accelerated this scouring process, and therefore, produced more annual load for high water years post-1990. This would also

explain why the average and low water years do not show an increase in computed annual load. The water flow was not powerful enough to accelerate scouring in the way high water flows can during high water years and flooding times did.

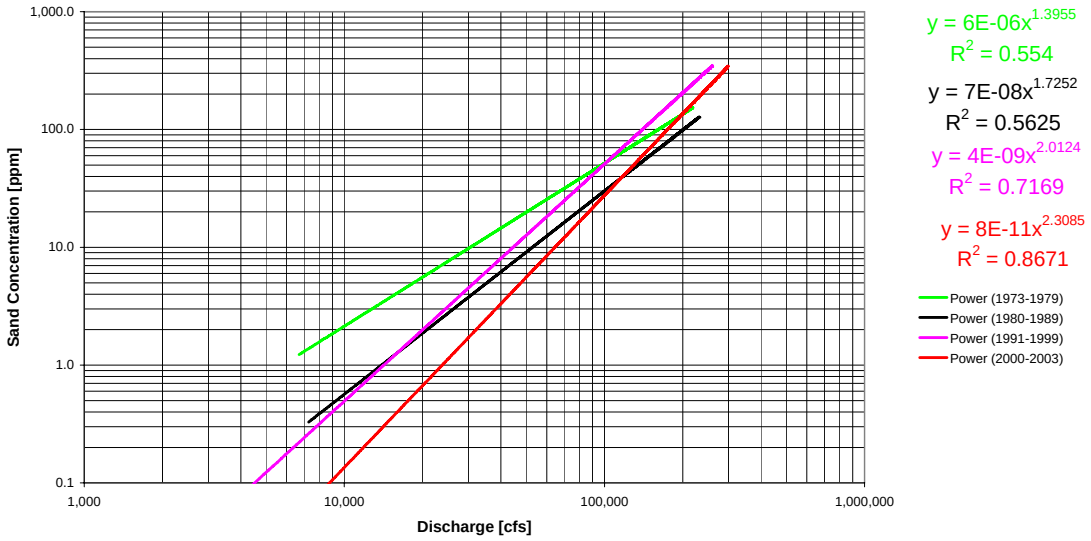


Figure 6 Combined Discharge-Sand Concentration Graph for Red River above Old River Outflow Channel

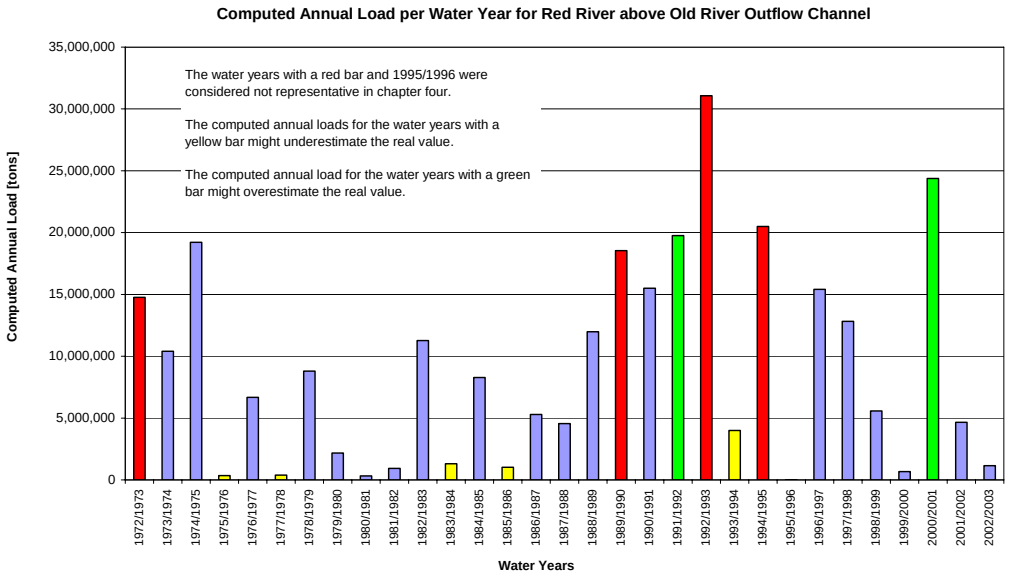


Figure 7 Computed Annual Load per Water Year for Red River above Old River Outflow Channel

To define more accurately how the locks and their operations correlate with the scour problems experienced in the Lower Red River, it is recommended, as a first step, for the ROMA Comprehensive Study to compare sediment sampling stations on the Red River below the locks and upstream of the sampling station Red River above Old River Outflow Channel with the observations from the sampling station Red River above Old River Outflow Channel. As a second step, if necessary, a more detailed study over the period of approximately a year, covering the stretch from the L.C. Boggs Lock to the Old River Outflow Channel, should be conducted. Sediment samples and discharges can be measured frequently throughout the year, especially after closures and openings of the L.C. Boggs Lock. This

information, along with a geomorphologic assessment, would help to analyze more specifically the sediment source/impact relationship, and help to produce management options for more environmentally sustainable and functional lock operations.

From the average power curve trendlines a chronological downward trend in sand concentration for discharges below approximately 100,000 cfs can be seen. At least 2/3 of all flows within one water year are below 100,000 cfs, implying that for most flows a downward trend in sediment concentration can be observed. For discharges higher than approximately 100,000 cfs, no clear trend could be observed. This could be the result of the construction of locks and dams on the Red River. These locks close during low flow times, which offers an explanation for the sand deficit at Red River above Old River Outflow Channel for low flows, because sediment becomes trapped in the pools. Conversely during high water and flood periods the locks are open and the suspended sediment can pass without any barriers, which explains why no explicit trend can be observed. Further investigations will have to be made to verify this trend conclusion.

In comparing the average grain size distributions of the bed material over time, a continuous decline in fines can be observed. The main flushing out of fines, which results in an armoring of the bed, occurred in the 1990's, and continues to the present. This is a potential problem because the fines provide the habitat for benthic organisms, which are the lowest members of the food chain in this system and their loss would overtime affect the rest of the food chain. Also, the fine bed material is where fish and other organisms place their eggs. Without the fines, the eggs would be lost in the gaps between the coarser particles, resulting in lower species reproduction. One explanation for the armoring is the sediment loss of the stream during closure periods of the locks. Closing the locks during low flows results in a sediment deficit downstream of the locks and encourages the uptake of downstream particles in order for the stream to return to its sediment equilibrium. Because the flow beyond the locks is not very powerful, the uptake of fine material versus coarse material is more likely to happen, explaining the experienced loss of fines. Based on the available data, more uptake of fines occurred in the 1990's, which was attributed to the completion of the construction of the five locks on the Red River between Shreveport and the Old River Outflow Channel, and the fact that more high water years and high average water years occurred in this period resulting in a more powerful stream with more capacity for sediment uptake. More data pertaining to the verification of these findings should be collected and analyzed to confirm these introduced conclusions. If supplemental data verifies that the locks are causing the experienced sediment deficit, it is recommended to manage the locks on the lower Red River as a system, making the passage of sediment more organized, and if necessary, to dredge material from the pool to the downstream end of the locks during closure periods to decrease the sediment deficit downstream.

No definite trend was found for the suspended sediment. The lack of a trend could result from much of the suspended sediment being wash load generated from particle uptake in the watershed. Because wash load is that part of the total sediment load that is composed of particles smaller than 0.0625 mm, smaller than the particles present in appreciable quantities in the stream bed, it is only present as suspended sediment. Because the watershed characteristics and their contributions to the suspended load have not changed significantly since the 1970's and because the locks are flushed frequently, the settling suspended material is the first material which continues its downstream transport leading to no detectible change in suspended sediment.

It should be stated, that in the Draft of the ROMA Study, the reason given for the experienced scouring in the Red River is inaccurate. It has been stated by the USACE that a decrease in sand load is causing the problems, but a decrease in sand load has not been observed in this research. It has been found that the load correlates with the discharge and stayed similar for average and low water years over time. However, a decrease in sand concentration has been observed, which is the reason for the scouring, because the sand concentration, not the sand load, is the important variable to measure in a river experiencing bed and bank erosion.

The most time consuming parts of the introduced analysis involved manually entering and verifying data. Recognizing that fact, the introduced study will be very work- and labor-intensive. To make the quality control of the existing data more efficient for the other four key stations in the vicinity of the ORCC, it is recommended that a statistical analysis be done with the data once it is summarized in the database spreadsheet. Also, because in the future all the new data will be in a 3pg format, one recommended action is to write a program to copy the important information from the 3pg file into the summary spreadsheet, which would minimize the needed labor for updates.

To improve and expedite quality control for the future, it is recommended that the people sampling in the field indicate the measurements that seem odd. An engineer in the office, familiar with the river and the collection procedures, can check the data before it is entered into the data summary. This way no further verification of the data would be necessary after it had been entered to the summary spreadsheet.

The station Red River above Old River Outflow Channel was established in 1963, but there are only 3pg-files available from the USACE starting in 1973. Data from 1963 to 1972 would be very valuable for this research because that decade precedes the construction of the locks and dams on the lower Red River and because it would add another decade to strengthen the conclusions and trend analyses presented here.

Because the data available for the Red River was not always consistent over time, and because the amount of samples throughout a water year has declined drastically (from 26 to 6), the analysis is limited and a certain variability has to be accounted for. Specific values, like the computed annual load, cannot be taken as 100% accurate numbers, which should always be in mind for further conclusions. To be able to draw overall and more complex conclusions for the Old River Control Complex and its vicinity, the analysis introduced has to be finished for Tarbert Landing, Coochie, Old River Outflow Channel and Simmesport. Only with the same type of analysis for all these stations can the data be comparable and adequate recommendations made. It should also be noted, however, that even with the results from all five stations, a more comprehensive analysis of channel geometry and geomorphology is required to fully interpret the trends identified with this sediment study.

REFERENCES

Catalyst-Old River Hydroelectric Limited Partnership d/b/a Louisiana Hydroelectric Limited Partnership, Vidalia, Louisiana, “Lower Mississippi Sediment Study - Volume I - V”, May 28 1999, Mississippi River Commission, New Orleans District, La.

http://biology.usgs.gov/s+t/SNT/noframe/ms137.htm.

http://users.stlcc.edu/jangert/oldriver/oldriver.html.

http://www.loyno.edu/lucec/mrdchar.html.

U.S. Army Corps of Engineers, Draft, “Red, Old, Mississippi, and Atchafalaya Rivers Comprehensive Study,” June 2004, New Orleans, LA.

AN APPARATUS FOR BED MATERIAL SEDIMENT EXTRACTION FROM COARSE RIVER BEDS IN LARGE ALLUVIAL RIVERS

Michael Bliss Singer, NRC Researcher, US Geological Survey, Water Resource Division, Menlo Park, CA, bliss@bren.ucsb.edu; Stacy Cepello Environmental Scientist, California Dept. of Water Resources, Northern District, Red Bluff, CA, cepello@water.ca.gov; Adam Henderson, Environmental Scientist, California Dept. of Water Resources, Northern District, Red Bluff, CA, admh@water.ca.gov

Abstract: Grain size distributions of bed material sediment in large alluvial rivers are required in applications ranging from habitat mapping, calibration of sediment transport models, high resolution sediment routing, and testing of existing theories of longitudinal and cross stream sediment sorting. However, characterizing bed material sediment from coarse river beds is hampered by difficulties in sediment extraction, a challenge that is generally circumvented via pebble counts on point bars, even though it is unclear whether the bulk grain size distribution of bed sediments is well represented by pebble counts on bars.

We have developed and tested a boat-based sampling apparatus and methodology for extracting bulk sediment from a wide range of riverbed materials. It involves the use of a ~36 x 23 x 28 cm stainless steel toothed sampler, called the Cooper Scooper, which is deployed from and dragged downstream by the weight of a jet boat. The design is based on that of a river anchor such that a rotating center bar connected to a rope line in the boat aligns the sampler in the downstream direction, the teeth penetrate the bed surface, and the sampler digs into the bed. The sampler is fitted with lead weights to keep it from tipping over. The force of the sampler 'biting' into the bed can be felt on the rope line held by a person in the boat at which point they let out slack. The boat then motors to the spot above the embedded sampler, which is hoisted to the water surface via a system of pulleys. The Cooper Scooper is then clipped into a winch and boom assembly by which it is brought aboard.

This apparatus improves upon commonly used clamshell dredge samplers, which are unable to penetrate coarse or mixed bed surfaces. The Cooper Scooper, by contrast, extracts statistically representative bed material sediment samples of up to 16 kg (dry weight) with an average sample size of ~6 kg. Not surprisingly, the sampler does not perform well in very coarse or armored beds (e.g. where surface material size is on the same scale as the sampler). The Cooper Scooper has been tested in mixed and coarse beds at ~60 cross sections of the Middle and Upper Sacramento River (usually 3 samples across each section) spanning ~160 river kilometers. The sampler and method have allowed us to characterize the grain size distribution for large portions of the river for which bed material data were previously unavailable. The data will enable assessment of habitat for anadramous and benthic species, computations of sediment transport and routing, and the testing of current theories of downstream fining.

ANALYZING SEDIMENT YIELDS IN THE CONTEXT OF TMDL'S

Mary Ann Madej, Research Geologist, U.S. Geological Survey Western Ecological Research Center, Arcata, CA, mary_ann_madej@usgs.gov; Randy Klein, Hydrologist, Redwood National and State Parks, Arcata, CA, randy_klein@nps.gov; Vicki Ozaki, Geologist, Redwood National and State Parks, Arcata, CA, vicki_ozaki@nps.gov, Tom Marquette, Hydrological Technician, Redwood National and State Parks, Arcata, CA, tom_marquette@nps.gov

Abstract: In 1998, the California Regional Water Quality Control Board established a Water Quality Attainment Strategy for Sediment and Total Maximum Daily Loads (TMDL) for Redwood Creek, California. In the TMDL, a 10-year rolling average of sediment yield of 1900 t of total sediment/mi^2/year (equivalent to about 500 Mg of suspended sediment/km^2/yr) was used as a threshold of concern. We investigate the relevance of this value by analyzing trends in suspended sediment yields at two gaging stations in Redwood Creek, north coastal California. The TMDL reported that at both the upstream and downstream gaging stations, the 10-year rolling average exceeded the threshold between 1973 and 1992, and was below threshold from 1993-1996. A comparison of suspended sediment-discharge rating curves shows a significant shift from higher sediment transport rates in the 1970's (following large storms and extensive landslide activity) to lower rates in the 1980's and 1990's, and even lower rates in the 2000's. In recent years the upstream and downstream gaging stations, monitoring sediment transport from drainage areas of 175 and 725 km^2, respectively, have similar sediment concentrations on a per unit area basis. This lack of a significant shift in sediment transport curves suggests that the trends in the TMDL rolling average are more dependent on flow magnitude rather than being indicative of changes in sediment transport relationships in the basin.

INTRODUCTION

Section 303(d) of the federal Clean Water Act of 1972 requires states to identify waterbodies that do not meet water quality standards and are not supporting their beneficial uses. These waters are placed on the Section 303(d) List of Impaired Waterbodies. This Act gave the State Water Resources Control Board and the US Environmental Protection Agency (EPA) the authority to establish a pollution control plan called a Total Maximum Daily Load (TMDL) for each water body and associated pollutant on the list. The Total Maximum Daily Load (TMDL) process leads to a "pollution budget" designed to restore the health of a polluted body of water. Many rivers and streams in north coastal California are listed as sediment impaired, and within the North Coast Region, sediment TMDLs have been established for 16 rivers (described at http://www.swrcb.ca.gov/rwqcb1). The sediment TMDL's calculate the maximum amount of sediment that a river can receive and still meet water quality standards, and outlines sediment reductions necessary to reach those goals.

The Redwood Creek Sediment TMDL (1998) identified major sediment sources to Redwood Creek as streamside landslides, gully erosion, and cutbank and fillslope failures on unpaved logging roads. Landslides are prominent sources during large floods. For example, Pitlick (1995) reported that 45 percent of the total landslide material delivered to 16 tributaries of

Redwood Creek between about 1936 and 1978 was generated during a 50-year flood that occurred in December, 1964, and another 23 percent was delivered during 25-year floods in the early 1970's. Kelsey et al. (1995) similarly found that the 1964 flood accounted for much of the volume generated by streamside landslides along the mainstem of Redwood Creek, with a secondary peak of landslide activity occurring during the 1972 and 1975 floods. A storm in 1997 (10-year flood) initiated an additional 365 landslides (Redwood National and State Parks unpublished data, Arcata, CA).

Sediment measurements and stream gaging on Redwood Creek did not commence until the early 1970's, so the sediment loads during the 1964 flood are unknown. Based on an analysis of sediment sources, the Redwood Creek TMDL recommends a total allowable sediment load of 665 $Mg/km^2/yr$, which includes both bedload and suspended sediment load. On average, 77% of the total load is transported as suspended sediment, so the TMDL target load is equivalent to about 500 $Mg/km^2/yr$ as suspended load. Now that the Redwood Creek TMDL is in place, it is an opportune time to evaluate sediment loadings measured at gaging stations to determine if and when sediment goals have been reached. This analysis examines changes in trends in the suspended sediment loads by comparing suspended sediment transport curves from the 1970's to the present.

FIELD AREA

Redwood Creek, north coastal California, drains an area of 725 km^2 (Figure 1). For much of its 108-km length, Redwood Creek flows along the trace of the Grogan Fault, which juxtaposes unmetamorphosed or slightly metamorphosed sandstones and siltstones against a quartz-mica schist of the Franciscan assemblage. The basin receives an average of 2,000 mm of precipitation annually, most of which falls between October and March. Total basin relief is 1,615 m; average hillslope gradient is 26 percent.

Aerial photographs taken in 1936 show that most of the basin was covered with old-growth redwood and Douglas-fir forests. Timber harvest began in earnest in the early 1950's, and by 1966, 55 percent of the old growth coniferous forest had been logged (Best, 1995). During this period, extensive landsliding and gully erosion, especially prominent on logging roads, resulted in widespread channel aggradation that affected most of the length of Redwood Creek. Currently 18 percent of the old growth forest remains, almost exclusively within Redwood National and State Parks (RNSP) in the downstream third of the basin. The old-growth redwood groves have been designated as a World Heritage Site and an International Biosphere Reserve, but the alluvial redwood groves have been threatened by sedimentation and bank erosion. In 1978, park lands were expanded in the downstream third of the watershed, timber harvest was terminated in this area, and a large-scale watershed restoration program was initiated. Due to the concern about accelerated erosion and sedimentation, RNSP, in cooperation with the U.S. Geological Survey (USGS), established a stream gaging network within the Redwood Creek basin. Two gaging stations have been operating on Redwood Creek for over three decades. "Redwood Creek near Blue Lake" (USGS Station "O'Kane" #11481500) monitors the upper basin, an area of 175 km^2, and "Redwood Creek at Orick" (USGS Station "Orick" #11482500) is located near the mouth of the river, where the basin is 720 km^2 in size (Figure 1).



Figure 1 Redwood Creek watershed in northern California showing streams and gaging stations.

METHODS

Stream gaging and sediment measurements are conducted by the USGS and RNSP. Between 1970 and 1992 suspended sediment samples were collected daily during high flows from October 1 to April 30, and from 1993 to 2004, sediment was measured intermittently, mostly during high flows. Sediment samples were analyzed in USGS and RNSP laboratories, and concentration results were used to construct suspended sediment concentration–discharge rating curves for the O'Kane and Orick stations. Sediment rating curves express the rates of suspended sediment transport as a function of flow magnitude. Differences in the slopes and intercepts of the rating curves for different time periods and between the two stations were tested using a multiple slopes model of the rating curves.

RESULTS

Floods: Large floods occurred in the Redwood Creek basin in 1861 and 1890, as reported in historical documents. Since the establishment of the Orick gaging station in 1953, annual peak flows in Redwood Creek have been recorded. They are highly variable, ranging from 66 cubic meters per second (cms) in Water Year 2001 to 1429 cms in December, 1964 (Figure 2). (A water year extends from October 1 to September 30). The period from 1953 to 1975 had five large floods, whereas the subsequent two decades were relatively mild in terms of floods. The

period of 1996-1999 again had some moderate events, but they were not as high as the earlier period. The largest flow since 1975 was in January, 1997, which had a recurrence interval of 10 years.

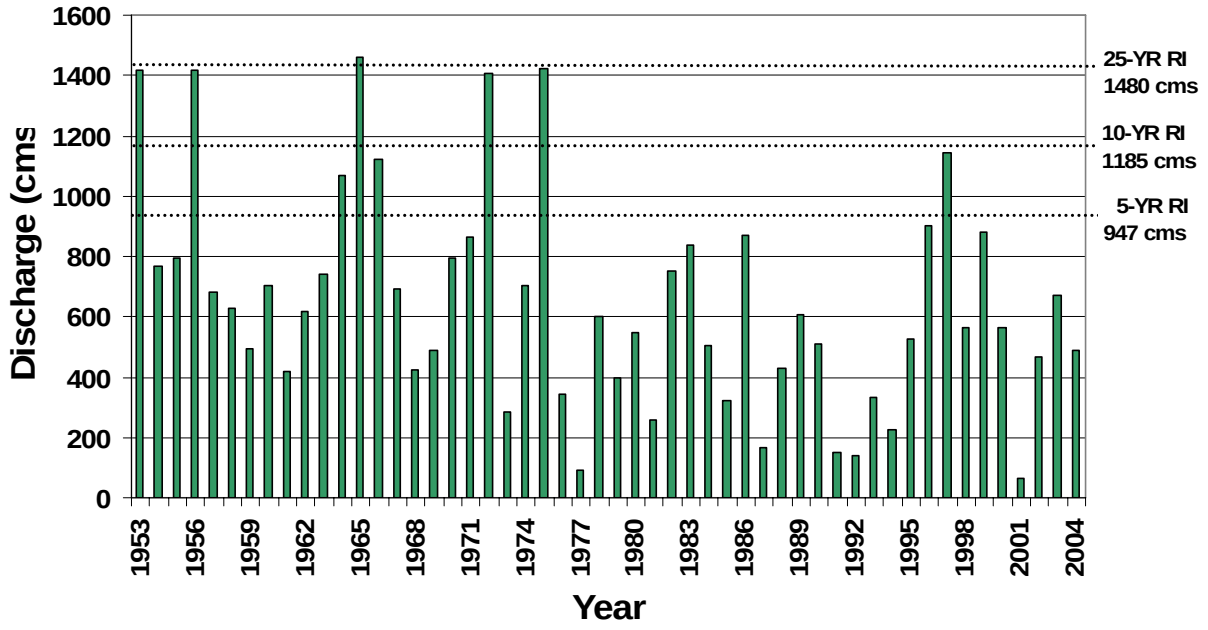


Figure 2 Annual peak flows at Redwood Creek at Orick, California (USGS Station #11482500).

The Redwood Creek TMDL target of 500 Mg/km^2/yr as a 10-year rolling average of suspended load was exceeded for two decades, from 1972 to 1992, then was below threshold until 1996. (Figure 3). It is unclear from the rolling average data, but important to determine, if the occurrences of TMDL target exceedence were a consequence of high flows, new hillslope erosion sources, or re-mobilization of channel-stored sediment. This question is important in terms of management issues in the watershed, such as the magnitude of hillslope destabilization from older and newer timber harvest and the role of watershed erosion prevention activities.

Sediment Transport: To examine trends in sediment transport, we compared suspended sediment rating curves for four periods at the two gaging stations (Figure 4 a and b). A downward shift in the intercept of the regression lines represents a lower sediment concentration for a given discharge, whereas a shift in the slope represents a change in the rate of sediment transport with increasing discharge.

From 1970 to 1975, sediment concentrations were significantly higher than in later years at the Orick and O'Kane gaging stations ($p < 0.001$ and < 0.02 for differences in intercepts, respectively). During this period, even at low flows Redwood Creek was transporting moderate levels of suspended sediment. This may be due to the high sediment supply delivered to the Redwood Creek channel during the large floods of 1972 and 1975. Between the periods of 1977-1995 (when no flows exceeded 850 cms) and 1996-1999, when several moderate flows

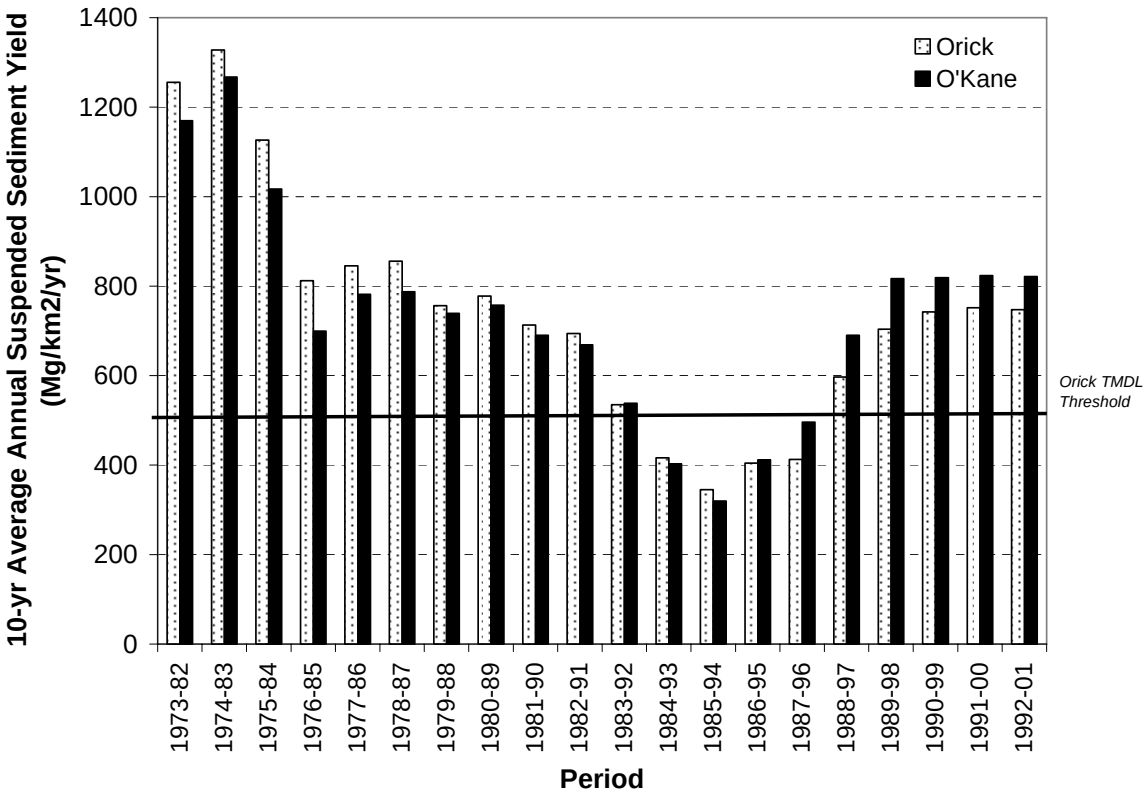


Figure 3 10-year rolling average of suspended sediment yield in Redwood Creek at Orick

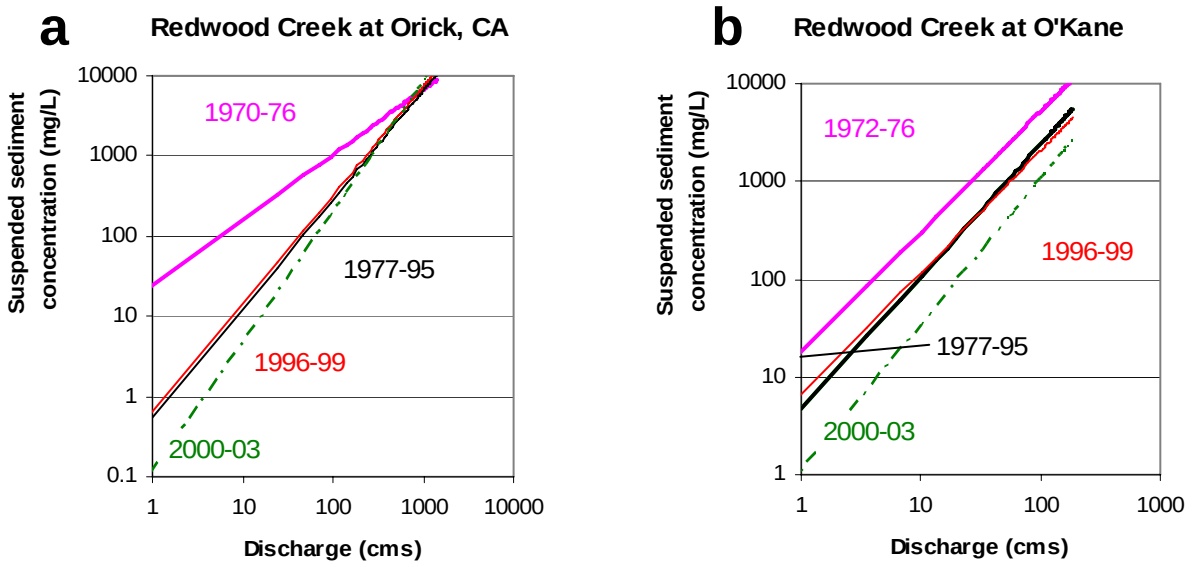


Figure 4 a and b: Suspended sediment rating curves for Redwood Creek near the mouth of the river (a) and at the upstream gaging station (b).

occurred, there were no significant differences in intercepts or slopes (Figure 4). However, in recent years (2000-2003), sediment concentrations for a specific discharge are significantly lower than in the period 1996-1999 for both stations ($p = 0.0161$ and $p < 0.001$ for difference in intercepts for Orick and O'Kane, respectively). At Orick, there were significant differences in slopes between the period 1970-1975 and later periods ($p<0.001$), but differences in slope between other periods were weak ($0.05 < p < 0.10$). At O'Kane, there was a difference in slopes between the periods of 1996-1999 and 2000-2003 ($p = 0.0348$) and a weaker difference between the earliest and latest periods ($p=0.0680$).

The moderately high flows of 1995 to 1999 provided the first 'test' since the flood of 1975 to see if there is a change in the sediment transport characteristics of the upstream basin (the location of active timber harvest and road construction) and the downstream basin (where more of the basin is revegetated and 300 km of abandoned logging roads have been removed through a watershed restoration program). Figure 5 compares the suspended sediment rating curves at the Orick and O'Kane stations. There is no significant difference between the two stations in either slope or intercept ($p> 0.10$ for both).

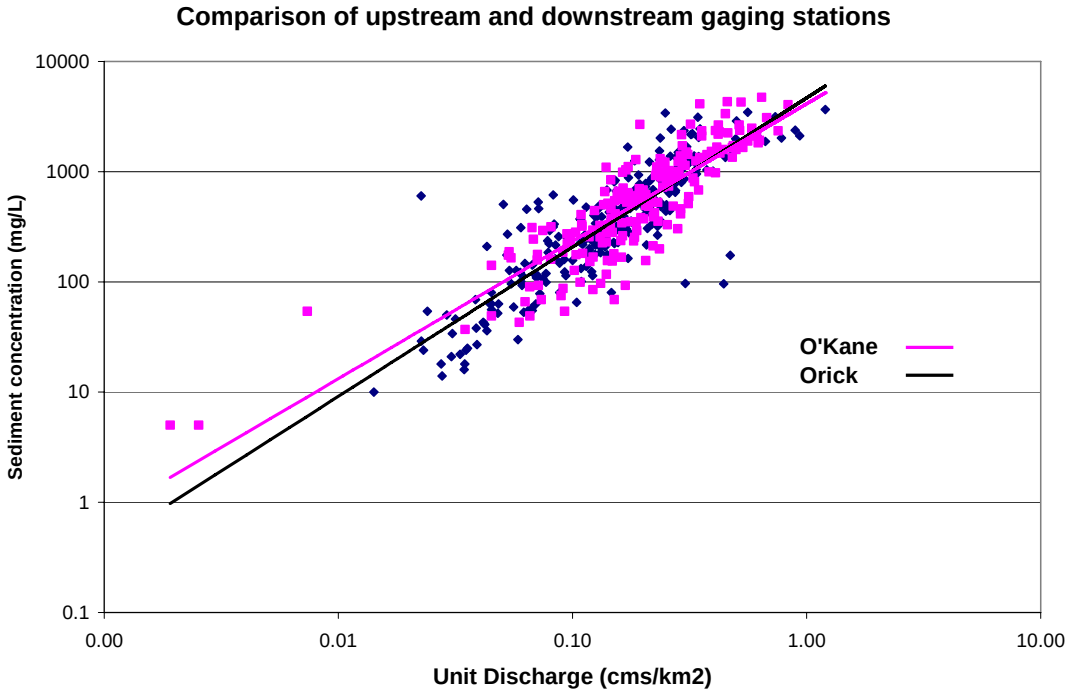


Figure 5 Comparison of upstream (O'Kane) and downstream (Orick) gaging stations for the period 1995-1999.

DISCUSSION AND CONCLUSIONS

We can examine suspended sediment data from two perspectives: changes at a single station through time, and differences between stations. The TMDL considers changes in sediment loads averaged over 10-year periods. Redwood Creek exceeded the threshold of concern in the 1970's, when sediment rating curves showed a significantly higher rate of sediment transport. The TMDL threshold of concern in Redwood Creek was not exceeded in the period of 1984 to 1995. At-a-station analysis shows that during this period there was a downward shift in the sediment rating curves at both the upstream and downstream gaging stations, but it was also a period of low flows (all less than a 5-year recurrence interval). Moderate flows during the 1996-99 period transported more total sediment than the previous decade, but this was not due to an increase in sediment concentrations for a given discharge. Instead, higher precipitation resulted in greater total water discharge and sediment yield. Data from the low flow period of 2000 to 2003 show a significant shift in the sediment rating curves at both stations, meaning that suspended sediment concentrations are now significantly lower than in any of the earlier periods. Whether or not this shift will continue through the next large flood, however, is a major question for land managers, but it must wait until further stream monitoring during high flows.

Between-station analysis shows that during the recent period of moderately high flows, from 1996 to 1999, the upstream and downstream gaging stations displayed similar suspended sediment rating curves on a per unit water discharge basis. The similarity of transport rates at the two stations is somewhat surprising because there was higher landslide sediment delivery to channels in the upper basin area. The Redwood Creek watershed experienced accelerated landsliding during the wet period of 1996-1999, particularly during the January, 1997, storm period. A landslide inventory, based on 1997 air photos and intensive field mapping, documented the location and size of 365 new landslides (unpublished data, RNSP, Arcata, CA). Total landslide mass as well as the portion of the total mass that was delivered to the stream system were determined for the watershed areas above each of the gaging stations. For the area above O'Kane (the upper basin area), landslide mass delivered to channels was about 173,000 Mg, or 990 Mg/km^2, and for the area above Orick (entire watershed), the mass delivered was about 485,000 Mg, or 676 Mg/km^2. The lower basin produced less landslide mass delivered to channels than the upper basin on an area-weighted basis. There are several possible explanations for the discrepancy between sediment transport and landslide activity. The middle portion of the basin, downstream of O'Kane but upstream of Orick, is also undergoing timber harvest, but contemporary erosion sources are unquantified there. In addition, sediment previously stored in the channel bed in the middle and lower basin is being reworked and remobilized (Madej and Ozaki, 2001), contributing to the downstream station's sediment yield. Sediment from landslides in the upper watershed may be stored in the channel.

We expect that as the sediment supply in the lower basin diminishes due to revegetation, road decommissioning, channel bed scour and the cessation of timber harvest, there will be a detectable shift in the sediment transport curve at the downstream, Orick station. No large flows (return period of 25 years or more) have occurred since 1975, however. Continued stream monitoring and field evaluation of hillslope erosion sources, especially during the next large flood, will be used to test this premise further.

The TMDL's use of a rolling average gives a general picture of sediment yields in the watershed, but it does not differentiate between decreases in sediment supply and decreases due to low water yield. Such a differentiation is critical in guiding land management decisions. The use of suspended sediment rating curves strengthens the interpretation of the TMDL threshold by comparing the relationship of sediment concentrations for a given discharge across several time periods. For example, the rolling average showed an increase in sediment yield in the late 1990's following several years of low flow and low sediment yields, but the rating curve analysis demonstrated that the increase was not due to lower sediment concentrations per unit discharge, rather to higher total runoff for the period.

REFERENCES

California Regional Water Quality Control Board North Coast Region. (1998). "Proposed Redwood Creek Water Quality Attainment Strategy for Sediment (Total Maximum Daily Loads and Implementation Plan)," Santa Rosa California.

Kelsey, H. M.,Coghlan, M., Pitlick, J. and Best, D. (1995). "Geomorphic analysis of streamside landslides in the Redwood Creek Basin, Northwestern California," Geomorphic Processes and Aquatic Habitat in the Redwood Creek Basin, Northwestern California. USGS Professional Paper 1454. K. M. Nolan, H. M. Kelsey, and D. C. Marron, eds.

Madej, M. A., and Ozaki, V. 2001. Redwood Creek, California, USA in Source to Sink Sedimentary Cascades in Pacific Rim Geo-systems. T. Marutani, G. J. Brierley, N. A. Trustrum, and M. Page, eds. Ministry of Land, Infrastructure and Transport, Nagano, Japan. 183 p.

Pitlick, J. (1995). "Sediment routing in tributaries of the Redwood Creek Basin, Northwestern California," Geomorphic Processes and Aquatic Habitat in the Redwood Creek Basin, Northwestern California, USGS Professional Paper 1454. K. M. Nolan, H. M. Kelsey, and D. C. Marron, eds.

OVERVIEW OF SELECTED SURROGATE TECHNOLOGIES FOR CONTINUOUS SUSPENDED-SEDIMENT MONITORING

John R. Gray, Hydrologist, U.S. Geological Survey, Reston, Virginia, jrgray@usgs.gov; Jeffrey W. Gartner, Research Oceanographer, U.S. Geological Survey, Tucson, Arizona, jgartner@usgs.gov

Abstract: Surrogate technologies for inferring selected characteristics of suspended sediments in surface waters are being tested by the U.S. Geological Survey and several partners with the ultimate goal of augmenting or replacing traditional monitoring methods. Optical properties of water such as turbidity and optical backscatter are the most commonly used surrogates for suspended-sediment concentration, but use of other techniques such as those based on acoustic backscatter, laser diffraction, digital photo-optic, and pressure-difference principles is increasing for concentration and, in some cases, particle-size distribution and flux determinations. The potential benefits of these technologies include acquisition of automated, continuous, quantifiably accurate data obtained with increased safety and at less expense. When suspended-sediment surrogate data meet consensus accuracy criteria and appropriate sediment-record computation techniques are applied, these technologies have the potential to revolutionize the way fluvial-sediment data are collected, analyzed, and disseminated.

INTRODUCTION

The U.S. Geological Survey (USGS) and several partners are evaluating instruments and methods that show promise for providing continuous and reliable—unbiased and quantifiably precise—data on selected fluvial-sediment characteristics in riverine and laboratory settings. Sedimentary phases of interest include characteristics of bed material and bed topography, size distributions and transport rates of sediments in suspension and as bedload, and suspended-sediment concentrations.

This paper describes the operational basis of some of the instruments and techniques being developed or tested (Gartner and Gray, 2003; Gray, 2005), and evaluates initial results of USGS research in bulk-optic, laser-diffraction, digital-optic, acoustic, and pressure-difference technologies (Gray et al., 2003) used to infer selected characteristics of suspended sediments without the need for routine collection and analysis of physical samples (Edwards and Glysson, 1999; Bent et al., 2001). Criteria for the accuracy of data produced by surrogate technologies are suggested, as is a method of using concurrent flow and surrogate data to compute reliable records of suspended-sediment discharge.

SUMMARY OF SURROGATE TECHNOLOGIES IN EVALUATION

Bulk Optics: Measurements of the bulk-optical properties of water are the most common means for determining water clarity and estimating suspended-sediment concentrations (SSC) in United States (U.S.) rivers (Pruitt, 2003). A number of optical instruments are commercially available.

Bulk-optic instruments can be categorized as:

- Transmissometers, which employ a light source beamed directly at the sensor. The instrument measures the light transmission.
- Nephelometers, which measure light scattered by suspended particles (rather than light transmission). Nephelometers generally measure 90° or forward scattering. An optical backscatter (OBS) instrument (Downing et al., 1981; Downing, 1983) is a type of nephelometer designed to measure backscattered infrared radiation in a small (concentration dependent) volume on the order of a few cm^3.

These instruments provide measurements from a single point. Both transmittance and scatterance are functions of the number, size, color, index of refraction, and shape of suspended particles.

These bulk-optical instruments are generally inexpensive, lack moving parts, and provide rapid sampling capability. The instruments rely on empirical calibrations to convert measurements to estimates of SSC. The technology is relatively mature, and has been shown to provide reliable data at a number of USGS streamflow-gaging stations (Schoellhamer and Wright, 2003; Melis et al., 2003; Uhrich, 2003; Rasmussen et al., 2003; Rasmussen, et al. 2005) and other sites (Pratt and Parchure, 2003; Lewis, 2003).

There are several drawbacks associated with use of bulk-optic instruments that include:

- Lack of consistency in instrument measurement characteristics (Ziegler, 2003; Landers, 2003)
- Variable instrument response to grain size, composition, color, shape, and coating,

- Biological fouling or damage to optical windows, and
- Nonlinear responses of sensors to sediment concentration (Downing, 1996).

Maximum concentration limits for these instruments depend in part on particle-size distributions. The OBS has a generally linear response at concentrations less than about 2 g/L for clay and silt, and 10 g/L for sand (Ludwig and Hanes, 1990), although Kineke and Sternberg (1992) describe the capability to measure very high concentrations up to about 320 g/L (in the non-linear region of the OBS response curve). The upper concentration limit for transmissometers depends on optical path length, but may be as low as about 0.05 g/L (D&A Instrument Co., 1991). Thus, transmissometers are more sensitive at low concentrations but OBS has superior linearity in turbid water. Sensor-output "drift," or the tendency for the output to shift from the calibration curve to spuriously higher values over timescales of days to weeks, remains a problem, particularly in warmer, microbiologically active waters.

Because of the relation between OBS gain and particle size, OBS (like all single-frequency instruments) is best suited for application at sites with relatively stable particle-size distributions. The OBS is minimally affected by changes in particle-size distribution in the range of 200-400µ, moderately affected by changes between 63-125µ, and greatly affected by changes when particles smaller than about 44µ (Conner and De Visser, 1992; Sutherland et al., 2000). Conner and De Visser (1992) caution against using OBS in environments where changes in size distributions occur and particle sizes are less than 100µ. Additionally, the OBS signal can vary as a function of particle color. Sutherland et al., (2000) found a strong correlation between observed and predicted OBS measurements of varying concentrations and ratios of black and white suspended sediment. They found the smallest OBS response for black sediment and the largest for white sediment, with other colors falling between. They suggest that the level of blackness of particles acts to absorb the near-infrared signal of the OBS, thus modifying its output. Hence, caution should be exercised in deployments under varying particle-size and –color conditions, unless the instrument is recalibrated for ambient conditions.

Laser Diffraction: Applications of laser diffraction in rivers is a relatively recent undertaking, having been originally developed in the 1990's for use in marine and estuarine environments. The USGS is testing in-situ and manually deployed versions of this technology in field and laboratory settings (Topping et al., 2006; Mark N. Landers, USGS, oral commun., 2005; Lawrence Freeman, USGS, oral commun., 2005). At present, this type of in-situ instrument is commercially available from a single manufacturer.

The instruments are designed for in-situ and laboratory determinations of suspended material particle-size distributions from which concentrations can be calculated. These instruments exploit Mie scattering theory: At small forward-scattering angles, laser diffraction by spherical particles is essentially identical to diffraction by an aperture of equal size (Agrawal and Pottsmith, 1994). Thus, this method of estimating concentration and size distribution is mostly insensitive to changes in particle color or composition. Departure from sphericity does produce as yet unknown changes in calibration, and in most cases distorts the fine particle end of the retrieved size distribution. New research is addressing this question empirically (Yogesh Agrawal, Sequoia Scientific, Inc., 2005, written comm.)

The in-situ LISST-100 (Laser In Situ Scattering and Transmissometry) (use of trade, product, or firm name is for descriptive purposes only and does not imply endorsement by the USGS) uses 32 ring detectors to determine particle-size distributions between 2.5-500µ or 1.25–250µ (Sequoia Scientific, Inc., 2004). The LISST-100, which has been field and laboratory tested, has been shown to successfully determine particle-size distributions of natural materials and the size of mono-sized particle suspensions within about a 10-percent accuracy (Traykovski et al., 1999; Gartner et al., 2001). The LISST-100 can also be used to determine SSC from volume concentration if particle density is known (Gartner et al., 2001). Unlike single-frequency optical backscatter instruments, these instruments are not subject to potential inaccuracies associated with changes in particle size if the particles sizes fall within the range of instrument sensitivity (Agrawal and Pottsmith, 2000). As is the case with all types of in-situ optical instruments, however, biological fouling can degrade measurements. This problem can be addressed with anti-fouling shutters that are now available for the LISST-100 (Yogesh Agrawal, Sequoia Scientific, Inc., 2005, written comm.).

In-situ versions of laser diffraction instruments may be deployed unattended to provide a time series of particle-size distributions. There are measurement limitations (in addition to size range), however, that are associated with multiple scattering in the presence of high SSC. Limitations associated with high SSC values are based on the laser-path length and SSC, ranging from tenths of a g/L (small particle sizes) to several g/L (large particle sizes). For suspensions of typical marine sediments, appropriate concentration levels range between about 0.15-5 g/L (Traykovski et al., 1999).

New instrument options and versions are being developed to address these problems and increase the range of applications. For example, reducing the optical path in water from the standard 5 cm to 3 mm has been effected to extend measurement limits to 2-3 g/l of fine material. For still higher concentrations, a LISST-Infinite was developed by Sequoia Scientific, Inc., as part of a research-and-development project with the USGS. The LISST-Infinite, a prototype of which is being tested by the USGS (Konrad et al. 2006), employs a pump to bring a water-sediment sample to the instrument, and then uses automated multi-stage dilution (as necessary) before measuring particle-size distributions and concentrations with a built-in LISST-100. Thus, the measurable concentration limit is, in theory, extended to the highest concentrations of material that can be pumped to the LISST-100 (Yogesh Agrawal, Sequoia Scientific, Inc., 2005, written comm.).

A simpler instrument—the LISST-25—has been developed for measuring a mean concentration and a mean particle size (Sauter mean size). Another instrument, the LISST-FLOC covers the size range from 7.5-1500µ.

A manually deployable cable-suspended streamlined version of the LISST-100 developed for riverine application—the LISST-SL—is in development and testing (Federal Interagency Sedimentation Project, 2005). The LISST-SL is designed to measure real-time velocities that in turn are used to control a pump to withdraw a filament of water and route it through the laser beam at a rate approximately equal to the ambient current velocity (Gray et al, 2002; Gray and Agrawal, 2004). Achieving isokinetic flow-through capability by the LISST-SL—considered by the Federal Interagency Sedimentation Project to be +/- 10 percent of the ambient stream velocity, although the actual sedimentological efficiency of any device that relies on the isokinetic-flow principle may also vary with changes in ambient particle-size distributions (Federal Interagency Sedimentation Project, 1941)—is a prerequisite for reliably ascertaining the suspended-sediment properties in all but the shallowest or most sluggish rivers (Edwards and Glysson, 1999; Agrawal and Pottsmith, 2006).

Digital Photo-Optics: Digital-imaging acquisition and analysis techniques pioneered by industry in the late 1970's became relatively sophisticated in the later 1980's following the advent of high-speed computers with ample storage capabilities. The initial focus of the technology's application included biomedical image processing (such as for enumerating blood cells), machine vision for manufacturing, and computer vision for use in robotics. Adaptation of the technology for in-situ determination of suspended-sediment size and shape followed in the 1990's (Eisma and Kalf, 1996). This technology is in development at the USGS Cascades Volcano Observatory (CVO) fluvial-sediment laboratory (U.S. Geological Survey, 2005; Gooding, 2001). Present equipment is designed for laboratory use, although the technology also is intended for in-situ applications.

A prototype for digital imaging acquisition and classification for suspended sediment analysis that utilizes an exclusively designed flow-cell enables discrete identification of particle attributes such as size and shape. Using software developed at CVO, a high-quality digital image of suspended-sediment particles is simplified by morphological transformation. The transformation retains the size and shape characteristics of the discretely imaged particles for quantitative analysis. Hardware enhancements have improved image quality for more reliable automated computer interpretations and extended the size range that can be resolved. Use of a multi-lens system will permit applications with sand-, silt-, and (or) clay-size distributions of suspended material.

There is no lower concentration limit. The upper limit is yet to be established, but tests up to 10 g/L have provided accurate results. The upper limit might be obviated in laboratory applications by a dilution system that is being designed to use optically sensed concentration values to automatically add and mix known amounts of de-ionized water to the sample to obtain concentrations within the measurable range (Daniel Gooding, USGS, 2005, written commun.).

Efforts are now focused on refining and testing computer software to determine particle concentration, size, and shape in real or near-real time. The system is presently designed for determining size distributions and turbidity; however future plans are to add capability to determine SSC from size-distribution information. Nevertheless, digital photo-optic systems requiring little or no calibration may ultimately replace visual accumulation tube and pipette laboratory techniques for analysis of particle-size distributions.

Acoustic Backscatter: The technique of using acoustic backscatter (ABS) intensity to estimate mass concentration of suspended material, first tested in the 1980's (Gartner, 2003), is the focus of research at about a dozen USGS streamflow-gaging stations (Gray et al., 2003). Results of some initial tests of single-frequency ABS are encouraging (Byrne and Patiño, 2001). Research has expanded into use of multi-frequency ABS that may provide continuous information on particle-size distributions in addition to concentrations (Topping et al., 2006; Mark N. Landers, USGS, oral commun., 2005).

The method, which utilizes the strength of the signal backscattered from suspended-sediment particles, is based on the sonar equation (Urick, 1975; Reichel and Nachtnebel, 1994). ABS applications require empirical calibrations to convert measurements to estimates of SSC. Post-processing algorithms are complex, requiring compensations for hydrologic properties of ambient water such as temperature, salinity, pressure, and suspended materials as well as instrument characteristics such as frequency, power, and transducer design (Thorne et al., 1991; Downing et al., 1995). Researchers generally develop their own software, for example Jay et al., 1999 or Gartner, 2004, although at least one commercial product is available (Land and Jones, 2001) but not yet widely used.

Instruments operating at a single acoustic frequency can provide estimates of SSC but lack information about particle-size distributions. The method appears appropriate for use in concentrations up to several grams per liter. Quantification of higher concentrations may be problematic, especially when using high acoustic frequencies that are more prone to attenuation from sediment. The result is a non-linear (backscatter intensity) response at high concentrations (Hamilton et al., 1998). Although a function of frequency, attenuation from sediment should be accounted for in the presence of as little as 0.1 g/L (Libicki et al., 1989; Thorne et al., 1991) and multiple scattering produces non-linear response when SSC is on the order of 10 g/L (Sheng and Hay, 1988; Hay, 1991).

The method has the advantage of being less susceptible to biological fouling than optical techniques and is non-intrusive. ABS also holds a distinct advantage over most other surrogate technologies in that, if an acoustic Doppler velocity profiler (ADCP) is used, it measures in a beam that may extend tens of meters laterally or vertically in the channel, thus integrating the sedimentary characteristics over an area. Additionally, when calibrated, the estimated SSC values enable calculations of suspended-sediment transport when coupled with river-discharge values, for example Topping et al., 2006 or Wall et al., 2006. The relation between acoustic frequency and particle size, however, limits the size range for which the method is appropriate (Hanes et al., 1988; Schaafsma et al., 1997). For example, with a 1200 kilohertz ADCP, the method is appropriate for particle-size distributions in which there is no significant concentration of particles larger than about 400µ. The method is increasingly less accurate as the percentage of particles approaching or larger than this limit increases. In addition, variations in size distribution increase errors associated with the ABS method, similar to all single frequency instruments, thus careful calibrations are critical. Estimates of SSC at accuracies similar to those for optical instruments are possible under some conditions (Thevenot and Kraus, 1993); comparisons with SSC values from water samples have been found to agree within about 10-20 percent (Thevenot et al., 1992; Thorne et al., 1991; and Hay and Sheng, 1992).

Pressure Difference: One of the first uses of the pressure-difference technique for measuring fluid density was applied to crude oil in pipes (William Fletcher, D&A Associates, 1999, oral commun.). The technology has laboratory and field applications (Lewis and Rasmussen, 1999). Information on the field performance of the technology is available from USGS streamflow-gaging stations in Puerto Rico, Georgia, and Arizona. Initial tests at concentrations ranging up to about 1.5 g/L at a USGS streamflow gaging station in Puerto Rico were encouraging, but were not unequivocally successful (Larsen et al., 2001). Results from subsequent tests at the Paria River at Lees Ferry, Arizona, streamflow-gaging station at concentrations of hundreds of g/L are encouraging (Gregory G. Fisk, USGS, oral commun., 2005).

The pressure-difference technique relies on simultaneous measurements from two precision pressure-transducer sensors arrayed at different fixed elevations in a water column. The difference in pressure readings is converted to a water-density value, from which SSC is inferred after correcting for water temperature (dissolved-solids concentrations in these fresh-water systems are inconsequential in the density computation). Implicit assumptions in the method are that density of water and sediment are known, and exceptionally sensitive pressure transducers are used. The technique has been applied in the laboratory with promising results of better than 3-percent accuracy (0.543 ± 0.014 g/L) for determining mass concentration of suspensions of glass microspheres (Lewis and Rasmussen, 1999). Application of this technique in the field can be complicated by low signal-to-noise ratio, turbulence, significantly large dissolved solids concentrations, and temperature variations. Additionally, analysis may be complicated by density variations in the suspended material. The differential pressure method generally has been successful in the field at concentrations greater than about 50 g/L but needs additional evaluation in the range of 10-50 g/L. The technique may not be reliable at lower concentrations. William Fletcher (D&A Associates, 2005, oral commun.) indicated that calculations based on a moving average of the pressure-difference data tended to provide a smoother concentration time series and render them more comparable to available concentration data derived from water-sediment samples obtained by methods described by Edwards and Glysson (1999).

RANGE AND ACCURACY CRITERIA

All of the preceding sediment-surrogate technologies are capable of providing a signal that can be empirically converted to a concentration value (in the case of laser-diffraction technology, LISST, concentration is inferred from summation of the measured particle-size distribution). However, a fundamental question remains: Can the technology provide reliable measurements over the full range of the sedimentary parameter of interest? Thus, it is important for a user to recognize the sensitivity of these systems to particles outside their measurement range.

A measurement range normally is confined by the expected extremes for the parameter of interest within the context of the monitoring program's objectives. For example, if the objective is to quantify mass transport, the instrument should be able to measure the concentration values that can occur at the site during the monitoring period, with particular emphasis on the larger concentrations and higher flows. If information on transport by size class is sought, then a sufficient number of particle-size distributions are needed; ergo, the instrument must be capable of characterizing the full range of particle sizes expected at the site.

Among the benefits of sediment-surrogate technologies—aside from not requiring routine collection of a physical sample for subsequent analysis—is the capability to compute estimates of uncertainty associated with the derived unit- and daily-value data. The subject of uncertainty estimates in concentration or particle-size distribution measurements, and particularly in flux measurements, is complex given that each measurement variable – the surrogate signal and the calibration, streamflow, and ancillary data – have non-zero variances. Until research provides a reliable means for such computations, uncertainties computed for sediment-surrogate measurements will be referenced to analytical results from periodically collected, representative water samples (Edwards and Glysson, 1999) which are widely considered to be the best such data available describing the sedimentary conditions of the Nation's rivers and streams.

Gray et al. (2002) developed accuracy criteria specifically for development of the LISST-SL. An updated version of those concentration and particle-size distribution criteria suggested for general use follows:

- Particle-Size Distributions: The instrument should be capable of measuring suspended-sediment particles ranging from 2-2,000μ median diameter within 25 percent of the actual size for 90 percent of the measured values.
- Suspended-Sediment Concentrations: The instrument should provide SSC from zero to the maximum expected concentration value for 90 percent of measured values to within:
  (a) 50 percent of actual SSC for SSC less than 0.01 g/L,
  (b) from 50 percent of actual SSC of 0.01 g/L to 25 percent of SSC of 0.1 g/L, computed linearly,
  (c) from 25 percent of actual SSC of 0.1 g/L to 15 percent of SSC of 1 g/L, computed linearly,
  (d) from 15 percent of actual SSC of 1 g/L to 10 percent of SSC of 10 g/L, computed linearly, and
  (e) 10 percent of actual SSC for SSC greater than 10 g/L.

Deviations from these criteria should not be skewed within a single size-distribution or in a concentration range, rather, they should be more or less evenly distributed throughout the measuring ranges.

SEDIMENT-RECORD COMPUTATION

Use of a reliable unit-value time series of SSC with paired discharge values represents the most accurate means for computing suspended-sediment loads on a sub-daily and daily basis. Record computation based on this technique was developed in the middle 20th century (Porterfield, 1972) and is used by the USGS today. In the late 1990's, the USGS developed the Graphical Constituent Loading Analysis System (GCLAS), a software package for computing daily discharge (load) records of suspended sediment and other water-quality constituents, to facilitate and enhance those computational techniques (Mckallip et al., 2001).

GCLAS features an interactive graphical user interface that permits easy entry of estimated constituent-concentration values and provides new tools to aid in making those estimates. It uses a water-discharge time series, and suspended-sediment values to determine daily suspended-sediment discharges and associated daily mean SSC. The program also is capable of computing discharges of any constituent expressed in terms of mass per volume.

GCLAS includes tools to aid in making estimates of constituent concentrations for periods when concentration data are missing or under-sampled. In addition, GCLAS facilitates analysis and application of cross-section coefficients, which are multipliers used to adjust concentration values obtained from samples collected at a fixed

point or vertical so that the concentration values are more representative of the discharge-weighted mean concentration at the cross-section and time of interest.

CONCLUSIONS

New river monitoring technologies being studied by the USGS and several partners show considerable promise for providing continuous and quantifiably accurate data describing selected characteristics of suspended-sediment. It is unlikely that any one technology will suffice for all monitoring needs of the USGS. An understanding of the sedimentary conditions in a given river coupled with knowledge of data requirements and the attributes of these technologies is needed to select an appropriate surrogate technology. Instruments that meet data-accuracy criteria will be deployed operationally, and new software will use the derivative data to compute quantifiably accurate records of suspended-sediment discharge.

REFERENCES

Agrawal, Y.C. and Pottsmith, H.C. 1994, "Laser diffraction particle sizing in STRESS," Con. Shelf Res., 14, pp. 1101-1121.

Agrawal, Y.C. and Pottsmith, H.C., 2000, "Instruments for particle size and settling velocity observations in sediment transport," Marine Geology 168 (2000), Elsevier Science Publishers, Amsterdam, pp. 89-114.

Agrawal, Y.C. and Pottsmith, H.C., 2006, "The isokinetic streamlined suspended sediment profiling LISST-SL - status and field results," Proceedings, 8th Federal Interagency Sedimentation Conference, April 2-6, 2006, Reno, NV.

Bent, G.C., Gray, J.R., Smith, K.P., and Glysson, G.D., 2001, "A synopsis of technical issues for monitoring sediments in highway and urban runoff," in The National Highway Runoff Data and Methodology Synthesis, Gregory E. Granato, Chester Zenone, and Patricia E. Cazenas, eds: U.S. Department of Transportation Publication No. FHWA-EP-03-054, Vol. 1, pp. 113-163. (http://ma.water.usgs.gov/fhwa/products/ofr00497.pdf).

Byrne, M.J., and Eduardo Patiño. 2001, "Feasibility of using acoustic and optical backscatter instruments for estimating total suspended solids concentrations in estuarine environments," Proceedings of the 7th Federal Interagency Sedimentation Conference, Reno, NV, March 25-29. Vol. I, III-135 to III-138. (http://pubs.usgs.gov/misc_reports/FISC_1947-2001/).

Conner, C. S., and De Visser, A. M., 1992, "A laboratory investigation of particle size effect on an optical backscatterance sensor," Marine Geology 108 (1992), Elsevier Science Publishers, Amsterdam, pp. 151-159.

D&A Instrument Company, 1991, "OBS-1&3: Suspended solids and turbidity monitor (rev 3/91)," Port Townsend, WA, D & A Instrument Company Instruction Manual, 41 p.

Downing, Andrew, Thorne, P. D., and Vincent, C. E., 1995, "Backscattering from a suspension in the near field of a piston transducer," J. Acoustical Society of America, 97 (3), pp 1614-1620.

Downing, J. P., 1996, "Suspended sediment and turbidity measurements in streams: What they do and do not mean. Automatic Water Quality Monitoring Workshop, Richmond, B.C., February 12-13, 1996.

Downing, J. P., Sternberg, R. W., and Lister, C. R. B., 1981, "New instrumentation for the investigation of sediment suspension processes in the shallow marine environment," Marine Geology 42 (1981), pp. 19-34.

Downing, J. P., 1983, "An optical instrument for monitoring suspended particles in ocean and laboratory," in OCEANS 1983, San Francisco, California, August 29-September 1, 1983, Proceedings. pp. 199-202.

Edwards, T. K., and Glysson, G. D., 1999, "Field methods for measurement of fluvial sediment," U.S. Geological Survey Techniques of Water-Resources Investigations Book 3, Chapter C2, 89 p. (http://water.usgs.gov/osw/techniques/sedimentpubs.html).

Eisma, D., and Kalf, J., 1996, "In situ particle (floc) size measurements with the NOIZ (Netherland Institute of Sea Research) in situ camera system," Journal of Sea research 36, (1/2) pp. 49-53.

Federal Interagency Sedimentation Project, 1941, "Laboratory investigation of suspended-sediment samplers: Iowa City," Iowa University Hydraulics Laboratory, Interagency report No. 5, 99 p.

Federal Interagency Sedimentation Project, 2005, Home page. (http://fisp.wes.army.mil/).

Gartner, J. W., Cheng, T.T., Wang, P.F., and Kenneth Richter, 2001, "Laboratory and field evaluations of the LISST-100 instrument for suspended particle size determinations," Marine Geology 175 (2001), Elsevier Science Publishers, Amsterdam, pp. 199-219.

Gartner, J. W., 2003, "Estimation of suspended solids concentrations based on acoustic backscatter intensity—theoretical background," Proceedings of the Federal Interagency Workshop on Turbidity and Other Sediment Surrogates, April 30-May 2, 2002, Reno, NV, J. R. Gray and G. Douglas Glysson eds.: U.S. Geological Survey Circular 1250, 136 p. (http://water.usgs.gov/pubs/circ/2003/circ1250/).

Gartner, J. W., 2004, "Estimating suspended solids concentrations from backscatter intensity measured by acoustic Doppler current profiler in San Francisco Bay, California<' Marine Geology 211 (2004), Elsevier Science Publishers, pp 169-187.

Gartner, J.W., and Gray, J.R., 2003, "Summary of suspended-sediment technologies considered at the Interagency Workshop on Turbidity and Other Sediment Surrogates," Federal Interagency Workshop on Sediment Monitoring Instrument and Analysis Research, September 9-11, 2003, Flagstaff, Arizona, 9 p. (http://water.usgs.gov/osw/techniques/sediment/sedsurrogate2003workshop/gartner_gray.pdf).

Gooding, D. J., 2001, "Photo-optical sedimentation tube," Proceedings of the 7th Federal Interagency Sedimentation Conference, March 25-29, 2001, Reno, NV, poster-29. (http://pubs.usgs.gov/misc_reports/FISC_1947-2001/).

Gray, J.R., (ed), 2005, "Proceedings of the Federal Interagency Sediment Monitoring Instrument and Analysis Workshop, September 9-11, 2003, Flagstaff, Arizona," U.S. Geological Survey Circular 1276, 46 p. (http://water.usgs.gov/pubs/circ/2005/circ1276/; Appendix 4 is available only online at: http://water.usgs.gov/osw/techniques/sediment/sedsurrogate2003workshop/listofpapers.html).

Gray, J.R., and Agrawal, Y.C., 2004, "The LISST-SL Streamlined Isokinetic Suspended-Sediment Profiler," Proceedings, 9th International Symposium on River Sedimentation, Oct. 18-21, 2004, Yichang, China, Vol. IV, pp. 2549-2555. (http://water.usgs.gov/osw/techniques/Lisst_Gray_Agrawal_Pottsmith.pdf).

Gray, J.R., Glysson, G.D., and Mueller, D.S., 2002, "Comparability and accuracy of fluvial-sediment data: A view from the U.S. Geological Survey," Proceedings of the American Society of Civil Engineers, Hydraulic Measurements and Methods Symposium, July-August, 2002, Estes Park, CO, 6 p. (http://water.usgs.gov/osw/techniques/asce.pdf).

Gray, J.R., Patiño, Eduardo, Rasmussen, P.P., Larsen. M.C., Melis, T.S., Topping, D.J., and Alamo, C.F., 2003, "Evaluation of sediment surrogate technologies for computation of suspended-sediment transport," Proceedings of the 1st International Yellow River Forum on River Basin Management, October 21-24, 2003, Zhengzhou, Henan Province, China, the Yellow River Conservancy Publishing House, Vol. III, pp. 314-323. (http://water.usgs.gov/osw/techniques/yrcc_surrogates.pdf).

Hamilton, L. J., Shi, Z., and Zhang, S. Y., 1998, "Acoustic backscatter measurements of estuarine suspended cohesive sediment concentration profiles," Journal of Coastal Research 14(4), pp. 1213-1224.

Hanes, D. M., Vincent, C. E., Huntley, D. A., Clarke, T. L., 1988, "Acoustic measurements of suspended sand concentration in the C2S2 experiment at Stanhope Lane, Prince Edward Island," Marine Geology 81 (1988), Elsevier Science Publishers, Amsterdam, pp. 185-196.

Hay, A. E., 1991, "Sound scattering from a particle-laden, turbulent jet," J. Acoust. Soc. Am., 90(4) pt. 1, pp. 2055-2074.

Hay, A. E. and Sheng, Jinyu, 1992, "Vertical profiles of suspended sand concentration and size from multi-frequency acoustic backscatter," Journal of Geophysical Research, Vol. 97, No. C10, pp. 15,661-15,677.

Jay, D. A., Orton, Philip, Kay, D. J., Fain, Annika, and Baptisa, A. M., 1999, "Acoustic determination of sediment concentrations, settling velocities, horizontal transports, and vertical fluxes in estuaries," Proceedings, 6th Working Conference on Current Measurement, March 11-13, 1999, San Diego, CA, pp. 258-263.

Kineke, G. C., and Sternberg, R. W., 1992, "Measurements of high concentration suspended sediments using the optical backscatterance sensor," Marine Geology, 108, pp. 253-258.

Konrad, C., Pottsmith, C., Melis, T., and Rubin, D., 2006, "Real-time analysis of concentrated fluvial suspended sediments," Proceedings, 8th Federal Interagency Sedimentation Conference, April 2-6, 2006, Reno, NV.

Land, J. M. and Jones, P. D., 2001, "Acoustic measurement of sediment flux in rivers and near-shore waters," Proceedings of the 7th Federal Interagency Sedimentation Conference, March 25-29, 2001, Reno, NV, pp. III 127-134. (http://pubs.usgs.gov/misc_reports/FISC_1947-2001/).

Landers, M.N., 2003, "Summary of blind sediment reference sample measurement session," Proceedings of the Federal Interagency Workshop on Turbidity and Other Sediment Surrogates, April 30-May 2, 2002, Reno, NV, J. R. Gray and G. Douglas Glysson, eds. U.S. Geological Survey Circular 1250, pp. 29-30 (http://water.usgs.gov/pubs/circ/2003/circ1250/).

Larsen, M.C., Alamo, C.F., Gray, J.R., and Fletcher, William, 2001, "Continuous automated sensing of streamflow density as a surrogate for suspended sediment concentration sampling," Proceedings of the 7th Federal Interagency Sedimentation Conference, March 25-29, 2001, Reno, NV, pp III 102-109. (http://pubs.usgs.gov/misc_reports/FISC_1947-2001/).

Lewis, A. J. and Rasmussen, T. C., 1999, "Determination of suspended sediment concentrations and particle size distributions using pressure measurements," J. Environ. Qual., 28, pp 1490-1496.

Lewis, Jack, 2003, "Estimation of suspended sediment flux in streams using continuous turbidity and flow data coupled with laboratory concentrations," Proceedings of the Federal Interagency Workshop on Turbidity and Other Sediment Surrogates, April 30-May 2, 2002, Reno, NV, J. R. Gray and G. Douglas Glysson eds.: U.S. Geological Survey Circular 1250, 3 p. (http://water.usgs.gov/osw/techniques/TSS/LewisTSS.pdf).

Libicki, Charles, Bedford, K.W., and Lynch, J.F., 1989, "The interpretation and evaluation of a 3-MHz acoustic backscatter device for measuring benthic boundary layer sediment dynamics," J. Acoust. Soc. Am. 85(4), April 1989, pp. 1501-1511.

Ludwig, K.A., and Hanes, D.M., 1990, "A laboratory evaluation of optical backscatterance suspended solids sensors exposed to sand-mud mixtures," Marine Geology 94 (1990), Elsevier Science Publishers, Amsterdam, pp. 173-179.

Mckallip, T.E., Koltun, G.F., Gray, J.R., and Glysson, G.D., 2001, "GCLAS – A graphical constituent loading analysis system," Proceedings of the 7th Federal Interagency Sedimentation Conference, March 25-29, 2001, Reno, NV, vol. II, VI-49 to VI-52. (http://pubs.usgs.gov/misc_reports/FISC_1947-2001/).

Melis, T.S., Topping, D.J., and Rubin, David M., 2003, "Testing laser-based sensors for continuous in situ monitoring of suspended sediment in the Colorado River, Arizona," in, Bogen, J., Fergus, T., and Walling, D.E. (eds), Erosion and Sediment Transport Measurement in Rivers, Technological and Methodological Advances. International Association of Hydrological Sciences Publication 283, pp. 21-27.

Porterfield, George, 1972, "Computation of fluvial-sediment discharge," U.S. Geological Survey Techniques of Water-Resources Investigations Book 3, Chapter C3, 66p. (http://pubs.er.usgs.gov/pubs/twri/twri03C3).

Pratt, Thad, and Parchure, Trimbak, 2003, "OBS calibration and field measurements," Proceedings of the Federal Interagency Workshop on Turbidity and Other Sediment Surrogates, April 30-May 2, 2002, Reno, NV, J. R. Gray and G. Douglas Glysson eds.: U.S. Geological Survey Circular 1250, 3 p. (http://water.usgs.gov/pubs/circ/2003/circ1250/).

Pruitt, B.A., 2003, "Uses of turbidity by States and Tribes," Proceedings of the Federal Interagency Workshop on Turbidity and Other Sediment Surrogates, April 30-May 2, 2002, Reno, NV, pp. 31-46 (http://water.usgs.gov/pubs/circ/2003/circ1250/).

Rasmussen, P.P., Bennett, Trudy, Lee, Casey, and Christensen, V.G., 2003, "Continuous in-situ measurement of turbidity in Kansas streams," Proceedings of the Federal Interagency Workshop on Turbidity and Other Sediment Surrogates, April 30-May 2, 2002, Reno, NV, J. R. Gray and G. Douglas Glysson eds.: U.S. Geological Survey Circular 1250, 3 p. (http://water.usgs.gov/pubs/circ/2003/circ1250/).

Rassmussen, T.J., Ziegler, A.C., and Rasmussen, P.P., 2005, "Estimation of constituent concentrations, densities, loads and yelds in lower Kansas River, northeast Kansas, using regression models and continuous water-qualtiy monitoring, January 2000 through December 2003," U.S. Geological Survey Scientific Investigations Report 2005-5165 (http://pubs.er.usgs.gov/pubs/sir/sir20055165).

Reichel, G., and Nachtnebel, H. P., 1994, "Suspended sediment monitoring in a fluvial environment: Advantages and limitations applying an acoustic Doppler current profiler," Wat. Res., Vol. 28, No. 4, pp. 751-761.

Schaafsma, A. J., Lafort, A. M., and Guyomar, Daniel, 1997, "Development of an acoustic method and prototype instrumentation for size and concentration measurement of suspended sediment," in, Proceedings of the First International Conference on EuroGOOS: 7-11 October, 1996, The Hague, The Netherlands (Elsevier), pp. 168-175.

Schoellhamer, D.H., and Wright, S.A., 2003, "Continuous measurement of suspended-sediment discharge in rivers by use of optical backscatterance sensors," in, Bogen, J., Fergus, T., and Walling, D.E. (eds), Erosion and Sediment Transport Measurement in Rivers, Technological and Methodological Advances: International Association of Hydrological Sciences Publication 283, pp. 28-36.

Sequoia Scientific, Inc., 2004, Home page: http://www.sequoiasci.com/default.aspx?SectionName=home.

Sheng, Jinyu and Hay, A. E., 1988, "An examination of the spherical scatter approximation in aqueous suspensions of sand," J. Acoust. Soc. Am. 83(2), February 1988, pp. 598-610.

Sutherland, T.F., P.M. Lane, C.L. Amos, J. Downing, 2000. "The calibration of optical backscatter sensors for suspended sediment of varying darkness levels," Marine Geology, 162: 587-597.

Thevenot, M. M., Prickett, T. L., and Kraus, N. C., 1992, "Tylers Beach, Virginia, dredged material plume monitoring project 27 September to 4 October 1991," Dredging Research Program Technical Report DRP-92-7, US Army Corps of Engineers, Washington, D.C, 204 p.

Thevenot, M. M., and Kraus, Nicholas C., 1993, "Comparison of acoustical and optical measurements of suspended material in the Chesapeake Estuary," J. Marine Env. Eng., Vol. 1, Gordon and Breach Science Publishers, pp. 65-79.

Thorne, P. D., Vincent, C. E., Harcastle, P. J., Rehman, S., and Pearson, N., 1991, "Measuring suspended sediment concentrations using acoustic backscatter devices," Marine Geology, 98, Elsevier Science Publishers, Amsterdam, pp. 7-16.

Topping, D. J., Wright, S. A., and Melis, T. S., 2006, "High resolution monitoring of suspended-sediment concentration and grain size in the Colorado River using laser diffraction instruments and a three-frequency acoustic system," Proceedings, 8th Federal Interagency Sedimentation Conference, April 2-6, 2006, Reno, NV.

Traykovski, Peter, Latter, R. J., and Irish, J. D., 1999, "A laboratory evaluation of the laser in situ scattering and transmissometry instrument using natural sediments," Marine Geology 159 (1999), Elsevier Science Publishers, Amsterdam, pp. 19355-367.

Uhrich, M.A., 2003, "Determination of total and clay suspended-sediment loads from instream turbidity data in the North Santiam River Basin, Oregon, 1998-2002," Proceedings of the Federal Interagency Workshop on Turbidity and Other Sediment Surrogates, April 30-May 2, 2002, Reno, NV, J. R. Gray and G. Douglas Glysson eds. U.S. Geological Survey Circular 1250, 3 p. (http://water.usgs.gov/pubs/circ/2003/circ1250/).

Urick, R. J., 1975, Principles of Underwater Sound: 2nd ed., McGraw Hill, N. Y., 384 p.

U.S. Geological Survey, 2005, Cascades Volcano Observatory sediment laboratory. (http://vulcan.wr.usgs.gov/Projects/SedLab/framework.html).

Wall, G. R., Nystrom, E. A., and Litten, Simon, 2006, "Use of an ADCP to compute suspended sediment discharge in the tidal Hudson River, NY," Proceedings, 8th Federal Interagency Sedimentation Conference, April 2-6, 2006, Reno, NV.

Ziegler, A.C., 2003, "Breakout session 1: Definition of optical methods for turbidity and data reporting," Proceedings of the Federal Interagency Workshop on Turbidity and Other Sediment Surrogates, April 30-May 2, 2002, Reno, NV, J. R. Gray and G. Douglas Glysson, eds. U.S. Geological Survey Circular 1250, pp. 9-13 (http://water.usgs.gov/pubs/circ/2003/circ1250/).

TURBIDITY SENSORS TRACK SEDIMENT CONCENTRATIONS IN RUNOFF FROM AGRICULTURAL FIELDS

Seth M. Dabney, Research Agronomist, USDA-ARS, Oxford, MS, sdabney@ars.usda.gov;
Martin A. Locke, Research Leader, USDA-ARS, MS, mlocke@msa-oxford.ars.usda.gov;
R. Wade Steinriede, Biologist, USDA-ARS, Oxford, MS, rsteinriede@ars.usda.gov

Abstract: Optical backscatter (OBS) turbidity sensors offer the opportunity to obtain a continuous record of soil loss if turbidity is well correlated with sediment concentration. The relationship between turbidity and sediment concentration depends on several factors, including: particle size, particle shape, and particle color. As watershed size is reduced to the scale of individual fields or plots, variability in particle composition is reduced and the relationship between turbidity and concentration may become stable. We undertook studies to determine this relationship for several fields using OBS-3 turbidity sensors. We compared concentration - turbidity relationships for both suspensions of dried soil samples and sequential natural rainfall runoff samples from three ~15-ha fields. We obtained strong correlations between turbidity and concentration, but the relationships differed between natural runoff and resuspended samples. Overall, turbidity explained 95% of the variability in sediment concentration observed in natural runoff samples from one of the fields that was used for calibration. When the resulting regression relationship was applied to two adjacent but independent fields, accuracy of prediction was similar. Prediction accuracy was only marginally improved by consideration of additional parameters including discharge, rate of change of discharge, and time within runoff event, indicating little hysteretic behavior. Peak turbidity usually preceded both peak flow rate and the time of collection of the first sequential sample. We conclude that calibrated optical backscatter turbidity sensors placed in edge-of-field grade control pipes have good potential for continuously monitoring soil loss and improving field-scale soil loss estimates with an expected accuracy estimated to be about 0.5 t ha^{-1} y^{-1}. When combined with measured concentrations, turbidity data they may provide an indication of the particle size distribution of sediment in transport.

INTRODUCTION

Turbidity has been shown to be strongly correlated with suspended sediment concentration, but calibration relationships often vary between locations, between events at a location, or even within an individual event hydrograph (Lewis, 1995). The main factors that influence the relationship between turbidity and suspended sediment concentration are: particle size, shape, spectral reflectivity, and bulk refractive index (Downing, 2005). Most testing of turbidity-suspended sediment relationships has been conducted in streams, estuaries, and oceans; much less experience exists relating turbidity to edge-of-field sediment concentration.

For conservation compliance, average annual erosion rates must be held below a “tolerable” level. To measure the effect of management on erosion, cumulative discharge is usually combined with sediment concentration determined on flow-weighted composite samples. Such samples provide no information of erosion dynamics.

We hypothesized that turbidity vs. suspended sediment calibration would become more stable as the size of drainage areas was reduced to individual agricultural fields because soils and contributing areas would become less variable. The objective of this study was to evaluate the utility of turbidity for improving assessment of erosion loss from agricultural fields.

METHODS

Submersible optical backscatter turbidity sensors (OBS-3[1], D & A Instrument Company Port Townsend, WA) calibrated using formazine so that 4000 NTU output 2 volts were used in this study. These sensors employ an 875 nm infrared LED light source and a detector made up of four photodiodes that integrate infrared light scattered between 140 and 160 degrees.

The sensors were deployed within 0.56-m diameter grade control pipes made of smooth steel (Fig. 1) draining three 15 to 17 ha agricultural fields (Fig. 2) at the Delta Demonstration Conservation Center <http://www.dcdcfarm.org/>. The predominant soil in the fields was Sharkey [Very-fine, smectitic, thermic Chromic Epiaquerts] clay, silty clay or very fine sandy loam. The fields were all precision graded during 2001 to between 0.1 and 0.15% slope (Fig. 2). Sampling was conducted between July 2002 and March 2004. Cotton (*Gossypium hirsutum* L.) was grown in field 7 in 2002 and 2003, in field 5 during 2002, and in field 3 during 2003. Corn (*Zea mays* L.) was grown in field 3 during 2002 and in field 5 during 2003. Both



Figure 1 Photographs illustrating instrument deployment in pipe and flow conditions with irrigation tailwater.

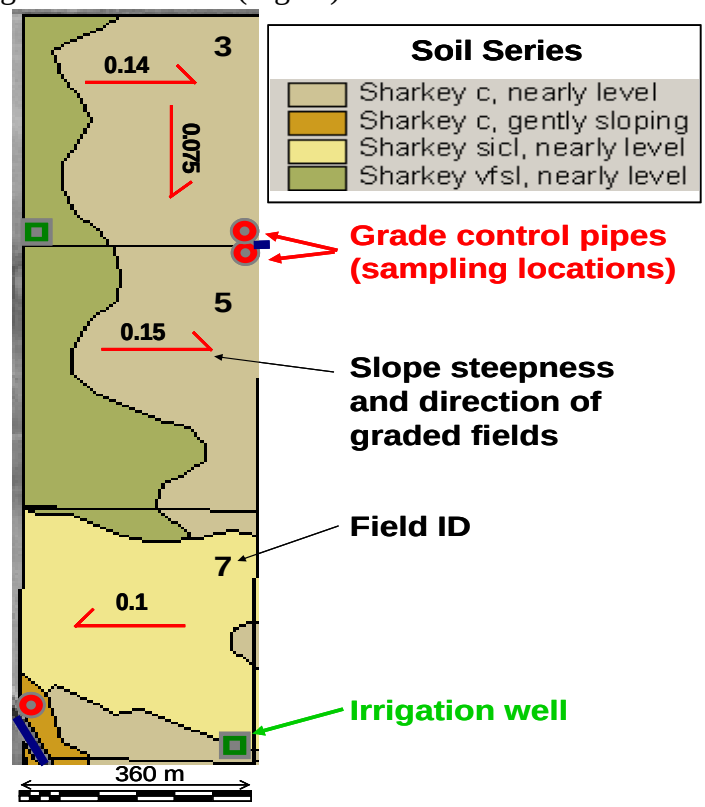


Figure 2 Soils, field grades, and locations of irrigation wells and sampling points of the three adjacent fields studied.

[1] Mention of trade names or commercial products in this article is solely for the purpose of providing specific information and does not imply recommendation or endorsement by the U.S. Department of Agriculture.

cotton and corn were planted on hipped rows spaced 0.97-m apart and running with the slope. Both crops were grown without tillage (no-till) each year after the initial row construction following grading. Runoff water was accumulated in a tail ditch graded toward the pipe outlet at the lower end of each field.

In addition to the turbidity meter, a Doppler flow meter (ISCO 4150), a 24-bottle sequential sampler (ISCO 3700), and a datalogger (Campbell Scientific 510) were deployed at each sampling site. All sensors were attached to a removable array that included a 7.5-cm high weir that increased depth during low flows (Fig. 1). The pump sampler intake tube was located just upslope of the weir and had five intake points distributed at depths between 1 and 6 cm. A sluice at the base of the weir provided a sediment outlet. Pipes were set at ~1% grade. The turbidity sensor was deployed at an angle that permitted the sensor head to be located close to the pipe wall while minimizing IR beam reflection off the pipe. This arrangement was designed to maximize the ability of the instrumentation to monitor low flow conditions. A fin was designed to help shed plant debris that might be wrap around the turbidity sensor.

Instruments were programmed to log depth, flow, and turbidity information at 1-minute intervals during flow periods, and to pump a 900-ml sample whenever 340 m^3 of flow had taken place. Sediment concentration was determined by flocculating the samples with 10 ml of 0.05 M $Al_2(SO_4)_3$, followed by settling, decanting, drying, and weighing.

Data were analyzed using a mixed linear model to determine relationships to predict sediment concentration based on turbidity and flow parameters at the same minute that samples were pumped. In this analysis, events were separated using the criterion that no discharge was observed for 5 hours. Event within a field was considered a random effect, and samples within events were considered repeated measure sub-samples with an exponential covariance structure based on sampling time after the start of the event. Flow parameters evaluated included discharge, rate of change of discharge, flow depth, flow velocity, time into the event and time relative to the first, largest, and last peak of the flow event. Rate of change of discharge was determined on a centered 2-hour moving average of the one-minute measurements in order to minimize the effect of short-term noise on discharge gradients. Turbidity measurements were collected as the average of 120 individual readings within each minute. Data from each field were analyzed separately in order to optimize prediction sediment concentration based on turbidity and flow parameters for each field. These results were then compared with the ability to predict concentration in fields 3 and 5 based only on the relationships derived from field 7. The Mixed procedure (SAS, 1996) was used to perform calculations.

In a preliminary study, soil collected from a nearby Sharkey silty clay soil was returned to the laboratory, dried, and crushed to pass a 2-mm sieve. Weighed amounts of this soil were added to 3 l of water in a stirred bucket at ~5-min intervals, and responses of two OBS-3 sensors were recorded. The final slurry was separated into particle (aggregate) size classes with a settling tube (Dabney et al., 2001), quantified with Imhoff cones, and the sensitivity of the OBS-3 to these separated size fractions was determined. Also, soil samples collected from fields 7, 5, and 3 were analyzed for texture using a pipet method to estimate clay after removing organic matter with hydrogen peroxide, dispersion by overnight shaking with Na-hexametaphosphate, and sand separation using a sieve (Gee and Or, 2002).

RESULTS

The sensitivity of the OBS-3 to increasing concentrations of Sharkey silty clay loam soil added to a mechanically stirred bucket is shown in Fig. 3A. A linear relationship existed up to ~30,000 mg l^{-1}, while at concentrations above ~60,000 mg l^{-1} response decreased. A 2.5 V voltage clamp may have limited the response of the instrument at intermediate sediment concentrations.

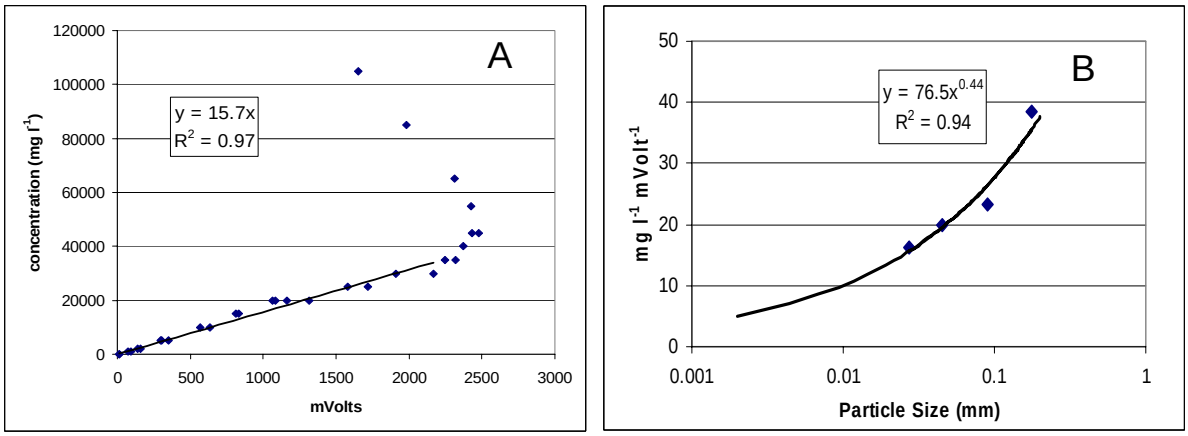


Figure 3 Turbidity measured in the laboratory when dried, ground soil samples of Sharkey sicl soil was sequentially added to a stirred bucket showed a linear response to concentrations up to 30,000 ppm (A). Instrument sensitivity to aggregate size class (plotted at geometric mean size) separated by settling showed a decreasing sensitivity of the calibration equation to increasing particle size (B).

Assessment of sensitivity to aggregated particle size fractions separated based on fall velocity demonstrated a 2.5 fold decrease in sensitivity between particle size classes of 0.028 and 0.18 mm geometric mean diameter (Fig. 3B). It is well known that finer particles produce more turbidity per unit mass than do coarser particles (Conner and DeVisser, 1992). The sensitivity to particle size seen here is similar to that reported by Sutherland et al. (2000). The sensitivity observed in the bulk stirred soil sample of 15.7 mg l^{-1} per mVolt suggests an effective sediment size of about 0.03 mm (Fig. 3B) for this laboratory test.

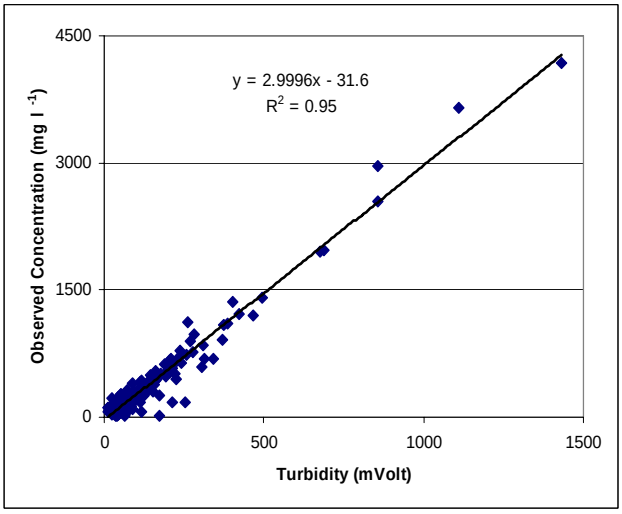


Figure 4 Regression of concentration vs OBS-3 turbidity for all samples taken in Field 7 with synchronous turbidity data collection.

Sensitivity of samples collected from Field 7 (Fig. 4), was five times greater than observed in the laboratory (discussed above), suggesting the field-generated sediment had a finer particle size distribution than that derived from dried, sieved soil samples. The regression equation (Fig. 4) estimated from 272 observations explained approximately 95% of the observed variation in sequential samples taken during the same minute that the turbidity readings were averaged. The standard error of the intercept estimate was 15.8 with 23 degrees of freedom and that of the turbidity coefficient was 0.0452 with 247 degrees of freedom. When the rate of change of discharge at the time of sampling was

added to the regression model, it was found to be a statistically significant effect, but its influence was so small as to be of no practical value. Therefore no significant or consistent hysteretic effects were observed in the relationship between turbidity and suspended sediment concentration in runoff leaving this 15-ha cotton field.

In order to test the utility of the regression equation developed in Field 7, it was applied to the 232 simultaneously measured turbidity and concentration samples available from Field 3 (90 samples) and Field 5 (142 samples). Figure 5 presents the observed and predicted concentrations for all three fields.

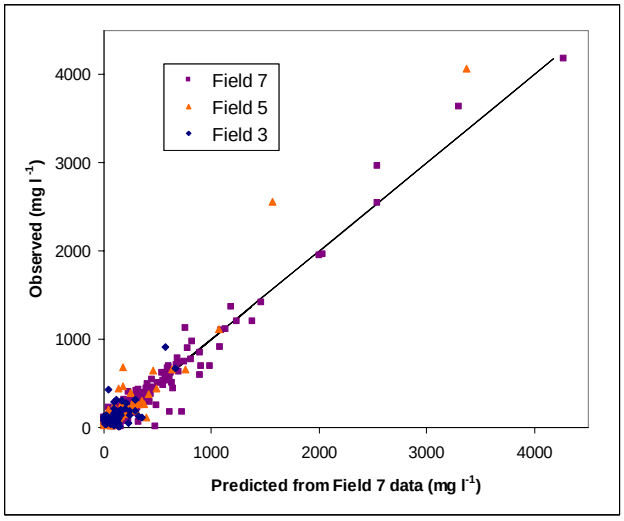


Figure 5 Observed concentrations from all fields plotted against the concentrations predicted from the regression equation derived from Field 7 data alone.

Examination of the difference between predicted and observed concentrations showed that prediction precision of sediment concentration in rainfall runoff was similar in all the fields (Table 1). In the calibrated Field 7, the mean of the differences between observed and predicted values was close to zero (-3 mg l^{-1}) with a standard deviation of 95 mg l^{-1}. For Field 3, the results were similar (mean difference 5 mg l^{-1} with standard deviation of 97 mg l^{-1}), although the range of observed concentrations was smaller. In Field 5 the mean difference of 35 mg l^{-1} with a standard deviation of 135 mg l^{-1} was significantly different from zero. The two large positive residuals for Field 5 (Fig. 5, 6) would be better predicted if a calibration had been optimized separately for that field because large values exert a large effect on regression parameters. However, as discussed below, some of these differences may be related to uncertain synchrony of sampling and turbidity measurement during periods of rapidly changing concentration.

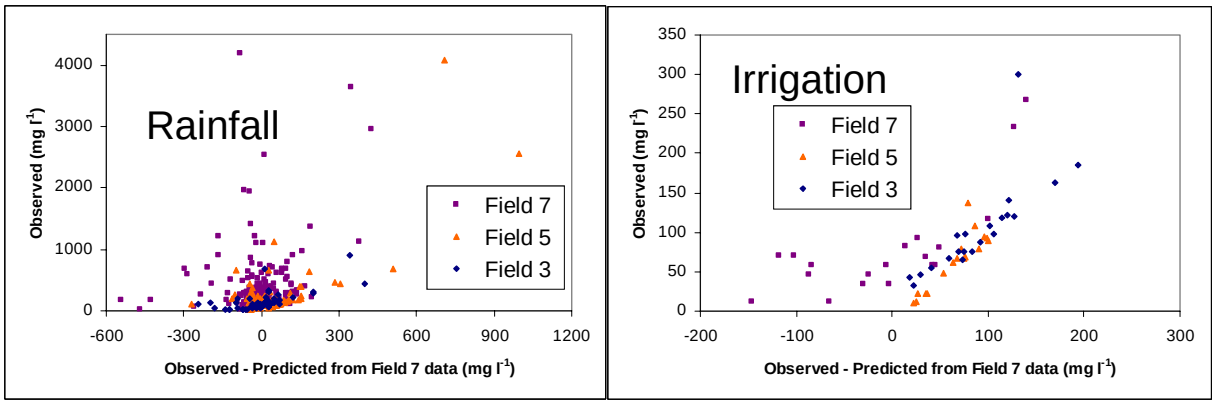


Figure 6 Differences between observed and predicted sediment concentrations plotted against observed concentration for samples derived from rainfall runoff or irrigation tailwater. Differences of rainfall samples are distributed around zero with 2 large positive outliers for Field 5. In contrast, differences for irrigation tailwater from fields 3 and 5 were uniformly positive, indicating that irrigation sediment concentrations, although low, were consistently underpredicted by the Field 7 turbidity calibration equation.

Table 1 Number of samples and mean and standard deviation of the difference between observed and predicted sediment.

Field	Source	n	Mean (mg l^{-1})	Std. Dev. (mg l^{-1})
3	Rainfall	69	5	97
	Irrigation	21	90	46
5	Rainfall	125	35	135
	Irrigation	17	65	27
7 (calibrated)	Rainfall	253	-3	95
	Irrigation	19	-4	82

Samples derived from irrigation tailwater (excess furrow irrigation water) in fields 3 and 5 had consistent higher suspended sediment concentrations than predicted from the Field 7 turbidity calibration (Table 1, Fig. 6). As discussed later, this may have been associated with coarser sediment derived from concentrated flow erosion (in the absence of raindrop impact).

Figure 7 illustrates the application of the calibration equation to produce a continuous predicted concentration trace that tracked observed concentrations in discrete sediment samples. Figure 7A shows some of the Field 7 data from the calibration dataset, while 7B shows results applied to an independent dataset from Field 5. Both hydrographs displayed in Fig. 7 illustrate the typically observed tendency for turbidity peaks to precede flow peaks and for turbidity and concentration to be highest at the beginning of runoff events and to increase briefly as new maximum event discharge levels were approached for the first time.

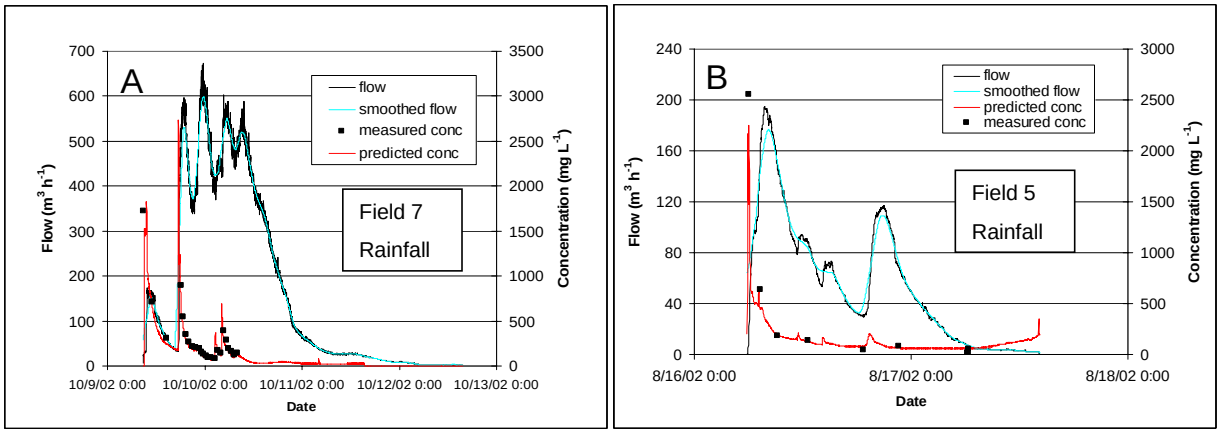


Figure 7 Selected hydrographs and sedigraphs derived from measured samples and from OBS-3 sensors using the calibration equation derived from Field 7 samples (Fig. 4). Both the raw flow and the smoothed (2-hr centered moving average) flow that was used to determine rate of change of flow are displayed.

All of the sampler bottles were used before the end of the large 3-day flow event of Fig. 7A, but the turbidity data provided information that the unsampled portion of the event had even lower sediment concentrations than that in the last sample bottle. Although the agreement between observed and turbidity-predicted concentrations was generally good for the event recorded in Fig. 7B, the difference between observed and predicted concentrations for the first sample of the event represents the largest deviation in the Field 5 record (Fig. 6). In fact, both DCDC5

differences exceeding 600 mg l^{-1} (Fig. 6) were associated with rapidly changing concentrations near the start of runoff events. The increase in predicted concentration at the end of Fig 7B, probably represents an artifact associated with sediment deposition around the turbidity sensor mounted near the bottom of the pipe (Fig. 1). Such artifacts have little effect on estimated event sediment yield but illustrate the need for routine sensor maintenance between events.

DISCUSSION

The systematic tendency for the turbidity to under predict suspended sediment concentration of irrigation events in fields 3 and 5 may be related to two factors. In these fields, unlike in Field 7, the grade control pipes were set at elevations that were from 15 to 30 cm lower that those of the adjacent fields. In contrast, the invert of the grade control pipe in Field 7 was about 5 cm higher than the adjacent field. The low grade control elevations in fields 3 and 5 allowed headcut or ephemeral gully erosion at the lower end of the tail ditch during flows that did not create flow depths in the pipes sufficiently deep to submerge the lower ends of the fields. Such erosion was evident in these fields and was progressive over time. During large storms that filled the pipes to capacity, these headcuts became submerged and were presumably less active. Because surface irrigation tail water did not reach submergence depths, headcut erosion could have occurred during the irrigation events, and may have added coarse aggregated sediment to flows that were otherwise relatively clear because irrigation runoff events also lacked the detachment of fine sediment that can be caused by raindrop impact. Thus, while the runoff leaving the fields due to irrigation had low suspended sediment concentrations, the sediment that was in transport probably had a coarser particle size distribution than was found in the rainfall runoff events that dominated the calibration relationship. Visual observations confirmed the presence of large soil aggregates and pieces of particulate organic matter rolling along the bed within relatively clear irrigation water runoff (Fig. 1).

The relatively high mean difference between observed and predicted sediment concentration (Table 1) for irrigation tailwater and the tendency for these differences to increase with increasing measured concentration (Fig. 6) suggests: (1) that the pump sampler was able to sample the coarse sediment moving through the pipe, and (2) that because of the low range of concentrations observed and the small response of turbidity to those concentrations, the turbidity sensor technique would not be well suited to monitoring soil loss in similar slow flows that transport sediment predominantly as bedload.

CONCLUSIONS

OBS turbidity sensors have proven useful for monitoring sediment yield from three agricultural fields. The fields studied were (selected to be) similar in many respects: 15 to 17 ha in size, 0.1 to 0.15 slope gradient, silty clay texture, and no-till management. Under these similar conditions, the calibration of one turbidity meter in one of the fields successfully predicted the suspended sediment concentration in runoff from the other two fields using different turbidity meters. Errors of prediction of suspended sediment concentration within the calibration and independent datasets were similar, with standard deviations of approximately 100 mg l^{-1} for individual rainfall runoff event samples. An error of ±100 mg l^{-1} applied to annual runoff volume of 500 mm per year implies an error of about ±0.5 t ha^{-1} in estimated annual soil loss, a level of uncertainty that is acceptable for assessing conservation practice effectiveness.

No within-event hysteretic or seasonal trends were observed in the relationship between sediment concentration and turbidity for rainstorm runoff. Turbidity and sediment concentration were found to be largest at the start of runoff events, with concentration peaks generally preceding flow peaks. Turbidity was not a good predictor of sediment concentration in irrigation tailwater runoff, but sediment concentrations were generally low during these events.

When watersheds are reduced to the scale of individual agricultural fields, and where soil and management are uniform, many of the factors that affect the OBS response to suspended sediment are minimized. Under these conditions, we suggest that calibrated OBS sensors have good potential for improving field scale sediment yield estimates. Further, the continuous records they provide give an indication of erosion process dynamics. Finally, we suggest that when turbidity measurements are combined with measured concentrations, deviations of observed and predicted concentrations provide an indication of the particle size distribution of the sediment in transport. In agricultural runoff at the field scale, much sediment is transported in the form of silt- and sand-sized aggregates (Meyer et al, 1992). The size distribution of these aggregates, as with that of the sediment "flocs" that develop in oceans and estuaries, alters sediment transport and turbidity relationships compared to those of completely dispersed primary particles. Knowledge of sediment particle size distribution and composition is important for predicting the efficiency of best management practices such as filter strips and detention basins that depend on sediment settling for improving water quality. Combining turbidity and concentration measurements at the field scale can provide an indication of the sediment size distribution if the other factors that affect the turbidity response to suspended sediment (particle mineralogy, shape, reflectivity, and bulk refractive index) vary within narrow limits. In this study, turbidity and concentration data suggested that sediment eroded during furrow irrigation was coarser and created less turbidity than sediment eroded by rain storms. Particle size analysis of eroded sediments would be needed to unequivocally prove this conclusion.

REFERENCES

Conner, C.S. and De Visser, A.M. (1992). "A laboratory investigation of particle size effects on an optical backscatterance sensor," Marine Geology 108, pp 151-159.

Dabney, S.M., Cullum, R.F., and Smith, S. jr. (2001). "Automated sediment size discriminator," Proc. of the Seventh Interagency Sedimentation Conference I, Reno, NV, pp 152-159.

Downing, J. (2005). "Turbidity monitoring," *In* Environmental Instrumentation and Analysis Handbook. John Wiley & Sons, New York. pp 511-546.

Gee, G.W., and Or, D. (2002). "Particle-size analysis," *In* J.H. Dane and Topp, G.C. (eds.) Methods of Soil Analysis. Part 4. Physical Methods. Soil Science Society of America Book Series No. 5, Soil Science Society of America, Madison, WI, pp 255-293.

Lewis, J. (1996). "Turbidity-controlled suspended sediment sampling for runoff-event load estimation." Water Resources Research 32(7), pp 2299-2310.

Meyer, L.D., Line, D.E., and Harmon, W.C. (1992). "Size characteristics of sediment from agricultural soils," J. Soil and Water Cons. 47(1), pp 107-111.

SAS. (1996). SAS/STAT Software: Changes and Enhancements Through Release 6.11. SAS Inst. Inc., Cary, NC.

Sutherland T.F., Lane, P.M., Amos, C.L., and Downing, J. (2000). "Calibration of optical backscatter sensors for suspended sediment of varying darkness levels." Marine Geology 162, pp 587-597.

A NEW SENSOR FOR TURBIDITY AND SEDIMENTATION ANALYSES IN NATURAL WATERS

Stuart Garner, P.E., Eureka Environmental Engineering, 2113 Wells Branch Parkway, Austin TX 78728, sgarner@EurekaEnvironmental.com

Abstract: Two traditional turbidimeters are used to analyze natural waters. The EPA 180.1 sensor, a white-light nephelometer, covers a wide range of particle sizes but is influenced by water color and is difficult to miniaturize. The ISO 7027 sensor, an infrared nephelometer, is not influenced by water color but has poor sensitivity to larger particles. Both methods are defined only for turbidities up to 40 turbidity units even though field turbidities often exceed 5000 NTU.

A new turbidity sensor uses four incident colors to reduce water-color and particle-size biases. The new sensor detects light scatter at 0 degrees and 90 degrees off the incident beam to extend the dynamic range of the sensor and obtain an inherent correction for lens fouling.

The eight data (four colors, two paths) collected in each measurement cycle can correlate with sediment loads and characteristics when used in a multivariable regression model built with empirical sediment characteristics. The resulting "signature" is useful not only for calculating continuous sediment loads, but also in comparing sediments from other locations or conditions.

THE PROBLEMS WITH TURBIDITY MEASUREMENTS

What is turbidity? Turbidity is a qualitative term for the influence of entrained foreign matter on water's optical properties. Field turbidity measurements help determine light available for photosynthesis, aesthetics (303d listings), and sediment transport. The closest thing to a quantitative turbidity definition is that one nephelometric turbidity unit (NTU) is 1/4000 of a set recipe for formazin.

Turbidity has several conflicting definitions and measurement methods. Early definitions did not specifically address absorption (capture of visible, ultraviolet, or infrared light energy by water and entrained foreign matter), scattering (deflection by foreign matter of light energy from its normal path), or fluorescence (light absorbed and then re-emitted at a different wavelength).

More recently, ASTM standard D 1889-00 calls turbidity "an expression of optical properties of a [water] sample that cause light rays to be scattered and absorbed rather than transmitted in straight lines through a sample". A USGS work group adds "any suspended or dissolved particle that is capable of causing light to be scattered or absorbed should be expressed in a turbidity measurement". This definition recognizes that optical turbidity sensors are not particularly selective – they can't separate different types of influences on light transmission in water.

What are the problems of turbidity measurement?

- EPA Method 180.1 turbidity measurement requires the incident radiation of a tungsten lamp (white light) and a light path for incident light and scattered light not to exceed 10 cm. The 180.1 nephelometer covers a wide range of particle sizes, but is influenced by

water color. The sensor's power requirements make it difficult to miniaturize, and so 180.1 is not often used for field measurements.

- ISO 7027 turbidity measurement requires an incident radiation of 860 nm (infrared light, IR) and a light path for incident light and scattered light not to exceed 1 cm. The ISO nephelometer is not influenced by water color, but has poor sensitivity to larger particles. Because ISO does not meet the regulatory definitions of 180.1, but can be accomplished with inexpensive, low-power LED's, ISO is used most often in field measurements.

- The ISO standard is defined only for the range of 0 – 40 NTU. Diluting samples into the 0 – 40 NTU range is expensive to apply to multiple samples in natural waters, and infeasible to apply when continuous turbidity data are desired.

- ISO 7027 sensors typically employ one light source and one light detector and so return only one datum per measurement cycle. This limitation of data, and the bias in that data (due to different sensitivities to different particles), make accurate estimates of other useful parameters (for instance total suspended solids) difficult to produce.

- Small variations in the different sensors from the different manufacturers, including linearity algorithms, can result in large measurement disagreements of up to 40% of reading or more, even when calibrated with the same solution.

- There are a dozen or more turbidity units (NTU, FTU, FTTU, RTU, etc.) that are similar but not equal. Each unit refers to a slightly different measurement technique, meaning those data are not directly comparable. A suggested reporting convention includes the turbidity-measurement method, light wavelength, detector orientation, and number of sources and detectors – quite a burden for large, water-quality databases.

- Formazin is difficult to prepare, has a short shelf life, and is a suspected carcinogen. Yet the calibration value of polymer beads is not defined analytically; it's referenced to a set formazin recipe as measured by a specific manufacturer's specific instrument model.

A NEW APPROACH TO TURBIDITY MEASUREMENT

The New Sensor in Theory: A new turbidity sensor adds three features to the traditional field turbidity-measurement technique (ISO 7027).

- First, the sensor uses the dual-beam, ratiometric measurement technique (Figure 1, showing four incident beams, four scattered beams, and four transmitted beams) often found in process-control turbidimeters. This method combines the benefits of transmitted light measurement and scattered-light measurement, providing a wider linear range, relative insensitivity to lens fouling, and better color rejection than the ISO technique.

- Second, the new sensor employs multiple wavelengths, covering IR and the visible range. The resulting data can be used to calculate an optical value which, though similar in concept to a traditional turbidity value, is less sensitive to (or biased by) water color and

particle size, shape, and color. The sensor has the ability to mimic both the white-light (EPA) and IR (ISO) turbidimeters if desired.

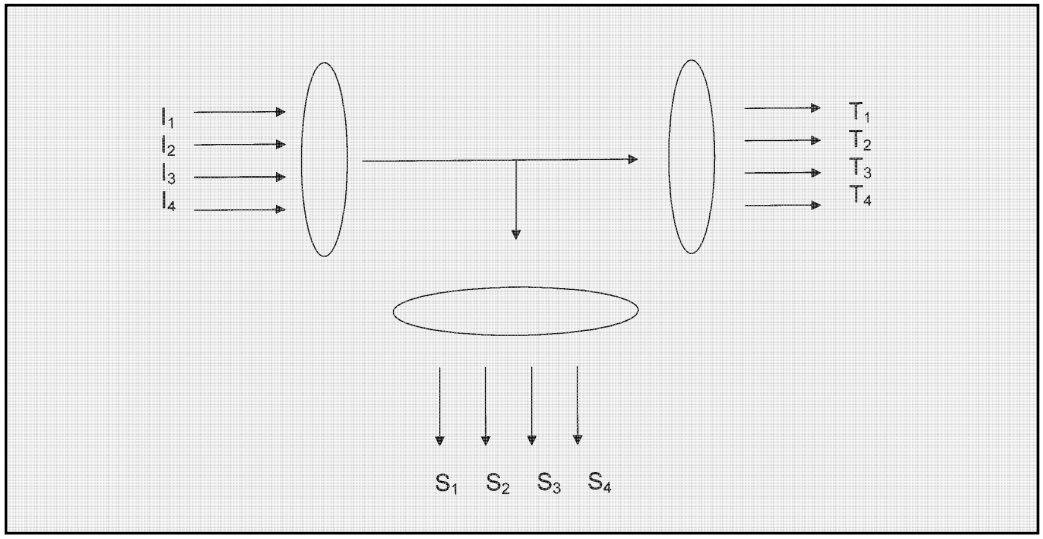


Figure 1 The New Sensor in Theory.

- Third, the new sensor has the rigorous construction and calibration methods that facilitate a new, well-defined optical index for water. Its materials, tolerances, etc. can be tightly specified so that Manufacturer A's sensor matches the performance of Manufacturer B's sensor when calibrated with the linearizing media (polymer beads) whose material, size, shape, color, etc. are specified unambiguously. This consistency produces the opportunity for a new, consistent optical index to replace the dozen or so measurement units in use today. The new measurement unit – call it the Environmental Optical Index - will be defined by linearity with linear dilutions of the absolute calibration solution.

- Fourth, the sensor produces a different combination of responses for different types of particles. These differences, carried in the eight data gathered per measurement cycle, can be used to characterize different combinations and concentrations of particles.

The New Sensor in Practice:

- The sensor uses sequentially-pulsed infrared, red, green, and blue light-emitting diodes (LED's) measured at 90 degrees and 0 degrees to produce eight data per measurement cycle to reducing particle-size bias while increasing accuracy and range. The configuration is shown below.

- The sensor is calibrated with white polymer beads with 1.0 µm mean size and 0.1 µm standard deviation, and linearized to any concentration or dilution of that calibration solution. This, along with specific construction specifications, ensures comparability of data taken with different individual sensors.

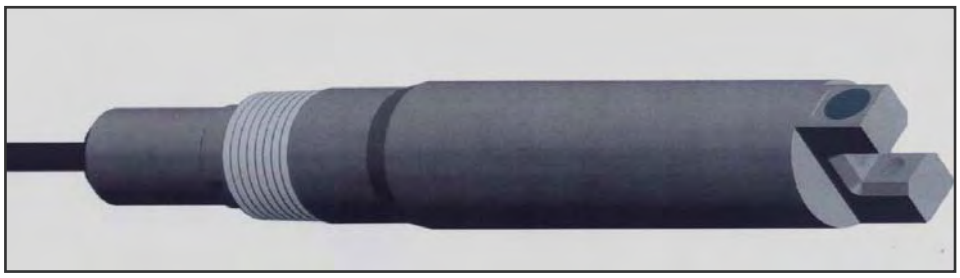


Figure 2 The New Sensor in Practice.

- The sensor uses all eight data per measurement cycle, combined in the expression shown in the figure above, to produce one turbidity reading. For convenience, a reading of 4000 environmental optical units is assigned the polymer-bead concentration corresponding to 4000 NTU.

- The sensor has an auxiliary function in which the eight data from each of several dilutions of a water sample are stored in memory, along with the sediment load (or other variable). A multivariable regression is used to create an algorithm for continuously estimating sediment loads (or other variable). The algorithm will be valid for dilutions of water containing the same type particles as did the calibration water, and may apply with various accuracies to waters with slightly different particle populations. Algorithms can be saved for different field conditions, for instance a certain stream after a rainfall event of a certain magnitude.

- The sediment "signature" resulting from the regression described above can also be used to compare sediments from different locations or conditions by comparing the correlation coefficients and other statistics available with multivariable regression models. For instance, clay suspensions may be explained primarily by a red light scattered at 90 degrees, secondarily by infrared light transmitted at 0 degrees, and not at all by either green signal – it can thereafter be inferred that other waters matching that "signature" may be similarly loaded with clay.

EXAMPLE DATA

Figure 3 shows the ratiometric measurements (90-degree response divided by 0-degree response) in Formazin solutions up to 2000 NTU. Note the differences in response slopes between the four light colors. The higher responses with the higher slopes are preferred for instrumentation as they represent larger electrical signals, but the other responses carry information, too. Also note the descending order of the light-color responses: blue, green, red, IR.

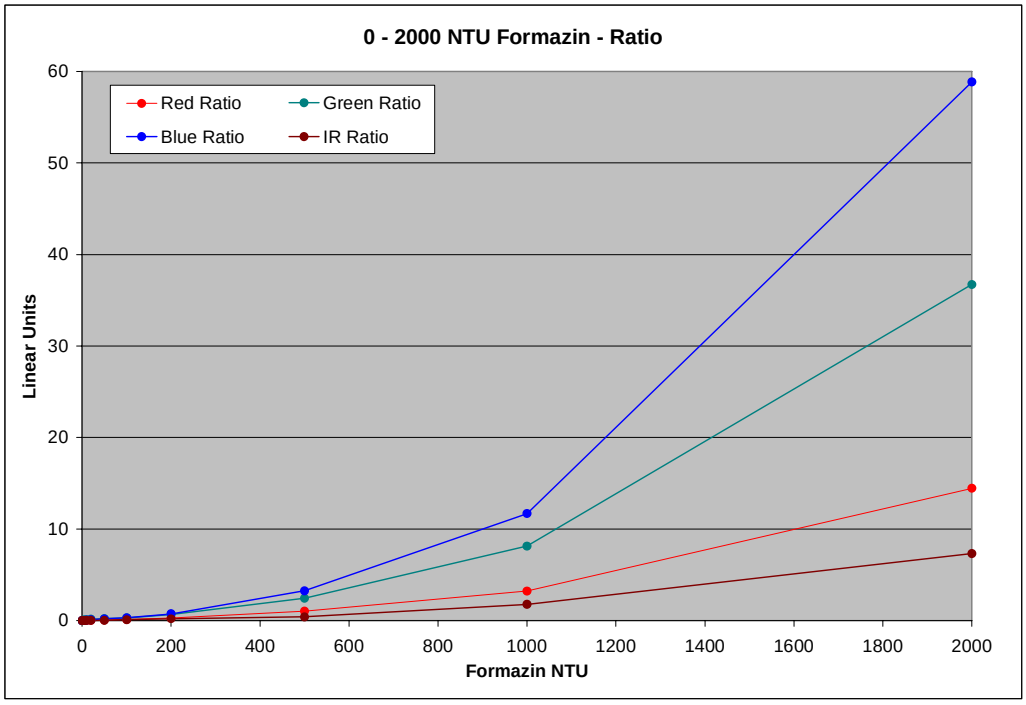


Figure 3 The New Sensor's Ratiometric Response to Formazin Dilutions.

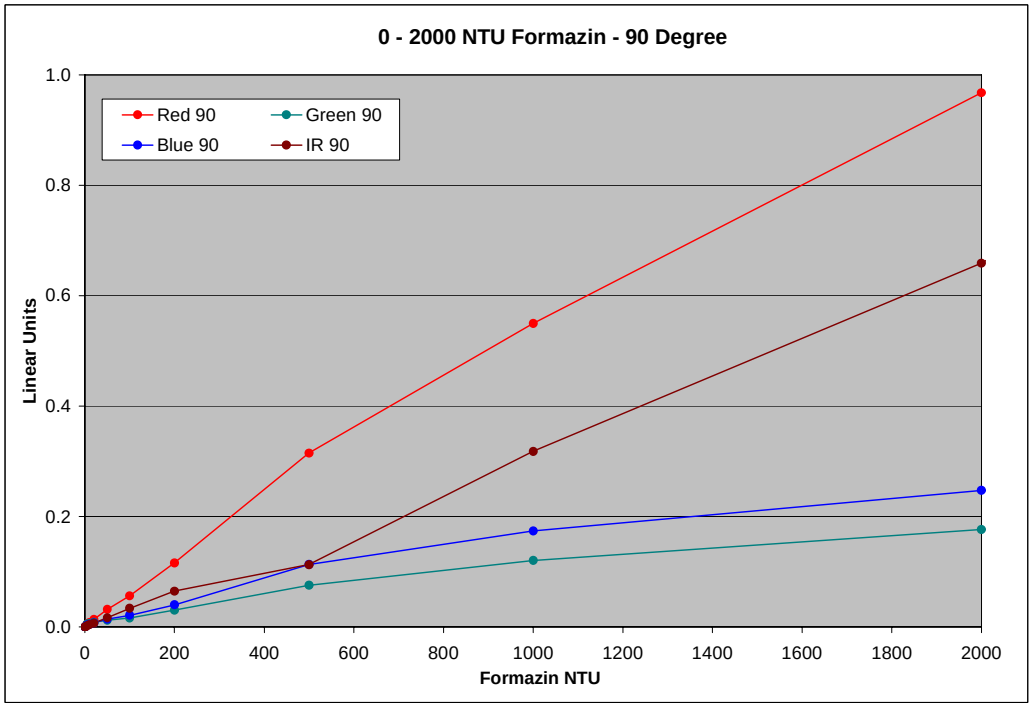


Figure 4 The New Sensor's 90-Degree Response to Formazin Dilutions.

Figure 4 shows the 90-degree (i.e., nephelometric response) of the sensor in Formazin solutions up to 2000 NTU. Again, note the differences in the response slopes of the four colors. But

notice also that the descending order of the light-color responses has changed to red, IR, blue green from blue, green, red, IR. This is the differential behavior indicates the desired sensor operation: different responses from the different colors and light paths. These different responses carry information useful in discriminating between different types or sizes of particles.

Formazin is relatively uniform white color with somewhat variable particle size and shape. It does not color its carrier water. "Dirt" mixed with water, on the other hand, can have a wide range of particle characteristics, and may impart color to its carrier water. Figure 5 shows the new sensor's responses in a mixture of brown, fine-particle garden soil and water. Unlike the more predictable Formazin, the responses of the different light colors are so different that they cross one another in the ratiometric mode – and appear in a different order. Figure 6 shows yet another behavior.

Does the new sensor carry any information not found in the traditional, 90-degree IR measurement? Figure 7 shows a section of a regression report (first-order, least-squares) using the IR 90 data from Figure 6. The adjusted R-squared value is 0.94 – not bad.

Figure 8 shows a multivariable regression (first-order, least-squares) using all four colors' 90-degree responses and all four colors' 0-degree responses. The adjusted R-squared value is 1.00, indicating a significantly better predictive power for the extra seven types of data provided by the new sensor.

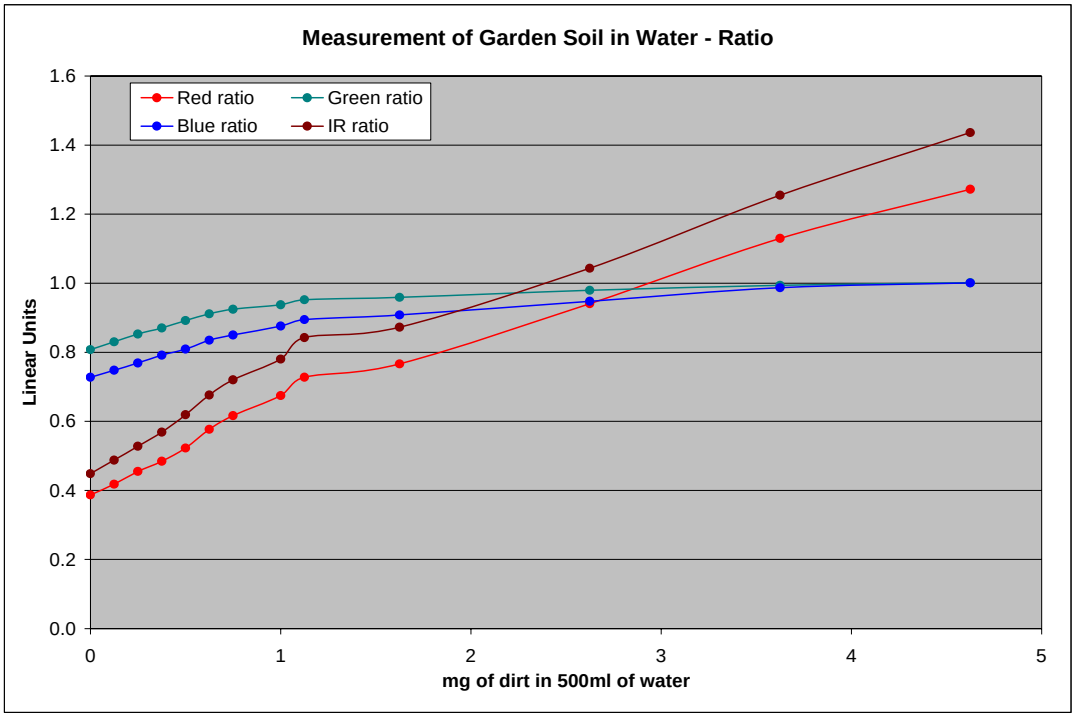


Figure 5 The New Sensor's Ratiometric Response to Dirt Dilutions.

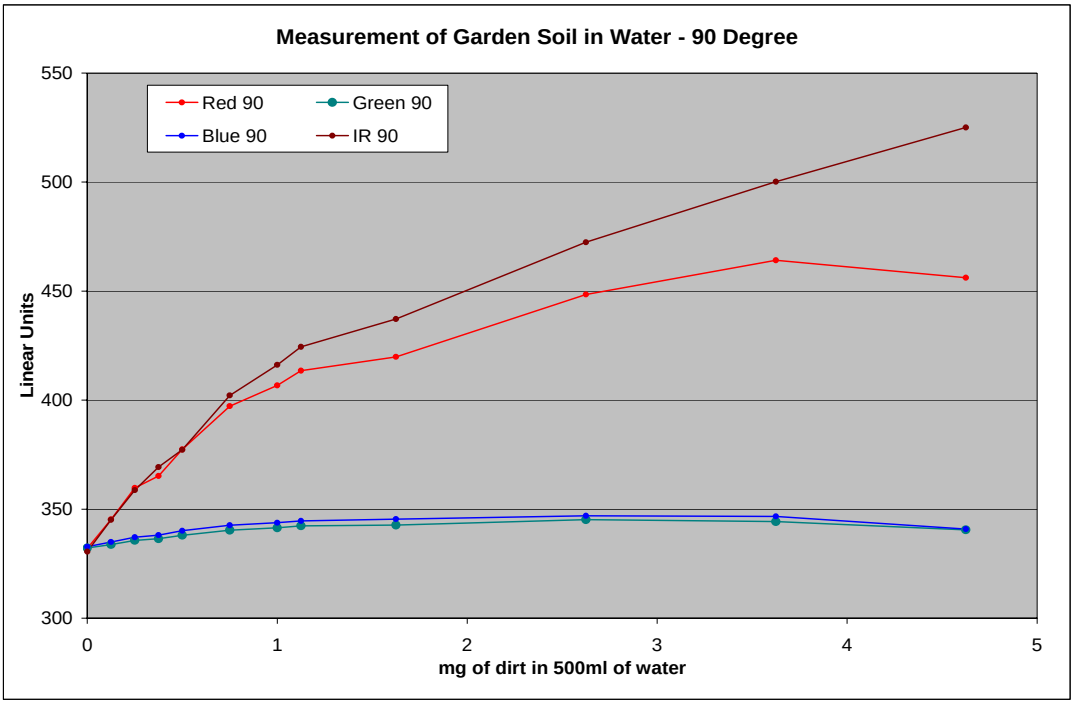


Figure 6 The New Sensor's 90-Degree Response to Dirt Dilutions.

Output for Soil mg

Regression Equation
Soil mg = - 8.15 + 0.02*IR 90

Summary Statistics

Criterion	Value
R^2	0.94
R^2 adj	0.94
R^2 predict	0.90
R^1	0.76
PRESS	2.37
s (est. err.)	0.36

ANOVA

	df	SS	MS	F	p-value
Regression	1	23.43	23.43	180.32	0.00
Residuals	11	1.43	0.13		
Total	12	24.86			

Coefficient Estimates

	Coefficients	Standard Error	t Stat	p-value	Lower 95%	Upper 95%	VIF
const	-8.153508	0.71	-11.43	0.00	-9.72	-6.58	
IR 90	0.022988	0.00	13.43	0.00	0.02	0.03	1.00

Figure 7 Regression Statistics for IR-90 Predictions of Soil Loading.

Notice that the regression outputs contain a listing of the coefficients due each light variable. Those coefficients provide a "fingerprint" unique to a particular empirical calibration curve.

Figure 9 shows the predictor curves for the IR-90 and Eight-Data predictors, along with a curve illustrating ideal behavior. The IR-90 predictor has an error of nearly 50% at 1 mg/l soil; the new sensor's predictor is nearly coincident with the ideal behavior.

Output for Soil mg

Regression Equation

Soil mg = 66.21 + 0.06*RED 90 - 0.01*RED 0 - 0.03*GREEN 90 - 0.00*GREEN 0 - 0.24*BLUE 90 - 0.02*BLUE 0 +
+ 0.00*IR 90 + 0.02*IR 0

Summary Statistics

Criterion	Value
R^2	1.00
R^2 adj	1.00
R^2 predict	0.98
R^1	0.97
PRESS	0.47
s (est. err.)	0.08

ANOVA

	df	SS	MS	F	p-value
Regression	8	24.83	3.10	480.49	0.00
Residuals	4	0.03	0.01		
Total	12	24.86			

Coefficient Estimates

	Coefficients	Standard Error	t Stat	p-value	Lower 95%	Upper 95%	VIF
const	66.21	51.09	1.30	0.26	-75.62	208.05	
RED 90	0.06	0.04	1.71	0.16	-0.04	0.17	5122.77
RED 0	-0.01	0.01	-0.77	0.48	-0.03	0.01	2267.25
GREEN 90	-0.03	0.19	-0.15	0.89	-0.54	0.49	1005.00
GREEN 0	0.00	0.03	-0.15	0.89	-0.08	0.07	695.63
BLUE 90	-0.24	0.22	-1.09	0.34	-0.84	0.36	1757.50
BLUE 0	-0.02	0.03	-0.62	0.57	-0.10	0.06	2123.95
IR 90	0.00	0.02	0.12	0.91	-0.06	0.06	3165.31
IR 0	0.02	0.01	1.78	0.15	-0.01	0.05	2830.14

Figure 8 Regression Statistics for Eight-Data Predictions of Soil Loading.

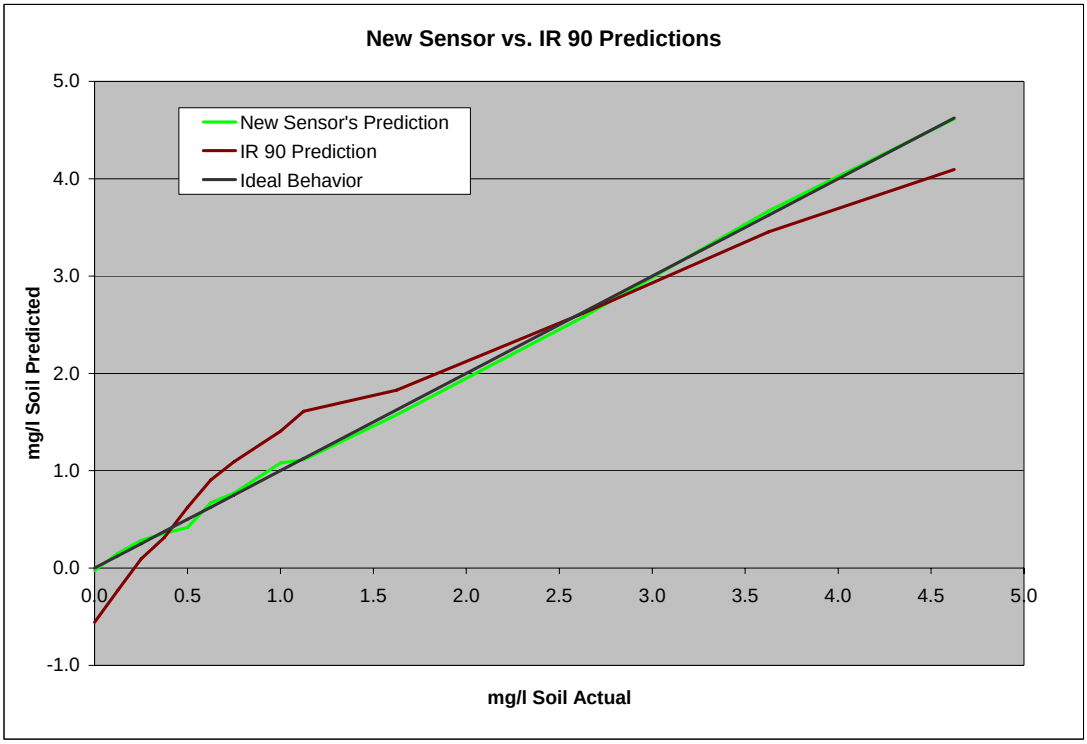


Figure 9 Differences in Predictive Models.

IMPACT OF THE ROSEWOOD CREEK RESTORATION PROJECT ON SUSPENDED SEDIMENT LOADING TO LAKE TAHOE: PRE-MONITORING AND YEAR 1

Richard B. Susfalk, Assistant Research Scientist, Division of Hydrologic Sciences, Desert Research Institute, Reno, NV, rick.susfalk@dri.edu

Abstract: Rosewood Creek is a small, urban creek in the northeastern part of the Lake Tahoe basin. In 2003, the creek was elongated by 975 linear meters to restore a historically sensitive environmental zone and to mitigate the delivery of suspended sediment from upland sources into Third Creek and ultimately into Lake Tahoe. Strategies to reduce suspended sediment loads included: 1) increasing the length of the channel, thereby increasing the distance that sediments must travel before discharging into the higher-velocity waters of Third Creek; 2) providing erosion control measures and a healthy riparian zone around the creek that are capable of mitigating poor water quality; and, 3) routing the creek through five flood-spreading basins.

The objectives of this research are to assess what impacts the Rosewood Creek Restoration Project has on the net transfer and particle-size distribution of suspended sediment. Data collected at each site included near-continuous measurements of water discharge, turbidity, specific conductivity, and water temperature. Discrete water samples were collected by an automated vacuum sampler and were analyzed for suspended sediment concentration (SSC) and particle-size distribution. In-stream turbidity was used as a surrogate for SSC by developing linear and sequential linear regression models to describe the relationship between turbidity and SSC. Particle-size distribution was used to assess the relative importance of suspended sediment loading, as the loading of finer-sized particles have played an important role in the historical decline of Lake Tahoe's optical clarity.

The ability of the restoration project to alter suspended sediment loads the first year after construction was variable and dependent on the type of hydrologic event. For example, suspended sediment loading leaving the restoration zone was half that entering the project during a series of small, low-elevation snowmelt and rain-on-snow events in early 2004. In contrast, sediment loads exiting the project during spring snowmelt were 60% greater than those entering the project. The restoration project did not alter the average particle-size distribution during snowmelt, with particles of less than 20 μm in diameter comprising 40% of suspended sediment samples. However, distinct periods of coarser-grained suspended sediment were observed and were attributed to the presence of unconsolidated sediments remaining from the project construction, and from sediment that had been previously eroded during an earlier, intense thunderstorm. The response of the restoration project during its first post-construction year should not be representative of its future ability to alter suspended sediment delivery due to the recent construction disturbance and the immature status of the newly planted riparian vegetation.

INTRODUCTION

Rosewood Creek is a small, urban tributary located within the Third Creek watershed in Incline Village, NV. Visual observations have suggested that the loading of suspended sediment from Rosewood Creek can significantly increase the load of suspended sediment carried by Third Creek into Lake Tahoe. Once in the lake, suspended sediment can have a direct negative impact

on visual water clarity (Jassby et al., 1999) and it can serve as a source of nutrients that may stimulate algal growth. Identification and reduction of sediment sources from the Third Creek watershed are important, as the historical average monthly yield of suspended sediment by Third Creek into Lake Tahoe has consistently been greater than the other streams monitored by the Lake Tahoe Interagency Monitoring Program (Rowe et al., 2002).

The Rosewood Creek Restoration Project was constructed during spring and summer 2003 to improve the quality of water discharged by the creek, as well as to restore an historically sensitive environmental zone. The project increased the overall length of Rosewood Creek by approximately 975 linear meters, resulting in the movement of its confluence with Third Creek from just south of State Route 28 to just north of Lakeshore Blvd. The restored channel ranged from 2 to 9% in gradient, and consisted of mostly Rosgen Type "E" channels, with some Type "A" channels in the upper areas of the restoration. The project was expected to improve the quality of water discharged from Rosewood Creek by: 1) increasing the distance that sediments and nutrients must travel before discharging into the higher-velocity waters of Third Creek; 2) providing erosion control measures and a healthy riparian zone around the creek that are capable of mitigating poor water quality; and 3) routing the creek through five flood-spreading basins, and constructing a storm detention basin to pre-treat water entering the creek above Incline Way.

Water flows into the completed project area are currently managed by the Incline Village General Improvement District. Peak flows are controlled by a new diversion structure located at the upstream end of the project. The particular positioning of head gate boards allows water to enter Rosewood Creek, or be diverted into Third Creek. Currently, the boards are positioned to restrict peak flows into the project to an estimated 4.1 cfs (Miller, 2004) with water in excess of 4.1 cfs diverted into Third Creek. This operating plan was designed to protect the project from damage from high flows during the establishment phase of recently planted riparian vegetation.

The overall objectives of this research were to: 1) ascertain the ability of Rosewood Creek to deliver suspended sediment into Third Creek; and 2) estimate the ability of the Rosewood Creek Restoration Project to alter the quantity (mass) and composition (particle-size) of suspended sediment delivered by Rosewood Creek into Third Creek. This monitoring was conducted between November 2002 and May 2004, and included the winter and snowmelt periods prior to and after the construction of the restoration project. Data collected at each site included continuous measurements of water discharge, turbidity, specific conductivity, and water temperature, and discrete measurements of suspended sediment concentration (SSC) and particle-size analysis.

METHODS

Field Sites, Equipment, and Sample Collection: A total of three monitoring sites were established within Incline Village, NV, in the northeastern section of the Lake Tahoe Basin. Two monitoring sites were established before the restoration project, with the third installed after completion of the restoration project. The Rosewood Creek site was installed above (RW-Abv) the restoration project area, 130 m prior to the creek's discharge into Third Creek. The Third Creek (3rd) site was another 0.8 km downstream near its outfall into Lake Tahoe. The 2003 restoration project extended the length of Rosewood Creek by 975 linear meters and moved the

creek's confluence downstream to a point just below the existing Third Creek monitoring site. A new monitoring site near the lower extent of the restoration project was added on Rosewood Creek (RW-Blw) prior to its discharge into Third Creek. Each site was equipped with an in-stream turbidimeter (OBS-3, D&A Instrument Co., Port Townsend, WA), conductivity and water temperature sensor (Campbell Scientific, Logan, UT), and pressure transducer (KPSI, Hampton, VA) to monitor stage. A datalogger (Campbell Scientific) collected data from these sensors every 10 minutes. An automated vacuum sampler collected discrete water samples when triggered by a modified version of the Turbidity Threshold Program (Lewis, 1996).

Suspended Sediment Concentration and Laser Particle Size Analyses: A subset of the samples collected by the automated vacuum samplers was analyzed for SSC by the Soil Characterization Laboratory at the Desert Research Institute following the ASTM D 3977-97 method. Laser particle-size analysis (LPSA) was conducted using the Micromeretics Saturn DigiSizer 5200® laser particle size analyzer following a procedure based on ASTM C 1070 – 01 for the particle-size determination of alumina and quartz powders by laser light scatter (ASTM, 2002). The DigiSizer 5200® determined the percentage of specific size-class fractions between 0.02 µm and 1,500 µm in diameter in a sediment sample (Gee and Or, 2002) based on the Mie theory of light scattering by a spherical particle.

Load Calculation: The instantaneous suspended sediment load (SSL) was the product SSC (in mg L^{-1}) and discharge Q (in L s^{-1}) summed over each 10-minute interval. Load calculations were done on a hydrologic-event basis. When in-stream turbidity exceeded the turbidimeter maximum (1,000 NTU), SSL was calculated using hourly SSC measurements collected during the events. Suspended sediment loads by particle-size group were calculated by multiplying the percentage particle-size fraction determined by LPSA by total SSL.

RESULTS AND DISCUSSION

The relationships used to estimate suspended sediment concentrations from in-stream turbidity are presented in Table 1. The predictive ability for RW-Blw was poor due to the limited number of samples since and the impacts of disturbance from the recent project construction. The predictive ability of this model should improve as more samples are collected while the restoration zone matures toward an ecological equilibrium. The 3rd model was stratified by turbidity value to reduce overestimation of SSC at lower turbidities that occurred in non-stratified models. The correlation between log(SSC) and the fitted log(SSC) was 0.71 for RW-Abv, 0.39 (P =0.0225) for RW-Blw, and 0.87 ($P \leq 0.0001$) for 3rd. These regression models are preliminary, and will be adjusted as new data are collected over the next two years.

Pre-restoration Project Monitoring: The objective of pre-project monitoring was to establish background data prior to construction and to assess the impact that suspended sediment delivery by Rosewood Creek had on Third Creek. Four events were monitored during this period including low- and high-elevation snowmelt events, and two rainstorms (Table 1). The geography of the two watersheds played an important role in the timing and magnitude of suspended sediment loading. The Rosewood Creek watershed is a low-elevation, urbanized watershed that responds rapidly to low-elevation/lake-level snowmelt and storm events. Approximately 55% of the 2.3 km^2 watershed lies within urbanized areas above lake level (1,800

m) to 2,300 m in elevation. The Third Creek watershed is larger in area, with a higher mean elevation, and responds primarily to high-elevation hydrologic events. Only 10% of this 13.3 km^2 watershed lies within lower-elevation urban areas.

Table 1 Relationships between suspended sediment concentration (SSC), turbidity (TU), water temperature (WT), and discharge (Q).

Site	Equation	R^2	P value
RW-Abv	$\log(SSC) = 0.0580 * \sqrt{TU} + 1.9313$	0.72	(TU) ≤0.0001
RW-Blw	$\log(SSC) = 0.7909 \times \log(TU) + 0.0924 \times WT + 0.9109$	0.56	(TU) 0.0197 (WT) 0.0378
3rd	$\log(SSC) = 0.6823 \times \log(TU < 12) + 0.0138 * Q + 0.3758$ $\log(SSC) = 0.6824 \times \log(TU \geq 12) + 0.0138 * Q + 0.9611$	0.88	(TU) ≤0.0001 (WT) 0.0007

Total suspended sediment delivered to Lake Tahoe from these watersheds was dominated by high-elevation, seasonal snowmelt originating from the upper Third Creek watershed (Event 2, Table 2). On an event basis, however, Rosewood Creek was capable of contributing significant suspended sediment loads to Third Creek during low-elevation events (Events 1 and 4).

Table 2 Suspended sediment loadings (SSL) and water discharge on an event basis.

Event	SSL (kg/event)			Water (10^6 L/event)			Duration
Description	RW-Abv	RW-Blw	3rd	RW-Abv	RW-Blw	3rd	(hours)
1. Low-elevation snowmelt (1/22-2/50/03)	6,922	--	3,694	41.6	--	155.7	351
2. High-elevation snowmelt (5/11-6/20/03)	7,056	--	339,877	33	--	2,346	960
3. Rainstorm (7/22-7/24/03)	236	--	867	0.9	--	10.7	41
4. Rainstorm (8/21-8/24/03)	9,966	--	12,530	5.6	--	19.4	73
5. Early season snowmelt (1/20-2/10/04)	3,419	1,651	6,033	24.2	27.14	313.4	522
6. Rain on snow (2/16-2/18/04)	2,700	1,345	764	6.3	3.67	16.8	47
7. Low-elevation snowmelt (3/1-4/27/04)	31,745	50,837	15,532	178.3	183.2	--	1,368

Particle-size analysis revealed that only 35% of the suspended sediment from Rosewood Creek was less than 20 μm in diameter, whereas over 85% of the suspended sediment from Third Creek was less than 20 μm in diameter (Figure 1). The delivery of fine-grained suspended sediment has important consequences to the clarity of Lake Tahoe, as fine-grained particles not only remain suspended in the water column for longer periods, but also have a greater potential to be a source of limiting nutrients, such as phosphorus. As a result, fine-grained particles adversely affect both near-shore clarity (Taylor et al., 2004) and long-term clarity at mid-lake (TRG, 2001). Regulatory agencies within the Lake Tahoe basin have placed a strong emphasis on the reduction of suspended sediment input to the lake as a way to restore Lake Tahoe's famed clarity.

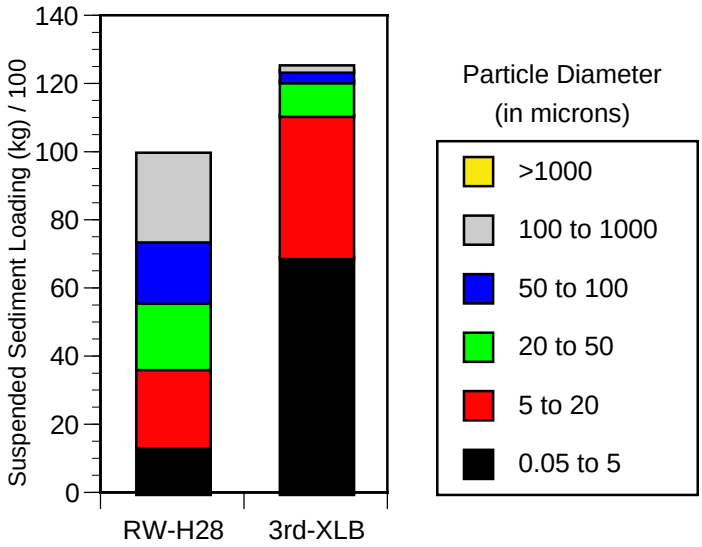


Figure 1 Total suspended sediment loading (SSL) by particle-size group for Event 4, a series of summer thunderstorms.

Post-Restoration Project Monitoring: The restoration project was constructed in the summer of 2003 and added 975 linear meters to the length of Rosewood Creek's channel. This resulted in the movement of the creek's confluence 800 m downstream to a point just below the existing Third Creek monitoring site. Three hydrologic events were monitored: early season snowmelt (Event 5), a rain-on-snow event (Event 6), and a low-elevation snowmelt (Event 7).

The effectiveness of the restoration project to reduce suspended sediment loading was judged by comparison of the calculated loadings entering (RW-Abv) and exiting (RW-Blw) the restoration project. During the two mid-winter events (Events 5 and 6), the restoration project acted as a sediment sink, reducing suspended sediment loads by about 50%. This was likely due to the relatively low water velocities resulting from flooding within the designed spreading zones that occurred due to the presence of snow and ice dams that partially blocked several sections of the restored creek.

The larger, low-elevation snowmelt event occurred between March 1 and April 27, 2004. During this time, the restoration project was a source of 335 kg/day of suspended solids and the total loading from Rosewood Creek comprised 77% of the suspended sediment delivered to Lake Tahoe by Rosewood and Third creeks. Hysteresis curves and particle-size analyses data were

used to gain insight on the possible sources of suspended sediment within the restoration project during the most intensive days in early snowmelt. For example, the concentration of suspended sediment entering the restoration project was found to be unimodal in distribution, elevated between 1.1 to 1.8 cfs (Figure 2). Although suspended sediment concentrations were elevated, the observed mean particle diameters between 35 and 53 μm were consistent with mean diameters observed during other hydrologic events at this site.

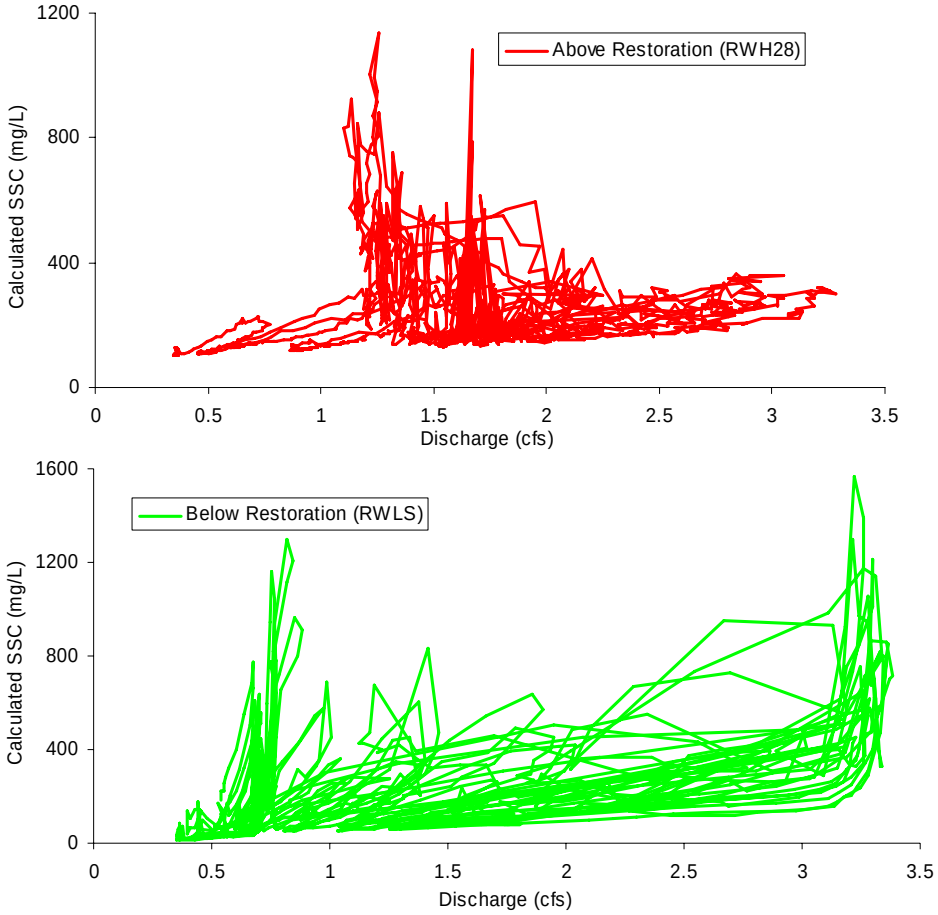


Figure 2 Hysteresis relationships above (top) and below (bottom) the Rosewood Creek Restoration Project observed between March 9 and March 16, 2004.

In contrast, the suspended sediment leaving the restoration project was observed to be bimodal in distribution, with elevated sediment concentrations between 0.5 to 0.9 cfs, and above 3.2 cfs. Mean particle size was found to vary, primarily during the early part of snowmelt when particles greater than 100 μm in mean diameter were mobile during relatively low flows (0.5 to 0.9 cfs). This suggested an easily mobile sediment source within the restoration project that was short lived, presumably as the source of this material was depleted. This coarser, mobile material was likely residual, unconsolidated material that remained from the project's construction and from severe erosion that occurred in response to an intense series of rainstorms on August 21, 2004, prior to the completion of the project. If this hypothesis is correct, then this pulse of coarse material should not be observed in subsequent years.

SUMMARY

The objectives of this project were to ascertain the ability of Rosewood Creek to deliver suspended sediment into Third Creek and to estimate the ability of the Rosewood Creek Restoration Project to alter the quantity and composition of suspended sediment delivered by Rosewood Creek into Third Creek. The data presented here included several months of pre-construction data and the first winter season following the completion of the restoration project.

The ability of Rosewood Creek to significantly increase suspended sediment loads in Third Creek was due to the geographical differences between the watersheds. Events such as lake-level snowmelt and low-elevation rainstorms resulted in the mobilization of sediment from the low-elevation Rosewood Creek watershed, but not from the higher-elevation Third Creek watershed. For example, lake-level snowmelt in 2003 resulted in Rosewood Creek transporting 6,922 kg of suspended sediment compared to just 3,694 kg in Third Creek. These values were dwarfed by the 339,877 kg of suspended sediment transported by Third Creek during spring thaw at higher elevations. However, Rosewood Creek was able to mobilize significant amounts of suspended sediment during summer thunderstorms, such as contributing 44% of the combined 22,496-kg load entering Lake Tahoe from the Third Creek watershed. However, suspended sediment delivery from Third Creek itself was more important, as suspended sediment from Third Creek had a finer particle-size distribution (85% < 20 μm diameter) than observed in Rosewood Creek (35% < 20 μm diameter).

The ability of the Rosewood Creek Restoration Project to alter the delivery of suspended sediment to Third Creek was mixed. Suspended sediment loading was reduced by approximately 50% during a series of small, low-elevation snowmelt events in January and February 2004, and during a rain-on-snow event in mid-February 2004. In contrast, suspended sediment loading within the project increased by 60% during low-elevation spring thaw. The restoration project did not affect the average particle-size distribution, as about 42% of the suspended sediment above and below the project was less than 20 μm in diameter. However, distinct periods were observed where the particle-size distribution of suspended sediment was skewed by the substantial presence of particles greater than 100 μm in diameter. This transport of coarser particles was attributed to the presence of unconsolidated sediments remaining from the construction, and from sediment remaining in the project that had eroded from the banks and channel failures during a previous thunderstorm. The response of the restoration project during its first post-construction year should not be representative of its future ability due to the disturbance caused by recent construction and the immaturity of recently planted riparian vegetation. Monitoring to determine the effectiveness of the restoration project will continue for at least two more years.

ACKNOWLEDGEMENTS

The author would like to thank the Nevada Division of State Lands' Lake Tahoe License Plate Program for funding the project. Additional funds for equipment were provided by the Desert

Research Institute, and the National Science Foundation's RING-TRUE Incline Creek Watershed Project.

REFERENCES

ASTM, 1999, "D 3977-97 Standard test method for determining sediment concentration in water samples," Annual Book of Standards, Water and Environmental Technology, 1999, Volume 1 I .02, pp 389-394.

ASTM, 2002, C 1070 – 01 Standard test method for particle size distribution of alumina and quartz powders by laser light scattering. http://www.astm.org.

Gee, G.W., and Or, D. (2002). "Particle-size analysis," in Dane, J.H. and G.C. Topp (eds.), Methods of Soil Analysis, Part 4, Physical methods, Soil Science Soc. Am., Inc., Madison, WI, pp 255-293.

Jassby, A.D., Goldman, C.R., Reuter, J.E., and Richards, R.C. (1999). "Origins and scale dependence of temporal variability in the transparency of Lake Tahoe, California-Nevada," Limnol. Oceanogr. 44(2) pp. 282-294.

Lewis, J. (1996). "Turbidity-controlled suspended sediment sampling for runoff-event load estimation," Water Resources Research 26, pp 2069-2077.

Miller, D. (2004). "Rosewood Creek Restoration Project: Operations and Maintenance Plan," Mainstream Restoration, Inc. March 23, 2004.

Rowe, T.G., Saleh, D.K., Watkins, S.A., and Kratzer, C.R. (2002). "Streamflow and water-quality data for selected watershed in the Lake Tahoe Basin, California and Nevada, Through September 1998," United States Geological Survey Water-Resources Investigations Report 02-4030.

TRG (Tahoe Research Group) (2001). "Annual Progress Report. Water Quality, Air Quality and Watersheds," Tahoe Research Group, Dept. of Civil and Environmental Engineering, Center for Ecological Health Research, Delta Group, Dept. Land, Air, and Water Resources. University of California, Davis, August 7, 2001.

Taylor, K., Susfalk, R., Shanafield, M. and Schladow, G. (2004). "Near-shore clarity at Lake Tahoe: Status and causes of reduction," Desert Research Institute Publication No. 41193.

IDENTIFYING SOURCES OF FINE-GRAINED SUSPENDED-SEDIMENT FOR THE POCOMOKE RIVER, AN EASTERN SHORE TRIBUTARY TO THE CHESAPEAKE BAY

Allen C. Gellis, U.S. Geological Survey, Baltimore, MD, 21237, agellis@usgs.gov; Jurate M. Landwehr, U.S. Geological Survey, Reston, VA 20192, jmlandwe@usgs.gov

Abstract: Sources of fine-grained suspended sediment in the Pocomoke River watershed draining above Willards, Maryland, were identified using a 'sediment-fingerprinting' approach. Potential sediment sources in the watershed were cropland, forest, channel and ditch banks, and ditch beds. Samples of fine-grained suspended sediment were obtained for seven storms between July 2001 and November 2002 and showed that the channel corridor (channel and ditch banks, and ditch beds) were significant sources averaging 76.5 % of the total sediment sources for the seven storms. Results indicate that sediment sources vary between events, and may be affected by seasonality and runoff conditions. Cropland was an important source of sediment for the two storms with the highest peak flow which occurred in the late summer and fall when harvesting began and vegetative cover was low. Ditch beds, which contributed an average of 46.1 % of sediment for the seven storms, were important sources of sediment over a range of peak flows (0.2 m^3/s to 15.7 m^3/s) and may also be important when crop areas have mature leaf cover.

INTRODUCTION

Fine-grained sediment is having an adverse effect on the habitat of the Chesapeake Bay and its watershed. To reduce sediment loadings to the Bay, it is helpful to identify the significant sources of the sediment. In 2002, the 157-km^2 watershed of the Pocomoke River above Willards, Maryland (MD), which drains part of the Eastern Shore of the Chesapeake Bay, was chosen as a watershed in which to identify sediment sources. The Pocomoke River was a focus area for previous and ongoing U.S. Geological Survey (USGS) studies (Phillips, 2001) on nutrients (Ator et al., 2004) and stream biologic health (Blazer et al., 1999). Because of the importance of fine-grained sediment in the transport of phosphorus (Walling, 2005) and its impact on water clarity (Landwehr, 2005), the identification of its sediment sources in the Pocomoke River is important to assist resource managers in development of strategies for its reduction.

BACKGROUND

The sediment-fingerprinting approach provides a direct method for quantifying watershed sources of fine-grained suspended sediment (Collins et al., 1997; Motha et al., 2003; Walling, 2005). This approach entails the identification of specific sources through the establishment of a minimal set of physical and/or chemical properties, i.e. tracers that uniquely define each source in the watershed. Suspended sediment collected under different flow conditions exhibits a composite, or fingerprint, of these properties that allows them to be traced back to their respective sources. Tracers that have successfully been used in the sediment-fingerprinting approach include mineralogy, radionuclides, trace elements, magnetic properties, and stable isotope ratios (^{15}N /^{14}N and ^{13}C /^{12}C) (Walling and Woodward, 1992; Collins et al., 1997; Motha et al., 2003; Papanicolaou et al., 2003). Sources of watershed sediment include upland sources (i.e. agriculture, urban construction, and forest) and the channel corridor (beds, banks, ditches,

and floodplains). Sampling sediment at these sources and linking the fingerprints to sediment in transport using a statistical mixing model enables quantification of the source(s).

STUDY AREA

The Pocomoke River drains entirely within the Coastal Plain Physiographic Province (Miller, 1967). Surficial geology in the watershed consists primarily of unconsolidated sand and some clay-silt of the Parsonburg Sand and Omar Formations (Denny et al., 1979). Land use in the Pocomoke River watershed in 1992 was 52 % agriculture (35 % in cultivated crops), 38 % forests, and 10 % wetland, and less than one percent urban (U.S. Geological Survey, 2003). Land-use categories considered to be relevant sediment sources for this study included cropland and forest. Cultivated crops in the Pocomoke River watershed are primarily corn and soy. Depending on soil moisture conditions, planting for corn and soy can occur from April to May and crop harvesting from August to September. The Pocomoke River has been channelized in selected portions as early as the 1600's and continuing into the 20th century (Ross et al., 2004). Ditching on agricultural lands in the Pocomoke River watershed is an extensive practice that has been used to drain wetlands (Fig. 1).

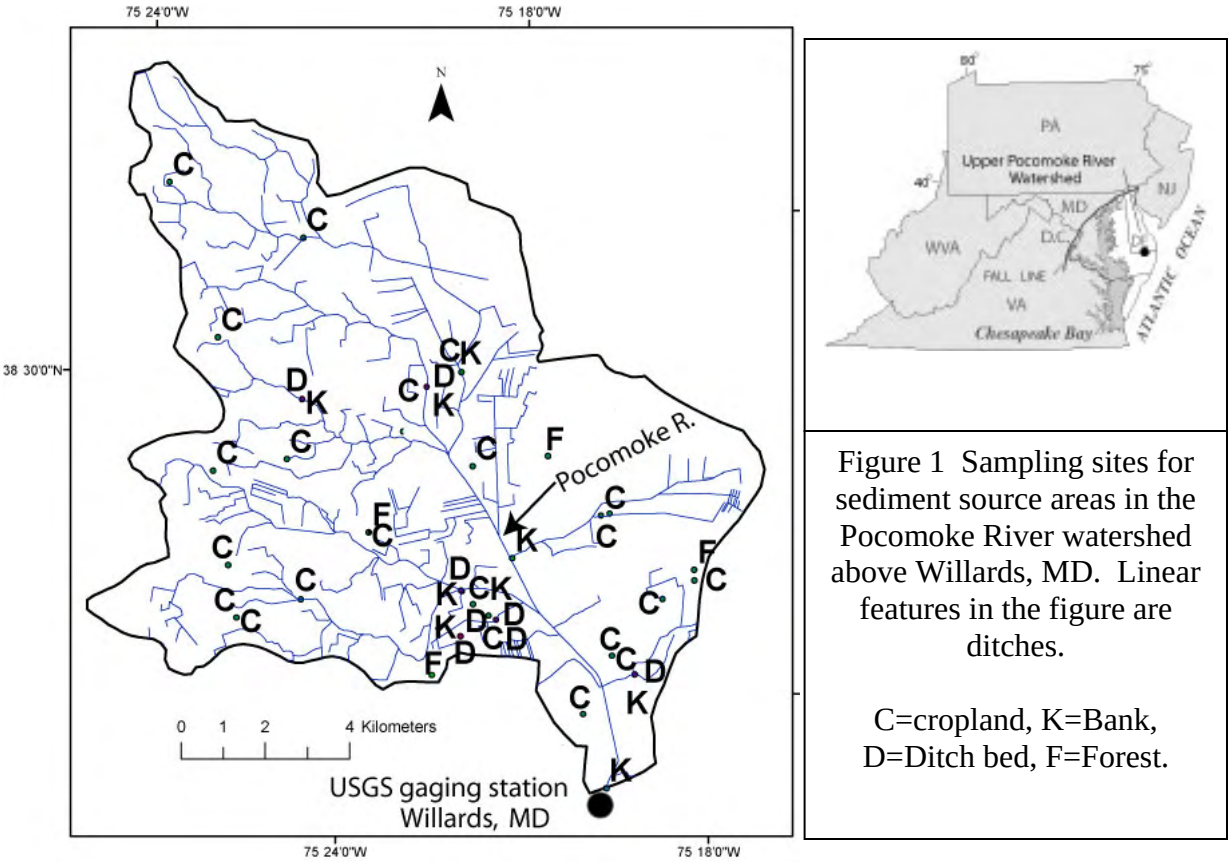


Figure 1 Sampling sites for sediment source areas in the Pocomoke River watershed above Willards, MD. Linear features in the figure are ditches.

C=cropland, K=Bank, D=Ditch bed, F=Forest.

Suspended-sediment samples were collected in the Pocomoke River near Willards, MD (USGS Station ID 01485000) from October 23, 2000, through April 29, 2002, for discharges ranging from 0.39 to 10.8 m^3/s. Samples were also collected in a tributary to the Pocomoke River, Nassawango Creek near Snowhill, MD (USGS Station ID 01485500), from October 28, 1998,

through April 18, 2000, for discharges ranging from 0.04 to 36.8 m^3/s (U.S. Geological Survey, 2005). These samples all had low suspended-sediment concentrations, which never exceeded 60 mg/L. These low suspended-sediment concentrations may be a function of the gradual slope of the Coastal Plain Province, as well as low streampower.

METHODS

Suspended sediment in the Pocomoke River at Willards, MD, was pumped into 83-L plastic containers using a submersible pump placed at mid-depth in the center of the channel. The sample was brought back to the laboratory and centrifuged with a continuous-flow centrifuge. The sediment obtained from the centrifuge was wet-sieved through a 63-micron sieve to remove sand and dried at 60C, with appropriate care taken to avoid cross-contamination.

Soil samples from cropland and forest areas were taken from the top 0.5 cm of the soil surface. Channel and ditch bank samples were sampled from the top to the bottom of the bank face. If banks were exposed on both sides of the channel, samples were taken on both banks and composited into one sample. Ditch-bed samples were taken from the top 0.5 cm of the ditch bed. The channel bed of the Pocomoke River was not considered to be a source in this study because this sediment may only represent temporary storage from upstream sources and is not a true source by itself. Because the ditch beds are deep and straight, dredged periodically, and extend over much of the watershed, they were considered a potential sediment source.

Upland and channel corridor samples were taken back to the laboratory, dried at 60^0C, disaggregated using a pestle and mortar, and dry-sieved through a 63-micron sieve to remove the sands. The silt and clay portion of suspended sediment, upland, and channel corridor samples was sent for analysis of radionuclides (^{137}Cs and unsupported ^{210}Pb), stable isotopes (δ^{13}C and δ^{15}N), and total carbon, nitrogen, and phosphorus. Unsupported ^{210}Pb refers the atmospheric deposition of ^{210}Pb and is reported in terms of disintegrations per minute per gram of sample (DPM/g).

The mass fraction of the sample that was composed by weight of total carbon, total nitrogen, and total phosphorus (*w*(C), *w*(N), *w*(P)) was analyzed at the University of Maryland's Chesapeake Biological Laboratory (Solomons, Maryland). Methods of analysis are accessible on the web at: *http://www.cbl.umces.edu/nasl/index.htm*. Stable isotopes (δ^{13}C and δ^{15}N) were analyzed at the USGS Stable Isotope Laboratory in Reston, Virginia and methods for analysis are described in the laboratory's web site at: *http://www.isotopes.usgs.gov.* Carbon-stable isotope ratios are reported relative to VPDB (Vienna Pee Dee Belemnite). Nitrogen isotopes are reported relative to nitrogen in air.

Radionculides were analyzed at three different laboratories: Case Western Reserve University in Cleveland, Ohio: the U.S Geological Survey Geologic Division Laboratory in Denver, Colorado: and the U.S Geological Survey Geologic Division Laboratory in St. Petersburg, Florida. At all three laboratories, radionuclides were analyzed by gamma spectroscopy using a Canberra HPGe

photon detector.** At Case Western Reserve University and the USGS lab in Denver, an EG&G Ortec** was also used. The technique used for counting efficiencies can be found in Wilson et al., (2003).

Statistical Methods: Several steps were taken to finalize which tracers were most appropriate to determine the relative contributions from each source for each sampled flow event. A requirement of sediment fingerprinting is that the fluvial tracers must be conservative and not change during transport from the source to the sampling point. Consequently, values for the fluvial tracers must be within the range of the tracer values measured for all sources. Any tracers that did not satisfy this constraint within measurement error were considered to be nonconservative and removed from further consideration. In addition, a Kruskal-Wallis H-test (Swan and Sandilands, 1995) was used to determine if there were significant differences ($p \leq 0.05$) between the medians of the measured tracer values in the source areas. Any tracers that did not satisfy this constraint were considered nondiscriminatory and removed from further consideration. Finally, each tracer should distinguish a specific source, but not necessarily separate all other sources. Conversely, each source should be statistically distinguishable from all others on the basis of at least one tracer. A students t-test (unpaired data with unequal variance) as well as a nonparametric Wilcoxon-Mann-Whitney test (Swan and Sandilands, 1995; Conover, 1999) were performed for each tracer between each pair of source areas (significance test at $p \leq 0.05$) to confirm that each source area was distinguished from all other source areas by at least one tracer and to identify redundant tracers for elimination.

The literature suggests many different mathematical forms by which the fingerprint may be decomposed into the relative contributions by source. In this study, the fluvial sample is considered to be composed of a mixture of sediment from the different source areas. To determine the relative source contributions to the fluvial samples, we defined an "unmixing" variable E (equation 1) in terms of normalized scores (Snedecor and Cochran, 1980). "E" is defined as the average absolute difference between each tracer value measured in the fluvial sample and as would occur in the proposed mixture, scaled by the relevant standard deviation of the mixture. The best model is considered to be that for which the set of the relative contributions from each source will provide the closest match to the fluvial tracer value, that is, provide a minimal value for E. The best mixture model was considered to be that set of fractional values (f_s, s=1 to 4) which minimizes the expression E as given below. Note that the f_s must sum to one. The minimizing function E, expressed in standard deviation units, is defined as

$$E = (1/T) \sum_{t=1}^{T} \left| \{ v_t - \sum_{s=1}^{S} f_s A_{st} \} \right| / \text{sqrt} \{ \sum_{s=1}^{S} f_s^2 VAR_{st} \} \qquad (1)$$

where t is a specific tracer, T is the total number of tracers, v_t is the value of the tracer t in the fluvial sample, s is a specific source area, S is the total number of source areas, and A_{st} and

** Any use of trade, product, or firm names in this publication is for descriptive purposes only and does not imply endorsement by the U.S. Government.

VAR_{st} are the estimated average and variance of the measured values of tracer t in source area s, respectively.

RESULTS

Seven storm suspended-sediment samples were collected from July 2001 to November 2002. The source data set consisted of a total of 43 samples from the 4 source areas (channel and ditch banks, ditch beds, croplands, and forest) with samples taken at n = 9, 8, 22, and 4 sites, respectively (Fig. 1). The amount of sand in the sources was high, averaging 70% + /- 27% for banks, 86 % +/- 20 % for ditch beds, 87% +/- 5% for croplands, and 94% +/- 2% for forest. The sand content in the source samples reflects the high abundance of sand composition in the Coastal Plain sediments.

Examination of the fluvial tracer values compared to the source samples showed that the measured values for three tracers, $m(^{137}Cs)$, $w(P)$, and $w(C)/w(N)$, were outside the range of measured values in 4, 6, and 5 cases, respectively. These tracers were deemed not conservative and were not used. One fluvial sample had a $\delta^{15}N$ value that was outside the range of the source $\delta^{15}N$ values, but it was within measurement error of a measured source site value and was retained. A Kruskal-Wallis test performed for each of the remaining five potential tracers (^{210}Pb, $w(C)$, $w(N)$, $\delta^{13}C$, and $\delta^{15}N$) confirmed that there were statistically significant differences between the medians of the measured tracer values in the four source areas.

Results were in agreement of the students t-test (unpaired data and not assuming equal variance) as well as a nonparametric Wilcoxon-Mann-Whitney test performed among all pairs of source areas for the five remaining tracers, namely ^{210}Pb, $w(C)$, $w(N)$, $\delta^{13}C$, and $\delta^{15}N$, were in agreement. The results confirmed that the tracers could distinguish between sources. $w(N)$ and $w(C)$ provided comparable distinctions between source areas, so that use of both tracers was redundant. Because $w(N)$ has a higher measurement error, particularly as grain size diminishes, this tracer was eliminated. The only tracer capable of significantly distinguishing between bed and bank was ^{210}Pb. Thus, the number of relevant tracers was T=4 (^{210}Pb, $w(C)$, $\delta^{13}C$, and $\delta^{15}N$). Results for one fluvial sample – that of August 29, 2002 – had an outlier for ^{210}Pb, however, and the analysis for this date was performed with T=3 tracers. The fluvial sample values for the final four tracers are shown in Table 1. Average tracer values for the four source areas are shown in Table 2. Variance of the tracer values is shown in Table 3. Results of the minimizing model are shown in Table 4. In using the minimizing model, the f values were incremented in steps of 0.025, computing over 69,000 possible solutions for E. Note that the E terms, expressed in standard deviation units, are all less than 2, which implies that we cannot reject the hypothesis that the fluvial sediment and the proposed mixture of sediment sources for each event are significantly different.

Averaging sediment sources for the seven events indicated that channel corridor (channel and ditch banks, and ditch beds) were major sources of sediment (76.5%), but the sources were variable over the seven sampled events (Table 4). Seasonality, rainfall intensity, and streamflow are some of the factors that may affect the contribution of a given sediment source for a given particular storm. For the two highest peak-discharge storms and the lowest peak-discharge storm, cropland was an important source of sediment (Table 4). For the range of peak flows (0.2

m^3/s to 15.7 m^3/s), the channel corridor (channel and ditch banks, and ditch beds) were important sources. Forests, as a sediment source, show up in the highest peak discharge event. Examination of source by season shows that for the late August, September, and November events, cropland was a sediment source. Corn and soy, which are grown in the Pocomoke River watershed, are harvested beginning in late summer. The depleted vegetative cover after harvesting combined with a rainfall event would make this a likely sediment source. The highest peak flow of the seven sampled events occurred in early September during this harvesting period.

CONCLUSIONS

Observed suspended-sediment concentrations in the Pocomoke River are less than 60 mg/L. Two factors make the Pocomoke River a minor contributor of fine-grained suspended sediment to the Chesapeake Bay. First, the abundance of sand in the unconsolidated Coastal Plain sediments limits the potential for transport of silt and clay. Second, the Pocomoke River watershed drains the Coastal Plain, which is relatively flat compared with other physiographic provinces in the Chesapeake Bay; this low gradient limits streampower for sediment transport. Periods of significant overland flow are rare in the upper Pocomoke River watershed, occurring only 20 % of the time when flows exceed 2.83 m^3/s (Ator et al., 2004). Analysis of storm-generated hydrographs by Ator et al., (2004) indicated that over 70 % of the flow is from ground-water discharge. Infrequent periods of overland flow in the Pocomoke River limit upland areas (cropland and forest) as significant sources of sediment, except under periods of high rainfall intensity or under saturated-soil conditions when overland flow may occur.

Samples of fine-grained suspended sediment were obtained during seven flow events between July 2001 and November 2002, to determine sediment sources using a sediment-fingerprinting technique. The seven sampled events had recurrence intervals ranging from 2 years to less than 1 year. Potential sediment sources in the Pocomoke River watershed were cropland, forests, ditch bed and banks, and channel banks. Statistical analysis indicated that the source areas could be differentiated in terms of four tracer parameters (^{210}Pb, w(C), δ^{13}C, and δ^{15}N).

Table 1 Tracer values for sampled flow events used in the sediment source identification, in order of peak-flow rate.

Date	Collection time	Peak discharge m^3/s	^{210}Pb (DPM/g)	$10^3\delta^{13}$C	$10^3\delta^{15}$N	w(C)	Peak-flow recurrence interval †
9/2/2002	11:15	20.0	5.886	-25.48	7.60	11.40	2 yrs
11/18/2002	15:15	15.7	2.454	-26.10	9.08	8.48	1.25 yrs
11/6/2002	11:30	6.3	6.96	-27.40	11.85	11.30	<1 yr
3/21/2002	9:45	2.5	0.001	-27.88	8.64	11.40	<1 yr
7/19/2001	10:00	1.6	0.001	-27.29	10.99	11.72	<1 yr
8/29/2002	14:00	0.3	*	-27.41	8.72	12.60	<1 yr
8/30/2002	9:00	0.2	0.001	-26.65	8.37	8.17	<1 yr

* *Data value in error,* † *Recurrence intervals of peak flow were determined using the USGS peak- flow program (PEAKFQ) (Thomas et al., 1998).*

Table 2 Average tracer values for the source samples used in sediment source identification.

Tracer Source Area	^{210}Pb DPM/g	Range ^{210}Pb (DPM/g)	w(C)	Range w(C)	$10^3\ \delta^{13}$C	Range $10^3\ \delta^{13}$	$10^3\ \delta^{15}$N	Range $10^3\ \delta^{15}$N
Bank	2.629	0.743 to 5.09	7.802	4.99 ro 11.8	-27.38	-27.76 to -26.78	7.203	4.57 to 10.6
Bed	1.075	0.001 ro 2.91	6.236	1.08 to 11.0	-27.683	-29.05 ro -25.95	8.414	6.63 to 9.83
Cropland	4.385	1.25 to 15.3	7.334	2.90 to 14.2	-24.005	-26.60 to -22.4	8.823	4.85 to 11.5
Forest	6.432	13.3 to 18.8	21.825	17.1 to 24.8	-27.268	-27.79 to -26.15	-1.238	-2.06 to -0.470

Table 3 Variance of tracer values for the source samples used in sediment source identification.

Tracer Source Area	^{210}Pb DPM/g	w(C)	$10^3\delta^{13}$C	$10^3\delta^{15}$N
Bank	2.57	4.59	0.15	3.85
Bed	0.85	10.22	1.57	1.10
Cropland	10.55	5.47	1.02	3.22
Forest	15.36	10.91	0.57	0.56

Table 4 Minimizing model results showing the contribution from each source area (in percent) for each of the seven sampled runoff events.

Date	Peak discharge m^3/s	Channel and ditch banks %	Ditch bed %	Cropland %	Forest %	Minimum E
9/2/2002	20	15	0	57.5	27.5	0.577
11/18/2002	15.7	0	57.5	42.5	0	0.350
11/6/2002	6.3	100	0	0	0	1.689
3/21/2002	2.5	0	100	0	0	0.789
7/19/2001	1.6	97.5	0	2.5	0	1.391
* 8/29/2002	0.3	0	95	5	0	0.812
8/30/2002	0.2	0	70	27.5	2.5	0.639
Average		30.4	46.1	19.3	4.3	

*This sample was fit using only 3 tracers, namely *w*(C), δ^{13}C, and δ^{15}N because the *unsupported* ^{210}Pb value was in error in the fluvial sample.

Results of applying an "unmixing" equation developed for this study indicated that the channel corridor (channel and ditch banks, and ditch beds) was a major source of sediment, averaging 76.5% of the total sediment sources for the seven sampled flow events; however, the contributions from the sources were variable between sampled events. Cropland was an important source for the two highest discharge events (peak flow of 20 m^3/s and 15.7 m^3/s) and was also a sediment source in late August and September. The channel corridor (channel and ditch banks, and ditch beds) were important sediment sources over a range of peak flows (0.2 m^3/s to 15.7 m^3/s).

From this limited data set, several conclusions on sediment sources for the Pocomoke River watershed above Willards, MD can be presented. One conclusion is that higher runoff events, presumably associated with higher rainfall, increase the potential for upland erosion, and cropland is a sediment source. Forests, which is another upland sediment source, also appeared as a sediment source in the highest peak-discharge event. At intermediate and lower peak flows, which are associated with moderate to low rainfall events, the channel corridor (channel and ditch banks, and ditch beds) is an important source. During periods when cropland is devoid of vegetation, such as before planting and after harvesting (late August to May), cropland is an important sediment source. When crop cover is mature, the ditch beds are an important sediment source.

REFERENCES

Ator, S.W., Denver, J.W., and Brayton, M.J., 2004, "Hydrologic and geochemical controls on pesticide and nutrient transport to two streams on the Delmarva Peninsula," U.S. Geological Survey Scientific Investigations Report 2004-5051, 34 p.

Blazer, V., Phillips, S.., and Pendleton, E., 1999, "Fish health, fungal infections, and Pfiesteria—The role of the U.S. Geological Survey," U.S. Geological Survey Fact Sheet 114-98, 4 p.

Collins, A.L., Walling, D.E., and Leeks, G.J.L., 1997, "Sediment sources in the Upper Severn Catchment – a fingerprinting approach," Hydrology and Earth System Sciences, v. 1, p. 509-521.

Conover, W.J., 1999, Practical Nonparametric Statistics, Third Edition: John Wiley and Sons, New York, 584 p.

Denny, C.S., Owens, J.P., Sirkin, L.A., and Rubin, M., 1979, "The Parsonburg Sand in the Central Delmarva Peninsula, Maryland and Delaware," U.S. Geological Survey, Professional Paper 1067-B, 16 p.

Landwehr, J. M., 2005, "Determining the "best" model for explaining water clarity variation during SAV seasons within the tidal tributary rivers of the Chesapeake Bay watershed," Conference Abstracts - Estuarine Interactions, 18th Biennial Conference of the Estuarine Research Federation, October 16-20, 2005 Norfolk, Virginia, p. 104.

Miller, F.P., 1967, "Maryland soils," University of Maryland, Cooperative Extension Service, College Park, Maryland, Extension Bulletin 212, 42 p.

Motha, J.A., Wallbrink, P.J., Hairsine, P.B., and Grayson, R.B., 2003, "Determining the sources of suspended sediment in a forested catchment in southwestern Australia," Water Resources Research, v. 39, p. ESG 2-1 –ESG 2.14.

Papanicolaou, A.N., Fox, J.F., and Marshall, J., 2003, "Soil fingerprinting in the Palouse Basin, USA using stable carbon and nitrogen isotopes," International Journal of Sediment Research, v. 18, p. 278-284.

Phillips, S.W., 2001, "The U.S. Geological Survey Chesapeake Bay Science Program," U.S. Geological Survey Fact Sheet 125-01, 4 p.

Ross, K.M., Hupp, C.R., and Howard, A.D. 2004. "Sedimentation in floodplains of selected tributaries of the Chesapeake Bay," in Bennett, S.J., and Simon, A., eds., Riparian Vegetation and Fluvial Geomorphology: American Geophysical Union, Water Science and Application Series. v. 8, 290 p.

Snedecor, G.W., and Cochran, W.G., 1980, Statistical Methods, Seventh Edition: The Iowa State University Press, 507 p.

Swan, A.R.H. and Sandilands, M., 1995, "Introduction to geological data analysis," Blackwell Science, 446 p.

Thomas, W.O., Jr., Lumb, A.M., Flynn, K.M., and Kirby, W.H., 1998, "User's manual for program PEAKFQ," annual flood frequency analysis using Bulletin 17B guidelines, written communication, 89 p.

U.S. Geological Survey, 2003, "National Land Cover Database 2001 (NLCD 2001)," U.S. Geological Survey, Sioux Falls, SD, assessed October 31, 2005 at http://www.mrlc.gov/mrlc2k_nlcd.asp.

U.S. Geological Survey, 2005, USGS National Water Information System (NWIS) water-quality data base, accessed August 15, 2005 at http://waterdata.usgs.gov/md/nwis/qw. Walling, D.W., 2005, "Tracing suspended sediment sources in catchments and river systems," Science of the Total Environment, v. 344, p. 159-184.

Walling, D.W., and Woodward, J.C., 2002, "Use of radiometric fingerprints to derive information on suspended sediment sources," International Association of Hydrological Sciences Publication 210, p. 153-164.

Wilson, C.G., Matisoff, G., and Whiting, P.J., 2003, "Short-term erosion rates from a ^{7}Be inventory balance" Earth Surface Processes and Landforms v. 28, p. 967-977.

THE USE OF TURBIDITY SENSORS FOR MONITORING SEDIMENT LOADS FOLLOWING WILDFIRE

Sandra E. Ryan, Research Hydrologist/Geomorphologist, USDA Forest Service, Rocky Mountain Research Station, 240 W. Prospect Rd., Ft. Collins, CO 80526 sryanburkett@fs.fed.us; Mark K. Dixon, Hydrologist, Fraser Experimental Forest, P.O. Box 117, Fraser, CO 80442, mdixon01@fs.fed.us; Kathleen A. Dwire, Research Riparian Ecologist, USDA Forest Service, Rocky Mountain Research Station, 240 W. Prospect Rd., Ft. Collins, CO 80526 kadwire@fs.fed.us

Abstract: Turbidity sensors (OBS-3 and OBS-5; D & A Instruments) were deployed to monitor sediment loads following a moderate-to-severe burn in the Little Granite Creek watershed near Bondurant, WY. The sensors were installed at the mouth of a burned tributary, in an adjacent reference tributary watershed, and at a longer-term study site on the main stem. Sensors were calibrated using depth-integrated samples taken with DH-48 suspended sediment samplers and from samples obtained using ISCO automated water samplers. The ISCO samplers were later programmed to collect samples once a threshold turbidity value was exceeded. This scheme allowed the collection of more samples during periods in which rapid changes in sediment loads were most likely to occur. Generally, the turbidity sensors characterized the sediment load at all sites very well during periods of snowmelt runoff, with good correspondence between turbidity values and measured suspended sediment concentrations. However, fouling problems were encountered at the 2 sites below the burned area during summer baseflow when slower and warmer water fostered the growth of algae on the sensors. The growth was quite rapid, with detectable fouling occurring within days after cleaning at one site. This likely could have been avoided with more frequent cleaning of the sensor or the use of a device with an automated cleaning wiper. In short, turbidity sensors showed promise as a surrogate for monitoring sediment loads following large-scale disturbance, such as wildfire. However, the results underscore the need for periodic and on-going collection of suspended sediment samples to calibrate the signal from the sensors and to identify shifts in relationships between turbidity and suspended sediment concentration.

INTRODUCTION

Substantial increases in sediment loads commonly occur in channels downstream of areas burned by wildfire. Rapid increases in sediment are typically associated with increases in runoff generated by high intensity rainfall. Such events are often short-lived, but can deliver a tremendous amount of sediment to the aquatic system and potentially to water supply systems further downstream. Monitoring sediment loads in these systems can provide information about sediment transport rates and processes occurring after large scale disturbances, as well as the precipitation intensity required to trigger sedimentation events. However, given the episodic nature of these pulses in sediment and flow, it is often difficult to adequately characterize sediment concentrations using a discrete water sampling scheme. Turbidity sensors, which measure light backscattering from particles suspended in water, have been utilized as a surrogate measure of suspended sediment concentration (SSC) (Kuhnle and Wren 2005). High turbidity generally indicates a high concentration of material, including organic and inorganic sediment. Turbidity sensors that have been programmed to measure on a relatively frequent basis (e.g., 15 minute interval) can provide highly detailed information on sediment transport, particularly when calibrated using periodic grab samples of SSC.

As part of a monitoring program following a wildfire, we deployed turbidity sensors to provide estimates of SSC at Little Granite Creek near Bondurant, WY. The monitoring was conducted in control and burned watersheds during snowmelt runoff and summer baseflow periods. The objectives were to determine 1) if there was a predictable relationship between turbidity and measured suspended sediment concentrations, and 2) whether the sensors worked with sufficient consistency so that they could be used to replace the discrete water collection program. Turbidity values were linked to sediment concentrations measured concurrently and regression relationships were developed. The quality of these statistical relationships and departure over time are discussed. Problems encountered with instrument fouling are also described, as are recommended methods for reducing these difficulties.

WATERSHED DESCRIPTION

Little Granite Creek, an upland contributor to the Snake River system, drains 21.1 miles^2 (54.6 km^2) of the Gros Ventre range near Bondurant, Wyoming, south of Jackson, Wyoming. A sediment sampling program at this site

began in 1982 as part of environmental monitoring in conjunction with planned exploration and extraction of fossil fuels in the upper basin. Though the exploratory effort was eventually abandoned, suspended sediment monitoring was continued by the USGS through 1993 (Ryan and Emmett 2002), providing an extensive dataset against which changes in sediment loads due to wildfire could be detected (Ryan et al. 2003). The area is administered by the USFS, Bridger-Teton National Forest, Jackson Ranger District. Over half of the basin is in the Gros Ventre Wilderness Area.

Detailed descriptions of the Little Granite Creek watershed are provided in Ryan and Emmett 2002 and Ryan et al. 2003. Briefly, the two main tributaries of Little Granite Creek are Boulder Creek (8.0 miles^2/20.7 km^2) and the upper basin of Little Granite Creek (7.6 miles^2/19.7 km^2). Approximately 80% of the forested area in Boulder Creek and less than 5% of that in upper Little Granite Creek burned in 2000 (Figure 1). Both basins face south and had similar pre-fire forest cover (Engelmann spruce, subalpine fir, and lodgepole pine) and geology (sedimentary formations of marine origin (Love and Christiansen, 1985)). Flow and rates of sediment transport were monitored at (1) the mouth of Boulder Creek (burned), (2) upper Little Granite Creek (reference), and (3) Little Granite Creek above the confluence with Granite Creek (site of previous work) (Figure 1). Site 3 is approximately 2.5 river miles (4 km) downstream of the burned area. The elevations of the monitoring sites are around 6,500 feet (1981 m.).

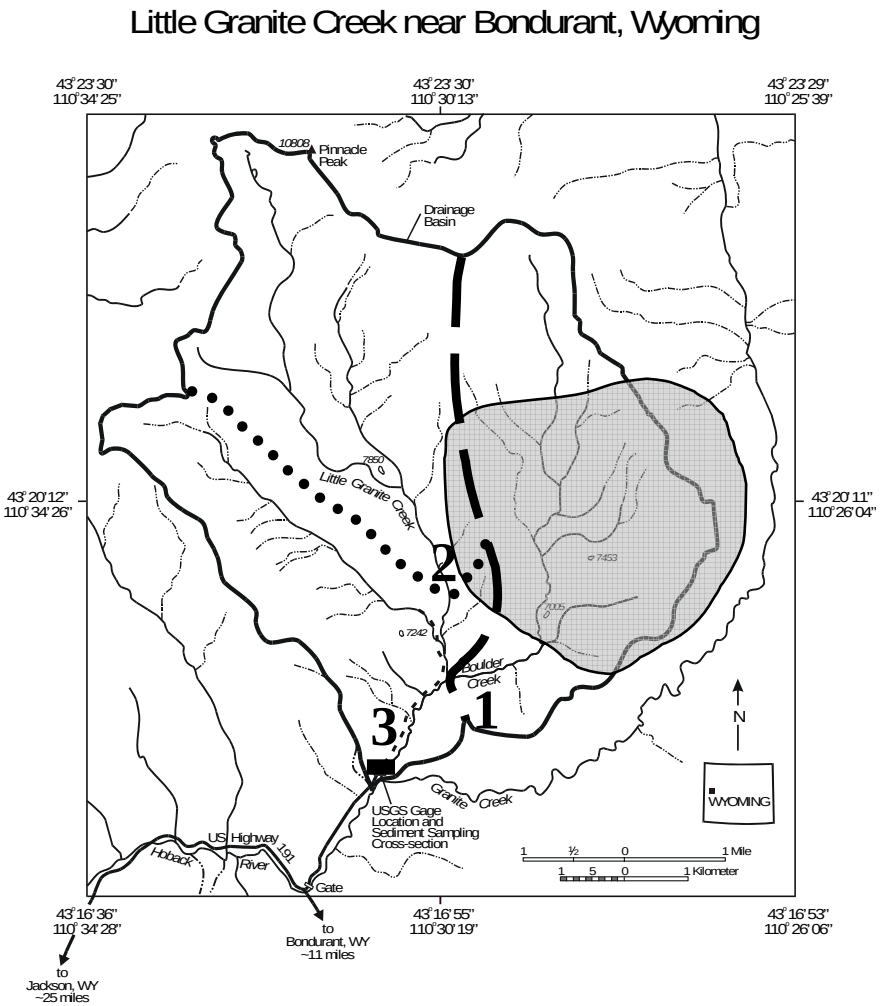


Figure 1 Map of Little Granite Creek watershed. Stipple pattern approximates the area burned by the Boulder Creek fire in 2000. An estimated ¾ of the area burned with moderate to high severity. The dark dashed line delineates the Boulder Creek watershed and the dotted line indicates the limits of the unburned watershed (upper Little Granite Creek). Numbers are described in text. The light dashed line represents an unimproved forest road.

The primary sources of sediment in the watershed come from mass wasting, including active earthflows from unstable hill slopes, and slumping from undercut terraces and road cuts. Baseline concentrations of suspended sediment at high flows are relatively high (between 100 and 1000 mg L^{-1}) because of the underlying marine sedimentary formations (Ryan and Dixon, in review). By comparison, similar measurements in streams in forested areas draining granitic terrain are rarely greater than about 100 mg L^{-1} (Andrews 1984).

METHODS

In 2002, an OBS-5 turbidity sensor (D & A Instruments 2005) was deployed at the Lower Little Granite Creek site, downstream of the burned area (Figure 1, site 3). This device was selected in anticipation of very high sediment loads following wildfire because particle concentration detected by this sensor are greater than those of many other sensors. The sensor was calibrated at the factory using a suspended sediment sample collected from the site in 2001. The device was attached to a metal post that had been driven into the channel bed adjacent to a sampling platform from which water and sediment samples were obtained. The device was adjusted for changing flow depth several times during the runoff season. The internal datalogger was programmed to take a reading and recorded an estimate of SSC once every 5 minutes. These values were later correlated with SSC's measured once every 4 hours by an ISCO automated water sampler (Teledyne ISCO 2005) and with samples taken with a DH-48 depth integrated sampler (Edwards and Glysson, 1998; Federal Interagency Sedimentation Project 2005) on an intermittent basis.

In 2003, OBS-3 turbidity sensors (D & A Instruments 2005) were deployed at each of the 3 sites in Little Granite Creek watershed (Figure 1). These devices were selected because results from the previous year indicated that the range of measured particle concentrations was within the limits established for this device. The sensors were installed on a metal post driven into the channel bottom at each of the monitoring stations. The height of the OBS-3 was manually adjusted during the flow season so that the sensor was seated at about ½ the depth of the flow (± depending on daily flow fluctuations). Data collection and instrument programming were performed using Campbell CR10x dataloggers (Campbell Scientific 2005). At 15-minute intervals, the dataloggers recorded the median of a series of 20 turbidity readings taken in rapid succession. Turbidity values (FTU) from the OBS-3 were calibrated using SSC determined from samples collected intermittently using a DH-48 sampler. Later in the season, automated water samplers were installed and programmed to collect water samples when a threshold turbidity value was exceeded (Eads and Lewis 2002). This sampling scheme permitted the collection of samples only when rapid changes in sediment concentrations were likely to occur, thereby reducing the overall number of samples collected and processed. The turbidity threshold above which collection was initiated varied by site due to differences in load characteristics (expected concentration range, color, etc.) in the burned and reference watersheds.

Stage data were collected at 15-minute intervals in both 2002 and 2003 using Aquarod stage recorders or pressure transducers. Intermittent discharge measurements were made at each of the 3 sites (about 25 per runoff season) and stage-discharge relationships were developed.

RESULTS

Turbidity and Suspended Sediment Measurements – 2002: An overall linear relationship between estimates obtained with the calibrated OBS-5 sensor and concentrations from the automated samplers was observed (Figure 2). However, the relationship differs for low and high ranges of concentrations and is never 1:1. Though not easily discerned at the scale shown, at low concentrations, estimates from the OBS-5 consistently overestimated measured concentrations by about 100 mg L^{-1}. This discrepancy did not appear to be related to fouling of the sensor and may reflect a limit in resolution at the lower end as this particular device is intended for use in flow with higher concentrations of sediment. There was better correspondence between measurements and estimates at higher concentrations (>500 mg L^{-1}) where differences were on the order of 10-40% of the measured values. A notable departure from the general trend was observed for samples following a storm on September 7, 2002 (shown in purple, Figure 2). The values from the OBS-5 over-predicted measured concentrations during this storm by a factor of 4 to 5. The differences for this short period are likely due to changes in the sediment characteristics following the rainstorm and, hence, visual qualities of the stream water. For instance, differences in organic matter content or particle sizes will change the amount of backscattered light received by the sensor, causing erroneous estimates from a pre-calibrated device. While the exact cause of this particular discrepancy is unknown, the results underscore the need for periodic and on-going collection of suspended sediment samples to calibrate the signal from turbidity sensors and to identify shifts in established relationships between turbidity and SSC.

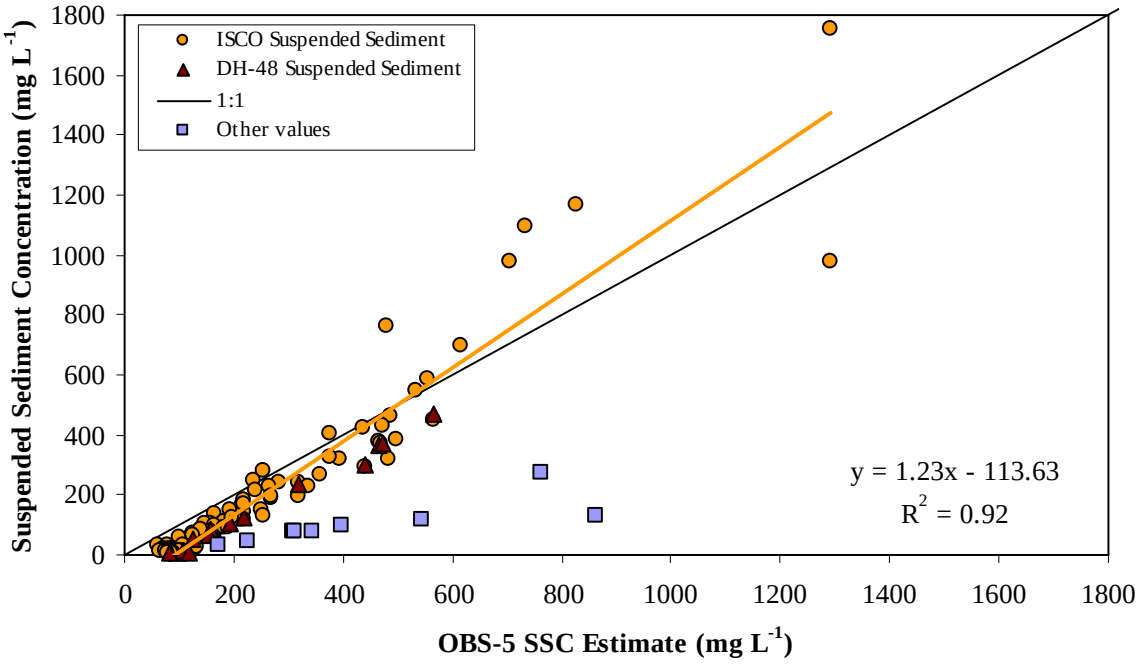


Figure 2 Relationship between estimates of suspended sediment concentration obtained with a (calibrated) OBS-5 turbidity sensor and measurements from ISCO automated samplers (orange circles) at Lower Little Granite Creek. Correspondence between samples obtained with automated and depth-integrated samplers was close to 1:1, as shown by the overlap between orange circles (ISCO) and red triangles (DH-48). This indicates that the flow was well-mixed and no correction factor for the automated sampler was required. Purple squares (excluded from the regression) depict a drift in the relationship between turbidity and ISCO samples following a rain storm in late summer.

Turbidity and Suspended Sediment Measurements – 2003: OBS-3 turbidity sensors were installed on the rising limb of the snowmelt hydrograph in 2003 and removed from the sites in early fall. Similar to that observed in 2002, there were linear relationships between measured (raw) turbidity values and SSC's at all 3 sites (Figure 3), though these relationships often varied over the course of the hydrograph (Figure 3, e.g., Boulder Creek). At Upper Little Granite Creek, the predictive relationship over the duration of the measurement period was quite good as the departure of individual measurements of SSC was relatively small (Figure 4a). The automated sampler was triggered to collect water samples during two storms in late summer and there was close correspondence between measured and predicted SSC during these events. At Lower Little Granite Creek, there was good correspondence from the period of late May to early June (Figure 4b). Shortly thereafter, there was notable departure on the falling limb of the seasonal hydrograph as the sensor became increasingly fouled due to the growth of algae over the lens. This occurred as flows became slower and warmer and the period of ambient light availability increased. Turbidity values returned to expected levels following sensor cleaning, but there continued to be fouling problems during June and July until a regularly scheduled cleaning program could be established. At Lower Little Granite Creek, this was achieved by cleaning the sensor on a weekly basis. At Boulder Creek, a more frequent program was needed. Here, the sensor often became fouled within days after cleaning, providing erroneous turbidity values that are difficult to discriminate from the main record (data not shown). The automated water sampler at Lower Little Granite Creek was triggered to collect samples during 5 higher concentration events, though one (September 12) appears to be a false trigger initiated, in part, by sensor fouling.

Estimates of peak concentrations during snowmelt runoff in 2003 ranged from about 450 to 3,330 mg L^{-1} at Upper Little Granite and 450 to 4,800 mg L^{-1} at the Lower site (Figure 4). This suggests that differences in SSC between the upper and lower sites were not substantial over the early part of the record. For comparison, concentrations in the first post-fire year (2001), measured using a discrete sampling program, ranged from 300 to 1,200 mg L^{-1} at Upper Little Granite and 350 to 5,700 mg L^{-1} at Lower Little Granite during the snowmelt period (Ryan et al. 2003).

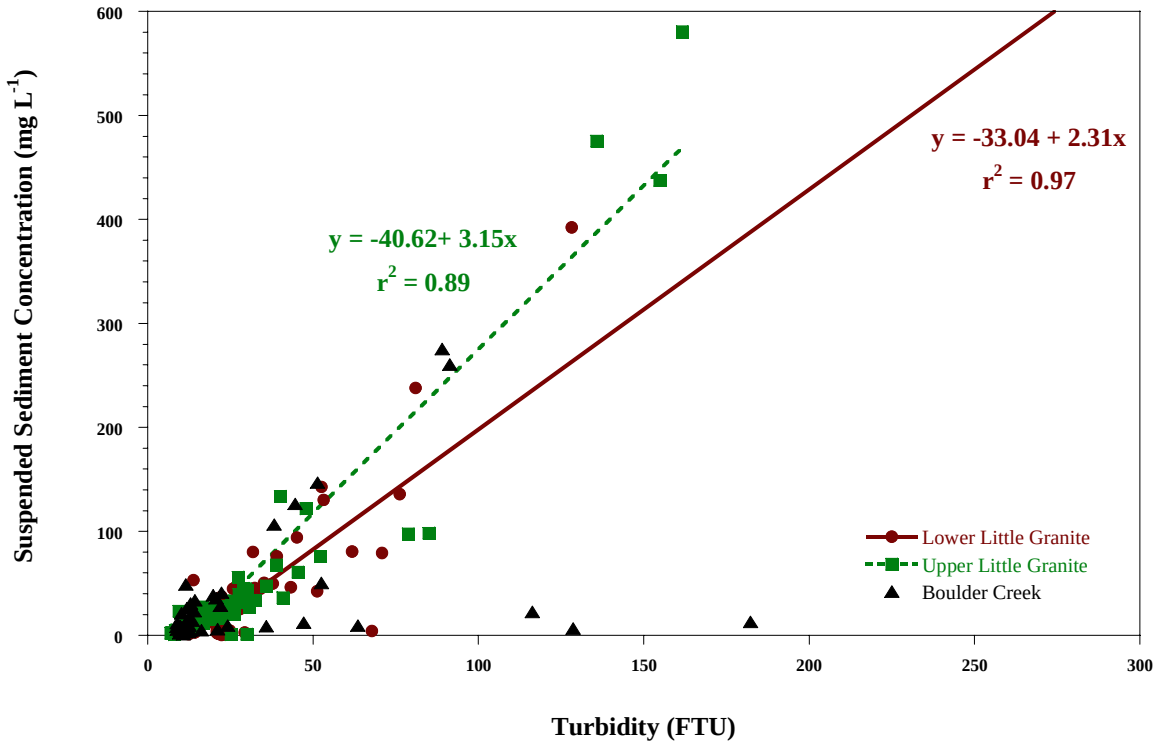


Figure 3 Relationships between turbidity values and measured SSC at 3 sites in Little Granite Creek watershed. Standard error of the residuals at Lower Little Granite was 30.1 and was 33.9 at Upper Little Granite. One additional data point for Lower Little Granite is beyond the limits of this plot, but is included in the regression. No single regression could be determined for the Boulder Creek site as the relationship between turbidity and SSC varied over the measurement period.

Most of the estimates of peak concentrations from the turbidity sensors fall within the range of those measured previously, suggesting that they are realistic values. Higher projected concentrations at Upper Little Granite in 2003 are likely due to the ability to obtain estimates from turbidity sensors during periods that were unsampled by the discrete sampling program. Notably, the peak concentrations from the turbidity record use a reliable statistical relationship, providing increased confidence in the estimate of SSC for these periods. To predict peak concentrations using the discrete data, one would need to establish a relationship between flow and SSC and extrapolate this relationship to higher discharges. Given that the relationship between flow and SSC varies greatly over different parts of the seasonal hydrograph (Ryan and Dixon, in review), this estimate has greater inherent uncertainty than that obtained using turbidity/SSC relationships.

Estimates of SSC obtained during baseflow and summer thunderstorms at Upper and Lower Little Granite were also comparable, though more variability was exhibited in the Lower Little Granite data (Figure 4b). This may be due, in part, to the crossing of more than 1 log cycle, which visually exaggerates small differences in SSC in the 0.1 to 1 range. The difference in ranges may also be an artifact of the model used to estimate concentration from turbidity. SSC estimates for Upper Little Granite ranged from 2 to 8 mg L^{-1} during baseflow and increased up to 200 mg L^{-1} during a single event in early September. SSC estimates for Lower Little Granite ranged from 0.2 to 10 mg L^{-1} and increased up to 120 mg L^{-1} during the same event.

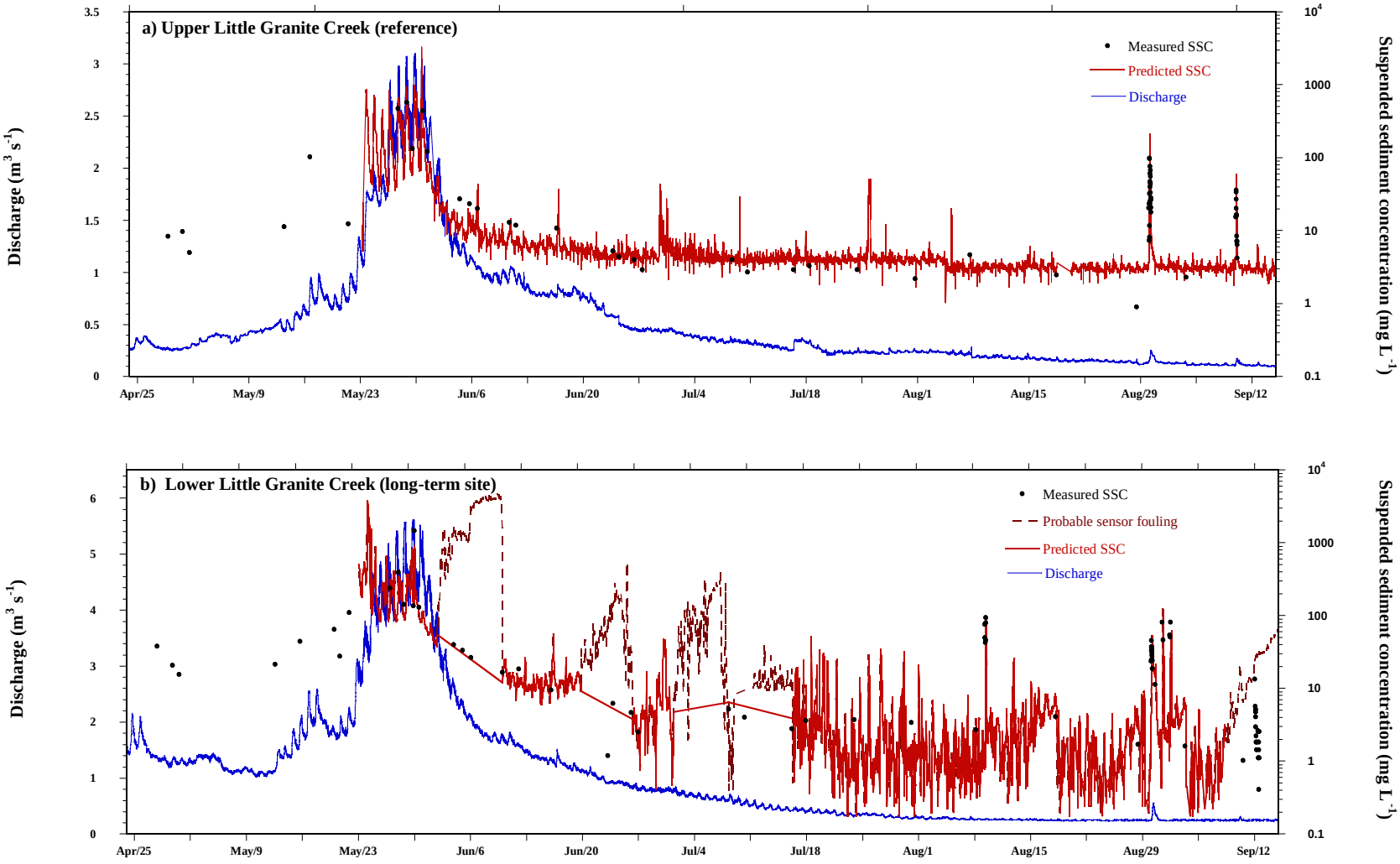


Figure 4 Suspended sediment concentration estimated from values of turbidity from OBS-3 sensors at a) Upper and b) Lower Little Granite Creeks in 2003 (red line). Individual DH-48 samples are shown as black circles and discharge is indicated as a blue line. SSC is plotted on a logarithmic scale to show better the correspondence between predicted and measured values. Though a slightly larger range of values exists for Lower Little Granite during baseflow, this appears exaggerated in (b) where the values cross more than 1 log cycle.

DISCUSSION AND SUMMARY

The purpose of this paper was to report findings on the relationship between measured SSC and turbidity values obtained under reference conditions and at sites below an area recently burned by wildfire. Generally, there was good correspondence between turbidity values and SSC and this relationship could be used to develop time-series data for sediment concentration. Such information can potentially improve the understanding of the timing and magnitude of instream sediment transport relative to changing hydrologic conditions or large-scale sediment inputs following disturbance. It also improves the understanding of the inherently variable nature of sediment concentrations over different ranges of timescale. Moreover, implementing a sampling scheme using a turbidity threshold permits the collection of water samples during periods of higher and more rapidly changing sediment conditions, potentially improving the predictive capabilities of the turbidity/SSC relationship(s). Automating the process allows sample collection during periods often missed by a discrete or intermittent sampling program when travel to a site is impossible or impractical.

As shown here and elsewhere, the use of turbidity sensors show great promise in supplementing a discrete water sampling program. However, in order to derive a meaningful record, it is imperative that the turbidity meters be kept free of debris, either by using an automated wiper for smaller materials (biological fouling) or frequent manual cleaning of the sensor surface (which may be impractical in remote locations). Frequent cleaning will help prevent erroneous measurements of turbidity and false triggering of sample collection due to sensor fouling. Our results also underscore the need for periodic and on-going collection of suspended sediment samples to calibrate the signal from the sensors and to identify shifts in relationships between turbidity and SSC.

ACKNOWLEDGEMENTS

Funding for this experimental monitoring effort was provided by the Bridger-Teton National Forest and by USDA Forest Service, Research Work Unit 4352. Helpful reviews of an earlier draft of this paper were made by Rudy King, Jack Lewis, and Dan Marion of the US Forest Service and Roger Kuhnle of the Agricultural Research Service. Any errors or omissions are solely the responsibilities of the authors.

REFERENCES

Andrews, E.D. (1984). “Bed-material entrainment and hydraulic geometry of gravel-bed rivers in Colorado.” Geological Society of America Bulletin, 95, pp. 371-378.

Campbell Scientific (2005). “ CR10X datalogger for measurement and control.” [On-line] Available: http://www.campbellsci.com/cr10x [August 22, 2005].

D and A Instruments (2005). “D and A Instrument Company.” [On-line] Available: http://www.d-a-instruments.com/ [August 22, 2005].

Eads, R., and Lewis, J. (2002). “Continuous turbidity monitoring in streams of Northwestern California.” Turbidity and Other Sediment Surrogates Workshop, April 30 – May 2, 2002, Reno, N. [On-line] Available: http://water.usgs.gov/osw/techniques/TSS/eads.pdf [August 22, 2005].

Edwards, T.K., and Glysson, G.D. (1998). “Field methods for measurement of fluvial sediment.” U.S. Geological Survey, Techniques of Water-Resources Investigations. Book 3, chapter C2.

Federal Interagency Sedimentation Project (2005). “US DH-48 Depth integrating suspended wading type sampler.” [On-line] Available http://fisp.wes.army.mil/Catalog_Page_US_DH-48.htm (August 22, 2005).

Kuhnle, R.A., and Wren, D.G. (2005). “Suspended sediment measurement: data needs, uncertainty, and new technologies.” Proceedings of the Federal Interagency Sediment Monitoring Instrument and Analysis Research Workshop, September 9-11, 2003, Flagstaff, AZ, U.S. Geological Survey Circular 1276, pp. 8-15.

Love, J.D., and Christiansen A.C. (1985). “Geologic Map of Wyoming.” U.S. Geological Survey, prepared in cooperation with the Wyoming Geologic Survey, 3 sheets.

Ryan, S.E., and Dixon, M.K. (in review). “Spatial and temporal variability in stream sediment loads using examples from the Gros Ventre Range, Wyoming, USA.” Gravel Bed Rivers 6, Lienz, Austria, September 5-9, 2005.

Ryan, S.E., Dixon, M.K., Dwire, K.A., and Emmett, W.W. (2003). “Historical and on-going hydrologic and sediment transport research at Little Granite Creek near Bondurant, Wyoming.” Proceedings of the First Interagency Conference on Research in the Watersheds, October 28-30, 2003, Benson, AZ. Agricultural Research Service, pp. 657-662.

Ryan, S.E., and W.W. Emmett. (2002). "The nature of flow and sediment movement at Little Granite Creek near Bondurant, Wyoming." U.S. Department of Agriculture, Forest Service, Rocky Mountain Research Station, General Technical Report RMRS-GTR-90. Ogden [Utah].

Teledyne ISCO (2005). "6712 Full-Size Portable Sampler." [On-line] Available: http://www.isco.com/products/products3.asp?PL=201101010 (August 22, 2005).

The use of trade or firm names in this publication is for reader information and does not imply endorsement by the U.S. Department of Agriculture of any product or service.

TURBIDITY MEASUREMENTS FOR DETERMINATION OF SEDIMENT SOURCE AND RETENTION IN RIVER AND MARSH ENVIRONMENTS.

A.P. Stubblefield, Research Associate, Dept. Geological Sciences, Case Western Reserve University, Cleveland, OH, aps12@case.edu; E.W. Larsen, Research Faculty, Dept. Landscape Architecture, Univ. California, Davis, CA, ewlarsen@ucdavis.edu; M.I. Escobar, Student, Dept. Hydrology, Univ. California, Davis, CA, mescobar@ucdavis.edu; J.E. Reuter, Research Faculty, Dept. Env. Sci. & Policy, Univ. California, Davis, CA, jereuter@ucdavis.edu; C.R. Goldman, Professor, Dept. Env. Sci. & Policy, Univ. California, Davis, CA.

INTRODUCTION

A key component of the conservation of water quality is the prevention of the introduction of excess suspended sediment (SS). Sediment is a major pollutant of U.S. waterways. (Nearly et al. 1989). In addition to impacting water clarity and quality for swimming and drinking purposes, sediment clogs spawning grounds and aquatic habitats. Agricultural practices, timber harvest and associated roads, are chief sources of suspended sediment. Water quality monitoring networks provide a means of identifying regions with high loading rates, comparing different land management practices and examining the roles of geomorphologic and hydrologic variables. This information can be used to guide management and permitting activities by identifying erosional "hot spots": specific soils, slope positions, or landscapes that are unstable when disturbed; and specific harvesting, road placement or agricultural practices that result in high sediment loading. Sediment loading can be episodic, dynamic and highly variable. Thus monitoring need to be either triggered by storm events or running continuously. If the intent is to compare loading rates between different landscapes and management practices, it is important to compare storm events of similar magnitude and intensity- optimally, the same event. This creates a need for monitoring simultaneously at several locations to compare responses. Networks of *in situ* turbidometers can greatly increase the resolution and power of monitoring networks by providing continuous water quality data at multiple locations.

The measurement of turbidity as a surrogate for suspended sediment is dependent on the consistency of the relationship between the two over the full range of sediment loading conditions at a site. If the intent of the study is to determine particle size variations over time, laser diffraction instruments (Topping 2000) would be more appropriate. However if an adequate calibration between SS and turbidity can be obtained the method offers an inexpensive means of recording and integrating SS flux over a wide range of time scales and spatial comparisons.

Lake Tahoe has shown a steady and steep decline in clarity over several decades (Goldman 2000) making studies of sediment source and retention critical. This paper presents three examples of the use of turbidometry in the Tahoe basin. The first application was the creation of a sediment budgets for subalpine forested and rockland watersheds of the west shore of Lake Tahoe (Figure 1). We compared subwatersheds draining metasedimentary and volcanic regolith, and headwater and valley stream reaches. Turbidometry was useful for this application because the majority of sediment loading occurs during the spring snowmelt. Access to the upper watersheds is difficult at this time because of deep snowpacks and rugged terrain, and the discharge varies dramatically due to snowmelt fluctuations.

The second application was the measurement of the retention of SS within a freshwater marsh. Most monitoring stations are located upstream of river deltas to avoid tidal or backwater effects on discharge measurements. The result is very little information on sediment retention of deltas. In South Lake Tahoe, California, the Upper Truckee River and Trout Creek come together in the Truckee Marsh before emptying into Lake Tahoe (Figure 2). Previous monitoring on both rivers had largely taken place above the marsh. Formerly one of the largest wetlands in the Sierra Nevada, the marsh has been extensively modified, with a marina and a housing development placed in the center. A canal was excavated to make the Upper Truckee River bypass the developed area. We installed turbidity monitors above and below the wetland portion of each river as a means of comparing sediment retention within the unimpacted and channelized rivers.

The third application was the detection of hysteresis, the variation in the relationship between SS and discharge over daily and seasonal time periods. By continually measuring SS and discharge, it was possible to observe flushing and sediment exhaustion, phenomenon that are important for understanding in channel storage of sediment, potential rates of recovery, and design optimal sampling protocols.

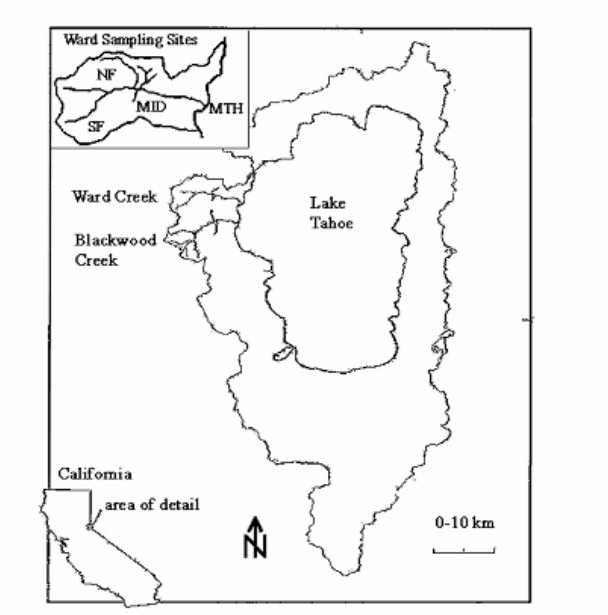


Figure 1 Ward Creek at Lake Tahoe. Inset: sampling locations.

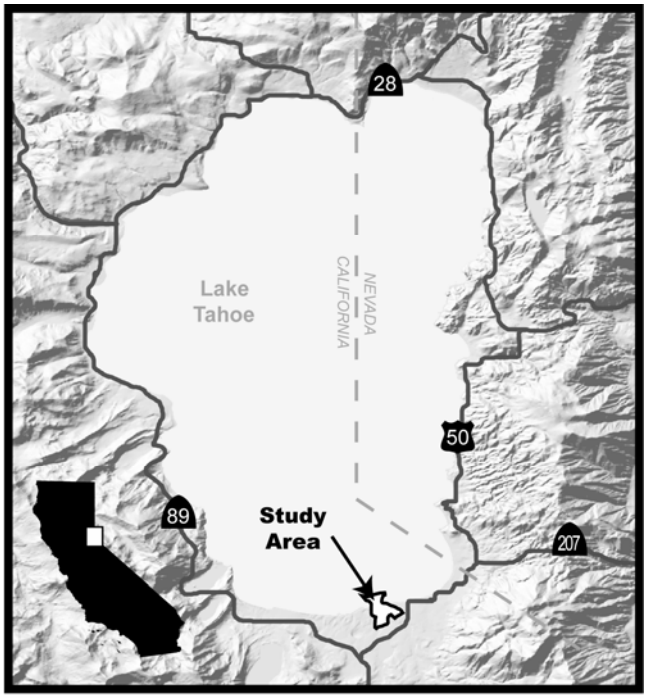


Figure 2 Truckee Marsh at South Lake Tahoe, CA. (Figure 2, 4; Table 2, 3 © Springer Science and Business Media, Stubblefield et al. 2005a).

METHODS

Ward Creek (25 km^2) extends from 1900 m at lake level to 2700 m at the watershed boundary. It is predominantly forested with conifers, with urban development at the lake shore and subalpine zones above treeline. The North Fork is predominantly regolith derived from metasedimentary rocks. The South Fork has volcanic and granitic outcrops, with its most notable feature a large mudflow breccia badlands. The main stem has a lower steep walled canyon section with cobble sized alluvium and occasional exposed bedrock. The upper section of the main stem opens into a broader valley with pebble-sized alluvium.

Sediment budgets are quantitative measurements of inputs, outputs and storage within a designated region. To create a sediment budget for Ward Creek on the west shore of Lake Tahoe we focused on quantifying SS loads entering and exiting river reaches. We installed a network of four turbidometers to quantify sediment loading in the South and North Forks of the watershed, and the upper and lower reaches of the watershed (inset, Figure 1). Data was collected for the spring snowmelt seasons of 1999, 2000, and 2001. Long term monitoring of Tahoe watersheds (Rowe 2002) indicate that the bulk of SS is transported during spring snowmelt. Optical backscatter nephelometers were connected to dataloggers. Twelve readings were made per minute, and the average stored every fifteen minutes. Grab samples of river water were taken weekly, and during peak flows. Samples were analyzed gravimetrically for TSS and compared to concurrent turbidity readings for calibration. Continuous discharge measurements were available from USGS monitoring stations at three locations within the watershed. Discharge in the North and South Forks were determined using standard gauging techniques and related to USGS station data from just below the confluence. Turbidity data was converted to SS concentration using the calibration data. SS concentration per 15 minute time step was then multiplied by flow volumes and summed over longer time periods to generate sediment loads at each site. Further details are provided by Stubblefield (2002).

The Truckee Marsh is approximately 400 ha. A barrier beach lies between the marsh and the lake. Vegetation is primarily grass and sedge, with some regions of willow and conifer. In 2003, the year of this study, the Trout Creek divided into two distributaries, one passing through a lagoon, and the other a beaver dam, before rejoining each other, and exiting into Lake Tahoe. The Upper Truckee River meanders through the upper marsh before reaching the straight canal reach and exiting into Lake Tahoe. The Trout Creek watershed has an area of 10,674 ha. The Upper Truckee Watershed has an area of 14,673 ha. Both rivers have sandy alluvium in the lower reaches.

For the measurement of SS retention on the Upper Truckee Marsh, turbidometers, and velocity and stage recorders were installed above and below the marsh reaches of the Trout and Upper Truckee rivers. Instrumentation was also installed at a mid-marsh station in Trout Creek. Sampling was focused on the spring snowmelt as this represents the bulk of sediment loading for subalpine Sierra watersheds. SS samples were collected with depth-integrated flow samplers. Sediment loads entering and exiting the marsh were compiled as described above for Ward Creek. Further description is provided by Stubblefield et al. (2005a).

In addition to creating a sediment budget from the Ward Creek data, we examined sediment transport dynamics. For specific flow events, we plotted the ratio of concentration at 15 minute intervals (C) as a fraction of peak concentration (Co) versus discharge at 15 minute interval (Q) as a fraction of peak discharge (Qo). The resulting graphs (C/Co versus Q/Qo) highlight changes in the relationship of SS and discharge over time. We also compared sediment yields estimated from turbidometry with estimates generated from a sediment rating curve method. Further description is provided in Stubblefield et al. (2005b).

RESULTS

Excellent correlations were found between suspended sediment and turbidity values for four Lake Tahoe basin tributaries: Ward Creek (1999-2001, r^2 =.95), Blackwood Creek (2001, r^2 =.91), Upper Truckee River and Trout Creek (2003, combined r^2 =.90). Turbidity and discharge data for Ward Creek in 1999 is shown in Figure 3. Turbidity fluctuations are closely linked to daily discharge peaks from snowmelt. Turbidity responses tend to be sharper peaks, occurring on the rising limb of the hydrograph, and falling faster than

the discharge falling limb. Turbidity response to discharge appears to lessen over the course of the season. For example, the turbidity response on May 13 is much greater than June 13, 1999 for roughly

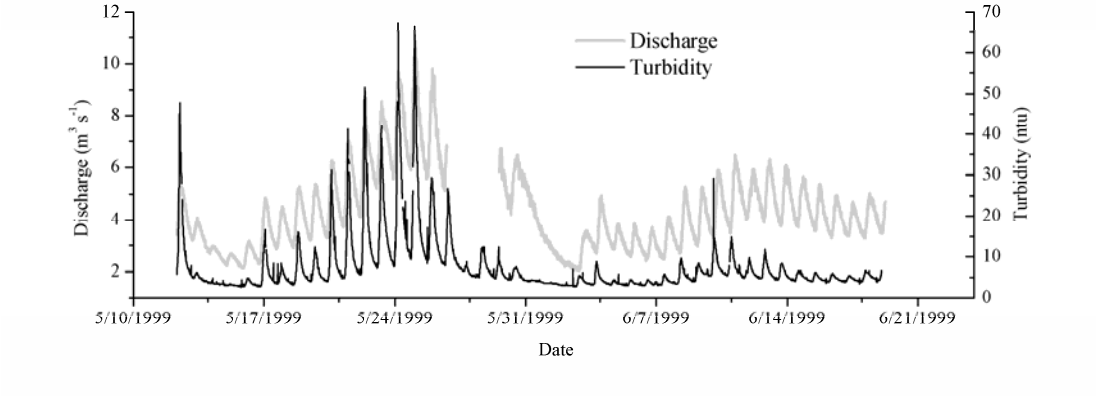


Figure 3 Turbidity and discharge. Ward Creek, 1999. (Figures 3, 5, 6 © John Wiley & Sons Ltd., Stubblefield et al. 2005).

equivalent discharge levels (Figure 3). Sediment budgets for 1999, 2000 and 2001, created from the SS turbidity regression, and the turbidity and discharge record for each site, are shown in Table 1a. Because of sensor blockages and electronic malfunction, the budgets are constructed for time periods in which all four sensors were operational, 6 days in 1999, 34 days in 2000 and 29 days in 2001. The short record of 1999 occurred during peak flow, when the bulk of SS was transported. Budgets indicate high specific sediment loads for the South Fork, and the Upper Main Stem of Ward Creek. A closer look at 3 distinct pulses in the snowmelt load for 2000 is shown in Table 1b. At different times within the season, the Lower Main Stem goes from storing sediment (negative values) to releasing sediment. The South Fork makes steady contributions, and the Upper Main Stem with a high initial load, drops steadily as the season progresses.

Table 1 Ward Creek sediment budget (kg/ha/d).

a. Specific Sediment Loads for 3 years (kg/ha/d)

Basin	1999	2000	2001*
North Fork	4.2	1.1	0.6
South Fork	7.1	3.0	
Upper Main Stem	19.6	2.4	0.1
Lower Main Stem	4.7	2.4	0.2
Duration (d)	6	34	29

* Single headwater station for 2001 below confluence.

b. Sediment Loads for 3 Events in Snowmelt 2000 (kg/ha/d)

	Event#			
Basin	1	2	3	Total
North Fork	0.1	2.0	0.6	1.1
South Fork	2.1	4.4	2.17	3.0
Upper Main Stem	8.6	3.9	0.73	2.4
Lower Main Stem	-4.6	7.8	-0.1	2.4
Duration (d)	2.3	12	20	34

Table 2 Trout Creek suspended sediment (SS) load.

	Time Period*	Above Marsh	Mid Marsh	Below Marsh	Retention
Discharge (m^3)	1	11,524,793	5,384,165	n/a	
	2	953,798	550,062	785,031	18%
	3	643,131	293,324	424,457	34%
SS Total Load (Mt)	1	260	89	n/a	
	2	39	18	12.5	68%
	3	33	10	3.4	90%
SS Load per Unit Volume (Mt/m^3)	1	2.3(-5)	1.7(-5)	n/a	
	2	4.1(-5)	3.3(-5)	1.6(-5)	
	3	5.1(-5)	3.4(-5)	8.0 (-6)	

*Sample period 1 was May 6 to June 17. Sample periods 2 and 3 are subsets of 1. They are May 21 to May 25, and May 27 to May 29 respectively.

Data for sediment retention for the spring snowmelt 2003 are shown for Trout Creek in Table 2 and the Upper Truckee River in Table 3. Retention of SS was 26% on average for the Upper Truckee River, with a daily range of 13-41%. Retention of SS was much higher for Trout Creek, ranging from 68-90%. The Trout Creek retention estimate was based on the peak flow period. Data from Mid and Above Marsh stations indicate similar retention trends for longer time periods. Discharge results indicate higher retention of water within the Trout Creek portion of the marsh, with 18-34% retention as compared to the Upper Truckee River with 6% retention. The Mid Marsh discharge values for Trout Creek are lower than the Mouth because a side channel, ungaged in this study, carried more flow than was predicted in designing the experiment. For this reason a measure of concentration, SS Load per Unit Volume, is presented in Table 2. It indicates that there was a reduction in SS concentration between the Above and Mid stations, but not as large as might be suggested by the Total Load results. Examining the SS Load per Unit Volume results, it is apparent that the greatest reduction in SS concentrations took place in the lowest reach of the marsh, between the Mid and Below stations. Turbidity data is supported by grab sampling results shown in Figure 4. SS concentrations at the two Mouth stations were consistently low, regardless of incoming SS concentrations measured at the Above and Mid stations.

Table 3 Upper Truckee River suspended sediment (SS) retention.

	Time Period*	Above Marsh	Below Marsh	Retention
Discharge (m^3)	Total	7,090,095	6,636,520	6%
SS Load (Mg)	May 12 - 14	14	8	41%
	May 15 - 16	6	5	24%
	May 16 - 17	24	21	13%
	May 17 - 22	177	130	26%
	May 28 - 28	20	15	26%
	May 29 - 29	22	15	32%
	Total	263	194	26%

A continuous record makes it possible to examine variations in the relationship between SS and discharge. Figure 5 is a hysteresis graph for a rain on snow event occurring on May 10, 2000 at the Mouth station of Ward Creek. During the rising limb the SS concentration rises quickly, achieving peak concentration at 80% of peak flow. The fall of SS is more precipitous, with concentrations at 40% of peak, while flow has only returned to 80% of peak level. Hysteresis is also observed at the seasonal level as described above for

Figure 4. As an evaluation of the effects of hysteresis on sediment load estimates, turbidity based daily loads were plotted against sediment rating curve loads for Ward Creek. Total SS load from the turbidity estimate was 80.2%, 98.5%, and 58.4% of rating curve estimates for the years 1999, 2000, 2001, respectively. The data for 1999 is shown in Figure 6 and inset. Rating curve estimates appear to underestimate turbidity loads during peak flow and overestimate loads during low flow periods.

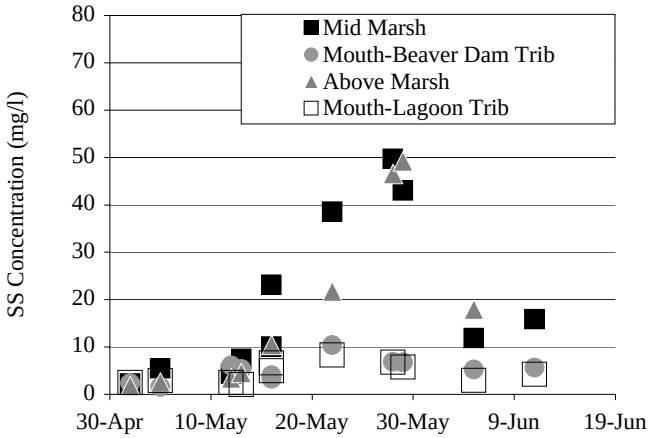


Figure 4 Trout Creek SS concentrations from grab-sampling, 2003.

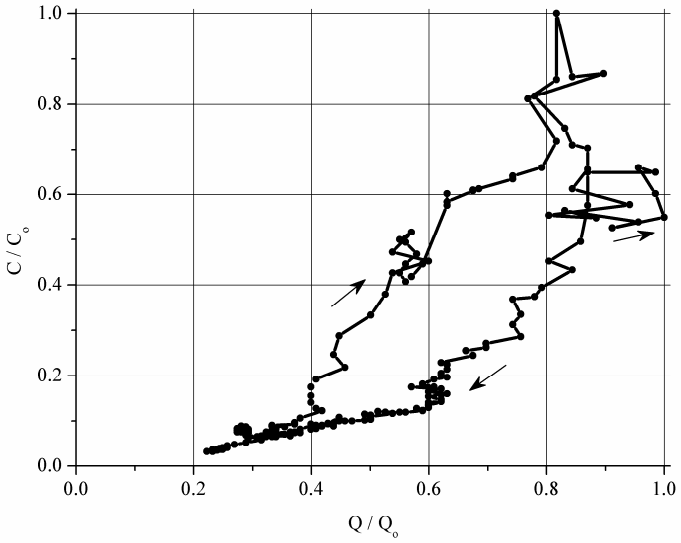


Figure 5 Hysteresis plot for Ward Creek, May 10, 2000.

DISCUSSION

The results presented here demonstrate the efficacy of turbidometry for determining sediment source and sediment retention characteristics for SS concentrations of 1-100 mg/l. The high-resolution data set generated by turbidometric measurements indicates sediment delivery dynamics with important implications for monitoring networks and rates of stream recovery.

The high SS loads from the South Fork of Ward Creek are likely the result of the badlands region. Within the subcatchment, other erosion sources are unlikely. Forested regions typically have low sediment outputs (ref). Visual inspection of the channel course indicates very little bank erosion. Other indications of high rates of erosion are pedestalled trees, with a 20 cm gap between the root crown and the current land surface, exposed bedrock surfaces without rock varnish, highly friable and unconsolidated regolith, and extensive

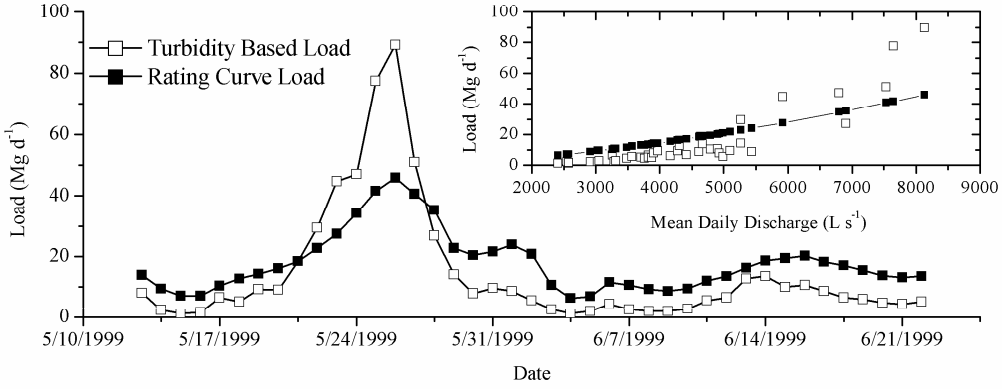


Figure 6 Comparison of turbidity and sediment rating curve-based load estimates. Ward Creek, 1999.

networks of rills and gullies. The Tahoe basin was heavily overgrazed by cattle and sheep (Holland 1987). It is possible the badlands were initiated by overgrazing. Cold thermal conditions and limited moisture in montane climates can limit revegetation of badland surfaces (Regues et al. 2000).

The Upper Main Stem also had high SS loads. A landslide on the south slope reached the stream course during a hundred year flood event in 1997. However during the average flows recorded during 1999-2001 (see Stubblefield, 2002) the landslide did not appear to contribute to SS loads. A few gravel tongues extended down to the channel, with no fines evident. Inspection of the channel course showed limited bank erosion. However it is difficult to visually assess the impact of bank erosion since a small increment over many kilometers of river can be significant. The other source of fines, suggested by inspection of the Upper Main Stem, is mud drapes deposited by summer and fall thunderstorms (Dunkerly and Brown 1999). During a high intensity rain event observed by the authors, large quantities of SS were washed into the channel. The sediment was traced to the badlands region of the South Fork. Thunderstorms typically occur during summer low flow periods, when sediment transport capacity may not be sufficient to transport it to the lake. The material remains as a coating on sands and gravels and in interstitial spaces. The decrease in specific sediment loads in the Upper Main Stem during 2000 (Table 1b) may represent the gradual winnowing of instream fine sediment deposits deposited during earlier events.

The sediment retention characteristics of the Truckee Marsh reflect floodplain connectivity. The Upper Truckee River is highly incised, with two meter high banks preventing movement of snowmelt flows out into the marsh. Constrained flows result in the reach acting like a pipe, directly transmitting SS with little retention. High rates of bank erosion can result in sediment yield rather than retention. Conversely in the Trout Creek section of the marsh, particularly the lower reach, flows spread out over a wide area. During late May, 2003, snowmelt waters moved out over much of the 80 area. Resulting low flow velocities and increased contact with the bottom sediments result in greater sediment retention. Channels are small, and stabilized by vegetation. By diverting flows to the north, the barrier beach creates a lagoon, backing up water and increasing marsh flooding. As the Upper Truckee River is the largest source of SS in the Tahoe basin, the results of this study indicate that restoration of floodplain connectivity has the potential to greatly reduce SS loading to Lake Tahoe.

Clockwise hysteresis is an indication of sediment exhaustion (Asselman 1999). It was observed in single events (Figure 5) and over the course of the snowmelt season (Figure 3). Hysteresis has two implications.

The first is that sediment rating curves dependent on a stationary relationship between SS and discharge may be subject to bias. Coats suggested that reduced grab sampling frequency during the falling limb of the seasonal hydrograph would result in a sediment rating curve that overestimated sediment loading (2002). Figure 6 gives an example of this bias, with rating curves overestimating during low flow and underestimating during peak flow events. The second implication of sediment exhaustion is the existence of a condition of limited sediment supply in relation to transport capacity. If loads from the upper watersheds and banks were reduced, Ward Creek would return to excellent water quality levels in a short time period.

REFERENCES

Asselman, N.E.M. 1999. "Suspended sediment dynamics in a large drainage basin," the River Rhine. Hydrological Processes 13: 1437-1450.

Coats, R.N., Liu, F., and Goldman, C.R. 2002. "A Monte Carlo test of load calculation methods, Lake Tahoe Basin, California-Nevada," Journal of the American Water Resources Association 38: 719-730.

Dunkerly, D., and Brown, K. 1999. "Flow behavior, suspended sediment transport and transmission losses in a small (sub-bankfull) flow event in an Australian desert stream," Hydrological Processes. 13: 1577-1588.

Goldman, C.R. 2000. Baldi lecture. "Four decades of change in two subalpine lakes," Verh. Int. Verein. theor. ang. Limnol. 27: 7–26.

Holland, A. 1987. "History of Blackwood Canyon," Unpublished Report. USDA Forest Service. Lake Tahoe Basin Management Unit, South Lake Tahoe, CA.

Neary D.G., Swank, W.T., and Riekerk, H. 1989. "An overview of nonpoint source pollution in the southern United States," In: Hook, D.D. and Lea, R. (Eds.) Proceedings of a Symposium: The Forested Wetlands of the Southern United States, p.1-17. Orlando, FL. July 12-15. USDA Forest Service General Technical Report SE-50. 168 pp.

Regues, D.R., Guardia, D., and Gallart, F. 2000. "Geomorphic agents versus vegetation spreading as causes of badland occurrence in a Mediterranean subhumid mountainous area," Catena. 40: 173-187

Rowe, T.G., Saleh, D.K., Watkins, S.A., and Kratzer, C.R. 2002. "Streamflow and Water-Quality Data for Selected Watersheds in the Lake Tahoe Basin, California and Nevada, Through September 1998," Water Resources Investigations Report 02-4030. U.S. Geological Survey: Carson City; 118 pp.

Stubblefield, A.P. 2002. "Spatial and Temporal Dynamics of Watershed Sediment Delivery, Lake Tahoe, California," Ph.D. Dissertation. University of California, Davis. 199 pp.

Stubblefield, A.P., Escobar, M.I., and Larsen, E.W. 2005a. "Retention of suspended sediment and phosphorus on a freshwater delta, South Lake Tahoe, California," In Press. Wetlands Ecology and Management.

Stubblefield, A.P., Reuter, J.E., Dahlgren, R.A., and Goldman, C.R. 2005b. "Suspended sediment flux and the use of turbidometry in the Lake Tahoe basin," In Press. Hydrological Processes.

Topping, D.J., Rubin, D.M., Nelson, J.M., Kinzel, P.J., and Corson, I.C. 2000. "Colorado River sediment transport 2. Systematic bed-elevation and grain–size effects of sand supply limitation," Water Resources Research. 36: 543-570.

RIVER RESTORATION USING A GEOMORPHIC APPROACH FOR NATURAL CHANNEL DESIGN

David L. Rosgen, Hydrologist/Geomorphologist, Wildland Hydrology, 11210 North County Road 19 North, Fort Collins, Colorado 80524, wildlandhydrology@wildlandhydrology.com

Abstract: River restoration based on the principles of natural channel design is most commonly accomplished by restoring the dimension, pattern and profile of a disturbed river system to emulate the natural, stable river. To "restore" rivers involves securing their physical stability and biological function, rather than the unlikely ability to return the river to a pristine state. Restoration is used synonymously with the term *rehabilitation*. Any river restoration design must first identify the cause and consequence of stream channel impairment (instability). The design must not only address the causes of instability, but also the rivers potential to balance the objectives, desires and benefits of the proposed restoration.

Natural channel design uses a geomorphic approach that incorporates a combination of *analog*, *empirical* and *analytical* methods for assessment and design. Because all rivers within a wide range of valley types do not exhibit similar morphological, sedimentological, hydraulic or biological characteristics, it is necessary to group rivers of similar characteristics into discrete stream types. Such characteristics are obtained from stable *reference reach* locations by discrete valley types, and are then converted to dimensionless ratios for extrapolation to disturbed stream reaches of various sizes. Hydraulic, sedimentological and morphological relations are obtained for both the reference and impaired conditions. Such values describe not only the average but the range of selected variables used for assessment as well as natural channel design. Sediment competence and capacity calculations are key to both the stability assessment and the design phases of the methodology.

The proper application of this approach requires extensive training and experience. A strong background in geomorphology, hydrology and engineering is required. The restoration specialist must also have the ability to integrate principles from fishery and plant science disciplines, and to implement the design in the field. The assessment methodology is broken into eight major sequential phases.

INTRODUCTION

The cumulative effects of long-term watershed development and "river works" have had extensive adverse impacts on our rivers. The effects of road construction, riparian vegetation change, in-channel gravel mining, logging, reservoirs/diversions, urban sprawl and other similar developments have significantly changed flow and sediment regimes and the boundary conditions associated with stable stream systems. Direct disturbance to channels by straightening, lining, draining, raising, lowering, clearing, dredging in the name of flood control, navigation and other single-purpose objectives have taken a serious toll on the physical and biological functions of our rivers.

Public awareness over the last decade has prompted federal, state, local jurisdictions and environmental groups to direct major efforts at preserving, protecting, enhancing, stabilizing, rehabilitating and restoring rivers throughout the United States. The pendulum is at least swinging the other way, albeit sometimes into a strong headwind. Great demands, as well as strong criticisms, are being directed to those who restore rivers. Society has spent the last 200 years changing landscapes: now, they want their rivers back. Often, the urgency to restore rivers comes at a price, as many rush into river restoration without the proper tools and/or the experience to properly use the tools. This paper provides a brief overview of the natural channel design method for river restoration. Space does not permit a full description of the methods here, nor does it allow for examples. Rather, this introduction is intended to build respect for the science and complexity behind river restoration using natural channel design procedures.

The river restoration dilemma reflects the complexity and uncertainty contained within the science. Although the study of rivers is not new, the science and art of river restoration is relatively recent in terms of addressing multiple objectives associated with physical, chemical and biological processes. Aesthetic considerations need to be balanced with efforts to provide a restoration that will be self-stabilizing over time. Some academics have become theoretical disciples of river restoration; others have become "prophets of doom." Many argue that rivers should be left alone to "do their thing." Others wonder, "What is the recovery potential of rivers? Are rivers really "trainable"? How do we define and implement ecological balance? If you cannot take care of the entire watershed, should local

problem river reaches be left alone? How should property, road fills and homes be protected from erosion, other than with standard "hard control" practices? Ideal solutions make good sense, but practical realities, ownership boundary constraints and economics often preclude their implementation.

"Natural channel design" is a geomorphic-based method that is an obvious departure from traditional river engineering. Critics have labeled this methodology a "simplified cook-book" procedure that ignores process (Kondolf, et al., 2003). For example, Simon et al. (2005) stated "that natural channel design, using 50 year old technology, was never intended for engineering design, and the inability of the method to quantify the very variables and processes that control channel processes and morphology." This dialog from those least familiar with the method will likely continue; however, it is increasingly important to familiarize those who are curious, yet unfamiliar, with the method.

The natural channel design method is continually updated based on post-project monitoring. The author has implemented this method on miles of rivers for more than 32 years. The method presently constitutes a chapter in the new *Stream Restoration Design Handbook* being developed by the USDA Natural Resources Conservation Service (NRCS, 2005; In review). The conceptual layout for the eight phases of the geomorphic approach to natural channel design is shown in Figure 1. The flowchart is indicative of the full extent and complexity associated with this method, including detailed, quantitative assessments of the cause(s) of river disequilibrium (stability); field measurements required to quantify hydraulic and sedimentological relations; and designs that implement *analog*, *empirical*, and *analytical* methods. The eight phases are detailed below.

METHODS

Sequential Phases: There are eight phases associated with the natural channel design method. Each phase is described below and corresponds to the outline in Figure 1.

Phase I: Restoration Goal/Objectives - *Define specific restoration objectives associated with physical, biological and/or chemical process*. It is very important to obtain clear and concise statements of restoration objectives in order to appropriately design the solution(s). The potential of a certain stream to meet specific objectives must be assessed early on in the planning phases, so that the initial restoration direction is appropriate. The following are common objectives: a) reduce flood levels; b) stabilize streambanks; c) reduce sediment supply, land loss and attached nutrients; d) improve visual values; e) improve fish habitat and biological diversity; f) create a "naturally stable" river; g) withstand floods; h) provide for self-maintenance; i) be cost-effective; j) improve water quality; and k) improve or create wetlands.

It is essential to fully describe and understand restoration objectives. There may be competing or even conflicting objectives. These conflicts must be mediated and can often be offset by varying the design and/or the nature of stabilization methods or materials planned. The assessment required must also reflect the restoration objectives, to ensure that all processes are thoroughly evaluated. For example, if improved fishery abundance, size, and species are desired, then a limiting factor analysis of habitat and fish populations must be linked with morphological and sedimentological characteristics.

Phase II: Regional and Local relations - *Develop regional and localized specific information on geomorphologic characterization, hydrology and hydraulics*. During Phase II, it is important to incorporate information on valley types, stream types and reference reach data representing the stable form in similar valley types. Preparation should include assessing regional hydrology curves (bankfull discharge and cross-sectional area versus drainage area) (Rosgen and Silvey, 2005) and hydraulic calculations and validation at gage stations using resistance relations and/or roughness values.

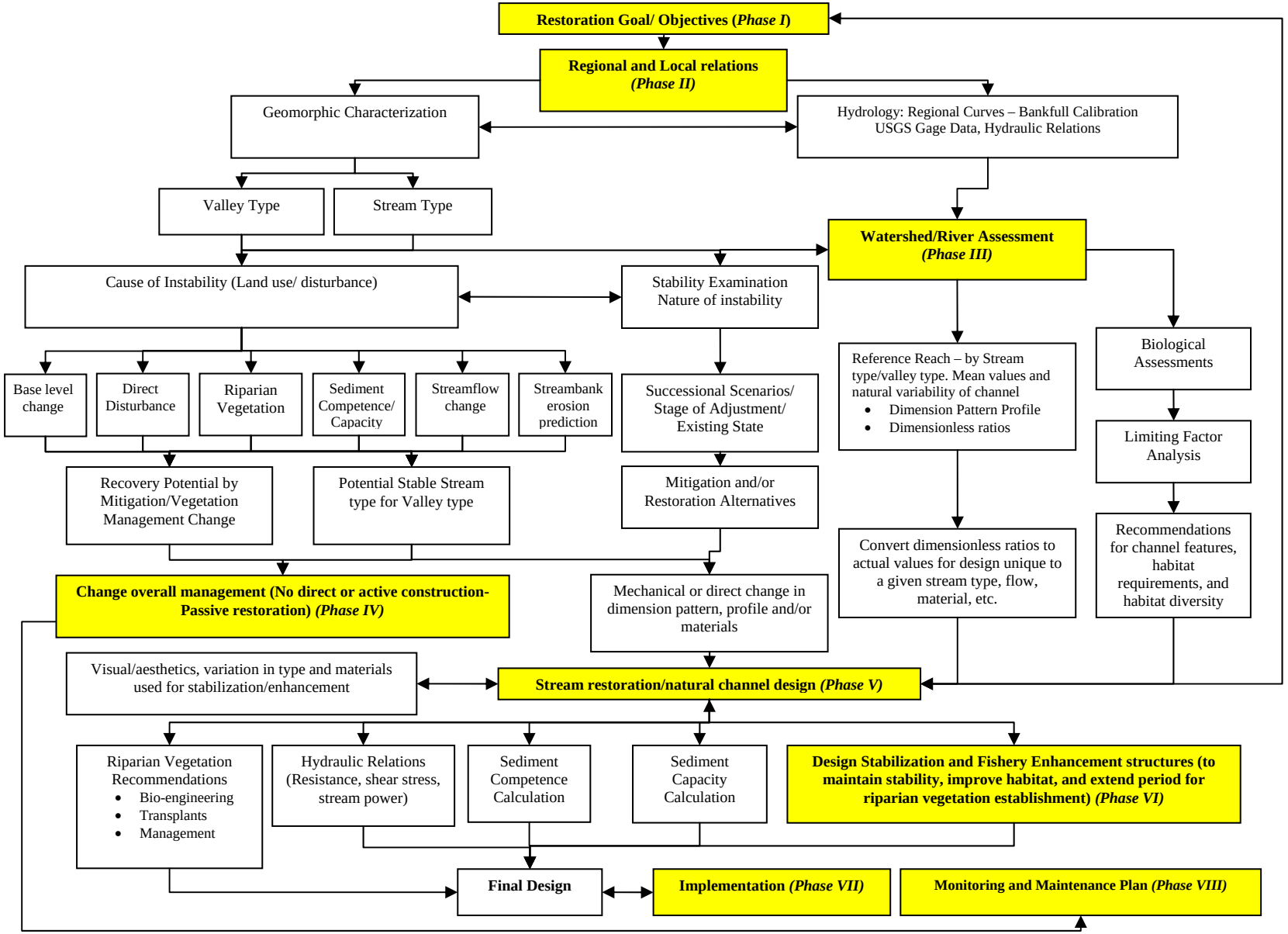


Figure 1 Flow chart depicting sequence of implementation of the eight sequence phases associated with natural channel design using a geomorphic approach.

Phase III: Watershed/River Assessment – *Conduct a watershed/river assessment to determine river potential, current state and the nature, magnitude, direction, duration and consequences of change.* Phase III, watershed/ river assessment, is one of the key procedural steps in a sound restoration plan because it identifies the causes and consequences associated with the loss of physical and biological river function. Phase III assesses the cause(s) and consequence(s) of change at both the micro and macro levels. During this phase, it is important to: a) review land use history and time-trends of river change; b) isolate the primary causes of instability and/or loss of physical and biological function; c) collect and analyze field data, including reference reach data, to define sedimentological, hydraulic and morphological parameters; d) obtain concurrent biological data (limiting factor analysis) on a parallel track with the physical data; and e) quantify streamflow and sediment regime changes.

It is important to realize the dynamic nature of streams, and the difference between the natural adjustment process and the acceleration of such adjustments. For example, bank erosion is a natural channel process; however, accelerated streambank erosion creates a disequilibrium condition. Many stable rivers naturally adjust laterally, such as the "wandering" river. While it may meet certain local objectives to stabilize high-risk banks, it would be unadvisable to try to "control" or "fix in place" such a river. In many instances, a braided river and/or anatomizing river type is the stable form. Designing all stream systems to be a single-thread meandering stream may not properly represent the natural stable form. Valley types are a key part of river assessment because geomorphic settings affect the characterization of a stable stream type. Further, reference reaches representing the stable form have to be measured and characterized for use with similar valley types. This prevents applying good data to the *wrong* stream type.

River stability (equilibrium or quasi-equilibrium) is defined as "the ability of a river, over time, in the present climate to transport the flows and sediment produced by its watershed in such a manner that the stream maintains its dimension, pattern and profile without either aggrading or degrading" (Rosgen, 1994, 1996, 2001a). To optimize river stability, one must take an inventory of riparian vegetation, identify changes in flow and sediment regime, compare limiting factor analysis to biological potential, and identify sources/causes of instability and adverse consequences to physical and biological function. Procedures for this assessment are described in detail by Rosgen (1996, Chapter 6; 2001a) and in the *Watershed Assessment and River Stability for Sediment Supply (WARSSS)* (Rosgen, 1999, 2006a, In press).

Streambank erosion rate (lateral erosion rate and sediment, tons/year) is predicted as part of the river stability assessment. The influence of vegetative change, direct disturbance and other causes of bank instability are quantitatively assessed. One of the major consequences of stream channel instability is accelerated streambank erosion and associated land loss. Fish habitat is adversely affected not only due to increased sediment supply, but also by changes in pool quality, substrate materials, imbrication and other physical habitat loss. Water temperatures are also adversely affected due to increases in width/depth ratio due to lateral accretion. The prediction methodology for streambank erosion is presented in Chapter 6 (Rosgen, 1996), and in Rosgen (2001a), using a Bank Erodibility Hazard Index and Near-Bank Stress calculations.

Time-trend data using aerial photography is very valuable for documenting channel change. Field evidence using dendrochronology, stratigraphy, carbon dating, paleochannels or evidence of avulsion and avulsion dates can help the field observer to understand the rate, direction and consequences of channel change. The field inventory and number of variables required for watershed and river stability assessment is substantial. Figure 2 represents a general summary of the elements used to assess channel stability in the natural channel design methodology. Detailed procedures for such assessments are provided in Chapter 6 of Applied River Morphology (Rosgen 1996) and in *WARSSS* (Rosgen, 2006b, In press).

Phase IV: Change overall management (Passive restoration) – *Consider passive restoration recommendations based on land use change prior to considering mechanical restoration.* A priority in restoration is to seek a natural recovery solution based on changes in the variables causing the instability and/or loss of physical and biological function. Changes in land use management can influence riparian vegetation composition, density and vigor, flow modifications (diversions, storage, reservoir release schedule modifications based on the operational hydrology),

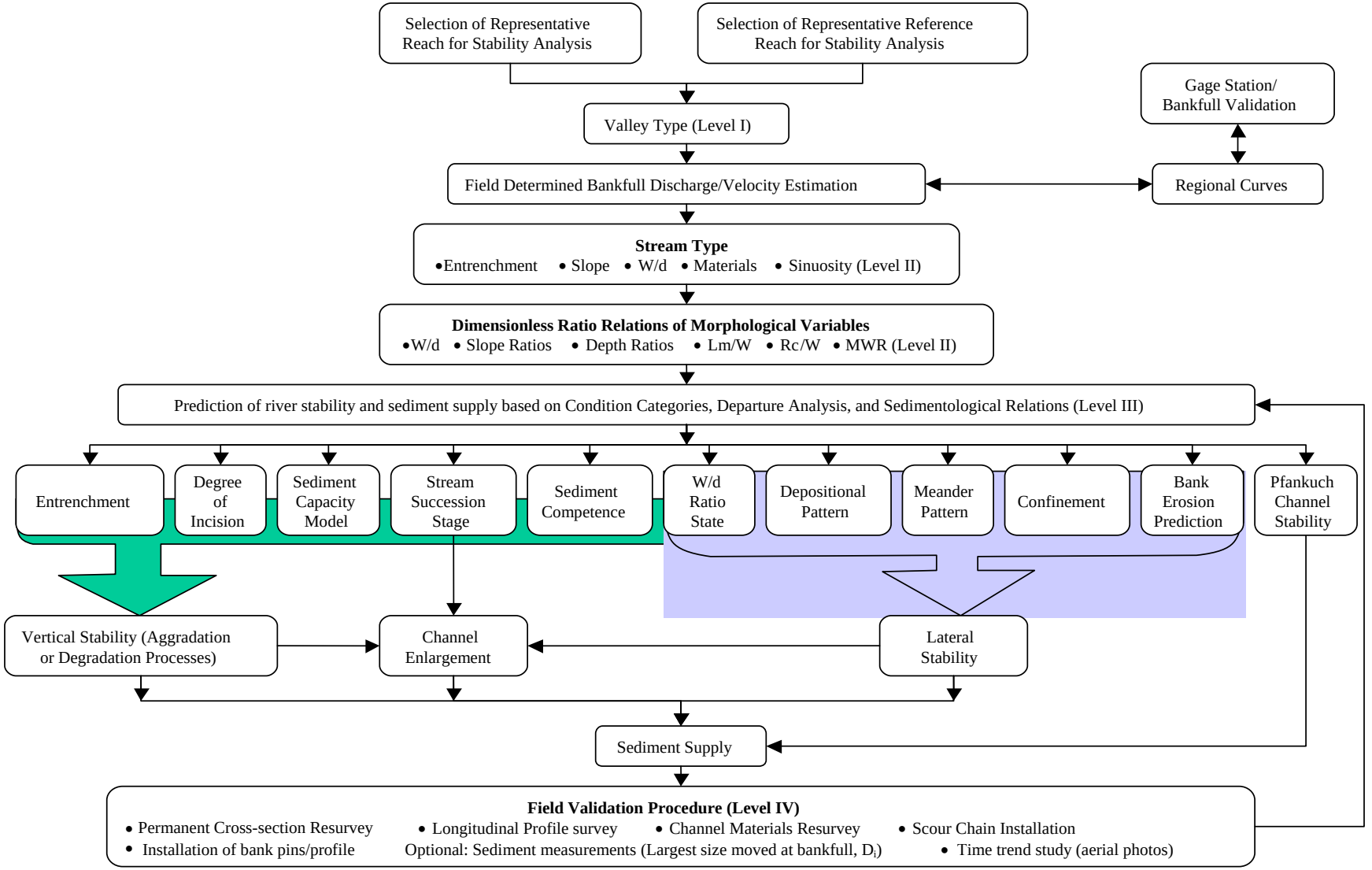


Figure 2 Generalized flowchart of application of various assessment levels of channel morphology, stability ratings, and sediment supply.

flood control measures, road closures/stabilization, hillslope erosional processes and other process influencing river stability. Changes in management strategies can be very effective in securing stability and function. This is determined based on the recovery potential of various stream types and the short- and long-term goals associated with the stated objectives, including costs.

The alternative to self-stabilization is always a key consideration in any stability assessment. The time-trend aerial photography from Phase III may help to provide insight into stream recovery potential following disturbance. Successional stages of channel adjustment can also provide clues to natural recovery potential. Passive restoration designs require effectiveness monitoring, including documentation of the nature, magnitude, rate and consequences of natural recovery, to ensure that objectives are met. If natural recovery potential is poor and/or does not meet specific objectives, then stream restoration/natural channel design (Phase V) is appropriate.

Phase V: Stream Restoration/Natural Channel Design – *Initiate natural channel design with subsequent analytical testing of hydraulic and sediment transport (competence and capacity) relations.* This phase combines the results from phases I through IV. It is important to remember that a good design stems from a good assessment. The goal of this phase is not to patch symptoms, but rather to provide restoration solutions that will offset the causes of the problem and allow the river be self-maintaining. To accomplish this goal, the practitioner must be very familiar with the processes involved in hydrology, hydraulics, sedimentology, geomorphology, soil science, aquatic habitat and riparian vegetation assessments. Due to the inherent complexity, it is usually necessary to obtain technical assistance for assessment and design, depending on the practitioner's experience and training.

The conceptual, generalized flowchart shown in Figure 3 depicts the general sequence of the mixed use of *analog*, *empirical*, and *analytical* methods in the natural channel design procedure. To determine the appropriate channel form, the existing valley type and potential stream type of the stable form must be available. The proposed natural channel design must be converted to a dimension, pattern and profile to determine if the hydraulic and sediment relations are compatible prior to completing the remaining procedural steps. A total of 40 analytical sequence steps generate and test restoration design specifications to determine dimension, pattern and profile relations as outlined in Chapter 11 of the NRCS (2005, In review). Sediment competence is determined with methods described in Rosgen (2001b, 2006a). Sediment capacity is calculated using FLOWSED and POWERSED models (Rosgen, 2006a) based on dimensionless sediment rating curve relations (Troendle et al., 2001). These models are programmed and made available by RIVERMorph$_{TM}$, version 4.0, FMSM Engineers, Inc., Louisville, KY.

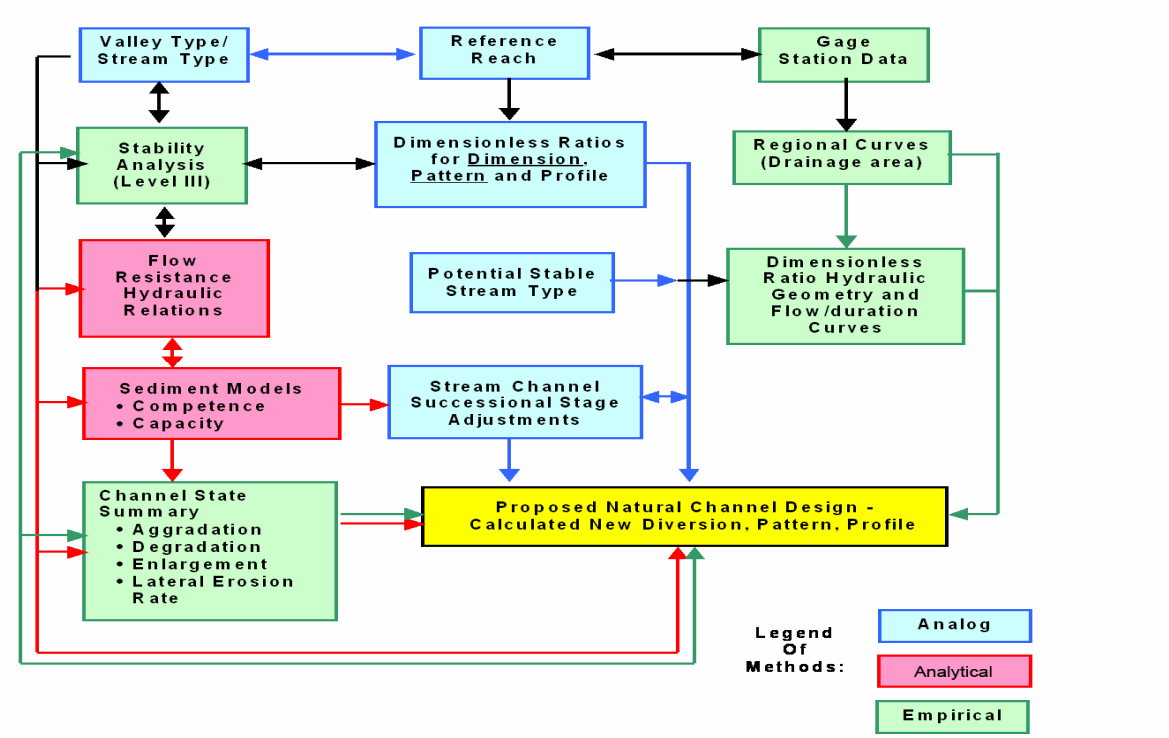


Figure 3 Flowchart representing natural channel design using analog, analytical and empirical methodologies.

Phase VI: Design Stabilization and Fisheries Enhancement Structures – *Select and design stabilization/ enhancement/vegetative establishment measures and materials to maintain dimension, pattern and profile to meet stated objectives*. Structures of native materials are used for energy dissipation, fish habitat enhancement, and near-bank stress reduction to extend time for vegetation response and establish bed pavement. Selection of designs, materials and methods are critical to meet multiple objectives including aesthetics. Various structures used for restoration are described by Rosgen, (2001c).

Phase VII: Implementation – *Implement the proposed design and stabilization measures involving layout, water quality control and construction staging.* River structures are often primarily designed to a) buy time to protect the new channel from excess erosion until significant riparian vegetation can become established; b) reduce accelerated streambank erosion; c) provide grade control; d) obtain stable flow diversions; e) enhance fish habitat, including in-stream cover, holding cover, spawning habitat, and habitat diversity, etc.; f) re-introduce and stabilize large wood for fishery, stability and aesthetic purposes; g) protect infrastructure adjacent to streams; h) protect bridges, culverts and drainageway crossings; i) reduce flood levels; j) transport sediment; and k) provide energy dissipation. Designs using native materials to meet these objectives are shown in Rosgen (2001c).

Phase VIII: Monitoring and Maintenance Plan – *Design a plan for effectiveness, validation and implementation monitoring to ensure stated objectives is met, prediction methods are appropriate and construction is implemented as designed*. Watershed and river assessments leading to restoration involve complex process interactions, making accurate predictions somewhat precarious. Continually measuring data after restoration will improve our understanding and prediction of sedimentological, hydrological, morphological and biological process relations. Additional benefits from monitoring include demonstration of the effectiveness of reduced sediment problems and improved river stability due to management/mitigation — the central purpose of watershed and sediment assessments and restoration. Without monitoring, the science behind river restoration cannot be advanced, nor can our understanding of these complex processes be improved.

The key to a successful monitoring program is to focus on the specific objectives of monitoring. Monitoring is generally recommended to: a) measure the *response of a system* from combined process interaction due to imposed change; b) document or observe the *response of a specific process* and compare it to a *predicted* response; c) prescribe treatment; d) define short-term versus long-term changes; e) document spatial variability of process and system response; f) ease the anxiety of uncertainty of prediction; g) provide confidence in specific management practice modifications or mitigation recommendations to offset adverse water resource impacts; h) evaluate effectiveness of stabilization or restoration approaches; i) reduce risk once predictions and/or practices are assessed; j) build a data base to extrapolate for similar applications; and k) determine specific maintenance requirements.

CONCLUSIONS

It is desirable that the individual(s) responsible for the project be involved in *all phases* of this methodology. If the same individual who conducts the assessment also completes the design, implementation and monitoring, then the desired restoration objectives are more likely to be accomplished. The complexity of this method requires great attention to detail, training and an understanding of processes. Involvement in the implementation, validation and effectiveness procedures is the best way to become experienced and knowledgeable about natural channel design methodology. Additional information regarding natural channel design river restoration methods can be found in Chapter 11 of the new USDA Natural Resources Conservation Service *Stream Restoration Design Handbook* (NRCS, 2005; in review).

REFERENCES

Kondolf, G.M., Montgomery, D.R., Piegay, H. and Schmitt, L. 2003. "Geomorphic classification of rivers and streams," In: Tools in Fluvial Geomorphology, (eds.), Kondolf, G.M. and Piegay, H. Wiley, Chichester, England, p171-204.

Rosgen, D.L., 1994. "A Stream Classification System," Catena Vol 22 169199. Elsevier Science, Amsterdam.

Rosgen, D.L., 1996. Applied River Morphology. Wildland Hydrology Books, Pagosa Springs, Colorado, and Ft. Collins, CO.

Rosgen, D.L., 1999. "Development of a River Stability Index for Clean Sediment TMDL's," In: Proceedings of Wildland Hydrology, Ed. D.S. Olsen and J.P. Potyondy, AWRA, Bozeman, Montana, pp. 25-36.

Rosgen, D.L., 2001a. "A Stream Channel Stability Assessment Methodology," 7th Federal Interagency Sedimentation Conference, March 25-29. Reno, Nevada.

Rosgen, D.L., 2001b. "A Hierarchical River Stability Watershed-based Sediment Assessment Methodology," 7th Federal Interagency Sedimentation Conference, March 25-29. Reno, Nevada.

Rosgen, D.L., 2001c. "The Cross-Vane, W-Weir and J-Hook Vane Structures: Their Description, Design and Application for Stream Stabilization and River Restoration," Amer. Assoc. Civil Engrs., Restoration Proceedings, Reno, Nevada, 22 pp.

Rosgen, D.L. and Silvey, H.L., 2005. The Reference Reach Field Book. Wildland Hydrology Books, Fort Collins, CO, 256 pp.

Rosgen, D.L., 2006a. WARSSS (A Watershed Assessment for River Stability and Sediment Supply). Wildland Hydrology Books, Fort Collins, CO. (In press). http://www.epa.gov/warsss/

Rosgen, D.L., 2006b. "FLOWSED/POWERSED – Prediction Models for Suspended and Bedload Transport," Proc. Joint 8th Federal Interagency Sedimentation Conference, April 2-6, Reno, Nevada.

Simon, A., Doyle, M., Kondolf, M., Shields Jr., F.D., Rhoads, B., Grant, G., Fitzpatrick, F., Juracek, K., McPhillips, M. and MacBroom, J., 2005. "How Well do the Rosgen Classification and Associated "Natural Channel Design" Methods Integrate and Quantify Fluvial Processes and Channel Response?" Proc. American Society of Civil Engineers, May 15-19, Anchorage, Alaska.

Troendle, C.A., Rosgen, D.L., Ryan, S., Porth, L. and Nankervis, J., 2001. "Developing a "Reference" Sediment Transport Relationship," Proc. 7th Federal Interagency Sediment Conference, March 24-29, Reno, Nevada.

USDA Natural Resources Conservation Service, 2005. Stream Restoration Design Handbook. (In Review).

THE HYDRAULICS OF BENDWAY WEIRS

C. I. Thornton, Colorado State University, Engineering Research Center, Fort Collins, CO 80523, thornton@engr.colostate.edu; D. C. Baird, U.S. Bureau of Reclamation, Denver Technical Service Center, P.O. Box 25007, D-8540, Denver, CO 80255-0007, dbaird@do.usbr.gov; S. R. Abt, Colorado State University, Engineering Research Center, Fort Collins, CO 80523, sabt@engr.colostate.edu; R. S. Padilla, U.S. Bureau of Reclamation, 505 Marquette NW, Suite 1313, Albuquerque, NM 87102-2162, rpadilla@uc.usbr.gov

Abstract: Design teams of the 21st Century must contend with multiple problems created as a result of channel migration and bank erosion. Protecting land and riverside facilities, while also improving habitat conditions for endangered species, has become a task of increasing frequency. To mitigate bend migration problems while considering industrial, recreational, biological, and environmental demands requires that innovative methods for bank stabilization be developed. One such technique is to construct transverse features designed to train flow away from channel banks. Bendway weir structures, also know as spur dikes, groins or jetties, have been successfully used to decrease bank erosion while promoting aquatic habitat and riparian vegetation. While bendway weir structures have been successfully used in many applications, quantifiable design guidance has not been readily available. Past projects utilizing bendway weirs have relied heavily on field experiences, site-specific flume studies, and engineering judgment, but have lacked general design guidelines. To accurately model flow conditions resulting from the placement of bendway weirs, an undistorted 1:12 Froude scale, hard boundary model was constructed at the Hydraulics Laboratory of the Engineering Research Center at Colorado State University. The model contained two bends, which exhibited unique geometric characteristics representative of those found in the Middle Rio Grande reach. Three-dimensional velocities and water surface profiles were recorded for a series of tests including variations of weir length, spacing, and angle. Using the data obtained from the test series, relationships relating resulting hydraulic conditions in the channel, around the weir field and in eddies between weirs have been developed.

RESEARCH, COORDINATION, AND OPEN-SOURCE MODELS TO IMPROVE STREAM RESTORATION PRACTICE

Peter Wilcock, Department of Geography and Environmental Engineering, Johns Hopkins University, Baltimore MD 21218, wilcock@jhu.edu; Gary Parker, Department of Civil and Environmental Engineering and Department of Geology University of Illinois, Urbana IL 61801, parkerg@uiuc.edu; through the National Center for Earth-surface Dynamics

Abstract: Most agree that there is room for improvement in the science and engineering basis for stream restoration. There is also a bewildering array of methods and models, the application of which requires a diverse range of expertise and effort with little clear indication of need, reliability, efficacy, and effort. There is a need for not only research and improved methods supporting stream restoration practice, but also for improved organization, distribution, and coordination of existing and emerging methods and training. The National Center for Earth-surface Dynamics (NCED), a Science and Technology Center funded by the National Science Foundation, has formed a Stream Restoration Group to organize and focus research relevant to stream restoration, to collaborate with agencies and practitioners in identifying knowledge gaps and developing improved tools for restoration practice, and to disseminate this knowledge to practitioners. Our goal is to move restoration practice to an analytical, process-based approach that will ultimately lead to better prediction and hence better design. Predictive understanding is needed in a number of key areas, including sediment routing at the reach to network scale, channel and floodplain response to watershed changes, and linkages between physical channel conditions and nutrient cycling, stream metabolism, primary production, and population dynamics. The broadest challenge facing restoration is placing projects in a watershed context. A central part of the Restoration Group's efforts involves support and interaction with a partners group consisting of agency and industry professionals. This group helps to define research needs, to identify and contribute useful models for restoration design, to evaluate restoration practice, and to coordinate training in restoration practice.

This paper outlines some efforts of the NCED Stream Restoration Group to support improved stream restoration practice, including our research priorities and examples of knowledge transfer. Research efforts focus on laboratory and field experiments on sediment transport and stream channel change. With its partners, NCED is conducting short courses and developing training materials and a web-based "toolbox" that provides numerical models and supporting information to improve evaluation of stream channels, design of restoration projects, and linkages between geomorphic design and ecological outcomes. The toolbox is intended to address the need for useful models of tested reliability and documented limitations that more immediately link research to practice. Toolbox programs are open source and address a wide range of practical problems, such as hydraulic geometry, transport and sorting in coarse-bedded streams, bed evolution below dams, and the delineation between threshold and alluvial channels. Although it is widely acknowledged that most predictions and design choices associated with stream restoration have large uncertainty, estimates of uncertainty are rarely incorporated into restoration design. We propose approaches by which uncertainty can be incorporated into stream restoration design and decision-making. Example toolbox applications are discussed in this paper.

RESTORATION PRACTICE

To be effective, research, models, and training must be developed in the context of current practice and understanding. Current stream restoration practice is based on analogy – a template is sought in a nearby channel, stream type, or hydraulic geometry relation that the designer judges to be suitable. The template channel is then scaled to the design site, typically using estimates of bankfull discharge (FISRWG, 1998). When scaling is accomplished via an estimated bankfull discharge, an implicit assumption of equilibrium is introduced: it is assumed that the disturbed channel is adjusting toward some 'stable' state and that evidence of this future condition can be found. But if a disturbed stream is adjusting to changes in essential controlling factors, particularly water and sediment supply, its future steady-state condition may not yet be evident. An appropriate template is unlikely to exist and would, in any case, be difficult to reliably demonstrate. The experience of designing stream channels when no suitable reference reach or identifiable bankfull discharge are available appears to be common (e.g. Sortman, 2004). Beyond its deficiencies in supporting channel design, an analogy approach does not efficiently support learning and cannot lead to true prediction because it provides no basis for linking cause and effect in a logically complete and testable framework.

An analogy approach may have some practical use in particular cases for which the channel disturbance is not driven by essential changes in forcing, but by changes internal to the channel and reversible. The primary examples are exclusion of livestock from the riparian corridor and restoring a natural geometry to artificially straightened stream channels. If no substantial changes in water and sediment supply are anticipated, a basis exists for transplanting the geometry of a similar stable channel.

What is the alternative to an analogy approach to stream restoration design? It must begin with specification of the materials and configuration of the stream valley and the water and sediment supply, including the variability and uncertainty in these quantities. In the essential next step, the specified conditions must be connected via predictive relations sufficient to link cause and effect. The predictive relations must satisfy general physical principles of mass, momentum, and energy conservation and will include empirical relations of demonstrated generality.

As all seem to acknowledge, streams adjust to the water and sediment supplied to them. To this must be added essential feedbacks between the physical channel and the chemistry and biology of its waters, flora, and fauna which can influence details of transport processes and broad expression of channel geometry. A predictive, science-based approach to stream restoration must be built on these essential inputs. An ability to predict water and sediment supply is needed, as is an ability to predict the patterns of erosion and deposition within a design reach. Although existing methods invoke sediment transport in their designs, even calculate transport at some stages of the design process, only recently has a logically complete structure for predicting inputs and outcomes in stream channels emerged (Shields et al., 2003).

There is good reason that an analogy approach dominates stream restoration practice: in most practical cases, current approaches do not permit predictions of sediment transport of sufficient accuracy to support channel design. This is particularly the case in gravel-bed streams, for which neither empirical nor theoretical approaches can provide suitable accuracy on a routine

basis (Wilcock, 2001). A predictive approach requires that the future supply of sediment can be adequately forecast. With current technology, this is possible only for threshold channels. In this case, a precise estimate of sediment supply is not needed, it is only necessary to determine that the supply will be smaller than a critical threshold amount. One NCED Stream Restoration tool provides a basis for estimating this threshold.

The primary challenges facing development of a predictive stream restoration science are:

1. Forecasting water and sediment supply. Stream channel change is driven by changes in water and sediment supply. Catastrophic failure of restoration projects can usually be attributed to a poor (or missing) estimate of the water and sediment supply. A reliable estimate of sediment supply is the essential threshold between analog and predictive design.

2. Variability and uncertainty. There is enormous uncertainty in virtually every aspect of channel design: historical trends, future forcing, and calculated water and sediment fluxes. Estimates of uncertainty in water and sediment supply are rarely made and incorporation of uncertainty in channel design is virtually absent. Ignoring uncertainty does not make its consequences disappear.

3. Watershed context. An adequate forecast of future water and sediment supply can only be done in a watershed context.

NCED RESTORATION ACTIVITIES

Research: NCED research addresses a wide range of erosion and sediment transport topics supporting improved restoration science and practice.

Routing and supply of sediment: Channels develop in response to their water and sediment supply. An inability to predict sediment supply (mean and variability) is the primary technical barrier to predicting future channel configuration and composition. Development of predictive sediment supply relations will require a means of determining sediment storage throughout the stream network and a reliable treatment of sediment storage in reach-scale transport models. We are currently developing models for routing sand and fine gravel through coarse immobile beds (Dietrich, et al., 2005; Grams, et al., 2005). Our goals are to develop reach-averaged transport models incorporating storage dynamics and to test these models at the watershed scale in different transport environments.

Transport, sorting, and morphodynamics of mixed-size sediment: The transport of streambed material drives channel change and the composition and configuration of the bed, which determines the essential, organism-scale template for the stream ecosystem. We now have in place surface-based transport models (Wilcock and Crowe, 2003) and a general framework for bed scour and aggradation (Parker, et al., 2000). Current NCED work (Blom and Parker, 2004; Dietrich, et al., 2005;Wilcock and DeTemple, 2004; Wong and Parker, 2005) focuses on rates of lateral and vertical sorting to provide the detail needed to complete a predictive mixed-size morphodynamic model.. With this model, our focus will shift to verification and application of

the model in different settings and scaling up to the reach and channel network and integration of the model into predictive relations for streambed ecology.

Size, shape, and planform of resilient, dynamically stable channels: The size, shape, composition and planform of the stream channel define the physical framework of a stream restoration project, but we still cannot predict channel geometry reliably. Current NCED activity focuses on channel geometry and channel change as it varies through a watershed, on morphodynamic models, and on the interaction between vegetation and channel dynamics. As improved predictions of sediment supply and its variability become available, we will develop methods that effectively incorporate variability and risk in channel design. Our goal is to develop predictive relations between valley slope, water discharge, sediment supply rate and caliber, riparian vegetation, and channel geometry.

Rates, mechanisms, and location of floodplain deposition: Floodplain "reconnection" is a common restoration objective in order to provide habitat, support riparian vegetation, sequester nutrients and contaminants, and protect delta shorelines. Current NCED work focuses on channel-floodplain exchange of sediment through overbank flow and via tie channels.

From grains to the reach and network scale – placing restoration projects in their watershed context: The most obvious and persistent cause of physical failure is ignoring, or predicting erroneously, the supply of water and sediment from the watershed. Current best practice includes a narrative watershed history identifying the timing and location of major watershed disturbances. A predictive restoration science will require transforming this history to a form suitable for providing quantitative predictions, including uncertainty.

NCED Stream Restoration Toolbox: A primary vehicle for our knowledge transfer is the online NCED Stream Restoration toolbox, a set of tools supporting channel assessment and design. Our goal is to make the latest research results readily available in a useable form. Both tools and documentation are open source. Not only is free use encouraged, but the code can be modified as needed by the user. Tools are developed to address particular topics and tasks and it is up to the user to determine the appropriate tools for the job. The principal overhead of this approach is that use of the tools requires an ability to understand their context, purpose, and function. The alternative would be complex 'black box' models that perform many interconnected calculations without requiring complete understanding of the supporting principles. We argue that the first approach is needed for informed application, but also to support development of a predictive restoration science. This latter approach works against informed application of the underlying principles and inhibits dissemination – and evaluation – and improvement – of methods. Complex black-box models with insufficient exposition of the underlying principles also limit discussion of assumptions, methods, and results and thereby reduce the opportunity for learning and improvement.

A range of tools have been developed and posted on the NCED web site (www.nced.umn.edu; Table 1) and the list will be updated during the FISC conference. We are eager to learn of information needs that could be addressed with the development of new tools. Contact either author regarding suggested tools and the availability of other useful, open source models.

Table 1 Partial List of NCED Stream Restoration Tools

Tool Name	Description
Bankfull Estimator	A 2-in-1 tool using dimensionless criteria to estimate channel geometry from a specified bankfull discharge and to estimate bankfull discharge from specified channel geometry. Currently implemented for gravel-bed streams; a general version for both sand-bed and gravel-bed streams available soon.
Spawning Gravel Refresher	Calculates changes in gravel bed composition, including fines content in the subsurface, in response to specified discharge and sediment supply, to support design of controlled dam releases and gravel augmentation to restore the integrity of spawning gravels.
The Dam Remover	This tool predicts the morphodynamic development of a dam deposit after the sudden or gradual removal of a dam. It implements a 1-D model flow and transport model that predicts the evolution of channel width and stream gradient as a channel incises into the reservoir deposit.
Monte Carlo Transport	Provides estimate of uncertainty in critical discharge for incipient motion and calculated transport rates based on specified uncertainty in the input variables. Gives guidance for incorporating this uncertainty in restoration design.
Monte Carlo Channel	A 2-in-1 tool. One tool provides an estimate of channel aggradation/degradation in response to changes in discharge, sediment supply rate and grain size, including uncertainty in the calculated result, to support historical analysis of channel change. The other tool estimates combinations of channel slope and width, and their uncertainty, that produce equilibrium transport of a specified water and sediment supply.
Threshold Channel Calculator	Provides a quantitative estimate of the boundary between threshold and alluvial channels, supporting a determination of whether a detailed analysis of sediment transport is necessary.
iSURF	Applies a surface-based transport model to predict equilibrium bed surface grain size for specified sediment transport rate and grain size, to support estimates of stream bed grain size changes.
Willow post velocity analyzer	Predicts depth-averaged velocity distributions in straight trapezoidal channels with newly constructed willow post systems, to support planting design for channel stabilization.
Bank Stabilization Diagnostic	This tool presents a methodology for evaluating the reduction in sediment yield possible from bank stabilization, to support analysis of one of the more expensive elements of a stream restoration project.
Channel Planform Statistics Tool	A GIS tool that develops a centerline and computes width and radius of curvature from specified banks locations and local channel shift from specified centerlines.

Tool Format: The tools are presented as Visual Basic modules embedded in Microsoft Excel documents in order to promote the broadest possible accessibility. The programs are accompanied by a Microsoft Powerpoint documents that explain the background and application of the module.

An example tool is the Bankfull Estimator, a 2-in-1 tool that uses dimensionless criteria to estimate channel geometry from a specified bankfull discharge and to estimate bankfull discharge from specified channel geometry. The tool is currently implemented for gravel-bed streams and a general version for both sand-bed and gravel-bed streams is forthcoming. The Powerpoint document includes background information, guidelines for measuring the bankfull channel, caveats about appropriate application, explanation of the underlying analysis, the data and their sources (Figure 1). The Excel workbooks that calculate bankfull properties are embedded in the Powerpoint document, allowing the user to go directly to the desired calculations (Figure 2).

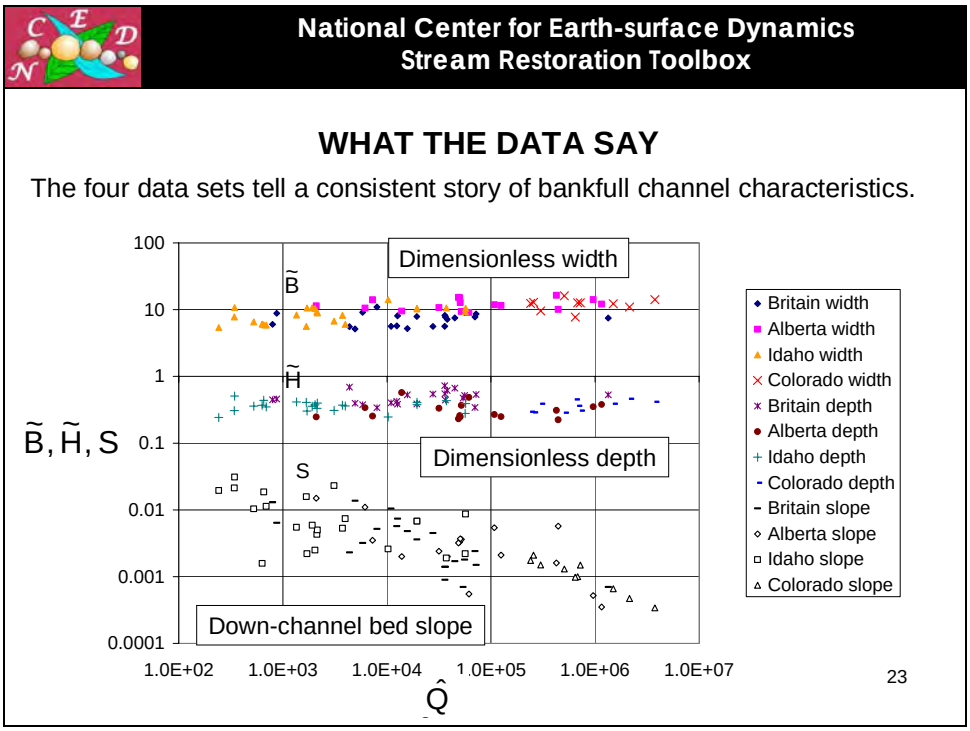


Figure 1 Example page from the Bankfull Estimator tool, showing the data used to develop the hydraulic geometry relations.

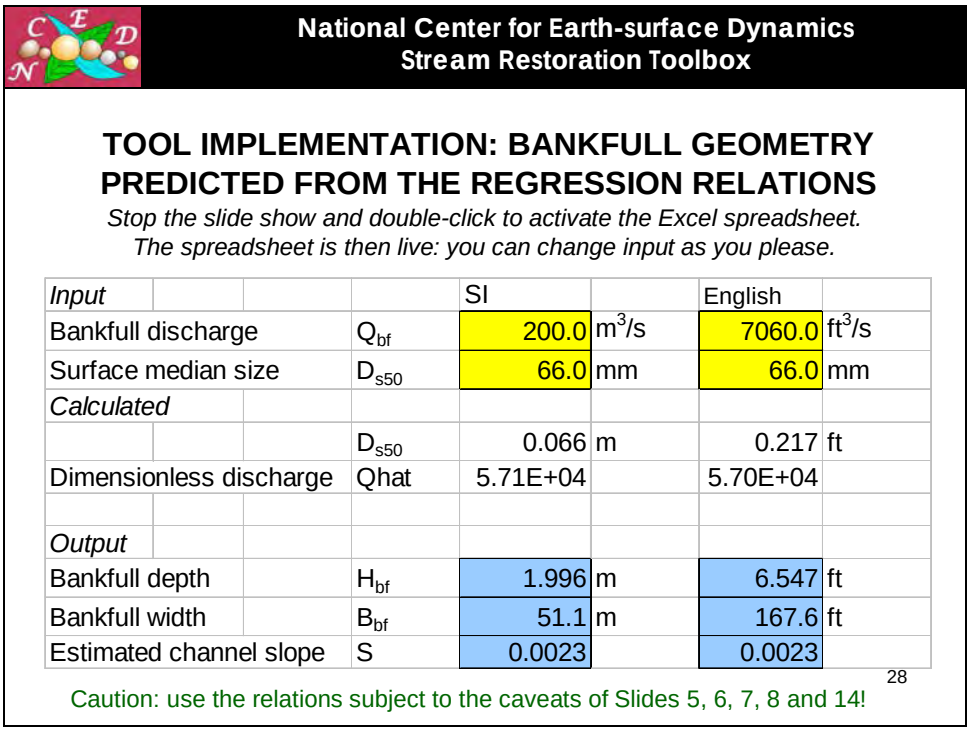


Figure 2 Example page from the Bankfull Estimator tool, showing embedded Excel workbook.

CONCLUDING REMARKS

Consider a project involving realignment of a stream and construction of a new highway bridge. The transportation industry has developed standards that require (correctly, we think) that those building bridges have specific and thorough training not only in the principles of structural statics and dynamics and the specifics of bridge design, but in the supporting science, mathematical, and engineering disciplines. Uncertainties are accounted for using safety factors associated with methods that have been developed in an organized and open approach allowing for testing, learning, and improvement. Despite the uncertainty in materials, traffic, and future flows, the design is predictive in the sense that the final product is developed via a sequence of decisions and calculations based on clear, logically complete and general principles within a tested application. Compare this with the design of the stream that flows beneath the bridge. What are the principles that the design is based on? Have the controlling factors been defined and incorporated in a thoroughly evaluated and truly predictive model? Has the uncertainty associated with future water and sediment supply and undetected variability in bed and bank materials been accounted for? We place our trust in the reliability of the design methods every time we drive over a bridge. Should the design of the stream and its ecosystem beneath the bridge be any different?

REFERENCES

Blom, A., and G. Parker (2004), "Vertical sorting and the morphodynamics of bedform-dominated rivers: a modeling framework," Journal of Geophysical Research Earth Surface, 109.

Dietrich, W. E., et al. (2005), "Sediment patches, sediment supply and channel morphology," paper in River, Coastal, and Estuarine Morphodynamics: RCEM 2005, edited by G. Parker and M. Garcia, pp. 131-139, Taylor and Francis Group, London.

Federal Interagency Stream Restoration Working Group (FISRWG) (1998) "Stream corridor restoration: principles, processes and practices," GPO Item No. 0120-A; SuDocs No. A 57.6/2:EN 3/PT.653. ISBN-0-934213-59-3.

Grams, P., P. Wilcock, and S.M. Wiele (2005), "Entrainment and nonuniform transport of fine sediment in coarse-bedded rivers," in River, Coastal, and Estuarine Morphodynamics: RCEM 2005, edited by G. Parker and M. Garcia, pp. 1074-1081, Taylor and Francis Group, London.

Parker, G., C. Paola, and S. LeClair (2000), "Probabilistic form of Exner equation of sediment continuity for mixtures with no active layer," Journal of Hydraulic Engineering, 126, 818-826.

Shields, F.D. Jr., R. R. Copeland, P. C. Klingeman, M. W. Doyle, and A. Simon (2003). "Design for Stream Restoration," J. Hydraulic Engineering, 129(8), 575-584.

Sortman, V.L. (2004). "Complications With Urban Stream Restorations, Mine Bank Run: A Case Study," in Clar, M., D. Carpenter, J. Gracie, and L. Slate (eds.), Protection and Restoration of Streams 2003, ASCE, pp. 431-436.

Wilcock, P.R., 1997. "Friction Between Science and Practice: The Case of River Restoration," Eos, Transactions, Am. Geophysical Union 78(41): 454

Wilcock, P.R., 2001. "Toward a practical method for estimating sediment transport rates in gravel-bed rivers," Earth Surface Processes and Landforms 26, 1395–1408.

Wilcock, P.R., 2004. "Sediment Transport in the Restoration of Gravel-bed Rivers," Proceedings, ASCE Environmental and Water Resources Institute Annual Congress, Salt Lake City.

Wilcock, P., and J. C. Crowe (2003), "A surface-based transport model for sand and gravel," Journal of Hydraulic Engineering, 129, 120-128.

Wilcock, P., and B. T. DeTemple (2005), "Persistence of armor layers in gravel-bed streams," Geophysical Research Letters.

Wong, M., and G. Parker (2005), "Flume experiments with tracer stones under bedload transport," in *River*, Coastal, and Estuarine Morphodynamics: RCEM 2005, edited by G. Parker and M. Garcia, pp. 131-139, Taylor and Francis Group, London.

EMPIRICAL AND ANALYTICAL APPROACHES FOR STREAM CHANNEL DESIGN

F. Douglas Shields, Jr., Research Hydraulic Engineer, USDA-ARS National Sedimentation Laboratory, PO Box 1157, Oxford, MS 38655-1157, dshields@ars.usda.gov; Ronald R. Copeland, Principal Hydraulic Engineer, Mobile Boundary Hydraulics, PO Box 264, Clinton MS 39060, mbh2o@aol.com

Abstract: Stream channel design has become a controversial topic, with different approaches favored by two main schools of thought. One approach, termed "natural channel design," features the use of stream classification, design analogs (reference reaches) and empirical relations (regional curves). Natural channel design is intended to result in planforms and cross sections thought typical of undisturbed systems, with flow conveyance matched to a "bankfull" or dominant discharge. Explicit sediment transport analyses are typically limited to issues of sediment-transport competence and initiation of motion. Below, we refer to "natural channel design" as the empirical approach. The other approach, termed "analytical," features the use of geomorphic assessments, process-based numerical models and sediment budgets. The analytical approach may be used to produce channel geometries that will accommodate any discharge. Varying amounts of erosion control and sediment management will be required. In fact, both approaches involve some empiricism and both contain certain analytical models. In this paper, differences and similarities between the two schools are further demonstrated in a case study of an alluvial channel carrying a significant load over a movable bed. In this case study the two approaches produce similar outcomes for channel base width and slope, but different channel depths and top widths. A sediment budget indicates adequate performance for the analytical design, but likely failure through erosion for the empirically-based design.

INTRODUCTION

Thirty to forty years ago, widely-used hydraulic engineering texts (e.g. Chow 1959, Henderson 1966) and design manuals (USACE 1970, USDA 1977) contained very limited discussions of stable channel design, particularly with regard to fully alluvial channels, preferring to emphasize fixed-boundary hydraulics (MacBroom 2004). Some guidance was provided for matching the boundary shear stress ("tractive stress") with channel boundary particle size so that the channel would not erode, but actual sediment transport computations and channel reach sediment budgeting were treated superficially. Further, aspects of then-current river geomorphology that were relevant, such as planform analyses and hydraulic geometry, were also covered lightly or not at all. Most analyses of channel stability assumed steady, uniform flow. As a consequence of ignoring the mobile boundaries of alluvial streams, many channelization projects experienced unforeseen instability, with long-lasting damage to stream corridor ecosystems, bridges and other riparian infrastructure (Brookes 1988, Wohl 2004). McCarley et al. (1990) reported results of a survey of flood control channel projects constructed by the U.S. Corps of Engineers: 39% of the reported post-construction problems were either vertical or horizontal channel instability and an additional 39% were classified as bank or toe failure. Biological effects of many of these projects were simply disastrous (Brookes 1988, National Academy of Sciences 1992). In fact, even channels that performed satisfactorily in terms of flood control or drainage often had extremely negative environmental effects because they featured uniform geometries (e.g., straight, prismoidal channels with trapezoidal cross sections) that departed strongly from natural stream morphologies that are necessary for quality aquatic habitat (Simpson et al. 1982).

In response to the unsatisfactory performance of many channels, new methods for channel design emerged. We arbitrarily categorize these approaches as empirical and analytical, combining the categories labeled "analog" and "empirical" by Skidmore et al. (2001) and "intuitive" and "empirical" by Shields (1997) into a single "empirical" category. Although the two approaches are contrasted below, others (Schwartz et al. 2003, MacBroom 2004) have noted that they are sometimes combined. Proponents of the empirical approach come from a wide variety of disciplinary backgrounds, education levels and professional affiliations, but include life scientists and hydrologists affiliated with consulting firms and public agencies. Proponents of the analytical approach include consulting engineers, fluvial geomorphologists, academics and researchers.

Empirical design approaches are based on form-based geomorphology (e.g., hydraulic geometry relations) as described by Leopold and Maddock (1953), Leopold and Wolman (1960) and others. In their original papers, these authors did not suggest that hydraulic geometry relationships be used to design channels, despite their similarity to older regime relations used for canal design. Rather they were advanced as indicators of fluvial channel form as a

function of discharge. In the empirical approach, however, regional regression relations based on hydraulic geometry have been advanced as a design tool. These greatly simplify fluvial processes by assuming that channel form can be predicted as a function of a single geomorphic variable. Typical descriptions of empirical design approaches include Newbury and Gaboury (1993), Rosgen (1996, 1997, 1998, 2005), Brookes and Sear (1996), Riley (1998), Hey (2004) and RiverMorph (2005). An example of a project based on this approach is described by Doll et al. (2001). Although these methods sometimes include incipient motion analyses based on a characteristic bed material size and average hydraulic conditions at a selected design discharge, they ignore questions of sediment continuity (e.g., Will the design channel transport the sediment supplied to it from upstream reaches?), sometimes with negative results (Shields 1997, Smith 1997, Soar 2000, Kondolf et al. 2001). Despite the fact that the core of these approaches is based on an aspect of fluvial geomorphology, current workers in that field almost uniformly reject them as outmoded (Miller and Ritter 1996, Wilcock 1997, Doyle et al. 1999, Juracek and Fitzpatrick 2003, Committee on Applied Fluvial Geomorphology 2004, Malakoff 2004, and Simon et al. 2005).

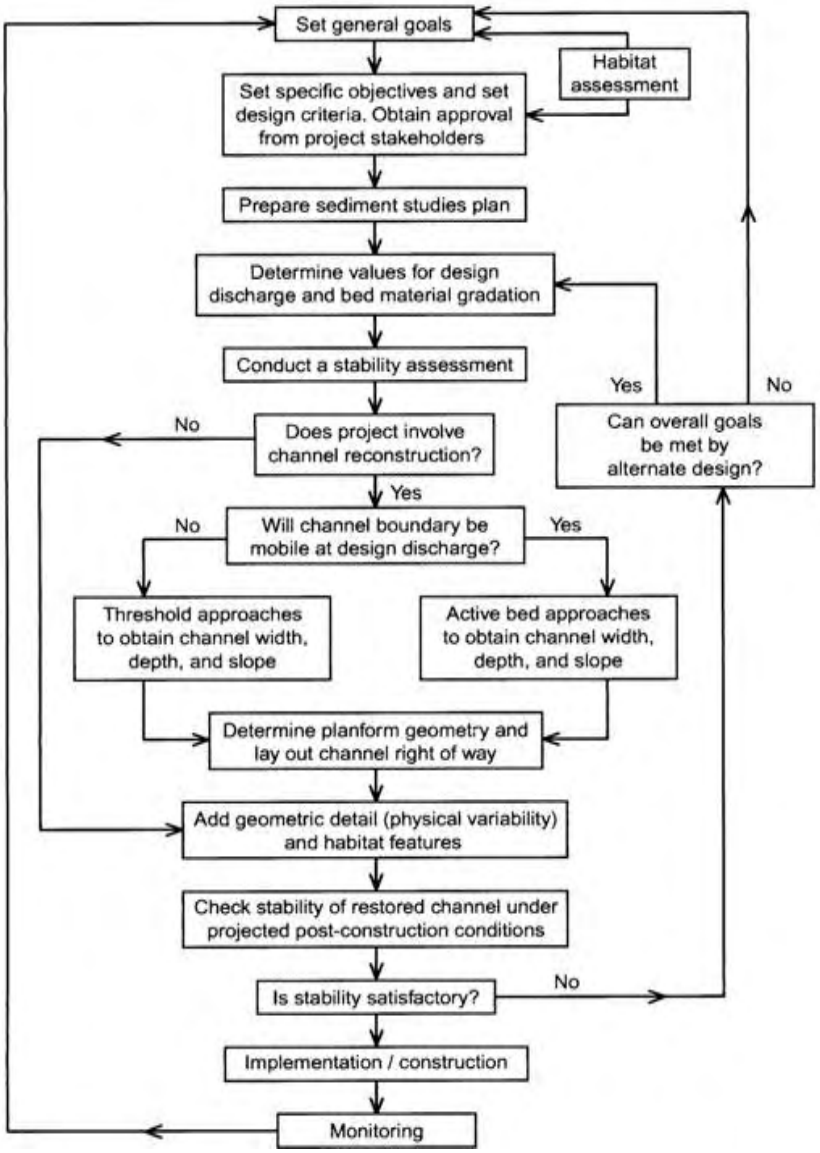


Figure 1 Analytical design approach for stream channel restoration projects from Shields et al. (2003).

Analytical approaches (e.g., Figure 1) involve more complex mathematical formulations to achieve joint solutions for water and sediment continuity and flow resistance, often using extremal hypotheses to achieve closure (Miller and Skidmore 2001). Analytical approaches are based on one- or two-dimensional representations of water flow and sometimes they include refinements such as sediment transport relations that handle a distribution of bed material grain sizes, unsteady flows, bank stability or flow-dependent flow resistance functions. Standard references with treatments of analytical alluvial channel design include Chang (1988), Millar and Quick (1998), Copeland et al. (2001), Eaton et al. (2004). Millar and MacVicar (1998), Schulte et al. (2000), Byars and Kelly (2001), Neary and Korte (2002), and Dierks et al. (2003) present examples of a design using the analytical approach. Johnson and Niezgoda (2004) argue that the analytical approach produces cost savings in terms of reduced failure risk, even though the initial costs for design are higher. For restoration, users of the analytical approach must incorporate ecological criteria ("habitat assessment," Figure 1) and a stability assessment that includes the important step of placing the project reach within

its spatial and temporal geomorphic context (Kondolf et al. 2001). Without these prerequisites, stream channel modifications are likely to fall far short of the goal of ecological restoration (Shields et al. in press, Gillilan et al. 2005).

Both analytical and empirical approaches are now represented by software tools that facilitate design computations. Below we use these tools to solve a simple, hypothetical design problem partially based on a real-world alluvial channel in an urban watershed in metropolitan Baltimore, Maryland.

METHODS

Empirical and analytical approaches were used to determine reach-mean channel width, depth and slope for a reach of Whitemarsh Run, Maryland. For simplicity, a minor tributary (North Fork Whitemarsh Run) that entered Whitemarsh Run between the project reach and the reference reach was ignored (Figure 2). The empirical approach was essentially the same as that presented by RiverMorph (2005), while the analytical approach follows Shields et al. (2003). The empirical approach produces different channel widths and depths for pools, runs and riffles; riffle geometry was used for comparison with reach-mean values computed by the analytical technique.

Whitemarsh Run is located in the Chesapeake Bay watershed and flows eastwards from a suburban zone north of Baltimore, through the town of White Marsh. The headwaters are located in the Piedmont, but the majority of the system is found in the Western Coastal Plain. A USGS gage was located immediately downstream from the project reach. The channel regime was characterized by Soar (2000) as “dynamic” due to a “high sediment load of fine gravel material pulsed through the system by a flashy flow regime.” The channel was relatively straight and uniform

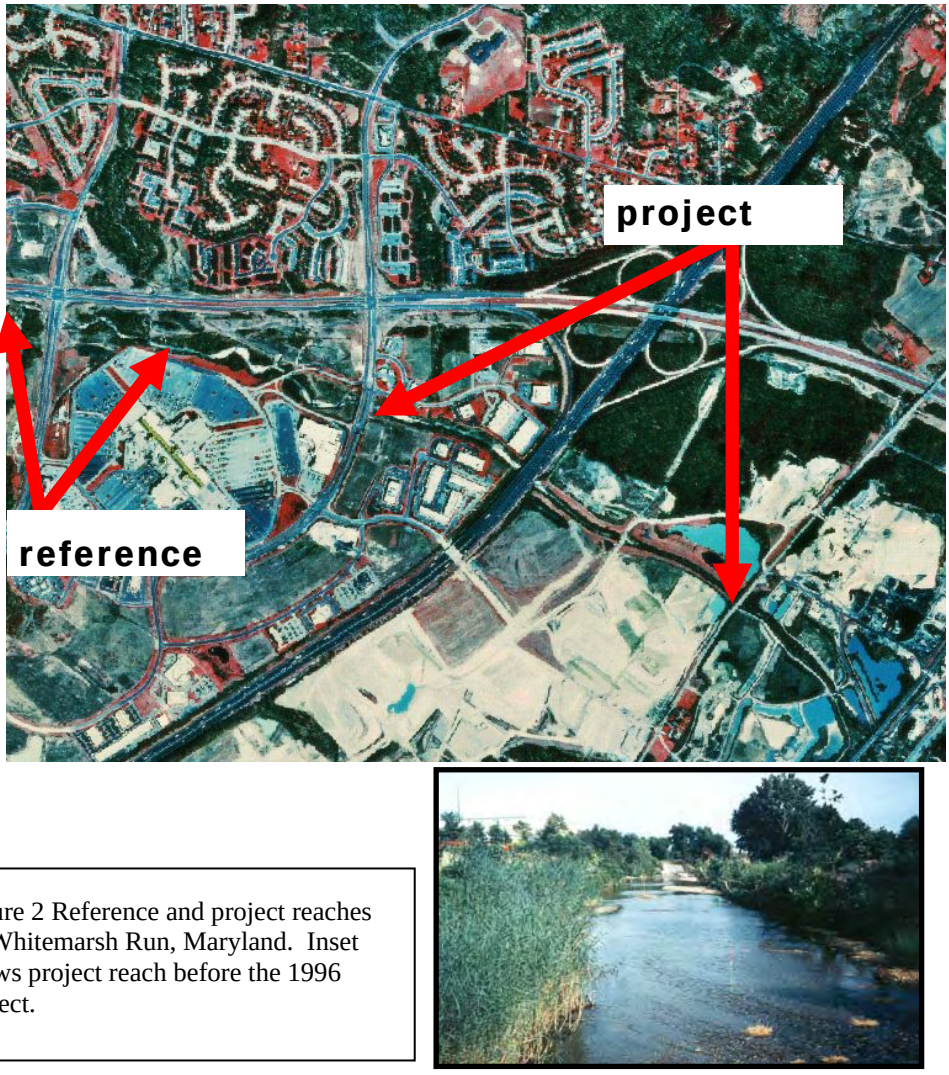


Figure 2 Reference and project reaches on Whitemarsh Run, Maryland. Inset shows project reach before the 1996 project.

(Figure 2). An empirically-based project was designed and constructed in the study reach of Whitemarsh Run in 1996 (Brightwater, Inc. 1994, 1995, 1997) and was later evaluated by Soar (2000); this paper does not attempt to evaluate that project, but merely uses some of the published data to furnish a hypothetical, simplified example. Results from this example should not be considered an actual design.

Empirical approach The basic steps for channel design using the empirical approach are (RiverMorph 2005):

1. Select a reference reach. The reference reach must be the same stream type (Rosgen 1994) as intended for the design project reach.
2. Compute bankfull discharge and associated channel dimensions for the reference reach.
3. Compute bankfull discharge and associated channel cross-sectional area for the project reach.
4. Compute design channel geometry by scaling up the reference reach geometry.
5. Check design channel for sediment-transport competency.
6. Lay out the channel alignment.

Limitations of the empirical design approach have been identified by RiverMorph (2005):

1. The method is primarily applicable to gravel-bed, meandering streams.
2. The largest particles normally transported by the stream begin to mobilize at bankfull flows.
3. A suitable reference reach of appropriate stream type must be utilized and dimensionless ratios based on the size gradation of a sediment sample collected from a bar[1] must fall within specified ranges for competency checks based on Andrews and Erman (1986) or Andrews and Nankervis (1995). Rosgen (2005) has proposed use of a shear stress-grain size curve when bed material gradations produce ratios outside these ranges.

Additional limitations on reference reach characteristics have been published by Hey (2004).

We selected a stable reach upstream from the project reach as a reference (Figures 2 and 3). Project and reference reach dimensions (Table 1) were obtained from cross-section surveys provided by Brightwater, Inc. (1995 and 1997) and Soar (personal communication, 2005), respectively. Contributing drainage areas were obtained from applicable USGS gage descriptions. Valley slope was unavailable for the reference reach and was assumed equal to that reported for the project reach. Bed material gradations were from sieve analyses of samples collected in 1998 by Soar (2000). Dimensionless ratios for the reference reach were within tolerances prescribed by Hey (2004) (Table 2).



Figure 3 Conditions in reference/supply reach of Whitemarsh Run, Maryland, 1998. **This**

[1]"The Rosgen modified procedure substitutes gradation parameters from a bar sample for the subpavement parameters used in the Andrews' equations. Typically, the bar sample is taken on the lower 1/3 of a point bar at an elevation halfway between the channel thalweg and bankfull elevation at the location of one of the largest particles on the bar. A good way to collect the sample is to scan the surface of the bar in this location for the largest particle and then place a plastic 5-gal bucket (with the bottom cut out) over the largest particle. The sample should be taken to a depth at least twice the size of the largest particle." RiverMorph (2005)

Table 1 Characteristics of Whitemarsh Run, Maryland, as of 1995. * = assumed quantity.

	Reference	Project
Location	Immediately upstream from North Fork confluence	Honeygo Rd. to State Route 7 neglecting North Fork tributary
Valley type	VIII	VIII
Valley slope	0.0043*	0.0043
Channel slope	0.0037	0.0038
Channel materials	Sand and gravel	Sand and gravel
Bed material D_{50}, mm	9.53*	9.53
Drainage area, km^2	14.0	16.2
Bankfull discharge, m^3/s	23.4	29.2
Annual sediment transport capacity, tonnes	7,680	12,500

Table 2 Reference reach evaluation using ratios proposed by Hey (2004). Subscript r denotes ratio of reference reach/design reach quantities. Q_s = bed material load estimated by the Parker et al. (1982) equation (kg/s), k_r = the ratio of bank vegetation factors (Hey and Thorne 1986). In this case k_r was assumed to be 1.0.

Quantity	Reference/ Design	Relationship (Hey 2004)	Recommended value for ratio
Bankfull Discharge, Q	1.16	$Q_r = k_r^{7.69} D_{50r}^{-0.846}$	1.00
D_{50}	1.00	$D_{50r} = D_{84r}^{0.555}$	1.00
Valley slope, S_v	1.00	$S_v = Q_r^{2.326} D_{50r}^{4.057} Q_{sr}^{0.542}$	1.75[2]

It is important to note that bankfull discharge does not directly enter the design when using software produced by RiverMorph (2005). Instead, the bankfull cross-sectional geometry (area and width-to-depth ratio) is used to develop the design cross section. The first computational step in the empirical approach (Table 3) involves calculating the design channel width (W_{bkf}) based on the design channel cross-sectional area (A_{bkf}) and the reference width-to-depth ratio (w_{bkf} / d_{bkf}). Therefore, a value of the design cross-sectional area at bankfull flow, A_{bkf}, must be generated using regional relations or by scaling up the value from the reference reach. RiverMorph (2005) advises that the reference reach cross section used as a template should be for "a stable riffle not under the effects of backwater other than the downstream stable pool." We generated the design A_{bkf} by multiplying the reference reach value by the ratio of project to reference reach drainage areas. Design channel geometry was then computed by substituting reference reach dimensions into the expressions given in Table 3 with the exception of meander amplitude and radius of curvature, which were based on a sine-generated curve function (RiverMorph 2005). RiverMorph (2005) produces a typical design cross section that may be modified by the user. Portions of the typical section higher than the bankfull discharge elevation are simply straight lines connecting the bankfull elevation with the existing ground surface (floodplain or channel banks) at an elevation 2 x bankfull depth higher than the thalweg. The slope of these lines is selected so that the entrenchment ratio (channel width at 2 x bankfull flow depth / bankfull width) equals the reference reach entrenchment ratio (Figure 4). For our design, we truncated the typical

[2] Within limits suggested by Hey (2004) based on data from UK restoration sites.

RiverMorph cross section where it intersected the existing ground surface, tying the new cross section into the current channel.

Even though the bankfull discharge is not used to determine design geometry, it may be used to check the sediment competency of the design. Bankfull discharge for the reference reach (Table 1) was determined using cross-section indicators of bankfull stage and the Limerinos (1970) formula for Mannings "n." The bankfull discharge for the project reach was obtained by multiplying the discharge for the reference reach by the ratio of contributing drainage areas. Resulting discharges were much greater than those shown on regional curves for non-urban watersheds (White 2001), but within 19% of those for urban areas in North Carolina (Doll et al. 2002). Sediment transport competency was checked and found adequate using D_{90} from the bed sediment gradation and modified Shields curves provided by Rosgen (2005).

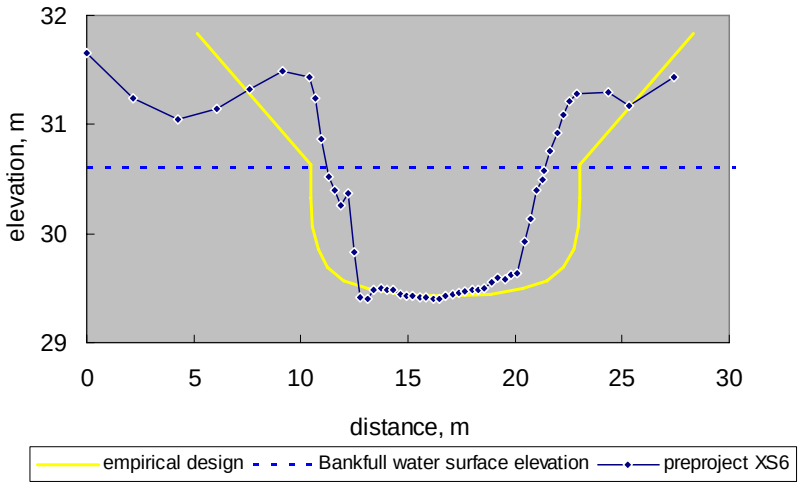


Figure 4 Typical empirical design cross section superimposed on typical preproject cross section.

Analytical approach: The basic steps in the analytical approach for sizing alluvial channels are

1. Locate the stable supply reach and determine bed gradation and roughness (Mannings) coefficients for bed and banks.
2. Determine channel-forming discharge and flow duration curve.
3. Calculate bed-material sediment inflow for the project reach.
4. Develop a family of slope-width solutions that satisfy resistance and sediment transport equations.
5. Reduce the range of solutions to meet site constraints such as maximum slope, width or depth.
6. Conduct sediment budget analysis to ensure sediment transport continuity for the full range of discharges.

It is very important that the supply reach be stable with no signs of active widening, degradation or aggradation, since the analytical approach produces a design that transports the same quantity of sediment as the supply reach. The supply reach was the same as the reference reach used for the empirical design (Figure 3). A rating curve for water surface elevation in the supply reach was calculated using the equal velocity method (Chow 1959) to composite bed and bank roughness. The Limerinos (1970) equation was used to calculate bed roughness and a Mannings roughness coefficient of 0.085 was selected for the banks and overbanks based on evaluation of photographs. Using this procedure allowed the composite roughness to vary with depth. The Meyer-Peter and Muller (1948) equation was selected based on the bed material size and used to calculate a sediment transport rating curve. The rating curves were used to calculate bankfull discharge, effective discharge and average annual sediment load.

A flow duration curve for the supply reach was developed using the regionalized duration curve method described in Copeland et al. (2001). Discharges from the gaged watershed were reduced by a constant (0.9) equal to the ratio of the two-year annual peak discharges. This ratio was developed using two-year annual peak flows calculated from regional regression equations presented by Dillow (1996) for the Western Coastal Plain of Maryland.

A preliminary or initial geometry for the project reach was selected to accommodate the channel-forming discharge. Three methods were used to estimate the channel-forming discharge. The effective discharge for the supply reach was determined by integrating the supply reach flow duration curve with the supply reach sediment transport rating curve. The midpoint of the discharge increment with the greatest sediment transport (27.5 m^3/s) was selected as the effective discharge (Figure 5). The effective discharge for the project reach was determined by increasing the supply reach effective discharge by the ratio of two-year annual peak flows. The project reach effective discharge was therefore 31.1 m^3/s, which corresponds to a return interval of 1.5 years. The supply reach bankfull discharge determined using field indicators of bankfull stage was 23.4 m^3/s (Table 1) and had a return interval of 1.3 years. The effective discharge was selected for use as the channel-forming discharge because its return interval was closer to that generally accepted for channel-forming discharge and because field indicators may be misleading in urban stream channels.

The next step in the analytical method is to determine a representative trapezoidal cross-sectional geometry with a combination of width, depth and slope for which the resultant hydraulic conditions are able to transport the incoming bed-material load without aggradation or degradation. The initial estimate for these dimensions was made for the channel-forming discharge in the project reach.

Table 3 Empirical Design for Whitemarsh Run, Maryland

	Relationship[3]	Reference C5	Preproject F4	Design C5
Width, m	$W_{bkf} = \sqrt{A_{bkf} \cdot (w_{bkf} / d_{bkf})}$	12.2	9.8	13.1
Depth, m	$D_{bkf} = W_{bkf} / (w_{bkf} / d_{bkf})$	0.8	0.8	0.8
Entrenchment ratio	$ER_d = ER_{ref}$	1.84	1.27	1.33[4]
Sinuosity	$K_d = K_{ref}$	1.17	1.13	1.17
Slope	$S_{bkf} = S_v / K$	0.0037	0.0038	0.0037
Wavelength, m	$L_m = W_{bkf} \cdot (l_m / w_{bkf})$	116	-	124
Amplitude, m	$W_{blt} = W_{bkf} \cdot (w_{blt} / w_{bkf})$	34	-	33
Radius of curvature, m	$R_c = W_{bkf} \cdot (r_c / w_{bkf})$	28	-	32

[3] Upper case letters are bankfull channel dimensions for the design channel, while lowercase letters are for the reference reach channel. All dimensions shown here are for riffles; the RiverMorph software also produces dimensions for pools and runs. W = channel width, D = channel depth, A = cross sectional-area, K = sinuosity, S_{bkf} = channel slope, S_v = valley slope, L_m = meander wavelength, W_{blt} = meander belt width or amplitude, R_c = meander radius of curvature.

[4] The design entrenchment ratio does not follow the prescribed relationship because the project reach is deeply incised, and when the design cross section is superimposed on the existing topography, it is not possible to attain the reference reach entrenchment ratio without prohibitive amounts of excavation and fill.

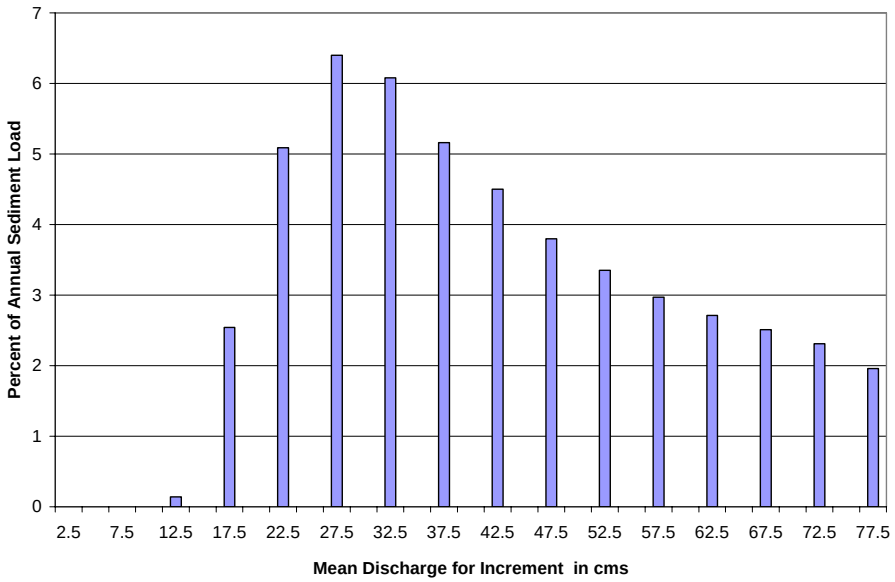


Figure 5 Effective discharge analysis for Whitemarsh Run, Maryland.

The design geometry was checked using the full range of expected discharges. One method for calculating the channel geometry with the channel-forming discharge is the Stable Channel Analytical Method in SAM (Thomas et al. 2002) and HEC-RAS (USACE-HEC 2002). This method solves sediment transport and resistance equations simultaneously, providing a family of width-depth-slope solutions that will pass the incoming bed-material sediment load. In this case, the incoming sediment load from the supply reach was calculated for a discharge of 27.5 m^3/s. The calculated stability curves are shown in Figure 6. These curves were calculated by assigning a channel side slope of 2.5 (a first estimate of slope needed for geotechnical stability) and a bank roughness of 0.085. Theoretically, any geometry represented by a point on the stability curve represents a stable design solution. Selected dimensions (Table 4) featured a slightly higher sinuosity than present in the existing channel to improve habitat characteristics.

Flow duration curves were developed for the project reach and the supply reach. The flow duration curve for the project reach was calculated directly from 39 years of mean daily flow records from the USGS gage located just downstream from the project reach. An annual peak-flow frequency curve was also developed from gage data. Since the stability curve ensures sediment transport stability for only the channel-forming discharge, the next step in the design process is to compute a sediment budget using the entire range of expected discharges. This is done by integrating the flow duration and the sediment transport curves for the supply reach and the project reaches to obtain average annual sediment loads for both reaches. If necessary, channel dimensions may be modified to ensure sediment loads are practically equal.

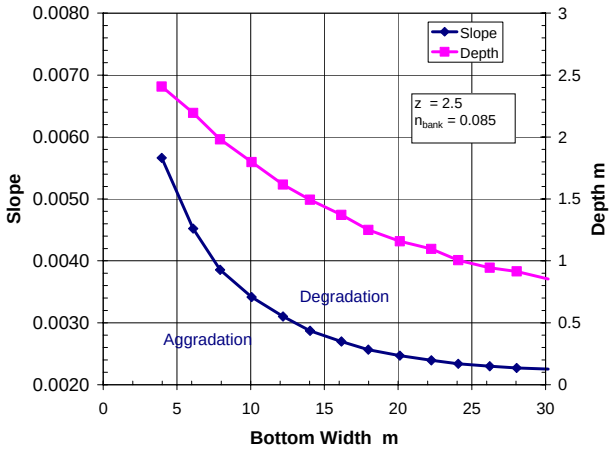


Figure 6 Slope-width-depth family of curves for project.

RESULTS

Empirical and analytical approaches differ in selection of design discharge. The effective discharge for the reference/supply reach (27.5 m^3/s) was 18% higher than the estimated bankfull discharge (23.4 m^3/s), probably due to the effects of urbanization-driven channel incision on cross-sectional morphology. Disturbed channels, such as those draining urban watersheds like this one, exhibit inconsistent relationships between bankfull and channel forming discharge and field indicators are subject to operator error (Williams 1978). Griffin (1998) measured bed material and bed material load gradations for storms spanning a range of peak discharges in the project reach during 1996 and found that the channel forming discharge was about three times as great as bankfull discharge estimated from field indicators by others.

Table 4 Comparison of Design Outcomes, White Marsh Run, Maryland

	Empirical	Analytical
Top Width, m	14.9[5]	18.5
Bottom Width, m	9.5	10.7
Flow Depth at Design Q, m	0.82	1.8
Channel Slope	0.0037	0.0034
Design Q, m^3/s	27.2	31.1
Design Mannings "n"	0.025	0.059
Mean annual sediment transport capacity, tonnes	10,800	8,360
Trap efficiency, %	-41	-9

The empirical design discharge was smaller and a lower Mannings "n" value was used to compute this discharge (Table 4). The Mannings "n" value used for the reference reach in the empirical approach (0.025) was simply based on the application of the Limerinos formula to the observed bed sediment gradation without increases for bends, bars, bank vegetation, or other boundary irregularities. This was justified based on the fact that the reference reach was rather straight and uniform and the analysis was limited to the lower part of the channel cross section that was unlikely to support woody vegetation. A single "n" value was used for the entire cross section since sophisticated techniques for compositing different bed and bank roughness values were not available within tools normally used for empirical design. The higher "n" value used for the supply reach within the analytical approach (0.059) was derived by compositing Limerinos-based values for the bed and a much higher value (0.085) assumed for the heavily vegetated banks.

Sediment budgets for the empirical and analytical designs were compared by computing their trap efficiencies:

$$TE = 100 \frac{Y_{Supply} - Y_{Project}}{Y_{Supply}}$$

Where TE = trap efficiency, %, and Y = mean annual sediment load for the supply and project reaches, as indicated by the subscripts.

For sediment load computations, composite roughness values were computed for both design cross sections using the Limerinos equation for the bed and 0.085 for the banks. The resulting trap efficiencies were fair for the analytical design (-9%), but very poor (-41%) for the empirical design, indicating excessive degradation potential.

[5] Width of channel at water surface elevation for analytical design discharge.

The degradation predicted for the empirical design reflects the effect of the steeper, narrower channel geometry on sediment transport at flows above bankfull. Similar analyses with Yang and Laursen-Madden sediment transport relations, which allow computation of transport by size class but do not consider armoring at low flows produced trap efficiencies of +12% for the analytical channel and -18% to -14% for the empirical channel. Interestingly, the empirical design project actually constructed at this site in 1994 suffered failure through excessive aggradation because the project design slope (0.0025) was much lower than required to transport the supplied load (Soar 2000). This slope was selected based on adoption of planform characteristics of the target stream type for the design channel without consideration of reference reach properties (Brightwater 1994). A reanalysis (Brightwater 1997) included data from a reference reach described as unstable by Soar (2000).

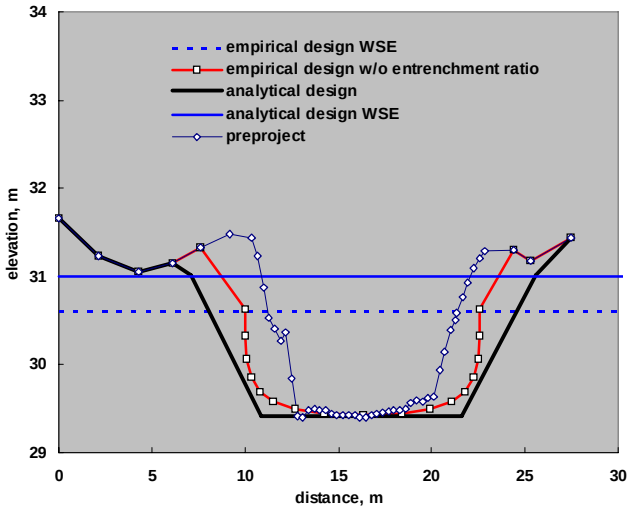


Figure 7 Cross sections for preproject conditions and empirical and analytical designs, White Marsh Run, Maryland.

Both designs produced cross sections larger than the preproject channel, but the analytical cross section was larger, consistent with a larger design discharge and larger Mannings "n" value (Figure 7). In Figure 7, preproject topography is used for overbank portions of both design cross sections. Although the empirical design flow depth at design discharge was only about half of the corresponding analytical depth, similar channel depths resulted when the design cross sections were superimposed on a typical preproject cross section. The analytical channel was about 5% wider at the bottom and 28% wider at the top. The empirical design channel, with a slope of 0.0037, had significantly more sediment transport potential than the analytical channel. The design slope for the empirical channel was taken directly from the reference reach where annual flows were about 10% less than the project reach. The analytical method allowed the designer to slightly reduce the slope and increase the sinuosity while retaining sediment continuity, which is attractive from aesthetic and habitat quality standpoints. The analytical design channel had a slope of 0.0034, which was chosen from the stability curve and had a corresponding base width of 10.7 m. If a design slope of 0.0037 had been selected, the channel base width for the analytical channel would have been 9.0 m. The narrower channel would have an increased composite roughness due to the influence of the vegetated banks.

Neither approach addresses complex properties of natural channels such as the effects of meandering; bank geometry, soils, and vegetation on bank stability and flow resistance; cohesive sediments; or armoring (MacBroom 2004). Changes in bed roughness due to bedform changes were not considered. Analytical approaches are based on sediment transport computations which have high levels of uncertainty (Dierks et al. 2003), but this problem may be addressed by using field observations to refine transport estimates or by simply using relative transport rates as a basis for design (Wilcock 2004).

CONCLUSIONS

Design of stream channels for restoration purposes involves many critical decisions, regardless of the approach involved. Design outcomes are sensitive to input parameters such as bed material size, design discharge, hydraulic roughness and cross-sectional shape. Even with new software to facilitate computation, an experienced, well-educated (rather than a trained) designer is needed.

Selection of the reference or supply reach has major effects on the outcome of both design approaches. Empirical design sediment continuity problems associated with inappropriate reference reach selection were minimized in this case by using the sediment supply reach as the reference reach. Selection of channel forming discharge should

include all three methods: determination of bankfull discharge based on field indicators of bankfull stage, analysis of flow frequency and effective discharge analysis. Calculation of hydraulic parameters in deep, narrow channels must account for the effects of bank roughness. When bank roughness differs strongly from bed roughness, channel hydraulics are very sensitive to cross-sectional shape.

The underlying philosophy of the empirical approach lends itself to habitat restoration, but it does not allow for designs where conveyance (flood control) issues act as constraints. It tends to be computationally less difficult and less process-based than analytical approaches. The empirical approach is targeted at coarse-bed streams and produces suspect results for streams with beds that are frequently mobile. The empirical approach, as currently practiced, contains checks for sediment competence, but not sediment continuity. Therefore even though a design may produce a channel that is competent to transport the larger bed material sizes found in samples from the pre-project reach, it may fail through aggradation or degradation.

ACKNOWLEDGMENTS

RiverMorph, LLC provided a copy of RiverMorph 3.1 and associated technical support. Inset of Fig. 2 furnished by Phil Soar. Sean Bennett, Munsell McPhillips and Andrew Simon read an earlier version of this paper and made many helpful comments.

REFERENCES

Andrews, E.D. and Erman, D.C. (1986). "Persistence in the Size Distribution of Surficial Bed Material During an Extreme Snowmelt Flood," Water Resources Research, 22(2), pp 191-197.

Andrews, E.D. and Nankervis, J. M. (1995). "Effective Discharge and the Design of Channel Maintenance Flows for Gravel-Bed Rivers," Natural and Anthropogenic Influences in Fluvial Geomorphology, Geophysical Monograph 89. American Geophysical Union. pp. 151-164.

Brightwater, Inc. (1994). "White Marsh Run." Report on establishing design discharge and criteria for stream restoration and wetland hydrology, Brightwater, Inc., Ellicott City, MD.

Brightwater, Inc. (1995). "White Marsh Run." Report on establishing design discharge and criteria for stream restoration and wetland hydrology, 1994 Revision, Brightwater, Inc. Ellicott City, MD.

Brightwater, Inc. (1997). "White Marsh Run." Report on concept design modifications to stream restoration construction project between Honeygo Blvd. and Route 7, Brightwater, Inc., Ellicott City, MD.

Brookes, A. (1988). Channelized Rivers: Perspectives for Environmental Management. John-Wiley & Sons, Chichester, U. K.

Brookes, A. and Sear, D. A. (1996). "Geomorphological principles for restoring channels," in River Channel Restoration: Guiding Principles for Sustainable Projects. John Wiley & Sons, New York.

Byars, M.S. and Kelly M. (2001). "Sediment transport in urban stream restoration design," Proc. 2001 Wetlands Engineering and River Restoration Conference, American Society of Civil Engineers, Reston, VA, pp.17-28.

Chang, H.H. (1988). Fluvial Processes in River Engineering. John Wiley & Sons, New York.

Chow, V. T. (1959). Open Channel Hydraulics, McGraw Hill, New York.

Committee on Applied Fluvial Geomorphology. (2004). Position statement on Applied Fluvial Geomorphology, Committee on Applied Fluvial Geomorphology, Quaternary Geology and Geomorphology Division, Geological Society of America. http://www.geo.wvu.edu/%7Ekite/QG&GFluvGeomPositionStatement22March2004.html

Copeland, R.R., McComas, D.N., Thorne, C.R., Soar, P. J., Jonas, M.M. and Fripp, J.B. (2001)."Hydraulic Design of Stream Restoration Projects," ERDC/CHL-TR-01-28, U.S. Army Corps of Engineers Engineer Research and Development Center, Vicksburg, MS.

Dierks, S., Gustavson, K., Schneider, J., Wilson, S. (2003). "Stream Restoration Design using the Stable Channel Analytical Model (SAM)," Proc. Protection and Restoration of Urban and Rural Streams Symposium 2003. Philadelphia, Pennsylvania. American Society of Civil Engineers, Reston, VA. (doi:10.1061/40695(2004)32)

Dillow, J.A. (1996). "Technique for Estimating Magnitude and Frequency of Peak Flows in Maryland," USGS Water Resources Investigations Report 95-4154, Towson, MD.

Doll, B.A., Clinton, D.R., Jenkins, J.W., Jr., Patterson, J.M., Coleman, N.J. (2001). "Urban Stream Restoration Using a Natural Channel Design Approach," Proc. Wetlands and River Restoration 2001. Reno, Nevada. American Society of Civil Engineers, Reston, VA (doi:10.1061/40581(2001)2).

Doll, B.A., Wise-Frederick, D.E., Buckner, C.M., Wilkerson. S.D., Harman, W.A., Smith, R.E. and Spooner, J. (2002). "Hydraulic Geometry Relationships for Urban Streams throughout the Piedmont of North Carolina." Journal of the American Water Resources Association. 38(3), pp. 641-651.

Doyle, M. W., Boyd, K.F. and Skidmore, P.B. (1999). "River Restoration Channel Design: Back to the Basics of Dominant Discharge." Proceedings, Second International Conference on Natural Channel Systems. Watershed Science Centre, Trent University, Peterborough, Ontario.

Eaton, B. C. Church, M. and Millar, R. G. (2004). "Rational regime model of alluvial channel morphology and response," Earth Surface Processes and Landforms 29:4, 511-529, doi: 10.1002/esp.1062

Gillilan, S., Hoitsma, B. T. and Kauffman, M. (2005). "Challenges in developing and implementing ecological standards for geomorphic river restoration projects: a practitioner's response to Palmer et al. (2005)," Journal of Applied Ecology (2005)42, pp. 223-227.

Griffin, D. (1998). "Channel Restoration Using Indicators of Bankfull." "Engineering Approaches to Ecosystem Restoration, Wetlands Engineering and River Restoration Conference 1998," Conf. Proc. 100, American Society of Civil Engineers Reston, VA. (doi 10.1061/40382(1998)178.)

Henderson, F. M. (1966). Open Channel Flow. New York: The MacMillan Company.

Hey. R.D. (2004). "Applicability of Geomorphological procedures for river restoration" Proc. Critical Transitions in Water and Environmental Resources Management, June 27-July 1, 2004, Salt Lake City, Utah, American Society of Civil Engineers, Reston, VA. (doi:10.1061/40737(2004)409).

Hey, R. D. and Thorne, C. R. (1986). "Stable channels with mobile gravel beds," Journal of Hydraulic Engineering 112(9), pp. 671-689.

Johnson, P. A. and Niezgoda, S. L. (2004). "Risk-based method for selecting bridge scour countermeasures." Journal of Hydraulic Engineering 130(2), pp.121-128.

Juracek, K. E. and Fitzpatrick, F. A. (2003). "Limitations and implications of stream restoration," Journal of the American Water Resources Association 39(3) pp 659-670.

Kondolf, G.M., Smeltzer, M.W. and Railsback, S.F. (2001). "Design and performance of a channel reconstruction project in a coastal California gravel-bed stream." Environmental Management 28(6), pg. 761.

Leopold, L. B. and Maddock, T., Jr. (1953). "The Hydraulic Geometry of Stream Channels and Some Physiographic Implications." U. S. Geological Survey Professional Paper 252, U.S. Government Printing Office, Washington, D. C., (252), pp 117-127.

Leopold, L. B. and Wolman, M. G. (1960). "River meanders." Bulletin of the Geological Society of America 71, pp. 769-794.

Limerinos, J. T. (1970). "Determination of the Manning Coefficient from Measured Bed Roughness in Natural Channels," Water Supply Paper 1898B, US Geological Survey, Washington, DC.

MacBroom, J.G. (2004). "Merging River Mechanics and Fluvial Morphology for River Management," Proc. World Water and Environmental Congress 2004. Salt Lake City, Utah. American Society of Civil Engineers, Reston, VA. (doi:10.1061/40737(2004)408).

Malakof, D. (2004). The River Doctor. *Science* 305(5686), pp. 937-939 [DOI: 10.1126/science.305.5686.937].

Meyer-Peter, E., and Müller, R. (1948). "Formulas for bed-load transport," Proc. 2nd Meeting of the IAHR, Stockholm, Sweden, pp 39–64.

McCarley, R.W., Ingram, J.J., and Brown, B.J. (1990). "Flood-Control Channel National Inventory," Miscellaneous Paper HL-90-10. U.S. Army Engineer Waterways Experiment Station.

Millar, R.G. and MacVicar, B.J. (1998). "An Analytical Method for Natural Channel Design," Proc. Wetlands Engineering and River Restoration Conference 1998. Denver, Colorado. American Society of Civil Engineers, Reston, VA. (doi:10.1061/40382(1998)65).

Millar, R. G. and Quick, M. C. (1998). "Stable width and depth of gravel-bed rivers with cohesive banks." Journal of Hydraulic Engineering 124(10), pp. 1005-1013.

Miller, J.R. and Ritter, J.B. (1996). "An Examination of the Rosgen classification of natural rivers." Catena 27, pp. 295-299.

Miller, D.E. and Skidmore, P.B. (2001). "Natural channel design: How does Rosgen classification-based design compare with other methods?" Proc. Wetlands and River Restoration 2001. American Society of Civil Engineers, Reston, VA. CD-ROM.

National Research Council, Committee on Restoration of Aquatic Ecosystems. (1992). Restoration of Aquatic Ecosystems: Science, Technology and Public Policy. National Academy Press, Washington, D. C.

Neary, V.S. and Korte, N. (2002). "Preliminary Channel Design: Blue River Reach Enhancement in Kansas City." Proc., 9th International Conf. on Urban Drainage. Portland, Oregon, September 8-13, 2002.

Newbury, R.W. and Gaboury, M.N. (1993). Stream Analysis and Fish Habitat Design: A Field Manual. Newbury Hydraulics Ltd., Gibsons, British Columbia.

Parker, G., Klingeman, P. C. and McClean, D. G. (1982). "Bedload and size distribution in paved gravel-bed streams," Journal of the Hydraulics Division, American Society of Civil Engineers, 103(HY4), pp. 544-571.

Riley, A. L. (1998). Restoring Streams in Cities: A Guide for Planners, Policymakers and Citizens. Island Press, Washington, D. C.

RiverMORPH (2005). RiverMORPH User's Manual Version 3.1. RiverMORPH, LLC, Louisville, Kentucky.

Rosgen, D.L. (1994). Applied River Morphology. Wildland Hydrology Books, Pagosa Springs, Colo.

Rosgen, D. L. (1997). "A geomorphological approach to restoration of incised rivers." In Wang, S.Y., Langendoen, E. and Shields, F. D. Jr., (eds.) Management of Landscapes Disturbed by Channel Incision, Stabilization, Rehabilitation and Restoration. Center for Computational Hydroscience and Engineering, University of Mississippi, University, Mississippi. pp 12-22.

Rosgen, D.L. (1998). "The Reference Reach – A Blueprint for Natural Channel Design," Proc. Wetlands Engineering and River Restoration Conference, Denver, Colorado, American Society of Civil Engineers, Reston VA., pp. 1009-1016. (doi: 10.1016/40382(1998)166)

Rosgen, D. L. (2005). "The Rosgen Geomorphic Approach for Natural Channel Design," Appendix 7-C, NRCS Draft Stream Design Guide, USDA-NRCS, Washington, D. C.

Schulte, M. A., Forman, S. M., Williams, D. T., Mashburn, G. and Vermeeren, R. (2000). A stable channel design approach for the Rio Salado, Salt River, Arizona," Proc. Building Partnerships - 2000 Joint Conference on Water Resource Engineering and Water Resources Planning & Management, American Society of Civil Engineers, Reston VA., CD-ROM, (doi:10.1061/40517(2000)362).

Schwartz, J.S., Carpenter, D.D., Slate, L.O., Sinha, S.K., Brennen, K. and MacBroom, J. (2003). "Research needs for improvement of principles and practices in urban stream restoration." Proc. Protection and Restoration of Urban and Rural Streams Symposium 2003. Philadelphia, Pennsylvania. American Society of Civil Engineers, Reston, VA. pp. 15-28.

Shields, F. D., Jr. (1997). "Reach-average dimensions for channel reconstruction." In Wang, S. Y., Carstens, T. (eds.) Environmental and Coastal Hydraulics: Protecting the Aquatic Habitat. Proceedings Theme B, Vol. 1, XXVII Congress of the International Association for Hydraulic Research, American Society of Civil Engineers, New York, pp. 388-393.

Shields, F. D., Jr., Copeland, R. R., Klingeman, P. C., Doyle, M. W. and Simon, A. In press. Stream restoration. Chapter 9 in Sedimentation Engineering, Volume 2, Manual 54, American Society of Civil Engineers, Reston, Virginia.

Shields, F. D., Jr., Copeland, R. R., Klingeman, P. C., Doyle, M. W. and Simon, A. (2003). "Design for stream restoration." Journal of Hydraulic Engineering 129(3), pp.575-584.

Simon, A., Doyle, M., Kondolf, M. Shields, F.D., Jr., Rhoads, B., Grant, G., Fitzpatrick, F., Juracek, K., McPhillips, M. and MacBroom, J. (2005). "How Well do the Rosgen Classification and Associated 'Natural Channel Design' Methods Integrate and Quantify Fluvial Processes and Channel Response?" Proc. World Water and Environmental Resources Congress. Anchorage, Alaska. American Society of Civil Engineers, Reston, VA. (doi: 10.1061/40792(173)584)

Simpson, P.W. (1982). "Manual of Channelization Impacts on Fish and Wildlife." Contract No. 14-16-0009-80-006. U. S. Fish and Wildlife Service, U.S. Department of the Interior, Washington, D. C.

Skidmore, P. B., Shields, F. D., Jr., Doyle, M. W. and Miller, D. E. (2001). "A categorization of approaches to natural channel design." Proc. Wetlands and River Restoration 2001. American Society of Civil Engineers, Reston, VA, CD-ROM.

Soar, P. J. (2000). "Channel restoration design for meandering rivers." Thesis submitted to the University of Nottingham for the degree of Doctor of Philosophy, Nottingham, U. K.

Soar, P.J. and Thorne, C.R.. (2001). "Channel Restoration Design for Meandering Rivers," ERDC/CHL CR-01-1. U.S. Army Corps of Engineers, Washington, D.C.

Smith, S.M. (1997). "Changes in the hydraulic and morphological characteristics of a relocated stream channel." MS thesis, University of Maryland, College Park.

Thomas, W.A., Copeland, R.R. and McComas, D.N. (2002). "SAM –Hydraulic Design Package for Channels," U.S. Army Corps of Engineers Engineer Research and Development Center, Coastal and Hydraulics Laboratory, Vicksburg MS.

U.S. Army Corps of Engineers (USACE). (1970). "Hydraulic Design of Flood Control Channels," EM 1110-2-1601, Office of the Chief of Engineers, Washington, D.C.

U.S. Army Corps of Engineer Hydrologic Engineering Center (USACE-HEC) (2002). "HEC-RAS River Analysis System," Users Manual, Version 3.1, Davis CA.

U.S. Department of Agriculture (USDA) (1977). "Design of Open Channels," Technical Release No. 25, Soil Conservation Service, Washington, D.C.

White, K. E. (2001). "Regional curve development and selection of a reference reach in the non-urban, lowland sections of the piedmont physiographic province, Pennsylvania and Maryland," U.S. Department of the Interior, U.S. Geological Survey Water-Resources Investigations Report 01-4146, USGS, New Cumberland, PA.

Wilcock, P.R. (1997). "Friction between Science and Practice: The Case of River Restoration." Eos, Transactions, Am. Geophysical Union 78(41), pg 454

Wilcock, P.R. (2004). "Sediment Transport in the Restoration of Gravel-bed Rivers," Proc. Critical Transitions in Water and Environmental Resources Management. Salt Lake City, Utah. American Society of Civil Engineers, Reston, VA. (doi:10.1061/40737(2004)433).

Williams, G.P. (1978). "Bankfull Discharge of Rivers," Water Resources Research 14(6), pp 1141-1154.

Wohl, E. (2004). Disconnected rivers: linking rivers to landscapes. Yale University Press. New Haven, Conn.

RESTORATION OF LOWER LAS VEGAS WASH – UPPER DIVERSION WEIR

Chris Bahner, Hydraulic Engineer, WEST Consultants, Inc., Salem, OR, cbahner@westconsultants.com; Gerry A. Hester, Facilities Manager, Southern Nevada Water Authority (SNWA), Las Vegas, NV, gerry.hester@snwa.com; Dr. Syndi Dudley, Director of Water Resources, Louis Berger Group, Inc., Las Vegas, NV, sdudley@louisberger.com

Abstract: Las Vegas Wash is a tributary to Colorado River that drains into Lake Mead. The Wash naturally would be an ephemeral system with the infrequent summer storms being primarily responsible for forming the channel and transporting sediment. However, the Wash has been a perennial system since the 1950s as a result of continuous effluent flows, which have increased fairly significantly over time due to increased urbanization. The increased flows resulted in the initiation of bed and bank erosion in the late 1960s, and severe headcuts and channel incision were evident in the 1970s. The progression of the headcuts and channel incision was accelerated when culverts near the downstream end of the wash were replaced with a bridge in 1978. Also, the Wash experienced multiple large storm events in the early 1980s. The Wash during this period degraded up to 35 feet and widened up to 520 feet, resulting in the destruction of most of the historical wetlands in the lower Wash, large amounts of sediment depositing into Lake Mead, and the decline of the Wash aesthetics. It has been estimated that approximately 4 million cubic yards of sediment eroded from the Wash during the 15-year period prior to 1984.

Due to growing concerns over water quality issues in Lake Mead and the Wash, the Nevada Division of Environmental Protection (NDEP) initiated the Lake Mead Water Quality Forum (Forum) in 1997. A Water Quality Citizens Advisory Committee (WQCAC) was established in 1997 by the Southern Nevada Water Authority (SNWA) to provide the Forum with public input and recommendations in the area of water quality. This committee recommended that a comprehensive adaptive management plan for the Wash be developed, with SNWA as the lead agency in implementing the plan. The Las Vegas Wash Coordination Committee (LVWCC) was established by SNWA to develop this plan.

The adopted plan includes the construction of twenty-two grade control structures and the establishment of wetlands habitat for the reach between Lake Las Vegas, which is just upstream of Lake Mead, and the Nature Center located about 6.6 miles upstream. The upstream most structure, Upper Diversion Weir, is currently being designed by Louis Berger Group, Inc. and WEST Consultants, Inc. This structure will be a concrete grade control structure that will divert water to the existing Wash and an outfall channel. As part of the design efforts, an HEC-6 model was developed for the upper 5.2 miles of the lower reach of the Wash. The model was used to evaluate the effect the grade control structures proposed in this reach would have on the stability of the wash and the impacts to the downstream sediment load for two hydrologic conditions: 20-year of effluent flows and flood series. The HEC-6 results indicate that (1) the proposed weir structures will significantly reduce the amount of degradation within the study reach and the sediment discharge passing the Pabco Weir; (2) the bed load sediment discharge will be reduced about 85%, and the suspended sediment discharge will be reduced about 60%; (3) significant aggradation will occur upstream of the weir structures; and (4) about 1 to 2 feet of sediment will deposit upstream of the Upper Diversion Weir in 20-years.

SIAM, SEDIMENT IMPACT ANALYSIS METHODS, FOR EVALUATING SEDIMENTATION CAUSES AND EFFECTS

David M. Mooney, Hydraulic Engineer, Bureau of Reclamation, Technical Service Center, Sedimentation and River Hydraulics Group D8540, P.O. Box 25007, Denver, CO 80225, dmooney@do.usbr.gov

INTRODUCTION

River restoration succeeds best when accounting for system interactions and restoring processes. Sedimentation effects can undermine, bury, or leave restoration efforts stranded. Traditional means of evaluating sediment impacts include sediment continuity analysis and mobile boundary hydraulic modeling. Sediment Impact Analysis Methods (SIAM) provides a framework for combining morphological, hydrologic, and hydraulic information. The results develop a quantitative picture of sediment movement through a watershed that are more detailed than a qualitative geomorphic evaluation, yet require less effort than a numeric mobile boundary model.

SIAM represents a network as a series of homogeneous reaches and defines the connectivity between reaches to create a geomorphic aware sediment linkage model from a sediment continuity perspective. The results map potential short- and long-term imbalances and instabilities in a channel network and provide the first step in identifying sediment related problem areas and designing or refining remediation. The procedures allow for a rapid assessment of dynamic equilibrium in channel networks to improve efforts to target the source of problems and develop solutions from a systems approach.

The following paragraphs describe the theory behind the SIAM model and then validate and compare against numerical models of Hickahala Creek, Mississippi and hypothetical mobile boundary numerical simulations. The SIAM techniques facilitate incorporating sediment movement into stream rehabilitation and management.

COMPUTATIONAL METHODS

Input Records: Constructing a SIAM model requires developing records to describe the bed material gradation, sediment characteristics, hydrology, hydraulics, transport potential, and local sediment sources of a dendritic network. The input records describe the driving sedimentation parameter for a regime static in space and time. Hydrology, hydraulics, and transport potential describe the magnitude, duration, and hydraulics, and theoretical transport capacity of a flow event. Bed material describes the composition of the channel boundary. Sediment characteristics describe how flow events interact with the channel boundary including cohesive scour, armored reaches, and the threshold between wash load and bed material load. Local sources describe sediment supply from features outside of the modeled reaches such as gullies, net bank failure, surface erosion, or augmentation.

Hydrology consists of flows and durations representing the range of events under a particular flow regime. SIAM acts independently from the methods used to generate input and can scale from coarse to very detailed definitions. A project may begin with a coarse survey and regional estimates and then fill in specific measurements where available. By separating the development of input records from the synthesis, the model retains the flexibility to vary techniques and procedures as the state-of-the-art improves or studies expand a database.

Local Sediment Accounting: SIAM models the movement of sediment through a watershed by dividing the range of grain classes into wash load or bed material load transport modes. A reach in SIAM contains a wash material reservoir and a channel material reservoir. Wash material passes through a reach without interacting with or modifying the channel boundary. A change anywhere upstream impacts all downstream reaches in connected grain classes. Channel material interacts with the channel bed and banks to impact the physical structure of the channel. A change to the channel material budget can only immediately impact the reach directly downstream. Impacting reaches farther downstream requires adjustment to the channel boundaries and may take many years to exert an impact. Grain classes can transition back and forth between reservoirs as the material moves to downstream reaches. A transition from wash material to channel material severs the connection to upstream wash load reservoirs. **Figure 1** shows the conceptual framework for a reach in the SIAM model.

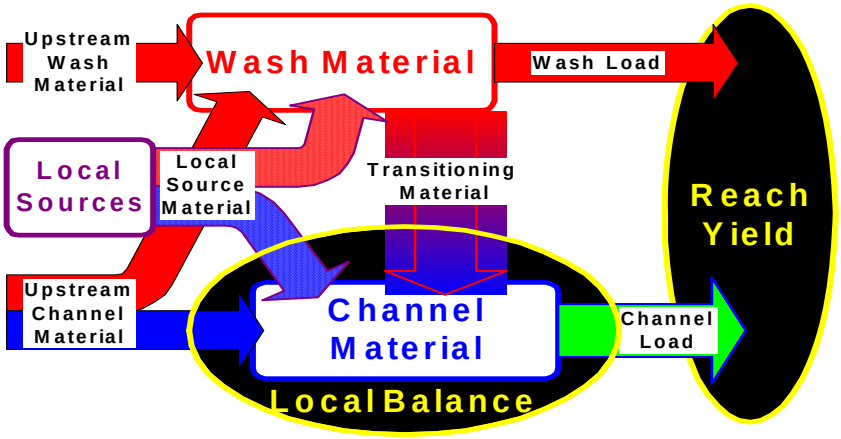


Figure 1 SIAM Reach Level Conceptual Framework.

Material enters a reservoir through upstream channels or local sediment sources. Local sources include material supplied to a reach from outside of the channel bed or upstream of the model boundary. Sources include inflows to the reaches at the upstream boundary of the model, bank failures, surface erosion, gravel mining, gully formation, and all other forms of external sediment production. Local sediment source records do not include material hydraulically supplied between modeled reaches through entrainment or bed scour. All material supplied to the wash reservoir must either transition to the channel reservoir or pass downstream. Material leaves the channel reservoir according to the channel load. Channel load entering a downstream reach either passes into the wash material reservoir or the channel material reservoir depending on the wash load threshold. Supply of material to the channel reservoir does not need to equal the channel load. When supply exceeds the load, a positive local balance occurs. When load exceeds supply a negative local balance occurs. SIAM tracks the individual supply constituents to identify causality. A large wash load may originate from gully formation high up in the basin or the cumulative effect of agriculture. Local accounting only links wash load impacts. Identifying impacts to or from channel load requires network accounting. Effects require adjustment to channel boundaries.

Network Accounting: The computation routines do not adjust channel boundaries, update sediment sources, or account for time dependent effects. Sediment supplies represent regime averaged properties, and average results over a regime to provide balances showing trends in a system, but not intermediate or final states. Network impacts from channel reservoir imbalances are computed through extrapolating trends in the channel reservoir according to geomorphic principles of channel response. A reach that cannot transport the supply of material is aggrading and will evolve to increase transport capacity. A reach transporting more than the supply of sediment is degrading and will evolve to reduce the sediment transport rate. For a single reach in a network otherwise at equilibrium, the evolution results in a permanent change to the upstream base level and a transitory change to the downstream sediment supply. An aggrading reach adjusts in order to increase transport capacity by either increasing slope, reducing width, and/or fining of boundary material. An aggrading reach will increase the base level of upstream reaches and temporarily reduce the supply to downstream reaches with no net change in transport capacity. A degrading reach must adjust to reduce transport capacity through a combination of reduction of slope, increase in width, or coarsening boundary material. The base level of upstream reaches lowers and the downstream reaches experience increased sediment supply with no net change in transport capacity. **Figure 2** shows an example adjustment.

The imbalanced reach acts as a pivot with upstream reaches moving one direction and downstream reaches moving the opposite. Multiple aggrading and degrading reaches create interference to attenuate or amplify geomorphic change. Reaches do not always adjust equally. Stream power and applied energy provide a means of distributing the change throughout a network. Reaches, which respond more to changes in sediment supply and transport capacity, will absorb more of the adjustment than less responsive reaches. The pivot point within a reach moves upstream or downstream depending on the responsiveness of the connected reaches.

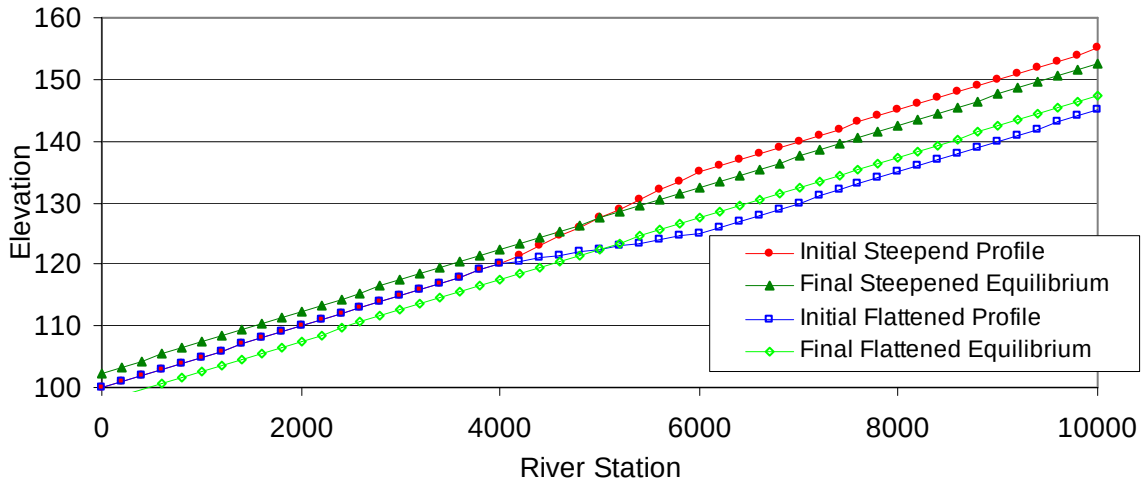


Figure 2 Adjustment Progressions of Aggrading and Degrading Reaches.

Applied Energy and Responsiveness: Bagnold (1966) postulated a link between stream power and sediment transport. His research suggested stream power provided an integrative parameter for relating sediment transport to channel hydraulics with an efficiency term defining the fraction of the total stream power expended in sediment transport. Other researchers use similar energy methods for total load (Yang 1973 and Parthenaides 1977). Equation 1 shows stream power in terms of shear stress and the hydraulic components of shear stress.

$$\Omega_T = \tau \cdot v \cdot P = (\gamma \cdot R \cdot S_f) \cdot v \cdot P \tag{1}$$

Where,

Ω_T = total stream power;
τ = shear stress;
P = wetted perimeter;
γ = unit weight of water;
R = hydraulic radius;
S_f = friction slope; and
v = average flow velocity.

The sediment load is related to the relative weight of sediment and the fraction of the total power expended in sediment transport. Bagnold defined an efficiency term as a linear function of the ratio between channel velocity and mean particle diameter. Using fall velocity as a surrogate for particle diameter, Equation 2 shows the hydraulic parameters controlling sediment transport rates.

$$Q_s \approx \Omega_A = \sum (e_b \cdot \Omega_T) = \sum \left(\gamma \cdot \left(\frac{v}{\omega} \right) \cdot (R \cdot S_f \cdot V \cdot P) \right) \tag{2}$$

Where,

Q_s = sediment load in mass or volume per time;
Ω_A = power expended in sediment transport over a flow event, applied power;
e_b = efficiency coefficient $\approx \left(\frac{v}{\omega} \right)$; and
ω = particle fall velocity in water.

Applied stream power represents a flux of force per time for a single flow event. The sediment load is also a flux, but of mass (or volume) per time. Geomorphic change occurs due to net transfer of material, yield, from a channel boundary. SIAM applies the stream power to a reach control volume. Application of the duration of an event to the stream power over the reach length results in work done on the channel boundary. Equation 3 applies the stream power over the longitudinal length of a channel for the duration of a flow event to derive an applied work term, Π_A.

$$Y_s \approx \Pi_A = \sum \left(\Omega_A \cdot t \cdot X \right) \tag{3}$$

Where,

Y_s = sediment yield;
Π_A = applied work;
t = duration of a flow event; and
X = longitudinal length of the channel.

Applied energy provides a measure of the resistance to adjustment due to changes in sediment load. Reaches requiring large changes in the amount of work required for altering sediment yields will respond more than a reach requiring small changes. The responsiveness is defined by the slope of the work versus yield curve, Equation 4.

$$\Psi = \frac{d}{dY_s} \Pi_A = \frac{d}{d\sum \left(Q_s \cdot t \right)} \sum \left(\Omega_A \cdot t \cdot X \right) \approx \frac{d}{dQ_s} \sum \left(\Omega_A \cdot X \right) \tag{4}$$

Where Ψ = response parameter.

Responsiveness measures the change in sediment transport capacity with a change in applied stream power, which represents the inverse of the slope of the sediment transport rating curve as a function of stream power. Half of imbalance moves upstream of the pivot point and half of the imbalance moves downstream. The stress from the imbalance on each side of the pivot point must be evenly distributed to maintain equilibrium. The imbalanced reach adjusts to accommodate some of the imbalance. The effect appears as a shift in the pivot point. The location of the pivot point depends on the ratio of responsiveness of the surrounding reaches. Estimates of the pivot point location neglect the internal responsiveness of the pivoting reach and bias the position towards predicting lower amounts of response in reaches relatively shorter than other reaches in the network. **Figure 3** shows an example of pivot movement and the impact on the network balance.

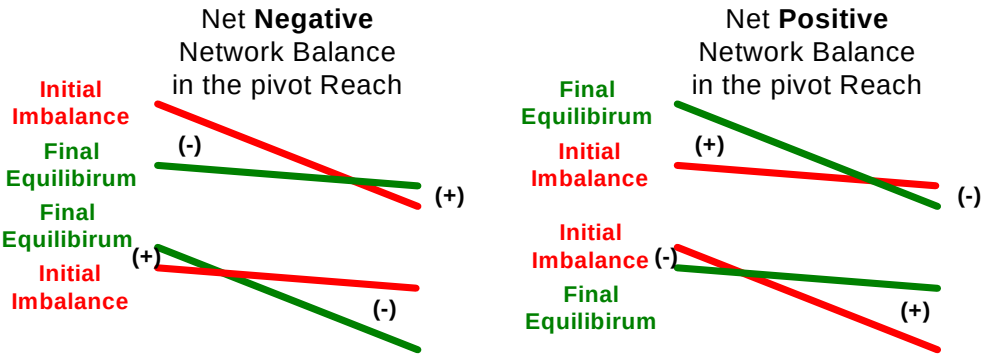


Figure 3 Pivot Reach Absorption of Network Balance Effects.

VALIDATION AND APPLICATION

Hickahala Creek, Mississippi, Demonstration Basin: Historic agricultural practices in the Hickahala Creek Basin (230 mi^2) in North Central Mississippi increased sediment yields and exacerbated flooding. Channelization in the 1960's initiated incision and widening and continued deposition in the lower reaches. A rehabilitation plan implemented grade control, bank stabilization, drop pipes, land treatment, and detention ponds. These actions stabilized the watershed and halted the downstream deposition. Geomorphic studies, numerical simulations, and

rehabilitation plans performed by Simons, Li and Associates, SLA, (1987a, b, and c) identified sediment sources and hydraulics in the Hickahala Basin as well as locations of geologic controls and the sediment budget. Channel boundaries consist of bedrock, erodible cohesive clays, silts, sands, and fine gravel. Armoring was not found to be significant. A SIAM model was developed for the Hickahala Basin consisting of 84 reaches spanning 15 tributaries nested to a 4th order for the purpose of validating the computational techniques.

Local Accounting on Hickahala Creek: The SLA investigations integrated field observations, sediment transport, and numerical modeling to classify reaches as under capacity (aggrading, positive local balance) or over capacity (degrading, negative local balance). SIAM results agreed in 25 cases and disagreed in 5 cases. The SIAM model broke the reaches into smaller lengths. Subsuming reaches to the SLA designation reconciled 1 case and inclusion of additional tributaries accounted for 3 cases. Sufficient information on SLA input was not available to determine the discrepancy in the last case.

Applied Energy Relationships on Hickahala Creek: Modeled reaches in the Hickahala Basin represent cohesive and sand bed channels with small gravel in a range of stages of adjustment processes. The channel evolution model of Schumm, Harvey, and Watson (1984) lists five stages of adjustment including initial imbalance, incision, widening, deposition, and equilibrium. The hypothetical regime was developed by adjusting flow-duration subject to passing an equivalent volume. The hypothetical regime curve was compared to the computed existing work and yield estimates. **Figure 4** shows example comparisons with yield in tonnes per year on the vertical axis and applied work in N-m on the horizontal axis.

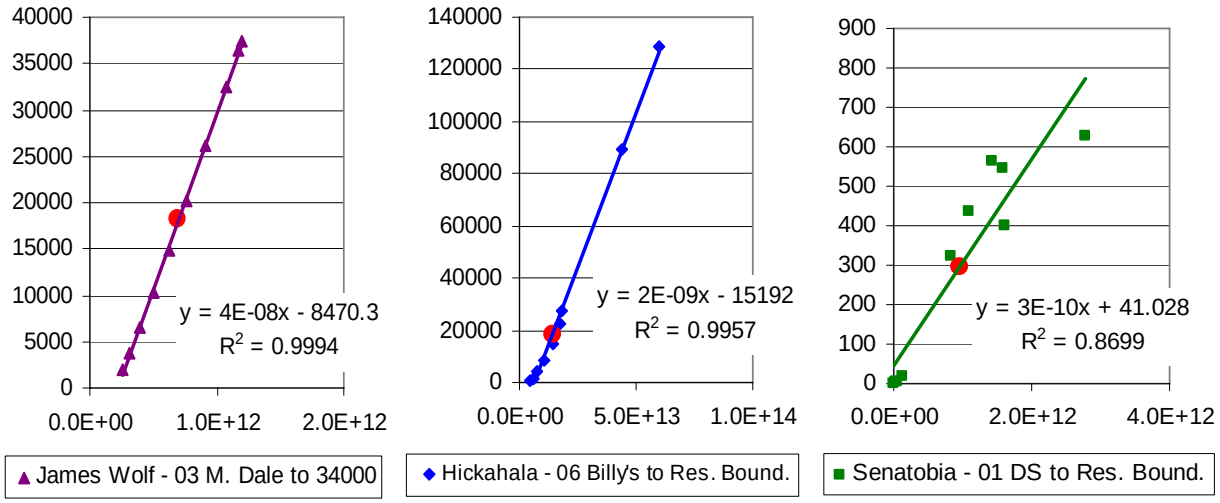


Figure 4 Example Existing and Hypothetical Regime Work Comparison.

R^2 values averaged 0.95 with a standard deviation of the residuals averaging 14% when normalized to the existing regime yield. The loosest fits occur in areas controlled by backwater from the reservoir at the basin outlet. Fits outside of the reservoir resulted in R^2 values around 0.99 and standard deviations on the residuals of 12 percent. Statistics on the difference between the existing computed sediment yields compared to the hypothetical regime relationship showed 93 percent of the data within 2 percent of the prediction curve. The spread of channel evolution stages validates applied work for predicting sediment yield from reaches based on discharge conditions for channels in a variety of adjustment phases. Hickahala creek represents a rainfall driven system with flashy floods and long periods of lower flows. For snow melt driven basins with rain on snow events, the fewer unsteady and transient sediment impacts might improve the correlation. However, the shift to coarser material is subject to all the additional uncertainties in gravel and cobble transport relationships and represents a shortcoming in the ability to predict sediment movement.

Channel geometry changes applied work through the hydraulic radius, wetted perimeter, and friction slope. Velocity is dependent. Two of the three parameters operate independently while the cross section shape (rectangular, trapezoidal, ovoid, and irregular, etc) fixes the third. Either a designer selects a channel shape or the

shape forms though interaction with the bed and bank material. Either case is external. Slope and perimeter were selected for comparison. The geomorphic evaluation of Hickahala provided partial hydraulics for the 1968 channelization plan under the 2 year recurrence discharge. Comparing yield to the hypothetical regime curve provided comparisons for adjustments to channel geometry. Normal depth and rectangular geometries were assumed. The duration was assumed equal to the time required to pass the entire annual volume. Only reaches outside of the reservoir boundary were included resulting in 11 test cases due to the inability to completely determine hydraulics under backwater influence from the given information. **Figure 5** shows some example comparisons with yield in tonnes per year on the vertical axis and applied work in N-m on the horizontal axis.

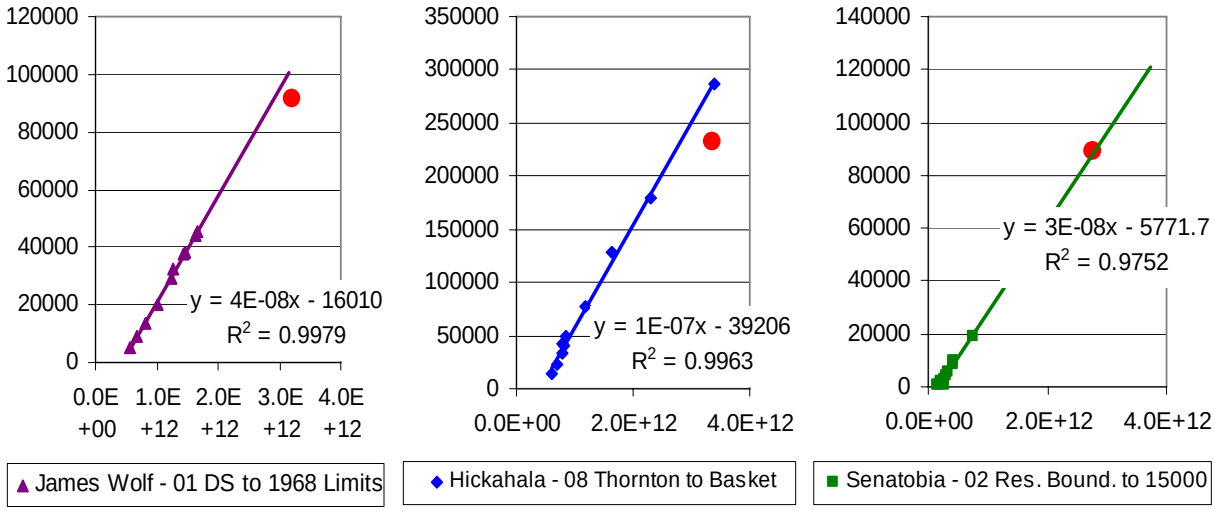


Figure 5 Example Historic Geometry Applied Work versus Hypothetical Regime.

Comparing the channelized work and yield results to the hypothetical regime curve showed an average error of 10 percent with a standard deviation of 100 percent for the errors. The largest error occurs under backwater and invalidates the normal depth assumption. Excluding the largest error reduces the standard deviation to 30 percent. Other inaccuracies include the general assumption of normal depth and the duration estimate using a representative discharge. In several cases, comparing to the 1968 plan required extrapolating the hypothetical regime curve. The order of magnitude agreement was considered adequate to not refute the applied work theory. Due to the limitations of empirical evaluation, universality cannot be demonstrated outside of the range of conditions provided by the Hickahala Creek channelization plans. Repeated surveys throughout channel evolution for a variety of systems would be required for more conclusive empirical confidence in the application to other basins.

Mobile Boundary Example Models **Figure 6** shows an example numerical boundary run with degrading reaches and a comparison to network balances. Comparison of SIAM to mobile boundary numerical simulation used GSTAR 1D. Relative adjustments under mobile boundary modeling were compared to the routed SIAM stresses. The GSTAR 1D model shows greater changes in the shorter sections. SIAM trend results agree with the GSTAR 1D simulation in direction. Magnitudes cannot be directly compared, but relative differences provide a means of understanding. Of the total 4.93 ft adjustment difference on each side of the pivot, the shortest reach (maximum change) comprised 71 percent. In the SIAM simulation, the shortest reach (maximum change) showed a 65 percent difference. The estimate of the pivot point location in SIAM uses the upstream and downstream reaches only and neglects additional weight from adjustment in the pivot reach. Accounting for the shift in the pivot reach would increase the difference and change SIAM results in the direction of the GSTAR 1D simulation.

Cases of GSTAR 1D and SIAM models were compared combining fixed and free boundaries, upstream and downstream shifts of the imbalanced reach, multiple imbalanced reaches of different directions and magnitudes, different grain diameters, and changes in width. Grain sorting and mixing changed the sediment transport rates resulting in geometries generally deviating from SIAM in magnitude, but matching in direction.

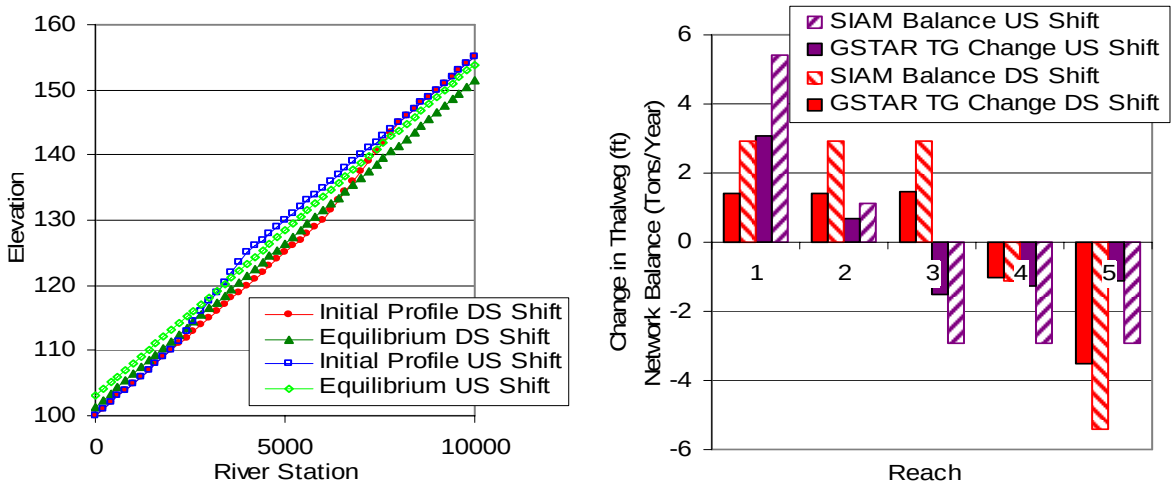


Figure 6 Comparison of SIAM Results to Mobile Boundary Modeling.

Additional SIAM Information on Hickahala Creek: The SIAM model of Hickahala Creek included several results not present in the geomorphic report including a relative breakdown of which sediment features provided the majority of the input to both sediment yield and geomorphic adjustment. For the purpose of identifying total sediment yield, wash load comprised the bulk of the material passing the outlet. **Figure 7** shows an example breakdown of the wash load.

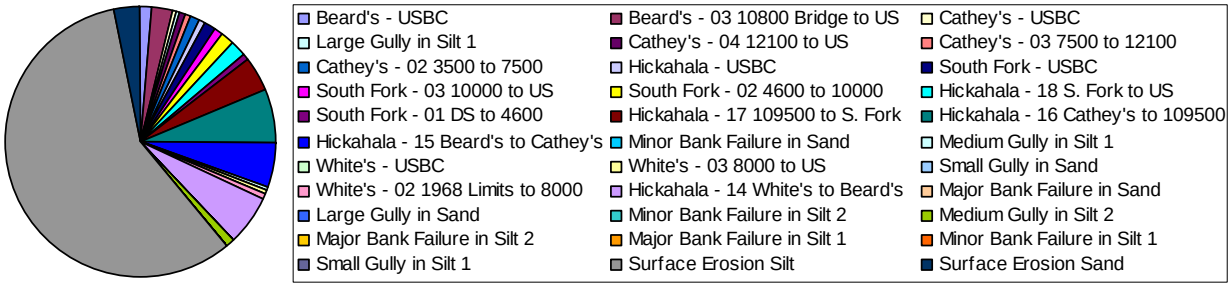


Figure 7 Wash Load Composition Entering Hickahala Creek at the Reservoir Boundary.

Wash material primarily originates from surface erosion in silty material. Secondary contributions include erosion of cohesive material in the upper reaches of the basin. Halting upstream degradation would reduce the wash load 21 percent. For the same reach, the most significant sources of channel material occurred through bank erosion in sandy material with 85 percent occurring in major sites and 14 percent occurring in minor sites. The results would suggest bank protection to reduce long term deposition in the reservoir.

DISCUSSION

A sediment continuity analysis compares the supply and transport capacity on a reach by reach basis. The wash load and local balance routines in the SIAM model improves upon the methodology by considering transport mode in linking reaches. Dividing sediment movement into wash and bed material transport modes differentiates between short-term yield effects and long-term geomorphic change. Targeting wash load can result in solutions with immediate improvements. Efforts impacting the structural component require longer time frames. Transitions between wash and channel reservoirs may isolate portions of the watershed from impacting goals at the outlet. In some cases a structural problem (aggradation or degradation) may result from transitioning material. Identifying transition material linkages can suggest immediately realizable benefits. The additional amount of effort in applying SIAM over a sediment continuity analysis is the specification of a wash load threshold.

The applied energy methods in SIAM provide a means of estimating the impact on sediment transport to changes in the hydraulic conditions including geometry, slope, discharge, and duration. The hypothetical regime curve provides a means of estimating how adjustments to the governing parameters can change yield. Alternately, a target yield can be obtained by adjusting the parameters to achieve the desired outcome. SIAM provides an estimate for a starting point. A mobile boundary numerical or physical model can verify and fine tune the procedure.

Applied energy also provides a means to route the impact of changes in one portion of the network to other reaches. Comparison in uniform grain sizes showed close agreement. The lack of an exact pivoting point location introduces error, but none of the hypothetical test cases found differences large enough to impact the direction of change. An exact evaluation requires a mobile boundary model. Comparisons of SIAM to GSTAR 1D under conditions of grain sorting showed larger deviations in the relative magnitude than the uniform gradation but generally agreed on direction. SIAM grain sorting requires interpretation of the results beyond the scope of this paper.

Advantages of the SIAM model include ease of setup and operation. Hydraulics and sediment transport are developed outside of the computational framework and may use a diverse array of techniques including regime relationships, regional hydrology, or other simplifications to fill in sparse data sets. Quality of the results is subject to the accuracy of the input. Time step and section spacing are present in SIAM computations. SIAM will always return a result, but quality depends on the appropriateness of the model. Numerical simulations for the simple 5 reach, 50 cross section comparisons took on average 1 hour. The Hickahala Creek model ran in 1 minute on a 1.6 GHz processor. An equivalent model within GSTAR 1D might take 1 or more days. The quick results allow consideration of multiple scenarios. When using sparse data sets, multiple scenarios can identify the sensitivity. SIAM returns less information on final channel geometry than a mobile boundary model. SIAM reports magnitude and direction of trends while a mobile boundary model reports states. Ultimate conditions remain unknown in SIAM. SIAM will not result in a final water surface profile and does not output the results from grain sorting. In a numerical model, the connection between sediment sources and impact becomes obscured. SIAM tracks the linkages in both wash and channel material load resulting in targeted recommendations for rehabilitation.

CONCLUSIONS

The SIAM model contributes to stream assessment and rehabilitation by facilitating the integration of sediment continuity. Considering sediment balances reduce the likelihood of system scour or deposition shortening the useful life of a project. By locating potential instabilities, detailed field investigative efforts can target the most crucial areas. Source tracking allows planners to focus mitigation efforts to the areas causing the most problems. In considering the transition from wash material to bed material load, immediate benefits may be realized through grain size specific design practices. The simplified formulation of continuity reduces some of the difficulties and data requirements present in numerical modeling efforts at a cost of less information. Future work on the SIAM model includes improvements to incorporate grain sorting and application to more systems including the Sacramento River, CA, Methow Basin, WA, and Rio Grande River, NM.

REFERENCES

Bagnold, R.A. (1966). An Approach to the Sediment Transport Problem from General Physics. U.S. Geological Survey Professional Paper 422-J.

Schumm, S.A., Harvey, M.D. and Watson, C.C. (1984). Incised Channel: Morphology, Dynamics and Control. Water Resources Publications, Littleton, Colorado, 200pp.

Parthenaides, E. (1977). "Unified View of Wash Load and Bed Material Load," Journal of the Hydraulics Division, Proceedings of the American Society of Civil Engineers, 103(9):1037-1057.

Yang, C.T. (1973). "Incipient Modtion and Sediment Transport," J. of the Hydraulics Division, ASCE 98:1679-1704.

Simons, Li & Associates, Inc. (1987a). Preliminary Field Data Collection and Sediment Continuity Analysis for the Hickahala/Senatobia Creek Watershed Yazoo River Basin Tate, Panola, and Marshall Counties, Mississippi. Report to the Army Corps of Engineers, Vicksburg, MS. February.

Simons, Li & Associates, Inc. (1987b). Detailed Field Data Collection and Sediment Continuity Analysis for the Hickahala/Senatobia Creek Watershed Yazoo River Basin Tate, Panola, and Marshall Counties, Mississippi. Report to the Army Corps of Engineers, Vicksburg, MS. May.

Simons, Li & Associates, Inc. (1987c). Final Report Quantitative Analysis of Baseline Conditions for the Hickahala/Senatobia Creek Watershed Yazoo River Basin Tate, Panola, and Marshall Counties, Mississippi. Report to the Army Corps of Engineers, Vicksburg, MS, October.

DESIGN OF A LOW FLOW CHANNEL FOR SALT RIVER RESTORATION

Dennis L. Richards, Vice President, WEST Consultants, Inc., Tempe, AZ 85284, drichards@westconsultants.com; Glenn Mashburn, Hydraulic Engineer, U.S. Army Corps of Engineers, Los Angeles, CA 90053, Glenn.M.Mashburn@spl01.usace.army.mil

Abstract: The U.S. Army Corps of Engineers, the City of Phoenix, and the Flood Control District of Maricopa County have been partnering in the planning, design, and construction of a habitat restoration project along the Salt River in Phoenix, Arizona. The project, known as the Phoenix Rio Salado Habitat Restoration Project, encompasses a 5.5 mile reach of the Salt River and is located approximately 1-mile south of downtown Phoenix. The initial design feature was the design of a low flow channel to convey a design discharge of 12,200 cfs without significant scour or deposition. The low flow channel was designed to maintain the flood carrying capacity of the Salt River throughout the project reach by balancing the loss of capacity from the introduction of plants and trees within the river, with additional capacity created by channel excavation.

The low flow channel design consisted of initially establishing the channel slope, channel geometry, and proposed grade-control structures locations by utilizing stable channel analysis. The stable channel slope was estimated using several analysis methods, and the initial channel cross-section geometry was determined using velocity constraints and normal depth methods. Sediment transport modeling was then performed to refine the channel geometry and determine the optimum location for grade control. The low flow channel analysis also included the design of guide dike structures to help maintain the low flow channel alignment and minimize formation of channels in the overbank areas.

Construction of the low flow channel and the associated hydraulic structures was completed in early 2001. Flows within the Rio Salado exceeded the 12,200 cfs low flow channel design discharge for extended periods in early 2005. This paper will present the approach utilized in the design of the low flow channel and discuss the performance of the low flow channel and associated features.

INTRODUCTION

The U.S. Army Corps of Engineers, the City of Phoenix, and the Flood Control District of Maricopa County have been partnering in the planning, design, and construction of a habitat restoration project along the Salt River in Phoenix, Arizona. The project, known as the Phoenix Rio Salado Habitat Restoration Project, encompasses a 5.5 mile reach of the Salt River which extends from Interstate 10 (I-10) to 19th Avenue. The project is located within the banks of the Salt River plus a 50-foot wide area at the top of each bank. **Figure 1** shows the Phoenix Rio Salado Habitat Restoration Project reach.

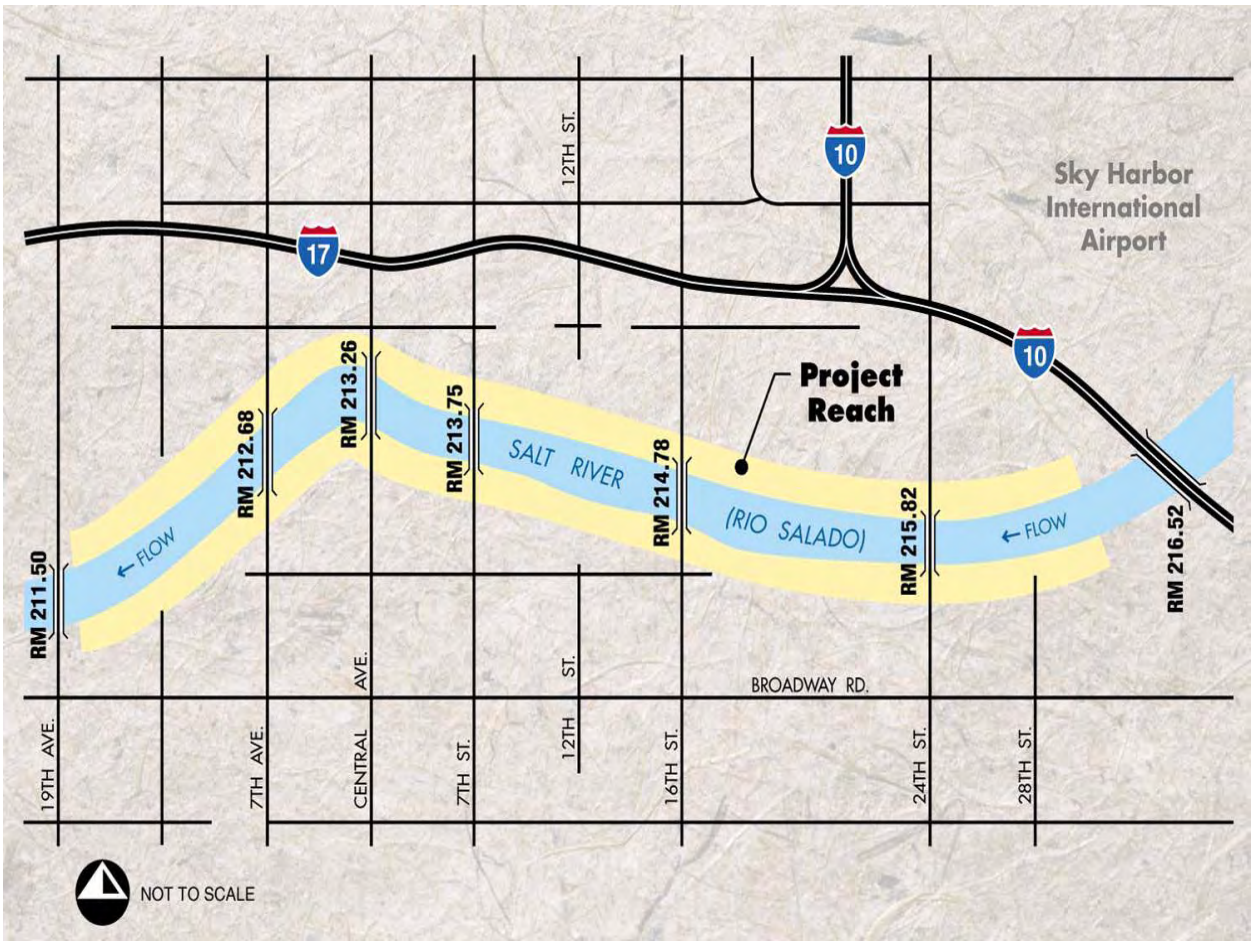


Figure 1 Phoenix Rio Salado habitat restoration project reach.

Key features of this restoration project include:

- A low flow channel constructed in the bottom of the present river, designed to pass the more frequent storm release;
- Wells and a water delivery system to bring water to the trees and other vegetation, wetlands, ponds, and the stream;
- Habitat elements such as riparian tree species, volunteer riparian grasses and shrubs, open water ponds, and a small flowing stream;
- A park located in the overbanks of the low flow channel; and
- A recreational and interpretive trail system.

LOW FLOW CHANNEL DESIGN PROCEDURE

The low flow channel is intended to replicate the low flow channel in a native river. It adds to the flood carrying capacity of the river through the project as well as balances the loss of capacity resulting from the introduction of plants and trees into the channel. There were many constraints on the design of the low flow channel. Because this was a habitat restoration project,

the low flow channel was required to have "soft" sides and bottom. This means that the channel should be earthen instead of being constructed out of concrete or soil cement. To maximize the area available for the park in the overbanks and the trail system, the footprint of the low flow channel was minimized. However, the low flow channel was still large enough to convey a design discharge of 12,200 cfs without significant scour or deposition. The low flow channel was sized to carry all long-term releases from Roosevelt Dam lasting over 30 days, thus preventing drowning of the habitat. Grade control structures were located throughout the low flow channel to minimize scour. In addition, guide dikes were proposed to help preserve the alignment of the low flow channel during flood events that exceeded the capacity of the channel. The construction of the low flow channel was completed in 2001. The invert of the low flow channel is 8 to 12 feet below the pre-project channel invert and the bottom width ranges from 160 feet to 205 feet (WEST 2000). **Figure 2** shows the low flow channel approximately one year after construction was completed.



Figure 2 Low flow channel looking upstream from 7th Avenue.

Design Approach: The low flow channel was initially designed using channel stability methods. First, the channel slope of the existing low flow channel was determined. Then, several slope stability methods were used to determine a range of stable design slopes and a design stable slope selected for design of the low flow channel. An initial estimate of the geometry of the low flow channel was determined using the normal depth method and the estimate of the stable slope. The U.S. Army Corps of Engineers' HEC-RAS v. 2.2 (1998) was used to confirm the channel capacity of the initial design. This initial design of the low flow channel was then refined using sediment transport modeling techniques. The sediment transport modeling was performed using HEC-6T v. 5.13.05 (Mobile Boundary Hydraulics 1999), which is an enhanced version of the U.S. Army Corps of Engineers' scour and deposition in rivers and reservoirs computer program HEC-6 v. 4.1 (1993).

Stable Channel Analysis: Several methods were used to establish an appropriate stable slope for the low flow channel. The existing channel slope was examined first, and then several slope stability methods were used to bracket an appropriate design slope for the low flow channel. The existing overall channel slope within the project reach was 0.0027. If a channel is in a quasi-equilibrium state, then the existing channel geometry is a good indication of the stable channel conditions. However, there were many factors in the Rio Salado project that suggested that the existing low flow channel was not in a quasi-equilibrium state. These factors include:

- Levee work and channelization both upstream and downstream of the project reach,
- A history of sand and gravel mining throughout the reach, and
- A reduced peak discharge as a result of the recent raising of Roosevelt Dam.

Three different stable slope methods were used: the U.S. Army Corps of Engineers' Engineering Manual (EM) No. 1110-2-1418 (USACE 1994), the Albuquerque Metropolitan Arroyo Flood Control Authority (AMAFCA) *Sediment and Erosion Design Guide* (Resource Consultants 1994), and U.S. Army Corps of Engineers' Hydraulic Design Package for Channels, or SAM (Thomas et al. 1995). Stable slopes resulting from the various methods are shown in **Table 1**.

Table 1 Results from stable slope analysis.

Stable Slope Method	Stable Slope
Existing Conditions	0.0027
EM-1418	0.0010
AMAFCA	0.0033
SAM	0.0087

Initial Channel Design: A design slope of 0.0025 was selected for the low flow channel. In order to determine the initial geometry of the low flow channel, the normal depth method was used subject to velocity constraints and the capacity of the channel was verified using HEC-RAS v. 2.2 (1998). In order to maintain the stable design slope, several grade control structures were proposed. The elevation drop at each grade control structure was limited to 3 feet in order to prevent the formation of dangerous hydraulic rollers.

The low flow channel was broken into two portions: an upstream reach and a downstream reach. The initial design for the upstream portion of the low flow channel had a channel bottom of 165 feet, a depth of at least 8 feet, side slopes of 3H:1V, and a channel slope of 0.0025. The initial design for the downstream portion of the low flow channel had a channel bottom of 205 feet, a depth of at least 8 feet, side slopes of 3H:1V, and a channel slope of 0.00125. The channel slope was reduced in the downstream reach of the low flow channel to complete the transition to the existing channel near 19th Avenue. The alignment of the low flow channel closely followed the existing channel thalweg. In addition, the proposed low flow channel maintained a similar sinuosity to the existing low flow channel. Total sinuosity for the existing low flow channel was 1.06 while the total sinuosity for the proposed low flow channel was 1.07.

Sediment Transport Modeling: Twenty-two long-term sediment transport simulations were completed using HEC-6T v. 5.13.05 (Mobile Boundary Hydraulics 1999) to refine the initial low flow channel design. The simulation results were also used to evaluate the grade control locations, determine over-excavation depths, determine annual maintenance requirements, and estimate the effects of the 25-year, 50-year, and 100-year discharge events.

FINAL LOW FLOW CHANNEL DESIGN

Channel Configuration: The final design of the low flow channel was very similar to the initial design. The appropriate geometric parameters of the proposed low flow channel are shown in Table 2.

Table 2 Final geometric parameters for low flow channel design.

Reach	Channel Slope	Bottom Width (ft)	Side Slopes	Channel Depth (ft)
Upstream Reach	0.0025	160	3H:1V to 4H:1V	> 8
Downstream Reach	0.0015	205	3H:1V to 4H:1V	> 8

Grade Control Structures: In order to maintain the stable design slope, grade control structures were needed along the low flow channel. The sediment transport simulations were used to determine the optimal number of grade control structures. The analysis suggests that four grade control structures were needed in addition to the grade control structure upstream of the project reach (downstream of I-10) and immediately downstream of the project reach (downstream of 19th Avenue). The grade control structures were designed for the 100-year flood event of 166,000 cfs and were located:

- At the upstream limit of the Rio Salado project,
- Immediately downstream of the 24th Street Bridge,
- Downstream of the 16th Street Bridge, and
- Immediately downstream of the Central Avenue Bridge.

The grade control structures located near bridges also provide scour protection for the bridges. The toe down depth for the grade-control structures is 27 feet. To help prevent the formation of hydraulic rollers, RCC aprons with steps 3 feet in height were constructed. The grade control structure at the 24th Street Bridge can be seen in **Figure 3**.

Guide Dike Structures: Guide dikes were incorporated into the project to help maintain the alignment of the low flow channel, protect the main channel banks from erosion, and reduce damage in the overbank areas. The dikes also help to prevent the development of secondary low flow channels in the overbanks. This was accomplished by directing flow toward the low flow channel during the period of receding flood flows, which help preserve the location of the original meander geometry and location of the low flow channel. Like the grade control structures, the guide dikes were designed to withstand a 100-year flood event (166,000 cfs).

There are 36 guide dike structures along the 5.5 mile Rio Salado project reach. The guide dikes extend from the banks of the low flow channel to the banks of the main Salt River channel. The guide dikes were constructed entirely of RCC.



Figure 3 Grade control structure at the 24th Street Bridge.

Bridge Scour Countermeasures: Of the five major bridges that cross the Salt River within the Rio Salado project reach, two of these bridges (the 24th Street Bridge and the Central Avenue Bridge) were found to be scour vulnerable with the construction of the low flow channel. Various hydraulic and structural scour countermeasures were evaluated for these two bridges. The selected scour countermeasure for both bridges was to construct an RCC apron within and immediately adjacent to the low flow channel. The RCC aprons protect the piers located within the low flow channel plus one pier on each overbank area. The RCC apron for the 24th Street Bridge can be seen in **Figure 3**.

PERFORMANCE DURING THE 2005 FLOOD EVENT

The winter of 2004/2005 was unusually wet in Arizona. The Granite Reef Diversion Dam released water into the Salt River and the first flows of the season at Priest Drive were recorded on December 31, 2004. Within the next few days, discharges as high as 20,000 cfs were recorded at the gage. Except for brief pauses, the river flowed continuously until early March. For a six day period from February 12 to February 18, 2005, the discharge exceeded the design discharge of 12,200 cfs. The highest recorded flows were on February 13, 2005, when the flow did not go below 20,000 cfs and a peak flow of 28,034 cfs was reached. **Figure 4** shows the maximum recorded daily flows from January 2005 through March 2005 at the Priest Road gage. **Figure 5** illustrates flow in the low flow channel during the February 2005 flow event. The low

flow channel performed very well with minor erosion of the "soft" banks occurring at a few locations, but no major failure of the banks.

Following the event, there was no noticeable scour of the channel bed with the exception of local scour immediately downstream of the grade-control structures. The guide dikes performed exceptionally well in maintaining the alignment of the low flow channel. In a few locations, erosion of the low flow channel bank exposed the end of the guide dike, but lateral movement of the low flow channel was minimized. **Figure 6** shows the exposed guide dike following the February 2005 event. In summary, the Rio Salado low flow channel effectively conveyed flow releases in excess of the flow releases for which the channel was designed.

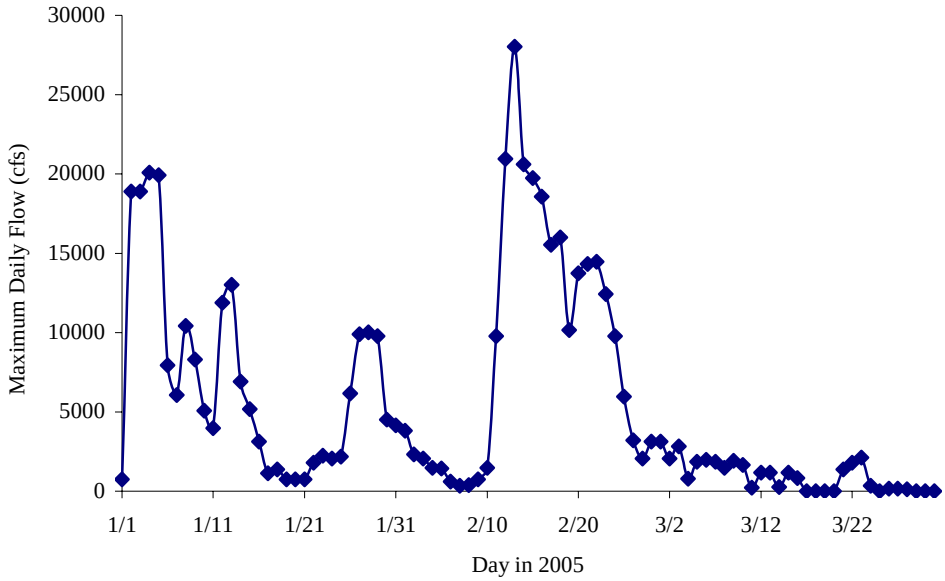


Figure 4 Maximum daily flows at the Priest Road gage.

REFERENCES

HEC-6 v. 4.1. (1993). Scour and Deposition in Rivers and Reservoirs. Hydrologic Engineering Center.

HEC-RAS v. 2.2. (1998). River Analysis System. Hydrologic Engineering Center.

Mobile Boundary Hydraulics. (1999). HEC-6T v. 5.13.05 Sedimentation in Stream Networks.

Resource Consultants and Engineers, Inc. (1994). AMAFCA Sediment and Erosion Design Guide. RCE Ref. No. 90.5560.

Thomas, W.A., Copeland, R.R., Raphelt, N.K., and McComas, D.N. (1995). Hydraulic Design Package for Channels (SAM). Waterways Experiment Station.

WEST Consultants, Inc. (2000). "Low Flow Channel Design Analysis for Rio Salado (Salt River), Arizona." Tempe, AZ.



Figure 5 February 2005 flow at a grade control structure.



Figure 6 Exposed guide dike following the February 2005 event.

JUDY'S BRANCH, ILLINOIS REHABILITATION PLAN

Chester C. Watson, Professor, Colorado State University, Engineering Research Center, Fort Collins, CO 80523, cwatson@engr.colostate.edu; David S. Biedenharn, Hydraulic Engineer, USACE, Engineer Research Development Center, Vicksburg, MS 39180, David.S.Biedenharn@erdc.usace.army; Moosub Eom, Hydraulic Engineer, CDM, Denver, CO 80202, eomm@cdm.com

Abstract: Judy's Branch is a tributary to Cahokia Canal, which is located near Glen Carbon, Illinois, (Madison County) and across the Mississippi River from St. Louis, Missouri. Cahokia Canal drains into Horseshoe Lake through an overflow feature at Horseshoe Lake State Park. The Judy's Branch watershed area is 8.64 sq mi and the total stream length of the project encompasses approximately 14.5 mi. The East St. Louis and Vicinity, Illinois Flood Protection Project was authorized through Congressional actions in 1965 and in 1974. The project authorization was again modified by the Water Resources Development Act of 2000. Section 304 of this Act states: *"The project for flood protection, East Saint Louis and vicinity, Illinois (East Side levee and sanitary district) authorized by section 204 of the Flood Control Act of 1965 (79 Stat. 1082), is modified to include ecosystem restoration as a project purpose*." The principal goal of the presently authorized project is to identify potential improvements that will enhance habitat quality and sustainability while also providing incidental ecosystem services, such as flood-damage reduction. This paper summarizes a report that provides a stream-rehabilitation plan for Judy's Branch to address goals of sediment reduction, stream stability improvement, and use as a demonstration and teaching vehicle by agencies and other interested parties.

INTRODUCTION

Judy's Branch is a tributary to Cahokia Canal, which is located near Glen Carbon, Illinois, (Madison County) and across the Mississippi River from St. Louis, Missouri. Cahokia Canal drains into Horseshoe Lake through an overflow feature at Horseshoe Lake State Park. The Judy's Branch watershed area is 8.64 sq mi and the total stream length of the project encompasses approximately 14.5 mi.

In 1801, Samuel Judy (Tschudi) acquired a 100-acre property along the bluff line and was instrumental in establishing the agriculture of the watershed. The history of Judy's Branch takes another step as the railroad and coal mining become established in the early 1880s, when channelization of the stream allowed low gradient routes for railways to climb from the valley to the general level of the Illinois prairie. The former rail routes now provide the right-of-way for bike trails (Cedeck et al. 1992). These early channelizations of Judy's Branch and Judy's Creek, along with the significant quantities of crushed rock used in maintaining the railroads, have significantly influenced the morphology and ecology of the streams. Also, land-use change in the Judy's Branch watershed, from existing rural and agricultural to suburban development, is presently pressuring channel and watershed stability.

This paper provides a stream-rehabilitation plan for Judy's Branch that will address goals of sediment reduction, improve stream stability, and will be used as a demonstration and teaching

vehicle for the U.S. Army Corps of Engineers (USACE), Illinois Department of Natural Resources personnel, and other interested parties. A specific sediment-reduction goal is to reduce sediment yield by 70%.

The original report was authorized under contract with the USACE. Dr. David Biedenharn was the primary technical contact at the USACE Engineer Research and Development Center (ERDC) for this contract. Ms. Deborah Roush was the Project Manager for the Ecosystem Restoration Project for the USACE St. Louis District.

BACKGROUND

The East St. Louis and Vicinity, Illinois Flood Protection Project was authorized through Congressional actions in 1965 and in 1974. The project authorization was again modified by the Water Resources Development Act of 2000. The principal goal of the presently authorized project is to identify potential improvements that will enhance habitat quality and sustainability while also providing incidental ecosystem services, such as flood-damage reduction. Two choices that are included in a range of alternatives for controlling sediment delivery to downstream wetlands are: (1) excavate a large basin to retain sediment, or (2) control the sediment sources upstream. A large sediment basin would require continuing maintenance to excavate the accumulating sediment and would require a disposal site. Control of the upstream sediment sources provides the opportunity to enhance instream aquatic and riparian habitat, and reduces the dependence on long-term maintenance. In addition, as the watershed urbanizes, larger flood peaks will exacerbate channel instability.

AVAILABLE DATA

In preparations for the analysis and design of Judy's Branch and related bluff line streams, Federal, State, and local agencies have developed valuable data and related analyses. Several of these studies are briefly reviewed in the following paragraphs.

The Illinois Office of Water Resources (IOWR) conducted a survey of Judy's Branch and tributaries, and provided the initial calibrated HEC-RAS model with roughness coefficients. This HEC-RAS model has served as the basis for the analysis of Judy's Branch. Straub (2004) collected sediment data at three Judy's Branch gages to determine the amount of suspended sediment being delivered from the Route 157 gage (8.33 sq mi) and two subwatersheds (0.23 and 0.40 sq mi) during the period of October 2000 to September 2003. The undeveloped subwatershed drainage area is 0.40 sq mi, and the urban subwatershed drainage area is 0.23 sq mi. The average suspended sediment yield from the two subwatersheds was reported to be 851 tons/sq mi/yr, and the suspended sediment yield at the downstream Route 157 gage was reported to be 2,188 tons/sq mi/yr. Straub (2004) emphasized that sediment yield concentration increases in the downstream, which can be caused by increasing rates of channel erosion and channel failure. He attributed the increase in these sources to greater flow rates caused by urbanization.

Thorne et al. (1997) defined bank erosion as being comprised of detachment, entrainment, and removal of bank material as individual grains, i.e., grain-by-grain removal and transport. He also defined bank failure as the collapse of larger blocks of the bank in mass, generally in response to

geotechnical instability processes. Straub et al. (2006) evaluated the geotechnical bank stability along Judy's Branch, and found three primary scenarios of alluvial bank materials: (1) alluvial clayey silt over glacial till, (2) alluvial clayey silt over glacial till with trees, and (3) alluvial clayey silt over glacial till with a sand lense at the interface between the clayey silt and the glacial till.

Straub et al. (2006) reported that the alluvial soil deposits consist primarily of consolidated medium to soft clayey silts. Glacial till regularly outcrops at the toe of the bank, sometimes extending up to mid-bank. They found that till strength varied depending on the amount of time the material had been exposed, and that the degree of weathering may be assessed by the height of the till on the bank. This suggests that the greater the degree of bank incision, the weaker the toe material (glacial till), which can have severe consequences for bank instability.

Bank failure during the recession limb of large-flow events and following prolonged periods of precipitation has been observed by many. Simon et al. (1999) assessed five reasons for this observation:

1. Partial withdrawal of lateral support and confinement by the receding water level after the event;
2. Increase in driving forces due to the saturation and increase in unit of the bank materials;
3. Infiltration of water reduces negative pore water pressure;
4. Generation of positive pore water pressure; and
5. Erosion of bank toe material that steepens the bank and removes previously failed material.

Providing storm-water detention in the basin can reduce the magnitude of the peak flow for a given precipitation event, and can reduce the rate of change of the falling limb of the hydrograph. Both of these result in greater bank stability.

Geotechnical modeling by Straub et al. (2006) indicated that saturated bank materials for bank heights in excess of 10 to 12 ft and at bank angle in excess of 60 to 70 degrees may be unstable. Numerous assumptions must be made in any attempt at estimating bank characteristics over a watershed. However, these computations together with field observations indicate that banks in excess of 10 to 12 ft are likely to be susceptible to geotechnical failure as the degree of saturation increases and as the bank angle approaches 60 to 70 degrees, which may be caused by toe scour. Figure 1 shows bank angle and bank heights for survey cross sections on Judy's Branch. Bank angles and heights for locations greater that 70 degrees and 12 ft, respectively, are shown in the box. The lack of a significant number of cross sections that exceed 12 ft in height and a bank angle of 70 degrees suggests that these characteristics describe a bank failure threshold condition.

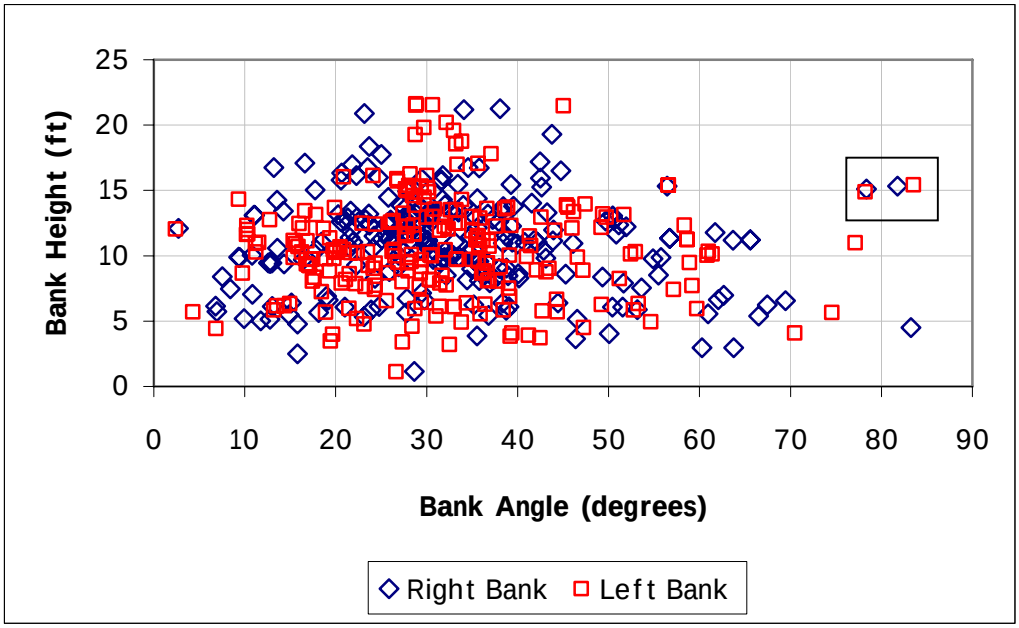


Figure 1 Bank angle and bank heights for surveyed cross sections along Judy's Branch. Only two cross sections (in box) exceed Straub et al. (2006) criteria for instability, which may indicate that most of the banks that exceed their criteria have already failed.

DESIGN PROCEDURES

Together with the original HEC-RAS provided by IOWR, several computer models were used in this design and analysis:

- HEC-RAS (Hydrologic Engineering Center - River Analysis System),
- HEC-HMS (Hydrologic Modeling System), and
- SIAM (Sediment Impact Analysis Model).

HEC-RAS was used to perform steady flow and unsteady flow calculations to estimate reduced discharge caused by planned dry sediment detention basins and to calculate hydraulic parameters. HEC-HMS was used to obtain the flow hydrographs used as the boundary conditions of the HEC-RAS unsteady flow analysis. SIAM is a newly developed program created at Colorado State University (CSU) in cooperation with ERDC that has been incorporated into RAS by HEC, and a version is expected to be available during the coming year. The SIAM model synthesizes quantitative geomorphic information for a watershed, including locations, magnitudes, and composition of watershed sediment sources; magnitudes and durations of discharges comprising the hydrologic regime; hydraulic performance of the stream network; and sediment transport characteristics of the channels. Model output provides sediment budgets, balances, and energy-transport relationships on a reach basis (Mooney 2003). Therefore, SIAM can be used to determine whether the reach will aggrade or degrade, and to predict the sediment yield in each reach.

The SIAM model represents a watershed as a series of linked sediment reaches dividing a channel network into segments at significant changes in bed composition, hydrology, hydraulics, sediment transport, or sediment sources. Sections upstream and downstream of a tributary junction must belong to separate reaches. The selection of sediment reaches determines the resolution of the model. Longer reach lengths can smooth small imbalances while shorter reach lengths amplify local effects. The network of the Judy's Branch model consists of 48 sediment reaches with a maximum of three levels of tributaries. Sediment reaches were created at tributary junctions and at points of significant change in hydrology.

In each SIAM sediment reach, the program keeps track of all the component sources to and transport from the sediment reach. A critical data set from the SIAM model is the *local sediment balance* for each reach, which is the sum of the wash material sediment supply plus the bed material sediment supply, minus the wash load and bed material load transported out of the reach. The wash material size is defined by the user based on field data as the D_{10} of the sediment found on the bed, and bed material is defined as sediment larger than the wash material.

If the local sediment balance for a reach equals zero, the reach is in balance and the reach has reached continuity. A negative local balance means the reach is degrading and a positive local balance means the reach is aggrading. For Judy's Branch, our goals are to achieve a zero local balance for each sediment reach and to reduce sediment yield.

The design procedure used in this rehabilitation design is as follows:

Step 1: Estimate the discharge from each potential site of dry sediment detention basins, using the unsteady flow analysis of HEC-RAS.
Step 2: Establish the flow-duration records including 50- and 100-yr discharges using the data measured at Route 157 gaging station and HEC-WMS.
Step 3: Estimate the sediment yield from the watershed using the sediment concentration data measured at Route 157 gaging station.
Step 4: Estimate the local sediment sources for the SIAM model input from the surface erosion and bank erosion data.
Step 5: Calibrate the local sediment sources using the estimated sediment yield (Step 3).
Step 6: Set a goal for the local sediment sources for each scenario.
Step 7: Design the drop structures and check if the local balance of each reach is within an acceptable tolerance after running the SIAM model.
Step 8: If the local balances of some sediment reaches are out of tolerance range, adjust the design of the drop structures of those reaches, and repeat Step 7 until the acceptable result is obtained.

Grade Control Design: Perhaps the simplest form of a grade control structure consists of dumping rock across the channel to form a hard point. These structures are often referred to as rock sills or bed sills. These types of structures are generally most effective in small-stream applications and where the drop heights are generally less than about 2 to 3 ft. A series of rock sills, each creating a head loss of about 2 ft, was used successfully on the Gering Drain in Nebraska (Stufft 1965). Whitaker and Jäggi (1986) report on design concepts for stabilizing the streambed with a series of rock sills. Abt and Johnson (1991), Newberry and Gaboury (1993),

Robinson et al. (1998), and EM 1110-2-1601 (USACE 1994 revisions on 1991 version) provide guidance for sizing stone for these structures.

Among many kinds of drop structures, the drop structures referred to as *Newbury riffles* (Newbury and Gaboury 1993) were modified and chosen for this design. The structures proposed for Judy's Branch were designed using the following criteria:

1. The crest stone is to be constructed of quarry stone (approximately 3 ft x 3 ft x 2 ft) with the approximate center of the structure at the crest elevation specified. The remainder of the crest stone should be constructed to form a shallow V-shape with 0.5 to 1.0 ft of relief. The bed for the crest should be excavated to firm material.
2. The crest should be keyed into both banks using a riprap-filled trench, which extends to the greater of the top bank elevation or the 2-yr flood. A desirable slope for the key trench is 1 vertical on 3 horizontal. A gravel blanket should be placed in the key trench and over the riprap if sandy material or piping of groundwater is observed.
3. Upstream and downstream of the crest is filled using riprap sized in accordance with EM 1110-2-1601 (USACE 1994 revisions on 1991 version). Upstream slope is 1 on 4, and downstream slope is 1 on 20.
4. Spacing of structures along the stream was based on an approximate height of 3 ft for each structure, spaced to provide the downstream crest elevation at or above the toe of the downstream face of the upstream structure.

Drop structures can be used to stabilize the channel and to reduce the bank erosion by decreasing the bank elevation. Therefore, grade control was planned for all of the reaches except tributaries in this design.

RESULTS

These initial four scenarios were analyzed:

1. Scenario with Existing Condition

2. Scenario with 21 Sediment Basins

3. Scenario with Sediment Basins and Vegetative Buffer Strips (VBS)

4. Scenario with Sediment Basins, VBS, and Drop Structures

At public meetings in Collinsville and Carbondale, Illinois, on 4 August 2004, the results of analyses of four initial scenarios were presented. These discussions lead to two additional scenarios that were analyzed. The discussion at those meetings included the consideration of the relatively rapid change in land use from agricultural to residential use. In addition, in previous field investigations the use of storm-water detention basins in the developing residential subdivisions had been noted. Therefore, two scenarios were developed that eliminated all or most of the Natural Resources Conservation Service (NRCS) proposed sediment basins:

5. Scenario with Drop Structures, No Sediment Basins, and No VBS

6. Scenario with Drop Structures, 6 Sediment Basins, and No VBS

Analyses indicated that in Scenario 6, channel stability was achieved with a balance of sediment supply and sediment transport, and that the sediment yield at the Route 157 gaging station is about 31% of the estimated sediment yield of 27,000 tons/yr, a reduction of an average of 69%.

REFERENCES

Abt, S.R., and Johnson, T.L. (1991). "Riprap design for overtopping flow," Journal of Hydraulic Engineering, ASCE, 117(8), pp 959-972.

Cedeck, M.J., Foster, J., Harris, L., Raffaelle, J., Smith, J.M., Wiechman, E., and Williams, J. (1992). A History of Glen Carbon. Published by Glen Carbon Centennial Inc.

Mooney, D. (2003). "SIAM Manual," Prepared for the USACE, Vicksburg, MS, by Colorado State University, Fort Collins, CO.

Newbury, R.W., and Gaboury, M.N. (1993). Stream Analysis and Fish Habitat Design. Newbury Hydraulics Ltd. (co-publisher, Manitoba Natural Resources), Gibsons, British Columbia, Canada.

Robinson, K.M., Kadavy, K.C., and Rice, C.E. (1998). "Rock chutes on slopes between 2 and 40 percent," Proc. 1998 ASAE Annual International Meeting.

Straub, T.D., Johnson, G.P., Roseboom, D.P., and Sierra, C.R. (2006). "Suspended-Sediment Yields and Stream-Channel Processes on Judy's Branch Watershed in the St. Louis Metro East Region in Illinois," Scientific Investigation Report 06-5016, U.S. Department of Interior, U.S. Geological Survey, Urbana, IL.

Simon, A., Curini, A., Darby, S.E., and Langendoen, E.J. (1999). "Streambank mechanics and the role of bank and near-bank processes in incised channels," in Incised River Channels, Processes, Forms, Engineering and Management, S.E. Darby and A. Simon (Eds.), John Wiley & Sons Ltd., Chichester, England, pp 123-152.

Straub, T.D. (2004). "St. Louis Metro East Region sediment and geomorphic study," Paper, U.S. Geological Survey, Urbana, IL, 12 pp.

Stufft, W.A. (1965). "Erosion control for Gering Valley," Proc. ASCE, Hydraulics Division Conference, Tucson, AZ.

Thorne, C.R., Hey, R.D., and Newson, M.D. (1997). Applied Fluvial Geomorphology for River Engineering and Management. John Wiley and Sons, Chichester, England.

USACE (1994). Hydraulic Design of Flood Control Channels, Engineering Manual 1110-2-1601, U.S. Government Printing Office, Washington, DC (updated 1991 version).

Whittaker, J., and Jäggi, M. (1986). "Blockschwellen." Mitteilungen der Versuchsanstalt fur Wasserbau, Hydrologie und Glaziologie, Nr. 91, an der Eidgenossischen Technischen Hochschule Zurich.

EVALUATING SEDIMENT SOURCES, EROSION, AND TRANSPORT PROCESSES IN THE UPPER YUBA RIVER WATERSHED, CALIFORNIA

Jennifer A. Curtis, Geologist, U.S. Geological Survey, Sacramento, CA, jacurtis@usgs.gov; Lorraine E. Flint, Hydrologist, U.S. Geological Survey, Sacramento, CA, lflint@usgs.gov; Charles N. Alpers, Chemist, U.S. Geological Survey, Sacramento, CA, cnalpers@usgs.gov; Scott A. Wright, Hydrologist, U.S. Geological Survey, Flagstaff, AZ, sawright@usgs.gov

Abstract: In this study a conceptual model of sediment sources, erosion, and transport processes was developed and sediment-transport studies were conducted in the upper Yuba River watershed located in northern California. Field observations of sediment production due to mass wasting, channel storage volumes, and the relative importance of sediment sources, erosion, and transport processes were used to develop the conceptual model. A geographic information system (GIS) was used to spatially distribute hillslope erosion potential and channel storage throughout the study area. The GIS-based hillslope erosion-potential model illustrates that landscapes with low potential evapotranspiration, sparse vegetation, steep slopes, erodible geology and soils, and high road densities display the greatest hillslope erosion potential. Although mass wasting was observed to be the dominant hillslope erosion process, fluvial erosion of stored sediment is the primary contributor to the annual sediment yield based on model assumptions and field observations.

Sediment-transport studies included development of suspended-sediment and bed-load rating relations and estimates of annual sediment discharge at two gaging stations, from October 1 to September 30 of water years (WY) 2001, 2002, and 2003. Seasonal suspended-sediment rating curves were developed using a group-average method and non-linear least-squares regression of measured data; whereas bed-load rating curves were estimated using an empirical bed-load transport model. Due to its larger drainage area, higher streamflow, and absence of man-made structures that restrict sediment movement in the lower basin, the South Yuba River (5 tonnes/km^2/yr) transports a greater and coarser sediment load than the Middle Yuba River (2 tonnes/km^2/yr). In both rivers, bed-load represented 1 percent or less of the total annual load throughout the three-year project period. Relatively dry conditions prevailed during the project period; therefore, the calculated average annual sediment transport may not represent longer-term conditions.

INTRODUCTION

This study is part of the California Bay-Delta Authority (CBDA) Upper Yuba River Studies Program (UYRSP), which is currently evaluating options for introducing spring-run Chinook salmon and steelhead trout upstream of Englebright Lake located in the foothills of the northwestern Sierra Nevada, CA (Figure 1). During the initial phase of the UYRSP, conceptual and GIS models (Curtis et al., 2005a) provided a means of identifying potentially important sediment sources and evaluating erosion and transport processes, and were further utilized to develop a deterministic watershed-scale sediment-transport model (Flint et al., 2004). Sediment rating curves (Curtis et al., 2005b) were used to assess the magnitude and duration of sediment loads that may impact the viability of long-term fish-introduction strategies (Curtis et al., 2004) and were further utilized to calibrate the watershed model.

Study Area: The Yuba River, a tributary to the Feather River in northern California, drains approximately 3,480 km^2 along the western slope of the Sierra Nevada (Figure 1). The study area is located within the upper Yuba River watershed, a heavily managed basin recovering from hydraulic gold mining (Gilbert, 1917), and includes two tributaries: the Middle Yuba River and the South Yuba River. The climate is Mediterranean with hot/dry summers and cool/wet winters. Runoff is typically generated by warm, winter Pacific storms, spring snowmelt, or occasionally by convective storms generated in the late summer or early autumn by subtropical air masses from the Gulf of Mexico. Beginning in November, Pacific frontal systems bring winter precipitation into northern California, resulting in about 85% of precipitation falling between November and April.

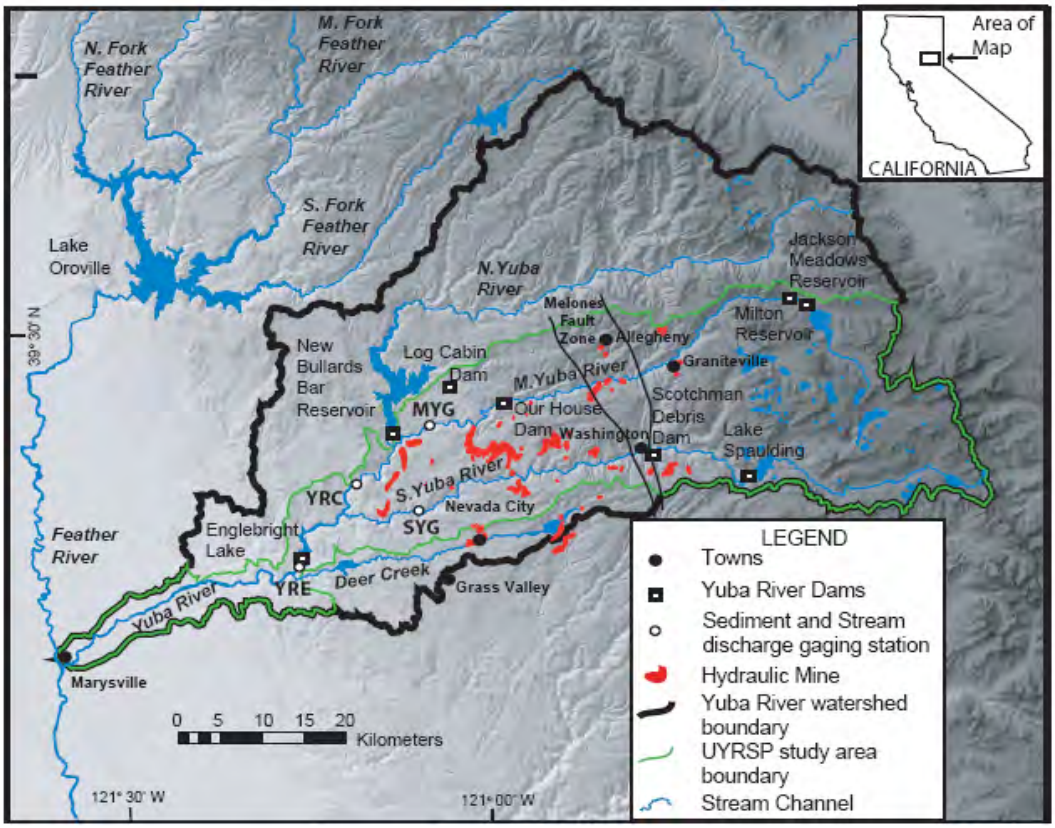


Figure 1 Study area map. MYG = Middle Yuba River gage; SYG = South Yuba River gage.

METHODS

Verifying, Refining, and Spatially Distributing Components of a Conceptual Model: An initial hypothesis of a conceptual model of upper Yuba River sediment dynamics was verified, refined, spatially distributed and used to discretize hillslopes units in the deterministic watershed model developed for this site (Flint et al., 2004). Subsequent aerial-photo and field observations clarified the relative importance of model components and identified sediment-source locations where key transport processes occur, thereby enabling verification and refinement of the model. As important sediment sources and transport processes were illuminated, components and linkages in the initial conceptual model were removed or moved, and line thicknesses indicating the relative magnitude of transport processes were defined (Figure 2).

Field measurements at mass-wasting sites (n=22) included scarp areas, mean evacuated depth, and sediment delivery (Figure 3). Surface erosion rates were not quantified; however the relative importance of surface and mass-wasting processes were evaluated at an additional 39-hillslope sites where the type and relative severity of hillslope erosion were documented. Field measurements at channel storage sites included length, width, and height of discrete channel storage elements (debris jams, channel bars, floodplains, and terraces).

The channel-storage and hillslope erosion-potential components of the conceptual model were spatially distributed using GIS. Development of the spatially distributed channel-storage component was a three-step process: 1) cumulative channel lengths for zero- through fifth-order stream channels were defined using a digital elevation model, 2) the arithmetic mean of storage volumes for individual storage elements (debris jams, bars, floodplains, and terraces) was calculated for each stream-order class, and 3) the arithmetic mean of storage volumes for each stream-order class were multiplied by channel lengths to provide basin-wide estimates. The spatially distributed hillslope erosion-potential component was developed using a raster-based map of hillslope erosion-potential generated at a 30-meter grid resolution. The first step in developing the hillslope erosion potential map was to

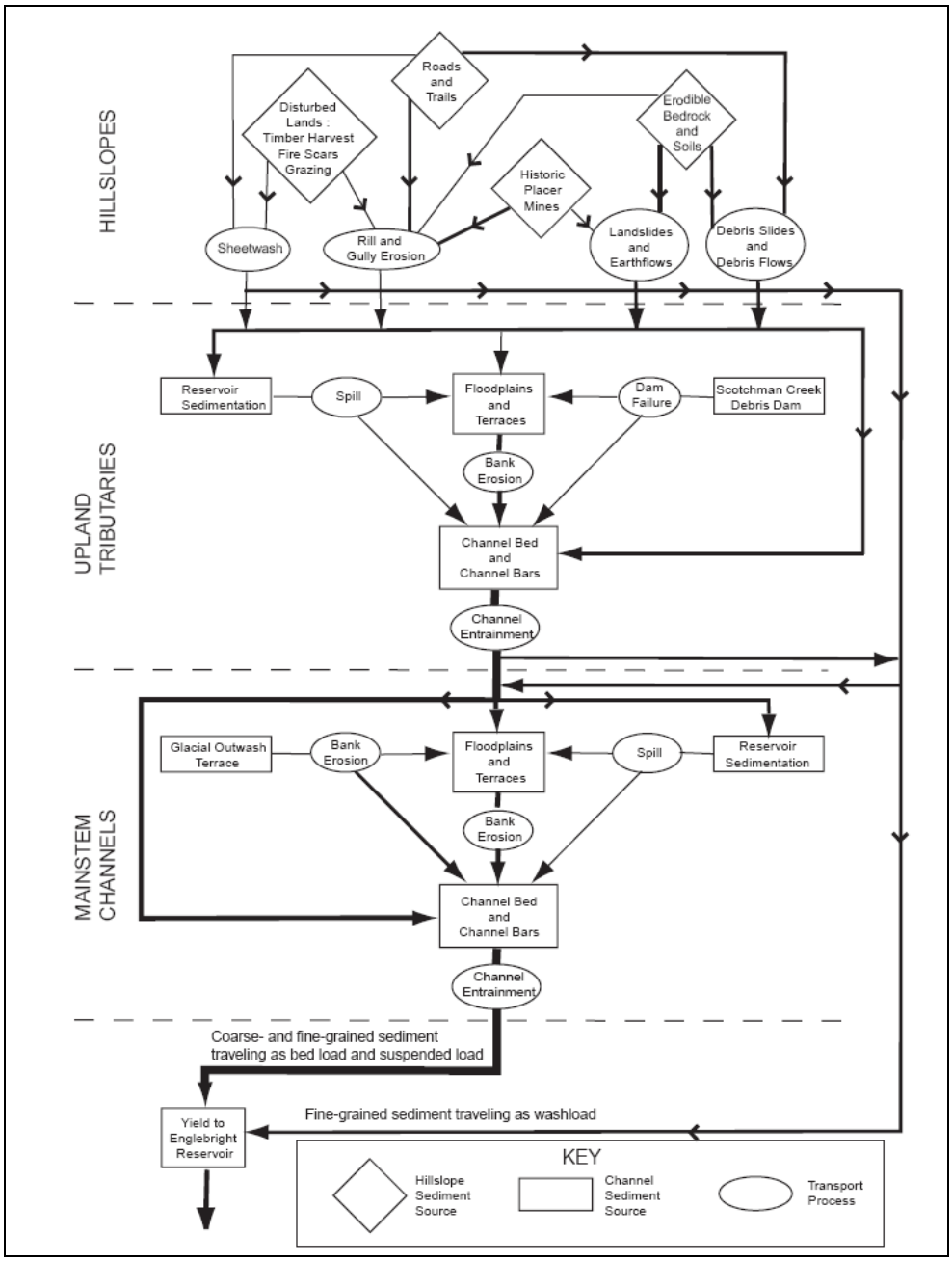


Figure 2 A conceptual model of sediment processes partitioned into three components: hillslopes, upland tributaries, and mainstem channels. The three components are further compartmentalized into hillslope sediment sources, channel sediment-storage elements, and transport processes. Arrows with variable line thickness denote linkages between compartments and transport directions. The hypothesized relative magnitude of basin-wide sediment transport is indicated by line thickness (i.e., thicker lines represent greater transport). Note: figure reproduced from Curtis et al. (2005a) Figure 3.

develop a matrix of landscape attributes governing hillslope erosion processes with scaling factors and relative multipliers assigned based on field observations. The scaling factors signify the inferred or measured range of values associated with each landscape attribute and the multipliers indicate the comparative importance, with larger values indicating greater importance. In the second step, landscape attributes were defined for each 30-meter grid cell using a digital elevation model and digital maps of geology, soils, vegetation, roads, hydrography, and mined

areas. An estimate of total potential evapo-transpiration (PET) for the month of April was simulated using climate data and the digital elevation model. In the final step, a calculation of hillslope erosion potential was developed that accounts for all contributing factors based on landscape attributes. The final calculation used to produce a hillslope erosion-potential map was additive, where hillslope erosion potential equals [elevation * 6]+ [(slope * geology + kfactor) * 9] +[(roads + mines + mass wasting sites + stream crossings) * 10] – [PET *4] - [vegetation cover * 6].

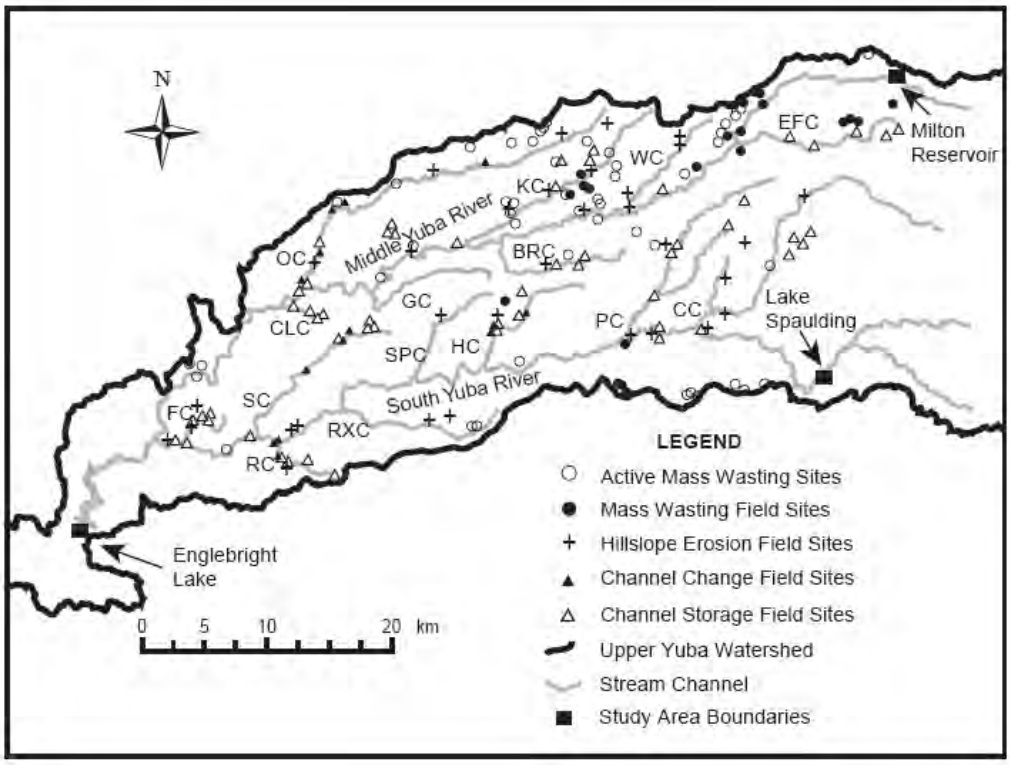


Figure 3 Map of study area showing field sites. Abbreviations for upland tributaries labeling are: FC, French Corral Creek; SC, Shady Creek; RXC, Rock Creek; SPC, Spring Creek; HC, Humbug Creek; PC, Poorman Creek; CC, Canyon Creek; CLC, Clear Creek; OC, Oregon Creek; GC, Grizzly Creek; BRC, Bloody Run Creek; KC, Kanaka Creek, WC, Wolf Creek; EFC, East Fork Creek.) Note: figure reproduced from Curtis et al. (2005a) Figure 4.

Sediment Rating Curves to Characterize Sediment Transport: To verify the conceptual model and help calibrate the deterministic watershed model developed for this study site, a series of seasonal suspended-sediment and bedload rating curves were developed for the Middle Yuba River and South Yuba River gaging locations shown in Figure 1 (Curtis et al., 2005b). Suspended-sediment rating curves that describe seasonal variations in suspended-sediment supply were developed using depth-integrated, single vertical suspended-sediment samples. The measured data indicate that seasonal variability in sediment supply dramatically influences sediment transport in the upper Yuba River watershed and that a single suspended-sediment rating curve cannot represent these varying conditions. Therefore, a series of group-average sediment rating curves that describe average, summer/fall, first flush, winter, and spring snowmelt conditions were developed for the Middle Yuba River and South Yuba River gage locations using non-linear least-squares regression.

Bed-load rating curves were estimated using an empirical bed-load transport relation (Wilcock and Crowe, 2003). Calculating the bed-load transport rate for a given stream discharge required estimates of the surface grain-size distribution, water-surface slope, and bed-shear velocities. Laboratory analyses of bed material from the Middle Yuba River and South Yuba River gage sites were used to define surface grain-size distributions. Water-surface slopes were determined from longitudinal surveys of water-surface elevations measured using a surveyor's transit level and a stadia rod along 500 feet of channel distance. Bed-shear stress can be partitioned into skin friction (the portion of stress that is exerted on individual grains and responsible for transport) and form drag (attributable to

large roughness elements, such as bedforms, boulders, bedrock outcrops, or large trees within the active channel). Because bed-shear stresses in the upper Yuba River include a significant component of form drag, this term was removed before computing the bed-shear velocities.

Annual sediment discharge was calculated at the Middle Yuba River and South Yuba River gage locations for water years 2001, 2002 and 2003 using sediment rating curves. Suspended-sediment discharge was calculated using seasonal suspended-sediment rating curves (developed using measured data) and mean daily streamflow data. Bed-load discharge was calculated using bed-load rating curves (developed using estimated data) and 15-minute streamflow data.

RESULTS

Field observations of hillslope sediment sources indicate low hillslope erosion rates throughout the study area. Based on field measurements, 95% of the upper Yuba River watershed exhibits negligible to moderate hillslope erosion potentials (Figure 4). Evidence of active hillslope erosion (rilling, gullying, and mass wasting) was documented at 44% of the 39-hillslope sites shown in Figure 3. Mass wasting was documented at 88% of the eroded sites and dominates surface erosion, which was observed at 41% of the eroded sites.

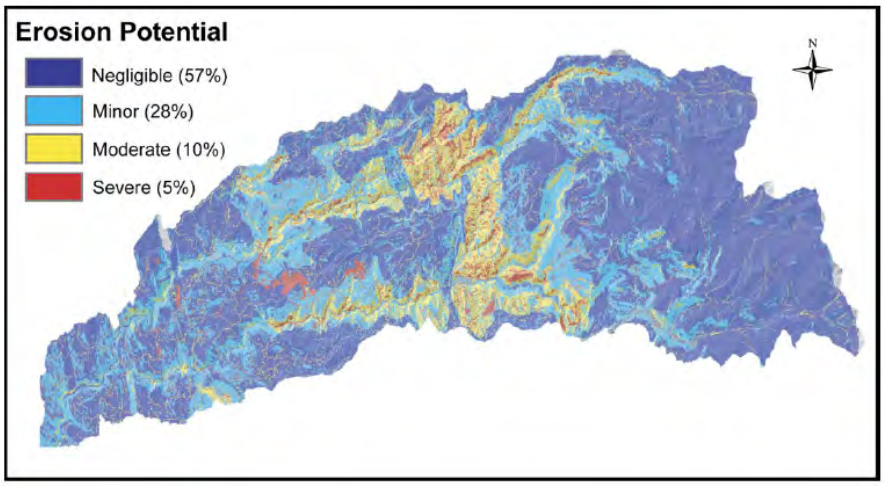


Figure 4 Hillslope erosion potential map generated using GIS calculations. The relative erodibility classes (negligible, minor, moderate, and severe) are based on field data from 39 hillslope sites. Note: figure reproduced from Curtis et al. (2005a) Figure 5.

Analysis of field measurements spatially distributed using GIS indicate that approximately 482 million m^3 of sediment is stored above the thalweg in zero- through fifth-order upper Yuba River channels. Debris jams store the majority of sediment in zero-order channels whereas 62% to 93% of alluvium in first- through fifth-order channels is stored in well-vegetated terraces that are for the most part inactive and stable. Large volumes of hydraulic mining sediment are stored in several low-order upland tributaries and an extensive glacial outwash terrace is preserved on the mainstem South Yuba River.

Suspended-sediment concentrations generally increase with increasing streamflow, however the slopes of seasonal suspended-sediment rating curves differ significantly (Figure 5). Variations in the slopes of the rating curves indicate changes in suspended-sediment supply throughout the water year. During average and below-average precipitation conditions such as those which occurred during the study period, sediment supply is greatest during the first flush of the water year; consequently the first-flush rating curves display the greatest slopes. Sediment supplies decreased following the first flush; thus, the slopes of the winter rating curves are lower than the first-flush curves. The spring and summer/fall rating curves had the lowest slopes, indicating lower sediment supplies during spring snowmelt conditions and throughout the dry summer and fall months.

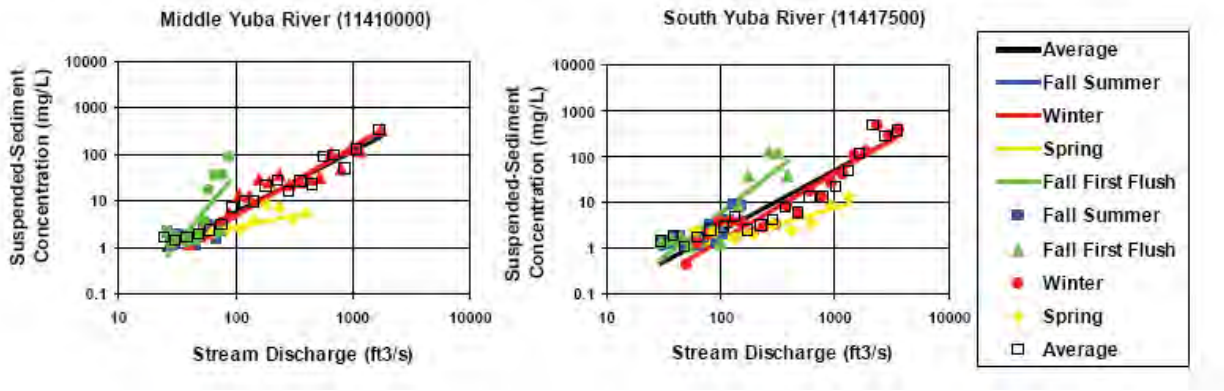


Figure 5 Group-average non-linear regressions between suspended-sediment concentration and instantaneous streamflow for the Middle Yuba River and South Yuba River gaging stations in the upper Yuba River watershed, California.

Estimated annual sediment discharges at the Middle Yuba River gage were significantly lower than those at the South Yuba River gage even when normalized by drainage area (Table 1). The main contributing factor to the difference in sediment loads is that 88 percent of the Middle Yuba River watershed lies upstream of Log Cabin and Our House Reservoirs. This effect is compounded by significant flow diversions above the Middle Yuba River gage, which resulted in a median daily flow for the project period of 1.6 m^3/s at the Middle Yuba River gage compared with 2.8 m^3/s at the South Yuba River gage. Because the South Yuba River has higher flows and no man-made restrictions to sediment movement in the lower basin, it is able to transport a greater and coarser sediment load. The percentage of annual sediment discharge transported as bed load was less than 1 percent throughout the study period, which was quite low and unexpected, given the abundance of bed material available for transport. Below-average to average precipitation conditions occurred throughout the project period, which likely influenced the volume of bed-load transport.

Table 1. Annual sediment discharge and bed-load estimates.

Year	Annual suspended-sediment discharge (tons/yr)	Annual bed-load discharge (tons/yr)	Total annual sediment discharge (tons/yr)	Annual sediment yield (tons/km^2/yr)
South Yuba River (SYG, Station ID 11417500 [drainage area 798 km^2])				
2001	660	1	661	1
2002	4,300	16	4,316	5
2003	6,900	89	6,989	9
Average annual sediment discharge			3,989	5
Middle Yuba River (MYG, Station ID 11410000 [drainage area 513 km^2])				
2001	140	0	140	0
2002	830	3	833	2
2003	1,800	19	1,819	4
Average annual sediment discharge			931	2

CONCLUSIONS

A conceptual model was used to evaluate sediment sources, erosion, and sediment transport in a dominantly bedrock basin impacted by hydraulic mining. Field observations and the conceptual model were used to develop a deterministic watershed-scale sediment-transport model. Sediment rating curves were used to assess the seasonal variability in sediment transport and to calibrate the watershed model. Field measurements indicate that mass wasting dominates surface erosion throughout the study area; however hillslope erosion rates are relatively low. The large volume of sediment stored in active to semi-active channel locations represents the dominant sediment source. GIS analyses further indicate that principal sediment sources are located in the central portion of the watershed

where the greatest hillslope erosion potential is displayed and large quantities of active alluvium are stored. During average and below-average precipitation conditions, such as those which occurred during the study period, sediment supply is greatest during the first flush of the water year. Sediment supplies decreased following the first flush; thus, the slopes of the winter rating curves are lower than those of the first-flush curves. The spring and summer/fall rating curves had the lowest slopes indicating relatively low rates of suspended-sediment transport during snowmelt conditions and during the dry season. Due to its larger drainage area, higher streamflow, and absence of man-made structures that restrict sediment movement in the lower basin, the South Yuba River (5 tonnes/km^2/yr) transports a greater and coarser annual sediment load than the Middle Yuba River (2 tonnes/km^2/yr). In both rivers, estimated bed-load represented 1 percent or less of the total annual load throughout the three-year project period. Owing to relatively dry conditions during the project period, the calculated average annual sediment transport rates may not represent longer-term conditions.

REFERENCES

Curtis, J.A., Flint, L.E, and Alpers, C.N., 2004, "Sediment transport in the upper Yuba River Watershed, 2001–03," Third Biennial CALFED Bay-Delta Program, Sacramento, Calif., October 4-6, 2004, Science Conference Abstracts, p. 48.

Curtis, J.A., Flint, L.E., Alpers, C.N., and Yarnell, S.M., 2005a, "Conceptual model of sediment processes in the upper Yuba River watershed, Sierra Nevada, CA," Geomorphology, v. 68, p. 149–166
doi:10.1016/j.geomorph.2004.11.019

Curtis, J. A., Flint, L.E., Alpers, C.N., Wright, S.A., and Snyder, N.P., 2005b, Use of Sediment Rating Curves and Optical Backscatter Data to Characterize Sediment Transport in the Upper Yuba River Watershed, California, 2001–03, U.S. Geological Survey Scientific Investigations Report 05-5246 [in press].

Flint, L.E., Guay, J.R., Flint, A.L., Curtis, J.A., and Alpers, C.N., 2004, "Spatially distributed model of flow and sediment transport in the upper Yuba River Watershed," Third Biennial CALFED Bay-Delta Program, Sacramento, Calif., October 4-6, 2004, Science Conference Abstracts, p. 78.

Gilbert, G.K. 1917. Hydraulic-mining debris in the Sierra Nevada. U.S. Geological Survey Professional Paper 105, 154 p.

Wilcock, P.R., and Crowe, J.C., 2003, "Surface-based transport model for mixed-size sediment," Journal of Hydraulic Engineering, v. 19, no. 2, p. 120–128.

EFFECTS OF CLIMATE ON FLOW AND SEDIMENT TRANSPORT IN THE UPPER YUBA RIVER BASIN, NORTHERN SIERRA NEVADA

Lorraine E. Flint, Joel R. Guay, Alan L. Flint, Jennifer A. Curtis, and Noah Snyder
U.S. Geological Survey, Sacramento, CA

Abstract: The Upper Yuba River basin is in a zone of the Sierra Nevada that is not reliably influenced by the major Pacific climate cycles (El Nino, La Nina, and the Pacific Decadal Oscillation), but which is expected to experience effects from future climate change. These effects will likely include increases in springtime temperatures, earlier snow melt, and associated increases in sediment transport. As part of CALFED's Upper Yuba River Studies to evaluate options for establishing salmonids above Englebright Dam, a flow and sediment transport model was developed for the Upper Yuba River watershed. This model was used to simulate the deposition of sediment in Englebright Lake for the 62 years since the dam was built. To evaluate the sensitivity of the hydrologic processes in the basin to differences in climate, simulated streamflow and transport of sediment from the watershed under the climate cycles that have occurred during the last 62 years were evaluated in light of the watershed management practices that took place in the early 1970's. The changes in the watershed due to installation of dams and diversions on the Middle Yuba River had a much larger influence on the simulated sediment loads than the climate cycles. The simulated flow and transport were also considered under a specified increase in annual-mean air temperatures representing future climate conditions. These simulations indicated that increases in mean annual and peak flows were negligible, as were changes in sediment loads. However, springtime snow melt and run off was initiated earlier in the season.

MODELING SYSTEMS FOR SEDIMENT MANAGEMENT AND BMP EVALUATION IN LARGE GREAT LAKES TRIBUTARY WATERSHEDS

Theresa Possley, Project Engineer, W.F. Baird & Associates, Madison, WI, tpossley@baird.com; Alex Brunton, Geoscientist, W.F. Baird & Associates, Oakville, ON, abrunton@baird.com; Rob Nairn, Principal, W.F. Baird & Associates, Oakville, ON, rnairn@baird.com; Jim Selegean, Hydraulic Engineer, U.S. Army Corps of Engineers - Detroit District, James.P.Selegean@lre02.usace.army.mil

Abstract: The identification of water and sediment sources, pathways and sinks is vital to sustainable management of watersheds worldwide. Numerical modeling approaches have been implemented to evaluate water and sediment movement in several large watersheds tributary to Lake Michigan. Numerical models of watershed hydrology and sediment delivery are valuable tools to assist in the planning of Best Management Practices (BMPs) for watershed sediment issues. The models aid in developing a general understanding of the hydrologic and geomorphic behavior of watershed systems, and they allow evaluation and prediction of the effects of changing land use and BMPs such as riparian buffer zone modification.

The semi-lumped parameter Soil and Water Assessment Tool (SWAT; USDA-ARS) has been applied on several Great Lakes watersheds to assess historic land use change at the watershed scale. SWAT is particularly suited to simulations on large watersheds over long periods of time. The two-dimensional, finite-difference, Gridded Surface-Subsurface Hydrologic Analysis model (GSSHA; USACE-CHL) was used to evaluate hydrologic and sediment transport processes in detail on subwatersheds nested within the domains of the SWAT model. Because of their detail, the GSSHA model simulations were limited to smaller areas and shorter time simulations. GSSHA allowed for detailed appraisal of modification to buffer strip morphology (such as different vegetation types and strip widths) on different land uses and crop types. A key feature of these studies was the synthesis of the different modeling activities into a single methodology that may be used for watershed management initiatives.

INTRODUCTION

Section 516(e) of the Water Resources Development Act (WRDA) of 1996 authorizes the US Army Corps of Engineers to develop sediment transport models for Great Lakes tributary watersheds contributing sediment to Federal Navigation Channels and Areas of Concern. These models and modeling systems are intended for use by local watershed managers to evaluate strategies to reduce sediment loading to the river systems, thus decreasing sediment transported to navigation areas and lessening the Corps' dredging requirements.

There are several challenging aspects of the 516(e) program. The tributary watersheds that are the greatest sediment producers are also some of the largest in the Great Lakes. To address sediment issues affecting the navigation areas, the whole watershed must be modeled, but model end-users (i.e. local watershed managers, county drain commissioners, watershed groups, etc.) are often concerned with issues on a smaller scale (i.e. locating and evaluating BMPs). Therefore, there is a large range of scale and resolution that must be addressed by these modeling systems. In addition, local entities that will use the models often have little or no modeling

expertise and lack the resources to run complicated models or to buy proprietary software. These factors must be considered during model selection. While the funding authority allows for model development, it does not allow for major data collection programs, which directly affects model calibration and validation.

With these issues in mind, a sediment transport modeling system was developed for the Clinton River Watershed in Michigan. The SWAT and GSSHA models were selected as complementary models to address the issues for which they are most appropriate: SWAT for watershed-wide land use and land management issues and GSSHA for small-scale BMP evaluation.

CLINTON RIVER WATERSHED

The Clinton River Watershed is located just north of Detroit in southeastern Michigan. The main channel travels 80 miles (128 km) from its western headwaters to Lake St. Clair near the city of Mt. Clemens. The watershed covers 760 square miles (1,968 km^2) of southeastern Michigan, including portions of Oakland and Macomb Counties and small areas of St. Clair and Lapeer Counties (Figure 1). The watershed is home to more than 1.6 million people in 56 municipalities. The southern portion of the watershed is dominantly urban, the middle section is undergoing rapid suburban development and the northern region is primarily agricultural and forested. The condition of the river system varies dramatically, from runoff and pollution problems in urban areas, to healthier waters with thriving trout fisheries in rural areas. A modeling system that can address both the watershed-wide issues of land use change and land management and the localized issues of specific BMP placement is required.

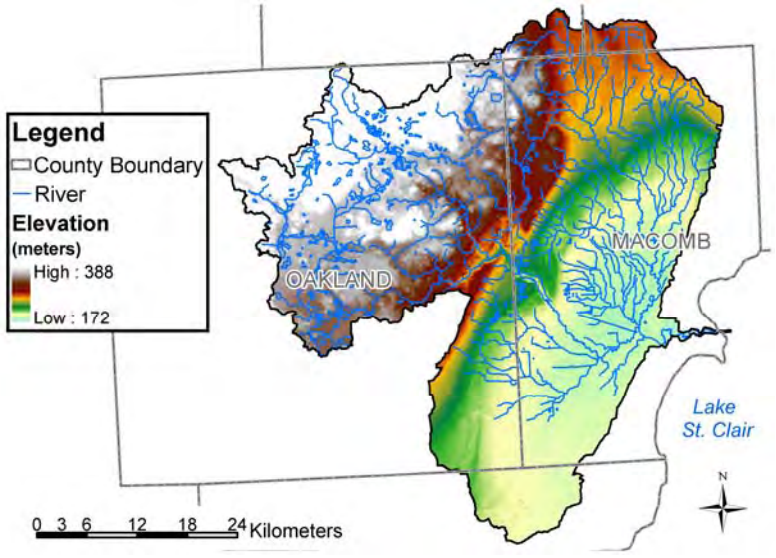


Figure 1 Clinton River Watershed topography map.

MODEL SYSTEM

"Simple models are sometimes incapable of giving desirable detailed results, and detailed models are inefficient and could be prohibitive for large watersheds. Therefore, finding an appropriate model for an application and for a certain watershed is quite a challenging task" (Borah and Bera, 2003).

The model selection phase was a very important part of this project. Issues that require consideration include data availability, specific questions to be addressed, watershed characteristics and end-user capabilities. All of these factors are combined, resulting in the selection of the optimal modeling tools. For the Clinton River Watershed, one of the most important considerations was the ultimate use of the modeling system – for both watershed-wide issues and detailed BMPs by local watershed managers. The SWAT and GSSHA models were chosen as a result of the selection process.

The Soil and Water Assessment Tool (SWAT) is a quasi-physically based, semi-empirical, watershed-scale numerical model for the simulation of water, sediment, nutrient and pesticide movement in surface and subsurface systems. SWAT aids in prediction of the impacts of climate and vegetation changes, reservoir management, groundwater withdrawals, water transfer, land use change and watershed management practices on water, sediment and nutrient dynamics in complex watershed systems. Land use and management conditions can be varied over long time periods, making the model a particularly useful tool to aid in the implementation of watershed-scale BMPs. SWAT is a continuous-time model, intended for the prediction of long-term water and sediment yields from a watershed. While SWAT is most appropriate for agricultural watersheds, it does have the capability to model urban areas, making it well suited to model the entire Clinton River Watershed.

SWAT is a semi-lumped parameter model that discretizes an area into Hydrologic Response Units (HRUs), based on land use, soil and management areas. Because of this lumping, SWAT cannot be used to target detailed, site-specific BMPs. The lumping of the watershed into HRUs and using a daily time step allows the SWAT model to simulate long time periods for large watersheds very quickly. This is important for evaluating the long-term impacts of land use and land management scenarios in a watershed.

SWAT is non-proprietary and is freely available to the public via the SWAT website (http://www.brc.tamus.edu/swat/). This is an important characteristic of the modeling system, due to the limited funding available to local watershed managers for modeling software. The AVSWAT extension interface is also free but requires ArcView GIS software. While ArcView is not free, local watershed management entities often have GIS software for other purposes and thus do not have to purchase it specifically for watershed modeling.

The GIS data layers necessary to create SWAT input files are a DEM, land use and soils coverages. The DEM was obtained from the National Elevation Dataset and was preprocessed using ArcHydro Tools, a non-proprietary package. Land use was taken from the 1992 National Land Cover Dataset (NLCD); each NLCD land use category was assigned a SWAT land cover/plant type. SWAT also requires climate data for the simulation period. For the Clinton

River Watershed SWAT model, daily rainfall data were obtained from Michigan's SEMCOG stations, and daily maximum and minimum temperature data were obtained from the Selfridge Air National Guard Base in Mt. Clemens.

Preliminary calibration of model hydrologic performance was undertaken using USGS streamflow measurements at USGS Gage # 04165500, the same location as the SWAT model outlet. A baseflow filter (Arnold and Allen, 1999) was used on the USGS streamflow data to determine the average annual ratio of baseflow to surface runoff for comparison to SWAT simulated baseflow. The Clinton River SWAT model was roughly calibrated to annual water yield and baseflow values and further calibrated to monthly water yields and daily values for particular events (Figure 2).

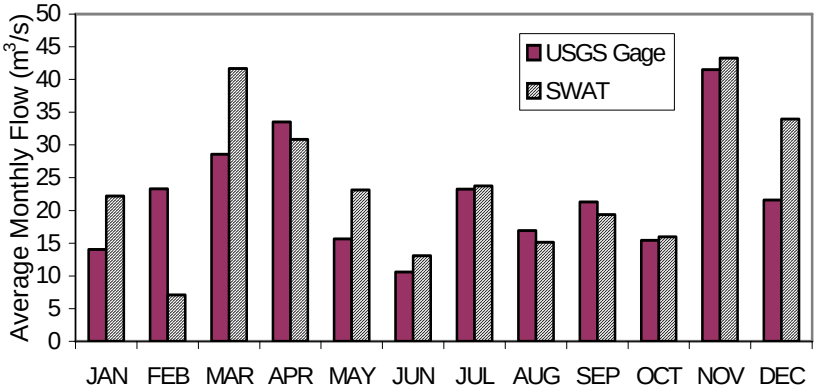


Figure 2 1992 measured and predicted discharge at model outlet.

The largest discrepancies between observed and predicted flows occurred in the winter and spring months. The Clinton River SWAT model does not replicate snowmelt events accurately; to improve these results, more detailed local temperature and precipitation data are required and modification to the frozen soil infiltration routines in SWAT may be necessary. Due to the lack of measured sediment transport data, the sediment component of SWAT was not calibrated. While this limits the model use for quantitative sediment loading estimates, the model can still be used in a relativistic manner, such as determining percent reduction in sediment yield or delivery between scenarios.

The SWAT model hydrology was also calibrated using the 1978 land use data and climate data from 1976 to 1980. With the calibrated model, climate data from 1990 to 1994 was run through the model with 1978 land use to determine the relative difference the change in land use from 1978 to 1992 had on sediment delivery. The 1978 and 1992 land use data sets had different resolutions, so the relative changes in specific land use types are approximate. There was little change from 1978 to 1992 in the percentage of urban/developed areas, the portion of the watershed used for agriculture increased by 10 %, and the percentages of forest and rangeland areas decreased (Figure 3).

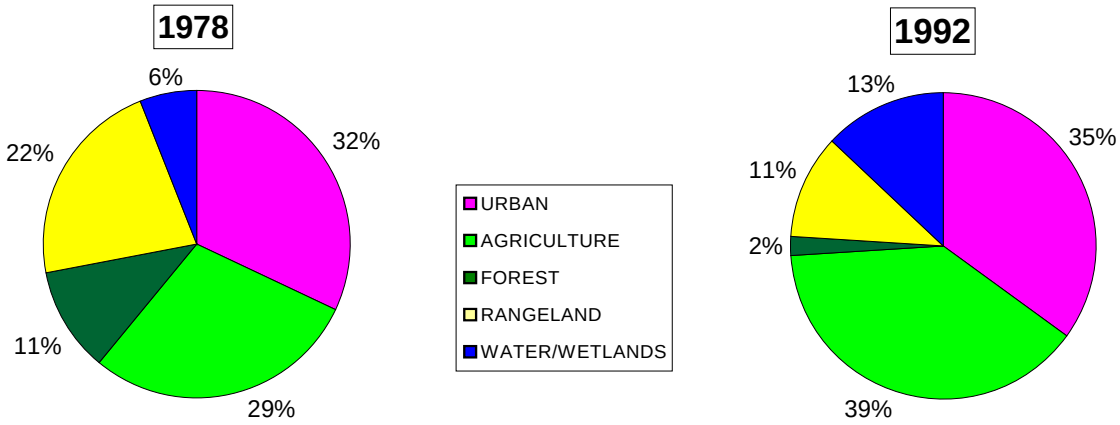


Figure 3 1978 and 1992 land use breakdown for the Clinton River Watershed.

Results for the average annual net soil erosion per unit area ($t/km^2.yr^{-1}$) for the 1978 and 1992 land use scenarios are shown in Figure 4. The annual values increased, on average, by 32%, resulting from only a 10% increase in agricultural land area. Scenario exercises such as this demonstrate how the SWAT model can be used to quickly evaluate the impact of land use change on watershed soil erosion.

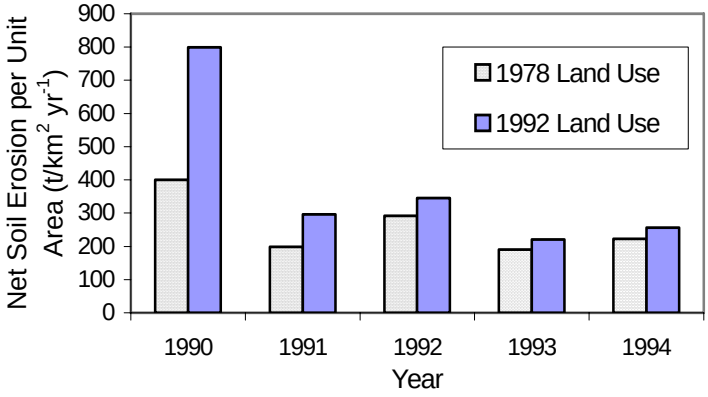


Figure 4 SWAT soil erosion results comparing different land use datasets.

SWAT can be used to model the entire Clinton River Watershed over long time periods, but it is not designed to simulate small-scale BMPs that were of interest to local watershed managers, so the GSSHA model was used to construct a detailed representation of small-scale BMPs. GSSHA (Gridded Surface Subsurface Hydrologic Analysis) is a physically based, distributed-parameter model that simulates the hydrologic response of small watersheds. Features include 2-D overland flow, 1-D streamflow, 1-D infiltration, 2-D groundwater, and full coupling between the groundwater, vadose zone, streams, and overland flow. The fully coupled groundwater to surface water interaction allows GSSHA to model both Hortonian (infiltration-excess) and Non-Hortonian (saturation-excess) areas. The model employs mass-conserving solutions of partial differential equations and closely links the hydrologic compartments to ensure an overall mass balance and correct feedback. GSSHA is a reformulation and enhancement of CASC2D (Ogden and Julien, 2002) and is supported by the US Army Corps of Engineers Engineer Research and Development Center (ERDC).

GSSHA is a fully distributed model so there is no requirement to lump areas according to their hydrologic characteristics. The watershed is divided into cells and water and sediment are routed from cell to cell according to topography. This feature makes GSSHA appropriate for simulating detailed BMPs on a subwatershed and smaller scale, providing the input data resolutions are appropriate to the processes being modeled. GSSHA can run in both single event and long-term modes but long-term simulations are often computationally impractical. For example, when using the full Richard's Equations in GSSHA, the time step needs to be less than one minute if the grid mesh size is less than 30 meters (Kalin and Hantush, 2003). The modeling for the Clinton River Watershed was therefore run for single events only.

Three HUC14 subbasins in the Clinton River Watershed were modeled with GSSHA. Choice of these basins was based on discharge data availability and identification of significant sources of watershed sediment according to anecdotal information. No sediment data were available for any of the subbasins, thus the sediment loads predicted by the model could not be considered as absolute values.

The Paint Creek subwatershed was one of the three areas modeled with GSSHA. Paint Creek covers an area of approximately 96 km^2 (37 mi^2), where approximately 23% is urban/developed, 32% agricultural, 33% forested and 11% wetlands, and the soil varies from loamy sand to sandy loam. The model was calibrated against flow discharge from USGS Gage #04161540 at Rochester, which has a temporal coverage from 1954 to present. Flow data from 1996 were utilized for the basin calibration (Figure 5).

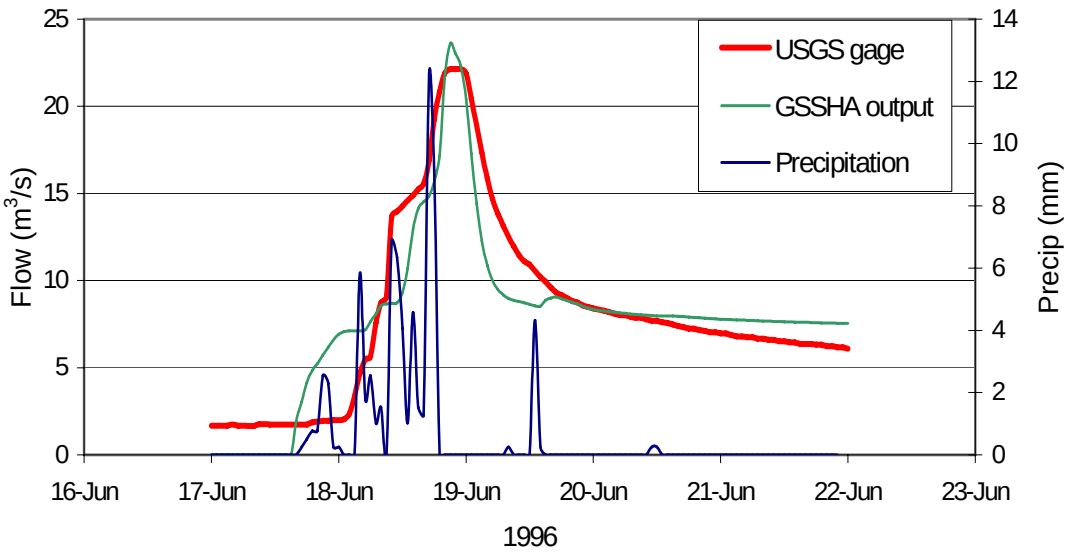


Figure 5 GSSHA flow calibration results.

The calibrated GSSHA model was used to simulate the hydrologic response of riparian buffer strips of varying width and vegetation type on a small area within Paint Creek. Buffer strips are areas of permanent vegetation that help control delivery of sediment and other pollutants to streams by reducing overland flow, velocity and discharge, causing sediment to drop out of suspension. This type of BMP could not be simulated with SWAT because it requires grid-to-

grid routing at a fine spatial resolution (a 5 m grid size was used in GSSHA). While the detailed physical processes simulated in GSSHA make it ideal for evaluating small-scale BMPs, the model is not specifically designed to facilitate BMP analysis and there are no built-in BMPs in GSSHA. In order to represent riparian buffers in GSSHA, land use and management characteristics in riparian grid cells were adjusted to represent buffer characteristics.

Three buffer widths were simulated (10, 20 and 30 m) along with five vegetation types and four land uses adjacent to the buffer strip. The objective of this exercise was to evaluate the potential of GSSHA for simulating buffer strips and to provide a buffer analysis tool and methodology that can be applied in different areas and circumstances within the Paint Creek watershed. The percentage reduction values were determined from scenarios without buffers for each land use type (Table 1).

Table 1 GSSHA percentage reduction in erosion results for riparian buffer scenarios.

Buffer Land Use	Buffer Width	Percent Reduction in Sediment			
		Land Use Adjacent to Buffer Strip			
		Bare ground	Row Crops	Small Grain	Residential
Short Grass	10 m	15.3 %	3.9 %	9.8 %	29.4 %
	20 m	26.9 %	6.6 %	16.4 %	36.2 %
	30 m	33.9 %	8.0 %	22.0 %	40.2 %
Long Grass	10 m	15.4 %	3.6 %	9.4 %	14.6 %
	20 m	26.4 %	5.7 %	13.0 %	17.1 %
	30 m	33.0 %	6.3 %	16.5 %	21.9 %
Forest	10 m	15.3 %	3.7 %	9.5 %	14.8 %
	20 m	26.4 %	5.7 %	13.2 %	17.6 %
	30 m	33.1 %	6.5 %	17.0 %	22.6 %
Bermuda Grass	10 m	15.7 %	3.6 %	9.7 %	30.3 %
	20 m	26.9 %	6.4 %	16.1 %	35.3 %
	30 m	33.6 %	7.2 %	21.3 %	39.0 %
Brush	10 m	15.3 %	4.0 %	9.8 %	27.5 %
	20 m	26.8 %	6.5 %	15.6 %	31.5 %
	30 m	33.8 %	7.7 %	20.5 %	34.1 %

CONCLUSIONS

The US Army Corps of Engineers has been authorized to develop sediment transport modeling systems for Great Lakes tributary watersheds to be delivered to local watershed managers to better manage sediment on the land, thus reducing Corps dredging costs in Federal Navigation Channels and Areas of Concern. The challenges posed by funding stipulations (multiple scales of application; complex processes yet the need for ease of use of the end product) were met by using multiple models. The models were set up and calibrated using readily available data, which did not include watershed sediment load data. While this limited model application for absolute quantitative assessments of watershed sediment loadings, the models were still useful to determine the relative effects of different BMPs on sediment yield and delivery.

The SWAT and GSSHA models together can address many challenges faced by watershed managers. Each model is applied at the appropriate scale to investigate both watershed issues and small-scale BMPs for sediment management. The models are non-proprietary and available to the public, though additional software is required for graphical pre- and post-processing. A user manual and custom ArcView extension facilitated use of these models by watershed managers. Table 2 summarizes the types of modeling activities most appropriate for the GSSHA and SWAT models.

Table 2 SWAT and GSSHA appropriate modeling scenarios.

SWAT	GSSHA
Long period simulations; climate change	Detailed (event) modeling
Large watersheds	Detailed erosion/sedimentation
Basin-wide management practices	Subbasin & small-scale BMP evaluation

In general, SWAT is more suited for long-term, large-scale modeling, while GSSHA is better for short-term, small-scale simulations. SWAT is useful in determining impacts of past and future land use/land management decisions in a watershed, and GSSHA is valuable in determining impacts of detailed small-scale BMPs such as buffer strips and rain gardens. SWAT has the ability to simulate both point and non-point sources of pollution as well as nutrient transport. Together SWAT and GSSHA cover the range of time and space scales required for watershed management.

REFERENCES

Arnold, J.G., Allen, P.M., Muttiah, R., and Bernhardt, G. (1995). "Automated Baseflow Separation Recession Analysis Techniques," Ground Water, NGWA, 33(6), pp 1010-1018.

Arnold, J.G., and Allen, P.M. (1999). "Automated Methods for Estimating Baseflow and Groundwater Recharge from Streamflow Records," Journal of the American Water Resources Association, AWRA, 35(2), pp 411-424.

Borah, D.K., and Bera, M. (2003). "Watershed-Scale Hydrologic and Nonpoint-Source Pollution Models: Review of Mathematical Bases," Transactions of the ASAE, ASAE, 46(6), pp 1553–1566.

Kalin, L., and Hantush, M.M. (2003). Evaluation of Sediment Transport Models and Comparative Application of Two Watershed Models. EPA National Risk Management Research Laboratory Report (EPA/600/R-03/139).

Ogden, F.L., and P.Y., Julien. (2002). CASC2D: A Two Dimensional, Physically-Based, Hortonian, Hydrologic Model. Mathematical Models of Small Watershed Hydrology and Applications (V.J. Singh and D. Freverts, eds.), Water Resources Publications, Littleton, Colorado, ISBN 1-887201-35-1, 972 pp.

DEVELOPMENT OF UPPER BOUNDARY CONDITIONS FOR A WATERSHED MODEL IN THE UPPER YUBA RIVER BASIN, NORTHERN SIERRA NEVADA

Alan L. Flint., Lorraine E. Flint, Research Hydrologists, U.S. Geological Survey, Sacramento, CA, **aflint@usgs.gov**

Abstract: A flow and sediment transport model was developed for the Upper Yuba River watershed as part of CALFED's Upper Yuba River Studies Program to evaluate options for establishing salmonids above Englebright Dam. This model was used to simulate the deposition of sediment in Englebright Lake for the 62 years since the dam was built. The upper boundary conditions were developed using sparse data (1 to 45 meteorological stations came in and went out of operation between 1941 and 2003). Point measurements of daily precipitation and minimum and maximum air temperature were spatially distributed throughout the watershed using gradient plus inverse distance squared calculations and a digital elevation model. In addition, solar radiation and potential evapotranspiration were modeled for the watershed, including the influence of clouds. A simple procedure was used to develop 15-minute precipitation data, which was adjusted by iteration to match peak flows during the day. Dew point temperature was assumed to equal the minimum daily temperature and wind was taken to be constant over the site from the single wind station in the area. By associating the upper boundary conditions with a digital elevation model we could use that information to develop the hydrologic response units in the watershed model (using the code HSPF; Hydrologic Simulation Program--FORTRAN) and easily extrapolate the boundary conditions to the developed hydrologic response units.

WATERSHED SIMULATION WITH AN ENHANCED DISTRIBUTED MODEL

Yong G. Lai, Hydraulic Engineer, Bureau of Reclamation, Denver, Colorado, ylai@do.usbr.gov

INTRODUCTION

Distributed watershed hydrological and erosion modeling is gaining popularity in recent years due to increased computing power and availability of detailed spatial hydrological data. Models of this type are widely believed to provide greatest opportunities to examine hydrologic impact of land use change and climate change (Sharika et al. 2000); they also have immense utility to forecast the movement of pollutants and sediments (Beven 1985). So far, quite a number of distributed models have been developed, and many were reviewed by Yang et al. (2003) and Lai and Yang (2004). Among them, WEPP (Nearing et al. 1989) and CASC2D (Julien et al. 1995; Johnson et al. 2000) are the two leading models used in the US.

Despite the consensus for their potential use and the need to develop distributed models, there have been a number of concerns. Ewen et al. (2000) pointed out three major outstanding issues: (1) True capabilities of distributed models are yet to be demonstrated in a convincing way; (2) Some important physical processes have not been included or modeled properly; and (3) There exists the so-called "scale problem" with the distributed models. Unrealistic results may be obtained when mesh size is too large, and a calibrated model at smaller-scale watersheds may not be extended to larger-scale ones.

This paper presents an enhanced distributed model, GSTAR-W (Generalized Sediment Transport for Alluvial Rivers and Watersheds), that is partially motivated by the scale issue. The model is based on the concept of CASC2D due to its popularity, ease of use and efficiency; but a number of improvements are made to extend the capability. One of the objectives is to partially address the scale problem. It is accomplished by developing a proper solution algorithm that guarantees mesh convergent solutions and a hybrid zonal modeling concept that allows mixed use of process models to achieve model scale-up.

MODEL CONCEPT AND METHOD

A significant departure from CASC2D is the geometric representation of a watershed. CASC2D uses the raster mesh while GSTAR-W adopts the zonal representation. With GSTAR-W, a watershed is partitioned into zones or polygons first. A zone may represent a sub-watershed or an arbitrary polygon, with the channel network as a special zone. Zonal partition lines may represent natural features based on topography, land use or soil types; or they may be arbitrary. Channel banklines are used as the partition lines in general applications and they form the channel network zone. This representation provides a more accurate coupling between overland and channel network in water and sediment exchange. In contrast, channels are 'approximated' in CASC2D by the raster mesh cells. The zonal modeling concept allows hybrid modeling: different methodologies or process models may be used in different zones. For example, one zone may use simple empirically based lumped modeling while another may select a physically based distributed modeling. In this regard, each zone may be viewed as a "building brick" of the

model and each zone may be modeled and validated separately. This provides an opportunity to alleviate scale issue number two discussed in the Introduction.

For a two-dimensional (2D) distributed zone, the zone is further divided into discrete mesh cells. Hydrological and erosion processes are modeled in detail on each mesh cell. The meshing strategy adopts the arbitrarily shaped element method of Lai (2000). Such a flexible mesh facilitates the implementation of the hybrid zonal modeling concept and encompasses most existing meshing methods in use. For example, the raster mesh is a special mesh representation. In addition, such a mesh allows a tight integration between watershed and channel network and a truly mesh convergent solution is achievable.

GSTAR-W offers both the diffusive wave and the dynamic wave solvers for water flow as it intends to extend the modeling capability beyond overland flows to river systems. It also offers both explicit and implicit solvers for solution efficiency and robustness. A detailed description of the mathematical formulation and the numerical methods has been reported by Lai and Yang (2004) and is not repeated here.

CASE STUDIES

Two-Dimensional Surface Runoff: A 2D runoff case is simulated which has an approximate analytical solution and previous numerical results for comparison. The geometry is displayed in Fig.1 in which a V-shaped overland is connected to a channel. The overland plane has a slope of 0.05 and the channel has a slope of 0.02 and a width of 20 m. The depth of the channel varies linearly from 1 m at the upstream end to 20 m at the downstream end. An unstructured mesh shown in Fig.2 is used. Simulation has been carried out under a constant rainfall intensity of 10.8 mm/hr and zero infiltration with the rainfall duration of 1.5 hr. The Manning's roughness coefficient is 0.015 for the overland and 0.15 for the channel. A number of simulations have been carried out using GSTAR-W with explicit or implicit schemes. Essentially identical solutions are obtained and they are compared with previous results in Fig.3. Note that DiGiammarco et al. (1996) used a central difference scheme that leads to an 'overshoot' of the solution during the rising limb of the hydrograph; while CASC2D used a first-order upwind scheme that is too dissipative. Overall, it is shown that GSTAR-W agrees with the analytical and previous numerical results quite well, indicating that the right equation has been solved.

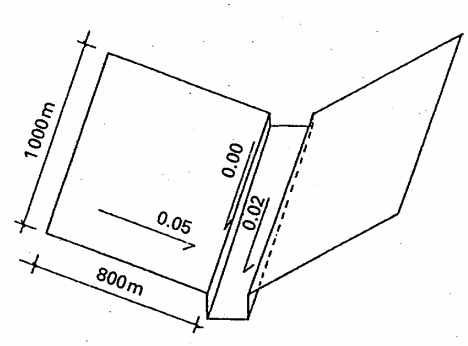


Figure 1 Geometry of the V-Shaped Catchment

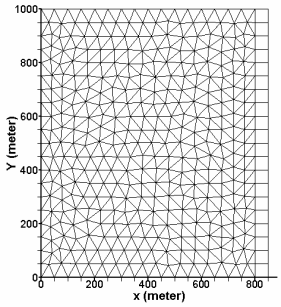
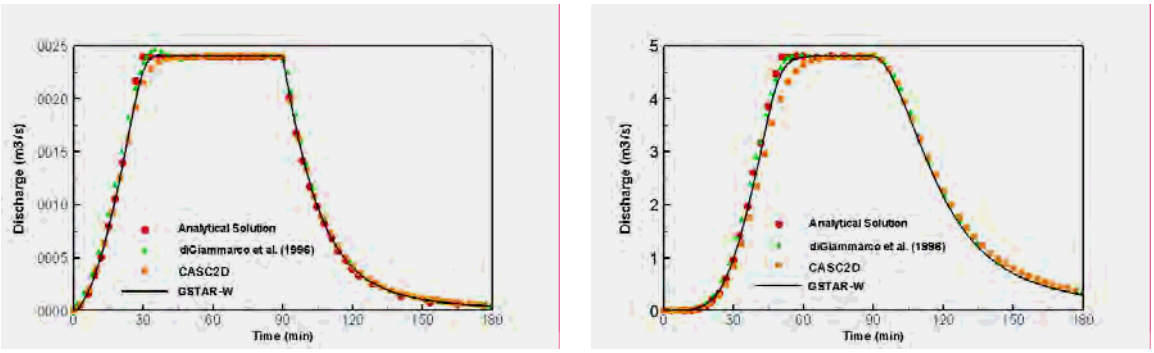


Figure 2 Unstructured Mesh Used

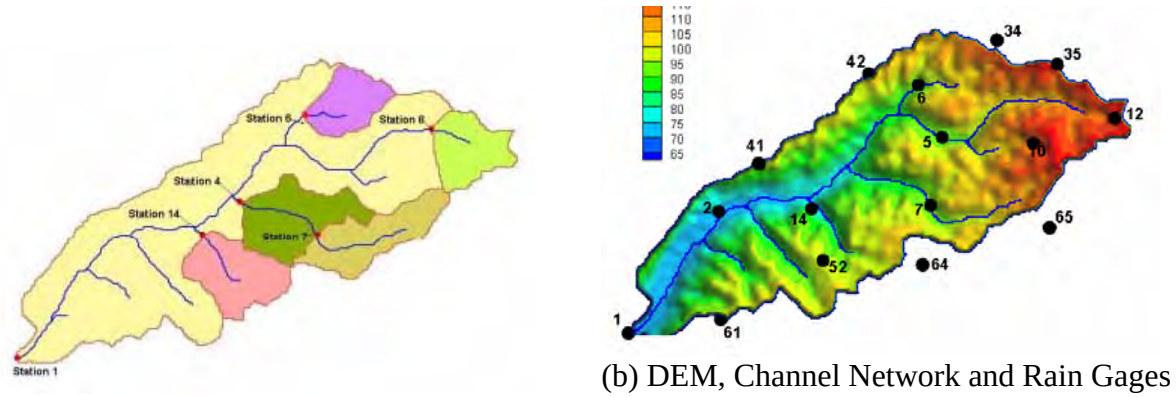


(a) at the Overland Exit into the Channel (b) at the Channel Exit

Figure 3 Comparison of Discharges for the 2D Runoff Case

Goodwin Creek Experimental Watershed: The runoff and erosion model is applied to the Goodwin Creek Experimental Watershed. Comparison is made between the GSTAR-W, CASC2D and the measured data at six gage stations shown in Fig.4a. A detailed presentation of the case is available in Lai and Yang (2004) with regard to the watershed and inputs to the model such as the digital elevation model, soil types, land use, precipitation, and others. They are only briefly described next while focus will be on the results and comparisons.

The digital elevation model (DEM) is available at 30-meter resolution and data are preprocessed first using TOPAZ to obtain a depressionless DEM (Sanchez 2002). The channel network and watershed are then delimited from the smoothed 30-meter DEM. Figure 4b shows the DEM and the channel network. Seven soil types are used based on the soil characteristics study by Blackmarr (1995). The land use is reclassified as forest (includes planted forest), pasture (includes idle land), water, and cultivated.



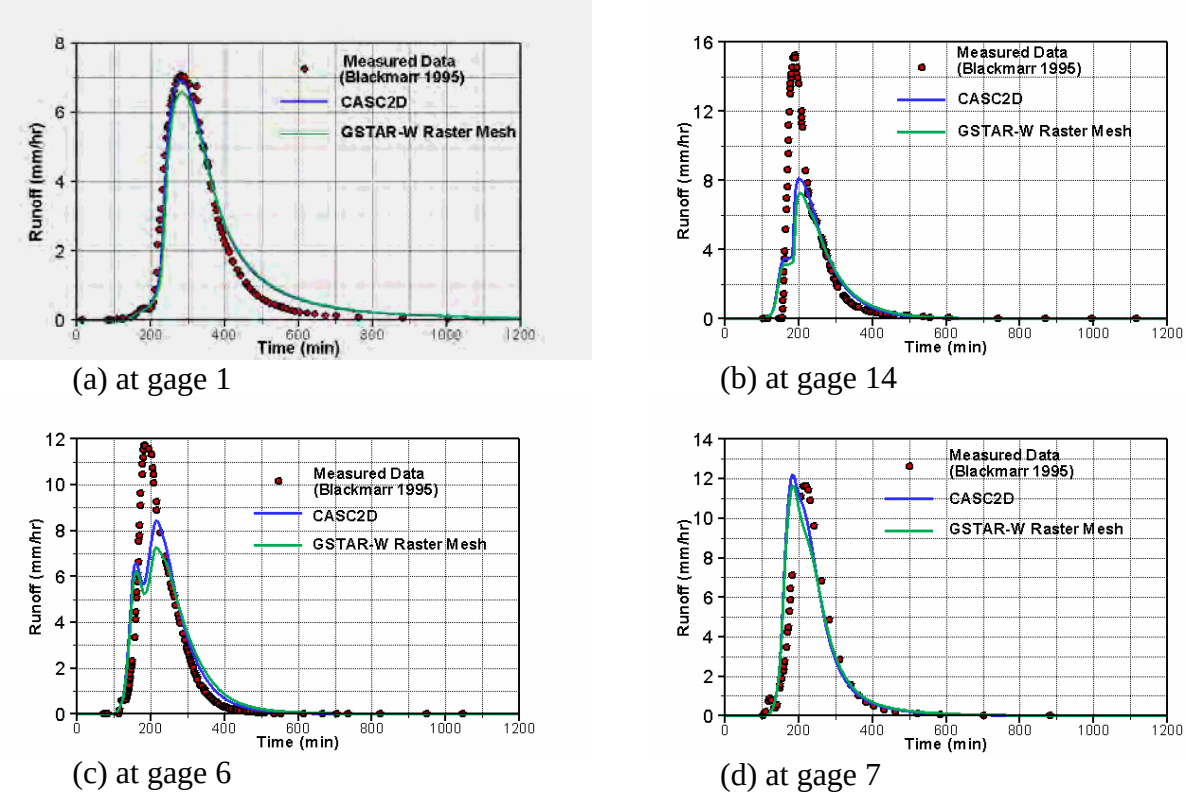
(a) Six Hydrograph Stations (b) DEM, Channel Network and Rain Gages

Figure 4 Goodwin Creek Watershed Information

The storm event of October 17, 1981 is chosen for simulation as the same event was also simulated by Sanchez (2002) with CASC2D. This event began at 9:19 pm and had a total rainfall duration of 4.8 hours with very little rainfall preceding this event. Precipitation data were taken from sixteen rain gages (see Fig.4b) that are located within and just outside the watershed. The entire watershed is divided into two zones: the overland zone solved with the distributed method

and the channel zone with the 1D diffusive wave solver. Two meshes are used: 30m-by-30m raster mesh the mixed element unstructured mesh. All input data and parameters used are the same as those of Sanchez (2002) unless otherwise stated. No attempt has been made to calibrate the parameters to fit the field measured data.

The first comparison in Fig.5 is between GSTAR-W and CASC2D with the raster mesh for flow hydrographs at four gage stations. The following are found: (1) The same results are predicted by GSTAR-W with the explicit and implicit solvers and with different time steps. Only one curve, therefore, is plotted with GSTAR-W; (2) Results from GSTAR-W and CASC2D are close but GSTAR-W results are consistently smaller than those of CASC2D. This may be attributed to the different resistance equations used. Smaller flow resistance was used by CASC2D even if the Manning's coefficients are the same for the two models; (3) It is noticed that a significant under-prediction of the peak occurred for stations 6 and 14. These are the smallest sub-catchments within the watershed (see Fig.4a) and therefore, errors may be attributed to sources such as the accuracy of precipitation and the delineated channel.



(a) at gage 1 (b) at gage 14

(c) at gage 6 (d) at gage 7

Figure 5 Comparison of Hydrographs with the 30-meter Raster Mesh.

The second set of comparisons is between the raster mesh and the mixed element unstructured mesh in order to see the difference between two mesh representations. Figure 6 shows the comparison when the channel Manning coefficient fixed at 0.035 for both mesh. It is seen that the predicted hydrograph at the watershed exit (station 1) is way off the measured one for the unstructured mesh, though the results are fine at other stations. It is found that this discrepancy is not due to the failure of the model but to the difference in channel representation of the two models. With the raster mesh, the channel is represented by the zigzagging mesh cells and as a

result, the channel length is longer than that of the unstructured mesh. If the channel length for each reach is increased for the unstructured mesh to the same value represented by the raster mesh, simulation results are obtained. This points out that the channel Manning coefficient was calibrated by the raster mesh using the wrong channel length! If the Manning coefficient is re-calibrated with the correct length, the Manning coefficient of 0.06 is obtained. Such re-calibrated results are shown in Figure 7. It is seen that agreement between the two meshes is much better. The difference at station 6 is hard to explain and it may be due to the difference of mesh size and density for the subcatchment. It is worthwhile to point out that the roughness coefficient of 0.06 is probably a more realistic value as the same roughness coefficient was found and used in applying the 1D CONCEPTS model to the channels of the Goodwin Creek watershed (Langendoen 2000). The above results show that a correction should be carried out to the channel length when a raster mesh is used to represent the channel. Without the correction, the calibrated roughness coefficient may be in error.

Next, predicted and measured sediment discharges at the six gage stations are compared in Figure 8. Overall the GSTAR-W results are similar to those of CASC2D by Sanchez (2002) as essentially the same input parameters and the same transport capacity equations have been used. In comparison with the field data, it is noted that significant under prediction at station 7 and 14 is observed. The reason is unclear and possibilities may include several. One of them may be that bank erosion and slide in the channel or gully erosion on the sub-catchment may occur that are not modeled.

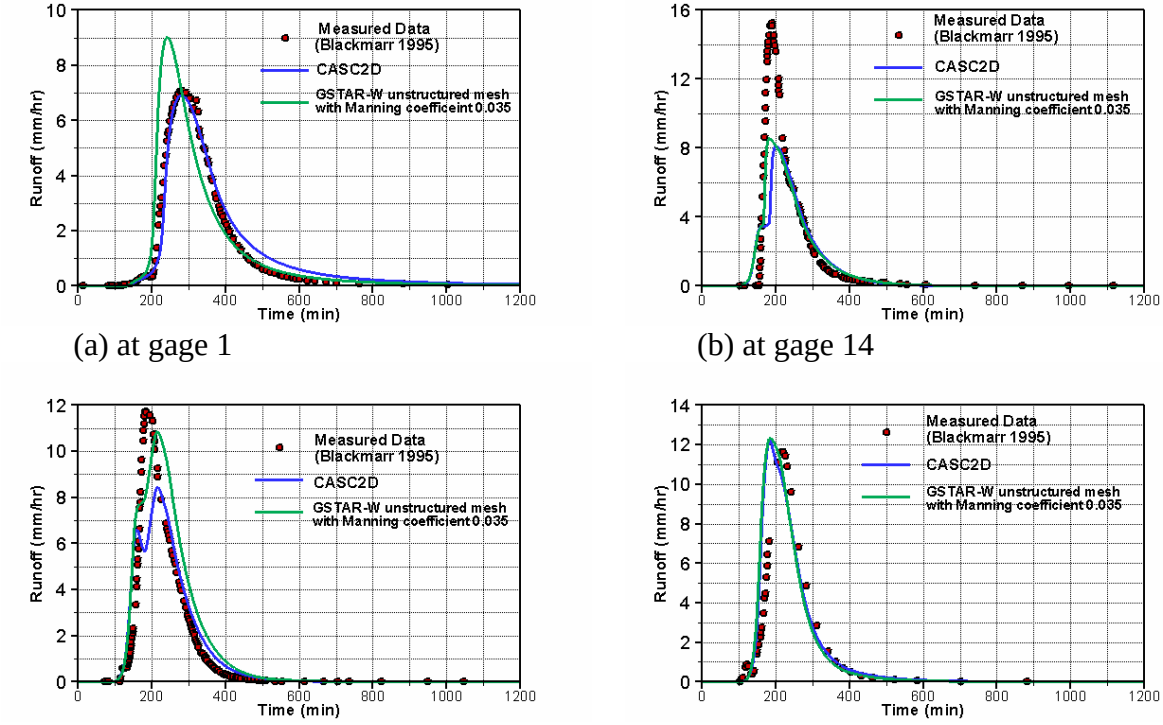
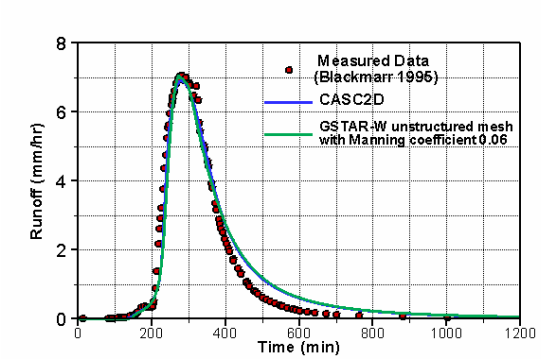
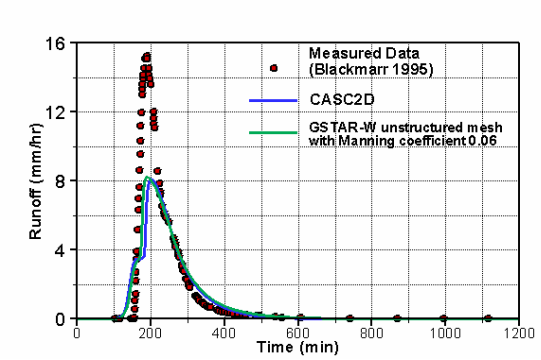


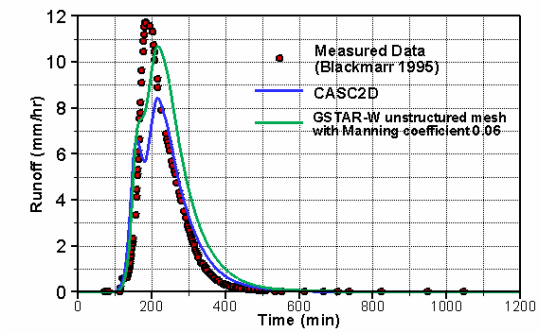
Figure 6 Comparison of Hydrographs with the Unstructured Mesh, n=0.035



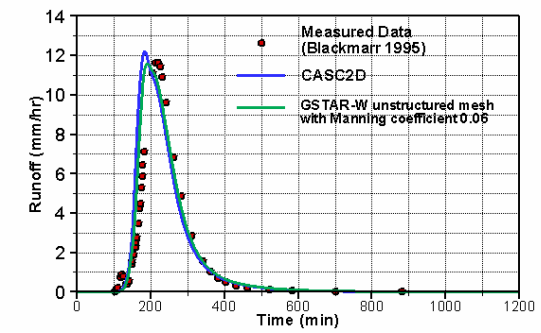
(a) at gage 1



(b) at gage 14

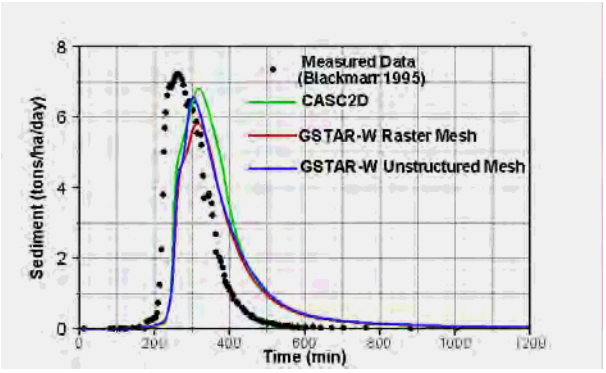


(c) at gage 6

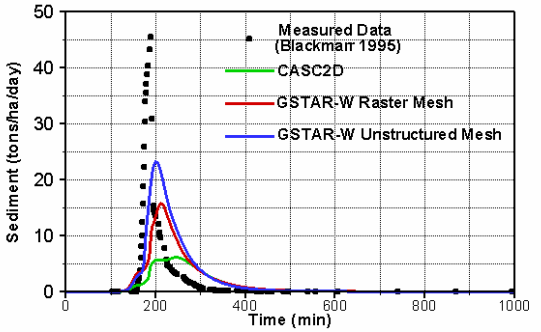


(d) at gage 7

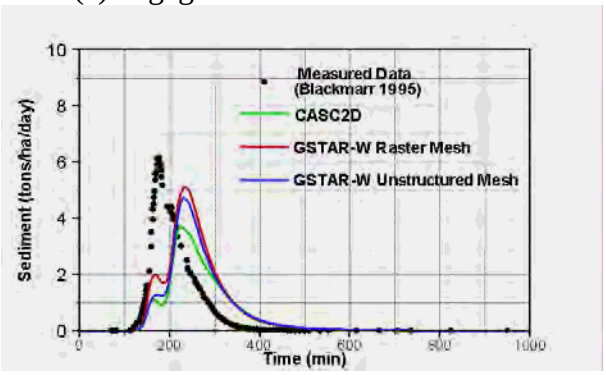
Figure 7 Comparison of Hydrographs with the Unstructured Mesh n=0.06



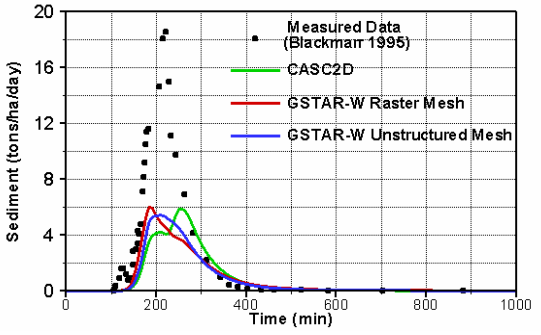
(a) at gage 1



(b) at gage 14



(c) at gage 6



(d) at gage 7

Figure 8 Comparisons of Sediment Graphs between CASC2D and GSTAR-W

One of the benefits of distributed modeling is its ability to predict flow and the erosion and deposition patterns. Such information may be used to assist the erosion management assessment and plan. The predicted water depth at 210 minutes and the predicted erosion and deposition pattern at 300 minutes after the storm event are displayed in Fig.9 and Fig.10. It clearly demonstrated the usefulness of the modeling as high erosion area could be identified graphically.

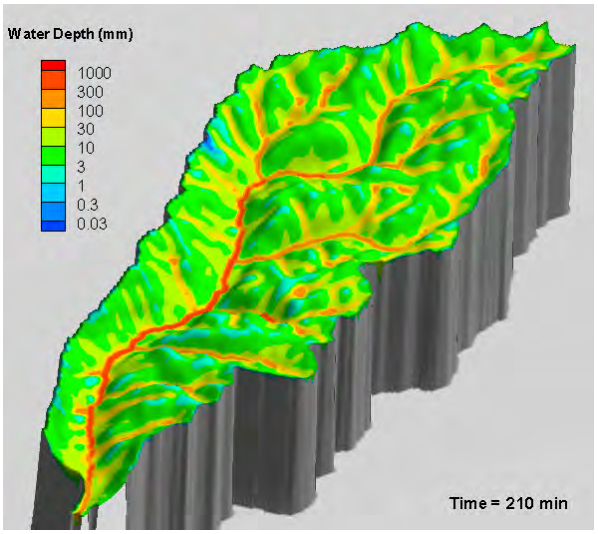


Figure 9 Water Depth at 210 Minutes

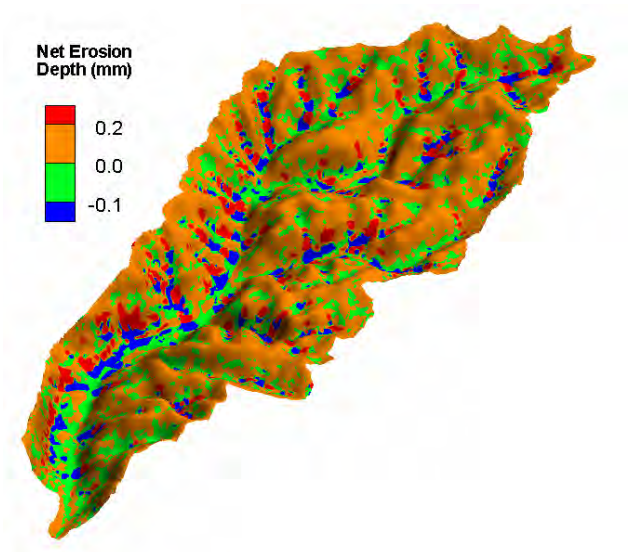


Figure 10 Net Erosion Depth at 300 Minutes

CONCLUDING REMARKS

An enhanced distributed model, GSTAR-W, has been developed to model the water runoff and soil erosion on watershed. The hybrid zonal modeling concept is proposed that is a major departure from the single zone raster mesh approach of most existing models. In addition, unstructured and implicit solution method is developed for the distributed zone that is more general and flexible than the raster mesh and more robust than the explicit method. Selected test cases of the model verify the model. Future work will focus on the demonstration of the hybrid zonal modeling capability and the ability of the model to resolve the scale issue, at least partially.

ACKNOWLEDGEMENTS

The author wishes to acknowledge assistance of John England at the Technical Service Center, Bureau of Reclamation, for CASC2D help. The peer review by Tim Randle is also acknowledged.

REFERENCES

Beven, K.J. (1985). Distributed Models in Hydrological Forecasting, edited by M.G. Anderson and T.P. Burt, John Wiley, NY, 425-435.

Blackmarr, W. A. (1995). Documentation of Hydrologic, Geomorphic, and Sediment transport Measurements on the Goodwin Creek Experimental Watershed, Northern Mississippi, for

the Period 1982-1993 - Preliminary Release. Research Report No.3 (CD-ROM), U.S, Dept. of Agriculture. Agricultural Research Service.

DiGiammarco, P., Todini, E., and Lamberti, P. (1996). "A Conservative Finite Element Approach to Overland Flow: the Control Volume Finite Element Formulation," J. Hydrology, 175, 267-291.

Ewen, J., Parkin, G., and O'Connell, P.E. (2000). "SHETRAN: Distributed river basin flow and transport modeling system," ASCE J. Hydrologic Engrg., 5(3), 250-258.

Johnson, B. E., Julien, P. Y., Molnar, D.K., and Watson, C.C. (2000). "The two-dimensional upland erosion model CASC2D-SED," Journal of The American Water Resources Association, 36(1), 31-42.

Julien, P. Y. , Saghafian, B., and Ogden, F. L. (1995). "Raster-based hydrologic modeling of spatially-varied surface runoff," Water Resource Bull., 31(3), 523-536.

Lai, Y.G. (2000). "Unstructured Grid Arbitrarily Shaped Element Method for Fluid Flow Simulation," AIAA Journal, 38(12), 2246-2252.

Lai, Y.G. and Yang, C.T. (2004). Development of a Numerical Model to Predict Erosion and Sediment Delivery to River Systems, Progress Report No.2: Sub-Model Development and an Expanded Review. Department of the Interior, Bureau of Reclamation, Technical Service Center, Denver, Colorado.

Langendoen, E. J. (2000). CONCEPTS – Conservational channel evolution and pollutant transport system: Stream corridor version 1.0. Research Report No. 16, US Department of Agriculture, Agricultural Research Service, National Sedimentation Laboratory, Oxford, MS.

Nearing, M. A., Foster, G.R., Lane, L.J., and Finker, S.C. (1989). "A Process-Based Soil Erosion Model for USDA-Water Erosion Prediction Project Technology," Transactions of the ASAE, 32(5), 1587-1593.

Sanchez, R. R. (2002). "GIS-based Upland Erosion Modeling, Geovisualization and Grid Size Effects on Erosion Simulations with CASC2D-SED," Ph.D. Thesis, Civil Engineering, Colorado State University, Fort Collins, CO.

Sharika, U., Senarath, S., Ogdon, F.L., Downer, C.W., and Sharif, H.O. (2000). "On the Calibration and Verification of Two-Dimensional, Distributed, Hortonian, Continuous Watershed Models," Water Resour. Res., 36(6), 1495-1510.

Yang, C.T., Lai, Y.G., Randle, T.J., and Dario, J.A. (2003), Development of a Numerical Model to Predict Sediment Delivery to River Systems in a Watershed: Project Progress Report No.1: Review and Evaluation of Erosion Models and Description of GSTAR-W Approach. Department of the Interior, Bureau of Reclamation Technical Service Center, Denver, Colorado.

ANNAGNPS: ACCOUNTING FOR SNOWPACK, SNOWMELT, AND SOIL FREEZE-THAW

Daniel S. Moore, P.E., Hydraulic Engineer, USDA-NRCS, Portland, OR, dan.moore@por.usda.gov; Ronald L. Bingner, Agricultural Engineer, USDA-ARS, Oxford, MS, Fred D. Theurer, Agricultural Engineer, USDA-NRCS, Beltsville MD

Abstract: The watershed model, AnnAGNPS (Annualized AGricultural Non-Point Source Pollution model) has been enhanced by incorporating winter climate algorithms that account for frozen soil conditions. The model includes snowpack accumulation and melt, and the freeze-thaw process in the soil. Three major improvements can be expected for watersheds with significant winter climates. First, the model will better account for the lag in runoff from precipitation held for months in snowpack. Second, the model will more accurately account for the movement of water through the soil layers and any resulting runoff. Third, the model will better account for the increase in sheet and rill erosion due to runoff over soil layers that have experienced the freeze-thaw process. These model improvements synthesize the science of the SHAW model (Simultaneous Heat and Water) by Gerald Flerchinger, Agricultural Research Service, Boise Idaho. SHAW, however, is a research model, while AnnAGNPS is a watershed model used by engineers and other practitioners for practical applications. In adapting SHAW, several modifications in computational procedures were made. For example, while the AnnAGNPS heat flux algorithm retains a simultaneous matrix solution of the temperature profile in soil and snow layers, the default timesteps and solution tolerances are larger than in SHAW. In addition, the first release of winter-enhanced AnnAGNPS will not include a full simultaneous matrix solution of soil moisture in thermal layers, as is done in SHAW. AnnAGNPS may adopt this in the future, but presently computes soil moisture in a more simplified manner. Also, SHAW includes a thermal layer for surface residue. This highly desired model component will be incorporated into AnnAGNPS in a future release. The AnnAGNPS winter enhancements improve modeling capability for many more geographic locations and will result in better sediment yield and pollutant loading estimates for water quality improvement in natural resources planning.

INTRODUCTION

The initial development and ongoing enhancement of water quality models is, of course, subject to considerable debate about appropriateness of scale, scope, complexity, and accuracy of results. Modeling the freeze-thaw process in the soil profile is inherently complex, and simplified procedures do not often produce meaningful results. The complexity of this natural process may be on a plane quite above the other modeled processes such as rainfall/runoff in many water quality models. The purpose of modeling the freeze-thaw process down into the soil profile, rather than merely at the surface, is that many watersheds, for example the Palouse area in the state of Washington, experience significant soil loss when a moderate rainfall event occurs on a thin layer of unfrozen soil, overlaying a deeper frozen layer. Other models similar to AnnAGNPS, such as SWAT, attempt to estimate soil surface temperature in an effort to better estimate winter runoff (Arnold and Fohrer, 2005). But sub-daily timesteps and an algorithm that takes into account heat and moisture fluxes in the soil profile are required for estimating the additional erosion

off of frozen sublayers. It may be suggested that coupling a highly complex soil profile algorithm with a very simple soil loss methodology, such as RUSLE, is a mismatch. Many water quality models have been designed to model complex hydrologic processes using simplified methods that were developed for entirely different purposes, such as single-event flood peak models for engineering uses. Whether or not both the curve number method for runoff and RUSLE for erosion are appropriate is a matter of some debate (Garen and Moore, 2005). But ongoing enhancement of models naturally involves this kind of leap-frogging, and there is no reason that improvement in the snowpack accumulation and melt, soil freeze-thaw, and soil moisture accounting cannot be followed by improvements of these other processes.

Adapting SHAW: The winter enhancements to AnnAGNPS are based on an elaborate research model that can be calibrated and sufficiently tested only with large amounts of empirical data. The Simultaneous Heat and Water Transfer Model, by Gerald Flerchinger of the Agricultural Research Service in Boise, Idaho, is a physical process model that simulates the movement of heat, water, and solutes through the soil column. It accounts for all the relevant thermodynamic processes such as shortwave and longwave radiation, conductance, and latent heat transfer. It accounts for snowpack accumulation, compaction, and melt. It captures the soil/snow temperature and moisture profile by analyzing it as a matrix of thermal layers for which heat and moisture flux equations are written and solved simultaneously. The model was originally verified and calibrated using data from twelve field plots, seven meter by thirty meter each, in which different types of tillage and different amounts of crop residue were applied. Weather data, including precipitation, air temperature, relative humidity, wind speed, and solar radiation were collected, as well as soil temperature and moisture data in the soil profile. Some necessary equation parameters were not measured but assumed from the empirical investigations and testing of other researchers. Flerchinger and colleagues concluded that the model performed well and showed “excellent agreement between observed and measured snow and frost depths, soil temperatures, and moisture contents” which were also “obtained with minimal calibration” (Flerchinger, 1987).

Available for several years, AnnAGNPS has undergone continual update and improvement. See Bingner (2001). The winter options include a matrix of thermal layers with finite difference equations for each to balance the heat fluxes. Sub-daily timesteps of default three hours are employed and air temperature is varied in the 24 hour time period between high and low. Snowpack settles and compacts over time, as is done in SHAW, and snow releases melt-water only after the liquid-holding capacity of the pack is satisfied. Moisture is percolated through the soil layers using hydraulic conductivity, varying by soil type and moisture content. Runoff is generated by either saturation excess or freezing of the topmost thermal layer, or saturation at the soil surface due to high intensity rainfall or rapid melt.

The details of the SHAW adaptation are given below, with discussion of assumptions, simplifications, increased timestep length, and relaxed solution tolerances of the heat balance iterative solution. Intended future enhancements are also discussed..

SOIL PROPERTIES

AnnAGNPS currently accepts as input a very detailed and complete set of soil properties for any multi-layered soil. The use of GIS and soil databases such as SSURGO (USDA-NRCS 2005a) or STATSGO (USDA-NRCS 2005b) facilitate the differentiation of soil parameters spatially and depthwise in any watershed. For the soil temperature profile important parameters are thermal conductivity and heat capacity, both highly dependent on soil type and moisture content. To determine thermal conductivity AnnAGNPS employs the method of Johansen, generally accepted as best by several researchers, which takes into account soil grain size, quartz content, and moisture (Johansen, 1975, Andersland and Ladanyi, 1994). Soil heat capacity in AnnAGNPS is a function of silt, sand, clay, and organic content (Andersland and Ladanyi, 1994).

The temperature at the bottom of the soil column is considered constant and assumed to be the average annual air temperature at the watershed location. The depth at which the annual temperature variation decreases markedly (called the damping depth) is dependent on the amplitude of the temperature variation at the surface and the soil thermal diffusivity. Normally, damping depth refers to the depth at which the amplitude of temperature variation is about one third that at the surface, but it can be determined for any amplitude variation. Thus, for AnnAGNPS, the damping depth is determined for an amplitude of plus or minus 2.5º C at the bottom of the soil profile. The thermal layers may not extend to that depth, but the initial temperature of each thermal layer is determined from an elliptical curve between air temperature at the top and damping depth.

SNOWPACK PROPERTIES

Air and dewpoint temperatures are adjusted with elevation, and precipitation is considered snow when both the average temperature of the day and the dewpoint are below zero degrees C. The snow density at time of snowfall is dependent on air temperature (Marks, et al., 1999). Density of the snowpack is adjusted with time as settling and compaction occur, following SHAW, citing Anderson (1976). Snow albedo is determined, based on snow "optical" grain-size and solar azimuth (Marks, et al., 1999) following the procedure provided in the web-based image processing workshop, "Software Tools for Hydro-Climatic Modeling and Analysis", (Frew and Dozier, 1986). The snowpack thermal layers are at most two in number, with the top layer varying in thickness up to a maximum of 20cm and the lower layer varying up to the total remaining depth of the snowpack. The maximum thickness of the top snow layer was set at 20cm, as this is generally the thickness for which the layer temperature can be affected by aerodynamic variables such as radiation and convection (Marks, et al., 1999). When no lower snow layer exists some shortwave solar is considered to reach through to the soil layer, attenuated with greater depth or density. Of course, snowpacks may be quite deep in mountainous regions, and although it may be suggested that more thermal layers would be needed to properly delineate the temperature profile for such depths of snow, the agricultural watersheds generally modeled by AnnAGNPS tend to have shallower snowpacks. The model tracks the age, settling, and compacting of up to a week's new snowfall, as well as that of the remaining pack. The liquid water holding capacity of each snow layer is tracked, meltwater drained, and thickness adjusted on a timestep basis.

CLIMATE DATA INPUT

AnnAGNPS currently uses six major daily climate data variables: precipitation, max & min temperature, dewpoint temperature, solar radiation, and wind speed. The winter algorithms employ several techniques to distribute this data through the 24-hour day. Temperature is varied on a sine curve from the high, assumed to occur at 4pm, to the low, assumed to occur at 4am. Air and dewpoint temperatures are also varied with elevation. Daily precipitation can be varied during the day by storm type distributions. Solar radiation is varied based on latitude, date, and sun angle, as well as the slope and aspect of the ground for each "cell" or subwatershed unit. None of these data requirements are new with the winter enhancements.

THERMAL LAYERS

As discussed above, the snow thermal layers vary in thickness, with the top layer no thicker than 20 cm and the lower layer the remainder of the snowpack. The soil thermal layers are of pre-determined and unchanging thickness. As shown in Figure 1, below, a residue layer belongs between the two, and this is a feature of SHAW, not yet incorporated into AGNPS.

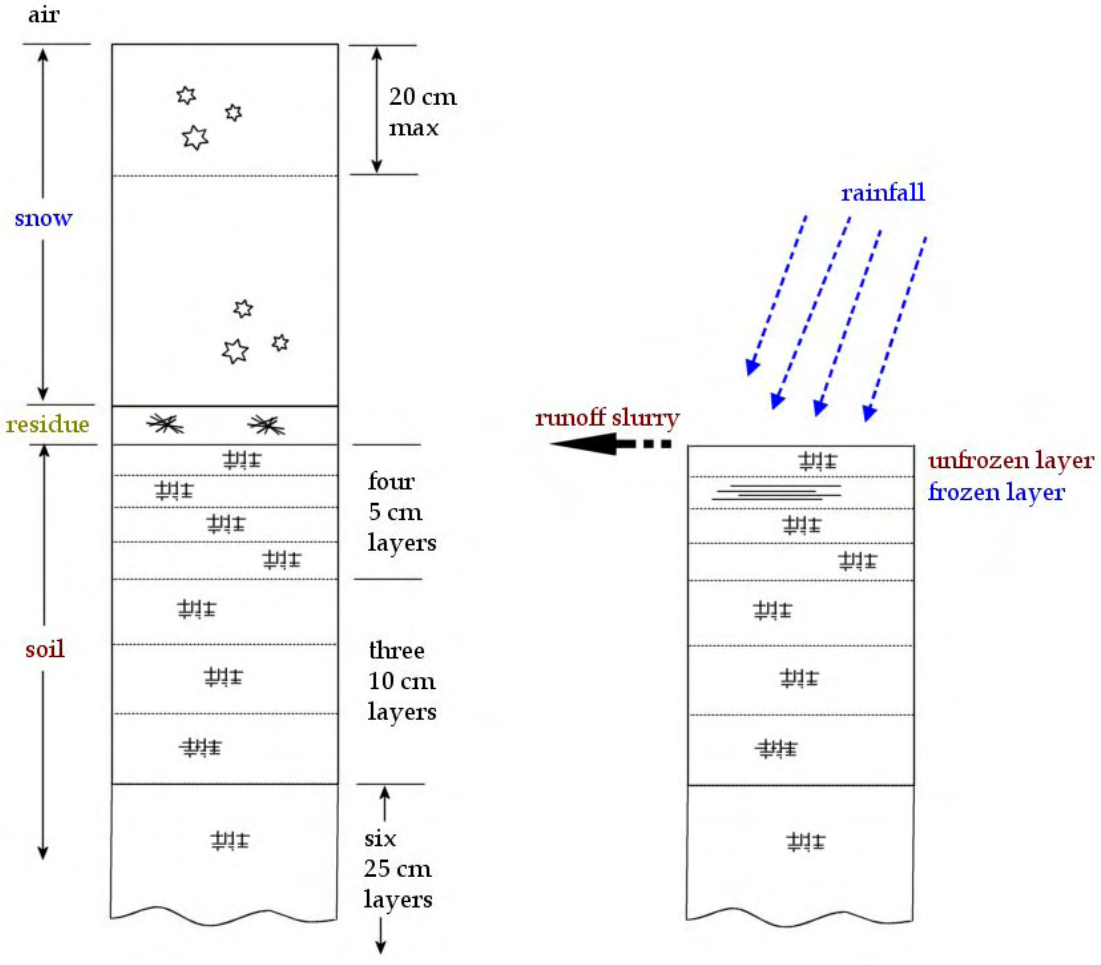


Figure 1 Snow-residue-soil thermal layers and an erosive runoff scenario.

The soil thermal layer thicknesses are thinner at the top and increasing down into the soil column because the upper layers experience more rapid temperature variation. In addition, thinner layers enable a more refined estimate of erosion over frozen soil. This latter scenario is also shown in Figure 1 above, in which the snowpack has melted or a significant rainfall is occurring while a thin top layer of soil is unfrozen, but a lower layer remains frozen. The frozen layer acts as something of a pavement, facilitating incorporation of soil from the unfrozen layer into the runoff stream. The deeper frozen layer, however, is not the only cause of the additional erodibility. As discussed in Gatto and Ferrick (2003), a good overall discussion of the phenomenon, the freeze-thaw process weakens the upper layers regardless of an underlying frozen layer.

For comparison, the center nodes of the soil layers used for the initial verification of SHAW were (in cm, not including a shallow top layer) 7.5, 15, 25, 38, 53, 68, 83, 107, 137, and 167. Many more recent articles exist concerning SHAW. See Flerchinger and Seyfried (1997) or Flerchinger, Hardegree, and Johnson (1998).

ENERGY BALANCE

Heat flow proceeds in the lower soil layers due to conduction between layers of different temperature, advection by moisture moving through the layers, and latent heat exchange due to phase change of the moisture. For the upper soil layer, or top snow layer, whichever is exposed to the atmosphere, additional significant heat flow is induced by radiation, convection due to wind, and advection from precipitation. As documented by Flerschinger (1987), second-order partial differential equations can be written for layers of infinitesimal thickness, with terms to represent each type of possible heat flux. To make practical application of these continuity equations, and apply them to thermal layers of finite thickness, they are reformulated as finite difference equations which approximate the partials. The solution of each layer's equation is dependent on the heat flux in neighboring layers, so the entire set of equations must be solved simultaneously.

A Key Assumption: Each thermal equation involves a number of unknowns related to either temperature or moisture content. Many references are available, for example, Marion (1995), which discuss the phenomenon of freezing point depression, and Flerchinger (1987) documents how the SHAW model takes into account the fact that the soil freezing temperature is dependent on, among other factors, solute concentration and matric potential. Freezing soil acts as a moisture sink, causing migration of water and solutes toward the freezing front. As the water freezes solutes are excluded and concentrate at the front. This phenomenon is not treated by the AnnAGNPS adaptation of SHAW. More significantly, neither is freezing point depression. By assuming a known temperature at which water freezes in the soil, the energy balance can compute ice content for layers in the process of freezing while simultaneously computing temperature for non-freezing layers. The AnnAGNPS winter algorithm could set this "known" phase change temperature at some subzero value, but currently it is assumed that soil water freezes at 0º C. Flerchinger indicated in conclusions from SHAW verification tests that "even very high concentrations of solutes seemingly have very little effect on soil freezing", while having a greater impact on salt redistribution.

Thus, if a soil layer contains no ice or is completely frozen then that layer's temperature is solved for. If the layer contains both ice and liquid, then the temperature of that layer is known (0º C) but the ice content of that layer becomes the unknown to solve for. For a snow layer, either the temperature is unknown or the layer contains meltwater and the temperature is known (zero), but the meltwater content becomes the unknown. Since each layer's equation also contains variables relating to its neighbors, the phase state of those layers also affects the given layer. The mechanics of the simultaneous solution of this matrix of equations is discussed in the Matrix Solution section below.

MOISTURE BALANCE

The percolation of moisture from one layer to another is dependent on hydraulic conductivity, matric potential, and moisture content of both layers, in addition to the moisture supply from above. Thus, a full moisture balance requires simultaneous solution of finite difference continuity equations written for the moisture flux of each layer. Keeping track of the moisture is a critical aspect of the energy balance, as well as for determining the instigation of runoff at the surface. Freezing and thawing involve the highly significant latent heat of fusion term. And the thermal conductivity of a soil layer depends on its moisture content. The SHAW model performs a full moisture balance of finite difference equations, solving either for matric potential, or ice content if the layer contains ice.

AnnAGNPS, however, simplifies the moisture accounting and avoids a simultaneous matrix solution. (A more complete moisture balance may be adopted in the future.) The simplified moisture accounting is accomplished as follows. Percolation through the thermal layers is computed by examining three layers at a time, starting at the bottom of the soil column at proceeding up, one layer at a time. Thus, the moisture content and percolation of two of the three layers can be adjusted twice, based on available incoming moisture from layers above. Percolation is assumed zero for layers more than 50% frozen and reduced for layers up to half frozen. This moisture accounting is computed at each timestep, but after the energy balance. For layers containing ice, liquid and ice content having been previously determined in each timestep by the energy balance, the liquid content only is adjusted for percolation into or out of that layer. Moisture loss due to evapotranspiration is accounted for in the top four thermal layers.

AnnAGNPS keeps track, on a timestep basis, of the infiltration or runoff of snowmelt or rainfall, accounting for a frozen or partially frozen top soil layer, and due to either saturation excess or infiltration excess. Surface saturation is computed by the Green-Ampt method, but should be coupled with the optional storm distribution capability which distributes daily rainfall into subdaily timesteps.

MATRIX SOLUTION

The equations for each thermal layer generally have three unknowns, relating to the given layer and its neighbors. A common method for solving indeterminate equations is the so-called Newton-Raphson method, a root-finding algorithm by which the first two terms (generally) of a Taylor Series expansion are used to continually improve on solution

estimates until an acceptable tolerance range is achieved. As long as the first estimate is "reasonably close" to the correct solution the method converges rapidly. In addition, since each thermal layer and its neighbors are a successive trio through the soil/snow profile, the equation set forms a "tri-diagonal matrix" for which very efficient programming algorithms exist. It remains to be determined what tolerance range is acceptable for the solution.

AnnAGNPS timesteps, tolerances, and iteration limits: The SHAW initial verification employed one-hour timesteps. Solution tolerances were 0.0001º C for temperature and a maximum of ten iterations were attempted before non-convergence was assumed. (In that case, SHAW would automatically halve the timestep and try again.) The AnnAGNPS adaptation uses similar thermal layer thicknesses (as mentioned above), a default timestep of three hours, increases the temperature tolerance to ±0.1 º C, and assumes non-convergence after eight iterations. The algorithm allows a decreasing of timestep size to one-hour and a re-attempt at convergence, but only after performing a check of phase condition. In testing, the AnnAGNPS matrix solution scheme usually converges very rapidly, within one or two iterations, unless it is contemplating a phase change. If non-convergence seems to be as a result of phase change in the layer, the checking algorithm looks at how close the convergence came and whether freezing or thawing should be expected. If meeting relaxed criteria for just that particular timestep, the solution is accepted.

Other Assumptions: The SHAW model includes a term in the snowpack thermal layers for heat exchange due to vapor transfer, which also enables the computation of snowpack mass loss due to sublimation. It includes a similar term for the soil layers. Both of these are neglected in the AnnAGNPS adaptation. The loss of soil moisture mass due to evapotranspiration, however, is not neglected.

PLANNED ENHANCEMENTS

AnnAGNPS gives the modeler significant capability to account for the impact of agricultural management practices, and since a residue thermal layer can be expected to significantly affect the freeze-thaw process in the soil, adding this feature is planned. AnnAGNPS can also model watersheds of greatly varying size, with over 100 years of simulated climate data. Using a cpu intensive feature such as the winter algorithm may not be feasible for very large watersheds. The current winter algorithm includes some attention paid to computational efficiency, such as not running winter calculations out of season.. Future enhancements will include further attention to computational efficiency. At the same time, adding the option of a full moisture balance will be explored.

SUMMARY

The NRCS watershed model AnnAGNPS has many features that enable an accounting of the water quality impacts of agricultural practices including crop types, field management practices, fertilizers, irrigation, and soil erosion mitigation measures. The addition of a winter algorithm to account for the runoff lag due to snowpack water storage, as well as infiltration and runoff over frozen soil, and the additional erosion from freeze-thaw impacts provides important new modeling capability.

REFERENCES

Andersland, O. and Ladanyi, B. (1994). Frozen Ground Engineering, Chapman and Hall, New York, NY.

Anderson, E.A. (1976). A point energy and mass balance model of a snow cover. US Dept. of Commerce, National Weather Service, NOAA Technical Report NWS 19.

Arnold, J.G. and Fohrer, N. (2005). "SWAT2000: current capabilities and research opportunities in applied watershed modeling," Hydrol. Processes 19(3), pp 563-572.

Bingner, R.L. and Theurer, F.D. (2001). "AnnAGNPS: estimating sediment yield by particle size for sheet & rill erosion," in Proceedings of the Seventh Federal Interagency Sedimentation Conference, Reno NV.

Flerchinger, G.N. (1987). "Simultaneous heat and water model of a snow-residue-soil system," Ph.D. Dissertation, Washington State University, Pullman WA.

Flerchinger, G.N. and Seyfried, M..S. (1997). "Modeling soil freezing and thawing and frozen soil runoff with the SHAW model," in Proceedings of the International Symposium on Physics, Chemistry, and Ecology of Seasonally Frozen Soils, Fairbanks AK, CRREL Special Report 97-10, US Army Cold Regions Research and Engineering Laboratory, Hanover, NH.

Flerchinger, G.N., Hardegree, S.P., and Johnson, G.L. (1998). "The simultaneous heat and water (SHAW) model: a research tool for management decisions," in Proceedings of the First Interagency Hydrologic Modeling Conference, Las Vegas, NV.

Frew, J., and Dozier, J. (1986). "The image processing workbench—portable software for remote sensing instruction and research," in Proceedings of the 1986 International Geoscience and Remote Sensing Symposium, European Space Agency, Paris, ESA SP-254, pp 271-276, see http://sevilleta.unm.edu/technology/reference/ipw/www/.

Garen, D.C. and Moore, D.S. (2005). "Curve number hydrology in water quality modeling: uses, abuses, and future directions," J. of the American Water Resources Association 41(2), pp 377-388.

Gatto, L.W. and Ferrick, M.G. (2003). Overland erosion due to freeze-thaw cycling. CRREL Technical Report 03-3, US Army Cold Regions Research and Engineering Laboratory, Hanover, NH.

Johansen, O. (1975). "Thermal conductivity of soils", Ph.D. Thesis, Norwegian Technical University, Trondheim, Norway, translated by R. Stone, 1977, in Draft Translation 637, US Army Cold Regions Research and Engineering Laboratory, Hanover, NH.

Marion, G.M. (1995). Freeze-thaw processes and soil chemistry. CRREL Special Report 95-12, US Army Cold Regions Research and Engineering Laboratory, Hanover, NH.

Marks, D., Domingo, J., Susong D., Link, T., and Garen, D. (1999). "A spatially distributed energy balance snowmelt model for application in mountain basins," Hydrol. Processes 13(12,13), pp 1935-1959.

USDA-NRCS (2005a). Soil Survey Geographic Database, SSURGO, National Soil Information System, http://nasis.nrcs.usda.gov/.

USDA-NRCS (2005b). State Soil Geographic Database, STATSGO, National Cartography and Geospatial Center, http://www.ncgc.nrcs.usda.gov/products/datasets/statsgo/.

WASH LOAD/BED MATERIAL LOAD CONCEPT IN REGIONAL SEDIMENT MANAGEMENT

David S. Biedenharn, Research Hydraulic Engineer, U.S. Army Corps of Engineers, U.S. Army Engineer Research Development Center, Coastal and Hydraulics Laboratory, Vicksburg MS; Colin R. Thorne, Professor, University of Nottingham, School of Geography, Nottingham, England; Chester C. Watson, Professor, Colorado State University, Department of Civil Engineering, Fort Collins, CO

Abstract: As water resource projects become more and more complex, there is a growing emphasis on the ability to implement effective regional sediment management. A common goal of many regional sediment management projects is the reduction of sediment loading from the watershed. This is usually accomplished by rehabilitation features such as grade control, bank stabilization, drop pipes, and land treatments. While these features are often implemented with the stated purpose of reducing sediment yields to downstream reservoirs, flood control channels, or wetlands, the spatial and temporal impacts of these features with respect to downstream sediment loads are far from straightforward, and often result in unanticipated morphologic adjustments and degradation of riverine habitats and ecosystems. Effective regional sediment management lies in identifying the sediment sources and sediment sinks in the watershed and understanding the processes responsible for transferring sediment along the pathways that link sediment sources and sinks at the reach and watershed scales. This paper describes how the concepts of wash load and bed-material load can be used to document how sediments are transported through channels systems, thereby, serving as the foundation for effective regional sediment management.

INTRODUCTION

Requirements for new water resource and river management projects to meet objectives in ways that are environmentally and economically sustainable have led to increasing attention on associated impacts on sediment dynamics and sedimentation in the fluvial system. Engineering works and management actions that fail to account for sediment dynamics risk disrupting sediment transfer in the fluvial system, triggering new patterns of erosion and sedimentation that require increased maintenance or further engineering interventions. Sediment impacts are seldom confined to the project reach, and may extend throughout the river network, which dictates the use of whole-system or watershed approaches that can underpin effective regional sediment management. While sediment impacts are increasingly taken into account at the design stage of new projects, many rivers bear the legacy of past schemes that inadvertently disrupted sediment dynamics, often to the detriment of riverine habitats and ecosystems or higher than expected life-cycle costs due to maintenance necessary to preserve the effectiveness of flood defense, navigation, or land drainage functions. Hence, the goal of many regional sediment management initiatives is to reduce elevated sediment loadings in previously disturbed river networks and restore connectivity in dysfunctional sediment transfer systems**.**

Regional sediment management is usually accomplished through channel rehabilitation that employs features such as grade control structures to control the longitudinal profile of the stream, bank stabilization to reduce sediment inputs, drop pipes to stabilize stream-side gullies, and soil

conservation measures to reduce watershed sediment yield (Hudson, 1997). However, while the primary purpose of a project may be to return the rate of sediment delivery to a reservoir, flood control channel, or wetland to some pre-disturbance level, it is still necessary to analyze the sediment impacts within a watershed perspective. This is essential because of complexity in the spatial and temporal dimensions of watershed sediment processes and morphological responses. In many rivers and streams, management of downstream sediment loads is far from straightforward, and the risk exists that a scheme designed without consideration of watershed sediment dynamics will solve one sediment-related problem at the expense of creating new sediment imbalances, and unintended morphological responses, elsewhere in the fluvial system.

The key to optimizing management of sediment dynamics in the fluvial system lies in identifying the sediment sources and sediment sinks in the watershed sediment system and understanding the processes responsible for transferring sediment along the pathways that link sediment sources and sinks at the reach and watershed scales. While a great deal has been written about sediment *transport*, there is much less in the literature concerning sediment *transfer* and there is surprisingly little published guidance on how sediment sources, pathways, and sinks can be identified and characterized within the context of project-related studies. Although detailed knowledge of the processes and mechanics of sediment transport serves as the foundation for many sediment transport studies, the complexity and large scale of watershed sediment dynamics preclude analysis using an approach that starts with the movement of individual grains. What is needed is a broader consideration of the sediment transfer system that supports higher-level treatment by reproducing the main functions and responses without attempting detailed replication of sediment transport processes. This paper describes how the concept of wash load and bed-material load can be applied to sediment transfer through the fluvial system for sediments derived from various bed, bank, gully, and watershed sources; and to provide a reliable analytical foundation for effective regional sediment management.

SEDIMENT DEFINITIONS

Historically, sediment moving in a stream has been defined on the basis of the method by which it is measured, the mechanism by which it moves, or the source from which it is derived (Simons and Sentürk, 1977). The distinctions between these classifications are not always obvious and there is often considerable confusion among the terms. Therefore, a brief description of the three classifications is provided.

Typically in the United States, sediment load data are collected at gaging stations based on measurements using a cable-suspended, nozzle sampler that is lowered and raised through the water column by a winch. This technique samples most of the suspended load, but the sampled zone does not extend all the way to the streambed and, consequently, the near-bed portion of the suspended load and the entire bed load are not sampled and remain unmeasured. Although the unmeasured load cannot be established by conventional sampling, it may subsequently be estimated based on the flow hydraulics and measured load using the Einstein-Brown sediment transport formula (Brown, 1950). Alternatively, the unmeasured load may be sampled using a specially designed device such as a Helley-Smith sampler, which is often thought of as a bedload sampler, although the original purpose was to sample the unmeasured load at U.S. Geological

Survey (USGS) gaging stations (Helley and Smith, 1971). The total sediment load at the station is made up of the measured load plus the unmeasured load.

Sediment in motion can also be classified as either bed load or suspended load, according to its transport mechanism. Bed load is made up of particles that are rolling, sliding or saltating and which are, therefore, in either continuous or intermittent contact with the bed. Suspended sediment moves in the water column above the bed and is rarely in contact with the bed. The distinction between bed and suspended loads is not obvious in the field, but it is physically significant and can be made on theoretical grounds. Bagnold (1966) demonstrated that the submerged weight of grains moving as bed load is supported solely by solid-to-solid contact at the bed, while that of suspended load is supported entirely by anisotropic turbulence due to fluid shear flow. The total load is the sum of the bed load and suspended load.

The third basis for classification of the sediment load is by the source of the sediment. The bed-material load is the sediment in transport that is comprised of particles that are found in appreciable quantities in the channel bed. Wash load is sediment in transport that is derived from sources other than the bed. It is finer than the bed-material load and is not found in appreciable quantities in the bed. The total load consists of the sum of the bed-material load and the wash load. With respect to channel morphology, the bed-material load is the more important component of the total load because it is derived from erosion of the channel bed, because bed-material load particles are constantly being exchanged with particles in the bed, and because it returns to the bed at the end of a transport event**.**

DEFINING THE WASH LOAD

The distinction between bed-material-load and wash-load components of the total load adopted here is that wash load is not found 'in appreciable quantities' in the bed of the channel. However, the precise definition of what constitutes an 'appreciable quantity' is unclear, meaning that the threshold grain size separating bed-material load and wash load may be defined in several ways. Einstein (1950, p. 7) defines wash load as the grain size of which 10 percent of the bed mixture is finer: "*This basically different behavior of the fine and the coarse particles in the same channel has led the author and collaborators to assume that the fine particles in the flow still behave like material called "wash load" in the concrete channel, whereas the coarse particles act like the sediment in a strictly alluvial channel. These investigators give the limiting grain size between wash load and alluvial or bed load in terms of the composition of the sediment deposit in the bed. They state that all particle sizes that are not significantly represented in the deposit must be considered as wash load. More specifically, the limiting size may be arbitrarily chosen from the mechanical analysis of the deposit as that grain size of which 10 percent of the bed mixture is finer. This rule seems to be rather generally applicable as long as low-water and dead-water deposits are excluded from the bed sediment.*" There is no theoretical justification for selecting D_{10} rather than some other percentile at the lower end of the bed material size gradation curve (the D_5, or D_{15}, might equally well be proposed), but the principle accepted here is that wash load may be defined on the basis of its *absence from the bed material* and that any size criterion used to define it must, therefore, be expressed in relative rather than absolute terms. It follows that while silt and clay would be defined as wash load in a sand-bed channel, the wash load in a gravel-bed channel would include the sand fraction of the

sediment load provided that the D_{10} of the bed was 2 mm or coarser.

It should be noted that the definition of wash load adopted here is by no means universally applied or accepted. For example, wash load has also been defined as consisting of particles smaller than 0.063 mm, corresponding to the division between sand and silt in the Wentworth scale (Yang and Simões, 2005; Knighton, 1998; Richards, 1982). Bettess (1994, p. 229) defines the wash load as: *"… sediment that moves in suspension in the flow but is not represented in the bed of the channel. It is generally assumed that the transport of the wash load is supply dependent and is independent of the local flow conditions*." Graf (1984) agrees with Einstein, pointing out that the wash load is made up of sizes finer than the bulk of the bed-material load, and states: *"The wash load rate can be related to the available supply of solid particles within the watershed; it enters the watercourse by sheet wash, bank caving, etc., but is merely washed through the sections.*" However, none of these definitions has the breadth of applicability of the definition adopted here. For example, as noted above, in gravel-bed rivers, sand may not be found in appreciable quantities in the bed and so it should be considered wash load as the source must lie away from the bed. Also, in laterally active channels, much of the wash load may be derived from erosion of the channel banks, rendering inappropriate a definition restricted to input from slopes outside the channel.

WASH-LOAD DYNAMICS

There is no universally accepted definition of wash load, yet despite this, the wider concept that sediment in transport that is finer than that making up the bed of the channel behaves differently and plays a different role in the sediment transfer system is widely perceived to have merit and has often proven useful in river engineering studies (Einstein, 1950). In this respect, there are three tenants within the wash load and bed-material load concept that are relevant from a practical regional sediment management perspective**.**

First, because wash load is fine relative to the bed-material load, the stream does not need to expend significant amounts of energy in transporting it through the fluvial system. It follows that changes in the quantity of wash load in transport (due to the addition or removal of wash-load sources) will seldom trigger significant morphological responses and marked changes to the stability of the channel. Conversely, imbalances in the bed-material load will usually drive local morphological response through channel scour (where transport capacity exceeds supply) or fill (where supply exceeds transport capacity).

Second, the quantity of wash load carried by a stream is limited not by the stream's sediment transport capacity, but by the available supply. It follows that it is only the bed-material load that most sediment transport equations can calculate on the basis of the transport capacity indicated by the local flow hydraulics. Wash-load transport cannot be predicted this way, but can only be estimated on the basis of comprehensive, quantitative assessment of wash-load sediment sources.

Third, the movement of wash load is relatively rapid compared to that of the bed-material load. In a sand-bed channel, where the wash load is composed of fine sands, silts and clays that are fairly evenly distributed throughout the water column, wash load may move through the channel

system at a speed approximating the mean flow velocity. It follows that fines moving as wash load may travel from upstream sources to downstream sinks during single transport events, so that variations in wash-load supply are quickly reflected in rates of downstream siltation. Conversely, in cobble and boulder-bed channels, the movement of gravel-sized wash load moving as bed load is much slower, resulting in longer travel times for coarse wash load moving from headwater sources to downstream sinks. Consequently, in coarse-bed systems, response times for the impacts of changes in wash-load sources to be realized might be measured in decades rather than the months or years evidenced in sand-bed rivers.

It must also be recognized that spatial variation in the wash load and bed-material load threshold grain size is inherent to most fluvial systems. Generally, the upper bound grain size for the wash load becomes finer in the downstream direction due to downstream "fining" of the bed material. Typical examples of this trend are shown in Figures 1 and 2, for D_{10} values from the Missouri and Mississippi Rivers, respectively. On the Missouri River, the bed material D_{10} value immediately downstream of the Garrison Dam is 0.2 to 0.25 mm, but decreases to less than 0.1 mm as the river encounters the backwater effects of Lake Oahe (Figure 1). In this case, fining of the wash load may be attributed largely to the pool effects of the lake, however, a similar trend can be found in an open river situation along the Lower Mississippi River. For example, D_{10} values along the Mississippi River decrease from about 0.25 mm in the New Madrid to Memphis reach to about 0.063 mm below Baton Rouge, Louisiana (Figure 2).

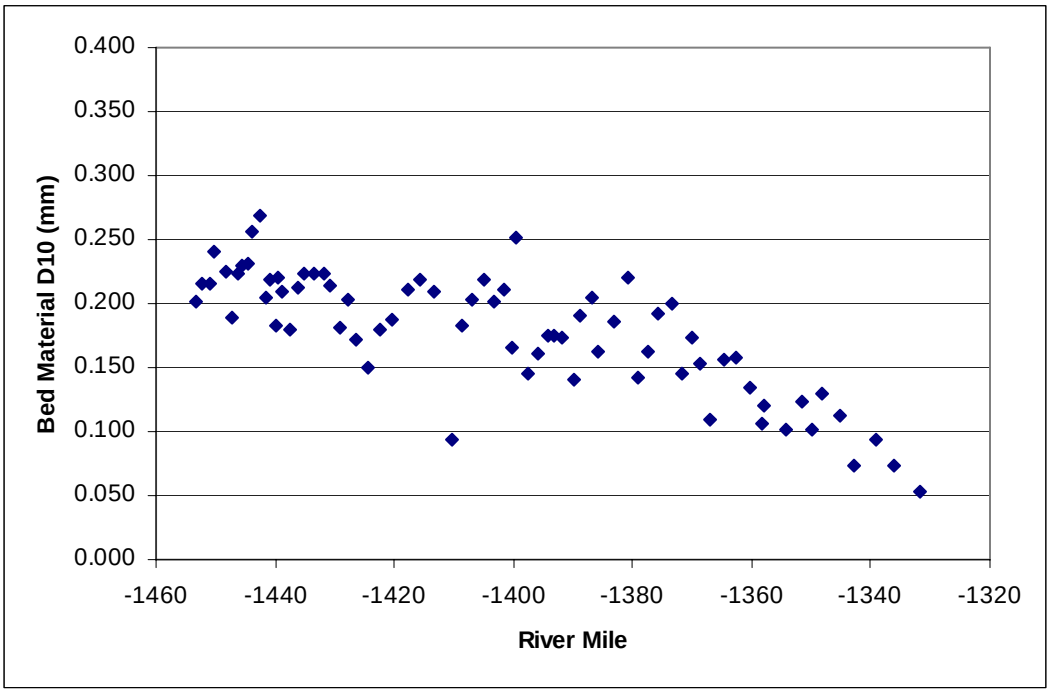


Figure 1 Bed material D_{10} values on the Missouri River below Garrison Dam.

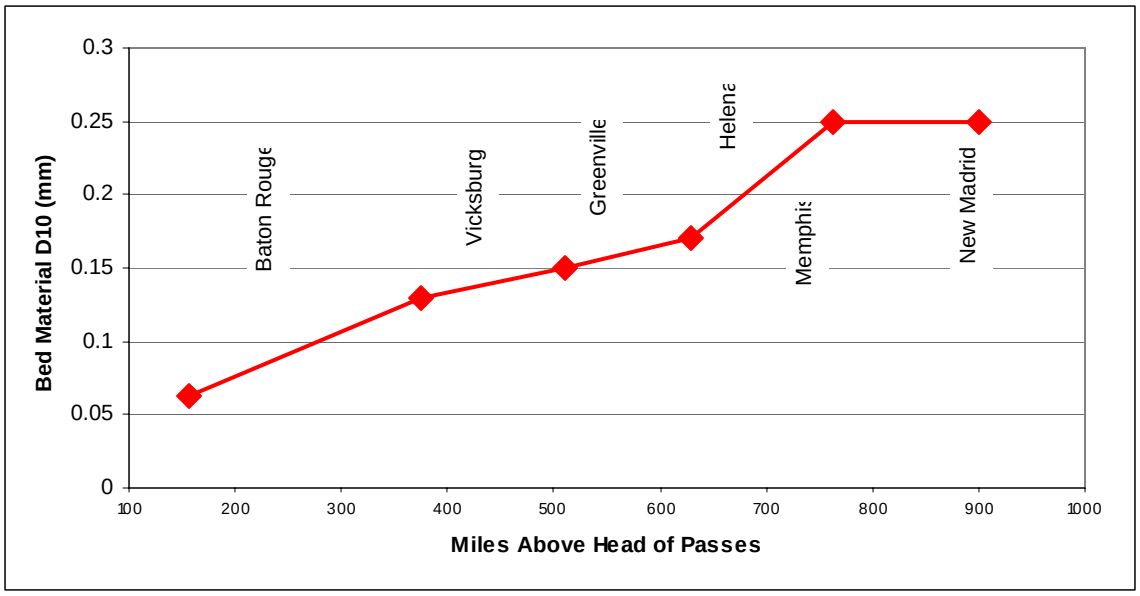


Figure 2 Bed material D_{10} along the Lower Mississippi River (adapted from Nordin and Queen (1989)).

Spatial changes in the upper limit of the wash-load size such as these have important implications for sediment dynamics in the fluvial system. For example, where the threshold size decreases in the downstream direction, as in the cases presented above, then the coarser fraction of wash load entering a reach from upstream must be re-classified as bed-material load in that reach. As a result, the behavior of this fraction of the total load switches from that characteristic of wash load to that of bed-material load, with consequential impacts on local sediment dynamics and morphological responses.

Temporal changes in the wash-load threshold grain size may also occur, but are more difficult to generalize. For example, the particle size distribution of the bed in some streams varies seasonally. In such cases, care would have to be taken to match the sampling strategy used to establish the D_{10} for the bed to the purpose of the study, which might be to investigate seasonal variability in sediment impacts or to characterize long-term sediment dynamics that are independent of seasonal fluctuations.

While these abstract arguments concerning the behavior of sediment load classed according to the wash load and bed-material load concept illustrate the general utility of the concept, application to regional sediment management can better be illustrated using an example based on the D_{10} plot in Figure 2. For this example, consider a sediment source from a streambank erosion site at River Mile 750 near Memphis TN, where the bank is comprised of material finer than 0.25 mm. Since the wash load – bed material load threshold in this reach is about 0.25 mm, all of the material eroded from the bank will be supplied to the river at this location as wash load. Consequently, stabilization of this bank would have a minimal morphological impact in this reach because the source material is all wash load within the reach, and not contributing significantly to the morphology of the reach. However, downstream near Vicksburg (River Mile 435) where the bed material-wash load threshold has decreased to about 0.14 mm, the channel

would realize a reduction in the supply of bed material in the range of 0.25 mm to 0.14 mm. Thus, the Vicksburg reach would realize an almost immediate reduction in bed material supply, and some sort of morphologic response would be expected. For instance, if the Vicksburg reach was experiencing aggradation, then the reduction in the bed material supply might lessen the aggradational trend. However, if the Vicksburg reach was in dynamic equilibrium, then the reduction in bed material supply could potentially shift the channel to degradation. Now consider what would happen if the bank material source near Memphis was comprised completely of material greater than 0.25 mm. In this instance, stabilization of the bank could have a more significant morphologic impact in the Memphis reach since a bed material source has been removed. However, the short-term impacts to the downstream reaches would be minimal. In fact, there could be a considerable time lag before the downstream reaches experience any sediment reduction, because these reductions would be purely a function of the morphologic adjustments in the Memphis reach. Obviously, these are hypothetical examples, and the actual response would depend upon the relative magnitude of the reduction in sediment supply and the morphologic characteristics of the river, but are presented to illustrate how the concept could be used to assess the potential impacts of sediment management activities.

SUMMARY

The sediment impact analysis methodology presented here provides a conceptual basis for developing, designing, and optimizing erosion control and channel-improvement plans. In practice, predicting the magnitude of sediment impacts and the nature of morphological responses to the changes in flow and sediment inputs would require development of a quantitative sediment budget for the channel system that includes and accounts for all the significant sediment sources in the watershed. To this end, the Sediment Impact Assessment Model (SIAM) was developed. SIAM incorporates the wash load and bed-material load concept discussed herein, and enables rapid assessment of the impacts of changes in flow and sediment input throughout the channel system.

REFERENCES

Bagnold, R.A., (1966), An approach to the sediment transport problem from general physics. U.S. Geological Survey Professional Paper 4221.

Bettess, R.,(1994), “Sediment transport and channel stability, In: The Rivers Handbook,” P. Calow and G.E. Petts (Eds.), Vol. 2, Blackwell Scientific Publications, pp. 227-253.

Brown, C.B., (1950), “Sediment transportation,” in: Engineering Hydraulics, H. Rouse (Ed.), Chap. XII, John Wiley and Sons, Inc., New York, NY.

Einstein, H.A., (1950), The bed-load function for sediment transportation in open-channel flows. U.S. Department of Agriculture, Soil Conservation Service, Technical Bulletin No. 1026.

Graf, W.L., (1984), “A probabilistic approach to the spatial assessment of river channel instability,” Water Resources Research. Vol. 20, pp. 953-962.

Helley, E.J., and Smith, W., (1971), Development and calibration of a pressure-difference bedload sampler. U.S. Geological Survey, Water Resources Division, Open-File Report 73-108, Menlo Park, CA.

Hudson, F.E., (1997), "Project formulation of the Demonstration Erosion Control Project," In: Proceedings of the Conference on Management of Landscapes Disturbed by Channel Incision, University of Mississippi.

Knighton, A.D., (1998), "Fluvial forms and processes: A new perspective," Arnold, London, 383 p.

Nordin, C.F., and Queen, B.S., (1989), "Particle size distributions of bed sediments along the thalweg of the Mississippi River, Cairo, Illinois, to Head of Passes," September 1989, Potamology Program (P-1) Report 7, U.S. Army Corps of Engineers, Lower Mississippi Valley Division, 93 p.

Richards, K.S., (1982), "Rivers: Form and process in alluvial channels," Methuen, London, UK, 361 p.

Simons, D.B., and Sentürk, F., (1977), "Sediment transport technology," Water Resources Publications, Fort Collins, CO.

Yang, C.T., and Simões, F.J.M., (2005), "Wash load and bed-material load transport in the Yellow River," J. Hydraulic Engineering. Vol. 131, No. 5, pp. 413-418.

ONE-DIMENSIONAL MODELING OF INCISION THROUGH RESERVOIR DEPOSITS

Blair P. Greimann and Jianchun Huang; Hydraulic Engineers, Sedimentation and River Hydraulics Group, Technical Service Center, Bureau of Reclamation, Denver, CO 80225; bgreimann@do.usbr.gov and vhuang@do.usbr.gov

Abstract: A one-dimensional sediment transport model (GSTAR-1D) is used to simulate a laboratory experiment of incision through a reservoir delta deposit. The model allows the user to specify the erosion width through the deposit as a function of the flow rate. The model is shown to predict the vertical incision and downstream sediment load with reasonable accuracy if the erosion width is specified correctly. Sensitivity tests to the transport equation parameters, erosion width, and angle of repose are conducted. The sediment loads exiting the dam are shown to be sensitive to the critical shear stress, but are relatively not sensitive to changes to the erosion width and angle of repose. Further work on modeling of bank erosion is necessary to more accurate predict the long term evolution of reservoir deposits.

INTRODUCTION

A reservoir draw down triggers many sediment processes. The initial drawdown causes an increase in hydraulic gradient that provides the energy for a rapid incision through the delta upstream of the dam. This incision may progress upstream as a head cut or as a diffusive front. The sediment eroded is then re-deposited into the receded delta. In some cases, the sediment eroded from the delta may form turbidity currents as it enters the reservoir. As the incision process continues, the steep banks can fail from becoming too steep or from undercutting. The dewatered delta sediments will begin to consolidate and significant changes in volume may result. If sufficient water is stored within the surrounding geology, there will be a hydraulic gradient through the sediments. The groundwater hydraulic gradient is transverse to the flowing water in the river and may cause slumping of the sediment towards the incising channel. Then, after the initial incision, a widening process may begin. The widening may occur through meandering processes and/or the occurrence of flood flows. A channel is eventually formed through the deposits that will be composed of a main channel and floodplains. However, depending upon the width of the reservoir delta, much of the original reservoir deposit may remain.

The above processes are quite complicated and presently no numerical model can reliably simulate all these processes. At this stage, a step-wise approach is suggested to develop models for these processes. As a first step, this paper presents a one-dimensional (1D) model for the incision process, and it is tested against laboratory data.

TEST OF 1D MODEL

The 1D model tested was GSTAR-1D (Generalized Sediment Transport for Alluvial Rivers – One Dimension), Reclamation (2005). GSTAR-1D is a hydraulic and sediment transport numerical model developed to simulate flows in rivers and channels with or without movable boundaries. It is able to compute water surface profiles in single channels, dendritic, and looped network channels. It has both steady and unsteady flow models, as well as steady and unsteady sediment models. GSTAR-1D uses standard step method to solve the energy equation for steady gradually varied flows and the Exner equation to solve the sediment routing equation. Internal boundary conditions, such as time-stage tables, rating curves, weirs, bridges, and radial gates are simulated. The notation of an active layer, which allows selective erosion, provides an appropriate framework to simulate the bed armoring. Non-cohesive sediment transport equations and cohesive sediment physical processes are applied to calculate the sediment deposition and erosion. The most recent version can be downloaded at: www.usbr.gov/pmts/sediment.

Experiment Description: Experimental data was used to test the validity of GSTAR-1D in predicting the erosion of reservoir deposits following dam removal or during reservoir sluicing. Cantelli et al. (2004) performed experiments at the University of Minnesota to simulate the removal of dam. A flume with a slope of 0.018 and a width of 0.061 m was filled with sediment to replicate the sediment deposit behind a dam. The sediment was uniform with a d_{50} of 0.8 mm, which is coarse sand. The maximum depth of the sediment deposit was approximately 0.12 m. A channel 1 cm deep and 27.5 cm wide was cut in the middle of the deposit to ensure that the erosion occurred in the middle of the channel. A flow of 0.3 l/s was allowed to erode the deposit. The sediment feed was continued at a rate of 0.002 kg/s during the experiment. This was calculated to be an equilibrium supply rate at the given slope and width.

A unique feature of these experiments was the precise measurement of the bed profile and cross section width upstream of the dam while the flow eroded the deposit.

Model Input: The input data for GSTAR-1D consists of geometry data, flow data, sediment boundary conditions, and sediment transport parameters. The geometry was taken from the description of the experimental set up. Cross sections were spaced 10 cm apart in the numerical model. Each cross section was represented by points spaced 1 cm transverse to the flow. The Manning's roughness coefficient was assumed to equal 0.025. A single sediment size of 0.8 mm was assumed. The flow rate and sediment feed rate were taken from the experiment values.

Parker's (1990) surface based transport formula was used to predict sediment transport capacity. Parker (1990) developed an empirical bed-load transport function based on the equal mobility concept and field data. However, a single sized sediment was used in these experiments and therefore the hiding and equal mobility features of this transport model are not important.

Two parameters must be defined by the user to use Parker's equation: the non-dimensional critical shear stress and the hiding factor (θ_c and α, respectively). Ideally, these values should be fit to data of the stream being simulated. However, in the absence of data, several references provide guidance, such as Buffington and Montgomery (1997). In the simulations performed here, a value of 0.03 was used for θ_c, which is near the values recommended in Buffington and Montgomery. As a sensitivity test, a value of 0.04 was also simulated for the value of θ_c. The value of α is not important because only a single size class is being simulated.

The erosion width is an important parameter in estimating the erosion details. Because one-dimensional models do not have a shear stress that varies across a cross section, it is difficult to estimate the non-uniform erosion that occurs during incision. Cantelli et al. (2004) observed a rapid narrowing of the channel followed by a gradual widening. The narrowing was caused because the vertical erosion in the middle of the channel was faster then the banks could supply additional sediment. The highest shear stresses were in the middle of the channel and therefore the highest erosion rates occur there. The banks initially do not supply sufficient sediment to maintain a wide section and the section narrows. Eventually, the rapid incision slows and the bank erosion continues and the section starts to widen.

GSTAR-1D does not directly simulate lateral transport of sediment because it is a one-dimensional model; however, it empirically accounts for the processes involved by using a relationship between erosion width and flow rate and an angle of repose condition for bank stability. The following equation is used in GSTAR-1D to determine the erosion width:

$$W_e = aQ^b \tag{1}$$

where W_e is the erosion width, Q is the stream flow, and a and b are user defined constants. The boundaries of the erosion width are determined by first finding the centroid of the cross section, then assuming that W_e is apportioned equally on either side. The erosion width for the experiments of Cantelli et al. (2004) began at approximately 26 cm. The width decreased rapidly to less than 5 cm near the dam face, but at about 40 cm upstream of the dam face the width was not less than 17 cm. After 2.5 minutes, the width throughout the entire flume was greater than 17 cm and began to gradually increase. For the simulation, the erosion width was set to 24 cm for the flow rate of 0.0003 m^3/s (a = 12, b = 0.5). As a sensitivity test, an erosion width of 20 cm was also simulated.

Bank failure is simulated using an angle of repose condition. GSTAR-1D requires an angle of repose below and above water. The angle of repose above water was set to 70 degrees because the banks were near vertical during the experiment. Because the sand was saturated before the experiment and the water was only a few centimeters below the banks, capillary forces were significant between the sand particles and enabled the banks to remain almost vertical. Based upon the video footage from the experiment, the bank collapse was seen to occur as the banks were undercut. The angle of repose below water is more difficult to determine. The shape of the below water channel is a function of the streamwise and transverse sediment transport. The below water angle of repose was set to 25 degrees. To test the sensitivity of the model to the angle of repose, simulations were also run for an angle of repose equal to 35 degrees above and below water.

A summary of the input parameter used in the simulations is given in Table 1. The simulations are referred to Simulations 1 through 4 with Simulation 1 being referred to as the base run.

Table 1 Summary of GSTAR-1D Input Parameters. Values changed from Base Run (Simulation 1) are italicized.

	Simulation			
Parameter (units)	**1**	**2**	**3**	**4**
Critical Shear Stress (-)	0.03	*0.04*	0.03	0.03
Erosion Width (cm)	24	24	*20*	24
Angle of Repose, Above Water (degrees)	70	70	70	*35*
Angle of Repose, Below Water (degrees)	25	25	25	*35*

Model Results: The simulated results from GSTAR-1D were compared against the experimental data of Run 6 of Cantelli et al. (2004). The simulated and measured bed elevations are shown in Figure 1. Overall, the agreement between the measured and simulated is satisfactory. It should be remembered, however, that the agreement was improved by calibrating the critical shear stress in Parker's bed load equation. The calibrated value (0.03) is a typical value applied in field situations but may vary based upon particle shape and form roughness in the river. The only significant disagreement between measured and predicted values is in the initial stages of channel formation where the initial incision rates were slightly under-predicted. Because the model does not simulate all processes involved in the erosional narrowing observed in the experiments, the simulated initial channel widths are larger than the measured ones. Therefore, the simulated bed elevations decrease more slowly than the measured ones.

The sediment loads are shown in Figure 2. Initially, the simulated sediment loads fit the measured relatively well. However, the simulated sediment loads at the dam face do not decrease as rapidly as the measured loads. The measured sediment loads decrease to approximately the feed rate values after approximately 600 seconds. This would indicate that after 600 seconds there is no net erosion or deposition between the location of the feed and the dam face. That conclusion is in contradiction to the bed profile and top width evolution. Both the bed profile and the top width indicate that erosion continues throughout the course of the experiment. Therefore, one would expect that the sediment discharge at the dam face should be higher than the feed rate. It is expected that there is a bias in the measured sediment discharges at the dam face.

The evolution of the wetted top width is shown in Figure 3. The 1D model does not predict erosional narrowing because no transverse sediment transport is modeled. The erosion is primarily vertical with only a minor widening because the angle of repose above water was assumed relatively large. There were no cross sectional data to compare the model against.

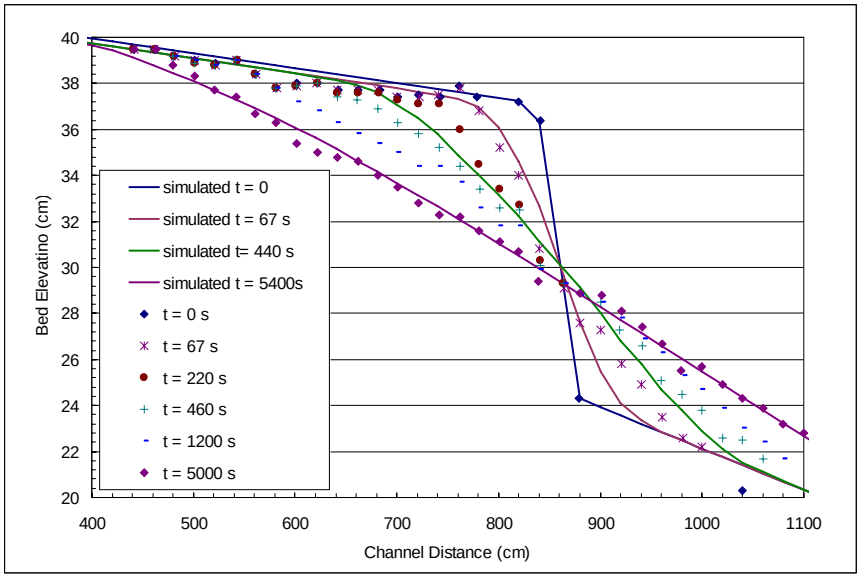


Figure 1 Comparison between Run 6 of Cantelli et al. (2004) and GSTAR-1D for the bed profile, base run, Simulation 1.

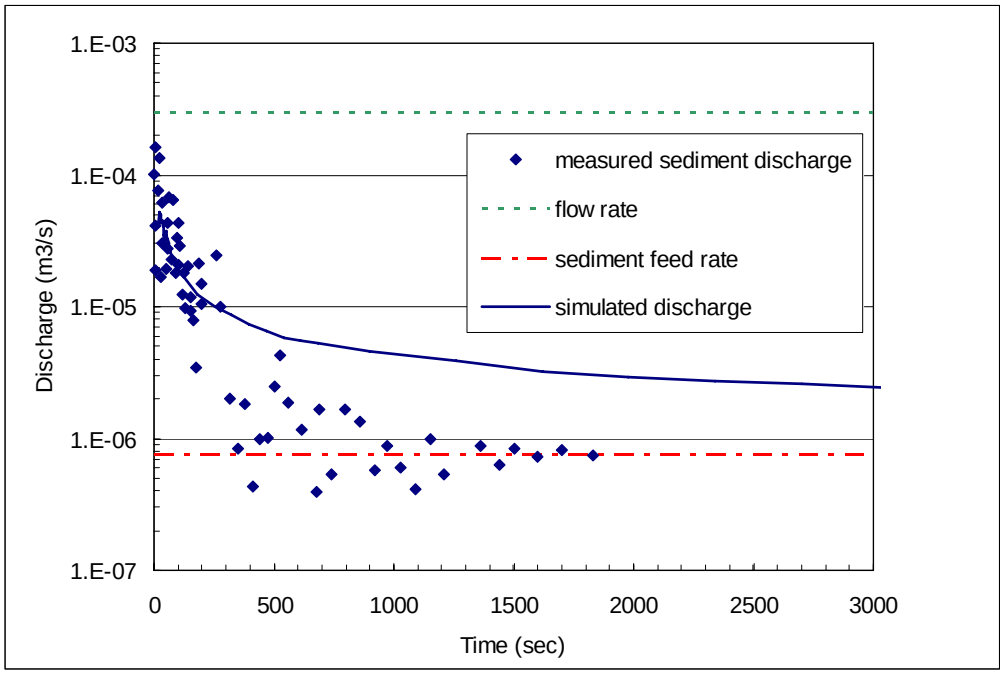


Figure 2 Comparison between Run 6 of Cantelli et al. (2004) and GSTAR-1D for the sediment discharge at the dam face, base run, Simulation 1.

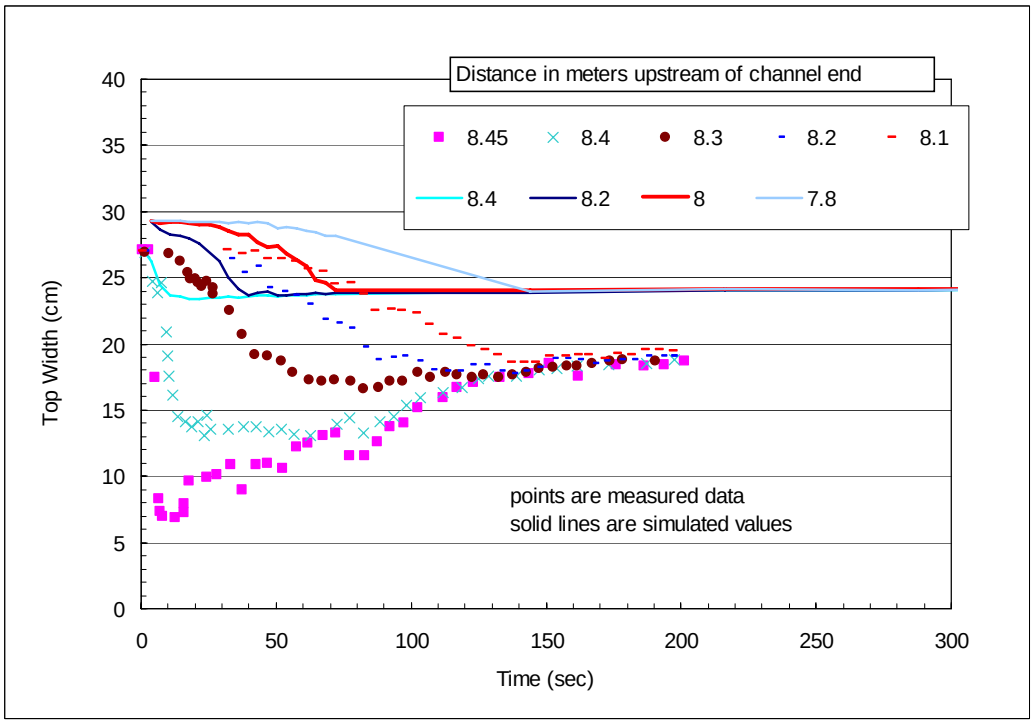


Figure 3 Comparison between Run 6 of Cantelli et al. (2004) and GSTAR-1D for the wetted top width, base run. Solid lines are simulated values. Points are measured. Simulation 1.

Sensitivity To Critical Shear Stress: The critical shear stress was increased to 0.04 and the same simulation was performed. This simulation is termed Simulation 2. A comparison of Simulations 1 and 2 is given for the bed profile (Figure 4) and for the sediment discharge at the dam face (Figure 5).

Because the critical shear stress enters directly into the sediment transport formula, Equation (1), raising the critical shear stress will decrease the simulated sediment transport rates. The decrease in the sediment transport rates causes sediment to erode more slowly. Therefore, the bed elevations of Simulation 2 are higher than for Simulation 1 upstream of the dam. The predicted sediment loads at the dam face are also lower in Simulation 2 than for Simulation 1.

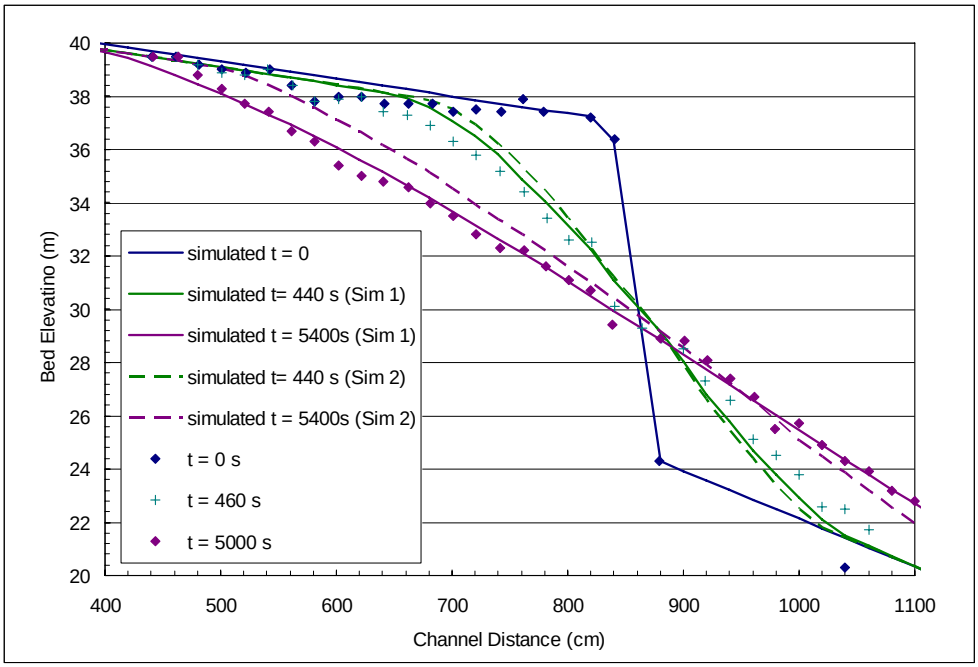


Figure 4 Sensitivity of bed profile to critical shear stress.

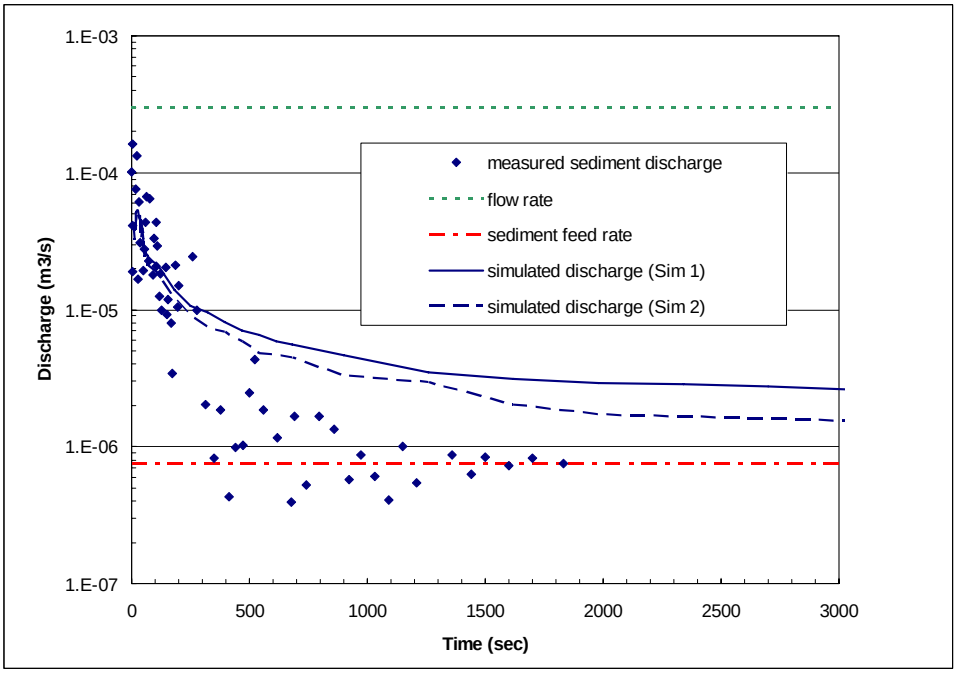


Figure 5 Sensitivity of sediment discharge at dam face to critical shear stress.

Sensitivity To Erosion Width: The erosion width was decreased to 20 cm and the simulation results from this simulation (Simulation 3) are compared against the base run, Simulation 1. Decreasing the erosion width causes the vertical incision to occur more rapidly (Figure 6). However, the sediment loads at the dam face are relatively unaffected by the decrease in erosion width. The sediment loads did not change significantly from Simulation 1 because even though the vertical incision occurred more quickly, the width of erosion was less and therefore approximately the same volume of sediment was removed (Figure 7).

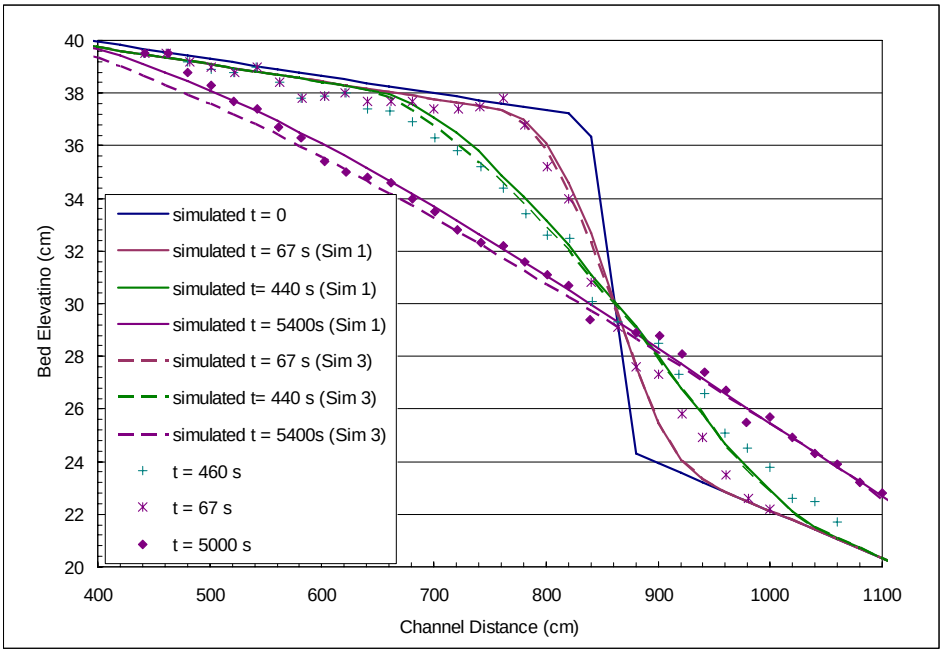


Figure 6 Sensitivity of bed elevation to erosion width.

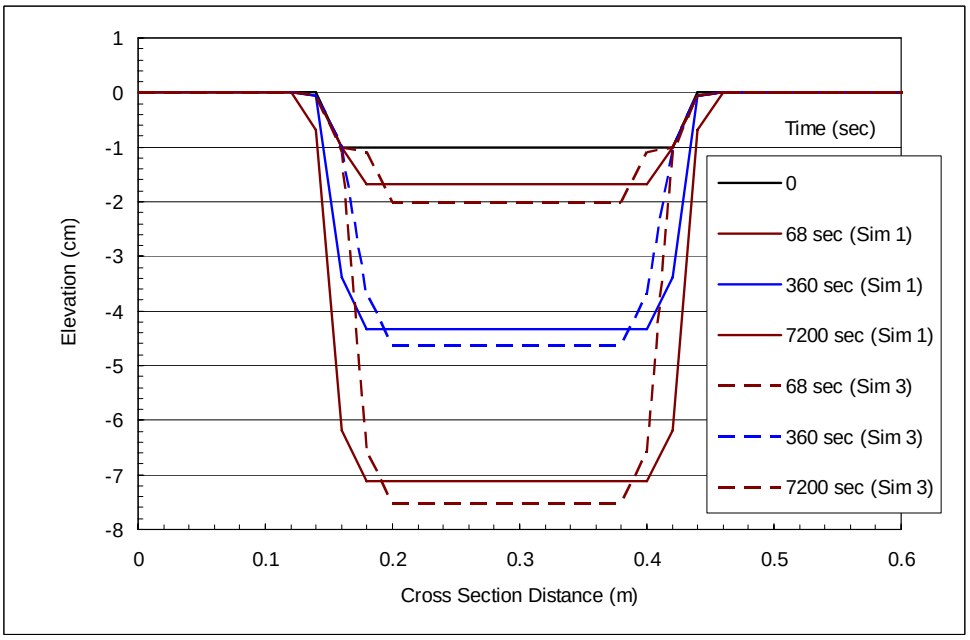


Figure 7. Sensitivity of cross section shape to erosion width.

Sensitivity To Angle Of Repose: The above and below angle of repose were set to 35 degrees. This simulation is termed Simulation 4 and is compared against Simulation 1. The difference in bed elevations was relatively small, 3 mm or less, but Simulation 4 consistently showed less erosion than the base run. However, the sediment loads at the dam face were relatively unaffected. The sediment loads were relatively unaffected because even though the vertical incision was less in Simulation 4, the horizontal widening was greater because of the smaller angle of repose.

DISCUSSION

Several important issues need to be addressed when applying a 1D model to simulate dam removal. Many sediment processes are ignored in a 1D model because the 1D model does not directly simulate transverse sediment movement and calculates a single average shear stress for a cross section. To empirically account for these factors, an appropriate erosion width and angle of repose should be specified. In GSTAR-1D, the erosion width is specified as a function of flow rate. HEC-6T (MBH Software, 2001) requires a similar specification and DREAM (Stillwater Sciences, 2002) requires a fixed base width. Often the erosion width is determined based upon the upstream and/or downstream river width. As a first estimate, Equation (1) could be fit to the upstream and downstream river channels. If the fit coefficients of Equation (1) for the upstream and downstream river channels are significantly different, some judgment may be necessary as to the most appropriate values.

The angle of repose can be specified based upon sediment type, while the angle of repose for non-cohesive sediments these values are relatively well bounded. However, for cohesive sediments, the angle of repose may be difficult to determine, or may not be a constant value. It is likely that the stable angle for cohesive soils will be a function of the groundwater gradients in the sediments. Future research is necessary to address this issue. Even though the transverse variation of shear stress and bed load are ignored, in many cases the loss of these details may not significantly alter the uncertainty of the erosion estimates. The greatest uncertainty may still reside in the calculation of the streamwise sediment transport.

Additional research is needed to develop appropriate models of the long-term bank erosion. It is important in determining the concentrations downstream of the dam. Because the reservoir is usually much finer than the river bed sediment, the reservoir may potentially act as a source of fine sediment for many years as the banks slowly erode. As shown in the experiments of Cantelli (2004), bank caving occurs after the initial channel incision as the flowing water undermines the steep banks. This process is difficult to model with a 1D model and no readily available model exists to do so. In most cases, it is assumed that bank erosion after the first few years will be limited to large storm events. However, there is often no quantitative method applied to determining which events will cause additional bank erosion. It may be feasible to use a method similar to that employed in CONCEPTS (Langendoen, 2000) where the geotechnical strength of the bank is evaluated as well as the shear stress applied to the bank.

REFERENCES

Buffington, J.M, and Montgomery, D.R. 1997 Resources Research, Vol. 40, W03304, 12 pp.

Langendoen, E. J., (2000). CONCEPTS – Conservational Channel Evolution and Pollutant Transport System. USDA-ARS National Sedimentation Laboratory, Research Report No. 16, December.

MBH Software (2001). Sedimentation in Stream Networks (HEC-6T). Users Manual, Mobile Boundary Hydraulics, http://www.mbh2o.com/index.html.

Parker, G. (1990). "Surface Based Bedload Transport Relationship for Gravel Rivers," Journal of Hydraulic Research, Vol. 28(4), 417–436.

Stillwater Sciences (2002). Dam Removal Express Assessment Models (DREAM). Technical Report, October.

Yang, C.T., Huang, J., and Greimann, B.P., (2005). User's Manual for GSTAR-1D 1.0.2 (Generalized Sediment Transport for Alluvial Rivers – One Dimension, Version 1.0.2). U.S. Bureau of Reclamation, Technical Service Center, Denver, Colorado.

PREDICTING WATERSHED IMPACTS OF FOREST FUEL MANAGEMENT WITH WEPP TECHNOLOGY

William J. Elliot, Project Leader, USDA Forest Service Rocky Mountain Research Station
1221 South Main, Moscow, ID 83843, welliot@fs.fed.us

Abstract: A new interface has been developed to specifically aid forest managers in evaluating hillslope sediment yields of fuel management activities in forested watersheds. From a single input screen, twelve computer runs are carried out, and the run results and a narrative are generated to aid the user in incorporating the results into an environmental analysis document. This tool will simplify synthesizing the watershed impacts of forest fuel management activities.

INTRODUCTION

One of the main products of many forests is surface water. The main pollutant in most forest streams is sediment. Upland management disturbances including fuel management activities and forest roads can cause erosion, leading to increased stream sedimentation and reduced water quality. Forest managers need to evaluate the impact of most forest activities on stream sedimentation, including fuel management. Fuel management activities include thinning and prescribed fire. With ground-based thinning operations, a road network must also be maintained.

A suite of Internet interfaces were developed to assist users in predicting soil erosion from disturbed forest hillslopes and forest roads (Elliot, 2004). As users were shown how to use these tools, they found the final synthesis of the information difficult to complete. Road erosion was in kg (lbs) sediment from a road section, and hillslopes in Mg/ha (tons/acre) in the year of the disturbance. Also, road segments generated sediment every year, whereas wildfire would only cause erosion for a year or two following the fire. Erosion from thinning and prescribed fire occurs every few decades. A tool was needed to synthesize the results of numerous erosion predictions, and aid users in interpreting those predictions.

To meet this need, a computer Internet interface was developed to assist with synthesizing soil erosion rates associated with fuel management activities in forests, named “WEPP FuMe”. This interface estimates background erosion rates, and predicts erosion associated with mechanical thinning, prescribed fire, and the road network. The interface uses the Water Erosion Prediction Project (WEPP) model to predict sediment yields from hillslopes and road segments to the stream network. The WEPP model is a physically-based soil erosion model developed over the past 15 years to predict soil erosion and sediment yields for agriculture, rangeland, and forest conditions (Laflen et al., 1997). The simple interface has a large database of climates, vegetation files, and forest soil properties. The soil databases for roads and disturbed forested hillslopes are based on rainfall simulation and natural rainfall studies carried out over the past 20 years (Elliot and Hall, 1997). To simplify the coding, the vegetation input to the WEPP model for WEPP FuMe was set to have a constant ground cover (no vegetation growth, no residue decomposition). A preliminary analysis to compare the effects of fixed cover showed that the impacts of this on predicted erosion was minimal for highly disturbed conditions, but may lead to over prediction of low erosion rates.

For this application, the WEPP hillslope version was used to model a single strip of hillslope (Figure 1). It was assumed that the sediment generated from this hillslope from a number of disturbances was routed through the watershed. In the year of the disturbance, there is likely to be deposition of sediment from the disturbed hillslope in the stream network. This sediment is gradually routed through the watershed in subsequent wet years. If the years are dry, there is unlikely to be any sediment routed. As the disturbed hillslope recovers, erosion from that hillslope will gradually decline. This application assumes that road erosion occurs every year, with the magnitude dependent only the level of traffic and the weather during the year. As more than one hillslope may be disturbed during a given sequence of fuel management activities, users will likely carry out the analysis for numerous hillslopes, and combine the final results.

DESCRIPTION OF WEPP FUME

The WEPP FuMe interface carries out erosion prediction runs for seven forest conditions:

1. Undisturbed mature forest
2. High severity wildfire
3. Prescribed fire
4. Thinning
5. No traffic roads
6. Low traffic roads
7. High traffic roads

In addition to the above runs, WEPP FuMe carries out an additional five runs for moderate and low severity wildfire, higher and lower severity prescribed fire, and lower impact thinning, such as cable logging.

The climate, soil texture, topography, road density, wildfire return interval, prescribed fire cycle and thinning cycle are specified by the user.

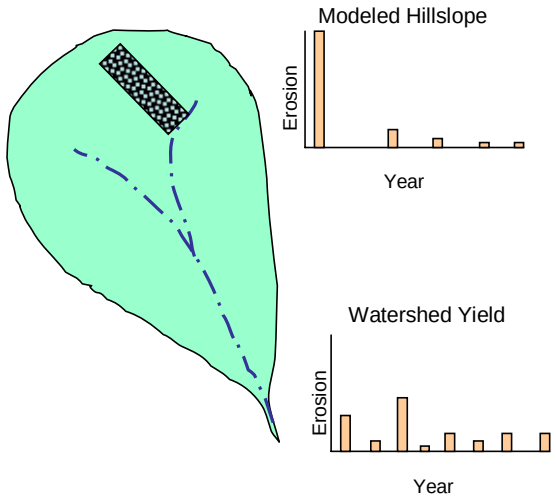


Figure 1 Diagram of a WEPP FuME hillslope within a watershed, and relationship of timing and magnitude of sediment generation from the hillslope and the watershed

Assumptions in WEPP FuMe: The WEPP FuMe interface makes a number of simplifying assumptions for the twelve runs. Table 1 shows some of the assumptions for the first seven runs. The five additional runs aid the user in developing alternative management scenarios. If users wish to consider disturbances other than those presented in Table 1 or the additional runs for disturbed forests, such alternatives can be evaluated with the Disturbed WEPP interface (http://forest.moscowfsl.wsu.edu/fswepp/).

Mechanics: From the online input screen, the input data files are formatted for the WEPP model for each of the seven runs. The WEPP model is then run on the server for each condition. The

results of the runs are converted into common units of tons sediment delivered per square mile per year and presented in tables with an accompanying summary narrative.

Table 1 Main assumptions for WEPP FuME runs

Run	Assumptions
Undisturbed forest	"20-yr forest" soil* Ground Cover 100 percent, including buffer All buffer slopes assumed to be half the hillslope steepness
Thinned forest	"5-yr forest" soil Ground cover 85% on treated hillslope, 100% on buffer
Prescribed fire	"Low Intensity Fire" soil Ground cover 85% on treated hillslope, 100% on buffer
Wildfire	"High Intensity Fire" soil Ground cover 30%, no buffer
No traffic road	Gradient = 1/10 of hillside slope, road length = 300 ft, width is 13 ft Treatment is insloped vegetated ditch, vegetated surface, no traffic Fillslope length is 30 feet, and steepness is twice the hillslope steepness Buffer length and steepness as specified
Low traffic road	Gradient = 1/10 of hillside slope, road length = 300 ft, width is 13 ft Treatment is insloped vegetated ditch, native surface, low traffic Fillslope length is 30 feet, and steepness is twice the hillslope steepness Buffer length and steepness as specified
High traffic road	Gradient = 1/10 of hillside slope, road length = 300 ft, width is 13 ft Treatment is rutted, gravel surface, high traffic Fillslope length is 30 feet, and steepness is twice the hillslope steepness Buffer length and steepness as specified

*Soils refer the nomenclature associated with the Disturbed WEPP database (Elliot, 2004)

For the road analysis, roads may deliver sediment to a stream crossing, or may have runoff and sediment diverted across the specified buffer before entering a stream. For "No Treatment," it is assumed that some roads will have no traffic, while others have low traffic, so the predicted sediment yield range is from no traffic with a buffer to low traffic with no buffer. For the treatment scenario, it is assumed that some of the roads will be low traffic and others will have high traffic with gravel. Therefore sediment yields will range from the lowest value from low traffic or high traffic with a buffer to the highest value from low traffic or high traffic with no buffer. The true road impact will be somewhere between these two values. Users who wish to make a more detailed analysis of road sediment generation can use either the WEPP:Road or WEPP:Road Batch interface (http://forest.moscowfsl.wsu.edu/fswepp/).

Background Sediment: Frequently "background sediment" is considered sediment eroded from undisturbed forests. Numerous studies on forests with even low levels of disturbance have shown that erosion rates from areas of minimal disturbance are near zero (Covert, 2003).

Generally, background rates measured at watershed scale are in the order of 10 t/ sq km (25 ton/sq mi). Some have attributed these numbers to landslides in the watershed, others to stream channel erosion. The WEPP FuMe technology attributes much of this sediment to the routing of sediment stored in watersheds following the last major wildfire. Following a wildfire, upland erosion rates can exceed the transport capacity of forest streams, causing an accumulation of sediments in upland channels. During the decades following the wildfire, this sediment is gradually routed the stream network. There will be high rates of sediment transport in years of higher runoffs, and low to no sediment transported during years of low runoff. An "average" background number can be estimated by dividing the estimated erosion following wildfire by the number of years between wildfire events, called the "fire return interval."

Currently, most forest watersheds have a significant network of roads. In the past, it was assumed that sediment from these roads was beyond any "background" value, and thus must be considered as excess sediment associated with any watershed planning. This assumption does not address the current realities, that the citizens expect to be able to access public lands. This means that at least a part of the current road network on public is now permanent, and managers may wish to incorporate sediment from the permanent network into the "background" sediment. The road network will contribute sediment to the stream network every year.

Scope of WEPP FuMe: The WEPP FuMe interface can be used anywhere within the U.S. using the existing climate database. It is intended to provide an overview of the sources of sediment on a given fuel management site. Users who want more detailed analysis will have to use more complex interfaces available online (http://forest.moscowfsl.wsu.edu/fswepp/) or standalone windows (USDA, 2004) or GIS interfaces (Renschler, 2004).

Sediment predictions from WEPP FuMe are for surface erosion only. In some watersheds, landslides may be a significant source of sediment, and in others, stream channels may be sources of sediment. Users will need to obtain estimates for these potential sources of sediment from local specialists.

Data Input Needs: The WEPP FuMe input screen has several input fields for selecting climate and soil, and specifying road density, hillslope and buffer lengths, hillslope steepness, wildfire return interval and frequencies of proposed treatments.

Climate Database: The climate database includes the statistics from over 2600 weather stations. In addition, the monthly precipitation estimates for every 4-km grid in the conterminous U.S. is also online (Scheele et al., 2001). Users also have the option of using their own monthly temperature and precipitation data.

Soil: The soil texture field contains four USDA soil textures, sandy loam, silt loam, clay loam, and loam. In the database behind the input screen, each of these textures includes the erodibility properties for each soil disturbance condition ranging from a native surface road to a wildfire and an undisturbed forest. Once a texture is selected, the appropriate erodibility values for that texture are used for all the soil components of the twelve runs. Research has found that small differences in texture are much less important than the nature of disturbance in determining forest soil erodibility (Robichaud et al., 1993).

Road Density: The road density is the length of road per unit area of forest. Typical values range from 0.8 to 2.4 km/sq km (2 to 6 miles/sq mi) of road in managed forests. In some cases, roads may be on ridge tops. Ridge top roads, greater than about 100 m (300 ft) from ephemeral channels, are unlikely to contribute sediment to the stream system. Users may wish to ignore these roads.

Topography: In the topography fields, the user is asked to input values for a typical horizontal slope length and steepness. Slope lengths and steepnesses can be obtained from field surveys or contour maps. Users may also have access to GIS topographic analysis tools to aid in estimating these values, providing average values, or determining a range of topographic values to consider. A special tool has been developed to obtain details of individual hillslopes developed by the GeoWEPP wizard (Renschler, 2004) for entering into the WEPP FuMe interface. Users also enter the horizontal length of any buffer strips of undisturbed forest between the treated areas and the stream system. These buffers are ignored for the wildfire run, and are the default distances used for the road erosion runs for the buffer estimates. Users may wish to evaluate several different buffer widths to determine the optimal width for their conditions. They may also wish to evaluate several different slope lengths or steepnesses to evaluate a range of conditions and determine which sites are likely to generate more sediment. In some of the wetter climates, the buffers may not reduce sediment delivery because they may become sources of sediment.

Disturbance Return Periods: Hillside disturbances do not happen every year. The user must specify the wildfire return interval, and the frequency of thinning and prescribed fire. The wildfire return interval will likely range from 20 years with low elevation, dry forests, to 200 years with high elevation moist forests, to 300 years with very wet forests on the west slopes of the Cascades or the Coastal ranges (McDonald et al. 2000). Prescribed fire return periods can vary from 2 to 40 years, or more, and thinning periods from 10 to 80 years.

WEPP FuMe OUTPUT

Once the twelve WEPP runs are complete, and the data are adjusted to common units, the input and output tables (Table 2) and narrative (Figure 2) are presented on the output screen. Details of all twelve runs are presented after the narrative. The user may wish to print this page, save it, or copy all or part of it for pasting into a spreadsheet or word processor.

On the output table (Table 2), the results from each of the four hillslope erosion runs are presented as average annual erosion rates, converted to tons/mi^2. The erosion rates for each of these hillside disturbances are divided by the frequency of the disturbances to get an average annual sediment yield expected from a watershed. The three road runs are summarized on a low access range (for no traffic and low traffic) and a high access range (for low traffic and high traffic with gravel). Road erosion is assumed to occur every year.

The narrative that follows (Figure 2) can serve as a basis for a report of the analysis. Users will likely want to incorporate information from some of the additional runs, carry out runs for other hillslopes or different buffer widths and modify the narrative to reflect what is learned from

those runs within a final report. Users may wish to add a value for sediment from landslides or from stream channel erosion to background or treatment values.

Table 2 Results table from a WEPP FuMe run for a climate in the Bitterroot National Forest.

Source of sediment	Sediment delivery in year of disturbance (ton mi^{-2})	Return period of disturbance (y)	"Average" annual hillslope sedimentation (ton mi^{-2} y^{-1})
Undisturbed forest		1	83.2
Wildfire	7622.4	40	190.6
Prescribed fire	1075.2	20	53.8
Thinning	147.2	20	7.4
Low access roads	2.0 to 14.5	1	2.0 to 14.5
High access roads	4.2 to 14.5	1	4.2 to 14.5

Additional Information: Details of inputs and outputs from the twelve runs are summarized at the end of the output page. The user can use these as guidelines to get additional information for any of the runs by clicking on the run description. Information includes surface runoff and probabilities associated with different amounts of erosion or sediment yield. The output information can also serve as a guide for the variables to enter into the Disturbed WEPP or WEPP:Road online interfaces so the user can use these interfaces to do a similar run, or to explore the sensitivity of the predicted sediment yields to the input variables.

The additional five runs can be used to present alternative options or outcomes, with the existing discussion serving as a guide for incorporating the results into an environmental analysis document. For example, the user may wish to present as an alternative to severe wildfire, a lower intensity wildfire plus impacts from the proposed fuel management activities. Another example might be to use the low impact thinning as an indication of the erosion associated with a cable thinning operation to compare to the erosion predicted from the assumed tractor logging operation in the main output to see if the extra costs associated with the cable operation are justified by reducing sediment generation.

VALIDATION

It is not possible to carry out an extensive validation of the predicted values. Validation of both the WEPP Road and Disturbed WEPP interfaces have been carried out (Elliot and Foltz, 2001). For example, the erosion rate presented in Table 1 for the Bitterroot National Forest can be converted to 27 t/ha for wildfire, and 4 t/ha for prescribed fire. These values can be compared to observed values in the Bitterroot National Forest of 31 Mg/ha (Spigel, 2002) following wildfire, and no erosion in the dry year (1994) following a prescribed fire (Covert, 2003). Running the prescribed fire scenario from the output screen showed that there was a 28 percent chance that there would be no erosion following wildfire.

Contents of Narrative

Background sedimentation.
Wildfire + Undisturbed Forests
With and without roads

Thinning effects.
With and without roads
Impacts on wildfire occurrence or severity

Prescribed fire effects.
Without roads
Impacts on wildfire occurrence or severity

Combined thinning and prescribed fire effects.
With and without roads
Impacts on wildfire occurrence or severity

Road Impacts
Effects of road design and management
Benefits of road removal

Multiple Hillslopes

Details of Inputs and Outputs for all 12 Runs

Figure 2 Outline of contents of the narrative section of the WEPP FuMe output.

SUMMARY

A new interface has been presented that was designed specifically to aid forest managers in evaluating watershed impacts of fuel management activities. From a single input screen, twelve computer runs are carried out, and the run results and a narrative are generated to aid the user in incorporating the results into an environmental analysis document.

REFERENCES

Covert, S. A. (2003) "Accuracy assessment of WEPP-Based erosion models for harvested and burned forest watersheds," MS Thesis. Moscow, ID: University of ID. 49 p.

Elliot, W. J. (2004) "WEPP internet interfaces for forest erosion prediction," *Jour. of the Amer. Water Res. Assoc*. 40(2):299-309.

Elliot, W. J., and Hall, D. E. (1997) Water Erosion Prediction Project (WEPP) forest applications. General Technical Report INT-GTR-365. Ogden, UT: USDA Forest Service, Rocky Mountain Research Station, 11 p.

Elliot, W. J. and Foltz, M. (2001) "Validation of the FSWEPP interfaces for forest roads and disturbances," Presented at the ASAE Annual International Meeting, Jul 30 – Aug 1, Sacramento, CA. St. Joseph, MI: ASAE. 13 p

Laflen, J. M., Elliot, W. J., Flanagan, D. C., Meyer, C. R., and Nearing, M. A. (1997) "WEPP–Predicting water erosion using a process-based model," Journal of Soil and Water Conservation 52(2), 96-102.

McDonald, G. I., Harvey, A. E., and Tonn, J. R. (2000) "Fire, competition and forest pests: Landscape treatment to sustain ecosystem function," in Neuenschwander, L. F., and K. C. Ryan (eds.). Proceedings from the Joint Fire Science Conference and Workshop, Boise, ID. June 15-17, 1999. Online at < http://jfsp.nifc.gov/conferenceproc/T-11McDonaldetal.pdf > Accessed June, 2004. 17 p.

Renschler, C. S. (2004) The Geo-spatial interface for the Water Erosion Prediction Project (GeoWEPP). Online at < http://www.geog.buffalo.edu/~rensch/geowepp/ >. Accessed June, 2004.

Robichaud, P. R., Luce, C. H., and Brown, R. E. (1993) "Variation among different surface conditions in timber harvest sites in the Southern Appalachians," in Larionov, J. A. and Nearing, M. A. (eds.). Proceedings from the Russia, U.S. and Ukraine international workshop on quantitative assessment of soil erosion. Moscow, Russia. Sep. 20-24. West Lafayette, IN: The Center of Technology Transfer and Pollution Prevention, Purdue University. 231-241.

Scheele, D. L., Elliot, W. J., and Hall, D. E. (2001) "Enhancements to the CLIGEN weather generator for mountainous terrain," Proceedings of the ASAE International Symposium on Soil Erosion Research for the 21st Century. Honolulu, HI. Jan. 3-5, 2001. St. Joseph, MI: ASAE, 4 p.

Spigel, K. M. (2002) "First year postfire erosion rates in Bitterroot National Forest, Montana," MS Thesis. Madison: University of Wisconsin. 147 p.

USDA ARS National Soil Erosion Research Laboratory. (2004) WEPP Software. Online at < http://topsoil.nserl.purdue.edu/nserlweb/weppmain/wepp.html >. Accessed June, 2004.

A GEOMORPHIC EVALUATION WITH CALIBRATED HYDRAULIC AND HYDROLOGIC MODELING OF THE HOP BROOK WATERSHED IN MASSACHUSETTS

Thomas Garday, Hydraulic Engineer, National Water Management Center - Natural Resources Conservation Service. Little Rock, Arkansas, Thom.Garday@ar.usda.gov.; Aaron Pugh, Hydrologist, National Water Management Center, US Geological Survey, Little Rock, Arkansas, apugh@usgs.gov

INTRODUCTION

The Hop Brook Watershed in Franklin County, Massachusetts was selected by NRCS for survey and analysis as part of a regional geomorphic and hydraulic geometry curve study of New England streams. The study area of 3.39 square miles is located within the Worchester Uplands of the New England Physiographic Province. The Worchester Uplands are characterized by rolling hills and rounded mountains, interrupted by numerous generally narrow valleys. The geology is igneous and meta-sedimentary Paleozoic and Pre-Cambrian crystalline rocks covered by glacial till. Hop Brook drains into the Quabbin Reservoir, a quality drinking water supply for central Massachusetts. Land management practices have limited development and logging to protect the watershed and runoff. The USGS established gage 01174000 on Hop Brook near New Salem in October of 1947 and operated a continuous recording gage until September 1982.

We are not often afforded the luxury of modeling watersheds that are already gaged. Initially, it would seem a waste of human resources to develop a hydrological model and calibrate it, when a flood frequency relationship was established by measurement. The Natural Resources Conservation Service (NRCS) has recently updated two (DOS version) hydrologic computer programs to window versions - WinTR-55 and WinTR-20. These computer programs are nearly always used on ungaged watersheds. Testing WinTR-55 on a gaged watershed would provide an opportunity to see how well the computation engine performs based on six input parameters of drainage area, time of concentration, curve number, rainfall amount, rainfall distribution, and dimensionless unit hydrograph. Comparing WinTR-55 results to measured flows from several storm events over several years would indicate the level of effort required to calibrate the model and the exercise would give indications of hydrologic parameter sensitivity; would the input parameters have to be changed on a storm by storm basis? Is there some natural variability of the input parameters over time? After calibrating the hydrologic model, would the model provide insight into NRCS design rainfall distributions?

CALIBRATION

There are three calibrations involved with this case study – a hydraulic calibration of the HEC-RAS model, a geomorphic calibration of the hydraulic geometry characteristics, and a hydrological calibration of the WinTR-55 model. The hydrologic calibration relies on the geomorphic calibration, which in turn relies on the hydraulic calibration. Each will be discussed, with major emphasis on the hydrologic calibration and results.

Hydraulic Calibration: Hydraulic calibration relies on good definition of the stream geometry that defines the model. Cross sections should be representative of the reach, extend across the floodplain, and be perpendicular to flow. Cross sections should also describe abrupt changes in conveyance; changes in width, depth, slope, and roughness. Good definition of the channel thalweg and water surface throughout the modeled reach facilitates the calibration process. Make note of stream discharge on the days surveying. If working on an ungaged stream, a discharge measurement at the beginning and at the end of the day will facilitate calibration. Once cross section data, reach lengths, and roughness coefficients are entered into HEC-RAS, first runs should try and match a computed water surface on the day(s) of survey with the water surface surveyed. This step usually entails adding in "interpolated" cross sections along the profile, where the bed profile changes, especially in pooled areas. What seems to work well is to take an existing surveyed cross section (either upstream or downstream) from the location of the interpolated cross section and translating the floodplain elevations up or down by the valley slope multiplied by the distance translated. Channel bottom elevations are adjusted up or down depending on the difference between the existing cross section thalweg elevation and the thalweg elevation on the profile for the interpolated location. All channel bottom elevations below bankfull are adjusted by this thalweg difference. Usually a good match between computed and measured water surface profiles can be made by inserting enough interpolated cross sections without altering Manning's n. The second phase of hydraulic calibration is to modify Manning's roughness coefficients starting at the downstream cross section (for sub-critical flows) and working up to the surveyed cross section that represents the USGS rating curve. Try and match the computed rating curve to the USGS rating curve working from low discharges up to higher discharges. However the roughness values are changed in order to create the match, a similar relative adjustment of Manning's n should be made to the cross sections upstream from the rating cross section.

Geomorphic Calibration: During the profile survey, there are usually three rodmen; one shooting channel bed features and one on each bank shooting left and right bankfull indicators respectively, this way there are up to three independent opinions on bankfull stage along the profile. Secondly, the reach is modeled in HEC-RAS. The hydraulic model is "calibrated" when two conditions are met; first HEC-RAS must produce a water surface profile that matches the water surface on the day(s) of survey and HEC-RAS must produce a rating curve for a cross section representing the USGS gage that matches the USGS rating curve. After calibration, the water discharge that produces a water surface profile that matches a best fit of bankfull indicators all along the reach is chosen as the bankfull discharge. The water surface elevations at bankfull discharge are examined more closely in each of the surveyed cross sections (usually in middle of riffles or at the downstream end of pools in the glides). The bankfull cross section dimensions are averaged for three or more cross sections. This gives an average value of hydraulic geometry dimensions more representative of the reach. Thirdly, mean shear stress is calculated at bankfull stage (using hydraulic radius and energy gradient at bankfull discharge), when dealing with gravel sizes, multiplying the shear stress calculation by a factor of two gives a likely particle size moved in inches, this size is converted to millimeters and this particle size is compared to the Wolman Pebble count. Usually, the particle size moved based on calculated shear stress and the D_{50} are within $^{+/-}$5 mm. Fourth and finally, the reach averaged hydraulic geometry at bankfull discharge are compared to the hydraulic geometry of stratified regime curves for the same stream classification. Eighty cubic feet per second produced a water surface that matched many of the

bankfull indicators. Average channel topwidth is 20.4 feet and mean depth is 1.18 feet, mean channel velocity is 3.3 feet per second, the stream classified as a C4 in Rosgen's Classification System.

Hydrologic Calibration: The strategy to calibrate the WinTR-55 hydrologic model was to "nail down" as many of the input variables as possible, starting with the most stable of the parameters (with respect to time). For instance drainage area is one input parameter that should not change over time, can be planimetered from a USGS topographic map and verified through the USGS gaging records. However road construction and culverts can alter flow paths and change drainage area size so even drainage area is not a guaranteed stable time invariant parameter.

Time of Concentration (Tc): Tc is a relatively stable hydrologic parameter, but it can vary due to changes in the flow path, development of roads, or debris in the conveyance system. The velocity method outlined in TR-55 was used to calculate Tc. The longest flow path from basin divide to the gage was delineated on a 7.5 minute USGS topographic map. The flow path was segmented into sheet flow, shallow concentrated flow, and channel flow. Channel flow was segmented into four reaches based on slope breaks. The hydraulics of Hop Brook were already modeled and calibrated during the geomorphic analysis, so estimates of channel velocities near the gage were taken from the HEC-RAS model at bankfull discharge. Channel velocities for upper reaches with smaller drainage areas were estimated from the New England Physiographic Regional Curves. Travel times are computed by dividing the lengths of the flow paths by the average velocity within the flow path, travel times are then summed and the time was converted to hours. Time of Concentration for the Hop Brook basin was computed to be 1.56 hours; the longest flow path from basin divide to gage is 16,100 feet, the average velocity throughout the basin is 2.5 feet per second, channel velocities of reaches varied from 2.9 to 4.1 feet per second.

Curve Number (CN): CN is probably the second most unstable hydrologic parameter with respect to time. Curve Number changes between growing and dormant seasons. CN can change due to antecedent rainfall, land use/management, land development or fire. The Hop Brook was a continuous recording gage, so mean daily discharge as well as peak discharge records are available from the USGS. Eight historical storms were modeled; six storm events occurred during the growing season and two storm events occurred during the winter. Each storm produced the peak annual discharge for their respective water year. Curve Number was calculated from gaged data – precipitation records and runoff measurements. For the six storms that occurred during the growing season, the CN varied between 71 and 72, the antecedent runoff condition was in either a II or III condition. Calculating CN from hydrologic soils groups, vegetation and land use would have resulted in a CN of 70. For the two storms that occurred in the winter, it is assumed that the ground was frozen (January and February). Curve Number changed drastically to 93 and 89 respectively. Peaks were matched for the two winter storms, but runoff volumes are a guess because it is not known how much snow or equivalent water was on the ground prior to the precipitation events.

Rainfall: twenty-four hour rainfall totals for the eight storms were taken from the New Salem Precipitation Station (195306). New Salem is approximately 1.5 miles from the USGS gage and is located just outside of the watershed boundary. With daily recording stations, possible

discrepancies in time series data may exist because any precipitation that falls after the observation time (in this case 8 am) is recorded under the next days rainfall total.

Rainfall Distribution: Historic storm distributions are probably the most unstable hydrologic parameter with respect to time. Storm distributions vary temporally and spatially, and need not repeat themselves. Good calibration requires using representative historical rainfall distributions. Erroneous rainfall distributions may affect CN and Tc calibration. Historical rainfall distributions were re-created from "nearby" hourly recording precipitation stations. NOAA's U.S. Hourly Precipitation Dataset (TD3240) CD and website were used to find stations with available data on the days of storm events. When one procedure doesn't always provide sufficient answers, we try another and then call the technique "art". There are four hourly recording stations within twenty miles from the New Salem precipitation gage; Petersham 3N – station 196322 is 9.6 miles east of New Salem, Barre Falls Dam – station 190408 is 15.3 miles away, Birch Hill Dam – station 190666 is 16.8 miles and West Brimfield – station 199093 is 19.9 miles south-southeast of New Salem. For each storm event, the precipitation recorded from New Salem was always used. The rainfall distribution was always made dimensionless by dividing each cumulative hour by the total amount recorded. To choose which station to use at New Salem was an art. The rainfall distribution either came from the station whose total was closest to New Salem's total or two rainfall distributions were made dimensionless, averaged together and then applied uniformly over the Hop Brook watershed.

Dimensionless Unit Hydrograph (DUH): The dimensionless unit hydrograph may be the second most stable hydrologic parameter with respect to time next to drainage area. The shape of the unit hydrograph is in some ways a measure of the watershed's storage characteristics and its' response time of shedding water once rainfall has hit the ground. It is not a parameter easily measured. The five other hydrologic parameters were measured or calculated, so in order to find a suitable DUH for the Hop Brook watershed, it was a matter of trial and error of running WinTR-55 and trying to match peak discharge and runoff volume without having to significantly change any of the other input parameters.

The first storm modeled was the June 6th, 1982 storm in which 2.72 inches of rain fell on the day the peak stream discharge was recorded, 0.56 inches on the day prior to the peak. The five day antecedent rainfall was 2.75 inches, ARC III was assumed. Peak discharge on June 6, 1982 was 168 cubic feet per second (cfs). The runoff was approximately 0.66 watershed inches. From daily mean discharge records, the three day runoff was approximately 1.04 watershed inches. From Figure 10.2 of NEH Part 630, the runoff curve number is approximately 70.

The hydrologic parameters used to model the 6/6/82 storm in WinTR-55 are as follows; drainage area (DA) is 3.39 square miles, Time of Concentration (Tc) is 1.56 hours, Curve Number (CN) is 70, the rainfall distribution was derived from Petersham 3N, an hourly recording gage 9.6 miles to the east of the watershed. The 24-hour precipitation total of 2.72 inches recorded from the New Salem gage on the edge of the watershed was applied over the one basin model. The DELMARVA Unit Hydrograph was selected. Computed peak discharge was 202 cfs and runoff was 0.564 inches, reducing CN lowered the peak but also reduced runoff volume.

A unit hydrograph with a peak rate factor (PRF) of 200 was selected from NEH Part 630 Chapter 16 – Hydrographs. Tc was increased to 1.6 hours, all other parameters remained the same; computed peak discharge was reduced to 181 cfs, but the runoff remained at 0.564 watershed inches.

A unit hydrograph with a PRF of 150 was selected, again from Chapter 16. Tc remained at 1.6 hours, CN was increased to 72, all other parameters remained the same; computed peak discharge was reduced to 171 cfs, and runoff increased to 0.646 watershed inches. Given the uncertainty of the average rainfall depth, the actual rainfall distribution, no further parameter adjustments were made. It was time to test these new parameters against a second storm event.

The second storm modeled was August 5th, 1969; 2.95 inches of rain fell in approximately 24 hours, 0.84 inches fell on the previous day and 2.20 inches in the previous five days. August being in the growing season, again the ARC III condition was assumed. The peak discharge recorded was 147 cfs and the runoff volume measured was approximately 0.78 watershed inches. Using a PRF of 150, a Tc of 1.6 hrs, CN of 72, Rainfall of 2.95 inches, and a rainfall distribution based on both the West Brimfield and the Petersham 3N stations, WinTR-55 computed a peak discharge of 141 cfs and a runoff volume of 0.778 watershed inches. Decreasing Tc to 1.5 hours and running WinTR-55 with all other parameters the same gave a computed peak discharge of 145 cfs. Changing Tc does not affect runoff volume. In a hydrologic sense, there are too many variables and uncertainties to try and refine the answer any closer. It appears that PRF, CN, and Tc are consistent enough to be “calibrated”, at least for the ARC III condition, however testing a third storm is advisable.

The third storm modeled was October 6th, 1962; New Salem precipitation gage recorded 1.60 inches on the day of peak (8 am observation time) and 2.90 inches of rain recorded 24 hours later. The antecedent rainfall is either 0.11 inches or 1.71 inches. The growing season is coming to an end and the ARC is in either a I or II condition. The peak discharge recorded at the gage was 199 cfs, 1-day runoff was approximately 0.42 inches, 2-day runoff was approximately 0.64 inches and the 3-day runoff volume measured was approximately 0.746 watershed inches. Using a PRF of 150, a Tc of 1.5 hrs, CN of 72, and a rainfall distribution based solely on the Birch Hill Dam (Station 190666), WinTR-55 computed a peak discharge of 181 cfs (-9 % off recorded peak) and a runoff volume of 0.749 watershed inches (+0.4% difference on 3-day runoff volume). A fourth storm was modeled to check for further variance in the hydrologic parameters.

After modeling three storms with good results and little change in hydrologic parameters, it was time to test the model against different climatic conditions. The January 23rd, 1973 storm was modeled because a low 1.28 inches of precipitation produced a high discharge of 246 cfs. Either this rain fell intensely over a short period (unlikely during winter) or the runoff condition may have changed (due to frozen ground?). The 24-hour rainfall value at New Salem was applied to a dimensionless rainfall distribution constructed from the Petersham 3N hourly measurements. Only Curve Number was varied to match peak discharge, a CN of 93 produced a peak discharge of 243 cfs and a runoff value of 0.677 watershed inches. The USGS gage recorded a peak of 246 cfs and 82 cfs-days mean daily discharge (runoff volume = 0.90 watershed inches. This event may have involved rain on snow, since there is evidence of runoff not accounted for due to rain.

The February 3rd, 1970 storm was modeled to test the dramatic change in Curve Number due to frozen ground conditions. The USGS recorded a peak discharge of 223 cfs and a mean daily discharge of 86 cfs (0.943 watershed inches) and a two-day runoff total, discounting base flow, of 1.224 watershed inches. Using a PRF = 150, Tc = 1.6 hrs, CN = 89 and 2.27 inches of rain applied to a dimensionless rainfall distribution based on Petersham 3N and Barre Falls Dam, WinTR-55 computed a peak discharge of 220 cfs and a runoff volume of 1.255 watershed inches.

Modeling the August 19th, 1955 storm shed light on major discrepancies between computed and recorded discharges; The New Salem precipitation station recorded 6.50 inches of rainfall. West Brimfield recorded 11.94 inches within a 24-hour period. The previous 5-day rainfall total was 6 inches (ARC III). The USGS gaging station recorded a peak discharge of 275 cfs. Modeling the storm event using a PRF = 150, Tc = 1.5 hrs, CN = 72, and 6.5 inches of rainfall applied to a dimensionless rainfall distribution constructed from the West Brimfield hourly recording station, WinTR-55 computed a peak discharge of 1,143 cfs. The runoff volume calculated (from the WinTR-20 computation engine) was 3.40 watershed inches however the actual 8-day runoff total recorded after the storm was 2.88 watershed inches. CN was reduced to 66 to better match runoff (2.82 watershed inches of runoff calculated). The corresponding computed peak discharge was 909 cfs, still a far ways off from 275 cfs published by the USGS. A new rainfall distribution was input into the model, in which the 6.5 inches of rain fell uniformly over 24 hours – this distribution minimizes intensities and therefore would minimize the computed peak discharge, given that the 6.50 inches of rainfall recorded was correct. The 24-hour uniform distribution with a CN = 66 and all other hydrologic parameters the same produced a peak of 421 cfs. The model has proven consistent up to this storm, so the USGS published value of 275 cfs seems doubtful. Sometimes even measured and published data are suspect to error.

The peak discharges generated from the August 19, 1955 storm from WinTR-55 were input into the HEC-RAS steady flow model. Computed water surface elevations indicates that a peak discharge of 915 cfs would overtop the road and bridge that are just upstream from the USGS gage by 1.4 feet. Ground observation in the vicinity of the gage also indicates that flows on the far right in the cross section would bypass the USGS gage before returning to the stream. Therefore it is possible that the gage did not record the true peak or volume for a storm of this magnitude. To resolve this discrepancy, the proper methodology would be to model the bridge and road embankment as a structure and run the WinTR-55 hydrographs in the HEC-RAS unsteady flow model.

The USGS gage is located on the downstream end of the bridge abutments. Modeling results indicate that the bridge will pass up to the 10-year flows without altering the peak, but the bridge significantly affects peak discharges of storms with longer recurrence intervals.

DESIGN STORMS

A new Weibull Distribution was plotted, based on changing the peak annual discharges for the October 24, 1959 storm (289 cfs measured changed to 537 cfs computed) and the August 19, 1955 storm (275 cfs measured changed to 915 cfs computed). Assuming these are the peak discharges just upstream of the bridge and gage. WinTR-55 was run using the Type I, Type IA,

Type II, and Type III design rainfall distributions and using the calibrated hydrologic parameters of CN = 72, Tc = 1.6 hrs and PRF = 150. The 2-year, 5-, 10-, 25-, 50-, and 100-year rainfall amounts were accepted from WinTR-55 for Franklin County, Massachusetts. Results are plotted in Figure 1. Discharges resulting from the Type I design rainfall distribution come closest to the new Weibull Distribution. In Massachusetts, the Type III design rainfall distribution is used. The Type I and the Type III rainfall distributions were then run with the standard design DUH, (which gives a peak rate factor of 484), CN was reduced to 71 and 70 respectively. Results are also plotted in the graphic below. Finally, WinTR-55 was run using a Type I rainfall distribution, a CN = 93 (for frozen ground conditions), a Tc = 1.6 hours, and a PRF = 150. Results were also plotted on the graphic below.

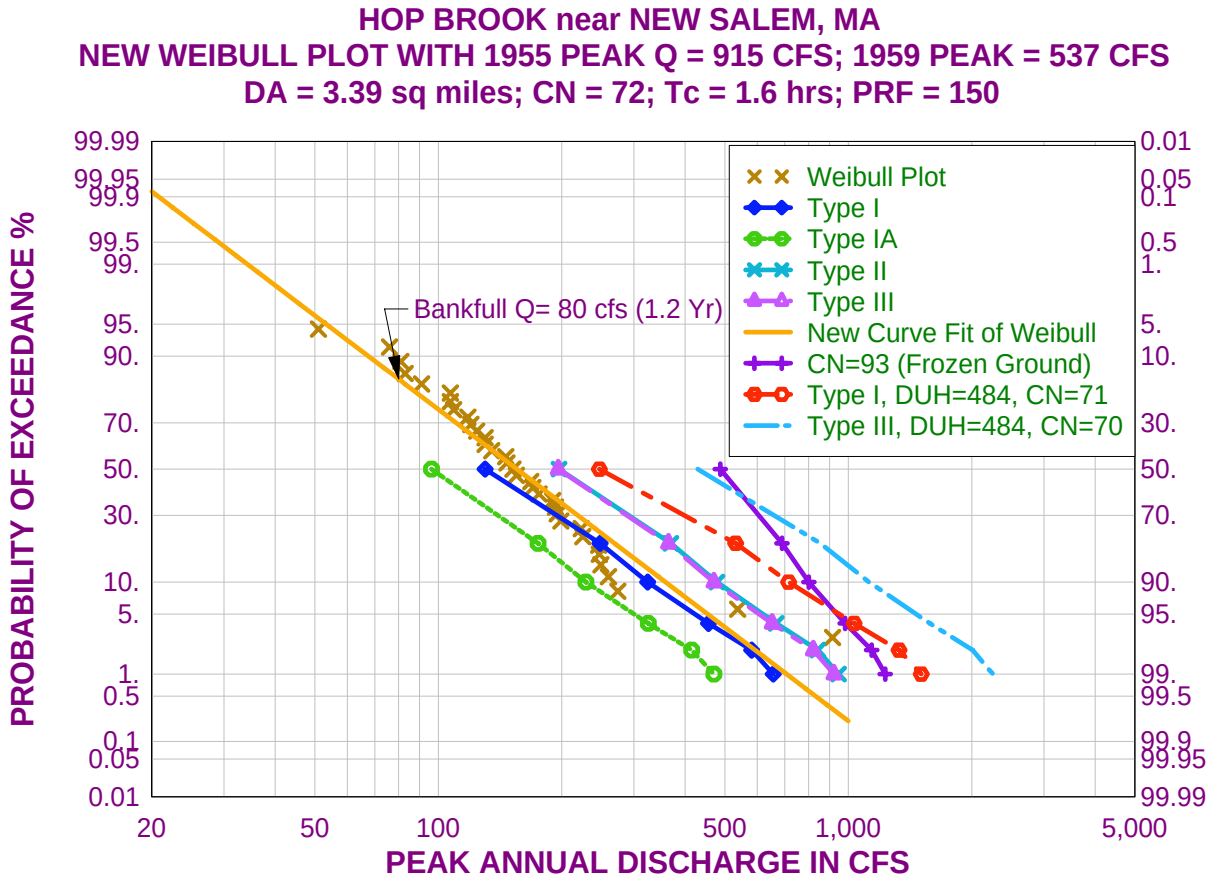


Figure 1 New Weibull distribution plot – Hop Brook near New Salem, MA.

What the graphic indicates is that the discharges generated using design parameters from WinTR-55 using the Type III rainfall distribution, along with the standard dimensionless unit hydrograph (PRF = 484) and a CN of 70, which would have been calculated from hydrologic soils groups, vegetation and land use maps, would be sufficient and even overly conservative to estimate discharges based on frozen ground conditions (CN of 93) had all the other parameters been calibrated correctly.

SUMMARY

The Table 1, below, shows the results of the WinTR-55 modeling effort. The storms are listed in the order of analysis and calibration. Comparisons of the recorded peak discharges and measured runoff volumes for the first four storms to computed values indicates that WinTR-55 (and the WinTR-20 computation engine) performs well given that a satisfactory job in calibrating the six hydrologic input parameters; of Drainage Area, Time of Concentration, Curve Number, Rainfall, Rainfall Distribution, and Dimensionless Unit Hydrograph. The largest difference between computed and measured peaks was -9 percent. It wasn't until the 6.5 and the 4.05 inch rains that major discrepancies arose in the computed results. It is the author's belief that the road and bridge above the gage acts as a dam that impounds water and reduces the peak discharge through the eleven-foot wide bridge abutments. There is also a discrepancy in runoff volumes. HEC-RAS modeling indicates that discharges above 900 cfs will overtop the road, and that flows that overtop will seek an alternate route around the gage, to which storm volumes will not be fully accounted for. All storms modeled produced the peak annual discharge for their respective water year. The last two storms modeled occurred in winter, when frozen ground and a dramatic change in Curve Number occurred, CN changes from a 70 during the growing season (72 in ARC III condition) to CN of 89 to 93. The modeling discrepancies in runoff volumes of the winter storms may be due to a melting of accumulated snow. Further detective work on nearby snotel sites may enlighten this theory.

Table 1 Results of the WinTR-55 modeling effort.

USGS Data			WinTR-55 Computed Results and Parameters				
		Volume		Volume			
Date	Peak Q	Watershed	Peak Q	Watershed	CN	Tc	PRF
	cfs	Inches	cfs	Inches			
6/6/1982	168	0.66	171	0.646	72	1.60	150
8/5/1969	147	0.779	145	0.778	72	1.50	150
10/6/1962	199	0.746	181	0.749	72	1.50	150
6/10/1961	247	0.548	244	0.547	71	1.60	150
10/24/1959	289	1.101	513	1.428	71	1.50	150
8/19/1955	275	1.906	915	3.829	72	1.50	150
1/23/1973	246	1.05	243	0.677	93	1.60	150
2/3/1970	223	1.367	220	1.255	89	1.60	150

REFERENCES

Forecast Systems Laboratory, Boulder, Colorado and National Climatic Data Center, Asheville, NC, (1998), US Hourly Precipitation Data. TD 3240 Vol. 1 and 2.

Hydrologic Engineering Center, (2003), HEC-RAS River Analysis System Computer program Version 3.1.1. U.S. Army Corps of Engineers

Rosgen, David L. (1994) "A Stream Classification System," Catena Vol. 22, pp 169-199. Elsevier Science, Amsterdam.

United States Department of Agriculture, Natural Resources Conservation Service (2003 draft), National Engineering Handbook; Part 630 Hydrology, Chapter 16 – Hydrographs. 42 pp

United States Department of Agriculture, Natural Resources Conservation Service (2003), Small Watershed Hydrology (WinTR-55) Computer program.

United States Department of Agriculture, Natural Resources Conservation Service (2004), National Engineering Handbook; Part 630 Hydrology, Chapter 10 – Estimation of Direct Runoff from Storm Rainfall. 79 pp

United States Department of Agriculture, Natural Resources Conservation Service (2004), Watershed Hydrology (WinTR-20) Computer program

Wolman, M.G. (1954), "A Method of Sampling Coarse River Bed Material," American Geophysical Union Transactions Vol. 35 pp 951-956.

MULTIPLE APPROACHES TO ASSESSING THE IMPACT OF DAMS ON SEDIMENT DELIVERY IN THE ST. JOSEPH RIVER WATERSHED, MICHIGAN/ILLINOIS

Rob Nairn, Principal, W.F. Baird & Associates, Oakville, ON, rnairn@baird.com; Alex Brunton, Geoscientist; W.F. Baird & Associates, Oakville, ON, abrunton@baird.com; Jim Selegean, Hydraulic Engineer, U.S. Army Corps of Engineers - Detroit District, James.P.Selegean@lre02.usace.army.mil

Abstract: The rates at which sediment moves through the St. Joseph River and its tributaries and watershed have been subject to significant human modification over the past 200 years. These modifications include logging, development of agricultural land, dam construction, urbanization and river channel alteration. The first major dam was constructed in 1850 and 66 large dams now exist in the watershed. Only 13% of the watershed now drains directly to the river mouth, and dams form a significant trap for sediment sourced from the remaining 87% of the watershed.

This study was undertaken as part of the US Army Corps of Engineers Great Lakes Tributary Modeling Program. A wide variety of techniques were used to assess the role of dams in altering sediment movement through the St. Joseph River watershed. Trap efficiency analysis was undertaken using the capacity-watershed and the capacity-inflow methods. Watershed sediment yield and delivery were under changing land uses were assessed using the Watershed Characterization System (EPA) and the Soil Water Assessment Tool (USDA-ARS). Acoustic bathymetric sediment surveys were taken of the larger downstream reservoirs in the watershed along with samples of trapped sediment. Historic dredging records of the navigable area of the lower river over a 150-year period were also evaluated to determine sedimentation rates in the lower river channel. A two-dimensional hydrodynamic and sediment transport model (RMA2-SED2D) was set up to examine the effects of modified upstream sediment delivery on the morphodynamics of the harbor and river mouth and to use the dredging data to test the sediment delivery model result over the last 150 years (i.e. by establishing the trapping rate of the harbor area).

The combination of the varied techniques outlined above allowed a detailed analysis of the role of dams in modifying watershed sediment movement in the face of changes to other watershed characteristics such as land use, BMPs and soil conservation practices. Evaluation using only one or two of the above techniques would have precluded identification of the role of dams in reducing sediment delivery to the lower river as their likely effect would not have been isolated from other factors. Dams were found to be effective in trapping up to 80% of sediment supplied from the upper watershed, with other factors such as in-channel sedimentation further reducing sediment supply to the river mouth. The merits of the various methods are discussed, along with challenges and benefits of their integration for assessment of sediment delivery.

INTRODUCTION

The U.S. Army Corps of Engineers is directed to develop sediment transport models for tributaries to the Great Lakes that discharge to Federal navigation channels or Areas of Concern (AOCs). These models are being developed to assist State and local resource agencies in evaluating alternatives for soil conservation and non-point source pollution prevention in the tributary watersheds. The ultimate goal is to support State and local measures that will reduce the loading of sediments to navigation channels and AOCs, and thereby reduce the costs for navigation maintenance and sediment remediation. A suite of models including the Soil and Water Assessment Tool, SWAT and the RMA2/SED-2D hydrodynamic and sediment transport models were developed to further understand sediment movement through the St. Joseph River Watershed. SWAT was constructed for the entire watershed so that significant sediment source areas could be identified, and the effects of land use change, best management practices (BMPs) and the impact of dams on sediment movement through the watershed could be evaluated. RMA2-SED2D model construction enabled upstream sediment delivery rates and harbor sediment trapping and throughput to be evaluated, allowing construction of a sediment budget, which formed the primary long-term sediment delivery calibration points for the SWAT model.

STUDY AREA

The St. Joseph River Watershed is a part of the Lake Michigan Basin, comprising 1.6 percent of its contributing area. The St. Joseph River main channel is 210 miles long and has over 1,641 miles of significant tributaries. The watershed covers 4,685 square miles-3,000 in Michigan and 1,685 square miles in Indiana. The river has a fall of over 600 feet from the source to its discharge into Lake Michigan.

METHODOLOGY

The Soil and Water Assessment Tool (SWAT) is a watershed-scale numerical model for the simulation of water, sediment, nutrient and pesticide movement in surface and subsurface systems. SWAT aids in prediction of the impacts of climate and vegetative changes, reservoir management, groundwater withdrawals, water transfer, land use change and watershed management practices on water, sediment and chemical dynamics in complex watershed systems. Land use and management conditions can be varied over long time periods, making the model a particularly useful tool to aid in the evaluation of BMPs. SWAT is a continuous-time model, intended for the prediction of long-term water and sediment yields from a watershed.

A detailed hydrodynamic model (RMA2) and an associated sediment transport model (SED2D) were set up to evaluate sediment movement through the harbor and into the nearshore zone. The main objectives of this exercise were to provide estimates of sediment movement through the harbor over long time periods and to evaluate the impact of dredging the inner harbor on sediment discharges to the nearshore zone. RMA2 is a two-dimensional, depth-averaged, finite element hydrodynamic numerical model. It computes water surface elevations and horizontal velocity components for subcritical, free-surface flow in two-dimensional flow fields. The original model was developed by Norton, King and Orlob (1973) for the US Army Corps of Engineers. Many subsequent enhancements have been made, culminating in the current version

of the code. The program has been applied to calculate water levels and flow patterns in rivers, reservoirs, and estuaries.

The sediment transport model, SED2D is coupled with the RMA2 model. SED2D is a sediment transport numerical model developed by the U.S. Army Corps of Engineers Waterways Experiment Station. It has the ability to compute sediment loadings and bed elevation changes when supplied with a hydrodynamic solution computed by RMA2. SED2D can be used to model sand bed types or clay/silt bed types. It is possible to model both steady-state and transient flow types, just as with RMA2. The RMA2-SED2D model domain was set up for an area including the lower St. Joseph River up to approximately 3 miles upstream from the inner harbor; the Paw Paw River for approximately 2 miles upstream from the inner harbor; the inner and outer harbor; and the lake for approximately 2.5 miles upstream and downstream from the harbor, and for 1 mile offshore. Full details of setup, calibration and verification of these models are available on request from the authors.

RESULTS

Effect of Land Use Change: The pre-European settlement delivery rate to the harbor was estimated by SWAT to be 28,000 cy/yr (Table 1). The estimate was generated with SWAT using land use circa 1800-1830 for Michigan, and an estimated 1830 land use for Indiana. The estimated pre-development sediment delivery value of 28,000 cy/yr suggests that sediment transport in the St Joseph watershed was much lower than modern values. Soil erosion and sediment delivery to the harbor mouth were much higher for the 1978 model runs than for the pre-European settlement scenario. Since the 1978 land cover data did not divide agricultural land into subcategories, two sets of model runs were created using this dataset. One run used a generic agriculture term and the second run categorized all unclassified agricultural land as row crops to provide the upper limit to soil erosion and sediment yield predictions. These two runs predicted sediment delivery to the inner harbor of 68,000 cy/yr and 79,000 cy/yr respectively.

Table 1 Summary of SWAT Model Output.

Year	Model Conditions	Total Soil Erosion in Watershed (cy per year)	Total Sediment at Inner Harbor (cy per year)
1830	Pre-development	72,000	28,000
1978	Generic Agriculture;	850,000	68,000
1978	Row Crops	1,118,000	79,000
1992	Reference Condition	884,000	57,000

For the 1992 land cover data (which was classified into component agricultural uses), sediment delivery was predicted to be 57,000 cy/yr. This is lower than the 1978 values because land has been taken out of agricultural production in the intervening years, causing a drop in soil erosion and sediment supply to the harbor.

Effect of Dams: There are 190 dams in the St. Joseph River Watershed (Michigan Department of Natural Resources, 1999). Since 1850, 65 major dams have been constructed in the St. Joseph

Watershed (Table 2). In 1850 the first major dam was constructed at South Bend, with 76% of the watershed located upstream of the dam. Dam construction continued from this time, with the large Twin Branch Dam in 1903, and the Berrien Springs Dam in 1908, resulting in the 87% of the watershed being above major impoundments (Figure 1).

Table 2 Number of dams categorized by reservoir size from EPA (2005).

Dam Size	Storage (ac-ft)	Normal Storage	Maximum Storage	High Hazard	Significant Hazard	Low Hazard
Small	1-100	20	12	2	3	7
Medium	100-10,000	43	51	19	12	20
Large	10,000-1,000,000	1	1	1	0	0
Very Large	>1,000,000	0	0	0	0	0
Unknown		2	2	0	2	0

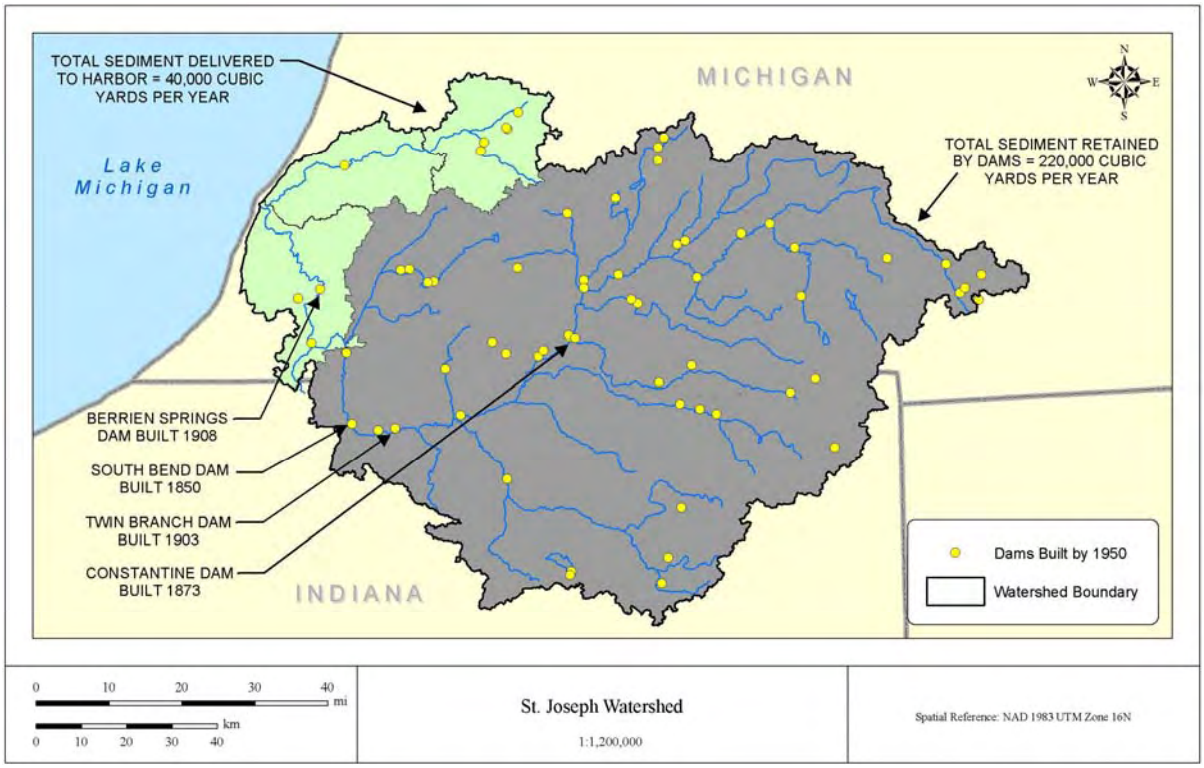


Figure 1 Influence of Dams on Sediment Supply From the River to St. Joseph Harbor.

These large dams are efficient sediment traps, regardless of whether they are underspill or overspill in construction. Either type of dam is an efficient trap because the sediment is not only trapped by the physical structure of the dam, but settles out in the slow moving water impounded for distances reaching several miles upstream from the dam. For example, the Twin Branch Dam impounds over 9 miles of main river, and has velocities that rarely exceed 1.5 ft/s. River flow data from 1930 was compared with a sediment transport capacity curve to determine an average annual sediment transport capacity of 20 tonnes per year in the Twin Branch Reservoir

for particles in excess of 0.25 mm diameter. This means that any sediment delivered in excess of this amount will be trapped in the reservoir above Twin Branch Dam.

In addition to using standard empirical relationships to examine trapping efficiency, the SWAT model was set up to evaluate the effect of dams on sediment movement through the watershed and sediment delivery to the harbor mouth. There are several options for estimating reservoir outflow in SWAT. The option used for simulating the effect of dams in the St. Joseph SWAT model requires an average annual spillway release rate. If the volume in the reservoir exceeds the principle storage, then water is released at the average annual rate. If the volume exceeds the emergency spillway, the difference between that and the principal volume is released within one day.

Table 3 shows a summary of the SWAT model results for the influence of dams on sediment delivery to the harbor mouth. These runs were undertaken for the 1992 land cover data as it is the most recent complete dataset. Table 3.3 shows that the presence of dams in the watershed reduces total sediment supply to the inner harbor from 283,000 cy/yr to 57,000 cy/yr: a reduction of 226,000 cy/yr, or 80%, between the two scenarios. Sediment supply from the Paw Paw River, a tributary to the harbour, remains at approximately 15,000 cy/yr due to the negligible influence of dams on this tributary. Figure 2 shows the effect of dams on sediment delivery downstream through the watershed, showing high amounts of sediment delivered downstream without the dams, but a low sediment delivery throughout the catchment with dams present.

Table 3 SWAT model output showing influence of dams on total sediment delivery to the St. Joseph harbor.

Year	**Model Conditions**	**Total Soil Erosion in the Watershed (cy/yr)**	**Total Sediment at Inner Harbor (cy/yr)**
1992	Reference Condition	884,000	57,000
1992	No dams or reservoirs	884,000	283,000

The estimate of reservoir sedimentation compares well with empirical estimates from other sources. Chanson (1999) provides reservoir sedimentation rates in the continental US with a mean value of 10,310 cy/mi^2/yr. With the surface area of BASINS dams in the St. Joseph watershed being 15.94 square miles, multiplication of these values gives an empirical estimate of reservoir sedimentation of 165,000 cy/yr. This value compares well to the 226,000 cy/yr predicted by the SWAT model.

In summary, 65 major dams now exist within the St. Joseph River and only 13% of the watershed is able to drain directly and carry sand freely to the river mouth area. According to the SWAT model output, of the current total supply from the entire watershed of about 884,000 cy/yr of sediment (of which about 50% is sand), 226,000 cy/yr is trapped by dams and reservoirs and 601,000 cy/yr is held in other sediment sinks, such as in-channel deposition. Only 57,000 cy/yr (of which about 50 % is sand) is able to reach the inner harbor and river mouth (with a

considerable portion of this delivered by the Paw Paw River tributary that feeds directly into the inner channel).

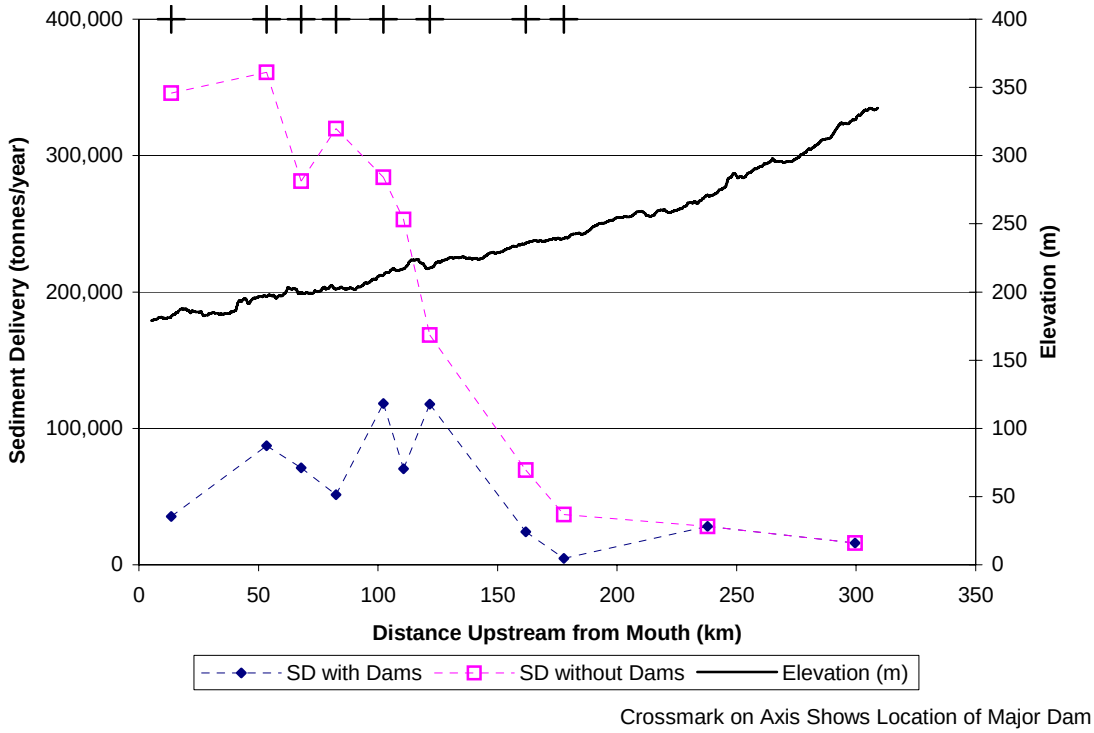


Figure 2 Effect of Dams on Watershed Sediment Delivery.

Harbor Sediment Trapping: A detailed hydrodynamic model (RMA2) and an associated sediment transport model (SED2D) were set up to evaluate sediment movement through the harbor and into the nearshore zone. In addition, an empirical analysis of river discharge and sediment load data produced a distribution of the amount of sediment transported by river flows of different magnitude. This showed that most sediment is transported in flows ranging from 3,500-4,900 ft^3/s. These flows have return periods in the range of 0.5-1.0 years.

Under mean flow conditions, most deposition is upstream from the inner harbor, and no sand reaches the harbor or lake (Figure 3). This is primarily due to the wide, deep, low gradient channel upstream from the harbor acting as a very efficient sediment trap under these conditions. It is only once flow is above the 1-year return period level that sand is transported into the inner harbor, and even at this stage, the amount deposited in the inner harbor is small compared to that deposited in the main channel upstream.



Figure 3 Velocity and Sediment Concentration in the St. Joseph Harbor.

Output from SED2D was then used to produce a set of look-up tables of sediment load for different flow and lake level scenarios. Daily sediment load from 1930 to present was derived by cross-referencing the look-up tables with the time series of river flows and lake level, thus giving a long-term prediction of sediment transport through the harbor. For the 2002 bathymetry, over the long term, the inner harbor traps approximately 50% of the sediment that enters, and 50% is transported to the outer harbor and lake. However, during the period from January 1988 to December 1997, the inner harbor trapped 67% of the entering sediment. This likely reflects an increased occurrence of flood events with a 1 to 3 year return period during this time.

CONCLUSIONS

Use of the SWAT model to evaluate watershed hydrology, sediment yield and sediment delivery in the St. Joseph Watershed greatly aided evaluation of a number of key topics in this watershed. Watershed sediment yield has increased approximately ten-fold since pre-settlement conditions, due to conversion of land from primarily forested to agricultural, and subsequently to urban land uses. Sediment delivery to the lake has approximately doubled as a result of these activities. However, watershed sediment delivery would be much higher were it not for the influence of many large dams and reservoirs in this watershed. SWAT proved to be a valuable tool in evaluating these parameters in such a large watershed. The use of harbor dredging data were vital as a measure of long-term sediment load in the St. Joseph River, and this provided valuable long-term calibration points for the SWAT model. However, it was only possible to link the

dredging data to watershed sediment delivery by the use of the RMA2-SED2D model system to evaluate harbor sediment dynamics and sediment trapping efficiency over a long-term period.

REFERENCES

Chanson, H. 1999. The Hydraulics of Open Channel Flow: An Introduction. Butterworth-Heinemann, Oxford. 495 pp.

EPA, 2005. BASINS data for the St. Joseph Watershed, HUC #04050001.

Michigan Department of Natural Resources. 1999. St. Joseph River Assessment. Michigan Department of Natural Resources Fisheries Division, Fisheries Special Report 24, Lansing, Michigan.

Norton, W.R., King, I.P. and Orlob, G.T. 1973. A Finite Element Model for Lower Granite Reservoir. Walla Walla District, U.S. Army Corps of Engineers, Walla Walla, WA.

CUMULATIVE WATERSHED EFFECTS ANALYSIS WITH THE GEOSPATIAL INTERFACE FOR THE WATER EROSION PREDICTION PROJECT (GEOWEPP)

Chris S. Renschler, Assistant Professor, National Center for Geographic Information and Analysis (NCGIA), University at Buffalo, Quad, Buffalo, NY, rensch@buffalo.edu, William J. Elliot, Project Leader, Rocky Mountain Research Station, Moscow, ID, welliot@fs.fed.us

Abstract: Hundreds of millions of dollars are spent each year on mitigation practices following wildfire. Additional hundreds of millions of dollars are proposed to be spent on fuel treatments - including prescribed fires - to reduce the likelihood of wildfires. One of the stated reasons for both of these large expenditures is that such investments are necessary to reduce (in the case of wildfire) or prevent (in the case of fuel management) damage to our nation's wildland watersheds. Wildland management agencies are frequently challenged by the public to demonstrate the watershed benefits of wildfire treatments, or watershed risks associated with fuel management treatments. Wildfire rehabilitation teams and fuel management teams require state of the art erosion prediction tools to aid in justifying or supporting such expenditures to Congress and to the general public. The development of a new tool focusing on wildfire treatments is currently funded by 2004 and 2005 Joint Fire Science Program (JFSP). The Geospatial Interface for the Water Erosion Prediction Project (GeoWEPP) (Renschler, 2003; Renschler and Lee, 2005) is based on the WEPP model (Laflen et al., 1997), a spatial erosion modeling tool that is widely accepted for soil erosion, runoff and sediment yield prediction in forests, woodlands, shrublands, grasslands, rangelands, and agricultural lands. In addition to assessing post-fire treatments, GeoWEPP can be used to perform a Cumulative Watershed Effects (CWE) analysis that allows fuel management activities to prevent fires. GeoWEPP received overwhelming positive response from fuel and watershed managers during several BLM and FS organized workshops. To meet these users' additional requests the development goals were expanded and implemented in the widely used Geographic Information System (GIS) ArcGIS. In particular the project targets applications to Burned Area Emergency Rehabilitation (BAER) for erosion analysis, postfire salvage logging analysis, and small scale CWE analysis of fuel management treatments including thinning and prescribed fire. The overwhelming positive response from fuel and watershed managers during several BLM and FS organized WEPP workshops and the successful GeoWEPP application for the largest US fire during the 2005 season use in confirmed that it is capable of answering crucial questions related to wildland fuel management. To meet the users' additional requests in ArcGIS, we will introduce more CWE analysis capabilities for much larger watershed scales that include roads and timber harvesting activities.

REFERENCES

Renschler, C.S. (2003). “Designing geo-spatial interfaces to scale process models: The GeoWEPP approach,” Hydrological Processes 17, p. 1005-1017.

Laflen, J.M., W.J. Elliot, D.C. Flanagan, C.R. Meyer, and M.A. Nearing (1997). “WEPP-Predicting water erosion using a process-based model,” Journal of Soil and Water Conservation 52(2), p. 96-102.

Renschler, C.S., and T. Lee (2005). "Spatially distributed Assessment of Short- and Long-term Impacts of Multiple Best Management Practices in Agricultural Watersheds," Journal of Soil and Water Conservation. 60(6), p. 446-456.

DEVELOPMENT OF AN ACOUSTIC SUSPENDED SEDIMENT MONITORING SYSTEM

Daniel E. Kleinert Jr., National Center for Physical Acoustics, University of Mississippi, University, MS, kleinert@olemiss.edu; Daniel Wren, USDA National Sedimentation Laboratory, Oxford, MS; Chris Smith and James P. Chambers, National Center for Physical Acoustics, University of Mississippi, University, MS

Abstract: Suspended sediments represent a serious worldwide pollutant which need to be monitored and ultimately controlled. Significant entrainment and transport of these sediments occur during adverse weather conditions and during relatively short time spans which make manual sampling and monitoring cumbersome, inefficient and dangerous. Toward that end, the development of a remote autonomous acoustic system to monitor suspended sediments in fluvial systems is considered. The system will transmit an arbitrary waveform via a Digital Analog Converter (DAC) and power amplifier using user defined inputs. This waveform can be any frequency up to 5 MHz. The receiver section is composed of two parts; 1) the modular pre-amplifier section which will incorporate the transmit/receive function, transducer impedance matching section and appropriate signal preconditioning in the form of voltage gain and 2) the Analog to Digital converter, which is a 12-bit 65 MSPS CMOS pipelined multi-stepped converter. The resulting A-D conversion is stored in the 16 MB of onboard RAM. The stored results are processed by an Analog Devices Blackfin ADSP-533 Digital Signal Processing chip. Other features of the unit include a serial port interface, a JTAG interface used in real-time emulation, a serial programming port which would allow real-time programming, a peripheral programming interface allowing easy changes to any of the control routines for the various peripherals and onboard power control and reset functions. The operation of the unit starts with a trigger from a stage height decision, either internally or externally, indicating that an event has occurred that warrants observation. The backscatter data is then collected for an amount of time depending on the determined depth. Multiple data sets are collected, processed using Fast Fourier Transforms and stored in memory at a rate of up to 3 times a second. Depending on the length of data capture, they are archived on board or sent to a host computer via serial port or wireless transfer. The unit is DC powered and may be put to sleep when there is no data to take to extend field deployments. This work has been supported by the USDA.

INTRODUCTION

Existing lab based systems to monitor suspended sediment are often based on personal computers (PC's) and 3rd party software and hardware for data acquisition. These types of systems have an advantage in that they are turn-key systems that usually require little if any modification. However they suffer two main disadvantages. The first is that even in a PC notebook configuration, they are not suited to long term exposure to the environment in which a suspended sediment monitoring system is deployed. The second disadvantage is one of cost. Unit costs may easily exceed several thousands of dollars when all factors are considered. The system under development seeks to alleviate both of these issues by being a rugged system that may be deployed in a variety of environments including the possibility of being submerged under water. With a per unit cost under $200USD, and the possibilty of becoming less expensive as

the individual integrated circuit technology matures, the unit under development will be far more affordable than current alternatives.

DESIGN CONSIDERATIONS

The primary design consideration that drove all other decisions was to make the system inexpensive due to the large number of potential data sites. This consideration eliminated any type of PC solution and suggested that some type of embedded system should be used. After an extensive review of available systems and integrated circuits it was decided to use an Analog Devices ADSP-BF533 Digital Signal Processing (DSP) integrated circuit (IC). This particular IC was designed to be used in video systems and high-end audio applications, such as cellular telephones. One of the challenges was the frequency range needed for the range of suspended sediments of interest. This application calls for a frequency range of approximately 500 kHz to around 5MHz (Kinsler et al.2000, Crocker 1998). The Nyquist Theorem calls for a sampling frequency of at least twice the highest frequency of interest (Smith, 2003), with a maximum frequency of 5 MHz yielding a 10 MSPS minimum acquisition rate. The chip chosen easily handles this data rate.

Other considerations included power consumption and portability. Since the IC chosen is used in cell phones and hand-held video devices it has a wide variety of power management modes, allowing long battery life and needing a minimum of external chips.

HARDWARE OPERATION

The system's primary function is to perform a Fast Fourier Transform (FFT) on the backscattered acoustic data. The FFT is a 1024 point complex radix-2 FFT. The routine takes 1024 points of data, performs the FFT on it and picks out the magnitudes for the three frequencies of interest. This process is done 392 times (representing a 1.28 mm range bin resolution for the anticipated creek depth of 5m) to complete one data set. Next the average of 20 data sets is found for each of the three frequencies. These averaged values are then transmitted back to the host Personal Computer (PC).

Setup of the system prior to field deployment will consist primarily of loading the flash memory unit with the desired programs. The flash memory unit has 1 MB available for program storage and must be programmed prior to deployment. Other issues are appropriate connections to peripheral systems such as specific transmit and communication connections. If desired, the unit may be placed in sleep mode such that the host computer may be used to wake the system via the serial port interface to start operations. Alternatively, an external power switch may be used. In some applications it may be desirous to minimize the number of openings in the system housing due to environmental concerns. Power and transmitting connections are relatively easy to harden against the environment but other connections such as switches could lead to increased cost and complexity.

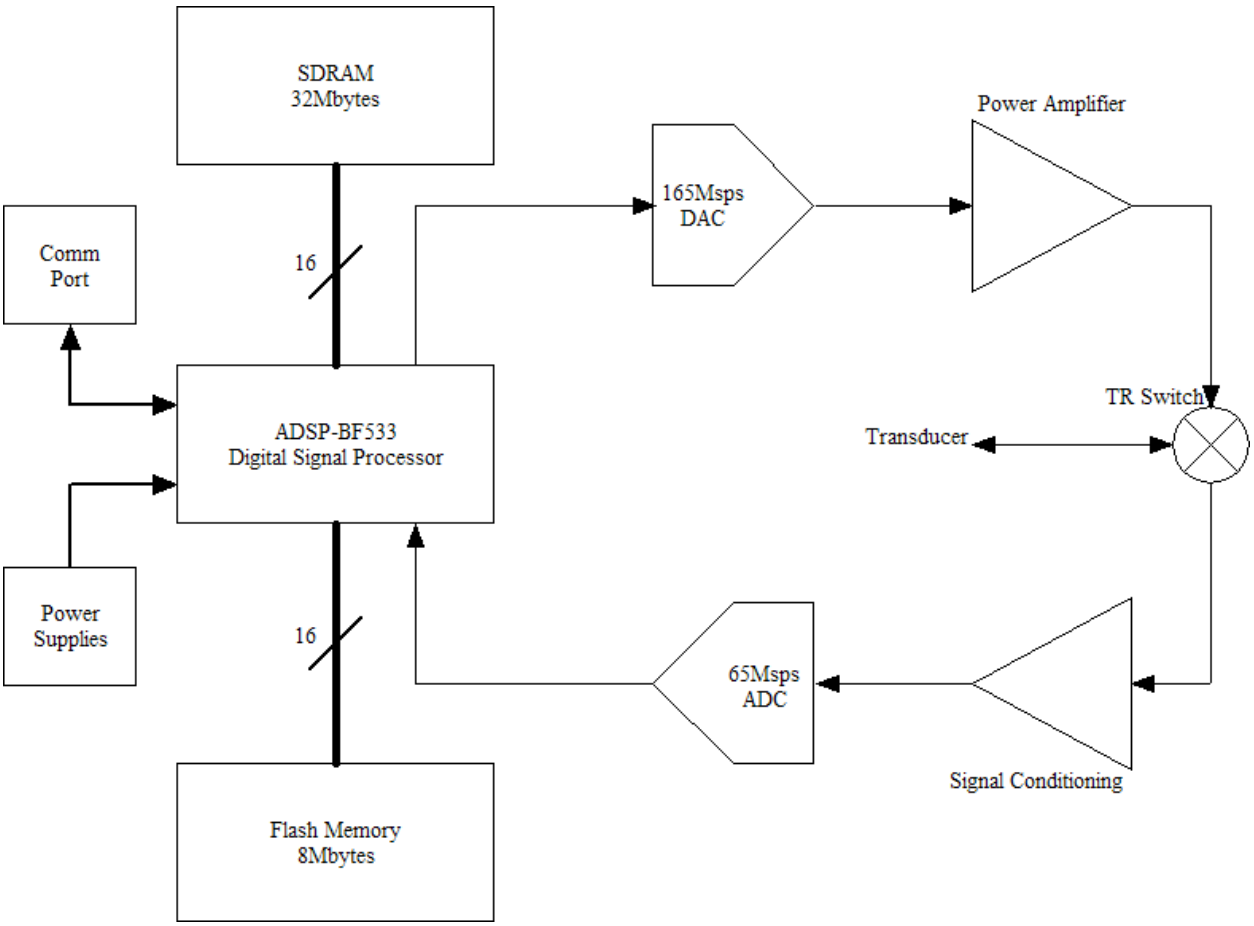


Figure 1 Block Diagram

Operation of the system begins with power being applied. At this time the DSP chip goes into a program loading mode called "boot loading" where the program stored in the onboard flash memory is loaded into the internal memory of the DSP and the system prepares to start taking data. After the boot operation is complete the first task performed is to check for connection to the land-based host computer. If communications are established the host computer will determine when data acquisition should begin. Generally this will be decided by a stage height monitoring system also connected to the host computer. Functions that may be performed while connected to the host computer include setting the data acquisition rate, transmitting of processed data, re-transmitting of processed data, initiating power saving modes and unit shutdown. In the event that communications are not established data acquisition will start automatically. The unit may also be instructed to wait for an activation signal directly from the stage height monitoring system. This is achieved through a hard wired connection to the stage height sensor. This data acquisition will continue until the memory buffer is full.

The data acquisition routine starts with a transmit pulse or chirp. The system has two transmit modes. The first mode is a single frequency mode which can generate any single frequency up to 20 MHz depending on transmitter power and transducer choices. The second mode is an arbitrary waveform mode which transmits a user defined waveform. The DSP chip has the capability to convert any mathematical expression into the necessary analog signals by

communicating with a 165 MSPS Digital to Analog Converter (DAC) chip. The output from the DAC is fed to the power transmitter circuitry which is chosen for a specific transducer type. The current transmitter circuitry is suited to transducers ranging in frequency from around 500 kHz to 5 MHz with impedances in the 50 ohm to 200 ohm range (Horowitz, 1989). Other transducers would require the appropriate transmitter circuitry.

After the transmitter pulse is generated and transmitted the system goes into a 134.04 μs wait state. This period allows time for the mechanical ring down of the transducer and to account for transducer near field effects. Depending on transducer type, impedance, and transmit levels this time may be adjusted. After the wait state is over, the system goes into receive mode. The time that the unit is receiving backscatter echoes is determined by the depth of the stream. This depth is determined in one of two ways. The first method is from the host computer which will relay depth information from the stage height sensor in the form of a status word. If the stage height information is not available the system can ping the bottom and acquire the depth itself by analyzing the return echoes. The second method is not as reliable since the algorithm for determining the bottom is affected by various factors, with the sediment flow being the primary one that could return a false bottom. There is also a default depth which is currently set at 5 meters.

The backscatter echoes from the entrained sediment are first sent to a signal conditioning circuit which matches impedance with the transducer, amplifies (if necessary) and anti-aliases the signal before it is applied to the Analog to Digital Converter (ADC). In the design phase an attempt was made to use standard parts for the amplifier section of the signal conditioner in order to accommodate various types of transducers, filter requirements, and gain. Also included in this stage is a diode clamp which acts as a transmit-receive switch to keep the high voltage of the transmitter stage out of the receiver stage. This section also converts the incoming transducer signal into a differential signal to drive the following ADC. In designing the signal conditioning stage, care was taken to insure that the IC's used were industry standard parts with standard pin outs. This decision was made to insure compatibility with as many types of transducers as possible. The bandwidth of the existing signal conditioning stage is approximately 10 MHz.

The ADC section is a 12-bit 65 MSPS integrated circuit with a Signal-to-Noise ratio of 72 dB. The ADC is configurable with a variety of input voltage levels and reference voltages to allow flexibility depending on the application. Some of the changes are software configurable by sending control words to the DSP and others are hardwired changes made during the board construction phase. The ADC digital output is fed directly to the synchronous dynamic ram under control of the SDRAM controller on the DSP. Both the control input and the analog signal inputs to the ADC are differential to reduce noise and jitter (Kester, 2003).

The DSP section is an Analog Devices ADSP-BF533 Digital Signal Processing integrated circuit. This chip is capable of running at a core clock speed of 756 MHz with a corresponding 1512 Million Multiply and Accumulate (MMAC) cycles. The prime function of the DSP is to take the raw backscatter data out of the SDRAM and perform a 1024-point complex radix-2 Fast Fourier Transform on that data and store the result back into the SDRAM. In addition to the core processing functions of the BF533, there are a number of other functions that it handles in controlling the system. One of these functions includes power management. By varying the

voltage and frequency significant power consumption reductions may be obtained. An example of where this might prove useful is during those times when a stream has too little water to maintain sediment flow. By utilizing the real time clock, you may dramatically reduce the power consumption of the chip by lowering the core voltage and since there is no processing to be done at the time, the clock speed as well. When the stage height monitoring system detects an event that needs observation the real time clock (RTC) can bring the processor back up to full speed. There are 5 modes of dynamic power management, each with a different power profile that can be used depending on needs and what types of external signals may be available to the system. With a real time clock subsection available, the processor can be put on an alarm system to awake once an hour or once a day to establish communications and make a determination if data collection is needed and if not, go back to sleep.

SOFTWARE AND MEMORY

The FFT routine is performed by dividing the raw data set into 1024 point bins, performing an FFT on each bin and picking out the magnitude of the frequency of interest. The number of bins will be determined by the depth of the measurement, e.g. a depth of 5 meters (the maximum depth available with the current system) would yield 392 bins. This number is arrived at by taking the number of raw data points and dividing by 1024. The number of raw data points is arrived at by taking the travel time of the acoustic signal times the ADC sampling rate. For 5 meters and a temperature of 20 degrees Celsius the equation would yielding a total number of raw data points of 402,220 (6.705 ms x 60 MSPS = 402,220). The 402,220 data points are then divided by the 1024 point FFT size to yield 392 individual bins. The number of data points may not be a multiple of 1024. In that case any left over data points are discarded. For three frequencies, the FFT routine needs 11,874 clock cycles. If the core speed of the DSP is set for 750 MHz the total FFT time would be 15.82 ms. This process is completed 20 times and the resulting FFT magnitudes are averaged together to create the final processed data set that is sent to the host computer. Including acoustic transmit and receive time, processing time and communications time, one processed event will take approximately 450 ms to complete. The amount of raw data collected for one processed event is approximately 320 MB while the processed event itself represents just a little over 2 KB of data. Depending on depth and sample rate there is enough onboard memory to store several minutes of processed data to insure that communication issues are not allowed to interfere with data collection and processing.

The routine that performs the FFT is 847 KB, while the communication routine is 77 KB. The routines are stored in the flash memory unit, separate from the SDRAM, and there is a total of 1 MB of storage in the flash memory. The communication routine and most of the FFT routine is common to any operation that the system may be asked to perform. The additional flash memory space may be used to store other possible profiles that the user may wish to run. These alternative profiles may be started by the host computer or by setting threshold conditions based on the processed data being accumulated. By allowing the user to pre-load various profiles and operating conditions a tremendous amount of flexibility is built into the system.

COMMUNICATION AND POWER

Communication between the host PC and the DSP system is provided by way of a serial port. The RS-232 standard was chosen due to the availability of standard and relatively inexpensive radios. At present the radio is an external component allowing each user to determine their best communication method. In current deployments both hard wired connections and radio links are used. Power is handled by onboard regulators that will accept an input voltage in the range of 5 VDC to 24 VDC. Power consumption is determined by the amount of time the unit is acquiring data and at what data rate the ADC is being operated. The higher the frequency of both the ADC and the DSP the more power consumed.

CONCLUSIONS

The system as described is both flexible and powerful. The DSP excels at performing FFT operations making the process of collecting and transmitting data a relatively simple one. The ability to communicate with the unit on the fly gives the user an opportunity to evaluate the data and make corrections or adjustments in the data collection routine without necessarily pulling the unit out of the experiment. Concerns and future improvements center on several areas. The first is power. Even with the different power modes available, this system will need approximately 1.5 Amp hours to run full-time. In meeting our current needs the system will not be processing data around the clock but only in instances where it is needed, such as storm events, renewable power sources will be needed. The primary consumers of power are the ADC and the DSP and both are optimized for power consumption. The second issue that will be addressed is communications. Currently the only communication method available is RS-232 to external radio or hard wired to a host computer. Investigations are underway concerning onboard radios and modems and also other serial standards, including differential standards for when communication must be hard wired and the cable runs are long. Another area that will be addressed is memory. Depending on communication issues, the system may be outfitted with sufficient memory to store days or weeks of data. This would facilitate remote locations where communication with a host computer may be impractical. It is anticipated that future systems will be even less expensive as the technology employed matures.

REFERENCES

Smith, Steven W. (2003) Digital Signal Processing, A Practical Guide for Engineers and Scientists. Newnes, Oxford

Horowitz, Paul, Hill, Winfield. (1989) The Art of Electronics. Cambridge, New York.

Kester, Walt. (2003) Mixed-Signal and DSP Design Techniques. Newnes, New York.

Kinsler, Lawrence, Frey, Austin, Coppens, Alan and Sanders, James. (2000) Fundamentals of Acoustics 4th ed. John Wiley and Sons, New York, New York

Crocker, Malcolm J. (ed.) (1998) Handbook of Acoustics. Wiley-Interscience Publication. New York, NY

ESTIMATION OF PARTICLE SIZES FOR A RANGE OF NARROW SIZE DISTRIBUTIONS OF NATURAL SANDS SUSPENDED IN WATER USING MULTI-FREQUENCY ACOUSTIC BACKSCATTER

Christopher K. Smith, Associate R&D Engineer, National Center for Physical Acoustics, University, MS, cksmith@olemis.edu; Daniel Wren, Hydraulic Engineer, USDA-ARS-NSL, Oxford, MS, wren@msa-oxford.ars.usda.gov; Jim Chambers, Senior Research Scientist, National Center for Physical Acoustics, University, MS, chambers@olemiss.edu

Abstract: The measurement of particle size using multiple, megahertz range acoustic frequencies has been focused on particles with radii of 50µm -150µm. The present study seeks to extend the applicability of the technique to particles with radii ranging from 50µm -425µm. A single acoustic transducer, transmitting a waveform with three peak frequencies, was used to measure backscatter from natural sand particles entrained in a turbulent jet. An approach similar to that taken by Sheng (1991) was used in the data processing, where particle size estimates were created by comparing theoretical ratios of the backscatter form factor and size density to measured ratios. It was found that the method produces 0.1%-36% error for particles with radii of 150µm - 425µm and 24%-160% error for particles with radii of 75µm - 150µm, depending on the concentration of the suspended particles. This work has been supported by the USDA.

INTRODUCTION

The use of single frequency ultrasonic acoustics to measure the concentration of suspended sediment is an established practice (Lynch, 1985, 1991; Hanes *et al*., 1988; Libiki *et al*., 1989; Thorne, 1993, 1994, 2000; Hardenberg *et al*., 1991; Lee and Hanes, 1995); however, this method requires previous knowledge of the sediment size characteristics to be accurate (Ma *et al*., 1983). To measure suspended sediment loads with no prior knowledge of the sediment sizes, a system that uses multiple frequencies must be used (Yu-shih Liu, 1965). Previous research using multi-frequency acoustics to estimate particle sizes has occurred primarily in shallow marine environments (Sheng, 1991; Crawford and Hay, 1993; Schat, 1997; Thosteen and Hanes, 1998) with sand of radii ranging from 50-150µm. Most of these studies used three single frequency transducers. The focus of the current study was to extend the measured range of radii of the sand particles to 50-425µm, and to establish the feasibility of using a single transducer with a composite waveform of three frequencies to estimate the size characteristics of the suspended sediment.

EXPERIMENTAL SETUP

The multi-frequency backscatter system was tested in a jet tank, Figure 1, similar to the one used by Hay (1991). The tank, hereafter referred to as the calibration tank, was constructed at the University of Mississippi National Center for Physical Acoustics. It was designed to produce a turbulent sediment carrying jet, by way of a pumping system that re-circulated sediment introduced into the tank. The pump speed could be varied to obtain optimum sediment jet conditions. A vacuum/j-tube system was also placed in the tank to collect physical samples for concentration measurements to be compared with acoustical backscatter data from a single transducer ultrasonic system.

The acoustic signals used by the backscatter system were produced by an arbitrary waveform generator. The composite waveform was created by adding together three different sine waves, each of a different frequency (1.4 MHz, 2.5 MHz, and 3.2 MHz). A broadband transducer with a center frequency of approximately 2.25 MHz was used to transmit and receive the signal. The transducer was placed 20cm from the centerline of the sediment jet. The input amplitude of each frequency was adjusted until the return echo from the back wall of the sediment free tank for each frequency was approximately equal. The return signal passed trough a 34 dB preamp and was then digitized by a 50 MHz oscilloscope card.

Backscatter data was taken before any physical samples, and consisted of 200 bursts from the transducer. Each burst was composed of twenty pings separated by a 5ms delay. Each ping was composed of ten cycles of the composite waveform. The jet's centerline concentration was then determined by collecting and analyzing an isokinetic sample of the fluid/particle mixture.

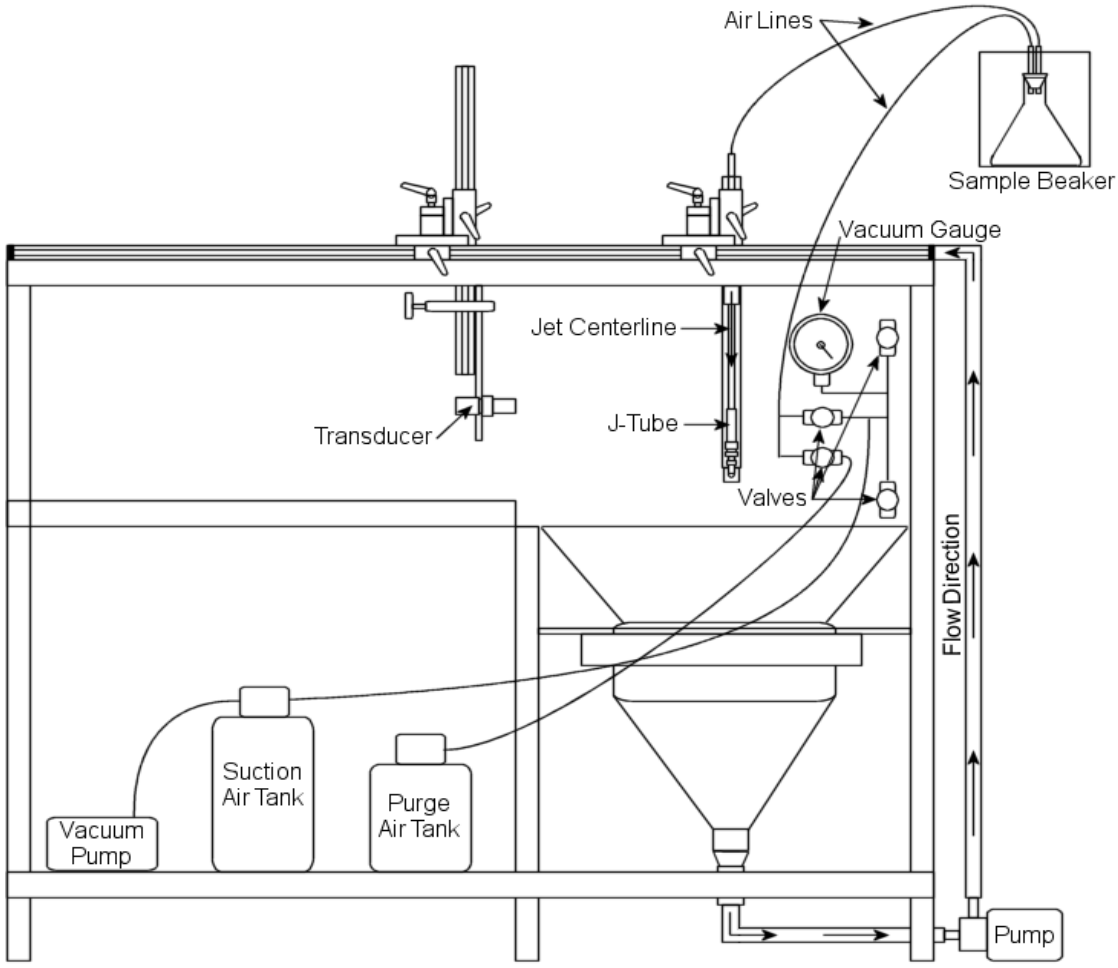


Figure 1. The calibration tank.

The sand used in the experiment was sieved into ten ranges of particle radius. Table 1 shows the ranges and their corresponding mean radii. The geometric standard deviation was equal to 1.05. Four different masses of each size range were used in the calibration tank: 5g, 10g, 20g, and 40g. The large size ranges yielded the highest concentrations for each mass of sand and the small size ranges yielded the smallest.

Table 1 The range of sand particle diameters and their corresponding mean radii.

Sand Particle Radius Range (μm)	Mean Sand Particle Radius (μm)
75.00-90.00	85.20
90.00-106.00	98.00
106.00-125.00	115.50
125.00-150.00	137.50
150.00-177.50	163.75
177.50-212.50	195.00
212.50-250.00	231.25
250.00-300.00	275.00
300.00-355.00	327.50
255.00-425.00	390.00

THEORY

The derivation of the acoustic equations used in this work has been established elsewhere (Sheng, 1991), and only the relevant equations are presented here. The backscatter voltage from the centerline of a sediment carrying jet (V_o) can be expressed by

$$V_o = B\sqrt{\frac{M_o}{\rho}}\frac{f\infty}{\sqrt{x}}\sqrt{\frac{\sinh\zeta}{\zeta}}\exp[-2\int_0^{r_0}\alpha_s dr], \tag{1}$$

where B is a system constant based on the frequency, directivity pattern, pulse duration, and beam-width of the acoustic system, M_o is the mass concentration at the centerline of the sediment jet, ρ is the density of the suspended sediment (2.65 g/cm^3), $f\infty$ is the backscatter form factor equation for uniformly sized suspended sediment, r_o is the range from the transducer to the centerline of the jet, and α_s is the attenuation due to the particles in the sediment jet. The term x is equal to the product of the wave number (k) and the particle radius (a).

The $\sqrt{\frac{\sinh\zeta}{\zeta}}$ term corrects for attenuation across the detected volume of the sediment jet (Hay, 1991). If the centerline concentrations of the sediment jet are small then the correction for attenuation across the detected volume and the attenuation due to the particles in the jet can be neglected (Sheng, 1991; Hay 1991). This gets rid of the $\sqrt{\frac{\sinh\zeta}{\zeta}}$ and $\exp[-2\int_0^{r_0}\alpha_s dr]$ terms, Equation (1) then becomes

$$V_o = B\sqrt{\frac{M_o}{\rho}}\frac{f\infty}{\sqrt{x}}. \tag{2}$$

The backscatter form factor equation is a rational fraction fit developed by Crawford and Hay (1993). The system constant, B can be solved for using Equation (2), if the backscattered voltages, sediment concentrations, and particle sizes at the centerline of the sediment jet are known.

A ratio of the backscattered voltages and system constants for two of the three frequencies (Equation 3) can be formed by rearranging and combining Equation (2) for each of the three frequencies.

$$\frac{V_{0i}B_j}{V_{0j}B_i} = \frac{f\infty_i\sqrt{x_j}}{f\infty_j\sqrt{x_i}},\ i \neq j;\ i = 2.5, 3.2, 3.2;\ j = 1.4, 1.4, 2.5, \tag{3}$$

where i and j are subscripts for each of the three frequencies. This equation no longer has a dependence on the mass concentration as does Equation (2).

The left-hand side of the equation is known from the backscattered voltage data, and the previously determined system constants. The right-hand side of the equation can be rewritten as

$$\frac{f\infty_i\sqrt{x_j}}{f\infty_j\sqrt{x_i}} = \frac{F(x_i,\sigma_g)}{F(x_j,\sigma_g)},\ i\neq j;\ i=2.5, 3.2, 3.2;\ j=1.4, 1.4, 2.5, \tag{4}$$

where $F(x, \sigma_g) = F[n(a),|f\infty|]$, which is a function of the size distribution and the backscatter form factor (Sheng, 1991), σ_g is the geometric standard deviation of the particle sizes and $n(a)$ is the size spectral density. $F[n(a),|f\infty|]$ can be written as

$$F\left[n(a),\left|f\infty\right|\right] = \frac{1}{\sqrt{k}}\left[\frac{\int_0^\infty a^2\left|f\infty\right|^2 n(a)da}{\int_0^\infty a^3 n(a)da}\right]^{\frac{1}{2}}. \tag{5}$$

Assuming a lognormal distribution of the sand particles yields

$$F\left[n(a),\left|f\infty\right|\right] = \frac{1}{\sqrt{k}}\left[\frac{\int_0^\infty a^2\left|f\infty\right|^2 \exp\left[\frac{-(\ln a - \ln a_g)^2}{2\ln^2\sigma_g}\right]da}{\int_0^\infty a^3 \exp\left[\frac{-(\ln a - \ln a_g)^2}{2\ln^2\sigma_g}\right]da}\right]^{\frac{1}{2}}, \tag{6}$$

where a_g is the mean particle radius and σ_g is equal to 1.05 in this experiment. Equation (6) can be solved to generate a set of theoretical values for each of the three frequencies used in the experiment using the rational fraction fit of the backscatter form factor and the known values of a_g, σ_g, and k. These theoretical values can then be used with Equation (4) to produce three theoretical ratios. A commercially available software package was used to produce an equation to fit the data points produced by each of the three theoretical ratios.

The method of estimating the size of the particle radius was to use one ratio (Equation 4) as a first estimate and one of the other two ratios (Equation 4) as a second estimate, depending on the estimated particle radius from the first estimate. This second estimate would then be averaged with the first to get the actual estimate of the particle's size. An experimental value using a ratio of backscattered voltages from the centerline of the jet and the system constants for two of the frequencies was substituted for the left hand side of Equation (4) and combined with the theoretical ratio to be used as the first estimate by substituting the ratio's curve fit equation for the right hand side of Equation (4). The roots of the resulting equation were then found. The polynomial equations used for the curve fits often resulted in more than one root being found. In order to account for this the median of the resulting roots was taken as the first estimate. This first estimate was then compared to a breakpoint. The breakpoint determined which of the other two ratios to use as the second estimate. If the first estimate was larger than the breakpoint a specific ratio was used, and if it was smaller than the breakpoint the other ratio was used. Estimates that were less than or equal to the breakpoint were considered "small". The second estimates were determined in the same manner as the first by finding the median of the roots for the second ratio's curve fit equation and the same experimental value used for the first estimate. Outlined below is the procedure using the 2.5/1.4 ratio as the first estimate, 164μm as a breakpoint, and the 3.2/1.4 ratio for estimating small particles, which is similar to the method described by Sheng (1991).

1. Determine a first estimate using the 2.5/1.4 ratio, a_1.
2. If $a_1 \leq 164\mu m$, determine a second estimate using the 3.2/1.4 ratio, a_2.
3. If $a_1 > 164\mu m$, determine a second estimate using the 3.2/2.5 ratio, a_2.
4. Average a_1 and a_2 to get the final estimate, a.

Unlike the theoretical values published in Sheng's paper the theoretical ratios produced with the combination of frequencies used in this experiment have multiple inflection points and overlap in some places. A likely breakpoint is not obvious from inspection of the equation plots. Consequently multiple combinations of the three ratios as first estimates and different breakpoints were tried until the best possible particle size estimates were realized. The breakpoint that produced the best estimates across all four masses of sand was 164μm.

RESULTS

The theoretical ratios produced using Equation (5) for each of the three ratio combinations used in the experiment and the corresponding curve fit equation are shown in Figure 2. All the curve fit equations had R^2 values greater than 0.9.

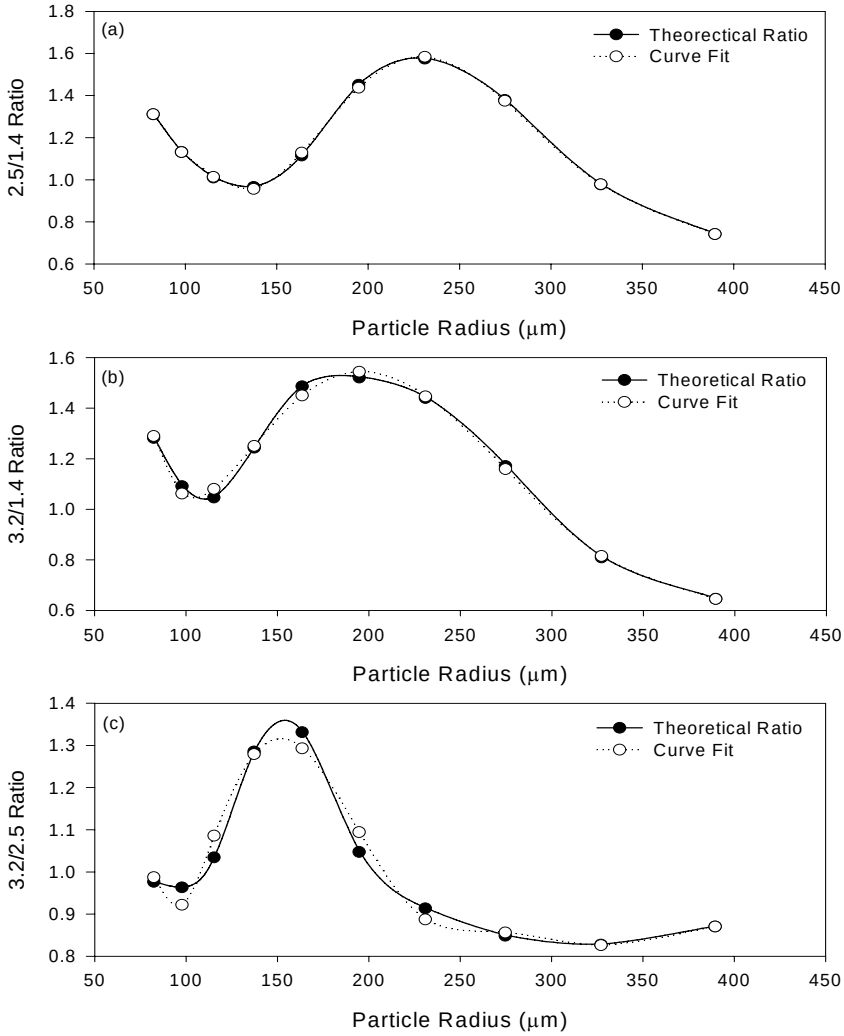


Figure 2 The theoretical values produced by Equation (5) for each of the three frequency ratios: (a) 2.5/1.4 Ratio, (b) 3.2/1.4 Ratio, (c) 3.2/2.5 Ratio.

The plots of true particle radius vs. estimated particle radius for each of the ratio combinations show the estimated particle radius for each of the four masses of sand, relative to a perfect agreement line, Figure 3. Each data point represents the mean estimated particle radius from a 200 burst experimental run for a particular mass of sand and size distribution, excluding radius estimates of zero. The exclusion of zero estimates caused the actual number of estimates for some of the size ranges be less than 200. The fewest number of estimates used to find a mean particle radius was 25, and the average number of estimates used to find a mean particle radius was 148. The previously established method estimates well the mean radius of particles in the range from 150μm - 425μm. However, the estimated mean radius for particles in the range from 75μm-150μm are larger than their actual mean particle radius. The combination of the 3.2/2.5 and 3.2/1.4 ratios, Figure 3(f), yields reasonable results for particles in the 125μm-

150µm range. The standard deviation of the estimates for all the ratio combinations ranged from 25 to 100, with a median of 54 and a mean of 56.

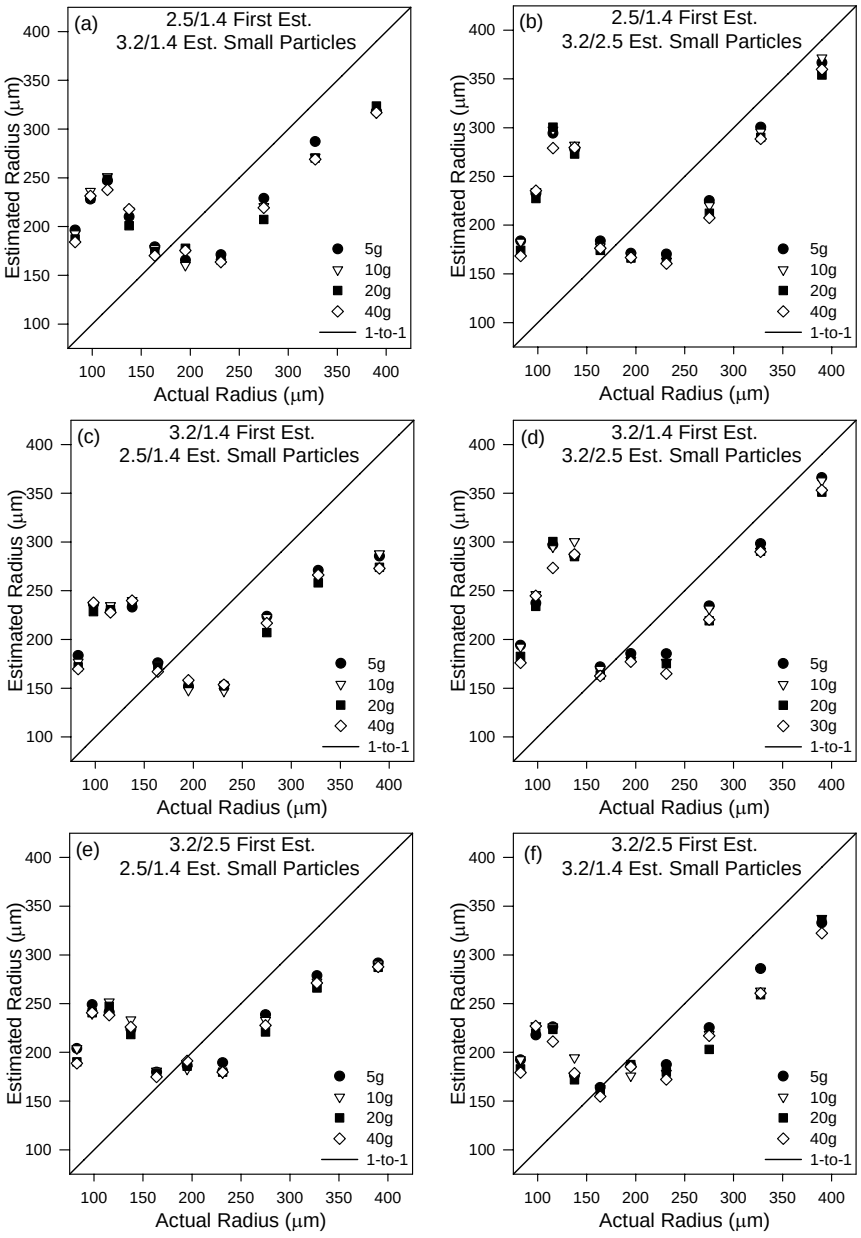


Figure 3 Actual mean particle radius compared to the estimated mean particle radius for each of the ratio combinations.

The plots of the true particle radius vs. percent error of the estimated mean particle radius for each of the ratio combinations show the percent error of the estimated particle radius for each of the four masses of sand, as well as a 0%, 20%, and -20% error lines, Figure 4. Each data point represents the percent error of the mean estimated particle radius of all the non-zero estimates from each experimental run for a particular mass of sand and size distribution. The majority of the estimates for particles in the 150µm - 425µm range fall within 20% of the actual mean particle radius. The error for estimates of the mean radius for particles in the range from 75µm-150µm are all between 25% and 160%. The combination of the 3.5/2.5 and 3.2/1.4 ratios, Figure 4(f), had errors from 25%-41% in the 125µm-

150µm range, depending on the mass of sand. This was the best of any of the ratio combinations at estimating particle sizes in this particular size range.

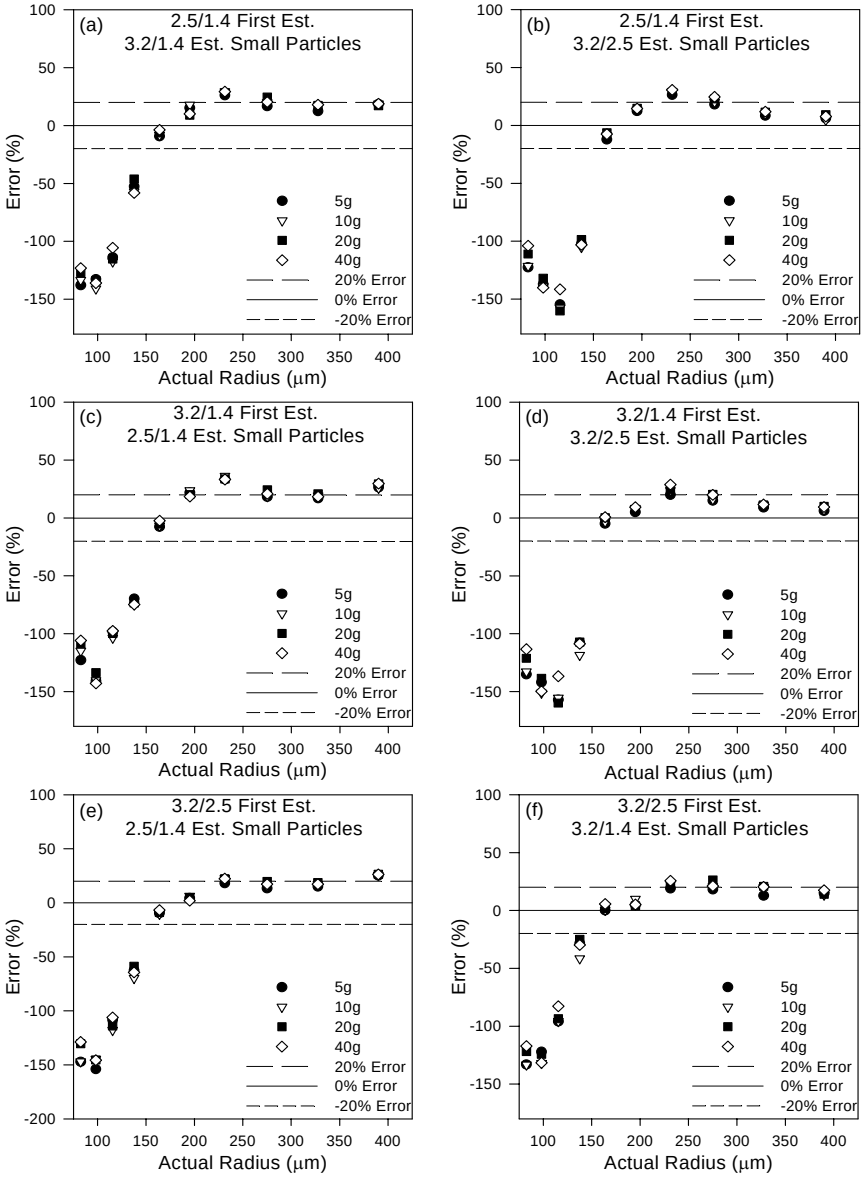


Figure 4 Actual mean particle radius compared to the percent error for the estimated mean particle radius for each of the ratio combinations.

CONCLUSIONS

The method of using ratios of backscattered voltages and system constants combined with theoretical ratios works well at estimating 150µm - 425µm particles, but overestimates 75µm - 150µm particles. This method yielded similar results for all four masses of sand used in the experiment which shows its robust nature in estimating mean particle radii for many different concentrations of suspended sediment composed of particles with radii larger than 150µm. The inability of the single transducer system to estimate particle sizes less than 150µm was problematic. Therefore, more work needs to be done on refining the method to reduce the error associated with smaller particles. One possible alternative will be to test different frequencies than the ones used in the experiment to produce theoretical ratio curves that have fewer inflection points. This may require the uses of two or more transducer

instead of a single transducer. This will allow lower order polynomials to be used as curve fit equations, yielding fewer possible roots.

REFERENCES

Crawford A. M. and Hay. A. E. (1993)"Determining suspended sand size and concentration from multifrequency acoustic backscatter," Journal of the Acoustic Society of America. Volume 94. Number 6. Pp. 3312-3324.

Hanes D. M. *et al*. (1988) "Acoustic measurements of suspended sand concentration in the C^2S^2 experiment at Stanhope Lane, Prince Edward Sound," Marine Geology. 81. Pp. 185-196

Hardenberg B. *et al*. (1991) "Field measurements of the vertical structure of suspended sediment," Coastal Sediments. Pp.300-312.

Hay A. E. (1991) "Sound scattering form a particle-laden turbulent jet," Journal of the Acoustic Society of America. Volume 90. Number 4. Pp. 2055-2074.

Lee T. H. and Hanes D. M. (1995) "Direct inversion method to measure the concentration profile of suspended particles using backscattered sound," Journal of Geophysical Research. Volume 100. Number C2. Pp. 2649-2657.

Libiki C. *et al*. (1989) "The interpretation and evaluation of a 3-Mhz acoustics backscatter device for measuring benthic boundary layer sediment dynamics," Journal of the Acoustic Society of America. Volume 85. Number 4.

Lynch J. F. (1985)"Theoretical analysis of ABSS data for HEBBLE," Marine Geology. 66. Pp. 277-289.

Lynch J. *et al*. (1991) "Sediment concentration profiling in HEBBLE using a 1-Mhz acoustic backscatter system," Marine Geology. 99. Pp. 361-385.

Ma Y. *et al*. (1983) "Multifrequency remote acoustic sensing of suspended materials in water," Journal of the Acoustic Society of America. Volume 74. Number 2. Pp. 581-585.

Schat J. (1997) "Multifrequency acoustic measurement of concentration and grain size of suspended sand in water," Journal of the Acoustic Society of America. Volume 101. Number 1. Pp. 209-217.

Sheng J. (1991) "Remote determination of suspended sediment size and concentration by multi-frequency acoustic backscatter," PhD. Dissertation. Memorial University. St. Johns, Newfoundland.

Thorne P. D. (1993) "Analysis of acoustics measurements of suspended sediment," Journal of Geophysical Reasearch. Volume 99. Number C1. Pp. 899-910.

Thorne P. D. *et al*. (1994) "On the use of acoustics for measuring shallow water suspended sediment processes," IEEE Journal of Oceanic Engineering. Volume 19. Number 1. Pp. 48-57.

Thorne P. D. (2000) "Acoustic measurements of boundary layer flow and sediment flux," Journal of the Acoustic Society of America. Volume 108. Number 4. Pp.1568-1581.

Thosteson E. D. and Hanes D. M. (1988) "A simplified method for determining sediment size and concentration from multiple frequency acoustic backscatter measurements," Journal of the Acoustic Society of America. Volume 104. Number 2. Pp. 820-830.

Yu-shih Liu E. (1965) "Ultrasonic measurement of the size distribution and concentration of natural sediments in suspension," M. S. Thesis. Utah State University. Logan, UT.

HIGH-RESOLUTION MONITORING OF SUSPENDED-SEDIMENT CONCENTRATION AND GRAIN SIZE IN THE COLORADO RIVER USING LASER-DIFFRACTION INSTRUMENTS AND A THREE-FREQUENCY ACOUSTIC SYSTEM

David J. Topping, Research Hydrologist, U.S. Geological Survey, Golden, Colorado, dtopping@usgs.gov; Scott A. Wright, Hydrologist, U.S. Geological Survey, Flagstaff, Arizona, sawright@usgs.gov; Theodore S. Melis, Physical Scientist, U.S. Geological Survey, Flagstaff, Arizona, tmelis@usgs.gov; David M. Rubin, Research Geologist, U.S. Geological Survey, Santa Cruz, California, drubin@usgs.gov

Abstract: In August 2002, we began testing a laser-acoustic system to monitor suspended-sediment transport on the Colorado River in Grand Canyon. This system consists of laser-diffraction, i.e., LISST[1] (Laser In-Situ Scattering and Transmissometry), instruments connected to an automatic pump sampler and an array of three sideways-looking acoustic-Doppler profilers at different frequencies. Stable functions have been developed relating the pump, laser-diffraction, acoustic-attenuation, and acoustic-backscatter measurements to cross-sectionally integrated measurements of suspended-sediment concentration and grain size. We relate acoustic attenuation to the concentration of suspended silt and clay; this approach yields accurate silt and clay concentrations over the range from less than 10 mg/l to about 20,000 mg/l. Suspended-sand concentration can then be computed as functions of the acoustic backscatter and acoustic attenuation; this approach yields accurate sand concentrations over the range from about 10 mg/l to over 3,000 mg/l. LISST-100 and three-frequency-acoustic measurements of the median grain grain size of the suspended sand are typically within 10% of the values of the median grain size measured by conventional methods. Silt and clay loads and sand loads computed by either the LISST-100, LISST-25X, or the three-frequency acoustic system are well within 5% of the values computed using conventional cross-section data (that have errors for silt and clay concentration of ~8% and errors for sand concentration of ~22%). This result, in conjunction with the fact that orders of magnitude more sediment-transport data can be collected each day by the laser-diffraction and acoustic instruments, indicates that a much more complete, and therefore more accurate record of suspended-sediment transport can be collected by the laser-acoustic instruments than by conventional methods alone.

INTRODUCTION

The grain-size distribution of suspended sediment in the regulated Colorado River below Glen Canyon Dam is bimodal, with a silt and clay mode (dominated by clay-sized particles) and a sand mode. Transport of both modes is limited by episodic resupply from tributaries. Transport of the sand mode is regulated by both the discharge of water and short-term changes in the grain size of sand available for transport. During tributary floods, sand on the bed of the river fines; this causes the suspended sand to fine and the suspended-sand concentration to increase, even when the discharge of water remains constant. Subsequently, the bed is winnowed of finer sand, the suspended sand coarsens, and the suspended-sand concentration decreases independently of discharge. This prohibits the computation of sand-transport rates in the Colorado River using stable relations between water discharge and sand transport, and therefore requires a more continuous method for measuring sand transport. To monitor sediment transport in the Colorado River in Grand Canyon, Arizona, we have designed and evaluated a laser-acoustic system for measuring the concentration and grain size of suspended sediment every 15 minutes. Earlier tests of this system were reported in Melis et al. (2003) and Topping et al. (2004).

TEST SITE AND EQUIPMENT

The instrument test site for this study is the Colorado River near Grand Canyon, Arizona, gaging station, hereafter referred to as the Grand Canyon gaging station (Fig. 1). At this test site, the laser-acoustic system consists of: (1) a Sequoia Scientific LISST-100 type C laser-diffraction instrument and a Sequoia Scientific LISST-25X type C laser-diffraction instrument, (2) an ISCO 6712 automatic pump sampler, and (3) three single-frequency Nortek acoustic-Doppler profilers. The ISCO pump sampler is triggered by either of the LISST instruments when laser transmission drops below a user-defined threshold (due to higher suspended-sediment concentrations) and then samples at a user-

[1] Use of brand and firm names in this paper does not constitute endorsement by the U.S. Geological Survey.

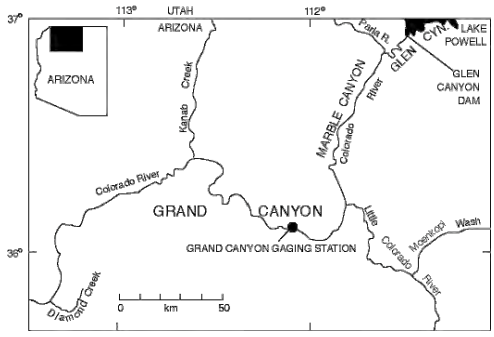


Figure 1 Map of the study area showing the location of the test site at the Colorado River near Grand Canyon, Arizona gaging station, U.S. Geological Survey (USGS) station number 09402500.

defined rate. This allows samples to be collected when the suspended-sediment concentrations exceed the upper sand limit for the LISST and the acoustic-Doppler profilers (around 2,000-3,000 mg/l). The two LISST instruments are suspended in the river from a steel cable on pulleys attached to a vertical cliff (Fig. 2a). The sampling path length of each LISST instrument is 1 cm. The LISST-100 averages 100 samples collected over 30 consecutive seconds out of every 15 minutes; output is volume concentration of suspended sediment in each of 32 log-spaced size classes from 0.0025 to 0.50 mm, water temperature, pressure, and laser transmission. The LISST-25X averages 1000 samples collected over 110 consecutive seconds out of every 15 minutes; output is volume concentration of suspended total sediment (0.0025 to 0.50 mm), volume concentration of suspended sand (0.0625 to 0.50 mm), Sauter mean sizes of suspended total sediment and sand, and laser transmission.

The three-frequency sideways-looking acoustic-Doppler profiler array is mounted on a cart attached to a vertical H-beam bracket anchored to a vertical concrete wall at the base of the gaging station stilling well (Fig. 2a). The cart is stationary at the base of the bracket during periods of data collection, and is raised to the surface (Fig. 2b) only to perform maintenance. The three acoustic-Doppler profilers mounted on this cart are a 1 MHz Nortek EZQ, 2 MHz Nortek EZQ, and a 600 kHz Nortek Aquadopp. These instruments were set to sample 13 out of every 15 minutes in the early phases of our tests; to conserve power, they are now set to sample 10 out of every 15 minutes.

The ISCO 6712 automatic pump sampler (Figs. 2a & 2c) has a capacity of 24 one-liter bottles. We designed the LISST-ISCO pump-sampler control circuit to allow data collection during periods when the river is so greatly enriched with suspended silt and clay that no usable data can be collected by either the LISST or acoustic-Doppler profilers. The protocol is as follows: when the LISST laser transmission is less than the user-defined threshold, the automated program of the ISCO pump sampler is enabled and samples are pumped at pre-defined intervals until either the laser transmission exceeds the user-defined threshold, or the supply of 24 one-liter sample bottles is exhausted.

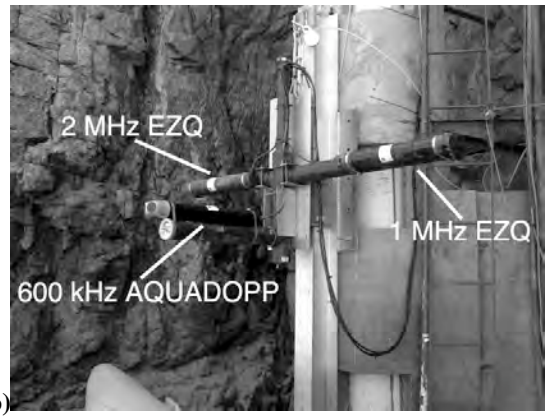
Data from the laser-acoustic system are downloaded over the internet via a two-way-broadband satellite system installed at the test site. This system was designed by Glenn Bennett and Tim Andrews (USGS, Flagstaff, Arizona) and consists of an on-site computer running the Symantec software "pcAnywhere," a satellite modem, a second computer that boots the system up each morning at a user-defined time for a user-defined duration, and a satellite dish (located on the cliff about 40 m above the gage house in Fig. 2a). The power supplies for the laser-acoustic system and the satellite system consist of 12V deep-cycle batteries (Fig. 2c) recharged by solar panels located on the cliff above the gage house.

DATA USED TO CALIBRATE THE LASER-ACOUSTIC MEASUREMENTS

Computation of cross-sectionally averaged suspended-sediment concentration and grain size from the automatic pump, LISST, and acoustic data was a two-step process. First, the at-a-point pump-measured values of concentration and grain size were calibrated to the corresponding velocity-weighted cross-sectionally averaged values measured at the cableway 200 m downstream (Fig. 2d) using the Equal-Discharge-Increment (EDI) method



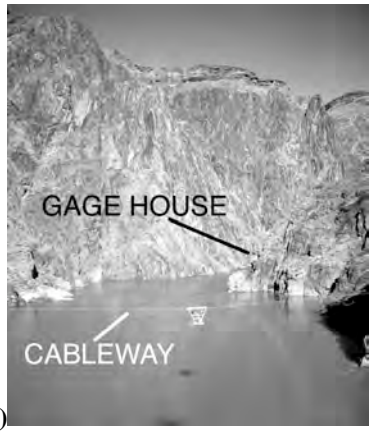
(a)



(b)



(c)



(d)

Figure 2 (a) Locations of instrument deployments at Grand Canyon gaging station. (b) Three-frequency acoustic-Doppler profiler array (out of water). (c) Contents of pump shelter in (a) showing automatic pump sampler (on right) and batteries. (d) Upstream view of reach showing measurement cableway and gage house in (a); cableway is 200 m downstream from gage house.

(described in Edwards and Glysson, 1999). The following point values measured with the pump were thus calibrated to the comparable cross-sectionally averaged values from the EDI measurements: the concentration of silt and clay (with $R^2 = 0.997$), the discharge-weighted concentration of total sand (with $R^2 = 0.971$), the discharge-weighted concentration of sand in three size classes [0.0625-0.088 mm (with $R^2 = 0.947$), 0.088-0.177 mm (with $R^2 = 0.967$), and 0.177-1.0 mm (with $R^2 = 0.891$)], and the median grain size of the suspended sand (with $R^2 = 0.826$). Calibration of the pump data for the three size classes of sand was conducted to aid in the calibration of the three single-frequency acoustic-Doppler profilers. This first step in the calibration process used 102 paired EDI and pump samples collected between January 2002 and November 2004 in discharges ranging from 190 to 1,210 m^3/s. Because depth-integrated samplers do not collect time-averaged samples (and therefore do not average over the fluctuating component of the flux due to the turbulent fluctuations in velocity and concentration), the errors associated with EDI measurements are large, i.e., about 8% for silt and clay concentration, 22% for sand concentration, and 12% for the median grain size of the suspended sand (Topping et al., *JGR*, in prep.). Therefore, to ensure that the combination of these large errors with a small sample size (i.e., if only the EDI measurements were used) did not bias the calibrations of the LISST and acoustic measurements, we calibrated the LISST and acoustic measurements to the much larger combined EDI and calibrated-pump dataset.

CALIBRATION OF THE LISST INSTRUMENTS

Calibration of the at-a-point LISST measurements to the "cross-sectionally averaged" (i.e., combined EDI and calibrated-pump) measurements depended primarily on sediment concentration, and secondarily on the discharge of

water (which affects how sediment is mixed between the main flow and the LISST deployment site). The data used for the LISST-100 calibrations were the 443 cross-sectionally averaged measurements made between January 2003 and November 2004; the data used for the LISST-25X calibrations were the 269 cross-sectionally averaged measurements made between June 2003 and November 2004. The LISST-100 and 25X measurements of concentration and grain size were calibrated to the cross-sectionally averaged concentration and grain-size data after segregating the data into five discrete discharge increments: <280 m^3/s, 280-420 m^3/s, 420-570 m^3/s, 570-850 m^3/s, and >850 m^3/s. Equations were then developed to relate the calibrations of suspended-silt and clay concentration, suspended-sand concentration, and suspended-sand median grain size among the five discharge increments. The equations relating the at-a-point silt and clay concentration measured by the LISST-100 and 25X to the cross-sectionally averaged silt and clay concentration were power laws, with exponents that increased non-linearly from 0.55 to 0.74 as a function of increasing discharge (with $R^2 = 0.960$ for the LISST-100 and $R^2 = 0.823$ for the LISST-25X). The equations relating the at-a-point sand concentration measured by the LISST-100 and 25X to the cross-sectionally averaged sand concentration were linear, with coefficients that increased linearly from 0.3 to 3.0 as a function of increasing discharge (with $R^2 = 0.971$ for the LISST-100 and $R^2 = 0.932$ for the LISST-25X). Finally, the equation relating the at-a-point median grain size of the suspended sand measured by the LISST-100 to the cross-sectionally averaged median grain size of the suspended sand was linear, with a coefficient that increased logarithmically from 0.2 to 0.4 as a function of increasing discharge (with $R^2 = 0.937$). No stable relation existed between the Sauter mean diameter of the suspended sand measured by the LISST-25X and either the median grain size of the suspended sand measured by the LISST-100 or the cross-sectionally averaged median grain size of the suspended sand. Therefore, although the LISST-25X accurately measures suspended-sediment concentration in two size classes (i.e, silt and clay, and sand), it does not provide accurate suspended-sand grain-size data at our test site.

CALIBRATION OF THE MEASUREMENTS OF ACOUSTIC ATTENUATION AND ACOUSTIC BACKSCATTER

Theory and measurements of underwater acoustics indicate that, for a given frequency of sound in water, bimodal grain-size distributions of suspended sediment such as those in the Colorado River can be segregated into two acoustic size classes: (1) a finer acoustic size class in which increasing concentration (or decreasing grain size at a constant concentration) results in increased attenuation of sound due to viscous losses (Urick, 1948; Flammer, 1962; Lohrmann, 2001; Gartner, 2004), and (2) a coarser acoustic size class in which increasing concentration (or increasing grain size at a constant concentration) results mainly in increased backscatter of sound (Thorne and Campbell, 1992; Thorne et al., 1993; Lohrmann, 2001; Thorne and Hanes, 2002; Gartner, 2004). At low concentrations of this second acoustic size class (<100 mg/l), concentration is related to backscattered sound pressure (in Pa) increased to the second power, or backscattered sound intensity (in decibels) increased to the fourth power (Thorne and Campbell, 1992; Thorne et al., 1993; Gartner, 2004). At higher concentrations of this second acoustic size class, however, increases in concentration result in increased attenuation of the acoustic energy due to scattering losses (Flammer, 1962; Gartner, 2004), and, at extremely high concentrations (>>1,000 mg/l), result in either no increase or a decrease in the backscattered acoustic energy (Thorne and Campbell, 1992; Thorne et al., 1993). The concentration threshold at which attenuation becomes important in this coarser acoustic size class depends on frequency, with this threshold being lower for higher frequencies of sound (Flammer, 1962). For example, Thorne and Campbell (1992) showed, using a 3 MHz transducer, that attenuation of acoustic energy resulted in substantial deviation from the power of two relation between backscattered sound pressure and sand concentration when the concentration exceeded about 100 mg/l. Power-law curves fit to the theoretically derived relations in Fig. 8 in Thorne and Campbell (1992) have exponents >10 (i.e., all much larger than two) as a result of the increased importance of attenuation relative to backscatter. The threshold grain size between the two acoustic size classes of sediment is negatively correlated with the frequency of sound (Flammer, 1962; Lohrmann, 2001). For a given concentration of sediment, lower frequencies of sound will return proportionately more backscatter from coarser sediment than finer sediment (Thorne and Hanes, 2002, Eqs. 7-10).

The approach employed builds on that in Topping et al. (2004) and takes advantage of the acoustical effects of the two acoustic size classes of sediment to: (1) relate increases in the attenuation of acoustic energy measured by the three single-frequency acoustic-Doppler profilers to increases in silt and clay concentration (this can be accomplished using any one of the three frequencies), (2) for small ranges in this acoustic attenuation due to silt and clay (expressed as a ratio of the acoustic signal strength in a far-field cell to the acoustic signal strength in a near-

field cell), relate increases in the amplitude of the acoustic signal strength to increases in the concentration of either total sand or a specified size class of sand (Fig. 3). The relation between the acoustic attenuation (expressed as this ratio) and silt and clay concentration is linear (Fig. 4a). At lower sand concentrations, the amplitude of the acoustic signal strength in a cell is dominated by backscattered acoustic energy, whereas at higher sand concentrations, the amplitude of the acoustic signal strength results from a combination of backscatter and attenuation. Because of the combined effects of backscatter and attenuation, the relation between the amplitude of the acoustic signal strength and sand concentration is a power law with an exponent that ranges between 10 and 20, depending on frequency and site geometry (Fig. 4b). At a fixed frequency at a given site, this exponent is constant and does not depend on silt and clay concentration. For small ranges in the above-described acoustic-attenuation ratio (arising from suspended silt and clay), a unique power-law relation will exist between the amplitude of the acoustic signal strength in a given cell and the concentration of sand. Thus, a family of power-law curves with identical exponents will exist over a broader range of silt and clay concentration. These curves are related to one another by a coefficient *k* that varies as a function of the acoustic-attenuation ratio. Next, the fact that the threshold grain size between the two acoustic size classes decreases as a function of increasing frequency of sound is used to develop empirical relations between

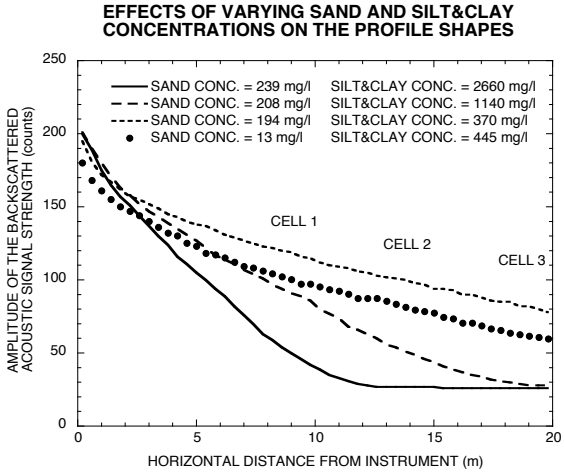
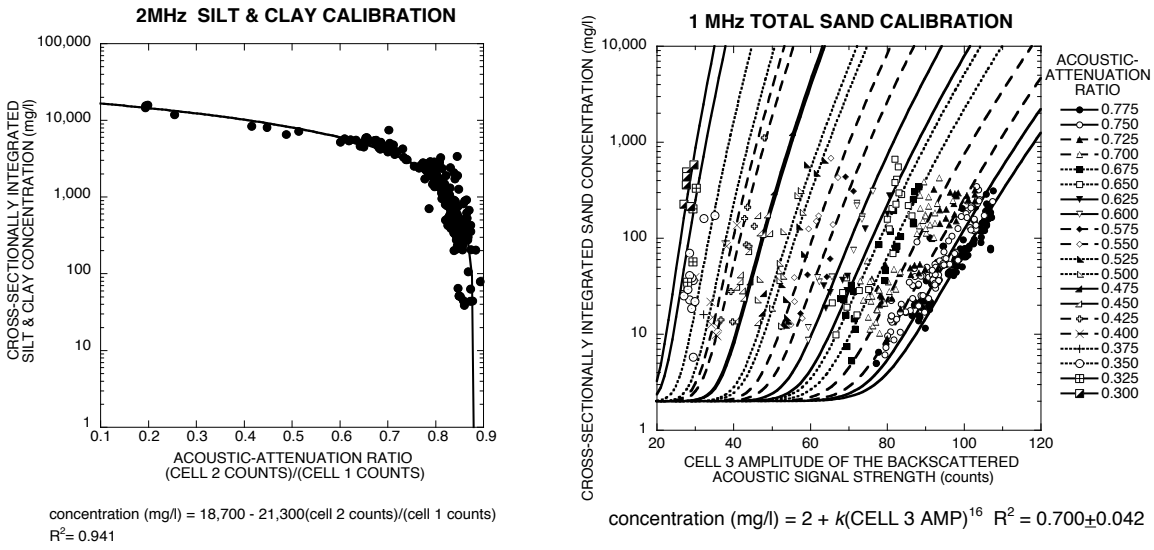


Figure 3 Effects of varying sediment concentration on acoustic profiles collected with the 1 MHz EZQ. Changes in silt and clay concentration mainly result in changes in the slope of the profile; changes in sand concentration mainly result in upward or downward shifts in the profile without changing the slope.

the amplitudes of the acoustic signal strength in a given cell at 600 kHz, 1 MHz, and 2 MHz to the concentration of sand in three size classes. These three size classes of sand were chosen on the basis of the minima in the attenuation-coefficient curves in Flammer (1962, Fig. 1) and are the same as those used above in the calibration of the pump data to the EDI measurements: 0.0625-0.088 mm, 0.088-0.177 mm, and 0.177-1.0 mm. Finally, logarithmic interpolation between the acoustically computed sand concentration in each size class is used to compute an "acoustic median grain size" (i.e., acoustic D_{50}) for the suspended sand.

The standard method for working with acoustic-attenuation and backscatter data is to convert the measured amplitudes of the signal strength in each cell (in counts) to sound intensity (in decibels) using the sonar equation of Urick (1975). This equation takes into account the two-way transmission losses due to beam spreading, the attenuation due to absorption by the water (which depends on pressure, temperature, and salinity), and the attenuation due to viscous or scattering losses by the suspended sediment. Because all of these terms are linear, and the pressure, temperature, and salinity do not vary greatly at the Grand Canyon gaging station test site, one does not gain much in the analysis by converting to sound intensity and using the sonar equation (besides determining that the values of the attenuation due to the suspended sediment fall in the normal range of about 0 to 20 dB/m). In the examples below, therefore, measured raw amplitudes in the acoustic signal strength (in counts) are used to compute the acoustic attenuation in terms of a ratio of counts in a far-field cell to counts in a near-field cell (Figs. 3 & 4).



(a) **(b)**

Figure 4 (a) Example of the relation between acoustic attenuation at 2 MHz (expressed as a ratio in counts between cells) and silt and clay concentration. (b) Example of the relations between the amplitude of the acoustic signal strength measured by the 1 MHz EZQ and total sand concentration for small ranges in the acoustic-attenuation ratio arising from silt and clay. The coefficient k relates the sand-calibration curves as a function of the acoustic attenuation ratio, i.e., silt and clay concentration (relation has $R^2 = 0.986$).

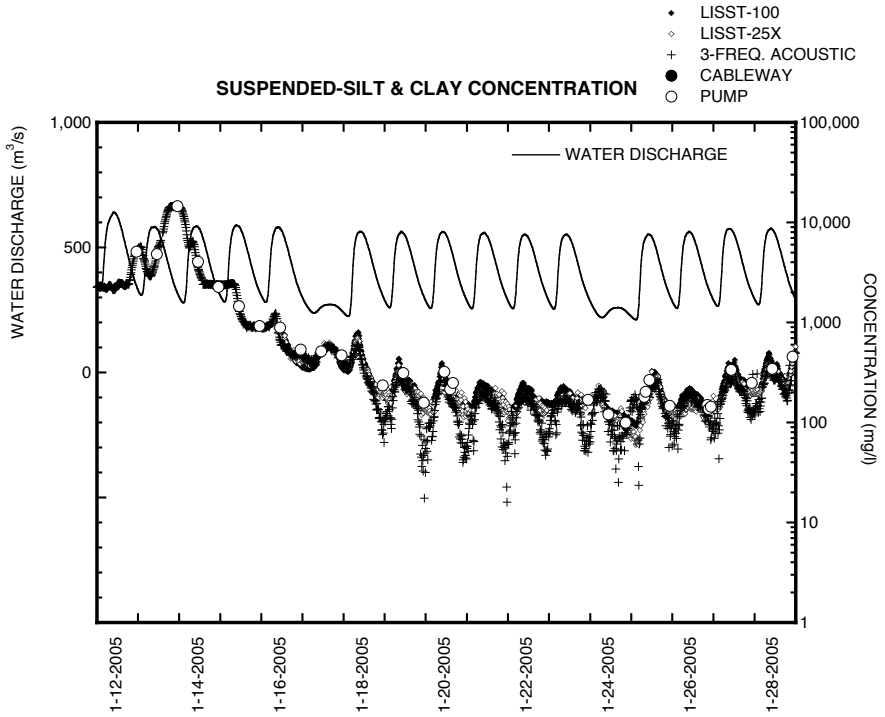
RESULTS

The laser-acoustic measurements are in excellent agreement with the EDI and calibrated pump measurements. The levels of agreement between the integrated loads (computed by summing the instantaneous loads) and integrated grain size are shown in Table 1. For comparison, errors associated with the EDI measurements against which the

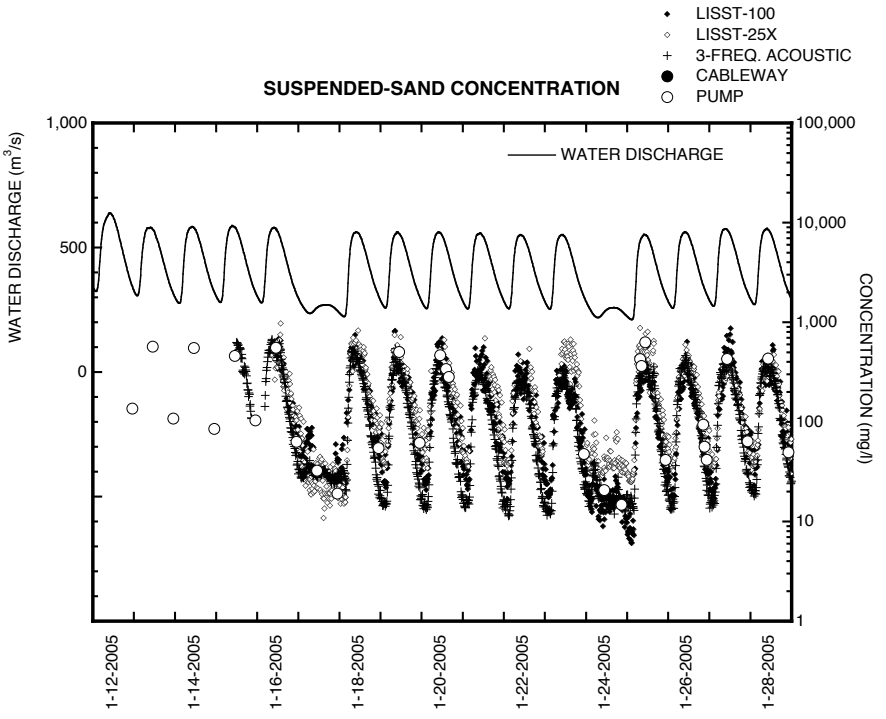
Table 1 Difference in the integrated laser-acoustic measurements relative to the integrated combined EDI, calibrated pump measurements (using both calibrated and uncalibrated laser-acoustic data).

	LISST-100	LISST-25X	1 MHz only	3-frequency
Silt and clay load	+5.0%	-0.5%	-2%	-2%
Total sand load	+0.4%	+1.0%	-4%	-3%
0.0625-0.088 mm sand load	Not analyzed	N/A	N/A	-10%
0.088-0.177 mm sand load	Not analyzed	N/A	N/A	-4%
0.177-1.0 mm sand load	Not analyzed	N/A	N/A	-1%
Suspended-sand D_{50}	+0.5%	N/A	N/A	+4.8%

laser-acoustic measurements were calibrated are much larger than the values in Table 1: ~8% for silt and clay concentration, ~22% for sand concentration, and ~12% for suspended-sand median grain size. Comparison of laser-acoustic, pump, and cableway measurements of silt and clay concentration, sand concentration, and suspended-sand median grain size beyond the calibration period ending in November 2004 are shown in Fig. 5. As shown in Fig. 5, the calibrations for concentration and grain size are stable for the pump, LISST, and acoustic measurements and the agreement remains excellent beyond the period used for calibration. Therefore, because of the larger errors associated with the EDI measurements, the stability of the laser-acoustic calibrations, and the fact that orders of magnitude more sediment-transport data can be collected each day by the laser-diffraction and acoustic instruments, a much more complete, and therefore more accurate record of suspended-sediment transport can be collected by the laser-acoustic instruments than by conventional methods alone.



(a)



(b)

Figure 5 Examples of the high-resolution laser-acoustic suspended-sediment data from beyond the period of calibration. No EDI measurements were made from the cableway during this 17-day period. Silt and clay concentrations were too high during the first 3 1/2 days of this period to get LISST or acoustic measurements of suspended-sand concentration or median grain size. (a) Silt and clay concentration, (b) Sand concentration, (c) Suspended-sand median grain size (D_{50}); on next page.

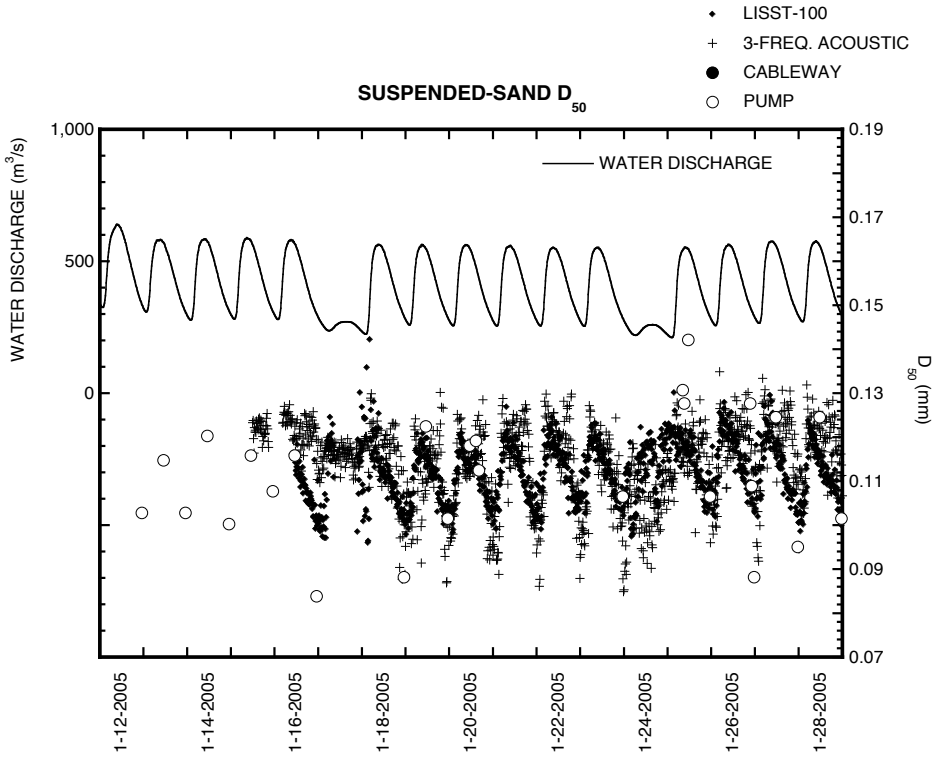


Figure 5 **(c)**

REFERENCES

Edwards, T.K., and Glysson, G.D., 1999, Field methods for measurement of fluvial sediment: *U.S. Geological Survey Techniques of Water-Resources Investigations Book 3, Chap. C2*, 89p.

Flammer, G.H., 1962, Ultrasonic measurement of suspended sediment: *U.S. Geological Survey Bulletin 1141-A*, 48 p.

Gartner, J.W., 2004, Estimating suspended solids concentrations from backscatter intensity measured by acoustic Doppler current profiler in San Francisco Bay, California: *Marine Geology*, v. 211, p. 169-187.

Lohrmann, A., 2001 Monitoring sediment concentration with acoustic backscattering instruments: *Nortek Technical Note No. 3*, 5 p., downloadable from http://www.nortek-as.com/.

Melis, T.S., Topping, D.J., and Rubin D.M., 2003, Testing laser-based sensors for continuous in situ monitoring of suspended sediment in the Colorado River, Arizona, *in* Bogen, J., Fergus, T., and Walling, D.E., eds., Erosion and Sediment Transport Measurement in Rivers: Technological and Methodological Advances: Wallingford, Oxfordshire, United Kingdom, IAHS Press, IAHS Publication 283, p. 21-27.

Thorne, P.D., and Campbell, S.C., 1992, Backscattering by a suspension of spheres: *Journal of the Acoustical Society of America*, v. 92, n. 2, p. 978-986.

Thorne, P.D., Hardcastle, P.J., and Soulsby, R.L., 1993, Analysis of acoustic measurements of suspended sediments: *Journal of Geophysical Research*, v. 98, n. C1, p. 899-910.

Thorne, P.D., and Hanes, D.M., 2002, A review of acoustic measurements of small-scale sediment processes: *Continental Shelf Research*, v. 22, p. 603-632.

Topping, D.J., Melis, T.S., Rubin, D.M., and Wright, S.A., 2004, High-resolution monitoring of suspended-sediment concentration and grain size in the Colorado River in Grand Canyon using a laser-acoustic system, *in* Hu, C., and Tan, Y, eds., Proceedings of the Ninth International Symposium on River Sedimentation, October 18-21, 2004, Yichang, China: People's Republic of China, Tsinghua University Press, p. 2507-2514.

Urick, R.J., 1948, The absorption of sound in suspension of irregular particles: *Journal of the Acoustical Society of America*, v. 20, n. 3, p. 283-289.

Urick, R.J., 1975, Principles of Underwater Sound for Engineers: New York, McGraw Hill, 384 p.

COMPARISON OF SUSPENDED-SEDIMENT LOAD ESTIMATES USING A TURBIDITY AND SUSPENDED-SEDIMENT CONCENTRATION REGRESSION AND THE GRAPHICAL CONSTITUENT LOADING ANALYSIS SYSTEM (GCLAS)

Mark Uhrich, Hydrologist, U.S. Geological Survey, Portland, OR, mauhrich@usgs.gov;
Heather Bragg, Hydrologic Technician, U.S. Geological Survey, Portland, OR, hmbragg@usgs.gov

Abstract Water withdrawn from the North Santiam River is treated to provide drinking water to the residents of Salem, Oregon, and surrounding communities. Turbidity testing is done at the water-treatment facility to determine whether the water meets drinking-water standards and to prevent excess sediment in the river water from damaging or clogging the filters. In an attempt to better understand the transport of sediment, a monitoring network was established in 1998 throughout the North Santiam River Basin. A regimen of continuous turbidity monitoring and selective suspended-sediment sampling over the hydrograph was implemented to determine the relation between turbidity and suspended-sediment concentration (SSC) at each of the monitoring stations. Using this relation, continuous turbidity measurements were used to estimate semihourly (every 30 minutes) concentrations of suspended sediment at each site.

Six years of turbidity and suspended-sediment concentration data have been analyzed for one of the network stations, the North Santiam River below Boulder Creek near Detroit, Oregon. The 1999 water year was chosen to illustrate the data, as well as a short period in 2003, as each were well represented by the collection of suspended-sediment samples over varying flow and turbidity conditions. A regression equation was developed between turbidity and SSC to estimate semihourly SSC. The Graphical Constituent Loading Analysis System (GCLAS), developed by the U.S. Geological Survey, was used to further adjust the estimated SSC values. The GCLAS visual interface and coefficient application software adjusted the estimated SSC curve to intersect the measured SSC sample data. Suspended-sediment loads were then calculated using both turbidity/SSC regressions and GCLAS-adjusted SSC estimation methods.

In most years, the highest sediment loads are transported during just a few large storm events. Hence, an accurate estimation of the SSC is critical in determining suspended-sediment loads for the few days during which most of the annual load occurs. Using GCLAS, adjustments were made to the SSC values for two high-turbidity and high-flow events in December 1998, and a summer high-turbidity event in September 2003. Both examples highlight the differences between using turbidity/SSC regressions with and without GCLAS-adjustment methods to compute suspended-sediment loads. The GCLAS adjustments in December 1998 resulted in a combined +35 percent change from the turbidity/SSC regression estimate for the month. The adjustments in September 2003 resulted in a -63 percent change. The December adjustments accounted for a 16 percent increase in annual load, and the September adjustments a 0.8 percent decrease in annual load. GCLAS can enhance turbidity/SSC regression methods during short periods when several measured samples are available during the period of adjustment. For longer time periods, and when fewer samples are collected, the turbidity/SSC regression alone provides a more reliable annual load as the instantaneous estimates are based on several thousand continuous turbidity measurements and the data fit around the regression line incorporates the entire suite of measured samples.

INTRODUCTION

The North Santiam River Basin is located on the western slopes of the Cascade Range in northwestern Oregon, east of Salem. The river flows west from Mount Jefferson to the Willamette River. The basin is 75 percent forested, with timber harvesting and recreation as the dominant land uses. Heavy precipitation is common in the Western Cascades mountain terrain. When rain combines with a melting snowpack, severe erosion can occur on the steep slopes. Geomorphic events, such as landslides, debris flows, and road failures, can supply tremendous volumes of suspended sediment into the river transport network. Slower moving earthflows can also move downslope when they become saturated during wet periods, impinging on streams and supplying fine-grained sediment that can cause persistent high turbidity.

Surface waters of the North Santiam River provide much of the drinking water for the 170,000 residents living in Salem, Oregon and surrounding communities. The City of Salem water-treatment facility is unusual in that it uses a slow-sand filtration system in conjunction with biological activity to treat raw river water. The water settles through an algal mat on the bottom substrate to remove organic contaminants and then through gravel and sand filters to remove inorganic particulates. Excessive sediment can damage these filters; consequently, daily turbidity testing is conducted at the water-treatment facility to assess the condition of the river water.

In 1998, the U.S. Geological Survey, in conjunction with City of Salem, established three sites in the upper North Santiam River Basin to measure water quality (specific conductance, pH, water temperature and turbidity) and streamflow. In 2005, the network expanded to nine continuously operating sites with telemetry, located throughout the basin. Eight additional non-telemetry sites are in operation to monitor turbidity downstream of suspected sediment sources. The monitoring network serves as an early-warning system to the Salem water-treatment personnel by providing near real-time river conditions upstream of the facility. The data allow plant operators to better regulate and control incoming surface waters, which might require application of costly particle settling chemicals during periods of high turbidity or closing intake gates to avoid damage to the sand filters. In addition, the monitoring network can be used to track the progress of high-flow and high-turbidity events from the subbasins in which they originated. This information also assists the appropriate land owners and regulatory agencies in managing their lands in such a way as to minimize or eliminate these high-turbidity occurrences by identifying potential sediment-source areas and activities.

Hence, turbidity monitoring provides useful water-quality data to both water-supply and land-management agencies within the North Santiam River Basin. Collection of streamflow data and suspended-sediment samples also can translate into useful quantitative data. In a previously-published report, Uhrich and Bragg (2003) demonstrated that turbidity is a better surrogate for suspended-sediment concentration than streamflow in the basin and outlined a procedure for estimating suspended-sediment loads. The use of GCLAS can enhance the usability and accuracy of the load data by matching these estimates to the measured field data, but the period of adjustment and number of samples available for analysis must be closely evaluated. The best application of GCLAS is when several samples are collected over a storm hydrograph; otherwise

when fewer samples are collected, the turbidity/SSC regression may provide the best annual suspended-sediment load estimate.

METHODS

Suspended-sediment loads were calculated for the gaging station at North Santiam River above Boulder Creek near Detroit, Oregon (14178000) for the 1999 water year (October 1, 1998, to September 30, 1999) and also for September 2003. The 216-square-mile basin upstream of this site is primarily forested and drains a mountainous terrain originating from glaciated volcanic peaks of the Cascade Range that top 10,000 feet elevation. Water year 1999 produced significantly high annual and peak flows in the North Santiam River Basin. The 1999 mean annual streamflow for the North Santiam site was near the 90th percentile for 80 years of record. The highest daily mean streamflow for this station was also above average, near the 70th percentile. There were several high turbidity events in water year 1999, yet only 4 percent of the 30-minute turbidity readings were at or above 10 FNU (formazin nephelometric units). Nonetheless, this short duration of increased turbidity accounted for almost 70 percent of the annual suspended-sediment load.

Estimating Suspended-Sediment Concentrations and Loads Instantaneous suspended-sediment concentrations were estimated for the North Santiam site by developing a regression relation between the instream turbidity recorded at the site (the explanatory variable) and the suspended-sediment sample concentrations (the response variable). The regression analysis used the entire suite of samples collected since the project inception. Regression equations are periodically revised as more samples are collected. The estimated suspended-sediment concentrations, along with their corresponding streamflow, are used to calculate suspended-sediment loads.

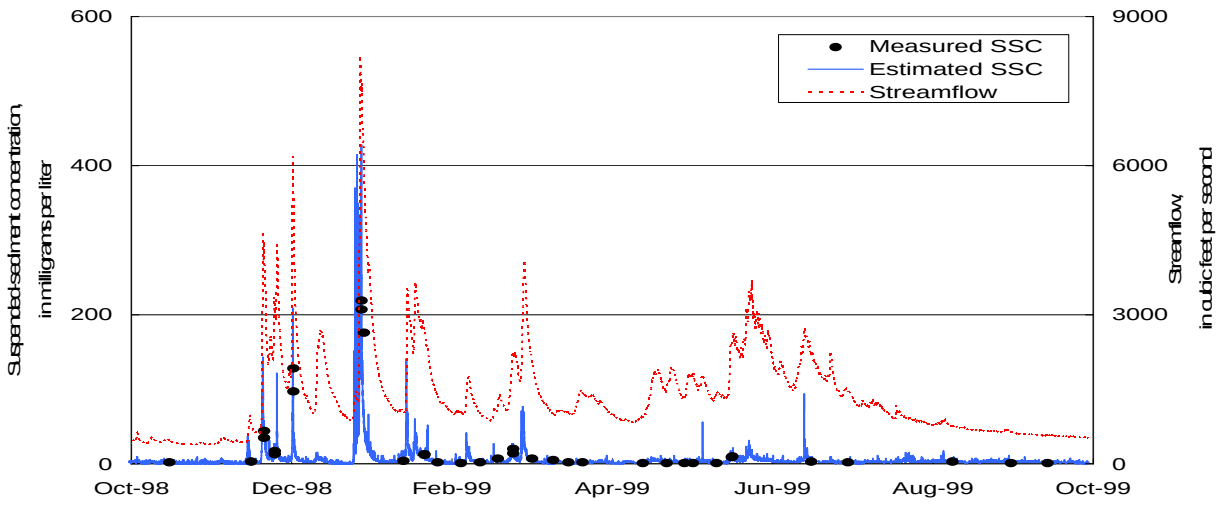


Figure 1 Instantaneous streamflow, measured SSC and estimated SSC, North Santiam River above Boulder Creek, 1999 water year

Instream turbidity and streamflow data were collected at 30-minute intervals, resulting in 17,520 values for water year 1999. Suspended-sediment samples have been collected at the North Santiam site over a range of hydrologic conditions from 1998 to 2004, resulting in 121 stream-width/depth-integrated samples. For each sediment sample, the 30-minute turbidity values were averaged over the duration of sample collection, providing a single turbidity value, in FNU. Each sample also was analyzed for suspended-sediment concentration, in milligrams per liter (mg/L). As a result, each suspended-sediment sample has two data values associated with it: turbidity and suspended-sediment concentration (SSC).

The paired data were used to develop a regression equation. The turbidity and SSC values were transformed to base-10 logarithmic values. The log values were then used to calculate a linear least-squares regression. The North Santiam site equation, converted to power form is:

$$SSC = 1.54 \text{ (turbidity)}^{1.04} \quad (1)$$

Transforming the data values to logarithmic values and back introduced a bias into the regression. This bias was corrected with a “smearing” estimator described by Helsel and Hirsch (1992). The final North Santiam regression equation including the bias correction factor is (figure 2):

$$SSC = 1.75 \text{ (turbidity)}^{1.04} \quad (R^2 = 0.893) \quad (2)$$

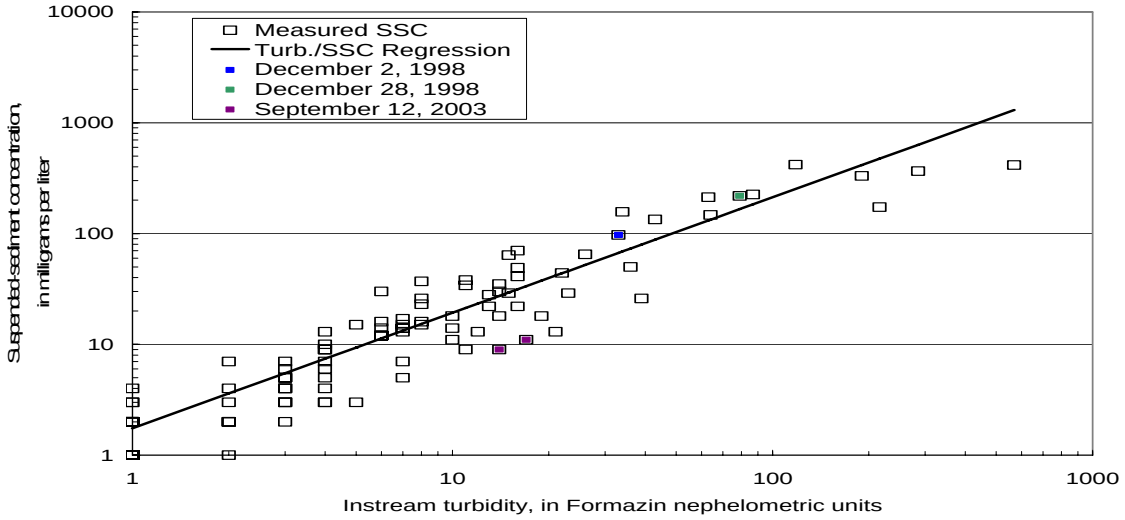


Figure 2 Turbidity and suspended-sediment concentration regression line

The SSC regression equation for the North Santiam site was used to calculate estimated suspended-sediment concentration for each 30-minute turbidity value logged for water year 1999 (figure 1). The instantaneous suspended-sediment load (SSL) values were then calculated using the corresponding streamflow with the following equation (Porterfield, 1972):

$$SSL \text{ (tons/day)} = SSC \text{ (mg/L)} \times Q \text{ (cfs)} \times c \quad (3)$$

where Q is instantaneous streamflow in cubic feet per second (cfs) and c = 0.00270, which converts the units to tons per day. The 48 SSD values calculated per day were averaged to provide a daily mean SSL (SSL is used here to represent Suspended-Sediment Discharge, although load is technically defined as a mass only and discharge as a mass per unit of time).

Graphical Constituent Loading Analysis System (GCLAS) The U.S. Geological Survey software program GCLAS (Graphical Constituent Loading Analysis System) can also be used to compute suspended-sediment loads, McKallip et al. (2001). The program is designed to use measured sample and streamflow data, along with estimated constituent concentrations to compute loads. The user normally selects a combination of measured and estimated SSC input values to compute loads. GCLAS provides a visual and interactive means to inspect and interpret the concentration data as it relates to the samples collected. The graphical interface of GCLAS can be used to portray the data at varying time and concentration scales, permitting a hands-on approach to adjusting the concentration data in relation to time or streamflow. On-the-fly computations of loads can be accomplished in GCLAS after each manipulation of the concentration curve. The changes can be compared numerically and visually to determine if adjustments are appropriate.

The instantaneous SSC estimated from the turbidity/SSC regression were imported into GCLAS. These estimated SSC values far outnumbered the measured values and therefore were selected instead of the measured SSC values to compute the suspended-sediment loads. The concentration and streamflow values of the measured sediment samples also were imported into GCLAS under a different classification and later used to make adjustments to the estimated SSC values. The suspended-sediment load for the North Santiam gaging station was calculated for two periods of record (table 1). Visual inspection of the estimated SSC curve was conducted by zooming in on the working graph and scrolling through the duration of each water year. In several instances, significant differences were noted between the estimated SSC (from the turbidity/SSC regression) and the measured SSC (from the sediment sample). GCLAS was used to apply coefficients to selected estimated SSC values to better correspond to measured values. Coefficients are multiplication factors applied to the estimated SSC values that adjust the SSC curve to intersect the measured SSC samples, along the sampled timeline. The examples shown in this report used both constant and time- or streamflow-varying coefficients. Suspended-sediment loads were calculated before and after each GCLAS adjustment for comparison.

RESULTS AND DISCUSSION

SSC estimates were evaluated for the 1999 water year at the North Santiam monitoring station. Analysis of the turbidity/SSC regression estimated SSC values and the measured SSC samples identified two periods requiring coefficient adjustments. The estimated SSC values during storm events on December 2, 1998, and December 27-29, 1998, were lower than the values of the stream width-/depth-integrated samples (figures 3 and 4). The GCLAS adjustment coefficients were calculated and applied over the selected time range. A total of 72 hours of SSC data was adjusted for December 2 and December 27-29. These adjustments resulted in an increase of nearly 2,500 tons in the December suspended-sediment load, or a 16 percent increase in the annual turbidity/SSC regression estimated load (table 1).

The entire adjustment period for each event was shifted to a single measured stream width-/depth-integrated SSC occurring on the declining portion of the hydrograph. Single vertical samples are shown, but were used only to verify the cross-sectional samples. GCLAS was used to recalculate the monthly and annual suspended-sediment load after each adjustment. Values for all other 1999 water year turbidity/SSC regression estimated periods were within 5 percent of the measured sample data and were not adjusted. An example of a nonadjustment period is shown in figure 3 for November 25-26, 1998. GCLAS adjustments to turbidity/SSC regression estimates work best for short time periods or for specific high-flow, high-sediment events when several samples are collected to define the changing load conditions. In addition, the measured samples collected during both December 1998 storm events were within the 95 percent confidence interval of the regression, and therefore would not normally be adjusted

Table 1 Adjusted Suspended-Sediment Loads (SSL).

Adjusted Dates	Estimated SSL	Adjusted SSL	Adjustment and percent change
December 2, 1998	940 tons	1360 tons	+ 420 tons (45%)
December 27-29, 1998	6240 tons	8300 tons	+ 2060 tons (33%)
Annual Suspended-Sediment Load Adjustments			+ 2,480 tons (16%)

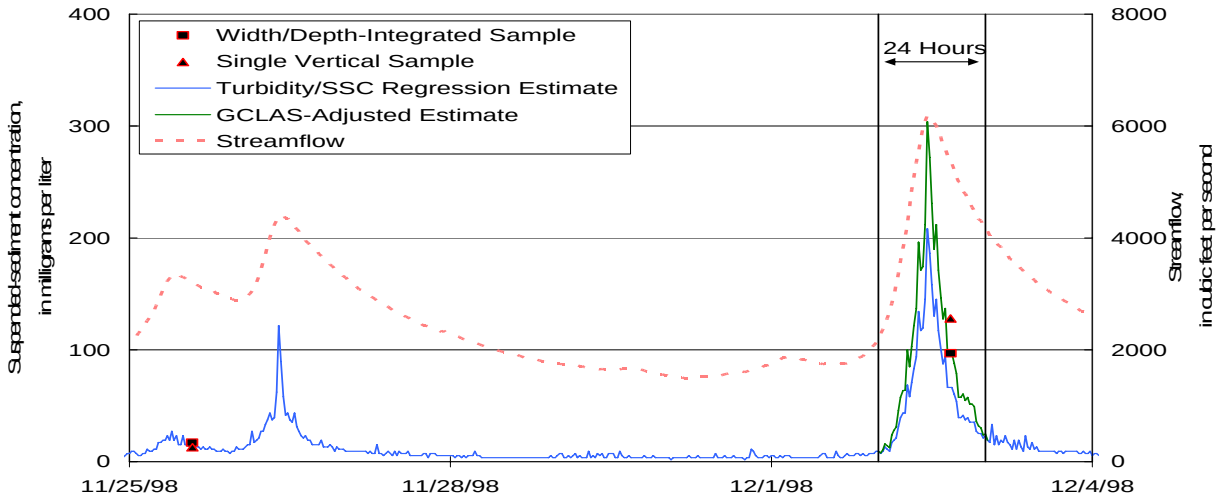


Figure 3 Adjustment of estimated suspended-sediment concentrations for December 2, 1998.

An example of a specific high-sediment event that fell outside the 95 percent confidence interval (figure 2) during which several samples were collected occurred in September 2003 and is shown in figure 5. In this case, two stream width-/depth-integrated samples were collected during this high-turbidity and low-flow period. At that time, an automatic pumping sampler was programmed to collect point samples based on the instream turbidity values. Fourteen point samples were collected before, during and after the collection of the two width-/depth-integrated

samples. The turbidity/SSC regression produced estimated SSC values higher than the samples collected. Such events can be common for the late summer season at the North Santiam site, and likely relate to a glacial or wilderness area disturbance in the basin headwaters.

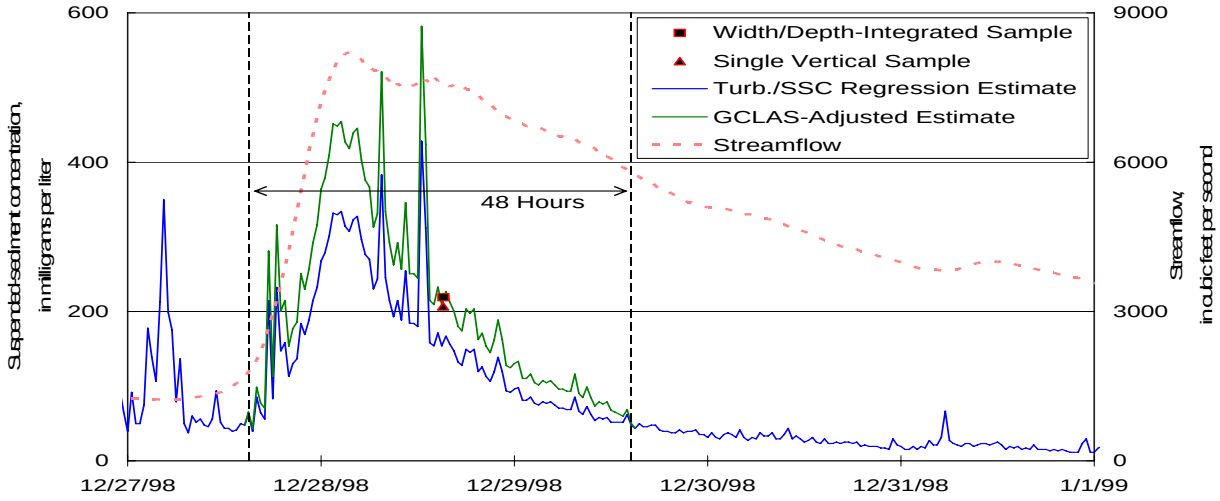


Figure 4 Adjustment of estimated suspended-sediment concentrations for December 27-29, 1998.

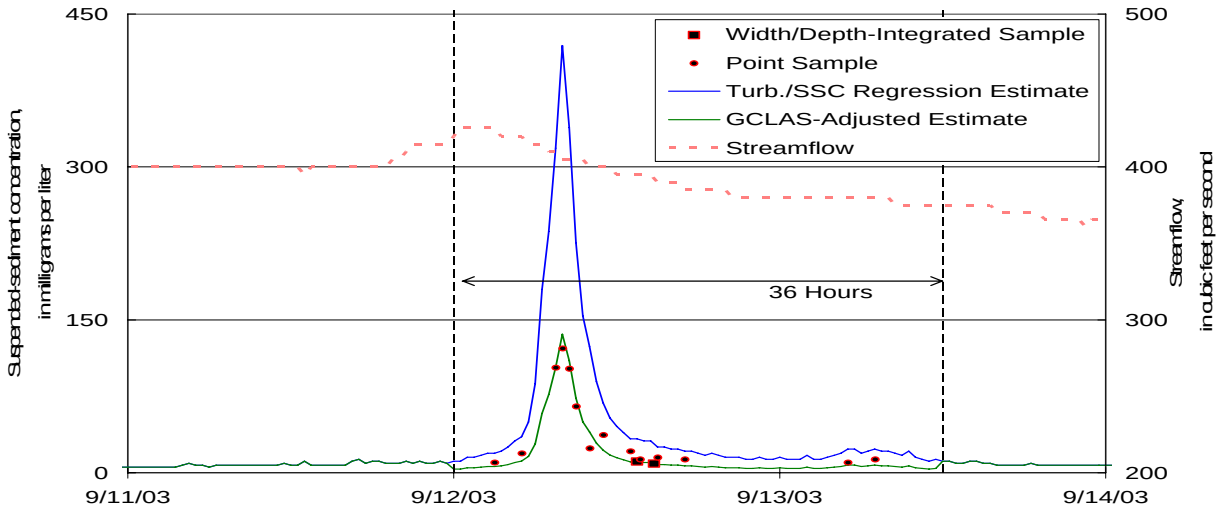


Figure 5 Adjustment of estimated suspended-sediment concentrations for September 2003.

Figure 5 shows the SSC values estimated by the turbidity/SSC regression for September 12-13, 2003. Using the estimated SSC, the suspended-sediment load for these 2 days is 84 tons. GCLAS was used to make adjustments encompassing the duration of the point-sample collection. The coefficients for the width-/depth-integrated samples were calculated and applied over 36 hours. The resulting SSC curve falls much closer to the point samples collected, providing additional support to the adjustment. Using the GCLAS-adjusted SSC values, the suspended-sediment load

for these 2 days is 32 tons. Although this represents a 63 percent decrease in these load values, the effect on the annual suspended-sediment load for water year 2003 is only -0.8 percent.

For these high-sediment events at the North Santiam site, the turbidity/SSC regression method appears to underestimate suspended-sediment loads during storm events and overestimate during low-flow periods, but this is entirely basin and event dependent, and may change both temporally and spatially as sediment sources change. Both periods of adjustment were relatively significant (+35 percent combined in December, and -63 percent in September), but the storm events obviously have the greatest impact in sediment transport. The 4 adjusted days in December comprise 47 percent of the annual suspended-sediment loads. The adjustments made with GCLAS can increase the reliability of turbidity/SSC regression derived SSC and load estimates for specific high-flow, high-sediment events when several samples are collected. When few samples are collected during a high-flow event, such as a single sample or samples that do not track the entire hydrograph, using GCLAS may shift the entire load curve, resulting in either an overestimation or underestimation. Use of the turbidity/SSC regression equation to estimate load when measured data are sparse may provide an estimate closer to the true value. When longer time periods are considered, the regression approach at the North Santiam site may better define the overall estimate of suspended-sediment loads under changing scales and degrees of flux.

SUMMARY

GCLAS permits adjustment of concentrations estimated by means of regression relationships developed between instream turbidity and measured suspended-sediment concentrations, which can enhance the use and applicability of the sediment-concentration regression equation. This fine tuning can provide a better estimate of suspended-sediment loads over short time frames or specific events when several samples are collected, since the estimated SSC values can be adjusted to agree with the measured concentration data. Over longer timescales, a turbidity/SSC regression approach, without adjusting with GCLAS, provides a better overall suspended-sediment estimate as it uses all the measured samples collected over several years and flow events, as well as the 17,520 per year readings of continuous turbidity to complete the sediment record. The continuous measurement of turbidity proves invaluable for providing information on concentration trends during periods without measured sediment data by documenting the timing of peak fluvial sediment flux that may not be detectable using streamflow alone.

REFERENCES

Helsel D.R., Hirsh R.M., 1992, Statistical methods in water resources; Studies in Environmental Science 49. New York, Elsevier, 522 p.

McKallip, T.E., Koltun, G.F., Gray, J.R., and Glysson, G.D., 2001, “GCLAS - a graphical constituent loading analysis system,” Proceedings of the 7th Federal Interagency Sedimentation Conference, Reno, Nevada, March 25-29, Vol. II, VI-49 to VI-52.

Porterfield, G., 1972, Computations of fluvial-sediment discharge. Techniques of Water-Resources Investigations of the U.S. Geological Survey, Book 3, Chapter C3, 66 p.

Uhrich, M.A., Bragg, H.M., 2003, Monitoring instream turbidity to estimate continuous suspended-sediment loads and yields and clay-water volumes in the Upper North Santiam River Basin, Oregon, 1998–2000. U.S. Geological Survey Water-Resources Investigations Report 03–4098, 43 p.

A METHOD FOR COMPARING THE LISST 100 TO THE USGS PIPETTE METHOD FOR SUSPENDED SEDIMENT PARTICLE SIZE ANALYSIS IN THE MARINA SEDIMENT LAB, U.S. GEOLOGICAL SURVEY CALIFORNIA WATER SCIENCE CENTER

Lawrence Freeman, Supervisory Hydrologic Technician, U.S. Geological Survey California Water Science Center, Marina, California, lfreeman@usgs.gov

Abstract: The Marina Sediment Lab of the USGS California Water Science Center has a need to automate and expand on the number of suspended sediment samples that can be processed for particle size analysis. Measuring the LASER scatter of sediment particles suspended in water is one method that shows promise for sediment lab application. The LISST 100 uses **L**ASER **I**n-**S**itu **S**cattering and **T**ransmissometry (LISST)[1] to determine particle size distribution in a water/sediment mixture sample volume. LISST is a Trademark of Sequoia Scientific, Inc. The technology represented by this instrument offers the potential to increase the number of samples that are submitted to the lab that can be processed for full particle size analysis, and at the same time, offers the potential for faster sample processing, along with improved data base entry. The LISST 100 is intended to operate as an in-situ time-series data collection instrument for monitoring suspended sediment concentration and particle size distribution in water bodies, Sequoia Scientific, Inc. (2002). A LISST 100 Type B was purchased by the Marina sediment lab.

INTRODUCTION

In order to broaden the range of samples that can be analyzed for particle size distribution, it is desirable to have the ability to accurately quantify the particle size distribution for samples with lower suspended sediment concentration than can be processed using the current USGS standard Pipette or Sedigraph methods. The LISST 100 is designed to determine particle size distribution in water having lower suspended sediment concentrations than either of these two methods. The Pipette method provides a theoretical particle size distribution with results for several size classes ranging from 2 to 62 microns in diameter. It requires a minimum dry weight of 0.8g of material for processing and provides a sediment concentration in terms of dry sediment weight in mg/l. The Sedigraph requires a 50 ml volume of condensed sediment mixture which is prepared by removing most of the native water from the sample, and then preparing the sub sample for analysis. The Sedigraph does not provide a sediment concentration value. The LISST 100 Type B produces results for 32 size ranges (bins). The 32 size ranges (fig. 1) are logarithmically incremented from approximately 1.25 – 250 microns in diameter. The particle size results for these increments are reported at the median point for each size class bin. These points range from 1.44 to 231 microns. Theoretically, the LISST 100 has no lower concentration limit. However, there may be a practical lower concentration threshold where a particle size distribution may have little meaning. The upper concentration limit is reported by the vendor to be approximately 500 mg/l, but higher concentration samples could be analyzed after careful splitting and/or dilution. The particle sizes are given as a volume percentage in terms of the total volume of particles in the sample. There is not a capability to produce a sediment concentration value that relates to a volume of water/sediment mixture. Testing will help determine the practical limits of using this technology in a production lab.

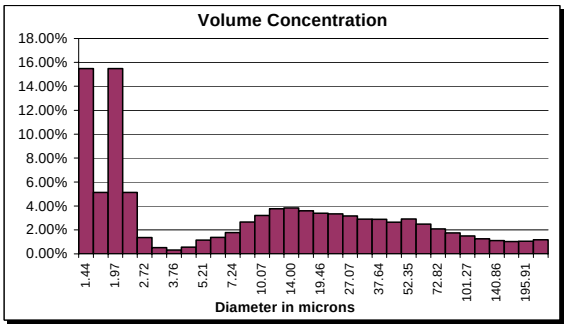
METHODS

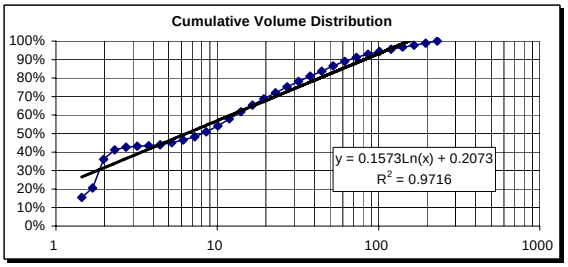
Samples designated for full particle size analysis will first have the sand fraction removed for separate analysis using the wet sieve method. Once this sand fraction has been removed, a trial aliquot will be drawn from the fully mixed fines to ascertain if sufficient material is present in the sample to use the pipette procedure. A duplicate trial aliquot will be run through the LISST 100. A dispersing agent is used to assure separation of fine particles. A dissolved solids correction is required when a dispersing agent is used. The correction is needed to adjust both the Pipette and LISST results. The above procedures were modified from initial test attempts which had several procedural issues. Problems with the initial procedures may or may have not had an impact on the sample data comparison, but the potential existed.

[1] Any use of trade, product, or firm names is for descriptive purposes only and does not imply endorsement by the U.S. Government.

Lab ID# C3503_lisst
Station number: SLQA
Collection Date: N/A
Technician: N/A
Sample Description: Full Size Particle Analysis

US Geological Survey
California District Sediment Lab
455 Reservation Rd. Suite F
Marina, Ca 93933
(831) 384 - 2143





Computed Statistics

D10 = #N/A
D50 = 7.24
D90 = 61.74
Dmean = 25.82
Specific Surface Area = 0.16 m^2/g

Total Instrument Results:

Size (microns)	Volume Conc (%)	Cumulative Volume
1.44	15.49%	15.49%
1.68	5.13%	20.62%
1.97	15.49%	36.11%
2.31	5.13%	41.24%
2.72	1.36%	42.60%
3.19	0.52%	43.12%
3.76	0.32%	43.44%
4.43	0.55%	43.98%
5.21	1.14%	45.12%
6.14	1.37%	46.50%
7.24	1.77%	48.27%
8.54	2.67%	50.93%
10.07	3.20%	54.14%
11.87	3.76%	57.90%
14.00	3.84%	61.74%
16.50	3.59%	65.33%
19.46	3.39%	68.72%
22.95	3.34%	72.06%
27.07	3.18%	75.24%
31.92	2.90%	78.13%
37.64	2.89%	81.02%
44.39	2.65%	83.67%
52.35	2.92%	86.59%
61.74	2.49%	89.08%
72.82	2.08%	91.16%
85.87	1.74%	92.90%
101.27	1.48%	94.38%
119.44	1.25%	95.64%
140.86	1.10%	96.74%
166.12	1.04%	97.78%
195.91	1.05%	98.83%
231.04	1.17%	100.00%

Comments: Dry sample was mixed with DI water and mixed in sample chamber. Background scatter included dispersing agent. Sample high concentration, was split twice (tag).

Analysis Performed by: TAG
Processing Date: 9/27/2005

Analysis performed using laser diffraction techniques as described in AWWA Standard No. 2560D. Instrumentation calibrated using NIST traceable standard particles.

USGS Standard Results

Size (microns)	Volume Conc (%)	Cumulative Volume
0.01 - 2.00	36.11%	36.11%
2.01 - 4.00	7.33%	43.44%
4.01 - 8.00	4.83%	48.27%
8.01 - 16.00	13.47%	61.74%
16.01 - 31.00	13.50%	75.24%
31.01 - 62.00	13.84%	89.08%
62.01 - 124	6.56%	95.64%
124.01 - 256	4.36%	100.00%

Figure 1 Example of LISST 100 data output format for one sample. Used by permission, Sequoia Scientific.

The Pipette Method: The Pipette procedure is the method used by the Marina sediment lab to determine full particle size. This procedure is based on Stokes Law which, when applied to the determination of sediment particle sizes, states that particles of different diameters fall through a given liquid at predictable rates (Guy 1969). The larger the size of a particle, the quicker its rate of fall through a fluid. A sample is stirred with a blender. The stirring is stopped and the settling process begins. Sample aliquots are taken using a pipette at specific depths and times during the duration of the settling process (which can last several days), theoretically capturing only specific particle sizes in each of the pipette withdrawals. Each withdrawal is dried and weighed to determine the percent of the total sample weight that is represented by each of these fall size classes.

The LISST 100 Method: A mixing chamber is attached to a flow through cell which is mounted to the optic head of the LISST 100. If concentration levels exceed the LISST 100 operational limits then the sample is accurately split, perhaps several times. Splitting is completed by using a standard laboratory silt/clay splitter. The final analysis begins with two instantaneous aliquot withdrawals made immediately at the starting time of the settling process. One aliquot is for the Pipette analysis, the other is used for the LISST 100. By performing the testing in this manner, all of the sediment material will be present in a fully dispersed state for both methods, thus, the direct comparison of sample results should be most valid.

Test Data Evaluation: Initial evaluation of results from the 2 methods was based on the analyses of 7 samples (Tables 1-7). The samples were provided to the Marina sediment lab by the USGS Sediment Lab Quality Assurance (SLQA) program. Each of the 7 samples was used twice. Each sample was processed using the Pipette method. After the drying and weighing the withdrawals, the sample was recovered, re-suspended in water and re-disbursed. Then a 20 ml aliquot was withdrawn. The LISST 100 analysis was performed on this aliquot. This was not an ideal method of comparison, as sample integrity and duplicity are not assured. The SLQA samples are composed of silica material (spark plug dust) with a specific gravity of 2.65, approximating that of quartz sediments.

Modified testing procedures described above have been implemented for a second round of testing currently in progress during December 2005. The second testing round uses duplicate sets of samples provided for each method by the SLQA program. One sample from the current round has been processed at the time of this writing. The Lab Chief has reported that the preliminary results still show a significant difference in the results of the two methods even when the revised procedure was used. The LISST 100 is still reporting a higher percentage of the finest and coarsest size material relative to the Pipette analysis. At this time, it is not clear what is causing the differences. More comparative testing is needed with SLQA samples and natural water samples. The revised methodology will also be reviewed and modified if necessary.

TABLES FOR RESULTS OF SLQA STUDY COMPLETED DECEMBER, 2004.

Table 1 Size distribution for SLQA sample ID C3503.

Particle size class range (microns)	Pipette results: Percent Finer Than	LISST 100 results: Percent Finer Than	SLQA Target Value
0.01-2.00	19.7	36.11	18
2.01-4.00	22.8	43.44	20
4.01-8.00	24.6	48.27	33
8.01-16.00	55.2	61.74	57
16.01-31.00	81.0	75.24	79
31.01-62.00	100	89.08	100
62.01-124		95.64	
124.01-256		100	

Table 2 Size distribution for SLQA sample ID C3504.

Particle size class range (microns)	Pipette results: Percent Finer Than	LISST 100 results: Percent Finer Than	SLQA Target Value
0.01-2.00	19.9	52.71	18
2.01-4.00	22.0	57.42	20
4.01-8.00	23.8	58.02	33
8.01-16.00	55.4	65.84	57
16.01-31.00	82.0	78.66	79
31.01-62.00	100	93.27	100
62.01-124		98.36	
124.01-256		100	

Table 3 Size distribution for SLQA sample ID C3505.

Particle size class range (microns)	Pipette results: Percent Finer Than	LISST 100 results: Percent Finer Than	SLQA Target Value
0.01-2.00	26.2	56.32	23
2.01-4.00	27.2	61.42	25
4.01-8.00	30.5	62.21	41
8.01-16.00	67.4	72.06	70
16.01-31.00	86.3	85.23	87
31.01-62.00	100	94.58	100
62.01-124		98.28	
124.01-256		100	

Table 4 Size distribution for SLQA sample ID C3506.

Particle size class range (microns)	Pipette results: Percent Finer Than	LISST 100 results: Percent Finer Than	SLQA Target Value
0.01-2.00	24.5	58.05	23
2.01-4.00	25.5	63.11	25
4.01-8.00	28.6	63.76	41
8.01-16.00	65.4	72.59	70
16.01-31.00	86.8	85.39	87
31.01-62.00	100	94.45	100
62.01-124		98.12	
124.01-256		100	

Table 5 Size distribution for SLQA sample ID C3507.

Particle size class range (microns)	Pipette results: Percent Finer Than	LISST 100 results: Percent Finer Than	SLQA Target Value
0.01-2.00	25.0	59.65	23
2.01-4.00	26.9	64.8	25
4.01-8.00	29.8	65.51	41
8.01-16.00	66.7	74.55	70
16.01-31.00	89.0	86.59	87
31.01-62.00	100	94.58	100
62.01-124		97.86	
124.01-256		100	

Table 6 Size distribution for SLQA sample ID C3508.

Particle size class range (microns)	Pipette results: Percent Finer Than	LISST 100 results: Percent Finer Than	SLQA Target Value
0.01-2.00	34.5	57.97	30
2.01-4.00	37.6	63.48	33
4.01-8.00	41.8	64.21	48
8.01-16.00	68.8	72.02	74
16.01-31.00	90.4	83.15	88
31.01-62.00	100	93.10	100
62.01-124		97.73	
124.01-256		100	

Table 7 Size distribution for SLQA sample ID C3509.

Particle size class range (microns)	Pipette results: Percent Finer Than	LISST 100 results: Percent Finer Than	SLQA Target Value
0.01-2.00	35.8	60.13	30
2.01-4.00	37.3	65.90	33
4.01-8.00	40.6	66.72	48
8.01-16.00	70.0	74.87	74
16.01-31.00	89.5	86.19	88
31.01-62.00	100	94.73	100
62.01-124		98.15	
124.01-256		100	

ISSUES TO CONSIDER FOR EVALUATION OF TEST RESULTS

1- The output of the LISST 100 does not provide particle size class information that corresponds directly with the class sizes historically used by the USGS.

2- A direct comparison of results for lower concentration samples (concentrations that fall in the LISST 100 operating range of <1 to ~500 mg/L) may not be possible. The Pipette method requires a substantial amount of sediment that is usually associated with samples of higher concentrations. The sediment concentrations of stream samples submitted to the lab for analysis that would characteristically fall within the operating range of the LISST 100 would most likely fall well below that of the samples that could be analyzed with the Pipette method. There may be little opportunity to compare samples having concentrations that overlap the limits of both methods.

3- The LISST 100 particle size determinations are based on 2 dimensional of the cross-sectional area of a particle. Measurements of the sediment particles are then converted mathematically to a 3 dimensional volume. The measurement is independent of the specific gravity of the particle. The Pipette method is based on theoretical fall rates of spherical particles through water. Thus, a large, but less dense particle could be classified by the Pipette method as having a size that is smaller than its true physical dimensions. The converse is true if the particle is composed of material with a high specific gravity.

4- Sediment concentration values are not generated by the LISST 100. The concentration of particles in a given class size is calculated as a volume percentage of the total of particle volume measurements of all the particles in the sample. This volumetric concentration is not related to the total particle volume in the water-sediment mixture of a sample. Determining a volumetric concentration (i.e. cc/ml) could be accomplished through use of a simple calculation by computing the ration of the total measured particle volume in cc versus the weight of the water/sediment mixture placed into the LISST 100 mixing chamber.

5- The Pipette method determines sediment concentration using the dry weight of all particles in a sample. If the additional analysis step in item 4 were used with the LISST 100 to determine sample concentration, it is probable that the sample concentration would be over estimated when samples contain organic materials or particles from sources where material is of low specific gravity. Conversely, there is also the potential for under estimating concentration where the sediment particles are composed of material with high specific gravity. Is this difference in determination of sediment concentration a significant problem? The implication of this difference has significant ramifications when computing suspended sediment transport. Calculations of suspended sediment transport are based on sediment concentrations expressed as dry sediment weight per unit volume of water, Porterfield (1972).

REFERENCES

Guy, H. P. (1969). “Laboratory Theory and Methods for Sediment Analysis” Techniques of Water Resources Investigations of the USGS, Book 5, Chapter C1, 89 pp.

Porterfield, G. (1972). “Computation of fluvial-sediment discharge” Techniques of Water Resources Investigations of the USGS, Book 3, Chapter C3, 66 pp.

Sequoia Scientific, Inc. (October 2002). Sequoia, LISST-100 Particle Size Analyzer, User’s Manual Version 4.2b, 75 pp.

USE OF AN ADCP TO COMPUTE SUSPENDED SEDIMENT DISCHARGE IN THE TIDAL HUDSON RIVER, NY

Gary R. Wall, Hydrologist, USGS New York Water Science Center, Troy, NY
Elizabeth A. Nystrom, Hydrologist, USGS New York Water Science Center, Troy, NY
Simon Litten, Research Scientist, NY State Department of Environmental Conservation, Albany, NY

Abstract: Acoustic Doppler current profilers (ADCPs) can provide data needed for computation of suspended-sediment discharge in complex river systems, such as tidal rivers, in which conventional methods of collecting time-series data on suspended-sediment concentration (SSC) and water discharge are not feasible. ADCPs are not designed to measure SSC, thus the software for such computation is limited, and considerable post processing is needed to correct and normalize ADCP data for use as a suspended-sediment surrogate. This paper describes the sampling design and procedure used to calibrate ADCP measures of echo intensity to SSC in the computation of suspended sediment discharge at the study site near Poughkeepsie, New York.

INTRODUCTION

Computation of instantaneous suspended-sediment discharge, or the mass of suspended sediment moving past a given river cross section per unit time, requires multiplying the average suspended sediment concentration (SSC) in the river cross section by the volume of water passing that cross section per unit time (water discharge). Computation of the suspended-sediment discharge over time, requires collection of SSC and discharge data at a frequency sufficient to permit a reasonable interpolation between data points (Potterfield, 1972). Environments in which SSC and discharge change little over time require fewer data than those environments in which flow conditions change rapidly such as a tidal river. Rapidly changing conditions require a surrogate for SSC because the large number of samples required becomes difficult and costly to obtain. Acoustic Doppler current profilers (ADCPs), however, can be used to provide surrogates for both discharge (Morlock and others, 2002) and SSC (Gartner and others, 2003) through measures of velocity and echo intensity (EI), respectively.

Limitations of an Acoustic Surrogate for SSC: Currently available ADCPs are single-frequency instruments, consequently changes in sediment concentration or particle size affect EI (Reichel and Nachtnebel, 1994); therefore interpretation of EI data requires additional measures or assumptions to resolve the cause of these changes. This limitation makes any relation between SSC and EI site specific. A second limitation of an acoustic surrogate is the relation between particle circumference and ADCP frequency (Reichel and Nachtnebel, 1994). Error in SSC estimates has been found to increase as the ratio of particle circumference to acoustic wavelength approaches 1 (Gartner, 2004). A third limitation is that ADCPs are designed to detect acoustic frequency changes in current profiles and are less accurate in measuring the amplitude changes associated with EI measurements (Schaafsma and others, 1997). Other factors that complicate the development of a relation between EI and SSC include the impossibility of collecting a water sample for SSC analysis and acoustic data from the same location at the same time, the need for data corrections to account for the loss of acoustic energy with distance from the ADCP, and normalizations for fixed and dynamic differences between instruments and instrument components over time.

Because of the many complications of applying this emerging SSC surrogate technology to a variety of river systems nationwide, the U.S. Geological Survey does not currently have a standard operating procedure for the use of ADCPs for estimation of suspended-sediment discharge. This paper is not intended to be such a procedure, but rather a documentation of how a specific pair of ADCPs were used at a specific site to compute suspended-sediment discharge. This paper may prove useful to others wishing to do similar work at other sites, but the procedure and assumptions described herein may not be appropriate for other sites.

Instrumentation: Two 614-kHz RD Instruments Workhorse Sentinel (Use of trade, product, or firm names in this publication is for descriptive purposes only and does not imply endorsement by the U.S. Government) ADCPs were used (referred hereafter as $ADCP_1$ and $ADCP_2$), each with four transceivers at a 20-degree angle to the instrument face. One ADCP was mounted to a stationary tripod on the river bottom in an upward-looking orientation about 65 cm above the bottom; the other was boat-mounted to measure discharge and develop a correlation between EI and SSC. Periodically the upward-looking ADCP was recovered for service and replaced with the other ADCP thus creating a rotation of the two instruments. Individual ADCP deployments ranged from 1 week to 7 months.

The upward-looking ADCP was set to transmit 100 acoustic pulses or "pings" every 15 min. The 100 pings were transmitted, and echoes were received, by the ADCP in a span of about 20 sec. Data from each bin in each beam were averaged into a single measurement. The size of the bins was set to 0.5 meters which resulted in 31 to 34 bins containing valid data in each beam. The exact number of bins used was computed from the depth of water above the ADCP at the time of each measurement and the cosine of the beam angle; this computation avoided the incorporation of bins with interference from acoustic reflections off the water surface (Simpson and Oltman, 1993).

COMPUTATION OF SUSPENDED SEDIMENT CONCENTRATION

Conversion of EI data recorded by the ADCP to suspended sediment concentration requires corrections for: 1) temporal changes in transmit power, transmit length, and the size of particles in the water, 2) spatial changes in the spreading of acoustic energy away from the transducer and the behavior of acoustic energy close to the transducer, 3) temporal and spatial changes in the sound absorption by water and suspended particles, and 4) variability between transducers. EI after normalization and (or) correction for all of the above factors except temporal changes in particle size is known as Acoustic Backscatter (ABS). A constant particle size distribution over the range of observed flow conditions indicates that changes in ABS can be attributed to changes in SSC. This relation is based on the sonar equation for sound scattering (Gartner, 2004) and takes the general form:

$$SSC = 10^{(A \times ABS + B)} \tag{1}$$

where A and B are the empirically derived slope and intercept of the regression of SSC against ABS. The following sections outline the steps used to convert EI to SSC.

Echo-Intensity Conversion to Decibels: EI is recorded by the ADCP in counts. Counts are extracted from the ADCP data and multiplied by an instrument-specific and beam-specific scale factor to produce EI in units of decibels (dB). These scale factors are available from RD Instruments by request.

Transmit-Power and Transmit-Length Normalization: Transmit Power (TP) is a measure of the acoustic energy transmitted by the instrument into the water column and TP is directly proportional to EI. TP can vary among instruments and through time. The measurements in this study were obtained from widely differing power-supply voltages because the upward-looking measurements were powered by an internal battery whereas boat-mounted measurements were made by direct connection of inverted AC power. This difference caused the transmit power to vary by a factor of 2.4 to 3.8 between upward-looking measurements (about 60-98 watts) and calibration measurements (about 25 watts). Additionally, the voltage of the upward-looking ADCP power-supply battery declined during individual deployments and resulted in a drop of as much as 25 watts (26 percent) in transmit power over an individual deployment.

TP in watts was calculated from transmit current and transmit voltage extracted from the ADCP data. All EI values were multiplied by a normalization factor (*TPn*) to adjust EI to a transmit power of 25 watts, the approximate value recorded during boat-mounted measurements, as expressed in eq. 2.

$$TPn = \frac{25}{TP} \tag{2}$$

Transmit Length (TL) in counts, is directly proportional to the length of the acoustic pulse and EI and was extracted from the ADCP data. Variability in TL over a deployment was generally less than 3 counts (~4 percent) and EI values were multiplied by a normalization factor (*TLn*) to adjust EI to a transmit length of 47 counts, the approximate value observed for most ensembles, as defined in eq. 3.

$$TLn = \frac{47}{TL} \tag{3}$$

Beam Normalization: ADCP beams are not factory calibrated to produce identical values of EI for a given ensonified volume (RD Instruments, oral commun., 2004). Adjusting for this variability entailed using data

gathered from a side-by-side deployment of both ADCPs over 4 weeks in October and November 2003 to normalize the beams on the two ADCPs to beam 1 on $ADCP_1$. $ADCP_1$ was set to collect a 100-ping ensemble every 15 min. and $ADCP_2$ collected 100-ping ensembles 1 min. before and 1 min. after each $ADCP_1$ ensemble. Each measurement took about 20 seconds to complete and allowed 40 seconds for the dissipation of any acoustic ringing from the previous measurements. The EI data from each $ADCP_2$ bin, collected immediately before the $ADCP_1$ measurement, were paired with data collected from the same bins immediately after the $ADCP_1$ measurement. These data pairs were first normalized to a 25-watt transmit power and a 47-count transmit length, then averaged to produce 1 value ($\overline{EI_{db}}$) for comparison with the EI value recorded by $ADCP_1$, which the data pairs bracketed. That computation is illustrated by the following equation:

$$\overline{EI_{db}} = 10 \times Log_{10}\left[\frac{\left(10^{\frac{EI_{dB}}{10}} \times TPn \times TLn\right) + \left(10^{\frac{EI'_{dB}}{10}} \times TPn' \times TLn'\right)}{2}\right] \quad (4)$$

where EI_{db} and EI'_{db} are the echo intensities in same beam and bin for the $ADCP_2$ measurement immediately before and after the $ADCP_1$ measurement

Acoustic Beam Spreading: The EI received by the ADCP is proportional to the range of the echo source particle from the ADCP. The two-way transmission loss due to beam spreading (*BS*) is:

$$BS = \psi \times 20 \times Log_{10}(R) \quad (5)$$

where R is the slant distance to the source of the return echo, in meters, defined by Deines (1999) and ψ is a transducer near-field correction (Downing and others, 1995), that accounts for the non-spherical spreading of acoustic energy close to the transducer.

Acoustic Absorption by Water: EI is also dependent on absorption of acoustic energy by the water (*WA*) according to the following equation (RD Instruments, 1996):

$$WA = 2\alpha R \quad (6)$$

where α is defined by Shulkin and Marsh (1962)

Acoustic Absorption by Sediment: Attenuation of an acoustic signal by suspended sediment can be divided into viscous, scattering, and diffraction energy loss components (Flammer, 1962). Based on Urick (1948), attenuation of 614-kHz acoustic signal is dominated by the viscous energy-loss component for particle sizes smaller than 200 microns and the scattering component dominates losses at sizes larger than this. SSC at the study site rarely exceeded 100 mg/L and silt and clay particles on average represented 96 percent of the material in suspension; therefore any attenuation due to suspended sediment was from the viscous component. The lack of information on particle size less than 62 microns, and the probability that a worst-case scenario would produce a signal loss of only a few dB over the full depth of water, led to the assumption that sound absorption by particles was negligible, and no correction was applied to account for this signal loss. The use of a higher frequency ADCP at this site could possibly invalidate this assumption, in that higher frequencies would result in greater attenuation.

Computation of Acoustic Backscatter (ABS): The 4-beam average ABS for the same bin in each beam, in decibels, is calculated by combining equations 5 and 6, which describe attenuation losses, with equations 2 (transmit-power normalization), and 3 (transmit-length normalization) and the beam-normalized factors, as follows:

$$ABS = 10 \times Log_{10}\left[\frac{\sum_{i=1}^{4}\left[10^{\frac{(EI_{dB}\times A+B)_i}{10}}\right]}{4} \times TPn \times TLn\right] + BS + WA \quad (7)$$

where A and B are the slope and intercept of the empirically derived beam-normalization factors relating observed data to data in $ADCP_1$ beam 1 and i is the beam number.

Relating Acoustic Backscatter (ABS) to Suspended Sediment Concentration (SSC): Water samples for SSC analysis and development of a relation between ABS and SSC were collected at known depths with a P-61 point-integrating isokinetic sampler suspended from the side of a boat. A downward-looking ADCP was mounted and run on the opposite side of the boat while the sample bottle filled (about 60 sec.). Echo-intensity data collected from the bin in each of the four transceiver beams closest to the depth of the P-61 sampler were averaged according to eq. 7.

River-water samples were collected at various times on the tidal cycle during several "calibration trips" when boating was possible between March and November. Typically, 3 to 6 samples were collected on these trips at different depths. Data from no more than 3 samples per trip were selected at random to avoid biasing the ABS to SSC relation toward any individual trip. The mean percentage of clay- and silt-size material (< 62 μm) in these samples was 96 percent with a standard deviation of 2.9 percent; this suggests that changes in ABS are attributable mainly to changes in SSC rather than to changes in particle-size distribution.

The relation between the base 10 logarithm of measured and predicted SSC is depicted in figure 1; predicted SSC is derived from a combination of two explanatory variables - ABS and water temperature (WT) in degrees C. Water temperature was found significant at the $p<0.001$ level and therefore included in the multiple regression equation. The coefficient of determination (R^2) between these variables is 0.86, and the standard deviation of the residuals (measured SSC minus retransformed-fit SSC) is 7.9 mg/L. SSC in mg/L for an individual bin after retransformation is expressed in eq. 8. The average of the retransformed regression residuals (1.033), known as the Duan smearing estimator (Helsel and Hirsch, 1992), is applied to the equation to account for bias (geometric as opposed to arithmetic means) introduced by the retransformation of SSC from logarithmic to arithmetic space.

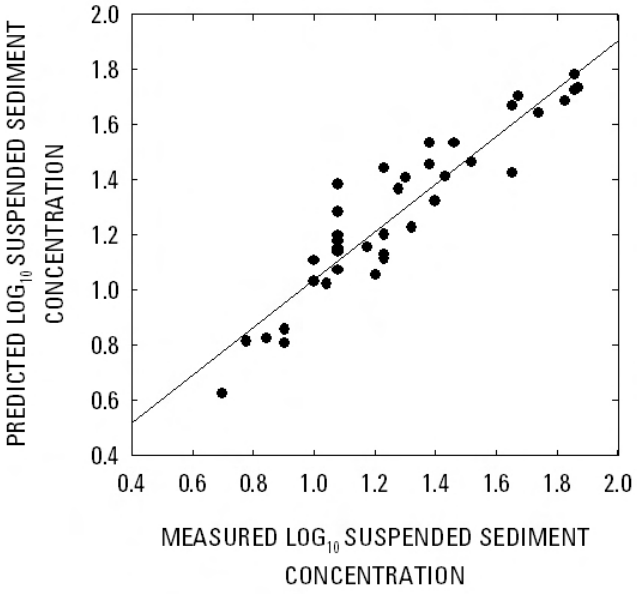


Figure 1: Relation between the base10 logarithm of suspended-sediment concentration and the predicted base10 logarithm of suspended-sediment concentration derived from acoustic backscatter and water temperature data measured at the same depth and time.

$$SSC_{bin} = 10^{ABS\times 0.034 - WT\times 0.019 - 1.018} \times 1.033 \quad (8)$$

Cross-Sectional Average Suspended Sediment Concentration (SSC): The ADCP-derived average SSC in the measured part of the water column above the upward-looking ADCP was compared with cross-sectional measurements of SSC to produce a cross-section correction factor. The average SSC measured above the upward-looking ADCP (SSC_{Pavg}) was computed as:

$$SSC_{Pavg} = \frac{\sum_{bin=1}^{n} \left(SSC_{bin} \times \left| Vp_{bin} \right| \right)}{\sum_{bin=1}^{n} \left| Vp_{bin} \right|} \quad (9)$$

where SSC_{bin} is the SSC in an individual bin defined by eq. 8,
Vp_{bin} is the projected downstream water velocity in an individual bin, and
n is the bin farthest from the ADCP.

The large size of the Hudson River at the site (~800m width) and constantly changing flow conditions, make conventional methods of sample collection in the full cross section, such as the equal-width or equal-discharge methods (U.S. Geological Survey, 1999) infeasible for accurate measurement of the average cross-sectional concentration (SSC_{Xavg}) for a given point in time. Boat-mounted cross-sectional ADCP measurements, however, provided sufficient data from which to calculate this value while minimizing time averaging measurements. The width of a given bin in an acoustic beam is dependent on the speed of the boat; therefore cross-sectional averaging of computed SSC values was weighted by the discharge, instead of velocity, in each bin or unmeasured zone and calculated as:

$$SSC_{Xavg} = \frac{\sum_{bin=1}^{n} \left(SSC_{bin} \times \left| Q_{bin} \right| \right) + \sum_{e=1}^{z} \left(\left(SSC_{top} \times \left| Q_{top} \right| \right)_e + \left(SSC_{bot} \times \left| Q_{bot} \right| \right)_e \right) + \left(SSC_l \times \left| Q_l \right| \right) + \left(SSC_r \times \left| Q_r \right| \right)}{\left| Q_{Total} \right|} \quad (10)$$

Where Q_{bin} is discharge in an individual bin,
n is the last measured bin in the cross section, and
Q_{Total} is the cross-section discharge.

Estimates of SSC in the unmeasured zones near the river bottom (SSC_{bot}) and water surface (SSC_{top}) of each ensemble (e) were made by fitting an ordinary least-squares line through the SSC_{bin} data from each ensemble and extrapolating to the center of the top and bottom of the respective unmeasured zones. Concentrations in these unmeasured zones were then weighted by the respective estimated discharges (Q_{bot} and Q_{top}) in each zone for each ensemble. Discharge estimates in the unmeasured near-surface zone were based on a 3-point solution (RD Instruments, 2003) when applicable and otherwise a constant-extrapolation method was used (RD Instruments, 2003). Discharge estimates for the unmeasured near-bottom zone were based on a power curve solution (RD Instruments, 2003).

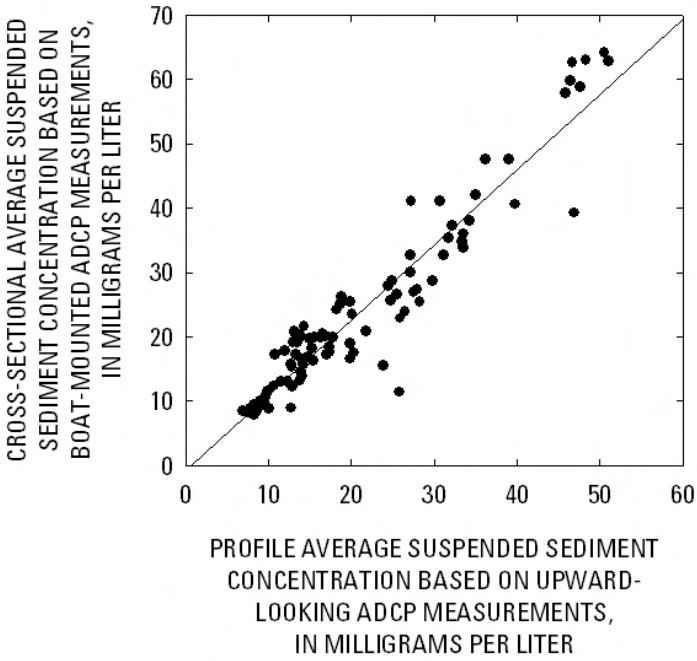


Figure 2: Relation between estimates of SSC based on upward-looking ADCP measurements and those based on boat-mounted ADCP measurements of full cross-section

SSC values for near-bank areas where the boat could not reach shore, or where the water was too shallow for the ADCP were estimated for the left and right banks (SSC_l and SSC_r); these terms represent the flow-weighted average SSC_{bin} values in the 10 ensembles closest to the left and right banks,

respectively. The SSC values for each bank were weighted by corresponding estimates of discharge (Q_l and Q_r) from the same 10 ensembles for each bank in accordance with standard methods (RD Instruments, 2003).

The estimated cross-sectional average SSC values are plotted against the velocity-weighted SSC average estimated by the upward-looking ADCP in figure 2. A linear regression equation relating these parameters was generated to adjust the upward-looking ADCP estimate to conditions in the full cross section. If necessary, an SSC value was interpolated between upward-looking ADCP measurements to correspond with the mean time of the cross-section measurement. The number of cross-section measurements made in each calibration trip varied; therefore, bias toward a particular calibration trip was avoided by a random sampling of no more than 4 measurements and no fewer than 3 from each trip (3 measurements were made on 2 trips). The resulting equation (eq. 11) represents 94 cross-section measurements made during 24 calibration trips between 2002 and 2004; it has an R^2 of 0.90 and a residual standard error of 4.55 mg/L.

$$SSC_{avg} = 1.17 \times SSC_{Pavg} - 0.75 \quad (11)$$

The percent error for each of the correction and normalization factors discussed above for these specific instruments at this site during a single 208-day deployment is summarized in table 1.

Table 1. Percent error resulting from omission of corrections and normalizations to data collected during a 208-day ADCP deployment in the Hudson River near Poughkeepsie, NY

Factor	Observed Range	Percent Error in Calculated Suspended-Sediment Discharge Without Accounting for Factor
Transmit power	71 to 65 watts	36 (-5.1)[1]
Transmit length	45-47 units	-1.0 (-0.3)[1]
Beam normalization	Slopes from 96 to 101% of $ADCP_1$ Beam 1	6.5
Beam spreading	~0.9 to 17.4m depth	-71
Near-field correction	Not applicable	0.8
Sound absorption	~0.9 to 17.4m depth	-18
Bias correction	Not applicable	-3.2
Cross section correction	Not applicable	-13

[1]First number accounts for both changes during deployment and differences between calibration and deployment. Numbers in parenthesis only include changes during the deployment

COMPUTATION OF SUSPENDED-SEDIMENT DISCHARGE

Instantaneous suspended-sediment discharge was computed by multiplying SSC_{avg} from equation 11 by the corresponding discharge, and converting units. Suspended-sediment discharge calculated for tidal settings, over periods other than tidal cycles, are biased with respect to one another, because the calculated difference between two periods of equal duration may be attributable to the part of the tidal cycle over which the respective periods were computed (fig. 3). Suspended-sediment discharge computation over successive tidal cycles, however, is awkward to manage in the context of a calendar day. Mathematically filtering the time-series data removes the semidiurnal tide signal from the data and the resulting bias from summing the discharge over incomplete tidal cycles. Similarly, computing long-term totals of instantaneous suspended-sediment discharge over periods much longer than a tidal cycle has the effect of minimizing this bias as indicated in fig. 3C. Therefore an annual suspended-sediment discharge, for example, computed either using a tidal filter or by simple summation of instantaneous data, should produce nearly identical results.

A low-pass digital filter was used to remove the semi-diurnal tide signal from the time series data. The filter residual represents the net, or downriver, suspended-sediment discharge. Each filtered data point was assumed to represent the instantaneous suspended-sediment discharge at any point in time over the next 15 minutes; therefore, each filtered value was multiplied by 15 to provide an estimate of the total sediment discharge over the 15 minutes that followed the measurement. Summation of the 96 15-min suspended-sediment discharge values for each day constitutes the net daily suspended-sediment discharge.

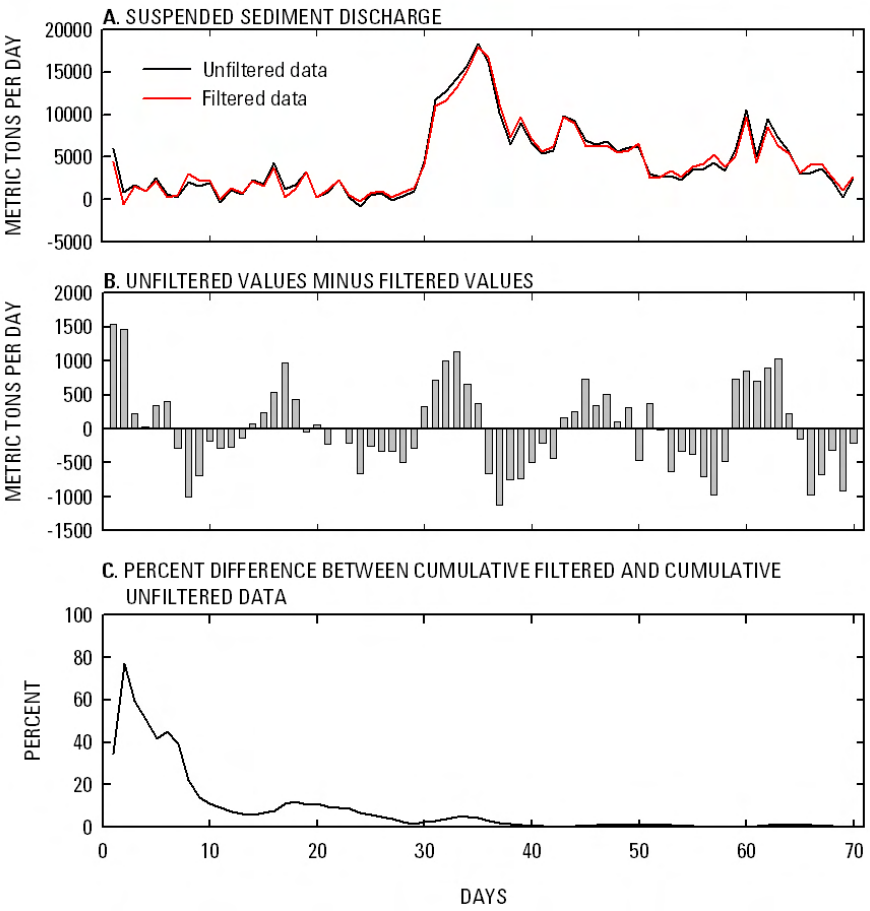


Figure 3: Differences between filtered and unfiltered suspended-sediment discharge data.

SUMMARY

Suspended-sediment discharge of a tidal river was computed using measures of echo intensity and velocity from an ADCP. Adjustments to EI data included an instrument and beam-specific EI conversion to decibels, normalizations for temporal and instrument variations in transmit power and length, beam-to-beam variability, and range-dependent corrections. Calibration of EI to SSC involved the collection of boat-mounted ADCP data from bins corresponding to the depth of a P-61 isokinetic water sampler lowered from the opposite side of the boat. Cross-sectional SSC estimates, based on boat-mounted ADCP measurements were used to adjust data collected by the fixed-position, upward-looking ADCP to conditions in the river cross section. Net suspended-sediment discharge was computed by filtering 15-minute time series data of instantaneous suspended-sediment discharge with a low-pass digital filter that used a fast-Fourier transform to remove the semidiurnal tidal signal in the data.

REFERENCES

Deines, K. L., 1999, Backscatter estimation using broadband acoustic Doppler current profilers: Oceans 99 MTS/IEEE Conference Proceedings, September 13-16, 1999.

Downing, A., Thorne, P. D., and Vincent, C. E., 1995, Backscattering from a suspension in the near-field of a piston transducer: The Journal of the Acoustical Society of America, v.97, no.3, p.1614.

Flammer, G. H., 1962, Ultrasonic measurement of suspended sediment: U.S. Geological Survey Bulletin 1141-A, 48 p.

Gartner, J., Mueller, D., Wall, G., and Gray, J., 2003, Breakout session 4: Other fluvial-sediment surrogates, *in*, Gray, J. and Glysson, D. (eds),.Proceedings of the Federal Interagency Workshop on Turbidity and Other Sediment Surrogates, , U.S. Geological Survey Circular 1250, 56 p.

Gartner, J., 2004, Estimating suspended solids concentrations from backscatter intensity measured by acoustic Doppler current profiler in San Francisco Bay, California: Marine Geology, v.211, p.169-187.

Helsel, D.R., and Hirsch, R.M., 1992, Statistical methods in water resources, studies in environmental science, v. 49., Elsevier Science B.V., 529 p.

Morlock, S.E., Nguyen, H.T., and Ross, J.H., 2002, Feasibility of acoustic Doppler velocity meters for the production of discharge records from the U.S. Geological Survey streamflow-gaging stations: U.S. Geological Survey Water-Resources Investigations Report 01-4157, 56 p.

Potterfield, G., 1972, Computation of fluvial-sediment discharge, techniques of water-resources investigations of the United States Geological Survey, Chapter C3, 66 p.

RD Instruments, 1996, Principles of operation: a practical primer, 158 p.

RD Instruments, 2003, WinRiver users guide – USGS version, 144 p.

Reichel, G., Nachtnebel, H. P., 1994. Suspended sediment monitoring in a fluvial environment: advantages and limitations applying an acoustic Doppler current profiler. Water Research., v. 28, no. 4, pp.751-761.

Schaafsma, A. J., Lafort, A. M., Guyomar, Daniel, 1997, Development of an acoustic method and prototype instrumentation for size and concentration measurement of suspended sediment: Proceedings of the First International Conference on EuroGOOS, 7-11 October, 1996, The Hague, The Netherlands (Elsevier), pp. 168-175.

Shulkin, M. and Marsh, H.W., 1962, Sound absorption in sea water: The Journal of the Acoustical Society of America, v. 34, no. 6, p. 864.

Urick, R.J., 1948, The absorption of sound in suspensions of irregular particles: The Journal of the Acoustical Society of America, v. 20, no. 1, p. 283-289.

U.S. Geological Survey, 1999, National field manual for the collection of water quality data: Chapter A4, Techniques of Water-Resources Investigations Book 9. 103 p.

CALCULATION OF SUSPENDED SEDIMENT AT GAGING STATIONS

Jason W. Kean, Hydrologist, USGS, Boulder, CO, jwkean@usgs.gov; J. Dungan Smith, Hydrologist, USGS, Boulder, CO, jdsmith@usgs.gov

Abstract: A method for calculating stage-discharge relations (rating curves) and suspended sediment concentrations in gravel bedded streams is presented and applied to a reach downstream from a U.S. Geological Survey (USGS) gaging station on Little Prickly Pear Creek, MT. The approach uses a fluid-mechanically based model to convert measurements of stage into discharge and boundary shear stress fields appropriate for determining sediment transport. The model does not use empirical roughness coefficients, such as the Manning coefficient, but rather determines channel roughness from field measurements of the channel geometry and the dominant physical and biological roughness elements in the modeled reach. The theoretical flow rating curve produced by the model is in excellent agreement with direct measurements of discharge made by the USGS. An empirical relation between the concentration of fine sediment near the bed and the rate of bedload transport is developed using station sediment data. This relation and a point measurement of concentration as a function of grain size are employed by the model to calculate suspended sediment concentration fields and fluxes in the reach. The approach also can be used to generate a sediment rating curve. Our method has the potential of providing accurate estimates of stream flow and suspended sediment loads less expensively than conventional gaging methods.

INTRODUCTION

The conventional USGS procedure for gaging discharge in rivers is to measure stage and then to calculate discharge from an empirically generated rating curve. Measuring stage is relatively easy using a pressure gage and is not particularly expensive. To determine an empirical rating curve, however, requires making discharge measurements at a wide range of stages and then fitting a curve to the stage-discharge data field. Although this approach has been used for over a century, attesting to its accuracy and robustness, procurement of the data necessary to generate an accurate empirical rating curve can be time consuming and expensive. By developing procedures that account for the fluid mechanical effects of all of the physical and biological roughness elements on the entire potentially wetted perimeter of a geomorphically stable reach of a stream or river, the resistance to flow can be explicitly determined as a function of stage, making possible a completely predictive model for the flow in that reach at all stages. Using such a fully predictive model (namely, one with no empirically adjusted coefficients) a “theoretical rating curve” can be constructed. We have developed such a model and tested the rating curves produced by it against the empirical rating curves at seven gaging stations [two in Kansas (Kean and Smith, 2005), three in Colorado, and two in Montana]. In all cases, the variance of the discharge measurements around our “theoretical rating curves” is comparable to or less than that around the empirical rating curves generated from the same data.

In addition to providing a less labor intensive and potentially more accurate means of calculating discharge at a gaging station, our model provides all of the fluid-mechanical parameters required to calculate bed-material (bedload and suspended-load) transport within the measurement reach. This paper describes how calculations of suspended sediment in a gravel bedded stream can be incorporated into the theoretical rating curve model. The approach is applied to a reach downstream from USGS gage station 06071300, Little Prickly Pear Creek at Wolf Creek, MT (Figure 1). Monitoring streamflow and suspended sediment concentrations on Little Prickly Pear Creek is particularly important for ecological reasons, because it is a major spawning tributary for migratory rainbow and brown trout from the Missouri River. Discharge measurements at the station are used to test the theoretical discharge rating curve calculated by our model. Daily values of suspended sediment concentrations recorded by the USGS from 1962-1967 are used to develop an empirical relation between the concentration of suspended sediment near the bed and the rate of bedload transport. This relation permits the calculation of accurate suspended sediment concentration fields using one or more point measurements of the sediment concentration as a function of grain size. The point sample is used to quantify the wash load and the amount of bed material of each sand size available for transport in suspension. The latter depends on the amount of fine sediment contributed to the channel and on the flow history of the stream. The combined flow and sediment transport model is then used to (1) reconstruct the flow and sediment transport fields for a high discharge in Little Prickly Pear Creek, and (2) demonstrate the effect that density stratification can have on the velocity and sediment concentration fields for flows with moderate to high concentrations of sand.



Figure 1 (a) Downstream view of Little Prickly Pear Creek from bridge. (b) View upstream from middle of the measured reach.

MODEL COMPONENTS

The model for calculating a theoretical stage-discharge relation is composed of two parts: a set of procedures for quantifying the various contributions to the total flow resistance in the channel and a flow model into which the results of these procedures are embedded. The description that follows is for the components necessary to calculate a rating curve and the suspended sediment transport fields for Little Prickly Pear Creek, which is relatively straight and which has a flow resistance due primarily to bed roughness and drag on the bank vegetation. A more detailed description of the model components required to develop a rating curve for narrow channels with these characteristics is given in Kean and Smith (2005). Their paper also outlines the procedures required to incorporate flow resistance caused by lateral stresses on irregularly shaped banks, which are not needed to address the flow and sediment transport in Little Prickly Pear Creek.

Bed roughness: In channels with gradually sloping banks, width-to-bankfull-depth ratios greater than about 10, and gravel beds that are devoid of significant form-drag-producing topographic elements, the vertically averaged velocity at any position in the channel ($\bar{u}$) can be related directly to the local boundary shear stress (τ_b) through the expression

$$\bar{u} = \left(\tau_b / \rho\right)^{1/2} \beta = u_* \beta \tag{1}$$

where ρ is the density of water, u_* is the local shear velocity, and β is a non-dimensional roughness coefficient that is a function of the size of the bed material, the flow depth (h), and the shape of the velocity profile. In this case, the boundary shear stress is that appropriate for calculating bed material transport, and is given by $\rho g h S_f$. Here g is the acceleration of gravity and S_f is the friction slope. Under these conditions, the velocity profile will be quasi-logarithmic in shape (see Wiberg and Smith, 1991), and β will have the form

$$\beta = \left[\ln\left(h/z_o\right) - 0.74\right]/\kappa \tag{2}$$

where κ is von Karmann's constant equal to 0.408 (Long et al., 1993). The roughness height, z_o, can be related to the moments of the particle size distribution for the gravel composing the bed. An adequate approximation is $z_o = 0.2D_{84Z}$, where D_{84Z} is the diameter at the 84th percentile of the size distribution for the vertically oriented axes (Wiberg and Smith, 1991). Alternatively, if the diameters of the vertically oriented axis are half of the nominal diameters (D_N), the approximation $z_o = 0.1D_{84N}$ (Whiting and Dietrich, 1989) can be used.

Vegetation roughness: In vegetated portions of the channel (edges), the velocity and boundary shear stress are reduced by drag on the plant stems, which can be calculated using the method of Smith (2001). The stems are modeled as a randomly distributed array of circular cylinders that have a mean stem diameter (D_s) and mean spacing (λ) specified from field measurements. In this application the stems are assumed to be rigid and extend throughout

the entire flow depth. Drag on the field of stems acts as body force on the fluid, and the average drag force on an individual stem (F) is given by

$$F = \tfrac{1}{2}\rho C_D D_s h\left(u_{ref}\right)^2 \tag{3}$$

where u_{ref} is reference velocity and C_D is the drag coefficient of a single stem, which for the flows of interest here is constant and equal to 1.2. The reference velocity is defined as $u_{ref} = [(_{z_o}\int^h u^2 dz)/h]^{1/2}$, where u is the local velocity within the field of stems. A suitable approximation for the reference velocity can be made using (1), (2), and a shear velocity that reflects the reduced boundary shear stress caused by the form drag on the stems (Smith, 2001 and 2004). By converting the drag force on a single stem into a drag stress (that is, by dividing (3) by λ^2) and separating it from the total boundary shear stress, Smith (2001) obtained an expression for the boundary shear stress within the stems, which is given by

$$\tau_b = \frac{\rho g h S_f}{1+\sigma_D} \text{ where } \sigma_D = \tfrac{1}{2} C_D \beta^2 \frac{h D_s}{\lambda^2} \tag{4}$$

Channel Flow Model: Owing to the fact that the study reach is relatively straight and does not contain large amplitude bars that would steer the high velocity core of the flow from side to side in the channel, a simple steady, one-dimensional model is sufficient to resolve the dominant flow accelerations in the reach. Application of such a model requires the average velocity for a cross-section, $(u)_{av}$, to be related to the perimeter-averaged shear stress, $(\tau_b)_{av}$. This is done using an expression analogous to (1), given by $(u)_{av} = \beta_r[(\tau_b)_{av}/\rho]^{1/2}$, where β_r is the non-dimensional roughness coefficient for the cross-section. The value of β_r varies as a function of stage and streamwise position, and this variation can be specified completely a priori using the roughness methods outlined in the previous sections. For a given stage and cross-section, β_r is calculated by integrating the unit discharge ($\bar{u}h$), obtained from (1), (2), and (4), across the cross-section and dividing this value by the area of the cross-section and the shear velocity computed from $(\tau_b)_{av}$. Specification of β_r in this manner differs from most applications of one-dimensional models, where β_r, or its equivalent Manning coefficient ($n = R^{1/6} g^{-1/2} \beta_r^{-1}$) or Chezy coefficient ($C = g^{1/2}\beta_r$), is either determined empirically by measuring the water discharge and water-surface elevations (e.g. Wiele and Smith, 1996) or is estimated from experience or the results of previous studies (e.g. Barnes, 1967; Limerinos, 1970).

The discharge for a given stage is determined iteratively by solving the one-dimensional model for the water-surface profile that matches both the stage and a measured water-surface elevation drop through the reach. In addition to discharge, the solution yields a quasi three-dimensional representation of the velocity field, meaning that values of velocity, shear stress, and eddy viscosity are provided by the solution for all points in the flow field. The theoretical rating curve for the reach is generated by repeating the calculation for different stages over the range of flows that can occur at the site. The calculated boundary shear stress fields with the effects of form drag on the shrubs removed are used in the next section to determine bedload and suspended sediment transport in the measurement reach.

Sediment Transport Model: The method of McLean (1992) can be used to calculate profiles of sediment volume concentration (C_s) given vertical distributions of shear stress and eddy viscosity and a reference sediment concentration ($C_a = C_s(z=a)$) and size distribution. For sand bedded channels, the concentration at the top of the saltation height of the particles is defined based on the work of Smith and McLean (1977). This formulation for C_a has been employed by Andrews (2000) to calculate suspended sediment concentrations in a predominately gravel bedded stream that had patches of sand on the bed. For gravel bedded streams that do not have distinct patches of sand, however, the Smith and McLean (1977) formulation for C_a is not applicable, because the fine sediment is located within the interstices of the pebbles, which shield the fine sediment from the flow processes that entrain the particles into the moving fluid. A second complication in calculating suspended sediment in gravel bedded streams is that fluid stresses below the level of the largest clasts are reduced due to the form drag on the clasts. This latter complication can be addressed by applying the method of Wiberg and Smith (1991) to calculate the profiles of stress and eddy viscosity down to the level of zero flow. Their method determines the momentum extracted from the flow by drag on each size class of the bed material. The former complication is addressed here for mobile beds without sand patches by developing an empirical model for C_a in a gravel bedded stream using data on daily sediment concentrations recorded at the USGS gaging station on Little Prickly Pear Creek between 1962 and 1967. We hypothesize that C_a is related to the non-dimensional rate of significant bedload transport (ϕ) by an empirical constant of proportionality (α) that depends on the concentration of fine sediment in the bed. Bedload transport is modeled here using a modified Meyer-Peter Müller equation

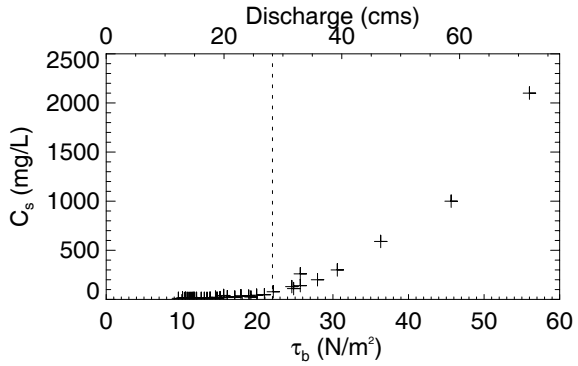


Figure 2 Daily suspended sediment concentration vs. daily discharge and boundary shear stress for the falling limb of the flood on 9 June 1964. The vertical dashed line corresponds to the critical boundary shear stress for significant motion.

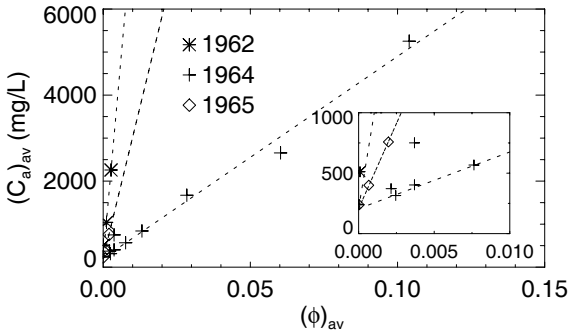


Figure 3 Empirically determined values of $(C_a)_{av}$ versus $(\phi)_{av}$ for selected spring flow events.

$$\phi = 8\left(\tau_* - \left(\tau_*\right)_{crt}\right)^{3/2} \tag{5}$$

where, τ_* and $(\tau_*)_{crt}$ are the non-dimensional shear stress and critical shear stress respectively. The reference level, a, is presumed to be related to the size of the bed material and is taken here to be D_{50N} /2, where D_{50N} is the median size of the probability distribution for the measured nominal grain diameters. Basically, when the clasts composing the river bed move, the sand from beneath is released into the flow by the method proposed here. In contrast, when the coarse bed material remains stationary or moves only as marginal transport, sand must build up in patches on the stream bed before significant sediment transport can occur in the manner described by Andrews (2000). These two cases are mutually exclusive and depend on whether the clasts move in significant transport or not.

An example of the dependence of suspended sediment concentrations on shear stress is shown in Figure 2. The figure contains daily values of suspended sediment concentration for the falling limb of the flood on 9 June 1964, which produced the highest measured discharge, as well as, the highest daily sediment concentration recorded in the station's history. The concentrations in the figure are plotted against both discharge and an estimate of the mid-channel boundary shear stress for that discharge. The estimate of boundary shear stress is obtained from application of the theoretical rating curve model to a measurement reach adjacent to the gage station. Although the model for the reach is based on recently measured topography, the reach averaged mid-channel boundary shear stress is assumed to be representative of the stress during the 1964 flood. The figure shows that sediment concentrations increase substantially after a threshold stress or discharge (denoted by the dashed line) is obtained. This threshold is thought to represent the critical shear stress (τ_{crt}) for significant motion of the gravel comprising the bed. The non-dimensional shear stress for this threshold based on the D_{50N} of the present bed is 0.036, which is within the range of observed values for $(\tau_*)_{crt}$ compiled by Buffington and Montgomery (1997). Plots of daily concentration and shear stress for the falling limbs of five other spring flow events exhibit the same trend shown in Figure 2 but have varying critical shear stress thresholds. The values of $(\tau_*)_{crt}$ determined visually for the other flows are 0.037, 0.041, 0.046, 0.037, 0.044. The mean $(\tau_*)_{crt}$ for the six flows is 0.040.

The hypothesis that C_a is linearly related to ϕ is tested as follows. For a given flow, where data on daily sediment concentration and discharge are available, the coupled flow and sediment transport model is inverted to find the distribution of C_a across the channel that yields the average concentration field that was recorded for that day. The concentration field is generated by computing concentration profiles at about 50 positions across the channel. The value of C_a for each vertical is specified by the product of the local ϕ and a fixed constant for the cross-section that is determined through iteration. Ancillary data on the size distribution for the daily values of concentration is not available, so a log-normal distribution composed of five size classes of sand (0.0625, 0.125, 0.25, 0.5, and 1 mm) is used to represent the fine bed material. The concentration fields are reconstructed for the falling limbs of six spring flows between 1962-1967. Spring flows are used for the analysis, because these flows have the highest discharge and sediment concentrations. Data from the rising limbs of the flows have been excluded, because the total

concentration during this time can have greatly varying percentages of wash load generated by initial runoff from the hillslopes and/or bank failures, and the grain size data necessary to separate the wash load from suspended bed-material load is not available.

The results of these calculations for three of the six floods are shown in Figure 3. The average of the back-calculated distribution of C_a across the cross-section, $(C_a)_{av}$, is plotted in relation to the cross-sectional average of the non-dimensional bedload transport rate, $(\phi)_{av}$. The data for each flow is fairly linear demonstrating that our model for C_a is appropriate. The volumetric concentration at $(\phi)_{av} = 0$ for these trends is nearly the same, and the mean for the six flows in units of mg/L is 266. This intercept ($(C_a)_o$) represents the value of C_a at the beginning of significant bedload transport. In the absence of wash load, $(C_a)_o$ represents the effects of marginal transport of the gravel on the availability of the fine bed material for transport. The value of $(C_a)_o$, however, is very small and consideration of the dependence of C_a for marginal transport is beyond the scope of this paper. If wash load were present, the volumetric concentration of silt and/or clay measured in a point sample, which would be representative of the value throughout the water column, would have to be added to the value of $(C_a)_o$ determined from the marginal transport regime. Based on the results shown in Figure 3, the expression for C_a in Little Prickly Pear Creek is given by

$$C_a = \alpha\phi + \left(C_a\right)_o \tag{6}$$

The value of α depends on the amount of sand in the bed, which, in turn, depends on the source of the fine sediment and the flow history. As is typical in most suspended sediment transport problems, it is easier and more accurate to specify α by one or more point measurements of concentration and a size distribution than to measure the concentration and size distribution of fine sediment in the riverbed during a flood. Although α can vary with time in a given stream, it represents the state of the bed after the last sand transporting event and there is no reason that it should vary with cross-stream position during a particular flood.

Table 1 Summary of channel characteristics for Little Prickly Pear Creek at Wolf Creek, MT

Reach Characteristics:	Roughness Characteristics:
Location: Lat. 47°00’19” Long. 112°04’10”	D_{50Z}: 21 mm D_{84Z}: 47 mm (vertical axis)
Drainage Area: 987 km^2	D_{50N}: 47 mm D_{84N}: 81 mm (nominal diameter)
Reach Length: 132 m	z_o: 0.009 m
Meas. water-surface slope at 1.1 cms: 0.0033	Mean willow stem diameter: 0.018 m
Meas. water-surface slope at 29 cms: 0.0035	Mean willow spacing: 0.258 m

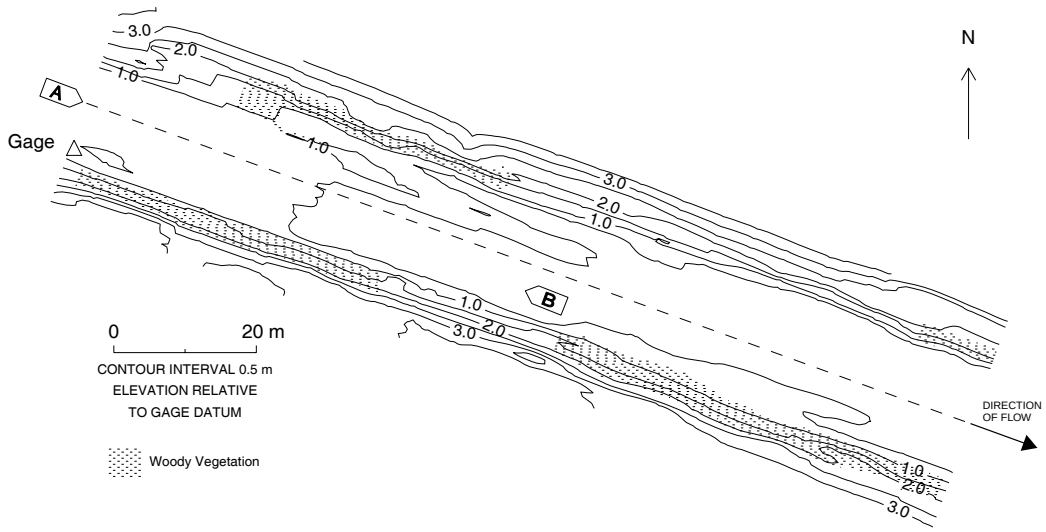


Figure 4 Map of surveyed reach. Arrows A and B indicate the approximate positions where the photos in Figure 2 were taken.

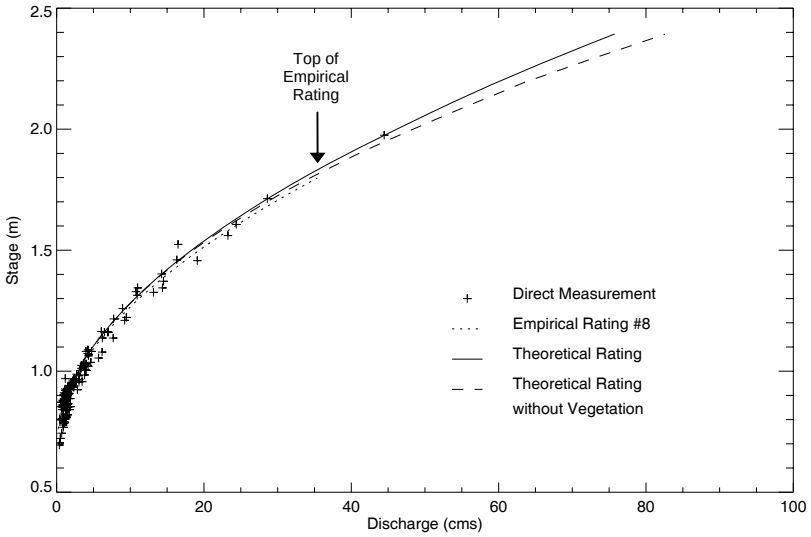


Figure 5 Comparison of rating curves and measurements for Little Prickly Pear Creek. Stage is relative to the USGS gage datum. Direct measurements of discharge are shown for the station's present location (established 1991).

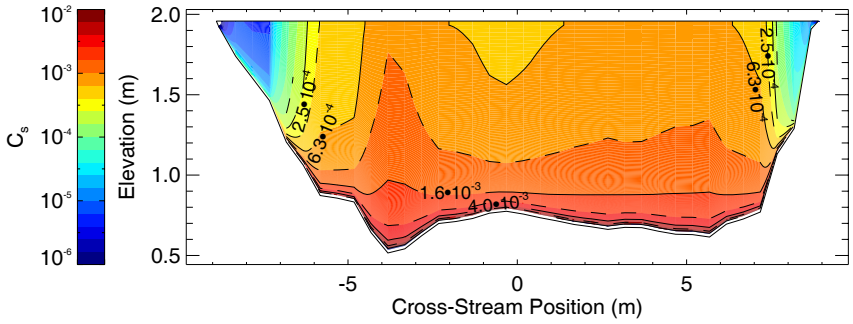
APPLICATION TO LITTLE PRICKLY PEAR CREEK

The field measurements required to make the model for the site were made by a two person crew on 26 October 2004. A summary of these measurements is given in Table 1.The shape of a reach downstream from the USGS gage was measured by surveying 22 cross-sections spaced about every 6 m using high-precision GPS surveying equipment (Figure 4). The size of the bed material was determined from Wolman pebble counts made at three locations in the reach (Wolman, 1954). The short, intermediate, long, and protrusion axis of each pebble was recorded. All four measurements are required to apply the model of Wiberg and Smith (1991), which is used in the computation of velocity and turbulence profiles. The stem density of the willows along the bank was determined by counting and recording the diameter of stems within two 3m x 3m plots adjacent to the channel. The location of the willows was mapped during the survey. The bed z_o for the reach is specified from the measured size distribution of the bed material through $z_o = 0.2D_{84Z}$. Water-surface profiles were surveyed at low flow at the time of the main field work and at high flow on 11 May 2005. These profiles show that the water-surface elevation drop across the reach, which is a boundary condition in the model, remains nearly constant as a function of stage.

A comparison of the theoretical rating curve with the USGS discharge measurements and empirical rating curve is shown in Figure 5. In general, there is good agreement between the theoretical rating curve and both the direct measurements and empirical rating curve. The theoretical rating curve calculated without the effects of drag on vegetation shows that this source of flow resistance is only important at very high stages. A quantitative comparison of the agreement of the empirical and theoretical rating curves with the measurements can be made by comparing the total weighted variance of the two curves about the measurements within the stage range shared by the two curves (see Hill, 1998; Kean and Smith, 2005). In general, the total weighted variances for the theoretical rating curve are comparable to the empirical rating curve.

The following example is given to illustrate how the theoretical rating curve method can be used together with one or more measurements of sediment concentration and size distribution to calculate suspended sediment concentration fields and fluxes. The example uses USGS sediment measurements made on 13 June 1967 in Little Prickly Pear Creek to reconstruct the concentration field. The measurements, which are given in Table 2, are used to specify both the size distribution of fine sediment in the bed and the value of α that sets C_a across the cross-section through (6). Initial guesses of these parameters are used to calculate the suspended sediment concentrations at the position(s) where measurements were made. Guesses of α and the size distribution of the fine sediment in the bed are improved iteratively until the calculation converges on the measured values. The measured sediment data used in this example is averaged over the cross-section. In practice, a small set of point measurements of concentration and size distribution in the same vertical is preferable, because it provides a better constraint on the calculation. Figure 6

a)



b)

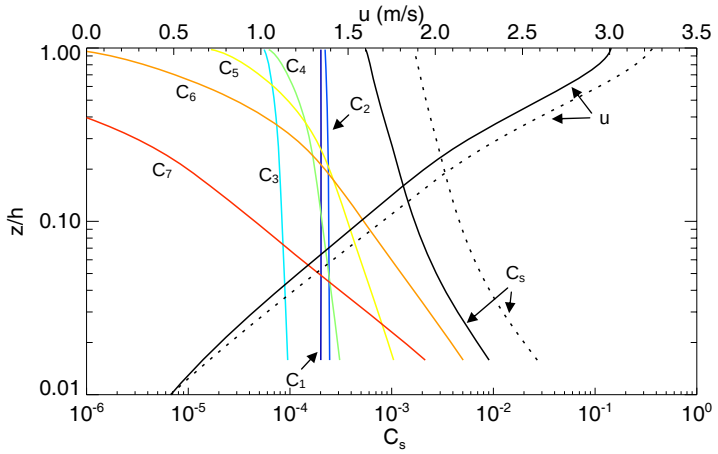


Figure 6 Calculated (a) concentration field and (b) and concentration and velocity profiles in the center of the channel for the 13 June 1967 high flow. The grain sizes of the concentration profiles C1 through C7 are: 0.010, 0.039, 0.094, 0.188, 0.375, 0.75, and 1.5 mm. The dotted lines are the velocity and total concentration profiles for a hypothetical event having 3 times the amount of fine sediment in the bed as in the 13 June 1967 flow.

shows the calculated concentration field at the gage cross-section and the calculated profiles of concentration and velocity in the center of the channel. The value of α determined for this flow is 0.11 and corresponds to a C_a in the center of the channel of 1%. The back-calculated size distribution of the fine material in the bed (listed in Table 2) is dominated by medium sand and differs greatly from the average distribution for the cross-section.

Vertical variations in sediment concentration produced by suspended grain sizes larger than silt create a density gradient that can, if sufficiently large, alter the velocity and turbulence fields. Although this effect is negligibly small in the present example, it can be appreciable for cases having larger amounts of sand. For example, given the same stage, boundary shear stress, and fine sediment size distribution in the bed, raising α by a factor of three creates a density gradient that increases the discharge by 8%. The velocity and concentration profiles in the center of the channel for this case are shown in Figure 6b. It is important to note that a single point measurement of total concentration is not sufficient to evaluate accurately the effects of density stratification, but a single point measurement that is separated into size classes is sufficient for this purpose.

Table 2 Meas. and calc. cumulative size distributions for the 1967 flow (Q = 45.6 cms, $(C_s)_{av}$ = 2780 mg/L).

Size (mm)	0.004	0.016	0.063	0.0125	0.25	0.5	1	2
Measured % finer for cross-section	8	20	43	50	63	78	97	100
Calculated % finer at $z = a$	-	2	5	6	9	21	76	100

SUMMARY AND CONCLUSIONS

This paper presents a method for calculating theoretical stage-discharge relations and suspended sediment concentrations and fluxes in gravel bedded streams. The approach utilizes a fluid-mechanically based model that does not rely on empirical roughness coefficients, such as Manning or Chezy coefficients, to convert measurements of stage into discharge, and it determines the distributions of boundary shear stress appropriate for sediment transport calculations. One or more point measurements of suspended sediment size and concentration are used to specify the amount of sand of each relevant size class in the bed and the percentage of silt and clay in the flow. For flows with significant gravel transport, the distribution of sediment concentration throughout the reach and its effect on the velocity field and water discharge are better left for the model to determine than to try to characterize them empirically. A combined calculation/measurement scheme, such as the one presented here, has the potential for substantially increasing the accuracy and reducing the cost of gaging streamflow and sediment. It also provides a foundation for calculating the transport of contaminants sorbed to sediment grains.

Acknowledgements: Peter McCarthy (USGS, MT) conducted the high precision GPS surveying for this study.

REFERENCES

Andrews, E.D. (2000). "Bed material transport in the Virgin River, Utah," Water Resour. Res., AGU, 36(2), pp. 585-596.

Barnes, H.H. Jr. (1967). "Roughness characteristics of natural channels," U.S. Geol. Surv. Water-Supply Pap. 1849.

Buffington, J.M. and Montgomery, D.R. (1997). "A systematic analysis of eight decades of incipient motion studies, with special reference to gravel-bedded rivers," Water Resour. Res., AGU, 33(8), pp. 1993-2029.

Hill, M.C. (1998). "Methods and guidelines for effective model calibration," U.S. Geol. Surv. Water Resour. Invest. Rep., 98-4005.

Kean, J.W., and Smith, J.D. (2004). "Flow and boundary shear stress in channels with woody bank vegetation," in Riparian Vegetation and Fluvial Geomorphology, edited by S.J. Bennett and A. Simon, AGU, pp 237-252.

Kean, J.W., and Smith, J.D. (2005). "Generation and verification of theoretical rating curves in the Whitewater River Basin, KS," J.Geophys. Res., AGU, 110, F04012, doi:10.1029/2004JF00250.

Limerinos, J.T. (1970). "Determination of Manning coefficient from measured bed roughness in natural channels", U.S. Geol. Surv. Water-Supply Pap., 1898-B.

Long, C.E., P.L. Wiberg, and Nowell, A.R.M. (1993). "Evaluation of von Karman's constant from integral flow parameters," J. Hydraul. Eng., ASCE, 119,pp 1182-1190.

McLean, S.R. (1992). "On the calculation of suspended load for noncohesive sediments," J. Geophys. Res., AGU, 97(C4), pp 5759-5770.

Smith, J.D., and McLean, S.R. (1977). "Spatially averaged flow over a wavy surface," J. Geophys. Res., AGU, 82, pp. 1735-1746.

Smith, J.D. (2001). "On quantifying the effects of riparian vegetation in stabilizing single threaded streams," in Proc. 7th Federal Interagency Sedimentation Conference, Reno, Nevada, 1(IV), pp 22-29.

Smith, J.D. (2004). "The role of riparian shrubs in preventing floodplain unraveling along the Clark Fork of the Columbia River in the Deer Lodge Valley, Montana," in Riparian Vegetation and Fluvial Geomorphology, edited by S.J. Bennett and A. Simon, AGU, pp 71-85.

Whiting, P.J. and Dietrich, W.E. (1989). "The roughness of alluvial surfaces; an empirical examination of the influence of size and heterogeneity and natural packing," EOS Trans. AGU, 70(43), p. 1109.

Wiberg, P.L. and Smith, J.D. (1991). "Velocity distribution and bed roughness in high-gradient streams," Water Resour. Res., AGU, 27(5), p. 825-838.

Wiele, S.M., and Smith. J.D. (1996). "A reach-averaged model of diurnal discharge wave propagation down the Colorado River through the Grand Canyon," Water Resour. Res., AGU, 32(5), pp. 1375-1386.

Wolman, M.G. (1954). "A method of sampling coarse river-bed material," Transactions of the American Geophysical Union, 35(6), pp. 951-956.

CROSS-SECTIONAL PROGRESSION OF APPARENTBEDLOAD VELOCITIES

Terry A. Kenney, Hydrologist, U.S. Geological Survey, Salt Lake City, Utah, tkenney@usgs.gov

Abstract: An acoustic Doppler current profiler was used to measure apparent bedload velocities as river discharge increased from 5,400 to 19,400 cubic feet per second at a cross section of the Green River near Green River, Utah. Apparent bedload velocities were obtained through the exploitation of the bottom-track bias of acoustic Doppler current profilers. A divergence in the progression of apparent bedload velocities along the cross section was identified. As discharges steadily increased, apparent bedload velocities on one side of the river channel increased while velocities on the other side initially increased and then approached zero. Average cross-sectional apparent bedload velocities were compared with river discharge and suspended-sediment conditions measured during the event.

INTRODUCTION

The dynamic processes associated with the transport of material along a channel bed are complicated. Bedload transport describes the movement of particles by flow through rolling, saltating, and (or) sliding along the channel boundary. Accurately determining the amount and rate of bedload transport in natural channels has proven to be an extremely daunting task. Rennie and others (2002) introduced a technique that utilizes an acoustic Dopper current profiler (ADCP) to measure apparent bedload velocities. Bedload-transport rates within a single cross section have been shown to vary with time and space under steady flow conditions, and rates of bedload transport are known to be greatest during large discharge events. Accurate collection and computation of bedload data under these conditions is necessary for the quantification of total bedload discharge. Further investigation into the variability of bedload processes within a single cross section under changing discharges is needed. In an effort to add some insight into these processes, this study, conducted by the U.S. Geological Survey (USGS), deployed an ADCP to measure apparent bedload velocities at nine stations across a single-channel cross section during a period of rising discharge and fluctuating suspended-sediment conditions.

BACKGROUND

Rennie and others (2002) identified four factors contributing to the difficulty in measuring bedload: (1) spatial and temporal variability is great in natural channels; (2) physical samplers are difficult and dangerous to deploy during channel-forming processes; (3) physical samplers disrupt the natural flow, thus biasing the transport; and (4) bedload sampling and processing is labor intensive. Conventionally, bedload has been collected by two methods: portable samplers or material traps. Material traps, such as slot or pit samplers, are semi-permanent installations that are designed to collect all material being transported along the bed during a set time period. Presently, the portable Helley-Smith bedload sampler is the most widely used. Portable physical samplers typically are lowered down to the streambed from cable-reel systems to collect material for a specified time interval. A series of point samples are collected within a cross section and integrated to compute total bedload discharge. The efficiency of material traps is close to 100 percent (Edwards and Glysson, 1999), and laboratory studies have determined the Helley-Smith

efficiencies to be 150 percent (Helley and Smith, 1971; Hubbell and others, 1985; Edwards and Glysson, 1999). The practicality of material traps limits their usage—they are notably difficult to install, retrieve, and maintain in large rivers, and the efficiency of the portable samplers is undesirably high. Fortunately, the nearly exclusive usage of the Helley-Smith samplers during the past 30 years allows for fair comparison of most of the bedload data that has been collected. These factors emphasize a need for new techniques for the measurement of bedload transport in natural channels. An ideal technique would possess a sampling efficiency close to 100 percent without disrupting the natural flow path of sediment particles. It would account for spatial and temporal variability of transport, and be safe to deploy during large discharge events. Recently, Rennie and others (2002) introduced a new technique to measure what they termed the apparent velocity of bedload with an ADCP. The study presented by Rennie and others (2002) shows strong agreement between the apparent bedload velocities and bedload transport rates obtained with conventional samplers in the Fraser River in British Columbia, Canada. To further advance this new technique, which appears to address many of the conventional bedload sampling shortcomings, more field and laboratory investigations will need to be conducted.

Cross-sectional variability of bedload transport can be large, especially under unstable flow conditions. Bedload transport is known to be greatest at large discharges, often experienced for only a small fraction of time throughout a water year. Acquisition of a valid annual bedload discharge requires the ability to quantify transport during these periods of unstable flow conditions, times in which the cross-sectional variability of bedload can be extreme. Moreover, natural channels commonly undergo complex hydraulic and geometric adjustments during these events. Most equations developed to predict bedload were derived under the theoretical assumption of an achieved equilibrium and do not account for the possibility of the channel undergoing aggradation or degradation (Graf, 1984). Applying these equations to periods of unsteady flow and extreme bedload variability can lead to gross errors. Empirical bedload-transport data, such as apparent bedload-velocity measurements, collected under unsteady flow conditions will lead to an improved understanding of certain components of bedload transport.

Use of the ADCP to measure apparent bedload velocities: The concept of exploiting the bias in the bottom tracking-feature of an ADCP to acquire apparent bed velocities was introduced by Rennie and others (2002). ADCPs measure water velocities relative to themselves. In order to determine true water velocities, the velocity of the ADCP is required. By assuming a stationary streambed and utilizing the principle of the Doppler effect, bottom tracking is the most common method of obtaining the velocity of the ADCP. Bottom tracking treats any shift in sound-wave frequency associated with the streambed as velocity of the ADCP. In the presence of a moving bed, a stationary ADCP in bottom-tracking mode will sense that it is moving in the opposite direction of the bed. Apparent bedload velocities (v_a) from stationary measurements are computed by dividing the distance "made good" reported by the ADCP in the bottom-track mode (d_{mg}) by the elapsed time of the measurement (t).

$$v_a = d_{mg} / t \tag{1}$$

The distance "made good" is equal to the straight-line distance from the initial to the final position of the ADCP. In the presence of a moving bed, the bottom-track mode distance "made

good" is equal to the straight-line distance from the initial to the final position calculated by the ADCP.

Rennie and others (2002) discussed some potential limitations of deploying an ADCP for bedload measurements. Most of these limitations are related to the geometric characteristics of the acoustic beams of the ADCP and how they sample the channel bed. Beam diameters increase with depth, as does the areal extent that the beams occupy (figure 1). Therefore, the region of the bed insonified by the ADCP varies with depth. Transducer geometry and angular orientation, the number of transducers in an array, and total water depth will have an effect upon how the channel bed is sampled. Greater depths allow for improved spatial averaging, but the geometry of the beams dictates the amount of channel material that is measured. There is also the potential for these instruments to possess an inherent preferential particle-size registration. Data indicate that different acoustic frequencies will register backscatters from different particle sizes in a dissimilar manner. This can lead to an instrument with one frequency identifying a moving bed while one of another frequency indicates no movement. Further study of how these limitations affect the measurement of apparent bedload velocities is needed.

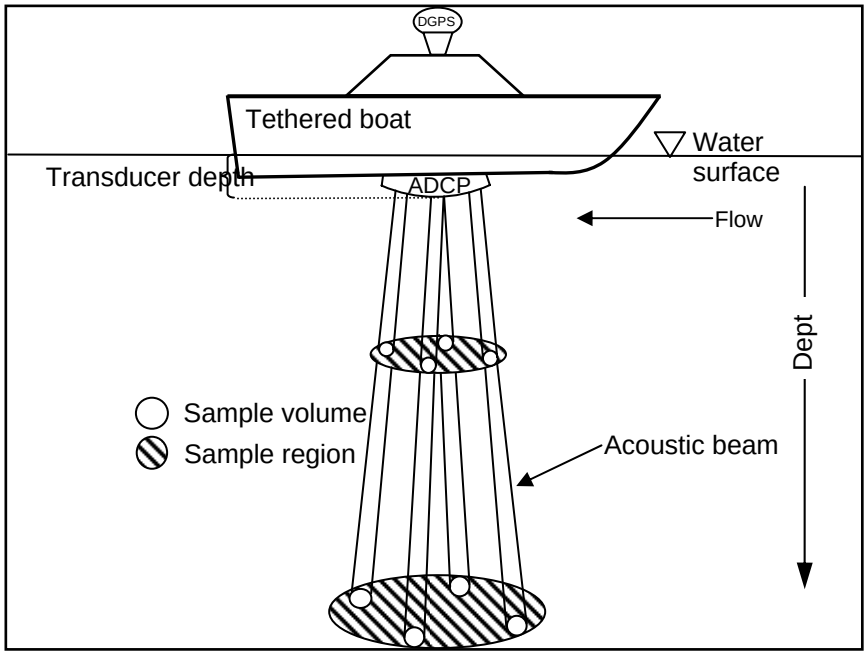


Figure 1 Schematic of ADCP showing increase in apparent bedload-velocity sample volume and sample region with depth.

The ADCP may prove to be a useful tool for acquiring bedload-transport data. There is no disruption of flow near the bed. Samples do not need to be sent away for analysis, decreasing cost and time, which allows for more samples to be acquired. Deployment of the instrument is rapid and safe because the ADCP remains on the water surface and is not submerged within the flow.

The apparent bedload-velocity data presented here should not be interpreted as bedload-transport rates. The data can be used only to identify regions of relatively high or low moving bed

velocities. For this investigation, the technique described for measuring apparent bedload velocities was not compared with any conventional bedload sampling data. No attempt was made to calibrate or determine the true relation between actual bedload transport and the apparent bedload velocities obtained during this study. The presence of bed forms can have an effect upon bedload-transport rates. From the methodologies employed during this study, appreciable bed form development was not recognized. This is not to say, however, that bed forms were not present.

SITE DESCRIPTION

The study site was located at the cross section defined by the cableway for USGS streamflow gaging station 09315000, Green River at Green River, Utah. The drainage basin of the Green River at Green River, Utah, is roughly 106,000 km^2. Average river slope of the reach containing the cross section is 0.0004 m/m, and bed materials consist of moderately sized gravels, sand, and silt.

DATA ACQUISITION METHODS

The bias associated with the bottom-tracking feature of an ADCP in the presence of a moving bed allows for a measurement of what Rennie and others (2002) termed apparent bedload velocity. Apparent bedload velocities were acquired at nine channel stations across a single-cross section on the Green River near Green River, Utah, as discharge increased from 5,400 ft^3/s on May 19, 2003, to 19,400 ft^3/s on May 29, 2003. One set of apparent bedload velocities was collected following the receding discharges on June 12, 2003. The ADCP and associated equipment were tethered from the USGS cableway. The ADCP was held in position at the desired channel station for between 60 and 300 seconds. This time span allowed a minimum of 90 subsets, known as ensembles, of data to be collected by the ADCP. The sampling interval of between 60 and 300 seconds was chosen to allow for the acquisition of a near-instantaneous cross-sectional condition. It is understood that longer sampling times would have resulted in improved time-averaged values at each station. The amount of times the ADCP samples the bottom during one ensemble, known as the bottom-track pinging rate, was increased to 3 from the default configuration of 1, to reduce the potential for bedload-velocity errors. A total of 14 sets of apparent bedload velocities were acquired during the study. The progression of apparent bed velocities based upon measurements at channel stations 17, 25, 33, 41, 47, 55, 63, 71, and 79 m is shown in figure 2.

RESULTS

Apparent bedload velocities in the early stages of the flow event, May 20, 2003, through May 21, 2003, were relatively uniform throughout the cross section. As flows continued to increase beyond 12,000 ft^3/s, velocities at channel stations 33 through 47 began to diverge from the velocities at stations on the right side of the cross section. Velocities at stations along the right side of the channel appear to rapidly drop off to near zero values with increasing discharge. The greatest apparent bedload velocity measured was 0.81 m/s at station 41 on May 29, 2003, at 10:05 hours. As would be expected, this velocity corresponded to the largest discharge observed during the study. However, the lowest measured apparent bedload velocities, not

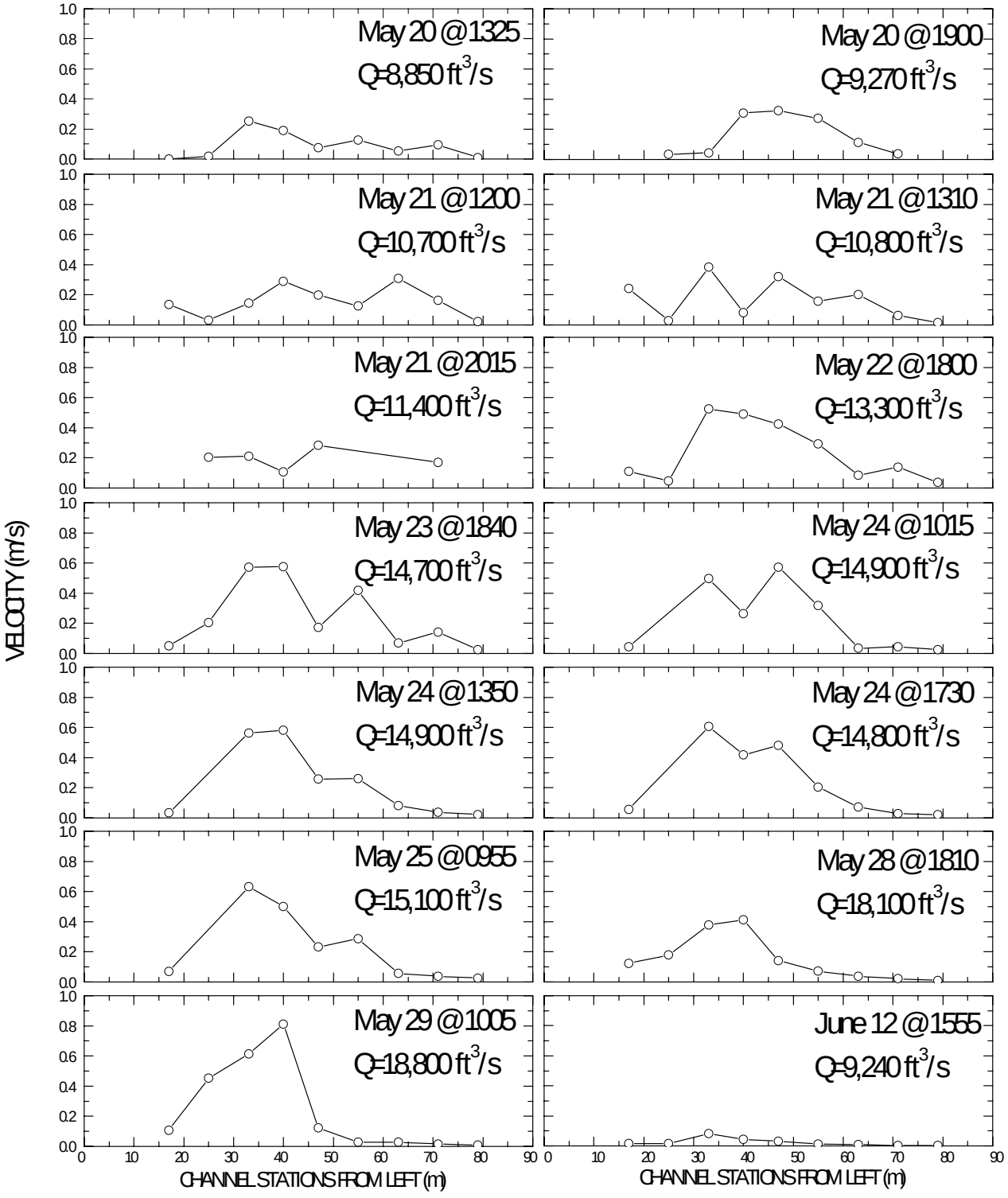


Figure 2 Apparent bedload velocities and corresponding discharge collected at specified channel stations from May 20 to June 12, 2003, at a cross section of the Green River near Green River, Utah.

including those of June 12, 2003, occurred at stations 55 through 79 at the same time. Sediment transport, in this case bedload transport, is dependent upon the availability of transportable materials. The timing of this divergence agrees with an increase in suspended-particle size and lower suspended-sediment concentrations. Prior to these changes, apparent bedload velocities were increasing in a somewhat uniform manner throughout the cross section. Another explanation for the divergence is that with the continued increase in discharge, erodible sediments along the right margin of the channel were exhausted, while the bed materials near the left-center were plentiful. It is not known how far up or downstream this phenomenon extended, but a gentle streamwise gradation into an area of nearly zero transport would be expected. The apparent bedload velocities acquired on June 12, 2003, following the peak of the snowmelt runoff, were the lowest measured. Apparent bedload velocities measured on May 20, 2003, and May 21, 2003, at discharges of 8,850 ft^3/s and 9,270 ft^3/s, respectively, were much greater than those of June 12 at a discharge of 9,240 ft^3/s. This is likely due to the removal of easily transportable sediments early on during snowmelt runoff.

Cross-sectional average apparent bedload velocities were computed from each of the 13 composite sets of apparent bedload velocities. In general, average cross-sectional apparent bedload velocities rapidly increased from 0.09 m/s on May 20, 2003, at 13:25 to as much as 0.25 m/s on May 23, 2003, at 18:40. As discharges remained relatively steady, average cross-sectional apparent bedload velocities did so as well. A plot of average cross-sectional apparent bedload velocities and discharge is shown in figure 3. Average apparent bedload velocities appear to increase in relation to suspended-sediment concentrations (Figure 4). The rapid rate of decrease in suspended-sediment concentrations does not seem to be reflected in the average apparent bedload velocities. A plot of average cross-sectional apparent bedload velocities and the percent of suspended material finer than 0.062 mm is shown in figure 5. This plot indicates that an increase in suspended-material size is related to an increase in average cross-sectional apparent bedload velocities. In general, the acquired apparent bedload velocities seem to show a relation to discharge and suspended-sediment conditions. However, it is difficult to evaluate the relations between apparent bedload velocities and these causal mechanisms after May 25 due to the extended temporal spacing of apparent bedload velocity measurements. The reasons for the low average apparent bedload velocity for May 28 are undetermined.

CONCLUSIONS

By exploiting the bottom-track bias common to ADCPs, apparent bedload-velocity data were acquired as river discharges increased from 5,400 ft^3/s to 19,400 ft^3/s at a cross section of the Green River in Utah. Although no calibration of the apparent bedload velocities to actual bedload-transport rates was conducted, the dataset acquired offers an interesting look at bedload behavior during unsteady flow and suspended-sediment conditions. Of particular significance is the cross-stream variability of apparent bedload velocities at the larger observed discharges.

With the shortcomings of physical bedload samplers and conventional techniques, further field and laboratory investigations into the utility of acoustic technology for the acquisition of bedload-transport data are needed.

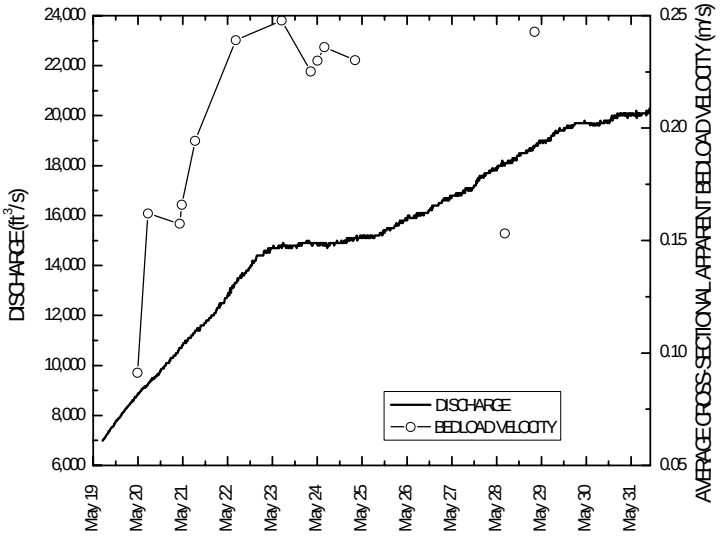


Figure 3 Average cross-sectional apparent bedload velocities in relation to discharge, at a cross section of the Green River near Green River, Utah.

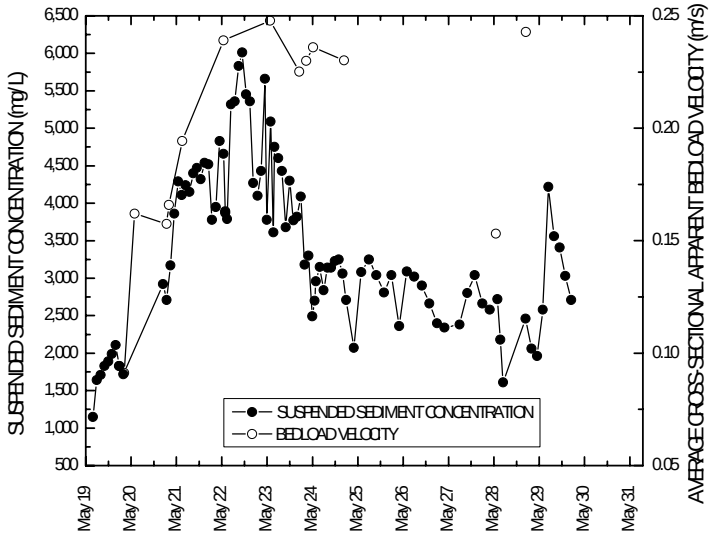


Figure 4 Average cross-sectional apparent bedload velocities in relation to suspended-sediment concentrations, at a cross section of the Green River near Green River, Utah.

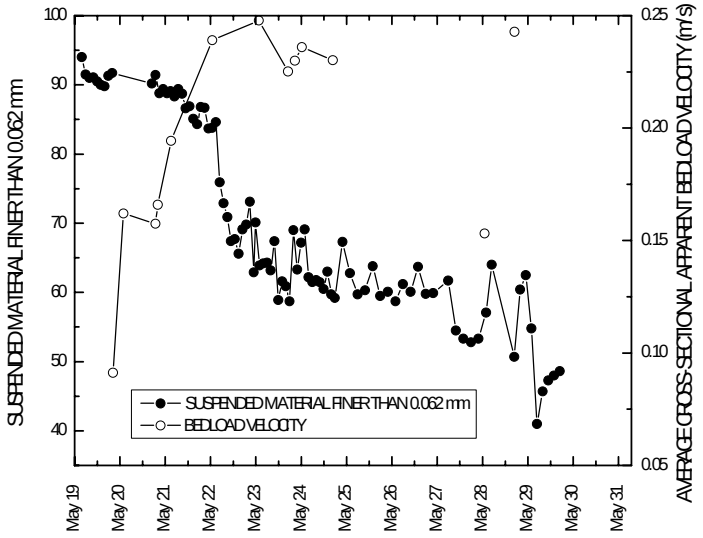


Figure 5 Average cross-sectional apparent bedload velocities in relation to percent of suspended material finer than 0.062 mm, at a cross section of the Green River near Green River, Utah.

REFERENCES

Edwards, T.K., and Glysson, G.D., 1999, Field methods for measurement of fluvial sediment. U.S. Geological Survey Techniques of Water-Resources Investigations, book 3, chap. C2, 89 p.

Graf, W.L. 1984, A probabilistic approach to the spatial assessment of river channel instability. Water Resources Research, v. 20, no. 7, p. 953-962.

Helley, E.J., and Smith, Winchell, 1971, Development and calibration of a pressure-difference bedload sampler. U.S. Geological Survey Open-File Report 73-108, 38 p.

Hubbell, D.W., Stevens, H.H., Skinner, J.V., and Beverage, J.P., 1985, "New approach to calibrating bedload samplers," American Society of Civil Engineers, Journal of Hydraulic Engineering, v. III, no. 4, p. 677-694.

Rennie, C.D., Millar, R.G., and Church, M.A., 2002, "Measurement of bed load velocity using an acoustic Doppler current profiler," Journal of Hydraulic Engineering, 128(5), p. 473-483.

CONTINUOUS IN-STREAM MONITORING TO ESTIMATE WATER-QUALITY CHARACTERISTICS AND SEDIMENT SOURCES IN THE LITTLE ARKANSAS RIVER, KANSAS

Andrew C. Ziegler, Supervisory Hydrologist, Lawrence, Kansas, aziegler@usgs.gov; Victoria G. Christensen, Hydrologist, Mounds View, Minnesota vglenn@usgs.gov; Patrick P. Rasmussen, Hydrologist, Lawrence, Kansas, pras@usgs.gov

Abstract: A continuous, in-stream water-quality monitoring system developed by the U.S. Geological Survey in Kansas provides real-time estimates of constituent concentrations and loads for sediment, major ions, selected nutrients and metals, atrazine, and indicator bacteria, and uncertainty and probability of exceeding criteria that improve the characterization of water quality compared to more traditional approaches (http://ks.water.usgs.gov/Kansas/rtqw/). Regression models are developed to relate constituent concentrations in laboratory-analyzed discrete samples to in-stream sensor measurements. An example from two sites in the Little Arkansas River, south-central Kansas, is presented comparing traditional and alternative approaches for estimation of sediment and sediment-associated constituents.

Comparisons of regression models for streamflow- and turbidity-estimated suspended-sediment concentrations and loads indicate that continuous turbidity measurement provides better defined estimates of concentrations and loads than those models developed using traditional streamflow-estimation techniques. From 1999-2004, annual suspended-sediment loads estimated using streamflow were 7 to 31 percent larger than those estimated using turbidity. Monthly suspended-sediment loads estimated using turbidity were larger than those estimated using streamflow during some spring and summer months.

Clockwise hysteresis has been demonstrated by other researchers to be related to depletion of available sediment from the streambed, channel, or areas near the channel. Clockwise hysteresis is a decrease in concentrations of suspended sediment corresponding with an increase in streamflow. Counterclockwise hysteresis is an increase in sediment concentrations corresponding to a decrease in streamflow. Counterclockwise hysteresis probably occurs when sediment is derived from sources that are more distant from the stream (overland flow, tributaries, or channel wasting). In the Little Arkansas River, examples of clockwise and counter-clockwise hysteresis of streamflow and turbidity are examined to infer sediment sources.

Despite implementation of practices to control sediment transport, an historical comparison in the Little Arkansas River Basin using streamflow-estimated concentrations and loads indicates that sediment transport and yield has changed little in the past 40 years considering the uncertainty in the estimation technique. Hysteresis variability of turbidity-estimated sediment concentrations with streamflow indicates that sources of sediment during storms are variable. Because of this variability, management of transport of sediment and sediment-associated constituents, such as nutrients and bacteria, may prove difficult given that the concentrations for some of these constituents frequently exceed their corresponding water-quality criteria even during the smallest of hydrologic events.

REAL-TIME ANALYSIS OF CONCENTRATED FLUVIAL SUSPENDED SEDIMENTS

Chris Konrad, Research Hydrologist, U.S. Geological Survey, Tacoma, WA, cpkonrad@usgs.gov; Chuck Pottsmith, Vice President, Sequoia Scientific Inc., Bellevue, WA, pottsmith@sequoiasci.com; Ted Melis, Integrated Science Program Manager, U.S. Geological Survey, Flagstaff, AZ, tmelis@usgs.gov; Dave Rubin, Research Geologist, U.S. Geological Survey, Santa Cruz, CA, drubin@usgs.gov

INTRODUCTION

Anthropogenic changes in sediment transport and deposition in rivers, lakes, and coastal waters is a global concern (Baca et al., 1982; Walling and Webb, 1996; Koebel et al., 1999; Wang et al., 2003; Langland et al., 2004). In the United States, over 5000 water bodies are listed as water-quality impaired due to sedimentation (U.S. EPA, 2005a). Human structures (for example, roads, dams, levees, revetments, and drainage networks) and activities (forestry, agriculture, urban development, water management) can either increase or decrease the amount and size of sediment delivered to and transported by rivers depending on the type of change and the location of interest in a river basin (Anderson, 1954; Guy and Ferguson, 1963; Brown and Krygier, 1971; Trimble, 1983; Williams and Wolman, 1984; Thoms, 1987; Syvitski et al., 2005). Changes in sediment loads affect management of water resources in many ways. For example, water supplies may require additional treatment before water can be used for out-of-stream municipal and industrial uses. Reservoirs may have to be dredged to restore their storage capacity. Increased sediment loads also impair in-stream uses of water, such as when physiological functions of aquatic organisms are affected by high sediment concentrations in the water column or when sediment deposits render the streambed inhabitable and reduce the available volume of low-velocity aquatic habitat. Conversely, anthropogenic reduction in the amount or size of sediment transported in a river may also impair in-stream uses where aquatic organisms are adapted to higher levels of turbidity and aquatic habitats are created by deposition of fluvial sediment.

THE NEED FOR SUSPENDED SEDIMENT DATA FROM STREAMFLOWS WITH HIGH CONCENTRATIONS

Sediment data are needed for informed management decisions to address the concerns about the effect of changing sediment loads on water resources (Pennisi, 2004; U.S. EPA, 2005b). Efforts to manage sediment loads in many rivers must proceed on the basis of few – if any - direct measurements of fluvial sediment in transport and, instead, use regional estimates of sediment yields or surrogates such as bank erosion (Tetra Tech, U.S. Environmental Protection Agency, and Tennessee Department of Environment and Conservation, 2002; Oregon Department of Environmental Quality, 2004; Thompson, 2005). In these cases, suspended sediment data for periods when streamflow and concentrations are high, would increase the precision of the estimated loads defining the problem and the precision of monitoring efforts to assess when the problem has been addressed.

In rivers, suspended sediment data are typically collected by periodic sampling at a point with a manual or automatic pump sampler and occasional manual collection of water samples over a

cross-section. The cross-sectional samples are used to develop a coefficient to relate the concentration of point samples to the mean sediment concentration across the river. This approach, however, cannot resolve changes in suspended-sediment concentration and particle-size distributions at time-scales shorter than the point sampling interval. For example, storm-scale hysteresis cannot be defined by daily samples in many rivers, so it must be inferred by analyzing data from individual storm events or from long time periods that include samples from both the rising and falling limbs of the hydrograph. Moreover, it is uncertain that interpolation of sediment concentrations between samples collected with a pump sampler accurately represents the changing sediment concentration during high flow events, particularly if the samples fail to capture peak concentrations during those events.

The paucity of sediment data, particularly when sediment concentrations are high, is not a trivial issue when calculating sediment loads. In many rivers, much of the long-term (years) sediment load is transported during only a few days or weeks of high flows (Leopold et al., 1964). The cumulative distribution of a river's sediment load can also be viewed in terms of the sediment concentration of flows transporting the load. The sediment load in 26 rivers in the U.S. with daily suspended-sediment records of at least 10 years (U.S. Geological Survey, 2005) was analyzed with respect to the sediment concentration. Flows with concentrations above 2000 mg/L carried a median value of 32 percent of the long-term load in these rivers (fig. 1). Although the distribution of the load depends on climate and basin physiography, suspended sediment data from flows with sediment concentrations on the order of 10^3 mg/L and higher are critical to accurate estimates of sediment loads in many rivers.

Monitoring of fluvial suspended sediment has advanced in recent years through the development of many different technologies that may be able to provide a continuous record of suspended sediment concentrations (Reichel and Nachtnebel, 1994; Lewis and Rasmussen, 1999). Optical technologies based on measurements of light scattering and diffraction are widely employed to provide a measure of macroscopic material suspended in water (van Wijngaarden and Roberti, 2002; Lewis, 2003; Thonon and van der Perk, 2003; Schoellhamer and Wright, 2003; Topping et al., 2005). Despite the advances in optical technologies, none currently are sufficient for continuous monitoring of high concentrations of suspended sediment ($> 10^3$ mg/L) for a number of reasons. For example, some turbidity meters can be used in flow with high suspended sediment concentrations, but they require calibration of the output to measured sediment concentrations (Urhich and Bragg, 2003). The operational range of laser diffraction is limited to concentrations around 3,000 mg/L because high concentrations of suspended sediment reduce the transmission of light or produce multiple scattering that obscures the relationship between sediment concentration and the signal from the instrument (Topping et al., 2005). As an alternative, optical technologies can be used to trigger pump sampling during periods when sediment concentration are out of range of the optical sensor (e.g., Lewis, 2003; Topping et al., 2005), but this approach still is limited by the pump sampling interval and may require frequent visits to collect samples that must be analyzed.

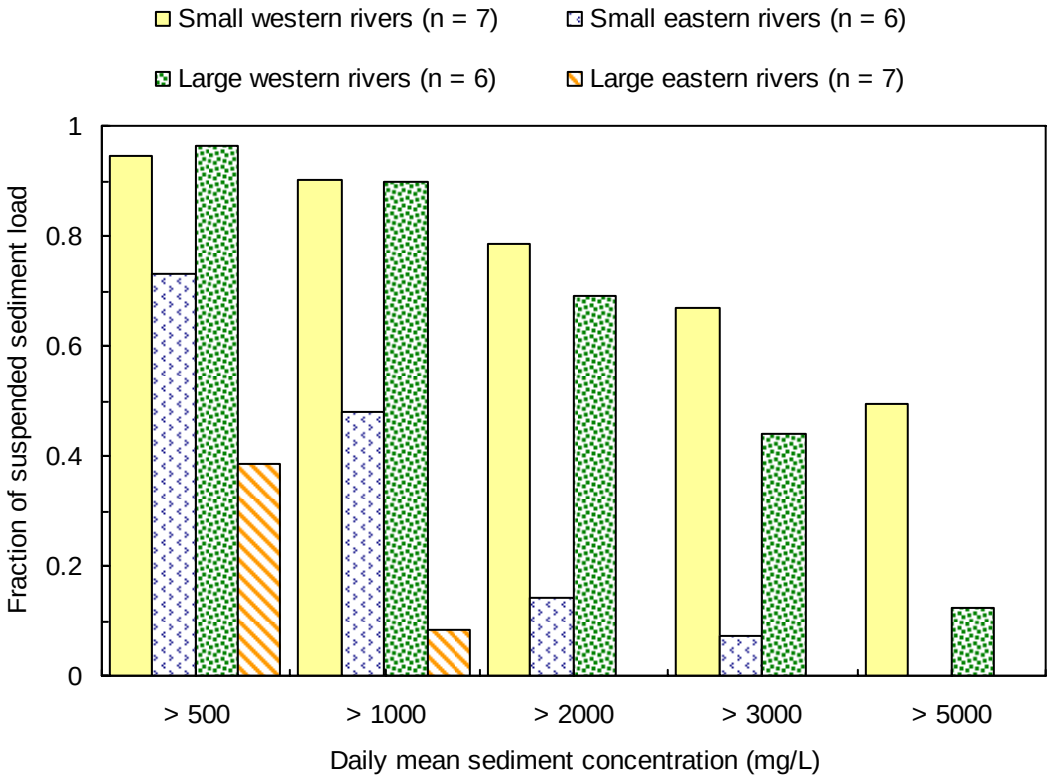


Figure 1 The fraction of suspended sediment load in 26 U.S. rivers carried by streamflow with high-concentrations of sediment. Minimum period of record is 11 years. Regional division is made at the Missippi River. Data source: U.S. Geological Survey, 2005.

A SYSTEM FOR REAL-TIME, CONTINUOUS ANALYSIS OF HIGH CONCENTRATIONS OF SUSPENDED SEDIMENT

A partnership of USGS scientists and Sequoia Scientific engineers has developed a suspended-sediment monitoring system (LISST-Infinite) with the goal of real-time analysis of highly concentrated suspended sediment. (Note that the use of a business or product name does not represent an endorsement by USGS.) The LISST-Infinite system integrates a laser diffraction sediment analyzer (LISST-25x) with an external pump, a dilution chamber and internal pump, and a digital controller that operates the pumps and eight valves. The LISST-25x is a self-contained, submersible instrument designed for in-situ measurements of the concentration and mean particle-size of suspended sediment (2.5 to 500 μm) and the concentration and mean particle-size of material greater than 62 μm. With the LISST-Infinite, the LISST-25X has been modified with an external pump and a dilution system for out-of-water deployment. Water passes through an optical cell, located in the laser path of the LISST-25x and connected to the external pump and dilution system with tubing (fig. 2).

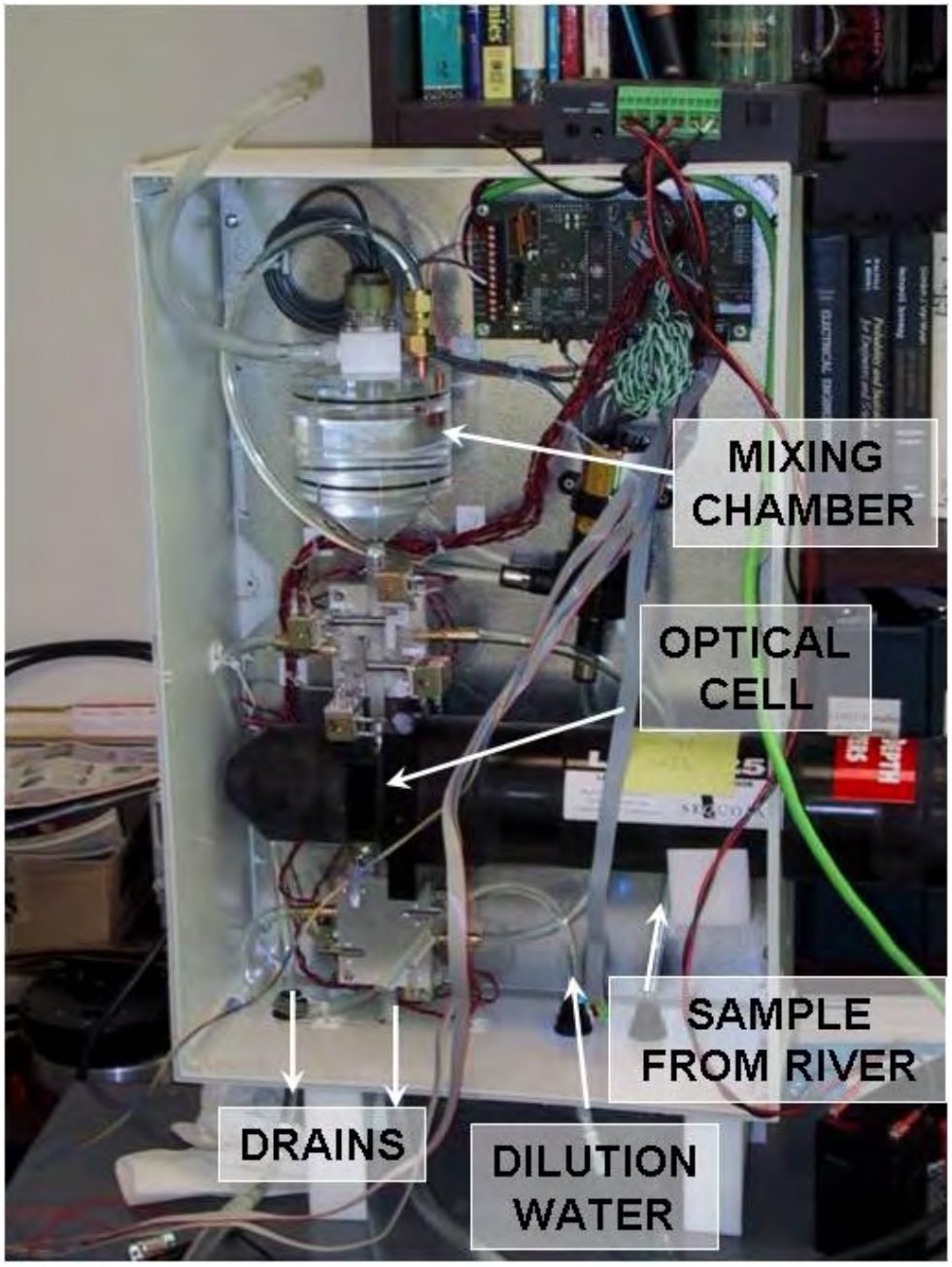


Figure 2 LISST-Infinite. Photo credit: Chuck Pottsmith.

At the beginning of each measurement cycle, filtered water from an external source (e.g., a water tank) drains into a dilution chamber with a volume of about 400 ml. Once the dilution chamber is filled, filtered water flows through the optical cell and the LISST-25x makes a background reading on the clear water. Once the background reading has been obtained, about 2,000 ml of water is pumped from the river through the cell in the LISST, purging any river water remaining in the intake line from the previous measurement cycle. After the intake line is purged, the LISST-25x obtains concentration and particle-size data while river water is circulated through the cell. If the laser transmission is less than 30%, the LISST-25x notifies the controller, which

then initiates a dilution cycle: pumping is stopped and an 8 ml sample is retained in the analyzer while the rest of the river water is drained. The filtered water in the dilution chamber is mixed with the retained sample and the resulting diluted sample is analyzed. The dilution step may be repeated until transmission is greater than 30%. Once the sample has been analyzed, the whole system drains, the dilution chamber is refilled with clean water, and the system is ready to pump the next sample from the river.

In addition to the limits imposed by high concentrations of suspended sediment, biological growth on the transmission or detection components of optical sediment sensors can also degrade their in-situ performance and necessitate frequent cleaning or recalibration of optical instruments. The LISST compensates for biofouling of its optics by using the background reading. Moreover, biofouling of the LISST-Infinite should be limited by light availability because the instrument will be housed in a closed instrument box (fig. 2).

The system is currently being tested in a laboratory setting. Initial tests have been conducted to assess the variability of the analysis of undiluted sediment-water mixtures. The variability of the analysis is critical to the validity of dilution of sub-samples at higher concentrations. For these tests, a churn-splitter was filled with sediment-laden water and churned while the LISST-Infinite pumps and analyzes the mixture. The mixture drained back into the churn-splitter creating a closed loop. The concentration and particle-size of the mixture was analyzed 10 times. Mixtures with concentrations ranging from 49 to 525 mg/L were tested. The median coefficient of variation of concentration was 0.07 (range 0.06 to 0.10). The median coefficient of variation of the mean particle-size was 0.04 (range 0.02 to 0.10). The variation of the results reflects both the heterogeneity of the sediment in the water and potential errors from analyzing sub-samples of the sediment-water mixture. Nonetheless, the variation does not appear to be substantial relative to other potential sources of error such as the effect of point sampling.

The initial test results provide only a limited assessment of the accuracy of sediment concentration and particle-size information provided by the LISST-Infinitie because the LISST reports the concentration and mean particle-size of sediment ranging from 2.5 to 500 microns and 63 to 500 microns, while laboratory analyses provides results in terms of the cumulative concentration of sediment <0.001 mm, < 0.002 mm, < 0.004 mm, < 0.008 mm, ... , < 1.0 mm. The median concentrations reported by the LISST for ¾ of the initial samples were within the expected range of concentrations based on laboratory analysis. For two samples with greater than 1 mg/L of sand, the LISST reported concentrations were 3.1 mg/L compared to 2.9 mg/L for the laboratory analysis and 36 mg/L compared to 38 mg/L. Future testing will evaluate the accuracy of the concentration and particle-size of diluted samples as determined by the LISST-Infinite.

Continuous suspended-sediment data is most difficult to collect at remote sites because of the limited capacity of automatic pump samplers. The LISST-Infinite will be deployed initially in the Elwha River in the Olympic Peninsula, Washington, where the Department of Interior is planning removal of two high dams. A modified version of the system that will provide the concentration of individual size-classes of suspended sediment has been proposed for use in the main channel of the Colorado River and in its major tributaries below Glen Canyon Dam in support of adaptive management of the Colorado River ecosystem. Currently, the only other

alternative would be frequent trips into these remote sites to retrieve water samples and replace sample bottles.

SUMMARY

Continuous, real-time suspended-sediment monitoring is vitally important for managing water resources but remains an elusive goal that will be achieved only with new technologies. Information on suspended sediment, particularly during periods of high sediment concentration, is needed for accurate calculation of sediment loads. The LISST-Infinite, which integrates laser-diffraction technology for sediment analysis with a dilution cycle, has been developed to analyze high concentrations of suspended sediments. It is being tested under both laboratory and field conditions. If successful, this approach could be used to collect continuous information on fluvial sediment transport, even at remote sites without the need for frequent maintenance.

REFERENCES

Anderson, H. W. (1954). "Suspended sediment discharge as related to streamflow, topography, soil, and land use," Eos, 35, pp. 268-281.

Baca, E., Bedient, P B, and Olsen, R. (1982). "Urban impacts of water supply reservoir," Journal of Environmental Engineering, 108, pp. 73-87. 1982.

Brown, G. W. and Kreygier, J. T. (1971). "Clear-cut logging and sediment production in the Oregon Coast Range," Water Resources Research, 7, pp. 1189-1198.

Guy, H. P. and Ferguson, G. E. (1963). "Sediment in small reservoirs due to urbanization," American Society of Civil Engineers Transactions, 128, pp. 982-992.

Koebel, J. W., Jones, B. L., and Arrington, D.A. (1999). "Restoration of the Kissimmee River, Florida: Water quality impacts from canal backfilling," Environmental Monitoring and Assessment, 57, pp. 85-107.

Langland, M. J., Phillips, S. W., Raffensperger, J. P., and Moyer, D. L. (2004). Changes in Streamflow and Water Quality in Selected Nontidal Sites in the Chesapeake Bay Basin, 1985-2003. U.S. Geological Survey Scientific Investigations Report 2004-5259.

Lewis, A. J., and Rasmussen, T. C. (1999). "Determination of suspended sediment concentrations and particle size distributions using pressure measurements," Journal of Environmental Quality, 28, pp.1490-1496.

Lewis, J. (2003). "Turbidity-controlled sampling for suspended sediment load estimation," Erosion and Sediment Transport Measurement in Rivers: Technological and Methodological Advances, IAHS Publication. 283, pp. 13–20.

Leopold, L. B., M. G. Wolman, and J. P. Miller (1964). Fluvial processes in geomorphology, Dover Publications, New York.

Oregon Department of Environmental Quality, Applegate Subbasin Total Maximum Daily Load HUC #17100309, 83 p.

Pennisi, E. (2004). "The Grand (Canyon) Experiment," Science, 306, pp. 1884-1886.

Reichel, G., and Nachtnebel, H. P. (1994). "Suspended sediment monitoring in a fluvial environment: advantages and limitations applying on Acoustic Doppler Current Profiler," Water Research, 28, pp. 751-761.

Schoellhamer, D. H. and S. A. Wright (2003). "Continuous measurement of suspended-sediment discharge in rivers by use of optical backscatterance sensors," Erosion and Sediment

Transport Measurement in Rivers: Technological and Methodological Advances, IAHS Publication 283, pp. 28–36.

Syvitski, J. P. M., Voeroesmarty, C J., Kettner, A. J., and Green, P. (2005). "Impact of Humans on the Flux of Terrestrial Sediment to the Global Coastal Ocean," Science, 308, pp. 376-380.

Tetra Tech, U.S. Environmental Protection Agency, and Tennessee Department of Environment and Conservation (2002). Total maximum daily load (TMDL) for Siltation & Habitat Alteration in the Harpeth River Watershed (HUC 05130204) Cheatham, Davidson, Dickson, Hickman, Rutherford, & Williamson County, Tennessee, 30 p.

Thompson, M. (2005). Beaver-Camas Subbasin Assessment and TMDLs, Idaho Department of Environmental Quality, 153 p.

Thoms, M. C. (1987). "Channel sedimentation within the urbanized River Thame, UK," Regulated Rivers, 1, pp. 229-246.

Thonon, I. and van der Perk, M. (2003). "Measuring suspended sediment characteristics using a LISST-ST in an embanked flood plain of the River Rhine," Erosion and Sediment Transport Measurement in Rivers: Technological and Methodological Advances, IAHS Publication 283, pp. 37–44.

Topping, D. J., Melis, T. S., Rubin, D. M., and Wright, S. A. (2005). "High-resolution monitoring of suspended-sediment concentration and grain size in the Colorado River in Grand Canyon using a laser-acoustic systems," Proceedings of the Ninth International Symposium on River Sedimentation, October 18-21, 2004, Yichang, China, pp. 2507-2514.

Trimble, S. W. (1983). "A sediment budget for Coon Creek basin in the Driftless Area, Wisconsin, 1985-1977," American Journal of Science, 283, pp. 454-474.

Walling, D. E. and Webb, B.W. (eds.) (1996). Erosion and Sediment Yield: Global and Regional Perspectives, IAHS Publication no. 236, 586 pp.

Wang, K. H., Jin, K. R., Tehrani, M. (2003). "Field measurement of flow velocities, suspended solids concentrations, and temperatures in Lake Okeechobee," Journal of the American Water Resources Association, 39, pp. 441-456.

Williams, G. P. and Wolman, M. G. (1984). "Downstream effects of dams on alluvial rivers," U.S. Geological Survey Professional Paper, 1286, 83 p.

Urhich, M. A. and Bragg, H. M. (2003). Monitoring instream turbidity to estimate continuous suspended-sediment loads and yields and clay-water volumes in the upper North Santiam River basin, Oregon, 1998-2000. U. S. Geological Survey Water-Resources Investigations Report 03-4098, 43 p.

U. S. EPA (2005a). "National Section 303(d) List Fact Sheet," http://oaspub.epa.gov/waters/national_rept.contr , accessed on September 15, 2005.

U. S. EPA (2005b). "Sediment Concentration Drastically Reduced in Las Vegas Wash," EPA 841-F-05-004G, http://www.epa.gov/owow/nps/Success319/state/pdf/nv_lvwash.pdf, accessed at on September 4, 2005.

U. S. Geological Survey (2005). "Suspended-Sediment Database Daily Values of Suspended Sediment and Ancillary Data," http://co.water.usgs.gov/sediment/seddatabase.cfm accessed on September 15, 2005

van Wijngaarden, M. and Roberti, J. R. (2002). "In situ measurements of settling velocity and particle size distribution with the LISST-ST," in Winterwerp, J. C. and Kranenburg, C. (eds.), Fine Sediment Dynamics in the Marine Environment, pp. 295-311.

PREDICTION OF THE GRAIN SIZE OF SUSPENDED SEDIMENT; IMPLICATIONS FOR CALCULATING SUSPENDED SEDIMENT CONCENTRATIONS USING SINGLE FREQUENCY ACOUSTIC BACKSCATTER

Roger A. Kuhnle, Research Hydraulic Engineer, National Sedimentation Laboratory, U. S. Department of Agriculture, Agricultural Research Service, Oxford, Mississippi 38655, rkuhnle@msa-oxford.ars.usda.gov; Daniel G. Wren, Research Hydraulic Engineer, National Sedimentation Laboratory, U. S. Department of Agriculture, Agricultural Research Service, Oxford, Mississippi 38655, dwren@msa-oxford.ars.usda.gov; James P. Chambers, Senior Scientist, National Center for Physical Acoustics, University of Mississippi, University, Mississippi 38677, chambers@olemiss.edu.

Abstract: The collection of samples of suspended sediment transported by streams and rivers is difficult and expensive. Emerging technologies, such as acoustic backscatter, have demonstrated the promise to decrease the cost and allow more thorough sampling of sediment in transport in the water column. One critical piece of information required to use single frequency acoustic backscatter to calculate the concentration of sand-sized sediment in the water column, is the vertical distribution of sediment particle size. In this study, techniques to predict the size of suspended sand particles are examined and their use with acoustic backscatter data to predict sediment concentration is explored. Methods to predict the size of sediment in suspension using bed sediment and flow criteria had mean absolute differences of from 7 to 50 percent as compared to measured values. When the sample nearest to the bed of the stream was used as a reference, the mean absolute differences between calculated and measured sizes were reduced to 5 percent. These errors in size determination translate into errors of 12 to 84 percent in the prediction of sediment concentration using backscatter data from 1 MHz single frequency acoustics.

INTRODUCTION

Knowledge of the amount of sediment being transported by streams and rivers is important for several reasons. The sediment transport rate at a given cross-section represents the net erosion rate from upstream sources. Sediment transported downstream can fill reservoirs, reduce channel capacities, and impair aquatic habitats. Sediment has been identified by the U. S. Environmental Agency as the largest single pollutant of the nation's waterways (1996 National Water Quality Inventory Section 305(b) Report to Congress). Detrimental effects to fish (Newcombe and MacDonald, 1991; Newcombe and Jensen, 1996) and aquatic invertebrates (Kuhnle et al., 2001) have been directly related to increases in the magnitude and duration of suspended sediment concentrations.

Yet, collection of suspended sediment transport data using standard techniques (Edwards and Glysson, 1999) requires a large financial investment for personnel to collect and analyze samples, and may put personnel in danger collecting samples during thunderstorms and floods (Kuhnle et al., 2000). Furthermore, collection of suspended sediment samples in the bottom 20 percent of the flow, where most of the bed derived suspended sediment is transported, is very difficult or impossible on streams and rivers with dunes or other bed forms on the bed. Conventional samplers collect a physical sample of the sediment and water mixture, which

requires each sample to be labeled, transported, and analyzed for sediment concentration and other sediment characteristics in a laboratory (Edwards and Glysson, 1999). The transport of sediment by streams and rivers is inherently variable in time and space and it is often difficult to collect a sufficient number of samples to define representative transport rates for the expected range of flows of a stream or river (Wren et al., 2005).

Recently efforts have been intensified to develop surrogate techniques to replace the conventional sampling techniques which collect a physical sample of the sediment and water mixture (Wren et al., 2000; Gray, 2005). Technologies that have been identified as being useful for measuring suspended sediment transport include: acoustic backscatter, digital-image analysis, laser diffraction, optical velocity, and pressure difference (Kuhnle and Wren, 2005). One technology that has been recognized as having promise for the automatic collection of suspended sediment concentration data is single frequency acoustic backscattering (Kuhnle and Wren, 2005). Commercially available instruments designed to measure velocity profiles in rivers have been successfully used to collect acoustic backscatter data that is proportional to the concentration of suspended sediment (Gartner and Cheng, 2001; Topping et al., 2004). Perhaps the most important limitation to calculating suspended sediment concentration using acoustic backscatter is the need for an independent measure of the sediment size with depth above the boundary (Wren et al., 2000; Gartner and Cheng, 2001; Kuhnle and Wren, 2005). This problem has been approached by using several frequencies of acoustic backscatter simultaneously to arrive at solutions of sediment size and concentration (Hay and Sheng, 1992; Crawford and Hay, 1993; Thorne et al., 1994). However, the range of grain sizes and concentrations commonly found in alluvial rivers continues to complicate solving for sediment size and concentration using only acoustic backscatter (Smith, 2004). This study will explore the available techniques to predict the size of sediment in suspension with application to calculating suspended sediment concentration using backscatter data from single frequency acoustics. The accuracy of employing this technique will be compared to physical samples of suspended sediment collected in a laboratory flume channel and from samples collected on two rivers.

METHODS TO PREDICT SUSPENDED SAND SIZES

If the flow is assumed to be steady and the average sediment concentration is constant at any level, the net vertical flow of sediment will be zero. In other words, the upward movement of sediment will be balanced by the settling of sediment through the water column. The rate of settling through a horizontal area may therefore be equated with the upward sediment movement due to diffusion:

$$Cw + \varepsilon_s \frac{dC}{dy} = 0 \tag{1}$$

where C is the concentration of sediment at a level y above the bed, ε_s is the sediment diffusion coefficient, and w is the fall velocity of the sediment. The sediment diffusion coefficient is generally assumed to be related to the coefficient of fluid momentum ε_m by:

$$\varepsilon_s = \beta\psi\varepsilon_m \tag{2}$$

where β is the difference in the diffusion of sediment and fluid, and ψ represents the damping of the turbulence by the sediment particles (Van Rijn, 1984). For the concentrations considered in this study $\psi = 1$ was assumed. The distribution of β was taken to be constant with distance above the bed but to vary with flow strength and grain size (Van Rijn, 1984):

$$\beta = 1 + 2\left[\frac{w}{U_*}\right]^2, \quad \text{for} \quad 0.1 < \frac{w}{U_*} < 1 \tag{3}$$

where $U_* = \sqrt{\frac{\tau_0}{\rho}}$, τ_0, and ρ are the bed shear stress and density of the water, respectively.

For low sediment concentrations for each i^{th} size group (C_i), and assuming a parabolic-constant distribution of ε_s (Coleman, 1970) the integration and separation of variables of (1) yields:

$$\frac{C_i}{C_{ai}} = \left(\frac{(a)}{(y)}\frac{(h-y)}{(h-a)}\right)^Z \quad \text{for} \quad \frac{y}{h} < 0.5 \tag{4a}$$

$$\frac{C_i}{C_{ai}} = \left(\frac{a}{h-a}\right)^Z e^{[-4Z(y/h-0.5)]}, \quad \text{for} \quad \frac{y}{h} \geq 0.5 \tag{4b}$$

(Van Rijn, 1984), where h is the depth of the flow, C_{ai} is the concentration of sediment of the i^{th} size group at the reference level a above the bed, and

$$z = \frac{w_i}{\beta \kappa U_*} \tag{5}$$

where w_i is the fall velocity of the i^{th} size sediment, and κ is the von Karman constant. Equation (4a) has been termed the Rouse equation (Rouse, 1937) and has been shown to fit the form of the variation of suspended sediment concentration with depth for a variety of data sets from field and laboratory situations (Vanoni, 1975, p. 80). The prediction of the relative concentration of suspended sediment requires a reference sample near the bed and the values of w_i, β, and κ. The value of κ for this study was assumed to be 0.4, fall velocities were calculated using the relation of Dietrich (1982), and β was calculated using equation (3).

The mean grain size at each distance above the reference elevation was calculated as:

$$\phi_m = \frac{\sum C_i \phi_i}{\sum C} \tag{6}$$

where ϕ_i and ϕ_m are the grain size expressed as the negative log of base 2 of the i^{th} size group and the mean grain size at a depth of y, respectively, and the mean grain size in mm for a given depth (D_m) is

$$D_m = 2^{-\phi_m} \tag{7}$$

Grain sizes in this study were predicted using the Rouse equation, with β defined by eq. 3 (Van Rijn, 1984), because of the close correspondence between suspended sediment grain size measured in laboratory flume experiments and predicted values. The experiments were conducted in a flume at the National Sedimentation Laboratory, which had an adjustable slope channel 30 m in length, 1.2 m in width and 0.6 m in height. The bed material sediment had a median size of 0.52 mm, $(D_{84}/D_{16})^{1/2}$ = 1.54, and a standard deviation of 0.67 ϕ. Dune bed forms with three dimensional plan forms were present on the bed in both the phase I (depth= 0.13 m) and phase II (depth =0.33 m) experiments (Table 1).

Table 1 Experimental conditions in laboratory flume experiments.

	Flow discharge (m^3/s)	Flow depth (m)	Water surface slope	Mean flow velocity (m/s)	Froude number	U_* (m/s)
Phase I	0.3403	0.3280	0.00304	0.851	0.47	0.0798
Phase II	0.08157	0.1273	0.00301	0.526	0.47	0.0558

Suspended sediment samples and bed elevation data were collected 23.5 m downstream of the inlet tank using "L" shaped samplers with inside diameters of 4.4 mm (11/64 in) and outside diameters of 6.4 mm (1/4 in). All samples were collected isokinetically (sampler intake velocity = mean channel flow velocity) to avoid bias in the sampling of the suspended sediment. Errors in the concentration of suspended sediment, assuming suspended sediment was 0.15 mm in diameter and the intake velocity of the samplers was within ±20% of the local flow velocity, would be expected to be within ± 5 % based on the testing reported in Report no. 5 (1941). Samples were collected at 2-minute intervals, for either 20 or 40 seconds over 2-hr periods at five different heights above the mean bed elevation. A continuous record of the bed height was collected at the same sites with a 1 MHz acoustic device at 30 Hz.

The suspended sediment samples were composited based on height above the bed for each of the two flow conditions. This yielded sufficient material to determine the size distribution of the sediment at the five heights using sieve analysis. The sample nearest the bed was used as a reference with eqs. 4, 5, and 6 to calculate the size of sediment in suspension. The correspondence between the mean measured (D_{mm}) and mean calculated (D_{mc}) grain sizes for the two experimental conditions was quantified by calculating the mean absolute percent difference:

$$M_{pd} = 100 * \frac{\sum\left(\frac{|D_{mc} - D_{mm}|}{D_{mm}}\right)}{N} \tag{8}$$

where N is the number of measurements of suspended grain size above the bed. Values of M_{pd} for the phase I and phase II experiments were 6.0 and 2.5 %, respectively. On this basis, the Rouse equation (eq. 4), with β from eq. 3 (Van Rijn, 1984), was chosen to calculate the sizes of suspended sediment using reference values.

Entrainment Relations: In many instances it is difficult or impossible to collect a sample of the suspended sediment near the channel bed for use as a reference sample with eq. 4. This is especially true when the bed material has been shaped into large three-dimensional dunes by the flow. To fill the need for reference data, entrainment relations have been developed by a number of researchers to calculate the near bed reference concentration of suspended sediment using information on the flow strength, bed material grain size distribution, and the fall velocity of the grains. Seven entrainment relations were evaluated by Garcia and Parker (1991). Of these relations the best predictors were those proposed by Smith and McLean (1977), and Van Rijn (1984). Based on the determinations of Garcia and Parker (1991), the relations of Garcia and Parker (1991), Smith and McLean (1977), and Van Rijn (1984) were evaluated for their ability to predict the size of suspended sediment. Of the three entrainment relations chosen, the only one explicitly developed to consider individual sizes is the relation of Garcia and Parker (1991). The relations of Smith and McLean (1977) and Van Rijn (1984) were modified to apply to each grain size individually and scaled by the fraction of each grain size class in the bed material.

FIELD DATA

Studies in which information on the size of suspended sediment originating from widely-graded bed material at several distances above the bed were sought for this study. The data collected on the Niobrara River (Colby and Hembree, 1955) and the Rio Grande River (Nordin and Dempster, 1963) have information on bed material, flow conditions, sediment concentrations and grain size distributions for multiple elevations for the same flow condition. Data used in this study were restricted to those which consisted of at least four samples of suspended sediment concentration and size distribution at different elevations above the bed for a given flow condition. To remove the effects of hindered settling, data with high concentrations of sediment less than 62 microns in diameter were not used in this study. The data that met the above criteria consisted of 19 verticals with 76 total samples from the Niobrara River (Colby and Hembree, 1955), and 17 verticals with 73 individual samples from the Rio Grande River (Nordin and Dempster, 1963). The sizes of the sediment in suspension ranged from 0.11 – 0.18 mm for the Niobrara, and 0.11 – 0.17 mm and 0.10 – 0.14 mm for the Bernalillo and Socorro reaches of the Rio Grande, respectively. The characteristics of the flows present during the collection of the suspended sediment data used are summarized in Table 2.

Table 2 Summary of conditions for field data.

River	Bed material D_{50} (mm)	Flow depth (m)	Mean flow velocity (m/s)	Water surface slope (x 10^{-3})	U_* (m/s)
Niobrara	0.28	0.46-1.10	0.84-1.34	1.3-1.9	0.077-0.11
Rio Grande Bernalillo reach Socorro reach	0.18, 0.31	0.43-0.78 0.20-0.47	0.58-0.95 0.72-0.88	0.83-0.86 0.76-0.98	0.061-0.080 0.044-0.065

Comparisons Between Calculated and Measured Sizes: The type of comparison desired is between instantaneous measurements and calculated values. This would correspond most closely to the type of information needed to calculate the sediment concentration from a given number of acoustic backscatter readings. The field data from the Niobrara and Rio Grande Rivers were collected sequentially over periods of several minutes for 4 or 5 points in the vertical. The scale of the processes in these channels indicates that changes in the local transport system were likely minor during that period of time.

The mean difference (eq. 8) between the calculated and measured mean grain sizes for each measured point for the Niobrara and Rio Grande Rivers were compared to sizes calculated using the Garcia and Parker (1991), Smith and McLean (1977), and Van Rijn (1984) entrainment relations combined with the modified Rouse equation (eq. 4). Comparisons were also made between calculated and measured sizes using the suspended sediment sample closest to the bed as the reference value for equation 4.

The mean differences for the three entrainment relations and Rouse equation yielded percent differences of 10.3, 17.5, and 37.0 for the Smith and McLean (1977), Garcia and Parker (1991), and Van Rijn (1984) relations respectively (Table 3). The percent differences for the Rio Grande data followed the same relative order (Table 4). In all cases using the sample collected closest to the bed yielded a better result for sediment size prediction than the three entrainment relations (Tables 3 and 4).

Table 3 Niobrara River grain size data (Colby and Hembree, 1955). Comparison between calculated and measured suspended sediment grain sizes.

Method of obtaining reference information for modified Rouse equation.	Mean absolute difference (mm)	Mean absolute percent difference
Garcia and Parker (1991)	0.026	17.52
Smith and McLean (1977)	0.014	10.28
Van Rijn (1984)	0.052	37.03
Reference sample (w/o ref. comparisons)	0.007 (0.010)	5.04 (6.70)

POTENTIAL ERRORS IN CONCENTRATION WITH ACOUSTICS

The potential errors that would result from calculating the concentration of the suspended sediment using acoustic backscatter data with incorrect sediment size information were analyzed. The concentration of suspended sediment from acoustic backscatter data may be calculated using Cheng and Hay's (1993) approach:

$$C = \frac{V_0 \rho}{B^2 f_\infty^2 x} \tag{9}$$

where V_0 is the voltage generated from acoustic backscattering, ρ is the particle density, B is the frequency dependent system constant, $x = kr$, where k is the wave number, r is the radius of the sediment particles, and f_∞ is the form factor which is a function of x.

Table 4 Rio Grande grain size data (Nordin and Dempster, 1963). Comparison between calculated and measured suspended grain sizes.

Method of obtaining reference information for modified Rouse equation.	Mean absolute difference (mm)	Mean absolute percent difference
Garcia and Parker (1991)	Bernalillo reach Socorro reach	0.018 0.017	14.18 14.68
Smith and McLean (1977)	Bernalillo reach Socorro reach	0.010 0.008	7.62 6.61
Van Rijn (1984)	Bernalillo reach Socorro reach	0.066 0.028	51.30 24.11
Reference sample	Bernalillo reach (w/o ref samples) Socorro reach	0.007 (0.009) 0.004 (0.005)	5.88 (7.56) 3.49 (4.60)

In Figure 1 the expected error in acoustically measured suspended sediment concentration caused by using an incorrect sediment particle size is depicted. These plots were prepared using data collected in a jet tank at the National Center for Physical Acoustics, University of Mississippi. The tank recirculated the water and sediment mixture and discharged a steady concentration of particles and sediment from a downwards oriented vertical jet (Smith, 2004). The data from the measurement volume of the jet consisted of backscatter amplitudes, sediment concentrations, and sediment particle sizes. The system constant (B) in equation 9 was solved for with the other variables being either known or measured. The two variables that depend on the sediment size in eq. 9 are f_∞ and x. In a channel with suspended sediment in transport, the sediment sizes at a level above the bed must be measured or estimated. Error in the concentration is introduced when incorrect particle sizes are used. Each line in Figure 1 results from assuming the particles in the insonified volume were of a given size. The x-axis represents the correct particle size with each line representing the assumed particle size. This results in an error of zero when the correct particle size is used. Achieving an error of zero percent was only possible because the system constant was calculated from the data used in the size estimate. The system constant is a weak function of sediment particle size and a mean value must be used in practice. The sensitivity of the calculation of sediment concentration using the acoustic backscatter technique is observed to be asymmetrical with the direction, negative or positive, of the error in sediment particle size

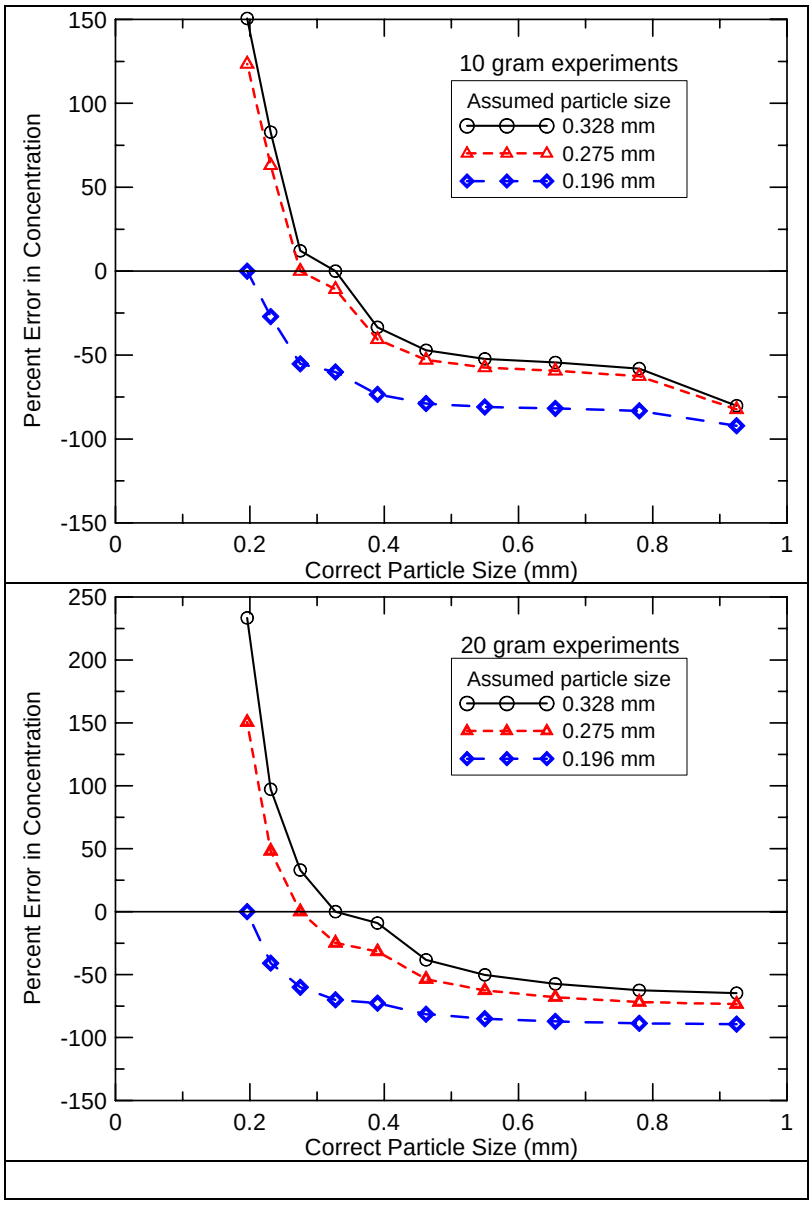


Figure 1 Errors in concentration due to incorrect grain size calculated using acoustic backscattering data from jet tank.

(Fig. 1). Therefore, mean errors between calculated and measured suspended sediment grain sizes were calculated separately for the negative and positive differences:

$$M_{di} = \frac{\sum (D_{mc} - D_{mm})}{N} \tag{10}$$

where the subscript i is either n for negative differences or p for the positive differences.Expected errors were calculated for the data from the Niobrara and Rio Grande Rivers using the error determinations from the laboratory jet experiments. If we assume that the actual size of the sediment in suspension is 0.196 mm, and that the errors by using the next

smaller grain size (0.165 mm) are 100%, the errors in concentration calculated using acoustic backscattering along with the calculated suspended sediment sizes from the four different methods of estimating sediment size may be calculated. The weighted mean errors for suspended sediment concentration calculated using acoustics for the Niobrara data ranged from 20 to 84% using grain sizes calculated with the three entrainment functions and reference sample coupled with the Rouse equation. Preliminary error determinations for the Rio Grande data ranged from 12 to 55%. The lowest errors were obtained using the reference sample with the Niobrara and Rio Grande data. More precise error determinations will be made following the completion of further jet tank experiments with finer sediment sizes.

It is notable that the greatest errors in predicted suspension concentration do not necessarily correspond to the greatest differences between calculated and measured values. This result occurs because of the asymmetrical nature of the error curves around zero (Fig. 1), which illustrate the greater magnitude of errors for particle sizes which are less than rather than greater than the actual sediment size. The suspended sediment size determinations have been shown as a potential source of significant errors in the determination of suspended sediment concentration and the method chosen to estimate the grain size needs to be checked with physical samples to establish its accuracy.

CONCLUSIONS

Methods to predict the size of widely graded bed material sediment in suspension transported by streams and rivers have been explored using laboratory and field data. The percent difference between grain sizes calculated using entrainment functions and a modified form of the Rouse equation yielded mean differences of 37, 18, 10 and 5% for the Niobrara River data for the Van Rijn (1984), Garcia and Parker (1991), Smith and McLean (1977), and reference sample methods respectively. For the Rio Grande River data mean differences were 51, 14, 8, and 6% for the Bernalillo reach and 24, 15, 7, and 3% for the Socorro reach, for the Van Rijn (1984), Garcia and Parker (1991), Smith and McLean (1977), and reference sample methods respectively. The size predictions of the four methods were coupled with acoustic backscatter data collected in a test tank with a vertical jet to arrive at sediment concentration. These concentrations had preliminary errors ranging from 12 to 84% with the most accurate predictions of concentration from the reference sample and the Smith and McLean (1977) methods.

REFERENCES

Cheng, H. and Hay, A. E. (1993). "Broadband measurements of the acoustic backscatter cross section of sand particles in suspension," Journal of the Acoustical Society of America. 94(4), pp 2247-2254.

Colby, B. R., Hembree, C. H., (1955). Computations of total sediment discharge Niobrara River near Cody, Nebraska. U. S. Geological Survey Water-Supply Paper 1357, 187 p.

Coleman, N. L., (1970). "Flume studies of the sediment transfer coefficient," Water Resources Research 6(3), pp 801-809.

Crawford, A. M. and Hay, Alex E., (1993). "Determining suspended sand size and concentration from multifrequency acoustic backscatter," Journal of the Acoustical Society of America. 94(6), pp 3312-3324.

Dietrich, W.E., (1982). "Settling velocity of natural particles," Water Resources Research, 18(6), pp.1615-1626.

Edwards , T. K., and Glysson, G. D. (1999). Field Methods for Measurement of Fluvial Sediment: U. S. Geological Survey Techniques of Water Resources Investigations, book 3, chapter 2, 89 p.

Garcia, M., Parker, G., (1991). "Entrainment of bed sediment into suspension," Journal of Hydraulic Engineering 1177(4), pp 414-435.

Gartner, J. W., Cheng, R. T., (2001). "The promises and pitfalls of estimating total suspended solids based on backscatter intensity from acoustic Doppler current profiler," Proceedings Seventh Federal Interagency Sedimentation Conference (III), p. 119-126.

Gray, J. R., ed. (2005). Proceedings of the Federal Interagency Sediment Monitoring Instrument and Analysis Research Workshop, September 9-11, 2003, Flagstaff, AZ, U.S. Geological Survey Circular 1276, 46 p.

Hay, A.E. and Sheng, J. (1992). "Vertical profiles of suspended sand concentration and size from multifrequency acoustic backscatter," Journal of Geophysical Research. 97(C10): pp 15661-15677.

Kuhnle, R. A., Bennett, S. J., Alonso, C. V., Bingner, R. L., and Langendoen, E., (2000). "Sediment transport processes in agricultural watersheds," International Journal of Sediment Research, 15(2): pp 182-197.

Kuhnle, R. A., Simon, A., Knight, S. S., (2001). "Developing linkages between sediment load and biological impairment for clean sediment TMDLs," Wetlands Engineering and River Restoration Conference, ASCE, Reno, Nevada.

Kuhnle, R. A., Wren, D. G., (2005). "Breakout Session I, suspended sediment measurement: data needs, uncertainty, and new technologies," In: Gray, J. R., ed., Proceedings of the Federal Interagency Sediment Monitoring Instrument and Analysis Research Workshop, September 9-11, 2003, Flagstaff, AZ, U.S. Geological Survey Circular 1276, p. 8-15.

Newcombe, C. P., Jensen, J. O. T., (1996). "Channel suspended sediment and fisheries: a synthesis for quantitative assessment of risk and impact," North American Journal of Fisheries and Management, 16(4), pp 693-727.

Newcombe, C. P., MacDonald, D. D., (1991). "Effects of suspended sediments on aquatic ecosystems," North American Journal of Fisheries and Management, 11, pp 72-82.

Nordin, C. R., Jr., Dempster, G. R., (1963). Vertical distribution of velocity and suspended sediment Middle Rio Grande, New Mexico. U. S. Geological Survey Professional Paper 462-B, 20 p.

Report No. 5, (1941). Laboratory Investigation of Suspended Sediment Samplers. Report No. 5, St. Paul U. S. Engineer District Sub-Office Hydraulic Laboratory, University of Iowa, Iowa City, Iowa, 97 p.

Rouse, H., (1937). "Modern conceptions of the mechanics of fluid turbulence," Transactions ASCE, 102, paper no. 1965, p. pp 463-543.

Smith, C. (2004). "Estimation of Particle Sizes for a Range of Narrow Size Distributions of Natural Sands Suspended in Water Using Multi-Frequency Acoustic Backscatter," Unpublished M. S. Thesis. National Center for Physical Acoustics, University of Mississippi.

Smith, J. D., McLean, S. R., (1977). "Spatially averaged flow over a wavy bed," Journal of Geophysical Research 82(12) pp 1735-1746.

Thorne, P. D., Hardcastle, P. J., Flatt, D. and Humphery, J. D. (1994). "On the use of acoustics for measuring shallow water suspended sediment processes," IEEE Journal of Oceanic Engineering. 19(1) pp 48-57.

Topping, D, J., Melis, T. S., Rubin, D. M., Wright, S. A., (2004). "High-resolution monitoring of suspended-sediment concentration and grain size in the Colorado River in Grand Canyon using a laser-acoustic system," Proceedings of the Ninth International Symposium on River Sedimentation, October 18-21, 2004, Yichang, China, pp 2507-2514.

Vanoni, V. A., ed. (1975). Sedimentation Engineering. Manual and Report on Engineering Practice – no. 54. American Society of Civil Engineers, Reston, Virginia, 745 p.

Van Rijn, L. C., (1984). "Sediment transport, part II: suspended load transport," Journal of Hydraulic Engineering 110(11): 1613-1641.

Wren, D. G., Barkdoll, B. D., Kuhnle, R. A., Derrow, R. W. II, (2000). "Field techniques for suspended sediment measurement," Journal of Hydraulic Engineering, 126(2), pp 97-103.

Wren, D. G., Bennett, S. J., Barkdoll, B. D., Kuhnle, R. A., (2005). "Variability in suspended-sediment concentration over mobile sand beds," Journal of Hydraulic Engineering 131(8), pp 733-736.

USING ACOUSTIC BACKSCATTER TECHNOLOGY TO MEASURE SUSPENDED SEDIMENT CONCENTRATIONS IN IDAHO STREAMS

Jon E. Hortness, P.E., Hydraulic Engineer, U.S. Geological Survey, Boise, Idaho, jehortne@usgs.gov

Abstract: The U.S. Geological Survey's Idaho Water Science Center is attempting to use the acoustic backscatter values from acoustic Doppler velocity meters to predict suspended sediment concentrations at four locations in Idaho. Lack of high suspended sediment concentrations at these locations over the past few years has somewhat limited the analyses. However, initial results based on the existing data are quite encouraging. Average absolute differences between the measured and predicted SSC values ranged from 7.1 to 32.2 percent.

INTRODUCTION

The standard techniques currently used to collect fluvial sediment data in the Nation's streams tend to be manually intensive, time consuming, and therefore quite costly. In addition, some of the data-collection techniques pose certain safety risks. As a result, the amount of daily-value sediment data being collected, primarily by the U.S. Geological Survey (USGS), has declined by more than two-thirds over the past two decades (Gray, 2005).

The need to safely and cost-effectively collect fluvial sediment data has led to the advancement of so-called sediment surrogate technologies. Among these techniques is the use of the acoustic backscatter strength from acoustic Doppler velocity meters. The strength of the acoustic backscatter signal increases as more particles are available in the water to reflect the acoustic pulse. Based on this fact, acoustic backscatter strength values can be related to suspended sediment concentrations on a site-by-site basis.

The USGS Idaho Water Science Center is attempting to use this surrogate technology to provide continuous suspended sediment data at locations in four streams across the State: Kootenai River, Coeur d'Alene River, St. Joe River, and Boise River. The channel and suspended sediment characteristics of these sites differ significantly; therefore, this work may also provide some insight as to what types of sites may be most amenable to this type of surrogate technology.

ACOUSTIC TECHNOLOGY

The primary purpose of an acoustic Doppler velocity meter (ADVM) is to measure the velocity of water by applying the Doppler principle. The ADVM emits an ultrasonic pulse from a transducer into the water, and the pulse bounces off small particles of sediment and other materials that are present. After the pulse is sent, the ADVM listens for the return echo from the particles in the water and calculates the resulting Doppler shift to determine the water velocity. Each ADVM computes an index of the strength of the pulse that is returned to the instrument. In theory this index value, called the acoustic backscatter strength (ABS), can be related to the concentration of particles (primarily suspended sediment) in the area sampled by the ADVM.

METHODS

Suspended sediment concentrations (SSC) were determined over a range of discharges using standard techniques, spanning several months at each of the four sites. Relations between the SSC and ABS values were determined using ordinary least squares regression techniques. Other variables such as water temperature and discharge were also included in the analyses and were found to help improve the relations in some instances.

Two different types of ADVMs, the Nortek EasyQ (Nortek USA, 2005) and the Sontek Argonaut-SL (Sontek/YSI, Inc., 2005) are deployed at the study sites. The configurations of the ADVMs vary based on site conditions and whether or not they are being used to estimate discharge using index velocity methods. The ADVMs being used for discharge were set up for optimal velocity sampling, and those settings were not altered for the sediment surrogate work.

ANALYSES

Relations between SSC and ABS values were determined at four sites in the Kootenai, Coeur d'Alene, St. Joe, and Boise rivers in Idaho. Upstream drainage areas for these sites range from about 1,500 mi^2 to 12,700 mi^2. The channel and suspended sediment characteristics vary by site. Two of the sites are located on regulated streams where dams trap sediments. The other two sites are located on unregulated streams with significantly more sources of sediment.

Kootenai River: This site is located at the USGS streamflow gaging station 12310100, Kootenai River at Tribal Hatchery near Bonners Ferry, Idaho. The upstream drainage area for this gaging station is approximately 12,700 mi^2, of which a significant portion is located in Canada. Most of the drainage area is mountainous, with much of the precipitation resulting from winter snowfall. As a result, most of the streamflow other than baseflow is a direct result of snowmelt runoff. Streamflow at this site is regulated by Libby Dam, located about 70 mi upstream near Libby, Montana; the annual mean discharge is approximately 15,000 ft^3/s. Because discharges are regulated at this site, mean cross-sectional water velocities are fairly stable and typically range from about 1.0 to 2.5 ft/s.

The portion of the Kootenai River below Libby Dam is essentially "sediment starved". A majority of the SSC values immediately downstream of Libby Dam ranged from 2 to 10 mg/l between 1972 and 2002 (Barton, 2004). Sediment is introduced to the system from several major tributaries between Libby Dam and Bonners Ferry. However, SSC values near Bonners Ferry are still relatively low, ranging from 1 to 100 mg/l or less in most instances. Based on limited data, the particle-size distributions seem to vary, as may be expected, by discharge and resulting water velocities. Silts and clays account for about 75 percent or more of the suspended sediments at low discharges (less than about 10,000 ft^3/s), while they only account for about 50 percent of the suspended sediments at high discharges (greater than about 25,000 ft^3/s).

For this project, suspended sediment samples were collected eight times at this site during the spring and summer of 2005. Samples were collected using the equal-width-increment (EWI) method. Analysis of the initial sample data and acoustic backscatter data from acoustic Doppler

current profiler (ADCP) discharge measurements indicate that the suspended sediments at this site are well mixed.

A 1.5 MHz Argonaut-SL (Sontek/YSI, Inc., 2005) ADVM is deployed at this location, primarily for the purpose of determining river discharges using index-velocity methods. Each of the two beams is configured to sample a volume of water from 0.5 to 15.0 meters horizontally outward from the ADVM. Velocity data, and thus ABS data, are recorded at 15-minute intervals. The ADVM continuously sends acoustic pulses into the water for one 5-minute period during each 15-minute interval. The ABS values from each beam measured during that 5-minute period are averaged to obtain the final ABS value for that beam. The values for the two beams are then averaged to obtain the final ABS for the site.

Multiple linear regression analyses were used to determine the best-fit relation between SSC and various parameters at this site. The final averaged ABS value (ABS_{avg}), the instantaneous temperature in degrees Centigrade (T), and the instantaneous discharge were all considered as possible variables for the final equation. Log transformations of all of the variables were used in the analyses. Based on the multiple linear regressions, an equation that includes ABS and temperature provides the best estimation results for SSC. Following a transformation back to linear units, the equation is as follows:

$$SSC = 4.0 \times 10^{-14} T^{-1.003} ABS_{avg}{}^{7.403}. \quad (1)$$

Based on the data used to develop the equation, a plot of predicted versus measured SSC values was derived (figure 1). The average absolute difference between the predicted and measured SSC values is 7.1 percent. The differences range from -19.3 to +14.8 percent.

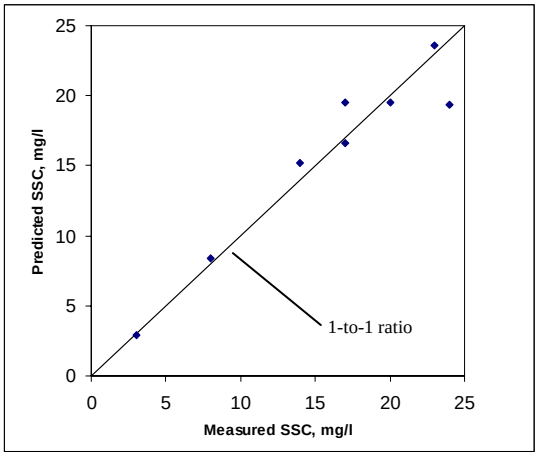


Figure 1 Measured versus predicted suspended sediment concentrations for the Kootenai River at Tribal Hatchery near Bonners Ferry, Idaho (12310100).

Coeur d'Alene River: This site is located at the USGS streamflow gaging station 12413860, Coeur d'Alene River near Harrison, Idaho. The upstream drainage area for this gaging station is about 1,475 mi^2. The gaging station is located at the mouth of the Coeur d'Alene River where it

flows into Coeur d'Alene Lake. Because of the proximity to the lake, backwater conditions are prevalent at this location. Most of the drainage area is mountainous, with much of the precipitation resulting from winter snowfall. As a result, most of the streamflow other than baseflow is a direct result of snowmelt runoff. Streamflows at this site are unregulated and generally unaffected by outside factors other than a few minor diversions for irrigation or mining uses. The annual mean discharge is approximately 2,500 ft^3/s. Mean cross-sectional water velocities at this site range from as little as about 0.02 ft/s during low discharges and high lake levels to as much as 3.0 ft/s or more during annual runoff events.

SSC values at this site typically range between 1 and 100 mg/l. Extreme runoff events have produced SSC values approaching 400 mg/l. Particle-size distributions from nearly 200 recent and historic samples vary significantly, ranging from less than 20 to more than 90 percent silts and clays. Based on these data, the particle-size distributions seem to vary, as may be expected, with discharge and resulting water velocities.

For this project, suspended sediment samples were collected 12 times at this site beginning in October of 2003. Samples were collected using the EWI method. Analysis of previous sample data and acoustic backscatter data from ADCP discharge measurements indicate that the suspended sediments at this site are well mixed.

A 2.0 MHz EasyQ (Nortek USA, 2005) ADVM is deployed at this location, primarily for the purpose of determining river discharges using index-velocity methods. Each of the two beams is configured to sample in three separate 1.5 meter "cells" extending from 0.8 meters to 5.3 meters horizontally outward from the ADVM. Velocity data, and thus ABS data, are recorded at 15-minute intervals. The ADVM continuously sends acoustic pulses into the water for one 10-minute period during each 15-minute interval. The ABS values for each cell in each beam are averaged over that 10-minute period to obtain the ABS values for each of the six cells. This configuration results in 6 separate ABS values for each 15-minute period.

Multiple linear regression analyses were used to determine the best-fit relation between SSC and various parameters at this site. The final averaged ABS values for each cell, the instantaneous temperature, and the instantaneous discharge were all considered as possible variables for the final equation. Log transformations of all of the variables were used in the analyses. Based on the multiple linear regressions, an equation that includes temperature in degrees Centigrade (T) and ABS values from cell 2, beam 2 (C2B2) and cell 3, beam 2 (C3B2) provides the best estimation results for SSC. Following a transformation back to original units, the equation is as follows:

$$SSC = 14.26T^{-0.730}C2B2^{-18.944}C3B2^{20.460} \quad (2)$$

Based on the data used to develop the equation, a plot of predicted versus measured SSC values was derived (figure 2). The average absolute difference between the predicted and measured SSC values is 32.2 percent. The differences range from -56.1 to +92.1 percent.

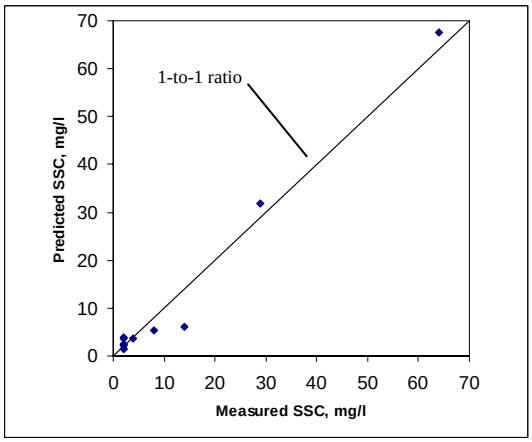


Figure 2 Measured versus predicted suspended sediment concentrations for the Coeur d'Alene River near Harrison, Idaho (12413860).

St. Joe River: This site is located at the USGS streamflow gaging station 12415140, St. Joe River near Chatcolet, Idaho. The upstream drainage area for this gaging station is about 1,720 mi^2. The gaging station is located at the mouth of the St. Joe River where it flows into Coeur d'Alene Lake. Because of the proximity to the lake, backwater conditions are prevalent at this location. Most of the drainage area is mountainous, with much of the precipitation resulting from winter snowfall. As a result, most of the streamflow other than baseflow is a direct result of snowmelt runoff. Streamflows at this site are unregulated and generally unaffected by outside factors other than a few minor diversions for irrigation. The annual mean discharge is about 2,700 ft^3/s. Mean cross-sectional water velocities at this site range from as little as about 0.05 ft/s during low discharges and high lake levels to as much as 2.5 ft/s or more during annual runoff events.

No historic SSC data are available for this site. Recent SSC values ranged between 2 and 18 mg/l. Particle-size distribution data are also extremely limited. Recent data (5 samples) indicate that silts and clays make up between 75 and 95 percent of the suspended sediments.

For this project, suspended sediment samples were collected 11 times at this site beginning in December of 2003. Samples were collected using the EWI method. General analysis of acoustic backscatter data from ADCP discharge measurements indicate that the suspended sediments at this site are well mixed.

A 2.0 MHz EasyQ (Nortek USA, 2005) ADVM is deployed at this location, primarily for the purpose of determining river discharges using index-velocity methods. Each of the two beams is configured to sample in three separate 1.5 meter "cells" extending from 0.5 meters to 5.0 meters horizontally outward from the ADVM. Velocity data, and thus ABS data, are recorded at 15-minute intervals. The ADVM continuously sends acoustic pulses into the water for one 10-minute period during each 15-minute interval. The ABS values for each cell in each beam are averaged over that 10-minute period to obtain the ABS values for each of the six cells. This configuration results in 6 separate ABS values for each 15-minute period.

Multiple linear regression analyses were used to determine the best-fit relation between SSC and various parameters at this site. The final averaged ABS values for each cell, the instantaneous temperature, and the instantaneous discharge were all considered as possible variables for the final equation. Log transformations of all of the variables were used in the analyses. Based on the multiple linear regressions, an equation that includes ABS values from cell 1, beam 2 (C1B2) and cell 3, beam 1 (C3B1) provides the best estimation results for SSC. Following a transformation back to original units, the equation is as follows:

$$SSC = 3.15 \times 10^{-20} C1B2^{19.540} C3B1^{-7.887} \quad (3)$$

Based on the data used to develop the equation, a plot of predicted versus measured SSC values was derived (figure 3). The average absolute difference between the predicted and measured SSC values is 24.6 percent. The differences range from -31.3 to +50.1.

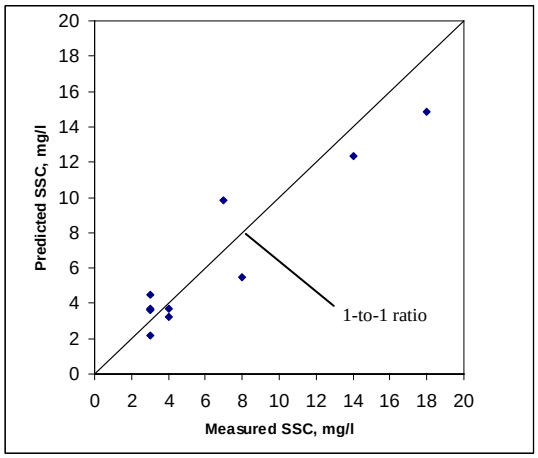


Figure 3 Measured versus predicted suspended sediment concentrations for the St. Joe River near Chatcolet, Idaho (12415140).

Boise River: This site is located at the USGS streamflow gaging station 13213000, Boise River near Parma, Idaho. The upstream drainage area for this gaging station is approximately 3,970 mi^2. Streamflow is regulated by Lucky Peak Dam located about 60 mi upstream. The upper portion of the basin (about 2,500 mi^2) is mountainous, with much of the precipitation resulting from winter snowfall. The lower portion of the basin lies in a broad, alluvium-filled area with several terraces. Most of the streamflow other than baseflow is a direct result of snowmelt runoff. The annual mean discharge is approximately 1,650 ft^3/s. Mean cross-sectional water velocities at this site typically range from about 1.5 to 2.5 ft/s.

The main channel of the Boise River below Lucky Peak Dam is essentially “sediment starved”. A majority of the SSC values about 5 mi downstream of Luck Peak Dam ranged from 2 to 5 mg/l between 1989 and 2002 (Hardy and others, 2005). Significant amounts of additional sediment are introduced to the system primarily from the several irrigation return drains located between Lucky Peak Dam and Parma. SSC values near Parma are significantly higher, ranging from about 5 to 250 mg/l between 1989 and 2002 (Hardy and others, 2005). Particle-size distributions (based on about 100 recent and historic samples) vary significantly, ranging from less than 10 to

more than 90 percent silts and clays. There is no significant relation between the particle-size distributions and discharges or stream velocities.

For this project, suspended sediment samples were collected 11 times at this site beginning in May of 2005. Samples were collected using the EWI method. Analysis of sample data indicate that the suspended sediments at this site are well mixed.

A 2.0 MHz EasyQ (Nortek USA, 2005) ADVM is deployed at this location. Each of the two beams is configured to sample in three separate 1.0 meter "cells" extending from 0.5 meters to 3.5 meters horizontally outward from the ADVM. Velocity data, and thus ABS data, are recorded at 15-minute intervals. The ADVM continuously sends acoustic pulses into the water for one 2-minute period during each 15-minute interval. The ABS values for each cell in each beam are averaged over that 10-minute period to obtain the ABS values for each of the six cells. This configuration results in 6 separate ABS values for each 15-minute period.

Multiple linear regression analyses were used to determine the best-fit relation between SSC and various parameters at this site. The final averaged ABS values for each cell, the instantaneous temperature, and the instantaneous discharge were all considered as possible variables for the final equation. Log transformations of all of the variables were used in the analyses. Based on the multiple linear regressions, an equation that includes temperature in degrees Centigrade (T) and the ABS values from cell 1, beam 1 (C1B1) provides the best estimation results for SSC. Following a transformation back to original units, the equation is as follows:

$$SSC = 5.78 \times 10^{13} T^{-3.422} C1B1^{-4.482} \quad (4)$$

Based on the data used to develop the equation, a plot of predicted versus measured SSC values was derived (figure 4). The average absolute difference between the predicted and measured SSC values is 24.5 percent. The differences range from -40.2 to +51.4 percent. The largest measured SSC value had one of the largest percent differences. Additional data collection and analyses are needed to determine if there are problems with predicting larger SSC values at this location.

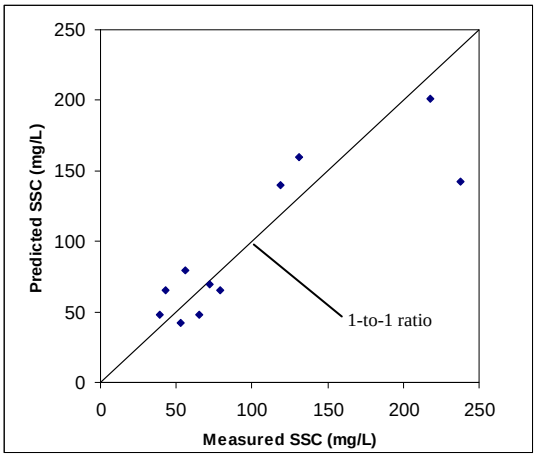


Figure 4 Measured versus predicted suspended sediment concentrations for the Boise River near Parma, Idaho (13213000).

CONCLUSIONS

Attempts to relate SSC to ABS values from ADVMs at four locations in Idaho have yielded initial results that are quite encouraging. Based on limited data (8 to 12 sample pairs per location), various combinations of ABS data or combinations of ABS and temperature data predicted SSC reasonably well. Average absolute differences between the measured and predicted SSC values ranged from 7.1 to 32.2 percent. Lack of SSC data at higher concentrations has limited the analyses. Additional data collection and analyses are needed to verify these initial results and to determine the applicability of the current relations at higher concentrations.

Because of the limited data, it is difficult at this time to determine whether site characteristics significantly influence the quality of the ABS vs. SSC relations. The relation for the Kootenai River site resulted in the smallest percent differences between measured and predicted values. More sand-sized particles seem to be transported in suspension at this site. However, this result was based on only 8 suspended sediment samples and 5 particle-size analyses.

The cost of sediment monitoring could be reduced if these relations are improved with additional data and if the error of prediction is acceptable. Sediment sampling may be only needed for quality control or extreme events that are outside the modeled measurements. In addition, this approach may be eventually acceptable for the prediction of chemical constituents whose concentration compares well with suspended sediment concentration.

REFERENCES

Barton, G.J., 2004. Characterization of Channel Substrate, and Changes in Suspended-Sediment Transport and Channel Geometry in White Sturgeon Spawning Habitat in the Kootenai River near Bonners Ferry, Idaho, Following the Closure of Libby Dam. U.S. Geological Survey Water-Resources Investigations Report 03-4324, pp 7-16.

Gray, J.R., ed., 2005. Proceedings of the Federal Interagency Sediment Monitoring Instrument and Analysis Research Workshop, September 9-11, 2003, Flagstaff, Arizona, U.S. Geological Survey Circular 1276, pp 1-15.

Hardy, M.A., Parliman, D.J., O'Dell, Ivalou, 2005. Status of and Changes in Water Quality Monitored for the Idaho Statewide Surface-Water-Quality Network, 1989 – 2002. U.S. Geological Survey Scientific Investigations Report 2005-5033, pp 1-67.

Nortek USA, 2005. EasyQ, River Velocity and Stage Monitor, accessed September 2005 at URL http://www.nortekusa.com/hardware/EasyQ.html

Sontek/YSI, Inc., 2005. Argonaut-SL Overview, accessed September 2005 at URL http://www.sontek.com/product/asl/aslov.htm

A COMPARISON OF TWO FIELD STUDIES OF ACOUSTIC BED VELOCITY: GRAIN SIZE AND INSTRUMENT FREQUENCY EFFECTS

David Gaeuman, Research Associate, USGS, Columbia Environmental Research Center, Columbia, MO, dgaeuman@usgs.gov ; Colin D. Rennie, Assistant Professor of Civil Engineering, University of Ottawa, Ottawa, ON, Canada.

INTRODUCTION

Recent studies (Rennie et al., 2002; Rennie and Villard, 2004) suggest that it may be possible to measure bedload transport rates using measurements obtained with an acoustic Doppler current profiler (ADCP) or similar instrument. The method is based on the ADCP's bottom-tracking capacity, by which relative motion between the ADCP and sediment particles on the stream bed is normally used to detect instrument motion when making water discharge measurements. Rennie et al. (2002) hypothesized that the difference between the apparent instrument trajectory according to bottom-tracking and the actual instrument trajectory is representative of the average velocity of sediment particles on the stream bed. They designated this corrected bottom-track measurement as the bed velocity (ν), and proposed that it can be used to estimate bedload transport rates via an empirical calibration.

Significant obstacles must be overcome before calibrated ADCP bed-velocity measurements can be generally applied for monitoring bedload sediment transport. Perhaps the most obvious difficulty is that physical bedload transport samples can be difficult to obtain under some field conditions, and are themselves often of uncertain accuracy. Thus, precise and reliable transport data with which to calibrate may be unavailable. Secondly, the acoustic response of a given instrument depends to some degree on site characteristics, including the sizes of sediment particles in transport. Bed material sizes can be spatially variable at multiple scales, from within-reach variability associated with element of channel morphology (Lisle et al., 2000) to transitions from gravel to sand at the segment scale (Sambrook Smith and Ferguson, 1995). Bed-material particle size distributions, and hence the sizes of bedload particles in transport, can vary systematically in time at a single location (Rubin and Topping, 2001). The sensitivity of ν to relatively subtle changes in sediment characteristics typical of sand-bed rivers has not been investigated. Consequently, the extent to which a calibration of ν obtained at a given site or at a given time can be transferred to similar sites or other times is unknown.

In this paper, we compare bed-velocity responses to bedload transport and flow changes measured with a 1500-kHz Doppler instrument in a sand-bed reach of the Fraser River (Rennie and Villard, 2004) to similar data collected with a 600-kHz instrument in the lower Missouri River. The Missouri River data was collected as part of a project conducted by the USGS Columbia Environmental Research Center (CERC). Our present objective is to explore the adequacy of existing theory for describing differences in bed-velocity responses arising from differences in instrument frequency and reach characteristics. A fundamental understanding of these effects is necessary for assessing the spatial and temporal stability of bed-velocity calibrations, and for the potential development of appropriate corrections to account for varying reach conditions.

CHARACTERISTICS OF THE STUDY REACHES

All Missouri River data were collected in the navigation channel between 1 and 3 km upstream from the US Interstate 70 bridge in central Missouri. The Missouri River study reach is henceforward referred to as MR. This part of the river contains wing dikes that maintain a deep, narrow navigation channel about 200 m wide between the dike tips. Thalweg depths range between about 7-10 m when the river is near flood stage. The reach-averaged water surface slope is consistently about 0.00016 irrespective of stage, and thalweg depth-averaged flow velocities frequently exceed 2.5 m/s. Bed material is primarily sand, with a median particle size (D_{50}) of about 0.0006 m in diameter and a 90th percentile particle size (D_{90}) of 0.0022 m. Most of the bed is covered with dunes that are 1-2 m high and between 10 and 60 m in wavelength. The 2-year annual peak discharge is 5,747 m^3/s (USACOE, 2003).

Sea Reach (designated SR below) is a sand-bed estuarine distributary of the Fraser River about 300 m wide and less than 5 m deep at low tide when the bed is mobile. Depth-averaged flow velocities are normally less than 1 m/s. D_{50} was found to be about 0.00025 m for all sample locations. A D_{90} of 0.002 m was recorded for 40 of the 68 samples, whereas 0.00035 m was recorded for the remaining 28 samples. The mean annual peak flow of the Fraser River at

the Hope gage (155 km upstream) is 8,800 m^3/s (Rennie and Villard, 2004). However, the study reach occupies a distributary arm in which discharge in not accurately known. The reach is tidal in nature, so that stages and water surface slopes lack consistent relationships to discharge. No evidence of salt wedge intrusion or flow reversal was observed during the sampling period.

METHODS

Field Methods: Both data sets compared in this paper consist of hydraulic and bed-velocity measurements recorded with commercially-available acoustic Doppler instruments while simultaneously collecting bedload sediment samples and global positioning system (GPS) data . Rennie and Villard (2004) recorded acoustic data in 2001 with a narrowband Sontek 1500-kHz acoustic Doppler profiler (ADP). Actual instrument velocities were tracked using differential GPS. MR data was obtained in 2004 and 2005 using a broadband RD Instruments 600-kHz Workhorse Rio Grande ADCP and real-time kinematic (RTK) GPS. Aside from the differences inherent in the use of instruments manufactured by different companies, the acoustic data collection procedures were similar. More complete discussions of bottom-tracking, bed velocity, and sources of errors in these measurements are available in Rennie et al. (2002), Rennie and Villard (2004), and Gaeuman and Jacobson (2005).

Bedload sampling was conducted from boats using similar Helley-Smith samplers in both studies. Helley-Smith samplers are pressure-difference samplers with a nozzle expansion ratio of 3.22 and a sampling efficiency of about 100-150% (Edwards and Glysson, 1999). CERC personnel collected 80 Helley-Smith bedload samples from MR during the 2004 field season, and Rennie and Villard (2004) collected 68 samples at their Fraser River site. All sampled transport rates are reported herein as bedload capture rates (c_B), defined as the mass of sediment caught in the sampler divided by the sampler residence time on the bed in seconds. Especially at MR, where flow is both deep and turbid, the position of the sampler on the bed with respect to bed topography could not be determined. High spatial variability in the bedload transport rate associated with bedform position (Gomez and Troutman, 1997) undoubtedly contributed to variability in the sampling results. Although sampler position on the bed was known only approximately, spatial averaging inherent in the acoustic measurements ensured that the concurrently-recorded acoustic data encompassed the sampler position. This spatial averaging is the result both of slight boat motions during the sampling period and because ADCP measurements are based on multiple acoustic beams directed radially outward from the instrument. Rennie et al. (2002) and Gaeuman and Jacobson (2005) describe the footprint characteristics of the respective instruments.

Flow conditions at the time of MR data collection were highly variable. Data were collected on a total of 28 different days at discharges ranging from about 1,110 to about 5,380 m^3/s. However, only selected subsets of these data are reported in this paper. Paired ν and Helley-Smith bedload samples were obtained in 2004 only. Although MR bedload samples were collected in 2005 as well, they were obtained using a BL-84 bedload sampler, and so are not directly comparable to the SR samples. A second subset of data was selected for comparing acoustic response characteristics, independent of the availability of Helley-Smith bedload samples. Depth-averaged flow velocities and ν were generally much larger at MR than at SR. The maximum sampled values of these variables at MR were 2.38 m/s and 0.62 m/s, whereas the corresponding maxima recorded at SR were just 1.06 m/s and 0.18 m/s. In order to compare data collected over a similar range of ν, only the 111 MR samples for which $\nu \leq 0.2$ m/s are included in the following comparisons of bed-velocity response to hydraulic conditions. The complete set of MR data indicates that the nature of the bed-velocity response may change at high transport stages; those data are reported elsewhere (Gaeuman and Jacobson, submitted). All Fraser River samples were collected on 4 consecutive days during the June, 2001 freshet (flood). Discharge through the reach was not measured.

Data Processing Method: Bed-velocity magnitudes for each sample location were computed as the square-root of the sum of squared east-west and north-south bed-velocity components. Each directional velocity component was obtained by averaging the results of a large number of acoustic pings collected over several minutes at each location. Time-averaged ADCP data were also used to determine depth-averaged downstream flow velocities (U) and flow depths (h) at all sampling locations. These measurements were then used to estimate additional hydraulic parameters, including the shear velocity (u_*) and shear stresses. To compare shear parameters from the two study locations, it is necessary to select a method for estimating them that will produce reasonable results at both sites. A simple means for estimating u_* is to apply the standard expression, $(ghS)^{0.5}$, where S is slope of the energy grade line, which is typically approximated by the slope of the water surface. This method can be conveniently applied at MR, since repeat surveys indicated that the reach-averaged water surface slope was essentially constant over a wide

range of discharges. However, SR is tidal, so that the energy slope changes constantly in response to sea level change. Together with generally low water surface slopes, the dynamic nature of the energy slope made it impractical to estimate the energy slope from the water surface slope. Thus, equations that require S to estimate shear stress or channel roughness cannot be directly applied to SR data. Rennie and Villard (2004) chose to estimate u_* with:

$$\frac{U}{u_*} = 2.5 \ln\left(12h \Big/ 3D_{90}\right) \tag{1}$$

A drawback of this approach is that the results are sensitive to the value chosen for the bed roughness height, which Rennie and Villard (2004) assumed to be equal to $3D_{90}$, This implies that the shape of the vertical velocity gradient is influenced primarily by grain resistance. This assumption may be appropriate for SR, where bedform development was minimal, but not for MR, where large bedforms were observed. Shear velocities used for the present analyses were therefore computed using an alternative method that can be applied to either site with equal validity. First, mean slopes were computed for both reaches using the Lacey formula, as presented by Raudkivi (1998):

$$U = 10.8 h^{\frac{2}{3}} S^{\frac{1}{3}} \tag{2}$$

in which U and h were replaced with their mean values for each reach, and the numeric constant was changed to 7.6 so that Equation (2) would yield the mean velocity measured at MR using the known mean slope of 0.00016. This adjustment is justified because the original Lacey analyses incorporate assumptions regarding the scaling of the channel geometry based on measurements of artificial canals in British India (Lacey, 1930). The mean depth for all MR acoustic samples included in this analysis was 7.0 m (σ, standard deviation, = 1.63 m), and the mean U was 1.51 m/s (σ = 0.30 m/s). Inserting the mean values for h (3.7 m, σ = 0.46 m) and U (0.69 m/s, σ = 0.17 m/s) at SR in Equation (2) using the coefficient calibrated with the MR data (7.6) produced an estimated mean slope for SR of 0.00005. Mean values for U, h, and S were then inserted into the definition of the Chezy roughness coefficient to yield a mean roughness coefficient for each study site:

$$\overline{C} = \overline{U} \Big/ (\overline{h}\,\overline{S})^{0.5} \tag{3}$$

where bars over the variables indicate mean values. For SR, the mean value of C was estimated to be 48.9. This value of C was used to compute u_* for each sample according to:

$$u_* = Ug^{0.5} \Big/ C \tag{4}$$

Repeating the application of Equations (3) and (4) to the MR data yielded an average Chezy coefficient of 45.2, and an average value of u_* that is nearly identical to the average value estimated from $(ghS)^{0.5}$ (0.1045 vs. 0.1041). Pronounced changes in bedform development noted at different discharges at MR strongly suggest that C is highly variable there, so that values of u_* computed as $(ghS)^{0.5}$ are probably more reliable for that site. Nonetheless, for consistency across sites, we use u_* based on constant C for the analyses presented below. Total boundary shears stresses (τ) for both sites were obtained from u_* using $\tau = \rho u_*^2$, and dimensionless shear stresses (τ^*) were calculated according to $\tau^* = \tau/g(\rho_s - \rho)D_{50}$, where ρ is the density of water and ρ_s is the density of the sediment particles. Some of the total boundary shear stress is expended in form drag associated with bedforms and turbulence in the water column, so only a portion of τ^* is available for entraining sediments at the bed. We estimated dimensionless shear stress at the bed, or skin friction, with the relation of Wright and Parker (2004).

$$\tau_{sk}^* = 0.05 + 0.7(\tau^* F^{0.7})^{0.8} \tag{5}$$

It is worth noting that a general model for accurately predicting skin friction has yet to be developed (McLean et al., 1999). Models that are reasonably successful for predicting skin friction in laboratory settings may be inadequate for evaluating the conditions found in large sand-bed rivers (Wright and Parker, 2004). Equation (5) was developed specifically for application in these types of environments.

CONCEPTUAL FRAMEWORK

It is assumed that the magnitude of the bed velocity can be related to the velocity of sediment particles in the bedload layer (u_b) by an equation of the form:

$$\nu = B u_b \tag{6}$$

where B is an unspecified function ranging between 0 and 1. Little can be said regarding the form of B, except that it is related to both particle entrainment and the strengths of acoustic backscatter from the entrained particles, i.e., $B = f(\tau_{sk}^*, k_s)$, where k_s is the normalized backscattering cross section (Thorne and Hanes, 2002):

$$k_s = \frac{f}{\sqrt{0.5 D \rho_s}} \tag{7a}$$

$$f = C_0 \left(\frac{1.1(0.5Dk)^2}{1 + 1.1(0.5Dk)^2} \right) \tag{7b}$$

$$C_0 = 1.1\left\{1 - 0.25\exp\left[-((0.5Dk - 1.4)/0.5)^2\right]\right\} \times \left\{1 + 0.37\exp\left[-((0.5Dk - 2.8)/2.2)^2\right]\right\} \tag{7c}$$

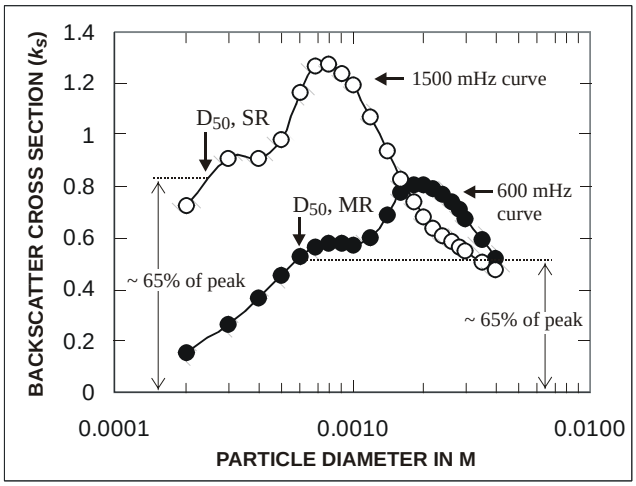


Figure 1 Normalized backscatter cross section as a function of particle diameter. Values of k_s for the median particle size are about 65% of the peak value at both sites.

In Equations (7a), (7b), and (7c), D is the diameter of the entrained particles and k is the acoustic wave number, defined as $k = 2\pi f_i/c$, where f_i is the frequency of the instrument and c is the speed of sound in water. k_s is thus primarily a function of the size of the sediment particles in motion and the acoustic frequency of the instrument being used. Figure 1 compares values of k_s as a function of particle diameter for instrument frequencies of 600 and 1500 kHz. The strength of a backscattered 1500-kHz signal from individual particles reaches a peak for particles less than 1 mm in diameter, whereas the backscatter strength for a 600-kHz signal reaches maximum values for particles larger than about 1.5 mm in diameter. The strength of the total backscatter signal from a population of discrete particles within a sampled volume of water is proportional to the product of k_s and the square root of the mass concentration of the particles (Thorne and Hanes, 2002). In the case of bed-velocity measurements, the relevant backscattering particles are presumed to be moving within the bedload layer or as concentrated suspended sediments moving immediately above the saltating bedload. However, it is also possible for ν to incorporate backscatter from suspended particle moving 10's of cm above the bed. The significance of this circumstance, which is commonly referred to as water bias (RD Instruments, 1996), will be considered later.

The expected behavior of Equation (6) is summarized as follows. If τ_{sk}^* is near the threshold for particle entraiment (τ_c^*), the concentration of particles in motion will be low, their total acoustic backscatter strength will be small relative to the backscatter reflected from the immobile bed surface, and ν will be << u_b. If τ_{sk}^* is increased to a

value many times larger than τ_c*, the concentration of moving particles will increase, their total acoustic backscatter strength will increase, and ν will increase. As the cross sectional density of the moving particles approaches 100%, ν will presumably approach u_b. Additionally, for a given bedload layer concentration, larger particles will generate stronger acoustic backscatter and larger values of ν.

HYDRAULIC COMPARISONS

Both MR and the SR data show an approximately linear relationship between U and ν for U greater than a threshold (Figure 2A). The threshold occurs at U ~ 1 m/s for the MR data and U ~ 0.5 m/s for SR. Similar relations emerge when ν is plotted versus τ_{sk}* (Figure 2B). The threshold for τ_{sk}* at which ν goes to zero is also approximately twice as large for the MR data (~ 0.2) as for SR (~ 0.1). The differences in the y-intercepts of the trend lines in both relations are consistent with the conceptual framework described in the previous section, but each of the two relations requires a slightly different explanation.

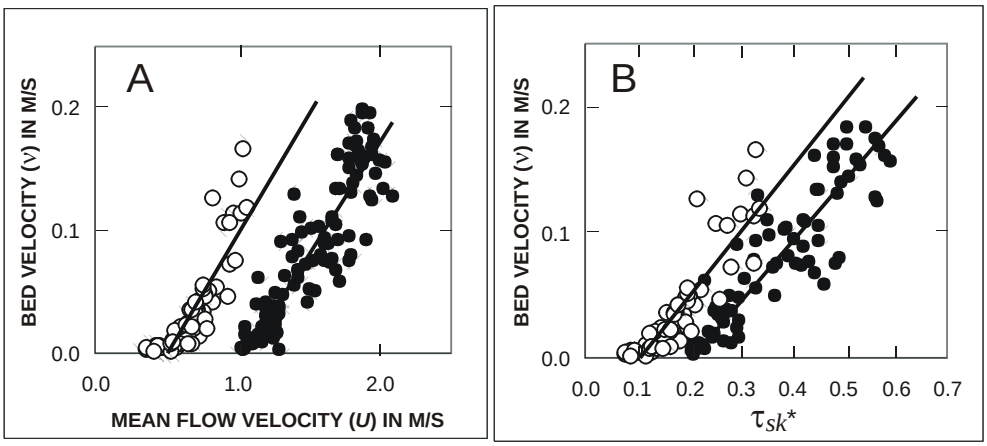


Figure 2 Graphs of A) bed velocity versus depth-average flow velocity and B) bed velocity versus dimensionless skin friction. MR data is shown in black; SR data is shown in white.

For the relation involving U (Figure 2A), the difference in the intercepts is best explained in terms of the difference in bed-material particle sizes in the two study areas. The D_{50} at SR is slightly less than half the D_{50} at MR. As a result, τ_c* at SR is about half that of the Missouri site. As can be seen by numerical experiments with Equations (4) and (5) or careful inspection of their form, τ_{sk}* scales approximately linearly with U. A decrease in grain size of 50% therefore translates directly into a corresponding 50% decrease in the threshold U at which ν becomes non-zero. In this case, instrument frequency is a secondary consideration. All that is required is that k_s is sufficiently large for the particle sizes considered and the instrument frequency to generate a measurable signal. It is unclear whether the 600-kHz ADCP would have begun to detect bed motion at SR when U reached 0.5 m/s. If it did, the relative backscatter strength per particle would have been weaker, so that the slope of the line would have presumably been flatter. The virtual equivalent of the slopes shown in Figure 2 are likely coincidental, and may reflect the fortuitous fact that the ratios of k_s for the D_{50} present at each site to the maximum k_s for the instrument frequency are similar for both sites (Figure 1).

The difference in the intercepts for the relation involving τ_{sk}* (Figure 2B) cannot be explained by a change in τ_c* because particles size effects are explicitly included in τ_{sk}*. As a preliminary explanation, it is worth pointing out that the acoustic response may be primarily keyed to a grain-size percentile other than the D_{50}. Indeed, Figure 1 indicates that for either site the maximum acoustic sensitivity occurs for grain sizes considerably larger than the D_{50}, so that somewhat larger grains exert a disproportionably large effect on the measured ν. In addition, incipient motion of the relevant particle size is unlikely to produce a measurable ν. It seems more reasonable to assume that particle motion must be relatively widespread and persistent, although the required degree of mobilization cannot presently be quantified. In any case, both of these considerations imply that the value of τ_{sk}* corresponding to the appearance of non-zero ν (denoted here as τ_ν*) is somewhat larger than τ_c*. There is, however, no reason to expect

τ_v* to vary as a function of bed-material particle size. Instead, the difference in τ_v* depicted in Figure 2B is related to the instrument frequency alone. The value of τ_v* is approximately twice as large as τ_v* for SR. When averaged over the relevant range of particle sizes (0.00025-0.0022 m) the ratio of k_s for the 600-kHz instrument to k_s for the 1500-kHz instrument is almost exactly 0.5. Thus, the particles sizes that must be entrained to produce an equivalent acoustic response are twice as large for the 600-kHz instrument; this translates directly to the observed doubling of τ_v*. In other words, τ_v* appears to be directly proportional to k_s.

These interpretations suggest a possible approach to adjusting ADCP bed-velocity data to account for differences in bed-material particle sizes and instrument frequencies. As a first step, it is useful to recast ν in the dimensionless form, ν/u_b. As u_b is generally unknown, we substitute U for u_b, i.e., ν/U is assumed to be roughly proportional to ν/u_b for flow conditions in which τ_{sk}* is significantly greater than τ_c*. The linear relationships shown in Figure 2A suggest that this is a reasonable approximation. The only noticeable departure from linearity in the figure is associated with a small cluster of points indicating locations at SR where ν exceeded 0.1 m/s. All these points correspond to locations where an atypical D_{90} of just 0.00035 was reported for the bed-material. The second step in adjusting the data involves normalizing τ_{sk}* to reflect differences in the signal strengths provided by the two instruments. As noted above, the backscatter signal strength at 1500 kHz is twice a great as at 600 kHz for the same transmit power. A direct comparison between the results from the two instrument can be obtained by comparing values of $K_s(\tau_{sk}*)$, where K_s is the average k_s for the particular instrument over the relevant range of particles sizes. When plotted against ν/U, this adjustment successfully merges the two data sets (Figure 3).

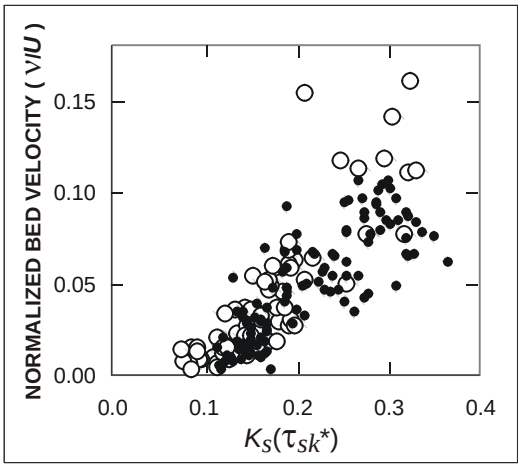


Figure 3 Normalized ν versus normalized τ_{sk}*. MR data is shown in black; SR data is shown in white.

BEDLOAD TRANSPORT COMPARISON

Bedload transport rates for all samples obtained at MR were at least an order of magnitude larger than transport rates sampled at SR for given values of ν (Figure 4). This difference overwhelms any possible discrepancies associated with differences in sampler efficiency or other sources of uncertainty. Instead, a large portion of the difference can probably be attributed to differences in the bed-material particle sizes at the two sites. This result suggests that empirical correlations between ν and bedload transport rates may be exceedingly sensitive to subtle changes in the size distribution of the bed-material. As previously noted, the 1500-kHz instrument is approximately twice as sensitive to particles of a given size as the 600-kHz instrument within the range of sizes present at these study sites. For a bed composed of a uniform particle size, it seems reasonable to assume that switching from a 600-kHz instrument to a 1500-kHz instrument would generate an approximate doubling of the ν associated with a given actual sediment transport rate. However, changes in grain size appear to have the potential to exert a much greater effect on the ν-transport relation.

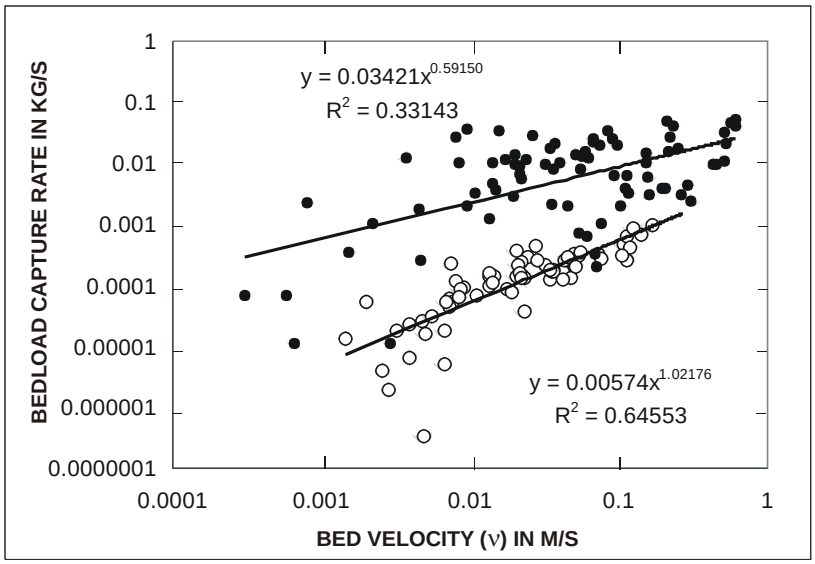


Figure 4 Bedload capture rates versus ν for MR samples (black) and SR samples (white). MR samples are between about 12-20 times larger for the same ν, as estimated from the best-fit power functions for $\nu \geq 0.1$.

Consider a uniformly-graded bed characterized by an arbitrary grain diameter of 0.0005 m and flow conditions given by a dimensionless skin friction based on the bed-material size ($\tau_{sk0.0005}$*) and U. If instrument frequency is held constant at 600 kHz and the grain size is doubled to 0.001 m, k_s would increase by approximately 25%. At the same time, assume that a constant dimensionless transport rate is maintained by increasing the skin friction to $2\tau_{sk0.0005}^* = \tau_{sk0.001}^*$. Because $\tau_{sk0.001}$* has an identical relation to the new stream bed as $\tau_{sk0.0005}$* had to the former bed, the resulting entrainment response should be invariant. There is no reason to suppose that any more or fewer particles would be entrained at any moment in the second situation than in the first. Nonetheless, the particles in transport would be larger by a linear factor of 2, which corresponds to an 8-fold increase in the transported volume. As the acoustic backscatter strength scales with the product of k_s and the square root of particle concentration, simultaneous doubling of the particle and flow scales would therefore produce a 3.5-fold increase in the backscatter strength ($1.25 \times 8^{0.5} = 3.53$). Assuming that ν is approximately proportional to backscatter strength, ν would increase by the same factor. However, the associated increase in the bedload transport rate would equal the concentration increase, i.e., a factor of 8.

We note here that the increase in τ_{sk} invoked in this thought experiment would be associated with increases in U and u_b, which would result in additional increases in both ν and the bedload transport rate. However, these changes would affect ν and the sediment transport rate in a similar manner, and so have no net effect on their ratio. The net result of the particle size doubling is therefore estimated to be an increase in the sediment transport rate associated with the same ν by a factor of about 2.25 (i.e., 8/3.5). Together with the instrument frequency effects incorporated into comparisons between the MR and SR data, bedload transport rates associated with a given ν should be expected to be about 4.5 times greater for the MR data. This accounts for about a third of the difference depicted in Figure 4. Although the remaining difference could plausibly be attributed to bedload sampling error, the possibility of additional acoustic effects cannot be ruled out. A fairly obvious candidate for an acoustic effect that might amplify the magnitude of ν for a given transport rate would be a greater sensitivity to water bias on the part of the 1500-kHz instrument. As is clear from the values of k_s plotted in Figure 1, a 1500-kHz instrument should be considerably more sensitive to the finer particles likely to be suspended high in the water column than is a 600-kHz instrument. The successful collapse of the data shown in Figure 3 was achieved with a simple scaling according to k_s that makes no assumptions regarding where in the water column the backscattering particles are located. This suggests that the cause of the unexplained difference in the relation between ν and c_B lies elsewhere. However, this analysis was limited to consideration of sand-sized particles only, and water bias effects may very well be dominated by the acoustic responses to particles in the silt range where k_s for a 600-kHz signal rapidly converges toward zero. We leave this question unresolved for the time being.

CONCLUSIONS

The relationship between ADCP bed-velocity measurements and the rate of bedload sediment transport is highly sensitive to changes in the sediment grain size distribution. Because bed-material grain sizes can be variable in both space and time, empirical calibrations for estimating bedload transport rates from ν cannot be assumed to be stationary, even when confined to a single measurement site. Equations describing backscatter strength as a function of particle size indicate that a two-fold increase in the diameter of sand-size particles will increase the ratio of the bedload transport rate to ν by a factor of about 2.25. Comparisons between ν measurements and bedload samples obtained at sites in the Missouri and Fraser Rivers suggest the actual effect of particle size changes on ν response may be even larger. The threshold dimensionless skin friction below which ν is zero is approximate twice as large at the Missouri River site than at Sea Reach on the Fraser River. Theoretical considerations suggest that this difference is due to the differences in the operating frequencies of the instruments used at the two sites. However, a similar difference in the threshold mean flow velocities required for non-zero ν is probably related to differences in bed-material particle sizes between the sites. The data from the two sites can be collapsed to a single relation using normalized versions of τ_{sk} and ν, in which shear stress is scaled by a frequency- and grain-size-dependent backscattering cross section parameter and ν is expressed as a fraction of the depth-averaged flow velocity. ADCP bed velocities are derived from a mixture of acoustic backscatter from the moving bedload layer and specular reflections from the immobile bed. The success of the data collapse presented here suggests that this complex acoustic information can nonetheless be interpreted in terms of relatively simple acoustic theory.

REFERENCES

Edwards, T.E., and Glysson, G.D. (1999), Field Methods for Measurement of Fluvial Sediment, U.S. Geological Survey Techniques of Water Resources Investigations 3-C2.

Gaeuman, D., and Jacobson, R.B. (submitted). "Acoustic bed velocity and bedload dynamics in a large sand-bed river," Journal of Geophysical Research, doi:101029/2005JF000411.

Gaeuman, D., and Jacobson, R.B. (2005). Aquatic habitat mapping with an acoustic Doppler current profiler: Considerations for data quality, U.S. Geological Survey Open File Report 2005-1163.

Gomez, B., and Troutman, B.M. (1997). "Evaluation of process errors in bed load sampling using a dune model," Water Resources Research 33(10), pp. 2387-2398.

Lacey, G. 1930. "Stable channels in alluvium," Proceedings of the Institution of Civil Engineers, London, 229, pp. 259-285.

Lisle, T.E., Nelson, J.M., Pitlick, J., Madej, M.A., and Barkett, B.L. (2000). "Variability of bed mobility in natural, gravel-bed channels and adjustments to sediment load at local and reach scales," Water Resources Research 36(12), pp. 3743-3755.

McLean, S.R., Wolfe, S.R., and Nelson, J.M. (1999). "Predicting boundary shear stress and sediment transport over bed forms," Journal of Hydraulic Engineering, ASCE, 125(7), pp. 725-736.

Raudkivi, A.J. (1998). Loose Boundary Hydraulics, A.A. Balkema, Rotterdam.

Rennie, C.D., Millar, R.G., and Church, M.A. (2002). "Measurement of bed load velocity using an acoustic Doppler current profiler," Journal of Hydraulic Engineering, ASCE, 128(5), pp. 473-483.

Rennie, C.D., and Villard, P.V. (2004). "Site specificity of bedload measurement using an acoustic Doppler current profiler," Journal of Geophysical Research 109, F03003, doi:10.1029/2003jf000106.

RD Instruments, Inc. (1996). Principles of Operation: A Practical Primer, 2nd Edition for Broadband ADCPs, RD Instruments, Inc., San Diego, CA.

Rubin, D.M., and Topping, D.J. (2001). "Quantifying the relative importance of flow regulation and grain size regulation of suspended sediment transport α and tracking changes in grain size of bed sediment β," Water Resources Research 37(1), pp. 133-146.

Sambrook Smith, G.H., and Ferguson, R. I. (1995). "The gravel-sand transition along river channels," Journal of Sedimentary Research A65(2), pp. 423-430.

Thorne, P.D., and Hanes, D.M. (2002). "A review of acoustic measurement of small-scale sediment processes," Continental Shelf Research 22(4), pp. 603-632.

USACOE (2003). Upper Mississippi River System Flow Frequency Study, Appendix E: Missouri River Hydrology and Hydraulic Analysis, U.S. Army Corps of Engineers, Kansas City District.

Wright, S., and Parker, G. (2004). "Flow resistance and suspended load in sand-bed rivers: Simplified stratification model," Journal of Hydraulic Engineering, ASCE, 130(8), pp. 796-805.

Using High Resolution Bathymetric Data for Measuring Bed-Load Transport

David Abraham, Research Hydraulic Engineer, USACE-ERDC-CHL, Vicksburg, MS, abrahad@wes.army.mil; Roger Kuhnle, Research Hydraulic Engineer, USDA-ARS, NSL, Oxford, MS, RKUHNLE@msa-oxford.ars.usda.gov

Abstract: A new methodology for measuring bed-load transport in sand bed rivers is presented. This methodology uses high-resolution multi-beam bathymetric data taken over discrete time intervals to infer a transport rate. The method is called ISSDOT, which stands for Integrated-Section Surface Difference Over Time. The paper will present a general overview of the concept, and some results obtained to date. These results come from a flume study carried out at the National Sedimentation Laboratory in Oxford Mississippi. A reference is also made to results obtained from actual field measurements on the Mississippi River. The preliminary results show close correspondence to bed load transport rates derived from ISSDOT and an independent measurement technique.

INTRODUCTION

The measurement of bed-load transport in large sand bed rivers has remained elusive and problematic to the present time. Many types of physical sampling methods have been devised and tested over the last century. For examples of such methods see Van Rijn, L. C., and Gaweesh M. (1994), USACE (1995), and Hubbell, D. W., (1964). No method is universally accepted and there is no standard against which to measure an outcome. Analytic and statistical techniques have also been developed to estimate bed-load transport, Nakato (1990). Although successful to varying degrees, even these methods are often sediment-type specific, and still without an absolute standard to measure against with regards to large rivers. A need remains for a methodology of quantifying bed-load transport that is consistent and repeatable. Recent advances in non-intrusive echo scanning devices have resulted in an ability to accurately measure and resolve bathymetric features, Saenz (1997). Thus the bottom of a river can be mapped in fine detail, accurately resolving all sand dunes and ripples. Under lower regime flow conditions much or all of the bed-load moves in dunes and ripples, thus it seems reasonable to try and measure the bed-load transport by measuring changes in the bedforms. The idea was pursued extensively in the past by studying 2-d sand waves, Simons D. B., Richardson E. V., Nordin C. F. Jr., (1965). Some studies were carried out on 3-d waves, Mahmood, Khalid, (1985) but the data were difficult to obtain and process. That is not the case anymore, and so a new methodology for the computation of bed load transport should be developed that will take advantage of the three-dimensional bathymetric data that is now available. This paper introduces the ISSDOT (Integrated Section Surface Difference Over Time) method.

METHODOLOGY

Definition: ISSDOT stands for Integrated Section Surface Difference Over Time.

Integrated Section simply means that the process divides the river or flume cross-section into many small divisions. A value of the transport rate difference across the upstream and downstream boundaries of the cell is computed for each small division. In cases when the bed load transport rate, or sediment flux across one boundary is near zero, this difference will approach the bed load transport rate at the location. At such locations the individual quantities are summed over the entire section. The values obtained can be taken as the total transport for the section, or averaged and presented as a rate per width of channel.

Surface Difference is the resulting surface obtained by mapping a portion of the surface of a sand wave at some initial time, then mapping the exact same location again at some second point in time, and finally subtracting surface-one from surface-two.

Over Time indicates that some measured time difference is allowed to elapse between the mapping of surface one and surface two. This change in time (ΔT) is necessary to infer rates of transport.

An Intuitive Approach to the ISSDOT Concept: The idea is to take the vertical difference of the two measured surfaces for a defined area of the concurrent surfaces, and to compute a volume. For ease of computations, a simple square is used. One square foot, meter, or any other unit can be used. However, a carefully selected size of surface area is important with regards to the sand wave speed and size. Figure 1 shows a schematic of the defined volume.

As can be seen, if surface one was the surface at t1, and surface two was the surface at t2, then the volume inscribed as surface one dropped to the level of surface two, is the area of the square (dY x dX) times the change in height, dη. In this case it would be the volume of scour that occurred in the time interval ΔT. These measurements indicate a change in volume for a given change in time. If this is multiplied by density, then at first glance it would appear that the process has defined a mass transport rate. But, these measured quantities constitute a difference of bed-load transport except in the special case when the fluxes through one boundary or the other may be taken as near zero. This topic will be addressed in more detail in a later paper. In the cases in which ISSDOT yields a value approaching the bed load transport rate, the entire surface of the river or flume was divided into 2-d square surface cells. The size of the cells was chosen such that two or more cells could be used to resolve the deposition side of the smaller waves. Thus in practice, for all the other waves, the resolution is much greater than that. All the cells together form a grid that covers the entire surface area of any selected study location. Some cells of the grid will be located over scour areas on the back side of dunes and ripples, and some will be located over the front side of the dunes. Additionally, some cells will also be located over the troughs of the dunes. Figure 2 shows an example of such a grid superimposed over actual Mississippi River bathymetric data. Though the bathymetric data is real, the grid is for demonstration purposes only and was not used in any calculation.

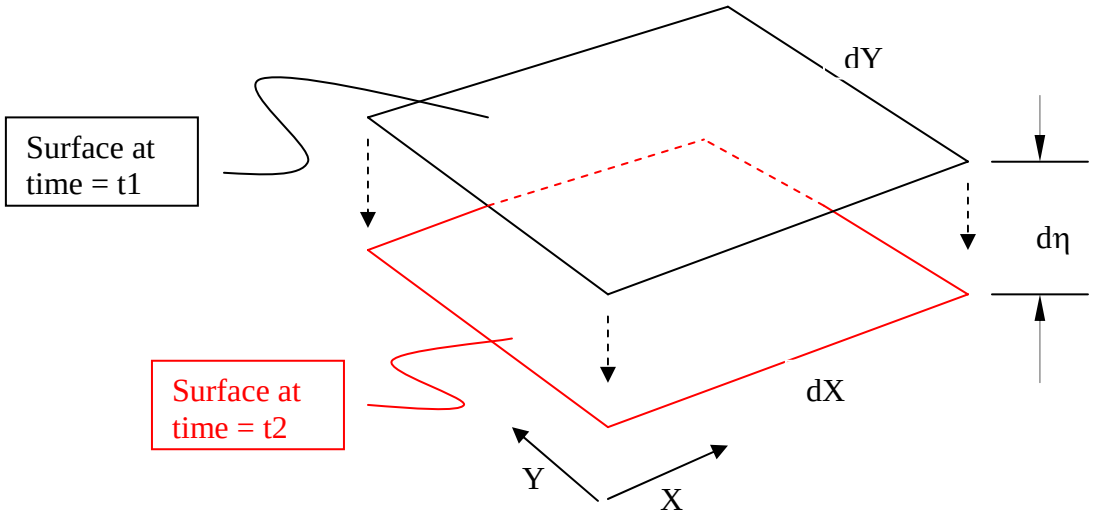


Figure 1 Schematic defining the scour volume.

The intuitive idea of ISSDOT is that each of these cells is an incremental measurement of the sediment transport at that location when the sediment flux through one boundary of the computational cell is near zero. It was found that the cells with negative changes in elevation (scour) approached the bed load transport rate. When the negative change in volume in each cell during a given time span is individually evaluated, then all the cells in any given row can be summed across the entire width of that row to give the total bed-load transport rate for that section. For example, in Figure 2, computations could be made for every cell in row 1. By summing all the cells in row 1 the total for the section can be determined. This is in a sense integrating across the section, thus the IS initials in ISSDOT. The computations for each cell stand alone as a transport measurement much the same way as any physical bottom sampler. For instance, the Helley-Smith or Dutch-Nile samplers are set on the channel bottom for a short period of time to allow sand to enter the collection bag. When the sample is retrieved the mass of sand collected during the time interval that the sampler was in place provides a direct measurement of mass per time per incremental channel width. The time interval must be short enough so that the bag does not completely fill; otherwise the time it took to fill it is unknown. When many samples are taken both laterally and longitudinally in a given channel study area, then some type of statistical average of all samples can be taken as the average transport for that part of the river. It is usually reported as mass per time per unit width of channel. In any case, each sample at each individual location stands alone as one measurement of the transport. A single cell in ISSDOT also stands alone as a single measurement of transport. So in this sense, it might be thought of as a virtual, non-intrusive

sampler. In order to test this concept, a flume study was devised. The details of the experimental plan and results are presented in the remainder of this paper.

FLUME STUDY

Proof of concept: Initial tests of ISSDOT on Pool 8 of the Upper Mississippi River indicated that this method showed promise as a non-intrusive technique to measure bed-load transport, Abraham and Hendrickson (2003). So it was decided to test this method under the controlled conditions of a laboratory flume. By doing so the problems of concurrently measuring the bed-load and the suspended load could be addressed. The flume study was conducted at the USDA-Agricultural Research Service, National Sedimentation Laboratory (ARS-NSL) in Oxford Mississippi from December 2002 to February 2003. The purpose of the flume study was to test the ISSDOT concept for measuring bed-load transport. As mentioned earlier, the ISSDOT method depends on being able to accurately measure or map the surfaces of sand waves at two different times. When this is possible, ISSDOT will provide an estimate of the transport of bed-material moving in the sand wave. In the flume, it was possible to measure the suspended bed material as well as the total bed-material load. Thus the basic idea to test ISSDOT was to measure the total bed-material load (Q_{BT}) and to concurrently measure the suspended bed material (Q_S). When the suspended is subtracted from the total, the remainder should be the bed material that is moving in the sand waves, Q_B. When the bed material moving in the sand waves is independently measured at the same time by the ISSDOT method, which we will call Q_{BI}, then Q_{BI} can be compared to Q_B. The foregoing discussion is shown by Equation 4.

$$Q_{BT} - Q_S = Q_B \cong Q_{BI} \tag{4}$$

Figure 3 shows the flume that was used for this study. This flume is 30.5 m (100 ft) long, 1.2 m (4 ft) wide and 0.6 m (2 ft) deep. The sediment-water mixture is recirculated from downstream to upstream via a return pipe running under the flume. Figure 4 shows a schematic diagram (not to scale) identifying the major features of the flume. To reduce clutter in the figure, the head bay, flow diffuser, pump, viewing window and other details are not shown.

The total bed-material load (Q_{BT}) was measured in the return pipe using a density meter. The density meter operated on the principle of vibration amplitude/frequency changes associated with density changes in a vibrating U-tube (Willis, 1977). The change in voltage from the density cell was proportional to the change in density. The density cell was calibrated by passing known concentrations of sand and water through the meter using a test stand similar to that used by Willis (1977). Total sediment load being transported through the flume channel was calculated from mean sediment concentrations measured with the density cell times the flow rate measured from the Venturi meter. The mean sediment concentrations in the return pipe were calculated from a 4-hour record of the density cell stored on a PC.

The suspended sediment (Q_S) was calculated using a combination of acoustic backscatter data collected over the lower 40% of the flow depth with isokinetic physical samples collected in the upper 60% of the flow. These were added together and multiplied by flow rate to yield the suspended load. The basis for the validity of these measurements is described in Kuhnle, Wren (2004). The suspended load was subtracted from the total load to yield a value for the bed load (Q_B) moving in the sand waves.

The bed material moving in the sand waves and computed using the ISSDOT method (Q_{BI}) was mapped with special sensors manufactured by SeaTek Instrumentation and Engineering (http://seatek.com/) and are discussed under the Flume Data heading.

Flume Data: To apply the ISSDOT concept it is necessary to accurately map the sand wave surfaces. This must be done several times over the same location and at known time intervals between each mapping. This was done in the flume by using two sets of sonic transducers. These are shown in Figure 5.

Each sensor bank consisted of 8 transducers for which the acoustic operating frequency was 5 MHz. A signal processing electronics package was also supplied to allow communication with a PC via a RS232 communications port. The electronics package is capable of running up to 32 transducers, and sampling up to 2 external analog channels. Three methods were used to test how well the sensors recorded the distance to the bottom. The results of

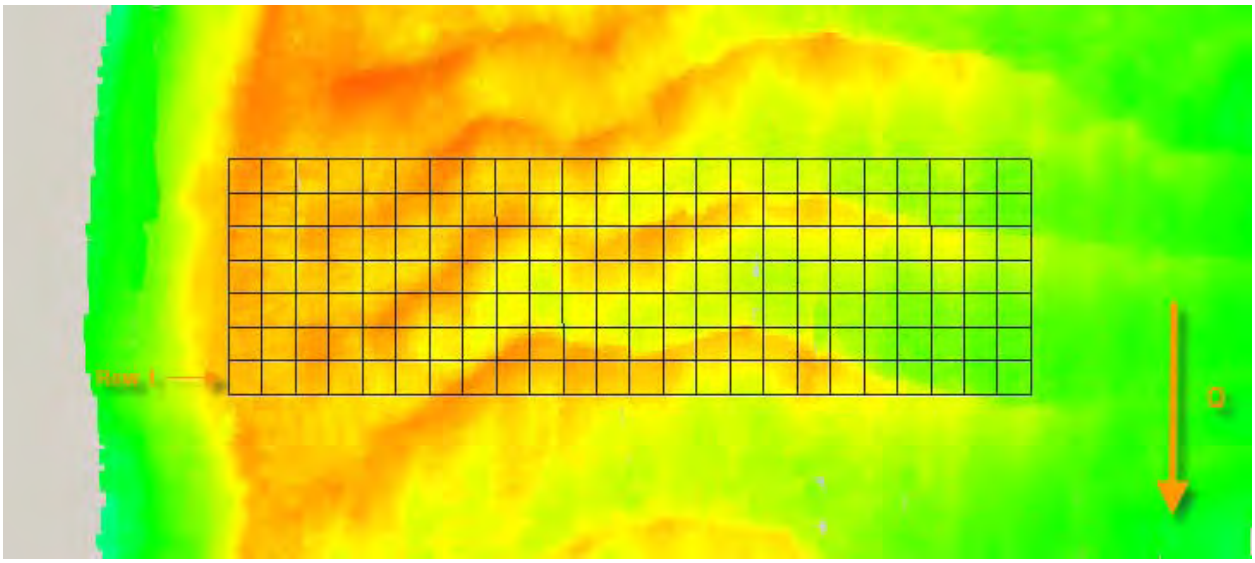


Figure 2 Sample grid superimposed over a plot of bathymetric data.

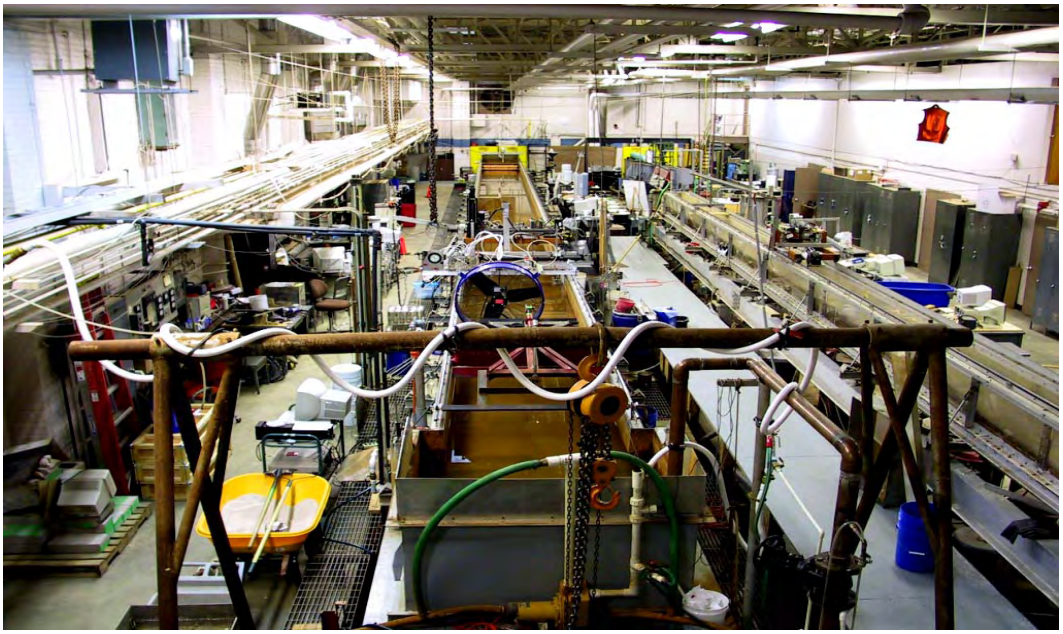


Figure 3 View of experimental flume.

these tests determined the instrument resolution and error. The tests consisted of the following scenarios; multiple depth measurement samples using stationary sensors in still water, two sensors each taking one sample at the same location in still water, and moving sensors in still water. The maximum average error of the eight sensor pairs was found to be about 2.2 mm. Additionally, the tests indicated that the speed at which the sensor banks traversed the flume did not influence the measurement error.

To map the bottom surfaces the two sensor banks were set a known distance from each other and moved across the flume at a known and constant speed. The bank 'A' of sensors (1 to 8) mapped the bed as it moved from left side to the right side of the flume looking downstream. Bank 'B' of sensors (9 to 16) followed bank A with a spacing of 15.24 cm (6 inches) between them. Thus sensor 9 mapped the same locations as sensor 1, separated by a known

change in time (Δt). Values of Δt were selected between 48 and 3 seconds. Likewise, sensor 10 followed sensor 2 and so on for eight pairs of sensors. This produced eight rows of sensor data. The overlap of sensors on bank A and B was the middle 0.76 m (30 in) of the flume cross section. The two sensor banks moved in this case from left to right, with B following A.

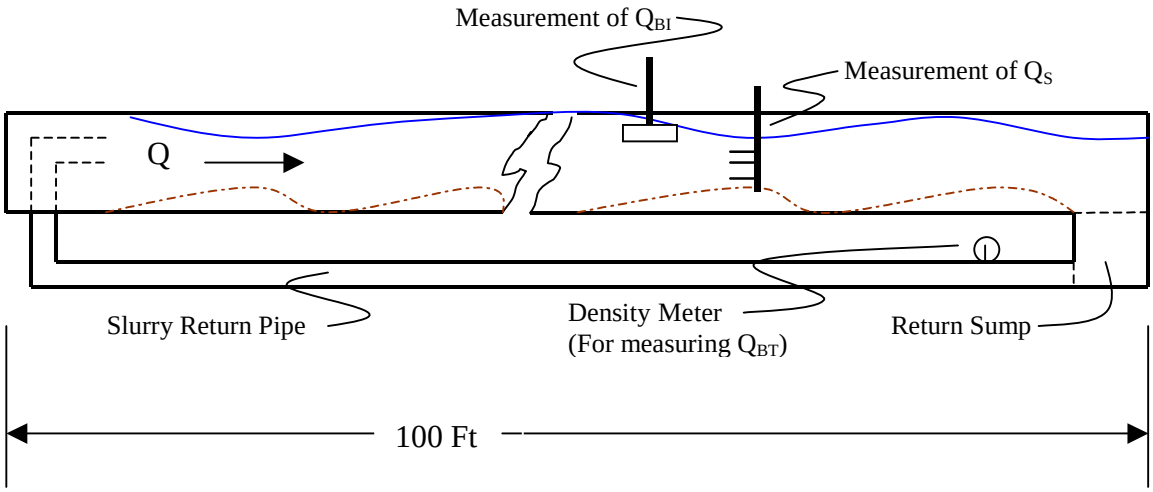


Figure 4 Schematic of experimental flume.

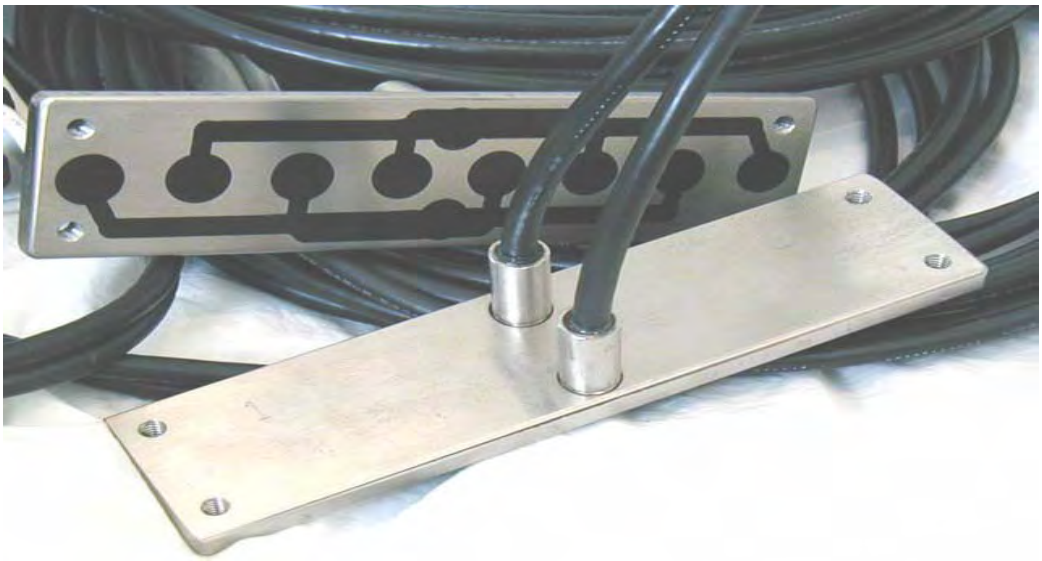


Figure 5 Acoustic sensor banks consisting of 8 transducers each.

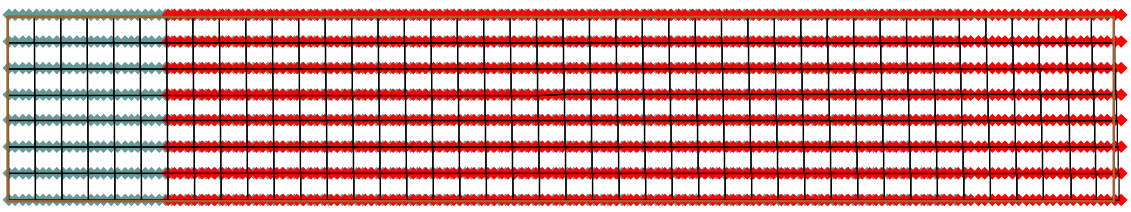


Figure 6 Plot of collected data points showing spacing and overlap on rectangular grid.

This can be seen in Figure 6. The first six inches are mapped by sensor bank B only, and the last six inches are mapped only by sensor bank A. Although shown superimposed one over another on the same grid, the data for each sensor bank were recorded and processed as separate files.

The eight lines of data traced by each sensor bank were processed to remove spurious data points and interpolated to a grid on 2.54 cm (1-in) squares. To apply the ISSDOT method, the nodal values on grid A were subtracted from those on grid B. An example of such a surface difference grid is shown in Figure 7. The overlapping computational cells are clearly visible in the center of the grid.

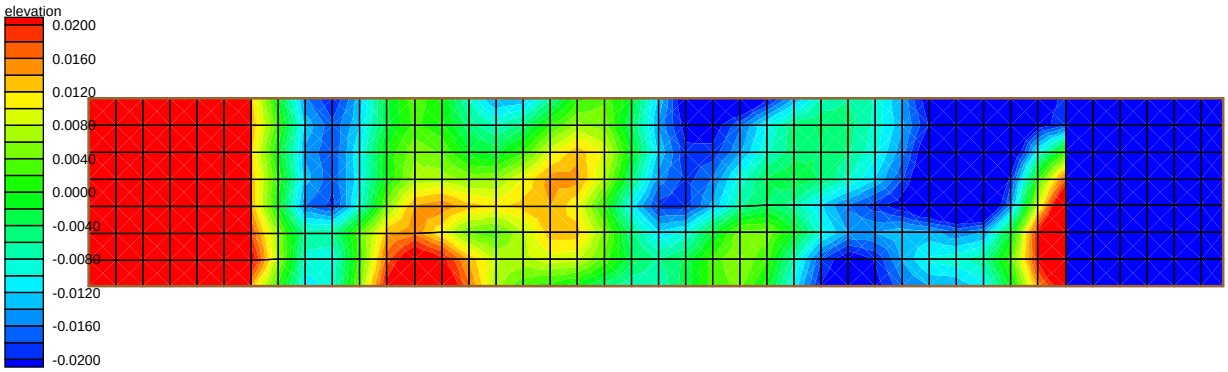


Figure 7 Contours of surface differences superimposed on computational grid.

At this point the processing of the raw data is complete and the grid is ready to be used in the ISSDOT computations. The computations are carried out on each element, or cell, in the grid. The cells consist of the four nodes that make up any square in the grid. It is these cells that form the individual computational units of this method as already described in the section, **An Intuitive Approach to the ISSDOT Concept.**

RESULTS

As explained above, the general idea was to determine the bed-load transport in the sand waves using the new methodology, and compare it to the measured bed-load transport of the same waves. This is quantitatively expressed in equation 4. The outcome of measurements to determine the total bed-material load, $Q_{BT,}$ showed a measured value of 0.0695 kg/s m (0.0467 lbs/s/ft). These data were obtained using the density meter. For the suspended load, its measured value was determined to be 58.6 percent of Q_{BT}. Thus the measured value of bed-material load moving in the sand waves (Q_B) must be 41.4 percent of Q_{BT}, or approximately 0.028 kg/s/m (0.019 lbs/sec/ft). For any computations of ISSDOT, this is the value to compare to.

Table 1 is a tabulation of computations for run six for the medium flow runs, and combined data points of all runs and sweeps. Only the scour elements were considered in all computations. The file name indicates the run and sweep number as well as the fact that it is a difference geometry file. The second column shows the number of scour elements for that file. The third column shows the number of scour elements whose change in elevation was less than the measurement error bound of 2.2mm. These elements were removed from the computations. DT, in the fourth column is the time increment used in the computations The average cell transport for the entire grid in the units specified for a given run and sweep are shown in the last two columns.

The top half of the table shows run 6 with 7 sweeps across the flume, and the DT for each sweep. All other runs (run 1 to run 5) used the same DT schedule. The time dependence of computed transport can be observed in the data. For the elements with negative changes in volume, (scour cells) ISSDOT predicted rates from 0.0044 to 0.046 kg/s/m (0.003 to 0.031 lbs/s/ft). The six runs that were analyzed covered a time span of about 2 hours. This ensured that many different wave configurations were measured and that the spatial variability of the sand waves was accounted for. The average value of all runs and sweeps was 0.019 kg/s/m (0.013 lbs/sec/ft), which compares well with the measured value of 0.028 kg/s/m (0.019 lbs/s/ft). This value is 31% lower than expected, and is without regards to the time difference between measurements.

If one considers bracketing DT, then slightly different values of average transport will be computed. These are shown at the bottom of Table 1.

Table 1 Results of run six and combined sweeps of all runs.

File Name	No. of scour elements	Removed elements	DT seconds	Avg. Trans. lbs/s/ft	Avg. Trans. kg/s/m
r6s1b-a.geo	173	13	48	0.003	0.004
r6s2b-a.geo	106	32	24	0.004	0.006
r6s3b-a.geo	87	29	12	0.008	0.012
r6s4b-a.geo	106	39	8	0.011	0.016
r6s5b-a.geo	81	62	6	0.014	0.021
r6s6b-a.geo	57	25	4	0.021	0.031
r6s7b-a.geo	47	9	3	0.031	0.046
Below data are for all runs and sweeps:					
Avg. of all data pts. for all sweeps				0.0128	0.019
Avg. of data pts.for sweep 2-6 [dt=24 through 4]				0.0126	0.019
Avg. of data pts.for sweep 3-5 [dt=12 through 6]				0.0127	0.019
Avg. of data pts. for sweep 2-7 [dt=24 through 3]				0.0144	0.021
Avg. of data pts.for sweep 3-7 [dt=12 through 3]				0.0162	0.024

CONCLUSIONS

Although the ISSDOT method in general yields the difference between the bed load transport rate at the upstream and downstream edge of each element, it has been found that the elements with negative changes (scour) closely approximate the bed load transport. This case has been shown with data from a laboratory flume with a sand bed (D50= 0.5 mm) with equilibrium dunes on the bed. While more testing is needed, this result indicates that a subset of the ISSDOT determined values may serve as a reliable indicator of the bed load transport on a channel bed with dunes as the stable bed form. Further studies should be carried out to further validate these conclusions and to formulate an analytic basis for the methodology as well as to explore its applications and limitations.

REFERENCES

Abraham, David D., and Hendrickson, Jon S. (2003). "Effects of drawdown and structures on bed-load transport in pool 8 navigation channel," USAE ERDC-CHL, Technical Note CHETN-VII-5, December 2003.

Hubbell, D. W. (1964). "Apparatus and techniques for measuring bedload," USGS Water-Supply Paper 1748, Washington, U.S. Govt. Printing Office.

Kuhnle, R. A., Wren, D. G. (2004). "Simultaneous side by side variability of sediment concentration over dunes," Proceedings of the Ninth International Symposium on River Sedimentation, Yichang, China, p. 2556-2562.

Mahmood, Khalid (1985). "Analysis of multi-channel bed profiles, Missouri River, near Omaha, July 27, 1982," U.S. Army Engineer Division, Omaha, Nebraska, MRD Sediment Series No. 36.

Nakato, Tatsuaki. (1990). "Tests of selected sediment-transport formulas," ASCE Journal of Hydraulic Engineering Vol 116, No. 3.

Saenz, Luis F. (1997). "Multibeam calibration and quality control," Survey and CAD Confrence, St. Louis, 1997.

Simons D. B., Richardson E. V., Nordin C. F. Jr. (1965). "Bedload equation for ripples and dunes," U. S. Geological Survey Professional Paper 462-H.

USACE (1995). "Engineer manual EM 1110-2-4000, sedimentation investigations of rivers and reservoirs, chapter 8, sediment measurement techniques," U.S. Army Corps of Engineers, Washington, DC.

Van Rijn, L. C. and Gaweesh, M. (1994). "Bed-load sampling in sand-bed rivers," J. of Hydraulic Engineering, ASCE, Vol.120 No.12.

Willis, J. C. and Kennedy, J. F. (1977). "Sediment discharge of alluvial streams calculated from bed-form statistics," Iowa Institute of Hydraulic Research, Report No. 202.

PASSIVE ACOUSTIC MONITORING OF COARSE BEDLOAD TRANSPORT ON THE TRINITY RIVER

Jonathan S. Barton, Doctoral Candidate in Geosciences, The Pennsylvania State University, University Park, PA, jbarton@geosc.psu.edu; Rudy L. Slingerland, Professor of Geosciences, The Pennsylvania State University, University Park, PA, sling@geosc.psu.edu; Smokey Pittman, M.S., Geomorphologist, Graham Matthews and Associates, Placerville, CA, smokey@gmahydrology.com; Thomas B. Gabrielson, Senior Research Associate, Applied Research Laboratory, The Pennsylvania State University, University Park, PA, tbg3@psu.edu

Abstract: Passive recording of acoustic pressure levels due to interparticle interactions has the potential to serve as a proxy for coarse-grained fluvial bedload, but the technique has never been tested using a fluvial dataset. Here we report a time-series of acoustic measurements taken in the Trinity River at Douglas City during the peak release flow from May 6 to 19, 2005, in Trinity County, California. Measurements were taken at the U.S. Bureau of Land Management campground at Douglas City, using a Geospace MP-18 hydrophone, a custom-built, variable-gain (1-800x) amplifier, a National Instruments DAQCard 6036E, and Mathworks' MATLAB Data Acquisition Toolbox. Data were recorded at 64 kHz for several hours each day on ten of the fourteen days in the study period. Estimates of actual bed material fluxes were obtained at the same cross-section by Graham Matthews & Associates GMA), who used pressure-differential bedload samplers: the 6x6" Helley-Smith and a 12 x 6" Toutle River (TR-2) sampler. Flow information is available from a USGS gauge (#11525854) about 150m upstream from the site. Results show that there is a statistically significant correlation between the coarse bedload flux measured by Graham Matthews & Associates and the total acoustic power. This correlation can be shown to be independent of third variables such as bubble collapse or turbulence. Acoustic power, and by inference, bedload flux, show interesting periodicity that needs further investigation, particularly in the 4 to 15 minute frequency range.

INTRODUCTION

There has long been a need to monitor bedload fluxes in mountain streams, but few practical methods for observation. Invasive systems, such as vortex (Klingeman et al. 1979) or Birkbeck (Reid et al. 1980) samplers, are one approach, and given small enough clast sizes, Helley-Smith type samplers (Helley and Smith, 1971) can provide an alternative. During high discharge flows, however, none of the present methods is effective, and all have difficulty measuring the spatial and temporal variability of transport rate.

Recent attempts to better understand bedrock erosion in steep mountain streams (e.g. Hartshorn, et al. 2002) have underscored the need for a better method to measure bedload accurately, especially during high-flow events. The prevailing view of fluvial bedrock erosion (e.g. Slingerland et al. 1997; Howard, 1998; Sklar and Dietrich, 1998) is of a process combining both hydraulic plucking and abrasion by bedload particles. Therefore, though the erosion rate will be a complex function of the bedload transport rate, in order to make predictions about downcutting in these channels, it is necessary to have accurate measurements of the rate of availability of abrasion tools.

Collisions between moving sediment grains and between moving grains and a stationary bed produce acoustic energy within the water. This paper will describe an experiment conducted in May 2005 to record the acoustic energy produced, and to relate that energy to bedload data obtained using traditional empirical methods.

BACKGROUND

Many methods have been used to measure bedload transport since the earliest basket samplers of Ehrenberger (1931). Acoustic methods represent an opportunity to obtain spatially-integrated and continuous measurements of bedload fluxes, even during extreme transport events. They have been proposed many times over the past century in various forms. The earliest work examined the impact of sediment on a plate (Mulhofer, 1933). Among the first to examine interparticle collisions were Johnson and Muir (1969), and later Twyoniuk and Warnock (1973), Anderson (1976) and Baenziger and Burch (1990). All of these studies reported that time-domain sound pressure levels measured by hydrophones increase with an increase in bedload transport rate. A variation on these techniques was reported by Govi (1993), who counted impulses from a passive geophone network caused by collisions of sediment grains with a poured concrete slab.

Work in the marine realm using hydrophones (e.g. Millard, 1976; Thorne, 1985, 1986; Thorne et al., 1984, 1989; Rouse, 1994; see Hardisty, 1993 for a review) has focused on wideband results, which predict a distribution of frequencies dependent on sediment size. Thorne (1986) reports that the centroid frequency of the wideband distribution decreases linearly with increasing particle diameter. Thorne (1986) also indicates that the particle size distributions calculated from this relationship relate well to visual estimates of number distributions of the mobile bed material, as determined from underwater video. According to Thorne's relationship, typical frequencies for gravel range from about 50 kHz for very fine (2mm) to about 2kHz for very coarse (64mm). Subsequent studies (e.g. Voulgaris et al., 1994, 1995) have reported extensive field-testing of this method.

This previous work provides a sound basis upon which to build a system for studying coarse bedload transport in mountain streams. Previous work has suggested that site-specific calibration will be necessary because of the dependence of the signal strength upon reach geometry.

STUDY SITE AND ANCILLARY DATA

Data were collected on the Trinity River at Douglas City, Trinity County, California during the peak release flow from Trinity Dam on May 6 to 19, 2005. Measurements were taken at the U.S. Bureau of Land Management campground at Douglas City using a hydrophone case lashed to the submerged trunk of a tree. The most important priority for instrument placement was proximity to ground-truth measurements carried out by Graham Matthews and Associates, and safety concerns relating to that proximity. The site selected was on the right bank of the river, four meters downstream from the cross-stream tether used for the GMA cataraft. Observations of the GMA samples led to the estimate that the closest moving coarse bed material was approximately 10-12 meters away from the instrument during the study.

Sediment sampling occurred from May 6 to May 31. Sampling was conducted from cataraft-based sampling platforms specifically developed for sampling at sites where other methods (bridge, cableway, etc.) were not available. The catarafts were attached to temporary, tensioned cable taglines securely anchored to large trees on either side of the channel. The cable passed through a modified version of the USGS standard quick-release boat rollers mounted on 6' towers on either side of the platform, allowing boat traffic to pass. Caution signage, flagging and safety kayakers were utilized. Crews consisted of two on-river personnel specifically trained in cataraft-based sediment data collection. All crew members attended a mandatory safety/sampling technique training session and crew leaders attended the USGS Sediment Data Collection Techniques course.

Bedload measurements were collected over a range of flows and at various positions on the hydrograph spanning the release period utilizing a 6" Helley-Smith sampler (through May 11), and the Toutle River-2 (TR-2) thereafter. Both used 0.5 mm mesh collection bags. Cross sections were sampled at 12-20 verticals following standard USGS procedures (Edwards and Glysson, 1999) for Single Equal Width Increment samples. Down-times of 60 seconds were usually used at each vertical. Two passes were generally completed for each sample. Samples were logged with site identifier, date, time, sampler-type, stage, moving bed width, sampler bottom time, and stationing information. Water surface slopes were recorded for each distinct stage and sites were photographed. Each sample pass was dried and sieved at ½ phi sizes to 1 mm, below which whole phi size classes were used. After each pass was analyzed, the data were composited into single-sample particle size distributions, reporting each size fraction as percent by weight of the total sample and reporting partial mass sub-totals for < 0.5 mm, 0.5-8 mm and > 8 mm fractions. Bedload samples were processed in the GMA Coarse Sediment Lab in Arcata. Quality assurance plans are available to interested parties. Transport rates were computed for each size fraction using the sample data and the standard methods utilized by the USGS as described in Edwards and Glysson (1999). A station analysis was developed for each sampling site and was submitted along with sample data and records to the USGS for review/approval/publication in the USGS California Science Center Annual Data Report Series.

SYSTEM DESIGN

The basis of the instrumentation is a Geospace, Ltd. MP-18 hydrophone. The hydrophone has been encased in a perforated three-inch PVC pipe, the interior of which is filled with pieces of permeable foam. The ends of the pipe are plugged with streamlined wooden caps, one of which can be removed for access. The cable to the hydrophone exits the pipe through the tip downstream cap, minimizing stress on the cable in a high-flow environment. The hydrophone is connected to an adjustable-gain amplifier, which allows for on-site adaptation to the sampling environment. For most of this experiment, the gain was set at 800x, but 325x was used for some of the early samples. This amplifier also includes an analog low-pass anti-aliasing filter that passes signals below 26 kHz. The filtered signal is fed to a 16-bit National Instruments NI-DAQCard 6036E analog-to-digital conversion card on a laptop computer. This card, controlled with Mathworks' Matlab Data Acquisition Toolbox, samples the amplified and filtered voltage at 62.5 kHz and records one-minute long samples. Each sample is separated by 2-5 seconds of time dedicated to file management. This arrangement is used because it results in sample sizes within

the memory constraints of a personal computer without subsetting or subsampling. The system is not designed to run unattended, but only minor modifications would be necessary to make it so.

RESULTS AND DISCUSSION

Theory predicts a linear relationship between acoustic power and the square-root of mass transported (Thorne, 1986). Total acoustic power was obtained by using Welch's algorithm, with 50% overlapping one-second rectangular windows, to obtain a power spectral density for each one-minute sample, which was then summed over frequency. The resulting power was then averaged over the period during which GMA were taking samples, and the resulting average powers were regressed against the square-root of the average mass tranport rates calculated by GMA. The regression was then applied to the sample data, and the results are plotted in Figure 1, along with the water discharge over the sample interval, and the GMA observations.

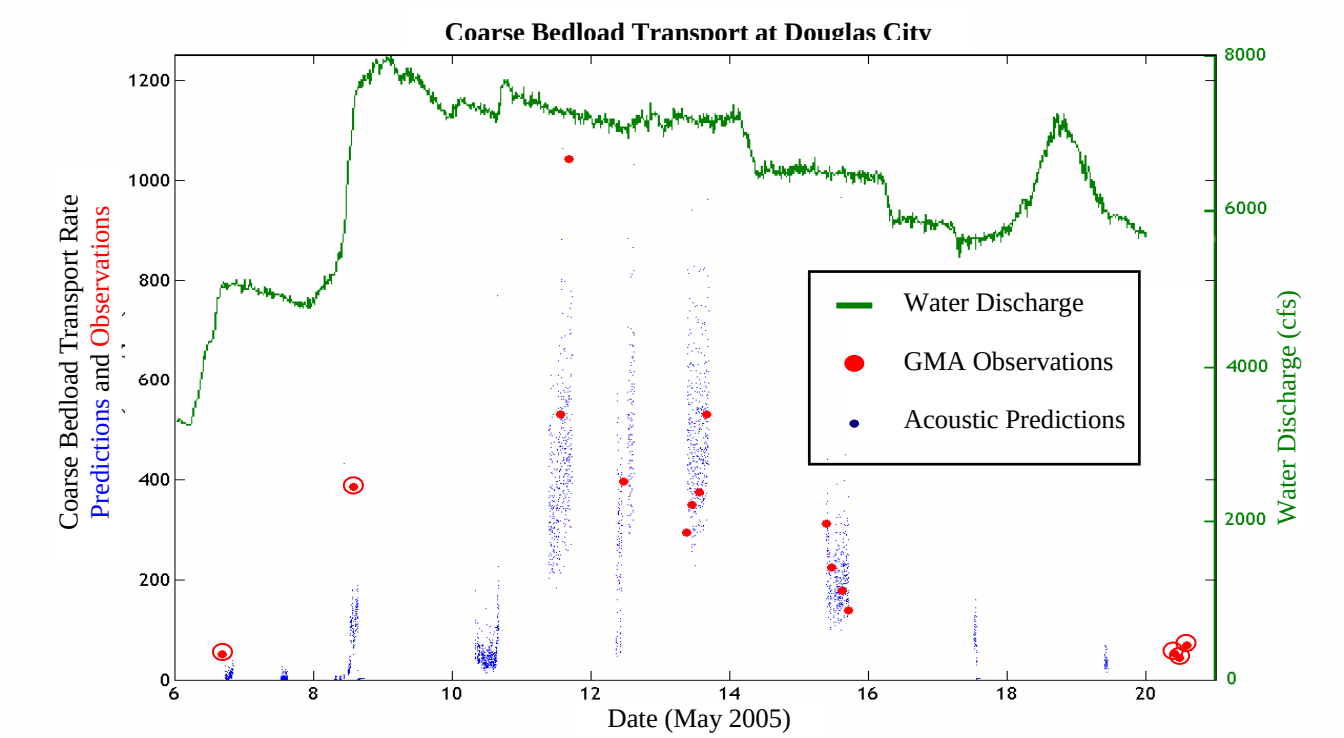


Figure 1 Predictions of coarse (>8mm) bedload transport rate from one-minute-averaged acoustic power (blue) over the study interval plotted with the water discharge (green) and GMA Helley-Smith and TR-2 observations (red). The circled GMA observations were excluded from the regression analysis because there were no contemporaneous acoustic data.

The regression used all 11 of the GMA observations for which contemporaneous acoustic data were available. Because of the paucity of data, it was impossible to reserve a test population to evaluate the effectiveness of the prediction. Figure 2 shows the regression plot, with the 95% confidence interval for the regression parameters (assuming Gaussian error). Note that the regression is linear with respect to the square-root of mass, and for clarity, the plot is drawn with respect to mass. The Pearson's correlation coefficient is 0.77, with a p-value of 0.005, indicating a significant correlation. To perform the regression, the acoustic power was averaged over the

entire GMA sampling period, which was typically about 40 minutes long, under the assumption that the GMA sampling technique provides an average transport rate over the sampling interval. The results from this regression were then used to produce the acoustic prediction values from the one-minute power data that were plotted in Figure 1.

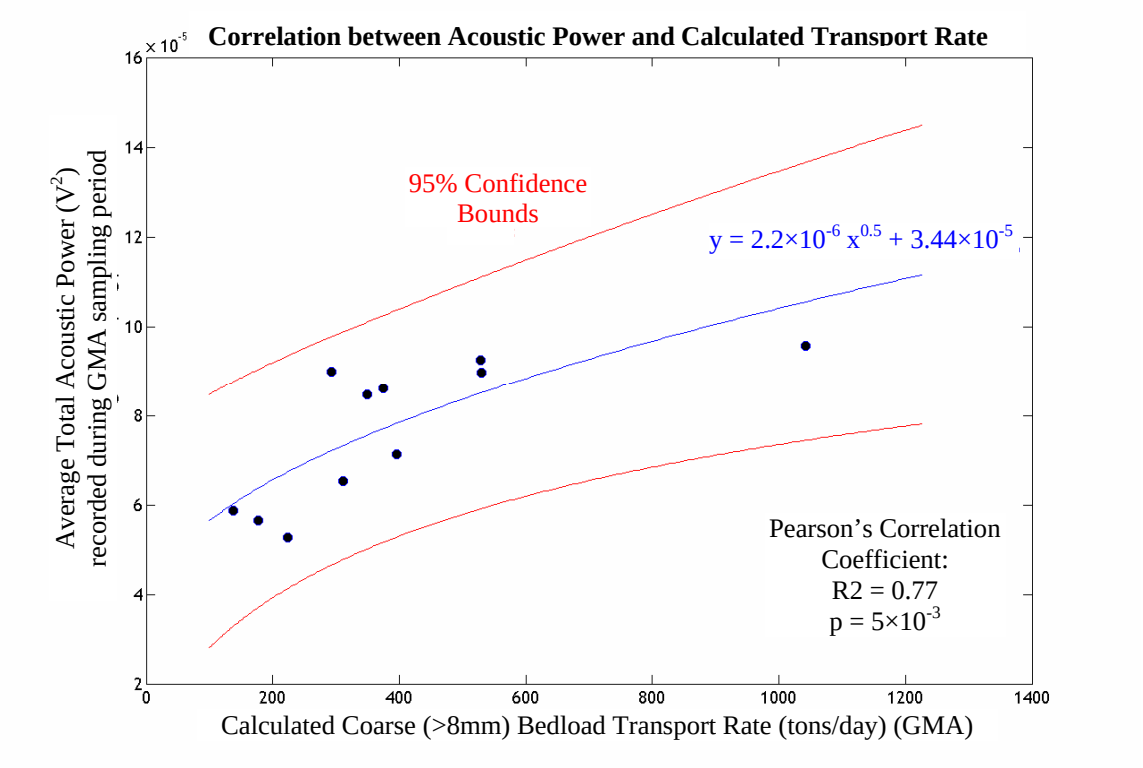


Figure 2 Correlation plot between average acoustic power and bedload transport rate.

It has been suggested (e.g. Hardisty, 1993) that acoustic noise will correlate strongly with discharge, because of bubble collapse and turbulence-induced noise. Figure 3 shows the relationship between discharge and acoustic power. The explanation for the dramatic rise in acoustic power well after the peak in water discharge cannot be attributed to water discharge, as the rising and falling limb values, for the same discharge, are distinct populations on this plot. We attribute this rise to bedload, although the hysteresis pattern in this plot is reversed when compared to the traditional view of sediment transport in a flood. A review of the GMA data from Douglas City during the 2004 release shows a similar pattern in the days immediately surrounding the peak flow. We conjecture that the coarse sediment sources for this site are the deltas of Indian and Weaver Creeks located from 2.5-3 miles upstream. Over the year, rain-event driven flooding progrades these deltas into the Trinity. It is only during the dam-release flows that this material gets transported downstream, and we speculate that this delay in the peak coarse-material transport rate corresponds with the arrival of the deltaic material. These distances and delays correspond to an average celerity of between 0.9 and 1.2 cm/s, which are well within the range given in the literature for bedload sheet migration.

Interpretation of the individual acoustic records reveals several interesting periodicities in the acoustic noise, and by inference, in the bedload transport (Fig. 4). In particular, the lowest

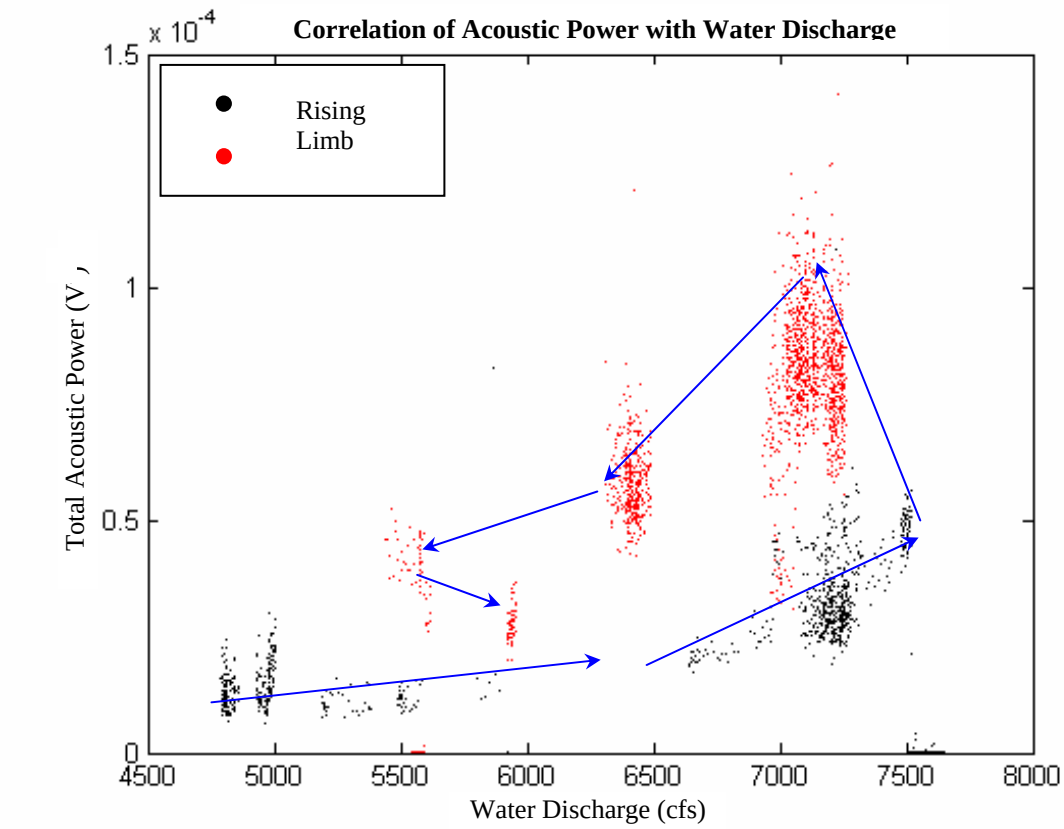


Figure 3 Relationship between acoustic power and discharge. The blue arrows indicate the approximate progression of time through the flood. The peak of the flood was assumed to fall

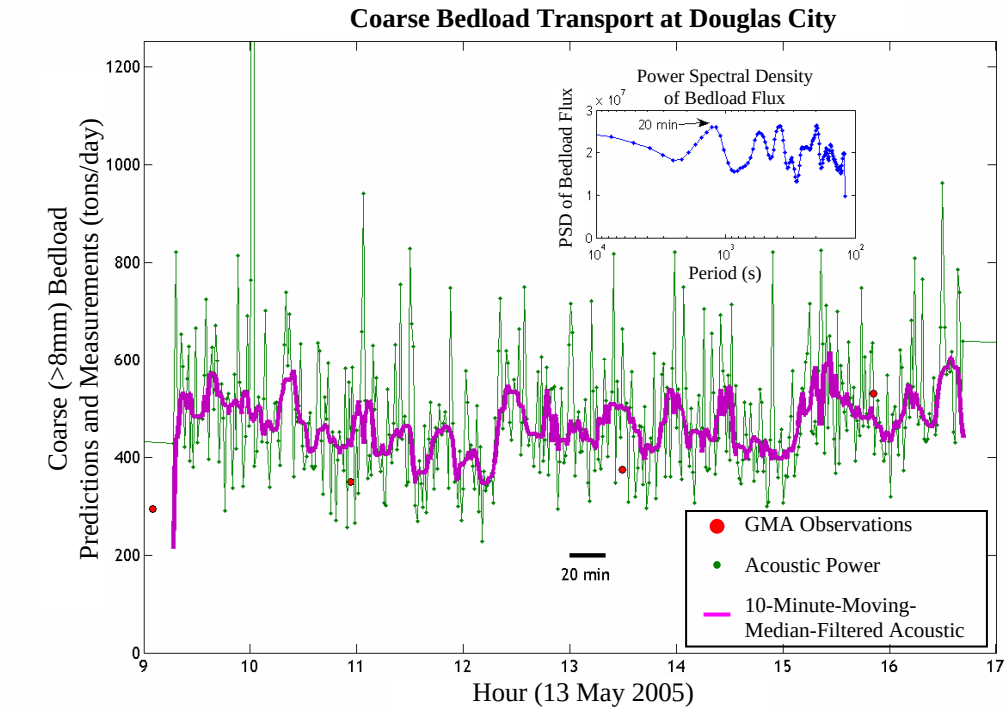


Figure 4 Detail of bedload transport predictions for 13 May 2005. The green dots are the predicted values, the lines are interpolations. The purple curve is the result of a 10-minute moving window median filter. Inset is the power spectral density of the one-minute data. Note that the horizontal axis is descending in period.

frequency peak that is captured by the spectral analysis, at a period of about 20 minutes, is consistent with those reported in the literature (e.g. Whiting et al, 1988) for periodic bedload sheets.

CONCLUSIONS

Although the data are limited, it is clear that there is a statistically significant correlation between acoustic power and bedload transport. The correlation cannot be attributed to a third variable dependent on discharge such as bubble collapse or turbulence, because the acoustic power during the rising limb was strongly separated from that during the falling limb.

The few data points of traditional data collected did not allow a test population for the relationship that was developed. However, there were five GMA samples that were not included in the regression analysis because there were no acoustic data acquired contemporaneously. Although no rigorous test is possible with this data, it is encouraging to note that these acoustic predictions are consistent with contemporaneous bedload transport observations.

REFERENCES

Anderson, M.G. (1976). "An inexpensive circuit design for the acoustic detection of oscillations in bedload transport in natural streams," Earth Surface Processes and Landforms, 1(3), pp 213-217.

Baenziger, R., and Burch, H. (1990). "Acoustic sensors (hydrophones) as indicators for bed load transport in a mountain torrent," in Lang, H., and Musy, A. (eds.), Hydrology in Mountainous Regions I — Hydrological Measurements; The Water Cycle: Proc. of Two Symposia Held at Lausanne, August, 1990, IAHS-AISH Publication 193, pp 207-214.

Edwards, T.K., and Glysson, G.D. (1999). Field Methods for Measurement of Fluvial Sediment, U.S. Geological Survey Techniques of Water Resources Investigation, Bk. 3 Ch. C2, 89 p.

Ehrenberger, R. (1931). "Direkte Geschibemessungen an der Donau be Wien und deren bischerige Ergehuisse," Die Wasserwirtschaft, 34, pp 1-9.

Govi, M., Maraga, F., Moia, F. (1993). "Seismic detectors for continuous bed load monitoring in a gravel stream," Hydrological Sciences Journal, 38, pp 123-132.

Hardisty, J (1993). "Monitoring and modeling sediment transport at turbulent frequencies," in Clifford, N.J., French, J.R., and Hardisty, J. (eds.), Turbulence: Perspectives on Flow and Sediment Transport, John Wiley and Sons, New York, pp 35-59.

Hartshorn, K., Hovius, N., Dade, W. B., and Slingerland, R. L. (2002). "Climate-driven bedrock incision in an active mountain belt," Science, 297, pp 2036-2038.

Helley, E.J. and Smith, W. (1971). Development and calibration of a pressure-difference bedload sampler. U.S.G.S. Open File Report.

Howard, A.D. (1998). "Long profile development of bedrock channels: Interaction of weathering, mass wasting, bed erosion, and sediment transport," in Tinkler, K. and Wohl, E.E., (eds) 1998, Rivers Over Rock: Fluvial Processes in Bedrock Channels, Geophysical Monograph Series 107, Am. Geophysical Union, Washington, D.C., pp 297-318.

Johnson, P., and Muir, T.C. (1969). "Acoustic detection of sediment movement," Journal of Hydraulic Research, 7, pp 519-540.

Klingeman, P.C., Milhous, R.T., and Heinecke, T.L. (1979). Oak Creek vortex bedload sampler. Oak Creek Sediment Transport Report F2, Water Resources Research Institute, Oregon State University, Corvallis.

Graham Matthews & Associates (2004). WY2004 Flow Release Sediment Transport Monitoring Report, Report for Trinity River Restoration Program, US Bureau of Reclamation, Shasta Lake, CA.

Millard, N.W. (1976). "Noise generated by moving sediments," in Proc. of the Conference on Recent Developments in Underwater Acoustics 31 March-1 April 1976, Institute of Acoustics, London, UK.

Mulhoffer L. (1933). "Untersuchungen uber der Schwebstoff und Geschiebefurung des Inn nachst Kirchbichl, Tirol," Wasserwirtschaft, pp 1- 6.

Reid, I., Layman, J.T., and Frostick, L.E. (1980). "The continuous measurement of bedload discharge," Journal of Hydraulic Research, 18, pp 243-249.

Rouse, H.L. (1994). "Measurement of bedload gravel transport; the calibration of a self-generated noise system," Earth Surface Processes and Landforms, 19, pp 789-800.

Slingerland, R., Willett, S.D., and Hennessey, H.L. (1997). "A new fluvial bedrock incision model based on the work-energy principle," EOS Transactions, Am. Geophysical Union 78(46), p F299.

Sklar, L.S. and Dietrich, W.E. (1998). "River longitudinal profiles and bedrock incision models: Stream power and the influence of sediment supply," in Tinkler, K. and Wohl, E.E., (eds) 1998, Rivers Over Rock: Fluvial Processes in Bedrock Channels, Geophysical Monograph Series 107, Am. Geophysical Union, Washington, D.C., pp237-260.

Thorne, P.D. (1985). "The measurement of acoustic noise generated by moving artificial sediments," Journal of the Acoustical Society of America, 78, pp 1013-1023.

Thorne, P.D. (1986). "Laboratory and marine measurements on the acoustic detection of sediment transport," Journal of the Acoustical Society of America, 80(3), pp 899-910.

Thorne, P.D., Heathershaw, A.D., and Triano, L. (1984). "Acoustic detection of seabed gravel movement in turbulent tidal currents," Marine Geology, 54, pp M43-M48.

Thorne, P.D., Williams, J.J., and Heathershaw, A.D. (1989). "In situ measurements of marine gravel threshold and transport," Sedimentology, 36, pp 61-74.

Tywoniuk, N., and Warnock, R.G. (1973). "Acoustic detection of bed-load transport," Proc. of Hydrology Symposium at University of Alberta, Edmonton, May 8 and 9, 1973, Department of Environment Natural Resource Council, Canada, pp 728-735.

Voulgaris, G., Wilkin, M.P., and Collins, M.B. (1994). "Shingle movement under waves & currents: An instrumented platform for field data collection," in Arcilla, A.S., Stive, M.J., Kraus, N.C. (eds.) Coastal Dynamics '94, American Society of Civil Engineers, pp 894-909.

Voulgaris, G., Wilkin, M.P., and Collins, M.B. (1995). "The in situ passive acoustic measurement of shingle movement under waves and currents: instrument (TOSCA) development and preliminary results," Continental Shelf Research, 15(10), pp 1195-1211.

Whiting, P.J., Dietrich, W.E., Leopold, L.B., Drake, T.G., and Shreve, R.L. (1988). "Bedload sheets in heterogeneous sediment," GEOLOGY, 16 (2), pp 105–108.

SEDIMENT TRACKING: A COMPLEMENTARY METHOD FOR MEASUREMENT OF SEDIMENT TRANSPORT IN RIVERS

Kevin Black, Sam Athey, Peter Wilson, Partrac Ltd., Glasgow, Scotland, info@partrac.com

Abstract: A range of techniques and methods are routinely used to provide insights into, and to quantify, the transport dynamics of sediments in rivers. These include high resolution flow speed or stage records, proxy-measurement of suspended solids concentration (e.g. using optical or acoustic sensors) and a variety of sediment traps. This presentation aims to introduce a complementary technique known as 'sediment tracking' to fluvial sediment studies. The sediment tracking method is a Lagrangian technique which utilizes uniquely labeled sediment analogs to determine the transport in time and across space. Historically, sediment tracking has encountered greater use in gravel-bed mountain streams but recent developments in the technique now permit useful data to be obtained for both sand and silt transport. Sediment tracking has several distinct advantages over conventional measurement approaches. It provides a direct indication of sediment transport rate, and is of particular use in defining specific source regions (e.g. stream bed, adjacent fields) an in-stream depo-centers. Moreover, it is a relatively cheap technique which simple to use. This paper presents the central factors involved in conducting a tracking study. We also describe a new, time-series suspended sediment sampler, which has been used in sediment tracking studies but which also forms a stand-alone sediment/contaminant flux monitoring instrument

GEOMORPHIC RESPONSE OF RIVERS TO DAM REMOVAL: NEW INSIGHTS FROM FLUME EXPERIMENTS AND FIELD STUDIES

Gordon E. Grant, Research Hydrologist, USDA Forest Service, Pacific Northwest Research Station, Corvallis, OR, ggrant@fs.fed.us ; Chris Bromley, Graduate Student, Department of Geography, University of Nottingham, Nottingham, UK, lgxjcb@nottingham.ac.uk; Gregory Stewart, Graduate Student, Department of Geosciences, Oregon State University, Corvallis, OR Gregory.Stewart@oregonstate.edu

Abstract: Faced with an aging national infrastructure of thousands of dams and reservoirs, dam removal is emerging as an option for restoring some semblance of natural fluxes of water, sediment, and organisms to rivers. Predicting geomorphic and ecologic response to dam removal is both an exciting research topic and important management and policy question. Until quite recently, however, scientific studies addressing the consequences of dam removal were rare.

New field and flume studies are providing the foundation for an analytical framework that predicts the geomorphic response of rivers to dam removal. A critical component of this framework is the distinction between reservoirs that are partially as opposed to fully filled with sediment. For reservoirs completely filled with sediment, dam removal initiates a cascade of geomorphic processes including knickpoint retreat, incision, and lateral migration within the former reservoir, leading to a rapid release of a pulse of sediment downstream. Migration of this pulse downstream promotes other geomorphic adjustments, including pool filling and bar and bed sedimentation and fining. Longevity of these changes is scaled to both the volume of sediment release and the post-removal sequence of flows.

For reservoirs only partially filled with sediment at the time of removal, a very different suite of geomorphic processes occur in the upstream reservoir, primarily delta incision and downstream progradation of accumulated sediment. Grain sorting of the migrating sediment, stranding and isolation of residual sediment as terraces, and armoring of the newly exposed channel bed, make prediction of sediment efflux from the former reservoir difficult (Fig 1). This efflux is further influenced by both the dam removal scenario employed (i.e., instantaneous versus staged removal) and flow sequence. A different downstream response is predicted than in the case of filled reservoirs, notably an initially fine sediment pulse followed by a supply of progressively coarser bedload as the delta migrates downstream.

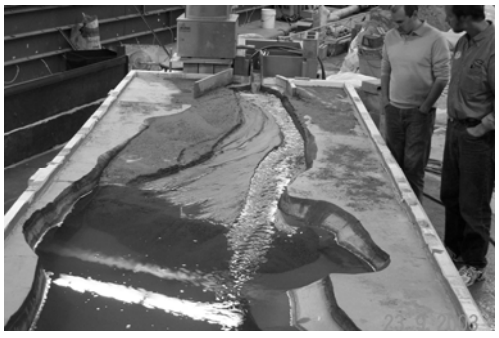


Figure 1 Laboratory model of Lake Mills, Elwha River, WA during experimental removal of Glines Canyon Dam. Note terraces abandoned during incision of the reservoir delta.

SEDIMENT DYNAMICS POST DAM REMOVAL: STATE OF THE SCIENCE AND PRACTICE

The EWRI/ASCE Task Committee on Sediment Dynamics Post Dam Removal: Laura Wildman, Chairman, Glastonbury, CT, lwildman@amrivers.org; Cassie Klumpp, Vice Chairman, Denver, CO, CKLUMPP@do.usbr.gov; Blaire Greiman, Secretary, Denver, CO, BGREIMAN@do.usbr.gov; James MacBroom, Committee Member, Cheshire, CT, jimm@miloneandmacbroom.com; Martin Doyle, Committee Member, Chapel Hill, NC, mwdoyle@email.unc.edu; Yantao Cui, Committee Member, Berkeley, CA, yantao@stillwatersci.com; Rollin Hotchkiss, Committee Member, Spokane, WA, rhh@wsu.edu

Abstract: In July 2005 the EWRI/ASCE Task Committee on Sediment Dynamics Post Dam Removal brought together the majority of the national experts, both in research and practice, on the specific topic of sediment dynamics post dam removal. 25 papers were presented regarding the state-of-the-science and state-of-the-practice in considering sediment remobilization and channel dynamics once a dam has been removed. Additional papers reflecting current approaches on this topic were then added to the initial 25 and compiled into a monograph. Authors included representation from federal agencies, universities, consulting firms, environmental non-profit organizations, federal and academic research laboratories, as well as state agencies, and included engineers, geomorphologists, academic researchers, hydraulic/hydrologic modelers, model developers, ecologists, and fish biologists. The papers compiled reflect the large regional and project specific variety relating to this topic. Subjects covered span from physical models, to numerical simulations, to specific case studies, to decision making processes, to individual dam scale issues, to geomorphic changes, to channel bed evolution, to downstream sediment transport, to ecological implications, to lessons learned, and to sediment quality, and encompass the wide variety in sediment composition, hydrologic region, and project scale. The monograph therefore represents the best compilation to date of data on this topic. Our paper will summarize the findings in the monograph papers, and therefore the many national ongoing efforts and the state-of-the-science/practice in the field of sedimentation as it relates to river dynamics post dam removal.

NATURAL RESOURCES CONSERVATION SERVICE WATERSHED REHABILITATION IN OKLAHOMA A GEOLOGICAL PERSPECTIVE

Glen B. Miller, Geologist, Natural Resources Conservation Service, 100 USDA, Suite 206, Stillwater, Oklahoma 74074, Glen.Miller@ok.usda.gov

Abstract: As floodwater control structures begin to approach the end of their functional life, Natural Resources Conservation Service (NRCS) must determine the best course of action to be taken to prevent potential damage to downstream facilities, such as mobile homes, church camps, and suburban residential areas, many of which have been built during the past few decades and since construction of the dams. NRCS continues to work with local communities to identify and rehabilitate dams that could become a threat to public health and safety. Rehabilitation will not only ensure that these flood control dams remain safe, but that they will continue to provide flood control, recreation and wildlife habitat for the next 50 to 100 years. It is the responsibility of the NRCS geologist in Oklahoma to provide the geological expertise to help ensure that these structures have adequate storage, foundations and appurtenances to function properly for the life of the structure.

Some geologic considerations that must be taken into account are:

1. Soluble geologic materials within the embankment, such as gypsum or anhydrite, which may contribute to dissolution and lead to seepage and/or structural failure.
2. Soils within secured easement areas adjacent to the existing structure or within the existing sediment pool must provide suitable borrow material and occur in adequate quantity for modification of the dam.
3. In cases where the auxiliary spillway must be widened to accommodate new discharge volumes, materials occurring there must be properly characterized to allow for a proper design.
4. Materials in the existing embankment foundation must be competent to withstand increased volumes of water should the dam height be raised to increase storage.
5. In cases where decommissioning is a viable option, effects on downstream facilities must be taken into consideration.
6. Dispersive and low plasticity soils and geologic materials, highly faulted geologic formations within the area, and karst features are just some of the geologic hazards that might have a significant impact on planning, design, and construction of dams.

A team of planning engineers, design and project engineers, surveyors, local field office and conservation district personnel must provide suitable alternatives for modification of these structures. As all parties work together, it is possible to achieve the desired effect: a safe and functional dam that will serve the local community for years to come.

INTRODUCTION

Background: The USDA Natural Resources Conservation Service (NRCS) has provided technical and financial assistance to local sponsors for the development of water resources projects since the 1940s. This assistance has been provided primarily through four programs: the

Flood Control Act of 1944 (P.L. 78-534), the Watershed Protection and Flood Prevention Act of 1954 (P.L. 83-566), the Pilot Watershed Program (transitional between P.L. 78-534 and P.L. 83-566) and the Resource Conservation and Development (RC&D) Program.

Watershed projects, which are organized and operated by local sponsors, provide flood control, municipal and irrigation water supply, recreation, erosion control, and wildlife habitat enhancement on more than 130 million acres nationwide.

Congress passed the Watershed Rehabilitation Amendments of 2000, authorizing NRCS to provide technical and financial assistance to watershed project sponsors in rehabilitating their aging dams. The purpose of rehabilitation is to extend the service life of the dams and bring them into compliance with applicable safety and performance standards or to decommission the dams so they no longer pose a threat to life and property.

DAM REHABILITATION TODAY

Needed Rehabilitation: Today, many project areas are in a far different setting than when they were originally constructed. Population has grown, residential and commercial development has occurred upstream and downstream from the dams, land use changes have taken place, sediment pools have filled with sediment, structural components have deteriorated, and many structures do not meet state dam safety regulations that have become more stringent through time.

Many of these dams lie in upstream agricultural areas and are unknown to the residents who are protected by them. Many are quietly deteriorating as time and weathering take their toll on the components. Unless something is done to rehabilitate these dams or, in some cases, to remove them, they pose a public safety concern.

As shown in Figure 1, 132 dams in Oklahoma (2005) were at or beyond design life. By the year 2015, 1090 dams in Oklahoma alone will be at or beyond design life. As of 1999, 2245 dams within 22 states were in need of rehabilitation. Many of these dams were designed to protect agricultural areas in downstream floodplains. In numerous communities, homes and businesses eventually were built downstream from the dams.

Nationally, two-thirds of the small flood control dams constructed to date are more than 30 years old. Many of the dams can function beyond the original design life with continued maintenance and rehabilitation.

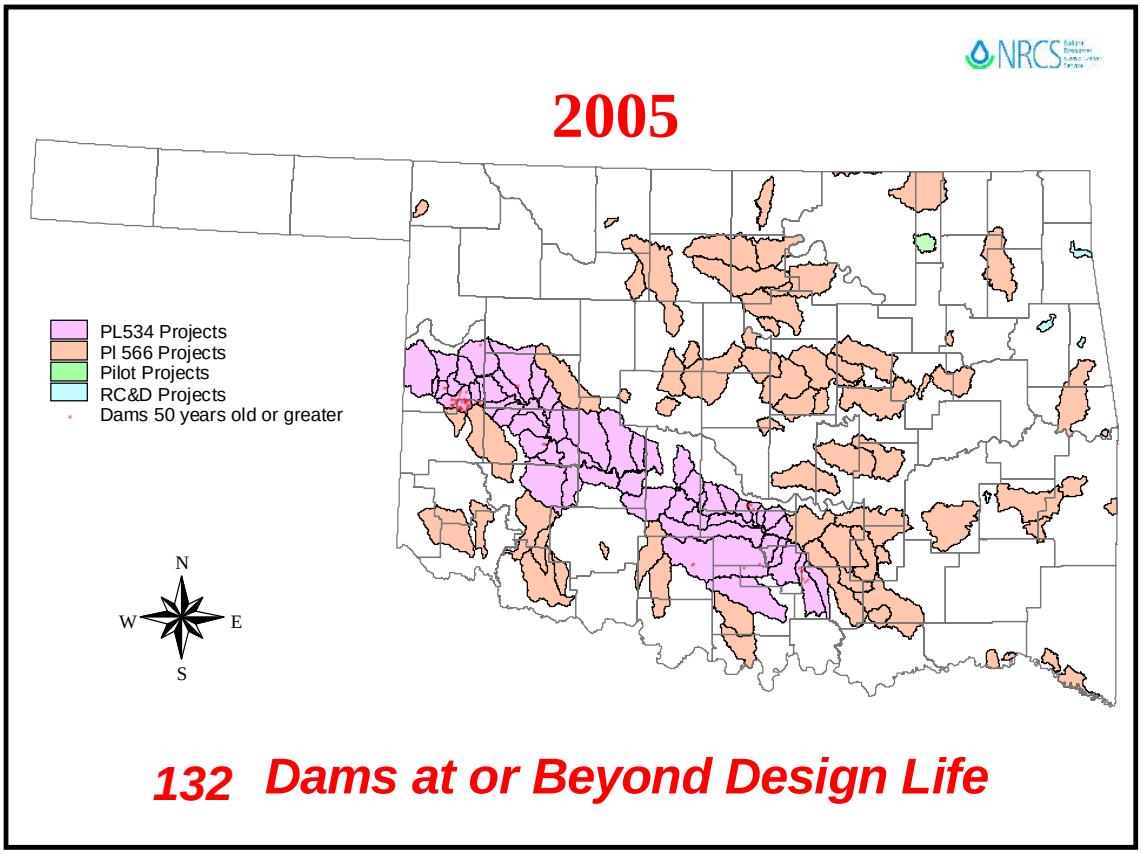


Figure 1 Status of dams needing rehabilitation in Oklahoma.

Common Rehabilitation Approaches: There are many approaches to rehabilitation of flood control dams. Any alternative considered and the final selected approach must be determined on the economic, environmental, and social merits of the site-specific project; there is no single solution for rehabilitation of all flood control dams. Common approaches to consider include the following:

- Remove sediment from the reservoir: Removing the sediment from the reservoir and disposing of it at an environmentally safe location can extend the life of a flood control dam. The sediment must be tested for potential contaminants, such as pesticides, oil field waste, and other toxins.

- Increase the height of the dam: Raising the embankment to provide additional storage for future sediment accumulation can extend the life of the dam and accommodate other resource needs.

- Remove the dam (decommissioning): In some projects, removal of the dam in an environmentally safe manner is an option. Obvious challenges include providing adequate grade control in the drainage way if significant sediment has been deposited in

the reservoir. Social, economic, and legal ramifications of the loss of downstream flood control must be evaluated.

- Increase the capacity of or replace the principal spillway: This approach would address greater amounts of runoff from the watershed above the dam due to residential and/or commercial development, or provide higher capacity discharge due to changed safety or design criteria. As above, social, economic, and legal ramifications of the increased flows downstream must be evaluated.

THE GEOLOGIST AND REHABILITATION

The geologist's role: The geologic investigation is crucial in determining alternatives for consideration in design of the dams targeted for rehabilitation. It forms the basis for the decisions that will be made, including soil mechanics analysis, design, construction, and operation and maintenance. The investigative procedures rely on the use of sound geomorphic, geologic, and investigative principles. With experience and conscientious effort, the geologist should be able to eliminate major surprises that can adversely affect the life and safety of the dam.

The objectives of geologic investigations are: 1) to determine and describe for other technical disciplines the geologic conditions at the specific site to be rehabilitated; 2) to interpret how these conditions will impact the design, construction, and operation of the structure; and 3) to provide representative field tests and collect samples for laboratory analysis (Fig. 2).



Figure 2 Collecting Split Tube Soil Samples, Oklahoma.

Geologic Site Considerations: Several geologic hazards or precautions have been noted within the state of Oklahoma as experience is gained through rehabilitation efforts state-wide. A few examples are provided:

- Soluble geologic materials within the embankment, pool areas, or other areas within the vicinity of the dam may cause concern. With time and continued seepage of water into the subsurface materials, gypsum or anhydrite is dissolved, and cavities or sinks form, providing avenues for water to seep through or under the embankment and eventually cause damage to the dam (Fig. 3).

- An adequate supply of usable soils must be located from within the borrow areas upstream and downstream of the dam, and quantified for use in the foundation, embankment, and auxiliary spillways. In Oklahoma, the existence of highly dispersive soils within formations of the Pennsylvanian and Permian bedrock materials and associated residual soils forming from these strata is a particular problem. It is, therefore, especially important to isolate, so far as possible, where these soils are located and in what quantity so they may be properly treated and placed in low risk zones within the embankment.

- In cases where the auxiliary spillway must be widened to accommodate potentially higher discharge velocities and volumes, materials occurring there must be properly characterized to allow for a proper design. The rock material properties are determined from examination of hand specimens, core sections, drill cuttings, outcrops, and disturbed samples.

- Many times, the existing dam must be replaced with properly compacted soil material in order to withstand increased volumes of water due to increased dam heights or greatly widened auxiliary spillways. More stringent engineering requirements due to hazard classification changes have been necessitated due to urban buildup downstream and within the watershed of many of these dams.



Figure 3 Sink Hole in Drained Sediment Pool, SW Oklahoma.

- Channel flow characteristics, changes in grade of the channel, and differing bed load will all be affected when the embankment is removed, and these impacts must also be carefully considered.

- Other considerations that may have a significant impact on planning, design, construction, and maintenance of the new dam are low plasticity soils, high shrink-swell soils (Fig. 4) and faulted geologic formations.



Figure 4 Desiccation Cracks in High Shrink-Swell Soils

CONCLUSIONS

Ultimately, it is incumbent upon the geologist to ensure that a professional geologic investigation is conducted and that the best, most cost effective tools available through training, experience and sound judgment are utilized. The geologist has the responsibility to gather not only the best tools available, but also to draw from the experience and judgment of engineers, water resource planners, contractors, local conservation district employees and NRCS field office personnel. Working as a team, these professionals are well equipped to provide a safe, economical, and socially acceptable dam that can serve the local community for years to come.

REFERENCES

Kearney, J.L. (1992). "Discoveries by a Geologist-No Surprises," Bulletin of the Association of Engineering Geologists,Vol. XXIX, No. 1, 1992, pp 87-90.

Natural Resources Conservation Service, USDA (2000). A Report to Congress on Aging Watershed Infrastructure. 15 p.

Natural Resources Conservation Service, USDA (2002). "Rock Material Field Classification System," National Engineering Handbook, 210-VI, Part 631, Chapter 12, 12 p.

Natural Resources Conservation Service, USDA (2003). Watershed Rehabilitation, A Progress Report. 4 p.

NUMERICAL SIMULATION OF CHANNEL ADJUSTMENT OF THE KALAMAZOO RIVER FOLLOWING THE REMOVAL OF TWO LOW-HEAD DAMS BETWEEN OTSEGO AND PLAINWELL, MICHIGAN

Eddy J. Langendoen, Research Hydraulic Engineer, USDA-ARS-NSL, Oxford, MS, elangendoen@msa-oxford.ars.usda.gov; Robert R. Wells, Research Hydrologist, USDA-ARS-NSL, Oxford, MS, rrwells@msa-oxford.ars.usda.gov

Abstract: The state of Michigan is interested in removing two low-head dams in an 8.8 km reach of the Kalamazoo River between Plainwell and Otsego, Michigan while minimizing impacts to the study reach and downstream reaches. The study was designed to evaluate the erosion, transport, and deposition of sediments over a 38-year period using the channel evolution model CONCEPTS for three simulation scenarios: Dams In, Dams Out, and Design. The total mass of sediment emanating from the channel boundary for the Dams In case shows net deposition of 8,760 T/y for the study reach, with net transport (suspended and bed load) of 10,500 T/y passing the downstream boundary. For the Dams Out case, there is net erosion of 9,180 T/y with net transport of 30,100 T/y passing the downstream boundary. For the Design case, net deposition was 9,070 T/y with transport of 14,200 T/y passing the downstream boundary. The most significant finding is that removal of the low-head dams will cause significant erosion of PCB-contaminated bed and bank material upstream of the dams.

INTRODUCTION

Between the mid 1800s and the early 1900s, four dams were constructed on the Kalamazoo River between Plainwell and Allegan, Michigan (see Fig. 1). Three hydroelectric dams (Trowbridge, Otsego, and Plainwell) were decommissioned as power generators in the mid 1960s, and by 1970 the Michigan Department of Natural Resources had assumed responsibility for the structures. The Otsego City Dam, which still remains in operation, was originally built to create freight business on the river but has since been providing a continuous industrial water supply for a papermill built in the 1880s. The impoundments have been the depositories of upstream sediment and industrial waste materials. Between 1957 and 1971, Kalamazoo area paper mills recycled carbonless copy paper containing polychlorinated biphenyls (PCBs) as ink solvent and incorporated these PCBs in their waste discharge. The paper wastes also included kaolinite clays, which were found in the impoundment sediments to contain concentrations of PCBs as high as 94 mg per kg (Blasland, Bouck & Lee 1994). During the 1960s, water levels behind the decommissioned hydroelectric dams were lowered, exposing the previously inundated material. In response to the lowering of water levels, the river began to erode the sediments and transport them downstream, but much of this waste clay remains impounded behind the dams mainly as floodplain deposits (Rheaume et al. 2002; 2004).

The state of Michigan is interested in removing the dams while minimizing impacts to the study reach and downstream reaches, and to provide for improved fisheries. Concerns over the fate of PCB-laden channel sediments in the Kalamazoo River between Plainwell and Otsego, especially its release by bank erosion, resulted in the U.S. Geological Survey (USGS) supporting a study by the USDA-ARS National Sedimentation Laboratory to simulate sediment loads and channel changes in the reach.

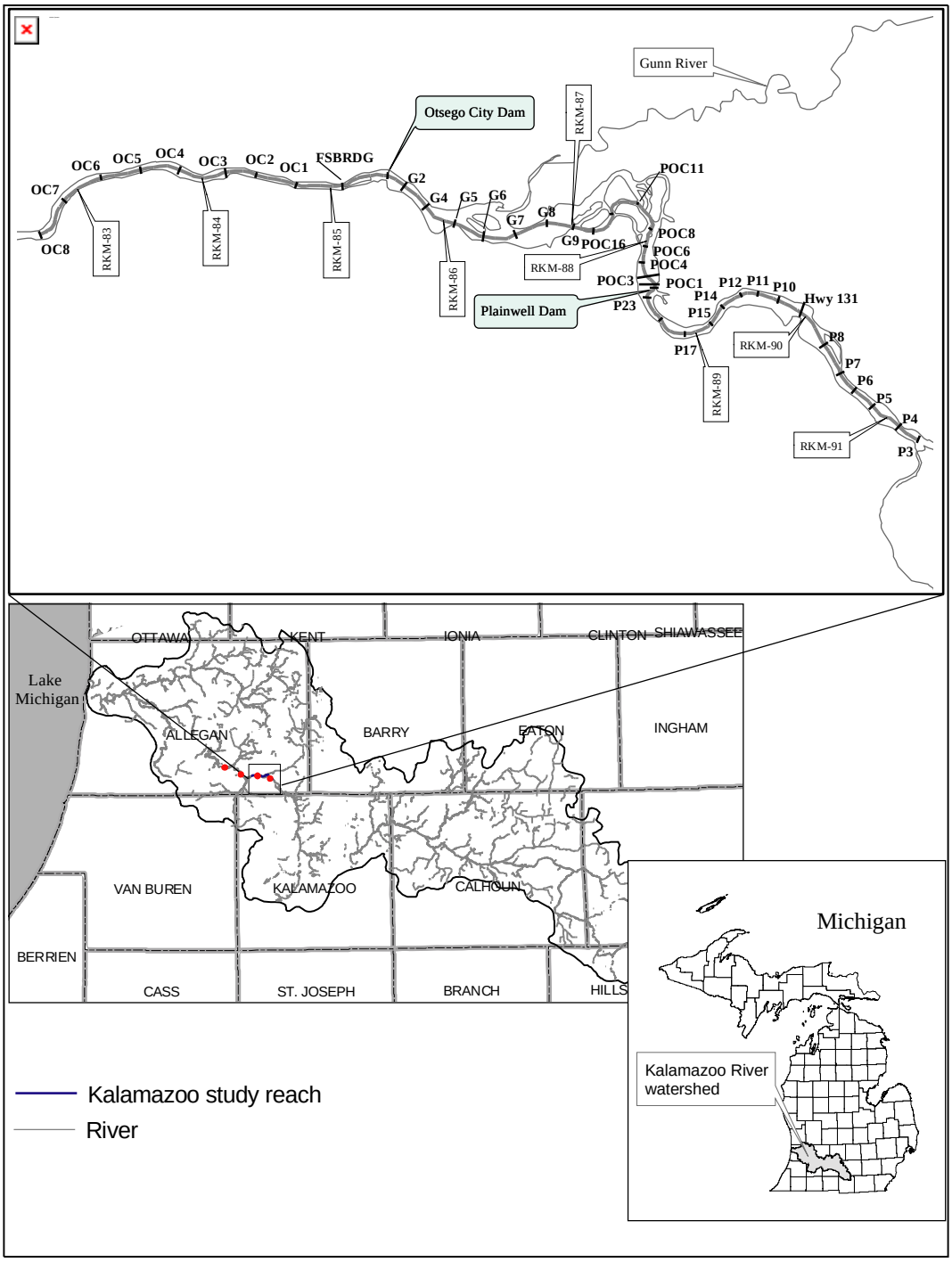


Figure 1 Map of study reach showing modeled cross sections and locations of the Plainwell and Otsego City Dams.

MODELING APPROACH

The PCBs between Plainwell and Otsego are mainly adsorbed onto fine-grained sediments comprising parts of the streambed, and most of the banks and floodplains. Prediction of the

erosion, transport and deposition of these materials after dam removal requires a model that can simulate streambank erosion processes as well as the conventional hydraulic and entrainment processes typical of non-cohesive sediments. The CONCEPTS (CONservational Channel Evolution and Pollutant Transport System) channel-evolution model, developed by the USDA-ARS National Sedimentation Laboratory (Langendoen 2000; 2002) provides for a deterministic simulation of these processes and allows for identification of sediment sources by particle-size class. In this way, river managers and action agencies involved with the Kalamazoo River can make informed decisions regarding stream rehabilitation measures. CONCEPTS has been successfully used in similar morphological studies of incised stream systems (Bingner and Langendoen 1997; Langendoen et al. 2000; Langendoen et al. 2002; Simon et al. 2002).

The one-dimensional model, CONCEPTS, simulates unsteady flow, graded-sediment transport, and bank-erosion processes in stream corridors (Langendoen 2000). Channel evolution is computed by tracking bed changes and channel widening. Bank erosion is a combination of flow-induced basal scour and mass wasting (slab or planar and cantilever type bank failures). Streambanks may be composed of soil layers with different material properties. Transport of cohesive and cohesionless sediments, both in suspension and on the bed, are simulated selectively by size class. CONCEPTS is limited to straight channels or channels of low sinuosity, 14 pre-determined sediment particle-size classes, homogeneous bed-material across the channel, and steady pore-water pressure in the streambank.

To estimate volumes and rates of sediment transport within the study reach and to address specific objectives of the study, three modeling scenarios were identified, one representing current channel conditions and two others representing alternative schemes. The three scenarios are termed: (1) “Dams In” (DI) or baseline, (2) “Dams Out” (DO), and (3) “Design” (D). The DI scenario assumes current channel geometries and boundary sediments as initial conditions. This simulation is used as a baseline by which to compare the two alternative scenarios in terms of gross amounts of channel change, the mass of material eroded from channel banks, and fine-grained sediment transport. The DO scenario also assumes current channel geometries as initial conditions but with the Plainwell and Otsego City Dams no longer in place, leaving 3 to 4 m-high knickpoints. This simulation does not model a dam breach, only the resulting hydraulic and sediment-transport processes associated with the “instantaneous” change resulting from removal of the non-erodable structures. Finally, the Design scenario also assumes that the two dams are no longer in place; however, a design channel geometry is used instead of the current channel geometry for initial conditions.

STUDY AREA

The modeling reach of the Kalamazoo River extends 8.8 km from approximately 82.4 km above the confluence with Lake Michigan (cross-section OC8), to cross-section P3, approximately 91.2 km above the confluence with Lake Michigan (Fig. 1). The study area can be separated into three distinct sub-reaches based on location relative to the Plainwell and Otsego City Dams. The Otsego (OC) reach extends from km 82.4 to the Otsego City Dam at km 85.3. The Plainwell-Otsego (POC) reach extends from the upstream end of the Otsego City Dam to the Plainwell Dam at km 88.3. The Plainwell (P) reach extends from the Plainwell Dam to the upstream boundary of the study reach at km 91.2.

Flows for all three simulation scenarios are based on a modified 17.7-year discharge record (October 1984 to June 2002) from the USGS gage on the Kalamazoo River at Comstock, Michigan (04106000). This period was selected because it provides the most recent continuous period of flow record. The discharge record was used to construct a time series of flow covering the simulation period from August 2000 through November 2037. The start of the simulation period coincides with dates the modeling reach was surveyed.

The Kalamazoo River is anastomosing along the upper half of the POC reach. CONCEPTS simulates flow in a single-thread channel. Velocity measurements by Rheaume et al. (2004) show the existence of a main thread carrying about 75 to 90% of the flow. The anastomosing segment is therefore simulated as a single thread, withdrawing: (1) 30% of the flow at section POC6 and returning it at section POC16; and (2) 20% of the flow at section G9 and returning it at section G6 (Fig. 1). The water is returned to the channel, whereas the sediment is deposited. This is supported by the study of Rheaume et al. (2004), which shows that the side channels are filling in.

Bed- and bank-material composition and geotechnical properties at each cross section were provided by testing and sampling conducted by the ARS, laboratory analysis by the USGS, and from historical data. Wells et al. (2004) tabulate the bank- and bed-material properties used in the simulations.

Roughness values (Manning's n) were assigned to bed, bank, and floodplain sections of each cross section based on visual inspection of the channel and using guidelines set forth by Chow (1959). Calibration was carried out to match observed water surface elevations along the modeling reach. In general, roughness values for the channel bed and banks ranged from 0.025 to 0.04; for the floodplain, values ranged from 0.05 to 0.1.

RESULTS AND DISCUSSION

Dams In Scenario: The DI modeling scenario represents a baseline condition with existing channel geometries (including the low-head dams) and boundary characteristics. Within the P reach, deposition upstream of the HWY 131 bridge crossing (rkm 90) is predicted. This deposition is predicted for all three scenarios; however, it is not supported by observations. As a result, simulated sediment loads at the downstream end of the P reach may be underpredicted. Fig. 2 further shows progressing simulated deposition upstream of the Plainwell Dam (rkm 88-89), but minor channel changes along the POC and OC reaches. Table 1 summarizes the mass of material eroded from (positive) or deposited on (negative) the channel boundary for the three reaches. Results shown in Table 1 are broken down by location (bed or banks) and by general particle-size class. The finer fractions (<63 μm and <10 μm) onto which the PCBs may be adsorbed are of particular interest. The simulated average-annual sediment load (suspended and bed load) at the downstream boundary of the study reach (OC8) is 10,500 T/y with 98% of this material (10,300 T/y) finer than 63 μm.

Dams Out Scenario: The Dams Out scenario has been evaluated using existing channel morphologies except for the removal of the non-erodable sections representing the Plainwell and Otsego City Dams. During the simulation, large-scale erosion of the channel bed in the

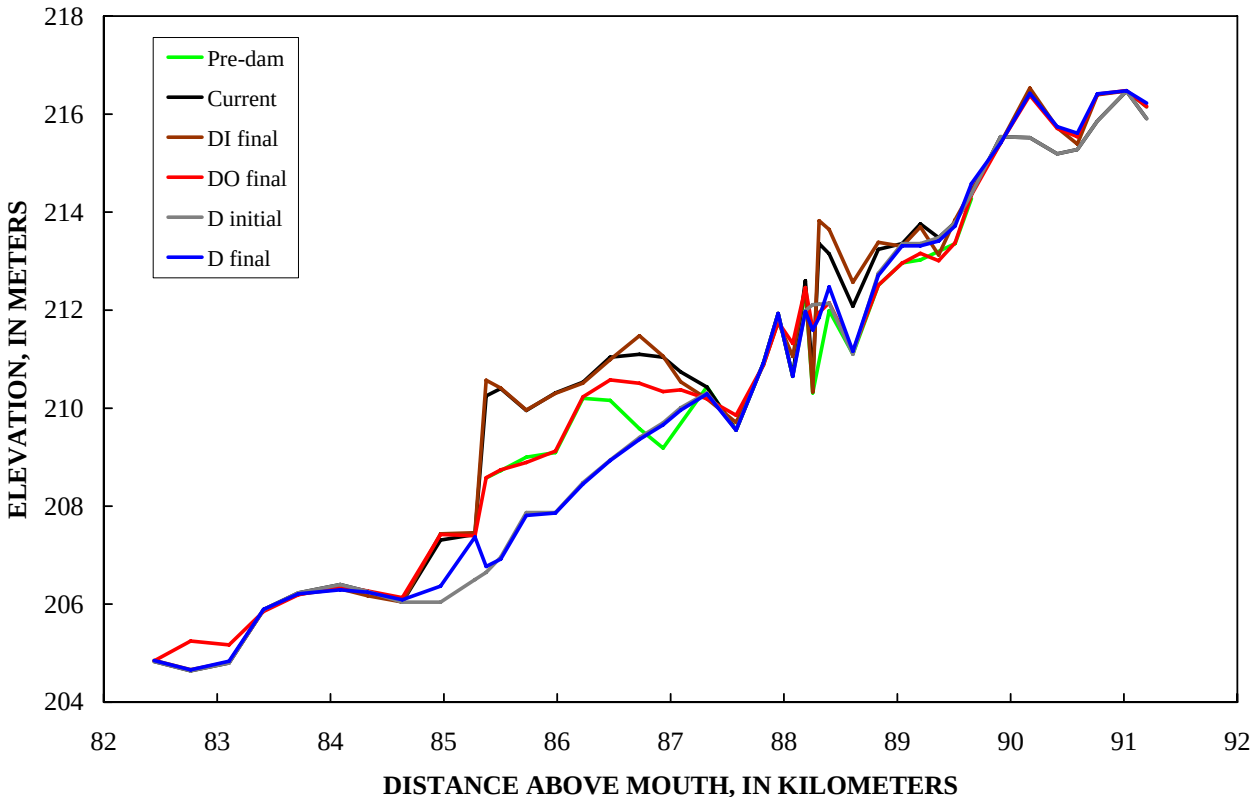


Figure 2 Initial and final thalweg profiles for the Dams In (DI), Dams Out (DO), and Design (D) modeling scenarios.

Table 1 Mass of sediment eroded (+) or deposited (-) in T/y for the Dams In modeling scenario.

	Total			Bank			Bed		
Reach	Total	<63 μm	<10 μm	Total	<63 μm	<10 μm	Total	<63 μm	<10 μm
P	(6,410)	(684)	341	0	0	0	(6,400)	(682)	341
POC	(4,070)	(2,910)	(311)	157	87.6	60.0	455	605	226
OC	1,720	2,000	631	0.061	0.014	0.009	1,730	2,000	631
Total	(8,760)	(1,590)	661	157	87.6	60.0	(4,220)	1,930	1,200

Plainwell and POC sub-reaches occurred as knickpoints migrated headward through these sub-reaches as a direct result of simulated dam removal (Fig. 2). Fig. 3 shows that the channel upstream of the Otsego City Dam rapidly incises to the coarse pre-dam bed-material and widens ensuingly. Table 2 shows bank erosion increased from 157 T/y for the DI scenario to 3,000 T/y, with an increase in eroded bed material of 20,500 T/y. Simulated average-annual sediment load at the outlet for the Dams Out case is 30,100 T/y, three times greater than the baseline case. However, the mass of fine-grained materials (finer than 63 μm) transported beyond the downstream boundary reduced to 8,860 T/y, which is caused by a coarsening of the bed-material resulting in an increase of the fraction of sand in transport.

Design Channel Scenario: The USGS designed a channel to minimize the scour of PCB-laden channel sediments after the removal of the Plainwell and Otsego City Dams. Fig. 2 shows that

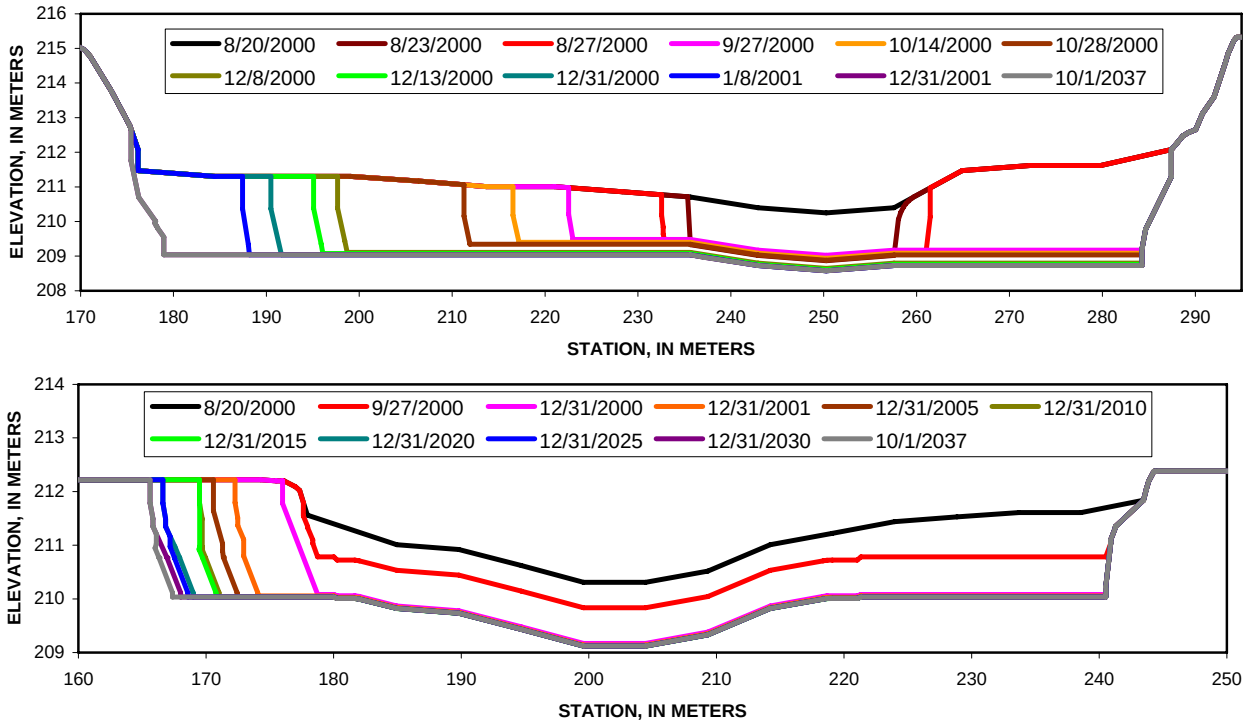


Figure 3 Simulated changes in geometry of cross section G1 (top, rkm 85.4) and cross section G5 (bottom, rkm 86.0)

Table 2 Mass of sediment eroded (+) or deposited (-) in T/y for the Dams Out modeling scenario.

	Total			Bank			Bed		
Reach	Total	<63 μm	<10 μm	Total	<63 μm	<10 μm	Total	<63 μm	<10 μm
P	512	(1,410)	340	232	98.1	51.7	289	(1,510)	288
POC	(719)	(3,950)	470	2,743	1,180	817	6,580	(547)	170
OC	9,390	637	30.1	22.6	5.13	3.29	9,380	638	27.1
Total	9,180	(4,720)	839	3,000	1,280	872	16,200	(1,420)	485

the thalweg profile of the design channel matches the pre-dam profile, except upstream of the Otsego City Dam where the design streambed is located within the pre-dam bed material. Multi-thread sections designed for the POC reach are handled identically to those sections in the DI and DO modeling scenarios. Streambeds of excavated cross sections are assigned material composition and properties found at the level of excavation.

Minor changes in streambed elevation are simulated (Fig. 2). Table 3 shows that the amount of bed and bank-material eroded along the modeling reach is similar to that of the DI scenario. The simulated average-annual total sediment load at the outlet (14,200 T/y) is slightly larger than that of the DI scenario. Similar to the DO scenario, fine-grained sediment loads at the downstream boundary (8,410 T/y) are slightly smaller than for the DI scenario.

Table 3 Mass of sediment eroded (+) or deposited (-) in T/y for the Design modeling scenario.

	Total			Bank			Bed		
Reach	Total	<63 μm	<10 μm	Total	<63 μm	<10 μm	Total	<63 μm	<10 μm
P	(4,580)	(349)	519	112	51.7	37.0	(4,680)	(397)	482
POC	(6,060)	(5,530)	(241)	272	59.6	36.6	176	(1,400)	3.58
OC	1,560	199	139	0	0	0	1,570	200	139
Total	(9,070)	(5,680)	417	385	111	73.5	(2,940)	(1,600)	624

Table 4 Average annual sediment load at the downstream boundary of the modeling reach.

	Sediment load in kilotonnes/year		
Scenario	< 63 μm	< 2 mm	Total
DI	10.4	10.5	10.5
DO	8.9	25.9	30.1
DO (year 1-3)	43.7	114.0	127.0
DO (year 4-38)	6.5	20.0	23.6
D	8.4	13.9	14.2

SUMMARY AND CONCLUSIONS

Three numerical simulations are carried out over a 38-year period to evaluate the response of the Kalamazoo River between Plainwell (rkm 91.2) and Otsego (rkm 82.4), Michigan to current channel conditions (DI), instantaneous removal of two low-head dams (DO), and a design channel without the low-head dams (D).

Sediments eroded from the channel boundary and downstream sediment load are similar and fairly low for the DI and D scenarios, indicating a stable stream system. Removal of the low-head dams induces severe channel bed and streambank erosion upstream of the former dam locations, significantly increasing sediment load. However, most of these sediments are eroded in the first three years (Table 4). The quantities of fine-grained material (< 63 μm) transported past the downstream boundary over the last 35 years of the simulation are similar to those of the DI and D scenarios. Therefore, most of the channel adjustment due to dam removal occurs in the first three years of the simulation.

If the dams have to be removed, mitigation measures should be considered to prevent PCB-contaminated sediment from being eroded. One mitigation measure is channel reconstruction based on the designed channel (D scenario). The designed channel appears to be stable. Some minor streambank erosion may occur between rkm 88.0 and 88.8 near the current location of the Plainwell Dam.

REFERENCES

Bingner, R. L., and Langendoen, E. J. (1997). "Impact of instream structures on channel evolution within Goodwin Creek Watershed," in Management of Landscapes Disturbed by

Channel Incision, S. S. Y. Wang, E. J. Langendoen, and F. D. Shields Jr., eds., University, MS, p. 765.

Blasland, Bouck & Lee (1994). Allied paper, Inc./Portage Creek/Kalamazoo River Superfund site remedial investigation/feasibility study. Tech. Memorandum 10, Sediment Characterization/Geostatistical Pilot Study, Vol. I-III.

Chow, V. T. (1959). Open-channel Hydraulics. McGraw Hill, New York, NY., 680p.

Langendoen, E. J. (2000). CONCEPTS - CONservational Channel Evolution and Pollutant Transport System. Research Rep. 16, U.S. Department of Agriculture, Agricultural Research Service, National Sedimentation Laboratory, Oxford, MS.

Langendoen, E. J. (2002). "CONCEPTS: A process-based computer model of instream hydraulic and geomorphic processes," Proc. Second Federal Interagency Hydrologic Modeling Conf., July 28-August 1, 2002 Las Vegas, NV, on CDROM.

Langendoen, E. J., Simon, A., and Alonso, C. V. (2000). "Modeling channel instabilities and mitigation strategies in eastern Nebraska," 2000 Joint Conf. on Water Resour. Eng. and Water Resour. Planning and Management, July 30-August 2, 2000, Minneapolis, MN, R. H. Hotchkiss and M. Glade, eds., ASCE, Reston, VA, on CDROM.

Langendoen, E. J., Thomas, R. E., and Bingner, R. L. (2002). "Numerical simulation of the morphology of the Upper Yalobusha River, Mississippi between 1968 and 1997." River Flow 2002, Proc. Int. Conf. Fluvial Hydraulics, 4-6 September, 2002, Louvain-la-Neuve, Belgium, D. Bousmar and Y. Zech, eds., A. A. Balkema Publishers, Lisse, The Netherlands, pp. 931-939.

Rheaume, S. J., Hubbell, D. L., Rachol, C. M., Simard, A., and Fuller, L. M. (2004). Sediment characteristics and configuration within the Otsego City Dam impoundment on the Kalamazoo River, Michigan, 2000-02. Water Resources Investigations Rep. 03-4218, U.S. Geological Survey, Lansing, MI.

Rheaume, S. J., Rachol, C. M., Hubbell, D. L., and Simard, A. (2002). Sediment characteristics and configuration within three dam impoundments on the Kalamazoo River, Michigan, 2000. Water Resources Investigations Rep. 02-4098, U.S. Geological Survey, Lansing, MI.

Simon, A., Bingner, R. L., Langendoen, E. J., and Alonso, C. V. (2002). Actual and reference sediment yields for the James Creek watershed - Mississippi. Research Rep. No. 31, U.S. Department of Agriculture, Agricultural Research Service, National Sedimentation Laboratory, Oxford, MS.

Wells, R. R., Langendoen, E. J., and Simon, A. (2004). Numerical simulation of sediment loads and channel changes along the Kalamazoo River between Plainwell and Otsego City, Michigan. Research Rep. No. 44, U.S. Department of Agriculture, Agricultural Research Service, National Sedimentation Laboratory, Oxford, MS.

IMPACT OF NON-ERODIBLE LAYER ON EPHEMERAL GULLY DEVELOPMENT

Robert Wells, Research Hydrologist, USDA-ARS-NSL, rrwells@msa-oxford.usda.ars.gov; Lee Gordon, Research Assistant, University at Buffalo, lmgordon@acsu.buffalo.edu; Sean Bennett, Associate Professor, University at Buffalo, seanb@buffalo.edu; Carlos Alonso, Supervisory Hydraulic Engineer, USDA-ARS-NSL, calonso@msa-oxford.usda.ars.gov

Abstract: As headcut erosion accelerates, the formation of ephemeral gullies can significantly increase the loss of topsoil and decrease the productivity of agricultural lands. Ephemeral gullies are erosional features, usually larger than rills, caused by concentrated flow that may be erased by normal tillage practices. Most researchers agree that a critical or threshold level of concentrated flow is required to initiate ephemeral gullies and once initiated, there is positive feedback between flow and erosion. The location and size of ephemeral gullies is controlled by the generation of concentrated surface erosion of sufficient magnitude and duration to initiate and sustain erosion for a particular soil. Once formed, ephemeral gullies tend to rejuvenate near or in the same location from year to year. Experiments were conducted to examine the effect of a non-erodible layer on growth, development, and upstream migration of headcuts typical in ephemeral gullies. During migration, the depth of the non-erodible layer impacted sediment yield and rate of upstream advance.

INTRODUCTION

Mildner (1983) presented a convenient working definition for ephemeral gullies as being "*usually larger than rills, occurring and recurring in depositional areas, forming a dendritic pattern unless another pattern is imposed by row alignment, and being partially or totally erased and filled in by normal tillage operations without the need for special equipment*." As pointed out by Thorne *et al.* (1986), this definition is dependent on farming practice and equipment, not environmental considerations, and is morphologically incomplete as to form, shape and size. Classifications merely focus our attention on a particular erosion form and, therefore, clarify the boundary conditions under consideration for a particular erosion feature. Poesen (1993) addressed the concerns of Thorne *et al.* (1986) by distinguishing ephemeral gullies based on a critical cross-sectional area criterion and Nachtergaele *et al.* (2002) used a mean width criterion; others have made similar distinctions based upon minimum depth and/or minimum width criteria.

Most researchers agree that a critical or threshold level of concentrated flow is required to initiate ephemeral gullies and once initiated, there is positive feedback between flow and erosion. In addition, most agree that the location and size of ephemeral gullies are controlled by the generation of concentrated surface erosion of sufficient magnitude and duration to initiate and sustain soil erosion. Logically, once initiated, surface flow becomes increasingly channelized and more flow leads to increased erosive power and further enlargement.

The photographs in Figure 1 depict classical forms of ephemeral gullies. In both figures, note the practice of contour farming. Concentrated flow in the furrows converge, flow tops the downhill furrow, and creates a cascade of water downslope, which leads to ephemeral gully development.



Figure 1 Photos of ephemeral gullies during the growing (top) and non-growing (bottom) season.

Smith (1993) identified four critical parameters of ephemeral gully development: (1) a critical slope length and gradient dependent upon slope characteristics and crop row direction, (2) occurrence and depth of a fragipan, (3) agricultural practices, such as crop row direction and timing of cultivation, and (4) timing and total amount of precipitation. Thorne (1984) suggests there are three requirements for the ephemeral gully development: (1) concentrated surface runoff, (2) erosion initiation, and (3) channelization. Both agree that it is not just the magnitude and duration of a storm that determines whether surface runoff is generated from a field, but also, the sequence of storms preceding and the timing in relation to the growing season.

Bennett (1999), Bennett *et al.*(2000), and Bennett and Casali (2001) reported experimental data showing that actively migrating ephemeral-gully headcuts display steady-state migration and self-similar organization in the absence of hardpans and upstream sediment supply. Alonso *et al.* (2002) combined jet impingement theory and conservation laws to predict soil losses due to headcut erosion and migration. Headcut erosion and migration rates were shown to depend on upstream flow depth and discharge, tailwater depth, and soil and fluid properties.

In this paper, the authors discuss laboratory experiments designed to examine the impact of a non-erodible layer on ephemeral gully development and migration, and discuss the impacts on morphology, migration rate and sediment yield.

MATERIALS AND METHODS

Using a constant bed slope (1%), initial headcut height (30 mm) and flow rate (71 l sec^{-1}), the impact of a constructed non-erodible layer at depths of 40 mm, 50 mm and 70 mm was examined. All experiments were conducted at the USDA-ARS National Sedimentation Laboratory in Oxford, MS using a tilting flume, designed for soil erosion studies, and simulated rainstorms of uniform intensity (21 mm h^{-1}). One run was performed in which no non-erodible layer was constructed to replicate the work of Bennett *et al.* (2000) and will be referred to as the baseline case in this paper.

Headcut Flume: A non-recirculating, 5.5 m tilting flume (Figure 2) was used to examine soil erosion processes associated with migrating headcuts. The flume was comprised of four compartments: inflow tank, false floor (1 m long and 0.165 m wide), soil cavity (2 m long, 0.165 m wide, and 0.25 m deep), and outflow pipe. A large reservoir was used to provide water for the inflow tank upstream of the false floor. Flow discharge was controlled by two adjustable intake valves and monitored with a point gage during experiments. A subsurface drainage system was installed along the base of the soil cavity and provided escape routes for both air and water during rainfall application.

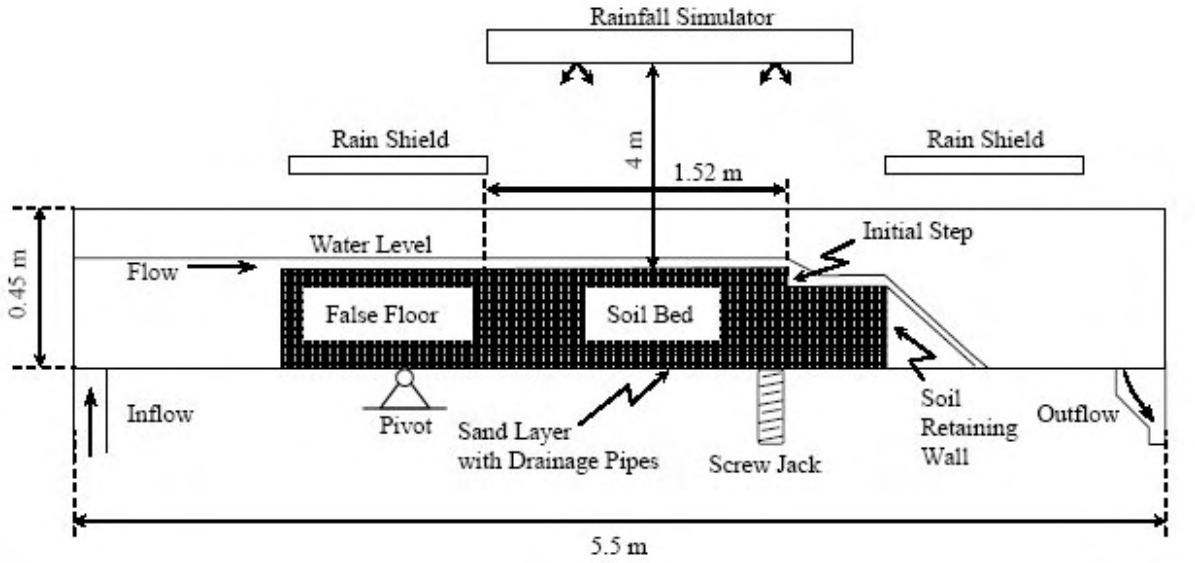


Figure 2 Schematic of headcut flume located at the USDA-ARS-NSL in Oxford, MS (Bennett *et al.*, 2000).

Soil and Step Plate: The soil used in the headcut experiments was a sandy loam to sandy clay loam textured soil (Ruston Series; fine-loamy, siliceous, thermic, Typic Paleudult; (Römkens *et al.*, 1997)), commonly found in the southeastern U.S. The soil consisted of 20.0% clay, 2.9% silt, and 77.1% sand. An appreciable amount of iron oxide in the soil greatly enhanced its stability (Rhoton *et al.*, 1998).

The soil was collected from a field site in Neshoba County, MS near Philadelphia in cooperation with the Natural Resources Conservation Service extension office. Following transport back to the laboratory, the soil was air dried, mechanically crushed, and passed through a 2 mm sieve.

Soil was packed incrementally in layers of about 0.02 m using a drop-weight of aluminum mounted to an aluminum frame, constructing uniformly packed soil beds with bulk densities ranging from 1403 to 1557 kg m^{-3}.

At depth, a non-erodible layer was constructed by subjecting a partially packed soil sample at 1% slope to a 21 mm h^{-1} rainstorm for 45 min, sprinkling sieved soil material (125 μm) on the surface and repacking the layer. Additional layers were packed incrementally to the preformed step depth (30 mm below the surface of the false floor). An aluminum frame with a 30 mm vertical face was placed 1.72 m downstream of the soil cavity entrance for the purpose of forming a headcut. After installation, soil was packed upstream of the frame producing a preformed vertical step in the bed profile. The soil material within the uppermost 0.02 m was treated with 0.75 cmol of $Ca(OH)^{2}$ per 100 g of soil (about 0.74 g per 1 kg of soil) to promote a physiochemically favorable condition for seal development (Römkens et al., 1995, 1997).

At 2 hour intervals during rainfall application, rainfall was interrupted for 5 minutes, additional sieved soil material (125 μm) was sprinkled across the surface and rainfall application was resumed. The additional sieved soil material was used to enhance surface seal formation.

Rainfall Simulation A multiple-intensity rainfall simulator consisting of two oscillating nozzles spaced 1.64 m apart (Meyer and Harmon, 1979; Figure 2) was suspended approximately 4 m above the flume. With the bed prepared and headcut-forming plate installed, a rainfall intensity of 21 mm h^{-1} was applied for 6 h to a bed slope of 5%. Following the application of simulated rain, a well-developed and reproducible surface seal formed.

Data Acquisition The soil cavity of the tilting flume contained a plexiglass wall which had a superimposed grid system allowing for visual observation of many morphologic and hydraulic parameters. A video camera mounted on a tripod during rainfall application and to a movable carriage during overland flow recorded each experimental run. From these images, the following information could be determined with sufficient accuracy: position and morphology of the headcut, overland flow depth, and angle of the overfall nappe. Upstream flow depth was monitored with a point gage and was in agreement with video recordings.

RESULTS AND DISCUSSION

Headcut Migration: As overland flow passed over the preformed step, flow impinged the surface seal just downstream of the step. The impinging overfall caused surface seal failure and soil erosion, initially migrating downstream, followed by scour hole development and upstream migration. After an initial period of scour hole development, scour hole length (horizontal length from brinkpoint to maximum scour depth) was dependent upon depth to the non-erodible layer (Figure 3). In each case, a headcut of similar geometry migrated upstream at a constant velocity, producing both a constant rate of sediment yield and a constant rate of sediment deposition in the downstream portion of the flume; however, the base of the scour hole was elongated and flattened due to the presence of the non-erodible layer. Figure 3D shows the characteristic shape of the scour hole for the baseline case, where no non-erodible layer was constructed, which was similar to experimental results reported by Bennett *et al.*, 2000.

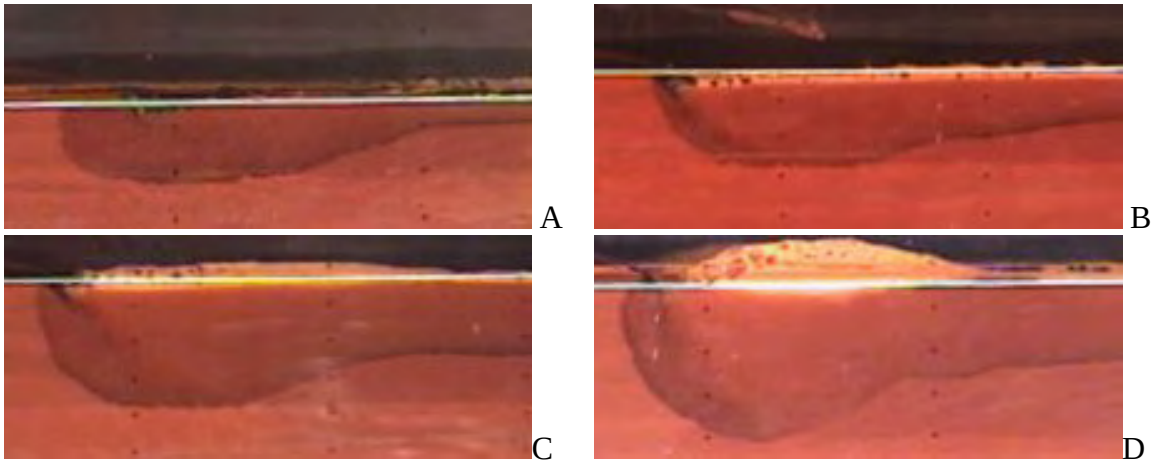


Figure 3 Photos of headcut geometry for (A) 40 mm layer, (B) 50 mm layer, (C) 70 mm and (D) baseline case.

After an initial period of growth, the headcut brinkpoint migrated upstream in a gradual and linear fashion in time (Figure 4). Headcut migration was constant in each case, ranging from 2.37 mm sec^{-1} to 2.86 mm sec^{-1}. The run in which the non-erodible layer was located 50 mm below the surface migrated at a reduced rate in comparison to other depths. The run in which the non-erodible layer was located 40 mm below the surface migrated upstream at an increased rate of 17% and 8.4% in comparison to the 50 mm or 70 mm depths. There was a 4% increase in migration rate when comparing the 40 mm run to the baseline case.

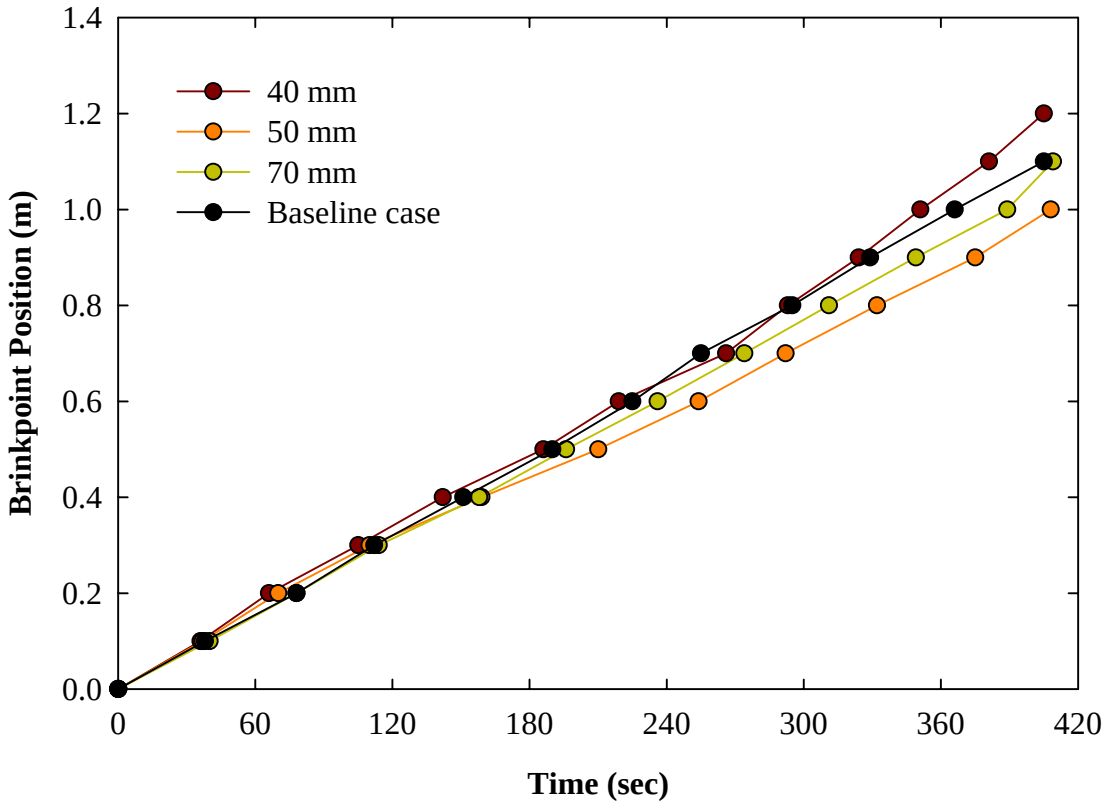


Figure 4 Time variation of headcut brinkpoint position for each run.

Sediment Yield: Water and sediment samples were collected at the outlet pipe (Figure 2) at 10 sec intervals until the headcut stabilized, and then sampling was reduced to 30 sec intervals. Sediment production increased rapidly after overland flow reached the preformed step and soil erosion was initiated. Peak sediment concentration coincided with upstream migration of the headcut and downstream deposition of eroded sediments. After this initial peak, sediment concentrations were reduced as the headcut migrated upstream (Figure 5).

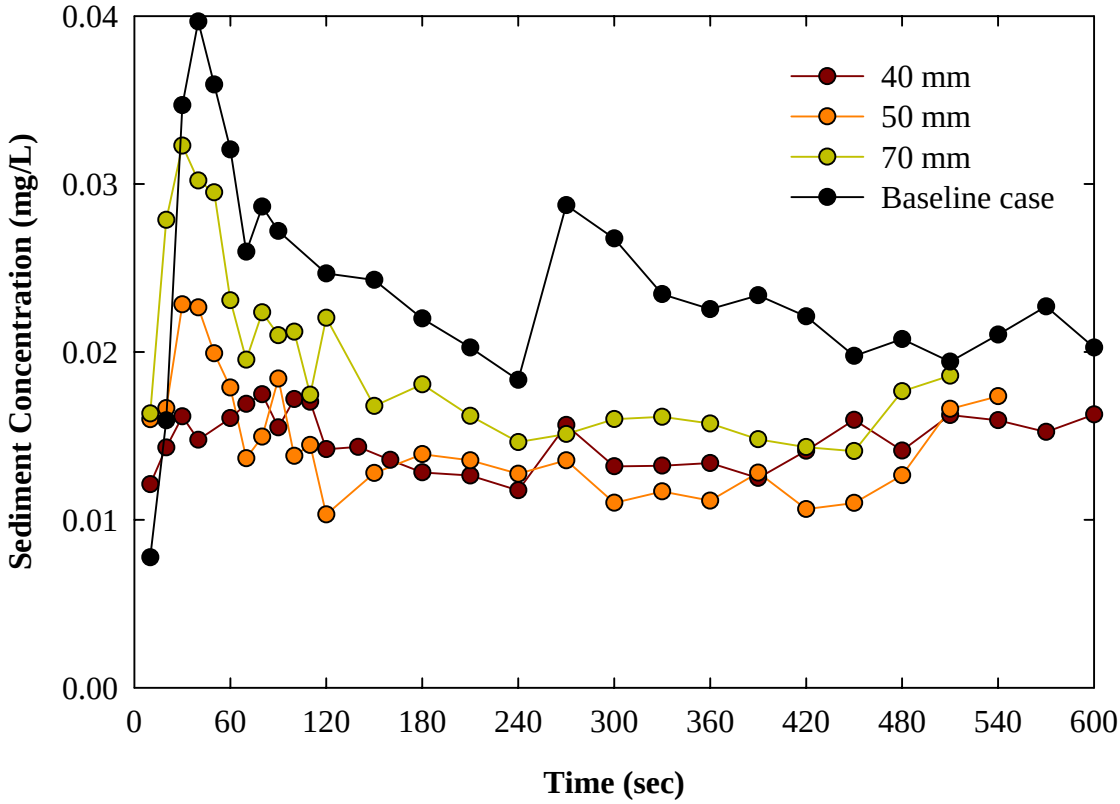


Figure 5 Time variation of sediment concentration for each run.

Peak sediment concentration increased by a factor of 2.3 (56%) when comparing results from the baseline case to the 40 mm non-erodible layer. Sediment peaks increased as the non-erodible layer was lowered in the soil profile. The run in which the non-erodible layer was 40 mm below the soil surface had an initial increase in sediment concentration that was sustained through the run. In the runs when the depth to the non-erodible layer was 50 mm and 70 mm, sediment trends were similar to those discussed by Bennett *et al.* (2000). There was a 43% increase in the sediment peak when comparing the baseline case to the 50 mm non-erodible layer and a 19% when comparing the baseline case to the 70 mm non-erodible layer.

Within individual experiments, the morphology of the headcut did not vary significantly during migration once steady-state conditions were achieved (Figure 3). Fluctuations (i.e. peak in 40 mm sediment concentration at 270 sec and the peak in baseline case at 270 sec (Figure 5)) from the mean were due to random spatial and temporal variations in the boundary conditions such as

bulk density, soil water content, matrix pore-water pressure, and physical, hydraulic, and chemical characteristics of the surface seal.

CONCLUSIONS

Migration rate appeared to be governed by the depth to the non-erodible layer; however, shallow and deep layers migrated similarly, median depths migrated at a reduced rate. The sediment concentration peak was also affected by the non-erodible layer. With the non-erodible layer closer to the surface, the peak concentration was greatly reduced. There was a reduction in sediment loss as the non-erodible layer approached the surface; however, the headcut migration rate accelerated as the non-erodible layer approached the surface. There was a definite point at which the depth of the non-erodible layer reached a reduced migration rate and, in this limited data set, the 50 mm depth was the slowest. Further work in this area is planned.

ACKNOWLEDGEMENT

Funding for this research was provided by USDA-ARS. The technique for constructing the non-erodible layer was created by Lee Gordon. Technical assistance during all experimental runs was provided by Lee Patterson.

REFERENCES

Alonso, C.V., S.J. Bennett, O.R. Stein, 2002. “Predicting headcut erosion and migration in upland flows,” Water Resources Research, 38(12), pp. 1-15.

Bennett, S.J., 1999. “Effect of slope on the growth and migration of headcuts in rills,” Geomorphology, 30, pp. 273-290.

Bennett, S.J., C.V. Alonso, S.N. Prasad, M.J.M. Romkens, 2000. “An experimental study of headcut growth and migration in upland concentrated flows,” Water Resources Research, 36(7), pp. 1911-1922.

Bennett, S.J. and J. Casali, 2001. “Effect of initial step height on headcut development in upland concentrated flows,” Water Resources Research, 37(5), pp.1475-1484.

Meyer, L.D., Harmon, W.C., 1979. “Multiple-intensity rainfall simulator for erosion research on row sideslopes,” Trans. ASAE 22, 100-103.

Mildner, W.F., 1983. Ephemeral cropland gullies. Draft Report to SCS, Washington, D.C.

Nachtergaele, J., J. Poesen, A. Sidorchuk, D. Torri, 2002. “Prediction of concentrated flow width in ephemeral gully channels,” Hydrological Processes, 16 (10), 1935-1953.

Poesen, J., 1993. Gully typology and gully control measures in the European loess belt. In: Wicherek, S. (Ed.), Farm Land Erosion in Temperate Plains Environment and Hills. Elsevier, Amsterdam, pp. 221-239.

Rhoton, F.E., Lindbo, D.L., Römkens, M.J.M., 1998. “Iron oxides erodibility interactions for soils of the Memphis catena,” Soil Sci. Soc. Am. J. 62, 1693-1703.

Römkens, M.J.M., Prasad, S.N.. Gerits, J.J.P., 1995. “Seal breakdown on a surface soil and subsoil by overland flow,” in So, H.B., Smith, G.D., Raine, S.R., Schafer, B.M., Loch, R.J. (Eds.), Sealing, Crusting and Hardsetting Soils: Productivity and Conservation. Australian Soc. Soil Sci., Brisbane, pp. 139-144.

Römkens, M.J.M., Prasad, S.N., Gerits, J.J.P., 1997. "Soil erosion modes of sealing soils: a phenomenological study," Soil Tech. 11, pp. 31-41.

Smith, L., 1993. Investigation of ephemeral gullies in loessial soils in Mississippi. US Army Corps of Engineers Technical Report GL-93-11, 58pp.

Thorne, C.R., 1984. Prediction of soil loss due to ephemeral gullies in arable fields. Report to the USDA-ARS and SCS, CER 83-84 CRT, 79pp.

Thorne, C.R., L.W. Zevenbergen, G.H. Grissinger, J.B. Murphey, 1986. "Ephemeral gullies as sources of sediment," Proceedings of the Fourth Federal Interagency Sedimentation Conference, (1) pp.3-152-161.

STUDY OF THE EFFECTS OF LATERAL SEEPAGE FORCES ON TENSION-CRACK DEVELOPMENT, BANK-FAILURE DIMENSIONS AND MIGRATION OF EDGE OF FIELD GULLIES

Andrew Simon, Research Geologist, USDA-ARS National Sedimentation Laboratory, P.O. Box 1157, Oxford, MS, asimon@ars.usda.gov; Robert R. Wells, Research Hydrologist, USDA-ARS National Sedimentation Laboratory, P.O. Box 1157, Oxford, MS, rrwells@ars.usda.gov

Abstract: Pore-water pressure is one of the most dynamic and important variables controlling geotechnical failure of streambanks and gully heads. Generation of positive pore-water pressures reduce frictional strength and the matric suction component of apparent cohesion. Pore-water pressure gradients, expressed as seepage forces, are counteracted by tensile and shear strengths. The effects of positive pore-water pressures, matric suction and lateral seepage forces on streambank failures and edge of field gullies are being investigated at the Goodwin Creek Experimental Bendway, Mississippi. Nine nests of digital tensiometers were installed in a radial pattern at depths of 30, 100, 150, and 270 cm, and spaced roughly 7, 60, 160, and 580 cm back from the gully head. Data were recorded at 10-minute intervals along with rainfall data from a tipping-bucket rain gage. Repetitive surveys of the gully head provide evidence of erosion events between February and September 2005. Results show that lateral seepage forces moving away from the gully face are greatest in the shallow (30 cm) zone closest to the gully face (7 – 60 cm) and generally decrease non-linearly with depth and with distance from the gully head. The vertical and horizontal distribution of these forces indicate a zone of strength that may determine failure-block dimensions during partial saturation of the soil mass. However, it is shown that mass failure of the headwall cannot occur unless the toe of the headcut has been previously undercut by hydraulic erosion or pop-out failures. Maximum seepage-force values of 13 kN/m^3 have been calculated, with values approaching zero at depths near 1.5 m. Infiltration via macropores and crack development behind the gully head may be important mechanisms in generating the positive pore-water pressures associated with saturation and mass failure.

INTRODUCTION

Erosion of cohesive materials is a complex phenomenon owing to the electro-chemical bonding between particles and because entrainment is, therefore, not controlled solely by particle size and weight. With respect to streambanks and edge-of-filed gullies (EFG), erosion of the bank top or gully headwall is governed by multiple processes and controls. Understanding and quantifying the controls of headcut migration is critical in predicting sediment losses, gully growth and gully control. Headcuts can migrate as a result of hydraulic erosion at the precipice, by geotechnical failure of the face and/or by undercutting of the face by either hydraulic erosion or seepage-induced pop-out failure and subsequent cantilever failure of the upper part of the headcut. Thus, headcut migration can be envisioned as the result of a triangle of processes with each apex representing a different process domain; hydraulic, geotechnical, and seepage (Figure 1). However, several recent field studies have reported that much of the material eroded from gullies and migrating headcuts is provided by failure of the gully face (Dietrich *et al*, 1985; Fernandez *et al*, 1995; Collison and Simon, 2001). This study aims to investigate the interaction of aspects of these three process domains on headcut migration of an EFG at the Goodwin Creek Experimental Bendway (GCEB), Mississippi (Figure 1).

The GCEB, has been monitored since 1996 to study streambank-erosion processes (Figure 2). Twelve monumented cross sections were surveyed after every major flow event (Figure 3). Pressure transducers placed at the upstream and downstream ends of the reach recorded stage. Geotechnical properties of the bank material were determined by *in situ* direct shear tests (Simon *et al*., 2000) and bank-toe erodibility was measured with a submerged jet-test device (Hanson, 1990). Pore-water pressure data were collected every 10 minutes using digital tensiometers at four depths. During 2004, an EFG developed at the head of a 1.3 m-high failure scar in the vicinity of cross section 4, providing an opportunity to monitor processes controlling migration of the headcut.

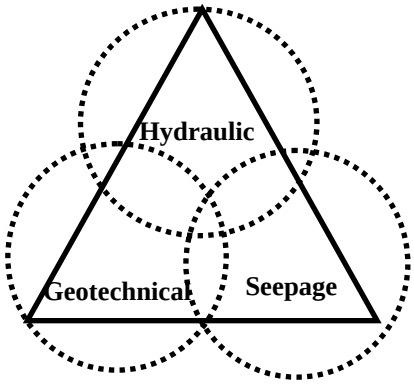


Figure 1 Conceptual drawing of the interaction of processes that can govern headcut migration.

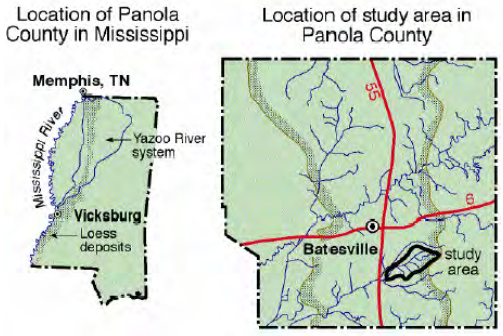


Figure 2 Location map of Goodwin Creek.

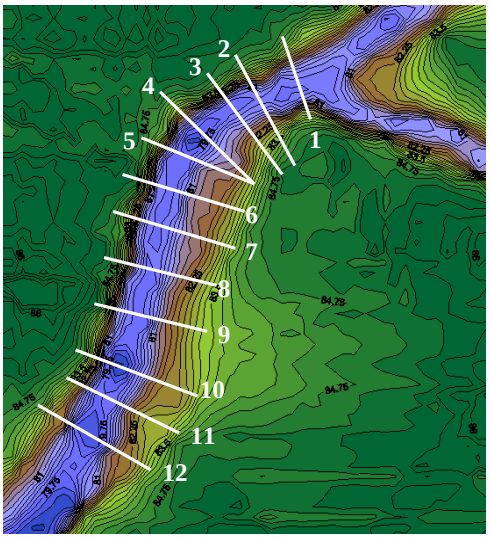


Figure 3 Location of cross sections at GCEB.

Based on previous observations and measurements of streambank processes at the GCEB, it was found that changes in pore-water pressure during rainfall events exert profound influences on bank-material shear strength and stability. Preliminary bank-stability analyses determined that migration of the headcut could not occur by mass failure even under worst-case, saturated conditions. Using a measured cohesive strength (c') and friction angle (ϕ') of 6.4 kPa and 34^o respectively, undercutting by hydraulic erosion or pop-out failure would be required to destabilize the headcut (factor of safety, $F_s < 1.0$) (Figure 4). Because of the cohesive nature of the materials and the presence of cropped grasses, hydraulic erosion by overland flow is not considered an important process in headcut migration of the Goodwin Creek EFG. The study was designed, therefore, to combine repeated surveys of the EFG with real-time measurements of precipitation amount and intensity, overland flow, pore-water pressures and lateral seepage gradients, and geotechnical strength to investigate those processes responsible for further headcut migration.

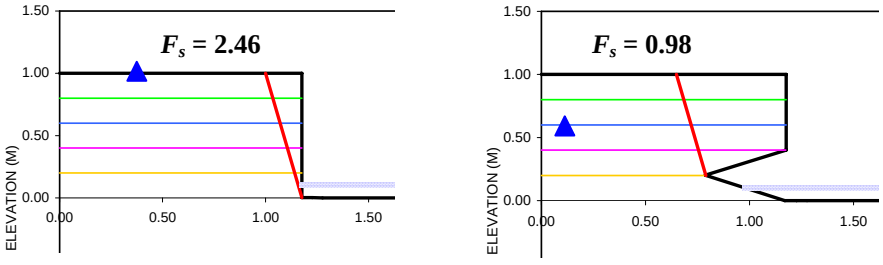


Figure 4 Bank-stability analysis of gully headwall showing destabilization by undercutting and partial saturation. F_s = factor of safety; blue triangles represent height of the phreatic surface.

FIELD AND ANALYTIC METHODS

An intital survey of the EFG was conducted in December 2004 with subsequent surveys conducted following significant storm events in February, April, July, and September of 2005. The effects of pore-water pressures and lateral seepage forces were measured by installing nine nests of digital tensiometers in a radial pattern from the headcut at depths of 30, 100, 150, and 270 cm. These nests were spaced roughly 7, 60, 160, and 580 cm back from the gully head and are referred to as edge, front, middle, and back, respectively. Precipitation was measured with a tipping-bucket rain gage and digitally recorded. All digital data were recorded at 10-minute intervals on data loggers starting on February 9, 2005. Overland flow was measured by a pressure transducer placed within a 12-inch diameter pipe where the downstream end of the gully drains down the bank face and into Goodwin Creek. Shear strength parameters of the headwall were measured *in situ* with an Iowa Borehole Shear Tester and the erodibility of the gully top edge was measured with a submerged jet-test device.

Tensiometer data, measuring both positive and negative (matric suction) pore-water pressures were downloaded on a weekly basis and plotted. Except for the deepest instruments, pore-water pressure values were generally negative indicating enhanced strength due to matric suction (Figures 5a and b). During and immediately following rainfall events the tensiometers reacted in a predictable manner with the shallow tensiometers (30 cm) generally responding over greater amplitudes than those set deeper. Those instruments installed at the "edge" (7 cm into the face) also showed a tendency towards greater amplitudes due to their proximity to the exposed face. Variations in pore-water pressure for all edge tensiometers showed a marked diurnal fluctuation of between 2 and 4 kPa, representing a 0.4 to 0.7 kPa change in cohesive strength (assuming $\phi^b = 10^o$; Simon *et al*, 2000).

Given the complexities of unsaturated flow in porous media, our calculations of lateral seepage gradients and seepage forces do not include changes in the coefficient of permeability and, therefore, represent approximations of this process. Pore-water pressure gradient is given by:

$$i = (h_1 - h_2)/L \tag{1}$$

where h_1 is the hydraulic head at point 1 in meters, h_2 is the hydraulic head at point 2 in meters, and L is the distance between the points, in meters. Seepage force per unit volume (j) is given by (Lambe and Whitman, 1969):

$$j = i\gamma_w \tag{2}$$

where j is the seepage force per unit volume, in kN/m^3, γ_w is the unit weight of water, in kN/m^3. This seepage force occurs by frictional drag as water moves through the soil skeleton. h_1 and h_2 generally represent vertically displaced points. In the analysis of lateral seepage forces however, h_1 and h_2 represent horizontally displaced points and imply movement of water towards the gully face (front to edge) or away from the gully face (edge to front).

To test the role that seepage forces play in headcut migration, lateral seepage gradients were calculated. Lateral seepage gradients were calculated by taking the difference between matric suction values (multiplied by -1) of two tensiometers set at the same depth and dividing by the horizontal distance between the instruments. An example is shown in Figure 5c where values from the edge tensiometers are subtracted from the associated values of the front tensiometers, then divided by L (approximately 0.6 m). Because the instruments are from the same depth (elevation), this is equivalent to evaluating differences in hydraulic head where the sign of the gradient implies the direction of a seepage force towards the headcut face (positive) or towards the floodplain (negative) (Figure 5c).

HEADCUT MIGRATION AND GULLY EROSION

The EFG at Goodwin Creek experienced several significant storms that produced overland flow during the monitoring period of February to October 2005. Rainfall associated with Hurricane Katrina (95.1 mm; August 29-30) was not sufficient to generate positive pore-water pressures 0.6 m back from the gully head owing to extremely dry conditions prior to the storm. In contrast, rainfall associated with Hurricane Rita (83.2 mm; September 25)

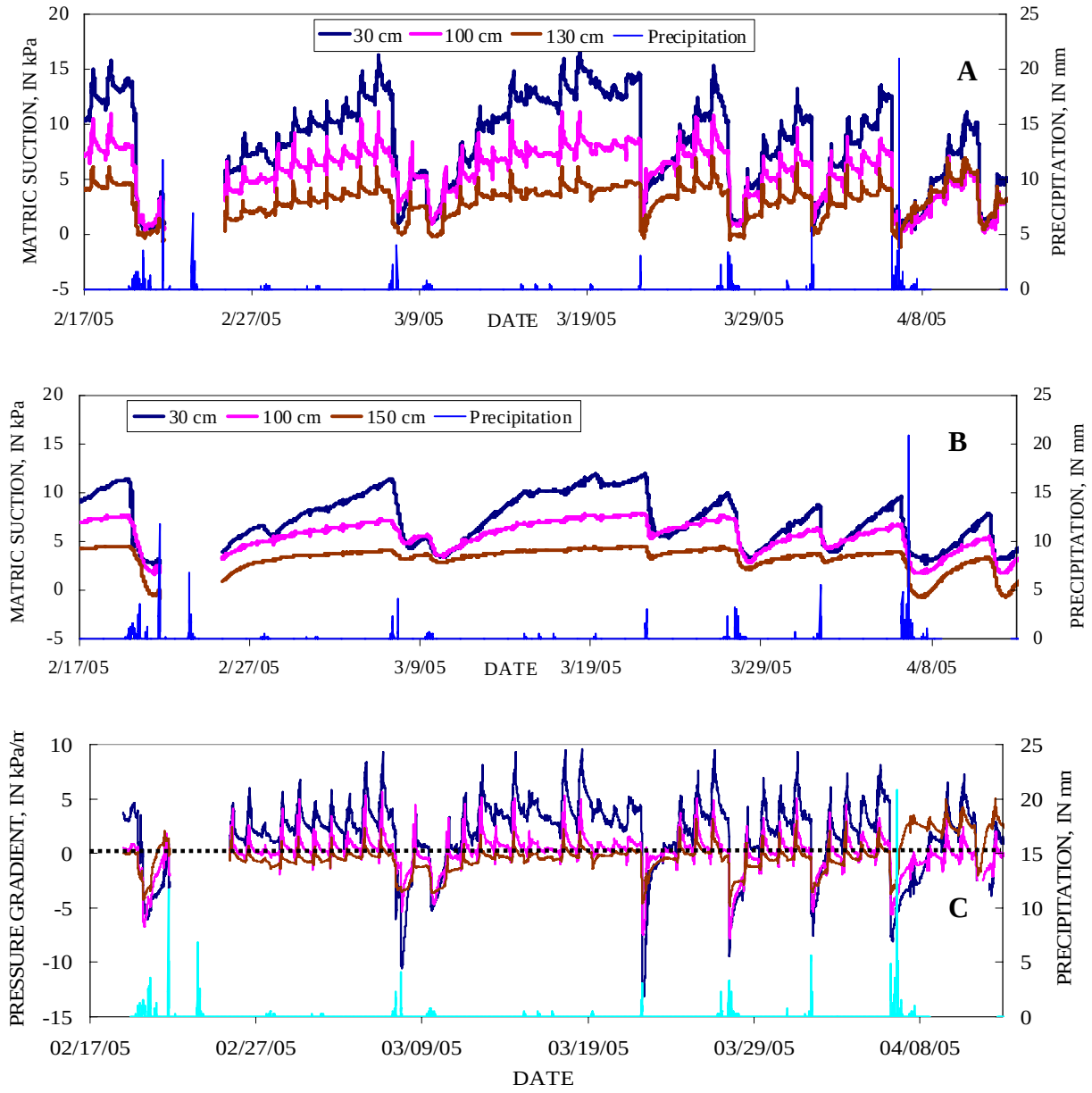


Figure 5 Data for the edge-center (A) and front-center (B) tensiometers nests, and pressure gradient between the front and edge nests (C) at three depths, all with associated rainfall.

caused considerable erosion of the EFG due to wetter antecedent moisture conditions. The most noteworthy events are shown in Table 1 and are all associated with mass failures of the gully face and migration of the headcut with the exception of the August 29-30 storm (Figure 6). None of the storm events resulted in headcut retreat by hydraulic erosion owing to relatively high, measured critical shear stresses of the surface material (6 Pa).

Views of headcut migration by mass failure, and the resulting morphology following the storm of September 25, 2005 are provided in Figure 7. Each of these events, with the exception of the August storm are associated with a complete loss of matric suction and generation of some positive pore-water pressures at both the edge and front tensiometers nests, particularly at depths between 1.3 and 1.5 m (Figure 5). This is just above an area of decreased permeability associated with a concentration of manganese nodules. Smaller rainfall events in March did not result in matric suction and shear strength reductions of the magnitude that occurred in February, April and September (Figure 5), rendering the headcut stable during March. These processes cannot, however, explain headcut migration

Table 1 Significant rainfall events and associated erosion of the EFG during the monitoring period.

Date(s) of precipitation	Total precipitation (mm)	Volume eroded from headcut (m^3)	Average headcut migration (m)
February 19-23, 2005	105	0.87	0.11
April 6 and 11, 2005	75.5	1.00	0.18
August 29-30, 2005	95.1	??	0.00
September 25, 2005	83.2	2.45	0.32

by mass failure at the EFG by themselves because, as we have seen with stability analyses (Figure 4), the headcut is stable under fully saturated conditions. Undercutting of the face must, therefore, be responsible for preparing the headcut for cantilever failure. Pop-out failures were observed to have emanated from an area 0.3 to 1.3 m-below the gully precipice on two occasions, forming triangular-shaped depressions at the base of the headcut. These failures could not be predicted from the observed pore-water pressure data probably because infiltration through macropores must be considerable. The pop-out failures that occurred in late August did not result in headcut failure for the reason stated above, but prepared the EFG for erosion by mass failure during Hurricane Rita three weeks later.

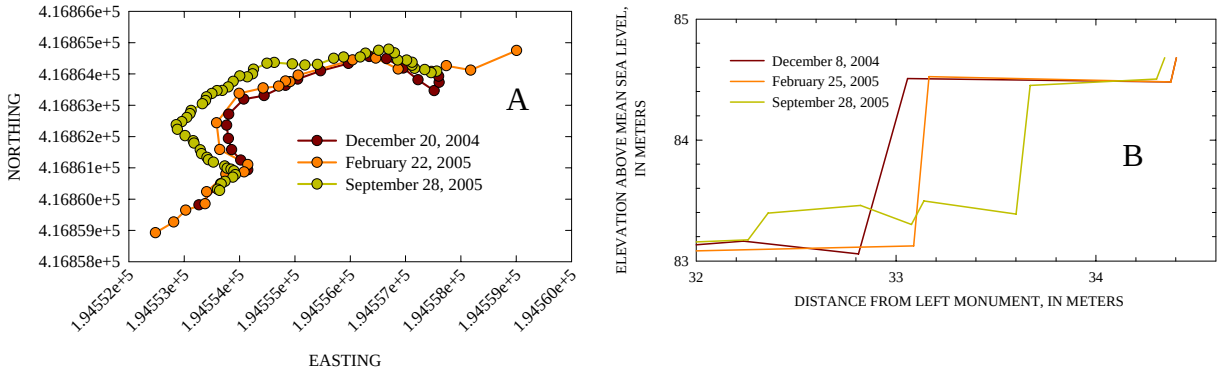


Figure 6 Time-series surveys of the EFG showing morphologic changes in plan (A) and in cross section (B).

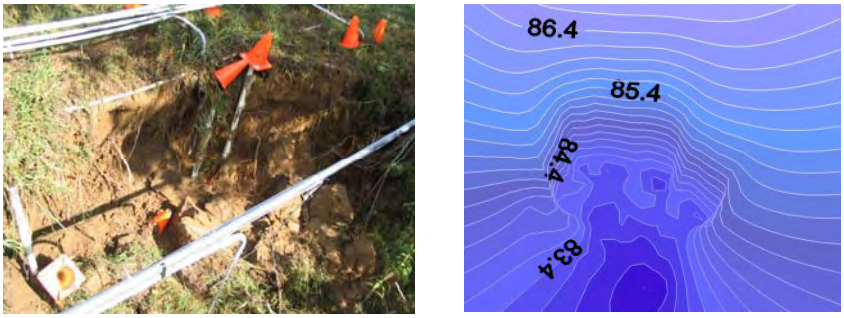


Figure 7 Photograph showing failed blocks and exposed tensiometers (left) and 3-D survey of EFG (right) following erosion event of September 25, 2005.

Using literature values to populate the finite-element stress-deformation model SIGMA/W, Collison and Simon (2001) showed that for typical loess-derived materials, high stresses are concentrated at two locations; at the base of the gully head and about 50 cm back from the gully head (Figure 8). Stress exceeded strength in these two areas with the shape of the potential pop-out failure at the base of the headcut looking strikingly similar to scars left by pop-out failures at the EFG and elsewhere. Results of the Collison and Simon (2001) study further indicate the potential importance of crack and macropore formation above the gully head to permit saturation of the headcut in a mass that is otherwise characterized by unsaturated conditions. This type of detail is not recorded by the tensiometers at the Goodwin Creek EFG that are measuring pore-water pressure at a point within the soil matrix.

DISCUSSION

Interaction of the seepage and geotechnical process domains involve viewing potential headcut failure over multiple spatial scales. At the particle scale, matric suction provides additional binding strength between grains, represented as an additional cohesion term (Fredlund *et al*, 1978). During dry periods, tensiometers some distance back from the bank face are wetter than at the edge, resulting in a considerable seepage force moving towards the gully face. In opposition to this tendency, however is the greater cohesive strength closer to the edge owing to heightened values of matric suction. During storms, infiltration of water results in a loss of matric suction and a weakening of the soil matrix. This process is amplified closer to the gully edge where overland flow over the gully precipice combines with infiltration via macropores to cause the edge of the headcut to wet faster and to lower values of matric suction relative to values some distance back from the headcut. This process leads to seepage gradients moving away from the headcut (up to 13 kN/m^3) at the very time when the tensiometers indicate that the soil is approaching saturation in a weakened state. This is also shown in the simulated data (Collison and Simon, 2001). At the block scale then, seepage forces are moving away from the gully face as indicated by calculated pressure gradients during storms (Figure 5c) creating a mechanism that can bind a block of soil together, thereby determining dimensions of potential failure blocks.

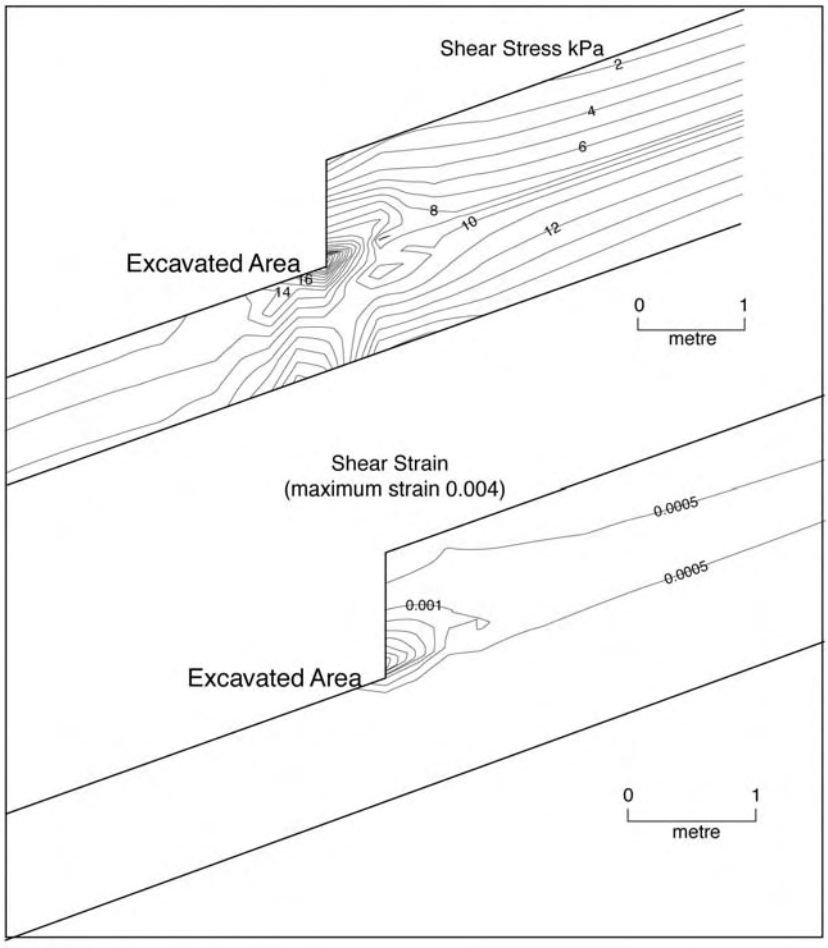


Figure 8 Distribution of shear stress and strain for a 1 m-high headcut in loess-derived materials. From Collison and Simon (2001).

These opposing tendencies are illustrated in Figure 9 but must be combined with a treatment of infiltration via macropores and stress-strain relations to better understand and predict this complex interaction of processes. The timing and magnitude of headcut migration by mass failure of the face (failure-block width) is at least partially

controlled by the juxtaposition of these processes; where wetting causes preferential weakening of the soil matrix and lateral seepage, combined with stress-strain deformation that can determine the dimensions of the block.

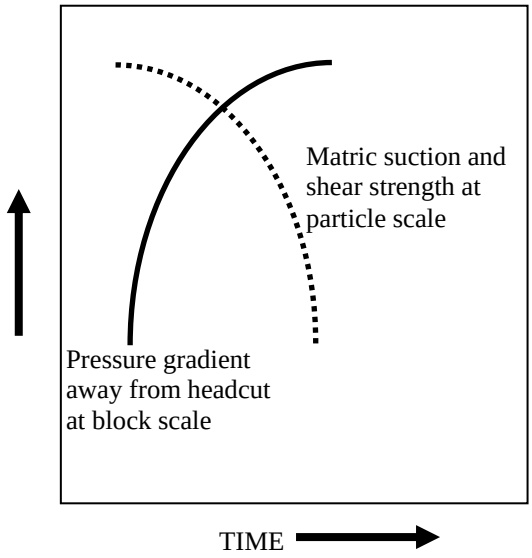


Figure 9 Conceptual illustration of opposing tendencies of seepage and geotechnical process domains during storms.

SUMMARY

Results of this study point to the interaction of hydraulic, geotechnical and seepage forces in controlling migration of an edge of field gully. Stability analysis has verified the need for undercutting to create conditions where mass failure of the gully headwall can occur with partial saturation of the face. These conditions were identified on several occasions at the Goodwin Creek EFG. The importance of cracks and infiltration via macropores remains to be further investigated using finite-element seepage and stress-deformation modeling. Measurements made in this study were not able to identify seepage forces moving towards the gully head (within the proximal 0.6 m) that would lead to pop-out failures although mass failures of this type were observed. However, previous simulations (Collison and Simon, 2001) of typical deposits do provide a mechanism for development of preferential zones of saturation and weakness that could explain undercutting by pop-out failures.

REFERENCES

Collison, A.J.C., and Simon, A. (2001). "Modelling gully head-cut recession processes in loess deposits," in, J.C. Ascough and D.C. Flanagan (Eds.) Soil Erosion Research for the 21st Century, Proc. Int. Symposium, Honolulu, HI, pp. 87-90.

Dietrich, W.E., Reneau, S.L., and Wilson, C.J. (1985). "The geomorphology of 'zero order basins'," Transactions of the American Geophysical Union 66 (46), p. 898.

Fernandez, N.F., Coelho Netto, A.L., and Lacerda, W.A. (1995). "Subsurface hydrology of layered colluvium mantles in unchanelled valleys of south-eastern Brazil," Earth Surface processes and Landforms, 19, pp. 609-626.

Fredlund, D.G., Morgenstren, N.R., and Widger, R.A. (1978). "The shear strength of unsaturated soils," Canadian Geotechnical Journal, 15, pp. 313-321.

Hanson, G.J. (1990). "Surface erodibility of earthen channels at high stresses. Part II-developing an *in situ* testing device," Transactions of the American Society of of Agricultural Engineers, 33, pp. 132-137.

Simon, A., Curini, A., Darby, S.E., and Langendoen, E.J. (2000). "Bank and near-bank processes in an incised channel," Geomorphology, 35, pp. 193-217.

EVALUATION OF THE IMPACT OF EPHEMERAL GULLIES ON SEDIMENT LOADING WITHIN WATERSHEDS USING AGNPS

Ronald L. Bingner, United States Department of Agriculture, Agricultural Research Service, National Sedimentation Laboratory, Oxford, Mississippi, RBingner@msa-oxford.ars.usda.gov; Fred Theurer, United States Department of Agriculture, Natural Resource Conservation Service, National Water and Climate Center, Gaithersburg, Maryland, Fred_Theurer@verizon.net; Jim Stafford, United States Department of Agriculture Natural Resource Conservation Service, Columbus, Ohio, jim.stafford@oh.usda.gov.

Abstract: The Maumee River Basin is a major watershed that drains into Lake Erie at Toledo Harbor in Ohio producing a significant amount of sediment into the harbor requiring periodic dredging. An evaluation of this watershed would help to determine recommended conservation practices that could control sediment entering into the harbor and reduce the associated dredging costs. The Upper Auglaize Watershed agricultural non-point source modeling project was an interagency effort to use a Geographic Information System (GIS) based modeling approach for assessing and reducing pollution from agricultural runoff and other non-point sources that eventually discharges into the Toledo Harbor. A significant source of sediment was identified from ephemeral gully processes and an approach was needed to assess this and determine its contribution to the total sediment load entering the harbor. This project applied the U.S. Department of Agriculture (USDA), Agricultural Research Service's AGricultural Non-Point Source (AGNPS) suite of models to the Upper Auglaize River Watershed and was conducted by an interagency team consisting of a partnership between the: (1) USDA, Agricultural Research Service (ARS); (2) USDA, Natural Resources Conservation Service (NRCS); (3) U.S. Army Corps of Engineers (USACE); (4) U.S. Geological Survey (USGS); (5) Ohio State University; (6) University of Toledo (UT); (7) Heidelberg College; (8) Ohio Department of Natural Resources (ODNR), Division of Soil and Water Conservation; (9) Ohio Environmental Protection Agency (OEPA); and (10) Allen, Auglaize, Van Wert, and Putnam Soil and Water Conservation Districts.

Ephemeral gullies were found to be the primary source of erosion (72 percent), sediment yield (73 percent), and sediment loading (73 percent) through the application of AGNPS. Controlling sediment load means controlling gully erosion and possibly trapping sediment yield before it reaches the stream system. Most BMPs (e.g., no-till, conversion of cropland, etc.) that reduce sheet and rill erosion and its sediment yield will also reduce gully erosion and its sediment yield. However, grassed waterways, which have no effect on sheet and rill erosion, are frequently an effective BMP to prevent ephemeral gullies. Riparian vegetation and sediment traps would also reduce the delivery ratios of all types of landscape erosion.

New techniques were developed by the team to quantify the ephemeral gully erosion within the model. When calibrated to available stream gage data the model demonstrated more (73% in the existing condition simulation) of the sediment load originated from ephemeral gully erosion rather than traditional sheet and rill erosion.

ASSESSING EPHEMERAL GULLY EROSION IN THE CHENEY LAKE WATERSHED USING GIS, REGEM AND THE ANNAGNPS MODEL

Lyle Frees, U.S. Department of Agriculture Natural Resource Conservation Service, Salina, KS, lyle.frees@ks.usda.gov; Jeffery Neel, Kent McVay, Daniel Devlin, Department of Agronomy, Kansas State University, Manhattan, Kansas

Abstract: Ephemeral gully (EG) erosion has been recognized as contributing significantly to sediment losses from agricultural fields, yet most methods for estimating soil erosion do not account for it. The Universal Soil Loss Equation (USLE), or revised and modified versions of it, evaluate soil loss as combined sheet and rill erosion, but do not include erosion due to concentrated flow channels, usually referred to as EGs in its estimates. Watershed models such as AnnAGNPS and SWAT, which are commonly used to evaluate non-point source (NPS) pollution in agricultural watersheds, are based only on combined sheet and rill estimates and do not account for EG erosion. Improved accuracy and adequate calibration of watershed models will likely require that EG erosion be considered as a contributor to sediment and nutrient loading to surface water bodies, especially if conservation practices are to be targeted to treat different NPS sources. We are engaged in a special emphasis, Conservation Effects Assessment Project (CEAP) in the Cheney Lake Watershed of south central Kansas, to study the influence of EG erosion on NPS loading to Cheney Reservoir and to integrate an EG erosion routine into the AnnAGNPS model which can account for this contribution. Preliminary assessment of soil losses in Cheney Lake Watershed suggest that EG erosion may deliver as much as 50 percent of the sediment load to the reservoir. Remote sensing and geographical information systems (GIS) have been used to quantify the occurrence and extent of EGs in the watershed and to extract gully profiles from a digital elevation model, and soil and engineering properties from NASIS soil data. The Revised Ephemeral Gully Erosion Model (REGEM) has been incorporated into AnnAGNPS, and an ArcView script and interface have been developed to populate AnnAGNPS with the necessary inputs to assess EG erosion in the watershed. Additionally, GIS procedures have been used to spatially analyze frequency and location of EGs as a function of soil, slope, tillage, contributing area, and cropping system. Better prediction of gully occurrence will help to locate field management and structure placement in the watershed. Addressing soil erosion from EGs may require a different suite of conservation practices than that required for sheet and rill erosion.

INTRODUCTION

Beta AGNPS/REGEM ARC VIEW INTERFACE: In an effort to capture the land features of ephemeral gully erosion in AnnAGNPS, a user-friendly data entry process is needed. Geographical Information Systems (GIS) have the capability to extract ephemeral gully features with a minimum requirement of user interaction. Currently AnnAGNPS has an AGNPS ArcView interface to aid in some data preparation for AnnAGNPS. Version 3.51, was used to integrate the Avenue Scripts needed for ephemeral gully data extraction. Tabs are added to the drop down menu, AGNPS DATA PREP, for generation of potential gully erosion flow paths, a tool to create and identify the gully mouth data set and create an ephemeral gully data set for export to AnnAGNPS. The only data entry needs from the user is the location of the ephemeral gully mouth. Location of the gully mouth, at this point, is as much an art as a science. The data

set, "Flow Accumulation", and digital-ortho photography can be used with an "on-screen" process to locate the gully mouth. The flow path characterized by the flow accumulation does not always overlay with the ephemeral gully location indicated on the ortho photo and some judgment is needed for the selection of the gully mouth locations. The Avenue Script routines are written to extract the gully profile, soils, land management and watershed properties from associated data layers. Ephemeral gully data can be appended to an existing annagps.inp file or a new annagnps.inp project can be created. An Arc View project (EG_AGNPS.apr) and User's Guide have been developed to assist the user in an AnnAGNPS project where ephemeral gully erosion concerns need evaluation. A special "Thank You" is extended to Ming-chieh Lee for his contribution to programming the Avenue Scripts in this project.

Cheney Lake Watershed Conservation Effects Assessment Program (CEAP): The purposes of the national CEAP assessment for cropland are, (1) estimate the environmental benefits for conservation practices applied to cropland, including cropland enrolled in the Conservation Reserve Program (CRP); (2) estimate the benefits of conservation practices currently present on the landscape; (3) estimate the need for conservation practices and the benefits that could be realized if appropriate conservation practices were implemented on all cropland; (4) simulate alternative options for implementing conservation programs on cropland in the future; and (5) incorporate science-based estimates of practice benefits into Natural Resource Conservation Service (NRCS) Performance Reporting System (PRS) to provide annual estimates of benefits for each program. Upon completion of validation and calibration of the AnnAGNPS model including REGEM, the following eight scenarios have been developed to estimate the benefits on conservation treatment within the Cheney Lake watershed:

1. **No Conservation Practices** – All land use is the same as 1997 land use but it is assumed there are no terraces, waterways, or CRP grass. All cropland will be assumed to be conventionally tilled for wheat and milo production. We will assume there is no irrigation.
2. **Ephemeral Gullies Treated** – It is assumed the same land use and all conditions from 1997 except the effect of all ephemeral gullies will be removed from the model.
3. **Conservation Tillage (1) –** It is assumed that all cropland is managed with no-till management practices. All land use, tillage, and conservation practices will be the same as the baseline in 1997.
4. **Conservation Tillage (2)** – It is assumed that all cropland is managed with mulch-till management practices. All land use, tillage, and conservation practices will be the same as the baseline in 1997.
5. **CRP** – It is assumed the same land use and all practices from 1997 except that Conservation Reserve Program grass will be replaced with conventionally tilled wheat and ephemeral gullies will be added in those crop fields.
6. **Native Grass -** The model will be run with the entire watershed planted to native grass.
7. **Split Applications of Atrazine** – It is assumed the same land use and all conditions from 1997 except a split application of Atrazine (half applied in the fall, half applied in early spring) will be included instead of applying the full rate at planting time in the spring.
8. **Irrigation scheduling –** It is assumed the same land use and all conditions from 1997 except that an irrigation trigger will be included when cropland reaches 50% of field capacity soil moisture instead of 70% of field capacity soil moisture.

RESULTS

The EG_AGNPS.apr Beta AGNPS/REGEM Arc View interface has successful extracted the input data for 989 identified ephemeral gullies within the Cheney Lake watershed and populated the AnnAGNPS input editor. As of October 15, 2005, the results of the eight conservation treatment scenarios have not been completed. Selected results will be presented at the conference in April 2006.

TERMINATION OF GULLY PROCESSES, SOUTHEASTERN NIGERIA

Peter P. Hudec, Emeritus Professor of Engineering Geology, University of Windsor Windsor, Ontario, Canada, hudec@uwindsor.ca, Frank Simpson, Professor of Geology, University of Windsor, Windsor, Ontario, Canada, franks@uwindsor.ca, Enuvie G. Akpokodje, Professor of Geology, University of Port Harcourt, Port Harcourt, Rivers State, Nigeria, enuvieak.b@ph.rcl.nig.com, and Meshach O. Umenweke, Associate Professor of Geology, Nnamdi Azikiwe University, Awka, Anambra State, Nigeria

Abstract: In southeastern Nigeria, gully erosion is responsible for the widespread destruction of transportation and communication systems, degradation of arable land, contamination of water supply, isolation of settlements and migration of communities. This account presents some of the results of a study of gully erosion, carried out during a period of eight years, in partnership with the rural people of twelve villages in Abia, Anambra, Enugu and Imo States.

The textural properties of the surficial deposits and horizontal to gently inclined bedrock make them susceptible to erosion. They are among the defining elements of a sensitive ecosystem, which undergoes rapid degradation, in response to surface runoff and human disruption. Gully processes are localized in the fine- to medium-grained Coastal Plain Sands (Pliocene-Recent) and Nanka Sands (Eocene) and the medium- to coarse-grained Nsukka Sandstone and Ajali Sandstone (Cretaceous) of the Anambra-Imo basin region. The most affected deposits are unconsolidated to poorly consolidated and with short dispersion times. The cleaner, more porous and weakly cemented sands are the most prone to gully advance, which increases directly with an increase in the proportion of grains, more than 1 mm. in diameter. Gully formation is enhanced by sliding, associated with a paleosol in the Nanka Sand, and by the rapid dispersion of clays in the interbedded shales.

Gully initiation is the result of localized erosion by surface runoff, associated with rainfall events of high intensity. Erosion is frequently focused, where the forest cover has been removed for agricultural purposes and also at the sites of uneven compaction of surface soils by foot (human and livestock) and wheeled traffic, in off-road locations. It also takes place, where soils and sediments abut against artificial materials, notably at poorly designed road culverts and roadside gutters. Gullies also occur, where springs issue from permeable sands, at contacts with less permeable deposits beneath. In general, the propagation of gullies is by sapping, caving and sliding at the gully head and sliding along the sides, accompanied by the down-slope transportation of gully-floor debris by storm runoff.

Termination of gully processes requires the integration of water-resource management, soil conservation and revegetation on the scale of a drainage basin. The technologies of water harvesting and spreading are necessary on hillsides, cleared for agricultural production. Some water harvesting technologies, such as roofwater harvesting, contribute to the control of runoff in settlements under threat. Spillways, diversion channels, culverts and gutters must be designed to accommodate runoff amounts at particular locations. For wider acceptance, termination strategies might take as their starting point design elements of indigenous technologies (terraces, barriers, diversion ditches, catchment ponds), which fell into disrepair as rural populations

increased. Public education is essential to a sustainable termination strategy. Different levels of government, donors, the private sector and the rural people must work together on solutions.

INTRODUCTION

In southeastern Nigeria, catastrophic gullies are formed by surface runoff from localized rainfall events of high intensity in the fine- to coarse-grained sands and sandstones of the Anambra-Imo basin region. Localized removal of soils, sediments and poorly consolidated sedimentary rocks by running water is augmented by processes of mass movement to form steep-sided ravines. The gully-forming processes ultimately yield a degraded "badlands" terrain, comprising knife-edge ridges, separated by deep ravines, and no longer amenable to agricultural use.

The World Bank (1990) recognized three main, environmental problems, facing Nigeria: soil degradation and loss, water contamination and deforestation. In addition, six other problem areas were specified: gully erosion, fishery loss, coastal erosion, wildlife and biodiversity losses, air pollution and the spread of the water hyacinth. Gully erosion contributes to each of the three main problems and causes damage with an annual cost to the nation, estimated at $100 million in 1990. In southeastern Nigeria, gully erosion is responsible for the destruction of transportation and communication systems, degradation of arable land, contamination of water supply, isolation of settlements and migration of communities. More than 2,500 gullies are active (Egboka, 2004).

The Food and Agriculture Organization of the United Nations summarized attempts to check gully erosion in southeastern Nigeria, from the establishment of the Udi Forest Reserve in 1918 to the formation of the Anambra State Task Force on Soil Erosion Control in 1990 (FAO, 1990). In general, these initiatives were "top down" in design and yielded some successful, mainly vegetative solutions, as well as largely unsuccessful, though expensive, engineered solutions. The FAO (1990) made reference to the "inherently unstable situation", in which gullying results from the action of heavy rainfall on surface Earth materials under a reduced or altered vegetation cover and proposed a number of vegetative and inorganic technologies as solutions.

The present account presents the view that the textural properties of the soils, sediments and sedimentary rocks are among the defining elements of a sensitive ecosystem, which undergoes rapid degradation, in response to surface runoff and human disruption. Simple, geotechnical tests, such as gradation analysis and soil dispersion rate, provide an indication of the susceptibility of Earth materials to gully erosion and also the rates and probable, preferred directions of gully enlargement. The results of such tests are essential to the safe and effective selection and siting of technologies to control and prevent gully erosion in southeastern Nigeria. Hudec (project leader) and Simpson were the Canadian project team; Akpokodje and Umenweke were the Nigerian project leaders at Port Harcourt and Awka, respectively. Umenweke died in a tragic automobile accident in March 2000.

PROJECT OUTLINE

The research project, Gully Erosion, Nigeria, involved the University of Windsor, Ontario, Canada, and the two Nigerian universities, the Nnamdi Azikiwe University, Awka, Anambra

State, and the University of Port Harcourt, Port Harcourt, Rivers State, working in partnership with villagers in Abia, Anambra, Enugu and Imo States, southeastern Nigeria. Twelve villages collaborated: Umenekwu and Uturu (Abia State); Ekwulobia, Oraukwu and Umuchu (Anambra State); Ngwo and Obufinia/Ndiono (Enugu State) and Amucha, Umuaka/Okwudor and Umuchima (Imo State). Participatory management and evaluation were essential elements of the research. The project goal was to reduce gully erosion in southeastern Nigeria. The purpose was (1) to explain the widespread occurrence of gullies in the area and (2) to design a strategy for the prevention and control of gully erosion. The project ran from 1992 to 2000; the joint work was interrupted during a hiatus in the democratic process in Nigeria from 1996 to 1999. The funding agency was the International Development Research Centre (IDRC), Ottawa.

The project research included detailed mapping of the gully systems at selected locations and revision of existing maps of surficial deposits and the solid geology at and around the main sites of gully erosion. These systematic observations yielded information on the mechanisms of gully formation and data on the rate and configuration of gully advance. Selected geotechnical tests were carried out on samples of soils, sediments and sedimentary rocks at Port Harcourt and Windsor. Close to the start of the project term, the people of several partner villages and outlying areas began emergency measures to halt the advance of gullies, which threatened parts of their settlements, as well as highways and communications systems. Collaboration of the research teams with the people produced improvements in the local approaches to remediation. The project outcomes were controlled runoff at the observation sites, sustainable control of gully erosion at the sites of emergency intervention, empowered village partners and pluralism in environmental awareness in the partner villages.

GEOTECHNICAL SYNTHESIS

In the project area, the bedrock consists of mainly siliciclastic strata, which exhibit different degrees of lithification. Upper Cretaceous sandstones and shales in the north and east give way to Tertiary clastic rocks and sediments in the south and west and Quaternary sands farther south, beneath a soil cover of variable thickness. Gully processes are localized in the fine- to medium-grained Coastal Plain Sands (Pliocene to Recent) and Nanka Sands (Eocene) and the medium- to coarse-grained Nsukka Sandstone and Ajali Sandstone (Cretaceous) of the Anambra-Imo basin region. Kogbe and Mehes (1986) summarized the age relations of these deposits. Laterite development is widespread in the surface materials, extending to depths of 2 to 20 m

The textural properties of these deposits to a large extent determine their responses to the erosive action of surface runoff. Hudec et al. (1998) described the results of gradation analysis and measurements of the dry bulk density, dispersivity and moisture content of samples from the main geological units, which are susceptible to gullying. Gradation analysis of the Nanka Sand, Ajali Sandstone and Nsukka Sandstone shows that they are all strikingly uniform. The combined percent passing curves for size analyses of the units follow closely similar trends. The coefficient of uniformity (d60/d10) shows relatively minor variation in size distribution, in the size range of fine to medium sand. A plot of changes in gully dimensions (length, depth and breadth) against the proportion of particles smaller than 1 mm. shows that gully advance in all three directions increases with the amount of coarse sand.

The degree of consolidation and the presence of interstitial and intercalated mudstone of the main sand and sandstone units also have a bearing on their susceptibility to gully erosion (Hudec et al., 1998). The amount and type of mineral cement, expressed as the oxides of Ca, Mg, Mn, Na and K, show negative correlations with the rate of gully growth: the smaller the amount of cement (decreasing consolidation), the greater the rate of gully advance. The iron oxide cements of the laterites show a reverse trend, with the rate of gully enlargement increasing with increases in the amount of iron cement. Rates of gully erosion also increase with decreases in the dispersion time of detrital materials, which is the time taken for a sample to disperse (disaggregate) in water. The Ajali Sandstone and the Nsukka Sandstone show the shortest dispersion times among the units, affected by gully erosion. The relationship between dispersion time and proportions of the finer size grades, passing through 0.15 and 0.075 mm. sieves, indicates that dispersion time increases with increasing proportions of fines. The cleaner sands show rapid dispersion and therefore are more susceptible to erosion.

The Nanka Sand contains subordinate shales. There is also a local development of a paleosol at Nanka, where it is responsible for landslides. The leaching of cements from the sands and the dispersion of the clays in the interbedded shales are regarded as the main factors, controlling localized erosion and gully formation. The underlying Imo Shale was not studied, but contains expanding clays, which are likely to show strong dispersion effects. The Nsukka Sandstone contains subordinate carbonaceous shales, sandy shales and coal seams. Dispersion of clays in the argillaceous layers probably also contributes to differential erosion of the unit.

GULLY INITIATION AND PROPAGATION

Grove (1951a, 1951b) recognized two main types of gully on the scarp slopes of the Udi plateau and the Awka-Orlu uplands: (1) spring gullies, where permeable sands and sandstones rest on less permeable deposits and (2) slope gullies, which originate as channels (for example, sunken footpaths) in bottom-of-slope locations. Spring gullies are enlarged by sapping, caving and landslips and slope gullies by pot-holing; both types are further enlarged by waterfall action at the rim and undercutting of the sides promotes earthfalls and landslips. Intensive rainfall clears the debris from the gully bottom and the more continuous rains saturate the bank materials and cause the slumping of larger blocks. Grove (1951b) noted a possible connection between gully erosion and the increased runoff, associated with the clearing of woodland and road-building. Nearly forty years later, the FAO (1990) concluded that most of the gully erosion in southeastern Nigeria is caused by badly designed roads and the clearance of vegetation from building sites.

These types of gully were observed during the present study. As well, it was noted that some gullies originate as narrow rills with a down-slope orientation, which undergo progressive widening and deepening, with successive rainfall events (Hudec et al., 2005). These features tend to occur on bare soil surfaces, created by human and animal foot traffic and wheeled traffic in off-road locations and also by the grading of soil along the sides of roads. A special case is provided by lateritic deposits, in which narrow, relatively deep gullies are eroded downwards to the more friable materials beneath the laterite layer, leading to caverning in the more easily eroded material and collapse. Measured rates of gully erosion in two to three months of a single rainy season were up to 157 m. in length, 50 m. in width and 4 m. in depth.

The largest rainfall events, observed in the region during the project term, were 250 to more than 350 mm. of rain, with intensities of more than 0.25 mm. per minute. Rainfall data, collected for the Nigerian researchers by area schools, and observations on the performance of road culverts and roadside gutters during periods of heavy rainfall revealed major flaws in the design of highway drainage throughout the four states. Gullies tend to form, where the concrete-lined drains and culverts are too small to accommodate peak surface runoff, are not terminated at base-of-slope locations and are allowed to decay and become clogged with debris. The overflowing water erodes beneath the roadside gutter or culvert, which eventually falls away to provide a site of localized erosion. Highway development and construction projects account for the erosion of up to 90 percent of the gully systems in southeastern Nigeria.

GULLY TERMINATION

The textural controls of rate and direction of gully erosion demand an important place in planning for the reduction of risks, associated with gully processes. Hudec et al. (2001) noted that risk reduction planning for gully erosion must take into account the management of large volumes of water in a setting of slope instability. Many of the risk reduction strategies, designed for floods (UNHDA, 1996) and different types of mass movement (Miller, 1997) are applicable to the formation of gullies. Indeed, landslides and related phenomena contribute to gully enlargement in southeastern Nigeria, while floods commonly occur at lower elevations, where river channels are choked with the sand from gullies in the adjacent uplands. Simpson et al. (2002) commented on the need to incorporate gully prevention and control into policies for the strategic management of water resources, in view of the threat posed by gully erosion to the fabric of rural society. .

The selection and siting of technologies for the prevention and control of gully erosion ideally would combine the analysis of satellite imagery with geotechnical and related investigations on the ground and in the laboratory. Simpson and Sohani (2001) outlined the relationships between straight-line ground features (lineaments), drainage and introduced measures for water conservation in a dryland region of Maharashtra, India. The lineaments are the surface traces of deep-seated fractures, seen on satellite imagery, which are conduits for ground water. In Nigeria, the wrench faults with east-northeasterly (dextral) and north-northwesterly (sinistral) orientations, described by Black and Girod (1970) over a wider area of West Africa, hold promise as a starting point for the understanding of possible, deep-seated controls of the surface processes, shaping the landscape. Sites of incipient gully formation in southeastern Nigeria are likely to have distinctive signatures for satellite observation, comparable to those presented by Hidalgo (2000) for landslides in northern South America. As noted by Grove (1951b), to be most effective, anti-erosion measures must be applied in the early stages of gully formation.

The termination of gully processes requires the integration of water-resource management, soil conservation and revegetation on the scale of a drainage basin. The technologies of water harvesting and spreading are necessary to reduce the velocity and erosive power of the runoff on hillsides, cleared for agricultural development. Water harvesting is the use of technologies for the capture at and near ground level and eventual extraction of fresh water, obtained from a particular catchment area. The catchment may be natural or artificial. Technologies for water spreading involve the diversion of water underground, into the interconnected pore systems of

shallow Earth materials. In general, water spreading requires the excavation of ridges and trenches, oriented parallel to contours of elevation above mean sea level; these are particularly effective on terraced hillsides. For example, water held at a particular terrace level by a terrace-margin ridge (bund) of soil infiltrates into the soil and this process may be accelerated through the additional use of trenches and infiltration pits. The FAO (1990) drew attention to the advantages, associated with the use of gabions (barriers comprising bundles of stones in galvanized iron chainlnk), strips of the grass Vetiver and alley cropping as approaches to the reduction of soil erosion on hillsides. Gabions are particularly suited to use on hillsides, composed of unstable materials, because of their flexibility.

In southeastern Nigeria, the rural people have a history of controlling surface runoff by means of minor hill-slope modifications, barriers and catchment basins. Hill farmers in the Mmaku area of the Udi plateau edge have traditionally used stone-faced terraces (FAO, 1990), though this practice appears to be isolated in extent. Barriers of interwoven branches and low walls of dried mud were used widely to control the movement of surface runoff around settlements and remain at many locations. These structures fell into disrepair, as a result of larger numbers of people crossing the hillsides, and for the most part are no longer maintained. Runoff is directed away from small roads and pathways in many parts of the project area by means of shallow diversion ditches, connected to catchment basins, located down-slope. These structures are generally effective in minimizing erosion along the roads.

The emergency measures for gully prevention and control, initiated by some of the partner villages and maintained by them, on the basis of consultations with the research teams, were effective over a period of eight years (Simpson et al., 2002). At the Okigwe-Uturu-Isiukwuato road junction, Uturu, near Abia State University, Abia State, the collapse of a roadside drain led to the formation of a deep gully that threatened the highway and disrupted the related telecommunication systems. A soil fill was introduced and then graded and a concrete drain diverted runoff down-slope, away from the highway. A dense cover of grasses and shrubs was established. At Ekwulobia, in Anambra State, the village and adjacent highway were at risk from a gully, resulting from a collapsed, concrete drain. The villagers constructed a concrete spillway at the gully head, leading to a concrete drain, which diverted the runoff away from the gully. Roofwater harvesting reduced the amount of surface runoff in the settlement, in the vicinity of the gully. At Amucha, in Imo State, the Nigerian researchers designed and constructed modifications to roadside drains, taking into account the volumes of runoff, received from local rainfall. There was no undercutting of the new section of gutter, even though the road itself previously had been eroded below the level of the drain in places.

The termination of gully erosion also may take place under entirely natural circumstances (Grove, 1951b). The headward erosion of deep ravines, associated with entrenched spring heads, is slowed down by the root systems of forested slopes and by slipped material, accumulated at lower levels. The erosion of slope gullies leads to the formation of badlands, in which erosion at an individual gully head slows, as it approaches the local water divide. Spring and slope systems commonly are stabilized by algal growth around the gully heads and the spread of ferns and mosses and later trees at lower levels. Recent observations of gullies at Ngwo, Enugu State, near the Enugu-Onitsha Expressway, showed that they had become inactive, as a result of the combined effects of lateritization and the growth of new vegetation.

The termination of gully processes on a significant scale in southeastern Nigeria will require unparalleled adjustments to lifestyle and professional outlook, encompassing such wide-ranging activities as highway construction and maintenance, agricultural practice and off-road movement of rural people and their livestock. This can be achieved only through close interaction of the affected communities, state and federal authorities, donors and private industry, working on the scale of a drainage basin. The project addressed this issue in an end-of-project workshop, held in Owerri, Imo State, on September 2, 1999. It brought together members of village erosion committees, traditional chiefs, government officials from each of the four states, individuals from private companies and the Canadian and Nigerian project teams, with faculty members and graduate students from each of the Nigerian partner universities.

CONCLUSIONS

In southeastern Nigeria, the textural properties of surficial deposits and the horizontal to gently inclined sands and sandstone, forming the bedrock, make them susceptible to gully erosion. Grain size, the distribution of mineral cements and dispersion rates are among the defining elements of a sensitive ecosystem, which undergoes rapid degradation, in response to surface runoff and human disruption. Localized erosion, leading to gully initiation and propagation, tends to occur at (1) textural heterogeneities and interruptions to the vegetation cover of granular surface materials; and (2) the unlined interfaces between such materials and artificial structures.

Trends in increasing proportion of well washed sands and of grains, exceeding 1 mm. in diameter, indicate where accelerated gully enlargement is most likely to occur and should be employed in the selection and siting of technologies for the termination of gully erosion. Success in gully prevention and control requires the careful integration of water-resource management, soil conservation and revegetation on the scale of a drainage basin. In particular, the technologies of water harvesting and spreading are essential to the control of surface runoff. Roofwater harvesting to reduce the surface runoff near dwellings and gabions, strips of Vetiver grass and alley cropping applications to arrest soil erosion on hill slopes are technologies that would make an immediate difference. Improvements to roadside drainage should have the highest priority.

ACKNOWLEDGEMENTS

The authors gratefully acknowledge funding from the International Development Research Centre, Ottawa, Canada. Simpson gratefully acknowledges helpful discussions on the gullies of southeastern Nigeria with A.T. Grove, in Kampala, Uganda, in 1993, and in later correspondence.

REFERENCES

Black, R., and Girod, M. (1970). “Late Paleozoic to Recent igneous activity in West Africa and its Relationship to basement structure,” in Clifford, T.N., and Gass, I.G. (Editors), African Magmatism and Tectonics. Oliver and Boyd, Edinburgh, pp. 185-210.

Egboka, B. (2004). "Gully erosion in Alaigbo," Osondu Newsletter, Online Edition, vol. 4. http://www.osondu.com/abec/erosionindex.htm.

FAO (1990). "Nigeria: land resources management study. Annex 6: proposals for improved soil and water management in representative (pilot) areas, Appendix 1: The very humid zone," Food and Agriculture Organization, Rome.

Grove, A.T. (1951a). "Land use and soil conservation in parts of Onitsha and Owerri provinces," Geological Survey of Nigeria, Bulletin No. 21, 79 p.

Grove, A.T. (1951b). "Soil erosion and population problems in south-east Nigeria," Geographic Journal, vol. CXVII, pt. 3, pp. 291-306.

Hidalgo, L.G., (1999). "Requirements for landslide signature observation by satellite," The Earth Observer, vol. 11, pt. 5 September-October 1999, pp. 11-13.

Hudec, P.P., Simpson, F., Akpokodje, E.G., and Umenweke†, M.O. (2001). "Risk reduction planning and gully erosion in southeastern Nigeria," in*:* Villacampa, Y., Brebbia, C.A., and Usó, J.L. (Editors), Ecosystems and Sustainable Development III, Advances in Ecological Sciences, Vol. 10 WIT Press, Southampton, pp. 283-289.

Hudec, P.P.H., Simpson, F., Akpokodje, E.G., and Umenweke†, M.O. (2005). "Anthropogenic contribution to gully initiation and propagation, SE Nigeria," in*:* Ehlen, J., Haneberg, W.C., and Larson, R.A. (Editors). Humans as Geologic Agents, Geological Society of America Reviews in Engineering Geology, v. XVI, Geological Society of America, Boulder, Colorado, pp. 149-158.

Hudec, P.P., Simpson, F., Akpokodje, E.G., Umenweke, M.O., and Ondrasik, M. (1998). "Gully erosion of coastal plain sediments of Nigeria," in*:* Moore, D., and Hungr, O. (Editors), Proceedings Eighth International Congress, International Association for Engineering Geology and the Environment, 21-25 September, 1998, Vancouver, Canada, A.A. Balkema, Rotterdam, pp. 1835-1841.

Kogbe, C.A., and Mehes, K. (1986). "Micropaleontology and biostratigraphy of the coastal basins of West Africa," Journal of African Earth Sciences, vol. 5, pt. 1, pp. 1-100. Miller, J.B. (1997). "Floods: people at risk, strategies for prevention," United Nations Department of Humanitarian Affairs, Geneva, 95 p.

Simpson, F., Hudec, P.P., Akpokodje, E.G., and Umenweke†, M.O. (2002). "Strategic water resource management, Nigeria (with Discussion)," in*:* Scott, R. (Editor), People and Systems for Water, Sanitation and Health, Proceedings of 27th WEDC Conference, 20-24 August, 2001, Lusaka, Zambia. WEDC (Water, Engineering and Development Centre), Loughborough University, Loughborough, U.K., pp. 402-404, 405.

Simpson, F., and Sohani, G.G. (2001). "Conjunctive water use, Maharashtra, India (with Discussion)," in*:* Pickford, J. (Editor) Water, Hygiene and Sanitation: Challenges of the Millennium. Proceedings of 26th WEDC Conference, November 5-9, 2000, Dhaka, Bangladesh. WEDC (Water, Engineering and Development Centre), Loughborough University, Loughborough, U.K., pp. 42-45, 56-58.

Simpson, F., and Sohani, G.G. (2002). "Best practice 13, India: Conjunctive use of water resources in Deccan Trap," in*:* Boven, K., and Morohashi, J. (Editors), Best Practices Using Indigenous Knowledge. Nuffic and UNESCO/MOST, The Hague, the Netherlands, and Paris, France, pp. 131-141.

UNDHA, (1996). Mudflows: Experience and lessons learned from the management of major disasters. United Nations Department of Humanitarian Affairs, Geneva, 139 p.

World Bank (1990). Towards the development of an environmental action plan for Nigeria. World Bank, Washington, D.C., 139 p.

ASPECTS OF GULLY EROSION RELATED TO EMBANKMENT OVERTOPPING AND BREACH

Greg Hanson, USDA-ARS-HERU, 1301 N. Western Stillwater OK, 74075, greg.hanson@ars.usda.gov; Darrel Temple, USDA-ARS-HERU, darrel.temple@ars.usda.gov

Abstract: Embankment erosion due to overtopping is one of the main causes for embankment accidents and failure. Seven large scale embankment overtopping tests using three material types from a silty-sand to a lean-clay have been conducted at the USDA-ARS Hydraulic Engineering Research Unit Laboratory in Stillwater, OK to observe the erosion processes, quantify erosion rates, and develop a computational breach model. Based on test observations, the erosion process has been broken up into four stages with one of the primary processes of erosion involving gully erosion (figure 1). The rate of gully headcut migration through the embankment was observed to vary several orders of magnitude, from 0.04 to 7.6 m/h, depending on the material type and placement. The rate of gully widening was observed to correlate to the headcut migration rate. The rate and episodic nature of the gully erosion was also observed to affect the timing and rate of water released during an embankment breach. The research conducted and observations made from the large physical testing described in this presentation provide an important basis for model development and validation.



Figure 1 Observed gully erosion during embankment overtopping test.

PIPE FLOW IMPACTS ON EPHEMERAL GULLY EROSION

G.V. Wilson, USDA-ARS National Sedimentation Laboratory, 598 McElroy Dr, Oxford, MS, gvwilson@ars.usda.gov; R.F. Cullum, USDA-ARS National Sedimentation Laboratory, 598 McElroy Dr, Oxford, MS, rcullum@ars.usda.gov; M.J.M. Römkens, USDA-ARS National Sedimentation Laboratory, 598 McElroy Dr, Oxford, MS, mromkens@ars.usda.gov.

Abstract: Rills and ephemeral gullies are major sources of sediment yet, their development is not well understood. Lateral flow through soil pipes over water-restricting horizons has been postulated to facilitate the development and head cut migration of ephemeral gullies. The objective was to determine the effect of subsurface pipe flow above a water-restricting horizon on ephemeral gully formation during rainfall events and specifically to quantify the effects of hydraulic head on ephemeral gully erosion. A rainfall simulator applied rainfall at 65 mm/h to a 1.5 m long by 1 m wide soil bed of 5% slope. Rainfall was applied for 1 hour on dry antecedent soil conditions, followed 30 minutes later by a 30 minute rainfall on wet soil, then 30 minutes later a final 30 minute rainfall on very wet soil. The soil profile consisted of 30 cm of Providence silt loam packed to a bulk density of 1.35 g cm^{-3} over a 5 cm thick water restricting layer packed to 1.57 g cm^{-3}. Pipe flow was simulated using a 2 cm diameter porous pipe that extended 50 cm into the soil bed from the upper end. Pipe flow was controlled under a constant head of 0 (no pipe flow) and 30 cm. Tensiometers with pressure transducers were inserted into the soil bed at 12 positions to monitor soil water pressure dynamics during flow events. Rainfall and pipe flow individually did not result in mass wasting, however, their combination did produce pop-out failures. The total soil losses by sheet erosion were 2-3 times higher with rainfall and pipe flow combined than by rainfall alone. The total soil loss by ephemeral gully erosion was 5 times higher than sheet erosion as a result of pipe flow combined with rainfall.

INTRODUCTION

Soil erosion by water remains a major problem in many regions of the US. More streams on the US EPA 303(d) list are impaired by sediment than by any other contaminant. Nutrients, heavy metals and pesticides are transported with sediment. Predicting and controlling the movement of sediment in a watershed requires a thorough knowledge and understanding of the runoff, erosion, and sediment transport processes. While substantial efforts have been made over the years to describe sheet erosion processes, there is an incomplete understanding of the basic mechanisms governing ephemeral gully erosion.

Ephemeral gullies can be a major source of sediment, yet the mechanisms of their development are not well understood. The relationship of gully erosion to rainfall, soil surface and subsurface conditions is poorly quantified. This knowledge gap hinders the development of accurate sediment delivery models and control techniques. Significant progress has been made in characterizing the role of surface flow processes on ephemeral gully development. The role of subsurface flow and soil water pressures has been shown to be important to rill initiation and growth (Römkens et al., 1997 and Froese et al., 1999). However, the contribution of subsurface flow to ephemeral gully erosion is less well known.

The two mechanisms of subsurface flow induced erosion are seepage flow and pipe flow (Dunne, 1990). Seepage flow is common, particularly at toe-slopes and streambanks (Wilson et al., 2005), where restriction of downward percolation results in lateral flow that emerges from the soil surface or streambank. Liquefaction of soil particles entrained in the seepage flow results in development and headward migration of gullies. Development of vertical gully faces enhances the process as undercutting of the gully face results in mass wasting or sapping of gully walls. In contrast, rapid and often turbulent preferential flow through macropores or soil-pipes erodes the periphery of the macropore when the shear forces exceed the frictional strength binding soil particles. Pipe erosion, also termed tunnel scour, can cause gully development when macropores collapse (Dunne, 1990).

Many studies have demonstrated the significance of subsurface flow through macropores to stream flow (Wilson et al., 1991a,b) and mass wasting (Sidle et al., 2000) under forested hillslope conditions. However, the contribution of macropore flow under agronomic conditions to ephemeral gully erosion is uncertain. Preferential flow can cause abrupt soil water pressure rises (Sidle et al., 200) and in loess soils with fragipans this results in perched water tables. In these soils it is common to observe ephemeral gullies eroded down to the fragipan. Soil pipes have been observed at the head of such ephemeral gullies as shown in Figure 1. Quantification of the conditions under which pipe flow contributes to ephemeral gully erosion is seriously lacking.



Figure 1 An ephemeral gully cut down to the surface of a fragipan horizon with a 3 cm diameter soil pipe at the head of the gully.

The objectives of this study were to quantify the soil physical and hydrologic properties under which preferential flow through soil-pipes results in ephemeral gullies. This paper reports preliminary analysis of the initial series of pipe flow experiments.

MATERIALS AND METHODS

Rainfall simulations were conducted on soil beds in a rectangular flume at 5 % slope with and without subsurface flow through an artificial soil-pipe. The flume (Figure 2) was 1.5 m long by 1

m wide by 50 cm high and constructed from 2 cm thick plexiglass. The endplate at the lower end was removed after packing the soil bed such that gully development would not be hindered by the endplate during flow events. The upper end had a port for connecting an artificial soil-pipe, at the topsoil-restrictive layer interface, to a water reservoir. The hydraulic head on the soil-pipe was controlled by a Mariotte device. The soil-pipe was a 2 cm i.d. soaker hose that extended 50 cm from the upper end into the soil bed with the end of the pipe left open.

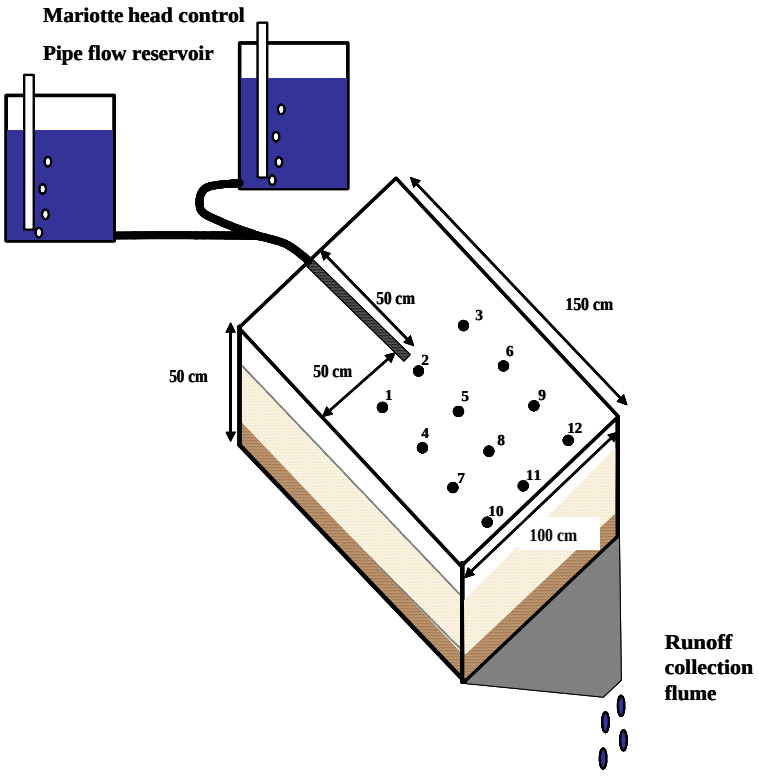


Figure 2 Illustration of the soil bed with a porous soil-pipe at the upper end and an open face lower end. Tensiometer locations are indicated by solid circles with their numbering scheme indicated. The water reservoir for the soil pipe has a Mariotte device for head control.

Bulk topsoil was collected from a depth of 0 to 10 cm from a Providence silt loam (fine-silty, mixed, active, thermic Oxyaquic Fragiudalfs) soil on the Holly Springs Experiment Station (HSES) of the Mississippi Agricultural and Forestry Experiment Station. Soil was sieved to < 2 mm and maintained in field-moist conditions (water content of 0.19 g g^{-1}) until packing. The bottom 5 cm of the soil bed mimicked a water restrictive layer by packing clay loam material to the average bulk density (1.57 g cm^{-3}) of fragipans in this area (Rhoton and Tyler, 1990). The topsoil was packed to a bulk density of 1.35 g cm^{-3} above the clay layer to form a 30 cm silt loam layer. Soil was packed in 2.5 cm lifts using field-moist soil after accounting for the measured water content.

Tensiometers were inserted vertically into the soil bed (Figure 2) such that the ceramic cup was positioned 1 cm above the water restrictive layer. Twelve tensiometers were installed in a 4 row

by 3 column array. The 4 rows were spaced 30 cm apart starting 5 cm from the end of the soil pipe at distances of 55, 85, 115, and 145 cm from the upper end. The middle column was positioned at the center of the soil, with a column on each side spaced 20 cm from the middle column (distances of 30, 50, and 70 cm from the side of the soil bed). Tensiometers were monitored by a CSI data logger.

Subsurface flow through the soil-pipe was simulated under a constant pressure head of 15 or 30 cm. The rainfall simulator (Meyer, 1960) consisted of a series of oscillating Veejet nozzles (80100) located approximately 3 m above the soil surface. Nozzles traversed the area horizontally in two dimensions in order to apply a uniform rainfall application with an impact energy of 211 kJ ha^{-1} mm^{-1}. Rainfall was applied at a rate of 65 mm h^{-1} for 1 h under antecedent soil-water conditions (dry run), followed 0.5 h later by a 0.5 h duration rainfall (wet run), and a final 0.5 h duration rainfall (very wet run) 0.5 h after the wet run. Ground water from wells on the HSES was used for soil-pipe and rainfall applications to mimic soil-water ionic strengths.

Four runs were made with the following combinations of treatments: (1) pipe flow only with 30 cm pressure head, (2) rainfall only, (3) rainfall and pipe flow with a 15 cm head, and (4) rainfall and pipe-flow with a 30 cm head. The time of runoff and/or seepage flow initiation was recorded and the runoff rate measured by collecting runoff for 15 sec every 3 minutes until rainfall was terminated, at which point runoff was collected for 15 sec every minute until runoff ceased. Runoff volume was recorded and sediment content analyzed by decanting excess water and then evaporating to oven-dryness (105° C). The timing and soil loss by mass wasting were recorded. Slumped material was collected, weighed, and sampled to determine water content. The dry mass of sediment loss by mass wasting was calculated after correcting for the water content.

RESULTS AND DISCUSSION

Pipe Flow Impact: Pieziometric observations on loess soils with a fragipan have indicated that perched water tables can reach the soil surface during winter storm events. The hydraulic head established will therefore be governed by the depth to the fragipan horizon. Fragipan depths are highly variable due to past erosion but typically range from 15 to 112 cm at the HSES (Rhoton and Tyler, 1990). This is typical of the loess region. Therefore, the simulated hydraulic head of 30 cm on the artificial pipe is clearly reasonable.

The tensiometers prior to establishment of the 30 cm pressure head for pipe flow alone exhibited a gradient from the upper end, just 5 cm downslope of the pipe outlet, of -35 cm to the lower end, just 5 cm from the open face, of -47 cm matric head. The first response to head establishment on the pipe for all four rows was by the middle tensiometers. The time to response was 2 min at T2, 15 min at T5, 47 min at T8, and 141 min at T11, Figure 3. Seepage began after 132 minutes of head. It is interesting to note that, seemingly contrary to Richards outflow law which states that positive matric heads are required for flow out of the soil through an open face, the tensiometers 5 cm from the face were still under negative matric heads. The last row of tensiometers had not begun to respond. The reason is likely due to the tensiometer cups being positioned 1 cm above the interface of the water restricting layer. Seepage response clearly indicated hydraulic non-equilibrium conditions caused by preferential flow immediately above

the surface of the restrictive layer. The observation of seepage occurring under apparently unsaturated conditions due to preferential flow over a restrictive layer is consistent with findings by Wilson et al. (2005) and Fox et al (2005) for streambank failure due to seepage erosion.

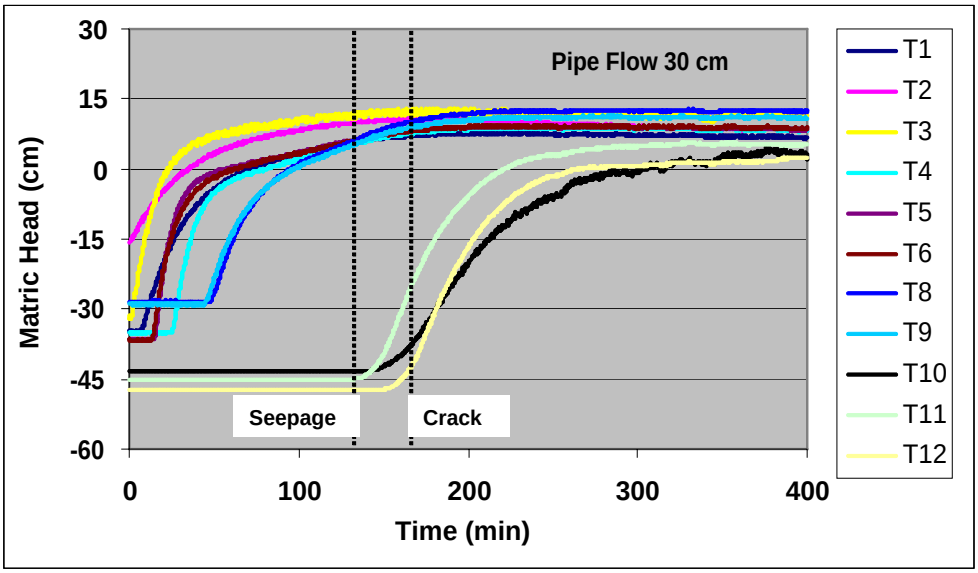


Figure 3 Tensiometer response to establishment of 30 cm head on the soil pipe. Vertical dashed lines indicate time to seepage initiation and tension crack development.

Wilson (unpublished data) observed an ephemeral gully on a loess soil in this region with a 3 cm diameter pipe at the head. Pipe flow rates entering the ephemeral gully following rainfall events, with rainfall and runon excluded from the gully, were typically around 33 L/d with sediment concentrations less than 1 g/L. Total soil losses from the pipe flow alone were typically less than 10 g over the course of a flow event. However, formation of the ephemeral gully constituted a soil loss of roughly 200 kg from a single event. The average pipe flow rate in the laboratory soil bed was 126 L/d. This value is higher than the field measurements, however, the conservative nature of the field measurements suggest that the laboratory flow rates were reasonable. Additionally, the laboratory pipe flow rate represents flow into the soil bed and not the seepage flow rate out of the bed. Pipe flow expressed on a per area basis using the known geometry of the soil bed (i.e., consistent with units for runoff/seepage rates) equaled 0.35 cm/h, Table 1. The seepage flow rate, i.e. runoff rate, out of the soil bed from pipe flow alone averaged 0.01 cm/h, which equates to a flux of 4 L/d. The difference between the pipe flow rate and the seepage rate is due to water storage within the soil bed.

Seepage flow rates for pipe flow alone were low, sediment concentrations were negligible and the soil bed did not exhibit mass wasting. Therefore soil loss in the runoff from pipe-flow alone was negligible. However, it did develop two tension cracks along the front face after 390 minutes of continuous flow through the soil-pipe. These cracks extended from the surface down to 5 and 11 cm depths at distances of 47 and 70 cm from the left side, respectively. This experiment was repeated with almost identical results. Tension cracks are commonly observed as precursors to bank failure (Fox et al., 2005).

Table 1 Hydrometric response to pipe flow and rainfall applications. The rates of runoff, Ro, and pipe flow, PF, and the sediment concentration are averages over the total time.

Trt	Seep Time	Ro Time	Pop-Out Time	Runoff Rate	PF Rate	Sed. Conc.	Ro Soil Loss	MW soil Loss
	min	min	min	cm/h	cm/h	g/L	kg	kg
1	132	na	na	0.01	0.35	0	0	0
2	na	4.5	na	5.30	na	128	2.22	0
3	110	2.0	144	5.88	0.08	238	4.92	18.04
4	128	15.0	162	6.17	0.35	376	6.61	37.42

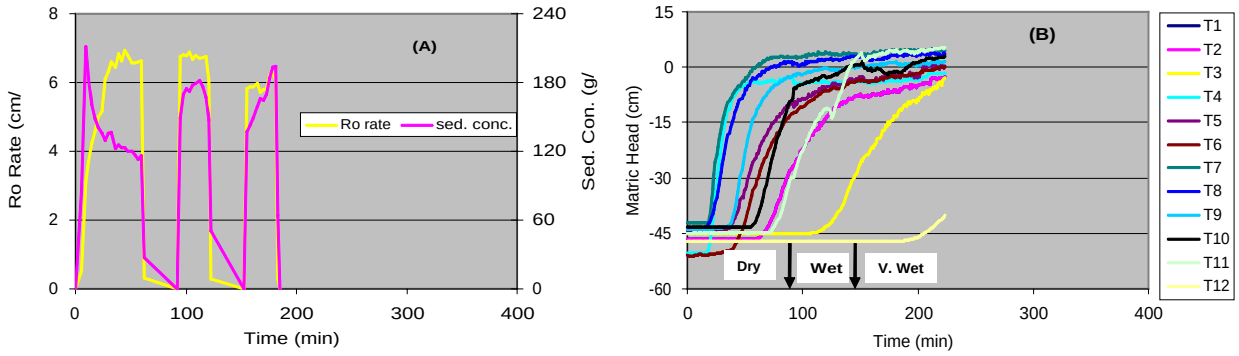
PF rate is the pipe flow rate as measured at the reservoir tanks.
MW is the total mass wasted by pop-out failures.

Rainfall Impact: The hydrologic response to rainfall alone was more dynamic than for pipe-flow alone. Surface runoff was initiated within 4.5 min of rainfall and the average runoff rate was 5.3 cm/h, Table 1. The antecedent conditions were similar to the pipe flow only experiment with matric heads between -43 to -51 cm. Unlike the pipe-flow experiment where tensiometric response sequentially tracked the arrival of a lateral wetting front, tensiometric response for the spatially uniform rainfall indicated random arrival of the vertical wetting front. The middle two rows of tensiometers were the first to respond, ranging from 24 to 37 minutes, and the last to respond was the most upslope (36 to 106 min) and downslope (56 to 188 min) rows, Figure 4. Perched water above the restrictive layer was not developed until after 57 minutes of rainfall. Thus, runoff was by Hortonian flow processes and not throughflow processes. The sediment concentrations in the surface runoff were fairly dynamic (Figure 4) during the first rainfall event, with a peak concentration of 210g/L at the initiation of runoff and decreasing to 116 g/L as runoff continued with an average of 130 g/L. The second event had stable sediment concentrations around 160 g/L, while the concentration increased during the third event from 137 to 194 g/L but averaged the same as the second event. The average sediment concentration over the three events was 129 g/L for a total soil loss by sheet erosion of 2.22 kg (6.6 ton/acre). Similar to pipe flow, rainfall alone failed to produce mass wasting of the soil bed.

Synergistic Effect of Pipe Flow with Rainfall: The synergistic effect of pipe flow with rainfall was simulated for a 15 cm pressure head and for a 30 cm head. The prescribed hydraulic head was established on the pipe until seepage from the soil bed was established before the three sequential rainfall events were initiated. The 15 cm head required 110 minutes to produce seepage whereas the 30 cm head required 128 minutes, Table 1, and the respective rainfall events were initiated at 120 and 135 minutes. The more rapid response to the lower head was due to wetter antecedent conditions (matric heads around -10 cm), however at the time of rainfall the soil beds had similar soil water conditions. The 30 cm head did have the higher pipe flow rate (flow into the pipe). The synergistic response of pipe flow with rainfall is clearly seen in the

runoff rates as the 15 cm head had higher average runoff than rainfall alone, and the 30 cm head had a higher runoff rate than the 15 cm head. As found by Wilson et al. (2004), the average sediment concentration by sheet erosion increased as the runoff rate increased. Soil losses by sheet erosion (14.6 and 19.6 ton/acre, respectively for 15 cm and 30 cm heads) were two to three times greater with pipe flow active during rainfall events.

Figure 4 (A) Runoff hydrograph and sedigraph for the rainfall only experiment. (B) Tensiometer



response to rainfall with no pipe flow. Arrows indicate time to start of the wet and very wet runs.

The main difference between rainfall or pipe flow alone and rainfall with pipe flow is in the mass wasting. Mass wasting failures occurred within 24 min and 27 min of rainfall initiation for the 15 and 30 cm heads, respectively (144 min and 162 min total time, respectively). The mass wasting from pipe flow occurred as pop-out failures. Mass wasting by pop-out failures is consistent with the findings of Simon et al. (1999) for soils with contrasting permeabilities that result in soil-water pressure increases. But it is in contrasts to cantilever type failures reported by Wilson et al. (2005) and Fox et al. (2005) where such contrasting layers resulted in seepage erosion that undercut gully banks. Rainfall with pipe flow under a 15 cm head produced two pop-out failures during the first (dry) rainfall event and two more during the third (very wet) rainfall event. The total soil loss by mass wasting, 18.0 kg (53.6 ton/acre), was almost five times greater than soil loss by sheet erosion. Rainfall with pipe flow under a 30 cm head was even more hydrodynamic with seven pop-out failures during the dry rainfall event. The total soil loss by mass wasting for the 30 cm head was 37.4 kg (111.2 ton/acre) which was more than five times greater than the sheet erosion losses.

CONCLUSIONS

Water restrictive layers, e.g. fragipans, which are common in loess soils, are known for causing perched water tables that result in lateral flow. Preferential flow through macropores above the restrictive layer can result in development of soil pipes. Soil pipes have been observed at the head of ephemeral gullies suggesting that pipe flow erosion by tunnel scour, is an important process of ephemeral gully development and head-cut migration. Flow through soil pipes can continue for days following a rainfall event. The impact of pipe flow alone, such as following a rainfall event, was investigated under a 30 cm head. The result of pipe flow alone was negligible soil loss. The impact of rainfall alone was investigated using three sequential rainfall events. Rainfall alone resulted in rapid runoff with soil losses by sheet erosion of 6.6 ton/acre but did not

result in ephemeral gully development or head-cut migration. In contrasts, rainfall with pipe flow produced a synergistic effect that not only resulted in two to three times higher sheet erosion but caused pop-out failures. The result of pipe flow during rainfall events was gully erosion rates of over 50 to 100 ton/acre for a single event. The degree of sheet and ephemeral gully erosion was highly dependent upon the hydraulic heads on the soil pipe. These findings demonstrate the potential significance of pipe flow on erosion when water-restricting layers perch water during rainstorms.

REFERENCES

Dunne, T. (1990). "Hydrology, mechanics, and geomorphic implications or erosion by subsurface flow," In Groundwater Geomorphology: The Role of Subsurface Water in Earth-Surface Processes and Landforms, Higgins CG and Coates DR (eds). Geological Society of America Special Paper 252: Boulder, CO.

Fox, G.A., G.V. Wilson, R. Periketi, and R.F. Cullum. (2005). "Sediment transport model for seepage erosion of streambank sediment," J. Hydrologic Engineering, ASCE (in review).

Froese, J.C., R.M. Cruse and M. Ghaffarzadeh. (1999). "Erosion mechanics of soils with an impermeable subsurface layer," Soil Sci. Soc. Am. J. 63:1836-1841.

Meyer, L.D. (1960). "Use of the rainulator on runoff plot research," Soil Sci. Soc. Am. Proc. 24:319-322.

Rhoton, F.E., and D.D. Tyler. (1990). "Erosion-induced changes in the properties of a fragipan soil,"Soil Sci. Soc. Am. J., 54:223-228.

Römkens, M. J. M. , S.N. Prasad and K. Helming. (1997). "Effect of negative soil water pressures on sediment concentration in runoff," In Management of Landscapes Disturbed by Channel Incision. Wang, S.S.Y., E.H. Langendoen and F.D. Shields (eds.), The University of Mississippi, Oxford, S. 1002-1007.

Sidle, R.C., Y. Tsuboyama, S. Noguchi, I. Hosoda, M. Fujieda, and T. Shimizu. (2000). "Stormflow generation in steep forested headwaters: a linked hydrogeomorphic paradigm," Hydrological Processes, 14:369-385.

Simon, A., A. Curini, S. Darby, and E.J. Langendoen. (1999). "Streambank mechanics and the role of bank and near-nbank processes in incised channels," In Incised River Channels, S.E. Darby and A. Simon (eds.), John Wiley & Sons Ltd.

Wilson, G.V., P.M. Jardine, R.J. Luxmoore, L.W. Zelazny, D.A. Lietzke and D.E. Todd. (1991a). "Hydrogeochemical processes controlling subsurface transport from an upper subcatchment of Walker Branch Watershed during storm events: 1. Hydrologic transport process," J. Hydrol. 123:297-316.

Wilson, G.V., P.M. Jardine, R.J. Luxmoore, L.W. Zelazny, D.E. Todd and D.A. Lietzke. (1991b). "Hydrogeochemical processes controlling subsurface transport from an upper subcatchment of Walker Branch Watershed during storm events: 2. Solute transport process," J. Hydrol. 123:317-336.

Wilson, G.V., S.M. Dabney, K.C. McGregor, and B.D. Barkoll. (2004)."Tillage and residue effects on runoff and erosion dynamics," Trans. ASAE 47:119-128.

Wilson, G.V., R. Periketi, G.A. Fox, S. Dabney, F.D. Shields, and R.F. Cullum. (2005). "Seepage erosion processes contributing to streambank failure," Earth Surface Processes and Landforms. (in review).

EPHEMERAL GULLY EROSION PROCESS AND MODELING ON THE LOESS PLATEAU OF CHINA

Fen-li Zheng, Prof., State Key Laboratory of Soil Erosion and Dryland Farming on Loess Plateau, Institute of Soil and Water Conservation, CAS and MWR, 26 Xinong Rd. Yangling, Shaanxi, P. R. China, flzh@ms.iswc.ac.cn; Zhong-shan Jiang, Prof., Institute of Soil and Water Conservation, CAS and MWR, 26 Xinong Rd. Yangling, Shaanxi, 712100, P. R. China; Min Wu, Assistant, Northwest A & F University, 22 Xinong Rd. Yangling, Shaanxi, P. R. China

Abstract: In recent 15 years, the large size of runoff plots with area of about 1000 m^2, located at the hilly-gully area of the Loess Plateau, and a dual-box system, consisted of a feeder box located at upslope and a test box located at downslope, have been established to quantify ephemeral gully erosion process and modeling. The results showed that different stages of ephemeral gully development were corresponded to different ephemeral gully headcuts advance, sidewall extension, and deep-cutting. In the earlier stage of ephemeral gully development, ephemeral gully headcuts were very active and played a crux role in sediment detachment; in the middle stage, sidewall extension, especially deep-cutting occupied predominant; and sidewall extension was dominant in the late stages. Sediment regime during ephemeral gully erosion process was always detachment-transport dominated. Upslope runoff discharging into downslope ephemeral gully area caused a great increase of sediment detachments. The net detachments at downslope caused by upslope runoff increased as either slope gradient, rainfall intensity, feeder runoff rate increased, or decreased as sediment concentration in upslope runoff increased. Soil erosion model included ephemeral gully at hillslope scale was developed on the Loess Plateau. The model validation indicated that the model had high-predicted precision for annual soil loss; the differences between the observed and predicted values on hilllospes with or without ephemeral gully erosion were less than 10%.

INTRODUCTION

Ephemeral gully, formed by erosion process and plough activities, are wider and deeper than rills, but they can be tilled across and filled in partially or completely (Zhu, 1956; Hutchinson and Pritchard, 1976). Ephemeral gully erosion causes severe soil loss on steep hillslopes. In the United States, ephemeral gully erosion contributes from 17 % of total soil loss at New York State to 73 % at Washington State (USDA-NRCS, 1977); in the loessial belt of Europe, ephemeral gully erosion contributes at least 10 % of the total soil loss (Robinson et al., 1998). In the hilly-gully region of the Loess Plateau, the ephemeral gully erosion takes up above 46% of total soil loss at steep hillslopes. Therefore, the understanding of ephemeral gully erosion process is important for erosion modeling and controlling.

Recently, WEPP, LISEM or EUROSEM has been applied to many areas in the world. However, due to terrain complexity and great contribution of ephemeral gully and classical gully erosion to sediment delivery from watersheds in China, especially on the Loess Plateau, application of WEPP, LISEM or EUROSEM to China meets great challenges. Therefore, it is necessary to develop a sound erosion prediction model in China according to regional conditions and erosion characteristics. Quantifying erosion process, especially ephemeral gully erosion process is the fundamental basis for development of an erosion prediction model.

This paper briefly introduces current researches of ephemeral gully erosion process and erosion prediction model development on the Loess Plateau of China. Especially, this paper focuses on discussing development of new approaches to study ephemeral gully erosion process and an erosion prediction model, including ephemeral gully at hillslope scale.

THE DEVELOPMENT OF NEW APPROACHES TO STUDY EPHEMERAL GULLY EROSION PROCESS

The Establishment of Natural Field Plots to Study Ephemeral Gully Erosion Process: The establishments of field plots, which covered the entire ephemeral gully catachment with are of 580-1144 m^2, were used to monitory ephemeral gully erosion process. Meanwhile, the field runoff plots without ephemeral gully were also established in order to identify the contribution of ephemeral gully erosion to sediment delivery (Zheng et al., 1998). Eight runoff plots were established at hillslopes in both regions of Ansai and Ziwuling, located at the hilly-gully regions on the Loess Plateau (Table 1).

Table 1 Establishment of natural runoff plots of ephemeral gully erosion.

Plot No.	Regions	With/without ephemeral gully (EG)	Length m	Width m	Area m^2	Slope gradient °
1	Ziwuling	Without EG	40.4	5.0	202	5-12
2		Without EG	40.8	5	203	5-12
3		With EG	86.3	13.6	995.2	5-32
4		With EG	99.2	13.8	1144.3	5-32
5	Ansai	Without EG	24	5.0	108	3-22
6		Without EG	25	5.0	112	3-22
7		With EG	50.2	12.6	580	3-30
8		With EG	49.5	12.6	576	3-30

The data from the field runoff plots showed that soil loss on the hillslopes with ephemeral gully erosion rates reached 10,000 to 12,000 t km^{-2} yr^{-1} and soil losses on the hillslopes without ephemeral gully were 5,000 to 6,800 t km^{-2} yr^{-1} (Table 2).

Table 2 Total soil loss, rill erosion and ephemeral gully erosion from the field plots.

Plot No.	Regions	With/without ephemeral gully (EG)	Total soil loss t km^{-2} yr^{-1}	Rill erosion (RE) t km^{-2} yr^{-1}	RE as percentage of total soil loss %	Ephemeral gully erosion (EGE) t km^{-2} yr^{-1}	EGE as a percentage of total soil loss %
1	Ziwuling	Without EG	6775	5311	78.4	0	0
2		Without EG	6859	5542	80.7	0	0
3		With EG	10448	2200	21.1	7200	68.9
4		With EG	10371	2400	23.1	7400	71.4
5	Ansai	Without EG	5148	3594	69.8	0	0
6		Without EG	5400	3910	72.4	0	0
7		With EG	11136	2138	20.8	7816	70.2
8		With EG	12048	2916	24.2	7976	66.2

The data in Table 2 showed that soil losses on the hillslopes with ephemeral gully were 1.51 to 2.34 times great than those on the hillslopes without ephemeral gully erosion. Moreover, the measured data of ephemeral gully erosion indicated that ephemeral gully erosion accounted for 66.2% to 71.4% of the total soil loss, indicating that ephemeral gully erosion had a great contribution to total soil loss. Soil erosion status on the hillslopes with and without ephemeral gully erosion demonstrated in Figure 1 and Figure 2. These two figures can simply identify soil erosion severity on the hilllsopes with and without ephemeral gully erosion.



Figure 1 Soil erosion status on the hillslope with ephemeral gully erosion



Figure 2 Soil loss status on the hillslope without ephemeral gully erosion

Design of A Dual-Box System to Study Ephemeral Gully Erosion Process and Sediment Regimes: For erosion studies, the traditional single-sized plot only produces total sediment delivery. Recently, we have developed a dual-box system, consisted of a feeder box located at upslope section and a test box with a miniature model of ephemeral gully shape located at downslope section to identify sediment detachment or deposition along the runoff route (Figure 3).

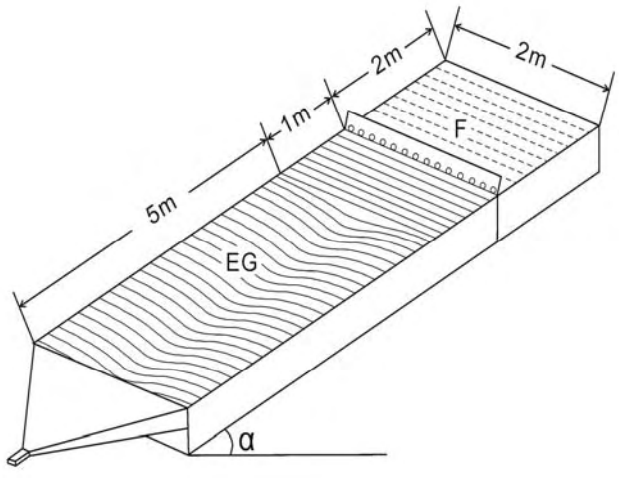


Figure 3 Schematic diagram of the dual-box system for stuffy ephemeral gully erosion (F is the feeder box; EG is the test box of ephemeral gully erosion)

The dual-box system was used to study the effects of run-on water and sediment on downslope ephemeral gully erosion process under different conditions. The experimental treatments included three slope degree of 26.8%, 36.4% and 46.6%, three rainfall intensities of 50, 75, 100 mm h-1, and six feeder runoff rates of 2, 4, 8, 12 and 16 L/min. The researched results demonstrated that sediment regimes were detachment-transport dominated on the hillslopes with ephemeral gully erosion. The upslope runoff always caused the net sediment delivery and the net sediment detachment at the downslope ephemeral gully area caused by the upslope runoff increased with a decrease of sediment concentration in upslope runoff or an increase of rainfall intensity, slope gradient or feeder runoff rate. The ephemeral gully erosion accounted for 52 % to 72.8 % of the total soil loss. These results showed the importance of understanding ephemeral gully erosion process.

EPHEMERAL GULLY EROSION PROCESS

The miniature model of ephemeral gully shape at initial stage was made to quantify the developing process of ephemeral gully, including ephemeral gully headcuts advance, sidewall extension and deep-cutting for the three rainfall intensities of 50, 75, 100 mm h^{-1}, the three slope gradients of 26.8%, 36.4% and 46.6%, and the six feeder runoff rates of 2, 4, 8, 12 and 16 L/min. In order to observe complete development of ephemeral gully, *i.e.*, the ephemeral gully experienced from the earlier stage (active stage), middle stage to late stage (stable stage), two to four continuous runs were made for each experimental treatment. For each treatment, after the first run was made, the soil box was set overnight, and then the second run was made on the eroded surface conditions formed by the first run. The same procedure was performed for the third and fourth run.

The experimental data showed that different stages of ephemeral gully development were corresponded to different ephemeral gully erosion process, *i.e.*, ephemeral gully headcuts advance, sidewall extension, and deep-cutting. Meanwhile, as rainfall intensity, slope gradient, and feeder runoff rates increased, the speeds of sidewall extension and deep-cutting, especially gully headcuts advance increased. For example, for the treatment of 100 mm $h^{-1}$of rainfall and 46.6% of slope degree, two continuous runs were made for the complete development of ephemeral gully. But for the treatment of 50 mm $h^{-1}$of rainfall and 26.8% of slope degree, four continuous runs were made for the complete development of ephemeral gully. Here the treatment of 50 mm $h^{-1}$of rainfall and 26.8% of slope degree was taken as an example for demonstrating the complete development of ephemeral gully.

The first run demonstrated that the ephemeral gully headcuts advance was fast (Table 3). The ephemeral gully length shifted from 315 cm at 9 min to 500 cm at 19 min of run duration. The speed of the headcuts advance was 11.1 m h^{-1}. After 19 min of run duration, the headcuts advance became slow and the speed of headcuts advance was 1.26 m h^{-1} from 19 min to 47 min of run duration. Meanwhile, the ephemeral gully sidewall extension and deep cutting were also active. For example, the ephemeral gully width changed from 8 cm at 12 min to 14.6 cm at 43 min of run duration and the ephemeral gully depth shifted from 5.6 cm at 12 min to 17.2 cm at 43 min of run duration; the speeds of sidewall extension and deep-cutting were was 0.13 m $h^{-1}$and 0.22 m h^{-1}, respectively. These results indicated that the development of ephemeral gully took place in the active stage and the headcuts advance and deep-cutting played a crux role to the sediment delivery.

The second run showed that the headcuts advance was very slow (Table 3). The speed of the headcuts advance was only 0.01m h^{-1}. But the sidewall extension was fast. The ephemeral gully width changed from 14.8 cm at 7 min to 30.6 cm at 56 min of run duration and the speed of the sidewall extension was 0.21, which was 1.6 times than that in the first run. Meanwhile, the deep-cutting was still active. The ephemeral gully depth shifted from 14.2 cm at 7 min to 23.6 cm at 23 min of run duration, and the speeds of the deep-cutting was 0.46 m h^{-1}, which was 2 times than that in the first run. After 23 min of run duration, the gully depth became shallow due to temporary sediment deposition in the ephemeral gully channels due to the active sidewall extension. These results indicated that the sidewall extension, especially deep-cutting were predominant in the sediment delivery and the development of ephemeral gully was still active during the secondary run.

Table 3 Average ephemeral gully length, width and depth during the each run.

The first run										
Run duration, min	9	12	19	24.5	31	36	43	47	53	59
Ephemeral gully length, cm	315	460	500	520	525	535	540	580	580	580
Ephemeral gully width, cm	-	8.0	8.6	9.7	11.0	13.8	14.6	14.6	14.6	14.6
Ephemeral gully depth, cm	-	5.6	5.8	7.0	11.8	16.0	16.3	16.8	16.9	17.0
The second run										
Run duration, min	7	15	19	23	28	35	42	46	52	56
Ephemeral gully length, cm	58.9	59.2	59.4	59.5	59.6	59.6	59.7	59.8	59.9	60.0
Ephemeral gully width, cm	14.8	15.1	15.3	15.6	21.4	22.4	25.2	26.2	30.4	30.6
Ephemeral gully depth, cm	18.4	22.1	23.2	23.6	18.4	19.8	19.2	18.4	19.6	20.4
The third run										
Run duration, min	8	14	19	23	30	34	40	45	51	56
Ephemeral gully width, cm	30.0	30.2	30.6	30	33.8	34.4	34.4	34.5	34.6	35.0
Ephemeral gully depth, cm	21.4	25.6	26.2	26.2	24.8	26.6	26.2	25.7	24.9	25.3
The fourth run										
Run duration, min	8	13	19	24.5	29	35	41	47	55	59
Ephemeral gully width, cm	36.6	36.8	36.8	36.8	37.0	37.2	40.6	41.0	42.4	42.6
Ephemeral gully depth, cm	25.7	26.1	26.3	25.8	25.6	26.2	25.6	25.8	25.6	25.8

In the end of the second run, the ephemeral gully head reached the top of the test box, the ephemeral gully headcuts advance ceased. This was similar to the filed phenomenon that the ephemeral gully head reached the watershed boundary (Zheng et al., 1998).

The third run showed that the speeds of the sidewall extension and deep-cutting were lesser than those in the second run (Table 3). The ephemeral gully width shifted from 30 cm at 8 min to 35 cm at 56 min of run duration, the speeds of the sidewall extension was 0.06 m h^{-1}, which was much smaller than that in the second run. The ephemeral gully depth shifted from 21.4 cm at 8 min to 25.3cm at 56 min of run duration, the speeds of the deep-cutting was 0.05 m h^{-1}, which was much smaller than that in the second run. These results showed that ephemeral gully development was relative stable.

The fourth run demonstrated that the speed of the sidewall extension was similar to the third run (Table 3). The ephemeral gully width shifted from 25.4 cm at 8 min to 42.6cm at 59 min of run duration, the speeds of the sidewall extension was 0.07 m h^{-1}. The ephemeral gully depth almost maintained constant. These results showed that ephemeral gully development took place in the stable state and the sidewall extension played a key role in the sediment delivery.

The measured data of ephemeral gully erosion for the four-times continuous runs indicated that gully erosion accounted for 48.5% to 70.2% of total soil loss (Table 4). These results were the same as we got from field study (Zheng *et al.*, 1998), indicating that ephemeral gully erosion plays an important role at steep hillslopes of the Loess Plateau. Therefore, soil erosion model on the Loess Plateau should cover ephemeral gully erosion.

Table 4 Ephemeral gully erosion as percentage of soil loss.

The four-continuous runs	Soil loss kg	Ephemeral gully erosion kg	Ephemeral gully as percentage of soil loss %
The first run	108.7	64.4	59.2
The second run	169.1	118.8	70.2
The third run	138.6	76.8	55.4
The fourth run	103.4	50.2	48.5

EROSION PREDICTION MODEL AT HILLSLOPE SCALE

In recent years, soil erosion model included ephemeral gully at hillslope scale has been developed on the Loess Plateau.

The Structure of Erosion Prediction Model: The structure of erosion prediction model is as follows:

$$A=RKLSGCP \tag{1}$$

Where A is annual soil loss (t ha^{-1} yr^{-1}) ; R is rainfall erosivity (MJ mm $ha^{-1}h^{-1}$ yr^{-1}) ; K is soil erodibility (t h MJ^{-1} mm^{-1}) ; L and S are slope gradient factor and slope length factor, respectively ; G is ephemeral gully erosion factor; C is crop cover and management (dimensionless); P is soil conservation measure factor.

Calculation of Each Factor:

Definition of the Standard Runoff Plot in China: The standard runoff plot in China is referred to as a runoff plot with 10°of slope degree, 20 m of slope length, 5 m of slope width, and continuous bare and fallow during the observation period.

Rainfall Erosivity (*R*): The formula for calculating R is as follows:

$$R_c = 16.4\left(\frac{P_c I_{60}}{100}\right)^{0.953} \tag{2}$$

Where R_c is rainfall erosivity in the certain year (MJ·mm ha^{-1} h^{-1} yr^{-1}) ; P_c is the yearly accumulative total of single rainfall amount equal or over 10 mm in the corresponding year (mm); I_{60} is maximum 60-min rainfall intensity selected from each single rainfall event in the corresponding year (mm h^{-1}).

Slope Length and Gradient Factors (*LS*): The formula for calculating *LS* is as follows:

$$LS = (\frac{\lambda}{20})^m (\frac{\theta}{10})^n \quad (3)$$

Where λ and θ are slope length (m) and slope degree (º), respectively ; *m* and *n* are slope length exponent and slope degree exponent, respectively.

The equation for calculating *m* is $m = 0.029 S_0^{0.69}$, where S_0 is slope degree (º)

The value of *n* is between 1.3 and 1.40, and the value of 1.35 is recommended.

Ephemeral Gully Erosion Factor (*G*): For slope gradient over 15ºand given rainfall data, the equation for calculating *G* is as follows:

$$G = 1 + \left(\frac{\theta - 15}{15} \right) \left[3.156 (\Sigma P I_{30})^{-0.167} - 1 \right] \quad (4)$$

Where θ is slope degree (º); *P* is the yearly accumulative total of single rainfall amount over 3 mm in the certain year (mm); I_{30} is maximum 30-min rainfall intensity selected from single rainfall event in the corresponding year (mm h^{-1}).

For slope gradient over 15ºand no rainfall data, the equation for calculating *G* is as follows:

$$G = 1 + 1.60 \sin(\theta - 15^\circ) \quad (5)$$

For the slope gradient less than or equal 15º, the equation for calculating *G* is as follows:

$$G = 1 + 1.20 (\sin\theta)^{0.5} \quad (6)$$

***K, C,* and *P* Factors:** K, C, and P factors were obtained from field observation and simulated rainfall experiments or were referred to as the data of USLE.

Validation of The Erosion Prediction Model: The data from the field runoff plots observed from 1991 to1998 were used to validate the erosion model. The results showed that predicted values were very close to the observed values (Figure 4). On the hillslopes with ephemeral gully erosion, the differences between predicted and observed values were less than 9.0%. The results indicate that the erosion model has high-predicted precision for annual soil loss.

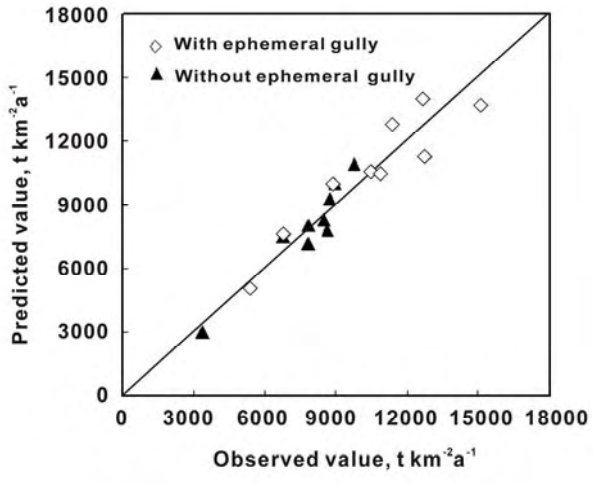


Figure 4 Comparison of the predicted values with the observed values on the hillslopes with and without ephemeral gully Erosion.

CONCLUSIONS

This paper presents the development of new approaches to study ephemeral gully erosion process and the erosion prediction model including ephemeral gully at hillslope scale. The following conclusions were derived:

The large size of runoff plots with area of about 1000 m^2, located at the hilly-gully area of the Loess Plateau were established on the Loess plateau to monitory ephemeral gully erosion process; and the dual-box system, consisted of a feeder box located at upslope section and a test box with a miniature model of ephemeral gully shape located at downslope section, was developed to quantify ephemeral gully erosion process.

Sediment regime during ephemeral gully erosion process was detachment-transport dominated. Soil losses on the hilllsopes with ephemeral gully erosion were 10,000 to 12,000 t km^{-2} yr^{-1}, which were 1.51 to 2.34 times great than those on the hillslopes without ephemeral gully erosion. The ephemeral gully erosion accounted for 48.5 to 72.8% of the total soil loss.

Upslope runoff discharging into downslope ephemeral gully area always caused the net sediment delivery in the downslope ephemeral gully section. The net detachments at the downslope ephemeral gully erosion area caused by upslope runoff increased as either slope gradient, rainfall intensity or feeder runoff rate increased, or decreased as sediment concentration in upslope runoff increased.

The development of ephemeral gully showed that the ephemeral gully headcuts played a crux role in sediment detachment in the earlier stage; in the middle stage, the sidewall extension, especially the deep-cutting occupied predominant; in the late stage, the sidewall extension were dominant.

Soil erosion model included ephemeral gully at hillslope scale was developed on the Loess Plateau. The results showed that predicted values were very close to the observed values. On

the hillslopes with and without ephemeral gully erosion, the differences between predicted and observed values were less than 10%, indicating that the model was suitable for the steep landscapes.

ACKNOWLEDGMENTS

This study was funded by CAS project (KZCX3-SW-422) and National Nature Science Foundation of China (40335050, 50239080).

REFERENCES

Hutchinson, D. E. and Pritchard H. W. (for Committee). (1976). "Resource conservation glossary," Journal of Soil and Water Conservation. 31(4):1-63.

Robinson, K. M., Bennett, S. J., and Casali, J. (1998). "Headcut dynamics and ephemeral gully erosion," ASAE Annual International Meeting, Orlando, Florida, USA, July 12-16, American Society of Agricultural Engineering, St Joseph, USA.

USDA-NRCS. (1977). "America's private land, a geography of hope," USDA-NRCS, Washington, D. C.

Zheng, F. and Kang, S. (1998). "Erosion and sediment yield in different erosion zone of the Loess Plateau," ACTA Geographica Sinica. 53(5):422-428 (in Chinese).

Zhu, X. (1956). "Soil erosion classification at the loessial region," ACTA Pedological Sinica. 4(2): 99-115 (in Chinese).

COMPARISON OF NUMERICAL HYDRAULIC MODELS APPLIED TO THE REMOVAL OF SAVAGE RAPIDS DAM NEAR GRANTS PASS, OREGON

Jennifer Bountry, Hydraulic Engineer, Bureau of Reclamation, Denver, CO, jbountry@do.usbr.gov; Yong Lai, Hydraulic Engineer, Bureau of Reclamation, Denver, CO, ylai@do.usbr.gov; Timothy Randle, Hydraulic Engineer, Bureau of Reclamation, Denver, CO, trandle@do.usbr.gov.

INTRODUCTION

Savage Rapids Dam is located in southwestern Oregon, on the Rogue River, 5 miles upstream from the town of Grants Pass (Figure 1). The dam, owned by the Grants Pass Irrigation District, is 39 feet high and has been diverting irrigation flows since its construction in 1921. Fish ladders on the dam are old, do not meet current National Marine Fisheries Service (NMFS) fisheries criteria, and delay migrating fish. In addition, the fish screens on the north side of the dam do not comply with current NMFS fisheries criteria. The Bureau of Reclamation (Reclamation) is designing the dam removal construction and a pumping plant to replace the existing dam to alleviate these fish passage problems. As part of the alternative analysis and design process, numerical models have been utilized to help predict the flow hydraulics, as well as the timing and magnitude of sediment release from the dam.

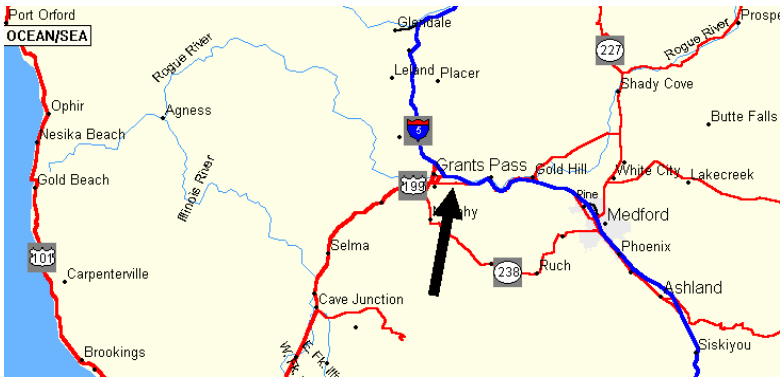


Figure 1 Location map.

OBJECTIVE

The objective of this paper is to present and compare the hydraulic results obtained with a number of numerical modeling tools utilized in the design of the Savage Rapids Dam removal project. The paper will focus the comparison to a calibration run of modeled data results to measured water surface elevation and velocity data. The paper will also discuss the critical input data and calibration parameters for each of the numerical models. Finally, the paper will discuss the modeling experience gained and what areas of modeling still need further research to answer dam removal project questions. It is hoped this case study will prove useful to future numerical model studies of dam removal projects and provide guidance to the appropriate use of numerical models.

METHODS

Numerical models utilized in the Savage Rapids Dam removal project are listed in Table 1. This paper will be limited to the hydraulic results only for water surface and velocity data. All models were run with flows based on discharges associated with the USGS gaging station located in Grants Pass, approximately five miles downstream. The simulation reach extends from the Savage Rapids Park, 0.5 mile upstream of the dam, to about 0.5 mile downstream of the dam for the two-dimensional models. The HEC-RAS and HEC-6t models were extended farther downstream to the Applegate River confluence, about 12 miles from the dam (USBR, 2001).

Table 1 List of numerical models applied to the Savage Rapids Dam removal project.

Model	Source	Description	Project Application
HEC-RAS	USACE Hydrologic Engineering Center (Brunner, 2002)	One-dimensional hydraulic model	Boundary conditions for two-dimensional models; fish passage velocity rating curves
HEC-6t	USACE Hydrologic Engineering Center (Thomas, 1996)	One-dimensional hydraulic and sediment routing model	Rate of reservoir sediment erosion and redistribution into the downstream river channel to evaluate potential impacts to flood stage, fish habitat areas, and downstream water users
MIKE-21	Danish Hydraulic Institute (DHI, 1996)	Two-dimensional finite-difference hydraulic model	Alternative assessment for 4 potential pumping plant locations based on potential for sediment deposition due to backwater eddies
GSTAR-W	Bureau of Reclamation (Lai, 2005)	Two-dimensional hydraulic model	Pumping plant intake and cofferdam design; dam removal alternative analysis

HEC-RAS was utilized to model one-dimensional sub-critical flow. Calibration parameters were limited to the Manning's roughness coefficient and it ranged between 0.035 and 0.040 which are typical for this type of river environment. The expansion coefficient was set at 0.3 and the contraction coefficient was set at 0.1, but not adjusted during calibration.

The MIKE-21 Flow Model is a two-dimensional finite-difference model that uses a square mesh of uniform size (DHI, 1996). Major input data and parameters are the representation of the channel bathymetry, boundary conditions at the upstream and downstream boundaries, channel roughness, eddy viscosity, and total simulation time. A uniform grid cell size of 2-by-2 meters (6.5-by-6.5 foot) was used to represent the channel and flood plain bathymetry. The final calibration resulted in a Manning's roughness parameter of 0.030. An eddy viscosity formulation is included in the 2D model computations to account for momentum fluxes due to turbulence, vertical integration, and sub-grid scale fluctuations. A final eddy viscosity of 1.0 was used.

GSTAR-W offers two-dimensional diffusive wave and dynamic wave solvers, as well as explicit and implicit solvers for solution efficiency and robustness. A detailed description of the

mathematical formulation and the numerical methods has been reported by Lai and Yang (2004) and Lai (2005). Both diffusive wave and dynamic wave solutions were obtained for this study so that a comparison may be made between the two solvers. GSTAR-W uses flexible unstructured mesh and the mesh used for this project consists of 20,145 elements and 20,468 nodes with a typical element size of 5 by 12 feet. The major calibration parameter is the flow loss coefficient that was determined to be 0.05 for the diffusive wave model and 0.04 for the dynamic wave model.

For both two-dimensional models, the upstream boundary conditions were a flow discharge of 2,800 ft^3/s where a uniform flow is assumed with flow velocity orthogonal to the boundary. The downstream boundary was a water surface elevation from the calibrated HEC-RAS model. In this study, the downstream elevation was based on the HEC-RAS model as described by Bountry and Randle (2003) and it was determined to be 935.53 ft.

MEASURED DATA DESCRIPTION

A river and floodplain survey was conducted in April 2002 (average discharge of 2,800 ft^3/s) by Reclamation to document the existing channel bottom and topography both upstream and downstream of the dam during a reservoir drawdown period. Data in the channel was collected by boat equipped with survey equipment and a depth sounder. In addition, velocity profile and discharge measurements were made in the river channel both upstream and downstream of the existing dam site. Some additional survey data for floodplain areas was also utilized for topography data, but did not contain any water surface elevation or velocity data.

The relative vertical elevations of the survey data collected should be accurate to the nearest centimeter because the survey was tied to a NGS monument using both global positioning system (GPS) equipment and total station. However, due to turbulence along the water surface in riffle and rapid sections, measurements from the boat can vary by a few tenths of a foot at any given location. This is considered acceptable due to the non-uniform channel bed that typically varies in elevation at least one bed-material particle size (cobble size material ranges from 0.2 to 0.8 feet). Measurements in pool sections do not tend to fluctuate as much as in riffle sections because velocities are slower and it is easier to hold a position.

A RD Instruments 1200 kHz Rio Grande acoustic Doppler current profiler (ADCP) was used to measure velocity, depth, and discharge. The standard deviation for an average velocity measurement was computed to be ±0.3 ft/s (Bountry and Randle, 2003). The average ADCP-measured discharge was about 2 % higher than the USGS reported discharge at Grants Pass.

COMPARISON OF RESULTS

Water Surface Elevation: Computed water surface elevations from different models are compared with the measured elevation along the thalweg in Figure 2. It is seen that all model results agree with the measured elevations well. This indicates that any model used in this project is appropriate in predicting the water surface elevation. Some minor discrepancies do exist among models but they are mostly limited to an area near the radial gates where a hydraulic

jump exists. As anticipated, the dynamic wave model predicts the existence of the jump, while the diffusive wave model is incapable of simulating the hydraulic jump.

For a more quantitative comparison, the computed water surface elevations from MIKE-21 was statistically compared to the measured water surface elevations at every point where a corresponding measured data point was available. Results were separated into three reaches: upstream of radial gate outlets, scour hole immediately downstream of the dam, and the downstream river channel from the scour hole to the end of the model (Table 2).

Table 2 Differences between computed (MIKE-21) and measured water surface elevation.

	Upstream of Dam (feet)	Scour Hole Just Downstream of Dam (feet)	River Channel Downstream of Scour Hole (feet)
Count	476	160	386
Mean	0.3	0.4	0.3
Maximum	1.2	0.8	1.0
Minimum	-1.5	0.0	-1.0
Range	2.7	0.7	2.0
Variance	0.0	0.0	0.0
Standard Deviation	0.4	0.1	0.4

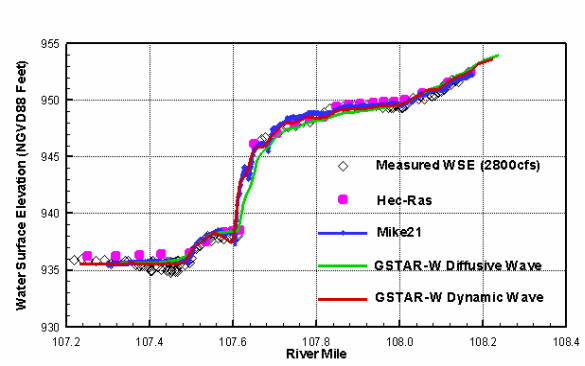


Figure 2 Comparison of predicted and measured water surface elevations for all models.



Figure 3 Velocity measurement points for the simulated river reach (points shown in red).

Velocities and Flow Patterns: The computed velocity vectors and flow patterns are compared with the measured data so that the flow hydraulics may be compared in greater detail. It is noted that a good prediction of the water surface elevation does not guarantee a good prediction of velocities and flow patterns.

The ADCP-measured and depth-averaged velocity data were compared for the measurement points displayed in Figure 3. Upstream of the dam, eight cross sections were compared along an

800-foot section of river. Downstream of the dam, two areas are compared: one is immediately downstream of the dam on the right side where a scour hole is present; another is downstream of the excavated channel used to bypass flow through the radial gates.

A comparison is first made between the GSTAR-W model results and measured velocity vectors at the eight cross sections upstream of the dam (Figures 4 and 5). Agreement is favorable for both diffusive and dynamic wave models except at a few locations. Overall, the difference between the two solutions is not appreciable. The dynamic wave model is capable of predicting the flow separation on the left bank of cross sections 3 and 4 while the diffusive wave model is not.

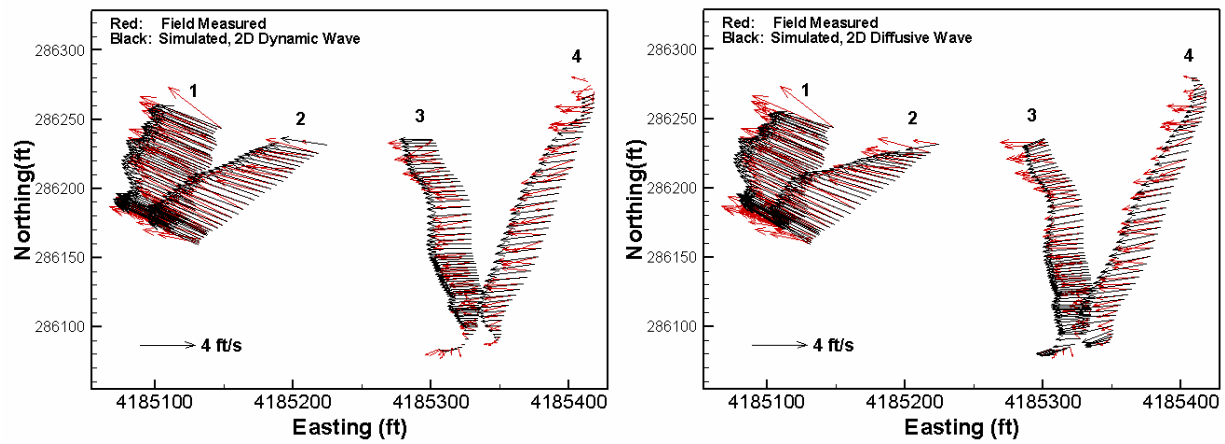


Figure 4 Comparison of predicted and measured velocity vectors at cross sections 1 to 4 upstream of the dam.

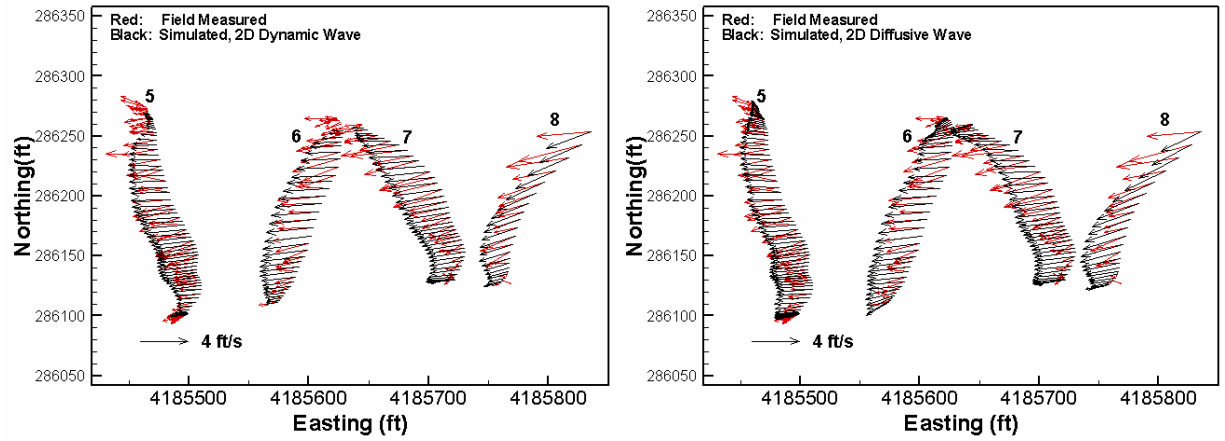
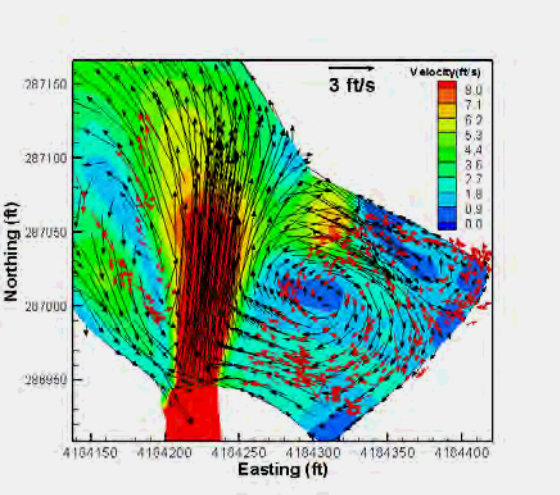


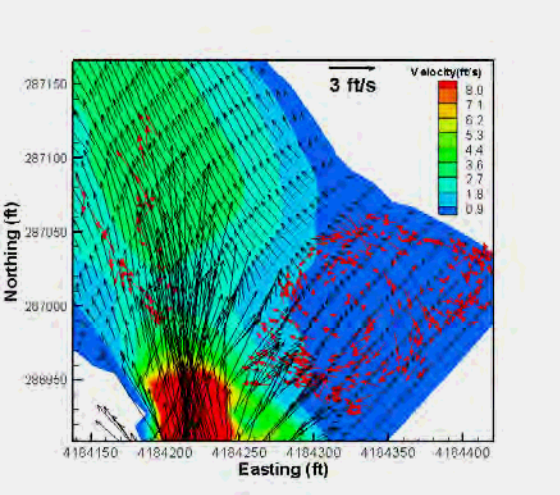
Figure 5 Comparison of predicted and measured velocity vectors at cross sections 5 to 8 upstream of the dam.

A comparison of velocities and flow patterns was done in a complex eddy area downstream of the dam where two different flow directions were measured (Figure 6c). It is clear that the diffusive model (Figure 6b) is incapable of predicting any eddies and therefore, the velocity

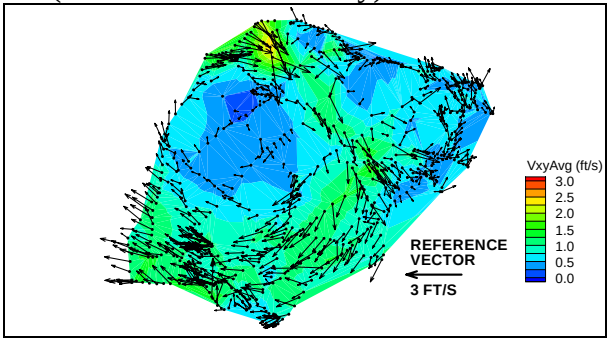
results in such areas are in gross error. On the other hand, the dynamic wave model of GSTAR-W is quite good in predicting the eddy structures (Figure 6a). It is noted that the two-eddy structure on the right of the jet stream from the excavated channel is well predicted both in terms of size and location. In addition, the eddy on the left of the jet stream is also predicted. However, the dynamic wave model of MIKE-21 failed to predict the two-eddy structure. The exact reason is unknown but one possibility could be due to the use of a square mesh. These results indicate that the dynamic wave model did the best overall representation of the complex eddies and flow separation present in this case study.



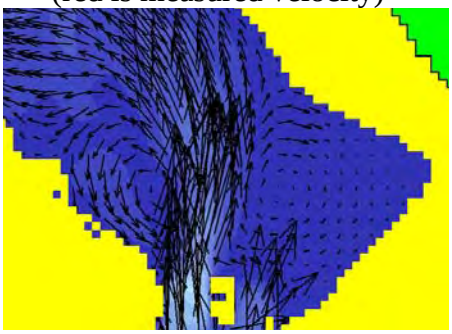
(a) GSTAR-W dynamic wave solution (red is measured velocity)



(b) GSTAR-W diffusive wave solution (red is measured velocity)



(c) Measured velocity vectors



(d) MIKE-21 solution (no scale)

Figure 6 Comparison of velocity vectors and flow patterns downstream of the dam.

More detailed comparisons were made between the MIKE-21 computed results and the measured results. The maximum computed velocity was compared to the maximum measured velocity for three reaches in the calibration model (Table 3). The range of computed velocities compared closely with measurements except for in the scour hole immediately downstream of the dam where measured velocities were higher than computed (see Figures 6c and 6d).

Statistics for a comparison of measured to computed velocities at all eight cross sections upstream of the dam are listed in Table 4. For a total of 418 measurements, the mean, minimum, and maximum computed velocities are very close to measured data and the average velocities are

within the ±0.3 ft/s accuracy of ADCP velocity measurements. The "mean difference" between computed and measured values is 0.2 ft/s, and the standard deviation is 0.8 ft/s.

Table 3 Comparison of measured to computed (MIKE-21) maximum velocities.

Reach Upstream of Dam (ft/s)		Scour Hole Just Downstream of Dam (ft/s)		River Channel Downstream of Scour Hole (ft/s)	
Computed Values	Measured Values	Computed Values	Measured Values	Computed Values	Measured Values
8.0	8.7	1.5	2.5	6.1	6.1

Table 4 Statistics for measured versus computed velocities for eight cross sections upstream of dam for calibration flow of 2,800 ft^3/s.

	Measured Velocity (ft/s)	Computed Velocity (ft/s)
Count	418	418
Mean	2.5	2.7
Maximum	6.2	5.8
Minimum	0.1	0.3

DISCUSSION AND CONCLUDING REMARKS

Based on this study, the most important input data and calibration parameters are summarized as follows:

1. A good bathymetric survey is important to represent the topography of the study area. If detailed flow hydraulics such as velocity and flow patterns is needed, local topography for the interested area should be surveyed accurately as local features influence local flows significantly.

2. The most critical calibration parameter is the Manning's roughness coefficient. It varies among different models due to differences in model assumptions, approximations and formulations.

3. Based on GSTAR-W simulations, we do not find the selection of turbulence models important, at least for the present study. It is recommended that it should be regarded as a secondary calibration parameter at the most.

Based on the results, following findings and recommendations may be drawn:

1. If water surface elevation along the thalweg is the major hydraulic variable of interest, any of the models used in this project may be suitable as far as a good calibration study is carried out. Use of two-dimensional models is warranted only for: (a) cases that require detailed flow velocity and/or flow patterns; or (b) require topography or flow features of 2D nature.

2. The diffusive wave solver is suitable for many applications that require the water surface elevation, water depth and bulk velocities. We found the dynamic wave solver necessary when eddies and flow separations is the interested outputs.

3. For the diffusive wave solver, the Manning roughness coefficient should be interpreted as the energy loss coefficient as extra losses due to eddies, separations, and hydraulic jumps are lumped together with the coefficient. So the coefficient used for the diffusive wave solver is usually higher than that for dynamic wave solver. Hydraulic jump can only be simulated with the dynamic wave model and a smooth transition will be predicted by the diffusive wave solver. If details around a jump are not important, the diffusive wave solution may still be used even if there are hydraulic jumps.

The currently available hydraulic modeling tools were sufficient for most design questions associated with the removal of Savage Rapids Dam. We found using a range of modeling tools worked well to meet a range of project needs while also complementing each other to improve confidence in results. Although not discussed in detail here, sediment modeling tools are still limited to one-dimensional scenarios and could use further development to address modeling sediment through riffle pool systems and erosion of reservoir sediment during dam removal.

REFERENCES

Bountry, J.A. and Randle, T.J. (2003). 2D Numerical model results at proposed intake sites for full dam removal. Project Final Report, Technical Service Center, Bureau of Reclamation, Denver, CO.

Brunner, G. (2002). HEC-RAS, river analysis system hydraulic reference manual. US Army Corps of Engineers, Davis, CA.

DHI. (1996). MIKE 21 hydrodynamic module users guide and reference manual. Danish Hydraulic Institute.

Lai, Y.G. and Yang, C.T. (2004). Development of a numerical model to predict erosion and sediment delivery to river systems, progress report no.2: sub-model development and an expanded review. Department of the Interior, Bureau of Reclamation, Technical Service Center, Denver, CO.

Lai, Y.G. (2005). "River and watershed modeling: current effort and future direction," US-CHINA Workshop on Advanced Computational Modeling in Hydroscience & Engineering, Sept. 19-21, 2005, Oxford, MS, USA.

Thomas, W.A. (March 1996). HEC-6T sedimentation in stream networks, user's manual, version h6tr514. Mobile Boundary Hydraulics, Clinton, Mississippi.

USBR. (February 2001). Savage Rapids Dam sediment evaluation study. Josephine County Water Management Improvement Study, Oregon, 23 pgs and appendices.

TEMPORAL AND SPATIAL TRENDS IN SEDIMENT CHEMISTRY IMPOUNDED WITHIN A FLOOD CONTROL RESERVOIR: GRENADA LAKE, MS

Sean J. Bennett, Associate Professor, Department of Geography, University at Buffalo, Buffalo, NY, seanb@buffalo.edu; Fred E. Rhoton, Research Soil Scientist, USDA-ARS National Sedimentation Laboratory, PO Box 1157, Oxford, MS, frhoton@msa-oxford.ars.usda.gov; ShuMin Hsu, Graduate Student, University at Buffalo, Buffalo, NY; Carlos V. Alonso, Supervisory Research Hydraulic Engineer, USDA-ARS National Sedimentation Laboratory, PO Box 1157, Oxford, MS, calonso@msa-oxford.ars.usda.gov

Abstract: Sedimentation issues were examined in a relatively large flood control reservoir in a highly unstable, cultivated watershed. Collected sediment cores were analyzed for ^{137}Cs and texture, which demarcated the as-built reservoir timeline, and the bulk chemistry of the sediments. The concentrations of select elements (As, Cu, Cr, Pb, Hg, and Zn) are positively correlated with clay composition and are not atypical for soils. Statistical analyses showed that since dam construction (1) select element concentrations normalized by clay and aluminum content do not vary vertically within each sediment core; and (2) depth-averaged concentrations of select element concentrations normalized by clay and aluminum content show no spatial variation within the sediment impoundment. These results suggest that sediment-associated chemical loadings to this reservoir have remained nearly invariant in time and evenly dispersed within the impoundment.

INTRODUCTION

There are more than 75,000 dams in the U.S., and these structures provide opportunities for navigation, hydroelectric power, irrigation, flood control, and water supply (Graf, 2001 and Bennett et al., 2002). These dams trap much of the incoming sediment loads from upstream sources, and these sediments may be of poor quality with respect to heavy metals and agrichemicals. This is especially true for the more than 11,000 small flood control structures built by the USDA-NRCS since 1948 in agricultural watersheds where trapping efficiencies typically exceed 80% (Dendy, 1974, 1982 and Bennett et al., 2002). These high sedimentation rates may be further exacerbated by unstable stream systems, erodible landscapes, poor land management, and inappropriate channel modifications (Simon and Thomas, 2002 and Simon et al., 2004).

The overall goal of the current research program was to assess recent sedimentation issues within a relatively large flood control reservoir in a highly unstable, cultivated watershed. The objectives of the present paper were to determine the concentrations of sediment-associated elements, notably Arsenic (As), Copper (Cu), Chromium (Cr), Mercury (Hg), Lead (Pb), and Zinc (Zn), trapped within the impoundment since dam construction and to ascertain if these chemical loadings show any temporal or spatial trends.

FIELD LOCATION AND METHODS

Field Location: Grenada Lake is a relatively large U.S. Army Corps of Engineers flood control reservoir located in north-central Mississippi (Figure 1). The reservoir has been in operation

since January 1954 and has a flood storage capacity of 1.605 km^3. Two major rivers drain into the lake. The Yalobusha River is a 4th-order stream system with an upstream drainage area of 1530 km^2, and this watershed has a long history of channel instability and sedimentation-related flooding. Agricultural development in the middle 1800s caused severe soil erosion and excessive sedimentation in the river channels of northern Mississippi, and measures taken by federal agencies further destabilized the river networks (Simon and Thomas, 2002). The watershed still maintains production of sweet potato, cotton, soybean, and corn (Cooper et al., 2002). The Skuna River is a 4th-order stream system with an upstream drainage area of 1127 km^2. Compared to the Yalobusha River, it is a more stable stream system and the primary land-use is silviculture (forestry).

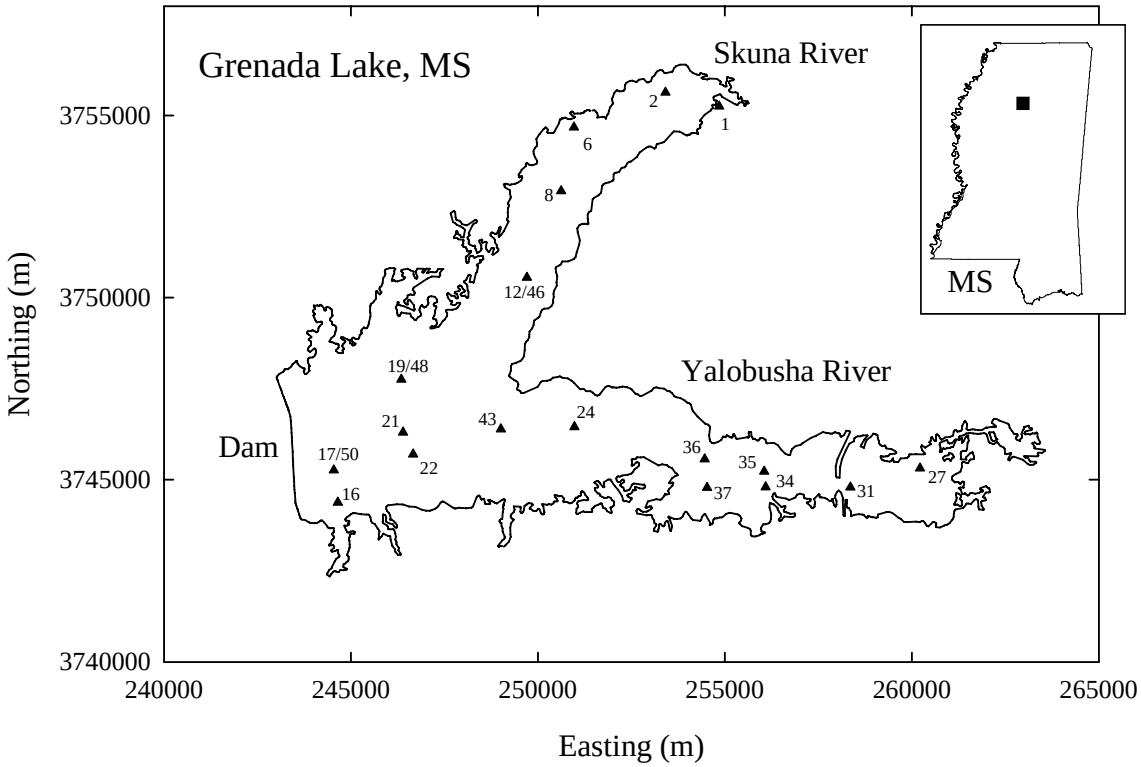


Figure 1 Map showing Grenada Lake in northern Mississippi (see inset), the location of select cores along the Skuna and Yalobusha River arms (numbers and symbols), and the position of the dam, which discharges to the west.

Sediment Coring and Chemical Analysis: Fifty sediment cores were collected and analyzed in this study, and only select cores will be discussed here (Figure 1). Cores were secured with a vibracoring system (Bennett et al., 2002), sealed, and returned to the laboratory where they were split, logged, and sampled incrementally. Bulk density was determined by weighing oven-dried samples of known core volumes. For particle size analysis, approximately 10 g of sediment was oven-dried at 70°C, crushed and sieved to less than 2 mm, treated with H_2O_2 to remove organic matter, and then shaken overnight in sodium hexametaphosphate for complete dispersion. Total clay (<2 μm) was determined by the pipette method (Method 3A1, Soil Survey Staff, 1992). Total sand (2000 to 53 μm) was determined by wet sieving the remaining sample though a 53-μm sieve and weighing the oven-dried fraction. Total silt (53 to 2 μm) was calculated by subtracting the sand and clay fractions from the original sample weight.

Selected cores were analyzed for radioactive cesium (^{137}Cs; 30-year half-life) for dating stratigraphic horizons. In the Northern Hemisphere, first deposition of ^{137}Cs occurred in 1954±2 due to above-ground nuclear testing and maximum deposition occurred in 1964±2 (Ritchie and McHenry, 1990). Approximately 50-g of dried, crushed, and sieved (2-mm) sediment samples were taken at 0.1-m increments from each core. All samples as well as the bulk sediment density data were sent to Flett Research Ltd., Winnipeg, Canada for analysis. Typical standard deviations for the measured ^{137}Cs emissions were about 0.08 pCi g^{-1}.

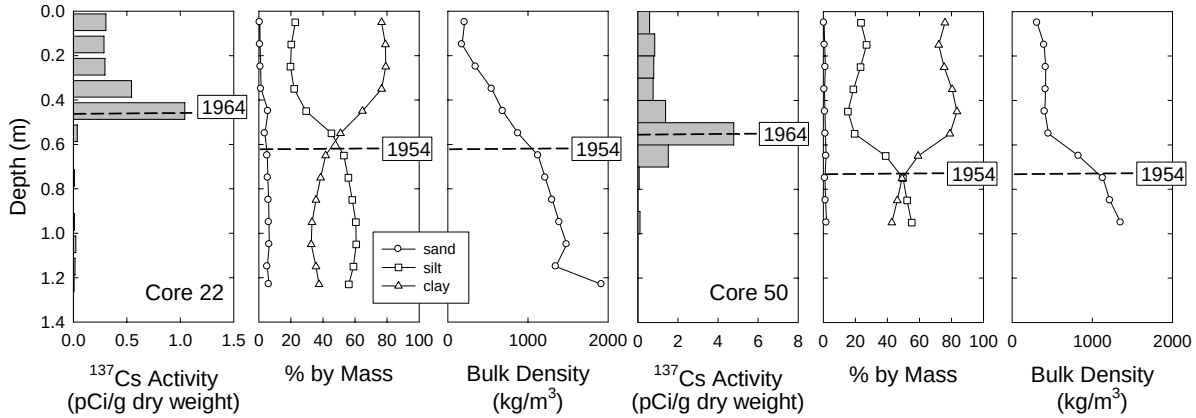


Figure 2 Vertical variations of ^{137}Cs emissions, sediment texture (sand, silt, and clay), and bulk density for Cores 22 (on left) and 50 (on right) in Grenada Lake (refer to Figure 1 for core locations). Also shown are the interpreted 1964±2 and dam construction (1954) timelines.

The bulk chemistry of sediment samples from select cores also was determined. Approximately 5 g of oven-dried, crushed sediment obtained from discrete layers were sent to Activation Laboratories, Ontario, Canada for analysis. A small subsample was digested using four acids (hydrofluouric HF, perchloric $HClO_4$, nitric HNO_3, and hydrochloric HCL; a near total digestion process) and analyzed for 48 elements using an inductively coupled plasma spectrometer and mercury using cold-vapor atomic absorption (cold vapor-flow injection mercury system). Only a small subset of these chemical results is presented here, which include Arsenic (As), Copper (Cu), Chromium (Cr), Mercury (Hg), Lead (Pb), Zinc (Zn), and Aluminum (Al).

RESULTS

Discriminating Post-impoundment Sedimentation: The most important interpretation of the sediment chemistry data within Grenada Lake is discriminating the post-impoundment sediment from the pre-existing or parent material. This interpretation is based on ^{137}Cs activity within the cores and variations in sediment texture with depth below the lake bottom.

The geochronologic results obtained for Cores 22 and 50 are plotted in Figure 2 alongside the variation of sediment texture and bulk density with depth. These cores show well-defined peaks in ^{137}Cs activity, which can be interpreted as the 1964±2 timeline. The reduced activities at depths greater than about 0.8 m correspond to dates earlier than this time (i.e., pre-dam construction). These timelines also correlate with variations in sediment texture and, to a lesser extent, bulk density with depth. For these cores, the post-impoundment sediments are markedly

enriched in clay and depleted in silt (and sand) as compared to the sediment located stratigraphically lower in these cores (Figure 2). Of the 19 cores analyzed for sediment texture, 11 of the cores or 58% showed this post-impoundment enrichment of clay and depletion of silt.

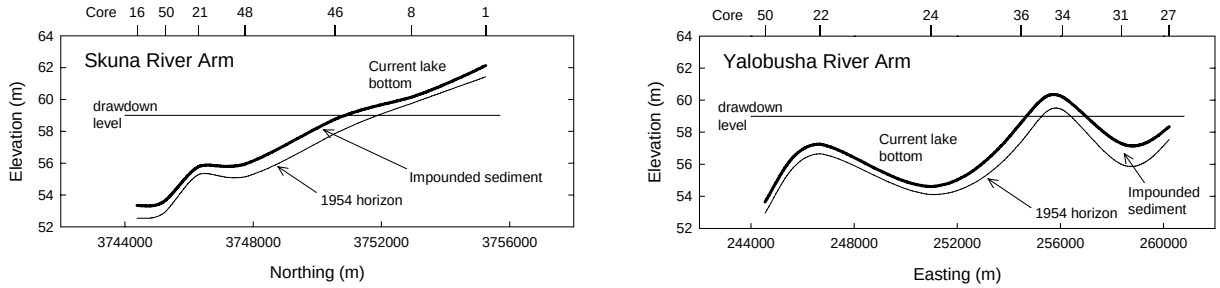


Figure 3 Profiles of current lake bathymetry and post-impoundment sediment thickness along the Skuna (left) and Yalobusha (right) River arms Grenada Lake based on ^{137}Cs emissions and vertical variations in sediment texture from select cores projected onto a line. Winter reservoir drawdown level also is shown, and refers to Figure 1 for core locations.

Bennett et al. (2005) used the geochronologic and textural results from these and other cores to define the 1954 stratigraphic horizon of dam construction. The thickness of the sediment impoundment in relation to current lake bathymetry is shown in Figure 3. These data show that the impounded sediment thickness changes monotonically along each arm of Granada Lake. The timeline is further extended here to include those cores having sediment chemical but no grain size data or ambiguous results.

Vertical Variations in Sediment Chemistry: For Cores 12, 16, and 34, the vertical variation of As, Cr, Hg, Pb, Zn, and Al concentrations, along with sand, silt, and clay content, are shown in Figure 4. For these sediments, concentrations for As range from 1 to 20 ppm, Cr ranges from 0 to 120 ppm, Pb ranges from 5 to 50 ppm, Hg ranges from 0 to 120 ppb, and Zn ranges from 10 to 140 ppm, and Al ranges from 1 to 15% by mass. These values are not atypical for element concentrations found in soils in the U.S. and worldwide (McBride, 1994).

The concentrations of these elements are strongly correlated with sediment texture, specifically clay content. Figure 5 shows that element concentrations can increase by orders of magnitude as sediment becomes increasingly rich in clay, and these increases clearly are related to mineralogy. Elements such as As, Pb, and Hg show more scatter than Cu and Zn, and this variability may be due to contributions from organic or atmospheric sources rather than mineralogic.

Because of these clear dependencies of element concentrations on soil texture, it is common to normalize chemical signatures by clay and/or Al content on the assumption that aluminosilicates dominate the clay-sized fractions (e.g., Schropp et al., 1990 and Abraham, 1998). Figure 6 replots these vertical variations in As, Cr, Hg, Pb, and Zn as normalized by the mass percent of Al and clay. Regression analyses performed on the vertical variations of these elements since dam construction, or post 1954 using the identified timeline, showed that none of the elements varied in any statistically significant way in any of the cores examined. Thus since dam construction, there has been no significant increase or decrease in the loadings of sediment-associated elements at-a-point within the reservoir.

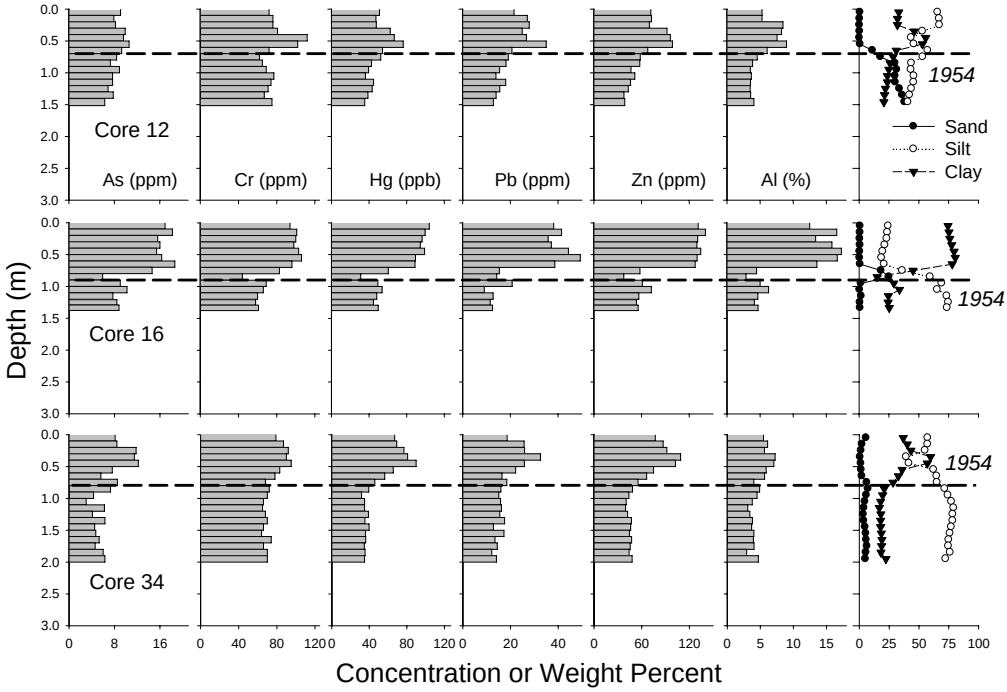


Figure 4 Vertical variations of Arsenic (As), Chromium (Cr), Mercury (Hg), Lead (Pb), Zinc (Zn), Aluminum (Al), and sediment texture (sand, silt, clay; from left to right) with depth for Cores 12 (upper), 16 (middle), and 34 (lower). Also shown are the interpreted dam construction (1954) timelines. Note variable units, and refer to Figure 1 for core locations.

Spatial Variations in Depth-averaged Sediment Chemistry: Since these sediment-associated chemical loadings showed no variation vertically within each core since the 1954 timeline, all sediment-associated chemical signals were depth-averaged and plotted simply as a function of downstream distance along the Skuna River arm (Figure 7) and the Yalobusha River arm (Figure 8), again normalized by Al and clay content. Interestingly, some trends show opposing tendencies depending upon the normalizing parameter (see Hg, Pb, and Zn, Figure 7; Cu, Cr, Hg, and Pb, Figure 8). Regression analyses performed on these spatial trends of depth-averaged concentrations showed that no element increased or decreased in concentration in any statistically significant way. Thus the depth-averaged sediment-associated concentrations of As, Cu, Cr, Hg, Pb, and Zn since dam construction show no spatial variation from the upstream arms of the Skuna and Yalobusha Rivers down to the pool region over distances of up to 16 km.

CONCLUSIONS

For Grenada Lake, a relatively large flood control reservoir in northern Mississippi, the discrimination of post-impoundment sedimentation was made possible through the combined use of ^{137}Cs emissions and vertical variations in sediment texture. This 1954 timeline then was used to segregate the post-impoundment sediment-associated chemical signatures from the pre-existing or parent material signatures.

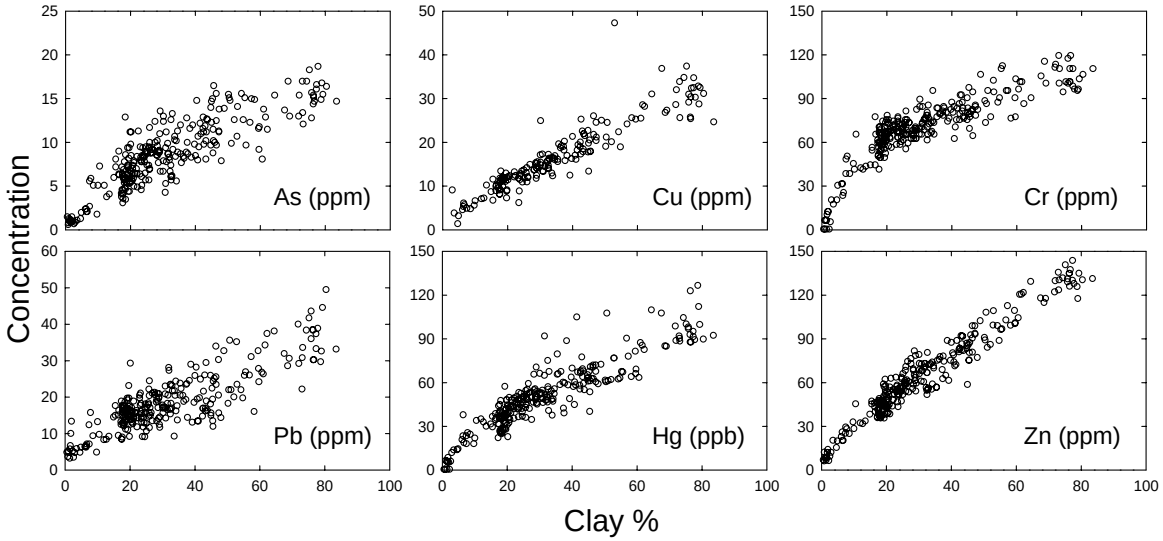


Figure 5 Concentration of Arsenic (As), Copper (Cu), Chromium (Cr), Lead (Pb), Mercury (Hg), and Zinc (Zn) for all sediment samples as a function of clay content. Note variable units.

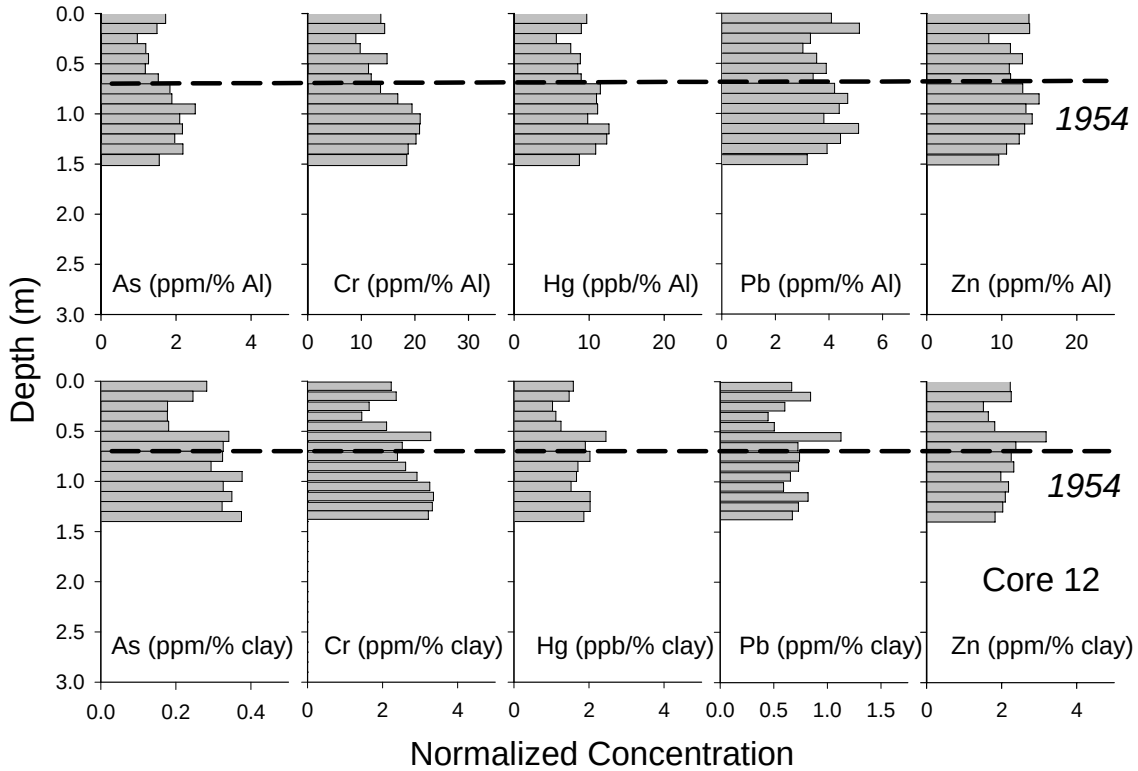


Figure 6 Vertical variations of Arsenic (As), Chromium (Cr), Mercury (Hg), Lead (Pb), and Zinc (Zn) (from left to right) with depth for Core 12 as normalized by mass percent of Aluminum (Al; upper) and clay (lower). Also shown is the interpreted dam construction (1954) timeline. Note variable units.

Concentrations of As, Cu, Cr, Hg, Pb, and Zn show a strong positive correlation with clay content, and all signatures were normalized by both mass percent of clay and Al. Regression analyses performed on each core, from the 1954 timeline to the present day or vertically within each sediment column, showed that none of these elements varied statistically in normalized

concentration. Moreover, regression analyses performed on the depth-averaged sediment-associated element concentrations since dam construction showed that none of these elements varied statistically in normalized concentration from the upstream areas within the reservoir to the pool region (upstream to downstream) over a 16 km distance. Thus since dam construction in 1954, sediment-associated loadings of As, Cu, Cr, Hg, Pb, and Zn were statistically invariant in time (at-a-point) and space (from upstream to downstream). These results suggest that the composition of the incoming sediments has not changed significantly over this time period and that the sediments are uniformly distributed in the reservoir.

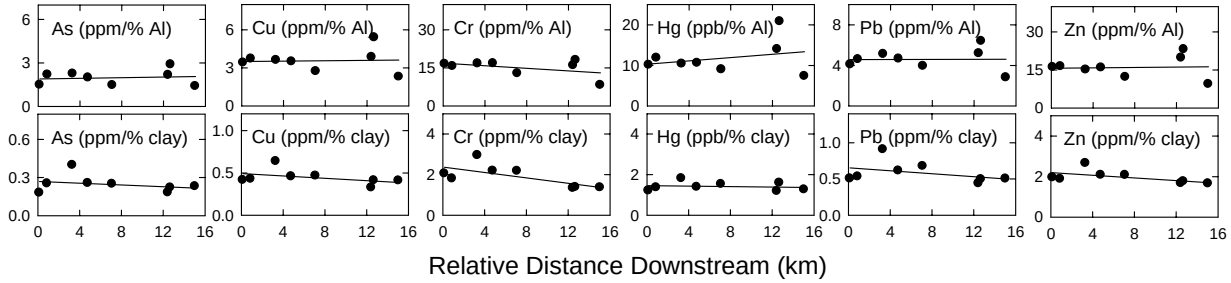


Figure 7 Spatial variations (from upstream to downstream) in depth-averaged concentrations of Arsenic (As), Copper (Cu), Chromium (Cr), Mercury (Hg), Lead (Pb), and Zinc (Zn) (from left to right) within the post-impoundment sediments along the Skuna River arm as projected onto a line, as normalized by mass percent of Aluminum (Al; upper) and clay (lower). Note variable units.

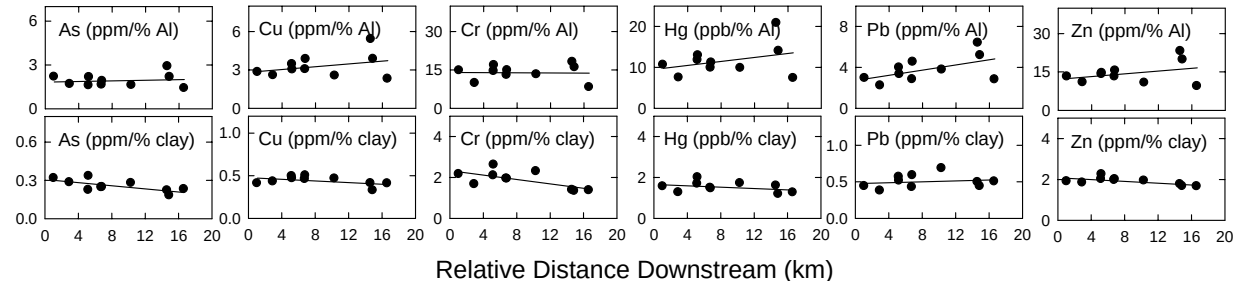


Figure 8 Spatial variations (from upstream to downstream) in depth-averaged concentrations of Arsenic (As), Copper (Cu), Chromium (Cr), Mercury (Hg), Lead (Pb), and Zinc (Zn) (from left to right) within the post-impoundment sediments along the Yalobusha River arm as projected onto a lime, as normalized by mass percent of Al (upper) and clay (lower). Note variable units.

ACKNOWLEDGEMENTS

We thank C. Anderson, W. Beard, V. Campbell, G. Gray, D. McChesney, and C. Patrick for technical assistance. Financial and programmatic support was provided by the USDA-ARS and Mr. Thomas L. Hengst, Senior Project Manager, Demonstration Erosion Control Project, U.S. Army Corps of Engineers, Vicksburg District, MS.

REFERENCES

Abraham, J. (1998). "Spatial distribution of major and trace elements in shallow reservoir sediments: An example from Lake Waco, Texas," Environmental Geology, 36, 349-363.

Bennett, S.J., Cooper, C.M., Ritchie, J.C., Dunbar, J.A., Allen, P.M., Caldwell, L.W., and McGee, T.M. (2002). "Assessing sedimentation issues within aging flood control reservoirs in Oklahoma," Journal of the American Water Resources Association, 38, 1307-1322.

Bennett, S.J., Rhoton, F.E., and Dunbar, J.A. (2005). "Texture, spatial distribution, and rate of reservoir sedimentation within a highly erosive, cultivated watershed: Grenada Lake, MS," Water Resources Research, 41(1), W01005, doi:10.1029/2004WR003645.

Cooper, C.M., Smith, S., Jr., Testa, S., III, Ritchie, J.C. and Welch, T. (2002). "A Mississippi flood control reservoir: Life expectancy and contamination," International Journal of Ecology and Environmental Sciences, 28, 151-160.

Dendy, F.E. (1974). "Sediment trap efficiency of small reservoirs," Transactions of the American Society of Agricultural Engineers, 17, 898-908.

Dendy, F.E. (1982). "Distribution of sediment deposits in small reservoirs," Transactions of the American Society of Agricultural Engineers, 25, 100-104.

Graf, W.L. (2001). "Damage control: Restoring the physical integrity of America's rivers," Annals of the Association of American Geographers, 91, 1-27.

McBride, M.B. (1994). Environmental Chemistry of Soils. Oxford University Press, New York, 406 pp.

Ritchie, J.C., and McHenry, J.R. (1990). "Application of radioactive fallout Cesium-137 for measuring soil erosion and sediment accumulation rates and patterns: A review," Journal of Environmental Quality, 19, 215-233.

Schropp, S.J., Lewis, F.G., Windom, H.L., Ryan, J.D., Calder, F.D., and Burney, L.C. (1990). "Interpretation of metal concentrations in estuarine sediments of Florida using aluminum as a reference element," Estuaries, 13, 227-235.

Simon, A., and Thomas, R.E. (2002). "Processes and forms of an unstable alluvial system with resistant, cohesive streambeds," Earth Surface Processes and Landforms, 27, 699-718.

Simon, A., Dickerson, W., and Heins, A. (2004). "Suspended-sediment transport rates at the 1.5-year recurrence interval for ecoregions of the United States: Transport conditions at the bankfull and effective discharge?" Geomorphology, 58, 243-262.

Soil Survey Staff (1992). Procedures for collecting soil samples and methods of analysis for soil survey, USDA-SCS Soil Survey Investigation Report 42. U.S. Government Printing Office, Washington, D.C.

ACOUSTIC PROFILING OF SEDIMENT ACCUMULATION IN THREE SMALL EROSION CONTROL RESERVOIRS IN NORTH MISSISSIPPI

Del Leary, R & D Engineer, National Center for Physical Acoustics, University, MS, dleary@olemiss.edu; Craig J. Hickey, Senior Scientist, National Center for Physical Acoustics, University, MS, chickey@olemiss.edu; Daniel G. Wren, Hydraulic Engineer, USDA-ARS, Oxford, MS, dwren@msa-oxford.ars.usda.gov

INTRODUCTION

In Northern Mississippi, as part of a preventative erosion control program, the Yazoo-Little Tallahatchie Project (YLTP) created a system of small dams and reservoirs to regulate stream flow and to stop the movement of sediment over large distances. These structures were designed to have a lifetime of approximately 50 years, depending on water flow and sediment accumulation. As these dams and reservoirs reach their lifetime expectancy, an assessment and decisions regarding their future must be addressed. More detail on this subject is given by Wren et al.(2006). Traditional sediment coring is a time consuming and expensive approach for determining accumulated sediment volumes and sediment characteristics. The National Center for Physical Acoustics (NCPA), in collaboration with the National Sedimentation laboratory (NSL), is developing acoustic methods to complement current methods of assessing sediment accumulation in these reservoirs. Three small reservoirs were chosen as the field sites. The small impoundments are approximately 4 hectares (10 acres) in area with water depths of 1–2 m and post-impoundment sediment accumulations on the order of 1m.

A number of complementing acoustic techniques have been used in the past for characterization and delineation of accumulated sediment. There is a vast amount of literature on marine studies showing the sensitivity of acoustics to sediment properties (Hamilton, 1982; Stoll, 1989). Acoustic methods for remotely measuring marine sediment properties include chirp sonar (Schock et al., 1989), parametric arrays (Muir et al., 1986), boomer source systems such as the Seistec[tm], and a variety of other systems employing vertical or horizontal receiver arrays in conjunction with airgun, sparker or boomer sources. These systems are designed to work best at frequencies less than 10 kHz and in water depths of tens of meters. All of these acoustic methods are pulse echo systems and measure the time it takes for an acoustic pulse to travel through the sediment, reflect at an interface, and return to the receiver. To extract the thickness of the layers between interfaces from the recorded time between echoes, an estimate of the velocity for each layer must be known. One way to measure the velocity within the layer is to use a core taken at some location along the survey. However, there are many logistical problems involved in keeping the sample in a pure state. In-situ methods, such as using acoustic probes to measure the velocity as a function of depth, could aid in this problem. In a large collaborative project known as SAX99, a number of probe-type instruments were developed to extract acoustic properties of marine sediments in-situ (Thorsos, 2001). An acoustic ‘lance’ consisting of receivers along a shaft has also been used in the past in a marine environment (Fu, 1996).

Small impoundments require acoustics systems that will work in water depths less than 1m, have higher resolution, and must be portable so that they can be deployed using small boats. A great deal of work in the development of such a sub-bottom profiler and some field tests has been

published (Dunbar et. al., 1998; Bennett et. al., 2002). Complementary acoustic systems will provide additional data for remotely measuring sediment properties.

This report will focus on the recent design and construction of a *sediment acoustic probe.* This probe consists of a rigid shaft having a series of piezoelectric receivers at 10 cm spacing and with a center frequency of 50 kHz. The source transmits a chirp signal while located in the water column and can be positioned at a number of known offsets. The data obtained from the acoustic probe will be used to obtain acoustic speed profiles. The speed profiles can in turn be used to convert time sections from the sub-bottom profiler to depth sections thereby allowing better estimates of sediment volumes. Another use of this tool is the measurement of in-situ acoustic attributes for correlation to physical parameters obtained from extracted cores. The advantages of the acoustic measurements are the speed of the data acquisition and the minimal disturbance of the sample. To date an acoustic probe along with an acquisition system has been constructed. Initial tests in a water tank have been completed to characterize and optimize the system. Initial fieldwork has been completed at selected field sites in conjunction with physical cores extracted by the NSL. Preliminary analysis indicates a good correlation between the bulk density profile and the acoustic speed profile measured at the same location. Further fieldwork and data collection are underway.

EQUIPMENT AND INITIAL TESTING

The sediment acoustic probe consists of a shaft approximately 2 cm in diameter with eight receiving piezoelectric ceramic elements spaced at 10 cm increments. The source signal is a chirp-type pulse having a typical bandwidth of 35 to 75 kHz and a pulse length of 0.3 ms. The signal is generated using an HP 33120a arbitrary waveform generator and then amplified using a Krohn-Hite 7500 amplifier. An omni-directional Reson[tm] hydrophone is used as the acoustic source converting the electrical signal to an acoustic signal by way of a piezoelectric element. The received pulses are filtered for aliasing frequencies and digitized using a NI 6070 DAQPad then saved on a portable PC. A flowchart of the system and a picture of the sediment probe being tested in the water tank are shown in Fig. 1.

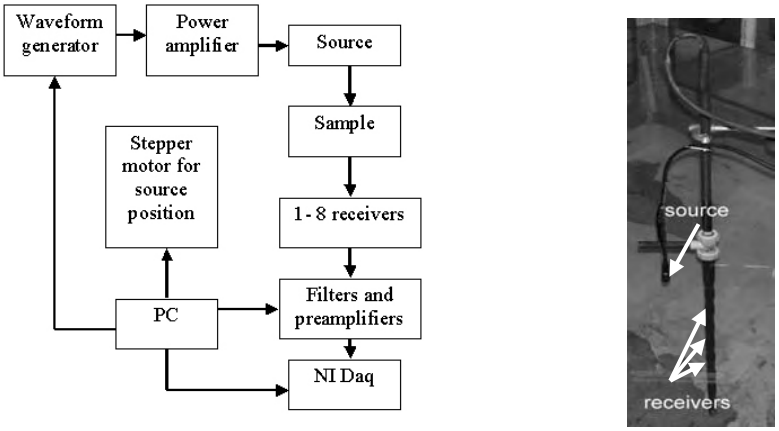


Figure 1 Flowchart of the sediment probe system and a picture of the probe in the water tank.

The raw time data collected in the water tank can be seen in Fig. 2. Each trace represents the amplitude of the receiver voltage as a function of time. The pressure of the acoustic signal arriving at the sensor produces the voltage. The chirp data are then cross-correlated with the reference electronic input chirp. The resulting waveforms are shown in Fig. 3. The travel times are determined by processing the cross-correlated data through an algorithm that takes a derivative of the enveloped data. The zero-crossings differentiated data were then 'picked' as the arrival time values. As a check, the measured value of the speed in water was confirmed to be 1490 m/s. Small deviations from this value were believed to be due to location of receivers, so distance calibrations were made. The boundaries of the water tank can be identified by investigating the direction and slope of the arrival time versus distance between the source and the receivers. For this test, the source was located near the surface and the time trace for the receiver nearest the source is the uppermost trace in Fig. 3. Downward traveling waves such as the direct wave have a slope from the upper-left to the lower-right. The reflection off the bottom of the water tank can be seen with an opposite slope indicating an upward traveling wave. The ghost wave refers to a wave that has reflected off the air-water interface and propagated downward to the receivers. The time difference between the direct and the ghost are related to the depth of the source and receiver in the water column. Acoustic waves reflecting off the wall of tank have a much greater slope since all the travel paths are nearly the same distance resulting in nearly equal arrival times at the receivers.

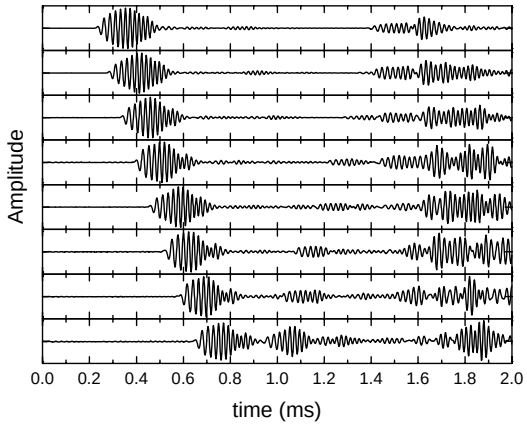


Figure 2 Raw data collected from all eight receivers. The uppermost trace is from the receiver nearest the water surface. The source is also located near the water surface.

FIELDWORK AND INITIAL RESULTS

The field measurements were collected from a pontoon style vessel built by connecting two small Jon-boats together. This provides a stable platform for measurements in very shallow water. Pictures of the research vessel are shown in Fig. 4. For this study a Global Positioning System (GPS) receiver was used locate sites that had been previously cored by the NSL. Once in position, a reference calibration was acquired in the water column and the probe was then inserted in the sediment.

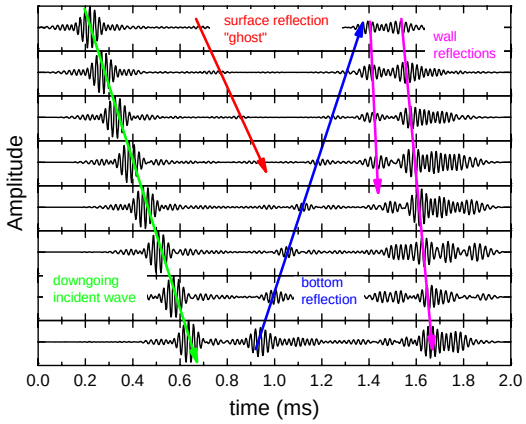


Figure 3 Cross-correlated data sharpens the waveform and the transit times can be easily measured. The arrivals of acoustic waves traveling different paths are annotated.



Figure 4 Pontoon style boat built by connecting two small Jon-boats together. This platform allows measurements to be taken in very shallow water.

Once the probe has been inserted the source is turned of and data are collected and averaged at each receiver. Since the source was very repeatable, many shots were averaged to improve the signal-to-noise ratio. A coherence threshold determined the number of averages for each receiver. Once the data is collected for all receivers, the source was moved to a new offset and the measurement repeated. An illustration of the probe and moving source for a layered sample is shown in Fig. 5. Figure 5 also shows a picture of the motorized source attached to the probe.

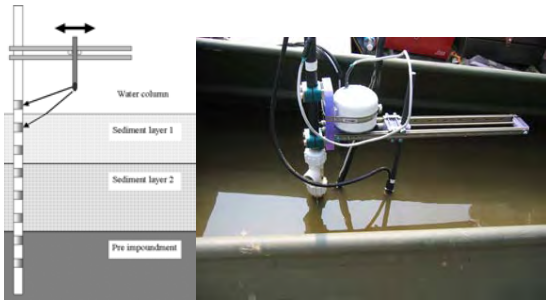


Figure 5 a.) An illustration of the variable offset source-receiver setup within a multi-layer. b.) The source-motorized-stage attached to the probe before being submerged.

Figure 6 is picture of a core extracted at location labeled Drewery #3. There is one obvious sediment layer above the pre-impoundment as indicated by the two different colors for each layer. From Fig. 6 the pre-impoundment depth is at approximately 26 cm below the water-sediment interface.



Figure 6 A picture of the vibracore sample at Drewery #3 after the aluminum casing has been split in half showing an interface at approximately 26 cm.

The cross-correlated acoustic data and arrival time picks taken at Drewery #3 are shown in Fig. 7. The first receiver was in the water column as a reference. Not surprisingly, the traces have more arrivals than the results shown for the water tank. When the acoustic signals get weaker due to absorption of acoustic energy by the sediment, coherent noise due to electromagnetic induction and the bar wave become visible. The bar wave is the acoustic wave traveling through the steel rod holding the receivers. To remove unwanted signals, the amplitude was muted in each channel up to the arrival time of the previous time picked. This was done so that the time picking routine only picks signals that propagate through the sediment. After the muting was applied, the routine was applied and arrival times were determined. This process was carried out on two sets of data from the same location but with source offsets of 23cm and 27cm. For each offset the average and instantaneous speeds were calculated by taking into consideration a simple source-receiver travel path. The average speed was calculated assuming the straight ray path distance divided by the arrival time. The interval speed was calculated as the difference in straight ray travel paths divided by the difference in time between two adjacent receivers. The bulk density was calculated as the dried solid mass divided by the total volume. The average speed, interval speed, and bulk density versus depth are shown in Fig. 8.

The bulk density profile shows a rapid increase up to a depth of about 5cm. The density then remains constant up to about 13 cm where it again starts increasing to a depth of about 26 cm. Depths below 26 cm show a much more gradual increases in bulk density. The 26 cm depth corresponds to noticeable change in color in the extracted core. The start of pre-impoundment sediment is at the 26 cm mark. The interval speeds show lower values in the shallow sediment than in the water. The very low speeds are not surprising and were associated with the presence of gas. There was a high level of gas due to biological activity during the time of year the acoustic data was collected. This was evident during fieldwork by the observation of gas released as the probe was inserted into the sediment. The interval velocity also shows a sharp increase at around the 26 cm depth. In theory, larger density should result in lower speeds. However, the post-impoundment materials are likely more compacted and have a higher stiffness that results in a higher speed. The 10cm increments of the speed profile do not show as much detail as the bulk density however; more data points at smaller intervals could be taken in the

future to increase the depth resolution. Refraction of the waves caused by layers having different speeds will increase the travel distances. In the analysis here only straight ray calculations (a straight line from the source to the receiver) are used for the travel distances and therefore all the speed values shown are lower than the actual propagation speed within the layer. The current results show promise and a collection of additional data would allow for more sophisticated processing techniques and the calculation of additional acoustic attributes other than speed.

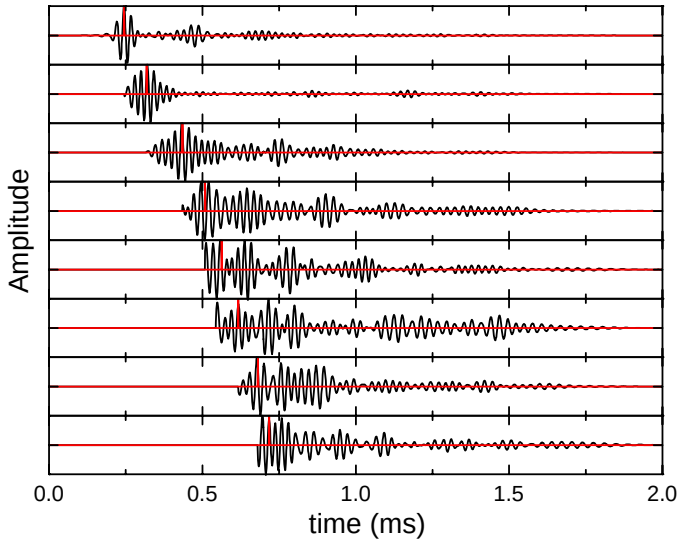


Figure 7: Travel time picks (in red) found from the cross-correlated data. The upper most waveform is nearest to the source and in the water column.

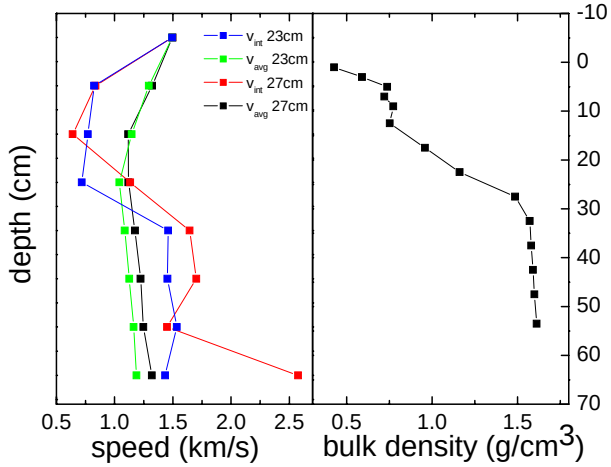


Figure 8: The depth profiles for the average and instantaneous velocities compared to the bulk density values for the same location in the reservoir.

CONCLUSION

An increasing number of impoundments throughout the country are approaching their predicted life expectancy. Sediment accumulations within the reservoirs need to be measured and characterized. Acoustics will play a key role in delineating sediment layers within the reservoirs and provide important information to assist future directions of remediation. The construction and development of an acoustic probe that can be used in shallow waters has been completed. The probe has eight 50 kHz piezoelectric transducers which spans over 70 cm. An omni-directional source sends a reproducible chirp signal from various offset distances. To date, initial field data has shown that the speed profile correlates well to the bulk density measured at the same location. Future plans include more field data measurements using the current system as well as more elaborate signal processing techniques.

REFERENCES

Bachman, Richard T. (1985). "Acoustic and Physical Property Relationships in Marine Sediments," Journal of the Acoustical Society of America. 78(2): pp 616-621.

Bennett, S. J., Cooper, C. M., Ritchie, J. C., Dunbar, J. A., Allen, P. M., Caldwell, L. W. and McGee, T. "Assessing Sedimentation Issues within Aging Flood Control Reservoirs in Oklahoma," Journal of the American Water Resources Association. 38(5): pp 1307-1322.

Dunbar, John A., Allen, Peter M., and Higley, Paul D. (1998). "Multifrequency Acoustic Profiling for Water Reservoir Sedimentation Studies," Research Methods Papers. 69:pp 521-527.

Fu, S. S., Wilkens, R. H., and Frazer, L. N. (1996). "Acoustic Lance: New in situ Seafloor Velocity Profiles," Journal of the Acoustical Society of America. 99(1): pp 234-242.

Hamilton, Edwin L., and Bachman, Richard L. (1982). "Sound velocity and related properties of marine sediments," Journal of the Acoustical Society of America. 72(6): pp 1891-1904.

Muir, T. G., Wyber, R. J., Lindberg, J. B., and Thompson, L. A., (1986) "Seismic Profiling with a Parametric, Self-Demodulated Ricker Wavelet," Proc. 12th International Congress on Acoustics, Associated Symposium on Underwater Acoustics, Halifax, Nova Scotia, Canada.

Schock, Steven G., LeBlanc, Lester R., and Mayer, Larry A. (1989). "Chirp subbottom profiler for quantitative sediment analysis," Geophysics. 54(4):pp 445-450.

Stoll, Robert D. (1989) Sediment Acoustics. Springer-Verlag New York.

Thorsos, Eric I., Williams, Kevin L., Chotiros Nicholas P., Christoff, James T., Commander Kerry W., Greenlaw, Charles F., Holliday, Vance D., Jackson, Darrell R., Lopes, Joseph L., MeGehee Duncan E., Piper John E., Richardson, Michael D., and Tang Dajun (2001). "An Overview of SAX99: Acoustic Measurements," IEEE Journal of Oceanic Engineering. 26(1): pp 4-25.

Wren, Daniel G., Wells, Robert R., Wilson, Chris, Cooper, Charles M., Leary, Del, Hickey, Craig J. (2006)."Sedimentation in Three Small Erosion Control Reservoirs in North Mississippi," Proc 8th Federal Interagency Sedimentation Conference and 3rd Federal Interagency Hydrologic Modeling Conference. Reno Nevada.

SEDIMENTATION IN THREE SMALL EROSION CONTROL RESERVOIRS IN NORTH MISSISSIPPI

Daniel G. Wren, Hydraulic Engineer, dwren@msa-oxford.ars.usda.gov; Robert R. Wells, Hydrologist, rrwells@msa-oxford.ars.usda.gov; Christopher G. Wilson, Hydraulic Engineer, cwilson@msa-oxford.ars.usda.gov; Charles M. Cooper, Ecologist, ccooper@msa-oxford.ars.usda.gov; National Sedimentation Laboratory, U. S. Department of Agriculture, Agricultural Research Service, Oxford, Mississippi, 38655 Del Leary, Research & Development Engineer, dleary@olemiss.edu; Craig J. Hickey, Principal Scientist, chickey@olemiss.edu National Center for Physical Acoustics, University, MS, 38677.

Abstract The water storage capacity and dam integrity of thousands of flood control reservoirs built in the last 50 years are compromised by excessive impounded sediments. The fate of these structures depends on the amount and characteristics of the impounded material. To aid in understanding the scope of this issue in the hill lands of northern Mississippi, physical sediment characteristics and reservoir holding capacity were evaluated in three small reservoirs (<20 acres) built 40+ years ago as part of the Yazoo-Little Tallahatchie erosion control project. A vibracoring system was used to collect continuous cores of impounded sediment and parent material. Particle size, bulk density, and a limited amount of ^{137}Cs data were used to define the pre-impoundment level. Sediment accumulation rates were found to range from 1 to 3 mm/year with reductions in storage capacity of 7% to 19%.

INTRODUCTION

There are approximately 11,000 flood control dams in the United States that have been constructed since the 1940's by the USDA-NRCS (Caldwell, 1999), and there are about 75,000 dams of various sizes in all (Graf, 1999). These structures, many of which have a design life of 50 years, are reaching a point in their lifespan where assessment is required so that informed decisions regarding the eventual fate of the reservoirs can be made.

Exploitative agricultural methods applied since in the 1830's resulted in excessive erosion in areas of west Tennessee and north-central Mississippi. Many of these upland areas were rendered almost completely unproductive, and the eroded sediments from upland areas buried fertile bottomlands as excessive runoff led to frequent flooding. During the years 1948-1976, the Yazoo-Little Tallahatchie Project (YLTP) was instituted to combat these erosion effects. The YLTP is credited with planting over 690,000,000 pine trees over 106,000 acres of highly eroded land (Ursick, 1963). As part of the project, numerous small erosion control dams were built.

In the work described here, three small lakes installed in North Mississippi's Holly Springs National Forest as part of the YLTP were chosen for investigation of the physical characteristics of impounded sediments (Figure 1). In related work, the same site is being used by the University of Mississippi National Center for Physical Acoustics (NCPA) for development of acoustic instrumentation to aid in reservoir sediment assessments. The field data from the present study will be used to augment the work being done at the NCPA. Lake schematics with core locations are shown in Figures 2-4, and Table 1 contains specific lake characteristics.

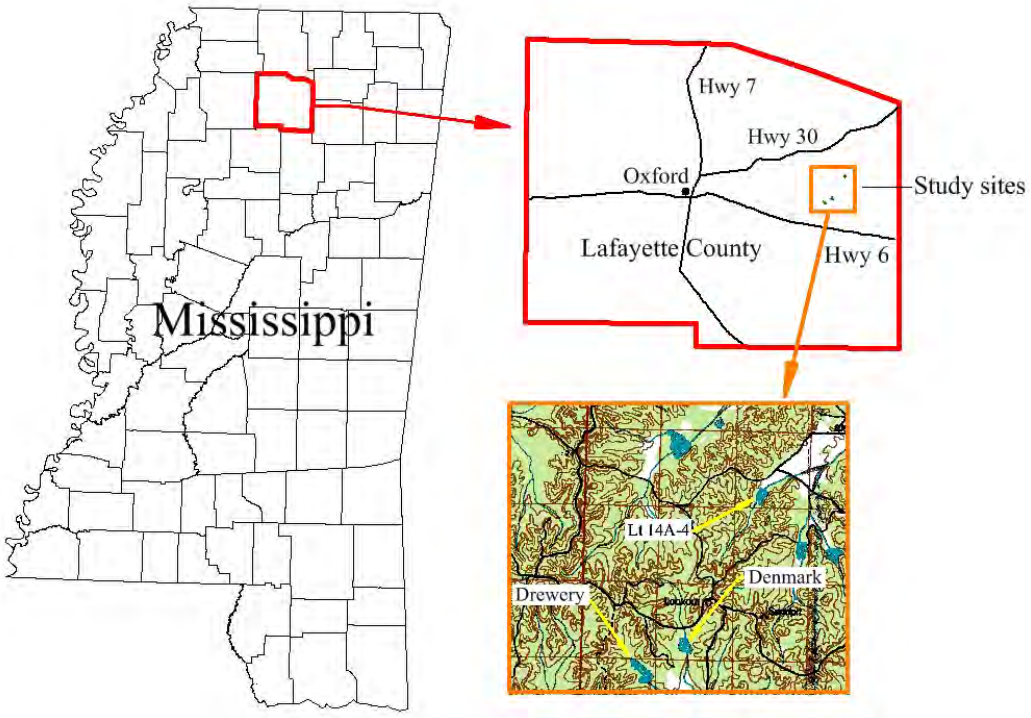


Figure 1 Location of study sites.

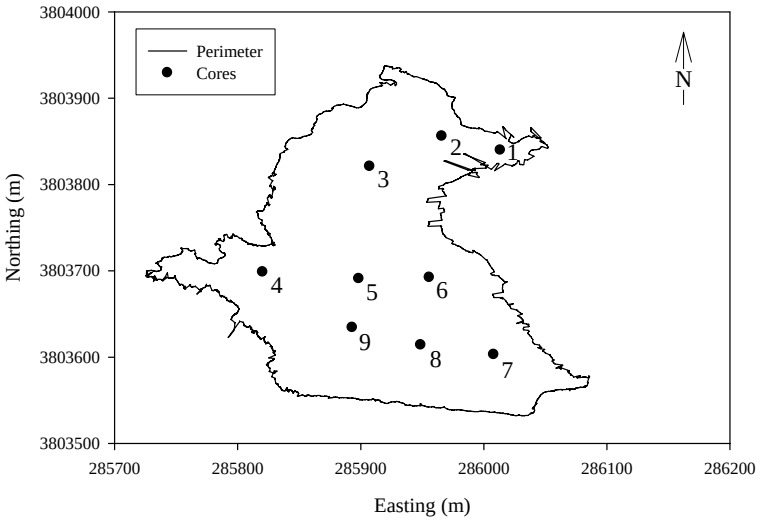


Figure 2 Denmark Lake.

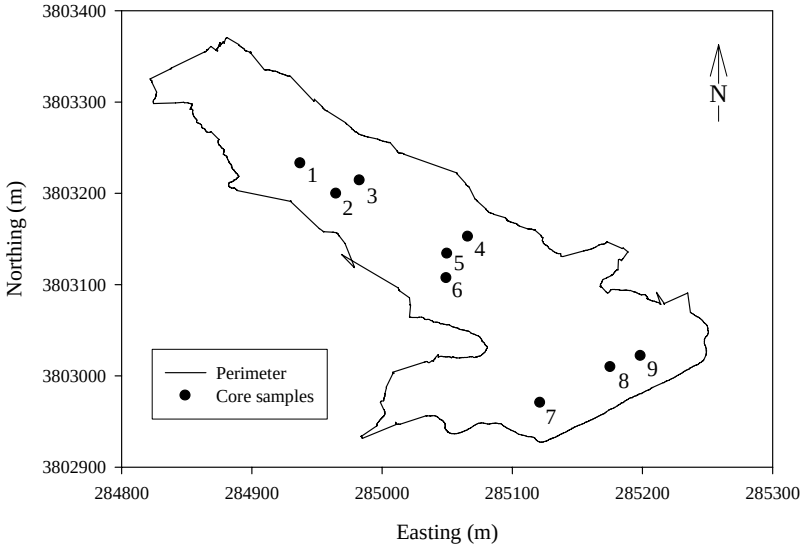


Figure 3 Drewery Lake.

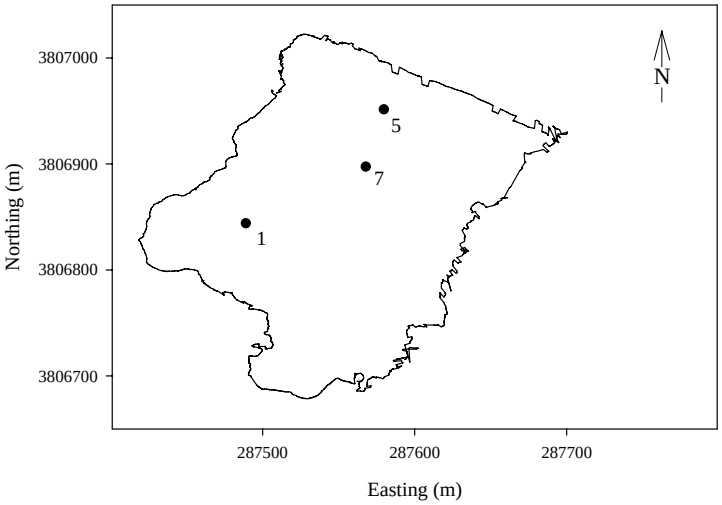


Figure 4 Lt 14A-4.

Table 1 Lake characteristics.

Lake	Year Built	Drainage area (ha)	Surface area (ha)	Reduction in storage	Mean accumulation rate (mm/yr)
Lt 14A-4	1962	280	3	19%	3
Drewery Lake	1965	171	7	7%	1
Denmark Lake	1965	284	4	9%	3

METHODS

A commercially available vibracoring system was used to collect a total of 21 sediment cores from the three lakes. The vibracoring system was suspended from an aluminum tripod with flotation provided by plastic drums connected to wooden platforms. The vibracorer was raised and lowered by an electric winch. The cores were collected in 76 mm diameter aluminum irrigation pipe that had a wall thickness of 1.5 mm. The vibracoring method has been shown to collect relatively undisturbed samples of bottom sediments due to liquefaction of the sediment at the vibrating interface between the sample pipe and sediment (Lanesky et al., 1979; Smith, 1984). It was assumed that minimal core compaction occurred. This was informally verified by observing the depth of penetration and resulting core length from selected cores. All cores were capped immediately after extraction and secured with duct tape. Care was taken to ensure that no air voids were present at the top of the cores. While awaiting processing, the cores were stored at 4^{o} C.

Each core was photographed after splitting the aluminum pipe longitudinally. The cores were sectioned at 2-cm intervals for the first 10-cm and 5-cm intervals for the remainder of the core. A portion of the top 20-cm of each sample was stored in airtight foil packs for use in pesticide analysis. Samples were initially weighed wet, dried at 60^{o}C for 48 hours and weighed again. Bulk densities for each depth interval were found as follows: Bulk density=dry mass/total volume, total volume=V_{voids}+$V_{particles}$, V_{voids}=(wet mass-dry mass)/1 g/cm^3), $V_{particles}$=dry mass/2.65 g/cm^3. Particle size fractions in each core increment were determined using an established pipette method (Method 3A1 (Soil Survey Staff, 1992)).

The depth of sedimentation was determined by locating the position in each core profile where clay began to be enriched relative to lower increments in the profile. This data was then checked against the bulk density data. The position in the core profile where a sharp decrease in bulk density was observed was used to augment the identification of the pre-impoundment sediment horizon. When the bulk density data showed a more clear trend than clay enrichment, the bulk density derived estimate was used. The depth of a marked depletion in % silts was also used as an identifier when possible, although these data generally did not show a clear trend. Limited comparison with photographs of cores also served to verify the determination of sedimentation depth. The minimum possible error in depth determination ranges from ±1 cm in the first 10 cm to ±2.5 cm in the rest of the core. A similar approach for determining the depth of sedimentation was used by Bennett et al. (2005).

In Denmark Core 1 and Lt 14A-4 core 1, ^{137}Cs was used to further check the selection of the pre-impoundment level. Gamma spectroscopy was used to determine the activity of ^{137}Cs in the lake core samples. Samples were counted in standardized geometries for at least 82,800 seconds on a High Purity Germanium (HPGe) gamma detector. Counting efficiencies for ^{137}Cs were established using two mixed radionuclide solutions (Bonniwell, 2001; Wilson, 2003). In cases where there was disagreement between the clay enrichment/bulk density decrease derived sedimentation depth and that derived from ^{137}Cs data, the former was used since ^{137}Cs data were only available for 2 cores.

RESULTS AND DISCUSSION

Bulk density, particle size, and preimpoundment levels for selected cores from each site are shown in Figure 5. Figure 5A is an example of a situation where bulk density and a small enrichment in % clay were in agreement on the depth of sedimentation. Figure 5D shows a strong trend in bulk density, which in this case was used to identify the pre-impoundment level. Overall, the agreement between clay enrichment and a downward trend in bulk density for identifying the depth of stored sediments was judged to be acceptable. The clear correlation of decrease in bulk density with clay enrichment differs somewhat from the findings of Bennett et al. (2005), where a weaker relationship was found.

^{137}Cs data was used to verify the pre-impoundment level in Denmark Lake core 1 (Figure 6) and Lt 14A-4 core 1 (Figure 7). Since these lakes were constructed so close to 1964±2 year peak in atmospheric nuclear testing, the peak in ^{137}Cs activity was taken to indicate the depth of sediment accumulation. Figure 6 shows good agreement of the ^{137}Cs peak with clay enrichment and reasonable agreement with decreasing bulk density. Here, % silt was not plotted because it showed no discernable trend and obscured the % sand and % clay plots. In Figure 7, the ^{137}Cs differs from the bulk density and clay enrichment derived bottom depth by 10 cm. Within the constraints and error bounds of the current sampling methodology, the ^{137}Cs data were in agreement with the clay enrichment/bulk density decrease for determining the depth of impounded sediments. Figure 7 also shows a significant depletion in % sand near the pre-impoundment level indicated by bulk density and % clay depletion.

The mean sedimentation rates shown in Table 1 were unexpectedly low. It was expected that high sedimentation rates early in the reservoirs' life spans would create an overall higher sedimentation rate. The methods used in the present study only allow average rates of sedimentation to be assessed, so positive identification of such a trend is not possible. The loss in storage data also shows little impairment of these structures. Lt 14A-4 shows the most loss in storage at 19%. This is not surprising since, of those examined here, it is the smallest lake and is part of the largest watershed. Lt14A-4 had a similar accumulation rate to Denmark Lake, but because of its increased area, Denmark shows only a 9% reduction in storage.

CONCLUSIONS

Sedimentation rates and loss in storage for 3 small erosion control lakes in the Holly Springs National Forest east of Oxford, Mississippi, were assessed. Sediment accumulation rates and reductions in storage caused by impounded sediments were found to be lower than expected. Accumulation rates were significantly less than those found by Bennett et al. (2005) in Grenada Lake. Using the method described by Bennett et al. (2005) for determining the depth of deposition appears to have been successful. Comparison with limited ^{137}Cs data shows reasonable agreement with % clay enrichment and decrease in bulk density data. An interesting divergence from the findings of Bennett et al. (2005) was the clear delineation of bulk density corresponding to ^{137}Cs peaks and % clay enrichment. Differences of this nature are likely to be associated with the smaller size and largely forested nature of the watersheds examined in the present study.

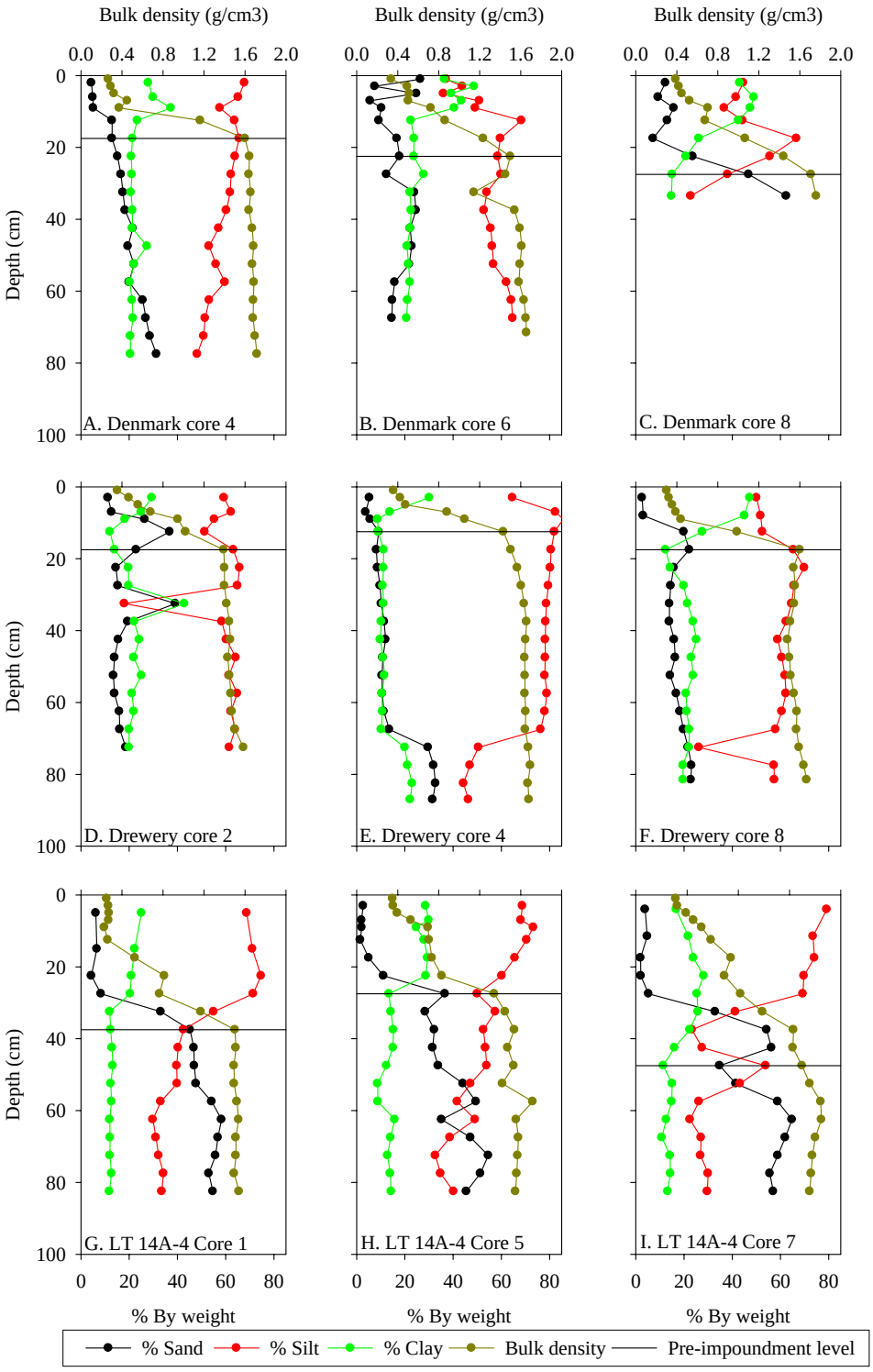


Figure 5 Selected particle size and bulk density data.

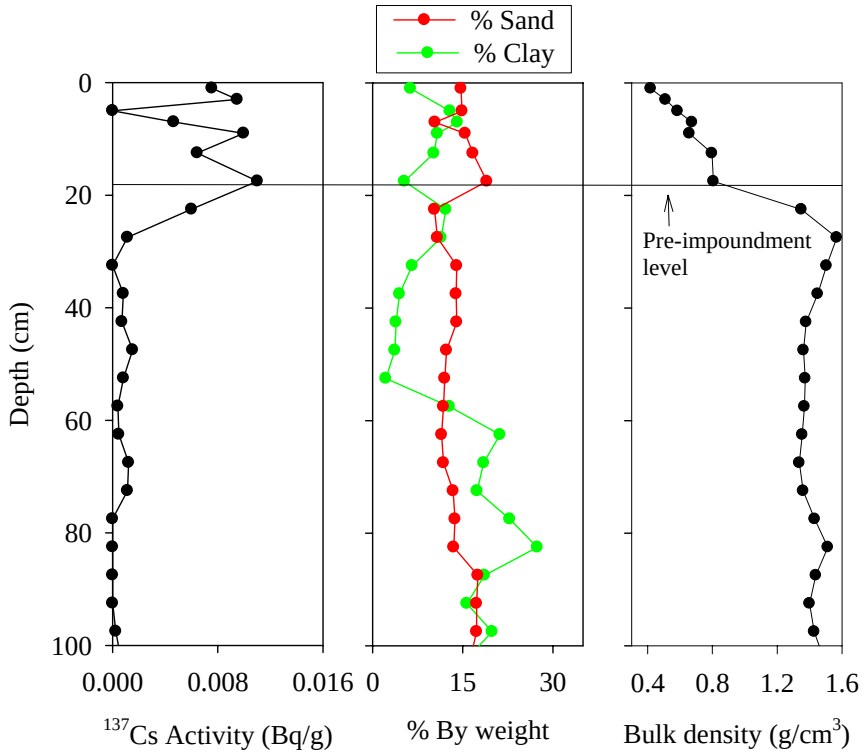


Figure 6 ^{137}Cs activity, % sand, % clay, and bulk density data from Denmark Lake core 1.

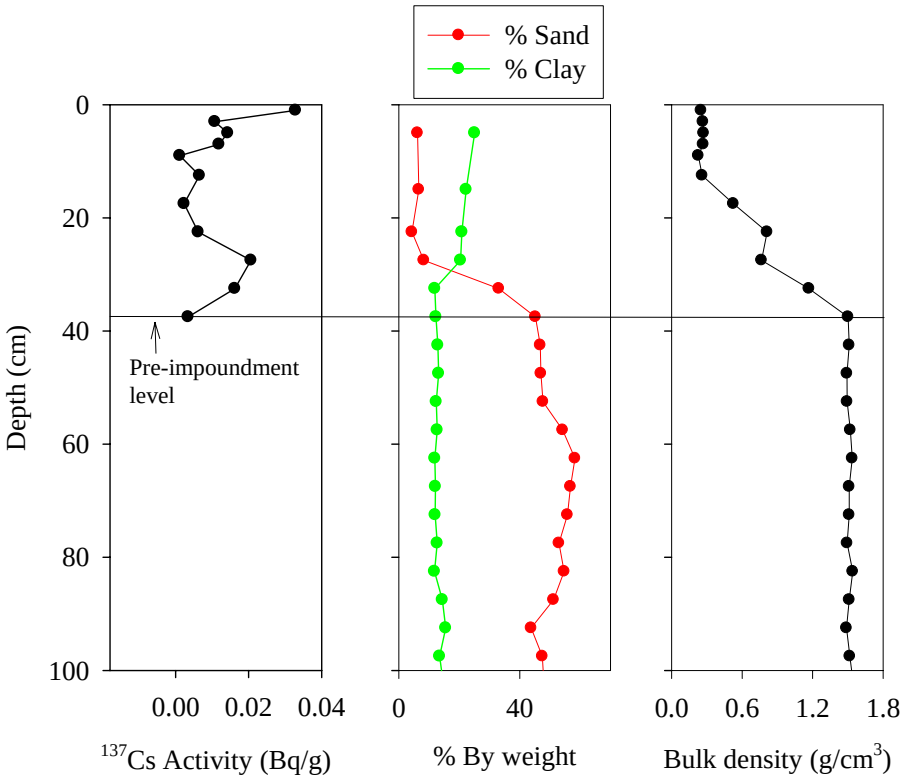


Figure 7 ^{137}Cs activity, % sand, % clay, and bulk density data from lake Lt 14A-4.

ACKNOWLEDGEMENTS

The authors would like to thank G. Gray for meticulous attention to detail in collection, storage, and preparation of core samples for analysis. J. Strickland, V. Joiner, and A. Smith also provided invaluable technical assistance without which this work would not have been possible.

REFERENCES

Bennett, S. J., Rhoton, F. E., and Dunbar, J. A. (2005). "Texture, spatial distribution, and rate of reservoir sedimentation within a highly erosive, cultivated watershed: Grenada Lake, Mississippi," Water Resources Research. 41, W01005, doi:10.1029/2004WR003645.

Bonniwell, E.C. (2001). Evaluating Soil Erosion and Sediment Transport with Radionuclides. Ph.D. Dissertation, Case Western Reserve University, Cleveland, OH.

Caldwell, L. W. (1999). "Rehabilitating our nation's aging small watershed projects," in Soil and Water Conservation Annual Conference, Biloxi, Mississippi.

Graf, W. L. (1999). "Dam nation: A geographic census of American dams and their large-scale hydrologic impacts," Water Resources Research. 35(4):1305-1311.

Lanesky, D. E., B. W. Logan, R. G. Brown, and A.C. Hine. (1979). "A new approach to portable vibracoring underwater and on land," Journal of Sedimentary Petrology. 49:654-657.

Smith, D. G. (1984). "Vibracoring fluvial and deltaic sediments: tips on improving penetration and recovery," Journal of Sedimentary Petrology. 54:660-663.

Soil Survey Staff (1992). Procedures for collecting soil samples and methods of analysis for soil survey. USDA-SCS Soil Surv. Invest. Rep. 42, U.S. Govt. Print. Office, Washington, D. C.

Ursick, Stanley J. (1963). Planting Loblolly pine for erosion control in North Mississippi. U. S. Forest Service Research Paper SO-3.

Wilson, C.G. (2003). The Transport of Fines Sediment Through Three NERR Estuaries Using Radionuclide Tracers. PhD. Dissertation. Case Western Reserve University. Cleveland, OH.

SEDIMENT CHEMISTRY OF THE COLORADO RIVER DELTA IN LAKE POWELL, UTAH

Robert J. Hart, Supervisory Hydrologist, U.S. Geological Survey, 2255 N. Gemini Dr., Flagstaff, Arizona 86001

Abstract: Sediment delta deposits in Lake Powell provide a repository for the potential accumulation of various natural and human-introduced contaminants. The Colorado River delta of Lake Powell extends for more than 50 kilometers from above Hite, Utah, to below Good Hope Bay. The greatest deposition occurs near and upstream from Hite. Owing to current (2005) low reservoir levels, a large segment of the delta is exposed in a reach near the former site of Hite marina near the mouth of the Dirty Devil River.

During the summer of 2001, the U.S. Geological Survey documented concentrations of major ions; trace and minor elements; organic compounds, including organochlorine pesticides, polychlorinated biphenyls, and polycyclic aromatic hydrocarbons; and radionuclides in the delta sediments of the Colorado River.

Three cores and several surface-sediment samples were collected near the Hite marina. Concentrations of major elements, such as calcium, aluminum, and iron, did not show any discernable patterns in concentrations within each core or among the different cores. Concentrations of several trace elements were correlative with sediment color and texture. Elements that are considered to be environmental contaminants, such as arsenic, uranium, selenium, and mercury, were detected in core samples. Some of these elements increased in concentration with core depth. In subsamples of the cores, organochlorine pesticides and polychlorinated biphenyls, except for p,p'-DDE, were not detected in concentrations greater than the laboratory detection limit. A total of 19 parent polycyclic aromatic hydrocarbons and multiple alkyl-polycyclic aromatic hydrocarbons were detected in all 3 core samples. All core samples contained concentrations of gross alpha and gross beta radionuclides; concentrations ranged from 11 to 17 picocuries per gram.

EFFECTS OF NONAGRICULTURAL HUMAN ACTIVITY ON SEDIMENT QUALITY: A COMPARISON OF TRACE ELEMENT CONCENTRATIONS IN EIGHT SMALL RESERVOIRS

Kyle Juracek, Research Hydrologist, U.S. Geological Survey, Lawrence, Kansas, kjuracek@usgs.gov;
Andrew Ziegler, Supervisory Hydrologist, U.S. Geological Survey, Lawrence, Kansas, aziegler@usgs.gov

INTRODUCTION

Small reservoirs are valued by the general public both as a source of drinking water and for recreational activities. In addition to information on water quality and sedimentation, effective reservoir management requires information on sediment quality. Sediment quality is an important environmental concern because sediment may act as a sink for some water-quality constituents and, under certain conditions, as a source of constituents to the overlying water column and biota (Baudo et al., 1990; Zoumis et al., 2001). Once in the food chain, sediment-derived constituents may pose an even greater concern because of bioaccumulation. An analysis of reservoir bottom sediments can provide historical information on sediment deposition as well as the occurrence of sediment-bound constituents. Such information may be used to partly reconstruct historical sediment-quality and water-quality records and to determine a present-day baseline with which to evaluate long-term changes in reservoir sediment and water quality that may be related to changes in human activity in the contributing basin (Charles and Hites, 1987; Van Metre and Callender, 1996; Van Metre and Mahler, 2004). Moreover, such information may be used to assist in the development, implementation, evaluation, and revision of total maximum daily loads (TMDLs) for sediment and associated constituents that contribute to the water-quality impairment of reservoirs.

To investigate the effects of nonagricultural human activity on sediment quality, sediment cores were collected from eight small reservoirs in eastern Kansas with basins of diverse land-use combinations. The sediment samples were analyzed for selected trace elements. Most, if not all, trace elements may be toxic in animals and humans if the concentrations are sufficiently large (Pais and Jones, 1997). Specific study objectives were to: (1) determine the occurrence and trends of trace elements in the reservoir bottom sediments, (2) assess sediment quality with respect to available guidelines, and (3) interpret the effects of nonagricultural human activity (in the basin or the reservoir) on sediment quality within and among the eight reservoirs.

The eight small reservoirs selected for the study were Bronson City Lake, Centralia Lake, Crystal Lake, Gardner City Lake, Lake Afton, Mission Lake, Otis Creek Reservoir, and Pony Creek Lake. The locations of the reservoirs are provided in Juracek (2004). Each of these reservoirs is used as a public water supply and (or) for recreation. All but Otis Creek Reservoir were listed under Section 303(d) of the Federal Clean Water Act of 1972 for eutrophication. The 303(d) list is a priority list that identifies water bodies that do not meet water-quality standards on the basis of the use of the water bodies. For each impaired water body on the 303(d) list, a State is required by the Clean Water Act to develop a TMDL, which is an estimate of the maximum pollutant load (material transported during a specified time period) from point and nonpoint sources that a receiving water can accept without exceeding water-quality standards (U.S. Environmental Protection Agency, 1991). Otis Creek Reservoir, which was not on the 303(d) list, was included in the study for the purpose of comparison.

Description of Reservoir Basins: The small reservoirs included in this study have completion dates ranging from 1879 (Crystal Lake) to 1993 (Pony Creek Lake). The reservoir basins range in area from less than 1 mi^2 (Bronson City Lake, Crystal Lake) to 14.0 mi^2 (Otis Creek Reservoir). The original water-storage capacities for the reservoirs range from 229 acre-ft (Crystal Lake) to 5,845 acre-ft (Otis Creek Reservoir). Available information indicated that the reservoirs have not been dredged. Table 1 provides the year completed, approximate basin area, and original water-storage capacity for each of the small reservoirs.

Long-term mean annual precipitation ranges from about 30 in. for the Lake Afton Basin to about 40 in. for the Bronson City Lake and Crystal Lake Basins (High Plains Regional Climate Center, 2002). Most of the annual precipitation is received during the growing season (generally April–September).

Table 1. Year completed, approximate basin area, original water-storage capacity, and number of sediment-core intervals analyzed for eight small reservoirs in eastern Kansas.[mi^2, square miles; --, not available]

Reservoir	Year completed	Approximate basin area (mi^2)	Original water-storage capacity[1] (acre-feet)	Number of sediment-core intervals analyzed
Bronson City Lake	1956	0.8	--	3
Centralia Lake	1990	12.5	4,769	3
Crystal Lake	1879	.6	229	10
Gardner City Lake	1940	5.5	2,301	5
Lake Afton	1942	10.4	3,264	5
Mission Lake	1924	8.6	1,866	5
Otis Creek Reservoir	1971	14.0	5,845	5
Pony Creek Lake	1993	6.6	2,367	3

[1]Sources of information for original water-storage capacity provided in Juracek (2004).

Land use (1988–90) in the basins is a mostly agricultural mix of cropland and grassland. Cropland is the dominant land use in the Bronson City Lake, Centralia Lake, Lake Afton, Mission Lake, and Pony Creek Lake Basins. Grassland is the dominant land use in the Crystal Lake and Otis Creek Reservoir Basins. The Gardner City Lake Basin is characterized by a mix of cropland, grassland, and urban land uses. Substantial urban land use also is present in the Crystal Lake Basin (Kansas Applied Remote Sensing Program, 1993).

Acknowledgments: This study was made possible in part by support from the U.S. Geological Survey (USGS) Cooperative Water Program, the Kansas State Water Plan Fund, the Kansas Department of Health and Environment, the U.S. Environmental Protection Agency (USEPA), the U.S. Department of Agriculture's Natural Resources Conservation Service, and the Fall River Watershed Joint District No. 21.

METHODS

Sediment-Core Collection, Sampling, and Analysis: The objectives of this study were accomplished through the collection and analysis of one bottom-sediment core from each of the eight reservoirs. The cores were collected in 2002 and 2003. Typically, each core was collected (using a gravity corer) from a site located in the downstream one-third of the reservoir relatively close to the dam. The near-dam site was selected because it is in relatively deep water where the sediment was least likely to be disturbed.

The number of intervals sampled for trace element analyses for each core ranged from 3 to 10 (table 1) and was dependent on reservoir age and sediment thickness. Samples were analyzed for arsenic, cadmium, chromium, copper, lead, nickel, and zinc. Elevated concentrations of these trace elements frequently are indicative of human activity. For example, elevated copper concentrations often reflect the historical application of copper sulfate to control algal blooms. Elevated lead concentrations often are indicative of the historical use of leaded gasoline. Trace element analyses were performed at the USGS Sediment Trace Element Partitioning Laboratory in Atlanta, Georgia, using the methods described by Fishman and Friedman (1989), Arbogast (1996), and Briggs and Meier (1999). Age dating of the bottom sediment in some cores was accomplished by determining the activity of cesium-137 (^{137}Cs) by gamma-ray spectrometry (American Society for Testing and Materials, 2000).

Sediment-Quality Assessment: MacDonald et al. (2000) developed consensus-based, sediment-quality guidelines (SQGs) that were computed as the geometric mean of several previously published SQGs. The consensus-based SQGs consist of a threshold effect concentration (TEC) and a probable effect concentration (PEC). The TEC represents the concentration below which harmful effects on sediment-dwelling organisms are not expected to occur, whereas the PEC represents the concentration above which harmful effects on sediment-dwelling organisms are expected to occur frequently. Generally, these guidelines are similar to USEPA adopted nonregulatory SQGs for threshold effects levels (TELs) and probable effects levels (PELs) (U.S. Environmental Protection Agency, 1997). An evaluation of the reliability of the consensus-based SQGs indicated that most of the individual TECs and PECs

provide an accurate basis for predicting the presence or absence of sediment toxicity (MacDonald et al., 2000). The TECs and PECs for the seven trace elements analyzed in this study are provided in table 2.

To provide a comparative assessment of the reservoirs in terms of the effects of nonagricultural human activity on sediment quality over the life of the reservoirs, two measures were used. First, the median concentration was determined for each trace element. Second, the percentage of samples that exceeded the TEC for each trace element was computed.

Table 2. Consensus-based sediment-quality guidelines, median trace element concentrations, and percentage of samples that exceeded the threshold effect concentration for eight small reservoirs in eastern Kansas.[As, arsenic; Cd, cadmium; Cr, chromium; Cu, copper; Pb, lead; Ni, nickel; Zn, zinc; TEC, threshold effect concentration; PEC, probable effect concentration; μg/g, micrograms per gram; --, not applicable]

Consensus-based sediment-quality guideline[1]/ reservoir	Trace element						
	As	**Cd**	**Cr**	**Cu**	**Pb**	**Ni**	**Zn**
TEC, μg/g	9.79	0.99	43.4	31.6	35.8	22.7	121
PEC, μg/g	33.0	4.98	111	149	128	48.6	459
Median concentration (μg/g) and percentage of samples that exceeded the TEC in parentheses ( )							
Bronson City Lake	15(100)	0.7(33)	74(100)	200(100)	34(33)	37(100)	150(100)
Centralia Lake	18(100)	.8(0)	77(100)	30(0)	19(0)	40(100)	110(0)
Crystal Lake	17(100)	.9(30)	79(100)	122(60)	49(70)	38(100)	220(100)
Gardner City Lake	18(100)	.6(0)	87(100)	77(100)	42(100)	43(100)	160(100)
Lake Afton	12(100)	.7(0)	71(100)	33(100)	45(80)	38(100)	130(60)
Mission Lake	15(100)	.3(0)	83(100)	32(60)	29(0)	41(100)	140(60)
Otis Creek Reservoir	11(100)	.5(0)	78(100)	21(0)	23(0)	36(100)	67(0)
Pony Creek Lake	14(100)	.5(0)	72(100)	26(0)	25(0)	37(100)	110(0)

[1]MacDonald et al. (2000).

RESULTS AND DISCUSSION

Bronson City Lake: In the bottom sediment of Bronson City Lake, arsenic, chromium, nickel, and zinc concentrations all exceeded the TECs but were less than the PECs. Cadmium and lead concentrations were either slightly greater than or slightly less than the respective TECs. Copper concentrations exceeded the PEC. The elevated concentrations of copper likely are due to the historical application of copper sulfate to control algal blooms in the reservoir (Ellen Harper, city of Bronson, oral commun., 2003). With the exception of a possible negative trend for lead, no trends in trace element concentrations were evident in the core samples.

Centralia Lake: Arsenic, chromium, and nickel concentrations in the bottom sediment of Centralia Lake all exceeded the TECs but were less than the PECs. All cadmium, copper, lead, and zinc concentrations were less than the TECs. No trends in trace element concentrations were indicated.

Crystal Lake: In the bottom sediment of Crystal Lake, arsenic, chromium, and zinc concentrations all exceeded the TECs but were less than the PECs. Most of the cadmium concentrations were less than the TEC. Copper concentrations ranged from less than the TEC for the bottom (oldest) four core intervals to larger than the PEC for the top (most-recent) five intervals (fig. 1*A*). With the exception of the bottom (oldest) three intervals, which were less than the TEC, lead concentrations exceeded the TEC but were less than the PEC. All nickel concentrations exceeded the TEC but were less than the PEC.

Trend analyses, with a significance level of 0.05, indicated a statistically significant positive trend (constituent concentration increased toward the top of the sediment core) for copper (fig. 1*A*), lead (fig. 1*B*), and zinc (fig. 1*C*).

Because the ^{137}Cs activity has a well-defined 1963–64 peak followed by a uniform, exponential decrease (fig. 1*D*), it was concluded that the bottom sediment in Crystal Lake is relatively undisturbed, and the trends may be considered representative of historical deposition. The indicated positive trends for copper, lead, and zinc do not appear to be caused by analytical variance as the majority of the concentrations were not within 10 percent of the mean concentration.

The indicated positive trends may be due to human activity in and near the Crystal Lake Basin. The elevated concentrations of copper in the upper one-half of the sediment core (fig. 1*A*) likely were caused by the historical application of copper sulfate (beginning in the 1940s or 1950s) to control algal blooms in the reservoir (Rick Doran, city of Garnett, oral commun., 2003). Increased concentrations of zinc (fig. 1*C*) may be attributed to increased vehicular traffic and associated tire wear over time (Callender and Rice, 2000).

For lead, there was a statistically significant positive trend over the life of the reservoir. However, inspection of figure 1*B* indicates that the initial positive trend leveled off and became a negative trend at the top of the core. This profile is consistent with the history of particulate lead emissions from leaded gasoline use in the United States. Leaded gasoline was introduced in the 1920s and quickly became standard (Davies, 1990). Use of leaded gasoline increased until its phase out, legislated by the Clean Air Act of 1970, began in the 1970s. From 1970 to 1990, total national lead emissions from vehicles decreased an estimated 99.8 percent (U.S. Environmental Protection Agency, 2000). Results indicated that, following the phase out of leaded gasoline, it will take at least several decades for lead in newly deposited reservoir bottom sediments to return to historical baseline concentrations.

Because Crystal Lake was completed in 1879, the trace element concentrations at the bottom of the sediment core likely provide an indication of historical baseline concentrations. Evidence in support of this interpretation is provided by the substantially smaller and relatively uniform concentrations of lead and zinc in the bottom three core intervals (figs. 1*B* and 1*C*).

For arsenic, chromium, nickel, and zinc, the historical baseline concentrations (likely represented by the bottom three core intervals) are substantially larger than the respective TECs (Juracek, 2004). This finding indicates that, for certain trace elements in certain areas, historical baseline concentrations may exceed the TECs prior to the effects of substantial nonagricultural human activity in the basin.

Gardner City Lake: Arsenic, chromium, lead, nickel, and zinc concentrations in the bottom sediment of Gardner City Lake all exceeded the TECs but were less than the PECs. Cadmium concentrations were less than the TEC.

All copper concentrations exceeded the TEC, and the top (most-recent) interval of the core had a concentration that also exceeded the PEC. Throughout the life of the reservoir, a positive trend in copper concentrations is evident in the bottom sediment. The positive trend is likely caused by frequent applications of copper sulfate (since the 1970s) to control algal blooms in the reservoir (Mike Howard, city of Gardner, written commun., 2003). The concentration profile for lead is consistent with the history of particulate lead emissions from leaded gasoline use in the United States. Because the ^{137}Cs activity has a well-defined 1963–64 peak followed by a uniform, exponential decrease (Juracek, 2004), it was concluded that the bottom sediment in Gardner City Lake is relatively undisturbed, and the trends may be considered representative of historical deposition.

Lake Afton: In the bottom sediment of Lake Afton, arsenic, chromium, copper, and nickel concentrations all exceeded the TECs but were less than the PECs. Cadmium concentrations were less than the TEC. Zinc concentrations were either slightly less than or larger than the TEC (but less than the PEC). For lead, four of five concentrations exceeded the TEC but were less than the PEC. The concentration profile for lead is consistent with the history of particulate lead emissions from leaded gasoline use in the United States. Because the ^{137}Cs activity has a well-defined 1963–64 peak followed by a uniform, exponential decrease (Juracek, 2004), it was concluded that the bottom sediment in Lake Afton is relatively undisturbed and the concentration profile for lead is representative of historical deposition.

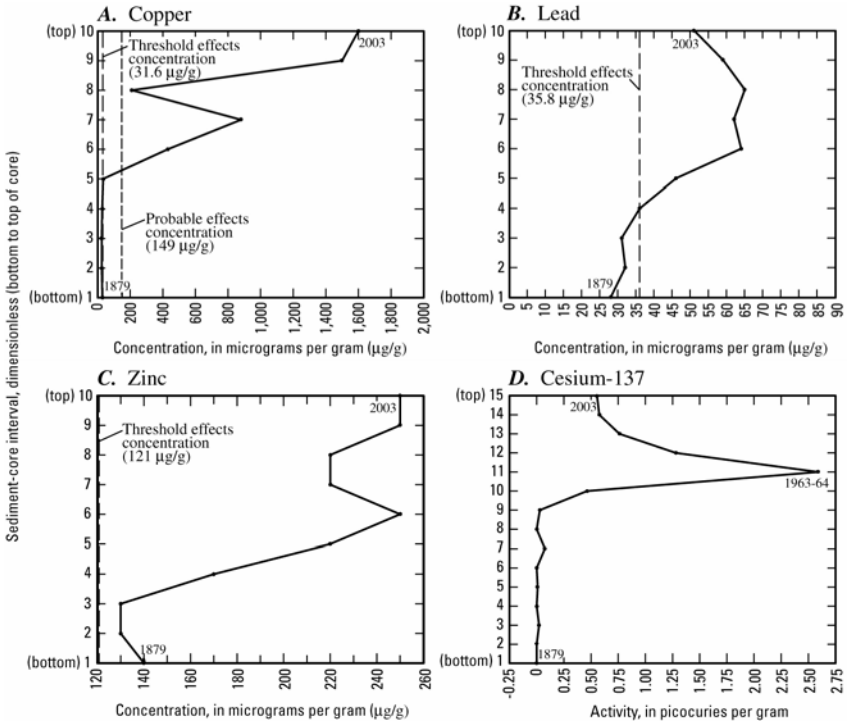


Figure 1. Variation in (A) copper concentrations, (B) lead concentrations, (C) zinc concentrations, and (D) cesium-137 activity with depth of bottom-sediment core samples collected from Crystal Lake, April 2003. Threshold and probable effect concentrations from MacDonald et al. (2000).

Mission Lake: Arsenic, chromium, and nickel concentrations in the bottom sediment of Mission Lake all exceeded the TECs but were less than the PECs. Copper concentrations were either slightly less than or slightly greater than the TEC. For lead, all concentrations were less than the TEC. The concentration profile for lead subtly reflects the history of particulate lead emissions associated with the use of leaded gasoline in the United States. For zinc, the two oldest intervals had concentrations that were slightly less than the TEC, whereas the remaining intervals had concentrations that exceeded the TEC but were less than the PEC. All cadmium concentrations were less than the TEC.

Otis Creek Reservoir: In the bottom sediment of Otis Creek Reservoir, arsenic, chromium, and nickel concentrations all exceeded the TECs but were less than the PECs. For cadmium, copper, lead, and zinc, all concentrations were less than the TECs. No trends for trace elements were indicated in the core.

Pony Creek Lake: Arsenic, chromium, and nickel concentrations in the bottom sediment of Pony Creek Lake all exceeded the TECs but were less than the PECs. All cadmium, copper, lead, and zinc concentrations were less than the TECs. No trends for trace elements were evident in the core.

Interlake Comparison: The eight small reservoirs were compared in terms of median trace element concentrations. Additionally, the reservoirs were compared using the percentage of samples that exceeded the TEC for each trace element.

Considered with respect to the SQGs, a comparison of the median trace element concentrations indicated that the eight reservoirs were similar in terms of arsenic, cadmium, chromium, and nickel concentrations (table 2). For arsenic, chromium, and nickel, every sediment sample for every reservoir had concentrations that exceeded the TECs but were less than the PECs. For cadmium, the sediment concentrations were typically less than the TEC. The generally similar concentrations and lack of trends over time (Juracek, 2004) may be indicative of a relative absence of effects of nonagricultural human activity on sediment quality for these four trace elements.

The effects of nonagricultural human activity on sediment quality were pronounced for copper, lead, and zinc. For copper, the effects of copper sulfate application were evident for Bronson City, Crystal, and Gardner City Lakes. Median copper concentrations for Bronson City and Crystal Lakes were substantially larger than for the other reservoirs (table 2). For these two reservoirs, at least one-half of the copper concentrations exceeded the PEC.

The history of leaded gasoline use apparently was documented by lead deposition in the bottom sediment of Crystal Lake (fig. 1*B*), Gardner City Lake, Lake Afton, and, to a lesser degree, Mission Lake (Juracek, 2004). That is, the reversal from an initial positive trend to a negative trend reflects the historical increase in consumption of leaded gasoline from the 1920s until the late 1970s when the phase out of lead from gasoline began (Callender and Van Metre, 1997; Callender and Rice, 2000). The fact that the largest median lead concentration was measured in the bottom sediment of Crystal Lake likely is because of the presence of the well-traveled U.S. Highway 59, which is located within the Crystal Lake Basin less than 100 ft upstream from the reservoir shore. In contrast, lead deposition in the bottom sediment of Otis Creek Reservoir was uniform through time with relatively small concentrations (Juracek, 2004). The lack of trend at this location may be attributable to the remote location of the Otis Creek Reservoir Basin, which is several miles from the nearest highway in every direction.

The variability of zinc concentrations in the bottom sediment of the reservoirs also likely was affected by human activity. A significant source of zinc is vehicular tire wear. Callender and Rice (2000) determined that increased zinc concentrations in sediment are related to increased vehicular traffic. The fact that the largest median zinc concentration was measured in the bottom sediment from Crystal Lake likely was because of its proximity to U.S. Highway 59. The fact that the smallest median zinc concentration was measured in the bottom sediment from Otis Creek Reservoir likely was because of the relative absence of vehicular traffic in and near its basin.

A comparison of the reservoirs in terms of the relative concentrations of trace elements in the bottom sediment also indicated effects of nonagricultural human activity. Typically, Crystal Lake and Gardner City Lake were among the reservoirs with the largest median sediment concentrations for the seven trace elements considered (table 2). Crystal Lake had the largest median concentrations for cadmium, lead, and zinc. Gardner City Lake had the largest median concentrations for arsenic (along with Centralia Lake) and chromium. Crystal Lake and Gardner City Lake are the only two reservoirs with a substantial percentage of urban land use in their basins.

Otis Creek Reservoir was included in this study for the purpose of comparison. Because of its relatively remote location and the fact that land use in its basin is almost exclusively grassland, Otis Creek Reservoir provided an opportunity to assess effects of nonagricultural human activity on the deposition of trace elements in the bottom sediment of the other reservoirs. For arsenic, cadmium, copper, lead, and zinc, the bottom-sediment concentrations in samples from Otis Creek Reservoir typically were the smallest or among the smallest measured. For chromium and nickel, the bottom-sediment concentrations in samples from Otis Creek Reservoir generally were comparable to samples from the other reservoirs (Juracek, 2004) (table 2).

A comparison of the overall effects of nonagricultural human activity on sediment quality over the life of the reservoirs, evaluated using the percentage of samples that exceeded the TEC for each of the seven trace elements, indicated that Bronson City Lake, Crystal Lake, Gardner City Lake, and Lake Afton were the most affected. Primary factors that contributed to increased trace element deposition in these reservoirs included vehicular traffic in the basins and copper sulfate application in the reservoirs. Urban land use likely was an additional contributing factor in the Crystal Lake and Gardner City Lake Basins. Among the remaining reservoirs, results indicated that the effects of nonagricultural human activity on trace element deposition were relatively moderate for Mission Lake and relatively minimal for Centralia Lake, Otis Creek Reservoir, and Pony Creek Lake (table 2).

SUMMARY AND CONCLUSIONS

To investigate the effects of nonagricultural human activity on sediment quality, sediment cores were collected from eight small reservoirs in eastern Kansas with basins of diverse land-use combinations. Samples from the sediment cores were analyzed for arsenic, cadmium, chromium, copper, lead, nickel, and zinc to assess changes in trace element deposition over the life of the reservoirs.

Results indicated that sediment concentrations of arsenic, cadmium, chromium, and nickel were similar among reservoirs and over time. Because the level of nonagricultural human activity in the eight basins varies considerably, its effects on the deposition of these four trace elements in the reservoirs were interpreted to be minimal. Substantial differences among the reservoirs were indicated for the sediment concentrations of copper, lead, and zinc. Relatively large concentrations of these three trace elements were attributed primarily to reservoir applications of copper sulfate to control algal blooms and vehicular traffic within the basins.

Sediment concentrations of arsenic, chromium, and nickel exceeded the consensus-based threshold effect concentration (TEC) for harmful effects on sediment-dwelling organisms in all samples from every reservoir. For copper, lead, and zinc, the results were more variable. In the case of copper, sediment concentrations frequently exceeded the probable effect concentration (PEC) for harmful effects on sediment-dwelling organisms in samples from the reservoirs that had been treated with copper sulfate. For lead, sediment concentrations frequently exceeded the TEC for several reservoirs and reflected the history of leaded gasoline use. Results for Crystal Lake indicated that, following the phase out of leaded gasoline, it will take at least several decades for lead in newly deposited reservoir bottom sediments to return to historical baseline concentrations. Sediment concentrations of zinc typically exceeded the TEC for several reservoirs and likely reflect inputs from vehicular tire wear. Cadmium concentrations in samples from all reservoirs typically were less than the TEC. Trace element concentrations in samples from a sediment core for Crystal Lake (long historical record) and Otis Creek Reservoir (relatively pristine basin) indicated that, for certain trace elements in certain areas, historical baseline concentrations may exceed the TECs prior to the effects of substantial nonagricultural human activity in the basin.

Overall, a comparison based on the percentage of samples that exceeded the TECs indicated that the sediment quality for Bronson City Lake, Crystal Lake, Gardner City Lake, and Lake Afton was most affected by nonagricultural human activity. The results indicated that the effects of nonagricultural human activity on sediment quality were relatively moderate for Mission Lake and relatively minimal for Centralia Lake, Otis Creek Reservoir, and Pony Creek Lake.

An analysis of sediment cores can provide information that may be used to partly reconstruct historical sediment-quality and water-quality records and to determine a present-day baseline with which to evaluate long-term changes in reservoir sediment and water quality that may be related to changes in human activity in the basin. Moreover, such information may be used to assist in the development, implementation, evaluation, and revision of total maximum daily loads for sediment and associated chemical constituents that contribute to the water-quality impairment of reservoirs.

REFERENCES CITED

American Society for Testing and Materials (2000). Standard Practice for High-Resolution Gamma-Ray Spectrometry of Water, *in* Annual Book of ASTM Standards, section 11, Water and Environmental Technology. ASTM, West Conshohocken, Pennsylvania, v. 11.02, D 3639–98a, pp 294–304.

Arbogast, B.F. (1996). Analytical Methods Manual for the Mineral Resource Surveys Program. U.S. Geological Survey Open-File Report 96–525.

Baudo, Renato, Giesy, J.P., and Muntau, Herbert, eds. (1990). Sediments—Chemistry and Toxicity of In-Place Pollutants. Lewis Publ., Ann Arbor, Michigan.

Briggs, P.H., and Meier, A.L. (1999). The Determination of Forty Two Elements in Geological Materials by Inductively Coupled Plasma-Mass Spectrometry. U.S. Geological Survey Open-File Report 99–166.

Callender, Edward, and Rice, K.C. (2000). "The Urban Environmental Gradient—Anthropogenic Influences on the Spatial and Temporal Distributions of Lead and Zinc in Sediments," Environmental Science & Technology, 34(2), pp 232–238.

Callender, Edward, and Van Metre, P.C. (1997). "Reservoir Sediment Cores Show U.S. Lead Declines," Environmental Science & Technology, 31(9), pp 424A–428A.

Charles, M.J., and Hites, R.A. (1987). "Sediments as Archives of Environmental Pollution Trends," chap. 12, *in* Hites, R.A., and Eisenreich, S.J., eds., Sources and Fates of Aquatic Pollutants. American Chemical Society, Washington, D.C., Advances in Chemistry Series 216, pp 365–389.

Davies, B.E. (1990). Lead, chap. 9, *in* Alloway, B.J., ed., Heavy Metals in Soils. John Wiley & Sons, New York, pp 177–196.

Fishman, M.J., and Friedman, L.C., eds. (1989). Methods for Determination of Inorganic Substances in Water and Fluvial Sediments. U.S. Geological Survey Techniques of Water-Resources Investigations, book 5, chap. A1.

High Plains Regional Climate Center (2002). Historical Data Summaries: Information available on the Web, accessed August 21, 2002, at http://www.hprcc.unl.edu/

Juracek, K.E. (2004). Sedimentation and Occurrence and Trends of Selected Chemical Constituents in Bottom Sediment of 10 Small Reservoirs, Eastern Kansas. U.S. Geological Survey Scientific Investigations Report 2004-5228.

Kansas Applied Remote Sensing Program (1993). Kansas Land Cover Data Base, 1:100,000 scale. Lawrence, Kansas, Data Access and Support Center, available on CD.

MacDonald, D.D., Ingersoll, C.G., and Berger, T.A. (2000). "Development and Evaluation of Consensus-Based Sediment Quality Guidelines for Freshwater Ecosystems," Archives of Environmental Contamination and Toxicology, 39, pp 20-31.

Pais, Istvan, and Jones, J.B., Jr. (1997). The Handbook of Trace Elements. St. Lucie Press, Boca Raton, Florida.

U.S. Environmental Protection Agency (1991). Guidance of Water Quality-Based Decisions—the TMDL Process. Office of Water, Washington, D.C., Report EPA440/4–91–001.

U.S. Environmental Protection Agency (1997). The Incidence and Severity of Sediment Contamination in Surface Waters of the Unted States, Volume 1—National Sediment Quality Survey. Office of Science and Technology, Washington, D.C., Report EPA823-R-97-006.

U.S. Environmental Protection Agency (2000). National Air Pollutant Emission Trends, 1990–1998. Office of Air Quality, Research Triangle Park, North Carolina, Report EPA454/R–00–002.

Van Metre, P.C., and Callender, Edward (1996). "Identifying Water-Quality Trends in the Trinity River, Texas, USA, 1969–1992, Using Sediment Cores from Lake Livingston," Environmental Geology, 28(4), pp 190–200.

Van Metre, P.C., and Mahler, B.J. (2004). "Contaminant Trends in Reservoir Sediment Cores as Records of Influent Stream Quality," Environmental Science & Technology, 38(11), pp 2978–2986.

Zoumis, Theofanis, Schmidt, Astrid, Grigorova, Lidia, and Calmano, Wolfgang (2001). "Contaminants in Sediments— Remobilisation and Demobilisation," The Science of the Total Environment, 266(1-3), pp 195–202.

SMALL ARTIFICIAL PONDS IN THE UNITED STATES: IMPACTS ON SEDIMENTATION AND CARBON BUDGET.

William. H. Renwick, Geography Department, Miami University, Oxford OH 45056. renwicwh@muohio.edu; Richard O. Sleezer, Earth Science Department Emporia State University, Emporia, KS 66801, sleezerr@emporia.edu; Robert W. Buddemeier, Kansas Geological Survey, University of Kansas, Lawrence, KS 66047, buddrw@ku.edu; Steven V. Smith, Departamento de Ecología, Centro de Investigación Científica y de Educación Superior de Ensenada, Ensenada, Baja California 22860, México, svsmith@cicese.mx.

Abstract: The proliferation of small artificial ponds constitutes a major human alteration of the hydrologic landscape. We have estimated the total number of such features across the conterminous United States to be between 2.6 and 9 million, with densities in some areas exceeding 5 per km^2. The majority of ponds have been built in agricultural settings, and densities are highest in the eastern Great Plains and the Southeast. Ponds intercept and temporarily store about 25% of runoff from the conterminous U.S., and in regions of high pond density that proportion may approach 100%. Ponds are a major sediment and carbon sink. Based on erosion and sedimentation rates typical of the mid-to late- 20th century they capture 0.2 to 1.8 x 10^9 tons of sediment and 4 to 36 x 10^6 tons of carbon annually. Case studies in eastern Kansas and southwestern Ohio indicate that while total numbers of ponds have increased steadily since the early 20th century, ponds are transient features on the landscape, with 30 to 90% of those present in the 1950s disappearing by 2000. Ponds disappear mainly by two processes: infilling with sediment, and replacement with other land uses. These processes are spatially variable with infilling by sediment being the dominant cause of disappearance in most areas. Trends in pond sedimentation rates are likely highly variable depending on local conditions. Erosion rates from lands used for row crop agriculture are declining, and ponds with these types of agricultural land uses in their headwater areas are the first to be affected by a reduction in sediment flux. The locus of pond construction appears to be shifting from agricultural to suburban settings, and the dominant rationales for pond construction are changing from provision of livestock water to aesthetic considerations and urban runoff management.

INTRODUCTION

In many parts of the world, especially in agricultural regions, small artificial impoundments (here called ponds) are common features of the landscape. They are built for a variety of purposes, both utilitarian and aesthetic. Despite their ubiquity and, in the U.S. at least, relatively recent appearance on the landscape, they have received little attention in the scientific literature. Individually they are small in comparison to the many named lakes and reservoirs that are generally better-studied, but they are much more numerous. Perhaps most importantly, they reach their highest densities in some areas that have virtually no natural standing surface water, and thus constitute a fundamental transformation of the hydrologic landscape. In this paper we: 1) discuss a recent continent-scale inventory of small ponds in the conterminous U.S.; 2) quantitatively estimate the cumulative impacts of these ponds on total fluxes of sediment and carbon; and 3) describe recent trends in pond construction and replacement and the relation of land-use and land-management trends to pond distribution and impacts.

INVENTORY

The publication of the National Inventory of Dams (NID) called attention to the proliferation of dams on the hydrologic landscape of the U.S. (Graf, 1999). The NID includes ~75,000 features exceeding specific height thresholds (2 m for capacity > 61,700 m^3; 8 m for capacity > 18,500 m^3). While the relatively large dams included in the NID represent the vast majority of total water storage volume in large and small impoundments, the actual number of artificial impoundments in the U.S. is 2 orders of magnitude higher. Smith and others (2002), using data in the satellite-derived National Land Cover Database (NLCD), inventoried small water bodies in the conterminous U.S. While their inventory does not distinguish between natural and artificial impoundments, it is clear from their distribution (Fig. 1) and a knowledge of the geomorphology of the continent that the vast majority of these features are artificial. The NLCD-based inventory concluded that there were ~2.6 million ponds in the early 1990s, the approximate date of the imagery used in the NLCD (Table 1). This number is a minimum estimate, however. Extrapolation from a ~1% sample of USGS 1:24,000 quadrangles suggested a total exceeding 8 million, and detailed analyses of parts of Kansas and Ohio using high-resolution aerial photography rather than the 30-meter Landsat

imagery used in the NLCD confirm that the NLCD inventory underestimates the total by a factor of 1-3. For example, in southwest Ohio, a count of ponds from recent (2000) aerial photographs in three counties found 1.0-3.3 times as many ponds as were identified from the NLCD inventory. In Kansas, identification of ponds on air photos found 0.9 to 1.9 times as many ponds as the NLCD inventory. Based on these data, the inclusion of small ponds in our inventory adds about 20% to the total water surface area of the conterminous U.S., although that number would be higher if we used a higher estimate of pond numbers.

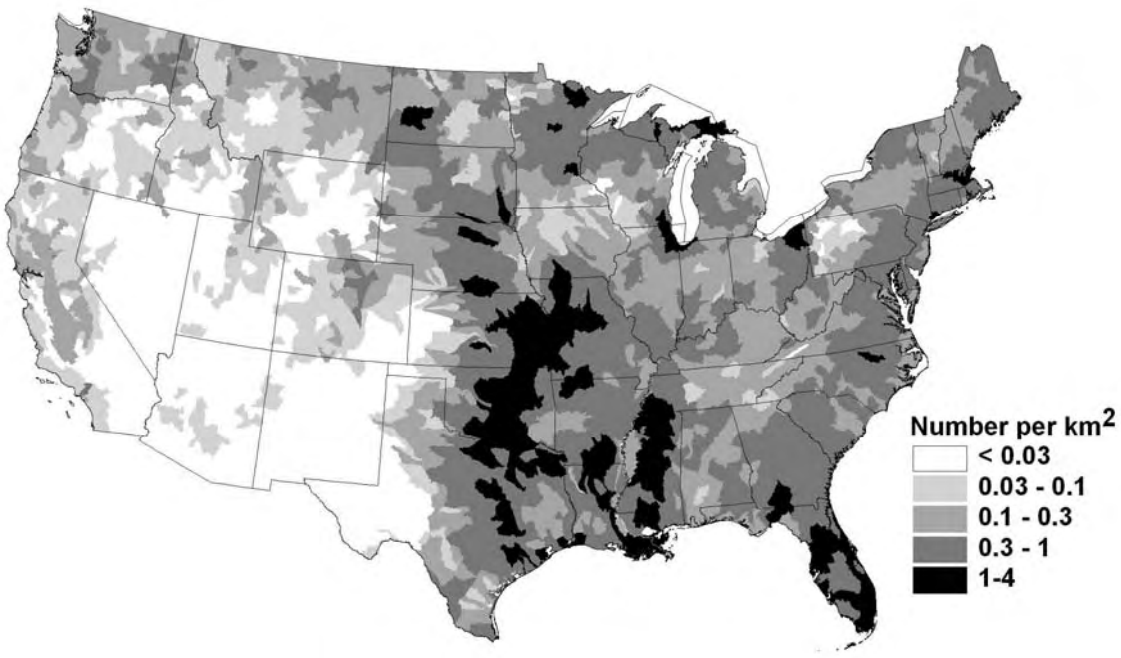


Figure 1 Density of small water bodies in the conterminous U.S., based on NLCD data (from Smith and others, 2002).

Table 1 Number and sizes of water bodies in the National Land Cover Data (NLCD), National Inventory of Dams (NID), and USGS 1:24,000 topographic quadragles (DLGs) (Smith and others, 2002).

Dataset	Number of water bodies (thousands)	Total surface area (1000 km^2)	Average area (m^2)	Maximum area (m^2)	Minimum area (m^2)
NLCD	2600	21	7×10^3	2.53×10^7	6.00×10^2
NID*	43	62	1.45×10^7	1.84×10^9	8.00×10^1
USGS DLGs	9000	--	--	--	2.5×10^1

* The National Inventory of Dams includes ~75,000 dams; a subset of these was used in our analysis. See text for details.

IMPACTS ON CONTINENT-SCALE MATERIAL FLUXES.

It is well documented that dams have profound effects on sediment fluxes through watersheds. For example, Meade and Trimble (1974) showed that dams constructed on the major streams draining eastward from the Appalachians have virtually shut off the flow of sediment to the Atlantic. In the Colorado system, the dramatic decrease in sediment flux is similarly well documented, (Carriquiry and Sanchez, 1999; Williams and Wolman, 1984; Collier and others, 1997). Until recently, however, the cumulative impact of millions of large and small dams on continental sediment flux has been unknown. Smith and others (2002), extrapolating from sedimentation rates in ~1600 reservoirs listed in the RESIS database (Steffen, 1996) have estimated the total volume of sediment deposited in ~43,000 large dams listed in the NID at $1.67 \times 10^9 m^3\ yr^{-1}$. Estimates of the total amount of sedimentation in the millions of smaller impoundments not included in the NID are more difficult to make, but appears to be in the range

of 0.1 to 1.8 x $10^9 m^3 yr^{-1}$ (Renwick and others, 2005). The total sedimentation in small ponds is thus apparently of similar magnitude to that occurring in the larger reservoirs in the NID. While the small ponds probably only account for a small percentage of the total water storage capacity, they are far more numerous and they exist higher in the drainage network, where sediment yields per unit drainage area are high. Based on relations between pond density and proportion of the landscape upstream of ponds we estimate that approximately 21% of land area of the conterminous U.S., representing 25% of runoff and 25% of total sheet and rill erosion, lies upstream of at least one pond. The total amount of sediment accumulating in impoundments in the 48 conterminous U.S. is thus in the range of 1.9 to 3.5 x $10^9 m^3 yr^{-1}$. For comparison, total sheet and rill erosion in the U.S. approximately 2.4 x $10^9 m^3 yr^{-1}$, based on the 1990 National Resource Inventory extrapolated to include Federal lands (Renwick and others, 2005). It appears that ponds and reservoirs are the dominant sink for soil eroded by water.

Table 2 Estimates of total sedimentation in ~2.6 million NLCD ponds ($10^9 m^3 yr^{-1}$) (Renwick and others, 2005).

Method		Sedimentation
Extrapolating from specific sedimentation rates	Regressions applied to all land using average drainage area = total area / number of impoundments	1.78
	Regressions applied to estimated drainage areas on impoundment-by-impoundment basis	0.22
Using erosion occurring on land tributary to impoundments and 80% trap efficiency		0.43

Several studies have shown that substantial amounts of carbon are accumulating in lakes and reservoirs (Stallard, 1998; Dean and Gorham, 1998; Mulholland and Elwood, 1982; Smith and others, 2001). The carbon content of sediment in ponds is variable, but similar to that of the soils that are being eroded (Ritchie, 1989). Smith and others (2005) estimated that the average carbon content of soils in the Mississippi basin is 1.5%. Applying this figure to our estimate of pond sedimentation suggests that 3 to 30 x 10^6 tons of carbon are accumulating in small ponds each year. A similar amount accumulates in larger reservoirs.

CHANGES IN POND NUMBERS OVER TIME

Although documentary evidence is scant, it appears that widespread pond construction in agricultural areas began in the early 20th century. Many ponds were first built for agricultural purposes—primarily livestock water—especially in areas of significant seasonal water shortage such as the Great Plains and southeast. Beginning in the 1940s and accelerating in the 1950s large numbers of ponds were built with technical and/or financial assistance from the Soil Conservation Service (Helms, 1992; ASCS, 1981). Ponds were encouraged as part of Farm Management Plans, and construction costs were subsidized. Ponds were seen as serving multiple uses including livestock water, sediment control, recreation, and emergency water supplies. Very large numbers of ponds were built in this period.
By the 1970s the rate of pond construction in agricultural settings declined in both Kansas and Ohio, but a new phase of pond construction began, especially in urbanizing areas. Two main purposes have dominated pond construction in the last 2-3 decades: aesthetics/recreation, and stormwater management. As suburban development expanded rapidly into surrounding rural areas, residential construction became more common on larger lots and at lower densities than was typical of the 1960s. With homes being built on lots of 1 hectare or more, there is room to include a pond on the lot. Ponds are attractive amenities for homes in semi-rural settings. At the same time, increased concern about the water quality and flood impacts of urban development has led local regulatory agencies to require construction of stormwater detention basins as part of higher-density suburban developments. Although a quantitative estimate of pond construction for this purpose is not available, it is likely that thousands of ponds are being built annually as part of stormwater management programs. In some areas aquaculture is also an important factor driving construction of ponds.

In order to gain a better understanding of pond distribution over time and space we mapped ponds from aerial photography for several time intervals in two regions of the U.S.: southwest Ohio and eastern Kansas (Figure 2). In both cases we assembled available historic aerial photography from the earliest imagery available (typically 1930s or 1940s) up to the most recent. In Ohio we mapped all the ponds in three counties that represent a transect of agricultural, suburban and urban landscapes. In Kansas we focused on four USGS 1:24,000 quadrangles that represent a range of environments. The Allen SE, Gridley, and Burlington quads are all in areas where livestock raising, particularly cattle grazing, was a dominant activity. The Gridley and Burlington quadrangles represent

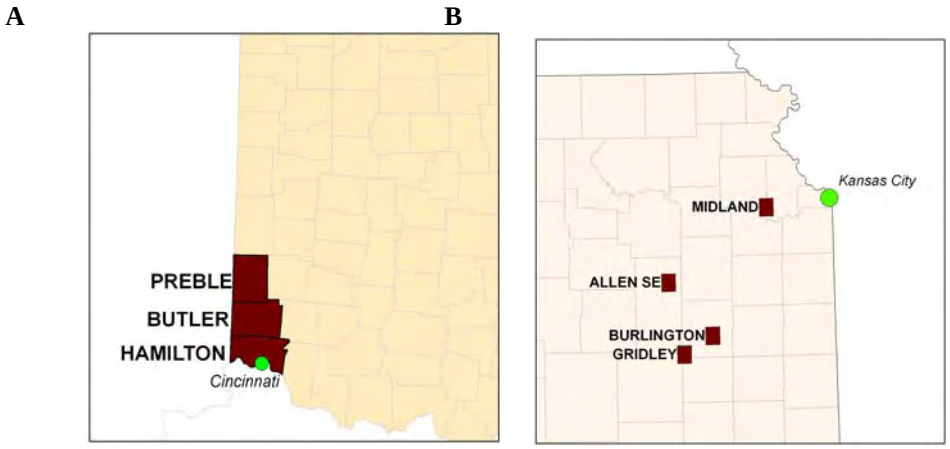


Figure 2 Case study regions where ponds were mapped from aerial photography at multiple time intervals from the earliest available imagery to the most recent. A) Three counties in southwest Ohio. B) Four USGS 1:24,000 quadrangles in eastern Kansas.

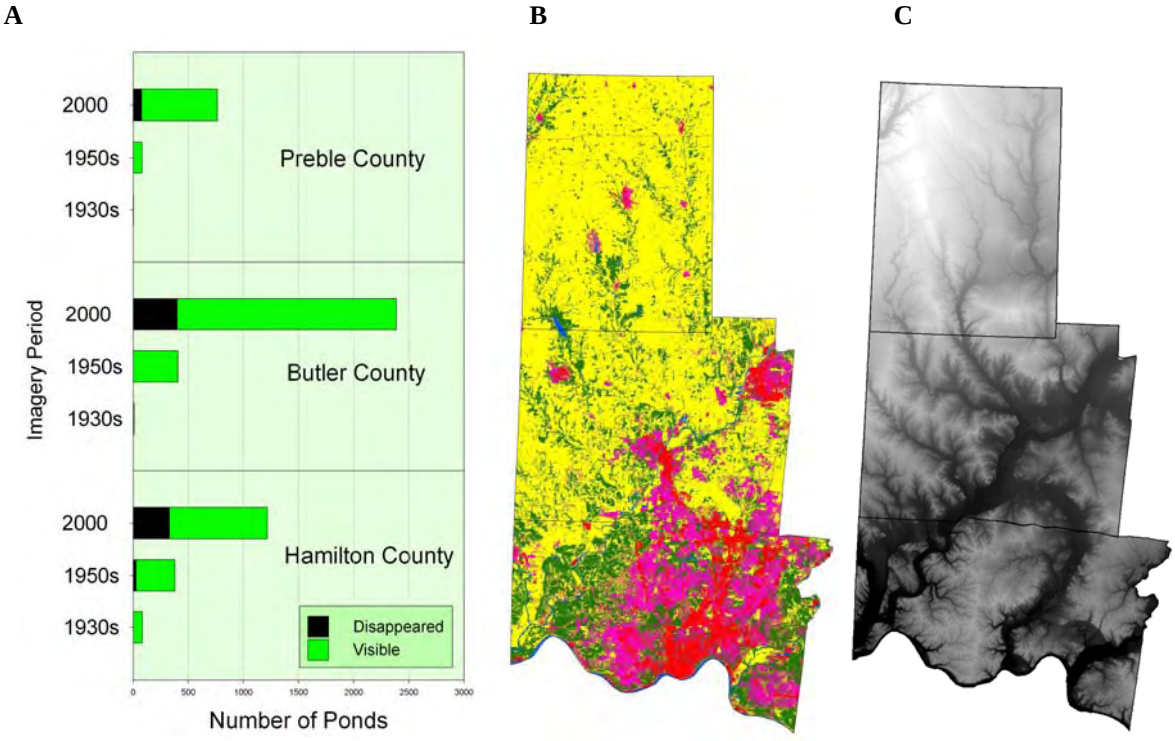


Figure 3 Numbers of ponds at three time periods in three counties in southwest Ohio. The three counties represent a transect from relatively low-relief topography and mostly agricultural land use in Preble County to relatively high relief and mostly urban and forest land use in Hamilton County (metropolitan Cincinnati). A) Pond densities are highest in Butler County, which is intermediate in topography and land use. B) Land use, from the National Land Cover Dataset (NLCD; http://landcover.usgs.gov/nationallandcover/html). Yellow is agricultural, green is forest, magenta is suburban and red is urban. C) Elevation, from USGS 30-meter DEMs. In general local relief increases from north to south, reaching a maximum near the Ohio River and its tributary valleys.

upland and floodplain-dominant landscapes. The Midland Quadrangle is an area which probably had fewer cattle and more row crop agriculture, and today it is in an area of urban growth. We also inventoried all ponds in four Kansas counties using aerial photography, as a comparison to the counts derived from the NLCD database.

In both cases the total number of ponds on the landscape has increased dramatically, from near zero in the earliest aerial imagery to thousands per county today (Figures 3 and 4). The data also show that ponds are dynamic features of the landscape, being both created and destroyed. For example, of a total of 867 ponds that existed in Preble, Butler and Hamilton Counties in the mid-1950s or earlier 810, or 93%, disappeared before 2000 (Figure 3). In the four quadrangles we sampled in Eastern Kansas, 292 of 520 or 57% of ponds disappeared between the first photographic record and 2002-03 (Figure 4). Thus average pond lifespan in these environments is in the range of a few to several decades.Based on the aerial photographic record two processes account for the long-term disappearance of ponds: sedimentation, and replacement with other land uses—principally urban uses. Infilling with sediment is especially common in agricultural areas undergoing accelerated erosion, and is dependent on erosion rates and the ratio of watershed area to pond volume. For example, consider a pond 0.5 hectare in size and averaging 1 m deep, and a drainage area of 80 hectares delivering 2 tons of sediment per hectare per year. Such a pond would fill completely in about 35 years. In areas undergoing significant urban and suburban development, land-use change is responsible for significant pond disappearance as well as construction of new ponds (Figure 5). In southwest Ohio urbanization is the dominant cause in urban and suburban areas, while sedimentation dominates in agricultural areas.

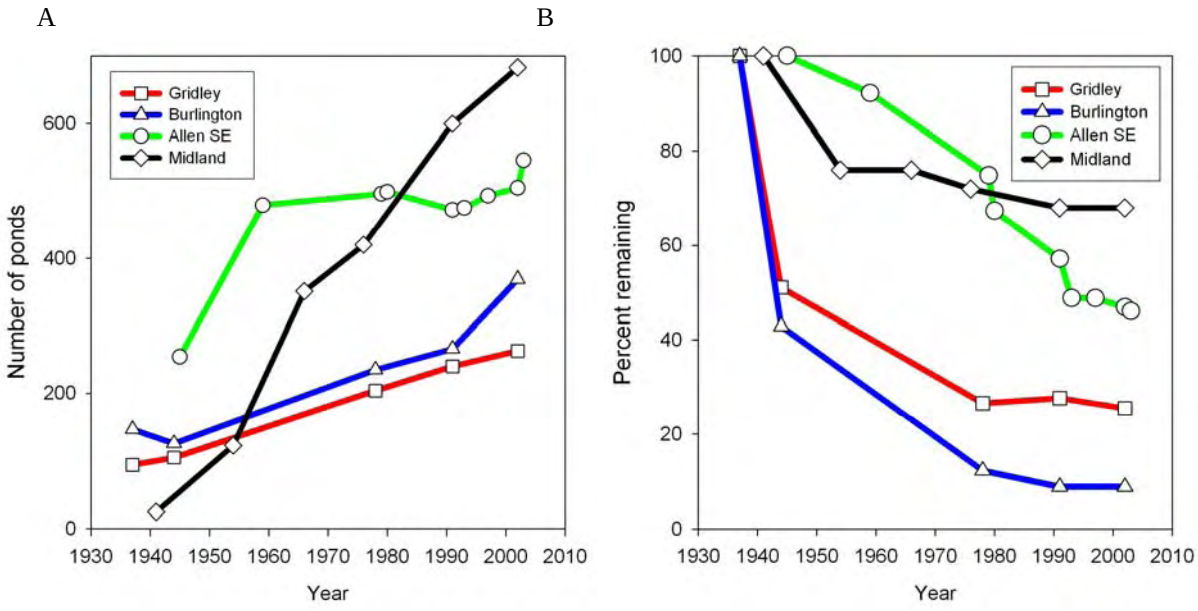


Figure 4 Construction and disappearance of ponds based on aerial photography for four sample quadrangles in eastern Kansas. A) Pond numbers increased through the last 60 years. The drop in pond numbers in the Allen SE quadrangle in the 1980s is attributable to a combination of drought and reduced profits in the cattle industry, which is particularly dominant in that area. In the Midland Quadrangle rates of pond were initially low because row-crop agriculture is more important in this area than in the other quadrangles. Pond construction there has been especially rapid in the last 2-3 decades as a result of urban/suburban development. B) Number of ponds mapped in the earliest aerial photography that remained in successive images for four 1:24,000 USGS quadrangles. The rates of pond disappearance vary considerably among the four quadrangles, but show that many ponds disappear in time scales of 10-50 years. In the Burlington and Gridley quadrangles the rate of pond disappearance was initially high, probably because the initial photography dates from a time when pond-building technology was poorly developed and sedimentation rates were high.

Pond construction is a form of land management and as such is intimately connected to the land use systems existing at any point in time. These systems are themselves linked to technologic, economic, political and cultural factors. A full understanding of the factors controlling pond construction and destruction is thus well beyond the scope of this

paper. However, it is instructive to place the history of pond construction in the context of historic changes in land use and land management, so that we can better understand recent and future trends in pond numbers and condition.

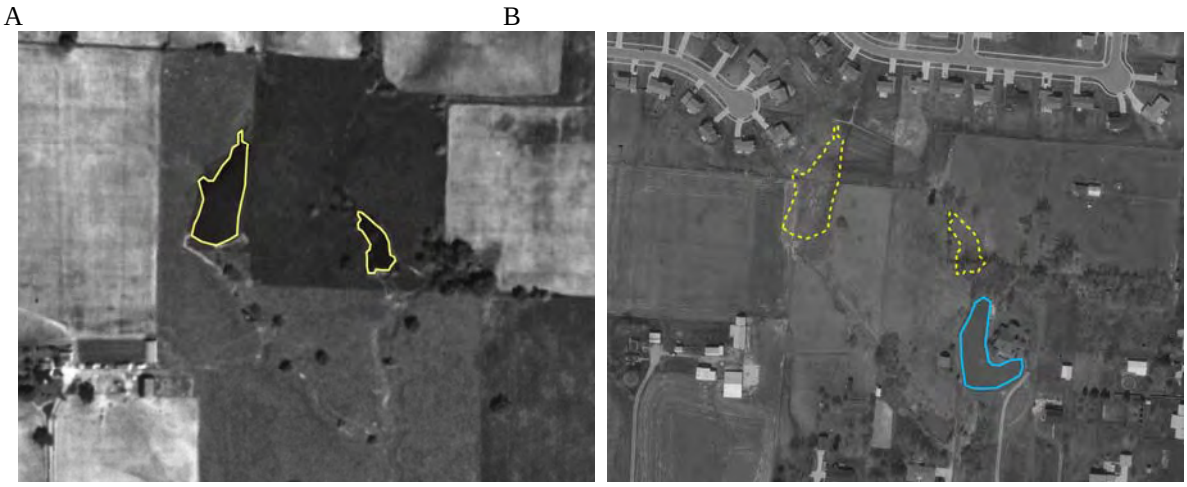


Figure 5 An area of Butler County, Ohio, in 1950 and 2000. A) In 1950 two ponds were present in what was then an agricultural landscape. B) By 2000 those two ponds had disappeared, presumably by sedimentation, and a third had appeared.

SUMMARY AND CONCLUSIONS

Artificial ponds, while individually small, have become so numerous that they represent a profound human alteration of the hydrologic landscape. Their impact is comparable in magnitude to that of larger reservoirs, both in terms of surface area and sedimentation. Because ponds occupy sites with small drainage areas they are close to source-areas for sediment and other substances moving in stormwater runoff, and hence have proportionately higher sedimentation rates than larger reservoirs. They appear to be a major carbon sink.

Ponds are dynamic features of the hydrologic landscape. They have appeared relatively recently—within the last 100 years—and their numbers have increased dramatically in that time period. Pond densities and dynamics are closely tied to both natural and human features of the landscape. The dominant purposes for which ponds are constructed appear to be shifting, but total pond numbers continue to increase.

Ponds that disappear from the landscape cease to be active sinks for sediment and carbon, but they retain the materials that accumulated when they were active. Ponds that remain on the landscape but are dredged also continue to accumulate sediment and associated materials. Although conditions will vary considerably among ponds, our observations indicate that dredged materials are typically buried and stabilized near the site of dredging so that they do not re-enter mass transport systems.

Changing land management upstream of ponds will affect their role as material sinks, with the magnitude and direction of change dependent on local circumstances. In areas where soil conservation technologies are reducing source-area erosion pond sedimentation rates can be expected to decline. In suburban areas ponds may temporarily serve as sinks for construction-period erosion, but thereafter sediment inputs are probably slow and pond lifespan is likely long. On the other hand, increased runoff from urban land will tend to mobilize sediment in and adjacent to streams, increasing sediment loads to ponds. Soil conservation and the shift in locus of pond construction from agricultural to suburban settings are likely to reduce rates of sediment accumulation in ponds.

The downstream effects of ponds are unclear. To the extent they reduce the magnitude of flood peaks they may help stabilize stream channels. On the other hand, reductions of sediment load caused by sedimentation in ponds may

encourage net erosion downstream. In any case, because of their high density and upstream position in the hydrologic system ponds will continue to exert a significant influence on biogeochemical cycles.

REFERENCES

Agricultural Stabilization and Conservation Service (1981). Agricultural conservation program: 45-year statistical summary, 1936 through 1980. Washington, D.C.: U.S. Dept. of Agriculture, Agricultural Stabilization and Conservation Service.

Carriquiry, J.D., and Sanchez, A. (1999). "Sedimentation in the Colorado River delta and upper Gulf of California after nearly a century of discharge loss," Marine Geology, 158, 125-145.

Collier, M., Webb, R., and Schmidt, J. (1997). Dams and rivers: Primer on the downstream effects of dams. U.S. Geological Survey Circular 1126.

Dean, W.E., and Gorham, E.(1998). "Magnitude and significance of carbon burial in lakes, reservoirs, and peatlands," Geology, 26, 535-538.

Graf, W. (1999). "Dam Nation: A geographic census of American dams and their large-scale hydrologic impacts," Water Resources Research, 35, 1305-1311.

Helms, D. (1992). Readings in the history of the Soil Conservation Service. U.S. Dept. of Agriculture, Soil Conservation Service, Economics and Social Sciences Division, NHQ, Historical Notes 1, 30pp.

Meade, R.H. & Trimble, S.W. (1974). "Changes in sediment loads in rivers of the Atlantic drainage of the United States since 1900," In Effects of Man on the Interface of the Hydrological Cycle with the Physical Environment. International Association of Hydrological Sciences, 113, 99-104.

Mulholland, P.J., and Elwood, J.W. (1982). "The role of lake and reservoir sediments as sinks in the perturbed global carbon cycle," Tellus, 34, 490-499.

Renwick, W.H., Smith, S.V. Bartley, J.D., and Buddemeier, R.W. (2005). "The Role of impoundments in the sediment budget of the conterminous United States," Geomorphology, 71, 99-111.

Ritchie, J.C. (1989). "Carbon content of sediments of small reservoirs," Water Resources Bulletin, 25, 301-308.

Smith, S.V., Renwick, W.H., Buddemeier, R.W., and Crossland C.J. (2001). "Budgets of soil erosion and deposition for sediments and sedimentary organic carbon across the conterminous United States.,"Global Biogeochemical Cycles, 15, 697-707.

Smith, S.V., Renwick, W.H. Bartley J.D., and Buddemeier R.W. (2002). "Distribution and significance of small, artificial water bodies across the United States landscape," The Science of the Total Environment, 299, 21-36.

Stallard, R.F. (1998). "Terrestrial sedimentation and the carbon cycle: coupling weathering and erosion to the carbon cycle," Global Biogeochemical Cycles, 12, 231-257.

Steffen, L.J. (1996). "A reservoir sedimentation survey information system – RESIS," Proceedings of the Sixth Federal Interagency Sedimentation Conference, Interagency Advisory Committee on Water Data, Washington. pp I29-I36.

Williams, G.P., and Wolman, M.G. (1984). Downstream effects of dams on alluvial rivers. USGS Professional Paper 1286.

MODELING SUSPENDED SEDIMENT AND WATER TEMPERATURE DETROIT LAKE, OREGON

Annett B. Sullivan, Hydrologist, USGS, Portland, OR, annett@usgs.gov; Stewart A. Rounds, Hydrologist, USGS, Portland, OR, sarounds@usgs.gov; Mark A. Uhrich, Hydrologist, USGS, Portland, OR, mauhrich@usgs.gov; Heather M. Bragg, Hydrologic Technician, USGS, Portland, OR, hmbragg@usgs.gov

Abstract: A water temperature and suspended sediment model of Detroit Lake, Oregon was constructed with CE-QUAL-W2 for 2002 and 2003. Input data for the model included lake bathymetry, meteorology, lake outflows, and tributary inflows, water temperature, suspended sediment concentration and total dissolved solids. An important model parameter is the light extinction coefficient. It is affected by suspended sediment in the lake and in turn affects water temperature and the lake heat budget. Three different methods of determining the light extinction coefficient for Detroit Lake are compared; one is derived from light meter measurements taken through the water column, the other two are based on measured Secchi depths. These data were collected at three sites in Detroit Lake at approximately three week intervals from April 2002 through October 2003. A seasonal variation in the light extinction coefficient was observed, with highest values in winter and lowest values in early spring and early fall. Algal blooms also produced higher light extinction coefficients in summer. Light extinction coefficients were similar between all three lake sampling sites when values were low; at higher values, there were larger differences between sites due to the heterogeneity of tributary sediment input and patchiness of algal blooms. The Secchi method, in particular the Williams et al. (1980) equation, was found to be an acceptable alternative to the light meter method for determining Detroit Lake extinction coefficients. The extinction coefficient for Detroit Lake water without suspended sediment (K_{H_2O}) was determined to be 0.21 m^{-1}.

INTRODUCTION

Detroit Lake (Figure 1) is a reservoir on the North Santiam River, 50 miles east of Salem, Oregon. The dam, a 463-foot high concrete structure, was finished in 1953, and the reservoir stores 455,000 acre-ft at full pool. It is used for recreation, flood control, irrigation, power generation and improvement of downstream navigation. The City of Salem takes its primary supply of drinking water from the North Santiam River approximately 28 miles downstream of Detroit Lake. High concentrations of suspended sediment in the river can impair the city's water filtration system, requiring the city to shut off its water intake or add coagulant during some large storms and periods of sustained high levels of turbidity in Detroit Lake. The U.S. Geological Survey has cooperated with the City of Salem since 1998 to monitor and study sediment and turbidity in the North Santiam watershed.

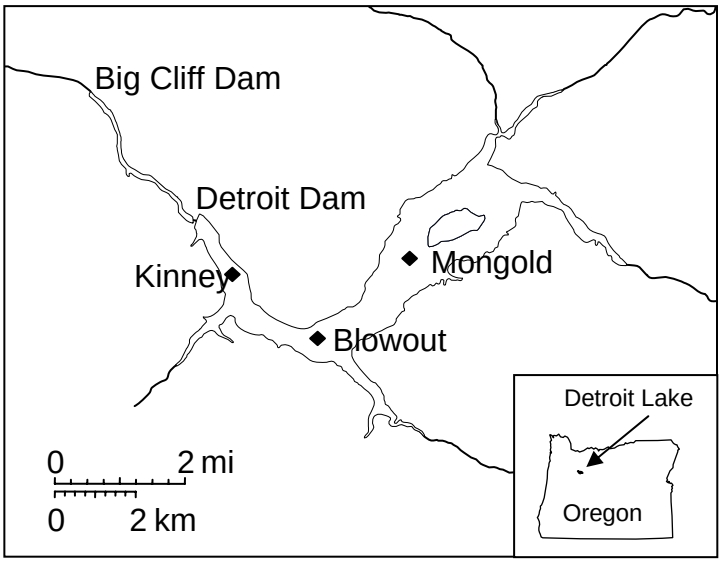


Figure 1 Map of Detroit Lake, Oregon showing the three lake sampling sites.

To help understand the transport and fate of sediment in Detroit Lake, a water temperature and suspended sediment model of the reservoir was constructed with CE-QUAL-W2 version 3.12, a two-dimensional, laterally averaged, hydrodynamic and water-quality model from the U.S. Army Corps of Engineers. Input data for the model included lake bathymetry, meteorology, lake outflows, tributary inflows, and tributary water temperature, suspended sediment and total dissolved solids. Suspended sediment in the tributary inflows was divided into three size classes, based on turbidity-suspended sediment relations developed in Uhrich and Bragg (2003).

One important parameter in reservoir temperature and sediment models is the light extinction coefficient, a measure of how light is attenuated through the water column. Higher light extinction coefficients mean that there is less light transmitted or that the water is less transparent. The coefficient is affected by suspended sediment and other dissolved and particulate materials in the water column, and in turn affects the heat budget and water temperatures. A low light extinction coefficient allows light to penetrate into deeper water, and less heat is lost in surface exchange. With higher light extinction coefficients, lake surface temperatures increase, deep waters stay cooler, the depth of the mixed layer decreases, and the total heat content of a lake decreases (Hocking and Straskraba, 1999).

There are several approaches to determining the light extinction coefficient. For Detroit Lake, the light extinction coefficient was determined by three methods: one method using a light meter, the other two using a Secchi disk. The light meter method is generally considered more accurate, but Secchi disk methods use less expensive equipment and only require one measurement versus many for the light meter method. In this paper, we compare results from the three methods and examine the seasonal and spatial variation in light extinction coefficients in Detroit Lake from April 2002 through October 2003.

METHODS

Data Collection: Measurements of light intensity in the water column as well as Secchi depths were part of the USGS monitoring program of Detroit Lake from April 2002 through October 2003, and were collected approximately every three weeks. Measurements were made from a boat at three sites in Detroit Lake: Mongold, Blowout, and Kinney (Figure 1).

Light meter measurements were made with a Licor LI-193SA spherical quantum sensor. A light intensity reading was first taken at the surface, then the instrument was lowered through the water column and readings were taken at approximately 1 m intervals until the readings were very low and constant. An example light profile is shown in Figure 2.

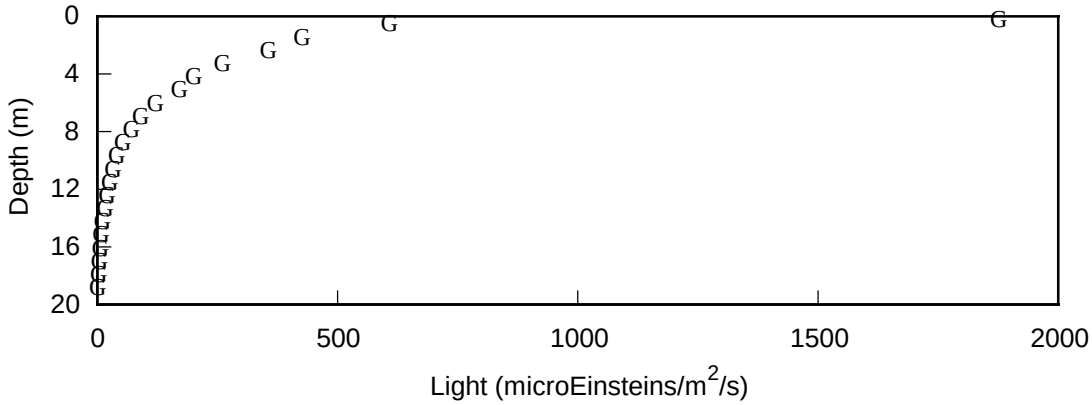


Figure 2 Light profile measured at Kinney in Detroit Lake on May 28, 2003.

Secchi depths were determined by lowering a metal Secchi disk with black and white quadrants into the water and noting the deepest depth at which it could still be distinguished. Typically, multiple measurements were taken and averaged.

Calculation of Light Extinction Coefficients Using light meter data, light extinction coefficients were calculated with the Beer-Lambert law:

$$I_z = I_o e^{-Kz} \tag{1}$$

or

$$\ln\left(\frac{I_z}{I_o}\right) = -Kz \tag{2}$$

where

I_z = light intensity at depth z

I_o = light intensity at water surface

K = extinction coefficient (m^{-1})

z = water depth measured from surface (m)

Using Secchi depth data, light extinction coefficients can be calculated with several equations. Two of these equations were applied to the Detroit Lake data. One commonly applied method is the Poole and Atkins equation (Poole and Atkins, 1929; Isdo and Gilbert, 1974):

$$K = \frac{1.7}{z_S} \tag{3}$$

where

z_S = Secchi depth

The other Secchi depth equation, referenced by the CE-QUAL-W2 manual, is by Williams et al. (1980):

$$K = \frac{1.1}{z_S^{0.73}} \tag{4}$$

All three of these methods calculate a light extinction coefficient that considers together the effect of all constituents (dissolved constituents, algae, suspended solids) that affect light extinction. The model CE-QUAL-W2 separates out these constituents as follows:

$$K = K_{H_2O} + K_{ISS} + K_{POM} + K_a \tag{5}$$

where

K_{H_2O} = extinction from water and dissolved constituents

K_{ISS} = extinction from inorganic suspended sediments

K_{POM} = extinction from suspended particulate organic matter

K_a = extinction from algae

To determine K_{H_2O} for Detroit Lake, a regression was calculated between light extinction coefficients and suspended sediment concentration (which includes inorganic suspended sediment, particulate organic matter and algae) in the top 10 m of the water column; K_{H_2O} is the extinction coefficient when suspended sediment concentration is zero. Measured suspended sediment concentration was determined from detailed turbidity profiles taken at the same time as light measurements, and regressions between suspended sediment and turbidity in Detroit Lake.

RESULTS

Results from the light meter method for the three Detroit Lake sites are shown in Figure 3. Light extinction coefficients were highest in December through February when winter storms brought suspended material into the lake. There were also some higher extinction coefficients in summer, probably due to algal blooms. Dissolved oxygen and pH profiles provided additional evidence for algal blooms in Detroit Lake at that time of year. The lowest light extinction coefficients occurred in late spring and early fall. When light extinction coefficients were low, there was very little difference in coefficients between sites. When light extinction coefficients

were higher, there were greater differences between the three sites in Detroit Lake, probably due to the spatial heterogeneity of sediment input from tributaries and patchiness of algal blooms.

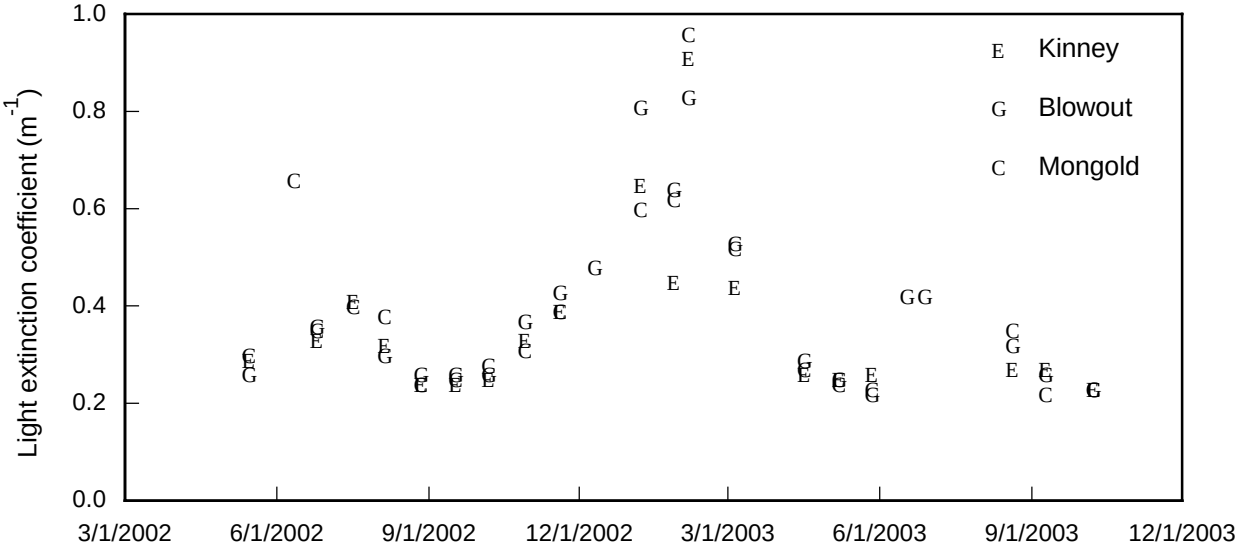


Figure 3 Light extinction coefficients at Detroit Lake sites using the light meter method.

Results of the Secchi methods were compared to results from the light meter (Figure 4) for the same date and location. At low values of the light extinction coefficient, both Secchi methods produced light extinction values close to those determined by the light meter method. At higher extinctions, the Williams et al. (1980) method produced values closer to those of the light meter method.

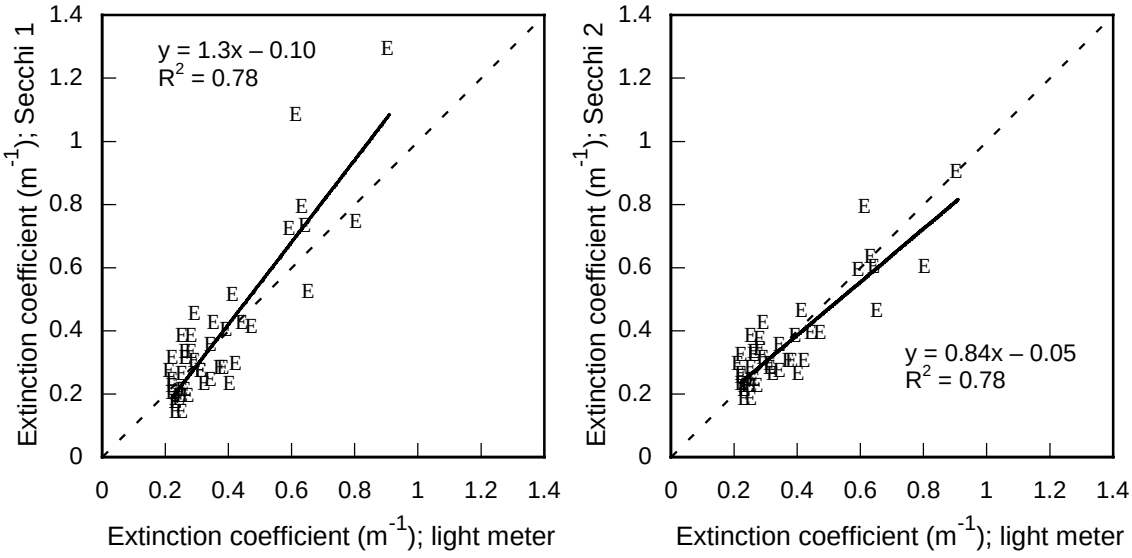


Figure 4 Light extinction coefficients by Secchi method 1 (Poole and Atkins, 1929) and Secchi method 2 (Williams et al., 1980) compared to those determined by the light meter method for the same date and location in Detroit Lake. The dashed line represents a one-to-one ratio.

The extinction coefficient for water, K_{H_2O}, was determined to be 0.21, 0.15, and 0.22 m^{-1} with the light meter, Poole and Atkins (1929), and Williams et al. (1980) methods, respectively. The extinction coefficients for the Williams et al. (1980) Secchi method and the light meter method were most similar.

SUMMARY

Light extinction coefficients are affected by suspended sediment and are critical for modeling water temperature in lakes. Light extinction coefficients in Detroit Lake were highest in winter due to tributary sediment input during storms, and also high during summer algal blooms. Low extinction coefficients were present in Detroit Lake in early spring and early fall. Light extinction coefficients were determined by three methods for purposes of comparison. The light meter method is generally thought to be most accurate, but the Secchi method, especially using the Williams et al. (1980) equation, was found to be an acceptable surrogate for the light meter method in Detroit Lake, and could be used if, for example, equipment or time was scarce. The extinction coefficient for water, 0.21 m^{-1} determined by the light meter method, was used in Detroit Lake water temperature and suspended sediment modeling.

ACKNOWLEDGEMENTS

Field data for this project was collected by a number of USGS technicians. Funding for this cooperative project was provided by the City of Salem and the USGS.

REFERENCES

Cole, T.M., Wells, S.A. (2002). CE-QUAL-W2: A two-dimensional, laterally averaged, hydrodynamic and water quality model, version 3.1. U.S. Army Corps of Engineers, Instruction Report EL-02-1, [variously paged].

Hocking, G.C., Straskraba, M. (1999). "The Effect of Light Extinction on Thermal Stratification in Reservoirs and Lakes," International Review of Hydrobiology, 84(6), pp 535-556.

Idso, S.B., Gilbert, R.G. (1974). "On the universality of the Poole and Atkins Secchi disk-light extinction equation," Journal of Applied Ecology, 11, pp 399-401.

Poole, H.H., Atkins, W.R.G. (1929). "Photo-electric measurements of submarine illumination throughout the year," Journal of the Marine Biological Association, 16, pp 297-324.

Uhrich, M.A., Bragg, H.M. (2003). Monitoring instream turbidity to estimate continuous suspended-sediment loads and yields and clay-water volumes in the upper North Santiam River Basin, Oregon, 1998-2000. U.S. Geological Survey, Water-Resources Investigations Report 03-4098, 43 p.

Williams, D.T., Drummond, G.R., Ford, D.E., Robey, D.L. (1980). "Determination of light extinction coefficients in lakes and reservoirs," In: Stefan, H.G. (Ed.), Proceedings of the Symposium on Surface Water Impoundments, June 2–5. Minneapolis, Minnesota. American Society of Civil Engineers, New York, pp 1329–1335.

ADAPTIVE MANAGEMENT CASE STUDIES FOR RIVER ENGINEERING AND RESTORATION PROJECTS ON THE MIDDLE RIO GRANDE, NEW MEXICO

Mark S. Nemeth, Hydraulic Engineer, U.S. Bureau of Reclamation, Albuquerque, NM, mnemeth@uc.usbr.gov; Kristi-Irene Smith, Hydraulic Engineer, U.S. Bureau of Reclamation, Albuquerque, NM, ksmith@fciol.com

Abstract: Applying adaptive management principles can provide flexibility to adjust to changing hydrologic and geomorphic conditions during and after construction of river rehabilitation projects. For three projects constructed by the Bureau of Reclamation along the Rio Grande in New Mexico, use of adaptive management resulted in a reduction of project costs and enhancement of wildlife habitat. Summaries of adaptive management practices are presented for each of the three projects. Primary project purposes are erosion control, improved water conveyance efficiency, restoration of fluvial processes, and wildlife habitat improvement. Activities associated with adaptive management practices encompass vegetation management, relocation of project features in response to changing groundwater levels, management of erosion and sedimentation, and modification of regulatory permits. Effective adaptive management requires timely response to unexpected developments and consideration of intermediate project conditions. It also requires that project participants understand adaptive management concepts and cooperate during implementation.

An erosion control and restoration project begun in 2000 at the Pueblo of Santa Ana includes a channel-wide bed elevation control structure, extensive floodplain lowering, and realignment of approximately 7,000 feet of river channel. An ongoing issue with this project has been the disposal of over 100,000 cubic yards of alluvial sediment generated by the floodplain lowering process. This material was originally placed adjacent to the realigned pilot channel with the intent that it would be removed by subsequent high flows during spring runoff periods. However, drought conditions have generally prevailed since the project's inception, so removal of this sediment has been much slower than expected. During the few periods when high flows have occurred, construction crews have been directed to continually reposition the material, concentrating it at points where erosion was most active,. As of late 2005, approximately two-thirds of the material has been removed. Another adaptive management action was redesigning two oxbow wetland areas to be intermittently flooded instead of being year-round stagnant pools when it was determined that the original design was not meeting habitat restoration goals. Finally, ongoing modifications to project features have been carefully planned to accommodate and sustain the development of cottonwood seedlings that were established by natural seeding due to an unintended breach of a berm in spring 2001.

At a restoration project begun in 2001 at the Bosque del Apache National Wildlife Refuge, the intent was to widen a 6,000-foot reach of the Rio Grande from an initial width of about 150 feet to 600 feet to provide improved habitat for the endangered Rio Grande silvery minnow. Owing partially to the absence of large spring runoff flows following the project's initial construction, the channel was unexpectedly slow to widen. In this case, patience and understanding from the Refuge management and other stakeholders was important in avoiding premature conclusions that the project had failed. The channel banklines were periodically cleared of vegetation to prevent them from stabilizing before larger flows occurred. Eventually, during the high spring runoff of 2005, the channel widened considerably, though not to the full 600-foot design width. Subsequent investigation revealed that a previously wider reach immediately upstream had narrowed because of changes in hydrologic conditions. This led to the conclusion that it was unrealistic to expect that the project reach would achieve the initial restoration goals; the final width would likely fall somewhere between the initial 150 feet and the intended 600 feet. It was decided that the remaining width would be managed to encourage development of desirable native vegetation in an area that had previously been monotypic saltcedar.

Construction began in 2000 on a temporary channel through the delta of Elephant Butte Reservoir to maintain connectivity between the Rio Grande and the upstream end of the reservoir pool. The project was seven miles long and took several years to construct, owing to its size and the difficult working conditions in the delta. Upon completion of the project, it was clear that maintaining a 250-foot-wide channel, as specified in the original design, would be excessively time consuming and costly. Field observations indicated that the channel was naturally developing a diverse habitat system of point bars and islands. An adaptive management plan was developed around the channel’s natural conditions to minimize maintenance while preserving the design capacity and flow connectivity to the reservoir pool. To that end, the plan called for dredging a narrower channel around the naturally

developed point bars and islands and for clearing vegetation from point bars and islands to prevent permanency of those features.

QUANTITATIVE LINKAGES BETWEEN SEDIMENT SUPPLY, STREAMBED FINE SEDIMENT, AND BENTHIC MACROINVERTEBRATES IN THE KLAMATH MOUNTAINS, NORTHERN CALIFORNIA

Matthew R. Cover, Department of Environmental Science, Policy and Management, University of California, Berkeley, CA, mcover@nature.berkeley.edu; Christine L. May, Department of Earth and Planetary Science, University of California, Berkeley, CA, cmay@seismo.berkeley.edu; William E. Dietrich, Department of Earth and Planetary Science, University of California, Berkeley, CA; bill@seismo.berkeley.edu; Vincent H. Resh, Department of Environmental Science, Policy and Management, University of California, Berkeley, CA; vresh@nature.berkeley.edu

Abstract: Predicting the cumulative watershed effects of forest management on stream ecosystems requires a quantitative understanding of the linkages between hillslope sediment supply, streambed response, and biological effects. Here we examine the relationships between sediment supply, streambed fine sediment, and benthic macroinvertebrate assemblages in six streams in the Klamath Mountains of Northern California. Sediment supply has increased by 2-4 times over background rates in some drainage basins. Reach-averaged V*, a measure of pool infilling by fine sediment that ranged from 5-20%, was strongly correlated with sediment supply, fine sediment in riffles, and excess transport capacity. Two biological metrics, Chironominae/Chironomidae (-, sign indicates response to fine sediment) and Orthocladiinae/Chironomidae (+), and four taxa, *Arctopsyche* (-), *Attenella delantala* (+), Chironominae (-), and Oligochaetea (+), responded as predicted in previous studies and were strongly related to fine sediment on the surface of the streambed. Many biological metrics commonly used in biomonitoring, such as taxonomic richness, exhibited poor or unexpected relationships with fine sediment. The quantitative relationships described in this study add to our understanding of the linkages between hillslopes, stream channels, and aquatic biota and identify areas where process-based understanding can be improved.

Key Words: sediment supply, V*, fine sediment, benthic macroinvertebrates, substrate, mountain streams, gravel-bed streams, cumulative watershed effects.

INTRODUCTION

Cumulative watershed effects are significant, adverse influences on water quality and biological resources that arise from the ways watersheds function and the ways that disturbances within a watershed can be transmitted and magnified within channels and riparian habitats downstream of disturbed areas (Dunne et al. 2001). Effects related to accelerated rates of erosion and sediment delivery to streams are of particular importance in mountainous, forested watersheds. In order to improve capabilities to predict cumulative watershed effects the quantitative linkages between sediment supply, channel conditions, and stream biota need to be better understood.

In this paper we examine the relationships between sediment supply, streambed fine sediment, and benthic macroinvertebrate assemblages in streams in the Klamath Mountains of Northern California. The objective of this study was to examine if increased rates of sediment supply result in increased levels of streambed fine sediment, and if this in turn is correlated with altered benthic assemblages. Additionally, we attempted to identify the quantitative relationships between hillslopes, streambeds, and biota, in order to examine whether there are thresholds at which increased sediment supply results in significant changes in stream condition and biotic communities. We examined the hypothesis that high sediment supply to mountain stream channels leads to high levels of fine sediment in the streambed, resulting in a reduction in benthic macroinvertebrate diversity and altered community composition.

METHODS

Study Area: Sampling of channel conditions and benthic macroinvertebrates was performed in 6 streams in the Klamath National Forest (KNF) in fall 2003 (Table 1). Streams were selected based on the following criteria: (1) moderate gradient (2-4%), (2) gravel and cobble substrate, (3) bedrock that produced abundant fine sediment (predominantly granitics), (4) no recent channel-scouring debris flows, (5) known anadromous fisheries, and (6) minimal human land use other than forest management activities. The sites were selected to reflect the endpoints of sediment supply, based on qualitative assessments of streambed fine sediment by KNF personnel and sediment

supply models developed by KNF geologist Juan de la Fuente (see below). Study reaches were 0.5 – 2.0 km in length, and contained a minimum of 15 pools.

Sediment Supply: The KNF has developed two models of sediment delivery to stream channels, one to predict episodic inputs from landslides and one to predict chronic inputs of fine sediment. The fine sediment model uses estimates of surface erosion from the Universal Soil Loss Equation based on the spatial distribution of roads, timber plantations, wildfires, and terrain and soil types. The landslide sediment supply model is based on empirical relationships derived from air photo landslide assessments in the Salmon River subbasin during the period 1970 – 1975, a moderately wet period following a period of intensive timber harvest across the forest (de la Fuente and Haessig 1993). Future sediment delivery is predicted for each of 11 geomorphic terrain types, based on the frequency and size of landslides during the reference period. Data from the Salmon River drainage are then extrapolated using GIS to predict sediment delivery rates throughout the west side of the KNF. Risk ratios, defined as the ratio of anthropogenic to background rates of sediment supply divided by a constant (2 for the landslide model and 8 for the USLE model), were used with the qualitative assessments of fine sediment to categorize each site as high or low sediment supply (Table 1). Thus, sediment supply was characterized using two quantitative variables (the USLE model surface erosion prediction and the landslide sediment delivery prediction) and one quantitative categorical variable (high/low sediment supply).

Table 1 Channel slope and estimated sediment supply conditions for the six study streams.

Stream	Slope (%)	Landslide Risk Ratio	USLE Risk Ratio	Qualitative Fine Sediment	Sediment Supply Category
Elk Creek	4.3	0.22	0.00	Low	Low
Little North Fork Salmon River	2.5	0.54	0.19	Low	Low
Upper South Fork Salmon River	1.6	0.07	0.03	Low-Medium	Low
Beaver Creek	2.3	1.24	1.01	Medium-High	High
Grouse Creek	2.8	1.98	1.00	Medium-High	High
Taylor Creek	3.4	0.39	0.39	High	High

Streambed Measurements: V* measurements were made in every pool in the study reach, following the methods of Hilton and Lisle (1993). Briefly, V* is a measure of the volume of pools filled in by fine sediment, and is determined by measuring the water depth and the depth of fine sediment deposited at multiple locations on the bottom of a pool (Lisle and Hilton 1999). V* values from all of the pools in a reach were averaged to obtain one reach-wide V* value.

The proportion of fine sediment on the surface of the bed was measured in four riffles in each reach. A modified soccer net (9'x 4' with 5" grid, containing 220 intersections) was used to determine the spacing of measurements. At each grid intersection a chaining pin was placed on the bed and the presence or absence of fines at the tip of the pin was recorded. Fine sediment measurements were made along three transects in each riffle, in the same locations where macroinvertebrates were sampled. For each reach we determined the percentage of the bed covered by fine sediment in each of four riffles.

Grain size was assessed in each riffle via transect-based pebble counts (Bunte and Abt 2001). Particle diameter was measured every 0.3 m along transects using a gravelometer. The number and spacing of transects was determined at each riffle to obtain a minimum of 200 grain measurements. The embeddedness of each grain was characterized using a three category qualitative scale of the effort required to remove the grain: (1) "pick" particles are unembedded, loose particles on the surface of the bed, (2) "pluck" particles are moderately embedded, and (3) "pry" particles are highly embedded by fine sediment. We are primarily concerned with the embeddedness of coarse gravel and cobble; thus, for each riffle we calculated the percentage of 16-256 mm grains that were sitting freely on the bed, moderately embedded, and highly embedded.

Benthic Macroinvertebrate Sampling: Benthic macroinvertebrates were sampled from the same locations where fine sediment was measured. A timed 4 minute sample was made at each of 3 transects per riffle by disturbing the substrate upstream of a 500 micron mesh D-frame kick net. The 3 transect samples were composited into one sample container. Samples were elutriated to separate the organic and inorganic portions of the sample, and large

leaves and woody debris was removed from the organic portion of the sample. The inorganic portion of the sample was carefully examined for benthic organisms such as cased caddisflies, which were added to the organic portion of the sample. The remainder of the organic sample was preserved in 95% ethyl alcohol.

In the laboratory benthic invertebrates were removed from the sample under a dissecting microscope at 10x magnification. The subsampled fraction ranged from 7-100%, and the number of identified organisms ranged from 541 to 1443. Organisms were identified to the lowest practical taxonomic level, usually genus or species, except for Chironomidae (subfamily), Collembola (order), Trombidiformes (order), Oligochaetes (class), Ostracoda (class), Turbellaria (class), and Nemata (phylum).

For analyzing relationships between individual taxa abundances and measures of fine sediment we excluded taxa that were present at less than half the sites or 40% of the samples. From the taxonomic abundance data we calculated 58 common biological metrics, including measures of richness, abundance, diversity, functional feeding groups, and pollution tolerance. To understand how altered benthic assemblages could affect prey availability for salmonids, we classified taxa by their availability to benthic-feeding fish. Following Suttle et al. (2004), each invertebrate taxa was classified as burrowing, armored, or vulnerable, based on sources of life history information (Merritt and Cummins 1996).

Statistical Analyses: We tested the hypothesis that high sediment supply is related to high levels of streambed fine sediment using three approaches. First, we examined whether measures of streambed fine sediment (V*, surface fine sediment, and embeddedness) were higher at the qualitatively ranked "high" sediment supply sites than the "low" sites using the nonparametric Mann-Whitney test ($\alpha = 0.10$ to increase power). Next, we examined whether there was a positive relationship between quantitative predictions of sediment supply (from the USLE and landslide models) and reach-averaged measures of streambed fine sediment (V*, riffle surface fine sediment, and embeddedness). Here we used linear regression to test whether the slope of the line was greater than zero (one-tailed, $\alpha = 0.05$). Finally, since V* has been shown to be a useful predictor of sediment yield (Lisle and Hilton 1999), we examined whether V* was positively related to riffle surface fine sediment and embeddedness using linear regression. No data transformations were required to satisfy criteria for normality and homoscedasticity of residuals.

To examine relationships between benthic macroinvertebrates and fine sediment we began by reviewing the available literature on this topic, with a focus on studies from the Pacific Northwest, USA. We identified relationships of three types (Waters 1995): (1) correlations between the presence or abundance of individual taxa with substrate size (e.g. grain size preferences), (2) changes in community metrics and taxa abundance following experimental additions of fine sediment, and (3) descriptive changes in taxonomic composition following changes in substrate conditions (Table 2). We examined each of the hypotheses identified in the literature by viewing bivariate plots of the biological variables versus riffle surface fine sediment. We choose not to examine biological variables relative to V* or embeddedness because V* is a reach-averaged value (n=6) and is well correlated with riffle surface fine sediment, and embeddedness is poorly correlated with any of the other measures of sediment supply or fine sediment. We used linear regression to test the significance of the hypothesized relationships between biological metrics or abundance of individual taxa and surface fine sediment (one-tailed, $\alpha = 0.05$). As the analysis progressed it became clear that many of the relationships between individual macroinvertebrate taxa and fine sediment were sub-optimally characterized by linear regression. Thus, in addition to linear regression we used partitioned linear regression, or factor-ceiling analysis (Thomson et al. 1996). Partitioned linear regression is a method using successive regressions through a cloud of data. The choice of the upper quantile is arbitrary; we used the upper quartile (75%) as a compromise between ability to identify the upper ceiling of the distribution and relatively few data points.

All of the tests described above are considered independent of one another, since individual hypotheses were made for each statistical test. The second phase of our analysis included identification of relationships between sediment and biological variables that were not explicitly tested above. Since these were multiple unplanned tests (two-tailed), the experiment-wise false positive rate ($\alpha_e = 0.05$) was adjusted using the Bonferroni Criterion, whereby the false positive rate for individual tests was $\alpha = 0.001$.

RESULTS AND DISCUSSION

Linkages Between Sediment Supply and Streambed Fine Sediment: Reach-averaged V* was significantly higher in streams judged to have high sediment supply (0.141 ± 0.029 (Mean $\pm$ SE)) than streams with low sediment supply (0.064 ± 0.008) (Mann-Whitney, $\alpha = 0.10$). Similarly, bed surface fine sediment was also significantly greater in streams with high sediment supply ($14.0\% \pm 2.1\%$ vs. $7.5\% \pm 1.9\%$). Thus, there are significant, measurable differences in streambed fine sediment levels between basins in the study area that were chosen as end-members of sediment supply. The three embeddedness categories, however, exhibited similar values at sites with high and low sediment supply.

Quantitative estimates of surface erosion from the USLE erosion model exhibited marginally significant positive linear relationships with V* ($p = 0.047$, $r^2 = 0.55$) and surface fines ($p = 0.052$, $r^2 = 0.52$), but were poorly related to measures of embeddedness. Estimates of sediment delivery from the landslide model exhibited positive relationships with V* and surface fines that were not statistically significant ($p = 0.08$ and $p = 0.21$, respectively). Fine sediment delivery in the USLE model is primarily a factor of road density, while the landslide model uses extrapolations of empirical observations of landslide delivery volumes in various terrain types, but does not explicitly consider roads. Since landslides in forested watersheds are often associated with roads, by accounting for watershed road density the USLE model may reflect both surface erosion and, indirectly, landslide delivery of sediment.

All three embeddedness categories were uncorrelated with categorical and model-based sediment supply estimates, as well as bed surface fine sediment. Of the three in-stream measures of fine sediment, V* and bed surface fine sediment reflect increased sediment supply fairly well while embeddedness measures were poorly related. Gravel and cobble embeddedness, as measured in this study, may reflect both embeddedness from fine sediment as well as the interlocking of grains with other large particles, and thus may not be the best measure of interstitial crevices.

Lisle and Hilton (1999) described a logarithmic increase in watershed sediment yield with increasing V*. Based on their relationship between V* and sediment yield, the range of V* values in this study implies at least an order-of-magnitude difference in basin sediment yield between the sites with the highest and lowest V*. Reach-averaged V* values exhibited a strong, statistically-significant linear relationship with bed surface fine sediment ($p = 0.016$, $r^2 = 0.72$) (Fig. 1). The linear regression model predicts approximately a 1:1 positive relationship (slope $= 76.5 \pm 23.8$) between volume of pools filled with fine sediment and surface area of riffles covered by fine sediment. Alternatively, the data also suggests the possibility of a riffle-surface fine sediment threshold near 15%, above which increases in sediment supply continue to cause infilling of pools but do not cause increased coverage of riffle surfaces (Fig. 1). As the volumetric fraction of sand in the bed increases to between 10 – 30%, pore spaces between coarser sediments can become completely filled in, creating localized patches of fine grained sediment (Wilcock and Kenworthy 2002). Based on our observations of streams in the study area, however, sand tends to be flushed through the turbulent, high velocity zones of steep gravel-bed streams, and is generally only deposited in the wakes and crevices of coarse grains. As flood flows decrease below the point of gravel entrainment, sand can be transported out of riffles and into pools (Lisle 1989). Fine sediment in riffles, then, is expected to increase rapidly as sediment supply increases, but plateau as interstitial spaces are filled with sand.

Increased sediment supply can cause a fining of the surface of the streambed as particle size adjusts to offer less resistance to transport (Dietrich et al. 1989, Lisle et al. 2000). The ratio of the median grain size predicted by the Shields equation (D_{50*}) (based on bankful depth measurements and assumed critical shear stress of 0.045) to the measured D_{50} is a relative indicator of excess transport capacity. The ratio of predicted D_{50*} to measured D_{50} exhibits a very strong positive linear relationship with V* ($p = 0.004$, $r^2 = 0.90$) (Fig. 2). This implies that the bed surface gets finer (and is mobilized more frequently) as V*, a proxy for sediment supply, increases.

Linkages Between Streambed Fine Sediment and Benthic Macroinvertebrates

From our survey of empirical relationships between benthic macroinvertebrates and fine sediment, we identified 8 metrics and 25 taxa that were common in our dataset (we excluded taxa occurring at less than half of the sites or less than 40% of samples) (Table 2). Of the 8 metrics we tested, four responded as predicted: total abundance, EPT abundance, Chironominae/Chironomidae, and Orthocladiinae/Chironomidae (Table 2). Our results are in strong agreement with the findings of Angradi (1999) with regards to the response of the Chironomidae to fine sediment.

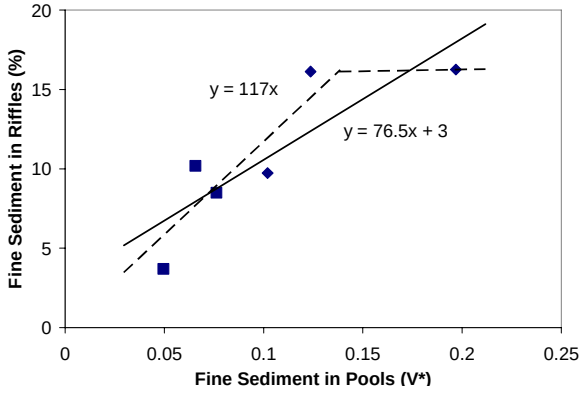


Figure 1 Percentage of riffle bed surface covered by sediment versus reach-averaged V*. Two models are presented, a linear regression (solid line) and a broken-stick regression (dashed line).

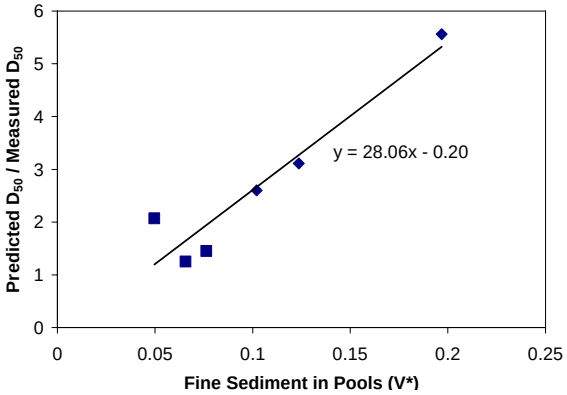


Figure 2 Ratio of predicted median grain size to fine measured median grain size, versus reach-averaged V*.

The fraction of chironomids composed of the sub-family Chironominae was negatively related to increasing fines, while the fraction made up of Orthocladiinae increased strongly (Table 2, Fig. 3). Although Orthocladiinae are often the dominant chironomid on gravel and cobble (Pinder 1986), they appear to be resistant to the filling of interstitial spaces, perhaps because they reside on the upper surfaces of stones rather than in crevices. Chironominae, common in organic-rich silt (Pinder 1986), respond negatively to deposits of fine sediment. In this study, fine sediment is primarily composed of inorganic deposits of coarse sand, suggesting that this substrate is not suitable for Chironominae. As predicted, total abundance and EPT abundance were negatively related to fine sediment, but the relationships were not statistically significant at $\alpha = 0.05$ (Table 2).

Four metrics responded in the opposite direction as predicted: taxa richness, EPT richness, percent burrowing and percent vulnerable (Table 2). Whereas other workers have observed decreased richness in response to large increases in deposited sand, especially in the Ephemeroptera, Plecoptera, and Trichoptera (EPT) insect orders (Angradi 1999), we observed strong positive relationships between both total taxa richness and EPT richness and fine sediment (Table 2, Fig. 4). When recalculated using a two-tailed test, both of these metrics exhibited statistically significant positive slopes (taxa richness: $p = 0.012$, EPT richness: $p = 0.022$). Rather than resulting in an overall reduction in taxa richness, higher levels of fine sediment in these steep mountain streams may provide habitat for many psammophilic taxa such as Oligochaeta, Gomphidae (Odonata), the ephemerellid mayflies *Attenell*a and *Serratella*, the stoneflies Yoraperla (Peltoperlidae) and Doroneuria (Perlidae), and the caddisfly Dolophilodes (Philopotamidae). Two caddisflies that build portable cases out of fine sediment, *Gumaga* (Sericostomatidae) and *Pedomoecus sierra* (Apataniidae), are more common at sites with high levels of fine sediment, suggesting that the availability of small mineral grains for case construction could be a limiting factor for these taxa. The percent burrowing metric exhibited a weak negative relationship with fine sediment, while percent vulnerable was weakly, positively related.

None of the metrics for which a priori predictions were not made were significant at the Bonferroni-corrected false-positive error rate of $\alpha_e = 0.001$. The strongest relationships among these metrics were the abundance of predators and the abundance of filter-feeding organisms, both of which decreased with increasing fine sediment. The declining trend in filter-feeders reflects low abundances of simulid blackflies and hydropsychid caddisflies in riffles with greater than 15% surface fine sediment. Likewise, decreasing predator abundance resulted from declines in perlid caddisflies, particularly *Calineuria californica*, and rhyacophilid caddisflies. Pollution tolerance metrics and other measures of community composition were weakly related to sediment supply and levels of fine sediment.

Of the 25 taxa with a priori predictions, only 14 responded in the expected direction with increasing fine sediment (Table 2). Of these, only four taxa had statistically significant relationships with fine sediment: the net-spinning caddisfly *Arctopsyche* (Hydropsychidae), the ephemerellid mayfly *Attenella delantala*, the midge subfamily Chironominae, and Oligochaetea, aquatic worms (Table 2, Figs. 5 and 6). *Arctopsyche* was identified by Relyea et

Table 2 Predicted and measured responses of biological metrics and benthic macroinvertebrate taxa to increased levels of fine sediment. The P-Value is calculated based on the predicted slope using a one-tailed test. Statistically significant relationships are in bold.

Metrics and Taxa (Predicted Response)	**Measured Response**	**Slope (SE)**	**Predicted Response P-Value**	**Source of Prediction**
Taxa Richness (-)	+	0.72 (0.27)	0.99	Waters 1995
Total Abundance (-)	-	-92.8 (66.3)	0.088	Angradi 1999
EPT Richness (-)	+	0.39 (0.16)	0.99	Angradi 1999
EPT Abundance (-)	-	-47.8 (54.2)	0.19	Waters 1995
% Burrowing (+)	-	-0.40 (0.25)	0.93	Suttle et al. 2004
% Vulnerable (-)	+	0.43 (0.38)	0.88	Suttle et al. 2004
Chironominae/Chironomidae (-)	-	-0.021 (0.008)	**0.004**	Angradi 1999
Orthocladiinae/Chironomidae (+)	+	0.022 (0.008)	**0.007**	Angradi 1999
Antocha spp. (-)	-	-0.46 (0.78)	0.28	Relyea et al. 2000
Arctopsyche spp. (-)	-	-1.50 (0.55)	**0.006**	Relyea et al. 2000
Attenella delantala (+)	+	2.00 (0.40)	**<0.0001**	Hawkins 1984
Caudatella spp. (-)	+	0.31 (0.79)	0.65	Relyea et al. 2000, Hawkins 1984
Chironomidae (+)	-	-29.1 (11.0)	0.99	Waters 1995
Chironominae (-)	-	-18.3 (6.3)	**0.004**	Angradi 1999
Cinygmula spp. (-)	+	1.34 (1.13)	0.88	Relyea et al. 2000
Dicranota spp. (+)	-	-0.34 (0.15)	0.98	Relyea et al. 2000
Drunella doddsi (-)	+	0.062 (1.22)	0.52	Relyea et al. 2000, Hawkins 1984
Epeorus spp. (-)	-	-4.95 (5.57)	0.19	Relyea et al. 2000
Glossosoma spp. (-)	+	1.20 (0.80)	0.92	Relyea et al. 2000
Hesperoperla pacifica (-)	-	-0.60 (0.52)	0.13	Relyea et al. 2000
Hexatoma spp. (+)	-	-0.026 (0.255)	0.54	Relyea et al. 2000
Isoperla spp. (+)	-	-0.66 (0.76)	0.80	Relyea et al. 2000
Lepidostoma spp. (+)	-	-3.59 (3.13)	0.87	Relyea et al. 2000
Malenka spp. (+)	+	0.32 (0.43)	0.76	Relyea et al. 2000
Neophylax spp. (-)	-	-0.13 (0.60)	0.59	Relyea et al. 2000
Oligochaeta (+)	+	1.19 (0.56)	**0.023**	Waters 1995
Optioservuis spp.(+)	-	-0.63 (0.37)	0.95	Relyea et al. 2000
Rhithrogena spp. (-)	+	4.45 (2.44)	0.96	Relyea et al. 2000
Rhyacophila Betteni grp. (-)	-	-0.20 (0.50)	0.65	Relyea et al. 2000
Rhyacophila Hyalinata grp. (-)	-	-0.17 (0.27)	0.27	Relyea et al. 2000
Simulium spp. (+)	+	0.06 (0.41)	0.56	Relyea et al. 2000
Zapada cinctipes (+)	+	0.03 (2.32)	0.51	Relyea et al. 2000
Zapada columbiana (+)	+	0.58 (0.75)	0.22	Relyea et al. 2000

al. (2000) as being very intolerant to fine sediment. The larvae build and reside in fixed retreats downstream of their coarse-meshed nets, where they remain unless disturbed. Voelz and Ward (1996) found that larvae and pupae of Arctopsyche *grandis* are found almost exclusively on the undersides of large cobble, usually in pairs, particularly during the winter and spring in the Rocky Mountains. The large size of the larvae necessitates large crevice spaces beneath stones, only found in streams with low levels of fine sediment. *Attenella delantala* had the most upstream distribution of 12 species of Epehemerellidae in the McKenzie River, Oregon, but was commonly found in patches of sand and gravel < 20 mm diameter (Hawkins 1984), suggesting a preference for fine sediment. As discussed

above, Angradi (1999) also found that Chironominae exhibited a strong negative response to fine sediment. Most oligochaetes are obligate burrowers in fine sediment; they are often reported to increase in abundance with fine sediment additions, although one group of Oligochaetes, the Lumbricina, are considered moderately intolerant (Relyea et al. 2000).

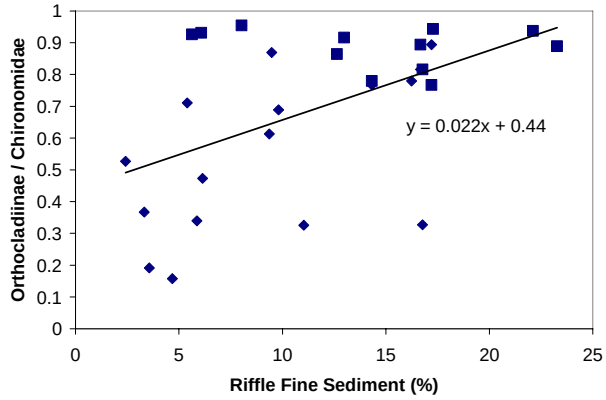


Figure 3 Fraction of Chironomidae composed of Orthocladiinae versus percentage of riffle bed surface covered by fine sediment.

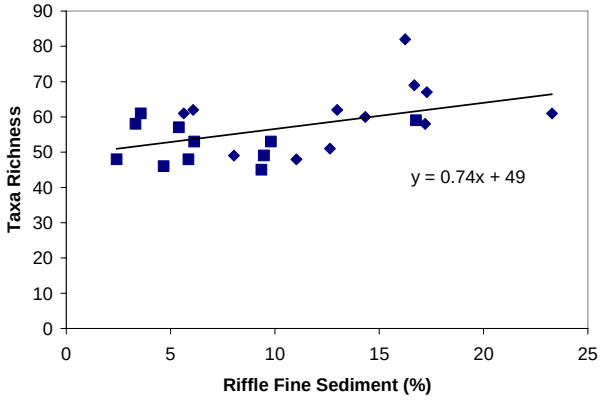


Figure 4 Benthic macroinvertebrate taxa richness versus percentage of riffle bed surface covered by fine sediment.

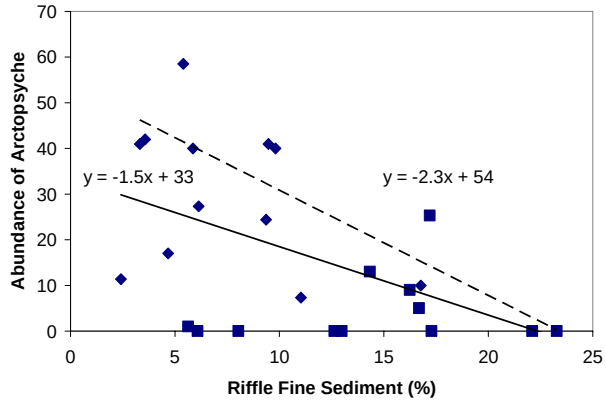


Figure 5 Abundance of *Arctopsyche* versus percentage of riffle bed surface covered by fine sediment. Two models are presented, a linear regression (solid line) and a partitioned linear regression (dashed line).

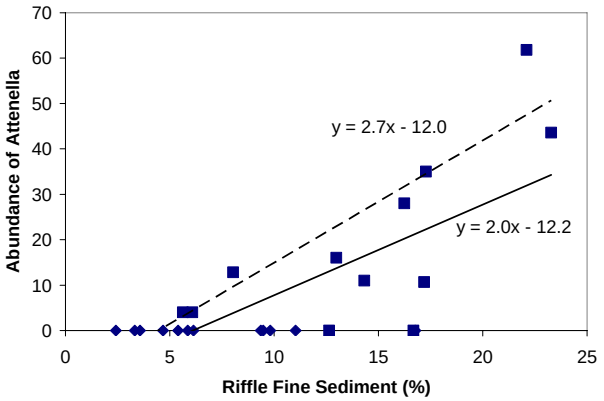


Figure 6 Abundance of Attenella versus percentage of riffle bed surface covered by fine sediment. Two models are presented, a linear regression (solid line) and a partitioned linear regression (dashed line).

CONCLUSIONS

Estimates of sediment supply from quantitative models and V* measurements suggests that sediment delivery to streams in the Klamath Mountains has increased several times over background rates in some drainage basins. Increases in sediment supply in steep, mountain streams can result in predictable increases in fine sediment in pools and riffles. Precise quantification of these relationships is hampered by the difficulty in accurately measuring sediment delivery to stream channels over decadal time scales, however. V*, bed surface fine sediment, and excess transport capacity all are potentially useful indicators for linking hillslopes and biota because they respond predictably to increased sediment supply and result in direct biological consequences.

The effects of increased sediment supply on benthic macroinvertebrate communities are more subtle than the effects of water quality impacts from urbanization or agriculture. Diversity and tolerance metrics that are useful for detecting the effects of water chemistry pollutants may not be useful for assessing the ecological impacts of increased sediment supply. Benthic invertebrate taxa such as Chironominae, Oligochaeta, *Attenella*, and *Arctopsyche* respond predictably to levels of fine sediment and offer potential for improved monitoring and increased understanding of stream ecosystems. The quantitative relationships described in this study add to our

understanding of the linkages between hillslopes, stream channels, and aquatic biota and identify areas where process-based understanding can be improved.

ACKNOWLEDGEMENTS

The field crew was led by Sue Maurer and composed of Jeremy Warner, John Bowman and Wind Beaver. Don Elder served as the KNF liaison and worked with the field crew. Juan de la Fuente (KNF) developed the landslide and surface erosion models and provided assistance with the study design. Al Olson (KNF) and Brian Staab (USFS Regional Office) provided project leadership and oversight. Tom Lisle (USFS Redwood Sciences Lab) provided insight that improved the study design and Sue Hilton (USFS Redwood Sciences Lab) trained the crews in measuring V*. The USFS funded this research in the form of a grant to W.E.D. and V.H.R.

REFERENCES

Angradi, T.R. (1999). "Fine sediment and macroinvertebrate assemblages in Appalachian streams: a field experiment with biomonitoring applications," Journal of the North American Benthological Society 18:49-66.

Bunte, K., and Abt, S. R. (2001). Sampling Surface and Subsurface Particle-size Distributions in Wadeable Gravel- and Cobble-bed Streams for Analyses in Sediment Transport, Hydraulics, and Streambed Monitoring. Gen. Tech. Rep. RMRS-GTR-74. Fort Collins,CO: U.S. Department of Agriculture, Forest Service, Rocky Mountain Research Station.

de la Fuete, J., and Haessig, P.A. (1993). Salmon Sub-Basin Sediment Analysis. U.S. Forest Service, Final Report, Yreka, California.

Dietrich, W.E., Kirchner, J.W., Ikeda, H., and Iseya, F. (1989). "Sediment supply and the development of the coarse surface layer in gravel-bedded rivers," Nature 340:215-217.

Dunne, T., Agee, J., Beissinger, S., Dietrich, W., Gray, D., Power, M., Resh, V., and Rodrigues, K. (2001). A Scientific Basis for the Prediction of Cumulative Watershed Effects. Wildland Resources Center, University of California, Berkeley, Report No. 46.

Hawkins, C. P. (1984). "Substrate associations and longitudinal distributions in species of Ephemerellidae (Insecta: Ephemeroptera) from western Oregon," Freshwater Invertebrate Biology 3:181-188.

Lisle, T. E. (1989). "Sediment transport and resulting deposition in spawning gravels, north coastal California," Water Resources Research 25: 1303–1319.

Lisle, T.E., Nelson, J.M., Pitlick, J., Madej, M.A., and Barkett, B.L. (2000). "Variability of bed mobility in natural, gravel-bed channels and adjustments to sediment load at local and reach scales," Water Resources Research 36: 3743–3755.

Lisle, T.E., and Hilton, S. (1999). "Fine bed material in pools of natural gravel bed channel," Water Resources Research 35:1291-1304.

Merritt, R. W., and Cummins, K.W., eds. (1996). An Introduction to the Aquatic Insects of North America. 3rd edition. Kendall/Hunt, Dubuque, Iowa.

Pinder, L.C.V. (1986) "Biology of freshwater Chironomidae," Annual Review of Entomology 31:1-23.

Relyea, C. D., Minshall, G.W., and Danehy, R .J. (2000). "Stream insects as bioindicators of fine sediment," Watershed Management 2000 Conference, Water Environment Federation.

Suttle, K.B., M.E. Power, J.M. Levine, and McNeely, C. (2004). "How fine sediment in riverbeds impairs growth and survival of juvenile salmonids," Ecological Applications 14: 969- 974.

Thomson, J.D., Weiblen, G., Thompson, B.A., Alfaro, S., Legendre, P. (1996). "Untangling multiple factors in spatial distributions: lilies, gophers and rocks," Ecology 77:1698–1715.

Voelz N.J. and Ward J.V. (1996). "Microdistributions of filter-feeding caddisflies (Insecta: Trichoptera) in a regulated Rocky Mountain River," Canadian Journal of Zoology 74: 654-666.

Waters, T.F. (1995). Sediment in Streams: Sources, Biological Effects and Control. American Fisheries Society, Bethesda, Md.

Wilcock, P.R. and Kenworthy, S.T. (2003). "A two fraction model for the transport of sand/gravel mixtures," Water Resources Research. 38: 1194 - 2003.

FLOWSED/POWERSED – PREDICTION MODELS FOR SUSPENDED AND BEDLOAD TRANSPORT

David L. Rosgen, Hydrologist/Geomorphologist, Wildland Hydrology, 11210 North County Road 19 North, Fort Collins, Colorado 80524, wildlandhydrology@wildlandhydrology.com

Abstract: FLOWSED and POWERSED are sediment transport models based on empirical and analytical methods used to predict both suspended load and bedload. The models predict changes in degradation and/or aggradation processes associated with impaired streams. The FLOWSED model involves the application of dimensionless sediment rating curves developed from reference streams that reflect sediment supply associated with a given stream type and stability rating. Measured bankfull discharge, as well as bankfull suspended and bedload sediment values are used as normalization parameters. Flow-duration curves from gage station data are also converted to a dimensionless form in order to develop localized flow-duration curves at ungaged sites. Measured bankfull values from the study stream are used to convert dimensionless to dimensional sediment rating and flow-duration curves. Annual sediment yields can then be determined using the predicted sediment rating and flow-duration curves.

Regionalized dimensionless sediment relations can be developed from measured data and tested against the dimensionless bedload and suspended sediment relations derived from the Colorado data presented in FLOWSED. Predicted sediment rating curves using this model are compared to observed values over a range of independent data sets representing small to large rivers in a variety of hydro-physiographic provinces.

The POWERSED model converts sediment rating curves from stream discharge to unit stream power. Changes in channel dimension, pattern, profile and velocity due to stability problems and/or proposed channel design options are evaluated in terms of sediment transport potential. Hydraulic geometry by stage is calculated to convert discharge to unit stream power. This conversion allows the user to predict sediment transport rates at different stages and channel response to changes in slope, depth and/or velocity for a given sediment supply. Sediment supply is determined from the dimensionless sediment rating curves stratified by stream type and stability using the FLOWSED model. Predicted annual suspended and bedload sediment yield values from both reference (stable) and impaired (unstable) reaches using POWERSED are compared to measured annual sediment yield. Applications of the models are presented for a) stability examinations; b) watershed and/or sediment supply assessments (WARSSS); c) fish habitat enhancement structures; d) flood level computations; e) bridge design; f) prediction of future reservoir capacity; and g) natural channel design for river restoration.

INTRODUCTION

Field practitioners must be able to accurately predict the sediment capacity of river channels in order to assess physical and biological function and stability. Recent stream restoration and fish enhancement projects have failed due to a lack of understanding of sediment transport and the importance of incorporating sediment transport into projects. For example, failure to include sediment transport estimates in calculating bridge hydraulics may result in the continued deposition of sediment in many of the bridge cells. Changes in the dimension, pattern, profile, materials and roughness of stream channels need to be assessed not only for sediment competency, but also for capacity. As channel boundary conditions and flow regimes change, it is imperative to ensure that the stream can transport the sediment made available from its catchment. Unfortunately, simple and accurate approaches to these problems are unavailable due to the inherent complexity and uncertainty of sediment transport prediction.

Using measured hydraulic and sediment data, Lopes et al. (2001) tested 7 bedload equations on 22 streams and concluded that the best overall sediment transport equations were developed by Schoklitsh (1962) and Bagnold (1980). Gomez and Church (1989) hypothesized that, when presented with limited hydraulic information, bedload is best predicted using equations incorporating the stream power concept. After testing 410 bedload events in gravel-bed rivers, however, Gomez and Church (1989) concluded that out of the 12 equations assessed, none performed consistently due to the limitation of the data and the complexity of the sediment phenomena. The authors concluded that sediment transport prediction involves 1) *"the need to collect localized bedload and suspended sediment rating curve data to establish sediment supply values; and, 2) the need to calibrate sediment transport models based on absolute values."* Without observed sediment values, predicted transport rates will continue to

differ significantly from actual transport rates. It is not uncommon for existing sediment transport models to overpredict or underpredict by two or three orders of magnitude, all on the same data sets (Parker, et al., 1982).

Purpose: Clearly, the need for a more accurate suspended and bedload transport model has not lessened. Since 1968, the author has measured suspended and bedload data on a wide range of flows for 160 rivers. The Rosgen data sets, combined with USDA Forest Service Rocky Mountain research data from sites in Colorado and Wyoming, were used to develop and test dimensionless relations of both suspended and bedload sediment rating curves by stream type/stability categories (Troendle, et al., 2001). The normalization parameter used to transform the sediment rating curves to dimensionless form was bankfull stage values of discharge, suspended and bedload sediment. With one exception, the relations found were power functions. The equations were tested and found to be statistically significantly ($p < 0.05$) different from one another, based on broad stream type groupings and associated "good/fair" versus "poor" stability ratings. Stream type alone was not significant, since stability ratings are needed to establish sediment supply (Rosgen, 2001). Where changes in stream type infer a stability shift, such as a change from an E5 to F5, there is an inferred relationship of not only a change in sediment supply with stream type change, but a shift in the sediment rating curve. The stream types are those described by Rosgen (1994), while the stability ratings are those by Pfankuch (1975), modified by Rosgen (2001). USGS sediment rating curves on Redwood Creek, California, were stratified into different sediment rating curves based on the Pfankuch stability ratings (USEPA,1980), explaining a range of 5 orders of magnitude in sediment supply for the same discharge. Bedload sediment rating curve data, published by Williams and Rosgen, (1989) were stratified by stream type to reduce the variability in the scatter of the data (Rosgen, 1996). The steeper slope of the sediment rating curves was related to a sediment supply condition and to channel processes described by stream type. Such relations eventually provide dimensionless sediment rating curves from measured values that represent the *supply* function in the sediment transport relations. Much like calibrating a model with measured values, bedload discharge, suspended and bedload sediment data are measured in order to convert the empirically derived dimensionless relation equation to a dimensional form for a given river reach. The FLOWSED model utilizes dimensionless sediment rating curves and dimensionless flow-duration curves. Dimensionless flow-duration curves were first presented by Emmett (1975).

One criticism of dimensionless ratio sediment rating curves offered by Kuhnle and Simon (2000) is that they will collapse into the same curve when the sediment rating curves of two rivers of different types are converted to a dimensionless form. This would be true if the stability/stream type/sediment supply relations were similar; however, tests of significance of "poor" versus "good/fair" stability were significantly different when made dimensionless (Troendle, et al., 2001). To demonstrate this point, USGS sediment rating curve data from Western Tennessee (Simon, 1986) from the Hatchie river (E5 stream type) and the South Fork of the Forked Deer river (F5 stream type), shown in Figure 1, indicate that for similar flows the South Fork of the Forked Deer river has 3 orders of magnitude higher sediment supply compared to the Hatchie river. When these relations were transformed to a dimensionless form, the curves did not collapse into one curve as asserted by Kuhnle and Simon (2000), but rather remained separate, as seen in Figure 1. If the curves had collapsed into the same relation, this would indicate a lack of statistically significant difference. In such a case, one dimensionless power function of discharge would then fit both streams.

The POWERSED model uses the output from FLOWSED, but simulates changes in stream power to predict transport relations due to stream channel dimension, pattern and profile changes. Thus, the combination of simple power functions from empirical and analytical relations of hydraulic geometry/stream power by stage are combined to provide a model that produces reasonable numbers. The empirical and analytical models and their validation over a wide range of geographic regions are presented below.

MODEL DESCRIPTION

FLOWSED: The framework for this model involves selecting streams of various types and stability ratings that have measured suspended and bedload sediment rating curves available. The streams selected should represent a "reference" condition for streams of various morphology and stability within a region. The sediment rating curves are then transformed to a dimensionless form over the entire range of flows using the bankfull stage values as the normalization parameter. Variations in the form of the relation describing the exponent and coefficient values depend on the nature of the streams in the region. Rivers of similar type and stability are grouped as in Troendle et al. (2001). Thus, the derived empirical relations can be extrapolated to similar rivers elsewhere. For the

development of dimensionless suspended sediment and bedload sediment rating curves, data from C4 stream types (gravel-bed, meandering, streams with floodplains, point bars, width/depth ratios >12, on slopes less than 0.02) (Rosgen, 1994) were selected to represent "good/fair" stability in the Pagosa Springs region of Southwestern Colorado. Two equations were established, one for suspended sediment and another for bedload sediment (Figure 2). Separate equations were developed for "poor" stability ratings for a region.

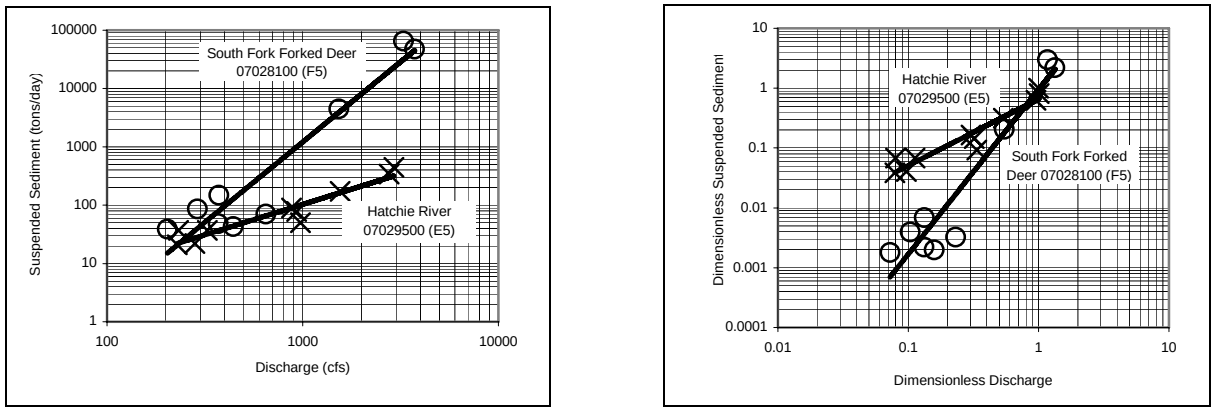


Figure 1 *Left graph*: Suspended sediment rating curves from West Tennessee for the South Fork forked Deer (F5 stream type) and Hatchie Rivers (E5 stream type). Data is from the USGS in English units as published by Simon, 1989. *Right graph:* Dimensionless ratio suspended sediment rating curves; separation of curves from one another.

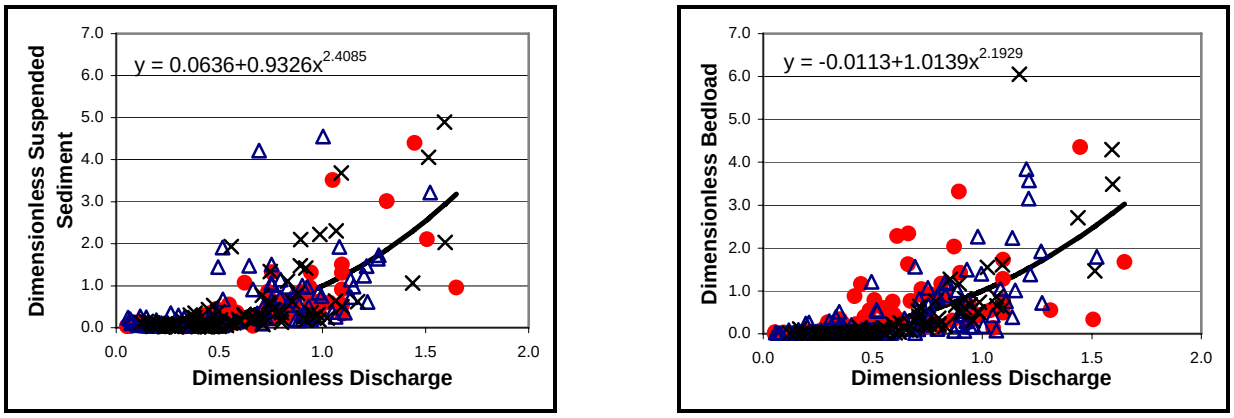


Figure 2 *Left graph*: Dimensionless ratio suspended sediment rating curves for "good/fair" stability categories. *Right graph*: Dimensionless bedload rating curves for "good/fair" stability categories. Both curves using data from Wolf Creek, the West Fork of the San Juan river and Fall Creek, Pagosa Springs, Colorado (1997 – 2001).

Flow-duration curves from USGS gage sites are also converted to dimensionless flow-duration curves using bankfull discharge as the normalization parameter. Since bankfull is a momentary maximum value, it must be converted to a "mean daily bankfull" value. USGS data is used to obtain the mean daily discharge on the day that the bankfull stage occurs. A ratio of mean daily discharge to the momentary maximum value is developed to establish the "mean daily bankfull" value. This value is used to normalize the flow-duration curve data. The use of dimensional flow-duration curves representing a hydro-physiographic province are used to obtain flow-duration curve data at ungaged sites once bankfull discharge is determined. Bankfull discharge is obtained from field investigations, measurement or extrapolation from regional curves for a hydro-physiographic region. The combination of sediment rating curves for both suspended and bedload sediment and flow-duration curves allows the calculation of total annual sediment yield. To convert the dimensionless sediment rating curve to dimensional values, measured suspended and bedload sediment must be obtained for the stream being studied. Regional bankfull sediment values such as those for suspended sediment (Simon, et al., 2004) could be used in the absence of locally measured values, but would require validation. Since direct measurements are necessary to calibrate

sediment models, then these same data can be used to convert a dimensionless relation in order to predict a sediment rating curve if the data collected is at or near the bankfull stage.

POWERSED: This model uses sediment supply data from the dimensionless suspended and bedload rating curves and dimensionless flow-duration cures in FLOWSED, but converts the full range of stream discharge into stream power. Stream power (ω) is defined as

$$(\omega) = \gamma QS \quad (1)$$

where, **γ** is the specific weight of the fluid, Q is stream discharge, and S is the water surface slope. Stream power is calculated for each stage from hydraulic geometry relations. The hydraulic geometry relations are predicted using various resistance equations and roughness coefficients for a wide range of flows. Thus, changes in slope, hydraulic radius (depth), and velocity by stage are reflected in an altered stream power and a corresponding altered sediment transport rate. The sediment consequences and resulting channel stability of over-widened streams, multiple cell bridges, and/or structures that alter the slope, depth and/or velocity of flow can be determined. The suspended sediment data for POWERSED is further separated into the sand portion of the suspended sediment sample and the wash load since the sand portion is more controlled by energy than the wash load. Washload is defined as a portion of the suspended load at sediment sizes less than .062mm, the remaining concentration represents the suspended sand material load. Ratios of suspended sand concentrations versus total suspended sediment concentrations are used in the analysis.

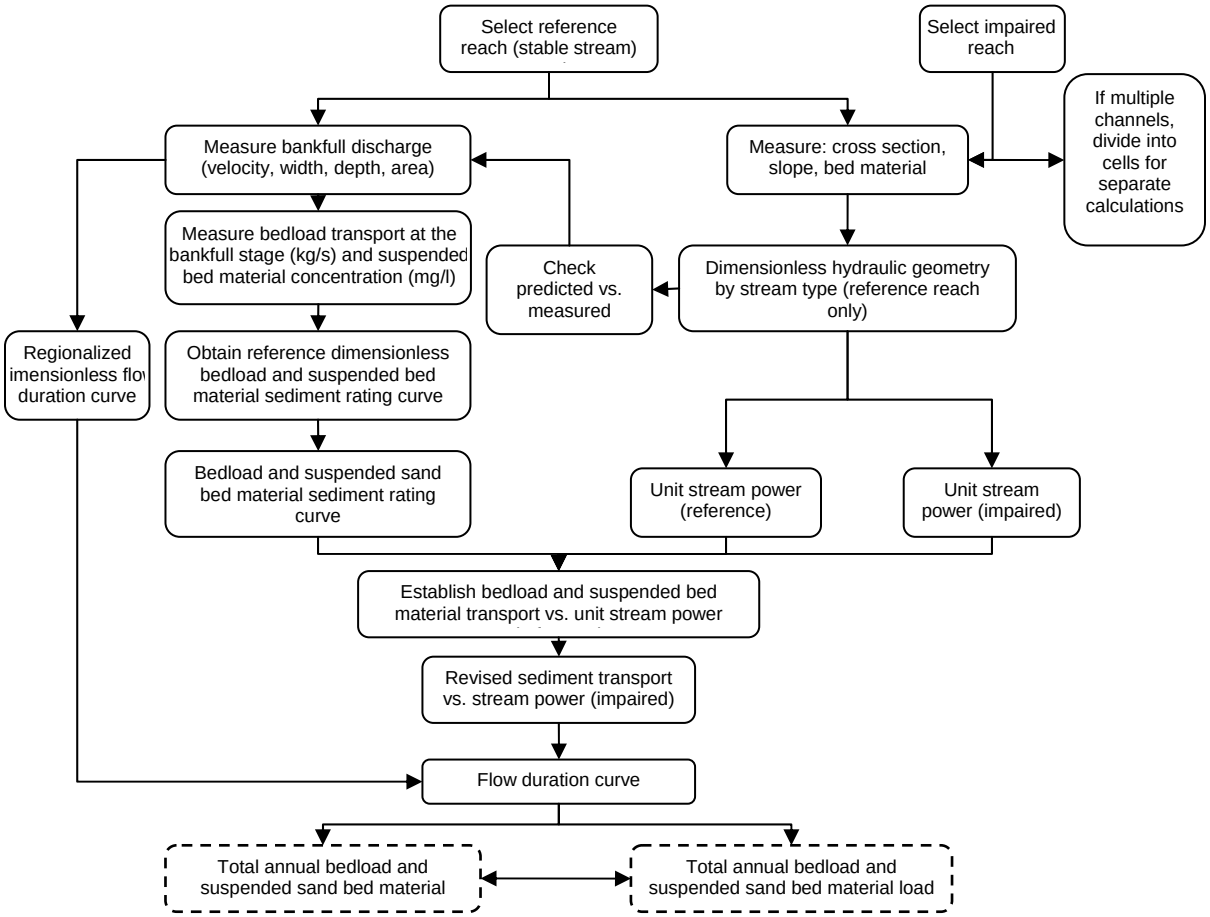


Figure 3 Flow chart for FLOWSED/POWERSED models when impaired and reference streams have the same discharge.

A flow chart depicting both models is shown in Figure 3. The user has an option to either route the same sediment supply through the impacted reach from the upstream reach or to measure sediment and flow at bankfull stage and re-enter the model to adjust sediment supply for the downstream reach. This option allows the user to insert locally

derived power function equations that best represent the altered stream. These models have been successfully used for river assessment, fish habitat structure evaluations and river restoration designs since 2001. The models are presently installed in a software program in RIVERMorph$_{TM}$ to assist users with rapid, multiple applications.

RESULTS AND DISCUSSION

Validation of both the FLOWSED and POWERSED models has been conducted using measured suspended and bedload data for a wide range of river sizes over diverse geographical areas. One measured data point representing discharge, suspended sediment and bedload sediment, all collected at the bankfull stage, was used to predict a sediment rating curve for each location. These rivers represented independent data sets, as none of the empirical dimensionless sediment rating curves tested were used to develop the relations. For validation, US Geological Survey data was obtained for measured bedload and suspended sediment in Alaska, Tennessee, Arkansas, Wyoming, Nevada, North Carolina and other states (Figure 4).

The reference dimensionless sediment rating curves for suspended and bedload sediment used for these predictions were the power function relations shown in Figure 2, from the Pagosa data. The comparison shows very good agreement between the predicted sediment rating curve and the measured values over a wide range of flows (Figure 4). The predicted sediment rating curves were derived from only one data point each representing the bankfull discharge, suspended sediment and bedload sediment values as depicted (dashed line) on each relation in Figure 4.

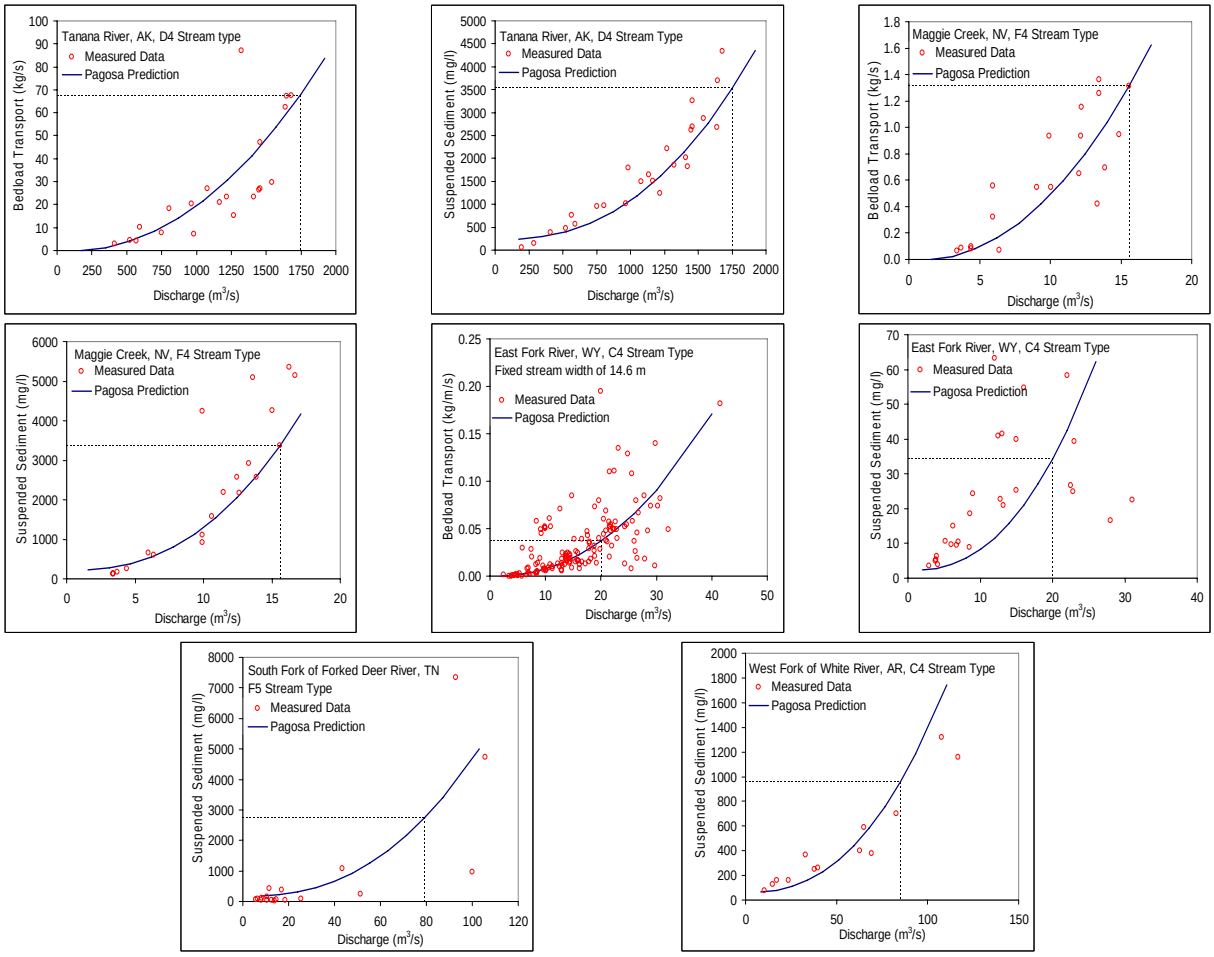
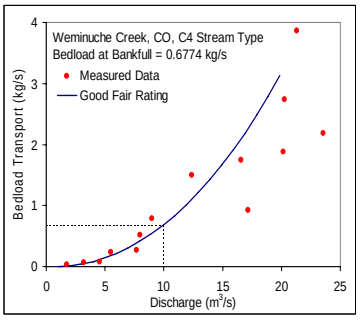


Figure 4 Predicted suspended and bedload sediment rating curves compared to observed data for a wide range of river sizes and geographical areas, using the FLOWSED model.

Field validation of the POWERSED model was recently conducted on Weminuche Creek in Southwestern Colorado. Annual suspended sediment and bedload sediment yield were measured at two locations on the same river for the same flows, but not the same stability. Bedload and suspended sediment, streamflow and hydraulic geometry data were collected concurrently on both reaches over a wide range of flows during snowmelt runoff. The upper reach was a C4 stream type with a width of 9.8 meters, width/depth ratio of 11, slope of 0.0047 and a D_{50} of 33 mm. The lower reach, 0.8 km downstream was a D4 (braided) stream type but of the same flow with a width of 72 meters, width/depth ratio of 412, slope of 0.0026 and a D_{50} of 22mm. The braided reach instability was caused by spraying willows and heavy grazing pressure, which caused excessive streambank erosion and channel aggradation. The braided channel sediment data included measuring 30 cells of individual verticals of suspended sediment and bedload data for a wide range of flows up to two times bankfull stage. Particle size analysis of each vertical was also collected and analyzed. The hydraulic geometry was also measured at each vertical including velocity, width, depth, and slope; used to calculate both discharge and stream power. This data was collected over the entire snowmelt runoff period in 2005 to calculate a transport rate for a range of flows on the braided channel by individual cell as well as for the total annual suspended, suspended sand and bedload transport. The same data was collected at the bridge site on the C4 stream type. Continuous streamflow data was also collected during the runoff season. A 152mm (6 inch) Helley Smith bedload sampler and a DH-48 depth-integrated suspended sediment sampler were used at both sites following standard field and lab analysis techniques. Due to an unusually heavy snowpack, stream flows reached twice the bankfull stage for Weminuche Creek in 2005.

Prediction of the measured suspended (sand) sediment and bedload rating curves for Weminuche Creek are shown in Figure 5. The prediction should be reasonable, as the reference dimensionless sediment rating curves were obtained from Southwestern Colorado, although not from Weminuche Creek. The next prediction represented annual sediment yield for both stream reaches. The same sediment supply function from the upstream C4 stream type was used for the downstream reach to determine how well the downstream reach could accommodate the sediment made available. In the case of the D4 stream type there was a major change in width, depth and velocity for the same discharge, thus a shift in stream power was predicted. The relation between stream discharge and stream power for the C4 and D4 stream type are depicted in Figure 6.



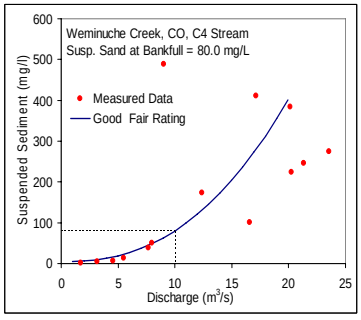


Figure 5 *Left graph*: Predicted suspended sand sediment rating curve compared to observed data. *Right graph*: Predicted bedload sediment rating curve compared to observed data using FLOWSED, C4 stream type, Weminuche Creek, Colorado, 2005.

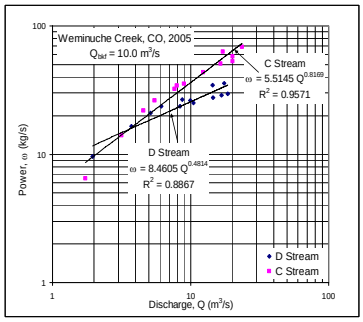


Figure 6 Relationship of stream discharge versus stream power for the C4 and D4 reaches of Weminuche Creek, Colorado, 2005.

The relationship between measured suspended sediment and bedload measurements versus stream power are shown in Figure 7 for each stream type. The D4 stream type stream power data reflects only reach averaged conditions rather than individual cells. The first POWERSED run using RIVERMorph$_{TM}$ on the braided reach did not separate the reach into cells across the section, but used reach averaged hydraulic geometry by stages to predict sediment transport. The resultant prediction was very low, (87 tons/year for bedload, 390 tons/year suspended sediment and a total of 477 tons/year, compared to an upstream supply on a C4 stream type of 2,557 tons/year of bedload, 1,852 suspended sediment tons/year, with a total of 4,452 tons/year). The next run, however on the braided reach was subsequently divided into three cells to develop hydraulic geometry and sediment transport separately.

The excellent results for both stream reaches of predicted versus measured values are shown in Table 1. The predicted total sediment yield for the C4 stream type was a 3.1% underestimate. The predicted annual sediment yield for the D4 stream type was 6.0% below the measured values. Predicted bedload was very close to that

produced for the C4 and the D4 stream type, as shown in Table 1. These results are very encouraging, as they suggest the field practitioner's ability to rapidly and accurately predict both sand-sized suspended and bedload transport rates and annual yields. The sand portion of the suspended sediment induced deposition on the stream bed when changing from a C4 stream type (1,895 tons/year measured versus 2,153 tons/year predicted), to a braided D4 stream type (878 tons/year measured versus 949 tons/year predicted) represents a reduction in sand size suspended

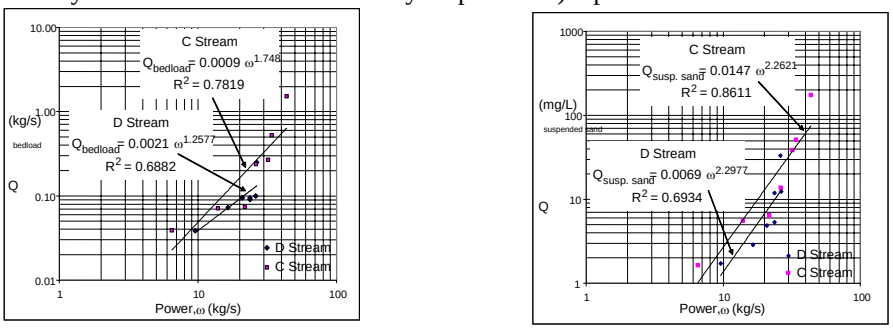


Figure 7 *Left graph*: Relationship of measured bedload sediment to stream power for C4 and D4 stream type. *Right graph*: Relationship of measured suspended sand sediment versus stream power – both relationships from Weminuche Creek, Colorado (2005).

sediment transport of 916 tons/year measured versus 1,275 tons/year predicted. The reduction in bedload transport when changing from a C4 stream type (2,557 tons/year measured versus 2,160 tons/year predicted), to a braided D4 stream type (636 tons/year measured versus 612 tons/year predicted) is 1,921 tons/year for the measured value and 1,548 tons per year for the predicted value. This excess deposition is the result of a reduction in stream power due to the consequence of an increased width to depth ratio (11 for the C4 stream type compared to 412 for the D4 stream type). The change in stream power for the braided D4 stream type was largely due to the reduction of mean depth and velocity. The hydraulic geometry by stage prediction of the POWERSED model closely approximates the measured values. In other words, the combined FLOWSED/POWERSED models not only predict the annual suspended sand and bedload yield, but they also accurately predict the channel consequence of aggradation rate (Table1).

A similar prediction was accomplished on the North Prong of the South Fork of the Mitchell River (12.6 km^2) near Jonesville, North Carolina from work initiated in 2004. The upstream stable reference reach cross-section was used to predict the suspended and bedload sediment using the Pagosa data (Figure 2). A very close agreement between the predicted and measured suspended and bedload data was observed. The downstream, impacted reach had a width/depth ratio of 24-29 compared to a width/depth ratio of 12 for the upstream reference. The POWERSED model indicated that approximately 40% of the total annual sediment yield would be deposited, including sand-sized particles. Twelve permanently monumented cross-sections were resurveyed one year later, all of which showed aggradation ranging from 0.06m to 0.18m and a shift to a higher percentage of sand. Interestingly, the competence of the river was maintained, as a 95-mm particle was predicted to be entrained and 100-mm particles were entrained in the bed, scouring down to 0.12m. The bed subsequently aggraded over the scour chains, depositing excess fine gravel and sand on the recession limb of the hydrograph over the previously installed scour chains. This study and model validation indicated that a stream may have adequate sediment *competence*, but lack the sediment *capacity* to maintain stability. The model was successful in that it predicted an aggradation process that matched field observations.

CONCLUSIONS

The close agreement between predicted versus observed data of both suspended and bedload sediment rating curves is very encouraging. Study results indicate that 1) a reference dimensionless sediment rating curve is appropriate to represent sediment supply in the region being studied; 2) a dimensionless flow-duration curve represents the hydro-physiographic province of the study site; and 3) near bankfull values are obtained in the field to transform the dimensionless relations to dimensional values. Researchers/practitioners could establish a range of dimensionless sediment rating curves for a given region and bankfull suspended and bedload sediment data by drainage area. Continued field measurements and comparisons of model prediction-to-observed values are recommended over a

wide range of regions. The initial development and testing of FLOWSED/POWERSED shows promise in predicting river behavior for stability assessment, fish habitat enhancements, bridge design, reservoir studies and river restoration applications.

Table 1 Comparison of predicted suspended (sand), bedload and total sediment loads to measured values for the C4 and D4 stream types on Weminuche Creek, Colorado, 2005.

STREAM LOCATION	PREDICTED VALUES (TONS/YEAR)	MEASURED VALUES (TONS/YEAR)	DIFFERENCE (%)
C4 Stream Type			
Bedload	2,160	2,557	
Suspended load (sand only)	2,153	1,895	
C4 Stream Type Total Sediment Load	**4,313**	**4,452**	**3.1% under**

STREAM LOCATION	PREDICTED VALUES (TONS/YEAR)	MEASURED VALUES (TONS/YEAR)	DIFFERENCE (%)
D4 Stream Type Cell 6.1			
Bedload	547	530	
Suspended load (sand only)	788	806	
Total	1,335	1,336	
D4 Stream Type Cell 6.2			
Bedload	65	104	
Suspended load (sand only)	83	141	
Total	148	245	
D4 Stream Type Cell 6.3			
Bedload	0	2	
Suspended load (sand only)	7	2	
Total	7	4	
D4 Stream Type Total			
Bedload	612	636	
Suspended load (sand only)	878	949	
D4 Stream Type Total Sediment Load	**1,490**	**1,585**	**6.0% under**

Acknowledgements: Special thanks to Dr. John Stamm for conducting and coordinating the field, lab and data analysis for the Weminuche Creek sediment study. Thanks to Brandon Rosgen, Keith Candelaria, Tiffany Thompson, Emily Davis, Christina Alvord, Josh Oberleas and Seth Kurt-Mason for field and lab work on Weminuche Creek, to Dr. William Emmett for supplying bankfull sediment data, and to George Athanasakes and Brian Belcher with FMSM Engineers, Inc., Louisville, KY (RIVERMorph$_{TM}$) for the FLOWSED and POWERSED programming and data analyses.

REFERENCES

Bagnold, R.A. (1980). "An empirical correlation of bedload transport rates in flumes and natural rivers," Proceedings of the Royal Society (London) 372, pp. 452-473.

Barry, J.J., J.M. Buffington, and J.G. King. (2004). "A general power equation for predicting bed load transport rates in gravel bed rivers," Water Resour. Res., 40, W10401.

Gomez, B. and M. Church. (1989). "An assessment of bedload sediment transport formulae for gravel bed rivers," Water Resour. Res., 25, 1161-1186.

Dietrich, W.E., J. Kirchner, H. Ikeda, and F. Iseya. (1989). "Sediment supply and the development of the coarse surface layer in gravel-bedded rivers," Nature, 340, 215-217.

Emmett, W.W. (1975). The channels and waters of the Upper Salmon River Area, Idaho. United States Geological Survey, Professional Paper 870A.

Kuhnle, R.A. and A. Simon. (2000). Evaluation of sediment transport data for clean sediment TMDL's. NSL Report No. 17, USDA, NSL, ARS, Oxford, Miss.

Lopes,V.L., W.R. Osterkamp, M.B. Espinosa. (2001). "Evaluation of selected bedload equations under Transport- and Supply-Limited Conditions," In: proceedings of the Seventh Interagency Sedimentation Conference, March 25 to 29, Reno, NV.

Parker, G.P., P.C. Klingeman and D.G. McLlea.. (1982). "Bedload and size distribution in paved gravel-bed streams," J. Hydraul. Div. Am Soc. Civ. Eng., 108, 544-571.

Pfankuch, Dale J. (1975). Stream reach inventory and channel stability evaluation. USDA Forest Service, R1-75-002. Govt. Printing Office, # 696-260/200, Washington, D.C., 26 pp.

Rosgen, D.L. (1994). "A stream classification system," Catena Vol 22 169199. Elsevier Science, Amsterdam.

Rosgen, D.L. (1996). Applied river morphology. Wildland Hydrology Books, Pagosa Springs, CO, pp. 6-42.

Rosgen, D.L. (2001). "A stream channel stability assessment methodology," in Proceedings, 7th Federal Interagency Sedimentation Conference. March 25-29. Reno, NV.

Simon, Andrew. (1989). "The discharge of sediment in channelized alluvial streams," Water Resources Bull., AWRA Vol. 25, No.6, pp. 1177-1188.

Simon, A., Dickerson, W., and Heins, A. (2004). "Suspended-sediment transport rates at the 1.5 year recurrence interval for ecoregions of the United States: transport conditions at the bankfull and effective discharge," Geomorphology 58, pp. 243-262.

Schoklitsch, A. (1962). Handbuch des Wasserbaues, 3rd edn. Springer-Verlag, Vienna.

Troendle, C.A., Rosgen, D.L., Ryan, S., Porth, L. and Nankervis, J. (2001). "Developing a 'reference' sediment transport relationship," in Proceedings, 7th Federal Interagency Sedimentation Conference. March 25-29. Reno, NV.

USEPA. (1980). (WRENSS). An approach to water resource evaluation of non-point silvicultural sources (A procedural handbook). EPA-600/8-80-012, Athens, GA.

Whiting, P.J., Stamm, J. F., Moog, D. B., and Orndorff, R. L. (1999). "Sediment transporting flows in headwater streams," Geol. Soc. Am. Bull., 111, 450-466.

Williams, G.P. and Rosgen, D.L. (1989). Measured total sediment loads (suspended and bedloads) for 93 United States streams. U.S. Geological Survey Open File Report 89-67, Denver, CO, 128 pp.

USE OF AERIAL INFRARED THERMOGRAPHY TO MAP EMERGENT RIVERINE SANDBARS

Ashley Heckman, Hydrologist, USGS, Golden, Colorado, aheckman@usgs.gov; Paul Kinzel, Hydrologist, USGS, Golden, Colorado, pjkinzel@usgs.gov; Jonathan Nelson, Hydrologist, USGS, Golden, Colorado, jmn@usgs.gov

Abstract: The Big Bend, a 145-kilometer reach of the Platte River in central Nebraska, has been designated by the US Fish and Wildlife Service as critical habitat for the endangered interior least tern and threatened piping plover. In the past, high flows occurring during spring runoff were capable of building ephemeral sandbars, which provided nesting and foraging habitat for these species. During the last century, regulation of upstream water resources has altered the flow in the central Platte River, which has in turn affected the seasonal cycle of sandbar formation. Currently, management efforts are focused on creating and maintaining in-channel habitat areas (artificial islands) and off-channel habitat areas (gravel pits). Future releases from upstream dams may be used to generate pulse flows with the objective of creating in-channel sandbar habitats.

As a means to quantify and evaluate the effect of pulse flows and channel management practices on sandbar creation and maintenance along the central Platte River, six 1-kilometer stream segments were chosen for geomorphic analysis. Two of the segments are located at bridges, two segments are located where the channel carries the total flow in the river, and two segments are located where a braided channel carries a portion of the flow. The discharges at the upstream and downstream ends of the Big Bend study reach are determined at two U.S. Geological Survey streamflow-gaging stations, providing flow information for each site.

Identifying the spatial extent of emergent sandbars is an essential component of the geomorphic analysis. Resolving these boundaries with traditional aerial photographic imagery such as natural color, black and white, and even color-infrared photography can be extremely difficult, because sufficient contrast between water and land surfaces is required. Mapping the sandbar perimeters using ground-based survey techniques can provide the required accuracy, but is labor-intensive and provides limited coverage. Aerial infrared thermography provided both the necessary contrast and the adequate spatial coverage needed for this purpose. The contrast in temperature between subaerial and submerged areas in this imagery provided a means to detect and isolate the emergent sandbars. Digital still-frames along the six sites were captured from the video and georeferenced to digital orthophotographs. For each year, and in some cases on consecutive nights within a given year, the emergent sandbars in each of the six sections were digitized within a geographic information system. It is our intent to incorporate imagery collected following future streamflow management activities as a means to document and quantify the effects on the area and distribution of emergent sandbars in these reaches.

INTRODUCTION

The Platte River valley is a combination of open, shallow, braided river channels, grasslands, and low wet meadows. All of these features contribute to the areas designated as critical habitat for the interior least tern and the piping plover, both of which rely on emergent ephemeral sandbars for nesting and foraging (Faanes and Lingle 1995). High discharge, large bed-sediment load, and increased channel width are conditions responsible for channel instability, which in turn creates emergent sandbars (Karlinger et al. 1983, Lyons and Randle 1988). Historically, spring runoff was capable of producing such conditions; since then, river flow has been increasingly regulated so that seasonal in-channel sandbar development has been insufficient for the needs of the species (U.S. Department of the Interior 2003). The absence of high flows and the subsequent decrease in transport of sediment during these flows have prevented the creation of new sandbars, as well as the redistribution of existing sandbars (Crowley 1981, Lyons and Randle 1988). Without the regular redistribution of sandbars and natural scouring, vegetation has stabilized sandbars, and created vegetated islands (Williams 1978, Eschner et al. 1983, Currier 1997, Faanes and Lingle 1995). These changes in the channel morphology have prompted channel mitigation measures, and while these efforts may help in the recovery of the river, as well as the recovery of the endangered species, results are less effective if they cannot be quantified. For this reason, aerial infrared thermography was employed as a technique for measuring, mapping, and evaluating emergent sandbars.

There have been many attempts to document the changes in the channel, as well as assess the effectiveness of management techniques along the Platte River. Williams (1978) illustrated the nature of the narrowing channel by comparing photographs from the early 1900's to photographs from 1977. Low-level aerial photographs were used by Crowley (1981) to supplement ground observations of channel characteristics; while Karlinger et al. (1983) investigated channel width changes by comparing 1860 map information to aerial photographs taken between 1971 and 1979. Water depth was measured by topographic surveys, and channel slope was measured from U.S. Geological Survey 7.5-minute topographic quadrangles. For the purposes of displaying changes in river geometry, Zelt and Frenzel (1996) surveyed habitat characteristics near Grand Island in 1993 through 1995.

More closely related to the work described in this paper, Sidle and Ziewitz (1990) described the use of an aerial videography system for quantifying habitat by determining total channel area, sandbar area, and permanent vegetation measured from video scenes that were selected and analyzed with image-processing tools. Currier (1997) used aerial videography collected between the years 1988 to 1994 to document both physical and biological changes in the Platte River. Furthermore, Tracy (2004) investigated the effects of river discharge on channel geometry by comparing the differences between two types of sandbars present in study sites on the Missouri River. Emergent sandbars were surveyed and mapped to measure their extent, and thus, determine available habitat for a variety of species.

SITE SELECTION

Six sections approximately 1-kilometer in length between Lexington and Grand Island were chosen for geomorphic analysis using aerial infrared thermography (figure 1). The sections were chosen for their proximity to river stage gages, and from west to east are: 1) Overton (at the bridge), 2) Kearney (also at the bridge), 3) Rowe Sanctuary (approx. 2 km west of the Gibbon bridge), 4) Prosser (approx. 5 km west of the Wood River bridge), 5) Doniphan (approx. 6 km east of the Alda bridge), and 6) Grand Island (approx. 0.5 km southwest from the U.S. 34 bridge). Of the six sites, two are located at bridges, (Overton and Kearney), two sites are located in areas where the channel carries the total flow of the river, (the Prosser and Grand Island reaches), and two sites are located in areas where a braided channel carries only a portion of the flow (the Rowe Sanctuary and the Doniphan reaches). The Overton and Kearney sites are located at bridges where the flow is constricted and the channels tend to be deeper. The Grand Island and Prosser sites are in reaches of river where the braided channels come together, and contain the total flow of the river. The Doniphan and Rowe sites are in reaches of the river where the flow is divided between multiple channels, and each only receives a fraction of the total flow.

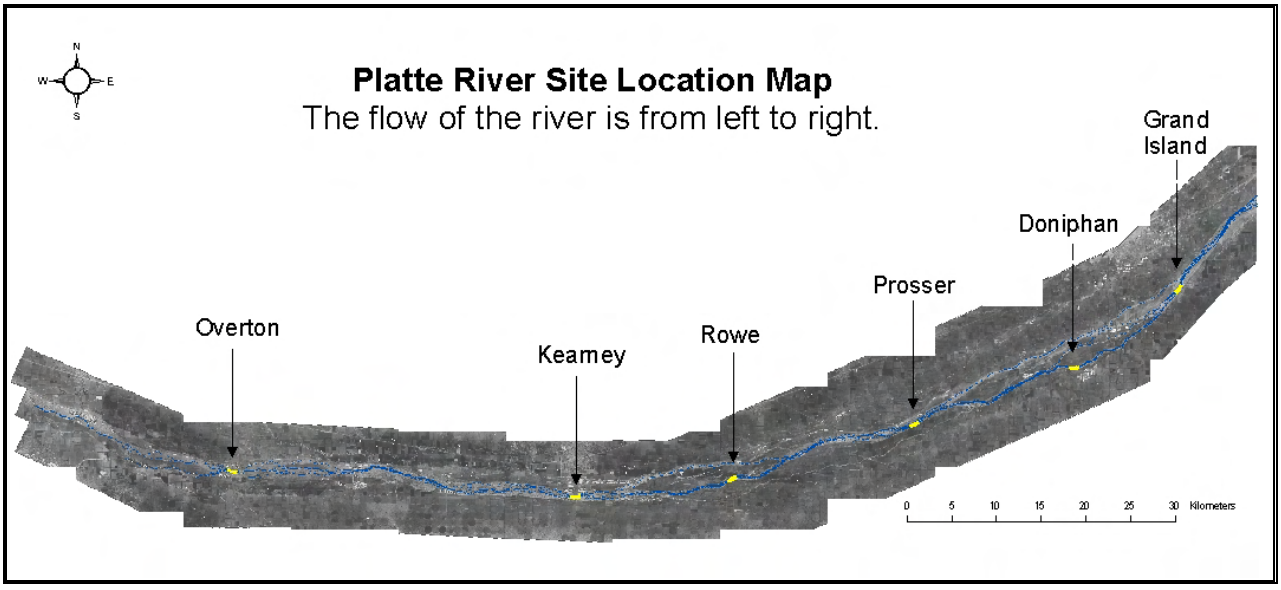


Figure 1 Map of the Big Bend reach of the Platte River. The selected sites for analysis are labeled and outlined in yellow. The USGS gaging stations are located at Overton and Grand Island.

METHODS

In shallow water depths such as those found in the Platte River, identifying the spatial extent of emergent sandbars requires sufficient contrast between water and land surfaces. Resolving these boundaries with traditional aerial imagery such as natural color, black and white, and even color infrared photography can be extremely difficult. Mapping the perimeters using ground-based survey techniques can provide the required accuracy, but the coverage can be spatially limited and the process is labor intensive. Aerial infrared thermography, however, provides both the necessary resolution of the land-water interface and the desired coverage with minimal labor.

Aerial thermal infrared video was collected from a Cessna 182 aircraft equipped with a 512 x 512 pixel camera mounted vertically in the underside of the aircraft. The camera had a Platinum Silicide Schottky_Barrier IRCSD detector with a detectable wavelength band of 3 to 5 microns and an infrared polarized f50 mm, F 1.2 lens with a field of view of 14 degrees horizontal by 11 degrees vertical. The image display was monochromatic with 256 gray levels. Images were displayed in a grayscale format where warm objects (such as water) appeared black to dark gray, while cold objects (such as land surrounding the river and wildlife) appeared white to very light gray.

The aerial thermal infrared video was collected in the third week of March each year from 2000 through 2003, and again in 2005. The aircraft was flown over the Big Bend, a 145-kilometer reach of the Platte River in central Nebraska, from Lexington to Grand Island throughout the night hours (figure 1). The pilot navigated over the river by noting his instantaneous position plotted on maps of the area. The pilot had control of the video output during the entire flight so that adjustments could be made to produce a clearer image at the pilot's discretion. In some instances, the black and white representations of object temperatures were reversed if it appeared that a better image could be generated. The flight altitude was roughly 1200 meters above the ground and parallel to the ground whenever possible to prevent any unnecessary distortion to the images. Video was stored on digital videocassettes, which were then viewed on a desktop personal computer with video-editing software where the individual images were captured and stored. The date, time, UTM coordinates, altitude, and air speed were displayed within the video frame, so that each frame was 'stamped' with this information (figure 2). The date and time on the image was later used to obtain streamflow data from gaging records for that particular moment.

After the images were captured from the video, they were then registered to a 2001 Platte River black and white digital orthorectified mosaic using geographical information system software. Each video image was anchored to the mosaic at four to six select points that fell within each quadrant of the image. The root mean square (RMS) of each registered image was less than 2.0 pixels, ensuring the best possible fit. Each registered image overlapped the next image to create a seamless mosaic for digitization.

Once the black and white images were registered, for each year and site, the river segment channel margins, vegetated sandbars, and emergent sandbars were digitized. The digitization process first involved defining the area considered as active channel. Areas within the channel having permanent vegetation were defined as vegetated bars. The areas considered as permanently vegetated were chosen from the 1998 Bureau of Land Management color infrared orthophotographs (U.S. Department of the Interior 1999). The areas devoid of permanent vegetation, or the total channel area minus the area of permanently vegetated bars, were defined as the active channel. Sandbars were defined as emergent features within the active channel identifiable in the thermal images by their contrasting white color in the dark gray river (figure 2). The features (total channel area, vegetated bars and sandbars) were then digitized by defining their boundaries with a series of points that once connected, formed a solid polygon area. Once digitization of all features was completed, the areas of each sandbar, vegetated bar, and active channel area for each site were tabulated.

Sandbar lengths and segment lengths were also tabulated for each night in order to compute the braiding index for each segment using a modification of Williams' (1978) definition for braiding index. William's definition sums the length of islands within the given reach divided by the length of the reach measured midway between the banks. The modified definition includes sandbars as well as vegetated bars (or islands) in the calculation because both contribute to the braiding. Consequently, the braiding indices appear to be quite high in recent years. The modified braiding index could be misleading in 2005, because as the sandbars integrate, fewer larger bars are created, replacing the numerous smaller bars. For this reason, only the relative degree of braiding between sites is considered here.



Figure 2 Aerial thermal infrared image from the Rowe Sanctuary site in 2003. The dark areas are wetted channel and the white areas are sandbar or vegetated bar.

RESULTS

By creating a series of time-lapse maps illustrating the progression of braiding and sandbar development, a geomorphic view of the river emerges over time. Because the video is able to capture a snapshot of the river over one night, the entire section of channel can be evaluated at that exact moment. Furthermore, the nighttime discharge into and out of the study reach is known at the Overton and Grand Island stream-gages, and when paired with the video images, allows evaluation of the sandbar morphology associated with a specific discharge through the study reach. The discharges into and out of the reach are presented in table 1.

Table 1 Instantaneous discharges reported at the upstream and downstream ends of the Big Bend study reach, Platte River, Nebraska.

Date (m/dd/yyyy)	Discharge at Overton (in cms)	Discharge at Grand Island (in cms)
3/27/2000	79.85	85.23
3/26/2001	25.63	41.63
3/27/2002	48.99	19.00
3/25/2003	11.07	18.49
3/27/2005	28.32	22.23

For the Rowe Sanctuary site, the channel morphology was captured by the video on more than one night for each year, displaying emergent sandbar development and braided channel behavior for multiple discharges (figure 3). Qualitatively, what was once a wide, single-thread channel has progressively narrowed and become braided with numerous smaller channels. Sandbars have emerged and begun to close off the channel in some areas. Quantifying attributes such as total sandbar area, sandbar area as a percent of the total area, and braiding index from the digitized features provides a numerical depiction of the changes occurring in the channel.

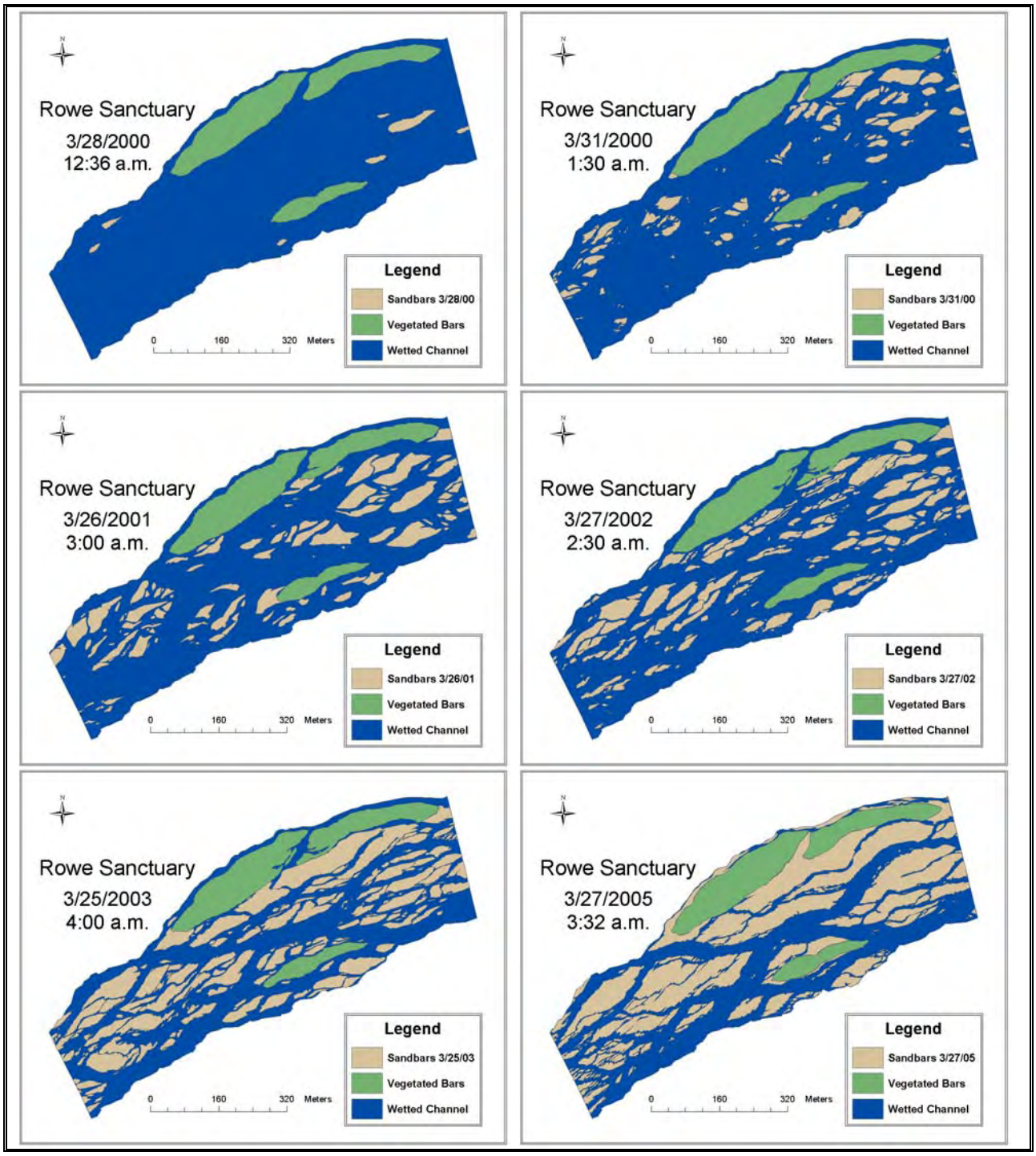


Figure 3 Changes in channel morphology of the Rowe Sanctuary site from 2000 through 2003, and 2005.

The total sandbar area was tabulated for each of the sites and then calculated as a percent of the total channel area. The results show that Rowe and Doniphan, both sites containing only part of the total flow, had a higher sandbar percent of total area than the other sites. Prosser and Grand Island, sites containing the total flow of the river, had a generally lower percentage of sandbars (figure 4). All but two sites (Overton and Prosser) had a progressive increase in sandbar area from 2000 to 2005.

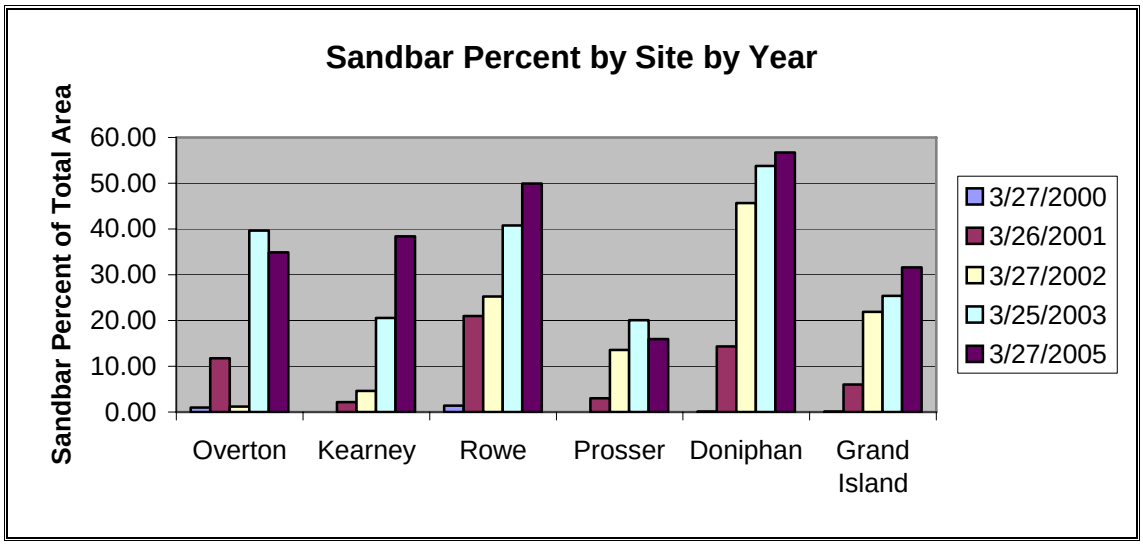


Figure 4 Chart displaying the percent of total area occupied by sandbars at each site by year.

The braiding index was also calculated for each year at each site using Williams' (1978) definition of total sandbar and vegetated bar lengths divided by stream segment length. These results showed that the channel morphology at both the Rowe and Doniphan sites was more braided than at the other sites, while the channel at Overton and Kearney, both at bridge segments, was less braided (figure 5). Most sites show a progressive increase in braiding index, at least through 2003.

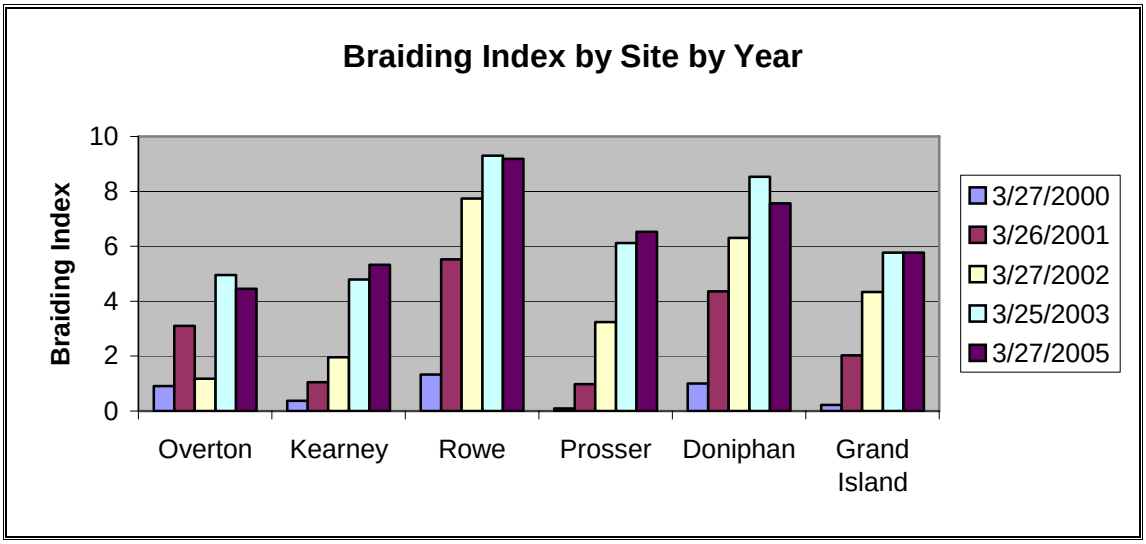


Figure 5 Chart displaying the braiding index at each site by year.

CONCLUSIONS

The use of aerial infrared thermography can be quite effective for mapping the spatial extent of emergent sandbars and consequently, the available habitat for endangered species. It is also a process by which a large amount of data can be collected and analyzed with a small amount of labor. When paired with other surveying techniques or other forms of aerial photography, it can be a very powerful tool.

The amount of subaerial sandbar area changes regularly as water-management practices in the Central Platte River change each year. This paper proposes a method of measuring that area for the purposes of habitat mapping and

evaluation. In the event of one or more scheduled pulse flows along the Platte River, aerial infrared thermography could be utilized as a means to detect changes in the geomorphology of the channel. By pairing this information with discharge and stage information, conclusions may be drawn about the effects of hydrology on channel morphology.

Any use of trade, firm, or product names is for descriptive purposes only and does not imply endorsement by the U.S. Government.

REFERENCES

Crowley, K.D., 1981, Large-scale bedforms in the Platte River downstream from Grand Island, Nebraska- structure, process, and relationship to channel narrowing. U.S. Geological Survey Open-File Report 81-1059, 32p.

Currier, P.J., 1997, "Woody vegetation expansion and continuing declines in open channel habitat on the Platte River in Nebraska," Proceedings of The North American Crane Workshop, v. 7, p. 141-152.

Eschner, T.R., Hadley, R.F. and Crowley K.D., 1983, Hydrologic and morphologic changes in channels of the Platte River Basin in Colorado, Wyoming, and Nebraska. A historical perspective: U.S Geological Survey Professional Paper 1277-A, 39 p.

Faanes, C.A., Lingle, G.R., 1995, Breeding birds of the Platte River Valley of Nebraska. Jamestown, ND: (Version 02SEP99) Northern Prairie Wildlife Research Center, accessed Feb 14, 2005 at URL http://www.npwrc.usgs.gov/resource/distr/birds/platte/platte.htm.

Karlinger, M.R., Eschner T.R., Hadley R.F., and Kircher J.E., 1983, "Relation of channel width maintenance to sediment transport and river morphology: Platte River, South-Central Nebraska," U.S. Geological Survey Professional Paper 1277-E, 19 p. 184-207, in Hydrologic and geomorphic studies of the Platte River Basin: U.S. Geological Survey Professional Paper 1277, 258 p.

Lyons, J.K., and T.J. Randle, 1988, Platte River channel characteristics in the Big Bend Reach - Prairie Bend Project. U.S. Department of the Interior, Bureau of Reclamation, Denver, Colorado, 28 p.

Sidle, J.G., and J.W. Ziewitz, 1990, Use of aerial videography in wildlife habitat studies. Wildlife Society Bulletin, v. 18, p. 56-62.

Tracy, E., 2004, "Effects of discharge on sandbar morphometry between two types of sandbars," in the 8th Annual Missouri River Natural Resources Conference 2004: Rediscovering Missouri River Connections, accessed February 9, 2005 at URL http://infolink.cr.usgs.gov/Events/Conferences/mrc04/abstracts/postexhib.asp.

United States Department of the Interior, 1999, Platte River color-infrared (CIR) digital orthophotos, Remote-sensing image. Denver, Colorado, June 3, 1999.

United States Department of the Interior, 2003, Platte River recovery implementation program draft environmental impact statement.

Williams, G.P., 1978, The case of the shrinking channels- the North Platte and Platte Rivers in Nebraska. U.S. Geological Survey Circular 781, 48 p.

Zelt, R.B., Frenzel, S.A., 1996, "Physical-habitat characteristics of the Platte River, Nebraska—assessment using surveys and spatial analyses," in Proceedings of the Sixteenth Annual ESRI User Conference, ESRI, 1996. Palm Springs, California, 1996.

MODELING OF SPECIAL HIGH-FLOW RELEASES ALONG PLATTE RIVER IN CENTRAL NEBRASKA

Mohammed A. Samad, Ph.D., P.E., Hydraulic Engineer, U.S. Bureau of Reclamation, Sedimentation and River Hydraulics Group, Denver, Colorado, msamad@do.usbr.gov, Timothy J. Randle, P.E., Supervisory Hydraulic Engineer, U.S. Bureau of Reclamation, Sedimentation and River Hydraulics Group, Denver, Colorado, trandle@do.usbr.gov

Abstract: The Platte River is a wide and shallow sand-bed river. Reservoirs in the watershed above the Platte River have reduced flows in the downstream river channel and trapped sediments. As a result, the river channel has narrowed and vegetation has encroached into the formerly wide channel. The reduction in channel width has reduced habitat for endangered migratory birds. Special high-flow releases are now being considered from certain local reservoirs to scour seedling vegetation from mechanically cleared areas of the river channel in an attempt to restore some habitat for the endangered migratory birds.

An unsteady flow model has been developed for the Platte River from Overton to Grand Island, Nebraska (from river miles 239.3 to 167.9), to route the special-high flow release along the river channel. The model predicts the magnitude and duration of peak flow and stage as the flow is routed downstream. The model uses the HEC-RAS computer program as a foundation for the unsteady flow modeling. This model was supplemented with a new procedure to simulate the losses to and gains from groundwater and bank storage. The model has been calibrated against measured fluctuating flow hydrographs near Kearney, Nebraska (river mile 215.0) by routing the measured flow hydrographs from the upstream end of the model reach near Overton, Nebraska. In the calibration process, it has been found that a hydraulic model that only considers unsteady flow routing, without losses to and gains from bank storage and groundwater can not replicate the measured flow hydrograph in a natural channel such as Platte River in central Nebraska. A new procedure has been developed to account for these losses and gains in the routing process. In addition, the calibration process has also taken into consideration the roughness in order to accurately match the lag time of the hydrographs. The model is being used to help design a special high-flow release planned for the future.

INTRODUCTION

The Platte River, flowing through the state of Nebraska, provides habitat for endangered migratory birds, including the whooping crane, interior least tern, and piping plover. The habitat of these migratory birds has degraded over the 20th century (National Research Council of the National Academies, 2005). As part of the habitat improvement program, the U.S. Fish and Wild Life Service is planning special high flow release from local upstream reservoirs to scour seedling vegetation from mechanically cleared areas of the Platte River in an attempt to restore the habitats of these endangered species (U.S. Department of the Interior, Bureau of Reclamation and Fish and Wildlife Service, 2003).

An unsteady flow model is being developed by Bureau of Reclamation to route the planned special high-flow release from local upstream reservoirs through the Platte River from Overton

to Grand Island, Nebraska (river miles 239.3 to 167.9). The results of this model development and its application to the Platte River are reported in this paper.

MODEL DEVELOPMENT

The HEC-RAS computer program (U.S Army Corps of Engineers, 2002) is used as the foundation for the unsteady flow model. Cross sections of the Platte River, in central Nebraska, have been surveyed during 1989, 1998 and 2002. The cross-section network was initially established and surveyed in 1989. A total of 90 cross sections were surveyed from North Platte to near Grand Island, Nebraska (river miles 310.5 to 157.1) with an average longitudinal spacing of 1.7 miles between two successive cross sections. A cross section was surveyed at each bridge crossing along with cross sections 0.1 mile upstream and 0.1 mile downstream from the bridge. Various subsets of the 1989 cross sections (excluding bridge cross sections) were resurveyed in 1998 and 2002. The bed and banks of the Platte River are composed primarily of sand and there are typically multiple channels separated by vegetated islands. The cross-section surveys include all channels of this sometimes braided, anastomosing, and anabranched river.

Initially, a Manning's *n* roughness coefficient of 0.035 was assigned to the main channel and a coefficient of 0.07 was assigned to the overbank area. The main channel roughness coefficient was revised during the calibration process. The cross sections from near Overton to near Grand Island, Nebraska (river miles 239.3 to 157.1) were used to construct the geometry of the river model. The most recent survey data were used to represent each river cross section. Cross-sections were interpolated every 500 feet in between measured cross sections to route unsteady flows without causing instability in the solution scheme of the HEC-RAS computer program. The upstream boundary condition of the model was the hydrograph near Overton, Nebraska and the downstream boundary condition was the assumption of normal depth at River mile 157.1 with average river slope of 0.00126.

The loss of flow to bank storage during the rising limb of the hydrograph and gain from bank storage during the falling limb of the hydrograph is accounted for by a special program developed by the authors. Also river losses to or gains from the surrounding groundwater table are accounted for by introducing a groundwater flow hydrograph that is separate from the flow to or from bank storage.

MODEL CALIBRATION

Fluctuating flow hydrographs were generated by the hydro-cycling operation from the upstream power plants. The two measured fluctuating flow hydrographs near Overton, Nebraska were used to calibrate the unsteady flow model:

1. March-April flows of 2002 and
2. February-March flows of 2005

First, the model was used to route the 2002 flow hydrograph with the initial Manning's *n* roughness coefficients of 0.035 and 0.07. With these roughness coefficients, the start of flow rise near Grand Island (71 miles downstream from Overton) was predicted to occur 15 hours after the measured start of rise flow (see figure 1). Therefore, the Manning's *n* roughness

coefficient was reduced to shorten this 15-hour lag time. Since the flow did not overtop the banks, only the main channel roughness coefficient was varied.

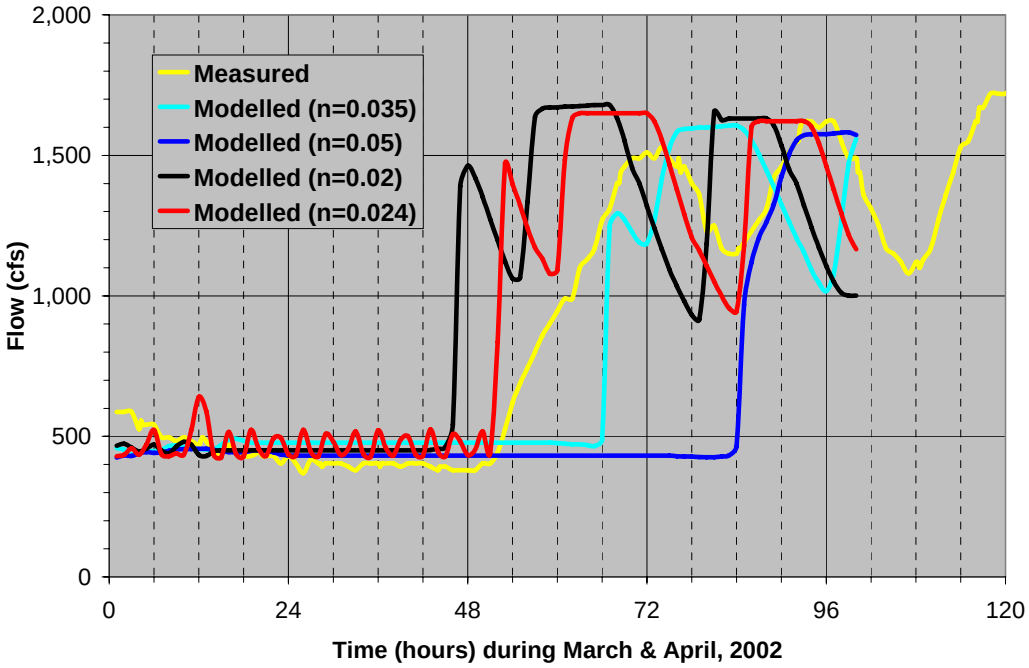


Figure 1 Comparison of measured and modeled hydrographs near Grand Island, Nebraska for various Manning's *n* roughness coefficients applied to the fluctuating flow period during March and April 2002

A regression analysis was then made between the lag time (time difference between predicted and measured start of rise) and main channel *n* values (see figure 2). The calibrated roughness coefficient corresponding to the desired lag time is 0.024. For verification, the predicted and measured start of flow rise was compared for the Platte River near Kearney, Nebraska (see figure 3). However, the peaks and volumes of the four routed discharge waves were over predicted.

Measured and modeled hydrographs near Kearney, Nebraska and the difference in flow between the two were plotted on the same time line (see figure 4, yellow and light-blue lines). A definite trend of losses to and gains from groundwater and bank storage was noticed. The losses to bank storage are associated with the start of rise of the first hydrograph wave, with maximum loss rate occurring just before the peak of each hydrograph wave. The gains from bank storage start after the river flow recedes and reach a maximum rate at about 50 percent of the peak stage above the base flow.

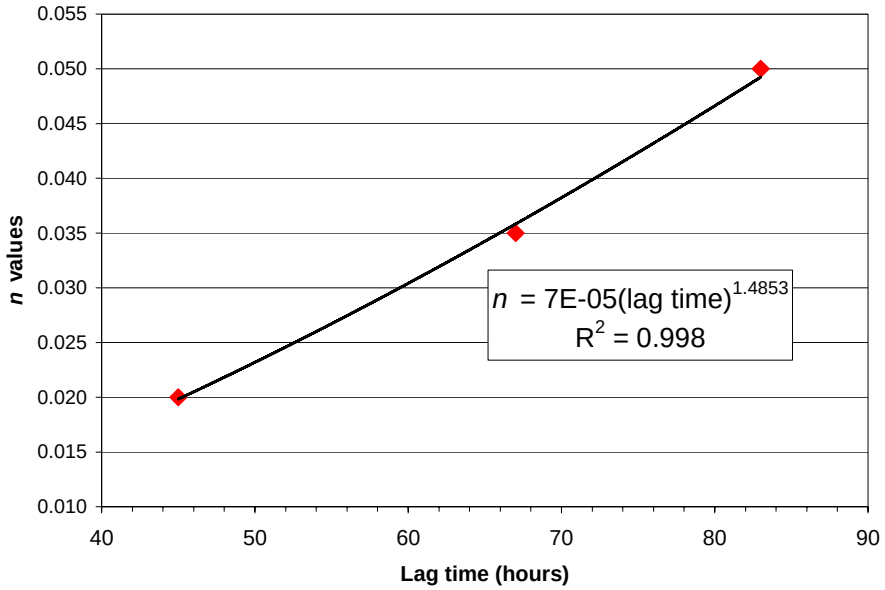


Figure 2 Lag Time near Grand Island, Nebraska versus Manning's *n* value

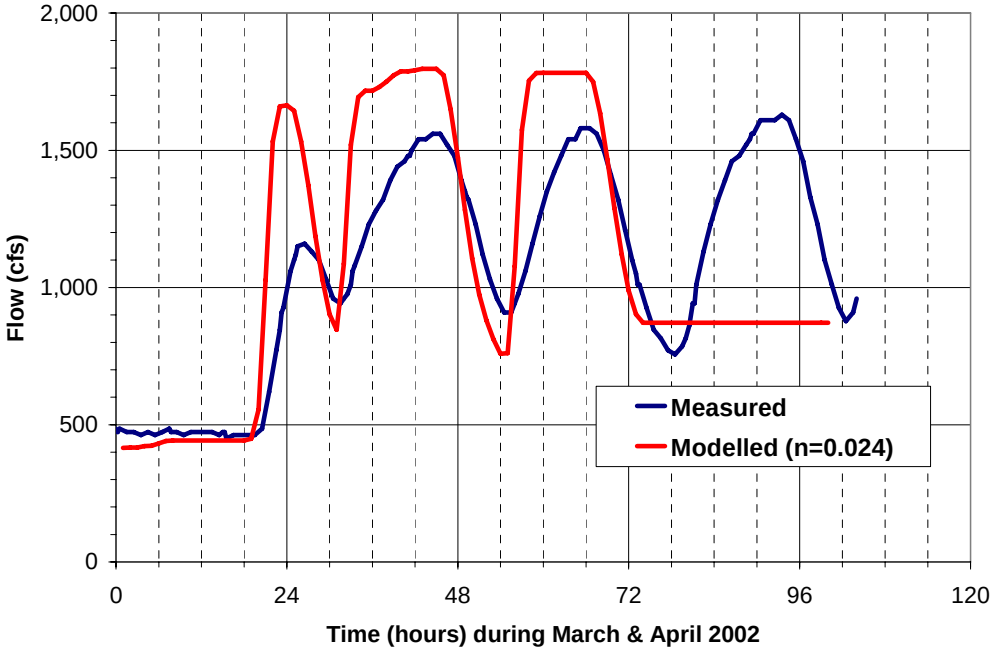


Figure 3 Comparison of measured and modeled hydrographs near Kearney, Nebraska applied to a fluctuating flow period during March and April 2002. The calibrated roughness coefficient of 0.024 was verified because the predicted start of flow rise matches the measured start of flow rise.

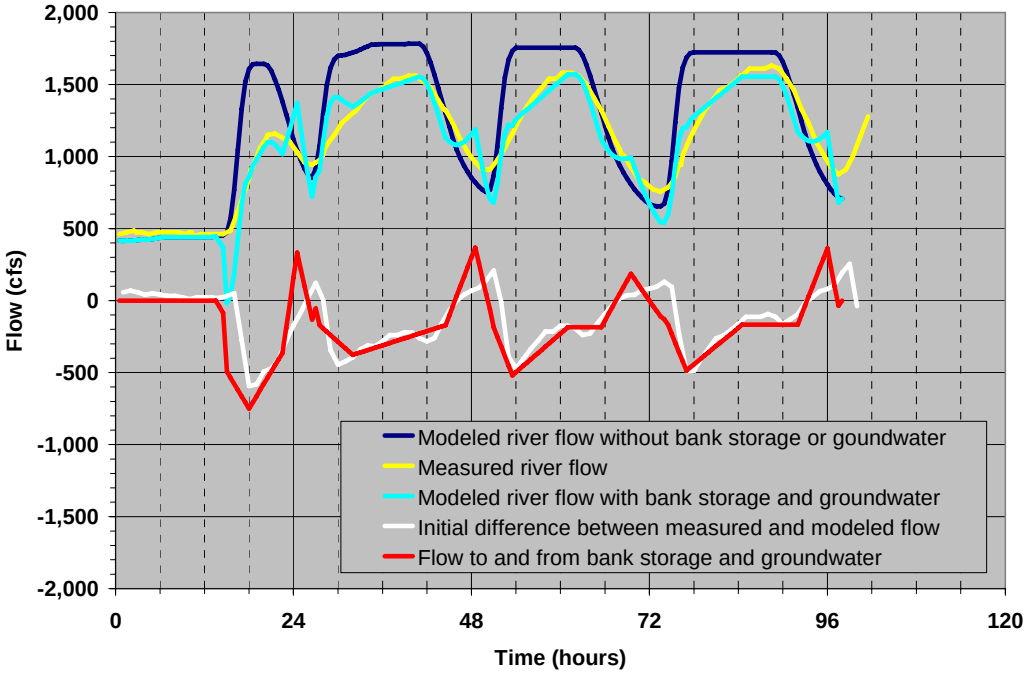


Figure 4 Comparison of measured and predicted unsteady flows on the Platte River near Kearney, Nebraska, March-April 2002

In order to match the modeled hydrograph with the measured hydrograph, two addition hydrographs are employed to simulate flow to and from bank storage and flow to or from groundwater:

1. A triangular hydrograph was to account for losses of river flow to bank storage during the rising limb of the river-flow hydrograph and gains to river flow during the falling limb of the river-flow hydrograph
2. A groundwater inflow or outflow hydrograph was used to account for river flow losses to or gains from the surrounding groundwater, independent from bank storage.

Losses to bank storage during the rising limb of the river-flow hydrograph were assumed to be equal to the gains from bank storage during the falling limb, so there is no net loss or gain in river flow over the period of simulation. When the losses to or gains from groundwater are added to the bank storage, the result is the net flow into and out of the river bank and groundwater.

The model procedure for flow to and from bank storage is presented in figure 5. The flow of river water to bank storage begins at t_0, which is has a lag time (Lag) of 1 or 2 hours after the start of rise in the river flow. The peak rate of flow to bank storage (Q_L) occurs at t_1, which corresponds to 97 percent of the maximum stage increase above the base flow. The end of river flow to bank storage occurs at t_2 ($\Delta t_2 = a\Delta t_1;\ a = 1 \text{ to } 3$). When the duration of the peak flow is long enough (Δt_3), there is no flow to or from bank storage. Flow return from bank storage begins at some lag time (t_3) after the decrease in river flow. The peak rate of return flow from

bank storage (Q_G) occurs at t_4, which corresponds to 45 percent of the maximum stage increase above the base flow. The end of return flow from bank storage occurs at t_5 ($\Delta t_5 = 5\Delta t_4$).

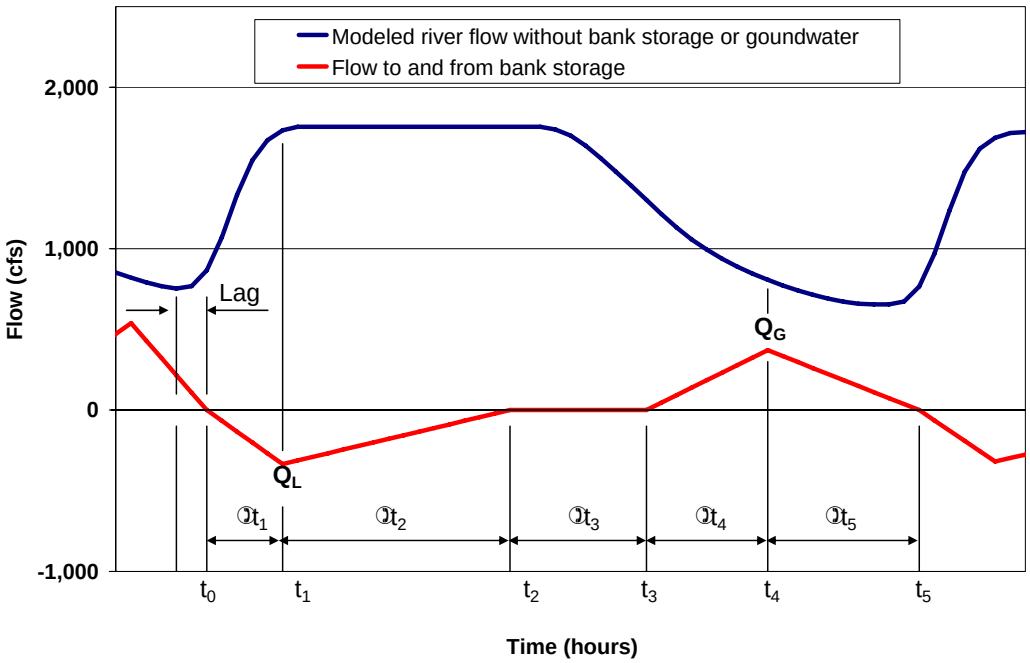


Figure 5. Model procedure of hydrograph flow to and from bank storage.

For the fluctuating flows of 2002, the discharge waves of the measured hydrograph near Kearney, Nebraska have less flow volume than the modeled hydrograph without considering bank storage or groundwater (see figure 4, yellow and blue lines). This volume difference means that there is a net loss to ground water. The actual bank storage volume is not precisely know, but, based on calibration, was found to be approximately equal to 50 percent of the flow volume difference between the measured hydrograph and the modeled hydrograph without bank storage or groundwater (see figure 4, white line). The net change in river flow due to bank storage and groundwater flow was determined (see figure 4, red line) and applied to the HEC-RAS model results to predict the final hydrograph (see figure 4, light blue line). The predicted hydrograph agreed well with the measured hydrograph (see figure 4, yellow line).

For the fluctuating flows of 2005, the discharge waves of the measured hydrograph near Kearney, Nebraska have more flow volume than the modeled hydrograph without considering bank storage or groundwater (see figure 6, yellow and blue lines). This volume difference means that there is a net gain from ground water. The bank storage volume was again modeled as equal to 50 percent of the flow volume difference between the measured hydrograph and the modeled hydrograph without bank storage or groundwater (see figure 6, white line). The net change in river flow due to bank storage and groundwater flow was determined (see figure 6, red line) and applied to the HEC-RAS model results to predict the actual hydrograph (see figure 6, light blue line). These predicted hydrograph results also agreed well with the measured hydrograph (see figure 6, yellow line).

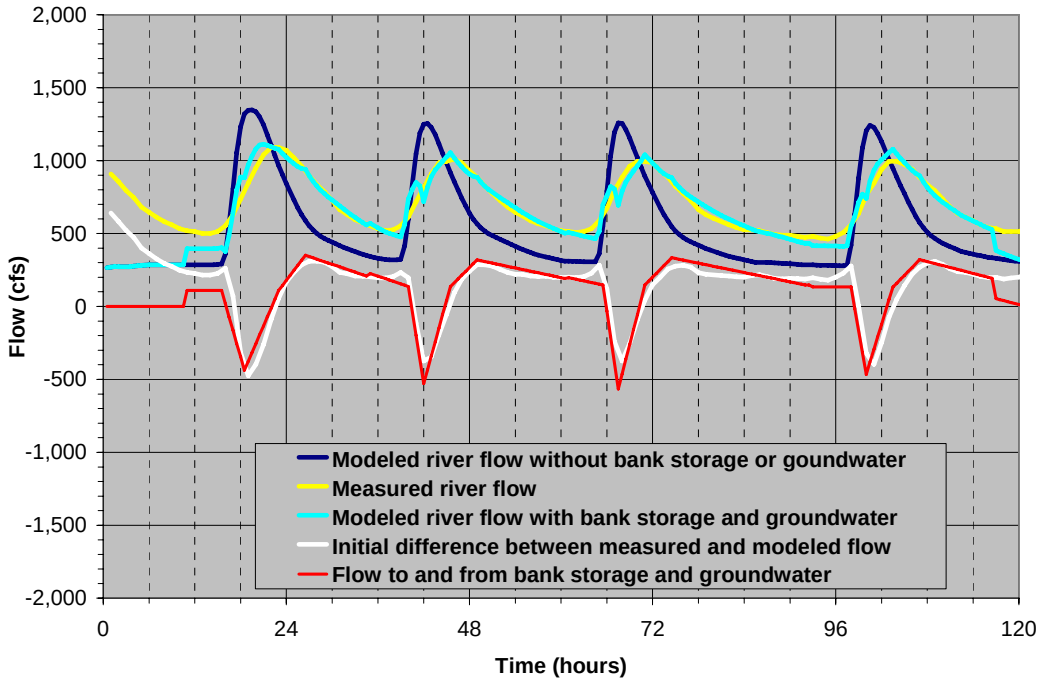


Figure 6 Comparison of measured and predicted unsteady flows on the Platte River near Kearney, Nebraska, February 2005

The model procedure was applied to the design of a preliminary special high-flow release hydrograph for the Platte River. This hydrograph was routed from Overton to Kearney, Nebraska using the HEC-RAS model (see figure 7, medium-blue line). The model procedure was then used to adjust the hydrograph predicted by the HEC-RAS model. A net loss of river flow to groundwater was assumed at a rate of 200 ft^3/s. The bank-storage volume that was calibrated for the 2002 fluctuating flows was increased by a scaling factor to account for the longer duration of the special high flow release.

The hydrographs representing the losses to and gains from bank storage and the resulting net losses to groundwater are also shown in Figure 7 (see green and red lines). The adjusted hydrograph near Kearney has lower peak flows and less volume than the hydrograph modeled without bank storage or groundwater (see figure 7, light-blue line).

CONCLUSIONS

The HEC-RAS model alone was found insufficient to route unsteady flow through a channel with significant bank storage and groundwater flow. For the Platte River in central Nebraska, bank storage and groundwater flow are important processes that need to be considered for unsteady flow modeling of flows less than the bank-full discharge capacity.

The use of a triangular hydrographs to account for the flow to and from bank storage and the specification of a separate hydrograph to account for flow to or from groundwater works well for the Platte River in central Nebraska. The model procedure was successfully calibrated for periods of fluctuating flow in 2002 and 2005 with nearly the same calibration parameters. The

model procedure worked well for the two different conditions of a net loss of river flow and a net gain river flow to and from groundwater. Application of the model procedure to the design of a special high-flow release to scour seedling vegetation along the Platte River looks promising. Additional work need to be conducted to extend the model procedure downstream from Kearney to Grand Island, Nebraska.

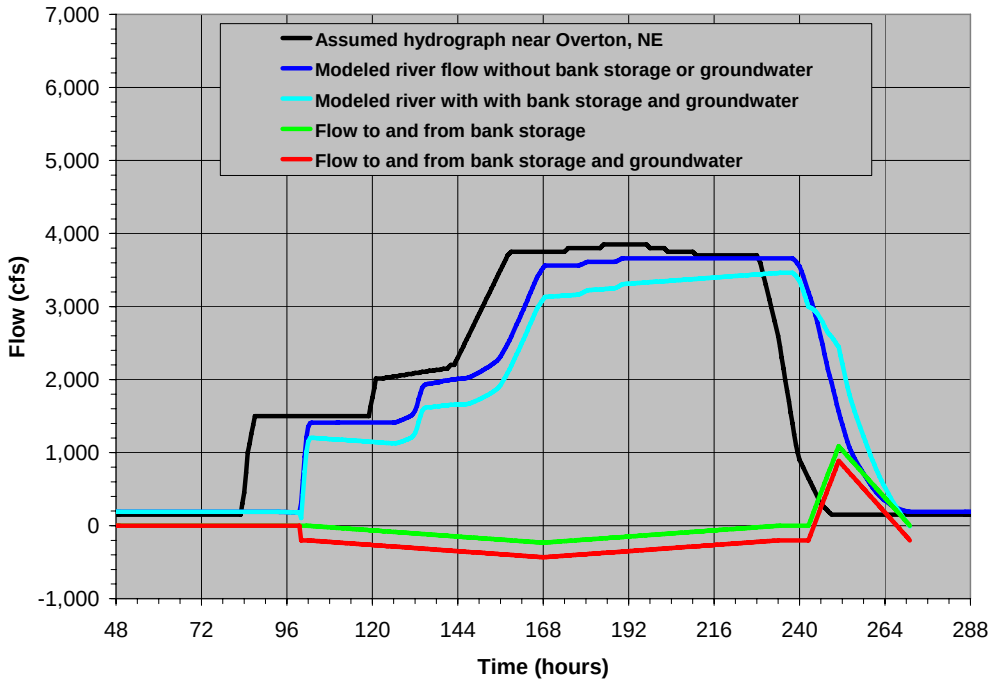


Figure 7 Predicted special-flow hydrograph routed 71 miles from Overton to Kearney, Nebraska.

REFERENCES

National Research Council of the National Academies (2005). Endangered and Threatened Species of the Platte River. Committee on Endangered and Threatened Species in the Platte River Basin, Board on Environmental Studies and Toxicology, Water Science and Technology Board, Division on Earth and Life Studies, The National Academies Press, Washington, DC.

U.S. Army Corps of Engineers (2002). HEC-RAS River Analysis System, Hydraulic Reference Manual, Version 3.1. Hydrologic Engineering Center, Davis, California.

U.S. Department of the Interior, Bureau of Reclamation and Fish and Wildlife Service, (2003). Platte River Recovery Implementation Program, Draft Environmental Impact Statement, Assessing Alternatives for Implementation of a Basinwide, Cooperative, Endangered Species Recovery Program. Denver, Colorado.

THE IMPLICATIONS OF RECENT FLOODPLAIN EVOLUTION ON HABITAT WITHIN THE MIDDLE RIO GRANDE, NEW MEXICO

Paul Tashjian, Hydrologist, Fish and Wildlife Service, Albuquerque, NM, Paul_Tashjian@fws.gov; Tamara Massong, Hydrologist, Bureau of Reclamation, Albuquerque, NM, tmassong@uc.usbr.gov

Abstract: Understanding the recent history (past 50 years) and current trends of river processes within the Middle Rio Grande (MRG) is important information for managing and restoring the current and future conditions of the MRG's fluvial-riparian habitat. During the past 50 years, flood control efforts have greatly reduced, and in many places eliminated, the connection between peak flows and floodplain surfaces. Pre flood-control processes include erosive banks, erosion of floodplain surfaces, and creation of floodplain surfaces. Disruption of these processes has affected the riparian community as well as the structure of native fish habitat.

Important physical factors determining the MRG's ability to maintain processes that create floodplain habitat include incision/aggradation rates, bankline mobility, sediment supply and the hydrograph. In order to assess the relative importance of these factors, a site-based physical habitat characterization of the MRG has been placed into sections defined by incision/aggradation rates. The MRG is divided into three of these sections, separated by transition zones, including: Section 1 (Sediment Supply Influenced Section) extends from Cochiti, NM to about Los Lunas, NM (~70 river miles), Section 2 (Uplift Influenced Section) extends from Arroyo Abo to Escondida, NM (~47 river miles), and Section 3 (Aggrading Section) constitutes the last 30 river miles is aggrading (Massong et al., 2006). Bankline complexity, bankline position and velocity distribution within the channel are used as surrogates for physical habitat characterization (Tashjian and Remshardt, 2005) in this study.

The majority of the historic floodplain within Section 1 is disconnected from the MRG at flows below 5000 cfs. Though often referred to as the "floodplain", this surface functions as a terrace and has been abandoned by river incision through flood and sediment control measures. Even when overbanking occurs, the flows do not contain the energy to disrupt the flooded surface. From Bernalillo, NM to Bernardo, NM (~75 river mile), jetty jack lines were placed in the mid 20^{th} century to stabilize bank locations. These structures, coupled with ensuing non-native vegetation, have 'frozen' the banklines creating a ~600 foot wide active channel corridor within the ~1800 foot wide "floodway". Within this corridor, active river processes are limited by upstream sediment supply and the hydrograph. The most vital modern habitat occurs in two parts of this Section; 1) south of Bernalillo in the transition from a multi to a single threaded channel, 2) from Isleta Diversion south where a floodplain-like surface has recently developed within the 600 foot wide corridor.

The most important shift for habitat within Section 2 is the cessation of the jetty jack defined river corridor and the input of sediment and high flows from unregulated tributaries. Where uplift of the Socorro Magma Body has produced a long history of river incision, the modern River has continued to create floodplain surfaces through bank erosion and bar growth associated with the occasional high discharge events. The result is complex in-channel fish habitat, and a

fairly complex age and class structure to the riparian community. The active river corridor for this Section is bound by uplifted terraces and ranges between 450 and 1200 feet.

Sections 3 contains some of the best habitat within the MRG, barring intermittence. Within these Sections, the MRG alternates between a wide, active channel and a narrow, channelized river with frozen banks. Connected floodplain surfaces within the wider sections include both in-channel bar and island surfaces and true floodplain surfaces, creating an active river corridor that ranges between 1200 and 6000 feet.

This assessment suggests that habitat quality within the Middle Rio Grande is primarily dependent upon sediment supply, the variability of the hydrograph and bank mobility. The physical processes associated with channel incision/aggradation are interrelated to, though not solely explained by these processes. In Section 1, where incision is associated with a reduction in sediment caused by reservoir operations, habitat quality is, in general, poor. The degradation associated with the incision in Section 1 is compounded by immobile banks and an altered hydrograph. In Section 2 where incision is associated with the uplift of the Socorro Magma body, sediment supply is sufficient, banks are more mobile, and the hydrograph is more variable in both low flow and peak flow variability than found in Section 1: the result is better habitat.

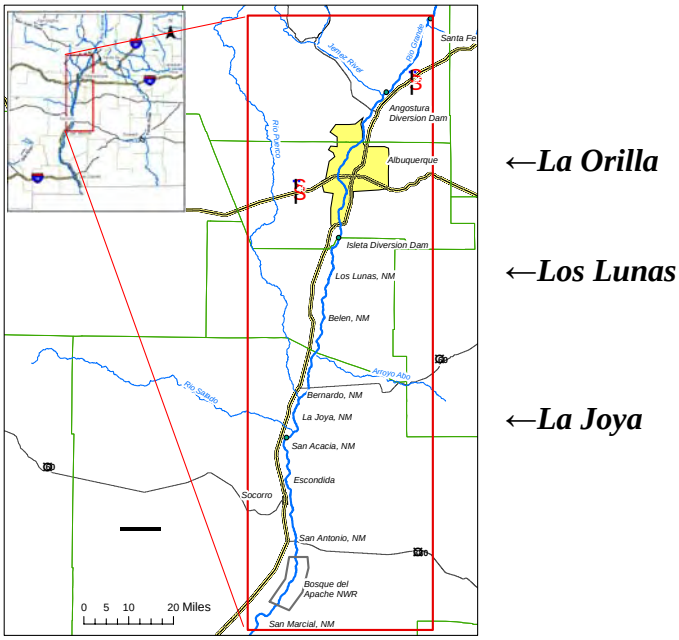


Figure 1 Location of the Middle Rio Grande within the State of New Mexico with locations of habitat sites.

INTRODUCTION

The Middle Rio Grande (MRG) of New Mexico encompasses roughly 170 river miles from the Cochiti Reservoir to the headwaters of Elephant Butte Reservoir and sits at a juncture between fairly intact mainstem Rio Grande ecosystems to the north and primarily denuded ecosystems to the south (Figure 1). There has been a considerable amount of focus on the physical-ecological functioning of the Middle Rio Grande over the past decade (Crawford et al., 1993: Robert,

2005). Recent work by Massong et al. (2006) describes recent incision patterns within the Middle Rio Grande. This paper discusses how habitat quality differs within the incision segments and relates any differences to the primary physical functions of sediment supply, hydrographic diversity and bankline stability.

DATA AND METHODS

Massong et al. (2006) utilize a variety of data to assess the degree of channel incision throughout the MRG which includes: terrace maps in the high incision areas, field observations of bank heights to assess degree of incision especially where terrace maps do not currently exist, review of historical and current bed elevation data, aerial photography to better define active floodplains, and GIS base layer/map. The incision based delineation of the MRG derived from the above analysis is used as a basis for weighing the importance of key physical processes for habitat quality within this paper.

The original and complete habitat data are found in Remshardt and Tashjian (2005), which describes habitat quality within the MRG in a variety of geomorphic provinces. Field collected data for habitat quality for this study included: 1) shoreline position and complexity as a function of discharge, 2) in-channel physical characteristics including velocity distribution, depth distribution, sediment distribution, and flow angle distribution, 3) cross sectional response to flow regime. Each site is roughly 0.75 miles length and contains 4 evenly spaced transects where physical characteristics are measured every 4 feet. Although 10 sites were surveyed in the original study, data from only three sites are presented here.

Remshardt and Tashjian (2005) describe habitat quality within the Middle Rio Grande using the above data, however, for this discussion we discuss bankline position and velocity distribution since these parameters can be easily compared and addressed. Shoreline position and complexity are meaningful habitat surrogates for the MRG since they demonstrate shoreline accessibility as a function of flow and complexity of the bank-floodplain interface. A reach that contains a mobile bankline and a complex bank-floodplain interface is considered better habitat as it represents areas where there is greater channel-floodplain connectivity. Greater amounts of active floodplain surfaces benefit both the native riparian species and native fish species (Remshardt et al., 2003; Crawford et al., 1993). In-channel velocity profiles are meaningful habitat surrogates for the MRG since they demonstrate the complexity of fish habitat. A reach that contains greater diversity of velocities within the channel at varying flow levels is considered better habitat since it satisfies the habitat requirements of native fish species and associated life stages (Remshardt et al., 2003). These data have been compared with the incision descriptions from Massong et al. (2006) to form a broader understanding of habitat.

RESULTS

The three sites selected for discussion in this paper are La Orilla, La Joya and Los Lunas (Figure 1). Each of these sites represents different habitat reaches of the Middle Rio Grande, as defined by Remshardt and Tashjian (2005), and have different incision character as defined by Massong et al. (2006).

The La Orilla Site which has a moderate-high incision character (Reach 3 from Massong et al., 2006) is located near Albuquerque, NM in the Albuquerque Valley Habitat Reach (Remshardt and Tashjian, 2005). This Site is typified by banks that are frozen in place by jetty jack lines (Figure 2), and a relatively tall abandoned floodplain. The site receives only a moderate amount of sediment supply and has a limited hydrograph. During the calendar years of 2000 through 2004, daily mean flows were between 100cfs and 1000cfs 95% of the days. Due to the frozen bank positions in this reach and an abandoned floodplain, flows in this range supply the in-channel habitat with very homogeneous velocity habitat availabilities (Figure 5). This site is considered poor habitat (Remshardt and Tashjian, 2005).

The La Joya Site is in the Sevilleta Habitat Reach of the MRG (Remshardt and Tashjian, 2005), has a high amount of incision (Reach 8 from Massong et al., 2006), however this site has good habitat. This Site is typified by bankline positions that vary with increasing flow (Figure 3) and associated floodplain surfaces at moderate (200cfs-500cfs) flow levels. Due to tributary input, this site has a larger sediment supply than the La Orilla Site and a hydrograph that is more diverse in the low, mid, and high flow ranges. The velocity profiles for the site are diverse at all flow ranges (Figure 6).

The Los Lunas Site is in the Isleta Habitat Reach of the MRG (Remshardt and Tashjian, 2005), has almost no incision (Massong et al., 2006), and contains good habitat. This Site is similar to the La Orilla Site in that it has banks that are frozen in place by jetty jack lines and a moderate amount of sediment supplied from upstream reaches (Figure 4). However, unlike the La Orilla Site, the hydrograph contains greater diversity at low to moderate flows which has caused the formation of bar and island floodplain surfaces that flood at moderate (200cfs to 500cfs) and high (>1000cfs) flow ranges. These in-channel floodplain surfaces contribute to diverse velocity profiles at all flow levels (Figure 7). Where the hydrographic diversity at this site assists in improved habitat, it is often at the cost of intermittency which is very damaging to native fish populations and riparian habitat (Remshardt et al., 2003; Crawford et al., 1993).

DISCUSSION

Based on the data at all ten sites, the most important factor in classifying the quality of habitat appears to be the existence of active floodplain processes regardless of incision. An example of this distinction is a comparison between the La Orilla and the La Joya Sites. Although both sites contain high banks due to incision, the La Orilla Site has very little to no subsequence floodplain development while the La Joya Site has a variety of flow dependant floodplain surfaces. The incision at the La Orilla Site is attributed primarily to the reduced sediment supply in the Rio Grande due to sediment capture in Cochiti Reservoir upstream of the Site. This sediment depredation is compounded by frozen banklines and a homogeneous hydrograph resulting in poor habitat. The incision at the La Joya Site, however, is caused by a more natural process of localized uplift created by a magma body located immediately downstream from the Site (Socorro Magma Body). Coupled with this process are mobile banklines and a diverse hydrograph resulting in quality habitat.

The Los Lunas Site provides an interesting insight into how the altered physical processes in the Albuquerque Reach (as represented by the La Orilla Site) could be adjusted to improve habitat.

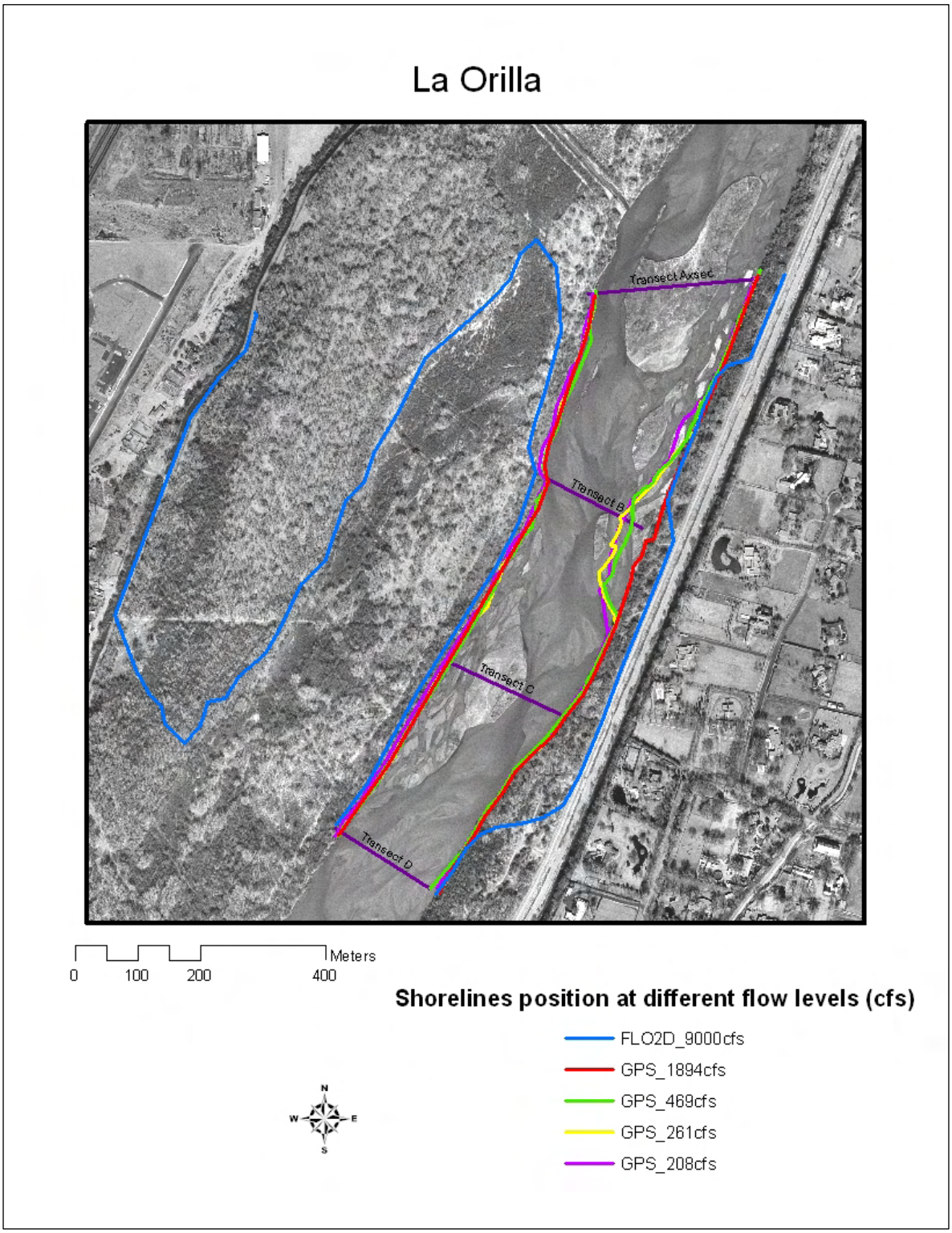


Figure 2: Shoreline position at various flow levels for the La Orilla Site. This site is considered to be have moderate to high incision, banks armored by jetty jack lines, moderate sediment supply with a relatively low diversity in the annual hydrograph. For flows above 2000cfs, the FLO2D model was used to estimate bankline position (Tetra Tech, 2004).

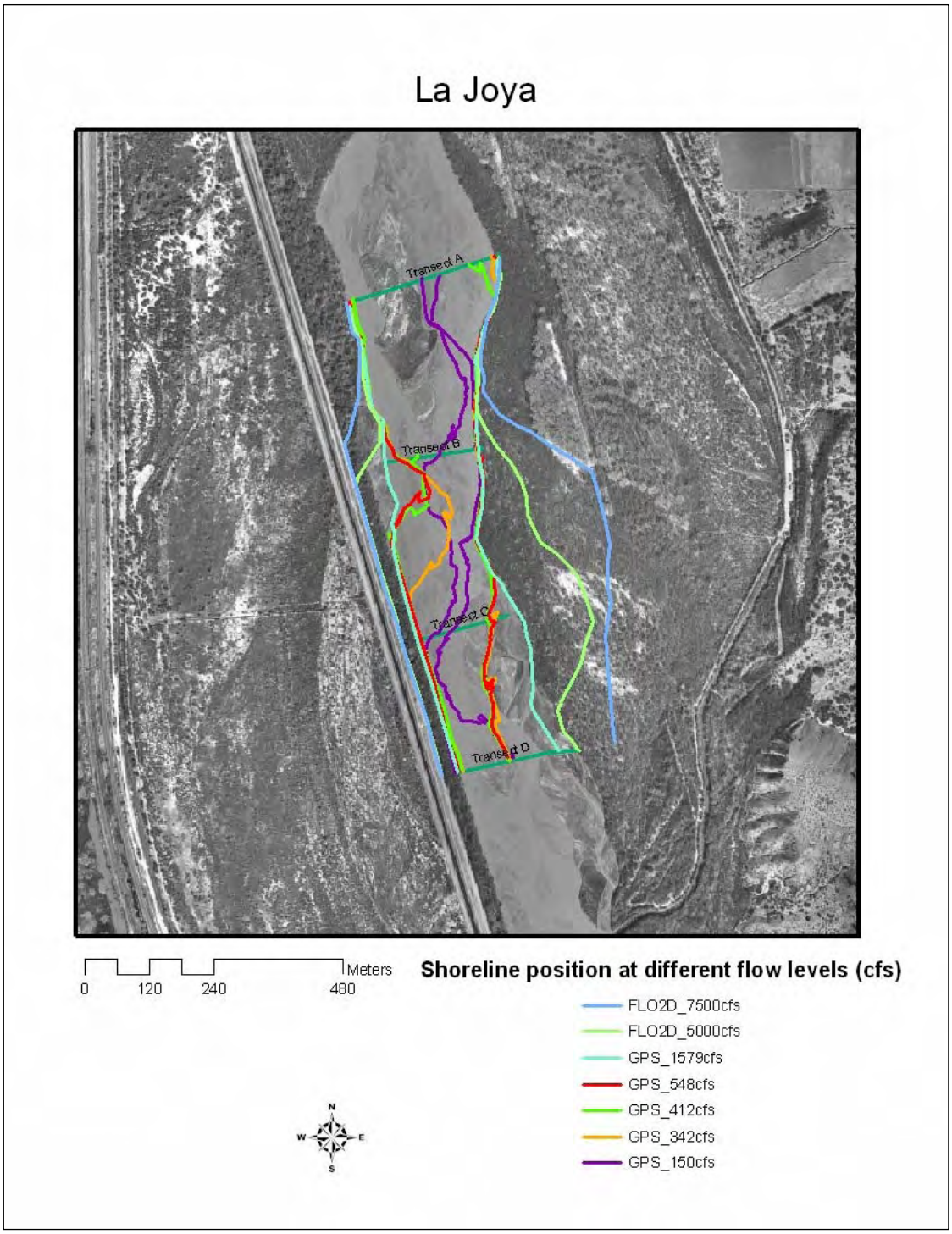


Figure 3: Shoreline position at various flow levels for the La Joya Site. This site is considered to be highly incised with a combination of banks that are both free and armored by jetty jack lines and a high sediment supply. This site also has a hydrograph that is diverse in low, mid and high flow ranges. For flows above 2000cfs, the FLO2D model was used to estimate bankline position (Tetra Tech, 2004).

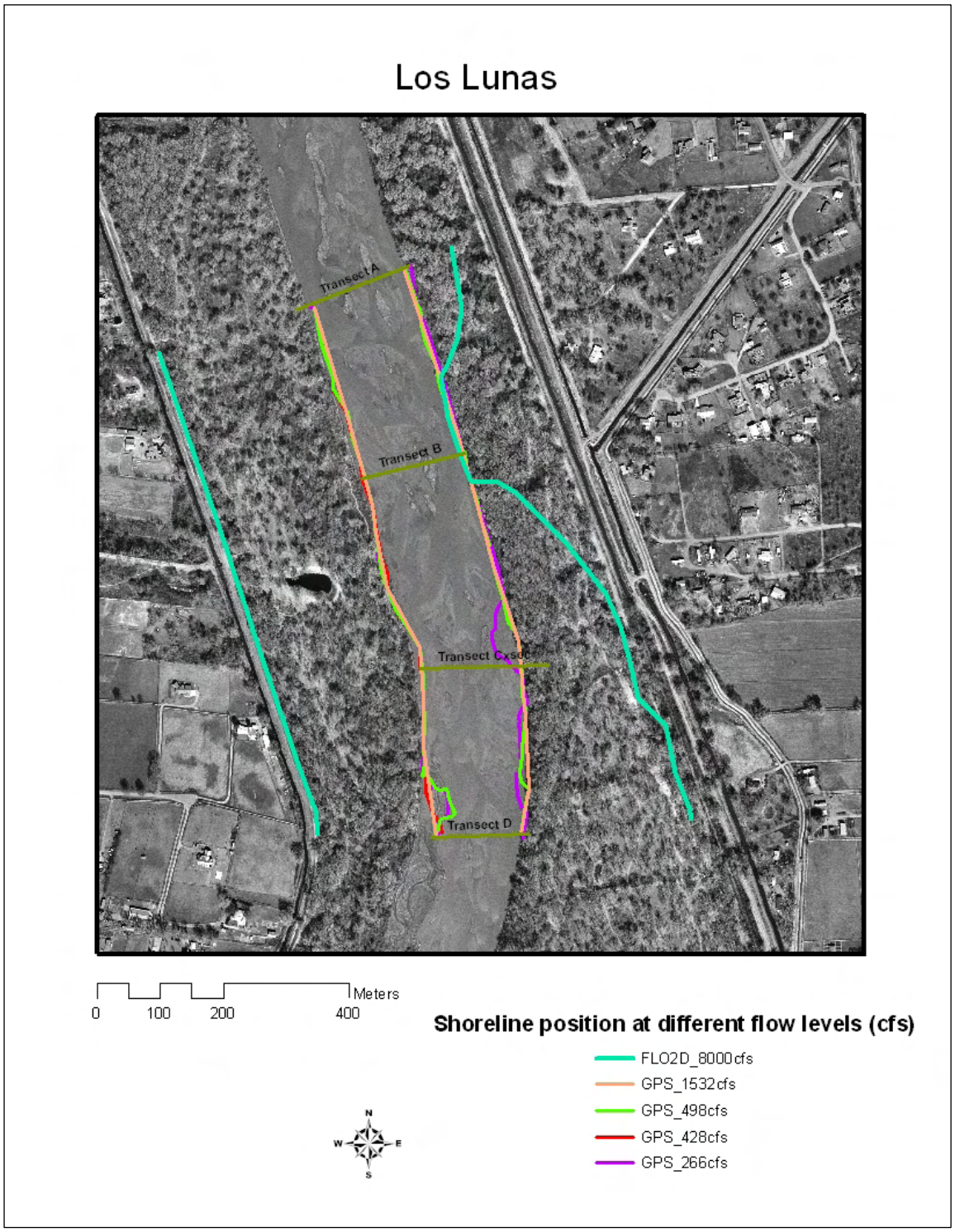


Figure 4: Shoreline position at various flow levels for the Los Lunas Site. This site is considered to be an area of no recent incision. The banks are armored by jetty jack lines and there is a moderate sediment supply. This site has a hydrograph that is diverse in low, mid and high flow ranges. For flows above 2000cfs, the FLO2D model was used to estimate bankline position (Tetra Tech, 2004).

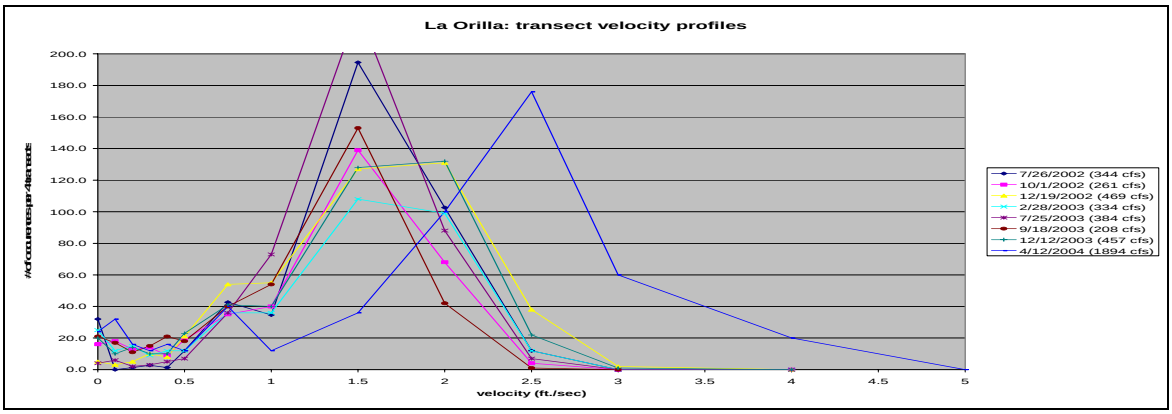


Figure 5: Velocity profiles for the La Orilla Site at various flow levels. These types of profiles are associated with poor habitat since there are very little in-channel velocity diversity at all flow levels.

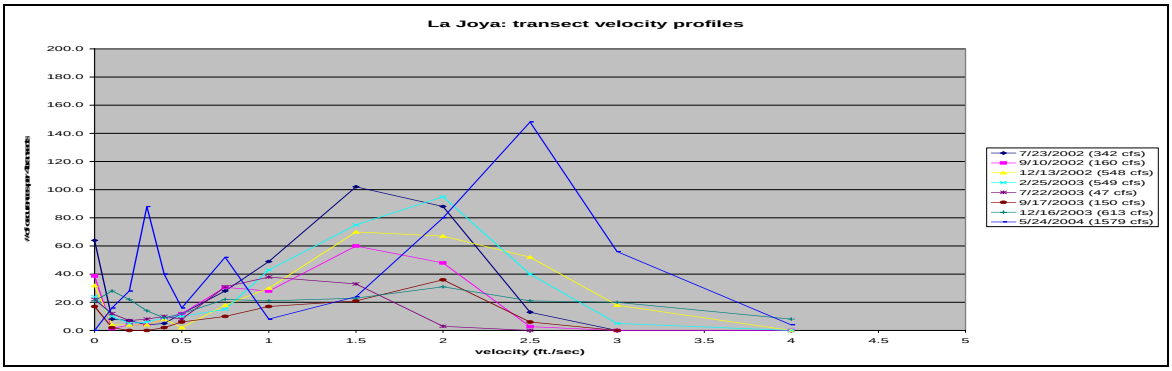


Figure 6: Velocity profiles for the La Joya Site at various flow levels. These types of profiles are associated with good habitat since there are diverse in-channel velocity diversity at all flow levels.

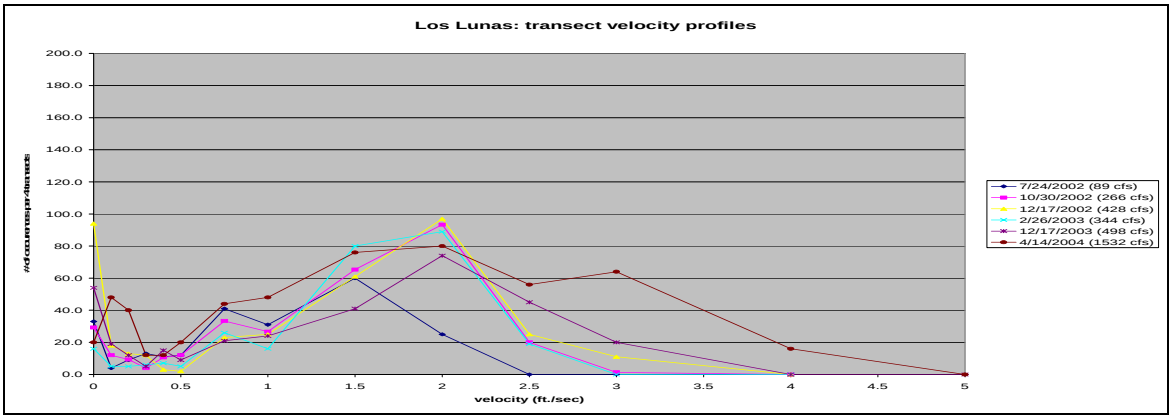


Figure 7: Velocity profiles for the Los Lunas Site at various flow levels. These types of profiles are associated with good habitat since there are diverse in-channel velocity diversity at all flow levels.

The primary difference between the La Orilla and Los Lunas Sites is that there is greater hydrographic diversity in the low and mid flow ranges at the Los Lunas Site. This diversity in the hydrograph, barring intermittence, has led to complex in channel habitats and modern bar and island floodplain surfaces, components of quality habitat.

ACKNLOWLEDGEMENTS

The authors wish to acknowledge Paula Maker and Jason Remshardt for their contributions to this paper.

REFERENCES

Crawford , C.S., A. Cully, R. Leutheuser, M. Sifuentes, L. White, and J. Wilbur, 1993. Middle Rio Grande Ecosystem: Bosque Biological Management Plan, U.S. Fish and Wildlife Service

Massong, T., P. Tashjian, and P. Makar, 2006. "Recent Channel Incision and Floodplain Evolution within the Middle Rio Grande, NM," Joint 8th Federal Interagency Sedimentation Conference and 3rd Federal Interagency Hydrologic Modeling Conference, Reno, NV.

Remshardt, W.J., J.R. Smith, and C.W. Hoagstrom. 2003. Fishes of the mainstem Rio Grande; Bernalillo to Fort Craig, New Mexico (1999-2001) with an emphasis on Rio Grande silvery minnow , *Hybognathus amarus* (Girard). Draft report to U.S. Army COE and City of Albuquerque; Albuquerque, New Mexico. 105 pp.

Remshardt, W.J. and Tashjian, P., 2005. Habitat Preferences of the Rio Grande silvery minnow in Relation to Fluvial Geomorphology and Flow Regime, Middle Rio Grande Valley, New Mexico: Interim Report for Funding Year 2003. Bureau of Reclamation, Albuquerque Area Office

Robert, Lisa, 2005. Middle Rio Grande Ecosystem Bosque Biological Management Plan; The First Decade: A Review and Update, U.S. Fish and Wildlife Service

Tetra Tech, Inc, 2004. Flo-2D Flood Routing Supporting URGWOPS. Tetra Tech, Inc. Surface Water Group, Albuquerque, New Mexico

SAFETY AND FISH PASSAGE FOR LOW-HEAD DAMS

Aaron W. Buesing, P.E., Hydraulic Engineer; U.S. Army Corps of Engineers, St. Paul District; 190 East Fifth Street, St. Paul, Minnesota 55101-1638; Aaron.W.Buesing@mvp02.usace.army.mil

Abstract: There are eight low-head dams on the Red River of the North that impede fish passage and create unsafe conditions for humans using the river. Already constructed and proposed dam modifications benefit the basin's eighty-four species of fish and will prevent people from drowning at these dams. The St. Paul District, Corps of Engineers, has been acting with state and local agencies to place fill downstream of several of these dams to allow fish passage and eliminate the hydraulic roller. The rock fill is generally placed at a 5% grade with rows of large boulders (boulder vanes) that dissipate energy and provide low velocity resting areas for fish. The boulder vanes are also designed to provide deeper water depths towards the center of the channel and to protect the downstream riverbanks from erosion during flood events. Three-dimensional hydrodynamic modeling has been conducted for two of the dams to address concern over whether the rock fill will increase upstream flood stages. For these two dams, the modeling has show that the 5% rock fill section does not increase the 100-yr flood elevation.

INTRODUCTION

Eight low-head dams exist on the Red River of the North within the United States. These dams were constructed in the twentieth century with the primary purpose of securing a supply of water during low flow conditions. The commonly used names for these dams, listed downstream to upstream and shown in the following figure, are:

1. Drayton Dam
2. Grand Forks Riverside Dam
3. Fargo North Dam
4. Fargo Midtown Dam
5. Fargo South Dam
6. Hickson Dam
7. Christine Dam
8. Wahpeton Kidder Dam

Safety Concerns: The dangerous flow conditions downstream of a low-head dam are not readily apparent to most people. Water plunging over the dam typically creates a deeper scoured region immediately downstream of the dam, which in turn supports the development of a hydraulic roller or undertow. Recreational users who approach the dam from the downstream side can be surprised by the deeper water and get caught up in the hydraulic roller. At moderate river flows, when the depth of flow allows for boat passage, traversing the dam looks like a fun whitewater ride, but the strength of the roller can easily trap boaters that fall overboard and can even trap the boat itself. A number of injuries and deaths have occurred at the low-head dams on the Red River of the North. The greatest number of fatalities has occurred at the Fargo Midtown Dam, where nineteen people have drowned since it was constructed in 1960.

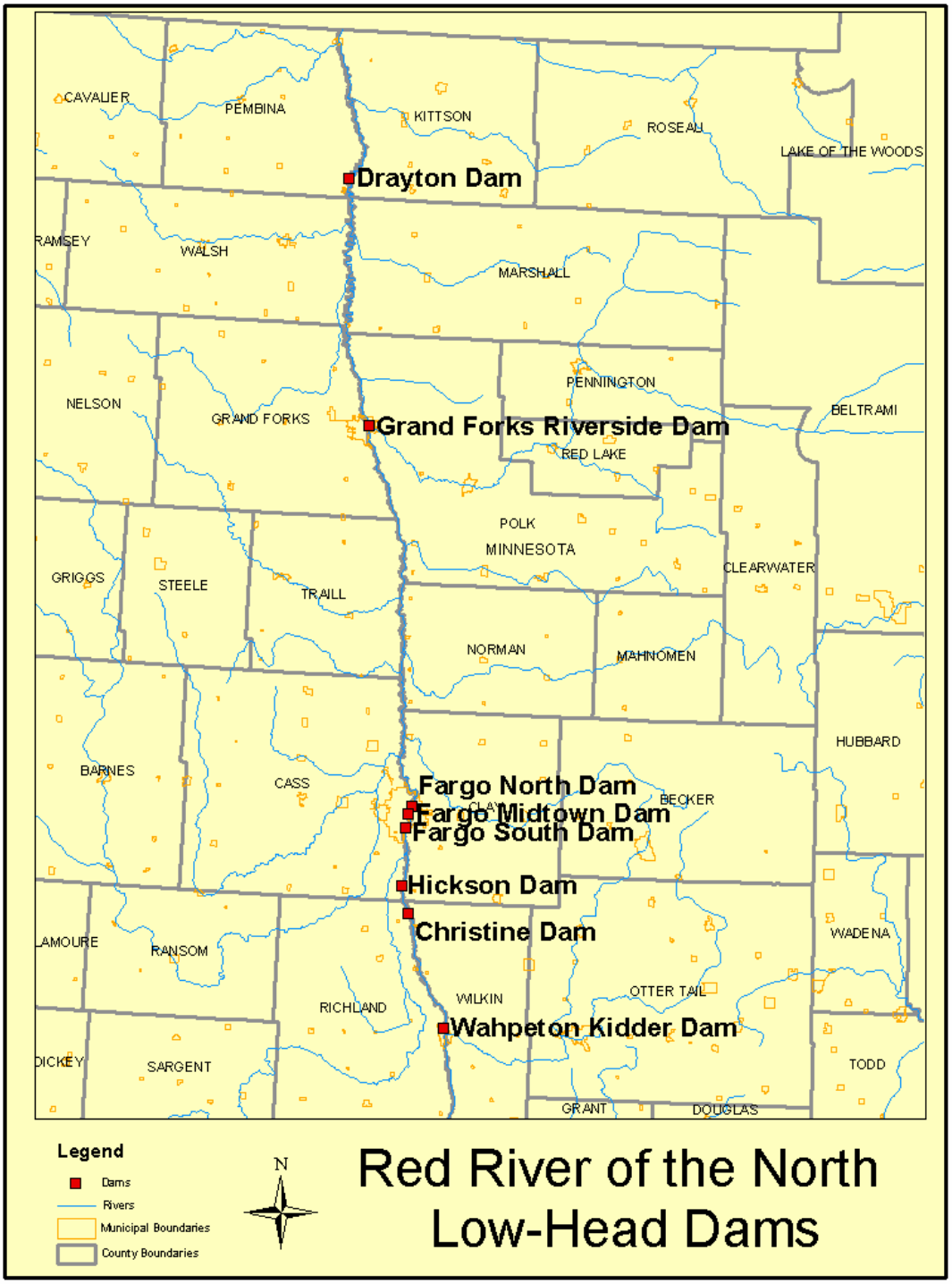


Figure 1 Location of Low-Head Dams on the Red River of the North



Figure 2 Grand Forks Riverside Dam Before Modifications

Fish Passage Concerns: According to data collected between 1892-1994, 77 native and seven introduced species of fish inhabit the Red River of the North and its tributaries in the United States (Peterka and Koel, 1996). By hindering the upstream and downstream movement of fish, these eight low-head dams limit access to important habitat and spawning areas. For example, data on fish migration indicate the Fargo South Dam is typically passable less than 10 percent of the time on the average from March through July, and even less during the fish spawning months of May through July. In some years, conditions favorable for upstream fish passage do not occur at the Fargo South Dam.

DESIGN

Low-Head Dam Modifications: Since 1999 five of the eight dams have been modified to address the safety and fish passage concerns. At each of these dams the fundamental design consists of a 20H:1V sloping rock fill section downstream of the dam crest with upstream-pointing concave boulder vanes incorporated into the rock fill to help dissipate energy, direct flow towards the center of the channel, and provide hydrodynamic diversity. The top-of-boulder elevation increases as you move from the channel centerline to the banks. This further protects the banks and provides a chute of deeper flow in the center of the channel that promotes recreational use. A plan view of the Grand Forks Riverside Dam design is shown in the following figure.

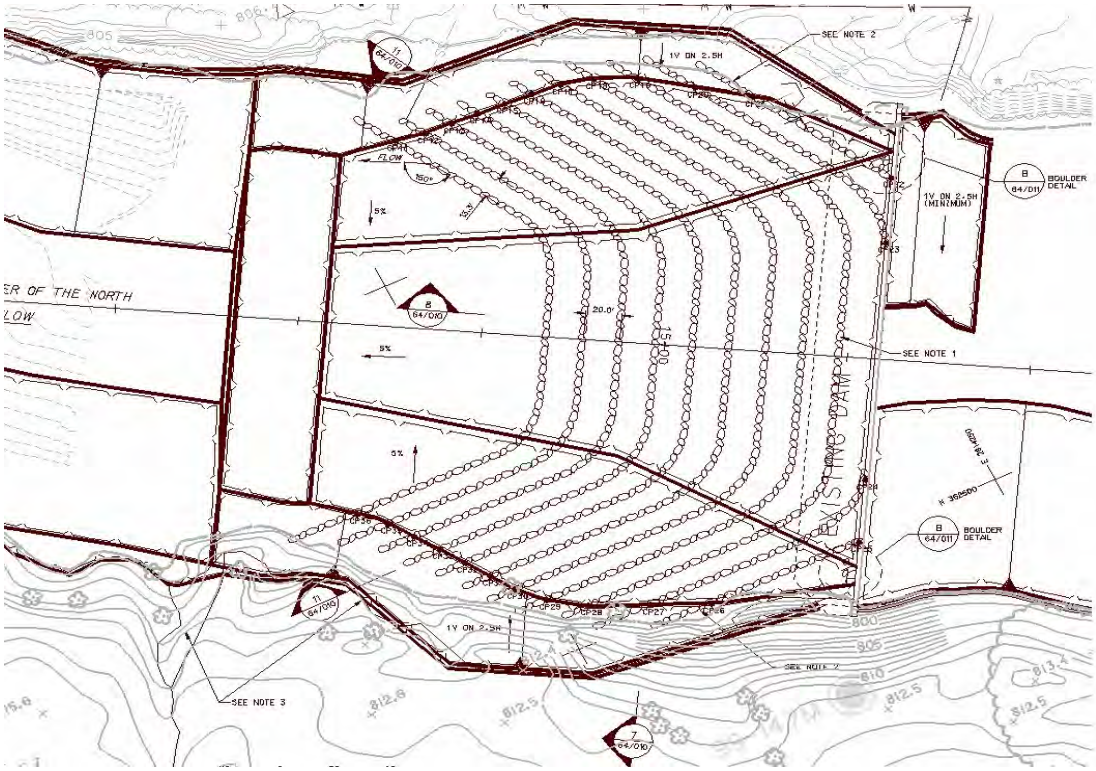


Figure 3 Grand Forks Riverside Dam Modification Plan

The rock fill section eliminates the vertical drop and hydraulic roller thereby improving the safety of the area. The 20H:1V slope and the boulder vanes provide velocity conditions and flow depths that allow many species of fish to navigate upstream and downstream across the dam. Table 1 summarizes the status of the effort to modify the eight low-head dams on the Red River of the North.

Rock Fill Design: For the Grand Forks and Fargo dams, an HEC-RAS model was developed to model existing and proposed conditions over a range of flow conditions. Because flow passes through critical depth during low to moderate flow conditions, HEC-RAS was run in its mixed flow mode. Using the maximum velocity obtained from the HEC-RAS model, the high turbulence curves of the Corps' Hydraulic Design Criteria, Sheet 712-1, were used to determine D_{50} minimum and W_{50} minimum for the rock fill. The steep slope riprap design equation of EM-1110-2-1601 was also used as a check of the sizes obtained from Sheet 712-1. The results of this analysis for the Grand Forks Riverside Dam rock fill design are provided in Table 2. The selected gradation is shown in Table 3. W_{50} of the selected gradation is slightly lighter than W_{50} minimum based on Sheet 712-1, but this is considered acceptable since the HEC-RAS model did not account for the roughness provided by the boulders placed throughout the area of rock fill.

Floodplain Impacts: Since the projects involve placing fill within the floodway, the North Dakota State Water Commission requires that these projects do not increase the 100-yr flood stage (a 0.01 ft. stage increase is considered unacceptable). Detailed modeling was not requested for the first three dam modifications, but it was required for the Fargo North Dam and the Fargo

South Dam. The initial HEC-RAS analysis for the Fargo North Dam indicated that the stage increase would be between 0.01 and 0.02 ft. Knowing that the HEC-RAS model might be underestimating the hydraulic losses in the hydraulic roller of pre-fill conditions, and therefore the 0.01 to 0.02 ft stage increase might be conservative, the St. Paul District recommended using a slightly higher expansion loss coefficient for pre-fill conditions. Not satisfied with this approach, the North Dakota Water Commission recommended physical or three-dimensional numerical modeling to more accurately compute the true stage increase. After exploring both options, all parties agreed to three-dimensional modeling performed by Corps' Engineer Research and Development Center (ERDC) in Vicksburg, Mississippi.

Table 1 Status of Work on Red River of the North Low-Head Dams

Name	Status	Volume of Rock (cubic yards)	Construction Cost
Fargo Midtown Dam	Completed – Feb 1999	4400	$261,000
Wahpeton Kidder Dam	Completed – Mar 2000	2700	$120,000
Grand Forks Riverside Dam	Completed – Nov 2001	150,000	$4,800,000
Fargo North Dam	Completed – Feb 2002	2600	$119,000
Fargo South Dam	Rock Placed – Project to be Completed in Spring 2004	14,400 (est.)	$810,000 (est.)
Hickson Dam	Preliminary Restoration Plan in Progress	N/A	N/A
Christine Dam	Preliminary Restoration Plan in Progress	N/A	N/A
Drayton Dam	Preliminary Restoration Plan in Progress	N/A	N/A

With the Fargo North Dam rock fill section in place and the Manning's n value raised from 0.035 to 0.050 in the rock fill section, the three-dimensional model computed the upstream 100-yr flood water surface elevation to be 0.05 ft lower than that of pre-fill conditions. For the Fargo South Dam the elevation decrease due to the rock fill was calculated to be even greater at 0.12 ft. The 20H:1V slope roughly follows the upper boundary of the hydraulic roller so the filled area is mostly an area of ineffective flow under pre-fill conditions. With the hydraulic roller eliminated by the rock fill, the overall energy losses are less, even with the greater bottom roughness. The result is a slightly lower upstream water surface elevation. The pre-fill and post-fill velocity vectors from the three-dimensional model of the Fargo North Dam are presented as Figures 4 and 5, respectively.

Performance of Dam Modifications: A major flood in 2001 tested the stability of the already completed dam modifications in Fargo and Wahpeton, and the partially completed modifications in Grand Forks. The rock fill performed very well with only minor movement of rock. No

repairs were required at the dams, and the configuration of the boulder vanes appears to reduce the amount of bank erosion downstream of the dams.

Table 2 Sizing Rock Fill for Grand Forks Riverside Dam (USACE, 2001)

Fish Passage Rockfill Bed Riprap Sizing based on Mixed Flow HEC-RAS Model Results					**Fish Passage Rockfill Bed Riprap Sizing based on EM-1110-2-1601**	
(HEC-RAS Model assumes a 5% riprap slope downstream of the dam crest and does not include the fish passage vanes/boulders. This results is conservative velocities and; therefore, a conservative riprap design/gradation.)					$D_{30} = (1.95 * S^{0.555} * q^{2/3})/g^{1/3}$ for Steep Slope Riprap Design (2 to 20 percent) Eq. 3-5 on page 3-8 of EM-1110-2-1601	
Discharge in cfs	Maximum Velocity in fps	D50 Minimum based on 712-1 High Turbulence	W50 Minimum based on 712-1 High Turbulence	Flow Conditions through Fish Passage Structure assuming 5% Slope (CONSERVATIVE ASSUMPTION THAT DOES NOT INCLUDE AFFECT OF BOULDERS ON FLOW)	q in cfs/ft	D_{30} in feet
1000	5.4	0.37	4	Supercritical with hydraulic jump	3.25	0.26
2000	6.9	0.61	20	Supercritical with hydraulic jump	6.49	0.4
3000	8.2	0.86	55	Supercritical with hydraulic jump	9.74	0.53
4000	9.1	1.06	103	Supercritical with hydraulic jump	12.99	0.64
5000	9.9	1.25	169	Supercritical with hydraulic jump	16.23	0.75
6000	10.6	1.44	258	Supercritical with hydraulic jump	19.48	0.84
7000	11.1	1.58	341	Supercritical with hydraulic jump	22.73	0.93
8000	7.7			Subcritical throughout		
9000	5.9			Subcritical throughout		
10000	5.1			Subcritical throughout		

Table 3 Selected Rock Fill Gradation for Grand Forks Riverside Dam (USACE, 2001)

Selected R270 Riprap Gradation D_{30}(min) of Gradation = 1.22 feet				
Percent Lighter by Weight	Limits of Stone Weight in pounds		Diameter based on Limits of Stone Weight and a spherical shape	
	Maximum	Minimum	Maximum	Minimum
100	1350	550	2.5	1.9
50	570	270	1.9	1.5
15	260	85	1.4	1.0
5	220	50	1.4	0.8

Luther Aadland, a research scientist with the Minnesota Department of Natural Resources and a key player in the design and monitoring of these dams, reports that about two dozen species of fish are making their way to upstream spawning areas because of these dam modifications. At one site he has observed walleyes and suckers spawning in the newly constructed rock rapids. Luther feels that all of the approximately 90 species of fish will benefit from the dam modifications. He is especially optimistic about the impact these projects will have on the once abundant lake sturgeon, which have declined in numbers drastically since these dams were built (Minnesota Department of Natural Resources, 2003).

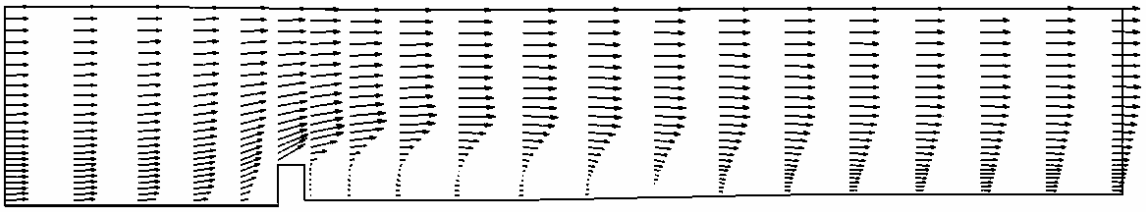


Figure 4 Velocity Vectors for Pre-Fill Conditions at Fargo North Dam (USACE, 2000)

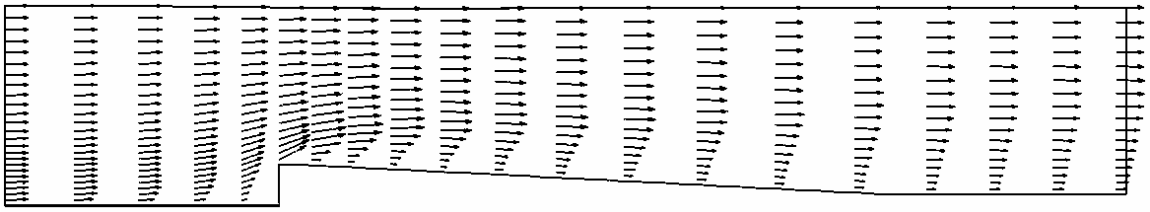


Figure 5 Velocity Vectors for Post-Fill Conditions at Fargo North Dam (USACE, 2000)

REFERENCES

Minnesota Department of Natural Resources (2003). "Rapid Changes on the Red River," Minnesota Conservation Volunteer, Nov-Dec 2003.

Peterka, John J. and Koel, Todd M. (1996). "Distribution and dispersal of fishes in the Red River basin." Report submitted to Interbasin Biota Transfer Studies Program, Water Resources Research Institute, Fargo, ND. Northern Prairie Wildlife Research Center, http://www.npwrc.usgs.gov/resource/fish/fishred/fishred.htm (Version 29AUG97).

United States Army Corps of Engineers, ERDC Waterways Experiment Station, Coastal & Hydraulics Laboratory (2000). Numerical Investigation of Changes in Water-Surface Elevation Induced by Modification of Channel Geometry.

United States Army Corps of Engineers, St. Paul District (2001). Red River of the North at East Grand Forks, MN / Grand Forks, ND, Riverside Dam / Bank Stabilization, Design Documentation Report, Hydraulic Design Attachment 2-F.

ASSESSING EFFECTS OF CONSERVATION AT THE WATERSHED SCALE

Tom Drewes, CEAP Watershed Coordinator, Resource Inventory & Assessment Division, Natural Resources Conservation Service, U.S. Department of Agriculture, Beltsville, MD, tom.drewes@wdc.usda.gov; Kelsi S. Bracmort, Ph.D., Agricultural Engineer, Conservation Engineering Division, Natural Resources Conservation Service, U.S. Department of Agriculture, Washington, DC, kelsi.bracmort@wdc.usda.gov ; Jerry Bernard, National Geologist, Conservation Engineering Division, Natural Resources Conservation Service, U.S. Department of Agriculture, Washington, DC, jerry.bernard@wdc.usda.gov

Abstract: CEAP, the Conservation Effects Assessment Project, will assess the effects of conservation practices at both the watershed and national levels. The focus of the national assessment is to track environmental effects of conservation practices installed on a national scale. The watershed assessment studies will complement the national assessment, provide additional field and watershed data, and develop a set of regionalized models for future national assessments. Three categories of watershed studies will be conducted as part of CEAP: Special Emphasis watersheds, Benchmark Research watersheds, and Competitive Grants watersheds. This paper introduces the eight CEAP Special Emphasis watersheds and their respective strategies for assessing the effects of conservation practices at a watershed scale. At the end of this coming year, these eight projects will provide early results and assessment of their modeling efforts.

INTRODUCTION

The U.S. Department of Agriculture (USDA) Natural Resources Conservation Service (NRCS) and the Agricultural Research Service (ARS) have joined with other USDA and Federal agencies to initiate studies that will quantify the environmental effects of conservation practices implemented through USDA conservation programs on retired and working cropland, grazing land, agro-forest land, and wetlands by way of the Conservation Effects Assessment Project (CEAP) (Table 1). CEAP addresses issues regarding the growing need to scientifically quantify natural resources effects of conservation practices. Moreover, CEAP comes at a time where there is a greater government-wide emphasis on performance outcome measures. Estimating environmental effects of the 2002 Farm Bill programs will allow policymakers and program managers to improve implementation of existing conservation programs and design new programs to meet the goals of Congress more effectively.

Table 1 CEAP Partners

USDA Partners	Non-USDA Partners
Natural Resources Conservation Service (NRCS)	U.S. Geological Survey (USGS)
Agricultural Research Service (ARS)	U.S. Environmental Protection Agency (EPA)
Cooperative State Research, Education and Extension Service (CSREES)	U.S. Fish and Wildlife Service (FWS)
National Agricultural Statistics Service (NASS)	Conservation districts
Farm Service Agency (FSA)	Local governments
Economic Research Service (ERS)	Universities
Office of Risk Assessment and Cost benefit Analysis (ORACBA)	Producers
	Agricultural and environmental organizations

A watershed studies assessment and national assessment comprise CEAP. The focus of the national assessment is to track environmental effects of conservation practices installed on a national scale. The watershed assessment studies will complement the national assessment, provide additional field and watershed data, and develop a set of regionalized models for future national assessments. This paper introduces eight CEAP Special Emphasis watersheds and their respective strategies for assessing the effects of conservation practices at a watershed scale.

CEAP WATERSHED STUDIES ASSESSMENT

The watershed studies component will provide more detailed assessments of environmental effects and benefits, a framework for evaluating and improving the performance of the national assessment models, and additional research on conservation practices and their expected effects at the watershed scale. The results of the watershed studies will be used to improve the performance of the national assessment models and to demonstrate that a richer set of benefits can be identified and measured when assessed at a finer scale. The watershed studies will demonstrate that an optimal collection and placement of conservation practices can achieve specific water quality and other environmental goals. NRCS, ARS and the Cooperative State Research, Education, and Extension Service (CSREES) will lead the effort for watershed assessment studies.

There are three categories of watershed studies that will be conducted as part of CEAP:
1. Special Emphasis Watersheds: Eight watersheds were selected to address specific resource concerns such as manure management for animal feeding operations and water use on irrigated cropland.

2. ARS Benchmark Research watersheds: In these 12 research watersheds, ARS already has long-term conservation effects research projects in progress. Development of regional watershed models is associated primarily with these research watersheds.

3. Competitive Grants watersheds: As of summer 2005, eight watersheds were selected through the CSREES Water Quality Initiative Competitive Grants Program. The ultimate goal of the program is to understand how to optimally locate and schedule the implementation of conservation practices within a watershed to achieve locally defined water quality and other environmental goals.

The five objectives for the CEAP watershed assessment studies are:
1. Assess water quality, soil quality, and water conservation effects and benefits of conservation practices at the watershed scale, and begin investigations into how to quantify wildlife and air quality benefits beyond the edge of the farm field;
2. Develop a set of regional watershed assessment models that can be used to address benefits of conservation practices and other environmental issues in the major agricultural regions of the nation and for use in future national assessments;
3. Develop water quality, soil quality, and water conservation databases that can be used to evaluate effects of conservation practices, and to compile air quality and wildlife habitat data for future assessment;

4. Develop indicators or performance measures for documenting water quality, soil quality, air quality, and aquatic and terrestrial habitat benefits from implementing conservation practices at selected watersheds; and
5. Expand research on the effects of conservation practices at the watershed scale for different soils, climates, topography, farming practices, cropping systems, and other land uses.

SPECIAL EMPHASIS WATERSHEDS

The Special Emphasis watersheds (SEW) will concentrate on the NRCS core four conservation practices (conservation buffers, nutrient management, pest management, and tillage management) plus irrigation management practices, manure management practices, establishment of wildlife habitat, and wetland protection and restoration. Environmental effects will be estimated for each of the five resource concerns (in priority order) that conservation programs are designed to address:

- Water quality (nutrient, pesticide, and sediment delivery to lakes, rivers, and streams)
- Soil quality (including soil erosion and carbon storage)
- Water conservation (including flood and drought protection)
- Air quality (including particulates and odors)
- Wildlife habitat (including aquatic and terrestrial habitats)

Benefits will be estimated separately for the four agricultural land use categories (in priority order) to which most conservation practices apply:

- Croplands, including croplands enrolled in CRP
- Grazing lands
- Wetlands
- Agro-forestry lands

The eight Special Emphasis watersheds selected in FY 2004 cover the Northeast, North Central, South Central, and Northwest major land resource areas. Figure 1 displays the general locations of the watersheds because the watershed boundaries shown on this map are at the 8-digit Hydrologic Unit Code resolution, which average over 700 square miles in drainage area. The Special Emphasis watersheds are generally focused on assessing the effects of conservation treatments in much smaller watershed drainage areas. Land use, conservation practice type and quantity, resource concerns, and pre-treatment data availability were the predominant criteria for watershed selection (Table 2). Watershed study objectives will be attained by water sampling, water quality monitoring, watershed hydrology modeling, and field trials. Financial support for the watersheds ranges from $200,000 to $600,000 per watershed study over three years, with an average of $330,000, excluding support received from non-USDA partners.

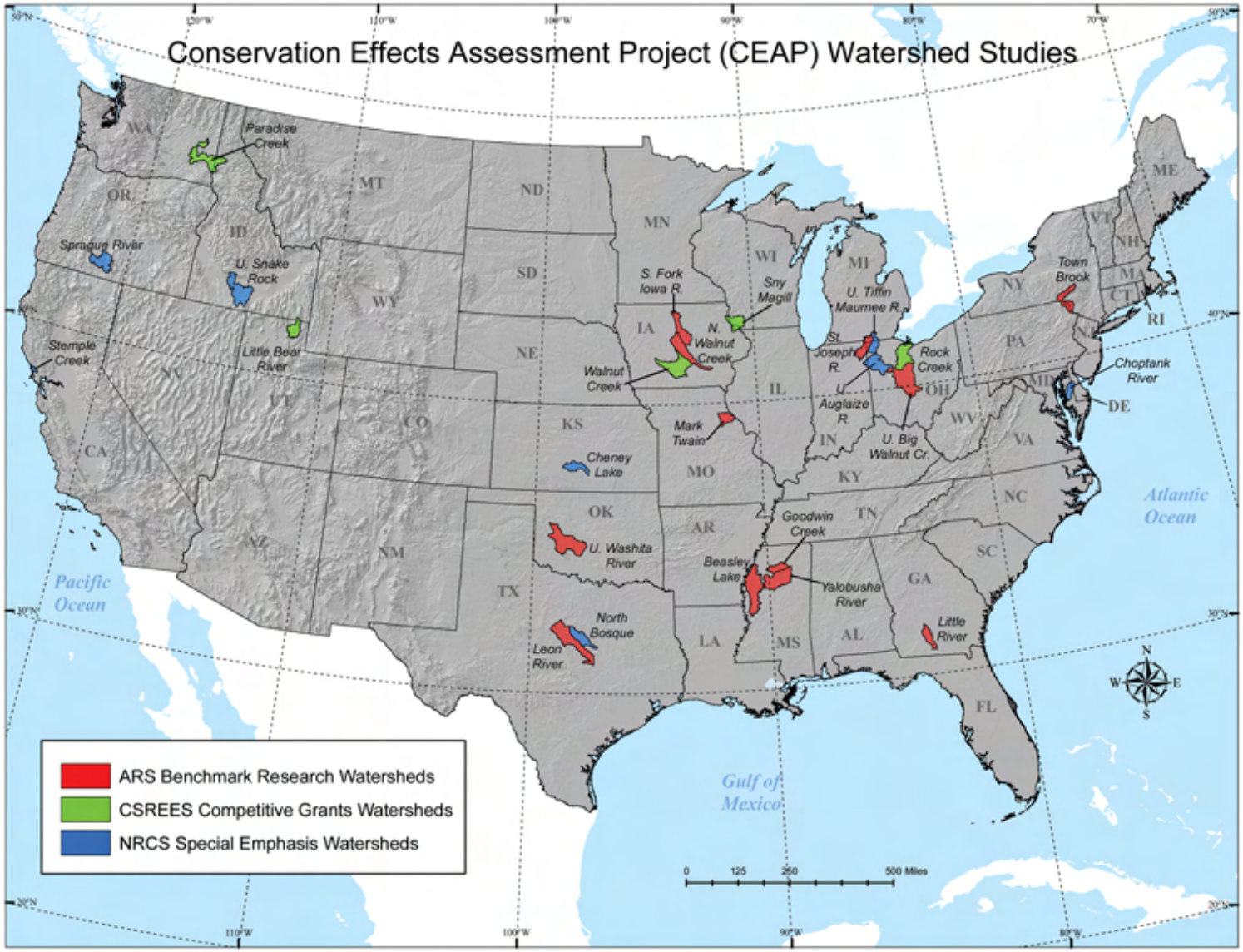


Figure 1 CEAP Watershed Studies Assessment Map

Table 2 Resource measurements, conservation practices, duration of records, and experimental approaches planned for CEAP Special Emphasis Watersheds

Special Emphasis Watershed	**Resource Measurements**			**Conservation Practices[4/]**	**Years of pre-treatment data available**	**Probable experimental design[5]**
	Water Quality[1/]	**Water Quantity[2/]**	**Economics [3/]**			
Stemple Creek, CA	S, N*, DO*, NH3*, TKN*, TU, pH*, W*, NO2*, BOD*, COD*,OPO4*	D, P	E	M, B, CM, LM	4	PP, UD
Upper Snake Rock, ID	S, P	D, I, P, G	P	B, C, D, N, T	Not provided	-
Cheney Lake, KS	pH*, DO*, TU*, W*, N, P	D, P	E, O	M, N, T, LM	5	PP, UD
Choptank River, MD	W*, pH*, DO*,P*, NH3* . Sa*, S*, N*, Se*, C*	D, I, G	E	B, N, CM	19	PP, UD
Maumee River, Upper Tiffin, MI	S*, N*, P*, DO*, Pa	A, D	E, O	D, M, T	26	PW, PP
Maumee River, Upper Auglaize, OH	S*, N*, P*, Pe*, M*	A, D, G	E	B, D, T	26	PP, UD
Upper Klamath River, OR	No specific parameters given, Sn	G, I	E	B, D, N, I	Not provided	PP
N. Bosque River, TX	P*, N*, S*	D, P	E	M, N, R	~14	PP

[1/]Water Quality Measurements:
DO - dissolved oxygen
N - nitrate-nitrogen
P – phosphorus
Pa – pathogens
Pe – pesticides
S – sediments
T – temperature
NH3 - ammonia
TKN – total kjeldahl nitrogen
TU - turbidity
pH - pH
W – water temperature
BOD – biological oxygen demand
COD – chemical oxygen demand
NO2- nitrogen dioxide
OPO4 – Orthophosphate
Sa – salinity
Se – Secci depth
C – chlorophyll
M – metals
Sn – SNOTEL site

[2/]Water Quantity Measurements:
A – Artificial drainage
C – Channel geomorphology
D – Discharge
I – Irrigation
G – Groundwater
P – Precipitation
S – Soil Water

[5]Probable experimental design
PW - Paired watersheds
PP - Pre and post studies and analysis of effects since initiation of CPs
UD – Upstream/downstream studies

[3/]Economic Measurements:
E – Program Efficiency
O – Optimal Placement
P – Profit

[4/]Conservation Practice Categories:
B – Buffers
C – Channel Management
D – Drainage Management
M – Manure Management
N – Nutrient Management
P – Pest
R – Range
T – Tillage
L – Land conversion
CM -Cover Management
LM - Livestock Management

* From previously collected data.

A synopsis detailing the more significant aspects for each of the Special Emphasis watersheds follows. Information furnished is current as of the fall of 2005. Additional information can be obtained by visiting the CEAP website at http://www.nrcs.usda.gov/technical/nri/ceap. Changes, some certainly to be unanticipated, to the goals and progress of CEAP watershed projects will be continually updated and available via the CEAP website. The website will also host materials that communicate project results, such as scientific and technical papers, outreach materials, and conference presentations.

Cheney Lake Watershed: The Cheney Lake watershed drains into the Cheney reservoir. Impacted with sediments and phosphorus, the reservoir provides the city of Wichita, Kansas with 70% of it daily water supply. Land use for the 630,000 acre watershed, is primarily cropland and range land. The primary objective of the watershed project is to evaluate downstream effects of current Conservation Reserve Program (CRP) and Environmental Quality Incentives Program (EQIP) practices.

Choptank River Watershed: The Choptank River watershed is located on the Delmarva Peninsula of the Chesapeake Bay. This poultry dominated region has major issues with accelerated eutrophication due to nutrients, seasonal hypoxia, soil management and carbon sequestration, air quality, and disappearance of submerged aquatic vegetation. The main goals for the project are to detect differences in nutrient concentrations in basins with similar amounts of agriculture but varying amounts of acres in Conservation Reserve Enhancement Program (CREP), cover crops, and Concentrated Animal Feeding Operations (CAFO) sites, and to determine the effect of land application of poultry litter on stream water quality.

North Bosque River Watershed: The 800,000-acre North Bosque River watershed contains the largest concentration of dairy animals in Texas. Mostly pasture and range, the watershed provides 75% of the drinking water for the city of Waco. The quality of water entering Lake Waco, air quality, and soil quality are all natural resource concerns for the watershed. A top priority for the study is to evaluate the ability of conservation practices to reduce phosphorus flow to Lake Waco.

Sprague River Watershed: The Sprague River watershed is experiencing issues with water shortages, irrigation water demands, water quality, streambank erosion, fish and wildlife habitat. One-million acres in size, the watershed consists of 56% public lands, 24% private forest lands, and 11% rangeland. The objectives of this watershed assessment are to evaluate effects of improving agricultural irrigation water management, restoring wetland/riparian areas, and conducting forest and range management on water quantity and quality.

Stemple Creek Watershed: The Stemple Creek watershed is a part of the Gulf of the Farallones National Marine Sanctuary. Natural resource issues for the 33,000 acre watershed include loss of riparian vegetation on over 70% of its waterways, nutrients in runoff from dairy manure, and sediment loads to the estuary, Estero de San Antonio. Land use for the watershed is about 90% grazing land. This watershed study will evaluate water quality and wildlife effects of dairy waste management systems, riparian restoration, and soil erosion control.

Upper Auglaize River Watershed: The Upper Auglaize River watershed contributes a significant amount of sediment to the Maumee River, which is then transported to Toledo

Harbor, Ohio. The watershed is 212,000-acres in size and more than 80% tile-drained. Effects of subsurface drainage and other related best management practices on water quality will be assessed.

Upper Snake Rock Watershed: The 1.5 million acre Upper Snake Rock watershed receives approximately 10 inches of precipitation per year. Primary land uses for the watershed are rangeland and cropland. Irrigation return flows laden with sediment and nutrients, runoff from dairies and feedlots, effluent from aquaculture, industrial and municipal facilities, and storm water runoff are significant natural resource concerns. The effects of changing surface to overhead irrigation systems on water quality of return flows and the effects of conservation practices on sediment and phosphorus in irrigation return flows will be evaluated.

Upper Tiffin Watershed: The Upper Tiffin watershed is utilizing a paired watershed approach to address issues of manure and nutrient loading from large livestock farms that are polluting waterways. The Lime Creek and Bean Creek watersheds, subwatersheds of the Upper Tiffin, are both representative of intensively drained watersheds in the Great Lakes region. Various manure management and drainage practice combinations will be compared to determine the best ways to reduce movement of manure via underground drainage tiles.

EARLY RESULTS

The Special Emphasis Watershed Studies will provide annual progress summaries for each of their respective three year activities. Generally the first year activities include collecting additional monitoring data for input to calibrate, validate and run the respective models. There are several models being utilized within the eight projects including Annualized Agricultural Non Point Source (AnnAGNPS), Soil and Water Assessment Tool (SWAT), Riparian Ecosystem Management Model (REMM), Conservation Channel Evolution and Pollutant Transport System (CONCEPTS), Agricultural Policy/Environmental Extender (APEX), MODular three-dimensional finite-difference ground-water FLOW model (MODFLOW), Distributed Hydrology Soil Vegetation Model (DHSVM), and MIKE SHE. The second year begins the running of models and the initial assessment of conservation practices effects. Year three reports will provide a summary of modeling results and assessment conclusions.

Each of these eight projects is studying a different set of resource issues with varying degrees of available data and modeling support. The Choptank River Watershed Study is progressing somewhat faster than the other studies. Like the others, it has established a strong collaboration of public and private organizations working within their watershed. In their work, AnnAGNPS is being used to study the role of practices, such as nutrient management, in reducing pollutant loads of nitrogen, phosphorus, and sediment. REMM is being utilized to evaluate the buffers within the subwatersheds. The outputs from these two models are then entered into SWAT to better understand the regional impacts to water quality. Remote sensing data for model inputs is also being explored to offer more time dynamic comparisons and evaluations.

ASSESSING THE NATIONAL EFFECTS OF CONSERVATION—FOR THE FIRST TIME (CEAP)

Robert L. Kellogg, CEAP Cropland Component Coordinator, Resource Inventory and Assessment Division, Natural Resources Conservation Service, U.S. Department of Agriculture, Beltsville, MD, robert.kellogg@wdc.usda.gov; Charles Rewa, CEAP Wildlife Component Coordinator, Resource Inventory and Assessment Division, Natural Resources Conservation Service, U.S. Department of Agriculture, Beltsville, MD, charles.rewa@wdc.usda.gov; Diane Eckles, CEAP Wetlands Component Coordinator, Resource Inventory and Assessment Division, Natural Resources Conservation Service, U.S. Department of Agriculture, Beltsville, MD, diane.eckles@wdc.usda.gov

INTRODUCTION

The Conservation Effects Assessment Project (CEAP) began in 2003 as a multi-agency effort to quantify the environmental benefits of conservation practices used by private landowners participating in U.S. Department of Agriculture (USDA) conservation programs. The project consists of three components:

- National Assessment - Providing national summary estimates of conservation practice benefits and assessing the potential for USDA conservation programs to meet the nation's environmental and conservation goals. Cropland, wetlands, wildlife and grazing lands will be assessed.
- Watershed Assessment Studies - Basic research on conservation practices in selected watersheds nationwide to provide a framework for evaluating and improving performance of national assessment models.
- Bibliographies and Literature Reviews - Current literature on conservation programs. Two literature reviews in progress will document what is known and not known about the environmental benefits of conservation practices and programs for cropland and wildlife.

The purpose of this paper is to briefly review the activities underway as part of the CEAP National Assessment. More information about CEAP can be found at www.nrcs.usda.gov/technical/NRI/ceap.

The National Assessment component of the Conservation Effects Assessment Project (CEAP) will provide scientifically credible estimates of the environmental benefits obtained from USDA conservation programs. The National Assessment component has two goals:

- Provide NRCS and the conservation community with quantitative estimates of the benefits of conservation practices for national and regional reporting.
- Assess the potential for existing conservation programs and future alternatives to meet the Nation's environmental and conservation goals.

Currently, there are four active components within the National Assessment:

- Wildlife component
- Wetlands component
- Grazing lands (pastureland and rangeland) component
- Cropland component

WETLANDS

The Wetlands Component of the Conservation Effects Assessment Project (CEAP) National Assessment quantifies the environmental, biological and ecological effects of wetland conservation practices and systems on agricultural landscapes. On-site and off-site conservation effects will be derived from collaborative regional assessments in the conterminous United States. Each assessment will focus on one or more wetland hydrogeomorphic classes dominant on agricultural landscapes in that region. Regional conservation effects will be interpreted by quantifying ecosystem services provided by each regional wetland class. The following wetland ecosystem services will be quantified, depending on the regional wetland class of interest:

- Biological conservation and sustainability
- Habitat quality
- Sediment and nutrient reduction
- Pesticide reduction
- Carbon sequestration in soils and vegetation
- Floodwater storage, reduction and attenuation
- Greenhouse gas emissions reduction
- Groundwater recharge

Regional assessments are developed in collaboration with researchers involved in ongoing or previous investigations complementary to the CEAP wetlands effort. Data gaps are identified, and new data are collected or measured at site and landscape scales using sampling designs developed for each regional class. A "reference-based" approach is used to quantify wetland ecosystem services and interpret conservation effects. USDA program wetlands and non-program wetlands that lie along an 'alteration gradient' are sampled in each region. Measures of conservation effects (i.e., the type of information to be quantified) and the specific variables to be collected or measured are identified for each regional wetland class ecosystem service. Data is collected or measured through field sampling, and using remote sensing data and Geographic Information Systems (GIS).

The regional assessments will provide the following types of products:

- Regional quantifiable estimates of wetland ecosystem services before conservation practice/system implementation (i.e., "baseline" conditions) and after practice/system implementation (i.e., "conservation" conditions) and the quantitative difference between the two conditions (i.e., "conservation effect");
- Regional predictive functional condition indicator models to identify site and landscape factors (i.e., variables) that influence wetland ecosystem service estimates;
- Estimates of modeled (i.e., simulated or predictive) conservation effects under varying environmental conditions or program scenarios;
- Analytical tools/models for selected ecosystem services.

WILDLIFE

The Wildlife Component of the Conservation Effects Assessment Project (CEAP) is an effort to quantify the effects of USDA conservation practices and programs on fish and wildlife in landscapes influenced by agriculture in the United States. The Wildlife Component links to and

complements the CEAP Cropland Component by addressing fish and wildlife population responses and habitat issues that are not obtainable through its sampling and modeling framework. Because fish and wildlife are affected by conservation actions taken on a variety of landscapes, the Wildlife Component also links to the Wetlands Component and Grazing Lands Component to the extent possible.

Since 1985, the wildlife conservation community -- state and federal agencies and non-governmental organizations (NGOs) -- viewed USDA conservation programs as a key element in effective fish and wildlife habitat management. These entities have spent considerable effort to help deliver these programs and to evaluate their effectiveness. The primary approach of the CEAP Wildlife Component is to engage these groups, apply information already collected on wildlife effects, and solicit their assistance in initiating additional work to fill remaining data gaps and develop modeling and other approaches to quantify conservation practice effects. A task force consisting of a diverse mix of agency and NGO representatives has developed an approach and a framework for developing a detailed work plan. This approach includes incorporation of numerous ongoing activities that can be used to explain conservation practice effects on fish and wildlife, as well as additional actions that will contribute to the effort.

GRAZING LANDS

The grazing lands component of the CEAP National Assessment will quantify the environmental effects of conservation practices used on pastureland and rangeland. A group of grazing lands scientists and conservation experts met in 2004 to discuss how best to proceed. A report was prepared that included the overall objectives, data availability, complimentary ARS research endeavors, and a possible analytical framework. The group suggested that the national assessment be based on the National Resources Inventory (NRI) and modeling (such as use of WEPP/SPUR to estimate erosion reductions), and that the first step should be a comprehensive literature review and synthesis of what is currently known about the effects of conservation practices on pastureland and rangeland. It is anticipated that the comprehensive literature review will be conducted in 2006. The literature review will be conducted in a manner similar to those currently underway for cropland and wildlife, and thus serve as the third in a series of CEAP literature reviews.

A research project has been initiated to determine how Sustainable Rangeland Roundtable (SSR) criteria and indicators could be used in conjunction with the NRI Rangeland Field Study data (collected during 2003-2005) to estimate the effects of conservation practices on grazing lands. This will include an investigation of the indicators to see which will be appropriate to include when addressing the effectiveness of conservation applied on grazing lands. Investigators will focus attention on about five conservation practices and five resource issues.

CROPLAND

The purpose of the national assessment for cropland is to estimate the environmental effects of conservation practices applied to cropland. The assessment has four specific goals:

- Estimate the benefits of conservation practices currently present on the landscape.

- Estimate the need for conservation practices and the benefits that could be realized if appropriate conservation practices were implemented on all cropland.
- Simulate alternative options for implementing conservation programs on cropland in the future.
- Incorporate science-based estimates of practice benefits into NRCS's Performance Reporting System (PRS) to provide annual estimates of benefits for each program.

A sampling and modeling approach is used to estimate the benefits of conservation practices. First, a subset of National Resources Inventory (NRI) sample points has been selected to serve as "representative fields." NRI sample points provide the statistical framework for the model as well as information on soils, climate, and topography.

Second, USDA developed and implemented a new farmer survey to collect the information needed at the selected NRI sample points to run field-level process models and assess the effects of conservation practices. The National Agricultural Statistics Service (NASS) interviews cooperating farmers to obtain current information on farming practices (crops grown, tillage practices, nutrient and pesticide application, conservation practices, etc.)

Third, the physical process model called APEX (Agricultural Policy Environmental Extender) is used to estimate field-level benefits. APEX is a variant of the EPIC (Erosion Productivity Impact Calculator) model that allows us to estimate the effects of buffers, grassed waterways, and other erosion control practices. APEX allows estimation of the reductions in soil loss, reductions in nitrogen loss, reductions in phosphorus loss, and reductions in pesticide loss from farm fields. Pesticide loss will be expressed as reductions in pesticide risk. APEX will also allow soil quality enhancement to be evaluated.

And finally, CEAP is integrating the model output from APEX with another model called SWAT/HUMUS (Soil and Water Assessment Tool / Hydrologic Unit Model of the U.S.) to assess off-site benefits for water quality. HUMUS includes databases on land use and sources of non-point and point source pollutants that are used with the SWAT model to simulate the transport of water and potential pollutants from the land to receiving streams, and routes the flow downstream to the next watershed and ultimately to the estuaries and oceans. SWAT/HUMUS allows estimation of the reduction in in-stream concentrations of sediment, nutrients, and pesticides attributable to implementation of conservation practices.

OVERVIEW OF THE MODELING APPROACH

A microsimulation model built on the National Resources Inventory (NRI) will provide the basis for estimating reductions in sediment, nutrients, and pesticides from farm fields, increased water use efficiency, and enhancement of soil quality. While the NRI is designed to provide statistical information on the natural resources on private lands, it can also be used as an analytical framework for simulation modeling. Data on field management activities are obtained from farmer surveys and integrated with the information on land use, climate, and soil characteristics at each NRI sample point. This information is then used in conjunction with a field-level fate and transport process model to estimate the loss of materials from farm fields and other outcomes such as accumulation of soil carbon. The statistical sample weight associated with

each sample point is used to aggregate the modeling results to the national or regional scale. The resulting simulation model captures the diversity of land use, soils, climate, and topography from the NRI, estimates the loss of materials from farm fields at the field scale where the science is best developed, and provides a statistical basis for aggregating results to the national and regional levels.

The CEAP Sample and Data Collection: A subset of about 30,000 NRI cropland and CRP sample points will be used to construct the simulation model for the national assessment on cropland, representing about 10 percent of the full NRI cropland sample. This sample constitutes the CEAP Farm Survey Database, and consists of a cropped subset and a CRP subset. Approximately 20 percent of the CEAP sample points will be fields enrolled in the CRP. In order to estimate the on-site effects of conservation practices, it is necessary to obtain information on farming practices (crops grown, tillage, nutrients and pesticides applied, conservation practices applied, etc.) at the selected NRI sample points. A farmer survey is being conducted to collect the needed information at CEAP sample points for the cropped subset. For the subset of points enrolled in the CRP, a link will be established to FSA's CRP database to obtain information on practices implemented. Since it is not possible to administer the survey for the full sample in a single year, survey data are collected over four years--2003 through 2006. The data are pooled for construction of the microsimulation model.

Field-Level Modeling: Field-level modeling will be conducted for the CEAP sample using the physical process model called APEX (Agricultural Policy/Environmental eXtender). APEX allows multiple land uses within a field to be simulated and includes a hydrologic component to route runoff from one land use to another. The EPIC routines are used in APEX to model outcomes for each land use within the field. EPIC is a continuous simulation model that has been widely used to determine the effects of management strategies on agricultural production and soil and water resources. For CEAP modeling, APEX will allow estimation of the effects of buffer strips and other conservation practices involving portions of the field that are not cropped. APEX simulates processes important in agricultural management as well as fate and transport of potential pollutants such as nitrogen, phosphorous, eroded soil, and pesticides. Recent versions of APEX and EPIC include carbon cycle routines from the Century model and pesticide fate and transport routines from GLEAMS. APEX operates on a daily time step, integrating daily weather data, soil characteristics, farming operations such as planting, tillage, and nutrient applications, and a plant growth model to simulate the growth and harvest of a crop. All farming operations that take place on the field throughout the year are taken into account. On a daily basis, APEX tracks the movement of water, soil erosion, the cycling of nitrogen, phosphorus, carbon, and pesticide loss. Model outputs represent pollutant and water movement to the bottom of the root zone and edge of the field. A wide variety of soil, weather, and cropping practice data input options allow simulation of most crops on virtually any soil and climate combination.

APEX model results will be obtained for each of the NRI sample points comprising the CEAP sample. Annual model output will include: volume of runoff, volume of percolate, soil erosion rate, sediment loss, nutrient loss, pesticide loss and an indicator of environmental pesticide risk, accumulation of carbon and phosphorus, and other related measures. Results will be aggregated to provide national and regional estimates of baseline conditions reflecting farming activities on

cropland for the time period 2003-2006, corresponding to the years of farm survey data collection.

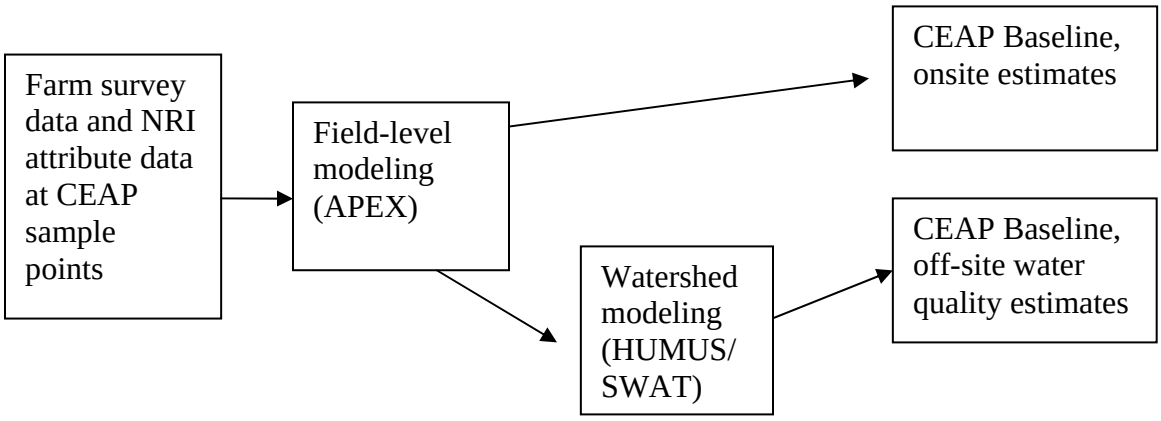


Figure 1. Flow Chart of Activities for Construction of the CEAP Baseline

Watershed-Level Modeling: Offsite estimates of water quality benefits will be assessed at the 8-digit hydrologic unit code watershed scale using a combination of models and databases called HUMUS (Hydrologic Unit Modeling for the United States). There are 2,263 8-digit watersheds in the U.S. The average size is about 10,000 square miles (or about 1.1 million acres). About two-thirds of these have significant cropland acreage. HUMUS includes databases on land use and sources of non-point and point source pollutants that are used with the SWAT model (Soil and Water Assessment Tool) to assess water quantity and water quality issues. SWAT simulates the transport of water, sediment, pesticides, and nutrients from the land to receiving streams and routes the flow downstream to the next watershed and ultimately to the estuaries and oceans. Outputs from the APEX model runs will be used to represent cultivated cropland in HUMUS. HUMUS/SWAT provides estimates of in-stream concentrations of potential pollutants at the outlet of each 8-digit watershed in agricultural regions.

Outcomes will be measured in terms of reductions in in-stream loadings and concentrations of nutrients, pesticides, and sediment attributable to implementation of conservation practices. The following outcome measures also will be estimated: 1) reductions in the number of days during the year that in-stream nitrogen concentrations exceed the drinking water standard, and 2) reductions in the number of days during the warm summer months that in-stream nitrogen and phosphorus concentrations exceed critical thresholds related to algal blooms and eutrophication.

Estimating Benefits of Conservation Practices: The CEAP Farm Survey Database, APEX, and HUMUS will be used to derive estimates of the CEAP Baseline Scenario as shown in figure 1. The CEAP Baseline represents the loss of potential pollutants from farm fields as represented by the farming practices reported in the CEAP Survey, including the presence or absence of conservation practices, and the instream concentrations associated with those farming activities.

In addition to the baseline, an alternative scenario will be constructed by assuming that no conservation practices were in use. For example, if a field associated with a sample point includes grassed waterways and a riparian buffer strip, the APEX model will be run for that sample point as if the grassed waterways and buffer strip were absent. By comparing this scenario to the CEAP baseline, the benefits of the conservation practices currently present on the landscape can be estimated.

EVALUATION OF THE IMPORTANCE OF CHANNEL PROCESSES IN CEAP-WATERSHED SUSPENDED-SEDIMENT YIELDS

Andrew Simon, Research Geologist, USDA-ARS National Sedimentation Laboratory, P.O. Box 1157, Oxford, MS; asimon@ars.usda.gov

Abstract: Sediment is one of the principle pollutants of surface waters of the United States. Efforts by the U.S. Department of Agriculture to quantify and control sediment erosion have historically focused on fields and upland areas. There is a growing body of evidence in agricultural areas of the mid-continent that the locus of sediment erosion has shifted from fields and uplands to edge of field gullies and channels. This is due in part to successful conservation efforts and the natural attenuation of erosion processes with time. Sediment, eroded historically from fields and uplands, was deposited in valley bottoms, filled channels, and accumulated on flood-plain surfaces, causing severe drainage problems. To convey floodwaters and to alleviate flooding problems, channels throughout the mid continent were dredged and straightened, resulting in de-stabilization of entire river systems, severe bank erosion and dramatic increases in erosion rates. This rejuvenation of channel systems results in a systematic series of processes and channel forms that can be identified as *stages of channel evolution*. Today, these channel-erosion processes are still active and can account for up to 85% of the suspended-sediment load in streams, much of this from streambank failures. A reconnaissance study of about 2,500 km of streams in western Iowa showed that 80% of the observed stream reaches were experiencing streambank failures (Hadish, 1994). Similar studies in southeastern Nebraska and western Tennessee showed that about 75% and 60% of stream reaches had unstable streambanks, respectively (Simon and Rinaldi, 2000; Bryan et al., 1995).

Rapid geomorphic assessments (RGAs) of benchmark watersheds in the Conservation Effects Assessment Program (CEAP) are used to determine the degree of instability and stages of channel evolution throughout the channel systems. The distribution of stages throughout the channel network identify local versus systematic disturbances and whether channels are important contributors of sediment. Stable, reference conditions are identified from stages I and VI and used as a means of comparing suspended-sediment yield data from the CEAP watersheds to regional values. Data from more than 2,900 sites across the United States were analyzed in the context of estimating flow and suspended-sediment transport conditions representing average, annual, and at the 1.5-year recurrence interval ($Q_{1.5}$) discharge. Data were sorted into the 84 Level III ecoregions to identify spatial trends in suspended-sediment concentrations and yields. Suspended-sediment yields for stable streams are used to determine “background” or “reference” sediment-transport conditions and to compare with values obtained from the monitored CEAP watersheds.

INTRODUCTION

The Conservation Effects Assessment Program is a collaborative effort between the USDA-Natural Resources Conservation Service, USDA-Agricultural Research Service (ARS) and other agencies and academic institutions. This national research effort aims to provide long-term, coordinated research across a range of hydrologic and agronomic settings for the purpose of improving models for national assessment and to develop policy planning tools. Twenty-four watersheds were initially selected for detailed investigation: 12 ARS Benchmark Watersheds and 8 NRCS Special Emphasis Watersheds and 4 Special Grants Watersheds (Figure 1). The impetus for this work stems from the need to evaluate the natural resource effects of conservation practices in a unified way. Historically these agencies have largely focused on issues involving the movement and transfer of water, pollutants and sediment attributed to “watershed” processes, or what has come to mean upland- and field-processes only. Channels, however, can be considered the “information highway” of the watershed, responsible for the transfer of energy and materials through and out of the watershed. This is particularly true for sediment and therefore requires attention.

Sediment is one of the principle pollutants of surface waters of the United States and has been positively correlated with negative impacts on aquatic ecosystems (Newcombe and MacDonald, 1991; Newcombe



Figure 1 CEAP research watersheds. Red denotes ARS Benchmark Watersheds; blue denotes NRCS Special Emphasis Watersheds; green denotes Special Grants Watersheds.

and Jensen, 1996; Kuhnle et al., 2001; 2002). Suspended sediment parameters have also been related to indices of biotic impairment. Efforts by the U.S. Department of Agriculture to quantify and control sediment erosion have historically focused on fields and upland areas.

There is a growing body of evidence in agricultural areas of the mid-continent that the locus of sediment erosion has shifted from fields and uplands to channels and edge of field gullies (Trimble, 1983; Simon and Rinaldi, 2000). This is due in part to successful conservation efforts (Trimble and Lund, 1983) and the natural attenuation of erosion processes with time. Sediment, eroded from fields and uplands, is deposited in valley bottoms, fills channels, and accumulates on flood-plains, causing severe drainage problems. To convey floodwaters and alleviate flooding problems, channels throughout the mid continent were dredged and straightened, resulting in de-stabilization of entire river systems and dramatic increases in erosion rates. This rejuvenation of channel systems results in a systematic series of processes and channel forms that can be identified as *stages of channel evolution* (Schumm et al., 1984; Simon and Hupp, 1986; Simon, 1989; Figure 1). A reconnaissance study of about 2,500 km of streams in western Iowa showed that 80% of the observed stream reaches were experiencing streambank failures (Hadish, 1994). Similar studies in southeastern Nebraska and western Tennessee showed that about 75% and 60% of stream reaches had unstable streambanks, respectively (Simon and Rinaldi, 2000; Bryan et al., 1995). Today, these channel-erosion processes, which include streambank failures, are still active and contribute a large proportion of sediment to the suspended load in streams. To evaluate the contributions of sediment from the landscape and stream banks to the suspended load, the innovative techniques discussed below are required.

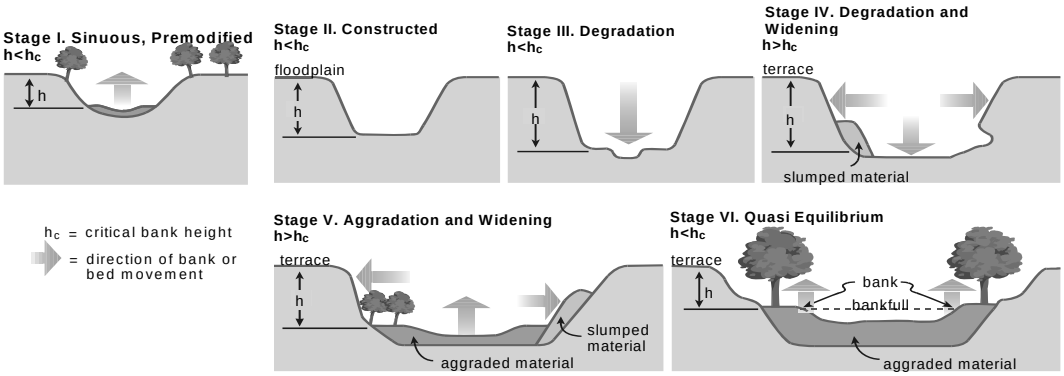


Figure 2 Six stages of channel evolution (from Simon and Hupp, 1986 and Simon, 1989) identifying Stages I and VI as "reference" conditions for Level III ecoregions.

Suspended-Sediment Concentrations, Loads and Yields at the National Scale: Recent research has shown that suspended-sediment yields can be distinguished by ecoregion for stable ("reference" conditions) and unstable streams differentiated by stage of channel evolution (Simon et al., 2002, 2004; Figure 2). This is accomplished using a three-step process:

1. Historical flow and sediment-transport data from sites across the United States are sorted by Ecoregion (Figure 3) and used to develop sediment-rating relations (Figure 4) and loads at the effective discharge by determining the $Q_{1.5}$ from peak-flow data (Figure 5). Mean-daily flow data are used with the transport relation to determine average annual suspended-sediment loads. Annual loads and those at the $Q_{1.5}$ are divided by drainage area to normalize the data for means of comparing values within a given ecoregion.

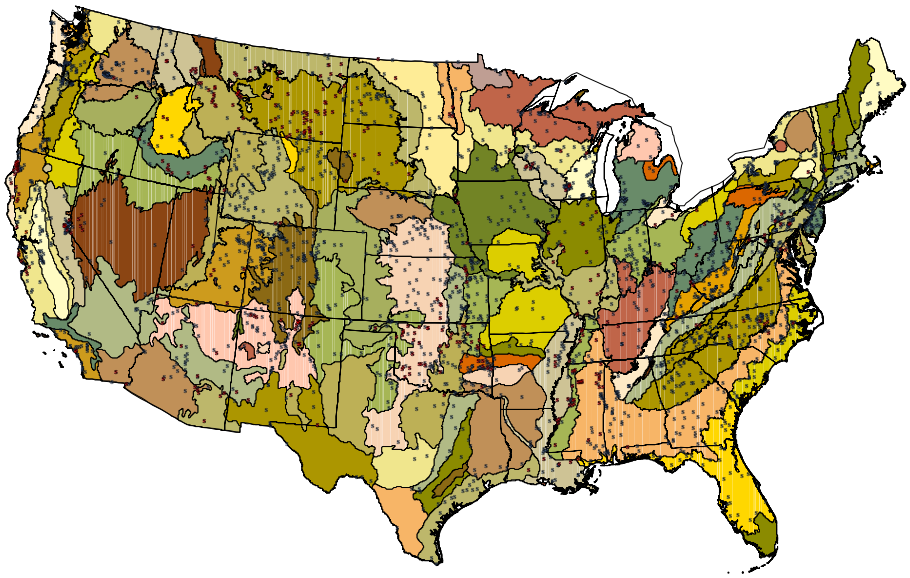


Figure 3 Map of Level III ecoregions of the continental United States showing locations of historical flow and suspended-sediment data.

2. Rapid geomorphic assessments and analysis of gaging-station records are used to determine the relative stability and stage of channel evolution of the site for the purpose of determining whether the calculated suspended-sediment loads reflect "natural", "background", or "reference" conditions, or whether they represent unstable, impacted conditions.

3. Suspended-sediment yield data for an ecoregion are then sorted into "reference" and unstable sites and plotted as histograms to determine the distribution of yields. A "reference" suspended-sediment yield is then determined as either the median value or as the inter-quartile range of the "reference" data (Figure 6). Results have provided an estimate of the range of suspended-sediment yields and concentrations for ecoregions of the continental United States (Figure 7).

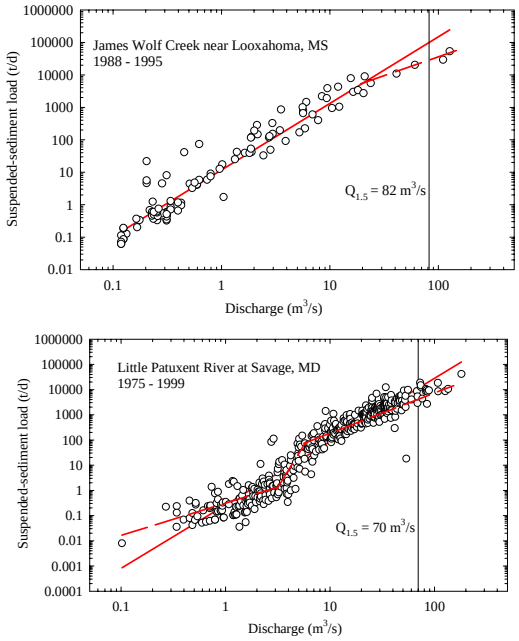


Figure 4 Suspended-sediment transport relation derived from historical data. Note the use of two- and three-stage relations to minimize error at high flows.

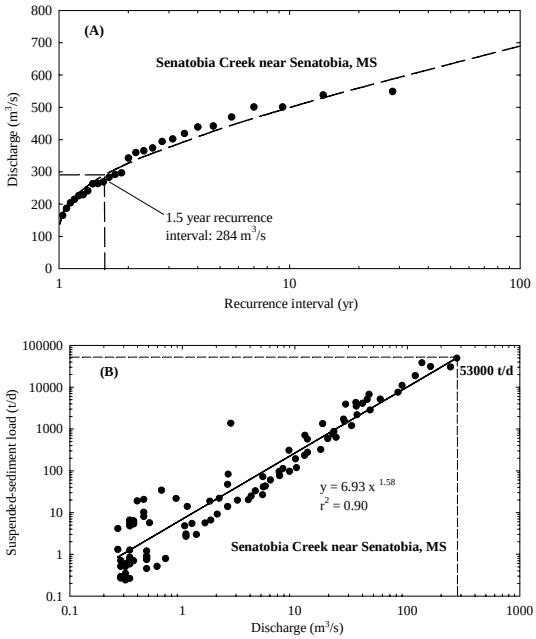


Figure 5 Determination of the $Q_{1.5}$ from peak flow data (A) and application to the transport relation for that site (B).

In addition, naturally occurring radionuclides (^{7}Be and ^{210}Pb) have been used as tracers to provide information regarding the sources of the sediment transported in streams (Wilson et al., 2003; 2005). Proportions of the two radionuclides can be used to differentiate between sediment delivered from the landscape and from streambank failures, gullies, or re-suspended bed material in the suspended sediment due to different half-lives and erosion mechanisms in each source area (Figure 3). They further provide a unifying set of measurements and analyses by which to compare sediment-transport rates and sources. During the 2004 CEAP meeting in Irving, Texas, 11 of the 12 CEAP watersheds (Beasley Lake to be excluded) representatives expressed needs for evaluation of channel erosion processes (Table 1). A number of these representatives indicated that they could aid in supporting this research effort to some degree.

Because the evaluation of conservation measures and best management practices in the CEAP watersheds must be aimed at addressing critical erosion sources, it is important to identify to what degree sediment yield from these watersheds are affected by both upland and channel erosion and if those loads represent impacted channel conditions.

APPROACH

The research approach includes three distinct phases of work that will provide parallel lines of evidence regarding magnitudes and sources of sediment emanating from 11 CEAP watersheds. These work phases follow the natural order of landscapes events from uplands through channels to watershed outlet:

1. Reconnaissance of trunk stream and major tributary channels using rapid geomorphic assessments (RGAs) to determine relative channel stability and stage of channel evolution;

2. Analysis of sediment-transport and flow data from the specific watershed and associated Level III ecoregion to compare rates of sediment transport between the watershed and stable and unstable streams in the ecoregion and to calculate magnitude, frequency, and duration of sediment concentrations; and

3. Quantification of the relative proportion of sediment from different sources in the suspended load of streams during runoff events using ^{7}Be and ^{210}Pb.

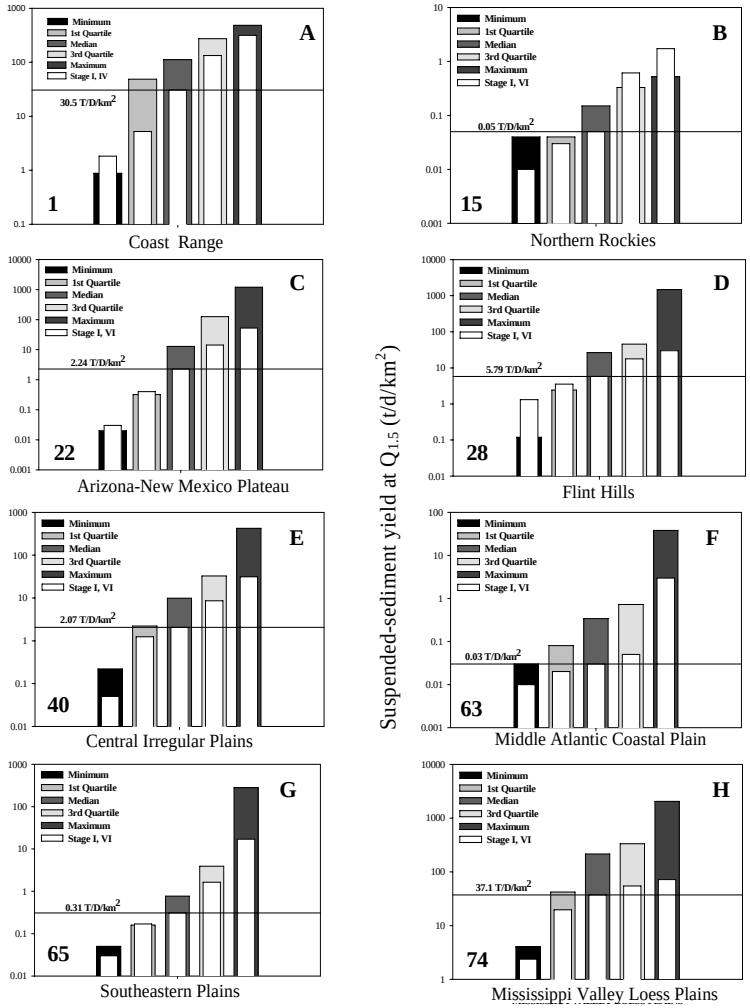


Figure 6 Examples suspended-sediment yield distributions (quartile values) for a range of ecoregions showing differences between stable and unstable sites. Numbers denote Level III ecoregion number.

Rapid geomorphic assessments: Relative channel stability and stage of evolution are determined by aerial and ground reconnaissance of main stem and tributary channels using diagnostic criteria of channel form to determine dominant channel processes. Rapid geomorphic assessments (RGAs) are conducted throughout the channel network and include a survey of channel gradient, bed-material sampling, photographs and an evaluation of attributes of channel erosion and deposition. A semi-quantitative index of channel stability is calculated by summing values of objectively ranked criteria such as type of bed material, degree of incision, existence and type of bank erosion, extent of reach experiencing streambank failures, prevalence of edge of field gullies, extent of bank and bar deposition, woody-vegetative cover, and stage of channel evolution. Mapping the channel-stability index, stage of channel evolution and stability conditions provides a means of determining the magnitude and extent of channel instabilities and erosion sources.

Actual and "reference" sediment-transport rates Annual suspended-sediment yields and those at the $Q_{1.5}$ (effective discharge) have been calculated for sites with USGS historical data in the ecoregion that contains each of the CEAP watersheds (Simon et al., 2004). Analysis of USGS discharge-measurement data combined with RGAs at sites that have not been previously visited in the appropriate ecoregions will be used to distinguish between stable and unstable conditions during the period of sediment sampling. Ranges of suspended-sediment yields for stable ("reference") and unstable sites will then be determined by sorting the data by stage of channel evolution. Flow and sediment-transport data available from CEAP-watershed gages will be used to calculate "actual" sediment-transport rates and compared with "reference" values to determine if the CEAP-watershed streams have been impacted by sediment. The same technique will be used to determine whether coarse-bedded streams are impacted by fine-sediment deposition, using the percentage of bed material finer than 2mm. Flow and sediment-transport data will also be used to calculate magnitude, frequency, and duration of various concentrations of suspended sediment to distinguish between stable and impacted conditions.

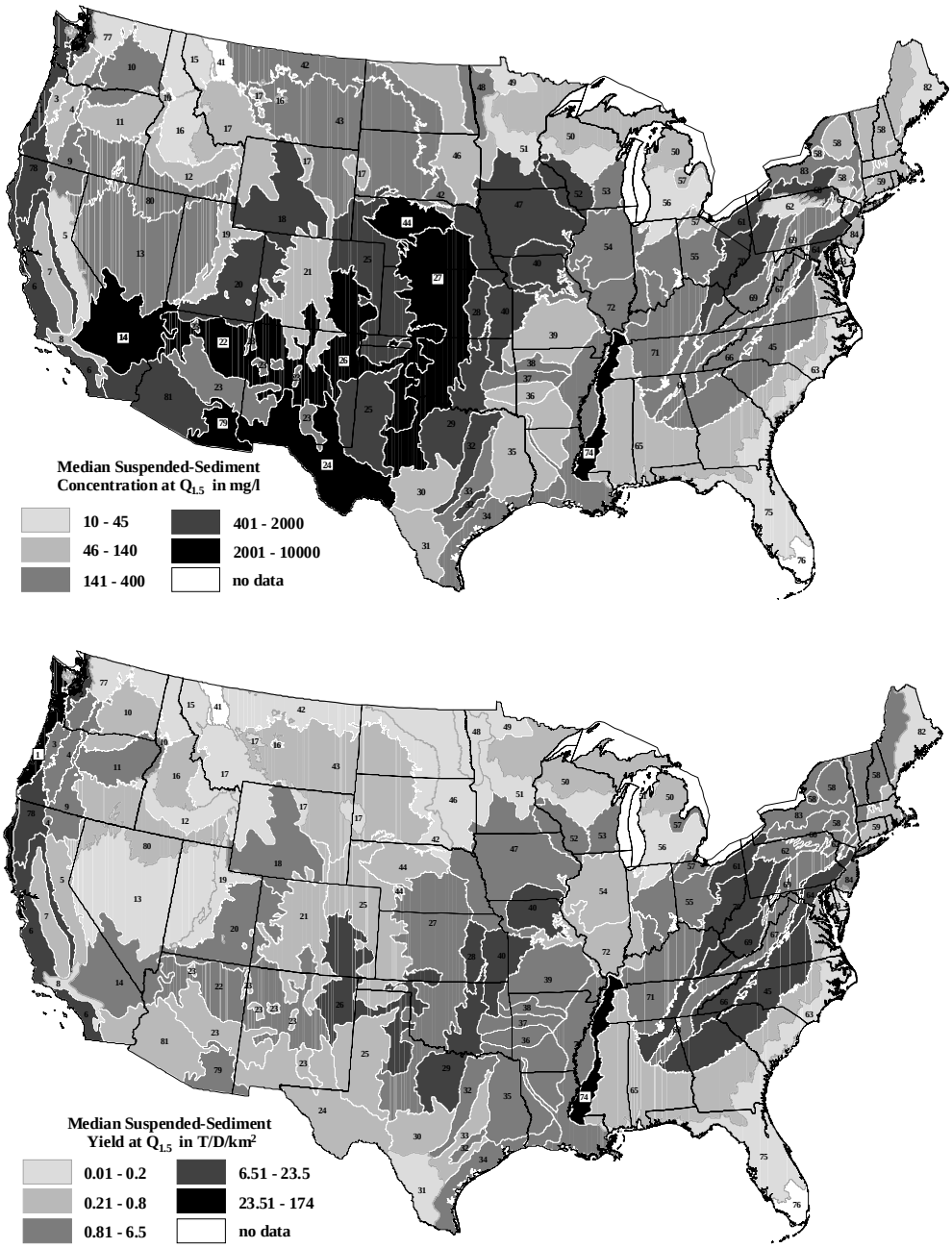


Figure 7 Distribution of median suspended-sediment concentrations and yields at the $Q_{1.5}$ for Level III ecoregions of the continental United States.

Sediment source areas: Activities of ^{7}Be and ^{210}Pb from soil, bank, and suspended sediments will be collected in the CEAP watersheds to determine the percent contribution from landscape erosion and bank collapse. Collection of the soil profiles of ^{7}Be and ^{210}Pb will focus in agricultural fields currently in use. Sampling of streambanks will require long cores to determine background activities of the radionuclides in the banks. Suspended-sediment samples will be collected during runoff events at the head and mouth of the designated stream reach. Sampling will be evenly spaced over the hydrograph. At least 1 g of sediment is required. Sampling during runoff events will also include collection of precipitation. Gamma spectroscopy will be used to determine the activities of ^{7}Be and ^{210}Pb at the NSL. High radionuclide activities suggest a large proportion of recently eroded landscape-derived material. Conversely, lower activities in the suspended sediment suggest dilution by bank material. A simple two-end

member-mixing model will determine the relative contribution of each source to the total sediment load. The radionuclide signature of suspended sediments would lie roughly along the mixing line between the signatures of the two end-member sources of sediment (Figure 8).

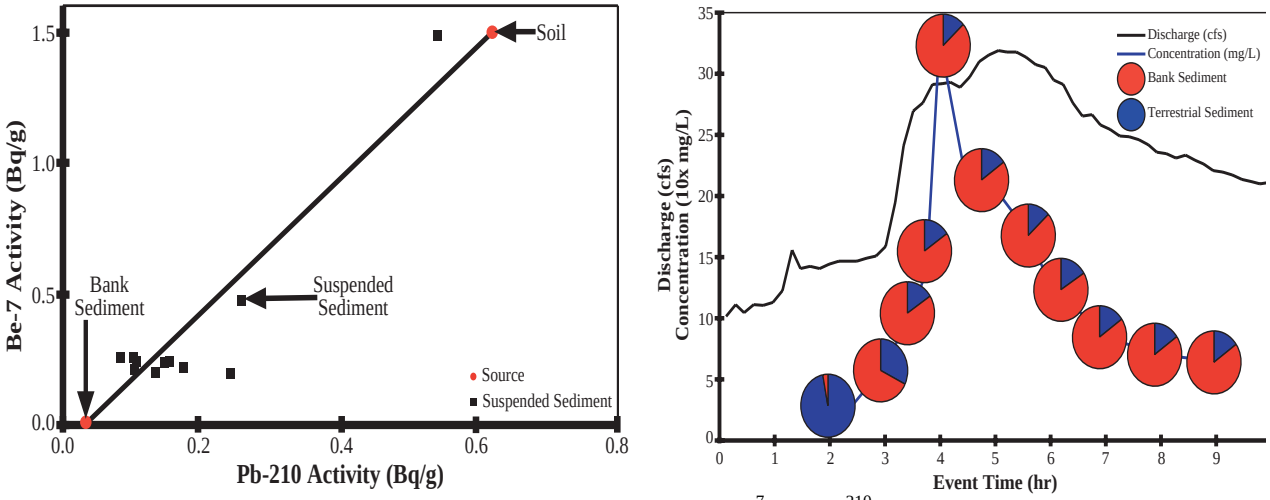


Figure 8 Example results from Goodwin Creek, MS showing ratios of ^{7}Be and ^{210}Pb in streambank, soil and suspended-sediment samples (A) and the percentage of eroded sediment emanating from streambank (red) and terrestrial (blue) erosion using ratios of ^{7}Be and ^{210}Pb in suspended sediment (B). From Wilson and Kuhnle (2006).

Table 1 Status of NSL work to determine suspended-sediment yields and "reference" conditions for Level III ecoregions encompassing the CEAP watersheds.

CEAP Watershed	Ecoregion #	Ecoregion Yields	"Reference" Yields	Watershed Interest
Upper Washita River, OK	27	Completed	Partial	Yes
Goodwin Creek, MS	74	Completed	Completed	Yes
Yalobusha River, MS	65	Completed	Completed	Yes
Beasley Lake	73	Completed	Completed	No
South Fork Iowa River, IA	47	Completed	Partial	Yes
Walnut Creek, IA	47	Completed	Partial	Yes
Town Brook, NY	58	Completed	Not Started	Yes
Upper Big Walnut Creek, OH	55	Completed	Not Started	Yes
Mark Twain Reservoir, MO	40	Completed	Completed	Yes
Little River, GA	45	Completed	Completed	Yes
Upper Leon River, TX	29	Completed	Partial	Yes
St Joseph River, IN	55	Completed	Not Started	Yes

EXPECTED RESULTS AND PRODUCTS

Results of the proposed cross-location research will provide a quantitative evaluation of the role of channel processes in CEAP watersheds. Series of maps will be produced distinguishing critical erosion areas in the stream network and determination of local versus system-wide instabilities. Comparison of watershed sediment yield with those for stable sites in the associated ecoregion will provide a basis to determine the relative magnitude of erosion-related sediment problems in the CEAP watersheds. The proportions of sediment eroded from fields and streambanks will be evaluated using radionuclide signatures and will assist in efficient development of management practices.

REFERENCES

Bryan, B.A., Simon, A., Outlaw, G.S., Thomas, R. (1995). Methodology for assessing channel conditions at bridges in Tennessee related to scour critical conditions. U.S. Geological Survey Water-Resources Investigations Report 94-4229. 54 p.

Hadish, G.A. (1994). Stream stabilization in western Iowa. Iowa DOT HR-352. Golden Hills Resource Conservation and Development. Oakland, Iowa. 198 p.

Kuhnle, R. A., Simon, A., Knight, S. S. (2001). "Developing linkages between sediment load and biological impairment for clean sediment TMDLs," Wetlands Engineering and River Restoration Conference, ASCE. Reno, Nevada. August.

Kuhnle, R. A., Simon, A., Knight, S. S. (2002). "Developing linkages between clean sediment indices and biological impairment," Proceeding of Central Plains Aquatic Bioassessment and Biocriteria Symposium.

Newcombe, C. P., Jensen, J. O. T. (1996). "Channel suspended sediment and fisheries: a synthesis for quantitative assessment of risk and impact," North American Journal of Fisheries and Management. 16(4): 693-727.

Newcombe, C. P., MacDonald, D. D. (1991). "Effects of suspended sediment on aquatic ecosystems," North American Journal of Fisheries and Management. 11: 78-82.

Schumm, S.A., Harvey, M.D., Watson, C.C. (1984). Incised Channels, Morphology, Dynamics and Control. Water Resources Publications. Littleton, Colorado. 200 p.

Simon, A. (1989). "A model of channel response in disturbed alluvial channels,"Earth Surface Processes and Landforms. 14(1): 11-26.

Simon, A., Dickerson, W., Heins, A. (2004). "Suspended-sediment transport rates at the 1.5-year recurrence interval for ecoregions of the United States: Transport conditions at the bankfull and effective discharge?" Geomorphology. 58: 243-262.

Simon, A., Hupp, C. R. (1986). "Channel evolution in modified Tennessee channels," Proceedings of the Fourth Interagency Sedimentation Conference. March 1986, Las Vegas, NV. 2(5) 5-71 to 5-82.

Simon, A., Kuhnle, R., Dickerson, W., Griffith, M. (2002). " 'Reference' and enhanced rates of suspended-sediment transport for use in developing clean-sediment TMDL's," In, Proceedings, ASAE Conference on TMDLs. Ft. Worth, TX. 12 p.

Simon, A., Rinaldi, M. (2000). "Channel instability in the loess area of the Midwestern United States.,"Journal of the American Water Resources Association. 36(1): 133-150.

Trimble, S.W. (1983). "A sediment budget for Coon Creek Basin in the Driftless Area, Wisconsin, 1853-1977," American Journal of Science. 283: 454-474.

Trimble, S.W., Lund, S.W. (1983). Soil conservation and the reduction of erosion and sedimentation in the Coon Creek Basin, Wisconsin. U.S. Geological Survey Professional Paper 1234. 35 p.

Wilson, C.G., and Kuhnle, R., (2006). Determining relative contributions of eroded landscape sediment and bank sediment to the suspended load of Goodwin Creek using radionuclides. This volume.

Wilson, C.G., Matisoff, G., Whiting, P.J. (2003). "Short-term erosion rates from a ^{7}Be inventory balance," Earth Surface Processes and Landforms. 28: 967-977.

Wilson, C.G., Matisoff, G., Whiting, P.J., Klarer, D.M. (2005). "Transport of fine sediment through a wetland using radionuclide tracers: Old Woman Creek, OH," Journal of Great Lakes Research. 31(1):56-67.

DETERMINATION OF SEDIMENT SOURCES ON THE CEAP BENCHMARK WATERSHEDS

Christopher G. Wilson, Research Scientist, NCCHE, University of Mississippi, Oxford, MS, CWILSON@olemiss.edu; Roger A. Kuhnle, Research Hydraulic Engineer, USDA-ARS, National Sedimentation Laboratory, Oxford, MS, RKUHNLE@msa-oxford.ars.usda.gov

Abstract: As part of the Conservation Effects Assessment Program (CEAP), 12 watersheds across the country have been designated as CEAP benchmark watersheds. These watersheds were chosen to evaluate the effectiveness of the conservation practices applied under various landscape and agricultural conditions in different parts of the country. Goodwin Creek, located in the north central part of Mississippi, is one of the CEAP benchmark watersheds where the effects of land use and management practices on sediment transport have been studied since 1982. Recently, technology to differentiate the source of fine sediments in the suspended load of streams using naturally occurring radionuclides has been applied within this watershed. Preliminary data from Goodwin Creek show that fine sediment is predominantly derived from the land surface during the initial part of a runoff event. The latter parts of the same runoff event indicated that the sources of fine sediment shifted to predominantly channel bank sources. Further measurements will provide information on the variations of sediment sources of fine sediments during different parts of the year and for different magnitude flows. This technique will be applied to other CEAP benchmark watersheds with the cooperation of the researchers from those watersheds. Knowledge of the sources of sediment in the different benchmark watersheds will provide critical information regarding sediment problems and the types of management practices that will most likely be effective in rectifying these problems.

INTRODUCTION

The 2002 Farm Bill and CEAP: Although erosion of surface soils from the landscape is a natural process, it has been considerably augmented by agricultural practices. This accelerated loss of topsoil can significantly lower crop yields. Moreover, anthropogenically increased erosion of fine sediment with sorbed nutrients and contaminants will have detrimental effects on the receiving waters below agricultural fields. These contaminants also can be transmitted through the food chain, causing further degradation of agricultural ecosystems.

The Farm Security and Rural Investment Act of 2002, more commonly known as the 2002 Farm Bill, was designed to curb increased soil erosion from agricultural fields by providing financial incentives for the implementation of conservation practices. The bill significantly increased overall spending for programs that support conservation of agricultural lands compared to previous initiatives. In addition, the 2002 Farm Bill expanded older programs and created new ones to promote Best Management Practices (BMPs). Understanding land use change and its effect on soil erosion is a crucial but daunting task for the development of efficient BMPs.

In response to the 2002 Farm Bill, the United States Department of Agriculture (USDA) created the Conservation Effects Assessment Project, or CEAP, to evaluate the environmental benefits of conservation practices. One of the primary objectives of CEAP is to develop a set of regional watershed assessment models that can be used to address benefits of conservation practices and other environmental issues in the major agricultural regions of the nation and for use in future national assessments (USDA-ARS, 2005). Several valuable models currently exist which attempt to evaluate the contributions of sediment from various sources within a watershed. However, limited data are available to validate these models. CEAP promises to provide validation data sets for these models that will be useful at the watershed and regional scales to evaluate the benefits associated with conservation practices and the effectiveness of current and proposed management practices (USDA-ARS, 2005).

The present study will assist CEAP in reaching the above objective. The ability to accurately assess the delivery of sediment from different parts of the watershed to the suspended load of a stream allows for better management of agricultural fields. An accurate determination of soil loss is crucial for validation of the models developed to evaluate conservation practices.

Project Objective: Agricultural fields are often considerable suppliers of fine sediment to the suspended load of streams because tillage practices loosen top soil making it more susceptible to erosion. Other processes, including

channel bank erosion and resuspension of bed sediment, which are not directly affected by anthropogenic influences, can also contribute to the fine sediment load of streams. Understanding the roles of these different processes controlling sediment transport within a watershed will provide valuable information for evaluating the effectiveness of BMPs. The ability to differentiate sediment contributed from different source areas is an important first step in calculating the relative contribution of different sources.

Each source of sediment must have a unique signature relative to the others to properly differentiate it from other sources and to quantify its contribution to the suspended load. Previous sediment sourcing studies have shown that the degree of precision in identifying major contributors of sediment and calculating their delivery is directly related to the number of sediment properties compared between the different source areas (Peart and Walling, 1986 and Walling and Woodward, 1992). However, the work load of the project also substantially increases with the number of studied sediment characteristics.

This study was developed to provide a simpler method of differentiating sediment from multiple sources within a watershed by examining only the activities of two naturally occurring radioisotopes, ^{7}Be and $^{210}Pb_{xs}$, and their ratio relative to one another. The simplified method does limit the precision of source identification. This method will provide only a relative contribution between eroded surface soils and collapsed bank sediment or resuspended bed material in the suspended load of a small stream during runoff events. The knowledge gained is extremely valuable for the validation of watershed assessment models developed by the USDA.

This paper will develop the novel method, which uses ^{7}Be and $^{210}Pb_{xs}$ for evaluating relative contributions of fine sediment from different source areas within agricultural watersheds, and its application to several agricultural systems identified by CEAP as benchmark watersheds. The theory behind the study and the methods used to conduct the research will be presented. Analysis of a case study at Goodwin Creek, MS, will be presented in an accompanying paper.

BACKGROUND

This study is designed to quantify the proportion of eroded surface soils relative to contributions from collapsed bank material and/or resuspended bed sediment in the fine suspended sediment load of streams within CEAP benchmark watersheds following runoff events using ^{7}Be and $^{210}Pb_{xs}$. Each source material must have a unique radionuclide signature relative to the other in order to quantify the contributions from the different source areas to the suspended sediment. Fallout radionuclides, namely ^{7}Be ($t_{1/2}$ = 53.3 days) and $^{210}Pb_{xs}$ ($t_{1/2}$ = 22.3 years), may provide the characteristic signature to differentiate sediments transported through streams. The two radionuclides relative to one another can be used to differentiate sediment sources due to differences in half-lives or erosion processes (Wilson, 2003; Matisoff et al., 2005 and Wilson et al., 2005).

The radioisotopes ^{7}Be and $^{210}Pb_{xs}$, which are attached to aerosol particles in the atmosphere, are delivered to the landscape mainly during precipitation events. The radionuclides quickly and strongly bond to surface soils. The binding nature of fallout radionuclides to sediment limits adsorption to only the finer silt and clay particles. The relatively high activities of ^{7}Be and $^{210}Pb_{xs}$ in the precipitation decrease as the two radionuclides are mixed with previously delivered ^{7}Be and ^{210}Pb in surface soils, which have undergone radioactive decay resulting in lower activities (Matisoff et al., 2005 and Wilson et al., 2005). Surface soils and absorbed radionuclides are eroded from the landscape as runoff initiates and are transported through streams. The eroded sediment from the landscape still has relatively high activities of ^{7}Be and $^{210}Pb_{xs}$ because sheet erosion removes only a thin layer (<1 cm) of surface soils, which contains the highest activities of the radionuclides from the strong and rapid bonding nature of the radionuclides (Bonniwell et al., 1999). Moreover, the preferential removal of clay particles that occurs during storm runoff (Rhoton et al., 1979) enriches the radionuclide activity of eroded sediment by concentrating the particles, to which the radionuclides sorb.

As the eroded sediment is transported downstream, sediment from stream banks and the bed are entrained into the flow. Additions of bed and bank material, which have low activities of ^{7}Be and $^{210}Pb_{xs}$, further decrease the radionuclide activities of the suspended fine sediment (Matisoff et al., 2005 and Wilson et al., 2005). Sediments from the bed have resided there for extended periods without radionuclide replenishment and have undergone substantial decay. Eroded bank sediments also will have relatively low activities of $^{210}Pb_{xs}$ and ^{7}Be because they receive little atmospheric input due to near-vertical slopes (Whiting et al., 2005). Moreover, stream bank failure

typically removes large volumes of material (Thorne, 1992). The high activity sediment from the soils at the top of the collapsed bank is diluted by a much larger volume of low activity sediment from deeper in the collapsed bank.

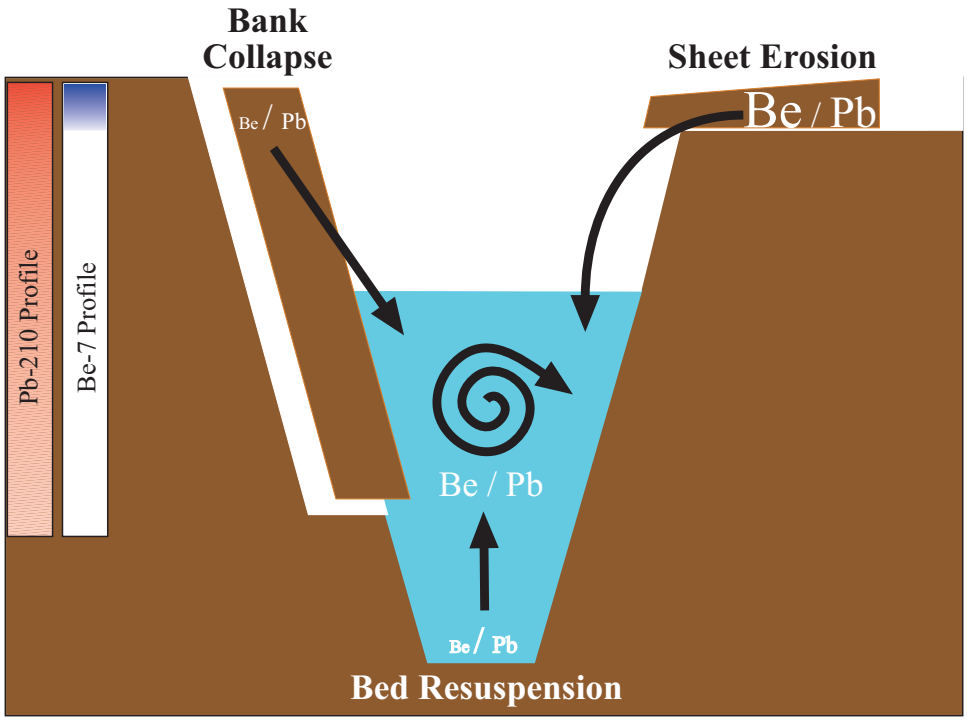


Figure 1 Radionuclide relationship of sources of sediment to suspended load of a stream.

Suspended sediment is a mixture of landscape derived sediment, bed sediment, and bank sediment (Figure 1). However, if one of those sources can be eliminated, as with sand and gravel bed streams, the fine suspended sediment has an intermediate radionuclide signature that is quantified in terms of the relative contribution of landscape derived and bank sediment. High radionuclide activities suggest a large proportion of recently eroded landscape derived material. Conversely, lower activities in the suspended sediment suggest dilution by bank material. The different erosion mechanisms affecting surface soils and bank sediments produce these different signatures.

The suspended sediment in the stream contains a mixture of the eroded surface soils and collapsed bank sediment. The resulting signature of the suspended sediment will reflect the mixture of the surface soils and the bank sediments. A simple two-end member mixing model would determine the relative contribution of each source area to the total fine sediment load. The radionuclide signature of suspended sediments would lie roughly along the mixing line between the signatures of the two end-member sources of sediment.

METHODS

Study Sites: Activities of ^{7}Be and $^{210}Pb_{xs}$ from precipitation samples, and soil, bank, and suspended sediments associated with individual runoff events will be collected within CEAP benchmark watersheds. The current CEAP benchmark watersheds (Table 1) are located primarily in the Central and Eastern parts of the United States. The sizes of individual watersheds in CEAP range from <1 km^2 to >8,000 km^2. The watersheds are all agricultural in nature, including mostly row crop farming, pastures, and feed lots. Nearly every watershed cites excess sediment, nutrients, and pesticides in storm runoff as chronic problems in the watershed. To counter these issues, several different BMPs have been implemented in these watersheds, which include conservation tillage, riparian buffers, grass waterways, constructed wetlands, drop pipes, and tile drains. A more complete description of each watershed can be found in USDA-ARS (2005).

Table 1 CEAP benchmark watersheds.

Watershed	Managing Laboratory Location
South Fork of the Iowa River	Ames, IA
Walnut Creek	Ames, IA
Salt River/ Mark Twain Reservoir	Columbia, MO
Upper Washita River	El Reno, OK
Goodwin Creek	Oxford, MS
Little Topashaw Creek	Oxford, MS
Beasley Lake	Oxford, MS
Leon River	Temple, TX
Little River	Tifton, GA
Town Brook/ Cannonsville Reservoir	University Park, PA
St. Joseph River	West Lafayette, IN
Upper Big Walnut Creek	Columbus, OH

Laboratory Methods: Gamma spectroscopy will be used to determine the activities of ^{7}Be and $^{210}Pb_{xs}$ in the soil, bank, and suspended sediments samples, as well as the precipitation samples. Samples are to be counted in standardized geometries for at least 82,800 seconds on a High Purity Germanium (HPGe) gamma detector and then for an additional 300 seconds with a standardized sealed source to account for self-adsorption of the ^{210}Pb photon (Cutshall et al., 1983). The counting efficiencies for ^{210}Pb were established using two mixed radionuclide solutions; ^{7}Be efficiencies were interpolated from the resulting curves of the efficiencies of the radionuclides present in the mixed solutions (Bonniwell, 2001 and Wilson, 2003).

Gamma spectroscopy provides a simple and non-destructive means of analyzing the radioactivity of each sample. Preparation of all samples for radionuclide analysis is minimal. Soil and sediment samples will be dried and separated into sand, silt, and clay size fractions because radionuclide sorption processes and preferential erosion mechanisms favor fine particles. The dissolved radionuclides in collected rain samples will be precipitated on a $Fe(OH)_3$ floc. The extraction procedure for the dissolved phase is detailed in Wilson (2003).

One limitation to this method is the substantial analysis time (~1 day), which is due to the low activities associated with environmental samples. Sediment particles are tagged with only the natural delivery of ^{7}Be and $^{210}Pb_{xs}$ from the atmosphere. The long analysis time constrains the number of collected samples. A gamma spectroscopy lab has been established at the National Sedimentation Laboratory (NSL) in Oxford, MS to facilitate the analysis of the required samples for this study.

Field Methods: Samples must first be collected from both the landscape and stream banks in each sampled watershed to determine the background activities of ^{7}Be and $^{210}Pb_{xs}$ of the potential source areas. Radionuclide activities on the landscape and in stream banks must be determined shortly before each sampled runoff event to ensure a strong relationship with the sampled runoff event. To accommodate the difficulty to predict adequate runoff events, radionuclide profiles less than two months old will be used, provided additions from the atmosphere and losses due to decay are accounted properly.

Soil sampling will be restricted to agricultural fields and pasture lands currently in use. The majority of erosion from the landscape will occur in fields with little vegetative cover where the soil has recently been loosened by tillage. Erosion on the landscape removes a thin layer of surface soils; therefore, high resolution soil profiles with sampling intervals of 0.5 cm will be taken to a depth of 5 cm. The soil profiles will have large surface areas (~200 cm^2) to ensure enough sediment is collected for analysis. Samples for gamma spectroscopy analysis at the NSL must be between 1 and 15 grams of sediment. Spatial variability of radionuclide activities on the landscape may be significant due to site specific characteristics; however, the number of samples is limited due to the long counting time and the relatively short half-life of ^{7}Be. Five soil profiles will be collected within each watershed.

Deeper cores from stream banks are required because bank failure removes larger volumes of sediment. To determine average activities of the bank material, the cores neither require the fine sampling resolution nor the large surface area of the soil profiles. The total depth of the cores will be 1 m and the sampling interval will be approximately 30 cm. Five bank cores also will be collected within each watershed.

The transport of fine suspended sediment in streams occurs most prominently during runoff events. Thus, suspended sediment samples will be collected during runoff events at each CEAP watershed. Suspended sediment samples will be collected at a designated site downstream of the soil surface and bank samples.

ISCO pump samplers can be used to collect suspended sediment. Fine suspended sediments in Goodwin Creek are well mixed (Kuhnle et al., 2001); therefore, point samples should provide adequate representation of the fine sediment load. Sampling should be evenly spaced throughout the hydrograph. ^{7}Be and ^{210}Pb tend to have higher concentrations when stage is rising as opposed to times when stage is falling or steady and is related to the timing of delivery of major sources of sediment from the landscape (Brigham et al., 2001). Much of the sediment removed from stream banks occurs as sloughs and toppling failures of banks particularly at decreasing stages (Thorne, 1992).

Sampling during runoff events will include collection of the precipitation to the watershed, as well as the suspended sediment in the streams. The radioisotopes ^{7}Be and ^{210}Pb are delivered in the precipitation, which produces the runoff event. The high partition coefficients of the radionuclides ($K_d \sim 10^4$ to 10^6; Wilson, 2003) result in rapid and strong bonding to the soil surface. The resulting radionuclide profile can be represented with an exponential fit (Owens et al., 1996; Wallbrink and Murray, 1996; and Wilson et al., 2003). The exponential fit can be used to determine the average expected activities of the radionuclides eroded from the landscape surface.

RESULTS

Each source material must have a unique radionuclide signature relative to the other in order to quantify the relative proportions from the different source areas in the suspended sediment. The activities of ^{7}Be and ^{210}Pb of the surface soils will be significantly higher than corresponding activities of the bank sediments. The radionuclide signature of the suspended sediment will lie intermediate along a mixing line between the signatures of the two end-member sources of sediment. Figure 2 is a graph of activities of ^{7}Be and ^{210}Pb of suspended sediments collected at a cross section of Goodwin Creek, MS, a CEAP benchmark watershed, relative to the average activities of the respective landscape and bank source materials. These data support the basic premise of the proposal. The suspended sediment lie along a mixing line, represented by the solid black line, between the average radionuclide signatures of the surface soils and the bank material. The mixing model allows determination of the relative contribution of sediment sources to the sediment load. Further interpretation of these data is in a following paper.

CONCLUSION

This study details a novel use of the activities of ^{7}Be and $^{210}Pb_{xs}$ to differentiate the relative contributions of surface soils eroded from the landscape and collapsed bank sediment to the suspended load of streams in agricultural watersheds during runoff events. The two source materials have distinct radionuclide signatures. The suspended load of the stream is a mixture of the two source materials and plot along a mixing line between the source activities. This study will be applied to several CEAP benchmark watersheds to provide validation for watershed assessment models that can be used to address benefits of conservation practices and other environmental issues in the major agricultural regions of the nation and for use in future national assessments.

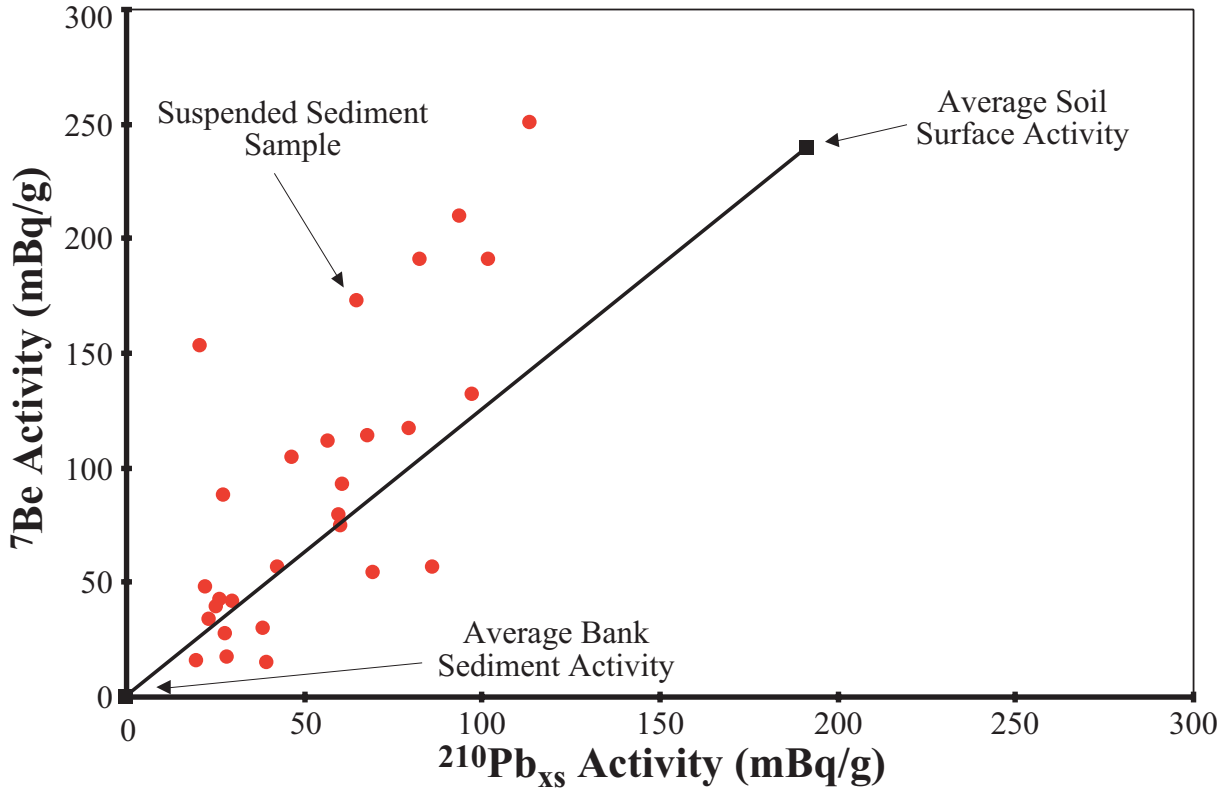


Figure 2 Activities of ^{7}Be and $^{210}Pb_{xs}$ for soil, bank, and suspended sediment samples collected in association with a runoff event at Goodwin Creek, MS.

REFERENCES

Bonniwell, E.C., Matisoff, G., and Whiting, P.J. (1999). "Determining the times and distances of particle transit in a mountain stream using fallout radionuclides," Geomorphology, 27, pp75-92.

Bonniwell, E.C. (2001). Evaluating Soil Erosion and Sediment Transport with Radionuclides. Ph.D. Dissertation, Case Western Reserve University, Cleveland, OH.

Brigham M.E., McCullough, C.J., and Wilkinson, P. (2001). Analysis of suspended-sediment concentrations and radioisotope levels in the Wild River Basin, Northwest Minnesota, 1973- 98. US Geological Survey Water-Resources Investigations Report, 01-4192, pp 1-21.

Cutshall, N.H., Larsen, I.L., and Olsen, C.R. (1983). "Direct analysis of ^{210}Pb in sediment samples: self-adsorption correction," Nuclear Instruments and Methods, 206, pp309-312.

Kuhnle, R.A., Bennett, S.J., Alonso, C.V, Bingner, R.L., and Langendoen, E. (2000). "Sediment transport in agricultural watersheds," .Journal of Sediment Research, 15(2), pp 182-197.

Matisoff, G., Wilson, C.G., and Whiting, P.J. (2005). "$^{7}Be/^{210}Pb$ Ratio as an indicator of suspended sediment age or fraction new sediment in suspension," Earth Surface Processes and Landforms, 30(9), pp 1191-1201.

Owens, P.N., Walling, D.E., and He, Q. (1996). "The behavior of bomb-derived cesium-137 fallout in catchment soils," Journal of Environmental Radioactivity, 32(3), pp 169-191.

Peart, M.R., and Walling, E.E. (1986). "Fingerprinting in sediment sources: The example of a drainage basin in Devon, UK," In Drainage Basin Sediment Delivery, IAHS Publication, 159, pp 41-55.

Rhoton, F.E., Smeck, N.E., and Wilding, L.P. (1979). "Preferential clay mineral erosion from watersheds in the Maumee River Basin," Journal of Environmental Quality, 8(4), pp 547-550.

Thorne, C.R. (1992). "Bed scour and bank erosion on the meandering Red River, Louisiana," In Carling, P.A. and Petts, G.E. editors, Lowland Floodplain Rivers; Geomorphologic Perspectives, John Wiley and Sons, Chichester, p. 95-115.

United States Department of Agriculture- Agricultural Research Service. (2005). Conservation Effects Assessment Project – The ARS Watershed Assessment Study. USDA-Agricultural Research Service Report, pp 1-163.

Wallbrink, P.J. and Murray, A.S. (1996). "Distribution and variability of ^{7}Be in soils under different surface cover conditions and its potential for describing soil redistribution processes," Water Resources Research, 32(2), pp 467-476.

Walling, E.E. and Woodward, J.C. (1992). "Use of radiometric fingerprints to derive information on suspended sediment sources," In Erosion and Sediment Transport Monitoring Programmes in River Basins, IAHS Publication, 210, pp 153-164.

Whiting, P.J., Matisoff, G., Fornes, W.F., and Soster, F.M. (2005). "Suspended sediment sources and transport distances in the Yellowstone basin," GSA Bulletin, 117, pp 515-529.

Wilson, C.G. (2003). The Transport of Fines Sediment Through Three NERR Estuaries Using Radionuclide Tracers. PhD. Dissertation. Case Western Reserve University. Cleveland, OH.

Wilson, C.G., Matisoff, G., and Whiting, P.J. (2003). "Short-term erosion rates from a ^{7}Be inventory balance," Earth Surface Processes and Landforms, 28(9), pp 967-977.

Wilson, C.G., Matisoff, G., Whiting, P.J., and Klarer, D.M. (2005). "Transport of fine sediment through a wetland using radionuclide tracers: Old Woman Creek, OH," Journal of Great Lakes Research, 31(1), pp 56-67.

MONITORING THE EFFECTS OF SEDIMENTATION FROM MOUNT ST. HELENS

Patrick S. O'Brien, P.E., Senior Hydraulic Engineer, U.S. Army Corps of Engineers, Portland District, P.O. Box 2946, Portland, OR 97208-2946, p.obrien@us.army.mil; Alan D. Donner, P.E., Senior Hydraulic Engineer, U.S. Army Corps of Engineers, Portland District, P.O. Box 2946, Portland, OR 97208-2946, alan.d.donner@usace.army.mil; Dr. David S. Biedenharn, PhD, P.E., Research Hydraulic Engineer, U.S. Army Engineer Research and Development Center, Coastal and Hydraulics Laboratory, 3909 Halls Ferry Road, Vicksburg, MS 39180, David.S.Biedenharn@erdc.usace.army.mil

Abstract: Sedimentation processes from Mount St. Helens eruption affect the channel capacities and morphology of the Toutle and Cowlitz rivers in southwest Washington State. Portland District Corps of Engineers must ensure that flood protection levels are maintained on the lower Cowlitz River at the communities of Longview, Kelso, Lexington, and Castle Rock.

Levees, dredging, and Sediment Retention Structure have maintained flood protection on the lower Cowlitz River. The annual monitoring program consists of data collection to assess the current channel capacity and geomorphic state of the Toutle and Cowlitz rivers. The current monitoring activities are river gages, periodic hydrosurveys, suspended sediment and bed material sampling. The Sediment Impact Assessment Model (SIAM) incorporates all the data collected and is used to verify the observed trends. The model is used in a predictive mode to determine the effects of dry, normal and wet periods on the river system.

DATA COLLECTION

Cowlitz River Gages: The Mount St. Helens Engineering Reanalysis (Portland District, April 2002) recommended a system of 7 stage gages to monitor sediment impacts to flow levels from the mouth of the Cowlitz River to the confluence of the Cowlitz River with the Toutle River. Five water level loggers were installed on the Cowlitz River during the month of October, 2002. These five gages along with USGS gage No. 14243000 (Cowlitz River at Castle Rock) and NWS gage No. 454131 (Cowlitz River at Kelso) make up the 7-stage gage system (Portland District, October 2005).

The system of gages on the Cowlitz River is intended to track potential changes in channel capacity due to sedimentation by specific gage analysis. The data collected from the gages to date has not shown any conclusive evidence of loss or gain of channel capacity. This was expected since the gages have been in operation a short time and there have not been any significant hydrologic events which could reduce the channel capacity in the Cowiltz River.

Toutle River Basin Gages: The Corps Portland District office operates two weather stations in the Toutle River Basin; at the Sediment Retention Structure [SRS] Coldwater Ridge in the North Fork Toutle basin. The SRS weather station records air/water temperature, precipitation, wind speed/direction and the water level at the spillway. The Coldwater Ridge weather station records air temperature, precipitation and wind speed/direction. The USGS operates two important stations in the Toutle River basin; Toutle River at Tower Road (14242580) and South Fork Toutle at Toutle, WA (14242580). These two gages provide stage, discharge and suspended

sediment data. The daily sediment discharge data measured by these gages is an important tool in monitoring the operation of the SRS and sedimentation processes in the Cowlitz and Toutle Rivers.

Bed Material Sampling: Bed material samples are collected in the Toutle and Cowlitz rivers during low water period by Portland District. Field observation of geomorphic changes in the rivers system is an important component of the monitoring effort and is part of the bed material sampling effort. Once collected, the samples are processed by the USGS Cascades Volcano Observatory into sediment gradation curves. The information from the sediment gradation at each location is used to estimate the wash load and sediment transport capacity of the river reach in which it was collected. Comparisons of the sediment gradation curves from bed material are made to monitor changes. Changes in the bed material at any given location, either to coarser or finer material are an indication of changes in sedimentation processes upstream. The sediment gradation curves (Figure 1) are also used in the SIAM model.

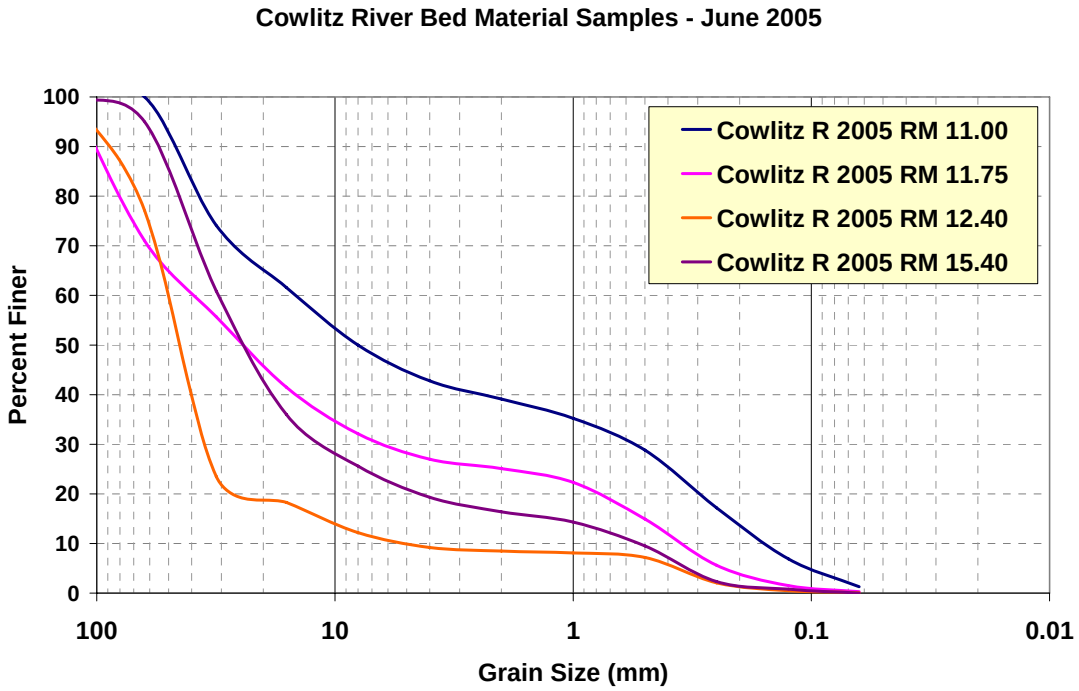


Figure 1 Sediment gradation curves - Cowlitz River bed material samples, June 2005.

SRS Deposition Monitoring: Estimates of sediment deposition (Figure 2) upstream of the SRS are made using elevation data collected using Light Detection and Ranging (LIDAR) techniques. The elevation data is used to develop a digital terrain model (DTM).

The volumetric change in the area of deposition was computed by spatial analysis of the WY 2003 and 2004 DTMs. The net deposition was estimated to be +0.7 million cubic yards (mcy) for WY 2004. This brings the total estimated sediment volume trapped behind the SRS to a total of 102.3 mcy.

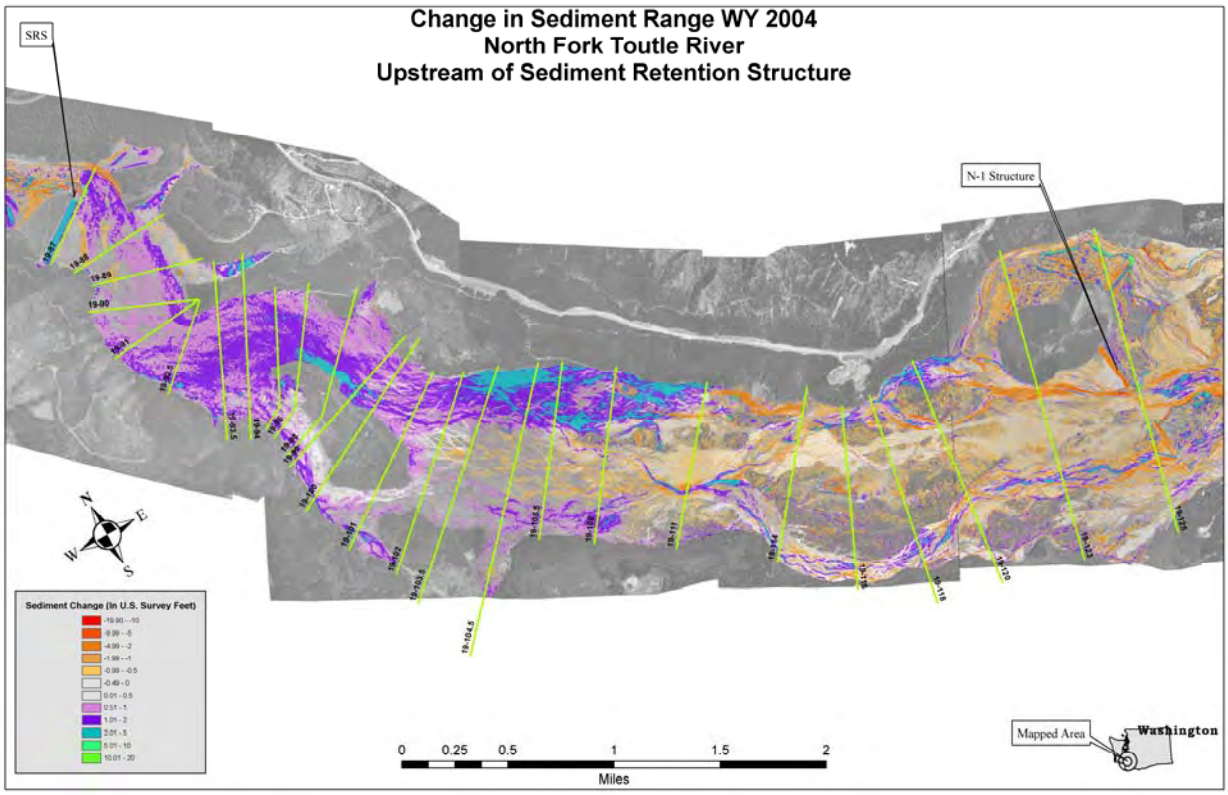


Figure 2 Sediment deposition upstream of the SRS comparing DTMs developed from LIDAR data from 2003 and 2004.

Cowlitz River Hydrosurveys: Hydrosurvey data for the lower Cowlitz River (river miles 0-20) was obtained in August 2003. The 2003 survey showed an aggradational trend in the lower 10 miles of the river from the last survey taken in 1996, and a slight degradation trend from about mile 10 to mile 20. The trend in the upper reach of the Cowlitz was confirmed by rating curve data from the USGS gage at Castle Rock (river mile 17.1).

The 2003 hydrosurvey data was used to update a HEC-RAS model developed with the 1996 survey data. The 2003 HEC RAS model for the Cowlitz was used as the basis for the WY 2004 SIAM model developed with a beta version of the software. Advances in the HEC-RAS model have greatly simplified data importation and manipulation of hydrosurvey data. The hydrosurvey data can be easily merged with data from LIDAR or conventional surveys. Portland District has recently acquired the capability to do acoustic river bed classification in conjunction with the conventional single beam hydrosurvey. The acoustical bed classification is obtained at no additional cost to provide the type of sediment on the bottom as well as the river cross sections. Bed material samples taken on the river are used to verify the sediment classification provided by the hydrosurvey. This combination of technological advances in software and data collection has greatly reduced costs making annual updates of channel bathymetry possible. This information can be used to monitor channel capacities and provide updates on levels of protection provided by the levees.

SEDIMENT IMPACT ASSESSMENT MODEL (SIAM)

ERDC and HEC (Gibson and Little, 2006) are currently developing a Sediment Impact Assessment Model (SIAM), which provides for rapid assessment of the impact of sediment management activities on downstream sedimentation trends. The model provides a framework to combine sediment sources and computed sediment transport capacities into a model that can evaluate sediment imbalances and downstream sediment yields for different alternatives. SIAM is incorporated into the Hydraulic Design module of HEC-RAS. Portland District has developed a SIAM model of the lower Cowlitz River using a beta version of the software and is participating in testing and implementation of the model.

INTEGRATION OF SIAM INTO MT ST HELENS DATA COLLECTION AND MONTIORING PROGRAM

The use of the SIAM model was recommended by the Corps Committee on Channel Stabilization during the December 2004 meeting on the Mt St Helens project at Portland District. The SIAM model utilizes all the data collected as part of the annual monitoring program and provides a platform for communication of the current and future effects of sedimentation from the eruption of Mt St Helens and the operation of the SRS. The model provides a practical means of developing a sediment budget and tracking sediment as it moves from the SRS through the Toutle and Cowlitz and into the Columbia River. Future sedimentation trends and their effect downstream based on changing hydrologic conditions may be evaluated in SIAM. The SRS has filled to the point where it may be passing more coarse sands and fine gravels downstream potentially affecting channel capacities on the lower Cowlitz.

Two SIAM models are proposed for incorporation into the Mt. St. Helens data collection and monitoring program; the Cowlitz River RM 0 to 20.8 and the SRS inflow/outflow to monitor deposition and trap efficiency. The model inputs and outputs may be used at a later date to develop a HEC-RAS mobile bed event based sediment transport model. The Cowlitz River model has been developed based on an existing HEC-RAS model updated with 2003 hydrosurvey data. The model will be updated annually with data collected for the monitoring program. Work on the SRS model will begin at a later date.

Cowlitz River SIAM model: SIAM was designed as a first order screening tool to provide reach averaged sediment transport and average annual sediment yields. Sediment yield in the program is computed on the basis of an average flow duration curve. SIAM is not an event-based sediment routing model, which limits its applicability to investigations where average annual sediment budget calculations are sufficient. The SIAM model developed for the Cowlitz River utilizes much of the data collected as part of the monitoring program. The Cowlitz River SIAM model (Figure 3) has 6 sediment reaches.

SIAM computations use an average flow duration curve which makes modeling of individual events impractical. The SIAM model for the Cowlitz uses an approach based on the annual hydrology and sediment discharge data published by the USGS. The “Water Year” approach uses a flow duration curve developed from the discharge records for the water year studied. Suspended sediment discharge data for the water year is used to estimate sediment supply. Bed

material samples and hydrosurvey data collected during the annual data collection cycle are incorporated into the model. The Cowlitz River SIAM application will be used to track sediment

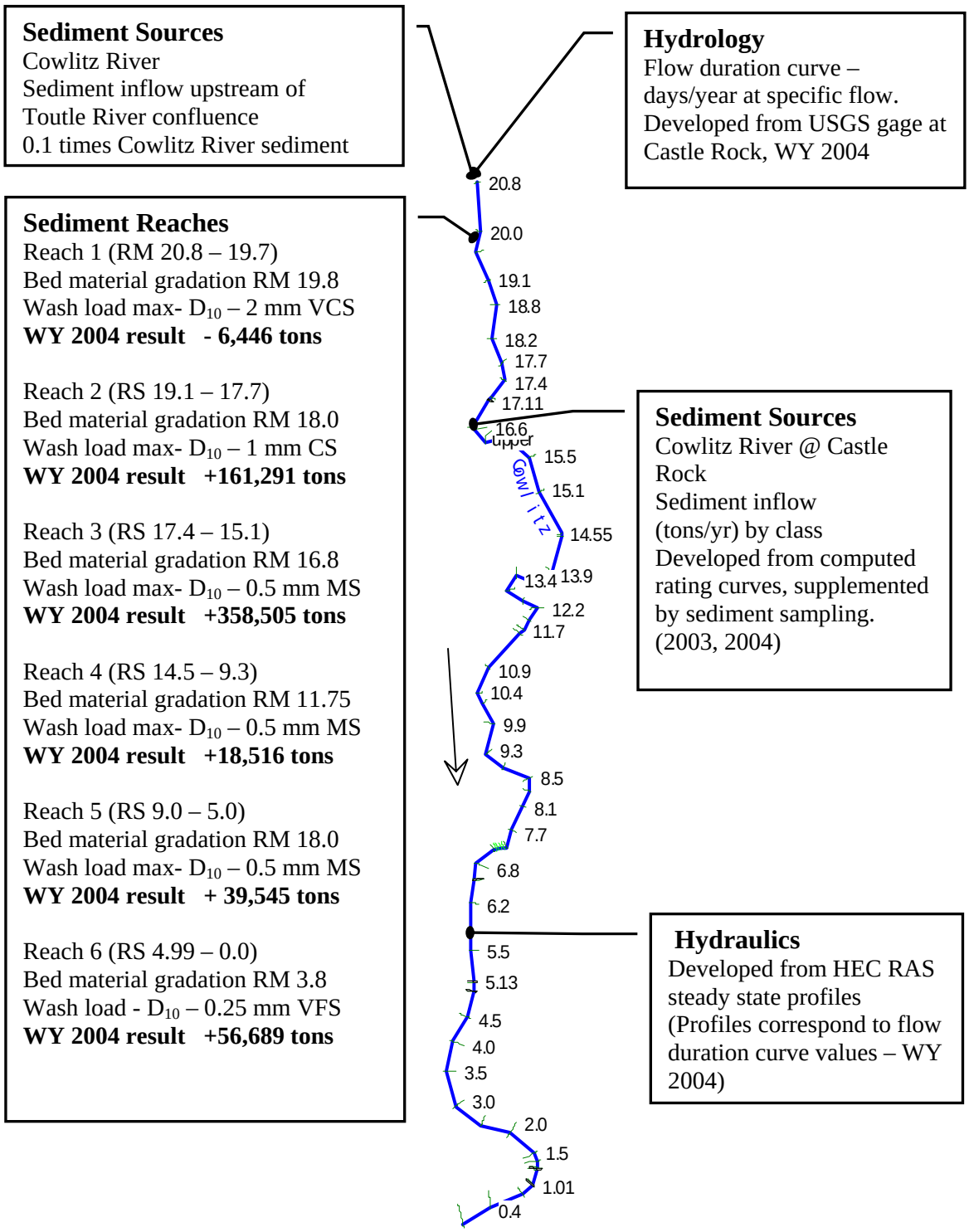


Figure 3 Cowlitz River SIAM model schematic, inputs, WY 2004 modeling results.

yield and geomorphic changes in the river on the water year cycle. Results of the model may be verified using data compiled and collected in the following water year.

WY 2004 Cowlitz River Sediment Supply: The sediment source load for WY 2004 was developed using suspended sediment data collected by the USGS at the Cowlitz River at Castle Rock, WA gage over the period from May 2003 to June 2004. The Modified Einstein method for computation of total sediment discharge was used to develop a sediment rating curve by grain size class. The total sediment supply for the water year was calculated by multiplying the sediment discharge by the fraction of the year for each flow in the SIAM flow duration curve (Figure 4).

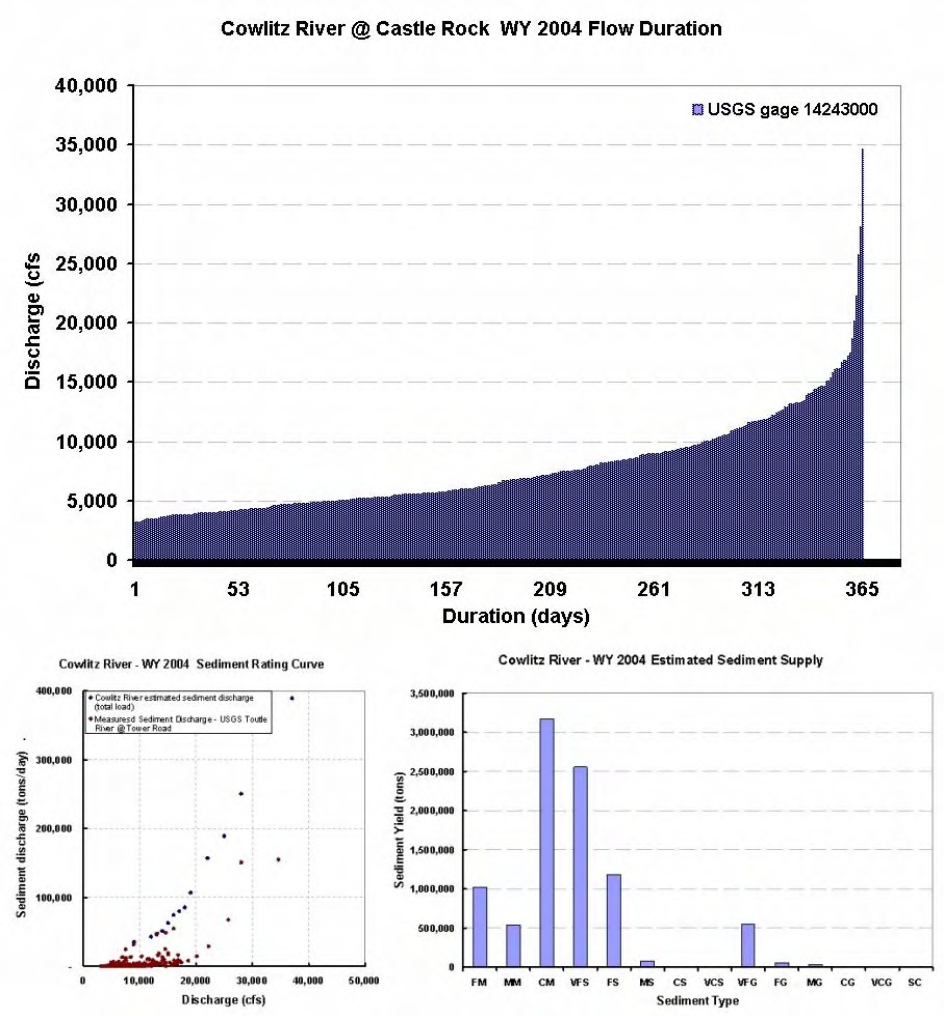


Figure 4 WY 2004 sediment supply estimation for Cowlitz River. Top - flow duration Cowlitz R @ Castle Rock, WA, WY 2004. Lower right - sediment rating curve WY 2004. Lower left - Sediment yield by grain size class for WY 2004, SIAM input.

Six sediment data sets were used to develop the sediment rating curve for WY 2004. Five contained sand – silt breaks and one contained a complete suspended sediment gradation. A bed material sample taken near the collection site was used in the computation. Total sediment

discharge estimates were made using a Modified Einstein program (O'Brien, 2000) developed in *Mathcad* (a mathematical software package).

Sediment Properties and Transport Function Used: Sediment properties are defined for each sediment reach. SIAM has six transport functions available to compute sediment transport capacity over the full range of particle sizes in the bed material gradation. For the Cowlitz River model, the Meyer-Peter Muller function was selected based on the HEC-RAS guidance given for grain size, velocity, and slope. The results are sensitive to the transport function. The maximum wash load threshold value for each sediment reach is derived from the bed material sediment gradation curves. The typical value used for maximum size class of wash load in bed material is the d_{10} fraction.

WY 2004 SIAM modeling results: The results of the initial SIAM modeling (Table 1) seem to fit with field geomorphic assessment, suspended sediment data, bed material sampling and rating curve data from the Castle Rock USGS gage.

Table 1 Cowlitz River SIAM model. Summary of WY 2004 modeling results, net of all six reaches.

Sediment type	d_g (mm)	Inflowing Sediment Supply (tons)	Bed Material Supply (tons)	Wash Material Supply (tons)	Net Deposition/ (Erosion) (tons)
FM	0.011	1,023,642		5,020,222	
MM	0.023	538,850		2,650,855	
CM	0.045	3,166,970		15,588,500	
VFS	0.088	2,556,077		12,593,000	
FS	0.177	1,181,417		5,800,600	
MS	0.354	81,500	81,500	400,834	(3,396)
CS	0.707	13,302	303,500	24,320	(25,991)
VCS	1.41	6,439	241,220	116	3,714
VFG	2.83	555,000	752,608		554,295
FG	5.66	61,050	171,608		61,057
MG	11.3	33,300	61,117		33,335
CG	22.6	3,885	3,885		3,885
VCG	45.3	250	250		250
SC	90.5	13	13		

The results shown are the net for all six reaches combined. Output by reach is available in graphical and tabular format. The model results by sediment reach (Table 2) indicate that the upper two sediment reaches of the Cowlitz (RM 19.1 to 15.1) show approximately 500,000 tons of net aggradation. The bulk of the deposition is in the fine gravel class (2 to 4 mm). Much of the material in this reach deposits in well established point bars. Although the number is large, the net effect in the 4 mile reach is small. The bulk volumetric estimate of the sediment is

400,000 cu yd. Model runs indicate that this result is sensitive to the derived estimate of supply (500,000 tons/year) used. The middle reach of the Cowlitz (RM 14.5 to 9.3) is a transport reach and had nominal deposition of 18,000 tons.

Table 2 Cowlitz River SIAM model. WY 2004 modeling results by sediment reach.

Sediment Reach (RM)	Net Deposition / (Erosion) (tons)	MS (tons)	CS (tons)	VCS (tons)	VFG (tons)	FG (tons)	MG (tons)	CG (tons)	VCG (tons)	SC (tons)
20.8 to 9.7	(6,446)	0	0	0	(4,407)	(2,100)	24	35	2	0
19.1 to 7.7	161,000	0	0	(158,000)	346,000	(33,700)	3,200	3,500	225	12
17.4 to 5.1	359,000	0	(86,600)	133,000	198,000	83,200	29,700	350	23	1
14.5 to 9.3	18,500	0	1,639	1,747	3,902	10,800	405	0	0	0
9.0 to 5.0	39,500	0	6,170	19,800	10,700	2,857	6	0	0	0
4.99 to 0.0	56,700	(3,396)	52,800	7,167	100	0	0	0	0	0

The net deposition in the lower two reaches of the Cowlitz (9.0 to 0) is approximately 100,000 tons in the coarse and very coarse sand fractions (0.5 to 2.0 mm). This indicates a slight aggradational trend in the lower Cowlitz. The amount of deposition is relatively small, but significant considering an average to below average water year. The results will be assessed during the next data collection cycle which will include new hydrosurvey data.

CONCLUSIONS

Sedimentation in the Cowlitz and Toutle Rivers below the SRS must be closely monitored so that the authorized levels of flood protection can be maintained on the Cowlitz River. The annual data collection program and SIAM modeling are cost effective measures which will ensure that these goals continue to be met.

REFERENCES

U.S. Army Corps of Engineers, Portland District, “ount St. Helens Engineering Reanalysis Hydrologic, Hydraulics, Sedimentation and Risk Analysis Design Documentation Report. April 2002, Portland, OR.

U.S. Army Corps of Engineers, Portland District, Hydrologic, Coastal, and River Engineering Section, Cowlitz River Basin Water Years 2003 and 2004 Hydrologic Summary. October, 2005, Portland, OR.

Gibson, S and Little, C. (2006) “Implementation of the Sediment Impact Assessment Model (SIAM) in HEC-RAS”, 8th Federal Interagency Sedimentation Conference, Reno, NV.

Colby, B. R., and Hembree, C. H., (1955) Computations of Total Sediment Discharge Niborara River Near Cody, Nebraska. Water Supply Paper 1357, USGS, Washington, DC.

O’Brien, P (2000) “Development of Techniques for Estimating the Unmeasured Load in Large Rivers”, Masters Thesis, University of New Orleans, December, 2000, New Orleans, LA.

MODELING SEDIMENT TRANSPORT DURING OVERBANK FLOW IN THE RIO PUERCO, NEW MEXICO

Eleanor R. Griffin, egriffin@usgs.gov; **J. Dungan Smith; Jason W. Kean; Kirk R. Vincent,U.S. Geological Survey, Boulder, CO**

Abstract: Reach-averaged in-channel flow within an 81-km segment of the lower Rio Puerco, New Mexico, has been modeled successfully using a physically based model for steady, horizontally uniform flow applied to reach-average channel shapes, bed gradients, and shrub characteristics. These characteristics were determined from survey data obtained in April 2002. Long segments of this channel have dense shrub willows or tamarisks growing on the banks and floodplain. Model results for three specific flows that left silt lines on the stream banks were found to be accurate as long as the shrubs on the stream banks were included, and they indicate rates of infiltration into the upper banks are high.

Prior to flow going overbank, the bed of the Rio Puerco is coated with a clayey silt, but once the flow reaches a bankfull depth, the cohesive layer of clayey silt is broken and the sand beneath goes into suspension. During overbank flows, form drag on the shrubs reduces flow velocities so that fine to very fine sand in suspension is deposited on the channel levees, and silt and clay are deposited on the floodplain, rather than sediment being carried back into the channel. As a result, the channel bed and floodplain have been aggrading since the 1970s, and the average annual sediment loads carried from the Rio Puerco into the Rio Grande have been reduced by about one-half. In contrast, prior to the 1970s the stream channel was wider and braided, and there were few shrubs along the banks, allowing much larger sediment loads to pass through the system into the Rio Grande. During this period, large amounts of sediment from the Rio Puerco ended up in Elephant Butte Reservoir.

In order to investigate the effectiveness of the riparian shrubs in promoting levee deposition and, thereby, maintaining a stable single channel morphology, we have added overbank flows to the above-described, in-channel flow model. The first step in this effort was the quantitative examination of weak overbank flows. Details of channel and floodplain stratigraphy mapped at two trench sites located at the upstream and downstream ends of a 27-km reach show that an overbank flow in August 1999 deposited very fine sand on the levee surfaces next to the channel to average depths of about 0.24 m. Flow discharge, suspended sediment concentration, volume of sediment scoured from the channel bed and volume of sediment deposited on the levees through the 27-km reach have been calculated for that overbank flow.

When sand is in suspension, a concentration gradient often exists in the water column, with concentrations decreasing away from the bed. Effects of density stratification due to the suspended sediment concentration gradient are included in the calculations. Woody vegetation on channel banks reduces near-bank flow velocities and boundary shear stresses, resulting in a lateral suspended sediment concentration gradient, with decreasing concentrations toward the edges of the channel. Turbulent diffusion of sand from the center of the channel into the near-bank area with shrubs causes a high rate of sand deposition on the steep (~30º) channel banks. Our hypothesis is that this results in mass movement of sediment down the bank toward the center of the channel, driving a secondary circulation that is toward the center of the channel at the bed, vertical (upward) near the center of the channel, and toward the banks near the surface. Velocities calculated for the secondary current using the rates of sand deposition initiated from lateral diffusion indicate that sand in the upper part of the flow is advected overbank onto the levees and deposited on levee surfaces next to the channel. Our calculations show that sand deposition on the levees is substantially enhanced by the presence of the shrubs. Efforts to remove riparian shrubs along the Rio Puerco currently are underway. Once the riparian shrubs are removed from the lower reaches, pre-1970 sediment transport rates are likely to resume.

THE EFFECTS OF ENSO PHASE ON THE OCCURRENCE OF COARSE PARTICLE MOTION IN CALIFORNIA COASTAL STREAMS

E. D. Andrews, U.S. Geological Survey, 3215 Marine Street, Boulder CO 80303, eandrews @usgs.gov; Ronald Antweiler, U.S. Geological Survey, 3215 Marine Street, Boulder CO 80303, antweil@usgs.gov

Abstract: The entrainment and transport of coarse gravel and cobble bed material is a relatively infrequent occurrence in most streams, typically a few to several tens of days per decade. Although infrequent, the movement of coarse bed material constructs and maintains the channel morphology, removes silt and sand that accumulates in the streambed during periods of stability and limits the encroachment of vegetation into the channel. Recent investigations have demonstrated a connection between the El Niño-Southern Oscillation (ENSO) and streamflows along the Pacific Coast of the U.S. The influence of ENSO phase is especially strong for relatively large flows, those equaled or exceeded <1% of the time, that are sufficient to move coarse bed particles.

In order to examine the effects of ENSO phase on the frequency of coarse bed-material motion, we determined the occurrence of initial motion and general motion of the median bed particle, d_{50}, in 17 California coastal gravel-bed streams with complete or nearly complete flow records for the period 1950-2005 and little or no flow regulation or depletion. There is a well-developed south-to-north pattern of particle motion depending on ENSO phase, as well as a significant increase from south-to-north in the total number of days when the daily mean discharge exceeds the threshold of initial and general motion of the median bed particles. In the southern most streams, 72-90 percent of all daily mean discharges sufficient to entrain the d_{50} particle occurred during an El Niño phase. Conversely, only 1-10 percent of all daily mean discharges sufficient to entrain the d_{50} occurred during a La Niña phase. A majority of the total number of days with either initial motion or general motion occurred during relatively few years, about 1 in 5 and then during one El Niño phase. Periods lasting 2-5 years with few or no days of discharge sufficient to exceed the initial motion threshold are common in the coastal streams of Southern California. The number of days with relatively large discharge during a La Niña phase gradually increases northward. Near 40°N, occurrences of bed particle motion are distributed about equally among the La Niña, Neutral, and El Niño phases. Accordingly, daily mean discharges sufficient to exceed the initial motion threshold typically occur, on average, a few to several days per year in the coastal streams of Northern California. General motion of bed material, however, is an uncommon occurrence even in these streams.

THE VALUE OF CONTINUOUS TURBIDITY MONITORING IN TMDL PROGRAMS

Teresa J. Rasmussen, Hydrologist, U.S. Geological Survey, Lawrence, Kansas, rasmuss@usgs.gov; Andrew C. Ziegler, Water Quality Specialist, U.S. Geological Survey, Lawrence, Kansas, aziegler@usgs.gov; Patrick P. Rasmussen, Hydrologist, U.S. Geological Survey, Lawrence, Kansas, pras@usgs.gov; Thomas C. Stiles, TMDL Manager, Kansas Department of Health and Environment, Topeka, Kansas, tstiles@kdhe.state.ks.us

Abstract: The Federal Clean Water Act requires States to establish total maximum daily loads (TMDLs) to meet water-quality criteria and to attain designated beneficial uses for each water body. Sediment and sediment-associated constituents, such as total nutrients and bacteria, are among the most common water-quality impairments in the Nation. The load of a contaminant introduced to a water body varies with both concentration and streamflow, requiring reliable information for both when implementing an effective TMDL program. In most TMDL programs, discrete water samples collected at periodic intervals are used to determine whether established criteria are being met and to determine loads from contributing sources. However, discrete samples do not adequately describe daily, monthly, or annual variability in load characteristics because both concentration and streamflow can fluctuate substantially between samples.

The ability to continuously measure water-quality constituents such as sediment, nutrients, and bacteria frequently is limited by technical and financial constraints. However, turbidity, which often is strongly correlated with sediment, nutrients, and bacteria, can be measured in-stream and on a continuous basis. By developing regression models to establish statistical relations between laboratory-analyzed samples and in-stream turbidity measurements, it is possible to provide continuous estimates of concentration and load under changing streamflow and seasonal conditions.

The information is valuable to State water-quality programs for several reasons. Continuous turbidity data lead to an improved understanding of in-stream processes affecting sediment and sediment-associated constituents. Regression models using turbidity to estimate sediment-associated constituents are better than those using streamflow because there is a better correlation between turbidity and sediment than between streamflow and sediment. Load and yield estimates that are based on continuous data may be more accurate than estimates that are based on discrete samples because the continuous data better capture variability. Continuous concentration estimates can be used to construct duration curves to determine the percentage of time that estimated concentrations exceed existing water-quality criteria or established goals. Because the full range of conditions are displayed, duration curves are a convenient tool for evaluating conditions during any selected time period and making comparisons between sites, seasons, years, and even particular periods of rainfall. In addition, when continuous data are transmitted in near real-time, the information can be used to optimize efforts to collect discrete samples. Continuous data collected over the long term may be used to help identify changes in water-quality conditions resulting from land-use changes and implementation of best-management practices in the watershed. Finally, continuous data lead to more effective strategies for developing and implementing TMDLs to protect water quality.

INTRODUCTION

The Federal Clean Water Act as amended in 1977 requires States to establish total maximum daily loads (TMDLs) to meet water-quality criteria and to attain designated beneficial uses for each water body. A TMDL is the maximum quantity of a contaminant that a water body can receive and still meet water-quality criteria (Kansas Department of Health and Environment, 2004). The load of a contaminant introduced to a water body varies with both concentration and streamflow, requiring reliable information for both when implementing an effective TMDL program. Typically, TMDLs are developed for water bodies identified by each State as impaired and included in the section 303(d) list required by the Clean Water Act. Sediment and sediment-associated constituents, such as total nutrients and bacteria, are among the most common water-quality impairments in the Nation (U.S. Environmental Protection Agency, 2005a).

Most State TMDL programs rely on analysis of discrete samples for constituent concentration information (Stiles, 2002). Although discrete samples are valuable for determining instantaneous constituent concentrations, they do not describe daily, monthly, or annual variability in constituent load characteristics because both concentration and streamflow can fluctuate substantially between samples. Continuous monitoring, on the other hand, does capture temporal variability and has become more common for many water-quality applications, including TMDL programs.

In-stream instruments designed to continuously measure specific conductance, pH, water temperature, turbidity, and dissolved oxygen are readily available. However, the ability to continuously measure water-quality constituents that are most commonly associated with impairments, such as sediment, nutrients, and bacteria, often is limited by technical and financial constraints. Fortunately, turbidity data can be used as a surrogate because it is strongly correlated with sediment, nutrients, and bacteria, and can be measured in-stream on a continuous basis. Turbidity is caused by the presence of suspended and dissolved matter such as clay, silt, organic matter, and microscopic organisms (ASTM International, 2003). These particulates in water provide attachment sites for nutrients, bacteria, and other potential contaminants (U.S. Environmental Protection Agency, 2005b). By developing regression models to establish statistical relations between laboratory-analyzed samples and in-stream turbidity measurements, it is possible to provide continuous estimates of concentration and load for sediment-related constituents under changing conditions.

The purpose of this paper is to describe methods for developing regression models that are used to continuously estimate concentration and load for sediment-related water-quality constituents and to demonstrate the utility of the resulting data for State water-quality monitoring efforts such as TMDL programs. Examples will be provided using water-quality data collected at three sites on the Kansas River in northeast Kansas from 2000 through 2004. Additional information can be found in Rasmussen et al. (2005), available at http://pubs.usgs.gov/sir/2005/5165, and on the U.S. Geological Survey Kansas Water Science Center Website at http://ks.water.usgs.gov/Kansas/rtqw/.

APPROACH

Data Collection: Three USGS streamflow-gaging stations on the Kansas River in northeast Kansas were equipped with water-quality monitors that provided continuous (hourly) measurements of turbidity. Monitor maintenance and data reporting followed standard procedures described in Wagner et al. (2000). In addition, about 20 discrete water samples were collected from each site throughout the range of recorded streamflow and turbidity conditions according to methods described by Wilde et al. (1999) and analyzed for suspended sediment, total nitrogen and phosphorus, *Escherichia coli* (*E. coli)* bacteria, and other selected constituents. Duration curves for streamflow and turbidity were used to evaluate sample distribution and adapt sampling strategies to fill voids in data along the curves. Continuous in-stream sensor data were compared to average cross-section data at the monitor locations to verify that the continuous data were representative of cross-section conditions.

Regression Models: Regression analysis through an overall model-building method (Helsel and Hirsch, 1992) was used to develop relations between the continuous turbidity measurements, streamflow, time, and discretely sampled constituent concentrations. Models were evaluated by using plots of each possible explanatory (independent) variable and the response (dependent) variable and visually and statistically examining the residual plots for patterns. The prediction error sum of squares (PRESS), which is a measure of goodness of fit of a regression model, coefficient of determination (R^2), which is the fraction of the variance explained by the regression, and the mean square error (MSE), which is a measure of the variance between the estimated and measured values, were used to evaluate the models. Explanatory and response variables (except time) were log transformed, if necessary, to develop linear relations. Although many possible models were evaluated, this paper focuses on the model that use turbidity as the explanatory variable because they generally were the best overall models for the Kansas River monitoring stations.

For variables that were log-transformed, retransformation of regression-estimated concentrations was necessary. Retransformation can cause bias (underestimation) in the constituent loads when adding individual load estimates over a period of time (Helsel and Hirsch, 1992). Therefore, the estimated hourly concentration and density values were multiplied by a log-transformation bias correction factor, or smear factor, to correct for this underestimation. Duan's smearing estimator (Duan, 1983) was used because it is the least complex and most easily applied correction method (Cohn and Gilroy, 1991).

Uncertainty of the estimates for the regression models was determined using 90-percent prediction intervals (Helsel and Hirsch, 1992). For a given explanatory variable, the 90-percent prediction interval represents the range of values expected for the response variable 90 percent of the time. Probabilities of exceeding water-quality standards, recommended criteria, or State and U.S. Environmental Protection Agency (USEPA) guidelines also can be used to evaluate uncertainty of the estimated values (Rasmussen and Ziegler, 2003).

Estimation of Loads and Yields: Constituent loads were calculated by multiplying hourly regression-estimated concentrations and densities by a bias correction factor (Duan smear factor; Duan, 1983) and by streamflow and then summing over the appropriate period of time. Constituent yields were calculated by dividing loads by corresponding drainage areas to determine constituent load per acre. Yields can be used to compare relative contributions of each drainage basin.

VALUE OF CONTINUOUS TURBIDITY DATA

Continuous Turbidity Data Lead to an Improved Understanding of In-Stream Processes: A fundamental knowledge of in-stream turbidity fluctuations leads to an improved understanding of processes affecting sediment and sediment-related constituents such as nutrients and bacteria. Streamflow data alone do not accurately characterize turbidity. For example, hourly turbidity measurements from the Kansas River at Wamego during the spring of 2001 (Figure 1A) indicate that turbidity peaks did not coincide with streamflow peaks. In fact, the turbidity peak occurred 4 days after the June 1 streamflow peak, but it preceded the streamflow peak 4 days later on June 5. In addition, the magnitude of the streamflow peak was not indicative of the magnitude of the corresponding turbidity peak. Turbidity values may be larger during either the rising or falling limb of the streamflow hydrograph, depending on the source of the suspended material. Sediment originating from the stream channel typically causes larger turbidity values as streamflow increases, and sediment originating from more distant basin sources may cause larger turbidity values as streamflow decreases because of the timing of the tributary inflows (Asselman, 1999). In addition, changes in turbidity often were much more abrupt than changes in streamflow. The increase in streamflow at the Kansas River at DeSoto that began on July 12, 2001 (Figure 1B), and peaked on July 14, 2001, occurred over about a 60-hour period. In contrast, the associated change in turbidity that peaked on July 13 increased within a 5-hour period and had nearly recovered about 7 hours later.

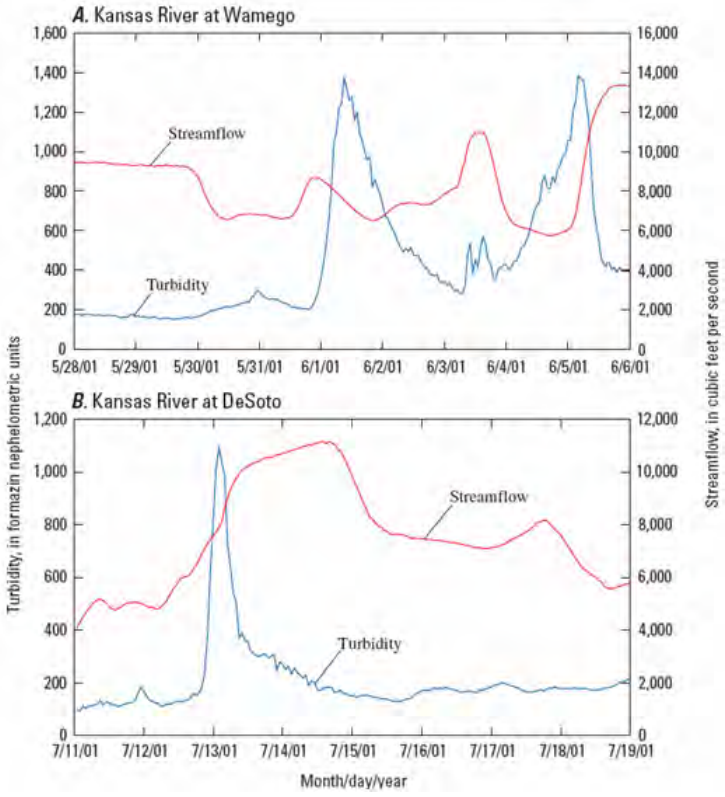


Figure 1 Comparisons of streamflow and turbidity for Kansas River at Wamego and DeSoto during the summer of 2001 (Rasmussen et al., 2005).

Regression Models Using Turbidity to Estimate Sediment-Related Constituents are Better than Those Using Streamflow: Regression models were developed for each of the three Kansas River sites to estimate suspended sediment using turbidity (Rasmussen et al., 2005). For comparison, regression models also were developed using streamflow to estimate suspended sediment. In each case, turbidity was a better explanatory variable for sediment-associated constituents than streamflow as indicated by larger R^2 values and smaller MSE values. For example, the turbidity model for estimating sediment at Wamego had an R^2 of 0.95 and MSE of 0.0158, compared to the streamflow model for sediment, which had an R^2 of 0.66 and MSE of 0.1361 (Rasmussen et al., 2005). Better statistical models result in better estimated values.

Regression models also provide information about relations between constituents of concern and variables that affect them. Generally, there was a one-to-one relation between turbidity and suspended sediment at the three Kansas River monitoring sites (Figure 2). The Topeka regression line had a steeper slope than the others, indicating that the relation between turbidity and suspended sediment at that site was different from the other sites. When turbidity was low, suspended sediment at Topeka was smaller than at the other two sites, and when turbidity was high, suspended sediment was larger than at the other two sites. In this river system, the different relation between turbidity and sediment may indicate a difference in sediment sources related to reservoir contributions (Rasmussen et al., 2005).

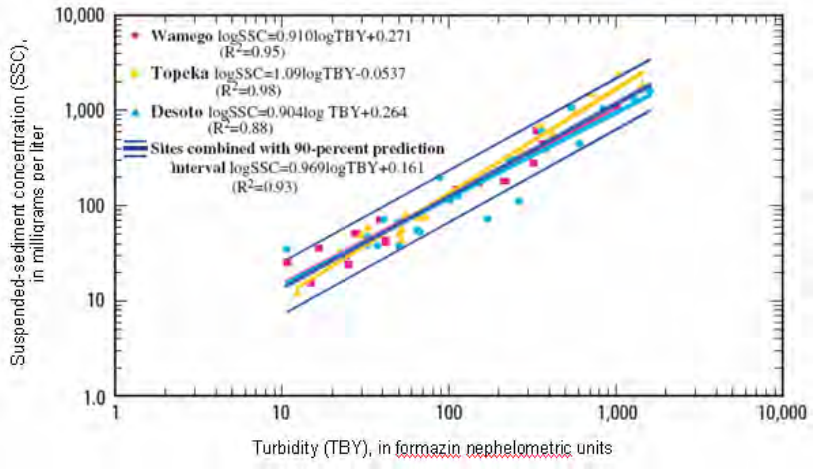


Figure 2 Comparison of turbidity (explanatory variable) and suspended-sediment concentration (response variable) in regression models developed for three Kansas River monitoring sites (Rasmussen et al., 2005).

Continuous Estimates, with Defined Statistical Uncertainty, Describe Variability of Water-Quality Constituents That Often Cause Impairments: Often, water-quality constituents that cause impairments, like sediment, nutrients, and bacteria, cannot be measured easily in-stream because of financial and technological limitations. In lieu of direct measurements, regression-estimated values provide important information about constituent variability throughout the year. Continuous monitoring helps identify climatic, seasonal, and hydrologic conditions during which sediment-related water-quality impairments occur. It is especially useful for characterizing nonpoint-source contributions associated with stormwater because it describes conditions throughout the duration of each runoff occurrence. Load and yield estimates that are based on continuous data may be more accurate than estimates made on the basis of discrete samples because the continuous data better capture temporal variability.

Hourly estimates of *E. coli* in the Kansas River at DeSoto in 2004 (Figure 3) indicate that, during normal flow conditions, water-quality criteria were not likely to be exceeded unless there was an unusual point source release upstream that increased *E. coli* load without increasing turbidity. *E. coli* densities were elevated during increased streamflow in March and June through August. Peaks in *E. coli* density tend to fall more quickly than corresponding streamflow peaks. *E. coli* densities can increase by several orders of magnitude within a short time. Statistical uncertainty of the estimates for the regression model is displayed in gray using 90-percent prediction intervals (Helsel and Hirsch, 1992). Probabilities of exceeding water-quality standards, recommended criteria, or guidelines also can be used as an alternative method of expressing statistical uncertainty. Examples can be found on the Web at http://ks.water.usgs.gov/Kansas/rtqw/.

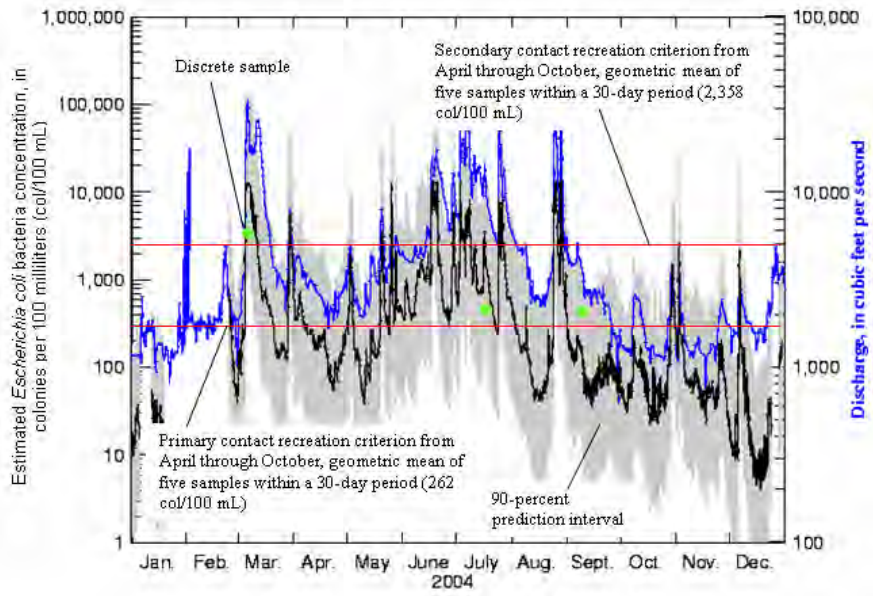


Figure 3 Estimated *Escherichia coli (E. coli)* bacteria densities at the Kansas River at DeSoto, Kansas monitoring site, 2004 (http://ks.water.usgs.gov/Kansas/rtqw/). Water-quality criteria from Kansas Department of Health and Environment (2003).

Duration Curves Have Many Uses: Continuous concentration or load estimates can be used to construct cumulative frequency distribution (duration) curves to estimate the frequency, duration, and magnitude of potential water-quality degradation. Because the full range of conditions are displayed, duration curves are a convenient tool for evaluating conditions during any selected time period and for making comparisons between sites, seasons, years, and even particular periods of rainfall. They also can be used to determine the percentage of time that estimated concentrations or densities exceed existing water-quality criteria, proposed criteria, and established goals.

Examination of differences in concentrations, densities, and loads at a series of sensor stations along a stream allows the analysis of upstream-to-downstream changes in water quality. Estimated *E. coli* densities at Topeka, the middle Kansas River monitoring site, were larger than estimated densities at the other two sites about 90 percent of the time (Figure 4). Duration curves also may be used to differentiate between base-flow and runoff conditions. The three *E. coli* duration curves in Figure 4 diverge at about 80-percent exceedance, which corresponds to about 50 col/100 mL (colonies per 100 milliliters of water). This also may be indicative of when stormwater runoff begins to affect base-flow conditions.

By summing hourly load values from a selected portion of the load duration curve or period of time and converting the calculated load to a percentage of the total load, it is possible to determine how much of the total annual load occurred during specified periods of time. For example, by summing hourly loads within the upper 10 percent of the load duration curve and converting to a percentage of the total load, it was found that, on average, 83 percent of the annual bacteria load in the Kansas River at DeSoto during 2000–03 occurred during 10 percent of the time in conjunction with the most intense runoff. The same method was used to estimate that 64 percent of the annual suspended-sediment load at the same site occurred during 10 percent of the time (Rasmussen et al., 2005).

Sampling Efforts Can Be Optimized: When continuous data are transmitted in near real-time, the information can be used to efficiently time discrete sampling efforts to collect important data during targeted water-quality conditions. In situations where discrete samples and constituent concentration or density data are necessary for regulatory requirements, monitoring by continuous sensor data allows regulatory agencies to optimize sampling efforts. In some cases it may be more cost effective to use continuous monitors for critical constituent monitoring rather than intensive discrete sampling.

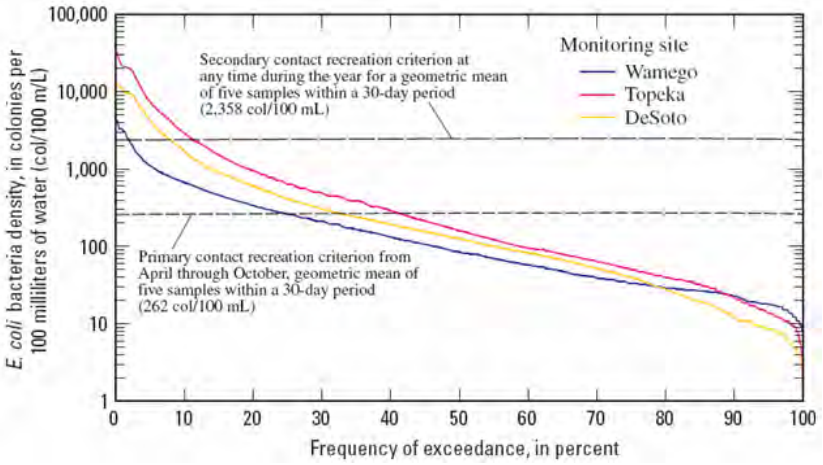


Figure 4 Duration curves for estimated *Escherichia coli (E. coli)* bacteria densities at three Kansas River monitoring sites, January 2000-December 2003 (Rasmussen et al., 2005). Water-quality criteria from Kansas Department of Health and Environment (2003).

Continuous Data Can Be Used to Monitor and Evaluate Changes Over Time: Temporal changes may be observed by evaluating hourly values over time and by evaluating changes in relations between explanatory and response variables in the regression models. Turbidity duration curves for the Kansas River at DeSoto during 2000-03 (Figure 5) indicate that turbidity generally was largest in 2001 and smallest in 2002. During low turbidity conditions corresponding with low streamflow, about 25 percent of the time, annual duration curves were similar from 1 year to the next. For the remaining 75 percent of the time, turbidity in 2001 was largest. Because duration curves show the entire range of conditions, they are more useful for evaluating changes than merely using summary statistics such as maximum, median, and minimum values. When continuous data are considered over the long term, it may be possible to identify changes in water-quality conditions resulting from land-use changes and implementation of best-management practices in the watershed (Rasmussen et al., 2005).

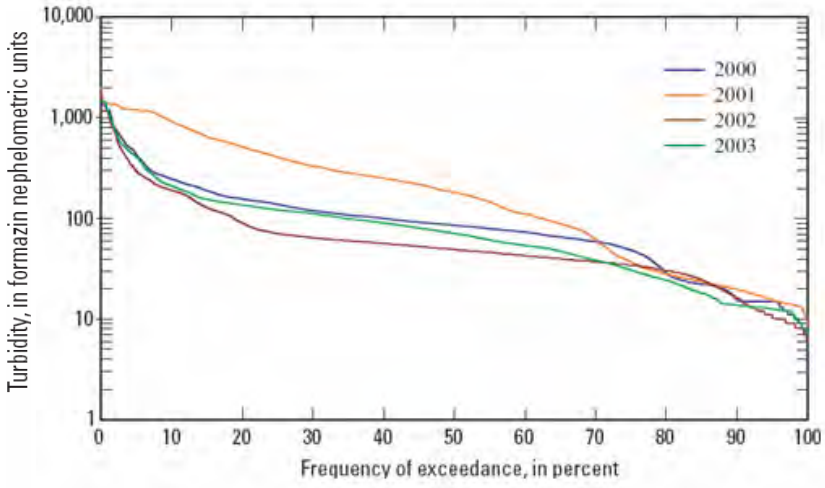


Figure 5 Annual duration curves for measured turbidity at Kansas River at DeSoto monitoring site, January 2000 through December 2003 (Rasmussen et al., 2005).

Continuous Data Lead to More Effective Strategies for Developing and Implementing TMDLs to Protect Water Quality: Understanding a particular stream system is the foundation for developing effective water-quality management plans. By knowing when conditions are likely to exceed criteria and what factors contribute to stream

degradation, cost-effective strategies can be developed to target particular conditions in each stream system rather than treating all systems uniformly.

CONCLUSIONS

The ability to continuously measure water-quality constituents such as sediment, nutrients, and bacteria, often is limited by technical and financial constraints. However, turbidity, which usually is strongly correlated with sediment, nutrients, and bacteria, can be measured in-stream and on a continuous basis. By developing regression models to establish statistical relations between laboratory-analyzed samples and in-stream sensor measurements, it is possible to provide continuous estimates of concentration and load under changing streamflow and seasonal conditions. The information is valuable to State water-quality management programs for the following reasons:

- Continuous turbidity data lead to an improved understanding of in-stream processes affecting sediment and sediment-related constituents such as nutrients and bacteria. Streamflow data alone do not accurately characterize turbidity because turbidity fluctuations do not coincide directly with streamflow fluctuations.
- Regression models using turbidity to estimate sediment-associated constituents are better than those using streamflow because there is a better correlation between turbidity and sediment than between streamflow and sediment.
- Continuous estimates, with defined statistical uncertainty, describe variability of water-quality constituents causing impairments. In addition, load and yield estimates that are based on continuous data may be more accurate than estimates that are based on discrete samples because the continuous data better capture variability.
- Continuous concentration and load duration curves have many uses for State water-quality monitoring programs. Because the full range of conditions are displayed, duration curves are a convenient tool for evaluating conditions during any selected time period and making comparisons between sites, seasons, years, and even particular periods of rainfall. They also can be used to determine the percentage of time that estimated concentrations or densities exceed existing water-quality criteria, proposed criteria, and established goals.
- When continuous data are transmitted in near real-time, the information can be used to optimize efforts to collect discrete samples.
- Continuous data can be used to monitor and evaluate changes by examining hourly values over time and by evaluating changes in statistical relations between explanatory and response variables.
- Continuous data lead to more effective strategies for developing and implementing TMDLs to protect water quality.

REFERENCES

Asselman, Nathalie, E.M. (1999). “Suspended Sediment Dynamics in a Large Basin—the Rhine River,” Hydrologic Processes, 13, pp 1437–1450.

ASTM International (2003). D1889-00 “Standard Test Method for Turbidity in Water,” *in* ASTM International, Annual Book of ASTM Standards, Water and Environmental Technology. West Conshohocken, Pennsylvania, American Society for Testing and Materials, v. 11.01.

Cohn, T.A., and Gilroy, E.J. (1991). Estimating Loads From Periodic Records. U.S. Geological Survey Branch of Systems Analysis Technical Memo 91.01.

Duan, N. (1983). “Smearing Estimate—A Nonparametric Retransformation Method,” Journal of the American Statistical Association, 78, pp 605–610.

Helsel, D.R., and Hirsch, R.M. (1992). Statistical Methods in Water Resources. Elsevier, New York.

Kansas Department of Health and Environment (2003). Kansas Register, Article 28-16-28e, Surface Water Quality Standards, Topeka, Kansas, Secretary of State.

Kansas Department of Health and Environment (2004). Basics of TMDLs. Information available on the Web, accessed July 30, 2004, at http://www.kdhe.state.ks.us/tmdl/basic.htm

Rasmussen, P.P., and Ziegler, A.C. (2003). Comparison and Continuous Estimates of Fecal Coliform and *Escherichia coli* Bacteria in Selected Kansas Streams, May 1999 Through April 2002. U.S. Geological Survey Water-Resources Investigations Report 03–4056.

Rasmussen, T.J., Ziegler, A.C., Rasmussen, P.P. (2005) Estimation of Constituent Concentrations, Densities, Loads,

and Yields in Lower Kansas River, Northeast Kansas, Using Regression Models and Continuous Water-Quality Monitoring, January 2000 Through December 2003. U.S. Geological Survey Scientific Investigations Report 2005-5165.

Stiles, T.C. (2002). "Incorporating Hydrology in Determining TMDL Endpoints and Allocations", Proc. National TMDL Science and Policy 2002 Specialty Conference, Watershed Environment Federation, Phoenix, Arizona.

U.S. Environmental Protection Agency (2005a). National Section 303(d) List Fact Sheet. Information available on the Web, accessed October 7, 2005, at http://oaspub.epa.gov/waters/national_rept.control

U.S. Environmental Protection Agency (2005b). Pollutants That Degrade Water Quality. Information available on the Web, accessed October 28, 2005, at http://www.epa.gov/region08/water/monitoring/pollutant.html

Wagner, R.J., Mattraw, H.C., Ritz, G.F., Smith, B.A. (2000). Guidelines and Standard Procedures for Continuous Water-Quality Monitors—Site Selection, Field Operations, Calibration, Record Computation, and Reporting. U.S. Geological Survey Water-Resources Investigations Report 00– 4252.

Wilde, F.D., Radtke, D.B., Gibs, J., Iwatsubo, R.T., eds. (1999). "Collection of Water Samples," *in* National Field Manual for the Collection of Water-Quality Data. U.S. Geological Survey Techniques of Water-Resources Investigations, book 9, chap. A4.

RESULTS OF A TWO-DIMENSIONAL HYDRODYNAMIC AND SEDIMENT-TRANSPORT MODEL OF THE CONSTRUCTION AND OPERATION OF THE OLMSTED LOCKS AND DAM, OHIO RIVER

Chad R. Wagner, Hydrologist, U.S. Geological Survey, North Carolina Water Science Center, cwagner@usgs.gov

INTRODUCTION

The Olmsted Locks and Dam hydrodynamic and sediment-transport model was developed by the U.S. Geological Survey (USGS) in cooperation with the U.S. Army Corps of Engineers, (USACE) Louisville District to evaluate the environmental effect of the construction and subsequent operation of the Olmsted Locks and Dam on the lower Ohio River. The Olmsted Locks and Dam will replace Locks and Dam 52 and 53 and be the final high-lift dam structure on the Ohio River. The modeling project was conducted in two phases; the first modeling phase focused on simulating the dam construction sequence while the second modeling phase focused on long-term effects of the fully operational locks and dam.

The Olmsted Locks and Dam model was developed to predict the change in sediment-transport patterns around the endangered orange-footed pearly mussel (*Plethobasus cooperianus*) induced by the construction and subsequent operation of the Olmsted Locks and Dam. There is evidence that indicates the orange-footed pearly mussels in the beds located in the lower Ohio River near the Olmsted Locks and Dam are reproducing, so any changes to the mussel habitat could threaten the survival of the species (U.S. Fish and Wildlife Service, 1993).

This paper describes the development and results of the Olmsted Locks and Dam hydrodynamic and sediment-transport model developed on the lower Ohio River (Locks and Dam 53 to Ohio River Mile 974.5). The field data and methodology used to develop and calibrate the models are also described herein.

MODELING APPROACH

The Olmsted Locks and Dam hydrodynamic and sediment-transport model was developed for a section of the lower Ohio River (Locks and Dam 53 to Ohio River Mile 974.5; fig.1). Floodplains were included in the model in order to accurately simulate high-flow conditions, which were thought at the onset of the project to induce the most significant habitat changes. The calibrated model was used to simulate sediment transport patterns for hydraulic conditions ranging from 1,100,000 cubic feet per second (ft^3/s) to 88,000 ft^3/s under a wide range of backwater and free-flowing conditions.

A Resource Management Associates–2 (RMA-2, version 4.53)[1] two-dimensional hydrodynamic model for the reach was calibrated to a middle-flow hydraulic survey (350,000 ft^3/s) and verified

[1] Any use of trade, product or firm names in this paper is for descriptive purposes only and does not imply endorsement by the U.S. Government.

with data collected during a low- and a high-flow hydraulic survey (72,500 ft^3/s and 770,000 ft^3/s, respectively). The calibration and validation process included matching water-surface elevations at the construction site and velocity profiles at 15 cross sections throughout the study reach. The sediment-transport aspect of the project was simulated with the Waterways Experiment Station's (WES) Sed2D model (version 4.52). The purpose of the construction modeling phase of the Olmsted sediment-transport simulation was to estimate the effect the phased in-the-wet construction sequence of the Olmsted Locks and Dam would have on sediment-transport patterns in the study reach and particularly over the mussel beds beginning approximately 2 miles downstream from the dam. The purpose of the operational modeling phase of the sediment-transport simulation was to evaluate the long-term effects of the fully operational Olmsted Locks and Dam would have on sediment-transport patterns in the reach and over the mussel beds.

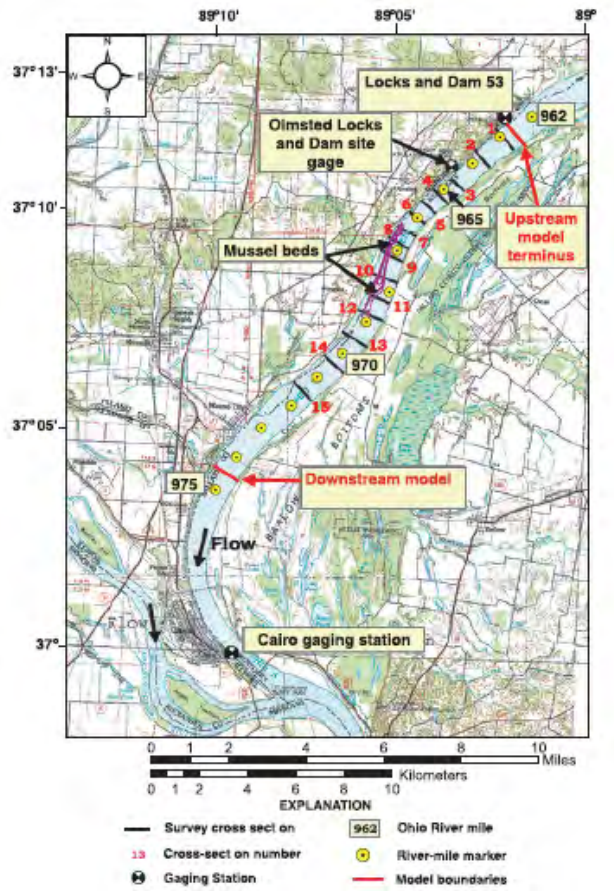


Figure 1 Location of the study area on the Ohio River, near Olmsted, Illinois.

A baseline scenario that included only the completed lock section was run concurrently with both the phased-construction and fully operational scenarios for the 9-year simulation period to compare to the sediment transport patterns induced by the dam construction and subsequent operation.

Hydrograph Development: Stepped annual hydrographs were used as input to drive the steady-state simulations. Representations of actual hydrographs from the USGS gaging station on the Ohio River at Locks and Dam 53 (03612500) were used instead of synthetic hydrographs in order to include the Mississippi River backwater conditions, which are common on the lower Ohio River.

The phased construction process was estimated to take 6 years to complete; therefore, the steady-state sediment-transport model simulated six annual stepped hydrographs. The hydrographs used were representative of conditions in 1996 (a typical annual hydrograph for the reach) and 1997 (a year of extreme high- and low-flow periods).

The fully operational locks and dam were simulated for 3 years, beginning at the end of the modeled 6-year construction phase, by three annual stepped hydrographs. In contrast to the hydrographs in the construction phase model, the hydrographs in operational phase modeling were representative of the hydrograph patterns that occur on a regular basis. The hydrographs used to model the 3-year operational phase were representative of data collected in 1985, 1986, and 1973 on the lower Ohio River.

HYDRODYNAMIC MODEL DEVELOPMENT AND CALIBRATION

At least two data sets are required to calibrate and validate a numerical model. The general procedure used to calibrate and validate the RMA-2 hydrodynamic model was to collect field data (bathymetry, roughness, etc.), which allowed the development of the computational mesh. The model then was calibrated to the water-surface elevations and velocities observed in the field for the initial mid-flow condition (350,000 ft^3/s). Both the low- and high-flow conditions were then simulated without changing the computational mesh or model parameters, and the simulated water-surface elevations and velocities were compared with those observed in the field for these additional flow conditions.

Field Data Collection and Interpretation: Water-surface elevations, channel bathymetry, and detailed water-velocity measurements were collected at the three different flow conditions. Water-surface elevations were measured at the Olmsted construction site and tailwater of Locks and Dam 53 concurrent with all three hydraulic surveys. Detailed water-velocity measurements and channel-bathymetry data were collected with an acoustic Doppler current profiler (ADCP) at 15 cross sections spaced from 2,000 feet to 5,000 feet (ft) apart during each of the hydraulic surveys.

Bathymetry data also were collected from a moving boat. The horizontal position of the boat was measured by use of a differential GPS (DGPS) receiver. Starting in 1993, bathymetric surveys were conducted annually by the USACE St. Louis District using a phased-array echo sounder. The phased-array system produced an extremely dense data set for a majority of the study reach. The raw bathymetry data were processed onto a 40 ft by 40 ft grid to make the file size more manageable, yet still provide high-resolution representation of the channel topography. The floodplains were digitized from USGS 7.5-minute quadrangle topographic maps with 5-ft contour intervals.

Calibration and Validation Results: Data from the mid-flow hydraulic survey were used to calibrate the model, and data from the low- and high-flow surveys were used to validate the model. The calibration and validation process consisted of comparing the simulated water-surface elevations (at the water-surface elevation stations) and cross-sectional velocity profiles with those surveyed in the field. A Manning's roughness coefficient (n) was assigned to each element and iteratively adjusted until the model most accurately simulated both the surveyed water-surface elevations and velocity profiles. A summary of the water-surface elevation calibration results is presented in Table 1.

Table 1 Summary of water-surface elevation calibration and validation for the Olmsted Locks and Dam study reach near Olmsted, Illinois.

	Olmsted Locks and Dam site		
Discharge (cubic feet per second)	Field water-surface elevation (feet above sea level)	Model water-surface elevation (feet above seal level)	Difference[1] (feet)
75,000	286.84	287.06	-0.22
350,000	305.94	306.00	-.06
750,000	322.34	322.10	.24

[1] Differences are determined by subtracting model from field data

The simulated-velocity magnitudes and distributions compared well with the field measurements. The shape of the field- and model-velocity distributions compared very well; on average, the differences in velocity magnitudes were within 0.25 feet per second (ft/s). The model also accurately reproduced the velocity directions, especially in areas of reverse flow experienced along the Kentucky bank just downstream from Locks and Dam 53 and in the shadow of the Olmsted cofferdam (fig. 2). Continuity also was checked throughout the model to ensure that mass was being conserved. The model conserved mass within +/- 0.7% throughout the reach under the low-, mid- and high-flow conditions.

Upon completion of the calibration and validation process, the proposed Olmsted Locks and Dam structures were added to the model without the ability to compare the model results with field data. The alternative to field data was to compare the numerical model to results from a physical model developed by the USACE Waterways Experiment Station in Vicksburg, MS. The flow fields for the numerical and physical models were consistent for a range of flow conditions.

SEDIMENT-TRANSPORT MODEL DEVELOPMENT AND RESULTS

Simulated velocities and water levels from the hydrodynamic simulations were used with the Waterways Experiment Station's (WES) Sed2D model and information on bed-material characteristics to simulate the effects of the Olmsted Locks and Dam on sediment deposition and erosion in the study reach.

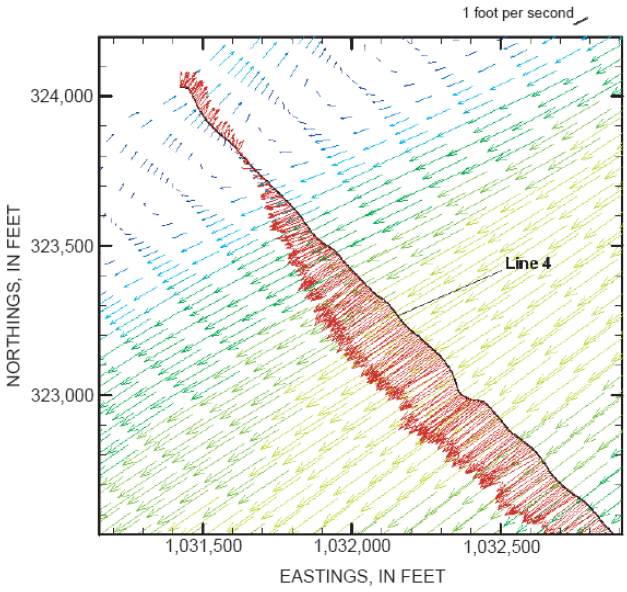


Figure 2 ADCP-measured and simulated low-flow velocity vectors at a cross-section in the Olmsted Locks and Dam study reach near Olmsted, Illinois (red arrows represent field data, multi-colored arrows represent model data)

Sediment-Transport Model Development: The following sections provide a discussion of the input data required to solve the governing equations of the Sed2D model as well as a brief explanation of the methods used to develop the input parameters.

Bed Material: The USACE St. Louis District collected bed-material data in the study reach on June 30, 1993 and February 13, 1994. These data were processed into a percent-finer format and geographically positioned to evaluate the composition of the bed material throughout the study reach. A summary of the D_{50} for all bed-material data collected in four cross sections over the mussel beds is illustrated in Figure 3 along with the position of each sample in the cross section. The data reveal that the mussel bed (located along the right bank) is primarily composed of gravel (average grain size around 10 millimeters (mm)), and the main channel is primarily composed of sand.

Selection of Representative Grain Size: The Sed2D model (version 4.52) currently (2003) considers only a single, effective grain size during each simulation. By entering the mussel-bed grain size (10 mm) into the Hydraulic Engineering Circular-18 (HEC-18) (Richardson and Davis, 2001) equation for critical velocity, it was estimated that the mussel bed would not scour at any of the hydraulic conditions being modeled; therefore, the representative grain size for the reach was determined by inspection of the D_{50} in the other areas of the reach. The field data shown in Figure 3 indicate that, aside from the mussel beds, the average grain size of the material comprising the channel bed is around 0.6 mm. A grain size of 0.6 mm was determined to be the most representative of the reach assuming that no scour of the mussel beds would occur for the hydraulic conditions being modeled.

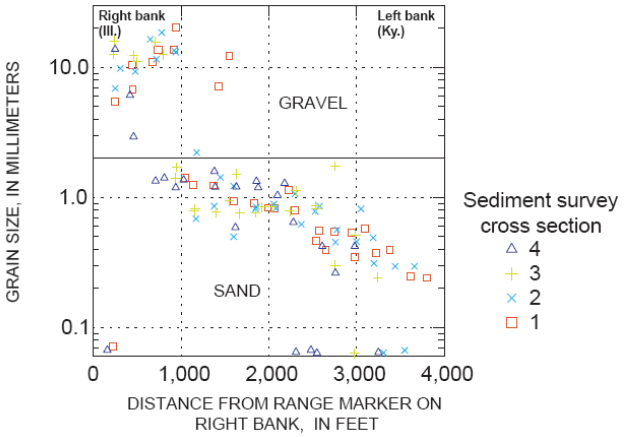


Figure 3 Summary of the bed-material D_{50} for sediment samples collected at four cross sections located around the mussel beds in the Olmsted Locks and Dam study reach near Olmsted, Ill.

Sediment-Inflow Concentration: The sediment-inflow boundary conditions for the annual hydrographs were established by a rating curve developed by Sed2D model runs. The various hydrograph steps were modeled with no sediment supply to the study reach to allow the river to reach equilibrium conditions. The equilibrium-sediment concentration for each step was used to build the bed-material inflow-rating curve. The absence of grain-size distributions for the suspended-sediment concentrations collected in the field and the inability of Sed2D to model multiple grain sizes prevented the use of empirical bed-load equations.

SEDIMENT-TRANSPORT MODEL RESULTS:

The results of the Olmsted modeling project are summarized according to the two modeling phases. The construction phase modeling will focus on results of the 6-year dam construction simulation and the operational phase modeling will focus on the long-term results of the 3-year fully operational locks and dam simulation.

Construction Phase Model - Sediment Transport: The cumulative difference in bed change between the baseline and construction phases at the end of the six annual hydrographs is shown in Figure 4. The amount and downstream extent of deposition caused by the dam construction progressively increases from year 1 through year 6. The initial concerns by U.S. Fish and Wildlife Service and USACE were that high-flow conditions would have the most effect on sediment-transport patterns in the study reach; however, the most significant bed change occurred during the low-flow period at the end of year 5 in which the wicket gates were closed and the flow of the river passed through the tainter gates (fig. 5). The maximum cumulative deposition on the mussel beds was approximately 1.5 ft, which occurred at the end of year 6. The greatest areas of deposition are shown to develop at the upstream section of the mussel beds as well as near the downstream end of the mussel beds, along the edge of the area where scour was prevented.

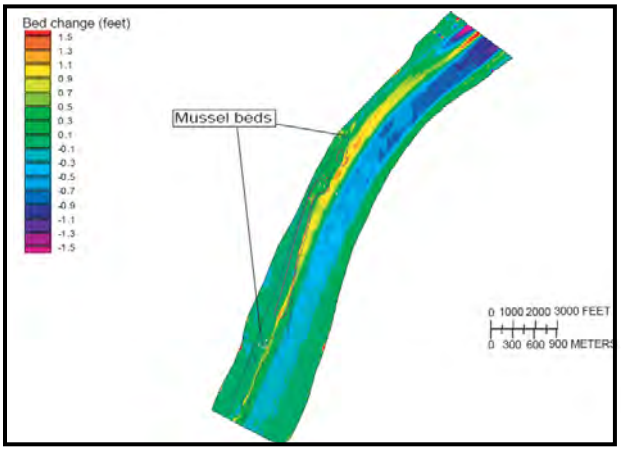


Figure 4 Difference in bed change between baseline and construction simulations after year 6 in the Olmsted Locks and Dam study reach near Olmsted, Illinois.

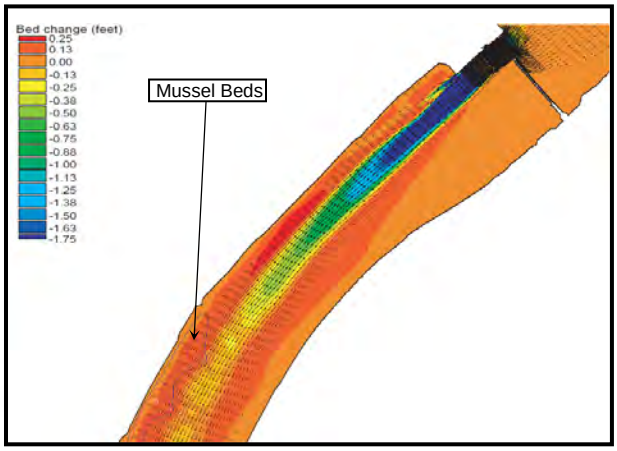


Figure 5. Difference in bed change between baseline and construction simulations after year 5, superimposed with hydraulics for a low-flow model simulation of Olmsted Locks and Dam.

Aside from these two sections, the majority of the mussel-bed area is expected to have little or no bed change that can be associated with the dam construction process over the 6-year simulation. Most areas of the mussel beds indicated less than 0.5 ft of bed change between the baseline and construction phases during the six annual hydrographs

Operational Phase Model - Sediment Transport: The cumulative difference in bed change between the baseline and operational dam scenarios at the end of the three annual hydrographs is shown in figure 6.

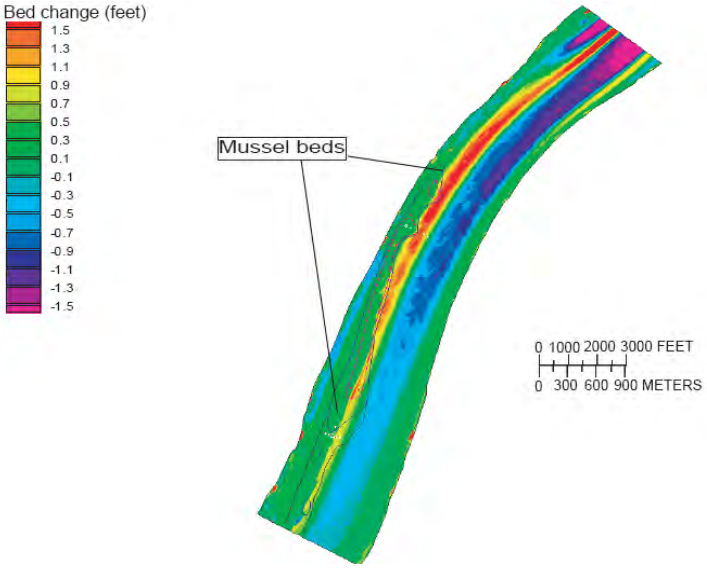


Figure 6 Difference in bed change between baseline and fully operational locks and dam simulation after year 9 in the Olmsted Locks and Dam study reach near Olmsted, Illinois.

The depth and downstream extent of scour and deposition caused by the dam operation progressively increases from year 7 through year 9. Although the depth of deposition continued to increase around the mussel beds in the operational phase modeling, the lateral migration of the deposition toward the mussel beds is limited. The spatial distribution of the depositional areas at the end of year 9 (fig. 6) is nearly identical to the spatial distribution simulated through year 6 in the construction phase model (fig. 4). As in the construction phase model, the most appreciable bed change during the operation phase model occurred during the low-flow periods when the wicket gates were closed and the flow of the river passed through the tainter gates. The maximum cumulative deposition on the mussel beds is approximately 2 ft occurring at the end of year 9.

SUMMARY AND CONCLUSIONS

The Olmsted Locks and Dam sediment-transport model was developed by the USGS incooperation with the USACE Louisville District to evaluate the environmental effect of the construction and subsequent operation of the Olmsted Locks and Dam on the lower Ohio River. Simulation of the phased Olmsted Locks and Dam construction and subsequent 3-year operation period resulted in a maximum additional deposition of approximately 2 feet when compared to the bed change simulated with baseline conditions. The areas of highest deposition are in the upstream section of the mussel beds and in the small area near the downstream extent of the beds. Aside from these two sections, the majority of the mussel bed area had minimal bed change that can be associated with the dam construction and (or) operation over the 9-year simulation. Most areas of the mussel beds had less than 0.5 ft of cumulative bed change between the baseline and construction phases during the nine annual hydrographs. Inspection of the scour and deposition patterns caused by the dam construction revealed a large scoured area in the channel downstream from the navigable pass and tainter gates (as a result of the flow contraction in those regions) and a section of high deposition located along the right descending (Illinois) bank, downstream from the tainter gates. The hydrodynamic changes are most prominent during low-flow conditions when the entire river flow passes through the tainter gates. The most appreciable increase in bed change between the baseline- and construction-phase conditions occurred during year-5 of the simulation because of an unusually extended low-flow period in which the entire flow for nearly 6 months passed through the tainter gates, which greatly altered the hydrodynamics of the river. The bed change over the 9-year Olmsted Locks and Dam simulation reveals a continuous downstream progression, deepening of the regions of scour in the main channel, and deposition along the right bank with limited lateral migration toward the more densely populated mussel-bed areas.

REFERENCES

Richardson, E.V., and Davis, S.R., 2001, Evaluating Scour at Bridges:Washington, DC, Federal Highway Admin., Hydraulic Engineering Circular No.18 FHWA-NHI-01-001, 378 p.

U.S. Fish and Wildlife Service, 1993, Supplemental biological opinion for the proposed Olmsted Locks and Dam, Ballard County, Kentucky: Cookeville, Tenn., 15 p.

A MULTIDIMENSIONAL MARKER-IN-CELL HYDRAULIC AND SEDIMENT TRANSPORT MODEL FOR BRAIDED RIVER FLOW

Robert Thomas, Schools of Geography and Earth Sciences, University of Leeds, Leeds, UK, r.thomas@earth.leeds.ac.uk; Stuart Lane, Department of Geography, University of Durham, Durham, UK, S.N.Lane@durham.ac.uk; Jim Best, School of Earth & Environment, University of Leeds, Leeds, UK, j.best@earth.leeds.ac.uk

INTRODUCTION

Recently, fluvial geomorphologists have expended a great deal of effort in developing numerical models to simulate braided rivers. Contingent upon limitations imposed by computing power (Nicholas (2003)) and a lack of integrated field and laboratory datasets at a suitable resolution (Lane and Richards (2001)), approaches have ranged in complexity in relation to the spatial and temporal scales to which they have been applied. For example, at the scale of individual braid bars or confluence units, two-dimensional depth-averaged and fully three-dimensional hydraulic models have been used to simulate flow patterns (e.g. Lane and Richards (1998), Lane et al. (1999)). At the braidplain scale, one-dimensional models of section-averaged flow and bedload transport (e.g. Paola (1996)), simplified two-dimensional cellular automata models (e.g. Murray and Paola (1994)) and, recently, two-dimensional models have been applied (e.g. Nicholas (2003)). However, only with the use of a fully three-dimensional model can the important secondary circulation processes that lead to the scour and deposition patterns seen in braided rivers be accurately represented.

Given the apparent dichotomy between the need for three-dimensional models and the associated computational and data limitations, this paper presents the formulation of a modified 2+ dimensional Marker-in-Cell model (Tetzlaff and Harbaugh (1989)). Lagrangian momentum tracers that have neither mass nor volume are tracked through an Eulerian mesh that characterizes the field variables (e.g. depth and bed elevation). For each tracer, the momentum equation is solved in its Lagrangian form to reduce numerical dispersion, whilst the continuity equation is solved in its Eulerian form to achieve improved mass conservation (e.g. Chin (1997)). As tracers accelerate and decelerate due to interactions with each other and topography, erosion and deposition are induced. The model presented here simulates fluid flow and sediment transport in the horizontal plane and depth and deposits in the vertical plane. Non-uniform total-load sediment transport is simulated by using a non-equilibrium approach, dividing the sediment mixture into size fractions and accounting for the effects of hiding and exposure. Historical erosion and deposition is represented by a mixing layer approach.

EQUATIONS OF TWO-DIMENSIONAL OPEN-CHANNEL FLOW

It is possible to obtain two key equation sets for a single fluid unit from Newton's laws of motion: (i) the law of conservation of mass for an incompressible fluid in Eulerian form and (ii) the Navier-Stokes momentum equations for an incompressible fluid (Lane (1998)). In two dimensions, and assuming that the fluid is homogeneous, incompressible and at constant temperature, the continuity or mass conservation equation can be expressed as:

$$\frac{\partial h}{\partial t}+\frac{\partial hU}{\partial x}+\frac{\partial hV}{\partial y}=0 \tag{1}$$

where h = flow depth, t = time, and U and V are depth-averaged velocities in the x and y directions, respectively.

In Cartesian coordinates, the simplified depth-averaged shallow water momentum equations may be written as:

$$\frac{\partial U}{\partial t}+\frac{\partial U^2}{\partial x}+\frac{\partial UV}{\partial y}=\frac{DU}{Dt}=-g\frac{\partial H}{\partial x}+\left(\frac{\mu}{\rho}+\nu\right)\left(\frac{\partial^2 U}{\partial x^2}+\frac{\partial^2 U}{\partial y^2}\right)-\frac{c_f UQ}{8h} \tag{2}$$

$$\frac{\partial V}{\partial t}+\frac{\partial UV}{\partial x}+\frac{\partial V^2}{\partial y}=\frac{DV}{Dt}=-g\frac{\partial H}{\partial y}+\left(\frac{\mu}{\rho}+\nu\right)\left(\frac{\partial^2 V}{\partial x^2}+\frac{\partial^2 V}{\partial y^2}\right)+-\frac{c_f VQ}{8h} \tag{3}$$

where $\frac{D(\ )}{Dt}$ = material or total derivative, g = gravitational acceleration, H = water surface elevation, μ = molecular viscosity, ρ = density of water, ν = turbulent eddy viscosity = $\frac{(e-1)}{e^2}\frac{\kappa hQ}{\left(8/c_f\right)^{1/2}}$, derived from the Kàrmàn-Prandtl law-of-the-wall, assuming the depth-averaged velocity occurs at h/e within the water column (where e is the base of natural logarithms), κ is the von Kàrmàn constant which has a value of ≈ 0.33 in suspended sediment-laden flows (Bennett et al. (1998)), c_f = Darcy-Weisbach friction coefficient, and $Q = \left(U^2+V^2\right)^{1/2}$.

In arriving at equations (2) and (3), a number of simplifying assumptions have been made. The Coriolis force, horizontal variations in atmospheric pressure and water surface wind stress terms have been neglected (e.g. Lane (1998)), and it has been assumed that the hydrostatic pressure distribution (e.g. Vreugdenhill (1994)) and constant density hold over the flow depth. In addition the shear stress and dispersion terms have been modeled very simply, assuming that dispersion dominates turbulent momentum diffusion, and terms involving cross-derivatives have been neglected (Westerink, 2003). In these equations, all velocities are time-averaged and uppercase letters denote depth-averaged velocities. Through the use of the material derivative, equations (2) and (3) express both the Eulerian and Lagrangian forms of the equations.

SEDIMENT EROSION, TRANSPORT AND DEPOSITION

Commonly, three main modes of sediment transport are distinguished: wash load, suspended load and bed load. This research is concerned with the latter two modes. The suspended load fraction is made up of particles that are held in suspension by turbulent eddies, whilst the bedload fraction is made up of particles that roll, slide, or saltate along the bed. In this research, the water column is treated as a single bed-material load layer, since computational efficiency is of key importance and because this technique is less reliant upon empiricism (Langendoen (2000)).

Non-equilibrium bed-material load transport model: Many early sediment transport models assumed that local equilibrium conditions applied when simulating bed-material transport. This sets the actual bed-material transport rate to be equal to the sediment transport capacity, the transported sediment load under equilibrium conditions (i.e. uniform flow and no net erosion or deposition) (Langendoen (2000)). However, this may lead to unrealistic predictions of bed deformation, especially in cases where flows are above (e.g. after urbanization, forest exploitation, channelization; Simon (1992), Stott et al. (2001), Trimble (1997)) or below (e.g. downstream of a reservoir; Sherrard and Erskine (1991)) capacity for much of the time. To overcome this limitation, a non-equilibrium transport model is implemented in this work.

For the determination of sediment transport in a non-uniform sediment mixture, it is convenient to divide the mixture into several size classes. For each size class k, the two-dimensional advection-diffusion equation of total load sediment transport can be derived (Wu et al. (2000a)):

$$\frac{\partial(hC_{tk})}{\partial t}+\frac{\partial(hUC_{tk})}{\partial x}+\frac{\partial(hVC_{tk})}{\partial y}=\frac{\partial}{\partial x}\left(\varepsilon_s h\frac{\partial C_{tk}}{\partial x}\right)+\frac{\partial}{\partial y}\left(\varepsilon_s h\frac{\partial C_{tk}}{\partial y}\right)+E_{bk}-D_{bk} \tag{4}$$

where C_{tk} = total load sediment concentration of the k^{th} size class, $\varepsilon_s = \nu/\sigma_s$ = eddy diffusivity of sediment (ν = eddy viscosity and σ_s = turbulent Prandtl-Schmidt number), E_b = entrainment rate of particles from the bed, and D_b = deposition rate of particles onto the bed. The net flux at the bed, $E_{bk} - D_{bk}$, equals the change in bed elevation due to erosion and deposition of each size fraction. The bed elevation change by size fraction can be formulated as:

$$E_{bk}-D_{bk}=(1-\lambda)\frac{\partial Z_k}{\partial t}=\alpha\omega_k(C_{tk}-C_{t^*k}) \tag{5}$$

where λ = bed porosity, Z_k = bed deformation of the k^{th} size class, α = non-equilibrium adaptation coefficient (Armanini and Di Silvio (1988)), ω = fall velocity (available from lookup tables published by, for example, USICWR (1957)), and C_{t^*} = the total load transport capacity.

Sediment transport capacity: Solution of equation (5) requires the determination of the sediment transport capacity. Sediment transport capacity is determined utilizing the formulations of Wu et al (2000b), which determine the fractional transport capacities of bed load and suspended load, and take into account hiding and exposure effects among different size classes. The total sediment transport capacity, C_{t^*}, is then defined as:

$$C_{t^*}=\sum_k p_k C_{*k} \tag{6}$$

where p_k = fraction of sediment in the k^{th} size class available for transport; and C_{*k} = sediment transport capacity of the k^{th} size class. The fraction p_k depends on the fractional content by volume of size class k in the surface layer and the fraction of sediment in the k^{th} size class entering the reach from upstream.

Representation of erosion and deposition- sediment layers: To represent historical erosion and deposition, the bed can be divided into a surface or active layer and a subsurface layer. These layers constitute the mixing layer (e.g. Hirano (1971)). Sediment particles are continuously exchanged between the water column and the surface layer. In contrast, sediment particles only exchange between surface layer and substrate when the bed scours or fills (Langendoen (2000). Variation in the bed material composition in the surface layer is determined from mass conservation:

$$\frac{\partial\left(\beta_k^s a\right)}{\partial t} = \frac{\partial z_{bk}}{\partial t} + \beta_k^*\left(\frac{\partial a}{\partial t} - \frac{\partial z_b}{\partial t}\right) \tag{7}$$

where β_k^s = bed material composition in the surface layer, a = thickness of the surface layer, $\partial z_b/\partial t$ = total bed deformation rate, β_k^* = β_k^s when $\partial a/\partial t - \partial z_b/\partial t \leq 0$, and β_k^* = the bed material composition in the subsurface layer when $\partial a/\partial t - \partial z_b/\partial t > 0$.

NUMERICAL SOLUTION OF FLOW AND SEDIMENT TRANSPORT EQUATIONS

In this research, a 'segregated' (Tannehill et al. (1997), Roache (1998)) or decoupled approach is utilized to solve the governing equations at each timestep. Two different solution methods for the equations are required- one for the Lagrangian momentum equations and one to solve the Eulerian continuity equation and sediment transport equation and to couple the solutions. This coupling is essential in order to ensure conservation of both mass and momentum (Tannehill et al. (1997), Roache (1998)).

Solution of the Lagrangian momentum equations: The simplified momentum equations in Lagrangian form are solved utilizing the second order in time, fourth order in space Runge Kutta method (e.g. Press et al. (1992)). Press et al. (1992) note that this method provides the maximum accuracy for the minimum of effort (in their words, "it gives the most bang for the buck" (p 716)). Since tracer positions do not necessarily coincide with grid nodes (which contain the values of flow depth and velocities), interpolation is required to determine h and $\partial H/\partial x$ and $\partial H/\partial y$. It is assumed that the water surface is made up of a series of hyperbolic paraboloids, whereby the water surface elevation is fitted exactly at each grid node and so avoids discontinuities at cell edges. A hyperbolic paraboloid degenerates to a plane when its four vertices are coplanar, which is justified by the fact that water surfaces tend to obtain minimum potential energy in the form of a plane (Tetzlaff and Harbaugh (1989)). The interpolation function is:

$$h = h_{x,y}(1-i)(1-j) + h_{x,y+1}(1-i)(j) + h_{x+1,y}(i)(1-j) + h_{x+1,y+1}(i)(j) \tag{8}$$

where i and j are the x- and y-coordinates of the tracer within the cell, respectively ($0 \leq i,j \leq 1$). It follows by differentiation that:

$$\frac{\partial H}{\partial x} = \frac{\left[\left(H_{x+1,y+1} - H_{x,y+1}\right)(j) + \left(H_{x+1,y} - H_{x,y}\right)(1-j)\right]}{\Delta x} \tag{9}$$

and:

$$\frac{\partial H}{\partial y} = \frac{\left[\left(H_{x+1,y+1} - H_{x+1,y}\right)(i) + \left(H_{x,y+1} - H_{x,y}\right)(1-i)\right]}{\Delta x} \tag{10}$$

Once the positions and velocities of all tracers have been updated, velocities at each grid node are updated by averaging the velocities of all the tracers within a grid cell. The accuracy of the flow representation is hence directly related to the number of tracers in each grid cell.

Solution of the Eulerian continuity equation and solution coupling: Comparison of the Eulerian two-dimensional shallow-water equations and the Euler equations of compressible isentropic gas dynamics indicate that they have the same mathematical structure (Majda (2002)). This suggests that numerical methods designed to solve compressible flows can be tailored to solve the shallow water equations. Several schemes have been devised to solve the decoupled continuity and momentum equations, such as the SIMPLE family (SIMPLE (Patankar and Spalding (1972)), SIMPLER (Patankar (1980))), PISO (Issa (1985)) and fractional step methods (e.g. Chorin (1968)). The SIMPLE method has been applied to compressible flows by, for example, Demirdžić and Perić (1990) and Ferziger and Perić (2002). PISO has been applied to compressible flows by Issa et al. (1986). Since the solution of the Lagrangian momentum equations should yield correct velocity fields, application of the SIMPLE method would lead to initial divergence and hence increase the required number of iterations for convergence (Patankar (1980)). To overcome this difficulty, Patankar (1980) developed the SIMPLER method, and hence it is adopted as the second solution method here.

Demirdžić and Perić (1990) detail the method to assemble the components of the algebraic equations in order to implicitly solve the transport equation for a scalar, ϕ. During solution, the velocities, U and V and the concentration C_{tk} can be considered as scalars. The discretized transport equation for a scalar quantity in integral form and a colocated finite volume grid is:

$$\Delta x^2 \frac{(h\phi)^{n+1} - (h\phi)^n}{\Delta t} + \Delta x \sum_l (h\phi)_l U_i \cdot n - \sum_l (\Gamma_\phi)_l \left(\phi_{l-\frac{1}{2}} - \phi_{l+\frac{1}{2}}\right) = \Delta x^2 q_\phi \tag{11}$$

where $U_i \cdot n$ is the velocity perpendicular to the cell face, l = 1,2,3,4 (east, south, west and north faces), Γ_ϕ is the relevant diffusion coefficient, and q_ϕ is the source term.

The method of Rhie and Chow (1983) to handle 'checkerboard' pressure distributions is implemented. By inserting the relevant scalar into the equation, a matrix equation results which can be solved iteratively for ϕ. In this research, the suggestion of Demirdžić and Perić (1990) is followed and Stone's (1968) SIP solver is implemented. The rate of convergence of this already efficient solver may, at a later date, be improved by utilizing it as a smoother within a multigrid framework (e.g. Ferziger and Perić (2002)).

The solution algorithm can be summarized as follows:

1. Employ the 4th order Runge Kutta solver to update the velocities and positions of the momentum tracers. Average all tracer velocities within each grid cell to determine nodal velocity values.
2. Assemble the coefficients for the discretized equation (11) and hence calculate pseudovelocities (Patankar (1980)). Assemble and solve the SIMPLER pressure equation resulting from the discretized equation (11) (Patankar (1980)).
3. Using this new pressure field, solve the discretized equation (11) with $\phi = U$ and then V to update the grid node velocities.
4. Calculate new mass fluxes using the updated grid node velocities, and determine the mass imbalance in each grid cell.
5. Assemble and solve the pressure correction equation resulting from the discretization. Apply SIP until the sum of absolute residuals is reduced by a factor of 5.
6. Correct the nodal velocity components utilizing the calculated pressure correction. Use the hydrostatic pressure equation to determine the flow depth.
7. Assemble and solve the sediment concentration equation resulting from the discretization, equation (11). Apply SIP until the sum of absolute residuals is reduced by a factor of 5.
8. Return to step 2 and repeat until the sum of the absolute residuals in the momentum and continuity equations has fallen by two orders of magnitude.
9. Advance the time by an increment Δt.

CONCLUSION

In this paper, the formulation of a modified Marker-in-Cell model has been presented. This technique entails tracking Lagrangian momentum tracers that have neither mass nor volume through an Eulerian mesh that characterizes the field variables. As tracers accelerate and decelerate due to interactions with each other and topography, erosion and deposition are induced. For each tracer, the momentum equation is solved by the fourth order in space Runge Kutta method, whilst the Eulerian continuity equation is discretized implicitly and solved by the SIMPLER method (Patankar (1980)) to achieve improved mass conservation and velocity-pressure coupling. The model operates in 2+ dimensions, whereby fluid flow and sediment transport are simulated in the horizontal plane and depth and deposits are simulated in the vertical plane. Non-uniform total-load sediment transport is simulated using a non-equilibrium approach, dividing the sediment mixture into size fractions and accounting for the effects of hiding and exposure. Historical erosion and deposition is represented by a mixing layer approach. It is believed that the use of the Marker-in-Cell method formulated in this paper may permit the simulation of some of the more stochastic features observed in braided rivers (e.g. Paola, 1996).

REFERENCES

Armanini, A. and Di Silvio, G. (1988). “A one-dimensional model for the transport of a sediment mixture in non-equilibrium conditions,” Journal of Hydraulic Research, 26, pp 275–292.

Bennett, S.J., Bridge, J.S. and Best, J.L. (1998). “The fluid and sediment dynamics of upper-stage plane beds,” Journal of Geophysical Research, 103, pp 1239–1274.

Chin, S. (1997). A three-dimensional numerical model for simulating flow and sediment transport processes in fluvial and deltaic environments. Unpublished PhD dissertation. Department of Geological and Environmental Sciences, Stanford University, Stanford.

Chorin, A.J. (1968). "Numerical solution of the Navier-Stokes equations," Mathematics of Computation, 22, pp 745–762.

Demirdžić, I. and Perić, M. (1990). "Finite volume method for prediction of fluid flow in arbitrarily shaped domains with moving boundaries," International Journal for Numerical Methods in Fluids, 10, pp 771–790.

Ferziger, J.H. and Perić, M. (2002). Computational methods for fluid dynamics, Third Edition. Springer-Verlag, Berlin.

Hirano, M. (1971). "River bed degradation with armoring," Proceedings Japan Society of Civil Engineers, 195, pp 55–65.

Issa, R.I. (1985). "Solution of the implicitly discretised fluid flow equations by operator-splitting," Journal of Computational Physics, 62, pp 40–65.

Issa, R.I., Gosman, A.D. and Watkins, A.P. (1986). "The computation of compressible and incompressible recirculating flows by a non-iterative implicit scheme," Journal of Computational Physics, 62, pp 66–82.

Lane, S.N. (1998). "Hydraulic modelling in hydrology and geomorphology. A review of high resolution approaches," Hydrological Processes, 12, pp 1131–50.

Lane, S.N. and Richards, K.S. (1998). "Two-dimensional modelling of flow processes in a multi-thread channel," Hydrological Processes, 12, pp 1279–1298.

Lane, S.N. and Richards, K.S. (2001). "The 'validation' of hydrodynamic models: some critical perspectives," Anderson, M.G. and Bates, P.D., (eds.), Model validation: perspectives in hydrological science. Wiley, Chichester, pp 413–439.

Lane, S.N., Bradbrook, K.F., Richards, K.S., Biron, P.A. and Roy, A.G. (1999). "The application of computational fluid dynamics to natural river channels: three-dimensional versus two-dimensional approaches," Geomorphology, 29, pp 1–20.

Langendoen, E.J. (2000). CONCEPTS - CONservation Channel Evolution and Pollutant Transport System. Research Report 16. USDA-ARS-NSL, Oxford, Mississippi.

Majda, A.J. (2002). Introduction to PDEs and waves for the atmosphere and ocean. Courant Lecture Notes 9. American Mathematical Society & Courant Institute of Mathematical Sciences, New York.

Murray, A.B. and Paola, C. (1994). "A cellular model of braided rivers," Nature, 371, pp 54–57.

Nicholas, A.P. (2003). "Investigation of spatially distributed braided river flows using a two-dimensional hydraulic model," Earth Surface Processes and Landforms, 28, pp 655–674.

Paola, C. (1996). "Incoherent structure: Turbulence as a metaphor for stream braiding", Ashworth, P.J., Bennett, S.J., Best, J.L. and McLelland, S.J., (eds.), Coherent Flow Structures in Open Channel Flows. Wiley, Chichester, pp 705–723.

Patankar, S.V. (1980). Numerical heat transfer and fluid flow. Taylor & Francis, London.

Patankar, S.V. and Spalding, D.B. (1972). "A calculation procedure for heat, mass and momentum transfer in three-dimensional parabolic flows," International Journal of Heat and Mass Transfer, 15, pp 1787–1806.

Press, W.H., Teukolsky, S., Vetterling, W. and Flannery, B. (1992). Numerical Recipes in C. Cambridge University Press, Cambridge, UK.

Rhie, C.M. and Chow, W.L. (1983). "Numerical study of the turbulent flow past an airfoil with trailing edge separation," AIAA Journal, 21, pp 1525–1532.

Roache, P.J. (1998). Fundamentals of computational fluid dynamics. Hermosa, Albuquerque.

Sherrard, J.J. and Erskine, W.D. (1991). "Complex response of a sand-bed stream to upstream impoundment," Regulated Rivers: Research and Management, 6, pp 53–70.

Simon, A. (1992). "Energy, time, and channel evolution in catastrophically disturbed fluvial systems," Geomorphology, 5, pp 345–372.

Stone, H.L. (1968). "Iterative solution of implicit approximations of multidimensional partial differential equations," SIAM Journal of Numerical Analysis, 5(3), pp 530–558.

Stott, T., Leeks, G., Marks, S. and Sawyer, A. (2001). "Environmentally sensitive plot-scale timber harvesting: impacts on suspended sediment, bedload and bank erosion dynamics," Journal of Environmental Management, 63, pp 3–25.

Tannehill, J.C., Anderson, D.A. and Pletcher, R.H. (1997). Computational fluid mechanics and heat transfer, Second Edition. Taylor & Francis, Philadelphia.

Tetzlaff, D.M. and Harbaugh, J.W. (1989). Simulating Clastic Sedimentation. van Nostrand Reinhold, New York.

Trimble, S.W. (1997). "Contribution of stream channel erosion to sediment yield from an urbanizing watershed," Science, 278, pp 1442–1444.

USICWR (1957). Some fundamentals of particle size analysis. A study of methods used in measurements and analysis of sediment loads in streams. Report No. 12. Sub-committee on Sedimentation, US Interagency Committee on Water Resources, Minneapolis.

van Doormal, J.P. and Raithby, G.D. (1984). "Enhancements of the SIMPLE method for predicting incompressible fluid flows," Numerical Heat Transfer, 7, pp 147–163.

Vreugdenhill, C.B. (1994). Numerical methods for shallow water flow. Kluwer Academic, Dordrecht.

Westerink, J.J. (2003). CE 344 Hydraulics Course Notes, Spring 2003. Department of Civil Engineering and Geological Sciences, University of Notre Dame, Notre Dame.

Wu, W., Rodi, W. and Wenka, T. (2000a). "3-D numerical modeling of water flow and sediment transport in open channels," Journal of Hydraulic Engineering, 126, pp 4–15.

Wu, W., Wang, S.S.Y. and Jia, Y. (2000b). "Nonuniform sediment transport in alluvial rivers," Journal of Hydraulic Research, 38, pp 427–434.

USE OF DIMENSIONLESS RATIOS IN STREAM RESTORATION PLANNING

W. Barry Southerland, PhD, Fluvial Geomorphologist-Hydrologist, USDA-Natural Resources Conservation Service, West National Technology Support Center, 1201 NE Lloyd Blvd. Suite 1000, Portland, OR 97232, barry.southerland@wa.usda.gov.

Abstract: Measuring the success of a restoration project for a natural stream channel can be difficult and subjective if there is no common frame of natural morphological reference for the evaluator. For this reason, the "geomorphic reference site (GRS)" is used as the basis for measuring the degree of departure of a given stream segment from the desired reference condition. A GRS is a stream segment that has natural morphologic stability within a specific valley type and climatic regime. Over time, it neither aggrades nor degrades, maintaining its profile, cross-section, and plan view within a range of natural variability. A set of morphometric measurements can be made in the field and developed into a template of dimensionless ratios for the GRS. This template can then be used to make quantifiable comparisons between segments of different streams or between segments of the same stream - provided the segments share similar hydrophysiographic characteristics with the GRS. Dimensionless ratios are also used as a basis for natural channel restoration. Examples are illustrated and discussed.

INTRODUCTION

The reference reach concept is based on the idea that there is a most probable form for any given stream reach (Leopold, 1994). A reference reach should reflect a minimum expenditure of energy moving toward an equal distribution of stream power. A major assumption used in natural channel restoration is that stream segments in similar hydrophysiographic areas and geologic settings evolve similar geomorphic dimensions within predictable ranges.

Geomorphic dimensions (e.g., bankfull width, depth) were described by Rosgen (1994) and combined into dimensional ratios (e.g., width to depth ratio) for use in his stream classification system. Rosgen (1998) expanded the original set of dimensionless ratios to more fully describe the longitudinal profile, cross-section and planview (planform) of a given stream reach.

RESOURCE CONCERN

Some of the more common reasons for design failures are due to the following:

1. Lack of stream and valley stratification;
2. Using one equation - analytical or empirical – to fit all stream types;
3. Lack of understanding of natural geomorphic potential and channel evolutionary stage;
4. Lack of understanding of dimension, longitudinal profile, and planform and how they integrate into stable bedload transport.

BACKGROUND

During summer-fall 2002, numerous sources (contour maps, aerial photos, etc.) and site visitations were used to select 218 potential GRS sites for streams flowing through 32 glacial-fluvial valleys in the Cascade Mountains of northern Washington State (Southerland, 2003). They were divided into west slope (high precipitation) and east slope (low precipitation) drainages. In each group, a random population was chosen for field review.

Morphologic measurements (using laser equipment), stream-gage data, and instream features were recorded for 58 of the most stable-appearing sites. The data were used to create templates of dimensionless ratios to describe the natural stable form for each site.

Dimensionless ratios can define reasonable ranges of physical variability for natural channel restoration for a proposed restoration site. The dimensionless ratios template from a GRS can be used to make quantifiable comparisons between different streams or between segments of the same stream - provided the GRS and the segment being compared share similar hydrophysiographic characteristics.

EXAMPLES

1. Dimensionless ratios used as a measure of departure from reference site conditions:

Table 1 includes a selection of dimensionless ratios for the two sites shown in Figures 1 and 2. The "reach of interest (ROI)" site is located just upstream of the GRS. Note the inclusion of root density and root matrix measurements in the table. Biological attributes such as fish, macro-invertebrates and native streambank vegetation could also be compared and indexed at the GRS and ROI sites. Stream morphometric measurements of longitudinal profile, dimension, planform, and root density measurements similar to the measured features described in Tables 1 and 2 can be surveyed over a given monitoring period. This data can be used to estimate the change in departure between the geomorphic reference and reach of interest sites.



Figure 1 Entiat River GRS

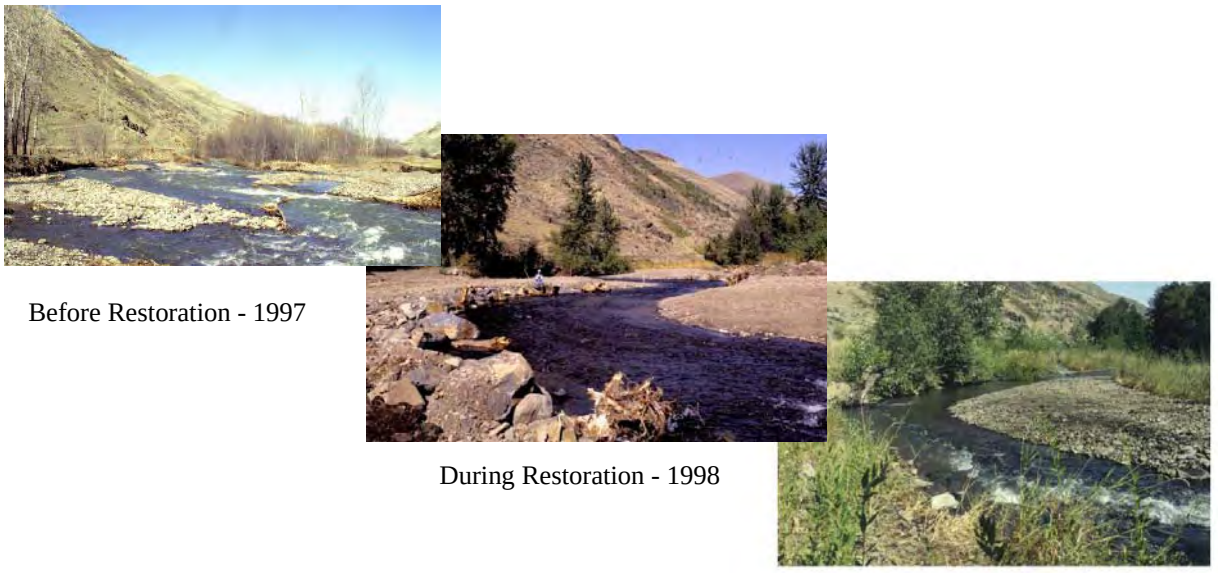


Figure 2 Entiat River ROI

Table 1 Selected Dimensionless Ratios for Entiat River				
Measured Feature (Apex of Meander)	**Reference Reach (GRS)**	**Reach of Interest (ROI)**	**Erosion Potential of ROI**	**Percent Departure of ROI**
Bank Height Ratio	1.07	1.25	Moderate	17%
Root Density	70%	25%	High	64%
Root Matrix	.78	.30	Low	62%
Width to Depth Ratio	19	42	High Lateral Shear Stress	121%
Mean Pool Depth/Mean Bankfull Depth	2.2	1.5	N/A	32%

2. Dimensionless ratios used to reconstruct a stable stream channel:

The mainstem of Asotin Creek as it flowed through the Frank Koch property had an unstable, braided channel. Steelhead trout, native to Asotin Creek, no longer spawned in this reach and riparian woody vegetation was not able to become established along most of its length (Figure 3). Using dimensionless ratios from Salmon Creek Table 2, similar hydrophysiographic area located on the East Cascade slope, this reach was restored to a single-thread, stable channel. Spawning steelhead and reds have since been documented at the site and woody vegetation is well-established.



Before Restoration - 1997

During Restoration - 1998

Post Restoration - 2003

Figure 3 Geomorphic Restoration of a Braided Stream System

Table 2 Sample Template of GRS Dimensionless Ratios for Koch Project

	Mean	Range
Profile		
Pool bankfull depth/Average bankfull depth, ft/ft	2.2	1.6-3.2
Riffle bankfull depth/Average bankfull depth, ft/ft	0.85	0.59-0.92
Run bankfull depth/Average bankfull depth, ft/ft	1.4	1.2-1.6
Glide bankfull depth/Average bankfull depth, ft/ft	1.2	1.1-1.5
Cross-sections		
Width to depth ratio, riffles	18	15-21
Width to depth ratio, pools	21	18-29
Width to depth ratio, runs	15	12-21
Width to depth ratio, glides	20	15-26
Plan-view		
Sinuosity, ft/ft	1.46	1.2-2.2
Radius of curvature/Meander belt width, ft/ft	2.2	1.8-2.7
Meander wavelength × Average bankfull width	12.2	8.9-14.8
Slope (water surface)		
Pool bankfull slope/Average bankfull slope, %/%	0.35	0.21-0.42
Riffle bankfull slope/Average bankfull slope, %/%	1.5	1.3-1.9
Run bankfull slope/Average bankfull slope, %/%	1.1	1.05-1.3
Glide bankfull slope/Average bankfull slope, %/%	0.40	0.26-0.45
Other		
Root Matrix = Root depth/ Bank height	0.78	0.54 -1.0
Bank Height Ratio = Bank height/Bankfull depth, ft/ft	1.07	1.01-1.21



1996: Incised – Post Flood

2002: Post Restoration

2003: Post Restoration

Figure 4 Geomorphic Restoration of an Incised Stream System

On the J-Bar Ranch (Figure 4), the channel of the South Fork Asotin Creek was straight and incised. Again, no steelhead spawning occurred there, and the riparian woody vegetation was non-existent. Meander reconstruction, using dimensionless ratio templates from a GRS in the same hydrophysiographic area, was very successful. Both of these Blue Mountain projects have successfully maintained their stability even though there have been some very high, out-of-bank flows.

DISCUSSION

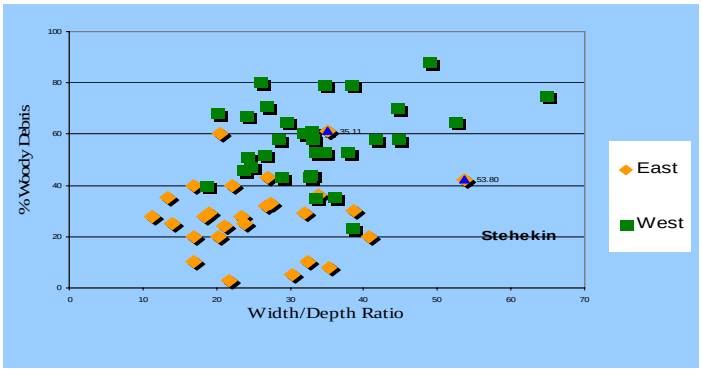


Figure 5 Width to Depth Ratio – East vs. West

Some dimensionless ratios may vary significantly within the same Rosgen geomorphic stream type if hydrophysiographic areas are different. In Figure 5, note that the width to depth ratio increases with the % woody debris, but at a higher rate on the west slope where there is more annual precipitation than the east slope. Thus, dimensionless ratios developed on one side of the mountains are likely not to work on the other side within the same geomorphic stream classification. However, in the above streams, the range of variability for each key classification parameter still falls within both the Rosgen and the Montgomery and Buffington (1993) classification systems.

To meet reference site conditions, a stream segment must have certain physically measurable attributes that are reproducible and meet specific criteria. These measurable attributes can be combined with others to develop dimensionless ratios that spatially describe the planview, profile, bedload, woody debris, and floodplain attachment of the stream system. Understanding the degree of departure that a reach of interest has from the reference site can aide the technician and/or land operator in identifying channel evolutionary changes such as those described in Schumm, Harvey, and Watson (1984).

CONCLUSION

To meet reference site conditions, a stream must manifest certain physically measurable attributes that are reproducible and meet specific criteria. These measurable attributes are relative ratios that are identifiable features in the field. Answers to approaches of management and restoration of streams and riparian communities can be acquired with a better understanding of the geomorphic processes, natural channel stability, and reference reach comparisons discussed in this paper. Dimensionless ratios are successfully being used for both stream restoration and a measure of departure from stable conditions.

REFERENCES

Leopold, L. B. (1994). A View of the River. Cambridge, MA, Harvard University Press.

Montgomery, D.R. and J.M. Buffington (1993). Channel Classification, Prediction of Channel Response and Assessment of Channel Condition. Seattle, WA, University of Washington: 84.

Rosgen, D. L. (1998). The Reference Reach - a Blueprint for Natural Channel Design

Rosgen, D. L. (1994). "A Classification of Natural Rivers," Elsevier Science, Catena Journal 22(No. 3: 169-199): 30.

Schumm, S. A., M. D. Harvey, and C. C. Watson, (1984). Incised Channels: Morphology, Dynamics and Control. Water Resources Publications, Littleton, Colorado.

Southerland, W.B. (2003). Stream geomorphology and classification in glacial-fluvial valleys of the North Cascade Mountain Range in Washington State. Unpublished doctoral dissertation. Washington State University, Pullman.

A MODEL OF STREAMBANK STABILITY INCORPORATING HYDRAULIC EROSION AND THE EFFECTS OF RIPARIAN VEGETATION

Andrew Simon, Research Geologist, USDA-ARS National Sedimentation Laboratory, Oxford, MS, asimon@ars.usda.gov; Natasha Pollen, Research Associate, USDA-ARS National Sedimentation Laboratory, Oxford, MS, npollen@ars.usda.gov

Abstract: Sediment is one of the principle pollutants of surface waters of the United States and sediment eroded from streambank failures has been found to be the single largest contributor to suspended-sediment loads to streams draining unstable systems in the mid-continent. With the recent focus on stream restoration, a quantitative means was needed to predict critical conditions for stability and the effects of riparian vegetation on attaining stable bank geometries. A deterministic bank-stability model was developed in the late 1990's at the USDA-ARS National Sedimentation Laboratory and has undergone substantial enhancements since that time. The original model (Simon et al. 1999) allowed for 5 unique layers, accounted for pore-water pressures on both the saturated and unsaturated parts of the failure plane, and the confining pressure from streamflow. The enhanced Bank Stability and Toe Erosion Model (BSTEM Version 4.1) includes a sub-model to predict bank-toe erosion and undercutting by hydraulic shear. This is based on an excess shear-stress approach that is linked to the geotechnical algorithms. Complex geometries resulting from simulated bank-toe are used as the new input geometry for the geotechnical part of the bank-stability model. The enhanced bank-stability submodel allows the user to select between cantilever and planar failure modes. In addition, the mechanical effects of riparian vegetation are included in Version 4.1, based on the RipRoot model developed by Pollen and Simon (2005). The model has been successfully tested in a diverse range of environments to predict bank failures and to investigate the effects of riparian vegetation on critical conditions for bank stability.

INTRODUCTION

Sediment is one of the principle pollutants of surface waters of the United States and sediment eroded from streambank failures has been found to be the single largest contributor to suspended-sediment loads to streams draining unstable systems in the mid-continent (Simon et al., 2004). With the recent focus on stream restoration, a quantitative means was needed to predict critical conditions for stability and the effects of riparian vegetation on attaining stable bank geometries. Streambank failure can occur by several mechanisms, including cantilever failures of undercut banks, toppling of vertically arranged slabs, rotational slumping, and wedge failures (Thorne et al., 1981). The type of failure reflects the degree of undercutting (if any) by fluvial scour or other mechanisms, and the nature of the bank materials.

In the late 1990's, a deterministic bank-stability model was developed at the USDA-ARS National Sedimentation Laboratory, and has undergone substantial enhancements since that time. The original model (Simon et al., 1999) allowed for 5 unique layers, accounted for pore-water pressures on both the saturated and unsaturated parts of the failure plane, and the confining pressure from streamflow. The enhanced model (Version 4.1) includes a sub-model to predict bank-toe erosion and undercutting by hydraulic shear. This is based on an excess shear-stress approach that is linked to the geotechnical algorithms. Complex geometries resulting from simulated bank-toe are used as the new input geometry for the geotechnical part of the bank-stability model. The enhanced bank-stability sub-model allows the user to select between cantilever and planar failure modes.

The Bank Stability Model combines three limit equilibrium-methods to calculate a Factor of Safety (F_s) for multi-layer streambanks. The methods simulated are horizontal layers (Simon et al., 2000), vertical slices with a tension crack (Morgenstern and Price, 1965) and cantilever failures (Thorne and Tovey, 1981). The model can easily be adapted to incorporate the effects of geotextiles or other bank stabilization measures that affect soil strength. This version of the model assumes hydrostatic conditions below the water table, and a linear interpolation of matric suction above the water table (unless the user's own pore-water pressure data are used).

The Bank Toe Erosion submodel can be used as a tool for making reasonably informed estimates of hydraulic erosion of the bank and bank toe by hydraulic shear stress. The model is primarily intended for use in studies where bank toe erosion threatens bank stability. The effects of erosion protection on the bank and toe can be incorporated to show the effects of erosion control measures. The model estimates boundary shear stress from channel geometry and considers critical shear stress and erodibility of two separate zones with potentially different materials at the

bank and bank toe; the bed elevation is assumed to be fixed. This is because the model assumes that erosion is not transport limited and does not incorporate, in any way, the simulation of sediment transport.

Streambank Stability: The shear strength of saturated soil can be described by the Mohr-Coulomb criterion:

$$\tau_f = c' + (\sigma - \mu_w) \tan \phi' \quad (1)$$

where τ_f = shear stress at failure (kPa), c' =effective cohesion (kPa), σ = normal stress (kPa), μ_w = pore-water pressure (kPa), and ϕ' = effective angle of internal friction (degrees).

In incised stream channels and in arid or semi-arid regions, much of the bank may be above the water table and will usually experience unsaturated conditions. Matric suction (negative pore-water pressure) above the water table has the effect of increasing the apparent cohesion of a soil. Fredlund et al. (1978) defined a functional relationship describing increasing soil strength with increasing matric suction. The rate of increase is defined by the parameter ϕ^b, which is generally between 10º and 20º, with a maximum value of ϕ' under saturated conditions (Fredlund and Rahardjo, 1993). The term ϕ^b varies for all soils, and for a given soil with moisture content (Fredlund and Rahardjo, 1993; Simon et al., 2000). Data on ϕ^b are particularly lacking for alluvial materials. However, once this parameter is known (or assumed) both apparent cohesion (c_a) and effective cohesion (c') can be calculated by measuring matric suction with tensiometers or other devices and by using equation 2. Apparent cohesion incorporates both electro-chemical bonding within the soil matrix and cohesion due to surface tension on the air-water interface of the unsaturated soil:

$$c_a = c' + (\mu_a - \mu_w) \tan \phi^b = c' + \psi \tan \phi^b \quad (2)$$

where c_a = apparent cohesion (kPa), μ_a = pore-air pressure (kPa), and ψ = matric suction (kPa).

Driving forces for streambank instability are controlled by bank height and slope, the unit weight of the soil and the mass of water within it, and the surcharge imposed by any objects on the bank top. The ratio of resisting to driving forces is commonly expressed as the Factor of Safety (F_s), where values greater than one indicate stability and those less than one, instability.

Streambank Stability Algorithms: 1.) Horizontal Layers: The Horizontal Layer method is a further development of the wedge failure type developed by Simon and Curini (1998) and Simon et al. (2000), which in turn is a refinement of the models developed by Osman and Thorne (1988) and Simon et al. (1991). The model is a Limit Equilibrium analysis in which the Mohr-Coulomb failure criterion is used for the saturated portion of the wedge, and the Fredlund et al. (1978) criterion is used for the unsaturated portion. In addition to positive and negative pore-water pressure, the model incorporates layered soils, changes in soil unit weight based on moisture content, and external confining pressure from streamflow. The model divides the bank profile into up to five user definable layers with unique geotechnical properties. The streambank Factor of Safety (F_s) is given by the equation:

$$F_s = \frac{\sum_{i=1}^{I} \left(c_i' L_i + S_i \tan \phi_i^b + \left[W_i \cos \beta - U_i + P_i \cos(\alpha - \beta) \right] \tan \phi_i' \right)}{\sum_{i=1}^{I} \left(W_i \sin \beta - P_i \sin[\alpha - \beta] \right)} \quad (3)$$

where c_i' = effective cohesion of ith layer (kPa), L_i = length of the failure plane incorporated within the ith layer (m), S_i = force produced by matric suction on the unsaturated part of the failure surface (kN/m), W_i = weight of the ith layer (kN), U_i = the hydrostatic-uplift force on the saturated portion of the failure surface (kN/m), P_i = the hydrostatic-confining force due to external water level (kN/m), β = failure-plane angle (degrees from horizontal), α = bank angle (degrees from horizontal), and I = the number of layers.

2.) Vertical Slices: The vertical slice method used only for failures with a tension crack is an adaptation of the method employed in the CONCEPTS model (Langendoen, 2000). As for the Horizontal Layer method, the analysis is a Limit Equilibrium analysis. In addition to the forces incorporated in the Horizontal Layer method, the Vertical Slice method evaluates normal and shear forces active in segments of the failure block. The confining force due to

the water in the channel is modeled by extending the slip surface vertically through the water and applying a horizontal hydrostatic force on the vertical portion of the slip surface. Figure 1 shows an assumed failure block configuration, which is subdivided into slices. The streambank is separated into vertical slices whereby there is an equal number of *J* slices and layers. Each slice is further divided into three subslices to increase the accuracy of the F_s calculations. The calculation of *Fs* is a 4-step iterative process: (1) vertical forces acting on a slice are summed to determine the normal force acting at the base of a slice, $N_{j;}$ (2) horizontal forces acting on a slice are summed to determine the interslice normal force, In *j*; (3) the interslice shear force, $I_{s\,j}$ is computed from $I_{n\,j}$ using the method of Morgenstern and Price (1965); and (4) horizontal forces are summed over all slices to obtain $F_{s.}$ During the first iteration, the interslice normal and shear forces are neglected and the normal force, N_j, equates to:

$$\frac{W_j}{\cos\beta} \tag{4}$$

where W_j is the weight of the j^{th} slice. This first iteration yields the Ordinary F_s. The interslice normal forces are then determined from:

$$I_{n_j} = I_{n_{j-1}} - \left(c_j^{'} L_j + S_j \tan\phi_j^b - U_j \tan\phi_j^{'}\right)\frac{\cos\beta}{F_s} + N_j\left(\sin\beta - \frac{\cos\beta\tan\phi_j^{'}}{F_s}\right) \tag{5}$$

and, in turn, the interslice shear forces are determined from:

$$I_{s_j} = {}^{0.4}\quad I_{n_j}\sin\left(\frac{\pi L_j}{\sum L_j}\right) \tag{6}$$

After the first iteration, for the j^{th} slice out of *J* slices. the normal force, N_j equates to:

$$\frac{W_j + I_{s_{j-1}} - I_{s_j} - \sin\beta\left(\dfrac{c_j^{'} L_j + S_j \tan\phi_j^b - U_j \tan\phi_j^{'}}{F_s}\right)}{\cos\beta + \dfrac{\tan\phi_j^{'}\sin\beta}{F_s}} \tag{7}$$

This completes the second iteration. Often, the calculated interslice normal forces are negative (tension) near the top of the failure block. Since soil is unable to withstand large tensile stresses, a tension crack is assumed to form at the last interslice boundary with tension. Factor of Safety is determined by the balance of forces in horizontal and vertical directions for each subslice and in the horizontal direction for the entire failure block. F_s is given by:

$$F_s = \frac{\cos\beta\sum_{j=1}^{J}\left(c_j^{'} L_j + S_j \tan\phi_j^b + \left[N_j - U_j\right]\tan\phi_j^{'}\right)}{\sin\beta\sum_{j=1}^{J}\left(N_j\right) - P_j} \tag{8}$$

The model then repeatedly iterates through equations 5 to 8 until the value of F_s converges.

3.) Cantilever shear failures: The cantilever shear failure algorithm is a further development of the method employed in the CONCEPTS model (Langendoen, 2000). Put simply, the F_s is the ratio of the shear strength of the soil to the weight of the cantilever. If the bank is submerged then the weight of the layers affected by the water are reduced to their submerged weight. By this method, the vertical hydrostatic confining force is included in the calculation. The F_s is given by:

$$F_s = \frac{\sum_{i=1}^{I}\left(c'_i L_i + S_i \tan\phi_i^b - U_i \tan\phi_i^{'}\right)}{\sum_{i=1}^{I}\left(W_i - P_i\right)} \tag{9}$$

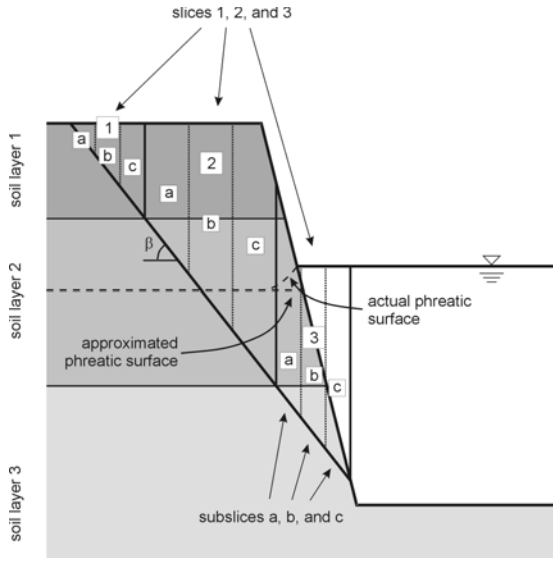


Figure 1 Subdivision of a failure block into slices (Langendoen, 2000).

Vegetation Component: Soil is generally strong in compression, but weak in tension. The fibrous roots of trees and herbaceous species are strong in tension but weak in compression. Root-permeated soil, therefore, makes up a composite material that has enhanced strength (Thorne, 1990). Numerous authors have quantified this enhancement using a mixture of field and laboratory experiments (see Pollen and Simon 2005). Wu et al. (1979) developed a widely used equation that estimates the increase in soil strength (c_r) as a function of root tensile strength, areal density and root distortion during shear:

$$c_r = T_r\,(A_r/A)\,(\cos\theta\tan\phi + \sin\theta) \qquad (10)$$

where c_r = cohesion due to roots (kPa), T_r = tensile strength of roots (kPa), A_r/A = area of shear surface occupied by roots, per unit area (root-area ratio), θ = shear distortion from vertical (degrees), and ϕ = friction angle of soil (degrees). The value of the second bracketed term has been shown to approximate 1.2 under most soil conditions (Wu et al.,1979)..

However, Pollen et al. (2004) and Pollen and Simon (2005) found that perpendicular root models such as those in Equation 10, tend to overestimate root-reinforcement in streambanks, by varying amounts depending on the driving forces acting on the bank, and the number and diameter-distributions of the roots present. To account for this overestimation, Version 4.1 of the model includes an option for the user to reduce the root-reinforcement estimates provided in the BSTEM (taken from Simon and Collison, 2002) by a user-defined percentage (reductions in the range of 20-50% are generally recommended). Future versions of the BSTEM will add a direct link to the RipRoot model developed by Pollen and Simon (2005). The RipRoot model calculates root reinforcement using a progressive breaking algorithm that is driven by the number and species of roots present in the bank, and the driving forces acting on the bank geometry being studied. In previous version of the BSTEM, vegetation was coded to act over the top layer of the streambank regardless of its depth. In Version 4.1, improvements have been made so that the vegetation always acts over the top meter of the bank profile, which fieldwork has shown generally includes the majority of fine roots that contribute to the reinforced root-soil matrix (Simon and Collison, 2002; Pollen et al., 2004).

In addition to stabilizing effects due to root reinforcement, vegetation can affect streambanks by increasing surcharge. Surcharge has both a beneficial and a detrimental effect; it increases the mass acting on a potential failure surface and increases normal stress and, therefore, shear strength due to friction. Whether the net effect is stabilizing or destabilizing depends on the slope of the shear surface and the effective friction angle (ϕ') of the soil, but in most cases it will be destabilizing due to steep shear-surface slopes of streambank failures.

Surcharge due to the mature riparian trees is calculated by multiplying the mass of trees by the stocking density (number of trees per unit area). Tree volume was estimated using the De Vries method (De Vries, 1974):

$$V = \frac{\pi L (d1^2 + d2^2)}{8} \quad (11)$$

where V = volume of wood (m^3), d1 = diameter of trunk at base (m), d2 = diameter of trunk at top (m), and L = length of trunk (m). Volume was converted to mass using an average density of 0.96 g/cm^3 measured for live sycamore, sweetgum and river birch trees in northern Mississippi (Shields et al., 2001). Mass was converted to surcharge by calculating the force per unit area, dividing the tree weight by the root plate area.

Toe Erosion model: Calculation of average boundary shear stress (τ_o): The average boundary shear stress (τ_o) acting on each node of the bank material is calculated using:

$$\tau_o = \gamma_w R S \quad (12)$$

where τ_o = average boundary shear stress (Pa), γ_w = unit weight of water (9.81 kN/m^3), R = local Hydraulic Radius (m) (calculated from the water depth) and S = channel slope (m/m).

The average boundary shear stress exerted by the flow on each node is determined by dividing the flow area at a cross-section into segments that are affected only by the roughness of the bank or bed and then further subdividing to determine the flow area affected by the roughness of each node. The line dividing the bed- and bank- affected segments is assumed to bisect the average bank angle and the average bank toe angle (see Figure 2). The hydraulic radius of the flow on each segment is the area of the segment (A) divided by the wetted perimeter of the segment (P_n). Fluid shear stresses along the dividing lines are neglected when determining the wetted perimeter.

Erodibility and critical shear stress of cohesive materials: A submerged jet-test device has been developed by Hanson (1990) to conduct soil erodibility tests *in situ*. This device has been developed based on knowledge of the hydraulic characteristics of a submerged jet and the characteristics of soil material erodibility. Utilizing this device, Hanson and Simon (2001) developed the following relation between critical shear stress (τ_c) and the erodibility coefficient (k) for cohesive silts, silt-clays and clays:

$$k = 2 \times 10^{-7} \ \tau_c^{-0.5} \quad (13)$$

This relation is very similar to observed trends reported by Arulanandan et al. (1980) in laboratory flume testing of streambed material samples from across the United States. Jet-testing on bank toes suggests that although the exponent is the same, the coefficient is instead 1×10^{-7}.

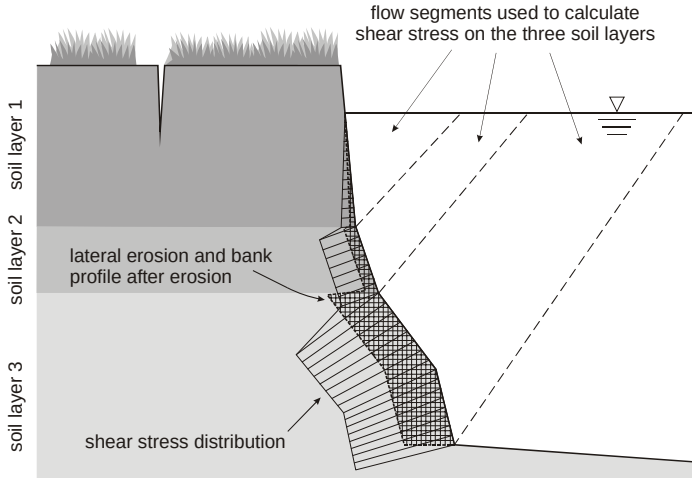


Figure 2 Segmentation of local flow areas and hydraulic radii.

Erosion rates and amounts: An average erosion rate (in m/s) is computed for each node by utilizing an excess-shear stress approach (Partheniades, 1965). This rate is then integrated with respect to time to yield an average erosion distance (in m). This method is similar to that employed in the CONCEPTS model (Langendoen, 2000) except that erosion is assumed to occur normal to the local bank angle, not horizontally:

$$E = k\,\Delta t\,(\tau_0 - \tau_c) \qquad (14)$$

where E = erosion distance (m), k = erodibility coefficient (m^3/N s), Δt = time step (s), τ_0 = average boundary shear stress (Pa), and τ_c = critical shear stress (Pa).

Erodibility and critical shear stress of non-cohesive materials: Resistance of non-cohesive materials is a function of bed roughness and particle size (weight), and is expressed in terms of a dimensionless critical shear stress (Shields 1936):

$$\tau^* = \tau_o / (\rho_s - \rho_w)\, g\, D \qquad (15)$$

where τ^* = critical dimensionless shear stress; ρ_s = sediment density (kg/m^3); ρ_w = water density (kg/m^3); g = gravitational acceleration (m/s^2); and D = characteristic particle diameter (m). Average boundary shear stress (τ_o) is the drag exerted by the flow on the bed and is defined as:

$$\tau_o = \gamma_w\, R\, S_b \qquad (16)$$

where γ_w = unit weight of water (N/m^3); and R = hydraulic radius (area/wetted perimeter)(m). Critical shear stress (τ_c) in dimensional form can be obtained by invoking the Shields criterion and, for hydrodynamically rough beds, utilizing a value of 0.06 for τ^*.

$$\tau_c = 0.06\,(\rho_s - \rho_w)\, g\, D \qquad (17)$$

Thus, the shear stress required to entrain a grain of diameter D can be estimated. Other commonly used values of τ^* are 0.03 and 0.047 (Vanoni and Brookes, 1957).

MODELING EXAMPLE AND SUMMARY

The example analysis provided in Figure 3 shows the BSTEM model run with simulated flow and pore-water pressure data for a site along the Missouri River, Montana (Collison, et al., 2002). In this case, bank-toe erosion (Figure 3a) and bank stability (Figure 3b) were modeled iteratively for a period of 70 days. The effects of decreasing shear strength and Factor of Safety due to loss of matric suction are apparent for the no bank erosion case. Modeling runs were repeated using the bank-toe erosion model. The difference in relative stability is clearly shown by contrasting the two lines plotted in Figure 3b. Simulations without the toe-erosion model would, therefore, have provided overly conservative estimates of bank stability.

The combined bank-stability and toe-erosion models have been used successfully in a variety of locations and alluvial environments in the United States to simulate streambank stability under different flow and pore-water pressure conditions. It has been widely distributed at short courses conducted by the authors at national technical meetings, regional practitioner workshops and for a geomorphology class at the USGS National Training Center. The revised model (Version 4.1) is available on the Web: http://www.ars.usda.gov?Research/docs.htm?docid=5044

Acknowledgement: Eddy Langendoen, USDA-ARS National Sedimentation Laboratory provided critical programming expertise in developing the cantilever failure option and in debugging.

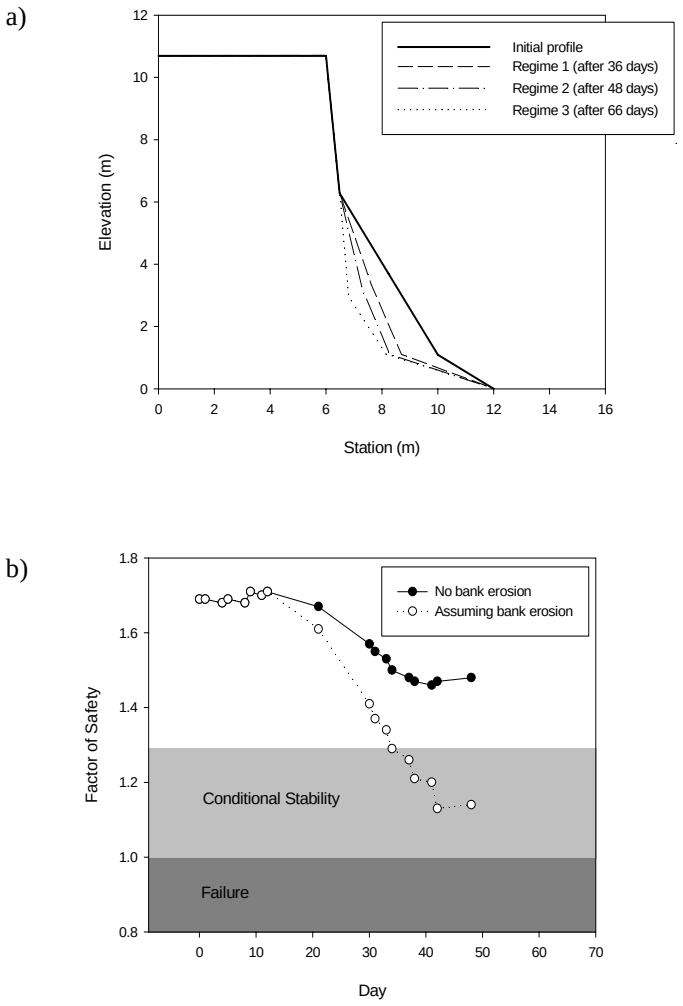


Figure 3 Impact of simulated flow regimes on bank erosion and resulting bank stability at River Mile 1624 (Tveit Johnson site) on the Missouri River, MT.

REFERENCES

Arulanandan K, Gillogley E, Tully R. (1980). "Development of a quantitative method to predict critical shear stress and rate of erosion of natural undisturbed cohesive soils." Technical Report GL-80-5. US Army Engineers Waterways Experiment Station: Vicksburg.

Collison, A.J.C., Layzell, T. and Simon, A. (2002). "Impact of Flow Releases on Bank Stability of the Missouri River, MT", Proceedings of ASCE-EWRI conference, Roanoke, Virginia, May 2002.

De Vries D.G. (1974). "Multi-stage line intersect sampling," Forestry Science 20(2): 129-133

Fredlund D.G, Morgenstern N.R, Widger RA. (1978). "The shear strength of unsaturated soils," Canadian Geotechnical Journal 15: 313-321.

Fredlund D.G, Rahardjo H. (1993). Soil Mechanics of Unsaturated Soils, John Wiley & Sons, Inc., New York.

Hanson G.J. (1990). "Surface erodibility of earthen channels at high stresses. Part II - Development of an in situ testing device," Transactions of the American Society of Agricultural Engineers 33(1): 132-137.

Hanson G.J, Simon A. (2001). "Erodibility of cohesive streambeds in the loess area of the midwestern USA". Hydrological Processes 15: 23-38

Langendoen E.J. (2000). "CONCEPTS - CONservation Channel Evolution and Pollutant Transport System", Research Report 16, US Department of Agriculture Agricultural Research Service National Sedimentation Laboratory, Oxford, MS.

Morgenstern N.R, Price, V.R. (1965). "The analysis of the stability of general slip surfaces." Geotechnique 15: 79-93.

Osman A.M, Thorne C.R. (1988). "Riverbank stability analysis. I: Theory", Journal of Hydraulic Engineering 114(2): 134-150.

Partheniades E. (1965). "Erosion and deposition of cohesive soils", Journal of Hydraulic Engineering 91(1): 105-139.

Pollen, N. and Simon, A. (2005). "Estimating the mechanical effects of riparian vegetation on stream bank stability using a fiber bundle model", Water Resour. Res., 41,No. 7, W0702510.1029/2004WR003801.

Pollen, N., Simon, A., and A. Collison (2004). "Advances in Assessing the Mechanical and Hydrologic Effects of Riparian Vegetation on Streambank Stability". In: S. Bennett and A. Simon, eds. Riparian Vegetation and Fluvial Geomorphology, Water Science and Applications 8, AGU, 125-139.

Shields, A.. (1936). "Anwendung der Aechlichkeitsmechanik und der Turbulenz Forschung auf die Geschiebebewegung", Mitteilungen der Pruessischen Versuchsanstalt fuer Wasserbau and Schiffbau, Berlin.

Shields Jr. F.D, Morin N, Cooper C.M. (2001). "Design of large woody debris structures for channel rehabilitation", Proceedings of the 7th Federal Interagency Sedimentation Conference, Reno, Nevada, 1: II-42 to II-49.

Simon A, Collison A.J.C.(2002). "Quantifying the mechanical and hydrologic effects of riparian vegetation on streambank stability", Earth Surface Processes and Landforms 27(5): 527-546.

Simon, A., Langendoen, E., Bingner, R., Wells, R., Yuan, Y., and Alonso, C. (2004). "Suspended-Sediment Transport and Bed-Material Characteristics of Shades Creek, Alabama and Ecoregion 67: Developing Water-Quality Criteria for Suspended and Bed-Material Sediment", U.S Department of Agriculture-Agricultural Research Service, National Sedimentation Laboratory Technical Report 43.

Simon A, Curini A. (1998). "Pore pressure and bank stability: The influence of matric suction", In Abt S.R, Young-Pezeshk J, Watson C.C (eds.), Water Resources Engineering '98, ASCE: Reston; 358-363.

Simon A, Curini A, Darby S.E, Langendoen E.J. (2000). "Bank and near-bank processes in an incised channel", Geomorphology 35: 183-217.

Simon, A., Curini, A., Darby, S., and Langendoen, E. (1999). "Stream-bank Mechanics and the Role of Bank and Near-Bank Processes in Incised Channels". In*:* Darby, S. and Simon, A., eds. Incised River Channels. John Wiley and Sons, New York. 123-152.

Simon A, Wolfe W.J, Molinas A. (1991). "Mass wasting algorithms in an alluvial channel model", Proceedings of the 5th Federal Interagency Sedimentation Conference, Las Vegas, Nevada, 2: 8-22 to 8-29.

Thorne C.R. (1990). "Effects of vegetation on riverbank erosion and stability", In Thornes JB (ed.), Vegetation and erosion: Processes and Environments, John Wiley & Sons: Chichester; 125-144.

Thorne C.R, Tovey N.K. (1981). Stability of composite river banks. Earth Surface Processes and Landforms 6: 469-484

Thorne C.R., Murphey J.B., Little W.C. (1981). "Bank Stability and Bank Material Properties in the Bluff Line Streams of North-west Mississippi", Appendix D, Report to the Corps of Engineers, Vicksburg District under Section 32 Program, Work Unit 7, USDA-ARS Sedimentation Laboratory, Oxford, Mississippi.

Vanoni, V. A. and Brooks, N. H. (1957). "Laboratory Studies of the Roughness and Suspended Load of Alluvial Streams", Report No. E-68, Sedimentation Laboratory, California Institute of Technology, Pasadena, California.

Wu T.H, McKinnell W.P, Swanston DN. (1979). "Strength of tree roots and landslides on Prince of Wales Island, Alaska", Canadian Geotechnical Journal 16(1): 19-33.

USE OF WET SIEVING TO IMPROVE THE ACCURACY OF SEDIMENT AND SEDIMENT-ASSOCIATED CONSTITUENT CONCENTRATIONS IN WHOLE-WATER SAMPLES

William Selbig, Hydrologist, U.S. Geological Survey, Madison, WI, wrselbig@usgs.gov; Roger Bannerman, Environmental Specialist, Wisconsin Department of Natural Resources, Madison, WI, banner@dnr.state.wi.us; George Bowman, Supervisory Chemist, Wisconsin State Laboratory of Hygiene, Madison, WI, *gtb@mail.slh.wisc.edu*

Abstract: Sand-size particles (greater than 63 microns) in urban runoff have the potential to produce substantial bias and/or poor precision both during sample splitting and laboratory analysis. New techniques were evaluated in an effort to overcome some of the limitations associated with sample splitting and analyzing whole-water samples containing sand-size particles. Wet sieving physically separates sand-size particles from a whole-water sample. Once separated, both the sieved solids and the remaining aqueous samples were analyzed for total recoverable metals using a modified version of EPA method 200.7 which digests the entire sample, rather than an aliquot, of the sample container. Using a total recoverable acid digestion on the entire contents of the sieved solid and aqueous samples improved the accuracy of sediment-associated constituent concentration. However, heterogeneities associated with coarser particle sizes may contribute to increased variability in concentration results.

INTRODUCTION

There is a growing body of evidence that demonstrates that using both churn splitting and aliquoting can introduce significant bias and/or poor precision into the sediment and sediment-associated constituent concentration results (Horowitz and others, 1997; Capel and Larson, 1996; Gray and others, 2000). Much of the variability can be attributed to the presence of sand-size particles found in many stormwater runoff samples. Whole-water samples collected from storm sewers frequently contain suspended sediment concentrations (SSC) exceeding 1,000 mg/L with a large percentage of sediment particles larger than 250 microns (Waschbusch, 2003; Sansalone and Buchberger, 1997; Furumai and others, 2002). Modifications to these sample splitting and laboratory analysis methods must be evaluated to ensure the future quality of stormwater contaminant concentration data.

Wet sieving the whole-water sample is one modification that could remove the bias and poor precision from both the sample splitting and laboratory analysis methods. To ensure the success of this modification, the proper sieve size must be selected. Two previous studies have observed two different particle sizes critical to reducing the errors associated with processing the whole-water sample with a churn splitter. Horowitz and others (1997) found unacceptable bias and precision when using churn splitters to process whole-water samples with suspended-sediment concentrations greater than 1,000 mg/L or particles greater than 250 microns. Other studies concluded that churn splitters are unable to adequately split particles greater than 63 microns since the stirring action is unable to overcome the tendency of sand grains to settle (Meade, 1985, cited in Capel and Larson, 1996). Other sample-splitting methods such as cone-splitters may produce less bias but demonstrate poor precision when dealing with sand-size particles (Horowitz and others, 1997). Based on these studies, selection of a 63-micron sieve should improve the quality of the splitting process, but wet sieving with a 63 micron sieve would add considerable time to the processing of most whole-water samples. The first objective of this study was to further evaluate the sieve size needed to reduce the bias and improve precision when splitting whole-water samples for SSC and total recoverable metal analysis.

Sub-sampling at the analytical laboratory is another potential source of error when determining sediment and sediment-associated constituent concentrations in samples with sand-size particles. Gray and others (2000) recognized that one of the more commonly used methods to quantify concentrations of solid-phase material in natural waters, total suspended solids (TSS), was “fundamentally unreliable”, especially when the majority of the material is in the sand-size fraction. This method measures the dry weight of sediment from a known volume of a subsample of the original. A better representation of solid-phase material in natural waters, regardless of the amount or percent of sand-sized material in the sample, measures the dry weight of all the sediment without subsampling (Gray and others, 2000).

One of the more commonly used methods to determine total recoverable metals concentrations in aqueous samples also recommends using a subsample of the water in the sample bottle submitted to the laboratory. Since most of the total recoverable metals in a stormwater sample are associated with the particulate matter (Bannerman and others, 1996), the sub-sampling procedure might under- or over-estimate the total recoverable metals concentration in the sample. As with the sediment analysis, the potential errors in the total recoverable metals analysis might be reduced by processing all the water in the sample bottle. A second objective of this study was to compare the results of a total recoverable analysis on a subsample from the sample bottle with a similar analysis on all the water in the bottle. The magnitude of the sub-sampling error is probed using two metals, zinc and copper, since they are two metals of concern in urban runoff (Bannerman and others, 1983; Bannerman and others, 1996)

MATERIALS AND METHODS

Experimental Design: The approach to both selecting the best sieve size for splitting whole-water samples and the best laboratory method for total recoverable metals analysis is based on comparing test results from water samples with known SSC and total recoverable metals concentrations when various modifications to these procedures are used. Results of the tests that best match the known values would provide guidance on the optimum sample splitting and laboratory analysis procedures.

Preparation of the Water Samples for Evaluation of Sieve Sizes: Reference samples with known sediment concentrations and particle sizes were created in the laboratory using sediment captured *in situ* by a storm sewer bedload sampler during a rainfall event. After the sediment was collected, it was dried and sieved into the following particle-size fractions: >2,000; 500–1,000; 250–500; 125–250; 63–125; and <63 microns.

Size-separated dry bedload material was added to deionized water in a tared, 14-liter, Teflon-lined churn splitter to create simulated urban runoff samples with known suspended sediment concentrations (figure 1). Two suspended sediment concentrations were made for each of three ranges of particle sizes (table 1). These samples were then well mixed for a period of approximately 1 minute using protocols developed by the USGS when processing whole-water samples in a churn splitter (USGS, 1999). Five aliquots of approximately 250 mL were transferred to laboratory bottles, placed on ice, and delivered to the State Laboratory of Hygiene (WSLH) for SSC analysis. Analysis results from these samples were compared to the known initial concentrations. The particle sizes that show the least amount of error after being processed in the churn splitter should indicate the sieve size to use on whole-water samples with sand-size particles.

Table 1 Prepared Suspended Sediment Concentrations for Selected Particle Size Ranges.

Particle Size Range, microns	Prepared Suspended Sediment Concentrations, mg/L		
63 to 125	1,000	--	5,000
250 to 500	--	2,000	5,000
500 to 1,000	--	2,000	2,000

Evaluation of Total Recoverable Metal Analysis Methods: Two analytical methods are used to determine total recoverable metals concentrations in aqueous samples. The whole-bottle analysis method uses an acid digestion on the entire contents of a 250-mL sample bottle submitted to the laboratory. The standard EPA method, on the other hand, performs the acid digestion only on a 25-mL aliquot taken from the sample bottle. When taking an aliquot from a sample containing sand-size particles, the particles that fall out of suspension quickly may be omitted from the sample analyzed. Tests comparing the results of these two methods were performed on a wide range of particle sizes and suspended sediment concentrations (table 2). Prepared sediment suspensions were split with a churn splitter and aliquots submitted to the laboratory.

The bedload material used to prepare the reference samples for these tests was processed in two different ways. Concentrations of zinc and copper were determined for both the dry bedload material and the sediments sieved from the sediment-water mixture in the churn splitter. The dry bedload material was used as a target because it precludes any bias or precision problems associated with the churn splitter. However, the concentration units from analysis on the dry material (mg/kg) are not directly comparable to the concentration units used for the water samples (mg/L).

Since the sieved sediment should have dry concentrations (mg/kg) of zinc and copper similar to the ones observed for the dry bedload material, the volume of the prepared sediment suspension was used to convert the dry weight concentrations to the concentrations in water.

Table 2 SSC Concentrations Prepared for Total Recoverable Metals Tests.

Particle Size Range, microns	Prepared Suspended Sediment Concentrations, mg/L		
63 to 125	2,000	5,000	--
250 to 500	--	5,000	10,000
500 to 1,000	--	5,000	10,000

A total of four aliquots were removed from the churn splitter for each particle-size range and corresponding suspended sediment concentration (figure 1): three aliquots of approximately 250 mL for the whole-bottle analysis and one 250-mL aliquot for the standard EPA analysis. The aliquots were then preserved with nitric acid, placed on ice, and delivered to the WSLH within 24 hours for analysis. The whole-bottle and standard EPA method samples were then analyzed for total recoverable zinc and copper (figure 2).

Wet Sieving Sediment in a Churn Splitter: The remaining sediment-water mixture was weighed using a large-capacity balance, then passed through a single 63-, 250-, or 500-micron nylon sieve to capture the remaining solid material for a specific particle-size fraction (figure 1). All material captured on the sieve was transferred into a 250-mL polypropylene container using deionized water. The container was then placed on ice and delivered to the WSLH within 24 hours. A total recoverable zinc and copper analysis was performed on the dried sieved sediment. To determine if any contaminants leached from the sediment particles in the churn splitter into the deionized water during the mixing process, a sample of the water passing through each sieve was submitted to the WSLH for total recoverable copper and zinc.

Dry Bedload Material Analysis: In addition to the aliquots from the splitter and sieved solid samples, a small amount of dry bedload material was sent to the WSLH for zinc and copper total recoverable metals analysis (figure 1). Deionized water was not added to the dry bedload sample.

Analytical Methods for Total Recoverable Metals: Figure 2 diagrams the procedures and methods used by the Wisconsin State Laboratory of Hygiene when analyzing the dry bedload material, sieved sediment, and aqueous samples from the splitter.

Split Water Samples: Historically, the USEPA has recommended the "total recoverable method" of sample preparation as an indication of the bioavailable pool of trace elements in sediments (U.S. Environmental Protection Agency, 1986a). We followed this approach as specified in EPA method 200.7 for liquids (U.S. Environmental Protection Agency, 2001) in the first of two approaches evaluated. The second method also used EPA method 200.7, but instead of sub-sampling the original sample, the entire contents of the 250-mL sample bottle (whole sample bottle method) were digested using a total recoverable acid digestion. Analyses for each method were performed in triplicate (figure 2).

The digestion protocol performed on all sediment suspensions was as follows: First, the samples were weighed to determine the volume. Nitric and hydrochloric acid were added to the entire contents of each vial to bring the concentration to 2.5 and 5 percent, respectively. Each vial was then heated in an Environmental Express Hotblock® at 95°C using EPA method SW846 3005A (U.S Environmental Protection Agency, 1993), and subsequently analyzed for zinc and copper by inductively coupled plasma emission spectroscopy (ICP) according to EPA method 200.7 (U.S. Environmental Protection Agency, 2001). Resulting concentrations were reported in mg/L.

Dry Bedload Material and Sieved Sediment: The sieved solid fraction was quantitatively transferred to an acid-washed, tarred porcelain evaporating dish with the aid of deionized water. The dish was dried at 103–105°C overnight, desiccated and brought to a constant weight. The dried bedload material did not go through this process since it was delivered to the laboratory as a dried solid. The dried solids were then transferred to a clean, dry 250 mL polypropylene bottle. A 0.25- to 2.0-gram portion of the dried solid was weighed directly into a 125-mL digestion vial and 10 mL of deionized water was added to re-hydrate the sample. Although a 0.5-gram sample is typically

used for this type of solids analysis, we used a 2.0-gram subsample where sample mass permitted. Using a 2-gram sample should improve reproducibility, as errors associated with heterogeneities are reduced when sub-sampling sediments with sand-size particles. The digestate protocols used for the aqueous samples were duplicated for the sieved solid samples. Resulting concentrations were reported in mg/kg.

Figure 1 Diagram of processes to prepare dry bedload, sieved sediment, and water samples for laboratory analyses.

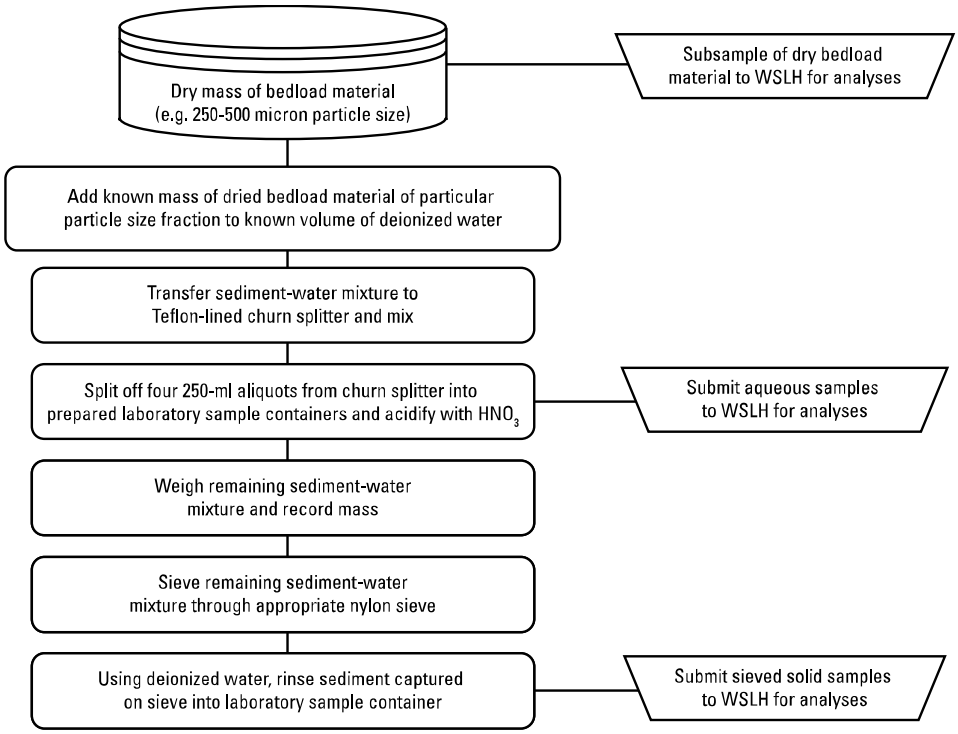
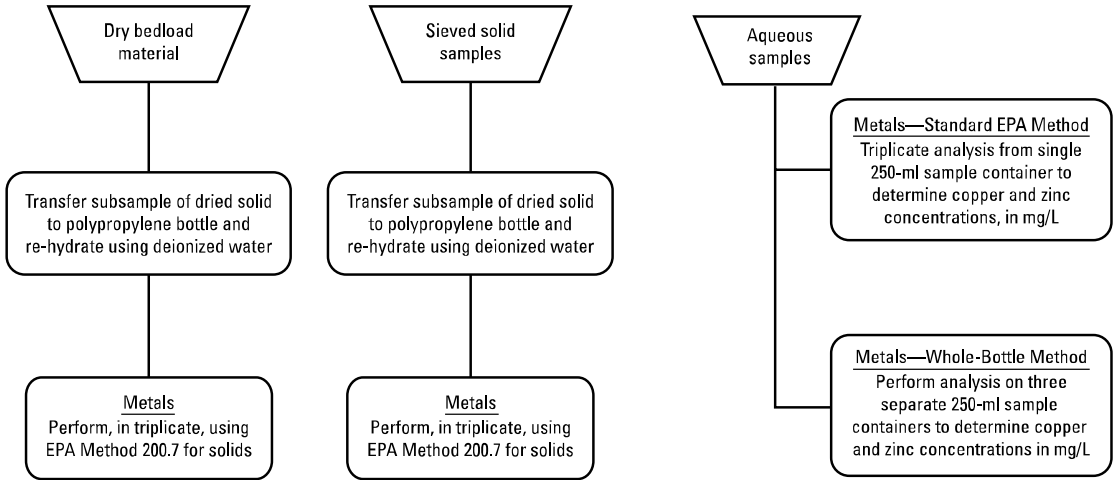


Figure 2 Diagram of analytical techniques used to determine total recoverable zinc and copper concentrations on dry bedload, sieved sediment, and water samples from the splitter.



RESULTS

Selection of Sieve Size for Processing Whole-Water Samples: Above a particle size of about 250 microns, a significant positive bias in the suspended sediment concentration (table 3) is observed in the churn split samples. For particles over 250 microns in size, the average percent difference between the target suspended sediment concentration and the split water samples ranges from 26 to 85 percent. In all the particle size ranges the bias is larger for the higher suspended sediment concentrations. A dramatic decrease in the degree of positive bias occurs for the samples in the particle size range of 63 to 125 microns. In this lower range, average percent differences ranged from only 1 to 6 percent. It is apparent that sieving a whole-water sample with a 125-micron sieve before using the churn splitter will greatly reduce the positive bias in suspended sediment concentrations for samples with sand size particles.

Sub-sampling precision was also degraded in water samples with larger particles. Coefficient of variation (COV) values increased from 0.01 for the 63 to 125 micron particles to 0.25 for the 500 to 1,000 micron particles. Removing particles greater than 125 microns from a whole-water sample before it is split will improve precision in the suspended sediment concentrations.

Table 3 Impact of Churn Splitter on SSC concentrations.

Particle Size (microns)	Replicate Number	SSC Target = 1,000 mg/L Result (mg/L)	SSC Target = 1,000 mg/L Percent Difference	SSC Target = 2,000 mg/L Result (mg/L)	SSC Target = 2,000 mg/L Percent Difference	SSC Target = 5,000 mg/L Result (mg/L)	SSC Target = 5,000 mg/L Percent Difference
	1	1,000	0%	--		5,350	7%
	2	1,020	2%	--		5,240	5%
63 - 125	3	1,020	2%	--		5,300	6%
	4	1,010	1%	--		5,330	7%
	5	1,010	1%	--		5,190	4%
Mean		**1,012**	**1%**			**5,282**	**6%**
Std. Dev.		**8**				**66**	
COV		**0.01**				**0.01**	
	1	--		3,340	67%	6,470	29%
	2	--		3,020	51%	8,140	63%
250 - 500	3	--		2,800	40%	8,600	72%
	4	--		2,540	27%	7,500	50%
	5	--		2,150	8%	7,760	55%
Mean				**2,770**	**39%**	**7,694**	**54%**
Std. Dev.				**454**		**800**	
COV				**0.16**		**0.10**	
	1	--		3,250	63%	6,600	32%
	2	--		2,700	35%	12,300	146%
500 – 1,000	3	--		1,850	-8%	11,000	120%
	4	--		2,450	23%	8,540	71%
	5	--		2,350	18%	7,740	55%
Mean				**2,520**	**26%**	**9,236**	**85%**
Std. Dev.				**512**		**2,354**	
COV				**0.20**		**0.25**	

Both the precision and bias errors observed for the larger particle sizes indicate the churn splitter is not able to keep all the large particles in suspension. Since the churn paddle is unable to distribute sand grains evenly, a gradient in concentration occurs inside the churn splitter where sand is more concentrated near the bottom (where the spigot is)

than the top (Mead, 1985, cited in Capel and Larson, 1996). This accumulation of larger particles near the bottom of the splitter would also be highly variable depending on the particle size, suspended sediment concentration, density of the particles, and the rate of mixing in the splitter. These errors caused by the churn splitter will obviously also impact measurements of particle-associated contaminant levels, both on a volumetric and mass basis.

Wet sieving a whole-water sample before splitting will require more effort to process a sample and more careful tracking of the volumes in the splitter. The mass of the sediment on the sieve will have to be added to the mass of sediment determined by the SSC analysis on the split samples. A final suspended sediment concentration will require knowledge of the volume of water in the splitter.

SELECTION OF METHOD FOR TOTAL RECOVERABLE METALS ANALYSIS

Concentrations of copper and zinc determined in the sieved sediment were reasonably close to those measured in the dry bedload material for each particle-size fraction (table 4). Therefore, we can assume the sieved solid concentrations, when converted to mg/L, are reasonable target concentrations for each method performed on the aqueous samples. Assuming 1 kilogram of water is equal to 1 liter of water, the following equation can be used to convert the concentration of copper and zinc as a solid, in mg/kg, to a concentration as a liquid, in mg/L:

$$C_l = \frac{\left(S_m / 1000\right) * C_s}{V} \tag{1}$$

where C_l = concentration of sieved solid represented in mg/L; S_m = mass of sieved solids after drying, in grams; C_s = concentration of sieved solid, in mg/kg; and V = volume of water sieved, in liters.

Concentrations of copper and zinc determined in the two methods evaluated are compared to the sieved sediment in table 5. In most cases, concentrations determined using the whole-bottle method came close to the target values established from the sieved sediment concentration. However, the standard EPA method 200.7 consistently produced lower copper and zinc concentrations than the sieved solid for each particle-size fraction. Though we cannot definitively determine the reason for the bias, it is likely that sedimentation or fractionation of particles within the bottle is the primary cause. Therefore, in aliquoting the bottle, the likelihood of unrepresentative sampling is great. Depending on where the aliquot is acquired from a sample container, the resulting concentrations could either be positively or negatively biased. For this reason, the whole-bottle version of EPA method 200.7 is recommended as the most appropriate technique for measuring metals concentration in an unfiltered water sample.

The observed bias for the zinc and copper concentrations was less than the large positive bias observed for the suspended sediment concentrations. This may partly be explained by the effect of increasing metal concentrations with decreasing particle sizes (table 5) (Bannerman and others, 1983). Smaller particles in each of the particle-size ranges might be transferred (aliquoted) with less error than the larger particles. Increasing the number of larger particles in the water sample has a significant impact on the suspended sediment concentrations, but a similar effect on metal levels is not observed because these large particles tend to have lower metals concentrations.

Table 5 also describes how a single value from the triplicate analysis can bias the average concentration away from the sieved solid target. The italicized value for zinc in the 500–1000 micron particle-size fraction can likely be attributed to heterogeneities in larger sand-sized particles. Due to laboratory error, only two concentrations were recorded for copper in the 63–125 micron particle-size fraction. Addition of a third value would have provided useful information to estimate the true value. While concentrations of copper and zinc appear somewhat more variable for the whole-bottle analysis compared to the standard EPA analysis, the improved accuracy of the whole-bottle analysis more than compensates for the difference in the precision.

Table 4 Comparison of dry bedload and sieved solid copper and zinc concentrations

Particle Size Range (microns)	SSC Concentration (mg/L)	Copper			Zinc		
		Raw Bedload (mg/kg)	Sieved Solid (mg/kg)	Absolute RPD (%)	Raw Bedload (mg/kg)	Sieved Solid (mg/kg)	Absolute RPD (%)
500-1,000	5,000	8.1	6.3	25%	20.2	30.2	40%
	10,000		6.0	30%		29.9	36%
250-500	5,000	4.3	3.7	14%	17.4	19.7	13%
	10,000		3.6	17%		17.9	3%
63-125	2,000	41.2	37.0	11%	151.0	138.3	9%
	5,000		41.7	1%		156.7	4%

Table 5 Triplicate concentration values for two sediment-associated metals using the whole-bottle and standard EPA methods for aqueous samples. All concentrations are expressed in mg/L.

Particle Size Fraction (microns)	SSC Concentration	Copper			Zinc		
		EPA 200.7 Method		Sieved Solid	EPA 200.7 Method		Sieved Solid
		Aliquot	Whole Bottle		Aliquot	Whole Bottle	
63 - 125	2,000	53	70	68	218	272	271
		49	69	74	204	291	252
		53	60	71	225	291	269
	Mean	**52**	**67**	**71**	**216**	**285**	**264**
	RPD	**-37%**	**-6%**		**-22%**	**7%**	
	5,000	111	*360*	190	606	698	764
		114	194	209	553	725	740
		72		202	508		754
	Mean	**99**	**277**	**200**	**556**	**712**	**753**
	RPD	**-102%**	**28%**		**-35%**	**-6%**	
250 - 500	5,000	12	23	19	45	123	111
		11	24	16	33	*88*	90
		11	26	18	35	133	78
	Mean	**11**	**24**	**18**	**38**	**115**	**93**
	RPD	**-56%**	**27%**		**-147%**	**19%**	
	10,000	11	38	35	52	201	159
		10	*62*	34	57	233	177
		11	40	32	52	191	166
	Mean	**11**	**47**	**34**	**54**	**208**	**167**
	RPD	**-216%**	**28%**		**-212%**	**20%**	
500 - 1,000	5,000	12	34	29	47	135	148
		11		29	47		175
		13	31	29	57	126	100
	Mean	**12**	**33**	**29**	**50**	**131**	**141**
	RPD	**-142%**	**11%**		**-180%**	**-8%**	
	10,000	16	56	59	55	*141*	271
		16	71	53	57	246	247
		15	77	50	58	299	280
	Mean	**16**	**68**	**54**	**57**	**229**	**266**
	RPD	**-245%**	**21%**		**-369%**	**-16%**	

CONCLUSION

Limitations associated with churn and cone splitters can be overcome by wet sieving sand-sized particles from the aqueous portion of a whole-water sample. This physical separation increases the efficiency of churn splitters and improves the overall accuracy of concentration data. Once sand-sized particles are removed from the sediment-water mixture, they can be analyzed independently using the same analytical methods as the parent aqueous sample. The process of transferring sieved solids from the nylon sieve to the sample container had negligible effects on metalsconcentrations. Analysis of the deionized water used after transferring solids indicated no leaching of metals from the solid particles into the residual water.

Digesting the entire contents of a sample container reduced bias normally associated with taking an aliquot from a sample containing sand-sized particles. Of the two analytical methods used to determine metals concentrations in an aqueous sample, those using an acid digestion on the entire contents of the sample container (the whole-bottle version of EPA method 200.7) produced concentrations that were closer to the sieved sediment concentration.

The presence of outliers in the concentration data using the whole-bottle version of EPA method 200.7 suggests difficulties in maintaining a high level of precision. The standard EPA method 200.7 produced results with high precision but lacked accuracy. The difference in precision is a function of subsampling an original sample. By taking an aliquot near the top of the sample container, particles that fall out of suspension quickly will be omitted from the sample analyzed. Similarly, an aliquot taken from the bottom of a sample container might acquire a sediment-enriched sub-sample. Therefore, in aliquoting a bottle, the likelihood of unrepresentative sampling is great. When compared to the corresponding sieved solid target concentrations, concentrations of copper and zinc using the whole-bottle version of EPA method 200.7 displayed greater accuracy over the standard EPA method 200.7.

REFERENCES

Bannerman, R.T.,Baun, K., Bohn, M., Hughes, P.E., and Graczk, D.A., 1983, Evaluation of Urban Nonpoint Source Pollution Management in Milwaukee County, Wi, Vol.1, EPA, Water Planning Division, PB84-114164.

Bannerman, R.B., Legg, A.D., and Greb, S.R., 1996, Quality of Wisconsin Stormwater, 1989-94, U.S. Geological Survey Open File Report 96–458, 26 p.

Capel, P.D. and Larson, S.J., 1996, Evaluation of selected information on splitting devices for water samples: U.S. Geological Survey Water-Resources Investigation Report 95–4141, 103 p.

Furumai, H., Balmer, H., Boller, M., 2000, Dynamic Behavior of Suspended Pollutants and Particle Size distribution in Highway Runoff, Water Science and Technology, v. 46, no. 11–12, p. 413–418.

Gray, J.R., Glysson, G.D.,Torcios, L.M., Schwartz, G., 2000, Comparability of Suspended-Sediment Concentration and Total Suspended Solids Data, U.S. Geological Survey Water Resources Investigation Report 00–4191, 14 p.

Horowitz, A. J., Hayes, T.S., Gray, J.R., Capel, P.D., 1997, Selected Laboratory Tests of the Whole-Water Sample Splitting Capabilities of the 14-Liter Churn and the Teflon Cone Splitters, U.S. Geological Survey Office of Water Quality Technical Memorandum No. 97.06, 28 p.

Mead, R.H., 1985, Suspended Sediment in the Amazon River and its Tributaries in Brazil during 1982-84: U.S. Geological Survey Open-File Report 85–492, 39 p.

Sansalone, J.J., Buchberger, S.G., 1997, Characterization of Solid and Metal Element Distribution in Urban Highway Stormwater, Water Science and Technology, v. 36, no. 8-9, p. 155–160.

Sansalone, J.J., Buchberger, S.G., 1997, “Partitioning and First Flush of Metals in Urban Roadway Storm Water,” Journal of Environmental Engineering, v. 123, no. 2, p. 134–143.

U.S. Environmental Protection Agency, 1986a, Quality Criteria for Water 1986: U.S. Environmental Protection Agency, EPA 440/5-86-001, variously paginated.

U.S. Environmental Protection Agency, 2001,Method 200.7: Trace Elements in Water, Solids, and Biosolids by Inductively Coupled Plasma-Atomic Emission Spectrometry, rev. 5, EPA-821-R-01-010, 57 p.

U.S. Environmental Protection Agency, 1993, Test Methods for Evaluating Solid Wastes, Physical/Chemical Methods, SW-846 Method 3005A, 3rd ed., Office of Solid Waste and Emergency Response, Washington D.C.

U.S. Geological Survey, 1999, National Field Manual for Collection of Water-Quality Data: Processing of Water Samples, Techniques of Water-Resource Investigation, 09–A5, 149 p.

Waschbusch, R.J., 2003, Data and Methods of a 1999-2003 Street Sweeping Study on an Urban Freeway in Milwaukee County, Wisconsin, U.S. Geological Survey Open File Report 03–93, 41 p.

Designing Log Erosion Barriers for Maximum Effectiveness: The Contour-Log-Basin Approach.

Larry J. Schmidt, Retired (Formerly with USDA Forest Service, Stream Systems Technology Center), 2904 La Cresta Circle, Minden, NV 89423, 775-267-6955, lpschmidt@gmail.com

Abstract: Controlling runoff from post wildfire storms is the key to reducing damaging erosion, sedimentation and flooding. In the interior West the use of contour trenches has proven effective if carefully designed and applied promptly. These structures detain runoff from high intensity short duration thunder storms providing for infiltration and delay in runoff. These are typically short term measures designed to be effective only for a few years while vegetation recovery occurs. Contour-Log-Basins (CLB) originated as a treatment that used essential principles for design of contour trenches developed by Reid Bailey and A.R. Croft at Intermountain Forest and Range Experiment Station in Utah. The principles governing the design of contour trenches are described in a paper by E.L. Noble presented at the 1963 Interagency Sediment Conference. CLB, by contrast, are designed to be constructed by hand crews taking advantage of available burned trees The expected runoff from the design storm in combination with feasible CLB capacity governs spacing of successive CLB courses applied from the top of the slope downward.

CLB's are designed to detain and infiltrate runoff captured in the basin behind the contour log. Sediment reaching streams requires first detachment of the soil by raindrop impact or overland flows and then transport by runoff or gravity (dry ravel) down slope to a channel. Accordingly, if flow is eliminated or reduced below the threshold needed for transport of eroded soil, then sediment and flood impacts will be substantially reduced.

CLB treatment functions by trapping, detaining and infiltrating runoff. When runoff from a design storm is detained on slope from the drainage divide to bottom of the slope unit, soil remains in place due to lack of transporting flows. One major advantage to this approach is that the basins may interdict several runoff events. By contrast once filled with sediment, log erosion barriers have completed their useful life, often in one storm. With CLB, only in treatments where the design storm runoff was exceeded would one expect to find sediment accumulated behind the CLB. Thus sediment accumulations are evidence of failure of the primary treatment either due to exceeding the design, improper design or application. In these cases, they will only function one time trapping of a small amount of sediment.

DESIGN PRINCIPLES

The following essential design principles should guide practitioners and researchers.

The CLB provides an interdependent network of basins to control runoff. Accordingly it needs to be designed and implemented from the top of the slope (ridge) down. Failure to follow this protocol risks exceeding runoff control capacity and ultimate failure of many successive structures down slope. Especially for storms that occur during construction. If unburned areas lie between the ridgeline and the burned area treatments could begin at the edge of the unburned area.

The CLB need to be implemented on the contour and in full contact with ground.

Effective CLB's require end sills and intermediate baffles to provide capacity for runoff detention and to reduce a risk of complete failure of a given contour log basin.

The CLB spacing and "brick coursing" is critical to effectiveness.

The infiltration behind the CLB in the basins can be enhanced by straw mulch to prevent soil puddling which reduces infiltration.

Recognize that the design is based on the ideal case and is unlikely to be fully achieved during implementation. The goal should be to approximate the capacity and spacing as closely as possible

Determine treatment slope spacing between contours where the spacing value is the distance in feet measured horizontally between courses of treatment contour log basins using the following formula:

Formula: Spacing in feet = Capacity $\frac{ft^3}{ft} x \frac{12}{\text{Rainfall in inches}}$

This prescription in terms of capacity and spacing when applied to slope units using proper construction techniques should effectively detain and infiltrate the design storm runoff

While the CLB are often effective, as in the emergency of burn rehab near Lowman, ID and near Helena, MT, there are many cases where the effectiveness has been questioned. The majority of cases where they were deemed ineffective can be explained by three factors: failures by practitioners to understand known principles, failure to implement fundamental design considerations and features, or storm which exceed the design. Success relies on proper design and implementation.

Also, understanding CLB systems design and implementation is fundamental to any effort of monitoring and evaluation. Any application of CLB should be predicated on a properly designed and implemented practice as the basis for evaluation of an effectiveness hypothesis.

USDA - NRCS STREAM RESTORATION DESIGN HANDBOOK

Kerry M. Robinson, Hydraulic Engineer, USDA-NRCS East National Technical Support Center, Greensboro, NC; kerry.robinson@gnb.usda.gov; Jerry Bernard, National Geologist, USDA-NRCS Conservation Engineering Division, Washington, D.C.; jerry.bernard@wdc.usda.gov; Jon Fripp, Stream Mechanics Engineer, USDA-NRCS National Design, Construction, and Soil Mechanics Center, Ft. Worth, TX; jon.fripp@ftw.usda.gov

Abstract: The USDA Natural Resources Conservation Service (NRCS) has worked with landowners to provide design solutions for eroding streambanks for over 70 years. The goals and objectives of these stream projects typically encompass restoring or rehabilitating a stream to address bed and bank stability and/or habitat enhancement. There is and has been a continued interest in improving and expanding the skill set in bank stabilization and stream restoration, as well as incorporating ecological needs into NRCS projects.

A previous NRCS-led effort resulted in 15 Federal agencies producing the document, "Stream Corridor Restoration: Principles, Processes, and Practices" in 1998 (FISRWG, 1998). This interagency document presents numerous approaches in planning stream restoration projects. The NRCS, other agencies, and local groups are using this document to plan stream corridor restoration projects. However, this planning document provides only an awareness level of understanding of the topic. It is not a design document. This presentation describes a new companion document that does address design issues. This new document, titled "NRCS Stream Restoration Design Handbook" will be part of the NRCS National Engineering Handbook series and is currently under final review.

This design document is currently divided into the following chapters:

Chapter	Title	Chapter	Title
1.	Introduction: Ecological and Physical Considerations for Stream Projects	10.	Two-Stage Channel Design
2.	Goals, Objectives and Risk	11.	The Rosgen Geomorphic Approach to Natural Channel Design
3.	Site Assessment and Investigation	12.	Channel Alignment
4.	Design Procedure	13.	Sediment Impact Assessments
5.	Stream Hydrology	14.	Techniques and Approaches
6.	Stream Hydraulics	15.	Project Implementation
7.	Channel Design: Basic Principles	16.	Maintenance and Monitoring
8.	Threshold Channels	17.	Permitting Overview
9.	Alluvial Channels		

This effort has involved the time and talents of over 100 authors and reviewers. These authors represent other Federal, State, and local agencies, universities, and private engineering firms, as well as many NRCS employees.

INFLUENCES OF OFF-HIGHWAY VEHICLES ON FLUVIAL SEDIMENT REGIMES

Mark S. Riedel, PhD, USDA Forest Service, Southern Research Station, Coweeta Hydrologic Laboratory, Otto, (current address: Baird & Associates, Madison, WI 53711), mriedel@baird.com

Abstract: A wealth of research quantifies forest road erosion and resultant sedimentation impacts on stream water quality; however, little is known about the impacts of off-highway vehicles (OHV) on stream sedimentation. We monitored OHV impacts on sediment for a trail system in northern Georgia. Suspended and bed load sediment transport in a control and OHV impacted stream were significant and both experienced massive transport following torrential rains. Bed load transport capacity was similar for the OHV and control stream. Sedimentation in the OHV stream occurred in the sand and gravel size classes. Suspended sediment concentrations and transport on the OHV stream was many times greater than the control stream.

INTRODUCTION

Multiple use management of USDA Forest Service (USFS) National Forests includes OHV use on designated trails that must comply with federal law. National Forests in the southern Appalachians are within a few hours drive of millions of potential OHV users (Figure 1).

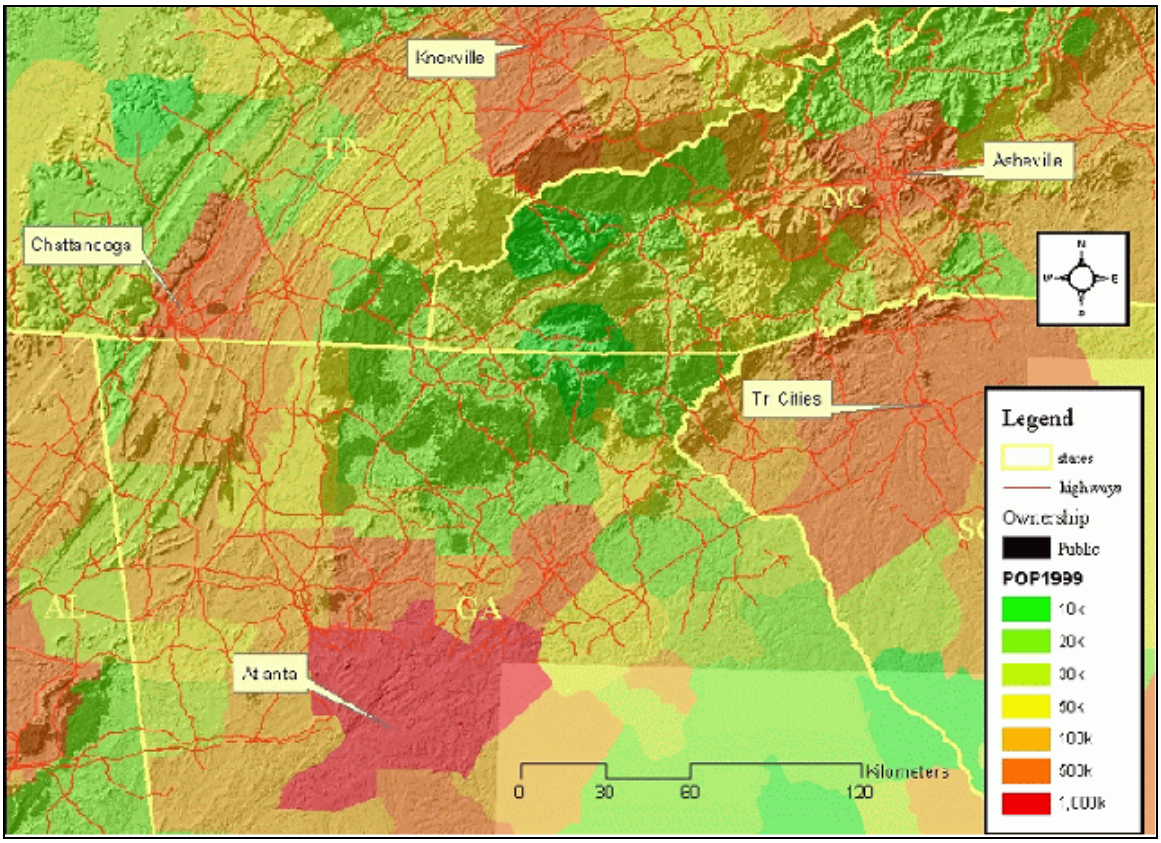


Figure 1 Population distribution on a per county basis for the southern Appalachians. Note, county borders are not indicated for neighboring counties (e.g., Atlanta metropolitan area is actually numerous counties).

While roads have been identified as a significant source of sediment in southern Appalachian streams (Riedel, et al, 2003), no research has investigated the influence of OHV trails and OHV use on stream sedimentation. While OHV trails are similar to roads, OHV trails have not been regularly maintained. In the southern Appalachians, average annual rainfall often exceeds 230 cm per year (Riedel, 2006) and fine grained micaceous soils are extremely sensitive to erosion (Riedel and Vose, 2005). Given these conditions, OHV trail has the potential to cause significant stream sedimentation in this region (Figure 2).



Figure 2 Typical erosion from an OHV trail in the southern Appalachians and resultant stream sedimentation.

The extent of OHV trail erosion on stream sedimentation in this region unknown (Riedel, et al, 2004). Given the widespread existence of illegal OHV trails, the extent of OHV trails on National Forests is also unknown. Consequently, Coweeta Hydrologic Laboratory and the Southern Region of the USFS initiated a study of erosion and sedimentation on an OHV Trail in the Chattahoochee National Forest of NE Georgia (Figure 3). This study was not designed to be a rigorous investigation of basic scientific principles; rather, the primary goal was to simply test and demonstrate field methods that may be easily used to rapidly assess and document the effects of OHV trails and OHV use on stream sedimentation.

Three sites were instrumented in a combined control vs. treatment and upstream vs. downstream design. We employed this approach as it allowed for determination of local and downstream impacts of OHV trails on stream sediment budgets. This was important because the Clean Water Act mandated cumulative effects (both offsite, and through time) be addressed when determining the impacts of a management activity on designated uses of water resources. The three sites were (Figure 3);

Site A: “OHV” treatment watershed (65 ha) with numerous trails and stream crossings,
Site B: “Control" watershed (35 ha) with no historic road or OHV impacts,
Site AB: “Downstream” watershed (104 ha) representing cumulative effects of site A.

OHV trails were in use during the study and no attempts were made to offset rider behavior, trail use or access to the trails. The trails affecting the sites in this study were official trails, and there were no illegal trails upstream of the sample sites.

METHODS

Discharge and Suspended Sediments: We installed automated pumping samplers and stage recorders on each study stream to monitor stream stage and collect water quality samples (Wagner, et al., 2000). We anchored inlets and pressure transducers to 1 m rebar pins driven into the streambed. Pressure transducers were placed in PVC stilling wells to minimize wave action.

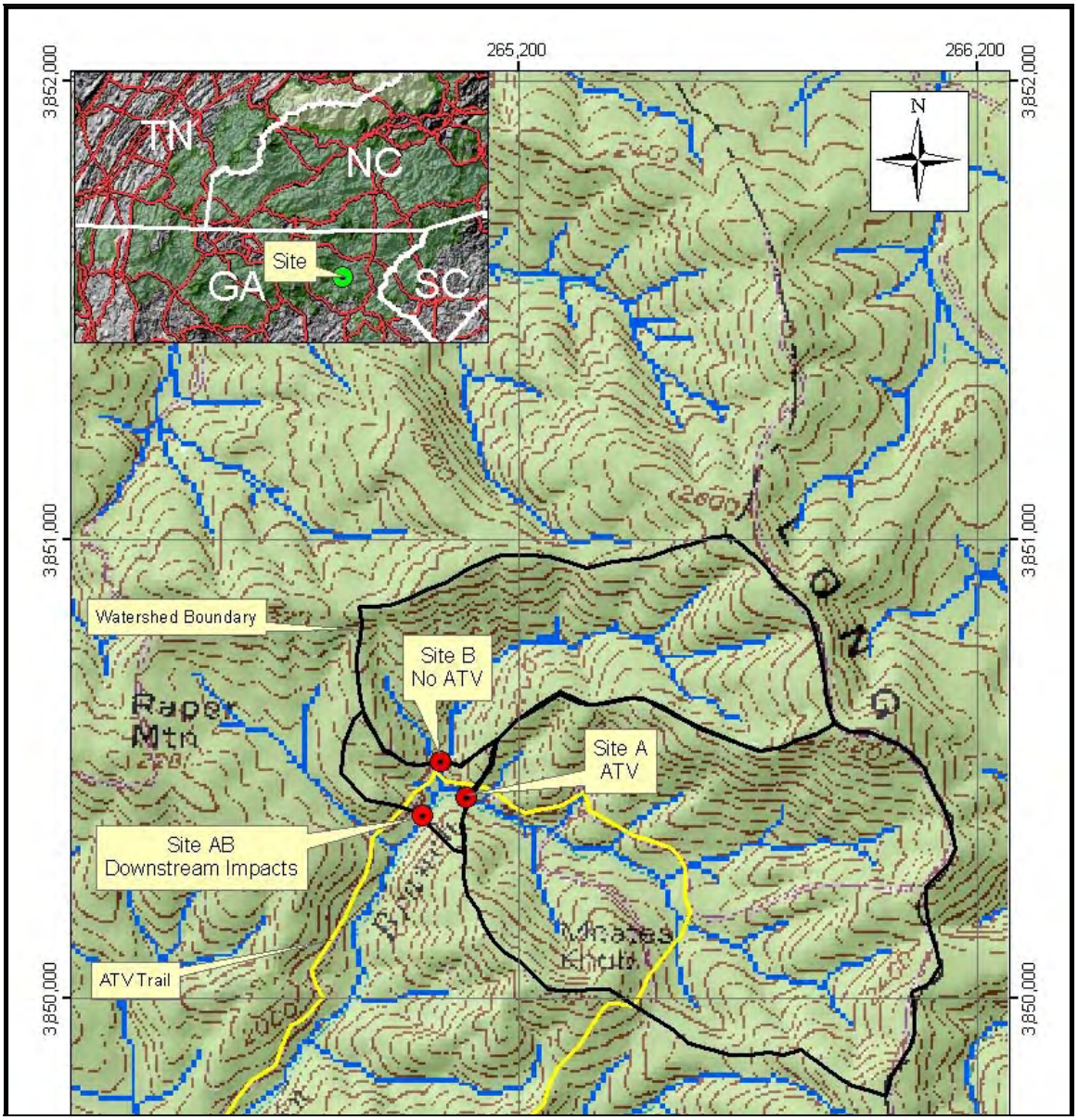


Figure 3 Location of OHV study sites. Here, ATV indicates all terrain vehicles (OHV).

Stage was recorded every 15 minutes and automatically corrected for variations in atmospheric pressure. Stage readings were validated weekly by manually surveying stage to each benchmark and measuring discharge (Buchanan and Somers, 1969). We developed stage discharge rating curves for each sampling site and programmed the pumping samplers to monitor stream flow using these rating curves. Samplers pumped samples to capture stream water quality during baseline conditions and storm flow conditions. The baseline regime collected samples on a flow proportional basis - sampling frequency increased with flow, whereas during storm flow, samples were pumped on a time proportional basis. We checked for bias in sampling via the fixed-point inlets using a DH-48 depth-integrated grab sampler to simultaneously collect depth-integrated grab samples on a weekly basis (Thomas, 1985). We then compared these to a simultaneously pumped sample. Total suspended solids (TSS) were analyzed to 1.5 μm by vacuum filtration (USGS, 1978a). Solids were combusted in a muffler furnace to determine clastic sediment as ash-free dry weight (USGS, 1978b).

Bed Load and Bed Material Sediments: Multiple pebble counts were replicated along each site. At least one hundred particles were measured with each sample. "Blindfolded" sampling was used to minimize sampling bias. Measurement of the intermediate particle axis to approximately 1 mm was obtained with a pebble chart and ruler. Sand particles smaller than this were simply lumped as fine sand. Silt size particles were determined using the "feel" method (Brady, 1990). Bed load transport was sampled across a range of flows using a Helley-Smith bed load sampler. Stream stage and discharge were simultaneously recorded. To track scour and deposition on each site, we installed multiple transects of scour and deposition pins (Figure 4).



Figure 4 Example showing scour and deposition pin transect – note: pins are elevated to show locations. Actual pins were installed nearly flush with streambeds to minimize flow disturbance.

Each pin consisted of a 12mm washer on a 9 mm x 0.5 m rolled steel pin. Pins were installed by drilling through stream bed armor into bedrock. Each pin was capped with a small nut to prevent the washer from being removed during high flows. We allowed multiple storms to reestablish stream bed sediments following installation of the pins. Then, we measured washer elevations and sediment deposition to quantify stream bed scour and deposition on an event basis. Scour and deposition pins were only used during the summer months. Data obtained in autumn were not useful as organic debris accumulated on the pins causing irregular scour and deposition in the transect area surrounding the pins.

RESULTS

Suspended Sediment: There was strong hysteresis in suspended sediment data for all sites (Figure 5a, Figure 5b). Peak suspended sediment concentrations over the study period were 30% and 10% higher for the OHV and Downstream sites, respectively. Over the course of samples, suspended sediment yields averaged 18% and 15% higher (Figure 6).

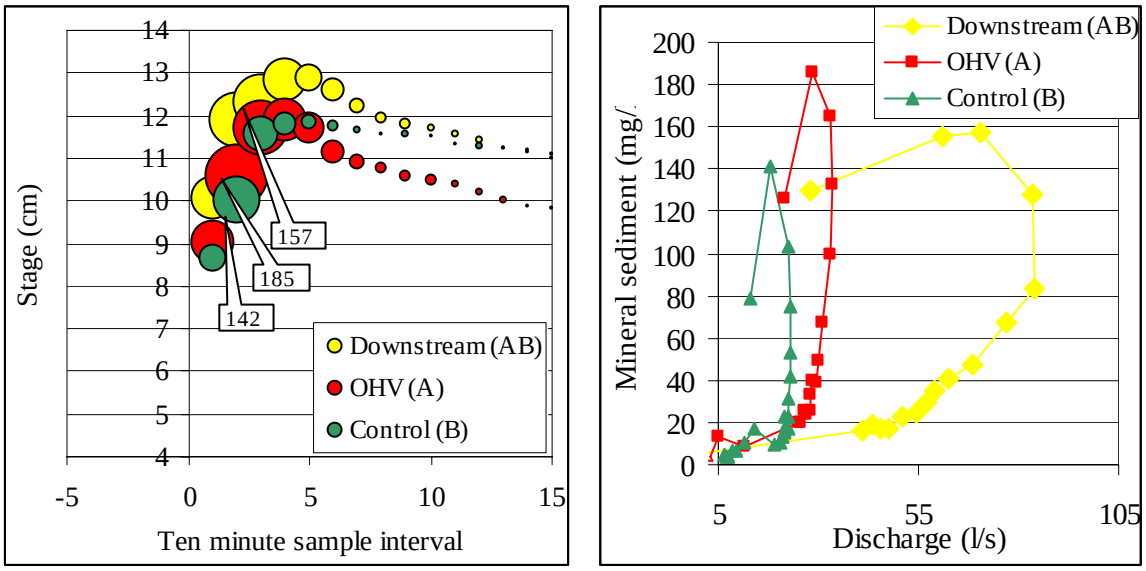


Figure 5a Sedigraph showing concentrations of sediment during a storm event. Bubble size indicates relative concentration and numbers show peak concentrations (mg/l).
Figure 5b: Sediment hysteresis loops for each site.

Bed Material and Bed Load Sediment: Stream beds in the OHV and Downstream sites included 3 fold more sand than the Control site (Figure 7). Differences in fine gravel and gravel were not significant. While bed load transport capacity (kg/s) was highest for the OHV site, transport on a per unit area basis was identical for the OHV and Control sites (Figure 8). Bed load transport capacity was sufficient to mobilize sand and fine gravel during typical events.

While extreme flows caused by Hurricane Ivan mobilized the entire streambeds, the beds returned to a form similar to that before being scoured (Figure 9).

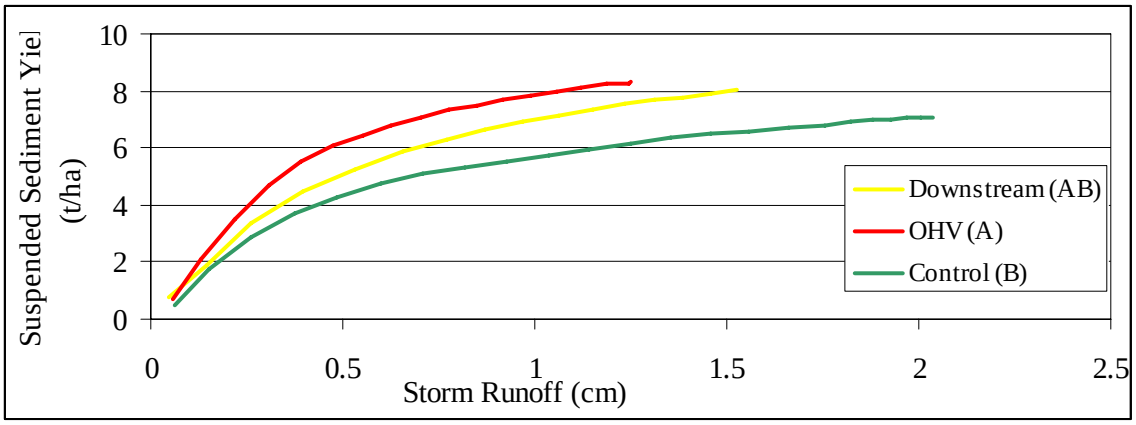


Figure 6 Example of suspended sediment yield over a single storm event.

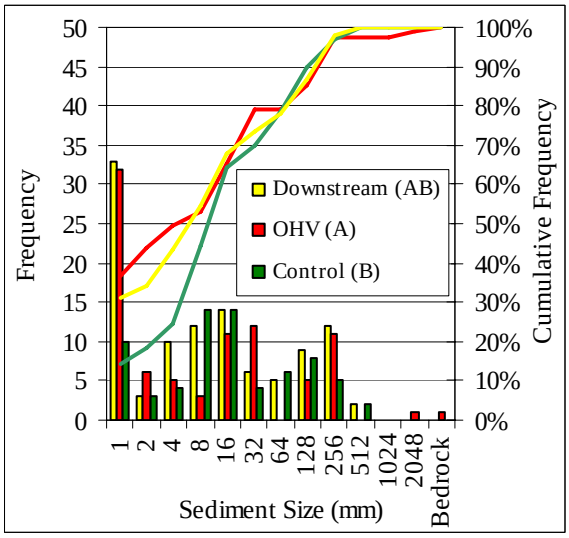


Figure 7 Particle size distributions of stream bed sediments.

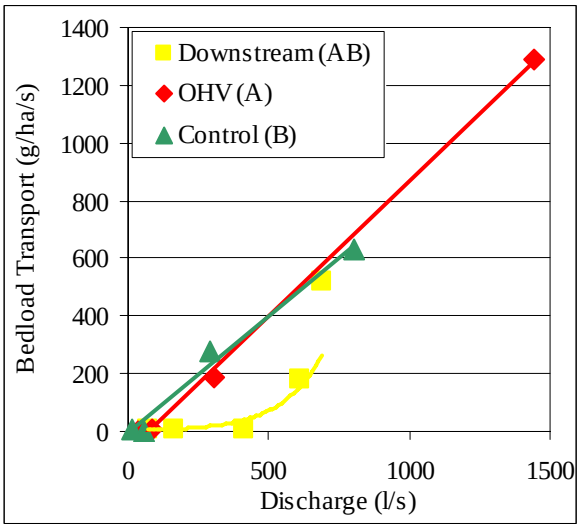


Figure 8 Bed load sediment transport for each reach.

DISCUSSION AND CONCLUSIONS

The results of this study, while preliminary, clearly indicate OHV trail use produced elevated concentrations and loadings of both suspended and fine bed load sediments in the OHV and Downstream reaches. Bed load transport for the Control and OHV sites was controlled by hydraulics (slope and depth). Hence, after accounting for watershed size, bed load transport capacity was similar between the two reaches. What appeared to be reduced transport capacity on the downstream reach was caused by two phenomena. First, flow on the downstream reach was the sum of the upstream reaches; e.g., when the upstream reaches contribute 200 and 300 l/s of runoff for Site A and B, respectively, Downstream (AB) flowed at > 500 l/s. Second, the Downstream (AB) reach had a lower slope so for a given flow, it had a lower transport capacity. Despite having sufficient bed load transport capacity, the OHV site (A) had elevated loading of fine bed load sediments in the sand and fine gravel size ranges. While these sediments were

readily flushed out by storm events, they were quickly replaced with sediments eroded from the OHV trails. Thus, implantation of OHV trail best management practices and runoff treatment methods that prevent sediments from reaching the stream would allow the stream to clear itself of excess sediments in the stream bed.

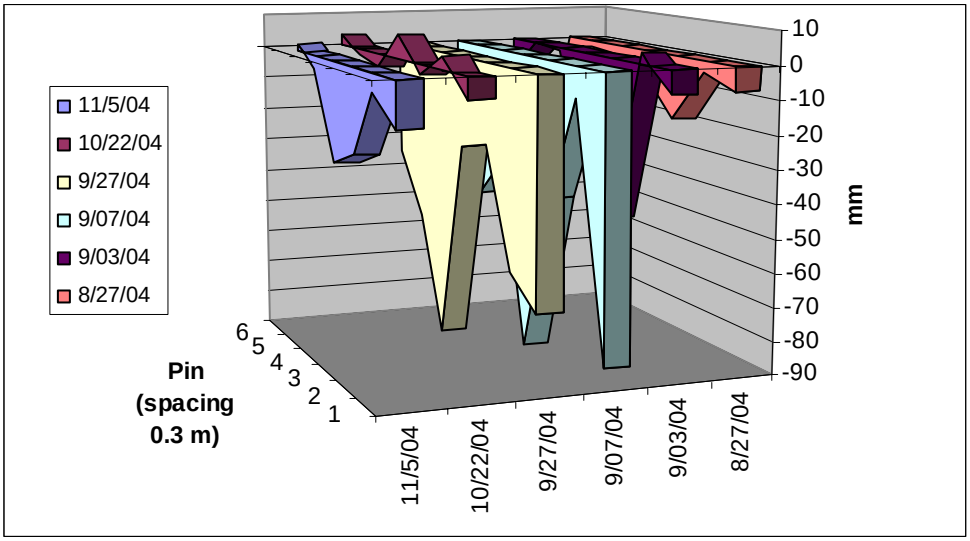


Figure 9 Scour and deposition of the stream bed at OHV Site A. Negative and positive values indicate event scour and deposition on a per event basis. Relative throughput of bed load sediment through the reach can be inferred from the area of each curve. The pre and post stream bed cross section elevations were quite similar following each event (no significant net change in bed elevation). October and November data are inaccurate from debris on pins.

The results indicate that simply collecting grab samples of water quality would not accurately characterize the impacts of OHV trails on stream sedimentation because the observed increases in suspended sediment loading came during storm events. Storm event sampling was necessary to characterize suspended sediment impacts. Bed load transport, stream bed scour and stream bed deposition were similar for the reaches. Only particle size analysis of stream bed sediments was useful in documenting OHV impacts on bed load / bed material load sediments.

ACKNOWLEDGEMENTS

This work would not have been possible without the support of Jack Holcomb, Hydrologist, USDA Forest Service, Region 8, Atlanta, GA. The author extends his gratitude to Charles Marshall, Derek Gregory, Erin Moore, Cindi Brown and Jim Deal for their assistance with the necessary field work and sample analysis to support this project. The author also thanks Dr. James Vose, Project Leader, Coweeta Hydrologic Laboratory, for his support in this research.

REFERENCES

Brady, N.C. (1990). "Determination of soil class. Chapter 4: Physical properties of mineral soils," The Nature and Properties of Soils. Macmillan Publishing Company, New York, NY. pp. 97 - 100.

Buchanan, T. J. and W. P. Somers. (1969). "Discharge measurements at gauging stations," Techniques of Water-Resources Investigations of the United States Geological Survey. U.S.G.S. Reston, VA.

Riedel, M.S. (2006). "North Atlantic oscillation influences on climate variability in the southern Appalachians," Proc. Federal Interagency Sedimentation and Hydrologic Modeling Conferences, Reno, NV, April.

Riedel, M.S. and Vose, J.M. (2005-In Review). "Prediction and management of sediment yields with restoration of southern Appalachian forest roads," Southern Journal of Applied Forestry.

Riedel, M.S., Vose, J.M., and Bolstad, P.V. (2004). "Characterizing hysteretic water quality in southern Appalachian streams," Proc. 2004 National Water Quality Monitoring Conference, United States Advisory Committee on Water Information, National Water Quality Monitoring Council, Chattanooga, TN, May.

Riedel, M.S., Vose, J.M. and Leigh, D.S. (2003). "The road to TMDL is paved with good intentions - Total Maximum Daily Loads for a Wild and Scenic River in the southern Appalachians," 2nd Conference on Watershed Management to Meet Emerging TMDL Environmental Regulations ASAE, Albuquerque NM, Nov.

Thomas, R.B. (1985). Measuring suspended sediment in small mountain streams. USDA Forest Service, Pacific Southwest Forest and Range Experiment Station General Technical Report PSW-83.

U.S.G.S. (1978a). "Laboratory Analysis – Suspended-Sediment Concentration," Section 3.F.2.a., Chapter 3, Sediment, the National Handbook of Recommended Methods for Water Data Acquisition. United Stages Geological Survey, Office of Water Data Coordination, Reston, VA.

U.S.G.S. (1978b). "Seston – Gravimetric (Ash-Free Dry Weight of Organic Matter)," Section 4.B.1.a.2.a., Chapter 4, – Biological Methods of the National Handbook of Recommended Methods for Water Data Acquisition. United Stages Geological Survey, Office of Water Data Coordination, Reston, VA.

Wagner, R.J., Mattraw, H.C., Ritz, G.F. and Smith, B.A. (2000). Guidelines and Standard Procedures for Continuous Water-Quality Monitors: Site Selection, Field Operation, Calibration, Record Computation, and Reporting. U.S. Geological Survey Water-Resources Investigations Report 00–4252

IDENTIFICATION OF SEDIMENT SOURCES IN A SEMIARID WATERSHED USING MULTIPLE DIAGNOSTIC PROPERTIES

Fred Rhoton, Soil Scientist, USDA-ARS, Oxford, MS, frhoton@ars.usda.gov; William Emmerich, Soil Scientist, USDA-ARS, Tucson, AZ, bemmerich@tucson.ars.ag.gov; Mark Nearing, Agricultural Engineer, USDA-ARS, Tucson, AZ, mnearing@tucson.ars.ag.gov; Jerry Ritchie, Ecologist/Soil Scientist, USDA-ARS, Beltsville, MD, jritchie@hydrolab.usdaars.gov; Christopher Wilson, Research Geologist, USDA-ARS, Oxford, MS, cwilson@ars.usda.gov; David DiCarlo, Research Physical Scientist, USDA-ARS, Oxford, MS, ddicarlo@ars.usda.gov

Abstract: The identification of sediment source areas in watersheds is important for the development of sediment budgets and for the design of management practices to reduce sediment and chemical loadings in receiving streams. This study was conducted to determine the primary sources of sediment at a watershed scale using a weighted means soil geomorphology approach to the characterization of soil properties that influence erodibility and sediment transport. Each major soil mapping unit in six subwatersheds (SW) was sampled along transects positioned to include the normal soil geomorphological features associated with a given mapping unit. At each sampling point, latitude-longitude, slope class, topographic position, and aspect were recorded. Soil samples collected from the surface 5.0 cm were characterized for a range of physical and chemical properties used for fingerprinting purposes. Suspended sediment samples collected from supercritical flumes at the mouth of each SW were analyzed identically. An aggregation index (AI) calculated for the soils in each SW as follows: 100 (1-water dispersible clay/total clay), served as a measure of soil erodibility. The physical and chemical signatures of the suspended sediment collected at the six flumes were used in a multivariate mixing model to identify the primary contributing source. The results suggested that the SWs with the lowest soil AI were contributing the greatest amounts of sediment.

INTRODUCTION

Two primary approaches are used in sediment source identification research in which detailed comparisons are made between suspended sediments transported in stream channels and watershed soils using a range of physical and chemical properties. Direct monitoring of potential source areas may be the most widely used approach (Slattery et al., 1995). These methods use technology such as erosion pins, runoff troughs, automated suspended sediment samplers, and manually collected grab samples (Sutherland and Bryan, 1989).The other approach to sediment source identification, commonly referred to as fingerprinting, is based on the analysis of suspended sediment properties for which equivalent values exist in the watershed soils (Slattery et al., 1995). These physical, chemical, and mineralogical properties include: clay mineralogy, sediment color, sediment chemistry, radionuclide concentrations, and magnetic susceptibility.

Clay mineralogy of suspended sediment has been used to infer source areas (Neiheisel and Weaver, 1967; Klages and Hsieh, 1975; Wall and Wilding, 1976), but these measurements have limitations since some clay minerals are preferentially eroded from soil surfaces at the expense of other species (Rhoton, et al., 1979). Likewise, the use of sediment color to separate channel and non-channel sediment sources (Grimshaw and Lewin, 1980) without the benefit of companion analytical measurements can lead to erroneous interpretations in soils with contrasting colors between the surface and subsurface horizons. Magnetic susceptibility measurements of watershed soils and sediment have been used extensively to identify source areas (Dearing et al., 1986; Oldfield et al., 1979). This approach is considered relatively successful especially at separating topsoil from subsoil sources on a field or small watershed scale, but in large watersheds with a wide variety of parent materials and soil types, the effects of soil geomorphology on magnetic susceptibility must be carefully evaluated. Fallout radionuclides (i.e., ^{7}Be, ^{210}Pb, ^{137}Cs) have been used in monitoring and fingerprinting suspended sediments in rivers and coastal waters (Walling and Woodward, 1992; Wallbrink et al., 1999; Bonniwell et al., 1999). In such studies, radionuclides, and their ratios to one another, can be used to differentiate between freshly eroded soil from the landscape and collapsed bank material due to differences in half-lives and the different delivery mechanisms of sediment to the stream (Whiting et al., 2005). In terms of sediment chemistry, Peart and Walling (1988) proposed a method for determining the origin of suspended sediments using their chemical properties as natural tracers. The chemical data, derived from the selective dissolution analysis of soil, stream bank, and suspended sediment samples are evaluated with a mixing model.

Soil geomorphology is critical to sediment source studies due to its influence on soil properties that determine soil erodibility and sediment characteristics. These soil properties, which include clay and organic matter contents and Fe and Al oxide contents, vary as a function of aspect, slope gradient, and topographic position (Schoenberger et al., 2002). The relationships between soil geomorphology and soil properties that influence erodibility have been addressed in previous studies. Franzmeier et al. (1969) reported greater organic C and darker soil colors on north-facing slopes that were attributed to lower temperatures and greater water contents. Particle size distributions were coarser on mid-slope positions, and basic cations were concentrated on the lower slope positions. In a similar study, Hanna et al. (1982) measured 20% more available water on north-facing slopes relative to south-facing slopes. East-facing slopes had the driest soils. Rhoton et al. (1998) indicated that water dispersible clay contents and soil erodibility were at a minimum on lower, wetter slope positions where the Fe oxide mineralogy was dominated by ferrihydrite, a poorly crystalline mineral that is most influential in aggregate stability.

The objective of this current research was to use fingerprinting techniques to identify primary sediment source areas in a large watershed by characterizing the distribution of several soil properties that determine the erodibility of watershed soils, and hence the characteristics of suspended sediments transported through the watershed.

MATERIALS AND METHODS

Site Characteristics: The research was conducted on the Walnut Gulch Experimental Watershed (WGEW) located at Tombstone, AZ (31 deg. 43 min. N. Lat., 110 deg. 41 min. W. Long.). The watershed covers approximately 150 km^2 with elevations ranging from 220 to 1890 m, a mean annual temperature of 17.6 ^{o} C, and an average annual precipitation of 324 mm (Renard et al., 1993). The WGEW is situated primarily in a high foothill alluvial fan portion of the larger San Pedro River Watershed. The soil complexes mapped occur largely on alluvium composed of Cenozoic age clastic clays and silts. Smaller areas of limestone, granite, granodiorite, and andesite parent materials occur throughout the watershed. The soils are generally well-drained, calcareous, gravelly loams containing large percentages of rocks and gravels at the soil surface (Breckenfeld et al., 1995). Land-use over the entire watershed is rangeland.

Study Approach: The subwatersheds (SW) selected for study were numbers 3, 7, 9, 10, 11, and 15. Each SW was instrumented with a supercritical flume (Renard et al., 1993). Suspended sediments were collected at these flumes using vertical samplers mounted on the face of the flume. This sampler was designed to collect suspended samples in 30.5 cm increments above the floor of the flume for the total flow depth of 122 cm. The sediment was collected through 6.4 mm diameter ports drilled into a 10.2 cm diameter (i.d.) aluminum tube. Plastic tubing was used to connect the ports to 500 ml plastic sample bottles mounted inside the sealed sampler. Also, a 2 L sample bottle was mounted on the bottom of the sampler to collect additional sediment at the 30.5 cm flow depth to ensure adequate sample for low flow events. Once filled, float valves sealed the sample bottles to prevent continuous flow-through of suspended sediments. All samples were combined to give one composite sample per flow event.

Soil samples were collected from the SWs on the basis of relative acreage occupied by individual soil mapping units. Initially, digitized soil surveys were superimposed on digital elevation models of each SW. A sampling transect length of 1000 m was arbitrarily chosen for each 200 ha of a given soil mapping unit. These transects were positioned by GPS-derived coordinates such that a range of surface morphometry factors (Schoeneberger et al., 2002) were represented by the samples. Specifically, soil samples were collected as a function of topographic position, slope class, and aspect along the transects. At each selected location, the surface 5.0 cm were sampled at three points, approximately 10 m apart and perpendicular to the slope. The three soil samples were then composited to form a single bulk sample, and sealed in a plastic bag. Data were recorded at each sampling location for latitude - longitude, topographic position, aspect, and slope steepness.

Laboratory Analyses: In the laboratory, all soil and sediment samples were air-dried or oven-dried at 60^{E} C, and sieved to < 2 mm. Particle size distribution was determined by standard pipette analysis following overnight dispersion in Na hexametaphosphate (USDA-NRCS, 1996). The water dispersible clay component of the total clay fraction was also estimated by this methodology using only distilled water as the dispersant. Soil pH was measured in a 1:1 soil/distilled water (v-v) suspension (McLean, 1982). Total C and N were determined by combusting 0.5 g samples in a Leco CN-2000 carbon-nitrogen analyzer (Leco Corp., St. Joseph, MI). The inorganic fraction of the total carbon was quantified by treating a separate 1 g sample with 5 N HC1 in a sealed decomposition vessel (200 mL) fitted with a rubber septum. Carbon dioxide pressure generated by the acid-decomposition of the sample was

measured with a Tensimeter (Soil Measurement Systems, Tucson, AZ) probe inserted through the septum. Pressure readings were converted to C contents using a standard curve, and subtracted from total C to give the organic C (OC) content. The Na pyrophosphate (p), acid ammonium oxalate (o), and Na citrate-bicarbonate-dithionite (d) extractable Fe and Mn contents of the soils and sediment were determined by the procedures of the USDA-NRCS (1996). Exchangeable cation contents were determined following extraction with ammonium acetate (USDA-NRCS, 1996). All extracts were analyzed by atomic absorption spectrophotometry. Radionuclide activities were measured using Gamma Spectroscopy similar to the methods of Whiting et al. (2005). Quantitative soil color was measured with a Minolta Chroma Meter (Minolta Corp., Ramsey, NJ). The total clay and WDC content data were used to calculate an aggregation index (AI) for the watershed soils based on the method of Harris (1971) as follows: AI = 100 (1- WDC/total clay).

The relative contribution of each SW to the sediment load leaving the WGEW at flume 1 was estimated using the multivariate mixing model methods of Walling and Woodward (1995), and the physical and chemical signatures for Fe_p, Fe_o, Fe_d, Mn_p, Mn_o, Mn_d, clay content, OC, and total N in the suspended sediment. This was done using the following linear optimization procedure. Each suspended sediment property was normalized by its standard deviation for each flume (SW). Thus, calling the vector of sediment properties obtained at flume *i* d_i, the linear optimization problem becomes finding the vector containing the proportion of sediment from each SW (**x**) which minimizes the function (**Cx-d**)$'$* (**Cx-d**), where **C** is the matrix consisting of the possible contributing SWs, and **d** is from the flume where the sediment is measured. This function is minimized with the constraints that the sum (**x**) = 1, (i.e., the total sediment signature is from the contributing SWs) and **x**>0 (i.e., a SW cannot contribute negative sediment). This routine was run in which the signature of sediment at flume 1 was expressed in terms of possible contributions from flumes 3, 7, 9, 10, 11, and 15.

All statistical analysis related to soil and sediment properties utilized the GLM and CORR procedures of SAS version 8 (SAS Institute, 1999).

RESULTS AND DISCUSSION

Watershed Soil Characteristics: The distribution of soil mapping units within WGEW (Breckenfeld et al., 1995) is shown in Table 1. The most extensive mapping unit in the watershed is the Luckyhills-McNeal complex, very gravelly sandy loam, which occupies approximately 4300 ha on a whole watershed basis. Other mapping units comprising substantial acreages are the Elgin-Stronghold complex, very gravelly fine sandy loam (1509 ha), McAllister-Stronghold complex, gravelly fine sandy loam (1363 ha), and Tombstone extremely gravelly sandy loam (1280 ha).

Selected physical and chemical properties of the soils are shown in Table 2. Again, the soil samples were collected from the surface 5 cm at each sampling point, irrespective of surface horizon thickness. In most cases, A-horizon thickness in these soils corresponds to our sampling depth according to the field descriptions of Breckenfeld et al. (1995). This sampling depth was considered representative of the portion of the profile most affected by erosion processes involving rill formation and infilling. These data, being from a composited depth sample include contributions from both A- and upper B-horizons in various proportions. Based on these data, some soil properties reflect differences in parent material composition between SWs. The most obvious differences exist between SWs 3 and 7, and the other SWs in terms of total clay, OC, AI, magnetic susceptibility, and hue. A large portion of the soils in SW 7 were formed on igneous residuum (i.e., granite, granodiorite) compared to limestone, andesite, and basalt parent materials in the other SWs. Consequently, SW 7 soils should have less clay and OC, and a lower AI. Similarly, the soils in SW 7 had the highest magnetic susceptibility readings, reflecting the higher magnetite contents of the igneous parent rocks. The higher Munsell color readings in SW 7 may be explained by the lighter colored, high quartz content granitic rocks, and lower OC contents. The calcareous alluvium parent materials in SW 3 contributed to somewhat similar soil conditions in terms of higher hue, value and chroma readings, a high pH, and low values for OC and AI. By contrast, SW 9 contained substantial acreages of soils formed from fine-grained igneous parent materials (i.e., andesite, basalt) which should weather to form soils with finer particle sizes. In fact, the soils in SW 9 had the highest total clay contents and AI, and relatively low average hue and value readings. Obviously, parent material has an important role in the physical and chemical behavior of soils in the WGEW.

The OC distributions varied significantly ($p \# 0.05$) between SWs, with SW 15 containing nearly twice the concentrations of SW 7. Total N distributions were closely related to OC contents, again, with SW 15 having

Table 1 Mapping unit acreages for the subwatersheds studied in Walnut Gulch Experimental Watershed.

Soil Mapping Unit	Subwatershed					
	WS 3	WS 7	WS 9	WS 10	WS 11	WS 15
	ha					
Baboquivari-Combate complex		19.5	188.7	190.1	6.7	
Blacktail gravelly sandy loam				245.5		
Budlamp-Woodcutter complex				64.6		
Chiricahua very gravelly clay loam		101.3				
Combate loamy sand	3.0	8.2				60.0
Elgin-Stronghold complex	120.2		881.7	283.7	75.3	
Epitaph very cobbly loam			71.9	18.1		152.7
Forrest-Bonita complex			12.6	18.7		103.2
Graham cobbly clay loam			175.7	13.8		66.8
Graham-Lampshire complex			122.1	9.1		113.4
Grizzle coarse sandy loam						81.6
Lampshire-Rock outcrop complex		28.4	52.5			
Luckyhills loamy sand		14.0	7.0			
Luckyhills-McNeal complex	443.4	286.8	44.6	1.1		740.1
Mabray-Chiricahua-Rock outcrop complex		295.8				36.3
Mabray-Rock outcrop complex		193.4				150.7
McAllister-Stronghold complex	273.0		317.4	229.3	61.4	144.8
Monterosa very gravelly fine sandy loam	12.7	15.6				248.6
Riverwash-Bodecker complex		8.1		12.6		
Schiefflin very stony loamy sand		190.2				
Stronghold-Bernadino complex	94.9		38.6	178.8	421.1	
Sutherland-Mule complex		65.7				
Sutherland very gravelly fine sandy loam		141.2				403.9
Tombstone very gravelly fine sandy loam			486.3	252.0	223.6	73.4
Woodcutter gravelly sandy loam				61.9		
	947.2	1368.1	2398.9	1579.4	788.2	2375.6

significantly ($p \# 0.05$) greater amounts than the other SWs. The C/N ratios exhibited more mean separation between SWs than the OC and N components taken individually. There were also significant differences identified in the pH values between SWs that ranged from 8.6 to 6.9. Again, these greater pH values are attributed to higher $CaCO_3$ contents in SWs 3 and 11, whereas, the lower readings in SWs 9 and 10 are probably related to higher acid clay contents in some of these soils. In terms of exchangeable cations, Ca was the dominant element, but there were few statistically significant differences in the concentrations between SWs. Extractable Fe and Mn contents were generally low and not significantly different between SWs with the exception of Fe_d which was significantly greater in SWs 7 and 10. The distribution of ^{137}Cs in the watershed soils appeared to be controlled by soil clay contents. The highest concentrations were found in SWs 9 and 10, which also had the greatest amounts of clay.

Sediment Characteristics: The physical and chemical properties of the suspended sediments (Table 3) indicate that the particle size distributions of suspended sediments were much finer than the watershed soils within SWs due to particle size selectivity created by soil erosion and sediment transport processes. However, there were basically no significant differences between SWs regardless of size fraction. Relative to color, the hue, value, and chroma of the suspended sediment were generally higher than the watershed soils, perhaps reflecting the differences in particle size distributions between the soils and sediment. Magnetic susceptibility of the sediments ranged from 103 (SW 3) to 226 10^{-8} m^3 kg^{-1} (SW 7). Organic C contents of the suspended sediments averaged 24.0 g kg^{-1} compared to 11.4 g kg^{-1} for the watershed soils. Total N content of the sediment was statistically similar between SWs, and was approximately 6% of the OC contents. The C/N ratios were generally slightly higher in the sediments. The pH of the

Table 2 Selected physical and chemical properties of soils for individual subwatersheds.

Property	Units	Subwatershed					
		3	7	9	10	11	15
Sand	g kg^{-1}	720a[†]	719a	653b	698a	731a	608c
Silt	g kg^{-1}	148c	162bc	184b	142c	136c	251a
Clay	g kg^{-1}	133bc	118c	163a	160a	133bc	141b
WDC	g kg^{-1}	108ab	91c	111ab	116a	102bc	98bc
AI		18.0c	22.8c	31.9a	28.1b	23.9c	28.2b
MS	$10^{-8}m^3kg^{-1}$	198b	800a	294b	189b	264b	217b
Hue[‡]		7.1b	8.2a	6.5d	6.4d	6.8c	6.9bc
Value		3.1ab	3.3a	2.9c	3.0c	3.1b	3.1b
Chroma		2.0ab	2.0a	1.7c	1.8c	1.5d	1.8bc
Organic C	g kg^{-1}	10.2bc	8.5c	12.1ab	11.5b	11.8b	14.2a
Total N	g kg^{-1}	0.62b	0.62b	0.76b	0.74b	0.64b	0.99a
C/N		17.4b	13.7c	16.8b	17.6b	19.1a	15.4c
pH		8.6a	7.9b	7.4c	6.9d	8.5a	7.9b
Exch. Ca	cmol kg^{-1}	32.2a	30.4a	27.2a	17.4b	32.4a	31.9a
Exch. Mg	cmol kg^{-1}	1.0b	1.3ab	1.7a	1.7a	1.0b	1.2ab
Exch. K	cmol kg^{-1}	0.7a	0.7a	1.0a	0.9a	0.6a	1.0a
Exch. Na	cmol kg^{-1}	0.02a	0.02a	0.03a	0.02a	0.01a	0.02a
Fe_p	g kg^{-1}	0.02b	0.03b	0.08ab	0.14a	0.01b	0.05b
Fe_o	g kg^{-1}	0.20a	0.71a	0.27a	0.40a	0.15a	0.28a
Fe_d	g kg^{-1}	3.76c	5.46ab	4.42bc	5.34a	3.43c	3.91c
Mn_p	g kg^{-1}	0.03b	0.03b	0.06ab	0.10a	0.03b	0.04ab
Mn_o	g kg^{-1}	0.16b	0.32a	0.23ab	0.24ab	0.20b	0.16b
Mn_d	g kg^{-1}	0.19b	0.40a	0.26ab	0.26ab	0.23b	0.24b
Cs	Bq kg^{-1}	11.2c	12.8bc	14.2b	16.5a	11.1c	12.8bc

[†]Values followed by the same letter are not statistically different at $p \leq 0.05$ based on Duncan's multiple range test.
[‡]All hues are yellow red (YR).

suspended sediments averaged slightly lower than the soils which may be the result of higher clay contents in the sediment. The activities of ^{137}Cs in the suspended sediments were low relative to the activities of the soils. This was unexpected considering the high clay enrichment in the sediment and the strong relationship between ^{137}Cs and soil clays. This may indicate clays are preferentially eroded from areas depleted in ^{137}Cs such as rills and gullies. The suspended sediment was so uniform relative to exchangeable cation concentrations that no significant differences occurred between SWs. The extractable Fe data show that the suspended sediment was substantially higher than the soils for all three extractants in all SWs. These higher Fe_p values for the sediment are explained by the higher OC contents in the sediment, and the increases in Fe_o and Fe_d can be largely attributed to the enhanced silt and clay contents of the sediment. The Fe_o component is primarily transported as a clay coating. The Fe_d is also transported as

clay coatings, but also as clay and silt-size discrete particles. The extractable Mn component only showed consistent increases in the suspended sediment phase for the Mn_d phase, and there were basically no differences between SWs.

Table 3 Selected physical and chemical properties of suspended sediments for individual subwatersheds.

		Subwatershed						
Property[†]	Units	1	3	7	9	10	11	15
Sand	g kg^{-1}	380ab[‡]	374ab	498ab	506ab	419ab	512a	423ab
Silt	g kg^{-1}	143a	409a	326a	337a	410a	320a	395a
Clay	g kg^{-1}	207ab	216ab	176ab	157b	171ab	168b	182ab
MS	$10^{-8}m^3kg^{-1}$	164b	103d	226a	176b	122cd	166b	116b
Hue		7.3b	6.7c	8.6a	6.8c	6.6c	7.0bc	6.8c
Value		3.6a	3.5ab	3.6ab	3.5ab	3.4b	3.6a	3.5ab
Chroma		2.0b	2.1a	1.9b	1.8c	1.9bc	1.8c	1.9bc
Organic C	g kg^{-1}	23.1ab	32.1a	24.9ab	19.9b	19.3b	21.6b	26.0ab
Total N	g kg^{-1}	1.44ab	1.90a	1.60ab	1.16b	1.21ab	1.24ab	1.58ab
C/N		16.0b	16.9ab	15.6b	17.2a	16.0b	17.4a	16.5ab
pH		7.6ab	7.8ab	7.5ab	7.7ab	7.6ab	7.8ab	7.8ab
Exch. Ca	cmol kg^{-1}	36.7a	37.3a	36.4a	37.7a	34.9a	39.1a	38.6a
Exch. Mg	cmol kg^{-1}	2.2a	2.1a	2.0a	2.1a	1.9a	1.8a	1.7a
Exch. K	cmol kg^{-1}	1.2a	1.2a	1.0a	1.5a	1.1a	1.0a	1.4a
Exch. Na	cmol kg^{-1}	0.05a	0.03a	0.04a	0.05a	0.04a	0.03a	0.05a
Fe_p	g kg^{-1}	0.11ab	0.11ab	0.10ab	0.09bc	0.14a	0.04d	0.06cd
Fe_o	g kg^{-1}	0.91b	0.71b	1.89a	0.48b	0.72b	0.34b	0.51b
Fe_d	g kg^{-1}	5.38abcd	5.60abc	6.47a	4.77cd	6.11ab	4.14d	4.99bcd
Mn_p	g kg^{-1}	0.04c	0.03c	0.04c	0.08b	0.13a	0.03c	0.03c
Mn_o	g kg^{-1}	0.18b	0.16b	0.30a	0.22ab	0.27a	0.15b	0.16b
Mn_d	g kg^{-1}	0.35b	0.32b	0.52a	0.33b	0.41ab	0.41b	0.34b
Cs	Bq kg^{-1}	8.9	8.1	11.9	7.6	8.0	6.7	12.1

[†]p, o, and d denote pyrophosphate, oxalate and dithionite extractable, respectively.
[‡]Values followed by the same letter are not significantly different at $p \leq 0.05$ based on Duncan's multiple range test.

The ratios determined for suspended sediment versus watershed soil properties indicate that, relative to the watershed soils, clay contents of the sediment were enriched by an average factor of 1.38. The greatest enrichment (1.67) occurred in SW 3, and the least (1.02) was recorded for SW 9. These two SWs had the lowest and highest AI, respectively (Table 2). This indicates that, overall, SW 3 had the most highly erodible soils in the WGEW, and SW 9 had the least erodible. These enrichment ratios (ER) of suspended sediment clays to soil clays were correlated against the SW soil AI for the six individual SWs. The resulting correlation coefficient (r) was -0.946 (p # 0.01). The only apparent discrepancy in the indicated strong relationship is the relatively high ER for SW 15 considering its high AI. However, SW 15 soils had the highest OC contents, suggesting that this sediment is transported in an OC stabilized, clay aggregate form as opposed to dispersed clay-size particles elsewhere. Further, suspended

sediments were more enriched in silt-size material, relative to the clay fractions, in most SWs by a factor of 2 to 3 times. Likewise, the OC contents of the suspended sediment were enriched by an average ratio of 2.13, relative to the watershed soils. The highest OC concentrations in the suspended sediments were associated with the lower AI soils, with the exception of SW 15. The magnetic susceptibility ratios for suspended sediments versus SW soils averaged 0.56 indicating the suspended sediments were depleted relative to the soils. This suggests that the soil magnetic fraction, primarily magnetite, is concentrated in the sand-size fraction which is also depleted in the suspended sediment. Since magnetic susceptibility is so particle size dependent, an accurate assessment of this soil property as a fingerprinting tool requires that similar particle size distributions be used when measuring soil and sediment samples.

Based on the highest ER for clay and the lowest soil AI (Table 2), both indicators of low aggregate stability/high erodibility, SW 3 would be expected to produce the greatest amounts of sediment in the runoff on a per unit area basis for a given rainfall event. Following SW 3, the order for ER is: 7 > 15 > 11 > 10 > 9. The order for AI by SW is: 9 > 15 $\geq$ 10 > 11> 7 > 3. These results may be substantiated by the average suspended sediment concentrations measured at each of the flumes which are reasonably close to expected results based on ER and AI. Specifically, the order of suspended sediment concentrations were: SW 7 (0.040 g ml^{-1}) > 3 (0.028 g ml^{-1}) > 11 (0.23 g ml^{-1}) > 9 (0.015 g ml^{-1}) > 10 (0.013 g ml^{-1}) > 15 (0.009 g ml^{-1}). Obviously, the relative land areas associated with the various slope factor components in each SW also have a strong influence on sediment yields measured at each flume, but the use of soil-sediment factors such as ER and AI appears to be a reasonable approach to estimating potential sediment yields in the SWs.

Sediment Source Estimations: Based on the results obtained from the multivariate mixing model as previously described, the percentage contributions of each SW to the sediment load monitored at flume 1 are as follows: SW 3, 54.2%; SW 7, 20.3%; SW 9, 12.6%; SW 10, 0%; SW 11, 12.9%; and SW 15, 0%. Obviously, these data present a number of questions. Specifically, how can we realistically assume no contributions from SWs 10 and 15 considering their size (Table 1)? Further, how realistic is the estimated 54.2 and 20.3% contributions of SW 3 and 7? Presently, such questions cannot be adequately addressed; however, there are some factors which make some of these source contributions seem reasonable. For example, SWs 10 and 15 had the two highest AI values after SW 9, which means that on the average, the soils in these SWs were relatively unerodible. Within this context, the 12.6% contribution by SW 9 is hard to explain since it had the third lowest average sediment concentration behind 10 and 15, and the lowest ER for clay content of all SWs. Of perhaps greater importance in this regard is the fact that 40.4 and 38.4% of the soils in SWs 9 and 11, respectively, occurred on E class (13-20%) slopes or steeper, compared to 35.5 and 17.4% for the soils in SWs 10 and 15, respectively.

In the case of SWs 3 and 7, the estimated greatest contributors of sediment leaving the watershed, the soils in these two SW had the lowest AI while the percent clay ER and sediment concentrations measured at these two flumes were the highest in the WGEW. All of these results correspond well with data expected from highly erodible watersheds. Additionally, these two SWs are closest to flume 1, thus the sediment contributed by these SWs to the main channel does not undergo as much sorting prior to its delivery at flume 1, relative to the other SWs. Also, the soils in the SW surrounding flume 1 are most similar to those in SW 3. This is a problem that could lead to an overestimation of the contribution from SW 3 which requires additional attention.

CONCLUSIONS

This preliminary study demonstrated that an approach of characterizing watersheds on the basis of soil geomorphology in conjunction with the use of a range of fingerprinting properties, digital elevation models, and digitized soil surveys has the potential to provide a reasonably accurate means of estimating which portions of a watershed are producing the greatest amounts of sediment. Additional research is necessary, however, to resolve questions related to the accuracy of multivariate mixing models used to calculate the relative contributions of sub-components of the watershed, and to determine which soil mapping units are the greatest sediment sources in individual SWs. Eventually, this ability to identify primary sediment sources in watersheds will contribute to a more efficient design of best management practices to affect maximum reductions in sediment and chemical contaminant loads in watersheds.

REFERENCES

Bonniwell, E.G., Matisoff,G.,and Whiting, P. J. (1999). "Determining the times and distances of particle transit in a mountain stream using fallout radionuclides", Geomorph. 27: 75-92.

Breckenfeld, D. J., Svetlik, W. A., and McGuire, C. E. (1995). Soil Survey of Walnut Gulch Experimental Watershed. U. S. Dept. of Agric., Soil Conservation Service, Washington, DC.

Dearing, J. A., Morton, R. A., Price, T. W., and Foster, I. D. L. (1986). "Tracing movements of topsoil by magnetic measurements: Two case studies", Phys. Earth Planet. Inter. 42: 93-104.

Franzmeier, D.P., Pedersen, E. J., Longwell,T. J., Byrne, J. G., and Losche, C. K. (1969). "Properties of some soils in the Cumberland Plateau as related to slope aspect and position", Soil Sci. Soc. Am. Proc. 33: 755-761.

Grimshaw, D.L., and Lewin, J. (1980). "Source identification for suspended sediments", J. Hydrol. 47: 151-162.

Hanna, A. Y., Harlan, P. W., and Lewis, D. T. 1982. "Soil available water as influenced by landscape position and aspect", Agron. J. 74: 999-1004.

Harris, S. (1971). "Index of structure: Evaluation of a modified method of determining aggregate stability", Geoderma 6: 155-162.

Klages, M. G., and Hsieh, Y. P. (1975). "Suspended solids carried by the Gallatin River of southwestern Montana: II. Using mineralogy for inferring sources", J. Environ. Qual. 1: 68-73.

McLean, E. O. (1982). "Soil pH and lime requirement", p. 199-204. *In* A. L. Page et al. (ed.) Methods of soil analysis. Part 2. 2nd ed. Agron. Monogr. 9. ASA and SSSA, Madison, WI.

Neiheisel, J. and Weaver, C. E. (1967). "Transport and deposition of clay minerals, southeastern United States", J. Sediment Petrol. 37: 1084-1116.

Oldfield, F., Rummery, T. A., Thompson, R., and Walling, D. E. (1979). "Identification of suspended sediment sources by means of magnetic measurements: Some preliminary results", Water Resour. Res. 15: 211-218.

Peart, M. R., and Walling, D. E. 1988. "Techniques for establishing suspended sediment sources in two drainage basins in Devon, UK; A comparative assessment", In, Sediment Budgets, Intl. Assoc. Hydrol. Sci. Publ. 174, pp. 269-279.

Renard, K. G., Lane, L. J., Simanton, J. R., Emmerich, W. E., Stone, J. J., Weltz, M. A., Goodrich, D. C., and Yakowitz, D. S. (1993). "Agricultural impacts in an arid environment: Walnut Gulch studies", Hydrol. Sci. Technol. 9: 145-190.

Rhoton, F. E., Smeck, N. E., and Wilding, L. P. (1979). "Preferential clay mineral erosion from watersheds in the Maumee River Basin", J. Environ. Qual. 8: 547-550.

Rhoton, F. E., Lindbo, D. L., and Römkens, M. J. M. (1998). "Iron oxides – erodibility interactions for soils for the Memphis Catena", Soil Sci. Soc. Am. J. 62: 1693-1703.

SAS Institute. (1999). The SAS system for windows. SAS Inst., Cary, NC.

Schoeneberger, P. J., Wysocki, D. A., Benham, E. C., and Broderson, W. D. (2002). Field book for describing and sampling soils, Version 2.0. Natural Resources Conservation Service, National Soil Survey Center, Lincoln, NE.

Slattery, M.C., Hurt, T. P., and Walden, J.(1995). "The application of mineral magnetic measurements to quantify within-storm variations in suspended sediment sources", IAHS Publ. No. 229: 143-151.

Sutherland, R.A., and Bryan, R. B. (1989). "Variability of particle size characteristic of sheetwash sediments and fluvial suspended sediment in a small semiarid catchment, Kenya", Catena 16: 189-204.

USDA-Natural Resources Conservation Service. (1996). Soil Survey Laboratory Methods Manual, Soil Survey Investigations Report No.42. U. S. Govt. Print. Office, Washington, DC.

Wall, G. J., and Wilding, L. P. (1976). "Mineralogy and related parameters of fluvial suspended sediments in Northwestern Ohio", J. Environ. Qual. 5: 168-173.

Wallbrink, P. J., Murray, A. S., and Olley, J. M. (1999). "Relating suspended sediment to its original soil depth using fallout radionuclides", Soil Sci. Soc. Am. J. 63: 369-378.

Walling, D. E., and Woodward, J. C. (1992). "Use of radiometric fingerprints to derive information on suspended sediment source", IAHS Publ. No. 215: 153-164.

Walling, D. E., and Woodward, J. C. (1995). "Tracing sources of suspended sediment in river Basins: A case study of the River Culm, Devon, UK", Mar. Freshwater Res. 46: 327-336.

Whiting, P. J., Matisoff, G., Fornes, W. F., and Soster, F. M. (2005). Suspended sediment sources and transport distances in the Yellowstone basin. GSA Bulletin, 117, pp 515-529.

TEXTURAL ANALYSIS OF MARINE SEDIMENTS AT THE USGS WOODS HOLE SCIENCE CENTER: METHODOLOGY AND DATA ON DVD

Lawrence J. Poppe, lpoppe@usgs.gov; S. Jeffress Williams, jwilliams@usgs.gov; and Valerie F. Paskevich, vpaskevich@usgs.gov, Coastal and Marine Geology Program, U.S. Geological Survey, Woods Hole, MA 02543

Abstract: Marine sediments off the eastern United States vary markedly in texture (i.e., the size, shape, composition, and arrangement of their grains) due to a complex geologic history. For descriptive purposes, however, it is typically most useful to classify these sediments according to their grain-size distributions. In 1962, the U.S. Geological Survey began a program to study the marine geology of the continental margin off the Atlantic coast of the United States. As part of this program and numerous subsequent projects, thousands of sediment grab samples and cores were collected and analyzed for grain size at the Woods Hole Science Center. USGS Open-File Report 2005-1001 (Poppe et al., 2005), available on DVD and online, describes the field methods used to collect marine sediment samples as well as the laboratory methods used to determine and characterize grain-size distributions, and presents these data in several formats that can be readily employed by interested parties. The report is divided into three sections. The first section discusses procedures and contains pictures of the equipment, analytical flow diagrams, video clips with voice commentary, classification schemes, useful forms and compiled and uncompiled versions of the data-acquisition and data-processing software with documentation. The second section contains the grain-size data for more than 23,000 analyses in two "flat-file" formats, a data dictionary, and color-coded browse maps. The third section provides a GIS data catalog of the available point, interpretive, and baseline data layers, with FGDC-compliant metadata to help users visualize the textural information in a geographic context.

INTRODUCTION

We have compiled the textural methods and data from the USGS Coastal and Marine Geology Program's Woods Hole Science Center and released them on DVD as Open-File Report 2005-1001 (Poppe et al., 2005). The purpose of that report is to describe the field methods used to collect marine sediment samples, primarily from along the U.S. east coast, and the laboratory methods used to determine and characterize the grain-size distributions. The report also provides a verified and well-documented sediment database in formats that can be readily employed by interested parties and supersedes a more limited report by Poppe and Polloni (2000).

Grain size is the most fundamental sediment property. Geologists use sediment grain size information to study trends in surface processes that are related to dynamic conditions of transportation and deposition, ecologists use it when studying benthic habitats, engineers use it to study permeability and stability of sediments under load, geochemists use it to study kinetic reactions and the affinities of fine-grained particles and contaminants, and hydrologists use it when studying subsurface fluid migration (Blatt and others, 1972; McCave and Syvitski, 1991). Furthermore, many scientific questions and policy issues related to the offshore require sediment data of historical and regional scope. Because data acquisition is both expensive and time consuming, existing data from different sources need to be compiled and coherently presented.

A detailed catalog of the sediment grain-size data produced at the Woods Hole Science Center provides users with a quantitative foundation for future work and a means of optimizing data acquisition strategies. As one example of value, the data from this report have been imported into usSEABED (Reid et al., 2005), a large data compilation and mining program, and used to provide regional information on sea-floor sedimentary character with applications to aggregate resources suitable for beach nourishment and coastal restoration, benthic habitat mapping, and sediment transport studies.

The new digital report (Poppe et al., 2005) provides an accessible, documented compilation of existing USGS east-coast sediment data and analytical techniques. It also provides the means for environmental managers, policy-makers, scientific researchers, and interested members of the public to gain access to this information.

PROCEDURES

Because many geological observations consist of measurements made on a large number of specimens, the techniques and equipment used for particle-size analysis must be fast, accurate, and yield highly reproducible results. However, the precision of these measurements is limited by the initial sampling techniques, storage conditions, analytical methods, equipment, and the capability of the operator. Therefore, we have incorporated a procedures section into the report to serve as a training manual and reference source for the analyst and as metadata for the scientist.

The procedures section describes field methods used to collect marine sediment samples and laboratory methods used to determine and characterize their grain-size distributions. The field methods section contains recommended sampling, handling, and storage protocols, as well as a pictorial gallery of common sampling devices including grabs, corers, dredges, bedload samplers, and sediment traps (Fig. 1A). The section on laboratory methods contains analytical flow diagrams, illustrated methodologies, instructional video clips with voice commentaries, pictures and schematics of the analytical equipment, classification schemes for grade scale and nomenclature, comments on quality assurance, useful forms, and software (Fig. 1B). Ancillary techniques, such as procedures for removing organics or calcium carbonate, are also included.

Compiled and uncompiled versions of the data acquisition and processing software are provided with documentation and information on system requirements. Although the data acquisition programs are necessarily dedicated to our analytical equipment, the newer data processing programs are not laboratory specific. These programs are written in Visual Basic, run under Windows 98/ME/2000/XP, provide a window to facilitate program execution, and accept input files in standard comma-delimited ASCII text. For example, the program GSSTAT generates statistics to characterize sediment grain-size distributions and can extrapolate the fine-grained end of the particle distribution. The input for the sediment fractions is weight percentages in whole-phi notation (Krumbein, 1934), and the program permits the user to select output in either method of moments or inclusive graphics statistics. The program SEDCLASS generates verbal equivalents to characterize sediment grain-size distributions. Inputs for this program are percentages of gravel, sand, silt, and clay in the Wentworth (1929) grade scale. The program

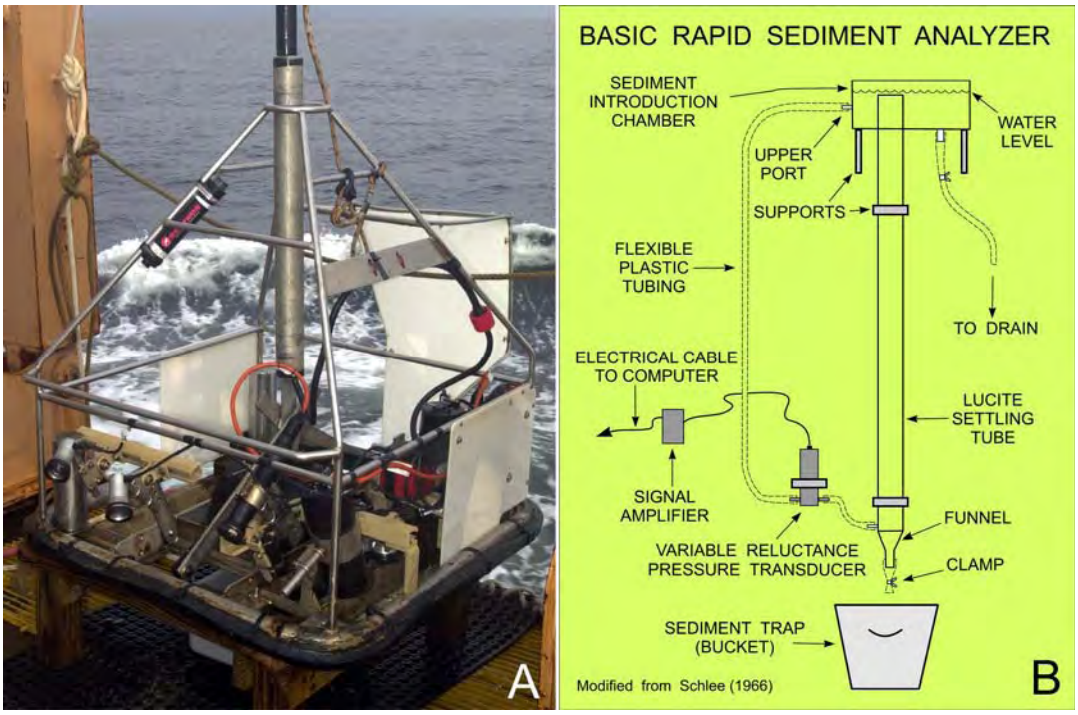


Figure 1. Browse graphics of field and laboratory methods. A. A Van Veen grab equipped with still and video camera systems that is part of the report's gallery of devices used to collect sediment samples. B. The basic design of a rapid sediment analyzer (i.e. settling tube) based on the design by Schlee (1966).

permits the user to select output in either the Shepard (1954) classification scheme, as modified by Schlee (1973), or the Folk (1974) scheme. Users of these programs select options primarily with mouse-click events or through interactive dialogue boxes.

DATABASE

The sediment database incorporates information on the collection, location, description, and texture of samples taken by numerous marine sampling projects, most of which are from off the east coast of the United States (Fig. 2). The database presently contains data for over 23,300 samples, which includes texture data for approximately 3,800 samples taken or analyzed by the Atlantic Continental Margin Program, a joint USGS/Woods Hole Oceanographic Institution project conducted from 1962 to 1970 (Emery and Schlee, 1963; Hathaway, 1971). Texture data for approximately 19,500 samples analyzed after 1980 in the Woods Hole Science Center's Sediment Laboratory make up the rest of the database. Although most records contain complete grain size analyses, some are simple bottom descriptions from rocky and bouldery locations where samples were not taken. Most of the samples were collected with some type of grab sampler, though a few were obtained by coring.

Database Platform and Formats: The basic structure of the sediment database is a matrix where rows are records representing individual samples and columns contain information on sample identification, navigation, classifications, analyzed parameters, and comments. This is a

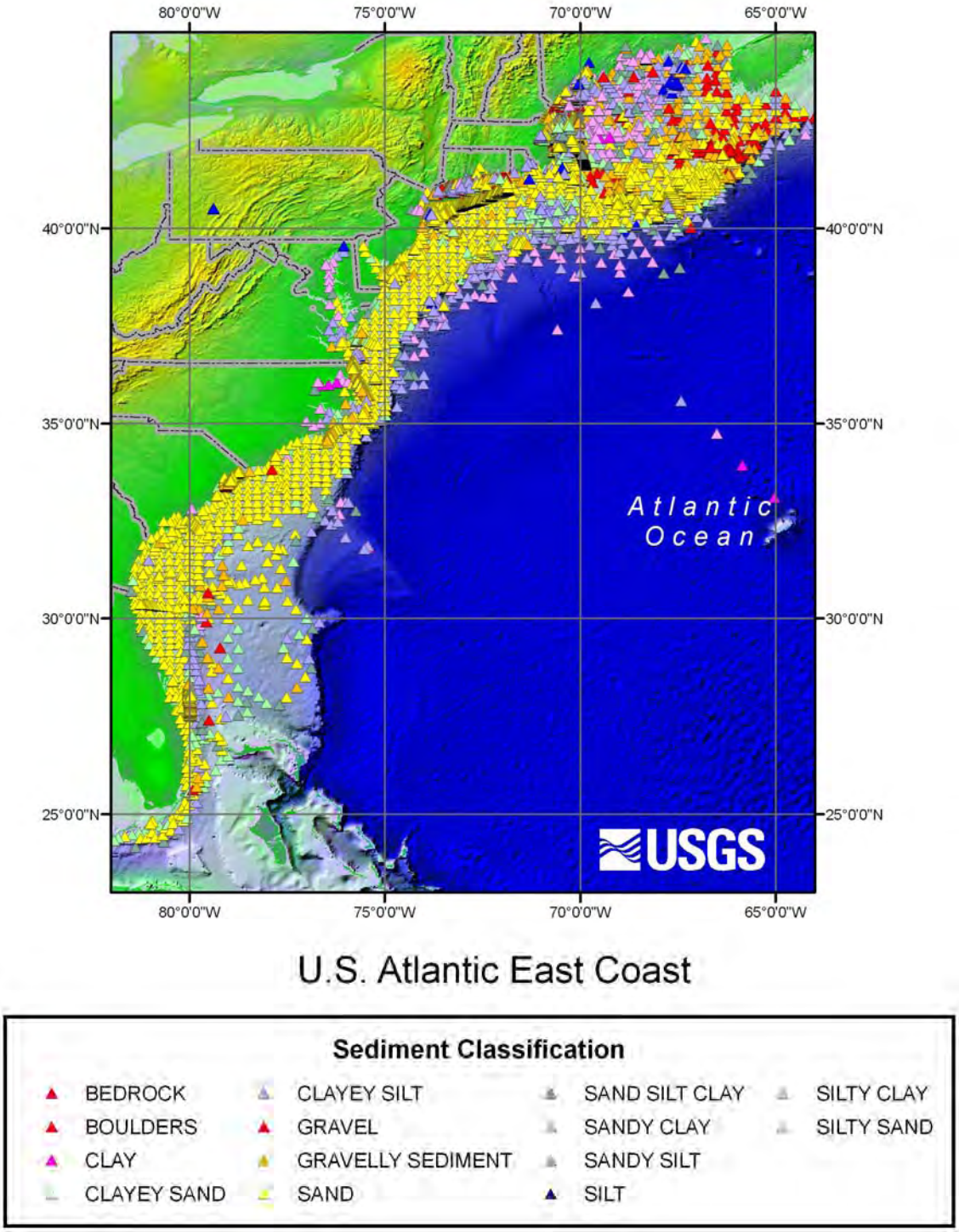


Figure 2. Graphic shows station locations in the USGS East-Coast Sediment Texture Database for those samples from off the U.S. east coast. Similar graphics are available for other areas (e.g. Carribean and Gulf of Mexico). Colors denote sediment classification, but, in cases where a sediment type is uncommon, colors may represent more than one class (e.g. silty sand and clayey sand are both light green).

"flat-file" format, which means that it is not "normalized" (i.e., of reduced redundancy). While this is considered inefficient from the point of view of database management, it is the most general way of presenting the basic data. This structure was chosen to avoid ambiguity, and to make the process of locating fields, entering data and validating simple yet comprehensive. Since neither the software capabilities of the user nor the probable uses of the data were known, no attempt was made to split the files or to reduce blank fields. If the user wishes to make the database more efficient through "normalization," we feel that it is better that this be done by the user to fit both the applications available to the user and the database structural logic that is familiar to the user. The price paid for the "flat-file" approach is additional storage space, exceptionally wide records, and the possibility that corrections made here at the source may fail to be carried through to all forms of the affected data. Browse graphics are supplied to help users visualize the geographic distribution of the stations and sediment types (Fig. 2).

The database is provided in two formats: Microsoft Excel 2000, a popular commercial software format, and tab-delimited ASCII text. The Excel file will open in the appropriate software if the user has this application installed and their web browser properly configured or if the file is downloaded and opened directly with Excel. The tab-delimited file contains data as well as headings for the tables of data in uncompressed ASCII format. This file is supplied for users who wish to import the data into applications that can accept ASCII character information. The database contains 58 fields and is supplied with a data dictionary that explains the structure and content of the database. The dictionary contains an index of the parameters measured and their definitions. Extracting data from the database is facilitated by reference to this document because it provides a means to keep track of abbreviations and field names. The specific fields and parameters were chosen based on the data produced in the sediment laboratory at the Woods Hole Science Center and the formats of information typically found in the literature. Most records do not have data in all of the available fields; however, additional fields, qualifiers, and data can be added in virtually unlimited fashion to accommodate specific needs.

GIS DATA

Data in the report are provided with geographic coordinates to facilitate their integration into a Geographic Information System (GIS). A GIS is defined as a system of hardware and software to display, manipulate, and analyze spatial data for mapping and complex data solving. This integrated package provides researchers the ability to combine, analyze, and map multiple datasets to help with economic and social policy-making decisions regarding the environment.

This report uses the Environmental Systems Research Institute's (ESRI) ArcView and ArcGIS software as its GIS mapping tools. Data layers archived here should not require additional processing to be utilized within ESRI software. This does not mean that a user will not wish to do additional processing, especially if utilizing a different GIS software package or ellipsoid, but that it is not necessary to do additional processing simply to utilize the data in its minimum archive format. For those who don't have the ESRI software or a compatible GIS data browser available on their computer, a free viewer, ArcExplorer, is available from ESRI. Although the report provides ArcView and ArcGIS project files, it contains no prepared project file for use with ArcExplorer. If the user chooses ArcExplorer, it will be necessary to add the selected data layers to their own defined project file.

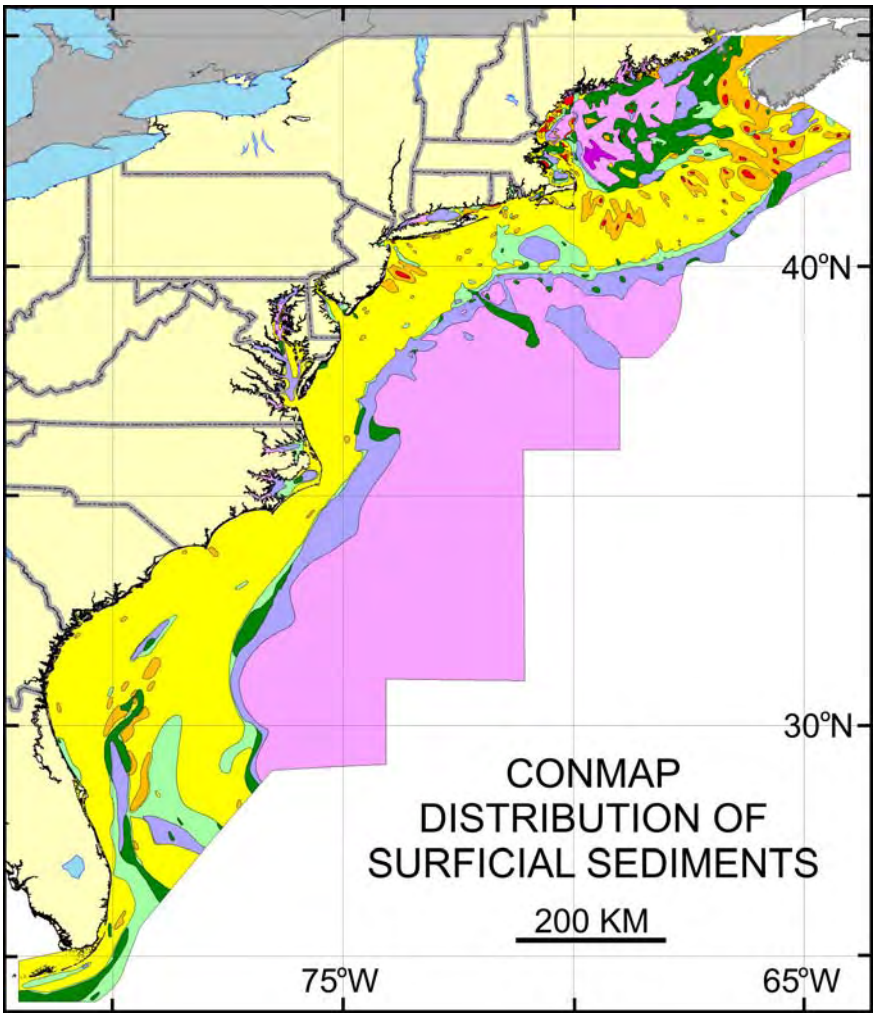


Figure 3. Polygon data layer of the Continental Margin Mapping Program (CONMAP) series composite map for surficial sediments off the U.S. east coast. Data layer is useful as a general overview and to show gross textural trends. See Figure 2 for a color key of classifications.

Data Catalog of GIS Layers: All GIS data layers in this report are available through a data catalog that includes browse graphics and FGDC-compliant metadata in FAQ, HTML, and text formats. These data layers include two sediment data layers and three basemap data layers. The two sediment data layers are the USGS East Coast Sediment Texture Database, which is supplied as a point shapefile, and the Continental Margin Mapping Project (CONMAP) series surficial-sediment maps, which are combined into one layer and supplied as a polygon shapefile (Fig. 3). The sediment maps in the CONMAP series (Klitgord and Hill, 1986; Poppe and others, 1989; Poppe and others, 1994) are regional syntheses of surficial sediment studies compiled from grain-size data produced at the Woods Hole Science Center and from earlier published and unpublished studies. Although old and inaccurate at large scales (e.g. less than 1:1,000,000), the CONMAP data layer is provided as a general overview and to show gross textural trends.

Supplied basemap data layers include internal U.S. state boundaries and color-encoded images of North American and world topography.

REFERENCES

Blatt, H., Middleton, G., and Murray, R., 1972, Origin of Sedimentary Rocks: Englewood Cliffs, New Jersey, Prentice-Hall, 634 p.

Emery, K.O., and Schlee, J.S., 1963, The Atlantic Continental Shelf and Slope, a program for study. U.S. Geological Survey Circular 481, 11 p.

Folk, R.L., 1974, The petrology of sedimentary rocks: Austin, Tex., Hemphill Publishing Co., 182 p.

Hathaway, J.C., 1971, Data File - Continental Margin Program. Woods Hole Oceanographic Institution Technical Report 71-15, 492 p.

Klitgord, K.D., and Hill, G.W., 1986, Continental Margin Mapping Project, U.S. Atlantic margin; a synthesis of geologic and geophysical data interpretations. American Association of Petroleum Geologists Bulletin, v. 70, p. 608.

Krumbein, W.C., 1934, "Size frequency distribution of sediments," Journal of Sedimentary Petrology, v. 4, p. 65-77.

McCave, I.N., and Syvitski, J.P.M., 1991, "Principles and methods of particle size analysis," In J.P.M. Syvitski (ed.), Principles, Methods, and Applications of Particle Size Analysis, New York, Cambridge University Press, p. 3-21.

Poppe, L.J., Schlee, J.S., Butman, B., and Lane, C.M., 1989, Map showing the distribution of surficial sediment, Gulf of Maine and Georges Bank. U.S. Geological Survey Miscellaneous Investigations Series Map I-1986-A, 1 sheet, scale 1:1,000,000.

Poppe, L.J., Schlee, J.S., Knebel, H.J., 1994, Map showing distribution of surficial sediments on the mid-Atlantic continental margin, Cape Cod to Albemarle Sound. U.S. Geological Survey Miscellaneous investigations Series Map I-1987-D, 1 sheet, scale 1:1,000,000.

Poppe, L.J., and Polloni, C.F. (eds.), 2000, USGS East-Coast Sediment Analysis. Procedures, Database, and Georeferenced Displays, U.S. Geological Survey Open-File Report 00-358, CD-ROM.

Poppe, L.J., Williams, S.J., and Paskevich, V.F., 2005, USGS East-Coast Sediment Analysis. Procedures, Database, and GIS Data: U.S. Geological Survey Open-File Report 2005-1001, DVD.

Reid, J.M., Reid, J.A., Jenkins, C.J., Hastings, M.E., Williams, S.J., and Poppe, L.J., 2005, us SEABED: Atlantic coast offshore surficial sediment data release, version 1.0. U.S. Geological Survey Data Series 118, CD-ROM.

Shepard, F.P., 1954, "Nomenclature based on sand-silt-clay ratios," Journal Sedimentary Petrology, v.24, p. 151-158.

Schlee, J., 1966, "A modified Woods Hole Rapid Sediment Analyzer," Journal Sedimentary Petrology, v. 30, p. 403-413.

Schlee, J., 1973, A"tlantic Continental Shelf and Slope of the United States sediment texture of the northeastern part," U.S. Geological Survey Professional Paper 529-L, 64 p.

Wentworth, C.K., 1929, "A scale of grade and class terms for clastic sediments," Journal Sedimentary Petrology, v. 30, p. 377-392.

LOWER CLEAR CREEK FLOODPLAIN REHABILITATION PROJECT: GEOMORPHIC MONITORING OF PHASE 3A

Smokey Pittman, M.S., Senior Geomorphologist, Graham Matthews and Associates, 4902 Cedar Ravine, Placerville, CA 95667, smokey@gmahydrology.com; Graham Matthews, M.S., Principal, Graham Matthews and Associates, PO Box 1516, Weaverville, CA 96063, graham@gmahydrology.com

Abstract: Three years of geomorphic monitoring of Phase 3A of the *Lower Clear Creek Floodway Rehabilitation Project* evaluated the effectiveness of reconstructing 0.5 miles of stream channel historically impacted by gravel mining, gold dredging and flow regulation. Sequential surveying, stream gaging, scour monitors, bulk sampling, suspended sediment and bedload sampling, photography and bed-mobility experiments were employed to evaluate floodplain function and in-channel geomorphic processes.

Large winter storm flows in December 2002 resulted in significant initial changes to the cross section, topographic and longitudinal geometry of the re-constructed channel. Point bars, mid-channel bars, new pools and transverse riffles began to develop. Riffle matrix particles initially mobilized at well below the design bankfull discharge of 3,000 cfs, but as the channel adjusted, the threshold of bed mobility increased to an average of 2,800 cfs. Gravel-injected banks eroded and some pools deepened. Further channel adjustment followed a rare sustained spill event in April 2003. Water years 2004 and 2005, with lower peak discharges, had a relatively smaller effect.

The design channel failed to flow over bank at flows above 3,000 cfs at the upstream end of the reach, thus contributing greater erosive energy to transport introduced gravels. However, at 6 of 8 cross sections, the channel functioned as designed, flowing over the banks above 3,000 cfs, resulting in fine sediment deposition on the floodplain. Increased roughness associated with floodplain plantings enhanced deposition of material (< 0.1 mm) in the desired size class.

Sediment transport curves for bedload and suspended load (generated from medium to high flow samples collected with a 6 inch Helley-Smith sampler deployed from a cataraft on a cableway) were applied to continuous discharge records to compute annual loads. Water Year 2003 produced 7,360 tons of bedload while Water Year 2004 produced 2,500 tons, illustrating the hydrologic differences in two consecutive years. Similarly, suspended sediment yield was computed using the relationships between suspended sediment concentration and discharge and/or turbidity: Water Year 2003 yielded 35,300 tons of suspended sediment compared to 8,460 tons in Water Year 2004.

The hydraulic design for Phase 3A may require modification to improve floodplain function and gravel injections may be required to provide desired geomorphic attributes.

THE USDA'S CONSERVATION EFFECTS ASSESSMENT PROJECT (CEAP)

Roberta Parry, USEPA, on detail with USDA-Natural Resources Conservation Service, Beltsville, MD; Roberta.parry@wdc.usda.gov

Abstract: The Conservation Effects Assessment Project (CEAP) is being carried out by the USDA, in coordination with USEPA, USGS, and others. This poster will present the key aspects of the ongoing project, which is focused on determining the effects of conservation programs and practices at the national scale, as well as at the watershed scale. The questions to be asked include (a) where are practices being applied, (b) what are their impacts, and (c) how can existing conservation programs be improved, including the conservation title of the 2002 Farm Bill. A total of 24 watersheds were included in the study in 2005, with more to be added in 2006. Nationally significant, scientifically defensible results will begin to be reported by the end of 2005. Individual watershed reports, assessments, and other products and tools, will be developed all through the life of the project, including locally calibrated models, as well as regionalized models (through modularization) to support the National Assessment of conservation practices and programs.

NUMERICAL STUDY OF THE RESPONSE OF A RESERVOIR DEPOSIT TO SUDDEN DAM REMOVAL

Alessandro Cantelli, Dept. of Civil & Environmental Engineering, Univ. of Illinois; Miguel Wong, St. Anthony Falls Laboratory, Univ. of Minnesota; Gary Parker, Depts. of Civil & Environmental Engineering, Univ. of Illinois

Abstract: Dams that are filled with sediment and serve no useful purpose may be targets for removal. A dam may be removed gradually or suddenly. Here the case of sudden removal, or "blow and go" is considered. Sudden removal leads to the incision of a channel into a reservoir deposit. In many cases the incision is so rapid that the channel first narrows as it incises before it widens. A 1D formulation of incisional narrowing and widening is presented. The degree of incisional narrowing plays a role in determining the short-term efficiency with which sediment is removed from the reservoir. The case of an homogeneous, non-cohesive sediment is considered. The results of a parametric study of the erosion process as a function of varying initial width of the incisional channel are reported. The results allow for tracking of short-term variation of a) sediment delivery, b) incisional channel width and c) disposition of sediment left in the reservoir. Long-term implications for sediment removal from the reservoir and downstream delivery are also discussed.

MONITORING AGGRADATIONAL AND DEGRADATIONAL TRENDS ON THE MIDDLE RIO GRANDE, NM

Robert Padilla, Bureau of Reclamation, Albuquerque Area Office, Albuquerque, NM;
Christi Young, Bureau of Reclamation, Technical Service Center, Denver, CO

Abstract: For nearly a century, topographic surveys of the river channel and floodplain associated with monitoring sedimentation trends have been conducted on the Middle Rio Grande valley extending from Cochiti Reservoir to the headwaters of Elephant Butte Reservoir. This 160-mile reach of alluvial river has some of the most problematic sedimentation issues in the United States. Reservoir sedimentation monitoring cross sections in Elephant Butte Reservoir have been resurveyed many times since they were established in 1916. The majority of sediment transported on the main stem Rio Grande is deposited in this reservoir. Analysis of the deposition along these cross sections shows over 600,000 acre-feet (23 percent) of storage were lost between 1916 and 1999 with the highest rate of reservoir sedimentation occurring prior to 1940. Additional cross sections in the upstream river have been established over time and field surveyed periodically by various federal and state agencies to monitor changes. The channel portion of many of these historical cross sections continues to be periodically field surveyed.

After an extensive period of construction of flood and sediment control facilities and channelization works, an aerial survey in 1962 established nearly 2000 photogrammetric aggradation/degradation (agg/deg) rangelines. These rangelines are spaced at about 500-foot intervals to monitor sedimentation and morphological changes of the river channel and floodplain for the entire Middle Rio Grande reach. Aerial surveys were conducted and data obtained for the same rangelines in 1972, 1992, and 2002. These cross section data have been analyzed to determine the rate and extent of sediment erosion and deposition. Trends are presented as average values for established sub-reaches and show significant differences in main channel volumetric changes over time among the sub-reaches. Conditions and responses vary along the study reach with the sediment deposition generally increasing downstream and decreasing over time. Historical main channel aggradational trends have in some cases reversed due to upstream dam construction and decreases in tributary sediment inflow.

Analysis of aggradational and degradational trends provides valuable evidence of the short- and long-term responses of the Middle Rio Grande to natural and anthropogenic influences. These trends are also used to evaluate river maintenance strategies, habitat recovery efforts, and estimate future processes and trends.

INTRODUCTION

A historical record of the aggradational and degradational trends of the 160-mile reach of the Middle Rio Grande has been compiled by Bureau of Reclamation in cooperation with other federal and state agencies. (USBR 1967, 1974; Young et al., 2005 draft). Arid and semi-arid watersheds of easily erodible sediments and steep-gradient ephemeral tributaries contribute to the high geological rate of erosion of the basin drainage areas. Flash floods on these tributaries carry loads greater than the main stem channel can normally transport and form delta fans at their confluences. Irrigation diversions contribute to accumulation of sediments in the river channel by decreasing discharge, and diversion

dams influence the river slope. Throughout the reach, the river is confined to a portion of its historical floodplain by levees associated with water delivery and drainage. About 90 miles of jetty fields are also present and previously encouraged sediment deposition in overbank areas and scour in the main channel. Excessive channel degradation disconnects the channel from the floodplain reducing the quality and quantity of in-stream and floodplain habitat and accelerating erosion of the bed and bank. Channel incision downstream of Cochiti Dam and corresponding increases in the potential for bank collapse are additional sources of sediments. Sediment deposition in the San Marcial area reduces channel capacity and water delivery efficiency, and it affects valley drainage, threatening the ability to effectively convey water through this reach. Historical losses involving sedimentation include the abandonment of productive lands, reduction in crop yields, increases in flood damages, and the inability of the State of New Mexico to deliver water required under the terms of the Rio Grande Compact while still providing sufficient water to meet normal irrigation demand (USBR 1967, 1974, and 2001).

Continued analysis and monitoring of the aggradational or degradational trends provides Middle Rio Grande river management agencies valuable quantifiable evidence of the short- and long-term responses of the Rio Grande to natural and anthropogenic influences. This additional understanding provides a useful basis for informed decision making regarding the effects of natural hydrologic variations, reservoir operations, habitat restoration, and channel maintenance activities on the river channel and floodplain.

DATA COLLECTION AND ANALYSIS

A variety of data collection and analyses techniques are being utilized by Reclamation to support its Middle Rio Grande river maintenance program, improve the effectiveness of maintenance design practices, and reduce uncertainties related to river hydraulics, sediment transport, and geomorphic channel response.

Hydrographic Surveys: This data collection includes river and reservoir cross section surveys, velocity and discharge measurements, sediment discharge measurements, and sediment sampling. The earliest comprehensive sedimentation survey of the entire Middle Rio Grande Valley was performed in 1936, corresponding to the completion of irrigation works constructed by the Middle Rio Grande Conservancy District. Subsequent sedimentation field surveys of limited cross sections were performed in 1940, 1941/42, 1944, and 1952/53. Data from these surveys have helped establish historical trends (USBR, 1967). Additional cross sections have been established and continue to be surveyed to support various river management goals by Reclamation and other agencies.

The Elephant Butte Reservoir rangelines are the oldest and most continuous cross section data sets available on the Middle Rio Grande. The original survey for Elephant Butte Reservoir was conducted between 1903 and 1908. A dozen resurveys have been conducted on the reservoir between 1916 and 1999. Resurveys are performed whenever there is an estimated 5 percent change in reservoir capacity based on historical trends. The 1999 resurvey estimated an average annual sediment accumulation rate for 84 years of record of about 7,200 acre-feet/year. The rates of reservoir capacity loss at Elephant Butte Reservoir provide reasonable estimates of the amount of sediment transported by the Rio Grande. Due to the length of the reservoir, virtually all sediment

entering the reservoir is trapped. Figure 1 shows how reservoir capacity and cumulative water inflow have varied over time. Over 600,000 acre-feet (23 percent) of storage were lost between 1916 and 1999 with the highest rate of reservoir sedimentation occurring prior to 1940 (Collins and Ferrari, 2000).

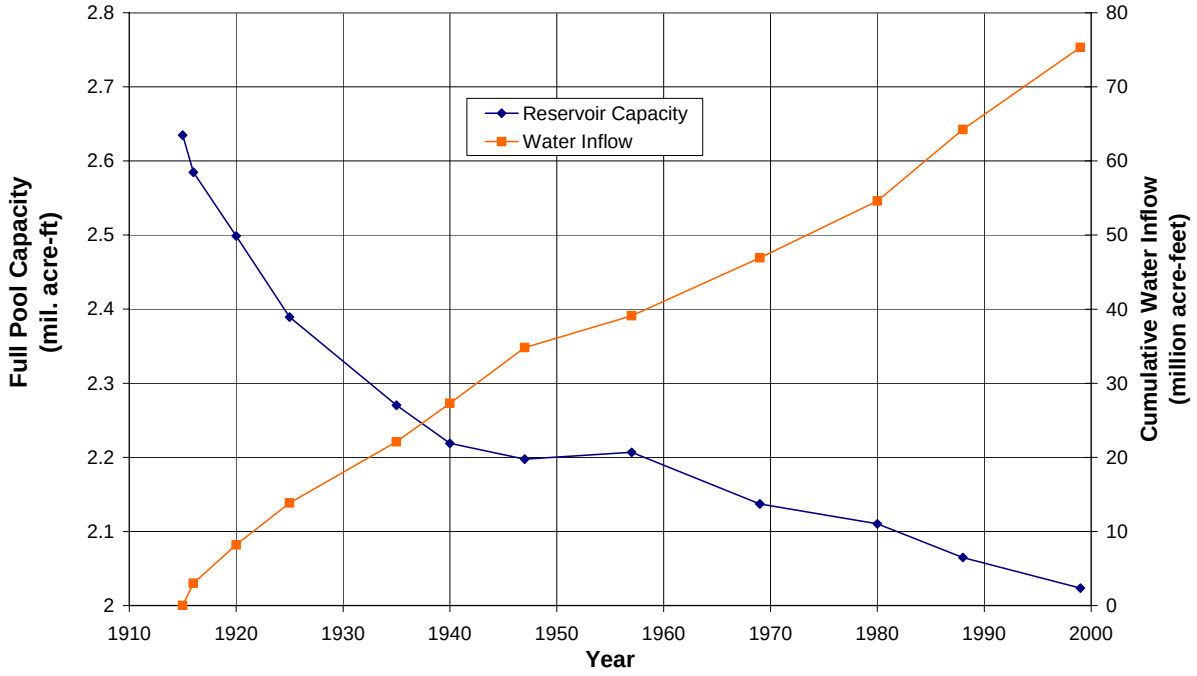


Figure 1 Elephant Butte Reservoir Capacity and Cumulative Water Inflow vs. Time

Field observations: These data include geomorphic observations such as mapping terrace and island formation, evaluating bank stability, classifying vegetation, and evaluating riverine and overbank habitat. The focus of this study is aggradational and degradation trends, more detailed analyses of the hydrologic and river process trends and documentation of planform changes including features such as terraces are available in other reports. (e.g., Bauer (1999); Makar and Strand (2002); Oliver (2004); Makar and Bauer (2004); Richard, Julien, and Baird (2005); Klawon and Makar (2002)) Generally over time, mean flows, channel and floodplain widths, and sediment transport rates have decreased, while channel depth, the number of islands and bars, and channel velocities have increased.

Aerial photography: This data collection includes mosaics of aerial photography and digital ratio-rectified or digital orthophotos that are the basis for deriving photogrammetric cross sectional data and developing digital terrain models and maps. Aerial photography data are typically collected for the river corridor between the levees in the months of January or February when foliage and river flows are at a minimum. Two to three ground control stations are located within every river mile using GPS survey equipment. Mapping, digital imagery, and cross sectional data are collected at the scale of 1:4800 or 1 inch equals 400 feet. Ground position accuracy for planimetric features are within ± 8 to 10 feet and within ± 0.5 feet for ground surface elevations.

The main focus of this study was the analysis of the current aggradation/degradation (agg/deg) photogrammetric cross sections between Cochiti Dam and Elephant Butte Reservoir. The cross

sections were established at roughly 500-foot intervals in 1962 to record the condition of the channel improvement works and serve as a basis for future evaluation of sedimentation and morphologic changes in the river channel and floodplain. The frequency of aerial surveys has been about every 10 years; photogrammetric data sets were collected in 1962 (Abram Aerial Survey Corporation), 1972 (Limbaugh Engineers, Inc.), 1992 (Koogle & Pouls Engineering, Inc.), and 2002 (Pacific Western Technologies, Ltd.).

A consequence of using conventional aerial photography to develop cross section data is that the underwater portion must be estimated. The elevation data obtained from the aerial photography for inundated portions represent the water surface, not the channel bottom. The underwater prism for each cross section is solved iteratively using backwater analysis with actual stream gage discharge data, photograph interpretation, and a rectangular prism assumption for the channel's underwater geometry.

For the data analysis, the river was divided into five sub-reaches based on historical geographic boundaries as described in the 1967 and 1974 Summary Reports. The most downstream San Marcial reach boundary was set to avoid any duplication of data obtained from the previously described reservoir sedimentation surveys. Table 1 below relates the divisions and the corresponding agg/deg cross sections that bound the reach divisions. Young et al. (2005) also provide similar data delineated by utilizing geomorphic reaches defined for water operation studies and further subdivision of the San Marcial reach into two sub-reaches.

Table 1 Middle Rio Grande Sub-Reach Divisions

Sub-Reach Name	Cross section number	
	Upstream Boundary	Downstream Boundary
Cochiti	17	236
Albuquerque	236	656
Belen	656	1207
Socorro	1207	1505
San Marcial	1505	1584

Computer programs and spreadsheets were applied in the analysis of cross section data for the 1962, 1972, 1992, and 2002 data sets. The accuracy of the river and floodplain volumetric changes and mean bed elevation comparisons was improved (when compared to the pre-1962 data sets) through the use of mathematical solutions based on a greater number of cross sections and a greater number of points representing each cross section. Other indicators used in this data analysis to evaluate the agg/deg trends include sub-reach slope, average bed elevation, and river and floodplain agg/deg volumetric changes. The sedimentation volumetric changes are reported for the main channel, flood plain, and total section, as shown in Figures 2a, 2b, and 2c, respectively. The main channel definition used in this study is the active channel, or the portion of the floodway the river has

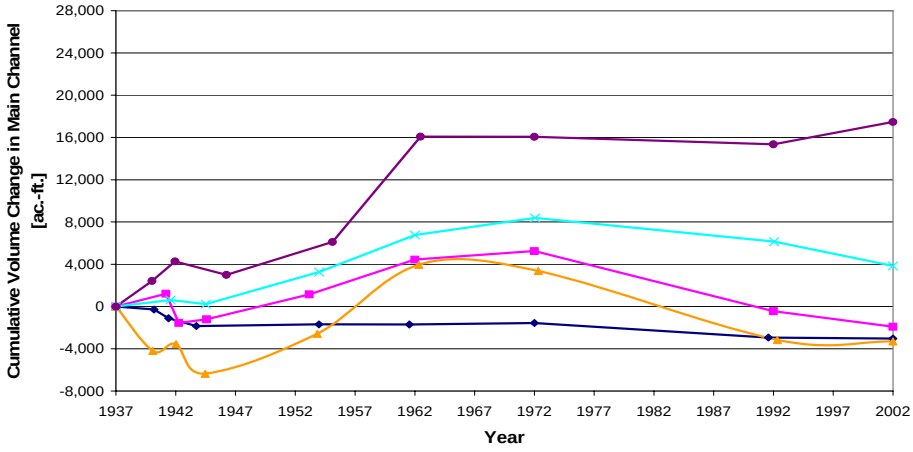
maintained clear of vegetation. The boundary for computing the volumetric change between the main channel and the overbanks for each cross section is determined according to the widest main channel definition combination obtained for the left and right main channel limits from both data sets for the period analyzed.

Comparison of the figures shows that the downstream-most San Marcial reach has experienced the most sediment accumulation, whereas the main channel of the upstream-most Cochiti reach has consistently lost sediment. The three middle reaches have varied between aggradation and degradation trends over the study period. The floodplains for all reaches experience most of the recorded accumulation prior to 1972 and have remained relatively steady since then.

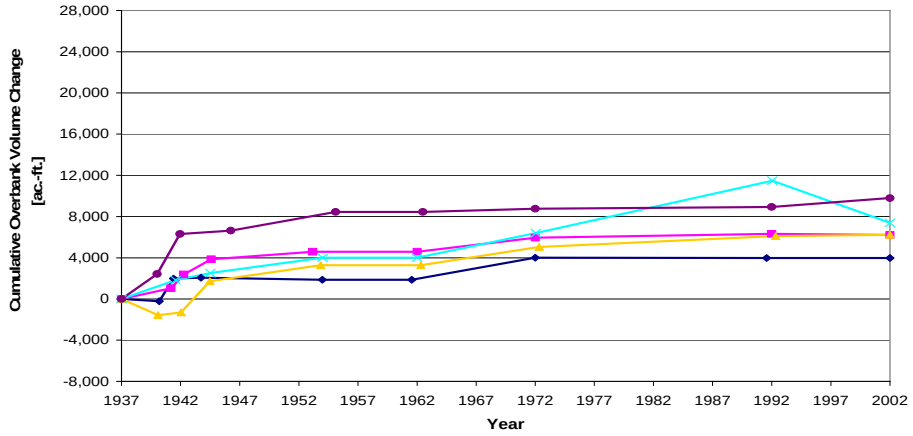
CONCLUSION

The Middle Rio Grande is a complex, dynamic system that experiences a myriad of resource management issues related to its aggradational and degradational trends. The efforts Reclamation and other agencies have made to the long-term collection of the agg/deg data on the Middle Rio Grande have provided significant benefits in supporting informed decisions related to reservoir operations, habitat restoration, and channel maintenance. The data are used to assess the response of the river channel to current and historical river management activities. Under the Middle Rio Grande Project activities of note include construction of flood and sediment control facilities such as Jemez Dam in 1953, Abiquiu Dam in 1963, Galisteo Dam in 1970, Cochiti Dam in 1973 and river channelization works from San Acacia Diversion Dam to Elephant Butte Dam and from Cochiti Dam to the Rio Puerco Confluence. The data provide substantial river morphological information such as channel width, floodplain width, river migration rates, river bed profile and changes over time in aggradation and degradation of the river and the floodplain. These trends are used to assess channel capacity, available aquatic and riparian habitats, channel stability, and the channel's response to flow releases from upstream dams. Most recently, the 2002 agg/deg cross section data and mapping were also utilized to analyze width trends by Makar et al. (2006), in geologic interpretation of channel incision and terrace formation in Massong et al. (2006); and as base geometry data for sediment transport modeling by Holmquist-Johnson (2006).

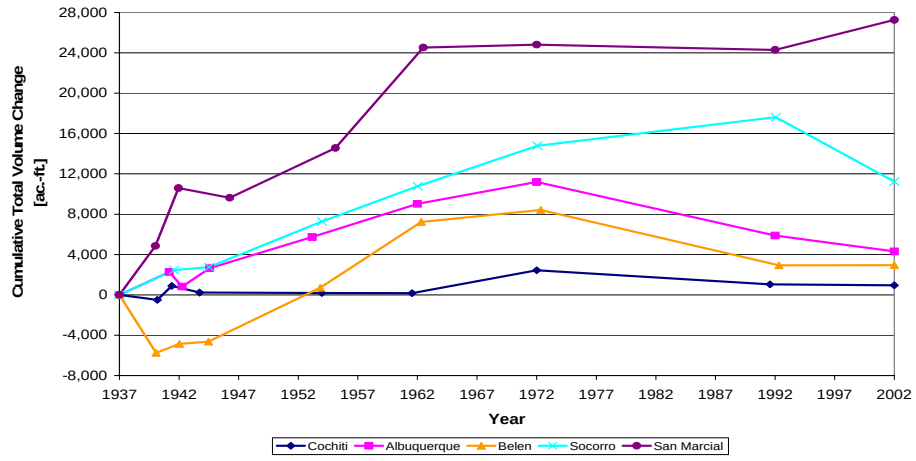
The need for ongoing data collection efforts and river and channel floodplain analysis related to the aggradation and degradation trends described will continue in the future to support informed maintenance decisions.



(a)



(b)



(c)

Figure 2 Cumulative Sediment Volumetric Change from 1937 – 2002
(a) Main Channel, (b) Overbank, and (c) Total

REFERENCES

Abram Aerial Survey Corporation, (1962). "Middle Rio Grande Project – Photogrammetry, Aggradation/Degradation Rangelines", prepared for U.S. Bureau of Reclamation and U.S. Corps of Engineers, Lansing, Michigan.

Bauer, T. R. (1999). "Morphology of the Middle Rio Grande from Bernalillo Bridge to the San Acacia Diversion Dam, New Mexico." MS thesis, Colorado State Univ., Fort Collins, Colo.

Collins, K. and Ferrari, R. (2000). "Elephant Butte Reservoir 1999 Reservoir Survey", U.S. Department of the Interior, Bureau of Reclamation, Technical Service Center, Sedimentation and River Hydraulics Group, Denver, CO

Holmquist-Johnson, C. (2006). "Application of GSTAR-1D Sediment Transport Model on the Middle Rio Grande, NM – San Acacia Diversion Dam to Elephant Butte Reservoir", Joint 8th Federal Interagency Sedimentation Conference and 3rd Federal Interagency Hydrologic Modeling Conference, Reno, NV.

Holmquist-Johnson, C. (2005). "Sediment Model for the Middle Rio Grande – Phase 1, San Acacia Diversion Dam to Elephant Butte Reservoir", U.S. Department of the Interior, Bureau of Reclamation, Technical Service Center, Sedimentation & River Hydraulics Group, Denver, CO

Klawon, J. and Makar, P. (2002). "Historical Terrace Mapping: Escondida Bridge to Pool of Elephant Butte Reservoir." U. S. Department of the Interior, Bureau of Reclamation, Technical Service Center, Flood Hydrology Group, Denver, CO.

Koogle & Pouls Engineering, Inc., (1992). "Middle Rio Grande Project – Photogrammetry, Aggradation/Degradation Rangelines", prepared for U.S. Bureau of Reclamation under contract No. 1425-2-CA-40-1077A, Albuquerque, New Mexico.

Limbaugh Engineers, Inc., (1972). "Middle Rio Grande Project – Photogrammetry, Aggradation/ Degradation Rangelines", prepared for U.S. Bureau of Reclamation under contract No.14-06-D-7229, Albuquerque, New Mexico.

Makar, P., Massong, T. and Bauer, T. (2006). "Channel Width Changes along the Middle Rio Grande, NM." Poster – Joint 8th Federal Interagency Sedimentation Conference and 3rd Federal Interagency Hydrologic Modeling Conference, Reno, NV.

Makar, P.W. and Bauer, T.R. (2004). "Middle Rio Grande Planform Characterization and Analysis." U. S. Department of the Interior, Bureau of Reclamation, Technical Service Center, Sedimentation and River Hydraulics Group, Denver, CO.

Makar, P.W. and Strand, R.I. (draft 2002). "Responses of the Middle Rio Grande: San Acacia to Elephant Butte." U. S. Department of the Interior, Bureau of Reclamation, Technical Service Center, Sedimentation and River Hydraulics Group, Denver, CO.

Massong, T., Tashjian, P. and Makar, P. (2006). "Recent Channel Incision and Floodplain Evolution within the Middle Rio Grande, NM." Joint 8th Federal Interagency Sedimentation Conference and 3rd Federal Interagency Hydrologic Modeling Conference, Reno, NV.

Oliver K.J., (2004). Middle Rio Grande Project – 1918-2002 Geomorphology Study for the Rio Grande from Velarde to the Narrows of Elephant Butte, New Mexico. U. S. Department of the Interior, Bureau of Reclamation, Technical Service Center, Remote Sensing and GIS Group, Denver, CO.

Pacific Western Technology, Ltd., (2002). "Cochiti to Elephant Butte – Aggradation/Degradation Rangelines", prepared for the Bureau of Reclamation under contract No. 1425-97-CA-40-2058B, Albuquerque, New Mexico

Richard, G.A., Julien, P.Y. and Baird, D.C. (2005). "Case Study: Modeling the lateral mobility of the Rio Grande below Cochiti Dam, New Mexico." Journal of Hydraulic Engineering, ASCE, 131(11).

United States Bureau of Reclamation, (2001). "Final Programmatic Biological Assessment of Proposed Bureau of Reclamation and Corps of Engineers Discretionary Actions and Related Non-Federal Actions Regarding Water Management in the Middle Rio Grande", Environmental and Lands Division, Albuquerque Area Office, Albuquerque , New Mexico. pp. 113 to 139.

United States Bureau of Reclamation, (1967). "Summary Report – Rio Grande, Aggradation or Degradation, 1936 – 1962, Middle Rio Grande Project", Sedimentation Section, Denver Office

United States Bureau of Reclamation, (draft 1974). "Summary Report – Rio Grande, Aggradation or Degradation, 1962 – 1972, Middle Rio Grande Project", Sedimentation Section, Denver Office

Young, C., Sailer, M., Collins, K. and Holmquist-Johnson, C. (2005 draft). "Sedimentation Studies of Aggradation or Degradation in the Middle Rio Grande Project", Bureau of Reclamation, Technical Service Center, Sedimentation and River Hydraulics Group, Denver, CO.

GEOMORPHIC CHANGE AND CONTROLLING VARIABLES IN AN EPHEMERAL ALLUVIAL CHANNEL

M. H. Nichols, Research Hydraulic Engineer, USDA-ARS, Southwest Watershed Research Center, 2000 E. Allen Rd., Tucson, AZ 85719; mnichols@tucson.ars.ag.gov , M. Nearing, Agricultural Engineer, USDA-ARS, Southwest Watershed Research Center, 2000 E. Allen Rd., Tucson, AZ 85719; mnearing@tucson.ars.ag.gov and B. Yuill, Graduate Student, Arizona State University, Temp, Arizona; brendan.yuill@asu.edu

Abstract: Channel form and adjustment are the result of complex interactions among bed sediment, geologic and vegetative controls, and flow hydraulics. In semiarid regions, where spatially varied thunderstorm rainfall produces discrete, high velocity flow events, temporal trends in flow characteristics, such as volume, peak runoff rate, and duration play a role in channel evolution. Channel geometry and patterns of spatially distributed channel vegetation were analyzed with respect to measured runoff on the main channel within the USDA-ARS Walnut Gulch Experimental Watershed in southeastern Arizona. Analyses of measured rainfall and runoff collected since 1956 on the WGEW reveal an increase in the proportion of winter rainfall and a decrease in annual runoff volume and annual peak. Cross sections measured in the 1960s were compared to those from 2004. In general changes in cross sections revealed aggradation as well as segments characterized by constricted low flow channel widths. Between 1935 and 1974 the spatial coverage of vegetation within the channel increased approximately 30% and increased an additional 150% from 1974 to 2003. Much of the vegetation has established on coarse sediment deposits. These changes in channel morphology indicate that sediment is currently being stored in the channel which may have an impact of sediment delivery to downstream receiving waters.

MONITORING COARSE SEDIMENT PARTICLE DISPLACEMENT USING A RADIO FREQUENCY IDENTIFICATION SYSTEM

M. H. Nichols, Research Hydraulic Engineer, USDA-ARS, Southwest Watershed Research Center, 2000 E. Allen Rd., Tucson, AZ 85719; mnichols@tucson.ars.ag.gov

Abstract: Coarse particles make up a relatively high contribution to overall sediment yield in ephemeral alluvial channels. A radio frequency identification system was developed and implemented to monitor the displacement of coarse particles following runoff in two upland, ephemeral channels on the USDA-ARS Walnut Gulch Experimental Watershed in southeastern Arizona. Sediment transporting flows are typically of short duration with rapidly rising and falling hydrographs. Commercially available radio frequency identification components including transponders, an antenna, a reader, and software were used to develop a system for locating particles under field conditions. During the 2003 field season 124 particles were located following four runoff events in two ephemeral channels. A total of 340 particle positions were measured with a differential geopositioning system after each particle was located with the radio frequency identification system. The overall recovery rate was 96%. The passive transponder system offers the advantages of low cost, consistent results under harsh environmental conditions, and no need for a power supply in the particle. Buried particles can be located and identified without disturbing channel bed material. The radio frequency identification system can be used to efficiently collect data for developing sediment transport equations and improving mathematical models for simulating sediment transport under natural runoff conditions.

INTRODUCTION

Sediment transport processes in normally dry channels in semiarid regions are generally poorly understood and difficult to quantify. In the southwestern US, channel runoff associated with intense summer thunderstorm rainfall is highly variable, turbulent, and often short lived, making measurement and data collection difficult. Because of the difficulties associated with collecting data, there are more data describing the relatively fine sediment that travels in suspension (Edwards and Glysson, 1999, Renard et al., 1976) as opposed to the coarse fraction that generally travels as bedload. Tracking individual particles is especially difficult

There is a need for field data coupling runoff measurements and sediment measurements to improve sediment transport prediction equations. Tracers have been used in sediment research to study the sediment movement for at least a century (Foster, 2000), with varying degrees of success. Tracers, traditionally in the form of painted rocks (Leopold et al., 1966, Wilcock, 1997), and more recently magnetic (Custer et al., 1987, Gintz, et al., 1996) and “radio” rocks (Ergenzinger at al., 1989, Emmett et al., 1990, Rosenfeld et al., 1996), have been used to study the movement of individual particles.

A radio frequency identification (RFID) system was developed to monitor the displacement of individual coarse, synthetic, sediment particles on the USDA-ARS Walnut Gulch Experimental Watershed as part of a long-term sediment transport experiment (Nichols, 2004). This paper describes the RFID system for monitoring individual coarse-grained particles and summarizes particle recovery rates for the 2003 measurement season. Additional detail can be found in Nichols 2004.

METHODS

Radio frequency identification (RFID) is a wireless, automatic identification system. RFID systems are employed in diverse applications from supply chain operations and inventory tracking in industrial settings, to toll road access and automatic gasoline payments in consumer settings. RFID systems consist of three parts, a transponder (derived from transmitter/responder), a reader, and an antenna. Each transponder can be coded with a unique alphanumeric string.

The particle tracking system (reader and antenna) is implemented in a manner similar to that of a metal detector. Particles are found by walking the channel and sweeping the antenna over the channel bed. The sweeper is powered by a battery pack made up of three 6V rechargeable batteries and consists of a gate antenna attached to one end of a pole and the reader mounted on the other end. A cable attaches the antenna to the reader, and a serial cable attaches the reader to a portable computer. When a transponder is detected, a buzzer sounds, and the computer displays the alphanumeric string stored within the transponder that indicates which particle was found.

Concrete spheres with a 5.72 cm diameter (95 cm^3), representing very coarse gravel, were cast from concrete with aggregate added to adjust the density. Transponders were placed into wet concrete during casting. The average density of cast spheres was 2.2 g/cm^3 (standard deviation = 0.1 g/cm^3), which was in close agreement with the natural rocks. In addition, synthetic cubes (98 cm^3) were cast. This analysis summarizes measurement of 124 transponder laden concrete particles that were set on channels 102-104 and 106-104 within the Lucky Hills Subwatersheds (Figure 1). A natural particle was removed from the channel for each particle added and the location of each particle was measured using a surveyor's total station. Particles were located by sweeping the channel with the antenna and locations were surveyed.

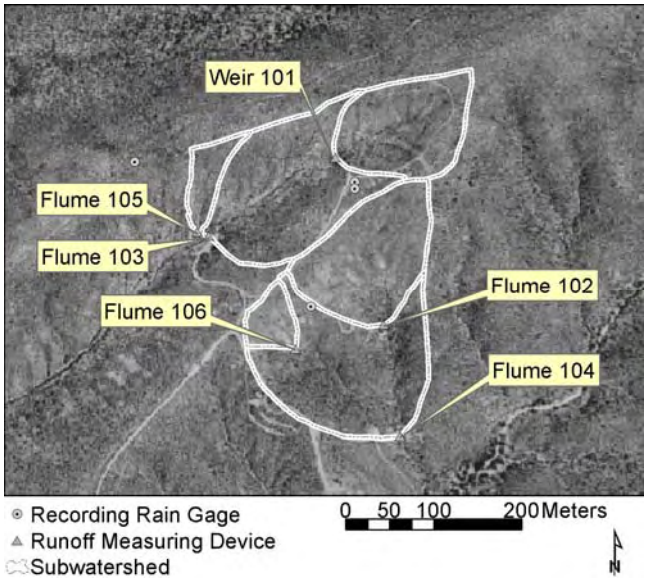


Figure1 Location of the Lucky Hills Subwatersheds and channels.

RESULTS

The RFID system was used to locate 96% of the particles searched for following four runoff events during the 2003 "monsoon" season. Without the RFID system, recovery of uniquely identifiable particles would have been limited to 79% of the particles in the 102-104 channel and 63% of the particles in the 106-104 channel (Table 1).

Table 1 2003 particle recovery characteristics.

Channel Number	Particle Position	Number of Particles
102-104	buried	28
	half buried	24
	less than half buried	21
	more than half buried	25
	surface	44
	missing	3
	total number of positions	145
	recovery rate	0.98
	maximum recovery rate without RFID system	0.79
106-104	buried	60
	half buried	15
	less than half buried	32
	more than half buried	34
	surface	42
	missing	12
	total number of positions	195
	recovery rate	0.94
	maximum recovery rate without RFID system	0.63

The field experiment is being conducted to monitor particle displacement following each flow event during three runoff seasons. Identifying buried particles is critical to maintaining continuity of particle travel data through successive flows. Given the high bed mobility and depth of alluvium in channels on the watershed, the state of burial of an individual particle is highly variable in response to runoff. Recovery of buried particles, and identifying the particles in situ has been a shortcoming of the use of painted rocks, or even magnetically tagged particles. The depth of alluvium in the 102-104 channels is variable ranging from zero (exposed hardpan) to approximately one meter in the fluvial deposit at the flume intake. During initial testing, several buried particles were dug up to verify their detection. With the RFID system, buried particles can be located and uniquely identified without disturbing the particle or the channel. However, a modified antenna configuration would be required if the system were used in a channel with deeper alluvium.

Although particles that were not classified as buried could be detected visually, particle detection was much more efficient with the RFID system. Often, particles were partially buried, obstructed by vegetation, or intermixed with particles of like color and size (Figure 2). Detecting the particles, particularly those particles under bank vegetation, was relatively easy by systematically sweeping the antenna below the vegetation. In addition, the synthetic particles employed in this experiment were intentionally of like shape and the RFID system was critical for uniquely identifying particles. When particles deposited in groups, additional care was taken when sweeping the antenna to ensure that the signal from any particular transponder did not dominate both the returned signal and the displayed identification string.



Figure 2 Typical channel segment with flag indicating a buried particle.

CONCLUSION

The radio frequency identification system provides reliable identification of tagged particles in a field setting. The tracking system consists of transponders, an antenna, a reader, and software. The passive transponder system offers the advantages of low cost, consistent results under harsh environmental conditions, and no need for a power supply in the particle. In addition, line of site is not required for locating particles.

The system was implemented and tested under natural runoff conditions. The RFID system was successful in locating 96% of the particles searched for following four runoff events. As RFID technology evolves, longer read ranges and lower costs will advance the feasibility of conducting field experiments based on radio frequency tracking. The radio frequency identification system has been used to collect particle displacement data for 3 summer runoff season. Collected data are being analyzed to improve sediment transport equations and mathematical models for simulating sediment transport under natural runoff conditions.

REFERENCES

Custer, S. G., Bugosh, N., Ergenzinger, P. J., and Anderson, B. C. (1987). "Electromagnetic detection of pebble transport in streams: a method for measurement of sediment transport waves," In: Etheridge, Flores (Eds) Recent Developments in Fluvial Sedimentology. Society of Paleontologists and Minerologists, pp. 21-26.

Edwards, T. K. and Glysson, G. D. (1999). Book 3, Chapter 2: Field Methods for Measurement of Fluvial Sediment. Techniques of Water-Resources Investigations of the U.S. Geological Survey. 89 p.

Emmett, W. W., Burrows, R. L., and Chacho, E. F., Jr. (1990). "Coarse-particle transport in a gravel-bed river." International Journal of Sediment Research, 11(2), 8-21.

Ergenzinger, P. J., Schmidt, K. H. and Busskamp, R. (1989). "The pebble transmitter system (PETS) – 1st results of a technique for studying coarse material erosion, transport, and deposition." Zeitschrift fur Geomorphologie, 33(4), 503-508.

Foster, I. D. (Ed.) (2000). Tracers in Geomorphology. Wiley, New York. 560 pp.

Gintz, D., Hassan, M. A., and Schmidt, K. H. (1996). "Frequency and magnitude of bedload transport in a mountain river." Earth Surface Processes and Landforms, 21(5), 433-445.

Leopold, L. B., Emmett, W. W., and Myrick, R. M. (1966). "Channel & Hillslope Processes in Semi-arid Areas, New Mexico." USGS Professional Paper 352-G.

Nichols, M.H. (2004). "A radio frequency identification system for monitoring coarse sediment particle displacement," ASAE Applied Engr. in Agric. 20(6):783-787.

Renard, K. G., Simanton, J. R., Donica, L. D. (1976). "A Time-Based Total-Load Automatic Sediment Sampler." Proc. 3rd Federal Interagency Sedimentation Conference, 7.17-7.29.

Rosenfeld, C. L., Castro, J. M., and Childers, E. S. (1996). "Individual Gravel Tracking Using a Passive Radio Transponder System," Proc. 6th Federal Interagency Sedimentation Conference, 5.47 – 5.51.

Smith, R. E., Chery, D. L. Jr., Renard, K. G., and Gwinn, W. R. (1982). Supercritical flumes for measuring sediment-laden flow. USDA Tech. Bull. 1655, 70 pp.

Wilcock, P. R. (1997). "Entrainment, Displacement and Transport of Tracer Gravels." Water Resources Research, 37(3), 813.

SPATIAL PATTERNS OF SOIL EROSION AND DEPOSITION IN TWO SMALL, SEMI-ARID WATERSHEDS

M.A. Nearing, Scientist, Agricultural Research Service, Tucson, AZ, mnearing@tucson.ars.ag.gov; Akitsu Kimoto, Agricultural Research Service, Tucson, AZ, akimoto@tucson.ars.ag.gov; Mary H. Nichols, Agricultural Research Service, Tucson, AZ, mnichols@tucson.ars.ag.gov; Jerry C. Ritchie, Agricultural Research Service, Beltsville, MD, jritchie@hydrolab.arsusda.gov

Abstract: This work investigates spatial patterns of hillslope erosion in a semiarid ecosystem considering influences of vegetation, slope, rocks, and landscape morphology. ^{137}Cs inventories were measured on one shrub and one grassed watershed in southeastern Arizona. Mean erosion rates in eroding areas were 5.6 and 3.2 t ha^{-1} yr^{-1}, and net erosion rates for the entire watershed, including depositional areas, were 4.3 and nearly zero t ha^{-1} yr^{-1} for the shrub and grass watersheds, respectively. Differences in hillslope erosion rates between the two watersheds were apparently due to vegetation and erosion rates within the watersheds and were not correlated to slope gradient or curvature, but were correlated to rocks in the upper soil profile. The study showed that measurement of sediment yield from a watershed can be a poor indicator of erosion taking place within the watershed.

INTRODUCTION

Surface cover associated with vegetation and rocks is known to be an important influence on the generation of sediment in semi-arid landscapes. Greater vegetative cover relates to a more protected soil surface and decreased erosion rates. In semi-arid regions it has been documented that in some cases greater patchiness translates to greater runoff and erosion. Slope gradient is generally considered to be a factor that influences soil erosion in most environments, but in uncultivated environments the situation is more complex. A part of the reason for this may be due to the mechanics of erosion caused by overland flow on relatively undisturbed sites. Studies of flow induced erosion in southeastern Arizona have indicated that the hydraulic roughness of slopes of different gradients may evolve in such a way that a slope-velocity equilibrium is established through differences in rock cover on different slopes (Nearing et al., 1999). Those measurements have shown that overland flow velocities became independent of slope gradient because of differential rock cover, which had evolved as a result of previous, preferential erosion of fine material.

The purpose of this study was to evaluate and compare the rates and spatial patterns of soil erosion and deposition in two small, semiarid watersheds by using ^{137}Cs measurements. ^{137}Cs was measured on a 1.9 ha grass-dominated watershed (Kendall), and a 3.7 ha shrub-dominated watershed (Lucky Hills), both located in the Walnut Gulch Experimental Watershed, southeastern Arizona, USA. A portion of the results of the study in the Lucky Hills watershed was reported previously [Ritchie et al., 2005]. In an attempt to understand the processes controlling the erosion and sediment yield in these watersheds, we also investigated the relationships between erosion and slope gradient, slope curvature, and the percent of rock fragments in the soils.

METHODS

The Lucky Hills watershed (3.7 ha) and the Kendall watershed (1.9 ha), which are sub-watersheds of the larger Walnut Gulch Experimental Watershed, are located in southeastern Arizona, USA, near Tombstone. Mean hillslope gradients of the Lucky Hills and Kendall watersheds are 7.7% and 12.3%, respectively. The Lucky Hills watershed is a shrub dominated, semi-arid rangeland with approximately 25% canopy cover. The Kendall watershed is largely vegetated with grass at approximately 35% canopy cover, with a trace of shrubs and forbs. Both of these watersheds have historically served as grazing land for cattle and horses. Managed grazing has occurred in the area since the establishment of Spanish ranches in the early 1800s, and intensive grazing in the area began in the 1880s. Lucky Hills is currently not being used for agriculture, while Kendall continues to be grazed.

Soil surface samples to measure ^{137}Cs inventories were collected at 68 sampling points in Lucky Hills and at 62 points in Kendall by using a bucket corer with 50 mm diam. to a depth of 25 cm. Sample locations were uniformly distributed over both watersheds. Twenty reference soil surface samples were also taken at sites with assumed negligible erosion in the area. Soil samples were dried and sieved. The less than 2-mm soil fraction was placed into beakers and sealed. Analyses for ^{137}Cs were made by gamma-ray spectrometry. Measurement precision for ^{137}Cs was $\pm$ 5%.

Soil erosion and deposition rates were calculated using the Diffusion and Migration Model for Erosion and Deposition on Undisturbed Soils [Walling and He, 1999], which compares ^{137}Cs of the samples to the ^{137}Cs of the un-eroded reference sites.

RESULTS

The spatial patterns of computed soil erosion rates in the two watersheds are shown in Figure 1. Basic results with respect to the measured erosion rates were:

1. 85% of all of the sampling points in Lucky Hills showed erosion, compared to 53% for Kendall, while 15% of all of the points in the Lucky Hills watershed showed deposition, compared to 47% for Kendall.
2. There was more net soil loss from the Lucky Hills watershed than from the Kendall watershed. The mean of the soil erosion and deposition in Lucky Hills was -4.3 t ha^{-1} yr^{-1}, while the mean in Kendall was +0.1 t ha^{-1} yr^{-1} (which was not significantly different from zero).
3. Erosion rates were greater in Lucky Hills than in Kendall. The mean for points of erosion in Lucky Hills was -5.6 t ha^{-1} yr^{-1} and for Kendall was -3.2 t ha^{-1} yr^{-1}.
4. Deposition rates were greater in Kendall. The mean for points of deposition in Lucky Hills was +3.4 t ha^{-1} yr^{-1} and for Kendall was +3.9 t ha^{-1} yr^{-1}.
5. There was a significant positive linear relationship between soil erosion and percent rock fragments in both Kendall and Lucky Hills (Fig. 2).

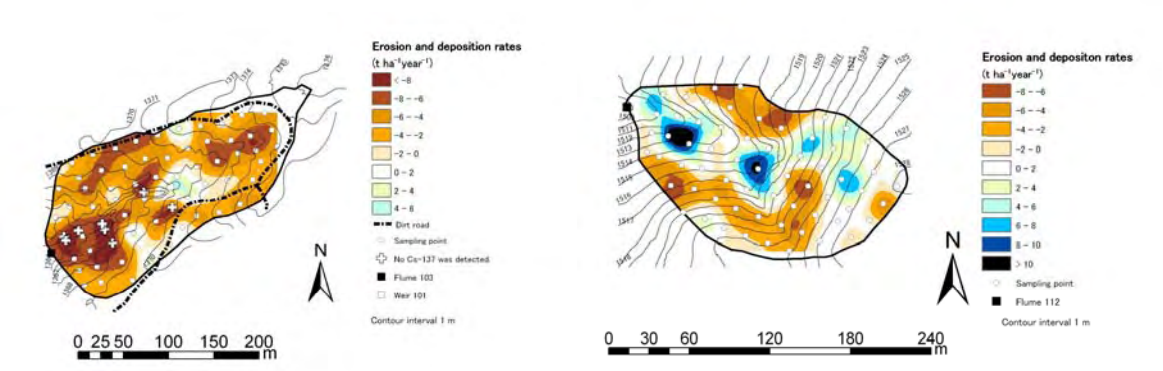


Figure 1 Spatial pattern of erosion and deposition in the Lucky Hills and Kendall watersheds.

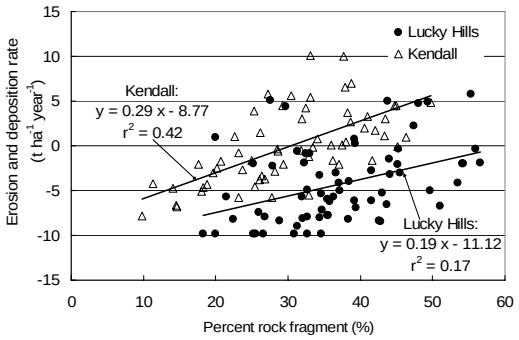


Figure 2 Relationships between percent rock fragments in the upper 25 cm of the soil profile and calculated erosion and deposition rates in the Lucky Hills and Kendall watersheds.

DISCUSSION

The evidence here suggests that the differences in hillslope erosion rates between the two watersheds were controlled largely by the vegetation differences, while within watersheds variation in hillslope erosion rates appeared to be dominated by rocks. The interpretation regarding vegetation is consistent with the interpretations related to the degree of patchiness of the vegetation. The grass cover in the Kendall watershed was certainly less patchy than that of Lucky Hills, wherein the shrubs were essentially lone plants separated by relatively wide inter-plant open spaces. Less erosion in the areas with higher percentages of rock fragments may be explained by the reduction of sediment transport capacity of flow with increasing hydraulic resistance on stony surfaces (Nearing et al., 1999; Poesen et al., 1999). Slope at sampling points and slope curvature did not appear to have a dominant influence on the hillslope erosion rates.

The delivery of eroded soil to the outlet of each watershed appears to have different controls than those controlling hillslope erosion rates. The difference in deposition between the two watersheds was due to differences in the watershed and drainage network morphology. The Lucky Hills watershed has a strongly incised channel network which facilitated transport of eroded sediments from the watershed. Conversely, the Kendall watershed had a swale area in which runoff slowed, allowing much of the sediment in the runoff from the hillslopes to deposit before it left the watershed outlet.

An important implication of the results of this study is that sediment yield from a watershed may have little to do with the rates of erosion within the watershed. The results from this study for the Kendall watershed are illustrative of the point. Even though the net erosion in the watershed was small, and even though past measurements show sediment yield rates to be quite small, there was net erosion taking place on 50% or more of the Kendall watershed area at rates as high as 7.9 t ha^{-1} yr^{-1}. Hillslopes at Kendall have been eroding over the past 40 years, even though very little sediment is being exported.

REFERENCES

Nearing, M.A., Simanton, J.R., Norton, Bulygin, S.Y., and Stone, J. (1999). "Soil erosion by surface water flow on a stony, semiarid hillslope", Earth Surface Processes and Landforms, 24, pp 677-686.

Poesen, J., De Luna, E., Franca, A., Nachtergaele, J., and Govers, G. (1999). "Concentrated flow erosion rates as affected by rock fragment cover and initial soil moisture content", Catena, 36, pp 315-329.

Ritchie, J.C., Nearing, M.A., Nichols, M.A., and Ritchie, C.A. (2005). "Patterns of soil erosion and re-deposition on Lucky Hills Watershed, Walnut Gulch Experimental Watershed, Arizona", Catena, 61, pp 122-130.

Walling, D.E., and He, Q. (1999). "Improved models for estimating soil erosion rates from cesium-137 measurements", Journal of Environmental Quality, 28, pp 611-622.

LANDSLIDE SEDIMENT PRODUCTION RATES IN THE MIDDLE FORK AND UPPER EEL RIVER BASINS, NORTHERN CALIFORNIA

Juan de la Fuente, Geologist, Klamath National Forest, Yreka, CA, jdelafue@fs.fed.us; Alisha Miller, Geologist, Shasta-Trinity National Forest, Redding, CA, alishamiller@fs.fed.us; Don Elder, Geologist, USFS Act 2 Enterprise Team, Yreka, CA, delder@fs.fed.us; Robert Faust, Hydrologist, Mendocino National Forest, Willows, CA, rfaust@fs.fed.us; William Snavely, Hydrologist, Klamath National Forest, Yreka, CA, wsnavely@fs.fed.us

Abstract: The Eel River basin of northwestern California has been identified as one of the highest sediment producing systems in the world. High quality water aquatic habitat, including that utilized by anadromous fish, and reservoirs are important natural resources in the basin. Human activities, such as logging, road construction, and grazing, can accelerate sediment production/delivery and adversely affect these resources. In 2003 and 2004 sediment source inventories were conducted in the Middle Fork Eel and Upper Eel sub-basins of the Eel River to support the development of sediment Total Maximum Daily Loads (TMDL) by the US Environmental Protection Agency (EPA). Both the Middle Fork Eel and Upper Eel watersheds are listed under section 303(d) of the Clean Water Act as impaired due to excessive sediment and temperature. The sediment source inventories examined sediment production/ delivery rates from landslides, smaller erosion sites and gullies, and channels and the magnitude of the effect of human activities on these rates. The studies were conducted by the US Forest Service (USFS), North State Resources, and Pacific Watershed Associates (PWA), funded and directed by the EPA, and in consultation with the California North Coast Water Quality Control Board. This paper focuses on the landslide element of the studies.

Air photo inventories along with field sampling were used to measure landslide-derived sediment in both the Middle Fork and Upper Eel sub-basins. A versatile GIS method (geodatabase) was used to capture and store multiple movement episodes of individual overlapping landslides. Methods for measuring small sources and channel-derived sediment were different in each basin, but both involved field sampling techniques. Determinations of natural vs. human-related sediment were made subjectively, according to a rule set developed prior to conducting the survey. For example: landslides which occurred in pre-existing clearcuts were classified as harvest-related, and landslides initiating at a road were classified as road-related. This classification does not imply cause, but rather that human activities were likely contributing factors. In the Middle Fork Eel and in the Upper Eel the majority of the landslide-related sediment production was found to be natural.

These studies provide invaluable information on local sediment production, including predominant sediment producing processes, impact of land management activities, changes in sediment production through time, and the impact of large storm events. This information is key to developing a sediment budget and to understanding how current watershed condition relates to past events. Further, it will eventually allow for extrapolation to adjacent basins and sediment modeling.

INTRODUCTION

The Middle Fork Eel and Upper Eel are 4th field watersheds located in northwestern California about 150 miles north of San Francisco (Figure 1). The Middle Fork Eel occupies about 750 square miles of which 51% is publicly owned. It includes five 5th field watersheds: Upper Middle Fork Eel, Black Butte River; Elk Creek, Williams/Thatcher, and Round Valley. The Upper Eel watershed is about 700 square miles of which 48% is publicly owned. In the Total Maximum Daily Load (TMDL) assessment prepared by the US Environmental Protection Agency (EPA), this watershed was referred to as the Upper Main Eel and Tributaries; however, we are using the naming convention of the United States Geological Survey (1981). The Upper Eel includes five 5th field watersheds: Upper Main Eel and Rice Fork (which together comprise the watershed of Lake Pillsbury), Soda Creek, Tomki Creek, and Outlet Creek (Figure 3).

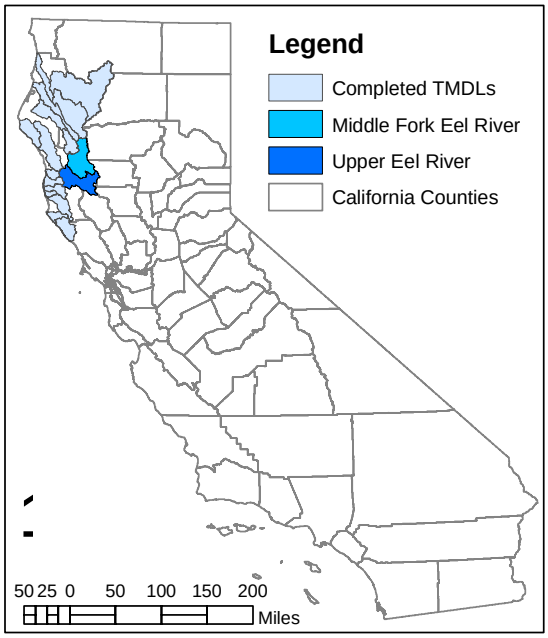


Figure 1 Location map for the Middle Fork and Upper Eel River sub-basins, along with other completed sediment TMDL's in northern California.

The primary beneficial use, as defined by the EPA, of the Eel River is salmonid habitat. Historically, both the Middle Fork and Upper Eel watersheds provided habitat to significant chinook salmon and steelhead populations. These salmonid populations are sensitive to excessive sediment and changes in sediment size distribution. The purpose of the sediment source analyses was to determine how sediment production rates have changed through time.

Bedrock: The Middle Fork and Upper Eel River are underlain primarily by Cretaceous rocks of the Franciscan Complex, including coastal belt rock, mélange, and metavolcanic rock. A relatively small proportion of the Middle Fork Eel watershed is occupied by Cretaceous rocks of the Great Valley Sequence, and sediments of the dominantly Tertiary Wildcat Group. Quaternary alluvium is exposed in the Upper Eel watershed in the vicinity of Willits, California.

Geomorphology: The Middle Fork and Upper Eel sub-basins are dominated by deep seated landslides, with higher elevation lands (>6,000 feet) sculpted by glaciers. Slump and earthflow deposits abound, and local reactivation of these features delivers a large proportion of the sediment which currently enters the stream system. Some of the slump and earthflow deposits occupy several square miles. Prominent inner gorges are developed in the lower reaches of most of the perennial streams.



Figure 2: Oblique aerial photograph of the Taliaferro landslide in the Middle Fork Eel sub-basin.

Management History: The Eel River basin was intensively grazed in the late 1800's and early 1900's (DWR, 1982). Much of the road system was in place prior to the 1964 flood. Regeneration harvesting (clearcutting) on National Forest lands was very limited until the 1980's; however, regeneration prescriptions were applied to some of the lands under other ownerships prior to the 1970's.

METHODS

Both TMDL's on the Middle Fork and Upper Eel utilized a time sequence of air photos to identify landslides over the entire basin, and a sampling method with field plots to identify other small sediment sources (EPA 2003, 2004). This paper addresses the results of the air photo landslide inventories only. The USFS conducted the photo inventories for all of the Middle Fork

and the eastern part of Upper Eel, while the western, privately-owned part of the Upper Eel was inventoried by Pacific Watershed Associates (Figure 4). This paper presents USFS data only, because of variations in mapping protocols further described below.

Middle Fork Eel: Air photos from 1952 through 2000 were used, and all landslides visible on the photos were mapped, down to a minimum dimension of 50 feet. Data recorded for each landslide included: landslide type, air photo year and number, length, width, depth, percent of the volume delivered to any channel, management association, certainty of identification, channel association, and comments. Approximately 5% of the inventoried landslides were examined in the field to calibrate estimates of depth and of the percent of material delivered to channels.

Upper Eel: Air photos from 1952, through 1998 were analyzed, using the same protocols as in the Middle Eel. In addition to landslides, gullies and altered channels were also mapped. The Pacific Watershed Associates (PWA) inventory excluded landslides smaller than 3,000 cubic yards (EPA, 2004). This variation in minimum landside dimension resulted in an order of magnitude difference in mapped landslide density in the two areas. In order to minimize variability introduced by different methodologies, we chose not to include the PWA data.

FINDINGS

Rates are given in tons per square mile per year for landslides and reservoir sedimentation and assume 1.5 and 1.25 tons per cubic yard respectively. Brown (1971) reported less than 1 ton per cubic yard for the fine sediment in the Lake Pillsbury.

Middle Fork Eel: The total landslide sediment delivery rate from 1940-2002 was estimated at 829 t/mi^2/yr, of which 4.3% is management-related (3.4% related to roads and 1.0% to harvest). The highest rate occurred during the 1940 to 1969 interval (Figure 3), which included the 1955 and 1964 flood events. A total of 4122 landslides were identified (de la Fuente et al. 2003).

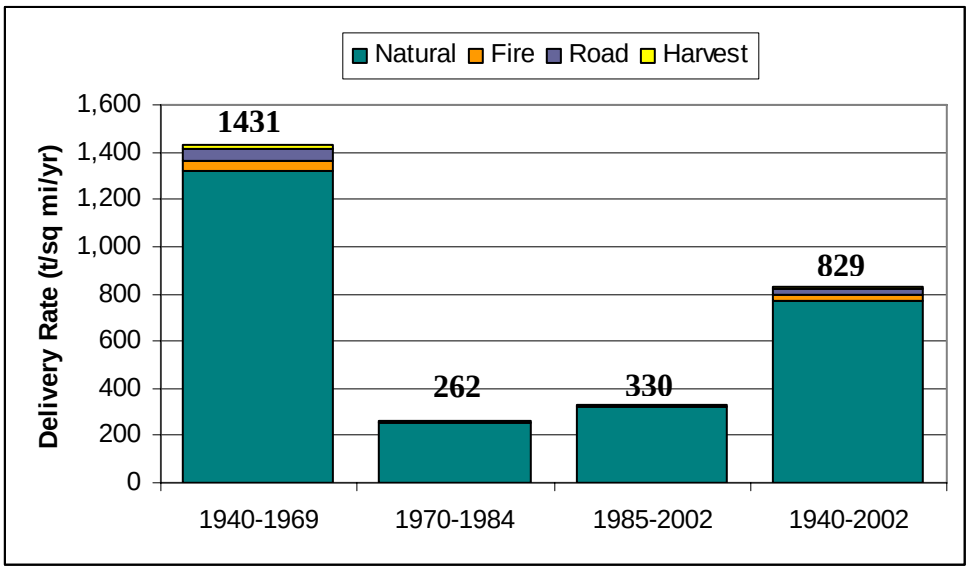


Figure 3 Middle Fork Eel landslide delivery rates by photo interval and disturbance class.

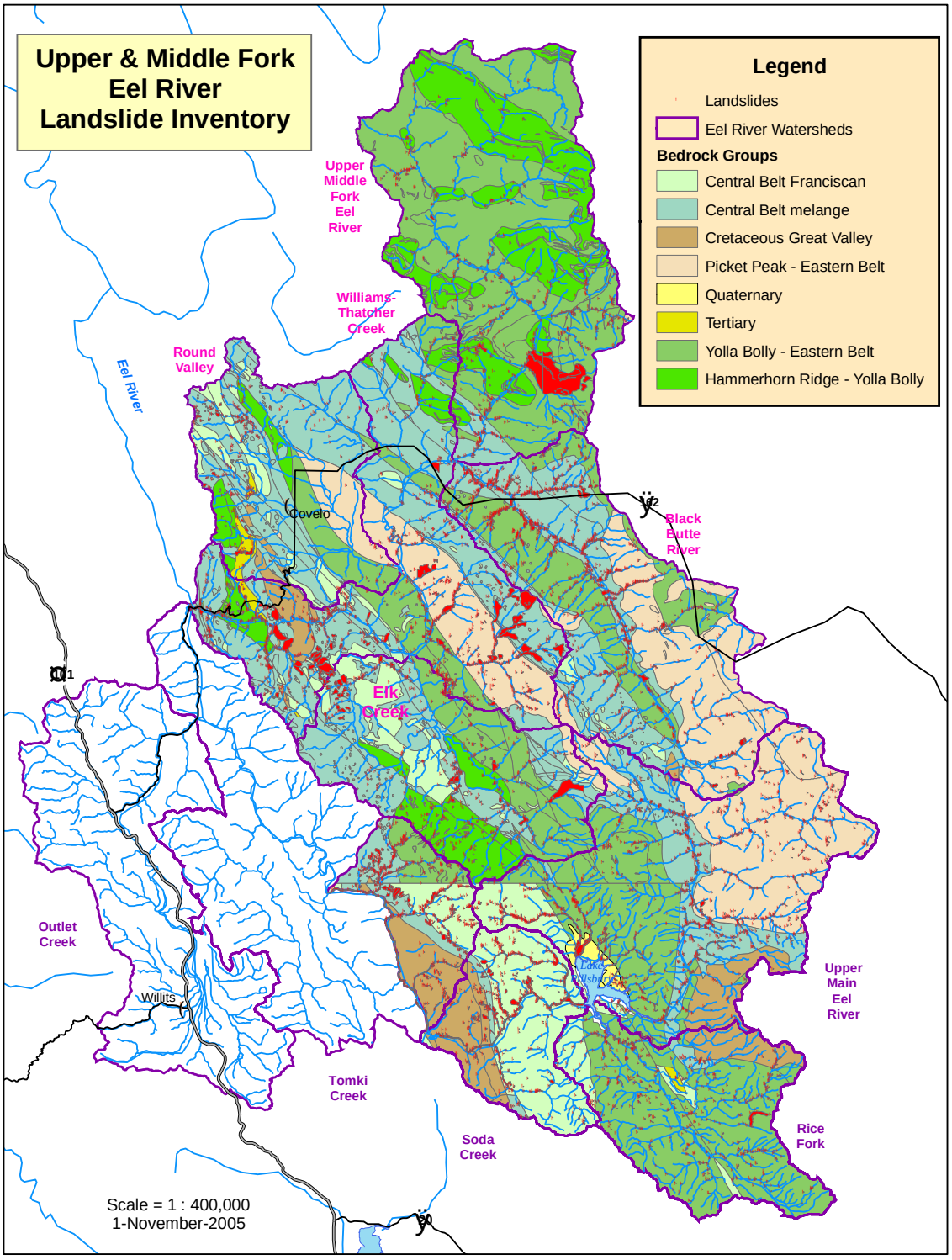


Figure 4 Map of landslides and altered channels mapped by the USFS for the Middle Fork and Upper Eel River watersheds. The southeast part of the sub-basin without mapping (Outlet and part of Tomki Creek) was inventoried by Pacific Watershed Associates.

Upper Eel: The total landslide sediment delivery rate from 1940-2004 was estimated at 531 t/mi^2/yr, of which 17% is management-related (12% related to roads and 4.7% to harvest). A total of 3129 landslides and altered channels were identified by Forest Service inventories.

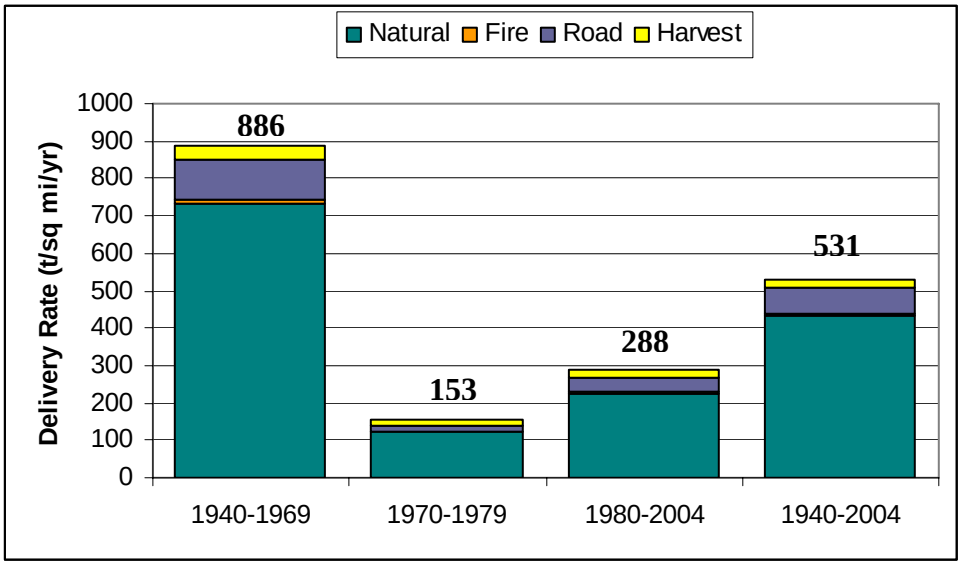


Figure 5 Upper Eel landslide delivery rates by photo interval and disturbance class.

Lake Pillsbury Bathymetry: In 2005, Pacific Gas and Electric conducted a bathymetric survey on Lake Pillsbury, and compared findings with previous surveys by USFS and California Department of Water Resources. The reservoir sedimentation rates increase through time and are significantly higher than our estimated landslide delivery rates (Figure 6).

Lake Pillsbury Drainage			
Bathymetric Survey		USFS Landslide Delivery	
Survey Interval	(t/mi^2/yr)	Photo Interval	(t/mi^2/yr)
1921-1959[1]	1400	1940-1969	535
1960-1984[1]	1737	1970-1979	86
1985-2005[1]	1898	1980-2004	307
1921-2005[2]	1625	1940-2004	369
[1]Buer et al., 1991			
[2]Eugene Geary, personal communication, Nov. 1, 2005			

Figure 6 Comparison of preliminary PG&E bathymetric survey data to USFS landslide sediment delivery rates for Lake Pillsbury basin.

Summary: The Middle Fork and Upper Eel sediment delivery rates follow a similar pattern through time. The 1940-1969 photo interval had by far they highest delivery rates, explainable by considering the large storm events in 1955 and 1964. Delivery rates decreased dramatically

during the middle photo interval, and then increased in the most recent photo interval. The recent increase could be explained by the 1997 flood event and the increase in management activities on USFS land starting in the 1980's. There is a large difference between the sedimentation rates in Lake Pillsbury and the estimated landslide delivery rates from hillslopes for the same watershed (Figure 6). This could be explained by contributions from mobilized channel material and chronic, non-landslide sediment sources such as surface erosion and gullies. The time period of 1985-2005 shows rapid deposition in Lake Pillsbury, but low landslide sediment delivery rates. This could be due to gradual transport of stored channel sediment to the reservoir from large storm events, such those in 1955 and 1964.

COMPARISON TO OTHER STUDIES IN NORTHERN CALIFORNIA

Study Comparison: Miller and de la Fuente (2004) compared the methodologies used in eighteen northern California sediment analyses, including those used to establish fifteen sediment TMDLs (Figure 1). They discovered a broad variability of sediment delivery rates, 600 to 12,500 t/mi^2/yr, and management-related contributions, 6 to 70%. The variability in these studies is due in part to physical differences between watersheds. However, an unknown proportion of the variability is introduced by differences in study methods. These numbers cannot be directly compared without consideration of time period of analysis, units of measurement, study methodology, and the physical variability of the watersheds.

Time Period: The relationship between the time period of a study and the timing of large storm events or changes in land management practices is important to consider. For example, refer to the impact of the 1955 and 1964 flood events on the sediment delivery rate of the Middle Fork Eel River (Figure 3). The 1940-2002 sediment delivery rate is 60% of the 1940-1969 interval, but about double the rates during the 1970-1984 and 1985-2002 intervals.

Units of Measurement: Additional consideration should be given to the units used in a study. All studies must be converted to the same units before a comparison can be made. If this requires converting between volume and mass an assumption of the sediment density must be made. Density can vary widely by bedrock, particle size, degree of weathering, and biotic activity.

Study Methodology: Sediment studies can generally be divided into three basic categories: reservoir bathymetric studies, suspended sediment/bedload measurements, and sediment source analyses. Sediment source studies typically use varying combinations of aerial photograph analysis, extrapolation based on field sampling, and published rates taken from the literature. Sediment source analyses are used in TMDLs because they enable categorization of sediment sources into management-related and natural. There are no set standards for field plot selection or density. There are also differences in what is considered to be management-related. This lack of consistency in methodology hinders our ability to review and compare analyses.

Physical Variability of the Watersheds: An accurate comparison of different sediment source studies needs to isolate the differences that are artifacts of the study methods or data used from those that result from real differences in physical characteristics of the landscape and geomorphic processes. Once this is done, bedrock and geomorphic mapping, river gage information, and a detailed management and fire history for each basin can be used to refine

comparisons of sediment production rates and management effects. In tectonically active areas, rates of uplift, subsidence, or movement along faults may also prove useful.

RECOMMENDATIONS:

There needs to be standardization of study methodologies so that individual studies can be analyzed and compared. Guidelines should be developed that specify: 1) sediment source categories; 2) what information is collected for each type of sediment source (i.e. time period, dimensions, mobilized vs. delivered volume, management association, etc.); 3) protocols for field sampling including plot size, plot density, and plot selection criteria; 4) criteria for distinguishing natural from management-related sources; and 5) standard reporting units and even standardized graphs, such as those in Figures 4 and 5.

CONCLUSIONS

Large storm events play a dominant role in landslide sediment production in the Middle Fork and Upper Eel, emphasizing the importance of knowing the storm history of a basin.

Sediment source studies help us understand watershed processes, and how they are affected by human activity, but caution must be exercised in comparing results with adjacent studies because of variability in study methodology.

Sedimentation rates in Lake Pillsbury were several fold higher than landslide sediment production rates measured on hillslopes. While expected, this finding points out the importance of understanding the entire erosion/deposition process, from hillslope generation, to channel transport, to reservoir deposition.

REFERENCES

Brown, W.M., III, and Ritter, J.R. (1971). Sediment transport and turbidity in the Eel River basin, California, U.S. Geological Survey Water-Supply Paper 1986.

Buer, K., Scott, R., and Gentry, W. (1991). Lake Pillsbury Watershed Erosion Study, California Department of Water Resources, Northern District.

de la Fuente, J.A., Miller, A.R., Snavely, W.P. (2003). Landslide Assessment Middle Fork Eel River Final Report, US Forest Service, Region 5, Internal Document.

Department of Water Resources, State of California (DWR) (1982). Middle Fork Eel River Watershed Erosion Investigation, DWR, Northern District, Red Bluff, CA.

Miller, A.R. and de la Fuente, J.A. (2004). A comparison of northern California sediment TMDLs [abs.], Advancing the Fundamental Sciences, A Forest Service Physical Scientists, Poster Guide, p. 8.

US EPA Region 9, (2003). Final Middle Fork Eel River Total Maximum Daily Loads For Temperature and Sediment.

US EPA Region 9, (2004). Upper Main Eel River and Tributaries (including Tomki Creek, Outlet Creek and Lake Pillsbury) Total Maximum Daily Loads For Temperature and Sediment.

US Geological Survey, (1981). US Geological Survey Data Standard Codes for the Identification of Hydrological Units in the United States and the Caribbean Outlying Area, Geological Survey Circular, pp. 878-A.

CHANNEL WIDTHS CHANGES ALONG THE MIDDLE RIO GRANDE, NM

Paula Makar, Hydraulic Engineer, Bureau of Reclamation, Denver, CO, pmakar@do.usbr.gov; Tamara Massong, Hydrologist, Bureau of Reclamation, Albuquerque, NM, tmassong@uc.usbr.gov; and Travis Bauer, Hydraulic Engineer, Bureau of Reclamation, Denver, CO, trbauer@do.usbr.gov.

INTRODUCTION

This paper describes the temporal and spatial characteristics of the river channel width of the middle Rio Grande during the twentieth century. The Rio Grande is an alluvial river that originates in the San Juan Mountains in southwestern Colorado and runs through New Mexico and Texas and along the border between Texas and Mexico. Historically, it had a wide, sandy, braided planform with a high sediment load and was aggrading (Scurlock 1998 and Lagasse 1980).

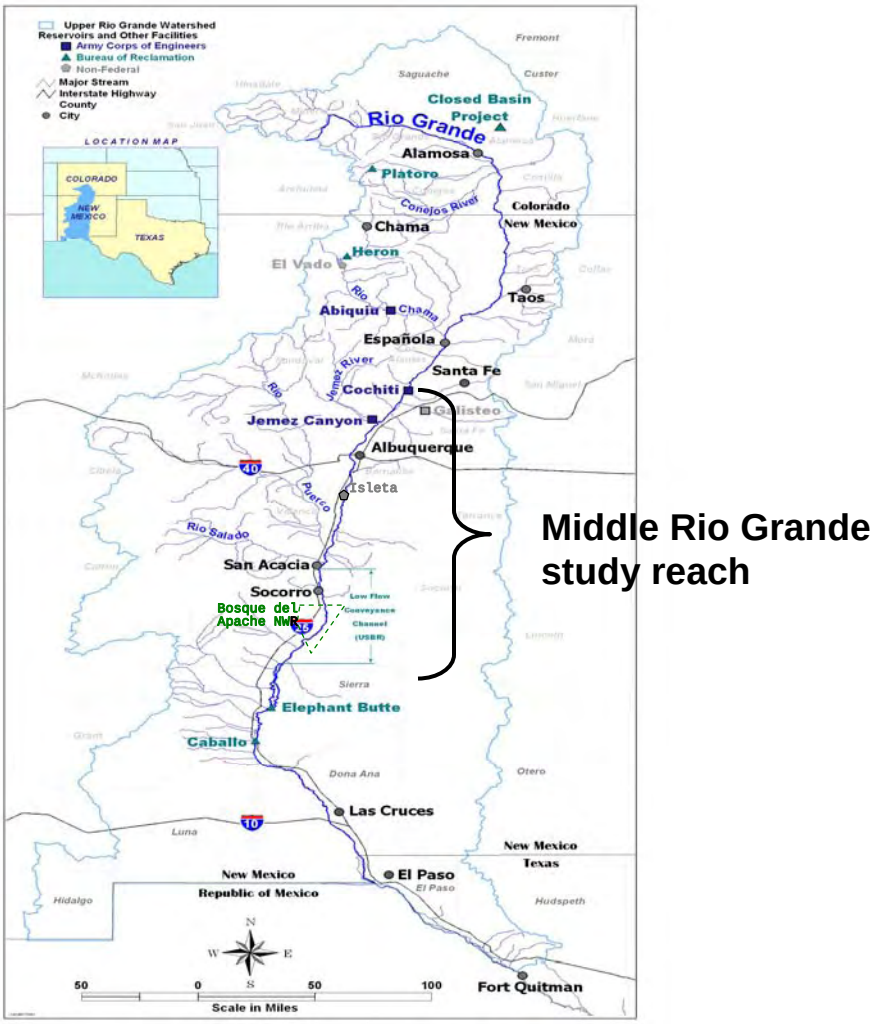


Figure 1 Middle Rio Grande study reach

The flow regime of the Rio Grande has varied over time. There are two primary sources of change: climate and water resource development. Periods of extended drought or wet hydrology have in particular influenced the magnitude, duration, and frequency of channel forming flows and the river morphology as have water delivery and flood control facilities. Figure 2 shows a timeline of these events. The general effect on the middle Rio Grande hydrology has been that peak flows have decreased in magnitude while the discharge has increased during winter base flow periods.

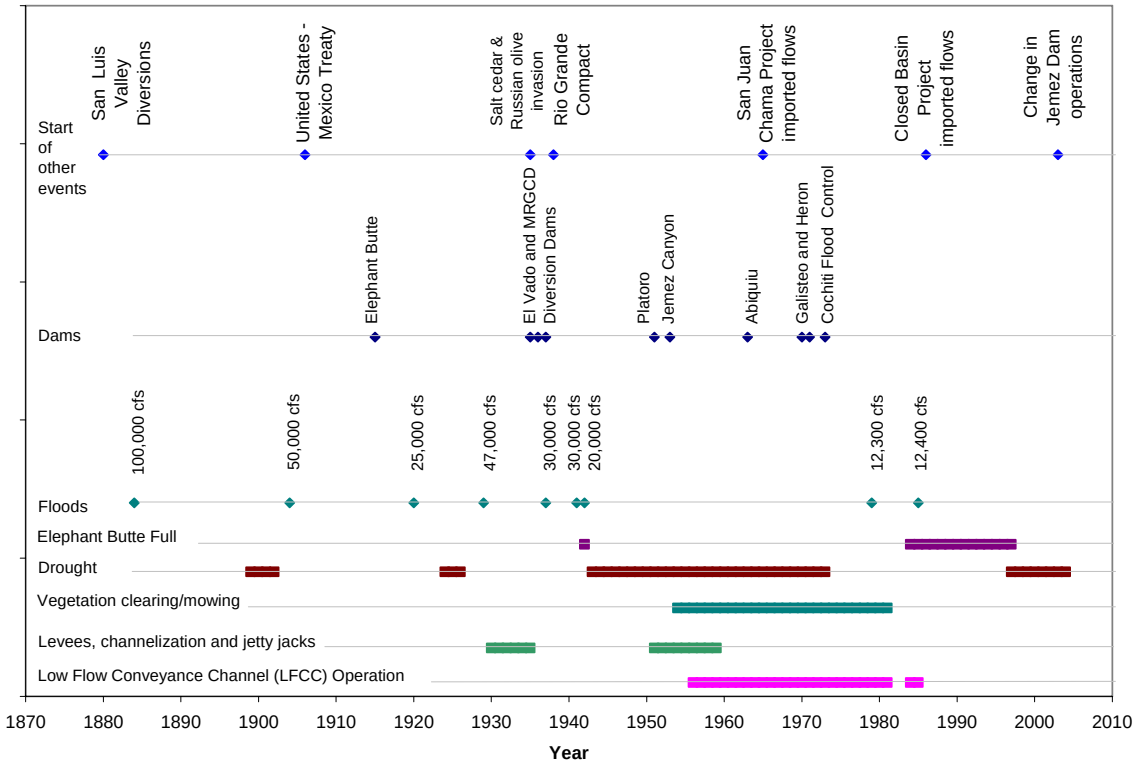


Figure 2 Timeline of significant events (adapted from Makar and Bauer 2004)

DATA AND METHODS

Planform data in the form of maps and aerial photographs are available in the Rio Grande GIS database (Oliver 2004) for nine data sets: 1908/18, 1935, 1949, 1962, 1972, 1984/85, 1992, 2001, and 2002. The earliest data are from hand-drafted linens while the rest are black and white aerial photography at various resolutions and were obtained from Reclamation's Albuquerque Area Office. Metadata that accompanies this database documents the categories of data and the limitations and sources of the data.

Active channel widths from Cochiti Dam to Elephant Butte Reservoir, at established cross sections with an approximate 500 foot spacing (cross section lines 19 through 1800 in Oliver 2004 and referenced by just the cross section number in this paper), are taken from digitized information in the GIS database. A few cross section lines are not perpendicular to the channel or the flow path, resulting in a small error in the channel widths. For this study, the active channel is the area of no or sparse vegetation cleared by the river which does not include vegetated islands or mechanically cleared areas. Figure 3 presents the widths for each set of

data. Data in Figure 4 is normalized to an average annual change and illustrates the rate of change in width between dates of photography.

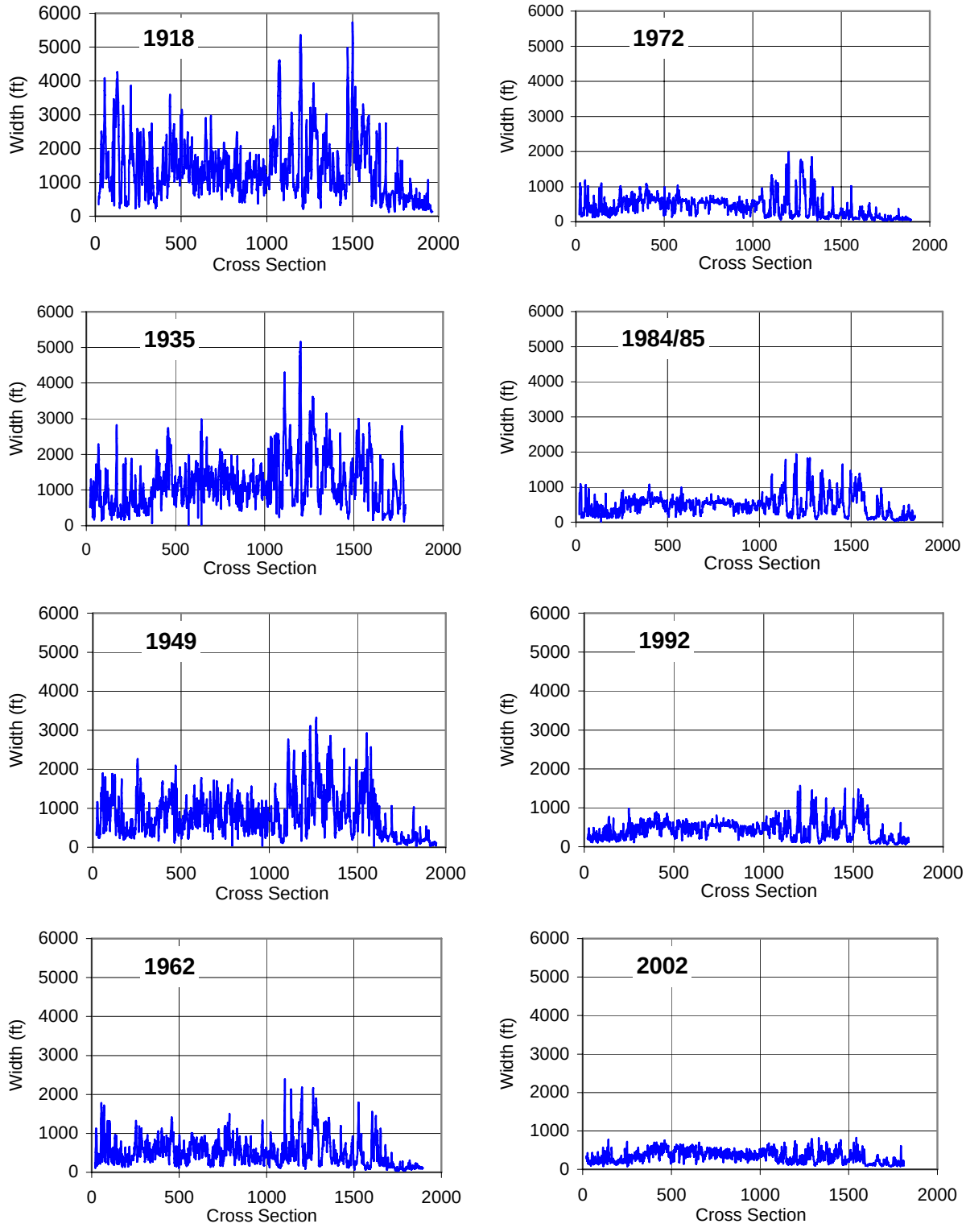


Figure 3 Active channel widths

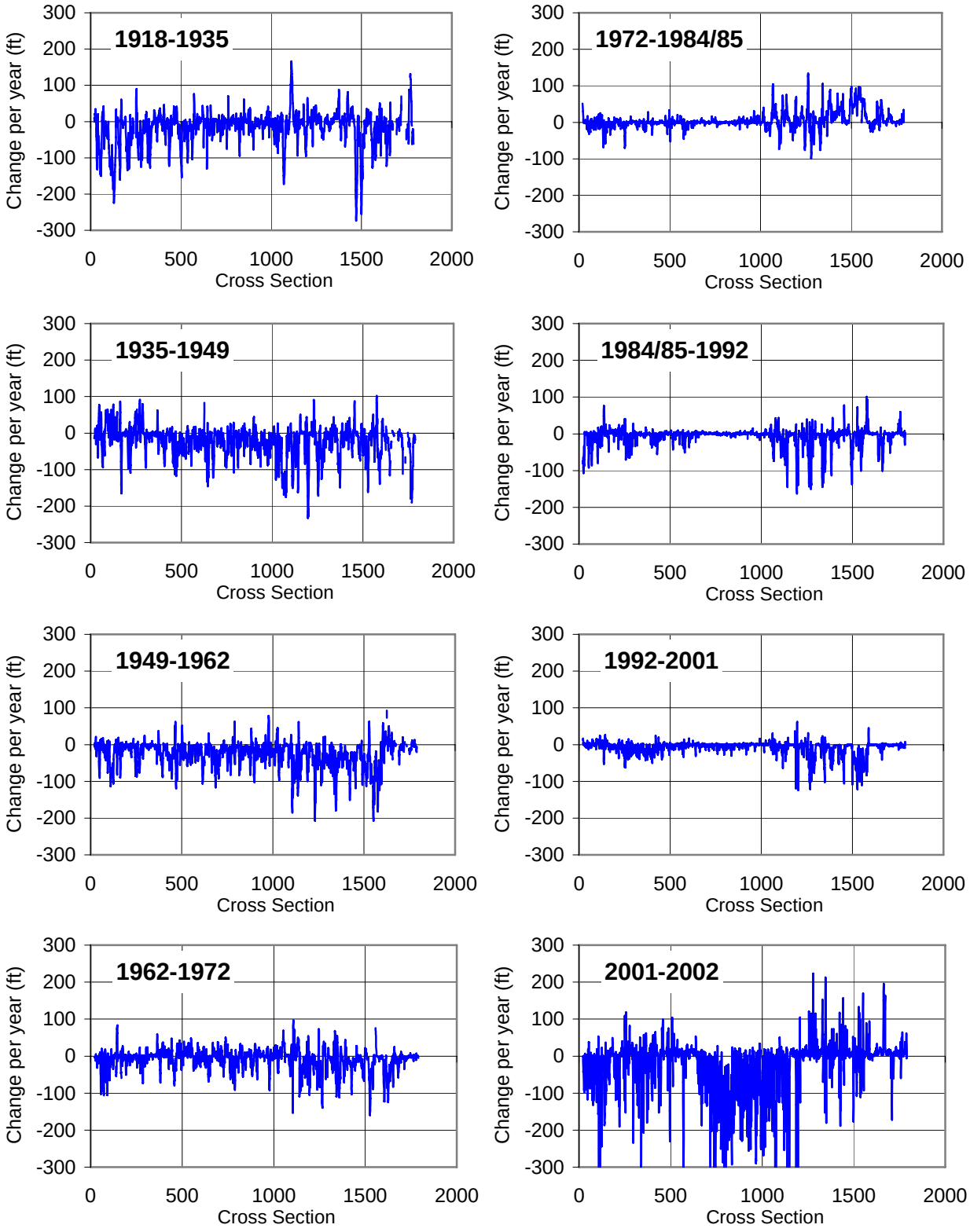


Figure 4 Average annual changes in active channel width

RESULTS AND DISCUSSION

Magnitude and rate of active channel width changes: On rivers like the Rio Grande, channel characteristics are often determined by major flood events (Knighton, 1998). These large events are followed by many years of adjustment, which may include narrowing, incision, and the formation of vegetated islands and bars. Previous studies (Richard et al. 2005, Makar and Bauer 2004, Makar and Strand 2003) have found a strong correlation between peak flows and active channel width. Some areas responded more strongly than others but decreased peak flows are associated with an overall decrease in the river channel width.

Figure 3 illustrates the general narrowing trend over time; such that channel widths in 1918 are the widest and 2002 the narrowest. Channel width data in 1918 shows that the reach was generally wider than 1,500 feet, with many areas in excess of 2,500 feet. By 1949, most of the reach was still wider than 1,000 feet, but few areas were greater than 2,000 feet and the extensive variability found in the 1918 channel width data is gone. The 1972 data set continues the decreasing width trend, such that nearly all the cross sections are less than 1,000 feet wide. The most recent data set from 2002 shows that at present, all of the cross sections have channel widths less than 1,000 feet, and that the majority are also less than 750 feet.

Decreases in width between 1918 and 1935 can be partially attributed to construction of riverside irrigation facilities such as drains and canals that are protected by levees. After 1941, there was an extended period of below average stream flows and peak flows. The river channel narrowed through vegetation encroachment on bars and islands that were no longer cleared by flooding. Drought conditions were still prevalent in 1962, but narrowing was also due to channelization. Beginning in the 1950s, large sections of the river were narrowed with jetty jacks to more efficiently transport water and sediment downstream. The jacks also trapped sediment and protected the banks. The Low Flow Conveyance Channel (LFCC) between San Acacia Diversion Dam and Elephant Butte Reservoir reduced flows by diverting up to 2,000 ft^3/s from the floodway from the late 1950s through the early 1980s. Widths continued to narrow through 1972, with vegetation encroachment during drought and channelization largely responsible for the narrowing.

Beginning in 1979 through the late 1980s, there were higher flows in the river. With minor exceptions, the LFCC has not been operated since the early 1980s, also increasing the flows in the river. In the 1960s through the 1980s, large sections of the river were mechanically cleared of vegetation to maintain flood capacity. By 1985, the active channel width widened to near the edge of the cleared floodway along much of the river. Low water levels were seen in the years around 1990 and after 1995 and mean channel width decreased more in the 1992, 2001, and 2002 photos.

Vegetation plays an important role in width adjustment on the Rio Grande. The majority of the widening that has occurred was where floodway clearing had taken place before periods of higher peaks. Vegetation continues to encroach when not scoured or cleared away. Once established, vegetation anchors deposited sediments and makes lateral adjustment difficult unless certain thresholds such as critical shear stress or root strength are exceeded. Rowntree and Dollar (1999) report riparian vegetation locally increases bank stability as a function of root mass

and depth and tends to reduce channel capacity through narrowing. Their evidence indicates that narrow stable reaches are associated with relatively thick vegetation and wider, unstable channels have more sparse riparian vegetation. In aggrading reaches, they postulate the reduced channel capacity results in increased overbank flooding which may lead to avulsion. This is similar to conditions seen on the Rio Grande just upstream of Elephant Butte Reservoir.

The trend of general narrowing is also evident in Figure 4 in that the majority of changes are negative. Note that the 2001-2001 data only represents one year of change, while the other figures are yearly averages of multiple years. The narrowing between 2001 and 2002 is still striking and generally a consequence of the drought and significant vegetation encroachment.

The persistence of the new vegetation was tested during the high peaks of the 2005 runoff and field observations show that while some areas widened many did not, as the runoff flows did not completely scour the vegetation from islands and bars. The next set of aerial photography is likely to be very important in estimates of future width changes. Close examination of Figure 4 shows that cross sections with significant narrowing in one photo stabilize or even widen in the next. Also of note is the appearance of a downstream progression in narrowing in some areas. Narrowing is likely related to the downstream progression of incision and bed material coarsening documented in Bauer (1999), Leon (1998), Makar and Strand (2002) and Massong et al. (2006). More detailed examination of this phenomenon is planned in the future.

Reach based changes: The reach boundaries of similar width and magnitude of change shift depending on the period and location examined but some large scale trends are evident. For example, the channel near the Bosque del Apache National Wildlife Refuge (BDANWR) area has always been the widest and immediately upstream of Elephant Butte Reservoir the narrowest. Four reaches are discussed below:

Cochiti Dam to Isleta Dam (63 river miles, cross sections 19 to 655): This reach was wide with a high amount of variability in 1918 and shows a fairly high level of channel width change through 1962. After 1962, the amount of narrowing decreases and the widths stabilized. The channelization and bank stabilization effort in the 1950s is a component of the uniformity. There was not a large change between the 1972 and later data, indicating Cochiti Dam (which closed in 1973) may not yet have had a large impact on width adjustment. It appears that major width adjustment in this reach had occurred by 1962 until the recent drought fostered significant vegetation growth and channel narrowing between 2001 and 2002. Richard et al. (2005) suggest the width of the Rio Grande in the upper portion of the reach may have been in equilibrium by 2001. When data become available, it will be interesting to compare widths after the high flows of 2005 to see whether they approach the previous condition.

Isleta Dam to Rio Puerco Confluence (42 river miles, cross sections 655 to 1099): There is less variability in widths in this reach, i.e. fewer very wide or very narrow cross sections. The amount of width change within a time period is also quite consistent in the reach; however, the channelization and bank stabilization effort in the 1950s resulted in the large reduction in width between 1949 and 1962. The narrowing continues at reduced rate through 1972, with very little change until 2002 when the largest amount of narrowing occurs between 2001 and 2002 throughout the reach. Field observations indicate the channel is shifting towards a single-thread

planform. The uniformity of both widths and width changes over time and the suddenness of the large change in 2002 indicate there has been a planform shift from braided to single thread. This reach has also shown little to no incision (Massong et al. 2006). It will bear watching for incision if the large reduction in width and the transition from braided to a single-thread channel are maintained.

Rio Puerco Confluence to mid-BDANWR (49 river miles, cross sections 1099 to 1580): This reach has generally had the most variability in width and the widest widths in the time periods examined. It also shows the highest widening rates (except in between 1935 and 1949). Despite the generalized narrowing in 2001 to 2002, this reach had the largest magnitude of widening while width reductions were smaller than that those upstream. Immediately downstream from San Acacia, NM, a section with the highest amounts of incision (Massong et al. 2006) rapidly widened in 2005 (Massong 2005), suggesting that discharge is still a major influence in determining channel width in this reach, especially in locations where the planform is single thread and the bank height is taller than root depth.

Mid-BDANWR to Elephant Butte Reservoir (18 river miles, cross sections 1099 to 1800): Always the narrowest and least variable, this reach generally shows lower amounts of width change. The historical pattern has included channel avulsions, consistent aggradation, and a perched riverbed (Makar and Strand 2002). Much of this reach was relocated when the river channel was moved to the east side of the valley during Low Flow Conveyance Channel construction. The cut channel with thickly vegetated banks has been generally stable, except for periodic avulsions that impinge on and sometimes breach the levees. The levee breaches have been repaired and the channel returned to the constructed alignment. This maintenance is certainly a factor in the stability of the widths in this reach.

CONCLUSIONS

Width changes of the Rio Grande have resulted from natural processes such as the response to large floods and drought but also have been influenced by anthropogenic modifications. The long dry periods with low peak flows facilitated vegetation encroachment and narrowing. Flood control dams that changed the timing and decreased the magnitude of upstream peaks plus channelization and bank stabilization activities have resulted in a narrower active channel. Photography from 2001, 2002, and 2004 shows that the development of well-established vegetated islands has increased in recent years. With uninterrupted and continued development of islands, the wetted channel width will continue to decrease. Eventually, the islands may become attached to the river bankline. The resulting river is likely to be single thread, narrow, high velocity, and incised with increased meandering tendencies. In aggrading reaches, thick vegetation locally stabilizes the channel at lower flows but channel avulsions may still occur during high peaks.

Planned future analysis on the Rio Grande includes integrating the width changes documented herein with the channel incision discussed in Massong et al. (2006), lateral mobility concepts in Richard et al. (2005) and the changing relationships between water and sediment loads documented in Bauer (1999), Leon (1998), Makar and Strand (2002), and MEI (2002).

AKNOWLEDGEMENTS

We'd like to thank others who contributed to this study: Chris Holmquist-Johnson, Jan Oliver, Christi Young, and Robert Padilla.

REFERENCES

Bauer, T. R. (1999). "Morphology of the Middle Rio Grande from Bernalillo Bridge to the San Acacia Diversion Dam, New Mexico." MS thesis, Colorado State Univ. Fort Collins, Colo.

Knighton, D., (1998). Fluvial Forms and Processes. Arnold, London, England.

Lagasse, P. F., (1980). An Assessment of the Response of the Rio Grande to Dam Construction-Cochiti to Isleta. A Technical Report for the U.S. Army Corps of Engineers. Albuquerque, NM.

Leon, C. (1998). "Morphology of the Middle Rio Grande from Cochiti Dam to Bernalillo Bridge, New Mexico." MS thesis, Colorado State Univ., Fort Collins, CO.

Makar, P.W. and T.R. Bauer, (2004). Middle Rio Grande Planform Characterization and Analysis. U. S. Department of the Interior, Bureau of Reclamation, Technical Service Center, Sedimentation and River Hydraulics Group, Denver, CO.

Makar, P.W. and R.I Strand, (draft 2002). Responses of the Middle Rio Grande: San Acacia to Elephant Butte. U. S. Department of the Interior, Bureau of Reclamation, Technical Service Center, Sedimentation and River Hydraulics Group, Denver, CO.

Massong, T. M., (2005). 2005 Bank Erosion Monitoring on the Rio Grande, San Acacia Reach. U. S. Department of the Interior, Bureau of Reclamation, Albuquerque Area Office, Environment Division, Albuquerque, NM.

Massong, T., P. Tashjian, and P. Makar, (2006). "Recent Channel Incision and Floodplain Evolution within the Middle Rio Grande, NM." Joint 8th Federal Interagency Sedimentation Conference and 3rd Federal Interagency Hydrologic Modeling Conference, Reno, NV.

Mussetter Engineering, Inc. (MEI). (2002). Geomorphic and Sedimentologic Investigations of the Middle Rio Grande between Cochiti Dam and Elephant Butte Reservoir. Submitted to New Mexico Interstate Stream Commission.

Oliver K.J., (2004). Middle Rio Grande Project - 1918-2002 Geomorphology Study for the Rio Grande from Velarde to the Narrows of Elephant Butte, New Mexico. U. S. Department of the Interior, Bureau of Reclamation, Technical Service Center, Remote Sensing and GIS Group, Denver, CO.

Richard, G.A., P.Y. Julien, and D.C. Baird, (2005). "Case Study: Modeling the lateral mobility of the Rio Grande below Cochiti Dam, New Mexico." Journal of Hydraulic Engineering, ASCE, 131(11).

Rowntree, K.M., and E.S.J. Dollar. (1999). "Vegetation Controls on Channel Stability in the Bell River, East Cape, South Africa. Earth Surface Processes and Landforms, 24.

Scurlock, Dan, (1998). From the Rio to the Sierra: An Environmental History of the Middle Rio Grande Basin. Rocky Mountain Research Station. Fort Collins, CO.

EVALUATION OF TECHNIQUES TO ESTIMATE SUSPENDED-SEDIMENT CONCENTRATIONS IN THE KANSAS RIVER

Casey J. Lee., Hydrologist , U.S. Geological Survey, Lawrence, KS, cjlee@usgs.gov; Patrick P. Rasmussen, Hydrologist , U.S. Geological Survey, Lawrence, KS, pras@usgs.gov; Andrew C. Ziegler, Hydrologist , U.S. Geological Survey, Lawrence, KS, aziegler@usgs.gov

Abstract: Continuous streamflow data are traditionally the surrogate used by hydrologists to estimate suspended-sediment concentration (SSC) and load in surface water because of its widespread availability. The U.S. Geological Survey in Kansas currently uses in-situ nephelometric (90-degree scatter) turbidity sensors to estimate SSC with less uncertainty than that associated with streamflow-based SSC estimation. Although in-situ nephelometric turbidity sensors have decreased the uncertainty associated with estimates of SSC, these sensors are prone to environmental fouling and have a maximum range of approximately 2,000 milligrams per liter. During 2004 and 2005, estimates of SSC using acoustic Doppler return signal strength, nephelometric turbidity, and optical backscatter were evaluated using data from a Yellow Springs Instruments model 6136 turbidity sensor currently deployed in the Kansas River at DeSoto, Kansas. These comparisons were done to find an SSC-estimator with increased range and minimal uncertainty.

The Sontek Argonaut 1.5 megahertz (Yellow Springs Instruments, Yellow Springs, Ohio) is a single-frequency acoustic Doppler instrument typically used to estimate streamflow velocity. However, recent studies by the U.S. Geological Survey have shown that acoustic signal strength can estimate SSC. The Sontek Argonaut was deployed from April to September 2004. Signal strength from the instrument did not correlate with YSI (Yellow Springs Instruments, Yellow Springs, Ohio) turbidity data. Signal strength truncated at a YSI-estimated SSC of 500 milligrams per liter, indicating the upper limit of the instrument's effectiveness. Limited SSC range and inability to measure small particle sizes preclude the Sontek Argonaut 1.5 megahertz from being an effective SSC estimator when small particle sizes and large sediment concentrations frequently occur.

The Forest Technology Systems (FTS) DTS-12 (Forest Technology Systems, Bellingham, Washington) is a nephelometric turbidity sensor with a manufacturer-determined range from 0 to 2,000 formazin nephelometric units. The DTS-12 was deployed from July 28 to October 1, 2004. The DTS-12 reported periods of inaccurate, spiking data values resulting in deletion of 31 percent of the total data reported during this period. Spiking data values were caused by a broken drive shaft that resulted in the wiper parking on or near the sensor optics. Although this monitor had wiper-parking problems, unaffected data correlated well with data reported by the YSI model 6136 turbidity sensor. The maximum value recorded by the FTS DTS-12 during the period of study did not exceed the 2,000 formazin nephelometric unit maximum, although YSI-estimated suspended-sediment concentrations reached 1,600 milligrams per liter.

The Hach optiquant TS-Line sensor (Hach, Loveland, Colorado) is a wiped optical backscatter sensor used to monitor sludge in wastewater-treatment operations, with a manufacturer-determined range of 0 to 50,000 milligrams per liter of suspended solids. The sensor was deployed in November 2004 and has been used continuously since February 2005. Data collection using the TS-Line sensor will continue through December 2005. The TS-Line sensor has only been tested thus far with a small range of estimated SSC (20-400 milligrams per liter), but results correlated well with YSI turbidity data.

The use of trade, product, or firm names is for descriptive purposes only and does not imply endorsement by the U.S. Government.

A FIVE-YEAR RECORD OF SEDIMENTATION IN THE LOS ALAMOS RESERVOIR, NEW MEXICO, FOLLOWING THE CERRO GRANDE FIRE

Alexis Lavine, Earth & Environmental Sciences Division, Los Alamos National Laboratory, Los Alamos, NM, 87545; Gregory A. Kuyumjian, U.S.D.A., Forest Service, Los Alamos, NM, 87544; Steven L. Reneau, Earth & Environmental Sciences Division, Los Alamos National Laboratory; Danny Katzman, Earth & Environmental Sciences Division, Los Alamos National Laboratory; Daniel V. Malmon, Western Earth Surface Processes Group, U.S. Geological Survey, Menlo Park, CA 94025

INTRODUCTION

The Cerro Grande fire of May 2000 burned approximately 17,400 ha in the eastern Jemez Mountains and the Pajarito Plateau in the vicinity of Los Alamos, New Mexico (BAER, 2000; Figure 1). Changes in surface characteristics caused by the fire resulted in significant increases in runoff and erosion relative to pre-fire conditions. This study documents five years of sedimentation in the Los Alamos Reservoir, providing a unique data set for examining post-fire erosion and sediment delivery in a montane watershed. The drainage basin above the dam has an area of about 16.6 km^2, elevations of 2320 to 3180 m, and supported a predominantly mixed conifer forest prior to the fire, dominated by ponderosa pine, Douglas fir, and white fir. Thirty-two percent of the basin experienced moderate to high burn severity, with complete loss of groundcover and development of hydrophobic soil conditions, including some of the steepest parts of the basin; 32% experienced low burn severity and 36% was unburned (Figures 1b, 1c). A variety of geologic units are present in the watershed above the reservoir, including dacite (the dominant rock type), nonwelded to welded tuffs, and conglomerate. Approximately 50% of the precipitation in the area is from high-intensity, short duration summer rainstorms (during the "summer monsoon") with most of the remainder from winter snowfall (Bowen, 1990).

The sedimentation record within the Los Alamos Reservoir offered a unique opportunity to study post-fire sediment delivery, including changes over time associated with watershed recovery, and to compare pre-fire and post-fire rates. The reservoir was built for water storage and supply in 1943. Serendipitously, it provided sufficient capacity to capture 15 months of delivered material from upstream burned areas after the fire, while allowing for draining and access for detailed surveys. Only a few overflows, carrying ash and suspended solids, occurred in the five years following the fire. Prior to the fire, the reservoir received minor amounts of sediment and had never been dredged, preserving a 57-year record of sedimentation. Because of concerns about potential post-fire flood damage to facilities downstream from the reservoir, it was drained several times and excavated when it was full of sediment to retain storage capacity. Subsequent partial excavation of a coarse-grained delta also occurred. We were able to coordinate our surveys with times when the reservoir was drained and before and after it was excavated, leading to a 5-year record of the amount and type of sedimentation following the fire. Local precipitation data allowed putting this record into the context of short-term and long-term precipitation, and examination of stratigraphy exposed in excavations allowed understanding of the effects of specific storm events.

METHODS

Total station surveys were performed annually at the Los Alamos Reservoir at the beginning of, or just before, the summer monsoon season, supplemented by additional surveys in other seasons. This allowed for yearly estimates of sedimentation. Eight surveys were performed: June 8 and 12, 2000; June 28-29, 2001; October 27-28, 2001; January 2002; April 2, 2002; July 23-25, 2003; June 30, 2004; and July 11, 2005. Total station survey measurements are accurate to within 3 mm/km in both horizontal and vertical directions (Geodimeter, 1998). Most surveys involved obtaining >300 points on the surface of the depositional packages in the reservoir. Surveyed points were gridded using kriging (Deutsch and Journel, 1992) to create surfaces for making contour maps (Figure 2). An additional contour map was provided from a detailed as-built survey from 1943. The volume of sediment deposited between surveys was determined using Surfer © software, by calculating the difference between surveys.

In October 2001, during excavation of sediments from the reservoir, we were able to study, survey, and sample the detailed stratigraphy of the first 15 months of post-fire sediments (Figures 3 and 4), which was when sedimentation rates were highest. Samples were collected for bulk density, particle size, and radiochemical analyses. The dates of some specific stratigraphic layers were determined by comparing elevations of surveyed points in the excavation

with previous surveys. Precipitation records from weather stations in and near the watershed (Figure 1b) assisted in relating the stratigraphic record to seasonal variations in precipitation and/or individual storms. Remote Automated Weather Stations (RAWS, http://www.losalamos.dri.edu/index.html) installed after the fire provide a record of short-duration precipitation for 2000 to 2003, and a snowpack telemetry (SNOTEL) site provides a longer term record (1981-2005, ftp://ftp.wcc.nrcs.usda.gov/data/climate/mtn_prec/table/history/new_mexico/06p01s.txt). The return periods of individual storms affecting the burn area were estimated using data for 1 and 2 hour rainfall recorded at the RAWS sites and locally-derived precipitation-frequency relations (Reneau et al., 2003). These estimates used Thiessen averages (Dunne and Leopold, 1978, p. 75) applied to the high and moderate burn severity parts of the watershed. Longer-term seasonal precipitation was estimated using the SNOTEL record (Table 1).

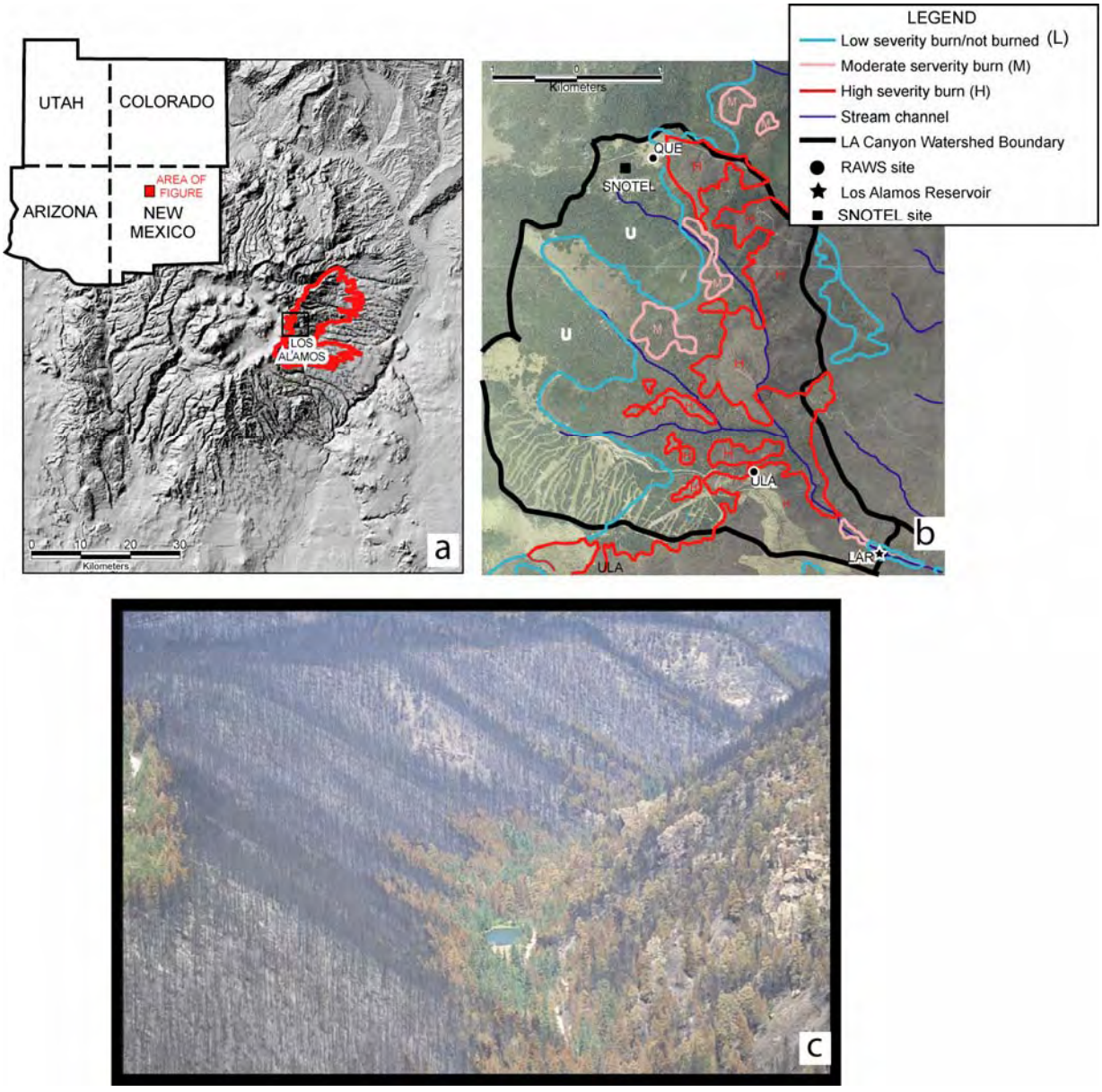


Figure 1 a) Map showing the location of the Cerro Grande fire in north-central New Mexico. Black outline shows area of Figure 1b. b) Aerial photograph showing burn severity in the Los Alamos Reservoir (LAR) watershed; QUE and ULA are RAWS sites; "U" indicates unburned areas; some of the high-severity burn areas have been treated with straw mulch (e.g., southeast of ULA RAWS). c) Oblique-aerial photograph of Los Alamos Canyon and reservoir, looking upstream, shortly after the Cerro Grande fire.

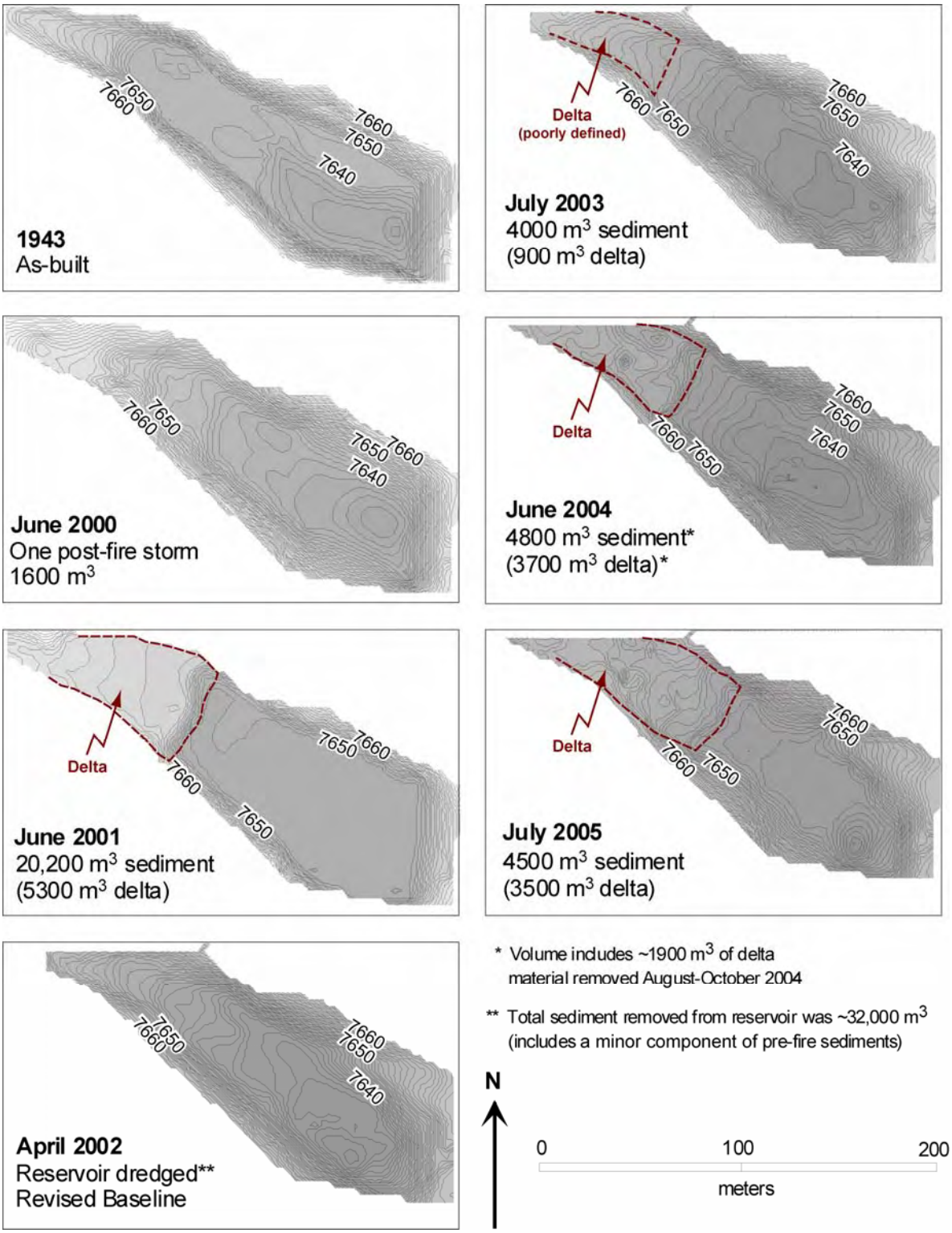


Figure 2 Series of contour maps showing changes in the topography of the reservoir basin based on total station surveys and an as-built survey (1943). Contour interval is 1 foot (0.3 m). Volumes shown reflect amount of sediment deposited between surveys.

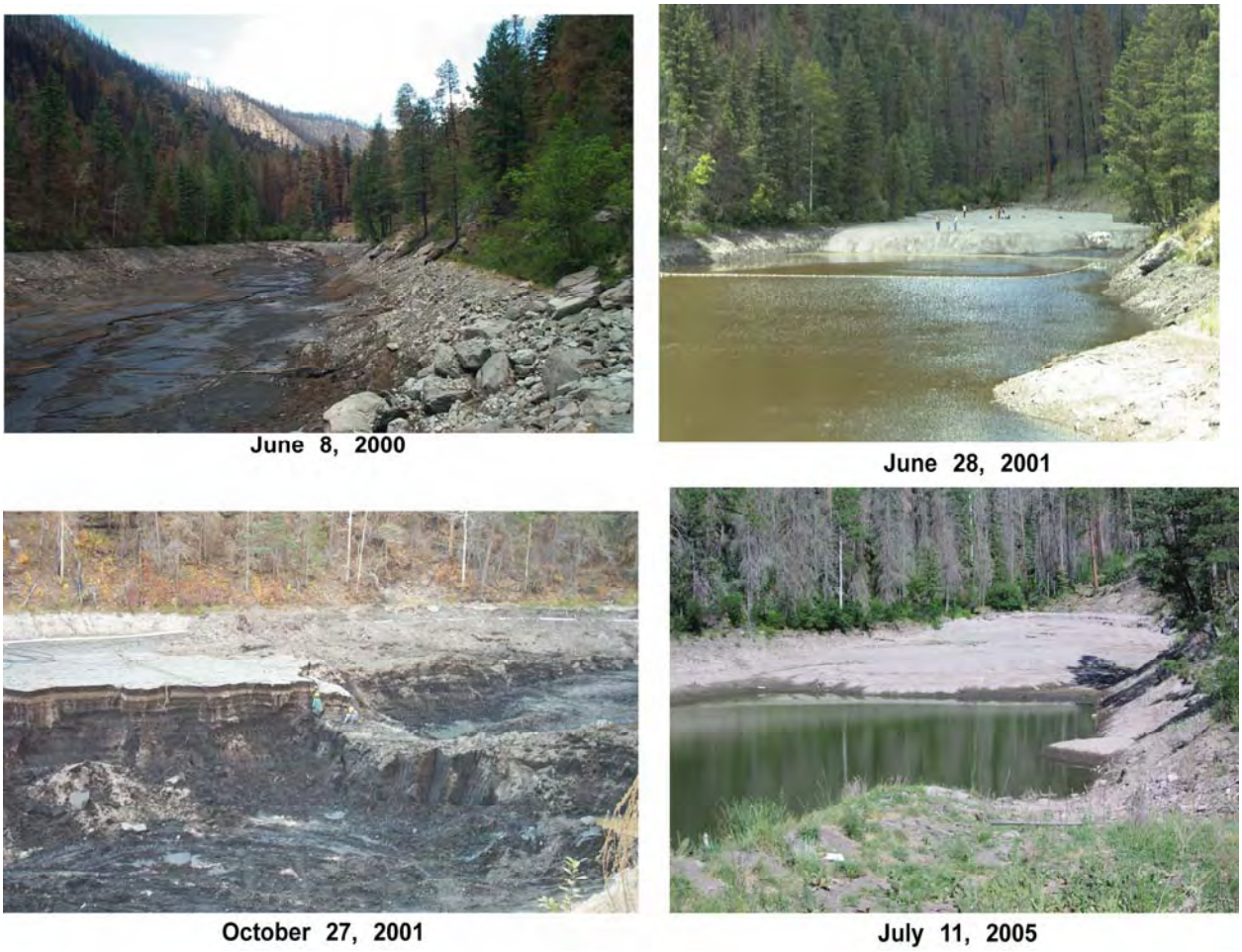


Figure 3 Photographs of the Los Alamos Reservoir: June 8, 2000, drained, after a single post-fire flood: June 28, 2001, showing a large coarse-grained delta that was formed during snowmelt runoff in spring 2001: October 27, 2001, partially excavated, showing fine-grained post-fire sediment deposits, people in center are describing stratigraphic section shown in Figure 4: July 11, 2005, showing delta formed during snowmelt runoff in spring 2005.

RESULTS

The initial total station survey of the Los Alamos Reservoir on June 8, 2000, in combination with the as-built drawings from 1943, indicated that approximately 10,200 m^3 of sediment had been deposited since construction of the reservoir (Table 2). The initial survey occurred after a single post-fire flood, on June 2, 2002, that deposited ~1,600 m^3 of sediment, with an average thickness of less than 0.3 m. This yields an estimate of ~8,600 m^3 of sediment accumulation in 57 years (Table 2), or an average of ~150 m^3/yr prior to the fire, equivalent to an average basin-wide denudation rate of ~0.009 mm/yr (assuming similar densities for reservoir sediments and hillslope soils). Observations in the drained reservoir indicated that the pre-fire sediment was dominated by fine-grained sediment that would have been carried in suspension. The sediment deposited during the June 2, 2000 event was predominantly silt and very fine sand with a large component of ash.

When total station surveys were repeated in June 2001, a large volume (5,300 m^3, Table 2) of medium to very coarse sand and gravel had formed a subaerial delta at the head of the reservoir (Figure 3). The distal subaqueous portion of the delta and deeper-water sediments were composed of finer sand, silt, and reworked ash (muck). Field observations document that the delta was formed during snowmelt runoff in early spring of 2001, which followed a winter with above-average precipitation (Table 1). The coarse-grained delta and fine-grained distal sediments together comprised approximately 21,800 m^3 of sediment accumulated in one year, of which about 75% consisted of fine-grained sediment. Excavation of reservoir fill began in August 2001, exposing a stratigraphic record of the first

15 months of sedimentation (Figure 3). Detailed stratigraphic studies and surveys completed in the excavation between October 2001 and January 2002 allowed for basin-scale correlation of discrete strata and identification of the dates of specific layers (Figure 4). A series of rainstorms recorded at the RAWS sites, with about 0.5 to 3 cm of

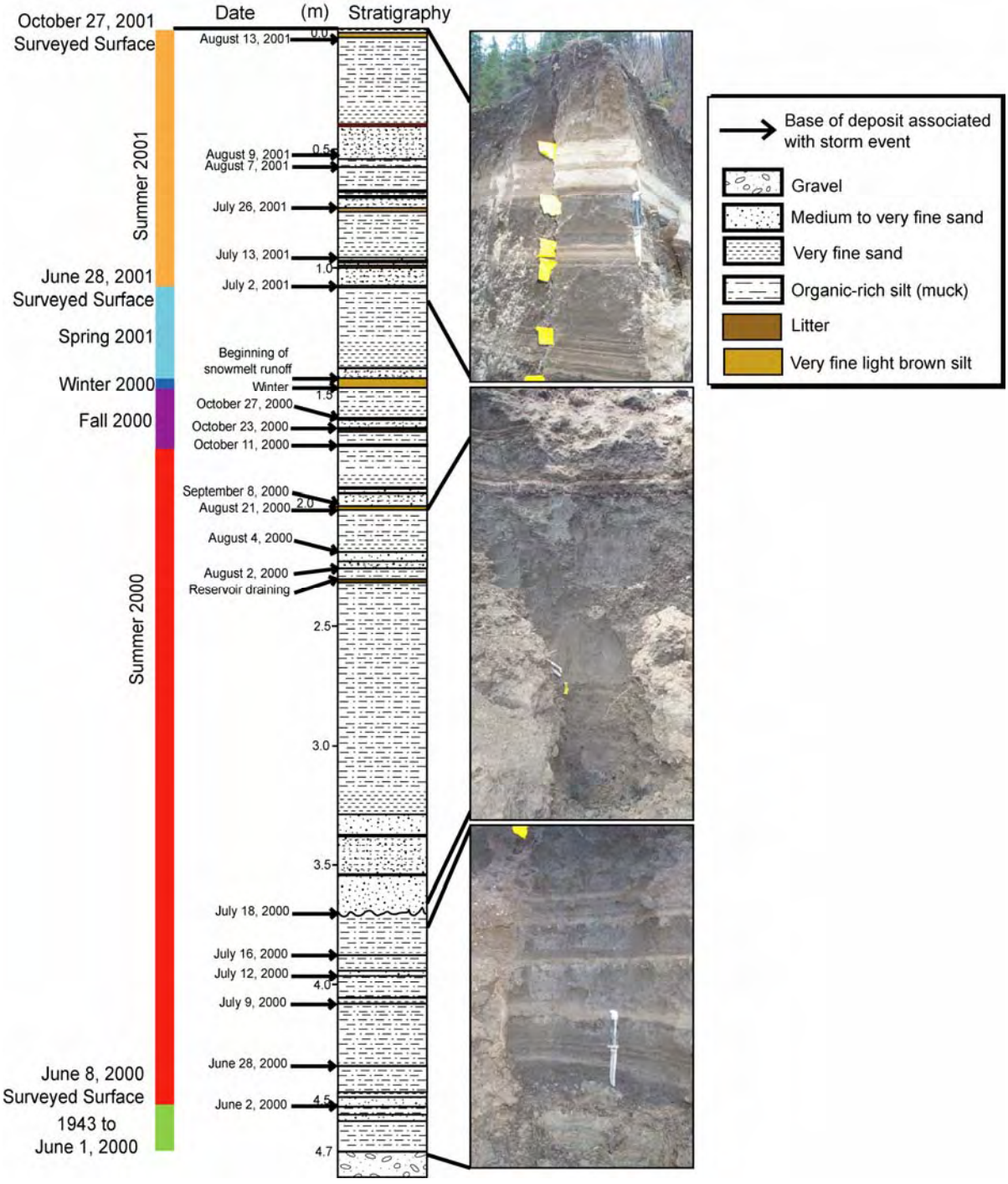


Figure 4 Stratigraphy exposed in excavation at the reservoir on October 27, 2001. Surveyed elevations, precipitation data, and field observations allowed correlation of individual layers to specific storms. More than 3 m of sediment were deposited during the first year following the fire, close to half of this following the July 18, 2000 storm, compared with ~0.2 m in the prior 57 years.

Table 1. Precipitation data.

Water Year	Precipitation at Quemazon SNOTEL		
Oct – Sept	Oct – Apr (cm)	May–Sept (cm)	Total (cm)
2000	21.59	24.13	45.72
2001	49.78	37.85	87.63
2002	12.70*	19.56	32.26
2003	30.23	27.94	58.17
2004	35.31	13.71	49.02
2005	49.28	--	--
1981 - 2004	35.86**	36.07**	71.93**

*Lowest in record. **Average values.

Table 2. Sediment data.

Sediment Volume in Reservoir		
Period	Total (m^3)	Delta (m^3)
1943 – 6/8/00	10,200*	0
6/8/00 – 6/28/01	20,200	5,300
6/28/01 – 4/2/02	8,000	0
4/2/02 – 7/23/03	4,000	900
7/23/03 – 6/30/04	4,800	3,700
6/30/04 – 7/11/05	4,500	3,500

* Includes 1,600 m^3 from 1 post-fire event.

rain falling in periods of no longer than 2 hours, could be correlated to specific strata exposed in the reservoir. The thickest sediment deposit in the center of the reservoir, ~1.4 m thick, resulted from a storm on July 18, 2000, that had an estimated average 2-hour rainfall on the burn area of 1.73 cm (an event with a return period of less than 1 year). This deposit fined upwards from fine to medium sand at the base to silty muck, a sequence typical of deposits from individual post-fire events. Overall, post-fire sediment in the center of the reservoir was about 1/3 very fine to fine sand (with minor medium sand), and about 2/3 silt and muck. Bulk density of the sand layers averaged 1.25 g/cm^3 and the silt and muck layers averaged 1.06 g/cm^3, similar to densities of surface soils on the Pajarito Plateau. It was not determined how much of the finer layers were ash versus mineral grains from the soil, although the muck layers were noticeably lighter in color in the upper 1 m of the section, indicating lower ash contents in the deposits from summer 2001 than summer 2000. In the fine-grained reservoir sediments that were exposed in October 2001, about 2/3 had been deposited in 2000 and 1/3 in 2001, despite the summer of 2001 being much wetter. In the first five summer monsoon seasons after the fire, 2001 was the only one with average precipitation totals, with the others being below average (Table 1). In addition, available data indicates the heaviest rainstorm in 2000 in the burn area in the upper Los Alamos Canyon watershed had a return period of less than 1 year, whereas at least two larger storms occurred in 2001 (July 13 and August 9, 2.51 and 2.97 cm in 2 hours, respectively), with estimated return periods of about 1-2 years. About 30% of the fine-grained sediment deposited in 2001 was apparently transported by snowmelt runoff, composing the surface that was surveyed on June 28, 2001, but overlying a distinctive light brown fine silt layer that records a period of minimal sediment input, probably representing deposition during the winter (Figure 4).

In 2002 to 2005, there was less sedimentation from summer precipitation relative to the first two years after the fire, and sedimentation was instead dominated by spring snowmelt runoff that formed coarse-grained deltas at the head of the reservoir (Table 2, Figure 5). Surveys performed in the second year after the fire record over 8,000 m^3 of sedimentation between June 2001 and January 2002, most of which occurred as a result of storms between July 2 and August 15, 2001. Minimal amounts of sediment were deposited in the reservoir between January and April 2002 due to limited snowmelt runoff associated with record low winter precipitation. The reservoir was completely excavated by April 2002, and a new baseline survey was completed. Subsequent surveys document reduced sedimentation as compared with the first two years, associated with intermediate levels of precipitation relative to 2000-2001 (Table 1). Between April 2002 and July 2003, ~4000 m^3 of sediment was deposited in the reservoir, with a small delta accounting for ~900 m^3. Between July 2003 and July 2004, ~4,800 m^3 of sediment was deposited, mostly consisting of a larger coarse-grained delta (~3700 m^3). This period included one of the two most intense storms in the watershed as recorded by the RAWS sites, August 23, 2003, with an estimated average 2-hour rainfall of 2.95 cm on the burn area, yet summer 2003 had relatively small amounts of fine sediment deposition relative to 2000 and 2001 (Figure 5). Between July 2004 and July 2005, ~4500 m^3 of sediment was deposited in the reservoir, with ~3500 m^3 comprising a delta. The 2005 delta, similar in size to the 2004 delta and smaller than the 2001 delta, was associated with the most prolonged snowmelt runoff period and the highest snowmelt peak after the fire.

The total amount of sediment deposited in the reservoir during the 5-year period after the fire was ~43,100m^3, ~70% fine-grained sediment and ~30% coarse-grained sediment. About half the post-fire sedimentation occurred in the first year, ~21,800 m^3 (Table 2), equivalent to an average basin-wide denudation rate of soil of ~1.3 mm/yr, or ~140

times the average pre-fire rate. Assuming that all of the sediment was derived from high and moderate severity burn areas (5.4 km^2) yields an average denudation rate of ~4.0 mm/yr for those areas, or ~450 times the pre-fire rate.

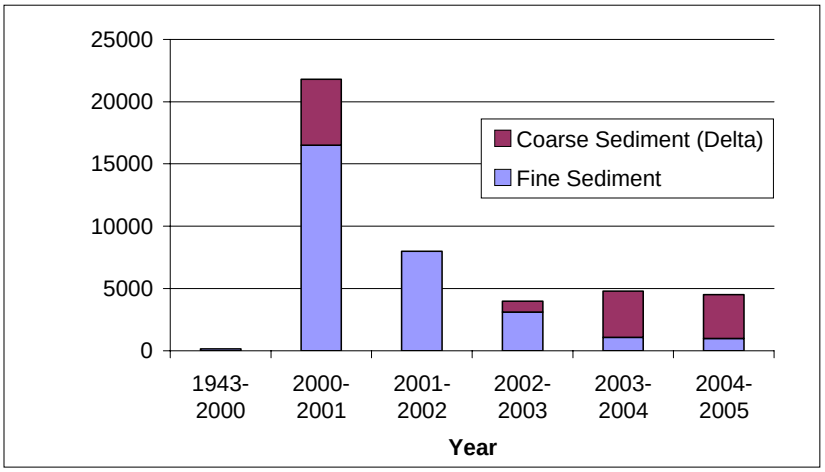


Figure 5 Plot of annual sedimentation in the reservoir, distinguishing coarse-grained sediment in the delta that predominantly reflects snowmelt runoff and fine-grained sediment that predominantly reflects suspended transport in summer floods. Note the overall annual decrease in the amount of fine sediments, and the relative increase in the percentage of coarse-grained to fine-grained sediments. 1943-2000 value is a 57-year average.

Calculated denudation rates using total sediment volumes declined rapidly over time, being about ~0.7-0.9 mm/yr in 2002 to 2004 (assuming a source in the high and moderate burn severity areas), or ~80-100 times the pre-fire rate.

Fine-grained and coarse-grained sediments, supplied largely by summer flash floods and spring snowmelt, respectively, show much different temporal patterns of deposition in the reservoir (Figure 5, Table 2). Fine-grained sediments show the highest depositional rates in the first year after the fire, and decline rapidly in subsequent years. Equivalent denudation rates were ~340 times pre-fire averages in 2000, declining to ~20 times pre-fire levels in 2003 and 2004. This trend is apparently independent of variations in summer precipitation. In contrast, coarse-grained sediment shows variations that relate more to the amount of winter precipitation and resultant snowmelt runoff than to time since the fire.

DISCUSSION AND CONCLUSIONS

The Los Alamos Reservoir has yielded an excellent record of post-fire erosion and sedimentation following a major wildfire. In addition to recording the magnitude of initial changes relative to pre-fire conditions and subsequent changes associated with watershed recovery, the effects of individual storms and variations in seasonal precipitation can be evaluated.

As recorded in the reservoir, erosion rates in the heavily forested watershed were extremely low in the 57 years prior to the Cerro Grande fire, averaging ~0.009 mm/yr. This low rate is consistent with field observations indicating the absence of extensive surface runoff and erosion prior to the fire, and is supported by stream gage records from nearby basins that show monsoon-season floods were rare in the eastern Jemez Mountains before the fire (Gallaher and Koch, 2004).

Erosion and sediment delivery into the reservoir were highest in the first year after the fire, accounting for about half the total sedimentation in the first five years, despite the occurrence of below-average summer precipitation and relatively low-intensity storms (<1 year return intervals). Adjusted for the area of high and moderate burn severity, equivalent denudation rates increased to ~4.0 mm/yr, ~450 times the pre-fire rate. Actual denudation rates in these areas may have been higher because of reduced sediment yield following treatments soon after the fire (1.5 km^2; e.g., straw mulch shown in Figure 1b). This exceeds an increase of 150-240 times reported by Moody and Martin

(2001) for an area with similar vegetation and climate in Colorado. Most of the sediment deposited in the first year was fine-grained and ash-rich, recording rapid stripping of hillslope soils by sheetwash and rill erosion and small debris flows in summer thunderstorms, common processes after fires (e.g., DeBano, 2000; Cannon et al., 2001). Sedimentation in the reservoir decreased by over half the second year after the fire, despite the occurrence of more summer precipitation and higher intensity storms that initiated gullying on the hillslopes. Sediment deposits in the second year were visibly lighter in color, containing lower ash contents, which is consistent with local stormwater analyses indicating lower concentrations of ash-derived constituents by the second year (Johansen et al., 2003; Gallaher and Koch, 2004). Sedimentation further decreased in the subsequent years, although remaining ~80-100 times higher than pre-fire levels in 2002-2005. A very slow return to pre-fire conditions in this region is similarly indicated by data from Frijoles Canyon, 8 km south, where peak stream discharge remained above pre-fire levels 22 years after the La Mesa fire (Veenhuis, 2002).

Significant differences occurred between delivery of fine-grained and coarse-grained sediment to the reservoir that are related to varying transport of these two components. The fine-grained sediment, carried in suspension, was largely transported quickly to the reservoir in flash floods, and deposition rates of fine sediment may closely track erosion rates on hillslopes in the burn area. In contrast, the coarse-grained sediment, transported as bedload, was largely delivered to the reservoir by snowmelt runoff, lagging behind upstream hillslope erosion. Studies downstream in Los Alamos Canyon showed that this seasonal difference in suspended versus bedload transport was also present before the fire (Malmon et al., 2004). Field observations after the fire confirm substantial deposition of coarse sediment along the main channel upstream from the reservoir during summer storms, and subsequent partial remobilization by snowmelt runoff. As inferred in other areas, much of this coarse sediment may remain in long-term storage upstream from the reservoir (e.g., Moody and Martin, 2001), although in the short term it may continue to be a major source of sediment reaching the reservoir.

ACKNOWLEDGMENTS

Funding was provided by the Department of Energy through the Los Alamos National Laboratory Environmental Restoration Project and as part of Cerro Grande recovery efforts, and by the USDA Forest Service. Los Alamos County was very helpful in coordination of draining and accessing the reservoir, and Bruce Gallaher and Rick Kelley provided reviews of this paper. Special thanks to all who assisted in the field with data collection.

REFERENCES

BAER (2000). Cerro Grande Fire, Burned Area Emergency Rehabilitation (BAER) Plan: Interagency Burned Area Rehabilitation Team.

Bowen, B. M. (1990). Los Alamos Climatology. Los Alamos National Laboratory report LA-11735-MS, Los Alamos, New Mexico.

Cannon, S.H., Bigio, E.R., and Mine, E. (2001). "A process for fire-related debris flow initiation, Cerro Grande fire, New Mexico," Hydrological Processes, 15, pp 3011-3023.

DeBano, L.F. (2000). "The role of fire and soil heating on water repellency in wildland environments; a review," Journal of Hydrology**,** 231-232, pp 195-206**.**

Deutsch, C.V., and Journel, A.G. (1992). GSLIB Geostatistical Software Library and Users Guide. Oxford University Press, New York, Oxford.

Dunne, T., and Leopold, L. (1978). Water in Environmental Planning. W. H. Freeman and Company, San Francisco.

Gallaher, B.M., and Koch, R.J. (2004). Cerro Grande Fire Impacts to Water Quality and Stream Flow near Los Alamos National Laboratory: Results of Four Years of Monitoring. Los Alamos National Laboratory report LA-14177, Los Alamos, New Mexico.

Geodimeter (1998) Geodimeter System 600 and 600 Pro User Manual, 10th Edition, Publ.Nr. 571 701 121. Larserics Digital Print Lab, Sweden.

Johansen, M.P., Hakonson, T.E., Whicker, F.W., and Breshears, D.D. (2003). "Pulsed redistribution of a contaminant following forest fire: Cesium-137 in runoff," Journal of Environmental Quality, 32, pp 2150-2157.

Malmon, D.V., Reneau, S.L., and Dunne, T. (2004). "Sediment sorting and transport by flash floods," Journal of Geophysical Research – Earth Surface, 109, F02005, doi:10.1029/2003 JF000067.

Moody, J.A., and Martin, D.A. (2001). "Initial hydrologic and geomorphic response following a wildfire in the Colorado Front Range," Earth Surface Processes and Landforms 26(10), pp 1049-1070.

Reneau, S.L., Kuyumjian, G.A., Malmon, D.V., and Tardiff, M.F. (2003). Precipitation-Frequency Relations on the Pajarito Plateau and in the Eastern Jemez Mountains, New Mexico, and Examples of Extreme or Flood-Producing Storms. Los Alamos National Laboratory report LA-UR-03-6484, Los Alamos, New Mexico.

Veenhuis, J.E. (2002). Effects of Wildfire on the Hydrology of Capulin and Rito de los Frijoles Canyons, Bandelier National Monument, New Mexico. U.S. Geological Survey Water-Resources Investigations Report 02-4152.

U.S. GEOLOGICAL SURVEY PILOT STUDY RESULTS FOR PARTICLE SIZE DISTRIBUTION ANALYSES OF QUALITY ASSURANCE SAMPLES

Natalie Latysh, Hydrologist, U.S. Geological Survey, P.O. Box 25046, Denver Federal Center, B. 95, M.S. 401, Denver, Colorado 80225, nlatysh@usgs.gov

Abstract: The United States Geological Survey (USGS) operates laboratories for the analysis of physical characteristics of fluvial sediment. The USGS Branch of Quality Systems (BQS) initiated the Sediment Laboratory Quality Assurance (SLQA) project in August 1996 to ensure that physical sediment data produced or used by the USGS are of a known quality and provide long-term comparability and consistency. The project quantifies bias and precision for suspended sediment concentration (SSC) and particle size distribution (PSD) analyses for participating laboratories. PSD analyses currently include determination of sand (>=0.063 mm) and fine (<0.063 mm) sediment portions only. USGS laboratories routinely produce PSD determinations for the fine sediment portion, in standard silt/clay size ranges (mm): <0.002, <0.004, <0.008, <0.016, <0.031, which are not being quality-assured by the SLQA project. Characterizing PSD aids investigators in identifying physical sediment transport mechanisms and deposition processes. Quantifying precision and bias of PSD analyses using SLQA performance evaluation samples would provide confidence limits for data interpretation.

During fall 2004, BQS conducted a pilot study using commercially-available test dust to determine its suitability for quality assurance (QA) samples intended for PSD analysis, in standard silt/clay size ranges, by SLQA project participants. The PSD for the test dust material was determined by the manufacturer using the Multisizer II Coulter Counter which measures particles individually by volume. During preparation of the test dust and water mixtures, BQS calculated the PSD for the QA samples using the manufacturer's PSD determinations. In the study, four USGS laboratories each received 3 sets of triplicate samples, with sediment mass ranging from 1,600 to 5,000 mg. The four laboratories have participated in the SLQA project since its inception and produce comparable data quality. Three of these laboratories used the pipette method and one laboratory used the SediGraph 5100 for PSD analysis. Prior to this study, PSD results for standard silt/clay size ranges produced by individual USGS laboratories have not been compared to each other.

Data submitted by the four participating laboratories were comparable. Ninety-seven percent of the analyses were within 10 percent of the target value determined by BQS during sample preparation. Results for the triplicate sample sets indicated precision was within 7 percent for each laboratory. The median values of reported percentages for particle size denominations 0.002, 0.004 and 0.031 mm were greater than the target values (positive bias) for all laboratories. Reported percentages for the 0.008 and 0.016 mm sizes were negatively biased for laboratories using the pipette method. The SediGraph method produced results that were positively biased for all particle sizes. Overall, pilot study results indicate small bias and variability among the laboratories for the test dust samples, comparable to bias and variability determined for suspended sediment concentration and fine/sand separation analyses in previous SLQA studies. The low variability and bias represented in the laboratory results indicate that BQS can formulate reproducible QA samples for laboratory analysis using the test dust. Dissolution of the material is minimal, and the manufacturer-specified PSD characteristics are accurate for calculating target properties for the SLQA project.

SOIL EROSION ON CROPLAND IN THE UNITED STATES: STATUS AND TRENDS FOR 1982-2003

Carla A. Kertis, Cartographer, U.S. Department of Agriculture-Natural Resources Conservation Service, Beltsville, MD, carla.kertis@wdc.usda.gov; Thomas A. Iivari, Watershed Planning Specialist, U.S. Environmental Protection Agency, Philadelphia, PA, iivari.tom@epa.gov

Abstract: Soil erosion is a natural process. However, accelerated erosion, often driven by anthropogenic activities, impacts agriculture, the infrastructure, and the environment. Cropland is particularly prone to erosion because many farming practices remove the protective vegetative cover. The National Resources Inventory (NRI) provides nationally consistent estimates of soil erosion resulting from water (sheet and rill) and wind processes on the Nation's cultivated cropland, non-cultivated cropland, and land enrolled in the Conservation Reserve Program (CRP). The NRI is a statistical survey designed to assess natural resource conditions and trends on non-Federal land in the United States. The NRI is conducted by the U.S. Department of Agriculture's Natural Resources Conservation Service in cooperation with Iowa State University's Center for Survey Statistics and Methodology. Data from the 2003 Annual NRI, the most up-to-date NRI information available, indicate that average soil erosion rates on all cropland and CRP land have decreased more than 38 percent since 1982. In 2003, the soil erosion rate was estimated at 4.5 tons per acre per year, compared to 7.3 tons per acre per year in 1982. Total soil erosion on all cropland and land in CRP declined since 1982 as well. Between 1982 and 2003, total soil erosion dropped from an estimate of over 3 billion tons per year to 1.7 billion tons. This is a decrease of 43 percent. Possible reasons for this decline include better management of the soil resource, prompted by land stewardship incentives and conservation compliance provisions in Federal farm legislation; increased use of conservation practices, such as conservation tillage; and an overall decline in cultivated cropland acres. A noteworthy trend indicated by the NRI data is a relative flattening of the decline in both soil erosion rates and total erosion since 1997. Although gains are still being made in reducing erosion, further reductions may require new approaches to addressing the soil erosion issue.

INTRODUCTION

Soil erosion is a natural process that contributes to the formation of fertile soils (e.g., in river deltas) and provides nutrients to water bodies for nourishing aquatic ecosystems. Accelerated soil erosion is a significant threat to soil quality and impacts agriculture, infrastructure, and the environment. Accelerated erosion is often driven by anthropogenic activities, such as cultivation of crops, urban development, deforestation, mining, etc. Cropland is particularly susceptible to erosion because many farming practices remove the protective vegetative cover. The United States Department of Agriculture (USDA) has estimated soil erosion and has addressed erosion issues since the 1930's. This paper discusses the impact of soil erosion and presents USDA data on soil erosion on cropland in the United States from 1982 to 2003.

THE SOIL EROSION PROCESS AND ITS IMPACT

Erosion is the breakdown, detachment, transport, and redistribution of soil particles by forces of water (rain, concentrated flow, streams, glaciers, etc.), wind, or gravity (Lal *et al*., 2004). As

falling raindrops impact the soil surface, they detach individual soil particles. When the topmost layers of soil become saturated, a film of water accumulates on the surface. This film captures the soil particles dislodged by raindrops and detaches additional soil particles as it moves down slope. Called "sheet erosion", this process removes a thin, fairly uniform layer of soil over the entire land surface. However, this type of erosion also carries away a high proportion of the lighter organic particles that are critical to soil fertility and health. Where sheet flow has increased thickness, flow is concentrated in small channels called rills. "Rill erosion" can remove considerable amounts of soil, because water becomes increasingly erosive when confined to these channels (Clark *et al*., 1985). Erosion caused by gullies, which are deep, often permanent, scours, can be severe enough to cause terrain deformation (Lal *et al*., 2004).

Wind erosion is the process of soil detachment and transport by forces generated by the wind. Regions of low precipitation, high temperatures, and elevated wind velocity are most prone to wind erosion. The risks of wind erosion are exacerbated by increased fetch as wind blows across long, bare fields. Soils of single-grain or weak structure and coarse-grained, loamy texture are particularly prone to wind erosion (Lal *et al*., 2004).

Soil erosion can negatively impact not only agriculture but also infrastructure and the environment. Soil erosion control practices historically have focused on preventing damage to farmland productivity as well as preserving land values. Accelerated erosion results in declining agricultural (biomass) productivity as organic matter is removed and effective root depth is decreased. Erosion also contributes to soil degradation and concomitant imbalances in the root zone, susceptibility to pests, and release of greenhouse gases (Lal *et al*., 2004). However, off-site effects of soil erosion may far exceed those experienced in the farm fields. As the soil is eroded, sediment, nutrients, pesticides, pathogens (bacteria and viruses), salts, and other pollutants are carried into the Nation's waterways and ultimately into the water supply. Wind erosion may cause sediment and pesticides, either in aerosol form or attached to soil particles, to be entrained in the atmosphere and deposited over vast areas.

The influx of sediment caused by erosion clogs drainage and irrigation ditches and canals, and navigational channels; degrades wildlife habitat and fisheries; infills water reservoirs; elevates water treatment costs; increases the need for dredging; and may indirectly contribute to flooding (Ribaudo *et al*., 1999). Siltation is the second leading cause of water quality impairment in the Nation's rivers and streams and the third leading cause in lakes (U.S. Environmental Protection Agency, 2002). Ribaudo (1989) estimated that sediment damage from agricultural erosion ranged between $2 billion and $8 billion per year. A survey of selected sediment damages to harbors, irrigation and agricultural drainage ditches, floodplain croplands, and water treatment facilities estimated annual damages at nearly $8 billion per year (Bernard and Iivari, 2000). Additional sediment damages to reservoirs, non-agricultural drainage ditches, pumping equipment, flooded buildings, and wildlife is estimated to be in excess of $10 billion annually (Iivari, 1996). McConnell (2001) puts the economic cost of soil erosion in the U.S. at $44 billion per year. This includes sediment damages and property damages, as well as on-site loss of productivity, lost nutrients, crop damages, increased energy demands, and replacement of water lost by erosion. Other references on the costs of soil erosion and erosion-related losses have been compiled by Sundquist (2005).

Nutrients, such as fertilizers and animal waste, fuel increased algal growth, which causes clogged pipelines, fish kills, reduced recreational opportunities, degraded aquatic ecosystems, and threats to human health. U.S. Environmental Protection Agency (EPA) studies have found that nutrient pollution is the primary cause of degraded water quality in lakes and is a significant cause of impairment in rivers (U.S. Environmental Protection Agency, 2002). Pesticide residues in surface water systems may harm aquatic organisms, damage fisheries, and pose a risk to human health. Additional costs are incurred for treatment of public water supplies in order to bring pesticide levels within health standards. Pesticides are the second leading cause of water quality impairment in estuaries (U.S. Environmental Protection Agency, 2002).

Some reports have identified agriculture as a leading contributor of non-point source water pollution in the United States (Pimental *et al.*, 1976; U.S. Environmental Protection Agency, 2002). However, with the establishment of soil conservation districts, widespread adoption of conservation tillage practices, implementation of measures outlined in recent Federal farm legislation, and increased participation in specific conservation programs, such as the Conservation Reserve Program (CRP) and Environmental Quality Incentives Program (EQIP), the agricultural sector has made significant advances in reducing soil erosion.

METHOD FOR ESTIMATING SOIL EROSION ON U.S. CROPLAND

Soil erosion rates and total erosion on cropland in the United States were estimated using data from the National Resources Inventory (NRI). The NRI is a statistical survey designed to assess natural resource conditions and trends on non-Federal land in the United States. This non-Federal land—including privately owned land, tribal and trust land, and land controlled by State and local governments—comprises approximately 78 percent of the Nation's total land area. The NRI is conducted by the U.S. Department of Agriculture's Natural Resources Conservation Service (NRCS) in cooperation with Iowa State University's Center for Survey Statistics and Methodology. The NRI covers all 50 States, Puerto Rico, the U.S. Virgin Islands, and some Pacific Basin locations (Goebel, 1998; U.S. Department of Agriculture, 2000).

Data from the NRI have been utilized for a variety of decision-making processes, scientific assessments, program evaluations, and other studies of soil and environmental issues. Examples of how data from the NRI have been applied include:

- Formulating agricultural and environmental legislation and policies to protect soil, water, and other related natural resources.
- Developing conservation programs and allocating USDA financial and technical assistance.
- Evaluating the effectiveness of existing policies, programs, and legislation that address or affect erosion, sediment, water quality, land-use, pollution prevention, and other related environmental issues.
- Identifying and/or targeting critical areas needing special emphasis, additional resources, or efforts to control erosion, protect water quality, or protect other related natural resources.
- Providing scientific data for land use planning.

- Supplying data for protecting soil quality or soil health in order to sustain long-term productivity and environmental protection.
- Aiding in estimating sediment yields and trends from landscapes and watersheds.
- Enhancing the public's understanding of natural resources and environmental issues.

During the period from 1977 to 1997, the NRI was conducted every 5 years. Data on land cover and use, soil erosion, prime farmland soils, wetlands, habitat diversity, selected conservation practices, and related resource attributes were collected at more than 800,000 randomly selected sample sites. Beginning in 2000, the NRI started a multi-year progression to an annual inventory. For the Annual NRI, data are gathered for a subset (approximately one-fourth) of the 800,000 sample sites that were established for previous NRI's. The data collection process for the Annual NRI is cumulative; that is, after several years of data collection, the reliability levels of the data will approximate those of the previous five-year cycle. For more information on the NRI, see the NRI Web site at www.nrcs.usda.gov/technical/NRI/.

The first release of Annual NRI data was from data collected during the 2001 NRI. Conclusions in this paper are based on data from the 2003 Annual NRI, the most up-to-date NRI information available. For national-level results, information is available for 1982, 1987, 1992, 1997, and 2003, so that trends and changes in land use and resource characteristics over a span of more than 20 years can be examined and analyzed. Soil erosion data from the 2003 Annual NRI presented in this paper are available only for the 48 conterminous States. Data derived from the NRI are estimates and not absolutes. This means that there is some amount of uncertainty in any result obtained using NRI information. Data in the tables in this paper are followed (in parentheses) by the estimated standard error for each value.

Present NRI data only describe the magnitudes of wind erosion and sheet and rill forms of water erosion. Gully, stream bank, mass wasting, channel scour, and other miscellaneous forms of water erosion or gravity-affected erosion are not included. However, data from some erosion studies (USDA, 1989; Bernard and Iivari, 2000) show that sheet and rill erosion on agricultural lands is the largest source of sediment contributed to small streams. Erosion from stream banks, gullies, road banks, construction sites, and other miscellaneous locations accounted for about 22 percent of total erosion on private lands (USDA, 1989). The NRI provides estimates of on-site erosion rates and does not estimate off-site sediment yield.

SOIL EROSION DATA FROM THE NRI, 1982-2003

The NRI estimates soil erosion on cultivated cropland, non-cultivated cropland, and land enrolled in the Conservation Reserve Program. Cropland is a land cover/use category in the NRI that includes areas used for the production of adapted crops for harvest. The subcategories of cultivated and non-cultivated cropland are utilized in the NRI. Cultivated cropland comprises land in row crops or close-grown crops as well as other cultivated cropland, such as hayland or pastureland that is in a rotation with row or close-grown crops. Non-cultivated cropland includes permanent hayland and horticultural cropland. CRP land includes land under a CRP contract.

NRI data show that between 1982 and 2003, total cropland acres declined, primarily due to a decrease in acres of cultivated cropland (Table 1). Some of this decline may be attributed to enrollment of land in the Conservation Reserve Program, initiated in 1985. In the same time interval, acres of non-cultivated cropland have increased.

Table 1 Acreage of Cultivated Cropland, Non-cultivated Cropland, and CRP Land by Year (millions of acres)

Year	Cultivated Cropland	Non-cultivated Cropland	All Cropland	CRP Land	Total—All Cropland and CRP
1982	375.7 (1.1)	44.1 (0.4)	419.7 (1.1)	0.0*(n/a)	419.7 (1.1)
1987	362.0 (1.1)	43.6 (0.4)	405.6 (1.2)	13.8 (0.1)	419.4 (1.2)
1992	334.5 (1.1)	46.9 (0.4)	381.3 (1.0)	34.0 (0.1)	415.4 (1.0)
1997	326.4 (1.1)	50.0 (0.5)	376.4 (1.0)	32.7 (0.0)	409.0 (1.0)
2003	310.1 (1.2)	57.8 (0.9)	367.9 (1.2)	31.4 (0.1)	399.3 (1.2)

*CRP established in 1985

Estimated standard errors are shown in parentheses.

Data from the 2003 Annual NRI indicate that average soil erosion rates on the total of all cropland and CRP have decreased significantly since 1982. In 2003, the soil erosion rate was estimated at 4.5 tons per acre per year, down from 7.3 tons per acre per year in 1982 (Table 2), a drop of more than 38 percent. In that same time interval, water erosion rates declined over 37 percent, from 4.0 to 2.5 tons/acre/year; corresponding wind erosion rates fell more than 39 percent.

Although not directly comparable to NRI data, estimates of historical erosion rates provide interesting and useful information on the magnitude of the soil erosion problem. Prior to 1930, it was common for soil in some areas to erode at rates in excess of 30 to 40 tons per acre per year (Trimble, 1974; Franzmeier, 1990; National Research Council, 1993; Trimble, 1999). The Dust Bowl catastrophe of the 1930's prompted farmers to implement conservation practices such as contouring and terracing. As a result, estimates of average erosion rates on U.S. cropland fell to under 15 tons per acre per year (Pimental, *et al*., 1976). Trimble (1999) gathered 140 years' of information about sediment buildup and erosion around Coon Creek Basin in Wisconsin and concluded that, overall, erosion in the watershed has been declining steadily, down to six percent of what it was in the 1930's. Many other references with historical soil erosion information have been compiled by Sundquist (2005).

Between 1982 and 2003, total soil erosion on all cropland and CRP land in the United States decreased from over 3 billion tons per year to 1.7 billion tons (Table 3). This is a decrease of nearly 43 percent. There are several likely reasons for this decline. Land stewardship incentives and conservation compliance provisions of the 1985, 1990, 1996 and 2002 Farm Bills led to better management of the soil resource. The Conservation Reserve Program, established by the 1985 Farm Bill, provided a mechanism and incentive for setting aside up to 34 million acres of highly erodible cropland that are now planted to permanent grass and/or trees. Increased use of conservation practices, such as conservation tillage and other Best Management Practices, has had a significant impact on reducing soil erosion. The use of conservation tillage has increased

from 1 percent of the planted land in 1963 to nearly 41 percent in 2004 (Uri, 1998; Conservation Technology Information Center, 2005). Finally, changes in land use, specifically, a decline in cultivated cropland acres, has affected national total erosion levels.

Table 2 Average Annual Rates of Soil Erosion on Cropland and Land in CRP, 1982-2003 (tons/acre/year)

	1982	1987	1992	1997	2003
Cultivated Cropland					
Water Erosion	4.4 (0.0)	4.0 (0.0)	3.4 (0.0)	3.1 (0.0)	3.0 (0.0)
Wind Erosion	3.6 (0.1)	3.5 (0.0)	2.9 (0.0)	2.5 (0.0)	2.4 (0.0)
Total	8.0 (0.1)	7.5 (0.1)	6.3 (0.0)	5.6 (0.0)	5.4 (0.0)
Non-cultivated Cropland					
Water Erosion	0.6 (0.0)	0.7 (0.0)	0.6 (0.0)	0.6 (0.0)	0.6 (0.0)
Wind Erosion	0.4 (0.1)	0.4 (0.0)	0.3 (0.0)	0.2 (0.0)	0.3 (0.0)
Total	1.0 (0.1)	1.1 (0.0)	0.9 (0.0)	0.8 (0.0)	0.9 (0.0)
All Cropland					
Water Erosion	4.0 (0.0)	3.6 (0.0)	3.1 (0.0)	2.8 (0.0)	2.6 (0.0)
Wind Erosion	3.3 (0.0)	3.2 (0.0)	2.6 (0.0)	2.2 (0.0)	2.1 (0.0)
Total	7.3 (0.1)	6.8 (0.0)	5.7 (0.0)	5.0 (0.0)	4.8 (0.0)
Land in CRP					
Water Erosion	--* (n/a)	2.0 (0.1)	0.6 (0.0)	0.4 (0.0)	0.4 (0.0)
Wind Erosion	--* (n/a)	6.7 (0.6)	0.6 (0.0)	0.3 (0.1)	0.5 (0.1)
Total	--* (n/a)	8.7 (0.6)	1.2 (0.1)	0.7 (0.1)	0.9 (0.1)
All Cropland and CRP					
Water Erosion	4.0 (0.0)	3.6 (0.0)	2.9 (0.0)	2.6 (0.0)	2.5 (0.0)
Wind Erosion	3.3 (0.0)	3.3 (0.0)	2.4 (0.0)	2.1 (0.0)	2.0 (0.0)
Total	7.3 (0.1)	6.9 (0.1)	5.3 (0.0)	4.7 (0.0)	4.5 (0.0)

*CRP established in 1985
Estimated standard errors are shown in parentheses.

The 2003 data show that the decline in total soil erosion has not been as dramatic since 1997, compared to the interval from 1982 to 1997. However, it is important to note that gains are still being made in this area. The significant reductions in soil loss that were made between 1982 and 1997 were not only sustained but slightly improved upon in the period between 1997 and 2003.

CONCLUSIONS

Results from the 2003 Annual NRI show that both soil erosion rates and total erosion on all cropland and land in CRP declined considerably between 1982 and 2003. Possible reasons for this decline include increased use of conservation practices, such as conservation tillage and other Best Management Practices, participation in land stewardship incentive programs, and

implementation of conservation compliance provisions outlined in Federal farm legislation. A noteworthy observation is that the decline in soil erosion rates and total erosion from 1997 to 2003 is not nearly as steep as for the interval from 1982 to 1997. The significant gains in soil erosion control that were made between 1982 and 1997 were sustained in the period between 1997 and 2003 and were improved upon slightly. As more data are accumulated with each successive year of the Annual NRI, soil erosion components and issues may be examined at finer levels of detail, such as on a regional basis, with greater degrees of reliability, and possibly with a deeper extent of resource information to attempt to explain the flattening in this trend. Further reductions in soil erosion may require new approaches to addressing the erosion issue.

Table 3 Total Annual Erosion on Cropland and Land in CRP, 1982-2003 (millions of tons)

	1982	1987	1992	1997	2003
Cultivated Cropland					
Water Erosion	1,637.8 (10.5)	1,436.9 (9.2)	1,139.8 (8.1)	1,010.1 (6.3)	935.5 (7.4)
Wind Erosion	1,367.5 (19.7)	1,275.0 (18.3)	972.5 (16.9)	828.1 (15.2)	757.6 (13.3)
Total	3,005.3 (21.4)	2,712.0 (19.9)	2,112.3 (17.2)	1,838.2 (15.1)	1,693.0 (15.2)
Non-cultivated Cropland					
Water Erosion	28.0 (1.1)	28.5 (1.2)	26.2 (0.8)	28.9 (0.7)	34.8 (0.9)
Wind Erosion	16.8 (2.8)	17.8 (2.0)	11.8 (1.3)	9.3 (1.0)	18.3 (1.6)
Total	44.8 (3.1)	46.4 (2.1)	38.0 (1.5)	38.2 (1.1)	53.2 (2.0)
All Cropland					
Water Erosion	1,665.8 (10.5)	1,465.4 (9.4)	1,166.0 (8.1)	1,039.0 (6.2)	970.3 (7.3)
Wind Erosion	1,384.3 (20.1)	1,292.9 (18.5)	984.3 (17.0)	837.5 (15.1)	775.9 (13.1)
Total	3,050.1 (21.8)	2,758.3 (20.4)	2,150.3 (17.5)	1,876.4 (15.2)	1,746.2 (14.9)
Land in CRP					
Water Erosion	--* (n/a)	27.7 (1.2)	19.4 (0.8)	12.1 (0.4)	11.4 (0.4)
Wind Erosion	--* (n/a)	92.9 (7.8)	20.1 (2.1)	10.3 (1.8)	14.2 (2.0)
Total	--* (n/a)	120.6 (8.0)	39.5 (2.4)	22.4 (1.8)	25.6 (2.0)
All Cropland and CRP					
Water Erosion	1,665.8 (10.5)	1,493.2 (9.6)	1,185.4 (8.4)	1,051.0 (6.3)	981.7 (7.3)
Wind Erosion	1,384.3 (20.1)	1,385.8 (19.8)	1,004.4 (17.1)	847.7 (15.6)	790.2 (13.0)
Total	3,050.1 (21.8)	2,879.0 (23.0)	2,189.8 (17.5)	1,898.7 (15.4)	1,771.8 (14.9)

*CRP established in 1985

Estimated standard errors are shown in parentheses.

ACKNOWLEDGEMENTS

The manuscript was improved through reviews by D. M. Moffitt, D. L. Lund, J. J. Goebel, and D. K. Brezinski. Important statistical data were supplied by S. M. Wallace.

REFERENCES

Bernard, J. M., and Iivari, T. A. (2000). Sediment damages and recent trends in the United States, International Journal of Sediment Research, vol. 15, No. 2, p. 135-148.

Clark, E. H. II, Haverkamp, J. A., and Chapman, W. (1985). Eroding Soils, The Off-Farm Impacts. The Conservation Foundation, Washington, DC.

Conservation Technology Information Center (CTIC) (2005). National Crop Residue Management Survey @ www.ctic.purdue.edu/Core4/CT/CT.html.

Franzmeier, D. P. (1990). "Soil landscapes and erosion processes," *in* Proceedings of Soil Erosion and Productivity Workshop, W. E. Larson, G. R. Foster, R. R. Allmaras, and C. M. Smith, eds., University of Minnesota, p. 81-104.

Goebel, J. J. (1998). "The National Resources Inventory and its Role in U.S. Agriculture," *in* Agricultural Statistics 2000: An International Conference on Agricultural Statistics, T. E. Holland and M. P. R. Van den Broecke, eds., International Statistical Institute, Voorburg, The Netherlands, p. 181-192.

Iivari, T. A. (1996). Resource Conservation Act Appraisal, Working Paper No. 15 (unpublished), U.S. Department of Agriculture-Natural Resources Conservation Service, Washington, DC.

Lal, R., Sobecki, T. M., Iivari, T., and Kimble, J. M. (2004). Soil Degradation in the United States. Lewis Publishers, Boca Raton, FL.

McConnell, D. A. (2001). The Good Earth, on-line textbook, version 1.5. McGraw–Hill Publishing, New York, NY.

National Research Council (1993). Soil and Water Quality: An Agenda for Agriculture. National Academy Press, Washington, DC.

Pimental, D., E. Terhune, R. Dyson-Hudson, S. Rochereau, R. Samis, E. A. Smith, D. Denman, D. Reifschneider, and M. Shepard (1976). Land degradation: Effect on food and energy resources, Science, vol. 194, p. 149-155.

Ribaudo, M. O. (1989). Water Quality Benefits from the Conservation Reserve Program, Agricultural Economic Report 606, U.S. Department of Agriculture-Economic Research Service, 38 pp.

Ribaudo, M. O., Horan, R. D., and Smith, M. E. (1999). Economics of Water Quality Protection from Nonpoint Sources, Agricultural Economic Report 782, U.S. Department of Agriculture- Economic Research Service, 106 pp.

Sundquist, B. (2005). Topsoil Loss—Causes, Effects, and Implications: A Global Perspective, on-line literature review, edition 6 @ http://home.alltel.net/bsundquist1/se0.html.

Trimble, S. (1974). Man Induced Erosion on the Southern Piedmont: 1700-1970. Soil Conservation Society of America, Ankeny, IA.

Trimble, S. (1999). Decreased rates of alluvial sediment storage in Coon Creek Basin, Wisconsin, Science, vol. 285, p. 1244-1245.

Uri, N. D. (1998). Conservation tillage in United States agriculture, Environmental Technology, vol. 19, p. 1017-1027.

U.S. Department of Agriculture (1989). The Second RCA Appraisal: Soil, Water, and Related Resources on Non-Federal Land in the United States. U.S. Department of Agriculture, Washington, DC, 280 pp.

U.S. Department of Agriculture (2000). Summary Report: 1997 National Resources Inventory. U.S. Department of Agriculture-Natural Resources Conservation Service, Washington, DC, and Iowa State University Statistical Laboratory, Ames, IA, 90 pp.

U.S. Environmental Protection Agency (2002). National Water Quality Inventory: 2000 Report. U.S. Environmental Protection Agency, Washington, DC, 207 pp.

SELF-SIMILARITY OF OPEN-CHANNEL TURBULENCE

Junke Guo, Assistant Professor, University of Nebraska, Omaha, Nebraska
e-mail: junkeguo@mail.unomaha.edu

Abstract: Based on our previous modified log-wake law in turbulent pipes and boundary layers, we invent two compound similarity numbers *(Y,U)* where *Y* is a combination of the inner variable y^+ and outer variable ξ, and *U* is the pure effect of the wall. The two compound similarity numbers can well collapse mean velocity profile data with different Reynolds numbers into a single universal profile. We then propose an arctangent law for the inner region and a general log law in terms of *(Y,U)* for the outer region. Using asymptotic matching method, we obtain a self-similarity law that describes the mean velocity profile from the bed to free surface, and embeds the existing knowledge of the linear law in the viscous sublayer, the quartic law in the bursting sublayer, the classic log lag in the overlap, the sine-square wake law in the wake layer, and the parabolic law near the free surface. In particular, the proposed self-similarity law can well reproduce the velocity dip phenomenon. The proposed arctangent law, the general log law in terms of *(Y,U)* and the self-similarity law have been confirmed with the high-quality data, with different Reynolds numbers, including those of Nezu and Rodi, Lyn, Muste and Patel, Sarma et al., and the measurements of the Mississippi River. The proposed law can be used to establish an accurate stage-discharge relationship and accurately study bedload velocity and suspended entrainments.

LOGARITHMIC MATCHING AND ITS APPLICATIONS IN DATA ANALYSIS

Junke Guo, Assistant Professor, University of Nebraska, Omaha, Nebraska
e-mail: junkeguo@mail.unomaha.edu

Abstract: Hydrological modeling is often based on observational data that often result in nonlinear relationships between variables. For example, the Manning equation is a typical power law; a stage-discharge relationship is often described with one or more power laws; turbulent velocity profile is described with one or more logarithmic or power laws; downstream hydraulic geometries are expressed with one or more power laws; and so on. Recently, Guo (2002) proposed a logarithmic matching that can be applied to analyze nonlinear data sets. It states that for a complicated nonlinear problem or an experimental curve, if one can find two asymptotes, in extreme cases, which can be expressed as logarithmic laws, power laws, exponential laws, or even linear laws, then the logarithmic matching can merge the two asymptotes into a single composite solution. The applications of the logarithmic matching have been successfully tried in several cases in open-channel flows, coastal hydrodynamics and sediment transport such as: 1) the inverse problem of Manning equation in rectangular open-channels, 2) the connection of different laws in computational hydraulics, 3) the solution of wave dispersion equation, 4) criterion of wave breaking, 5) wave-current turbulent model, 6) sediment settling velocity, 7) velocity profiles of sediment-laden flows, and 8) sediment transport capacity. All these applications agree very well with numerical solutions or experimental data. Although the examples are all for hydraulics and sediment transport, the method can be applied to many other nonlinear analyses.

INTEGRATED RIVER MORPHOLOGY AND VEGETATION MODELING OF THE SACRAMENTO RIVER

Blair P. Greimann, bgreimann@do.usbr.gov, Jennifer Bountry, Yong Lai, David Mooney, and Timothy Randle, Hydraulic Engineers, Sedimentation and River Hydraulics Group, Technical Service Center, Bureau of Reclamation, Denver, CO 80225

Abstract: Reclamation is considering altering water supply management in the Sacramento River Basin. Because the Sacramento River is integral to the aquatic and riparian habitat as well as to the water supply of California, it is necessary to understand the impact of alternative water supply management on the Sacramento River corridor. For this objective, the Mid-Pacific Region and the Technical Service Center of Reclamation are developing an integrated suite of predictive models that can be used to evaluate the effects of the proposed water supply management scenarios on the geomorphic conditions of the Sacramento River between Red Bluff and Colusa, California.

The models will include a watershed scale sediment budget and analysis tool called SIAM (Sediment Impact Analysis Model). It simulates the movement of sediment through a drainage network from source to outlet to assess the connectivity of sediment sources and sinks and so estimate the effect of sediment dynamics on channel morphology. Results identify areas of short and long term instability and provide information on the quantity and source of sediment loads in selected reaches of the fluvial system.

A one-dimensional sediment transport model called GSTAR-1D (Generalized Sediment Transport for Alluvial Rivers – One Dimension) will model the sediment transport and vertical channel changes at a reach scale. It will also simulate the river stage.

The migration process will be analyzed using analytical methods in conjunction with historical aerial photography. The detailed hydraulics and sediment transport in particular meander bends will also be analyzed using U2RANS (Unsteady and Unstructured Reynolds Averaged Navier-Stokes solver). It will be able to assess areas of scour and deposition in a bend.

Vegetation growth and survival will be simulated using results from an unsaturated flow model that tracks soil moisture content. It will use the river stage results from GSTAR-1D as a boundary condition. It will also account for the extensive groundwater pumping in the area.

The linked models will be used collaboratively to evaluate the benefits and impacts of proposed operational strategies including:

- Natural river processes (channel migration and point bar formation)
- Riparian vegetation establishment and survival
- Erosion and deposition processes on Tribal Trust Lands

The suite of models will be used to predict future geomorphic trends, including cottonwood recruitment, under various operational, hydrologic, and land use scenarios. The study will

evaluate the potential reasons that cottonwood recruitment has been successful at some locations, but not others, during specific years.

This poster will describe the conceptual models of river, groundwater and vegetative processes that occur on the Sacramento River. It will also describe data linkages between the models, and how output from each model will be used to support the impact analysis.

ALLUVIAL FAN EROSION AND SEDIMENTATION INVESTIGATIONS USING THE HYDRAULIC MODELING TOOL FLO-2D

Joseph Gasperi, Geologist, USDA-Natural Resources Conservation Service, 316 W. Boone Avenue, Spokane, Washington 99201, joe.gasperi@wa.usda.gov; John McClung, Hydraulic Engineer, USDA-Natural Resources Conservation Service, 101 South Main, Temple, Texas 76501, john.mcclung@tx.usda.gov

Abstract: FLO-2D offers a useful planning and evaluation tool for addressing sediment related resource concerns by providing information on the spatial distribution of erosion and deposition of sediment. This poster presents an example of how FLO-2D may be used for watershed scale evaluations of erosion and soil loss on alluvial fans. The model has been applied to four scenarios with different soil types and vegetative cover conditions to represent a range of conditions. Each scenario was evaluated using six different storm runoff events. Two-dimensional plots of the model output identify the spatial distribution of overland flow, maximum flow velocities, scour, and deposition. Processing of the model output permits the development of sediment-frequency curves and the determination of average annual soil loss rates. The soil loss rates have been compared to demonstrate the sensitivity of the watershed to differences in vegetative cover conditions and soil type.

INTRODUCTION

The Natural Resources Conservation Service (NRCS) has a long history of using physical process models to estimate erosion and transport of sediment by wind and water. FLO-2D, developed by James S. O'Brien of FLO-2D Software, Inc., continues this tradition by adding to the options available to NRCS and its partners for evaluating the impact of overland flow on erosion and deposition of sediment on alluvial fans.

FLO-2D is a two-dimensional watershed model with a sediment transport component. Model simulations describe the spatial distribution of erosion and deposition within the modeled area. Processing of the model output provides information on the relative severity of erosion in terms of average annual soil loss. O'Brien (2001) defined the sediment transport component in this way:

> FLO-2D can compute sediment transport in channels, streets and overland flow. A multiple regression sediment transport equation for sand bed channels or alluvial floodplains is used in the model. This empirical equation is a computer generated solution of the Meyer-Peter, Muller bed-load equation applied in conjunction with Einstein's suspended load integration (Zeller and Fullerton, 1983). The bed material discharge, $q_{s,}$ is calculated in cfs per unit width as follows:
>
> $$q_s = 0.0064\, n^{1.77}\, V^{4.32}\, G^{0.45}\, d^{-0.30}\, D_{50}^{-0.61}$$
>
> where n is Manning's roughness coefficient, V is mean velocity, G is the gradation coefficient, d is the hydraulic depth and D_{50} is the median sediment diameter. All units in this equation are in the ft-lb-sec system except D_{50}, which is in millimeters.

This poster presents an example that demonstrates how FLO-2D can be applied for watershed-scale sedimentation investigations.

RESOURCE CONCERN

Overland flooding and flood plain scour deliver sediment to a river with a recreational fishery that is important to the local economy.

UNKNOWNS

- Area subject to overland flow.
- Maximum overland flow velocities.
- Location of scour and deposition.
- Rate of soil loss.
- Sensitivity of soil loss rates to land use changes.

APPROACH

NRCS completed an analysis on a sub-part of the watershed (Figure 1) by running FLO-2D for the 100-, 50-, 25-, 10-, 5- and 2-year runoff events with two different soil types and two different cover conditions. The two soils represent the range of soils, from fine (silty sand, SM) to coarse (poorly-graded sand, SP), found in the subwatershed. Cover conditions assume either a fully vegetated state with grasses, shrubs and trees approximating an undisturbed condition (Good) or one with no vegetative cover (Poor).

The two soil types (SM and SP) and cover conditions (Good and Poor) represent extremes of conditions found within the study area. The model could also be modified to compare different vegetative and/or structural land treatment alternatives, but in this case we wanted to evaluate conditions that were most likely and least likely to erode. In this way, watershed planners are provided a basis (i.e. upper and lower limits of soil loss rates) for establishing numerical targets for managing for soil loss.

ANALYSIS

Output from FLO-2D was plotted in ArcView to show the spatial distribution of scour, deposition, overland flow and maximum flow velocities. Examples of output for the 100-year runoff event are shown in Figures 2 and 3. Flow is from the bottom of the page towards the top.

The sediment output files were used to develop sediment-frequency curves (Figure 4) and to calculate average annual soil loss (Figure 5). These numbers give planners representative estimates of the relative volume of soil that may be transported off-site following different storm events and under a range of cover conditions.

These data were also converted to units of tons/acre/year and the values plotted against geologic rates of erosion (Figure 5) to demonstrate the sensitivity of the different soil types to changes in cover conditions.

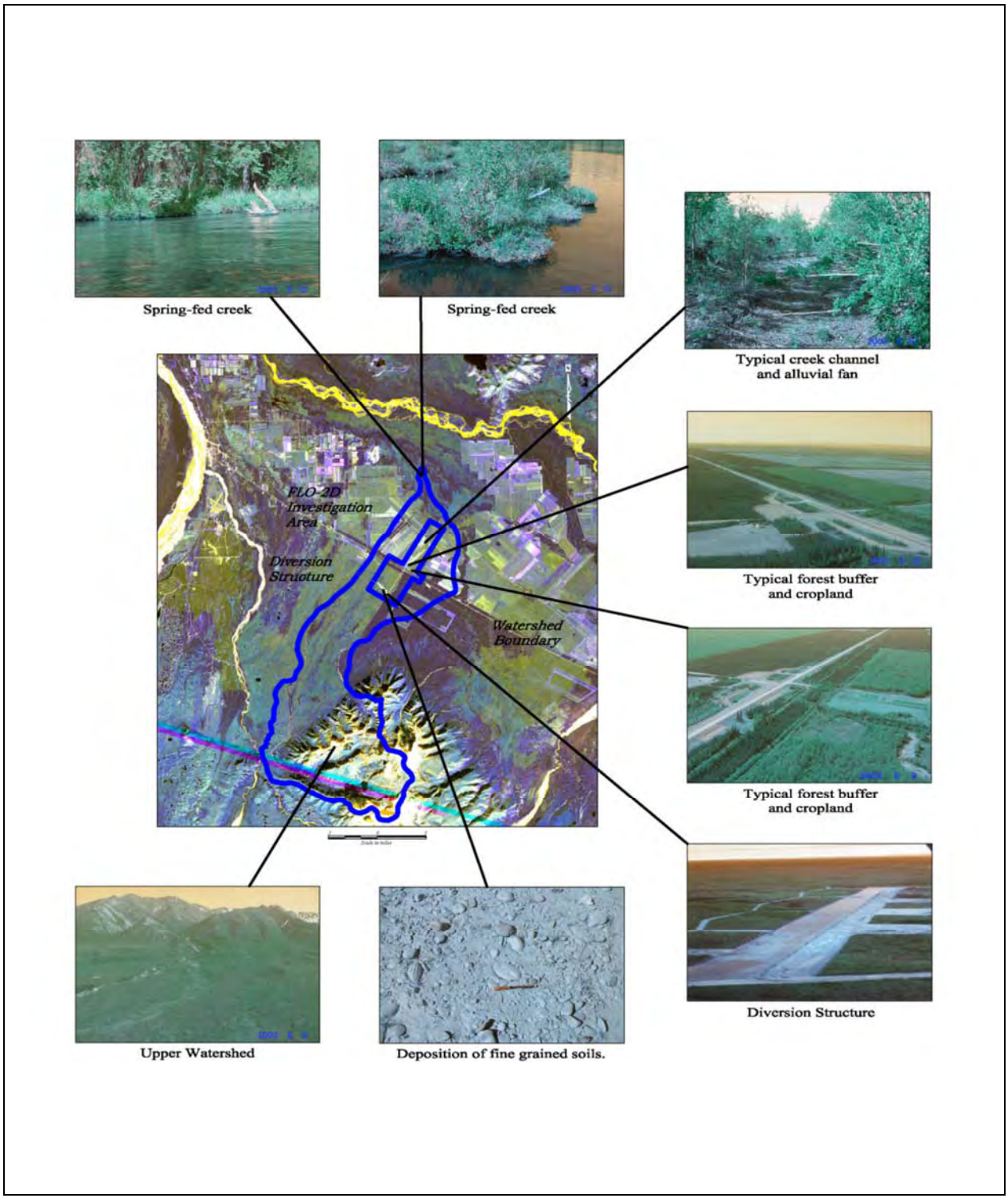


Figure 1. FLO-2D investigation area beginning at a diversion structure in the watershed. Water drains to the north and under a major interstate highway which lies about midway through the study area.

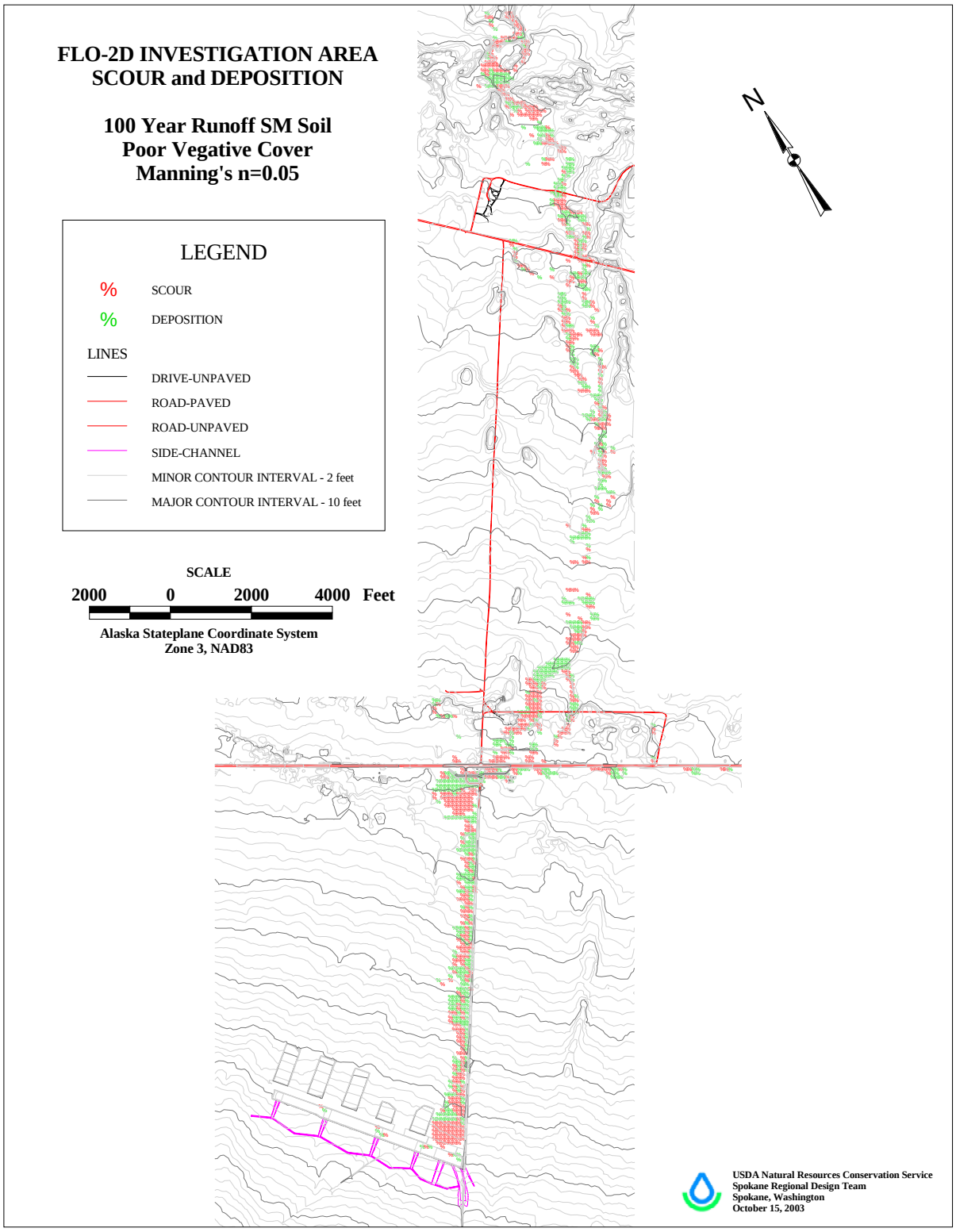


Figure 2 Scour and deposition for the 100-year runoff event; flow is from the bottom of the page towards the top.

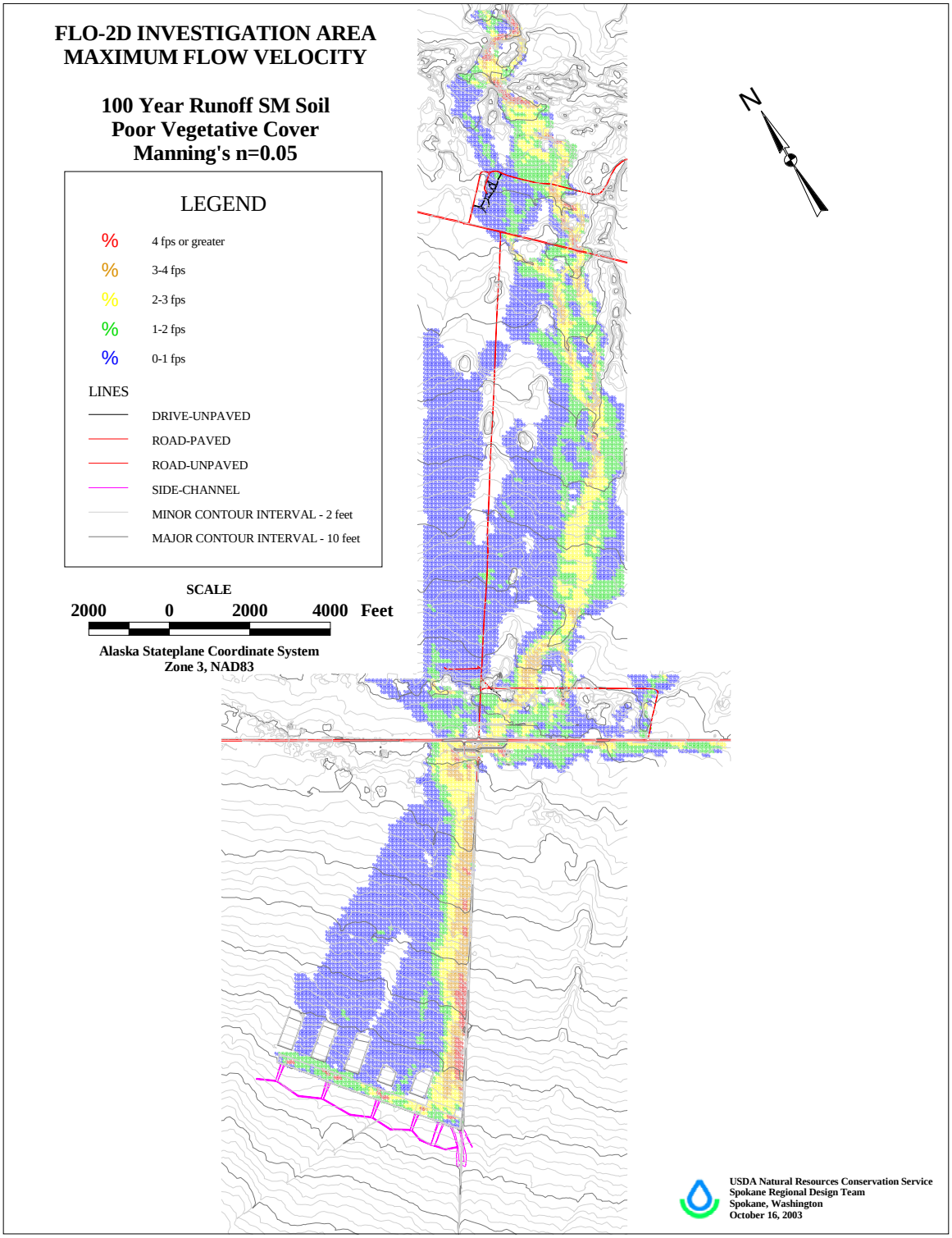


Figure 3 Maximum flow velocity for the 100-year runoff event; flow is from the bottom of the page towards the top.

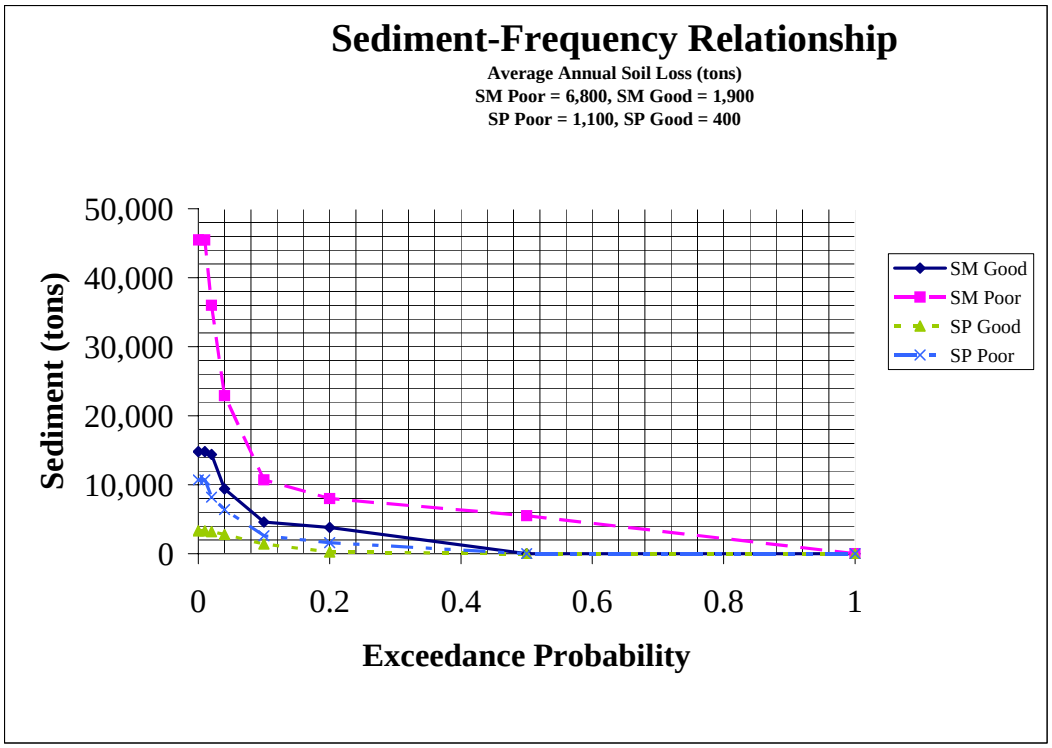


Figure 4 Sediment-frequency curves.

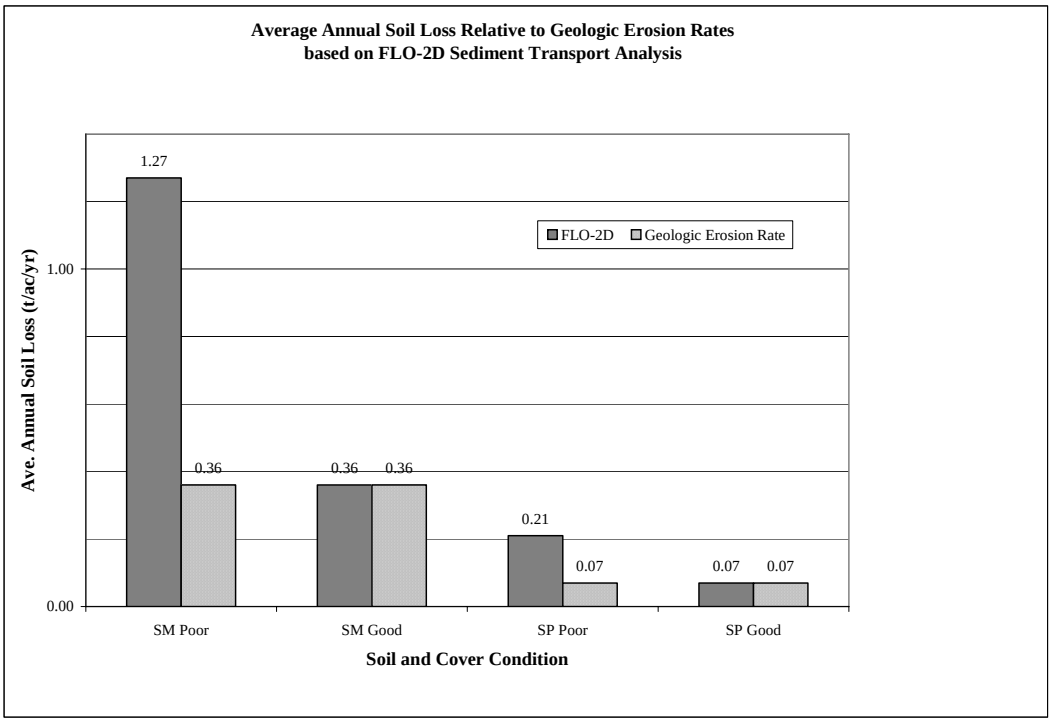


Figure 5 Average annual soil loss vs. geologi rates of erosion.

DISCUSSION

FLO-2D provides valuable information on where erosion and deposition occur and also information on the distribution of overland flows and flow velocities.

Plots of average annual soil loss relative to geologic rates of erosion reinforce the notion that ground cover plays a significant role in slowing overland flow and trapping sediment before it can be transported off-site.

Particle size too is critical to the gross erosion rate. Finer soils are more sensitive to watershed disturbances than coarser soils and are more likely to be scoured than coarser soils under the same runoff conditions.

CONCLUSION

Plots of output can help watershed planners and the public to better understanding the spatial distribution of overland flows and how flow velocities influence where scour and deposition of soils occur.

Processing of the model output and displaying it graphically demonstrates how the size of the runoff event, the coarseness of soil particles and the quality of cover conditions influence the volume of soil transported off-site and the rate of soil loss.

Appropriately designed watershed sensitivity analyses can provide a basis from which to establish numerical targets for the management of soil loss.

REFERENCES

O'Brien, J.S. (2001). "FLO-2D Users' Manual," Version 2001.06, FLO-2D Software, Inc., Nutrioso, Arizona, pp113.

FURTHER INFORMATION

FLO-2D Software, Inc., can be found on the web at: http://www.flo-2d.com/

RECONNAISSANCE TECHNIQUES FOR RESERVOIR SURVEYS

Ronald Ferrari , Hydraulic Engineer, Bureau of Reclamation, Technical Service Center, Sedimentation and River Hydraulics, P.O. Box 25007, D-8540, Denver, CO 80225-0007, rferrari@do.usbr.gov; Kent Collins, P.E., Hydraulic Engineer, Bureau of Reclamation, Technical Service Center, Sedimentation and River Hydraulics, P.O. Box 25007, D-8540, Denver, CO 80225-0007, kcollins@do.usbr.gov

Abstract: The reconnaissance survey technique is described then applied to two large U.S. reservoirs to update bottom topography and compute sediment deposition volumes and storage capacities. Known areas of accumulated sediment were surveyed using multibeam technology. The multibeam data was analyzed to determine the locations and volumes of sediment deposits in the surveyed reaches of the reservoirs. Using state of the art collection equipment and field reconnaissance techniques can greatly reduce collection and analysis costs and still produce accurate results. Recommendations are made for expanded application of reconnaissance techniques to larger areas and more detailed study of results where applied.

INTRODUCTION

Reservoir sedimentation is an ongoing natural depositional process that can remain invisible for a significant portion of the life of a reservoir. However, lack of visual evidence does not reduce the potential impacts of reservoir sedimentation on functional operations of a reservoir (Lin, 1997). As sediment deposition depletes reservoir storage volume, periodic reallocation of available storage at various pool levels may be necessary to satisfy operational requirements of water users.

Reclamation conducts reservoir surveys with the purpose of updating the area-capacity relationship and computing annual sediment inflow to project useful operation of their existing facilities. Evaluation of reservoir sediment deposition usually involves extensive field data collection, requiring significant time and resources to complete. A complete hydrographic survey provides an accurate contour map of the reservoir bottom, current surface area and reservoir capacity, and sediment accumulation since previous surveys. However, a complete survey for larger reservoirs can be expensive, limiting the frequency of surveys.

Currently, Reclamation oversees more than 400 storage reservoirs, but only thirty percent have been resurveyed since initial filling. Of those resurveyed, about thirty percent have had multiple surveys for monitoring high sediment inflow rates. Reclamation's Sedimentation and River Hydraulics Group (Sedimentation Group) has monitored reservoir sedimentation over the last century following the closure of several dams in the early 1900's. The monitoring methodology has varied from reconnaissance level studies to detailed field data collection and analysis. The reconnaissance collection and analysis techniques presented here use modern instrumentation and analysis tools to accurately update reservoir sedimentation information in a timely and cost effective manner.

RESERVOIR SEDIMENTATION

Reservoirs come in all shapes and sizes and are designed for purposes such as retention for flood control, debris/sediment storage, irrigation and municipal water supply, power production, recreation, navigation, conservation, and water-quality control. The reservoir size, shape, and operation affect the location and nature of the sediment deposits. As rivers and streams enter a reservoir, the flow depth increases and the velocity decreases, reducing the sediment transport capacity of the flow. Decreased sediment transport capacity and the damming effect of the reservoir may cause deposition of sediment in the stream channels above the reservoir water surface and in the upper reservoir area (Figure 1).

The sediment deposition process in reservoirs generally follows the same basic pattern; coarser sediments settle first in the upstream reservoir area as the river inflow velocities decrease, forming a delta. Deposition continues in the downstream direction, with the sediment gradation becoming finer as the deposition progresses toward the dam, until the inflowing sediment is deposited throughout the length of the reservoir. Some of the inflowing fine sediments (silts and clays) typically stay in suspension and may discharge through the dam outlets. As sediments deposit near the dam outlets, they eventually will be discharged downstream as releases are made from the dam.

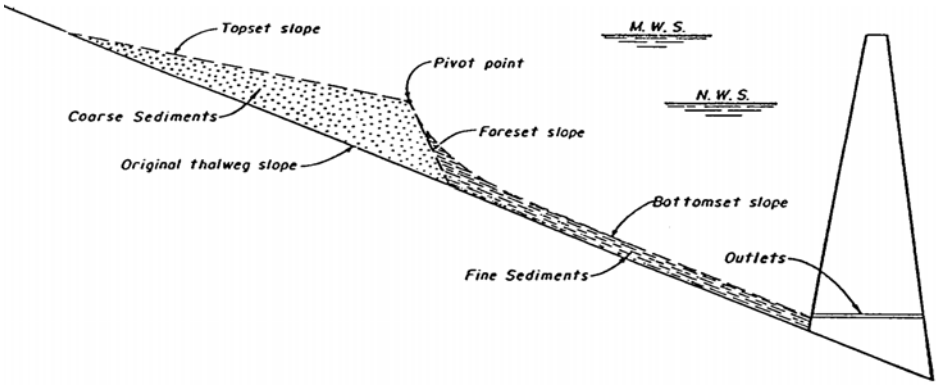


Figure 1 Profile of reservoir delta formation

Reservoir sedimentation seldom receives attention until the capacity has been significantly reduced, or the operation and surrounding area is effected. The primary objective of a reservoir survey is to measure the current area-capacity. Loss of storage capacity is generally caused by sediment deposition or shoreline erosion. Typical results from a reservoir survey and analysis include measured sediment deposition since dam closure and previous surveys, sediment yield from the contributing drainage, and future storage-depletion trends. Survey results can also include location of deposited sediment (lateral and longitudinal distribution), sediment density, reservoir trap efficiency, and evaluation of project operation.

RECONNAISSANCE SURVEY TECHNIQUE

The reconnaissance survey technique directly surveys the reservoir areas where most of the sediment is known to accumulate and uses that data to update reservoir topography and compute sediment deposit volumes for the entire reservoir. Using engineering judgment, sediment deposition in areas of the reservoir not covered by the survey can be extrapolated from the bathymetric survey data collected.

Survey data from hundreds of Reclamation reservoirs demonstrate that sediment tends to deposit along the alignment of the original river channel which is the deepest area (thalweg) of the reservoir. During a reconnaissance survey, longitudinal profiles are surveyed along the original reservoir thalweg using digital contours from the original reservoir topography to guide the survey vessel. Data from multiple profiles are used to compute the transverse slope of the sediment deposits. The measured transverse slope (which may be level) is extrapolated over the areas of the reservoir not surveyed to produce a complete surface of the existing reservoir bottom. The reservoir sediment deposit volume is computed by subtracting the original reservoir bottom surface from the new surface created from the survey data.

A complete hydrographic survey of the entire reservoir provides the most accurate means of measuring the reservoir bottom, sediment accumulation, and current reservoir capacity. However, a complete reservoir survey can be expensive and time consuming, especially for large reservoirs, sometimes limiting the feasibility and frequency of reservoir surveys. Survey technology has changed significantly over recent decades with dramatic increases in the speed of data acquisition and computer processing. These changes have reduced field data collection and analysis time and costs considerably while improving accuracy.

Following is a summary of the field collection techniques and analysis methods used for the 2001 Lake Mead and the 2004 and 2005 Lake Powell partial resurveys. In 2001, the Sedimentation Group conducted the first known multibeam survey of Lake Mead and in 2004 conducted the first known multibeam survey on portions of Lake Powell. In 2005, the Sedimentation Group participated in a Lake Powell multibeam survey that covered a larger portion of the submerged sediment deposits. The University of New Brunswick in cooperation with the National Park Service (Hughes Clarke, 2005) conducted the 2005 survey. Through reconnaissance analysis techniques, data from these surveys can be used to develop updated area and capacity tables for Lake Mead and Lake Powell.

Lake Mead 2001 Reconnaissance Survey: Reclamation's Sedimentation Group surveyed Lake Mead Reservoir in the spring of 2001 to develop a present storage-elevation relationship. This was the first multibeam survey conducted by the Sedimentation Group and the first known extensive multibeam survey of Lake Mead. Due to the size of the reservoir and the limited budget, only the areas of known sediment accumulation were surveyed. Between 1999 and 2002, extensive sidescan sonar images, seismic-reflection profiles, and bottom sediment samples were collected on Lake Mead by the USGS from Woods Hole, Massachusetts and the Lake Mead/Mojave Research Institute of the University of Nevada at Las Vegas. This data verified that the post-impoundment sediment deposits mainly covered the floors of the former streambeds of Lake Mead (Twichell, 1999).

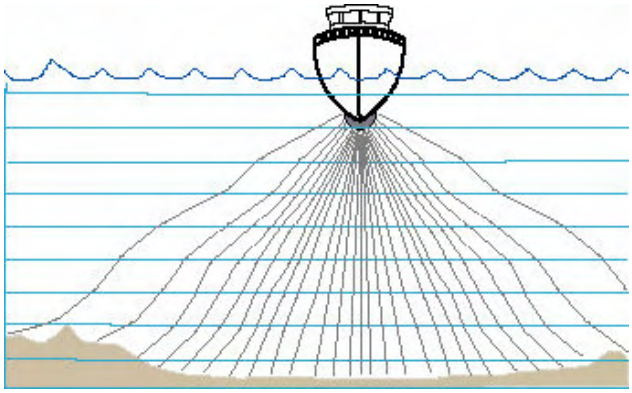


Figure 2 – Multibeam collection system

The Lake Mead multibeam underwater survey was conducted over 22 days in April and May of 2001. The Sedimentation Group used multibeam sonic depth recording equipment interfaced with GPS to obtain continuous sounding positions throughout the underwater portions of the reservoir covered by the survey vessel. The 2001 survey utilized a high-resolution multibeam mapping system for collecting x,y,z data of the Lake Mead bottom from depths of 3 meters in the upper portions of the lake to greater than 140 meters near Hoover Dam. The system consisted of a single transducer that was mounted on the center bow or forward portion of the boat. From the single transducer a fan array of narrow beams generated a detailed cross section of bottom geometry as the survey vessel passed over the areas to be mapped (Figure 2). The survey found the majority of the reservoir bottom sediment lying very flat.

The survey data analysis required digitizing the 1935 (original) Lake Mead surface topography into electronic format. These digital images were used during the survey to ensure the vessel was collecting data in the original river channel area. The new topographic map was developed from a combination of 2001 underwater measured topography and original USGS quad contours. The x,y,z data collected in 2001 were merged into the 1935 digital surfaces and provided the final 2001 surface images. Comparison of the original surface and the 2001 surface provided the quantity and location of sediment that has deposited in Lake Mead since the closure of Hoover Dam in February of 1935. The 2001 data were superimposed onto the 1935 data with the assumption that no change has occurred at elevations above the 2001 bottom survey since 1935. Reclamation's Lower Colorado Regional Office completed the GIS analysis of Lake Mead, resulting in digital images of the original and 2001 reservoir topography along with the sediment accumulation and reservoir storage volume for the areas studied. Figure 3 is a digital map developed from the 2001 Lake Mead multibeam survey data only (1935 topography not included).

The Sedimentation Group proposed to compute the 2001 Lake Mead area-capacity by measuring the storage changes on the 45 individual reservoir maps due to sediment accumulation (assuming no original surface area changes above the 2001 surveyed elevations). Even though most of the area is lost due to siltation, the 40 miles of surface area in the upper contours upstream of Pierce Basin should be included in the proposed analysis. Due to time and budget constraints, the proposed area-capacity computations were not performed. Compared to the 2001-2002 approach, this method would not likely produce a major change in the computed sediment inflow

volume since dam closure, but would provide a complete reservoir volume for all reaches of the original reservoir. The only means to truly measure the current storage volume of the reservoir would be to conduct a combined above and below water survey.

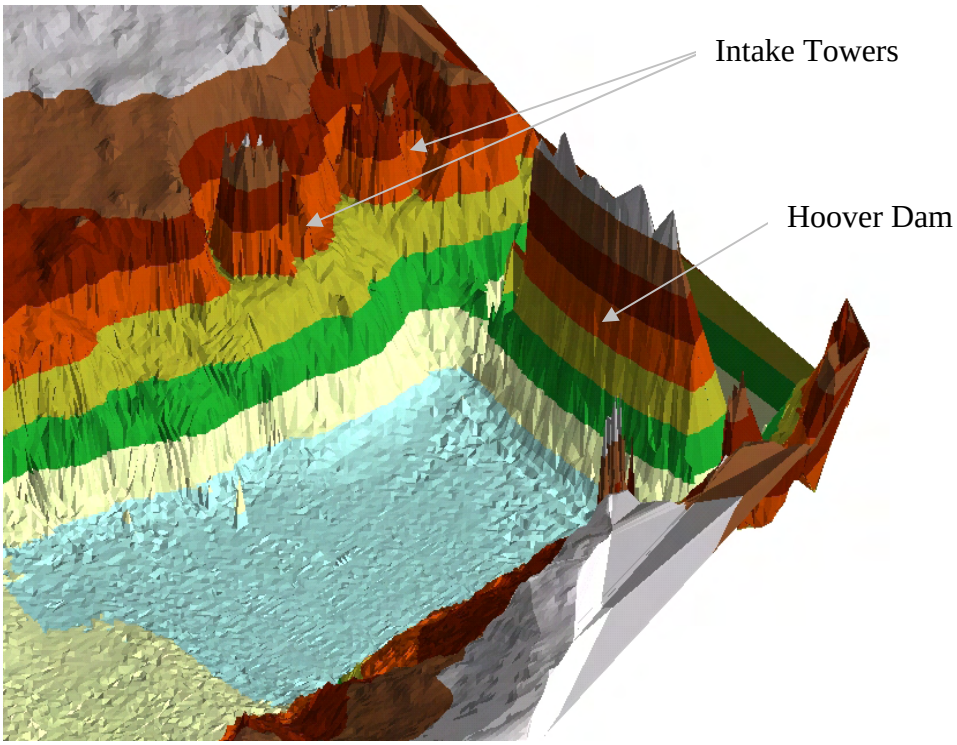


Figure 3 Multibeam image of Hoover Dam and intake towers

The Lake Mead longitudinal profile in Figure 4 compares results of the 1935, 1948, 1963 and 2001 Colorado River surveys. The 2001 profile of the Lower Granite Gorge above Pierce Basin was developed from cross section data collected by a regional contractor for studying the effects of the Colorado River and Lake Mead on bird nesting habitat. These cross sections were not tied to a true vertical datum, but with engineering judgment they were used to complete the thalweg profile from Pierce Ferry upstream (about 40 miles of the upper reservoir). On Figure 4, the 2001 bottom data plots lower than the 1948 and 1963 longitudinal profiles in the lower reservoir area. Reclamation's 2001 surveyed bottom data were verified by other data collected from 1999 through 2002 in the same areas. It is assumed that consolidation of the previously accumulated bottom sediments has occurred over time, resulting in lower elevation measurements in 2001. There are mathematical means to compute the consolidation rate over time (Strand and Pemberton, 1982), but the limited budget did not allow the Sedimentation Group to investigate further these findings.

Lake Powell 2004 and 2005 Reconnaissance Surveys: In October 2004, the Sedimentation Group used their multibeam system to map the Colorado River thalweg from Glen Canyon Dam to Antelope Marina. This was the first known multibeam survey of Lake Powell. The boat mounted multibeam system was able to map the level sediment deposits from bank to bank with

just two passes along the river channel. The 1986 Lake Powell Sedimentation survey covered 580 miles of the reservoir, including the total length of all the tributaries surveyed, in 6 months. Using the reconnaissance collection techniques employed in 2004, the multibeam system could survey the same area as the 1986 survey in less than 30 days. In cooperation with USGS Flagstaff Office, the Sedimentation Group mapped the Colorado River channel from Antelope Marina to the San Juan confluence, the San Juan River to the upper reservoir reach, and Navajo Canyon in December 2004. Reconnaissance analysis techniques were only applied to the Navajo Canyon reach of Lake Powell, but could be applied to the whole reservoir.

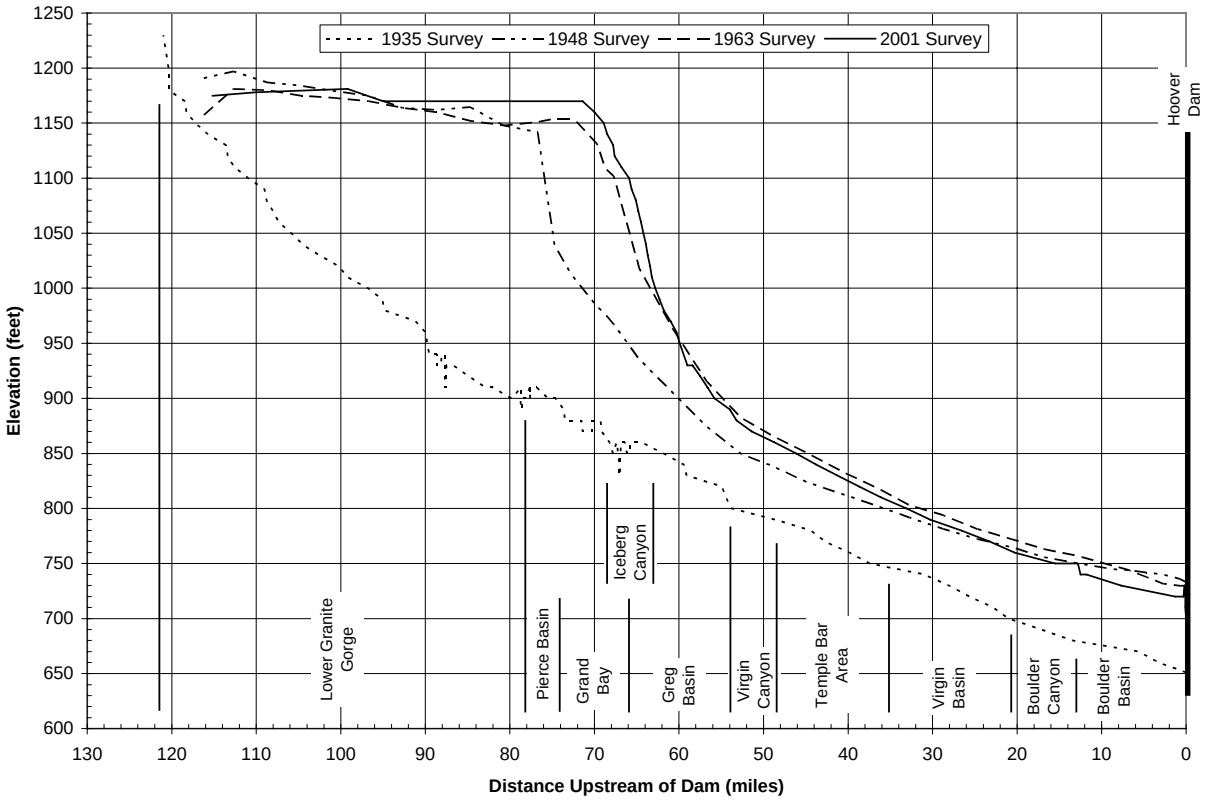


Figure 4 1935, 1948, 1963, and 2001 Colorado River profiles through Lake Mead

Navajo Canyon Area Computation: The Navajo Canyon drainage joins the Colorado River a few miles upstream of Antelope Marina and was determined by 1986 survey results to be a significant source of sediment. The survey boat was navigated along the thalweg as it maneuvered upstream and downstream in Navajo Canyon. The course along the thalweg was maintained using digitized map contours as a guide in the collection software. Figure 5 is a TIN image developed from the raw x,y,z points collected during two multibeam profiles along the canyon. The image clearly shows Navajo Canyon wall details and flat sediment deposition along the original river alignment.

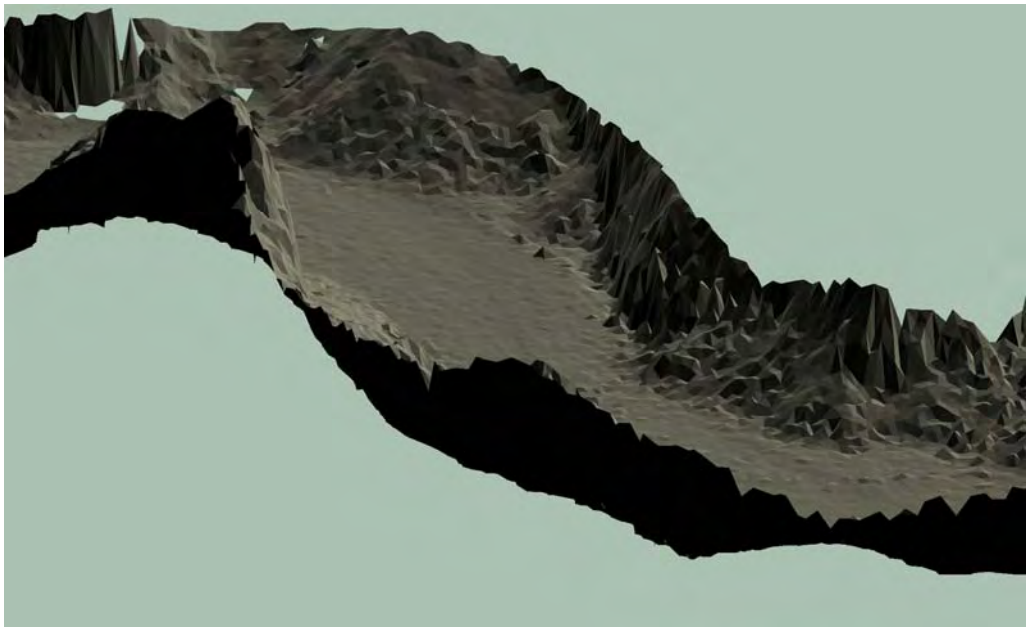


Figure 5 Navajo Canyon TIN generated from multibeam data only

The Navajo Canyon reconnaissance analysis was conducted using the original canyon topography (12 maps), cross sections surveyed in 1986, and the 2004 multibeam data. Using ARC software, cross sections were cut through the original digital contours and the 2004 multibeam x,y,z data set. The cross sections were cut in the same locations as the 1986 Lake Powell cross sections. Cross section locations were estimated using copies of the marked maps from the 1986 field collection. The resulting cross section plots show that the sediment deposition in Navajo Canyon is nearly level, with an even lateral distribution across the reservoir bottom. Figure 6 is an example of the lateral sediment distribution in Navajo Canyon.

Sediment deposit volumes in Navajo Canyon were computed from the 2004 cross sections and the original maps that form the boundary around the canyon to determine the 2004 surface areas at 20-foot elevation increments for each of the 12 maps. The original surface areas at 20-foot contour intervals were digitized and summed to determine the original reservoir surface area by elevation. The original surface areas represent contours not affected by sediment deposition. The 1963, 1986, and 2004 cross section results were used to determine the surface area changes, by map, for the 20-foot elevation increments. On some maps, the cross sections showed total loss of a 20-foot contour area due to sediment deposition. ARC GIS mapping tools were used to develop a TIN and resulting contours from the 2004 multibeam bottom data. This information was used to locate the upper end of the new 20-foot contours for each map. The resulting surface areas of the 2004 contours represent the zone affected by sediment deposition. This process was completed for each map and the summation of the surface area at each 20-foot contour interval became the 2004 surface areas for Navajo Canyon. The 2004 final surface areas provided the input for computing the new capacity of the Navajo Canyon arm of Lake Powell. According to the results, after 40 years of reservoir operation, 29,000 acre-feet of sediment has deposited in the Navajo Canyon study area from the Colorado River confluence upstream, an average of 725 acre-feet of sediment per year. Examination of Navajo Canyon and Colorado

River profiles indicates that a portion of the sediment from the Navajo Canyon drainage has deposited downstream towards Glenn Canyon Dam, outside of the Navajo Canyon study area.

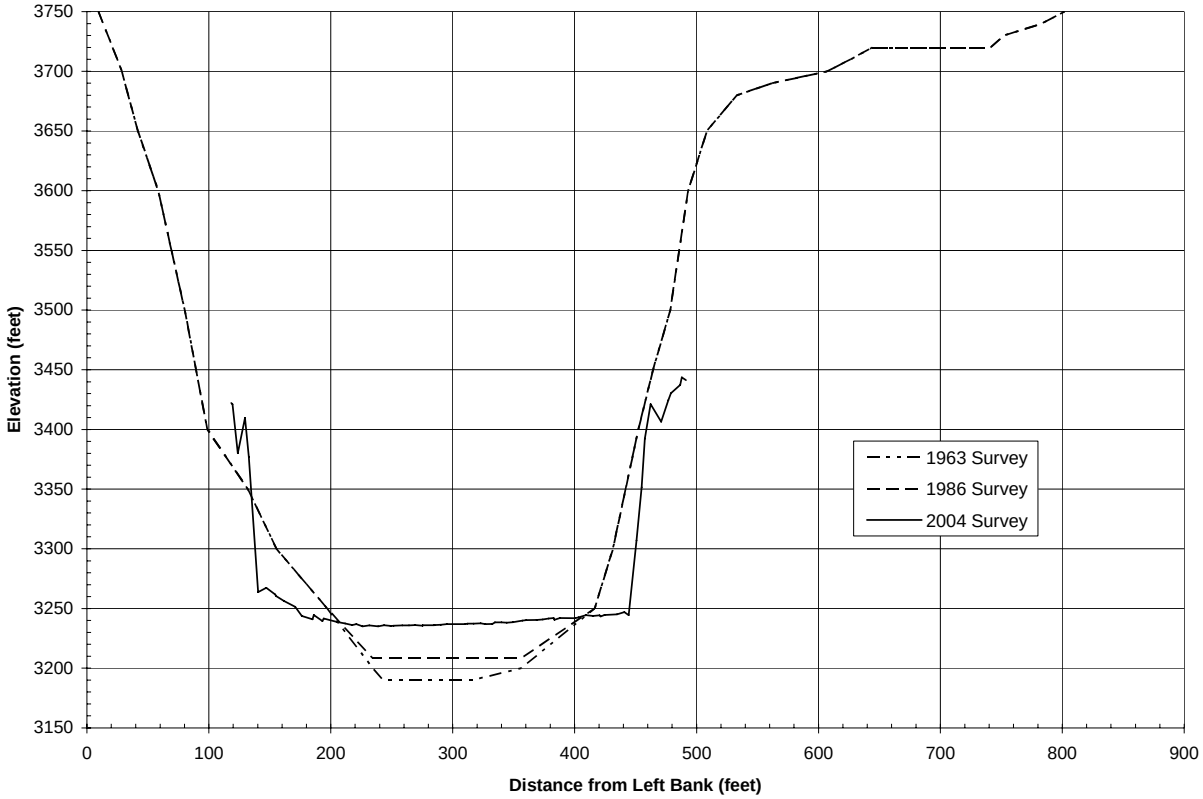


Figure 6 Navajo Canyon Range Line 422

Colorado River Analysis: Longitudinal average bed profiles for the original (1963), 1986, and 2004 Colorado River surveys were plotted from the dam upstream to the Lake Powell headwaters (over 180 miles), Figure 7. The 2004 profile ends just upstream of the San Juan River confluence where the 2004 field data collection concluded. The 1986 profile versus the 1963 (original) illustrates the upstream sediment deposition typical for this type of reservoir configuration and operation. The 2005 Hughes Clarke multibeam survey mapped from the dam upstream nearly to Hite Marina and was limited to this area due to the low lake level during their survey (around elevation 3,570 feet). The Sedimentation Group proposes to analyze the 2004-2005 data using a process similar to that used on the Navajo Canyon data, providing a complete longitudinal profile to elevation 3,570. Using results from previous studies, such as the Lake Mead and Lake Powell surveys, engineering judgment can extend the profile beyond the available 2005 data to update the current volume of Lake Powell.

SUMMARY

Reconnaissance survey and analysis techniques were outlined and applied to portions of two large U.S. reservoirs to generate updated bottom topography and to compute current area-capacity values. Compared with original reservoir topography and storage capacities, the reconnaissance survey method provides dam operators with accurate information for best

reservoir sediment management practices in a shorter time at reduced cost. The reconnaissance methodology used at Navajo Canyon can be applied to the 2001 Lake Mead and the 2004-2005 Lake Powell data to compute updated area – capacity values for both reservoirs.

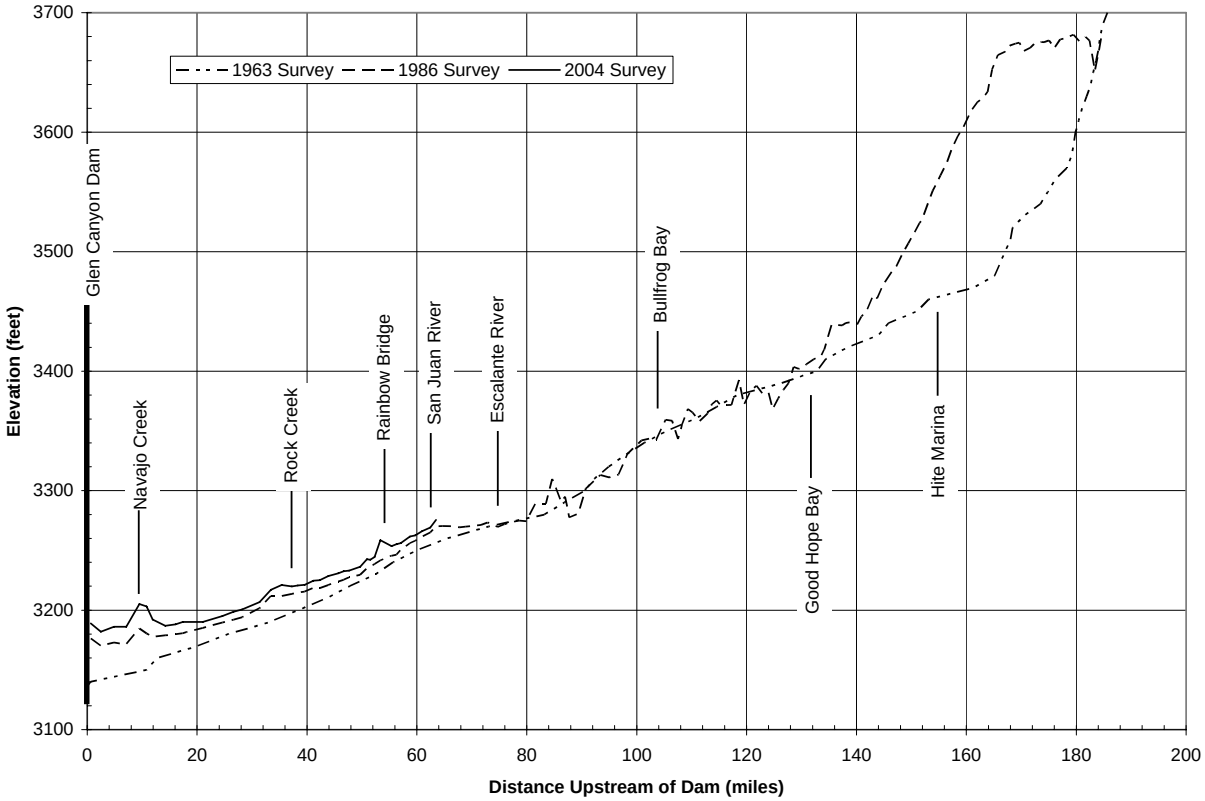


Figure 7 1963, 1986, and 2004 Colorado River Profiles through Lake Powell

REFERENCES

Hughes Clarke , J. E., (2005) Lake Powell Multibeam Mapping 2005. University of New **B**runswick, Canada. (Draft).

Collins, K. and Ferrari, R., (2000). Elephant Butte Reservoir 1999 Reservoir Survey. U.S. Bureau of Reclamation, Sedimentation and River Hydraulics Group, Denver, Colorado.

Ferrari, R.L. (1988). 1986 Lake Powell Survey. REC-ERC-88-6. Bureau of Reclamation, Sedimentation and River Hydraulics Group. Denver, Colorado.

Lin, S.S., 1997. Strategies for Management of Reservoir Sedimentation. Virginia Dam Safety Program, Richmond, Virginia.

Strand, R.I., and E.L. Pemberton, Reservoir Sedimentation. U.S. Bureau of Reclamation, Sedimentation and River Hydraulics Group, Denver, Colorado. October 1982.

Twichell, D.C., Cross, V.A., and Belew, S.D., (2003). Mapping the Floor of Lake Mead. USGS Open-File Reports 99-581 and 03-320.

PRELIMINARY SEDIMENT BUDGETS FOR FOUR WATERSHEDS AT THE KINGS RIVER EXPERIMENTAL WATERSHED IN THE SOUTHERN SIERRA NEVADA

Sean Eagan, Hydrologist, USDA Forest Service, Pacific Southwest Research Station, Sierra Nevada Research Center, 2081 E. Sierra Avenue, Fresno, CA 93710, seagan@fs.fed.us; Dr. Carolyn Hunaker, USDA Forest Service, chunsaker@fs.fed.us; Abbey Korte, Colorado State University, akorte02@aol.com; Sarah Martin, University of California, Merced., smartin@ucmerced.edu; Dr. Lee McDonald, Colorado State University, leemac@cnr.colostate.edu

Abstract: The Kings River Experimental Watershed (KREW) was initiated in 2000 to quantify the variability in characteristics of small stream ecosystems and their associated watersheds in the Sierra Nevada of California. The primary management questions to be answered are the effects of prescribed fire and mechanical harvest on the riparian and stream physical, chemical, and biological conditions. Soil erosion and sediment loads affect stream organisms, forest health and human water users. The magnitude and contribution from roads, undisturbed areas and headcuts is not well understood for the southern Sierra Nevada.

The Providence site contains four 100-hectare watersheds at 5,800 feet on the Sierra National Forest. One watershed will receive no treatment (control), one will be burned, one will be harvested, and one will be harvested and then under-burned. This presentation will focus on sediment movement during the pretreatment baseline period.

KREW staff has collected annual sediment catchment data and continuous discharge data since 1October 2002. We also have data on head cut recession and sediment delivery from natural slopes and roads. In October of 2005 we began collecting turbidity data on these same streams. These data allow us to develop a preliminary sediment budget.

TURBIDITY THRESHOLD SAMPLING: INSTRUMENTATION AND METHODS

Rand Eads and Jack Lewis, USDA Forest Service, Pacific Southwest Research Station, Redwood Sciences Laboratory, Arcata, California,

Abstract: Traditional methods for determining the frequency of suspended sediment sample collection often rely on measurements, such as water discharge, that are not well correlated to sediment concentration. Stream power is generally not a good predictor of sediment concentration for rivers that transport the bulk of their load as fines, due to the highly variable routing of sediment to the channel from hillslopes, roads, and landslides. A method, such as Turbidity Threshold Sampling, that employs a parameter well correlated to suspended sediment concentration can improve sampling efficiency by collecting samples that are distributed over a range of rising and falling concentrations. The resulting set of samples can be used to estimate sediment loads by establishing a relationship between concentration and turbidity for any sampled period and applying it to the continuous turbidity data. All river systems, particularly smaller watersheds that respond very quickly to rainfall, benefit from automated data collection.

A data logger, under direction of the Turbidity Threshold Sampling program, collects stage and turbidity data at 10 or 15-minute intervals, depending on the drainage size, then triggers an automatic pumping sampler to collect a sample whenever the turbidity passes selected thresholds, if the stage is above a specified minimum and temperature is above freezing. The program distinguishes rising from falling conditions and uses different sets of turbidity thresholds for each. When the measured turbidity exceeds the calibrated range of the sensor, the program collects pumped samples at a fixed rate specified by the operator. At each recording interval, the program records the median of 60-100 high-frequency turbidity readings. To avoid over-sampling, the program logic attempts to distinguish brief spikes caused by fouling from true rises in turbidity. Future improvements in program logic will provide a mechanism to limit the number of occurrences and frequency at which thresholds can be triggered without user intervention.

The turbidity probe, mounted inside a housing, and the sampler intake are usually attached to the end of an articulated sampling boom. Booms are most suited to sites that have adequate depth of flow. The boom and housing reduce contamination from organics by shedding debris, protecting the sensor from direct impacts by woody material, and when properly designed they reduce hydrodynamic noise caused by turbulence and the entrainment of air or re-suspension of sediment close to the sensor. Field personnel can retrieve the bank or bridge-mounted boom to remove debris during high flows. The boom controls the depth of the turbidity probe and sampler intake in the stream to maintain their position above bedload transport and below the water surface.

THE CHALLENGES OF SAMPLING SUSPENDED SEDIMENT IN A MOBILE CHANNEL WITH HIGHLY DYNAMIC TRANSPORT

Rand Eads, USDA Forest Service, Pacific Southwest Research Station, Redwood Sciences Laboratory, Arcata, California,

Abstract: Establishing a new gage site for the measurement of turbidity and suspended sediment can be technically challenging, but most sites can be successfully measured after making minor adjustments to the procedures and instrumentation during the initial phase of data collection. Highly erosive watersheds, however, demand a higher level of technical skills and fortitude to achieve success. Cuneo Creek, a 10.8 km^2 tributary to Bull Creek, in Humboldt Redwoods State Park, near Weott California, is an example of a gravel-bed stream that produces large sediment loads in a watershed with steep topography and very erosive soils. High frequency sediment pulses from hillslope failures and floodplain erosion are often poorly related to water discharge. In addition, elevated sediment transport rates create unstable bed forms through the process of aggradation-degradation, making it nearly impossible to establish a stable stage-discharge relationship. Shallow flow depths and velocities of 3.7 m/s or more create turbulent conditions that complicate sensor deployment and sample collection.

A Turbidity Threshold Sampling (TTS) station was installed during February 2004, utilizing a cable-mounted sampling boom, a DTS-12 turbidity sensor, an ultrasonic stage sensor, and two automatic pumping samplers. The cable-mounted boom can be adjusted both vertically and horizontally to reposition the turbidity sensor and sampler intakes within the measurement cross-section, but this must be accomplished manually by field personnel. Changes to the streambed elevation during runoff events resulted in the loss of data when the boom became stranded on newly formed sediment bars. It is common for the streambed elevation to change by 1 m or more during a moderate runoff event. When stream velocities were above 2.5 m/s, the boom hydroplaned on the water surface, overcoming the gravitational force of the counter weight placing the sensor near the water surface. We replaced the cable-mounted boom with a depth-proportional boom mounted to a large boulder in the thalweg of the channel.

Turbidities exceeding the range of the sensor (approximately 2000 FNU) are common during larger events. The sampling logic in TTS program was modified to control two pumping samplers, providing additional sample bottles for fixed-time sampling when the turbidity exceeded the sensor's range. A subset of samples collected within the sensor's range, and all samples collected above the sensor's range, were measured in the laboratory with a Hach 2100AN turbidimeter. During extreme transport events, the highest measured laboratory turbidity was 7485 NTU, and the highest measured SSC (1.0 µ filter) was 9194 mg/l. Sand fractions (> 0.63 µ) were determined from a subset of all pumped samples (577). The average sand fraction was 1.7%, and maximum was 14% of the total SSC. Instantaneous discharge measurements at the gage site were well correlated (R^2=0.95) to the continuous discharge records at the USGS Bull Creek gage, 4.4 km downstream. A stage-discharge rating was not developed for Cuneo Creek, but an average lag time was calculated from the stage peaks and applied to the Bull Creek discharge data to produce estimated 10-minute discharge values for Cuneo Creek.

EFFECTS OF THE 1997 FLOOD ON THE KLAMATH NATIONAL FOREST, NORTHERN CALIFORNIA: LESSONS LEARNED & IMPLICATIONS TO FUTURE FOREST MANAGEMENT

Juan de la Fuente, Geologist, Klamath National Forest, Yreka, CA, jdelafue@fs.fed.us; Don Elder, Geologist, USFS Act2 Enterprise Team, Yreka, CA, delder@fs.fed.us; Alisha Miller, Geologist, Shasta Trinity National Forest, Redding, California, alishamiller@fs.fed.us

Abstract: The Klamath National Forest occupies about 1.7 million acres (0.7 million hectares) in the Klamath Mountains of Northern California. This rugged terrain includes four arcuate belts of accreted oceanic terranes intruded by numerous plutons. Landsliding and debris flows are dominant slope processes, strongly influenced by the presence of steep slopes, abundance of older landslide deposits, and weathered and dissected granitic plutons. The storm of December 26, 1996 through January 1, 1997 delivered up to 17 inches of precipitation to parts of the study area. At the onset of the storm, the above average snowpack extended down to about 3,100 feet in elevation. The warm storm produced rain up to 7,500 feet in elevation. One station recorded 5 inches in the last 18 hours of December 31. Total precipitation for December ranged from 170% to 420% of normal for that month. Happy Camp, California received 28 inches of warm rain with about 3 inches per day coming on December 30th, 31st, and January 1st. Estimates of recurrence intervals for 1997 peak stream flows range from 9 to 37 years: (Scott River - 14 years; Salmon River - 37 years; Klamath River at Orleans - 18 years). Peak flows ranged from 51-84% of the 1964 flood (largest on record).

Landslides, debris flows, and altered channels were concentrated in a SW-NE band, about 20 miles wide by 40 miles long. Infrastructure damage (primarily to roads and bridges) exceeded $27 million. Effects were greatest in the Walker, Grider, Elk, Tompkins, Kelsey, Deep, and Ukonom Creek watersheds. Abundant debris flows were initiated by landslides at elevations over 3,800 feet. These flows scoured upper channel reaches, removed riparian vegetation, and deposited sediment and large logs in lower reaches. Air photo and field investigations identified a total of 1,543 landslides (including road-related landslides). Of these, 415 occurred on older landslide deposits, with 270 classed as debris slides, 97 deep-seated landslides, and 48 combinations. These 415 slides delivered about 1.3 million cubic yards of sediment to streams (34% of the total). Many of the 270 debris slides were associated with reactivation of deep landslides.

This event provided a unique opportunity to better understand the interactions between forest management practices and slope/channel processes. A model was developed which closely predicted the proportion of 1997 flood sediment (landslides) originating from undisturbed land, harvested or burned land, and road corridors. Similarly, it predicted the increase in landslide rates on disturbed land relative to undisturbed land. The model over-predicted total landslide sediment production several fold.

INTRODUCTION

The Klamath National Forest is located in northernmost California, adjacent to the border with Oregon (Figure 1). The flood of 1997 primarily affected the western portion of the Forest.



Figure 1 Location map of the Klamath National Forest.

Precipitation: The event which caused the flood was a warm tropical storm which occurred from December 26, 1996 through January 3, 1997, and traversed the forest in a northeasterly direction. This storm caused flooding from Idaho and Oregon to the Sierra Nevada Mountains (California Department of Water Resources, 1997). Prior to the beginning of this storm, precipitation was above normal for most recording stations on the Forest. November precipitation ranged from 90% to 170% of normal, while that for the water year from October 1, 1996 through January 3, 1997 was 150% to 220% of normal. December precipitation was about double the norm for the month of December, ranging from 170% to 420% of normal. Most of the early December precipitation accumulated during a storm which occurred from December 5-10. Another cold storm brought snow below 2,000 feet from December 21-23, and set the stage for the New Years storm and flood. From December 26 to January 3, a series of warm storms traversed the Pacific northwest in an E-NE direction, and brought rain above 7,000 feet in elevation on the Forest, and above 10,000 feet in the Sierra Nevada Mountains. Beginning December 30, rainfall intensified on the Forest.

Snow Melt: Snow pillow gages recorded intensities of 0.38-0.42 inches per hour at four stations over the last six hours of 1996, producing 6-hour totals of over 2 inches. During the last 18 hours of December 31, totals of four to over five inches were recorded at stations in Big Flat, Mumbo Basin, Scott Mountain, and Highland Lake. This intensity and duration of precipitation exceeds that identified in several studies as necessary for the initiation of debris slides (Cannon, 1985). The shallow debris slides which occurred in Deep Creek and in the granitic portion of Elk Creek were of this type. Data from the snow pillow recording stations suggest that snow melt may have contributed an additional 1-3 inches of water (or more) to the storm runoff at elevations below 6,000 to 6,500 feet. Since an average of ~10 inches of precipitation was recorded from December 30 through January 1 at these snow pillow stations, snow melt may have contributed an additional 20-30% (or more) to 3-day

totals in the vicinity of the stations (de la Fuente and Elder, 1997). Intense precipitation came to an abrupt halt on January 3, and no significant storms occurred during the spring of 1997. Had more storms occurred that spring, it is likely that more large slumps, activated by the flood, would have failed catastrophically.



Figure 2 Slump South Fk Salmon River (left); Earthflow on road, Walker Creek (right).

Peak Stream Flows: Peak flows in rivers and streams on the Forest ranged from second to fifth highest on record. This compares to record flows in some rivers of the Sierra Nevada Mountains, and possibly on Sacramento River tributaries. Estimated recurrence intervals for these peaks ranged from 16 years at Indian Creek (near Happy Camp), to 37 years at Salmon River. The recurrence interval for the 1997 Flood was 14 years on Scott River, 32 years on the Shasta River, 15 years on the Klamath River at Seiad, and 18 years on the Klamath River at Orleans. These intervals were computed by the Federal Emergency Management Act (FEMA) method: Recurrence interval T= (period of record + 1)/ranking. In the case of the Salmon River, the computation is: (73+1)/2 = 37.

Management Effects: The effect of human activities on landslide rates is a key issue in the management of western forests. In the Klamath Mountains, sedimentation has been identified as a key issue relative to anadromous fish habitat, and landslides contribute up to 90% of the total (de la Fuente and Haessig, 1993).

METHODS

Landslide Inventories: A landslide inventory was done on color infrared air photos (1:40,000 scale) flown after the flood in May of 1997 (Figure 3). These photos allowed an area-wide assessment of landslides and altered channels. Altered channels are those where the beds had clearly experienced recent scour or deposition and loss of vegetation rendered them visible on the air photos. These were associated with either debris flows or simply high water flows. Landslides as small as 20 feet wide were visible under optimal conditions, such as in open areas where barren soil contrasted with vegetated slopes. Densely timbered areas obscured smaller landslides, and field inventories were conducted in sample watersheds to augment the air photo work. All roads were examined as part of the damage assessments done for the Emergency Relief Federally Owned program (ERFO). Lastly, the Forest also conducted comprehensive road

inventories identifying potential problem sites, such as where culverts were at high risk of failure in the future. All visible landslides and altered channels were mapped and classified as natural, associated with roads, timber harvest, or fire, and then, the amount of sediment delivered to the stream system was estimated.

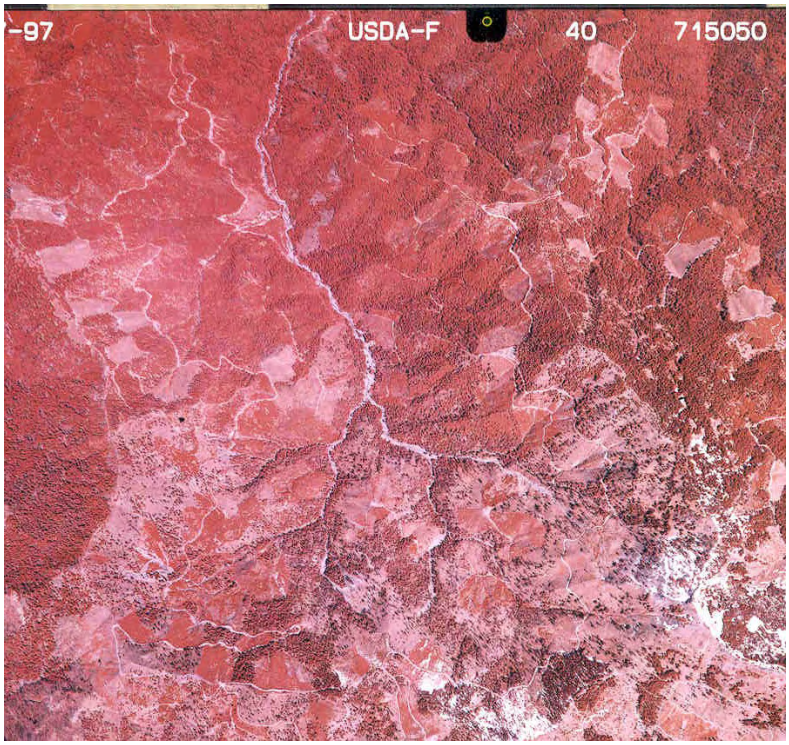


Figure 3 Color infrared air photo (1:40,000 scale) of Walker Creek, May, 1997.

GIS Coverage: A GIS coverage with all identified landslides and altered channels was created and linked to a data base with information on management association, volume of sediment delivered to the stream system, etc.

Geomorphic Terranes: The landscape was stratified into 12 geomorphic terranes (Figure 4) on the basis of geomorphic type, bedrock, and slope gradient. Polygon size ranged from a few acres for active landslides, to several thousand acres for other terranes such as granitic and non-granitic mountain slopes.

Predicting Landslide Sediment Production: An empirical model was used to estimate the amount of sediment landslides would deliver to the stream system on the west side of the Forest. A landslide production rate was assigned to each geomorphic terrane for undisturbed, harvested or burned, and roaded conditions. These rates were based on air photo/field inventories of landslides which occurred in the Salmon River basin, a 751 square mile tributary to the Klamath River, from 1965-1975 (de la Fuente and Haessig, 1993).

Landslide Coefficients for the 1997 Flood: A GIS was used to overlay the new active landslide inventory with other GIS coverages such as roads, timber harvest, and fire. This was done to

measure the amount of landslide sediment delivered to the stream system by each geomorphic terrane by disturbance class (natural, fire/harvest, road) during the 1997 Flood. Coefficients were then developed for each terrane.

GEO Mass-wasting model **1997 FLOOD** [Values represent model-estimated sediment delivery in cubic yards / **DECADE**]

Code	Description	Background (undisturbed)	Roads	High impact fire or harvest 1/	Moderate impact fire or harvest 2/
0	unknown				
1	Active Landslides	27.75	506.25	33.91	30.83
2	Toe Zone of Dormant Slides	1.01	84.06	8.65	4.83
3	Dormant Landslides	1.01	84.06	8.65	4.83
4	Granitic Mtn. Slopes, Steep Slopes (>65%)	0.30	165.32	8.88	4.59
5	Granitic Mtn. Slopes, Low to Moderate Slopes (<65%)	0.47	32.72	4.10	2.29
6	Non-Granitic Mtn. Slopes, Steep Slopes (>65%)	0.32	230.88	0.98	0.65
8	Non-Granitic Mtn. Slopes, Low to Moderate Slopes (<65%)	0.15	17.38	1.91	1.03
9	Inner Gorge on Unconsoildated Deposits	6.85	174.40	24.56	15.70
10	Inner Gorge on Granitic Slopes	4.44	197.61	37.10	20.77
11	Other Inner Gorge	0.99	51.82	3.96	2.48
12	Debris Basins	0.66	0.00	0.41	0.54
13	Surficial deposits (e.g., glacial moraines, terraces and fan deposits)	0.04	4.25	3.57	1.81

1/ Includes clear-cuts and equivalent silvicultural prescriptions and high/moderate burn intensity wildfire
2/ Includes partial cuts and other moderate impact silvicultural prescriptions

Figure 4: Landslide production coefficients for Geomorphic Terranes (1997 Flood data)

FINDINGS

General Findings: Figure 5 shows the distribution of landslides and altered channels across the west side of the Forest. Landslides were concentrated at elevations of 4000-6000 feet above sealevel, and in the north central part of the Forest. Debris slides (shallow rapid landslides) were abundant, but many deep slow moving landslides were also activated.

1. **Sensitive Lands-** Certain geomorphic terranes displayed particularly high landslide and debris flow rates under flood conditions, particularly inner gorges, previously active landslides, and older landslide deposits (Figure 7a). The influence of older landslide deposits has been reported for other storm events elsewhere (Nilsen 1975);
2. **Roads-** Roads exhibited the largest directly observable effects on flood processes (Figure 7b);
3. **De-vegetation-** Watersheds devegetated by a combination of wildfire and timber harvest experienced high rates of landslides and debris flows, particularly on devegetated sensitive geomorphic terranes (Figure 7b).

Predictive Ability of the Landslide Model: It was found that undisturbed land produced 34% of the landslide sediment volume in 1997 (Figure 6) compared to a model prediction of 39%. For

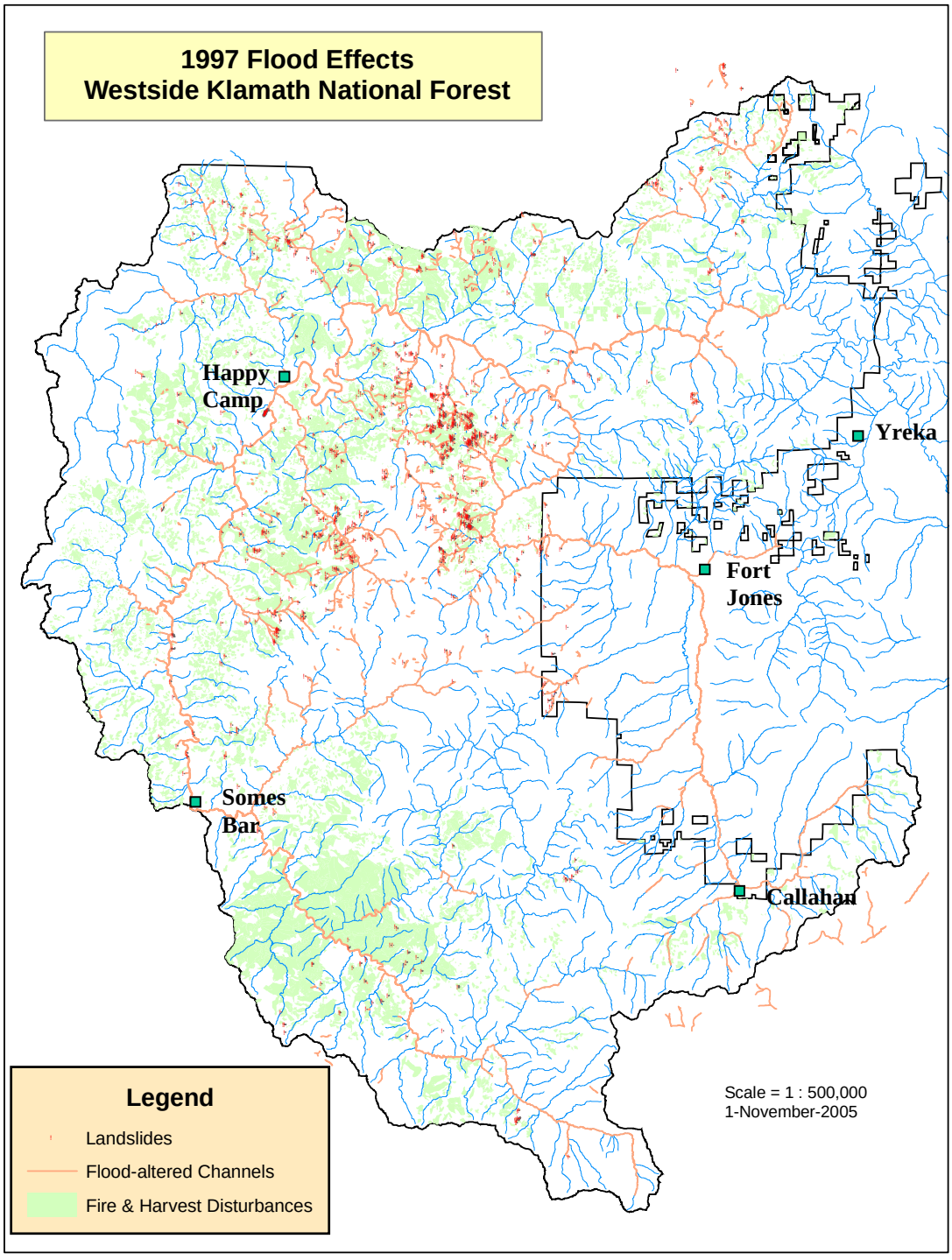


Figure 5 Active landslides and altered channels mapped following the 1997 flood event

road corridors, it was 40% versus the model prediction of 39%, and for harvested or burned lands, it was 27%, versus 21%. Similarly, the increases in sedimentation rate for harvested and roaded areas over undisturbed rates measured after the 1997 flood were very similar to those

predicted by the model. For example, data from 1997 revealed an increase of 4.5 times for harvested or burned land over undisturbed rates, while the model predicted 3.6 times. For road corridors, the increase was 62.7 times, compared to 58.3 predicted by the model. Landslide sediment delivery rates (cubic yards/acre/year) measured from 1997 data. This was based on the assumption that the 1997 event had a return interval of roughly 10 years return (measured sediment volumes were divided by 10). The result for undisturbed land was 0.09, 0.39 for harvested or burned land, and 5.39 for road corridors. This compares to 0.28, 1.01, and 16.33 respectively for modeled values. Thus, the modeled rates were 3.3, 2.6, and3.0 times higher for these categories respectively, than the rates measured following the 1997 flood.

Some subwatersheds in the southern part of the study area produced no measurable landslide sediment (Figure 5). The lack of landslides in these watersheds was verified by intensive field-based road inventories in these watersheds. This could have been due to local high intensity storm cells, differences in geomorphic characteristics, roading or logging practices. We were not able to resolve this question.

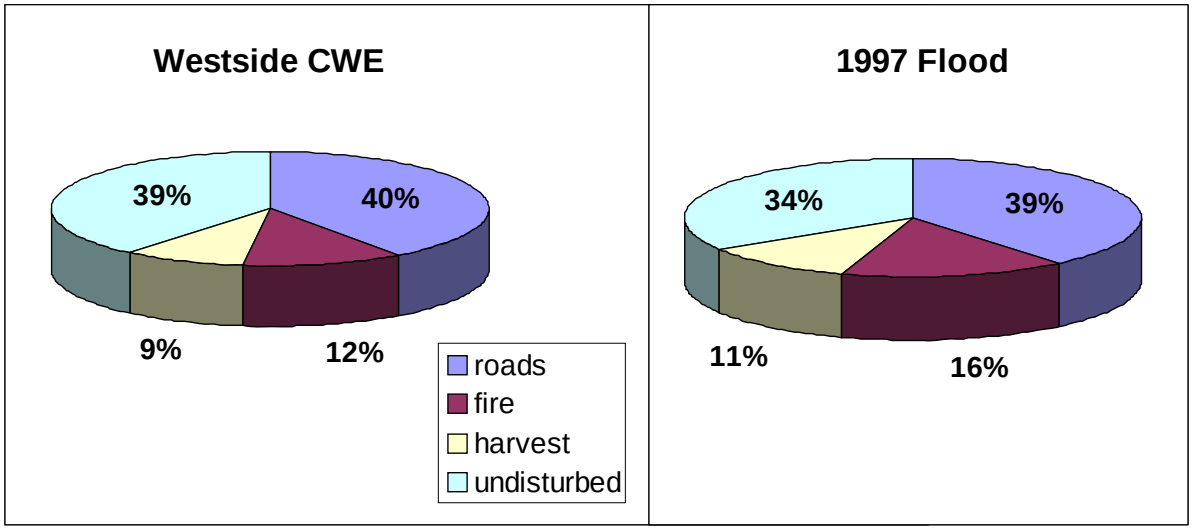


Figure 6 Comparison of sediment sources: CWE model, and 1997 Flood assessment

CONCLUSIONS

1. A model based on geomorphic terranes reasonably predicted the proportion of landslide sediment delivery to streams during the 1997 Flood associated with roads and devegetation.
2. The landslide model over-predicted landslide sediment delivery rate (cubic yards per acre per year) by a factor of 2 or 3, suggesting that it may not be suitable for predicting actual effects of future storms.
3. Knowing the relative contribution of undisturbed, harvested/burned, and roaded lands to the total sediment budget provides a sound foundation for prioritizing restoration activities to maximize efficiency in reducing the management-related contribution to the sediment budget.
4. The concentration of landslides in certain geographic areas lacking unique characteristics suggests that there were sharp local variations in storm intensity.

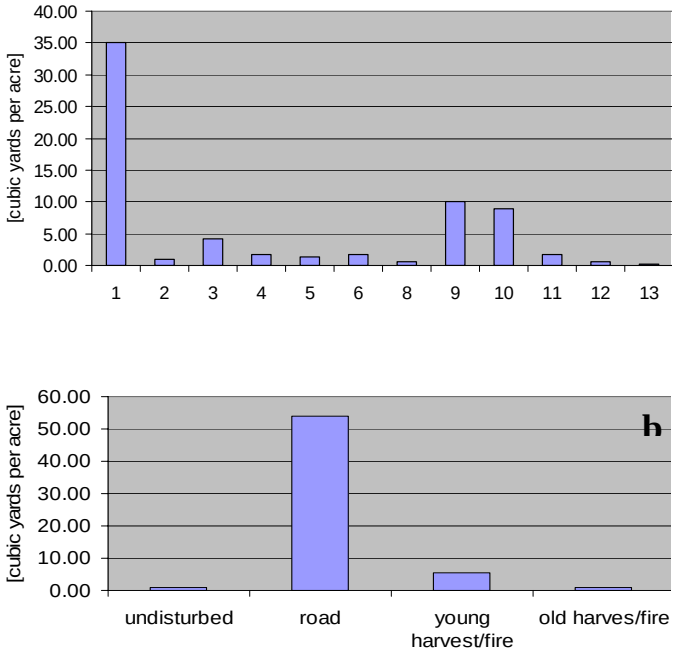


Figure 7 Landslide delivery rate by geomorphic terrane (a) and disturbance class (b)

REFERENCES

California Department of Water Resources. 1997. California Water Supply Outlook, May 19, 1997. Compiled by: Division of Flood Management, Flood Management, Flood Operations and Hydrology Branches, Department of Water Resources, State of California.

Cannon, Susan H., and Ellen, Stephen 1985. Abundant Debris Avalanches San Francisco Bay Region, California. California Geology, December 1985, v.38, no.12, p 267-272

de la Fuente, Juan, and Elder, Don, 1997. The Flood of 1997 Klamath National Forest Phase 1 Final Report: November 24, 1998 USDA Forest Service Klamath National Forest, Internal Document

de la Fuente, Juan, and Haessig, Polly.1993. Salmon Sub-basin Sediment Analysis. Revised in March, 1994. USDA Forest Service, Klamath National Forest Service Internal Document.

Nilsen, Tor H.1975. Influence of Rainfall and Ancient Landslide Deposits on Recent Landslides (1950-71) in Urban Areas of Contra Costa County. Geological Survey Bulletin 1388

Geomorphic Terranes

DETERMINING RELATIVE CONTRIBUTIONS OF ERODED LANDSCAPE SEDIMENT AND BANK SEDIMENT TO THE SUSPENDED LOAD OF GOODWIN CREEK USING RADIONUCLIDES

Christopher G. Wilson, Research Scientist, NCCHE, University of Mississippi, Oxford, MS, CWILSON@olemiss.edu ; Roger A. Kuhnle, Research Hydraulic Engineer, USDA-ARS, National Sedimentation Laboratory, Oxford, MS, RKUHNLE@msa-oxford.ars.usda.gov

Abstract: Identifying the major contributors to the fine suspended sediment load of a stream allows for better focus of Best Management Practices. This study was designed to quantify the relative proportion of eroded surface soils and collapsed bank sediment in the fine suspended sediment load of multiple runoff events in Goodwin Creek, MS using activities of ^{7}Be and $^{210}Pb_{xs}$. Each source material must have a unique radionuclide signature relative to the other to quantify the contributions from the different source areas to the suspended sediment load. Due to different erosion processes controlling the sediment delivery to streams, namely sheet erosion and bank collapse, eroded surface soils will have higher activities of the ^{7}Be and $^{210}Pb_{xs}$ than collapsed bank sediment. The fine suspended sediment, which is a mixture of eroded surface soils and collapsed bank sediment, will have an intermediate radionuclide signature that is quantified in terms of the relative contribution from both source materials. A simple two-end member mixing model would determine the relative contribution from each source area to the total fine sediment load. The radionuclide signature of suspended sediments would lie roughly along the mixing line between the signatures of the two end-member sources of sediment. Data presented here focus on one runoff event and suggest that eroded surface soils are more abundant in the suspended sediment early in the runoff event; however, collapsed bank sediment dominates the suspended load later in the runoff event.

INTRODUCTION

The anthropogenically enhanced delivery of sediment to streams leads to detrimental problems both on the landscape and within the channel. The loss of topsoil can significantly lower crop yields. In addition, increased sediment loads can diminish water quality and ecosystem health. Sediment-bound nutrients and contaminants are transmitted through the food chain resulting in depleted fish stocks (Smith et al., 2001) and eutrophication, as in the Gulf of Mexico (Rabalais et al., 1991). Finally, the deposition of this sediment fills reservoirs and waterways, polluting drinking supplies and limiting ship traffic. Identifying the major contributors of the sediment would allow better focusing of Best Management Practices (BMPs) to curb these increased sediment loads.

A sediment budget is a common practice of evaluating sediment loads to a system; however, most budgets merely provide a net balance and can not identify major sources of sediment. If each source of sediment had a unique signature associated with it, then these sources could be differentiated in the budgets and individually accounted. This study was designed to differentiate sediment sources to the fine suspended sediment load of a sand and gravel bed stream in Northern Mississippi, Goodwin Creek. In this system, freshly eroded surface soils from the landscape and collapsed bank sediment comprise the fine suspended sediment load. The activities of two naturally occurring radionuclides, ^{7}Be and $^{210}Pb_{xs}$, relative to one another will provide the unique signature of both sediment contributors. Because of the limited number of sediment characteristics used to differentiate the sediment, only relative proportions of the eroded surface soils and collapsed bank sediment will be determined in the sediment load of a sampled runoff event.

BACKGROUND

A more detailed explanation of the theory behind the use of ^{7}Be and $^{210}Pb_{xs}$ to quantify the proportion of eroded surface soils relative to the amount of collapsed bank material and/or resuspended bed sediment in the fine suspended sediment load of streams is presented in the following references: Wilson (2003); Matisoff et al. (2005); Wilson et al. (2005). A brief summary of the theory is presented within this paper, which focuses on a case study of the technique in Goodwin Creek, MS.

^{7}Be and $^{210}Pb_{xs}$, which are attached to aerosol particles in the atmosphere, are delivered to the landscape mainly during precipitation events. The radionuclides quickly and strongly bond to surface soils. The relatively high activities of ^{7}Be and $^{210}Pb_{xs}$ in the precipitation decrease as the two radionuclides are mixed with previously

delivered ^{7}Be and $^{210}Pb_{xs}$ in surface soils, which have undergone radioactive decay (Matisoff et al., 2005; Wilson et al., 2005). Surface soils, which still have relatively high activities of ^{7}Be and $^{210}Pb_{xs}$, are eroded from the landscape as runoff initiates and transported through streams. As the eroded sediment is transported downstream, sediment from stream banks is entrained into the flow. Additions of bank material, which have low activities of ^{7}Be and $^{210}Pb_{xs}$, further decrease the radionuclide activities of the suspended fine sediment (Matisoff et al., 2005; Wilson et al., 2005). Collapsed bank sediments will have relatively low activities of $^{210}Pb_{xs}$ and ^{7}Be because they receive little atmospheric input due to near-vertical slopes (Whiting et al., 2005). Moreover, stream bank failure typically removes large volumes of material (Thorne, 1992). The high-activity soil at the top of the bank is diluted by a much larger volume of low activity soil from deeper in the soil column of the bank.

Suspended sediment in Goodwin Creek is a mixture of eroded surface soils and collapsed bank sediment. The fine suspended sediment has an intermediate radionuclide signature that is quantified in terms of the relative contribution of the two source materials. High radionuclide activities suggest a large proportion of recently eroded landscape-derived material. Conversely, lower activities in the suspended sediment suggest dilution by bank material. The different erosion mechanisms affecting surface soils and bank sediments produce these different signatures. A simple two-end member mixing model would determine the relative contribution of each source area to the total fine sediment load. The radionuclide signature of suspended sediments would lie roughly along the mixing line between the signatures of the two end-member sources of sediment.

METHODS

Study Site: Activities of ^{7}Be and $^{210}Pb_{xs}$ from precipitation samples and soil, bank, and suspended sediments collected in the Goodwin Creek, MS, watershed (Figure 1) will be used to accomplish the objective identified above. The Goodwin Creek watershed is an experimental watershed situated in the bluff hill region of north central Mississippi, administered by the National Sedimentation Laboratory of the U.S. Department of Agriculture's Agricultural Research Service in Oxford, MS. The watershed is well instrumented to measure stream flow, sediment load, precipitation, channel characteristics, soil and land use characteristics, and other watershed parameters.

The 21.24-km^2 Goodwin Creek watershed consists of broad ridges and relatively narrow valleys filled with alluvial deposits. Soils are silty loams, which erode readily when surface cover is removed. The average annual precipitation in the watershed is 1400 mm/y. Major runoff events associated with intense erosion are commonly a result of severe thunderstorms in late winter or spring. The flow regime at Goodwin Creek is flashy, and over 77% of the annual runoff amount comes during the wet period between December and May. The watershed is mostly rural but with only 13% of its total area being cultivated. These agricultural lands are located predominantly in the lower half of the watershed (Kuhnle et al., 1996). A more complete description of the watershed can be found in USDA-ARS (2005).

Runoff Event: The sampled runoff in the Goodwin Creek watershed occurred on January 7, 2005. During the three months prior to the runoff event, 550 mm had fallen over the study area. Rainfall associated with the sampled runoff event totaled 27.69 mm and began shortly after 00:00 CST, lasting until 17:30 CST. The most intense rainfall occurred between 12:00 and 15:00 CST. Discharge in Goodwin Creek began to increase at approximately 04:00 CST and peaked at 11.78 m^3/s at 15:21 CST. This peak stage has a recurrence interval of approximately 0.5 yr (Kuhnle et al., 1999).

Field Methods: Samples were collected from both the landscape and stream banks to determine the background activities of ^{7}Be and $^{210}Pb_{xs}$ of the potential source areas. Profiles of the radionuclide activities in the soil column were collected in two fields, which contained soybeans the previous growing season, 9 days before the sampled runoff event. These fields were located immediately adjacent to the stream banks. Three locations were sampled in each field. High resolution profiles were developed by inserting a three-sided box corer with uniform sampling intervals every 0.4 cm and a sampling area of 232.83 cm^2 into the side of a soil pit in the field. The box core was removed and sampled at the 0.4-cm interval to a depth of 4.0 cm. Only the top 1.2 cm was used to establish soil profiles because of the limited penetration of ^{7}Be (Wallbrink and Murray, 1996; Bonniwell et al., 1999). These samples were dried at 60^{o} C, ground to a fine consistency, and passed through a 63 μm sieve. The samples were analyzed using gamma spectroscopy to determine activities of ^{7}Be and $^{210}Pb_{xs}$.

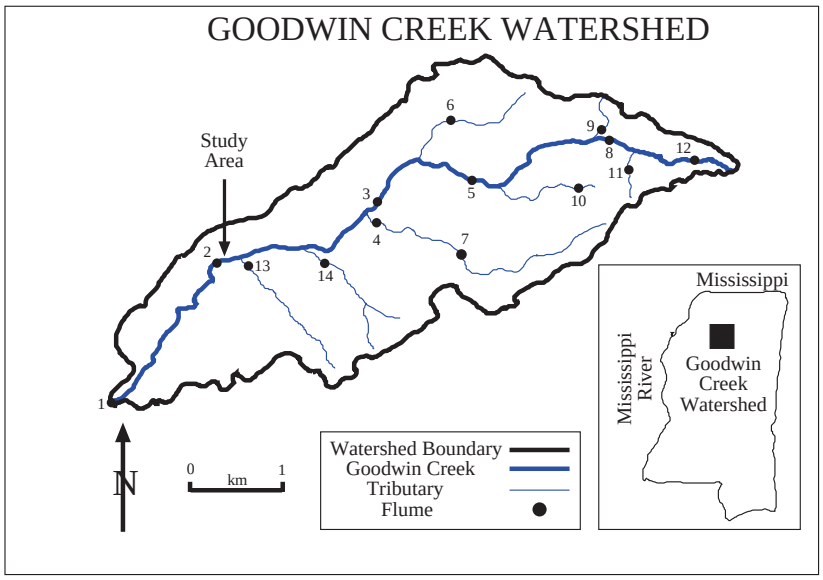


Figure 1 Map of the Goodwin Creek watershed.

A set of six more soil profiles were collected at similar locations after a later rain event. These soils were dried, weighed, and lightly crushed to less than 2 mm. A dispersant, $(NaPO_3)_6$, was added to each sample, and each mixture was placed on a shaker overnight. The sand particles were removed using a 53 μm sieve. The remaining mixture was placed in an automated, large-volume, particle size separator, similar to that in Rutledge et al. (1967) to separate the silt and clay fraction. All three size samples were dried, weighed, and placed in a standardized geometry for analysis using gamma spectroscopy to determine their radionuclide activities. Enrichment coefficients were determined for each size fraction relative to the total activity of the bulk sample. The enrichment coefficients were applied to the soil radionuclide profiles to account for the preferential erosion of the clays (Rhoton et al., 1979).

Three vertical cores of 1-m length and a surface area of 5.07 cm^2 were collected from an actively eroding stream bank upstream of the fields containing the soil profiles. Cores were collected in 33 cm intervals. Each interval was dried at 60° C and separated into size fractions using the automated, large-volume, particle size separator mentioned above. The samples are currently being analyzed by gamma spectroscopy to determine activities of ^{7}Be and $^{210}Pb_{xs}$.

Water and suspended sediment were collected from Goodwin Creek during the above mentioned runoff event. Plastic buckets, with a sampling volume of 20 L, were lowered from a bridge into the center of a supercritical flume in Goodwin Creek just downstream of the soil and bank samples. Sampling in the super critical flume insured the samples would be well mixed. An average of 15.5 L of water and suspended sediment was collected 28 times at regularly spaced intervals during the runoff event. Samples were sieved with a 63 μm sieve, dried, and weighed. The finer (silt and clay, combined) samples were analyzed using gamma spectroscopy to determine activities of ^{7}Be and $^{210}Pb_{xs}$.

Precipitation samples were collected at four locations near the sampling area. Buckets with a surface area of 630 cm^2 were placed atop a 1-m stand immediately after the soil profiles were collected. The buckets were retrieved immediately after the suspended sediment samples were collected. The four precipitation samples were pooled. The radionuclides were retrieved by precipitating them on a $Fe(OH)_3$ floc. The floc was collected in a standardized sampling geometry and analyzed for its radionuclide activity using gamma spectroscopy.

The resulting radionuclide activities of the precipitation samples were distributed exponentially to a depth of 1.2 cm over an average soil profile to determine the activity of the eroded sediment (Wilson et al., 2003). The high partition coefficients of the radionuclides ($K_d \sim 10^4$ to 10^6; Wilson, 2003) result in rapid and strong bonding to the soil surface. The resulting radionuclide profile can be represented by an exponential function (Owens et al., 1996;

Wallbrink and Murray, 1996; Wilson et al., 2003). The exponential function can be used to determine the average activities of the radionuclides eroded from the landscape surface.

Gamma spectroscopy was used to determine the activities of ^{7}Be and $^{210}Pb_{xs}$ in the soil, bank, and suspended sediments samples, as well as the precipitation samples. Samples were counted in standardized geometries for at least 82800 seconds on a High Purity Germanium (HPGe) gamma detector and then for an additional 300 seconds with a standardized sealed source to account for self-adsorption of the ^{210}Pb photon (Cutshall et al., 1983). Counting efficiencies for ^{210}Pb were established using a standard radionuclide solution; ^{7}Be efficiencies were interpolated from the resulting curves of the efficiencies of the radionuclides present in a mixed solution (Bonniwell, 2001; Wilson, 2003).

RESULTS

The atmospheric fluxes of ^{7}Be and $^{210}Pb_{xs}$ to the Goodwin Creek watershed measured during the sampled runoff event were 7.70 ± 0.30 mBq/cm^2/d and 0.463 ± 0.055 mBq/cm^2/d, respectively. The ^{7}Be / $^{210}Pb_{xs}$ ratio of the precipitation during this event, 16.6 ± 2.1, is very close to an observed global average of 16 (Baskaran et al., 1997; Matisoff et al., 2005). Moreover, plotting the atmospheric influxes of ^{7}Be and $^{210}Pb_{xs}$ to Goodwin Creek between January and June 2005 (Figure 2) show the general ratio is maintained over time with the slope of the linear fit being approximately 15. The strong correlation between the ^{7}Be and $^{210}Pb_{xs}$ in the atmospheric influx supports the use of the two radionuclides relative to one another as a tracer.

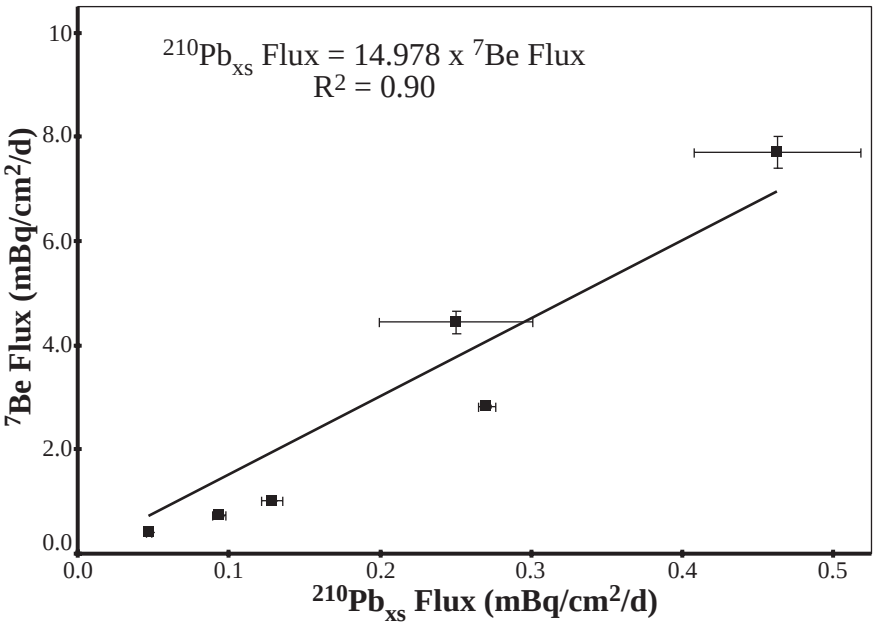


Figure 2 Atmospheric influxes of ^{7}Be and $^{210}Pb_{xs}$ to the Goodwin Creek watershed.

The activities of ^{7}Be and $^{210}Pb_{xs}$ from the samples collected in the soybean fields adjacent to the stream were averaged to develop a composite profile for the landscape (Figure 3a). The atmospheric influxes of ^{7}Be and $^{210}Pb_{xs}$ were distributed exponentially over these profiles (Figure 3b). From these constructed profiles, the activities of the eroded surface soils were assumed to be the surface activity, or the activity at depth = 0 cm suggested from an exponential fit through the data (Wilson et al., 2003). The surface activities (^{7}Be: 239 ± 31 mBq/g; $^{210}Pb_{xs}$: 192 ± 2 mBq/g) were used as the signature of the eroded surface soils. Enrichment coefficients, or the ratio of the activity of the clay particles relative to the activity of the bulk sample averaged 5.13 ± 0.82 and 5.28 ± 0.58 for ^{7}Be and $^{210}Pb_{xs}$, respectively.

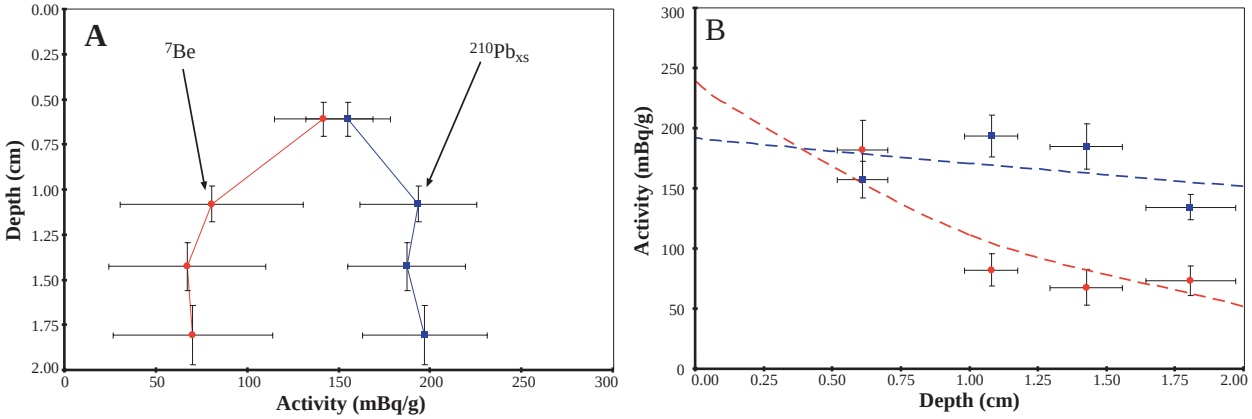


Figure 3 (a) Composite profiles of ^{7}Be and ^{210}Pb$_{xs}$ on the Goodwin Creek landscape prior to the sampled runoff event. (b) Composite profiles with exponential fits of ^{7}Be and ^{210}Pb$_{xs}$ on the Goodwin Creek landscape with atmospheric influxes added.

The activities of ^{7}Be and ^{210}Pb$_{xs}$ from the bank cores are assumed to be zero. This is because integration of activities over the length of the bank face would incorporate a vast majority of soil particles deficient in ^{7}Be and ^{210}Pb$_{xs}$. Cores are currently being counted to confirm this assumption. In support of this assumption, ^{7}Be is found only within the top few centimeters of the soil column, and the total ^{210}Pb is dominated by supported ^{210}Pb at depth, i.e., ^{210}Pb$_{xs}$ is near zero (Wallbrink and Murray, 1996; Bonniwell et al., 1999; Wilson et al., 2003).

As a result of the runoff event, discharge (Figure 4a) at the sampling site peaked at 11.78 m^3/s nearly 15 hours after the precipitation commenced and returned to base flow approximately 33 hours later. Fine suspended sediment concentration nearly mimicked the flow hydrograph. The concentration peaked at 1161 mg/L almost simultaneously with the flow discharge. There was enrichment in clay particles in the suspended sediment relative to the soils (Figure 4b). The percent clay in the suspended sediment ranged from 15% to 34%. The highest fractions were observed at the beginning and end of the event. Clay fraction in the soils averaged 10 ± 1%, based on the samples used for the radionuclide enrichment coefficient.

The activities of ^{7}Be and ^{210}Pb$_{xs}$ in the fine suspended sediment collected during the runoff event average 91.4 ± 54.6 mBq/g for ^{7}Be and 12.3 ± 5.3 mBq/g for ^{210}Pb$_{xs}$. The two radionuclides follow a similar pattern over the runoff event (Figure 4b). Activities generally increase during the initial stage of the rising limb of the hydrograph (Brigham et al., 2001). However, as the flow discharge and fine suspended sediment concentration sharply increase approximately 14 hours after the runoff event began, the radionuclides decrease substantially. The activities then begin a rise throughout the remainder of the sampling period, but the activities do not reach similar values to the activities at the beginning event. Changes in the clay fraction of the fine suspended sediment correspond to those of the radionuclide activities.

DISCUSSION

The average activities of ^{7}Be and ^{210}Pb$_{xs}$ of the eroded surface soils and collapsed bank sediment were plotted relative to each other in Figure 5a. The two source areas plot at different ends of the figure suggesting the two activities used in relation to one another can provide a unique signature for each source material. When the activities of ^{7}Be and ^{210}Pb$_{xs}$ of the fine suspended sediment collected during the event are added to the graph, each sample plots between the two average source activities. Moreover, they plot along a mixing line between the two source materials. Each fine suspended sediment sample was projected at right angles on the mixing line. The position where each sediment sample projects onto the line dictates the relative percentage of each source material contained in that sample.

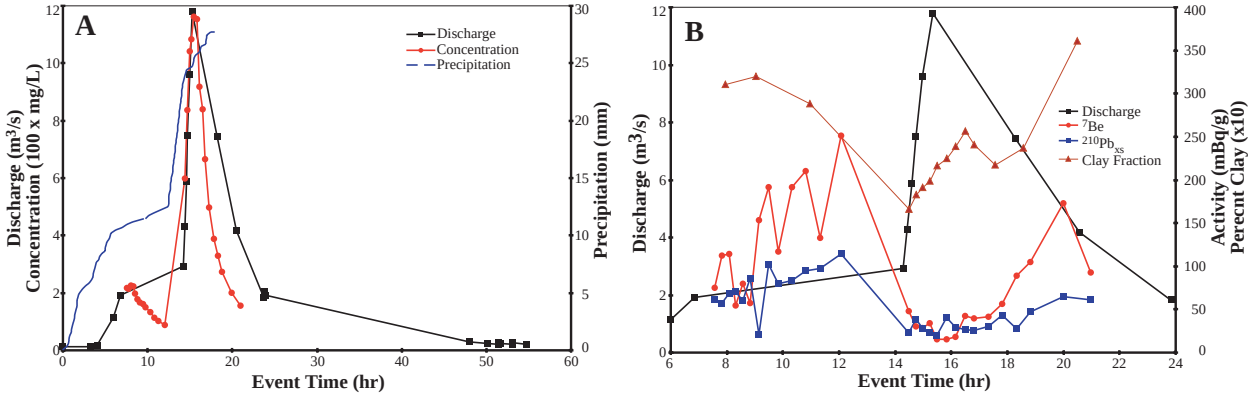


Figure 4 (a) Flow discharge, fine suspended sediment concentration and precipitation for the sampled runoff event on January 7, 2005 at Goodwin Creek and (b) ^{7}Be, $^{210}Pb_{xs}$, and clay content of the fine suspended sediment collected during the same runoff event.

The results of the two end-member mixing model are presented in pie charts in Figure 5b. The red and blue portions of the pie charts represent the proportions of collapsed bank sediment and eroded surface soils in the fine suspended sediment samples, respectively. Due to the limited spacing on the figure in the early stages of the rising limb and the peak of the hydrograph, select samples were plotted to show the general trend of the results.

The proportion of eroded surface soils increases through the beginning stages of the rising limb of the hydrograph to dominate the sample. As the stage, discharge, and fine suspended sediment concentration sharply increases (only flow discharge is represented in Figure 5b), the mixing model suggests that the proportion of eroded surface soils decreases substantially. This decrease corresponds to decreases in activities of ^{7}Be and $^{210}Pb_{xs}$ and clay content of the fine suspended sediments (Figure 4b). An increase in discharge would allow for suspension and transport of coarser and less reactive silt particles prompting the decreases in radionuclide activity and clay content. In addition, the increase of water in the channel and resulting shear stresses would engulf more bank material prompting collapse and entrainment into flow.

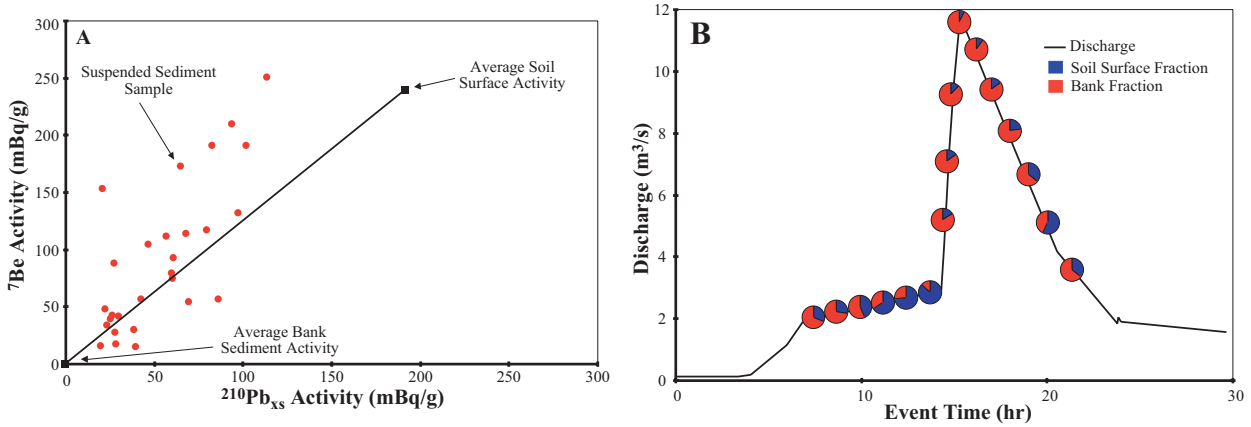


Figure 5 (a) Two end-member model for determining relative proportions of eroded surface soils and collapsed bank sediment in the suspended load of the sampled runoff event on January 7, 2005 at Goodwin Creek, which relates activities of ^{7}Be and $^{210}Pb_{xs}$ in the fines suspended sediment to the activities of the source areas, and (b) Results of the two end-member model.

CONCLUSION

Previous studies in determining sediment sources (Peart and Walling, 1986; Walling and Woodward, 1992) have shown that precision in identifying sources increases with the number of site characteristics used in the analysis.

This study is greatly simplified using only activities of ^{7}Be and $^{210}Pb_{xs}$ in its analysis. Therefore, results presented here are only relative contributions of eroded surface soils and collapsed bank sediment. This novel method shows promise but future comparison to more complex sediment source studies is warranted.

The results presented within this study suggest that eroded surface soils were in a greater proportion relative to bank sediments in the early stages of the runoff event. As discharge and suspended sediment rapidly increased through the peak of the runoff event, radionuclide activities, clay content of the fine suspended sediment, and relative proportion of eroded surface soils decreased. These results are for a single runoff event. More runoff events need to be sampled before the frequency of this pattern can be established.

REFERENCES

Baskaran, M., Ravichandran, M., and Bianchi, T.S. (1997). "Cycling of ^{7}Be and ^{210}Pb in a high DOC, shallow, turbid estuary of south-east Texas," Estuarine, Coastal, and Shelf Science, 45, 165-176.

Bonniwell, E.C., Matisoff, G., and Whiting, P.J. (1999). "Determining the times and distances of particle transit in a mountain stream using fallout radionuclides," Geomorphology, 27, pp 75-92.

Bonniwell, E.C. (2001). Evaluating Soil Erosion and Sediment Transport with Radionuclides. Ph.D. Dissertation, Case Western Reserve University, Cleveland, OH.

Brigham M.E., McCullough, C.J., and Wilkinson, P. (2001). "Analysis of suspended-sediment concentrations and radioisotope levels in the Wild River Basin, Northwest Minnesota, 1973- 98," US Geological Survey Water-Resources Investigations Report, 01-4192, pp 1-21.

Cutshall, N.H., Larsen, I.L., and Olsen, C.R. (1983). "Direct analysis of ^{210}Pb in sediment samples: self-adsorption correction," Nuclear Instruments and Methods, 206, pp309-312.

Kuhnle, R.A., Bingner, R.L., Foster, G.R., and Grissinger, E.H. (1996). "Effect of land use changes on sediment transport in Goodwin Creek," Water Resources Research, 32(10), 3189-3196.

Kuhnle, R.A., Simon, A., and Bingner, R.L. (1999). "Dominant discharge of the incised channels of Goodwin Creek," Procedings of the International Water Resource Engineering Confrerence, Seattle, WA, pp. 1-10.

Matisoff, G., Wilson, C.G., and Whiting, P.J. (2005). "$^{7}Be/^{210}Pb$ Ratio as an indicator of suspended sediment age or fraction new sediment in suspension," Earth Surface Processes and Landforms, 30(9), pp 1191-1201.

Owens, P.N., Walling, D.E., and He, Q. (1996). "The behavior of bomb-derived cesium-137 fallout in catchment soils,". Journal of Environmental Radioactivity, 32(3), pp 169-191.

Peart, M.R., and Walling, E.E. (1986). "Fingerprinting in sediment sources: The example of a drainage basin in Devon, UK," In Drainage Basin Sediment Delivery, IAHS Publication, 159, pp 41-55.

Rabalais, N.N., Turner, R.E., Wiseman, Jr., W.J., and Boesch, D.F. (1991). "A brief summary of hypoxia on the northern Gulf of Mexico continental shelf: 1985-1988," In Tyson, R.V. and Pearson, T.H., Eds., Modern and Ancient Continental Shelf Anoxia, Geological Society Special Publication, 58, pp 35-47.

Rhoton, F.E., Smeck, N.E., and Wilding, L.P. (1979). "Preferential clay mineral erosion from watersheds in the Maumee River Basin," Journal of Environmental Quality, 8(4), pp 547-550.

Rutledge, E.M., Wilding, L.P., and Elfield, M. (1967). "Automated particle size separation by sedimentation," Soil Science Society of America Proceedings, 31, pp 297-288.

Smith, G.F., Greenhawk, K.N., Bruce, D.G., Roach, E.B., and Jordan, S.J. (2001). "A digital presentation of the Maryland oyster habitat and associated bottom types in the Chesapeake Cay (1974-1983)," Journal of Shellfish Research, 20,192-206.

Thorne, C.R. (1992). "Bed scour and bank erosion on the meandering Red River, Louisiana," In Carling, P.A. and Petts, G.E. editors, Lowland Floodplain Rivers; Geomorphologic Perspectives, John Wiley and Sons, Chichester, p. 95-115.

United States Department of Agriculture- Agricultural Research Service. (2005). "Conservation Effects Assessment Project – The ARS Watershed Assessment Study," USDA-Agricultural Research Service Report, pp 1-163.

Wallbrink, P.J. and Murray, A.S. (1996). "Distribution and variability of ^{7}Be in soils under different surface cover conditions and its potential for describing soil redistribution processes," Water Resources Research, 32(2), pp 467-476.

Walling, E.E. and Woodward, J.C. (1992). "Use of radiometric fingerprints to derive information on suspended sediment sources," In Erosion and Sediment Transport Monitoring Programmes in River Basins, IAHS Publication, 210, pp 153-164.

Whiting, P.J., Matisoff, G., Fornes, W.F., and Soster, F.M. (2005). "Suspended sediment sources and transport distances in the Yellowstone basin," GSA Bulletin, 117, pp 515-529.

Wilson, C.G. (2003). The Transport of Fines Sediment through Three NERR Estuaries Using Radionuclide Tracers. PhD. Dissertation. Case Western Reserve University. Cleveland, OH.

Wilson, C.G., Matisoff, G., and Whiting, P.J. (2003). "Short-term erosion rates from a ^{7}Be inventory balance," Earth Surface Processes and Landforms, 28(9), pp 967-977.

Wilson, C.G., Matisoff, G., Whiting, P.J., and Klarer, D.M. (2005). "Transport of fine sediment through a wetland using radionuclide tracers: Old Woman Creek, OH," Journal of Great Lakes Research, 31(1), pp 56-67.

COMPARISON BETWEEN CONCEPTUAL PHYSICAL MODEL OF RESERVOIR SEDIMENTATION AND A 3D NUMERICAL MODEL

Omid Reza Safiyary, Ph.D candidate, Civil Engineering Department, University of Tehran, P.O.BOX 11345/4563, Tehran, Iran, o.safiyary@sazeh.co.ir; Amin Chegenizadeh, MS student, Civil Engineering Department, University of Tehran, P.O.BOX 11345/4563, Tehran, Iran, achegenizadeh@yahoo.com

Abstract: Morphological changes in dam reservoirs are one of the complicated phenomena which are controlled by different parameters in nature. Rivers deposit deltas wherever they reach standing water, i.e. a reservoir. In general, the sand tends to deposit out to form a fluvial Topset and an avalanching Foreset, and the fine material tends to deposit out as a Bottomset. Conventionally numerical models together with field measurements are applied to predict reservoir sedimentation. Another efficient methodology for studying sediment transport in nature is physical models, which are small scale or conceptual form of prototypes. In this research program a 3D-flume with expanded width was designed, as a conceptual model of dam reservoir. The flume is 20m long, varying in width from 30cm to 180cm and has a constant bed slope. Delta progression phenomenon has been monitored using 29 tests; for each test different effective parameters were considered. Also, SSIIM-3D has been used as a numerical model for simulation of sedimentation in the reservoir with the same geometry of physical model. Finally the results have been compared and the results are presented as tables and graphs.

EAST CHICAGO SEDIMENT REMEDIATION DEMONSTRATION PROJECT

David F. Bucaro, Environmental Plan Formulator, david.f.bucaro@usace.army.mil; Kirston Buczak, Project Manager, kirston.a.buczak@usace.army.mil, U.S. Army Corps of Engineers - Chicago District, 111 N. Canal Street, Suite 600, Chicago, IL 60606

Abstract: The U.S. Army Corps of Engineers (USACE), Chicago District, in partnership with the East Chicago Sanitary District (ECSD) has proposed to conduct a project that will demonstrate an approach for remediation of contaminated bottom sediments in the non-Federal portions of the Indiana Harbor Canal (IHC) and the Grand Calumet River (GCR) located in northwest Indiana. The IHC/GCR is listed as one of 43 Areas of Concern in the Great Lakes and holds impairments on all 14 beneficial use categories, an indication of the significant environmental contamination present. The main cause of impairment to the IHC/GCR is contaminated bottom sediments. Habitat restoration of the area cannot occur without management of the contaminated sediment.

The proposed demonstration project site encompasses a 600 by 40-foot channel that carries discharge from the ECSD water reclamation facility into the GCR. This site is representative of the conditions within the GCR, including contaminated sediment and similar overbank conditions. The proposed demonstration project includes the dredging of contaminated sediments, installing a sediment recontamination barrier, creating a new meandering channel, and resloping and replanting the banks of the channel. After completion of construction activities, the project will undergo a three-year monitoring program. Finally, a report on the demonstration project, monitoring results, and lessons learned will be prepared and presented to Congress.

Work completed to date includes coordination, environmental sampling, baseline biological monitoring, and preliminary design and formulation of construction methods. An environmental sampling activity was conducted. Samples were taken from five locations; in general, the results gave elevated levels of polychlorinated biphenyls (PCBs) and polycyclic aromatic hydrocarbons (PAHs), and determined the material is toxic to benthic organisms. Baseline biological monitoring activities including inventories of fish, benthic, and flora species were conducted at the site to determine the species present at the site prior to the implementation of the proposed demonstration project, and to help develop the post-construction monitoring plan.

Design features include a barrier to prevent sediment recontamination that will be of great importance in the developing a much larger study (referred to as the GCR Feasibility Study) to investigate and recommend alternatives for management of contaminated sediment in the non-Federal portions of the IHC and the GCR, and subsequently identify areas for potential habitat restoration. The GCR Feasibility Study is aimed at managing the contaminated sediment, which will most likely include partial dredging of the entire river system and isolating remnant contaminated sediments in a channel after dredging. The sediment barrier will be located just upstream of the confluence of the channel and the GCR and will separate the remediated channel from contaminated sediment migrating from the GCR. Due to the size of the GCR and extent of contamination present, the remediation activities proposed in the GCR Feasibility Study will most likely be approached in a series of reaches with sediment barriers preventing

recontamination by separating the reaches that are contaminated from the reaches that have been remediated. The proposed sediment barrier design consists of a series of vertical precast concrete panels, installed across the width of the channel. The vertical panels are supported on both sides by horizontal panels placed along the channel bottom.

Dredging is a critical feature to the success of the demonstration project; contaminated sediments present in the channel are the most severe impediment to developing a healthy aquatic ecosystem at the project site. The dredging activities will demonstrate how the removal of contaminated sediment alleviates environmental impairments. The remaining features of the project include the installation of the natural streambed, resloping and replanting of the channel banks, and post-construction monitoring. These features will demonstrate environmental restoration and habitat improvement, and will provide valuable knowledge and tools that can be applied throughout the development and implementation of the GCR Feasibility Study. The installation of the natural streambed will feature a series of pools and riffles and will demonstrate the feasibility of in-stream capping and the creation of aquatic habitat. The proposed meandered channel will function similar to a natural riverine system, but at a much smaller scale. The natural streambed features will be constructed of sand and stone similar to those originally found in the region, and will isolate the remnant contamination from the biological communities in the channel. The channel banks will be resloped and replanted with native species to demonstrate bank stabilization, recontamination avoidance, and improvement of terrestrial habitat. The three-year post construction-monitoring program will evaluate the effectiveness of project features to restore water quality and aquatic habitat and to resist recontamination.

The proposed demonstration project strives to achieve environmental sustainability, and seeks ways and means to assess and mitigate cumulative impacts to the environment. The project will provide a direct environmental enhancement; the sediment remediation will effectively remove a considerable source of sediment contamination, and the installation of the natural streambed and resloping and replanting of the banks will add a significant source of habitat enhancement and diversity. The proposed demonstration project will build and share an integrated scientific, economic, and social knowledge base. The project will demonstrate technologies that can be applied to the GCR Feasibility Study and to other Great Lakes Areas of Concern, and the project holds interdisciplinary partnerships with various agencies and organizations. By holding the partnerships, the project respects and esteems the views of individuals and groups interested in Corps activities.

The proposed demonstration project holds interdisciplinary partnerships with various agencies and organizations, including the U.S. Environmental Protection Agency, Indiana Department of Natural Resources, Indiana Department of Environmental Management, The City of East Chicago, Indiana, The Nature Conservancy, Aquatic Research Interactive, Chicago State University, John G. Shedd Aquarium, U.S. Army Engineer Research and Development Center, and Tetra Tech Environmental Management, Inc.

SEDIMENT ANALYSIS OF A GRADUAL DAM REMOVAL ON BREWSTER CREEK NEAR ST. CHARLES, ILLINOIS

Authors: **Timothy D. Straub, P.E., Hydrologist, U.S. Geological Survey, Urbana, IL, tdstraub@usgs.gov; Donald P. Roseboom, Hydrologist, U.S. Geological Survey, Urbana, IL, roseboom@usgs.gov; Gary P. Johnson, Hydrologist, U.S. Geological Survey, Urbana, IL, gjohnson@usgs.gov; Robert R. Holmes, Jr., PhD, P.E., Hydrologist, U.S. Geological Survey, Urbana, IL, bholmes@usgs.gov; Chester C. Watson, PhD, P.E., Civil Engineer, Colorado State University, Fort Collins, CO, cwatson@engr.colostate.edu; Dave Schrader, Hydrologist, U.S. Geological Survey, Dekalb, IL, dlschrad@usgs.gov**

INTRODUCTION

The Illinois Department of Natural Resources, Office of Water Resources (IDNR-OWR) classified the dam on Brewster Creek near St. Charles, Illinois (figs. 1 and 2) a Class I structure. This classification indicates a high probability for causing loss of life and/or substantial economic loss in the event of a catastrophic failure (Kosky and others, 2004). The dam was built in 1929 and through the years structural deficiencies have developed in the dam. Repairing the dam was cost prohibitive and the owners decided to remove the dam. Possible environmental effects and costs of removing dams, and managing or removing the impounded sediment also can be prohibitive. In Illinois, State regulations require complete sediment containment during any construction project. Project engineers developed a first design for the total removal of Brewster Creek dam that complied with these regulations. The projected construction, oversight, and restoration costs of the dam-removal under this first design were $1.17 million, which exceeded available funds (Kosky and others, 2004).

The Illinois Environmental Protection Agency (IEPA) granted permission for a pilot gradual dam-removal project, consisting of cutting five 12–18 inch notches, over approximately a 9-month period, across the length (or some portion of the length) of the dam. The projected construction, oversight, and restoration cost for the gradual dam removal was $330,000 (Kosky and others, 2004). The benefits of gradually removing the dam at this site using multiple notches included reducing the removal cost and reducing possible effects on downstream sedimentation, upstream erosion, and overall aquatic habitat and water quality by allowing the impounded sediment to slowly move downstream and a stable stream and revegetated flood plain to form upstream.

Effects of gradually removing dams are not well known. In 2002, the U.S. Geological Survey (USGS), in cooperation with the Kane County Division of Environmental Management (KCDEM), the Illinois Environmental Protection Agency (IEPA), and the Northeastern Illinois Planning Commission (NIPC), began a cooperative investigation to monitor, analyze, and interpret environmental conditions before, during, and after gradual removal of a dam on Brewster Creek near St. Charles, Illinois. The USGS monitored and analyzed water-quality, precipitation, streamflow, and sediment data. The USGS and

Colorado State University (CSU) have monitored and analyzed stream-channel evolution and stability, and aquatic habitat. The IDNR and the Shedd Aquarium in Chicago (SAC) monitored and analyzed aquatic organisms. The U.S. Fish and Wildlife Service, Chicago Illinois Field Office (USFWS-CIFO) monitored and analyzed the vegetation in the exposed lake bed and stream riparian area, and IDNR-OWR completed an initial conditions, cross-sectional survey of the lake and stream channel upstream and downstream of the dam. The interpretation of these analyses is being used by the USGS to evaluate the effectiveness of the gradual dam-removal methodology and develop notching criteria for future application on similar watersheds.

This study advances the knowledge and understanding of environmental effects on gradual dam removal on stream systems in northeastern Illinois, with potential application to similar watersheds throughout the Nation. The notching criteria developed in this study may be expanded to other watersheds so that permitting agencies can develop a technical basis for gradually removing dams.

The suspended-sediment data collection and results from June 2002 through September 2005 (pre-notching, notching, and post-notching) on Brewster Creek near St. Charles, Illinois (fig. 1) are presented in the following sections. Data collection will continue through September 2006.

DATA COLLECTION

Suspended-sediment concentrations and loads are being monitored at two stations [one upstream (station number 05551029) and one downstream (station number 05551030) of the dam] (fig. 2 and table 1). Suspended-sediment data are useful in quantifying the sediment yield into and out of Willow Lake on Brewster Creek. Suspended-sediment data are also useful in the analysis of stream-channel evolution and stability, aquatic habitat and organisms, and vegetation.

All suspended-sediment samples were collected following protocols outlined in Edwards and Glysson (1999). Methods used in the computation of sediment records are described in Guy (1970) and Porterfield (1972). During periods of rapidly changing flow, samples are collected more frequently (generally, multiple times on the rising and falling limbs of the storm hydrograph). Stage-weighted event, suspended-sediment samples were collected by electronically connecting the automatic suspended-sediment collector to the streamflow station datalogger. When possible, USGS personnel collected depth-integrated samples using isokinetic samplers to compare and adjust the fixed-point samples to compute the mean suspended-sediment concentration at the cross section.

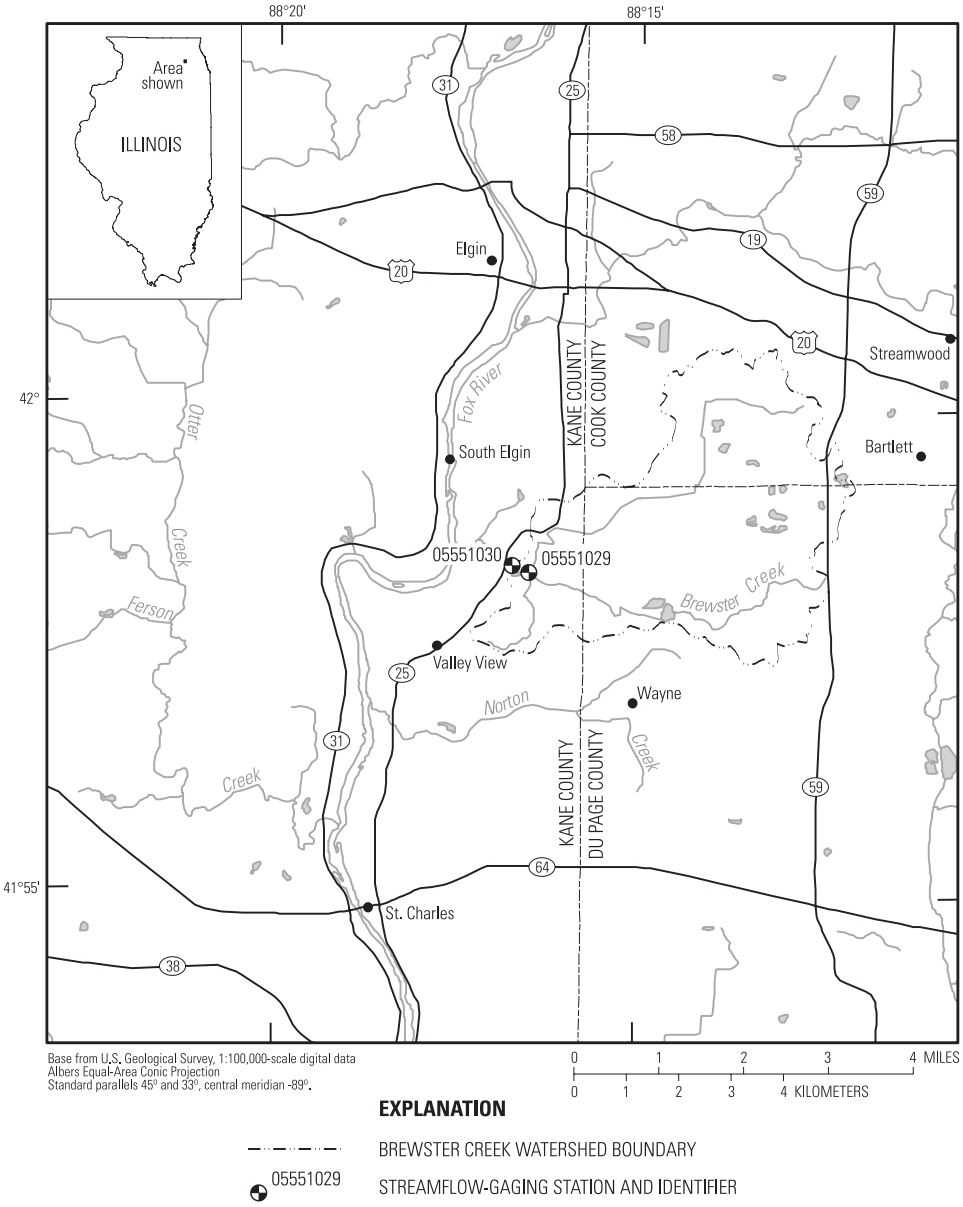


Figure 1. Location of Brewster Creek watershed and the U.S. Geological Survey streamflow and suspended-sediment stations near St. Charles, Illinois.



Figure 2. Location of the study area including Brewster Creek dam on Willow Lake and the U.S. Geological Survey streamflow and suspended-sediment stations on Brewster Creek near St. Charles, Illinois.

Table 1. Streamflow and suspended-sediment stations used in the study and corresponding drainage areas, Brewster Creek near St. Charles, Illinois. [mi^2, square miles]

Station	Station Number (fig. 2)	Drainage Area (mi^2)
Upstream	05551029	13.88
Downstream	05551030	14.00

SUSPENDED-SEDIMENT LOADS

Suspended-sediment loads for two discrete time periods: pre-notching (June 15, 2002, through June 14, 2003), and both the notching and post-notching (June 15, 2003, through September 30, 2005) are presented in the following paragraphs. The last notch was completed in February 2004.

During the pre-notching time period, the total suspended-sediment load at the downstream station (397 tons) is less than the upstream statoin (459 tons). The backwater effects from the dam (slowing the water and allowing for settling of sediment particles) trapped sediment in the pre-notching time period.

The total suspended-sediment load for the combined notching and post-notching time periods equals 2,293 tons at the downstream station as compared to 1,236 tons at the upstream-gaging station. The difference in the two loads (1,057 tons) is a result of streamflow eroding the sediment to form a channel through the old lakebed (fig. 3).

Once the stream channel becomes more stable the downstream load would be expected to be similar to the upstream load. The suspended-sediment load (at the upstream and downstream stations) did not exceed the expected regional estimate of annual suspended-sediment load for a similar sized watershed, thus limiting downstream impacts.



Figure 3. Top Left: Notching procedure during the fourth notch (November 2003). Top Middle: Dewatering of lake and channel formation after first notch (June 2003). Top Right and Bottom Left: Channel formation and headcut progression (May 2004). Bottom Right: Vegetated channel and riparian area (August 2005).

REFERENCES

Kosky, K. M., Straub, T. D., Roseboom, D. P., and Johnson, G. P., 2004, Preliminary Results of a Dam-Removal Analysis on Brewster Creek near St. Charles, Illinois, 2002-2004, Proceedings of the American Society of Agricultural Engineers, Self-Sustaining Solutions for Streams, Wetlands & Watersheds Conference, St. Paul, Minnesota, http://asae.frymulti.com/ (last accessed in October 2005)

MULTI-DISCIPLINED APPROACH ON THE UPPER QUINAULT RIVER GEOMORPHIC STUDY, 18 KM REACH UPSTREAM OF LAKE QUINAULT

Jennifer Bountry, Hydraulic Engineer, Bureau of Reclamation, Denver, CO, jbountry@do.usbr.gov; Lucille A. Piety, Geologist, Bureau of Reclamation, Denver, CO, lpiety@do.usbr.gov; Timothy Randle, Hydraulic Engineer, Bureau of Reclamation, Denver, CO, trandle@do.usbr.gov; Edward W. Lyon, Jr., Geologist, Bureau of Reclamation, Boise, ID, elyon@pn.usbr.gov; Tim Abbe, Herrera Environmental Consultants, Seattle, WA, tabbe@herrerainc.com; Chase Barton, Herrera Environmental Consultants, Seattle, WA, cbarton@herrerainc.com; Galen Ward, Herrera Environmental Consultants, Seattle, WA, gward@herrerainc.com; Kevin Fetherston, Herrera Environmental Consultants, Seattle, WA, kfetherston@herrerainc.com; Bill Armstrong, Biologist, Quinault Indian Nation, Taholah, WA, barmstro@quinault.org Larry Gilbertson, Biologist Quinault Indian Nation, Taholah, WA, lgilbe@quinault.org

Abstract: A team of scientists with backgrounds in fluvial engineering, geology, geomorphology, woody debris, and biology worked together to evaluate whether human disturbances along 18 km of the Upper Quinault River had adversely impacted river processes and sockeye salmon habitat. At the start of the study, many believed the Upper Quinault River was pristine because the north side of the river is managed by Olympic National Park (ONP) and there are no major dams or levees along the river. Our study found that near valley-wide logging and removal of large woody debris from the river channel area in the early 1900s (by 1939) did alter river processes. This occurred prior to the establishment of ONP. Since 1939, the mature vegetated islands and large woody debris have not yet been restored to the system in enough quantity to recreate the reference conditions in the late 1800s. The lack of mature terrace forest has resulted in rapid rates of terrace bank erosion and limited large woody debris in the channel of large enough size to slow channel migration, form large pools, and serve to generate floodplain surfaces that can form into vegetated islands. LiDAR data and comparison of historical information to the present river setting were two key data sets that allowed the study findings to be determined. Working with a multi-disciplined team facilitated an integrated study that allowed a geomorphic analysis to be successfully applied to biological management issues. A reach-based restoration strategy has been proposed to protect remaining sockeye habitat and begin to recover lost habitat in the system. This strategy was designed to work with river processes and existing land use to make projects more feasible and sustainable.

INTRODUCTION

Biologists have documented a decline in the number of sockeye salmon in the Upper Quinault River on the Olympic Peninsula in northwest Washington State (Figures 1 and 2) (QIN, 2002). In an effort to better understand what opportunities exist to restore sockeye salmon habitat, the Bureau of Reclamation was asked to undertake a geomorphic evaluation of the river (Bountry et al., 2005). The primary goal of restoring fish habitat in the Upper Quinault River is to increase the quantity and quality of sockeye spawning habitat; i.e., increase the capacity of the habitats to hold more spawning sockeye and produce greater numbers of emergent juveniles for recruitment into Lake Quinault. Funding for the study was provided by Reclamation and a Salmon Recovery Fund Grant that was part of a cooperative agreement with the Quinault Indian Nation, Reclamation, and the Salmon Recovery Fund Board.



Figure 1 Location of the Upper Quinault River.

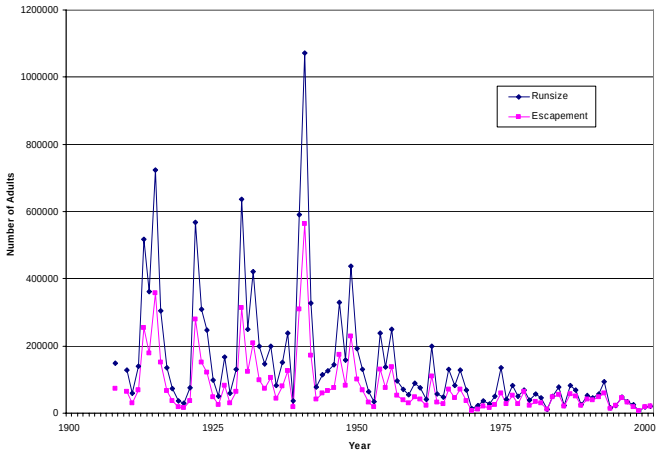


Figure 2 Annual sockeye data for last hundred years from Quinault Department of Fisheries.

STUDY QUESTIONS

Questions addressed in the geomorphic study about the Upper Quinault River are:

1. What were the natural river processes on the Upper Quinault River before settlement in the valley in the late 1800s and early 1900s?
2. Is the existing system different from that which existed prior to human settlement?
3. If differences exist, has the magnitude and frequency of change steadily increased with time, or has it varied in a more complex fashion?
4. What natural or human activities have taken place in the watershed and valley, and to what extent has each of these altered the system?
5. What might the river and its adjacent floodplain look like during the next 50 to 100 years?
6. If river conditions today differ from pre-settlement conditions and if today's land-use practices remain the same in the valley for some time into the future, what is the potential that the river will recover on its own? How long might recovery take?
7. On the basis of information gathered in this study, what restoration strategies for improving fish habitat are feasible, and which locations in the Upper Quinault would they most greatly increase habitat?

METHODS

A multi-disciplinary team with backgrounds in geology, geomorphology, fluvial engineering, and biology worked together on the project to address the stud y questions. Data collection and analysis techniques utilized by the team are summarized as follows:

- Bathymetric survey data combined with light distance and ranging (LiDAR) data to develop digital elevation map and to delineate channels in vegetated areas
- 1D hydraulic model to estimate the hydraulic properties of the river channel
- Timeline of the geologic history using radiocarbon dating and LiDAR data to evaluate potential age of surfaces binding river and erodibility, and identify any controls that naturally limit river migration or downcutting
- Woody debris analysis (Herrera Environmental Consultants) to assess the size and density of wood accumulation necessary to form stable hard points that would help limit channel migration.
- Time-lapse photography during a winter flood season to qualitatively characterize transport and deposition patterns of woody debris and their relation to growth or removal of gravel bars.

- Mapping of dominant vegetation species and general age class to see if terrace forests were of sufficient age and native species type needed to help resist bank erosion at presumed natural levels present prior to disturbance
- Sediment transport analyses included using a sediment budget, stream power (energy) computations, observations of sediment sizes present in the river bed, channel planform and active channel width between 1939 and 2002, and a longitudinal profile comparison between 1929 and the present (2002) measured channel slope.
- Mapping of channel position, width, and sediment bars in decadal spaced historical aerial photography between 1939 and 2002 and historical maps dating back to 1897 to look for trends over time.
- Flood peak analysis to look at possibility of trends over period of record of USGS gaging data
- Stability analysis of side and terrace channels utilized by sockeye to look for any response to human disturbances in basin

RIVER PROCESS FINDINGS

At the start of the study, some researchers felt human disturbances could have altered habitat conditions but others felt the Upper Quinault was in pristine condition because the north side of the river was mainly managed by the National Park Service. Based on journal accounts and historical geologic mapping, it is proposed that the Quinault River functioned as a natural, undisturbed river system through most of the 1800s. The river has changed markedly since the late 1800s. We propose the river was in a state of transition to a new "altered" condition in the early 1900s in response to the removal of large woody debris and increased sediment load from vegetated islands and terraces that were eroded. River process changes during the early part of the twentieth century in response to human-caused disturbance along the study reach were based on historical journal accounts, anecdotal accounts, reports, and maps up to 1939:

1. Homesteading and logging activities cleared forested islands and large woody debris in the active floodplain, which in turn led to rapid erosion of the islands and an increased sediment supply.
2. Once the sediment stored in the islands was available to the river, deep pools and channel areas quickly filled in to accommodate the increased sediment supply.
3. Even with pool storage utilized, the river could still not accommodate the increased sediment supply and the active channel widened and aggraded, causing the river to evolve to a more braided planform.
4. The largest flood of record occurred between 1900 and 1939, which would have resulted in substantial reworking of the channel area.
5. The braided channel was overly wide and unstable, so the low-flow channels rapidly migrated across the new braid plain. Large, wide gravel bars were frequently reworked by floods.
6. As the channel widened and shifted across the floodplain more rapidly, it put more pressure on adjacent terrace banks that historically bound the channel migration zone. Concurrent removal of mature vegetation on these terrace banks made them more vulnerable to erosion and less stable, leading to significant loss of property and infrastructure.
7. As the sediment supply from the eroding islands began to reduce, the width of the active channel would have tended to narrow within the wider floodplain, but this tendency was at least partially offset by the increase in terrace bank erosion.
8. On the 1929 map, the channel appears to be relatively confined and has only one or two flow paths. This configuration is as would be expected given the accounts of late-1800s expeditions. On the other hand, the 1929 map illustrates few of the vegetated islands that are described in expedition accounts of 40 to 50 years earlier. There do appear to be several side channels, although these are not detailed in the mapping to a great extent.
9. By 1939 (first aerial photograph available), the active channel was wide, braided, and flanked by very little mature riparian vegetation or side channels within the active area of the floodplain.
10. Because there was very little mature vegetation in the floodplain, it is assumed the channel migrated across the floodplain at a rapid rate, hence the reason for very few vegetated side channels in 1939.

A quote from a 1936 fisheries survey describes the changes thought to have occurred in the early part of the Twentieth Century:

> The early settlers and inhabitants of this region describe the Upper Quinault River as a large stream that flowed between two rather narrow heavily wooded banks. This condition, however, does not prevail at the present time for the logging off of the watersheds of the river has caused excessive washing to the extent that there is no definite river bed but a wide river valley through which the stream frequently changes its course with the winter and spring freshets. At the present time the devastated area caused by shifting of the channels varies in width from one-quarter to one-half mile and is noticeable the entire distance of twelve miles to the main forks. (Davidson and Barnaby, 1936)

Since 1939, our analysis indicates the river has remained relatively consistent in this altered channel state and has not recovered back to a natural state. The mature vegetated islands and large woody debris have not yet been restored to the system in enough quantity to recreate the reference conditions (Figure 3). The lack of mature terrace forest has resulted in rapid expansion of the historic channel migration zone (HCMZ). The HCMZ is defined as the area containing the active channel and floodplain most frequently reworked over at least about the last 100 years. Additionally, the channel continues to rework the area within the HCMZ with limited large woody debris of large enough size to slow channel migration, form large pools, and serve to generate floodplain surfaces that can form into vegetated islands (Figure 4). Large flood peaks have not changed in magnitude, but the 2-year flood has increased in magnitude in recent decades. Sediment loads to the river are believed to be accelerated to the rapid erosion rates of the terrace surfaces binding the HCMZ. However, increased HCMZ area has also increased the storage area for sediment. Although localized areas experience fluctuations in the channel bed elevation as the river erodes and fills the floodplain as a result of lateral shifting and migration, no long-term aggradation of more than a few feet is predicted to have occurred over the last century. In contrast to the changes in floodplain forest and channel response, no significant, measurable changes have occurred in mass wasting in the upper watershed above the confluence of the two forks of the Quinault River, or in geologic processes (such as uplift or the influence of Lake Quinault) during the twentieth century. A summary of the changes are presented in Table 1.

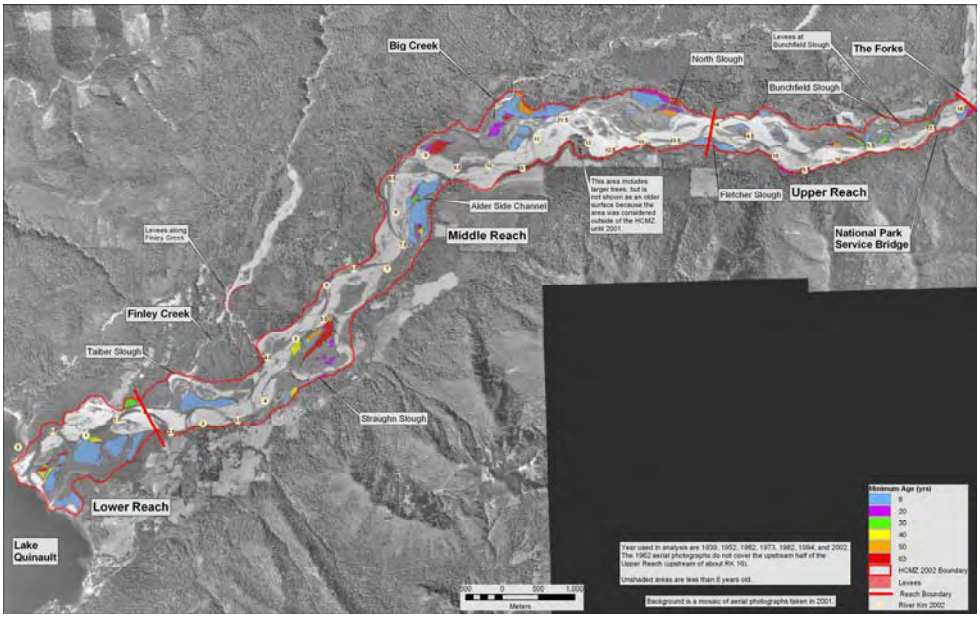


Figure 3 Minimum age of areas containing trees within the 2002 HCMZ. Note the area at RK 12 does have mature trees of significant age but did not get captured in the raster age analysis because it was considered terrace until the main channel recently punched through one of the terrace channels.

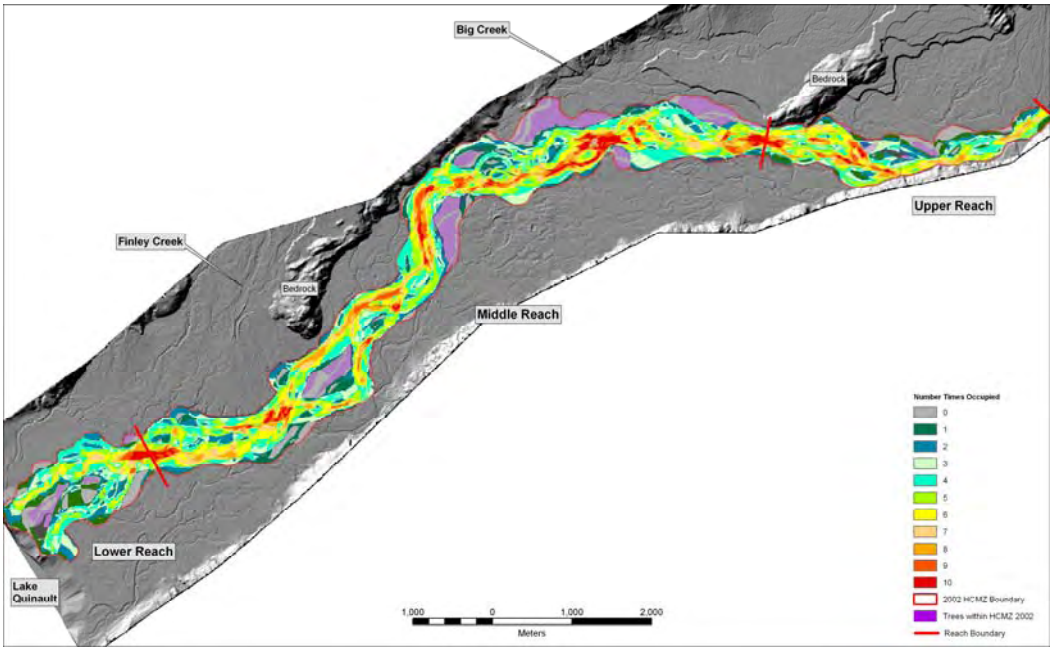


Figure 4 The number of times the active, unvegetated channel of the Quinault River has been located at a particular location as observed on aerial photography spaced about a decade apart. Red and orange areas within the HCMZ are areas where the unvegetated channel has been the most. Gray areas within the HCMZ area are where the unvegetated channel has not been in at least 64 years.

SOCKEYE RESPONSE TO CHANGES IN RIVER PROCESSES

Monitoring data show the Quinault sockeye produced cyclic, but substantial runs in the first fifty years of the twentieth century, but beginning in the 1950s experienced a decline that has not yet recovered. It is not known why the overall sockeye population numbers continued to be high into the 1950s when the most significant response of the main river to disturbance is thought to have peaked in the 1920s to 1930s and remained relatively consistent since that time. It is possible that remaining tributary channels and protected terrace channels provided sufficient premium habitat to sustain the sockeye population at high levels until cumulative effects of river disturbance degraded the overall habitat productivity.

In addition to cumulative effects of river channel instability and migration, the decline of sockeye population size after 1950 could have been influenced by increasing frequencies of channel reworking flood events. The more frequent and slightly larger flood flows occurring on a disturbed, unstable floodplain could have eliminated any remaining premium habitats for sockeye, and would have further degraded the over all habitat productivity in the system.

Increased channel migration, channel bank and terrace erosion, and the consequent reduction of the number of spawning salmon in the Upper River would also cause a decline in water quality and trophic productivity within the rearing environment of Lake Quinault. This is a critical phase for over all productivity of the system, and poor conditions in the Lake would act as a bottleneck that would limit production. Deteriorating conditions in Lake Quinault likely occurred simultaneously with changes occurring in the Upper River to affect and limit the capacity of the system to produce sockeye salmon.

The river can no longer sustain the same quantity of quality sockeye habitat for decades to centuries as it did in the reference conditions. Tributary channels that are less susceptible to river processes presently provide the most stable habitat in the present system. Terrace channels that were historically stable for several decades to centuries are now at a higher risk to erosion by the river. The presently wide, shallow river with a general lack of large, stable woody debris does not provide adequate holding pools that can remain wetted during low flow periods. These pools are

essential for sockeye survival to help them survive between hatching and migration down to Lake Quinault. The few areas that are available are at high risk for being washed out by the river during subsequent high flows.

Table 1. Summary of comparison of the characteristics of the reference conditions and present conditions on the Quinault River.

Property	Characteristics of Quinault River	
	Reference Conditions[1]	**Present Conditions**
Main Channel	One or two dominant low-flow channels; in places, the channel is confined by vegetated surfaces	Multiple low-flow channels; unvegetated bars common adjacent to the channel
Unvegetated Channel	Relatively confined by mature, dense vegetation on either side	Relatively wide and not bound by mature vegetation in most areas
Vegetated Surfaces	Range in age from pioneer bars to mature terraces	Range in age, but limited mainly to pioneer bars and developing floodplain; only a few transitional terraces; mature terraces are virtually absent
Woody Debris	Numerous large logs available to be recruited as key members, which in some cases initiate the formation of large jams	Few large logs available, so the river system lacks large jams because potential key members are absent
Side Channels Within HCMZ	Variable location within the river system; stability ranges from only a few years to tens of years; mature vegetation along boundaries limits the rate at which the main channel erodes into the side channel; large woody debris at entrances can help limit the rate at which the main channel shifts into the side channel	The wider HCMZ allows for more side channels to persist but generally with less stability than reference conditions due to more rapid shifting of main channel and less large woody debris; a few side channels appear to have lower risk than reference conditions due to wider HCMZ with more places for main channel to occupy
Terrace Side Channels	Stable for several centuries; very slow erosion and reworking rates of these areas	Large portion of the network of terrace channels has been lost and not replaced because of expansion the HCMZ; remaining terrace channels are at risk for erosion due to cleared banks; many terrace channels modified at entrances and at road crossings
Habitat Quality and Quantity	Diverse network of interconnected side and terrace channels that provided a wide range of habitat sustained from only a few years to centuries	Remaining habitat areas generally have less complexity and higher risk of being lost over a faster timeframe than in reference setting

[1]Reference conditions have been inferred from historical accounts and photographs and from the present characteristics of the Queets River

LAND MANAGEMENT CONSIDERATIONS

Landowners whose property and infrastructure directly abut the active channel have also suffered from a change in river processes because they run a greater risk of bank erosion and loss of land than previously. Surfaces on the south shore near Lake Quinault may contain old lake bed deposits (clay) that have more ability to resist erosion than upstream, more erodible, alluvial terrace surfaces (Figure 5). Over the last century river-front landowners have responded to loss of property and endangered infrastructure by re-arranging or removing large woody debris and log jams in the river and placing cabled logs and rock riprap along the river bank to try to limit erosion. This approach

has worked in places, but can also cause unanticipated effects to other land across or downstream from the site protected.

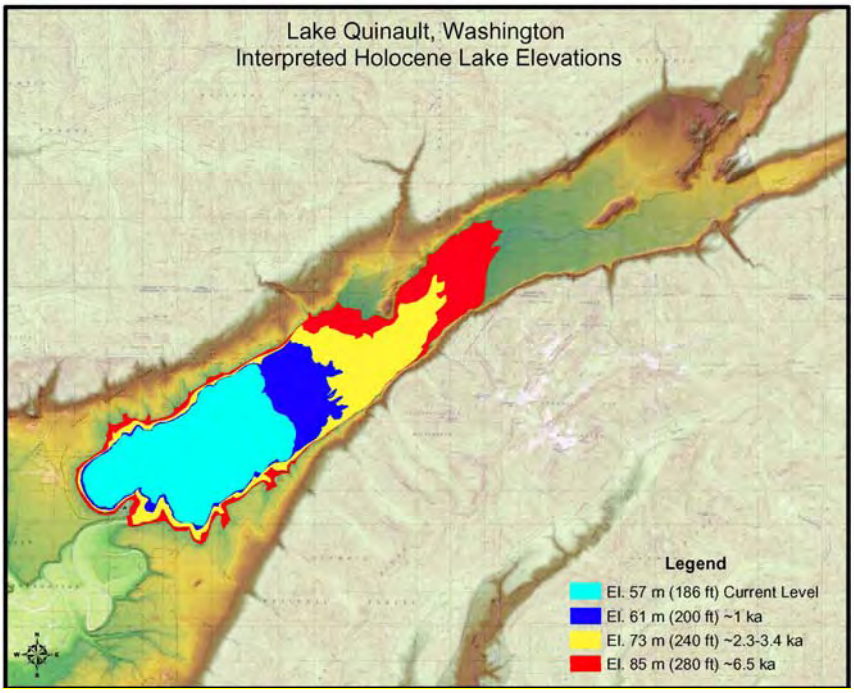


Figure 5 Interpretation of Quinault Lake's rate of regression based on radiocarbon ages and the elevation of where the sample was obtained.

RESTORATION STRATEGY

We propose both short-term and long-term restoration strategies to improve the ability of the river to sustain habitat features vital to sockeye salmon and to protect adjacent property. Short-term strategies would protect the most vulnerable terrace banks and sockeye side channel and terrace habitat areas. Long-term strategies would restore the mature forest on both terrace banks and patches within the active floodplain to provide an adequate recruitment source of large woody debris. This would re-establish the ability of the river to build stable hard points and terrace surfaces that have been lost over the last century. A reach-based restoration approach is recommended that will lead towards a more self-sustaining system, but also consider upstream and downstream implications of any actions. The long-term restoration strategy includes:

1. Restore floodplain conifer reproduction to slow rates of bank erosion and channel migration to match the interpretation of reference conditions from the late 1800s.
2. Restore stable wood jam-generated forested islands.
3. Restore mature (late-successional stage) floodplain forests.
4. Restore the sources of large woody debris (mature floodplain forests).
5. Restore stable wood jam and floodplain forest to create a deeper, narrower channel with more morphological complexity than the wide, shallow channel that exists today.
6. Modify existing infrastructure (roads, bridges, levees) that cut off historical channel paths and floodplains to allow natural flow paths to occur.

Within the vicinity of each side channel and terrace channel complex, specific short-term restoration actions include:

1. Engineered log jams at channel entrances to slow rate of being overtaken by the main channel (some rate of reworking is necessary over several decades)
2. Protection (engineered log jams and/or rock) of young vegetated bars within the active floodplain that have a chance at developing into mature forest (stable hard points)
3. Replanting (long-term) and protection (short-term) of cleared terrace surfaces most at risk to erosion, mainly on the south side of the active floodplain
4. Further evaluation of any infrastructure that could be modified to enhance sockeye habitat areas and manage flooding issues

REFERENCES

Bountry, J. A., Piety, L. A., Randle, T., Lyon, Jr., E.W., Abbe, T., Barton, C., Ward, G., Fetherston, K., Armstrong, B., Gilbertson, L. (2005). Geomorphic Investigation of Quinault River, 18 km Reach of Quinault River Upstream of Quinault Lake, unpublished, developed by Bureau of Reclamation, Herrera Environmental Consultants, and Quinault Indian Nation Fisheries Department.

EQUATIONS FOR ESTIMATING BANKFULL-CHANNEL GEOMETRY AND DISCHARGE FOR STREAMS IN THE NORTHEASTERN UNITED STATES

Gardner C. Bent, Hydrologist, U.S. Geological Survey, 10 Bearfoot Road, Northborough, MA, 01532 gbent@usgs.gov

Abstract: Equations for estimating bankfull-channel geometry (stream width, mean depth, and cross-sectional area) and discharge were developed for streams in the northeastern U.S. Bankfull-channel geometry and discharge information are needed by government agencies and private organizations involved in stream restoration projects that use a natural-channel design approach. Bankfull-channel geometry and discharge information are also useful in addressing issues related to fish habitat, the design of culverts and bridges, and the regulation of stream-buffer zones.

Bankfull-channel geometry and discharge data from for 204 natural-flowing streams in the northeastern U.S. were used in this analysis. Data were from 11 published and 1 ongoing field studies mainly in the following states: Maryland (McCandless and Everett, 2002 and 2003; and McCandless, 2003), Massachusetts (ongoing study), New York (Miller and Davis, 2003; Mulvihill and others, 2005; and Westergard and others, 2005), Pennsylvania (White, 2001; Cinotto, 2003; and Chaplin, 2005), and Vermont (Jaquith and Kline, 2001), with some additional data from adjacent states (U.S. Department of Agriculture, Natural Resources Conservation Service, National Water Management Center, 2004). Coefficients of determination (R^2) for the regression analyses relating bankfull stream width, mean depth, cross-sectional area, and discharge data to drainage area were 0.82, 0.76, 0.90, and 0.80, respectively. The unified regional equations for the northeastern U.S. were:

$$\text{bankfull stream width (ft)} = 13.2635[\text{drainage area (mi}^2)]^{0.4459}, \quad (1)$$

$$\text{bankfull stream mean depth (ft)} = 0.9951[\text{drainage area (mi}^2)]^{0.3012}, \quad (2)$$

$$\text{bankfull stream cross-sectional area in (ft}^2) = 12.8552[\text{drainage area(mi}^2)]^{0.7537}, \text{ and} \quad (3)$$

$$\text{bankfull discharge (ft}^3/\text{s}) = 40.9545[\text{drainage area (mi}^2)]^{0.8448}. \quad (4)$$

To investigate possible subregional differences in the relations of bankfull-channel geometry and discharge to drainage area, individual state and hydrologic-region studies' regression equations were systematically compared to versions of the unified regional regression equation that omitted data from that state or hydrologic region. No statistically significant differences were found between the slopes or intercepts of state or hydrologic-region studies' regression equations and the unified regional equations, with a few exceptions. The exceptions were the intercept of the regression equation for bankfull stream width and bankfull discharge in the Coastal Plain hydrologic region of Maryland (McCandless, 2003) and the intercept of the equation for bankfull discharge in the Piedmont hydrologic region of Maryland (McCandless and Everett, 2002). This analysis indicates that the northeastern U.S. can be adequately represented by one set of regional equations for estimating bankfull-channel geometry (stream width, mean depth, and cross-sectional area) and discharge on the basis of drainage area at natural flowing stream sites.

PRIMARY FACTORS AFFECTING WATER CLARITY AT SHALLOW WATER SITES THROUGHOUT THE CHESAPEAKE AND MARYLAND COASTAL BAYS

Julie M. Baldizar, Ecologist, U.S. Geological Survey, Reston, VA, baldizar@usgs.gov; Nancy B. Rybicki, Hydrologist, U.S. Geological Survey, Reston, VA, nrybicki@usgs.gov

INTRODUCTION

The Chesapeake Bay and its tributaries, which constitute the largest estuary in the United States, stretch approximately 290 km along the Nation's mid-Atlantic Coast. The total estuarine system (open bay and tidal tributaries) traverses six States (New York, Pennsylvania, Maryland, West Virginia, Virginia, and Delaware) and the District of Columbia. Historically, the shallow water portions of this estuary (< 2 m) supported a diverse and abundant community of submerged aquatic vegetation (SAV), which provided critical habitat for juvenile fish and shellfish, contained one of the world's most important spawning grounds for striped bass (*Morone saxatilis*), provided food for migratory birds, and stabilized bottom sediments (Phillips 2002). Since the 1960's, SAV acreage has decreased dramatically in the Chesapeake and Coastal Bays. This decline has been attributed to reductions in light availability caused by increased levels of sediment and nutrients entering the bays. To address this issue, scientists and resource managers established threshold levels for the primary water quality parameters that affect water clarity. Thus, SAV habitat requirements were established for active chlorophyll-a (Chla) (an indicator of phytoplankton biomass), total suspended solids (TSS), dissolved inorganic nitrogen (DIN), dissolved inorganic phosphorus (DIP), and light attenuation (K_d) for both the tidal fresh/oligohaline and mesohaline/polyhaline portions of the bay (Dennison et al. 1993; Kemp et al. 2000). Of these factors, light attenuation is considered the primary requirement for SAV growth and survival (Dennison 1987). In addition, minimum light requirements (MLR) are greater for SAV species that inhabit meso- (5 to 18 psu) to polyhaline (18 to 30 psu) portions of the bay. The MLR for SAV survival at a 1.0 m depth is a $K_d \leq$ 2.0 (13% of surface irradiance) in tidal fresh (0 to 0.5 psu) and oligohaline (0.5 to 5 psu) areas and a $K_d \leq$ 1.5 (22% of surface irradiance) in mesohaline (5 to 18 psu) and polyhaline (18 to 30 psu) areas.

The amount of surface irradiance available at a given depth is a function of the absorption and scattering of light photons by water itself, colored dissolved organic matter (CDOM), Chla, and TSS (Gallegos 1994, Gallegos and Moore 2000). The amount of light available to SAV is further diminished by aquatic plants' requirement for photosynthetically active radiation (PAR), a small bandwidth of light from 400 to 700 nanometers. Underwater quantum sensors often are used to measure PAR and calculate the diffuse attenuation coefficient of downward propagated irradiance (K_d). Once K_d is established, radiative transport equations can be used to calculate the percent of surface light (% light) available to SAV at a given depth (Kirk 1994; Gallegos and Moore 2000). Percent light calculations are used to evaluate the suitability of a site to meet the water clarity requirements for SAV growth. However, the need to better assess the duration and spatial extent over which criteria are met (US EPA 2003) has spurred the use of new sampling technologies to measure the light levels available to SAV.

Turbidity, an optical property that measures the scattering by light at 90° from an incident beam, increasingly is being used to assess water clarity. In recent years, the Chesapeake Bay Program's water quality monitoring efforts have expanded from mid-channel sites to include the near-shore, shallow water areas that support SAV. In an effort to better understand the light environment in these areas, *in situ* water quality meters measure turbidity continuously throughout the SAV growing season (April-October). Turbidity data eventually may be used to determine if Chesapeake Bay River segments are in compliance with the water clarity standards set forth in the Clean Water Act (US EPA 2003). However, it is unclear if turbidity is a good predictor of K_d in the Chesapeake and Coastal Bays.

In 2002, the Maryland Department of Natural Resources (MDDNR), in conjunction with the U.S. Geological Survey (USGS), expanded the scope of their *in situ* program to include weekly PAR measurements. We analyzed weekly water quality data to determine if water quality during the growing season met the five SAV habitat criteria at each site and to determine if compliance with these criteria related to the presence/absence of SAV. Furthermore, we analyzed the ability of turbidity to predict K_d values and determined primary factors other than turbidity that explained variability in K_d at individual sites. Finally, we evaluated the utility of an optical model, which partitions light attenuation due to TSS and Chla, to predict K_d and to provide further insight into the need for nutrient or sediment reduction strategies at individual study sites.

MATERIALS AND METHODS

Study Area: In 2002, MDDNR's *in situ* program assessed water quality at 10 sites within the following Chesapeake and Maryland Coastal Bay River Segments: Pocomoke River (Rehobeth, Cedar Hall Wharf, and Shelltown), Fishing Bay (Drawbridge Road), Severn River (Ben Oaks and Sherwood Forest), Magothy River (Whitehurst and Stonington Station), and Isle of Wight Bay (Bishopville Prong and Turville Creek) (Figure 1). Three of the sites (Sherwood Forest, Stonington Station, and Whitehurst) were vegetated in 2002.

***In Situ* Sampling:** MDDNR installed YSI Environmental's 6600 multi-parameter instruments at each of the 10 sites to measure temporal variability in water quality during the SAV growing season. At the eight Chesapeake Bay sites, a single YSI sonde floated within a perforated PVC housing unit that was attached to a dock, pier, or piling. At the two Coastal Bay sites, which were shallower than the Chesapeake Bay sites, housing units were anchored 0.3 m above the bottom sediments. The placement of the housing units in both bays allowed the field probes attached to the sondes to float approximately 1 m below the surface of the water. Data loggers recorded the following environmental parameters at 15 minute intervals: dissolved oxygen concentration (DO, mg l^{-1}), dissolved oxygen saturation (DO%), salinity, water temperature (°C), pH, turbidity (ntu), and total chlorophyll (µg l^{-1}). Throughout the growing season, the multi-parameter instruments were downloaded and replaced weekly with freshly calibrated units.

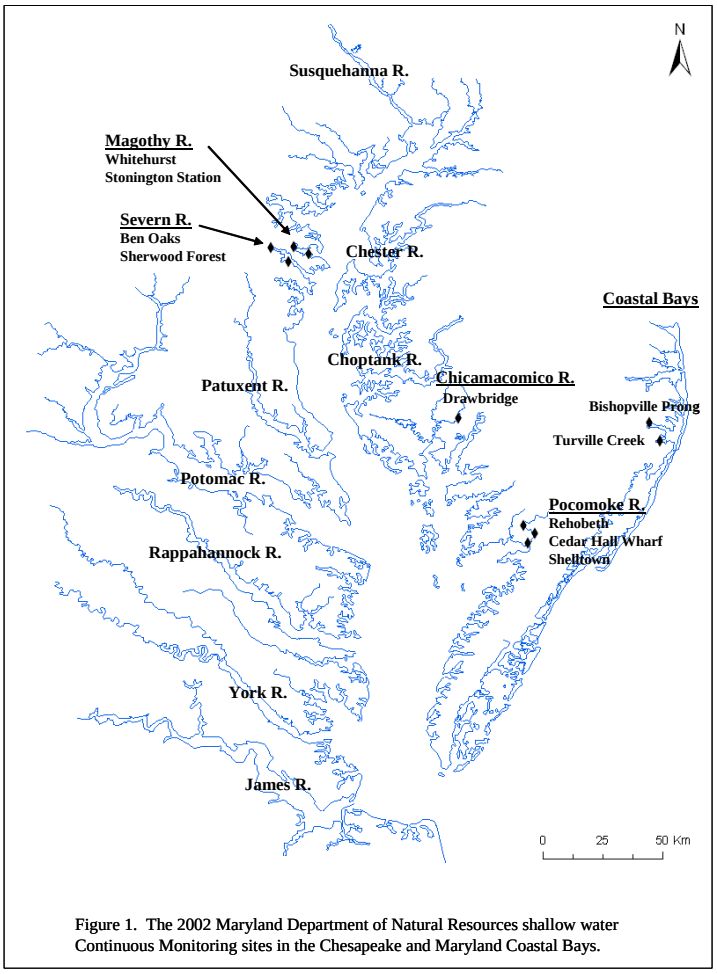


Figure 1. The 2002 Maryland Department of Natural Resources shallow water Continuous Monitoring sites in the Chesapeake and Maryland Coastal Bays.

In 2002, PAR was measured weekly at each site, although initiation of measurements at individual sites varied from April to July. Downwelling PAR was measured simultaneously at two depths (0.05 m and 0.55 m or 0.05 m and 1.0 m) with two LI-COR LI-193 Underwater Spherical Quantum Sensors. From these data, K_d was calculated as

$$K_d = (-(\ln(PAR_max_z)-\ln(PAR_min_z)))/(max_z-min_z) \quad (1)$$

where PAR_min_z is irradiance at 0.05 m and PAR_ max_z is irradiance at either 0.55 m or 1.0 m.

Laboratory Analysis: During the weekly site visit to service the YSIs, discrete water samples were collected from the same depth as that of field probes. The Nutrient Analytical Services Laboratory (NASL) at the Chesapeake Biological Laboratory (CBL) analyzed the dissolved and particulate constituents of these samples. Turbidity and Chla were analyzed by the Maryland Department of Health and Mental Hygiene (DHMH). The MDDNR collection methods, and the CBL and DHMH analytical procedures, can be found in Michael et al. (2004).

Statistical Analysis: Median seasonal values for K_d, Chla, TSS, DIN, and DIP were calculated to determine whether the 10 sites met the previously established SAV water clarity requirements for growth during 2002 (Dennison et al. 1993; Kemp et al. 2000; Figure 2). In addition, total volatile solid (TVS) medians were calculated for each site to compare TSS and its organic component (TVS) (Figure 2).

Data were log-transformed prior to their use in regression analyses. Using S-Plus 6.1, simple linear regression models were developed to determine if turbidity was a good predictor of K_d at each of the 10 sites, and collectively when all 10 sites were combined. Both simple and all possible regression analyses were used to determine the primary factors, other than turbidity, that affected K_d in 2002. The following explanatory variables were tested: TSS, TVS, total fixed solids (TFS), Chla, YSI chlorophyll (Fluor), DIN, DIP, total nitrogen (TN), total phosphorus (TP), dissolved organic carbon (DOC), and salinity. The all possible regression procedure tested for multicolinearity among the variables through a comparison of the variance inflation factors (VIF). Any multiple variable models whose coefficients possessed VIF scores greater than five, or were not significant at $p<0.05$, were excluded from consideration for the overall best-fit multiple variable model.

We also evaluated the relative importance of Chla and TSS in attenuating light using the Optical Model for Determining Water Quality Goals for SAV Habitat Restoration (Gallegos 1994, download the model @ www.chesapeakebay.net/cims/). This model uses raw Chla and TSS values to estimate a seasonal median K_d value for a site and then predicts the suitability of water clarity for SAV growth at 0.5 m, 1.0 m, and 2.0 m depths. Additionally, the optical model produces multiple management options that indicate how reductions in Chla and TSS together, TSS alone, or Chla alone, might meet the SAV water clarity requirements at a given depth.

RESULTS

SAV Habitat Criteria: The three vegetated sites (Sherwood Forest, Stonington Station, and Whitehurst) met the SAV habitat criteria for TSS and K_d in oligohaline SAV communities (Figure 2). Sherwood Forest, additionally, met the SAV water clarity goals for Chla and K_d in meso- to polyhaline SAV communities (Figure 2). The seven unvegetated sites did not meet the habitat criteria for K_d, TSS, or Chla; although, some sites met one or both of the requirements for DIN and DIP (Figure 2). The TVS concentrations were low with minimal ranges at the three vegetated sites and at the two un-vegetated lower Pocomoke River sites (Figure 2).

Turbidity as a Surrogate for K_d: Turbidity was a significant predictor of K_d at 6 of 10 sites: Cedar Hall Wharf (r^2=0.34, p=0.019), Ben Oaks (r^2=0.40, p<0.001), Sherwood Forest (r^2=0.32, p=0.003), Whitehurst (r^2=0.23, p=0.011), Stonington Station (r^2=0.62, p<0.001), and Bishopville Prong (r^2=0.36, p=0.008) (Table 1). Both simple and all possible regression analyses revealed that turbidity was the best single variable predictor of K_d at Ben Oaks, Sherwood Forest, Whitehurst, Stonington Station, and Bishopville Prong (Table 1). Turbidity was also the best single variable predictor of K_d (r^2=0.63, p<0.001) bay-wide (Figure 3).

Primary Factors Influencing K_d: An all possible regression analysis, excluding turbidity, was used to identify the best-fit single and multiple parameter models that explained the most variance in K_d during 2002 (Table 2). Total phosphorus was the best single predictor for K_d at: Whitehurst (r^2=0.17, p=0.031), Stonington Station (r^2=0.32, p=0.003), and Turville Creek (r^2=0.47, p=0.003); DOC at Sherwood Forest (r^2=0.18, p=0.033) and Bishopville Prong (r^2=0.33, p=0.012); salinity at Shelltown (r^2=0.25, p=0.034) and Drawbridge Road (r^2=0.50, p<0.001); TN at Rehobeth (r^2=0.30, p=0.019); DIN at Cedar Hall

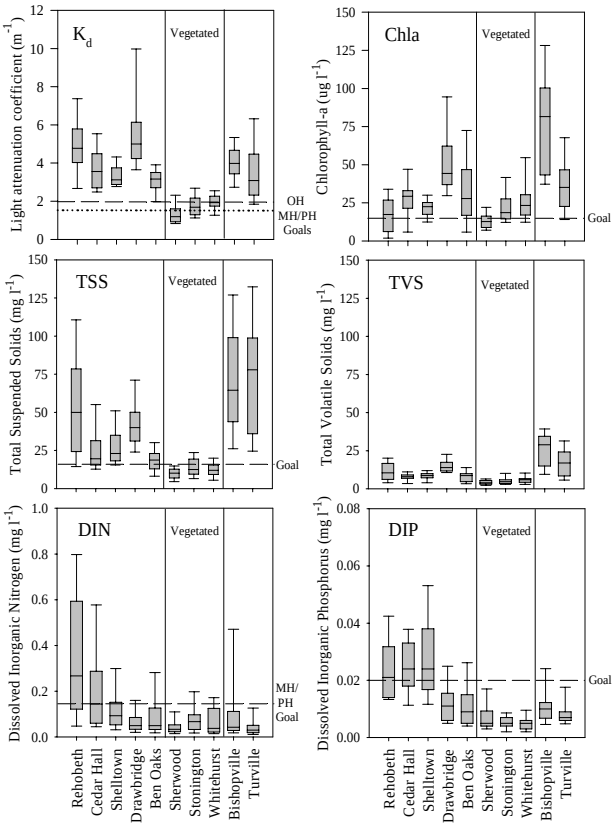


Figure 2. Box plots of median seasonal values for K_d, Chla, TSS, TVS, DIN, and DIP are shown for the 2002 sites. Each box represents 50% of the data; whiskers indicate the 10th and 90th percentiles. There are no established criteria for TVS. SAV habitat criteria are shown for the oligohaline (OH), mesohaline (MH), and polyhaline (PH) salinity zones in the Chesapeake and Maryland Coastal Bays, 2002.

Wharf (r^2=0.61, p<0.001); and TVS at Ben Oaks (r^2=0.20, p=0.020) (Table 2).

The best regression models for Rehobeth, Whitehurst, and Turville Creek contained a single predictor variable. For the other seven sites (Cedar Hall Wharf, Shelltown, Drawbridge, Ben Oaks, Sherwood Forest, Stonington Station, and Bishopville Prong) the best models were multiple regressions (Table 2).

Table 1 Results of the simple linear regression analyses describing the relation between K_d and turbidity in the Chesapeake and Maryland Coastal Bays, 2002. The sites where turbidity was a significant predictor of K_d are in bold. An * indicates that turbidity was the best single variable predictor of K_d when included in an all possible regression analysis.

River	Site	Salinity regime	F-statistic	r^2	p-value
Pocomoke	Rehobeth	oligohaline	1.48	0.08	0.242
	Cedar Hall Wharf	oligohaline	**7.07**	**0.34**	**0.019**
	Shelltown	oligohaline	0.05	0.00	0.834
Chicamacomico	Drawbridge	mesohaline	2.65	0.11	0.118
Severn	**Ben Oaks ***	mesohaline	**16.68**	**0.40**	**<0.001**
	Sherwood Forest *	mesohaline	**11.43**	**0.32**	**0.003**
Magothy	**Whitehurst ***	mesohaline	**7.61**	**0.23**	**0.011**
	Stonington Station *	mesohaline	**38.71**	**0.62**	**<0.001**
St. Martin	**Bishopville Prong ***	polyhaline	**9.10**	**0.36**	**0.008**
Turville Creek	Turville	polyhaline	3.49	0.20	0.083

The Impact of TSS on K_d: In 2002, TSS and its organic (TVS) and inorganic (TFS) fractions explained a small portion of the variability in K_d. However, TVS was the primary factor affecting light attenuation at Ben Oaks (r^2=0.20, p=0.020) (Table 2). TSS and TFS were not the best single variable descriptors of K_d at any of the sites. However, TSS was significantly related to K_d at Stonington Station (r^2=0.23, p=0.013) and Turville Creek (r^2=0.27, p=0.041); TVS at Cedar Hall Wharf (r^2=0.37, p=0.023), Ben Oaks (r^2=0.20, p=0.020), Stonington Station (r^2=0.17, p=0.035), and Turville Creek (r^2=0.39, p=0.013); and TFS at Cedar Hall Wharf (r^2=0.46, p=0.010).

Optical Model for Determining K_d

An Exact Wilcoxon Signed-Rank Test was used to compare the K_d values estimated by the Gallegos optical model (1994) to those calculated from PAR measurements (Figure 4). This analysis revealed that the estimated K_d values were not significantly different from the calculated K_d values (signed-rank statistic V =22, p=0.625) (Figure 4).

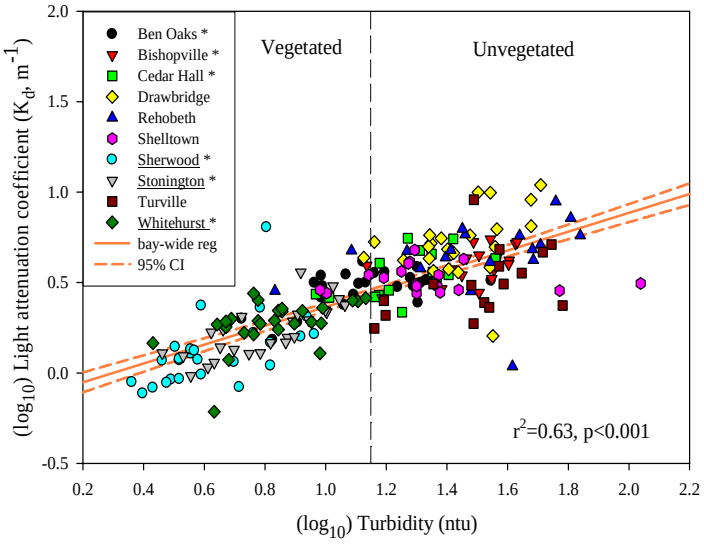


Figure 3. The regression line, 95% Confidence Interval (CI), and test statistic (r^2) for the bay-wide regression of K_d and turbidity. Each site is identified by an individual color. An * indicates those sites at which turbidity was significantly (p<0.05) related to K_d; sites with SAV present in 2002 are underlined. The turbidity at the vegetated sites was <11.1 ntu ($\log_{10}$ 1.15).

Table 2 Results of the best simple (SLR) and multiple (MLR) linear regression analyses describing the relation between K_d and total suspended solids (TSS), total volatile solids (TVS), total fixed solids (TFS), active chlorophyll-a (Chla), YSI chlorophyll (Fluor), dissolved inorganic nitrogen (DIN), dissolved inorganic phosphorus (DIP), total nitrogen (TN), total phosphorus (TP), dissolved organic color (DOC), and salinity (Sal) in the Chesapeake and Maryland Coastal Bays, 2002. At Rehobeth, Whitehurst, and Turville Creek, none of the multiple regression models were significant at $p \leq 0.05$. As a result, the best regression models were single variable models (shown in bold).

Site	Type of Regression Model	Parameters	F-statistic	r^2	p-value
Rehobeth	**SLR**	**TN**	**6.84**	**0.30**	**0.019**
Cedar Hall Wharf	SLR	DIN	21.78	0.61	<0.001
	MLR	TFS+Fluor	31.63	0.86	<0.001
Shelltown	SLR	Sal	5.39	0.25	0.034
	MLR	TFS+TN+TP+Sal	5.70	0.66	0.008
Drawbridge	SLR	Sal	22.39	0.50	<0.001
	MLR	Sal+TVS	12.45	0.55	<0.001
Ben Oaks	SLR	TVS	6.23	0.20	0.020
	MLR	TVS+TFS+DIP+TN	8.79	0.62	<0.001
Sherwood Forest	SLR	DOC	5.13	0.18	0.033
	MLR	DIP+Sal+DOC	5.01	0.43	0.009
Whitehurst	**SLR**	**TP**	**5.25**	**0.17**	**0.031**
Stonington Station	SLR	TP	11.06	0.32	0.003
	MLR	TP+TN+Fluor	6.26	0.46	0.003
Bishopville Prong	SLR	DOC	8.03	0.33	0.012
	MLR	Fluor+TFS	7.72	0.51	0.005
Turville Creek	**SLR**	**TP**	**12.60**	**0.47**	**0.003**

According to the model, six sites met requirements for SAV growth at 0.5 m: Cedar Hall Wharf, Shelltown, Ben Oaks, Sherwood Forest, Whitehurst, and Stonington Station; three sites (Sherwood Forest, Whitehurst, and Stonington Station) met requirements for SAV growth at 1.0 m (Table 3). No sites met the water clarity requirements for growth at 2.0 m. Four sites (Rehobeth, Drawbridge, Bishopville, and Turville) were not predicted to support SAV growth at any depth in 2002.

Reductions in both Chla and TSS levels at all 10 sites are expected to have resulted in water clarity improvements that favored SAV growth at 0.5 m, 1.0 m, and 2.0 m (Table 3). However, the magnitude of the recommended reductions varied greatly among sites and among depths at the same site. All sites, except for Drawbridge Road and Bishopville Prong at 2.0 m, could meet the habitat requirements for SAV by reducing TSS levels and maintaining current Chla levels (Table 3). Based on the model, no sites were expected to meet SAV water clarity requirements for growth through reductions in Chla alone.

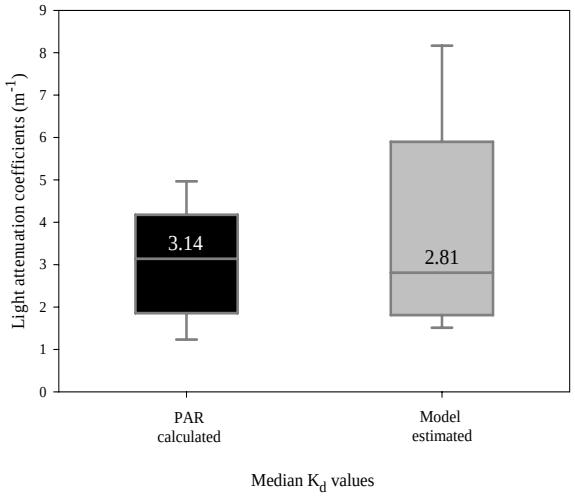


Figure 4. Box plots of the PAR calculated and model estimated (Gallegos 1994) combined median K_d values (n=10) for the 2002 Chesapeake and Maryland Coastal Bay sites. Each box represents 50% of the data; whiskers indicate the 10^{th} and 90^{th} percentiles. An Exact Wilcoxon Signed-Rank Test revealed that the estimated K_d median was not significantly different from the calculated K_d median ($p<0.05$).

Table 3 The PAR calculated and model estimated K_d values for the 10 Chesapeake and Maryland Coastal Bay sites, 2002. Based on the estimated K_d value, the optical model predicted whether or not a site met the water clarity habitat requirements for SAV growth at 0.5 m, 1.0 m, and 2.0 m depths. No sites met the water clarity requirements at 2.0 m. The sites and depths that met the SAV water clarity goals are shown in bold. The management options that would allow each site to meet the water clarity goals for each depth are shown (X). In 2002, no sites would have been expected to meet the water clarity habitat requirements through reductions in Chla alone.

Site	SAV (YES/NO)	PAR calculated medain K_d (m^{-1})	Model estimated median K_d (m^{-1})	Depth (m)	SAV habitat requirements (met/not met)	Reduce Chla & TSS	Reduce TSS only
Rehobeth	NO	4.77	5.3	0.5	not met	X	X
				1.0	not met	X	X
Cedar Hall Wharf	**NO**	**3.56**	**2.52**	**0.5**	**met**		
				1.0	not met	X	X
Shelltown	**NO**	**3.12**	**3.10**	**0.5**	**met**		
				1.0	not met	X	X
Drawbridge Road	NO	4.99	4.79	0.5	not met	X	X
				1.0	not met	X	X
Ben Oaks	**NO**	**3.16**	**2.46**	**0.5**	**met**		
				1.0	not met	X	X
Sherwood Forest	**YES**	**1.19**	**1.48**	**0.5**	**met**		
				1.0	**met**		
Whitehurst	**YES**	**1.93**	**1.82**	**0.5**	**met**		
				1.0	**met**		
Stonington Station	**YES**	**1.63**	**1.79**	**0.5**	**met**		
				1.0	**met**		
Bishopville Prong	NO	3.98	7.69	0.5	not met	X	X
				1.0	not met	X	X
Turville Creek	NO	3.09	8.22	0.5	not met	X	X
				1.0	not met	X	X

DISCUSSION

We found that the minimum light requirements were a good indicator of SAV presence at the near shore sites (Figure 2). The three vegetated sites (Sherwood Forest, Stonington Station, and Whitehurst), located in the mesohaline portion of the bay, met the oligohaline SAV water clarity criteria (13% of surface irradiance). Additionally, Sherwood Forest met the mesohaline light requirement (22% of surface irradiance). These results indicate that water clarity at Stonington Station and Whitehurst may have been adequate to support freshwater and oligohaline species but not meso- or polyhaline species. The species consistently present at the vegetated sites were widgeon grass (*Ruppia maritima*), redhead grass (*Potamogeton perfoliatus*), sago pondweed (*Potamogeton pectinatus*), and horned pondweed (*Zannichellia palustris*) (Orth et al. 2003). These species typically survive fluctuating salinity conditions in oligo- to mesohaline environments (Davis and Reel 2001). We also found that weekly turbidities at vegetated sites were less than 11.1 NTUs, and that unvegetated sites showed turbidity values exceeding 11.1 NTUs (Figure 3). As additional sites and years of data accumulate, the near shore, *in situ* data could be used to develop turbidity criteria for SAV growth, as was done for other SAV habitat criteria (Kemp et al. 2000).

During the 2002 growing season, turbidity was significantly related to K_d at six of the *in situ* sites (Table 1); however, it explained $\leq$ 40% of the temporal variability in K_d at five of those sites and ~63% of the spatial and temporal variability when all 10 sites were combined (Table 1, Figure 3). The low explanatory ability and large degree of variability in the regression models for K_d and turbidity indicate that the relation between the two variables needs to be better defined before turbidity can be used to predict water clarity or determine the interval during the growing season that a site meets established water clarity criteria (US EPA 2003).

We developed simple regression models to determine the primary factors, other than turbidity, that influenced K_d. Total phosphorus was the best predictor of Kd at three sites, nitrogen at two sites, DOC at two sites, salinity at two sites, and TVS at one site (Table 2). These results indicate that nutrient reduction and subsequent Chla reduction would have a greater effect on water clarity than TFS (mineral sediment) reductions.

Due to the low predictive abilities (r^2) of the single variable models, we developed multiple regression models of K_d and 11 independent variables. For Rehobeth, Whitehurst, and Turville Creek, the inclusion of additional variables in the regression model did not improve upon the results of the best single variable model (Table 2). For the remaining sites, the overall best-fit models included a combination of total nutrients (TP and TN), components of TSS (TVS, TFS, and Fluor), and dissolved constituents (DIP and salinity). These regression results are consistent with previous studies that have shown that TSS and/or Chla were good predictors of K_d in the Potomac River and Estuary (Carter and Rybicki 1990), the Chesapeake Bay (Gallegos 1994), and the Indian River Lagoon in Florida (Gallegos and Kenworthy 1996).

Total nitrogen (TN) and total phosphorus (TP) affected water clarity at various sites. Previous work in the Potomac River has shown that TP positively and TN negatively correlate to Chla and TSS, which in turn negatively correlate with secchi depth (Carter et al. 2000). These results indicate that TP and TN are indirectly involved in light attenuation, possibly through their relationships to Chla and TSS. An analysis of additional parameters, such as particle size, particle density, and chemical composition, may enhance our understanding of the relation among nutrients, suspended particulate material, and light attenuation.

The positive relationship between K_d and salinity may be an indirect effect of flow and its impact on the delivery of particulates to the sites. When river discharge is low, as it was in 2002 (Langland et al. 2004), the estuarine turbidity maximum (ETM) carries more saline waters upstream. As the ETM moves across a site that otherwise is located near, but upstream, of the turbidity maximum, turbidity and K_d may increase. The ETM is typically located downstream of both Shelltown and Drawbridge (US EPA 2003); perhaps low-flow conditions and the migration of the ETM upstream explain the positive relation between K_d and salinity at those two sites.

Finally, we compared our simple and multiple regression models with the output of the Gallegos (1994) optical water clarity model. The model predictions of the sites that met the SAV water clarity habitat requirements at 1.0 m matched the three sites (Sherwood Forest, Stonington Station, and Whitehurst) that supported SAV in 2002. In addition, the Gallegos model (1994), which computes an estimated K_d value for a site based on TSS and Chla values, was a good overall predictor of K_d at the shallow water sites during 2002. These results indicate that the optical model is a useful tool for estimating seasonal median K_d values when only Chla and TSS values are available. Additionally, the model reliably predicted the water clarity requirements for SAV growth.

The optical model indicated that TSS reduction alone, but not Chla reduction alone, would lower K_d to meet the minimum light requirements. This finding does not necessarily indicate sediment reduction is a better strategy than nutrient reduction at these sites. It is problematic to use the Gallegos model (1994) to distinguish between the relative importances of sediment or nutrients in attenuating light using only TSS and Chla values. TSS is composed of the dry weight of all particulate matter including both TVS (phytoplankton, heterotrophic plankton, bacteria, and particulate organic detritus) and TFS (clay, silt, and sand). Although TVS was a substantial portion of the TSS at some sites (especially sites with low TSS and TFS) (Figure 2), the optical model would determine that Chla had a greater effect on water clarity than TSS only if a site was affected by prolonged algal blooms (Gallegos and Moore 2000). The habitat criteria for Chla (15 $\mu g\ l^{-1}$ seasonal median), however, suggests that algal bloom conditions are not necessary to inhibit SAV growth. Increased understanding of the type and size of material (TFS), and species of plankton composing TVS will enhance understanding of the appropriate strategies needed to improve water clarity. Future research to determine factors causing light attenuation, based on ecological models (Cloern 2001), sediment nutrient flux, process oriented studies, and regression analyses, will improve our understanding and serve as a guide in determining the effectiveness of management strategies to establish nutrient and sediment loading rates that allow for restoration of SAV.

REFERENCES

Carter, V. and N.B. Rybicki. (1990). "Light attenuation and submersed macrophytes distribution in the tidal Potomac River and Estuary," Estuaries 13:441-452.

Carter, V., N.B. Rybicki, J.M. Landwehr, and M. Naylor. (2000). Light requirements for SAV survival and growth, in Chesapeake Bay submerged aquatic vegetation water quality and habitat-based restoration targets: A second technical synthesis: U.S. Environmental Protection Agency, Chesapeake Bay Program, p. 11-33.

Cloern, J.E. (2001). "Our evolving conceptual model of the coastal eutrophication problem," Marine Ecology Progress Series 201:223-253.

Davis, R.C. and J.T. Reel. (2001). Chesapeake Bay submerged aquatic vegetation identification guide. J.W. Boarman Co.

Dennison, W.C. (1987). "Effects of light on seagrass photosynthesis, growth, and depth distribution," Aquatic Botany 27:15-26.

Dennison, W.C., R.J. Orth, K.A. Moore, J.C. Stevenson, V. Carter, S. Kollar, P.W. Bergstrom, and R.A. Baituk. (1993). "Assessing water quality with submersed aquatic vegetation. Habitat requirements as barometers of Chesapeake Bay health," Bioscience 43:86-94.

Gallegos, C.L. (1994). "Refining habitat requirements of submersed aquatic vegetation: role of optical models," Estuaries 17:198-219.

Gallegos, C.L. and W.J. Kenworthy. (1996). "Seagrass depth limits in the Indian River Lagoon (Florida, U.S.A.): application of an optical water quality model," Estuarine, Coastal, and Shelf Science 42:267-288.

Gallegos, C.L. and K.A. Moore. (2000). Factors contributing to water column light attenuation, in Chesapeake Bay submerged aquatic vegetation water quality and habitat-based restoration targets: A second technical synthesis: U.S. Environmental Protection Agency, Chesapeake Bay Program, p. 35-54.

Kemp, M., R.A. Batiuk and P.W. Bergstrom. (2000). SAV, water quality, and physical habitat relationships in Chesapeake Bay submerged aquatic vegetation water quality and habitat-based restoration targets: A second technical synthesis: U.S. Environmental Protection Agency, Chesapeake Bay Program, p. 3-9.

Kirk, J.T.O. (1994). Light and photosynthesis in aquatic ecosystems. Cambridge University Press, Cambridge.

Langland, M.J., United States Environmental Protection Agency, Chesapeake Bay Program, Maryland Dept. of Natural Resources, Virginia Dept of Environmental Quality, U.S. Geological Survey. (2004). Changes in streamflow and water quality in selected nontidal sites in the Chesapeake Bay basin, 1985-2003. U.S. Geological Survey Scientific Investigations Report number 2004-5259.

Michael, B., E.L. Ebersole, M. Trice and C.J. Heyer. (2004). Quality assurance project plan for the Maryland Department of Natural Resources Chesapeake Bay shallow water quality monitoring program. Maryland Department of Natural Resources.

Orth, R.J., D.J. Wilcox, L.S. Nagey, A.L. Owens, J.R. Whiting and A. Serio. (2003). 2002 distribution of submerged aquatic vegetation in the Chesapeake and Coastal Bays. VIMS Special Scientific Report Number 139. Final report to U.S. EPA, Chesapeake Bay Program.

Phillips, S.W. (2002). The U.S. Geological Survey and the Chesapeake Bay-the role of science in environmental restoration. U.S. Geological Survey Circular 1220.

United States Environmental Protection Agency. (2003). Ambient water quality criteria for dissolved oxygen, water clarity, and chlorophyll a for the Chesapeake Bay and its tidal tributaries. U.S. Environmental Protection Agency, Chesapeake Bay Program and Region 3 Water Protection Division.

MEASUREMENTS OF VELOCITY PROFILES AND SUSPENDED-SEDIMENT CONCENTRATIONS IN A COLORADO RIVER EDDY DURING HIGH FLOW

Scott A. Wright, Hydrologist, U.S. Geological Survey, Flagstaff, AZ, sawright@usgs.gov; Jeffrey W. Gartner, Oceanographer, U.S. Geological Survey, Tucson, AZ

Abstract: Measurements of velocity profiles and suspended-sediment concentration were made in a recirculating eddy along the Colorado River in Grand Canyon during a high flow release from Glen Canyon Dam in November 2004. The objectives of the measurements were to test an acoustic Doppler current profiler (ADCP) within these environments, to roughly characterize the velocity and concentration structure in the eddy, and to test some assumptions of previous numerical modeling approaches. Results indicate that ADCPs can be useful tools for characterizing the velocity structure of recirculating eddies. The velocity profiles are useful for evaluating some of the assumptions that have been made in previous modeling efforts. In particular, the measurements indicate significant rotation of horizontal velocities vertically through the water column as well as significant vertical velocities; neither process can be simulated with depth-averaged, two-dimensional flow models. However, it is still unknown how important these features are for sediment transport and eddy morphology.

INTRODUCTION

Fine-sediment deposits along the Colorado River below Glen Canyon Dam (fig. 1) have been the subject of numerous studies because of their importance to recreational river users, riparian vegetation, and potential importance as physical habitat for juvenile native fish. Completion of Glen Canyon Dam in 1963 greatly reduced the fine sediment supply to Grand Canyon and has resulted in erosion of these deposits (Rubin et al., 2002, Wright et al., 2005); as a result, restoration and maintenance of fine sediment deposits in Grand Canyon is a primary goal of the Glen Canyon Dam Adaptive Management Program (U.S. Department of the Interior, 1996).

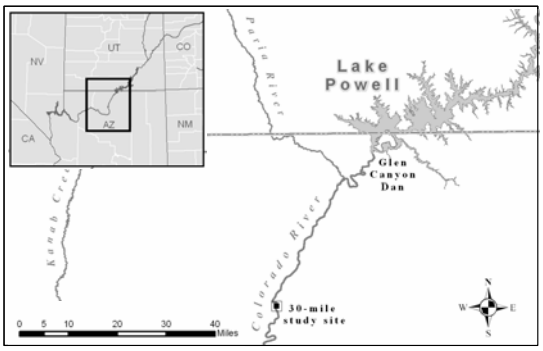


Figure 1 Location map showing 30-mile study site (45 miles from Glen Canyon Dam).

Fine-sediment deposits typically occur downstream from channel constrictions created by tributary debris fans. Flow separates immediately downstream from the constriction and reattaches to the bank at some point downstream, forming a recirculating zone (eddy) near the shore with relatively low velocity that is conducive to sediment deposition. Schmidt (1990),

Schmidt and Graf (1990), and Rubin et al. (1990) described the basic processes of recirculating flow and sedimentation along the Colorado River in Grand Canyon; Schmidt et al. (1993) documented an experimental investigation of similar processes.

Along with the considerable field and laboratory efforts to characterize fine-grained depositional areas, several modeling studies have been undertaken that attempt to simulate the fate of fine-grained sediments in the Colorado River under varying discharges and sediment supply conditions. Wiele et al. (1996) and Wiele (1998) describe development of a numerical model and its application to simulate deposition in reaches of the Colorado River below the confluence with the Little Colorado River (river mile 62, 77 miles below Glen Canyon Dam) following significant flooding and sediment inputs from this tributary in 1993. The model simulates the flow field as two-dimensional and vertically averaged; suspended sediment is modeled through use of the advection-dispersion equation which yields the three-dimensional concentration field, though it is not a full three-dimensional solution because of the two-dimensional depth-averaged flow field. Bed evolution is obtained from flux divergences in suspended- and bed-load transport. Model predictions were found to be in relatively good agreement with measured changes in topography. This model has been subsequently applied to study the effects of sand concentration on deposition rates (Wiele et al. 1999) and to study sand deposition in archaeologically significant reaches of the Colorado River (Wiele and Torrizo 2005).

Nelson and McDonald (1996) and Nelson et al. (1994) presented a modeling approach that stresses the need to model secondary flows in addition to the two-dimensional depth-averaged flow field. They argue that advective transport of sediment into the eddy near the bed can be an important mechanism that can only be accounted for by including secondary flows. This transport is a result of tilting of the vortices (by the vertical velocity gradient) that are shed from the separation point, leading to rotational structures with flow out of the eddy near the surface and into the eddy near the bed. Since sediment concentration is highest near the bed and lowest near the surface (when Rouse number is low), this leads to a net advective transport of sediment into the eddy. McDonald and Nelson (1996), McDonald et al. (1994), and Nelson (1991) document field and laboratory studies that demonstrate this transport mechanism. Also, Nelson and McDonald (1996) present numerical simulations with and without secondary flows and show that the simulations with secondary flows yield better agreement with laboratory measurements. Though transport by secondary currents must certainly be important under some conditions, it is not yet clear that it is an important transport mechanism for Colorado River eddies during high flow. Indeed, the model of Wiele et al. (1996), which relies solely on turbulent dispersion to transport sediment into and out of eddies, was shown to perform well for the cases studied; it is noted that these cases were quite large depositional events. Further investigation is required to better constrain these transport mechanisms for Colorado River eddies. Recent modeling efforts using large eddy simulation (Akahori and Schmeeckle, 2005) provide a promising start.

Despite the considerable efforts to characterize and model the fine-grained sediment deposits along the Colorado River in Grand Canyon, relatively few detailed field measurements of the velocity and concentration structure of recirculating eddies have been made. Schmidt (1990) presented a comparison of main channel and within eddy average velocities based on measurements at three sites on the Colorado. McDonald and Nelson (1996) and McDonald et

al. (1994) document measurements of flow velocities in three recirculating zones by employing a system of mechanical current meters designed to collect velocity profiles and turbulence intensities. While enough good data were collected to characterize mean depth-averaged recirculating flow patterns, significant contamination from suspended organic matter precluded analysis of vertical velocity profiles and turbulence intensities. These data were also used by Rubin and McDonald (1995) to document nonperiodic pulsations in velocity resulting from the vortex shedding.

The study described herein details the collection of velocity and suspended-sediment-concentration data during a high-flow experiment on the Colorado River at a single site approximately 45 miles downstream from Glen Canyon Dam (30-mile site, fig. 1). The high-flow experiment consisted of a 60-hour peak-flow release from the dam of about 1,160 m^3/s (41,000 ft^3/s). The experiment was designed to redistribute sand from the channel bed to eddy sandbar environments that have been eroding since construction of the dam (Webb et al., 1999, Wright et al., 2005, U.S. Department of the Interior, 2004). The objectives of the study described here were to: 1) test the application of an acoustic Doppler current profiler (ADCP) within these environments, 2) roughly characterize the velocity and suspended-sediment-concentration structure at the study site, and 3) use the data to evaluate some of the assumptions of previous modeling approaches. It was, however, beyond the scope of this investigation to quantify the effects of secondary flows on sediment transport in Colorado River eddies during high flow.

METHODS

A 600 kHz ADCP manufactured by RD Instruments[1] was used to collect vertical profiles of three-dimensional velocities at three locations within the eddy. Depth-integrated suspended-sediment samples (Edwards and Glysson 1999) were collected simultaneously at each location; main-channel suspended-sediment samples were also collected on an hourly basis during this time period. All measurements were made mid-day on November 23 which was the second day of the high-flow experiment peak. The ADCP was programmed to sample using Water Mode 1 (RD Instruments, 2003) utilizing a 30 cm resolution bin size.

The three locations for stationary measurements were selected in order to characterize velocity structure and sediment concentration at locations expected to exhibit a range in hydrodynamic and sediment-transport conditions (fig. 2). Sample locations shown in fig. 2 are approximate and based on field landmarks and aerial photographs. Station 1 was located in the return channel (which exhibited upstream flow near the bank); station 2 was located near the eddy fence (i.e. the interface between the main channel and eddy); and station 3 was located near the reattachment point. Because river conditions precluded anchoring, positions were maintained during measurements by maneuvering the boat. This resulted in some variations in position locations especially at station 2. Bottom tracking was used to remove boat motion from the velocity data. Also, station 2 had to be located further into the eddy than desired due to large depths, high suspended-sediment concentration, and moving bed

[1] Use of trade, product, or firm name is for descriptive purposes only and does not imply endorsement by the U.S. Geological Survey.

conditions directly within the eddy fence which precluded reliable velocity profiles at the desired sample location.

RESULTS

Measurements of single-ping ADCP velocity profiles were averaged to provide vertical profiles of mean horizontal velocity and direction, vertical velocity, and error velocity (horizontal/vertical orientation and direction from true north were determined by roll, pitch, and heading sensors internal to the ADCP). Averaging times were as follows: 308 sec at station 1, 422 sec at station 2, and 315 sec at station 3. The ADCP sample rate was about 2.2 Hz. Error velocity is an estimate of measurement quality; it is the difference between the two vertical velocities calculated using two different three-beam solutions (the ADCP has four beams). Profiles with error velocities greater than 0.81 m/s (three times the expected single-ping standard deviation of 0.27 m/s) were discarded prior to averaging. Because ADCPs cannot measure all the way to the bottom nor very near the surface (Gartner and Ganju, 2002), the center of the shallowest measurement bin was about 1 m below the water surface and the deepest measurement bin was at least 6 percent of total water depth above the bottom.

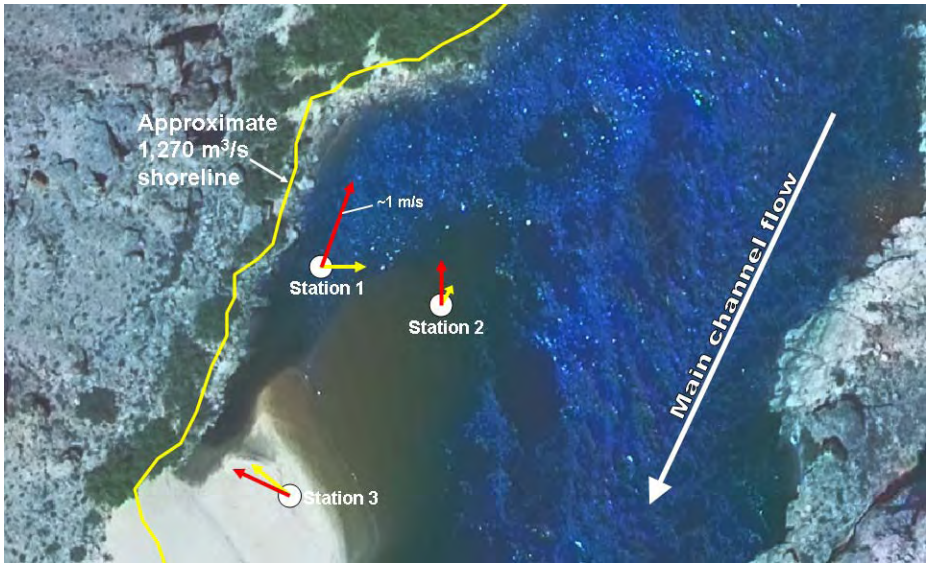


Figure 2 Aerial photograph (May 2002, at 227 m^3/s) showing the measurement locations.

Results of the ADCP measurements are shown in figs. 2 through 5. In fig. 2, arrows indicate approximate near-surface (red) and near-bed (yellow) horizontal velocities. Velocity profiles measured at station 1 (return channel) indicate that flow is primarily parallel to the bank in a direction opposite to main-channel flow. Near-surface horizontal velocity is approximately twice the near-bed velocity and, interestingly, the horizontal velocity rotates clockwise about 70º through the vertical such that near-surface velocity is approximately parallel to the bank while near-bed velocity is nearly perpendicular to the bank, directed toward the main channel (fig. 2). Vertical velocities ranged from about 7 to 15 cm/s directed downward, increasing slightly from surface to bed (fig. 3). Depth was approximately 6 m.

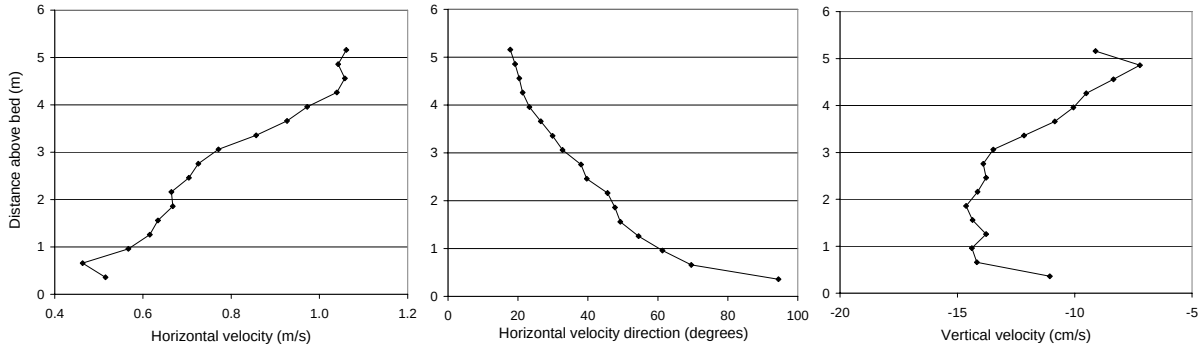


Figure 3 ADCP measured velocity profiles at station 1.

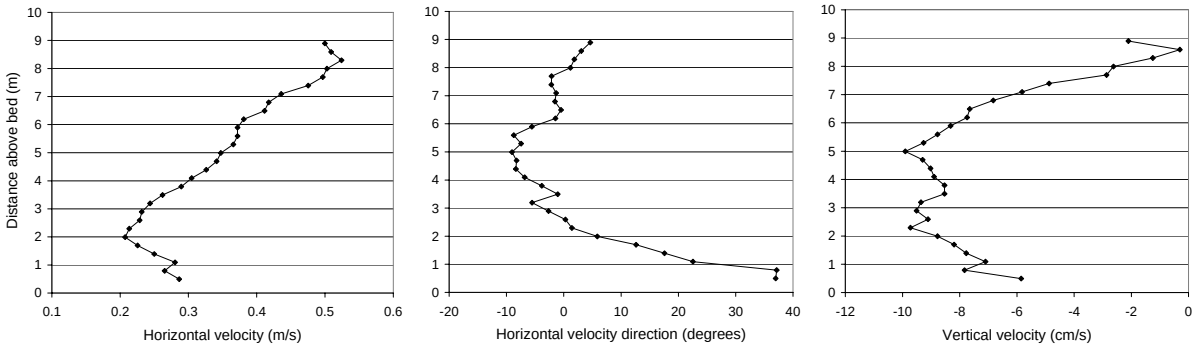


Figure 4 ADCP measured velocity profiles at station 2.

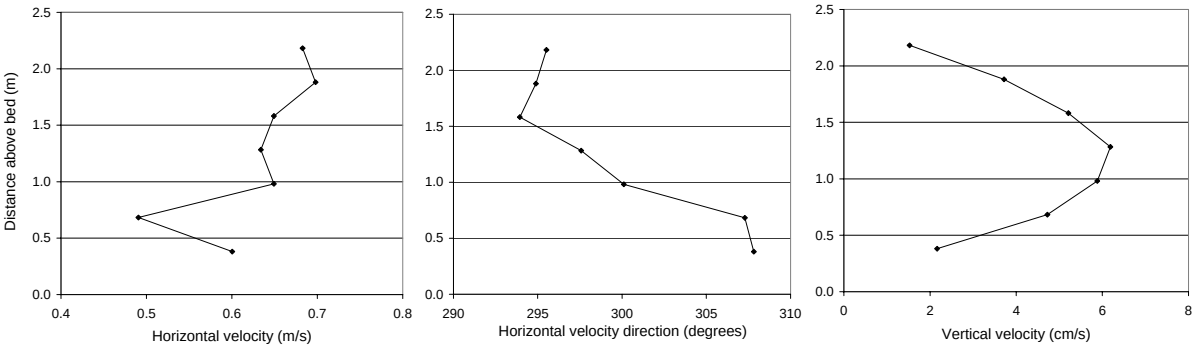


Figure 5 ADCP measured velocity profiles at station 3.

Velocity profiles at station 2 (eddy fence) indicate that it was located inside of the recirculation zone such that horizontal velocity is directed opposite to the main-channel flow. Horizontal velocities were approximately half those at station 1 with a similar decrease from surface to bed. About 30º of clockwise rotation from surface to bed was measured, primarily in the bottom 1-2 m of the profile. Vertical velocities ranged from almost zero near the surface to 6-10 cm/s in the lower half of the profile, oriented downward. Depth was approximately 10 m.

Station 3 (near reattachment point) velocity profiles indicate that horizontal flow was toward the bank, perpendicular to main-channel flow. In contrast to stations 1 and 2, horizontal

velocity was nearly constant in the vertical with little rotation occurring from surface to bed (<15º). Vertical velocities were directed upward (opposite to those at stations 1 and 2) and show a peak of about 6 cm/s at mid-depth. Depth at this location was about 3 m.

Caution must be used in interpreting the vertical velocities. At station 1 the calculated error velocities (not shown) were generally small and random except near bottom where values approached those of the measured vertical velocities. Station 2 error velocities show values in the bottom 3 m of water to be of the same order of magnitude as vertical velocities and, rather than being random, they include a clear positive bias. Error velocities at station 3 were small and without bias with the exception of the bottom bin. Thus, vertical velocities very near the bottom at station 1 and in the bottom 3 m at station 2 may not reflect actual water velocities. Further, some of the measured vertical velocity may be due to sediment particles settling through the measurement volumes. One of the assumptions of ADCP operation is that the water is flowing at the same speed and direction as the materials providing the backscattered signal for Doppler information. It is known that fine sediment accumulated in this eddy during this period. While the two effects (real water motion and settling sediment particles) cannot be reliably separated, it is noted that the calculated settling velocity of suspended sediment typical of this location (~0.1 mm) is only about 1 cm/s, significantly less than most measured vertical velocities.

Results of the depth-integrated suspended-sediment-concentration measurements are shown in fig. 6. For silt and clay, concentrations in the eddy correspond closely with those in the main channel; the maximum difference is only about 10%. Silt and clay concentrations within the eddy also show very little variability. This indicates that these sizes were being transported into and out of the eddy at approximately equal rates such that very little deposition was occurring at the time of the measurements. Sand concentrations exhibit significantly more variability, though is it difficult to know if this is real or measurement error. As with silt and clay, sand concentrations within the eddy are similar to main channel concentrations. Sand concentrations within the eddy do exhibit a structure that could be interpreted as reflecting deposition in the eddy. Concentration (and grain-size) was highest at stations 2 and 3 and drops off significantly at station 1 (>50 percent difference between stations 2 and 1). This suggests that sand was depositing in the eddy center during this time period. Sand at station 1 was also finer than at stations 2 and 3 suggesting that the coarsest material was settling out of suspension. Again, it is difficult to interpret these data in the context of measurement error (not known precisely for this environment), particularly given the degree of scatter in the main-channel sand concentrations evident in figure 6. A more rigorous sampling approach is required to better understand the temporal and spatial variability of the concentration field, possibly utilizing optical or acoustic techniques; however, those approaches may also be limited by inherent measurement errors.

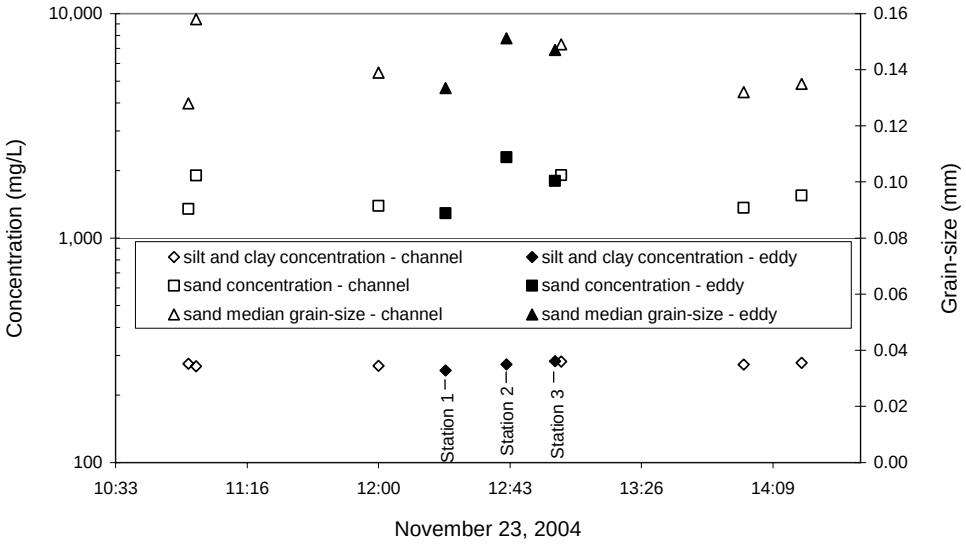


Figure 6 Measured silt/clay and sand concentrations and median sand grain-size in the main channel and at three locations within the recirculating eddy.

CONCLUSIONS

The ADCP can be a useful tool for characterizing the velocity structure of recirculating eddies. Difficulties with velocity measurements were encountered near the eddy fence due to large water depths in combination with high suspended-sediment concentrations and a moving bed. The moving-bed problem can be overcome through use of a differential global positioning system, a technology that is becoming more feasible in remote canyon environments such as Grand Canyon. The combination of large depth and high suspended-sediment concentration resulted from the unusually high flow; measurements during more typical conditions would likely be more successful in the eddy fence, a region critical to understanding sediment-exchange mechanisms. The study succeeded in roughly characterizing the velocity and suspended-sediment structure within the recirculating zone; however, significantly more effort would be required to fully characterize the suspended-sediment field, in particular, and results may still be difficult to interpret due to the combination of small differences in concentrations and inherent measurement errors. Finally, the velocity profiles indicate that 2D flow models may be too constrained under some conditions such that fully 3D flow and sand transport models would yield more accurate results. In particular, the measurements indicate significant rotation of horizontal velocities vertically through the water column (~70º at station 1, ~30º at station 2) as well as significant vertical velocities, also with some vertical structure. Depth-averaged, two-dimensional flow models, such as that developed and applied by Wiele et al. (1996), by definition cannot simulate these flow features. However, it has not yet been determined how important these features are for sediment transport and morphology within recirculating eddies. Further field investigations in combination with more rigorous modeling approaches (e.g. Akahori and Schmeeckle, 2005) are required to improve our understanding of these mechanisms.

REFERENCES

Akahori, R., and Schmeeckle, M.W. (2005). "Numerical analysis of secondary-flow around a spur dike using a three-dimensional free water surface LES," in River, Coastal, and Estuarine Morphodynamics: RCEM 2005, edited by G. Parker and M. Garcia.

Edwards, T.K. and Glysson, G.D. (1999). "Field methods for measurement of fluvial sediment," in Techniques of Water-Resources Investigations of the U.S. Geological Survey, Book 3, Chapter C2, 89 pages.

Gartner, J.W. and Ganju, N.K. (2002). "A preliminary evaluation of near transducer velocities collected with low-blank acoustic Doppler current profiler," Proceedings, ASCE 2002 Hydraulic Measurement and Experimental Methods Conference, Estes Park, CO, July 2002, Published as CD without page numbers.

McDonald, R.R., Nelson, J.M., Andrews, E.D., Campbell, D.H., and Rubin, D.M. (1994). "Field study of the mechanics of flow in lateral separation eddies in the Colorado River," (abstract), Eos Trans. AGU, 75(44), p 268.

McDonald, R.R., and Nelson, J.M. (1996). Field measurements of flow in lateral separation eddies on the Colorado River in Grand Canyon. USGS Director's Approved report submitted to the USGS Grand Canyon Monitoring and Research Center and available at: http://www.gcmrc.gov/library/reports/GCES/Physical/hydrology/McDonald1996.pdf

Nelson, J.M. (1991). "Experimental and theoretical investigation of lateral separation eddies," (abstract), Eos Trans. AGU, 72(44), pp 218-219.

Nelson, J.M., McDonald, R.R., and Rubin, D.M. (1994). "Computational prediction of flow and sediment transport patterns in lateral separation eddies," (abstract), Eos Trans. AGU, 75(44), p 268.

Nelson, J.M., and McDonald, R.R. (1996). Mechanics and modeling of flow and bed evolution in lateral separation eddies. USGS Director's Approved report submitted to the USGS Grand Canyon Monitoring and Research Center and available at: http://www.gcmrc.gov/library/reports/GCES/Physical/hydrology/Nelson1996.pdf

RD Instruments, Inc. (2003). WinRiver users guide – USGS Version. RD Instruments, Inc, San Diego, California, 152 pages.

Rubin, D.M., Schmidt, J.C., and Moore, J.N. (1990). "Origin, structure, and evolution of a reattachment bar, Colorado River, Grand Canyon, Arizona," Journal of Sedimentary Petrology, 60(6), pp 982-991.

Rubin, D.M., and McDonald, R.R. (1995). "Nonperiodic eddy pulsations," Water Resources Research, 31(6), pp 1595-1605.

Rubin, D.M., Topping, D.J., Schmidt, J.C., Hazel, J., Kaplinski, M., and Melis, T.S. (2002). "Recent sediment studies refute Glen Canyon Dam hypothesis" Eos Trans. AGU, 83(25), pp 273, 277-278.

Schmidt, J.C. (1990). "Recirculating flow and sedimentation in the Colorado River in Grand Canyon, Arizona," Journal of Geology, 98, pp 709-724.

Schmidt, J.C. and Graf J.B. (1990). Aggradation and degradation of alluvial sand deposits, 1965 to 1986, Colorado River, Grand Canyon National Park, Arizona. U.S. Geological Survey Professional Paper 1493, 74 pages.

Schmidt, J.C., Rubin, D.M., and Ikeda, H. (1993). "Flume simulation of recirculating flow and sedimentation," Water Resources Research, 29(8), pp 2925-2939.

U.S. Department of the Interior (1996). Record of Decision, Operation of Glen Canyon Dam. Office of the Secretary of Interior, 13 pages, Washington, D.C.

U.S. Department of the Interior (2004). Proposed experimental actions for water years 2005-2006 Colorado River, Arizona, in Glen Canyon National Recreation Area and Grand Canyon National Park. Draft Supplemental Environmental Assessment, Bureau of Reclamation, Upper Colorado Region, Salt Lake City, 26 pages.

Webb, R.H., Schmidt, J.C., Marzolf, G.R., and Valdez, R.A. (1999). The Controlled Flood in Grand Canyon. Geophysical Monograph 110, AGU, Washington, D.C., 367 pages.

Wiele, S.M., Graf, J.B., and Smith, J.D. (1996). "Sand deposition in the Colorado River in the Grand Canyon from flooding of the Little Colorado River," Water Resources Research, 32(12), pp 3579-3596.

Wiele, S.M. (1998). Modeling of flood-deposited sand distributions in a reach of the Colorado River below the Little Colorado River, Grand Canyon, Arizona. U.S. Geological Survey, Water-Resources Investigations Report 97-4168, 15 pages.

Wiele, S.M., Andrews, E.D., and Griffin, E.R. (1999). "The effect of sand concentration on depositional rate, magnitude, and location in the Colorado River below the Little Colorado River," in The Controlled Flood in Grand Canyon, Geophysical Monograph 110, edited by R.H. Webb, J.C. Schmidt, G.R. Marzolf, and R.A. Valdez, pp 131-145.

Wiele, S.M., and Torizzo, M. (2005). "Modelling of sand deposition in archaeologically significant reaches of the Colorado River in Grand Canyon, USA," in Computational Fluid Dynamics: Applications in Environmental Hydraulics, edited by P.D. Bates, S.N. Lane, and R.I. Ferguson, pp 357-394.

Wright, S.A., Melis, T.S., Topping, D.J., and Rubin, D.M. (2005). "Influence of Glen Canyon Dam Operations on Downstream Sand Resources of the Colorado River in Grand Canyon," in The State of the Colorado River Ecosystem in Grand Canyon, edited by S.P. Gloss, J.E. Lovich, and T.S. Melis, U.S. Geological Survey Circular 1282, pp. 17-31.

ALTERED DYNAMICS OF KOOTENAI RIVER WHITE STURGEON SPAWNING HABITAT AND FLOW MODELING

By Gary Barton, USGS, Boise, ID, gbarton@usgs.gov, Richard McDonald, USGS, Golden, CO, *rmcd@usgs.gov*, Jonathan Nelson, USGS, Golden, CO, *jmn@usgs.gov*, Charles Berenbrock, USGS, Boise, ID, *ceberenb@usgs.gov*, Mary Donato, USGS, Boise, ID, mdonato@usgs.gov, Pete VanMetre, USGS, Austin, TX, *pcvanmet@usgs.gov*, and Barbara Mahler, USGS, Austin, TX, *bjmahler@usgs.gov*

ABSTRACT

In 1994, the Kootenai River white sturgeon (*Acipenser transmontanus*) was listed as an Endangered Species. In response to the listing, the Kootenai River White Sturgeon Recovery Team was established to find and implement ways to improve spawning and rearing habitat used by white sturgeon. The team identified the need to develop and apply a multidimensional flow model to certain reaches of the river to quantify physical habitat in a spatially-distributed manner. The U.S. Geological Survey has addressed these needs by using the agency's MultiDimensional Surface-Water Modeling System (MD_SWMS) to construct a flow model for the critical-habitat reach of the Kootenai River white sturgeon near Bonners Ferry, Idaho. This paper describes the altered white sturgeon habitat and the model, presents the results of a few simple simulations, and demonstrates how the model can be used to link physical characteristics of streamflow to biological or other habitat data. This study was conducted in cooperation with the Kootenai Tribe of Idaho, the Idaho Department of Fish and Game, and the Bonneville Power Authority.

INTRODUCTION

Many local, State, and Federal agencies are concerned about the declining population of the endangered white sturgeon (*Acipenser transmontanus*) in the Kootenai River in Idaho (fig. 1). Biologists have observed an overall decline in recruitment of juvenile sturgeon beginning in the 1950s with an almost total absence of recruitment after 1974. Consistent annual recruitment of large year-classes has not been observed since before 1960 (Paragamian and others, 2005). Lack of Kootenai River white sturgeon recruitment has been attributed, at least in part, to changes in the natural streamflow regime, sediment transport, and water clarity of the Kootenai River after emplacement of Libby Dam, near Libby, Montana, in 1972 (U.S. Fish and Wildlife Service, 1999). Other changes could have affected sturgeon recruitment include the construction of dikes on natural levees, changes in the level of Kootenay Lake and in backwater conditions near Bonners Ferry, loss of wetlands in the river valley, and reduction of the river's nutrient load (Duke and others, 1999), and over fishing. The Kootenai River White Sturgeon Recovery Team was established to find and implement ways to improve spawning and rearing habitat used by white sturgeon. The team identified the need to develop and apply a multidimensional flow model to certain reaches of the river to quantify physical habitat in a spatially distributed manner. The U.S. Geological Survey (USGS) has addressed these needs by using a multidimensional flow model to simulate streamflow and sediment mobility in the critical habitat.

Kootenai River is 721 kilometers (km) long. Beginning in British Columbia, Canada, the river flows through Montana and Idaho, and then turns northwest back into British Columbia (fig. 1). The model reach lies within the designated critical habitat for white sturgeon nears Bonners Ferry, Idaho (fig 1; U.S. Fish and Wildlife Service, 1999). Since 1994, spawning has occurred in the model reach between river kilometers (RKM) 228.7 and 245.7 (Paragamian and others, 2002). River width in the model reach ranges from about 65 to 255 m and near the downstream boundary, Shorty Island divides the flow into main and secondary channels.

The model reach is subdivided into two reaches based on the primary sediment forming the river substrate: (1) a straight reach (Tetra Tech, Inc., 2003) between the upstream model boundary at RKM 245.9 and the upstream end of Ambush Rock at RKM 244.6 with a sand, gravel, and cobble substrate, and (2) a meandering reach between the upstream end of Ambush Rock and the downstream model boundary at RKM 228.4 consisting primarily of a sand substrate and dunes with minor amounts of lacustrine clay and silt. Seismic subbottom profiles and vibracores (fig. 2) of the river substrate show that isolated areas in the meander reach could be suitable for egg incubation where gravel, cobble, and riprap is present, but is partly buried by thin layers of sand, such as in the meander bend below the mouth of Myrtle Creek between RKM 234.20 and 234.60 (Barton, 2004; McDonald, and others, in press). Habitat suitability curves for white sturgeon in the Lower Columbia River (Parsley and Beckman, 1994), suggest that the particle size of substrate in the braided reach and the straight reach has poor to moderate suitability for egg incubation and in the meander reach has poor suitability (fig. 3) with moderate suitability in a few small areas such as RKM 233.9 to 234.6 near Myrtle Creek.

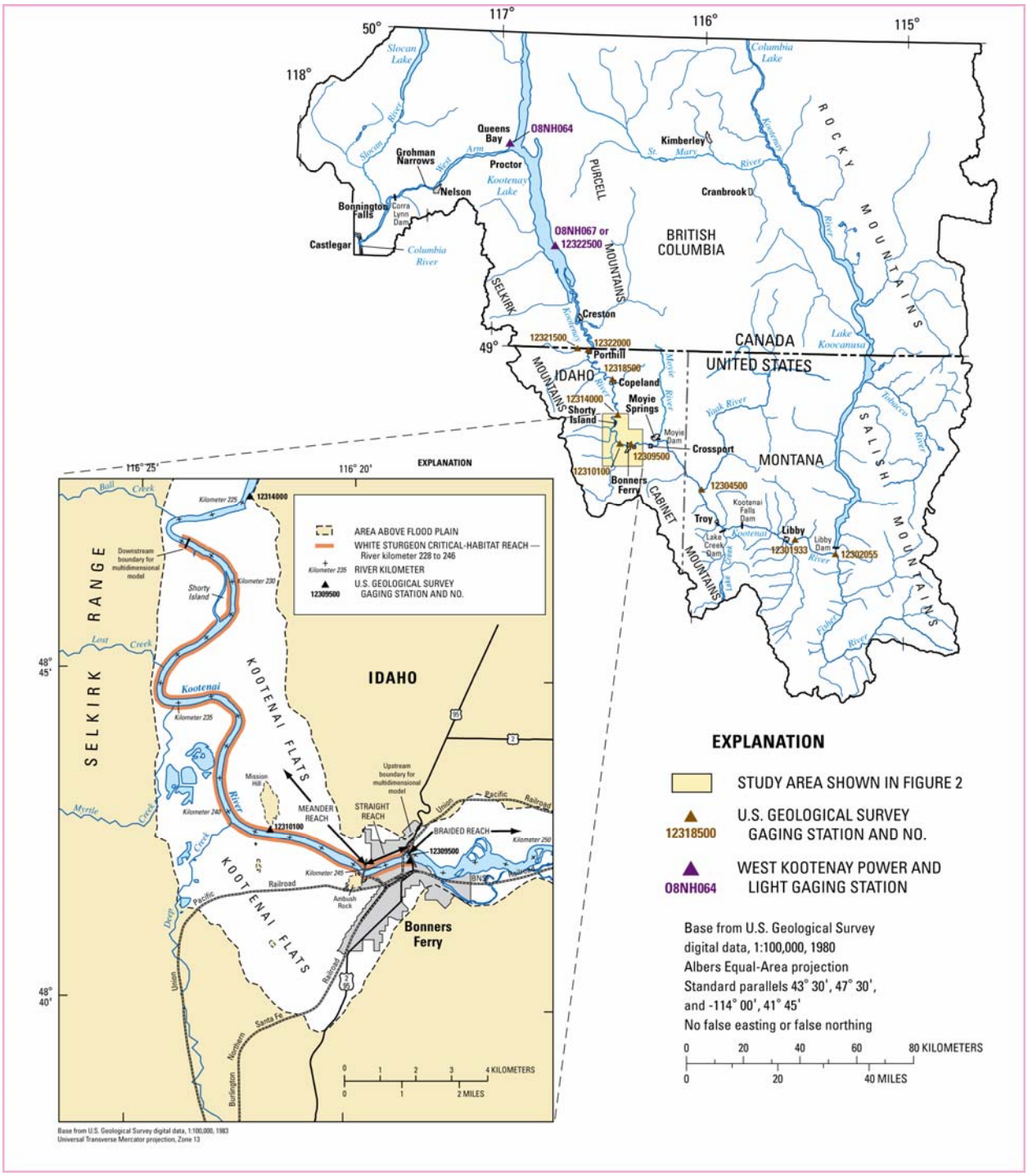


Figure 1. Map showing the location of the study area, near Bonners Ferry, Idaho, and selected streamflow-gaging stations and dams in the Kootenai River drainage basin, Idaho, Montana, and British Columbia, Canada. (modified from Barton and others, 2005)



Figure 2. U.S. Geological Survey personnel collecting a 3.7-meter-long vibracore sample of riverbed sediments in the Kootenai River, Idaho. (from Barton, 2004)

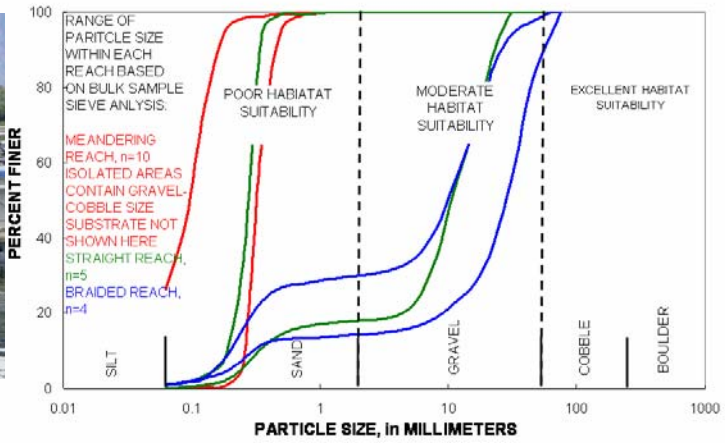


Figure 3. Range of riverbed particle size in the meandering, straight, and braided reaches near Bonners Ferry, Idaho. (modified from Berenbrock and Bennett, 2005, and from Barton and others, 2005)

ALTERED DYNAMICS IN THE WHITE STURGEON CRITICAL HABITAT REACH

The altered dynamics of streamflow are described for 1966-83 when suspended-sediment concentrations were measured daily at the Copeland gaging station (12318500, located 31 km downstream of spawning reach) and described for 1994 -2005. Copeland is the most complete and consistent data available for describing sediment transport before the dam and during the dam era. Prior to the emplacement of Libby Dam, the flow regime of the Kootenai River during the period of suspended sediment record at the Copeland gaging station (12318500), 1966-71, was characterized by peak streamflows resulting from spring snowmelt from late April through mid-July. Median annual peak streamflow was about 2,240 m^3/s. A slow recession of streamflow generally started in mid-June and stabilized in September. The annual median base streamflow during October through February was 88.0 m^3/s. The average cross-sectional velocity for 62 measurements from the cableway at the Copeland gaging station ranged from 0.06 to 1.21 m/s.

After the dam was constructed in 1972, the flow regime of the Kootenai River during the period of suspended-sediment record at the Copeland gaging station, 1973-83, was characterized by median annual peak streamflows of about 600 m^3/s, less than one-third of the pre-Libby Dam value. Long periods of sustained higher flows occurred during the autumn and winter, reflecting the greater demand for hydroelectric power generation and water storage in Lake Koocanusa. Average cross-sectional velocity during 83 measurements from the cableway at the Copeland gaging station ranged from 0.11 to 0.80 m/s. Since the mid-1990s, the U.S. Fish and Wildlife Service has requested that Kootenai River flows be increased during white sturgeon spawning in May and June to help re-establish recruitment. Kootenai River flows are augmented with additional releases of water from Libby Dam. However, instantaneous flow during spawning season is less than one-half that of the pre-Libby Dam era (Barton, 2004).

Kootenay Lake levels and Kootenai River backwater conditions have changed over time due to the operation of Corra Linn Dam and Libby Dam, and these conditions possibly influence white sturgeon spawning patterns (Duke and others, 1999). During the spawning season prior to the emplacement of Libby Dam, higher peak plows resulted in backwater extending further upstream into the braided reach where the substrate is more suitable for sturgeon egg incubation. Kootenay Lake creates backwater conditions in Kootenai River to a variable point upstream of the mouth of Deep Creek (RKM 240.2) near Bonners Ferry. During May, June, and early July, when lake water-surface elevation and river discharge are high, backwater conditions can extend several kilometers upstream of Bonners Ferry. During periods of low streamflow, backwater conditions diminish and free-flowing water may extend a few kilometers downstream of the bridge (Berenbrock, 2005). Corra Linn Dam was completed in 1931, and it affects water levels in Kootenay Lake and, consequently, in the backwater-affected reach of the Kootenai River (Duke and others, 1999). After the river channel at Grohman Narrows upstream of Corra Linn Dam was deepened in 1939, the lake level remained stable at an intermediate elevation for longer periods of the calendar year, probably in response

to the operation of Corra Lynn Dam. Seasonal fluctuations still occurred, but over a shorter period of time. From 1940 to 1972 (prior to the construction of Libby Dam), monthly median lake elevations ranged from 529.6 to 536.4 m, from 1973 to 1998 (after the dam was in place), elevations ranged from 529.9 to 534.2 m (Barton, 2004). The lower lake levels during the Libby Dam era indicate that backwater did not extend as far upstream as during the pre-Libby Dam era.

During snowmelt runoff in the pre-Libby Dam era, sediment data collected at the USGS gaging station at Copeland (12318500) indicate that large amounts of suspended sediment were transported through the white sturgeon critical-habitat reach. The annual suspended-sediment load leaving the Kootenai River critical-habitat reach decreased dramatically after the closure of Libby Dam in 1972. During the pre-Libby Dam era, annual average load at the Copeland gaging station from 1966 to 1971 was 1,740,000 metric tons (mt), and annual median daily load ranged from 14 to 48,700 metric tons per day (mt/d). Most of the sediment load was transported during May and June when streamflow and suspended-sediment concentrations were highest. In contrast, after dam closure the annual average load from 1973 to 1983 was 190,000 mt and the annual median daily load ranged from 53 to 1,560 mt/d.

Suspended-sediment transport during the Libby Dam era has been about 11 percent of the pre-Libby Dam era amount. This reduction was caused by the influence of Libby Dam on the flow regime and on the reduction of sediment in the river below the dam due to its sediment trapping characteristics. In addition to the effects of changes in streamflow, less sediment was available for transport because 70 percent of the basin is upstream of Libby Dam (Barton, 2004).

Prior to the closure of Libby Dam, when sediment transport was greater, minor amounts of gravel and cobble may have been exposed on the riverbed in the spawning reach just below the mouth of Myrtle Creek in the critical-habitat reach (Barton, 2004). The large reduction in suspended–sediment concentration after the closure of Libby Dam (Barton, 2004, fig. 14) has caused an increase in water clarity during May and June. Residents in Idaho and Montana have reported the river becoming much less turbid in the months of May-July (present day white sturgeon spawning season) after the closure of Libby Dam (Bob Hallock, U.S. Fish and Wildlife Service, oral commun. 2005). Additional information about the hydraulics and sediment transport can be found in Berenbrock (2005) and Berenbrock and Bennett (2005). Gadomski and Parsley (2005) reported that significantly more embryos may be preyed upon at lower turbidity.

METHODS

The USGS MultiDimensional Surface-Water Modeling System, MD_SWMS, was used to construct a flow model for the critical-habitat reach of the Kootenai River. The computational grid was 17,525 m in length with 3,505 nodes in the downstream direction and 800 m in width with 161 nodes in the cross-stream direction, forming an approximately 5.0-by-5.0-m grid. MD_SWMS was used to simulate water-surface elevation, velocity (stream-wise and cross-stream velocity components), boundary (bed) shear stress, and in conjunction with subsidiary methods, the incipient motion of sediment on the riverbed. MD_SWMS is a graphical user interface (GUI) developed by the USGS (McDonald and others, 2001) for hydrodynamic models. FaSTMECH is one computational model within MD_SWMS; it was developed at the USGS (Nelson and McDonald, 1997; Thompson and others, 1998; Nelson and others, 2003). FaSTMECH includes a 2-dimensional, vertically-averaged model and a sub-model that calculates vertical distribution of the primary velocity and the secondary flow about the vertically-averaged flow. Calibration, sensitivity analysis, and validation of the model are discussed in detail in Barton and others (2005).

The model's ability to simulate the velocity flow field, bed shear stress, and sediment mobility is constrained largely by (1) the accuracy and level of channel geometry detail, especially regarding errors that could arise because topography was measured during varying streamflows and different streamflows were used in the model, and because the accuracy of the current topography available for Shorty Island is not known (Barton and others, 2004), (2) the way the relation between streamflow and bedforms was characterized, and (3) the potential errors incurred by applying a steady-state model to unsteady flow situations. Although strong evidence indicates that pre-dam era and dam era channel geometry generally are similar, the accuracy of streamflow simulations for pre-dam peak flows is expected to be less than streamflow simulations for dam era peak flows (Barton and others, 2005).

RESULTS

The model was used to simulate water-surface elevation, depth, velocity, bed shear stress, and sediment mobility in the Kootenai River for streamflows of 170, 566, 1,130, 1,700, and 2,270 m^3/s. The range of simulated streamflows was selected to span river conditions typical of those before and since the construction of Libby Dam. The three lowest streamflows represent a range of conditions that have occurred throughout the historical record. The highest streamflow represents a discharge that is approximately equal to the annual median peak streamflow (2,237 m^3/s) prior to emplacement of Libby Dam in 1972. A few simple simulations are presented here to demonstrate how the model can be used to link physical characteristics of streamflow to biological or other habitat data. Some measures of depth, velocity, and substrate composition generally are considered when assessing sturgeon spawning habitat (Parsley and others, 1993). Discussions of the model simulation include relating the model results to observed patterns of spawning and egg locations, specifically the number of spawning events per unit of effort (SEPUE) during 1994-2001.

Depth

Spawning depth habitat suitability in the model is evaluated with the model using the research of Parsley and Beckman (1994): the straight reach ranges from poor to excellent, and the meandering reach is generally excellent (fig. 4). Parsley and Beckman (1994) showed that depths for spawning white sturgeon in the Lower Columbia River ranged from 3.5 to 25 m; and they rated habitat suitability as poor for depths less than 2 m, moderate for depths of 2 to 4 m. Model simulated median and maximum river depth for all wet nodes for the lowest and highest streamflow simulations, 170 and 2,270 m^3/s, ranged from 4.5 to 10.4 m and from 20.0 to 27.8 m, respectively. The model also simulated average and maximum water depth for the five streamflows at cross sections every 100 m along the modeled reach (fig. 4). Included in this figure is spawning depth habitat suitability from Parsley and Beckman (1994). The river depth is shallowest in the upper kilometer of the straight reach and here spawning habitat suitability is poor at the lowest streamflow. In this area, the average depth for the lowest and highest streamflow simulations is 2.5 and 8.7 m, and the maximum depth is 4.3 and 12.0 m. Below Ambush Rock, in the meandering reach, the average depth is 6.8 and 14.6 m, and the maximum river depth is 15.6 and 23.1 m (Barton and others, 2005).

Velocity

Higher velocities are associated with more suitable substrate for white sturgeon egg incubation, greater egg dispersal, and reduction of egg predation. A general description of the river velocity structure can be developed by examining variation of the median and maximum values of simulated velocity for all model nodes. Median and maximum velocity ranged from 0.25 and 1.07 m/s for the lowest streamflow to 1.0 and 1.8 m/s for the highest streamflow. The model reach can be divided into three velocity zones on the basis of simulated maximum velocity for cross-sections located every 100 m along the length of the model reach (fig. 5). Zone A, between the upstream model boundary and Ambush Rock, is a region of high velocity. Maximum velocities in zone A generally are higher than those in the rest of the model reach, but the differences decrease with increasing streamflow. Zone B, between Ambush Rock and the first sharp meander below the mouth of Deep Creek at RKM 237.5, has uniform maximum streamflow velocities compared to the rest of the model reach. One notable exception is near the deep hole and lateral recirculation eddy above Deep Creek. Zone C, downstream of zone B and extending to the downstream model boundary at RKM 228.4, shows variations in the maximum velocity that increase with increasing streamflow. The spatial variation in velocity across the river channel has been quantified using the standard deviation of velocity at cross sections positioned every 100 m along the length of the model reach. The greatest variability in velocity shown by the standard deviation is a reflection of both the complex channel geometry through the S-shaped meander and the flow divergence around Shorty Island. The greatest occurrence of white sturgeon spawning is in zone C.

Spawning habitat suitability for streamflow velocity in the model is evaluated here using the research of Parsley and Beckman (1994): in the meander reach the average velocity at streamflow of 1,700 m^3/s and less is classified as poor and in the straight reach only a streamflow of 170 m^s/s is classified as poor (fig. 5). Figure 5 shows the relation between simulated velocity results and sturgeon spawning habitat. McDonald and others (2004) showed a correlation between the model's maximum cross-sectional velocity and white sturgeon spawning location. In other studies, lake sturgeon were found to spawn in tributary rapids (Auer, 1996; LaHaye and others, 1992). Streamflow velocities equal to or greater than 1.0 m/s are believed to greatly reduce or eliminate predation of white sturgeon

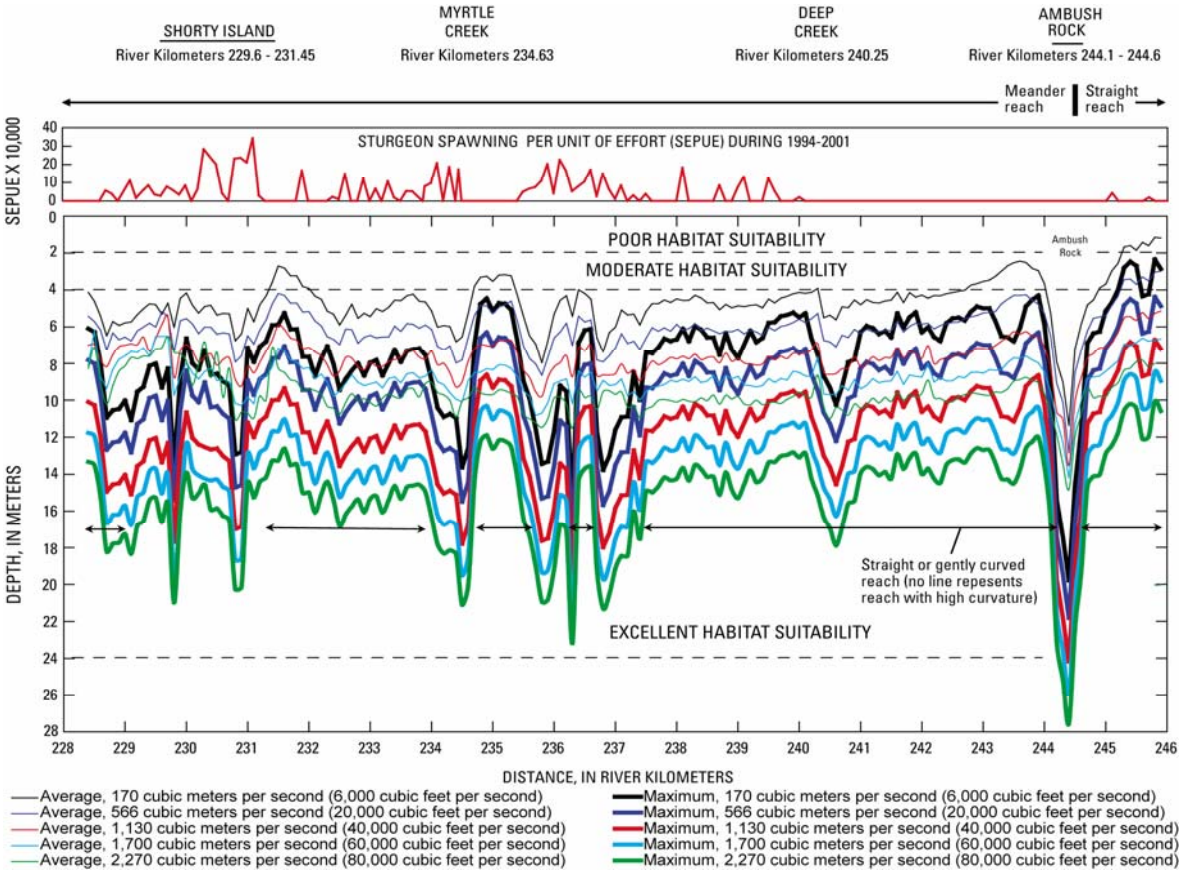


Figure 4. Simulated average and maximum depth for five streamflows at cross sections positioned every 100 meters along the white sturgeon critical-habitat reach of the Kootenai River near Bonners Ferry, Idaho, and spawning event locations. (modified from Barton and others, 2005; spawning habitat suitability from Parley and Beckman, 1994)

eggs (Bob Hallock, U.S. Fish and Wildlife Service, oral commun., 2005). The simulated average velocity in the main channel at Shorty Island, where white sturgeon most frequently spawn (Paragamian and others, 2002), does not approach 1.0 m/s until streamflow is 2,270 m^3/s, and this only occurs for portions of the reach between RKM 230.3 and 231.1 (fig. 5). However, the maximum simulated velocity in this reach (fig. 5) is greater than 1.0 m/s for flows equal to and greater than a streamflow of 1,130 m^3/s (Barton and others, 2005).

DISCUSSION

Many biologists believe that some or many of the altered dynamics in the Kootenai River have contributed to the lack of sustainable white sturgeon recruitment. Habitat suitability curves developed for white sturgeon in the Lower Columbia River (Parsley and Beckman, 1994) were used to characterize conditions in the Kootenai River spawning habitat. Requirements for Kootenai River white sturgeon spawning habitat may vary from that in the Lower Columbia; however, both rivers are highly regulated systems. Substrate suitability for egg incubation is poor to moderate in both the braided and straight reach and generally poor in the meander reach with moderate suitability in a few small areas such as RKM 233.9 to 234.6 near Myrtle Creek. Model simulations showed that depth suitability ranges from poor to excellent in the straight reach and is generally excellent in the meandering reach, and that average-velocity suitability is generally moderate in the straight reach and poor in the meander reach. Overall habitat suitability is better in the straight reach rather than the meander reach due to coarser substrate and higher velocities.

White sturgeon seldom spawn in the straight reach and avoid the adjacent braided reach; avoidance may be related to light attenuation--function of depth and clarity. Both reaches are significantly shallower and have more suitable substrate for egg incubation than the meandering reach. Perhaps during the pre-Libby Dam era when the river was

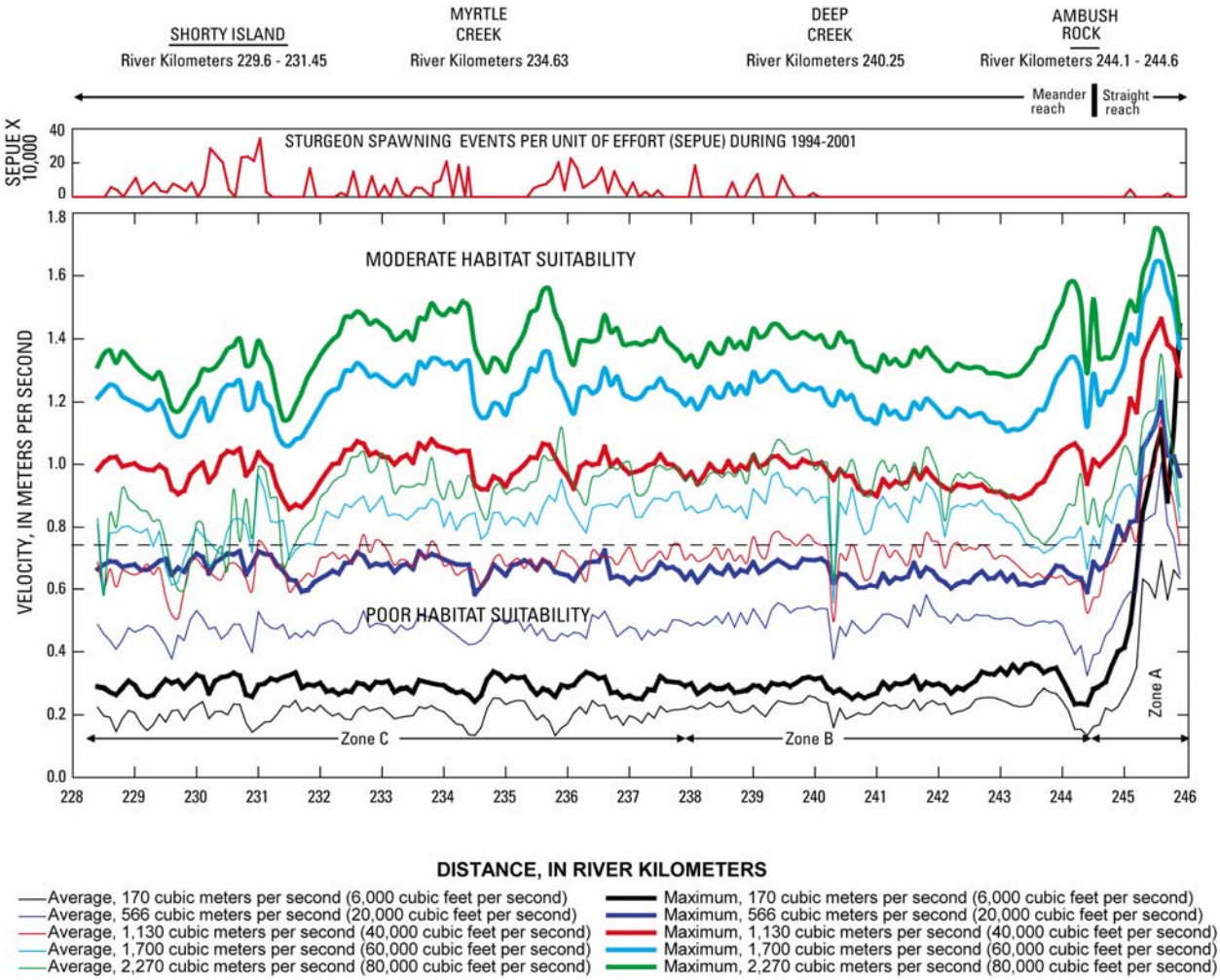


Figure 5. Simulated average and maximum velocity for five streamflows at cross sections positioned every 100 meters along the white sturgeon critical-habitat reach of the Kootenai River near Bonners Ferry, Idaho, and spawning event locations. (modified from Barton, 2005; spawning habitat suitability from Parley and Beckman, 1994)

more turbid and deeper the sturgeon spawned frequently in the shallow straight and braided reaches. Large reduction in suspended–sediment concentration after the closure of Libby Dam caused an increase in water clarity during the spawning season. (Perrin and others (2003) pointed out that water clarity as a factor affecting white sturgeon spawning patterns has not been examined on the Kootenai River. If white sturgeon are generally photophobic because of evolutionary history, light attenuation may be an important factor affecting spawning location and depth. Suspended-sediment concentration is one of the controlling factors on the amount of ultraviolet radiation penetrating the water column and Zagarese and Williamson (2001) have shown that the range of potential effects include DNA damage resulting in egg and larval mortality. The photophobic and ultraviolet radiation issues might explain why the white sturgeon avoid spawning in the shallow braided reach and seldom spawn in the straight reach.

ACKNOWLEDGEMENTS

The authors thank Sue Ireland of the Kootenai Tribe of Idaho for providing storage facilities for USGS equipment. Vaughn Paragamian, Diane Wakkinnen, and Peter Rust of the Idaho Department of Fish and Game provided white sturgeon spawning location and egg location data. Rick Backsen, John Gralow, and Russ Christensen of the USGS in Post Falls, Idaho, and Edward Moran of the USGS in Anchorage, Alaska, worked long hours collecting data for this project. Sandra Ball of the USGS in Post Falls, Idaho, helped with many logistical issues.

REFERENCES

Auer, N.A, 1996, Response of spawning lake sturgeon to changes in hydroelectric facility operations: Trans. Am., Fish. Soc. 125, p. 66 – 77.

Barton, G.J., 2004, Characterization of channel substrate, and changes in suspended sediment transport and channel geometry in white sturgeon spawning habitat in the Kootenai River near Bonners Ferry, Idaho, following the closure of Libby Dam: U.S. Geological Survey Water-Resources Investigations Report 03-4324, 102 p.

Barton, G.J., McDonald, R.R., Nelson, J.M., and Dinehart, R.L., 2005, Simulation of flow and sediment mobility using a multidimensional flow model for the white sturgeon critical-habitat reach, Kootenai River near Bonners Ferry, Idaho: U.S. Geological Survey Scientific Investigations Report 2005-5230, 75 p.

Barton, G.J., Moran, E.H, and Berenbrock, C., 2004, Surveying cross sections of the Kootenai River between Libby Dam, Montana, and Kootenay Lake, British Columbia, Canada: U.S. Geological Survey Open-File Report 2004–1045, 34 p.

Berenbrock, Charles, 2005, 1D Simulations of hydraulic characteristics in the white sturgeon spawning habitat of the Kootenai River near Bonners Ferry, Idaho: U.S. Geological Survey Scientific Investigations Report 2005-5110, 30p.

Berenbrock, Charles, and Bennett, J.P., 2005, Simulation of flow and sediment transport in the white sturgeon spawning habitat of the Kootenai River near Bonners Ferry, Idaho: U.S. Geological Survey Scientific Investigations Report 2005-5173, 43 p.

Duke, S., Anders, P., Ennis, G., Hallock, R., Hammond, J., Ireland, S., Laufle, J., Lauzier, R., Lockhard, L., Marotz, G., Paragamian, V., and Westerfhol, R., 1999, Recovery plan for Kootenai River white sturgeon (*Acipenser transmontanus*): J. of Applied Ichthyology, v. 15, p. 157-163.

LaHaye and others, 1992, Reproduction , early life history, and characteristics of the spawning grounds of lake sturgeon (*Acipenser transmontanus*) in Des Prairies and L'Assomption rivers, near Montreal, Quebec, Can. J. Zool. 70, p. 1681–1689.

McDonald, R.R., Barton, G.J., Nelson, J.M., and Paragamian, V., in press, Modeling hydraulic and sediment transport processes in white sturgeon spawning habitat on the Kootenai River: proceeding in the Joint 8th Federal Interagency Sedimentation and 3rd Federal Interagency hydrologic modeling conference, 8 p.

McDonald, R.R., Bennett, J.P., and Nelson, J.M., 2001, The USGS multi-dimensional surface water modeling system, in Proceedings, 7th U. S. Interagency Sedimentation Conference, Reno, Nev., p. I-161-I-167.

McDonald, R.R., Nelson, J.M., Barton, G., and Paragamian, V., 2004, Flow and sediment-transport modeling of Kootenai River White Sturgeon spawning habitat: Eos Trans., American Geophysical Union, v. 85, no. 47, Abstract H53B-1239.

Nelson, J.M., Bennett, J.P., and Wiele, S.M., 2003, Flow and sediment-transport modeling, *in* Kondolf, G.M., and Piegay, H., eds., Tools in fluvial geomorphology: England, Wiley, p.539-576.

Nelson, J.M., and McDonald, R.R., 1997, Mechanics and modeling of flow and bed evolution in lateral separation eddies: Bureau of Reclamation, Glen Canyon Environmental Studies Report, 69 p.

Parsley, M.J., and Beckman, L.G., 1994, White sturgeon spawning and rearing habitat in the lower Columbia River: North American J. of Fish Management, v. 14, p. 812-827.

Parsley, M.J., Beckman, L.G., and McCabe Jr., G.T., 1993, Spawning and rearing habitat used by white sturgeon in the Columbia River downstream of McNary Dam: Trans. of the American Fisheries Soc., v. 122, 10 p.

Paragamian, V.L., Wakkinnen, V.D., and Crews, G., 2002, Spawning locations and movement of Kootenai River white sturgeon: J. of Applied Ichthyology, v. 18, 9 p.

Paragamian, V.L., Beamesderfer, R.C., and Ireland, S.C., 2005, Status, population dynamics, and future prospects of the endangered Kootenai River white sturgeon population with and without hatchery intervention: spawning locations and movement of Kootenai River white sturgeon: Trans. of the American Fisheries Soc., v. 134, 14 p.

Perrin, C.J., Rempel, L.L., and Rosenau, M.L., 2003, White sturgeon spawning habitat in an unregulated river: Fraser River, Canada: Trans. of the American Fisheries Soc., v. 132, p. 154-165.

Tetra Tech, Inc., 2003, Kootenai River geomorphic assessment: Seattle, Washington, 114 p.

Thompson, D.M., Nelson, J.M., and Wohl, E.E., 1998, Interactions between pool geometry and hydraulics, Water Resources Research, v. 34(12), p. 3673-3681.

U.S. Fish and Wildlife Service, 1999, Recovery plan for the Kootenai River population of the white sturgeon (*Acipenser transmontanus*): Portland, Oregon, variously paginated.

Zagarese H.E., and Williamson, C.E., 2001, The implications of solar UV radiation exposure for fish and fisheries: Fish and Fisheries v. 2, no. 3, p. 250-260.

MODELING HYDRAULIC AND SEDIMENT TRANSPORT PROCESSES IN WHITE STURGEON SPAWNING HABITAT ON THE KOOTENAI RIVER, IDAHO

Richard McDonald, Hydrologist, USGS, Golden, CO rmcd@usgs.gov; Gary Barton, Hydrologist, USGS, Boise, ID gbarton@usgs.gov; Jonathan Nelson, Hydrologist, USGS, Golden, CO jmn@usgs.gov; Vaughn Paragamian, Fisheries Biologist, Idaho Department of Fish and Game, Coeur d'Alene, ID vparagam@idfg.state.id.us

Abstract: The Kootenai River white sturgeon currently spawn (2005) in an 18-kilometer reach of the Kootenai River, Idaho. Since completion of Libby Dam upstream from the spawning reach, there has been only one successful year of recruitment of juvenile fish. Where successful in other rivers, white sturgeon spawn over clean coarse material of gravel size or larger. The channel substrate in the current spawning reach is composed primarily of sand and some buried gravel; within a few kilometers upstream there is clean gravel. We used a 2-dimensional flow and sediment-transport model and the measured locations of sturgeon spawning from 1994-2002 to gain insight into the paradox between the current spawning location and the absence of suitable substrate. Spatial correlations between spawning locations and the model simulations of velocity and depth indicate the white sturgeon tend to select regions of highest velocity and depth within any river cross-section to spawn. These regions of high velocity and depth are independent of pre- or post-dam flow conditions. A simple sediment-transport simulation suggests that high discharge and relatively long duration flow associated with pre-dam flow events might be sufficient to scour the sandy substrate and expose existing lenses of gravel and cobble as lag deposits in the current spawning reach.

INTRODUCTION

The Kootenai River white sturgeon is both physically isolated and genetically distinct from other white sturgeon populations in the Columbia River. Following the completion of Libby Dam, Montana, in 1972, the only year of significant recruitment in the population occurred in 1974, one year prior to full power plant operation in 1975. In ensuing years, a small number of juvenile fish have been found but their abundance is not enough to sustain the population. In 1994 the Kootenai River white sturgeon were listed as endangered and further protection was obtained in 2001 through the designation of 18 river kilometers (rkm) of Critical Habitat downstream from Bonners Ferry, Idaho (rkm 228-246). Monitoring of both the physical location of adult white sturgeon through telemetry studies and the spawning locations by the collection of eggs has shown this reach to be the main region of spawning (Paragamian and others, 2001).

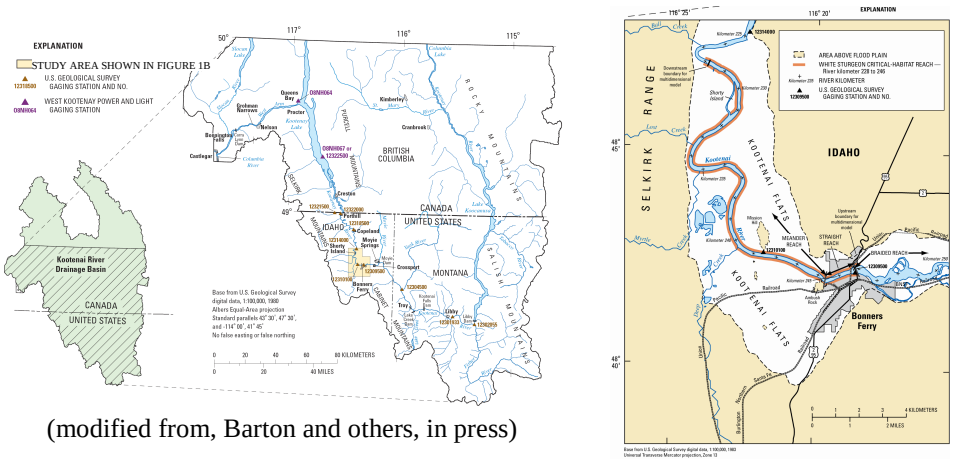
White sturgeon spawn by broadcasting their eggs which become adhesive shortly after exposure to water. Where successful spawning occurs in other river systems, these eggs attach to coarse substrate composed of gravel and larger-sized sediment. While the sturgeon are documented to successfully spawn in the Critical Habitat reach, the exposed river substrate under most flow conditions is dominantly composed of fine sand with large migrating dunes. Spawned eggs are presumed to settle onto the bed, become covered in the fine sand, or buried in the trough of migrating dunes resulting in suffocation. Interestingly, within a few kilometers upstream from the current (2005) spawning locations, the river is braided, relatively shallow, and has suitable substrate composed mostly of gravel and cobble.

Successful spawning and recruitment of Kootenai River white sturgeon is a complicated biologic process with the hydraulic and sediment-transport characteristics playing a contributing role to the success of hatching after deposition. Several hypotheses relating to the hydraulic and sediment transport characteristics of the Kootenai River have been put forth as possible explanations to the decline of successful recruitment (Duke and others, 1999) in this system. First, in the post-dam period, the loss of naturally occurring high spring flow in addition to lower Kootenay Lake stages may have shifted the hydraulic cues the fish use to initiate spawning further downstream into the current spawning reach. In other words, prior to Libby dam, higher lake levels or greater backwater extent and river stage encouraged the fish to spawn further upstream in the braided reach. Second, the higher pre-dam discharge may have mobilized and scoured the bed sufficiently in the existing spawning reach to expose coarse-grained substrate suitable for egg hatching. In this paper we use the results from a preliminary set of 2D computational simulations of flow within the 18-kilometer Critical Habitat reach to gain insight into the hydraulic cues the fish might use for spawning and the affect of flow management (Kootenay Lake Stage and Libby Dam discharge) on those cues. In addition we also use some very simple sediment transport simulations to gain insight into the role of pre- and post-dam flows in regulating the nature of the sediment substrate in the existing spawning reach.

BACKGROUND

Physical Setting: The Kootenai River originates in Kootenay National Park, British Columbia, Canada, and flows south into Montana and Lake Kookanuska formed by Libby Dam (Figure 1a). The river then flows east into northern Idaho and back north into British Columbia and Lake Kootenay. Bonnington Falls is between the confluence with the Columbia River and Lake Kootenay and provides natural barrier to fish migration that has isolated the Kootenai River white sturgeon from the rest of the Columbia River basin since the last glacial period approximately 10,000 years ago (Duke and others, 1999).

Geomorphology: The reach of interest to this study can be separated into three different geomorphic reaches including: a 16-rkm low-gradient, sandy, deep, and gently meandering reach downstream from Bonners Ferry, Idaho (rkm 244-228); a 10-rkm, high-gradient, gravel-cobble, shallow and braided reach upstream from Bonners Ferry (rkm 258-246); and a 2-rkm straight transition reach of high gradient and mixed sand and gravel substrate (rkm 246-244) (Figure 1b).



(modified from, Barton and others, in press)

A

B

Figure 1. (A) General location of study area and (B) detail location of study reach and Critical Habitat reach.

The river gradient changes dramatically in the transition reach from about 0.0006 in the braided reach to 0.00002 in the meandering reach. In addition, Kootenay lake levels vary from approximately 532-539 meters above the North American Vertical Datum of 1988 (NAVD88), in the pre-dam era to 532-535 meters in the post-dam era. These lake levels intersect the Kootenai River longitudinal profile between the upstream end of the meandering reach and into the braided reach. Consequently, the meandering reach is entirely in backwater. The backwater transition zone (Berenbrock and Bennett, 2005a) identifies the region of transition between free-flowing and backwater flow conditions over the range of potential discharge and Kootenay Lake stage conditions (Figure 2). Both the local gradient of the river and the backwater conditions lead to sharp change in hydraulic characteristics between the meandering and braided reach. Based on 1D model simulations, cross-sectional average velocities range from 0.25 – 1.0 and 0.75 – 2.0 meters per second and average depths range from 5 – 10 and 2 – 5 meters in the meandering and braided reaches respectively over a range of flows from 170 – 2125 cubic meters per second (Berenbrock, 2005b). In general, the meandering reach is twice as deep and half as fast as the braided reach.

Spawning Habitat: To document the timing and location of spawning events, artificial substrate mats were placed on the bed of the river during the period 1994-2002 (Paragamian and others, 2001 and Paragamian pers. com., 2004). Figure 3 shows the cumulative effort, reported as the number of hours the egg mats were deployed at each monitoring location, the number of spawning events, and the spawning events per unit of effort (SEPUE), which is the number of spawning events normalized by the cumulative effort. A spawning event simply represents the presence of eggs at the specific location. Eggs found on the substrate mats were aged to identify the potential presence of multiple spawning events. Several distinct groupings of spawning locations are noticeable and are broadly associated with the outside of meander bends (Figure 4).

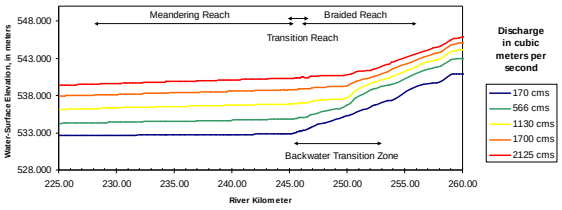


Figure 2. Simulated water-surface elevations in the study area from a 1-Dimensional flow model from Berenbrock (2005b).

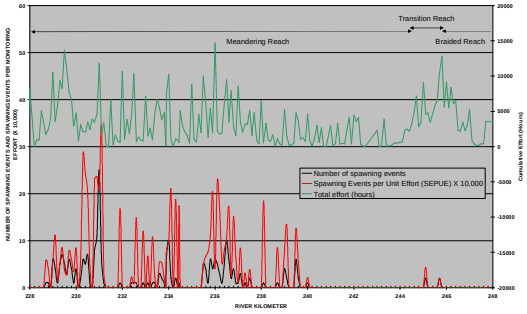


Figure 3. Location and magnitude of spawning events in the study reach

Studies of sturgeon spawning habitat in other river basins in the western United States where spawning and rearing are successful, including the Sacramento River, the Columbia River, and the Fraser River, generally describe the location of spawning sites as having relatively high velocity and a substrate that is composed of gravel and larger-sized material (Paragamian and others, 2001; Perrin and others, 2000; and Parsley and others, 1993). However, there are some site-specific differences from these idealized habitat values. Spawning sites on both the Sacramento and Fraser Rivers are associated with some sand as well as coarser material and on the Fraser River generally are located in shallower water. As previously noted, spawning sites in the Kootenai River are located in lower velocity compared to other rivers and are predominantly over sand-sized material. In all systems spawning tends to occur near the peak or descending limb of the hydrograph.

In this study we will address the paradox between the current (2005) spawning locations in the Kootenai River, even though there is a region of what appears to be a more suitable habitat for spawning in terms of higher velocity and coarser substrate a few kilometers upstream.

Channel Substrate: Several studies have been conducted to characterize the channel substrate in Kootenai River in the existing spawning reach. Barton (2004) used vibra- and piston-cores collected uniformly through the length of the Critical Habitat reach. Based on the grain-size and stratigraphy of the these cores, the river was classified into three broad zones; a sand-gravel-cobble zone in the transition reach downstream from Bonners Ferry; a buried gravel-cobble zone between 241-244.5 rkm; and a sand zone with isolated lenses of buried cobble downstream from 241 rkm. A subsequent vibra-core study in 2004 to better characterize the stratigraphy of the buried grave-cobble zone for 1D-sediment transport modeling (Berenbrock, 2005b) found that this zone is characterized by smaller lenses of buried coarse material. Figure 5 shows the locations of cores containing gravel or cobble sized material for the two studies above.

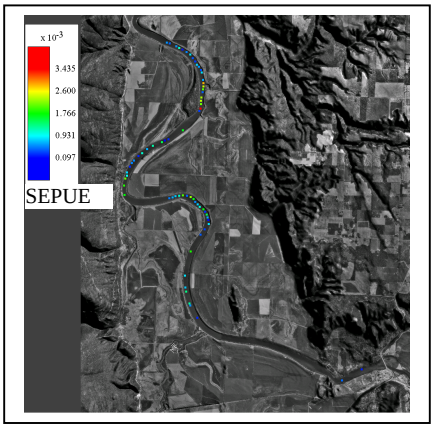


Figure 4. Spatial location of spawning events

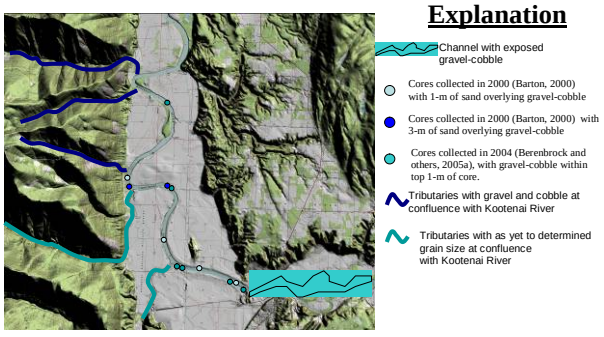


Figure 5. Location of gravel and cobble within existing spawning reach

In addition to the coring studies, informal field observations have identified that gravel-cobble sized material occurs at the confluence of three small tributaries with the Kootenai River in the downstream region of the study area (Figure 5). Presumably, periodic large floods would provide a limited supply of coarse material from these small tributaries to the river. The two larger tributaries, Deep Creek and Myrtle Creek (Figure 1), have gravel-cobble size

material in their upper reaches. However, their potential for delivering coarse material to the river is yet to be determined, particularly as both travel significant distances over the broad and relatively flat floodplain, and are backwatered by the river itself before their confluence with the Kootenai River. Clearly, the gravel-cobble substrate within both the transition and braided reaches provide a potential source of coarse material to the meandering reach. Of interest to this study is the potential of the greater magnitude and duration of pre-dam flows to expose the buried coarse substrate in the existing spawning reach.

2-DIMENSIONAL FLOW MODEL

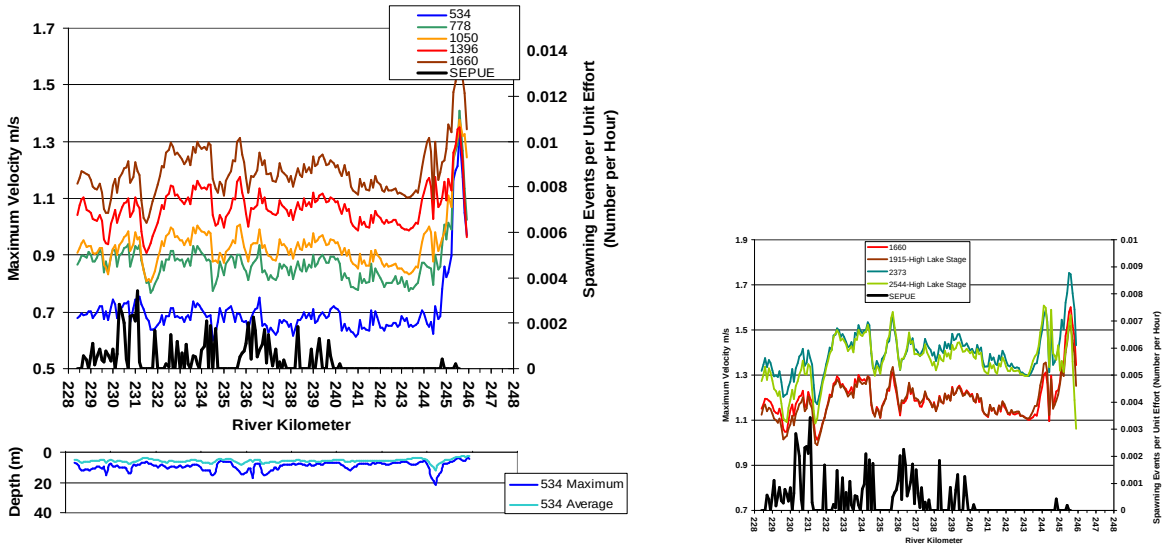
The USGS multidimensional surface-water modeling system (MD_SWMS) was used to simulate water-surface elevation, velocity, and boundary (bed) shear stress throughout the 18-rkm Critical Habitat reach (figure 1b). Subsidiary methods are used to simulate both the motion of sediment and morphologic evolution of the riverbed. MD_SWMS is a Graphical User Interface (GUI) developed by the USGS (McDonald and others, in press) for hydrodynamic models. FaSTMECH is one computational model within MD_SWMS and was developed at the USGS (Nelson and others, 2003). FaSTMECH includes a 2-dimensional, vertically averaged model and a sub-model that calculates vertical distribution of the primary velocity and the secondary flow about the vertically averaged flow. This so-called 2.5-dimensional approach has been shown to adequately simulate the velocity field, bed shear stress, and resulting patterns of erosion and deposition where secondary flows are significant, such as meander bends, without the complexity of a fully 3-dimensional model. Details of the model development, calibration and verification for the Kootenai River can be found in Barton and others (in press) .

MODEL SIMULATIONS OF VELOCITY AND DEPTH AND THE SPATIAL CORRELATION WITH SPAWNING LOCATIONS

As previously stated, one of the goals of this study is to look at the potential hydraulic cues the sturgeon are keying on for spawning site selection. A conceptual model of sturgeon spawning behavior based on hydraulic parameters in the current spawning reach might also lead to a better understanding of why sturgeon do not appear to spawn further upstream in the braided reach.

Typically, models of spawning habitat are developed based on the suitability of velocity and depth in terms of hydraulics and grainsize in terms of substrate (Parsley and others, 1993). For example, spawning suitability is generally described in terms of a range of desired magnitude for velocity or depth from values measured near the time of spawning at egg-collection locations. Spawning in any river basin typically occurs over a range of discharges, so the suitability of velocity developed in this way often reflects a wide range in velocity that to some degree simply reflects the range of discharge. The advantage of using a spatially distributed model such as the one used here is the entire river can be simulated at any particular point in time. Thus when looking at the suitability of spawning habitat based on velocity, the spatial distribution of velocity throughout the river for the discharge at the time of spawning is used rather than a range of velocity magnitude measured at various points in space and time in which discharge may substantially vary.

Model Results: Spawning in the Kootenai River during the time period 1994-2002 occurred over a range of discharges between approximately 500 – 1500 cubic meters per second (cms). To compare model simulations of depth and velocity over a similar range we picked five periods of time from the historical record where the discharge was both relatively constant for 2 or more days and fell within the range of spawning events. The solution for velocity and depth at each of the five modeled discharges was probed at an interval of 0.1 rkm along the thalweg and the minimum, average, maximum, and probed point were recorded. The maximum velocity for each of the five discharges is shown in Figure 6A along with the SEPUE and the average and maximum depth for the lowest discharge.



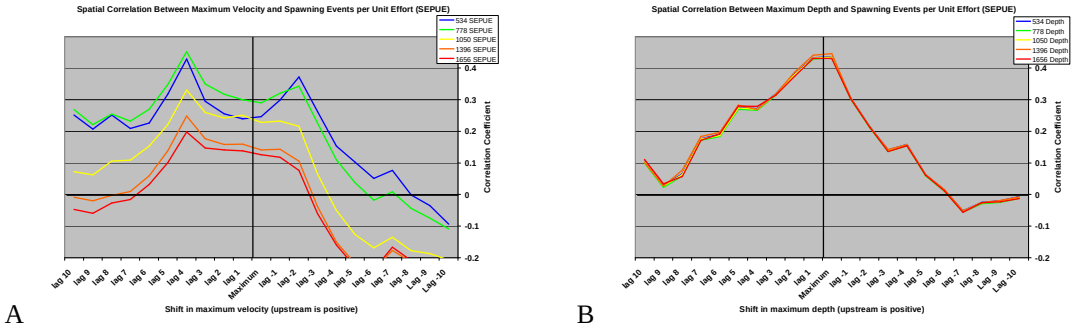
A B

Figure 6. (A) Model results of maximum cross-sectional velocity every 0.1 rkm at five discharges (the number in the explanation of each graph corresponds to the discharge value) which span the range of discharge during spawning are shown along with SEPUE. The maximum and average depth at each cross-section also is shown. (B) Model results of maximum cross-sectional velocity for simulation of discharges near the pre-dam mean annual peak flow of 2200 cubic meters per second at both high (labeled) and low Kootenay Lake stages.

Hydraulic and Habitat Spatial Correlations: Qualitatively (Figure 6A) there appears to be a positive correlation between spawning location and both high maximum velocity and high maximum depth. To test this observation we performed a spatial correlation between spawning location and maximum velocity and maximum depth by shifting velocity and depth each over a 1.0 rkm range both upstream and downstream by 0.1 rkm increments (Figure 7). The resulting correlations, reported as R^2 values and with significance at the 99^{th} percentile, while not particularly robust show broad regions of positive correlation centered on the position of maximum velocity and depth. In addition, the correlations fall off faster when shifting the velocity and depth downstream. Correlations calculated between the average velocity and average depth but not reported here, were not as conclusive. The correlation results suggest that the sturgeon are keying in on regions of highest velocity and greatest depth. This relationship has been presented in many other studies of sturgeon spawning habitat. However, in this study we present a slight modification by suggesting that there is not a particular threshold velocity or even a specific range of velocity sturgeon key on, rather, all other things considered such as sufficient discharge and temperature, they appear to key in on the highest velocity and depth within the spawning region for the given discharge that is occurring when the fish are physiologically ready to spawn. This apparent behavior suggests that fish, when ready to spawn, will seek out the best perceived location to deposit eggs given the current environmental conditions. Under current flow conditions the sturgeon must move through many of these high velocity or high depth regions before entering the braided reach.

Figure 6B shows simulated maximum velocity for four modeled discharges (values reported in figure explanation) which represent a range of flows close to the pre-dam mean annual peak flow (2200 cms) with both pre-dam high and low Kootenay Lake stages. Prior to this study it has been hypothesized that higher pre-dam Kootenay Lake stages damped velocities in the meandering reach and encouraged sturgeon to move into the braided reach. The limited number of simulations performed in this study shows that while the velocity may be slightly reduced in the meandering reach under higher lake stages compared to lower lake stages, the variability in velocity remains. However another interesting pattern emerges from the simulations; the maximum velocity in the meandering reach under the highest flows approach that of the maximum velocity in the transition reach thereby reducing the velocity contrast that exists between the two reaches at lower flows. This reduction in velocity contrast is enhanced under higher Kootenay Lake stages. Perhaps the additive affect of high discharge and high lake levels reducing the velocity contrast in the transition reach rather than reducing the velocity in the current spawning reach encouraged the fish to move up into the braided reach during pre-dam flow conditions where there was extensive suitable substrate.

Discussion of Modeling Results: Paragamian and others (2002) reported on the movement of reproductively mature Kootenai River white sturgeon from staging reaches between 203 - 216 rkm to the Critical Habitat reach (228 – 246 rkm) in the spring, within one to two weeks from the onset of spring high runoff and rising water temperatures. During the period 1994 – 1999, no tagged sturgeon were recorded upstream from Bonners Ferry in the braided reach. If the sturgeon are indeed keying on regions of high velocity, then as they move into and through the current spawning reach there are numerous potential spawning locations all of which appear to be used. In addition, at the lower flows there is a sharp velocity contrast at the boundary of the meandering reach with the transition reach and at all flows the maximum velocity is significantly higher in the transition reach. Perhaps the combination of several potential spawning locations and the sharp change in velocity at the transition zone prevent the sturgeon from moving further into the braided reach. Here our discussion is limited to the river hydraulics, however other biologic factors such as photophobia, which, with severely reduced turbidities and lighted bridges and buildings, may preclude sturgeons from migrating into the relatively shallow braided reach (M. J. Parsley, written communication, 2005).



A B

Figure 7. (A) the spatial correlation between streamwise maximum velocity and SEPUE, and (B) the spatial correlation between streamwise maximum depth and SEPUE. The lag is the shift in the velocity or depth profile respectively at 0.1 rkm increments (positive is upstream).

The results of our analysis suggest that sturgeon are spawning in the existing reach due to available habitat in the form of high velocity and depth over a range of flows. The affect of relatively high backwater conditions on velocity and depth is small, resulting in slight decreases and increases in the magnitude of velocity and depth respectively, but the spatial variability, which appears to be important based on the analysis presented here, remains intact. A possible hydraulic explanation to the lack of sturgeon spawning in the braided reach is the high velocity contrast at the boundary between the meandering reach and the braided reach. The affect of higher pre-dam discharges and Kootenay Lake levels is a damping of this contrast which may have lead spawning sturgeon to migrate up into the braided reach.

SEDIMENT TRANSPORT SIMULATIONS

The only year with measurable survival to the juvenile stage for Kootenai River white sturgeon during the post-dam period was 1974. Uniquely this year had both high discharge (~1300 cms) and relatively long duration (14 days) compared to any other year in the post-dam record (Figure 8A). Both 1991 and 1997 (Figure 8B) showed signs of some limited but unsuccessful recruitment (Duke and others, 1999). Flow regulation has long been postulated as a potential player in the lack of successful recruitment by decreasing the transport of fine-grain sand in the system and leaving potential coarse material buried. As noted previously, there are sources of suitable substrate identified in the Critical Habitat reach but most if not all is buried to some degree by sand. To explore the potential of high flows to periodically remove the sand and expose coarse gravel or a suitable substrate for egg adhesion we used the 1974 hydrograph as a test case in a sediment-transport simulation. We idealized the hydrograph to a steady-flow period of 14 days at a constant discharge of 1300 cms, corresponding to the high-flow period prior to the usual spawning season, to evaluate the spatial pattern and magnitude of erosion and deposition in the Critical Habitat reach.

Sediment-Transport Model: Details of the sediment transport model can be found in Nelson and others (2003). We note here several of the specific assumptions used in the model; the transport was assumed to be in equilibrium with the bed, a mean grain-size (0.2 mm) equivalent to the existing bed was used, only a single grain-size is considered, and we used the Engelund - Hansen total load equation to determine the transport rate.

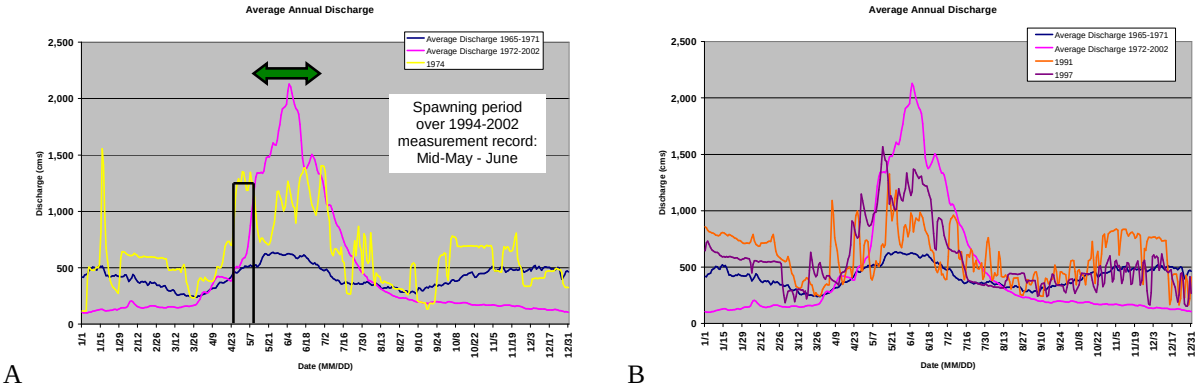


Figure 8. (A) Average discharge during the pre-dam period from 1965-1971, post dam conditions from 1972 – 2002, and 1974 hydrograph; the only year of successful recruitment in the post-dam period. The rectangular bracket shows the period and magnitude of the sediment-transport simulation. The green arrow represents the measured spawning period. (B) Avearage discharge for 1991 and 1997 each with limited recruitment.

Sediment-Transport Model Simulation: Figure 9 A-C shows the beginning, ending, and change in topography respectively for a small reach of meandering river at 234-235 rkm. This reach lies within the historically active spawning reach. Note that there is generalized scour of approximately 1 meter as shown by the negative change in elevation on Figure 9C throughout the outside of the meander bend and more locally extensive scour of up to approximately 3 meters near the apex of the meander bend. Based on the core records as shown in Figure 5 the scour would be sufficient to at least partially expose some buried gravel and cobble.

These results should be viewed with some degree of caution. While we have relatively good confidence in the pattern of scour and deposition as shown in Figure 9C, the magnitude of the change is much less certain for several reasons. As stated earlier the transport is assumed to be in equilibrium with the bed shear stress at the upstream cross-section of the model reach. However, depending on the upstream sediment supply the scour could be greater or less. The elevation of the topography at any point in time depends on the preceding history of flow and sediment supply and we started with the topography as measured at a specific point in time. The results clearly indicate the potential for flow with magnitude and duration as that in 1974 to scour the bed and expose limited patches of suitable substrate.

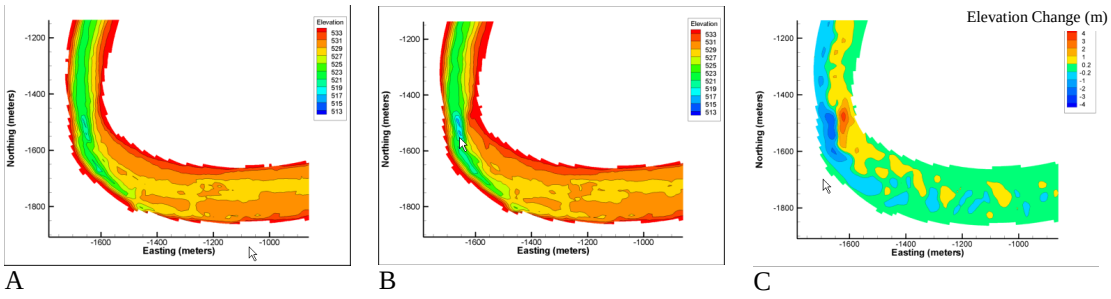


Figure 9. (A) Beginning topography, (B) ending topography and (C) change in topography for the 2-dimensional sediment transport simulation with constant magnitude of 1300 cms and duration of 14 days.

SUMMARY

Why Kootenai River white sturgeon do not spawn in the braided reach remains an open question. Based on the analysis presented here we identified that a velocity contrast exists between the relatively high velocity braided reach and the low velocity meandering reach. At the highest discharges associated with pre-dam peak flows, the difference between the existing post-dam managed flow regime and the natural pre-dam flow regime may have encouraged the white sturgeon to migrate further upstream and spawn over suitable substrate. Unfortunately, there is no historical evidence to show whether or not white sturgeon ever spawned within this reach. However, there is evidence that white sturgeon occupied areas within the braided reach, therefore spawning may have occurred here.

Our study adds to the understanding of spawning site selection in the current spawning reach. The sturgeon appear to seek the highest velocity and depth regions within the meandering reach to spawn as indicated by the spatial correlation analysis. The spatial location of these regions remains relatively constant at all flows though the region with highest velocity changes depending on the discharge. In the post-dam period most of the channel substrate in the spawning reach is composed of sand and despite the current levels of spawning, the sandy substrate likely remains a major bottleneck by increasing mortality of eggs which may require a coarser substrate to successfully incubate.

Paragamian and others (2001) noted that the Kootenai River white sturgeon use a longer reach of river to spawn than white sturgeon elsewhere. Perhaps this is an adaptation to Kootenai River where the natural variability in flow magnitude and duration from one year to another was at times sufficient to scour the bed and expose coarse substrate and depending on the downstream transport of coarse material from the locations upstream and local inputs of coarse material from tributaries, the location of suitable substrate varied from one year to another. Metapopulation theory suggests that dispersal of progeny over large areas has adaptive value to long-term persistence of populations. It is possible that the Kootenai River population of white sturgeon, once they became geographically isolated, adapted a strategy of spawning widely over marginally suitable habitats. However, human development within the Kootenai River basin has degraded these habitats. Although historically these areas may have been marginally suitable for spawning and egg incubation, they no longer are capable of providing all the requirements leading to successful hatching and production of enough free-swimming embryos to sustain the population.

REFERENCES

Barton, G.J. (2004). "Characterization of Channel Substrate, and Changes in Suspended-Sediment Transport and Channel Geometry in White Sturgeon Spawning Habitat in the Kootenai River near Bonners Ferry, Idaho, Following the Closure of Libby Dam," U.S. Geological Survey Water-Resources Investigations Report 03–4324, 102 pp

Barton, G.J., McDonald, R.R., Nelson, J.M., and Dinehart, R.L. (in Press) "Simulation of flow and sediment mobility using a multidimensional flow model for the white sturgeon critical-habitat reach, Kootenai River near Bonners Ferry, Idaho," U.S. Geological Survey Scientific Investigations Report, 100 pp.

Berenbrock, Charles, and Bennett, J.P., (2005a). "Simulation of flow and sediment transport in the white sturgeon spawning habitat of the Kootenai River near Bonners Ferry, Idaho," U.S. Geological Survey Scientific Investigations Report 2005-5173, 72 pp.

Berenbrock, Charles (2005b). "Simulation of Changes in Hydraulic Characteristics of the Kootenai River, Idaho, in Response to Alternatives of September 2005," U.S. Geological Survey Scientific Investigations Report, 10 pp.

Duke, S., Anders, P., Ennis, G., Hallock, R., Hammond, J., Ireland, S., Laufle, J., Lauzier, R., Lockhard, L., Marotz, B., Paragamian, V., Westerhof, R. (1999). "Recovery Plan for Kootenai River White Sturgeon," Journal of Applied Ichthyology. v.15, 7 pp.

McDonald, R.R., Nelson, J.M., and Bennett, J.P. (in press) "Multi-dimensional Surface-water modeling system user's guide", U.S. Geological Survey Techniques in Water Resources Investigations 11-B2, 136 pp.

Nelson, J.M., Bennett, J.P., and Wiele, S.M. (2003). "Flow and sediment-transport modeling", Tools in Fluvial Geomorphology, Wiley, England, pp.539-576.

Paragamian, V.L., Wakkinnen, V.D., and Kruse, G. (2002). "Spawning Habitat of Kootenai River white sturgeon," Journal of Applied Ichthyology, v. 18, pp. 9

Paragamian, V.L., Kruse, G., and Wakkinnen, V.D. (2001). "Spawning locations and movement of Kootenai River white sturgeon post libby-dam," North American Journal of Fisheries Management, v. 21, 11 p.

Parsley, M.J., Beckman, L.G., and McCabe Jr., G.T., (1993). "Spawning and rearing habitat used by white sturgeon in the Columbia River downstream of McNary Dam," Transactions of the American Fisheries Society, v. 122, pp. 217-227.

Perrin, C.J., A Heaton, and M.A. Laynes. (2000). "White Sturgeon (*Acipenser transmontanus*) spawning habitat in the lower Fraser River, 1999," Report prepared by Limnotek Research and Development Inc. for BC Fisheries. 72pp.